FINAL REPORT

Novel Whisker Mitigating Composite Conformal Coat Assessment

SERDP Project WP-2213

DECEMBER 2017

Dr. Stephan Meschter
BAE Systems

Distribution Statement A
This document has been cleared for public release

SERDP
DOD ▪ EPA ▪ DOE

Page Intentionally Left Blank

This report was prepared under contract to the Department of Defense Strategic Environmental Research and Development Program (SERDP). The publication of this report does not indicate endorsement by the Department of Defense, nor should the contents be construed as reflecting the official policy or position of the Department of Defense. Reference herein to any specific commercial product, process, or service by trade name, trademark, manufacturer, or otherwise, does not necessarily constitute or imply its endorsement, recommendation, or favoring by the Department of Defense.

Page Intentionally Left Blank

REPORT DOCUMENTATION PAGE

Form Approved
OMB No. 0704-0188

Public reporting burden for this collection of information is estimated to average 1 hour per response, including the time for reviewing instructions, searching existing data sources, gathering and maintaining the data needed, and completing and reviewing this collection of information. Send comments regarding this burden estimate or any other aspect of this collection of information, including suggestions for reducing this burden to Department of Defense, Washington Headquarters Services, Directorate for Information Operations and Reports (0704-0188), 1215 Jefferson Davis Highway, Suite 1204, Arlington, VA 22202-4302. Respondents should be aware that notwithstanding any other provision of law, no person shall be subject to any penalty for failing to comply with a collection of information if it does not display a currently valid OMB control number. **PLEASE DO NOT RETURN YOUR FORM TO THE ABOVE ADDRESS.**

1. REPORT DATE *(DD-MM-YYYY)*	**2. REPORT TYPE**	**3. DATES COVERED** *(From - To)*
26/12/2017	SERDP Final Report	Jan. 2012 - Dec. 2017

4. TITLE AND SUBTITLE Novel Whisker Mitigating Composite Conformal Coat Assessment	**5a. CONTRACT NUMBER** W912HQ-10-C-0052
	5b. GRANT NUMBER
	5c. PROGRAM ELEMENT NUMBER
6. AUTHOR(S) Meschter, Stephan J.	**5d. PROJECT NUMBER** WP2213
	5e. TASK NUMBER A006
	5f. WORK UNIT NUMBER
7. PERFORMING ORGANIZATION NAME(S) AND ADDRESS(ES) BAE Systems Controls 1098 Clark Street Endicott, NY 13760	**8. PERFORMING ORGANIZATION REPORT NUMBER** PM-LF-2017-12
9. SPONSORING / MONITORING AGENCY NAME(S) AND ADDRESS(ES) SERDP/ESTCP PROGRAM OFFICE ROBIN NISSAN Program Manager for Weapon Systems and Platforms 4800 Mark Center Drive, Suite 17D08 Alexandria, VA 22350-3605	**10. SPONSOR/MONITOR'S ACRONYM(S)** SERDP/ESTCP **11. SPONSOR/MONITOR'S REPORT NUMBER(S)** WP-2213

12. DISTRIBUTION / AVAILABILITY STATEMENT Approved for public release; distribution is unlimited

13. SUPPLEMENTARY NOTES

14. ABSTRACT European Union RoHS compliant commercial lead-free electronics use in DoD electronics have an increased failure risk due to tin whisker short circuits unless properly mitigated by design. The current project focused on enhancing liquid coating conformal materials and processes for tin whisker mitigation on coupons and assemblies. The project evaluated increasing strength by adding functionalized nanoparticles to rigid polyurethane coatings and improving coverage with sequential dip and spray layer processing. Coating microstructure and properties evaluations in combination with coverage assessments, environmental whisker tests, and finite element analysis were used. Successful coating rework was also demonstrated. Thicker and higher strength coating improved mitigation, but where thickness was excessive, coating cracking was observed and, solder joint thermal cycling reliability could be reduced. In addition to the new coating development, the samples from the WP1753 project were in exposed to additional simulated power cycling thermal cycling from +50 to +85C for 6,000 cycles and the polyurethane acrylate coating developed some cracks, but still had significantly better whisker mitigation than the uncoated samples .

15. SUBJECT TERMS Tin Whiskers, Conformal Coating, Coating Coverage, Coating Thickness, Short Circuits, Lead-Free Solder, Electronic Assembly, Humidity, Thermal Cycling

16. SECURITY CLASSIFICATION OF:			**17. LIMITATION OF ABSTRACT**	**18. NUMBER OF PAGES**	**19a. NAME OF RESPONSIBLE PERSON**
a. REPORT	**b. ABSTRACT**	**c. THIS PAGE**			Stephan Meschter
U	U	U	UU	179 Main report 866 Appendices	**19b. TELEPHONE NUMBER** *(include area code)* 607-770-2332

Standard Form 298 (Rev. 8-98)
Prescribed by ANSI Std. Z39.18

Page Intentionally Left Blank

SERDP WP-2213 Final Report
Novel Whisker Mitigating Composite Conformal Coat Assessment
26 December 2017

Dr. Stephan Meschter, Principal Investigator, BAE Systems

Abstract

European Union RoHS compliant commercial lead-free electronics use in DoD electronics have an increased failure risk due to tin whisker short circuits unless properly mitigated by design. The current project focused on enhancing liquid coating conformal materials and processes for tin whisker mitigation on coupons and assemblies. The project evaluated increasing strength by adding functionalized nanoparticles to rigid polyurethane coatings and improving coverage with sequential dip and spray layer processing. Coating microstructure and properties evaluations in combination with coverage assessments, environmental whisker tests, and finite element analysis were used. Successful coating rework was also demonstrated. Thicker and higher strength coating improved mitigation, but where thickness was excessive, coating cracking was observed and, solder joint thermal cycling reliability could be reduced. In addition to the new coating development, the samples from the WP1753 project were in exposed to additional simulated power cycling thermal cycling from +50 to +85C for 6,000 cycles and the polyurethane acrylate coating developed some cracks, but still had significantly better whisker mitigation than the uncoated samples.

Key words

Tin Whiskers, Conformal Coating, Coating Coverage, Coating Thickness, Short Circuits, Lead-Free Solder, Electronic Assembly, Humidity, Thermal Cycling

Supporting Investigators

BAE Systems, Endicott, NY
Modeling
Stephen McKeown

Celestica, Toronto, Ontario, Canada
Assembly soldering and coating, coverage analysis, whisker testing and inspection
Co-PI Polina Snugovsky, Ph.D.
Co-PI Jason Keeping
Eva Kosiba
Jeffery Kennedy
Marianne Romansky
Zohreh Bagheri
Andrea Delhaise

Henkel, LLC, Irvine, CA
Coating formulation development
Co-PI: David Edwards
Dale Starkey
Mario Gomez

Covestro (previously Bayer Material Science), LLC Pittsburgh PA
Nanoparticle suspension development
Co-PI Kevin Elsken
Abdullah Ekin, Ph.D.

Polymaterials AG, Kaufbeuren, Germany
Hans-Georg Herz, Ph.D
Michael Hunt

Binghamton University, Mechanical Engineering Dept., Binghamton, NY
Material characterization
Co-PI: Junghyun Cho, Ph.D.
Fei Deng
Suraj Maganty
Maria Roma
Ryan Roeder

Table of Contents

1. Extended abstract / Executive summary 1
1.1 Objectives 1
1.2 Technical approach 1
1.3 Results 2
1.4 Benefits 5
2. Structure of the document 6
3. Background 6
3.1 Industry response 7
3.2 Conformal coating whisker mitigation 8
4. Materials and methods 10
5. Summary of results and discussion 11
5.1 Overall 11
5.2 Nanoparticle suspension and coating formulation 11
5.3 Fluid properties 12
5.3.1 Viscosity 12
5.3.2 Gap flow test 13
5.4 Solid material microscopic examination 15
5.4.1 PC18M structure 15
5.4.2 PC18M with XP2742 nanosilica 16
5.4.3 PC18M with Nanophase X11102PMA nanoalumina 18
5.4.4 PC40-UMF and PC40-UMF with XP2742 Nanosilica 19
5.4.5 PC40-UMF with Polymaterials nanoalumina 20
5.4.6 Film microstructure summary 21
5.5 Solid mechanical properties results 21
5.5.1 Fluid compatibility 22
5.5.2 PC18M glass transition temperature and CTE TMA test 22
5.5.3 PC40-UMF Coefficient of thermal expansion 22
5.5.4 Water vapor transmission 22
5.5.5 Hydrolytic stability 23
5.5.6 Thermal shock 23
5.6 Nanoindentation test results 23
5.6.1 PC18M-mod baseline 23
5.6.2 PC18M + XP2742 nanosilica 24

5.7 Tensile test 25
5.7.1 PC18M with N3300 and XP2742 26
5.7.2 PC18M final coating comparison 27
5.7.3 PC40-UMF with XP2742 28
5.8 Adhesion testing 30
5.9 Assembly coating process 32
5.9.1 Dip coating 32
5.9.2 Spray process considerations 33
5.9.3 Automatic spray machine set – up 34
5.10 SEM Assembly coverage: Reference coatings 37
5.10.1 Reference coating Parylene ™ C 37
5.10.2 1B31-LOC Acrylic 39
5.11 SEM Assembly coverage: PC18M Baseline (dip + 50 micron spray) 39
5.11.1 Baseline PC18M base coating bubble observations 42
5.12 SEM Assembly coverage: PC40-UMF Baseline (dip + 50 micron spray) 43
5.12.1 PC40-UMF Batch A and B (dip+ 50 micron spray) 43
5.12.2 PC40-UMF Batch C and D spray coating, standard and high viscosity 43
5.13 SEM Assembly Coverage: Enhanced layered coating (dip + 25 micron spray + 25 micron spray) 47
5.13.1 Initial dip coating coverage 47
5.13.2 Dip + one 25 micron spray 47
5.13.3 Dip + 25 micron spray + 25 micron spray 47
5.13.4 Baseline and enhanced layered coating coverage comparison 53
5.14 Vertical cross - section thickness: PC18M Baseline (dip + 50 micron spray) 53
5.15 Vertical cross – section thickness: Enhance layered coating (dip + 25 micron spray + 25 micron spray) 60
5.15.1 Baseline and enhanced layer vertical comparison 60
5.16 Horizontal cross – section thickness: PC18M Baseline (dip + 50 micron spray) 64
5.17 Horizontal cross – section thickness: Enhanced layer (dip + 25 micron spray + 25 micron spray) 66
5.18 FE – SEM and microtome section thickness: Enhanced layer (dip + 25 micron spray + 25 micron spray) 70
5.18.1 Section one and two 70
5.18.2 Section three 77
5.19 Assembly whisker testing: PC18M Baseline (dip + 50 micron spray) 82
5.19.1 Uncoated control assembly test results 83

5.19.2 PC18M based coatings whisker test results 87
5.20 Assembly whisker testing: PC40-UMF Baseline (dip + 50 micron spray) 95
5.20.1 Baseline (dip +50 micron spray) PC40-UMF based coating whisker test results 95
5.21 Assembly whisker testing: Enhanced layered coating 104
5.21.1 Enhanced layered coating QFP board whisker growth 104
5.21.2 Enhanced layered coating BGA board whisker growth 106
5.21.3 Enhanced layered coating whisker growth discussion 109
5.22 Assembly whisker testing: Reference coatings 109
5.22.1 Parylene reference coating during baseline PC18M whisker test results 109
5.22.2 Humiseal 1B31-LOC reference coating 112
5.23 Coupon whisker test: Layered coatings 114
5.23.1 Experimental Procedure 114
5.23.2 Results 115
5.23.3 Microstructure evolution of polyurethane coated coupons with zero hours, 2,500 hours and 5,250 hours HTHH storage 117
5.23.4 Discussion 121
5.23.5 Summary of layered coating coupon whisker test results 132
5.24 Coating rework 132
5.24.1 Rework coating thickness 133
5.24.2 SEM examination after environmental exposure 135
5.25 Coating rupture modelling 137
5.26 Long term PCTC cycling 138
5.26.1 Whisker statistics discussion 139
5.26.2 Metallurgical observations discussion for uncoated 6,000 PCTC samples 140
5.26.3 Coating integrity and whisker mitigation discussion for 6,000 PCTC cycle test 143
5.27 General discussion 145
5.27.1 Whisker testing summary 145
5.27.2 Novel aspects of nanoparticle enhanced coatings 145
5.27.3 Process considerations with coatings having large viscosity changes with solvent concentration 145
5.27.4 Layered coating coverage enhancement 147
5.27.5 Potential improvements for coating stress analysis 149
5.27.6 Improvements to liquid coating technology deficiencies 149
5.27.7 Nanoparticle enhanced coating material commercial availability and adoption 150
6. Conclusions and implications 151

6.1 Whisker mitigation 151
6.2 High strength coatings and adhesion 151
6.3 Coating evaluation and test methods 151
6.4 Nanoparticle coating additions 152
6.5 Enhanced layered coating 152
6.6 Unique tin nodule microstructure evolution under coating and the importance of coating adhesion 153
6.7 Liquid coating application processes 153
6.8 Industry implementation of whisker mitigating coatings 153
7. Literature cited 155
8. Description of appendices 157

List of Figures

Figure 1: Whisker growth on an electronic assembly after environmental exposure; (A) SEM image of a whisker (see red arrow) between leads of a copper alloy lead 64 pin quad flat pack after 4,000 hours at 85 °C/85 %RH, 100x, and (B) an overall isometric optical image of the quad flat pack test board [9]. 7

Figure 2: Sources of compressive stress contributing to whisker growth. 7

Figure 3: Coating whisker mitigation modes. 8

Figure 4: Hybrid conformal coating with nanoparticles in a polyurethane matrix (segmented block copolymer). 11

Figure 5: Viscosity versus spindle speed of PC18M, PC18M+20%XP2742, PC18M+20%X11102PMA, and PC40-UMF. Measurements were made using the Brookfield small sample adaptor. 12

Figure 6: Viscosity versus total solvent percentage for PC18M and PC40-UMF. 13

Figure 7: Viscosity of coatings used in the gap flow test. 14

Figure 8: Contact angle, after one minute, of coatings used in the gap flow test. 14

Figure 9: Glass slide gap penetration experiment. 14

Figure 10: Gap filling time versus gap spacing for various viscosity PC18M and PC40-UMF coatings. 15

Figure 11: (a) AFM height image of 1 x 1 µm region of plain PC18M polyurethane coatings. (b) SEM cross-sectional image of the plain coating. 15

Figure 12: SEM cross-sectional images of cryo-fractured nanosilica filled PC18M coatings: (a) 20% XP2742, (b) 30% XP2742, (c) 50% XP2742 filled. 17

Figure 13: TEM images of polyurethane with 50% XP2742 nanosilica suspension addition; (a) particle distribution at one end of the coating, and (b) an example of the agglomeration. 17

Figure 14: Cross-sectional SEM images of polyurethane films with (a) 4% X11102PMA (b) 20% X11102PMA Al_2O_3. 18

Figure 15: Cross-sectional TEM image of nanoalumina-filled PU coating. 18

Figure 16: Cryo-fractured cross-section of a plain PC40-UMFcoating showing: (a) the entire thickness; (b) high magnification view inside the circled domain. 19

Figure 17: High resolution SEM image of cryo-fractured PC40-UMFcoating filled with 30% XP2742. 19

Figure 18: Microtome cross-section of plain PC40-UMFcoating, showing (a) entire thickness, inset: sub-micron sized void; (b) the network structure at higher magnification. 20

Figure 19: Cross-sectional overview image of WTA996 with PC40-UMF; (a) overall, (b) region of settled particles at one end of the coating, and (c) PU and nanoparticles in the settled layer. 21

Figure 20: Water vapor transmission for various XP2742 or X11102PMA concentrations in PC40-UMF and PC18M. 23

Figure 21: Nanoindentation testing results from PC18M films: (a) elastic modulus; (b) nanohardness. 24

Figure 22: Nanoindentation testing results of PC18M filled with XP2742 (nanosilica); (a) elastic modulus, and (b) nanohardness. 24

Figure 23: Nanoindentation testing results of PC18M+20% XP2742 at room temperature, 50˚C, 85˚C, and 125˚C; (a) elastic modulus, and (b) nanohardness. 25

Figure 24: A crack grown from a defect site embedded in PU film; (a) bright field optical micrograph, and (b) C-differential interference contrast (DIC) image. Arrows indicate tensile loading direction. 26

Figure 25: Effect of XP2742 (nanosilica+isocyanate) and N3300 (isocyanate) suspension on tensile properties; (a) elastic modulus, (b) yield strength, (c) tensile strength at break, and (d) percent elongation. 27

Figure 26: PC18M Stress versus strain comparison with Parylene C; (a) overall and (b) strain up to 15 percent. 28

Figure 27: Representative tensile stress-strain plots of UV-curable PC40-UMF filled with XP2742 SiO_2 suspension. For reference an unfilled PU film (PC40-UMF) case is also included. 29

Figure 28: Tensile properties of PC40-UMF family (filled with NNN2835 equivalent to XP2742, N3300); (a) Elastic modulus, and (b) Tensile strength. 30

Figure 29: Typical force versus displacement curve for the four point bend test. (PU (PC18M) on Sn shown). 31

Figure 30: Critical interface energy (Gc) for the coating to tin interface adhesion. The PU (PC18M) adhesion is considerably better than the PUA (PC40-UMF). The APTES silane treatment improved the adhesion on the PUA samples. 31

Figure 31: Dip coating process flow. 32

Figure 32: Dip coating machine; (A) Front of machine with one board shown on immersion bar and (B) boards partially immersed in the coating reservoir. 33

Figure 33: Dip coat samples on a tray in the drying chamber. 33

Figure 34: Schematic of spray process. 34

Figure 35: Coating film formation from spray coating process. 35

Figure 36: Spray coating machine; (A) Samples in the spray machine and (B) the small volume reservoir fitted to the rear of the spray machine. View (A) also shows a flat steel process control coupon centered between the boards. 35

Figure 37: Typical machine spray pattern. 36

Figure 38: Curing oven 36

Figure 39: SEM image of Parylene ™ C coated QFP44, 60x (ref. Board 2, U5, lead 24). 37

Figure 40: Optical overall cross-section image of Parylene ™ C with Adpro + coated QFP44, left lead, 25x 38

Figure 41: SEM cross-section image of the Parylene ™ C with Adpro + coated QFP44, left lead, lead tip, 150x (ref. Board 1). 38

Figure 42: SEM image of 1B31-LOC coated QFP44, 60x (ref. Board 82). Light regions are where the coating is thinner than approximately three microns. 39

Figure 43: SEM image of baseline PC18M dip + PC18M+20%X11102PMA nanoalumina 50 micron spray showing full coverage of QFP44 leads, 60x (Ref. board 28, U2, lead 23, no environmental exposure). 40

Figure 44: SEM image of baseline PC18M dip + PC18M-20%X2742 nanosilica 50 micron spray coating on QFP44 leads showing isolated thin coverage regions less than 50 microns long, 60x (ref. Board 39, U2, lead 23, image taken after thermal cycling exposure). 40

Figure 45: SEM image of baseline PC18M dip + PC18M-mod 50 micron spray on QFP44 leads showing extended thin coverage regions, 60x (ref. Board 15, U2, lead 23, 60x, image take after thermal cycling and 1000 hours of HTHH)..... 41

Figure 46: SEM image of baseline PC18M dip + PC18M-mod 50 micron spray on QFP44 leads showing extended thin coverage regions with measurements, 80x (ref. Board 11, U2, lead 12, no environmental exposure). 41

Figure 47: PC18M-mod SOT board 233 with large bubble density, 10x, after ATC+1000HTHH. The color change in the second image is an artifact of the illumination used to highlight the bubbles. 42

Figure 48: PC18M+20%X1102PMA, SOT board 226, 10x, small/no bubble density, milky appearance. 43

Figure 49: Batch A and B QFP44 SEM images of PC40-UMF coating based coating; (A) PC40-UMF dip coat, (B) PC40-UMF (no plasma between dip and spray), and the following spray coated samples with plasma etch between the dip and the spray layers: (C) PC40-UMF batch 2 with plasma, (D) PC40-UMF+10%NNN2835 nanosilica, (E) PC40-UMF+30%NNN2835 nanosilica, (F) PC40-UMF+50%NNN235 nanosilica, and (G) PC40-UMF+15.54%N3300. Image (H) shows an uncoated control board. 45

Figure 50: SEM cross – section showing separation between the PC40-UMF dip layer and PC40-UMF + 10%NNN2835 nanosilica spray layer processed with plasma etching after dip coating cure,1,000x. (ref. Board 62, QFP44, location T). Arrow highlights delamination between the dip and spray layers. 46

Figure 51: Batch C SEM image of PC40-UMF coated QFP44 leads, 40x; (A)standard viscosity (ref. Asymtech 8-2015) and (B) high viscosity coated QFP44, 40x (ref. Asymtech 8-2015). 46

Figure 52: SEM image of PC18M dip coated QFP44, board A261, with the light gray color revealing thin coating coverage areas, 30x. 48

Figure 53: Optical image showing example of coating bridging between leads on the board A261, dip only, QFP44, 25x. 48

Figure 54: SEM image of PC18M dip + two (PC18M+20%XP2742) sprays board A336, QFP64, 40x, with coating bridging. 49

Figure 55: Cross-section optical image of PC18M dip + two (PC18M+20XP2742) sprays, board A225, U1203, QFP44, lead 6-7 showing coating bridging, 100x. 49

Figure 56: SEM image of PC18M dip + 25 micron spray, QFP44, board A156, exhibiting thin coating lead edges and backside of pad as well as surface roughness, 30x. 50

Figure 57: SEM image of PC18M dip + 25 micron (PC18M+20%XP2742) spray, board A348, QFP44, thin coating on edges and vertical surfaces of the leads and the printed wiring board vias, 30x... 50

Figure 58: SEM image of PC18M dip + two 25 micron PC18M sprays, board A191, QFP44, with good overall coverage but still exhibiting surface roughness, 40x. 51

Figure 59: SEM image of PC18M dip + two (PC18M+20%XP2742) sprays, board A336, QFP44, 15KV, with good coverage on different leads than those shown in Figure 60, 60x. 51

Figure 60: SEM image of PC18M dip + two (PC18M+20%XP2742) sprays, board A336, QFP44, 15KV, good thick coverage, but arrows indicate small thin coverage areas, 40x. 52

Figure 61: Photographs illustrating the surface luster of QFP board; (A) PC18M dip only, (B) PC18M dip + two PC18M sprays, and (C) PC18M dip + two (PC18M+20%XP2742) sprays. Image B shows the increased dullness due to the high microbubble roughness of the PC18M spray layer build up. 52

Figure 62: Typical SEM image of a coating cross-section, 60x (Ref. Baseline PC18M-mod, board 12, QFP44, left lead). 54

Figure 63: Vertical cross-section thickness measurement locations. 54

Figure 64: Lead tip cross-section showing thin coverage. SEM image of baseline PC18M dip + PC18M-mod unfilled 50 micron spray, board 12, QFP44, left lead, location T, 150x and 2,000x. 57

Figure 65: Cross-section SEM view of baseline PC18M dip + PC18M-20%XP2742 nanosilica 50 micron spray coated QFP, left lead, location T, SEM, 150x (ref. Board 20)..... 58

Figure 66: Lead tip cross-section showing thicker coverage. SEM image of baseline PC18M dip + PC18M-20%X11102PMA nanoalumina 50 micron spray coated QFP, right lead, location T, 150x (ref. Board 12). 58

Figure 67: Cross-section SEM view of baseline PC18M dip + PC18M-20%X1102PMA nanoalumina 50 micron spray coated QFP, left lead, location E, 150x (ref. Board 12). 59

Figure 68: SEM cross-section image of the Parylene ™ C with Adpro + coated QFP44, left lead, location T, 150x (ref. Board 1). 59

Figure 69: Cross-section SEM image of PC18M dip only, board A179 U6 left T, 1,000x. 60

Figure 70: Cross-section SEM image of PC18M dip + PC18M spray layers on QFP44 lead tip (location T), 1000x; (A) one 25 micron spray (ref. board A012, U1, left) and (B) two 25 micron spray layers (ref. Board A191, U1, right)..... 61

Figure 71: Cross-section SEM image of PC18M dip + PC18M+20XP2742 spray layers on QFP44 lead tip (location T), 1,000x; (A) one 25 micron spray (ref. board 334 U1 left), two 25 micron spray layers (ref. board A225, U1, right)..... 61

Figure 72: Vertical section comparison of location T coating thickness for the enhanced layered coating dip + 25 micron spray + 25 micron spray for a P18M dip with PC18M spray (left) or PC18M+20%XP2742 nanosilica spray (right)..... 61

Figure 73: Enhanced layered coating vertical section thickness plots comparing dip only, dip + 25 micron spray, and dip + 25 micron spray + 25 micron spray for a PC18M dip coating and PC18M+20%XP2742 nanosilica spray coating; (A) front of lead side and (B) back side. 62

Figure 74: Vertical section comparison of the dip + baseline 50 micron spray and the enhanced layered dip + 25 micron spray + 25 micron spray for a PC18M dip coating and PC18M+20%XP2742 nanosilica spray coating; (A) front of lead side and (B) back side. 63

Figure 75: Horizontal cross-section plane location for coating thickness evaluation. 64

Figure 76: QFP44 pin numbering..... 64

Figure 77: Horizontal cross section, SEM, board 11, baseline PC18M-mod, QFP44, U1, lead 23, 200x. 65

Figure 78: Horizontal cross section, SEM, board 21, baseline PC18M+20%XP2742, QFP44, U1, lead 23, 200x..... 65

Figure 79: Horizontal cross section, SEM, board 28, baseline PC18M+20%X11102PMA, QFP44, U1, lead 23, 200x. 65

Figure 80: Horizontal cross section, SEM, board 11, PC18M-mod, QFP44, U1, lead 6, 1,000x. Back side coating coverage is four microns. 66

Figure 81: Horizontal cross-section, SEM, board 21, PC18M+20%XP2742, QFP44, U1 lead 6, 1,000x. Back side coating coverage is one micron. 66

Figure 82: Horizontal cross-section SEM image of corner leads, PC18M dip + two (PC18M+20XP2742) sprays, board A225, U3, 200x (enhancement added to highlight coating). 67

Figure 83: Cross-section SEM image of PC18M dip + two (PC18M+20XP2742) sprays, board A225, U3, lead 6; (A) 200x, and (B) upper back corner, 900x (enhancement added to highlight coating). 68

Figure 84: Cross-section SEM image of PC18M dip + two (PC18M+20XP2742) sprays, board A225, U3, lead 28; (A) overall, 200x, and, (B) back center and bottom corner, 900x (enhancement added to highlight coating). 69

Figure 85: QFP from board A225 examined using microtome sectioning. 70

Figure 86: Schematic showing microtome section locations. 70

Figure 87: Microtome section perpendicular to lead schematic; (A) materials and (B) locations examined. 71

Figure 88: FE – SEM images of microtome sections (A) section one, and (B) section two. The lighter coating color is the nanoparticle spray layer. Note that there is a dip coating web on the right side of the image (B) lead. 72

Figure 89: FE – SEM of microtome section one at higher magnification; (A) top and (B) bottom. 73

Figure 90: FE – SEM of microtome section two at higher magnification; (A) front and (B) back. 74

Figure 91: FE – SEM of microtome section two right back along the dip coating web to the adjacent lead. Arrow highlights particle filled spray coating droplets on the dip coating. 75

Figure 92: High magnification FE – SEM images of microtome section two front showing particle uniformity and a well adhered knit line between the two spray layers. 75

Figure 93: High magnification FE – SEM images of microtome section top of lead showing spray coating to dip coating interface. 76

Figure 94: Section one dip coat and spray coating thicknesses. 76

Figure 95: Section two dip coat and spray coating thicknesses. Note that a coating bridge between leads prevented measurements on the right side of the lead. 77

Figure 96: Microtome section three examination areas 78

Figure 97: Overall FE – SEM image of microtome section three lead and coating. 78

Figure 98: Typical FE – SEM image showing uniform particle distribution (Area C base shown). 79

Figure 99: Section three Area A FE – SEM image; (A) top, and (B) bottom. 80

Figure 100: Section three Area B FE – SEM image; (A) overall, (B) front, and (C) back with arrows showing the first spray layer covered by the second spray layer. 81

Figure 101: Section three Area C FE – SEM image; (A) overall, (B) back of lead, (C) second location on back of lead with arrow indicating spray coating drop covered with additional spray coating. 82

Figure 102: SEM image of an uncoated SOT6 lead, ATC, 180x (ref. board 237). Whiskers growing from top and lower solder fillet regions. 83

Figure 103: SEM image of an uncoated SOT6 lead, ATC, 1,000x (ref. board 237). 84

Figure 104: SEM image of an uncoated SOT5 lead (lead 2), ATC+ HTHH1000, 100x (ref. board 238). Corrosion near the bottom of the joint and whisker growth from the boundary between tin grains were observed. 85

Figure 105: SEM image of an uncoated QFP44 lead, ATC+HTHH2000, 100x (ref. board 46). 86

Figure 106: SEM image of uncoated QFP64 lead toes, HTHH2000, 100x (ref. Board 48). 86

Figure 107: SEM image of an uncoated QFP64 lead whisker growth, HTHH2000, 1500x (ref. Board 48). 87

Figure 108: SEM image of PC18M-mod coated SOT6 leads, ATC. 60x, small bubble density (ref. Board 211). 88

Figure 109: SEM image of PC18M-mod coated QFP44 leads, ATC, U2, Lead 17, 80x, large bubble density (ref. Board 34). 88

Figure 110: SEM image of PC18M-mod coated QFP44 leads, U2, Lead 14-15, ATC + 1000HTHH, 60x, small bubble density (ref. Board 15). 89

Figure 111: SEM image of PC18M-mod coated SOT package and leads, ATC+ HTHH1000, 40x (ref. Board 233). Large bubble density condition causing the coating to obscure the SOT leads. 89

Figure 112: SEM image of PC18M-mod coated SOT6 lead (lead 3), ATC + 2000HTHH, 150x, small bubble density (ref. Board 215). 90

Figure 113: SEM image of PC18M+20%XP2742 nanosilica coated SOT6 leads, ATC, 60x, medium coating bubble density (ref. Board 217). 91

Figure 114: SEM image of PC18M+20%XP2742 nanosilica coated chip resistor, ATC, 80x, medium coating bubble density (ref. Board 217). 91

Figure 115: SEM image of PC18M+20%XP2742 nanosilica coated SOT3 lead (lead 2), ATC+HTHH2000, 100x and 300x, medium bubble density (ref. Board 235). 92

Figure 116: SEM image of PC18M+20%XP2742 nanosilica coated SOT6 leads, ATC+ 2000HTHH, 40x, medium bubble density (ref. Board 235). 93

Figure 117: SEM image of PC18M+20%X11102PMA nanoalumina coated SOT6 leads, ATC, 60x, small/no bubble density (ref. Board 222). 93

Figure 118: SEM image of PC18M+20%X11102PMA nanoalumina coated SOT6 lead, ATC + 2000HTHH, 40x, small/no bubble density (ref. Board 228). 94

Figure 119: SEM image of PC18M+20%X11102PMA nanoalumina, SOT6, lead 4 (center lead from Figure 113), ATC+HTHH2000, 100x, small/no bubble density (ref. Board 228). 94

Figure 120: SEM image of baseline PC40-UMF coated QFP44 lead, HTHH1767, 90x (ref. Board 60). A discontinuous film of discrete droplets and coating pull – away from the metal were observed. 96

Figure 121: SEM image of baseline PC40-UMF coated QFP44 lead, HTHH1767, QFP44, 1,000x (ref. Board 60). Higher magnification view of coating pull away. 97

Figure 122: SEM image of baseline PC40-UMF coated QFP44 lead side, HTHH1767, QFP44, U4, lead 12, 1,000x (ref. Board 60). 97

Figure 123: SEM image of baseline PC40-UMF coated SOT5 leads, HTHH1767, U01, 40x (ref. Board 256). 98

Figure 124: SEM image of baseline PC40-UMF coated SOT6 leads, HTHH1767, 40x (ref. Board 256). 98

Figure 125: SEM image of baseline PC40-UMF+10%NNN2835 nanosilica coated QFP64 lead toe, HTHH1767, 700x, (ref. Board 65). 99

Figure 126: SEM image of baseline PC40-UMF+10%NNN2835 nanosilica coated SOT3 leads, HTHH1767, U06, 40x (ref. Board 284). 100

Figure 127: SEM image of baseline PC40-UMF+10%NNN2835 nanosilica coated SOT6 lead, HTHH1767, U65, lead 2, 300x (ref. Board 284). 100

Figure 128: SEM image of baseline PC40-UMF+10%NNN2835 nanosilica coated SOT6 lead, HTHH1767, U65, lead 2, 4,500x (ref. Board 284). 101

Figure 129: SEM image of baseline PC40-UMF+30%NNN2835 nanosilica coated QFP44 lead, HTHH1767, U5, lead 44, 120x (ref. Board 70). 101

Figure 130: SEM image of baseline PC40-UMF+30%NNN2835 nanosilica coated QFP44 lead, HTHH1767, U5, lead 44, 1800x (ref. Board 70). 102

Figure 131: SEM image of baseline PC40-UMF+30%NNN2835 nanosilica coated QFP44 lead, HTHH1767, U5, lead 44, 4,000x (ref. Board 70). 102

Figure 132: SEM image of baseline PC40-UMF+30%NNN2835 nanosilica coated SOT5 leads, HTHH1767, U04, 40x (ref. Board 269). 103

Figure 133: SEM image of baseline PC40-UMF+30%NNN2835 nanosilica coated SOT5 lead, HTHH1767, U15, lead 5, 250x (ref. Board 269). 103

Figure 134: Uncoated board 48 QFP64 after 2,000h of HTHH; (A) 100x and (B) 1,500x. 104

Figure 135: SEM images comparing layer coated unfilled PC18M spray and PC18M+20%XP2742 nanosilica filled sprays in the dip + two 50 micron spray QFP44 parts after HTHH testing for 3,030h. Images (A) (B) (C) are of unfilled PC18M dip + two unfilled PC18M sprays (board A023) and images (D) (E) (F) are of unfilled PC18M dip + two (PC18M+20%XP2742) nanosilica filled sprays (board A347). Image magnifications are: (A) (D) overall lead at 40x, (B) (E) lead top at 100x, and (C) (D) lead bottom at 100x. 105

Figure 136: SEM images of PC18M+20%XP2742 nanosilica spray layered coated BGA pads with increasing number of layers at various magnifications after HTHH testing for 3,030h.(A) (B) (C) dip, (D) (E) (F) dip + one spray, and (G) (H) (I) dip + two sprays with (A) (D) (G) 40x, (B) (E) (H) 180x and (C) (F) (I) 2,500x. 106

Figure 137: SEM images of layered coated BGA pads with increasing number of layers for unfilled PC18M sprays and PC18M+20%XP2742 nanosilica filled sprays after HTHH testing for 3,030h, 180x. (A) (B) (C) unfilled spray run and (D) (E) (F) nanosilica filled spray run with (A) (D) dip, (B) (E) dip + one spray, and (C) (D) dip + two sprays. Image (A) unfilled PC18M dip processed with unfilled PC18M spray run (U808, B3, Board A377), (B) unfilled PC18M dip + two unfilled PC18M spray (U606, A2, Board A307), (C) unfilled PC18M dip + two unfilled PC18M sprays. (U501, A1, Board A296), (D) unfilled PC18M dip processed with the PC18M+20%XP2742 nanosilica filled spray run (U508, G3, Board A596), (E) unfilled PC18M dip + one (PC18M+20%XP2742) nanosilica filled spray (U805, K1, Board A593), and (F) unfilled PC18M dip + two (PC18M+20%XP2742) nanosilica filled sprays (U501, A1, Board A392). Note that the image (H) bright spot is debris and the dark spot is a hole. 107

Figure 138: SEM image and electrodispersive x-ray (EDX) analysis of some nodules found on BGA pads from board A377, PC18M dip only. Note that the nodules in locations one and two are Ag_3Sn intermetallic with the surrounding Sn corroded away. 108

Figure 139: SEM image of Parylene™ C SOT3 leads, ATC + 2000HTHH, 40x (ref. Board 209).... 110

Figure 140: SEM image of Parylene™ C with Adpro+ coated SOT6 leads, ATC+ 2000HTHH, 40x (ref. Board 206)..... 110

Figure 141: SEM image of a Parylene™ C & Adpro+ coated SOT3 lead, ATC+HTHH1000, 100x and 350x (ref. Board 204). Small coating crack evident at lead-to-package interface. 111

Figure 142: SEM image of 1B31-LOC acrylic coated QFP44 lead, HTHH1767, U5, lead 44, 120x (ref. Board 85)..... 112

Figure 143: SEM image of 1B31-LOC acrylic coated QFP44 lead, HTHH1767, U5, lead 44, 1,200x (ref. Board 85)..... 113

Figure 144: SEM image of 1B31-LOC acrylic coated QFP44 lead, HTHH1767, U5, lead 44, 4,000x (ref. Board 85)..... 113

Figure 145: (a) Schematic of a panel showing 18 individual tin-plated copper coupons attached with break-off tabs. (b) An individual coupon photograph. 114

Figure 146: SEM images of whisker growth (a) uncoated region thin whisker formation (initial stage) at 1500 hours HTHH storage, and (b) thin coverage vs. uncoated regions of the same coupon. 116

Figure 147: Over cross – sections of 20 micron thick PU conformal coating with (a) 0 hours HTHH storage, (b) 2,500 hours storage, and (c) 5,250 hours storage..... 118

Figure 148: Zero hour cross – section SEM image of 20 micron thick unfilled PU; (a) overall view with various regions labelled (b) delamination between the coating and the tin indicative of poor adhesion, and (c) interfacial Cu_6Sn_5 formation noted between tin and copper. 119

Figure 149: Cross – section SEM image of 20 micron thick unfilled PU following 2,500 HTHH storage; (a) Cross – section of coating-tin-copper with revealed space (in box) between coating and tin (b) Close-up SEM image of delamination at coating-tin interface and attached tin on coating. 119

Figure 150: Cross – section SEM BSE images of IMC particles within tin under 20 micron PU; (a) 2,500 hours HTHH storage and (b) 5,250 hours storage; showing larger IMCs with time and interface IMC thickening. 120

Figure 151: 5,250 hours HTHH storage coupon cross – section with various key features labelled.. 121

Figure 152: Cross – section examination of a representative coating-tin-copper interface in a coupon coated with 20 micron PU following 5,250 hours HTHH storage; (a) BSD image and (b) EDS spectrum obtained from the top (brighter) tin layer, and (c) EDS spectrum obtained from the bottom (darker) tin layer..... 123

Figure 153: Cross – section SEM images of seven micron thick PC18M+30%XP2742 over bright tin on copper after 2,500 hours 60°C/60%RH (Celestica cross – section of the cantilever beam coupon); (a) SE image with yellow arrow shows coating delamination from tin and red arrows shows fracturing in the tin region below the coating and (b) BSE image showing the Cu_6Sn_5 intermetallic formation near the coating surface. 124

Figure 154: SEM cross – section image of a protrusive tin growth beginning to impinge on the conformal coating. 125

Figure 155: SEM cross – section images of tin growth under coating; (a) example of two well-developed protrusive growths from tin being deflected laterally by a conformal coating and (b) left branch of lateral growth from location ‘1’ in (a)..... 126

Figure 156: A mechanism of lateral protrusive tin growth from electroplated tin on copper substrate. 127

Figure 157: (a) Representative SEM cross – section of PU coated coupon following 4,000 HTHH storage and (b) a high magnification image of the well-adhered coating-tin interface. 128

Figure 158: Coating-tin interface in 4,000 hour HTHH storage coupon cross – section with oxide layer visible. 129

Figure 159: Thickness measurements of primary tin plating and interfacial IMC formation from zero to 5,250 hours HTHH storage. 130

Figure 160: Representative cross – sectional microstructure developments in coated tin coupons following 4,000 hour HTHH storage; (a) 20 micron thick PC18M + 20%XP2742 nanosilica and (b) 20 micron thick unfilled PUA. 131

Figure 161: Cross – sectional microstructure development in a bilayer (filled PU on unfilled PU) coated coupons following 4,000 hour HTHH storage; (a) Tin plating on copper with secondary (lateral) growth and IMC formation and (b) Magnified view of unfilled and filled coatings with deformation noted at protrusion sites. 131

Figure 162: Coating thickness measurement locations. 133

Figure 163: Optical cross-section image, unfilled PC18M QFP-A023 U1002, Lead 6 measurement, location C, 500x. Coating thickness was 10.5 microns..... 133

Figure 164: SEM cross-section image, filled PC18M+20%XP2742 QFP-A312 U902, Lead 6 measurements, location B, 1,930x. Coating thickness was 3.4 microns..... 134

Figure 165: Individual value plot comparing rework coating thickness by location, lead and side (front/back) for unfilled PC18M and filled PC18M+20%XP2742 (PC18M+NanoSi)..... 134

Figure 166: Box plot comparing rework coating thickness by lead and side (front/back) for unfilled PC18M and filled PC18M+20%XP2742 (PC18M+NanoSi). 135

Figure 167: SEM BSE filled PC18M+20%XP2742 QFP-A312 non-reworked U903 adjacent to U902 pins 23 to 26, 67x. 136

Figure 168: SEM image of the PC18M+20%XP2742 brush coat reworked QFP after 100 -55 to +125°C thermal cycles and 10 days of MIL-STD-810 humidity, 69x (ref. Board A312 U902 pins 1 to 3). Note some cracks present in reworked coating adjacent to leads. 136

Figure 169: Coating strength required versus coating thickness. 137

Figure 170: Cantilever beam coupon SEM inspection of thin coating region, areas after 2,500 (500+2,000) hours 60°C/60%RH showing a tin nodule under thicker coating and tin eruptions through thin coating. 138

Figure 171: Cantilever beam coupon longitudinal cross-section through thin coating region areas after 2,500 (500+2,000) hours 60°C/60%RH; (a) and (b) eruption through three micron coating, (c) cross-section region on sample, (d) nodule under seven micron coating and (e) nodule under 30 micron coating. The thinner coating areas had smaller nodule diameters. 138

Figure 172: Box plot comparing whisker length (microns) after 1,797 and 6,000 PCTC cycles for lead alloy, part contamination and board contamination combinations; (A) 1,797 PCTC cycles and (B) 6,000 PCTC cycles. 139

Figure 173: SOT3 maximum whisker length for the three last PCTC inspection intervals. 140

Figure 174: Competing mechanisms of stress relaxation (SOT3, 0-0 contamination level after 1,797 PCTC cycles shown). 141

Figure 175: High magnification SEM image comparison of whisker growth at 1,797 and 6,000 cycles SOT6 (A) after 1797 cycles, and (B) after 6,000 cycles 2,500x (ref. Image B A-SOT-PC-1-0-ncc-3, SOT6, U71, lead 4). 141

Figure 176: Close up SEM image of grain boundary slip regions, cracks, grain recrystallization, and whisker growth after 6,000 cycles on a SOT3 lead region with increasing amount of solder cracking; (A) no cracks, 3,000x, (B) small cracks, 2,500x and (C) large crack, 3,000x (ref. A-SOT-PC-1-1-ncc-1, SOT3, U31 lead 1 and A-SOT-PC-1-0-ncc-1, SOT3, U27, lead 3). 142

Figure 177: SEM image of the SOT3, U20, lead 1, no conformal coating, 1-0 contamination level after 6,000 PCTC cycles; (A) 100x and (B) high magnification image of pad edge growth highlighted by arrow, 1,000x (ref. A-SOT-PC-1-0-ncc-3)..... 142

Figure 178: Close up SEM image of growth after 6,000 cycles along the grain boundary on the front of a SOT3 lead, 3,000x, (ref. A-SOT-PC-1-0-ncc-1, SOT3, U27, lead 3). 142

Figure 179: Higher magnification SEM image of coating on right SOT6 lead shown in Appendix N after 6,000 PCTC cycles, 1,000x. Some whisker nucleation is evident (ref. B-SOT-PC-1-1-cc-3, SOT6). 143

Figure 180: Higher magnification SEM image of coating on a SOT6 lead from board 2 with interdendritic solder spaces filled with coating and no whiskers 6,000 cycles , 1,000x (ref. B-SOT-PC-1-1-cc-2, SOT6). 144

Figure 181: SEM image of coating on SOT6 leads from board 2 after 6,000 PCTC cycles, 45x (ref. B-SOT-PC-1-1-cc-2, SOT6). Arrows highlight coating cracks near the lead knee. 144

Figure 182: SEM image of the three layer PC18M dip with two PC18M sprays, board A191, QFP44, with good overall coverage but still exhibiting surface roughness, 40x. 146

Figure 183: PC18M-mod SOT board 233 with large bubbles around the leads, 10x (note the photograph was taken after thermal cycling and 1,000 hours of 85°C/85%RH humidity (ATC+1000HTHH) environments). The color change is an artifact of the illumination used to highlight the bubbles. 146

Figure 184: Coating film formation from spray coating process. 147

Figure 185: Spray drop deposition resulting in bubbles in the coating; (A) three deposited drops, (B) a fourth drop deposited on top of the initial three trapping some gas, (C) drop coalescence with a small entrained bubble, (D) multiple groups of the coalesced drops containing small bubbles, (E) during the heated portion of the cure there is a coalescence of small bubbles into larger bubbles, and (F) with drier films, having a higher some bubbles escape but the coating surface does not smooth out. 147

Figure 186: Cross-section view of coated QFP lead (a) one layer with thin coating on corners and (b) multiple layers with increased buildup around corners. 148

List of Tables

Table 1: Summary of PC18M+XP2742 glass transition temperature, coefficient of thermal expansion and hardness 22

Table 2: Batch A and B assembly coating thickness observations of PC40-UMF, PC40-UMF+NNN2835 and PC40-UMF+N3300 from cross-sectioning. (Note NNN2283 is equivalent to XP2742) 44

Table 3: QFP44 SEM baseline and enhanced layered coating coverage inspection results. 53

Table 4: Coating thickness measurements for baseline (PC18M dip + 50 micron spray) process PC18M based coatings on QFP44 leads. 55

Table 5: Baseline (PC18M dip + 50 micron spray) PC18M based coated QFP44 minimum and maximum thicknesses from Table 4. 56

Table 6: PC40-UMF base coating assembly whisker inspection summary. 95

Table 7: 1B31-LOC acrylic reference coating assembly whisker inspection summary. 112

Table 8: Coating types for the 10, 20 and 50 micron schemes 115

Table 9: Coating types for the bilayer 10 + 10 micron thickness scheme 115

Table 10: Compiled summary of the PU, PUA and PU+nanosilica coating performance at various time-steps 117

List of Appendices

Appendix A: List of Scientific/Technical Publications

Appendix B: Suspension and Coating Formulation

Appendix C: Coating Evaluation Methods

Appendix D: Coating Characterization Results

Appendix E: Assembly Test Vehicle Coating Process

Appendix F: Coating Coverage Baseline Results

Appendix G: Coupon Whisker Testing for Baseline Coating Process

Appendix H: Assembly Whisker Testing for Baseline Coating Process

Appendix I: Coating Coverage Layered Coating Results

Appendix J: Layered Coupon Whisker Testing

Appendix K: Assembly Whisker Testing for Layered Coating Process

Appendix L: Rework Evaluation

Appendix M: Coating Tin Whisker Mitigation Modeling

Appendix N: Simulated Power Cycling Thermal Cycling (PCTC)

Acronyms

Acronym	Definition
AFM	Atomic Force Microscope
Alloy-42	Fe42Ni composition lead material (composition is in weight percent)
ATC	Accelerated Thermal Cycles
BGA	Ball Grid Array
BSD	Back Scatter Detector
CALCE	Center for Advanced Life Cycle Engineering, University of Maryland
COTS	Commercial-off-the-Shelf
cps	Centipoise
CTE	Coefficient of Thermal Expansion
DoD	Department of Defense
FE – SEM	Field Emission SEM
HDI	Hexamethylene diisocyanate
HTHH	High Temperature High Humidity
IMC	Intermetallic
IPC	IPC Association Connecting Electronics Industries
IR	Infra-Red
MDI	Methylene diphenyl diisocyanate
MPa	Mega Pascal
OEM	Original Equipment Manufacturer
OSE	Odd Shaped Eruptions
PCTC	Simulated power cycling thermal cycling
PMA	Propylene glycol methyl ether acetate
PU	Polyurethane
PUA	Polyurethane acrylate
QFP	Quad-flat-pack Electronic Packages
RH	Relative Humidity
RoHS	Reduction of Hazardous Substances
SAC	Sn-Ag-Cu alloy lead free solder
SAE	Society of Automotive Engineers
SCS	Specialty Coating Systems Company
SDS	Chemical Safety Data Sheet
SEM	Scanning Electron Microscope
SERDP	Strategic Environmental Research and Development Program
SMT	Surface Mount Assembly
SMTA	Surface Mount Technologies Association
SOT	Small Outline Transistor Electronic Packages
TMA	Thermomechanical Analysis
TEM	Transmission Electron Microscope
UV	Ultraviolet
VOC	Volatile organic compound

Acknowledgements

The investigators wish to thank the Strategic Environmental Research and Development Program (SERDP) office for providing funding for this research and David Kayser, NAVAIR, for being the project Department of Defense (DoD) technical point of contact and for his military electronics systems perspective on the tin whisker research.

In addition, the principle investigator would like to thank S. Cronk from BAE Systems for her administrative and cost tracking efforts and V. Gordon from BAE Systems, for her help compiling the final report. Further, this program would not have been successful without the lab support of Z. Bagheri, David Yang, and A. Delhaise from Celestica for assembly sample inspection, cross – sectioning, and whisker photo documentation and the data compilation. Also, thanks go out to R. Brush from Celestica for supporting the many months of thermal cycling testing.

They also appreciate the efforts by the Binghamton University graduate students, F. Deng, S. Maganty, M. Roma and R. Roeder, for the extensive coupon whisker testing, coating characterization, microtome sectioning, field emission scanning electron microscopy, and transmission electron microscopy needed to examine the nanoparticles in the coating films. The investigators would also like to thank Dr. Eric Chason and F. Pei from Brown University for their attempts at trying to measure coating stress on the tin surface.

The investigators would also like to thank Dr. Cotts from the Binghamton University Physics Department for rolling the SnAgCu+Ce coupon foils, Dr. Kumar from Specialty Coating Systems for Parylene™ coating the test assemblies, and R. Adcock from BAE Systems, for Parylene™ coating the pull test samples. The investigators also appreciate the work done by L. Snugovsky, University of Toronto, on ion beam milling and SEM microscopy of the various cross-sections. The investigators would also like to thank, W. Rollins, Raytheon Retired, H. Leidecker, J. Brusse, and L. Panashchenko from NASA Goddard, Dr. Boettinger, Dr. Williams, Dr. Gilman, Dr. Holmes, and Dr. Lin from NIST in Gaithersburg MD, and Dr. Michael Osterman from the University of Maryland CALCE center for their thoughtful discussions throughout this project.

1. Extended abstract / Executive summary

1.1 Objectives

An electronic assembly is created by integrating thousands of parts from multiple suppliers utilizing a host of circuit card manufacturing processes. With the lead elimination from electronics resulting from the European Union Reduction of Hazardous Substances (RoHS) legislation, many of the heritage aerospace and defense commercial – off – the – shelf solder materials with tin – lead have become obsolete. Most notably there has been an increasing cost and schedule pressure to use commercially available pure tin part finishes and lead – free solders in Aerospace and Defense electronic systems.

Since these materials have an increased tendency to grow tin whiskers that can cause short circuit failures and decrease reliability, original equipment manufacturers are relying on multiple mitigation methods to manage the tin whisker risk. One of the main mitigations is the use of conformal coating to prevent tin whisker electrical shorting. Current widely used low cost coating spray processes used for humidity protection generally provide incomplete coverage and insufficient coating thickness for whisker mitigation or no coating at all on many tin surfaces. The most challenging areas are the back side of the leads, vertical surfaces and edges. There are vapor deposited coatings that provide complete coverage, but have yet to demonstrate complete whisker mitigation, are difficult to repair, and have a high manufacturing cost.

There continues to be increasing risk to DoD systems reliability and affordability due to the growing gap between consumer electronics designs and DoD electronics needs. The DoD benefits greatly by using consumer parts directly or using them with modification. Environmental compliance, cost, and miniaturization continually drive consumer designs, reducing unnecessary design margins, as long as the relatively short consumer warrantees are satisfied. As a result, significant DoD risk associated continues to accumulate and evolve with lead-free, conversion to greener chemistry, and other design changes accompanying each generation of consumer electronic parts and materials.

The main objectives of project were to (1) develop and evaluate nanoparticle filled conformal coatings designed to provide long term whisker penetration resistance and coverage on tin rich metal surfaces prone to whisker growth in modern DoD electronic assemblies containing commercial lead-free consumer electronics, (2) utilize enhanced liquid coating application processes to improve coverage, (3) perform fundamental studies into the mechanisms by which conformal coatings provide tin whisker penetration resistance and inhibit nucleation/growth, and (4) evaluate coating reworkability. An objective added later was to evaluate the impact of long term simulated power cycling thermal cycling on coating whisker mitigation.

1.2 Technical approach

Desired coating qualities that will exhibit superior whisker mitigation include complete coverage, high strength to buckle whiskers and/or high elongation prior to breaking to capture whiskers within the coatings. The key elements being evaluated are (1) coating and particle chemistry, (2) coating microstructure and mechanical properties enhancement, (3) coverage quality, (4) layered coating application, (5) coating rupture resistance on whisker test samples, and (6) reworkability. Coating microstructural evaluation, nanoindentation, tensile, and adhesion testing were used to characterize the coatings and select candidates for lead – free electronic assembly coating and testing. Finite element modeling was used in conjunction with the experimental observations and the measured coating properties to determine when coatings are expected to rupture from tin whisker or tin nodule growth.

Nanoparticle suspension and coating formulation: For the coating development activity, the base coating was selected to be a polyurethane based chemistry that meets the requirements of IPC-CC-830 and MIL-I-46058. The nanoparticle filled coating development began with making a suspension with

functionalized nanoparticles which could covalently bond to the polyurethane matrix. A basic challenge with functionalized nanoparticles is preventing particle agglomeration and keeping them dispersed. After the suspension was mixed into the base material and cured, the nanoparticle surface modification bonding sites would tightly bind the particles to the resin matrix and have uniform dispersion without agglomeration. The initial evaluation of the suspension chemistry, particle size and loading was based on viscosity, transparency and pot life. Select suspensions were mixed with the base coating and cured films were fabricated for microstructural evaluation using the atomic force microscope, microtome sectioning, cryo-fracturing, scanning electron microscope examination, and transmission electron microscopy to assess nanoparticle agglomeration and resin adhesion. Then sample coupons were developed to facilitate nanoindentation and mechanical testing in order to determine the particle loading that yielded optimal tensile and elongation properties for whisker mitigation.

Coating application process enhancement and whisker mitigation evaluation: For the process evaluation effort, dip coating and spray coating process were used as the baseline coating application method since it provided good coverage and manufacturability. The experimental and analytical assessment evaluated various thicknesses and layer combinations of filled and unfilled coatings on idealized coupons and real electronic assemblies. The coverage and thickness on various metal features were assessed using scanning electron microscopy and cross-sectioning. In addition, whisker penetration resistance was assessed using high whisker propensity coupons and the lead – free assemblies developed in SERDP project WP1753 in traditional high temperature/high humidity and thermal cycling. These assemblies were also evaluated for coating reworkability after the layered coating tin whisker environmental high temperature high humidity testing.

Extended power cycling thermal cycling (PCTC): The approach used to evaluate the extended power cycling thermal cycling test assemblies from the SERDP WP1753 project was to first perform an inspection of the assemblies remaining at the of the original 1,797 cycle test (note that the longest whiskering samples were cross – sectioned). The initial inspection recorded whisker growth statistics on uncoated and coated assemblies as well as the condition of the conformal coating. Additional thermal cycling was performed until a total of 6,000 cycles was accumulated, then a final inspection was performed. The whisker statistics will contribute to the current database of over 120,000 whiskers counted in the total WP1753 project.

1.3 Results

Nanoparticle suspension and coating formulation: Two IPC-CC-830 conforming base coatings that had polyurethane isocyanate functionality were selected. The first was a moisture cure solvent thinned polyurethane (PU – PC18M from Henkel). The second was a moisture and ultraviolet (UV) dual cure 100% solids low volatile organic compound (low VOC) polyurethane acrylate (PUA – PC40-UMF from Henkel). The nanosilica and nanoalumina particle suspension were evaluated. The nanosilica suspension with a 20 nm particle size (XP2742 from Covestro) was superior in many respects to the nanoalumina suspension. It had good shelf life, particle size uniformity, particle isocyanate functionality, particle size uniformity, and particle dispersion. Upon mixing into the base coatings, the nanosilica had good particle dispersion with little agglomeration, good particle bonding to the polyurethane matrix, and it increase the coating strength. The disadvantage of using the XP2742 is that the addition of silica brings a certain amount of N3300 Hexamethylene diisocyanate, HDI, trimer along with it. And while this HDI functionality easily reacts with both the PC18M and PC40-UMF systems, it brings physical properties that are different from the base formulations, which may or may not be desirable. When the XP2742 was mixed with the PC18M, some Dabco T 12 was needed to accelerate the cure slightly to maintain a 2 hour cure. This was also added to the PC18M and called PC18M-mod.

The nanoalumina particles were not functionalized, had poor pot life after mixing with the PU, a broad particle size distribution and upon mixing with the PU had particle agglomeration and did not increase the PU strength. Even though the nominal particle size was 40 nm according to the specification data,

the average particle diameter was confirmed to be about 70 nm, with a range from 20 to 200 nm. During spray trials the nanoalumina had somewhat better coverage than the nanosilica or the unfilled PU. The nanoalumina supplier was a smaller company and after a few improvement attempts, was not interested in further developing the nanoalumina suspension to be isocyanate compatible. Mechanical testing identified the optimal suspension concentration to obtain an increase in strength without impacting the elongation significantly. Mechanical testing was used determine the optimum suspension concentration for the assembly spray coating evaluation.

Coating application process enhancement and whisker mitigation: A baseline dip/partial cure/ 50 micron spray was performed first with a thickness goal of 25 to 75 microns on a flat surface. The following coatings were evaluated: PC18M-mod, PC18M+20%XP2742 nanosilica, PC18M+20%X11102PMA nanoalumina, unfilled PC40-UMF, PC40-UMF+10%XP2742, and PC40-UMF+30%XP2742. The PC18M base coatings exhibited better coverage than the PC40-UMF. Some, but not all, baseline spray coated PC18M assemblies had extensive coating bubbling after curing. The PC40-UMF based spray coatings had spreading and adhesion issues on the cured PC40-UMF dip coating, which were not resolvable by using plasma etching or reduced UV exposure partial curing. Whisker testing of the baseline process samples showed no whisker growth or coating rupture where the coating was greater than approximately three microns (the coating thickness the SEM beam can penetrate through and examine the underlying metal). Where the coating thickness was excessive, the coating cracked and/or pulled-way from the part features. Some thin areas had corrosion. The reference coatings, vacuum deposited Parylene C and the Parylene C with the Adpro plus adhesion promoter, had excellent uniform coverage and did not have any corrosion, whisker growth, or coating ruptures. The acrylic 1B31 reference coating test did grow whiskers where the coating was approximately three microns for the exposure times tested.

Although the PC18M+20%X11102PMA had the best coverage, based on suspension availability, the PC18M and the PC18M+20%XP2742 were selected for the enhanced layered coating development. The enhanced layered coating used a dip/partial cure/25 micron spray/partial cure/25 micron spray/cure combination with reduced individual spray layer thicknesses so the overall target thickness was still 25 to 75 microns on a flat surface. There was an issue with the dip coat viscosity increase resulting in excessive coating thickness and pooling around the part bodies. The layered spray coating surface was very rough probably due to a spray coating process that was too “dry”. The lead surface had craters where microbubbles appear to have burst and the surface did not flow and level out. The layered assembly coating coverage was better than the baseline dip/partial cure/spray/cure in that there were no vertical edges and fewer lead tips with thin coating. There was no whisker growth on the layered polyurethane samples.

A key finding was that processing coatings where the viscosity depends on the solvent concentration requires monitoring and tight controls. The PC18M had high viscosity dependence on solvent concentration. As the solvent concentration decreased, the PC18M viscosity became like molasses. During dip coating, the coating viscosity can increase with time due to solvent drag out causing excessive coating build up. During spray coating, either bubbles or a rough surface can result. However, this could be useful attribute to control coating thinning on vertical surfaces and increase corner thickness. Future application techniques might leverage methods to secure deposited material and reduce gravity and surface tension thinning effects.

Unique tin nodule microstructure evolution under coating and the importance of coating adhesion: During this project, several unique tin whisker/nodule growth observations were made. In the presence of a sufficiently thick rigid coating, either growth was suppressed or the tin formed nodules rather than whiskers. During the high temperature high humidity (HTHH) whisker growth testing of bright tin plating over copper after ~2,500 hours of 60°C/60%RH, the presence of a rigid coating suppressed whisker growth, but tin nodule growth developed instead. The following conditions were observed (1) no growth under the coating where the coating was ~100 micron thick and well adhered,

(2) where the coating was three to 30 microns thick nodules were observed with larger Cu_6Sn_5 intermetallic (IMC) islands forming in the tin under the coating, and (3) the seven to 30 micron thick coating regions formed domes that stretched the coating, but where the coating was three microns the coating ruptured. Interestingly, the tin nodule dome diameter decreased as the coating thickness decreased which inspired energy based models for coating rupture and coating adhesion during nodule growth. The models, in combination with the measured coating mechanical properties, were in reasonable agreement with the rupture and dome formation observations.

Another set of observations related to coating adhesion. In the 20 micron polyurethane 85°C/85%RH whisker test, bright tin plated samples with high coating adhesion did not form nodule growth, but samples having lower adhesion regions formed nodules and developed tin/coating separation. Like the 60°C/60%RH samples, large Cu – Sn IMC islands formed near the coating surface, that were not attached to the Cu substrate. The higher magnification SEM imaging suggested that the Cu was transported from the Cu substrate interstitially through the tin and along the grain boundaries toward the coating interface and nucleating Cu_6Sn_5 IMC grains. Larger Cu_6Sn_5 IMC islands probably were formed from Cu_6Sn_5 particle coarsening during HTHH aging. Notably present was a complex layer of tin, Cu, and Cu – Sn IMC which formed where the original plated tin layer was located. In samples with greater aging, the coating redirected the complex tin growth laterally along the coating/tin delamination zone.

In some of the delaminated areas, tin was still attached to the coating indicating that coating adhesion to the tin depends not only on the coating/tin reaction layer but the strength of the tin near the coating, which could be impacted by sub – surface phenomena or increased stresses. The stresses in the coating area increased tin oxide layer growth and the accumulation of Cu_6Sn_5 IMC near the coating and increasing interfacial stress due the volumetric increase these compounds compared to tin.

Systematic annealing studies of tin and adhesion promoter (e.g., silane treatment) may be useful to assess the nature of this relationship between the adhesion and the tin whisker/nodule growth.

Layered coating rework: Environmentally aged assemblies from the enhanced layered coating whisker experiments were used to evaluate rework. The old coating could be removed with standard shop practices. Then a low viscosity thinned PC18M coating was syringe applied, cured, and then a higher viscosity PU coating was applied and cured. Cross-sections of assemblies showed that the reworked coating had good adhesion to the new replacement part and to the old coating adjacent to the rework site. The adhesion was confirmed on a flat section of a board with a tape test. The brush coating applied excessive material and cracking was observed after environmental testing. The coating materials have the basic adhesion characteristics for successful rework, but further work is needed to refine the method.

Coating rupture modeling: A unique energy based coating rupture model was developed with a combination of classical analysis and finite element modeling. The model predicted that larger nodules are more likely to rupture the coating layer than smaller diameter whiskers. A coating delamination model versus nodule diameter and coating thickness was also developed. The model results were in reasonable agreement with observed coating rupture and delamination by nodules.

Extended simulated power cycling thermal cycling of the WP1753 samples: The coating on the WP1753 cards was an ultraviolet and humidity dual cure polyurethane acrylate (Humiseal UV40) applied with an automated spray coating machine. After a total of 6,000 power cycling thermal cycling (PCTC) cycles, no whiskers penetrated coating where it was thicker than approximately three microns (e.g the approximate coating thickness where the SEM beam cannot penetrate through the coating and image the underlying solder). Although the coating obscured the majority of the tin surface from SEM examination, it was thin enough (less than approximately three microns) on the knee and at the toe to examine the metal. The solder areas with thin coating did have some whisker nucleation on the Alloy-42 (Fe42Ni) leads. Some coating cracking was also observed. On assemblies without coating, the whisker length did increase with additional cycling, but still were less than ~40 microns. A number of unique thin wide tin growths were observed. These appeared mainly between the lead-free solder and

the copper board pads on both copper and Alloy-42 lead material terminations. While these growths were short, they could impact coating integrity.

1.4 Benefits

The knowledge developed in the current project on whisker mitigation will result in increased aerospace and defense electronic assembly reliability while hopefully preventing overly conservative design practices. The approach used to characterize, analyze and characterize these coatings can be extended to any coating intended for tin whisker mitigation applications. Including a particle enhanced coating to the tin whisker mitigation tool box will be useful because if the particles are used for strengthening, thinner layers could be used. Alternatively, the particles can be used to alter the liquid coating rheology and improve corner coverage, as was observed in nanoalumina case. Layering with a filled layer over an unfilled layer could provide optimal adhesion to the tin while providing a stronger more penetration resistant top coat. In addition, by alternating nanoparticle filled and unfilled layers, the nanoparticles can make it easier to validate the thickness of the various layers applied. A list of publications and briefings generated from this project are provided in Appendix A. Over the five years of study, many references were collected and complied in the reference section here and in the appendices.

The results of this work have been briefed to both the IPC and SAE committees responsible for lead – free risk management and conformal coating of Aerospace and Defense electronics. Recommendations were made for improvement to GEIA-STD-0005-2, Tin whisker mitigation for Aerospace and High Performance Electronics and discussion have been underway on potential changes to IPC-CC-830 and IPC J-STD-001 when conformal coatings are used for whisker mitigation.

The results of this work were also flowed into ESTCP – WP – 201573T2 project training webinars to help educate the program management and systems communities and available on line for future use. This project highlights a means of effective systems risk mitigation by having research in place to understand how and if consumer parts changes impact DoD systems reliability. The immediate reflex is to flow down of reliability requirements all the way down the supply chain to make sure “high reliability” is obtained. Unfortunately these requirements end up at suppliers who are furthest from the DoD integration tier, which are often the weakest links in the supply chain. The suppliers in the lower supply chain levels have narrow margins with little or no R&D money. The main way R&D happens in these communities is leveraged investments and consortia activities. Consortia often have foreign participation, making it more difficult for the DoD interests satisfied. Achieving year over year product cost reductions can negatively impact long term reliability without significant research. The DoD and all levels of its supplier chain must actively collaborate on research to evaluate new consumer electronic parts and materials to ensure proper design and manufacturing standards are in place. The methods developed here can be applied to evaluate and monitor fielded assemblies containing lead-free parts and materials for continued reliability improvement.

2. Structure of the document

In the remaining document, the background is presented in Section 3. Then an overview of the materials and methods is given in Section 4, which is followed a summary of result and discussion in Section 5. Then an overall conclusion is provided in Section 6. Most of the detailed observations and supporting images are given in the appendices described in Section 8.

3. Background

With the advent of lead-free electronics from the European Union Reduction of Hazardous Substances (RoHS) legislation and other lead reduction initiatives, there is concern over tin whisker formation [1]-[6]. Tin whiskers can cause erratic system operation [7] and undesired shut downs [8].

Tin whiskers are conductive crystalline structure of tin growing from tin rich surfaces. The whiskers are formed through addition of atoms at the base, not the tip and their shape can be straight, kinked, or curled. The whisker diameter is typically one to 10 microns in diameter. Whiskers can have long incubation times and lengths vary greatly, from 10s of microns to 10s of mm. Whiskers are best observed with a scanning electron microscope (SEM). Whisker growth can bridge between electrical conductors and form short circuit failures (Figure 1). Failure modes include intermittent, soft and hard shorts circuits and metal vapor arcing is possible in power circuits.

Compressive stresses are believed to promote whisker growth (Figure 2). Whisker growth is more pronounced in thin tin and lead-free solder films up to 50 to 75 microns thick. Bulk lead-free solder, e.g. 300 micron Ball Grid Array (BGA) balls, do not grow whiskers. Electrical bias is not required for whisker growth. The whisker nucleation and growth clock starts after plating or is restarted after lead-free reflow. Many DoD applications have all four whisker stress sources. Even if an assembly uses tin-lead assembly solder, there is still a significant tin whisker risk due to tin plated part leads. Generally the industry part level tin whisker testing is insufficient for long term DoD applications. Programs are also advised to watch for tin (and zinc) plated electrical part bodies and mechanical items.

One of the challenges accompanying real electronic systems is understanding the details associated with the components, product design, manufacturing process and service environments that contribute directly or conspire with one another to exacerbate whisker growth. On the SERDP WP1753 program [9], BAE Systems, in partnership with Celestica, performed tin whisker testing to assess the key manufacturing and environmental variable combinations hypothesized to contribute to whisker growth. In total, over 120,000 whiskers were observed on uncoated assemblies. In addition to the testing, whisker short circuit risk modeling was performed to assist in the quantification of the overall electronic system risk.

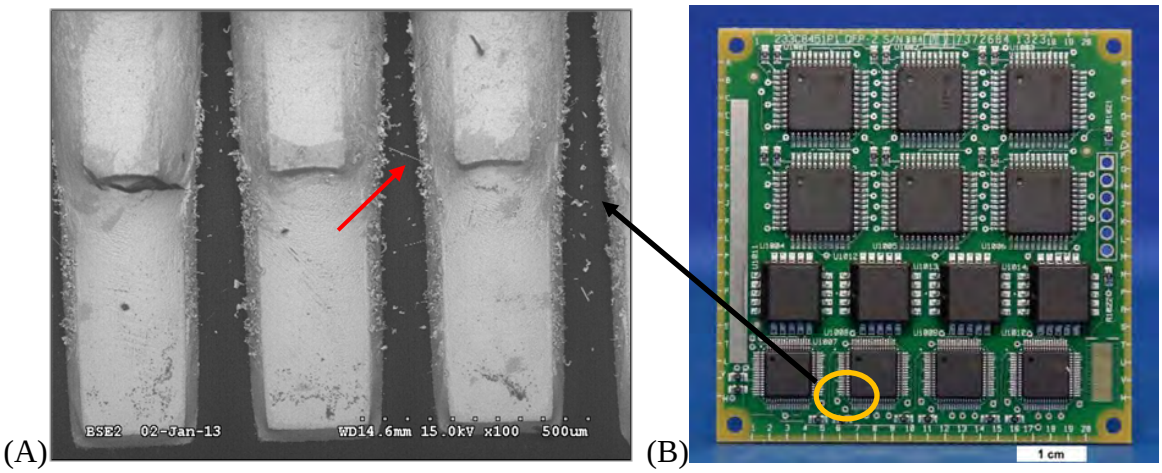


Figure 1: Whisker growth on an electronic assembly after environmental exposure; (A) SEM image of a whisker (see red arrow) between leads of a copper alloy lead 64 pin quad flat pack after 4,000 hours at 85 °C/85 %RH, 100x, and (B) an overall isometric optical image of the quad flat pack test board [9].

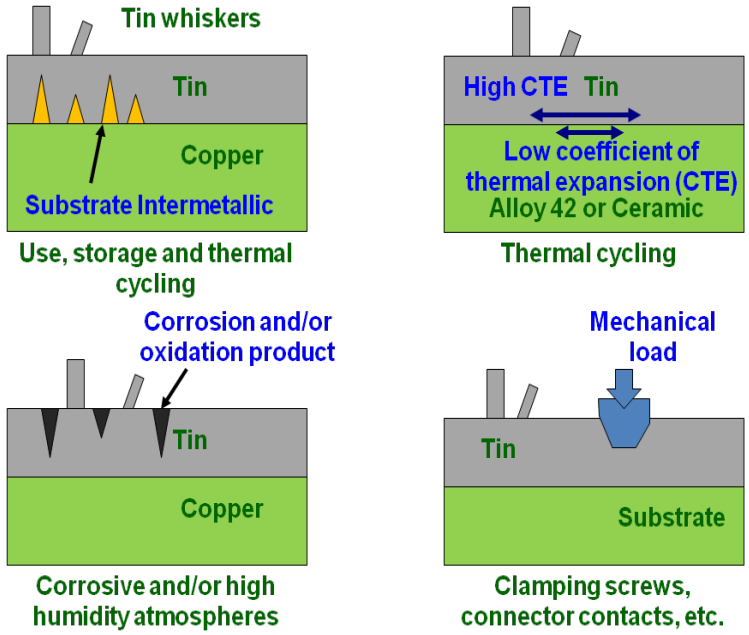


Figure 2: Sources of compressive stress contributing to whisker growth.

3.1 Industry response

It is a Systems Engineering best practice to require any electronics supplier, including commercial–off–the–Shelf (COTS) item users, to provide a lead-free control plan meeting GEIA-STD-0005-1 [1] and GEIA-STD-0005-2 [2]. Lead-free materials risk awareness to program management and systems engineering efforts continue [10].

The GEIA-STD-0005-2 industry standard for mitigating tin whisker risk in aerospace, defense and high performance systems leverages multiple mitigations such as lower whisker propensity material combinations, conformal coating, and electrical/systems design. One of the most commonly used

whisker mitigations is conformal coating because it has been used for years to provide moisture protection [11] – [14]. While the current coating application and coverage requirements contained in J-STD-001 [15], the assembly specification intended for high reliability systems, is entirely based on heritage humidity performance lessons learned. Requirement developments are continuing for coatings intended for use as whisker mitigation [2]. Coating remains one of the more practical approaches to pursue because these materials and processes are within the DoD suppliers control.

3.2 Conformal coating whisker mitigation

Conformal coating mitigates whisker/nodule growth by reducing oxidation and corrosion, modifying the tin surface, capturing whiskers, and preventing contact from adjacent surface whisker growth (Figure 3). Rupture and penetration resistance of the coating is achieved by having an optimal combination of coating strength, modulus, elongation and adhesion. As the coating stretches, the coating strength can increase as the coating polymer chains align. However, it is important to note that nodules and odd shaped eruptions have also been observed. In contrast to tin whiskers that are typically one to ten microns in diameter, nodules can be 50 to 200 microns in diameter, grow 50 microns or more in height, and impart significant rupture stress when growing under conformal coatings. Furthermore, if a nodule ruptures the coating, whisker growth can then continue from the nodule surface.

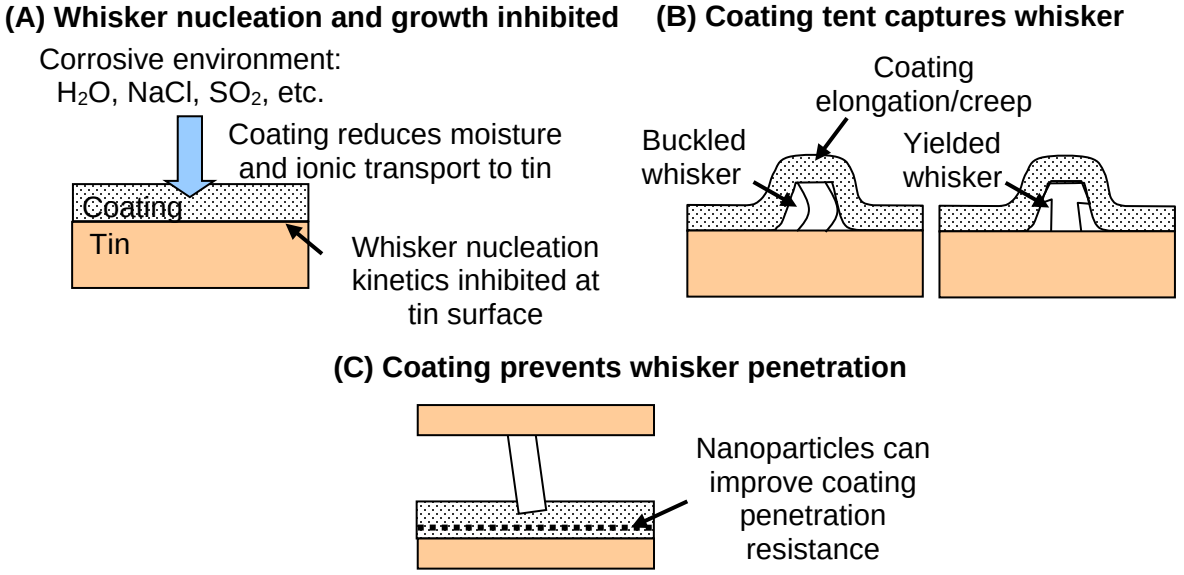


Figure 3: Coating whisker mitigation modes.

Some of the earliest coating whisker mitigation evaluations started in 1998 [16] using test coupons of "bright" tin plated brass (with and without a copper under plating) coated with Arathane™ polyurethane (PU). (Note: Bright tin plated brass was selected because of its rapid whisker growth characteristics.) These coupons were recently re-evaluated after 11 years by Panashchenko [18] and found that Arathane™ PU provided effective room temperature whisker mitigation if the coating was at least 50 microns thick.

A test comparing the whisker mitigation of acrylic, acrylic-polyurethane, silicone, and Parylene™ coatings on tin plated brass coupons was performed by Woodrow [19] [20] [21]. This test found that urethane-acrylic and Parylene™ conformal coatings provided the best whisker mitigation, while the first

coatings to be penetrated by whiskers and odd shaped eruptions were silicone and acrylic (thermoplastic).

While tin plated brass rapidly grows whiskers, its use is typically limited to connector contacts or mechanical hardware. Electronic assemblies have many other substrates under the tin and/or lead-free solder. Parts use alloys such as C110, C194, C7025, C151, BeCu, Phosphor-bronze, and alloy-42 (Fe42Ni). In addition, printed wiring boards use plated copper with finishes such as hot air solder leveled solder, immersion tin, immersion silver, electrolytic nickel/electrolytic gold, and electroless nickel/immersion gold. Woody [22] recently reported on conformal coating mitigation on tin plated C110 and alloy-42 coupons after 9.5 years at 50°C/50%RH. Although uncoated specimens exhibited whisker growth after the first 1,000 hours, many years elapsed before whiskers penetrated some of the conformal coated samples. The alloy-42 substrate exhibited whisker protrusion through 50 micron thick acrylic coating but whiskers remained tented under 50 micron polyurethane.

Less testing has been performed on coated electronic assemblies [23] [24]. Tin parts on tin-lead soldered assemblies with various conformal coatings were evaluated by the Center for Advanced Life Cycle Engineering (CALCE) [23]. The coated assemblies were exposed to a sequence of thermal cycling, high humidity and mixed flowing gas environments. The inspection of the leads revealed that the spray coated assemblies exhibited whisker growth through the acrylic-polyurethane coating where it thinned at the lead corners and vertical surfaces. Rohwer and Martin [24] from Sandia evaluated using composite coatings comprised of Ni and MgF_2-coated Al/Ni/Al platelets in epoxy or silicone in a study in 2015 (after much of the WP2213 work had been completed). Tin whisker growth on control capacitors and transistors was monitored as a function of aging condition. The whiskers did not typically grow longer than 20 microns, regardless of aging condition. The longest whisker was 75 microns and found on a temperature cycled capacitor. After 500 temperature cycles (-55 to 85°C), tin whiskers had penetrated both the silicone and the epoxy coatings on capacitors. The polymer composite coatings, which were comprised of Ni or MgF_2-coated Al/Ni/Al platelets in epoxy and silicone, withstood 1,500 temperature cycles and 4,000 h at 60°C, 93% RH without whisker penetration.

The current project added functionalized nanoparticles to spray process compatible polyurethane conformal coatings which are less expensive to apply than vacuum deposited coatings. The goal was to enhance the coating properties, allowing a thinner coating to be used, and improve coverage characteristics, particularly on corners and vertical surfaces.

4. Materials and methods

The materials and method details are provided in Appendix B and Appendix C and highlights are presented next.

The two base coating materials evaluated were polyurethane (PU) and polyurethane acrylate (PUA). The first base coating was moisture curable solvent-based polyurethane previously qualified to MIL-I-46058 and conforms to IPC-CC-830 (PC18M, from Henkel). The second coating was an ultraviolet (UV) moisture dual cure low volatile organic compound (VOC) that conforms to IPC-CC-830 (PC40-UMF, from Henkel). The moisture cure isocyanates in the PC18M and PC40-UMF will bind to the nanosilica particles which were designed to have isocyanate functionality. For low viscosity dip coating, the PU and PUA could be diluted as low as 30 cps with the Henkel AC0305 solvent and still form a continuous film upon curing.

The nanoparticle suspensions selected for incorporation into the coatings were: (1) Desmodur XP2742 suspension (N3300 Hexamethylene diisocyanate (HDI), trimer with 20 nm mean diameter functionalized silica nanoparticles) from Covestro (formerly Bayer Material Science (Pittsburgh, PA)) and (2) X11102PMA (Nanophase Technologies, Romeoville, IL) containing non – functionalized alumina nanoparticles (40 nm mean diameter in methylene diphenyl diisocyanate (MDI) and propylene glycol methyl ether acetate (PMA)). The functionalized nanosilica covalently bond to with the polyurethane during curing while the non – functionalized nanoalumina are not chemically bound to the resin.

Coating films were cast into substrates for the microstructure and mechanical properties evaluation and coupon whisker testing. The coating was removed from a glass substrate if a free film was needed. The assemblies were coated with combinations of dip and spray processing to obtain a built up layer structure.

Material and microstructure characterization was performed by examining cast film surfaces and microtome cross – sectioning with infra – red analysis techniques and atomic force, field emission scanning electron, and transmission electron microscopes. Mechanical properties were obtained using nanoindentation, tensile testing, thermomechanical analysis, and differential scanning calorimetry.

Flat test coupons and electronic assemblies were used for whisker testing. The majority of the whisker test coupons were bright tin plated copper with slot features to capture coating thinning over corners. The assemblies had tin finished part leads soldered with Sn3.0Ag0.5Cu lead – free solder and were cleaned with normal production processes used for aerospace products.

Whisker testing for the new coatings was mainly performed using 85°C/85%RH high temperature high humidity (HTHH) aging for up to 5,000 hours. For the simulated power cycling thermal cycling a +50 to +85°C thermal cycle was used to obtain a total of 6,000 cycles on the previously tested WP1753 samples.

5. Summary of results and discussion

5.1 Overall

The coating fluid characteristics were quantified in support of the coating application process development. With the conformal coating used in a dual role of humidity protection and whisker mitigation, the mechanical behavior of the coating was also evaluated. New coating formulations were compared to the vacuum deposited Parylene ™ C, the current industry best performing material for complete coverage, thickness and mechanical properties and the 1B31 acrylic, the most widely used coating due to its ease of application and rework. Solvent free coating materials were included as part of the investigation, but the performance did not match the solvent based materials and these materials require further work to improve wetting, interlayer adhesion and mechanical properties.

Unique mechanical test and evaluation were performed beyond current coating characterization practices to understand critical material properties related to prevention of whisker and nodule penetration. In addition, new techniques were used to evaluate the microstructure of the materials that provided a unique understanding on how the microstructure related to mechanical properties. Combinations of coating properties and thickness were identified as important for future tin whisker mitigation coating development.

The result highlights are presented here of the detailed work performed in Appendix B to Appendix N.

5.2 Nanoparticle suspension and coating formulation

The suspension and coating formulation details are provided in Appendix B, with some highlights presented next. Historically, micro-particles were used as inert fillers to modify the mechanical properties of potting and coating materials. One of the drawbacks with micron sized particles is that the viscosity increases dramatically with increased particle concentration. Nanoparticle additions result in lower viscosity increases than micro-particles. The innovation with the present work is to add functionalized nanoparticles that are covalently bonded to the polymer matrix (Figure 4) in an effort to improve physical response of the coating for the containment of whiskers and coverage characteristics.

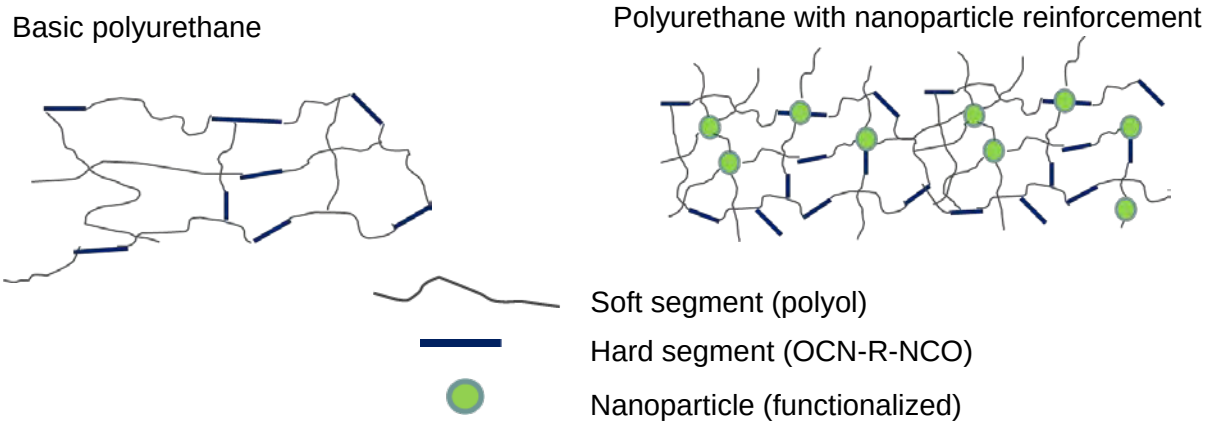


Figure 4: Hybrid conformal coating with nanoparticles in a polyurethane matrix (segmented block copolymer).

Nanosilica and nanoalumina particles were evaluated. The XP2742 nanosilica suspension from Covestro performed well, resulting in uniform particle dispersion and no agglomeration in the cured PU or PUA films.

The X11102PMA nanoalumina was only mixed into the PU for spray coating tests. The nanoalumina particles varied in size, exhibited agglomeration, did not bond to the PU, and had a short shelf life; however had the best coverage in the assembly spray coating test. The short shelf life was believed to be due to trace amounts of water or alcohol from the nanoalumina synthesis that reacted with the isocyanate in the coating upon mixing. After a few unsuccessful improvement attempts, the nanoalumina suspension provider no longer was interested develop the suspension to make it isocyanate compatible. A follow on effort with another supplier, Polymaterials, proved unsuccessful as well.

5.3 Fluid properties

The fluid properties results are given in Appendix D, with some highlights presented next.

5.3.1 Viscosity

The production PC18M viscosity is between 300 and 400 cps but is easily adjusted with the addition of solvent. The production PC40-UMF viscosity is 250 cps and since it is a solvent-free formulation, its viscosity is typically not tailored with a solvent. The coatings exhibit non-Newtonian rheology and the measured viscosity depends upon the shear rate. It was found that the viscosity decreases with increasing the spindle speed (Figure 5). This is a useful condition because it means that while the fluid is flowing during application, it can spread more easily. When the flow velocity decreases, the viscosity increases and the coating will tend to stay in place.

The PC18M liquid has solvent in it even before AC0305 is added, while the PC40-UMF does not. The PC18M liquid without any solvent has the consistency of molasses and its viscosity will increase considerably above 300 cps as the final portions of solvent evaporate. The coating viscosity versus total solvent curves for the PC40-UMF and the PC18M are shown in Figure 6. The Desmodur N3300 is solvent-free and has a nominal viscosity of 3,000 cps, which is much higher than the PC40-UMF. Thus it is expected that the viscosity of PC40-UMF mixed with XP2742 will increase more than PC40-UMF alone as solvent evaporates.

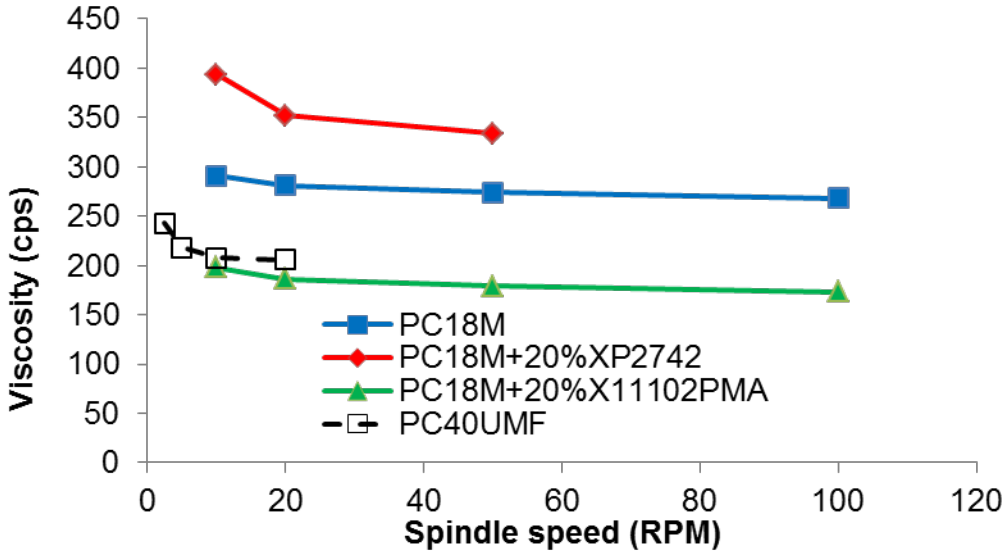


Figure 5: Viscosity versus spindle speed of PC18M, PC18M+20%XP2742, PC18M+20%X11102PMA, and PC40-UMF. Measurements were made using the Brookfield small sample adaptor.

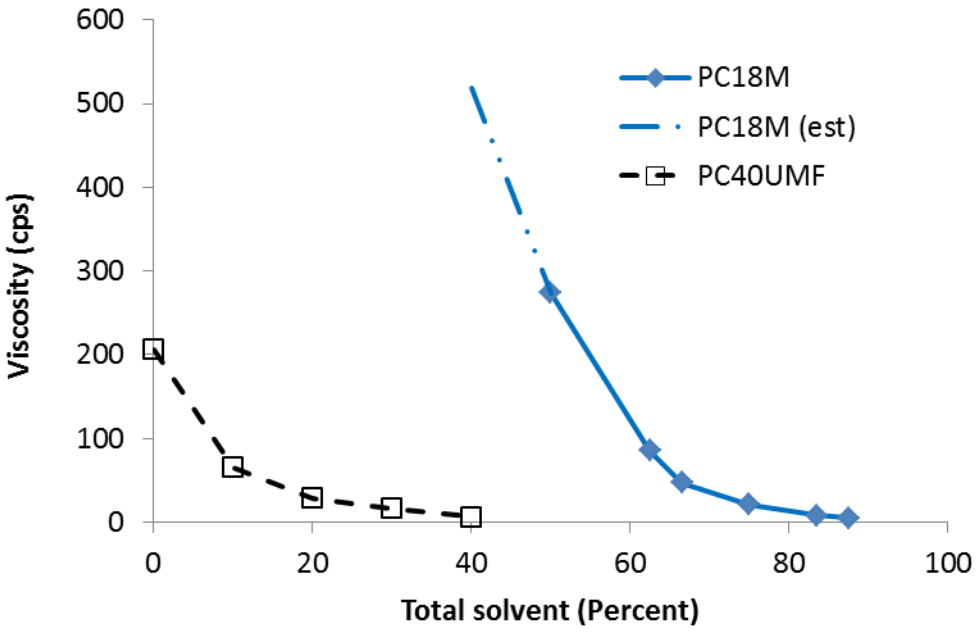


Figure 6: Viscosity versus total solvent percentage for PC18M and PC40-UMF.

5.3.2 Gap flow test

The tendency of the coating to fill gaps between the parts and the board were evaluated using a pair of glass slides separated by shims to establish gaps from 50 to 635 microns (Figure 9). Four coating variants were evaluated. The normal PC40-UMF base viscosity is typically 250 cps. The base PC40-UMF viscosity was increased further by decreasing the monomer with respect to the oligomer in the liquid. A modified PC40UM with a viscosity of 500 cps was formulated. The PC18M viscosity was reduced to 100 cps by adding AC0305 solvent (Figure 7). The contact angles of six drops were measured on glass slides. The addition of solvent to the PC18M resulted in a slight reduction of contact angle (Figure 8). In contrast, the PC40-UMF surface tension did not change with decreasing monomer.

The samples were dipped into the coating reservoirs using the dipping machine at Celestica Toronto at a rate of 76 mm/minute (machine minimum rate). The flow into the gaps could be examined visually during the immersion process. As the gap size decreased, the tendency to form a void in the gap increased. The time to fill the gap increased with decreasing gap spacing (Figure 10).

From this work, it was determined that the dip coat viscosity needed to be much thinner than originally anticipated, as discussed in the assembly coating process development section.

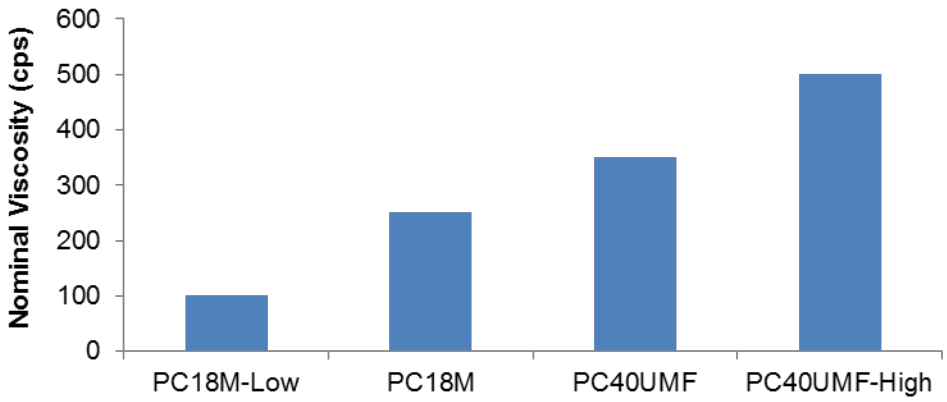


Figure 7: Viscosity of coatings used in the gap flow test.

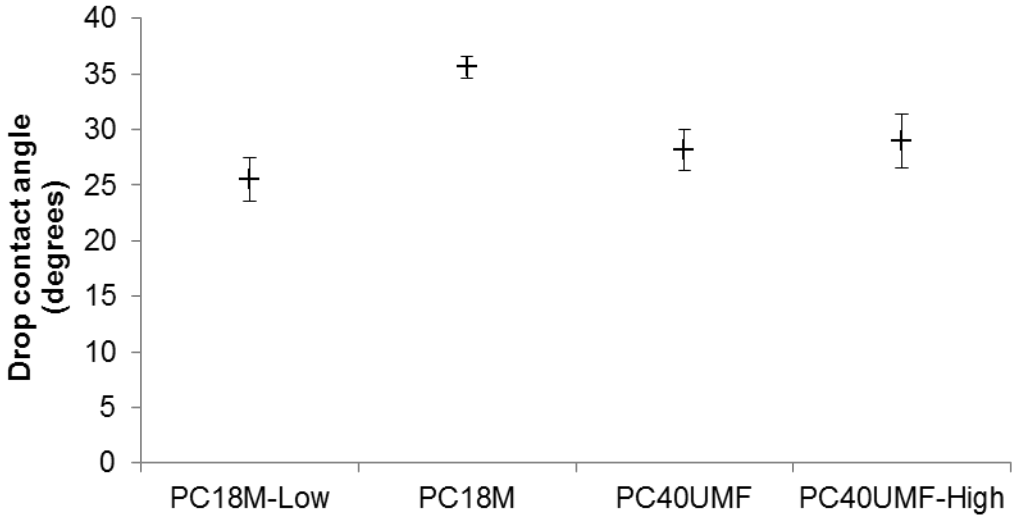


Figure 8: Contact angle, after one minute, of coatings used in the gap flow test.

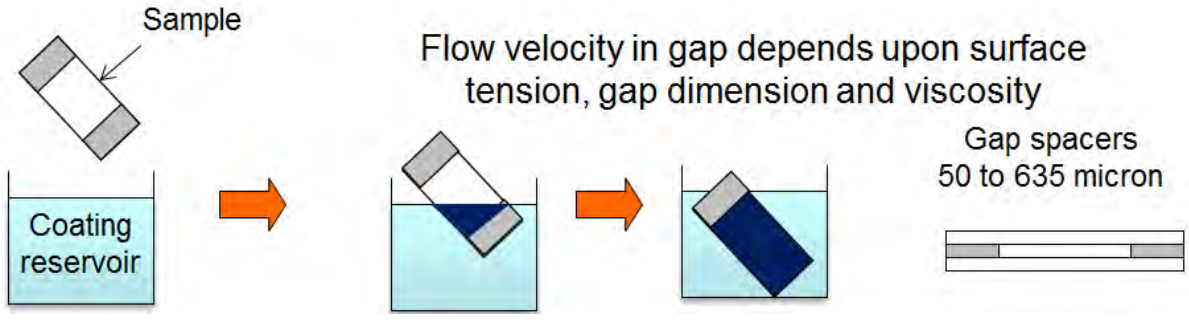


Figure 9: Glass slide gap penetration experiment.

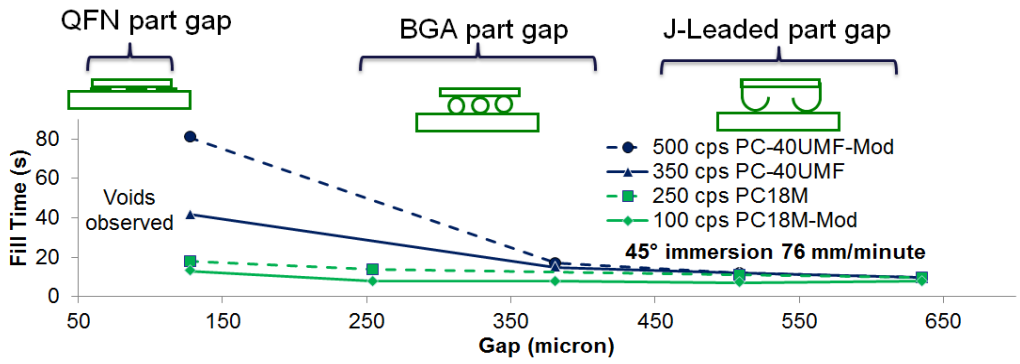


Figure 10: Gap filling time versus gap spacing for various viscosity PC18M and PC40-UMF coatings.

5.4 Solid material microscopic examination

The results of the solid coating microscopic examination are given in Appendix D, with some highlights presented next. The performance of the conformal coatings is strongly influenced by nano- and microstructural features. To gain insight into the material behavior, the structural variations due to the nanoparticle addition were examined by a wide range of characterization methods including Atomic Force Microscope (AFM), Scanning Electron Microscope (SEM) and Transmission Electron Microscope (TEM). The microstructural characterization results generated through this study in relation with the concurrent results through chemical (IR spectroscopy) and mechanical testing combine to determine an optimum concentrations of nanoparticle addition to the coating which would in turn provide an ideal mitigation ability to tin whisker growth.

5.4.1 PC18M structure

The microstructure of PU (PC18M) consists of hard and soft segmented domains. The relative amount of these domains present in each coating is dependent on the amount of isocyanate hardener added. In Figure 11(a) networked structures are visible in the AFM height image, which are also shown in the cross sectional SEM image in Figure 11(b). These structures are soft domains of the polyurethane which are expected to evolve with changing amounts of isocyanate added with the nanoparticle suspension.

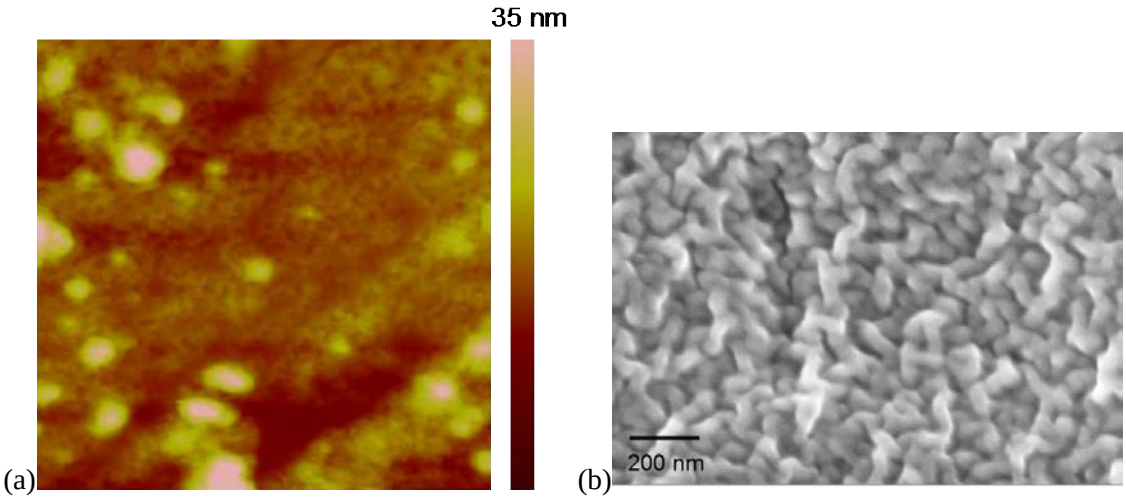


Figure 11: (a) AFM height image of 1 x 1 µm region of plain PC18M polyurethane coatings. (b) SEM cross-sectional image of the plain coating.

5.4.2 PC18M with XP2742 nanosilica

With an addition of nanosilica particle suspension (XP2742) that also contains isocyanate, the microstructure of the PU changes, in which hard segments become more segregated to have hard domains more separated from the network.

The structural changes in the PC18M with XP2742 additions were also evident in the cross-sections. When 20%XP2742 nanosilica suspension was added, the microstructure changed such that the dimpled domains were surrounded by the network (Figure 12(a)). Well dispersed nanosilica particles were also seen in this image. The relative amounts of the hard and soft domains present in each coating were dependent on the amount of isocyanate hardener added. Increasing amounts of the nanosilica suspension consequently increased the added isocyanate (HDI trimer), thereby resulting in higher hard segment concentration in the coating. This increase in hard segments within the coating leads to small hard domains forming in the PU matrix microstructure.

A similar network structure, although much finer, was seen for the 30% suspension case in Figure 12(b). The increased hard segment concentration in the coatings began to show the brittle microstructure with more than 30%XP2742 suspension. This was noticeably demonstrated in the 50%XP2742 addition case by small and localized nanocracks as shown in Figure 12(c). These cracks might have formed during the sample fracture process (also, shown during the microtome slicing process). This is a consequence of not only the increased isocyanate concentration, resulting in the hard segment increase, but also a result of an increased formation of polyurea in the coating with an increase in the isocyanate content. The polyurea serves as another hard segment in the polyurethane network that can provide the defect sites. Furthermore, this polyurea formation generates carbon dioxide gas as a by-product resulting in inclusions such as gas bubbles in the coating.

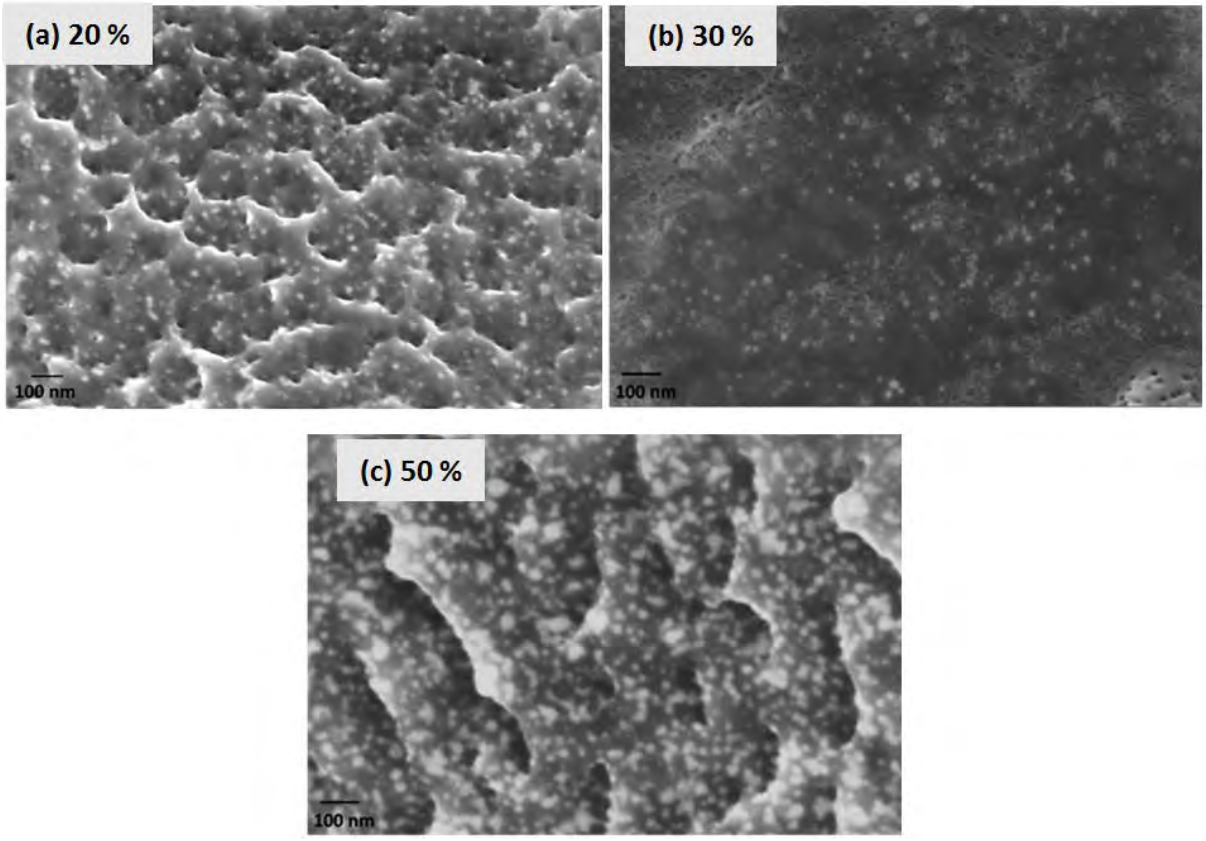


Figure 12: SEM cross-sectional images of cryo-fractured nanosilica filled PC18M coatings: (a) 20% XP2742, (b) 30% XP2742, (c) 50% XP2742 filled.

Individual nanosilica particle size was ~20 nm in diameter for all compositions and there was no significant agglomeration. It confirms proper surface functionalization of the nanoparticles with an isocyanate group (-NCO). TEM analysis confirms this finding and further facilitates viewing of individual nanoparticles. In Figure 13, particles were seen to be well distributed as well as monosized. Further, there was very little agglomeration behavior noticed, even though the suspension addition was 50% XP2742. In some isolated regions, there were agglomerations observed as shown in Figure 13(b), but were very rare across the whole film region.

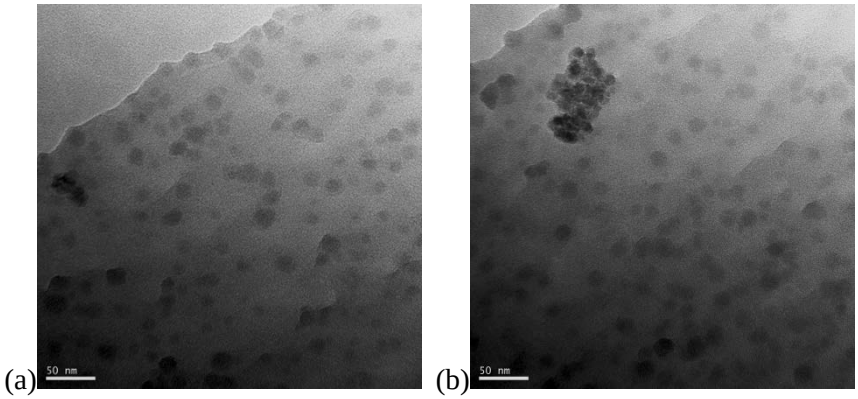


Figure 13: TEM images of polyurethane with 50% XP2742 nanosilica suspension addition; (a) particle distribution at one end of the coating, and (b) an example of the agglomeration.

5.4.3 PC18M with Nanophase X11102PMA nanoalumina

For the nanoalumina-filled PU coating case, since these particles (Nanophase X11102PMA) were not functionalized, a strong agglomeration behavior was observed in Figure 14 even with the 4% suspension. Those agglomerated particle clusters were still sub-micron sized in most of cases but were in stark contrast with the nanosilica case, which exhibited dispersed individual particles with no significant agglomeration (even at the 50% silica suspension). On the other hand, microcracks that were present in PU coating with 50% XP2742 (Figure 12(c)) were not observed, indicating that PU matrix did not become brittle with increasing the amount of particle suspension with X11102PMA Al_2O_3. The voids between the particles and the PU in the microtome sliced nanoalumina sample indicated that the particles were not bonded to the PU matrix (Figure 14(a)).

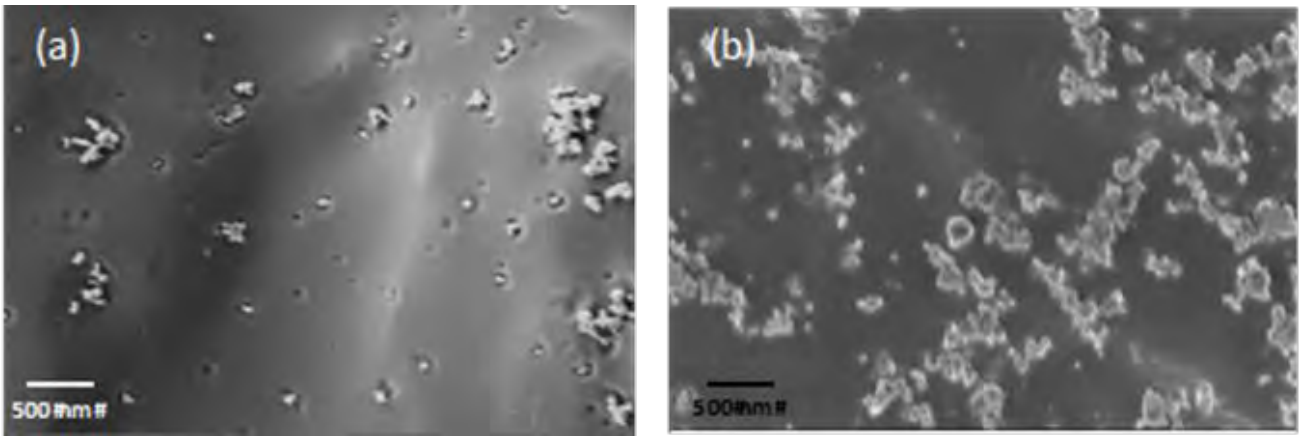


Figure 14: Cross-sectional SEM images of polyurethane films with (a) 4% X11102PMA (b) 20% X11102PMA Al_2O_3.

In an effort to observe individual nanoparticles more clearly within the agglomerated clusters, cryo-TEM observation was done using a cold stage. Figure 15 shows a cross-sectional TEM image of a nanoalumina-filled PU film, where individual nanoparticle shapes and sizes were visible within those clusters. The particle size distribution was much wider than the nanosilica case. Based upon multiple TEM images, many particles have the sizes greater than 100 nm, as well as about ~ 10 nm, even though the nominal particle size was 40 nm according to the specification data. The average particle diameter was confirmed to be about 70 nm, with a range from 20 to 200 nm, based upon the dynamic light scattering measurements of the suspensions.

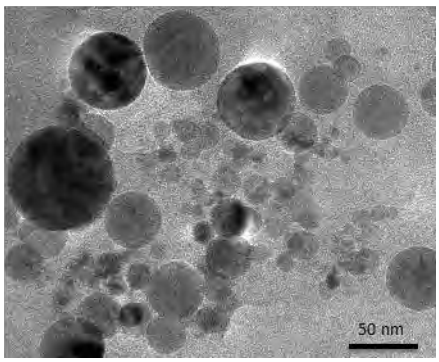


Figure 15: Cross-sectional TEM image of nanoalumina-filled PU coating.

5.4.4 PC40-UMF and PC40-UMF with XP2742 Nanosilica

Figure 16(a) shows the cross-sectional overview of a cryo-fractured plain (unfilled) PUA (PC40-UMF) coating. Toward the top of the cross-section, fracture pattern of domains about ~10µm in size is noted which transition into a smoother region toward the mid-region. A ridge that appears pulled out during the fracture is shown toward the bottom of the coating. The domain structure, bound by crack growth paths, clearly indicates a brittle fracture near the top portion, as the fracture direction was from top to bottom part of this image, where some tearing occurred near the end of the fracture. Such domains were not clearly defined for the PC18M case, which was more ductile. In addition, high-resolution images of each domain exhibit the 'wormy' network structure as shown in Figure 24(b). This network structure is finer, compared to that for PC18M, which is again indicative of more brittleness. Both smaller domain size and finer network structure are consistent with a limited ductility shown on the PC40-UMFcoatings that have total elongation less than 10%.

In order to improve mechanical properties, 10 to 50% XP2742 SiO_2 suspension was added to PC40-UMFresin. It corresponds to 1.88 to 10.7 wt.% of the nanosilica particles added. Figure 17 shows the microstructure of PC40-UMFcoating filled with 30% XP2742 SiO_2 suspension (6.0 wt.% nanosilica particles). Well-distributed nanosilica particles (~20 nm in size) are visible without much agglomeration in this SEM image. The network structure still remains even with the addition of the nanoparticle suspension. A void is also present at the bottom of the image.

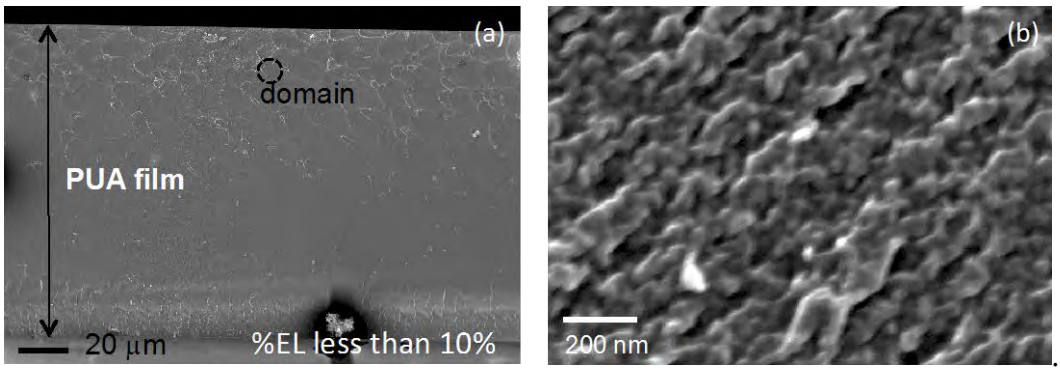


Figure 16: Cryo-fractured cross-section of a plain PC40-UMFcoating showing: (a) the entire thickness; (b) high magnification view inside the circled domain.

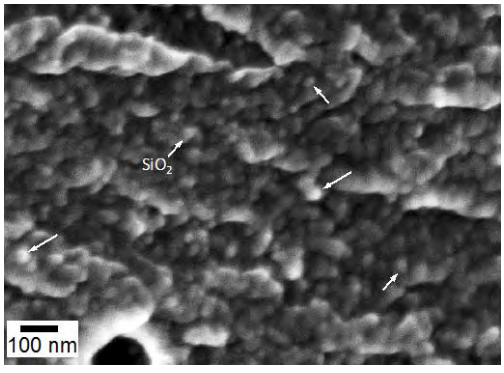


Figure 17: High resolution SEM image of cryo-fractured PC40-UMFcoating filled with 30% XP2742.

The microtome sliced cross-section of the same PUA coating is shown in Figure 18(a). The coating section is interfaced with the epoxy encapsulation used for sample preparation. Scratch lines from the diamond knife are seen; oriented mostly vertical in the image. Some artifacts of the slicing process known as 'chatter' lines, running as broken lines perpendicular to the scratches, are also detectable but mostly within the epoxy region surrounding the coating. A sub-micron sized void is also shown, believed to be caused by trapped carbon dioxide (Figure 18(a), inset). Similar features were also observed on the cryo-fracture cross-section in the middle of the fracture features of PC40. High resolution imaging of the microstructure of this plain (unfilled) coating again reveals a 'wormy' networked structure as shown in Figure 18(b).

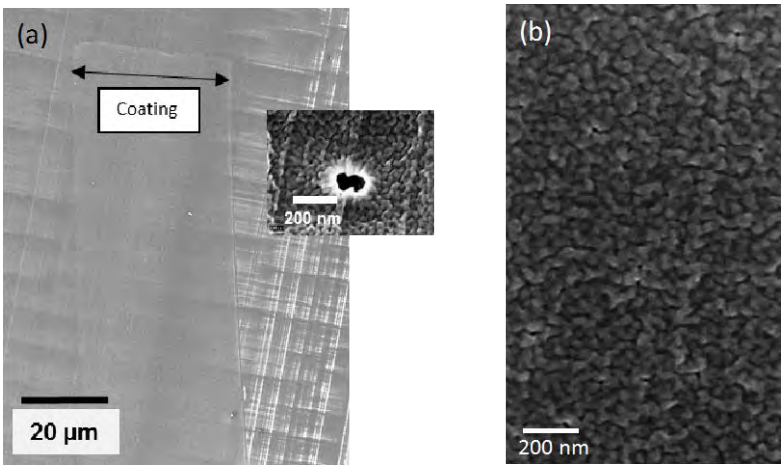


Figure 18: Microtome cross-section of plain PC40-UMFcoating, showing (a) entire thickness, inset: sub-micron sized void; (b) the network structure at higher magnification.

5.4.5 PC40-UMF with Polymaterials nanoalumina

In an effort to achieve faster process time, lesser energy consumption, and more energy friendly process for the coating application, UV-curable films can be adopted. Since the coatings have a much higher curing speed than conventional water or solvent based coating technologies, higher production throughput is expected. This throughput is also supplemented by energy and cost savings from using such UV-curable polymer coatings. For investigating the applicability of such polymer systems to whisker mitigation coatings, PC40-UMF, a dual cure (UV + water curing) polyurethane acrylate system was used. Nanoalumina suspensions were added to this polymer resin to provide increased mechanical properties. To avoid the particle agglomeration, similar to those used in case of PC18M, two functionalization schemes were employed: i) dispersant addition followed by functionalization (WTA996); ii) functionalization followed by dispersant addition (WTA997).

Good dispersal of the nanoparticles within the polymer matrix was noted in the PU coating cross-section in case of the WTA996 samples (Figure 19). However, a continuous layer of settled particles was also observed. The inclusion of PU within the particle clusters (in the settled particle layer) was, however, suggestive of some amount of dispersion of the nanoparticles taking place within the polymer resin.

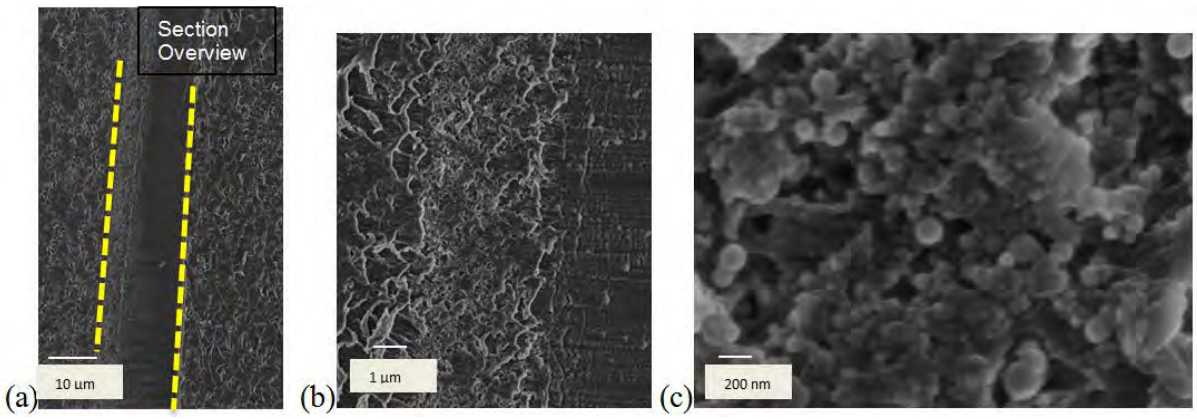


Figure 19: Cross-sectional overview image of WTA996 with PC40-UMF; (a) overall, (b) region of settled particles at one end of the coating, and (c) PU and nanoparticles in the settled layer.

5.4.6 Film microstructure summary

Nanoparticle-filled PC18MPU conformal coatings were analyzed using a combination of high-resolution and analytical tools for structural characterization. Plan-view AFM and cross-sectional microstructure characterization showed the presence of networked 'wormy' patterns and domain structures. These features disappeared beyond the 30%XP2742 addition of nanosilica suspension. This is consistent with the brittleness and premature failure observed in such compositions. The distribution of nanoparticles within the matrix was homogeneous at the 20%XP2742 suspension or lower, but it showed the particle settlement after 30%XP2742 suspension. There was no significant particle agglomeration observed even for the 50% nanosilica suspension case, which suggests that more particle addition could be possible if the brittleness observed in the PU matrix were prevented.

For the Nanophase nanoalumina-filled PC18M PU coating case (X11102PMA suspension), the particles were not functionalized, which resulted in strong agglomeration. Those agglomerated particles that are still sub-micron sized in most of cases are in stark contrast with the nanosilica case, which was rather individually populated with no significant agglomeration. Clustered particle groups were also clearly visible in TEM studies.

To reduce the agglomeration tendencies of the Polymaterials nanoalumina filled PU films, two improved surface functionalization schemes were attempted by Polymaterials; one by adding a dispersant followed by functionalization and another by functionalization followed by the dispersant addition. Higher polyurethane content with adequate dispersant content in case of the first scheme proved better in reducing the agglomeration behavior, but could not completely eliminate it. Further it reduced large micron sized settling of nanoparticles within the coating cross-section. The same scheme used with a UV-cured polymer base (PC40-UMF) with the Polymaterials nanoalumina suspension addition also showed similar effects.

5.5 Solid mechanical properties results

The results of the solid coating mechanical properties are given in Appendix D, with some highlights presented next.

5.5.1 Fluid compatibility

The jet fuel fluid resistance was evaluated for both the PC18M and PC40-UMF sets of PU materials. The PC18M family underwent slight softening after exposure. It was also noted that the PC18M coating regions touching the Skydrol hydraulic fluid crazed. The P40UMF micro hardness was unchanged.

5.5.2 PC18M glass transition temperature and CTE TMA test

The thermomechanical analysis (TMA) was used to measure the glass transition temperatures and coefficient of expansion (CTE) of the PC18M + XP2742 2.2 mm thick cast coatings. In addition, the hardness was recorded for the samples. The T_g for the base PC18M was 68°C and with the addition of the Dabco T 12 accelerant was 107 °C (Table 1). Note the Dabco T 12 accelerant was added to reduce the cure time of the PC18M+XP2742 mixtures, but it also impacts the mechanical properties. The addition of the XP2742 reduced the T_g to the 44 to 46 °C range because of the lower T_g of the N3300 isocyanate.

Table 1: Summary of PC18M+XP2742 glass transition temperature, coefficient of thermal expansion and hardness

	PC18M Control	PC18M Control with Dabco T 12	90%PC18M+ 10%XP2742 Dabco T 12	70%PC18M+ 30%XP2742 Dabco T 12	50%PC18M+ 50%XP2742 Dabco T 12
First Tg single scan (°C)	-53.2	-71.2	-60.1	-63.1	-78.4
Second Tg single scan (°C)	68.1	107.3	58.2	46.4	44.0
Coefficient of thermal expansion (ppm/C) (-140 to -100C)	61.2	67.5	60.6	68.0	63.1
Hardness Shore D	60	64	62	65	65

5.5.3 PC40-UMF Coefficient of thermal expansion

Due to the moisture cure nature of the coatings, it was difficult to cast PC40-UMF films that were sufficiently thick without defects. More work is needed to determine a reliable film casting method.

5.5.4 Water vapor transmission

The water vapor transmission testing was performed for various concentrations of XP2742 in PC18M and PC40-UMF and for various concentrations of X11102PMA in PC18M. Increasing the XP2742 concentration in PC40-UMF increased the water vapor transmission rate slightly. In contrast, increasing the XP2742 concentration in PC18M resulted in a decrease in water vapor transmission rate (Figure 20).

The curing method impacted the moisture transmission of the PC40-UMF. The PC40-UMF moisture cure only (no UV) transmission rate of 0.2422 g/(100cm^2-day) was higher than the PC40-UMF with the standard UV and moisture cure value of 1.112 g/(100cm^2-day).

In summary, the best performer, having the lowest vapor transmission rate, was the PC40-UMF coating with the standard UV and moisture cure.

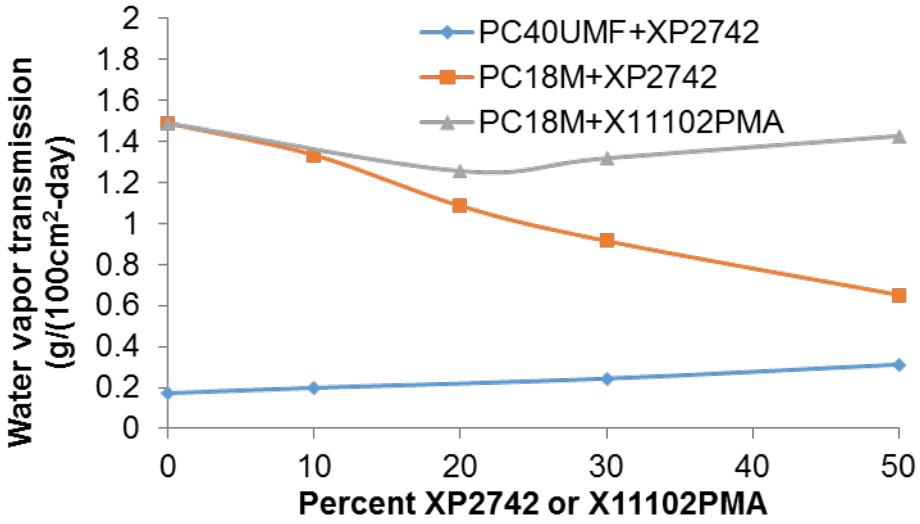


Figure 20: Water vapor transmission for various XP2742 or X11102PMA concentrations in PC40-UMF and PC18M.

5.5.5 Hydrolytic stability

Board coupons coated with PC18M+20%XP2742 and PC18M+20%X11102PMA passed the 120 day 85°C/95%RH hydrolytic stability test.

5.5.6 Thermal shock

Board coupons coated with PC18M+20%XP2742 and PC18M+20%X11102PMA passed 100 cycles from -55 to 125°C using an air-to-air transfer shuttle.

5.6 Nanoindentation test results

The results from the nanoindentation testing are provided in Appendix D, with some highlights presented next. An example of the nanoindentation analysis on the PC18M base coatings is given next. The PC40-UMF was evaluated in a similar manner.

5.6.1 PC18M-mod baseline

Mechanical properties were evaluated via a small-force nanoindentation. In particular, the depth-sensitive nanoindentation testing can emulate the whisker penetration behavior by examining local deformation of PU around an indenter tip. Figure 21 shows the nanoindentation results from unfilled polyurethane (PC18M). The original PC18M has a viscosity of ~250 cps and the modified version has a reduced viscosity of ~ 100 cps and Dabco T12 addition. Mechanical properties did not show much difference with the modified PC18M version.

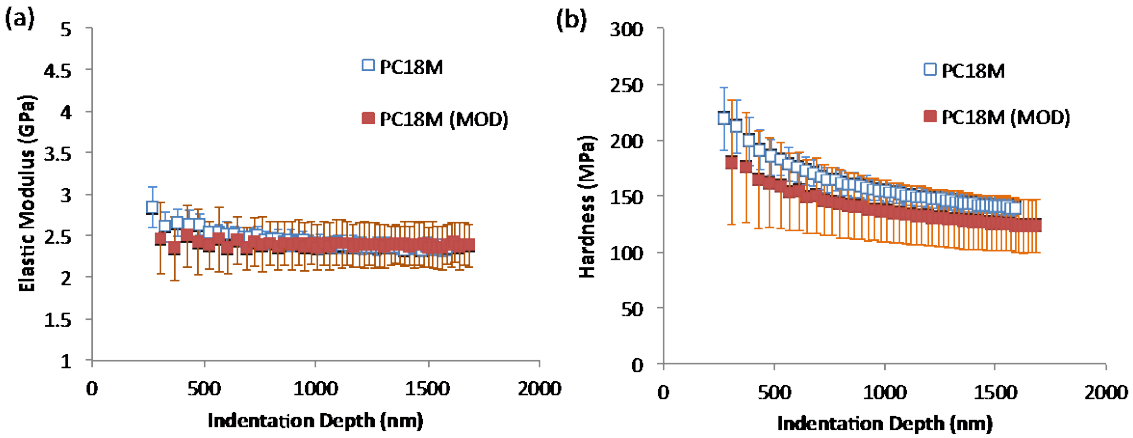


Figure 21: Nanoindentation testing results from PC18M films: (a) elastic modulus; (b) nanohardness.

5.6.2 PC18M + XP2742 nanosilica

After adding nanoparticle suspensions (XP2742) to the PU base resin, mechanical properties of the filled PU coatings were improved as shown in Figure 22. Both elastic modulus and nanohardness increased after 10% XP2742 SiO_2 (which corresponds to 3.5 wt.% SiO_2). These properties decreased with indentation depth, which has been found in moisture-cured polymers. Nanosilica-filled PU coatings displayed decreasing hardness values near the surface region (< 500 nm range). Mechanical properties of those nanosilica-filled PU coatings, however, did not show any improvement with 30% XP2742 addition (corresponding to 9.8 wt.% SiO_2) or 50% XP2742 addition (to 15.2 wt.% SiO_2). In fact, there was a decrease as seen in the modulus of 30% XP2742 case due to its greater dependence on indentation depth.

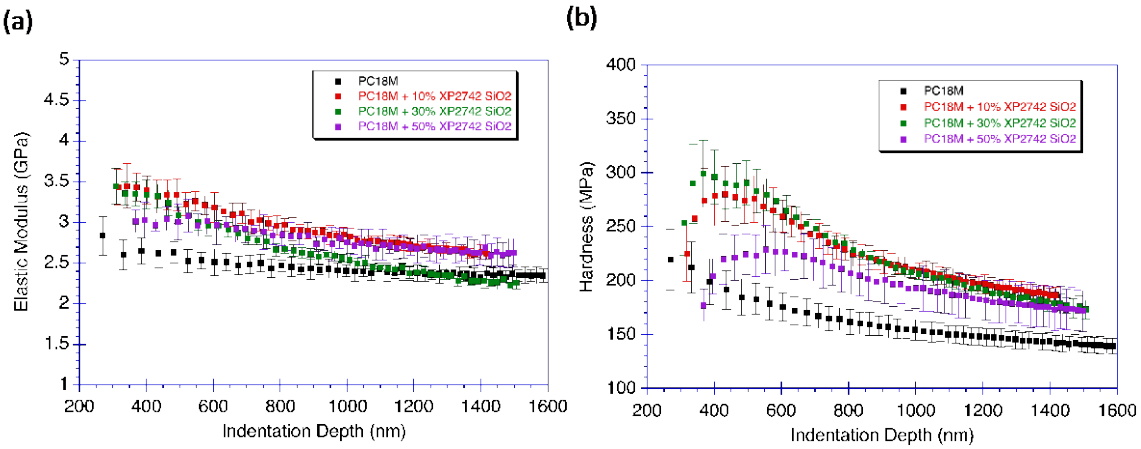


Figure 22: Nanoindentation testing results of PC18M filled with XP2742 (nanosilica); (a) elastic modulus, and (b) nanohardness.

The majority of the tin whisker testing is performed at elevated temperature. In addition DoD electronics often encounter temperatures up to 125°C. Nanoindentation testing of PC18M with the XP2742 suspension at elevated temperatures up to 125˚C is shown in Figure 23. Dramatic reduction in mechanical properties occurs even at 50˚C, which can be related to the presence of the glass transition temperature below this temperature. This also confirmed the TMA result that the addition of the XP2742 to the PC18M caused a glass transition temperature decrease.

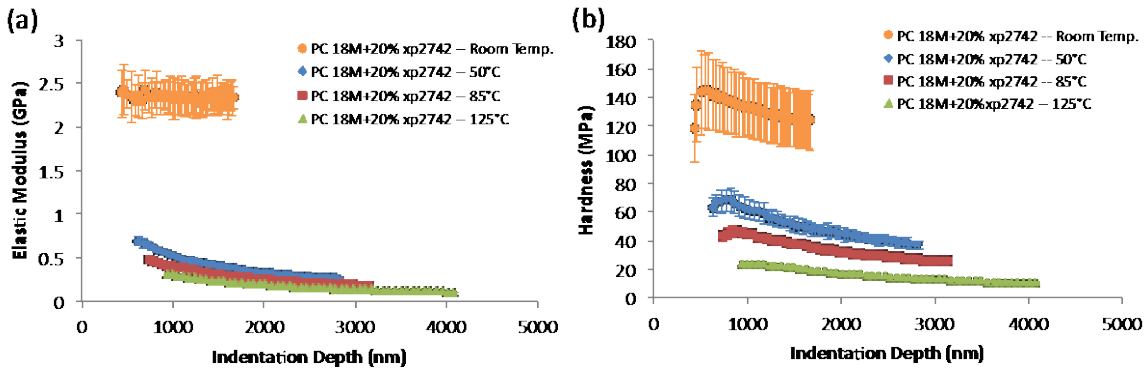


Figure 23: Nanoindentation testing results of PC18M+20% XP2742 at room temperature, 50˚C, 85˚C, and 125˚C; (a) elastic modulus, and (b) nanohardness.

5.7 Tensile test

The results of the tensile tests are provided in Appendix D, with some highlights presented next. Examination of ruptured PU films after tensile testing (Figure 24) indicates the failure origin at the bubbles (or voids). These defect locations provide a stress concentration site, where the crack initiates and propagates. Shear bands that extended from this location with about 45˚ angle from a tensile loading axis were also observed. Because of the presence of these defects, there was premature failure, as well as data scattering. It ultimately made the polymer film quite brittle. Therefore, it will be necessary to have the defect concentration reduced to increase ductility, which can be comparable to that of the Parylene film.

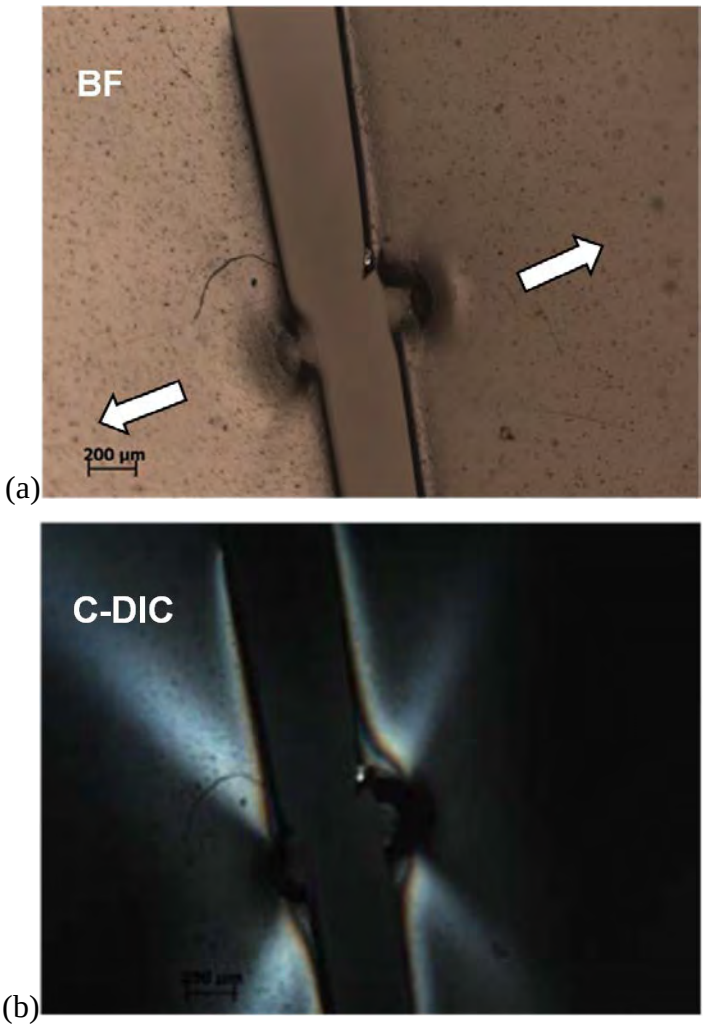


Figure 24: A crack grown from a defect site embedded in PU film; (a) bright field optical micrograph, and (b) C-differential interference contrast (DIC) image. Arrows indicate tensile loading direction.

5.7.1 PC18M with N3300 and XP2742

As was previously mentioned, XP2742 is made up of nanosilica particles in N3300 isocyanate. In order to differentiate the effect of nanosilica particles from the hard segments, mechanical properties of the PC18M PU coatings were compared as a function of the amounts of nanosilica+isocyanate and the corresponding isocyanate percentage as shown in Figure 25. The thicker the sample the more defects it can have and could have reduced elongation as a result. The elastic responses of the polyurethane coatings, both with nanosilica+isocyanate and only isocyanate, show a trend of increasing modulus with an increase in those additions; that is, increasing up to the 30% suspension case and then decreasing with more suspension, as observed by the elastic modulus chart in Figure 25(a). A higher value in the elastic modulus was, however, observed when nanosilica particles were added besides the addition of isocyanate.

This is indicative of particulate reinforcement provided by the nanosilica, beyond the strengthening effect of the hard segments in the polyurethane matrix that restrict chain alignment in the axial stress direction. However, a degradation of the elastic modulus was also observed after 30% nanosilica suspension (also, 15.54 % isocyanate). The drop in elastic modulus was more significant with the

nanoparticle suspension case, indicating that the brittleness of PU matrix results in more dramatic impact when combined with the defects resulting from the nanoparticle addition.

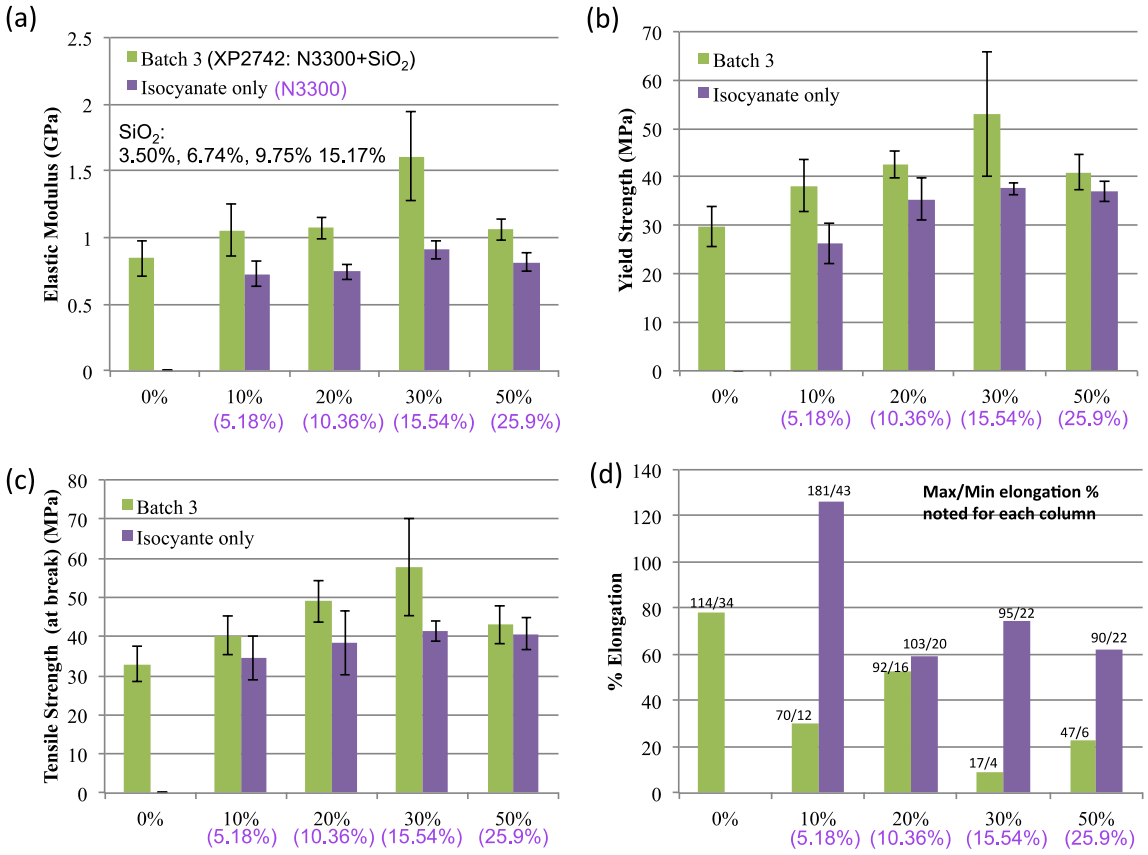


Figure 25: Effect of XP2742 (nanosilica+isocyanate) and N3300 (isocyanate) suspension on tensile properties; (a) elastic modulus, (b) yield strength, (c) tensile strength at break, and (d) percent elongation.

5.7.2 PC18M final coating comparison

The coating formulations selected for whisker testing were PC18M + 20%XP2742 nanosilica and PC18M + 20%11102PMA nanoalumina. The nanoparticles resulted in an improvement of properties over the PC18M and the PC18M+N3300 isocyanate (Figure 26). It is likely that the nanoalumina formulation could have had better performance if the particles had been functionalized as originally planned. In the low strain region, the properties of the nanoparticle filled coatings approach those of Parylene C.

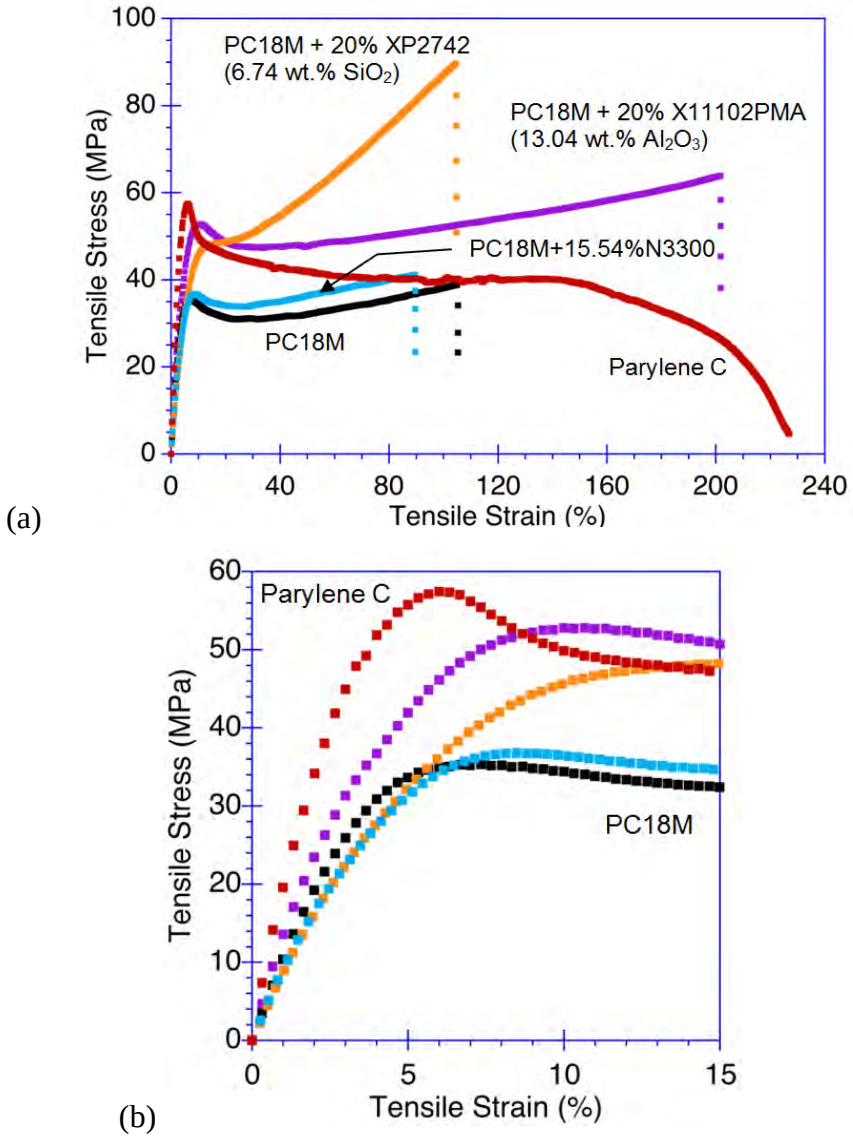


Figure 26: PC18M Stress versus strain comparison with Parylene C; (a) overall and (b) strain up to 15 percent.

5.7.3 PC40-UMF with XP2742

Tensile properties of the PC40-UMF dual curing system (UV+moisture) are shown in Figure 27. Unlike the 'localized' nanoindentation behavior, macroscopic tensile behavior of PC40-UMF was much lower than PC18M (moisture cured). In addition, there was no improvement in mechanical properties by adding the XP2742 SiO2 suspension. More importantly, total elongation was too low, which might result from the defect population. Indeed, the PU film thickness was thicker (around 100 microns for most of cases) and bubble defects were clearly visible. (Note: During the PC40-UMF family film casting, the thinner films were difficult to remove from the glass without tearing, so thicker films were made.) Moisture-only cured PC40-UMF films displayed the highest ductility among these samples, but still much lower elongation than the PC18M counterparts.

Effects of the particle suspension (XP2742) and isocyanate (N3300) on elastic modulus and tensile strength of PC40-UMF are shown in Figure 28. PC18M properties are shown as a dashed line for comparison. In all cases of unfilled and filled PC40-UMF, the properties were less than PC18M. In particular, moisture only cured samples showed very low modulus and strength since the acrylate domain included in the polymer network was not cured under thermal/moisture treatments.

It would be beneficial to further improve the resin formulation to restore the ductility (also, toughness) of this UV curable polyurethane film taking care to ensure that the attributes needed to pass IPC-CC-830 and solvent resistance are still retained.

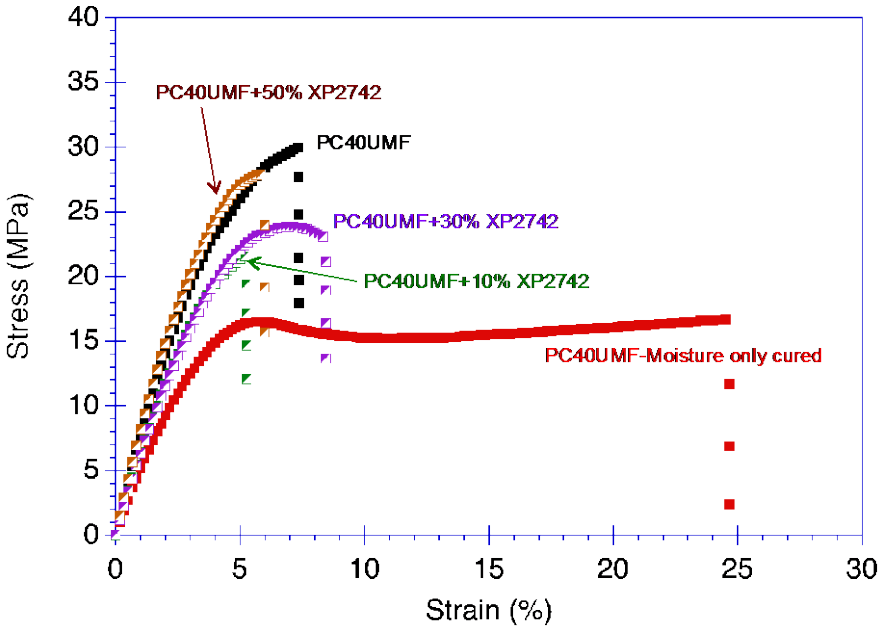


Figure 27: Representative tensile stress-strain plots of UV-curable PC40-UMF filled with XP2742 SiO_2 suspension. For reference an unfilled PU film (PC40-UMF) case is also included.

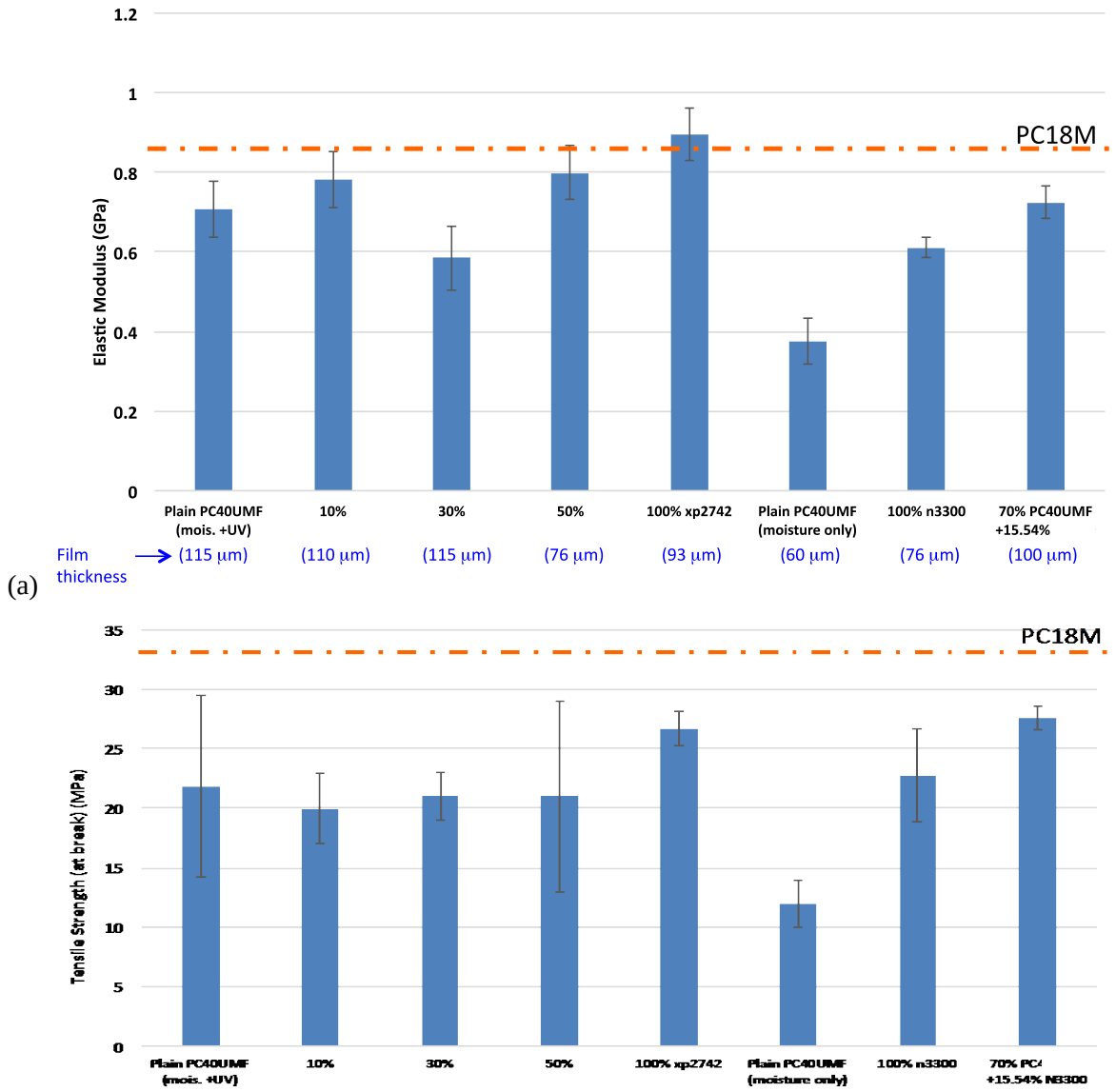


Figure 28: Tensile properties of PC40-UMF family (filled with NNN2835 equivalent to XP2742, N3300); (a) Elastic modulus, and (b) Tensile strength.

5.8 Adhesion testing

The result of the adhesion tests are provided in Appendix D, with some highlights presented next. The coating adhesion to tin was evaluated using a four point bend test. Adhesion tests were performed on the polyurethane PC18M (PU) and the polyurethane acrylate PC40-UMF (PUA). The adhesion between coating and Sn was improved:

- PU and PUA: O_2 plasma treatment on Sn surface
- PUA only: (3-Aminopropyl) triethoxysilane (APTES) treatment on Sn surface – 2% APTES in water with acidified environment (pH=5)

A typical force versus displacement curve is shown in Figure 29. On the PC18M samples, the critical interfacial energy increased to 57.8 J/m^2. For the PC40-UMF, the siliane adhesion promoter in addition to the plasma treatment improved the adhesion from 12 J/m^2 t for the plasma alone to 22.4 J/m^2 for the plasma and the APTES silane treatment (Figure 30).

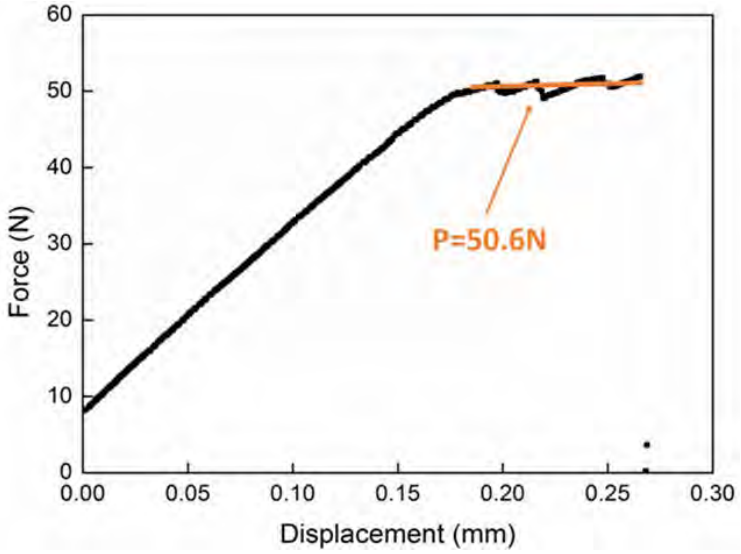


Figure 29: Typical force versus displacement curve for the four point bend test. (PU (PC18M) on Sn shown).

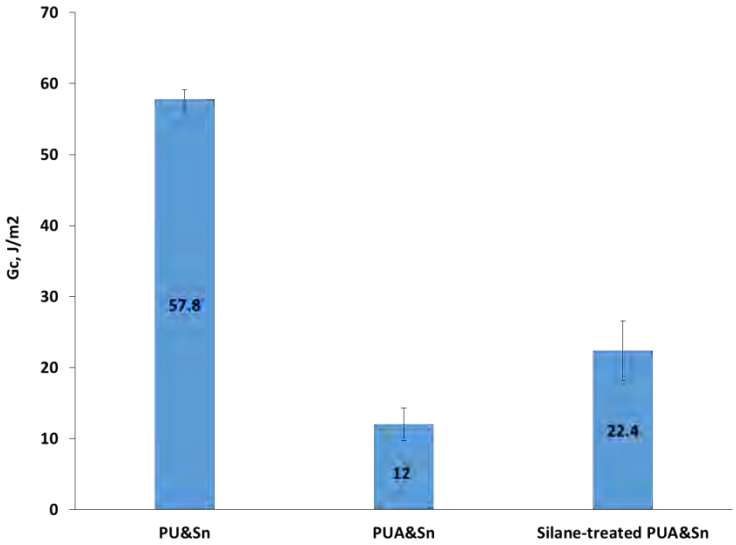


Figure 30: Critical interface energy (Gc) for the coating to tin interface adhesion. The PU (PC18M) adhesion is considerably better than the PUA (PC40-UMF). The APTES silane treatment improved the adhesion on the PUA samples.

5.9 Assembly coating process

The assembly process development is outlined in Appendix E, with some highlights presented next.

5.9.1 Dip coating

The dip coating process is outlined in Figure 31. The immersion rate, immersed hold time, withdrawal rate, and vertical drain time are controlled by the dipping machine and the operator. After the vertical drain time has finished, the assemblies are placed horizontally on a tray and air dried to allow the solvent to evaporate. The dip capillary flow into gaps and behind leads is primarily controlled by (1) surface energies of the solid assembly materials, (2) the wetting contact angle between the coating and assembly surfaces, (3) coating viscosity, (4) the lead/part geometry (e.g. spacing between leads, sharp lead corners, bend radii, etc.), and (5) the gap size under the parts. Typically, solvent additions to the coating significantly improve wetting by decreasing the viscosity, contact angle and sensitivity to surface contamination. During the withdrawal and vertical draining phases, the coating solvent is evaporating, resulting in increased coating viscosity and slower coating flow.

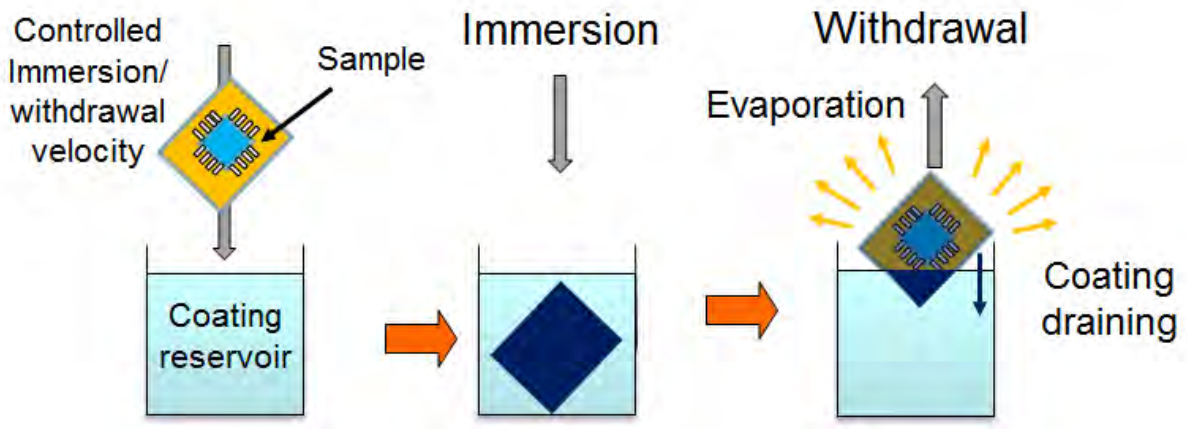


Figure 31: Dip coating process flow.

The Specialty Coating Systems (SCS) PL-3201 dipping machine used for dipping is shown in Figure 32. The coatings were typically diluted to 30 cps and the dip coating immersion and withdrawal speeds were 76 mm/minute. The board immersion time after contact with the coating was approximately 70 seconds. After complete immersion, the withdrawal was immediately started (no dwell), after approximately 70 seconds the boards were clear of the coating, the boards were then allowed to drip for approximately 90 seconds and then placed on a horizontal tray and air dried overnight in a chamber with low velocity air flow (Figure 33).

It was noted that the samples dipped later in the day had thicker dip coating. The thicker coating was attributed to viscosity increase due to solvent drag-out and evaporation over the three to four hour dipping session. It is recommended that the coating viscosity monitored during the dipping process.

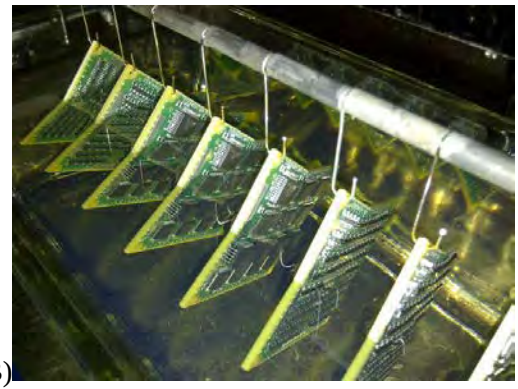
(A)  (B) 

Figure 32: Dip coating machine; (A) Front of machine with one board shown on immersion bar and (B) boards partially immersed in the coating reservoir.

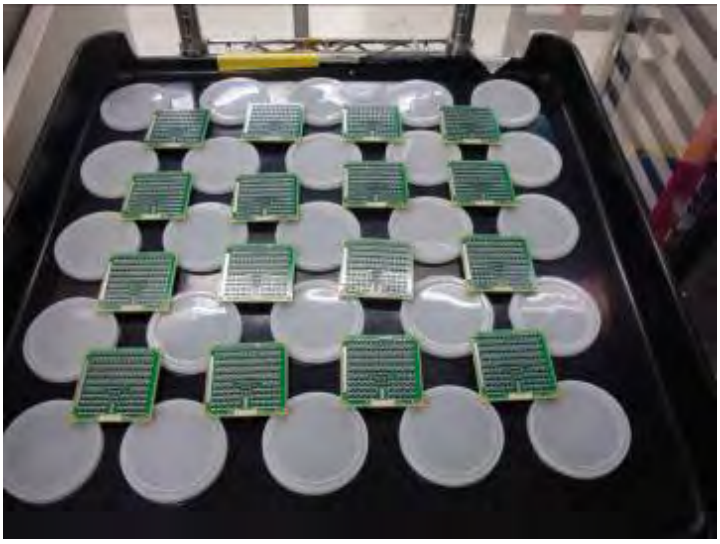


Figure 33: Dip coat samples on a tray in the drying chamber.

5.9.2 Spray process considerations

The liquid conformal coat and solvent mixture is drawn from a reservoir and combined with pressurized nitrogen gas flow in the nozzle to form atomized liquid droplets which are directed onto the board (Figure 34). Some key spray coating parameters are (1) surface energies of the solid assembly materials, (2) the wetting contact angle between the coating and assembly surfaces, (3) coating viscosity, (4) the spray droplet size, (5) the lead/part geometry (e.g. spacing between leads, sharp lead corners, bend radii, spacing between leads, part height, etc.), (6) nozzle height, (7) coating flow micro-adjust, (8) nozzle speed, (9) atomization pressure, (10) number of X-Y spray layers, (11) spray delta X and delta Y jog increments, and (12) tall parts that can block the spray particles or limit nozzle position.

The spray droplet coalescence steps to form a continuous film are shown in Figure 35. During spraying and after the coating is sprayed on the board, the coating droplets combine, the solvent evaporates and the film levels out. If the viscosity is too high or the film spray is too dry the film cannot level out properly and the assembly surface is uneven.

To have effective tin whisker mitigation, further work is required to obtain better coverage consistency. Techniques such as high speed photography to study droplet size and patterning, UV partial cure to secure material in place, and a method for penetrating into low component height gap spacing areas of electronic assemblies would be beneficial.

5.9.3 Automatic spray machine set – up

In the present work, the test board coupons were spray coated at Celestica in Toronto using an Asymtek SL-940 spray coater with a EFD 781S conical atomizing spray nozzle and a 591 ml (20 oz.) low volume coating reservoir (Figure 36). A combination of paper grid sheets and metal coupons were used to define the initial atomization pressure and spray pattern to obtain the desired flow and thickness. The thickness was measured on the steel panels after solvent evaporation using an eddy current meter. The eddy current was a PosiTector 6000 NS Probe, SN167346, Date Oct/31/2011 with a thickness range of 0 to 60 mils and an accuracy of ±(0.05mil+1%) for thickness of 0–2 mils and ±(0.1mil+1%) for thicknesses greater than 2 mils.

The spray pattern used an alternating X and Y pattern with a 4.4 mm step size (Figure 37). A typical nozzle speed of 250 to 350 mm/second was used and the nozzle height above the board was approximately 75 mm.

After the initial spray parameters were established, a test board was coated and visually examined for coverage and flow. The spray parameters were adjusted as needed to achieve the desired appearance. After any spray adjustments, the coating thickness on the steel panels was measured again.

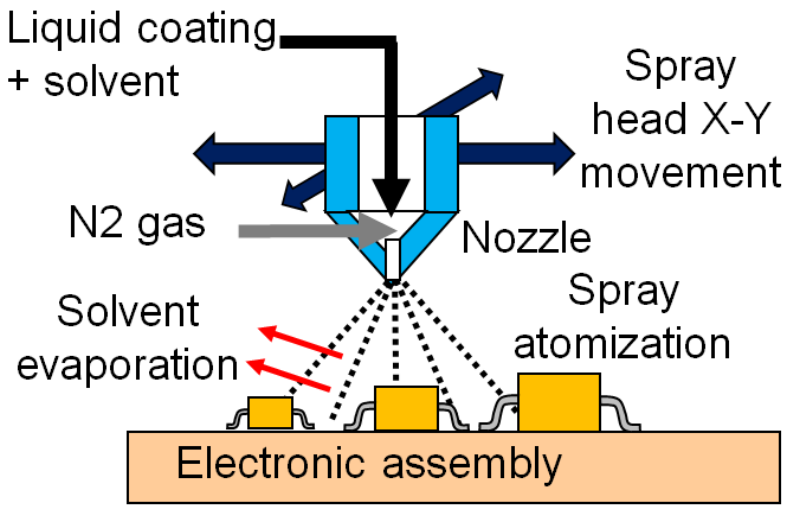


Figure 34: Schematic of spray process.

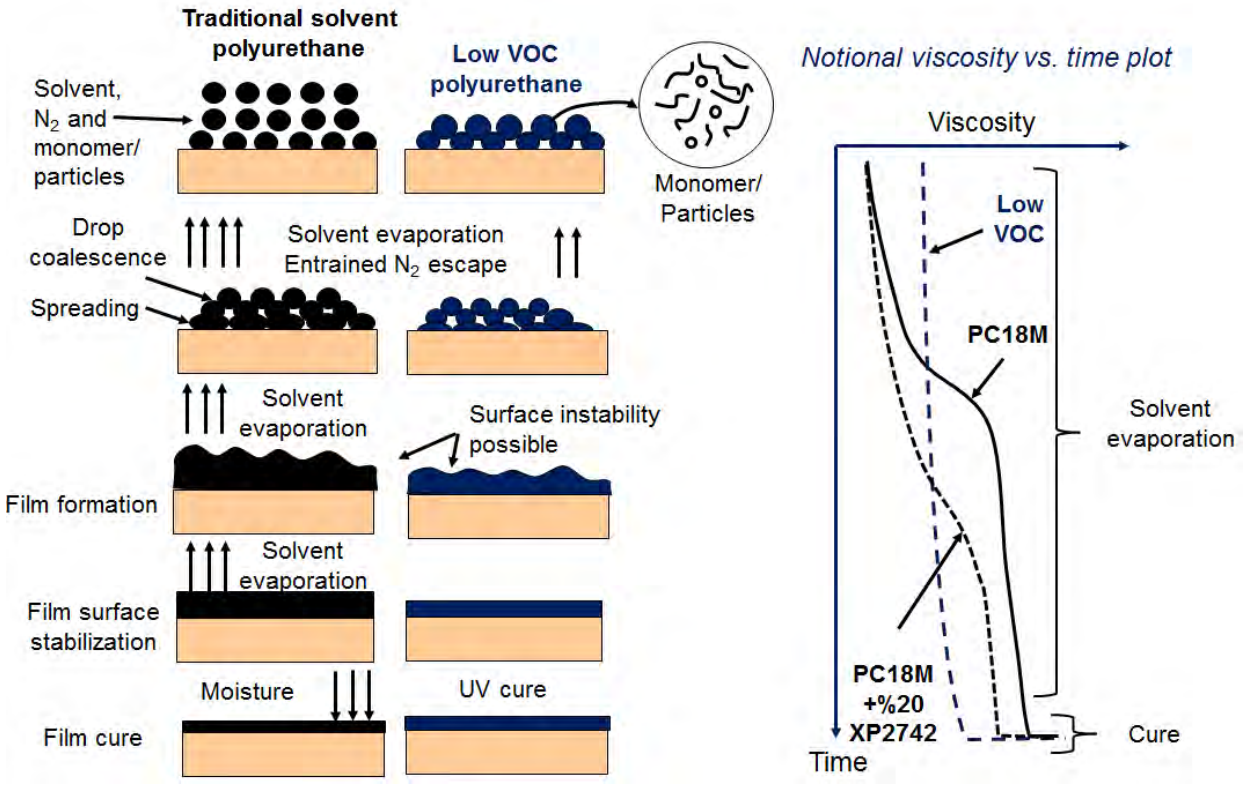


Figure 35: Coating film formation from spray coating process.

(A) (B)

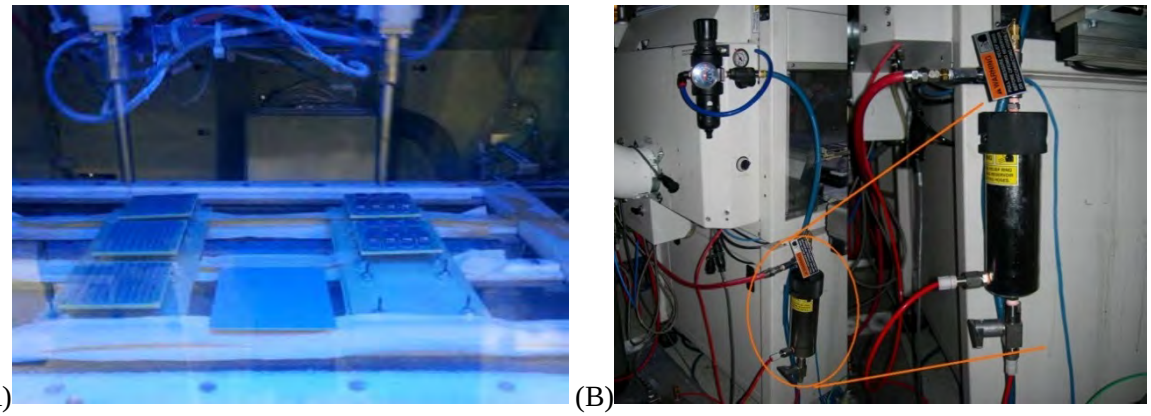


Figure 36: Spray coating machine; (A) Samples in the spray machine and (B) the small volume reservoir fitted to the rear of the spray machine. View (A) also shows a flat steel process control coupon centered between the boards.

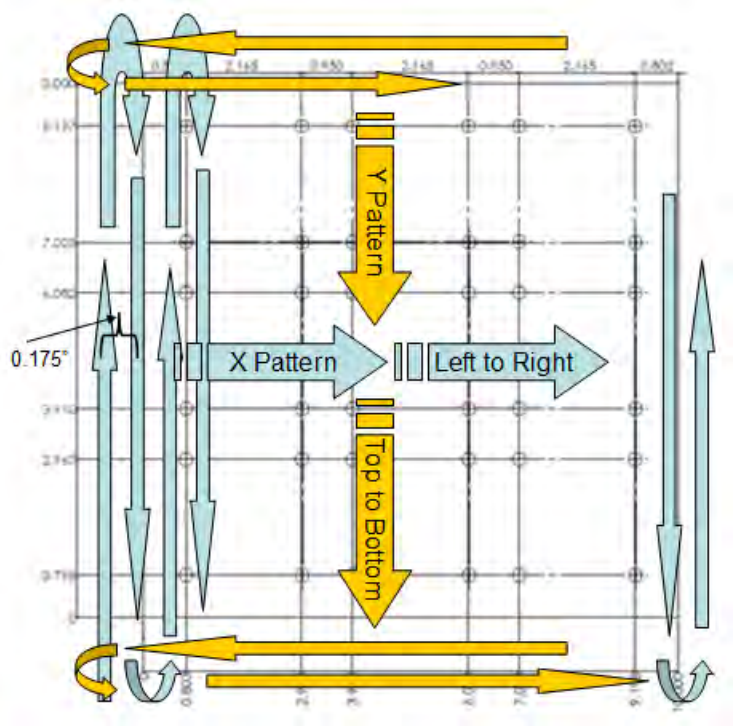


Figure 37: Typical machine spray pattern.

5.9.3.1 Coating curing

After spray coating, the assemblies were placed horizontally in a solvent drying cabinet.

The PC18M based coating samples were then placed in an oven for curing (Figure 38). The samples were then maintained at room temperature/humidity for approximately a week to obtain full properties.

The PC40-UMF coating samples were UV light cured after spray and the PC40-UMF+nanoparticle suspension coatings were solvent dried then UV cured.



Figure 38: Curing oven.

5.10 SEM Assembly coverage: Reference coatings

The details of the reference coating process SEM coverage analysis for the Parylene ™ C coating and the 1B31-LOC coating are given in Appendix F, with some highlights presented next.

5.10.1 Reference coating Parylene ™ C

The Parylene ™ C and Parylene ™ C with Adpro + coatings were very uniform on the leads and the package body (e.g. Figure 39). The vacuum deposited Parylene™ C with Adpro+ was the most uniform, with a thickness range from 27 to 30 microns (Figure 40 and Figure 41). (Note Parylene™ C was not sectioned in the present evaluation, because it had previously shown excellent thickness uniformity). Vacuum deposition is the only known process to ensure full coverage on the back side of the leads and the gaps under the parts.

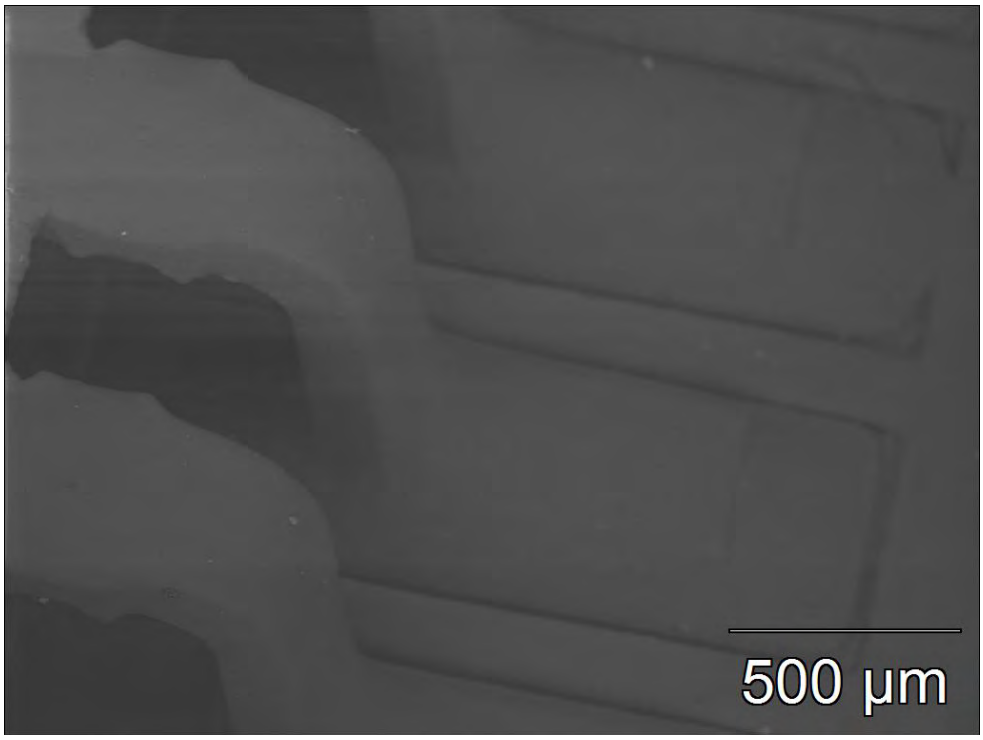


Figure 39: SEM image of Parylene ™ C coated QFP44, 60x (ref. Board 2, U5, lead 24).

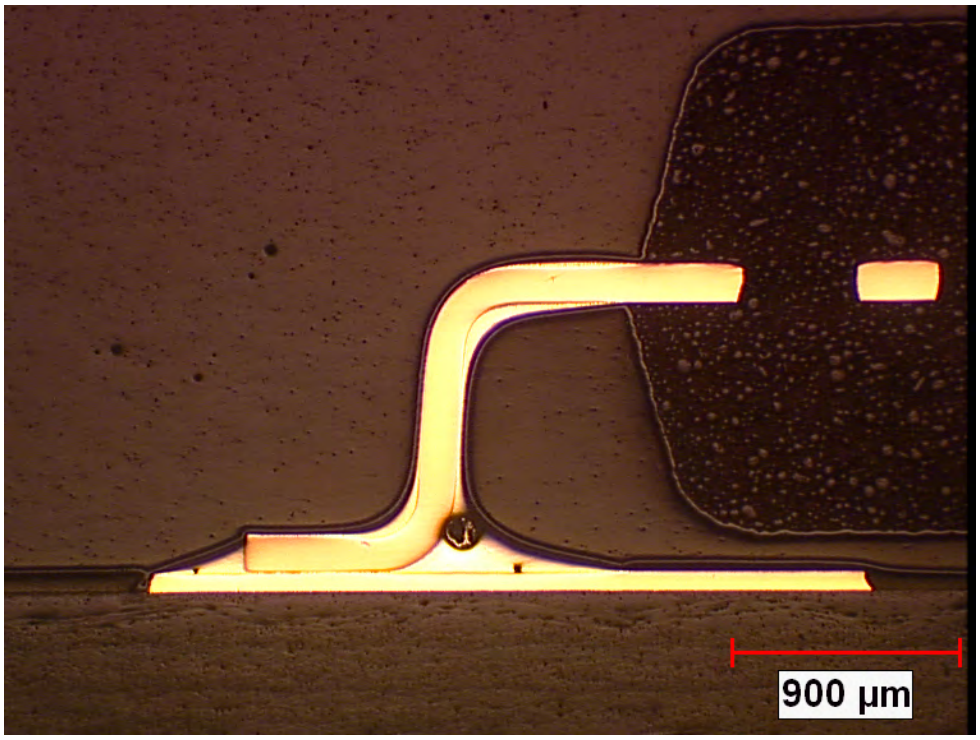


Figure 40: Optical overall cross-section image of Parylene ™ C with Adpro + coated QFP44, left lead, 25x.



Figure 41: SEM cross-section image of the Parylene ™ C with Adpro + coated QFP44, left lead, lead tip, 150x (ref. Board 1).

5.10.2 1B31-LOC Acrylic

Some assemblies were spray coated with Humiseal 1B31-LOC acrylic coating. The target coating thickness was 25 to 75 microns on a flat surface. SEM images were obtained on QFP44, QFP64, and PLCC devices. Some thinning of the coating along the lead edges and corners was observed (e.g. Figure 42).

The cross – sections of the 1B31 was not successful because the solvents in the section potting compound attacked the coating.

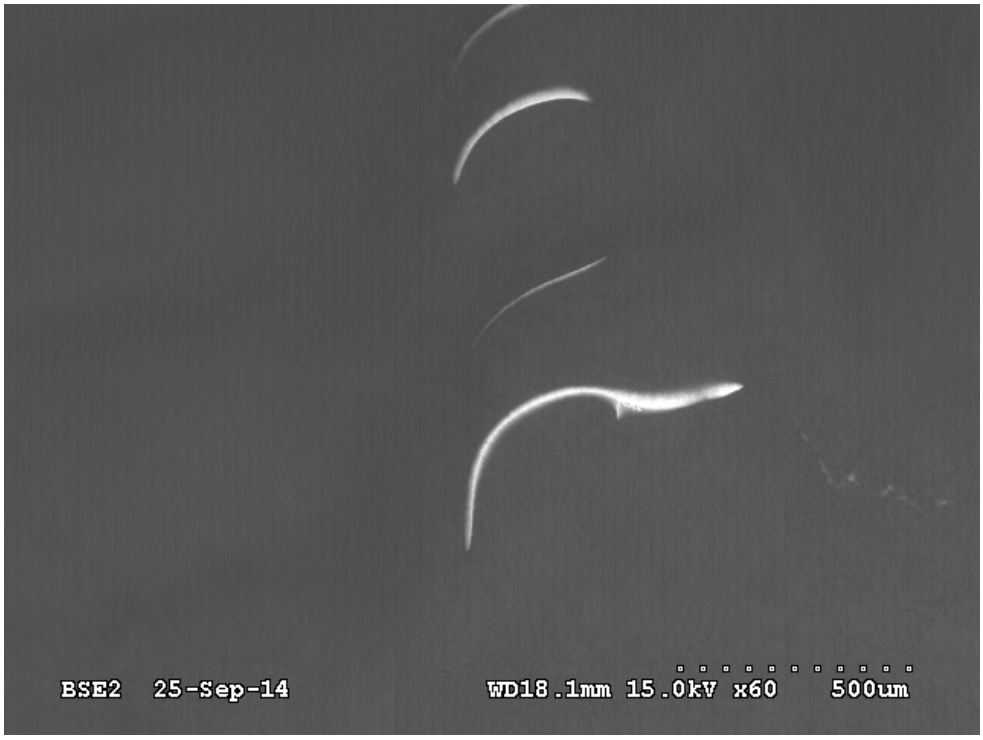


Figure 42: SEM image of 1B31-LOC coated QFP44, 60x (ref. Board 82). Light regions are where the coating is thinner than approximately three microns.

5.11 SEM Assembly coverage: PC18M Baseline (dip + 50 micron spray)

The details of the baseline coating process SEM coverage analysis are given in Appendix F, with some highlights presented next. The QFP assemblies were examined in the scanning electron microscope (SEM) to obtain overall coverage information. The images presented next focus on the QFP44 parts, but selected examinations of the PLCC and QFP64 parts were also made (Appendix F). The spray coating had greater coverage variability. The SEM image spray coating coverage classifications were (1) complete coverage (Figure 43), (2) isolated thin regions less than 50 microns (Figure 44), and (3) extended thin coverage regions longer than 50 microns (Figure 45 and Figure 46). The inspection results from the QFP44 (Table 3) revealed that the PC18M-mod had the greatest number of thin coating areas and the longest exposed edges. The PC18M+20%X11102PMA nanoalumina exhibited the best corner coverage of the spray coated samples. The PC18M+20%X2742 nanosilica coating had similar coverage to the PC18M-20%X11102PMA except that it had more corners with thin coverage. Further work is needed to determine if the coating coverage difference is due to the difference in spray passes used during coating.

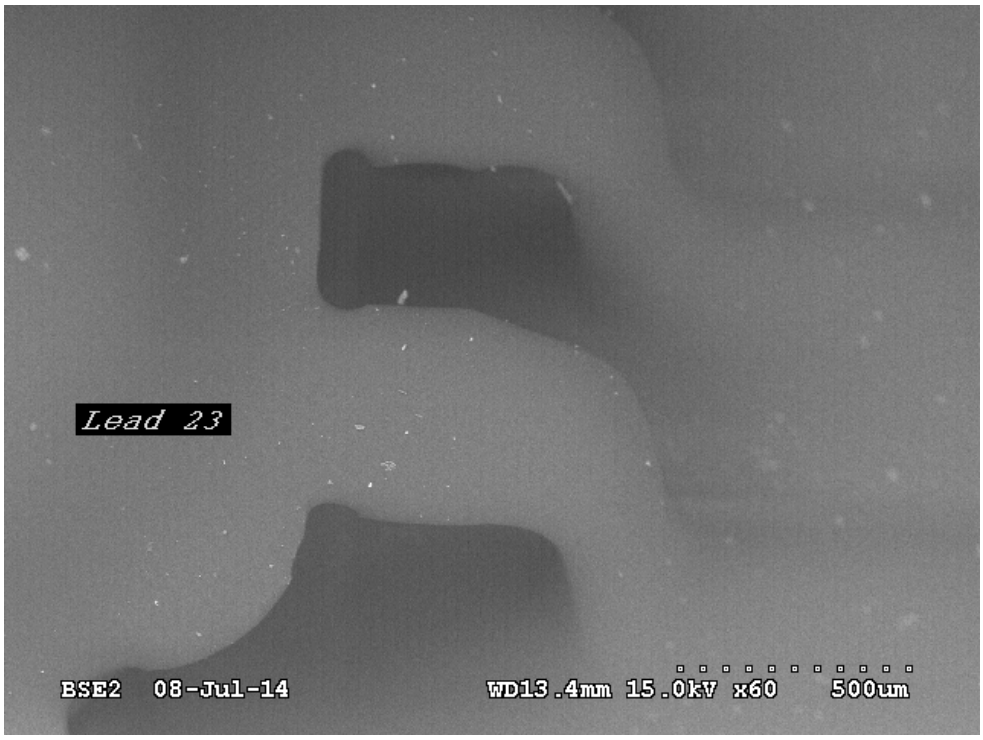


Figure 43: SEM image of baseline PC18M dip + PC18M+20%X11102PMA nanoalumina 50 micron spray showing full coverage of QFP44 leads, 60x (Ref. board 28, U2, lead 23, no environmental exposure).

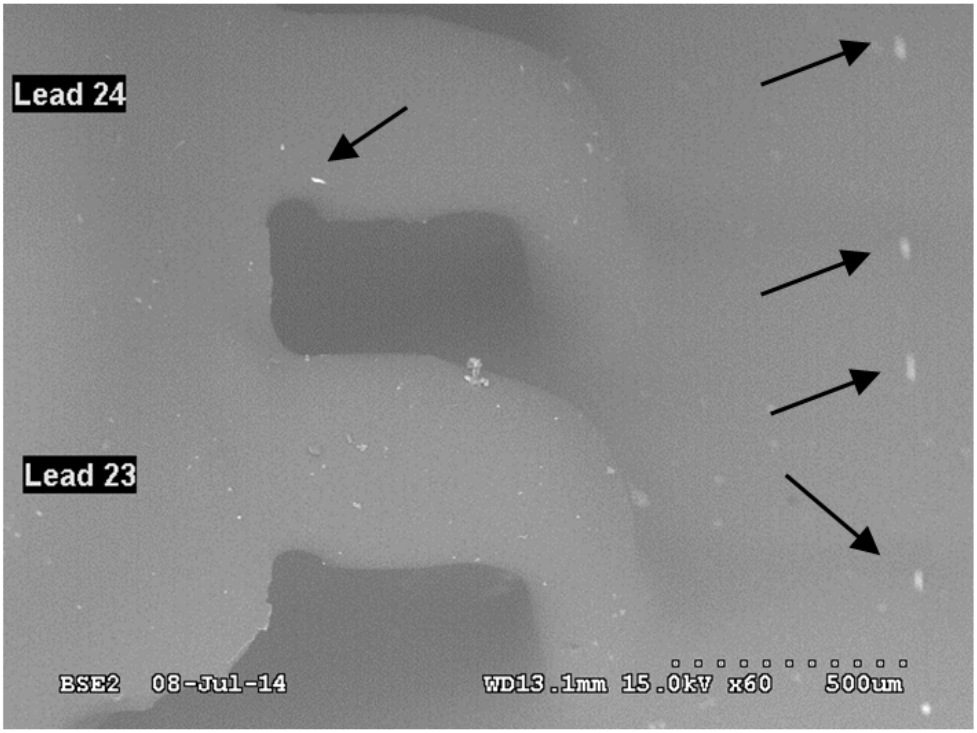


Figure 44: SEM image of baseline PC18M dip + PC18M-20%X2742 nanosilica 50 micron spray coating on QFP44 leads showing isolated thin coverage regions less than 50 microns long, 60x (ref. Board 39, U2, lead 23, image taken after thermal cycling exposure).



Figure 45: SEM image of baseline PC18M dip + PC18M-mod 50 micron spray on QFP44 leads showing extended thin coverage regions, 60x (ref. Board 15, U2, lead 23, 60x, image take after thermal cycling and 1000 hours of HTHH).

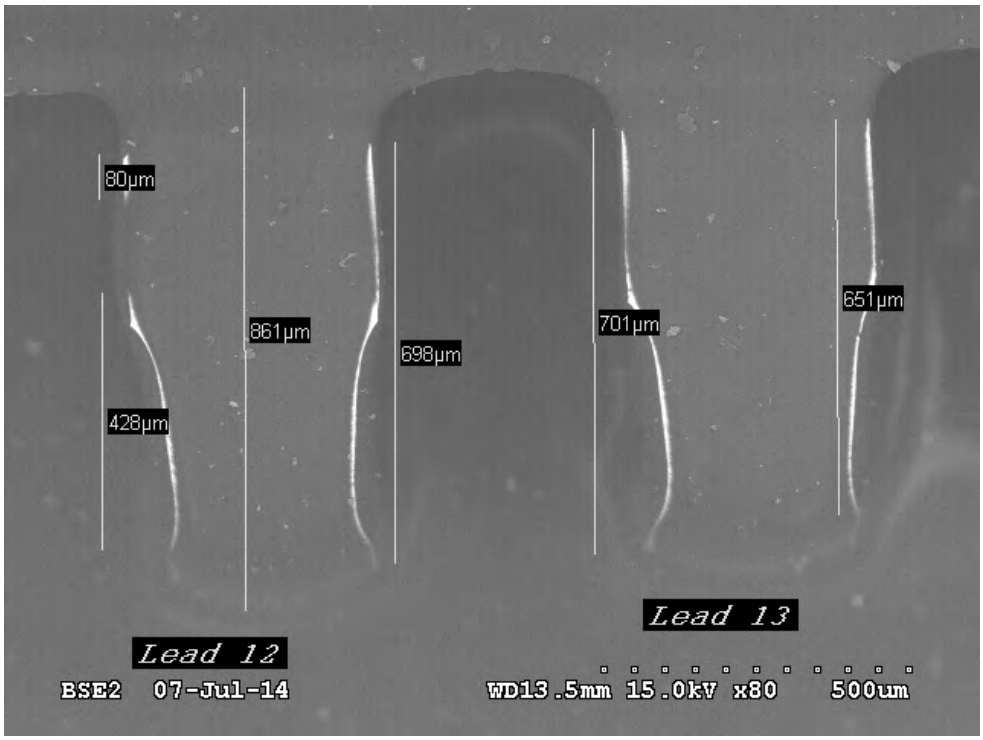


Figure 46: SEM image of baseline PC18M dip + PC18M-mod 50 micron spray on QFP44 leads showing extended thin coverage regions with measurements, 80x (ref. Board 11, U2, lead 12, no environmental exposure).

5.11.1 Baseline PC18M base coating bubble observations

Another production process risk observed on the tin whisker test assemblies was the presence of bubbles in some of the coatings during the baseline processing. For example, the PC18M-mod (Figure 47) and PC18M+20%XP2742 boards had the higher bubble density while the PC18M+11102PMA had few if any bubbles (Figure 48). However, bubble formation did not seem to depend on part type. It also was not consistent amongst PC18M and PC18M+20%XP2742 coated assemblies because some of these had few if any bubbles. There were few or no bubbles on any of the PC18M+20%X11102PMA nanoalumina coated assemblies.

Several attempts to form bubbles with very thick cast films under various temperature humidity cure conditions were unable to reproduce the condition. It was noted that PC18M has very high viscosity when no solvent is present. Since the bubble formation was observed on both the 2X-2Y PC18M-mod spray coating and the 2X-2Y PC18M+20%XP2742 spray coating but not on the 4X-4Y PC18M+20%X11102PMA boards, the thickness of material applied during each spray pass and the manner that the solvent escapes may be related to the bubble formation. The bubble formation is discussed further in Section 5.27.3 and Appendix F.

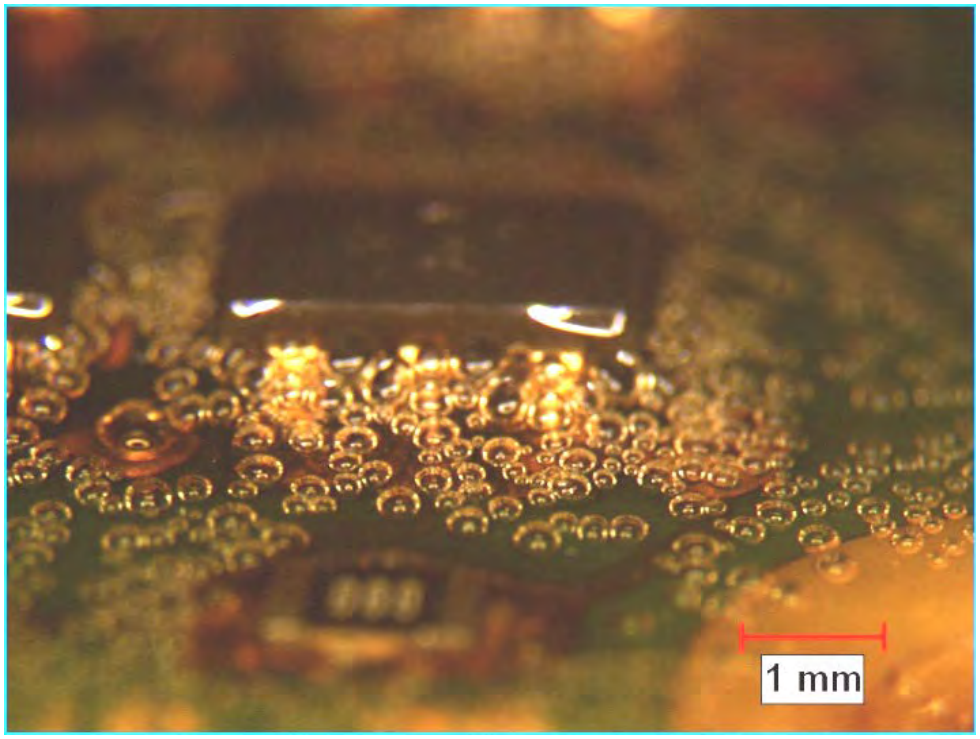


Figure 47: PC18M-mod SOT board 233 with large bubble density, 10x, after ATC+1000HTHH. The color change in the second image is an artifact of the illumination used to highlight the bubbles.

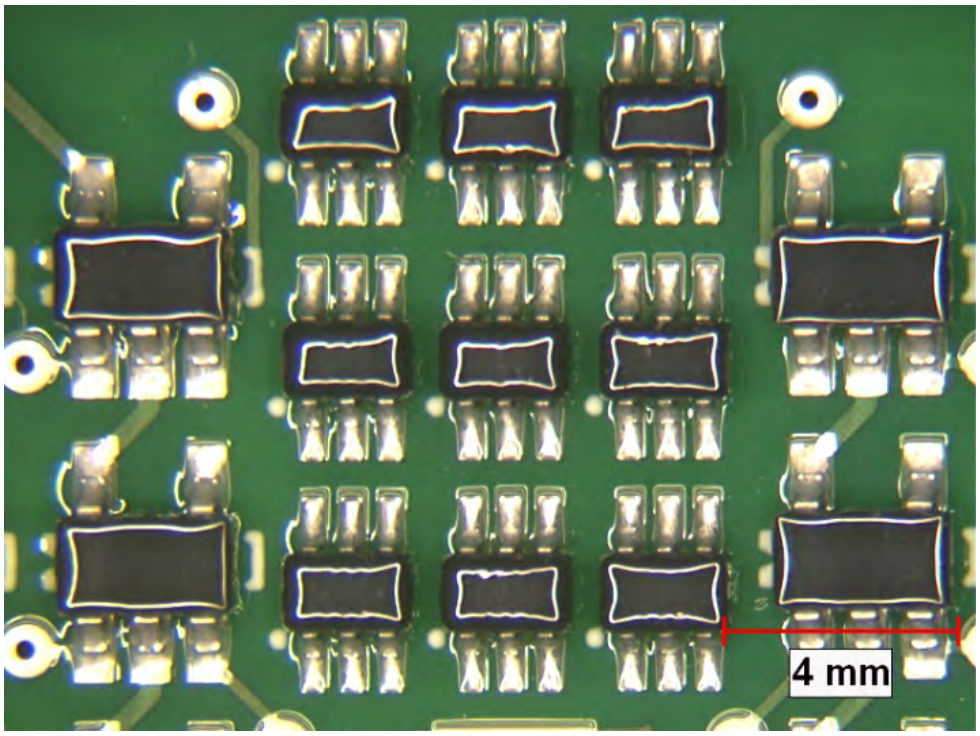


Figure 48: PC18M+20%X1102PMA, SOT board 226, 10x, small/no bubble density, milky appearance.

5.12 SEM Assembly coverage: PC40-UMF Baseline (dip + 50 micron spray)

The details of the baseline coating process SEM coverage analysis are given in Appendix F, with some highlights presented next. When processing the PC40-UMF based coatings with and without nanosilica filler, interlayer adhesion, wetting and coverage issues were encountered. Four spray batches were processed in an effort to evaluate improvements in interlayer adhesion and coverage. The first two batches used a dip + spray combination coating without (Batch A) and with (Batch B) plasma etching between the dip and spray layers. The second two batches evaluated spray coating only without a dip of unfilled standard viscosity PC40-UMF (Batch C) to high viscosity PC40-UMF (Batch D) (ref. viscosity was same as gap flow test coatings given in Figure 7).

5.12.1 PC40-UMF Batch A and B (dip+ 50 micron spray)

The PC40-UMF coated leads had poor coating coverage (Figure 49) as compared to the PC18M samples (e.g. Figure 43). Even with the addition of plasma etching between the dip and the spray layer (Batch B), there was little or no additional thickness provided by the PC40-UMF based coating spray coating layer if the leads. The plasma etching did not sufficiently increase the surface energy of the cured PC40-UMF dip coat to get good wetting without pooling of the PC40-UMF spray coating.

The coating thickness varied considerably as is summarized in Table 2. Typical delamination observed between the dip and the spray coating is shown in Figure 50.

5.12.2 PC40-UMF Batch C and D spray coating, standard and high viscosity

The standard viscosity PC40-UMF batch C coverage was considerably better without the initial dip (Figure 51A) as compared to the PC40-UMF spray coating over an initial PC40-UMF dip (Figure 49 (B) or (C)). The higher viscosity PC40-UMF batch D (Figure 51B) was not significantly better than the standard viscosity.

Table 2: Batch A and B assembly coating thickness observations of PC40-UMF, PC40-UMF+NNN2835 and PC40-UMF+N3300 from cross-sectioning. (Note NNN2283 is equivalent to XP2742)

Coating	Front of lead thickness	Continuous corner coverage	
		Vertical section	Horizontal section
PC40-UMF low viscosity dip	breaks in coverage	minimal	Little or none except if coating bridging occurred.
PC40-UMF batch A (no plasma etch between dip coat and spray coat)	breaks in coverage, consistently very thin	minimal	
Plasma etch implemented between dip coat and spray coat			
PC40-UMF batch B	very thin to 7.7µm	N/A	
PC40-UMF+10% NNN2835	very thin (not measureable) to 7.7µm	thin top layer (not complete coverage of bottom layer)	
PC40-UMF+30% NNN2835	breaks in coverage	very thin, bottom layer only	
PC40-UMF+50% NNN2835	complete coverage, 1.4 to 15µm	minimal	
PC40-UMF+15.54%N3300	complete coverage, 0.55 to 1.8µm	little or none	

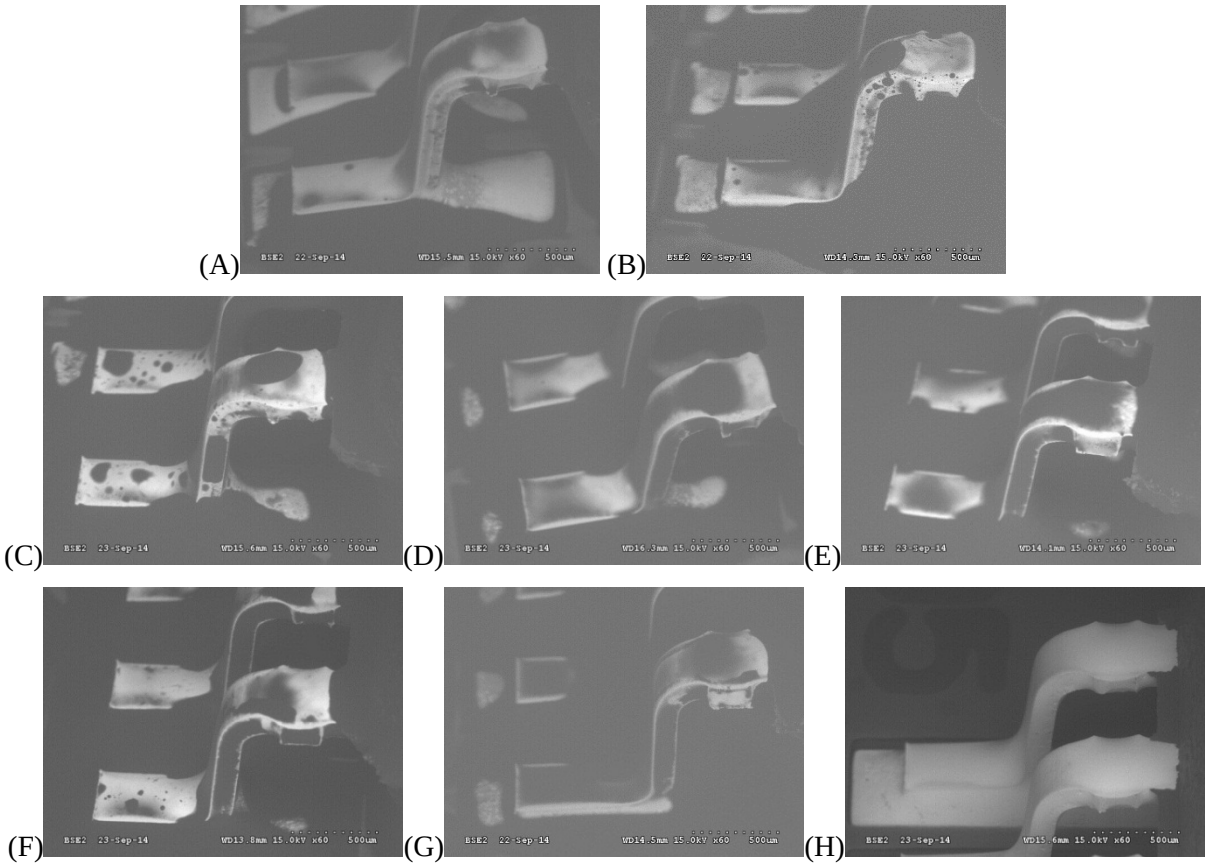


Figure 49: Batch A and B QFP44 SEM images of PC40-UMF coating based coating; (A) PC40-UMF dip coat, (B) PC40-UMF (no plasma between dip and spray), and the following spray coated samples with plasma etch between the dip and the spray layers: (C) PC40-UMF batch 2 with plasma, (D) PC40-UMF+10%NNN2835 nanosilica, (E) PC40-UMF+30%NNN2835 nanosilica, (F) PC40-UMF+50%NNN235 nanosilica, and (G) PC40-UMF+15.54%N3300. Image (H) shows an uncoated control board.

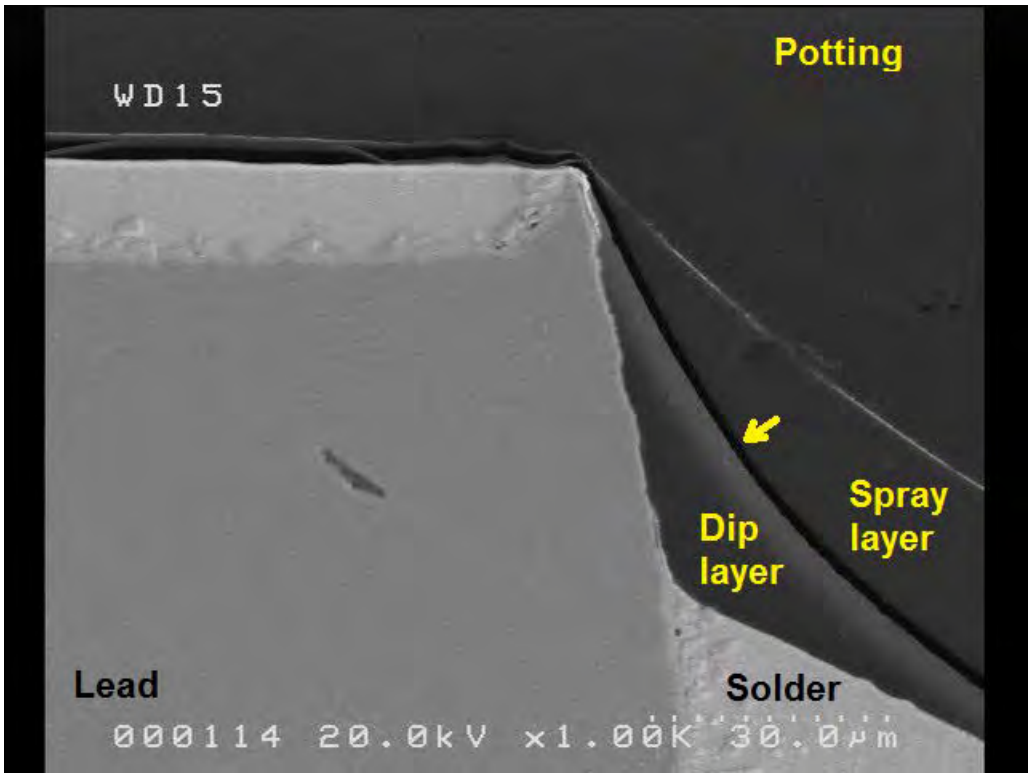
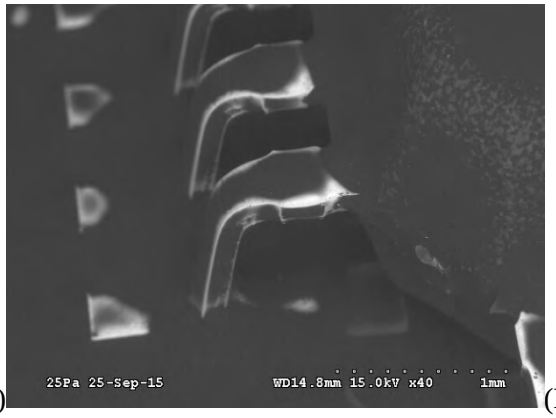


Figure 50: SEM cross – section showing separation between the PC40-UMF dip layer and PC40-UMF + 10%NNN2835 nanosilica spray layer processed with plasma etching after dip coating cure,1,000x. (ref. Board 62, QFP44, location T). Arrow highlights delamination between the dip and spray layers.

(A) 

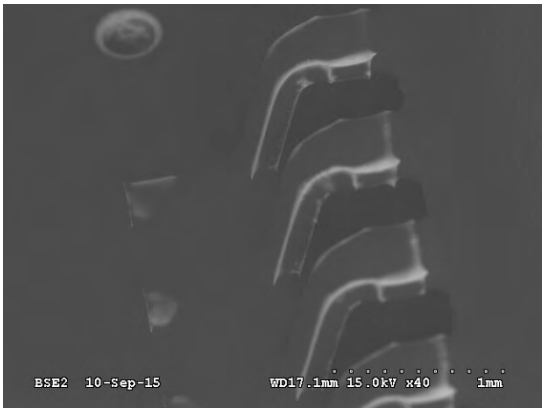
(B) 

Figure 51: Batch C SEM image of PC40-UMF coated QFP44 leads, 40x; (A)standard viscosity (ref. Asymtech 8-2015) and (B) high viscosity coated QFP44, 40x (ref. Asymtech 8-2015).

5.13 SEM Assembly Coverage: Enhanced layered coating (dip + 25 micron spray + 25 micron spray)

The details of the enhanced layered coating process SEM coverage analysis are given in Appendix I, with some highlights presented next.

5.13.1 Initial dip coating coverage

SEM examination of the “dip only” QFPs showed that the front and portions of the lead sides had coating thicker than approximately three microns (darker areas in Figure 52), while the corners and edges of the leads and the board pads were thin (light areas in Figure 52). The dip coating resulted in some bridging of the QFP44 and QFP64 leads (Figure 53 to Figure 55). Cross – sectioning showed that the coating webs between leads were generally thin.

Bridging is undesirable because it adds stress to the solder joints during thermal cycling.

5.13.2 Dip + one 25 micron spray

One spray layer of PC18M over the PC18M dip coating exhibited good coverage, but was rough (Figure 56).

The PC18M dip + one 25 micron spray (PC18M+20%XP2742) nanosilica resulted in good coverage (Figure 57) and was smoother than the PC18M coating.

5.13.3 Dip + 25 micron spray + 25 micron spray

The additional spray and cure step in the PC18M dip + 25 micron spray + 25 micron spray (two 25 micron sprays) layer build up improved coverage for both the PC18M spray (Figure 58) and the PC18M+20%XP2742 nanosilica filled spray (Figure 59). Although coverage was improved, there were some very small thin coating areas on some of the lead tips (Figure 60).

The degree of surface roughness was greater with the two 25 micron PC18M spray layers than with the two 25 micron PC18M+20%XP2742 nanosilica spray layers. The PC18M spray surface appeared to have pits and craters that looked like popped microbubbles. Optically the PC18M spray was duller than the PC18M dip and the PC18M+20%XP2742 nanosilica spray coatings (Figure 61).

Roughness due to microbubbles would likely reduce film strength by adding stress concentration sites. The factors contributing to the observed roughness is discussed further in Section 5.27.3 and Appendix F.

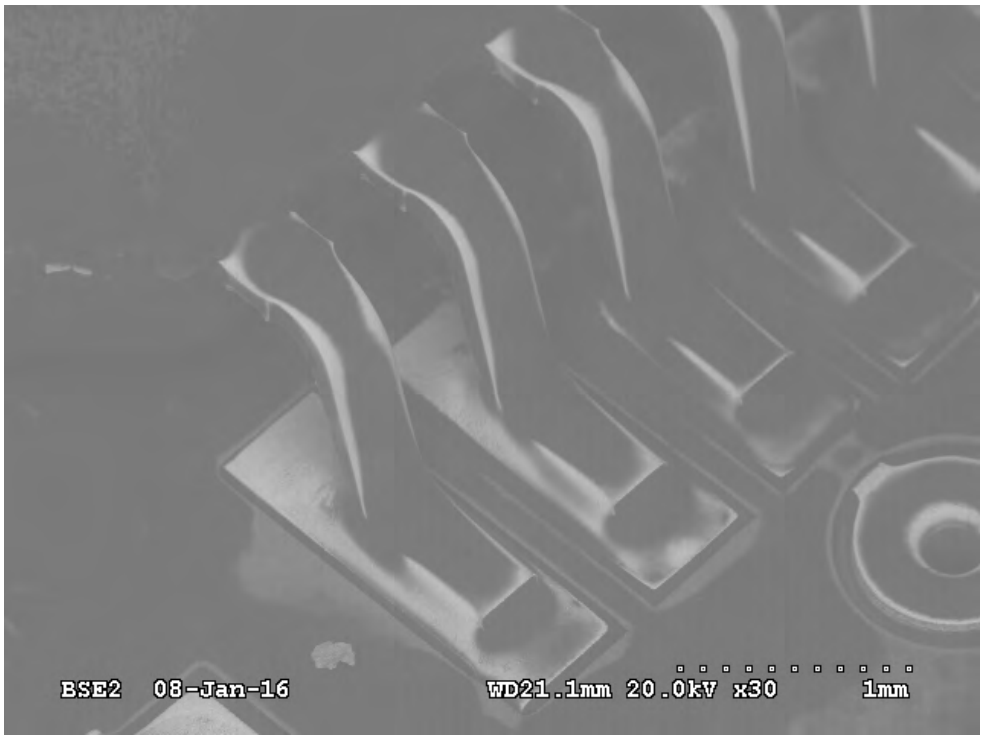


Figure 52: SEM image of PC18M dip coated QFP44, board A261, with the light gray color revealing thin coating coverage areas, 30x.

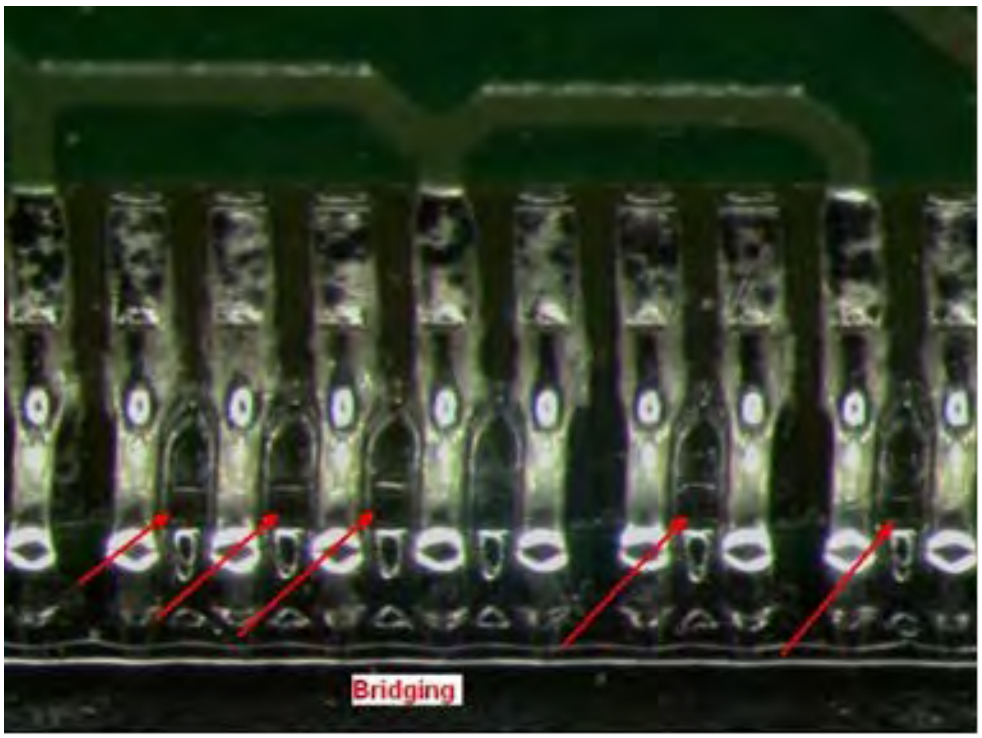


Figure 53: Optical image showing example of coating bridging between leads on the board A261, dip only, QFP44, 25x.

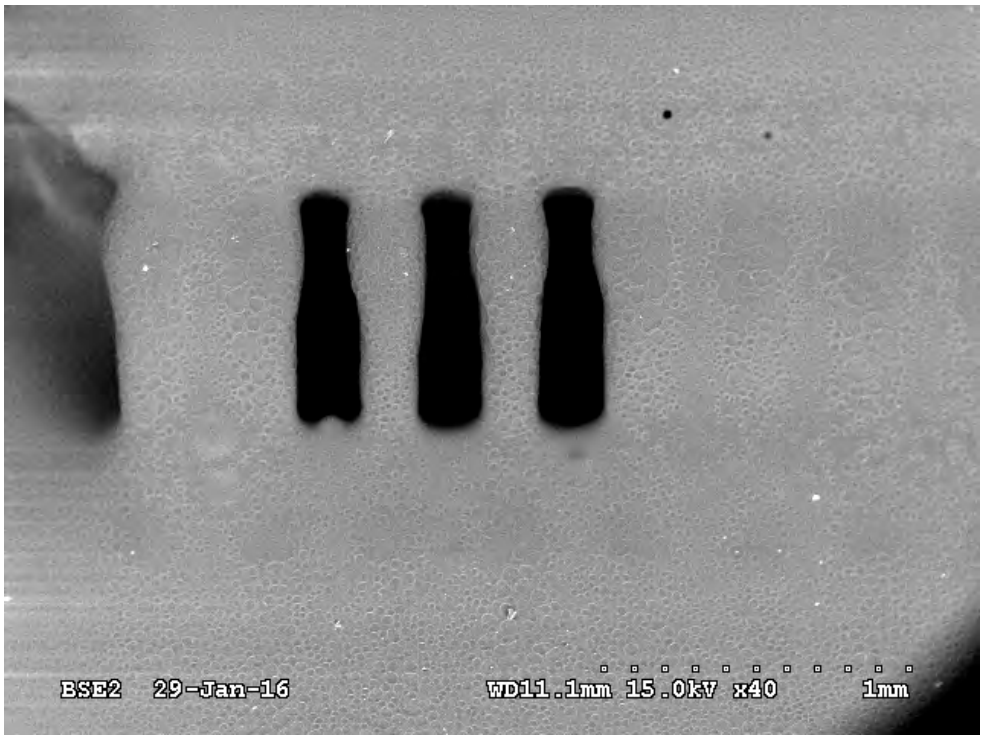


Figure 54: SEM image of PC18M dip + two (PC18M+20%XP2742) sprays board A336, QFP64, 40x, with coating bridging.

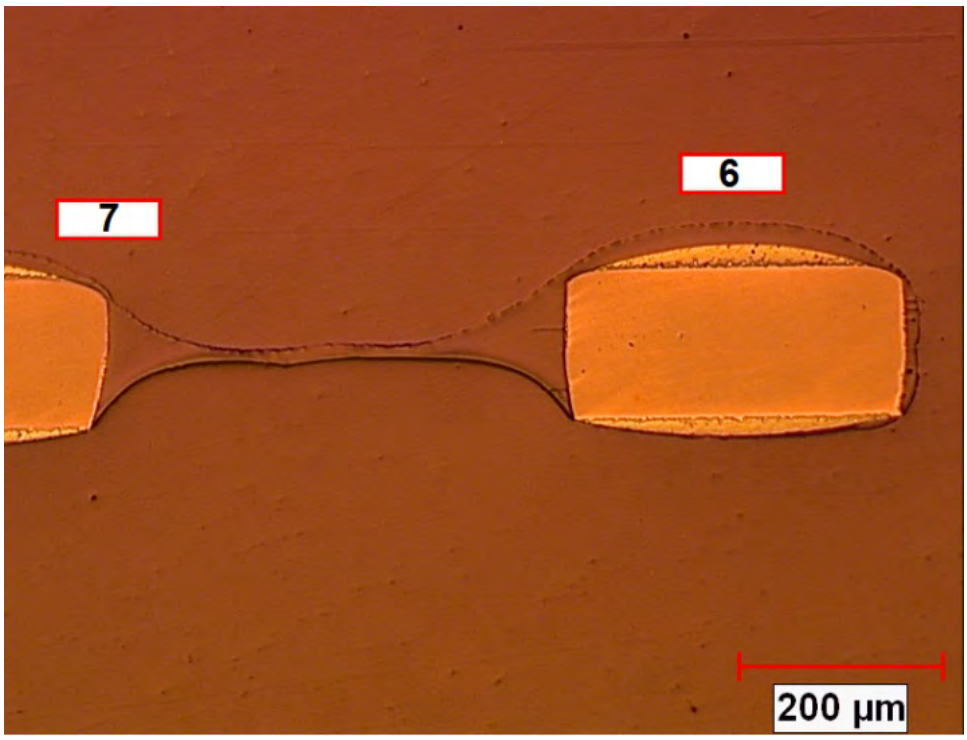


Figure 55: Cross-section optical image of PC18M dip + two (PC18M+20XP2742) sprays, board A225, U1203, QFP44, lead 6-7 showing coating bridging, 100x.

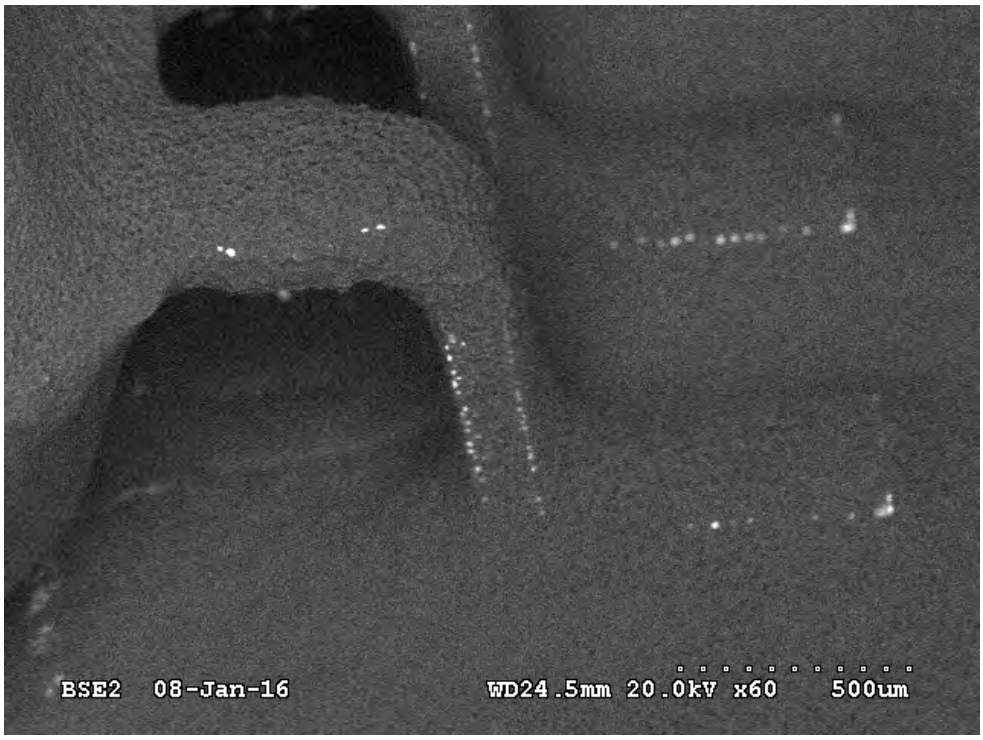


Figure 56: SEM image of PC18M dip + 25 micron spray, QFP44, board A156, exhibiting thin coating lead edges and backside of pad as well as surface roughness, 30x.

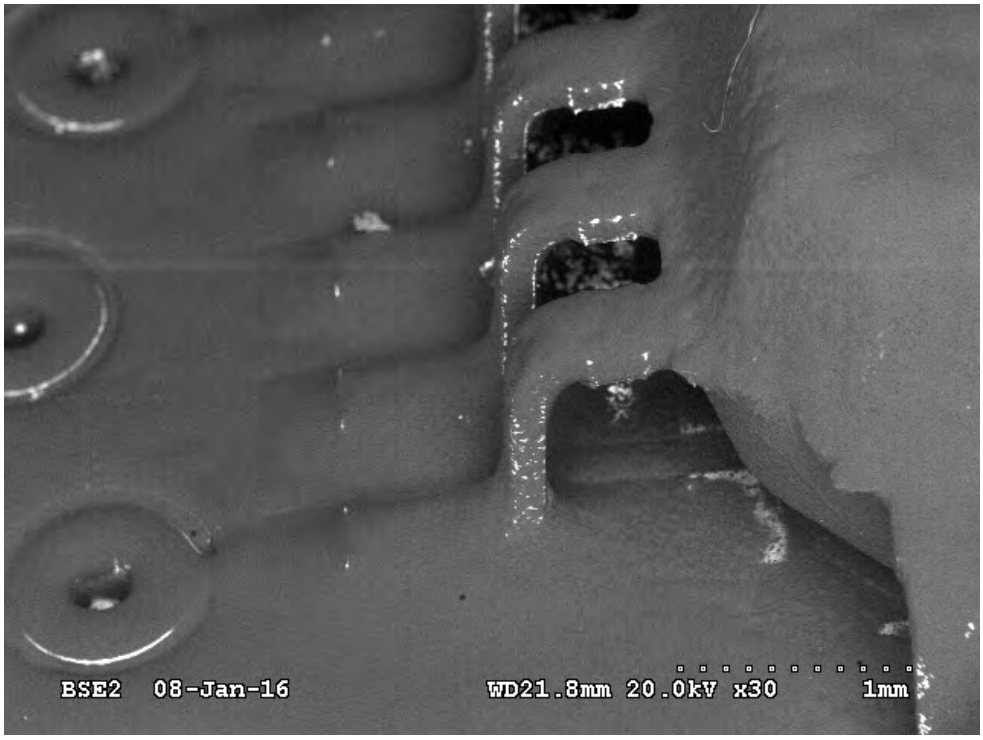


Figure 57: SEM image of PC18M dip + 25 micron (PC18M+20%XP2742) spray, board A348, QFP44, thin coating on edges and vertical surfaces of the leads and the printed wiring board vias, 30x.

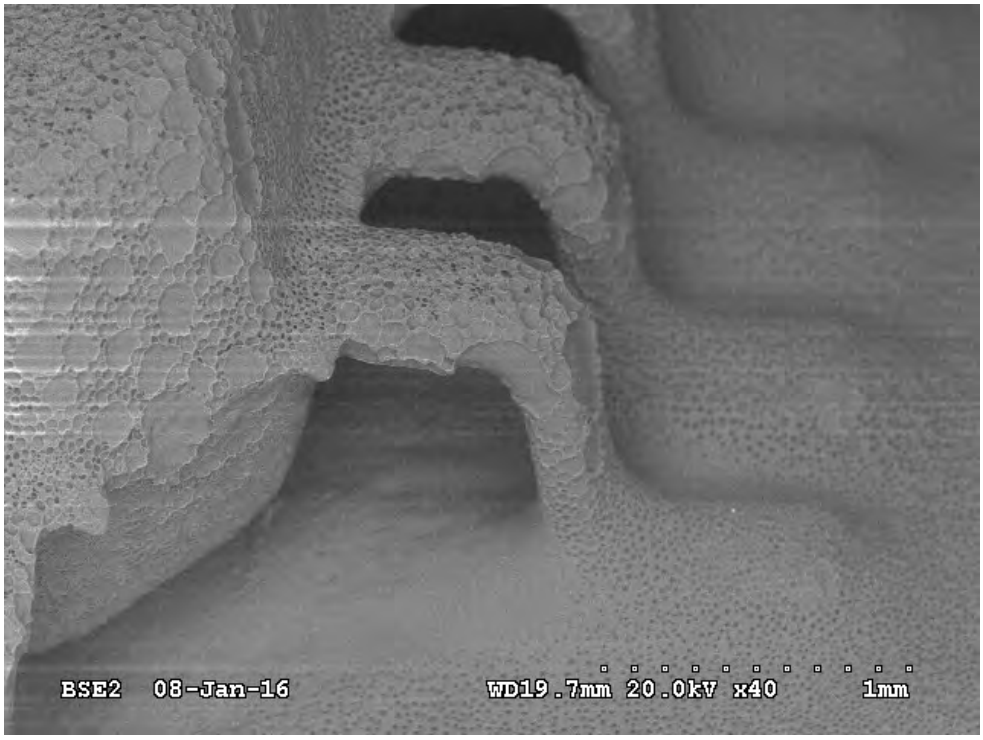


Figure 58: SEM image of PC18M dip + two 25 micron PC18M sprays, board A191, QFP44, with good overall coverage but still exhibiting surface roughness, 40x.

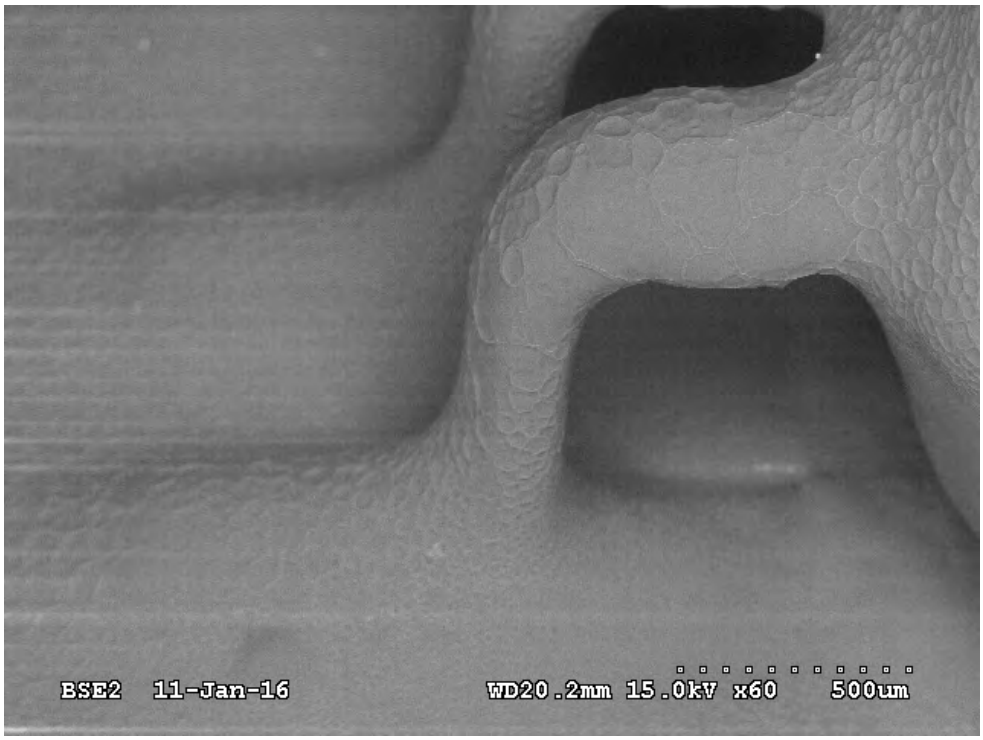


Figure 59: SEM image of PC18M dip + two (PC18M+20%XP2742) sprays, board A336, QFP44, 15KV, with good coverage on different leads than those shown in Figure 60, 60x.

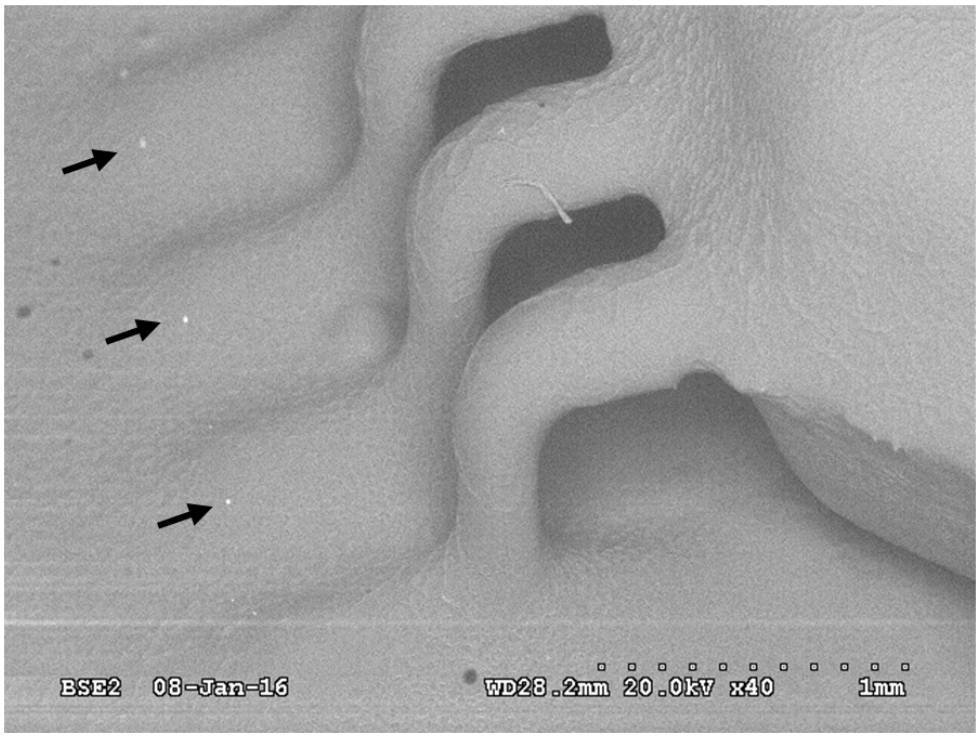


Figure 60: SEM image of PC18M dip + two (PC18M+20%XP2742) sprays, board A336, QFP44, 15KV, good thick coverage, but arrows indicate small thin coverage areas, 40x.

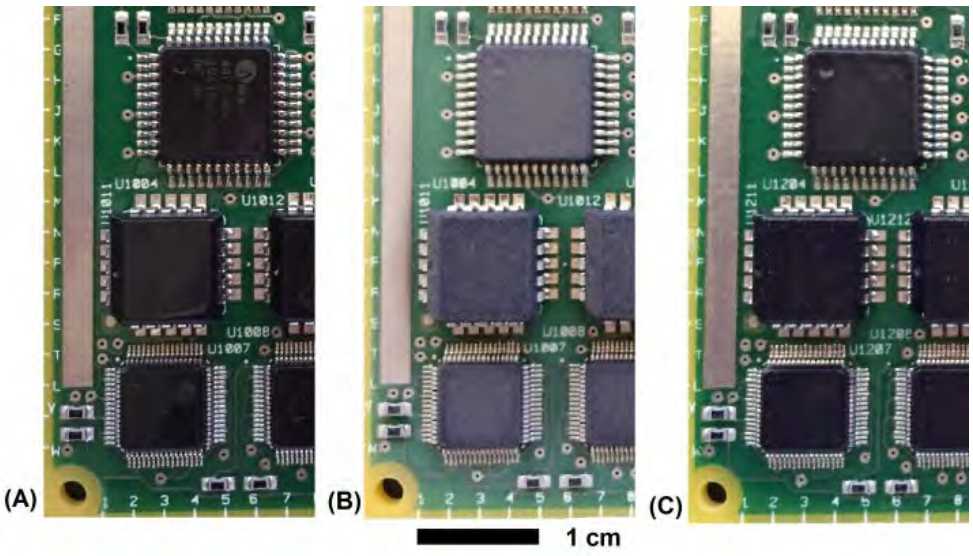


Figure 61: Photographs illustrating the surface luster of QFP board; (A) PC18M dip only, (B) PC18M dip + two PC18M sprays, and (C) PC18M dip + two (PC18M+20%XP2742) sprays. Image B shows the increased dullness due to the high microbubble roughness of the PC18M spray layer build up.

5.13.4 Baseline and enhanced layered coating coverage comparison

The layered coating coverage was generally better than the coverage obtained earlier with the baseline PC18M dip followed by a baseline 50 micron spray coating process.

By counting the number of thin coating regions for various coatings, the layered spray coatings were measurably better than the baseline coatings (Table 3). While the current SEM results favor the PC18M without the nanoparticles, the roughness of the PC18M surface made it more difficult to examine the lead tips areas.

Table 3: QFP44 SEM baseline and enhanced layered coating coverage inspection results.

Coating	Total leads inspected (1)	Total thin areas	Total less than 50 µm	Total greater than 50 µm
Baseline PC18M dip + 50 micron PC18M spray	14	43	15	28
Baseline PC18M dip + 50 micron PC18M+20% XP2742 spray	17	10	10	1
Enhanced layered PC18M dip + two 25 micron PC18M sprays (1)	11	3	3	0
Enhanced layered PC18M dip + two 25 micron PC18M+20%XP2742 sprays	11	11	11	0
Note 1: The rough surface on the PC18M sprayed samples made it difficult to examine for thin coating.				

5.14 Vertical cross - section thickness: PC18M Baseline (dip + 50 micron spray)

The details of the baseline process vertical sectioning is given in Appendix F, with some highlights presented next. The vertical cross-section coating thickness analysis was performed on the QFP44 components. A typical overall cross – sections images is shown in Figure 62. The measurement locations are given in Figure 63 to provide thickness characterization over the entire lead, not just the flat part of the board.

For the baseline dip + 50 micron spray, the PC18M based coating vertical cross-section evaluation showed that coating thickness ranged from between 0.06 to 76 microns on the front of the lead and 0.5 to 103 microns on the back of the lead (Table 4). The minimum and maximum for each coating type is given in Table 5.

Location T in the front always had the thinnest coating; ranging from 0.06 to 37 microns for the PC18M-mod spray and from 13 to 29 microns for the PC18M+20%XP2742 nanosilica spray. Coating surface tension effects during spray coating resulted in thin coating over sharp corners, but the amount of thinning depended upon the coating type. The PC18M-mod did not cover the lead toe corners well (Figure 64). The PC18M+20%XP2742 had good lead tip coverage (Figure 65).The PC18M+20%X11102PMA coating also provided good lead tip coverage (Figure 66). Even though the PC18M+20%X11102PMA coating had good corner coverage, the back of lead coverage was dependent upon the dip coat which was thin (Figure 67). The Parylene ™ C reference coating had the best coverage (Figure 68).

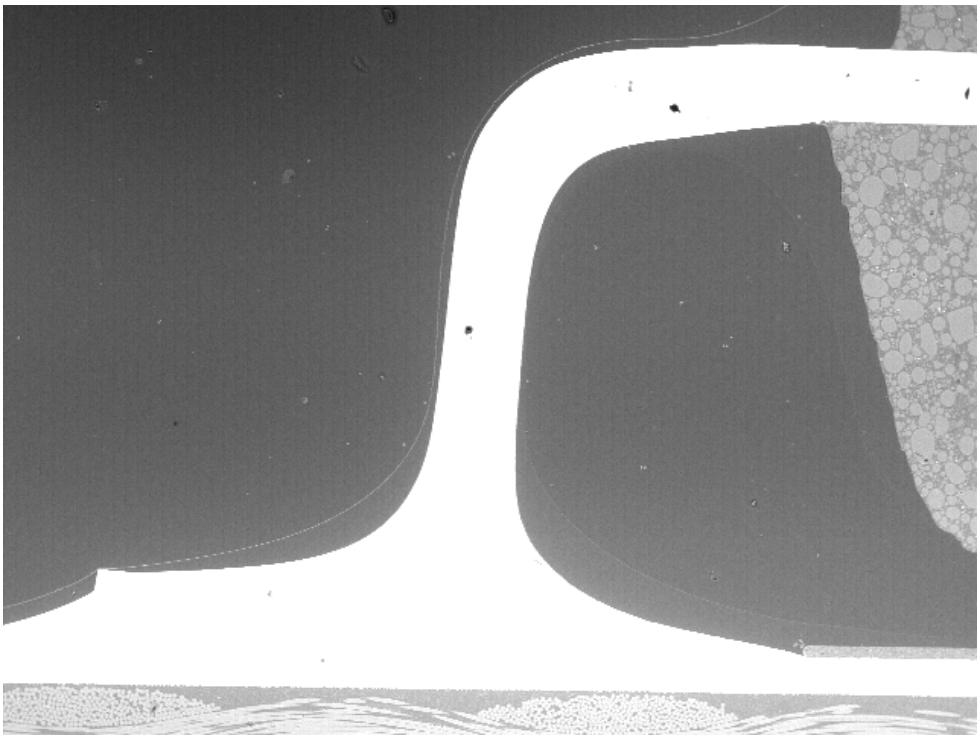


Figure 62: Typical SEM image of a coating cross-section, 60x (Ref. Baseline PC18M-mod, board 12, QFP44, left lead).

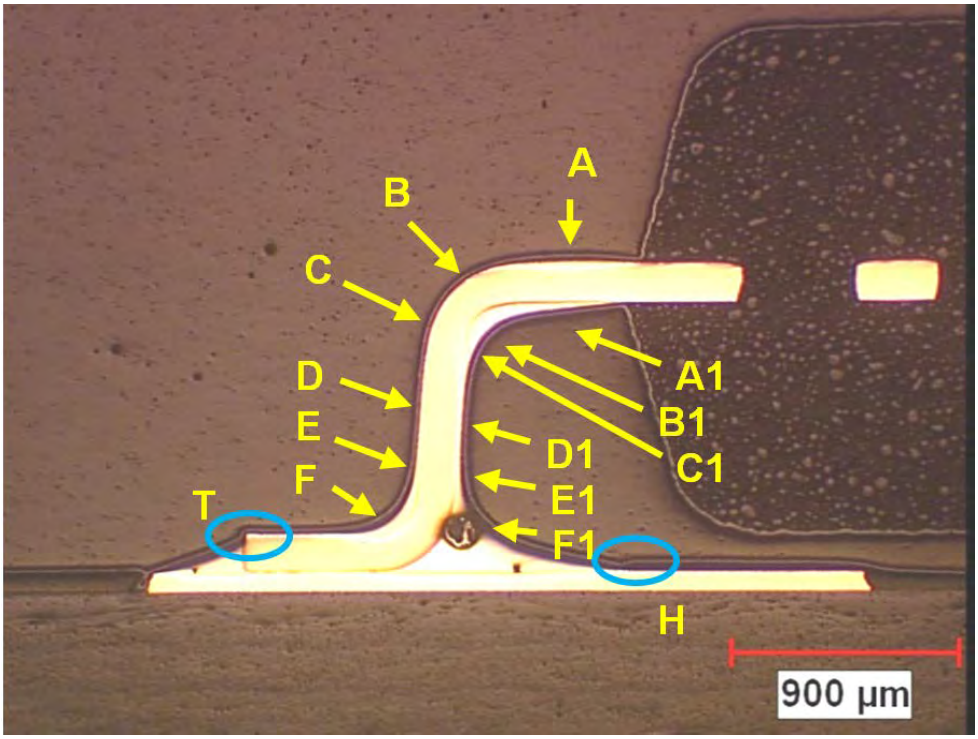


Figure 63: Vertical cross-section thickness measurement locations.

Table 4: Coating thickness measurements for baseline (PC18M dip + 50 micron spray) process PC18M based coatings on QFP44 leads.

Sample	Lead	Coating Thickness (microns)													
		A	B	C	D	E	F	T	A1	B1	C1	D1	E1	F1	H
PC18M-mod spray	R	28	32 36 42	45	42	32	32 37 38	2 0.06 37	1.6 0.8 1.4	31 34 29	18	13	7	22 42 46	7 25 20
	L	19	14 15 13	23	21	17	48 71 76	13 0.56 36	26	33 32 29	16	9	3.2	74 103 100	62 70 45
PC18M +20% XP2742 spray	R	65	52 50 53	50	31	28	33 36 43	20 13 36	0.5 0.6 0.8	7 6 7	2.2	7	5	8 6 8	10 14 9
	L	66	60 45 43	42	39	37	49 59 58	20 18 29	8	14 20 19	10	5	0.8	4 4.2 3.7	4 10 8
PC18M +20% X11102 PMA spray	R	73	69 67 66	71	64	60	62 62 58	14 10 37	5	10 15 10	9	5	2.4 1.8 4	4 3.5 4	7 15 12
	L	52	54 54 48	43	40	38	39 48 52	15 17 45	1.2 1.8 2.2	18 17 16	12	9	3.7 2.4 1.5	4.3 5.5 6.8	8 12 8
Parylene C with Adpro+	R	28	28 28 28	28	28	28	29 29 28	31 28 29	28	27 28 28	27	28	28	28 28 29	30 29 30
	L	29	29 30 29	28	28	27	30 30 30	29 28 27	28	27 30 28	28	27	28	29 28 29	27 27 29

Table 5: Baseline (PC18M dip + 50 micron spray) PC18M based coated QFP44 minimum and maximum thicknesses from Table 4.

Coating	Min/Max	Front (micron)	Back (micron)
PC18M-mod spray	Min	0.06	0.8
	Max	76	103
PC18M+20%XP2742 spray	Min	13	0.5
	Max	66	20
PC18M+20%X11102PMA spray	Min	10	0.5
	Max	73	18
Parylene C with Adpro+	Min	27	27
	Max	31	30

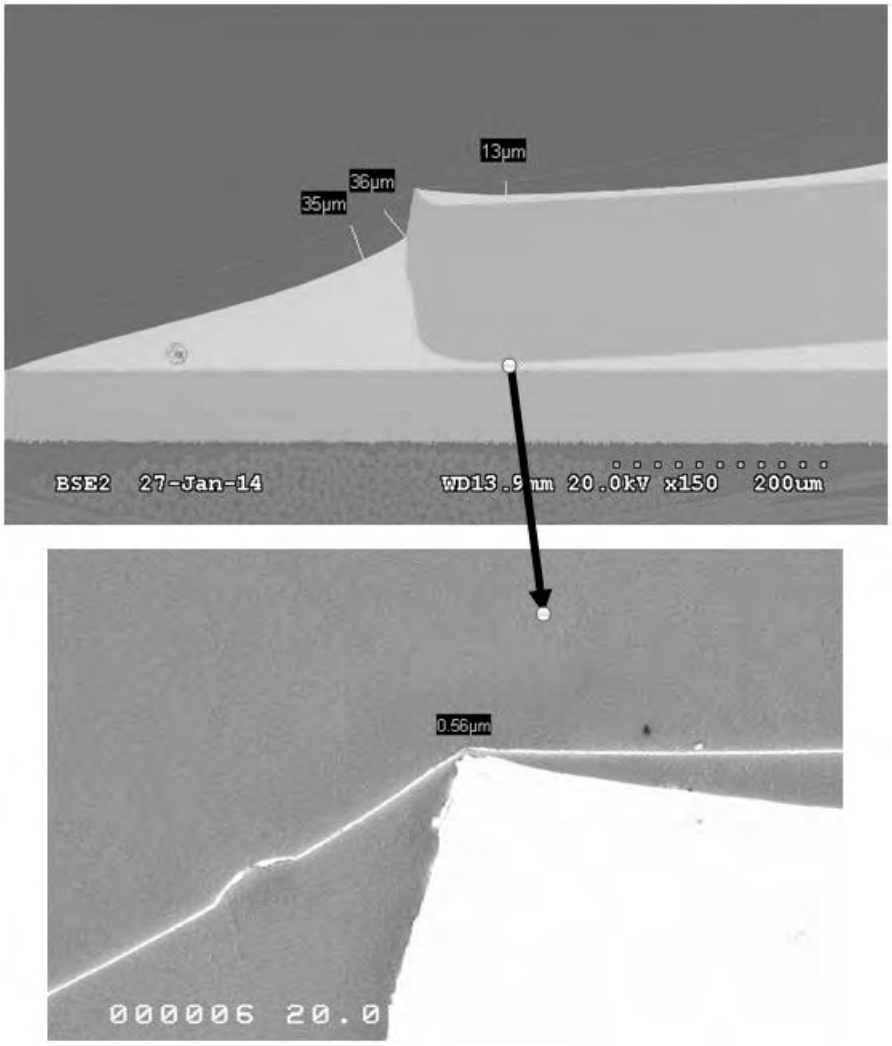


Figure 64: Lead tip cross-section showing thin coverage. SEM image of baseline PC18M dip + PC18M-mod unfilled 50 micron spray, board 12, QFP44, left lead, location T, 150x and 2,000x.

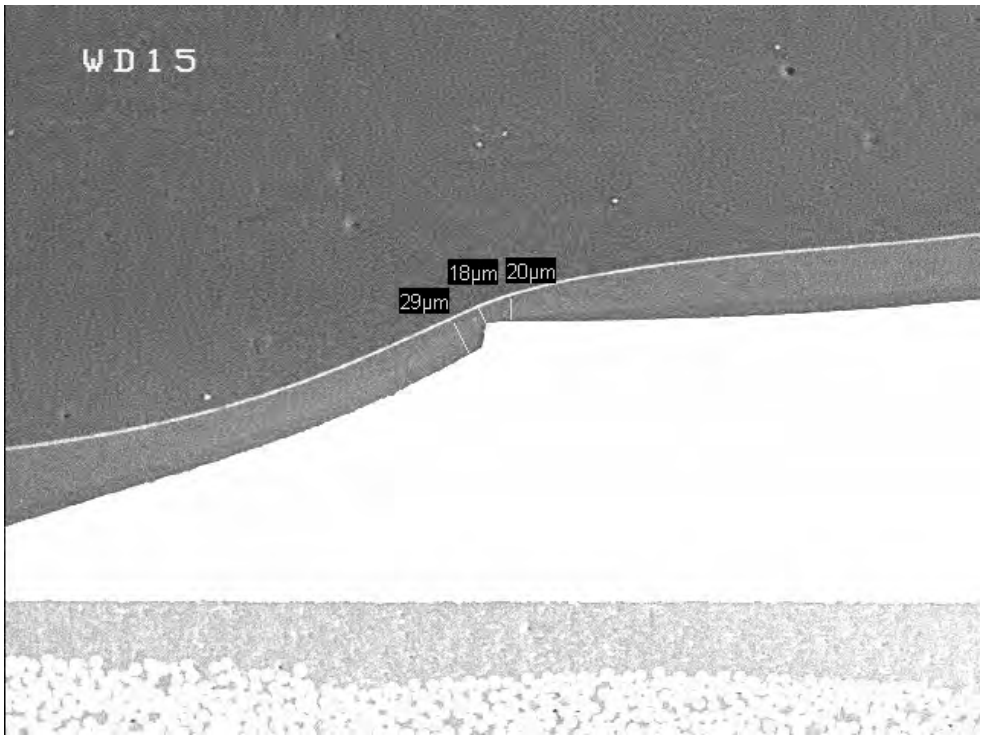


Figure 65: Cross-section SEM view of baseline PC18M dip + PC18M-20%XP2742 nanosilica 50 micron spray coated QFP, left lead, location T, SEM, 150x (ref. Board 20)

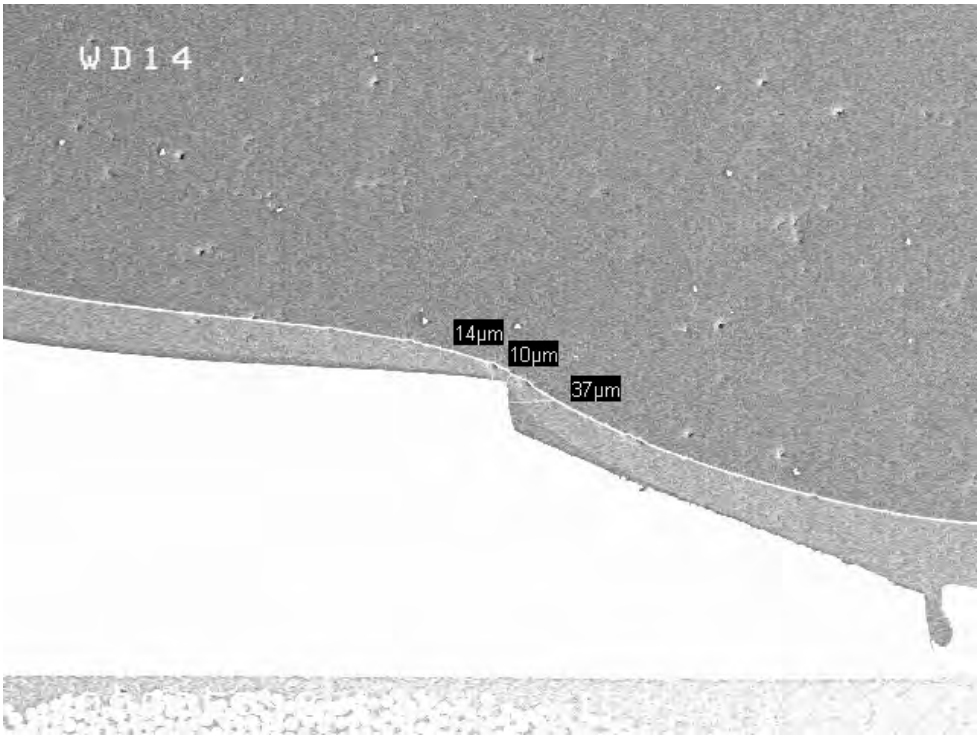


Figure 66: Lead tip cross-section showing thicker coverage. SEM image of baseline PC18M dip + PC18M-20%X11102PMA nanoalumina 50 micron spray coated QFP, right lead, location T, 150x (ref. Board 12).

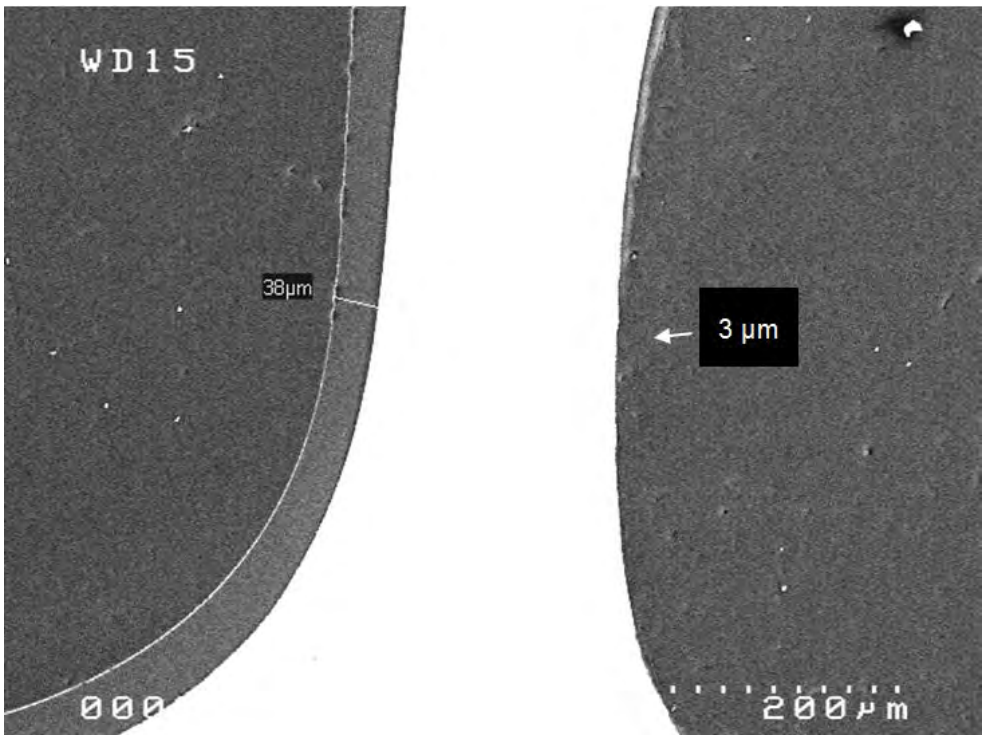


Figure 67: Cross-section SEM view of baseline PC18M dip + PC18M-20%X1102PMA nanoalumina 50 micron spray coated QFP, left lead, location E, 150x (ref. Board 12).



Figure 68: SEM cross-section image of the Parylene ™ C with Adpro + coated QFP44, left lead, location T, 150x (ref. Board 1).

5.15 Vertical cross – section thickness: Enhance layered coating (dip + 25 micron spray + 25 micron spray)

The details of the enhanced layer process vertical sectioning is given in Appendix I, with some highlights presented next. The goal for the enhanced layered coating (PC18M dip + 25 micron spray + 25 micron spray) was to have the minimum coating thickness of 10 microns on the front and side lead surfaces, less pooling at the bottom of the lead and/or package, and less coating thickness variation, both lead to lead and along the lead.

The coating thickness on the lead tip after the initial PC18M dip is minimal, but the coating filled in between the lead tip and the pad and began to build up on top of the lead (Figure 69).

The subsequent build up after successive 25 micron spray layers is less uniform with PC18M spray layers (Figure 70) than the PC18M+20%XP2742 nanosilica spray layers (Figure 71). The improved location T uniformity for the PC18M+20%XP2742 nanosilica sprays is reflected in the measured values (Figure 72).

Due to the roughness of the enhanced layered PC18M spray samples, the subsequent thickness graphs focused on the layered PC18+20%XP2742 samples.

The measured coating build up with increasing layers for the layered PC18+20%XP2742 samples is shown in (Figure 73). The minimum coating thickness on the lead front was above 20 microns and the maximum was approximately 85 microns in location A.

5.15.1 Baseline and enhanced layer vertical comparison

Figure 74 compares the baseline (dip + 50 micron spray) thickness with the enhanced (dip + 25 micron spray + 25 micron spray) layered coating. The average thickness on the back side of the leads for the layered coating was greater than the baseline. Although the thickness variation was larger for the layered coating, there might be a slight trend showing the layered coating having a tighter grouping of average thicknesses at the different lead the locations.

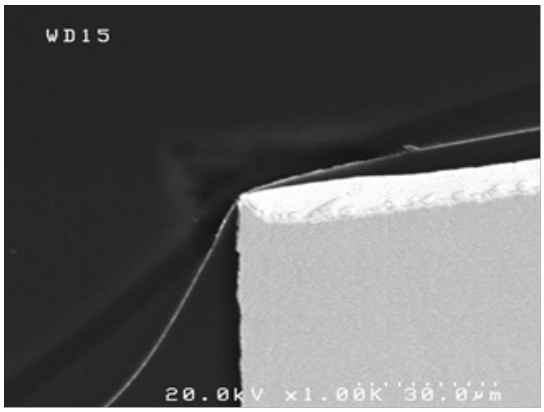


Figure 69: Cross-section SEM image of PC18M dip only, board A179 U6 left T, 1,000x.

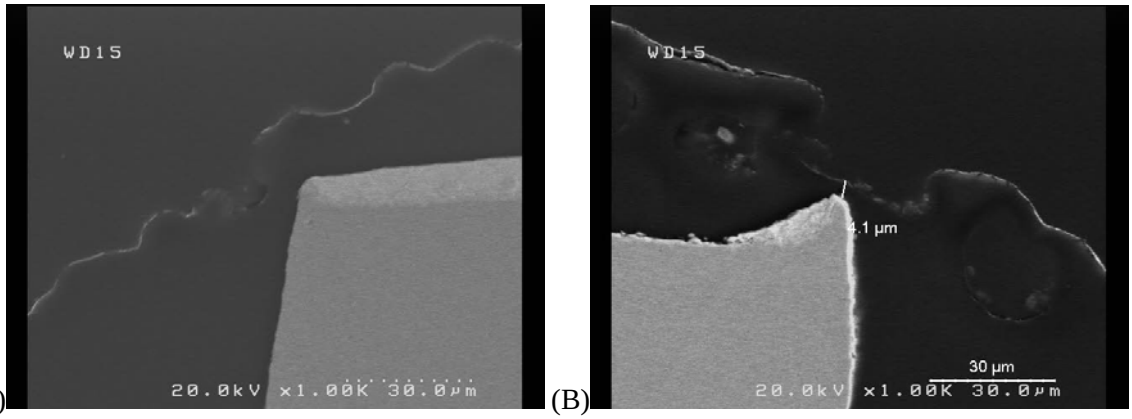


Figure 70: Cross-section SEM image of PC18M dip + PC18M spray layers on QFP44 lead tip (location T), 1000x; (A) one 25 micron spray (ref. board A012, U1, left) and (B) two 25 micron spray layers (ref. Board A191, U1, right).

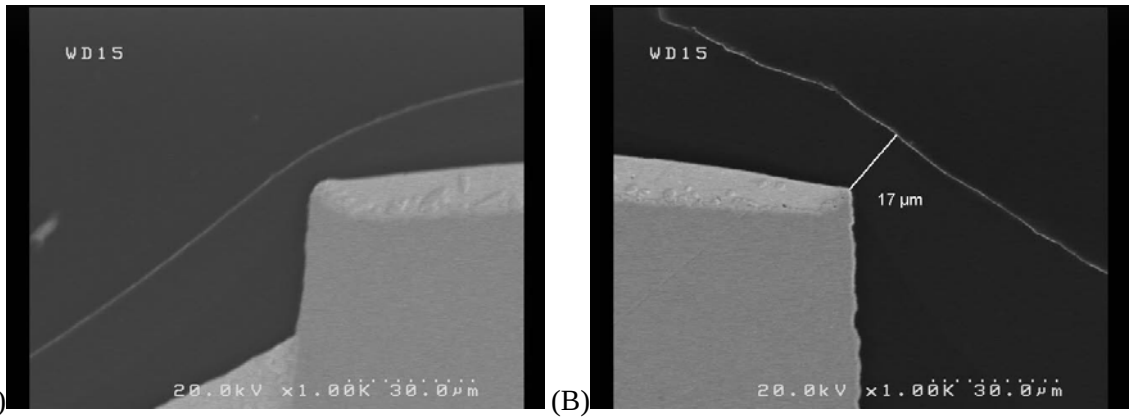


Figure 71: Cross-section SEM image of PC18M dip + PC18M+20XP2742 spray layers on QFP44 lead tip (location T), 1,000x; (A) one 25 micron spray (ref. board 334 U1 left), two 25 micron spray layers (ref. board A225, U1, right)

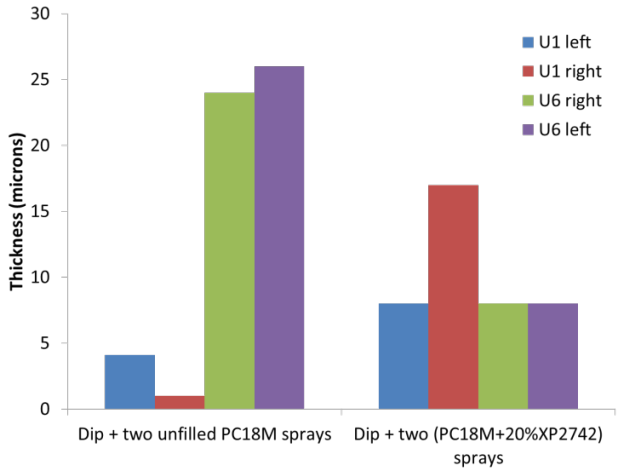
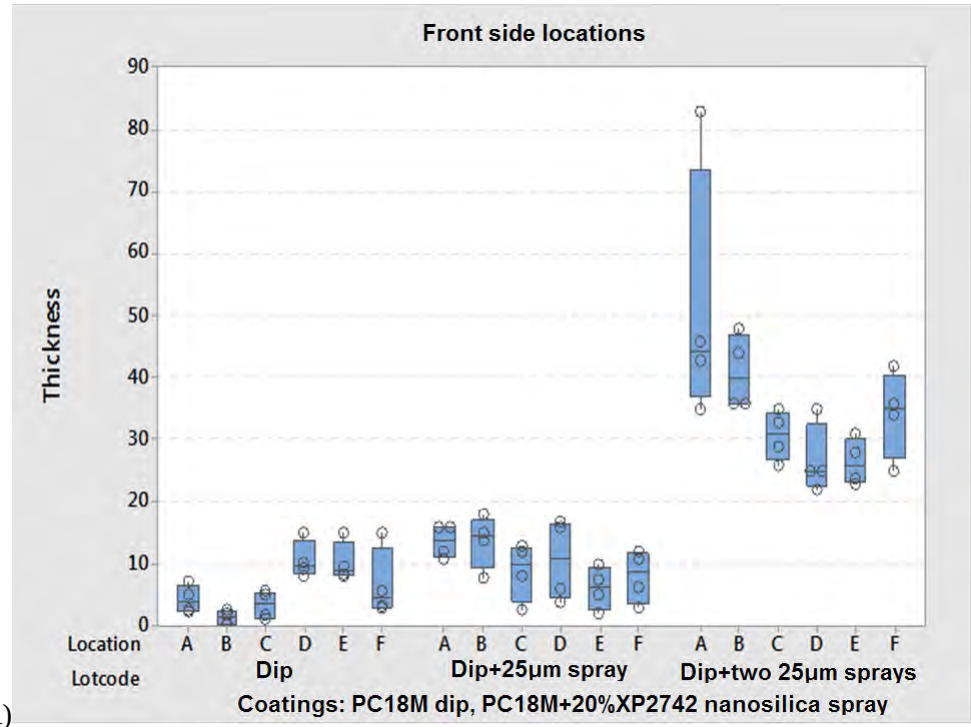


Figure 72: Vertical section comparison of location T coating thickness for the enhanced layered coating dip + 25 micron spray + 25 micron spray for a P18M dip with PC18M spray (left) or PC18M+20%XP2742 nanosilica spray (right).

(A)



(B)

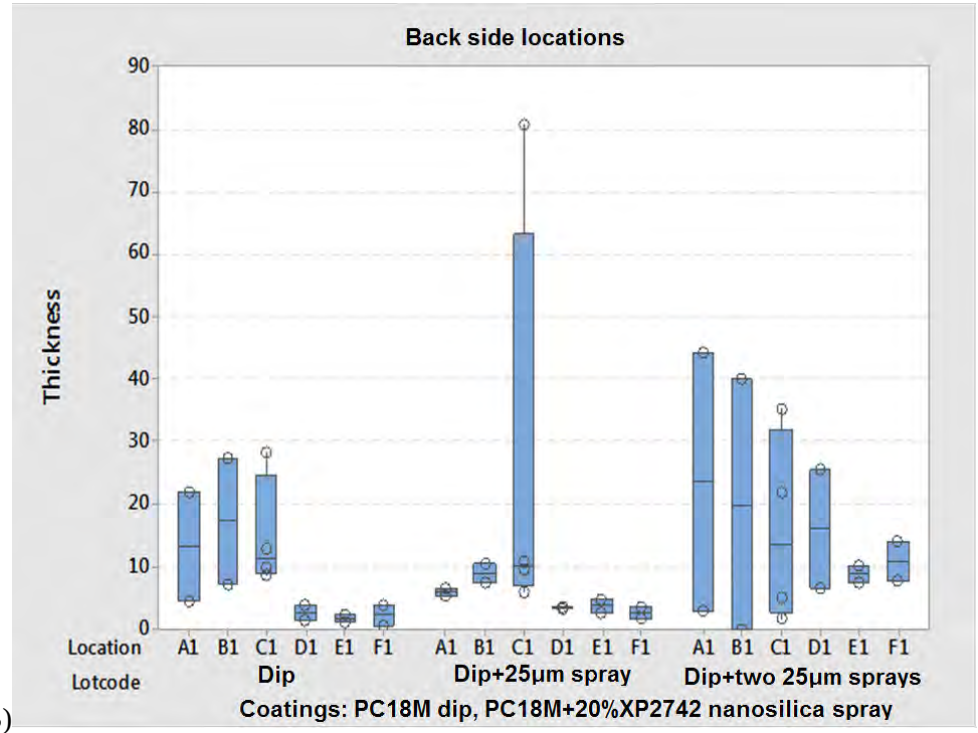
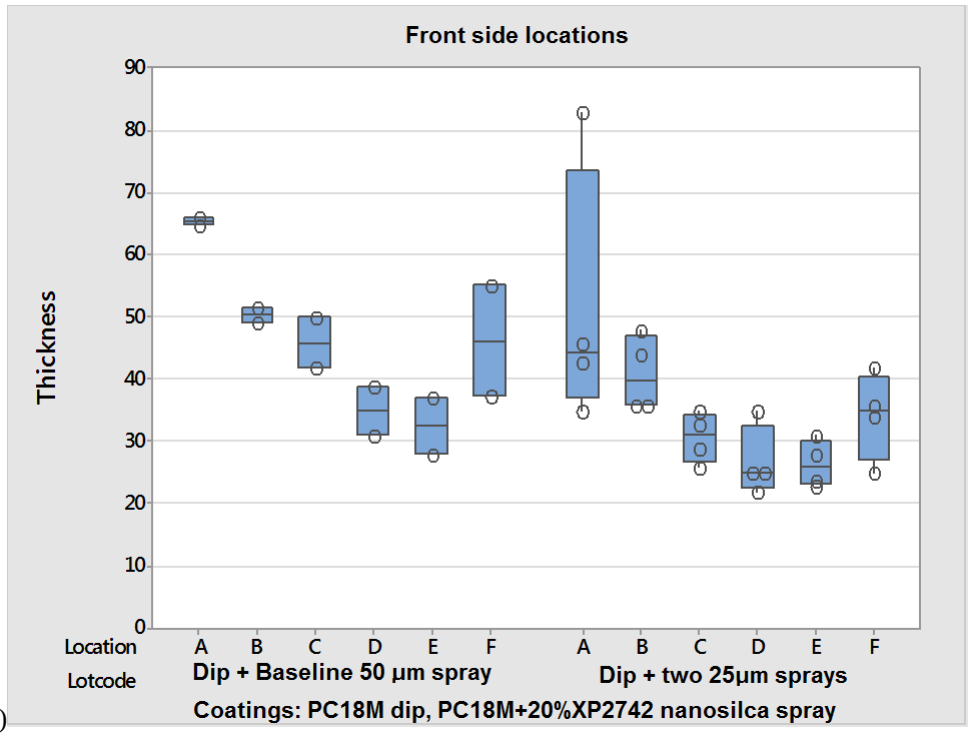


Figure 73: Enhanced layered coating vertical section thickness plots comparing dip only, dip + 25 micron spray, and dip + 25 micron spray + 25 micron spray for a PC18M dip coating and PC18M+20%XP2742 nanosilica spray coating; (A) front of lead side and (B) back side.

(A)



(B)

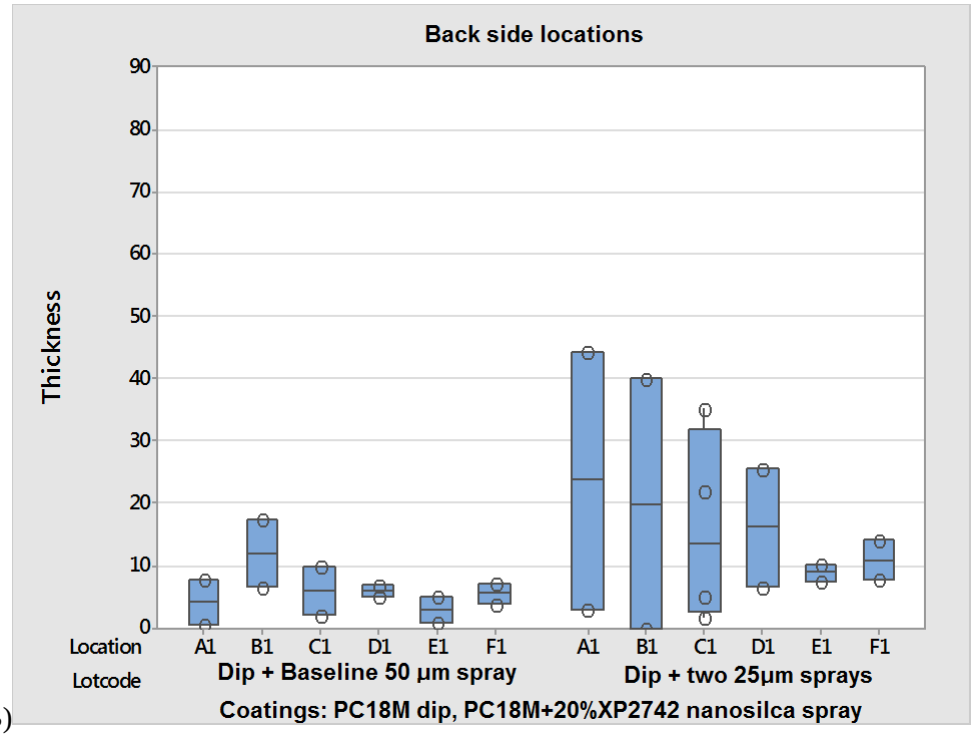


Figure 74: Vertical section comparison of the dip + baseline 50 micron spray and the enhanced layered dip + 25 micron spray + 25 micron spray for a PC18M dip coating and PC18M+20%XP2742 nanosilica spray coating; (A) front of lead side and (B) back side.

5.16 Horizontal cross – section thickness: PC18M Baseline (dip + 50 micron spray)

The details of the baseline process horizontal sectioning is given in Appendix F, with some highlights presented next. The thickness of the coating on the vertical lead section between the package exit and the lead foot was evaluated on the QFP44 parts with a horizontal section plane near region E (Figure 75). The top of the chip resistors were used as a reference to keep the section plane parallel to the board and at a consistent height for the various boards that were sectioned. An x-ray image of the potted cross-section mount confirmed that the section plane was just above the main part of the solder fillet. For the analysis, SEM images were obtained from leads 6, 11, 17, 23, 28 34 and 39 to represent corner and center leads on each side of the QFP (Figure 76). Sometimes the back side of the lead had little or no gold sputtered over the conformal coating on the center leads, making it more difficult to differentiate between the coating and the potting compound. Due to potting shrinkage, the coating separated slightly from the lead.

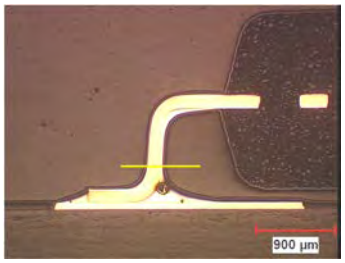


Figure 75: Horizontal cross-section plane location for coating thickness evaluation.

Overall the coating thickness varied from approximately one micron on back side to 50 microns on front side. Generally, the front of the leads exhibited thicker coating than the back side and that back side coating thickness was better on the corner leads than the middle leads. The spray process uses an overlap spray pattern and the location of the overlap may have influenced the amount of deposited coating. The nanoparticle filled coatings had better corner coverage, but back side coverage could be improved. There are many variables that could affect this result, but the nanoparticle filled coating coverage performance is encouraging.

All coating types exhibited good front of the lead coverage (e.g. Figure 77 – Figure 79). The front coating nanoparticle filled coating thickness was greater on the right side of the part (leads 23 – 33) than the left (leads 1 – 11). The leads on the lower side (leads 12 – 22) had comparable coverage to the left and right sides, except for the thick coating coverage of the PC18M-mod coating on lead 17.

Sometimes on the corner leads, the coating was thicker on the side adjacent to the neighboring lead (top of Figure 77) and thinner on the side facing the open corner.

Greater back side coating thickness variation was observed from lead-to-lead. Sometimes on a given lead, the back side coating thicknesses were comparable (Figure 80 – Figure 81), but on the PC18M-mod, there were cases where relatively thick back side coating was observed (Figure 77).

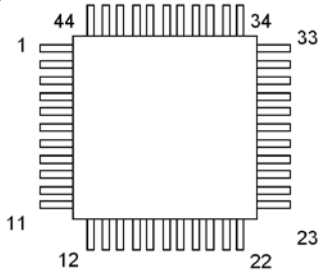


Figure 76: QFP44 pin numbering.

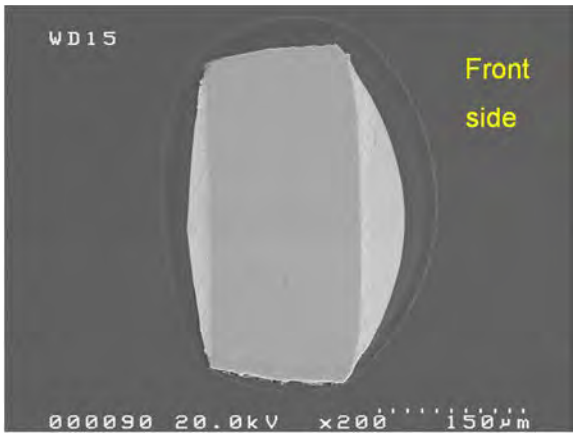


Figure 77: Horizontal cross section, SEM, board 11, baseline PC18M-mod, QFP44, U1, lead 23, 200x.

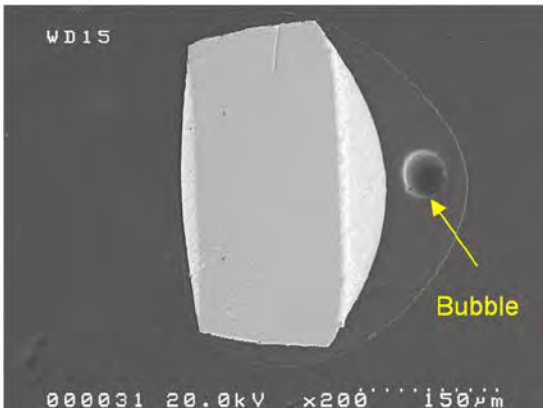


Figure 78: Horizontal cross section, SEM, board 21, baseline PC18M+20%XP2742, QFP44, U1, lead 23, 200x.

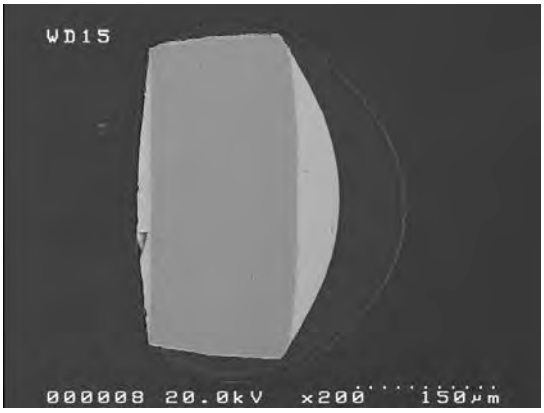


Figure 79: Horizontal cross section, SEM, board 28, baseline PC18M+20%X11102PMA, QFP44, U1, lead 23, 200x.

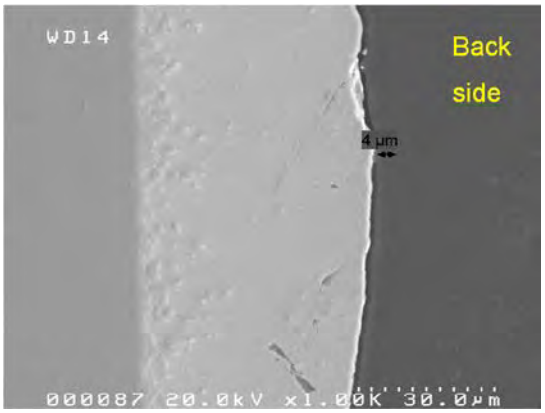


Figure 80: Horizontal cross section, SEM, board 11, PC18M-mod, QFP44, U1, lead 6, 1,000x. Back side coating coverage is four microns.

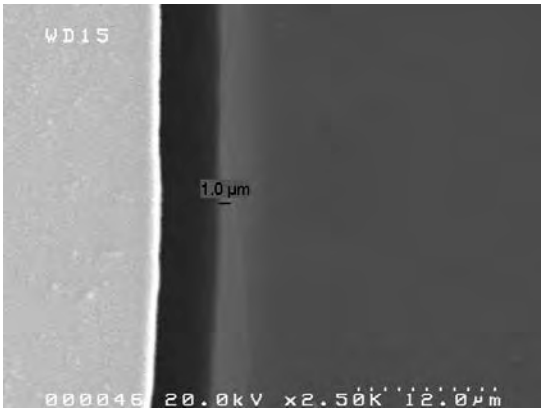


Figure 81: Horizontal cross-section, SEM, board 21, PC18M+20%XP2742, QFP44, U1 lead 6, 1,000x. Back side coating coverage is one micron.

5.17 Horizontal cross – section thickness: Enhanced layer (dip + 25 micron spray + 25 micron spray)

The details of the enhanced layer process horizontal sectioning is given in Appendix I, with some highlights presented next. The PC18M dip + two (PC18M+20XP2742) sprays enhanced layered coating was evaluated with a horizontal section as is described in Section 5.17. The coating coverage on the front and the sides of both the corner and center leads was good. The coverage on the back was more variable (Figure 82 to Figure 84).

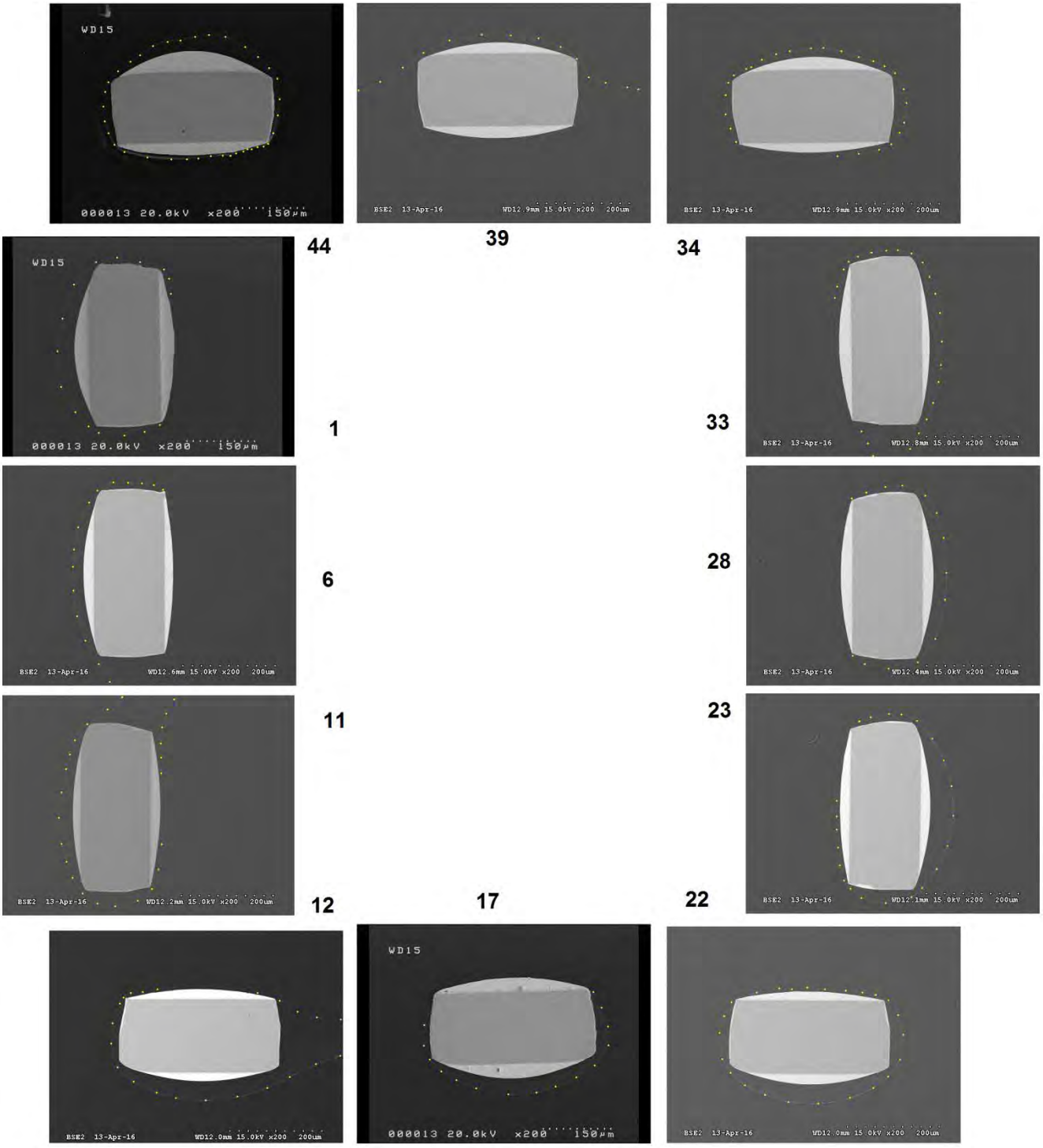
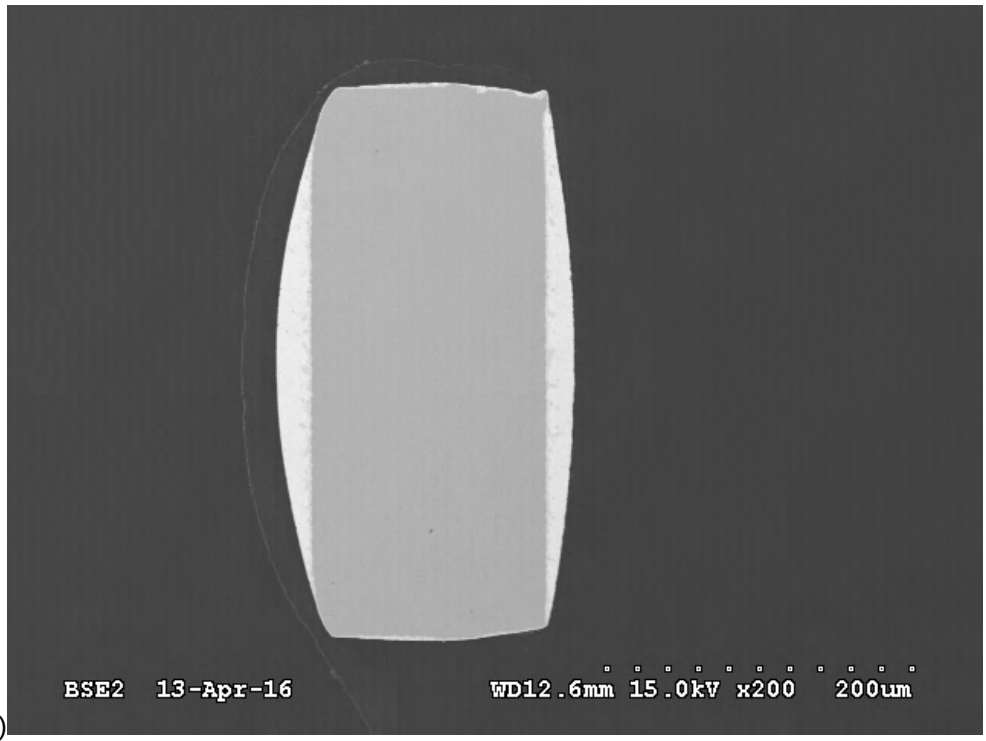


Figure 82: Horizontal cross-section SEM image of corner leads, PC18M dip + two (PC18M+20XP2742) sprays, board A225, U3, 200x (enhancement added to highlight coating).

(A)



(B)

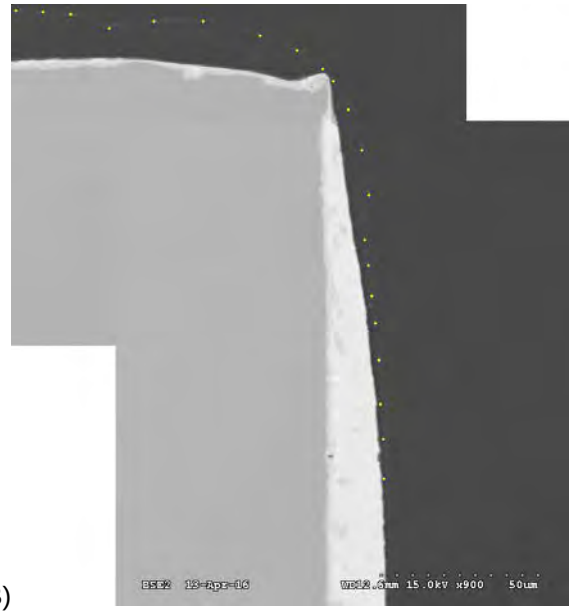
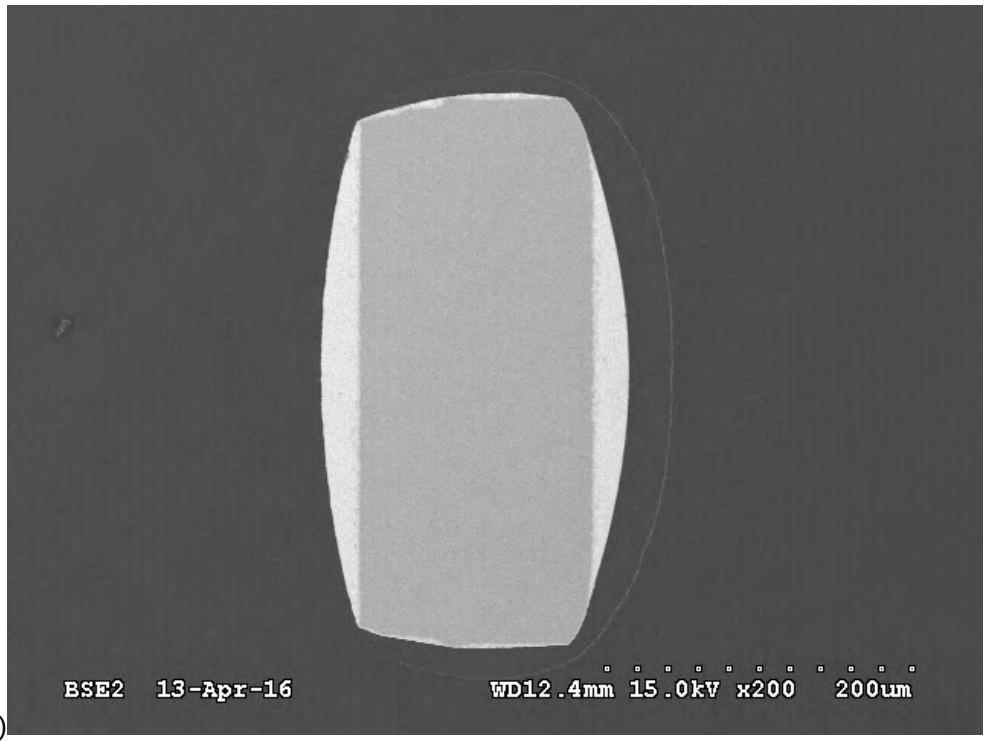


Figure 83: Cross-section SEM image of PC18M dip + two (PC18M+20XP2742) sprays, board A225, U3, lead 6; (A) 200x, and (B) upper back corner, 900x (enhancement added to highlight coating).

(A)



(B)

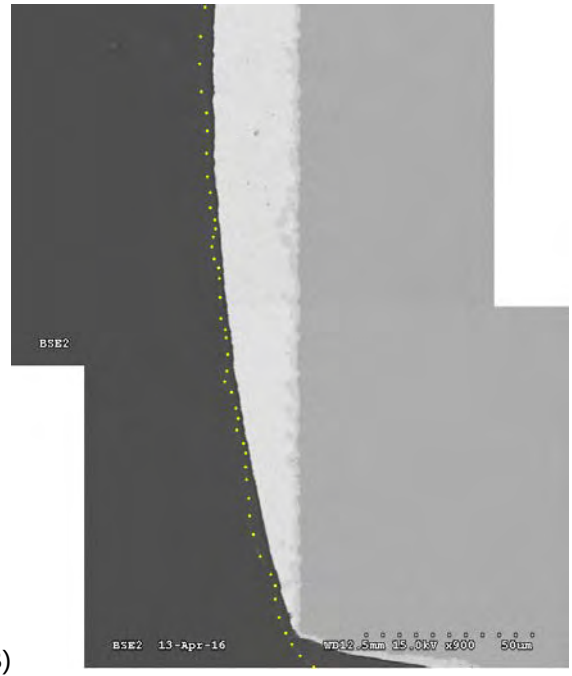


Figure 84: Cross-section SEM image of PC18M dip + two (PC18M+20XP2742) sprays, board A225, U3, lead 28; (A) overall, 200x, and, (B) back center and bottom corner, 900x (enhancement added to highlight coating).

5.18 FE – SEM and microtome section thickness: Enhanced layer (dip + 25 micron spray + 25 micron spray)

The extra coating coverage details of the enhanced layered coating obtained by microtome sectioning and field emission SEM (FE – SEM) examination are given in Appendix I, with some highlights presented next. These techniques were used to examine the nanoparticles and layer thickness variation along the lead on a QFP44 with PC18M dip + two (PC18M+20%XP2742) sprays (Figure 85). Sections one and two are perpendicular to the lead and section three is along the length of the lead (Figure 86).

5.18.1 Section one and two

Section one and two locations correspond to locations A and D in the conventional vertical cross-sectioning (Figure 63). Leads from the middle of the row (not corner leads) were used for each section. The perpendicular section examined the sides and corners of the lead (Figure 87).



Figure 85: QFP from board A225 examined using microtome sectioning.

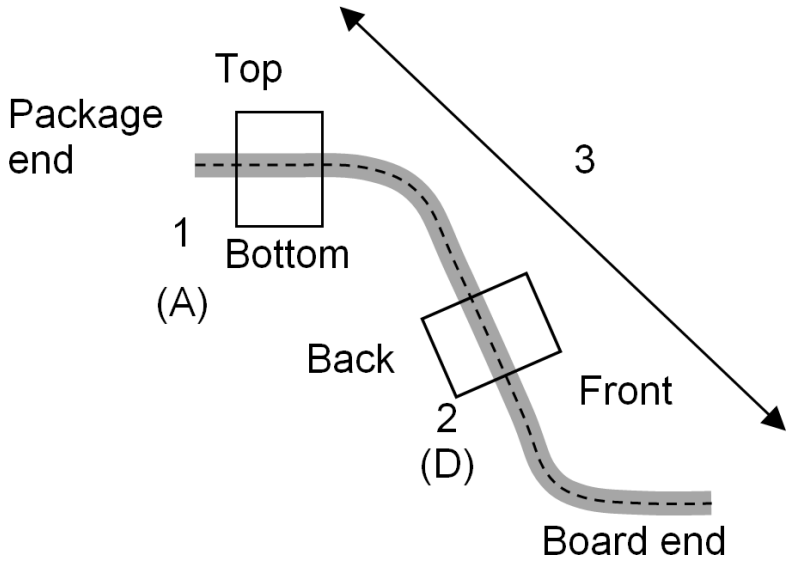


Figure 86: Schematic showing microtome section locations.

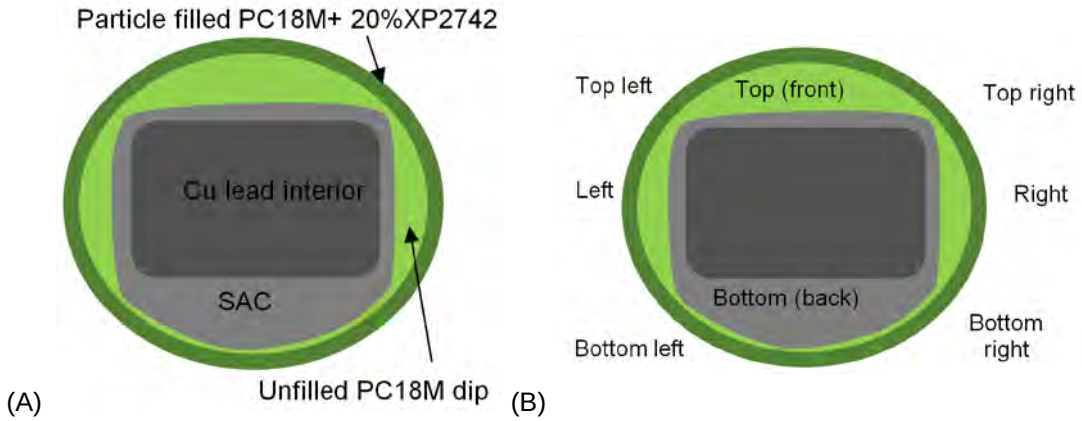


Figure 87: Microtome section perpendicular to lead schematic; (A) materials and (B) locations examined.

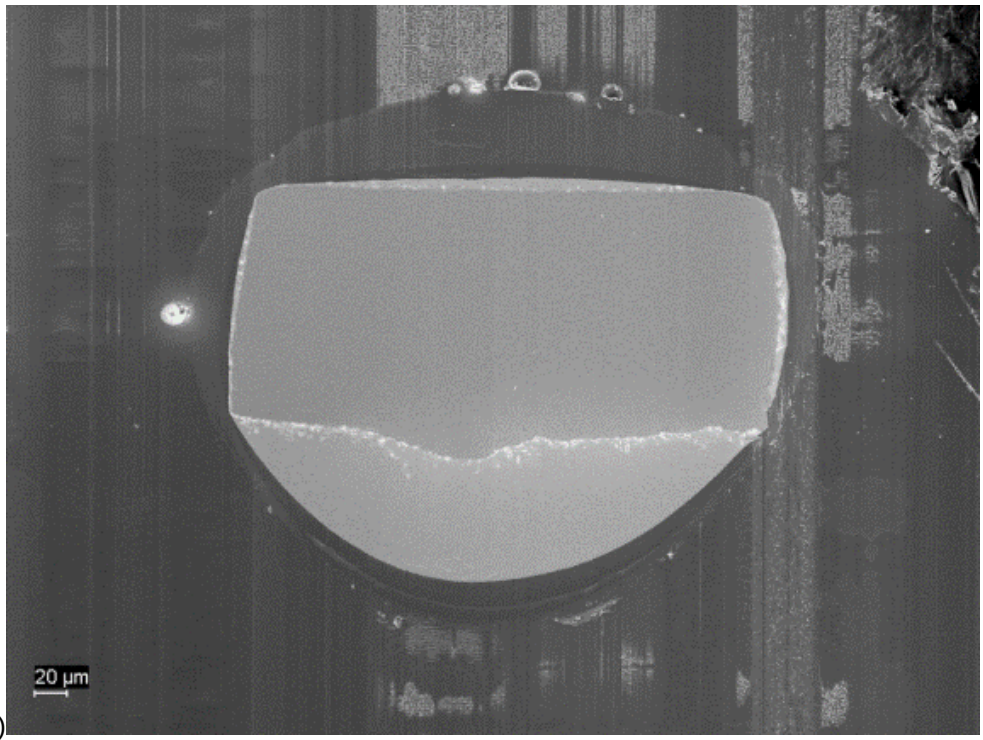
Generally, the nanosilica particles were well distributed with no agglomeration and good adhesion between layers and to the metal. The overall perpendicular cross-sections of section one and two (Figure 88) and the higher magnification images of top and bottom (Figure 89 and Figure 90) show that the side with the direct line-of-sight to the spray nozzle (top or front) has greater particle filled spray coating thickness than the shadowed side (bottom or back). Even though the right side of section two has a coating web bridging to the next lead, particle filled coating from the spray process was evident.

As expected, the corner coverage was better on the top and front side corners. The dip coating on the corners was approximately one micron thick. The spray coating added considerable the thickness build-up to the corners. The coating thickness on the side consisted mostly of the particle filled spray coating build-up. The spray coating on the right side of section two along the back of the dip coating web had droplets of spray coating (Figure 91).

The particle uniformity and the knit line between the layers, both spray – to – spray layers and spray – to – dip layers, exhibited good adhesion (Figure 92 and Figure 93). The particle filled microstructure consisted of uniformly dispersed nanosilica particles (white specks) chemically bonded to an isotropic network structure in the polyurethane matrix (Figure 93). This has the benefits of increased flexibility and isotropic mechanical properties.

Measurements of the dip and spray coating thicknesses on sections one and two show that the top (or front) of the leads had the greatest amount of spray coating (Figure 94 and Figure 95). The sides and top (front) had a minimum of 10 microns of coating except in some instances of the bottom (back) corners. The very thin dip coating in the corners was covered by spray coating on the top (or front) and to a lesser extent bottom (or back) corners. In addition, there were often a few microns of spray coating on the bottom (back) in both sections.

(A)



(B)

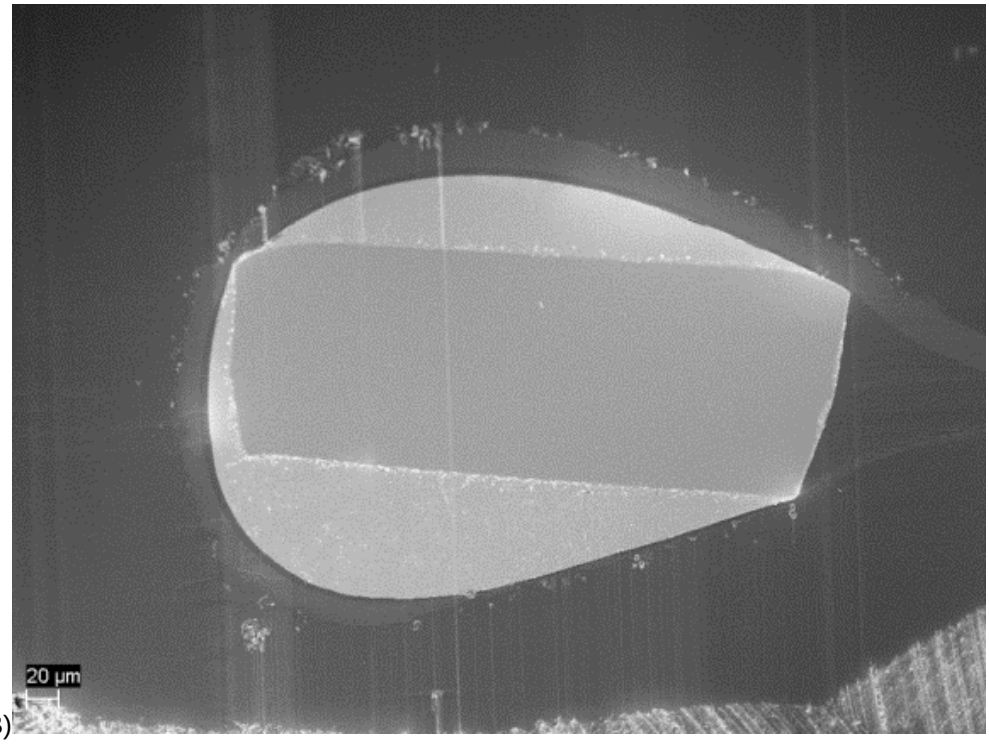
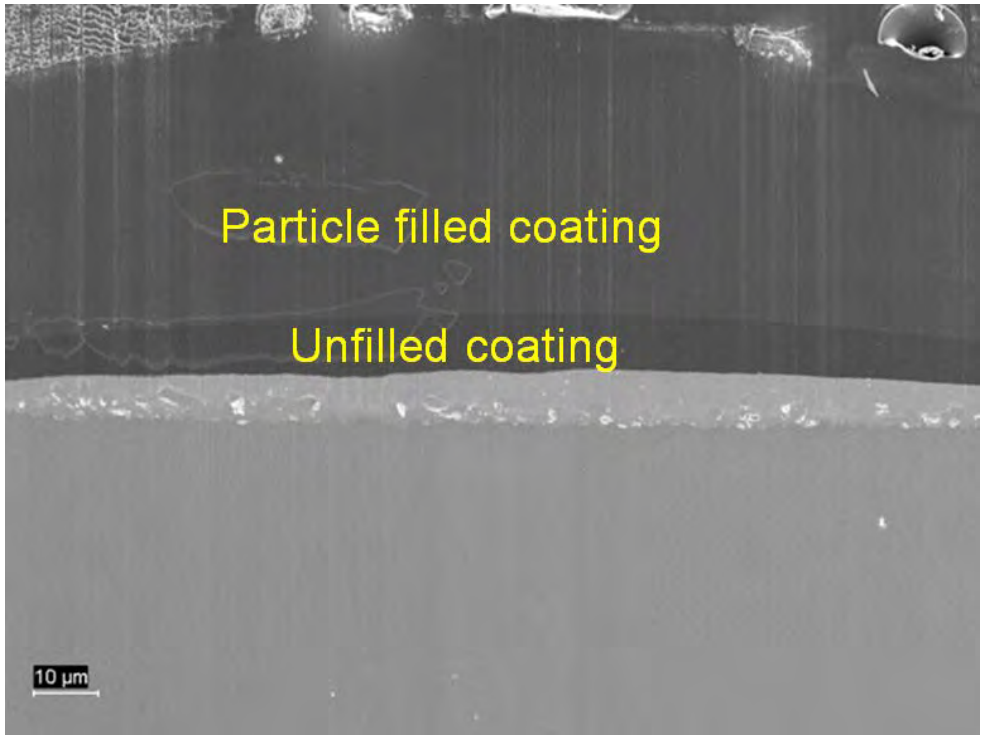
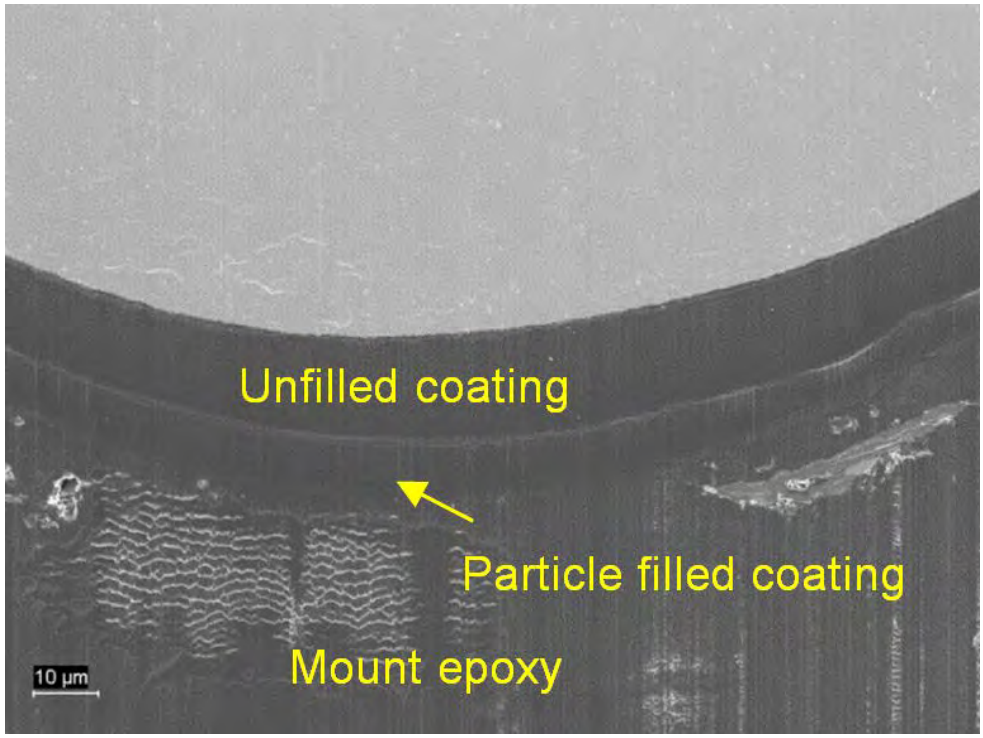


Figure 88: FE – SEM images of microtome sections (A) section one, and (B) section two. The lighter coating color is the nanoparticle spray layer. Note that there is a dip coating web on the right side of the image (B) lead.



(A)



(B)

Figure 89: FE – SEM of microtome section one at higher magnification; (A) top and (B) bottom.

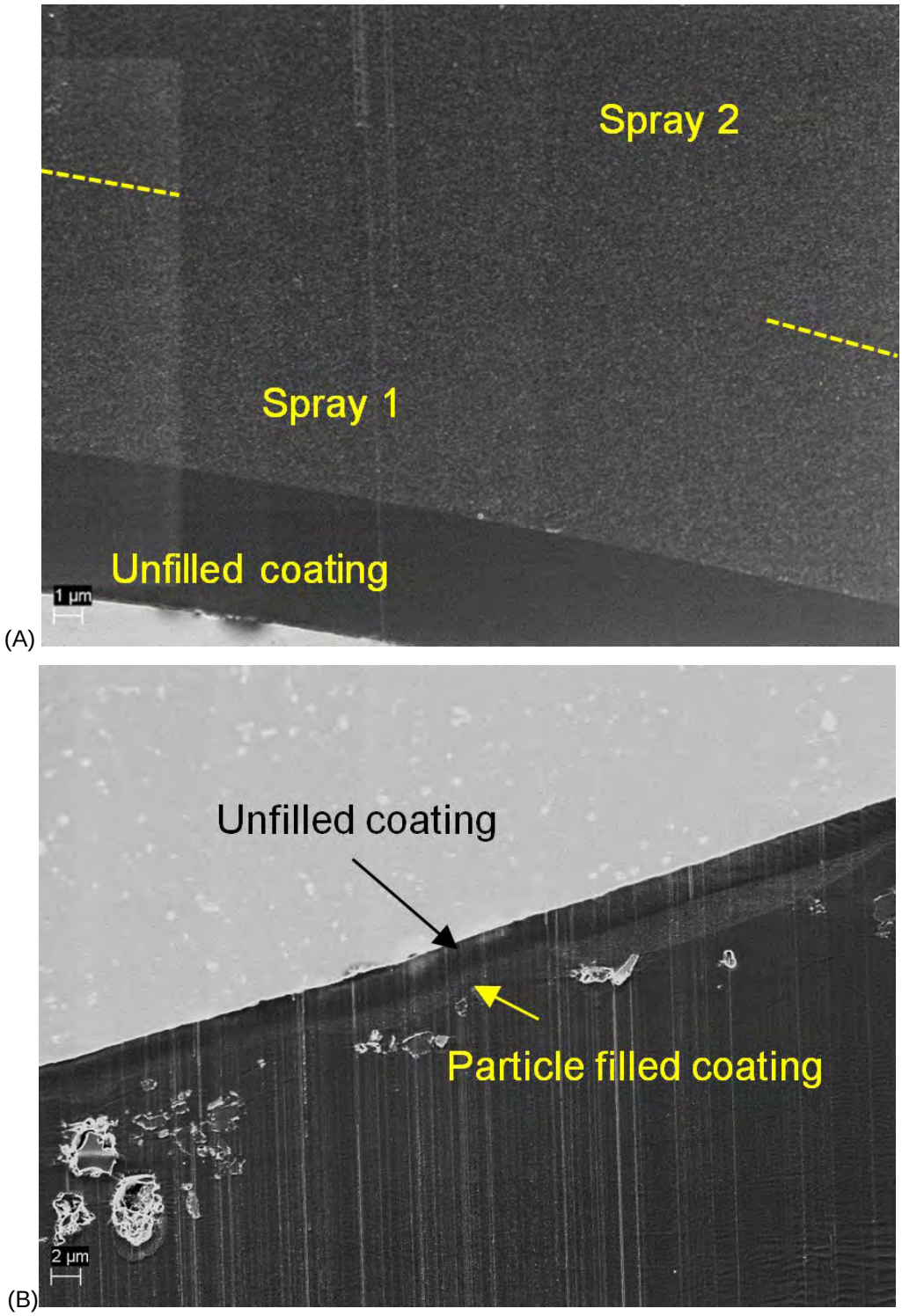


Figure 90: FE – SEM of microtome section two at higher magnification; (A) front and (B) back.

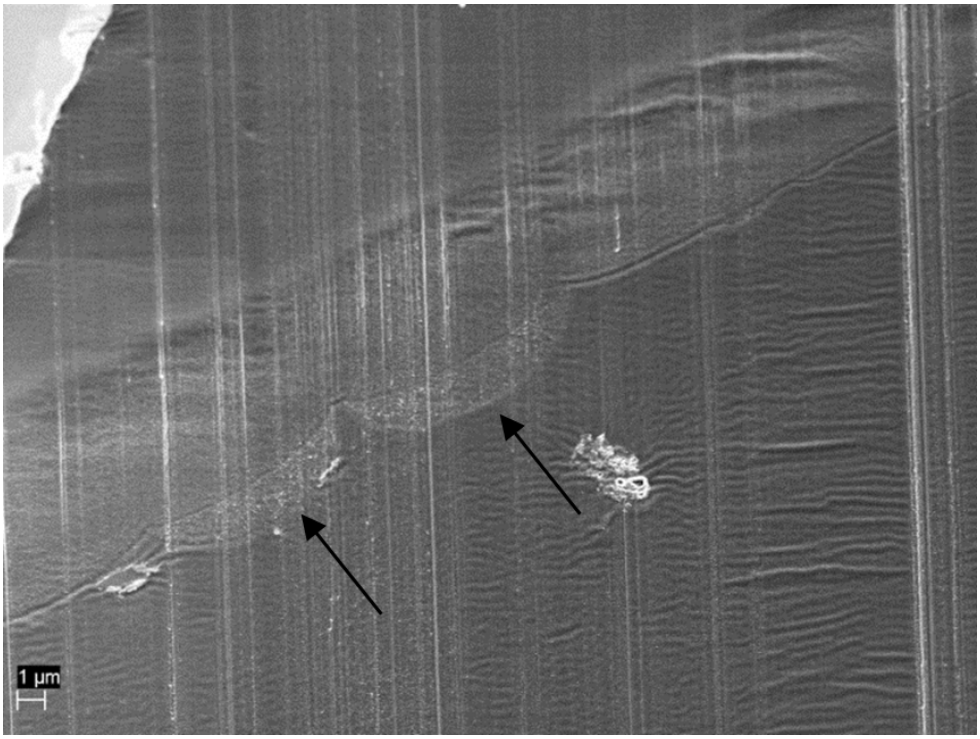


Figure 91: FE – SEM of microtome section two right back along the dip coating web to the adjacent lead. Arrow highlights particle filled spray coating droplets on the dip coating.

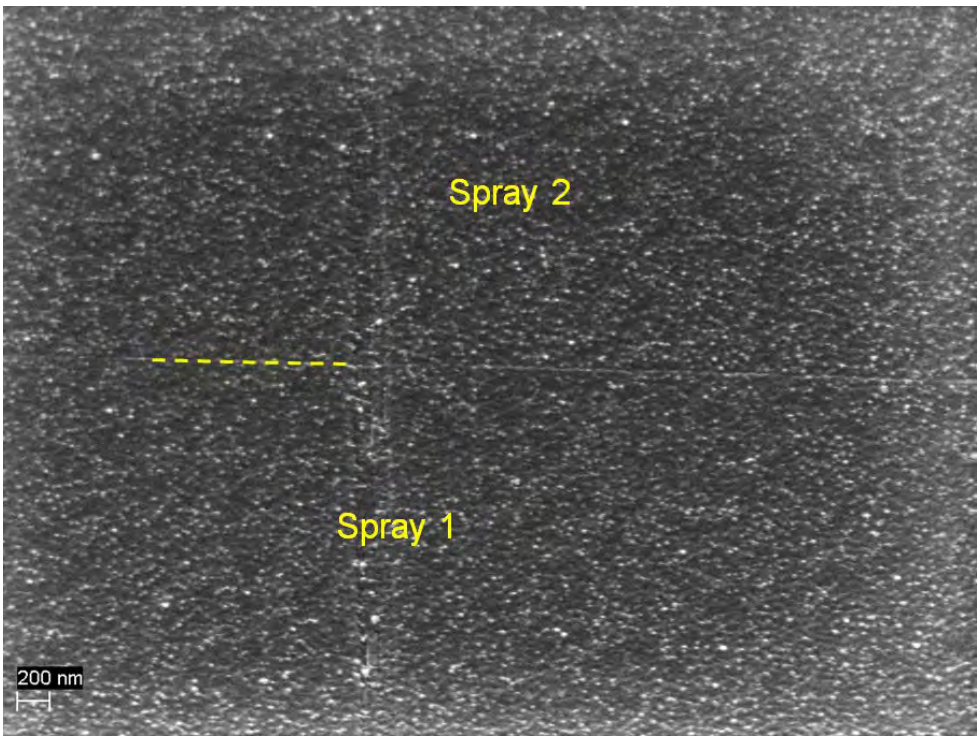


Figure 92: High magnification FE – SEM images of microtome section two front showing particle uniformity and a well adhered knit line between the two spray layers.

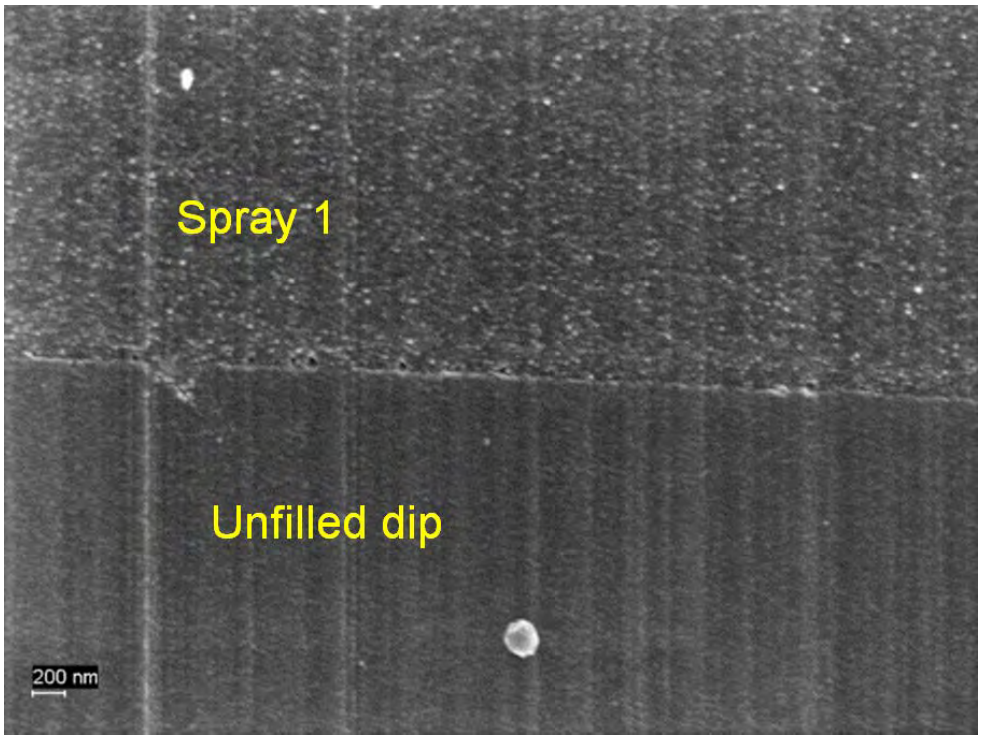


Figure 93: High magnification FE – SEM images of microtome section top of lead showing spray coating to dip coating interface.

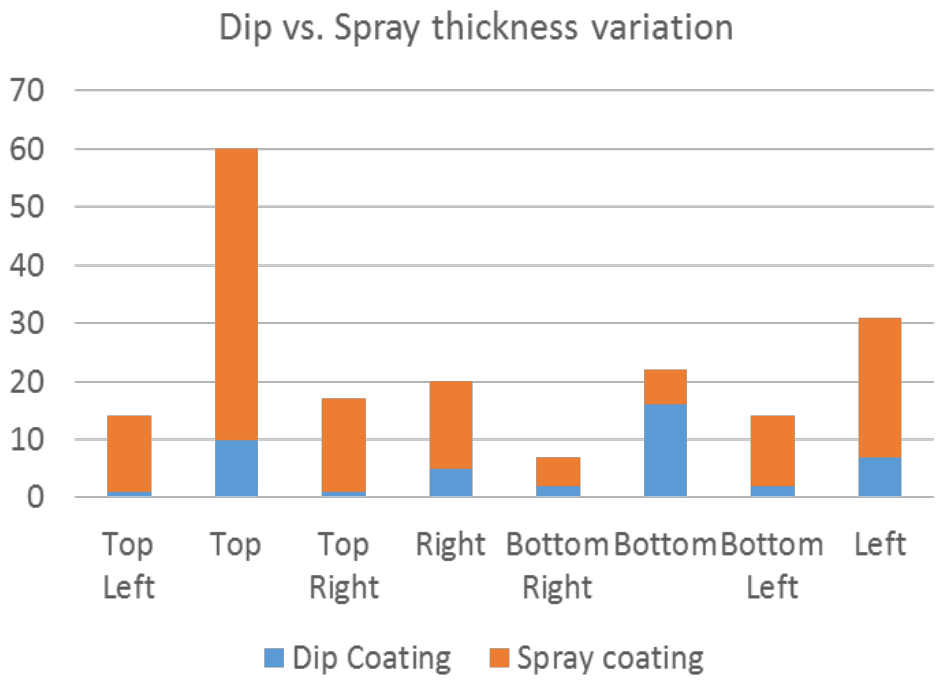


Figure 94: Section one dip coat and spray coating thicknesses.

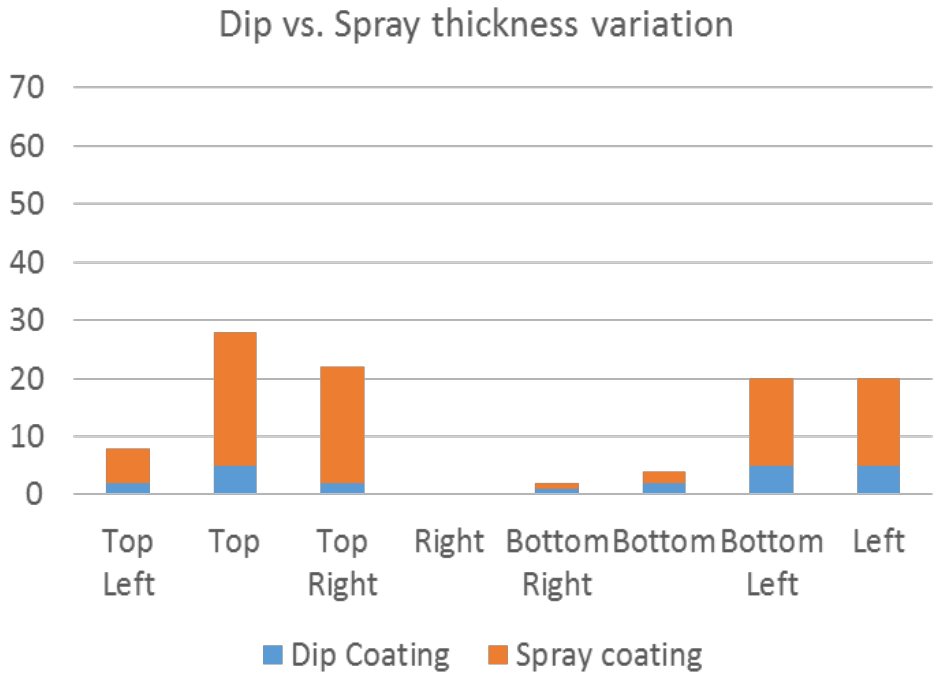


Figure 95: Section two dip coat and spray coating thicknesses. Note that a coating bridge between leads prevented measurements on the right side of the lead.

5.18.2 Section three

Microtome section three along the length of the lead was used to examine three areas (Figure 96). Note that the location of Area C aligns to microtome section 2 (Figure 86) which also approximately aligned to vertical section location D (Figure 63).

The overall section with the markers highlighting the coating thickness is shown in Figure 97. The thickest coating is in inside corners between the lead and the package and the inside radius made between the vertical part of the lead and the lead foot. The overall particle distribution throughout the section was uniform (e.g. Figure 98). Generally, the particle filled coating was thicker on the top or front of the lead than the bottom or back in all areas (Figure 99 to Figure 101).

At the lead – to – package region, area A (Figure 99), the coating fillet between the underside of the lead and the package was primarily unfilled dip coating with a thin layer of nanosilica spray coating. On the top side of the lead and the package corner, the fillet was smaller. In this area, the unfilled dip coating formed a fillet in the corner and became progressively thinner at locations further along the lead toward the knee. The top side nanosilica filled spray coating formed a relatively uniform layer on top of the dip coat layer.

At the lead knee, area B (Figure 100), the thickness of the unfilled dip on the back side of the lead was greater than the front side; while the nanosilica filled spray coat was thicker on the front than the back. There were also some distinct cured nanosilica droplets from the first spray layer that were covered over by additional nanosilica coating from the second spray layer. This may indicated that the first spray layer facilitated wetting behind the lead of the second spray layer.

At the midpoint of the lead, area C (Figure 101), there were more instances where nanosilica filled coating droplets from the first spray layer were covered by additional nanosilica filled coating from the

second spray layer. In some areas the unfilled (dip) coating layer showed delamination from vertical portions of the back side of the lead, but that may have been from cutting motion of the microtome.

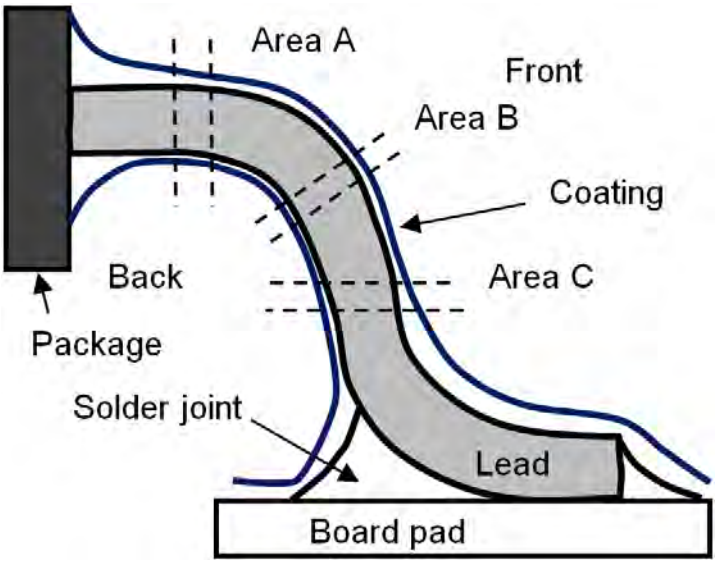


Figure 96: Microtome section three examination areas.

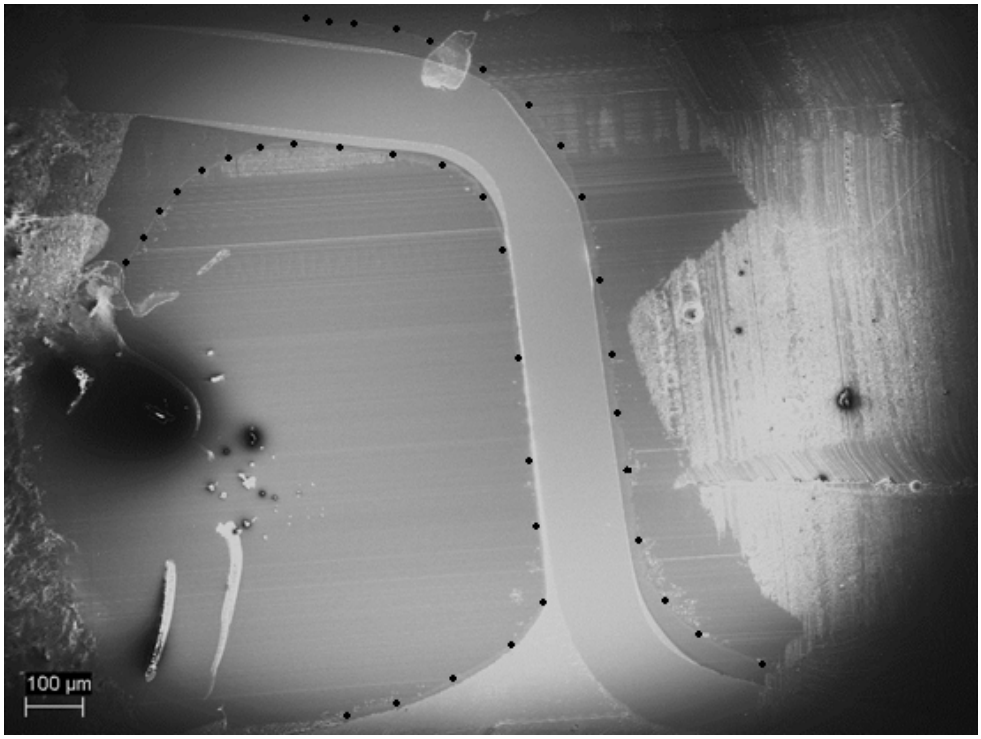


Figure 97: Overall FE – SEM image of microtome section three lead and coating.

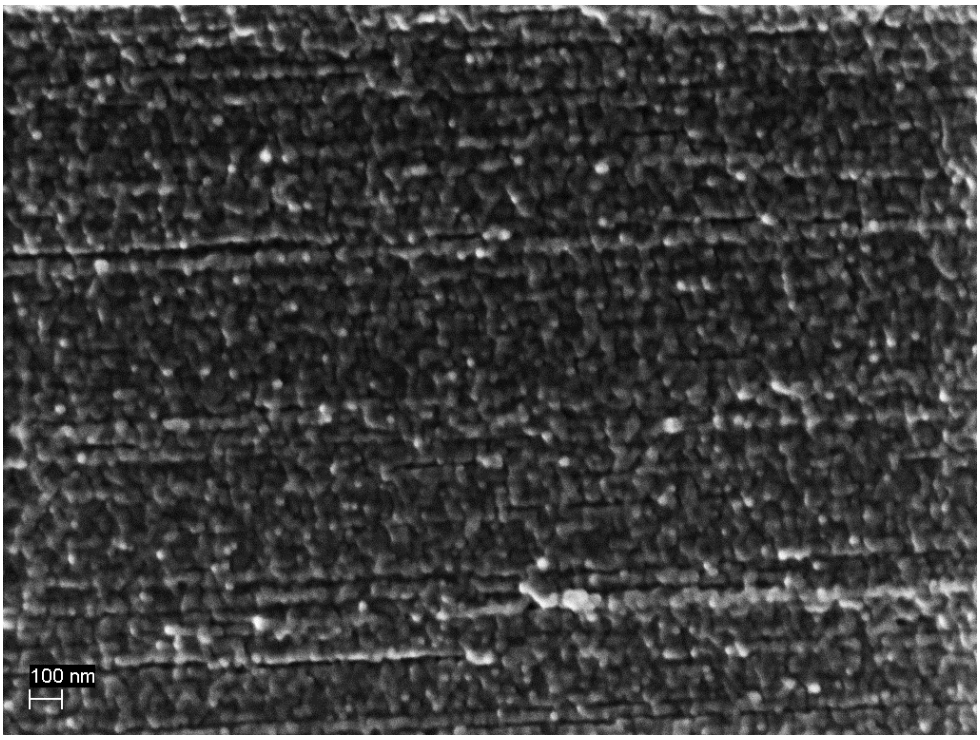
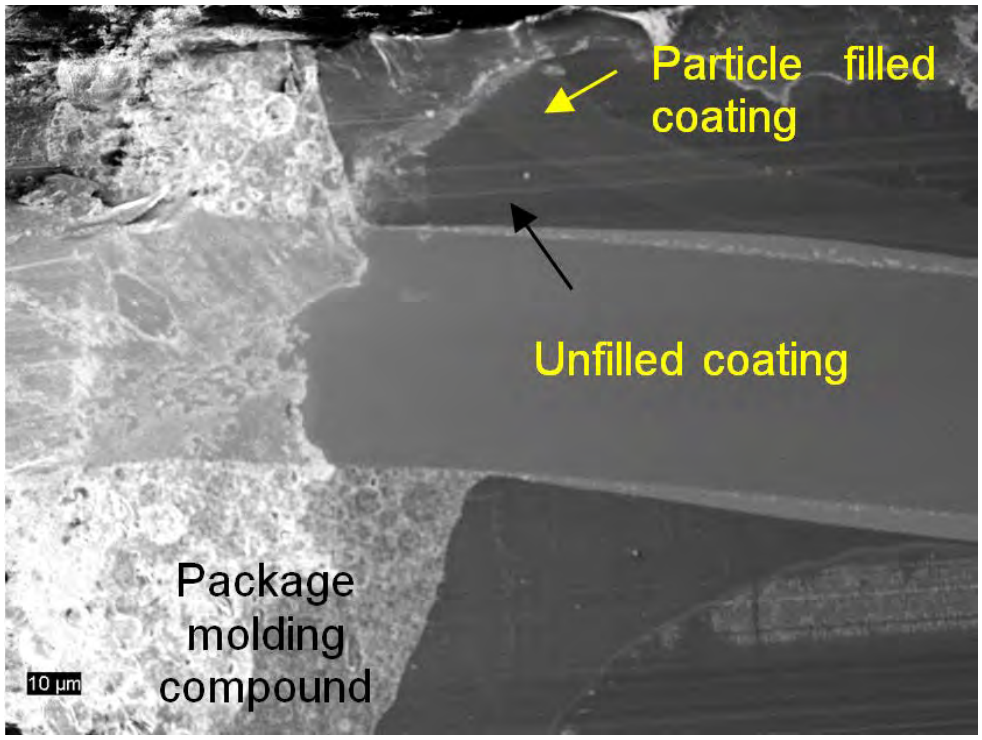


Figure 98: Typical FE – SEM image showing uniform particle distribution (Area C base shown).

(A)



(B)

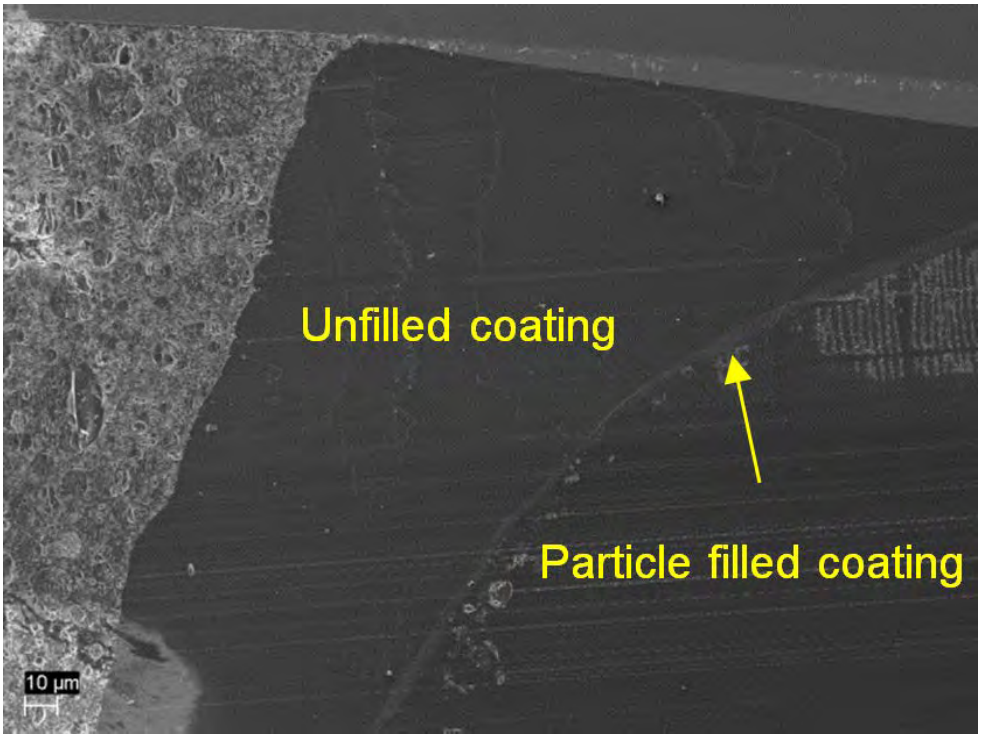
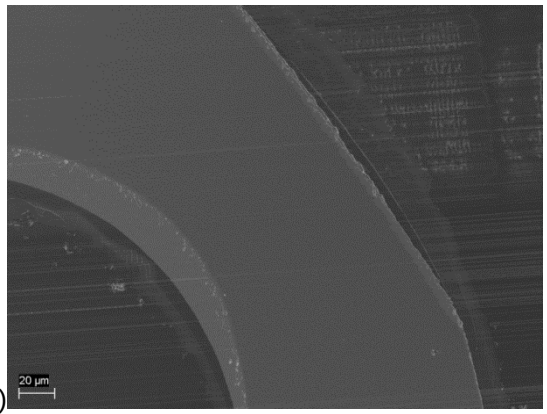
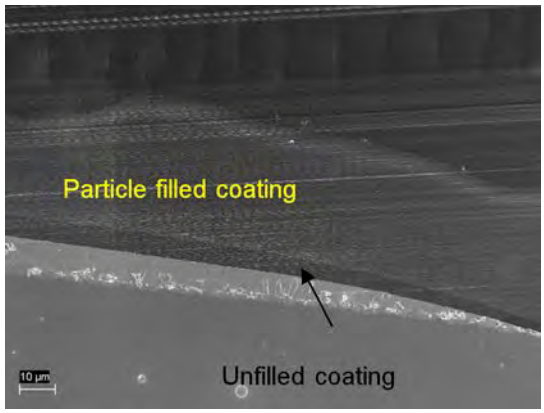


Figure 99: Section three Area A FE – SEM image; (A) top, and (B) bottom.

(A)



(B)



(C)

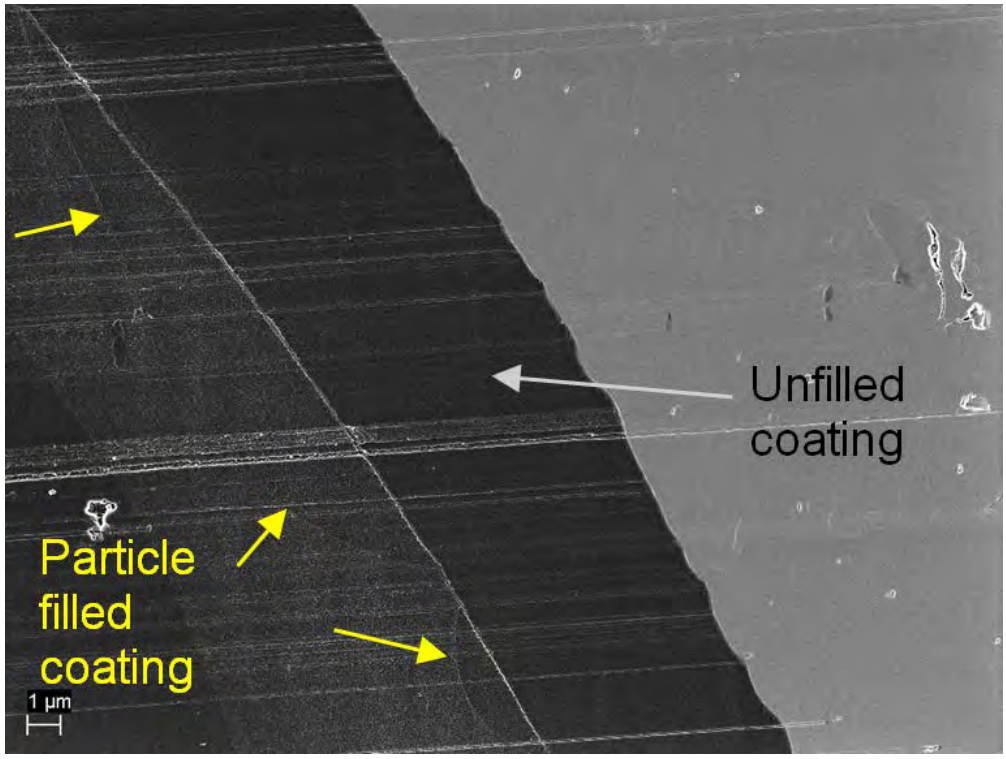


Figure 100: Section three Area B FE – SEM image; (A) overall, (B) front, and (C) back with arrows showing the first spray layer covered by the second spray layer.

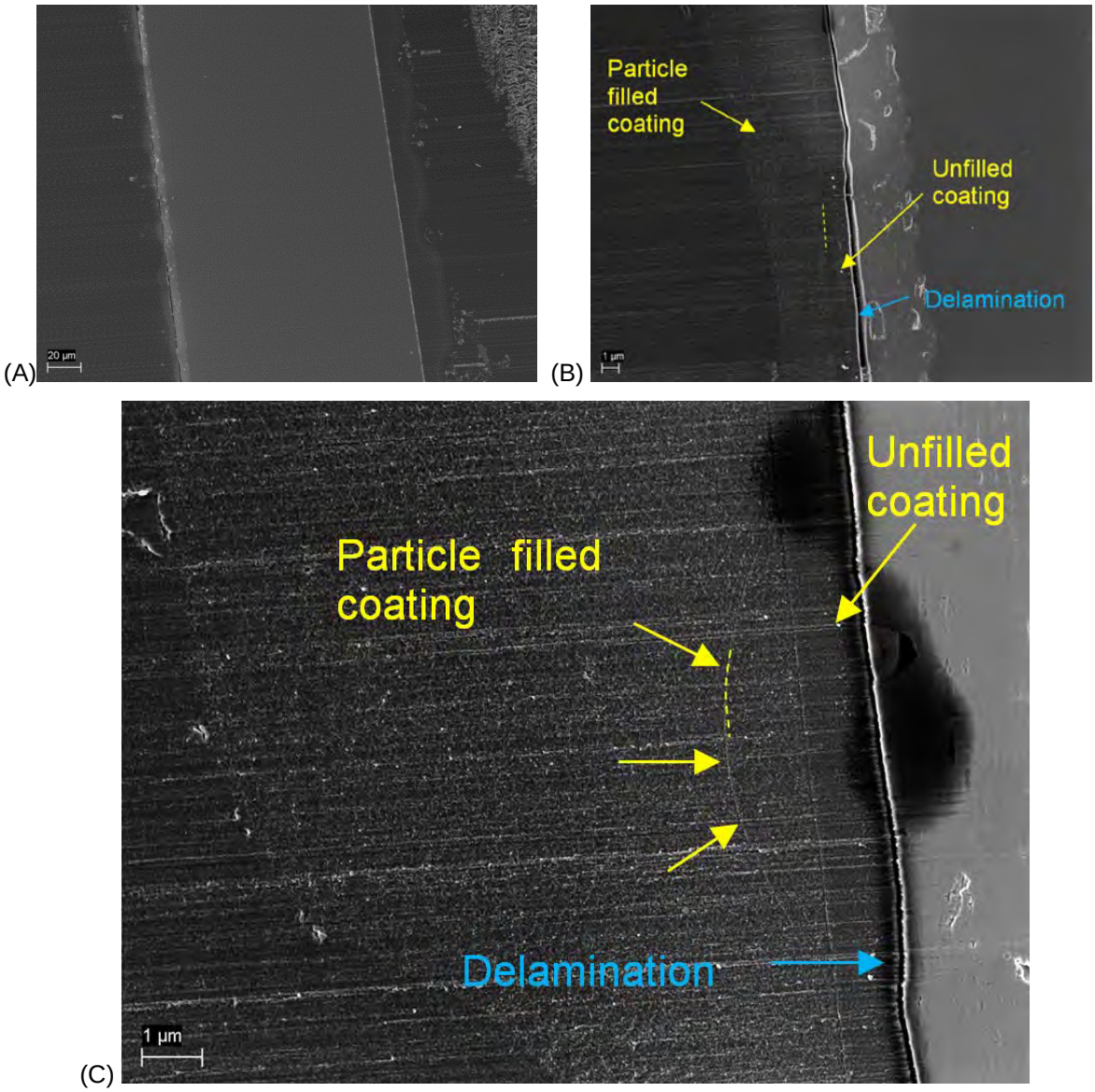


Figure 101: Section three Area C FE – SEM image; (A) overall, (B) back of lead, (C) second location on back of lead with arrow indicating spray coating drop covered with additional spray coating.

5.19 Assembly whisker testing: PC18M Baseline (dip + 50 micron spray)

The baseline coating process assembly whisker testing details are provided in Appendix H, with some highlights presented next. The three PC18M-mod coating variations evaluated, each having an initial thinned PC18M-mod dip that was partially cured. Then the following spray coatings were applied on the dip coating layer; (1) PC18M-mod, (2) PC18M-mod+20%XP2742 nanosilica, and PC18M+20%X11102PMA nanoalumina coating. The following reference assemblies were tested at the same time: (1) uncoated and (2) Parylene C ™ coated assemblies with and without the Adpro + adhesion promoter. The boards were exposed to accelerated thermal cycling (ATC) and/or high temperature high humidity (HTHH). The following nomenclature was used to describe the conditions:

- **ATC:** 100 cycles -55 to +125°C followed by 233 cycles -20 to +80°C

- **ATC+HTHH1000:** 100 cycles -55 to +125°C followed by 233 cycles -20 to +80°C followed by 1,000 hours 85°C/85% Relative Humidity (RH)
- **ATC+HTHH2000:** 100 cycles -55 to +125°C followed by 233 cycles -20 to +80°C followed by 2,000 hours 85°C/85%RH
- **HTHH2000:** 2,000 hours 85°C/85%RH

5.19.1 Uncoated control assembly test results

The SEM images from the whisker inspection are shown in Figure 102 to Figure 107. The examination after ATC of the uncoated control boards showed that the alloy-42 lead terminations had more tin growths and solder steps (Figure 102 – Figure 103) than the Cu lead terminations. Inspections after the addition of 1,000 hours HTHH after ATC showed increased corrosion (Figure 104) that resulted whisker growth at the boundaries between tin grains even without a significant solder step (Figure 104). When ATC was followed by longer humidity exposure (ATC+HTHH2000), the lead terminations exhibited more whisker growth and more corrosion (Figure 105). Only performing humidity, HTHH2000, was sufficient for whisker growth (Figure 106 and Figure 107).



Figure 102: SEM image of an uncoated SOT6 lead, ATC, 180x (ref. board 237). Whiskers growing from top and lower solder fillet regions.



Figure 103: SEM image of an uncoated SOT6 lead, ATC, 1,000x (ref. board 237).

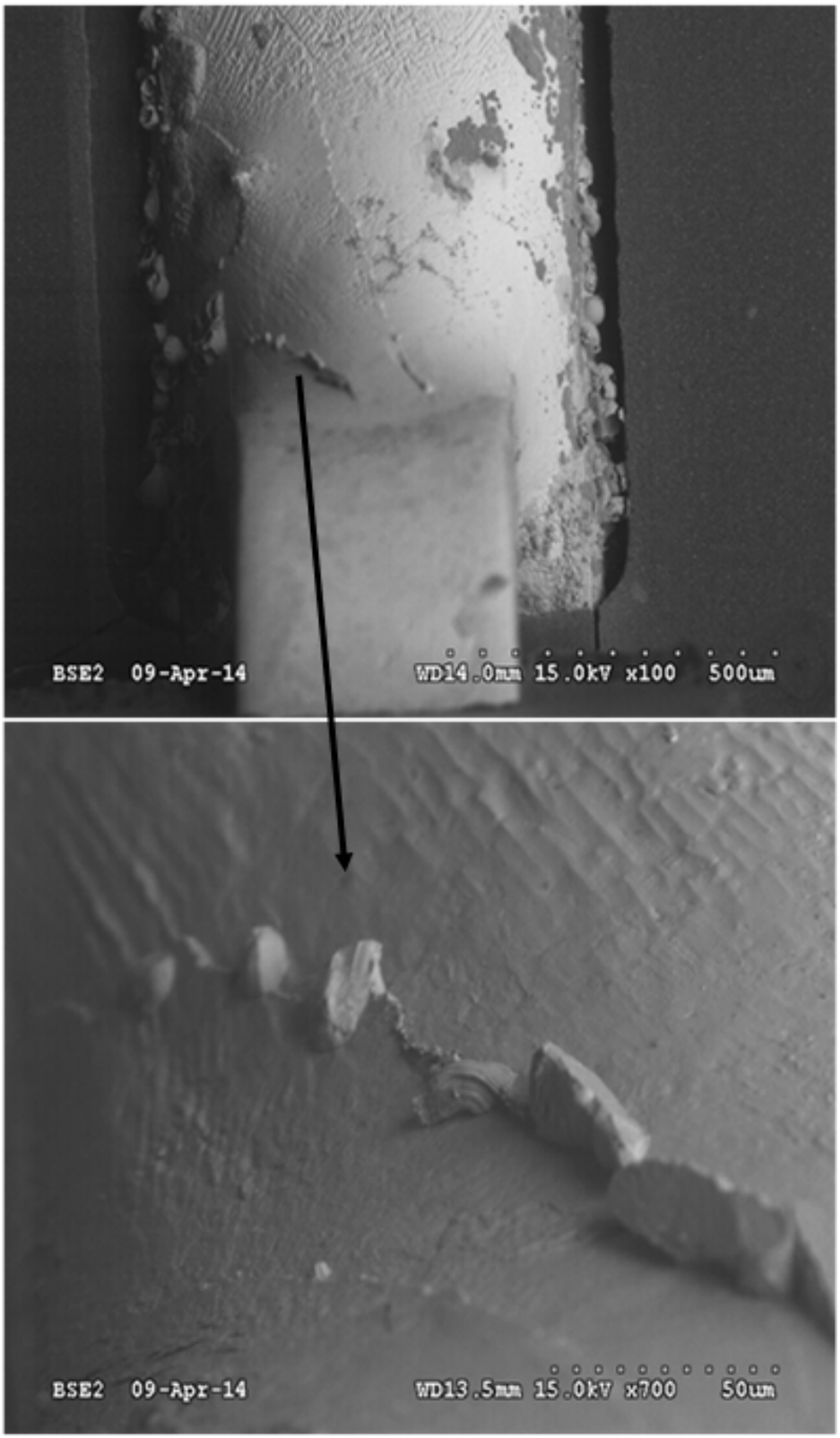


Figure 104: SEM image of an uncoated SOT5 lead (lead 2), ATC+ HTHH1000, 100x (ref. board 238). Corrosion near the bottom of the joint and whisker growth from the boundary between tin grains were observed.

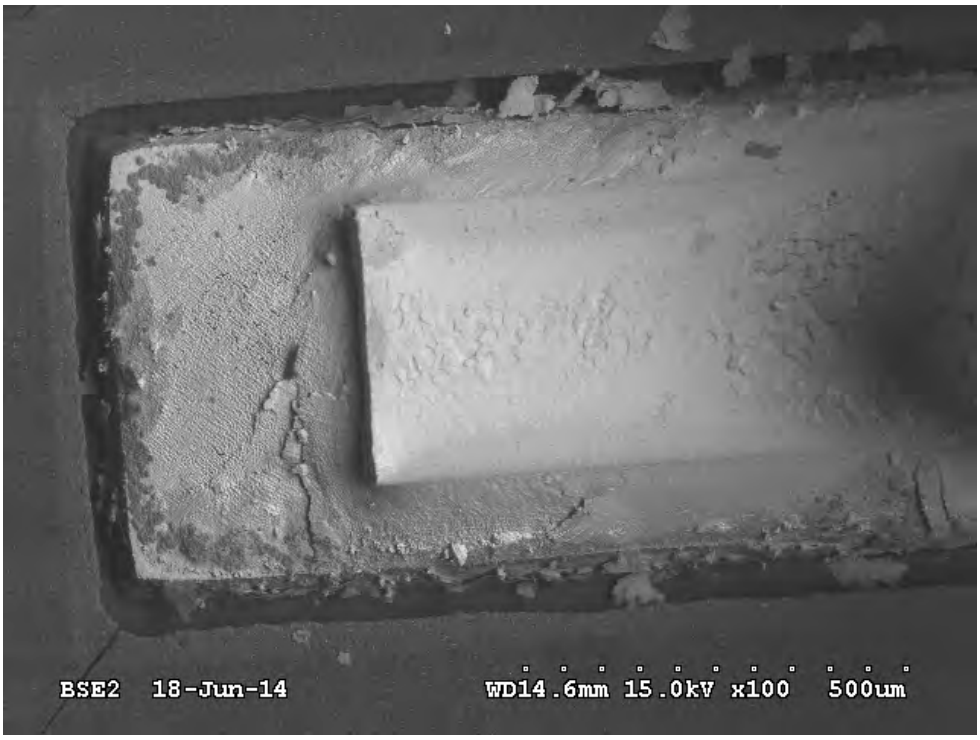


Figure 105: SEM image of an uncoated QFP44 lead, ATC+HTHH2000, 100x (ref. board 46).

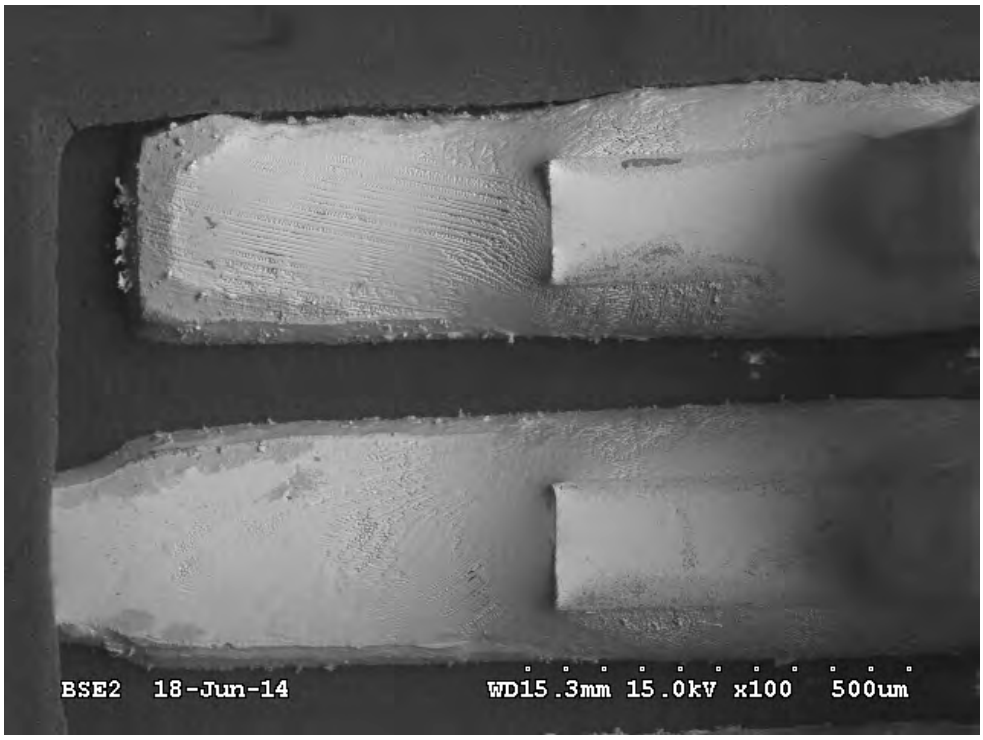


Figure 106: SEM image of uncoated QFP64 lead toes, HTHH2000, 100x (ref. Board 48).



Figure 107: SEM image of an uncoated QFP64 lead whisker growth, HTHH2000, 1500x (ref. Board 48).

5.19.2 PC18M based coatings whisker test results

The selected images from the SEM inspection results are given in Figure 108 to Figure 112 for the PC18M-mod, Figure 113 to Figure 116 for the PC18M+20%XP2742 nanosilica, and Figure 117 to Figure 119 for the PC18M+20%X11102PMA nanoalumina. The coated assemblies exhibited very little whisker growth or corrosion on the boards that went through ATC or ATC followed by HTHH. As was observed with the coupon tests, the whisker growth occurred where the coating was thin around the lead corners on the spray coated Polyurethane (PU) samples. Some of the spray coatings exhibited cracking after environmental exposure. The PC18M+20%X11102PMA nanoalumina did not crack, the PC18M+20%XP2742 nanosilica exhibited some cracking, and the PC18M-mod had greatest numbers of cracked coating regions. Generally, samples with good coverage without coating cracks showed no whisker growth or corrosion after ATC (Figure 117 and Figure 113) or after ATC+HTHH2000 (Figure 118).

In some cases of conformal coat crack widths up to 100 microns were observed. The majority of the cases were on the unfilled PC18M-mod coated low thermal expansion leads after ATC (Figure 109 and Figure 108). After ATC+HTHH, coating cracking was observed both on alloy-42 lead and on Cu lead terminations (Note that large bubble density caused stress concentrations that resulted in more cracking) (Figure 111). The coating cracks did not generally grow from the exposed metal regions. Note that the thin coating over the lead tip had instances of tin growth through the surface (Figure 112). Not all lead termination coated with the PC18M-mod coating exhibited cracking (Figure 110).

Less cracks formed in the PC18M+20%XP2742 nanosilica coating. After ATC, a chip resistor (low thermal expansion ceramic) exhibited cracks around the perimeter (Figure 114), but there were no cracks on the alloy-42 SOT6 (Figure 113). A small crack was observed in the PC18M+20%XP2742 nanosilica coated alloy-42 SOT3 after ATC+HTHH2000 (Figure 115).

There were no cracks observed during the SEM examination on any of the PC18M+20%X11102PMA nanoalumina samples.

5.19.2.1 SEM inspection of unfilled PC18M-mod

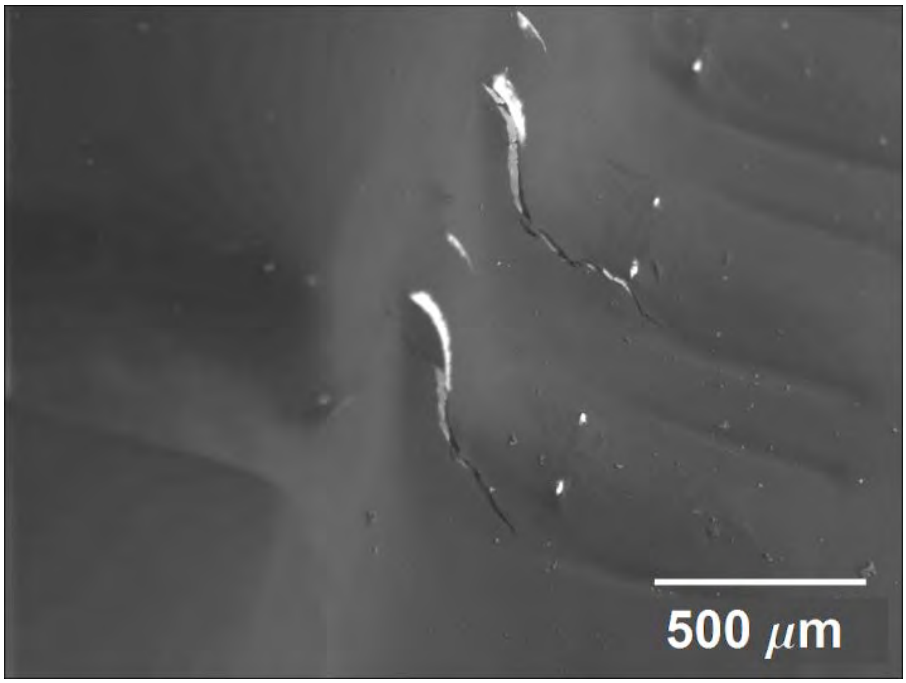


Figure 108: SEM image of PC18M-mod coated SOT6 leads, ATC. 60x, small bubble density (ref. Board 211).

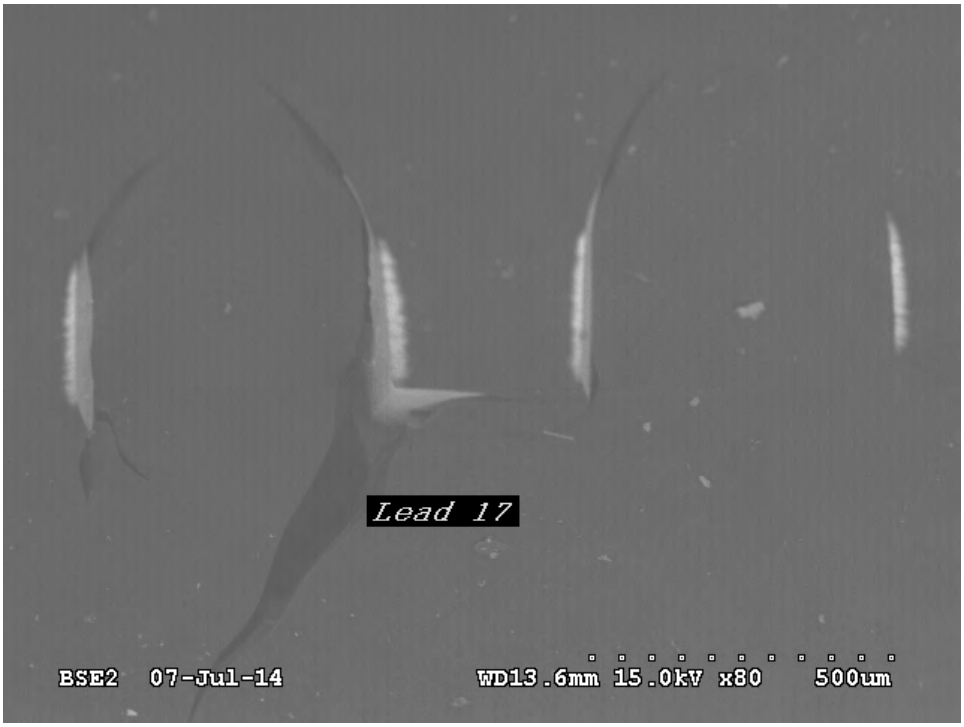


Figure 109: SEM image of PC18M-mod coated QFP44 leads, ATC, U2, Lead 17, 80x, large bubble density (ref. Board 34).



Figure 110: SEM image of PC18M-mod coated QFP44 leads, U2, Lead 14-15, ATC + 1000HTHH, 60x, small bubble density (ref. Board 15).



Figure 111: SEM image of PC18M-mod coated SOT package and leads, ATC+ HTHH1000, 40x (ref. Board 233). Large bubble density condition causing the coating to obscure the SOT leads.

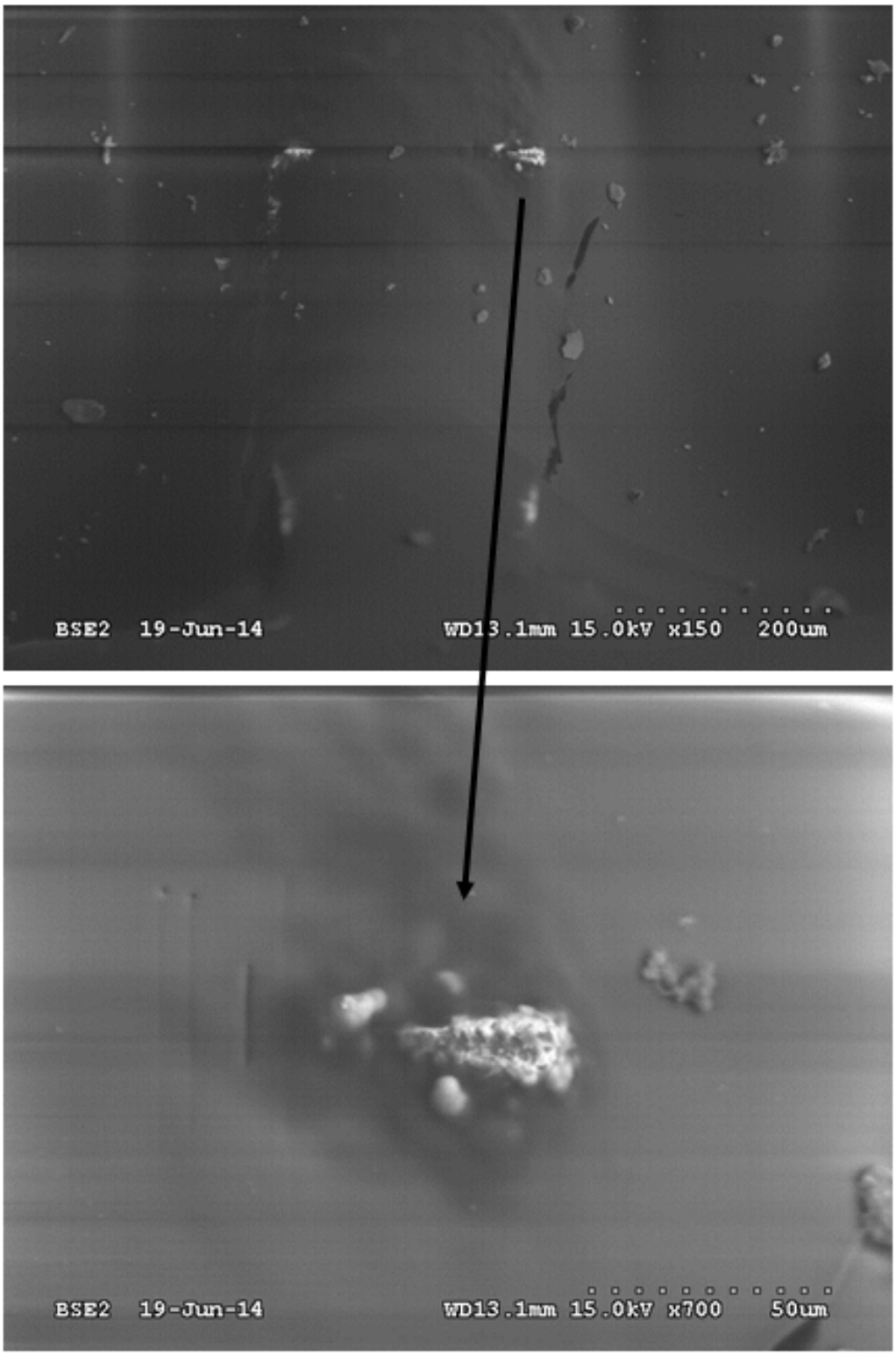


Figure 112: SEM image of PC18M-mod coated SOT6 lead (lead 3), ATC + 2000HTHH, 150x, small bubble density (ref. Board 215).

5.19.2.2 SEM inspection of PC18M+20%XP2742 nanosilica

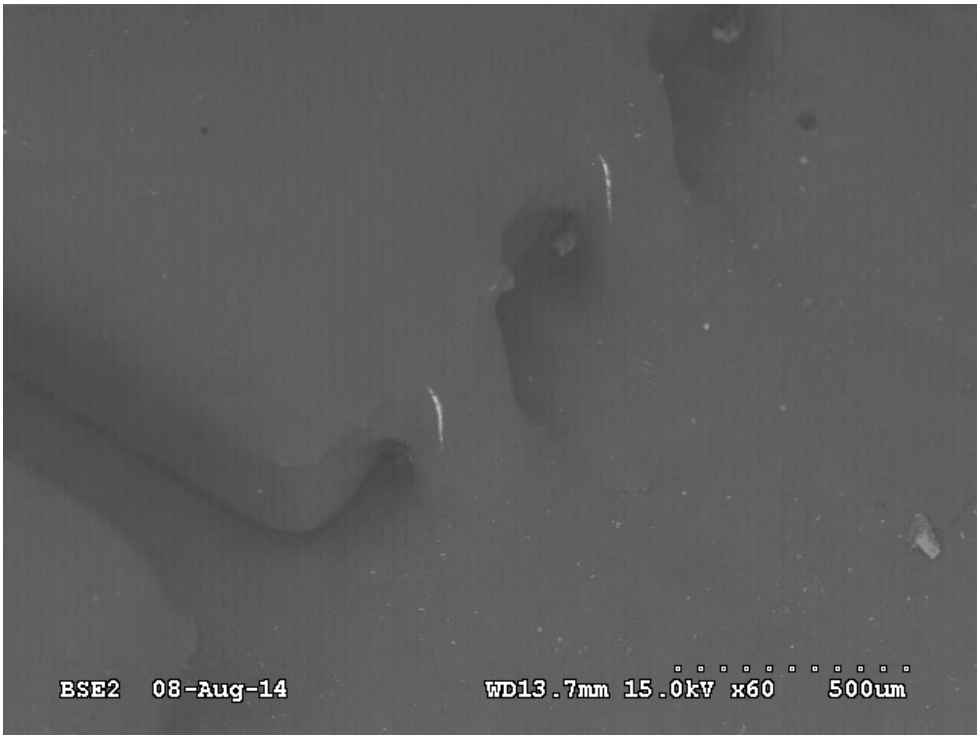


Figure 113: SEM image of PC18M+20%XP2742 nanosilica coated SOT6 leads, ATC, 60x, medium coating bubble density (ref. Board 217).

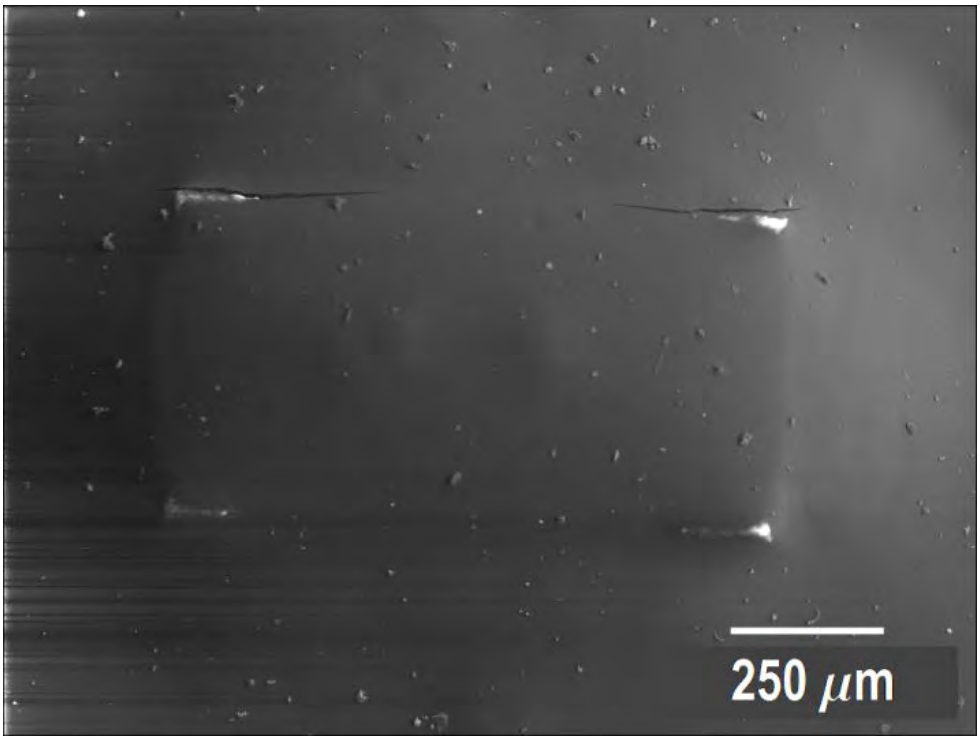


Figure 114: SEM image of PC18M+20%XP2742 nanosilica coated chip resistor, ATC, 80x, medium coating bubble density (ref. Board 217).

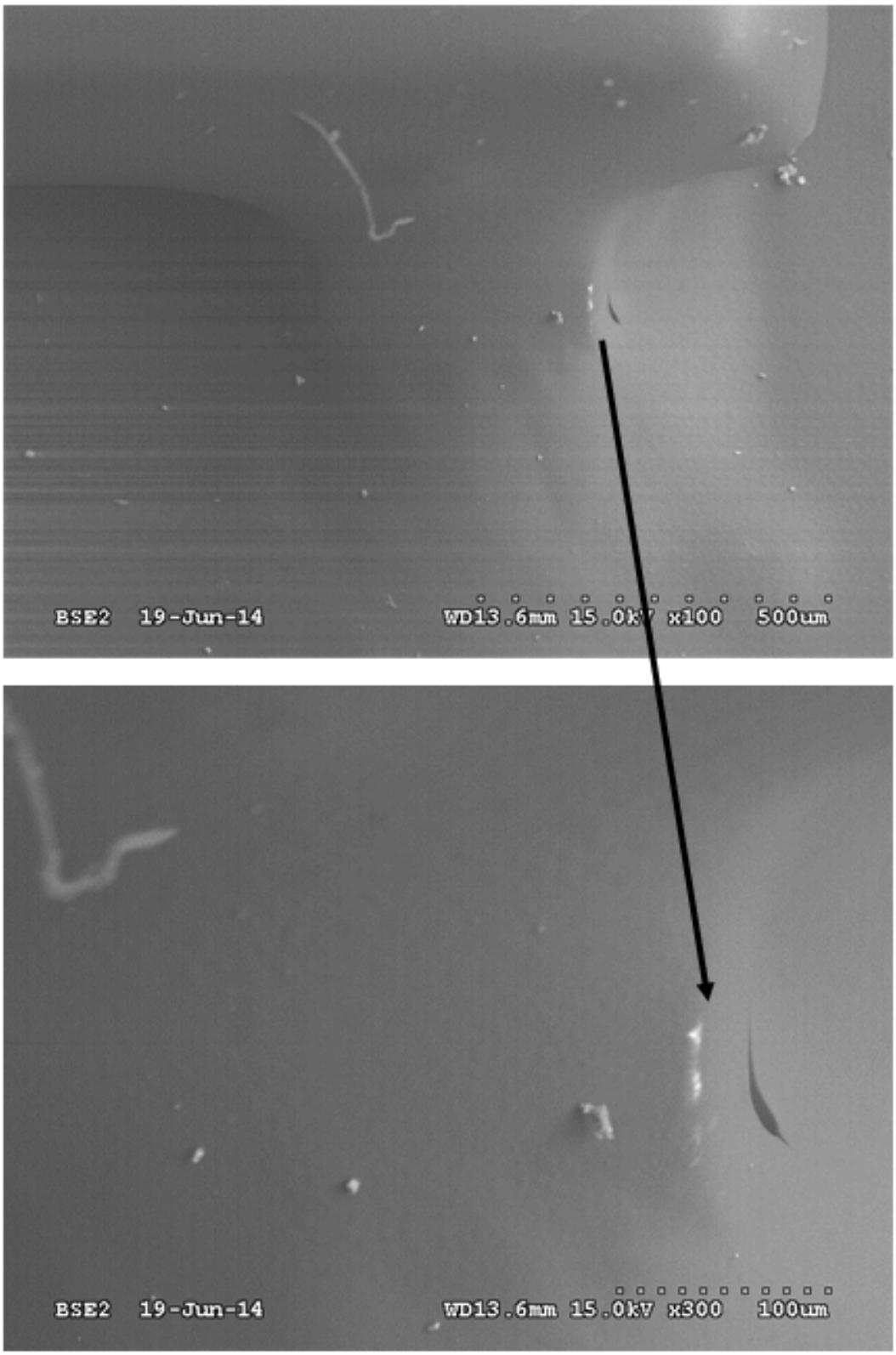


Figure 115: SEM image of PC18M+20%XP2742 nanosilica coated SOT3 lead (lead 2), ATC+HTHH2000, 100x and 300x, medium bubble density (ref. Board 235).

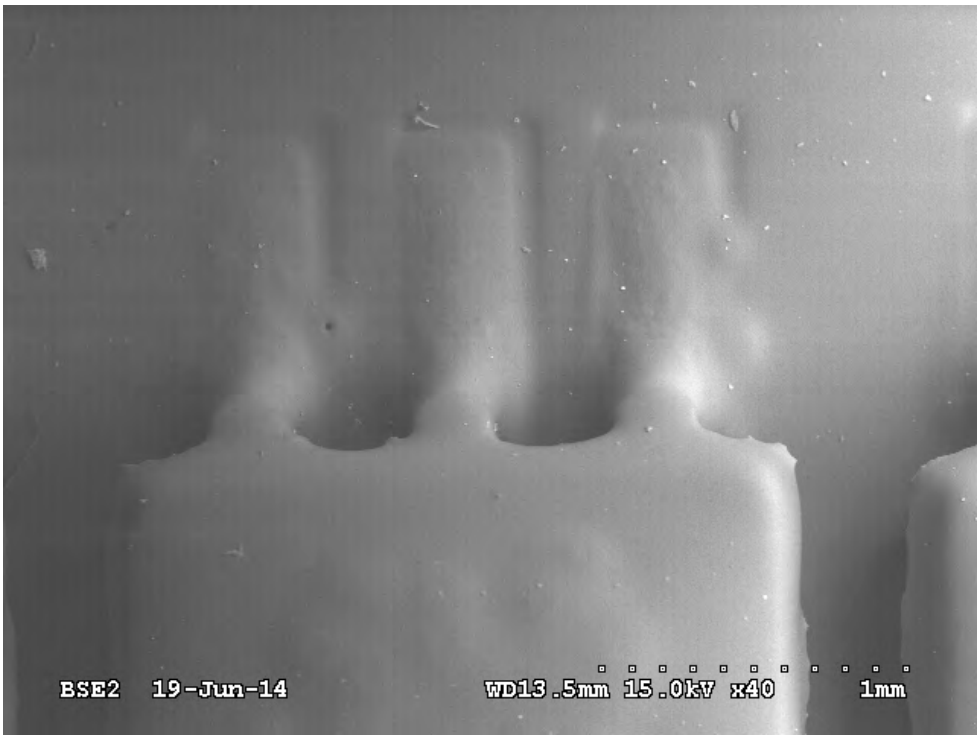


Figure 116: SEM image of PC18M+20%XP2742 nanosilica coated SOT6 leads, ATC+ 2000HTHH, 40x, medium bubble density (ref. Board 235).

5.19.2.3 SEM inspection of PC18M+20%X11102PMA nanoalumina

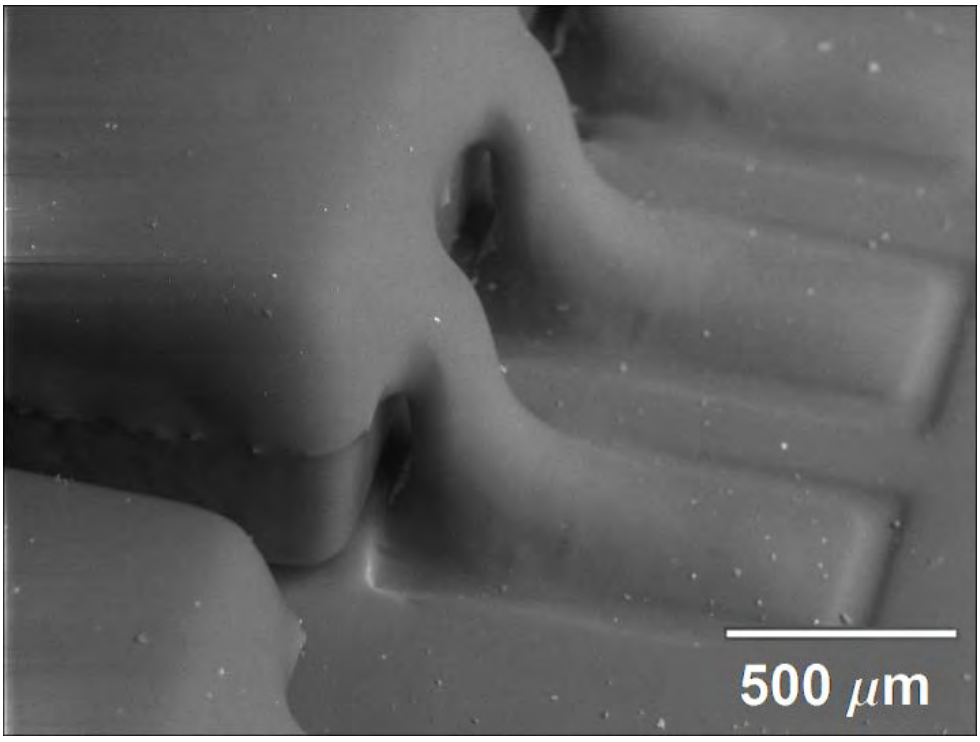


Figure 117: SEM image of PC18M+20%X11102PMA nanoalumina coated SOT6 leads, ATC, 60x, small/no bubble density (ref. Board 222).

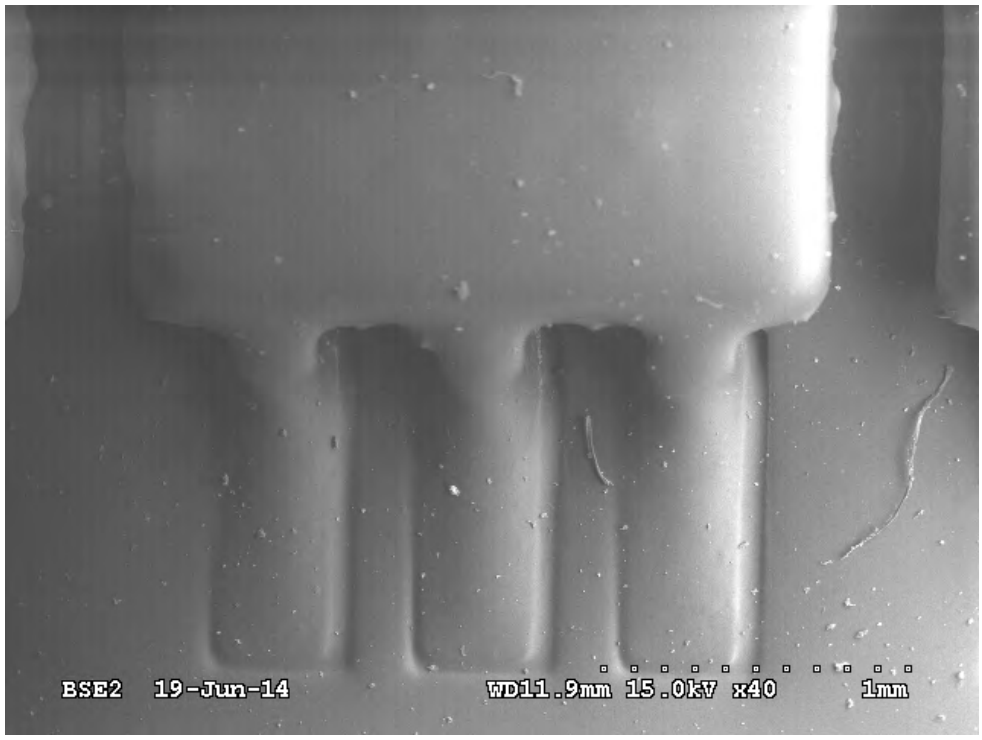


Figure 118: SEM image of PC18M+20%X11102PMA nanoalumina coated SOT6 lead, ATC + 2000HTHH, 40x, small/no bubble density (ref. Board 228).



Figure 119: SEM image of PC18M+20%X11102PMA nanoalumina, SOT6, lead 4 (center lead from Figure 113), ATC+HTHH2000, 100x, small/no bubble density (ref. Board 228).

5.20 Assembly whisker testing: PC40-UMF Baseline (dip + 50 micron spray)

The PC40-UMF assembly whisker testing details are provided in Appendix H, with some highlights presented next. The three PC40-UMF coating variations evaluated, each having an initial thinned PC40-UMF dip followed by plasma etching, were as follows; (1)PC40-UMF, (2) PC40-UMF+10%NNN2835 nanosilica, or (3) PC40-UMF+30%NNN2835 nanosilica. Note that the NNN2835 nanosilica suspension was made by Covestro (formerly Bayer Material Science) to be equivalent to the XP2742, but was prepared at a later time. Assemblies coated with 1B31 acrylic were tested at the same time for reference.

During the PC40-UMF coating process development, coverage and adhesion issues were encountered with the PC40-based coatings during the dip and spray process. Limited whisker testing was performed on these samples. The assemblies were part of the baseline coating build and test in the 2013-2014 time frame with the baseline PC18M samples, but not inspected. Then in 2015, these samples were included in the layered coating exposure for an additional 767 hours of 85C/85%RH and then inspected. The following nomenclature was used to define conditions:

- **HTHH1767:** 1,000 hours 85°C/85% RH then an additional 767 hours of 85°C/85% RH (Note: due to personnel changes and time elapsed, the records are unclear as to whether the samples were exposed to 100 cycles of -55 to +125°C and 200 cycles of -20 to +80°C thermal cycling)

5.20.1 Baseline (dip +50 micron spray) PC40-UMF based coating whisker test results

The PC40-UMF based coatings included PC40-UMF (Figure 120 to Figure 124), PC40-UMF+ 10%NNN2835 nanosilica (Figure 125 to Figure 128), and PC40-UMF+30%NNN2835 nanosilica (Figure 129 to Figure 133). Whisker growth observations are summarized in Table 6. The summary of the SEM inspection results follows.

Table 6: PC40-UMF base coating assembly whisker inspection summary.

Board Label	Coating identifier	Board Type	Observations
60	2014 - Main (PC40-UMF)	QFP	Most whisker growth on QFP44; none on QFP64 and PLCC
65	2014 - Main (PC40-UMF+10% NNN2835 nanosilica)	QFP	On QFP44, no difference between 10% & 30% filler levels; no growth on QFP64 and PLCC
70	2014 - Main (PC40-UMF+30% NNN2835 nanosilica)	QFP	On QFP44, no difference between 10% & 30% fillers; no growth on QFP64 and PLCC, but some corrosion on QFP64
256	2014 - Main (PC40-UMF)	SOT	SOT5s show more growth than SOT3s and SOT6s.
284	2014 - Main (PC40-UMF+10%NNN2835 nanosilica)	SOT	SOT5s show more growth than SOT3s and SOT6s.
269	2014 - Main (PC40-UMF+30%NNN2835 nanosilica)	SOT	SOT5s show more growth than SOT3s and SOT6s.

5.20.1.1 Coating thickness

The PC40-UMF spray coating did not form a continuous thin film on the dip coating and formed discrete droplets. The droplets were especially pronounced on the knee and the vertical surfaces (Figure 120).

No whisker growth was observed where the coating was thicker (greater than approximately three microns). Where the coating was thinner, whiskers and nodules were seen (e.g. Figure 122, Figure 128, and Figure 131). A range of corrosion was observed where the coating was thin. The majority was considered low, but sometimes it was extensive (Figure 125)

Some parts had very thick coating (greater than approximately 150 microns) and in some cases the coating nearly encapsulated the parts, especially of the lower profile SOT3 (Figure 123) and QFP64 (Figure 124). Also, when the coating was thick, it often pulled away from the lead leaving a substantial gap (e.g. Figure 120 and Figure 121) and cracked near the package body (Figure 124). The pull-away was less evident with the PC40-UMF+30%NNN2835 nanosilica spray coating Figure 133).

5.20.1.2 Coating type

All whiskers and corrosion were observed in thin areas that were of the initial PC40-UMF dip coating where the spray coating dewet. No significant differences in whisker mitigation were observed between the thick PC40-UMF and PC40-UMF with 10% or 30% nanosilica regions.

5.20.1.3 Part type

As is expected in a high humidity environment, the copper lead material exhibited greater whisker growth and corrosion than the alloy – 42 lead materials on the SOT3 and SOT6 devices. QFP44s had the more whisker growth than QFP64s and PLCCs. SOT5s had more growth than SOT3s and SOT6s.

5.20.1.4 SEM inspection of baseline PC40-UMF assemblies

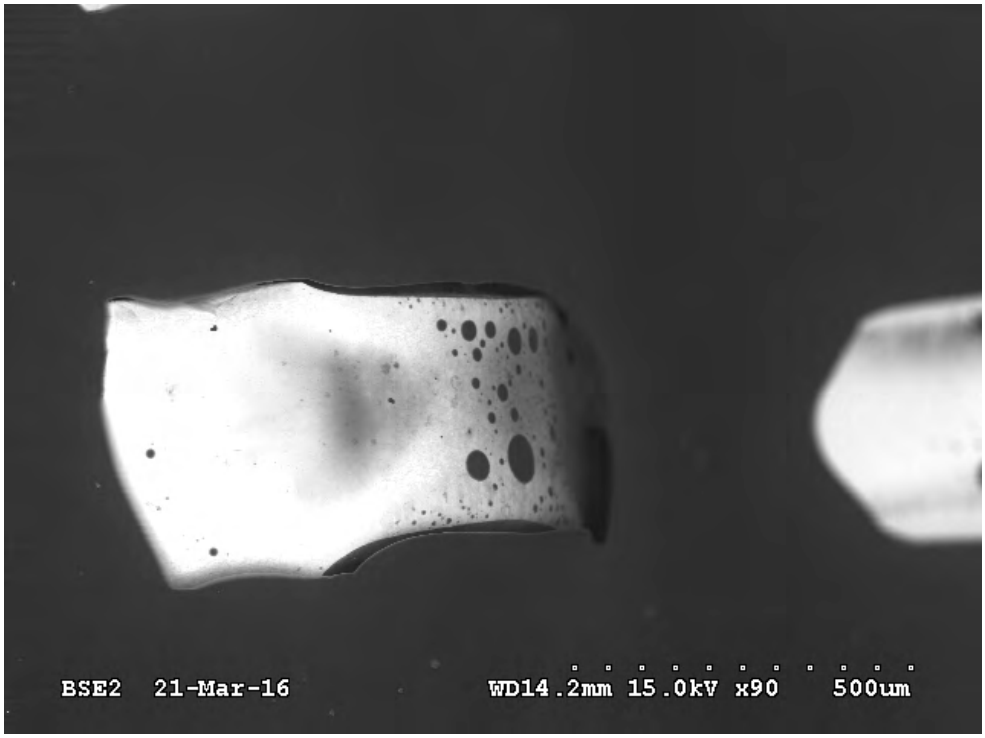


Figure 120: SEM image of baseline PC40-UMF coated QFP44 lead, HTHH1767, 90x (ref. Board 60). A discontinuous film of discrete droplets and coating pull – away from the metal were observed.

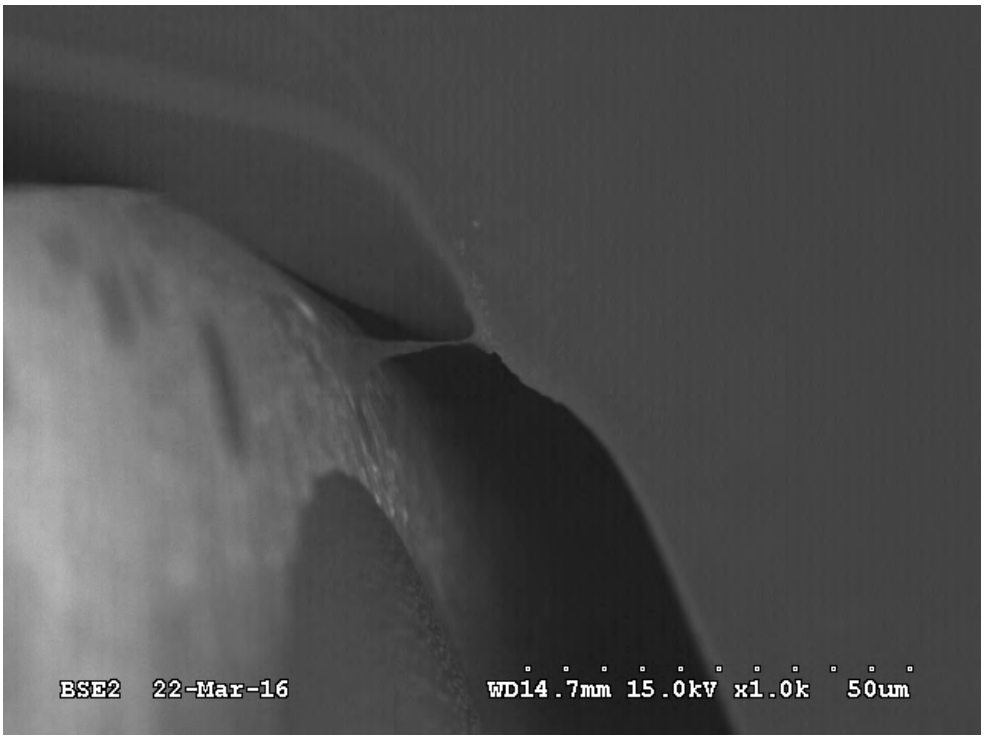


Figure 121: SEM image of baseline PC40-UMF coated QFP44 lead, HTHH1767, QFP44, 1,000x (ref. Board 60). Higher magnification view of coating pull away.

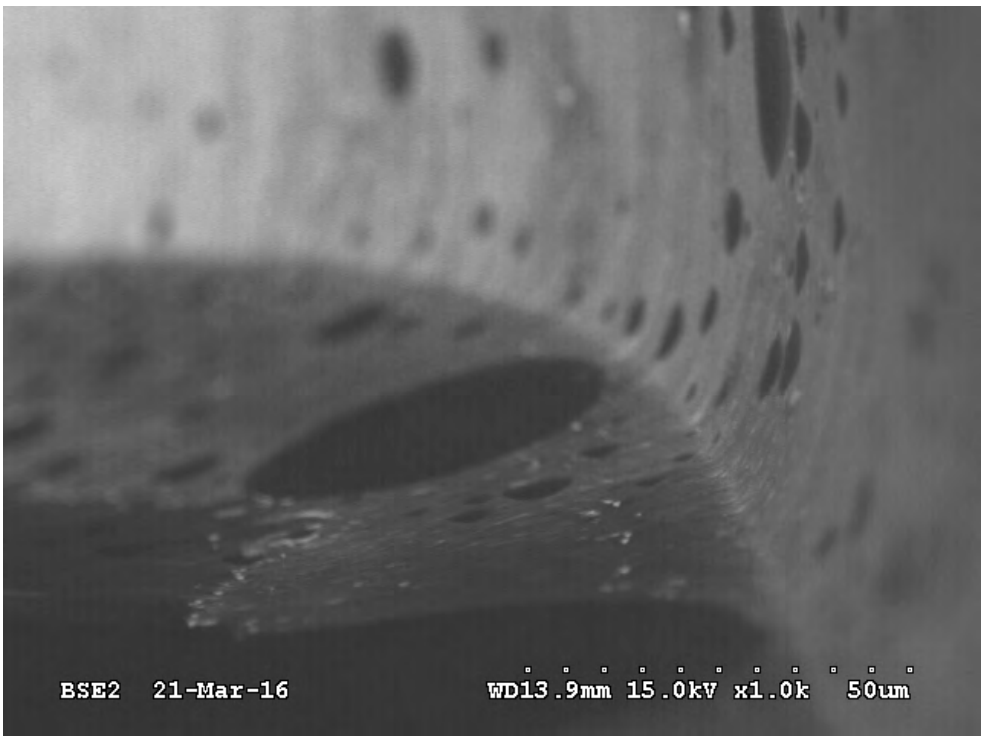


Figure 122: SEM image of baseline PC40-UMF coated QFP44 lead side, HTHH1767, QFP44, U4, lead 12, 1,000x (ref. Board 60)**.**

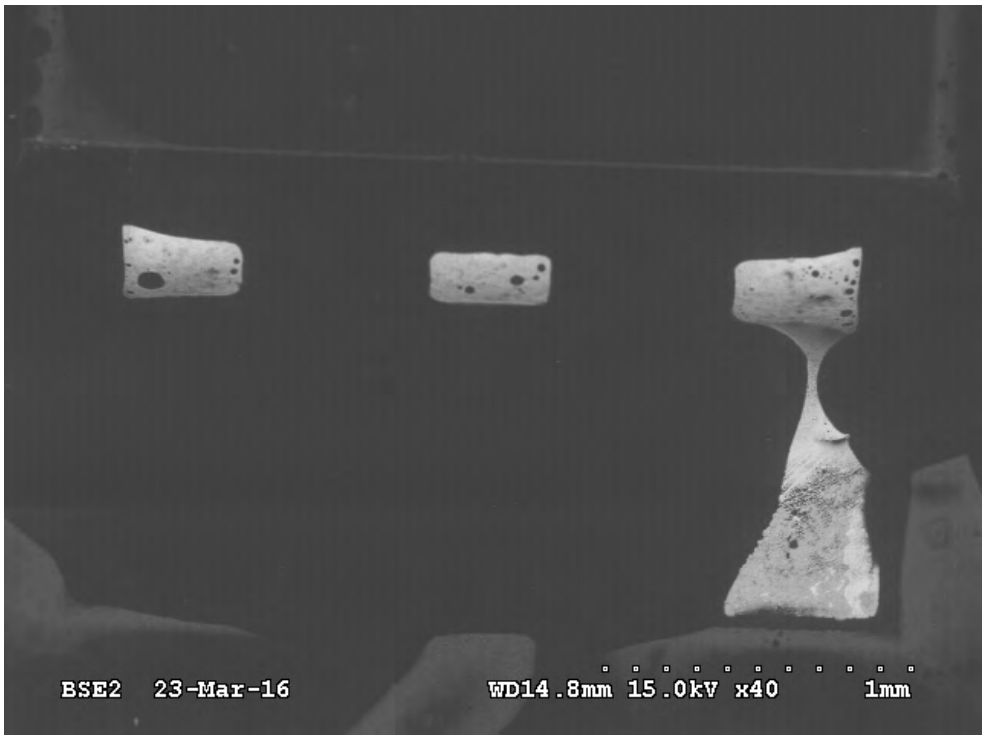


Figure 123: SEM image of baseline PC40-UMF coated SOT5 leads, HTHH1767, U01, 40x (ref. Board 256).

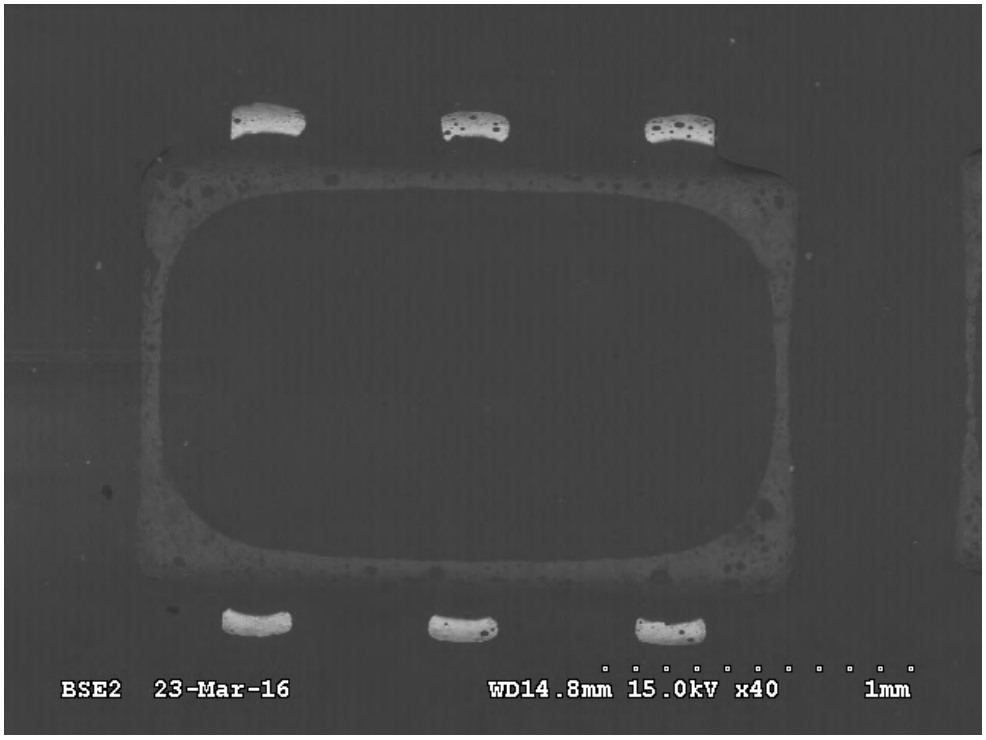


Figure 124: SEM image of baseline PC40-UMF coated SOT6 leads, HTHH1767, 40x (ref. Board 256).

5.20.1.5 SEM inspection of baseline PC40-UMF+10%NNN2835 nanosilica assemblies

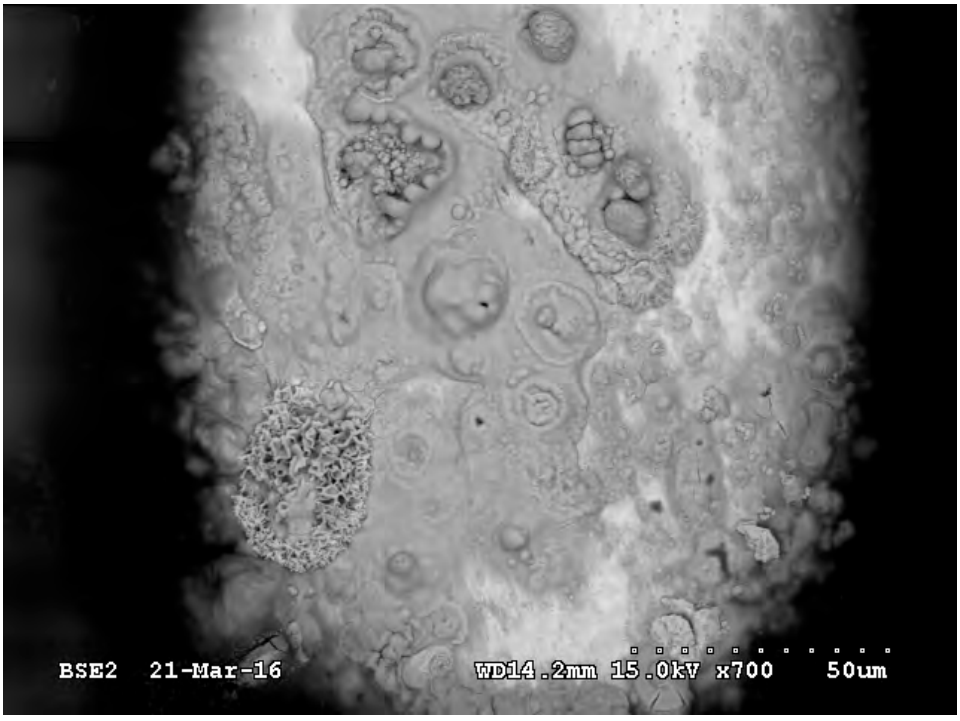


Figure 125: SEM image of baseline PC40-UMF+10%NNN2835 nanosilica coated QFP64 lead toe, HTHH1767, 700x, (ref. Board 65).



Figure 126: SEM image of baseline PC40-UMF+10%NNN2835 nanosilica coated SOT3 leads, HTHH1767, U06, 40x (ref. Board 284).

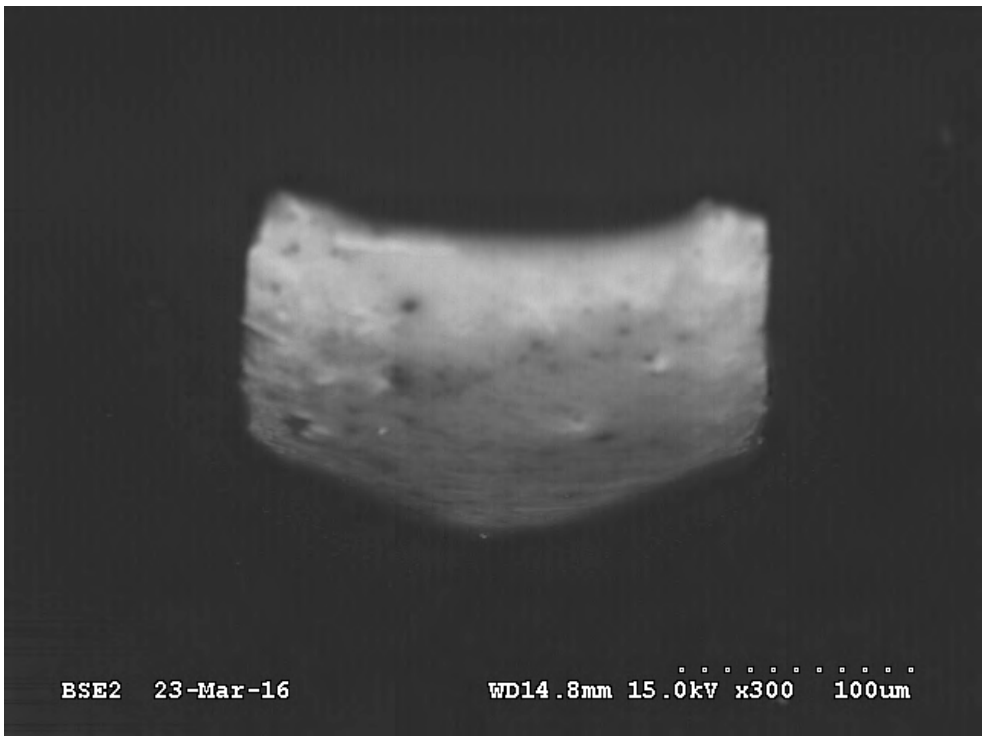


Figure 127: SEM image of baseline PC40-UMF+10%NNN2835 nanosilica coated SOT6 lead, HTHH1767, U65, lead 2, 300x (ref. Board 284).

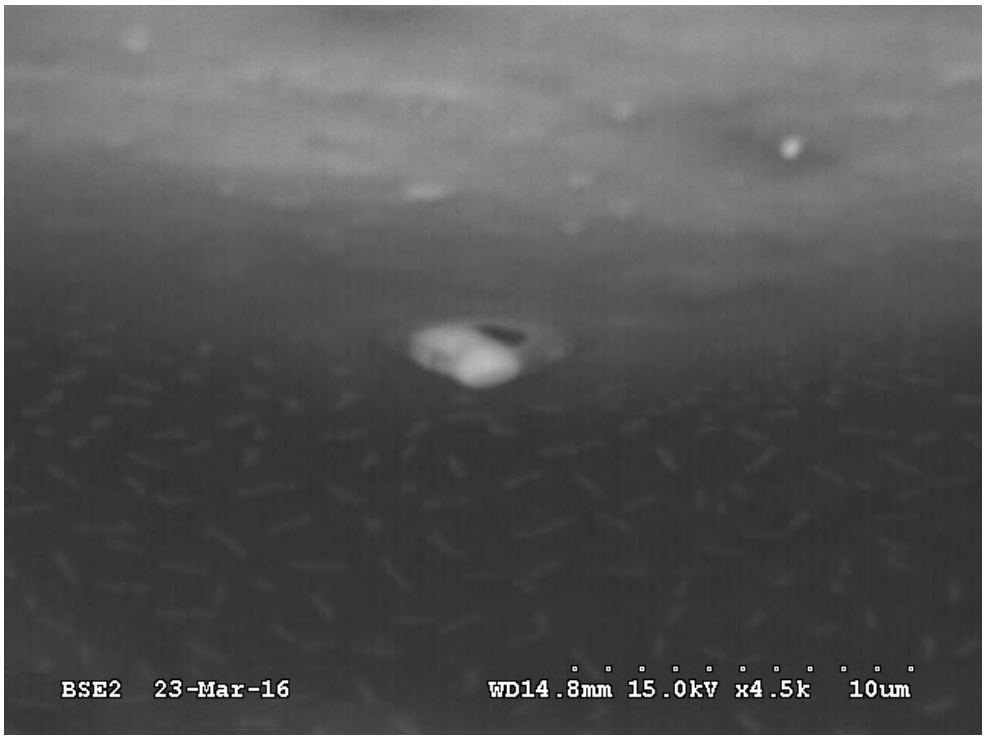


Figure 128: SEM image of baseline PC40-UMF+10%NNN2835 nanosilica coated SOT6 lead, HTHH1767, U65, lead 2, 4,500x (ref. Board 284).

5.20.1.6 SEM inspection of baseline PC40-UMF+30%NNN2835 nanosilica assemblies



Figure 129: SEM image of baseline PC40-UMF+30%NNN2835 nanosilica coated QFP44 lead, HTHH1767, U5, lead 44, 120x (ref. Board 70).

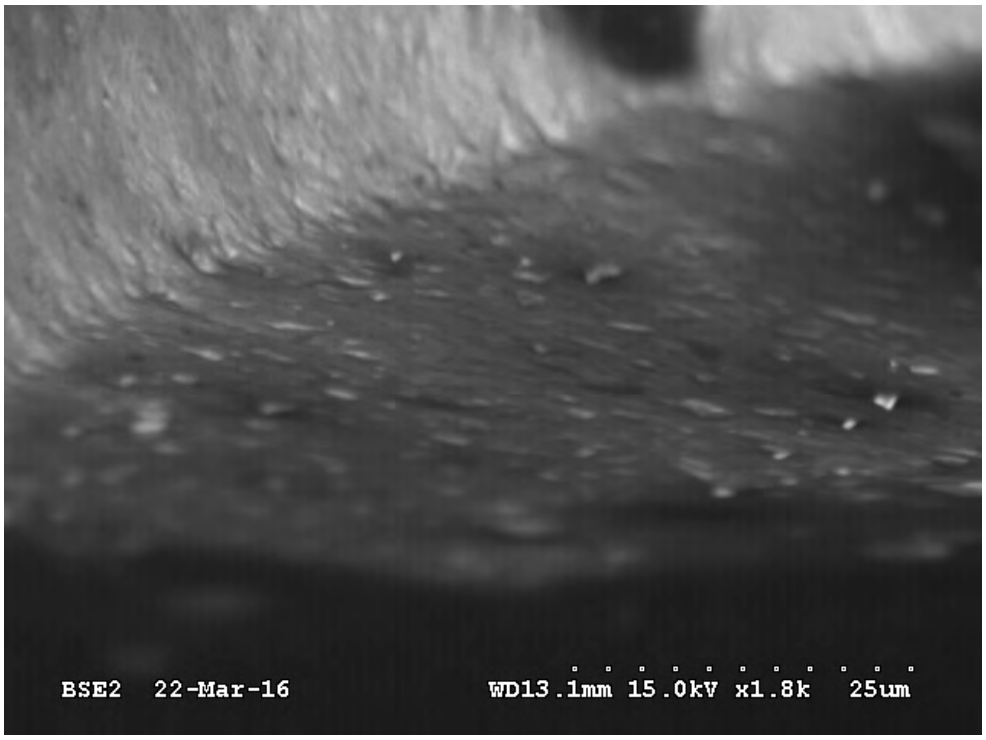


Figure 130: SEM image of baseline PC40-UMF+30%NNN2835 nanosilica coated QFP44 lead, HTHH1767, U5, lead 44, 1800x (ref. Board 70).



Figure 131: SEM image of baseline PC40-UMF+30%NNN2835 nanosilica coated QFP44 lead, HTHH1767, U5, lead 44, 4,000x (ref. Board 70).

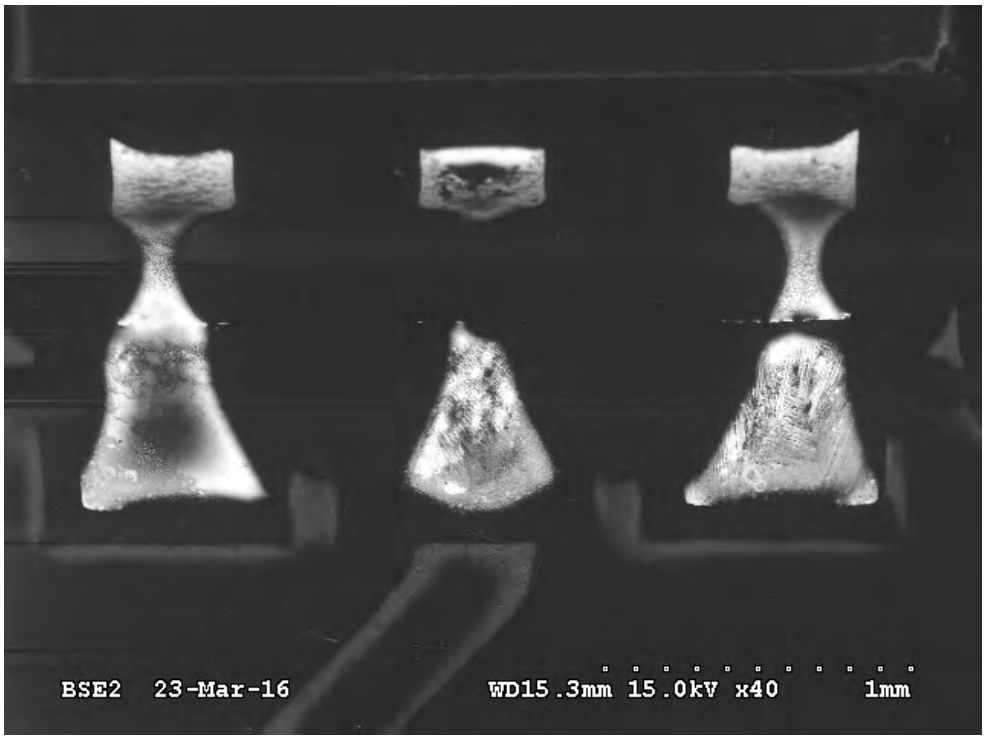


Figure 132: SEM image of baseline PC40-UMF+30%NNN2835 nanosilica coated SOT5 leads, HTHH1767, U04, 40x (ref. Board 269).



Figure 133: SEM image of baseline PC40-UMF+30%NNN2835 nanosilica coated SOT5 lead, HTHH1767, U15, lead 5, 250x (ref. Board 269).

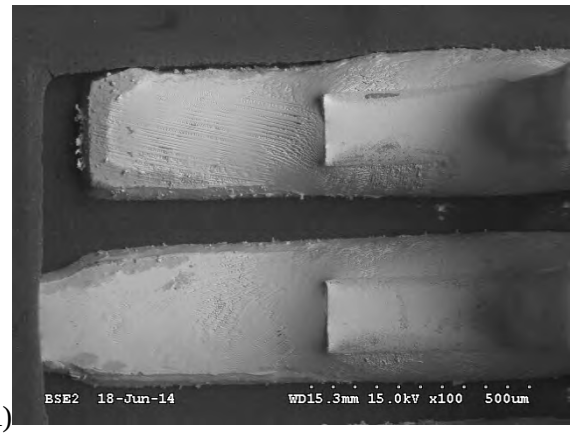
5.21 Assembly whisker testing: Enhanced layered coating

The enhanced layered coating tin whisker testing is presented in Appendix K, with some highlights presented next. Layered coatings were applied in an effort to improve the coating coverage on corners, edges, behind leads and on vertical surfaces. The detailed materials and processes are given in Appendix E. Briefly, the layered coatings were formed through sequential dip or spray coating applications with partial cures between them. The base layer of both the unfilled and the nanosilica filled coatings is a low viscosity initial dip layer. Then additional layers are sprayed on using either unfilled PC18M or nanosilica filled PC18M+20%XP2742. The dip only boards were dipped then fully cured. The one spray layer coating sequence was: dip, partial cure, spray, and then full cure. The two spray layer coating sequence was: dip, partial cure, spray, partial cure, spray, and then full cure.

This Appendix Kcompares the whisker mitigation of layered unfilled and layered nanosilica filled coatings. The assemblies were exposed to an 85°C and 85 percent relative humidity (%RH) high temperature high humidity (HTHH) environment and examined after 3030 hours in the SEM. The inspection focused on the quad flat pack (QFP) because it contained part with the longest leads and the BGA boards because of the large number of solder bumps and the ease of inspection. A summary of the inspection is given next.

5.21.1 Enhanced layered coating QFP board whisker growth

During the baseline whisker testing, uncoated SAC305 soldered QFPs were exposed to high temperature humidity. These boards exhibited corrosion and whisker growths after 2,000 hours of 85C/85%RH (Figure 134). In contrast to the uncoated boards, no corrosion or whisker growth was observed on the layer coated QFP44s assemblies using either the unfilled PC18M or the nanosilica filled PC18M+20%XP2742. The presence of a rough coating surface and surface bubbles did not appear to impact whisker growth propagation to the surface, but continues to cause risk for material embrittlement and cracking.

(A) 

(B) 

Figure 134: Uncoated board 48 QFP64 after 2,000h of HTHH; (A) 100x and (B) 1,500x.

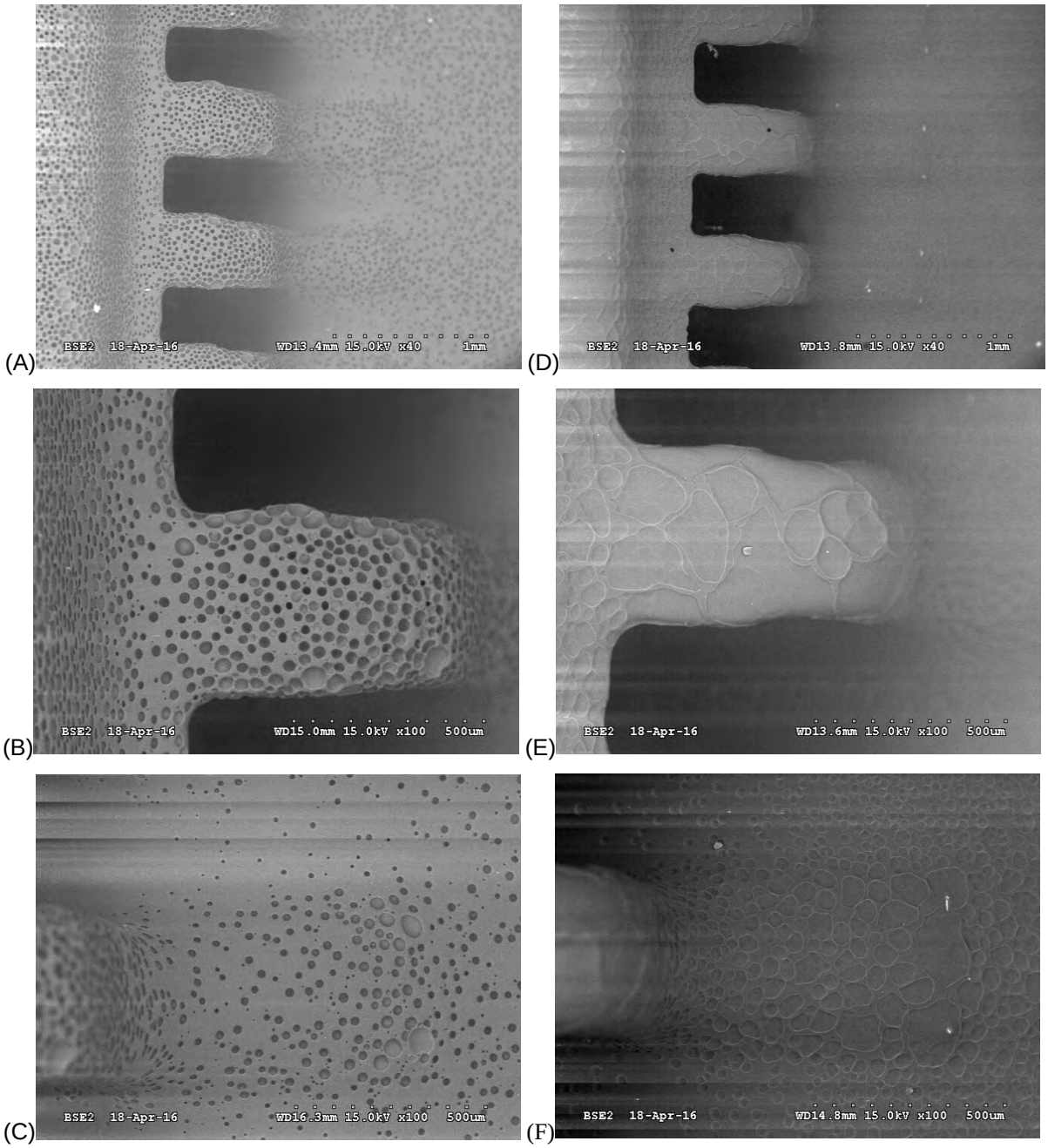


Figure 135: SEM images comparing layer coated unfilled PC18M spray and PC18M+20%XP2742 nanosilica filled sprays in the dip + two 50 micron spray QFP44 parts after HTHH testing for 3,030h. Images (A) (B) (C) are of unfilled PC18M dip + two unfilled PC18M sprays (board A023) and images (D) (E) (F) are of unfilled PC18M dip + two (PC18M+20%XP2742) nanosilica filled sprays (board A347). Image magnifications are: (A) (D) overall lead at 40x, (B) (E) lead top at 100x, and (C) (D) lead bottom at 100x.

5.21.2 Enhanced layered coating BGA board whisker growth

The BGA pads on this board were printed with a SAC305 solder paste and refllowed to form a small solder dome which caused thin coating areas when fewer layers were applied. The dip coat alone had the thinnest coating coverage. The dip/partial cure/spray layer combination increased the coating thickness, but there were still thin regions. The dip/partial cure/spray/partial cure/spray further increased the coating thickness. By increasing the number of layers a decrease in corrosion and whisker growth were observed (Figure 136). The PC18M "dip only" boards resulted in less than approximately three microns of coating on the BGA solder domes and exhibited extensive corrosion and whisker growth. In contrast, the PC18M dip + two sprays of either unfilled PC18M or (PC18M+20%XP2742 nanosilica filled) material had no corrosion or whisker growth (Figure 137).

In some instances, Ag_3Sn intermetallic nodules were observed because the surrounding tin had corroded away; reinforcing the importance of EDX verification when counting tin whiskers/nodules (Figure 138).

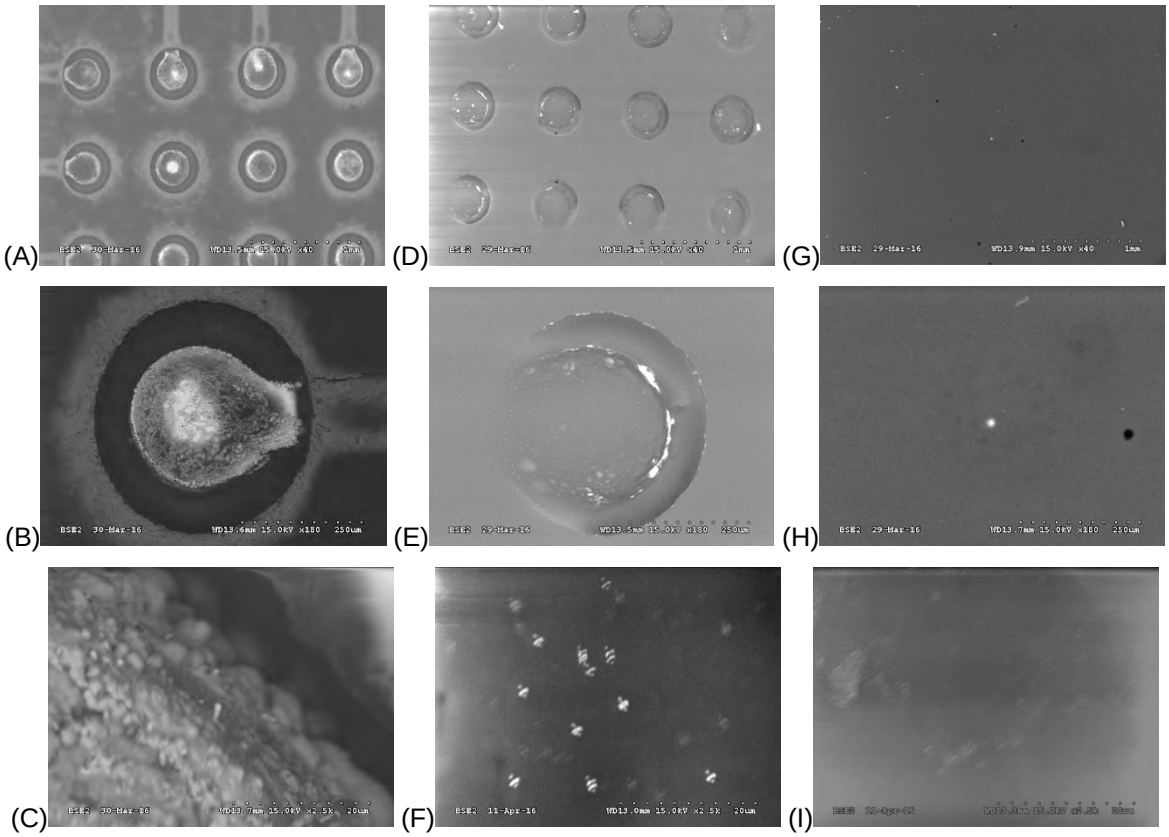


Figure 136: SEM images of PC18M+20%XP2742 nanosilica spray layered coated BGA pads with increasing number of layers at various magnifications after HTHH testing for 3,030h.(A) (B) (C) dip, (D) (E) (F) dip + one spray, and (G) (H) (I) dip + two sprays with (A) (D) (G) 40x, (B) (E) (H) 180x and (C) (F) (I) 2,500x.

Extended Figure 136 caption: (A) (B) (C) unfilled PC18M dip (board A596); (D) (E) (F) PC18M dip + one (PC18M+20%XP2742) nanosilica filled spray (board A593); (G) (H) (I) PC18M dip + two (PC18M+20%XP2742) nanosilica filled sprays (board A392). Note that the image (H) bright spot is debris and the dark spot is a hole.

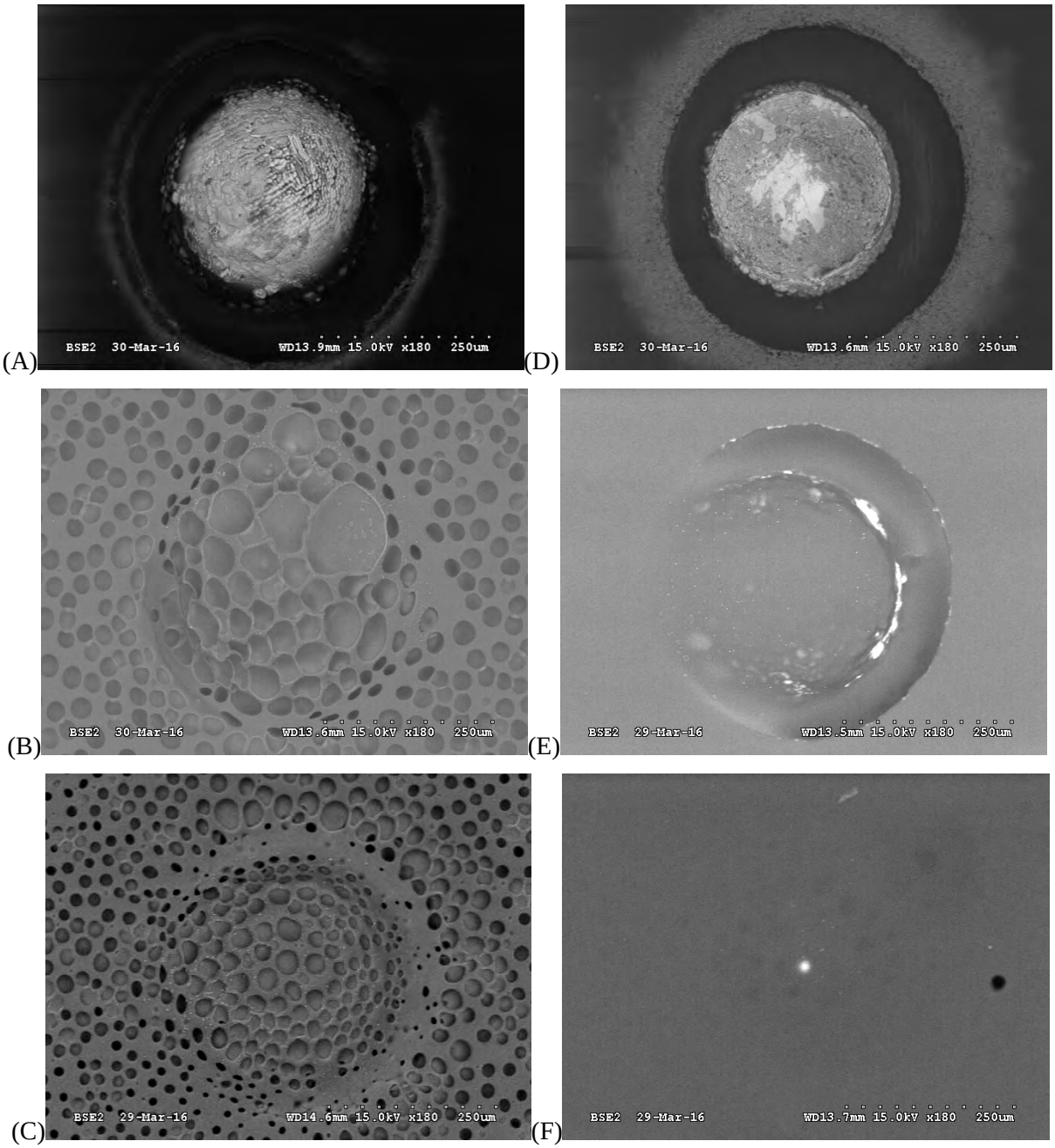


Figure 137: SEM images of layered coated BGA pads with increasing number of layers for unfilled PC18M sprays and PC18M+20%XP2742 nanosilica filled sprays after HTHH testing for 3,030h, 180x. (A) (B) (C) unfilled spray run and (D) (E) (F) nanosilica filled spray run with (A) (D) dip, (B) (E) dip + one spray, and (C) (D) dip + two sprays. Image (A) unfilled PC18M dip processed with unfilled PC18M spray run (U808, B3, Board A377), (B) unfilled PC18M dip + two unfilled PC18M spray (U606, A2, Board A307), (C) unfilled PC18M dip + two unfilled PC18M sprays. (U501, A1, Board A296), (D) unfilled PC18M dip processed with the PC18M+20%XP2742 nanosilica filled spray run (U508, G3, Board A596), (E) unfilled PC18M dip + one (PC18M+20%XP2742) nanosilica filled spray (U805, K1, Board A593), and (F) unfilled PC18M dip + two (PC18M+20%XP2742) nanosilica filled sprays (U501, A1, Board A392). Note that the image (H) bright spot is debris and the dark spot is a hole.

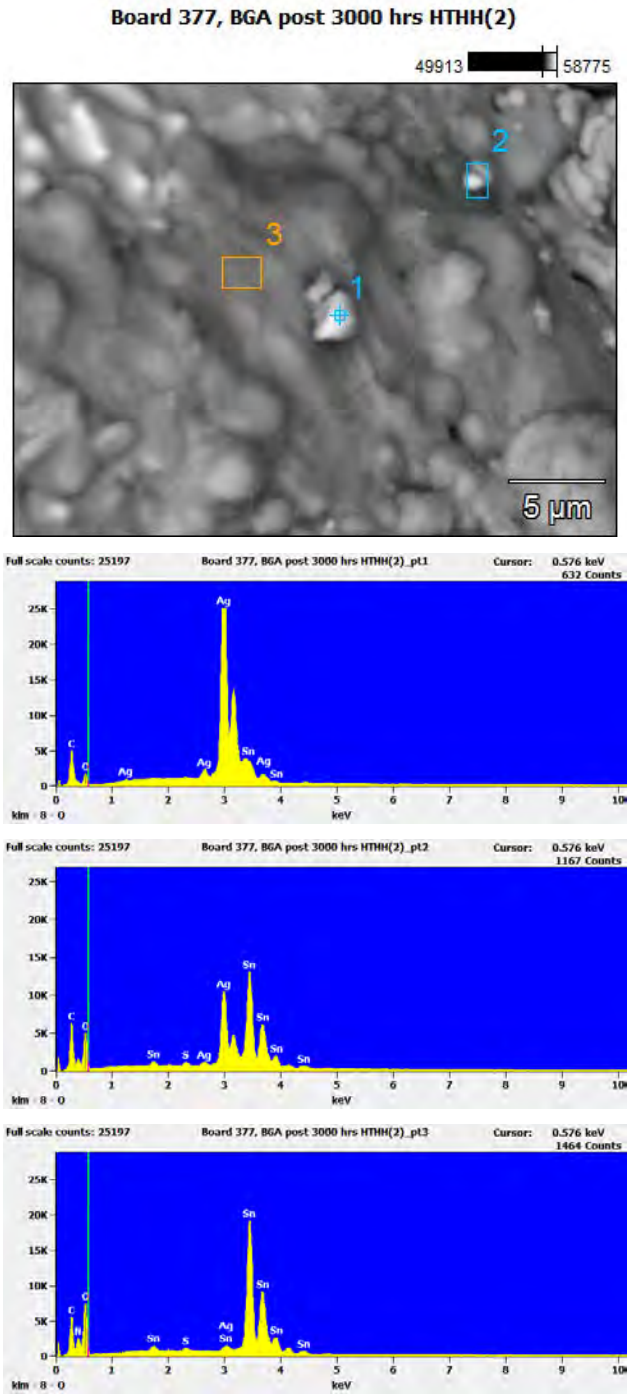


Figure 138: SEM image and electrodispersive x-ray (EDX) analysis of some nodules found on BGA pads from board A377, PC18M dip only. Note that the nodules in locations one and two are Ag_3Sn intermetallic with the surrounding Sn corroded away.

5.21.3 Enhanced layered coating whisker growth discussion

No whisker growth or corrosion was observed where there was at least one layer of spray coating over the dip. Only the dip coated PC18M samples exhibited whisker growth or corrosion (Figure 136C). The successive layer thickness build-up from the dip/partial cure, to the first spray/partial cure, then the second spray/partial cure resulted in progressively better coverage. As the coverage improved, there were fewer areas where the SEM beam could examine the tin though the coating (e.g. the coating was less than approximately three microns). The presence of a rough coating surface and surface bubbles did not appear to negatively impact whisker mitigation effectiveness.

Even one additional spray layer significantly improved the coverage and the whisker/corrosion resistance. For example, the PC18M dip + one spray of PC18M+20%XP2742 nanosilica significantly improved the performance of the BGA pads. The PC18M dip + one spray of PC18M+20%XP2742 nanosilica only had a few areas of thin coating along the BGA PWB pad edge and a few solder tin dendrite tips (Figure 136 E and F).

On the QFP parts with the dip + 2 spray layer coating, only the lead tips had thin coating when examined with the SEM and the BGA pads were fully covered (Figure 136 H and I). No whisker growth or corrosion was observed on the QFP lead tips.

The layered coating method provided good coverage. Increasing the number of layers, decreased the thin coating sites. No whisker growth or corrosion was observed on any of the dip + one or two spray layered assemblies regardless as to whether an unfilled PC18M spray or a filled PC18M+20%XP2742 nanoparticle spray was used.

5.22 Assembly whisker testing: Reference coatings

The results from the reference coating assembly testing are provided in Appendix H, with some highlights presented next.

5.22.1 Parylene reference coating during baseline PC18M whisker test results

During the baseline coating whisker testing Parylene ™ C coatings were evaluated at the same time. The results showed that good coating integrity and no whisker growth was observed on both the Parylene ™ C or the Parylene ™ C with Adpro+ (Figure 139 and Figure 140). However, the Parylene™ C with Adpro+ exhibited some instances of very small cracking (approximately one micron wide) at the lead-to-package interface (Figure 141) after thermal cycling. There were no whiskers or eruptions present in the microcrack region, and the crack may not go all the way to the underlying metal. The coating supplier indicated that small cracks can occur during assembly thermal cycling from the stresses arising from the various material thermal expansion coefficients. The enhanced Parylene™ C adhesion from the Adpro+ causes the substrate stresses to be transferred into the coating. Without the Adpro+, small regions of Parylene™ C debonding from the surface would likely occur in the high stress regions. A thinner Parylene™ C would be less susceptible to this type of cracking. Microcracking might be avoided with a 10 – 15 micron, rather than a 25 micron, thick coating when coated parts are subjected to high stress accelerated aging conditions.

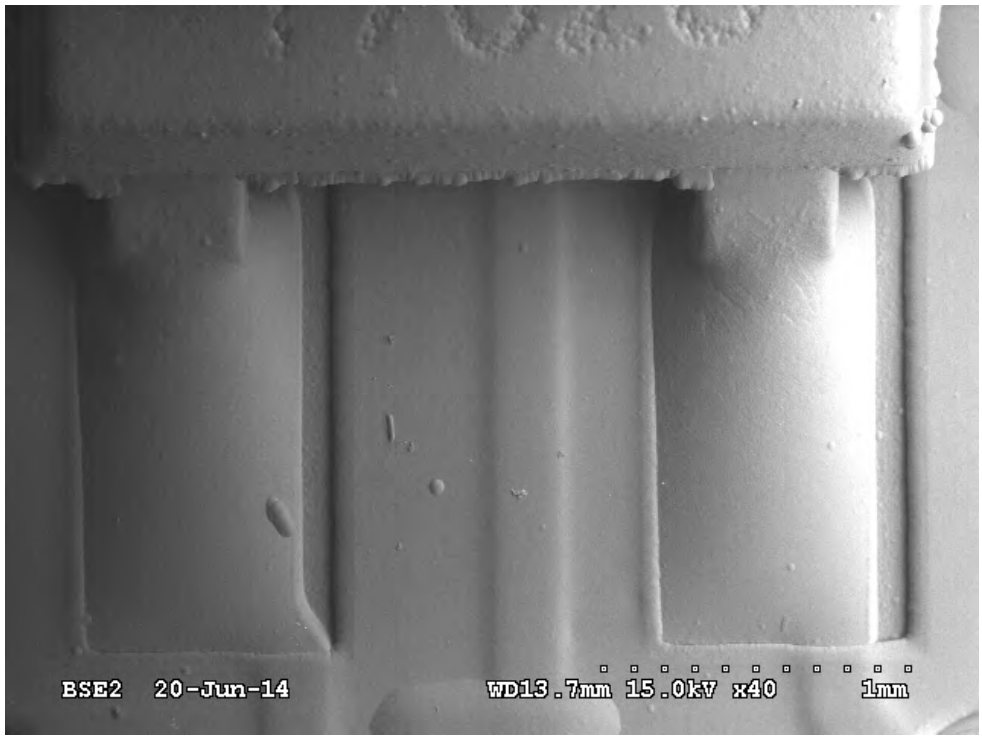


Figure 139: SEM image of Parylene™ C SOT3 leads, ATC + 2000HTHH, 40x (ref. Board 209).

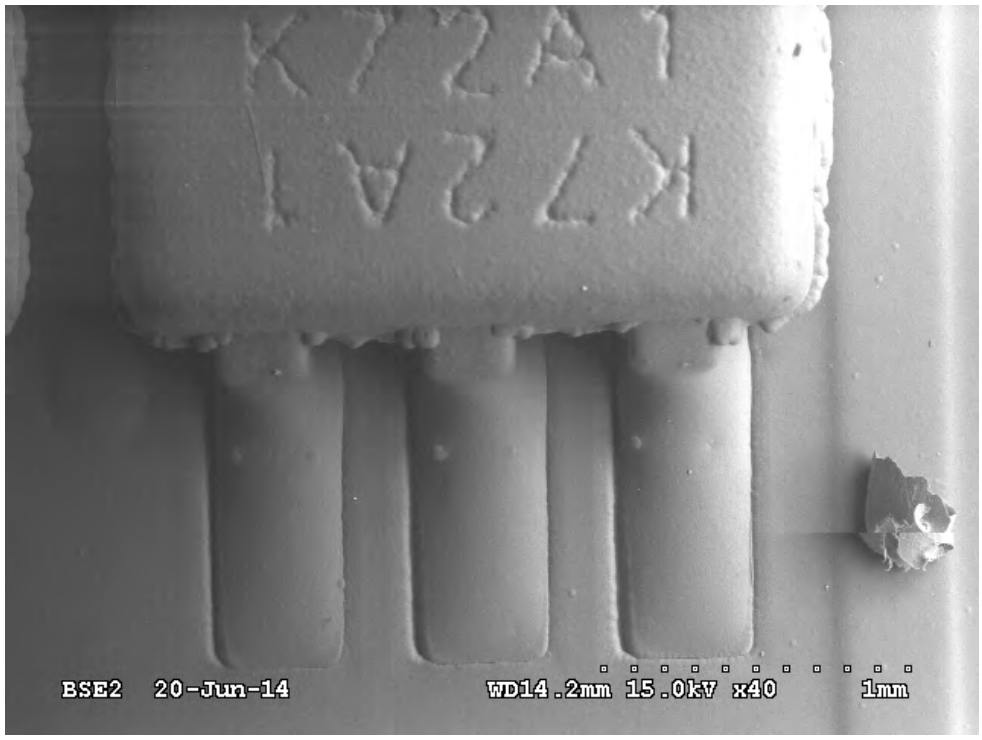


Figure 140: SEM image of Parylene™ C with Adpro+ coated SOT6 leads, ATC+ 2000HTHH, 40x (ref. Board 206).

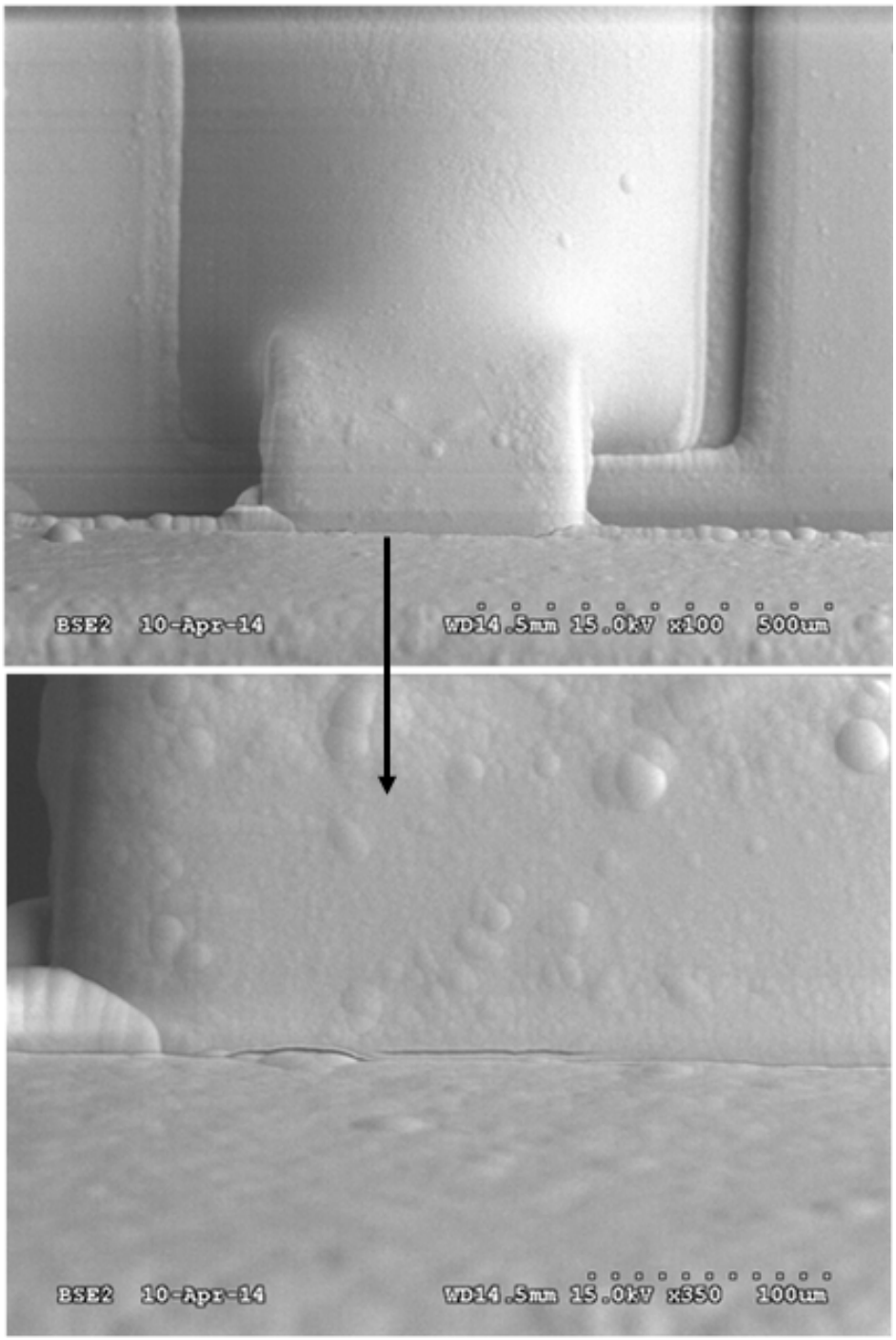


Figure 141: SEM image of a Parylene™ C & Adpro+ coated SOT3 lead, ATC+HTHH1000, 100x and 350x (ref. Board 204). Small coating crack evident at lead-to-package interface.

5.22.2 Humiseal 1B31-LOC reference coating

The 1B31-LOC acrylic reference coating was tested at the same time as the enhanced layered coating whisker testing. Some typical SEM inspection images are shown in Figure 142 to Figure 144. The complete inspection results are summarized in Table 2. Although the 1B31-LOC coated boards samples size was limited (one QFP and SOT board), whisker growth was observed where it was thin (Figure 144). The 1B31 coated samples had less whisker growth than PC40-UMF based coatings, mostly because of the large thin areas due to the dewetting of the PC40-UMF spray coat from the thin dip coat layer.

Table 7: 1B31-LOC acrylic reference coating assembly whisker inspection summary.

Board label	Board type	Observations
85	QFP	Some whisker growth on QFP44 but less than PC40-UMF; none on QFP64 and PLCC
288	SOT	No growth, but debris seen.

5.22.2.1 SEM images Humiseal 1B31-LOC reference coating

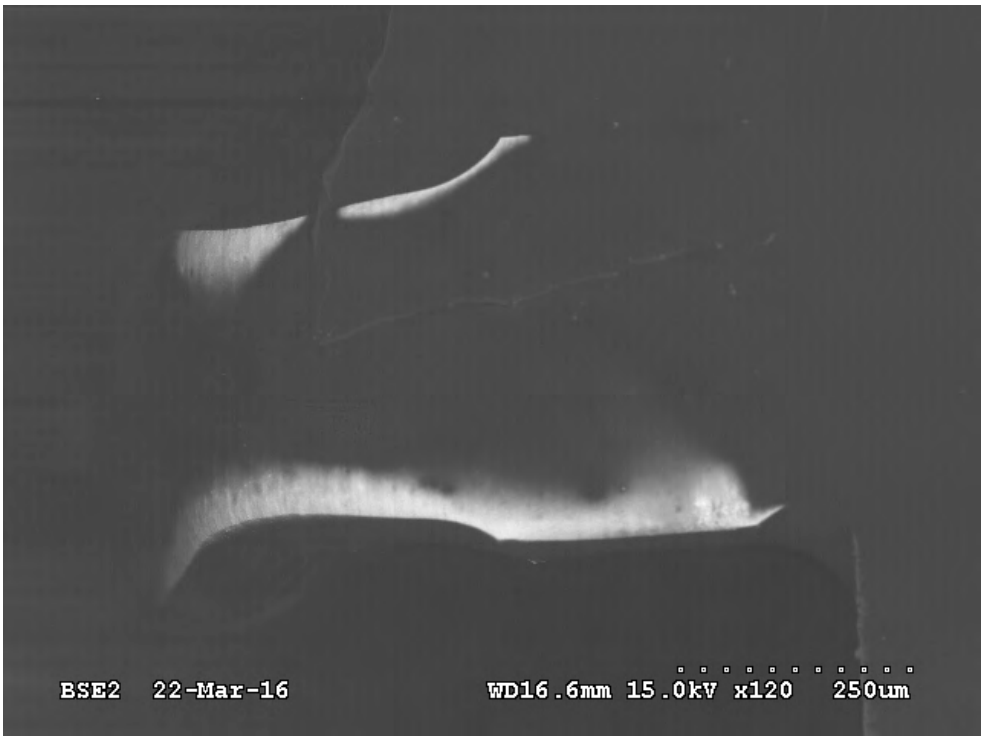


Figure 142: SEM image of 1B31-LOC acrylic coated QFP44 lead, HTHH1767, U5, lead 44, 120x (ref. Board 85).

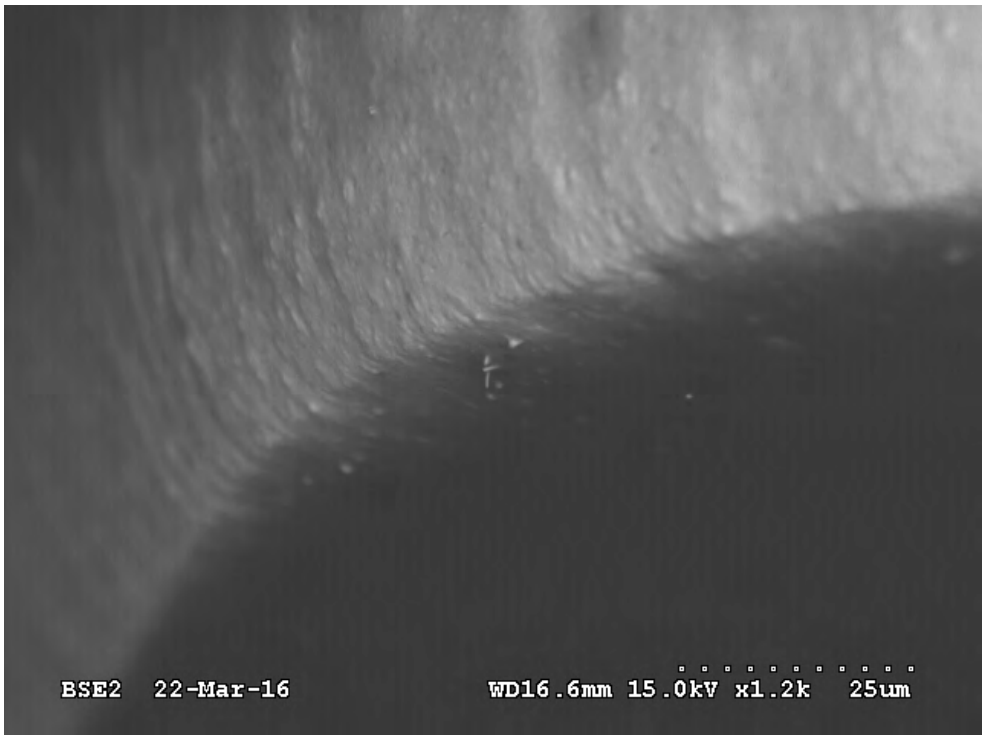


Figure 143: SEM image of 1B31-LOC acrylic coated QFP44 lead, HTHH1767, U5, lead 44, 1,200x (ref. Board 85).



Figure 144: SEM image of 1B31-LOC acrylic coated QFP44 lead, HTHH1767, U5, lead 44, 4,000x (ref. Board 85).

5.23 Coupon whisker test: Layered coatings

The layered coating coupon evaluation performed at Binghamton University is given in Appendix J and highlights are provided next.

5.23.1 Experimental Procedure

5.23.1.1 Samples and materials description

All the HTHH storage tests were performed on flat slotted test coupons, which were copper alloy sheets in accordance with ASTM B152, Type 110, 1/2 hard, 0.635 mm thick with waterjet cut slots finished by electroplating with bright acid tin in accordance with ASTM B545 paragraph 4.3.2 five to eight microns thick. The flat coupon allows precise coating thickness to be cast in place and the slots provide corners for the coating to flow over and thin.

The as-plated tin finish verified by cross – sectioning was confirmed to be around 8 microns thick. For the tin electrodeposition, panels containing 18 individual coupons attached by break-off tabs to a frame were used, as shown in the schematic in Figure 145(a). Individual coupons were 25.4 mm x 12.7 mm in dimension and are shown in Figure 145(b).

Before conformal coating and HTHH test initiation, the coupons were rinsed with alcohol and acetone followed by deionized water and dried with pure dry nitrogen gas. The tin-plated copper coupons were coated with PU and PUA resins of pre-determined thicknesses and subjected to HTHH storage after curing. The performance of the coatings and the tin coupons were studied in parallel by examining the cross – sections of the copper-tin-coating interface at various time steps.

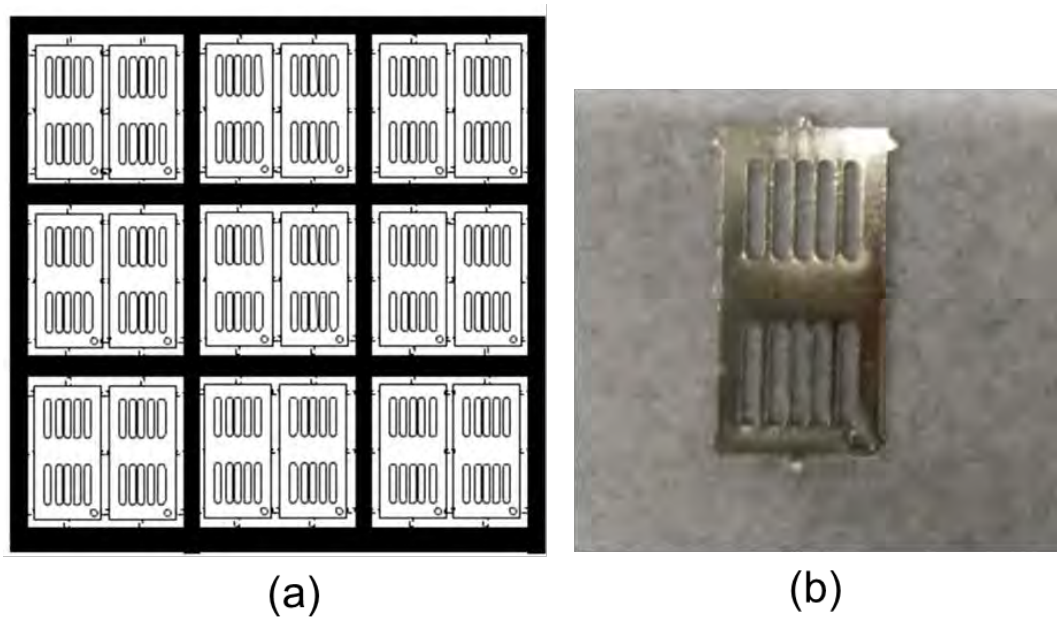


Figure 145: (a) Schematic of a panel showing 18 individual tin-plated copper coupons attached with break-off tabs. (b) An individual coupon photograph.

Two different commercially available polymer coatings, a PU – PC18M, and a PUA – PC40-UMF, were used for this study. Additionally, a third coating composition, PC18M+20%XP2742 nanosilica, was also used. Different coating thicknesses were achieved by using polyimide (Kapton™, 3M Inc., St. Paul, Minnesota) tapes of varying thickness as walls on the sides of the coupons. The polymer resin was dispensed and spread through a manual doctor blade process using sharp edged glass slides. Three coating thicknesses of 10, 20 and 50 micron each with the fourth coating scheme of a dual coated layer of 10 micron thickness coated on a 10 micron pre-cured conformal coating were prepared. Table 8 shows the coating types for the 10, 20 and 50 micron thicknesses. Table 9 shows the fourth coating thickness type (10 + 10 micron) with a dual coating scheme.

Table 8: Coating types for the 10, 20 and 50 micron schemes

10 micron thick	1) Unfilled PU	3) PU + 20% nanosilica	5) Unfilled PUA
20 micron thick	2) Unfilled PU	4) PU + 20% nanosilica	6) Unfilled PUA
50 micron thick	7) Unfilled PU	8) PU + 20% nanosilica	9) Unfilled PUA

Table 9: Coating types for the bilayer 10 + 10 micron thickness scheme

10) PU + 20% nanosilica on PU only base layer
11) PU + 20% nanosilica on PUA only base layer
12) Unfilled PUA on Unfilled PU base layer

Prepared coupons were transferred to the high-temperature and high-humidity chamber (Despatch® Ecosphere™) maintaining a steady condition of 85°C and 85% relative humidity (RH). These conditions of HTHH storage were chosen due to previously demonstrated ability to promote whisker growth in lead-free solder alloys. Selected coupons were removed from storage and examined at various time steps which are reported along with their associated results throughout this study. Samples removed at the pre-designated time intervals were all stored at room temperature in a humidity controlled environment (below 10% RH). HTHH storage was terminated at the 5,250 hour mark (219 days).

The samples were evaluated using optical microscopy, microtome cross – sectioning, scanning electron microscopy, and energy dispersive x-ray spectroscopy.

5.23.2 Results

5.23.2.1 Assessment of whisker mitigation ability of various coating schemes at different time steps

Following initial coating of the coupons with the required resin, and the required curing steps, multiple coupons of similar type were placed in the HTHH chamber for each of the 12 compositions listed in Table 8 and Table 9. One coupon each from the 12 types tested was removed at time ‘0’ without exposure to HTHH conditions and examined in an optical microscope to evaluate the coverage and other surface features for the specific composition. While the PU compositions (filled and unfilled) appear to have a homogeneous coverage on the tin surface, the PUA coated sample has poor coverage around the edges of the slots.

Following the confirmation of coverage, each coupon was analyzed subsequently at 500, 1500, 2,500, and 4,000 hours to verify coating performance (rupture, or cracking) with respect to time of storage and coating condition. After 500 hours of HTHH storage, while whisker formation was not noted at the

surface of the tin, the entire surface of the coupon was mostly convered by oxidation products of different thickness, as can be distinguished through the color variation under optical microscope inspection.

SEM imaging of the coated coupons was performed at the succesive time-steps following HTHH exposure above 500 hours (1500 through 4,000 hours). Tin whisker formation in uncoated areas of coupons was first revealed at the 1500 hour time step. Figure 146 (a) shows uncoated regions of a 20 micron thick PU coated coupon with tiny whisker growth. Whisker aspect ratios are considerably large (filament-like), as can be seen in Figure 146; however, the diameter of the tin whisker is very small (<100 nm diameter), such that it would not be visible through optical microscopy. This is also indicative of being in its initial stage of the growth. Spillover patches also formed while spreading the resin during the doctor blading process and were noted in the areas surrounding the polyimide tape walls on the coupon. These areas were much thinner (~3 micron in Figure 146 (b)) than the other coated areas but still showed no prortusions or rupture following 1500 hours storage.

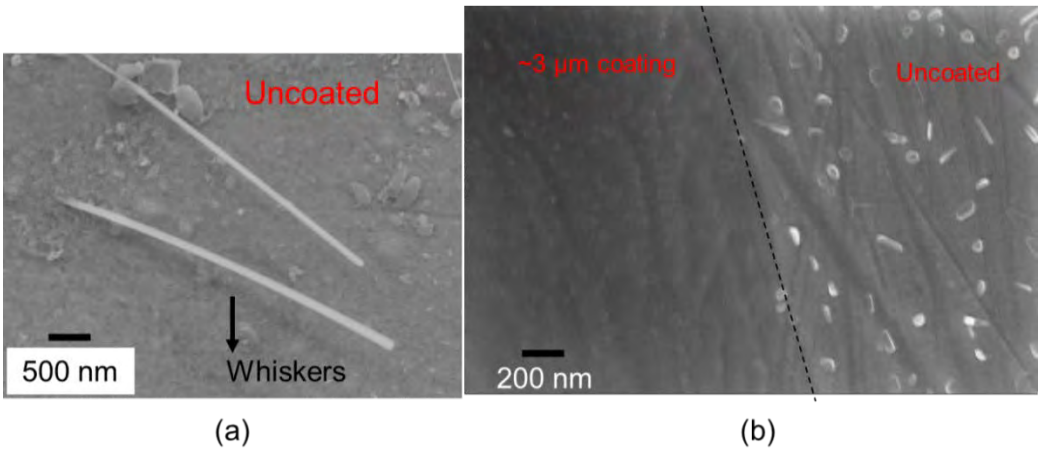


Figure 146: SEM images of whisker growth (a) uncoated region thin whisker formation (initial stage) at 1500 hours HTHH storage, and (b) thin coverage vs. uncoated regions of the same coupon.

The coarse wormy networks noted in the unfilled PU cases were also noted in the PU cases with the nanoparticle additions. The PUA coated coupons with 4,000 hour HTHH storage showed no discernable difference on the top coating surface in the 20 micron thick coating case, even though some isolated tented areas were observed in the 10 micron case.

From the 4,000 hour assessments of the tin coupons, it was clear that the 10 micron thick conformal coatings of three different compositions showed robust performance at least with respect to rupture resistance at the extreme storage conditions tested. A comprehensive tabular report summarizing critical features noted for each time step is listed in Table 10. Further cross – sectional analysis on selected coupons from these compositions in addition to the bilayer (10-micron filled PU on top of 10-micron unfilled PU) coupon were performed and results are discussed in the forthcoming sections.

Table 10: Compiled summary of the PU, PUA and PU+nanosilica coating performance at various time-steps.

10, 20 and 50 µm thick coatings	500 hours	1500 hours	2500 hours	4000 hours
Plain PC18M	• Surface oxidation noted at 500 hours • No whisker formation in uncoated regions	• Whiskers noted at uncoated regions • No protrusions/tenting or rupturing in coated regions	• Whiskers noted at uncoated regions • No protrusions/tenting or rupturing in coated regions	• No whisker growth through the coatings • One 20µm sample showed tenting (candidate for cross-section)
Plain PC40UMF	• Surface oxidation noted at 500 hours • No whisker formation in uncoated regions	• Whiskers noted at uncoated regions • No protrusions/tenting or rupturing in coated regions	• Whiskers noted at uncoated regions • No protrusions/tenting or rupturing in coated regions	• 10 µm case shows tenting – not seen in 20 µm thickness • Isolated tenting noted; no rupture noted
PC18M + 20% XP2742	• Surface oxidation noted at 500 hours • No whisker formation in uncoated regions	• Whiskers noted at uncoated regions • No protrusions/tenting or rupturing in coated regions	• Whiskers noted at uncoated regions • No protrusions/tenting or rupturing in coated regions	• Similar performance as Plain PC18M case – no rupture/protrusions

5.23.3 Microstructure evolution of polyurethane coated coupons with zero hours, 2,500 hours and 5,250 hours HTHH storage

From the copper-tin phase diagram there is a possibility of two distinct intermetallic (IMC) phases forming at lower (below 505K) temperatures, an η-phase (Cu_6Sn_5) and an ε-phase (Cu_3Sn). During the initial stages of reaction between tin and copper, Cu dissolves rapidly into the Sn and forms a Cu_6Sn_5 phase at the Sn/Cu interface. The Cu_3Sn layer is formed between the Cu substrate and the Cu_6Sn_5 layer as the Cu atoms at the Cu/Cu_6Sn_5 interface react with Cu_6Sn_5 to form Cu_3Sn. After a homogeneous Cu3Sn layer forms, Cu atoms, continuously diffuse through the Cu3Sn layer and react with Cu6Sn5 to grow more Cu3Sn at the Cu3Sn/Cu6Sn5 interface through the consumption of some of the Cu6Sn5. There is also some Sn diffusion through the interfacial region, but Cu diffusion rates are shown to be higher, so Sn diffusion can be assumed to be negligible.

Figure 147 shows a schematic representation of cross – sectional microstructure development between a coating and a copper substrate following storage in 85°C/85%RH, ranging from 0 to 5,250 hours. Of the examples considered, the growths of intermetallics in tin-plated copper coupon cross – sections with 20 micron thick polyurethane (PU – PC18M) conformal coating after HTHH storage are shown. With an increase in HTHH storage time, significant intermetallic growth (of varying thickness) into the tin layer continuously along the interface between tin and copper was noted in every coupon. Additionally, some particulate - IMC growth was noted, which had no connection to bulk IMC at the interface. Some IMC particles were noted leading vertically toward the coating surface (Figure 147 (b) and (c)). A dramatic increase in total thickness (intermetallics and tin layer) of plating was observed.

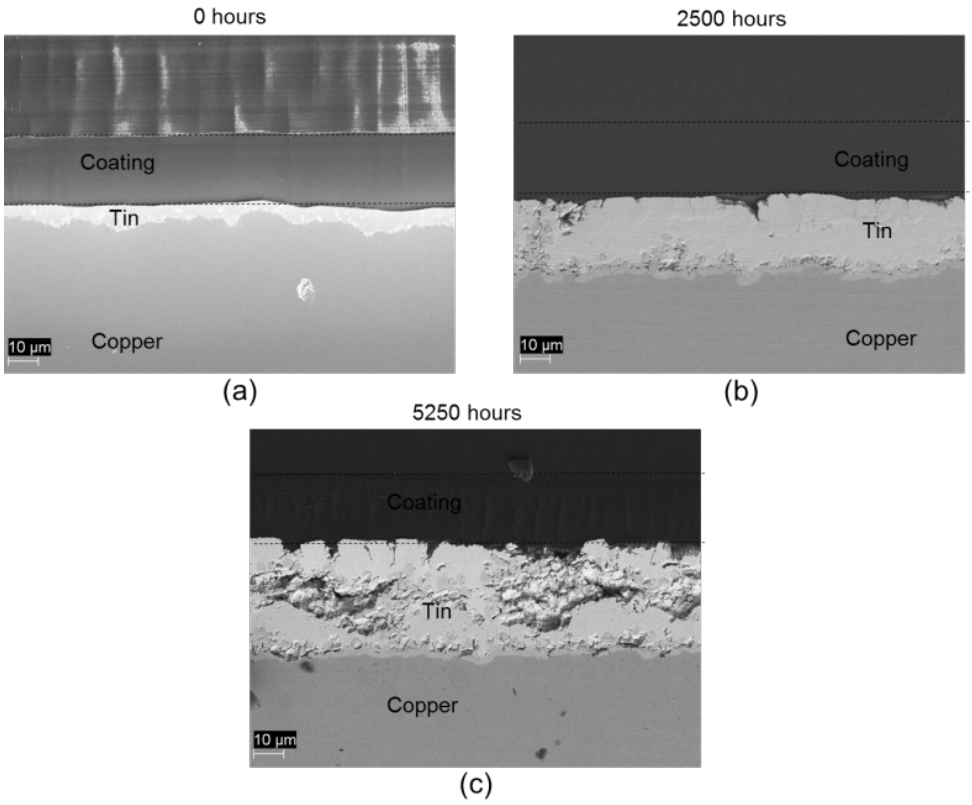


Figure 147: Over cross – sections of 20 micron thick PU conformal coating with (a) 0 hours HTHH storage, (b) 2,500 hours storage, and (c) 5,250 hours storage.

Figure 148(a) shows a more detailed cross – sectional image of the coating at the zero hour HTHH storage time step, with all the major regions denoted. Examination of this sample showed a homogeneous intermetallic layer at the interface of the copper and the plated tin. The high magnification SEM of the interface of the coating and the tin surface (Figure 148(b)) shows a continuous delamination of 100 to 200 nm. This split of the coating from the surface could have been caused during preparation of the cross – section, which involves a slicing operation using a sharp diamond edge and is indicative of weak adhesion between the coating and the tin layer in this case.

Following 2,500 hours HTHH exposure, a similarly prepared PC18M coated coupon, i.e., with 20 micron thickness, was removed from storage and examined. As noted in the zero hour coupon cross – section, a continuous interfacial intermetallic layer was observed; however, in this case with both Cu_6Sn_5 and an additional Cu_3Sn phase between the copper and the tin plating. In addition to this continuous layer, discrete Cu_6Sn_5 particles were noted interspersed within the tin layer. A concurrent increase in the interfacial IMC (Cu_6Sn_5 + Cu_3Sn) thickness is also noted. Some regions between the tin layer and the conformal coating appeared to have tin preferentially removed during microtome slicing, leaving spaces between the coating and the remaining tin layer. Further, such cracks which result in tin removal, propagated through the tin – coating interfacial region with a thin layer of tin remaining attached to the underside of the coating, indicative of weak interfacial adhesion due to formation of the reaction products at the interfacial region (Figure 149).

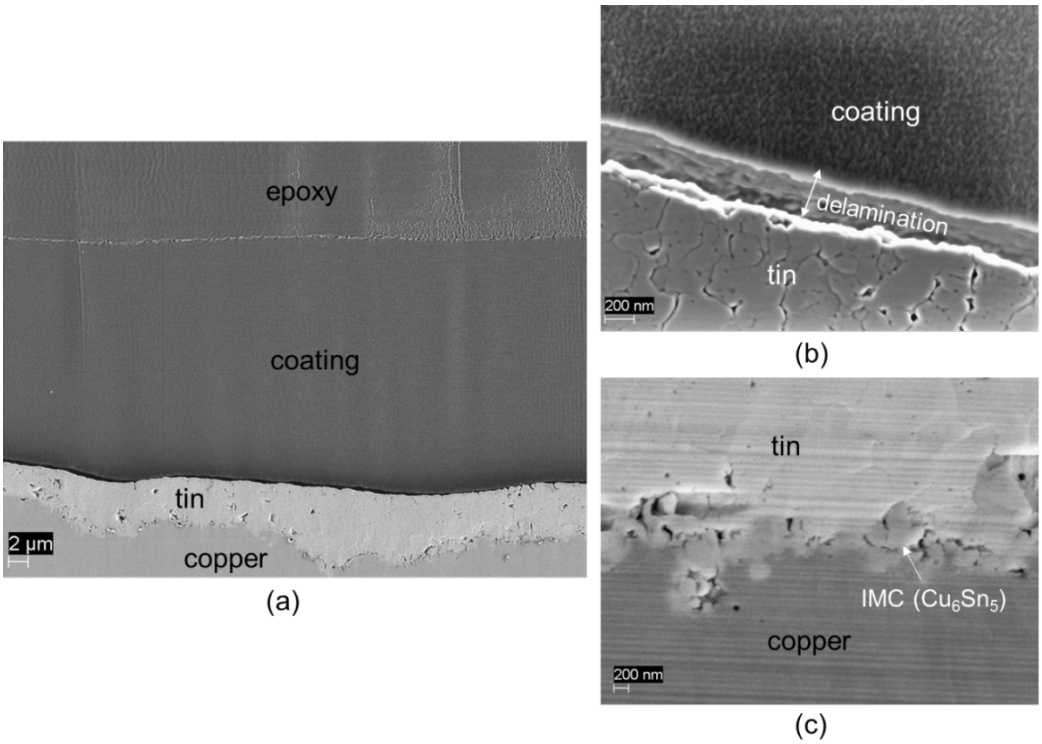


Figure 148: Zero hour cross – section SEM image of 20 micron thick unfilled PU; (a) overall view with various regions labelled (b) delamination between the coating and the tin indicative of poor adhesion, and (c) interfacial Cu_6Sn_5 formation noted between tin and copper.

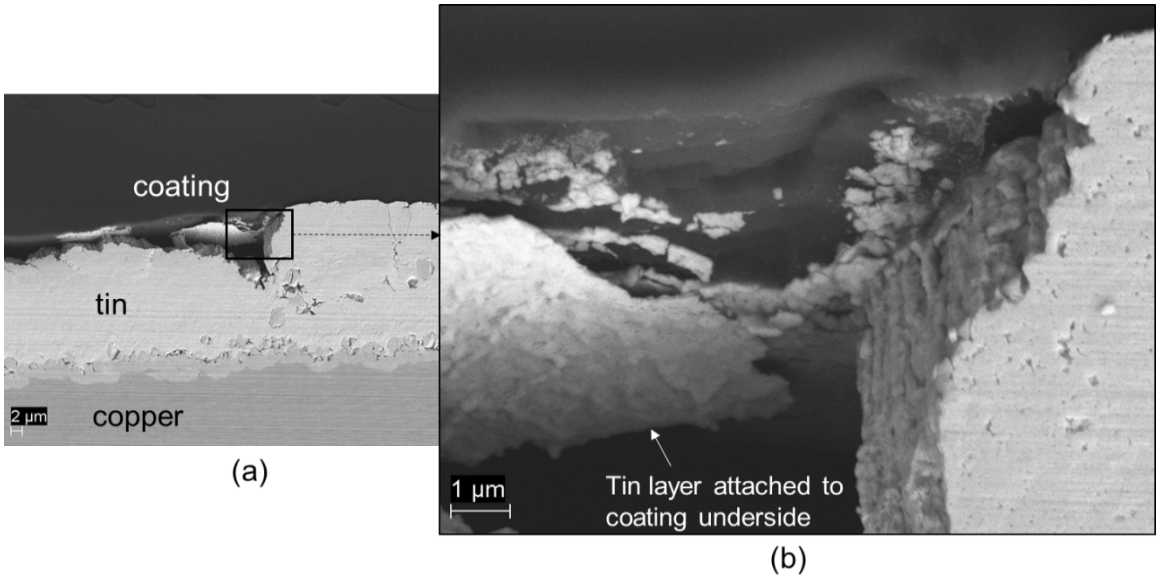


Figure 149: Cross – section SEM image of 20 micron thick unfilled PU following 2,500 HTHH storage; (a) Cross – section of coating-tin-copper with revealed space (in box) between coating and tin (b) Close-up SEM image of delamination at coating-tin interface and attached tin on coating.

Comparative back scatter electron (BSE) imaging of similarly located isolated IMC particles (with respect to Cu substrate) in Figure 150 of two coupons, following 2,500 hours and 5,250 hours storage, shows a larger intermetallic isolated particle size in the latter case, while a concurrent increase in the thickness of the interfacial IMC region can also be discerned. Red arrows in Figure 150 note IMC particles within the tin plating on the copper substrate. The interfacial region between the tin and the copper substrate can also be seen to ripen, with the more uniform Cu_3Sn forming between the Cu_6Sn_5 and the copper side of the interfacial region, and the scallop-like Cu_6Sn_5 forming into the tin plating.

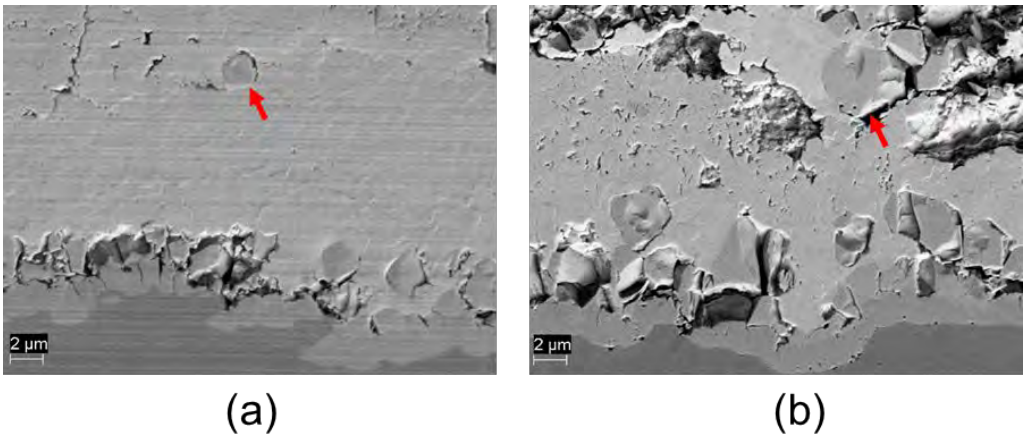


Figure 150: Cross – section SEM BSE images of IMC particles within tin under 20 micron PU; (a) 2,500 hours HTHH storage and (b) 5,250 hours storage; showing larger IMCs with time and interface IMC thickening.

Figure 151 shows a comprehensive view of the cross – section with 5,250 hours storage (point of experiment termination), with several critical features denoted. An additional development and coarsening of the discrete IMC's to form a layer of IMC's within the bulk tin as seen in Figure 151. A significant increase in the tin thickness from the original tin plating (< 10 micron) can be clearly observed. In contrast with the 2,500 hour storage case where discrete particle-like IMC's were noted interspersed within the tin layer, a more completely developed cluster of IMC's is visible above the original thickness of the tin layer plated on the copper substrate. Additionally, similar to the previous 2,500 hour storage case, the regions of removed tin were seen with a thin layer remaining attached to the underside of the coating. This is indicative of uneven adhesion at certain regions between the tin and the conformal coating with other regions having delamination initiated by the slicing motion of the microtome knife.

From the initial microstructural analysis of the corresponding stages of HTHH storage (time zero through 5,250 hours), it is evident that the nature of the IMC formation *within* the tin layer, in addition to interfacial IMC formation reactions, the nature of thickness increase in the tin plating, and the secondary layer of tin above the isolated clusters of IMC's noted in certain sections; all necessitate a more detailed analysis.

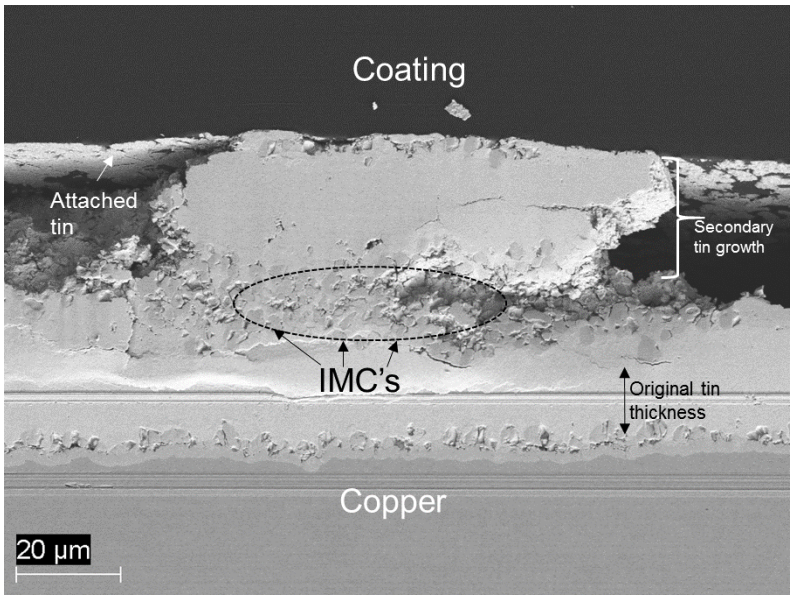


Figure 151: 5,250 hours HTHH storage coupon cross – section with various key features labelled.

5.23.4 Discussion

5.23.4.1 Effect of HTHH storage on the tin-copper microstructure

From Figure 150 and Figure 151, it is evident that there was a sustained growth of intermetallics, both at the interface of copper and tin and within the bulk tin with HTHH storage. In addition to this observation, a concurrent increase in the total thickness of the complex tin layer (including voids, intermetallics and pure tin) on the underlying copper substrate is seen. A closer look is therefore warranted at the various cross – sections to propose suggested mechanisms for this behavior, which includes the growth of intermetallics and a 'lateral' outward growth of tin away from the original tin layer and guided by the conformal coating.

It is well known that an atom such as Cu may diffuse easily into Sn by a rapid, interstitial mechanism, whereas Sn diffuses in Cu by a slower, substitutional mechanism. This is further supported by considerations of the lattice parameters of tin, which is a relatively less densely packed tetragonal structure (a=b= 5.83Å & c= 3.18Å) and easily facilitates the accommodation of diffusing copper atoms within its lattice. Consequently, there is a concentration gradient established between the copper and tin layers which act as a diffusion couple stressed under high temperature and high humidity conditions. First, Cu_6Sn_5 formation was noted at the interface of tin and copper. As a result of the effects of continuing copper diffusion under increasing storage time from zero to 5,250 hours at 85°C and 85% RH, this was followed by thickening of the interface intermetallics along with increased incidence of copper within the bulk tin adjacent to growing Cu_6Sn_5. Reaction of copper with the Cu_6Sn_5 at the Cu/Cu_6Sn_5 interface eventually leads to Cu_3Sn formation first noted at the 2,500 hour examination step.

At the 2,500 hour time step, discrete particles of Cu_6Sn_5 begin to appear on the surface of tin plating. While copper diffusion on the whole is not restricted to grain boundaries but is rather throughout the bulk tin structure, an earlier work on the coupled copper-tin systems at room temperature has shown IMC (Cu_6Sn_5) growths to preferentially nucleate at triple junctions of tin grain boundaries and other regions of free surface availability. In the case of the 2,500 and 5,250 hours HTHH storage samples, there is a significant availability of free surfaces at the interface between the coating and the tin layer caused due to the poor adhesion of the coating to the tin surface, as shown in Figure 148 and Figure 149. While there is in general an increased diffusion of copper atoms interstitially through the tin lattice, free surfaces and grain boundaries see an increased likeliness of intermetallic formation due to its

accumulation. At such locations, the concentration of copper atoms within the tin is sufficient to initiate nucleation of the Cu_6Sn_5 intermetallic compound. Further, these particles continue to coarsen while newer particles nucleate and grow during the continual storage up to 5,250 hours as seen previously in Figure 151, forming more populated intermetallics at the coating-tin interface. Such a discrete layer of intermetallics is seen to significantly increase with the storage time.

Figure 152 (a) shows a backscattered electron detector (BSD) image of a cross – section after 5,250 hours HTHH storage. BSD facilitates atomic number contrast imaging with regions of darker contrast representing the presence of lower atomic number elements and can have different contrast with different grain orientation. As noted above, the formation of intermetallics in the bulk tin is preceded by a fast interstitial diffusion of Cu atoms into the Sn lattice. A clear demarcation in contrast can be noted from the copper substrate at the bottom toward the coating on the tin layer at the top. A complex tin 'band' of tin and IMC with higher copper concentration adjacent to the interfacial IMCs can be distinguished. Within the band, discrete particulate IMCs within the bulk tin, a region of the complex tin band showing a brighter contrast, and the unfilled PC18M coating at the top can all be noted in the BSD imaging.

EDS plots of the two different regions of tin, one adjacent to the coating (brighter contrast) and one adjacent to the copper (darker contrast) are shown in Figure 152(b) and Figure 152(c) respectively. Distinct peaks at 0.93 keV and 8.04 keV representing the copper Lα and Kα line, respectively in the X-ray spectrum were seen in the bottom tin layer, providing the confirmation of the presence of diffused copper in the tin region. Further, semi-quantitative analysis of the spectrum indicated a presence of around 3.7% Cu with a smaller amount detected from the upper tin layer (brighter contrast in BSD). It should be noted that the solubility of copper in tin at 85°C is very low (much less than 3.7 wt. %). The copper detected in the darker region of the band is likely to be primarily from the presence of nano – sized IMCs like those in Figure 150.

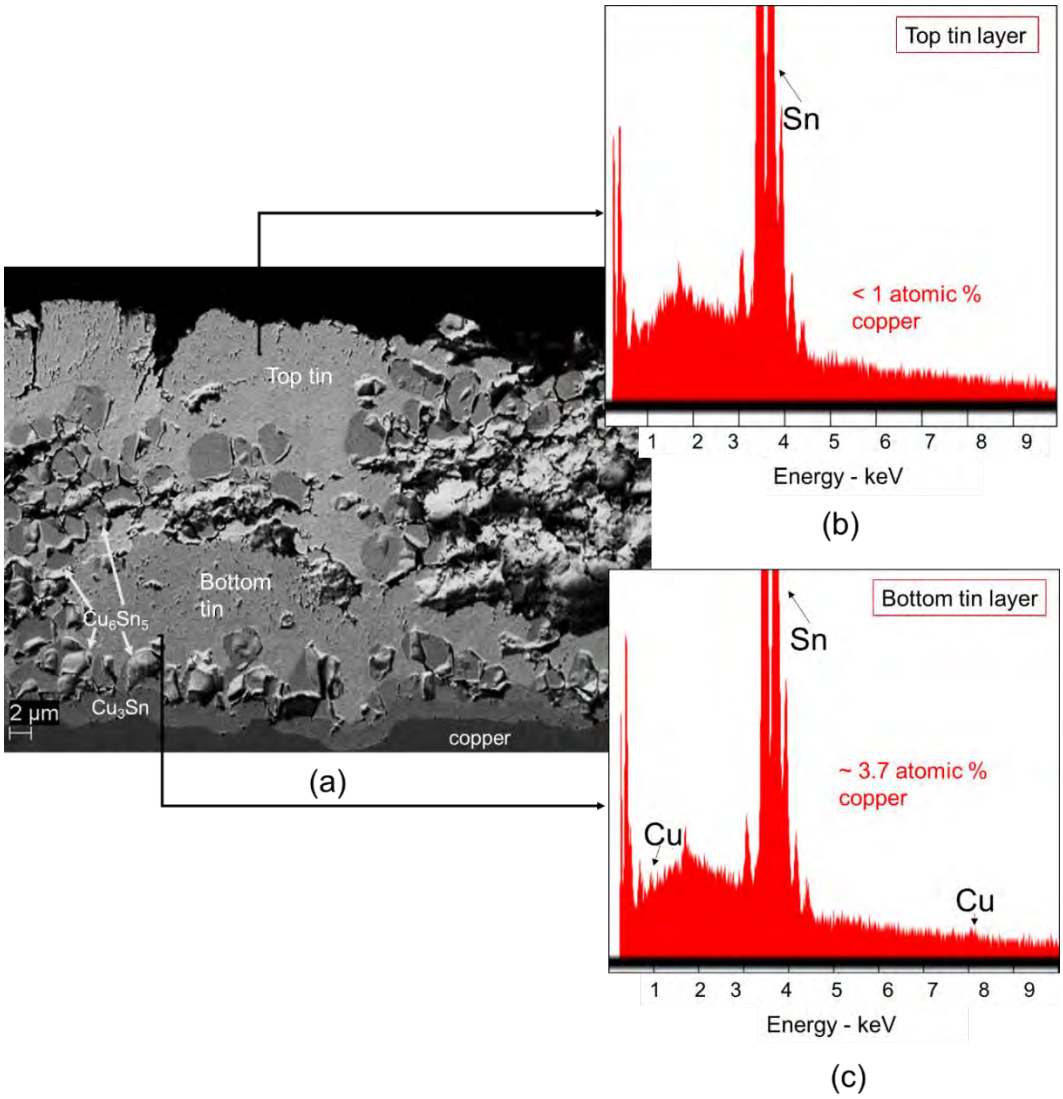


Figure 152: Cross – section examination of a representative coating-tin-copper interface in a coupon coated with 20 micron PU following 5,250 hours HTHH storage; (a) BSD image and (b) EDS spectrum obtained from the top (brighter) tin layer, and (c) EDS spectrum obtained from the bottom (darker) tin layer.

In 2014, similar tin and coating features were also observed during the cantilever beam coupon testing (see Appendix G). An ion polished conventional metallurgical cross – section of a typical tin nodule growing under PC18M+30%XP2742 nanosilica filled coating after 2,500 hours of 60°C/60%RH is repeated here in Figure 153. In this figure, the nodule is in an area where the PC18M+30%XP2742 nanosilica filled coating was seven microns thick and was bulging the coating. There is some coating delamination from the tin on the left side of the nodule (Figure 153a) where the tin is no longer adhered to the coating (yellow arrow). Adjacent to this delamination, the tin fractured one to five microns below the coating (black arrows). In these regions, some tin remained adhered to the coating. Also on this sample, there were large Cu_6Sn_5 IMCs in the tin layer away from the copper interface and near the coating (Figure 153b).

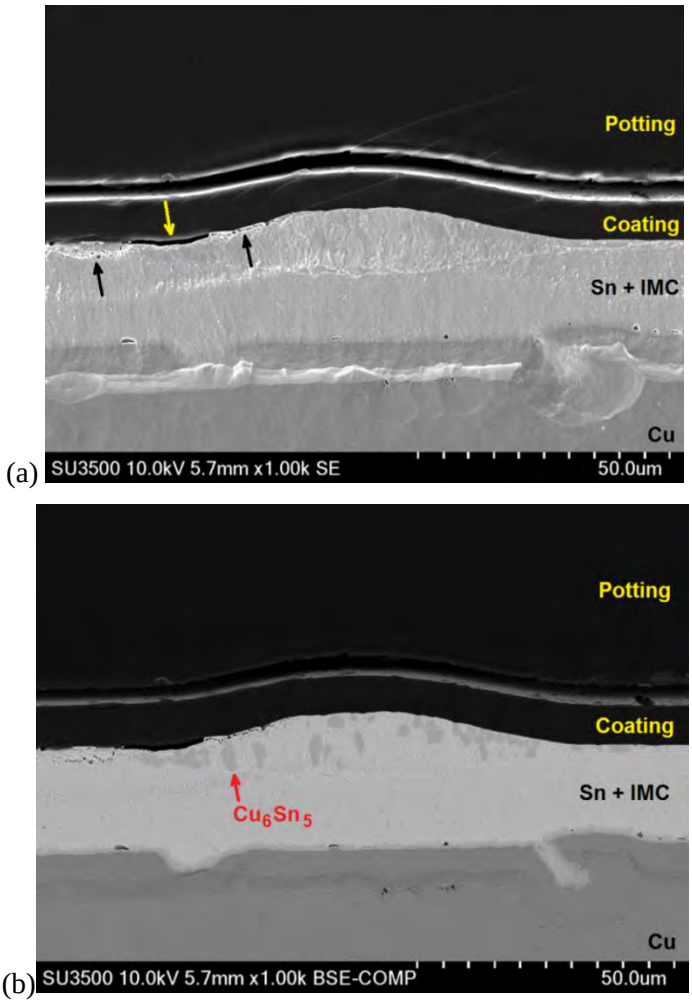


Figure 153: Cross – section SEM images of seven micron thick PC18M+30%XP2742 over bright tin on copper after 2,500 hours 60°C/60%RH (Celestica cross – section of the cantilever beam coupon); (a) SE image with yellow arrow shows coating delamination from tin and red arrows shows fracturing in the tin region below the coating and (b) BSE image showing the Cu_6Sn_5 intermetallic formation near the coating surface.

5.23.4.2 Mechanism of lateral growth of tin protrusions

One of the most noted and commonly discussed sources of compressive stress in electroplated tin on copper is intermetallic compound (IMC) formation due to the reaction of Sn with Cu in the substrate metal. Here, in the case of tin plated copper coupons, there is a clearly increasing presence of intermetallics and diffused copper regions in the tin plating with HTHH storage. Together with this, it is also observed that a secondary tin layer, above the complex tin and intermetallic layer formed from the original tin plating (discussed above), grows in thickness with storage time. The nature of this thickness increase is specifically due to an outward growth of tin and tin – copper intermetallic from the original plating layer region pushed laterally due to a barrier to vertical growth caused by the conformal coating. Figure 154shows the initial stage of a protrusive tin growth beginning to interact with the conformal coating. The initial layer of IMC's formed on the top of the tin surface are also visible in this image.

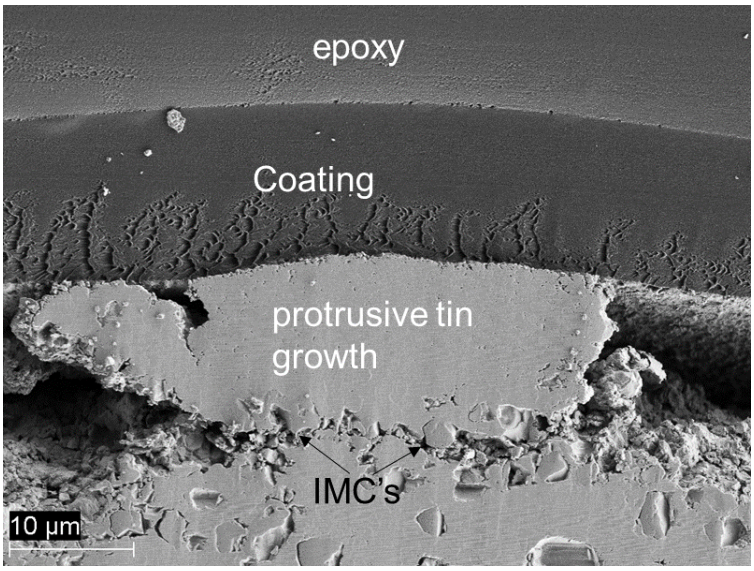


Figure 154: SEM cross – section image of a protrusive tin growth beginning to impinge on the conformal coating.

Figure 155(a) shows a BSD image of a tin plated copper coupon cross – section following 5,250 HTHH storage. A conformal coating of 20 micron unfilled PU - PC18M was applied to tin plated copper coupons prior to storage. In this micrograph, two locations shown by the numerals '1' and '2' in the tin layer denote regions which are the roots of outward tin protrusions originating from the original tin plating. Compared to Figure 154 this protrusion was in a much more advanced state of growth, leading to its advancement along the coating-tin interface.

The thickness of the original (pure tin) region is labelled as 'time zero' thickness in Figure 155(a). It is seen that along with interfacial IMC developments which are expected and have been explained previously, there is also IMC formation on the top surface of the tin plating. The combined effect of steadily increasing compressive stress in the tin film from the effects of copper diffusion and intermetallic formation causes the outward protrusive growth of tin. These growths are subsequently deflected laterally due to the blocking from conformal coating and follow a growth direction parallel to the surface of the original tin surface along the coating-tin interface.

Figure 155(b) shows the coupon cross – section adjacent to root location '1' in Figure 155(a). Laterally grown tin is continually pushed along the original tin plating and continues to grow in this orientation with continued storage. Empty spaces between this lateral protrusive growth and the tin layer correspond to IMC's which have been displaced during sample preparation.

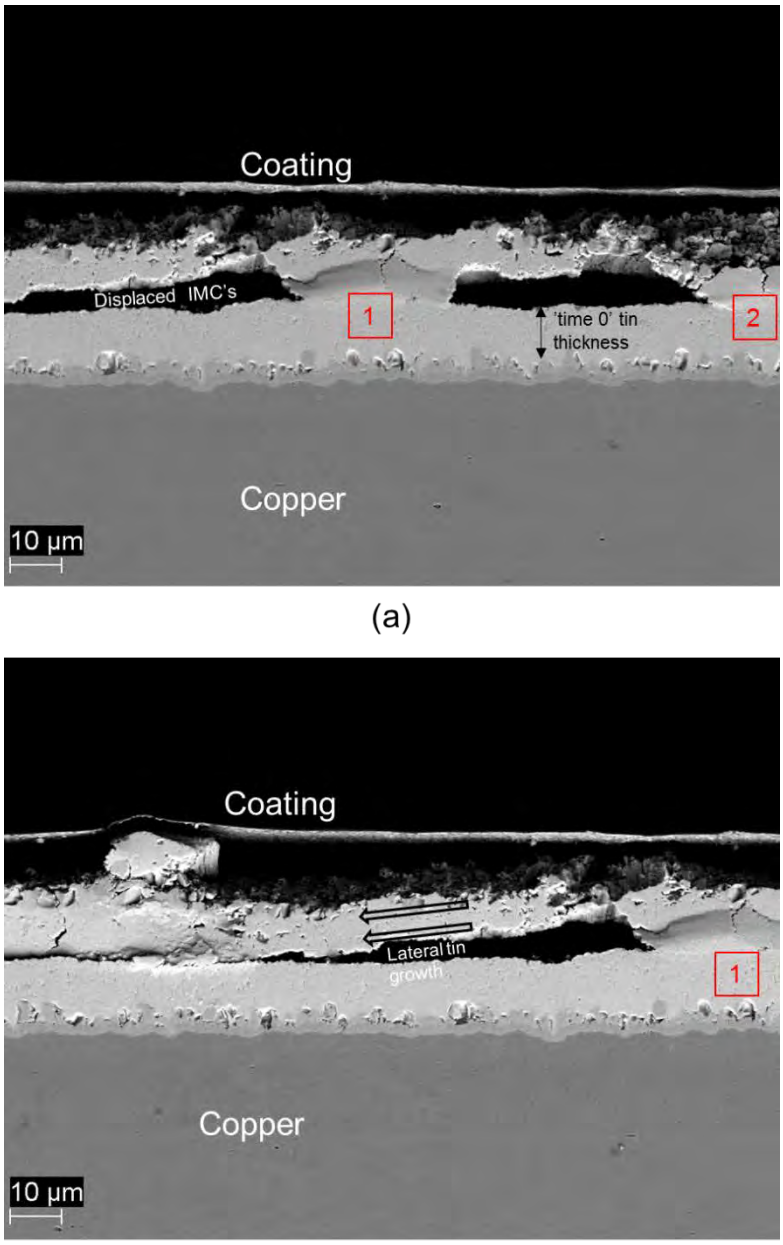


Figure 155: SEM cross – section images of tin growth under coating; (a) example of two well-developed protrusive growths from tin being deflected laterally by a conformal coating and (b) left branch of lateral growth from location '1' in (a).

A schematic of the lateral growth mechanism is shown in Figure 156 by way of integrating the factors explained above. With no exposure to the HTHH conditions, i.e. immediately following the conformal coating, the cross – section consists simply of tin plated on copper. This microstructure eventually evolves at the interface to form an IMC layer consisting of the two phases, Cu_6Sn_5 and Cu_3Sn. The conformal coating is at the top of the tin surface. With sustained storage at the HTHH conditions

(85°C/85%RH), copper diffusion is increased into the adjacent tin layer with IMC nucleation and growth with sufficient copper availability. In addition to these surface intermetallics, an embedment of copper atoms at the tin grain boundaries even without consequent IMC formation results in further compressive stress on the tin layer which needs to be relaxed. Concurrently, tin atoms are driven outward due to compressive stresses caused due to diffusion of copper as well as the steady growth of the intermetallics. A flux of mostly pure tin atoms is pushed upward and thus overall thickness is increased as a result of lateral growth of tin due to the restriction in further vertical growth due to the barrier in the form of the conformal coating.

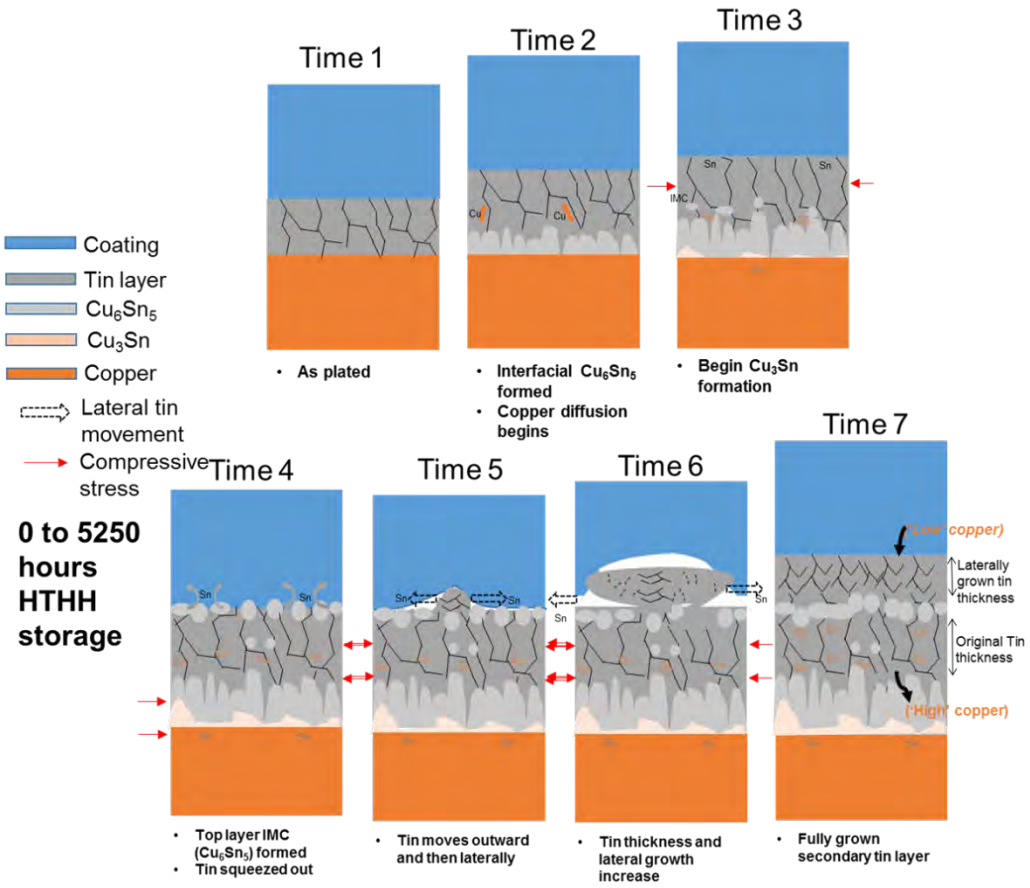


Figure 156: A mechanism of lateral protrusive tin growth from electroplated tin on copper substrate.

5.23.4.3 Effect of well-adhered conformal coating on tin: Cross – sectional analysis of Sn-plated Cu coupon with 4,000 hours HTHH storage

Cross – sectional analysis of 4,000 hour HTHH storage coupon coated with unfilled polyurethane (PU – PC18M) while demonstrating an increase of interfacial IMC thickness and a corresponding increase in the pure tin layer, did not show discrete particulate IMC formation within the bulk tin or a secondary lateral growth of plated Sn. This was an exception to the trend previously noted in coupons exposed up to even 2,500 hours of HTHH storage. A more detailed look at the cross – section was undertaken in an attempt to understand the unusual (with respect to other coupon sections examined) microstructural characteristics.

At first, it may be recalled that similar coating thicknesses of the unfilled PU (PC18M) conformal coating, for 0, 2,500 and 5,250 hour HTHH storage, showed visibly poorer adhesion with delamination noted at the tin-coating interface. In this regard, Figure 157(a) shows an overview cross – section of the

4,000 hour HTHH section. As seen in this representative SEM micrograph, no delamination was visible between the tin layer and the conformal coating or in regions in the tin plating. High magnification imaging of the tin-coating interface also confirmed this observation, with homogeneous and consistent adhesion apparent between the coating and the tin at the sub – micron scale. The characteristic wormy networked microstructure of the PU is also noticeable (Figure 157(b)). Specifically, in this coupon, coating adhesion to the tin plating appeared to be robust and without delamination.

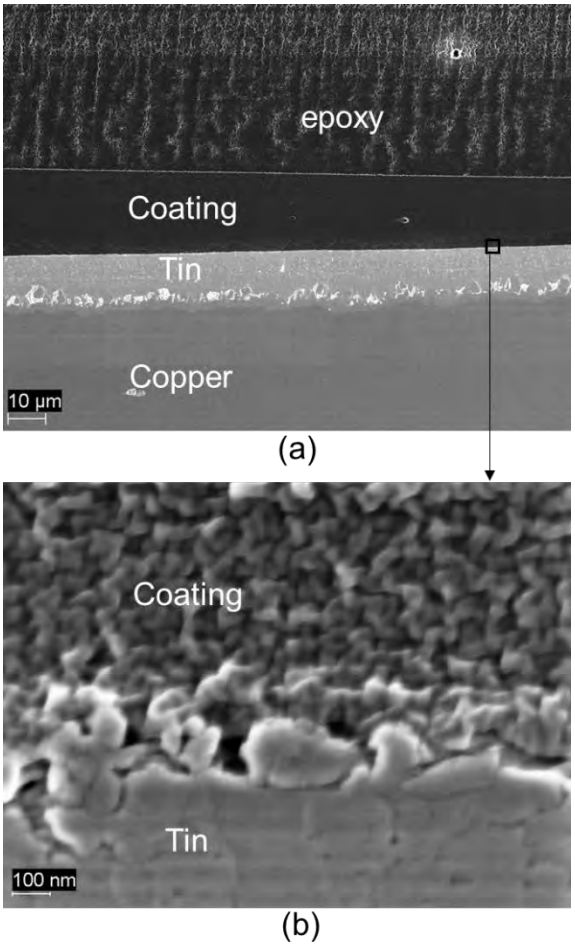


Figure 157: (a) Representative SEM cross – section of PU coated coupon following 4,000 HTHH storage and (b) a high magnification image of the well-adhered coating-tin interface.

Therefore, to better evaluate this well adhered interface, SEM imaging was performed using a BSD which is particularly sensitive to atomic numbers and therefore provides elemental contrast (Figure 158**).** This confirmed the presence of a clearly delineated, relatively thick and homogeneous layer of oxide (~30 nm) at the tin surface under the coating.

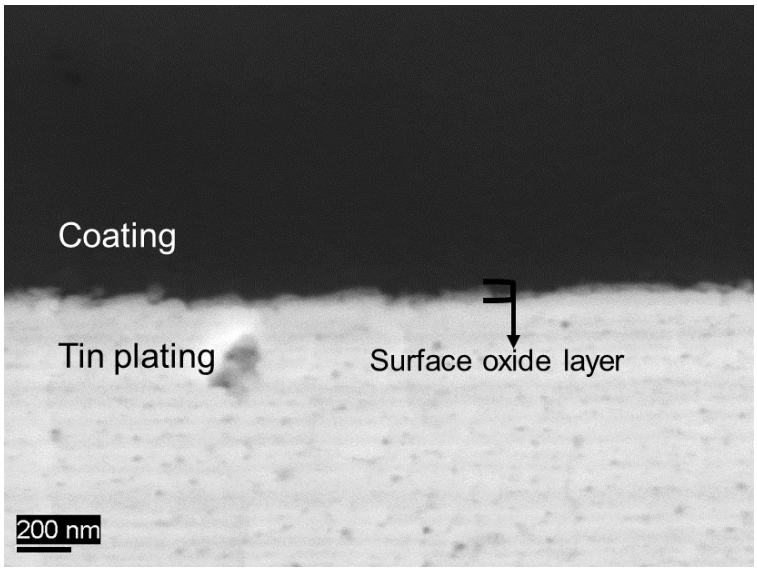


Figure 158: Coating-tin interface in 4,000 hour HTHH storage coupon cross – section with oxide layer visible.

A similar oxide layer was not observed for the other unfilled PC18M coated coupons examined in this study. Increased adhesion due to the presence of the very thin oxide layer could explain the lack of lateral tin growth and IMC formation in the tin plating layer. While the mechanisms of adhesion between metal surfaces and polyurethanes are not entirely understood, there is evidence in the case of aluminum and copper to show that the occurrence of native oxides plays a significant role in enhancing the adhesion of polyurethanes. Due to the enhanced adhesion there is a reduced availability of free surfaces for, i) sufficient accumulation of copper atoms, and ii) the subsequent nucleation of the intermetallics following reaching a requisite concentration of the copper.

Figure 159 is the thickness comparison among primary tin layer and interfacial IMC layers at various time steps of the HTHH storage. The linear trend line (considering only the thickness of 0, 2,500 and 5,250 tin thickness; R^2= 94%) was plotted to compare *expected* thickness of primary Sn layer with the *measured* thickness, in the 4,000 hour storage case. While an increase in measured primary Sn thickness (i.e. original plating on copper) was noted in the 0, 2,500 and 5,250 hours HTHH storage coupons, in the 4,000 hour case, this measured thickness was significantly smaller (~23%) than predicted (from linear trend).

However, the interfacial IMC growth rates incorporating all four time steps (0 to 5,250 hours) were well matched with the growth rate exponents of Cu_6Sn_5 and Cu_3Sn (n = 0.17 and n = 0.46 respectively). The difference in tin thickness increase in the 4,000 hour cross – section between measured and expected values may therefore be attributed to the relative lack of volume expansion in the tin layer by the formation of discrete IMC's within the tin layer, as in the 2,500 and 5,250 hour cases. Diffusion of copper atoms into the tin lattice and accumulation at tin grain boundaries can also increase its thickness. The relative lack of compressive stress caused by the surface IMC growth reduces the need for pure tin atoms to push outward thereby negating the formation of protrusive growths in this case. Therefore, in comparison with the varying amounts of delamination noted in the other sections (0, 2,500 and 5,250 hours of HTHH storage) of same coating thickness and composition examined in this study, the better adhesion and lack of IMC formation afforded in part by the presence of the oxide layer in the 4,000 hour sample tended to restrict lateral tin layer growth.

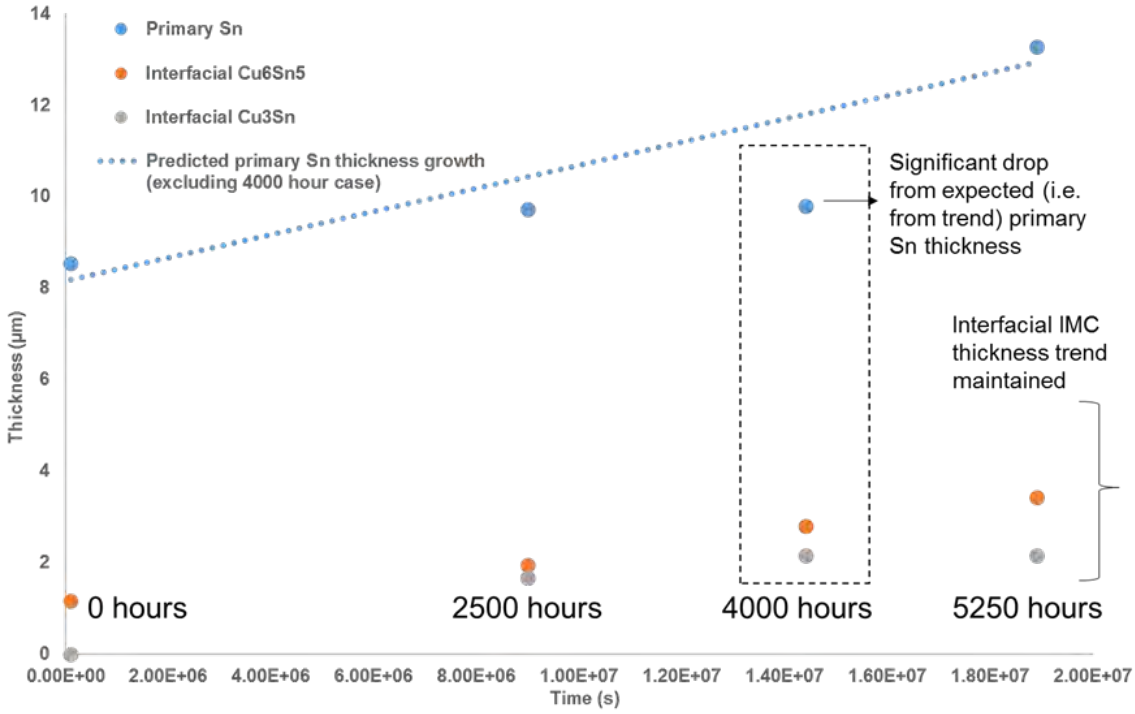


Figure 159: Thickness measurements of primary tin plating and interfacial IMC formation from zero to 5,250 hours HTHH storage.

5.23.4.4 Effects of HTHH storage on polyurethane acrylate (PUA – PC40-UMF™), nanoparticle filled PC18M™, and bilayer (filled on unfilled PC18M™) conformal coatings

In addition to unfilled polyurethane (PU – PC18M) coatings, HTHH storage tests were also conducted on unfilled polyurethane-acrylate (PUA – PC40-UMF) coatings as well as silica nanoparticle (20% suspension weight) filled PU coatings on the tin plated copper coupons. Another coupon, a bilayer conformal coating of 10 micron filled on 10 micron unfilled PU coating was also tested. On microelectronic components, the bilayer coating configuration may be used to afford more complete surface coverage; with the second coating run covering any ‘pinholes’ or other artefacts caused in the first coat. Further, an important effect of using two coatings with distinct mechanical properties is that the desirable properties of both the coatings may be utilized advantageously. For instance, in the bilayer configuration with a nanoparticle filled coating applied over unfilled coating layer, the filled coating may provide enhanced strength and stiffness while the unfilled coating could give more flexibility and ductility during plastic deformation.

The Figure 160 shows cross – sections show coupons coated with 20 micron filled PU and unfilled PUA following 4,000 hours HTHH storage. In both of these cases, similar to the unfilled PU cases, extensive interfacial IMC formation followed by tin growth was noted. The amount of lateral tin growth, however, is thicker in the case of PC40-UMF coated sample, compared to the filled PU coated sample. These differences could be caused due to adhesion effects and oxidation on the surface of the tin plating as explained in the earlier sections.

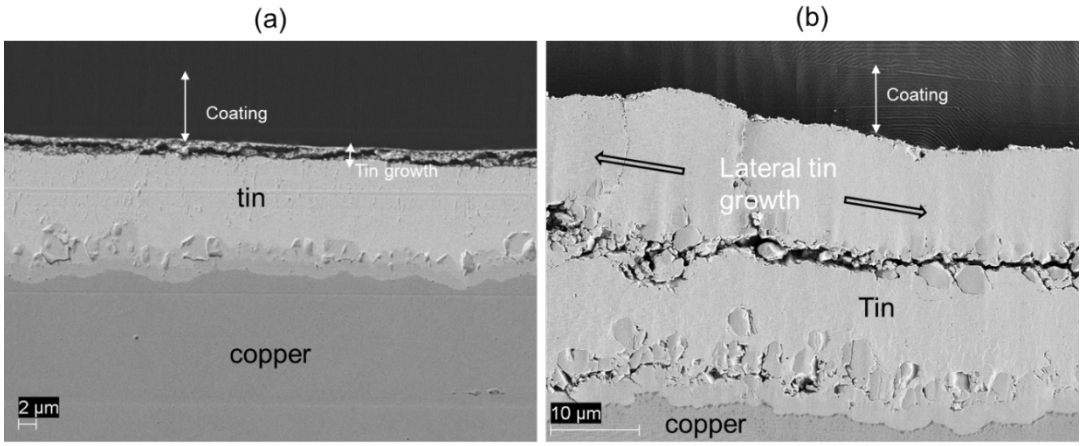


Figure 160: Representative cross – sectional microstructure developments in coated tin coupons following 4,000 hour HTHH storage; (a) 20 micron thick PC18M + 20%XP2742 nanosilica and (b) 20 micron thick unfilled PUA.

The lateral tin growth accompanied by the IMC formation at the interface was also noted in the case of bilayer coating coupon cross – section, as seen in Figure 161. Higher magnification images of the coating/tin interface showed a relatively higher deformation locally of the unfilled PU coating (PC18M) which was the first coating on tin (10 micron thickness). The second layer of filled PU of similar thickness was relatively less displaced. This may be explained by our previously reported nanoindentation measurements for the 'localized' matrix properties of the polyurethane coatings with and without nanoparticle additions which showed an increase of nanohardness in the case of 20% nanosilica suspension addition, to 210 MPa from about 160 MPa in the case of unfilled polyurethane, at a depth of one micron (see Appendix D).

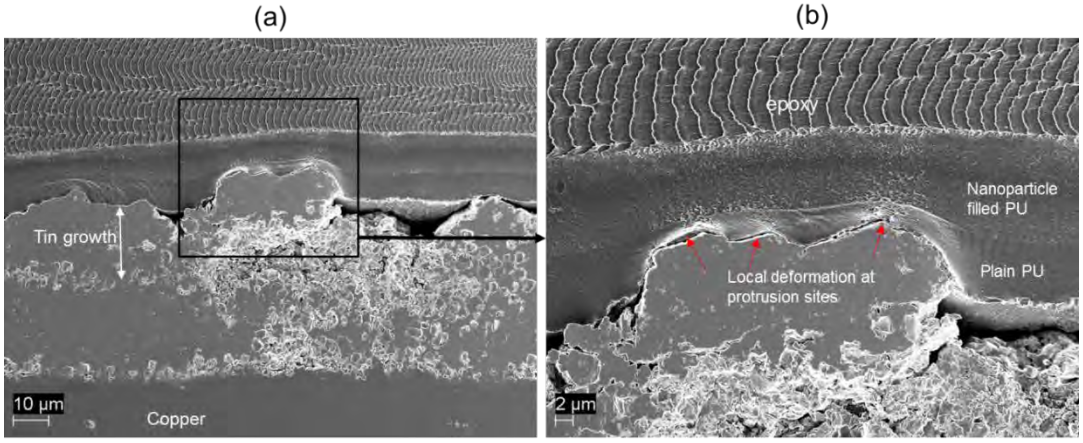


Figure 161: Cross – sectional microstructure development in a bilayer (filled PU on unfilled PU) coated coupons following 4,000 hour HTHH storage; (a) Tin plating on copper with secondary (lateral) growth and IMC formation and (b) Magnified view of unfilled and filled coatings with deformation noted at protrusion sites.

5.23.5 Summary of layered coating coupon whisker test results

High-temperature and high-humidity (HTHH @ 85°C/85%RH) storage testing of various conformal coatings applied to tin plated copper coupons was conducted for different time steps ranging from zero to 5,250 hours. The behavior of the conformal coatings was reported with respect to the mitigation of tin whisker and nodule growths originated from the surface of the tin plating as well as unique microstructural developments and features caused by the long-term storage. The effects of copper diffusion into the tin layer, followed by the formation of intermetallics in the tin-copper system was a critical factor in initiating protrusion-like growths from the surface of the tin plating.

All the polyurethane (PU) and polyurethane acrylate (PUA) coatings tested demonstrated their protection capabilities under HTHH storage up to 5,250 hours by showing no penetration of the tin whiskers or nodules through the coating layer. Cross-sectional analysis of selected coated coupons, however, showed that the poor adhesion due to the reaction between PU coatings and the top of the tin plating facilitated an availability of free surfaces at that interface, thereby causing diffused copper concentrations to reach critical levels necessary for intermetallic formation. Compressive stresses in the tin beneath this interface region (between coating and tin surface) and the growing interfacial intermetallic compounds caused protrusive growths to form and grow with increased storage time. Furthermore, the protrusive growths impinged upon the conformal coating which acted as a barrier to the vertical growth and forced the tin to grow into the interface between the coating and the tin, resulting in lateral growth.

Analysis of the lateral growth showed that extended storage (from 2,500 to 5,250 hours) resulted in an increase in the thickness of such secondary growth. The original tin plating thickness also showed an increasing linear trend with sustained storage time (0, 2,500 and 5,250 hours storage). However, when this trend was compared with the well-adhered coating case (4,000 hours HTHH storage) which showed no discrete intermetallic formation in bulk tin and no subsequent protrusions, the increase in tin plating thickness was significantly lower. The primary tin thickness increase can therefore have a critical dependence on the intermetallic formation at the tin surface (coating-tin interface) as well as diffused copper embedment along the grain boundaries of tin.

Other distinct coating compositions including PUA, nanosilica filled PU and bilayer (filled PU on unfilled PU) coatings all demonstrated similar tin microstructural developments (at 4,000 hours) with HTHH storage as in the unfilled PU cases although they displayed more substantial interfacial failure and tin lateral growth. The difference is believed to be due to interfacial adhesion, for which PU showed the highest adhesion. The beneficial effects of using coatings with different properties to construct bilayers was demonstrated via the distinct deformation behavior of filled PU versus unfilled PU coating under the stress during the tin protrusions.

5.24 Coating rework

The coating rework study is given in Appendix L and a summary is presented next. The PC18M and newly developed PC18M+20%XP2742 nanosilica coatings were both removable by standard manufacturing methods. Using the thermal removal and the media blaster removal method, the rework coating adhesion to both the solder and the adjacent old coating was acceptable. Localized re-coatings or replaced parts using syringe flooding of a 50 cps PC18M followed by a typical brush coating application was successful.

After part rework, selected samples were exposed to 100 thermal cycles -55 to 125°C and 10 days of humidity. The thermal ccycle used a dwell time of 30 minutes and a ramp rate of 10 °C/min for a total cycle time of 96 minutes. A modified MIL-STD-810 method 507 humidity test was used with a 24 hour cycle, consisting of a ramp from 38 °C to 65 °C in 2 hours, then a hold at 65 °C for 6 hours, followed by a ramp from 65 °C to 38 °C in 16 h while continually maintaining 95 percent relative humidity. The samples were inspected after environmental exposure in the SEM.

5.24.1 Rework coating thickness

The rework coating thickness was measured on the QFP center leads six and 28. The coating thicknesses at the locations shown Figure 162 were measured. When the coating was sufficiently thick, high magnification optical images were used for the measurement. In cases where the coating thickness could not be resolved, the sample was examined in the SEM (note that the sample was Au sputter coated prior to potting so that the coating surface could be distinguished from the potting when imaged in the SEM). Typical optical and SEM measurements are shown in Figure 163 and Figure 164.

Plots of coating thickness are shown in Figure 165 and Figure 166. Locations B, T and H had the thinnest coating. Significant coating build-up on the inside of the bend radius above the foot (locations D to F) was evident on several leads.

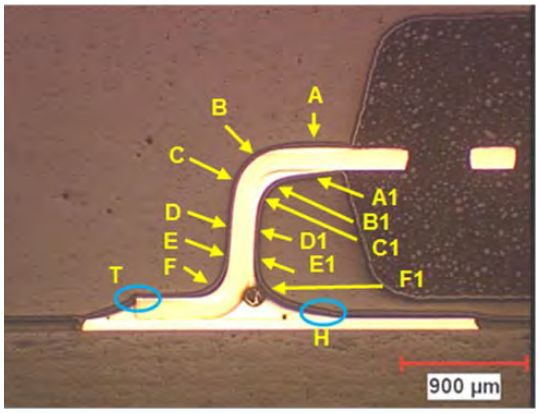


Figure 162: Coating thickness measurement locations.

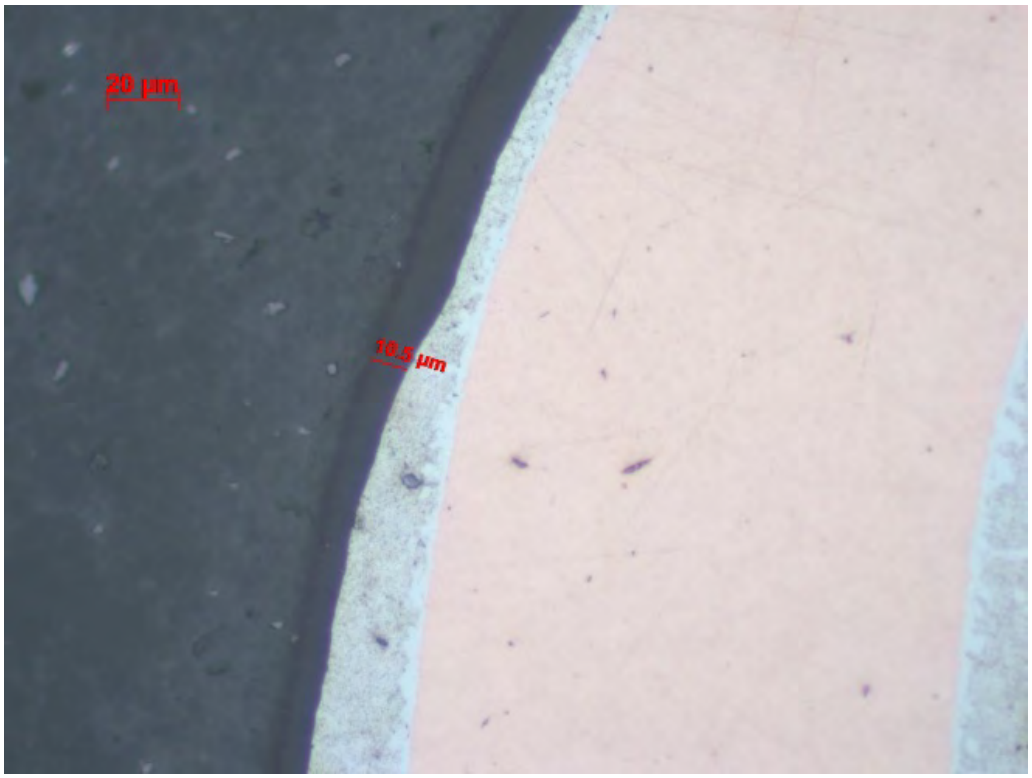


Figure 163: Optical cross-section image, unfilled PC18M QFP-A023 U1002, Lead 6 measurement, location C, 500x. Coating thickness was 10.5 microns.

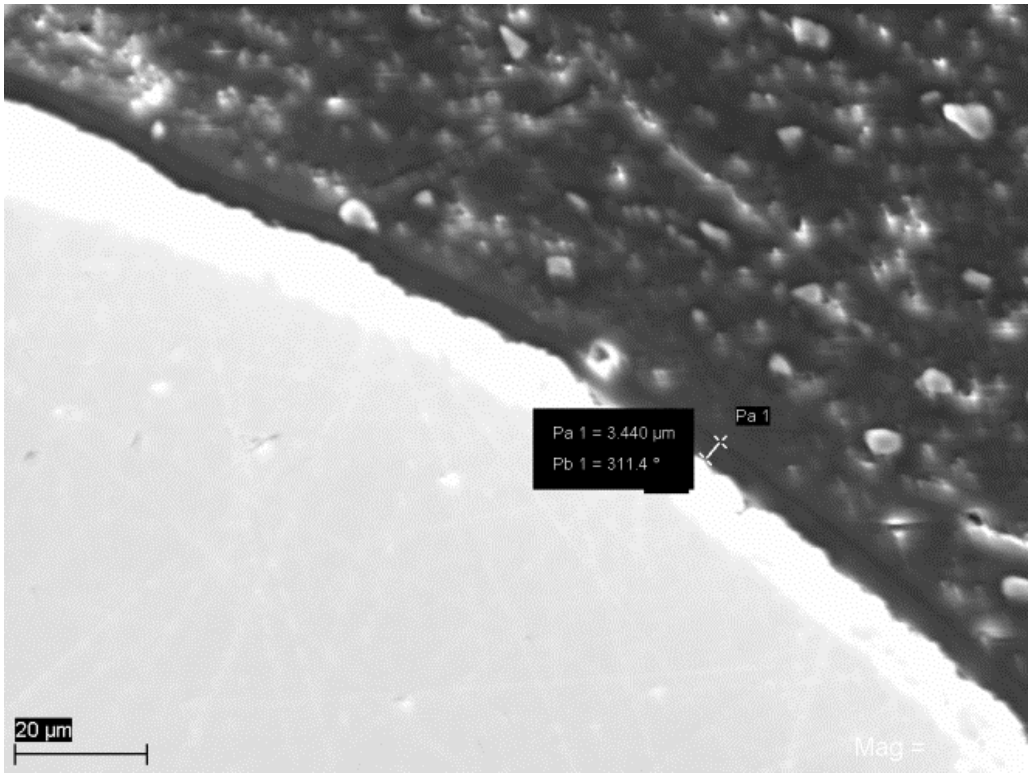


Figure 164: SEM cross-section image, filled PC18M+20%XP2742 QFP-A312 U902, Lead 6 measurements, location B, 1,930x. Coating thickness was 3.4 microns

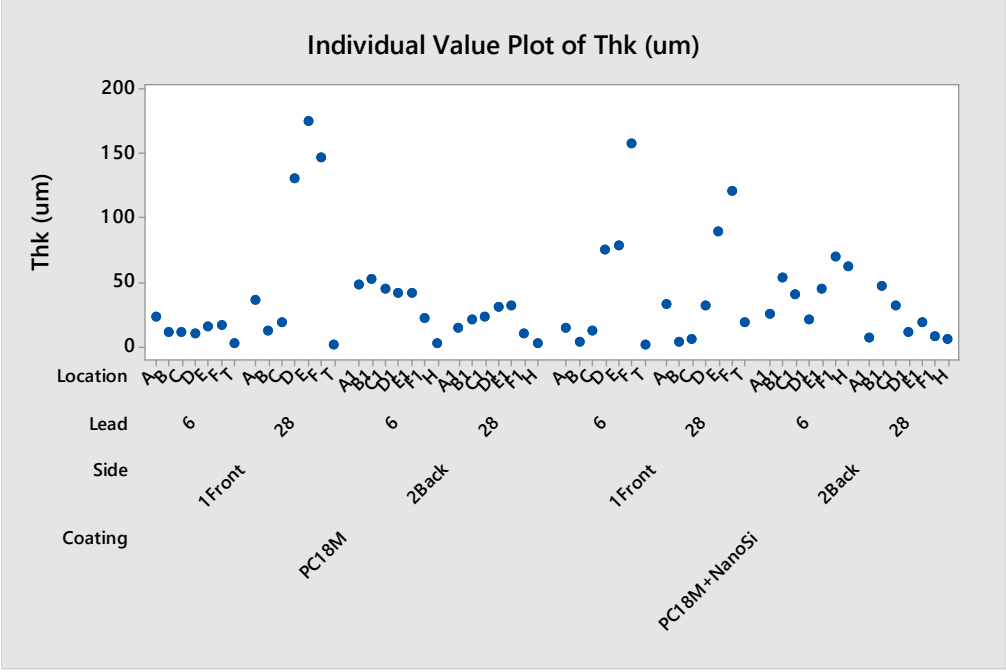


Figure 165: Individual value plot comparing rework coating thickness by location, lead and side (front/back) for unfilled PC18M and filled PC18M+20%XP2742 (PC18M+NanoSi).

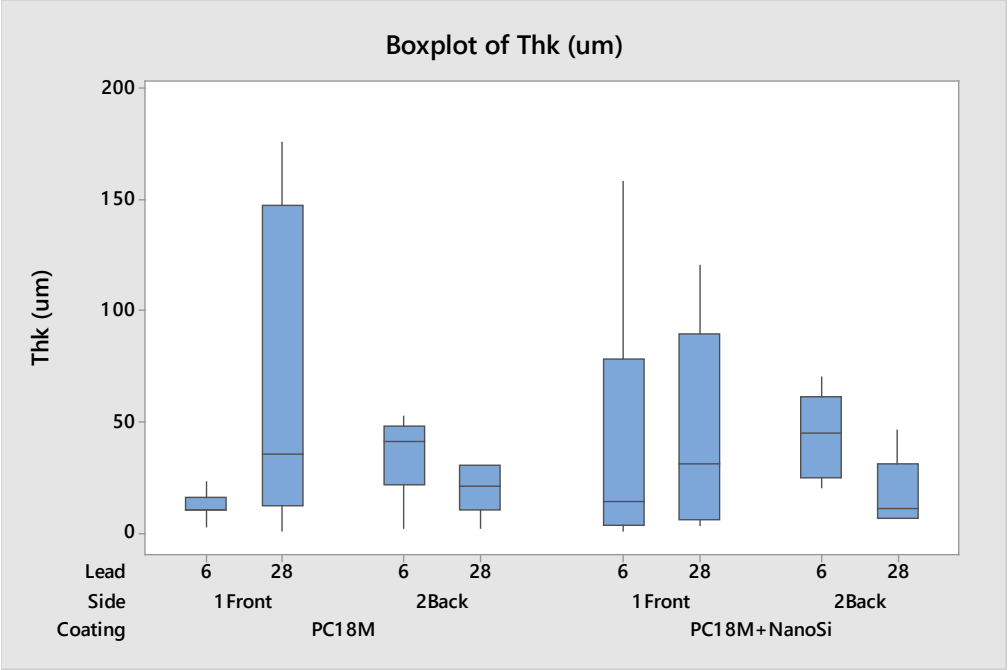


Figure 166: Box plot comparing rework coating thickness by lead and side (front/back) for unfilled PC18M and filled PC18M+20%XP2742 (PC18M+NanoSi).

5.24.2 SEM examination after environmental exposure

The SEM inspection after environmental exposure showed that the rework coating wet well onto the original coating (Figure 167) but that the thickness around the leads was excessive and cracked after environmental exposure (Figure 168). In addition, the lead edges had thin coating even though a relatively high viscosity (350 cps) was used for the brush coat.

The coating materials have the basic adhesion characteristics for a successful rework, but further work is needed to refine the method to improve coverage and prevent excessive coating thickness which caused cracking after environmental exposure.

5.24.2.1 Comment on the original layered coating performance on the rework samples

The rework coating wet into the original rough layered coating surface. This confirms the hypothesis that the initial cause for the roughness was burst microbubbles and not poor wetting.

The microbubbles in the enhanced layered coating exhibited cracking after the rework environmental exposure (Figure 167), suggesting that the microbubbles contributed to coating brittleness. (Note: This was a PC18M dip + two 25 micron PC18M+20%XP2742 spray coated board A312 which did not see prior environmental aging).

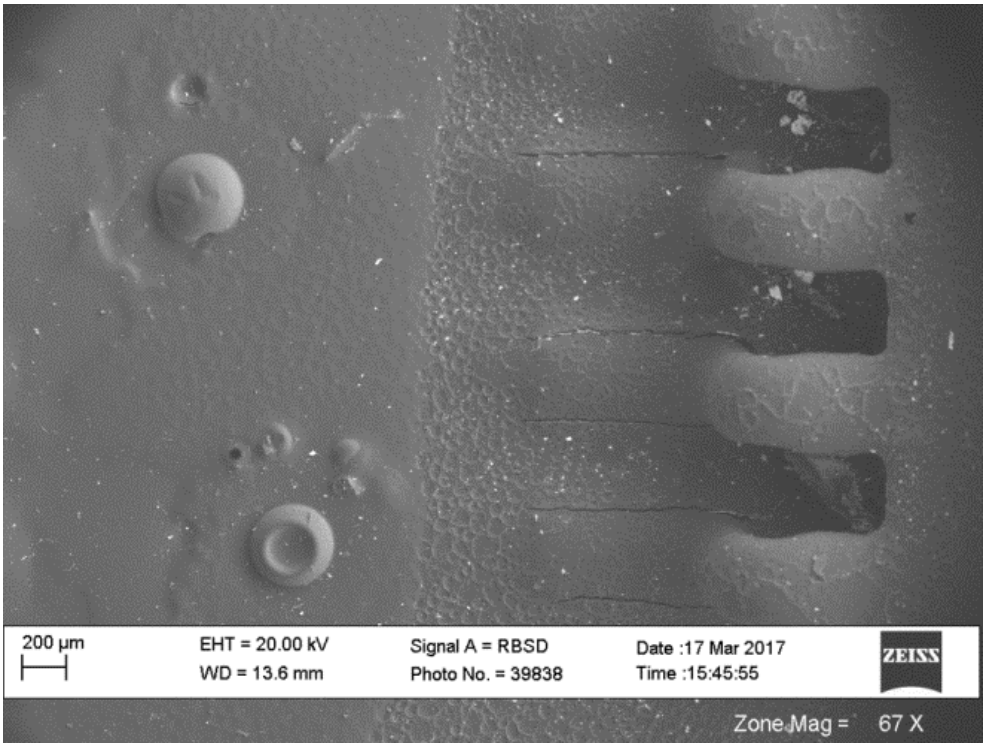


Figure 167: SEM BSE filled PC18M+20%XP2742 QFP-A312 non-reworked U903 adjacent to U902 pins 23 to 26, 67x.

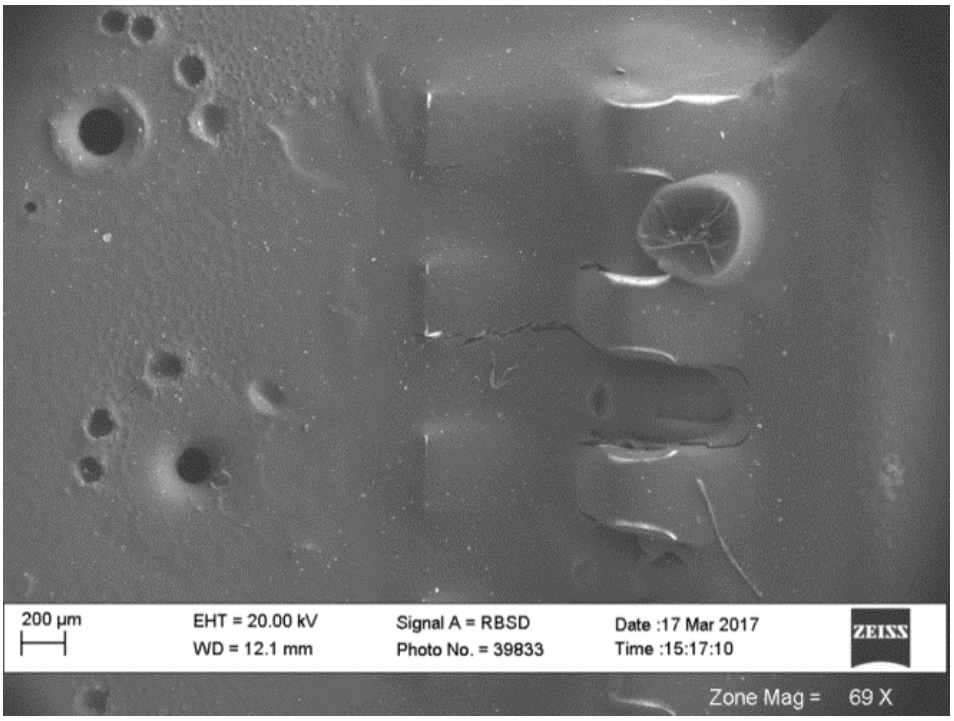


Figure 168: SEM image of the PC18M+20%XP2742 brush coat reworked QFP after 100 -55 to +125°C thermal cycles and 10 days of MIL-STD-810 humidity, 69x (ref. Board A312 U902 pins 1 to 3). Note some cracks present in reworked coating adjacent to leads.

5.25 Coating rupture modelling

In addition to the experimental work, an energy based model was developed to predict coating rupture (Appendix M). The input parameters are coating thickness, coating tensile properties, critical crack energy between the coating and the tin and the pressure in the tin during the nodule/whisker formation. Rupture predictions were computed for various eruption/whisker diameters. In the model, a circular area was established that would apply pressure to a coating film. The maximum pressure applied was taken to be equal to the tin yield strength. The tin energy was balanced with the elastic and plastic deformation coating energy. Both the classical and finite element model analysis encountered and instability in the solution. The classical solution yielded an algebraic expression for the coating rupture critical pressure. Finite element modeling was used to obtain model constants for the expression. Interestingly, for a given strength, as the coating film thickness increased, a large tin nodule was needed to cause rupture (Figure 169), which was in general agreement with experimental observations for the 34.5 MPa coating shown in Figure 170 and Figure 171. A coating strength of 40 MPa and a thickness of 10 microns would just rupture with a 60 micron diameter nodule but a thickness of 30 microns would resist rupture by a 120 micron diameter nodule.

A model that evaluates adhesion and delamination by various diameter nodules was also created. The results suggest that increasing adhesion results better mitigation which was also observed experimentally. For example an energy release rate of 10 J/m^2 and a coating thickness of six microns would be required to not have delamination of a 30 micron diameter nodule.

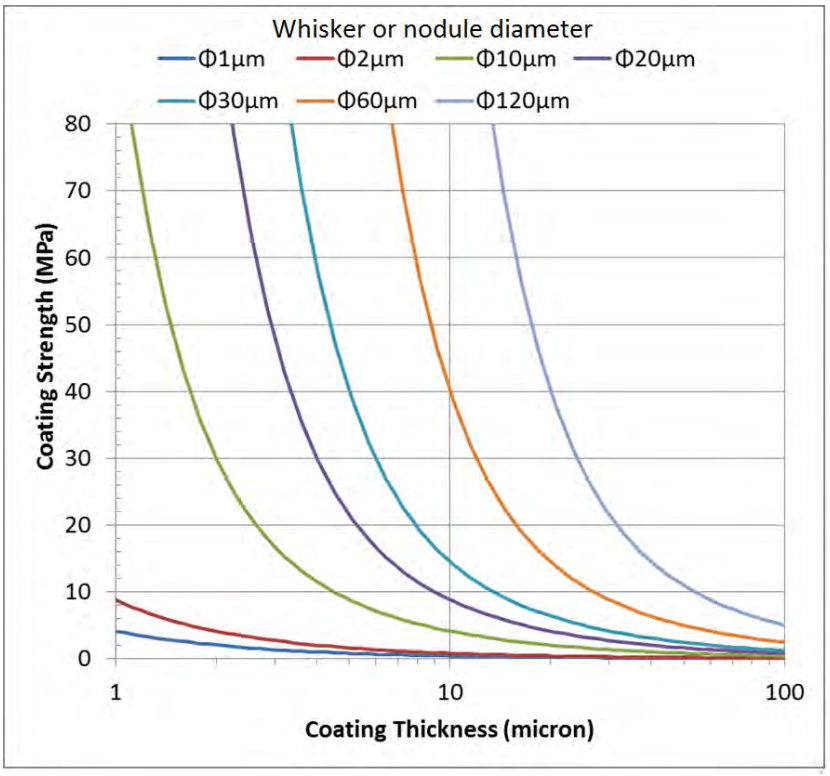


Figure 169: Coating strength required versus coating thickness.

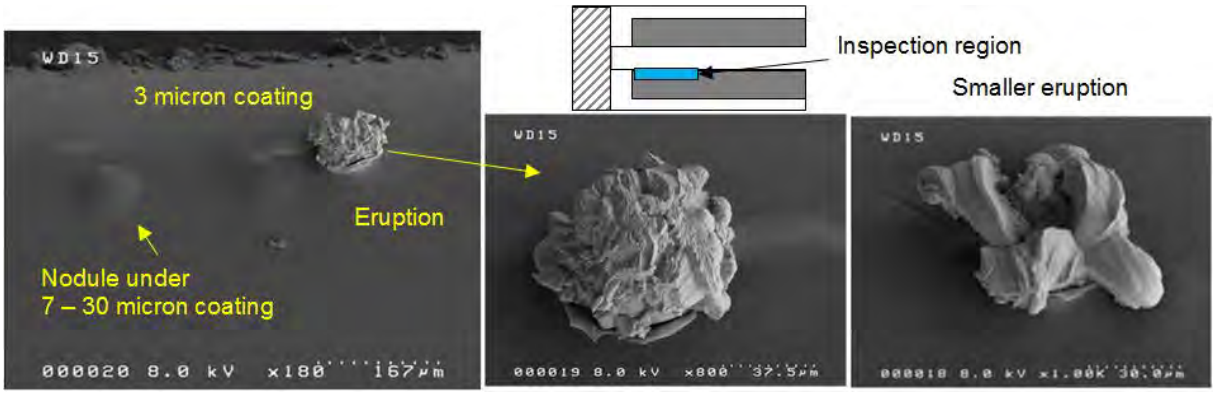


Figure 170: Cantilever beam coupon SEM inspection of thin coating region, areas after 2,500 (500+2,000) hours 60°C/60%RH showing a tin nodule under thicker coating and tin eruptions through thin coating.

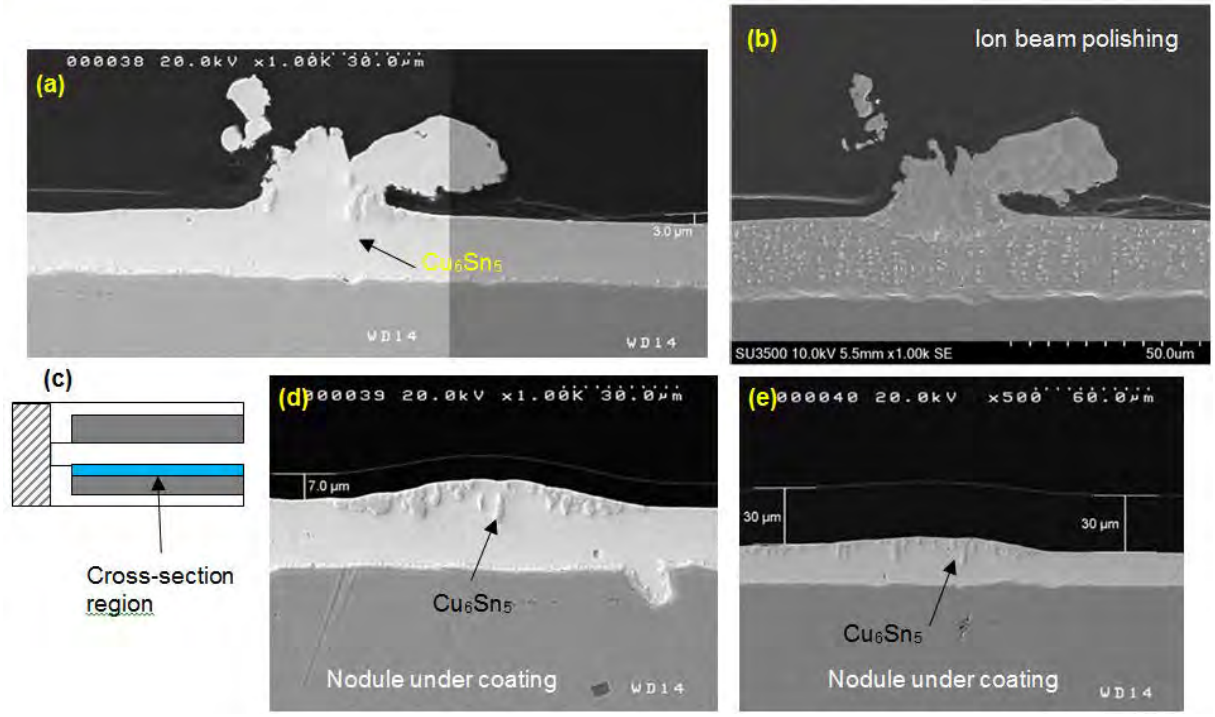


Figure 171: Cantilever beam coupon longitudinal cross-section through thin coating region areas after 2,500 (500+2,000) hours 60°C/60%RH; (a) and (b) eruption through three micron coating, (c) cross-section region on sample, (d) nodule under seven micron coating and (e) nodule under 30 micron coating. The thinner coating areas had smaller nodule diameters.

5.26 Long term PCTC cycling

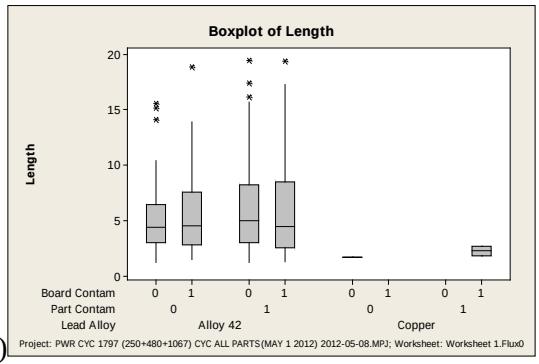
The details are provided in Appendix N and summarized here. The coating on the WP1753 cards was an ultraviolet and humidity dual cure polyurethane acrylate (Humiseal UV40) applied with an automated spray coating machine. The coating thickness cross – section results during the coating process development were documented in the present work for two coating viscosities. Thin coating was observed along the lead edges similar to the PC40 coating batches C and D (Appendix F). After a total of 6,000 power cycling thermal cycling (PCTC) cycles from +50 to +85°C, no whiskers penetrated

coating where it was thicker than approximately three microns (e.g the approximate coating thickness where the SEM beam cannot penetrate through the coating and image the underlying solder).

5.26.1 Whisker statistics discussion

During PCTC cycling, the uncoated reference sample whisker growth was primarily from the Alloy-42 lead-frame materials, but not as prominent as whisker growth during HTHH environments. The PCTC whisker growth stress was predominantly from the coefficient of thermal expansion differences between the low expansion leads and higher expansion lead-free solder and tin. Over the interval from 1,797 to 6,000 PCTC cycles, some whiskers remained unchanged, some grew longer, and some new whiskers grew. The box plots in Figure 172 show that mean and the maximum whisker length increased between 1,797 PCTC cycles to 6,000 cycles. It should be noted that the whisker length reported at 6,000 cycles did not include board with the longest whiskers at 1,797 cycles which was removed for sectioning. The trend of increasing whisker length with increasing cycle count continued through the 6,000 PCTC cycles (Figure 173). The 0 – 0 contamination level had shorter maximum whisker lengths throughout the test and the 1 – 1 contamination level had the longest.

(A)



(B)

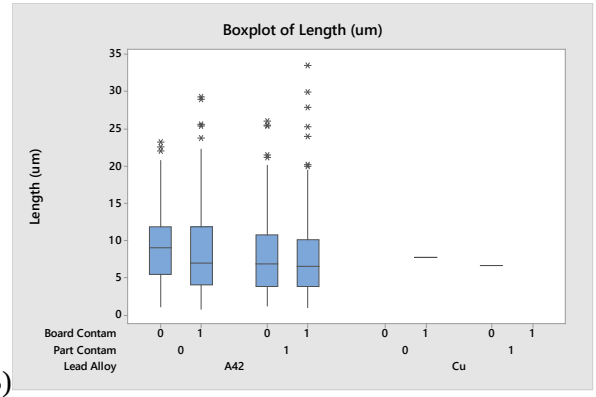


Figure 172: Box plot comparing whisker length (microns) after 1,797 and 6,000 PCTC cycles for lead alloy, part contamination and board contamination combinations; (A) 1,797 PCTC cycles and (B) 6,000 PCTC cycles.

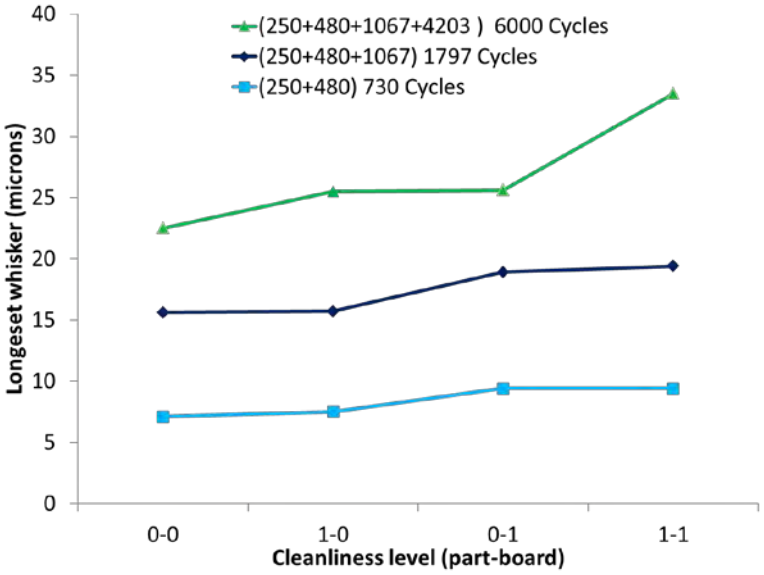


Figure 173: SOT3 maximum whisker length for the three last PCTC inspection intervals.

5.26.2 Metallurgical observations discussion for uncoated 6,000 PCTC samples

The whiskers mainly grow where the solder is thin at the lead above the main solder joint and around the toe. During PCTC cycling, there are several stress relaxation mechanisms occurring. In addition to whisker growth, there is grain boundary sliding, crack formation and grain recrystallization (Figure 174). The dynamic recrystallization theory proposed by Vianco and Rejent [25] [26] suggests that there is an optimal combination of stress, strain rate, grain size and temperature conditions for whisker growth. If the stresses are too high other non-whisker growth stress relaxation mechanisms occur if the stresses are too low, whiskers would not form.

The whisker growth between tin dendrites at 1,797 PCTC cycles was similar in some cases to the 6,000 PCTC (Figure 175). As was seen initially at 1,797 PCTC cycles, sometimes the whiskers were observed next to small solder cracks between tin grains. At the 6,000 PCTC cycle inspection, larger cracks were also observed suggesting that the cyclic stresses promoting whisker growth, while small, can eventually result in solder fatigue cracks. A progression of whisker growth and crack formation during thermal cycling is postulated as follows: (1) initial tin grain recrystallization, whisker nucleation, and whisker growth in the region between tin grains (Figure 176A), (2) then after more cycling the initiation of solder cracks less than a micron wide which could result in decreased whisker growth rate due to reduction of stress from the crack gaps (Figure 176B), and (3) then after more cycling the formation of very large cracks (~ 5 microns) where a whisker growth slows significantly or stops due to a reduction in stress and/or a reduction in mass tin transport to the whisker (Figure 176C).

Unique pad edge growths were also observed at the 6,000 PCTC inspection. The thin flat tin sheets were growing laterally from the interface region between the solder and the copper pad (Figure 177). They were similar in appearance to flat tin growths observed between grains (Figure 178). The pad edge growths were on the order of 10 microns long, 20 microns wide and a few microns thick. Pad edge growth was observed on both Alloy-42 and copper lead terminations.

Although the vast majority of whisker and pad edge growth occurred on the Alloy-42 lead terminations, the SOT5 copper lead terminations did exhibit some growth. The SOT5 whisker growth could be due to different coefficients of thermal expansion (CTE) between the different tin grain orientations. The β-tin is a very anisotropic metal. The CTE varies between 15 (a- and b-axes) and 30 ppm/K (c-axis) at 25 and

between 20 and 40 ppm/K at 125^{0}C. The elastic modulus varies between 22 (a- and b-axes) and 69 GPa (c-axis) at 25^{0}C. Tin is stiffest in the direction in which it also expands the most.

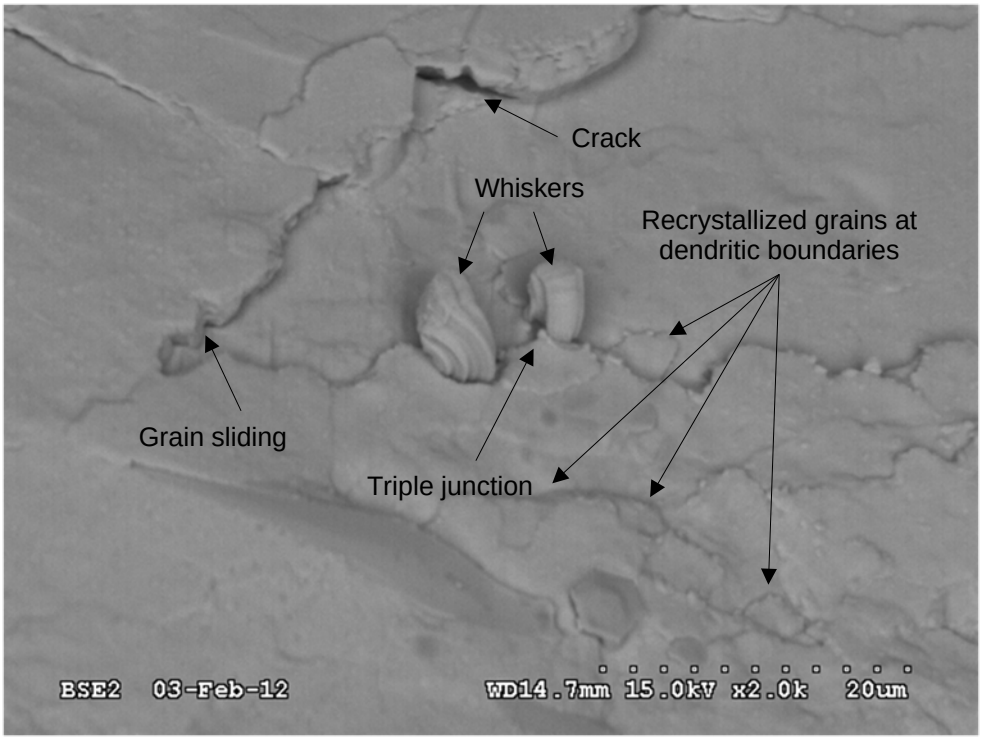
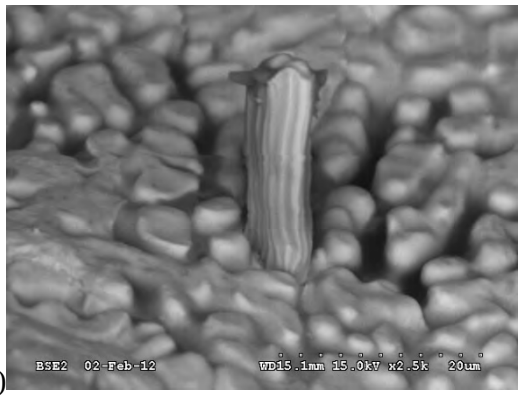


Figure 174: Competing mechanisms of stress relaxation (SOT3, 0-0 contamination level after 1,797 PCTC cycles shown).

(A) 

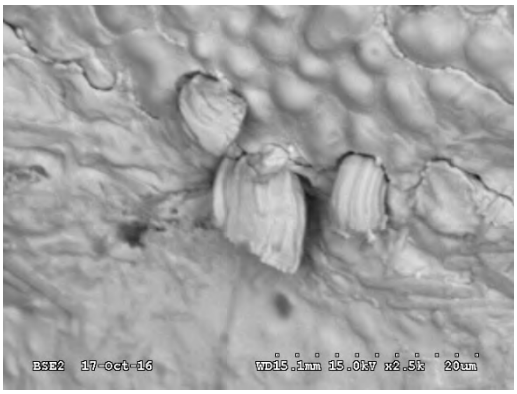
(B) 

Figure 175: High magnification SEM image comparison of whisker growth at 1,797 and 6,000 cycles SOT6 (A) after 1797 cycles, and (B) after 6,000 cycles 2,500x (ref. Image B A-SOT-PC-1-0-ncc-3, SOT6, U71, lead 4).

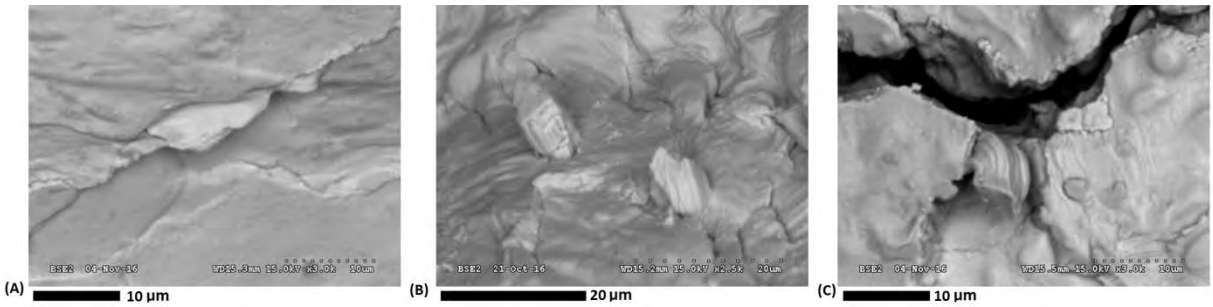


Figure 176: Close up SEM image of grain boundary slip regions, cracks, grain recrystallization, and whisker growth after 6,000 cycles on a SOT3 lead region with increasing amount of solder cracking; (A) no cracks, 3,000x, (B) small cracks, 2,500x and (C) large crack, 3,000x (ref. A-SOT-PC-1-1-ncc-1, SOT3, U31 lead 1 and A-SOT-PC-1-0-ncc-1, SOT3, U27, lead 3).

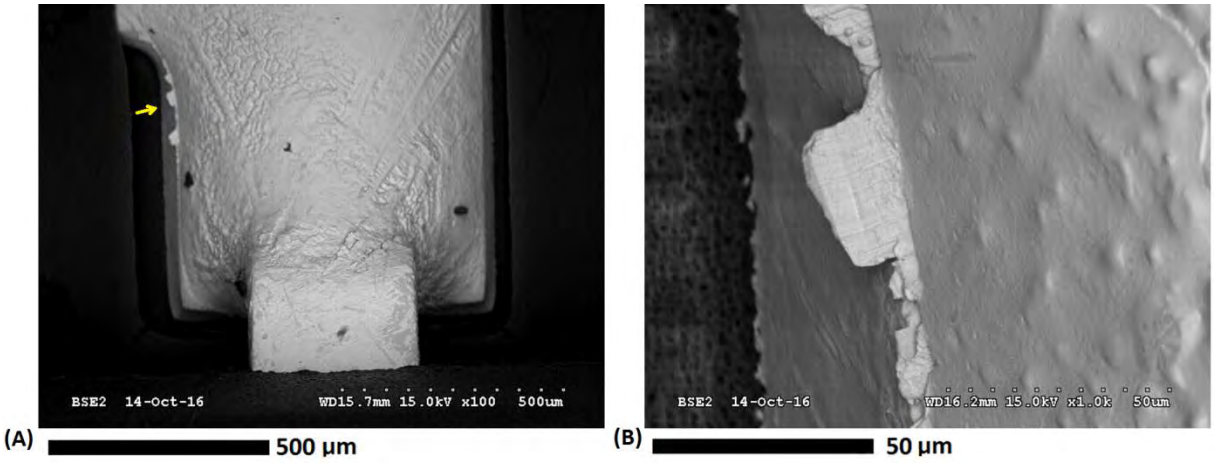


Figure 177: SEM image of the SOT3, U20, lead 1, no conformal coating, 1-0 contamination level after 6,000 PCTC cycles; (A) 100x and (B) high magnification image of pad edge growth highlighted by arrow, 1,000x (ref. A-SOT-PC-1-0-ncc-3).

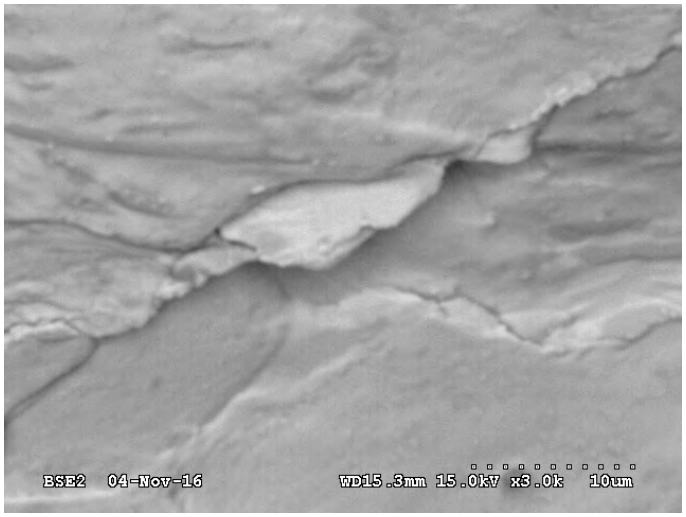


Figure 178: Close up SEM image of growth after 6,000 cycles along the grain boundary on the front of a SOT3 lead, 3,000x, (ref. A-SOT-PC-1-0-ncc-1, SOT3, U27, lead 3).

5.26.3 Coating integrity and whisker mitigation discussion for 6,000 PCTC cycle test

Although the coating obscured the majority of the tin surface from SEM examination, it was thin enough (less than approximately three microns) on the knee and at the toe to examine the metal. The solder areas with thin coating did have some whisker nucleation on the Alloy-42 (Fe42Ni) leads (Figure 179).

The coating wicked thoroughly into the solder interdendritic grooves (Figure 180). The coating adhesion in these areas is both mechanical and chemical.

Some coating cracking was also observed. The cracks were located along the lead near the lead knee where the coating fillets were thick (Figure 181). The cracks were sometimes accompanied by separation of the coating from the lead.

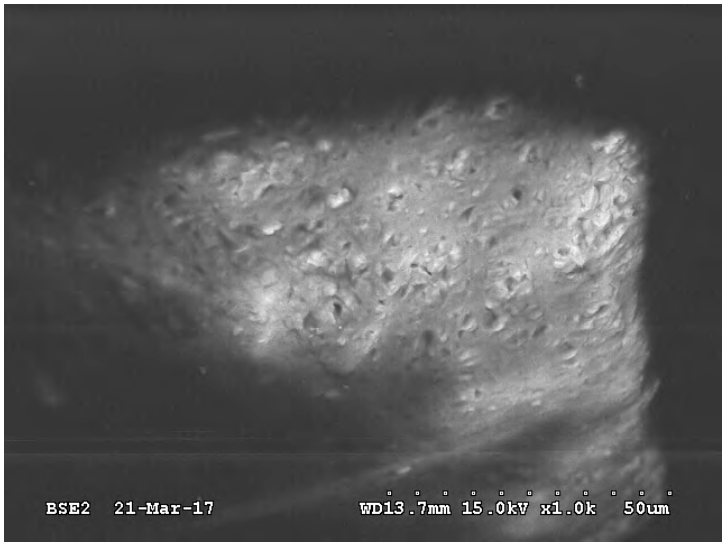


Figure 179: Higher magnification SEM image of coating on right SOT6 lead shown in Appendix N after 6,000 PCTC cycles, 1,000x. Some whisker nucleation is evident (ref. B-SOT-PC-1-1-cc-3, SOT6).

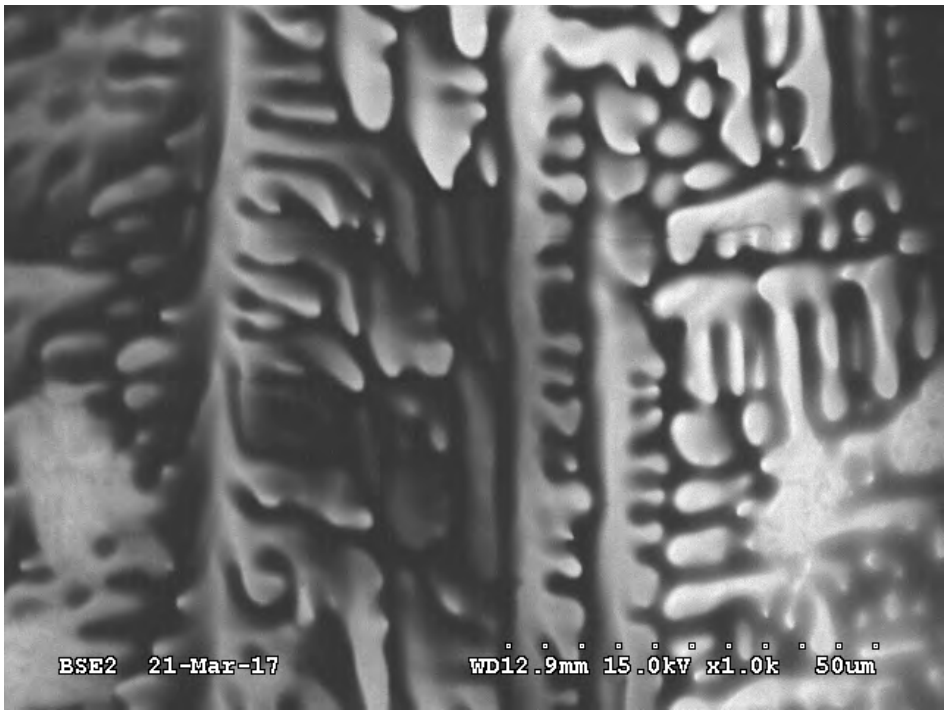


Figure 180: Higher magnification SEM image of coating on a SOT6 lead from board 2 with interdendritic solder spaces filled with coating and no whiskers 6,000 cycles , 1,000x (ref. B-SOT-PC-1-1-cc-2, SOT6).

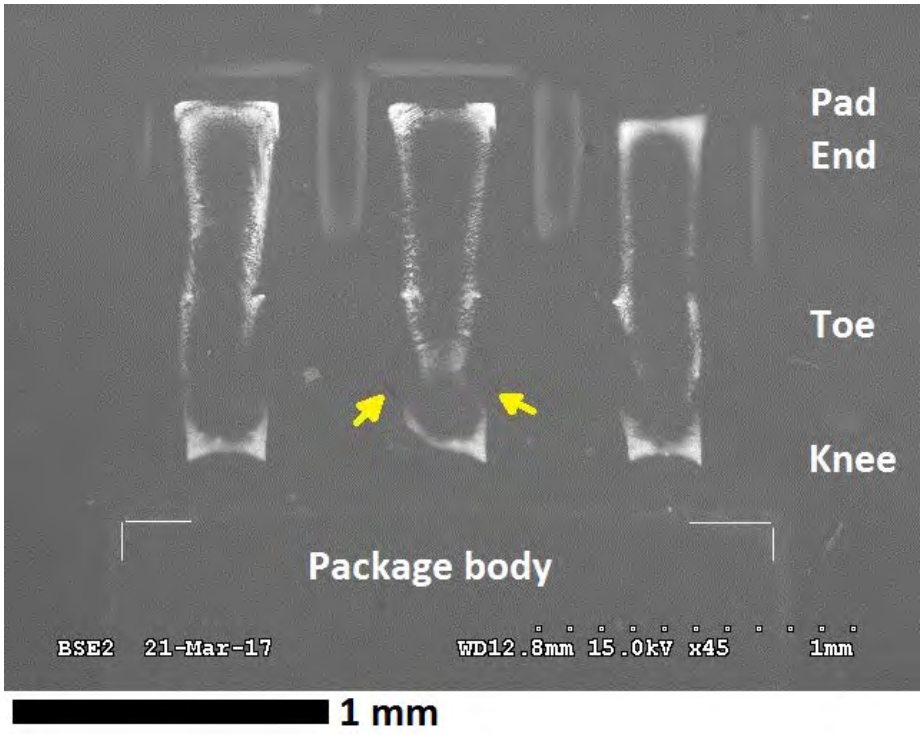


Figure 181: SEM image of coating on SOT6 leads from board 2 after 6,000 PCTC cycles, 45x (ref. B-SOT-PC-1-1-cc-2, SOT6). Arrows highlight coating cracks near the lead knee.

5.27 General discussion

5.27.1 Whisker testing summary

For the relatively rigid coatings evaluated in this work, no whiskers penetrated through any coating that was thicker than approximately 10 microns in either the coupon or assembly tests. Even where the coating was very thin (less than approximately three microns), the corrosion and whisker resistance was greatly improved over uncoated samples. For comparison the PU and PU nanoparticle coatings performed better than the 1B31 acrylic coating, but not as good as the Parylene C™ coating reference samples.

While providing insight into the coating performance, the extended HTHH testing had difficulty differentiate between the various hard coatings. Further increasing test times could exceed the basic coating material qualification standards.

5.27.2 Novel aspects of nanoparticle enhanced coatings

Use of nanoparticles may improve layered coating performance by leveraging a unique combination of properties. The SEM contrast difference from the nanoparticles can make it easier to validate the thickness of the various layers (see Appendix I). In addition, by alternating nanoparticle filled and unfilled layers can have mechanical benefits by having a high adhesion unfilled layer on the tin with a harder filled cap layer on a more elastic foundation to improve rupture resistance (Appendix J).

5.27.3 Process considerations with coatings having large viscosity changes with solvent concentration

The PU – PC18M coating presented challenges during both the dip and spray processes due in part to the large viscosity change as the solvent concentration is reduced. The PC18M coating family generally exhibited better coverage than the PC40-UMF coating family. Comparing the coatings, one factor influencing coverage is the solvent dependent viscosity characteristics of the PC18M and the XP2742. Particularly for the PC18M based coatings, the coating starts with a high solvent concentration and low viscosity allowing the coating to flow readily behind the leads. Then as the solvent evaporates, the viscosity increases rapidly and to a high value, which tends to prevent the coating from flowing down and away from the vertical sides of the leads. The PC18M viscosity without solvent is very high (like molasses). The solvent dependent viscosity was also present in the PC40-UMF based coatings, but to a lesser extent.

In the dip process solvent is lost due to solvent evaporation from the reservoir surface with time. In addition solvent is lost as it is “dragged out” when the coated samples are withdrawn. Increased dip coating viscosity caused some assemblies to have excessive coating pooling around the parts and coating bridging between leads.

The coating film formation during spray processing has a direct impact on the coating smoothness (Figure 182) and bubble formation (Figure 183). The solvent evaporates as the spray droplets coalesce after deposition (Figure 184). Further work is needed, but the following bubble formation process is postulated. During the spray process, the coating droplets proceed from the nozzle to the assembly surface and loose solvent along the way. If the atomized droplet loses too much solvent, it might have a high enough viscosity to prevent micro air/solvent bubbles from escaping as the spray coating thickness is built up. Particularly for the PC18M based coatings, the coating starts with a high solvent concentration and low viscosity. Then as the solvent evaporates, the viscosity increases rapidly and to a high value, since the PC18M viscosity without solvent is very high (like molasses). Upon heating during

the cure, the small gas bubbles coalesce to form larger bubbles that either remain trapped under the surface or partially escape leaving a rough surface (Figure 185).

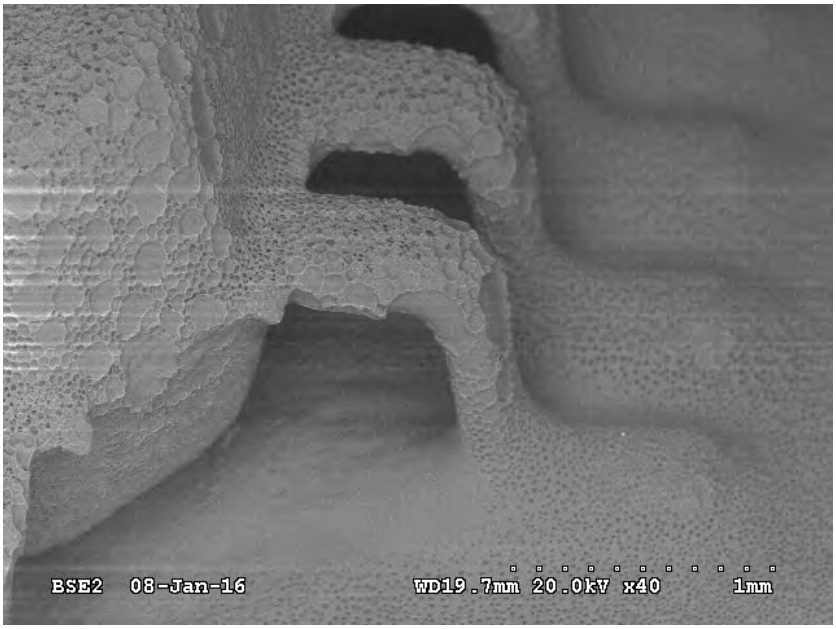


Figure 182: SEM image of the three layer PC18M dip with two PC18M sprays, board A191, QFP44, with good overall coverage but still exhibiting surface roughness, 40x.

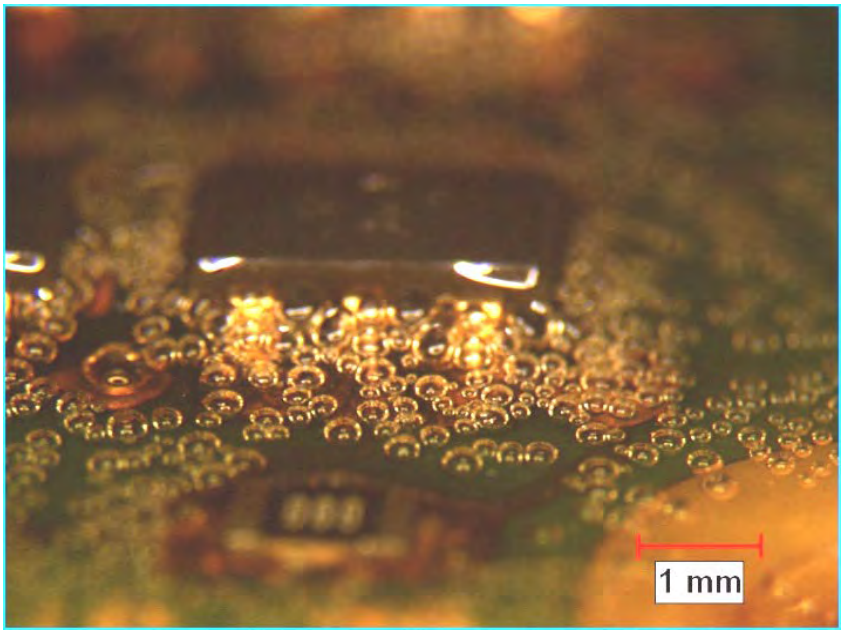


Figure 183: PC18M-mod SOT board 233 with large bubbles around the leads, 10x (note the photograph was taken after thermal cycling and 1,000 hours of 85°C/85%RH humidity (ATC+1000HTHH) environments). The color change is an artifact of the illumination used to highlight the bubbles.

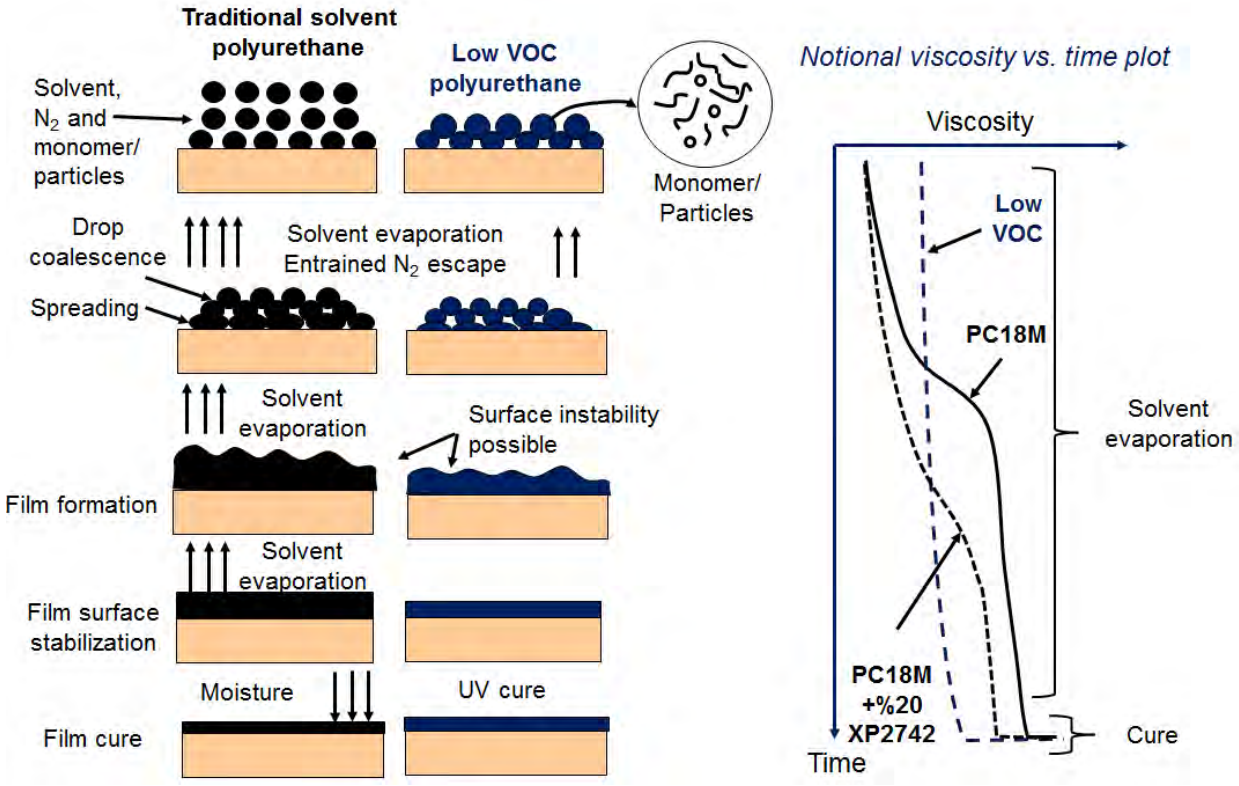


Figure 184: Coating film formation from spray coating process.

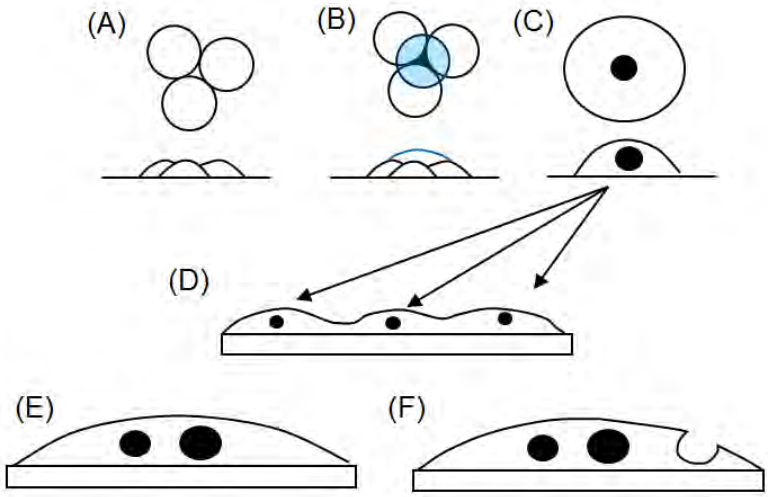


Figure 185: Spray drop deposition resulting in bubbles in the coating; (A) three deposited drops, (B) a fourth drop deposited on top of the initial three trapping some gas, (C) drop coalescence with a small entrained bubble, (D) multiple groups of the coalesced drops containing small bubbles, (E) during the heated portion of the cure there is a coalescence of small bubbles into larger bubbles, and (F) with drier films, having a higher some bubbles escape but the coating surface does not smooth out.

5.27.4 Layered coating coverage enhancement

The layered coating process improves coverage on corners as shown in Figure 186. The coating capillary action tends to build up the flat region between the corners and reduce the sharpness of the corner. By

building up multiple layers, the coating thickness on the corner will increase and whisker mitigation will be improved.

A two layer build up, a dip and spray combination, was evaluated in the baseline coating test for the PU and PUA base coatings. The PUA spray coat over the PUA dip exhibited poor film formation on the cured PUA dip material on the leads even when plasma etching was used after the dip cure. Where the PUA spray did coat the dip layer it exhibited poor adhesion. Additional experiments were performed to reduce the UV exposure during cure, but there was no lower exposure that would sufficiently gel the PUA surface and still have a low enough surface energy to permit the spray to wet and adhere.

As a result the PU based coatings were used for the enhanced layer process seeking to improve coverage. The enhance layer process was a three layer build up comprised of a PC18M dip + 25 micron spray + 25 micron spray. The three layer structure had improved coverage compared to the two layer dip + 50 micron spray structure.

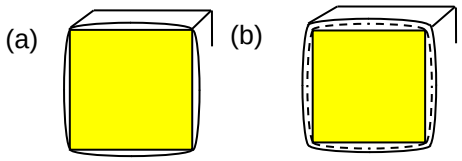


Figure 186: Cross-section view of coated QFP lead (a) one layer with thin coating on corners and (b) multiple layers with increased buildup around corners.

Tight process controls are important for good coverage. The solvent evaporation time during dip coating sample withdrawal needs careful monitoring to avoid lead-to-lead and lead-to-package coating bridging. A high degree of spray atomization can impact the coating surface smoothness, particularly when the coating material has a high viscosity that is strongly dependent upon solvent concentration.

The enhanced inspection techniques used in this project are more comprehensive than standard industry practices and address the coating performance aspects associated with tin whisker mitigation. The following observations were made during the examination:

- Layered coating provided better coverage and thickness uniformity and increased thickness on corners than conventional spray without an excessive coating build-up around the packages
- The spray coating contributed to an increased thickness on the front, front corners, and sides of the leads
    - All front and side areas had at least 15 micron thick coating
    - Some lead tips had small areas, less than 50 microns long and ~ five microns wide, of thin coating less than approximately three microns thick.
    - Coating thickness on the vertical part of the lead was less than on the horizontal part near the package body due in part to a coating fillet between the lead and the package body.
    - Spray coating built up the thinner dip coating at the corners and sides
- The coating build-up on the back of the leads was primarily from the dip coat
- There was incomplete spray coverage (droplets and discontinuities) on the back of the leads
- There was no discernable variation in nanoparticle distribution, even within thin or discontinuous coating regions
- Some interfaces between the first spray layer and the second spray layer were visible from high resolution FE – SEM imaging of the microtome sections; however, there was no indication of delamination
- The horizontal sectioning of the leads showed that the coating coverage was uniform lead-to-lead around the perimeter of the QFP (corner leads versus center leads).

- Further work is need on coating viscosity control during dipping to reduce coating webbing between fine pitch leads.
- The maximum coating thickness was 66 microns which is below the 75 micron thickness rule of thumb for rigid coatings to avoid coating cracking during thermal cycling

5.27.5 Potential improvements for coating stress analysis

There is an opportunity for DoD and Industry collaboration to leverage work at Sandia and NIST Gaithersburg on the stresses in the coating, the complex tin layer, and the interface between them. The dynamic recrystallization model developed by Dr. Vianco for tin whisker growth indicates that there is a sweet spot in stress for a given layer thickness, grain size, strain rate and temperature for whisker growth, which will be impacted by the presence of a coating. In addition, the recently developed taggant and fluorescence imaging developed by Dr. Gilman [27], surface stress techniques developed by Dr. Stafford [28] and others at NIST may be able to show changes in coating stress and coating adhesion. Also, there may be an opportunity to extend the stress measurements obtained during whisker growth by Dr. Chason [29] at Brown University to coated samples.

5.27.6 Improvements to liquid coating technology deficiencies

Improved liquid coating science is needed for advanced electronic packaging to provide enhanced whisker mitigation and moisture protection, particularly for low volatile organic compound (VOC) coatings. Improvements in low VOC coating rheology to optimize spray coating coverage and improvements in cured coating toughness are desirable.

This area would be an excellent candidate for further SERDP research.

The low VOC coatings evaluated in the WP 2213 exhibited the following deficiencies compared to the heritage solvent coating:

- Low wetting and coverage on the lead, particularly when the leads were narrow
- Low interfacial adhesion between cured layers
- Low elongation during tensile pull testing

The SERDP WP2213 demonstrated that liquid conformal coatings can provide substantial whisker risk mitigation. However, there remains a fundamental lack of understanding of the spray process parameters and coating rheological properties needed to obtain effective and consistent coating coverage on electronic assembly metallic conductors. In the current “top-down” spray coating processes, it is necessary to overcome deficiencies such as thin coating on corners and vertical surfaces and inconsistent coverage behind leads and other areas shadowed to provide enhanced whisker mitigation and moisture protection It is important to understand the factors influence coverage effectiveness such as the spray coating droplet size, droplet velocity, liquid rheology (viscosity) and surface tension, droplet impact angle, free surface instability , solvent evaporation effects, solid surface geometry and solid surface tension (both metal and polymer). Often multiple coating layers are applied to obtain the desired final thickness. The material build-up often obtained through deposition of multiple liquid spray passes or spray/partial cure/spray layering and the interlayer effects such as dissolution and adhesion are important to understand.

A key element is effective validation of coating coverage/thickness on electronic assemblies. Lack of a low cost quick validation technique remains a significant impediment to ensuring consistent mitigation. Development of representative coating validation test vehicles and rapid coating coverage/thickness measurement techniques are needed for process control.

The low VOC coatings exhibited low surface energy and low bond strength when the liquid was over coated on a previously cured layer. The low interlayer adhesion is an impediment to rework and using

multilayer build-up techniques to increase coating thickness. In addition, it was found that low VOC compounds exhibited considerably less toughness than the traditional solvent based coatings.

High elongation, penetration resistance, and strength combine to provide whisker mitigation and coating durability during thermal cycling. The addition of nanoparticles to enhance whisker tended to reduce elongation further. Improvements in toughness are desirable.

5.27.7 Nanoparticle enhanced coating material commercial availability and adoption

Under WP2213, the basic idea of incorporating functionalized covalently bonded nanoparticles into electronic conformal coating to improve the coating mechanical properties has been demonstrated and published. The most promising formulation developed to date, Henkel PC18M with 20%XP2742, approaches Parylene ™ properties. Adoption of this specific coating would require qualification to IPC-CC-830 and MIL-I-46058 and the creation of a commercial chemical safety data sheet (SDS) (currently it has an experimental SDS).

Some original equipment manufacturers (OEMs) of electronic assemblies may want to add functionalized nanoparticles to base coatings they have already qualified on product (e.g. other base coatings from Henkel, Humiseal, Electrolube, Cytec, Dymax, Huntsman, etc.) to reduce impact on current production processes. Adoption into other coatings would likely require variations in particle functionalization or a tailoring of the suspension media (e.g. N3300). In addition, it would be highly desirable for OEMs to have a single coating, so the new coating would need to be qualified for use on heritage product production and rework, which can require additional product qualification to obtain end customer approval.

The U.S. Patent Office did not grant BAE System's patent application for a particle enhanced conformal coating for whisker mitigation citing prior art in patents US2007295530 Jackson and Humphrey (Honeywell) and US2008216704 Eisenbeis and Strong (Fisher Controls International LLC). Commercialization of a particle enhanced coating for whisker mitigation will likely require agreements with one or both of these companies.

While electronic assembly producers may be able to mix a functionalized nanoparticle suspension to any coating they choose, it would be more desirable to have a coating manufacturer provide the material already mixed. To do this, the coating manufacturers will need to determine the commercial potential of a nanoparticle filled coating material. It should be noted that the nanoparticle suspension would be a fraction of the coating volume (e.g. 20% by volume for the current XP2742 mixture). It is likely that this volume of material is too small for Covestro to effectively manufacture; however licensing the XP2742 technology patent to a low volume manufacturer is an option. Polymaterials with a U.S. office in Greensboro, NC might be one such supplier.

6. Conclusions and implications

6.1 Whisker mitigation

All rigid coatings evaluated here that were at least 10 microns thick inhibited rupture by nodules or whiskers during long term high temperature high humidity aging. Parylene ™ C vacuum deposited is still the best baseline material for best whisker risk mitigation performance. For liquid coatings, polyurethane materials are more effective than acrylic materials for whisker mitigation based on prior industry testing [18] to [21] and the results obtained here.

Continued coverage and thickness improvements for liquid coatings are needed. When solvents are used in the coatings, careful monitoring of viscosity is needed to ensure sufficient, but not excessive, coating thickness and a minimization of coating cracking and bubble defects. Applying successive layers of coatings with partial cures between them is an effective means of improving coverage and thickness on edges and corners. Consider use of coupons or scrap parts with three dimensional features that can be processed along with actual assemblies to be used for coating coverage and thickness analysis on the leads.

6.2 High strength coatings and adhesion

The incorporation of nanoparticles into the coating can increase the coating strength and as a result a thinner coating would be needed to accomplish the same level of tin whisker mitigation. Balancing coating strength, while minimizing the reduction in toughness/elongation characteristics, remains a challenge. Where the coating was thick or had void defects, it cracked more easily. Application method improvements are needed.

The low VOC PC40-UMF moisture permeability results were good, but strength and elongation were limited by micro – voids within the cured coating structure. Further work is needed to reduce the formation of these voids during curing. In addition, research is needed to improve low VOC coating wetting and interlayer adhesion to enable use in multilayered structures.

The presence of a higher strength coating, like those tested here, of sufficient thickness changes the nature of the tin growth from whiskers to nodules. The modeling indicates that large nodule diameters are more difficult to contain than smaller diameter whiskers and would require greater coating thickness. The results also indicate that adhesion is important for nodule formation prevention and whisker mitigation. The factors impacting coating separation from the tin are the chemical and mechanical bond strength of the coating to tin reaction layer, the development of voids in the tin structure below the coating which can result in a crack immediately below the initial reaction layer and the increased stresses near the coating interface due to the accumulation of intermetallic and oxide/corrosion products, which both have a larger volume than the Sn.

The actual tin surfaces on real electronic assemblies contain matte tin, reflowed tin, and lead-free solder, which are considerably different than the bright tin used during the coupon whisker investigations. While the mechanisms of adhesion between metal surfaces and polyurethanes are not entirely understood, there is evidence in the case of aluminum and copper to show that the occurrence of native oxides plays a significant role in enhancing the adhesion of polyurethanes (see references in Appendix J). Additional coating adhesion work on surface representing electronic assemblies is needed.

6.3 Coating evaluation and test methods

The knowledge developed in the current project on whisker mitigation will result in increased aerospace and defense electronic assembly reliability. The approach used to characterize, analyze and characterize these coatings can be extended to any coating intended for tin whisker mitigation applications. Physical analysis of a coating prior to selection should include the following tests (ref. Appendix C):

- Viscosity for various shear rates and solvent concentrations
- Surface tension and contact angle on glass reference slides and on cured coating films
- Adhesion testing of films
- Microstructure evaluation, e.g. micro-voiding, particle agglomeration, settling, and adhesion to matrix, hard segment and soft segment, chemical bonds, etc.
- Tensile strength, modulus, and elongation of films using nanoindentation and classical tensile tests
- Spray coating characterization including droplet size, spray patterning and overlap
- Ability to form sequential layers for partial cure/coating/partial cure layering
- Evaluation of coverage and thickness on three dimensional lead surfaces using cross-sectioning and SEM

6.4 Nanoparticle coating additions

Including functionalized particles in enhanced coating will be useful because stronger coatings can provide mitigation with a thinner layer. Alternatively, the particles can be used to alter the liquid coating rheology and mechanical properties to improve corner coverage and to prevent whisker penetration.

Attention to the nanoparticle suspension is critical to ensure compatibility with the polyurethane coating. In contrast to larger micron sized particles, greater concentrations of nanoparticles can be added into coatings without significantly increasing viscosity and reducing spray-ability. Study of the mechanical properties using cast films is needed to determine the particle concentration for balancing elongation and tensile strength (see Appendix D).

Use of nanoparticles may improve layered coating performance by leveraging a unique combination of properties. The SEM contrast difference from the nanoparticles can make it easier to validate the thickness of the various layers (see Appendix I). In addition, by alternating nanoparticle filled and unfilled layers can have mechanical benefits by having a high adhesion unfilled layer on the tin with a harder filled cap layer on a more elastic foundation to improve rupture resistance (Appendix J).

6.5 Enhanced layered coating

The layered coating method with intermediate partial cures steps is a promising method for obtaining enhanced thickness uniformity and control (Appendix E, Appendix I, Appendix J, and Appendix K). The developed method can be used for polyurethane coatings with and without nanoparticles. The low viscosity dip provided some electrical insulation on all surfaces on the small features behind leads and in low gap spacing. The risk with dip coating is that if the viscosity is not low enough (~ less than 50 cps), bridging between and filling behind leads can occur, which may cause solder thermal cycling fatigue reduction.

The layered spray coating provided significant additional coating coverage on all lead surfaces except for the back of the lead. The additional front and side lead coating thickness was obtained without excessive coating build-up around part bodies. When using coating with a very high solvent dependent viscosity, process and material process controls have increased importance to avoid bubble entrapment and rough coating surfaces. It would be desirable to further reduce variation and increase back side thickness, but process/machine optimization or an entirely new liquid deposition technique may be needed.

Layered coating process can improve coating coverage, but excessively thick coating regions pooling at the base of the packages, between the leads, and between the leads and the packages needs to be avoided to prevent coating cracking. Another issue with excessive coating is the possible impact to solder joint fatigue life in applications requiring extensive thermal cycling.

6.6 Unique tin nodule microstructure evolution under coating and the importance of coating adhesion

The layered coating coupon testing provided insight into the coating impact on the progression of nodule formation and subsequent complex tin layer growth (Appendix J). A new IMC formation phenomenon was observed in the tin regions where nodules developed under the rigid coating:

- Large Cu_6Sn_5 intermetallic grain growth occurred near the coating/tin interface that was not attached to the lower copper substrate to tin interface
- A complex layer of tin and IMC developed from original plated tin
- Within the complex tin and IMC layer both small and large IMC grains as well as voids were observed

- Coating adhesion to the tin is important
  - PU showed the highest adhesion
  - Poor adhesion due to the reaction between PU coatings and the top of the tin plating facilitated an availability of free surfaces at that interface, thereby causing diffused copper concentrations to reach critical levels necessary for intermetallic formation.
  - Compressive stresses in the tin beneath this interface region (between coating and tin surface) and the growing interfacial intermetallic compounds caused protrusive growths to form and grow with increased storage time
  - The protrusive growths impinged upon the conformal coating which acted as a barrier to the vertical growth and forced the tin to grow into the interface between the coating and the tin, resulting in lateral growth available at the interface for IMC growth in that region
- The coating adhesion to the tin appeared to be limited by
  - Interfacial strength between the coating and the tin oxide on the tin surface
  - Strength of the tin below the coating, possibly impacted by voiding
  - Additional stress near the interface due to increased tin oxidation and the accumulation of Cu_6Sn_5 IMC near the coating/tin interface both which have greater volume than tin

Systematic annealing studies of tin and adhesion promoters (e.g., silane treatment) may be useful to assess the nature of this relationship between the adhesion and the tin whisker/nodule growth. The can be facilitated by leveraging work at Sandia, NIST and other researchers on the coating stresses, development the complex tin and intermetallic layer of the nodule, and the adhesive interface between them.

6.7 Liquid coating application processes

To have effective tin whisker mitigation, further work is required to obtain better coverage consistency. A greater fundamental understanding of film formation in a spray process is needed. Attention to surface energy and wetting of partially cured, cured, and aged coatings is needed for layered coating and rework processes. Use of alternating X-Y spray patterning reduces shadowing and provides more consistent coverage. Adhesion promotion techniques such as silane treatment or plasma cleaning will improve whisker mitigation.

Techniques such as high speed photography to study droplet size and patterning, UV partial cure to secure material in place, measurement of the volume/time/pressure relationship during spraying, and a method for penetrating into low component height gap spacing areas of electronic assemblies would be beneficial.

6.8 Industry implementation of whisker mitigating coatings

An understanding of materials, application processes, and validation beyond current industry standards is required when using coating for long term whisker mitigation. The existing coating qualification [11],

coating application guidelines [12], and coverage/inspection requirements [13] require significant updates to include the coating coverage, thickness, and verification requirements. Three dimension coupons and assemblies will need to be an integral part of coating process monitoring and should be incorporated into IPC-CC-830 coating materials and J-STD-001 Class 3 assembly requirements.

Additional DoD and industry collaboration will be needed to develop new coating materials leveraging nanomaterials and/or rheology changes for improved tin whisker mitigation. New coating development, production and adoption needs to have industry/customer consensus, test data, and modification to existing specifications to enable their use.

Further work is needed to quantify the coating mechanical properties and adhesion strength to allow these parameters to be correlated to the stress developed in the coating film during tin nodule and complex tin layer growth.

The results from field monitoring and a broader range of whisker tests can be used to improve the whisker risk modeling initially developed in WP1753, which is now hosted on-line by the University of Maryland Center for Advance Life Cycle Engineering (CALCE) which is now available for anyone to use.

Whisker test methodologies are needed beyond the consumer part tests currently in place like JESD-201. Longer exposure times and sequential exposures to thermal cycling and humidity may be required for coating evaluations to simulating product operating environments. The thermal cycling will tend to cause cracking if the coating is too thick. The high temperature high humidity will increase corrosion, altering the tin surface stresses and promoting whisker growth. Additional research is needed to establish assembly level tin whisker coating qualification protocols.

7. Literature cited

[1] GEIA-STD-0005-1, Performance Standard for Aerospace and High Performance Equipment using Lead-free Solder, SAE International, Warrendale, PA.

[2] GEIA-STD-0005-2, Standard for Mitigating the Effects of Tin Whiskers in Aerospace and High Performance Electronic Systems, SAE International, Warrendale, PA.

[3] The Lead-free Electronics Manhattan Project Reports, Completed under U.S. Government Contract No. N00014-08-D-0758, The Benchmarking and Best Practices Center of Excellence at ACI Technologies, Inc., Philadelphia, PA, Phase 1: July, 30 2009 and Phase 2: February 10, 2010.

[4] S. Meschter, P. Snugovsky, Z. Bagheri, E. Kosiba, M. Romansky, J. Kennedy, L. Snugovsky, and D. Perovic, Whisker Formation on SAC305 Soldered Assemblies, J. of Metals, (DOI) 10.1007/s11837-014-1183-9, to appear in the Nov. 2014 issue, available on line at http://www.springer.com/home?SGWID=0-0-1003-0-0&aqId=2737780&download=1&checkval=c6d6cb73aec6cca572a5b064f23677b9

[5] G.T. Galyon, Annotated Tin Whisker Bibliography and Anthology, IEEE Trans. Packag. Manuf. Vol. 28, No. 1, January 2005, pp. 94-122.

[6] T. Shibutani, Q. Yu, M. Shiratori, M. Pecht, Pressure-induced tin whisker formation, Microelectronics Reliability, Vol, 48 (2008) pp. 1033–1039.

[7] B. Sood, M. Osterman and M. Pecht, Tin Whisker Analysis of Toyota's Electronic Throttle Controls, Circuit World, Vol. 37, No. 3, 2011, pp. 4–9.

[8] P. Daddona, Reactor Shutdown: Dominion Learns Big Lesson From A Tiny ‘Tin Whisker', TheDay.com, New London, CT, July 4, 2005 (from the NASA Goddard Tin Whisker Home Page https://nepp.nasa.gov/whisker).

[9] S. Meschter and P. Snugovsky, Tin Whisker Testing and Modeling, SERDP WP-1753 Final Report, November 2015.

[10] S. Meschter, M. Osterman, P. Borgesen and I. Dutta, Enabling Lead-Free Interconnects in DoD Weapon Systems Final Presentation and Webinars, ESTCP Project WP-201573-T2, September 2017 (available on line).

[11] IPC-CC-830, Qualification and Performance of Electrical Insulating Compound for Printed Wiring Assemblies, IPC-Association Connecting Electronics Industries, Bannockburn, Illinois, USA, September 2008.

[12] IPC-HDBK-830A, Guidelines for Design, Selection and Application of Conformal Coatings, IPC-Association Connecting Electronics Industries, Bannockburn, Illinois, USA, August 2013.

[13] MIL-I-46058, Military Specification, Insulating Compound, Electrical (for Coating Printed Circuit Assemblies), U.S. Department of Defense, Original issue 1966, last revised 1998 (inactive for new designs).

[14] L. Zou and C. Hunt, Protection Performance of Conformal Coatings in Harsh Environments, National Physical Laboratory (NPL) Report DEPC MPR 054, July 2006.

[15] J-STD-001 Requirements for Soldered Electrical and Electronic Assemblies, Joint JEDEC Solid State Technology Association/IPC Association Connecting Electronics Industries document, April 2010

[16] J.S. Kadesch and H. Leidecker, “Effects of Arathane Conformal Coating on Tin Whisker Growth”, Proceedings of IMAPS Nordic, The 37th IMAPS Nordic Annual Conference, pp. 108-116, September 10-13, 2000.

[17] S. McKeown, J. Kane and S. Meschter, Whisker Penetration into Conformal Coating, Proc. IPC APEX Conference 2007.

[18] L. Panashchenko, J. Brusse and H. Leidecker, Long Term Investigation of Urethane Conformal Coating Against Tin Whisker Growth Tenting of 2mil conformal coating, IPC Tin Whisker Conference Dec. 7, 2010.

[19] T. Woodrow and E. Ledbury, "Evaluation of Conformal Coatings as a Tin Whisker Mitigation Strategy", IPC/JEDEC 8th International Conference on Pb-Free Electronic Components and Assemblies, San Jose, CA, April 18-20, 2005.
[20] T. Woodrow, E. Ledbury, Evaluation of Conformal Coatings as a Tin Whisker Mitigation Strategy, Part 2, Proceedings of the SMTA International Conference, September 24-28, 2006.
[21] T. Woodrow and E. Ledbury, "Evaluation of Conformal Coatings as a Tin Whisker Mitigation Strategy, Part 3", Symposium on Reprocessing Tin Whisker Mitigation, and Assembly Rework, University of Maryland, November 11-12б 2008.
[22] L. Woody and W. Fox, Tin Whisker Risk Management by Conformal Coating, SMT magazine, July 2014, pp. 40-58.
[23] S. Han, S. Meschter, M. Osterman and M. Pecht, Evaluation of Effectiveness of Conformal Coatings as Tin Whisker Mitigation, Journal of Electronic Materials, DOI: 10.1007/s11664-012-2179-2, July 6, 2012.
[24] L. Rohwer and J. Martin, Platelet composite coatings for tin whisker mitigation, Sandia National Laboratories Report, SAND2015-8335J, 2015
[25] P.T. Vianco, and J.A. Rejent, “Dynamic Recrystallization (DRX) as the Mechanism for Sn Whisker Development Part I: A Model”, Journal of Electronic Materials, Volume 38, Number 9, pp. 1815-1825, September 2009.
[26] P.T. Vianco, and J.A. Rejent, Dynamic Recrystallization (DRX) as the Mechanism for Sn Whisker Development. Part II: Experimental Study, Journal of Electronic Materials, Volume 38, Number 9, pp 1826-1837, September 2009.
[27] J. W. Woodcock, R. Beams, C. S. Davis, S. J. Stranick, D. U. Shah, F. Vollrath, J. W. Gilman, Interfacial damage sensing and cure monitoring in a silk-epoxy composite using a mechanochromic probe, Advanced Materials, March 19, 2017.
[28] J.Y. Chung , A. J. Nolte , and C. M. Stafford, Surface Wrinkling: A Versatile Platform for Measuring Thin-Film Properties, Adv. Mater., Vol 23, 2011, pp 349–368.
[29] Chason, E., Jadhav, N. & Pei, F. Effect of layer properties on stress evolution, intermetallic volume, and density during tin whisker formation, JOM (2011) 63: 62. https://doi.org/10.1007/s11837-011-0178-z

8. Description of appendices

Appendix Name and Title	Area	Description	Total Number of Pages
Appendix A: List of Scientific/Technical Publications	Publications	Summary of publications published as a result of the work done in the WP2213 project. (Included within the summary report file)	3
Separate files			
Appendix B: Suspension and Coating Formulation	Coating materials and coupon test methods	Describes the development details associated with the nanoparticle suspensions and the coating formulations.	19
Appendix C: Coating Evaluation Methods		Describes the detailed materials and procedures used in the evaluation of the coatings.	27
Appendix D: Coating Characterization Results	Coating properties	Provides the detailed examination of the fluid and solid materials characterization. Solid coating film evaluations included microstructure evaluation, particle dispersion, and mechanical coating characterization	52
Appendix E: Assembly Test Vehicle Coating Process	Assembly dip and spray coating process	Describes the development of the dip and spray coating processes used to coat the assemblies.	41
Appendix F: Coating Coverage Baseline Results	Assembly coating: Baseline coating dip + 50 micron spray	Provides the coverage evaluation for the dip + spray baseline coating process for PC18M, PC18M+nanosilica, PC18M+nanoalumina, PC40-UMF, PC40-UMF+nanosilica(two concentrations) coated assemblies. Coverage is qualitatively assessed with a SEM and thickness is quantified with vertical and horizontal cross – sectioning.	190
Appendix G: Coupon Whisker Testing for Baseline Coating Process		Provides the inspection results of coated coupons after high temperature and high humidity exposure that promotes whisker growth	33
Appendix H: Assembly Whisker Testing for Baseline Coating Process		Provides the inspection results of baseline coated assemblies evaluated for coverage in Appendix F after high temperature and high humidity exposure whisker testing	84

Appendix Name and Title	Area	Description	Total Number of Pages
Appendix I: Coating Coverage Layered Coating Results	Assembly coating: Enhanced layered coating dip + 25 micron spray + 25 micron spray	Provides the coverage evaluation for the dip + spray + spray enhanced layer coated assemblies for the PC18M and the PC18M+nanosilica coated assemblies. Coverage is qualitatively assessed with a SEM and thickness is quantified with vertical and horizontal cross – sectioning. It also includes microtome sectioning of QFP44 leads and FE-SEM imaging to show the thickness of the unfilled dip and nanosilica filled spray layers	70
Appendix J: Layered Coupon Whisker Testing		Provides the details of the layered coupon high temperature high humidity whisker testing with cross-sections showing unique complex tin and IMC nodule growths structures trapped under the coating.	31
Appendix K: Assembly Whisker Testing for Layered Coating Process		Provides the inspection results of baseline coated assemblies evaluated for coverage in Appendix I after high temperature and high humidity exposure whisker testing	44
Appendix L: Rework Evaluation		Provides the evaluation of coating rework on layered PC18M+nanosilica aged assemblies. The evaluation includes coating removal, part removal and replacement, and recoating. In addition, BGA boards without parts were used in a tape test adhesion study quantify the reworked coating adhesion.	162
Appendix M: Coating Tin Whisker Mitigation Modeling	Modeling	Describes the development of a coating rupture model based using both classical and finite element modeling	23
Appendix N: Simulated Power Cycling Thermal Cycling (PCTC)	PCTC	Provides the results from the extended simulated power cycling thermal cycling from +50 to +85C on the WP1753 samples to obtain a total of 6,000 cycles. Whisker growth on coated and uncoated assemblies was examined.	109
		Total	866

SERDP WP2213

Final report

Appendix A: List of Scientific/Technical Publications

Number	Publication
1	F. Dong, S. Maganty, S. Meschter, J. Cho, Effects of curing on structural evolution and mechanical properties of UV-curable polyurethane acrylate coatings, Progress in Organic Coatings, V114, January 2018, pp 58-67. https://doi.org/10.1016/j.porgcoat.2017.09.018
2	S. Meschter, SERDP/ESTCP Lead-free project overview, IPC Lead(Pb)-free Electronics Risk Management (IPC-PERM) Meeting 32, Stockholm Sweden, 4/5/2017
3	S. Meschter, SERDP ESTCP Working Session/Tin Whiskers Users Group 8-81H, Lead(Pb)-free Electronics Risk Management (IPC-PERM) Meeting 30, Melbourne, FL, 11/2/2016
4	S. Meschter , SERDP Project Update, 29th IPC PERM (Virtual Conference), Virtual Web Meeting 7/27/2016
5	S. Meschter, Tin Whisker Testing and Modeling, Circuit Insight, 6/30/2016 on-line http://www.circuitinsight.com/programs/53796.html
6	S. Meschter, J. McMahon, P. Snugovsky, M, Romansky, J. Kennedy, J. Keeping, Z. Bagheri, J. Cho, S. Majaty, D. Edwards. K. Elsken, Strategic Environmental Research and Development Program (SERDP) Layered Conformal Coating for Whisker Mitigation, 2016 SMTA International Conference on Soldering and Reliability, Toronto Canada, 5/10/2016
7	S. Maganty, F. Dong, S. J. Meschter, and J. Cho, Microstructure and Property Assessments of UV-Curable Conformal Coatings for Pb-Free Electronics, 2016 SMTA International Conference on Soldering and Reliability, Toronto Canada 5/10/2016
8	S. Maganty, S. Meschter, and J. Cho, Conformal Composite Coatings for Tin Whisker Mitigation, 17th IMAPS Symposium on Polymers for Microelectronics, Wilmington DE,4/25/2016
9	S. Maganty, M. Roma, S. Meschter, D. Starkey, M. Gomez, D. Edwards, A. Ekin, K. Elsken, J. Cho, Enhanced mechanical properties of polyurethane composite coatings through nanosilica addition, Progress in Organic Coatings, Vol 90 (April 2016), pp. 243-251
10	S. Meschter, P. Snugovsky, M, Romansky, J. Kennedy, J. Keeping, Z. Bagheri, J. Cho, D. Edwards. K. Elsken, Coverage evaluation of layered coatings for whisker mitigation, IPC PERM Council Meeting Phoenix, AZ 2/22/2016
11	S. McKeown, S. Meschter, P. Snugovsky, J. Kennedy, Z. Bagheri, J. Keeping, J. Cho, D. Edwards, K. Elsken, SERDP WP2213 Project: Conformal coat modeling for tin whisker mitigation, IPC Europe Forum Innovation for Reliability, Essen Germany 10/13/2015
12	S. Meschter, P. Snugovsky, J. Kennedy, and Z. Bagheri, Whiskers on SAC305 Soldered assemblies, IPC Europe Forum Innovation for Reliability Essen Germany 10/13/2015

Number	Publication
13	S. McKeown, S. Meschter, P. Snugovsky, J. Kennedy, Z. Bagheri, J. Keeping, J. Cho, D. Edwards, K. Elsken, Modeling of Coating Rupture by Tin Nodule and Whisker Growth, Surface Mount Technology Association (SMTA) International Conference Rosemont, Illinois 9/27/2015
14	S. Meschter and P. Snugovsky, Conformal coating whisker penetration resistance, 23nd IPC Lead-free(Pb) Electronics Risk Management (PERM) Council meeting Dayton, OH 7/22/2015
15	J. Cho, S. Meschter, and S. Maganty, Development of Polyurethane-based Conformal Coatings for Pb-free Electronics, 2015 SMTA International Conference on Soldering and Reliability Toronto, Canada 5/19/2015
16	S. Meschter, P. Snugovsky, Nanoparticle Enhanced Conformal Coating Lead Coverage Evaluation, 22nd IPC Lead-free Electronics Risk Management (PERM) Council meeting, Binghamton, NY 11/4/2014
17	J. Cho, S. J. Meschter, S. Maganty, D. Starkey, M. Gomez, D. G. Edwards, A. Ekin, K. Elsken, J. Keeping, P. Snugovsky, J. Kennedy, and M. Romansky, Development of Polyurethane Composite Coatings for Tin Whisker Mitigation, 8th International CALCE-IPC Symposium on Tin Whiskers Raleigh, NC 10/28/2014
18	M. Penafrancia Roma, S. Maganty, R. Roder, S. J. Meschter, and J. Cho, Evaluation of interfacial adhesion of polyurethane conformal coatings used for tin whisker mitigation, MS&T'14 Conference, Pittsburgh, PA 10/12/2014
19	S. Maganty, M. Roma, S. J. Meschter, and J. Cho, Nanoparticle-filled Conformal Coatings for Tin Whisker Mitigation, MS&T'14 Conference Pittsburgh, PA 10/12/2014
20	S. Meschter, J. Cho, S. Maganty, D. Starkey, M. Gomez, D. Edwards, A. Ekin, K. Elsken, J. Keeping, P. Snugovsky, and J. Kennedy, Nanoparticle Enhanced Conformal Coating for Whisker Mitigation, SMTA International 2014, Rosemount, IL 9/28/2014 (Won the Best Paper Award)
21	S. Meschter, P. Snugovsky, SERDP Whisker Project Thermal Cycling, 21st IPC Lead-free Electronics Risk Management (PERM) Council meeting, Toronto, Ontario Canada 7/22/2014
22	J. Cho, S. J. Meschter, S. Maganty, D. Starkey, M. Gomez, D. G. Edwards, A. Ekin, K. Elsken, J. Keeping, P. Snugovsky, J. Kennedy, and M. Romansky, Polyurethane Conformal Coatings Filled with Hard Nanoparticles for Tin Whisker Mitigation, SMTA International Conference on Soldering and Reliability (ICSR) Toronto Ontario Canada, 5/13/2014
23	J. Cho, S. Meschter, and S. Maganty, Characterization of Nanoparticle Enhanced Conformal Coatings for Whisker Mitigation, IPC/CALCE International Tin Whisker Symposium, Costa Mesa, CA,11/13/2013
24	S. Maganty, S. Meschter, and J. Cho, Nanoparticle-Filled Conformal Coatings for Tin Whisker Mitigation, Materials Science & Technology 2013 Conference, Montreal, Quebec, Canada,10/27/2013
25	S. Maganty, S. Meschter, and J. Cho, Conformal Composite Coatings for Tin Whisker Mitigation, 2013 Electronic Packaging Symposium, Binghamton University, Binghamton, NY 10/15/2013

Number	Publication
26	J. Cho, S. Meschter, S. Maganty, D. Starkey, M. Gomez, D. Edwards, A. Ekin, K. Elsken, J. Keeping, P. Snugovsky, and J. Kennedy, Characterization of Hybrid Conformal Coatings Used for Mitigating Tin Whisker Growth, presented at Analog Devices, Inc., Wilmington, MA, 7/25/2013
27	J. Cho, S. Meschter, S. Maganty, D. Starkey, M. Gomez, D. Edwards, A. Ekin, K. Elsken, J. Keeping, P. Snugovsky, and J. Kennedy, Characterization of Hybrid Conformal Coatings Used for Mitigating Tin Whisker Growth, SMTA 2013 International Conference for Soldering and Reliability, Toronto, Ontario Canada, 5/14/2013
28	S. Meschter and P. Snugovsky, Conformal coating panel discussion: Nanoparticle enhanced conformal coating for whisker mitigation, AIA-PERM Meeting, Salt Lake City, Utah, 2/5/2013
29	S. Meschter, P. Snugovsky, J. Keeping, J. Kennedy, E. Kosiba, D. Starkey, D. Edwards, M. Gomez, A. Ekin, K. Elsken4 J. Cho, and S. Maganty, Novel nanoparticle enhanced conformal coating for whisker mitigation, 6th International Symposium on Tin Whiskers, Henry Ford College, Loughborough University UK, 11/27/2012

FINAL REPORT
SERDP WP-2213
Appendix B: Suspension and coating formulation

Appendix B: Table of Contents

1. Introduction 1

1.1 Nanoparticle formulation background: 1

1.2 Coating formulation background: 1

2. Suspension development results and discussion 3

2.1 Bayer MaterialScience Desmodur XP2742 nanosilica suspension 3

2.2 Nanophase 11102PMA nanoalumina suspension 5

2.3 Polymaterials nanoalumina suspension 5

3. Coating formulation development 10

3.1 PC18M based coating formulation 10

3.2 PC40-UMF based coating 11

3.3 Summary of coating compositions 11

4. Summary and conclusions 13

5. Literature cited 14

Appendix B: List of Figures

Figure 1: Chemical structure of N-3300. 3

Figure 2: Nanosilica incorporation into the N3300 isocyanate through the compatibilizer [1] [Zou 2008] H. Zou, S. Wu, and J. Shen "Polymer/Silica Nanocomposites: Preparation, Characterization, Properties and Applications" Chem. Rev., 108, 3893-3957, 2008. 4

Figure 3: Chemical structure of H12 MDI. 5

Figure 4: Particle settling observations; (a) no settling after 30 minutes, (b) slurry with no dispersant, sample 0, showed settling after 45 minutes, and (c) only samples II through V show no settling after 12 hours. 7

Figure 5: Polymaterials nanoalumina suspension samples of both the D/F and F/D approaches mixed with Henkel PC18M. 9

Figure 6: Polymaterials nanoalumina suspension samples of nanoalumina with PC40-UMF. 9

Appendix B: List of Tables

Table 1: Dispersant addition levels 6

Table 2: Summary of Polymaterials nanoalumina suspension “functionalize then disperse” (F/D) mixing trials with PC18M. 8

Table 3: Summary of nanoalumina suspension “disperse then functionalize” (D/F) mixing trials with PC18M. 8

Table 4: Summary of particle concentrations in the various coating formulations. 12

Acronyms

Acronym	Definition
AFM	Atomic Force Microscope
AG	German designation for a corporation
BGA	Ball Grid Array
D/F	Disperse then functionalize
DoD	Department of Defense
F/D	Functionalize then disperse
HDI	Hexamethylene diisocyanate
MDI	Methylene diphenyl diisocyanate
NCO	Nitrogen Carbon Oxygen functionality
PM	Propylene Glycol Monomethyl Ether
PMA	Propylene Glycol Monomethyl Ether Acetate solvent
PTSI	p-Toluenesulfonyl Isocyanate
PU	Polyurethane
QFP	Quad Flat Pack Electronic Packages
SOT	Small Outline Transistor Electronic Packages
UV	Ultraviolet
VOC	Volatile organic compound

1. Introduction

1.1 Nanoparticle formulation background:

A key technical issue with nanoparticle fillers is preventing particle agglomeration by enhancing compatibility via surface modification. Unmodified silica particles are hydrophilic due to their surface hydroxyl groups, and when dispersed into a nonpolar polymer media, the particles agglomerate resulting in hazy / opaque films and reduced efficacy in increasing mechanical properties. Hydrophobic surface treatments aid in the particles compatibility with the polymer matrix, and reactive treatments provide functional groups that can covalently bond into the polymer network. The most studied compatibilizers are alkoxysilanes that react with silanols on the particles, yielding a surface that can be covalently bonded to the polymer network [1]. The reactive coupling agents are selected to have an appropriate functional group that is covalently bonded during polymerization. Another method to compatibilize the two phases is by modifying the monomers to make them compatible with the silica surface. For example, a silane-modified isocyanate from Bayer Material Science has been shown to be effective in stabilizing nanoparticles in polyurethane coatings [2].

Silica particles having a relatively large "micron size" diameter are known to impart a substantial viscosity increase to the coating that can have a major effect on the coating's application and coverage characteristics. In contrast, at low loadings (e.g., <10 wt. %), hydrophobically modified nanosilicas have been shown to have a moderate effect on the coating's viscosity and this project targeted loadings of 5 – 20 wt. % nanosilica [3].

The major advantages of silica nanoparticles in coatings is increased mechanical and barrier properties while generating transparent films due to their refractive index (ca. 1.55) being close to most polymers (ca. 1.50). Mechanical properties such as improved abrasion, scratch, and nanoindentation of coatings have been observed using a variety of polymeric binders due to the addition of the hard, nanosilica particles [1][4]. Barrier properties have also been shown to reduce gas permeation through the coating by reducing vapor solubility in the coating and decreasing free volume. Furthermore, it has been shown that the coefficient of thermal expansion (CTE) could be reduced from 75 ppm/K down to 30 ppm/K with 20 wt. % nanosilica and still maintains excellent optical properties [5].

Two key properties that could affect tin whisker growth are modulus and toughness. It has been shown that as silica nanoparticles are increased, the Young's modulus also increased [Hsieh 2010]. In the same study it was found that the presence of the silica nanoparticles always led to an increase in toughness of the epoxy polymer [6]. In another study was shown that the fracture toughness increased from 100 J/m2 for the unmodified epoxy, to 460 J/m2 for the epoxy with 13 vol.% of nanosilica [7].

The inclusion of hard, nanoparticles into the coating matrix will impede or prevent tin whiskers penetration due to their growth mechanisms being retarded by a containment effect imposed by the particles hardness and density. An increase in the coating's yield stress with the incorporation of nanosilica, allowing more stress to be applied before unrecoverable elastic flow occurs in the film. A plausible fracturing mechanism could occur at the polymer / nanosilica particle interface and particle surface, thus particle surface modification will be altered to enhance the mechanical properties of the organic / inorganic interface.

1.2 Coating formulation background:

Conformal coatings are polymeric coatings, applied at low coat-weights, to printed circuit boards to provide protection from the end-use environment. Common functions of conformal coatings are to inhibit current leakage due to environmental contamination, inhibit corrosion, improve fatigue resistance of solder joints, inhibit arcing and corona, and provide mechanical support. There are several chemistries commonly used as conformal coatings. Acrylics and silicones are easily repairable,

but have poor whisker penetration resistance [8][9][10]. Urethanes have good thermal shock resistant, are generally repairable, have good solvent resistance and can be used at temperatures up to 110 or 130°C. The polyurethane resin possesses both thermoset and thermoplastic capabilities that can potentially be adjusted to obtain the optimal whisker mitigation properties. Hybrid urethane acrylate dual cure resins cure with both ultraviolet light (UV) and moisture, and provide good solvent resistance, moderate reworkability, and fast cure. The starting point for the base coating was to select polyurethane base coatings that meet the IPC-CC-830 and MIL-I-46058 requirements for DoD equipment.

2. Suspension development results and discussion

Silica (SiO_2) and alumina (Al_2O_3) were identified as materials of interest due to their combination of physical hardness as well as their optical properties, i.e., the potential to create a suspension that, when added to an existing conformal coating system, would result in a film that was still optically transparent, at least to the degree that circuit board markings could still be read through the coating.

In order to bond the particles to the coating system it is necessary to modify their surface with chemical functionality that is compatible with the chosen coating system. The systems chosen for this project were Henkel's PC18M (moisture cure polyurethane) and PC40-UMF (dual cure, ultraviolet (UV) and moisture cure polyurethane acrylic blend), which are both compatible with the use of an isocyanate (-NCO) functionality. The challenge this presents is the requirement that the functionalization process be free of any –NCO reactive materials such as water, amines, or alcohols. This requirement significantly limits the selection of potential reagents.

2.1 Bayer MaterialScience Desmodur XP2742 nanosilica suspension

Desmodur XP2742 is an experimental product developed by Bayer MaterialScience AG. It was designed as an additive to impart scratch and abrasion resistance to polyurethane based coating systems [1] [Zou 2008] H. Zou, S. Wu, and J. Shen "Polymer/Silica Nanocomposites: Preparation, Characterization, Properties and Applications" Chem. Rev., 108, 3893-3957, 2008.

[2]. The material is made by modifying Desmodur N-3300, which is an aliphatic polyisocyanate trimer based on hexamethylene diisocyanate (HDI) (see Figure 1). The synthesis of Desmodur XP2742 is cover by US patent 2009/0124727A1 [11].

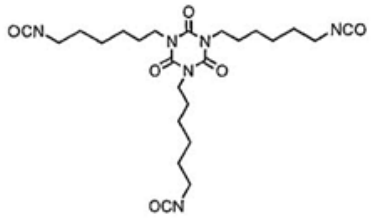


Figure 1: Chemical structure of N-3300.

Desmodur XP2742 is synthesized using specialized silane coupling agents; molecules that have isocyanate functional groups on one end and silanol groups on the other. For Desmodur XP2742, the isocyanate functional groups are initially reacted onto a fraction of the available –NCO sites on the N-3300, followed by the addition of silica sol nanoparticles with a mean diameter, D50, of 15 nm and 90 percentile particle diameter, D90, of 20.8 nm [1] [Zou 2008] H. Zou, S. Wu, and J. Shen "Polymer/Silica Nanocomposites: Preparation, Characterization, Properties and Applications" Chem. Rev., 108, 3893-3957, 2008.

[2].

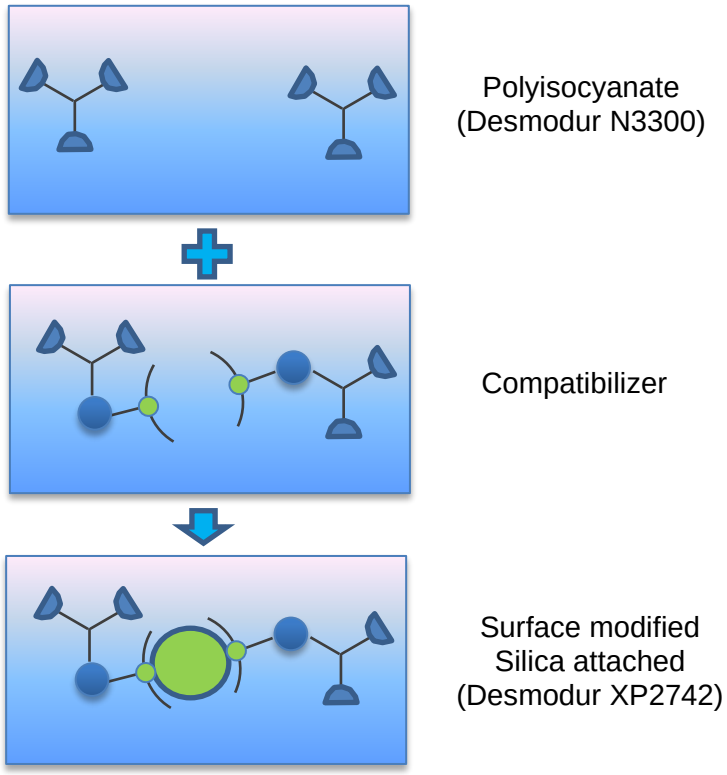


Figure 2: Nanosilica incorporation into the N3300 isocyanate through the compatibilizer [1**] [Zou 2008] H. Zou, S. Wu, and J. Shen "Polymer/Silica Nanocomposites: Preparation, Characterization, Properties and Applications" Chem. Rev., 108, 3893-3957, 2008.**

[2].

The product XP2742 is supplied at 70% by weight in butyl acetate. The nominal product specifications are:

NCO Content: 9%

Alumina:	18% by weight, as supplied
	26% by weight, solids/solids
Viscosity:	~500 mPas
Particle Size:	5 to 50 nm (90% < 21 nm, 50% < 15 nm)

The advantages of this product include excellent stability, shelf life, and ease of use. It performs very well, resulting in PC18M and PC40-UMF based films with excellent distributions of silica particles. The disadvantage of this approach is that the addition of silica brings a certain amount of the HDI isocyanate along with it. And while this HDI functionality easily reacts with both the PC18M and PC40-UMF systems, it brings physical properties that are different from the base formulations, which may or may not be desirable. (Note: During the course of the characterization and spray coating experiments, additional XP2742 was needed and another batch was ordered. It was designated NNN2835 and is supposed to be equivalent to XP2742)

2.2 Nanophase 11102PMA nanoalumina suspension

Nanophase Technologies Corporation is a manufacturer of metal oxide particles in a variety of particle diameters. Their products are supplied in either powdered form or dispersed in solvent. Of particular interest is the aluminum oxide (Al_2O_3) with an advertised diameter of 40 nm. Upon inquiry Nanophase indicated they could supply a 40 nm isocyanate functionalized aluminum oxide particles dispersed in 1-methoxy 2-propanol acetate (PMA). In addition to the opportunity to evaluate a different particle material, it was also an opportunity to develop an additive with a higher loading of nanoparticles, relative to the isocyanate content.

Nanophase supplied the 11102PMA material and numerous technical issues were identified. From a user standpoint, the most problematic was unexpected gelation of the coating system after the addition of the 11102PMA. At first the problem was attributed to the selection of a standard grade of PMA rather than a special low water version. Low water versions are recommended because the residual moisture will react with isocyanates. However, the use of low water PMA did not completely alleviate the problem. It is known that alumina is quite hygroscopic, and there was concern that the moisture on the alumina might be reacting, though this could not be proven. The trials that were run with the 11102PMA resulted in films with significant particle agglomerations, and the particles were not well adhered to the polymer matrix.

These results led to a more detailed discussion of Nanophase's approach to functionalization. The coupling agent used by Nanophase was 3-(triethoxysilyl)propyl isocyanate. The reaction of this coupling agent with the hydroxyl functionality of the aluminum oxide liberates ethanol, which likely reacted with the available isocyanate, thereby eliminating the functional groups. This explains the poor adhesion found between the alumina to the polymer matrix, and the short pot life which was due the gelation contribution by residual ethanol.

Following this discovery, Nanophase declined to provide further resources to develop functionalized alumina.

2.3 Polymaterials nanoalumina suspension

A search was conducted to identify potential methods to functionalize alumina, and the following paper described a "direct functionalization" method by Eroglu [12] that would be very useful.

Boehmite is an oxide of aluminum very closely related to the alumina. The paper describes mixing the alumina and isocyanate in the presence of a catalyst, and allowing the reaction to proceed for five hours. For compatibility with the coating systems, it was requested the alumina be dispersed in PMA, therefore it was first necessary to evaluate the solubility of various isocyanates in PMA. Aromatic isocyanates were the first choice, since they are known to exhibit the highest isocyanate reactivity; however it was found that these were not soluble in PMA. Although there were a variety of potential aliphatic isocyanates to choose from, hydrogenated H12 methylene diphenyl diisocyanate (MDI) (Figure 3) was selected due to its solubility in PMA, reasonable reactivity, and commercial availability.

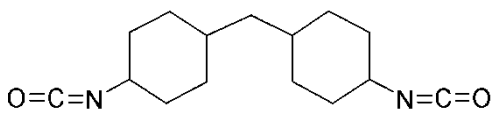


Figure 3: Chemical structure of H12 MDI.

Two routes were taken in the initial synthesis. The first used NanoArc Al-2405, alumina powder with a claimed 40 nm particle size. The powder was initially dried at high heat and vacuum to remove

excess moisture, then 25 weight percent was added to PMA and mixed in a high efficiency stirrer. H12 MDI and tin catalyst were then added and the mixture was heated to 80°C and stirred for 5 hours. The resulting material was supplied for analysis as WTA940.

Samples of WTA940 were centrifuged and washed three times with PMA and the resulting solids were analyzed by IR-spectroscopy. This analysis suggested that limited isocyanate functionality was created, though urea groups were identified. Urea could potentially hydrogen bond with the PC18M or PC40-UMF polymer. The isocyanate on the particle would result in the particle anchoring to the urethane matrix that was desired.

The second synthesis used NanoArc Al-2425, a product from Nanophase consisting of 40 nm alumina pre-dispersed in PMA. NanoArc Al-2425 also contains a proprietary dispersant. Since this was already dispersed, the process involved adding catalyst and isocyanate at levels equivalent to the WTA940 development, and then stirring under heat for five hours. This sample was supplied for analysis as Al-2405. The material did not yield separate particles after the centrifuging and as a result no IR work was performed.

Following the evaluation of films made from the above dispersions, a second round of synthesis was undertaken. This effort was directed at improving the relative dispersion of the particles in the finished film. Toward this end, a literature search was undertaken to find an appropriate dispersant that was both soluble in PMA and non-reactive to isocyanate species. Work was discovered that identified Paraloid B99N as a dispersant that worked with aluminum oxide in PMA. Paraloid B99N is a block co-polymer of methyl and butyl methacrylate.

In order to estimate the amount of dispersant that might be need, a sedimentation test was developed. Varying levels of dispersant (Table 1) were added to a 5 weight percent solution of alumina in PMA. The solutions were allowed to sit and the amount of settling was noted over time. As seen in Figure 4, all solutions were stable for thirty minutes, but after 45 minutes the sample with no dispersant showed signs of separation. After 12 hours, only samples II to V showed no signs of settling.

Table 1: Dispersant addition levels

#	Wt.% Paraloid B-99N
0	0
I	3
II	7
III	15
IV	25
V	35

(a)



(b)



(c)

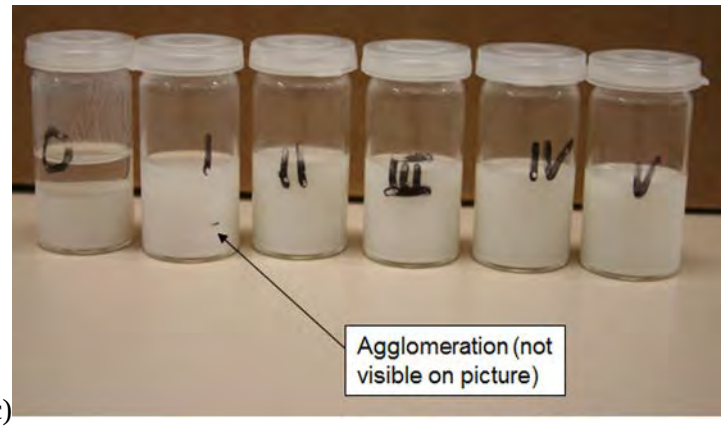


Figure 4: Particle settling observations; (a) no settling after 30 minutes, (b) slurry with no dispersant, sample 0, showed settling after 45 minutes, and (c) only samples II through V show no settling after 12 hours.

This work was repeated with 20% and 30% weight solutions of alumina. At 20% samples II through V remained stable for several hours after mixing, but the 30% weight samples were not stable for more than one hour.

From this work the conclusion was made that it would be reasonable to work with alumina levels in the 8% to 16% range, and dispersant levels in the 7% to 25% range.

Next, two functionalization approaches were taken. In the first approach, particles would be first mixed with the PMA and functionalization would be carried out, followed by the addition of the dispersant (F/D). In the second approach, the dispersant would be added prior to the functionalization step (D/F).

The dispersions that were made were further mixed with the Henkel PC18M liquid resin and cured into a film for analysis. Table 2 and Table 3 summarize the various mixtures that were made. Figure 5 shows samples of both the F/D and D/F approaches mixed with Henkel PC18M. The D/F approach showed much less settling and separation.

Table 2: Summary of Polymaterials nanoalumina suspension "functionalize then disperse" (F/D) mixing trials with PC18M.

WTA995 & WTA997	% Alumina	8	8	8	16	16	16
	% Dispersant (based on Al)	7	15	25	7	15	25
Al-Dispersion (g)	**Stock solution**	4.13	4.13	4.13	4.13	4.13	4.13
	Dispersant	0.07	0.15	0.25	0.07	0.15	0.25
	PMA	8.30	8.22	8.12	2.05	1.97	1.87
Composition of Al-Dispersion (%)	**Alumina**	8.0	8.0	8.0	16.0	16.0	16.0
	Dispersant	0.6	1.2	2.0	1.1	2.4	4.0
	OCN + Sn	1.0	1.0	1.0	2.1	2.1	2.1
	PMA	90.4	89.8	89.0	80.8	79.5	77.9
Resin Dispersion for Curing (g)	**Σ Al-Dispersion**	12.50	12.50	12.50	6.25	6.25	6.25
	Hysol PC18M	16.06	17.13	18.47	16.06	17.13	18.47

Table 3: Summary of nanoalumina suspension "disperse then functionalize" (D/F) mixing trials with PC18M.

WTA996	% Alumina	8	8	8
	% Dispersant (based on Al)	15	15	15
	% Hysol PC18M in cured film	93	87	80
Al-Dispersion (g)	**OCN + Sn**	0.13	0.13	0.13
	Dispersant	0.15	0.15	0.15
	PMA	11.22	11.22	11.22
Composition of Al-Dispersion (%)	**Alumina**	8.0	8.0	8.0
	Dispersant	1.2	1.2	1.2
	OCN + Sn	1.0	1.0	1.0
	PMA	89.8	89.8	89.8
Resin Dispersion for Curing (g)	**Σ Al-Dispersion**	12.50	12.50	12.50
	Hysol PC18M	34.01	17.13	10.24

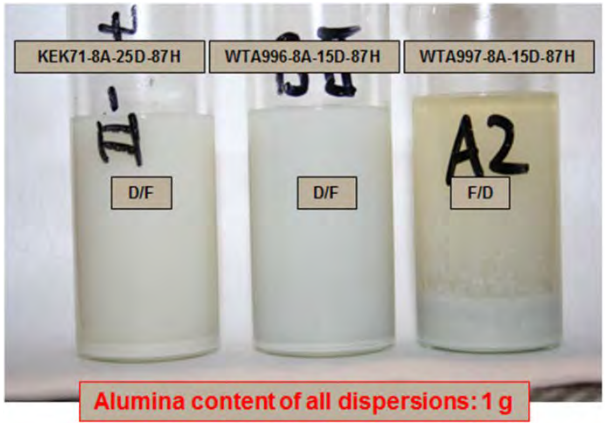


Figure 5: Polymaterials nanoalumina suspension samples of both the D/F and F/D approaches mixed with Henkel PC18M.

It was further noted that the composition of PC18M includes a significant amount (up to 30%) of non-polar solvents such as xylene and ethylbenzene. It is expected that these solvents would have a negative effect on the solubility and stability of mixtures made with a PMA based dispersion. Since it was also noted that the PC40-UMF material contained no solvent, mixtures of the dispersions were made with PC40-UMF. Figure 6 shows that these mixtures maintained much better stability (note the lines highlight the settled height).

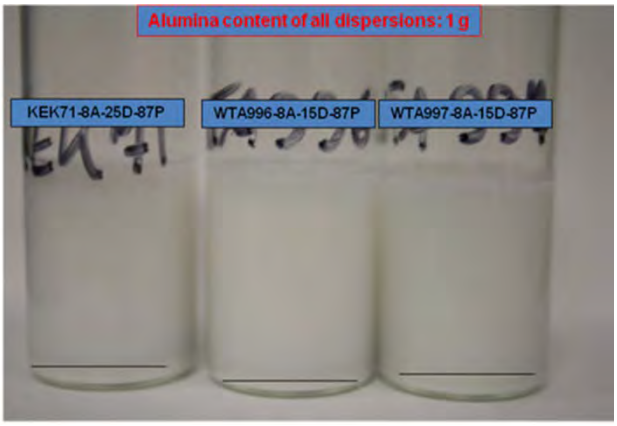


Figure 6: Polymaterials nanoalumina suspension samples of nanoalumina with PC40-UMF.

3. Coating formulation development

The conformal coating formulations were prepared by mixing polyurethane resin with a nanoparticle suspension. High-speed dispersion or sonication was employed to facilitate particle dispersion in the suspension medium. The polyurethane (PU) resin system was chosen because it is commonly used in Department of Defense systems and can be formulated to have a wide range of liquid viscosity and solid physical properties. The base coatings were initially screened for jet fuel fluid compatibility. It was also desirable to have two coatings that could use the same nanoparticle suspensions to allow an easier comparison between formulations.

The first base coating was moisture curable solvent-based polyurethane previously qualified to MIL-I-46058 [13] and conforms to IPC-CC-830 [14] (PC18M, from Henkel). It is an established coating with a nominal viscosity of 300 cps and can be readily thinned to lower viscosities with a solvent. The moisture cure isocyanates in the PC18M will bind to the nanosilica particles which were designed to have isocyanate functionality.

The second coating was an ultraviolet (UV) moisture dual cure low volatile organic compound (VOC) that conforms to IPC-CC-830 [14] (PC40-UMF, from Henkel). The material is a polyurethane acrylic blend with UV reactive sites and isocyanate functionality. The isocyanate moisture cure ensures cure in UV shadowed areas under parts. The moisture cure isocyanates in the PC40-UMF will bind to the nanosilica particles which were designed to have isocyanate functionality.

The nanoparticle suspensions selected for incorporation into the coatings were: (1) Desmodur XP2742 suspension (N3300 Hexamethylene diisocyanate, HDI, trimer with 20 nm mean diameter functionalized silica nanoparticles) from Covestro (formerly Bayer MaterialScience (Pittsburgh, PA)) and (2) X11102PMA (Nanophase Technologies, Romeoville, IL) containing non – functionalized alumina nanoparticles (40 nm mean diameter in methylene diphenyl diisocyanate (MDI) and propylene glycol methyl ether acetate (PMA)). The functionalized nanosilica covalently bond to with the polyurethane during curing while the non – functionalized nanoalumina are not chemically bound to the resin.

3.1 PC18M based coating formulation

The PC18M based formulation preparation details are also described in [15] [16]. The PC18M was mixed with both the nanosilica and nanoalumina particle suspensions.

The silica nanoparticles were dispersed in a hexamethylene diisocyanate (HDI) system (Desmodur® XP2742, from Bayer MaterialScience) that was chemically compatible with the base PU systems (see Section 2.1). With the addition of XP2742 to the PC18M, it was found that the cure rate was reduced. As a result, an accelerant was added (Dabco T 12) such that a nominal cure time of two hours at 60°C/60%RH would be obtained. A version of unfilled PC18M with the Dabco T 12 accelerant (designated PC18M-mod) was formulated for the baseline coating testing. During the layered testing developed later in the project, the commercially available non – modified PC18M polyurethane was used. PC18M based coatings with a 10 to 50 percent XP2742 suspension range were used.

The alumina nanoparticles were dispersed in propylene glycol methyl ether acetate (PM acetate) suspension (X11102PMA, from Nanophase) that is also compatible with the base PU resins (see 2.2). A four to 40 percent X11102PMA suspension range was used. When the X11102PMA was initially mixed with the PC18M, the pot life gel time was very short so some p-Toluenesulfonyl Isocyanate (PTSI) was added to scavenge residual moisture in the suspension. As was previously mentioned, there was also residual alcohol in the suspension that contributed to a short gel time and a loss of particle functionality (see 2.2). The PTSI increased the pot life sufficiently to allow sufficient time to send the material to Celestica and coat the assemblies.

For low viscosity dip coating, the PC18M could be diluted as low as 30 cps with the Henkel AC0305 solvent and still form a continuous film upon curing.

3.2 PC40-UMF based coating

The second formulation, PC40-UMF-UMF from Henkel, was compatible either the nanosilica or nanoalumina suspensions, but was only mixed with nanosilica.

For the initial dip coating, the PC40-UMF could be diluted as low as 30 cps with the Henkel AC0305 solvent and still form a continuous film upon curing.

3.3 Summary of coating compositions

Several combinations of polyurethane (PU – PC18M) and polyurethane acrylate (PUA – Henkel PC40-UMF) were mixed with nanoparticle suspensions to obtain a range of properties. Since the nanosilica suspension has N3300 isocyanate, special mixtures of PC18M or PC40-UMF and N3300 were formulated to provide comparative resin properties without the functionalized nanosilica.

A summary of the coating formulations is given in Table 4.

Table 4: Summary of particle concentrations in the various coating formulations.

No.	Coating	wt% isocyanate in suspension (N3300 HDI trimer)	wt% nanoparticle after cure	Comment
1	PC18M-mod	0.00%	0	
2	PC18M+10%XP2742	5.18%	3.50% nanosilica	
3	PC18M+20%XP2742	10.36%	6.74% nanosilica	
4	PC18M+30%XP2742	15.54%	9.75% nanosilica	
5	PC18M+50%XP2742	25.90%	15.17% nanosilica	
6	PC18M+5.18%N3300	5.18%	0	Same as 2 without nanosilca
7	PC18M+10.36%N3300	10.36%	0	Same as 3 without nanosilca
8	PC18M+15.54%N3300	15.54%	0	Same as 4 without nanosilca
9	PC18M+25.90%N3300	25.90%	0	Same as 5 without nanosilca
10	PC18M+4%11102PMA	Not applicable	2.44% nanoalumina	
11	PC18M+12%11102PMA	Not applicable	7.56% nanoalumina	
12	PC18M+20%11102PMA	Not applicable	13.04% nanoalumina	
13	PC18M+40%11102PMA	Not applicable	28.57% nanoalumina	
14	PC40-UMF	0.00%	0	
15	PC40-UMF+10%XP2742	5.18%	1.88% nanosilica	
16	PC40-UMF+30%XP2742	15.54%	6.0% nanosilica	
17	PC40-UMF+50%XP2742	25.90%	10.7% nanosilica	
18	PC40-UMF+5.18%N3300	5.18%	0	Same as 15 without nanosilca
19	PC40-UMF+15.54%N3300	15.54%	0	Same as 16 without nanosilca
20	PC40-UMF+25.9%N3300	25.90%	0	Same as 17 without nanosilca
21	100%N3300	100.00%	0	
22	100%XP2742	51.80%	26% nanosilica	

4. Summary and conclusions

The advantages of the XP2742 include excellent stability, shelf life, and ease of use. It performs very well, resulting in PC18M and PC40-UMF based films with excellent distributions of silica particles. The disadvantage of this approach is that the addition of silica brings a certain amount of the HDI isocyanate along with it. And while this HDI functionality easily reacts with both the PC18M and PC40-UMF systems, it brings does bring physical properties that are different from the base formulations, which may or may not be desirable.

The nanoalumina particle suspension made by Nanophase has adsorbed moisture or alcohol which is reacting with the isocyanate and significantly reducing pot life. Nanophase was not interested in doing further research to improve compatibility with the isocyanate at this time. In addition, the Polymaterials efforts to develop a nanoalumina suspension were largely unsuccessful. Some characterization and spray coating was eventually performed, but further work with the nanoalumina filled coating was limited by pot life issues and material availability.

5. Literature cited

[1] [Zou 2008] H. Zou, S. Wu, and J. Shen "Polymer/Silica Nanocomposites: Preparation, Characterization, Properties and Applications" Chem. Rev., 108, 3893-3957, 2008.

[2] O. Pyrlik, A. Nennemann, R. Maleika, Bayer Materials, "Nanoparticle-modified coating raw materials for high performance PU coatings," Eurocoat 2009, Barcelona, Spain, Sept. 29, 2009 – October 1, 2009.

[3] [Zhou 2002] S-X Zhou, L-M Wu, J. Sun, and W-D Shen "Effect of Nanosilica on the Properties of Polyester-based Polyurethane", J. Applied Poly. Sci., 88, 189-193, 2003.

[4] [Ranjbar 2010] Z. Ranjbar and S. Rastegar "Nano mechanical properties of an automotive clear-coats containing nano silica particles with different surface chemistries", Prog. Org. Coat., 2010, Available online 13 December 2010.

[5] [Winkler 1999] Winkler, "New UV-Curable Adhesive with Variable Refractive Index Based on Inorganic-Organic Nanocomposites (Nanomer R)for Optical Components" 9th Cimtec – World Ceramics Conference, 1999.

[6] [Hsieh 2010] Hsieh, The mechanisms and mechanics of the toughening of epoxy polymers modified with silica nanoparticles. Polymer. 2010.

[7] [Kinloch 2007] A.J. Kinloch, B.B. Johnsen, R.D. Mohammed, A.C. Taylor, and S. Sprenger "Toughening mechanisms in novel nano-silica epoxy polymers". Proceedings of the 5th Australian Congress on Applied Mechanics, 441-446, Brisbane, Australia 2007.

[8] [Woodrow 2005] T. Woodrow and E. Ledbury, "Evaluation of Conformal Coatings as a Tin Whisker Mitigation Strategy", IPC/JEDEC 8th International Conference on Pb-Free Electronic Components and Assemblies, San Jose, CA, April 18-20, 2005.

[9] [Woodrow 2006] T. Woodrow and E. Ledbury, "Evaluation of Conformal Coatings as a Tin Whisker Mitigation Strategy, Part 2", SMTAI, Sept. 2006.

[10] [Woodrow 2008] T. Woodrow and E. Ledbury, "Evaluation of Conformal Coatings as a Tin Whisker Mitigation Strategy, Part 3", Symposium on Reprocessing Tin Whisker Mitigation, and Assembly Rework, University of Maryland, November 11-126 2008

[11] A. Nennemann, Bayer MaterialScience Ag, Nanoparticle-modified polyisocyanates, US patent 20090124727 A1, May 14, 2009.

[12] G. Eroglu "Isocyanate Functionalization of Nano-Boehmite for the Synthesis of Polyurethane Organic-Inorganic Hybrid Materials" Master of Science Thesis in Polymer Science and Technology Middle East Technical University (Turkey) January 2011.

[13] MIL-I-46058, Insulating Compound, Electrical (for Coating Printed Circuit Assemblies), Military Specification, July 1972. Note that the Qualified Providers List (QPL) is still active, but MIL-I-46058 is inactive for new designs.

[14] IPC-CC-830, Qualification and Performance of Electrical Insulating Compound for Printed Wiring Assemblies, IPC-Association Connecting Electronics Industries, Bannockburn, Illinois, USA, Sept. 2008.

[15] J. Cho, S. Meschter, S. Maganty, D. Starkey, M. Gomez, D. Edwards, A. Ekin, K. Elsken, J. Keeping, P. Snugovsky, and J. Kennedy, Characterization of Hybrid Conformal Coatings used for Mitigating Tin Whisker Growth, SMTA International Conference on Soldering and Reliability, Toronto, Ontario, Canada, May 14-17, 2013.

[16] J. Cho, S. Meschter, S. Maganty, D. Starkey, M. Gomez, D. Edwards, A. Ekin, K. Elsken, J. Keeping, P. Snugovsky, J. Kennedy, and M. Romansky, Polyurethane Conformal Coatings Filled with Hard Nanoparticles for Tin Whisker Mitigation, SMTA International Conference on Soldering and Reliability, Toronto, Ontario, Canada, May 13-15, 2014.

[17] Appendix E of the current report: Assembly Test Vehicle Coating Processes.

[18] S. Meschter and P. Snugovsky, SERDP WP1753 Final Report: Tin whisker testing and modeling, November 2015.

SERDP WP2213
Final Report
Appendix C: Coating evaluation methods

Appendix C: Table of Contents

1. Liquid coating characterization methods 1

1.1 Viscosity 1

1.2 Contact angle 1

1.3 Gap flow 1

1.4 Dynamic light scattering 2

1.5 Thermogravimetric analyzer 2

1.6 Photo differential scanning calorimeter 2

2. Coating materials, cure, and sample fabrication processes 3

2.1 Coating materials and cure 3

2.1.1 PC18M based coating materials 3

2.1.2 PC40-UMF based coating materials 3

2.1.3 Reference coatings (Parylene, 1B31, and UV40) 3

2.2 Coating processes 4

2.2.1 Coupon coating application 4

2.2.2 Test vehicle assemblies 5

3. Solid coating microscopic examination 6

3.1 Coating application method overview 6

3.2 Film structure and particle distribution using AFM, cross-sectioning, FE-SEM imaging, and TEM imaging. 6

3.2.1 AFM 6

3.2.2 Cross-sectioning 6

3.2.3 FE SEM 6

3.2.4 CryoTEM 7

3.3 Fourier transform infrared (FTIR) spectroscopy 7

4. Solid coating mechanical evaluation methods 8

4.1 Fluid compatibility 8

4.2 Glass transition temperature 9

4.3 Coefficient of thermal expansion 9

4.4 Water vapor transmission rate 9

4.5 Hydrolytic stability 10

4.6 Thermal shock 10

4.7 Nanoindentation hardness and modulus 10

4.8 Tensile test 10

4.9 Adhesion 10

5. Whisker mitigation effectiveness evaluation 13
5.1 Coating coverage and whisker inspection methods 13
5.1.1 Optical Inspection 13
5.1.2 SEM Inspection 13
5.1.3 Cross-sectioning 14
5.2 Whisker test methods 14
5.2.1 Cantilever beam coupon test procedure 14
5.2.2 SAC+REE Coupon test procedure 15
5.2.3 Slotted flat coupons 16
5.2.4 Assembly test vehicles 18
5.2.5 Assembly coverage evaluation method 20
5.2.6 Assembly whisker test procedure 21
6. Literature cited 23

Appendix C: List of Figures

Figure 1: Parallel plate glass slide coating fill test; (A) side view of glass slides with spacers and (B) immersion of sample into coating bath. 2

Figure 2: Board coupon. 9

Figure 3: MTS Mini Bionix tester used for the four point bend testing 11

Figure 4: Four point bend sample schematic. The four mandrels are 2-mm diameter 11

Figure 5: Schematic diagram of the four point bend test force versus deflection output. The force regimes are: (1) elastic loading, (2) crack initiation, (3) interface delamination, and (4) steady state crack growth. 12

Figure 6: Four point bend sample fabrication and fracture path. 12

Figure 7: Sample layer thicknesses. 12

Figure 8: Cantilever beam whisker coupon; (A) coated cantilever beam, and (B) cantilever beam installed in fixture. 15

Figure 9: EDX analysis of $CeSn_3$ intermetallic in master alloy cross-section. 16

Figure 10: SAC+REE whisker coupon (dimensions in mm). 16

Figure 11: Slotted flat whisker test coupon, mm (inch). 17

Figure 12: Flat slotted coupon panel layout, mm (inch). 18

Figure 13: SOT board. 19

Figure 14: QFP Board. 19

Figure 15: BGA Board. 20

Figure 16: Example of assembly coating integrity and tin whisker evaluation conditions 22

Figure 17: Screening test showing coating cracks in PC18M+30%XP2742 after 1,610 thermal shock cycles from -55 to +85°C (three cycles per hour) 22

Appendix C: List of Tables

Table 1: Liquid coating measurements 1
Table 2: Mechanical evaluation of cured coating samples. 8
Table 3: Four point bend test parameters. 11
Table 4: Test vehicles for coverage evaluation and whisker testing 13

Acronyms

Acronym	Definition
ATC	Accelerated Temperature or Thermal Cycling
AFM	Atomic Force Microscope or Microscopy
APTES	(3-Aminopropyl)triethoxysilane
BGA	Ball Grid Array
Cryo	Cryogenic
DLS	Dynamic Light Scattering
DSC	Differential Scanning Calorimeter
EDX	Energy Dispersive X-ray
FE-SEM	Field Emission Scanning Electron Microscope or Microscopy
FTA	First Ten Angstroms
FTIR	Fourier Transform Infrared
HALT	Highly Accelerated Life Test
HTE	High Temperature Elongation
IPC	IPC Association Connecting Electronics Industries
JEOL	Scanning electron microscope manufacture
JESD	Joint Electronic Semiconductor Device council
MTS	Material Test Systems (MTS Systems Corporation)
Photo-DSC	Photo Differential Scanning Calorimeter
PLCC	Plastic Leaded Chip Carrier Electronic Package
PU	Polyurethane
QFP	Quad Flat Pack Electronic Packages
REE	Rare Earth Element (Note only RE is used in a chemical formula)
RH	Relative Humidity
RVT	Room temperature vulcanizing silicone rubber
SAC	Tin(Sn) – Silver (Ag) – Copper(Cu) solder alloy
SEM	Scanning Electron Microscope or Microscopy
SERDP	Strategic Environmental Research and Development Program
SOT	Small Outline Transistor Electronic Packages
TA	Thermomechanical Analyzer
TEM	Transmission Electron Microscope or Microscopy
TGA	Thermogravemetric Analyzer
TMA	Thermomechanical Analyzer
TQFP	Thin Quad Flat Pack Electronic Packages

1. Liquid coating characterization methods

A summary of the typical liquid coating tests is given in Table 1.

Table 1: Liquid coating measurements

Parameter	**Test method**
Viscosity	Brookfield (small sample adaptor)
Contact angle	Goniometer contact angle of a coating drop on a glass slide
Gap flow	Parallel plate glass slide dip test
Particle size	Dynamic light scattering
Solvent evaporation	Thermal gravimetric analyzer (TGA)
UV Cure	Photo Differential Scanning Calorimeter (DSC)

1.1 Viscosity

The viscosity measurements used a Brookfield RVT DV-II with the small sample adaptor to minimize consumption of coating material. Spindle 18 was used at speeds ranging from 2.5 to 50 rpm depending upon the coating viscosity range. The tests were performed at room temperature.

1.2 Contact angle

A qualitative evaluation of the liquid-vapor surface tension measurement was obtained by measuring the contact angle of the coating on a glass slide. The measurement was performed at 25 °C using a FTA200 by First Ten Angstroms (FTA) video capture goniometer using a 25 gage dispense needle 25.4 mm long. Video goniometer provides video-based contact angle and surface tension measurements. Prior to performing the measurement, the coating viscosity was measured and the glass slide was cleaned with acetone. The contact angles of manually dispensed drops were measured at 30 seconds and one minute.

1.3 Gap flow

The parallel plate glass slide dip test (see Figure 1) was used evaluate coating flow into a narrow gap. Microscope slides 25 by 75 mm were spaced apart on each end with metal shims and taped together. The gap was approximately 50 mm wide by 25 mm deep at the thickness determined by the shims. The immersion test was performed with the sample oriented at approximately 45° at an immersion velocity of 76 mm/minute (the minimum machine velocity). The ability of the coating to flow into the gap without void formation was evaluated.

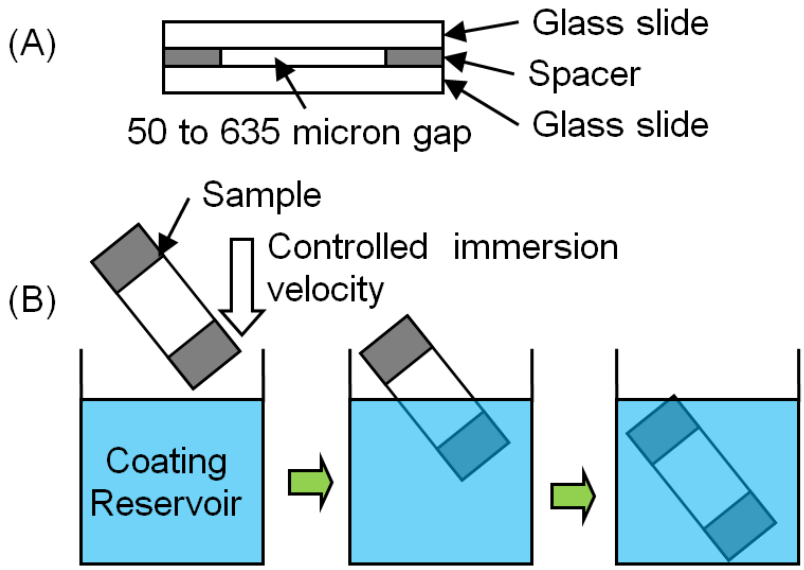


Figure 1: Parallel plate glass slide coating fill test; (A) side view of glass slides with spacers and (B) immersion of sample into coating bath.

1.4 Dynamic light scattering

Dynamic light scattering (DLS) techniques using a Malvern Zetasizer Nano-ZS (Malvern Instruments Ltd., U.K.) were utilized to analyze the nanoparticle suspensions prior to integrating them into the polyurethane base resin to quantify the particle size and distribution. This technique can characterize the particle size ranges from ~ 1 nm to 6 microns.

1.5 Thermogravimetric analyzer

A thermogravimetric analyzer (TGA) TA TGA-500 was used to determine the time required for solvent evaporation from the coating at room temperature. A liquid coating film 75 to 125 microns thick using the drawn down method was used.

1.6 Photo differential scanning calorimeter

A photo differential scanning calorimeter (Photo-DSC) was used to verify the cure of the PC40-UMF family of coatings with the nanoparticles. The instrument is a Netzsch DSC 204 F1 with Delolux 04 using an Hg bulb, a 320-500nm UVA+ Blue filter, and a 2-mm aperture operating in air. The sample was a 10 mg sample in open aluminum pan that was tested isothermally at 25 °C. The samples were exposed 3 consecutive times for 45 seconds with 3 minutes between exposures. The resultant peak was integrated to obtain the exothermal energy during the cure.

2. Coating materials, cure, and sample fabrication processes

The mechanical characteristics were obtained for a number of coating and nanoparticle suspensions combinations developed in Appendix B [1] and some reference coatings commonly used in industry. The mechanical evaluations required various cured coating sample geometries. An overview of the coating materials, coating cure and sample preparation process is given next.

2.1 Coating materials and cure

Microstructural and mechanical properties were obtained for the base polyurethane with increasing amounts of nanoparticles and determine the optimum nanoparticle concentration(s) for assembly testing.

2.1.1 PC18M based coating materials

PC18M polyurethane was mixed with both nanosilica and nanoalumina suspensions (see Appendix B [1]). PC18M-mod, PC18M + 20%XP2742 nanosilica and PC18M + 20%11102PMA nanoalumina were eventually selected for spray coating assemblies in the baseline coating test. The PC18M and the PC18M + 20%XP2742 were then selected for the enhanced coverage layered assembly testing.

Unless otherwise noted, all PC18M family samples were air dried for a minimum of 30-45 minutes and then cured for a minimum of two hours at 60 ºC (140 ºF) in an oven having a minimum relative humidity of 30 percent in accordance with the PC18M datasheet.

2.1.2 PC40-UMF based coating materials

PC40-UMF polyurethane acrylate was mixed with the nanosilica suspension. The PC40, PC40-UMF + 10%NNN2835 and the PC40-UMF + 30%NNN2835 were selected for assembly level testing. (Note: NNN2835 is equivalent to XP2742 but processed in different batch at Covestro) The PC40-UMF based materials were not used in the enhanced layer coating evaluation due to interlayer adhesion issues. NNN2835 nanosilica

The PC40-UMF base material cure schedule had to be modified to account for the solvent in the nanoparticle suspension. For the mechanical pull test, nanoindentation, and SAC+REE coupon samples was: (1) initial solvent evaporation for 30 minutes, (2) UV exposure using Hg bulb, and (3) moisture cure 60°C/60%RH for two hours. In some cases, a longer high humidity cure was used or an extended room temperature hold was used after high humidity curing to ensure complete curing prior to performing certain testing.

2.1.3 Reference coatings (Parylene, 1B31, and UV40)

Several commercially available coatings were also tested for comparison. Prior testing has shown Parylene C ™ to be among the best coatings for coverage and whisker penetration resistance and an acrylic coating was selected because it had lower whisker mitigation performance. The reference coatings are MIL-I-46058 and IPC-CC-830 qualified [3] [4]. (Note: using any qualified coating significantly improves whisker mitigation over not having a coating.)

2.1.3.1 Parylene

For reference, samples of Parylene™ C and Parylene™ C with an Adpro+ adhesion promotion under layer were coated. The Parylene™ C is a thermoplastic that is vacuum deposited.

The Parylene™ C tensile test specimens were formed by depositing the coating onto 12.5 mm wide stainless steel shims using DiX (Chiba, Japan) Parylene™ C dimer at BAE Systems in Ft. Wayne, Indiana.

The Parylene™ C and Parylene™ C with an Adpro+ whisker test samples were coated to a nominal thickness of 25 microns after plasma etching at using SCS Parylene™ C dimer at Specialty Coating Systems in Indianapolis, Indiana.

2.1.3.2 Humiseal 1B31

The Humiseal 1B31 is a noncross-linked acrylic coating manufactured by Chase Corporation. The coating is thinned to the desired viscosity and applied. The solvent is evaporated to solidify the film. The coating was deposited using an automated spray machine to a nominal thickness of 25 to 75 microns as measured on a flat surface, allowed to air dry overnight and cured according to the manufacturer's recommendations.

2.1.3.3 Humiseal UV40

The Humiseal UV40 was used to coat the WP1753 test vehicles in the PCTC cycling test [5]. The UV40 is a VOC free cross-linked urethane acrylic blend coating that has a dual UV and humidity cure. The UV40 is manufactured by Chase Corporation. It is not solvent thinned. Any UV light shadowed areas cure with humidity over time. The coating was spray coat deposited using an automated spray machine to a nominal thickness of 25 to 75 microns as measured on a flat surface. The coating was then UV cured in accordance with the manufacturer's recommendations.

2.2 Coating processes

Coupons and electronic assemblies were coated for evaluation. The coupons were used for mechanical properties evaluation and tin whisker testing. The electronic assemblies were used for coverage evaluation and tin whisker testing.

2.2.1 Coupon coating application

Flat coupons were coated using a spread film coating or a drawn film coating process.

The spread film coating method begins by depositing a volume of liquid coating with a plastic pipet along an edge of the substrate. Then a grooved steel mandrel is used to spread the coating to a thickness of 20 to 40 microns. This method was used for the fluid compatibility board coupon coating.

The drawn film coating process is a casting process that begins by securing two parallel shims to the edges of the substrate to be coated. A volume of liquid coating is deposited on the substrate and a squeegee blade is then drawn across the liquid to form the layer. The thickness of the film is controlled by the two shims which set the height of a squeegee blade. It was difficult in some cases to prevent bubble entrainment in the coating when the squeegee blade was drawn over the liquid. The drawn film method was used to coat glass slides for the nanoindentation, atomic force microscope (AFM) and structure evaluation. It was also used for coating the flat whisker test coupons. Thicknesses ranging from 40 to 300 microns were obtained.

A free film of coating was needed for the tensile test coupons and cross – section microstructural evaluations. In this case, the film was drawn coated onto a larger glass plate and cured. The film was then removed from the glass plate and cut to the final size.

Unlike thermal cure materials that can utilize conventional casting techniques, the present sheet casting process requires the coating film remain relatively thin and have a large free surface that is open to atmospheric moisture.

2.2.2 Test vehicle assemblies

The test vehicle assemblies used to evaluate coating coverage and tin whisker growth were coated with a combination of dip coating and machine spray coating. The tin whisker assembly coating targeted a nominal coating thickness of 50 microns. A baseline coating evaluation was performed using the PC18M and PC40-UMF based coatings that exhibited the best mechanical properties. The results from the baseline tests were used to select coatings for an enhanced layered coating process. The assembly processes are provided in Appendix E [2].

3. Solid coating microscopic examination

3.1 Coating application method overview

For evaluations requiring a coating film, a draw down method was used to cast the films. The thickness of the film was controlled using two shims to set the height of a squeegee blade that was drawn across the deposited liquid coating. It was difficult in some cases to prevent bubble entrainment in the coating when the squeegee blade was drawn over the liquid. Thicknesses ranging from 40 to 300 microns were obtained. The tensile test and the cross-section samples were peeled from glass substrates after curing.

3.2 Film structure and particle distribution using AFM, cross-sectioning, FE-SEM imaging, and TEM imaging.

3.2.1 AFM

AFM was used to characterize the top surface of cured polyurethane (PU) coatings (both filled and unfilled) to understand the morphological features of the polymer structure underneath. Cured coatings on glass slides were utilized in the AFM under tapping mode (Dimension 3100 and Nanoscope-V AFM Veeco Instruments, USA) which provided a surface analysis of the coating with a nanometer resolution.

3.2.2 Cross-sectioning

For the examination of particles within the film, cross-sectional sides of the PU coatings were exposed by cryo-fracturing after freezing the samples in liquid nitrogen, or sectioning through with an ultramicrotome tool. The former method provided the samples for low-kV SEM (at 2 kV) while the latter provided the samples for both low-kV SEM and cryo-TEM observations.

Cryofracture:

Peeled PU films were fractured to expose the inside of the films through the cross-sectional viewing in the SEM. For this, the coatings were immersed in liquid nitrogen for a few minutes, followed by rapid bending to fracture. Fracture surfaces were then coated with a conductive carbon or Cr coating for negating an accumulation of charge during SEM characterization. Before a conductive coating is deposited, ion etching on fracture surface can generate more topographic contrast.

Microtome:

To obtain thin slices which are around 50-90 nm in thickness for TEM analysis, microtome methods, which enable slicing of very thin sections of the sample were utilized. Before slicing, PU films were mounted in the epoxy resin and cured. PU films set in epoxy were sliced using a diamond knife set stationary against the sample moving in a regulated stroke motion in the microtome (Leica Instruments Ltd., USA) to generate sections of the coating surrounded by epoxy. Additionally, the remaining epoxy blocks for generating these slices were also used for SEM viewing of the cross section. This cross-sectioning also enabled a qualitative evaluation of the interfacial strength between the polyurethane and the nanoparticles.

3.2.3 FE SEM

Low-kV (~2kV) field emission SEM (Zeiss Supra 55 FESEM, Carl Zeiss GmbH, and Germany) was utilized to obtain high resolution images of the cross-sectional surface. The cross-section of the PU film prepared either via cryo-fracture or microtome was observed to characterize PU matrix, particle

distribution and agglomeration, and the interaction of the PU with the nanoparticles. To avoid the charging, SEM samples were ion-etched and coated with a thin Cr or C film while TEM samples were coated with a thin carbon film. The TEM was operated at 120kV on a cold stage at ≤ -176 ˚C in order to avoid electron beam damage.

3.2.4 CryoTEM

In an effort to see individual nanoparticles and their distribution and agglomeration more clearly, Cryogenic (cryo-) TEM observation was done using a liquid nitrogen cooled stage on a JEOL 2100F Field Emission TEM (JEOL Ltd, Japan). The cold stage was maintained below -175˚C. It was also possible to observe the inside of the clustered particle agglomerations in terms of individual particle size and distribution. Further analysis of the nanoparticle-polymer matrix interface was also facilitated by this means.

3.3 Fourier transform infrared (FTIR) spectroscopy

The Spectrum 100R from Perkin Elmer was used to examine the types of chemical bonds within the film.

4. Solid coating mechanical evaluation methods

The mechanical behaviour of the coating needs to be well understood when the coating is being used for whisker mitigation. Parameters and attributes such as those in Table 2 are important for the coating evaluation. Often the coating data sheets focus on moisture resistance and electrical performance and often do not include parameters such as glass transition temperature, modulus, strength and adhesion strength, which are necessary for the analysis. In addition, one purpose of this study was to select the optimum concentration of nanoparticles based upon microstructural observations and associated mechanical properties. Mechanical properties were evaluated via macroscopic tensile testing as well as nanoindentation.

Table 2: Mechanical evaluation of cured coating samples.

Parameter	**Test method**
Fluid compatibility	Microhardness
Glass transition temperature (T_g)	TMA and/or DSC
Coefficient of thermal expansion (CTE)	TMA
Hydrolytic stability	Visual assessment
Thermal shock	Visual assessment
Hardness	Nanoindentation
Modulus	
Strength	Tensile test
Modulus	
Elongation	
Adhesion	4 point bend
Film structure and particle distribution	Cryo-FE SEM
	Cryo-TEM
	AFM
Chemical bonds	FTIR
Water vapor transmission	Mocon™ tester
Coating coverage	WP1753 SOT Assembly
	WP1753 QFP Assembly
Whisker mitigation	Cantilever beam whisker coupon
	SAC+Rare Earth Element (REE) whisker coupon
	WP1753 SOT and QFP assemblies in thermal cycling and high temperature/high humidity

4.1 Fluid compatibility

Some coatings undergo significant softening after fluid exposure. Fluid compatibility is an important consideration in the selection of a coating for whisker mitigation. In the present work, microhardness was measured before and after fluid exposure using a Fischerscope H100C on coated board coupons (Figure 2). The glass epoxy board coupons (4 inches x 2.75 inches) with copper traces were coated

with approximately 50 micron thick coatings. The cure for the PC18M family of coating was (1) initial solvent evaporation for 30 minutes at room temperature, (2) moisture cure 60°C/60% Relative Humidity (RH) for two hours, and (3) hold samples at room temp for 72 hours prior to test to complete curing. For the PC40-UMF family of materials the cure was (1) initial solvent evaporation for 30 minutes at room temperature, (2) UV exposure using a Hg bulb, (3) moisture cure 60°C/60%RH for two hours, and (4) then hold samples at room temperature for 72 hours to complete curing.

One set of samples were immersed in JP8 jet fuel for 168 hours at room temperature and a second set of samples were suspended in the vapors above Skydrol™ hydraulic fluid for 168 hours at room temperature. Microhardness measurements were performed between four and five hours after removal from the environment. The hardness measurement was performed by applying a known force to the coating surface and the penetration depth was not more than ten percent of the coating thickness (five microns). The estimated measurement variation is +/-3%. Three coupons were used for jet fuel and four coupons were used for the Skydrol™ test.

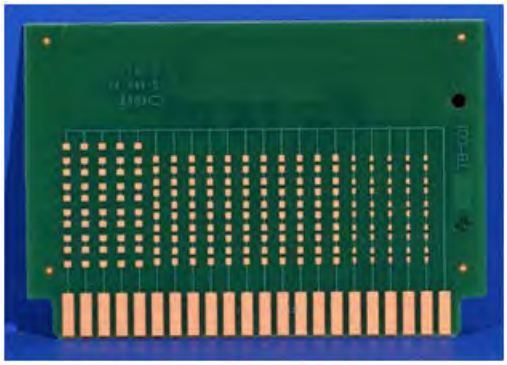


Figure 2: Board coupon.

4.2 Glass transition temperature

The glass transition temperature was measured either with a themomechanical analyzer (TA) Instruments TMA Q400)) or a differential scanning calorimeter (TA Instruments DSC Q20). The TMA samples size was approximately 2.2 mm and the DSC sample size was approximately 18 mg.

4.3 Coefficient of thermal expansion

The coefficient of thermal expansion was measured using a TA Instruments TMA Q400. For the CTE measurement a cast sample approximately 2.2 mm thick is desired.

4.4 Water vapor transmission rate

A Mocon PERMATRAN-W^{TM} Model 3/33 tester was used to measure moisture permeability of the coating film. The area of the film tested was 5 cm^2 (2.54 cm diameter circle). PC18M family samples were air dried for a minimum of 30-45 minutes and then cured for a minimum of two hours at 60 ºC (140 ºF) in an oven having a minimum relative humidity of 30 percent. The following cure for the PC40-UMF+XP2742 cast films was used: (1) solvent evaporation three hours at 40°C on hotplate, (2) UV exposure – 3.5 joules/cm^2, and (3) overnight (16 hours) in 60°C/60% RH. Coating film thicknesses between 50 and 120 microns were used. The PC40-UMF+15.54%N3300 having the same composition as the PC40-UMF+30%XP2742 except it has no nanosilica particles. One sample of the PC40-UMF and the 100%XP2742 were made using only a moisture cure with no UV. Typically, three or more days elapsed before testing was performed.

4.5 Hydrolytic stability

The hydrolytic stability test was performed in accordance with the IPC-CC-830 [IPC Association Connecting Electronics Industries, Bannockburn, Illinois] conformal coating qualification requirements. Board coupons with metal traces (Figure 2) were coated and exposed to the long-term humidity 120 day 85°C/95%RH test.

4.6 Thermal shock

The thermal shock test was performed on selected coatings applied to board coupons to evaluate adhesion. The coupons were cycled 100 times from -55 to 125°C using an air-to-air transfer shuttle providing nearly instantaneous temperature changes (Ref IPC-CC-830 qualification requirements). Note that the assembly testing described in the whisker test section uses temperature ranges of -55 to +125°C and a -20 to 80°C with ramp rates of 10°C/minute for the long-term testing. Prior coated assembly testing found that -55 to +85°C thermal shock testing (20 minute dwells, three cycles per hour) in accordance with JESD201 [6] was too severe and cracked the coatings and board laminates [7].

4.7 Nanoindentation hardness and modulus

A Hystron TriboIndenter™ was used to evaluate nanohardness and elastic modulus of the PU matrix. The depth-sensitive nanoindentation testing can emulate the whisker penetration behavior by examining local deformation of PU around an indenter tip. Hardness and modulus were obtained for various indenter penetration depths.

4.8 Tensile test

The tensile test provides macroscopic properties to compliment the nanoindentation testing. Testing was performed in accordance with ASTM D882 [ASTM International, West Conshohocken, PA] except the sample size was 63.5 x 12.7 mm (2.5 x 0.5 inch) with a gauge length of 12.7 mm (0.5 inch) and the displacement rate was 2.54 mm/minute (0.1 in/min). Ultimate tensile strength, yield strength, and modulus were obtained.

4.9 Adhesion

The coating adhesion to tin was evaluated using a four point bend test (see Figure 3 and Figure 4). The sample sandwiches the coating/tin interface between pieces of silicon. The critical strain energy release rate, G_c (J/m^2) for debonding, can be found using the relationship:

$$\frac{21(1-\upsilon^2)P^2L^2}{16Eb^2h^3} \qquad \text{Eq. 1}$$

where E and ν are the Young's modulus and Poisson's ratio of the silicon, P is the steady crack growth force (Figure 5), b is the substrate width, and L and h are given in Figure 4 and Table 3. Force versus displacement data was obtained for three to five samples at a loading rate of 0.01 mm/min.

An overview of the sample fabrication and crack propagation path is given in Figure 6. The silicon pieces were cut from a wafer then rinsed with acetone, isopropyl alcohol, and deionized water. The silicon pieces were then dried and plasma etched prior to Ti/Sn sputtering. The sample layer thicknesses are given in Figure 7.

The coating films were formed using a manual doctor-blade process and the following cures were used:

- PU or PU+nanosilica (Henkel PC18M or PC18M+20%XP2742): 30 to 45 minute room temperature cure followed by a moisture cure for two hours at 60°C
- PUA (Henkel PC40-UMF): 20 minute ultraviolet cure (4800 µW/cm2, UV-A) followed by moisture curing for four hour at 60°C

In a second set of tests, additional adhesion improvement techniques were implemented; roughening of the Si prior to epoxy bonding using EPO-TEK 375, Epotek Corp., and plasma etching (Si prior to sputtering, the tin prior to coating, cured coating prior to epoxy bonding, Si prior to epoxy bonding). In addition, the polyurethane acrylate coating sample was evaluated with and without a silane treatment using (3-Aminopropyl)triethoxysilane (APTES) treatment of Sn surface. A two percent APTES water solution with that was slightly acidified (pH=5) was used.



Figure 3: MTS Mini Bionix tester used for the four point bend testing.

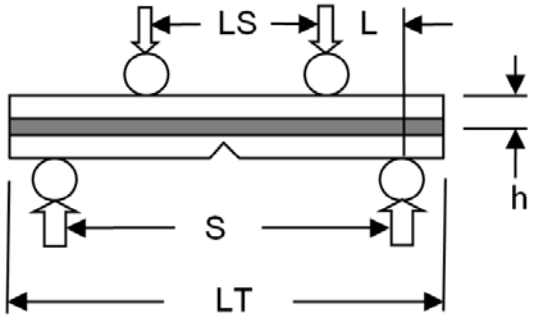


Figure 4: Four point bend sample schematic. The four mandrels are 2-mm diameter.

Table 3: Four point bend test parameters.

Description	Designation	Value
Sample Length	LT	38.1 mm
Sample Width	b	9.545 mm
Sample half thickness	h	Measured (~0.60 mm)
Support Span	S	24 mm
Load Span	LS	12 mm
Silicon Poisson's ratio	ν	0.22
Silicon Young's Modulus	E	160 GPa
Force Plateau	P	Measured

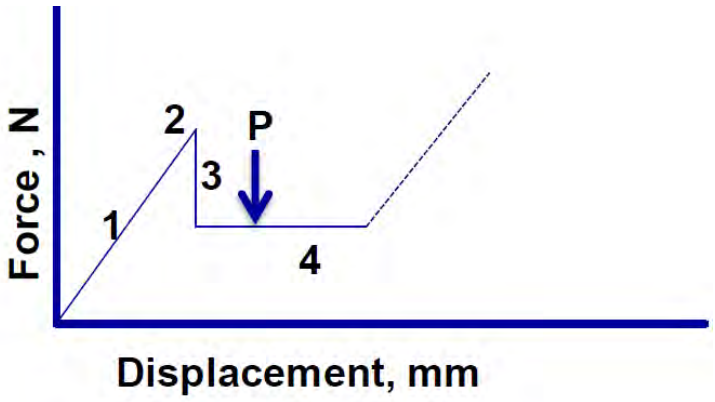


Figure 5: Schematic diagram of the four point bend test force versus deflection output. The force regimes are: (1) elastic loading, (2) crack initiation, (3) interface delamination, and (4) steady state crack growth.

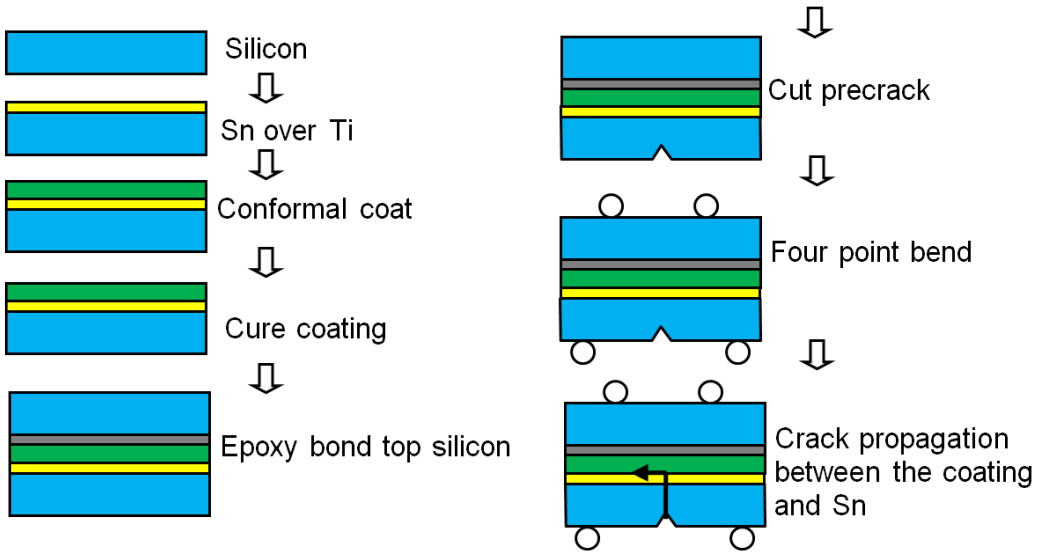


Figure 6: Four point bend sample fabrication and fracture path.

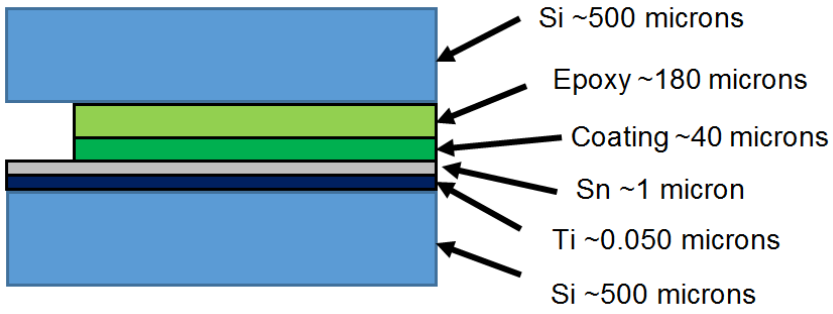


Figure 7: Sample layer thicknesses.

5. Whisker mitigation effectiveness evaluation

The whisker mitigation considered conformal coating coverage, coating thickness and testing on whisker prone test samples as summarized in Table 4. The whisker testing was done on two types of rapid whisker growth coupons and SAC305 soldered assemblies. The coupons provide relatively consistent coating thickness and are easy to inspect. The assembly coupons contain real electronic components with a diverse materials and real manufacturing process factors. A detailed SEM and cross-section coverage/thickness evaluation was performed on the on the assemblies to capture the coverage variation associated with the three dimensional aspects of the part leads, solder joints and part bodies.

Table 4: Test vehicles for coverage evaluation and whisker testing

Test vehicle	Coverage evaluation	Whisker test environment
Cantilever beam	Optical, SEM and Cross-section	High temperature/ high humidity (HTHH)
SAC+REE Coupon	Optical, SEM and Cross-section	HTHH
SAC305 SOT Assy	Optical and SEM	Accelerated thermal cycling (ATC) alone, ATC+HTHH and HTHH alone
SAC305 QFP Assy	Optical, SEM and Cross-section	

5.1 Coating coverage and whisker inspection methods

A combination of optical and scanning electron microscopy inspection in conjunction with cross-sectioning was used to evaluate the coupons and assemblies. The coupons and assemblies were inspected for coating cracks, whisker growth and coating bumps. Coating bumps can indicate tin whisker/nodule growth under the coating. However, sometimes the bumps were due to debris under the coating or irregularities in the coating.

5.1.1 Optical Inspection

Optical inspection up to 100x was used. An advantage of the optical inspection is that it can see through the transparent coatings. Unfortunately it lacks the resolution and depth of field to effectively observe whiskers. A heritage MIL-I-46058 requirement for conformal coating is that the coating has sufficient transparency so as not to obliterate the identification markings on the electrical components.

5.1.2 SEM Inspection

SEM imaging is an effective means of evaluating coating coverage over the metal surfaces, coating cracking, and tin whiskers. SEM imaging has the advantage of high resolution and large depth of field; however the electron beam cannot penetrate through the thick coating regions to evaluate whiskers under the coating. SEM inspection was typically performed with a beam voltage of 15 kV at magnifications of 50 to 100x with increased magnification used as needed. With regard to coating coverage over metal, the SEM images can provide qualitative thickness information. The SEM image is dark when the coating is greater than approximately three microns thick and the electron beam cannot penetrate though the coating to the underlying metal. The SEM image becomes gray when the beam penetrates through the coating and interacts with the underlying metal. In this case, the coating is

less than approximately three microns thick. The SEM image is brightest when directly imaging metal that either has no coating or very thin coating that the beam can easily penetrate. Note that some bright image regions on the leads evaluated with electron dispersive x-ray (EDX) were found to have a significant carbon peak, suggesting that some coating was present. Also, in a particular image the darkness also increases due to the incident electron beam angle with respect to the coating surface. So even if the coating thickness has not changed, some regions of the lead could be darker or lighter depending upon the orientation of the lead surface. In addition, comparing different images can be problematic because incident electron beam energy and brightness/contrast settings change for each image. In addition, non-conductive debris often appears as bright regions and can be difficult to differentiate from metal whiskers.

5.1.3 Cross-sectioning

Cross-sectioning was used to evaluate coating coverage and thickness, coating adhesion, and metal microstructure. Since it is difficult to differentiate between the potting compound and the conformal coating, the sample was first sputtered with a layer of gold prior to potting. This technique enables coating thickness resolution of less than a micron.

5.2 Whisker test methods

5.2.1 Cantilever beam coupon test procedure

The cantilever beam coupon was five to eight micron thick bright tin plated C110 copper (see Figure 8). Note that a bright tin plated C110 alloy also was used in the long-term test by Woody [8] and on Hillman's Strategic Environmental Research and Development Program (SERDP) whisker testing [9]. The coating was applied with a drawn film process. The tape used to set the draw height also provided the masking for the uncoated tin area.

In the present work, the cantilever beam was placed in an aluminum fixture that clamped one end and raised the other end. The 0.38 mm free end displacement resulted in a bending preload of 11.4 MPa near the clamp. The compressive stress in the tin had been thought to increase whisker growth, but did not seem to make a difference in the present experiments.

Four sets of cantilever beam samples were coated with PC18M+30%XP2742 and then placed into high humidity testing. The samples were exposed to 60°C/60%RH for 500 hours and removed for SEM examination. Then the samples were returned to the humidity environment. The four samples were then sequentially removed at the following times:

- Sample 1: 1,000 hours (500 + 500 hours)
- Sample 2: 1,500 hours (500 +1,000 hours)
- Sample 3: 2,000 hours (500 + 1,500 hours)
- Sample 4: 2,500 hour (500 + 2000 hours)

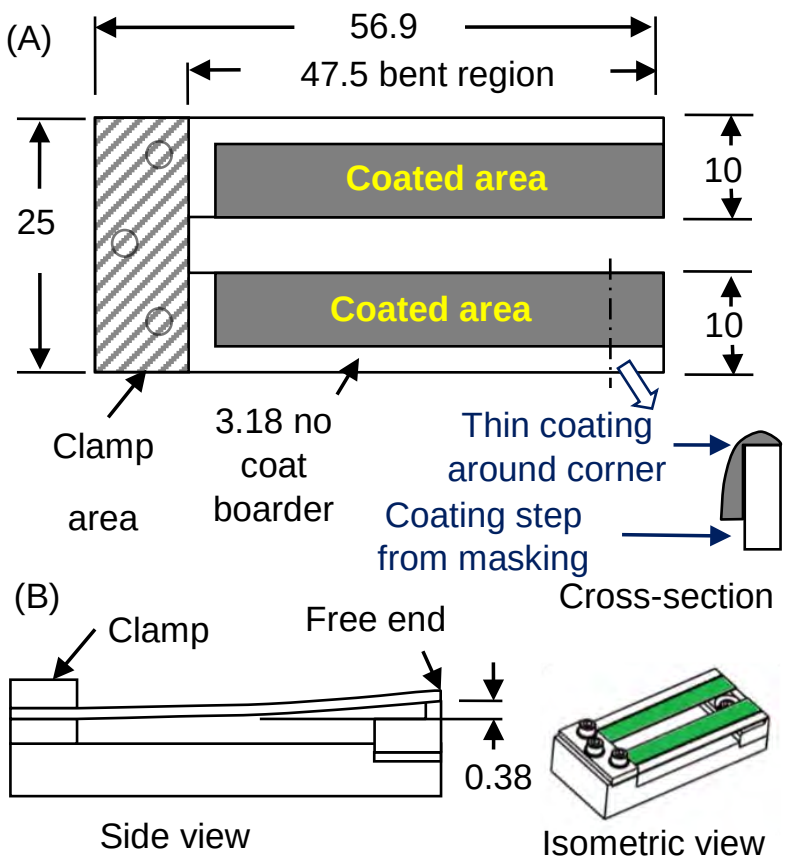
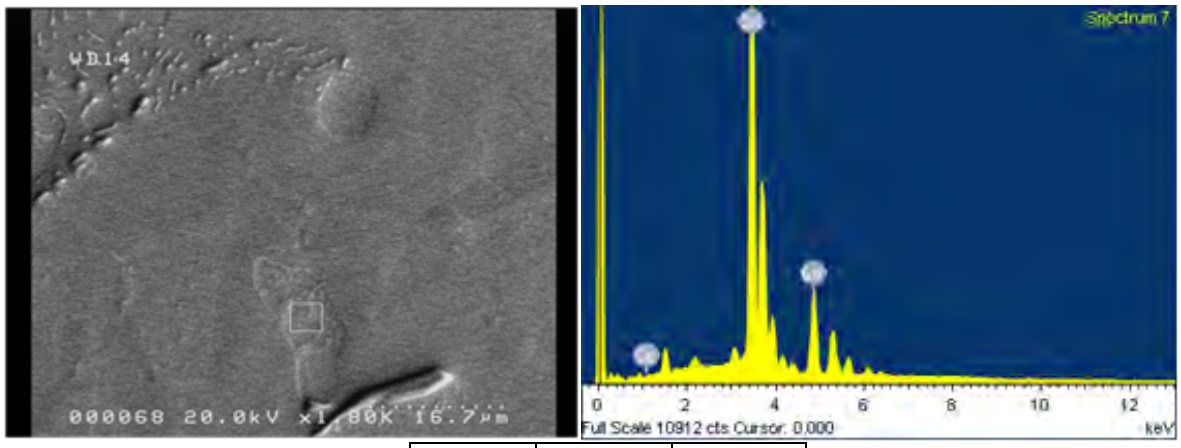


Figure 8: Cantilever beam whisker coupon; (A) coated cantilever beam, and (B) cantilever beam installed in fixture.

5.2.2 SAC+REE Coupon test procedure

The SAC+REE coupon is made from an alloy of SAC305+0.1Ce solder that had a final composition measured to be Sn-2.6%Ag-0.5%Cu-0.1%Ce. An electron dispersive x-ray analysis (EDX) examination of the master alloy cross-section microstructure shows $CeSn_3$ intermetallic (Figure 9). The SAC+REE intermetallic corrodes/oxidizes liberating tin and creating compressive stress [10]. A rolling process was used to prepare the foil prior to machining. First the master alloy ingot was cut into two mm thick slices approximately 12x25 mm, then the material was placed between cleaned steel plates and compressed in an arbor press to a thickness of 0.8 to 1.3 mm. The flattened samples were then placed in stainless steel sleeves and rolled in a rolling mill until the final thickness was obtained. The samples were then machined to the final shape.



Element	Weight%	Atomic%
Sn L	70.56	73.89
Ce L	29.44	26.11
Totals	100	

Figure 9: EDX analysis of $CeSn_3$ intermetallic in master alloy cross-section.

The SAC+REE coupon (Figure 10) was 0.2 to 0.3 mm thick and had notches to simulate coating lead edges, a hole for coating dipping and a corner chamfer to facilitate with sample orientation. The surface and edges were lightly abraded with silicon carbide sandpaper to remove machining burrs. Minimal deburring was performed in the notches to ensure that the corners were not rounded. To facilitate machining, copper backing pieces were used to support the foil.

Prior to coating, the samples were cleaned with a solvent and dried. Although, some embedded particles of SiC, Al, and stainless steel were observed in the SAC+REE coupons, these did not impact coating adhesion or the ability of SAC+REE to form whiskers. The PU application and cure followed the same process as the assemblies except that no initial dip was done. The SAC+REE samples were exposed to 85°C/85%RH high temperature high humidity (HTHH) for 1,000 hours.

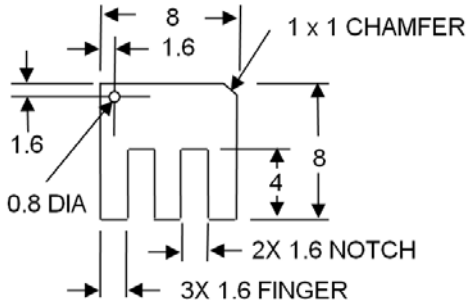


Figure 10: SAC+REE whisker coupon (dimensions in mm).

5.2.3 Slotted flat coupons

Slotted flat coupons were added later to evaluate tin whisker mitigation on substrate with multiple slots simulating lead edges where coating can thin (Figure 11).

The coupon material is copper alloy sheet in accordance with ASTM B152 Type 110, 1/2 hard, 0.635 MM (0.025 INCH) thick finished with ASTM B545 bright acid tin plating (see para 4.3.2 bright tin electrodeposits), five to eight microns thick. The coupons were cut with a waterjet SiC abrasive cutter and plated on a panel of 18 pieces (Figure 12). After cutting prior to plating, the panel was deburred using 600 grit silicon carbide paper until top and bottom surfaces were smooth. Then the slots were gently deburred using a scotchbright pad. Finally, the top and bottom surfaces were sanded with 600 grit silicon carbide paper.

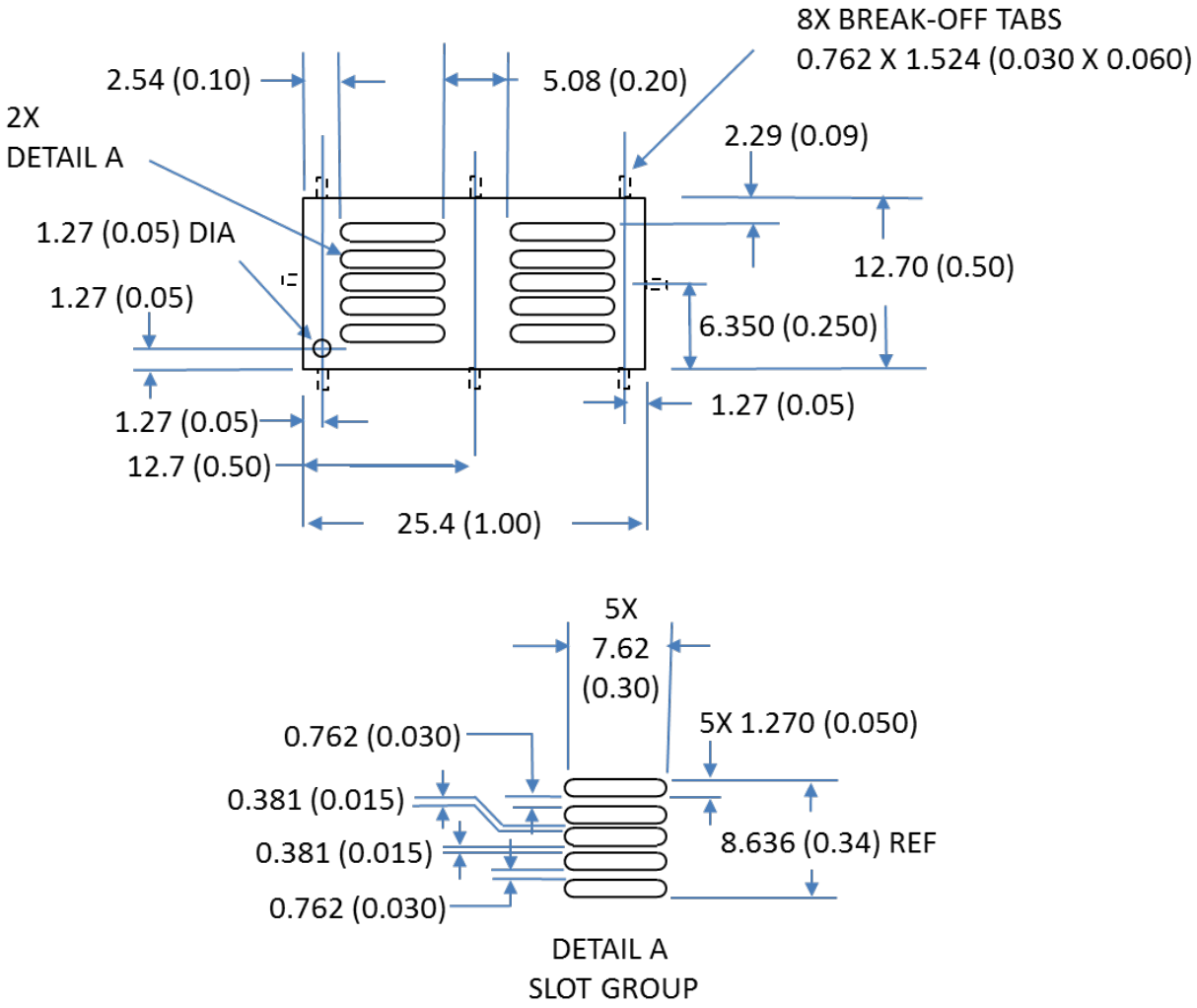


Figure 11: Slotted flat whisker test coupon, mm (inch).

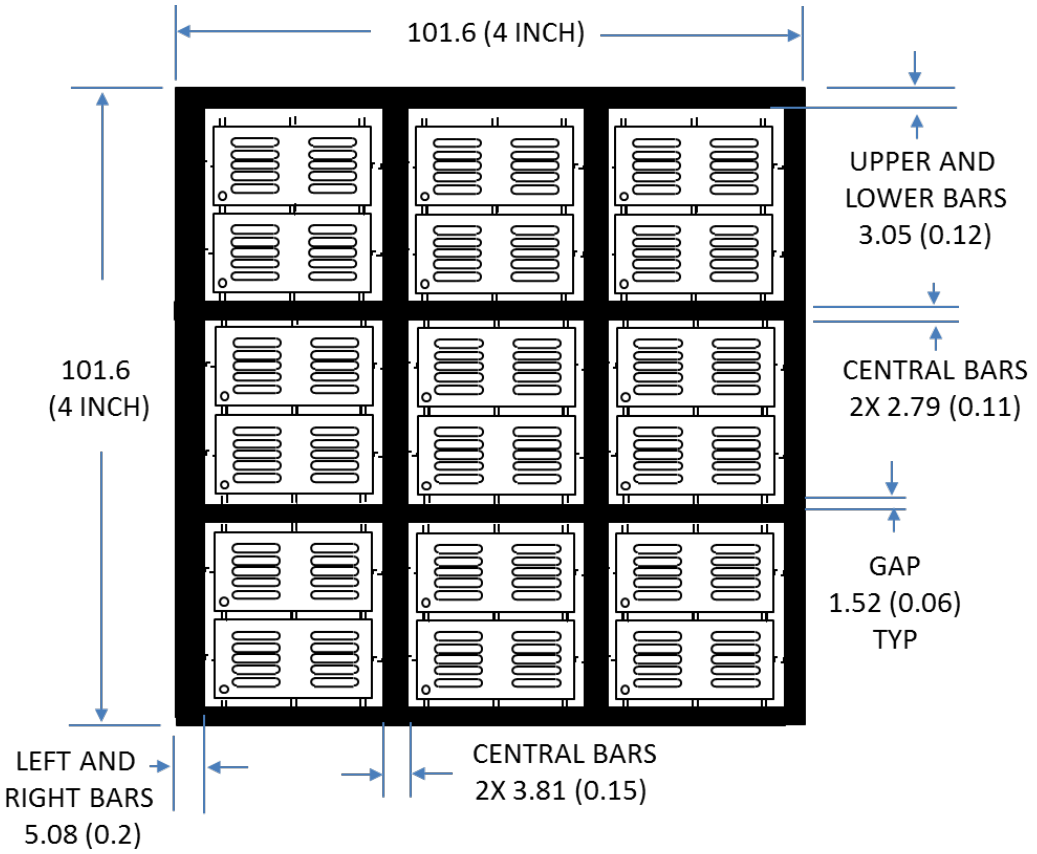


Figure 12: Flat slotted coupon panel layout, mm (inch).

5.2.4 Assembly test vehicles

Custom designed test boards from the SERDP WP1753 project were used for the lead-free soldered assembly whisker growth testing [5]. The small outline transistor (SOT) board (Figure 13) has three, five and six leaded SOT parts with C194 Cu alloy and alloy-42 alloy leads. The quad flat pack (QFP) board (Figure 14) has C7025 Cu alloy high pin count QFPs with two lead pitches and a C151 Cu alloy plastic leaded chip carrier (PLCC). The ball grid array (BGA) board (Figure 15) contains 0.8 and 0.4 mm pitch BGAs. The test vehicles for this study are small boards 6 cm x 6 cm in size processed together 12-up on a panel with handling edges. The boards were separated after surface mount soldering, inspected, coated, and then exposed to the environments.

The individual boards were found to be well suited for inspection by SEM, since the boards fit easily into the SEM's sample chamber. The placement area was limited to 5 cm x 5 cm to ensure all leads of interest were contained in a region that could be viewed by the SEM. The boards are 0.24 cm thick and are a double layer design manufactured in accordance with IPC-6012 Class 3, Type 2 with high temperature woven E glass epoxy laminate (IPC-4101/126), one ounce base Cu foil (IPC-4562/3 Type E Grade 3 (HTE)) with an additional 25 microns of plating on the outer layers from the hole plating process, solder mask over bare Cu (IPC-SM-840 Class H liquid photoimageable), with immersion tin over Cu finish (IPC-6012, Type IT) [IPC Association Connecting Electronics Industries, Bannockburn, Illinois].

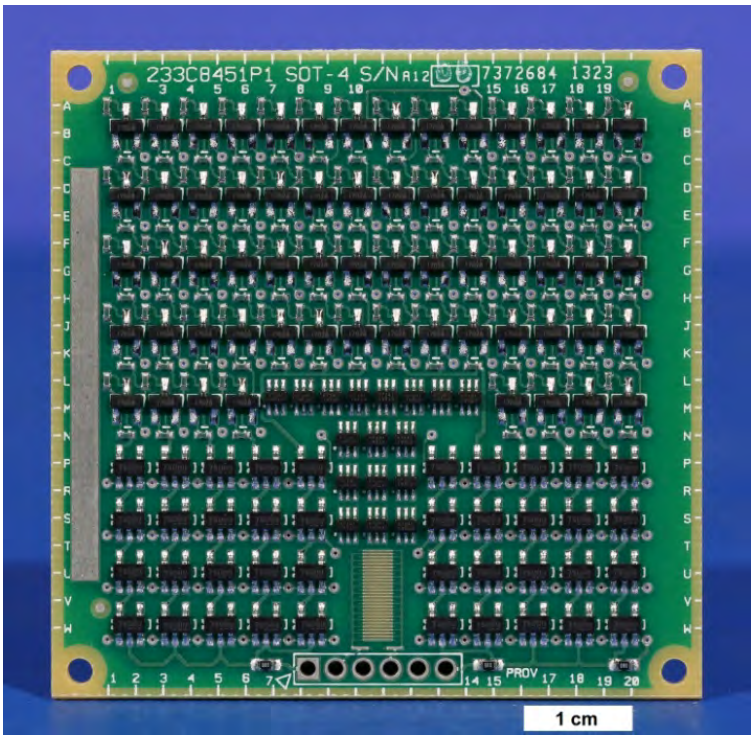


Figure 13: SOT board.

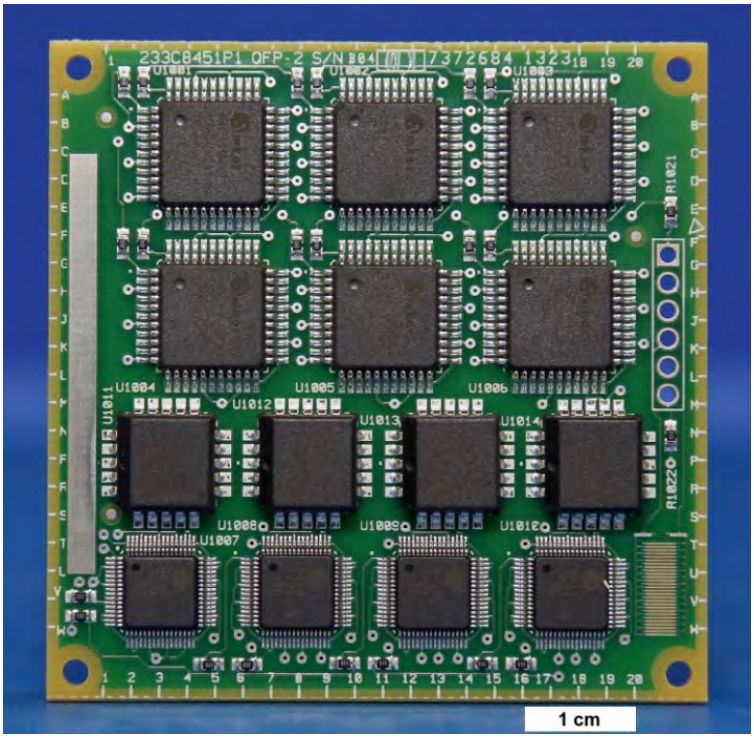


Figure 14: QFP Board.

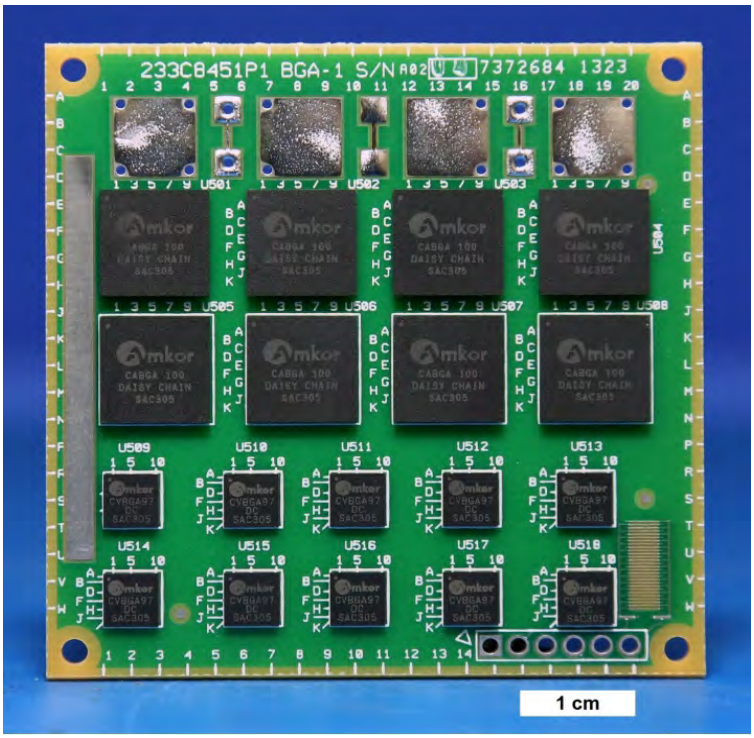


Figure 15: BGA Board.

The SOT board has 64 alloy-42 lead material SOT3 Fairchild 2N7002 parts, 40 C194 lead material SOT5 Fairchild NC7S08M5X parts and 17 alloy-42 lead material SOT6 Diodes Inc. 2N7002DW-7-F parts. The lead composition for the alloy-42 is Fe-42Ni and the Cu alloy C194 is Cu2.1-2.6Fe-0.015-0.15P-0.05-0.2Zn.

The Quad Flat Pack (QFP_ board has the following Practical Component Inc. Amkor Cu alloy lead material parts: six C7025 lead material QFP44 A-QFP44-10mm-.8-3.2-DC-Sn (0.8 mm pitch) parts, four C151 lead material PLCC20 A-PLCC20T-DC-Sn (1.25 mm pitch) parts with and four C7025 lead material Thin Quad Flat Pack Electronic Packages (TQFP)64 A-LQFP64-.7mm-.4mm-2.0-DC-Sn (0.4 mm pitch) parts. The lead composition for the C7025 is Cu2.2-4.2Ni0.25-1.2Si0.05-0.3Mg and for the C151 is Cu0.1Zr.

The BGA board contains the following Practical Components Inc. Amkor BGA components: eight SAC305 A-CABGA100-.8mm-10mm-DC-LF-305 BGAs and ten SAC305 A-CVBGA97-.4mm-5mm-DC-LF-305 BGAs.

The parts were not electrically biased on any of the boards during the whisker testing.

5.2.5 Assembly coverage evaluation method

The coating quality, coverage, and thickness after cure were dependent upon the liquid properties, the application method, and the assembly geometry. The initial coating quality was evaluated in accordance with the visual assessment in J-STD-001 [IPC Association Connecting Electronics Industries, Bannockburn, IL]. The J-STD-001 requirements are used for coating process control. It states that the coating (1) be completely cured and homogeneous, (2) be free of blisters or breaks that could affect the operations of the assembly or sealing properties of the conformal coating, and (3) be

free of cracks, crazing, voids, bubbles, mealing, peeling, wrinkles, or foreign material which expose component conductors, printed circuit conductors, (including ground planes) or other conductors and/or violates design electrical clearance (Note that there are no J-STD-001 requirements for coating used tin whisker mitigation). The current J-STD-001 inspection is an unaided visual appraisal unless magnification is needed on fine features to determine if the defect affects form, fit, or function. If magnification is used in the J-STD-001 inspection, it is limited to 4x.

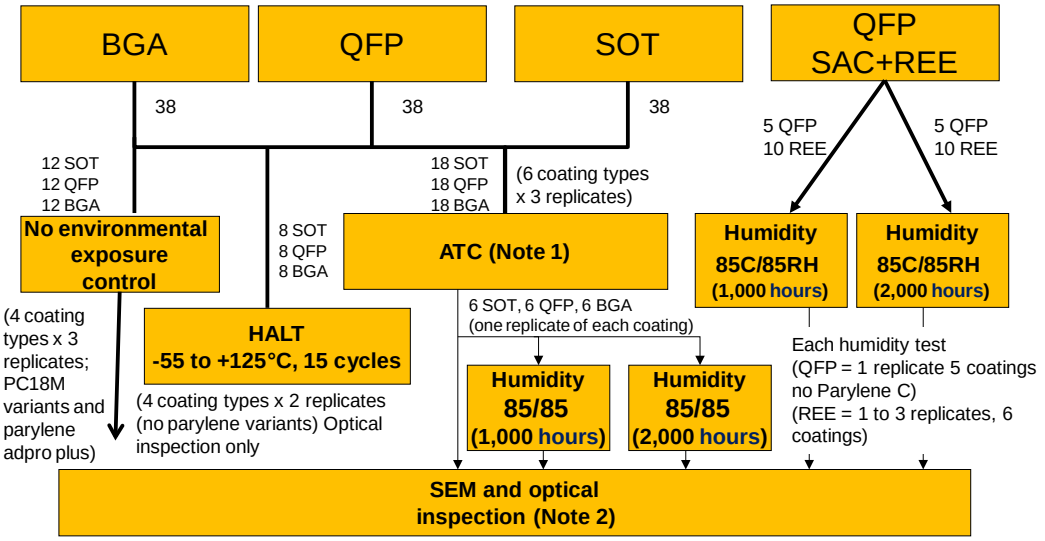
In the present work, the assemblies were evaluated from a mitigation perspective using a combination of optical and SEM inspection at magnifications up to 5,000x in conjunction with cross-sectioning.

5.2.6 Assembly whisker test procedure

The SERDP 1753 SOT, QFP and BGA test vehicles were used for the whisker testing. Test assemblies were coated with modified PC18M-mod (no nanoparticles), 80%PC18M+20%XP2742 (6.74% functionalized nanosilica), 80%PC18M+ 20%X11102PMA (13.04% non-functionalized nanoalumina), Parylene™ C and Parylene™ C with an Adpro+ adhesion layer (Ref. Specialty Coating Systems, Indianapolis, Indiana USA). A nominal coating thickness of 50 microns was targeted for the PU coatings and 25 microns for the Parylene C.

The environmental tests are summarized in Figure 16. Highly Accelerated Life Test (HALT) testing of 15 cycles of thermal shock from -55 to +125°C was used to verify adhesion of the coatings to the boards. A combination of accelerated thermal cycling (ATC) and 85°C/85%RH (HTHH) was used to evaluate whisker growth and coating integrity. During the WP1753 thermal cycling testing [5], it was found that the -55 to +85°C (20 minute dwells, three cycles per hour) thermal shock testing defined by JESD-201 was too severe for assembly level testing because it induced coating and board laminate fractures not typically observed in service. In addition, the stresses on the alloy-42 lead termination solder joints were too large for optimal whisker growth. A screening experiment on alloy-42 SOT3 parts soldered to a test board and coated with PC18M+30%XP2742 without plasma etch exposed to 1,610 cycles from -55 to +85°C (three cycles per hour) confirmed that significant coating cracking would occur with the thermal cycle shocks (Figure 17).

In the current work, a set of serial thermal cycles was used. The cycle combination has a lesser number of cycles over the full range of airborne military equipment temperatures and a larger quantity of less extreme temperature cycles selected by the NASA-DOD lead-free solder testing program [11]. The cycling consisted of 100 cycles from -55 to +125°C (10 minutes cold and 30 minutes at hot with 18 minute ramps) followed by 200 to 400 cycles from -20 to +80°C (30 minutes at cold and hot with 10 minute ramps). The cycling is more severe than the set used by Han and Osterman to evaluate conformal coating whisker mitigation [12].



Coating types are : No coat, PC18M, PC18M+20%XP2742, PC18M+20%X11102PMA, Parylene C, Parylene C+Adpro plus
Note 1: ATC was 100 cycles -55 to +125°C followed by 200 cycles (233 actual) -20 to +80°C
Note 2: Sample inspection of random parts performed

Figure 16: Example of assembly coating integrity and tin whisker evaluation conditions.

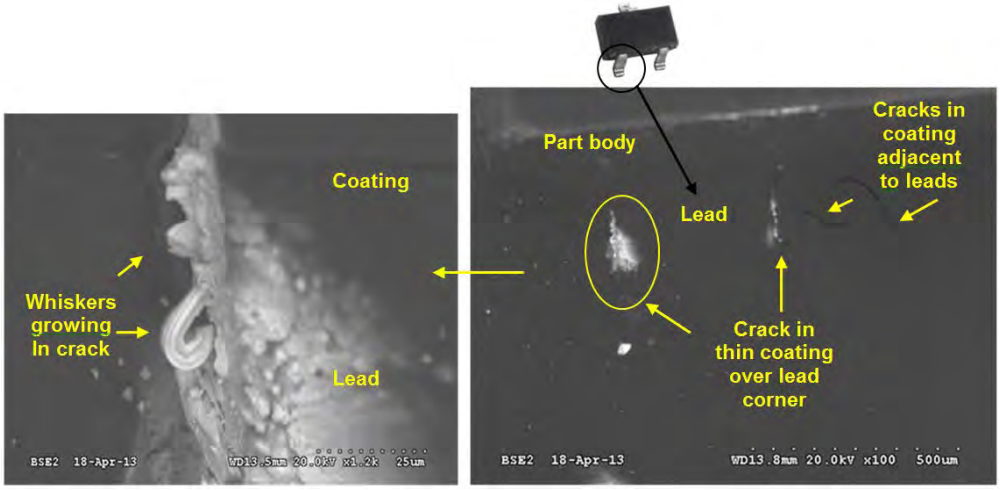


Figure 17: Screening test showing coating cracks in PC18M+30%XP2742 after 1,610 thermal shock cycles from -55 to +85°C (three cycles per hour).

6. Literature cited

[1] Appendix B of the current report: Suspension and coating formulation.

[2] Appendix E of the current report: Assembly Test Vehicle Coating Processes.

[3] MIL-I-46058, Insulating Compound, Electrical (for Coating Printed Circuit Assemblies), Military Specification, July 1972. Note that the Qualified Providers List (QPL) is still active, but MIL-I-46058 is inactive for new designs.

[4] IPC-CC-830, Qualification and Performance of Electrical Insulating Compound for Printed Wiring Assemblies, IPC-Association Connecting Electronics Industries, Bannockburn, Illinois, USA, Sept. 2008.

[5] S. Meschter and P. Snugovsky, SERDP WP1753 Final Report: Tin whisker testing and modeling, November 2015.

[6] JESD201A, Environmental Acceptance Requirements for Tin Whisker Susceptibility of Tin and Tin Alloy Surface Finishes, JEDEC Solid State Technology Association, Arlington, VA, September 2008.

[7] S. Meschter, P. Snugovsky, J. Kennedy, Z. Bagheri, and E. Kosiba, Strategic Environmental Research and Development Program (SERDP) Tin Whisker Testing and Modeling: Thermal Cycling Testing, SMTA International Conference on Soldering and Reliability Toronto, Ontario, Canada; May 13-15, 2014.

[8] L. Woody and W. Fox, Tin Whisker Risk Management by Conformal Coating, SMT magazine, July 2014, pp. 40-58.

[9] D. Hillman, Tin Whiskers Inorganic Coating Evaluation, 7th International Symposium on Tin Whiskers, Nov. 12-13, 2013, Costa Mesa, CA.

[10] D. Perovic, L. Snugovsky, J. Rutter, P. Snugovsky, Z. Bagheri, and S. Meschter, Microstructure and Whisker Growth of SAC Solder Alloys with Rear Earth Additions in Different Environments, SMTA International Conference on Soldering and Reliability, Toronto, Ontario, Canada May 2011.

[11] K. Kessel, NASA-DoD Lead-Free Electronics Project, SMTA International Conference, October 28, 2010.

[12] S. Han, S. Meschter, M. Osterman and M. Pecht, Evaluation of Effectiveness of Conformal Coatings as Tin Whisker Mitigation, Journal of Electronic Materials, DOI: 10.1007/s11664-012-2179-2, July 6, 2012.

SERDP WP-2213
Final Report
Appendix D: Coating characterization results

Appendix D: Table of Contents

1. Introduction 1

2. Fluid properties and flow 1

2.1 Viscosity 1

2.2 Viscosity and contact angle for gap flow test 3

2.3 Gap flow 4

2.4 Solvent evaporation 5

2.5 PC40-UMF+XP2742 PhotoDSC cure testing 6

3. Solid material microscopic examination 8

3.1 PC18M structure 8

3.2 PC18M with XP2742 nanosilica 8

3.3 PC18M with Nanophase X11102PMA nanoalumina 11

3.4 PC18M with Polymaterials nanoalumina initial evaluation 13

3.5 PC40-UMFstructure 16

3.5.1 PC40-UMFwith XP2742 Nanosilica 16

3.6 PC40-UMFwith Polymaterials nanoalumina 19

3.7 Film microstructure summary 20

4. Solid mechanical properties results 21

4.1 Fluid compatibility 21

4.2 PC18M glass transition temperature and CTE TMA test 21

4.3 PC40-UMF Coefficient of thermal expansion 24

4.4 Water vapor transmission 24

4.5 Hydrolytic stability 25

4.6 Thermal shock 25

4.7 Nanoindentation 25

4.7.1 PC18M 25

4.7.2 PC40-UMF 28

4.8 Tensile testing 30

4.8.1 PC18M 30

4.8.2 PC18M final coating comparison 35

4.8.3 PC40-UMF with XP2742 36

4.9 Adhesion testing 39

4.9.1 Initial adhesion tests [4] 40

4.9.2 Enhanced coating adhesion test [5]. 40
4.10 Solid mechanical properties conclusion 41
5. Literature cited 43

Appendix D: List of Figures

Figure 1: Viscosity versus spindle speed of PC18M, PC18M+20%XP2742, PC18M+20%X11102PMA, and PC40-UMF. Measurements were made using the Brookfield small sample adaptor. 2

Figure 2: Viscosity versus %AC0305 solvent addition to the PC18M and PC40-UMF coating families. Measurements were made using the Brookfield small sample adaptor at 20 RPM for the PC40-UMFfamily and 50 RPM for the PC18M family of coatings. 2

Figure 3: Viscosity versus total solvent percentage for PC18M and PC40-UMF. 3

Figure 4: Viscosity of coatings used in the gap flow test. 3

Figure 5: Contact angle, after one minute, of coatings used in the gap flow test. 4

Figure 6: Parallel glass plate immersion test results. 5

Figure 7: Solvent evaporation at 27 °C of PC40-UMF+30%AC0305 and PC40-UMF+50%XP2742 drawn liquid coating films 75 to 125 microns thick. 5

Figure 8: PC40-UMF nanosilica coating family photoDSC output exotherm (mW/mg) versus time. 6

Figure 9: Photo DSC results for the cure time characteristics for PC40-UMF, PC40-UMF+10%XP2742, PC40-UMF+30%XP2742, and PC40-UMF+50%XP2742. 7

Figure 10: Photo DSC exotherm results for PC40-UMF, PC40-UMF+10%XP2742, PC40-UMF+30%XP2742, and PC40-UMF+50%XP2742. 7

Figure 11: (a) AFM height image of 1 x 1 µm region of plain PC18M polyurethane coatings. (b) SEM cross-sectional image of the plain coating. 8

Figure 12: AFM height image of 1 x 1 µm region of PC18M + 20% XP2742 (6.7 wt. % SiO_2). (Inset) Phase image of a 5x5 µm region of the same coating. 9

Figure 13: SEM cross-sectional images of cryo-fractured nanosilica filled PC18M coatings: (a) 20% XP2742, (b) 30% XP2742, (c) 50% XP2742 filled. 10

Figure 14: Polyurethane with 30% XP2742 nanosilica suspension addition; (a) particle distribution in the top region of the coating, and (b) particle distribution in the bottom region. 10

Figure 15: TEM images of polyurethane with 50% XP2742 nanosilica suspension addition; (a) particle distribution at one end of the coating, and (b) an example of the agglomeration. 11

Figure 16: AFM height image of a 1 x 1 µm region of PC18M + 4% X11102PMA nanoalumina filled polyurethane coating. 11

Figure 17: Cross-sectional SEM images of polyurethane films with (a) 4% X11102PMA (b) 20% X11102PMA Al_2O_3. 12

Figure 18: Cross-sectional TEM image of nanoalumina-filled PU coating. 12

Figure 19: Size distributions of nanoalumina suspensions: (a) AL2425-non-functionalized and (b) WTA940-functionalized. 14

Figure 20: Cross-sectional SEM images of microtome sectioned nanoalumina-filled PC18M: (a) AL2425; (b) WTA940. 15

Figure 21: Cross-sectional SEM images (high magnification view and the entire thickness overview) of PU films filled with nanoalumina; (a) WTA996-8A-15D-87H and (b) KEK71-8A-25D-87H. 15

Figure 22: Cross-sectional SEM images of PU films filled with nanoalumina; (a) WTA997-8A-25D-87H and (b) KEK71-8A-25D-87H. 16

Figure 23: Cross-sectional SEM images of WTA996-8A-15D-93H at various magnifications. 16

Figure 24: Cryo-fractured cross-section of a plain PC40-UMFcoating showing: (a) the entire thickness; (b) high magnification view inside the circled domain. 17

Figure 25: High resolution SEM image of cryo-fractured PC40-UMFcoating filled with 30% XP2742... 17

Figure 26: Cryo-fracture surface of PC40-UMFcoatings: (a) plain PC40; (b) PC40-UMFfilled with 30% XP2742. 18

Figure 27: Cryo-fractured PC40-UMFcoatings filled with (a) 10% XP2742 SiO_2 suspension and (b) 30% XP2742 SiO_2 suspension. 18

Figure 28: Microtome cross-section of plain PC40-UMFcoating, showing (a) entire thickness, inset: sub-micron sized void; (b) the network structure at higher magnification. 19

Figure 29: Cross-sectional overview image of WTA996 with PC40-UMF; (a) overall, (b) region of settled particles at one end of the coating, and (c) PU and nanoparticles in the settled layer. 19

Figure 30: Cross-sectional overview image of WTA997 with PC40-UMF; (a) overall, (b) agglomeration within the PU film, and (c) particle agglomeration with very little PU in it. 20

Figure 31: Fluid compatibility results for PC18M based materials. 21

Figure 32: Fluid compatibility results for PC40-UMF based materials. 21

Figure 33: TMA measured expansion of (a) PC18M (control), (b) PC18M-modified with Dabco T 12, (c) PC18M+10%XP2742, (d) PC18M+30%XP2742 and (e) PC18M+50%XP2742. 23

Figure 34: Water vapor transmission for various XP2742 or X11102PMA concentrations in PC40-UMF and PC18M. 24

Figure 35: Nanoindentation testing results from PC18M films: (a) elastic modulus; (b) nanohardness. ... 26

Figure 36: Nanoindentation testing results at room temperature, 50˚C, 85˚C, and 125˚C; (a) elastic modulus, and (b) nanohardness. 26

Figure 37: Nanoindentation testing results of PC18M filled with XP2742 (nanosilica); (a) elastic modulus, and (b) nanohardness. 27

Figure 38: Nanoindentation testing results of PC18M+20% XP2742 at room temperature, 50˚C, 85˚C, and 125˚C; (a) elastic modulus, and (b) nanohardness. 27

Figure 39: Nanoindentation testing results of PC18M filled with N3300; (a) elastic modulus, and (b) nanohardness. 28

Figure 40: Nanoindentation testing results of PC18M filled with X11102PMA (nanoalumina); (a) elastic modulus, and (b) nanohardness. 28

Figure 41: Nanoindentation testing results from PC40-UMF films; (a) elastic modulus and, (b) nanohardness. 29

Figure 42: Nanoindentation testing results of PC40-UMF at room temperature, 50˚C, 85˚C, and 125˚C; (a) elastic modulus, and (b) nanohardness. 29

Figure 43: Nanoindentation testing results of PC40-UMF with NNN2835/XP2742 (nanosilica); (a) elastic modulus, and (b) nanohardness. 30

Figure 44: Nanoindentation testing results of PC40-UMF filled with N3300; (a) elastic modulus, and (b) nanohardness. 30

Figure 45: Representative tensile stress-strain plots of PU films with different amount of XP2742 SiO_2. For reference an unfilled PU film (PC18M) case is also included. 31

Figure 46: A crack grown from a defect site embedded in PU film; (a) bright field optical micrograph, and (b) C-differential interference contrast (DIC) image. Arrows indicate tensile loading direction. 32

Figure 47: Effect of XP2742 (nanosilica+isocyanate) and N3300 (isocyanate) suspension on tensile properties; (a) elastic modulus, (b) yield strength, (c) tensile strength at break, and (d) percent elongation. 33

Figure 48: Tensile stress-strain plots of PU films with different amounts of X11102PMA Al_2O_3. For reference, unfilled PU film (PC18M) and PU film with 20 wt.% XP2742 SiO_2 are also included. 35

Figure 49: PC18M Stress versus strain comparison with Parylene C; (a) overall and (b) strain up to 15 percent. 36

Figure 50: Representative tensile stress-strain plots of UV-curable PC40-UMF filled with XP2742 SiO_2 suspension. For reference an unfilled PU film (PC40-UMF) case is also included. 37

Figure 51: Tensile properties of PC40-UMF family (filled with NNN2835 equivalent to XP2742, N3300); (a) Elastic modulus, and (b) Tensile strength. 38

Figure 52: MTS Mini bionix tester used for the four point bend testing. 39

Figure 53: Four point bend sample schematic. The four mandrels are 2-mm diameter 39

Figure 54: Sample layer thicknesses. 40

Figure 55: Critical interfacial adhesion energy for PC18M+0%XP2742 and PC18M+20%XP2742. 40

Figure 56: Typical force versus displacement curve for the four point bend test. (PU (PC18M) on Sn shown). 41

Figure 57: Critical interface energy (Gc) for the coating to tin interface adhesion. The PU (PC18M) adhesion is considerably better than the PUA (PC40-UMF). The APTES silane treatment improved the adhesion on the PUA samples 41

Appendix D: List of Tables

Table 1: Unfilled PC18M and PC40-UMF viscosity, density and contact angle. 4

Table 2: Photo DSC data for PC40-UMF+10%XP2742, PC40-UMF+30%XP2742, and PC40-UMF+50%XP2742. 6

Table 3: Sample names and compositional information for Polymaterials initial functionalized nanoalumina suspensions evaluated in the cross-sections. 13

Table 4: Summary of PC18M+XP2742 glass transition temperature, coefficient of thermal expansion and hardness 23

Table 5: Water vapor transmission test sample thicknesses. 25

Table 6: PC18M tensile test set sample thicknesses. 33

Table 7: Four point bend test parameters. 39

Acronyms

Acronym	Definition
AFM	Atomic Force Microscope
cps	centipoise
DLS	Dynamic Light Scattering
DSC	Differential Scanning Calorimeter
IR	Infra-Red
KEK	Supplier material designation
QFP	Quad flat pack
RPM	Revolutions Per Minute
SEM	Scanning Electron Microscope
TEM	Transmission Electron Microscope
TGA	Thermogravimetric analysis
TMA	Thermomechanical analysis
UV	Ultraviolet

1. Introduction

The fluid and solid coating property results are presented in the following document. The test methods are given in Appendix C [1]. Much of the data was presented to the industry in 2014 when the testing was completed to support assembly whisker testing down selection [2][3].

2. Fluid properties and flow

2.1 Viscosity

The production PC18M viscosity is between 300 and 400 cps but is easily adjusted with the addition of solvent. The production PC40-UMF viscosity is 250 cps and since it is a solvent-free formulation, its viscosity is typically not tailored with a solvent. The coatings exhibit non-Newtonian rheology and the measured viscosity depends upon the shear rate. It was found that the viscosity decreases with increasing the spindle speed (Figure 1). This is a useful condition because it means that while the fluid is flowing during application, it can spread more easily. When the flow velocity decreases, the viscosity increases and the coating will tend to stay in place.

In the present work, the PC18M and PC40-UMF viscosities were modified by adding Henkel AC0305 solvent (Figure 2). A viscosity of 150 cps was used as the spray coating baseline and a viscosity of approximately 30 cps was used for dip coating. For the dip coating, the goal was to ensure that a thin coating layer was on all the surfaces without filling the gaps behind the leads. Note that as solvent was added, the percentage of polymer was reduced resulting in thinner cured coatings. Even at the lowest viscosity a continuous cured coating film was obtained.

The PC18M liquid has solvent in it even before AC0305 is added, while the PC40-UMF does not. The PC18M liquid without any solvent has the consistency of molasses and its viscosity will increase considerably above 300 cps as the final portions of solvent evaporate. The coating viscosity versus total solvent curves for the PC40-UMF and the PC18M are shown in Figure 3. The Desmodur N3300 is solvent-free and has a nominal viscosity of 3,000 cps, which is much higher than the PC40-UMF. Thus it is expected that the viscosity of PC40-UMF mixed with XP2742 will increase more than PC40-UMF alone as solvent evaporates.

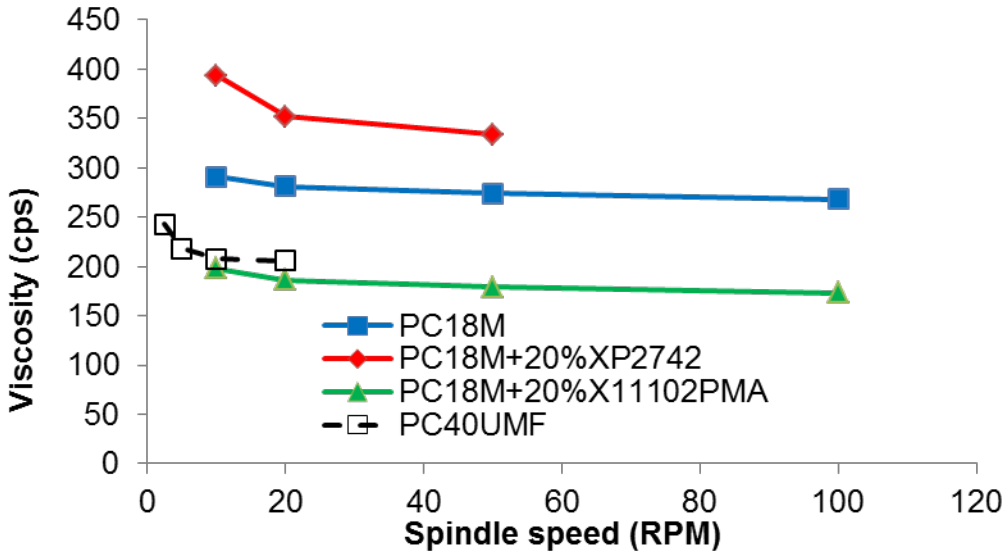


Figure 1: Viscosity versus spindle speed of PC18M, PC18M+20%XP2742, PC18M+20%X11102PMA, and PC40-UMF. Measurements were made using the Brookfield small sample adaptor.

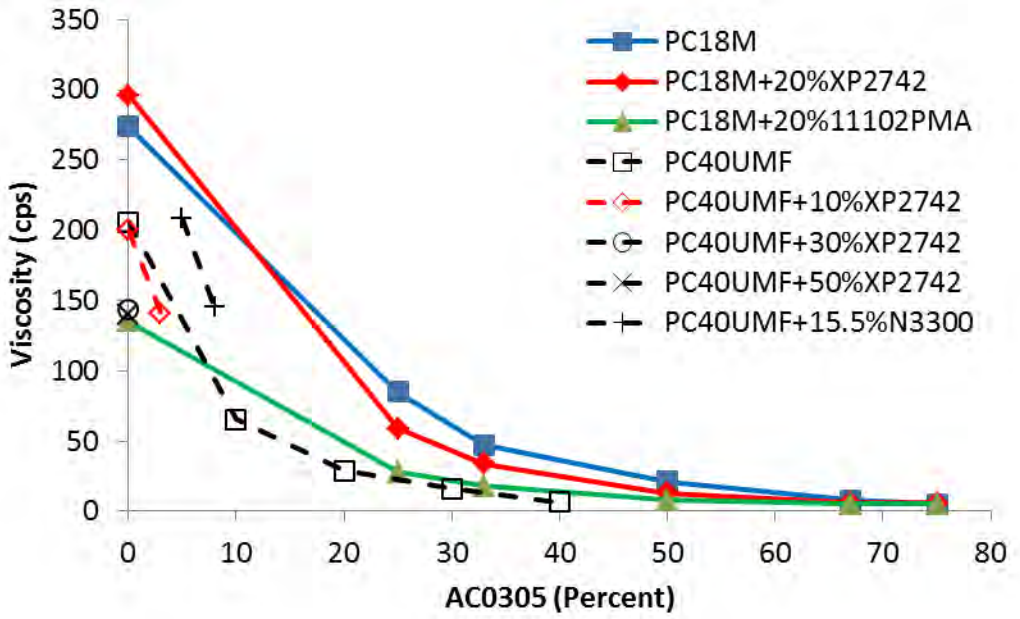


Figure 2: Viscosity versus %AC0305 solvent addition to the PC18M and PC40-UMF coating families. Measurements were made using the Brookfield small sample adaptor at 20 RPM for the PC40-UMFfamily and 50 RPM for the PC18M family of coatings.

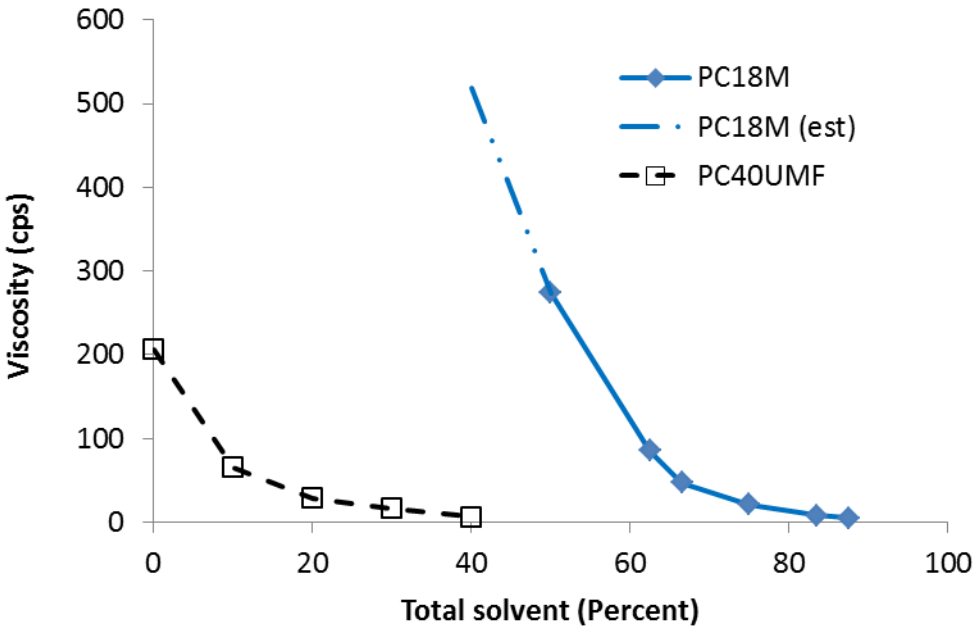


Figure 3: Viscosity versus total solvent percentage for PC18M and PC40-UMF.

2.2 Viscosity and contact angle for gap flow test

The normal PC40-UMF base viscosity is typically 250 cps. The base PC40-UMF viscosity was increased further by decreasing the monomer with respect to the oligomer in the liquid. A modified PC40UM with a viscosity of 500 cps was formulated. The PC18M viscosity was reduced to 100 cps by adding AC0305 solvent (Figure 4).

The contact angles of six drops were measured on glass slides. The addition of solvent to the PC18M resulted in a slight reduction of contact angle (Figure 5). In contrast, the PC40-UMF surface tension did not change with decreasing monomer. The viscosity, density and contact angles for the preliminary coating dip experiment are summarized in Table 1.

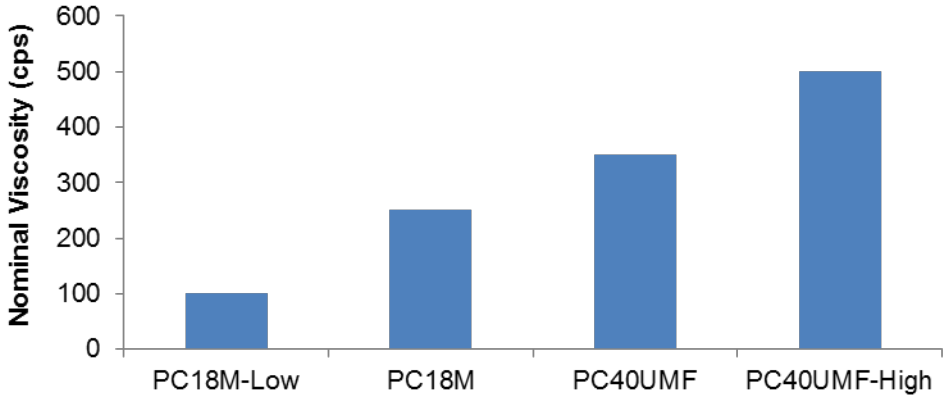


Figure 4: Viscosity of coatings used in the gap flow test.

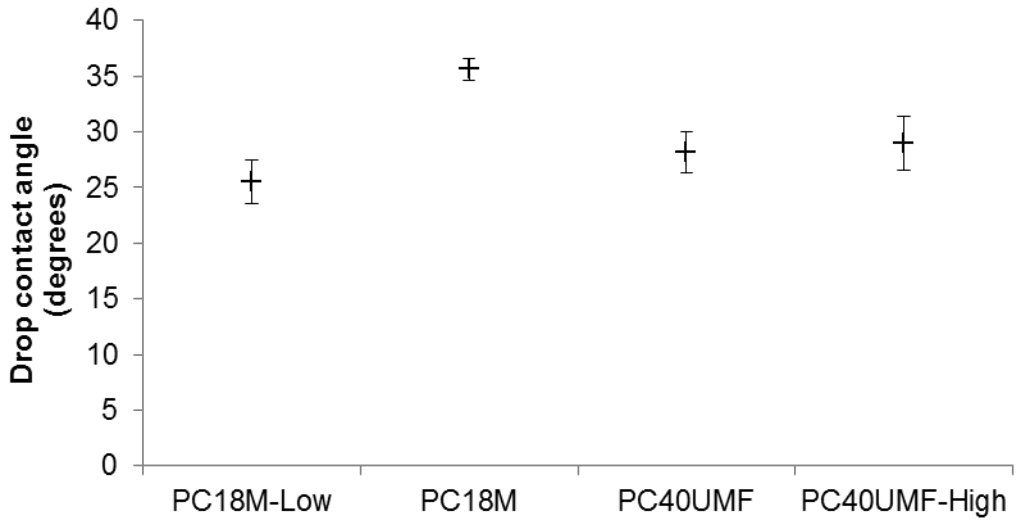


Figure 5: Contact angle, after one minute, of coatings used in the gap flow test.

Table 1: Unfilled PC18M and PC40-UMF viscosity, density and contact angle.

Coating	Viscosity (cps)	Viscosity (cps)	Density (g/cc)	Contact Angle (degrees)			
	Nominal	Measured		30 sec.	std dev	60 sec.	std dev
PC18M-Low Mod	100	102	1.035	26.21	1.88	25.56	1.96
PC18M	250	238	1.029	36.36	1.06	35.61	0.99
PC40-UMF	250	273	1.098	30.03	2.64	28.18	1.83
PC40-UMF- High Mod	500	570	1.130	30.36	1.29	29	2.4

2.3 Gap flow

The results of the parallel glass slide immersion test showed that at the 127 micron gap spacing voids formed for coatings ranging in viscosity from 100 to 500 cps (see Figure 6). This data suggested that dip coating at these viscosities would not be satisfactory because the coating would not be able to coat behind the leads without filling the entire region between the lead and the package body. When coating fills this region, low solder joint thermal cycling reliability can occur. These results were validated on a test board where the QFPs were dip coated. After coating the leads were cut on three sides and the package peeled up to reveal a lack of coating behind the leads. It was decided that a combination of a low viscosity dip and a spray coat would be used for the whisker test assemblies.

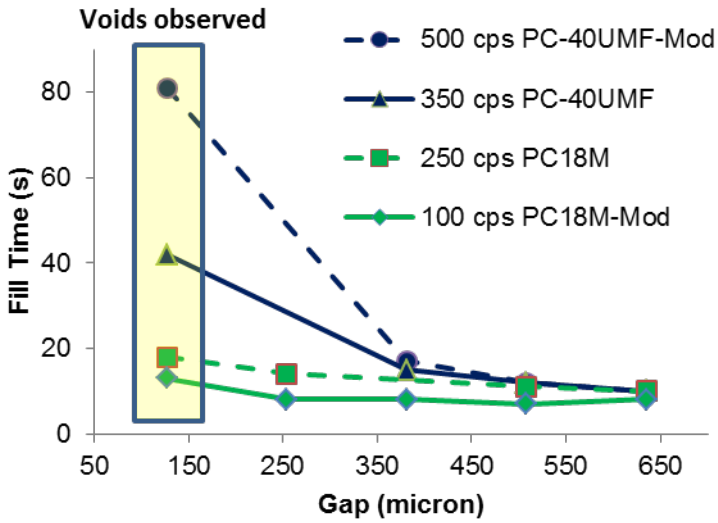


Figure 6: Parallel glass plate immersion test results.

2.4 Solvent evaporation

To guide the solvent evaporation time before UV exposure in the cure process, the solvent evaporation characteristics of PC40-UMF with 30%AC0305 and PC40-UMF+50%XP2742 were measured with the Thermogravimetric analysis (TGA) (Figure 7). After ~120 minutes, the weight changed very little indicating the remaining material is mostly PU resin. Another way to look at the data is to examine the amount of solvent in the sample over time. The residual solvent percentage was computed by subtracting the final weight percentage from the current weight percentage.

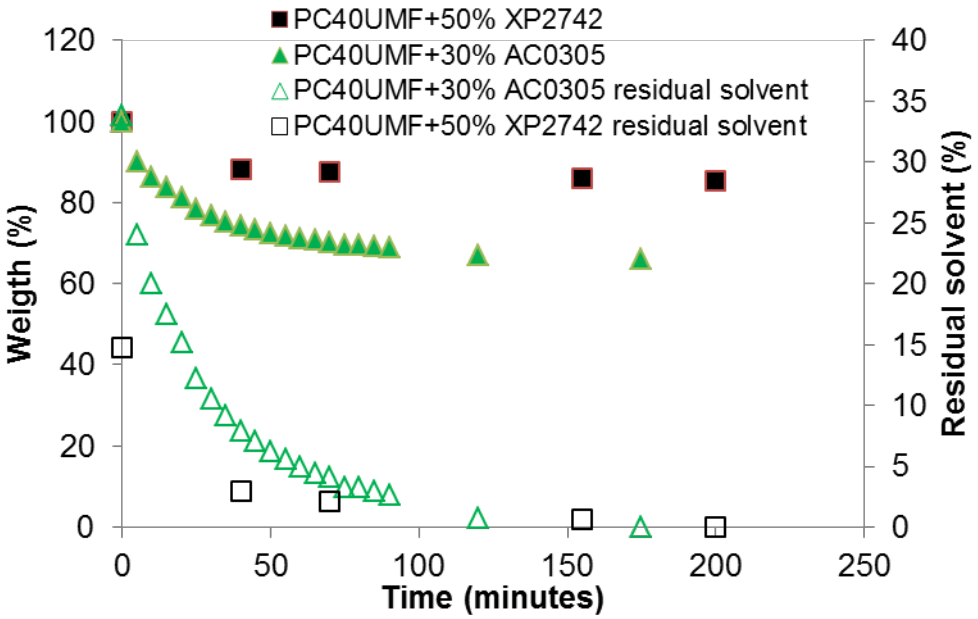


Figure 7: Solvent evaporation at 27 °C of PC40-UMF+30%AC0305 and PC40-UMF+50%XP2742 drawn liquid coating films 75 to 125 microns thick.

2.5 PC40-UMF+XP2742 PhotoDSC cure testing

The photo DSC was performed on the PC40-UMF + X2742 coating mixtures (Figure 8, Table 2, Figure 9, and Figure 10). Values for the onset of cure time, t_{onset}, the time at the exotherm maximum, t_{max}, and the time difference, t_{max} minus t_{onset}, were similar for all samples. This shows no reduction in cure speed. Exotherm values decreased with increased % XP2742. This is expected as XP2742 is not photo reactive and thus the addition reduced the amount UV sensitive acrylate components. Based on these Photo DSC results it can be concluded the introduction of nanosilica-particles had little or no impact on Ultraviolet (UV) cure of PC40-UMF.

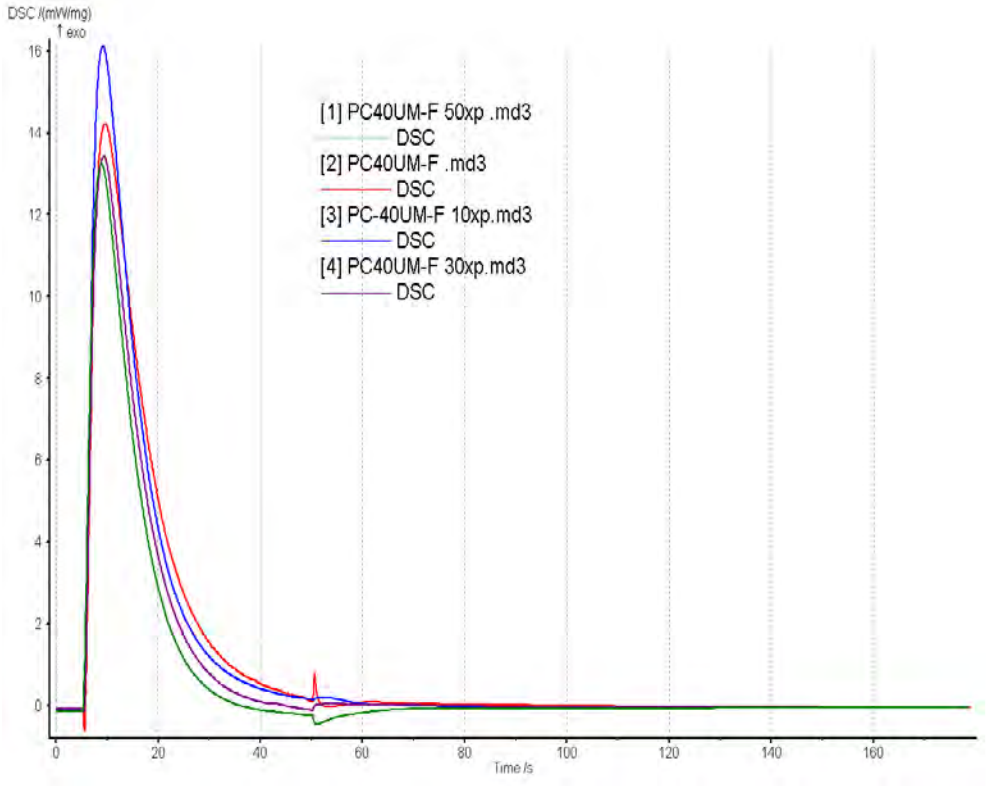


Figure 8: PC40-UMF nanosilica coating family photoDSC output exotherm (mW/mg) versus time.

Table 2: Photo DSC data for PC40-UMF+10%XP2742, PC40-UMF+30%XP2742, and PC40-UMF+50%XP2742.

Sample	Replicate	t_{onset} (s)	t_{max} (s)	t_{max}-t_{onset} (s)	Exotherm (J/g)
PC40-UMF	1	5.9	9.4	3.5	186
PC40-UMF	2	6	9.8	3.8	182
PC40-UMF	Average	6	9.6	3.7	184
PC40-UMF+10%XP2742	1	5.7	9.3	3.6	197
PC40-UMF+10%XP2742	2	5.9	9.3	3.4	181
PC40-UMF+10%XP2742	Average	5.8	9.3	3.5	189
PC40-UMF+30%XP2742	1	6	9.5	3.5	150
PC40-UMF+30%XP2742	2	5.9	9.5	3.6	148

Sample	Replicate	t_{onset} (s)	t_{max} (s)	t_{max}-t_{onset} (s)	Exotherm (J/g)
PC40-UMF+30%XP2742	Average	6	9.5	3.6	149
PC40-UMF+50%XP2742	1	5.8	9.9	4.1	126
PC40-UMF+50%XP2742	2	5.6	9	3.4	136
PC40-UMF+50%XP2742	Average	5.7	9.5	3.8	131

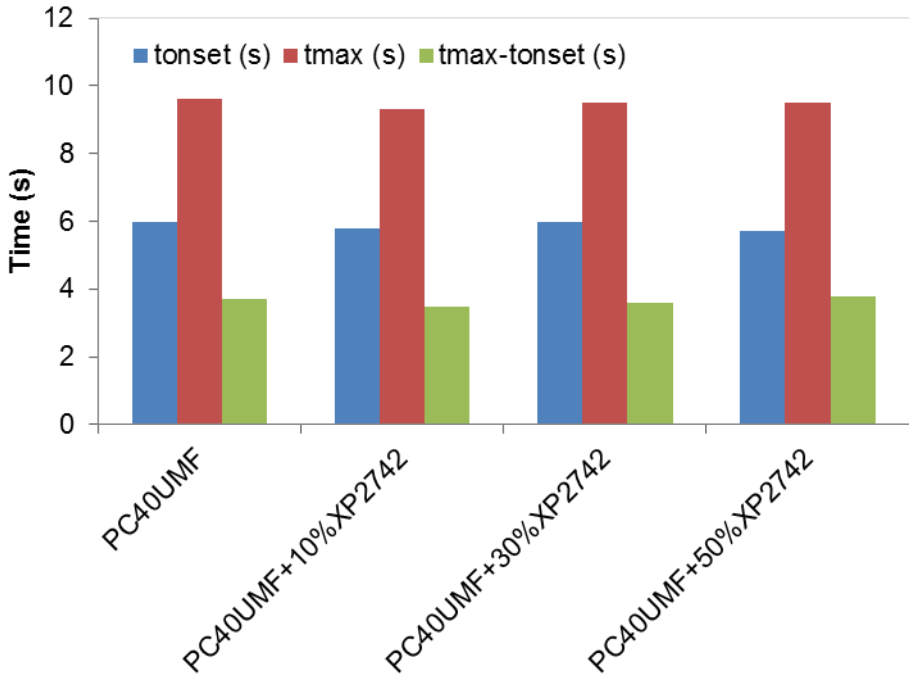


Figure 9: Photo DSC results for the cure time characteristics for PC40-UMF, PC40-UMF+10%XP2742, PC40-UMF+30%XP2742, and PC40-UMF+50%XP2742.

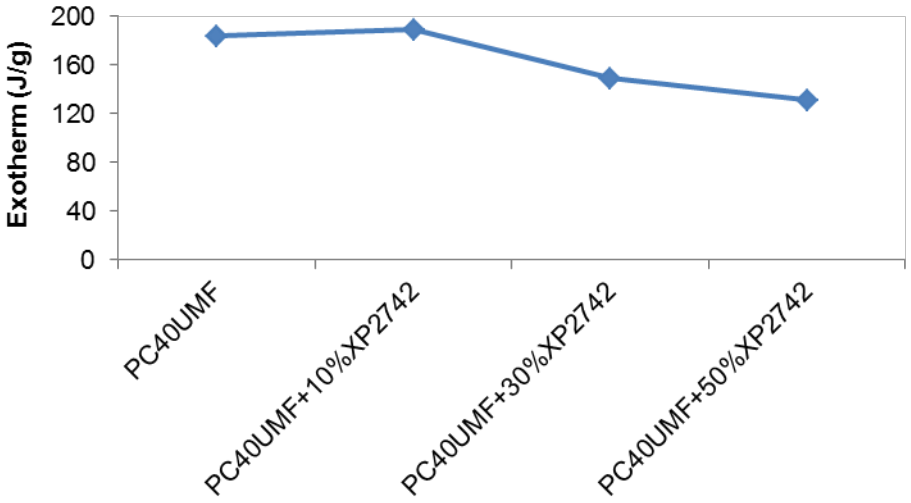


Figure 10: Photo DSC exotherm results for PC40-UMF, PC40-UMF+10%XP2742, PC40-UMF+30%XP2742, and PC40-UMF+50%XP2742.

3. Solid material microscopic examination

The performance of the conformal coatings is strongly influenced by nano- and microstructural features. To gain insight into the material behavior, the structural variations due to the nanoparticle addition were examined by a wide range of characterization methods including Atomic Force Microscope (AFM), Scanning Electron Microscope (SEM) and Transmission Electron Microscope (TEM). The microstructural characterization results generated through this study in relation with the concurrent results through chemical (IR spectroscopy) and mechanical testing combine to determine an optimum concentrations of nanoparticle addition to the coating which would in turn provide an ideal mitigation ability to tin whisker growth.

3.1 PC18M structure

The microstructure of PU (PC18M) consists of hard and soft segmented domains. The relative amount of these domains present in each coating is dependent on the amount of isocyanate hardener added. In Figure 11(a) networked structures are visible in the AFM height image, which are also shown in the cross sectional SEM image in Figure 11(b). These structures are soft domains of the polyurethane which are expected to evolve with changing amounts of isocyanate added with the nanoparticle suspension.

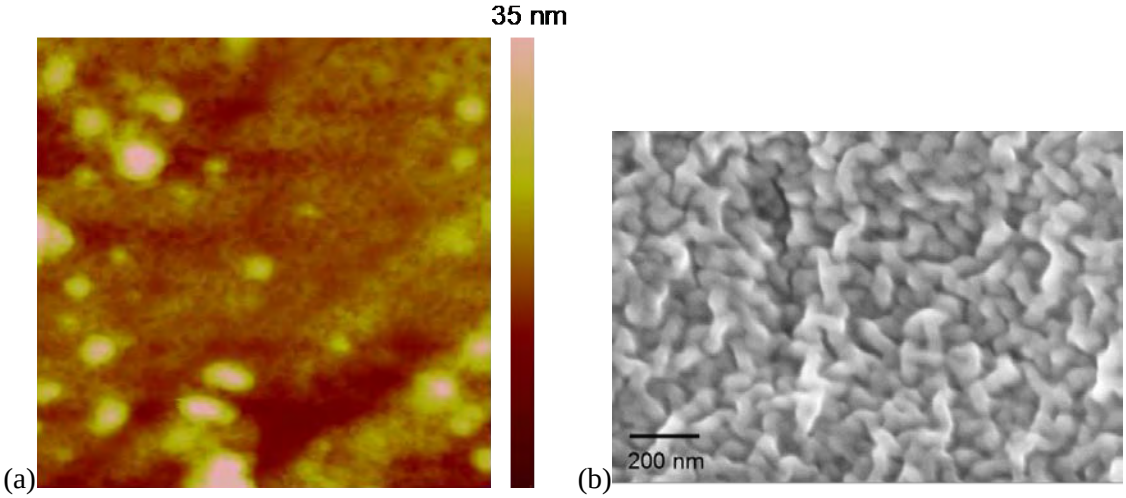


Figure 11: (a) AFM height image of 1 x 1 µm region of plain PC18M polyurethane coatings. (b) SEM cross-sectional image of the plain coating.

3.2 PC18M with XP2742 nanosilica

With an addition of nanosilica particle suspension (XP2742) that also contains isocyanate, the microstructure of the PU changes, in which hard segments become more segregated to have hard domains more separated from the network. These domains (more clearly visible in the phase image) were observed until the addition of XP2742 reached to ~ 30%. Figure 12 shows two AFM images with such hard domains noted in bright contrast.

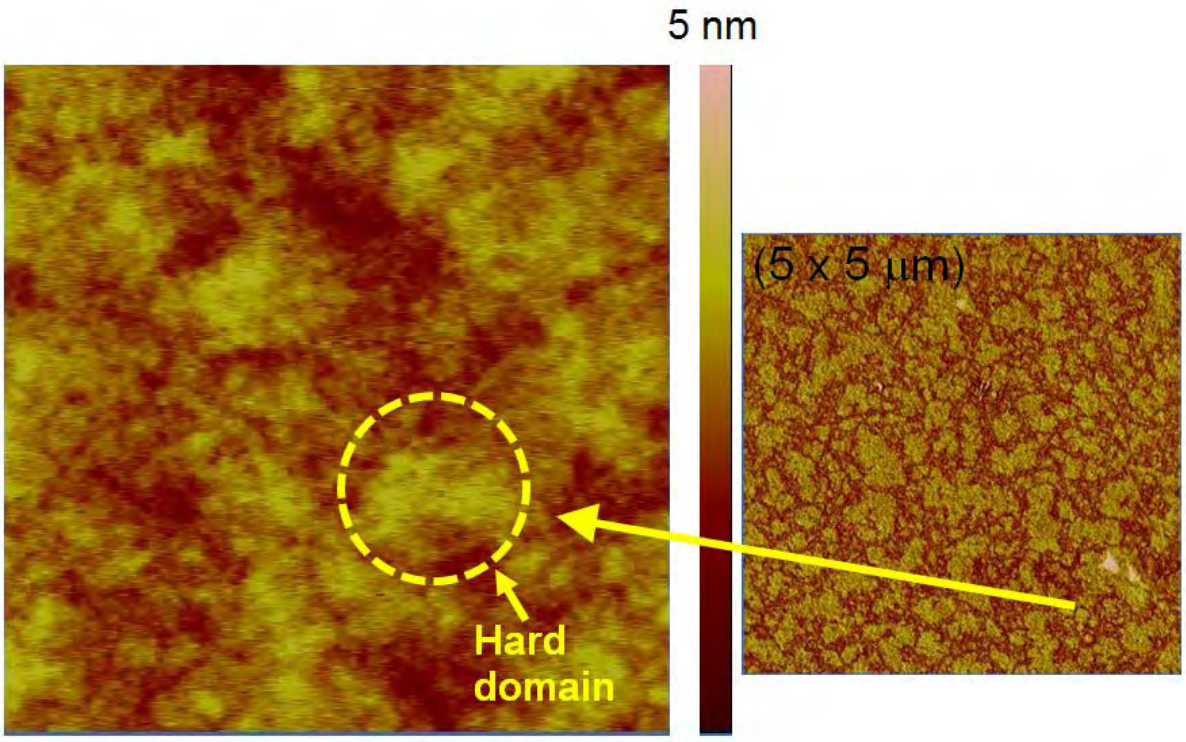


Figure 12: AFM height image of 1 x 1 µm region of PC18M + 20% XP2742 (6.7 wt. % SiO_2). (Inset) Phase image of a 5x5 µm region of the same coating.

The structural changes in the PC18M with XP2742 additions were also evident in the cross-sections. When 20%XP2742 nanosilica suspension was added, the microstructure changed such that the dimpled domains were surrounded by the network (Figure 13(a)). Well dispersed nanosilica particles were also seen in this image. The relative amounts of the hard and soft domains present in each coating were dependent on the amount of isocyanate hardener added. Increasing amounts of the nanosilica suspension consequently increased the added isocyanate (HDI trimer), thereby resulting in higher hard segment concentration in the coating. This increase in hard segments within the coating leads to small hard domains forming in the PU matrix microstructure.

A similar network structure, although much finer, was seen for the 30% suspension case in Figure 13(b). The increased hard segment concentration in the coatings began to show the brittle microstructure with more than 30%XP2742 suspension. This was noticeably demonstrated in the 50%XP2742 addition case by small and localized nanocracks as shown in Figure 13(c). These cracks might have formed during the sample fracture process (also, shown during the microtome slicing process). This is a consequence of not only the increased isocyanate concentration, resulting in the hard segment increase, but also a result of an increased formation of polyurea in the coating with an increase in the isocyanate content. The polyurea serves as another hard segment in the polyurethane network that can provide the defect sites. Furthermore, this polyurea formation generates carbon dioxide gas as a by-product resulting in inclusions such as gas bubbles in the coating.

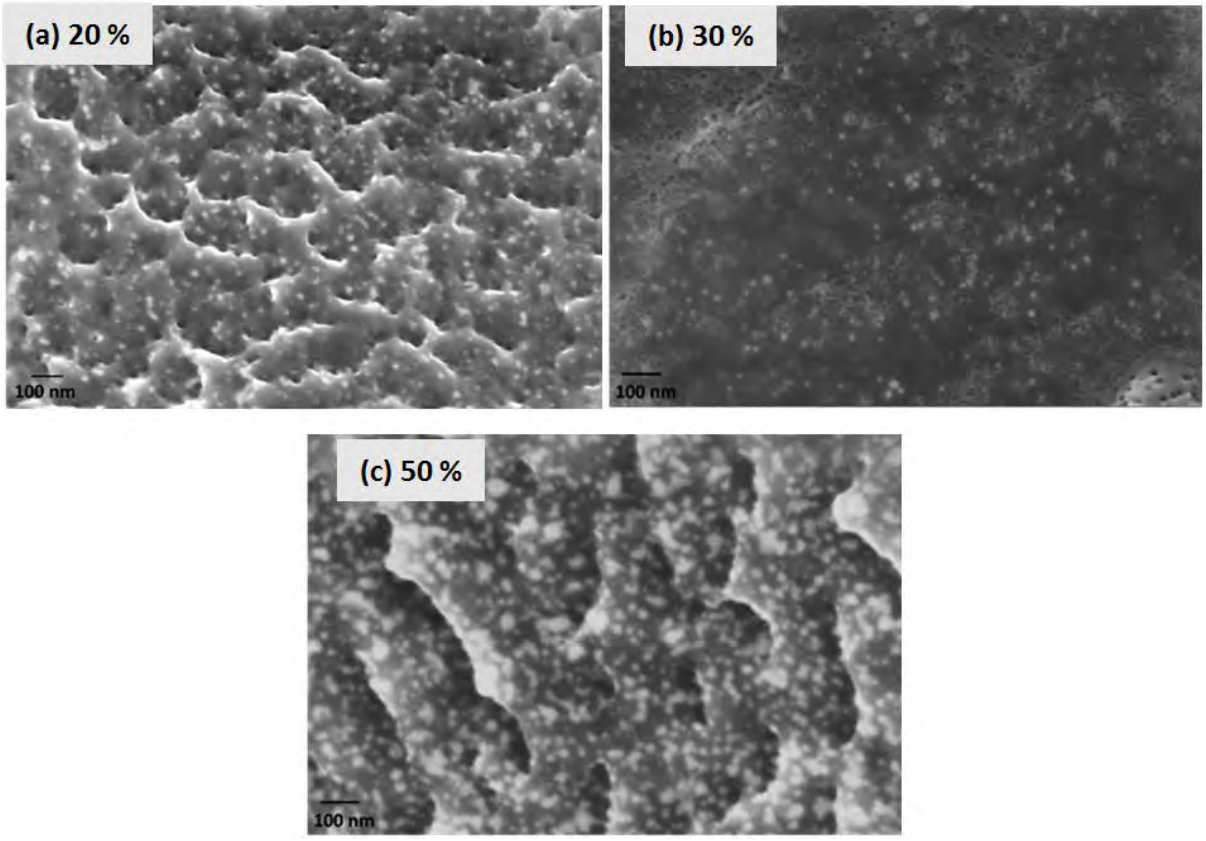


Figure 13: SEM cross-sectional images of cryo-fractured nanosilica filled PC18M coatings: (a) 20% XP2742, (b) 30% XP2742, (c) 50% XP2742 filled.

The distribution of nanoparticles within the polymer matrix was in general uniform with no evidence of extensive settling up to the 20% XP2742 suspension. However, some settling began to occur when 30% suspension or more was added, as shown in Figure 14. The bottom side of the PU coating shows more nanosilica particles than the top side. Even with the particle settling, particle agglomeration was largely absent in all compositions as confirmed by TEM studies.

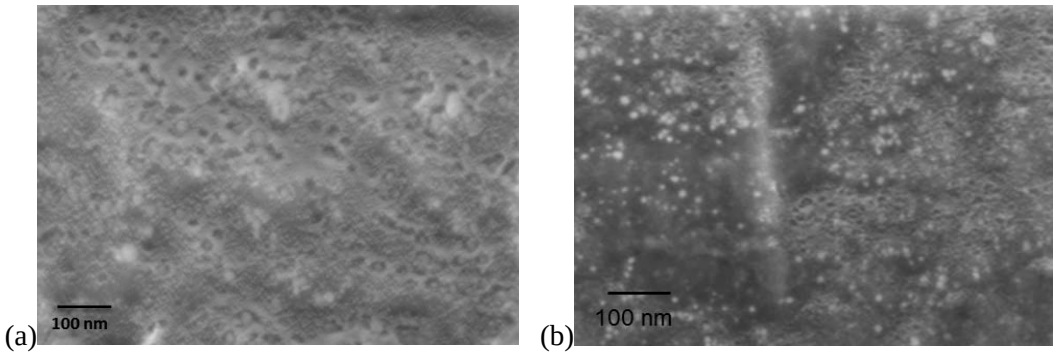
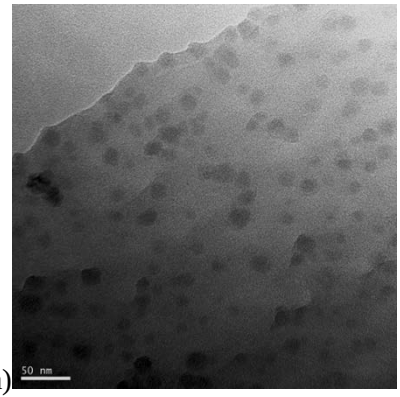


Figure 14: Polyurethane with 30% XP2742 nanosilica suspension addition; (a) particle distribution in the top region of the coating, and (b) particle distribution in the bottom region.

Individual nanosilica particle size was ~20 nm in diameter for all compositions and there was no significant agglomeration. It confirms proper surface functionalization of the nanoparticles with an isocyanate group (-NCO). TEM analysis confirms this finding and further facilitates viewing of

individual nanoparticles. In Figure 15, particles were seen to be well distributed as well as monosized. Further, there was very little agglomeration behavior noticed, even though the suspension addition was 50% XP2742. In some isolated regions, there were agglomerations observed as shown in Figure 15(b), but were very rare across the whole film region.

(a) 

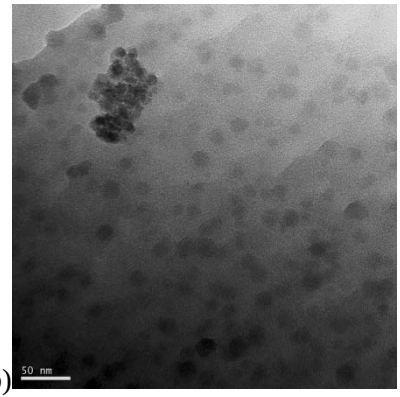
(b) 

Figure 15: TEM images of polyurethane with 50% XP2742 nanosilica suspension addition; (a) particle distribution at one end of the coating, and (b) an example of the agglomeration.

3.3 PC18M with Nanophase X11102PMA nanoalumina

The PU films filled with the nanoalumina suspension (X11102PMA) show a networked structure similar to the unfilled PU films for a 4% suspension addition of alumina (Figure 16). Unlike the nanosilica-filled PU films, hard domains are not clearly visible in the AFM images.

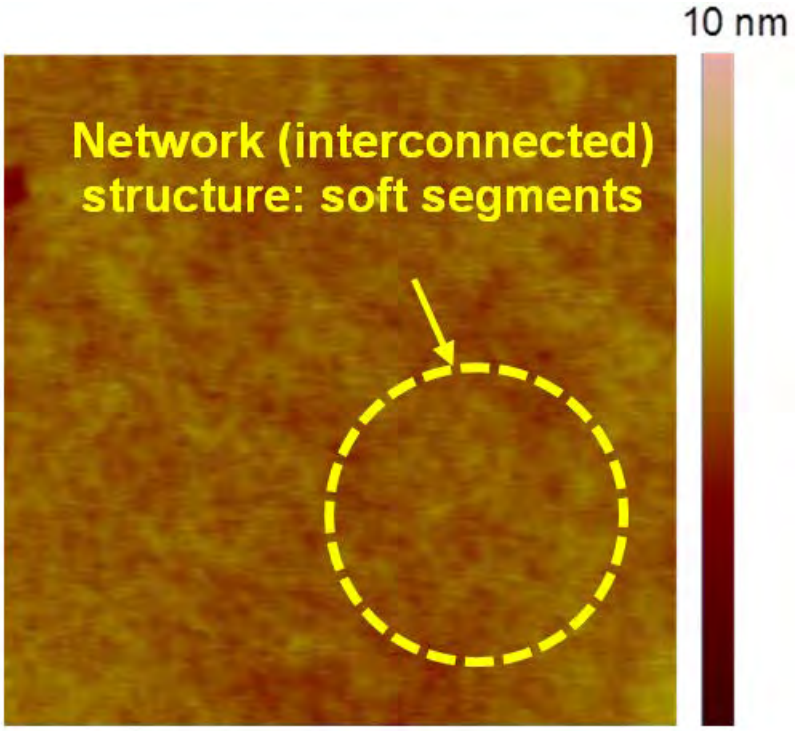


Figure 16: AFM height image of a 1 x 1 µm region of PC18M + 4% X11102PMA nanoalumina filled polyurethane coating.

For the nanoalumina-filled PU coating case, since these particles (Nanophase X11102PMA) were not functionalized, a strong agglomeration behavior was observed in Figure 17 even with the 4% suspension. Those agglomerated particle clusters were still sub-micron sized in most of cases but were in stark contrast with the nanosilica case, which exhibited dispersed individual particles with no significant agglomeration (even at the 50% silica suspension). On the other hand, microcracks that were present in PU coating with 50% XP2742 (Figure 13(c)) were not observed, indicating that PU matrix did not become brittle with increasing the amount of particle suspension with X11102PMA Al_2O_3. The voids between the particles and the PU in the microtome sliced nanoalumina sample indicated that the particles were not bonded to the PU matrix (Figure 17(a)).

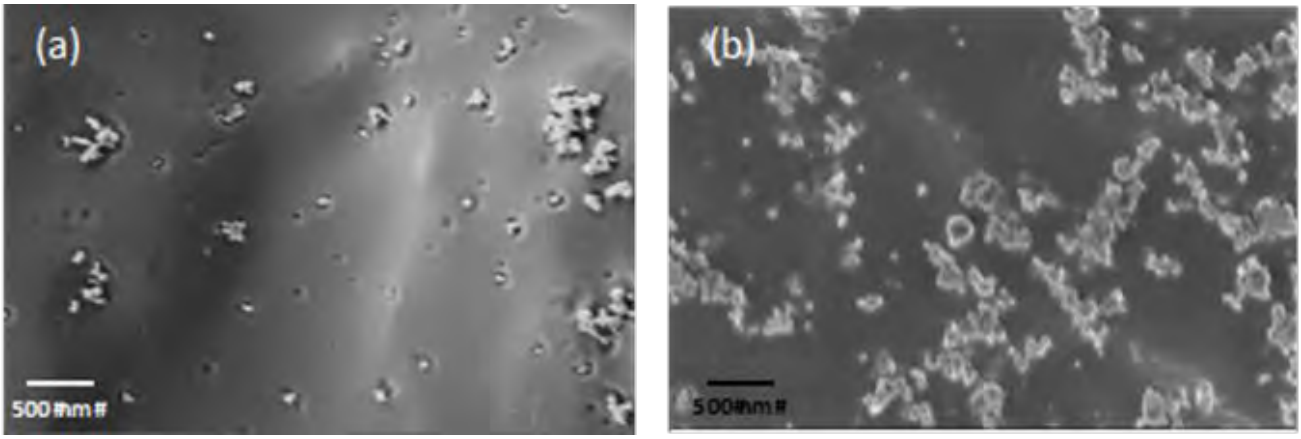


Figure 17: Cross-sectional SEM images of polyurethane films with (a) 4% X11102PMA (b) 20% X11102PMA Al_2O_3.

In an effort to observe individual nanoparticles more clearly within the agglomerated clusters, cryo-TEM observation was done using a cold stage. Figure 18 shows a cross-sectional TEM image of a nanoalumina-filled PU film, where individual nanoparticle shapes and sizes were visible within those clusters. The particle size distribution was much wider than the nanosilica case. Based upon multiple TEM images, many particles have the sizes greater than 100 nm, as well as about ~ 10 nm, even though the nominal particle size was 40 nm according to the specification data. The average particle diameter was confirmed to be about 70 nm, with a range from 20 to 200 nm, based upon the dynamic light scattering measurements of the suspensions.

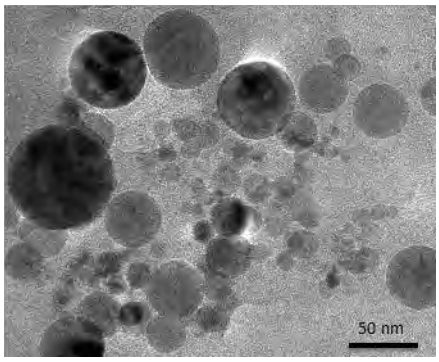


Figure 18: Cross-sectional TEM image of nanoalumina-filled PU coating.

3.4 PC18M with Polymaterials nanoalumina initial evaluation

During the development of the Polymaterials nanoalumina, the lessons learned from the Nanophase suspension development were applied. All solvents were specified to be PU grade and no chemistry that evolved alcohol was used. In addition, sample films of PC18M and PC40-UMF were made and examined in cross-section to evaluate particle bonding and dispersion.

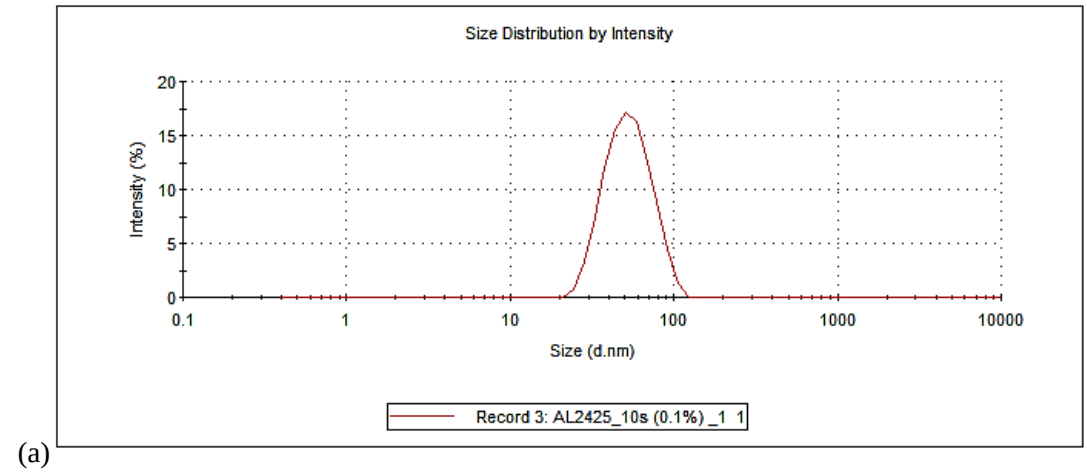
With the objective to better integrate and disperse alumina nanoparticles within the polyurethane matrix, suspensions of several different compositions of nanoalumina particles were created for microstructural examination. These suspensions were mixed with dispersion agents and the surface of the particles was functionalized to provide their enhanced integration into the PU matrix. Two sets of samples, one set with nanoparticles dispersed before functionalization in the suspension (WTA996 and KEK071) and another with functionalization prior to dispersal (WTA997) were prepared for cross-sectioning as shown in Table 3.

Table 3: Sample names and compositional information for Polymaterials initial functionalized nanoalumina suspensions evaluated in the cross-sections.

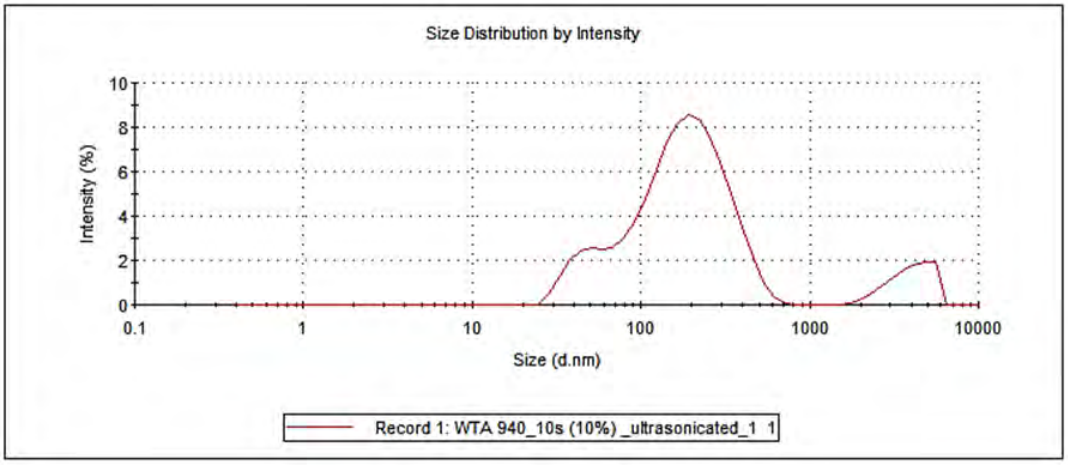
Sample Name	% Base Polyurethane (PC18M)	% addition of Nanoalumina suspension	% addition dispersant	% of solid nanoalumina in finished coating
Dispersed then functionalized				
WTA996-8A-15D-80H	80	8	15	15.6
WTA996-8A-15D-87H	87	8	15	10.2
WTA996-8A-15D-93H	93	8	15	5.50
KEK71-8A-25D-87H	87	8	25	9.40
KEK71-8A-25D-80H	80	8	25	14.5
Functionalized then dispersed				
WTA997-8A-7D-87H	87	8	7	10.8
WTA997-8A-25D-87H	87	8	25	9.40

For an estimation of particle distribution in the suspensions, two suspensions of nanoalumina, AL2425 (non-functionalized; only with a dispersant) and WTA940 (functionalized) were both diluted in propylene glycol monomethyl ether acetate (PMA) and then analyzed using a dynamic light scattering (DLS) technique. Figure 19(a) shows the size distribution with respect to the intensity of the scattering in case of the AL2425 suspension.

The size distribution in case of the non-functionalized AL2425 suspension shows a singular peak with a distinct maximum at ~54 nm while in case of the functionalized WTA940 suspension three local maxima were noted at 46nm, 205nm, and 4047nm (Figure 19(b)). For the functionalized case agglomeration of the nanoparticles was responsible for the two maxima (at 205 nm, 4047 nm) and the wider distribution compared to that of the AL2425. It also suggests that singly distributed particles were sparsely present but most of the particle agglomerations were still in the sub-micron range in this particle suspension. Very large particle sizes shown around the third peak (above > 1 micron range) could be due to the particle settling out of solution which is located at the bottom of the cuvette.



(a)



(b)

Figure 19: Size distributions of nanoalumina suspensions: (a) AL2425-non-functionalized and (b) WTA940-functionalized.

One function of the dispersant in the nanoparticle suspension is to negate the possibility of agglomeration of nanoparticles in order to disperse them well and obtain a uniform particle distribution. Surface functionalization of the nanoparticles has a similar function, but the organic molecule is bonded to a particle that ends with a specific functional group (isocyanate). Properly prepared surface end group prevents the particle agglomeration while having them well integrated to the polymer network that has a matching group to be bonded to. Two nanoalumina cases were compared in cross-sections: i) AL2425 – non-functionalized, only being added with a dispersant; ii) WTA940 – particle functionalized with no dispersant added. As seen in Figure 20, AL2425 (with a dispersant) exhibited well distributed particles in the PU matrix but showed extensive delamination (due to microtome slicing) between nanoparticles and PU matrix, as shown in Figure 20(a). On the other hand, WTA940 (functionalized, but without a dispersant) exhibited strong agglomeration as shown in Figure 20(b), indicating the surface functionalization scheme was not optimized yet. WTA940 did, however, show a stronger bonding between the nanoparticles and the PU matrix.

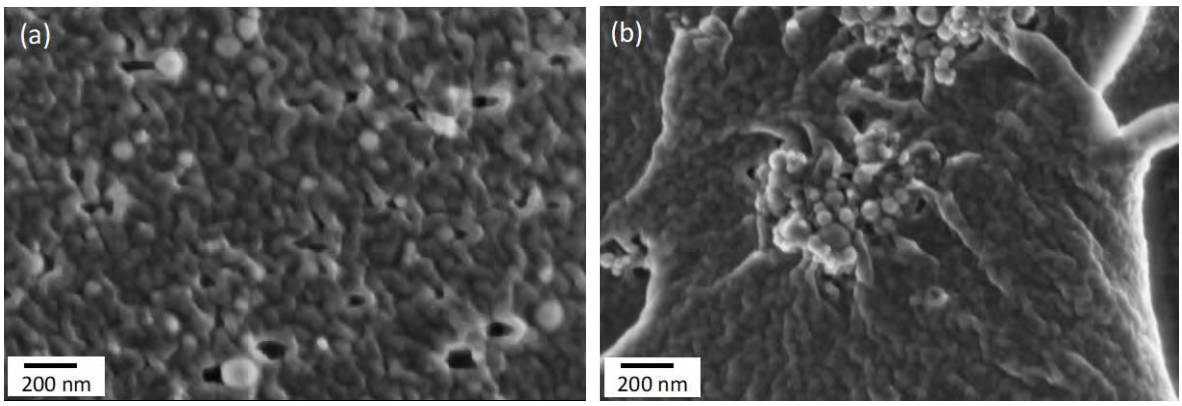


Figure 20: Cross-sectional SEM images of microtome sectioned nanoalumina-filled PC18M: (a) AL2425; (b) WTA940.

Dispersed nanoalumina suspensions were further treated with surface functionalization to evaluate the nanoparticle performance. In Figure 21, a microtome sliced cross-section of WTA996-8A-15D-87H is compared to a sample with more dispersant (KEK71-8A-25D-87H) to analyze the effects of increasing dispersant. Both samples show certain amounts of agglomeration with the former having extensive settling and large agglomerates (~ 10 microns). Despite some settling, the higher amount of dispersant (25%) showed much less agglomeration and settling behavior.

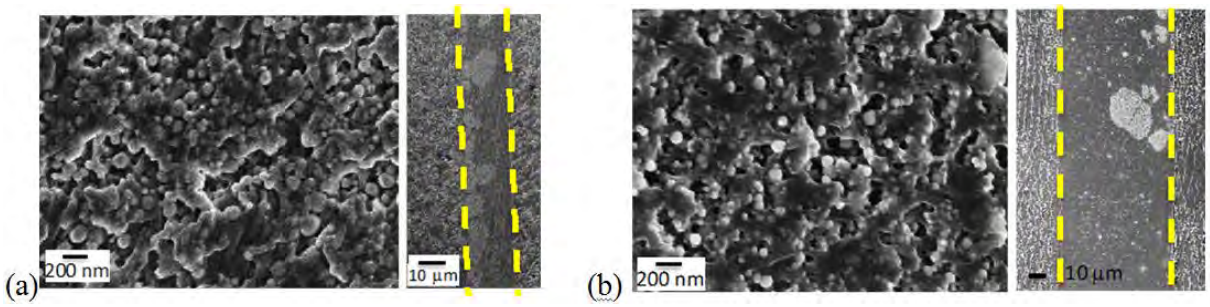


Figure 21: Cross-sectional SEM images (high magnification view and the entire thickness overview) of PU films filled with nanoalumina; (a) WTA996-8A-15D-87H and (b) KEK71-8A-25D-87H.

Previous PU films filled with functionalized nanoalumina (WTA940) did not display good dispersion as shown above. Thus, the dispersant was added to the functionalized suspension (WTA997 batch), and one example is shown in Figure 22(a). This batch showed slight improvement in terms of the particle dispersion (due to the addition of the 25% dispersant after a functionalization treatment) but still had the agglomeration behavior in the PU film. Compared to that of the reversed formula (i.e., KEK batch; adding the dispersant, followed by the surface functionalization), it showed stronger agglomeration behavior. The KEK batch seemed to disperse the particles better (Figure 22(b)). WTA997 batch (functionalized then dispersed), however, lessened the agglomeration behavior, as compared to WTA940, but the particle adhesion to the PC18M PU was generally not as good as the KEK71 or the WTA996 suspensions.

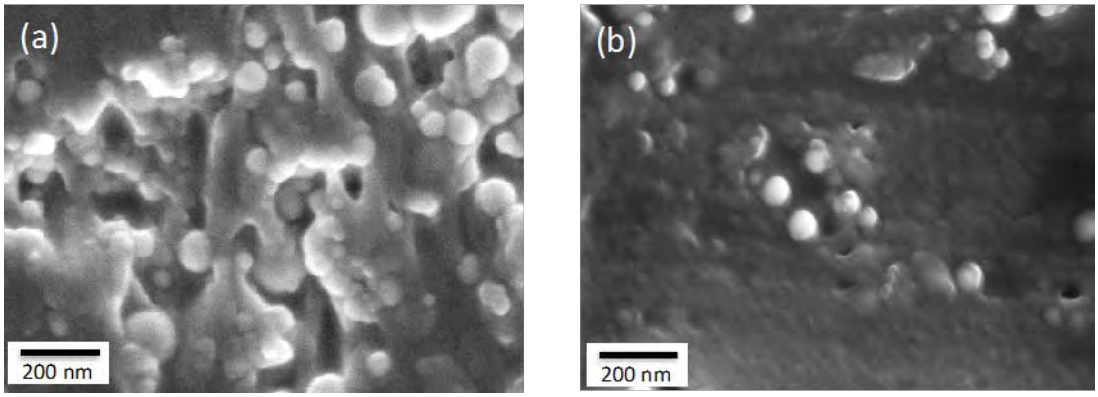


Figure 22: Cross-sectional SEM images of PU films filled with nanoalumina; (a) WTA997-8A-25D-87H and (b) KEK71-8A-25D-87H.

The best dispersion and the least settling of the particles occurred in the batch WTA996-8A-15D-93H that is shown in Figure 23. It is noted that the trend of increasing dispersant (25%) coupled with the higher amount of PC18M content (93%) in this case causes better distribution and less agglomeration of particles. Higher concentrations of PC18M have the lower number of the nanoalumina particles present in the given PU volume, which results in less agglomeration behavior. More polyurethane appears between particles indicating better dispersion. But the WTA996-8A-15D-93H batch appeared to have more delamination around the particles from the microtome slicing.

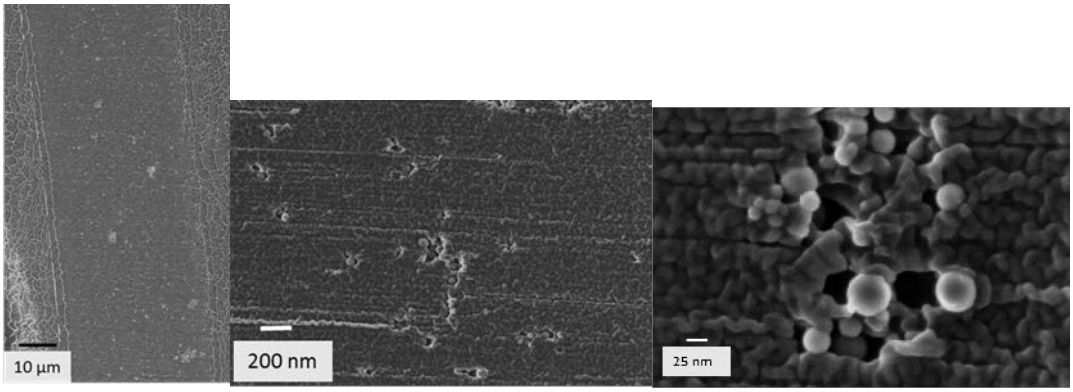


Figure 23: Cross-sectional SEM images of WTA996-8A-15D-93H at various magnifications.

Higher dispersant amounts were noted to make the particles more separated, but do not appear to prevent agglomeration effectively. So far, WTA996-8A-15D-93H (best) and KEK71-8A-25D-87H appear to have the better particle dispersion compared to that of other batches. In both cases adding the dispersant prior to particle functionalization seems to make the prevention of agglomeration more effective.

3.5 PC40-UMFstructure

3.5.1 PC40-UMFwith XP2742 Nanosilica

Figure 24(a) shows the cross-sectional overview of a cryo-fractured plain (unfilled) PUA (PC40) coating. Toward the top of the cross-section, fracture pattern of domains about ~10µm in size is noted which transition into a smoother region toward the mid-region. A ridge that appears pulled out during the fracture is shown toward the bottom of the coating. The domain structure, bound by crack growth paths, clearly indicates a brittle fracture near the top portion, as the fracture direction was from top to bottom part of this image, where some tearing occurred near the end of the fracture. Such domains

were not clearly defined for the PC18M case, which was more ductile. In addition, high-resolution images of each domain exhibit the 'wormy' network structure as shown in Figure 24(b). This network structure is finer, compared to that for PC18M, which is again indicative of more brittleness. Both smaller domain size and finer network structure are consistent with a limited ductility shown on the PC40-UMFcoatings that have total elongation less than 10%.

In order to improve mechanical properties, 10 to 50% XP2742 SiO_2 suspension was added to PC40-UMFresin. It corresponds to 1.88 to 10.7 wt.% of the nanosilica particles added. Figure 25 shows the microstructure of PC40-UMFcoating filled with 30% XP2742 SiO_2 suspension (6.0 wt.% nanosilica particles). Well-distributed nanosilica particles (~20 nm in size) are visible without much agglomeration in this SEM image. The network structure still remains even with the addition of the nanoparticle suspension. The void is also shown at the bottom of the image.

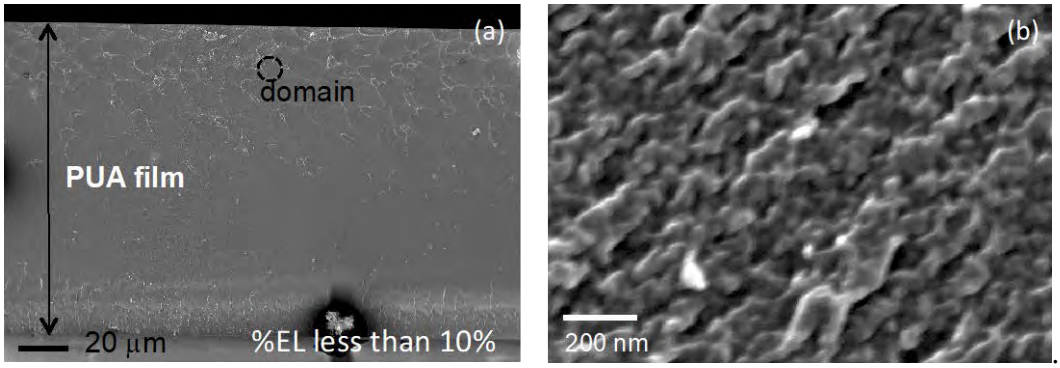


Figure 24: Cryo-fractured cross-section of a plain PC40-UMFcoating showing: (a) the entire thickness; (b) high magnification view inside the circled domain.

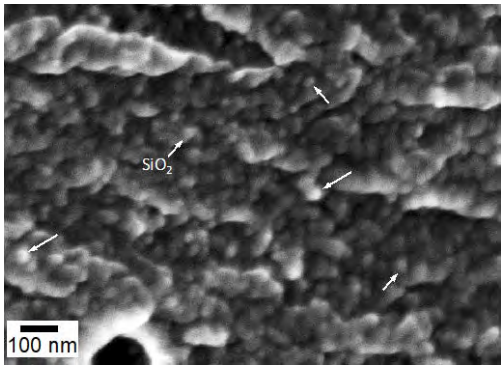


Figure 25: High resolution SEM image of cryo-fractured PC40-UMFcoating filled with 30% XP2742.

With the addition of XP2742 suspension that also contains isocyanate, PC40-UMFcoating microstructure becomes more brittle (Figure 26). As seen here, the domain size on the fracture surface decreases and the air bubbles (voids) became larger and more abundant with XP2742 suspension, compared to those on plain PC40-UMFcoating. The domain size is an indicative of the brittleness and the voids in the microstructure can lead to the crack initiation and the reduction in total elongation.

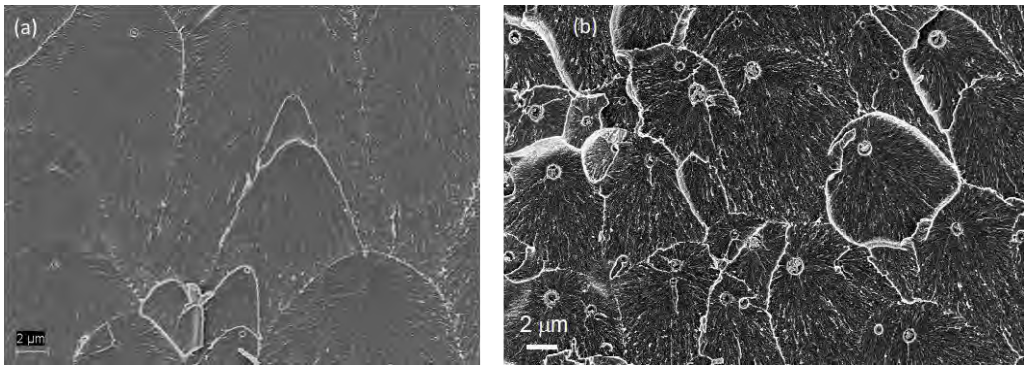


Figure 26: Cryo-fracture surface of PC40-UMFcoatings: (a) plain PC40; (b) PC40-UMFfilled with 30% XP2742.

The microstructures of nanoparticle-filled PC40-UMFcoating are shown in Figure 27 in more detail. Figure 27(a) shows an SEM image of a cryo-fractured cross-section of PC40-UMFcoating filled with 10% XP2742 suspension (3.5 wt.% nanosilica). PUA microstructure displays a network structure that is retained after adding the XP2742 suspension. This network structure appears finer than the plain PUA case. With increased addition of the XP2742 suspension to PC40-UMFcoating (Figure 27(b)), the microstructure appears to show more nanosilica which is well distributed and without agglomerations. The network structure is significantly finer than the plain or 10% cases. Furthermore, with nanosilica additions, more voids were observed, compared to the plain case, which were caused by the addition of more isocyanate via the XP2742 suspension.

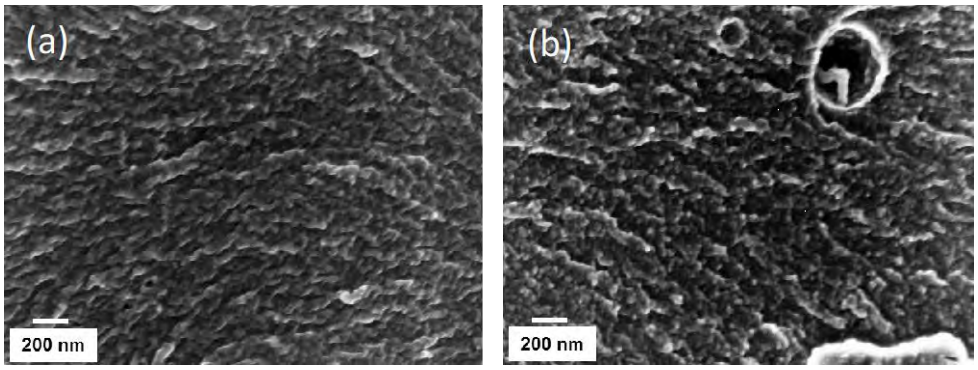


Figure 27: Cryo-fractured PC40-UMFcoatings filled with (a) 10% XP2742 SiO_2 suspension and (b) 30% XP2742 SiO_2 suspension.

The microtome sliced cross-section of the same PUA coating is shown in Figure 28(a). The coating section is interfaced with the epoxy encapsulation used for sample preparation. Scratch lines from the diamond knife are seen; oriented mostly vertical in the image. Some artifacts of the slicing process known as 'chatter' lines, running as broken lines perpendicular to the scratches, are also detectable but mostly within the epoxy region surrounding the coating. A sub-micron sized void is also shown, believed to be caused by trapped carbon dioxide (Figure 28(a), inset). Similar features were also observed on the cryo-fracture cross-section in the middle of the fracture features of PC40. High resolution imaging of the microstructure of this plain (unfilled) coating again reveals a 'wormy' networked structure as shown in Figure 28(b).

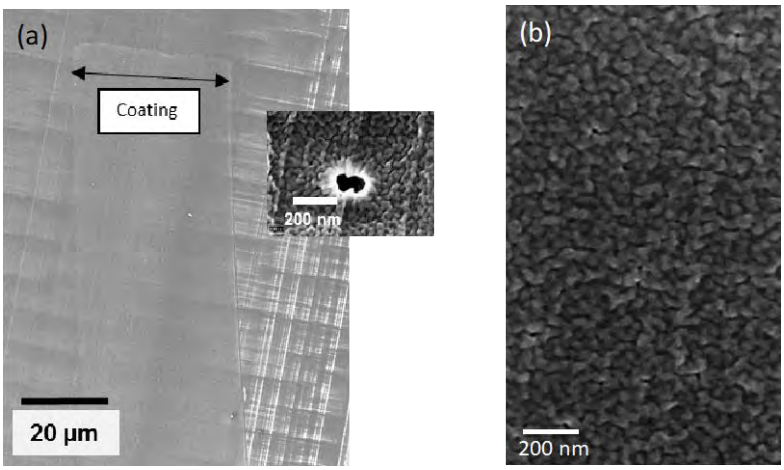


Figure 28: Microtome cross-section of plain PC40-UMFcoating, showing (a) entire thickness, inset: sub-micron sized void; (b) the network structure at higher magnification.

3.6 PC40-UMFwith Polymaterials nanoalumina

In an effort to achieve faster process time, lesser energy consumption, and more energy friendly process for the coating application, UV-curable films can be adopted. Since the coatings have a much higher curing speed than conventional water or solvent based coating technologies, higher production throughput is expected. This throughput is also supplemented by energy and cost savings from using such UV-curable polymer coatings. For investigating the applicability of such polymer systems to whisker mitigation coatings, PC40-UMF, a dual cure (UV + water curing) polyurethane acrylate system was used. Nanoalumina suspensions were added to this polymer resin to provide increased mechanical properties. To avoid the particle agglomeration, similar to those used in case of PC18M, two functionalization schemes were employed: i) dispersant addition followed by functionalization (WTA996); ii) functionalization followed by dispersant addition (WTA997).

Good dispersal of the nanoparticles within the polymer matrix was noted in the PU coating cross-section in case of the WTA996 samples (Figure 29). However, a continuous layer of settled particles was also observed. The inclusion of PU within the particle clusters (in the settled particle layer) was, however, suggestive of some amount of dispersion of the nanoparticles taking place within the polymer resin.

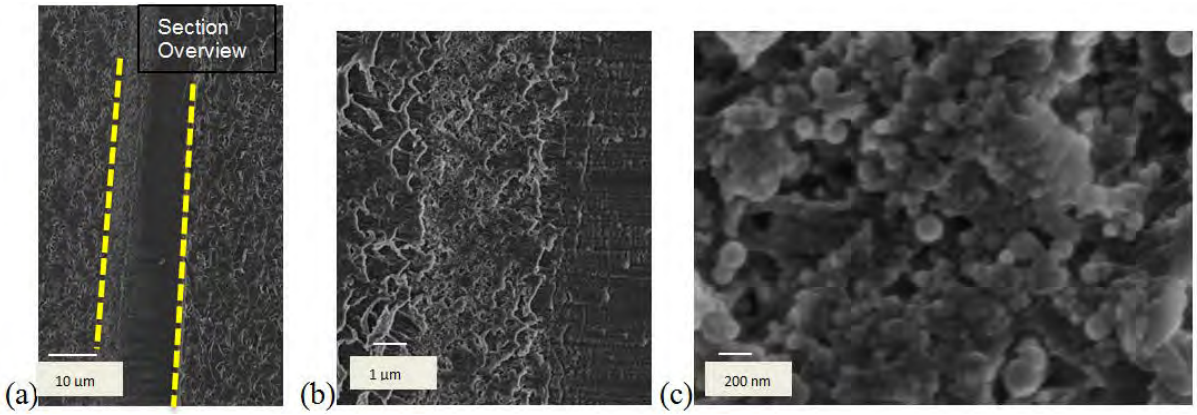


Figure 29: Cross-sectional overview image of WTA996 with PC40-UMF; (a) overall, (b) region of settled particles at one end of the coating, and (c) PU and nanoparticles in the settled layer.

In case of the PC40-UMF coating with the WTA997 suspension added, several micron sized agglomerates were noted across the cross-section, Figure 30. Although no significant settling was noted in the cross-section, the particle dispersion was observed to be poor in comparison with the WTA996 case. The appearance of PU within the particle clusters in this case was also less compared to the WTA996 case. This trend was similar to the case of functionalized nanoalumina added to the PC18M, in that the dispersal followed by functionalization scheme appeared to give better dispersion, although with still some residual settling and small scattered agglomerates.

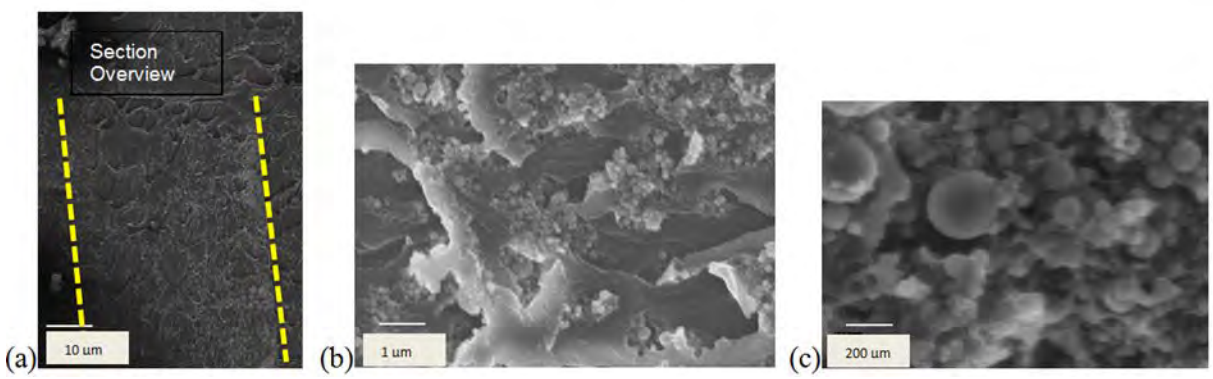


Figure 30: Cross-sectional overview image of WTA997 with PC40-UMF; (a) overall, (b) agglomeration within the PU film, and (c) particle agglomeration with very little PU in it.

3.7 Film microstructure summary

Nanoparticle-filled PC18MPU conformal coatings were analyzed using a combination of high-resolution and analytical tools for structural characterization. Plan-view AFM and cross-sectional microstructure characterization showed the presence of networked 'wormy' patterns and domain structures. These features disappeared beyond the 30%XP2742 addition of nanosilica suspension. This is consistent with the brittleness and premature failure observed in such compositions. The distribution of nanoparticles within the matrix was homogeneous at the 20%XP2742 suspension or lower, but it showed the particle settlement after 30%XP2742 suspension. There was no significant particle agglomeration observed even for the 50% nanosilica suspension case, which suggests that more particle addition could be possible if the brittleness observed in the PU matrix were prevented.

For the Nanophase nanoalumina-filled PC18M PU coating case (X11102PMA suspension), the particles were not functionalized, which resulted in strong agglomeration. Those agglomerated particles that are still sub-micron sized in most of cases are in stark contrast with the nanosilica case, which was rather individually populated with no significant agglomeration. Clustered particle groups were also clearly visible in TEM studies.

To reduce the agglomeration tendencies of the Polymaterials nanoalumina filled PU films, two improved surface functionalization schemes were attempted by Polymaterials; one by adding a dispersant followed by functionalization and another by functionalization followed by the dispersant addition. Higher polyurethane content with adequate dispersant content in case of the first scheme proved better in reducing the agglomeration behavior, but could not completely eliminate it. Further it reduced large micron sized settling of nanoparticles within the coating cross-section. The same scheme used with a UV-cured polymer base (PC40-UMF) with the Polymaterials nanoalumina suspension addition also showed similar effects.

4. Solid mechanical properties results

4.1 Fluid compatibility

The fluid resistance was evaluated for both the PC18M and PC40-UMF sets of PU materials. The PC18M family underwent slight softening after exposure (Figure 31). It was also noted that the PC18M coating regions touching the Skydrol liquid crazed. The P40UMF micro hardness was unchanged (see Figure 32).

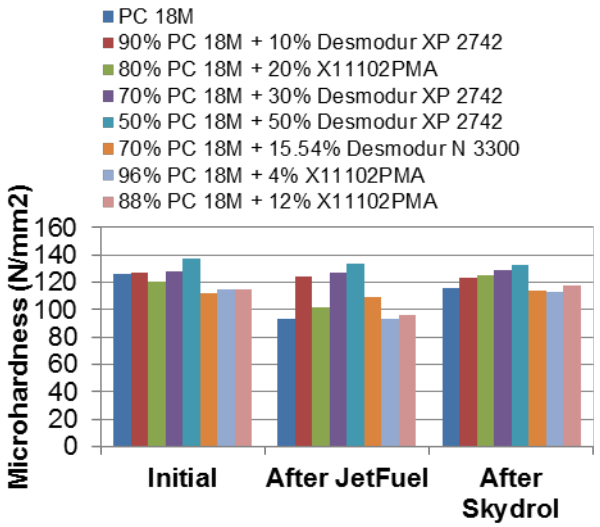


Figure 31: Fluid compatibility results for PC18M based materials.

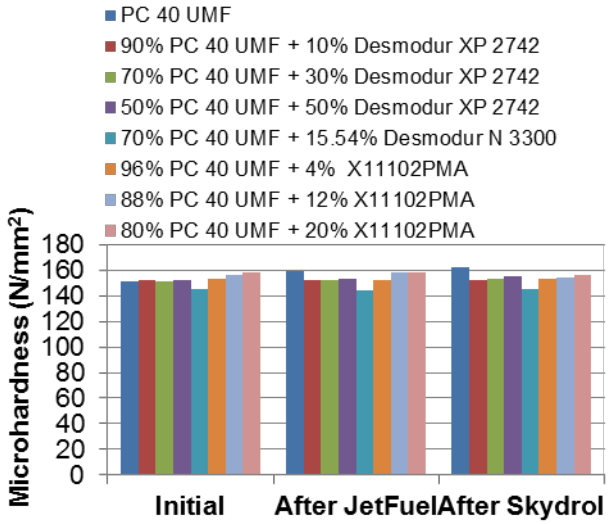


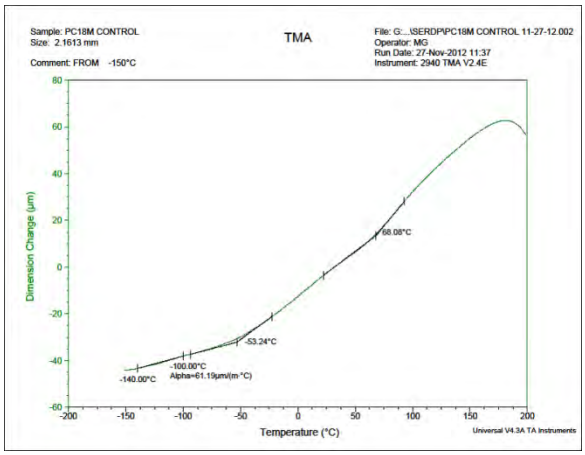
Figure 32: Fluid compatibility results for PC40-UMF based materials.

4.2 PC18M glass transition temperature and CTE TMA test

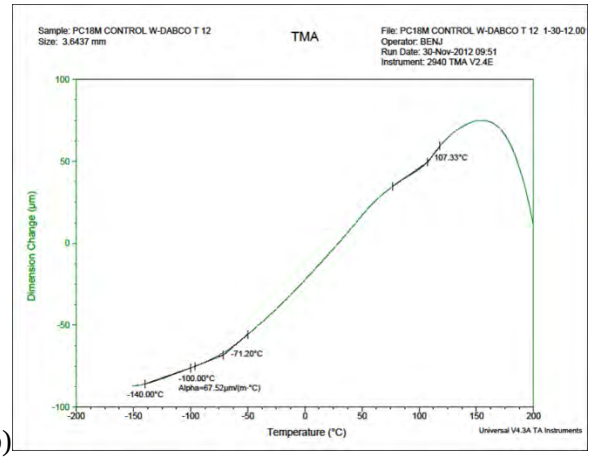
The thermomechanical analysis (TMA) was used to measure the glass transition temperatures and coefficient of expansion of the PC18M + XP2742 2.2 mm thick cast coatings. In addition, the hardness was recorded for the samples. The T_g for the base PC18M was 68°C and with the addition of the

Dabco T 12 accelerant was 107 °C (Figure 33, Table 4). Note the Dabco T 12 accelerant was added to reduce the cure time of the PC18M+XP2742 mixtures. The addition of the XP2742 reduced the T_g to the 44 to 46 °C range because of the lower T_g of the N3300 isocyanate.

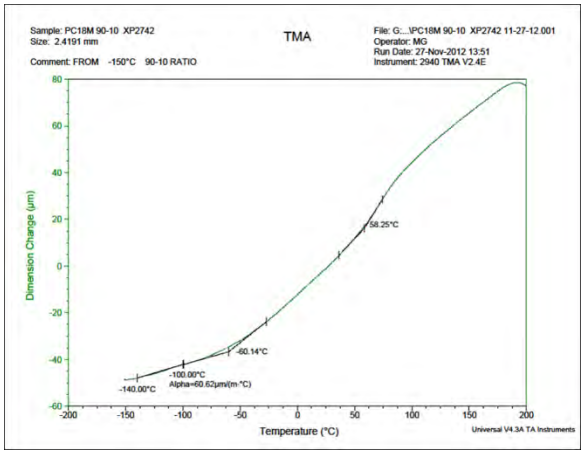
(a)



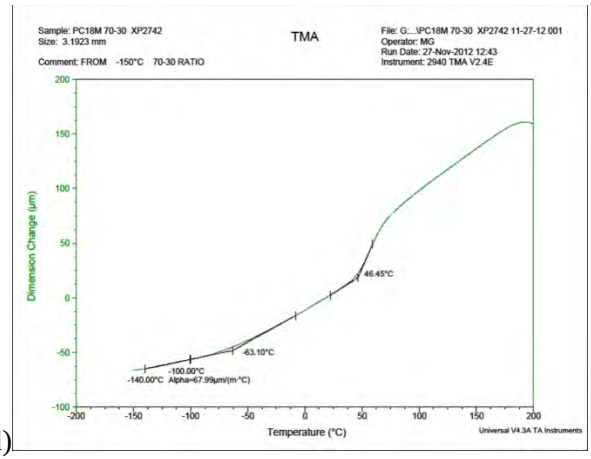
(b)



(c)



(d)



(e)

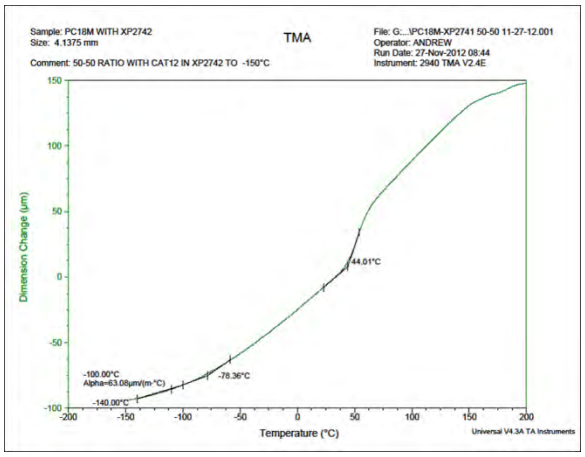


Figure 33: TMA measured expansion of (a) PC18M (control), (b) PC18M-modified with Dabco T 12, (c) PC18M+10%XP2742, (d) PC18M+30%XP2742 and (e) PC18M+50%XP2742.

Table 4: Summary of PC18M+XP2742 glass transition temperature, coefficient of thermal expansion and hardness

	PC18M Control	PC18M Control with Dabco T 12	90%PC18M+ 10%XP2742 Dabco T 12	70%PC18M+ 30%XP2742 Dabco T 12	50%PC18M+ 50%XP2742 Dabco T 12
First Tg single scan (°C)	-53.2	-71.2	-60.1	-63.1	-78.4
Second Tg single scan (°C)	68.1	107.3	58.2	46.4	44.0
Coefficient of thermal expansion (ppm/C) (-140 to -100C)	61.2	67.5	60.6	68.0	63.1
Hardness Shore D	60	64	62	65	65

4.3 PC40-UMF Coefficient of thermal expansion

Due to the moisture cure nature of the coatings, it was difficult to cast PC40-UMF films that were sufficiently thick without defects. More work is needed to determine a reliable film casting method.

4.4 Water vapor transmission

The water vapor transmission testing was performed for various concentrations of XP2742 in PC18M and PC40-UMF and for various concentrations of X11102PMA in PC18M. Increasing the XP2742 concentration in PC40-UMF increased the water vapor transmission rate slightly. In contrast, increasing the XP2742 concentration in PC18M resulted in a decrease in water vapor transmission rate (Figure 34). For reference the sample thicknesses are provided in Table 5. Since the 100%XP2742 has a 0.2083 g/(100cm^2-day) transmission rate, adding XP2742 to the PC18M (1.488 g/(100cm^2-day) rate) reduces the overall mixture transmission rate. Since the PC40-UMF base material water vapor transmission rate is already low (0.172 g/(100cm2-day)), the addition of the XP2742 tended to increase the value.

Evaluating the role of isocyanate contribution alone to the water vapor transmission rate, the PC40-UMF+15.54%N3300 (comparable to PC40-UMF+30%XP2742 without the nanosilica particles) value was 0.2123 g/(100cm^2-day), This was slightly less than the PC40-UMF+30%XP2742 value of 0.243 g/(100cm^2-day). This suggests that the nanosilica particles tended to increase the water vapor transmission rate.

The PC40-UMF cure impacted the water vapor transmission rate. The PC40-UMF moisture cure only (no UV) transmission rate of 0.242 g/(100cm^2-day) was higher than the PC40-UMF with the standard UV and moisture cure value of 0.172 g/(100cm^2-day).

A 20% concentration of X11102PMA non-functional nanoalumina particles in the PC18M resulted in a slight decrease in the water vapor transmission rate. Increasing the nanoalumina suspension concentration further, increased the transmission rate.

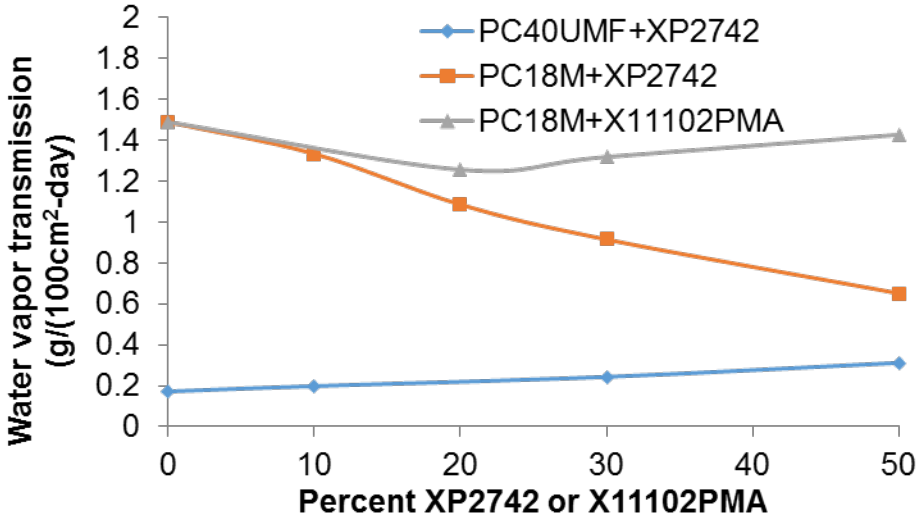


Figure 34: Water vapor transmission for various XP2742 or X11102PMA concentrations in PC40-UMF and PC18M.

Table 5: Water vapor transmission test sample thicknesses.

Coating	Thickness (microns)
PC40-UMF UV + Moisture (1)	116
PC40-UMF Moisture only (2)	55
PC40-UMF XP2742 90/10 (1)	104
PC40-UMF XP2742 70/30 (1)	87
PC40-UMF XP2742 50/50 (1)	64
PC40-UMF N3300 70-15.54 (2)	98
100% XP2742 + cat (2)	101
Note (1) Moisture + UV cure; (2) Moisture only cure	
PC18M	54
PC18M+10%XP2742	52
PC18M+20%XP2742	60
PC18M+30%XP2742	64
PC18M+50%XP2742	65
PC18M+20% X11102PMA	59
PC18M+30%X11102PMA	49
PC18M+50%X11102PMA	44

4.5 Hydrolytic stability

Board coupons coated with PC18M+20%XP2742 and PC18M+20%X11102PMA passed the 120 day 85°C/95%RH hydrolytic stability test.

4.6 Thermal shock

Board coupons coated with PC18M+20%XP2742 and PC18M+20%X11102PMA passed 100 cycles from -55 to 125°C using an air-to-air transfer shuttle.

4.7 Nanoindentation

4.7.1 PC18M

4.7.1.1 PC18M-mod baseline

Mechanical properties were evaluated via a small-force nanoindentation. In particular, the depth-sensitive nanoindentation testing can emulate the whisker penetration behavior by examining local deformation of PU around an indenter tip. Figure 35 shows the nanoindentation results from unfilled polyurethane (PC18M). The original PC18M has a viscosity of ~250 cps and the modified version has a reduced viscosity of ~ 100 cps and Dabco T12 addition. Mechanical properties did not show much difference with the modified viscosity version.

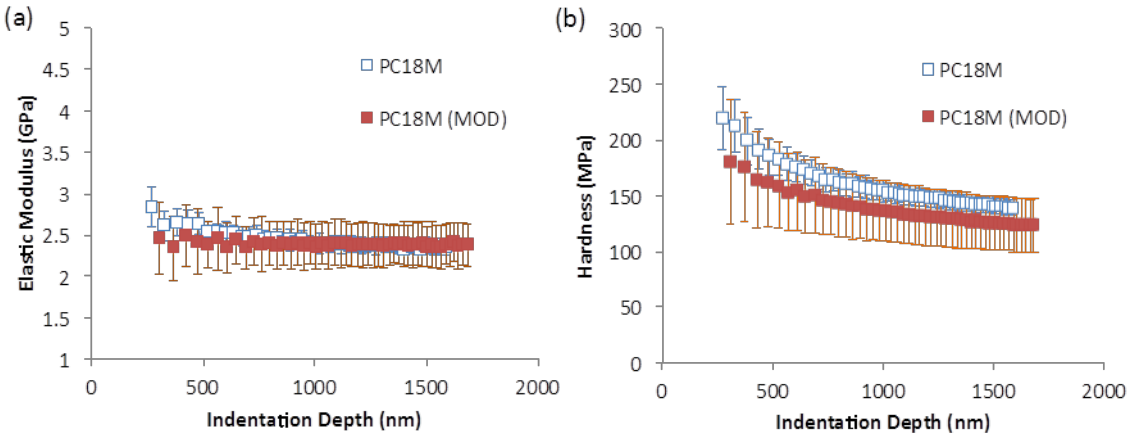


Figure 35: Nanoindentation testing results from PC18M films: (a) elastic modulus; (b) nanohardness.

The majority of the tin whisker testing is performed at elevated temperature. In addition DoD electronics often encounter temperatures up to 125°C. Nanoindentation testing at elevated temperatures up to 125˚C is shown in Figure 36. Dramatic reduction in mechanical properties occurs between 50 and 85˚C, which can be related to the presence of the glass transition temperature in this temperature range.

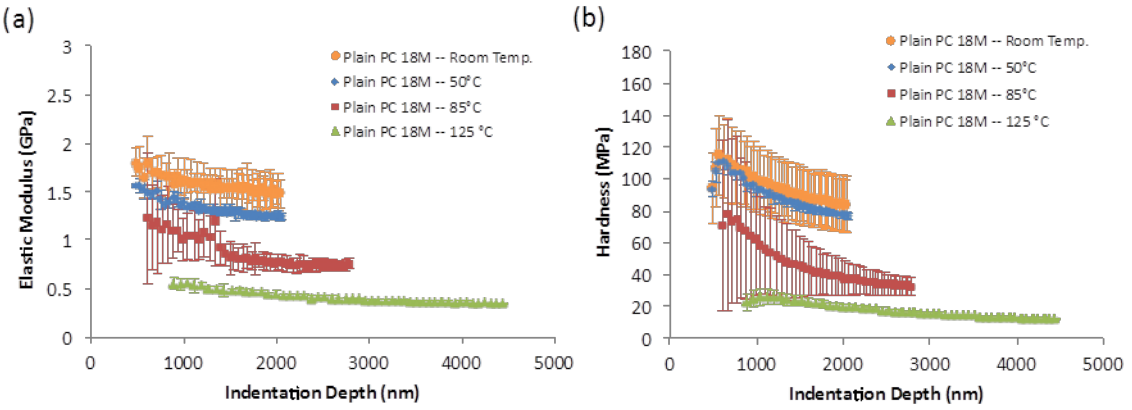


Figure 36: Nanoindentation testing results at room temperature, 50˚C, 85˚C, and 125˚C; (a) elastic modulus, and (b) nanohardness.

4.7.1.2 PC18M + XP2742 nanosilica

After adding nanoparticle suspensions (XP2742) to the PU base resin, mechanical properties of the filled PU coatings were improved as shown in Figure 37. Both elastic modulus and nanohardness increased after 10% XP2742 SiO_2 (which corresponds to 3.5 wt.% SiO_2). These properties decreased with indentation depth, which has been found in moisture-cured polymers. Nanosilica-filled PU coatings displayed decreasing hardness values near the surface region (< 500 nm range). Mechanical properties of those nanosilica-filled PU coatings, however, did not show any improvement with 30% XP2742 addition (corresponding to 9.8 wt.% SiO_2) or 50% XP2742 addition (to 15.2 wt.% SiO_2). In fact, there was a decrease as seen in the modulus of 30% XP2742 case due to its greater dependence on indentation depth.

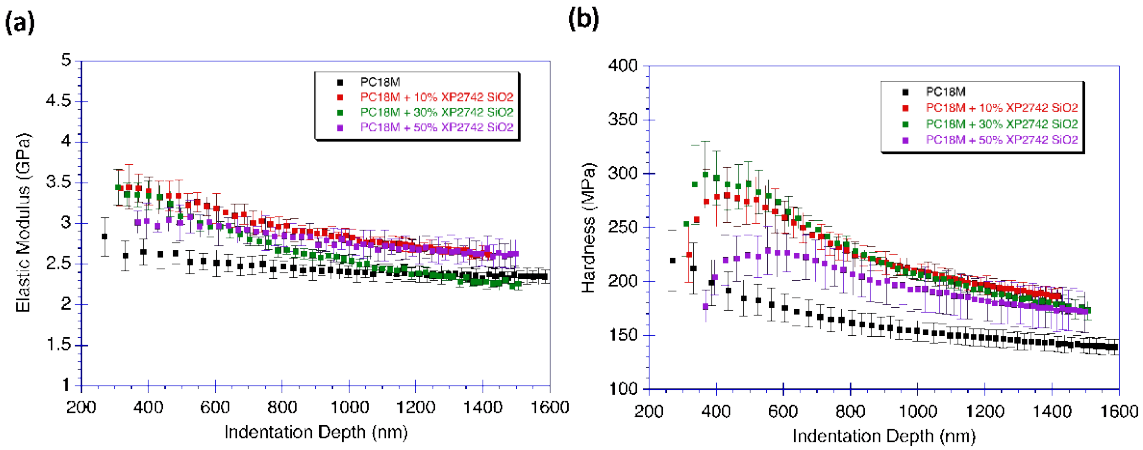


Figure 37: Nanoindentation testing results of PC18M filled with XP2742 (nanosilica); (a) elastic modulus, and (b) nanohardness.

Nanoindentation testing of PC18M with the XP2742 suspension at elevated temperatures up to 125˚C is shown in Figure 38. Dramatic reduction in mechanical properties occurs even at 50˚C, which can be related to the presence of glass transition temperature below this temperature. Confirming that the addition of the XP2742 to the PC18M caused a glass transition temperature decrease (see 4.2).

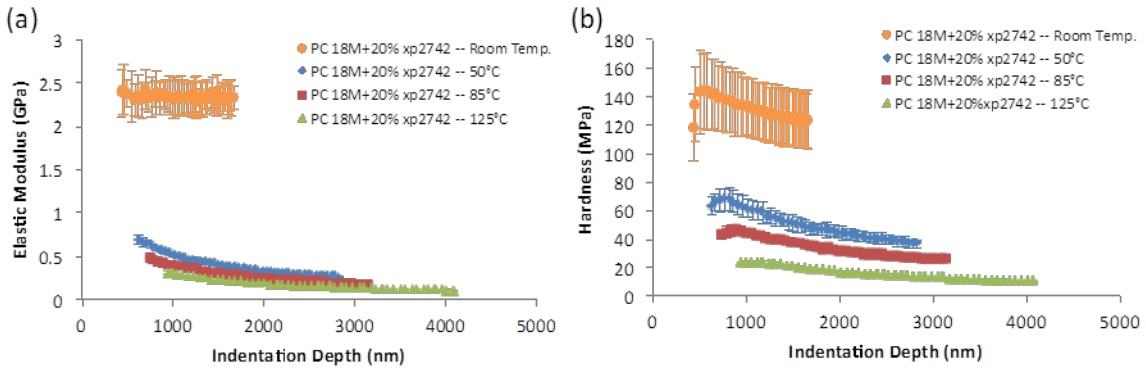


Figure 38: Nanoindentation testing results of PC18M+20% XP2742 at room temperature, 50˚C, 85˚C, and 125˚C; (a) elastic modulus, and (b) nanohardness.

4.7.1.3 PC18M + N3300

The particle suspension, XP2742 contains a hexamethylene diisocyanate trimer (N3300) in addition to the nanosilica particles. In order to evaluate the effect of the isocyanate addition on mechanical properties, the N3300, without nanosilica particles, was added to the base polyurethane. Figure 39 shows the nanoindentation result from the PU with the N3300 alone, compared with that of the nanosilica suspension (XP2742) that has the same amount of a diisocyanate (that is, 15.54 %). Only the shallow indentations (< 0.8-1 μm) showed the influence of nanosilica on both elastic modulus and nanohardness.

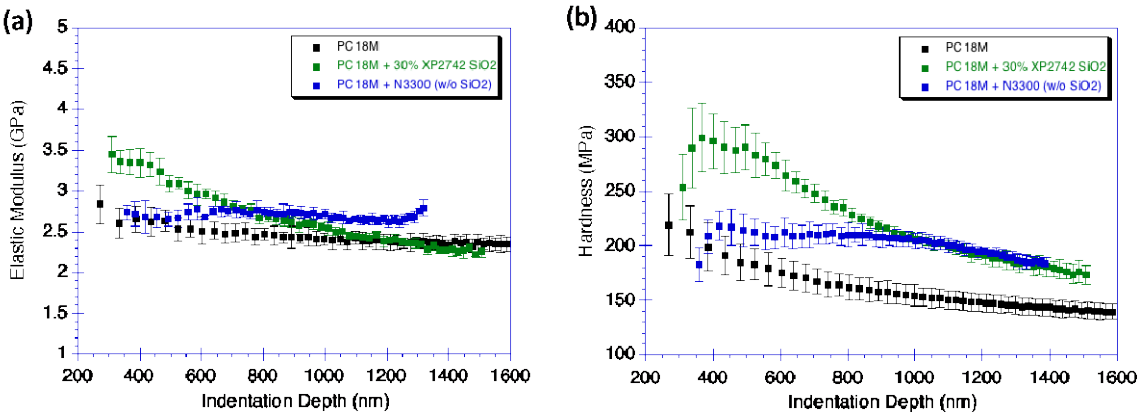


Figure 39: Nanoindentation testing results of PC18M filled with N3300; (a) elastic modulus, and (b) nanohardness.

4.7.1.4 PC18M + 11102PMA nanoalumina

Nanoindentation testing results of PC18M PU coatings with 0 – 40% X11102PMA Al_2O_3 suspensions are shown in Figure 40. Elastic modulus from the nanoindentation increased with increasing nanoalumina suspension concentration, having the highest modulus at 40% X11102PMA. Nanohardness also seemed to saturate at 40% X11102PMA, but no clear degradation was observed. This trend confirms that the PU matrix was not degraded from the addition of the nanoalumina particle suspension unlike the nanosilica case.

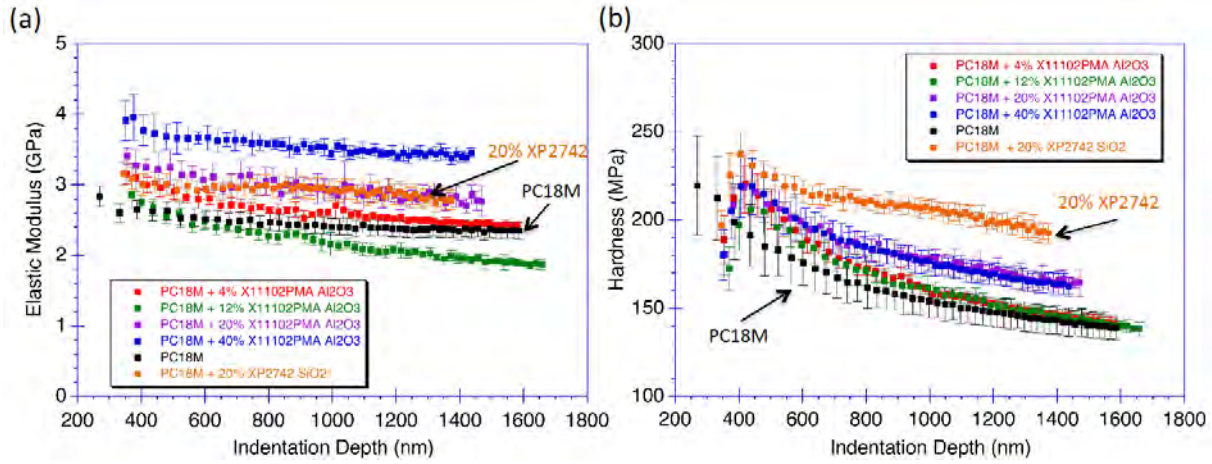


Figure 40: Nanoindentation testing results of PC18M filled with X11102PMA (nanoalumina); (a) elastic modulus, and (b) nanohardness.

4.7.2 PC40-UMF

PC40-UMF is a UV curable polyurethane acrylate system, which can also be cured through exposure to the moisture. Figure 41 shows the nanoindentation results from PC40-UMF, which was cured with both UV and moisture exposure. Hardness was shown to be less dependent upon the indentation depth, compared to that of PC18M.

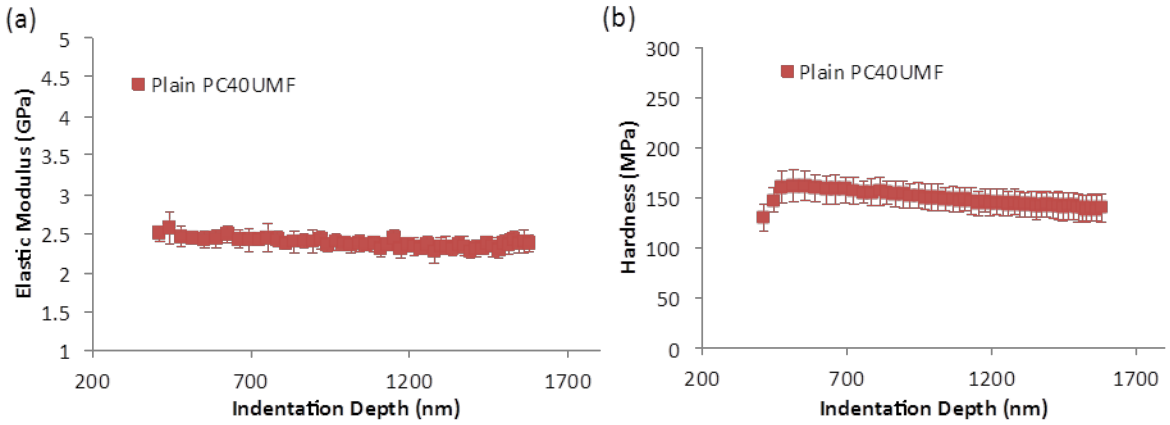


Figure 41: Nanoindentation testing results from PC40-UMF films; (a) elastic modulus and, (b) nanohardness.

Nanoindentation testing of UV-curable PU films at elevated temperatures up to 125˚C is shown in Figure 42, where mechanical properties of PC40-UMF are compared with increasing temperature. A dramatic reduction in mechanical properties occurs between 50˚C and 85˚C, which can be related to the presence of a glass transition temperature in this range.

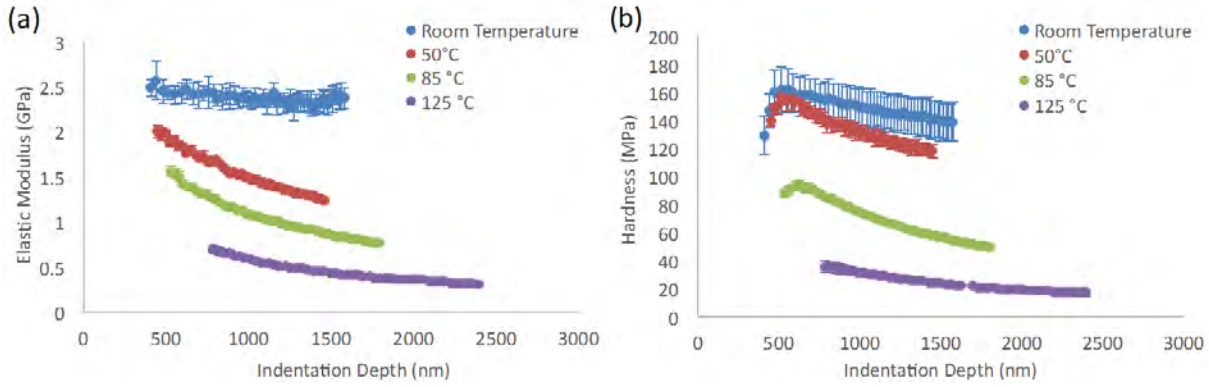


Figure 42: Nanoindentation testing results of PC40-UMF at room temperature, 50˚C, 85˚C, and 125˚C; (a) elastic modulus, and (b) nanohardness.

4.7.2.1 PC40-UMF + XP2742 nanosilica

Nanosilica particles were added to the base PC40-UMF polymer through the XP2742/NNN2835 suspension. 10% NNN2835 (which is equivalent to XP2742) shows an increase in both elastic modulus and hardness, but its improvement did not continue beyond 30% NNN2835 (Figure 43). In fact, 50% XP2742 suspension case showed a significant reduction, so both modulus and hardness were even lower than unfilled PC40-UMF.

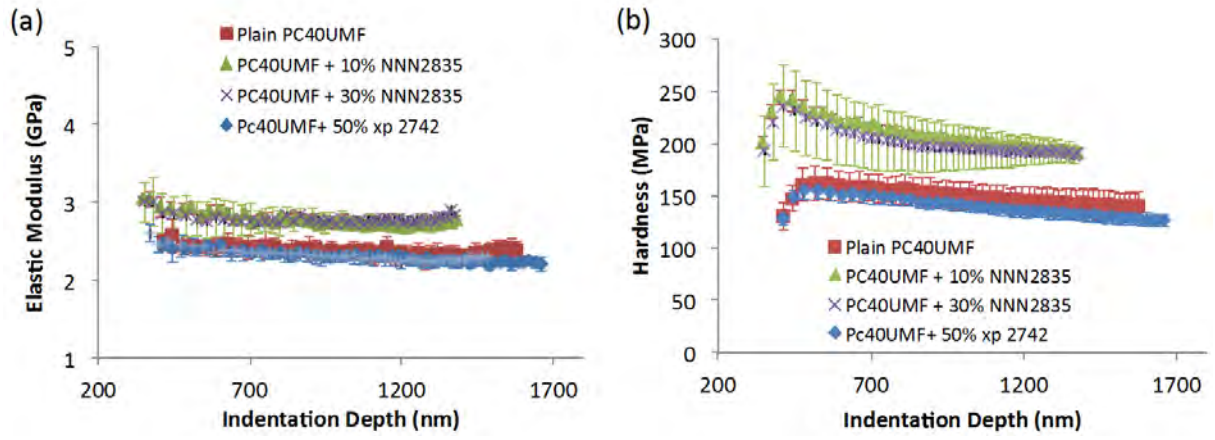


Figure 43: Nanoindentation testing results of PC40-UMF with NNN2835/XP2742 (nanosilica); (a) elastic modulus, and (b) nanohardness.

4.7.2.2 PC40-UMF + N3300

Figure 44 shows the nanoindentation testing result from the PC40-UMF mixed with N3300 (isocyanate). Elastic modulus did not show much change while nanohardness increased from the addition of N3300. Even though a large amount of N3300 was added to PC40-UMF, the mechanical properties did not degrade unlike the PC18M case with the N3300.

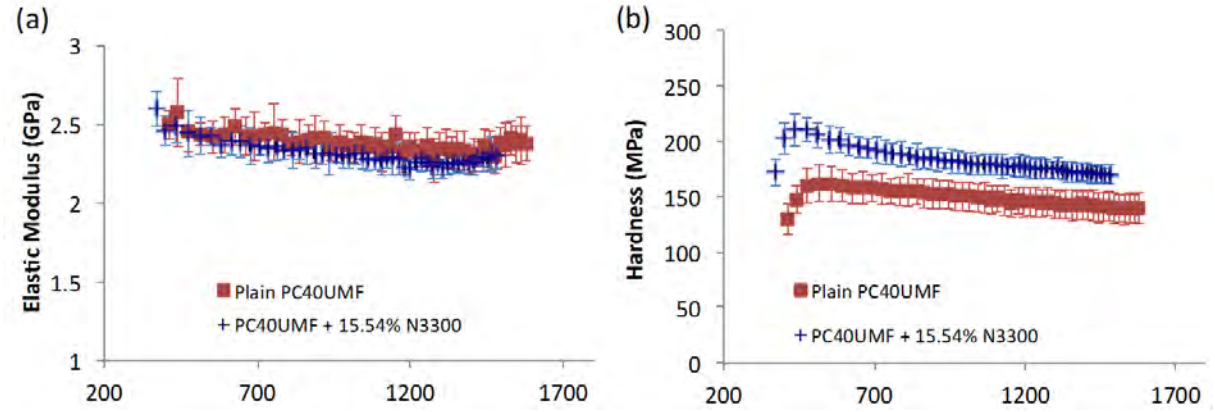


Figure 44: Nanoindentation testing results of PC40-UMF filled with N3300; (a) elastic modulus, and (b) nanohardness.

4.8 Tensile testing

4.8.1 PC18M

4.8.1.1 PC18M with XP2742 nanosilica

While nanoindentation data represent local deformation behavior near the surface of the PU coatings, tensile testing results assess the bulk behavior of nanosilica-filled PU composite coatings. Figure 45 shows representative tensile behavior of filled PU, as compared to those of unfilled PU. The tensile specimen was 2.5 inch x 0.5 inch cut from the cast material with a gauge length of 0.5 inch. Testing was performed on an Instron instrument with a displacement control of 0.1 inch/min. Large sample-

to-sample variation was observed partly due to the defect population embedded during the sheet casting process. As was the case for the nanoindentation test, PU coating with 30% XP2742 or more exhibited a decrease in modulus and strengths. The 50% XP2742 case was rather brittle, thereby showing a limited total elongation. This brittleness resulted from the bubble defects that existed in the PU sheets. Also, the urea formation with the presence of moisture constitutes other hard segments in the PU network, which can add the brittleness to the PU.

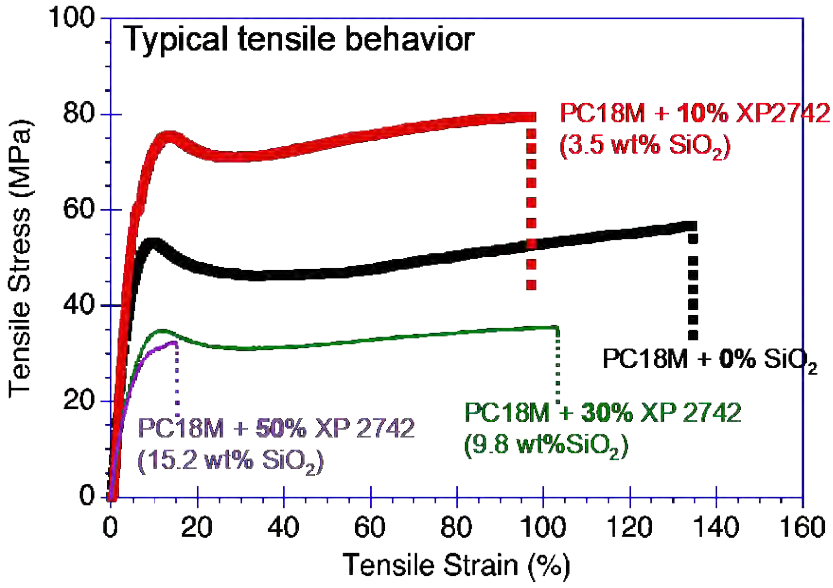


Figure 45: Representative tensile stress-strain plots of PU films with different amount of XP2742 SiO_2. For reference an unfilled PU film (PC18M) case is also included.

Examination of ruptured PU films after tensile testing (Figure 46) indicates the failure origin at the bubbles (or voids). These defect locations provide a stress concentration site, where the crack initiates and propagates. Shear bands that extended from this location with about 45˚ angle from a tensile loading axis were also observed. Because of the presence of these defects, there was premature failure, as well as data scattering. It ultimately made the polymer film quite brittle. Therefore, it will be necessary to have the defect concentration reduced to increase ductility, which can be comparable to that of the Parylene film.

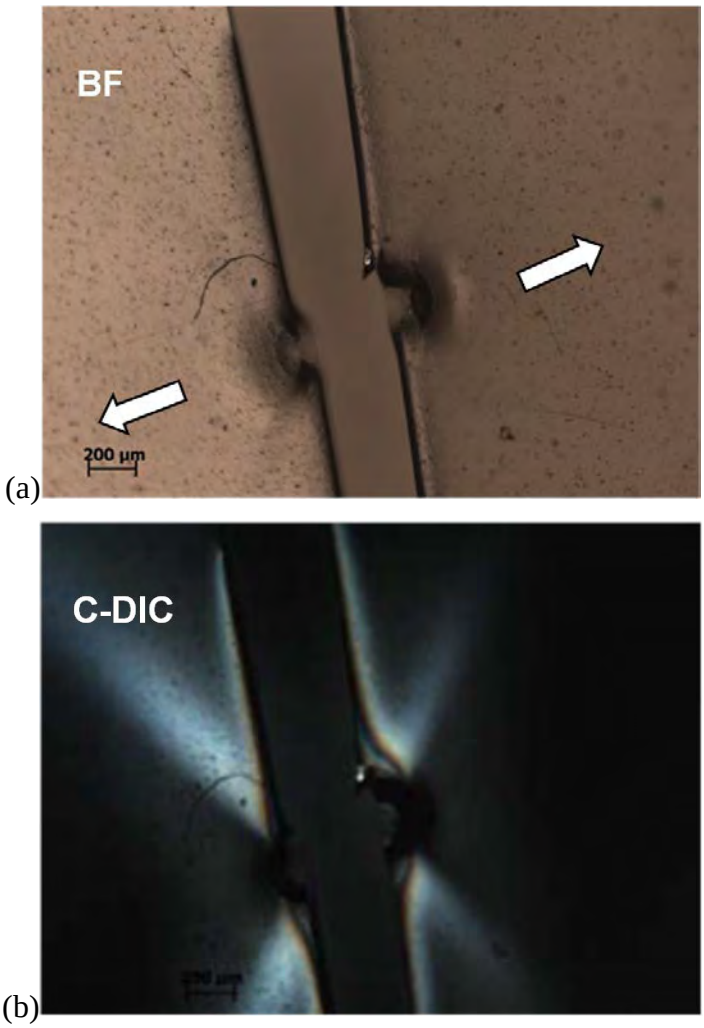


Figure 46: A crack grown from a defect site embedded in PU film; (a) bright field optical micrograph, and (b) C-differential interference contrast (DIC) image. Arrows indicate tensile loading direction.

4.8.1.2 PC18M with N3300 and XP2742

As was previously mentioned, XP2742 is made up of nanosilica particles in N3300 isocyanate. In order to differentiate the effect of nanosilica particles from the hard segments, mechanical properties of the PC18M PU coatings were compared as a function of the amounts of nanosilica+isocyanate and the corresponding isocyanate percentage as shown in Figure 47. The thicker the sample the more defects it can have and could have reduced elongation as a result. For reference, the sample thicknesses are given in Table 6. The elastic responses of the polyurethane coatings, both with nanosilica+isocyanate and only isocyanate, show a trend of increasing modulus with an increase in those additions; that is, increasing up to the 30% suspension case and then decreasing with more suspension, as observed by the elastic modulus chart in Figure 47(a). A higher value in the elastic modulus was, however, observed when nanosilica particles were added besides the addition of isocyanate.

This is indicative of particulate reinforcement provided by the nanosilica, beyond the strengthening effect of the hard segments in the polyurethane matrix that restrict chain alignment in the axial stress direction. However, a degradation of the elastic modulus was also observed after 30% nanosilica suspension (also, 15.54 % isocyanate). The drop in elastic modulus was more significant with the nanoparticle suspension case, indicating that the brittleness of PU matrix results in more dramatic impact when combined with the defects resulting from the nanoparticle addition.

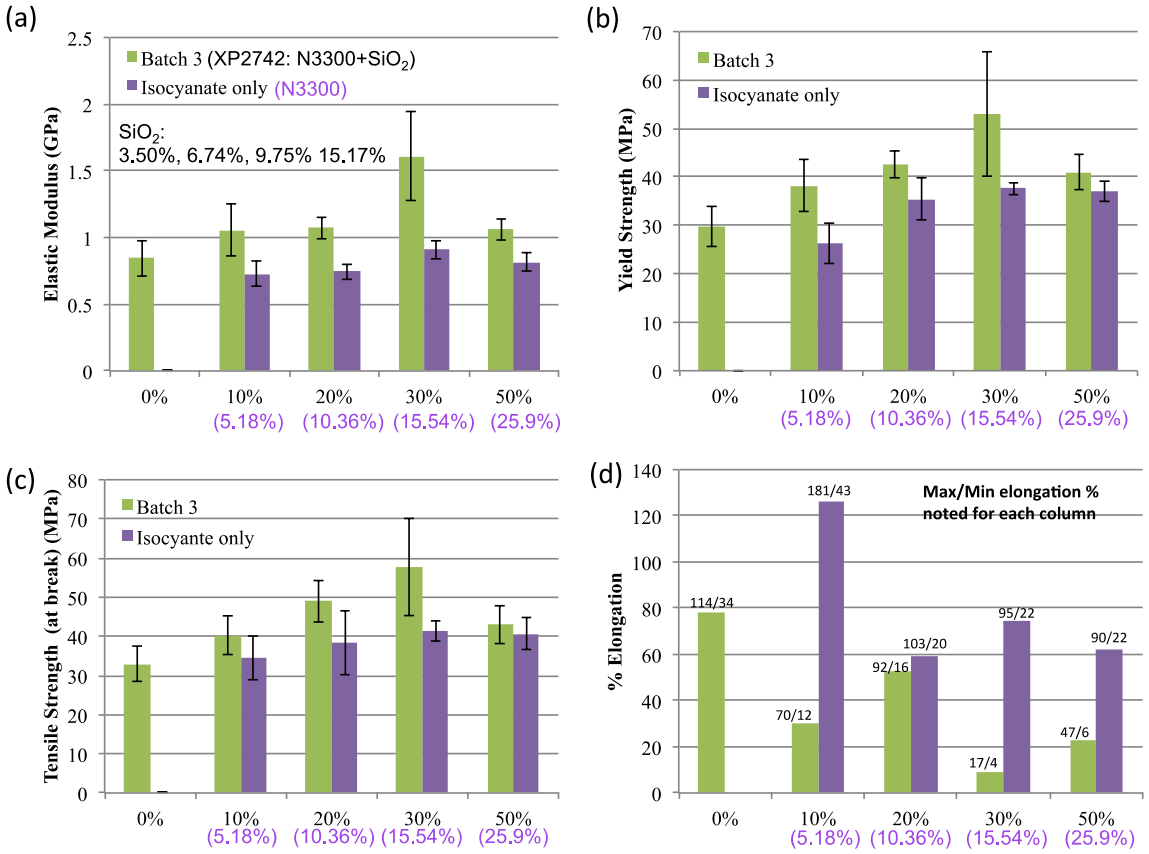


Figure 47: Effect of XP2742 (nanosilica+isocyanate) and N3300 (isocyanate) suspension on tensile properties; (a) elastic modulus, (b) yield strength, (c) tensile strength at break, and (d) percent elongation.

Table 6: PC18M tensile test set sample thicknesses.

XP2742 (fraction in PC18M)	Thickness (micron)	N 3300 (fraction in PC18M)	Thickness (micron)
0	36-44		
0.1	28-38	0.0518	66-99
0.2	42-47	0.1036	61-99
0.3	41-46	0.1554	69-114
0.5	67-72	0.259	86-99

This trend of increase and a subsequent decrease in the mechanical property is mirrored in the yield strength and the tensile strength of both sets of samples. Again, a significant increase in the case of nanosilica addition is observed, in the yield strength and the tensile strength, which cannot be matched by the addition of N3300 isocyanate alone (Figure 47(b) and (c), respectively). As the hard domains act as a barrier for chain movement and uncoiling following the yield point, the nanoparticles can also suppress the chain motion because the functionalization of the nanoparticles make the strong bonding with the PU network. However, as noted previously, the urea formation in the polyurethane matrix from the reaction of isocyanate in the resin with water proceeds rapidly, and forms regions of urea along with the interspersed hard and soft domains. These urea domains become defect sites acting as stress concentration points that can facilitate premature failure as shown in the 30% and 50% suspension cases. In the case of 50% nanosilica suspension (with 25.90 % isocyanate addition), this mechanism negates the strengthening effect of the hard domains and the reinforcement by the nanoparticles leading to degradation in the properties.

The 20% nanosilica addition showed the highest total elongation (ductility) among nanoparticle blended coatings with comparable modulus and strength with the 30% case. In general, isocyanate only samples display more elongation in comparison. However, the extent of elongation of the coatings showed a significant dependence on sample preparation and defect density in the coatings. Voids, bubbles and other macro-sized defects served as crack initiators and caused pre-mature failure.

4.8.1.3 PC18M with Nanophase 11102PMA

Nanoalumina-filled PU coatings were also investigated for tensile properties. With little increase of an isocyanate amount in the particle suspension (X11102PMA), the PU matrix did not contain the trace of polyurea formation unlike with the XP2742 suspension (as confirmed by FT-IR). Tensile strengths and total elongation began to degrade when reaching at 40% X11102PMA, which corresponds to 28.57% Al_2O_3 (Figure 48). Therefore, the degradation in mechanical properties seems to be more related to the strong agglomeration of alumina that causes the PU coatings to be more brittle and susceptible to inhomogeneous deformation. Tensile modulus was, however, not degraded even at 40% X11102PMA. Compared to the aforementioned 20% XP2742 SiO_2, 20% X11102PMA Al_2O_3 showed more extensive drawing after neck formation, but had less strain hardening behavior (Figure 48). This may be attributed to more flexibility in aligning the polymer chain structure with respect to tensile load.

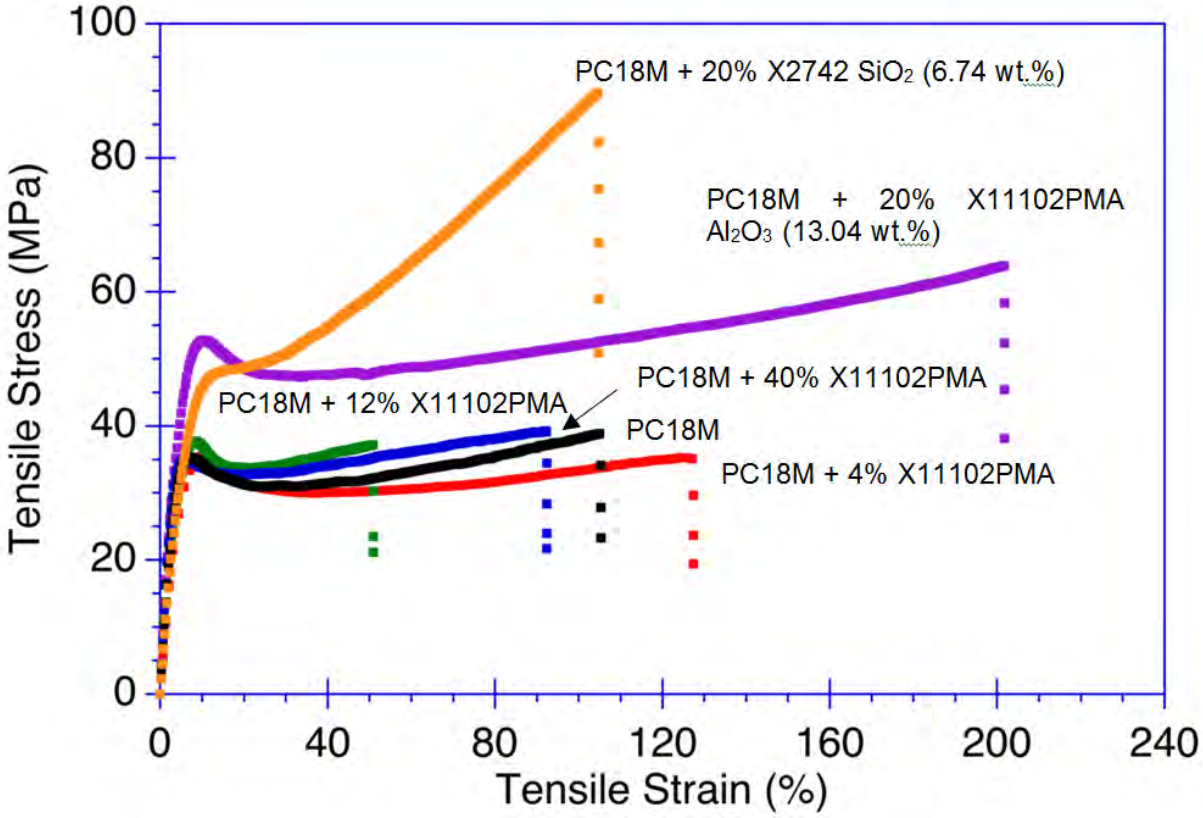


Figure 48: Tensile stress-strain plots of PU films with different amounts of X11102PMA Al_2O_3. For reference, unfilled PU film (PC18M) and PU film with 20 wt.% XP2742 SiO_2 are also included.

4.8.2 PC18M final coating comparison

The coating formulations selected for whisker testing were PC18M + 20%XP2742 nanosilica and PC18M + 20%11102PMA nanoalumina. The nanoparticles resulted in an improvement of properties over the unfilled PC18M and the PC18M+N3300 isocyanate (Figure 49). It is likely that the nanoalumina formulation could have had better performance if the particles had been functionalized as originally planned. In the low strain region, the properties of the nanoparticle filled coatings approach those of Parylene C.

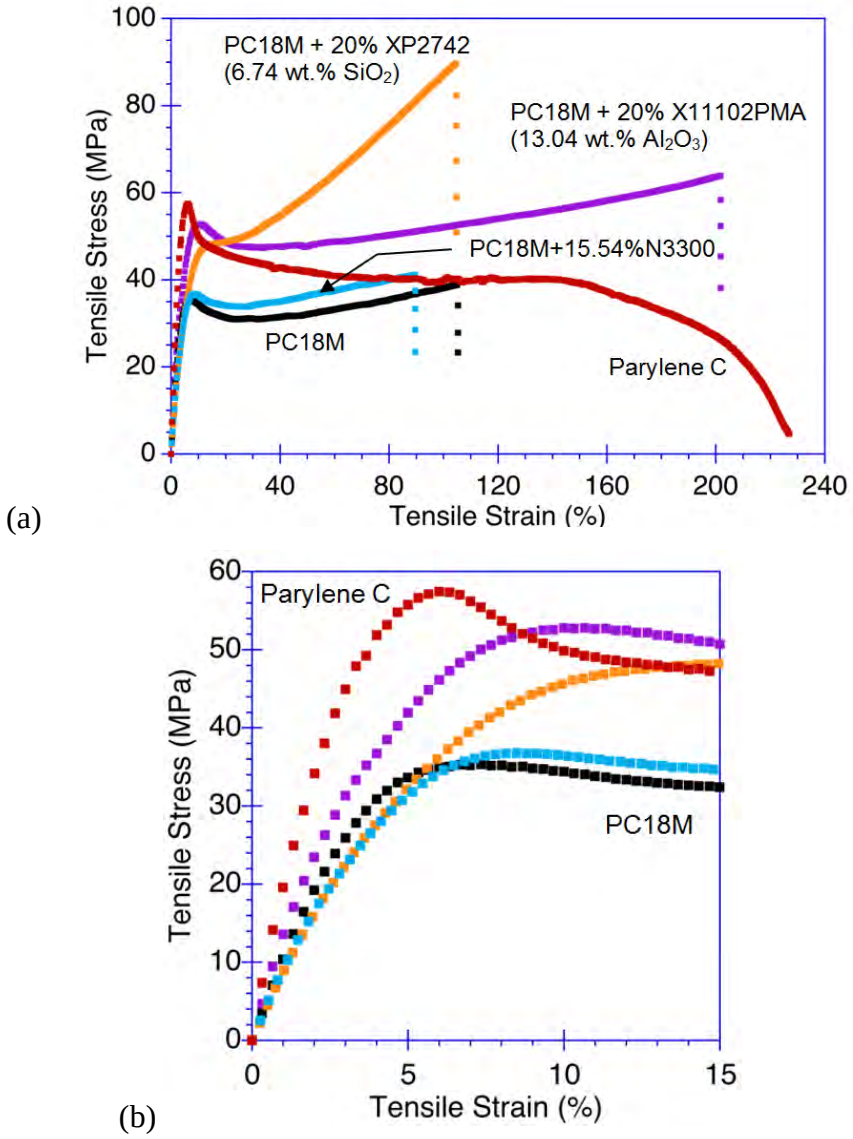


Figure 49: PC18M Stress versus strain comparison with Parylene C; (a) overall and (b) strain up to 15 percent.

4.8.3 PC40-UMF with XP2742

Tensile properties of the PC40-UMF dual curing system (UV+moisture) are shown in Figure 50. Unlike the 'localized' nanoindentation behavior, macroscopic tensile behavior of PC40-UMF was much lower than PC18M (moisture cured). In addition, there was no improvement in mechanical properties by adding the XP2742 SiO2 suspension. More importantly, total elongation was too low, which might result from the defect population. Indeed, the PU film thickness was thicker (around 100 □m for most of cases) and bubble defects were clearly visible. (Note: During the PC40-UMF family film casting, the thinner films were difficult to remove from the glass without tearing, so thicker films were made.) Moisture-only cured PC40-UMF films displayed the highest ductility among these samples, but still much lower elongation than the PC18M counterparts. It would be beneficial to further improve the resin formulation to restore the ductility (also, toughness) of this UV curable

polyurethane film taking care to ensure that the attributes needed to pass IPC-CC-830 and solvent resistance are still retained.

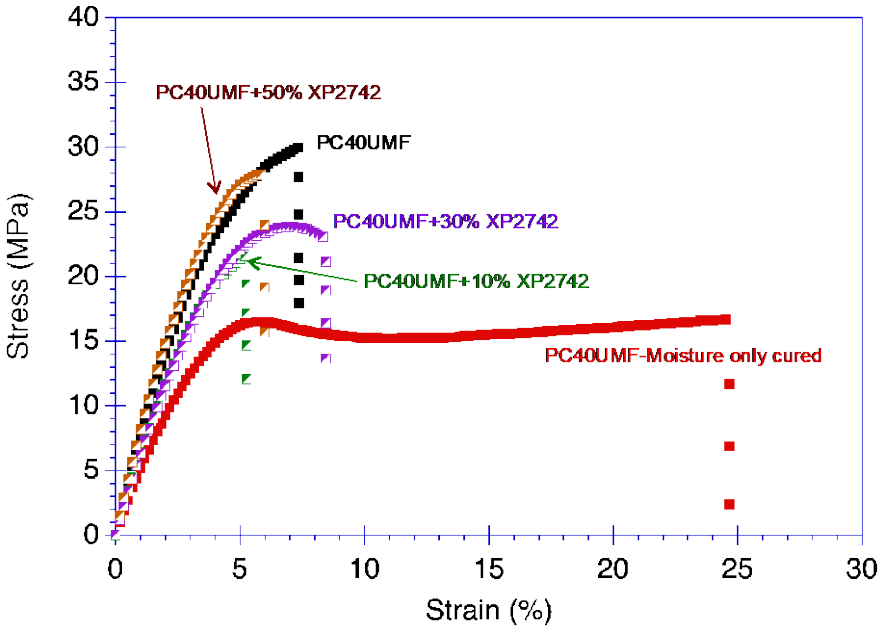
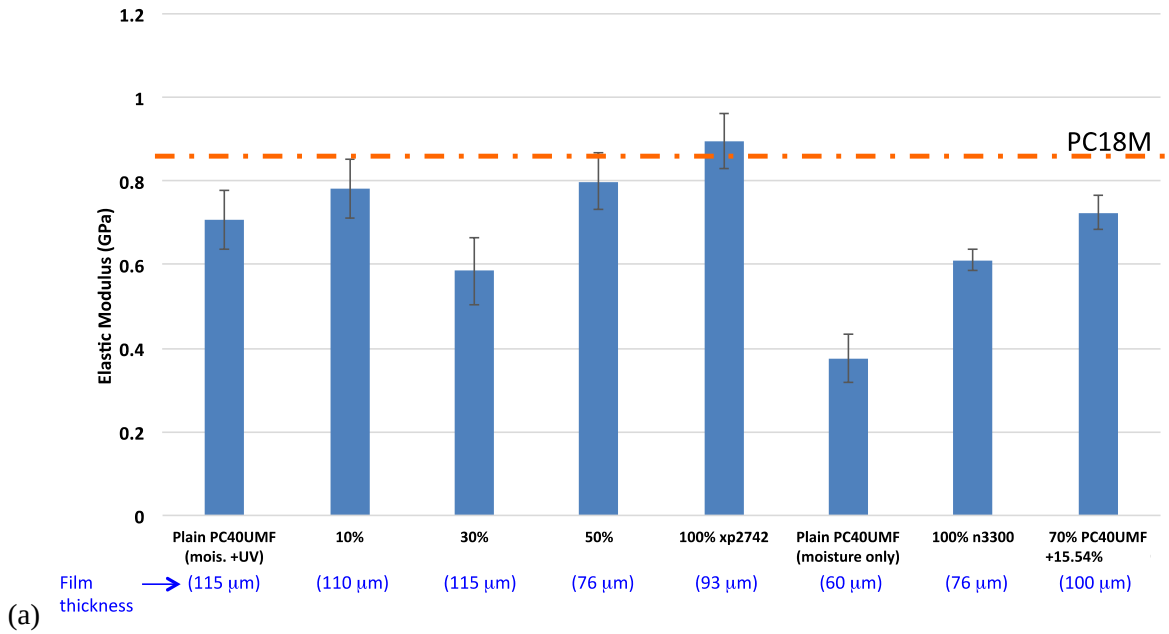


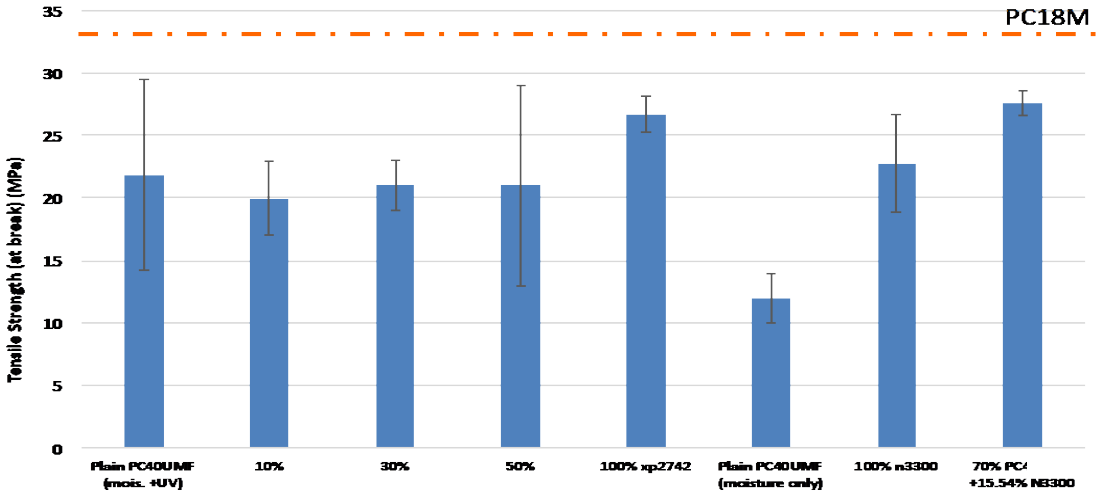
Figure 50: Representative tensile stress-strain plots of UV-curable PC40-UMF filled with XP2742 SiO_2 suspension. For reference an unfilled PU film (PC40-UMF) case is also included.

4.8.3.1 PC40-UMF Family (including XP2742, N3300)

Effects of the particle suspension (XP2742) and isocyanate (N3300) on elastic modulus and tensile strength of PC40-UMF are shown in Figure 51. Unfilled PC18M properties are shown as a dashed line for comparison. In all cases of unfilled and filled PC40-UMF, the properties were less than PC18M. In particular, moisture only cured samples showed very low modulus and strength since the acrylate domain included in the polymer network was not cured under thermal/moisture treatments.



(a)



(b)

Figure 51: Tensile properties of PC40-UMF family (filled with NNN2835 equivalent to XP2742, N3300); (a) Elastic modulus, and (b) Tensile strength.

4.9 Adhesion testing

The coating adhesion to tin was evaluated using a four point bend test (see Figure 52 and Figure 53). The sample sandwiches the coating/tin interface between pieces of silicon. The critical strain energy release rate, G_c (J/m^2) for debonding, can be found using the relationship:

$$\frac{21(1-\upsilon^2)P^2L^2}{16Eb^2h^3} \qquad \text{Eq. 1}$$

where E and ν are the Young's modulus and Poisson's ratio of the silicon, P is the steady crack growth force, b is the substrate width, and L and h are given in Figure 53 and Table 7. Force versus displacement data was obtained for three to five samples at a loading rate of 0.01 mm/min. The sample layer thicknesses are given in Figure 54.



Figure 52: MTS Mini bionix tester used for the four point bend testing.

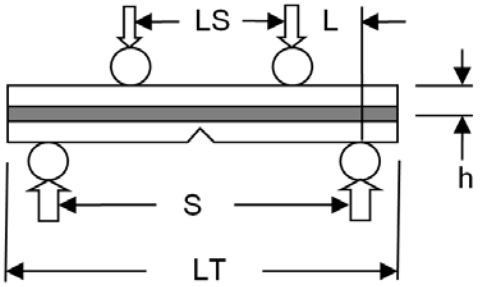


Figure 53: Four point bend sample schematic. The four mandrels are 2-mm diameter.

Table 7: Four point bend test parameters.

Description	Designation	Value
Sample Length	LT	38.1 mm
Sample Width	b	9.545 mm
Sample half thickness	h	Measured (~0.60 mm)
Support Span	S	24 mm
Load Span	LS	12 mm
Silicon Poisson's ratio	ν	0.22
Silicon Young's Modulus	E	160 GPa
Force Plateau	P	Measured

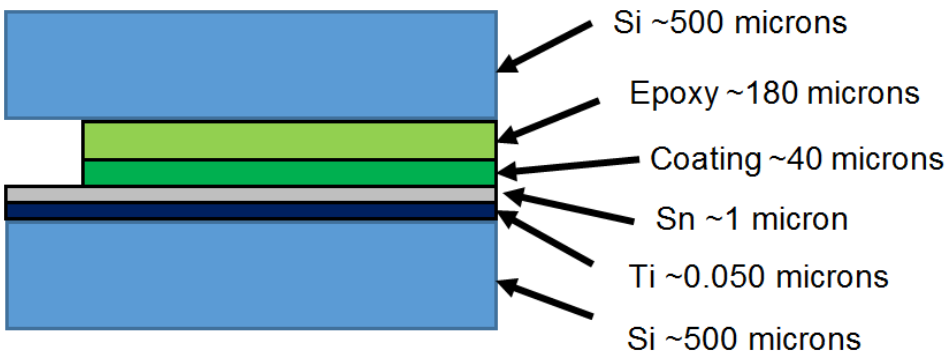


Figure 54: Sample layer thicknesses.

4.9.1 Initial adhesion tests [4]

Initial polyurethane to tin adhesion tests were performed on the PU coatings PC18M and PC18M+20%XP2742 nanosilica. The resulting computed critical interfacial adhesion energies are given in Figure 55. In the test, various interfaces failed, but not the PU to Sn interface. The largest values were obtained for epoxy to PU interface. Thus the interfacial adhesion energy of polyurethane coating to tin surface is must be greater than 14-15 J/mm^2.

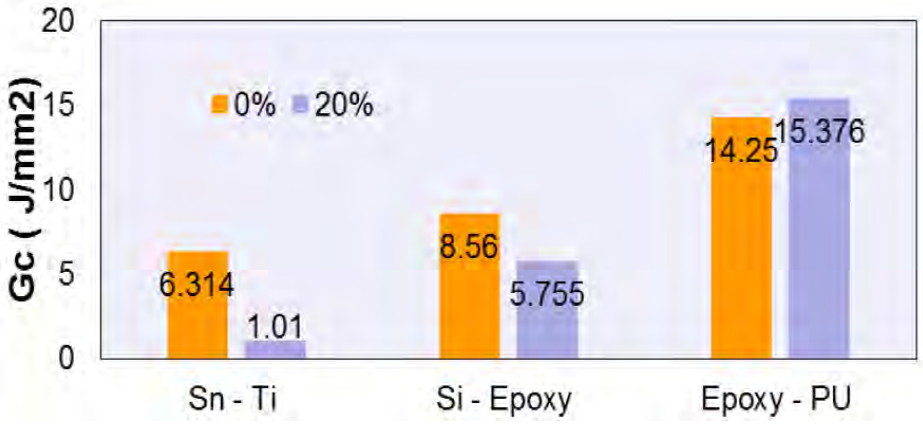


Figure 55: Critical interfacial adhesion energy for PC18M+0%XP2742 and PC18M+20%XP2742.

4.9.2 Enhanced coating adhesion test [5].

Adhesion tests were performed on the polyurethane PC18M (PU) and the polyurethane acrylate PC40-UMF (PUA). The adhesion between the coating and the epoxy was improved by roughening and plasma etching the Si and the coating prior to epoxy bonding. The adhesion between coating and Sn was improved by:

- PU and PUA: O_2 plasma treatment on Sn surface
- PUA only: (3-Aminopropyl)triethoxysilane (APTES) treatment on Sn surface – 2% APTES in water with acidified environment (pH=5)

A typical force versus displacement curve is shown in Figure 56. On the PC18M samples, the critical interfacial energy increased to 57.8 J/m^2. For the PC40-UMF, the siliane adhesion promoter in addition to the plasma treatment improved the adhesion from 12 J/m^2 t for the plasma alone to 22.4 J/m^2 for the plasma and the APTES silane treatment (Figure 57).

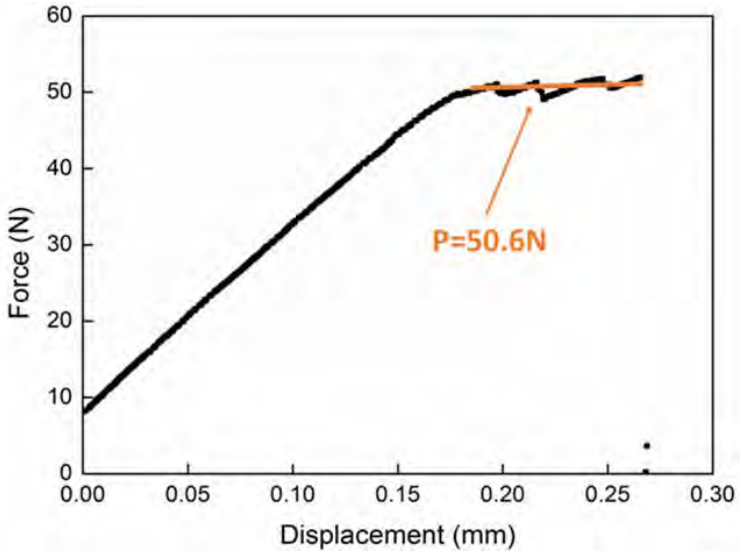


Figure 56: Typical force versus displacement curve for the four point bend test. (PU (PC18M) on Sn shown).

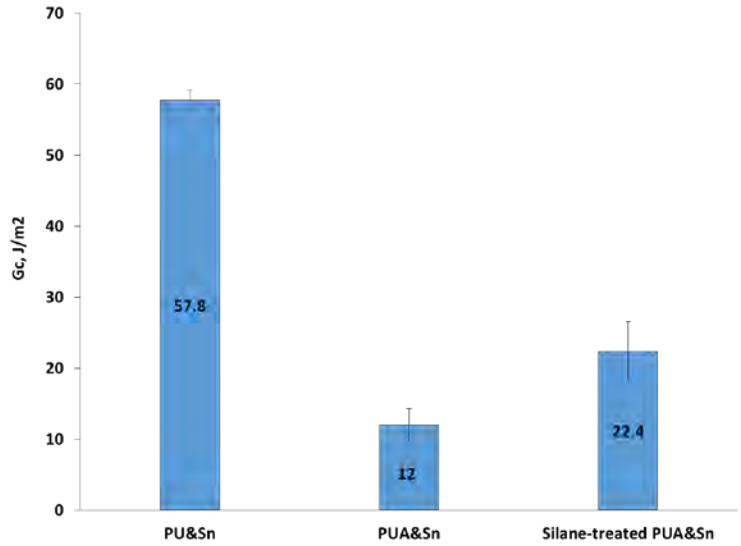


Figure 57: Critical interface energy (Gc) for the coating to tin interface adhesion. The PU (PC18M) adhesion is considerably better than the PUA (PC40-UMF). The APTES silane treatment improved the adhesion on the PUA samples.

4.10 Solid mechanical properties conclusion

Functionalized nanosilica particles, approximately 20 nm in diameter, were integrated into a PU coating in an attempt to attain its optimum mechanical properties for mitigating tin whisker growth. Due to excellent surface functionaliza1tion, nanosilica particles were well dispersed with no significant agglomeration. It was shown that mechanical properties do not continuously increase with the XP2742 nanosilica suspension concentration. This was due to the polymer structure change with added nanoparticle suspensions, which resulted in polyurea formation and microdefects created during film processing. Higher levels of XP2742 also made the coating quite brittle having limited ductility.

Because of this, the maximum allowable nanosilica concentration was obtained with the 20% XP2742 suspension that resulted in ~6.74 wt.% SiO_2 in PU.

On the other hand, the surface of nanoalumina particles were not functionalized, thereby resulting in very strong agglomeration that leads to sub-micron sized secondary particles. The addition of X11102PMA to PC18M was not producing the brittleness in the matrix, so it was possible to add more nanoparticles (up to 13.04 wt.% Al_2O_3).

Mechanical properties of the PC40-UMF (UV-curable polyurethane acrylate) were quite brittle, resulting in lower modulus, strength, and very limited ductility. Because of this, the XP2742 nanosilica addition did not show much improvement in mechanical properties of polyurethane. Nanoindentation results, however, not only showed the comparable properties with non-filled and filled PC18M (moisture curable) but also demonstrated the effect of the nanosilica addition. It suggests that the defects resulted from the resin formulation and the film casting were mainly responsible for the degradation in macroscopic mechanical properties. It is therefore necessary to restore the toughness and ductility of PC40-UMF by reducing the flaws via optimized processing.

The adhesion of the PC40-UMF was improved by treating the Sn with APTES.

Future work will involve more systematic establishment of the structure – property relationships of the nanoparticle-filled PU, which will be linked to the tin whisker mitigation performance to identify optimum mechanical properties of the PU coatings. For this, the coating adhesion on the Sn surface will also be of importance, and is under investigation using a four-point bending test to measure the interfacial debond energy. Surface functionalization of nanoalumina particles that will address the particle agglomeration issue and its related drawbacks is also currently in process. UV curing will provide significant energy savings and also reduce environmental impact by lowering greenhouse gas emissions and volatile organic compounds (VOC). It is thus important to develop UV-curable polyurethane-based polymers that can work as a ‘reliable’ conformal coating for tin whisker mitigation.

5. Literature cited

[1] Appendix C of the current report: Coating evaluation methods

[2] S. Meschter, J. Cho, S. Maganty, D. Starkey, M. Gomez, D. Edwards, A. Ekin, K. Elsken, J. Keeping, P. Snugovsky, Eva Kosiba, Zohreh Bagheri, and J. Kennedy Strategic Environmental Research and Development Program (SERDP) Nanoparticle Enhanced Conformal Coating for Whisker Mitigation, SMTA International Conference, Rosemont, IL, Sept. 28 – Oct. 2, 2014.

[3] J. Cho, S. Meschter, S. Maganty, D. Starkey, M. Gomez, D. Edwards, A. Ekin, K. Elsken, J. Keeping, P. Snugovsky, J. Kennedy, and M. Romansky, Polyurethane Conformal Coatings Filled with Hard Nanoparticles for Tin Whisker Mitigation, SMTA International Conference on Soldering and Reliability, Toronto, Ontario, Canada, May 13-15, 2014.

[4] M. Roma, S. Maganty, R. Roeder, J. Cho, S. Meschter, "Evaluation of Interfacial Adhesion of Polyurethane Conformal Coatings Used for Tin Whisker Mitigation", Materials Science and Technology 2014 Conference and Exhibition, October 12-16, 2014, Pittsburgh, PA

[5] F. Dong, S. Meschter, J. Cho, Study of Tin Whisker Growth under Polyurethane Based Conformal Coatings, Materials Science and Technology 2017 Conference and Exhibition, Oct. 8 – 12, 2017, Pittsburg, PA.

SERDP WP-2213
Final Report
Appendix E: Assembly test vehicle coating process

Appendix E: Table of Contents

1. Introduction 1

2. Materials 2

3. General process development 3

3.1 Coating viscosity 3

3.2 Dip coating 5

3.2.1 Dip coating process - initial viscosity evaluation 6

3.2.2 Dip coating 7

3.3 General spray coating process development 8

3.3.1 Spray process considerations 8

3.3.2 Automatic spray machine set – up 9

3.3.3 Coating curing 9

4. PC18M Baseline dip + spray coating method 12

4.1 PC18M bubble observations 12

5. PC40-UMF coating 14

5.1 Batch A and B PC40-UMF Baseline dip + spray 14

5.1.1 Excessive thickness of PC40-UMF dip coat 14

5.2 Batch C and D PC40-UMF Interlayer adhesion and Coverage Improvement Experiments 16

5.2.1 Objective 16

5.2.2 Planned analysis after coating 16

5.2.3 Coating experiment participants 16

5.3 Equipment and materials 16

5.3.1 Location and environment 16

5.3.2 Coating materials 17

5.3.3 Surface energy measurement 17

5.3.4 Assembly boards and pre-coating preparation 17

5.3.5 Coating Equipment 18

5.4 Test and experimental procedures 19

5.4.1 Development of UV cure process for Henkel PC40-UMF Conformal Coating 19

5.4.2 Coated surface energy measurements 20

5.4.3 Modification of UV cure to provide UV flash between coating layers 20

5.4.4 Development of Coating Process to Apply Henkel PC40-UMF (100% Coating) 20

5.5 Coating and curing of assemblies 21

5.5.1 STI assemblies 21
5.5.2 WP1753 assemblies 21
5.6 RESULTS 23
5.6.1 Coating process setup and validation summary 23
5.6.2 Final assembly coating summary 24
5.7 Discussion of results 25
5.7.1 Wet and dry coating thickness measurement discussion 25
5.7.2 Additional UV Intensity development (UV flash cure) 25
6. PC18M+20%XP2742 Dip+layered spray coating 27
6.1 Assembly preparation 27
6.2 Dip+layered spray 28
6.3 Layered spray surface roughness observation 30
7. Comparative reference coatings 32
7.1 Parylene ™ coating material 32
7.2 Humiseal 1B31 acrylic coating 32
7.3 Humiseal UV40 low VOC acrylic – urethane coating 32
8. Summary and conclusion 33
9. Literature cited 34

Appendix E: List of Figures

Figure 1: Process flows for the baseline dip+spray and dip+layered spray coatings. 1

Figure 2: Viscosity of PC18M based coatings versus AC0305 solvent addition. Note: CCP20601-30 = PC18M+20%XP2742 and CCP20601-31 = PC18M+20%X11102PMA. 4

Figure 3: Viscosity of PC40-UMF coating versus AC0305 solvent addition. 4

Figure 4: Solvent evaporation versus time for PC40-UMF and PC40-UMF+50%XP2742 drawn films 75 to 125 microns thick. 5

Figure 5: Dip coating process flow. 6

Figure 6: Glass slide gap penetration experiment. 6

Figure 7: Gap filling time versus gap spacing for various viscosity PC18M and PC40-UMF coatings. 6

Figure 8: Coating draining after pipette application of PC18M having various viscosities. 7

Figure 9: Dip coating machine; (A) Front of machine with one board shown on immersion bar and (B) boards partially immersed in the coating reservoir. 8

Figure 10: Dip coat samples on a tray in the drying chamber. 8

Figure 11: Schematic of spray process. 9

Figure 12: Coating film formation from spray coating process. 10

Figure 13: Spray coating machine; (A) Samples in the spray machine and (B) the small volume reservoir fitted to the rear of the spray machine. View (A) also shows a flat steel process control coupon centered between the boards. 10

Figure 14: Typical machine spray pattern. 11

Figure 15: Curing oven. 11

Figure 16: PC18M-mod SOT board 233 with large bubble density, 10x, after ATC+1000HTHH. The color change in the second image is an artifact of the illumination used to highlight the bubbles. 13

Figure 17: PC18M+20%X1102PMA, SOT board 226, HALT, 10x, small/no bubble density, milky appearance. 13

Figure 18: SEM image of PC40-UMF Dip, Board 292, SOT5, 60x. 15

Figure 19: SEM image of PC40-UMF Dip coat, Board 292, SOT6, 40x. 15

Figure 20: Thinned PC40-UMF dip coating viscosity change during processing. 15

Figure 21: Cutting pattern for STI assembly. 18

Figure 22: Wet Film Gage. 19

Figure 23: WP-1753 Coupons (A) Optical photograph and (B) coupon layout. 22

Figure 24: Spray pattern on WP1753 coupons. 22

Figure 25: Recommended UV cure for PC40-UMF from the datasheet. 26

Figure 26: UVICure Plus radiometer. 26

Figure 27: Boards in the plasma etch machine. 27

Figure 28: Spray fixture for locating individual assembly coupons with respect to the spray machine; (A) Without coupons and (B) with coupons. 28

Figure 29: Typical board tooling hole masking. Yellow tape dots cover the tooling holes in three locations on both sides of the board. 28

Figure 30: Assemblies partially immersed into the dip coating reservoir..... 29

Figure 31: SEM image of PC18M dip + two PC18M sprays, board 191, QFP44, with good overall coverage but still exhibiting with surface roughness, 40x [6]. 30

Figure 32: SEM image of PC18M dip + two (PC18M+20%XP2742) sprays, board 336, QFP44, 15KV, good thick coverage, 60x [6]. 31

Appendix E: List of Tables

Table 1: Test vehicle assembly coating materials. 2
Table 2: Environmental conditions during evaluation 17
Table 3: Raw material information 17
Table 4: Dyne Pen Summary 17
Table 5: Plasma etch equipment 18
Table 6: Conformal Coating Application Equipment 18
Table 7: Conformal Coating Thickness Measurement Tools. 19
Table 8: Conformal coating process evaluation summary 23
Table 9: Conformal coating application summary 24
Table 10: UV Intensity and resulting coating surface energy. 26
Table 11: Sample coating 29

Acronyms

Acronym	Definition
BGA	Ball Grid Array
DOE	Design of Experiment
EFD	Supplier designation for a nozzle type
HDI	hexamethylene diisocyanate
NPI	New Product Introduction
PCTC	Power Cycling Thermal Cycling
PM	propylene glycol methyl ether
PU	Polyurethane
PTSI	p-Toluenesulfonyl Isocyanate
QFP	Quad Flat Pack
REE	Rare Earth Element
RVT	Supplier designator for a viscometer type
SAC	Sn-Ag-Cu alloy lead free solder
SCCM	Standard cubic centimeters per minute
SCS	Specialty Coating Systems Equipment Manufacturer
SEM	Scanning Electron Microscope
SOT	Small Outline Transistor
STI	Test board manufacturer (STI Electronics)
UV	Ultraviolet
VOC	Volatile Organic Compound

1. Introduction

Conformal coating has been used for many years for moisture and corrosion protection of electronic circuit boards. Many coating selection considerations and best practices are provided in IPC-HDBK-830 [1]. The current coating approach utilizes a low viscosity dip coat followed by spray coating. The low viscosity dip provides some, albeit thin, coating on all surfaces including surfaces difficult to coat during spraying (e.g. behind leads). The spray coat provides additional coating on the sides, top and front of the leads.

The initial phase compared the solvent based heritage urethane coatings to acrylic – urethane low VOC coatings with and without nanoparticle additions. A baseline dip+spray process was used. The results of the baseline evaluation showed that the PC18M and the PC18M+functionalized nanosilica were the most promising in terms of whisker mitigation.

The next phase sought to further improve coverage by using a layered spray process in addition to the initial dip. The PC18M and the PC18M+20%XP2742 functionalize nanosilica were selected for the layered spray coat process evaluation. The two process flows are summarized in Figure 1.

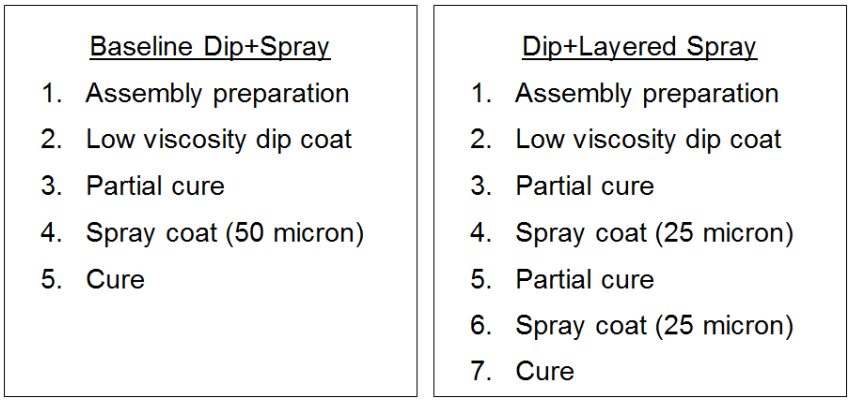


Figure 1: Process flows for the baseline dip+spray and dip+layered spray coatings.

2. Materials

The formulation preparation details are described in Appendix B [3]. Briefly, the first base coating was moisture curable solvent-based polyurethane previously qualified to MIL-I-46058 [4] and conforms to IPC-CC-830 [5] (PC18M, from Henkel). It is an established coating with a nominal viscosity of 300 cps and can be readily thinned to lower viscosities with a solvent. The moisture cure isocyanates in the PC18M will bind to the nanosilica particles which were designed to have isocyanate functionality.

The second coating was an ultraviolet (UV) moisture dual cure low volatile organic compound (low volatile organic compound (VOC)) that conforms to IPC-CC-830 [5] (PC40-UMF, from Henkel). The material is a polyurethane acrylic blend with UV reactive sites and isocyanate functionality. The isocyanate moisture cure ensures cure in UV shadowed areas under parts. The moisture cure isocyanates in the PC40-UMF will bind to the nanosilica particles which were designed to have isocyanate functionality.

The nanoparticle suspensions selected for incorporation into the coatings were: (1) Desmodur XP2742 suspension (N3300 Hexamethylene diisocyanate, HDI, trimer with 20 nm mean diameter functionalized silica nanoparticles) from Covestro (formerly Bayer MaterialScience (Pittsburgh, PA)) and (2) X11102PMA (Nanophase Technologies, Romeoville, IL) containing non – functionalized alumina nanoparticles (40 nm mean diameter in methylene diphenyl diisocyanate (MDI) and propylene glycol methyl ether acetate (PMA)). The functionalized nanosilica covalently bond to with the polyurethane during curing while the non – functionalized nanoalumina are not chemically bound to the resin.

A summary of the coating formulations used to coat the test vehicle assemblies is given in Table 1.

Table 1: Test vehicle assembly coating materials.

Use	Coating	wt% isocyanate in suspension (N3300 HDI trimer)	wt% nanoparticle after cure	Comment
Baseline dip + spray coating				
Dip or spray	PC18M-mod	0.00%	0	Thinned for dip
Spray	PC18M+20%XP2742	10.36%	6.74% nanosilica	
Spray	PC18M+20%11102PMA	Not applicable	13.04% nanoalumina	
Dip or spray	PC40-UMF	0.00%	0	Thinned for dip
Spray	PC40-UMF+10%XP2742	5.18%	1.88% nanosilica	
Spray	PC40-UMF+30%XP2742	15.54%	6.0% nanosilica	
Layered				
Dip or spray	PC18M	0.00%	0	Thinned for dip
Spray	PC18M+20%XP2742	10.36%	6.74% nanosilica	

3. General process development

3.1 Coating viscosity

The PC18M as received coating viscosity can be modified through the addition of AC0305 solvent. The as–received PC18M contains approximately 50 percent solvent. The solvent addition to the as-received PC18M is indicated in Figure 2. For reference, the PC18M with all the solvent completely evaporated is very thick with a molasses like consistency.

The viscosity versus solvent addition curves for the PC18M, the PC18M+20%XP2742 nanosilica and the PC18M+20%X11102PMA nanoalumina are also shown in Figure 2. The XP2742 functionalized nanosilica suspension is comprised of nanosilica particles in N3300 isocyanate. Functionalized particles have reactive groups that allow the particles to be covalently bonded to the urethane chains. The XP2742 viscosity is dominated by the 1752 to 3250 cps N3300. As a result there is a slight increase in viscosity to the PC18M when the XP2742 is added.

The X11102PMA nanoalumina suspension is approximately 70% propylene glycol methyl ether acetate (PMA) having a very low viscosity of 0.8 cps. Thus there is a substantial decrease in viscosity to the PC18M when the X11102PMA is added.

The nominal PC40-UMF base coating viscosity according to the data sheet is 250 cps. The PC40-UMF is a VOC free material with no solvent. It was necessary to thin the material for dip coating. The viscosity of the PC40-UMF with various percentages of AC0305 solvent is shown in Figure 3. Since the PC40-UMF is not typically used with a solvent, a recommended solvent evaporation time of three hours prior to ultraviolet cure was established based on the measurements shown in Figure 4.

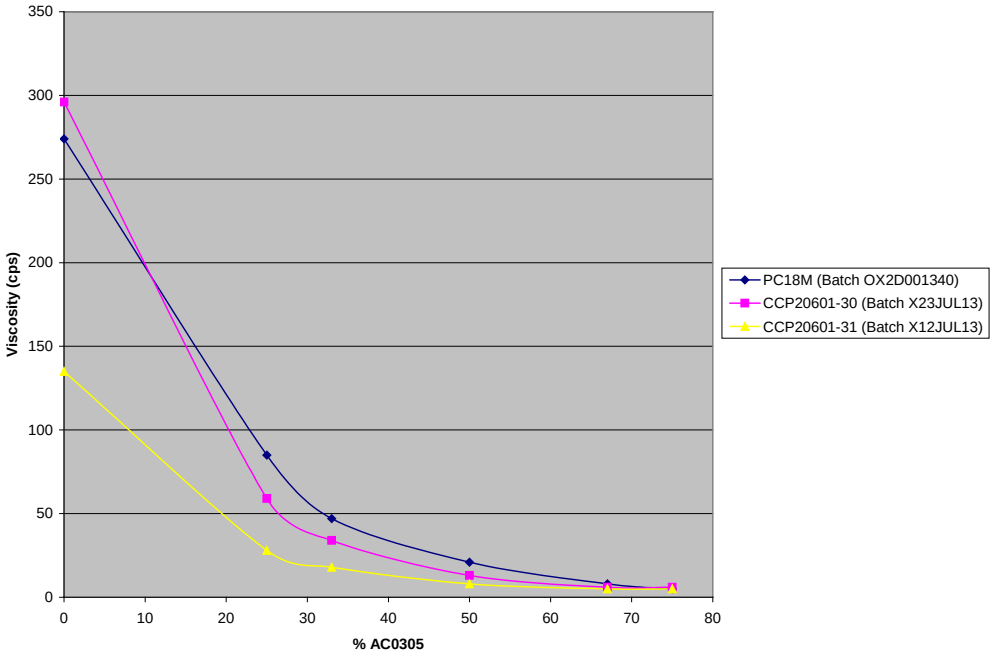


Figure 2: Viscosity of PC18M based coatings versus AC0305 solvent addition. Note: CCP20601-30 = PC18M+20%XP2742 and CCP20601-31 = PC18M+20%X11102PMA.

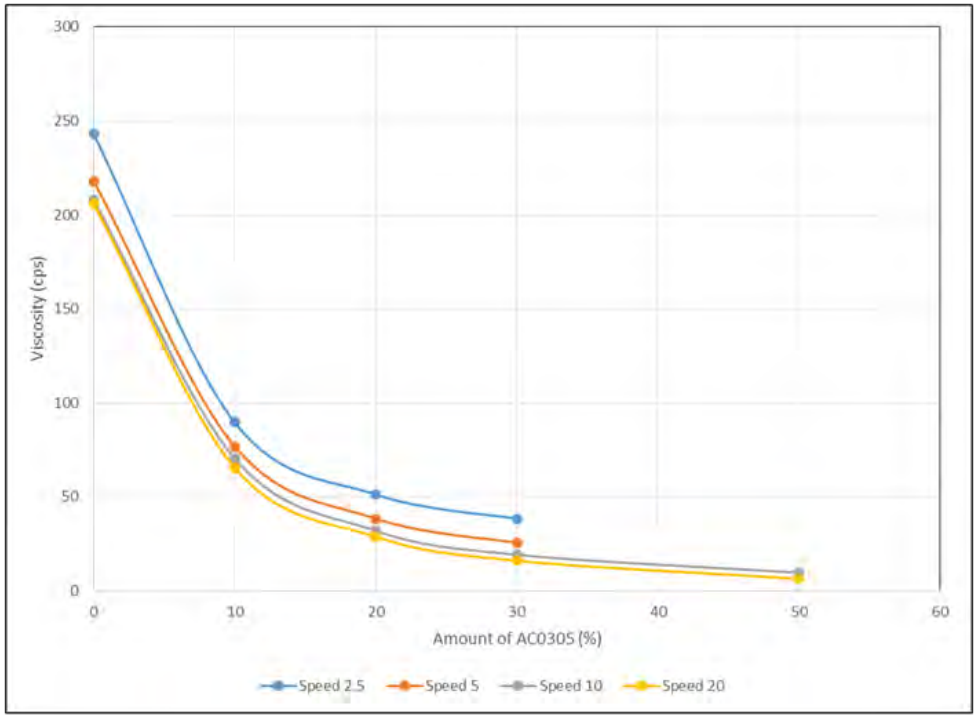


Figure 3: Viscosity of PC40-UMF coating versus AC0305 solvent addition.

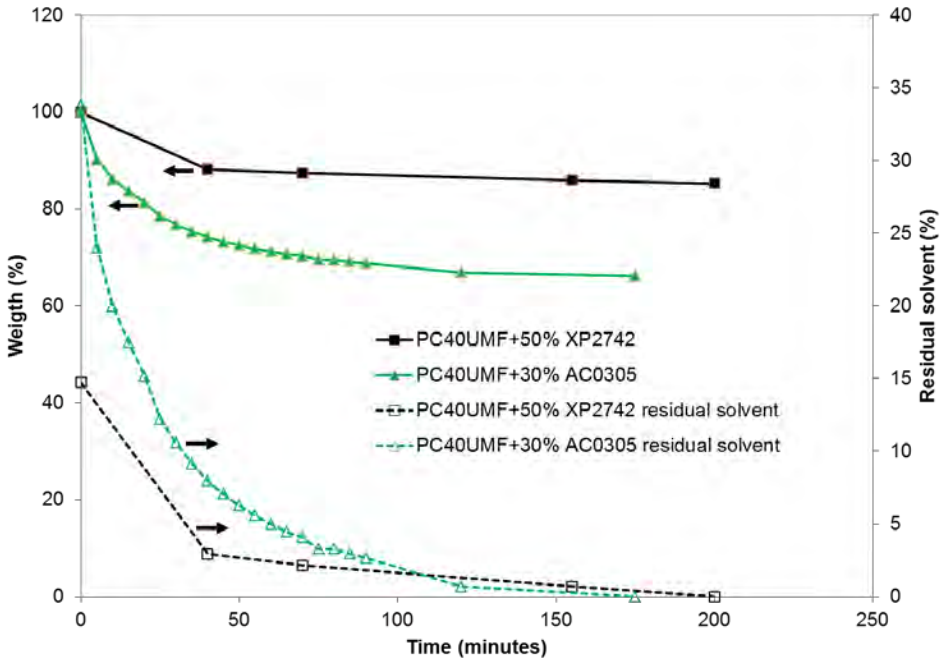


Figure 4: Solvent evaporation versus time for PC40-UMF and PC40-UMF+50%XP2742 drawn films 75 to 125 microns thick.

3.2 Dip coating

The dip coating process is outlined in Figure 5. The immersion rate, immersed hold time, withdrawal rate, and vertical drain time are controlled by the dipping machine and the operator. After the vertical drain time has finished, the assemblies are placed horizontally on a tray and air dried to allow the solvent to evaporate. The dip capillary flow into gaps and behind leads is primarily controlled by (1) surface energies of the solid assembly materials, (2) the wetting contact angle between the coating and assembly surfaces, (3) coating viscosity, (4) the lead/part geometry (e.g. spacing between leads, sharp lead corners, bend radii, etc.), and (5) the gap size under the parts. Typically, solvent additions to the coating significantly improve wetting by decreasing the viscosity, contact angle and sensitivity to surface contamination. During the withdrawal and vertical draining phases, the coating solvent is evaporating, resulting in increased coating viscosity and slower coating flow.

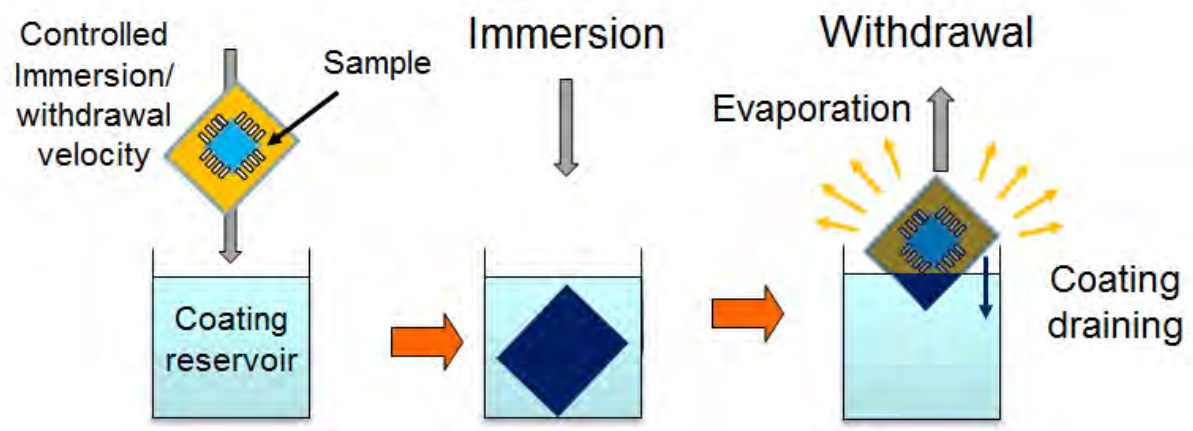


Figure 5: Dip coating process flow.

3.2.1 Dip coating process - initial viscosity evaluation

The tendency of the coating to fill gaps between the parts and the board were evaluated using a pair of glass slides separated by shims to establish gaps from 50 to 635 microns (Figure 6). The samples were dipped into the coating reservoirs using the dipping machine at Celestica Toronto at a rate of 76 mm/minute (machine minimum rate). The flow into the gaps could be examined visually during the immersion process. As the gap size decreased, the tendency to form a void in the gap increased. The time to fill the gap increased with decreasing gap spacing (Figure 7).

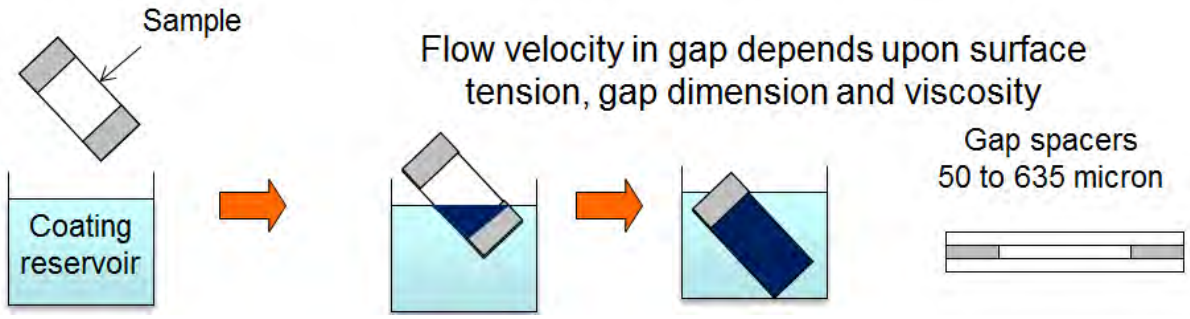


Figure 6: Glass slide gap penetration experiment.

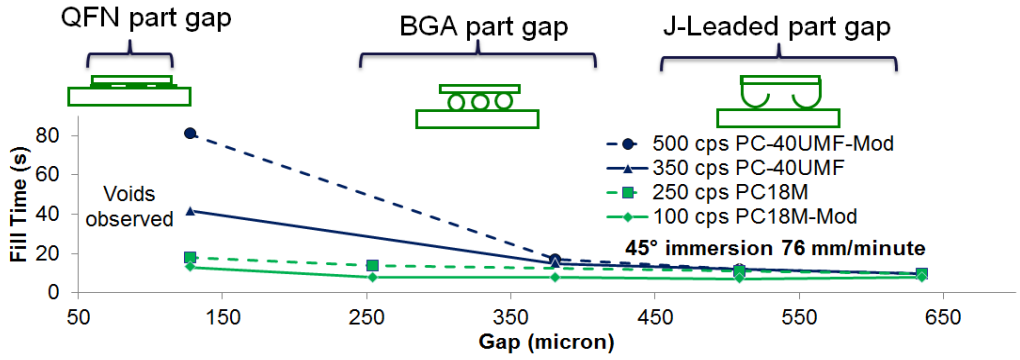


Figure 7: Gap filling time versus gap spacing for various viscosity PC18M and PC40-UMF coatings.

The dip coating flow on an assembly was initially evaluated by dispensing coating manually using a pipette. Two full pipettes were used to coat each part. The assembly was placed at an incline of approximately 30 degrees from vertical. The coating was allowed to drain for one hour. The lower viscosity resulted in better coating draining as shown in Figure 8 (Note the greater fluorescence intensity indicates a greater coating concentration of Ultraviolet (UV) tracer, i.e. thickness of the coating).

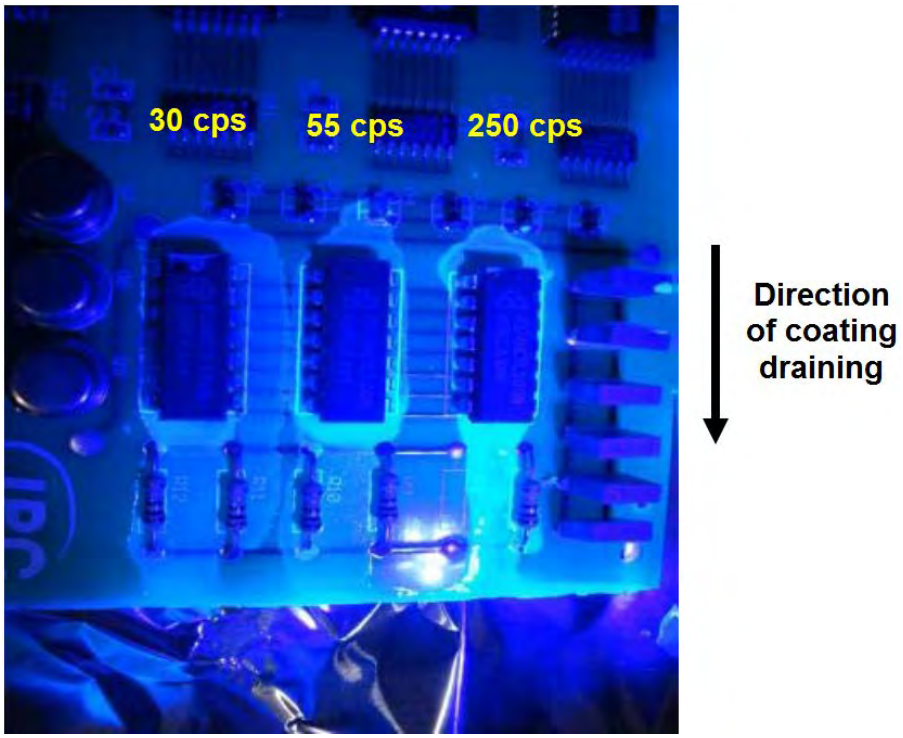


Figure 8: Coating draining after pipette application of PC18M having various viscosities. Photograph used ultraviolet light illumination. The 30 cps was a 50% dilution, the 55 cps was a 33% dilution, and the 250 cps was undiluted as received PC18M.

3.2.2 Dip coating

3.2.2.1 Initial dip coat for the 2013 dip+spray assemblies

For the baseline dip+spray assemblies, the initial assembly dip coating was completed Aug. 2013 at the Celestica Toronto facility. The Specialty Coating Systems (SCS) PL-3201 dipping machine used for dipping is shown in Figure 9. The local conditions were 22-23C at 60-61% R.H. The coating was PC18M / Lot OX3F009496 / Expiration Aug. 22, 2014 and the solvent was AC0305 / Lot X29JUL13 / Expiration Oct. 29, 2013. The PC18M was diluted to 30 cps. The dip coating immersion and withdrawal speeds were 76 mm/minute. The board immersion time after contact with the coating was approximately 70 seconds. After complete immersion, the withdrawal was immediately started (no dwell), after approximately 70 seconds the boards were clear of the coating, the boards were then allowed to drip for approximately 90 seconds and then placed on a horizontal tray and air dried overnight in a chamber with low velocity air flow (Figure 10).

It was noted that the samples dipped later in the day had thicker dip coating. The thicker coating was attributed to viscosity increase due to solvent drag-out and evaporation over the three to four hour dipping session. It is recommended that the coating viscosity monitored during the dipping process.

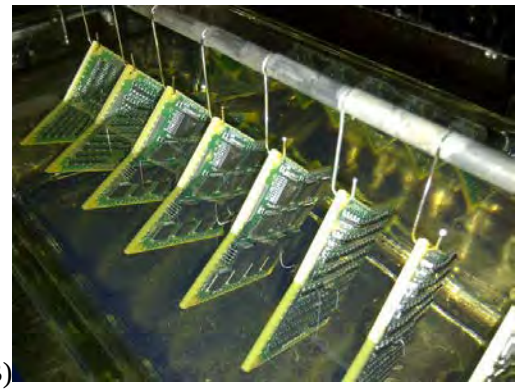
(A)  (B) 

Figure 9: Dip coating machine; (A) Front of machine with one board shown on immersion bar and (B) boards partially immersed in the coating reservoir.

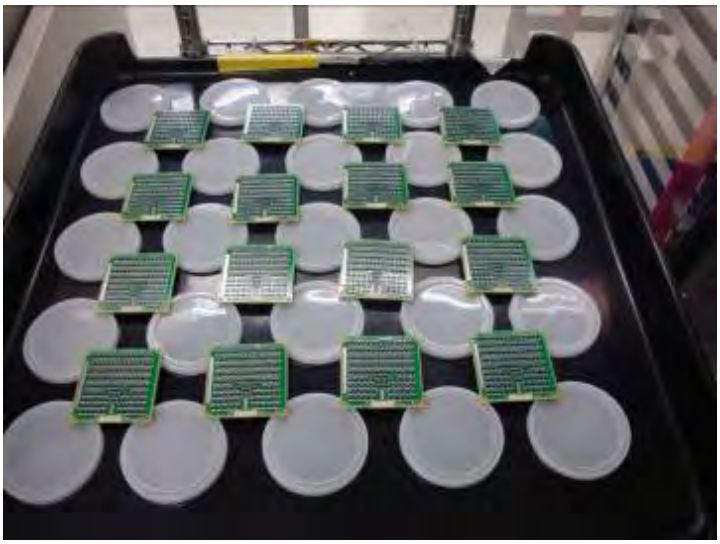


Figure 10: Dip coat samples on a tray in the drying chamber.

3.3 General spray coating process development

3.3.1 Spray process considerations

The liquid conformal coat and solvent mixture is drawn from a reservoir and combined with pressurized nitrogen gas flow in the nozzle to form atomized liquid droplets which are directed onto the board (Figure 11). Some key spray coating parameters are (1) surface energies of the solid assembly materials, (2) the wetting contact angle between the coating and assembly surfaces, (3)

coating viscosity, (4) the spray droplet size, (5) the lead/part geometry (e.g. spacing between leads, sharp lead corners, bend radii, spacing between leads, part height, etc.), (6) nozzle height, (7) coating flow micro-adjust, (8) nozzle speed, (9) atomization pressure, (10) number of X-Y spray layers, (11) spray delta X and delta Y jog increments, and (12) tall parts that can block the spray particles or limit nozzle position. The spray droplet coalescence steps to form a continuous film are shown in Figure 12.

During spraying and after the coating is sprayed on the board, the coating droplets combine, the solvent evaporates and the film levels out. If the viscosity is too high or the film spray is too dry the film cannot level out properly and the assembly surface is uneven.

3.3.2 Automatic spray machine set – up

In the present work, the test board coupons were spray coated at Celestica in Toronto using an Asymtek SL-940 spray coater with a EFD 781S conical atomizing spray nozzle and a 591 ml (20 oz.) low volume coating reservoir (Figure 13). A combination of paper grid sheets and metal coupons were used to define the initial atomization pressure and spray pattern to obtain the desired flow and thickness. The thickness was measured on the steel panels after solvent evaporation using an eddy current meter. The eddy current was a PosiTector 6000 NS Probe, SN167346, Date Oct/31/2011 with a thickness range of 0 to 60 mils and an accuracy of ±(0.05mil+1%) for thickness of 0–2 mils and ±(0.1mil+1%) for thicknesses greater than 2 mils.

The spray pattern used an alternating X and Y pattern with a 4.4 mm step size (Figure 14). A typical nozzle speed of 250 to 350 mm/second was used and the nozzle height above the board was approximately 75 mm.

After the initial spray parameters were established, a test board was coated and visually examined for coverage and flow. The spray parameters were adjusted as needed to achieve the desired appearance. After any spray adjustments, the coating thickness on the steel panels was measured again.

3.3.3 Coating curing

After spray coating, the assemblies were placed horizontally in a solvent drying cabinet.

The PC18M based coating samples were then placed in an oven for curing (Figure 15). The samples were then maintained at room temperature/humidity for approximately a week to obtain full properties.

The PC40-UMF coating samples were ultraviolet (UV) light cured after spray and the PC40-UMF+nanoparticle suspension coatings were solvent dried then UV cured.

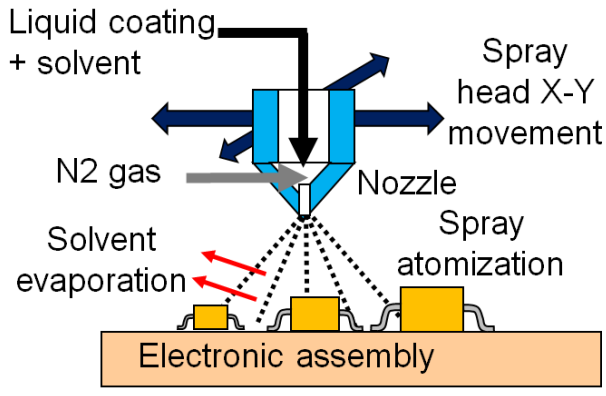


Figure 11: Schematic of spray process.

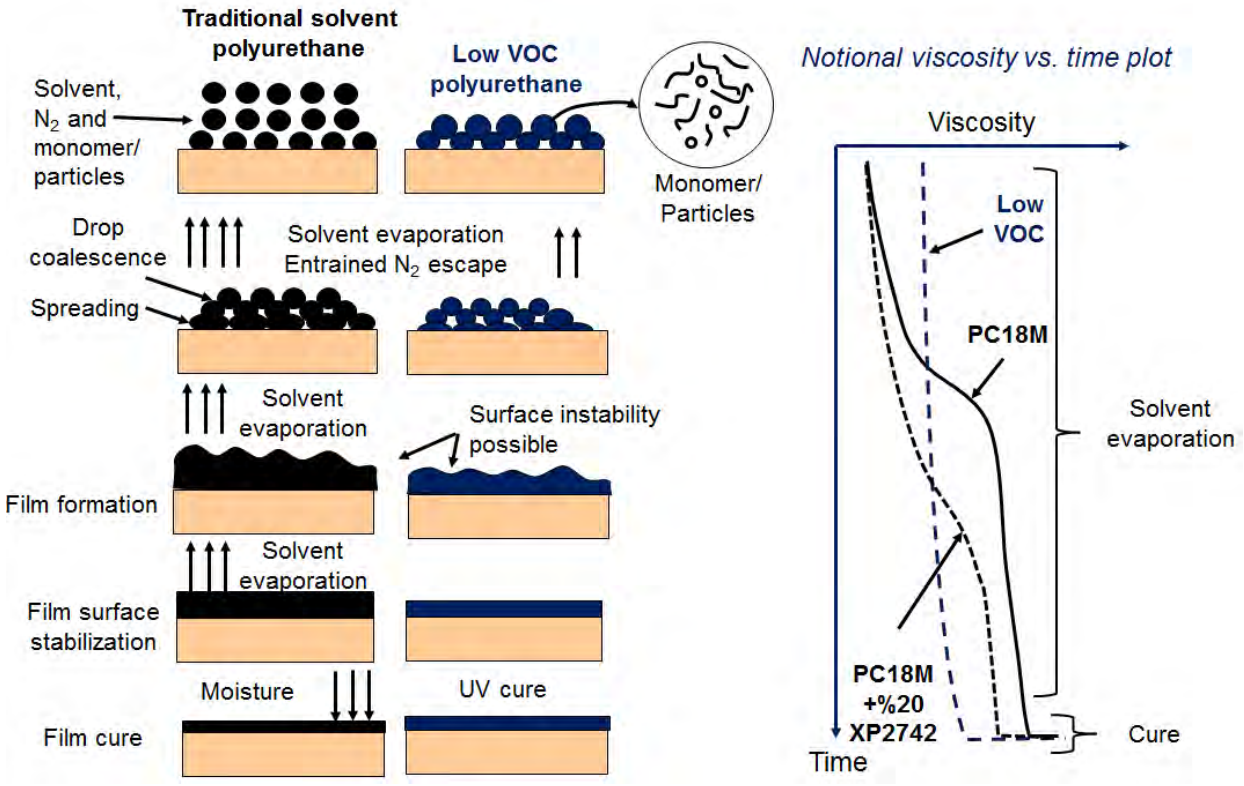


Figure 12: Coating film formation from spray coating process.

(A) (B)

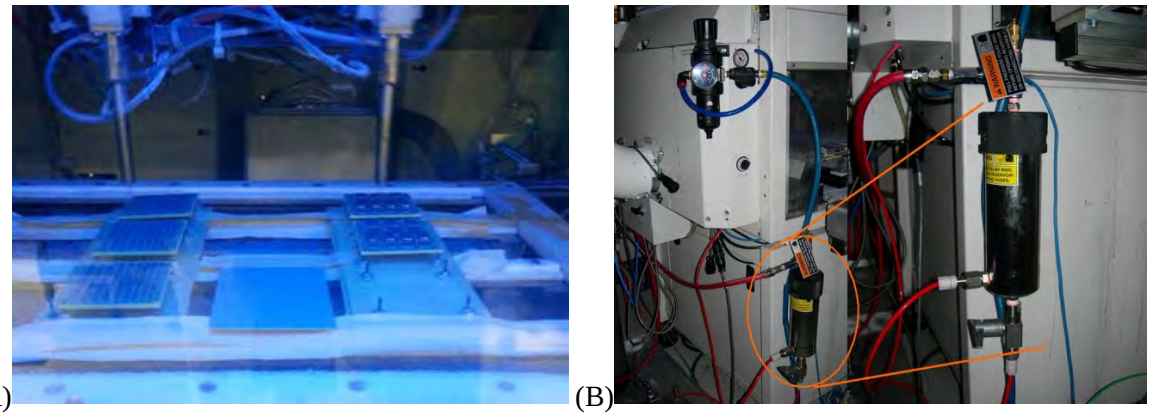


Figure 13: Spray coating machine; (A) Samples in the spray machine and (B) the small volume reservoir fitted to the rear of the spray machine. View (A) also shows a flat steel process control coupon centered between the boards.

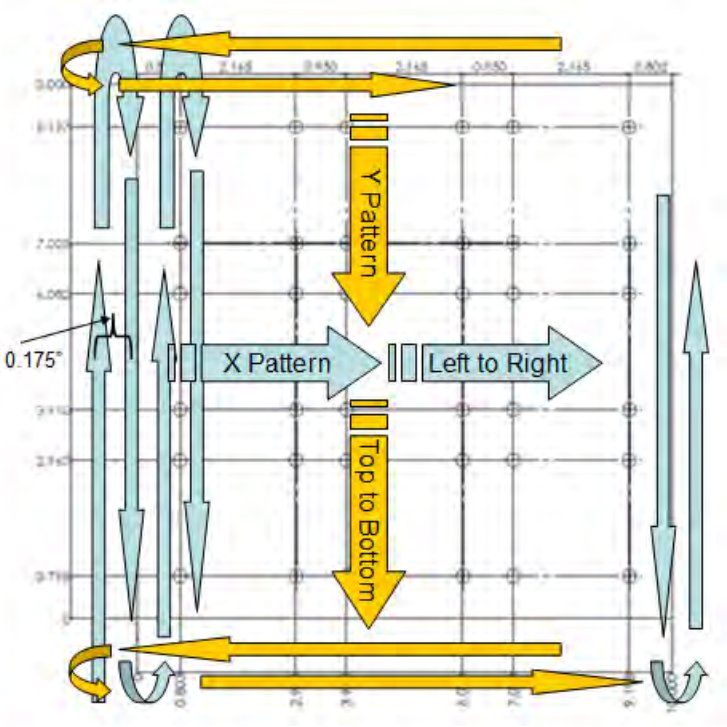


Figure 14: Typical machine spray pattern.



Figure 15: Curing oven.

4. PC18M Baseline dip + spray coating method

The baseline dip+layered spray process consists of a low viscosity dip, partial cure, 50 micron nominal thickness spray, and final cure (Figure 1). For low viscosity dip coating, the PC18M could be diluted as low as 30 cps with the Henkel AC0305 solvent and still form a continuous film upon curing.

Unless otherwise noted, all PC18M family samples were air dried for a minimum of 30-45 minutes and then cured for a minimum of two hours at 60 ºC (140 ºF) in an oven having a minimum relative humidity of 30 percent in accordance with the PC18M datasheet.

The tin whisker assembly coating targeted a nominal coating thickness of 50 microns PC18M-mod, PC18M+20%XP2742, and the PC18M+20%X1102PMA coatings.

The PU coatings were applied to the Small Outline Transistor (SOT), Quad Flat Pack (QFP), and Ball Grid Array (BGA) whisker test assemblies at Celestica in Toronto with the following process: (1) prior to coating the assemblies were cleaned using standard manufacturing in-line cleaning processes and plasma etched to ensure good adhesion; (2) low viscosity dip coat with PC18M-mod thinned to 30-50 cps followed by an solvent evaporation air cure of 30-45 minutes at room temperature with 30-40 percent RH, then two hours at 60 °C (note no added moisture in oven); (3) the samples waited for 72 hours at room temperature with 30-40%RH prior to spray coating; (4) automated spray coating applied PU; (5) then solvent evaporation for two hours at room temperature at 30-40%RH; (6) followed by two hours at 60°C (note no added moisture in oven).

The viscosity of the PC18M-mod, PC18M+20%XP2742 and the PC18M+20%11102PMA coatings were all approximately 150 cps, but there was a difference in the way that the coating thickness built up during spray coating. The PC18M-mod and PC18M+20%XP2742 build-up was such that the nominal 50 micron thickness was accomplished with two x-direction and two y-direction spray passes (a total of four coating layers). In contrast, the PC18M+20%X11102PMA could be coated with four x-direction and four y-direction spray passes (a total of eight coating layers), which generally improves coverage. The time between PC18M family spray coating and the assembly whisker testing was 10 days room temp 30-40%RH followed by two months nitrogen cabinet moisture (moisture content was estimated to be less than 5%RH).

4.1 PC18M bubble observations

Another significant finding on the tin whisker test assemblies was the presence of bubbles in some of the coatings. A range of bubble density and size was observed as will be discussed further in [6]. For example, the PC18M-mod (Figure 16) and PC18M+20%XP2742 boards had the higher bubble density while the PC18M+11102PMA had few if any bubbles (Figure 17). However, bubble formation did not seem to depend on part type. It also was not consistent amongst PC18M and PC18M+20%XP2742 coated assemblies because some of these had few if any bubbles. There were few or no bubbles on any of the PC18M+20%X11102PMA nanoalumina coated assemblies.

Several attempts to form bubbles with very thick cast films under various temperature humidity cure conditions were unable to reproduce the condition. It was noted that PC18M has very high viscosity when no solvent is present. Since the bubble formation was observed on both the 2X-2Y PC18M-mod spray coating and the 2X-2Y PC18M+20%XP2742 spray coating but not on the 4X-4Y PC18M+20%X11102PMA boards, the thickness of material applied during each spray pass and the manner that the solvent escapes may be related to the bubble formation (Figure 12).

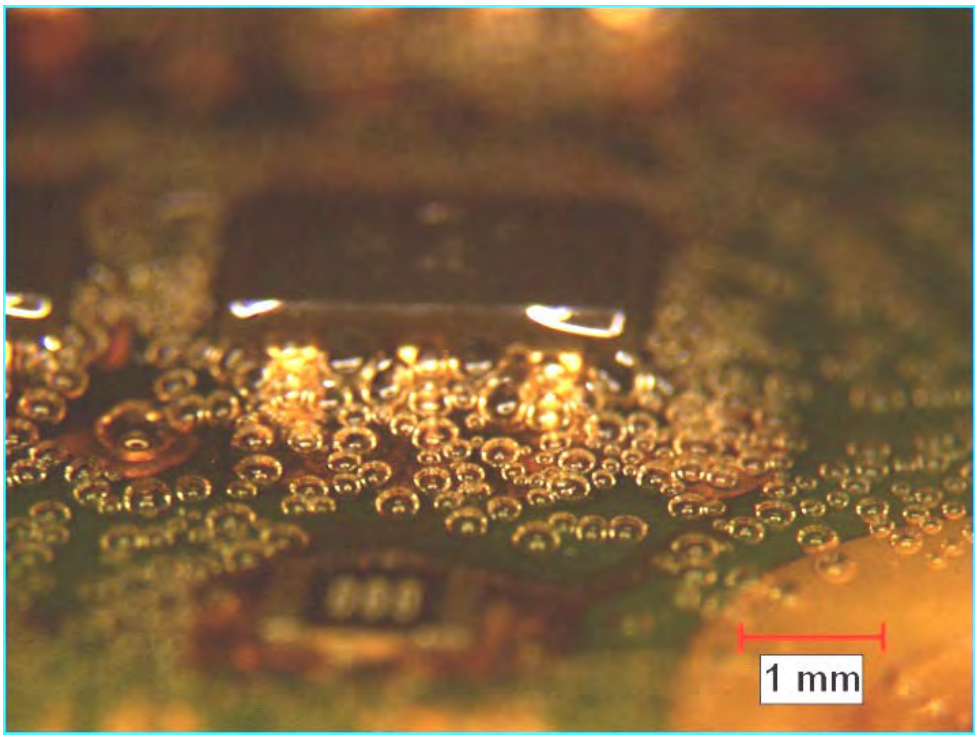


Figure 16: PC18M-mod SOT board 233 with large bubble density, 10x, after ATC+1000HTHH. The color change in the second image is an artifact of the illumination used to highlight the bubbles.

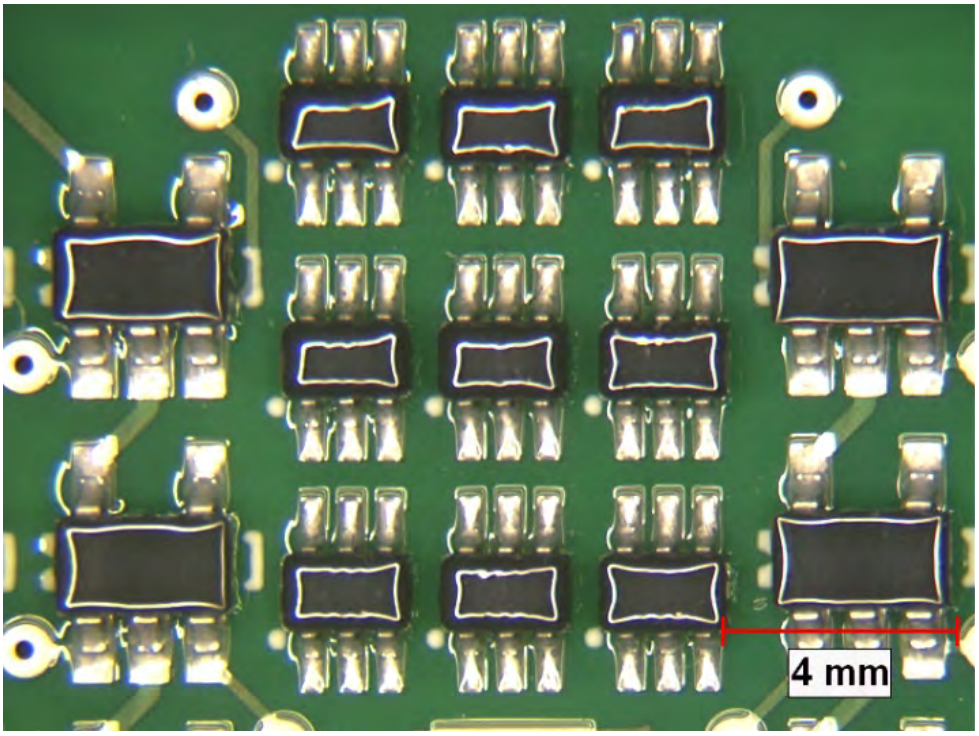


Figure 17: PC18M+20%X1102PMA, SOT board 226, HALT, 10x, small/no bubble density, milky appearance.

5. PC40-UMF coating

5.1 Batch A and B PC40-UMF Baseline dip + spray

The second formulation, PC40-UMF from Henkel, is compatible with all the nanoparticle suspensions. A summary of the PC40-UMF coating nanoparticle concentration based on solids is given in Table 4. For the initial dip coating, the PC40-UMF could be diluted as low as 30 cps with the Henkel AC0305 solvent and still form a continuous film upon curing.

The PC40-UMF material family cure schedule had to be modified to account for the solvent in the nanoparticle suspension. For the mechanical pull test, nanoindentation, and Sn-Ag-Cu alloy lead free solder (SAC) + Rare Earth Element (REE) coupon samples was: (1) initial solvent evaporation for 30 minutes, (2) UV exposure using Hg bulb, and (3) moisture cure 60°C/60%RH for two hours. In some cases, a longer high humidity cure was used or an extended room temperature hold was used after high humidity curing to ensure complete curing prior to performing certain testing.

The initial whisker test assemblies were coated with PC40-UMF diluted to 30 cps with AC0305 solvent using a dip process, 60 minute solvent evaporation, UV cure, six days at room temperature/humidity, spray coat PC40-UMF, then UV cured again. Unfortunately, de-wetting was observed between the initial dip layer and the spray layer so another set of samples needed to be made.

The next group of samples was plasma etched to increase the surface energy of dip coat layer and improve the wetting. The plasma etch was for 900 seconds using a 50/50 oxygen/argon gas mixture. The samples had now been at room temperature/humidity for six days prior to plasma etching and spray coating. Samples were then spray coated with PC40-UMF, PC40-UMF+10%XP2742, PC40-UMF+30%XP2742, PC40-UMF+50%XP2742 and PC40-UMF+15.54%N3300. The spray coating exhibited better wetting, but tape testing and cross-sectioning revealed that there was still low adhesion between the dip and spray layers. Follow-up testing by Henkel showed that better interlayer adhesion was obtained on coupons confirmed that lower adhesion was obtained when a UV+moisture cure was used between layers. Using only a UV cure between successive layer applications provided a slight improvement to the adhesion, but was still not at satisfactory levels for this project.

5.1.1 Excessive thickness of PC40-UMF dip coat

Inspection of PC40-UMF dipped samples in thinned PC40-UMF revealed that some of them had significant build-up of the coating (Figure 18 and Figure 19). The higher than expected coating build-up indicates that viscosity increase during the dipping session (Figure 20) resulted in decreased coating draining. After 4-hours the viscosity increased two to four times and after eight hours increased 13 to 15 times. This is the reason for the thicker dip coating layer for the SOT as compared to the QFP samples, as all of the QFP samples were run first then the SOT samples.

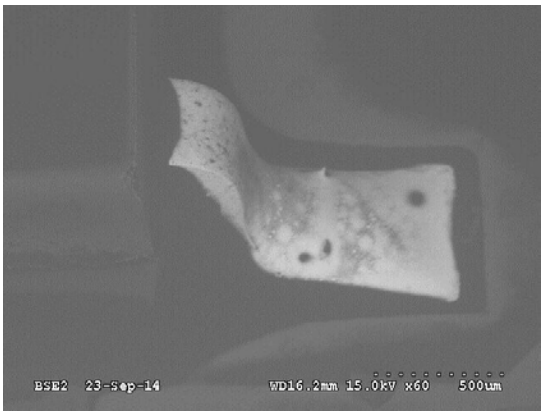


Figure 18: SEM image of PC40-UMF Dip, Board 292, SOT5, 60x.

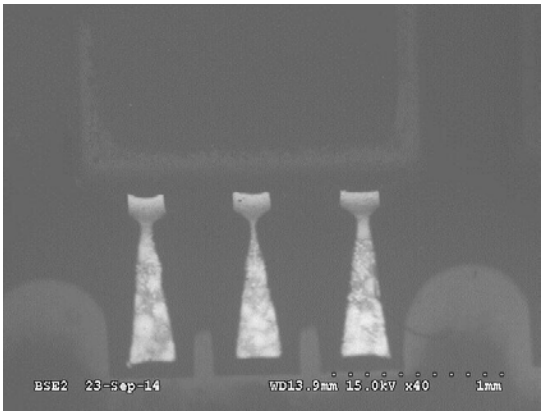


Figure 19: SEM image of PC40-UMF Dip coat, Board 292, SOT6, 40x.

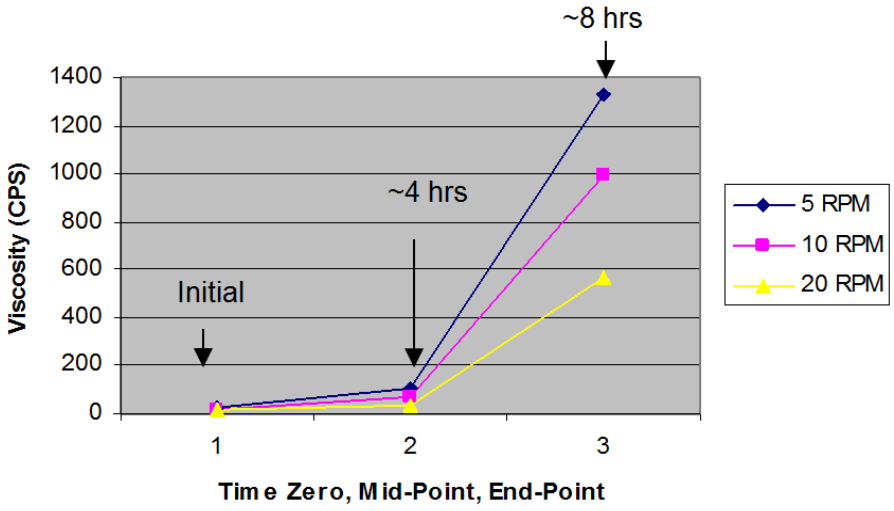


Figure 20: Thinned PC40-UMF dip coating viscosity change during processing.

5.2 Batch C and D PC40-UMF Interlayer adhesion and Coverage Improvement Experiments

5.2.1 Objective

Due to the de-wetting and interlayer delamination issues observed during the PC40-UMF Batch A and B board processing, a detailed evaluation that included surface energy, viscosity, various thickness measurements, and various interlayer UV curing conditions was performed. The goal was to determine the conditions under which PC40-UMF could be sprayed and provide good assembly coverage. For this requirement the initial PC40-UMF dip coating was than eliminated. With a new lot generated to meet the target thickness for flat surfaces of 50 microns. A process window of 25 to 75 microns was expected, based on typical industry experience due to varying component heights (distance to the nozzle) and sizes.

Both STI (PN SST-7711-K1 STI Electronics, Madison, AL) and BAE Systems WP1753 cards were coated at Asymtek in California on April 20, 2015, with Henkel and Celestica participating in the experiments. The intent was to confirm that good coating coverage could be achieved with PC40-UMF conformal coating, using the application expertise from all three companies together at once.

5.2.2 Planned analysis after coating

After coating at Asymtek, STI cards were sent to BAE Systems for immediate Scanning Electron Microscope (SEM) analysis. The WP1753 cards were sent to Celestica for optical, SEM, and cross section analysis.

The purpose of the visual inspections and SEM imaging was to determine the extent of coverage, with the thickness measurements to be confirmed by cross section as needed.

Cross sectioning was done to ascertain the coating thickness on some areas of interest from the SEM examination. This was done to get a quantitative measurement value of the coating thickness whereas the SEM can only give a qualitative measurement estimation of value.

5.2.3 Coating experiment participants

Celestica

Jason Keeping – Project Manager, Conformal Coating & Underfill

Henkel Electronic Materials LLC

Dave Edwards – Senior Technical Service Engineer

Nordson Asymtek

Mike Szuch – Senior Applications and Process Engineer

“Jaynie” Heakyoung Park – Applications Engineering Manager

Benjamin Quintero – Senior Technical Product Specialist, Americas

5.3 Equipment and materials

5.3.1 Location and environment

Nordson Asymtek Carlsbad, CA Office
2747 Loker Ave W Carlsbad, CA, 920106601
April 20, 2015
Henkel Electronic Materials Irvine, CA Office
14000 Jamboree Rd Irvine, CA, 926061730
April 20, 2015

The ambient environmental conditions are shown in Table 2. There was a small change in temperature and RH over the time of the coatings application, however, it was not considered significant for this coating type. The temperature and humidity levels were acceptable for this material and spray coating application.

Table 2: Environmental conditions during evaluation

Time	Temp (°C)	Relative Humidity (%)
8:30 am	19	50
2:30 pm	21	49

5.3.2 Coating materials

The conformal coating material was packaged in a 1-Gallon container, opened on site and inspected. The inspection was to see if there were any gelled or cured material in the container prior to usage; none was found. A time zero sample of the coating material was taken, sealed and retained by Henkel for viscosity testing. The coating material was then placed in the conformal coating dispenser.

Table 3: Raw material information

Material >>	Henkel coating PC40-UMF	Henkel solvent AC0305
Batch #	OX5C005615	INV IR36893
MFG Date	March/31/2015	
EXP Date	Sept/30/2015	
Initial Viscosity	256 cps	n/a
Final Viscosity	268 cps	n/a

AC0305 was determined to be compatible with PC40-UMF by Henkel. This solvent was used to flush the lines to ensure no prior material remained in the lines. After completion of the flushing process, compressed air was used to ensure that there was no residual solvent remaining in the lines.

Viscosity testing was done by Henkel at the Irvine lab prior to coating at Asymtek. The viscosity measurements were made using the small sample adaptor Spindle SC4-21 10rpm on the Brookfield RVT DV-II. The small sample adaptor was used to minimize consumption of coating material. The tests were performed at room temperature.

5.3.3 Surface energy measurement

Dyne Pens used for the board surface energy measurement ranged from 36 to 60 dynes/cm^2, as shown in Table 4.

Table 4: Dyne Pen Summary

Expiration Date	Dyne Pen Name
Sept. 30, 2015	38, 40, 44
Oct. 5, 2015	36, 48, 52, 60

5.3.4 Assembly boards and pre-coating preparation

The STI assemblies were pre-cut and cleaned at Henkel. The assembled boards were numbered one through six. Boards one through four were cut as and numbered as shown in Figure 21.

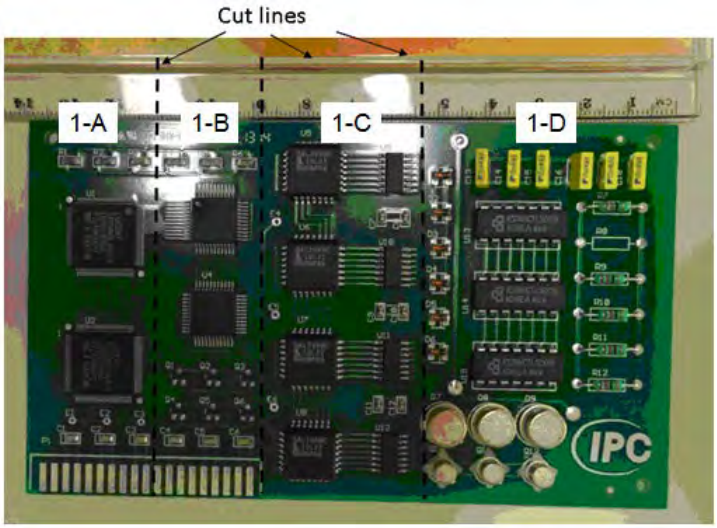


Figure 21: Cutting pattern for STI assembly.

A STI card was tested, and the solder mask surface energy was found to be between 36 and 37 dynes/cm^2 (the sample passed the 36 dyne pen test, but failed the 38 dyne pen test). The target surface energy for good coating is over 40 dynes/cm^2, therefore plasma etching was required. STI assemblies were plasma etched on site at Asymtek, using a March Plasma AP-600 system with a 50/50 Air to Oxygen mixture. Machine settings were: RF power of 400 Watts, base pressure of 80 mTorr and cycle time of 600 seconds.

After plasma etching, the same card was tested and it passed the 60 dynes/cm^2 pen test for surface energy.

Table 5: Plasma etch equipment

Equipment	Plasma Etch
Model	AP-600
Serial #	AP600212
MFG Date	July/31/2014

WP1753 boards were cleaned in the in-line cleaner at Celestica prior to shipment to Asymtek. They were not plasma etched because they were delivered to the coating area in the last hour of machine time. There was no surface energy measurement taken due to time constraints.

5.3.5 Coating Equipment

An Asymtek spray dispenser with a conical atomizing spray nozzle was used to coat all the samples (see Table 6).

Table 6: Conformal Coating Application Equipment

Equipment	Asymtek Dispenser	Nordson Nozzle	Reservoir
Model	SL-940E	EFD 781S	Semco 6 oz. cartridge and retainer
Serial #	S24515		None
MFG Date	Mar/31/2014		None

Wet coating thicknesses were measured with a wet film gauge (Figure 22). Dry coating thicknesses were measured with an eddy current meter. The thickness measurement instrument details are given in Table 7.

Table 7: Conformal Coating Thickness Measurement Tools.

Tooling	Wet Film Gauge	Eddy Current	Micrometer	Drop Gage
Model	Paul N. Gardner Co. Inc.	PosiTector 6000 NS Probe	Centech	Mitytoyo
Serial #	None	167346	47257	7326
MFG Date	None	Oct/31/2011	None	None
Range, mils	0.5 to 20 mils	0 to 60 mils	n/a	n/a
Accuracy, %	0.5 mils	±(0.05mil+1%) 0–2mils ±(0.1mil+1%) >2mils	n/a	n/a



Figure 22: Wet Film Gage.

5.4 Test and experimental procedures

5.4.1 Development of UV cure process for Henkel PC40-UMF Conformal Coating

Asymtek had a small in-line UV cure oven on-site. The UV cure oven information is:

- Model: UV-9
- Serial Number: 2472
- MFG Date: 2014
- Bulb Type H.
- No maintenance or calibration required. Performance is per the manufacturer's specifications that were available on Asymtek's website.

The UV intensity process control tool information is:

- Model: UVICURE Plus
- Serial Number: 7414

- Calibration Done: Sept. 26, 2014 / Due: Sept. 26, 2015

The requirement provided by Henkel for a full cure of the PC40-UMF coating was a complete exposure and *build-up* of at least 3.0 J/ cm^2. Build-up is the value of the UV intensity that is provided in a single pass of the cure conveyor.

The initial conveyor speed that was used for this testing was 60 cm/min, which resulted in a value of 5.063 J/cm^2 that was well above the 3.0 J/ cm^2 target. The conveyor belt speed was increased from 60 to 100 cm/min, which resulted in a 3.050 J/ cm^2 buildup, meeting the full cure requirements.

5.4.2 Coated surface energy measurements

After the UV Flash cure, the surface energy of the partially cured conformal coating was measured using the dyne pens. The reading was less than 30 dynes/ cm^2 and confirmed that even a 100% solids coating of the PC40-UMF would require additional surface treatment for a multi-layer application. (Note the higher the Dyne value achieved the better for adhesion. The Celestica minimum threshold for acceptance is 40 dynes/ cm^2that is in-line with industry standards noted in IPC-HDBK-830.

When the Dyne pen mark was wiped off with a Kimwipe, the dye in the Dyne pen remained on the PC40-UMF surface. The impact the pen residue could have had an impact on the adherence of any additional coating layers on top of it. It was recommended by Henkel that using a Dyne pen on a coating surface should be considered to be a destructive test, and samples should not be re-used for production due to this residue.

5.4.3 Modification of UV cure to provide UV flash between coating layers

In order to build up the coating material in an effort to improve coverage on the corners and edges of the leads, a layered coating approach of the PC40-UMF was attempted. The idea was to use as little UV flash as possible to simply make the first layer stay in place. The same Asymtek small in-line UV cure oven was used for this testing.

To generate a value of 50% UV intensity to provide an in-between flash cure, a conveyor speed double the production setting, i.e. 200 cm/min, was used and a UV intensity of 1.561 J/ cm^2 was obtained.

A first pass spray coating deposited 2x-2y layers, which was then flash cured using the 200 cm/sec conveyor speed. Then more coating was deposited using a 1x-1y spray application over the flash cure, however a high level of dewetting was observed.

To determine whether the 1x-1y layer was just too thin, another sample metal coupon was prepared, this time the first pass coating deposited was 1X – 1Y layers. The UV cure oven 200 cm/sec conveyor speed was used again for flash curing. After flash curing, a spray coating application of 2X – 2Y passes was applied, and dewetting was noticed again. Since both trials resulted in dewetting of the second coating application, the in-between cure of the PC40-UMF testing was terminated.

Henkel performed further work to evaluate if any UV flash for partial cure could be done between the layers of coating application. See Section 5.7.2 for the discussion.

(Note – there was no plasma etching between layers due to time constraint of the lab availability and would have to be evaluated on the UV flash cure before committing to experimental plans.)

5.4.4 Development of Coating Process to Apply Henkel PC40-UMF (100% Coating)

The initial step was to review the machine settings and process parameters developed during prior testing at Celestica with “PC40-UMF modified”. These parameters did not work well with PC40-UMF 100% solids, and resulted in “striping” on metal coupon #1 that was validated using 4x

magnifications, so a modification to the process parameter "width" (spacing between lines) was made from 10.2 to 5.1 mm. A uniform coating application was observed on Metal coupon #2. The resulting machine parameters used for this round of testing are listed below in Table 8.

The next steps were structured iterations performed on metal coupons. The objective was to find a set of machine parameters that would achieve the highest layer count and final conformal coating thickness between 25 and 75 microns (one to three mils). The main machine variables altered were: coating flow micro-adjust and layers. The nozzle speed and atomization pressure variables were determined in previous testing at Celestica, to be at the upper limits and could not extend further. The nozzle z-height was also held constant to reduce the evaluation matrix and provide the largest application window for various component height profiles that might be encountered future production.

Once a set of machine parameters gave good consistent results on the flat coupons, an STI assembly coupon was sprayed to confirm the settings. It was observed on the assembly that the coating was going on too "wet" and "blowing" the layer below it (i.e. this pattern could be seen moving the previous layer). Modification to the machine settings to reduce the "wet" effect was done and confirmed on both the flat coupons and the STI assembly.

The following parameters were confirmed as the go-forward coating application process:

- Direct material usage; no PC40-UMF dilution.
- Pattern performed 3X – 3Y alternating x and y patterns.
- Air Assist approximately 80 PSI
- Fluid Pressure approximately 8 PSI
- Nozzle Head Speed 609.6 mm/sec (24 inch/sec)

The parameters and resulting thicknesses are listed in Table 8.

5.5 Coating and curing of assemblies

5.5.1 STI assemblies

The dispenser applied the coating from A to D across each card. Refer to Figure 21: Cutting pattern for STI assembly. After the coating application; these cards were sent directly to the in-line UV cure system utilizing the 100 cm/min cure profile developed in Section 5.4.1.

The parameters and resulting thicknesses are listed in Table 9.

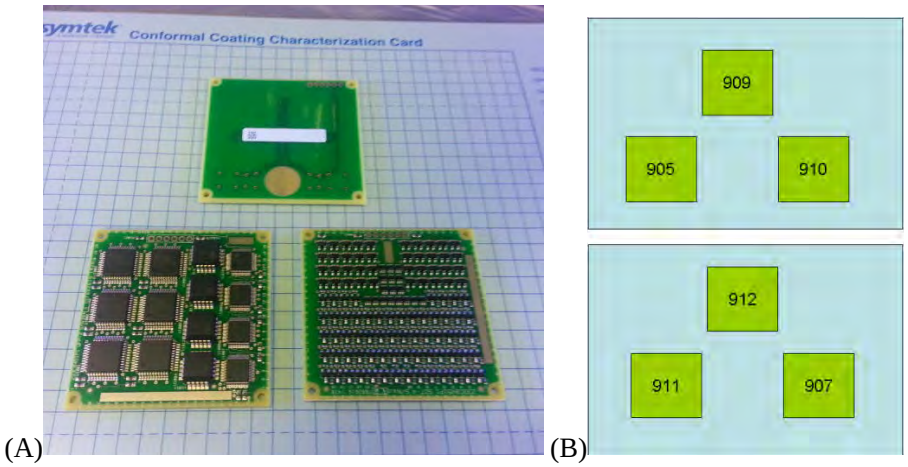
After cure, all samples were allowed to return to room temperature. Once at room temperature, all samples were packaged for shipment to BAE Systems, where an additional cure of 60 °C for 2 hours was to be completed upon arrival prior to any further inspection.

5.5.2 WP1753 assemblies

Samples were received in the coating area towards the end of the allotted line time. Due to this late material arrival and location of the plasma etch equipment, the WP-1753 SOT & QFP samples were not plasma etched prior to conformal coating.

The same dispensing and curing machine settings were used as for the STI card coating, shown in Table 8.

The WP-1753 SOT & QFP samples were coated in two lots; as per Figure 23. 909 and 912 show the unpopulated BGA backside, 905 and 911 are the QFP cards, and 910 and 907 are the SOT cards. The spray pattern was characterized using the paper back drop (Figure 24).



(A) (B)

Figure 23: WP-1753 Coupons (A) Optical photograph and (B) coupon layout.

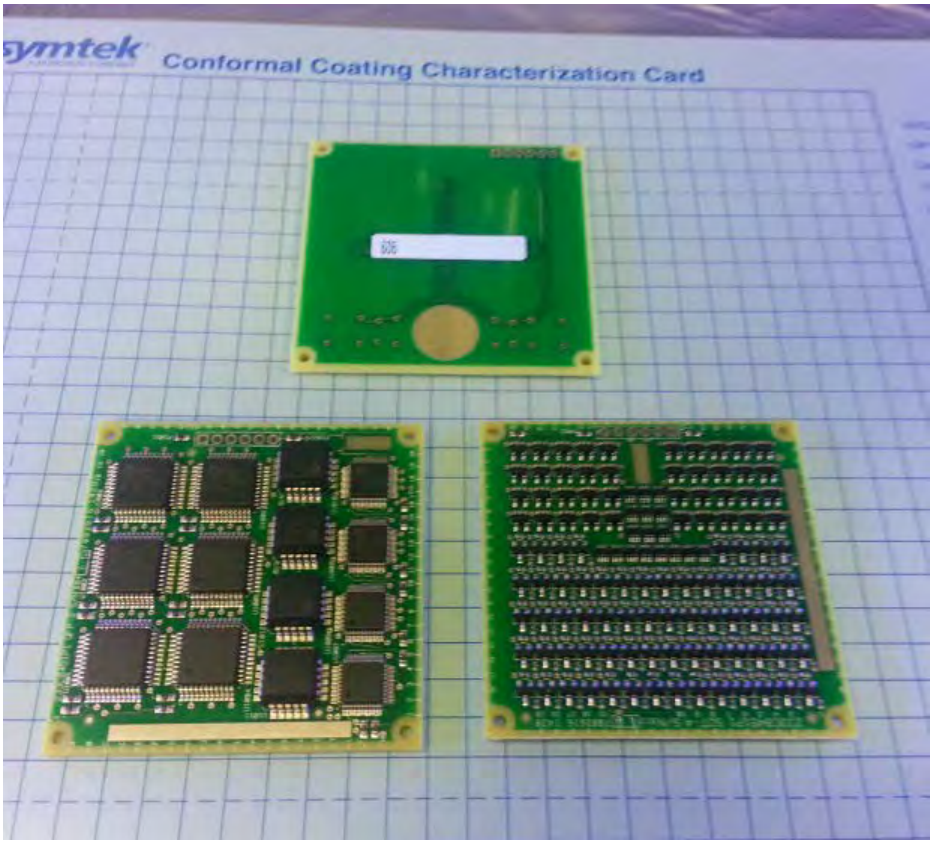


Figure 24: Spray pattern on WP1753 coupons.

After coating application, these cards were sent directly to the in-line UV cure system utilizing the same cure profile that was used for the STI cards of 100 cm/min providing at least 3.0 J/cm2 of UV intensity. After cure, all samples were allowed to return to room temperature. The parameters and resulting thicknesses are listed in Table 9.

Once at room temperature, all samples were packaged for shipment to Celestica for post coating bake at 60 °C for 2 hours prior to any further inspection.

5.6 RESULTS

5.6.1 Coating process setup and validation summary

The resulting machine parameters used for the paper and metal coating evaluation are listed in Table 8.

Table 8: Conformal coating process evaluation summary

Coupon Type	Coupon ID	Pattern Overlap (mm)	Micro-Adjust Aperture (value)	Layers	Observations	UV cure intensity (J/cm2)	UV cure conveyor (mm/min)	Eddy Current thickness (mils)	Wet Film gauge (mils)
paper	0	10.2	9	4					
Metal	1	10.2	9	4	Stripe formation	3.05	100	0.35	
Metal	2	5.1	9	4		3.05	100	0.50	
Metal	3	5.1	11	4		3.05	100	0.65	
Metal	4	5.1	15	4		3.05	100	1.00	
Metal	5	5.1	15	6	Wetness	3.05	100	1.50	3.50
Metal	6	5.1	13	6		3.05	100	1.20	
Metal	7	5.1	12	8	Wetness	3.05	100	1.35	
Metal	8	5.1	12	6		3.05	100	1.10	
Metal	9	5.1	12	6	Micrometer 2.0 mils / Drop Gage 1.25 mils	3.05	100	1.10	3.50
Metal	10	5.1	10	8		3.05	100	1.00	
Metal	11	5.1	10	10	9th good; 10th wet; Micrometer 2.0 mils / Drop Gage 1.25 mils	3.05	100	1.30	3.50
STI board	repeat 11	5.1	10	10	Too wet on PCBA	3.05	100		
metal	**12**	**5.1**	**12**	**6**	**Final Process Validation (same as run 9)**	**3.05**	**100**	**1.15**	**3.25**
STI board	B6	5.1	12	6		3.05	100		
STI board	B5	5.1	12	4	Dewetting of top layer; 4 layers then flash cure / 2 layers final cure	1.56 3.05	200 100		

5.6.2 Final assembly coating summary

The assembly spray parameters are listed in Table 9. Note that eddy current measurements could not be done directly on the STI or WP1753 cards because these boards lacked a large metal area on the component side for the eddy meter to properly measure the coating thickness. The reference coupon 12 (Table 8) was run using the same patterns as the program used for both the STI and WP1753 samples.

Table 9: Conformal coating application summary

Coupon Type	Coupon ID	Pattern Overlap (mm)	Micro-Adjust Aperture (value)	Layers	Observations	UV cure intensity (J/cm2)	UV cure conveyor (mm/min)
STI	B-1A	5.1	12	6		3.05	100
STI	B-1B	5.1	12	6		3.05	100
STI	B-1C	5.1	12	6		3.05	100
STI	B-1D	5.1	12	6		3.05	100
STI	B-2A	5.1	12	6		3.05	100
STI	B-2B	5.1	12	6		3.05	100
STI	B-2C	5.1	12	6		3.05	100
STI	B-2D	5.1	12	6		3.05	100
Metal	13	5.1	12	6	2 layers then flash cure	1.56	200
Metal	13	5.1	12	6	4 layers Dewetting	3.05	100
STI	B-3A	5.1	12	6		3.05	100
STI	B-3B	5.1	12	6		3.05	100
STI	B-3C	5.1	12	6		3.05	100
STI	B-3D	5.1	12	6		3.05	100
STI	B-4A	5.1	12	6		3.05	100
STI	B-4B	5.1	12	6		3.05	100
STI	B-4C	5.1	12	6		3.05	100
STI	B-4D	5.1	12	6		3.05	100
WP-1753	909	5.1	12	6		3.05	100
WP-1753	905	5.1	12	6		3.05	100
WP-1753	910	5.1	12	6		3.05	100
WP-1753	912	5.1	12	6		3.05	100
WP-1753	911	5.1	12	6		3.05	100

Coupon Type	Coupon ID	Pattern Overlap (mm)	Micro-Adjust Aperture (value)	Layers	Observations	UV cure intensity (J/cm2)	UV cure conveyor (mm/min)
WP-1753	907	5.1	12	6		3.05	100

5.7 Discussion of results

5.7.1 Wet and dry coating thickness measurement discussion

A wet film mechanical gauge was used to measure the "as applied" conformal coating. Post cure coating thicknesses were measured using an eddy current meter. The film thickness seemed to have decreased by 50% post cure from the initial wet coating thickness. The thickness measurement tools were investigated for accuracy. The eddy current meter was re-calibrated against the calibration samples. It was shown that the meter was in control. There was no tooling on-site to confirm any of the other three thickness process control tools. An additional study will be required to fully understand this thickness measurement variation and corresponding impacts to the process parameters.

Henkel completed cross sectional analysis of a flat, unencumbered area on an STI card and found the thickness to be around the 1.0 mil mark (25 µm), which aligned with the values obtained by the other cured measurements, shown in Table 8, coupons Metal 9 and Metal 11. Celestica also sectioned flat areas, and found thicknesses averaging in the high 30's micron range. Additional thickness evaluations are provided in the coating coverage analysis appendix.

Further review needs to be done on the wet film gauge and 100% "solids" polyurethane coating materials to understand why wet film thickness measurements are so much greater than dry film measurements.

5.7.2 Additional UV Intensity development (UV flash cure)

Henkel performed additional testing with the PC40-UMF 100% at various UV intensity levels. The goal was to determine the minimum UV exposure that would gel or tack the coating and have sufficiently high surface energy to permit wetting and adhesion of an additional spray layer. After UV cure the coating surface energies at different levels of cure. Glass-epoxy FR-4 coupons were used.

The recommended UV cure for PC40-UMF is shown in Figure 25. On-site at Asymtek, Henkel confirmed that a total of at least 3.0 J/cm^2 of UVA was required to cure the PC40-UMF conformal coating. The UV energy was validated with the UV cure monitor meter (Figure 26).

First, to baseline all the bare FR-4 coupons surface energies, all coupons were plasma treated with O_2 100 SCCM, Ar 100 SCCM, RW watt 250, pressure 400 mTorr with a process time of four minutes to ensure a surface energy of at least 40 dynes/cm^2. The coating was then drawn down coated using a doctor blade on the FR-4 surface to obtain a 75 micron liquid thickness.

The range of UV intensities evaluated and the resulting surface energies are shown in Table 10.

A low level UV intensity was not found that yielded a surface energy above 40 dyne/cm^2 without a plasma treatment.

Recommended UV Cure

Light Source and Condition:

Ultraviolet (UV) light:

10 seconds @ 300 to 600 mW/cm²

UV Wavelength, nm 365

Figure 25: Recommended UV cure for PC40-UMF from the datasheet. Note: J = W/s; so this requirements can be re-written as 3 to 6 J/cm^2.

Table 10: UV Intensity and resulting coating surface energy.

UV Intensity (J/cm2)	Surface Energy (Dyne/cm2)	Comments
0.35	32	
0.7	< 30	
1.2	< 30	
3	< 30	
5.1	< 30	
1.2	48	After Plasma Treatment



Figure 26: UVICure Plus radiometer.

6. PC18M+20%XP2742 Dip+layered spray coating

The dip+ layered spray process consists of a low viscosity dip, partial cure, 25 micron nominal thickness (layer one) spray, partial cure, 25 micron nominal thickness (layer two) spray, and final cure (Figure 1). The layered assembly spray coating work was completed September and October 2015. Each atomized spray process, including spray parameter design of experiment (DOE) evaluation, was completed within four hours. Each DOE consisted of metal coupon thickness validation of liquid layer build-ups between four and 10 layers (material dependent). All BGA, QFP and SOT samples were randomized within coating type. The complete cycle time to spray one panel of boards was approximately 10 minutes. Prior to spraying, the assemblies were dip coated and air dried overnight. Then the first spray layer was applied to a nominal thickness of 25 microns and partially cured. Then the second spray layer of an additional 25 microns was applied an a final cure was performed which consisted of a two hour air cure to allow the release of solvent followed by a two hour at 60C at 40% relative humidity.

6.1 Assembly preparation

All assemblies were built by Celestica's new product introduction (NPI) factory, labeled and stored within nitrogen cabinets. Assembly washing and plasma etch (prior to dip coating) was completed Sept, 2015. The local conditions were 24C and 51% R.H. A plasma mixture used 50% Argon / 50% Oxygen (Figure 27).



Figure 27: Boards in the plasma etch machine.

During the September 2015 spray session applying the layered PC18M dip with two PC18M+20%XP2742 spray coatings, it was found that the initial dip coating of PC18M partially filled the tooling holes needed for the board alignment to the fixture. For the Oct. 13, 2015 unfilled PC18M layered spray batches, the QFP, SOT and BGA assembly cards had three of the four tooling holes masked with tape dots during dip coating. The top hole used to hang the boards, drained the most and required minimal cleaning after dipping.

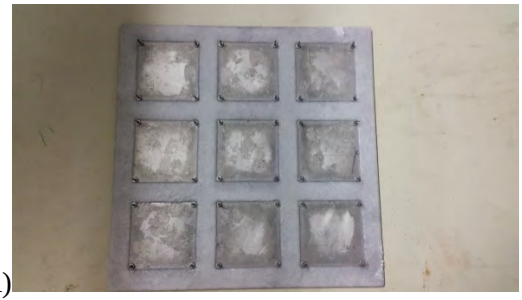
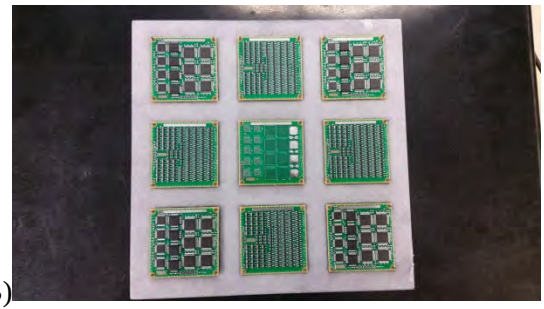
(A)  (B) 

Figure 28: Spray fixture for locating individual assembly coupons with respect to the spray machine; (A) Without coupons and (B) with coupons.



Figure 29: Typical board tooling hole masking. Yellow tape dots cover the tooling holes in three locations on both sides of the board.

6.2 Dip+layered spray

The dip+layered spray samples were processed in two sessions at the Celestica Toronto facility. The PC18M+20%XP2742 samples were processed on Sept. 24 – 25, 2015. The PC18M samples were processed October 13-14, 2015.

A total of 196 assemblies were coated (Table 11). The SOT, QFP, and BGA whisker test assemblies were coated with the following process: (1) prior to coating the assemblies were cleaned using standard manufacturing in-line cleaning processes and plasma etched to ensure good adhesion; (2) low viscosity dip coat with thinned PC18M; (3) followed by a solvent evaporation air cure overnight at room temperature with 30-40 percent RH; (4) automated spray coating applied PC18M or PC18M+20%XP2742; (5) then solvent evaporation for two hours in room temperature air with 30-40%RH; (6) automated spray coating applied PC18M or PC18M+20%XP2742; (7) followed by a final cure of a 2-hour room temperature solvent out-gas followed by 2-hours 60C/60%RH.

Table 11: Sample coating

Coating Dates	Spray material	No. of spray layers	SOT	QFP	BGA	**Total**
Sept. 24-25, 2016	NA	Dip only	10	13	7	**30**
	PC18M+ 20%XP2742	1	19	19	3	**41**
		2	25	25	1	**51**
Oct. 13-14, 2016	NA	Dip only	14	10	2	**26**
	PC18M	1	6	9	2	**17**
		2	12	13	6	**31**
		Total	**86**	**89**	**21**	**196**

Coating viscosity was checked before and after processing board lots using the small sample adaptor Spindle SC4-21 at 10 rpm on the Brookfield RVT DV-II. The coating viscosity was adjusted by adding Henkel AC0305 solvent.

The dip coating was performed into a 2.5L coating reservoir with a Specialty Coating Systems SCS PL-3201 with controlled immersion, dwell and withdrawal (Figure 30). The boards were hung from the top left hole (e.g. near U1). The September dip coat had two dip lots (1 – 9 and 10 – 17), each an hour long with an hour in between them. At the end of the first dip lot, the PC18M and solvent was found to be having a low degree of mixing and was estimated to have a 10 cps viscosity at the top of the dip tank where the solvent was added and 50 cps at the bottom. Between the first and the second dip lots, the reservoir was thoroughly mixed. The viscosity was 35 cps and did not change after an additional hour of dipping. The October 2015 dip lot (18 – 28) started at 20 cps and increased to 30 cps after 2 hours of dipping. Note: Board 179 used for the dip coat coverage and thickness cross-sectioning was dipped in October 2015.

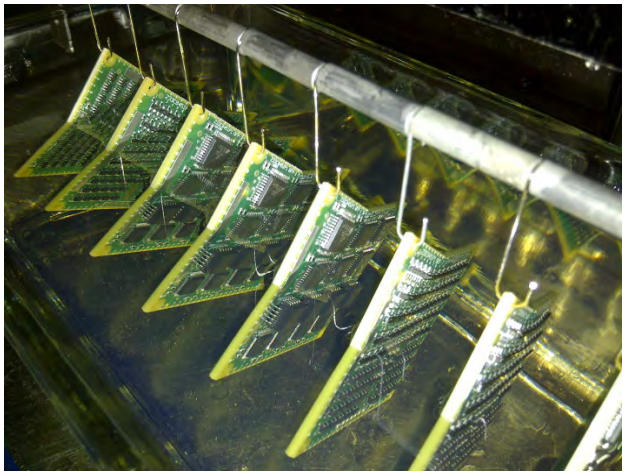


Figure 30: Assemblies partially immersed into the dip coating reservoir.

The layered spray build-up was targeted to achieve a 25 micron build-up with two x-direction and two y-direction spray passes (applied as 1x – 1y – 1x – 1y for a total of four passes). The thickness goal after a dip + spray + spray combination was 50 microns.

The spray coating was performed using an Asymtek SL-940 spray coater with a small reservoir. The lines were purged with AC0305 solvent between spray batches to ensure that all the material was fresh. A fixture was used to locate the boards consistently with respect to the machine X-Y spray pattern. The boards were oriented such that the board part number faced the left side of the machine. Coating was done the day following the dip coating. Initially the spray settings (spray pressure, atomization pressure, spray passes, spray overlap, etc.) were established experimentally to obtain the desired thickness. Then the first spray was applied to the boards. Then approximately half of the boards were sprayed with a second spray layer. New coating material was used for the second spray coating, to reduce the impact of viscosity increases over time. The PC18M+20%XP2742 viscosity in September spray coating session initial viscosity was 159 cps and increased to 226 cps at the completion of the spray setting experiments over three hours. The first assembly spray layer had an initial viscosity of 226 cps which increased to 328 cps over 2.5 hours. The second spray layer (using a new batch of material) initial viscosity was 158 cps and increased to 210 cps after 1.5 hours.

For the PC18M processed in October, the initial spray layer coating material started at 90 cps and increased to 123 cps after 6 hours in the coating tank. (Note: It was decided to start at 90 cps instead of 150, because a greater increase in viscosity with time was expected for the PC18M, based on the behavior of the PC18M+20%XP2742.). The viscosity for the second spray layer started at 165 cps and was completed in an hour (final viscosity was not recorded).

For reference, the original 2013 PC18M and PC18M+20%XP2742 spray build-up was such that a nominal 50 micron thickness was accomplished with two x-direction and two y-direction spray passes (applied as 1x – 1y – 1x – 1y for a total of four passes).

6.3 Layered spray surface roughness observation

Although not evident during optical inspection, during the SEM examination [6], a rough coating surface was observed (Figure 31). The PC18M+20%XP2742 samples were somewhat smoother (Figure 32).

Typically, rough surfaces are due to a “dry” spray where the solvent evaporates and a high coating viscosity state occurs before the surface tension can smooth the surface. It is likely that increased spray wetness would result in improved the coating self–leveling and smoothness. However, the “wetter” coating would have increased solvent and lower viscosity which would tend to reduce corner coverage and increase pooling.

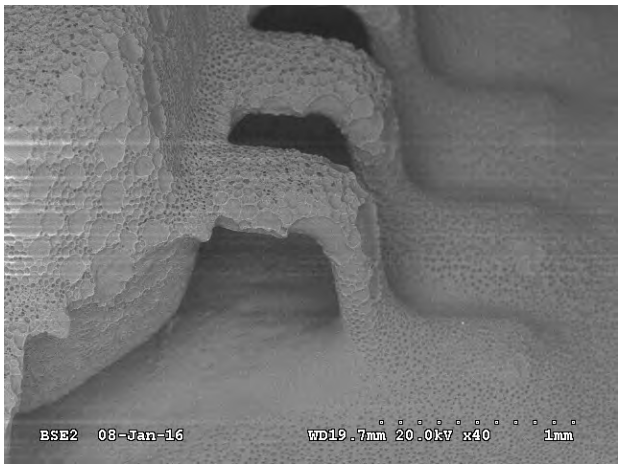


Figure 31: SEM image of PC18M dip + two PC18M sprays, board 191, QFP44, with good overall coverage but still exhibiting with surface roughness, 40x [6].

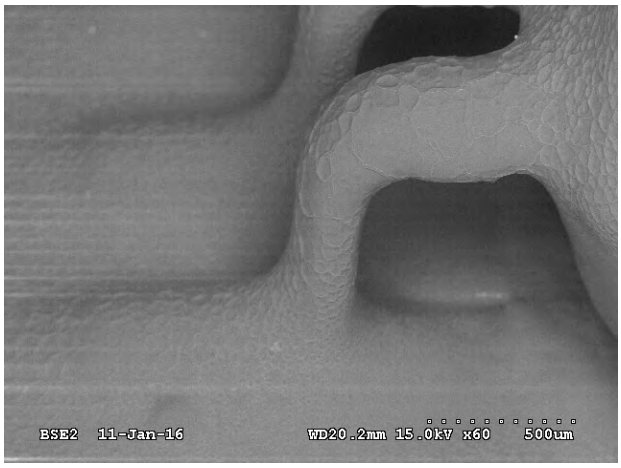


Figure 32: SEM image of PC18M dip + two (PC18M+20%XP2742) sprays, board 336, QFP44, 15KV, good thick coverage, 60x [6].

7. Comparative reference coatings

Assemblies and coupons were coated with common conformal coatings used in high reliability systems requiring additional humidity protection.

7.1 Parylene ™ coating material

For reference, samples of Parylene™ C and Parylene™ C with an Adpro+ adhesion promotion under layer were coated. The Parylene™ C is a thermoplastic that is vacuum deposited.

Tensile test specimens utilized Parylene™ C deposited onto 12.5 mm wide stainless steel shims using DiX (Chiba, Japan) Parylene™ C dimer at BAE Systems facility in Ft. Wayne, Indiana. The coating peeled readily off the shims for the tensile test specimen fabrication.

The assemblies used for whisker testing and coverage evaluation were coated with Parylene™ C and Parylene™ C with an Adpro+ were coated to a nominal thickness of 25 microns after plasma etching at using SCS Parylene™ C dimer at Specialty Coating Systems in Indianapolis, Indiana.

7.2 Humiseal 1B31 acrylic coating

The Humiseal 1B31 coating was machine sprayed onto whisker test assemblies to a nominal thickness of 50 microns using standard processes at the Celestica facility in Toronto Ontario Canada.

7.3 Humiseal UV40 low VOC acrylic – urethane coating

As was previously described in the WP-1753 final report [2], selected simulated power cycling thermal cycling (PCTC) whisker test assemblies were coated with the low volatile organic compound (VOC) UV cure Humiseal UV40. In the present work, additional PCTC thermal cycling from +50 to +85C was performed to increase the cyclic exposure from 1,797 to 6,000 thermal cycles. The coating was applied using machine spray process to a nominal thickness of 50 microns at the Asymtek facility in Ohio.

8. Summary and conclusion

The PC18M based heritage solvent containing urethane coating exhibited the greatest processing versatility. Sequential layers were built-up using a coat, partial cure, coat methodology with good wetting and adhesion between layers. There were issues with excessive thickness, bubbles and surface roughness. Careful monitoring of coating viscosity changes during processing is important because solvent drag-out during dipping and evaporation during spray coating can unexpectedly increase viscosity.

Coating with the UV cure VOC free PC40-UMF was more challenging. The lack of solvent in the coating reduces coating wettability and requires high assembly surface cleanliness, and high solid surface energy. The low VOC coating wets considerably better and more uniformly on the many material types encountered in an electronic assembly when a plasma etch pretreatment is used. Sequential application coating using a coat, partial cure, coat process was not successful in the present PC40-UMF work and requires further work.

9. Literature cited

[1] IPC-HDBK-830, Guidelines for Design, Selection and Application of Conformal Coatings, Association Connecting Electronics Industries, IPC, Bannockburn, Illinois, USA, Aug 2013.
[2] S. Meschter and P. Snugovsky, Tin whisker testing and modeling, SERDP WP-1753 Final report, Dec. 2015 https://serdp-estcp.org/content/download/40066/384515/file/WP-1753%20Final%20Report.pdf
[3] Appendix B of the current report: Suspension and coating formulation
[4] MIL-I-46058, Insulating Compound, Electrical (for Coating Printed Circuit Assemblies), Military Specification, July 1972. Note that the Qualified Providers List (QPL) is still active, but MIL-I-46058 is inactive for new designs.
[5] IPC-CC-830, Qualification and Performance of Electrical Insulating Compound for Printed Wiring Assemblies, IPC-Association Connecting Electronics Industries, Bannockburn, Illinois, USA, Sept. 2008.
[6] Appendix F of the current report: Coating coverage baseline results

SERDP WP-2213
Final Report
Appendix F: Coating coverage baseline results

Appendix F: Table of Contents

1. PC18M based coatings 1

1.1 PC18M optical coating inspection 1

1.2 PC18M SEM coverage inspection 7

1.3 PC18M vertical cross-section coating thickness evaluation 9

1.4 PC18M horizontal cross-section coating thickness evaluation 17

2. PC40-UMF based coatings 26

2.1 PC40-UMF Batch A and B (dip+spray) 28

2.1.1 Optical inspection of batch A and B (dip+spray) PC40-UMF + NNN2835 (nanosilica) 28

2.1.2 SEM inspection of Batch A and B (dip+spray) PC40-UMF + NNN2835(nanosilica) 30

2.1.3 PC40-UMF Batch A PC40-UMF vertical cross-section thickness evaluation 38

2.1.4 PC40-UMF Batch B vertical cross-section thickness evaluation 56

2.1.5 PC40-UMF Batch B horizontal section 86

2.2 PC40-UMF Batch C and D spray coating, standard and high viscosity 110

2.2.1 Optical inspection of Batch C and D of PC40-UMF standard and high viscosity 110

2.2.2 SEM inspection of Batch C and D with PC40-UMF standard and high viscosity 111

2.2.3 Vertical cross-section inspection of Batch C and D with PC40-UMF and PC40-UMF high viscosity spray coating without initial dip coat 115

3. Reference coatings 132

3.1 Parylene C ™ 132

3.1.1 Parylene C ™ SEM 132

3.2 Parylene C ™ with Adpro plus 135

3.2.1 Parylene C ™ with Adpro plus SEM 135

3.2.2 Parylene C ™ with Adpro plus vertical cross-section coating thickness evaluation 136

3.3 1B31LOC Acrylic 143

4. Reference coating Parylene ™ 146

4.1.1 Cross-section inspection of Parylene C with Adpro+ coating 149

5. Coating coverage summary 159

5.1 Coverage and thickness 159

5.2 Role of coating solvent and coverage 159

5.3 Bubble formation 160

5.4 Interlayer adhesion 166

5.5 Dewetting spray coating over cured dip coat in the PC40-UMF system 169

5.6 Comparison with published work 170

6. Conclusions **171**

7. Literature cited **172**

Appendix F: List of Figures

Figure 1: Marking readability test for pipet flood coated PC18M+50%XP2742 (15.17 wt. % 20 nm nanosilica). 1

Figure 2: Marking readability test for pipet flood coated PC18M+20%X11102PMA (13.04 wt. % 40 nm nanoalumina). 1

Figure 3: PC18M-mod, board 15, QFP44, 50x after ATC&HTHH1000. 2

Figure 4: PC18M-mod board 15, PLCC20, 30x 3 after ATC&HTHH1000. 2

Figure 5: PC18M-mod SOT board 234 with large bubble density, no exposure, 10x. 2

Figure 6: PC18M-mod, SOT board 233, ATC 1000HTHH, 10x, large bubbles, darkened coating. 3

Figure 7: PC18M-mod SOT board 233 with large bubbles, 10x, after ATC+1000HTHH. The color change in the second image is an artifact of the illumination used to highlight the bubbles. 3

Figure 8: PC18M-mod QFP board 35 with large bubble density, 10x. 4

Figure 9: PC18M-mod SOT board 213, no exposure, with small/no bubble density, 10x. 4

Figure 10: PC18M-mod QFP board 11, with small/no bubble density, no exposure, 10x. 4

Figure 11: PC18M+20%XP2742 SOT board with medium bubble density, no exposure, 10x. 5

Figure 12: PC18M+20%XP2742 QFP board with medium bubble density, no exposure, 10x. 5

Figure 13: PC18M+20%XP2742 QFP board with small/no bubble density, 10x. 5

Figure 14: PC18M+20%X1102PMA, SOT board 226, HALT, 10x, small/no bubble density, milky appearance. 6

Figure 15: PC18M+20%X11102PMA, QFP board 23, no exposure, 10x, small/no bubble density. 6

Figure 16: Parylene, SOT board 201, no exposure, no bubbles, 10x. 6

Figure 17: SEM image of Parylene™ coated QFP44, 60x (ref. Board 2, U5, lead 24). 7

Figure 18: SEM image of PC18M dip + PC18M+20%X11102PMA spray showing full coverage of QFP44 leads, 60x (Ref. board 28, U2, lead 23, no environmental exposure). 7

Figure 19: SEM image of PC18M dip + PC18M-20%X2742 spray coating on QFP44 leads showing isolated thin coverage regions less than 50 microns, 60x (ref. Board 39, U2, lead 23, image taken after thermal cycling exposure). 8

Figure 20: SEM image of PC18M dip + PC18M-mod spray on QFP44 leads showing extended thin coverage regions, 60x (ref. Board 15, U2, lead 23, 60x, image take after thermal cycling and 1000 hours of HTHH). 8

Figure 21: SEM image of PC18M dip + PC18M-mod spray on QFP44 leads showing extended thin coverage regions with measurements, 80x (ref. Board 11, U2, lead 12, no environmental exposure). 8

Figure 22: Typical SEM image of a coating cross-section, 60x (Ref. PC18M-mod unfilled, board 12, QFP44, left lead). 9

Figure 23: Coating cross-section thickness measurement locations. Optical image of Parylene™ C coated QFP44 shown. 10

Figure 24: SEM cross-section view of PC18M-mod coated QFP44 lead, top of lead, 150x (ref. Board 12, right lead, location A). 11

Figure 25: Coating cross-section SEM view of PC18M-mod unfilled, board 12, QFP44, left lead, location A, SEM, 150x. 12

Figure 26: Lead tip cross-section showing thin coverage. SEM image of PC18M-mod unfilled, board 12, QFP44, left lead, location T, 150x and 2,000x. 13

Figure 27: Lead tip cross-section showing thicker coverage. SEM image of PC18M dip + PC18M-20%X11102PMA nanoalumina spray coated QFP, right lead, location T, 150x (ref. Board 12). 14

Figure 28: Cross-section SEM view of PC18M-20%X1102PMA nanoalumina coated QFP, left lead, location E, 150x (ref. Board 12). 14

Figure 29: Cross-section SEM view of PC18M-20%XP2742 nanosilica coated QFP, left lead, location T, SEM, 150x (ref. Board 20). 15

Figure 30: Horizontal cross-section plane location for coating thickness evaluation. 17

Figure 31: X-ray images of cross-section mounts used in the horizontal section evaluation; (a) PC18M-mod board 11, (b) PC18M+20%XP2742 board 21, and (c) PC18M+X11102PMA board 28. 18

Figure 32: QFP44 pin numbering. 18

Figure 33: SEM image of horizontal cross section, board 11, PC18M-mod, QFP44, U1, lead 6, 200x. ... 19

Figure 34: Horizontal cross-section SEM board 21, PC18M+20%XP2742, QFP44, U1, lead 6, 200x. 19

Figure 35: Horizontal cross-section, SEM, board 28, PC18M+20%X1102PMA, U1, lead 6, 200x. 19

Figure 36: Horizontal cross section, SEM, board 11, PC18M-mod, QFP44, U1, lead 23, 200x. 20

Figure 37: Horizontal cross section, SEM, board 21, PC18M+20%XP2742, QFP44, U1, lead 23, 200x. 20

Figure 38: Horizontal cross section, SEM, board 28, PC18M+20%X11102PMA, QFP44, U1, lead 23, 200x. 20

Figure 39: Horizontal cross section, SEM, board 11, PC18M-mod, QFP44, U1, lead 17, 200x. 21

Figure 40: Horizontal cross section, SEM, board 21, PC18M+20%XP2742, QFP44, U1, lead 17, 200x. 21

Figure 41: Horizontal cross section, SEM, board 28, PC18M+20%X11102PMA, QFP44, U1, lead 17, 200x. 21

Figure 42: Horizontal cross section, SEM, board 11, PC18M-mod, QFP44, U1, lead 6, 1,000x. Back side coating coverage is four microns. 22

Figure 43: Horizontal cross-section, SEM, board 21, PC18M+20%XP2742, QFP44, U1 lead 6, 1,000x. Back side coating coverage is one micron. 22

Figure 44: Horizontal cross-section, SEM, board 28, PC18M+20%X11102PMA, QFP44, lead 6, 1,000x. Back side coating coverage is approximately three microns. 23

Figure 45: Horizontal cross section, SEM, board 11, PC18M-mod, QFP44, U1, lead 6, 1,000x. No coating on the back corner. 24

Figure 46: Horizontal cross-section, SEM, board 21, PC18M+20%XP2742, QFP44, U1 lead 6, 1,000x. 24

Figure 47: Horizontal cross-section, SEM, board 28, PC18M+20%X1102PMA, QFP44, lead 6, 2,000x. 25

Figure 48: Horizontal cross-section, SEM, board 28, PC18M+20%X1102PMA, QFP44, U1, lead 39, 1,000x. 25

Figure 49: Batch A and B QFP44 SEM images of PC40-UMF coating based coating; (A) PC40-UMF dip coat, (B), PC40-UMF (no plasma between dip and spray), and the following spray coated samples with plasma etch between the dip and the spray layers: (C) PC40-UMF batch 2 with plasma, (D) PC40-UMF+10%NNN2835(nanosilica), (E) PC40-UMF+30%NNN2835(nanosilica), (F) PC40-UMF+50%NNN235(nanosilica), and (G) PC40-UMF+15.54%N3300. Image (H) shows an uncoated control board. 27

Figure 50: Optical image of QFP assembly after low viscosity PC40-UMF dip coating. 28

Figure 51: Optical images of QFP boards after PC40-UMF coating; (A) no coating control, (B) batch A (no plasma between dip and spray coating), (C) batch two (plasma etch between dip and spray coating). 28

Figure 52: Optical images of batch 2 dip with (A) PC40-UMF+10%NNN2835(nanosilica) spray, (B) PC40-UMF+30%NNN2835(nanosilica) spray, (C) PC40-UMF+ 50%NNN2835(nanosilica) spray, and (D) PC40-UMF+15.54%N3300 spray. 29

Figure 53: SEM image of PC40-UMF dip only QFP44 leads, 60x (ref. Board 87, Batch B). 30

Figure 54: SEM image of a PC40-UMF dip-only coated QFP44 lead tip, 100x (ref. Board 87, Batch B). 31

Figure 55: SEM image of PC40-UMF dip-only coated QFP44 leads, top view, 45x (ref. Board 87, Batch B). 32

Figure 56: SEM image of PC40-UMF dip-only coated QFP64 leads, 60x (ref. Board 87, Batch B). 32

Figure 57: SEM image of PC40-UMF dip-only coated QFP64 leads, top view, 45x (ref. Board 87, Batch B). 33

Figure 58: SEM image of PC40-UMF dip-only coated PLCC leads, front view, 30x (ref. Board 87, Batch B). 33

Figure 59: SEM image of PC40-UMF dip-only coated PLCC leads, side view, 40x (ref. Board 87, Batch B). 34

Figure 60: Batch A SEM image of PC40-UMF dip+spray coated QFP44 leads, 60x (ref. Board 57). 34

Figure 61: Batch A SEM image of PC40-UMF dip+spray coated QFP64 leads, 60x (ref. Board 57). 35

Figure 62: Batch A SEM image of PC40-UMF dip+spray coated PLCC leads, side view, 40x (ref. Board 57). 35

Figure 63: Batch A SEM image of PC40-UMF dip+spray coated PLCC leads, front view, 40x (ref. Board 57). 36

Figure 64: Batch B SEM image of PC40-UMF dip+plasma+spray coated QFP44 leads, 60x (ref. Board 66). 36

Figure 65: Batch B SEM image of PC40-UMF dip+plasma+spray coated QFP64 leads, 60x (ref. Board 66). 37

Figure 66: Batch B SEM image of PC40-UMF dip+plasma+spray coated PLCC leads, front view, 40x (ref. Board 66). 37

Figure 67: Batch B SEM image of PC40-UMF dip+plasma+spray coated PLCC leads, side view, 40x (ref. Board 66). 38

Figure 68: Batch A SEM cross-section image of PC40-UMF dip only coated QFP44, toe region, 100x (ref. Board 87). 39

Figure 69: Batch A SEM cross-section image of PC40-UMF dip only coated QFP44, middle of lead region, 100x (ref. board 87). 39

Figure 70: Batch A SEM cross-section image of PC40-UMF dip only coated QFP44, heel region, 100x (ref. Board 87) 40

Figure 71: Batch A SEM cross-section image of PC40-UMF dip only coated QFP44, toe region, 100x (ref. board 87). 41

Figure 72: Batch A SEM cross-section image of PC40-UMF dip only coated QFP44, location A, 3,500x (ref. 87). 41

Figure 73: Batch A SEM cross-section image of PC40-UMF dip only coated QFP44, location B, 1,000x (ref. Board 87). 42

Figure 74: Batch A SEM cross-section image of PC40-UMF dip only coated QFP44, behind knee, 5,000x (ref. Board 87). 42

Figure 75: Batch A SEM cross-section image of PC40-UMF dip only coated QFP44, location between F and T location, 2500x (ref. Board 87). 43

Figure 76: Batch A SEM cross-section image of PC40-UMF dip only coated QFP44, location C, 5,000x (ref. Board 87). 43

Figure 77: Batch A SEM cross-section image of PC40-UMF dip only coated QFP44, location D, 3,500x (ref. Board 87). 44

Figure 78: Batch A SEM cross-section image of PC40-UMF dip only coated QFP44, location E, 1000x (ref. Board 87). 44

Figure 79: Batch A SEM cross-section image of PC40-UMF dip only coated QFP44, location F, 1000x (ref. Board 87). 45

Figure 80: Batch A SEM cross-section image of PC40-UMF dip only coated QFP44, location G, 5000x (ref. Board 87). 45

Figure 81: Batch A SEM cross-section image of PC40-UMF dip only coated QFP44, location H, 1000x (ref. Board 87). 46

Figure 82: Batch A SEM cross-section image of PC40-UMF dip only coated QFP44, location T, 2500x (ref. Board 87). 46

Figure 83: Batch A SEM cross-section image of PC40-UMF dip + spray coated QFP44, foot location, 100x (ref. Board 57). 47

Figure 84: Batch A SEM cross-section image of PC40-UMF dip + spray coated QFP44, knee location, 100x (ref. Board 57). 47

Figure 85: Batch A SEM cross-section image of PC40-UMF dip + spray coated QFP44, toe location, 100x (ref. Board 57). 48

Figure 86: Batch A SEM cross-section image of PC40-UMF dip + spray coated QFP44, heel location, 100x (ref. Board 57). 48

Figure 87: Batch A SEM cross-section image of PC40-UMF dip + spray coated QFP44, upper heel location, 1,000x (ref. Board 57). 49

Figure 88: Batch A SEM cross-section image of PC40-UMF dip + spray coated QFP44, location A, 3,000x (ref. Board 57). 49

Figure 89: Batch A SEM cross-section image of PC40-UMF dip + spray coated QFP44, location A, 5,000x (ref. Board 57). 50

Figure 90: Batch A SEM cross-section image of PC40-UMF dip + spray coated QFP44, location B, 3,000x (ref. Board 57). 50

Figure 91: Batch A SEM cross-section image of PC40-UMF dip + spray coated QFP44, behind the knee, 1,000x (ref. Board 57). 51

Figure 92: Batch A SEM cross-section image of PC40-UMF dip + spray coated QFP44, between location T and F, 1,000x (ref. Board 57). 51

Figure 93: Batch A SEM cross-section image of PC40-UMF dip + spray coated QFP44, location C, 5,000x (ref. Board 57). 52

Figure 94: Batch A SEM cross-section image of PC40-UMF dip + spray coated QFP44, location D, 3,000x (ref. Board 57). 52

Figure 95: Batch A SEM cross-section image of PC40-UMF dip + spray coated QFP44, location E, 1,500x (ref. Board 57). 53

Figure 96: Batch A SEM cross-section image of PC40-UMF dip + spray coated QFP44, location F, 2,000x (ref. Board 57). 53

Figure 97: Batch A SEM cross-section image of PC40-UMF dip + spray coated QFP44, location T, 1000x (ref. Board 57). 54

Figure 98: Batch A SEM cross-section image of PC40-UMF dip + spray coated QFP44, location G, 1,000x (ref. Board 57). 54

Figure 99: Batch A SEM cross-section image of PC40-UMF dip + spray coated QFP44, location H, 500x (ref. Board 57). 55

Figure 100: Batch A SEM cross-section image of PC40-UMF dip + spray coated QFP44, location H, 1,000x (ref. Board 57). 55

Figure 101: Batch B SEM cross-section image of PC40-UMF dip+spray coated QFP44, heel location, 100x, (ref. Board 66). 56

Figure 102: Batch B SEM cross-section image of PC40-UMF dip+spray coated QFP44, foot location, 100x, (ref. Board 66). 57

Figure 103: Batch B SEM cross-section image of PC40-UMF dip+spray coated QFP44, knee location, QFP44, 100x, (ref. Board 66). 57

Figure 104: Batch B SEM cross-section image of PC40-UMF dip+spray coated QFP44, toe location, 100x, (ref. Board 66). 58

Figure 105: Batch B SEM cross-section image of PC40-UMF dip+spray coated QFP44, location A, 1,000x (ref. Board 66). 58

Figure 106: Batch B SEM cross-section image of PC40-UMF dip+spray coated QFP44, location A, 3,000x (ref. Board 66). 59

Figure 107: Batch B SEM cross-section image of PC40-UMF dip+spray coated QFP44, location A, 6,000x (ref. Board 66). 59

Figure 108: Batch B SEM cross-section image of PC40-UMF dip+spray coated QFP44, location B, 1000x (ref. Board 66). 60

Figure 109: Batch B SEM cross-section image of PC40-UMF dip+spray coated QFP44, behind the knee, 1000x (ref. Board 66). 60

Figure 110: Batch B SEM cross-section image of PC40-UMF dip+spray coated QFP44, between location F and T, 1000x (ref. Board 66). 61

Figure 111: Batch B SEM cross-section image of PC40-UMF dip+spray coated QFP44, location C, 2000x (ref. Board 66). 61

Figure 112: Batch B SEM cross-section image of PC40-UMF dip+spray coated QFP44, location D, 1,000x (ref. Board 66). 62

Figure 113: Batch B SEM cross-section image of PC40-UMF dip+spray coated QFP44, location D, 8,000x (ref. Board 66). 62

Figure 114: Batch B SEM cross-section image of PC40-UMF dip+spray coated QFP44, location E, 1,000x (ref. Board 66). 63

Figure 115: Batch B SEM cross-section image of PC40-UMF dip+spray coated QFP44, location F, 3,500x (ref. Board 66). 63

Figure 116: Batch B SEM cross-section image of PC40-UMF dip+spray coated QFP44, location F, 5,000x (ref. Board 66). 64

Figure 117: Batch B SEM cross-section image of PC40-UMF dip+spray coated QFP44, location G, 1,000x (ref. Board 66). 64

Figure 118: Batch B SEM cross-section image of PC40-UMF dip+spray coated QFP44, location H, 1,000x (ref. Board 66). 65

Figure 119: Batch B SEM cross-section image of PC40-UMF + 10%NNN2835 nanosilica dip+spray QFP44, lead knee location, 100x (ref. Board 62). 65

Figure 120: Batch B SEM cross-section image of PC40-UMF + 10%NNN2835 nanosilica dip+spray QFP44, lead toe location, 100x (ref. Board 62). 66

Figure 121: Batch B SEM cross-section image of PC40-UMF + 10%NNN2835 nanosilica dip+spray QFP44, behind the knee, 2000x (ref. Board 62). 66

Figure 122: Batch B SEM cross-section image of PC40-UMF + 10%NNN2835 nanosilica dip+spray QFP44, back side, 3500x (ref. Board 62). 67

Figure 123: Batch B SEM cross-section image of PC40-UMF + 10%NNN2835 nanosilica dip+spray QFP44, location F, 1,000x (ref. Board 62). 67

Figure 124: Batch B SEM cross-section image of PC40-UMF + 10%NNN2835 nanosilica dip+spray QFP44, location T, 200x (ref. Board 62). 68

Figure 125: Batch B SEM cross-section image of PC40-UMF + 10%NNN2835 nanosilica dip+spray QFP44, location T, 1,000x (ref. Board 62). 68

Figure 126: Batch B SEM cross-section image of PC40-UMF + 10%NNN2835 nanosilica dip+spray QFP44, location T, 3,500x (ref. Board 62). 69

Figure 127: Batch B SEM cross-section image of PC40-UMF + 10%NNN2835 nanosilica dip+spray QFP44, location G, 2,500x (ref. Board 62). 69

Figure 128: Batch B SEM cross-section image of PC40-UMF + 30%NNN2835 nanosilica dip+spray QFP44, foot location, 100x, (ref. Board 67). Note coating sequence is PC40-UMF dip + (PC40-UMF + 30%NNN2835 nanosilica) spray. 70

Figure 129: Batch B SEM cross-section image of PC40-UMF + 30%NNN2835 nanosilica dip+spray QFP44, knee location , 100x, (ref. Board 67). 71

Figure 130: Batch B SEM cross-section image of PC40-UMF + 30%NNN2835 nanosilica dip+spray QFP44, toe location, 100x, (ref. Board 67). 71

Figure 131: Batch B SEM cross-section image of PC40-UMF + 30%NNN2835 nanosilica dip+spray QFP44, toe location, 500x, (ref. Board 67). 72

Figure 132: Batch B SEM cross-section image of PC40-UMF + 30%NNN2835 nanosilica dip+spray QFP44, heel location, 100x, (ref. Board 67). 72

Figure 133: Batch B SEM cross-section image of PC40-UMF + 30%NNN2835 nanosilica dip+spray QFP44, location A, 500x, (ref. Board 67). 73

Figure 134: Batch B SEM cross-section image of PC40-UMF + 30%NNN2835 nanosilica dip+spray QFP44, location A, 1,000x, (ref. Board 67). 73

Figure 135: Batch B SEM cross-section image of PC40-UMF + 30%NNN2835 nanosilica dip+spray QFP44, location B, 2,000x, (ref. Board 67). 74

Figure 136: Batch B SEM cross-section image of PC40-UMF + 30%NNN2835 nanosilica dip+spray QFP44, behind the knee, 1,000x, (ref. Board 67). 74

Figure 137: Batch B SEM cross-section image of PC40-UMF + 30%NNN2835 nanosilica dip+spray QFP44, between location F and T, 1500x, (ref. Board 67). 75

Figure 138: Batch B SEM cross-section image of PC40-UMF + 30%NNN2835 nanosilica dip+spray QFP44, location C, 3,500x, (ref. Board 67). 75

Figure 139: Batch B SEM cross-section image of PC40-UMF + 30%NNN2835 nanosilica dip+spray QFP44, location D, 3,500x, (ref. Board 67). 76

Figure 140: Batch B SEM cross-section image of PC40-UMF + 30%NNN2835 nanosilica dip+spray QFP44, location E, 3,000x, (ref. Board 67). 76

Figure 141: Batch B SEM cross-section image of PC40-UMF + 30%NNN2835 nanosilica dip+spray QFP44, location F, 2,000x, (ref. Board 67). 77

Figure 142: Batch B SEM cross-section image of PC40-UMF + 30%NNN2835 nanosilica dip+spray QFP44, location T, 1,000x, (ref. Board 67). 77

Figure 143: Batch B SEM cross-section image of PC40-UMF + 30%NNN2835 nanosilica dip+spray QFP44, location T, 2500x, (ref. Board 67). 78

Figure 144: Batch B SEM cross-section image of PC40-UMF + 30%NNN2835 nanosilica dip+spray QFP44, location G, 1,000x, (ref. Board 67). 78

Figure 145: Batch B SEM cross-section image of PC40-UMF + 30%NNN2835 nanosilica dip+spray QFP44, location H, 1,000x, (ref. Board 67). 79

Figure 146: Batch B SEM cross-section image of PC40-UMF + 30%NNN2835 nanosilica dip+spray QFP44, location H, 1,800x, (ref. Board 67). 79

Figure 147: Batch B SEM cross-section image of PC40-UMF + 30%NNN2835 nanosilica dip+spray QFP44, location H, 3,000x, (ref. Board 67). 80

Figure 148: Batch B SEM cross-section image of PC40-UMF + 50%NNN2835 nanosilica dip+spray QFP44, lead foot location, 100x (ref. Board 72). 80

Figure 149: Batch B SEM cross-section image of PC40-UMF + 50%NNN2835 nanosilica dip+spray QFP44, lead toe location, 100x (ref. Board 72). 81

Figure 150: Batch B SEM cross-section image of PC40-UMF + 50%NNN2835 nanosilica dip+spray QFP44, location F, 500x (ref. Board 72). 81

Figure 151: Batch B SEM cross-section image of PC40-UMF + 50%NNN2835 nanosilica dip+spray QFP44, location, F, 2,500x (ref. Board 72). 82

Figure 152: Batch B SEM cross-section image of PC40-UMF + 50%NNN2835 nanosilica dip+spray QFP44, location T, 1,000x (ref. Board 72). 82

Figure 153: Batch B SEM cross-section image of PC40-UMF + 50%NNN2835 nanosilica dip+spray QFP44, location G, 2,000x (ref. Board 72). 83

Figure 154: Batch B SEM cross-section image of PC40-UMF + 50%NNN2835 nanosilica dip+spray QFP44, location H, 1,000x (ref. Board 72). 83

Figure 155: Batch B SEM cross-section image of PC40-UMF + 15.54%N3300 nanosilica dip+spray QFP44, lead foot location, 100x (ref. Board 77). 84

Figure 156: Batch B SEM cross-section image of PC40-UMF + 15.54%N3300 nanosilica dip+spray QFP44, lead toe location, 100x (ref. Board 77). 84

Figure 157: Batch B SEM cross-section image of PC40-UMF + 15.54%N3300 nanosilica dip+spray QFP44, location F, 1,000x (ref. Board 77). 85

Figure 158: Batch B SEM cross-section image of PC40-UMF + 15.54%N3300 nanosilica dip+spray QFP44, location T, 1,000x (ref. Board 77). 85

Figure 159: Batch B SEM cross-section image of PC40-UMF + 15.54%N3300 nanosilica dip+spray QFP44, location T, 5,000x (ref. Board 77). 86

Figure 160: QFP44 pin numbering. 87

Figure 161: Batch B SEM image of the horizontal cross-section of PC40-UMF coating on a QFP44, lead 11, 200x (ref. Board 66, U3). 87

Figure 162: Batch B SEM image of the horizontal cross-section of PC40-UMF coating on a QFP44, lead 11, 1,000x (ref. Board 66, U3). 88

Figure 163: Batch B SEM image of the horizontal cross-section of PC40-UMF coating on a QFP44, lead 11, 1,000x (ref. Board 66, U3). The middle of the back of the lead is shown. There is a thin spray coating layer with delamination between the dip and the spray layers. 88

Figure 164: Batch B SEM image of the horizontal cross-section of PC40-UMF coating on a QFP44, lead 11, 1,000x (ref. Board 66, U3). Bump of spray coating on the dip coating with delamination between the dip and the spray layers. 89

Figure 165: Batch B SEM image of the horizontal cross-section of PC40-UMF coating on a QFP44, lead 11, 1,000x (ref. Board 66, U3). Delamination is present between the dip and the spray layers. 89

Figure 166: Batch B SEM image of the horizontal cross-section of PC40-UMF coating on a QFP44, lead 11, 2,000x (ref. Board 66, U3). 90

Figure 167: Batch B SEM image of the horizontal cross-section of PC40-UMF coating on a QFP44, lead 11, 2,500x (ref. Board 66, U3). 90

Figure 168: Batch B SEM image of the horizontal cross-section of PC40-UMF coating on a QFP44, lead 11, 3,500x (ref. Board 66, U3). 91

Figure 169: Batch B SEM image of the horizontal cross-section of PC40-UMF coating on a QFP44, lead 19, 200x (ref. Board 66, U3). Dip coating is bridging between the lead and the part at the image upper center. Spray coating appears to be bridging between leads at the image lower center. It is unclear what caused the large separation around the sides and the rear of the lead. 91

Figure 170: Batch B SEM image of the horizontal cross-section of PC40-UMF coating on a QFP44, lead 33, 200x (ref. Board 66, U3). Dip coating is bridging between the lead and the part at the image left center. Spray coating appears to be bridging between leads at the image right center. 92

Figure 171: Batch B SEM image of the horizontal cross-section of PC40-UMF coating on a QFP44, lead 34, 200x (ref. Board 66, U3). Coating is bridging between leads on the lower part of the image. 92

Figure 172: Batch B SEM image of the horizontal cross-section of PC40-UMF coating on a QFP44, lead 34, 2,500x (ref. Board 66, U3)..... 93

Figure 173: Batch B SEM image of the horizontal cross-section of PC40-UMF coating on a QFP44, lead 34, 1800x (ref. Board 66, U3)..... 93

Figure 174: Batch B SEM image of the horizontal cross-section of PC40-UMF coating on a QFP44, lead 44, 200x (ref. Board 66, U3)..... 94

Figure 175: Batch B SEM image of the horizontal cross-section of PC40-UMF coating on a QFP44, lead 44, 1,000x (ref. Board 66, U3)..... 94

Figure 176: Batch B SEM image of the horizontal cross-section of PC40-UMF coating on a QFP44, lead 44, 1,000x (ref. Board 66, U3)..... 95

Figure 177: Batch B SEM image of the horizontal cross-section of PC40-UMF coating on a QFP44, lead 44, 2500x, 2 (ref. Board 66, U3)..... 95

Figure 178: Batch B SEM image of the horizontal cross-section of PC40-UMF coating on a QFP44, lead 44, 2500x (ref. Board 66, U3)..... 96

Figure 179: Batch B SEM image of the horizontal cross-section of PC40-UMF+10%NNN2835 coating on a QFP44, lead 11, 200x (ref. Board 62, U3). 96

Figure 180: Batch B SEM image of the horizontal cross-section of PC40-UMF+10%NNN2835 coating on a QFP44, lead 11, 1,000x (ref. Board 62, U3). 97

Figure 181: Batch B SEM image of the horizontal cross-section of PC40-UMF+10%NNN2835 coating on a QFP44, lead 11, 1,000x (ref. Board 62, U3). 97

Figure 182: Batch B SEM image of the horizontal cross-section of PC40-UMF+10%NNN2835 coating on a QFP44, lead 11, 1,000x (ref. Board 62, U3). 98

Figure 183: Batch B SEM image of the horizontal cross-section of PC40-UMF+10%NNN2835 coating on a QFP44, lead 11, 1,000x (ref. Board 62, U3). 98

Figure 184: Batch B SEM image of the horizontal cross-section of PC40-UMF+10%NNN2835 coating on a QFP44, lead 11, 2,000x (ref. Board 62, U3). 99

Figure 185: Batch B SEM image of the horizontal cross-section of PC40-UMF+10%NNN2835 coating on a QFP44, lead 11, 3,000x (ref. Board 62, U3). 99

Figure 186: Batch B SEM image of the horizontal cross-section of PC40-UMF+10%NNN2835 coating on a QFP44, lead 19, 200x (ref. Board 62, U3). Dip coating is bridging between the lead and the part on the upper part of the image. Spray coating is bridging between leads in the image lower center. There is delamination between the dip and the spray layer along the bridging between leads. The delamination between the coating and the back of the lead (upper part of image) could be due to PC40-UMF shrinkage during cure..... 100

Figure 187: Batch B SEM image of the horizontal cross-section of PC40-UMF+10%NNN2835 coating on a QFP44, lead 33, 200x (ref. Board 62, U3). 101

Figure 188: Batch B SEM image of the horizontal cross-section of PC40-UMF+10%NNN2835 coating on a QFP44, lead 33, 1000x (ref. Board 62, U3). 101

Figure 189: Batch B SEM image of the horizontal cross-section of PC40-UMF+10%NNN2835 coating on a QFP44, lead 33, 1,000x (ref. Board 62, U3). 102

Figure 190: Batch B SEM image of the horizontal cross-section of PC40-UMF+10%NNN2835 coating on a QFP44, lead 33, 1,000x (ref. Board 62, U3). 102

Figure 191: Batch B SEM image of the horizontal cross-section of PC40-UMF+10%NNN2835 coating on a QFP44, lead 33, 1,000x (ref. Board 62, U3). 103

Figure 192: Batch B SEM image of the horizontal cross-section of PC40-UMF+10%NNN2835 coating on a QFP44, lead 33, 1,000x (ref. Board 62, U3). 103

Figure 193: Batch B SEM image of the horizontal cross-section of PC40-UMF+10%NNN2835 coating on a QFP44, lead 33, 2,000x (ref. Board 62, U3). Delamination is present between the dip and spray layers. 104

Figure 194: Batch B SEM image of the horizontal cross-section of PC40-UMF+10%NNN2835 coating on a QFP44, lead 34, 200x (ref. Board 62, U3). Dip coating is bridging to the package at the image left and bottom. Spray coating is bridging to the next lead on the left. 104

Figure 195: Batch B SEM image of the horizontal cross-section of PC40-UMF+10%NNN2835 coating on a QFP44, lead 34, 2,500x (ref. Board 62, U3). 105

Figure 196: Batch B SEM image of the horizontal cross-section of PC40-UMF+10%NNN2835 coating on a QFP44, lead 34, 2,500x (ref. Board 62, U3). 105

Figure 197: Batch B SEM image of the horizontal cross-section of PC40-UMF+10%NNN2835 coating on a QFP44, lead 39, 200x (ref. Board 62, U3). Dip coating bridging is bridging to the part body and the spray coating on top of it is bridging between leads. Epoxy to coating is highlighted by the added black line 106

Figure 198: Batch B SEM image of the horizontal cross-section of PC40-UMF+10%NNN2835 coating on a QFP44, lead 39, 1,000x (ref. Board 62, U3). 106

Figure 199: Batch B SEM image of the horizontal cross-section of PC40-UMF+10%NNN2835 coating on a QFP44, lead 39, 2,000x (ref. Board 62, U3). 107

Figure 200: Batch B SEM image of the horizontal cross-section of PC40-UMF+10%NNN2835 coating on a QFP44, lead 39, 2,500x (ref. Board 62, U3). 107

Figure 201: Batch B SEM image of the horizontal cross-section of PC40-UMF+10%NNN2835 coating on a QFP44, lead 44, 200x (ref. Board 62, U3). Coating is bridging to the next lead and to the package body on right side of the image. 108

Figure 202: Batch B SEM image of the horizontal cross-section of PC40-UMF+10%NNN2835 coating on a QFP44, lead 44, 1,000x (ref. Board 62, U3). 108

Figure 203: Batch B SEM image of the horizontal cross-section of PC40-UMF+10%NNN2835 coating on a QFP44, lead 44, 2000x (ref. Board 62, U3). 109

Figure 204: Batch B SEM image of the horizontal cross-section of PC40-UMF+10%NNN2835 coating on a QFP44, lead 44, 2,000x (ref. Board 62, U3). 109

Figure 205: Optical image of PC40-UMF standard viscosity, SOT3, 25x (ref. Asymtech 8-2015). 110

Figure 206: Optical image of PC40-UMF high viscosity, SOT3, 25x (ref. Asymtech 8-2015). 110

Figure 207: Batch C SEM image of PC40-UMF standard viscosity coated QFP44, 40x (ref. Asymtech 8-2015 QFP44 40x 4). 111

Figure 208: Batch C SEM image of PC40-UMF standard viscosity coated QFP64, 60x (ref Asymtech 8-2015). 112

Figure 209: Batch C SEM image of PC40-UMF standard viscosity coated PLCC44, 40x (ref. Asymtech 8-2015). 112

Figure 210: Batch D SEM image of PC40-UMF high viscosity coated QFP44, 40x (ref. Asymtech 8-2015). 113

Figure 211: Batch D SEM image of PC40-UMF high viscosity coated QFP64, 60x (ref. Asymtech 8-2015). 113

Figure 212: Batch D SEM image of PC40-UMF high viscosity coated PLCC, 40x (ref. Asymtech 8-2015). 114

Figure 213: Thickness summary for the PC40-UMF standard and high viscosity spray coatings without an initial low viscosity dip. 115

Figure 214: Optical cross-section image of the PC40-UMF standard viscosity coating on the QFP44 lead toe, 100x (ref. U2, lead 11). 116

Figure 215: Optical cross-section image of the PC40-UMF standard viscosity coating on the QFP44 lead foot, 100x (ref. U2, lead 11). 116

Figure 216: Optical cross-section image of the PC40-UMF standard viscosity coating on the QFP44 lower lead location, 100x (ref. U2, lead 11). 117

Figure 217: Optical cross-section image of the PC40-UMF standard viscosity coating on the QFP44 upper lead location, 100x (ref. U2, lead 11). 117

Figure 218: Optical cross-section image of the PC40-UMF standard viscosity coating on the QFP44 heel location, 100x (U2, lead 11). 118

Figure 219: SEM Cross-section image of PC40-UMF standard viscosity coated QFP44, U2, lead 11, location A, 13,000x. 118

Figure 220: SEM Cross-section image of PC40-UMF standard viscosity coated QFP44, U2, lead 11, location B, 9,000x. 119

Figure 221: SEM Cross-section image of SEM Cross-section image of PC40-UMF standard viscosity coated QFP44, U2, lead 11, location C, 5,000x. 119

Figure 222: SEM Cross-section image of PC40-UMF standard viscosity coated, QFP44 U2, lead 11, location D, 2,500x. 120

Figure 223: SEM Cross-section image of PC40-UMF standard viscosity coated QFP44, U2, lead 11, location E, 1,800x. 120

Figure 224: SEM Cross-section image of PC40-UMF standard viscosity coated QFP44, U2, lead 11, location F, 600x. 121

Figure 225: SEM Cross-section image of PC40-UMF standard viscosity coated QFP44, U2, lead 11, location G, 1,000x. 121

Figure 226: SEM Cross-section image of PC40-UMF standard viscosity coated QFP44, U2, lead 11, location H, 792x. 122

Figure 227: SEM Cross-section image of PC40-UMF standard viscosity coated QFP44, U2, lead 11, location T, 2000x. Coating is 10 microns in the fillet in front of the tip and two to three microns at the tip (Figure 228). 122

Figure 228: SEM Cross-section image of PC40-UMF standard viscosity coated QFP44, U2, lead 11, location T, 4000x. 123

Figure 229: SEM isometric image of PC40-UMF high viscosity coated QFP44, 40x (ref. U2, leads 1-3). 123

Figure 230: Optical cross-section image of the PC40-UMF high viscosity coating on the QFP44 lead toe, 100x (ref. U2, lead 11). 124

Figure 231: Optical cross-section image of the PC40-UMF high viscosity coating on the QFP44 lead foot, 100x (ref. U2, lead 11). 124

Figure 232: Optical cross-section image of the PC40-UMF high viscosity coating on the QFP44 middle lead location, 100x (ref. U2, lead 11). 125

Figure 233: Optical cross-section image of the PC40-UMF high viscosity coating on the QFP44 upper lead location, 100x (ref. U2, lead 11). 125

Figure 234: Optical cross-section image of the PC40-UMF high viscosity coating on the QFP44 heel location, 100x (ref. U2, lead 11). 126

Figure 235: SEM cross-section image of the PC40-UMF high viscosity coated QFP44, U2, lead 11, location A, 3,500x. 126

Figure 236: SEM cross-section image of the PC40-UMF high viscosity coated QFP44, U2, lead 11, location B, 900x. 127

Figure 237: SEM cross-section image of the PC40-UMF high viscosity coated QFP44, U2, lead 11, location C, 1,000x. 127

Figure 238: SEM cross-section image of the PC40-UMF high viscosity coated QFP44, U2, lead 11, location D, 2,000x. 128

Figure 239: SEM cross-section image of the PC40-UMF high viscosity coated QFP44, U2, lead 11, location E, 3,500x. 128

Figure 240: SEM cross-section image of the PC40-UMF high viscosity coated QFP44, U2, lead 11, location F, 450x. 129

Figure 241: SEM cross-section image of the PC40-UMF high viscosity coated QFP44, U2, lead 11, location G, 300x. 129

Figure 242: SEM cross-section image of the PC40-UMF high viscosity coated QFP44, U2, lead 11, location H, 600x. 130

Figure 243: SEM cross-section image of the PC40-UMF high viscosity coated QFP44, U2, lead 11, T, 3,500x. Coating is 6.1 microns in the fillet in front of the tip and 0.4 microns at the tip not including the small burr location where it essentially zero (Figure 244). 130

Figure 244: SEM cross-section image of the PC40-UMF high viscosity coated QFP44, U2, lead 11, location T, 15,000x. 131

Figure 245: SEM image of Parylene C coated QFP44, U5, lead 23, 60x (ref. Board 2) (image taken after accelerated thermal cycling ref. Board 2). 132

Figure 246: SEM image of Parylene C coated QFP44, U5, lead 24, 60x (image taken after accelerated thermal cycling ref. Board 2). 133

Figure 247: SEM image of Parylene C coated SOT3, 60x (image taken after accelerated thermal cycling ref. Board 207). 133

Figure 248: SEM image of Parylene C coated SOT5, 60x (image taken after accelerated thermal cycling ref. Board 207). 134

Figure 249: SEM image of Parylene C coated SOT6, 60x (image taken after accelerated thermal cycling ref. Board 207). 134

Figure 250: SEM image of Parylene C with Adpro plus coated SOT5, 60x (image taken after accelerated thermal cycling ref. Board 202). 135

Figure 251: SEM image of Parylene C with Adpro plus coated SOT6, 60x (image taken after accelerated thermal cycling ref. Board 202). 136

Figure 252: Optical cross-section view of Parylene C ™ with Adpro plus coated QFP44 lead, overall, 25x (ref. Board 1, left lead). 137

Figure 253: Optical cross-section view of Parylene C ™ with Adpro plus coated QFP44 lead, location A, 100x (ref. Board 1, left lead). 137

Figure 254: Optical cross-section view of Parylene C ™ with Adpro plus coated QFP44 lead, location F, 100x (ref. Board 1, left lead). 138

Figure 255: Optical cross-section view of Parylene C ™ with Adpro plus coated QFP44 lead, location H, 100x (ref. Board 1, left lead). 138

Figure 256: Optical cross-section view of Parylene C ™ with Adpro plus coated QFP44 lead, location T, 100x (ref. Board 1, left lead). 139

Figure 257: SEM cross-section view of Parylene C ™ with Adpro plus coated QFP44 lead, location A, 150x (ref. Board 1, left lead). 139

Figure 258: SEM cross-section view of Parylene C ™ with Adpro plus coated QFP44 lead, location B, 150x (ref. Board 1, left lead). 140

Figure 259: SEM cross-section view of Parylene C ™ with Adpro plus coated QFP44 lead, location E, 150x (ref. Board 1, left lead). 140

Figure 260: SEM cross-section view of Parylene C ™ with Adpro plus coated QFP44 lead, location F, 150x (ref. Board 1, left lead). 141

Figure 261: SEM cross-section view of Parylene C ™ with Adpro plus coated QFP44 lead, location F, 150x (ref. Board 1, right lead). 141

Figure 262: SEM cross-section view of Parylene C ™ with Adpro plus coated QFP44 lead, location H, 150x (ref. Board 1, left lead). 142

Figure 263: SEM cross-section view of Parylene C ™ with Adpro plus coated QFP44 lead, location T, 150x (ref. Board 1, left lead). 142

Figure 264: SEM cross-section view of Parylene C ™ with Adpro plus coated QFP44 lead, location T, 150x (ref. Board 1, right lead). 143

Figure 265: SEM image of 1B31LOC coated QFP44, 60x (ref. Board 82). 144

Figure 266: SEM image of 1B31LOC coated QFP64 showing thin coating on the lead knees, 60x (ref. Board 82). 144

Figure 267: SEM image of 1B31LOC coated PLCC, 30x (ref. Board 82). 145

Figure 268: SEM image of Parylene ™ C coated QFP44, 60x (ref. Board 2, U5, lead 24). 146

Figure 269: SEM image of Parylene ™ C coated SOT3, 60x (ref. Board 207). Note image taken after thermal cycling. 147

Figure 270: SEM image of Parylene ™ C coated SOT5, 60x (ref. Board 207). Note image taken after thermal cycling. 147

Figure 271: SEM image of Parylene ™ C coated SOT6, 60x (ref. Board 207). Note image taken after thermal cycling. 148

Figure 272: SEM image of Parylene ™ C with Adpro+ coated SOT6, 60x (ref. Board 202). Note image taken after thermal cycling. 148

Figure 273: Optical overall cross-section image of Parylene ™ C with Adpro + coated QFP44, left lead, 25x. 149

Figure 274: Optical cross-section image of Parylene ™ C with Adpro + coated QFP44, left lead, location A, 100x. 150

Figure 275: Optical cross-section image of Parylene ™ C with Adpro + coated QFP44, left lead, location B, 100x. 150

Figure 276: Optical cross-section image of Parylene ™ C with Adpro + coated QFP44, left lead, location C, 100x. 151

Figure 277: Optical cross-section image of Parylene ™ C with Adpro + coated QFP44, left lead, location D, 100x. 151

Figure 278: Optical cross-section image of Parylene ™ C with Adpro + coated QFP44, left lead, location E, 100x. 152

Figure 279: Optical cross-section image of Parylene ™ C with Adpro + coated QFP44, left lead, location F, 100x. 152

Figure 280: Optical cross-section image of Parylene ™ C with Adpro + coated QFP44, left lead, location T, 100x. 153

Figure 281: Optical cross-section image of Parylene ™ C with Adpro + coated QFP44, left lead, location G, 100x. 153

Figure 282: Optical cross-section image of Parylene ™ C with Adpro + coated QFP44, left lead, location H, 100x. 154

Figure 283: SEM overall cross-section image of the Parylene ™ C with Adpro + coated QFP44, left lead, 60x (ref. Board 1). 154

Figure 284: SEM cross-section image of the Parylene ™ C with Adpro + coated QFP44, left lead, location A, 150x (ref. Board 1). 155

Figure 285: SEM cross-section image of the Parylene ™ C with Adpro + coated QFP44, left lead, location B, 150x (ref. Board 1). 155

Figure 286: SEM cross-section image of the Parylene ™ C with Adpro + coated QFP44, left lead, location C, 150x (ref. Board 1). 156

Figure 287: SEM cross-section image of the Parylene ™ C with Adpro + coated QFP44, left lead, location D, 150x (ref. Board 1). 156

Figure 288: SEM cross-section image of the Parylene ™ C with Adpro + coated QFP44, left lead, location E, 150x (ref. Board 1). 157

Figure 289: SEM cross-section image of the Parylene ™ C with Adpro + coated QFP44, left lead, location F, 150x (ref. Board 1). 157

Figure 290: SEM cross-section image of the Parylene ™ C with Adpro + coated QFP44, left lead, location T, 150x (ref. Board 1). 158

Figure 291: SEM cross-section image of the Parylene ™ C with Adpro + coated QFP44, left lead, location H, 150x (ref. Board 1). 158

Figure 292: PC18M-mod SOT board 233 with large bubbles around the leads, 10x (note the photograph was taken after thermal cycling and 1,000 hours of 85°C/85%RH humidity (ATC+1000HTHH) environments). The color change in the second image is an artifact of the illumination used to highlight the bubbles (ref. Figure 7). 161

Figure 293: PC18M-mod QFP board 35 with large bubble density on top of the package, 10x (ref. Figure 8). 162

Figure 294: Horizontal cross-section, SEM, board 28, PC18M+20%X1102PMA, QFP44, U1, lead 39, 1,000x (ref. Figure 48). 163

Figure 295: Horizontal cross section, SEM, board 21, PC18M+20%XP2742, QFP44, U1, lead 23, 200x (ref. Figure 37). 163

Figure 296: Coating film formation from spray coating process. 164

Figure 297: Spray drop deposition resulting in bubbles in the coating; (A) three deposited drops, (B) a fourth drop deposited on top of the initial three trapping some gas, (C) drop coalescence with a small entrained bubble, (D) multiple groups of the coalesced drops containing small bubbles, (E) during the heated portion of the cure there is a coalescence of small bubbles into larger bubbles, and (F) with drier films, having a higher some bubbles escape but the coating surface does not smooth out. 164

Figure 298: SEM image of PC18M dip two PC18M sprays, board A191, QFP44, with good overall coverage but still exhibiting surface roughness, 40x. 165

Figure 299: PC18M dip + two PC18M sprays, Board A023, QFP44 lead; (A) 40x and (B) top of lead, 100x, and (C) bottom of lead. 166

Figure 300: Batch A and B with interlayer delamination evident in the vertical section SEM image of PC40-UMF+30%NNN2835 nanosilica coating on QFP44 with a dip coat/plasma etch/spray coat; (a) overall of lead tip location T, (b) lead tip, and (c) between board pad and solder mask. Yellow arrows show delamination between dip and spray layers. 167

Figure 301: Batch B with interlayer delamination evident in the vertical section SEM image of PC40+15.54%N3300 coating on QFP44 location T; (a) 100x, (b) 1,000x, and (c) 5,000x. Yellow arrows highlight delamination between the dip and spray layers. 168

Figure 302: Batch A and B interlayer delamination (arrow) evident in the horizontal section SEM image of PC40-UMF coating on QFP44 with a dip coat/plasma etch/spray coat on U3, lead 11, 1,000x... 169

Figure 303: SEM image of PC40-UMF coatings; (A) spray coated PC40-UMF directly on QFP44 leads showing no dewetting, 40x, and (B) dewetting on the knee and side of the lead of PC40-UMF spray coating over UV cured PC40-UMF dip coating on the side of a QFP44 lead, 1,000x (Ref for A: Batch C coating of PC40-UMF Asymtech 8-2015, and Ref. for B: baseline coating QFP44, U4, lead 12, Board 60 after HTHH1767). 170

Appendix F: List of Tables

Table 1: PC18M based coating QFP44 SEM coating coverage inspection results. 9

Table 2: Coating thickness measurements for PC18M based coatings on QFP44 leads. 16

Table 3: PC18M based coatings QFP44 minimum and maximum thicknesses from Table 2. 16

Table 4: Batch A and B assembly coating thickness observations of PC40-UMF, PC40-UMF+NNN2835 and PC40-UMF+N3300 from cross-sectioning. 26

Table 5: PC18M based coatings QFP44 minimum and maximum thicknesses (repeated from Table 3). 159

Acronyms

Acronym	Definition
BGA	Ball Grid Array
PLCC	Plastic Leaded Chip Carrier Electronic Package
QFP	Quad Flat Pack Electronic Packages
SEM	Scanning Electron Microscopy
SOT	Small Outline Transistor Electronic Packages

1. PC18M based coatings

1.1 PC18M optical coating inspection

The nanoparticle filled coated parts were visually inspected and were found to have sufficient transparency so as not to obliterate the identification markings on the electrical components (a MIL-I-46058 requirement). A screening experiment was performed on a memory card component where a pipet was used to flood coat the board while horizontally oriented. The board was then tipped up on edge and allowed to drain. The nanosilica filled coating was more transparent (Figure 1) than the nanoalumina filled coating (Figure 2). In the pictures, the right sides of the samples were oriented downward during coating draining. The PC18M+11102PMA nanoalumina coating was milky while the other PC18M+XP2742 nanosilica was more transparent. The nanoalumina filled coating was increasingly milky when it became thicker. The milky appearance was due in part to an index of refraction mismatch between the nanoalumina particles and the polyurethane matrix and possibly due to the some of the particle clustering. Inspection of the whisker test assemblies coated with PU coatings exhibited some darkening after ATC+HTHH environmental exposure but generally had good coating transparency (Figure 3 to Figure 4).



Figure 1: Marking readability test for pipet flood coated PC18M+50%XP2742 (15.17 wt. % 20 nm nanosilica).



Figure 2: Marking readability test for pipet flood coated PC18M+20%X11102PMA (13.04 wt. % 40 nm nanoalumina).

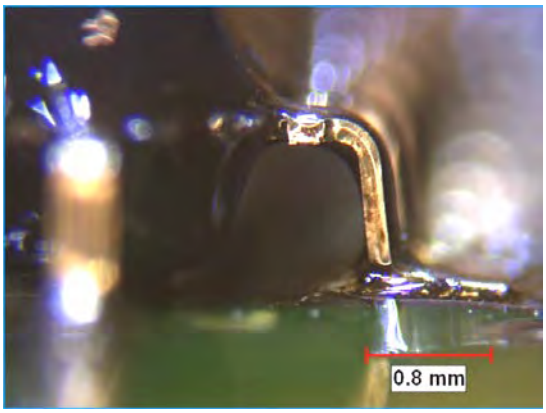


Figure 3: PC18M-mod, board 15, QFP44, 50x after ATC&HTHH1000.

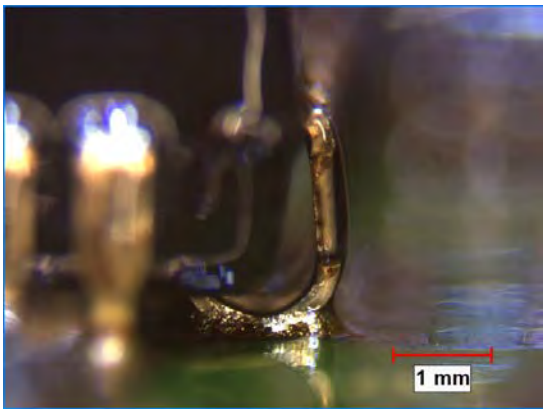


Figure 4: PC18M-mod board 15, PLCC20, 30x 3 after ATC&HTHH1000.

Another significant finding on the tin whisker test assemblies was the presence of bubbles in some of the coatings (Figure 5 to Figure 7). The PC18M-mod and PC18M+20%XP2742 boards had the highest bubble density while the PC18M+11102PMA had few if any bubbles.

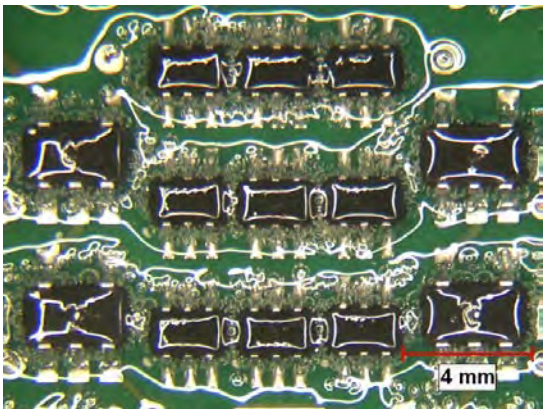


Figure 5: PC18M-mod SOT board 234 with large bubble density, no exposure, 10x.

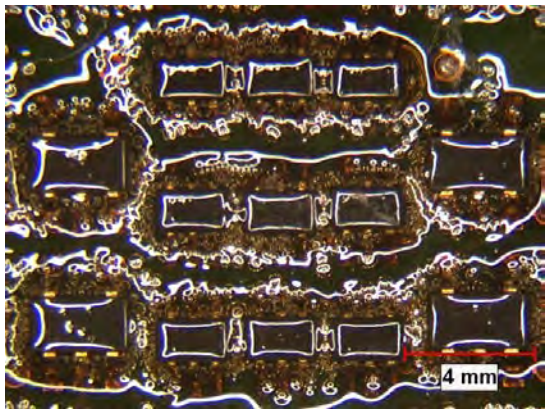


Figure 6: PC18M-mod, SOT board 233, ATC 1000HTHH, 10x, large bubbles, darkened coating.

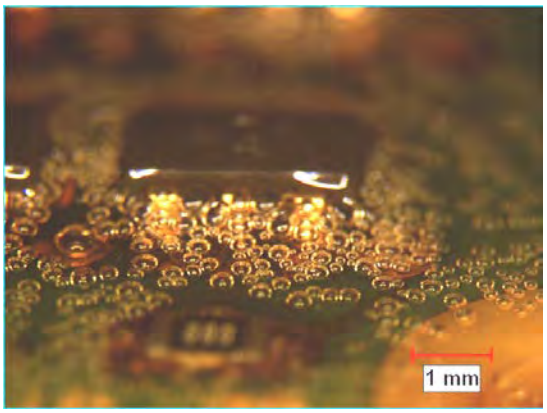


Figure 7: PC18M-mod SOT board 233 with large bubbles, 10x, after ATC+1000HTHH. The color change in the second image is an artifact of the illumination used to highlight the bubbles.

For the PC18M-mod coated boards two of seven Small Outline Transistor Electronic Packages (SOT) and four of nine Quad Flat Pack Electronic Packages (QFP) boards exhibited large bubble density (Figure 5, Figure 6, and Figure 8), with the rest having small/no bubble density (Figure 9 and Figure 10). For the PC18M+20%XP2742 all 25 of the SOT boards exhibited medium bubble density and four of the nine QFP boards had medium bubble density, while the rest had small/no bubble density (Figure 11 - Figure 13).

The bubble density was greater where the coating was thick on top of the part and in the fillet around the part. The PC18M+11102PMA coated boards had very few if any bubbles (Figure 14 and Figure 15). The Parylene™ C boards had no bubbles (Figure 16). It was decided to continue testing with the assemblies having bubbles in the coating and distribute the boards with the greatest bubble density throughout the environments.

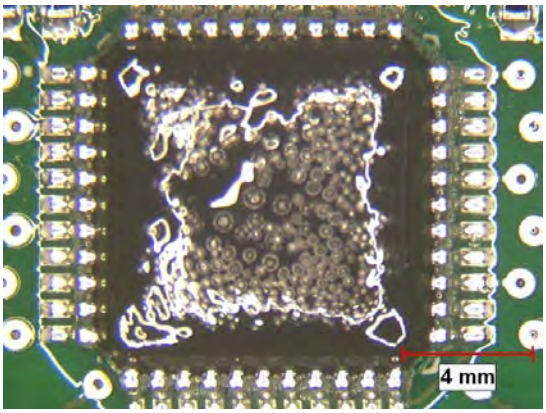


Figure 8: PC18M-mod QFP board 35 with large bubble density, 10x.

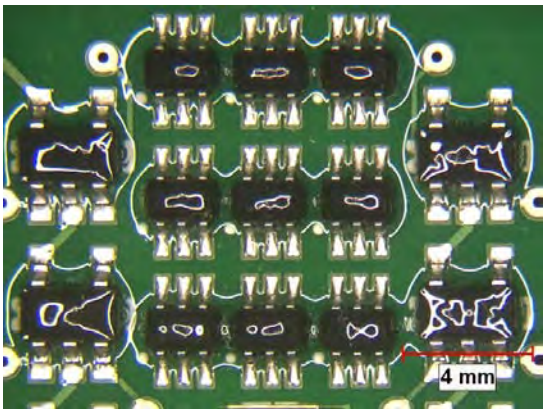


Figure 9: PC18M-mod SOT board 213, no exposure, with small/no bubble density, 10x.

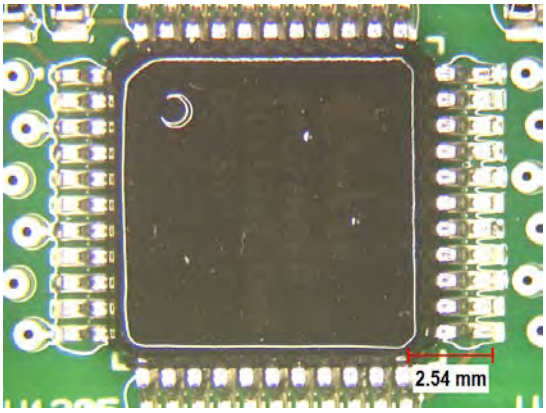


Figure 10: PC18M-mod QFP board 11, with small/no bubble density, no exposure, 10x.

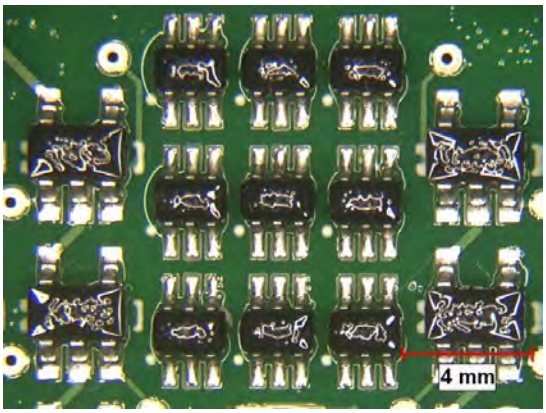


Figure 11: PC18M+20%XP2742 SOT board with medium bubble density, no exposure, 10x.

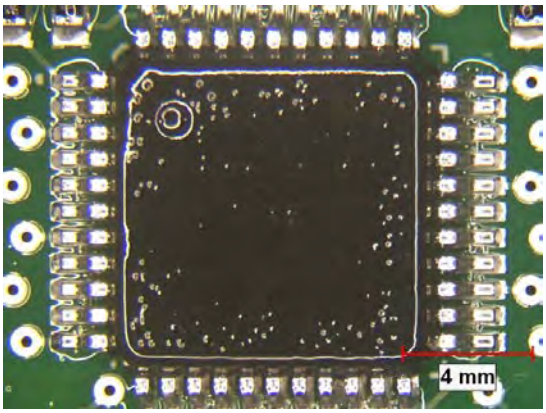


Figure 12: PC18M+20%XP2742 QFP board with medium bubble density, no exposure, 10x.

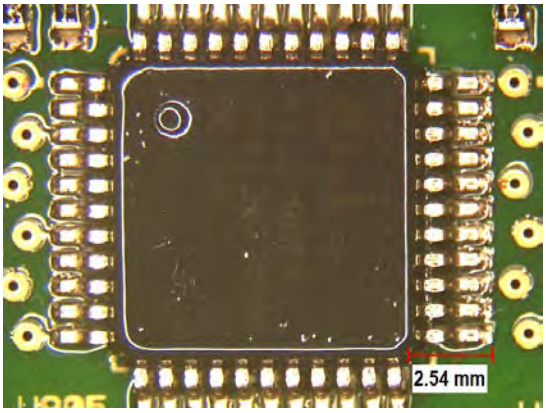


Figure 13: PC18M+20%XP2742 QFP board with small/no bubble density, 10x.

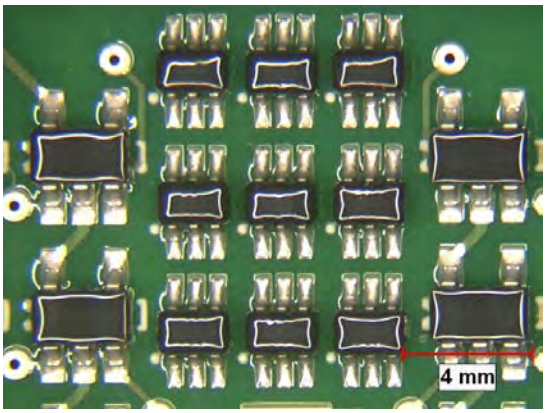


Figure 14: PC18M+20%X1102PMA, SOT board 226, HALT, 10x, small/no bubble density, milky appearance.

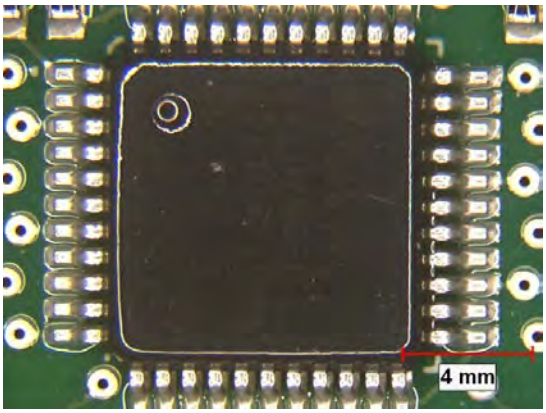


Figure 15: PC18M+20%X11102PMA, QFP board 23, no exposure, 10x, small/no bubble density.

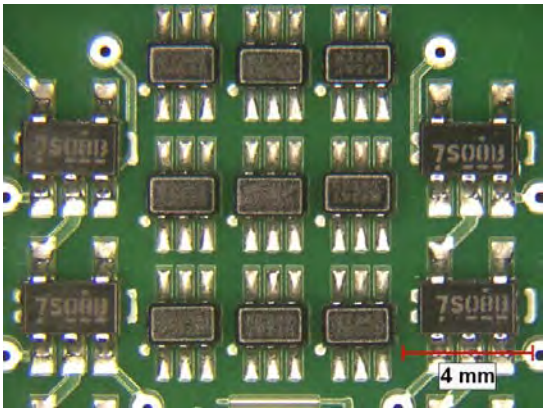


Figure 16: Parylene, SOT board 201, no exposure, no bubbles, 10x.

1.2 PC18M SEM coverage inspection

The SOT and QFP assemblies were examined in the scanning electron microscope (SEM) to obtain overall coverage information. The most complete and consistent coating coverage was observed on the Parylene™ coated samples (Figure 17). The spray coating had greater coverage variability. The SEM image spray coating coverage classifications were (1) complete coverage (Figure 18), (2) isolated thin regions less than 50 microns (Figure 19), and (3) extended thin coverage regions longer than 50 microns (Figure 20 and Figure 21). The inspection results from the QFP44 (Table 1) revealed that the PC18M-mod had the greatest number of thin coating areas and the longest exposed edges. The PC18M+20%X11102PMA nanoalumina exhibited the best corner coverage of the spray coated samples. The PC18M+20%X2742 nanosilica was similar in coverage to the PC18M-20%X11102PMA except that it had more corners with thin coverage. Further work is needed to determine if the coating coverage difference is due to the difference in spray passes used during coating.

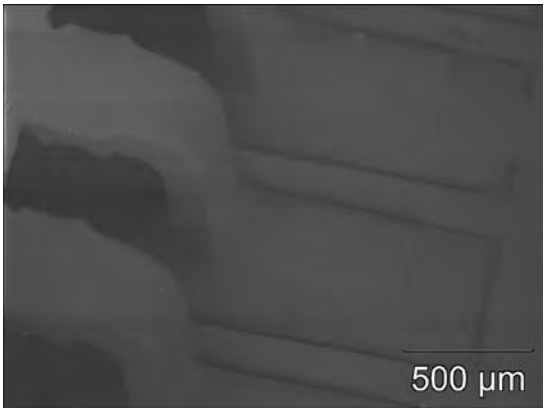


Figure 17: SEM image of Parylene™ coated QFP44, 60x (ref. Board 2, U5, lead 24).

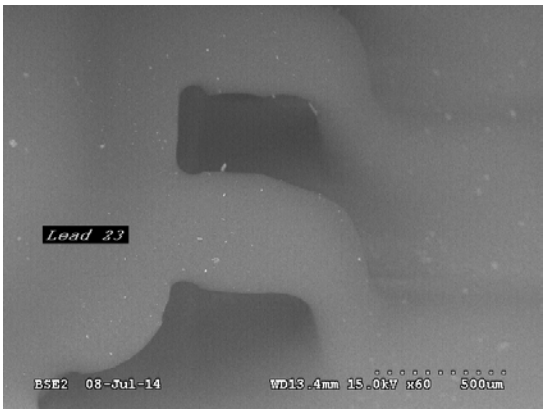


Figure 18: SEM image of PC18M dip + PC18M+20%X11102PMA spray showing full coverage of QFP44 leads, 60x (Ref. board 28, U2, lead 23, no environmental exposure).

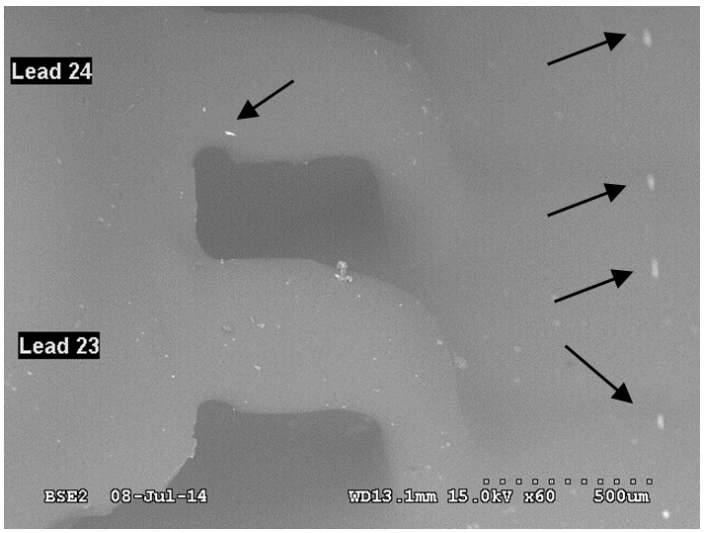


Figure 19: SEM image of PC18M dip + PC18M-20%X2742 spray coating on QFP44 leads showing isolated thin coverage regions less than 50 microns, 60x (ref. Board 39, U2, lead 23, image taken after thermal cycling exposure).



Figure 20: SEM image of PC18M dip + PC18M-mod spray on QFP44 leads showing extended thin coverage regions, 60x (ref. Board 15, U2, lead 23, 60x, image take after thermal cycling and 1000 hours of HTHH).

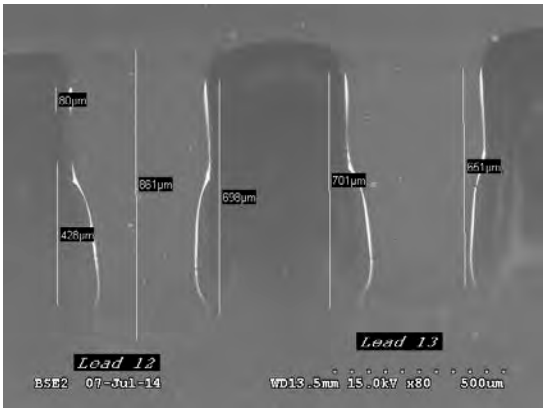


Figure 21: SEM image of PC18M dip + PC18M-mod spray on QFP44 leads showing extended thin coverage regions with measurements, 80x (ref. Board 11, U2, lead 12, no environmental exposure).

Table 1: PC18M based coating QFP44 SEM coating coverage inspection results.

Coating	Total leads inspected (1)	Total thin areas	Total less than 50 µm	Total greater than 50 µm
PC18M-Mod	14	43	15	28
PC18M+20% XP2742 (1)	16	10	10	0
PC18M+20% X11102 PMA	16	0	0	0
Note (1): Select leads on U2 were inspected on two boards. Note (2): All thin coating areas occurred on one board.				

1.3 PC18M vertical cross-section coating thickness evaluation

The vertical cross-section coating thickness analysis was performed on the QFP44 components. A typical overall cross – section is shown in Figure 22. The measurement locations are given in Figure 23. The results summarized in Table 2 shows that the coating thickness ranges from between 0.06 to 76 microns on the front of the lead and 0.5 to 103 microns on the back of the lead. The minimum and maximum for each coating type is given in Table 3. Location T in the front always had the thinnest coating; ranging from 0.06 to 37 microns for the PC18M-mod spray and from 13 to 29 microns for the PC18M+20%XP2742 nanosilica spray.

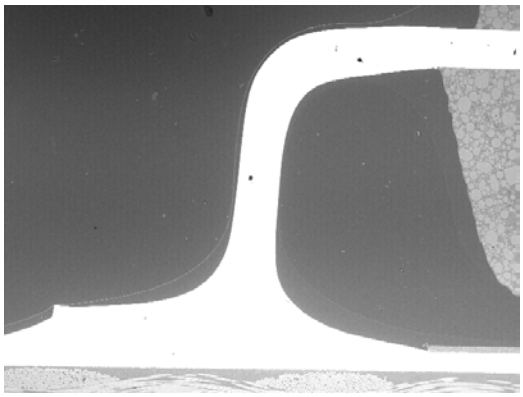


Figure 22: Typical SEM image of a coating cross-section, 60x (Ref. PC18M-mod unfilled, board 12, QFP44, left lead).

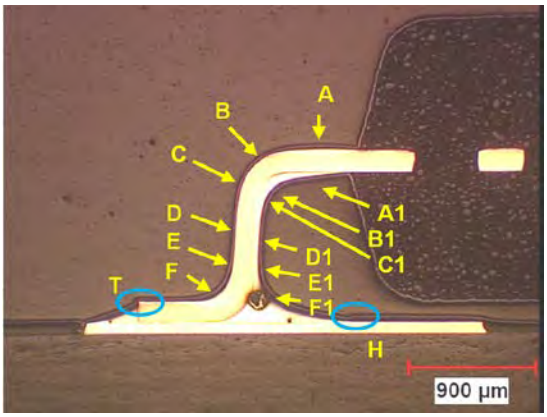


Figure 23: Coating cross-section thickness measurement locations. Optical image of Parylene™ C coated QFP44 shown.

The spray coating thickness was generally thicker on surfaces with good line-of-sight with the coating spray nozzle. Shadowed regions behind the leads were more difficult to cover, but in several cases substantial coating thickness was observed. The combination of an initial low viscosity dip coating, and alternating X-Y spray passes with a conical spray nozzle were used to minimize shadowing effects and achieve some back side coverage. Back side coating coverage is an important aspect of tin whisker risk.

The spray coated sample coverage depended upon location and coating type. Generally, a coating fillet formed in region A between the lead and the package (Figure 24) and was relatively uniform over the outside of the lead knee (location B). At the underside, A1 location, the coating thinned to a few microns between the package-side and the knee-side coating fillets. The A1 location generally had thin coverage, but in one case there appeared to be sufficient coating volume to join the underside coating fillets together and the coating was thick (Figure 25). Location B1 on the inside of the lead knee exhibited the thickest coating of all the back side locations.

Coating surface tension effects during spray coating resulted in thin coating over sharp corners, but the amount of thinning depended upon the coating type. The unfilled PC18M-mod did not cover the lead toe corners well (Figure 26). The PC18M+20%X11102PMA coating provided the best lead tip coverage (Figure 27). Even though the PC18M+20%X11102PMA coating had better corner coverage, coating on the back of the lead was thin (Figure 28). The PC18M+20%XP2742 also had good lead tip coverage (Figure 29).



Figure 24: SEM cross-section view of PC18M-mod coated QFP44 lead, top of lead, 150x (ref. Board 12, right lead, location A).

An additional interesting observation was made regarding the role of solder flow in improving subsequent coating coverage. The surface tension of the liquid tin and solder during reflow reduced the sharpness of inside lead bend radii corners (Figure 25), smoothed out irregularities from burrs (Figure 26) and formed menisci on the lead flats (see Horizontal cross-sectioning evaluation). In the areas where solder flow smoothed out the lead asperities, coating thickness uniformity was improved.

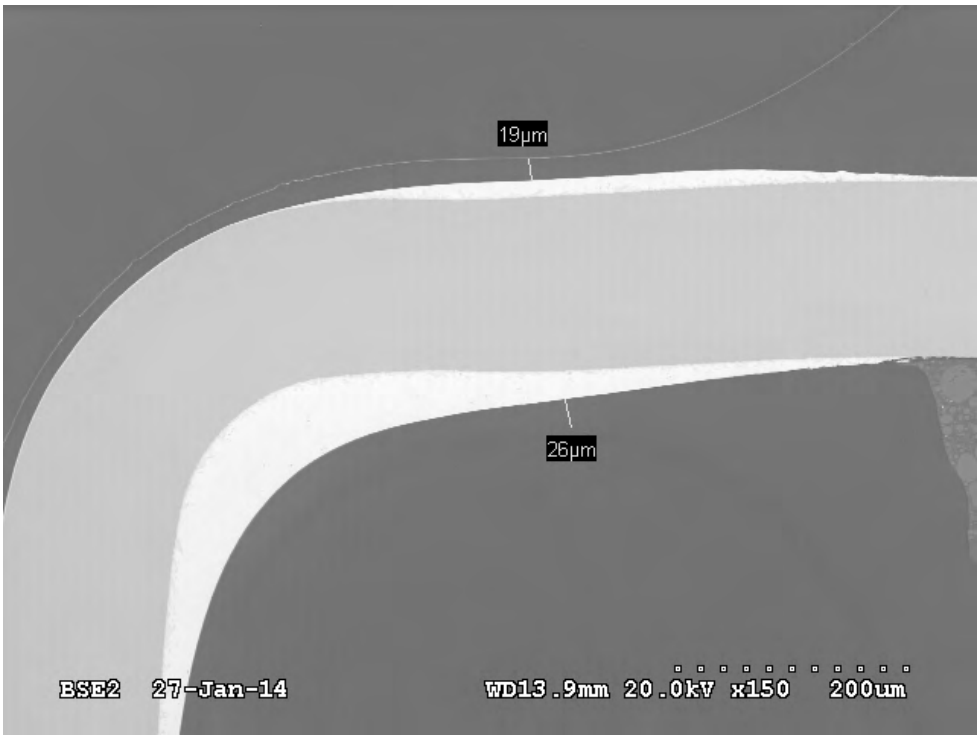


Figure 25: Coating cross-section SEM view of PC18M-mod unfilled, board 12, QFP44, left lead, location A, SEM, 150x.

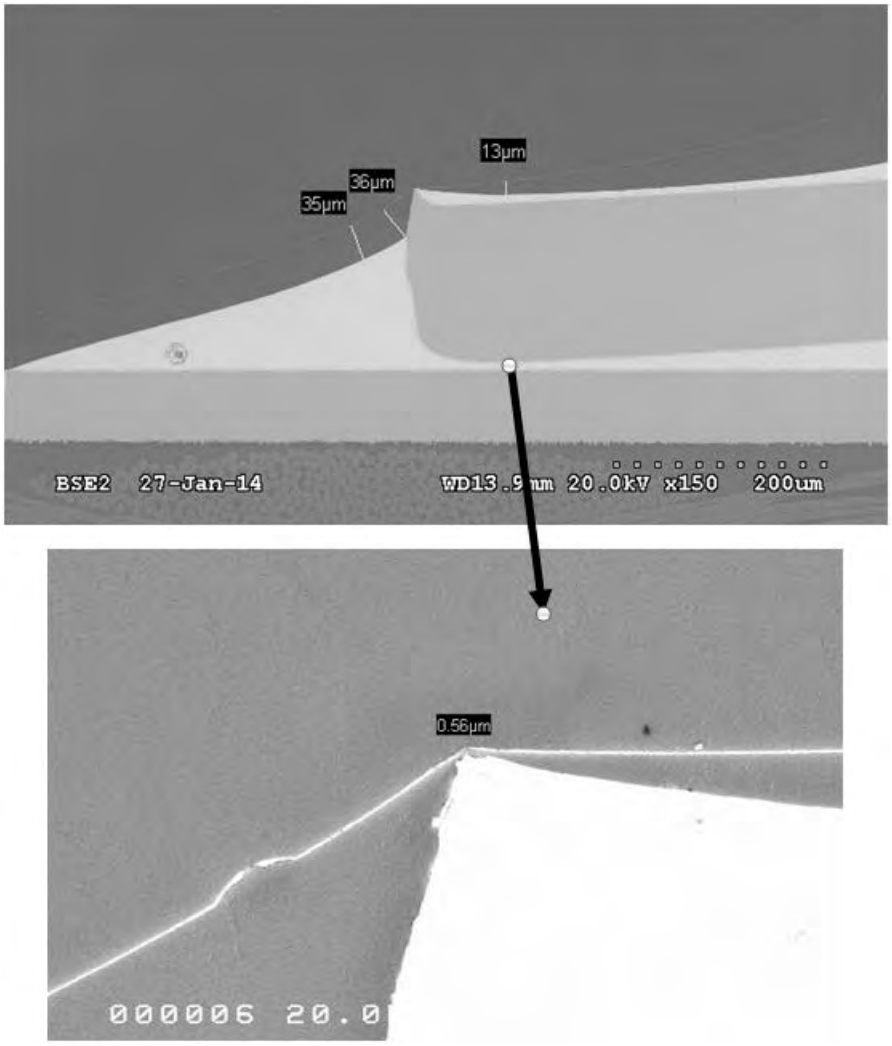


Figure 26: Lead tip cross-section showing thin coverage. SEM image of PC18M-mod unfilled, board 12, QFP44, left lead, location T, 150x and 2,000x.

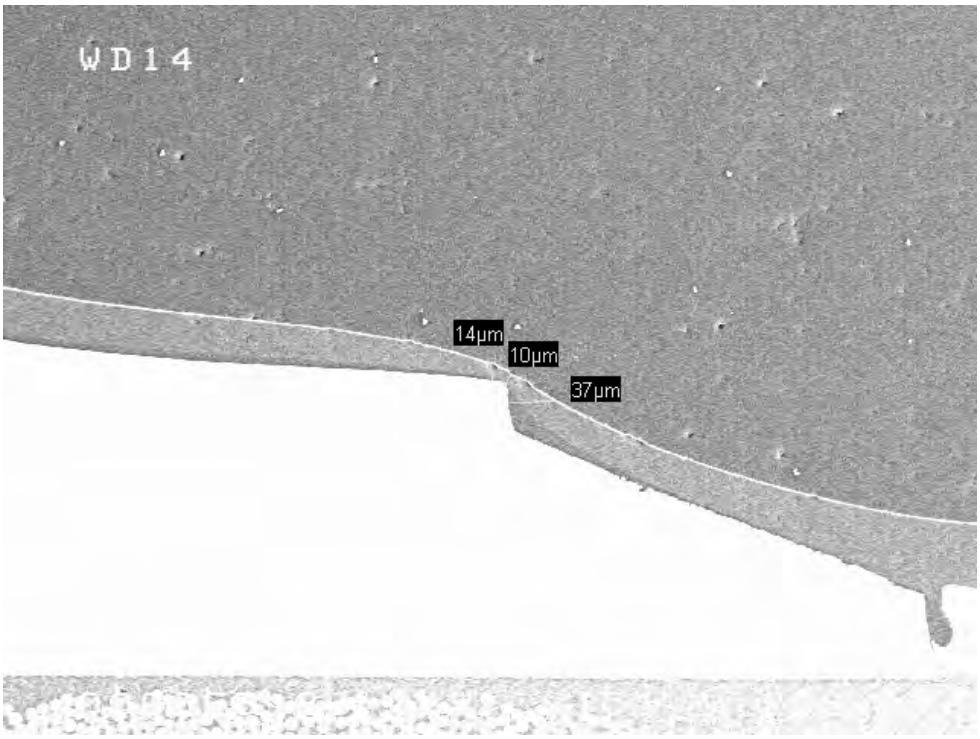


Figure 27: Lead tip cross-section showing thicker coverage. SEM image of PC18M dip + PC18M-20%X11102PMA nanoalumina spray coated QFP, right lead, location T, 150x (ref. Board 12).

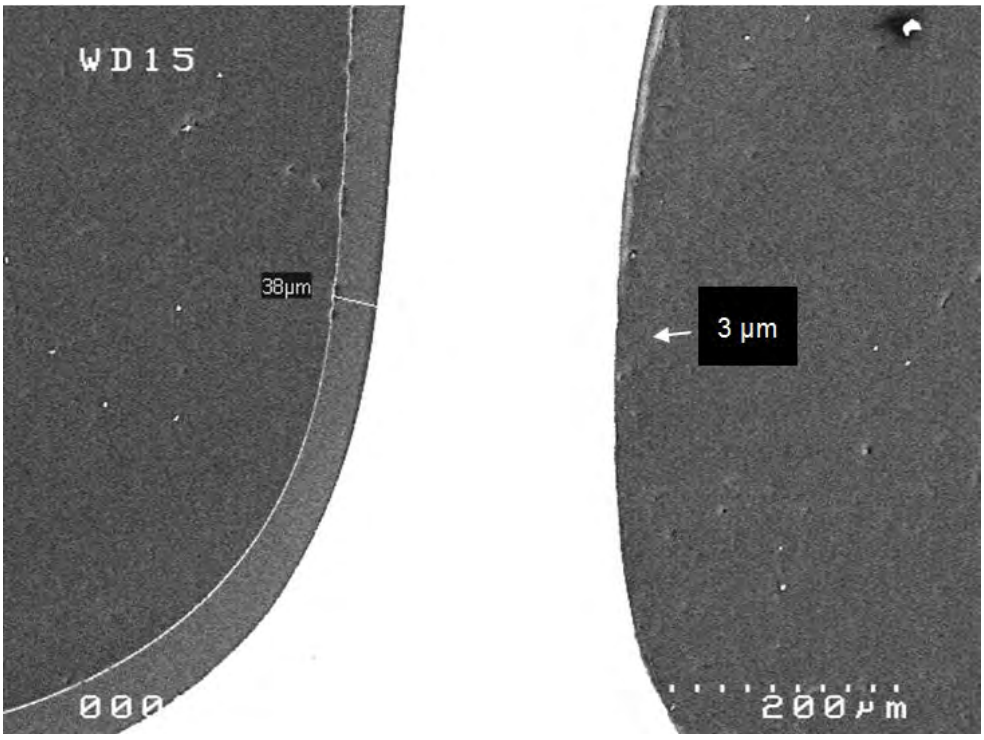


Figure 28: Cross-section SEM view of PC18M-20%X1102PMA nanoalumina coated QFP, left lead, location E, 150x (ref. Board 12).

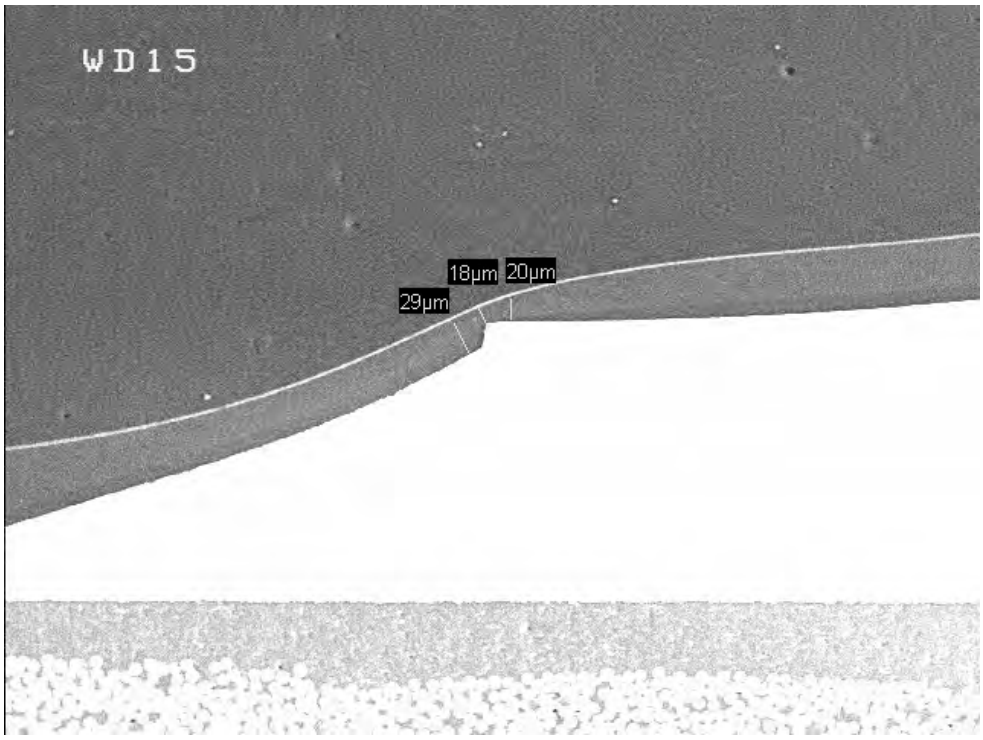


Figure 29: Cross-section SEM view of PC18M-20%XP2742 nanosilica coated QFP, left lead, location T, SEM, 150x (ref. Board 20).

Table 2: Coating thickness measurements for PC18M based coatings on QFP44 leads.

Sample	Lead	Coating Thickness (microns)													
		A	B	C	D	E	F	T	A1	B1	C1	D1	E1	F1	H
PC18M-mod	R	28	32 36 42	45	42	32	32 37 38	2 0.06 37	1.6 0.8 1.4	31 34 29	18	13	7	22 42 46	7 25 20
	L	19	14 15 13	23	21	17	48 71 76	13 0.56 36	26	33 32 29	16	9	3.2	74 103 100	62 70 45
PC18M +20% XP2742	R	65	52 50 53	50	31	28	33 36 43	20 13 36	0.5 0.6 0.8	7 6 7	2.2	7	5	8 6 8	10 14 9
	L	66	60 45 43	42	39	37	49 59 58	20 18 29	8	14 20 19	10	5	0.8	4 4.2 3.7	4 10 8
PC18M +20% X11102 PMA	R	73	69 67 66	71	64	60	62 62 58	14 10 37	5	10 15 10	9	5	2.4 1.8 4	4 3.5 4	7 15 12
	L	52	54 54 48	43	40	38	39 48 52	15 17 45	1.2 1.8 2.2	18 17 16	12	9	3.7 2.4 1.5	4.3 5.5 6.8	8 12 8
Parylene C with Adpro+	R	28	28 28 28	28	28	28	29 29 28	31 28 29	28	27 28 28	27	28	28	28 28 29	30 29 30
	L	29	29 30 29	28	28	27	30 30 30	29 28 27	28	27 30 28	28	27	28	29 28 29	27 27 29

Table 3: PC18M based coatings QFP44 minimum and maximum thicknesses from Table 2.

Coating	Min/Max	Front (micron)	Back (micron)
PC18M-mod	Min	0.06	0.8
	Max	76	103
PC18M+20%XP2742	Min	13	0.5
	Max	66	20
PC18M+20%X11102PMA	Min	10	0.5
	Max	73	18
Parylene C with Adpro+	Min	27	27
	Max	31	30

1.4 PC18M horizontal cross-section coating thickness evaluation

The thickness of the coating on the vertical lead section between the package exit and the lead foot was evaluated on the QFP44 parts with a horizontal section plane near region E (Figure 30). The top of the chip resistors were used as a reference to keep the section plane parallel to the board and at a consistent height for the various boards that were sectioned. An x-ray image of the potted cross-section mount shows that the section plane was just above the main part of the solder fillet (Figure 31). For the analysis, SEM images were obtained from leads 6, 11, 17, 23, 28 34 and 39 to represent corner and center leads on each side of the QFP (Figure 32). Sometimes the back side of the lead had little or no gold sputtered over the conformal coating on the center leads, making it more difficult to differentiate between the coating and the potting compound. Due to potting shrinkage, the coating separated slightly from the lead.

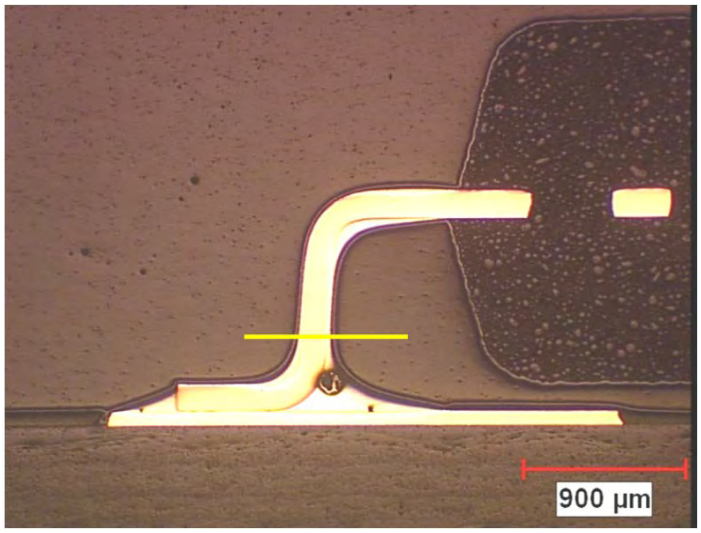


Figure 30: Horizontal cross-section plane location for coating thickness evaluation.

Overall the coating thickness varied from approximately one micron on back side to 50 microns on front side. Generally, the front of the leads exhibited thicker coating than the back side and that back side coating thickness was better on the corner leads than the middle leads. The spray process uses an overlap spray pattern and the location of the overlap may have influenced the amount of deposited coating. The nanoparticle filled coatings had better corner coverage, but back side coverage could be improved. There are many variables that could affect this result, but the nanoparticle filled coating coverage performance is encouraging.

All coating types exhibited good front of the lead coverage (Figure 33 – Figure 41). The front coating nanoparticle filled coating thickness was greater on the right side of the part (leads 23 – 33) than the left (leads 1 – 11). The leads on the lower side (leads 12 – 22) had comparable coverage to the left and right sides, except for the thick coating coverage of the PC18M-mod coating on lead 17.

Sometimes on the corner leads, the coating was thicker on the side adjacent to the neighboring lead (top of Figure 36) and thinner on the side facing the open corner.

Greater back side coating thickness variation was observed from lead-to-lead. Sometimes on a given lead, the back side coating thicknesses were comparable (Figure 42 – Figure 44), but on the PC18M-mod, there were cases where relatively thick back side coating was observed (Figure 36 and Figure 39).

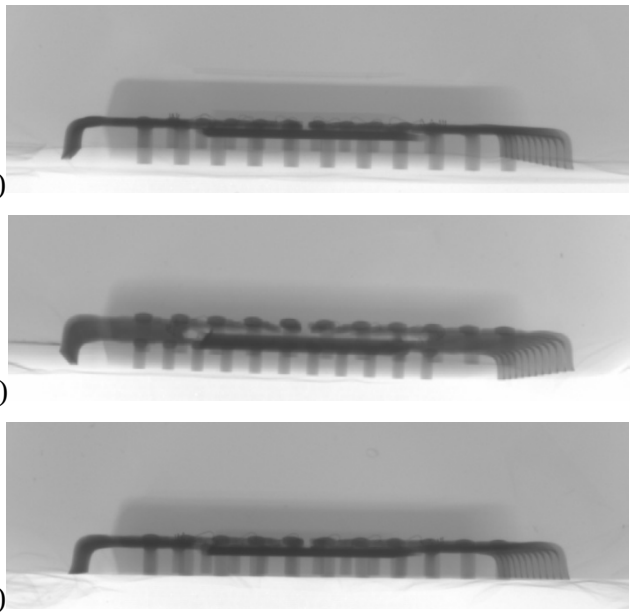


Figure 31: X-ray images of cross-section mounts used in the horizontal section evaluation; (a) PC18M-mod board 11, (b) PC18M+20%XP2742 board 21, and (c) PC18M+X11102PMA board 28.

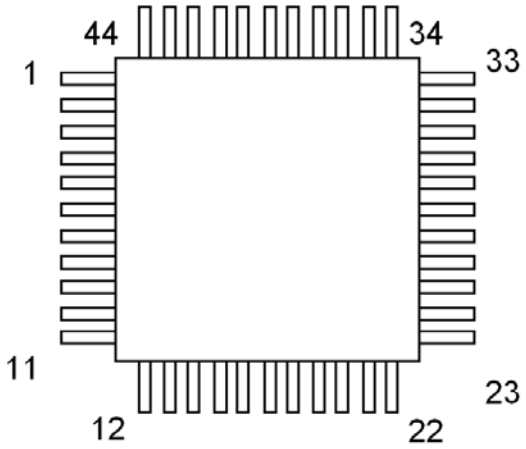


Figure 32: QFP44 pin numbering.

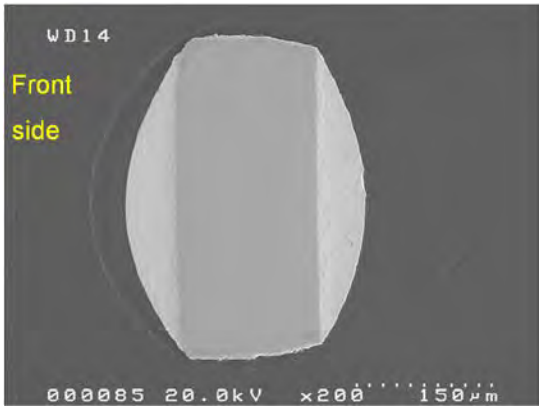


Figure 33: SEM image of horizontal cross section, board 11, PC18M-mod, QFP44, U1, lead 6, 200x.

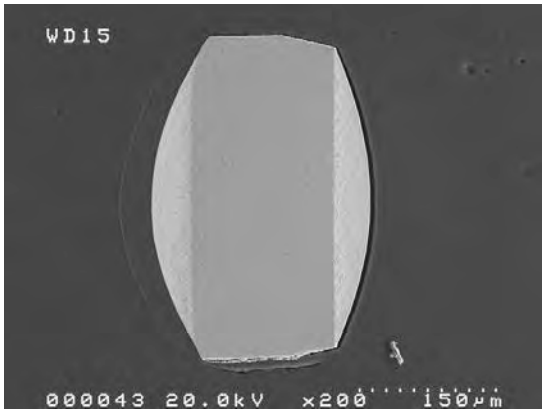


Figure 34: Horizontal cross-section SEM board 21, PC18M+20%XP2742, QFP44, U1, lead 6, 200x.

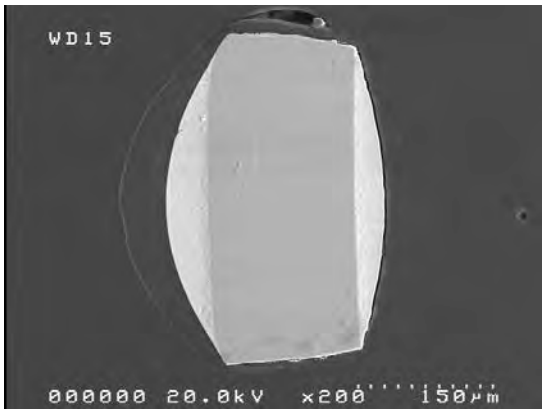


Figure 35: Horizontal cross-section, SEM, board 28, PC18M+20%X1102PMA, U1, lead 6, 200x.

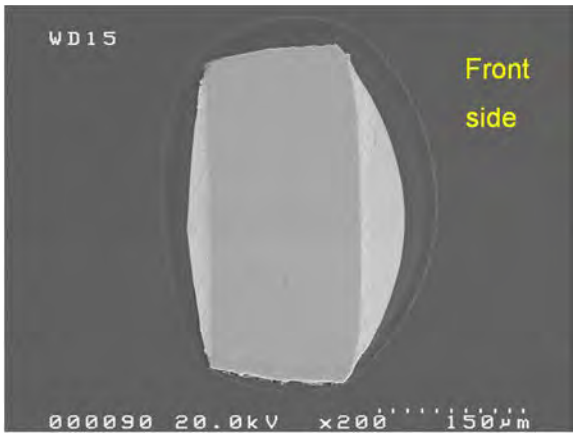


Figure 36: Horizontal cross section, SEM, board 11, PC18M-mod, QFP44, U1, lead 23, 200x.

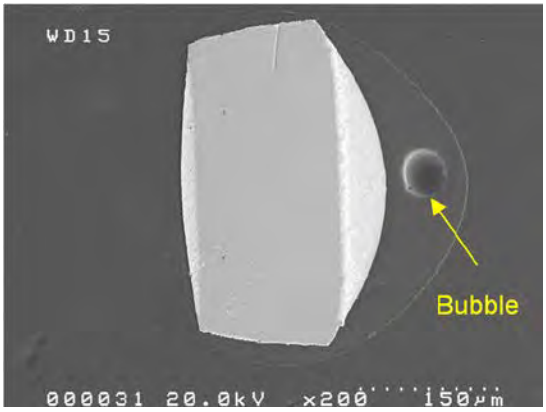


Figure 37: Horizontal cross section, SEM, board 21, PC18M+20%XP2742, QFP44, U1, lead 23, 200x.

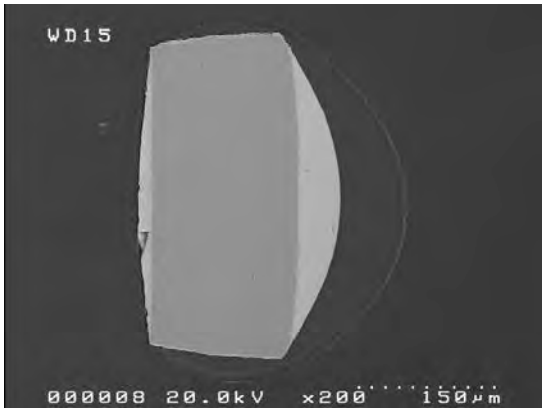


Figure 38: Horizontal cross section, SEM, board 28, PC18M+20%X11102PMA, QFP44, U1, lead 23, 200x.



Figure 39: Horizontal cross section, SEM, board 11, PC18M-mod, QFP44, U1, lead 17, 200x.

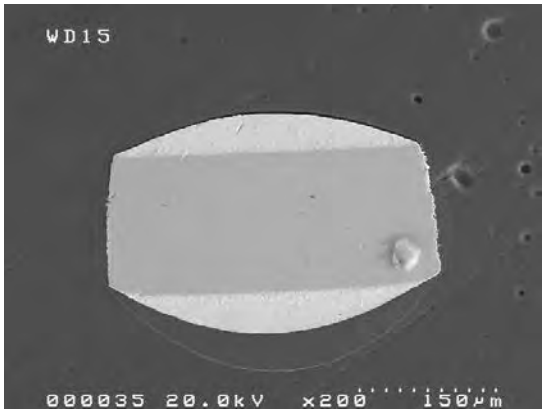


Figure 40: Horizontal cross section, SEM, board 21, PC18M+20%XP2742, QFP44, U1, lead 17, 200x.

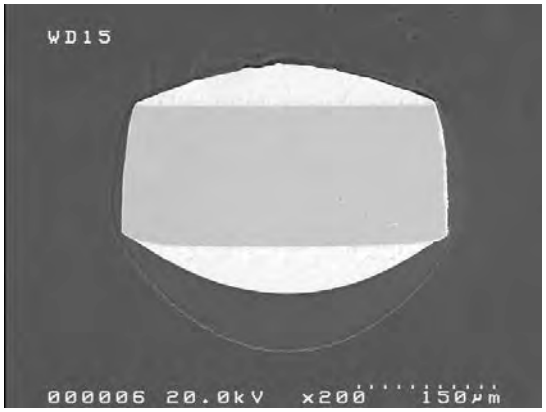


Figure 41: Horizontal cross section, SEM, board 28, PC18M+20%X11102PMA, QFP44, U1, lead 17, 200x.

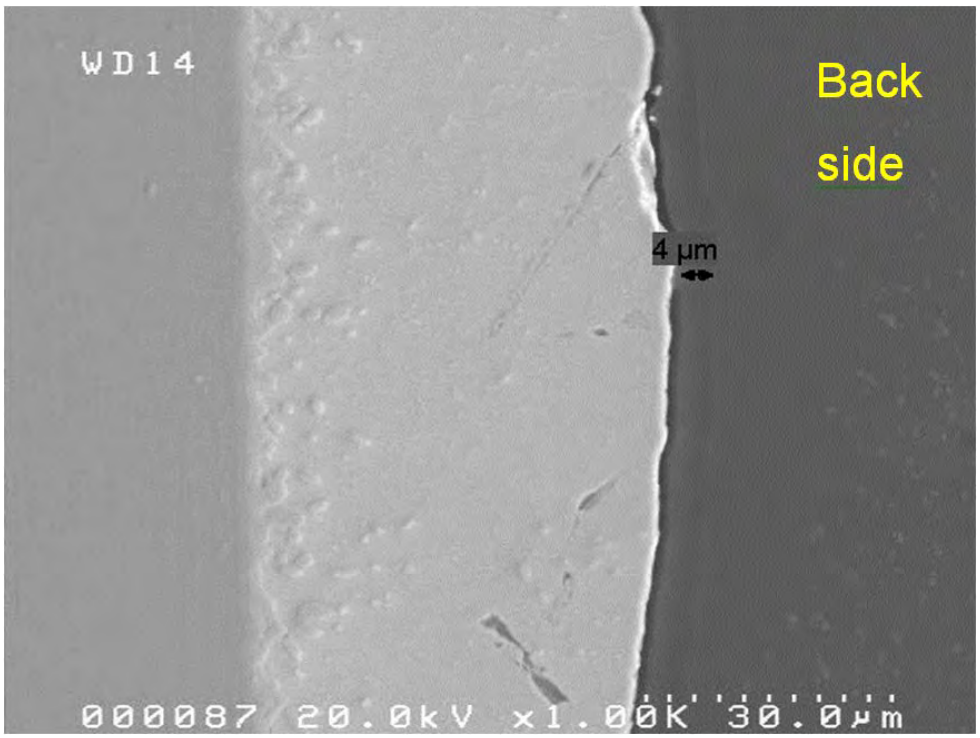


Figure 42: Horizontal cross section, SEM, board 11, PC18M-mod, QFP44, U1, lead 6, 1,000x. Back side coating coverage is four microns.

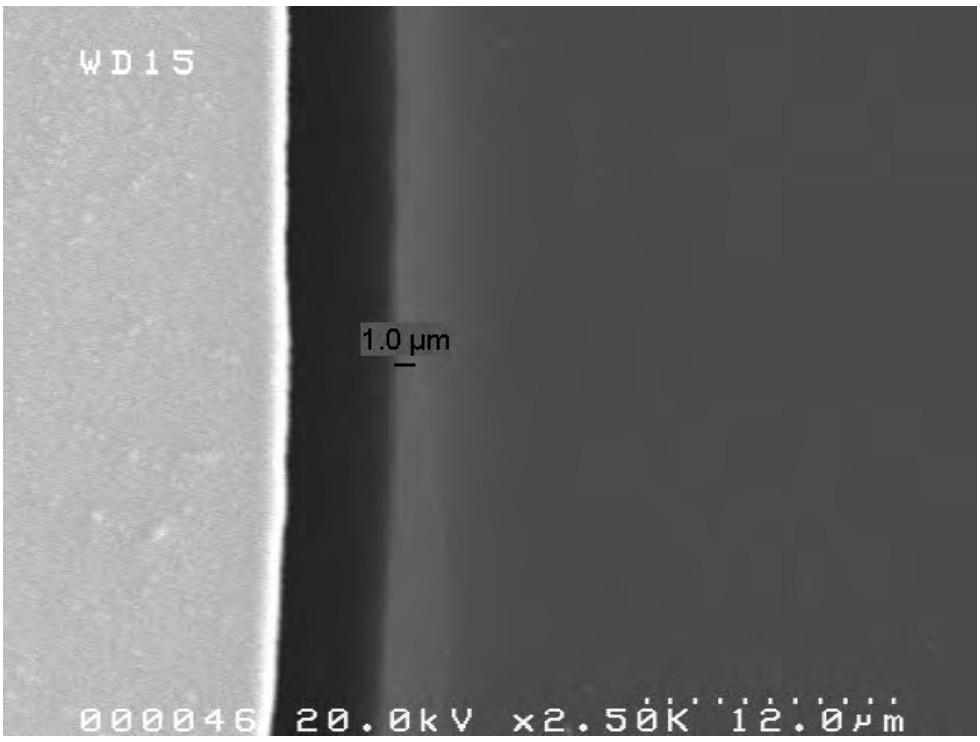


Figure 43: Horizontal cross-section, SEM, board 21, PC18M+20%XP2742, QFP44, U1 lead 6, 1,000x. Back side coating coverage is one micron.

Consistent with the overall SEM inspection from the previous section, the PC18M-mod coating tended to have more cases where the lead corner had no coating (Figure 45), but the nanoparticle filled coatings had better corner coverage (Figure 46 and Figure 47). There may be a trade-off between the ability of the coating to stay on the corners, while at the same time be able to flow onto the back side of the lead.

It was noted that two types of bubbles in the coating were observed in cross-sections; bubbles attached to the solder (Figure 48) and bubbles in the middle of the coating film (Figure 37) (see discussion in 1).

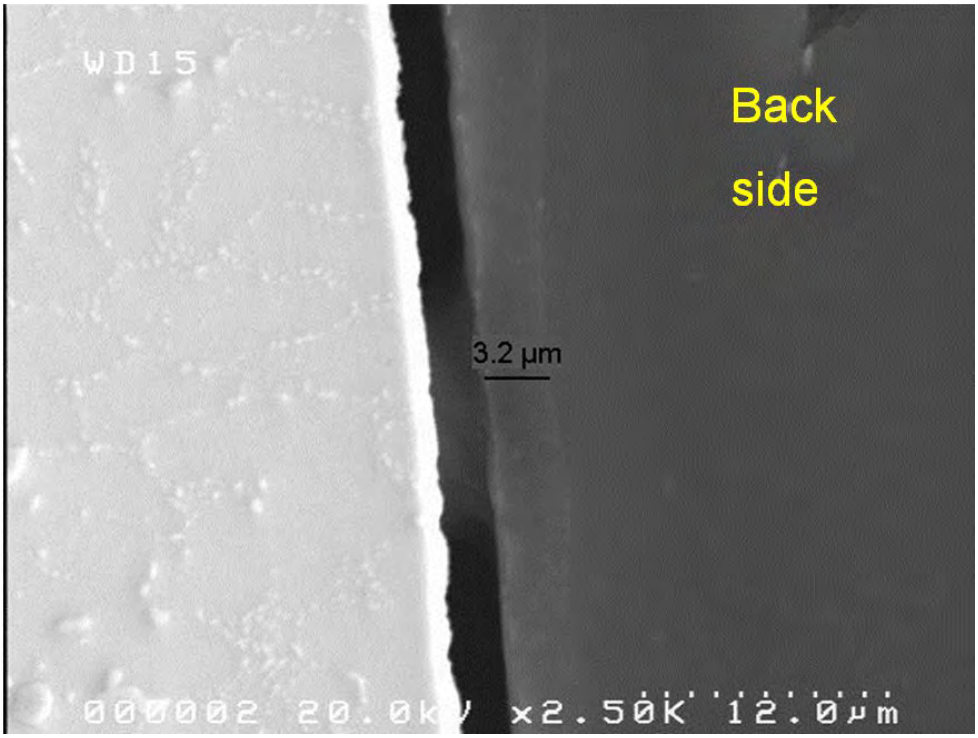


Figure 44: Horizontal cross-section, SEM, board 28, PC18M+20%X11102PMA, QFP44, lead 6, 1,000x. Back side coating coverage is approximately three microns.

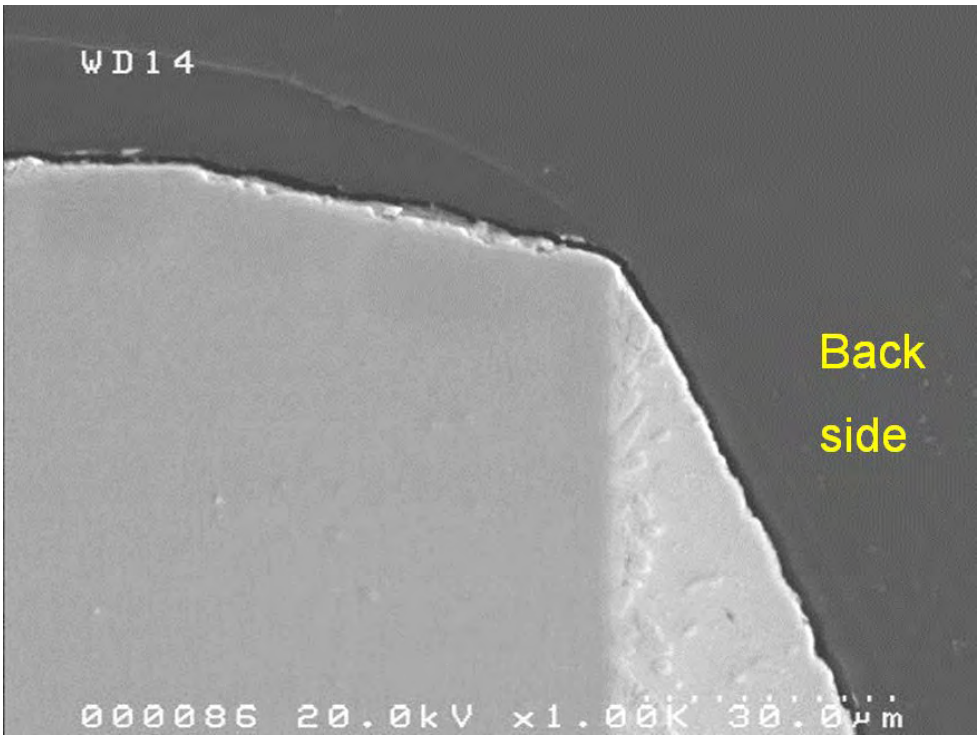


Figure 45: Horizontal cross section, SEM, board 11, PC18M-mod, QFP44, U1, lead 6, 1,000x. No coating on the back corner.

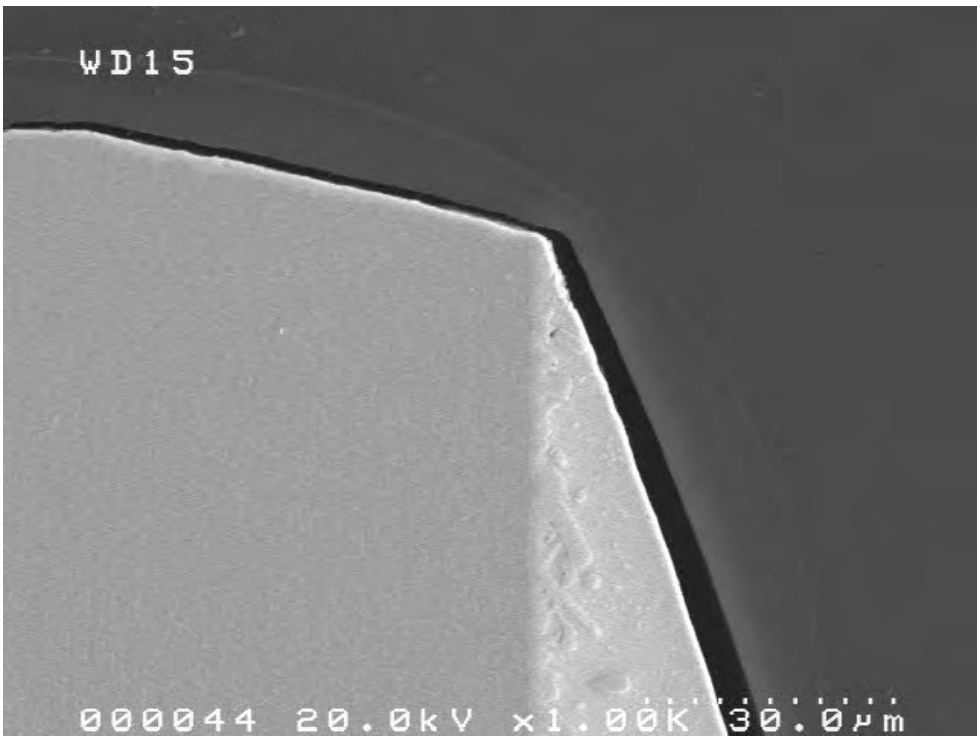


Figure 46: Horizontal cross-section, SEM, board 21, PC18M+20%XP2742, QFP44, U1 lead 6, 1,000x.

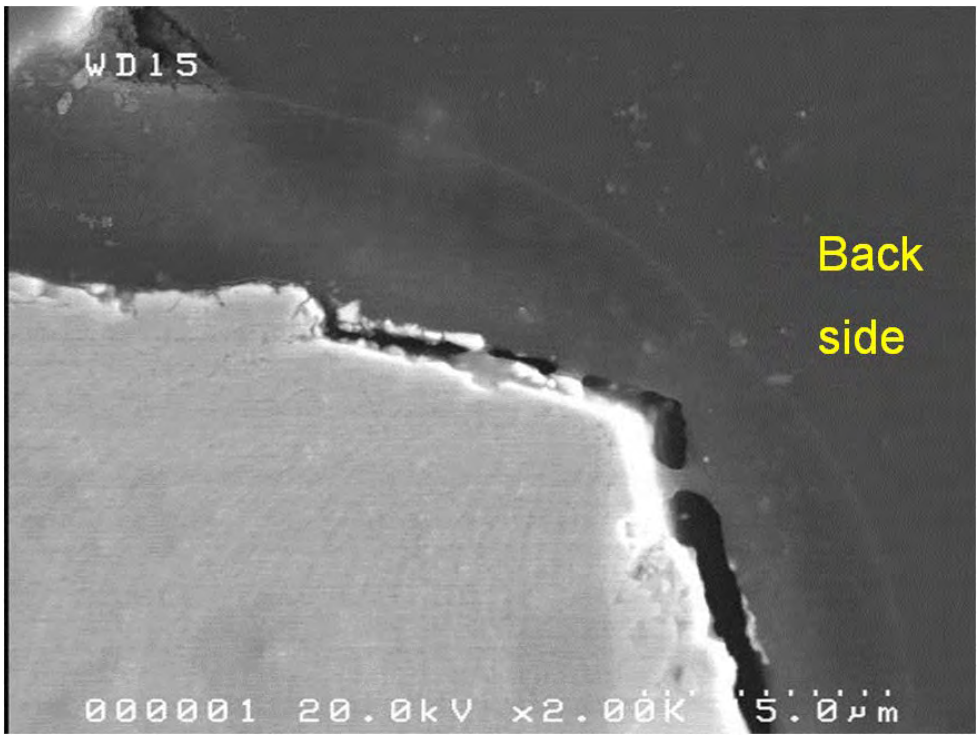


Figure 47: Horizontal cross-section, SEM, board 28, PC18M+20%X1102PMA, QFP44, lead 6, 2,000x.

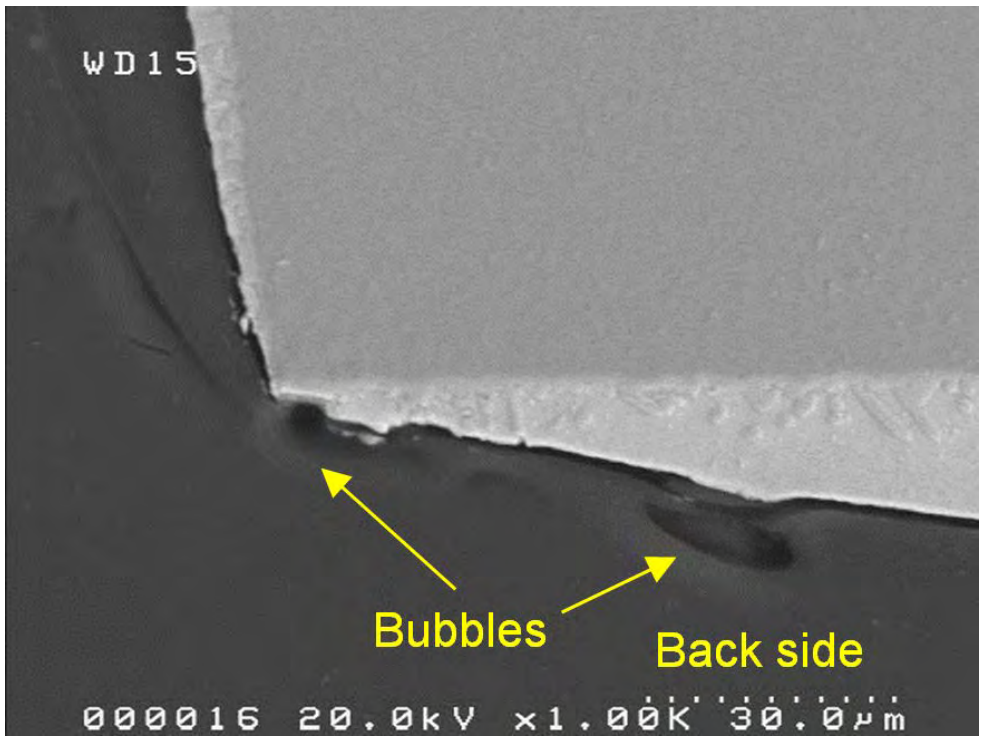


Figure 48: Horizontal cross-section, SEM, board 28, PC18M+20%X1102PMA, QFP44, U1, lead 39, 1,000x.

2. PC40-UMF based coatings

When processing the PC40-UMF based coatings with and without nanosilica filler, interlayer adhesion, wetting and coverage issues were encountered. Four spray batches were processed in an effort to evaluate improvements in interlayer adhesion and coverage. The first two batches used a dip + spray combination coating with and without plasma etching between the dip and spray layers. The second two batches evaluated spray coating (no dip) of unfilled standard viscosity PC40-UMF to high viscosity PC40-UMF. Note that without an initial low viscosity dip, there would not be coating behind the leads.

The following sections give the optical, SEM, vertical cross-section and horizontal cross-section coating evaluations.

In summary, the PC40-UMF coated leads had poor coating coverage (Figure 49) as compared to the PC18M samples (e.g. Figure 18). Even with the addition of plasma etching between the dip and the spray layer, there was little or no additional thickness provided by the PC40-UMF based coating spray coating layer if the leads. The coating thickness varied considerably as is summarized in Table 4.

Table 4: Batch A and B assembly coating thickness observations of PC40-UMF, PC40-UMF+NNN2835 and PC40-UMF+N3300 from cross-sectioning.

Coating	Front of lead thickness	Continuous corner coverage	
		Vertical section	Horizontal section
PC40-UMF low viscosity dip	breaks in coverage	minimal	Little or none except if coating bridging occurred.
PC40-UMF batch A (no plasma etch between dip coat and spray coat)	breaks in coverage, consistently very thin	minimal	
Plasma etch implemented between dip coat and spray coat			
PC40-UMF batch B	very thin to 7.7µm	N/A	
PC40-UMF+10% NNN2835	very thin (not measureable) to 7.7µm	thin top layer (not complete coverage of bottom layer)	
PC40-UMF+30% NNN2835	breaks in coverage	very thin, bottom layer only	
PC40-UMF+50% NNN2835	complete coverage, 1.4 to 15µm	minimal	
PC40-UMF+15.54%N3300	complete coverage, 0.55 to 1.8µm	little or none	

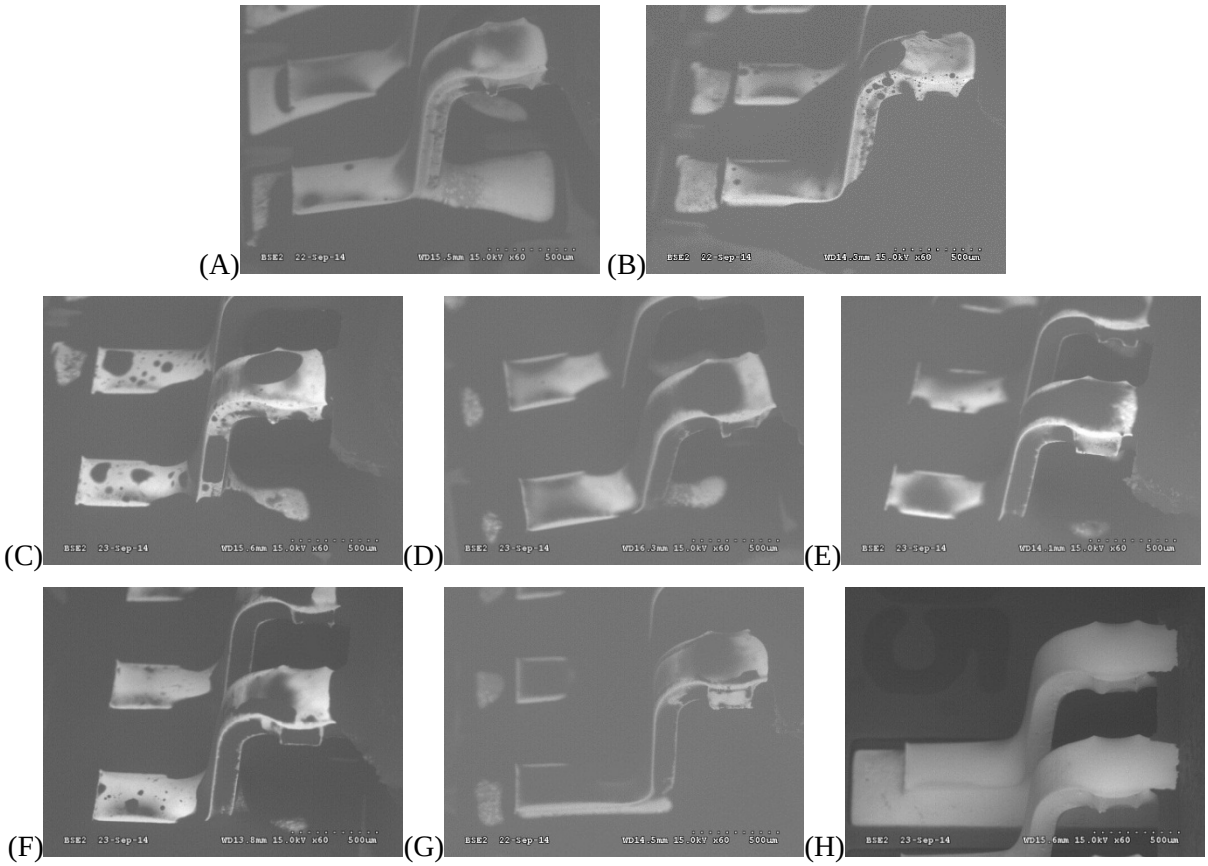


Figure 49: Batch A and B QFP44 SEM images of PC40-UMF coating based coating; (A) PC40-UMF dip coat, (B), PC40-UMF (no plasma between dip and spray), and the following spray coated samples with plasma etch between the dip and the spray layers: (C) PC40-UMF batch 2 with plasma, (D) PC40-UMF+10%NNN2835(nanosilica), (E) PC40-UMF+30%NNN2835(nanosilica), (F) PC40-UMF+50%NNN235(nanosilica), and (G) PC40-UMF+15.54%N3300. Image (H) shows an uncoated control board.

2.1 PC40-UMF Batch A and B (dip+spray)

The first two batches (A and B) used a dip coat of solvent thinned low viscosity PC40-UMF followed by a spray coat of PC-40-UMF or PC-40UMF+ (10%, 30% or 50%) NNN2835 (nanosilica) (Note the NNN285 is equivalent to XP2742).

Prior to dip coating, the bare assemblies were cleaned using standard in-line cleaning and plasma etched.

2.1.1 Optical inspection of batch A and B (dip+spray) PC40-UMF + NNN2835 (nanosilica)

The initial dip coat exhibited good wetting (Figure 50). The first batch of PC40-UMF coated assemblies (Batch A) revealed significant de-wetting of the spray coat layer from the initial dip coat layer, particularly on the top of the packages. A second batch was coated (Batch B) with a plasma etch between the dip and spray, which made an improvement to the spray coating wetting to the package (Figure 51). However, as will be shown in the SEM inspection section (see 2.1.2), the plasma etch between the dip and spray coatings only slightly improved coverage on the leads.

The nanosilica filled versions of the coating with the plasma etch tended to also exhibited better wetting on the package bodies (Figure 52).

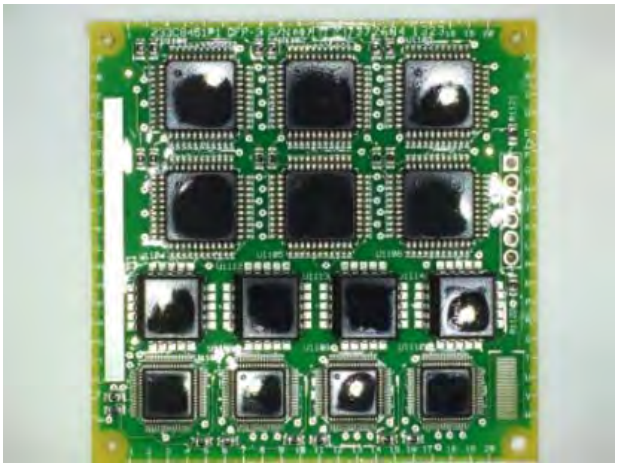


Figure 50: Optical image of QFP assembly after low viscosity PC40-UMF dip coating.

(A) (B) (C)

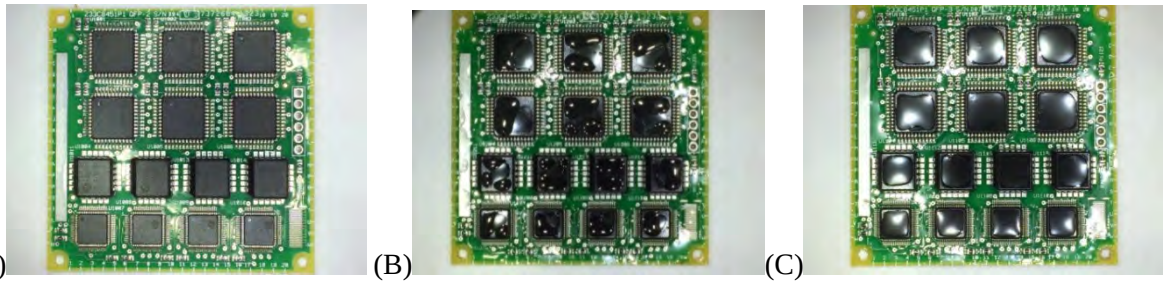
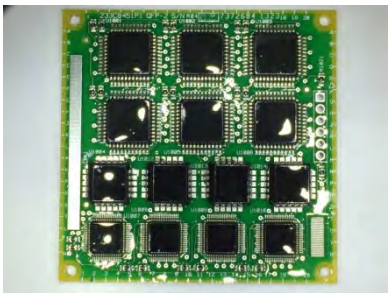


Figure 51: Optical images of QFP boards after PC40-UMF coating; (A) no coating control, (B) batch A (no plasma between dip and spray coating), (C) batch two (plasma etch between dip and spray coating).

(A)  (B) 

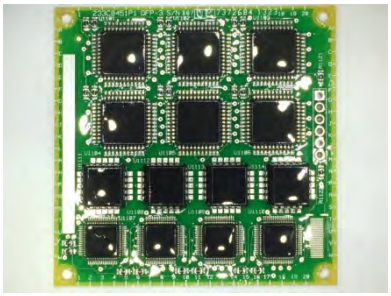
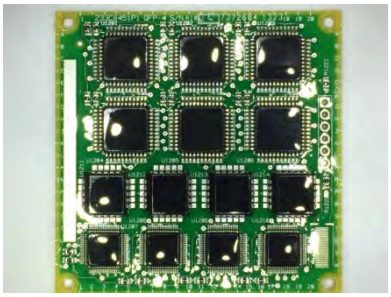
(C)  (D) 

Figure 52: Optical images of batch 2 dip with (A) PC40-UMF+10%NNN2835(nanosilica) spray, (B) PC40-UMF+30%NNN2835(nanosilica) spray, (C) PC40-UMF+ 50%NNN2835(nanosilica) spray, and (D) PC40-UMF+15.54%N3300 spray.

2.1.2 SEM inspection of Batch A and B (dip+spray) PC40-UMF + NNN2835(nanosilica)

Detailed images of for the QFP44, QFP64 and the Plastic Leaded Chip Carrier Electronic Package (PLCC) after dipping are shown in Figure 53 to Figure 59. Coating fill around and between the leads on these samples was unexpectedly high, especially for the thinner QFP64. This was due to the coating viscosity increase toward the end of the dip processing run as an increasing amount of solvent was dragged out. The images of the dip+spray with and without plasma are shown in Figure 60 to Figure 67. The plasma etching between the dip and the spray did not significantly improve coverage of the PC40-UMF on the leads.

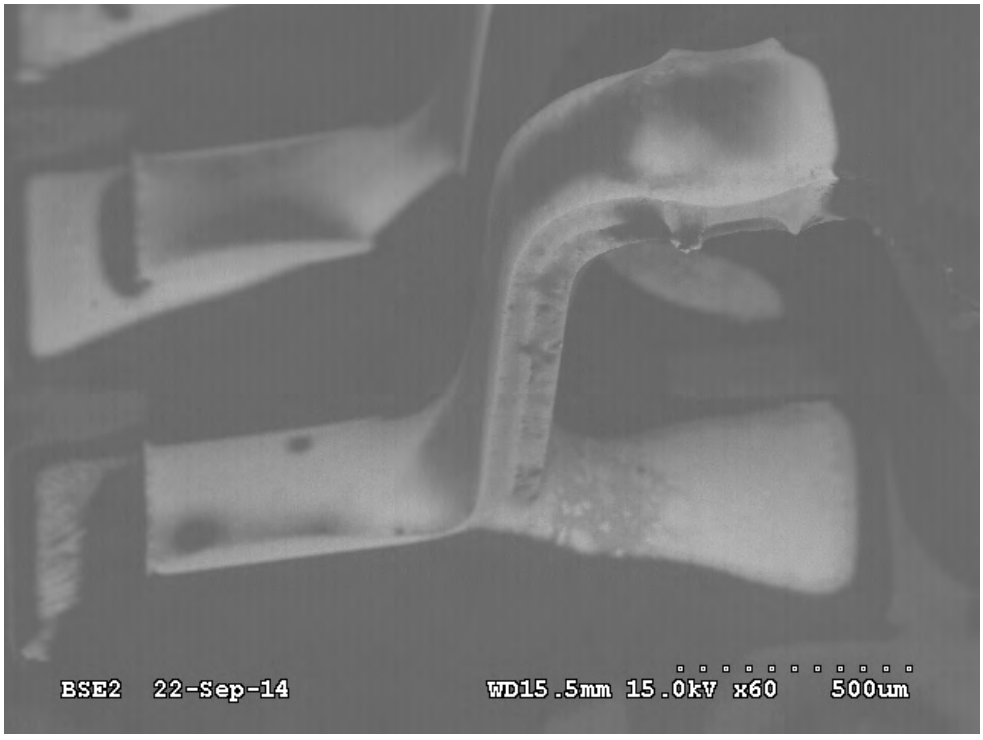


Figure 53: SEM image of PC40-UMF dip only QFP44 leads, 60x (ref. Board 87, Batch B).



Figure 54: SEM image of a PC40-UMF dip-only coated QFP44 lead tip, 100x (ref. Board 87, Batch B).



Figure 55: SEM image of PC40-UMF dip-only coated QFP44 leads, top view, 45x (ref. Board 87, Batch B).

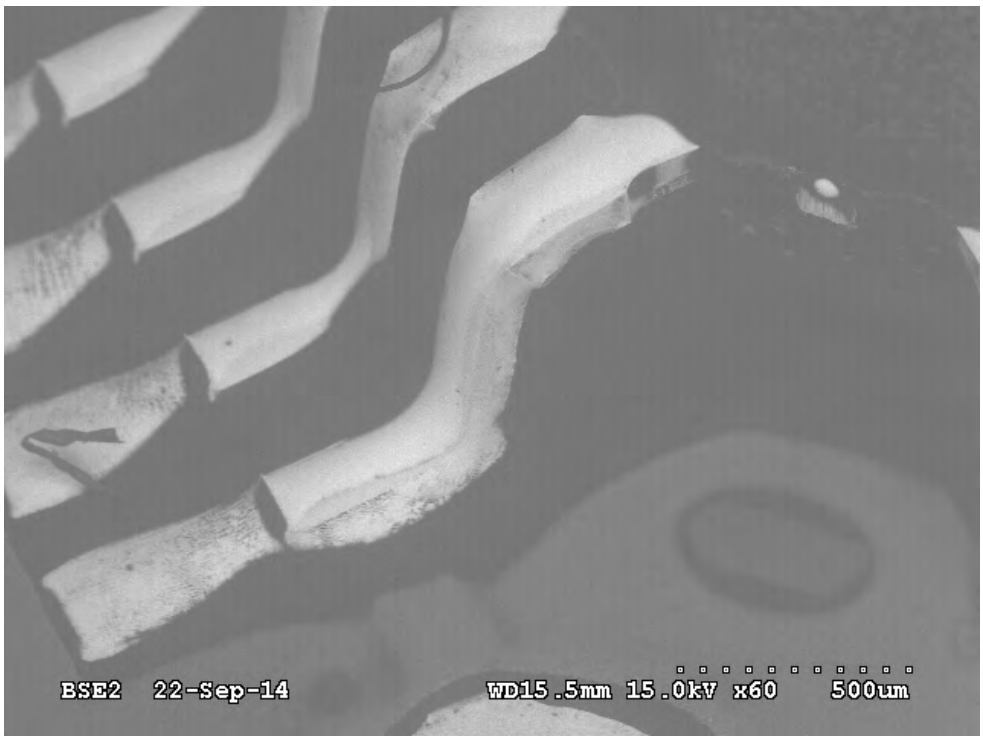


Figure 56: SEM image of PC40-UMF dip-only coated QFP64 leads, 60x (ref. Board 87, Batch B).

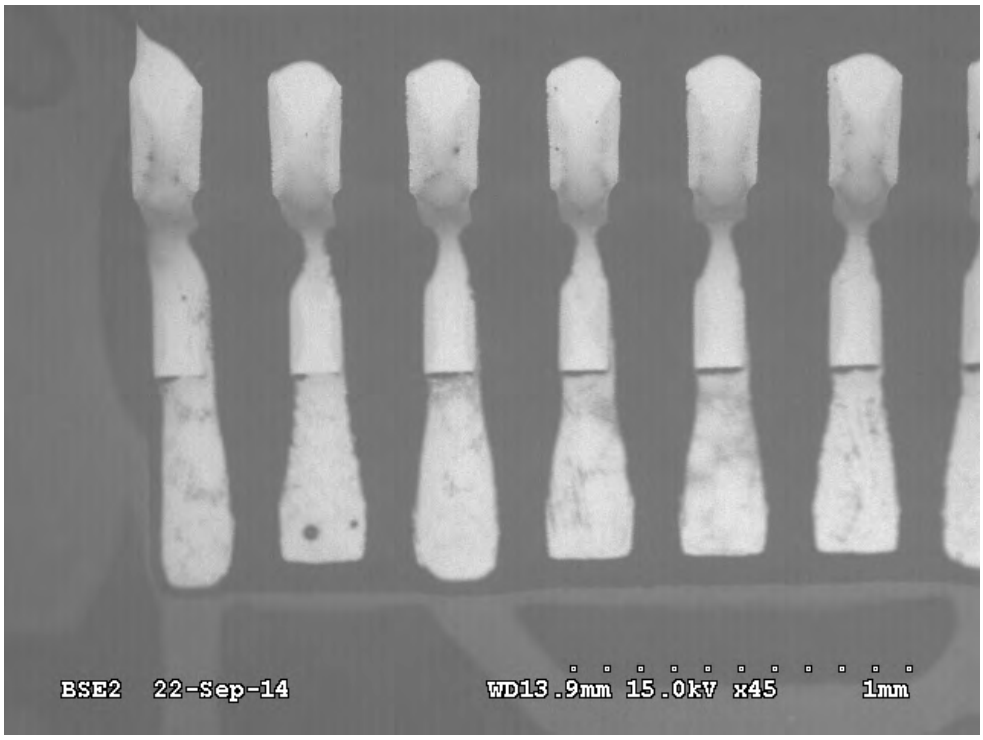


Figure 57: SEM image of PC40-UMF dip-only coated QFP64 leads, top view, 45x (ref. Board 87, Batch B).



Figure 58: SEM image of PC40-UMF dip-only coated PLCC leads, front view, 30x (ref. Board 87, Batch B).



Figure 59: SEM image of PC40-UMF dip-only coated PLCC leads, side view, 40x (ref. Board 87, Batch B).



Figure 60: Batch A SEM image of PC40-UMF dip+spray coated QFP44 leads, 60x (ref. Board 57).



Figure 61: Batch A SEM image of PC40-UMF dip+spray coated QFP64 leads, 60x (ref. Board 57).



Figure 62: Batch A SEM image of PC40-UMF dip+spray coated PLCC leads, side view, 40x (ref. Board 57).

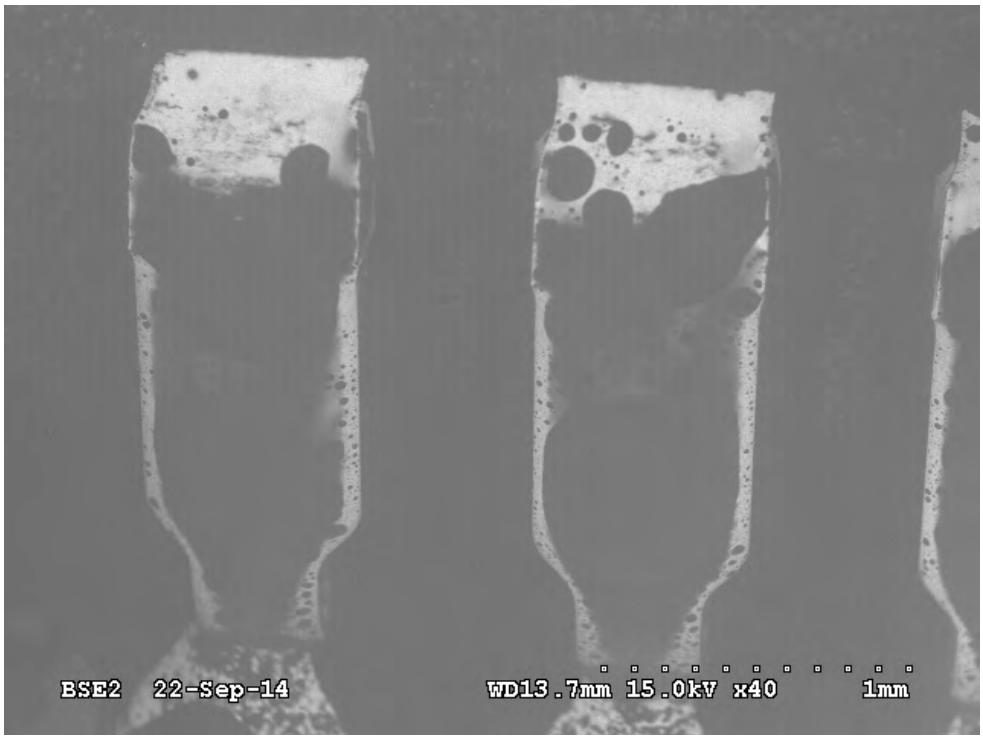


Figure 63: Batch A SEM image of PC40-UMF dip+spray coated PLCC leads, front view, 40x (ref. Board 57).

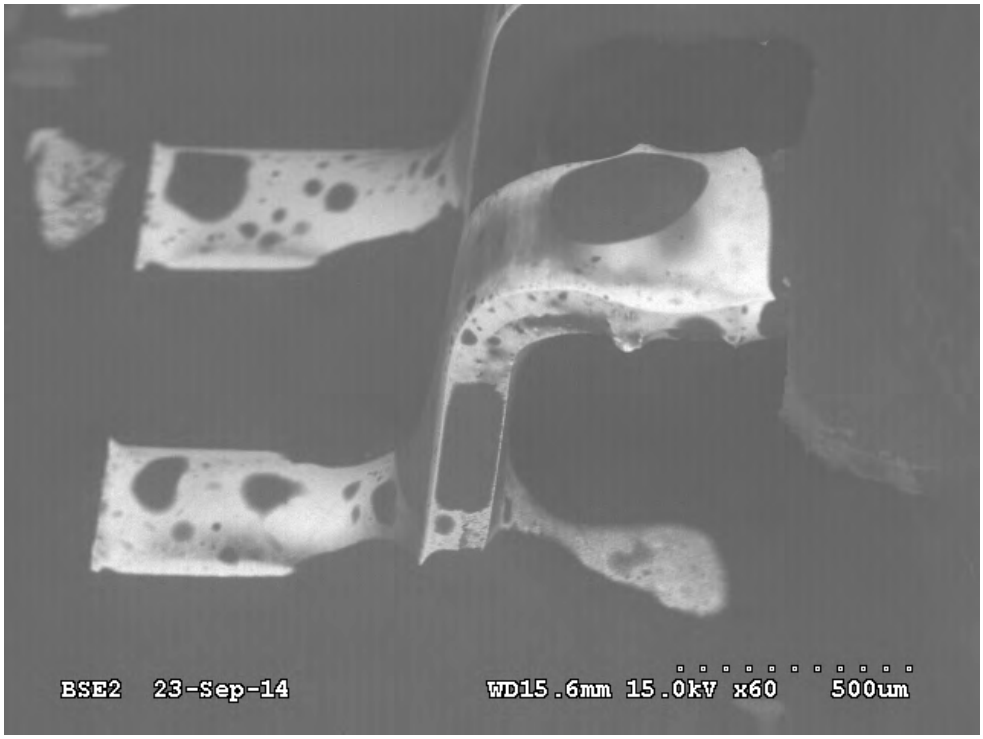


Figure 64: Batch B SEM image of PC40-UMF dip+plasma+spray coated QFP44 leads, 60x (ref. Board 66).



Figure 65: Batch B SEM image of PC40-UMF dip+plasma+spray coated QFP64 leads, 60x (ref. Board 66).

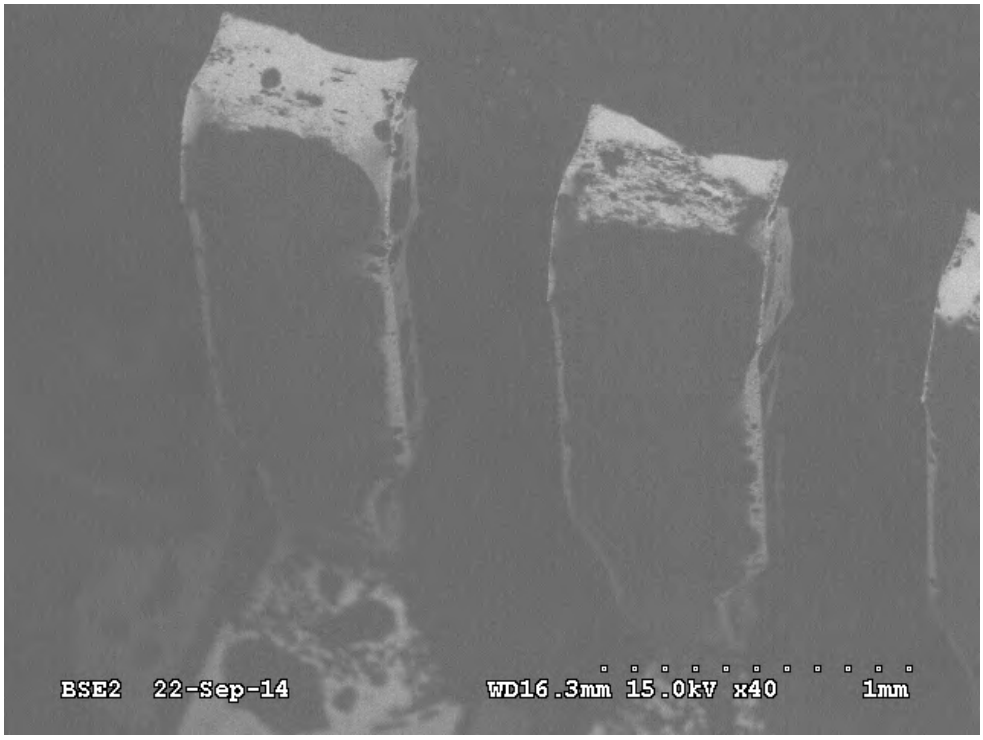


Figure 66: Batch B SEM image of PC40-UMF dip+plasma+spray coated PLCC leads, front view, 40x (ref. Board 66).



Figure 67: Batch B SEM image of PC40-UMF dip+plasma+spray coated PLCC leads, side view, 40x (ref. Board 66).

2.1.3 PC40-UMF Batch A PC40-UMF vertical cross-section thickness evaluation

The batch A cross-sections for the PC40-UMF "dip only" coated QFP44 are given in Figure 68 to Figure 82. The dip coating thickness ranged from no-detectable coating to less than two microns. The batch A cross-sections for the PC40-UMF dip+spray (no plasma etch between layers) coated QFP44 are given in Figure 83 to Figure 100.

2.1.3.1 PC40-UMF Batch A PC40-UMF dip only

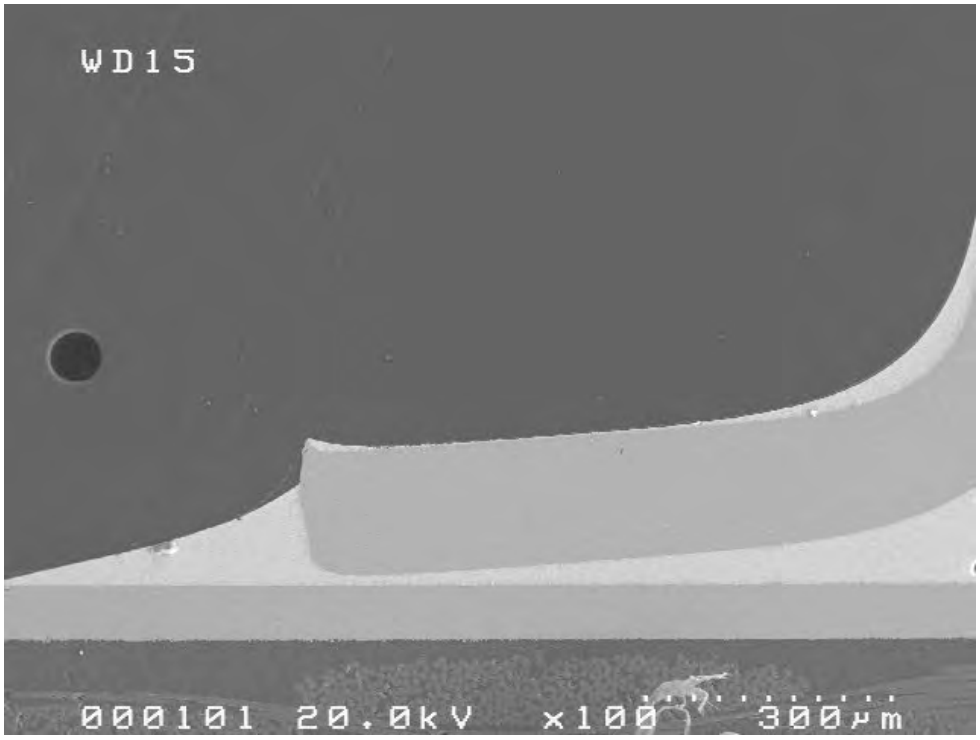


Figure 68: Batch A SEM cross-section image of PC40-UMF dip only coated QFP44, toe region, 100x (ref. Board 87).

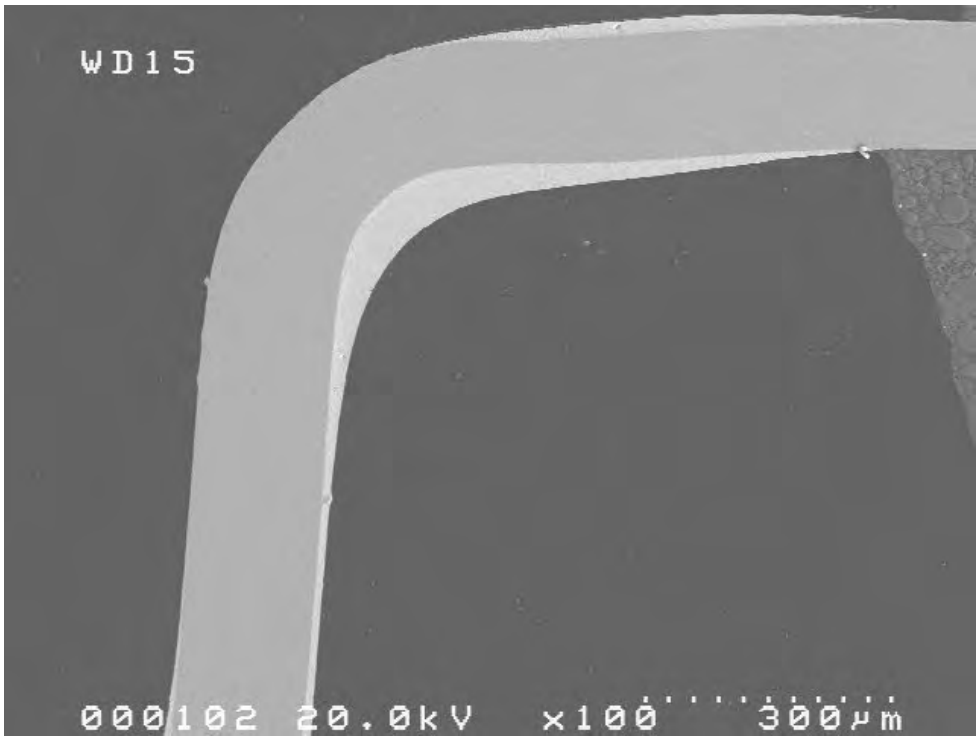


Figure 69: Batch A SEM cross-section image of PC40-UMF dip only coated QFP44, middle of lead region, 100x (ref. board 87).

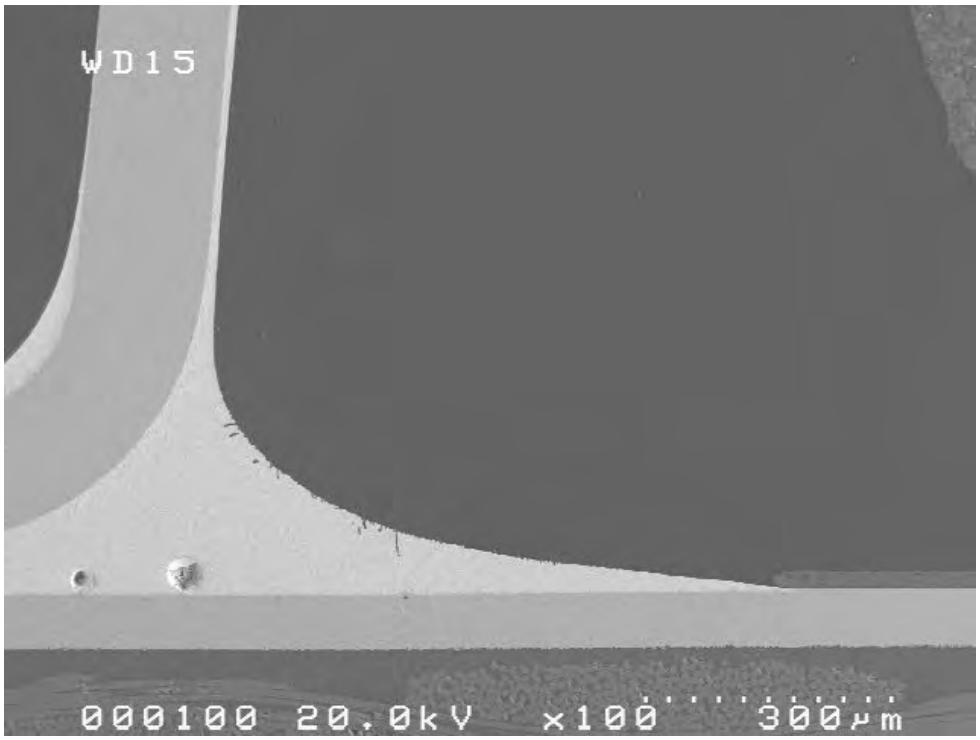


Figure 70: Batch A SEM cross-section image of PC40-UMF dip only coated QFP44, heel region, 100x (ref. Board 87)

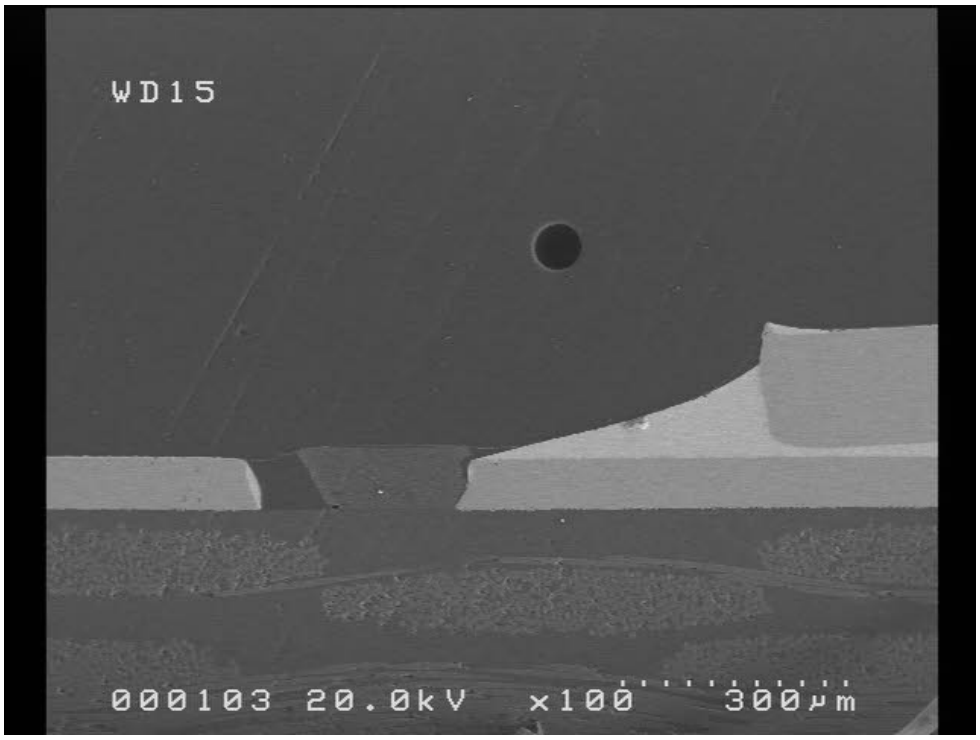


Figure 71: Batch A SEM cross-section image of PC40-UMF dip only coated QFP44, toe region, 100x (ref. board 87).

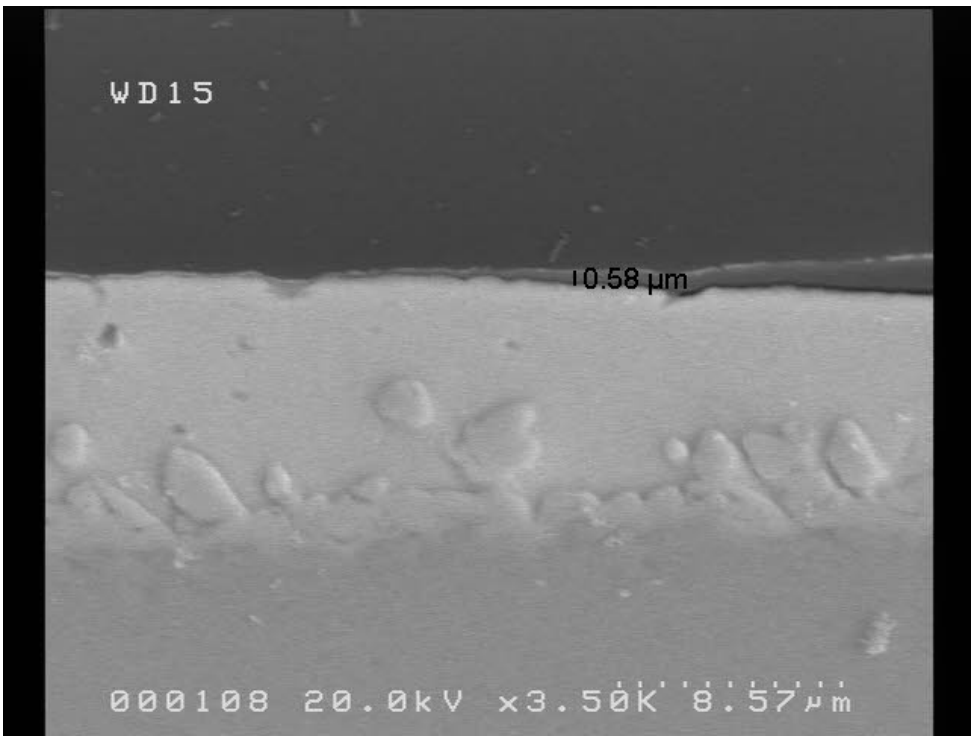


Figure 72: Batch A SEM cross-section image of PC40-UMF dip only coated QFP44, location A, 3,500x (ref. 87).

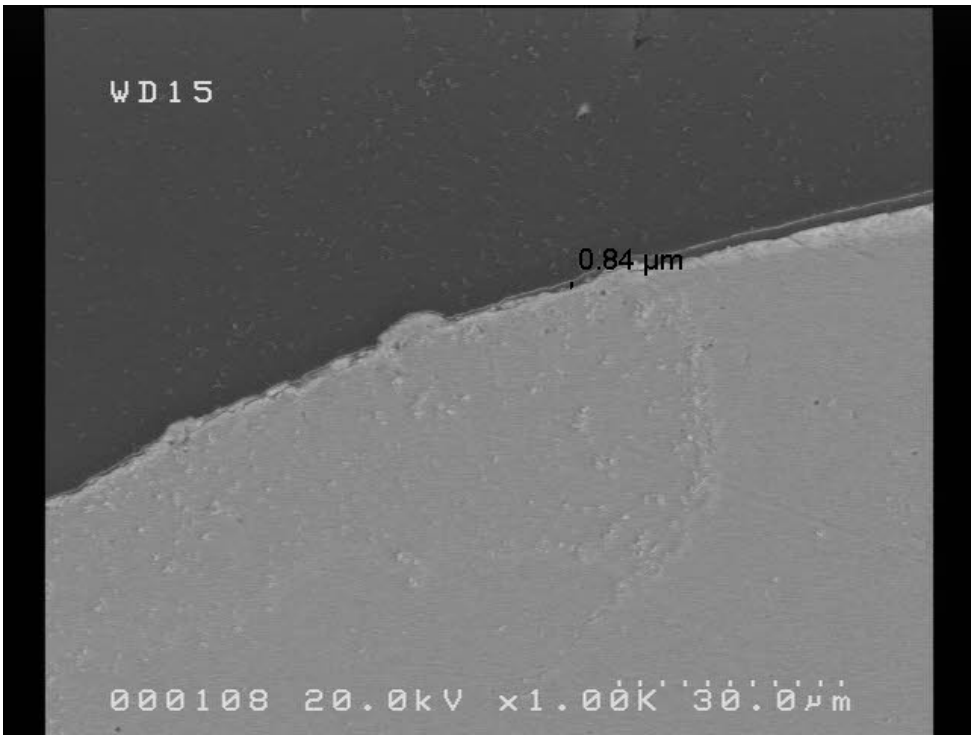


Figure 73: Batch A SEM cross-section image of PC40-UMF dip only coated QFP44, location B, 1,000x (ref. Board 87).

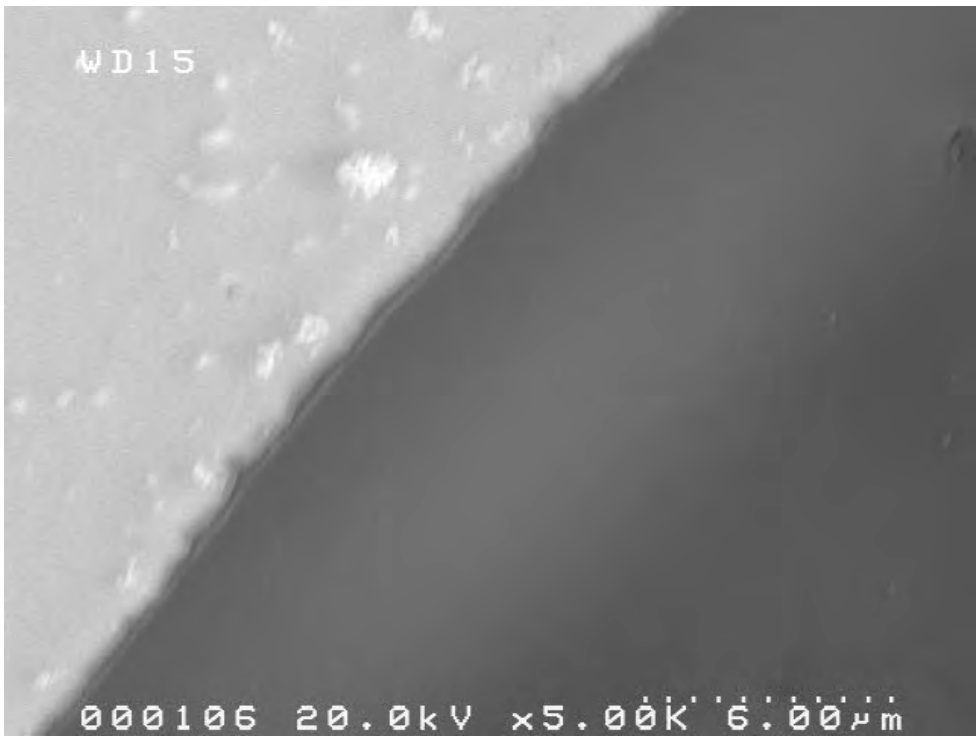


Figure 74: Batch A SEM cross-section image of PC40-UMF dip only coated QFP44, behind knee, 5,000x (ref. Board 87).

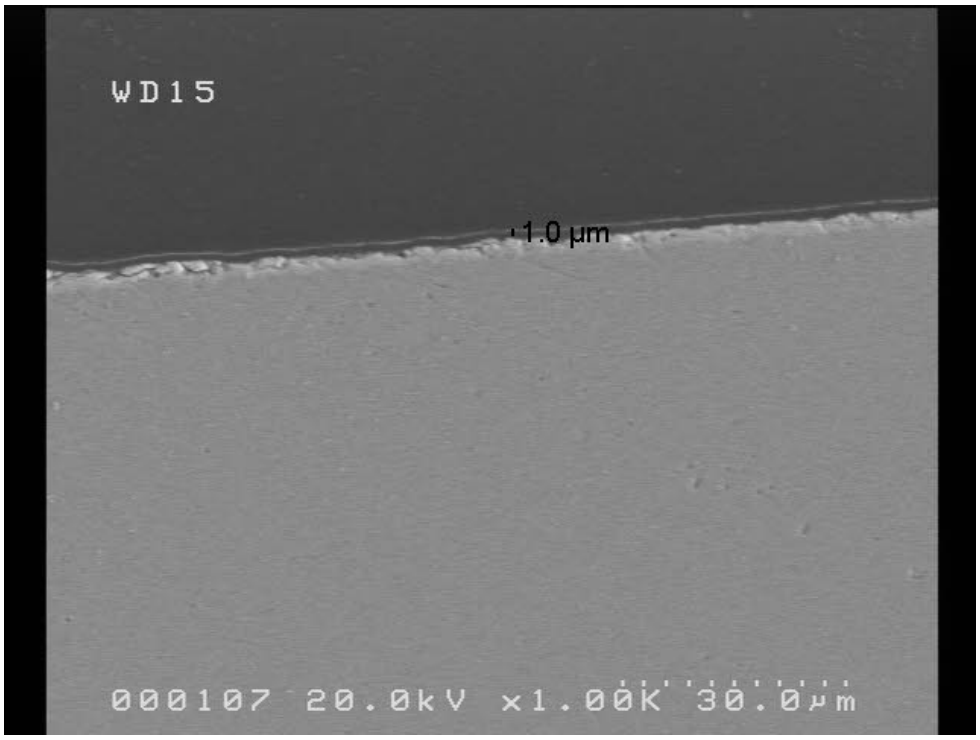


Figure 75: Batch A SEM cross-section image of PC40-UMF dip only coated QFP44, location between F and T location, 2500x (ref. Board 87).

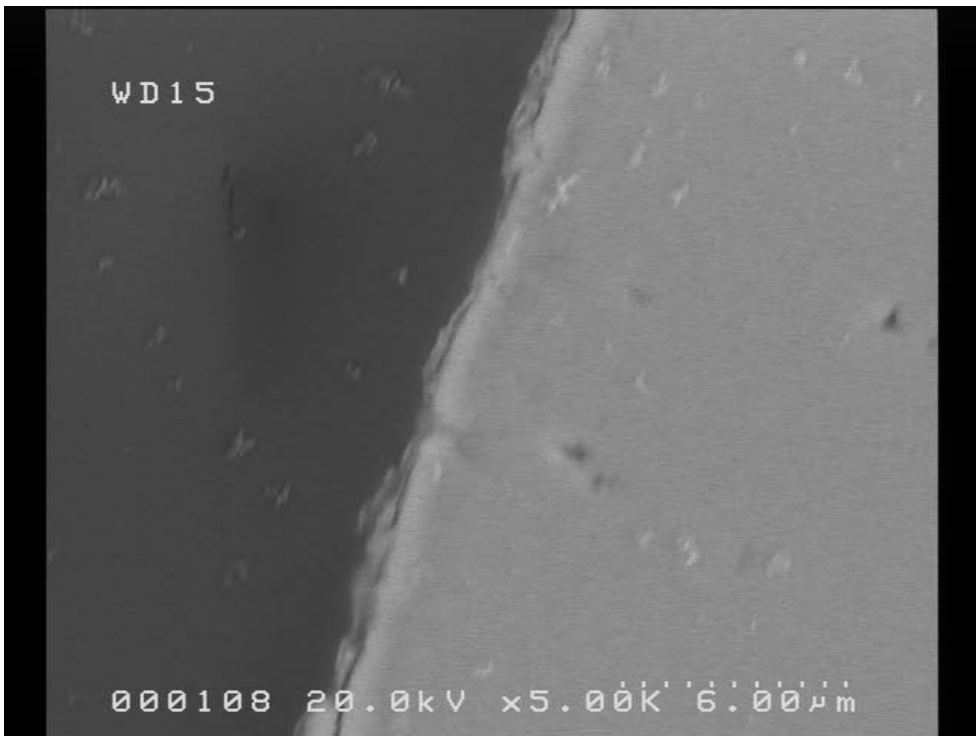


Figure 76: Batch A SEM cross-section image of PC40-UMF dip only coated QFP44, location C, 5,000x (ref. Board 87).

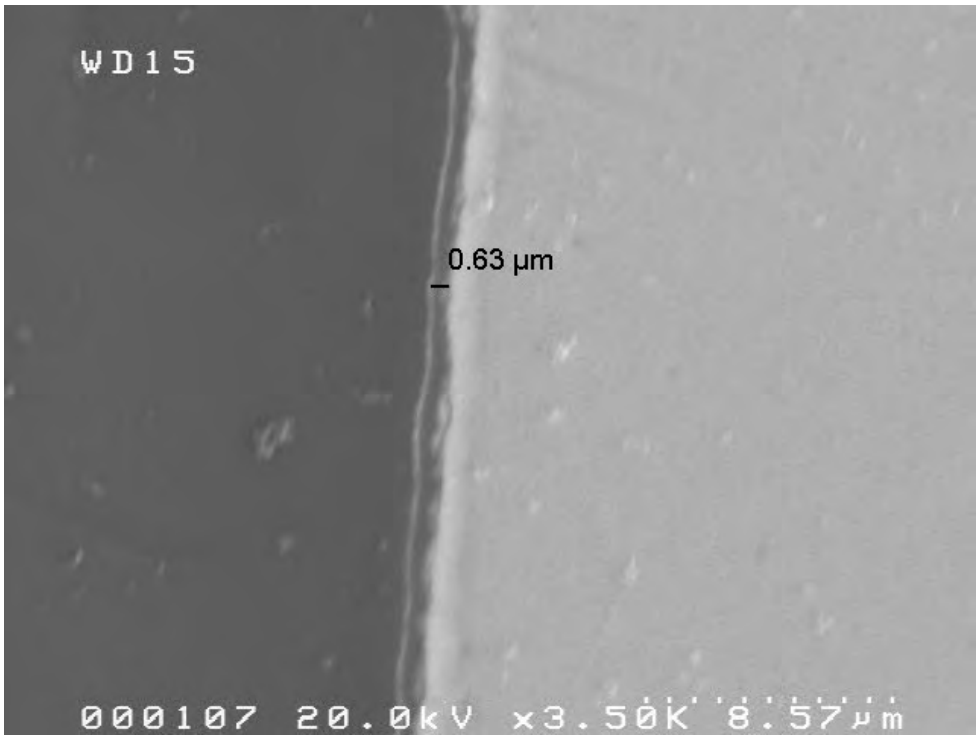


Figure 77: Batch A SEM cross-section image of PC40-UMF dip only coated QFP44, location D, 3,500x (ref. Board 87).

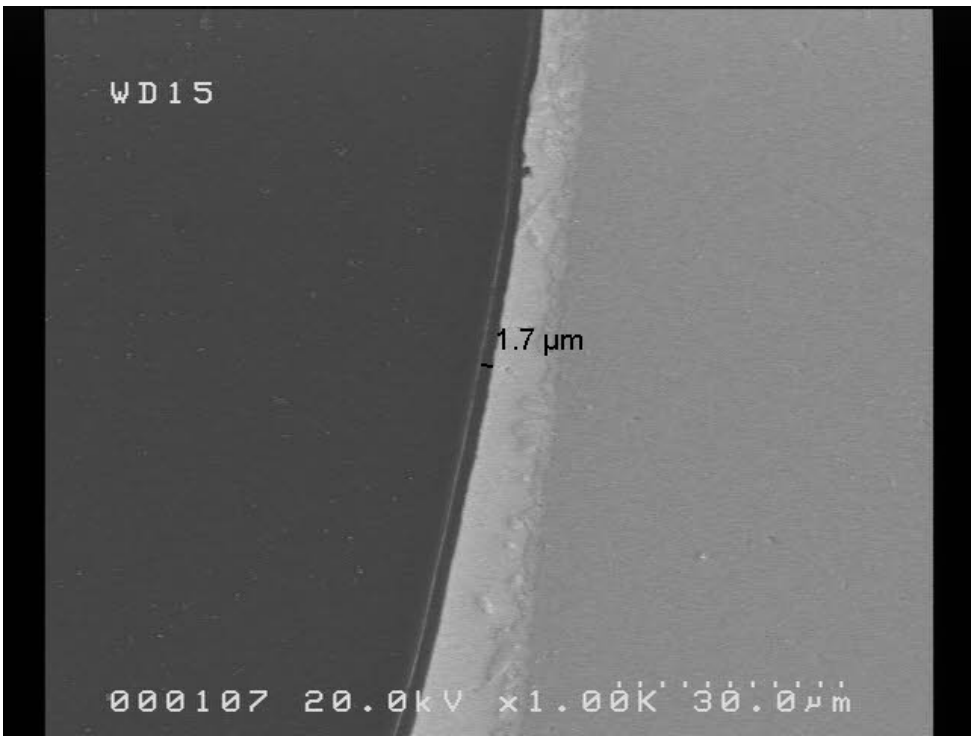


Figure 78: Batch A SEM cross-section image of PC40-UMF dip only coated QFP44, location E, 1000x (ref. Board 87).

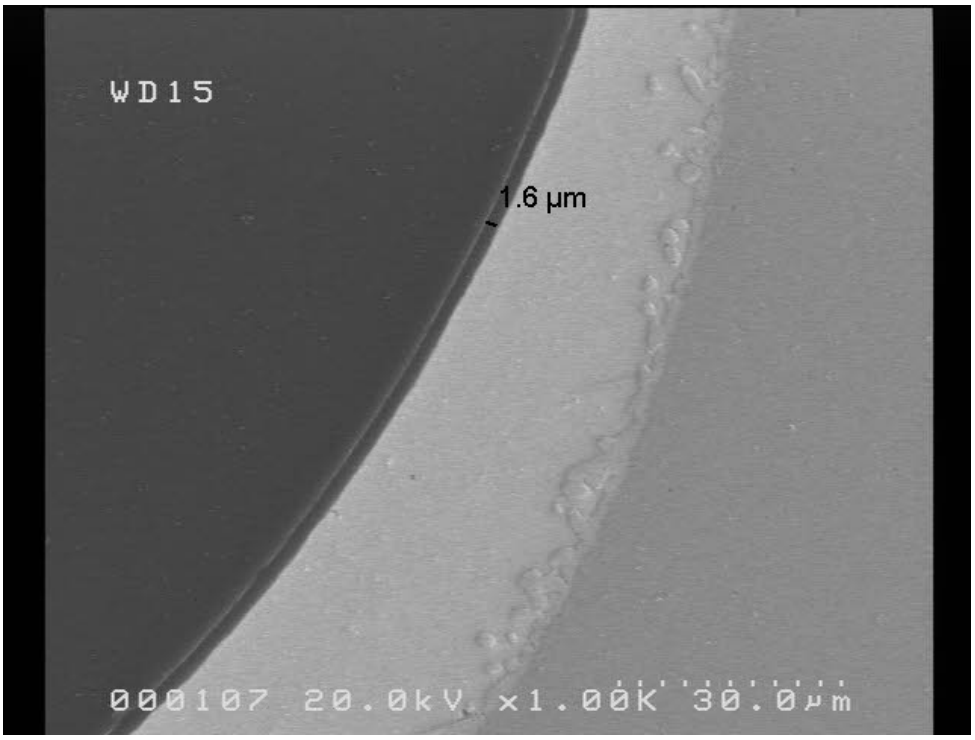


Figure 79: Batch A SEM cross-section image of PC40-UMF dip only coated QFP44, location F, 1000x (ref. Board 87).

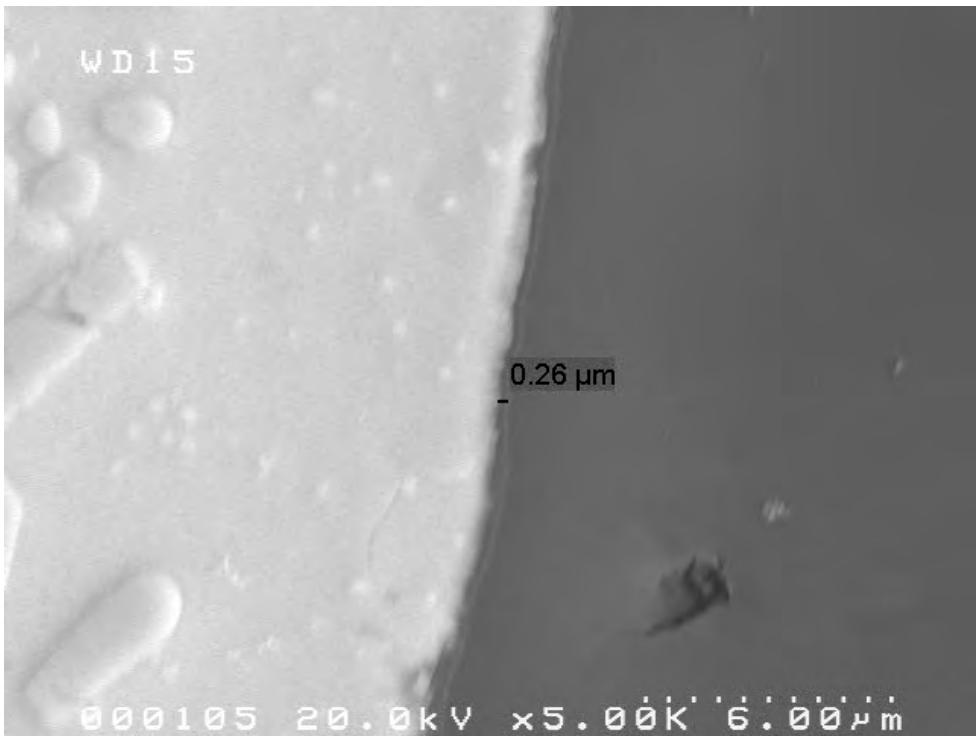


Figure 80: Batch A SEM cross-section image of PC40-UMF dip only coated QFP44, location G, 5000x (ref. Board 87).

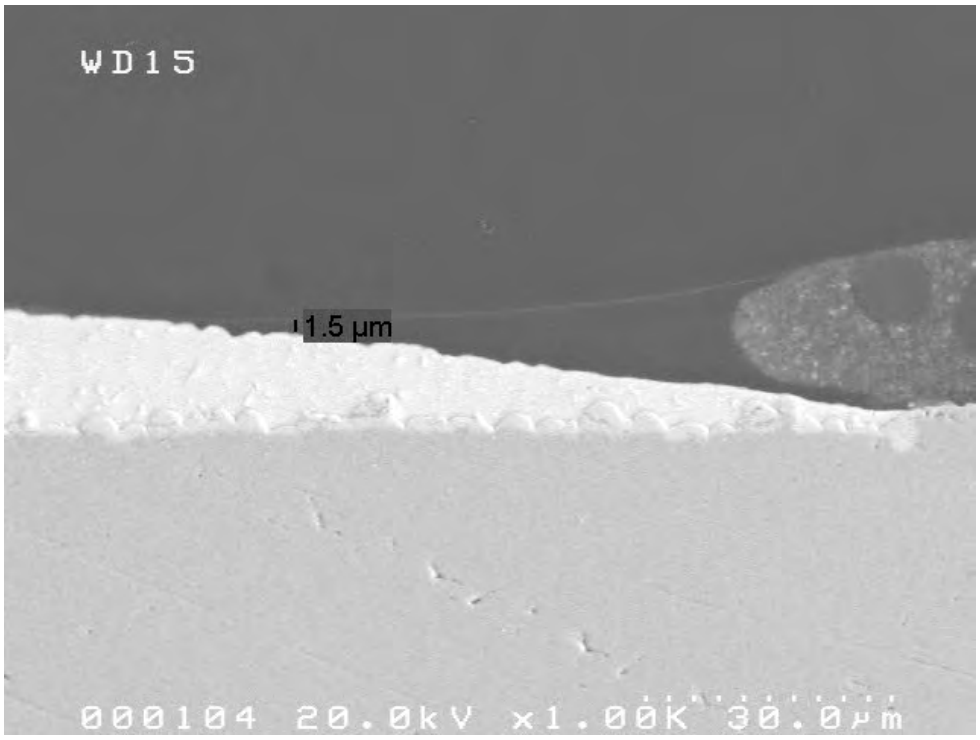


Figure 81: Batch A SEM cross-section image of PC40-UMF dip only coated QFP44, location H, 1000x (ref. Board 87).

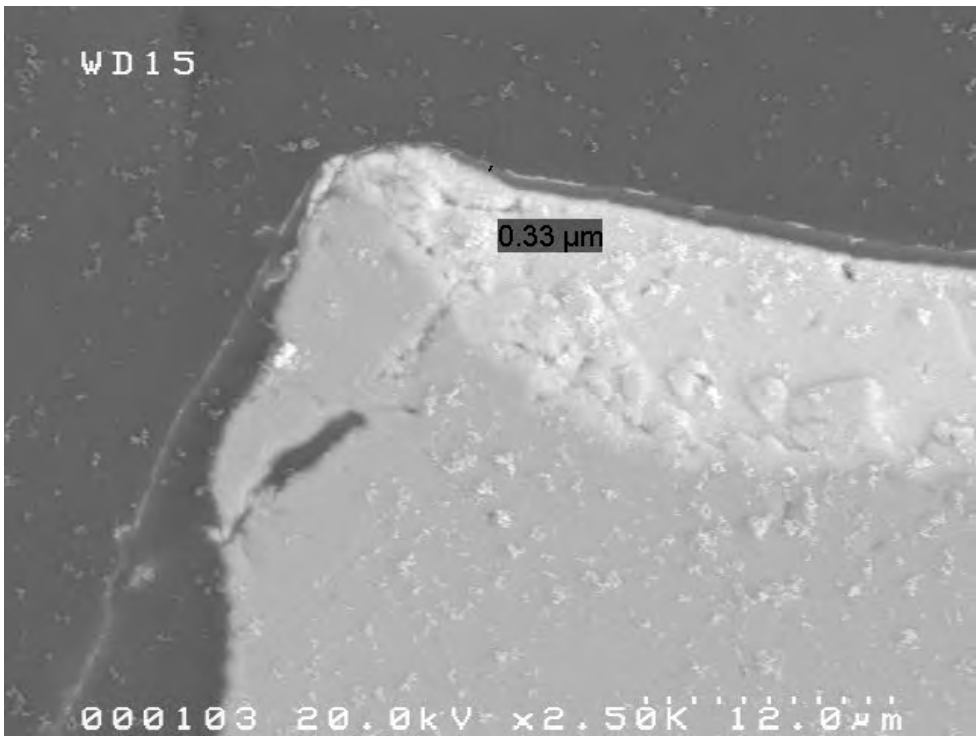


Figure 82: Batch A SEM cross-section image of PC40-UMF dip only coated QFP44, location T, 2500x (ref. Board 87).

2.1.3.2 PC40-UMF Batch A PC40-UMF dip + spray

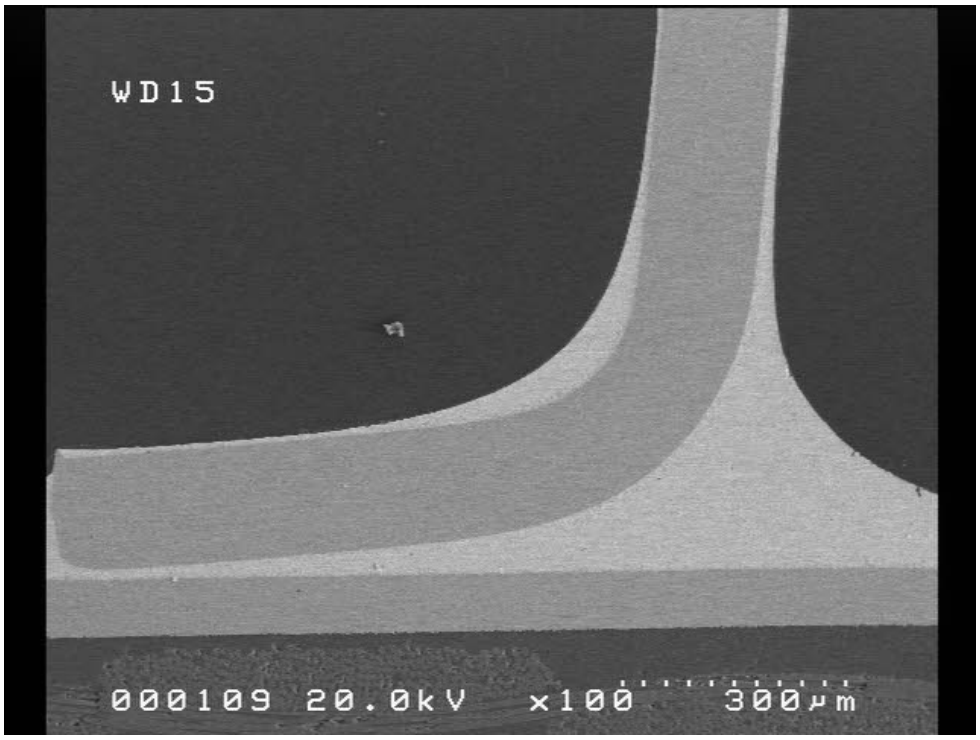


Figure 83: Batch A SEM cross-section image of PC40-UMF dip + spray coated QFP44, foot location, 100x (ref. Board 57).

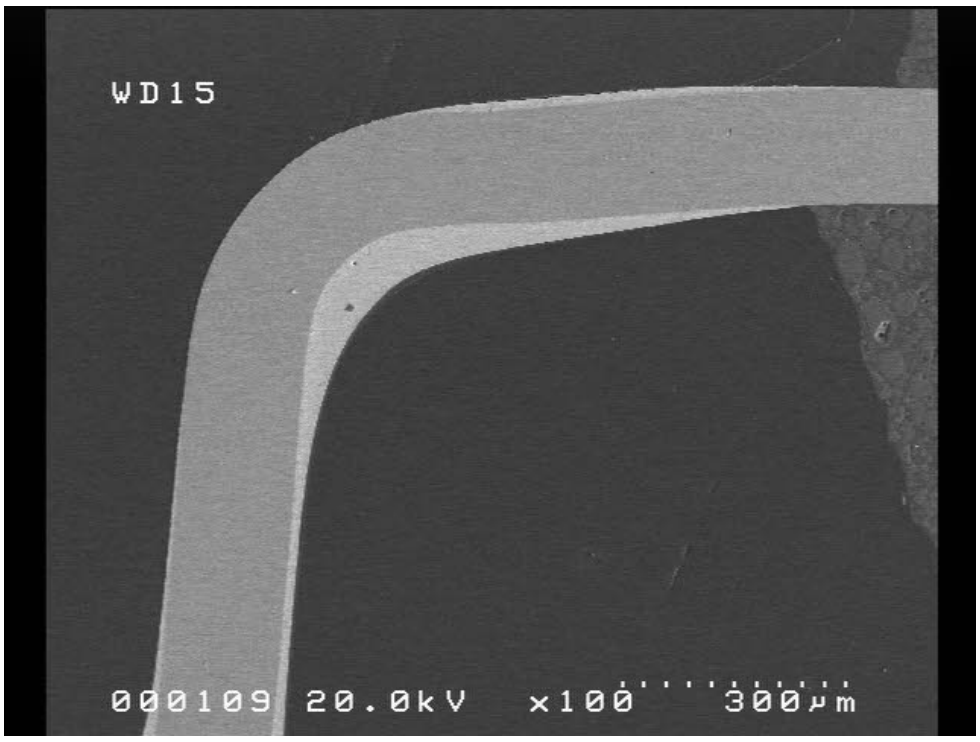


Figure 84: Batch A SEM cross-section image of PC40-UMF dip + spray coated QFP44, knee location, 100x (ref. Board 57).

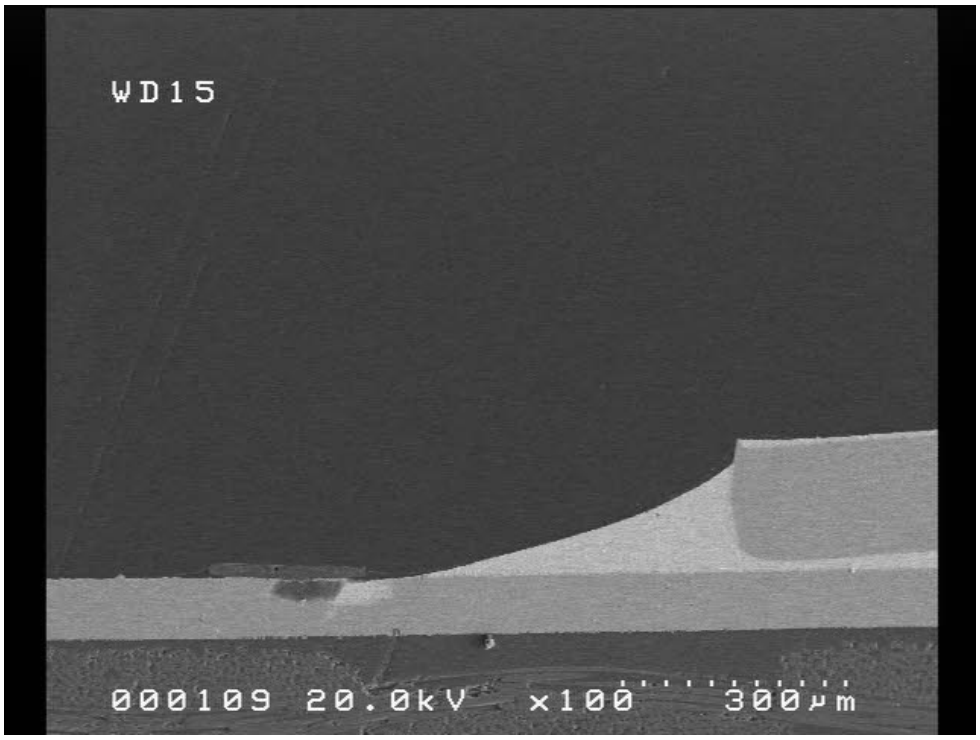


Figure 85: Batch A SEM cross-section image of PC40-UMF dip + spray coated QFP44, toe location, 100x (ref. Board 57).

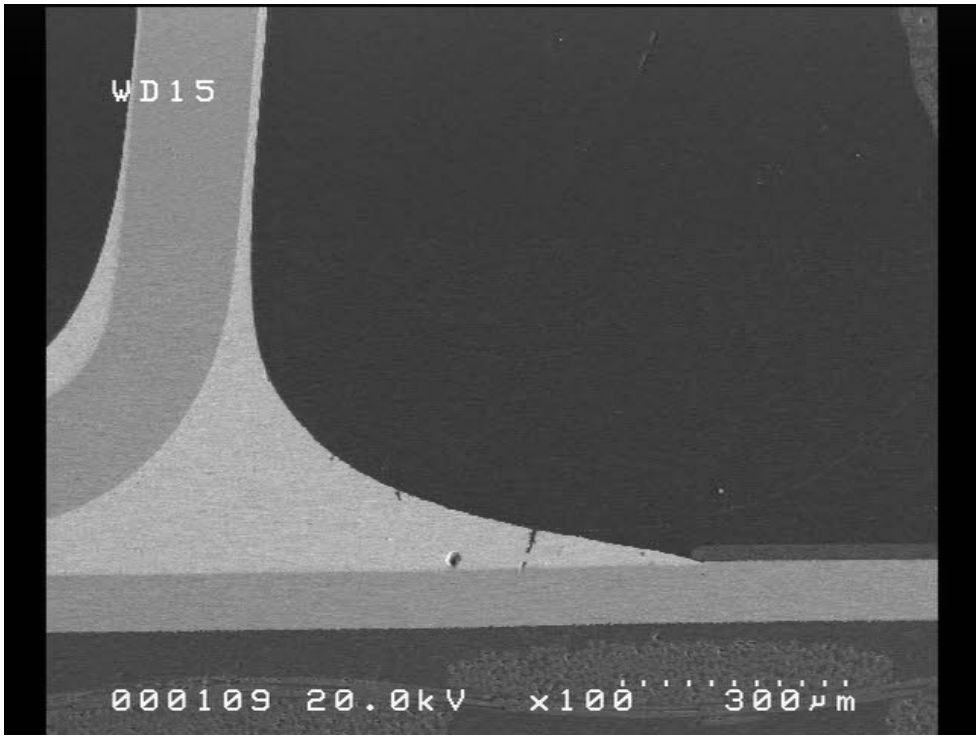


Figure 86: Batch A SEM cross-section image of PC40-UMF dip + spray coated QFP44, heel location, 100x (ref. Board 57).

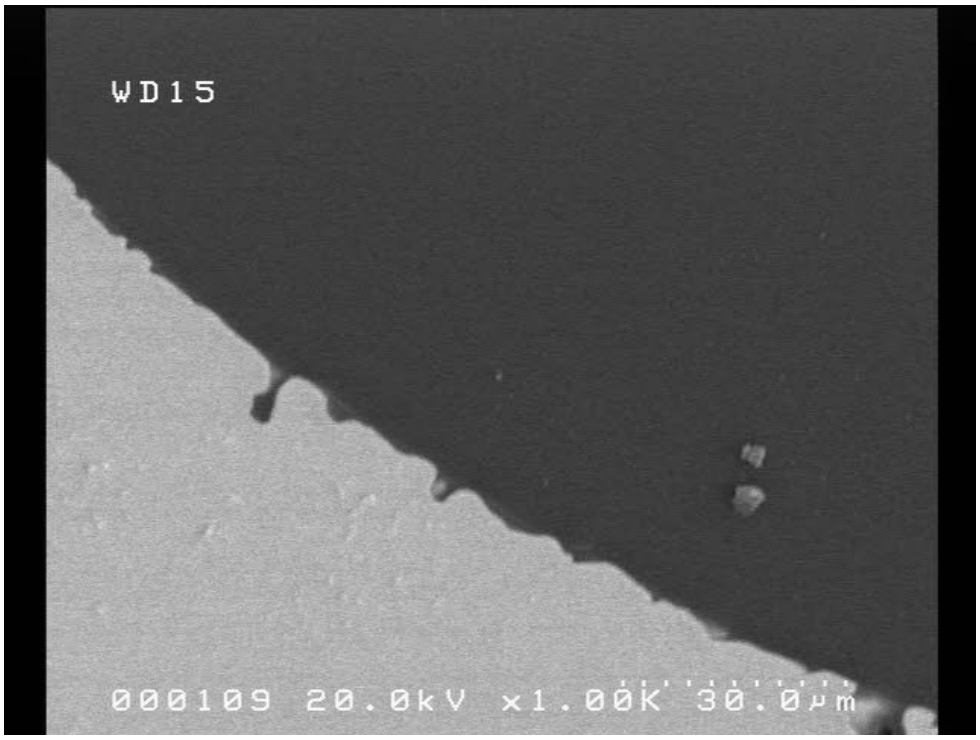


Figure 87: Batch A SEM cross-section image of PC40-UMF dip + spray coated QFP44, upper heel location, 1,000x (ref. Board 57).

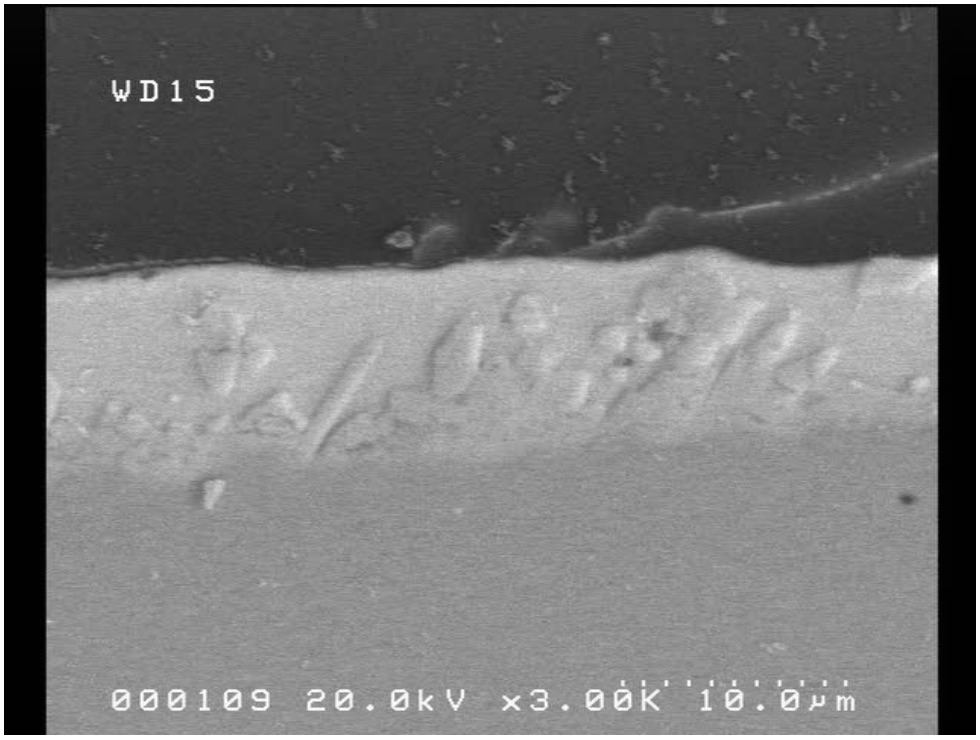


Figure 88: Batch A SEM cross-section image of PC40-UMF dip + spray coated QFP44, location A, 3,000x (ref. Board 57).

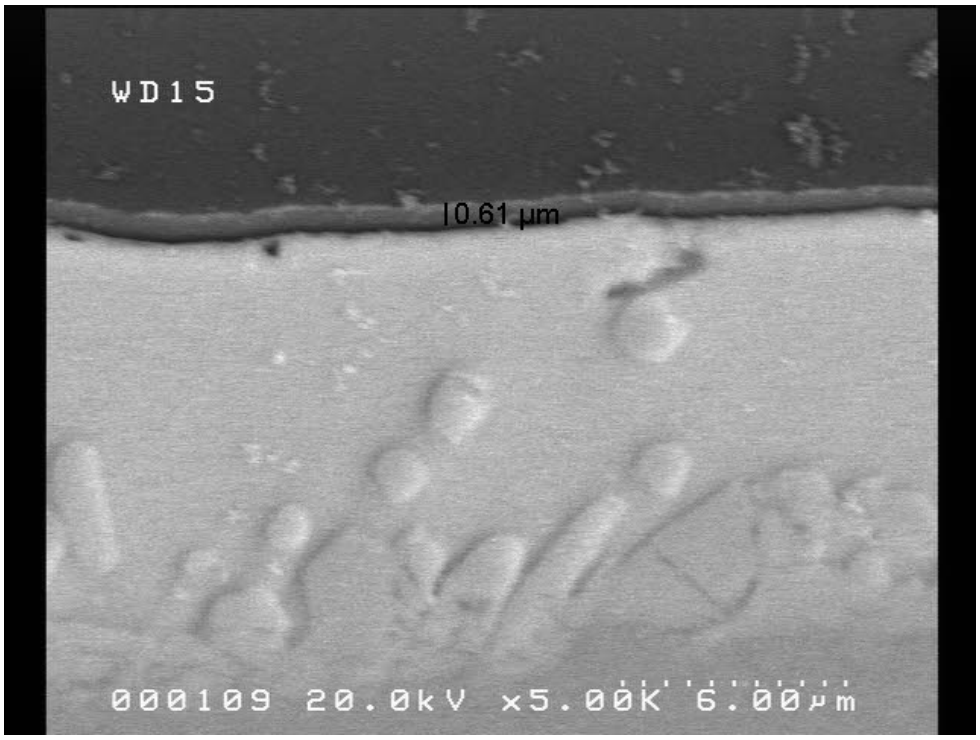


Figure 89: Batch A SEM cross-section image of PC40-UMF dip + spray coated QFP44, location A, 5,000x (ref. Board 57).

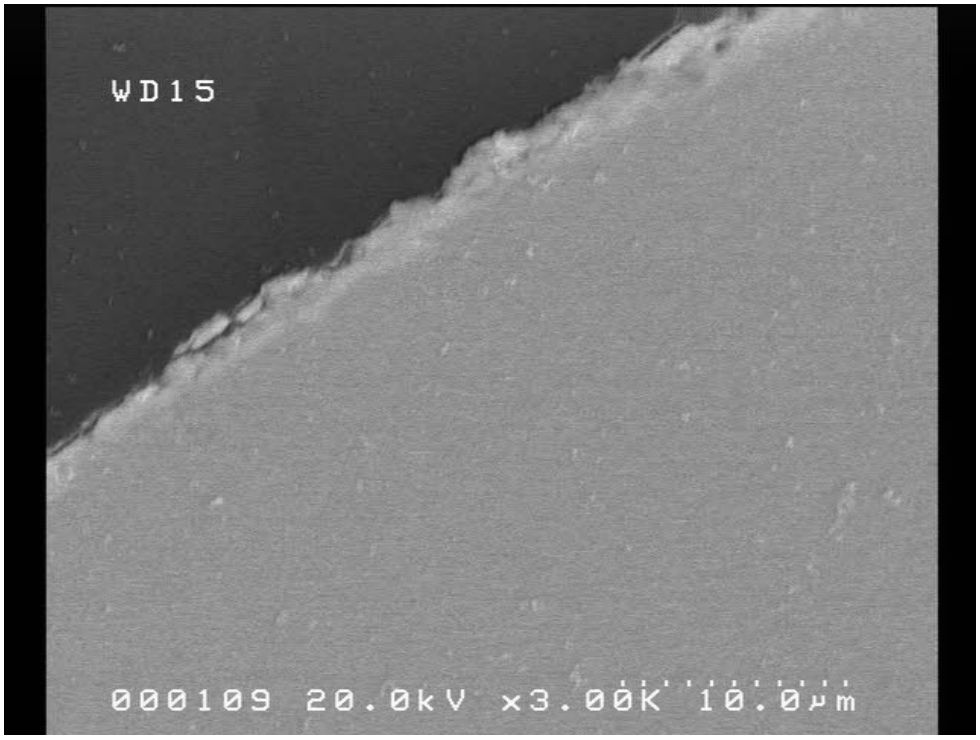


Figure 90: Batch A SEM cross-section image of PC40-UMF dip + spray coated QFP44, location B, 3,000x (ref. Board 57).

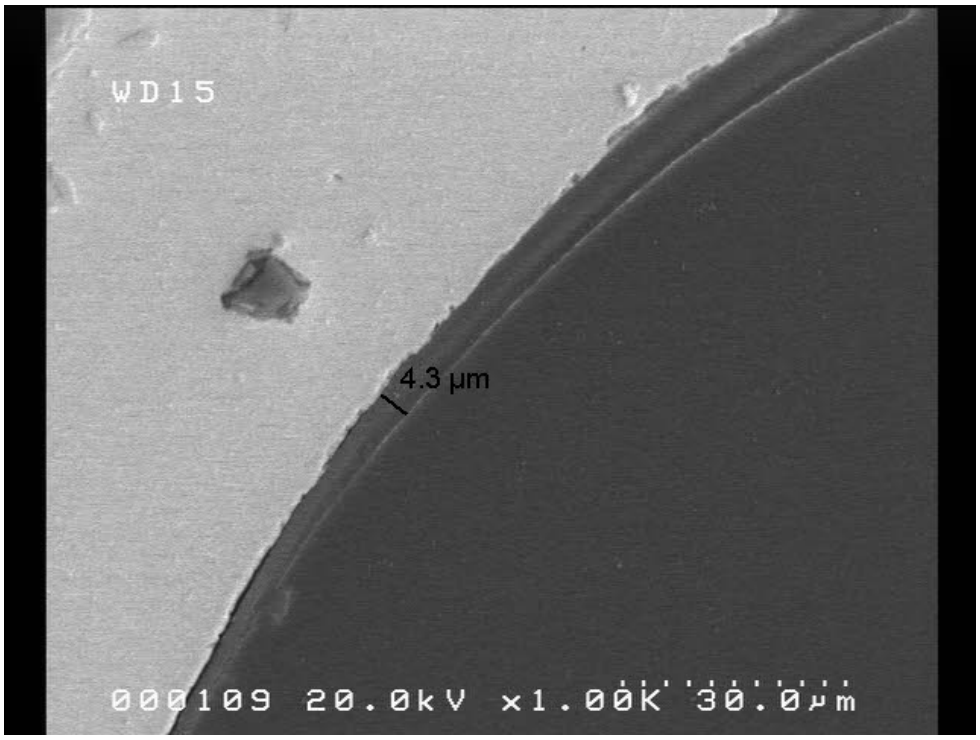


Figure 91: Batch A SEM cross-section image of PC40-UMF dip + spray coated QFP44, behind the knee, 1,000x (ref. Board 57).

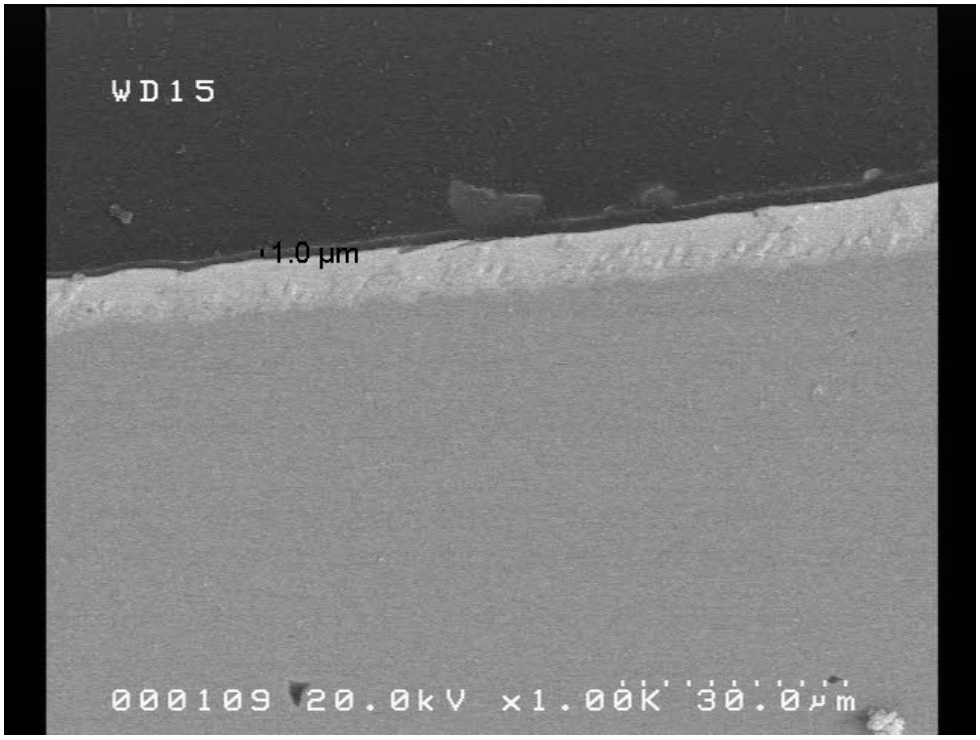


Figure 92: Batch A SEM cross-section image of PC40-UMF dip + spray coated QFP44, between location T and F, 1,000x (ref. Board 57).

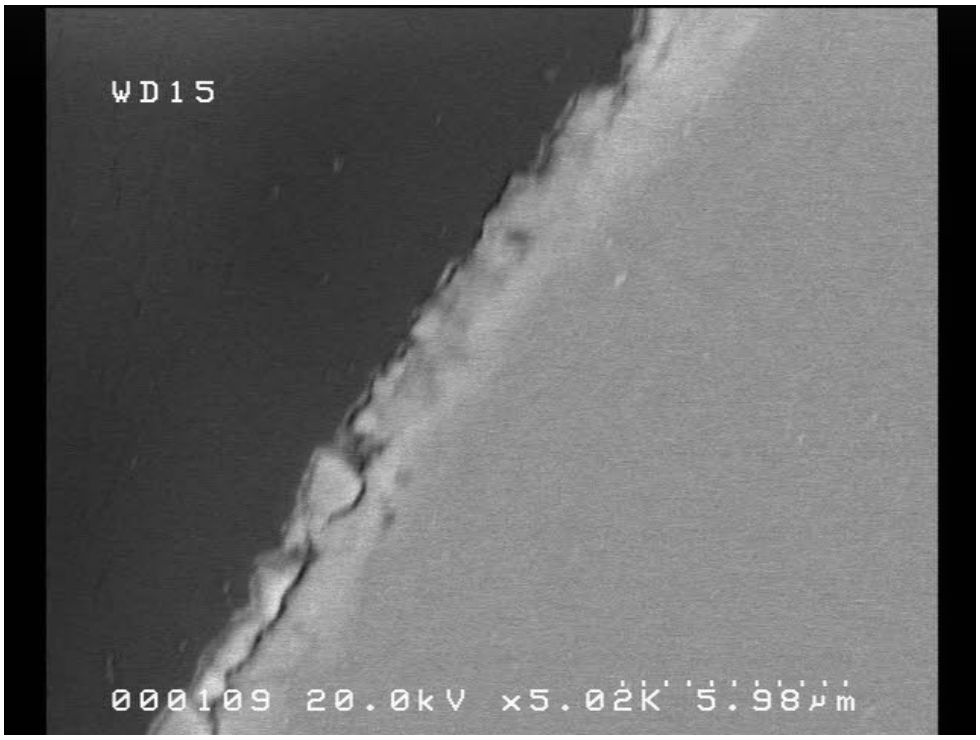


Figure 93: Batch A SEM cross-section image of PC40-UMF dip + spray coated QFP44, location C, 5,000x (ref. Board 57).

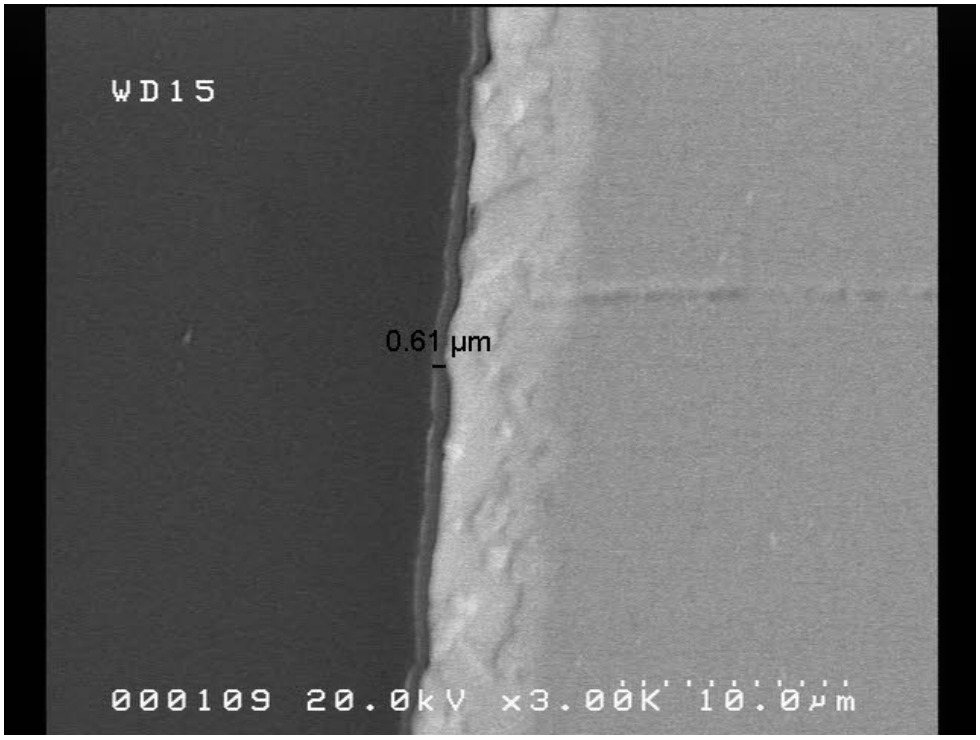


Figure 94: Batch A SEM cross-section image of PC40-UMF dip + spray coated QFP44, location D, 3,000x (ref. Board 57).

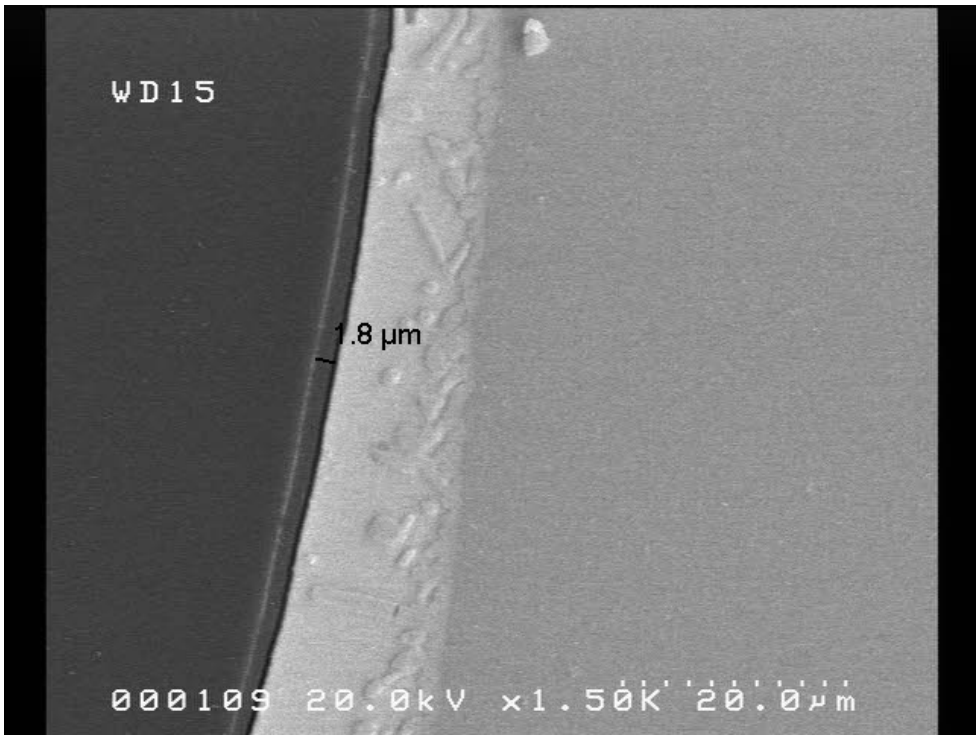


Figure 95: Batch A SEM cross-section image of PC40-UMF dip + spray coated QFP44, location E, 1,500x (ref. Board 57).

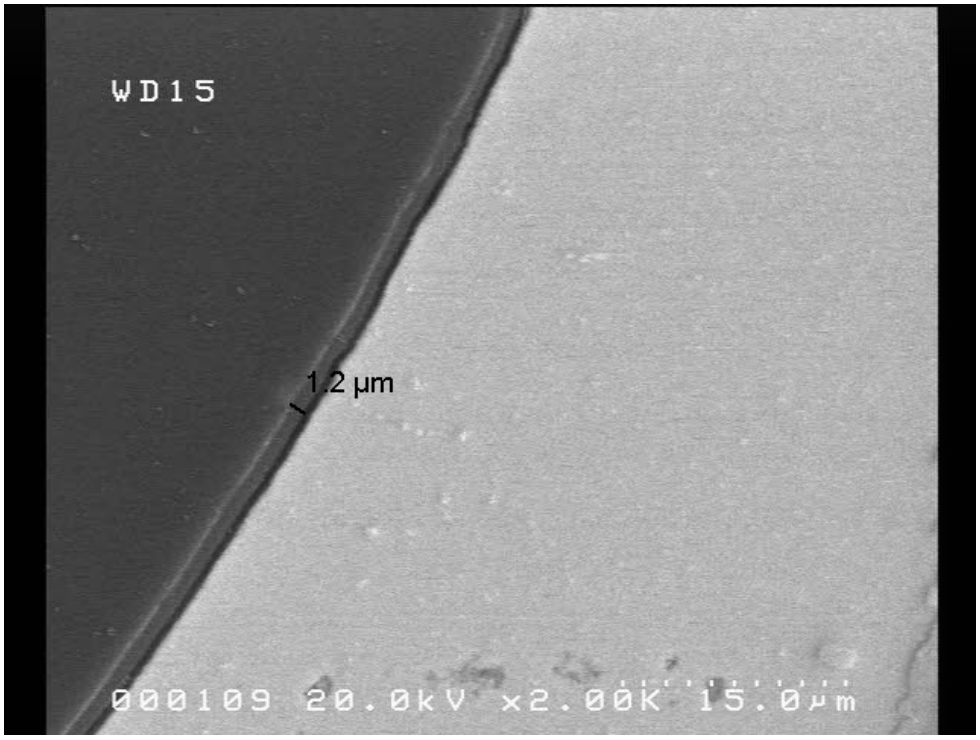


Figure 96: Batch A SEM cross-section image of PC40-UMF dip + spray coated QFP44, location F, 2,000x (ref. Board 57).

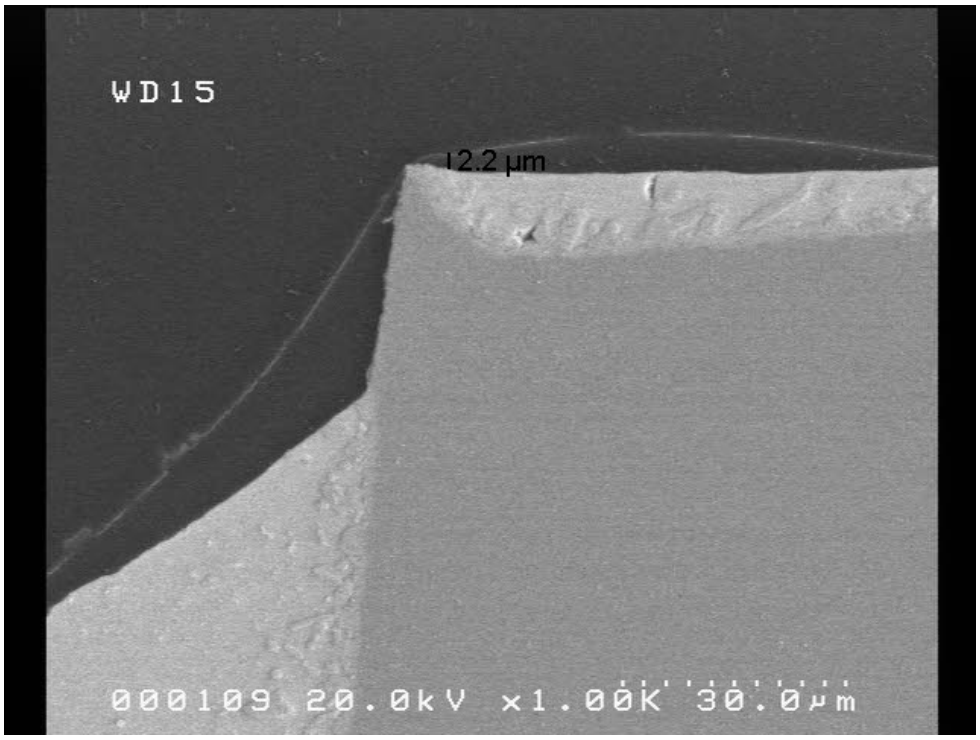


Figure 97: Batch A SEM cross-section image of PC40-UMF dip + spray coated QFP44, location T, 1000x (ref. Board 57).

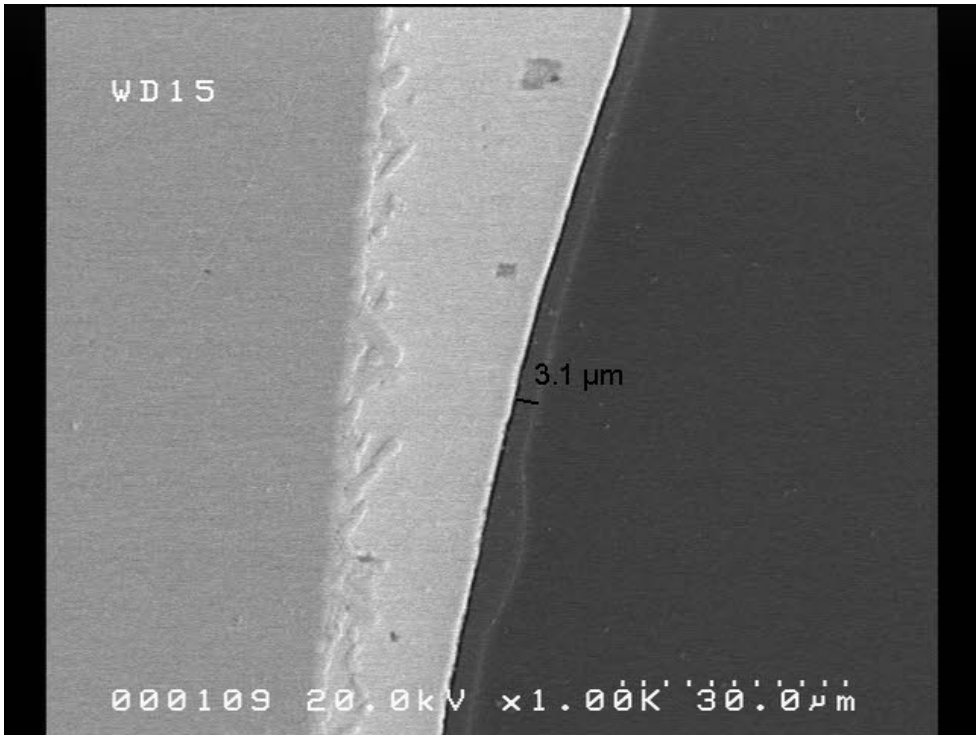


Figure 98: Batch A SEM cross-section image of PC40-UMF dip + spray coated QFP44, location G, 1,000x (ref. Board 57).

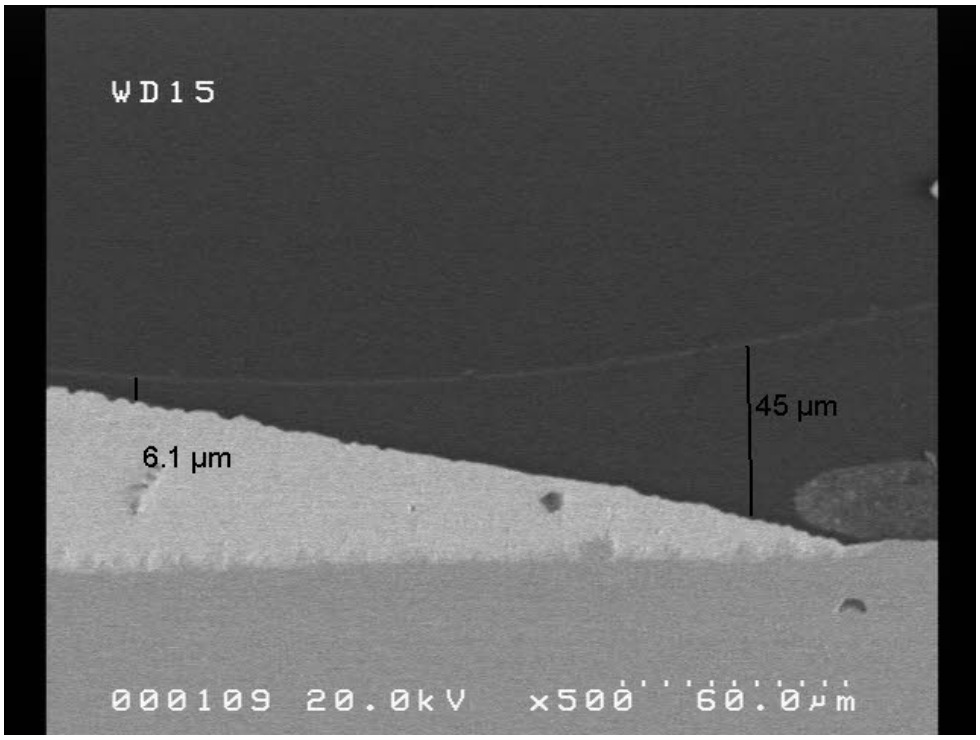


Figure 99: Batch A SEM cross-section image of PC40-UMF dip + spray coated QFP44, location H, 500x (ref. Board 57).

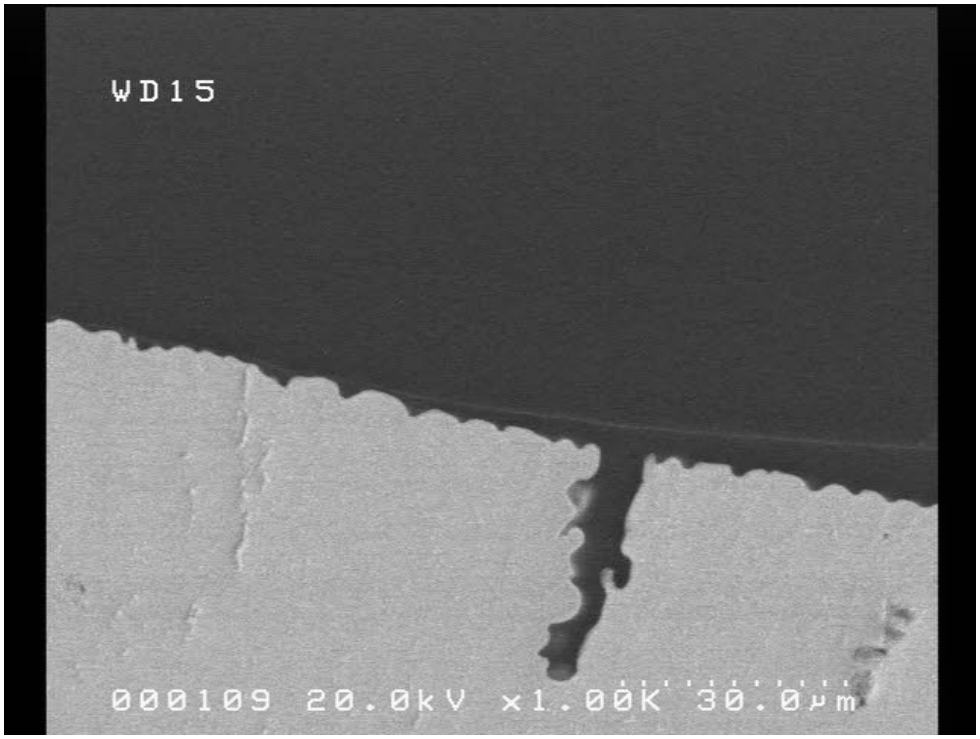


Figure 100: Batch A SEM cross-section image of PC40-UMF dip + spray coated QFP44, location H, 1,000x (ref. Board 57).

2.1.4 PC40-UMF Batch B vertical cross-section thickness evaluation

The vertical cross-sections for the batch B dip+spray with a plasma etch between layers were made for the PC40-UMF (Figure 101 to Figure 118), PC40-UMF + 10%NNN2835 nanosilica (Figure 119 to Figure 127), PC40-UMF + 30%NNN2835 nanosilica (Figure 128 to Figure 147), PC40-UMF + 50%NNN2835 nanosilica (Figure 148 to Figure 154), and PC40-UMF+15.54%N3300 (comparable to PC40-UMF+30%XP2742 without the nanosilica particles) (Figure 155 to Figure 159).

Note the nanosilica filled spray coating was always applied over an unfilled PC40-UMF dip, e.g. PC40-UMF dip, plasma etch, then (PC40-UMF + 30%NNN2835 nanosilica) spray.

2.1.4.1 PC40-UMF Batch B dip+spray

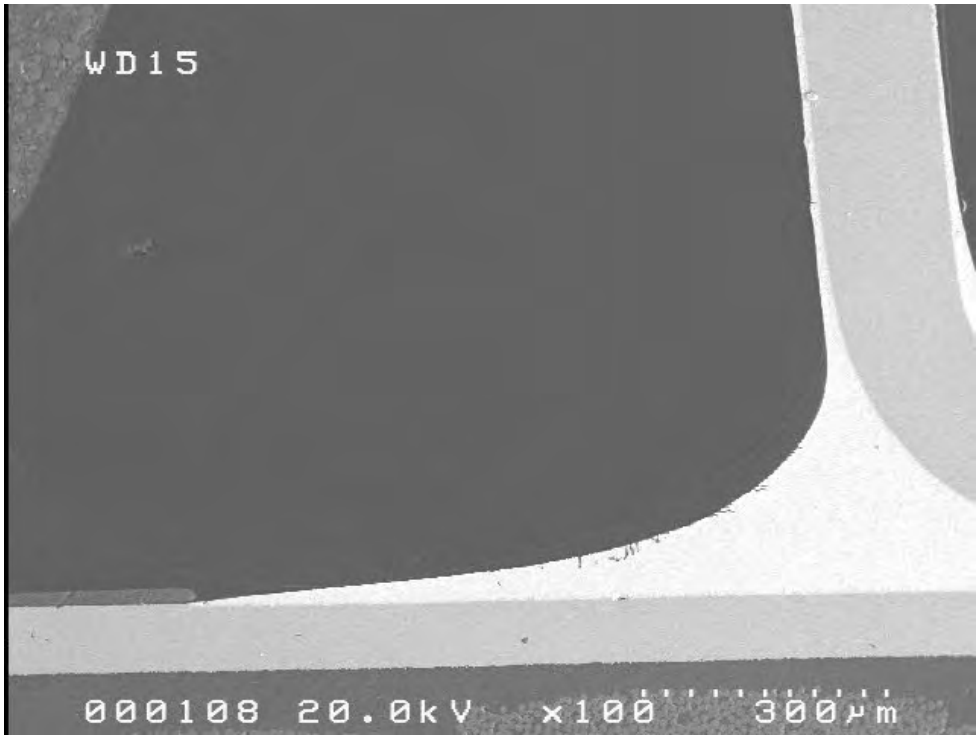


Figure 101: Batch B SEM cross-section image of PC40-UMF dip+spray coated QFP44, heel location, 100x, (ref. Board 66).

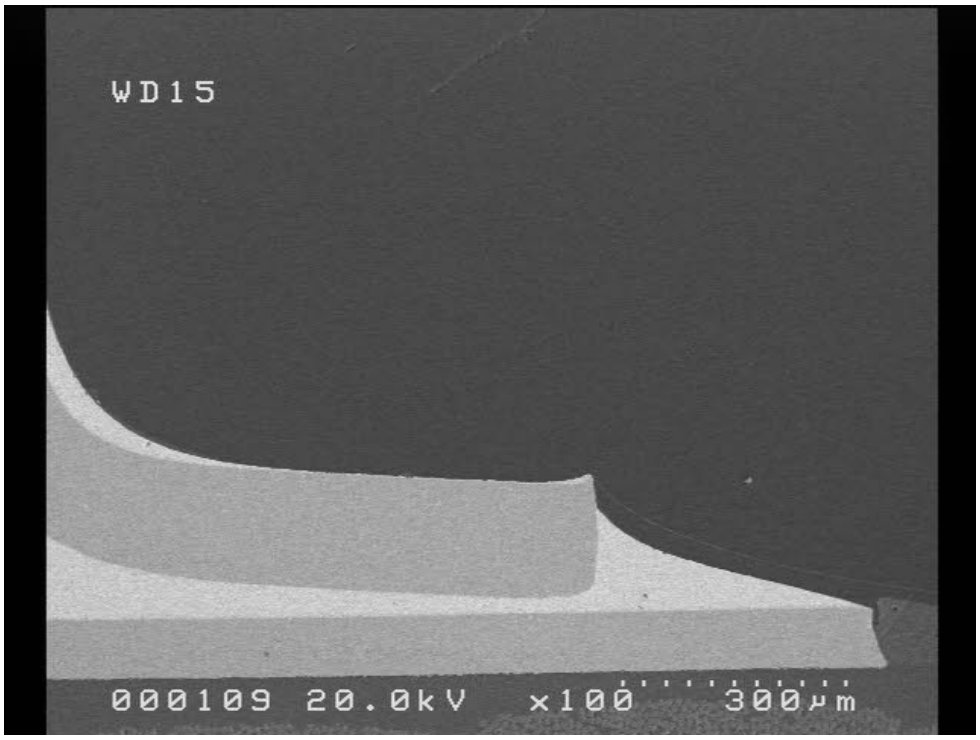


Figure 102: Batch B SEM cross-section image of PC40-UMF dip+spray coated QFP44, foot location, 100x, (ref. Board 66).

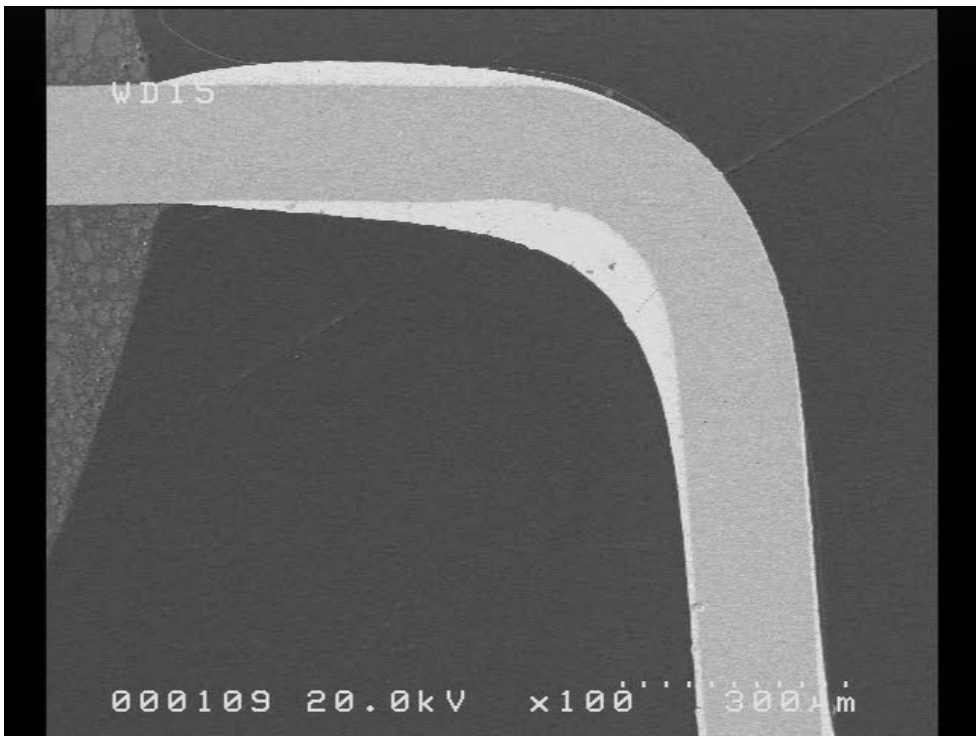


Figure 103: Batch B SEM cross-section image of PC40-UMF dip+spray coated QFP44, knee location, QFP44, 100x, (ref. Board 66).



Figure 104: Batch B SEM cross-section image of PC40-UMF dip+spray coated QFP44, toe location, 100x, (ref. Board 66).

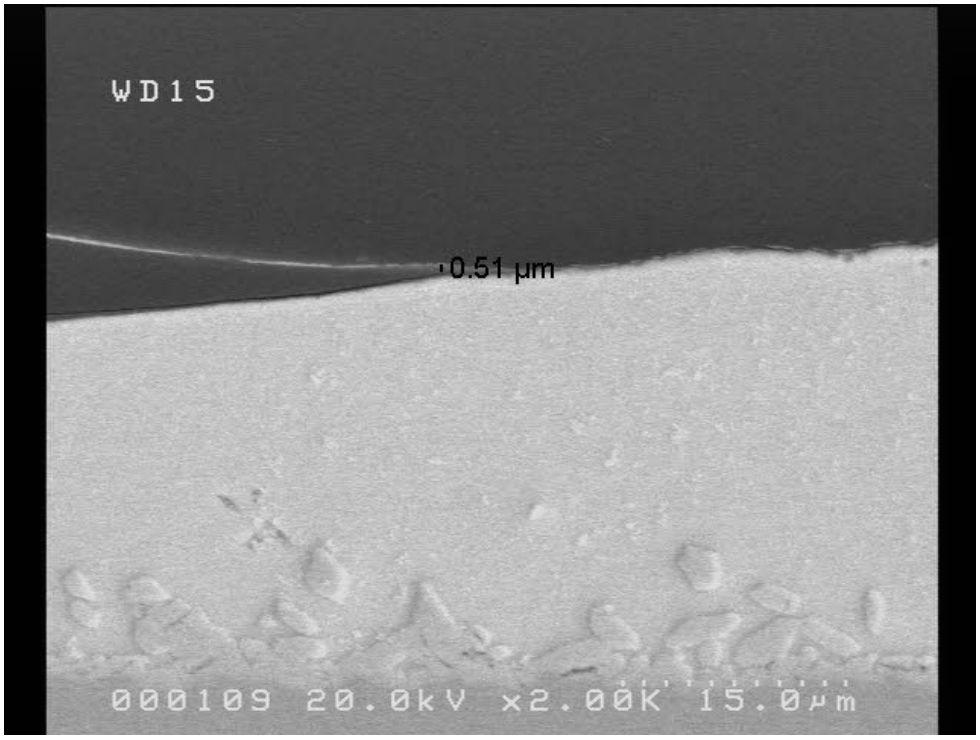


Figure 105: Batch B SEM cross-section image of PC40-UMF dip+spray coated QFP44, location A, 1,000x (ref. Board 66).

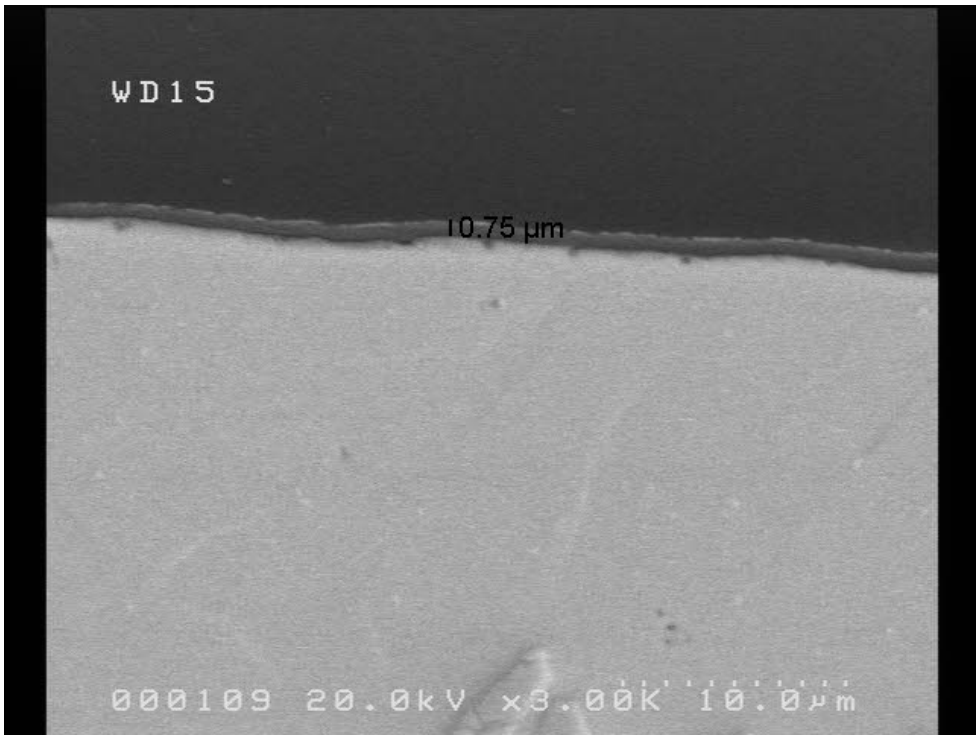


Figure 106: Batch B SEM cross-section image of PC40-UMF dip+spray coated QFP44, location A, 3,000x (ref. Board 66).

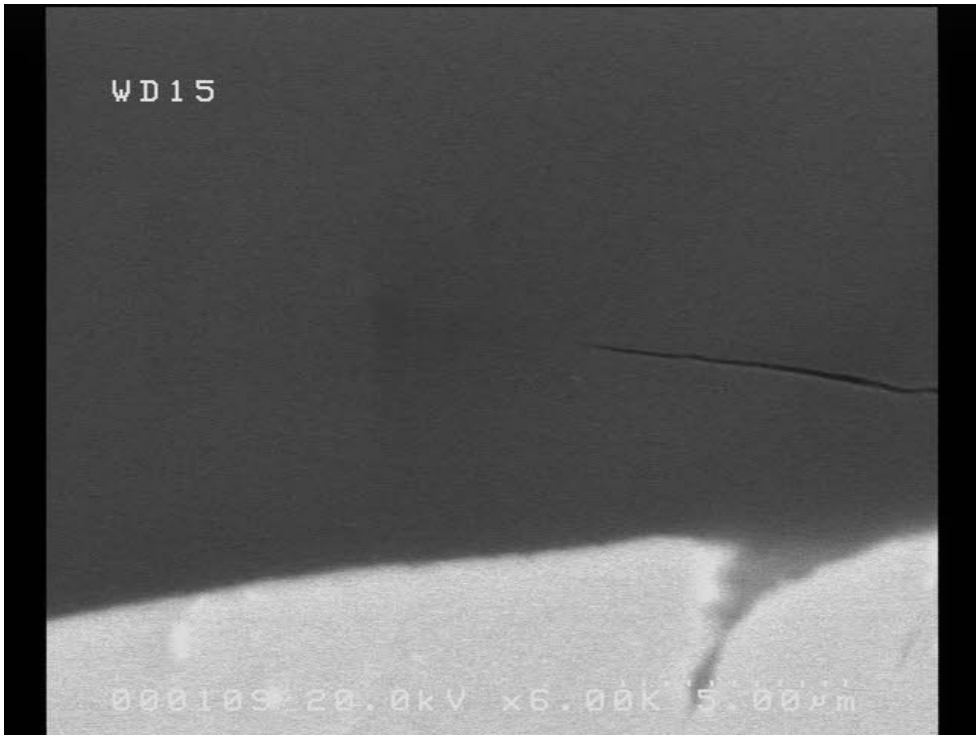


Figure 107: Batch B SEM cross-section image of PC40-UMF dip+spray coated QFP44, location A, 6,000x (ref. Board 66).

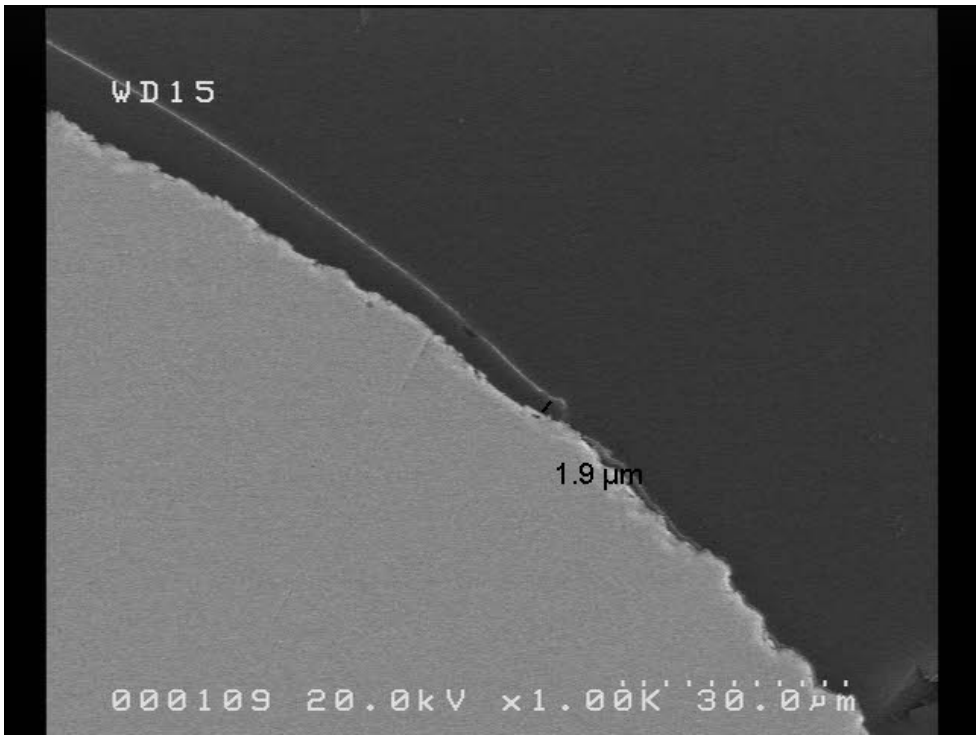


Figure 108: Batch B SEM cross-section image of PC40-UMF dip+spray coated QFP44, location B, 1000x (ref. Board 66).

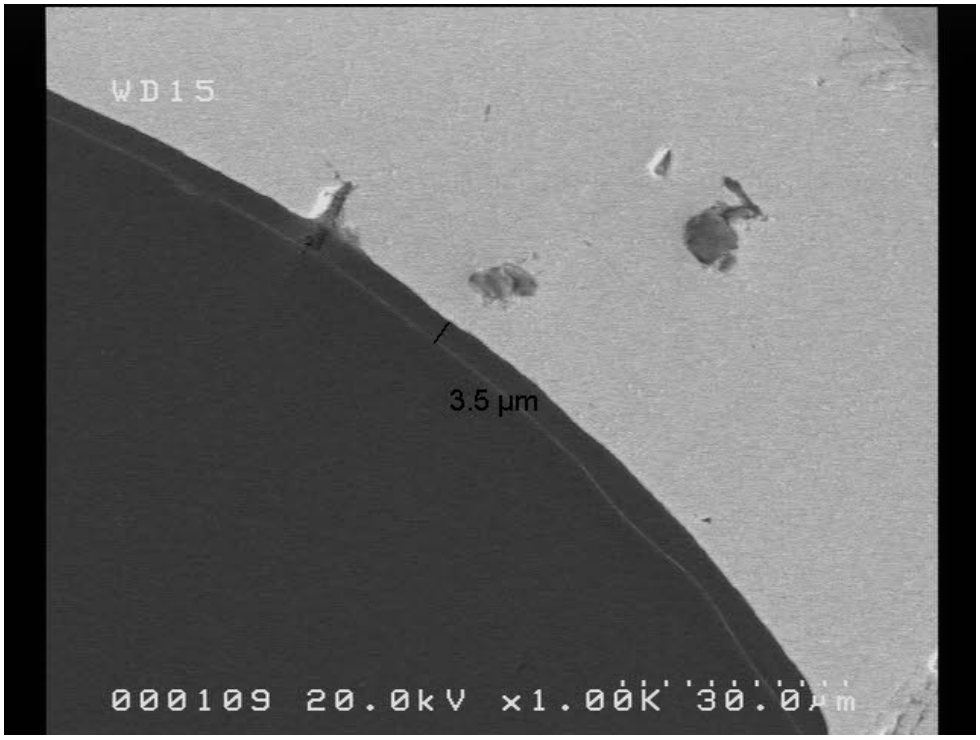


Figure 109: Batch B SEM cross-section image of PC40-UMF dip+spray coated QFP44, behind the knee, 1000x (ref. Board 66).

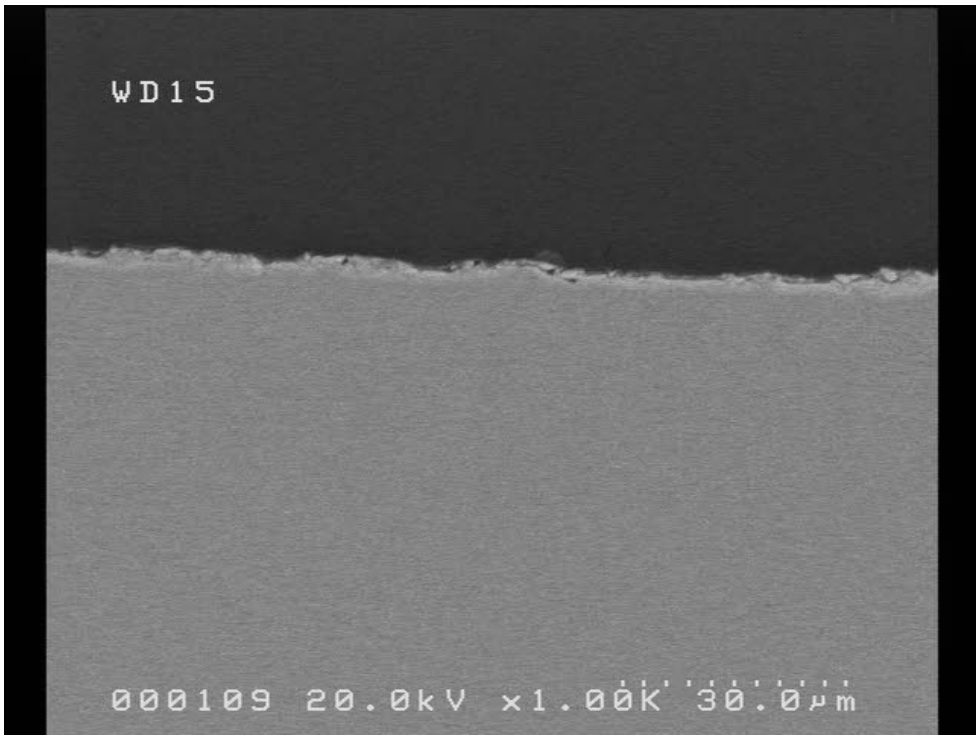


Figure 110: Batch B SEM cross-section image of PC40-UMF dip+spray coated QFP44, between location F and T, 1000x (ref. Board 66).

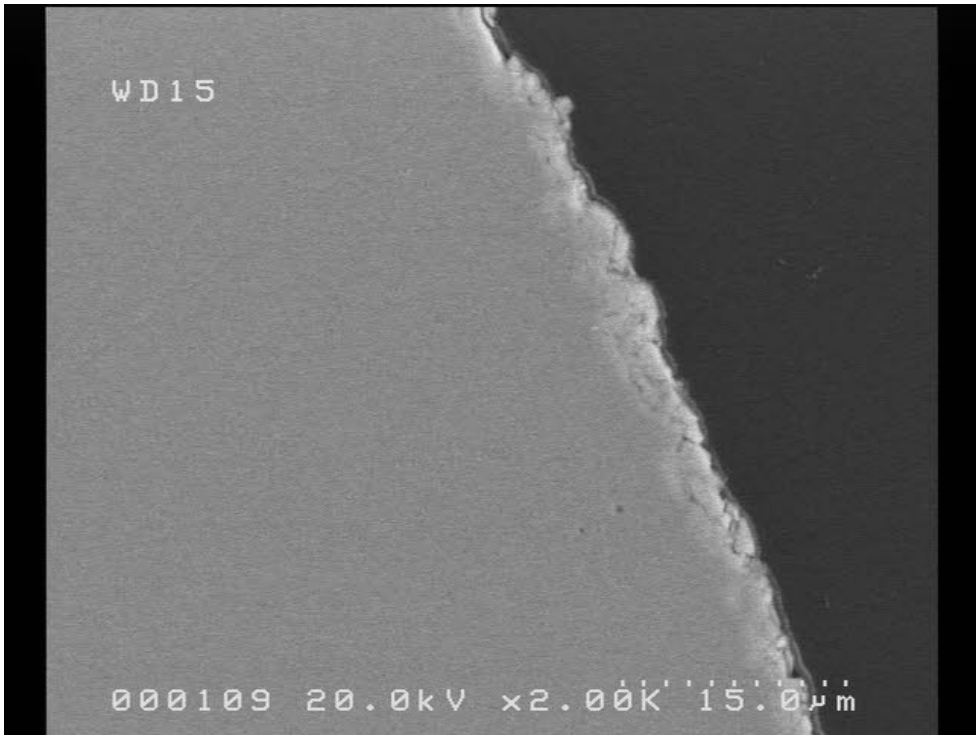


Figure 111: Batch B SEM cross-section image of PC40-UMF dip+spray coated QFP44, location C, 2000x (ref. Board 66).

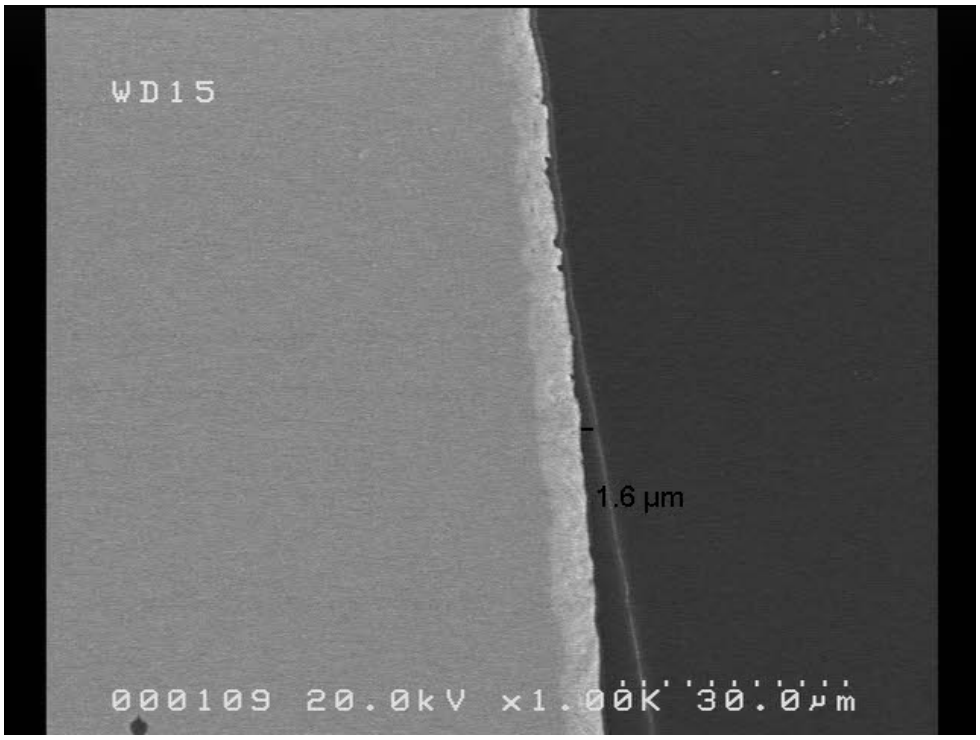


Figure 112: Batch B SEM cross-section image of PC40-UMF dip+spray coated QFP44, location D, 1,000x (ref. Board 66).

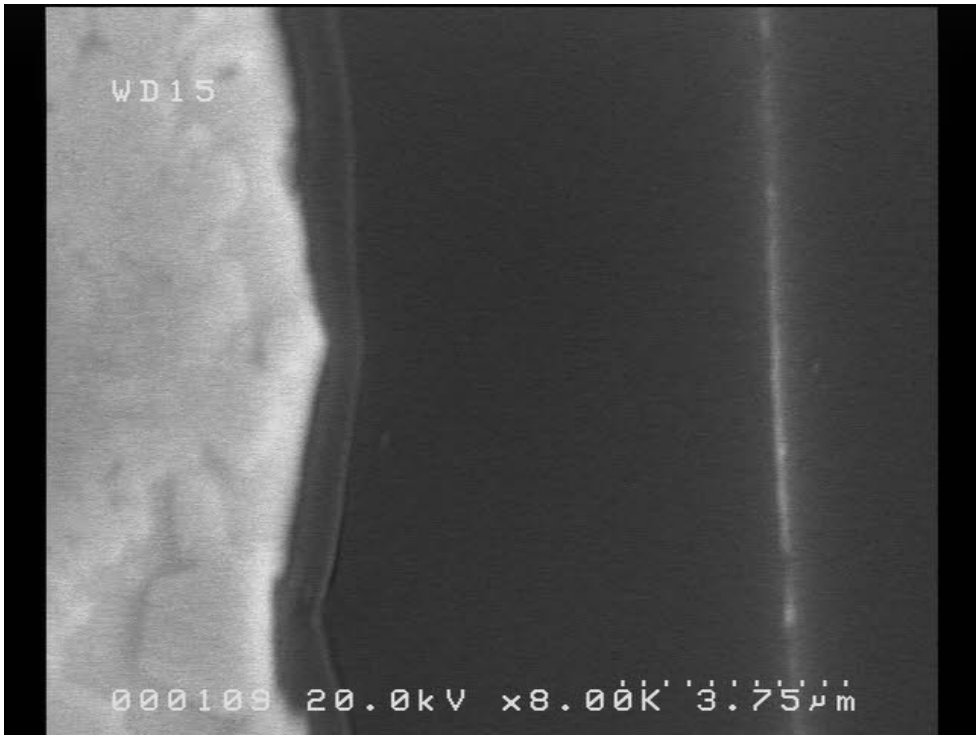


Figure 113: Batch B SEM cross-section image of PC40-UMF dip+spray coated QFP44, location D, 8,000x (ref. Board 66).

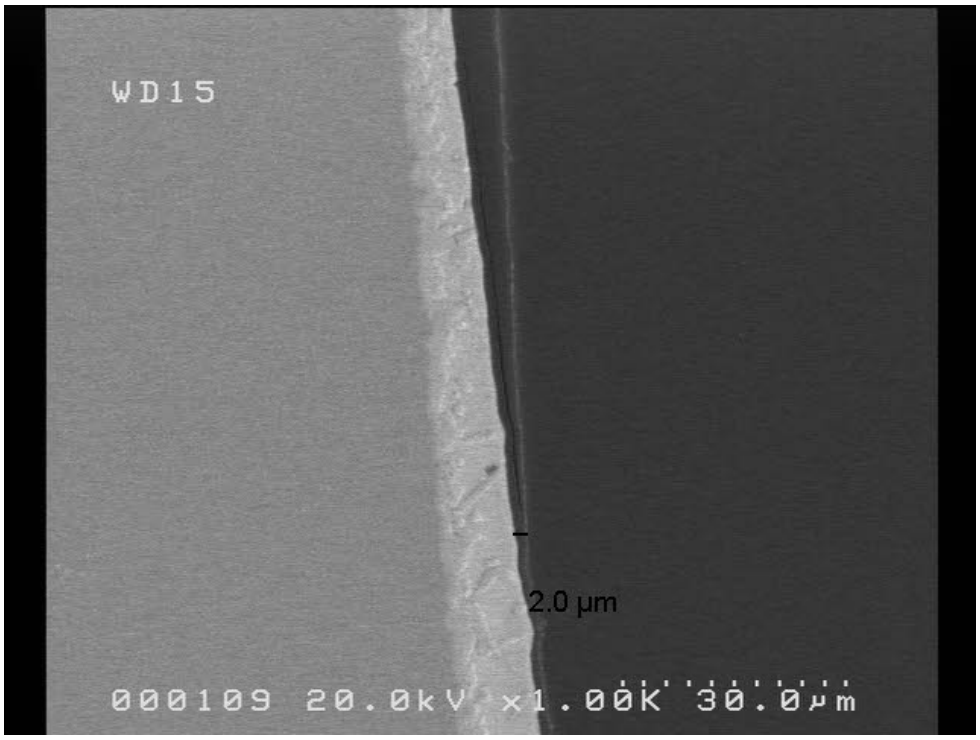


Figure 114: Batch B SEM cross-section image of PC40-UMF dip+spray coated QFP44, location E, 1,000x (ref. Board 66).

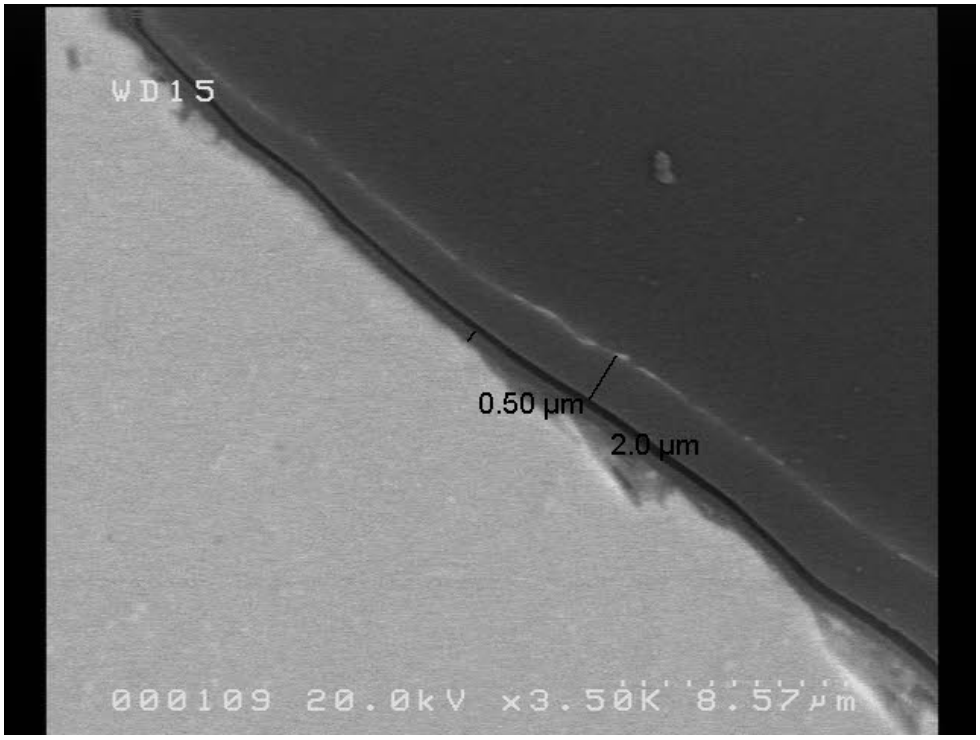


Figure 115: Batch B SEM cross-section image of PC40-UMF dip+spray coated QFP44, location F, 3,500x (ref. Board 66).

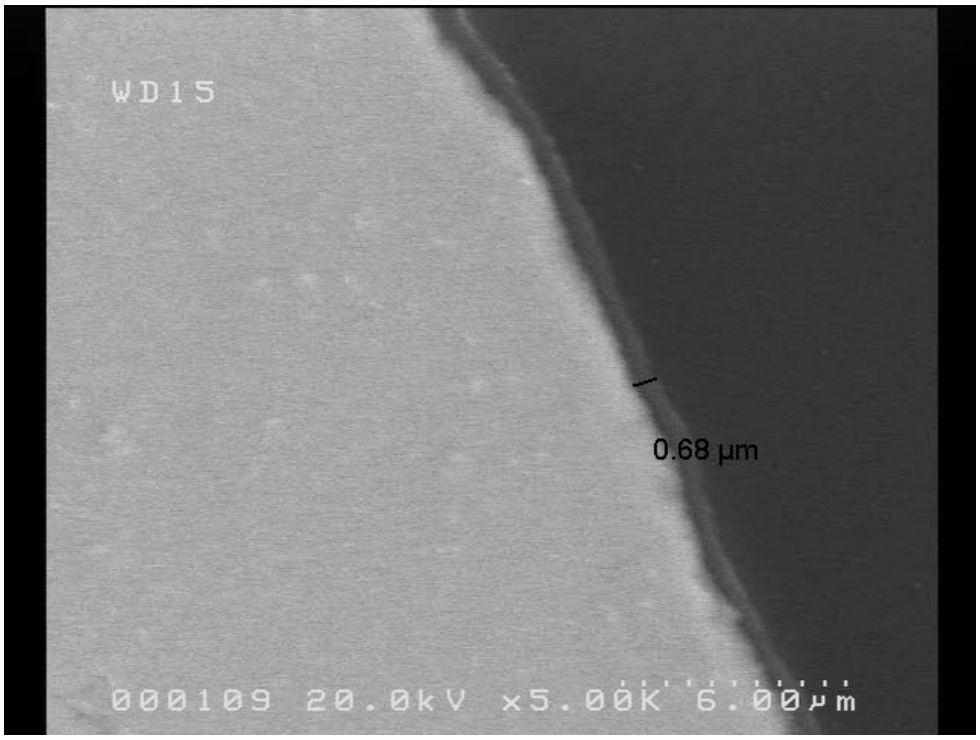


Figure 116: Batch B SEM cross-section image of PC40-UMF dip+spray coated QFP44, location F, 5,000x (ref. Board 66).

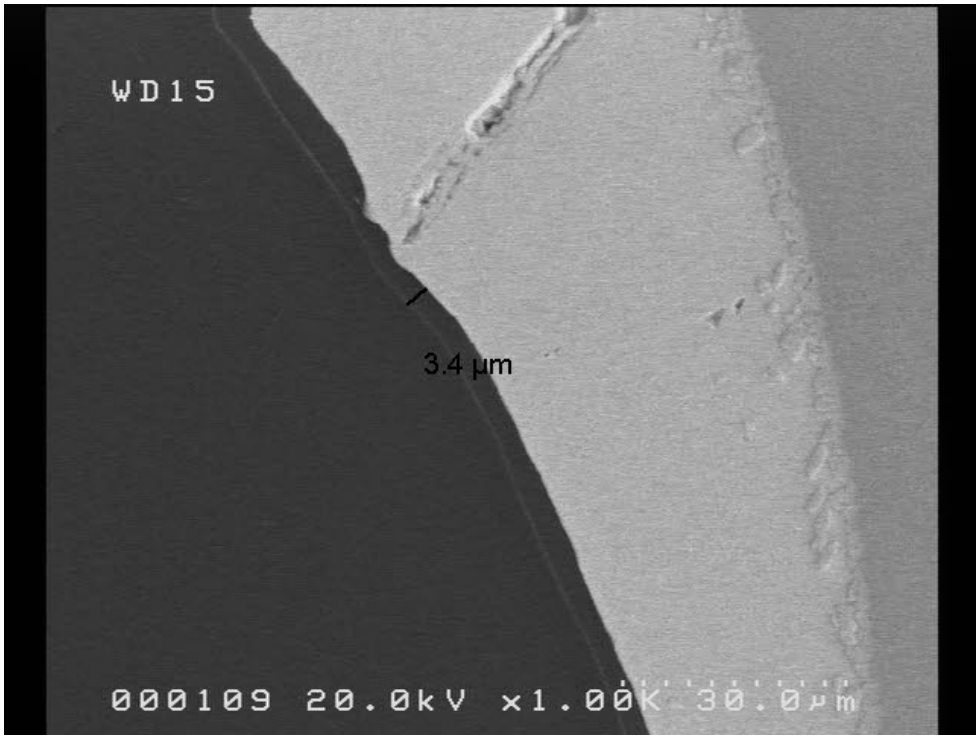


Figure 117: Batch B SEM cross-section image of PC40-UMF dip+spray coated QFP44, location G, 1,000x (ref. Board 66).

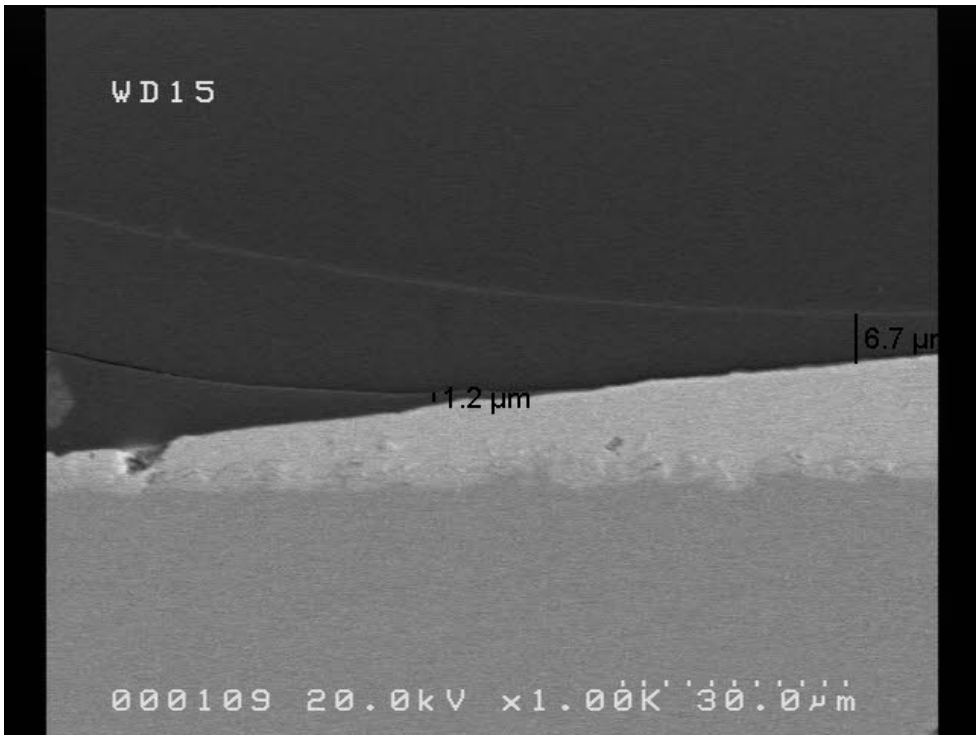


Figure 118: Batch B SEM cross-section image of PC40-UMF dip+spray coated QFP44, location H, 1,000x (ref. Board 66).

2.1.4.2 PC40-UMF+10%NNN2835 nanosilica

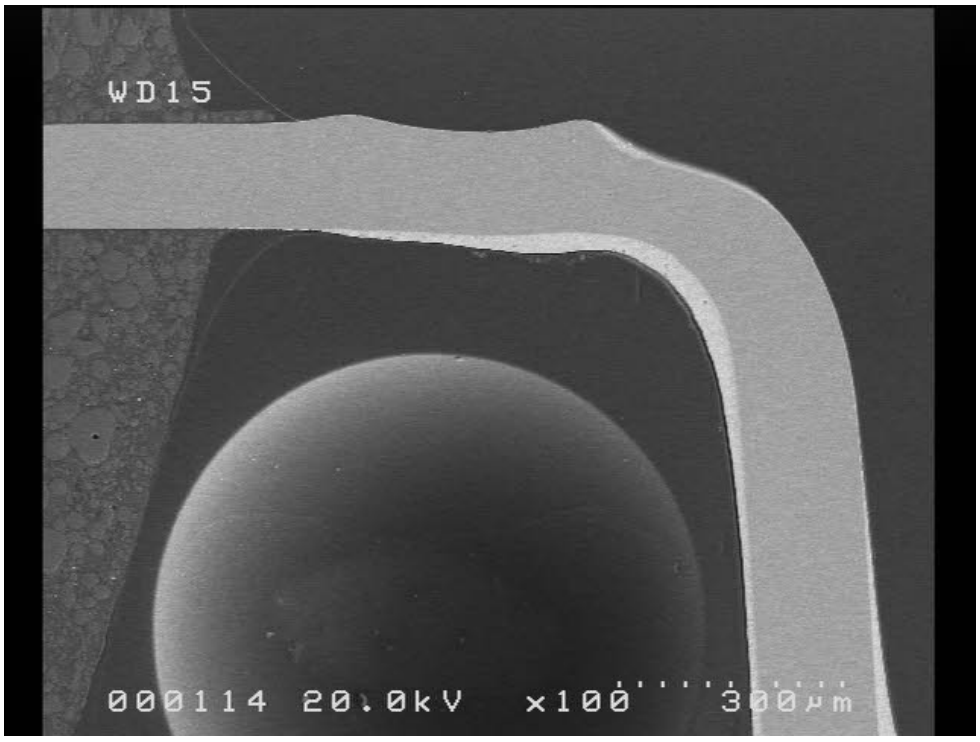


Figure 119: Batch B SEM cross-section image of PC40-UMF + 10%NNN2835 nanosilica dip+spray QFP44, lead knee location, 100x (ref. Board 62).

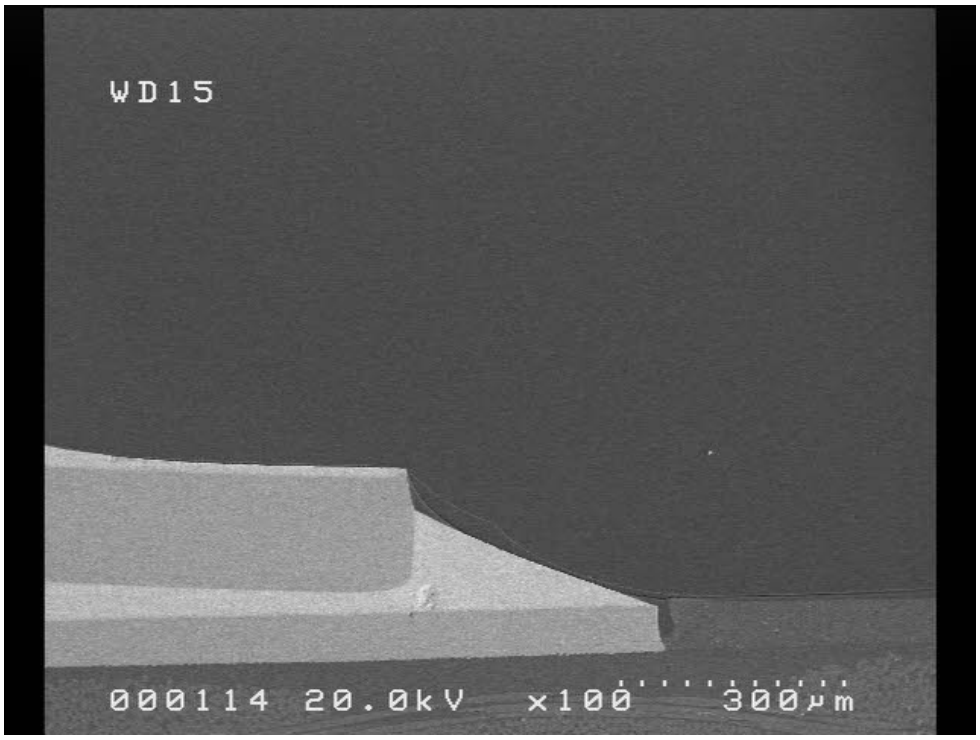


Figure 120: Batch B SEM cross-section image of PC40-UMF + 10%NNN2835 nanosilica dip+spray QFP44, lead toe location, 100x (ref. Board 62).

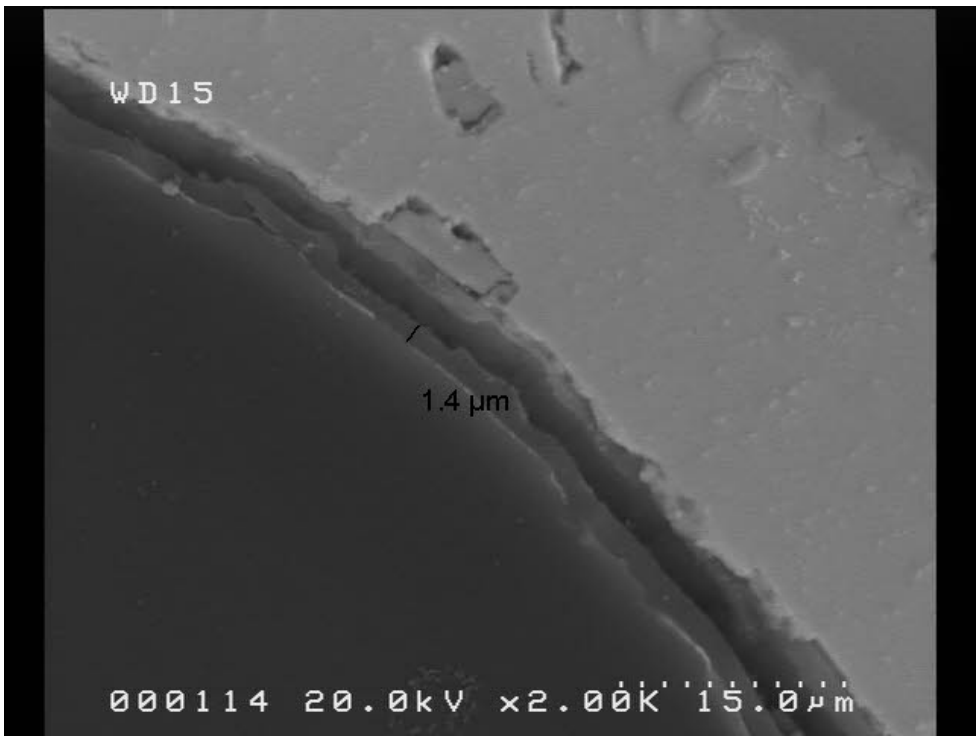


Figure 121: Batch B SEM cross-section image of PC40-UMF + 10%NNN2835 nanosilica dip+spray QFP44, behind the knee, 2000x (ref. Board 62).

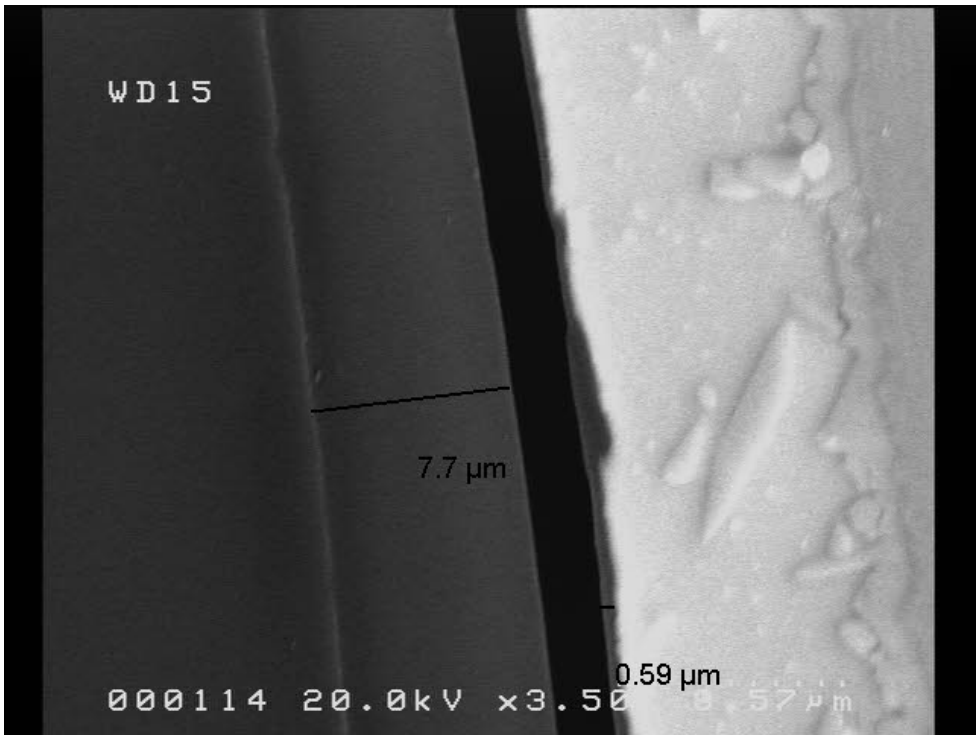


Figure 122: Batch B SEM cross-section image of PC40-UMF + 10%NNN2835 nanosilica dip+spray QFP44, back side, 3500x (ref. Board 62).

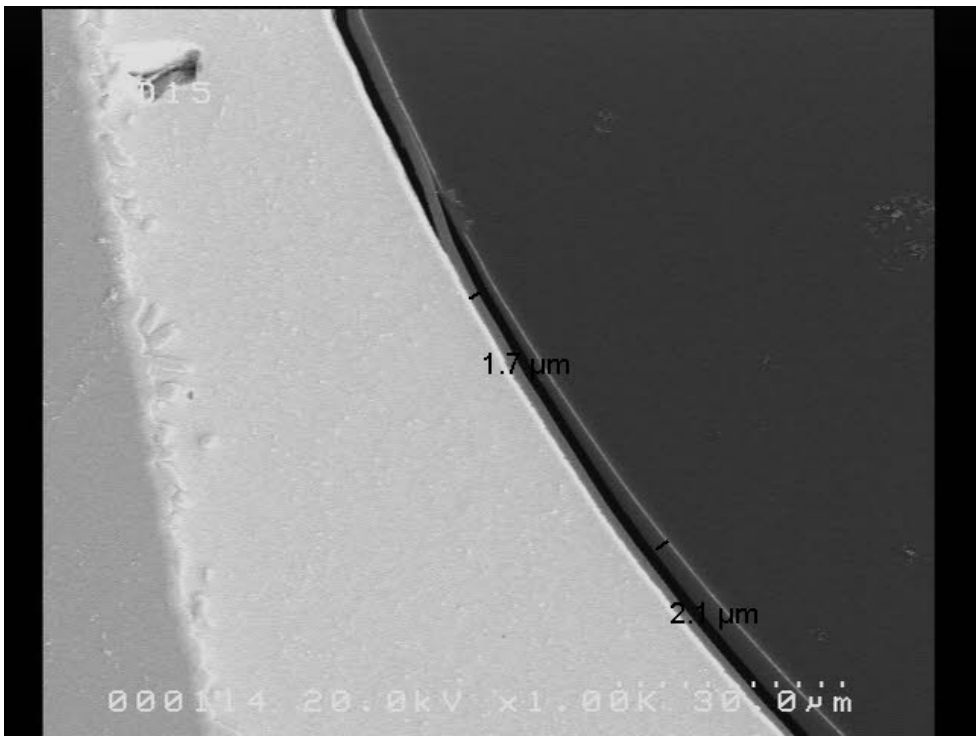


Figure 123: Batch B SEM cross-section image of PC40-UMF + 10%NNN2835 nanosilica dip+spray QFP44, location F, 1,000x (ref. Board 62).

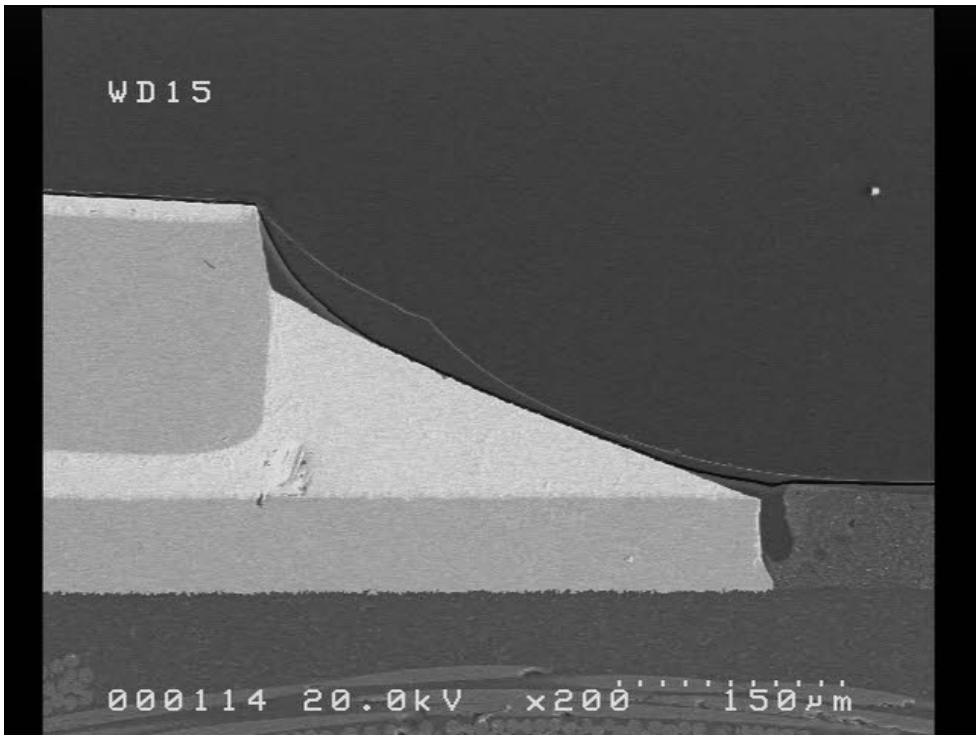


Figure 124: Batch B SEM cross-section image of PC40-UMF + 10%NNN2835 nanosilica dip+spray QFP44, location T, 200x (ref. Board 62).

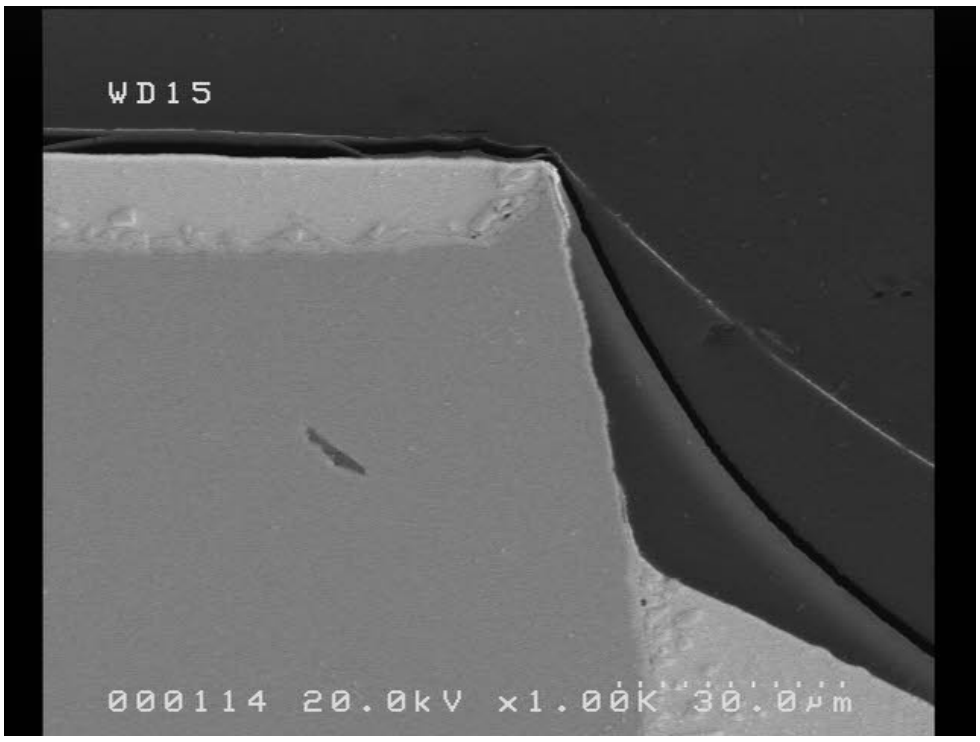


Figure 125: Batch B SEM cross-section image of PC40-UMF + 10%NNN2835 nanosilica dip+spray QFP44, location T, 1,000x (ref. Board 62).

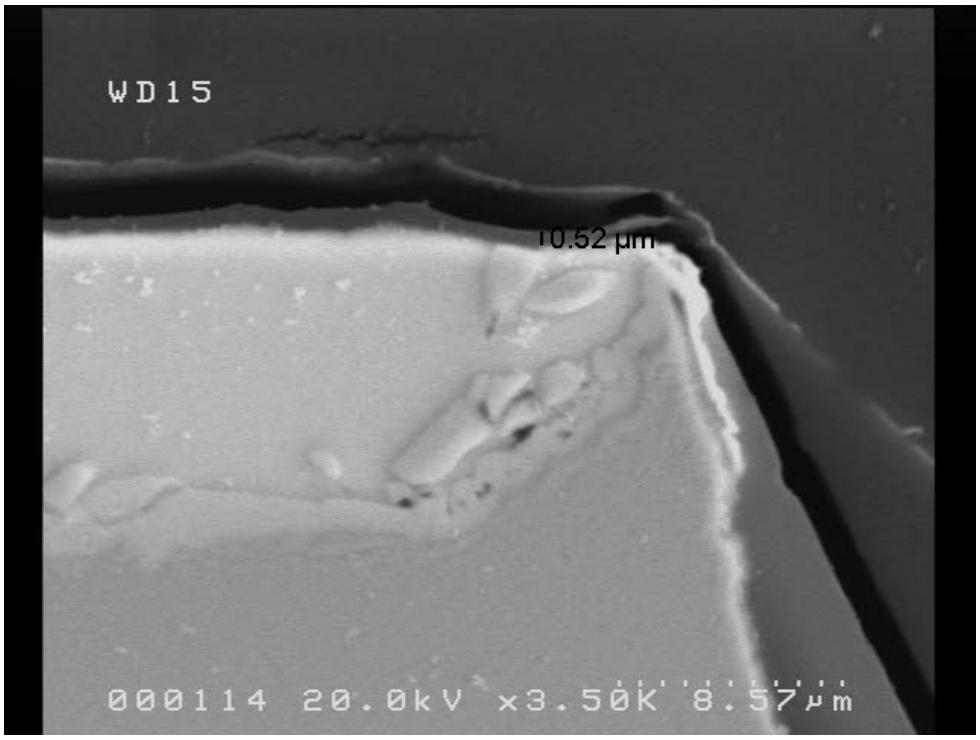


Figure 126: Batch B SEM cross-section image of PC40-UMF + 10%NNN2835 nanosilica dip+spray QFP44, location T, 3,500x (ref. Board 62).

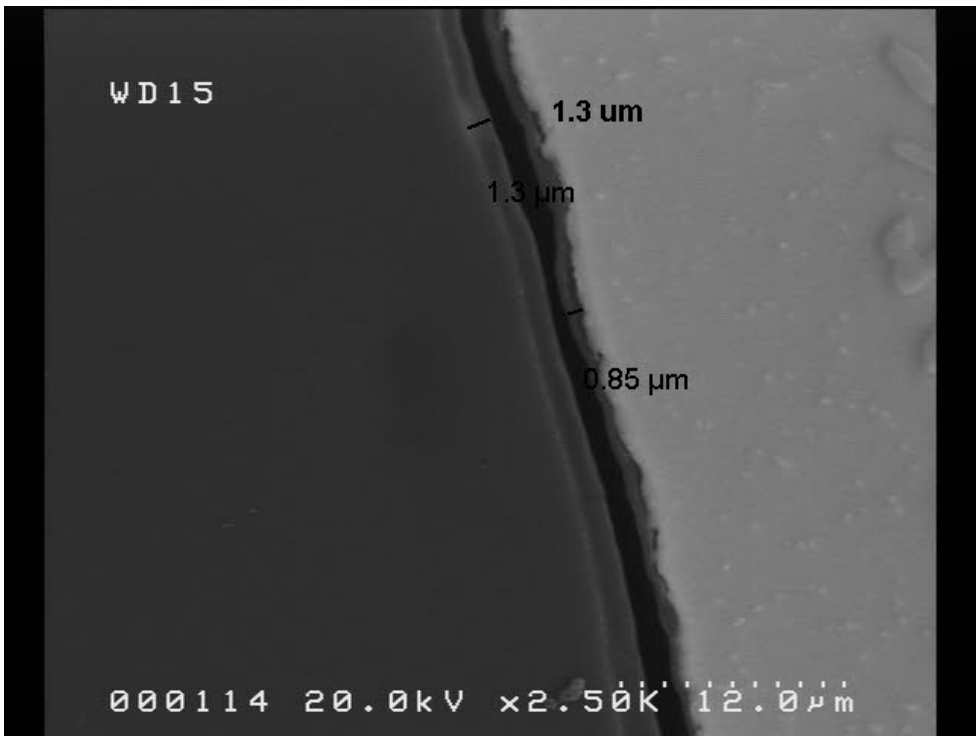


Figure 127: Batch B SEM cross-section image of PC40-UMF + 10%NNN2835 nanosilica dip+spray QFP44, location G, 2,500x (ref. Board 62).

\

2.1.4.3 PC40-UMF+30%NNN2835 nanosilica

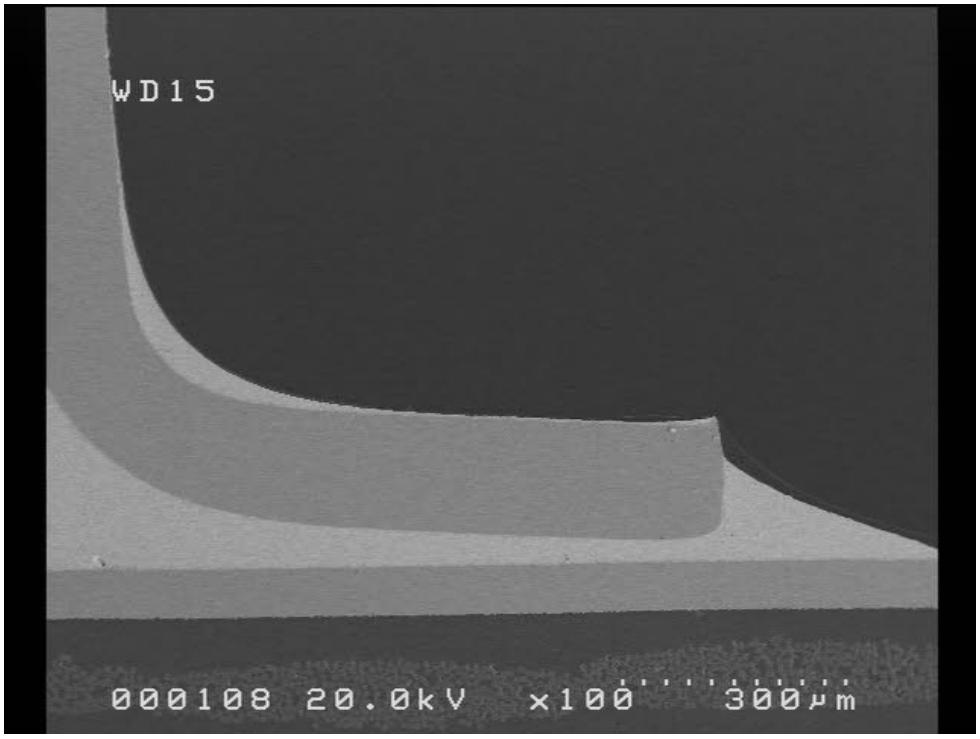


Figure 128: Batch B SEM cross-section image of PC40-UMF + 30%NNN2835 nanosilica dip+spray QFP44, foot location, 100x, (ref. Board 67). Note coating sequence is PC40-UMF dip + (PC40-UMF + 30%NNN2835 nanosilica) spray.

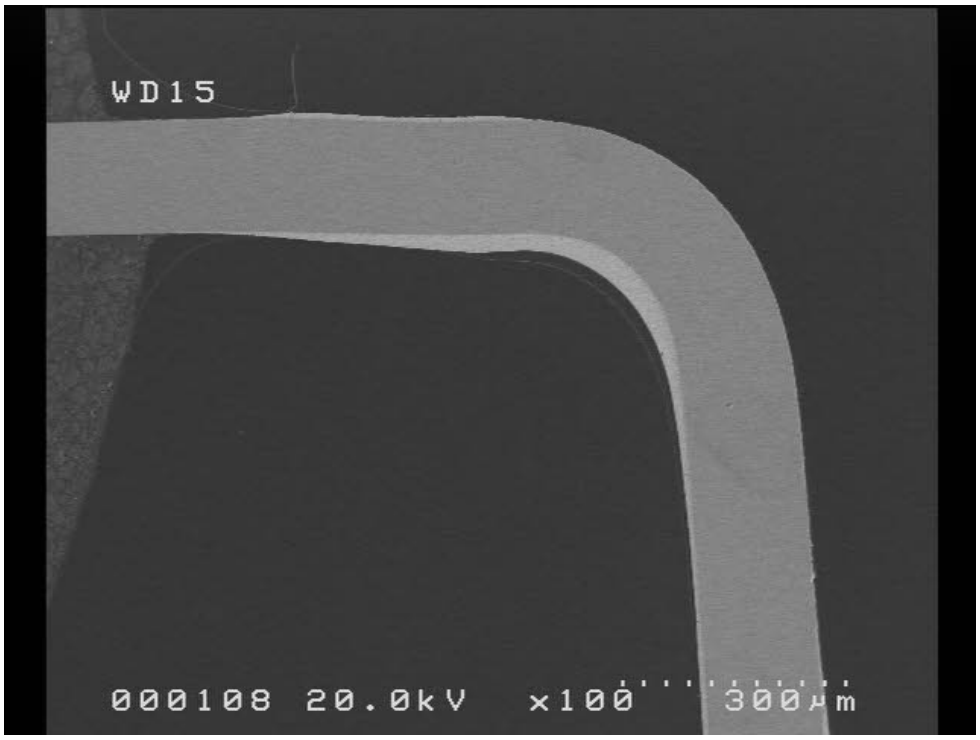


Figure 129: Batch B SEM cross-section image of PC40-UMF + 30%NNN2835 nanosilica dip+spray QFP44, knee location , 100x, (ref. Board 67).

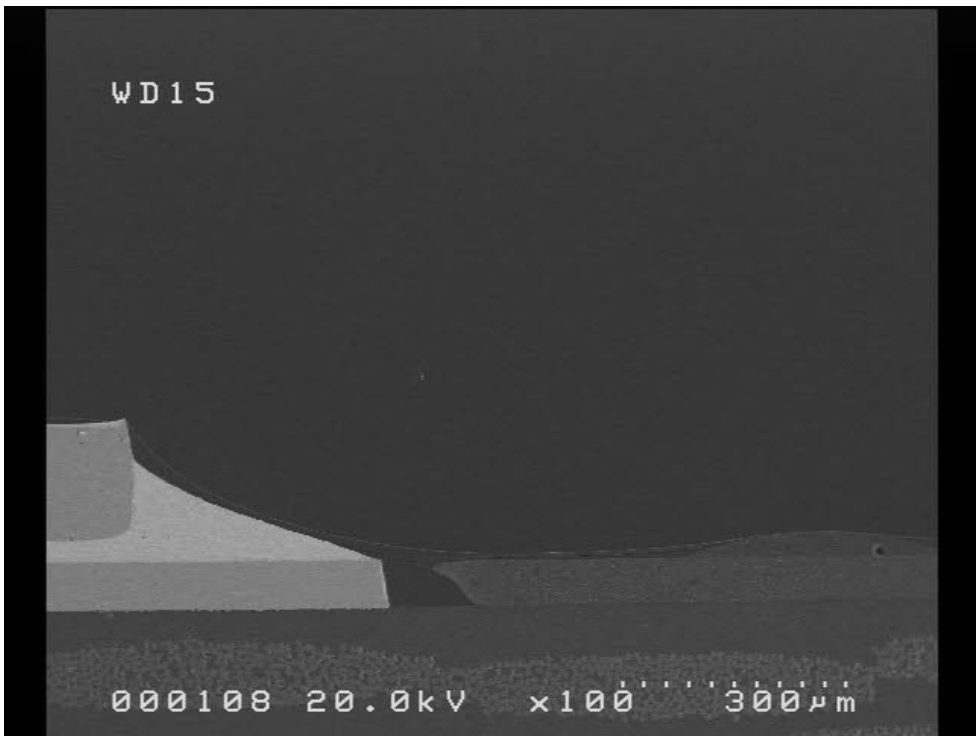


Figure 130: Batch B SEM cross-section image of PC40-UMF + 30%NNN2835 nanosilica dip+spray QFP44, toe location, 100x, (ref. Board 67).

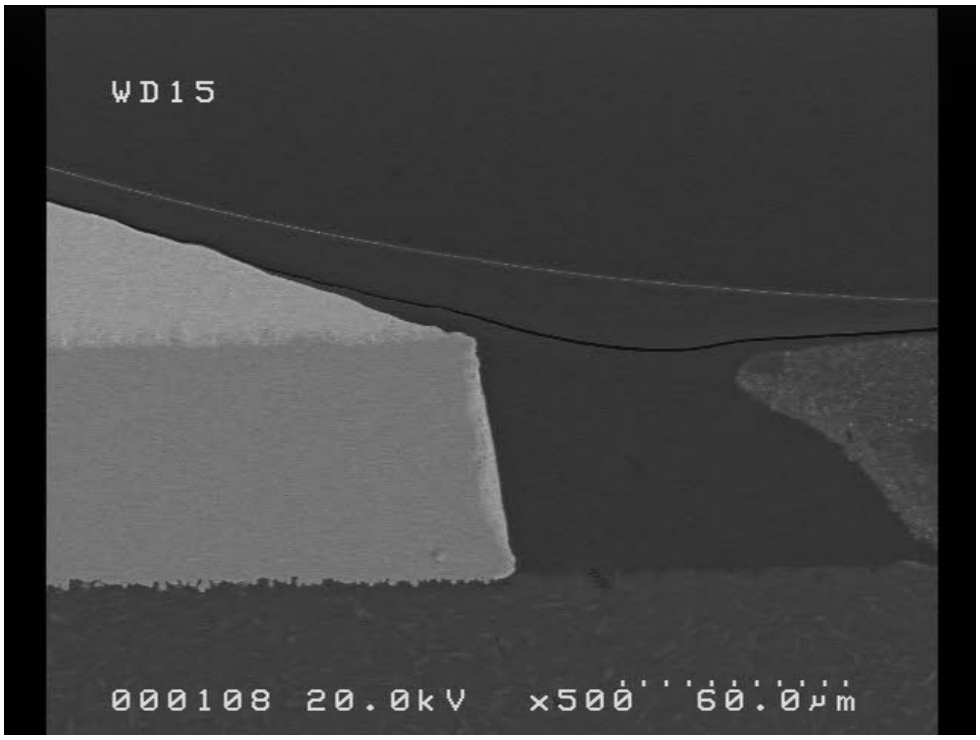


Figure 131: Batch B SEM cross-section image of PC40-UMF + 30%NNN2835 nanosilica dip+spray QFP44, toe location, 500x, (ref. Board 67).

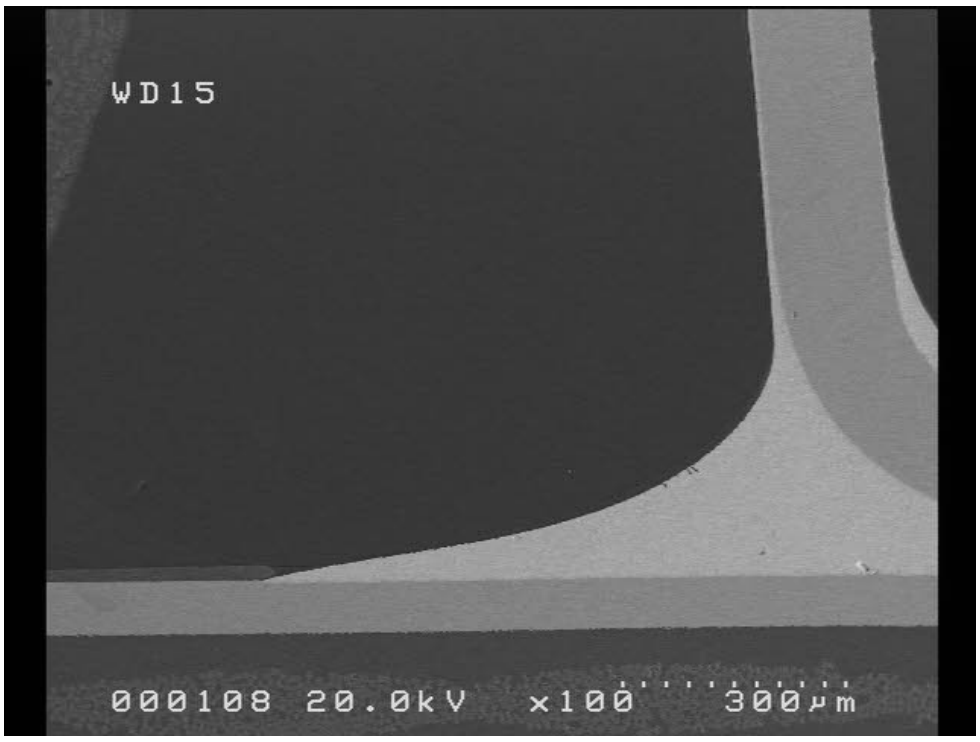


Figure 132: Batch B SEM cross-section image of PC40-UMF + 30%NNN2835 nanosilica dip+spray QFP44, heel location, 100x, (ref. Board 67).

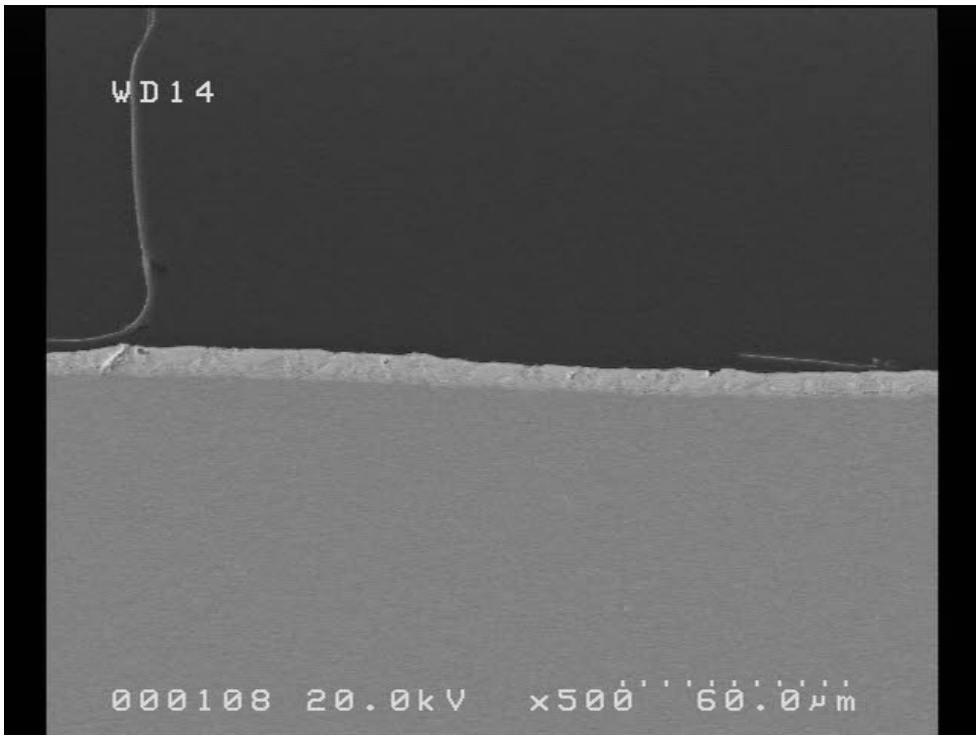


Figure 133: Batch B SEM cross-section image of PC40-UMF + 30%NNN2835 nanosilica dip+spray QFP44, location A, 500x, (ref. Board 67).

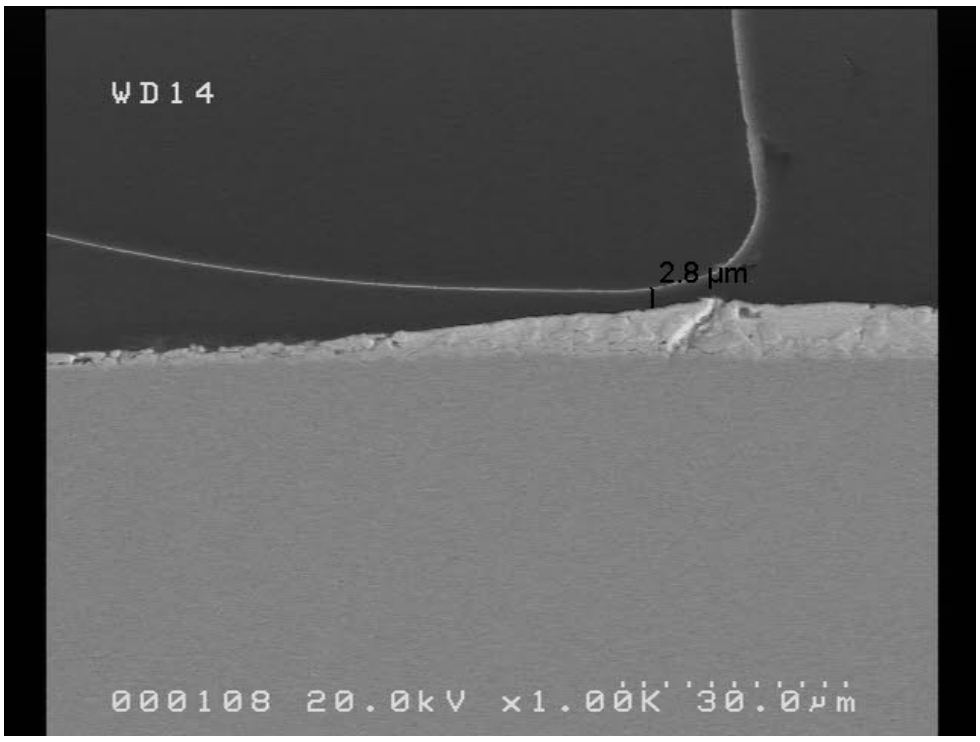


Figure 134: Batch B SEM cross-section image of PC40-UMF + 30%NNN2835 nanosilica dip+spray QFP44, location A, 1,000x, (ref. Board 67).

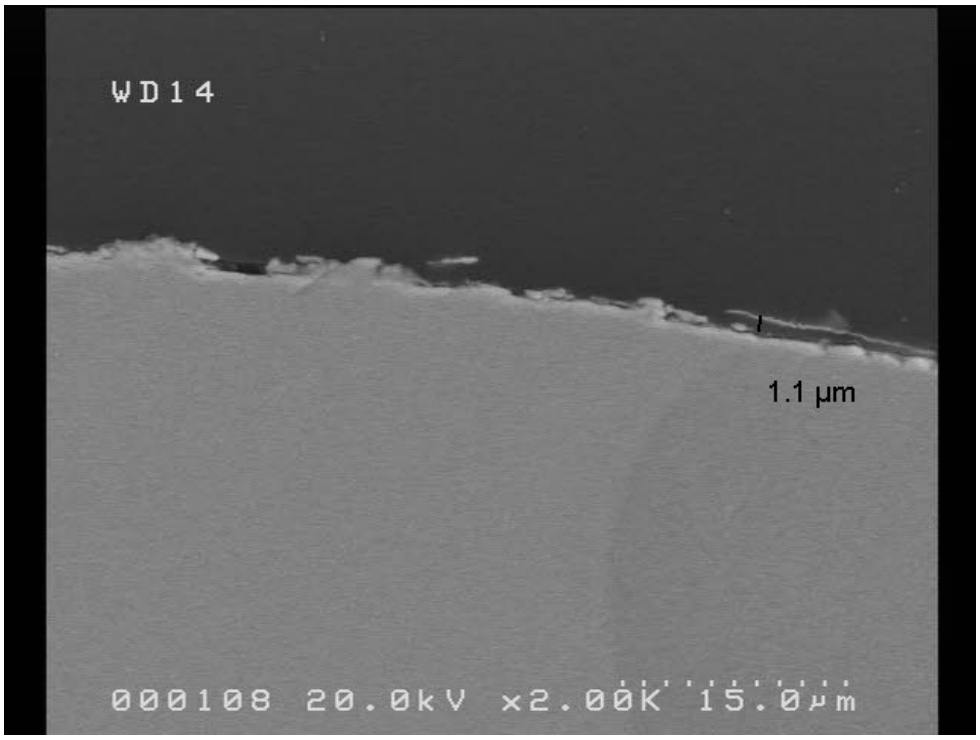


Figure 135: Batch B SEM cross-section image of PC40-UMF + 30%NNN2835 nanosilica dip+spray QFP44, location B, 2,000x, (ref. Board 67).

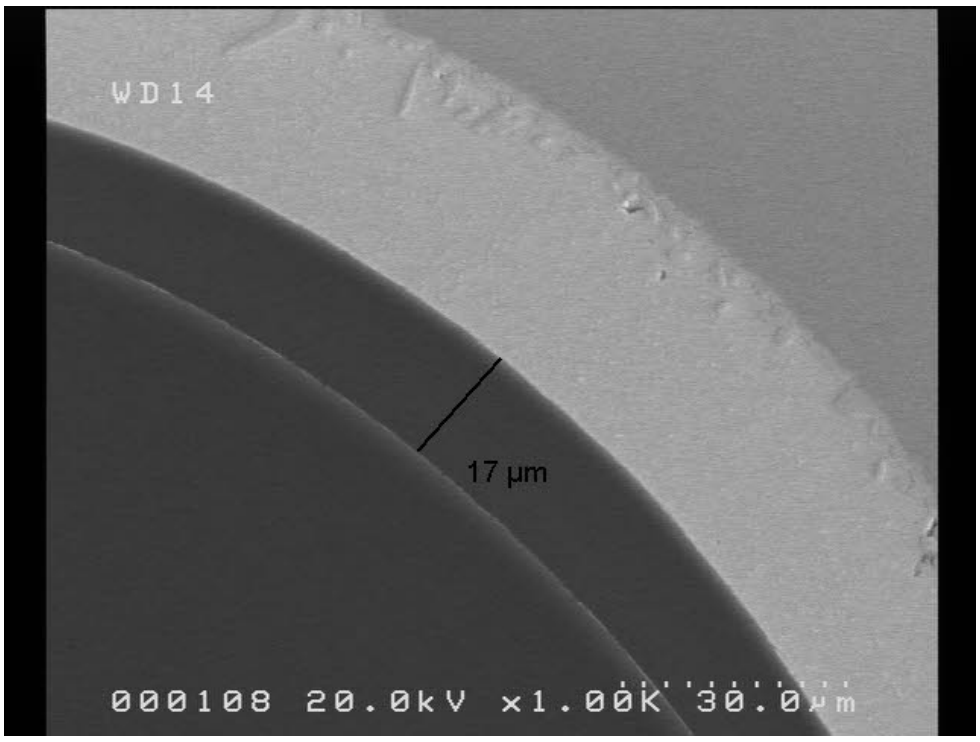


Figure 136: Batch B SEM cross-section image of PC40-UMF + 30%NNN2835 nanosilica dip+spray QFP44, behind the knee, 1,000x, (ref. Board 67).

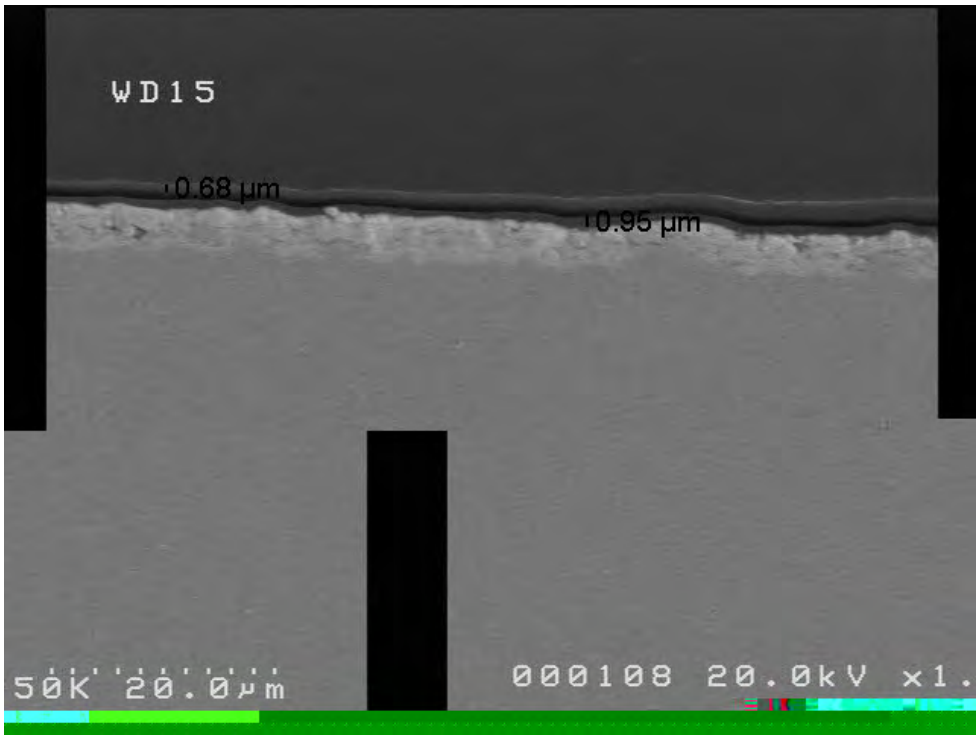


Figure 137: Batch B SEM cross-section image of PC40-UMF + 30%NNN2835 nanosilica dip+spray QFP44, between location F and T, 1500x, (ref. Board 67).

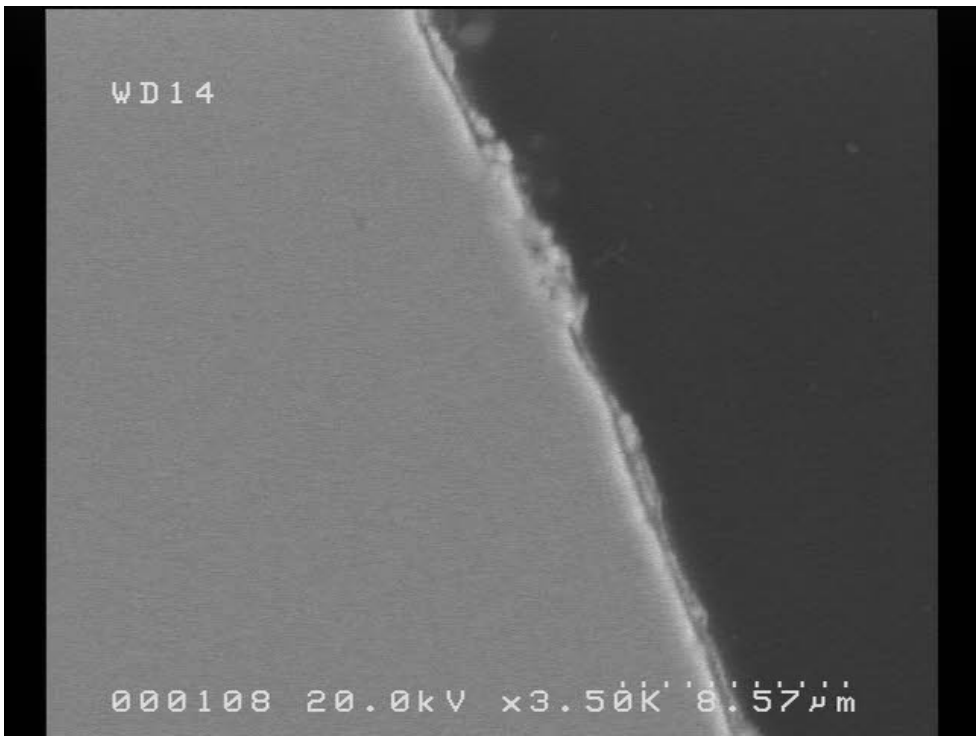


Figure 138: Batch B SEM cross-section image of PC40-UMF + 30%NNN2835 nanosilica dip+spray QFP44, location C, 3,500x, (ref. Board 67).

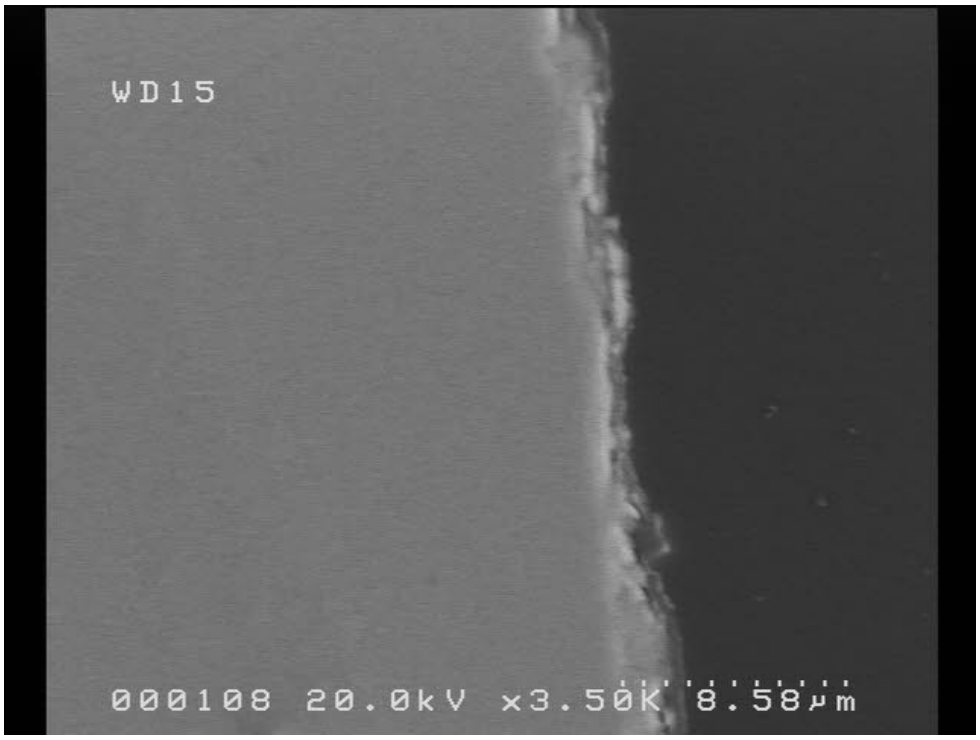


Figure 139: Batch B SEM cross-section image of PC40-UMF + 30%NNN2835 nanosilica dip+spray QFP44, location D, 3,500x, (ref. Board 67).

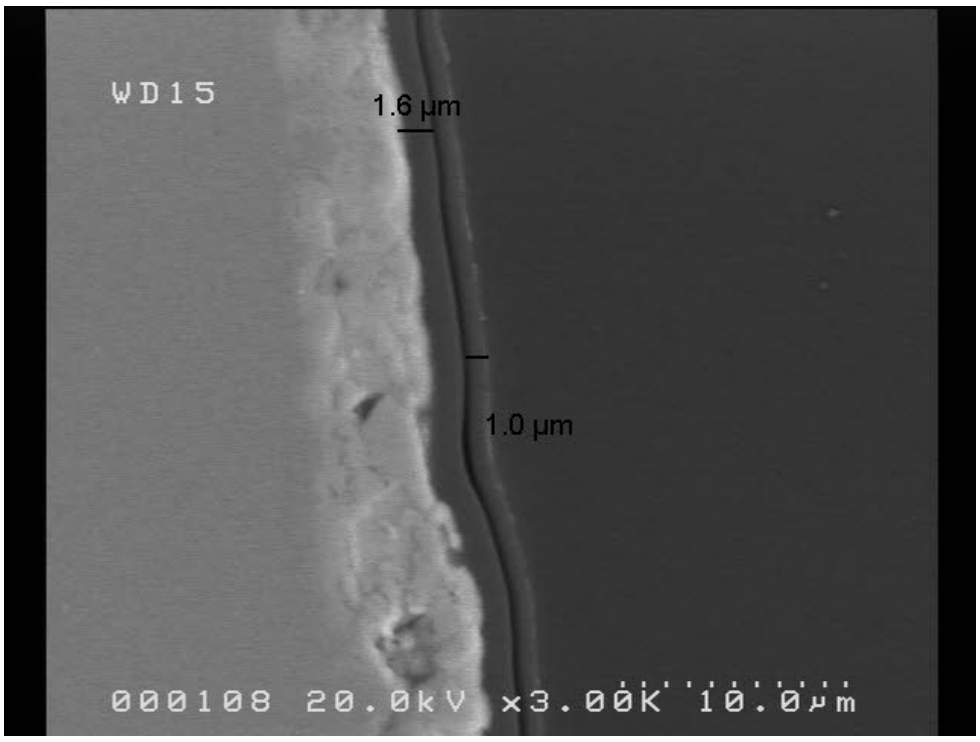


Figure 140: Batch B SEM cross-section image of PC40-UMF + 30%NNN2835 nanosilica dip+spray QFP44, location E, 3,000x, (ref. Board 67).

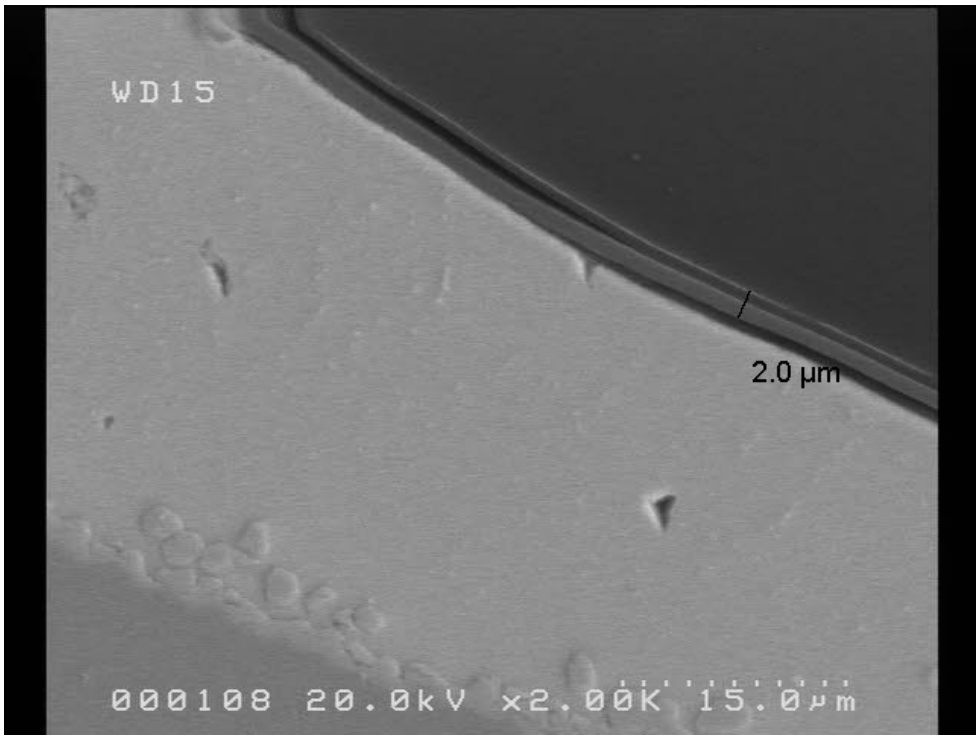


Figure 141: Batch B SEM cross-section image of PC40-UMF + 30%NNN2835 nanosilica dip+spray QFP44, location F, 2,000x, (ref. Board 67).

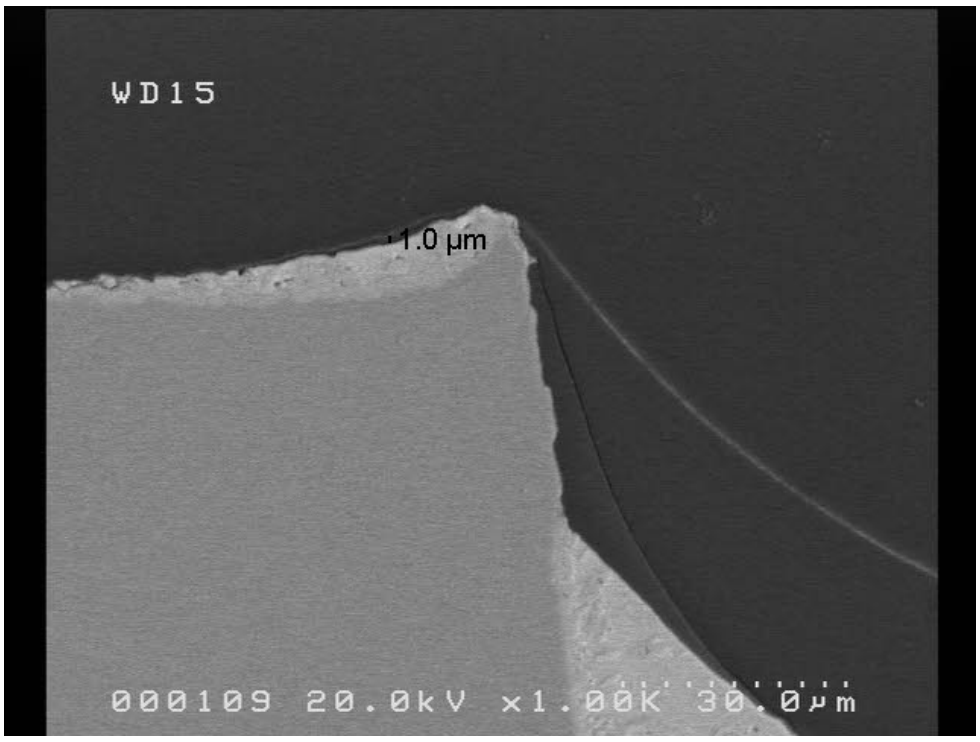


Figure 142: Batch B SEM cross-section image of PC40-UMF + 30%NNN2835 nanosilica dip+spray QFP44, location T, 1,000x, (ref. Board 67).

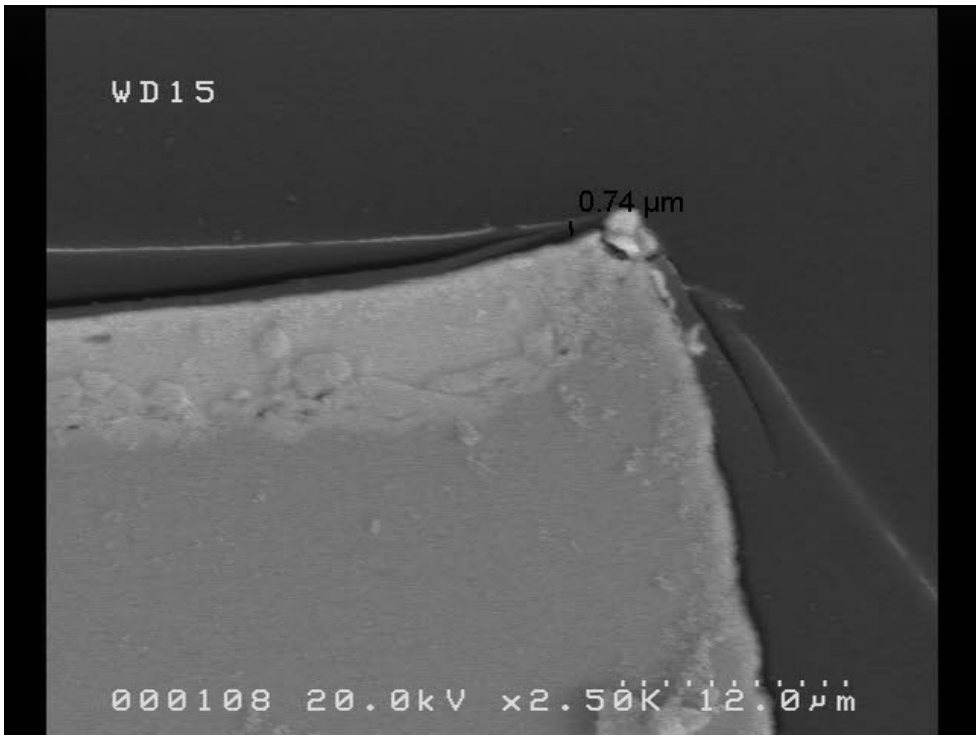


Figure 143: Batch B SEM cross-section image of PC40-UMF + 30%NNN2835 nanosilica dip+spray QFP44, location T, 2500x, (ref. Board 67).

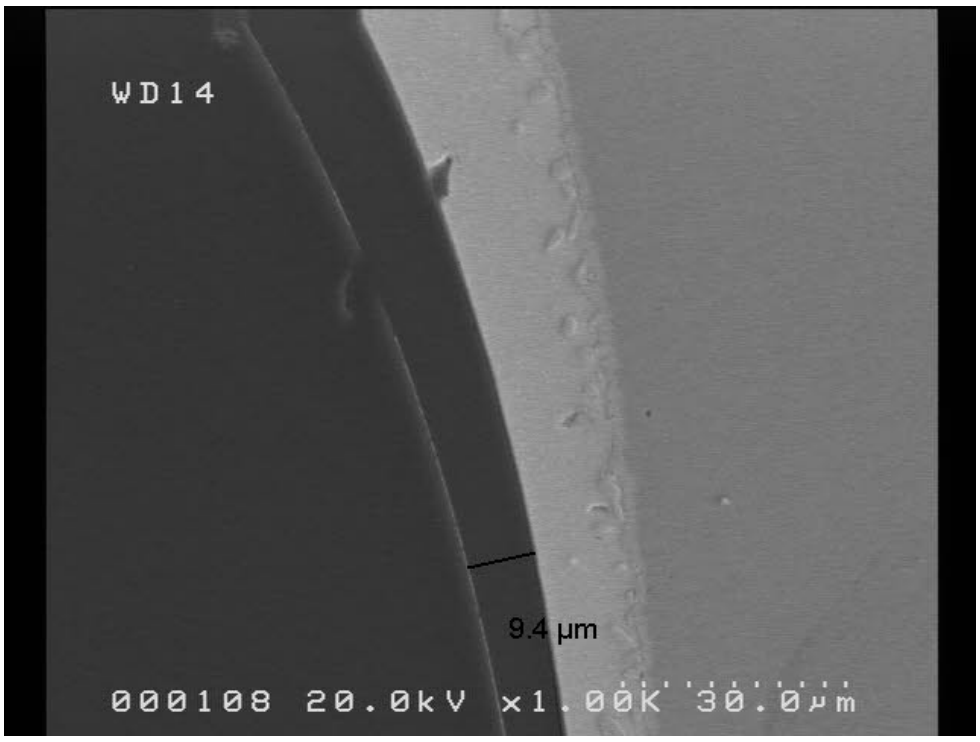


Figure 144: Batch B SEM cross-section image of PC40-UMF + 30%NNN2835 nanosilica dip+spray QFP44, location G, 1,000x, (ref. Board 67).

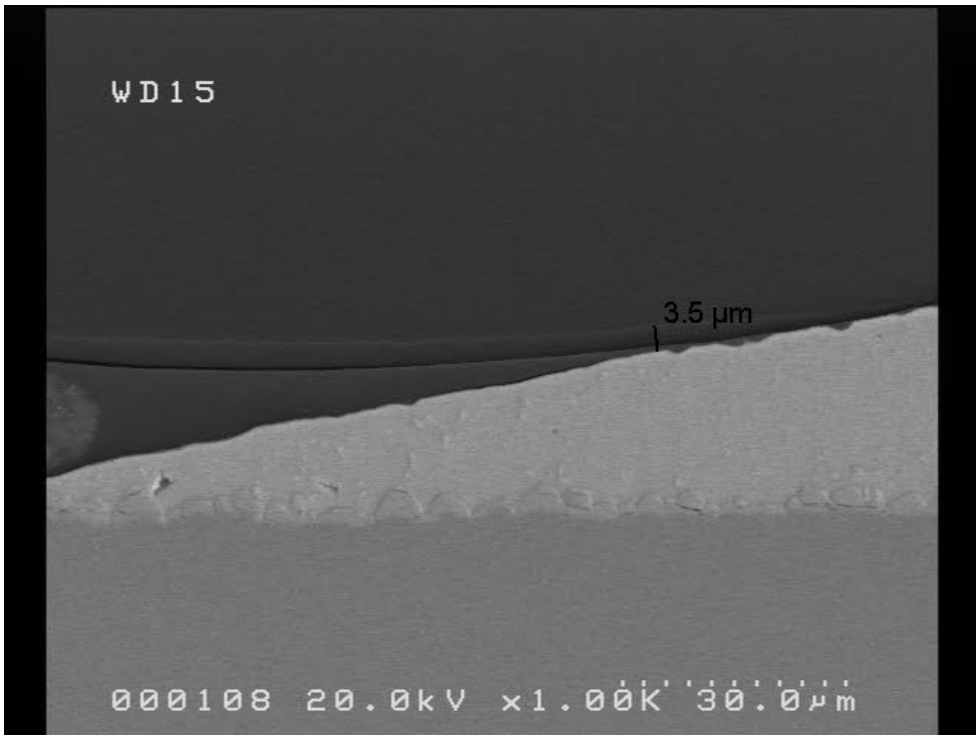


Figure 145: Batch B SEM cross-section image of PC40-UMF + 30%NNN2835 nanosilica dip+spray QFP44, location H, 1,000x, (ref. Board 67).

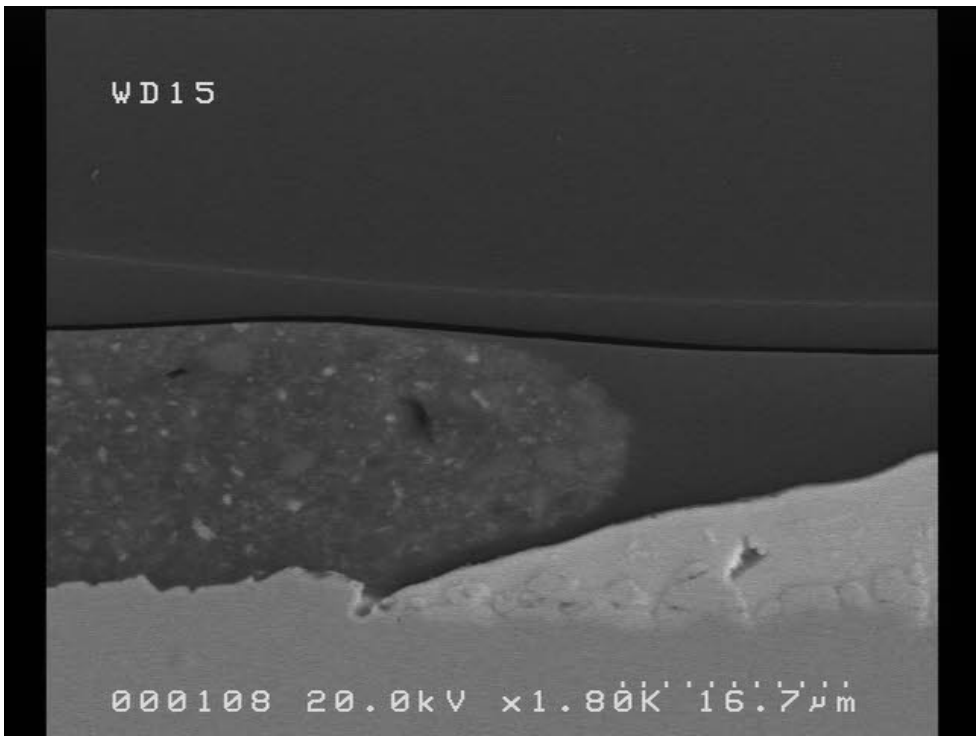


Figure 146: Batch B SEM cross-section image of PC40-UMF + 30%NNN2835 nanosilica dip+spray QFP44, location H, 1,800x, (ref. Board 67).

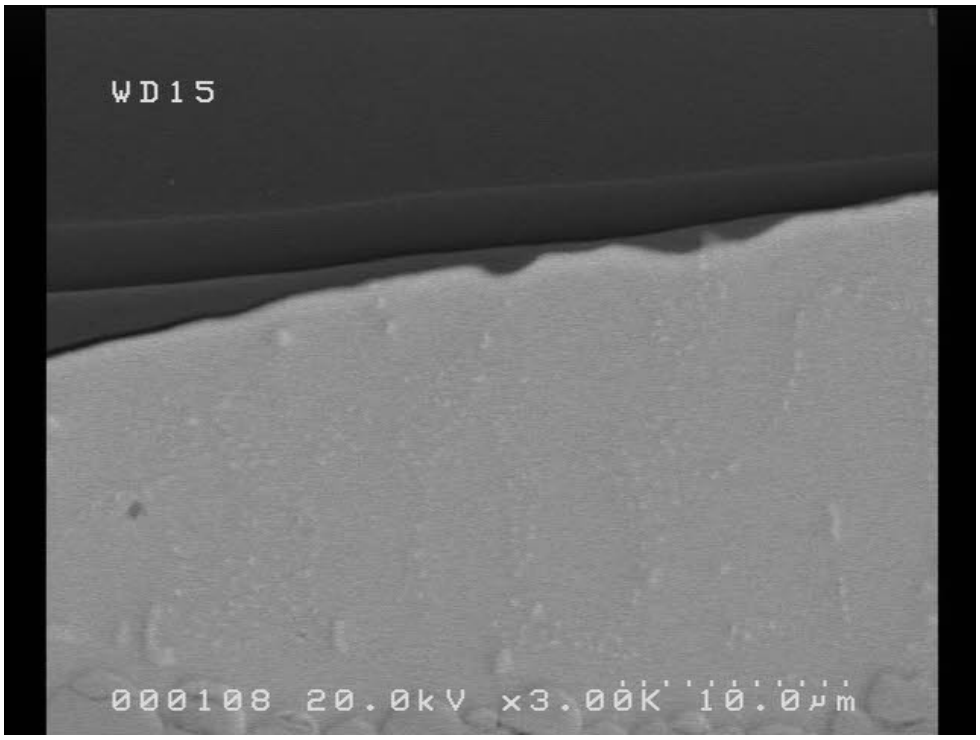


Figure 147: Batch B SEM cross-section image of PC40-UMF + 30%NNN2835 nanosilica dip+spray QFP44, location H, 3,000x, (ref. Board 67).

2.1.4.4 PC40-UMF+50%NNN285 nanosilica

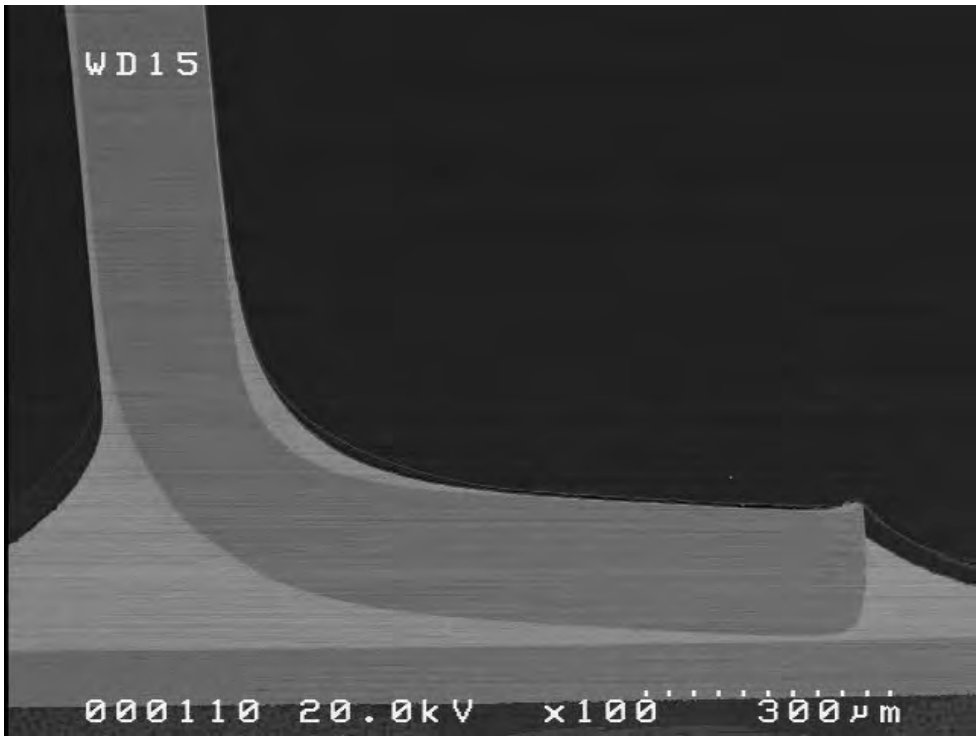


Figure 148: Batch B SEM cross-section image of PC40-UMF + 50%NNN2835 nanosilica dip+spray QFP44, lead foot location, 100x (ref. Board 72).



Figure 149: Batch B SEM cross-section image of PC40-UMF + 50%NNN2835 nanosilica dip+spray QFP44, lead toe location, 100x (ref. Board 72).

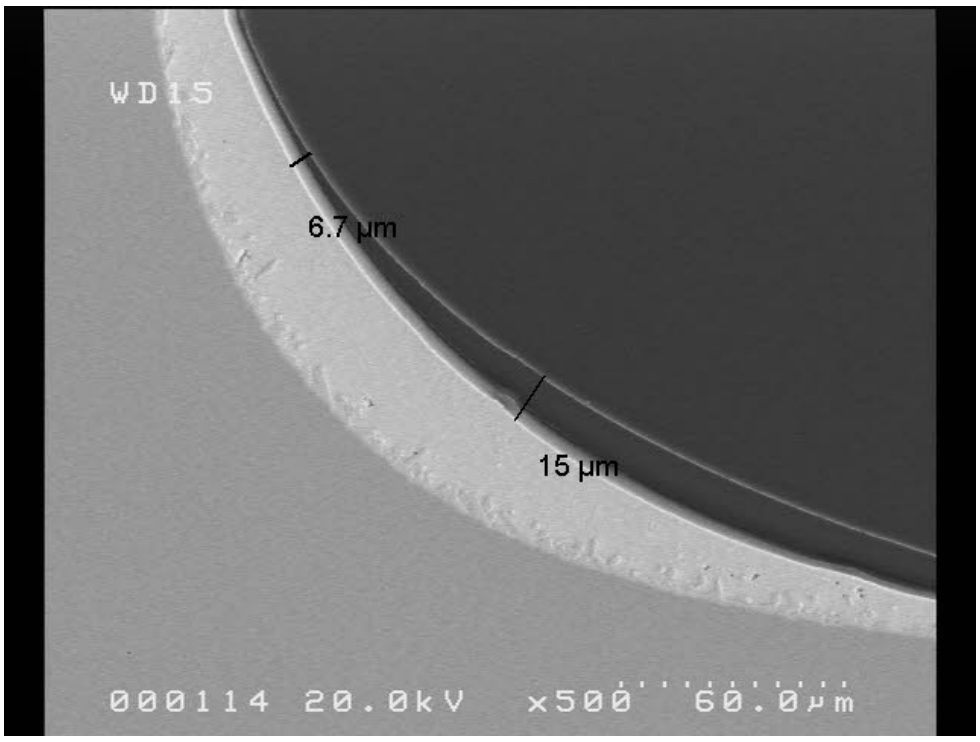


Figure 150: Batch B SEM cross-section image of PC40-UMF + 50%NNN2835 nanosilica dip+spray QFP44, location F, 500x (ref. Board 72).

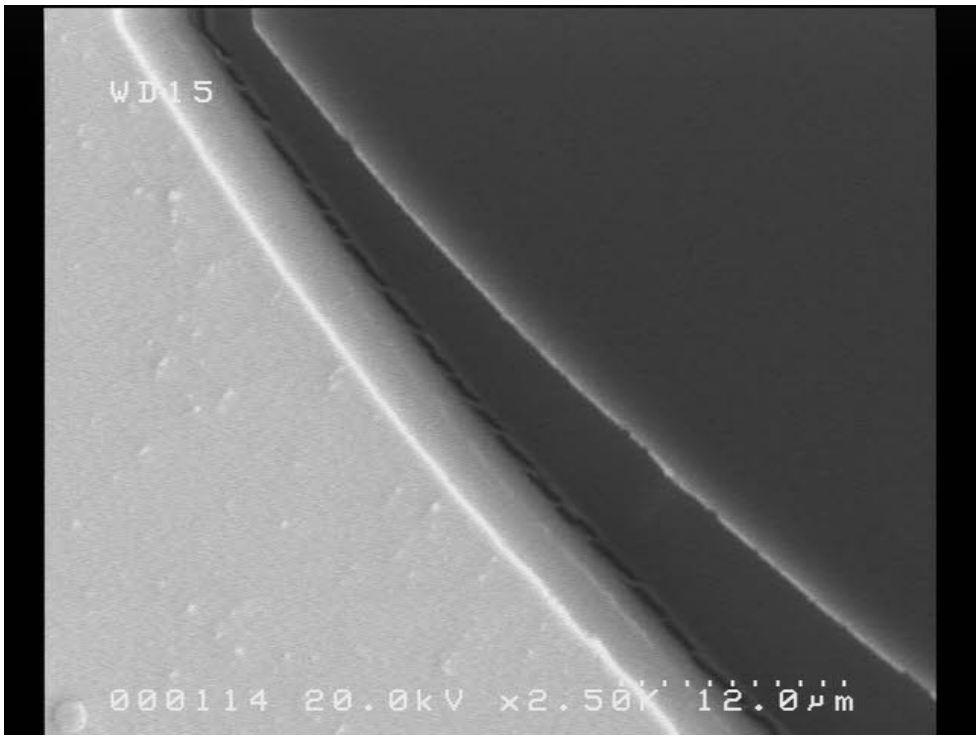


Figure 151: Batch B SEM cross-section image of PC40-UMF + 50%NNN2835 nanosilica dip+spray QFP44, location, F, 2,500x (ref. Board 72).

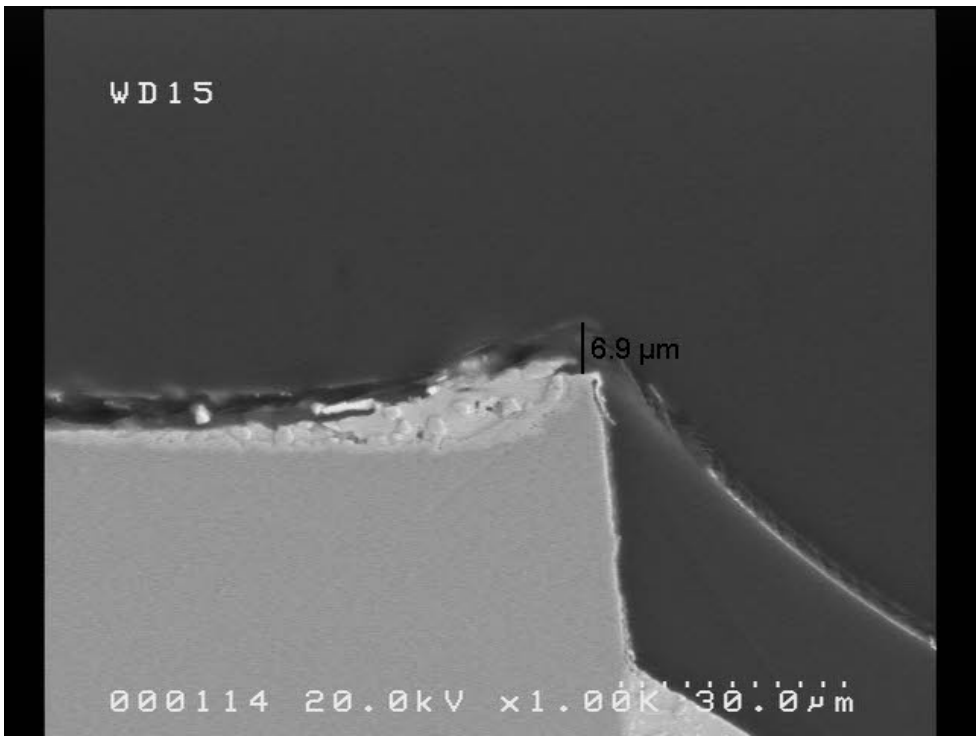


Figure 152: Batch B SEM cross-section image of PC40-UMF + 50%NNN2835 nanosilica dip+spray QFP44, location T, 1,000x (ref. Board 72).

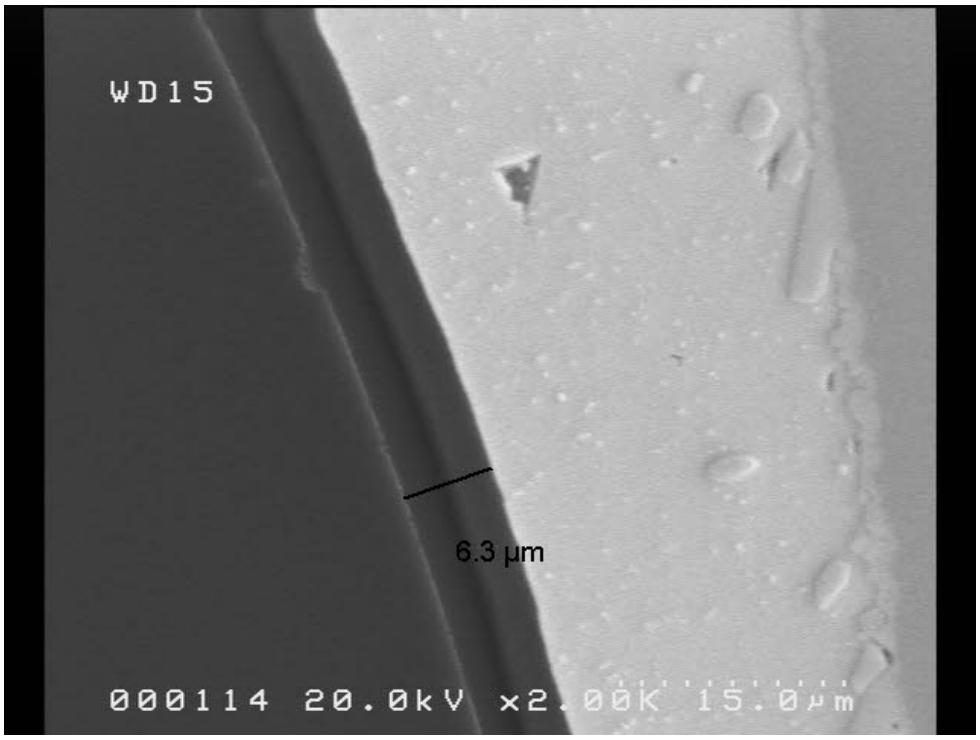


Figure 153: Batch B SEM cross-section image of PC40-UMF + 50%NNN2835 nanosilica dip+spray QFP44, location G, 2,000x (ref. Board 72).

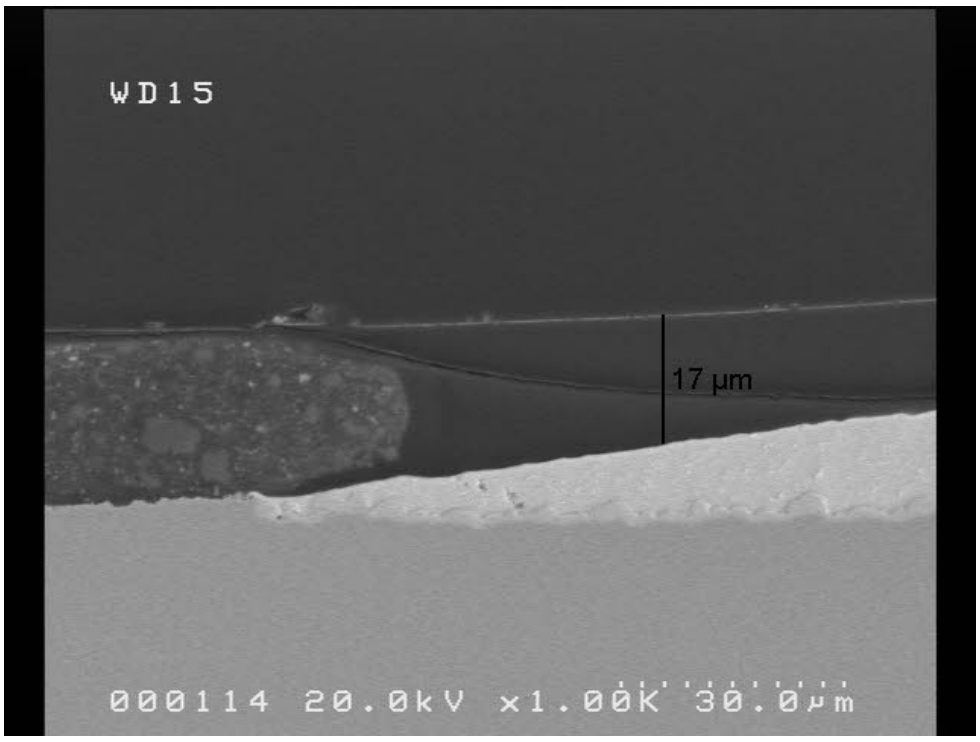


Figure 154: Batch B SEM cross-section image of PC40-UMF + 50%NNN2835 nanosilica dip+spray QFP44, location H, 1,000x (ref. Board 72).

2.1.4.5 PC40-UMF+15.54%N3300 (no nanosilica)

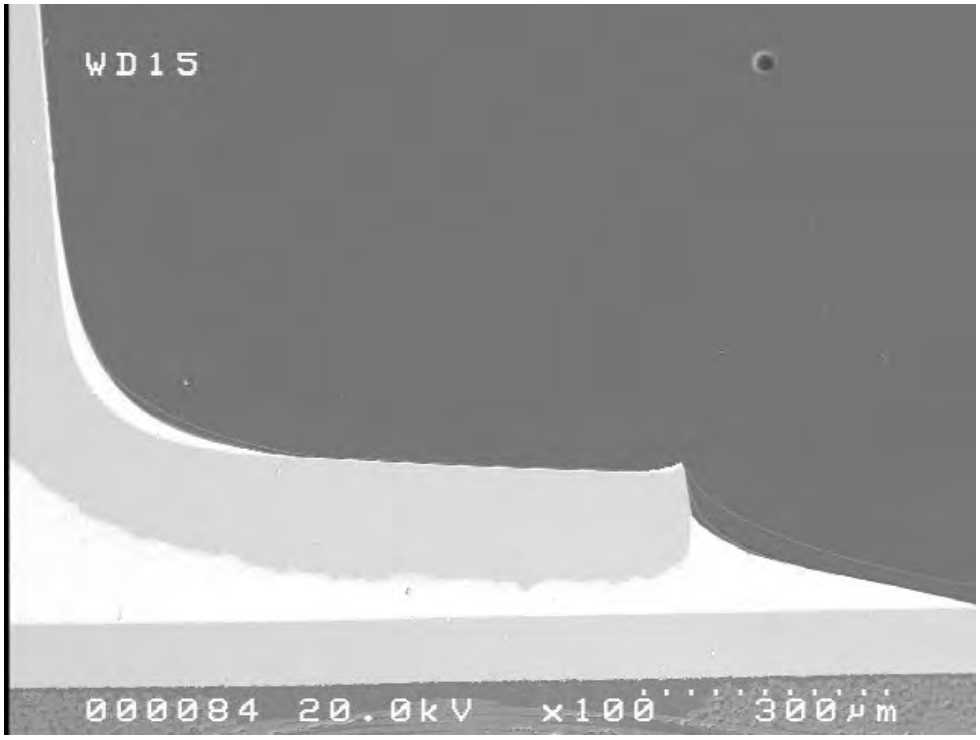


Figure 155: Batch B SEM cross-section image of PC40-UMF + 15.54%N3300 nanosilica dip+spray QFP44, lead foot location, 100x (ref. Board 77).

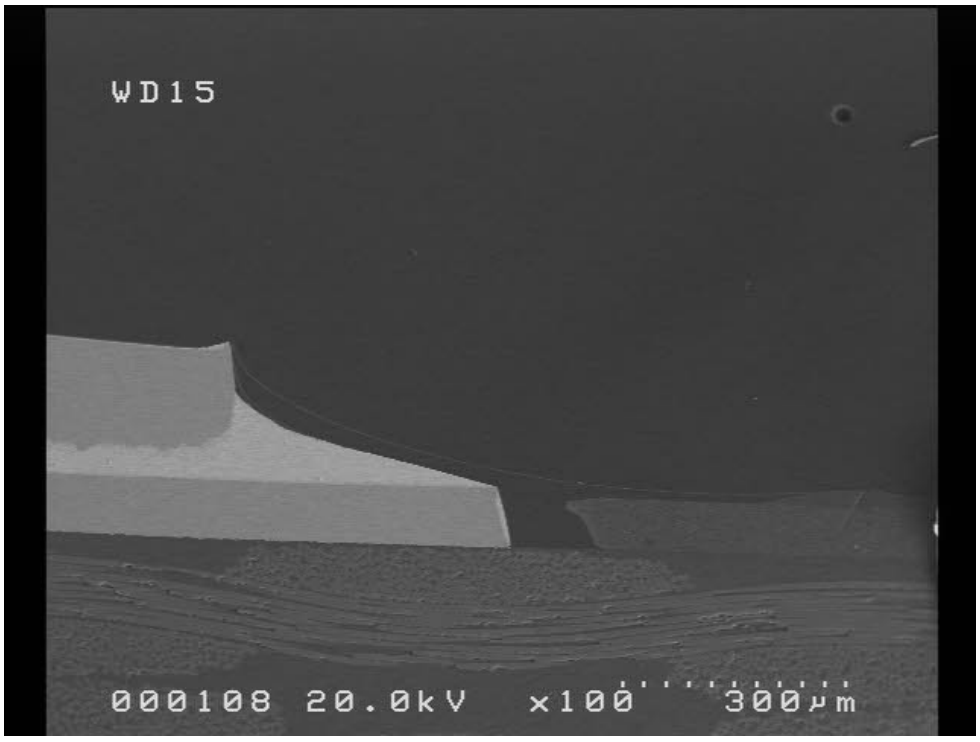


Figure 156: Batch B SEM cross-section image of PC40-UMF + 15.54%N3300 nanosilica dip+spray QFP44, lead toe location, 100x (ref. Board 77).

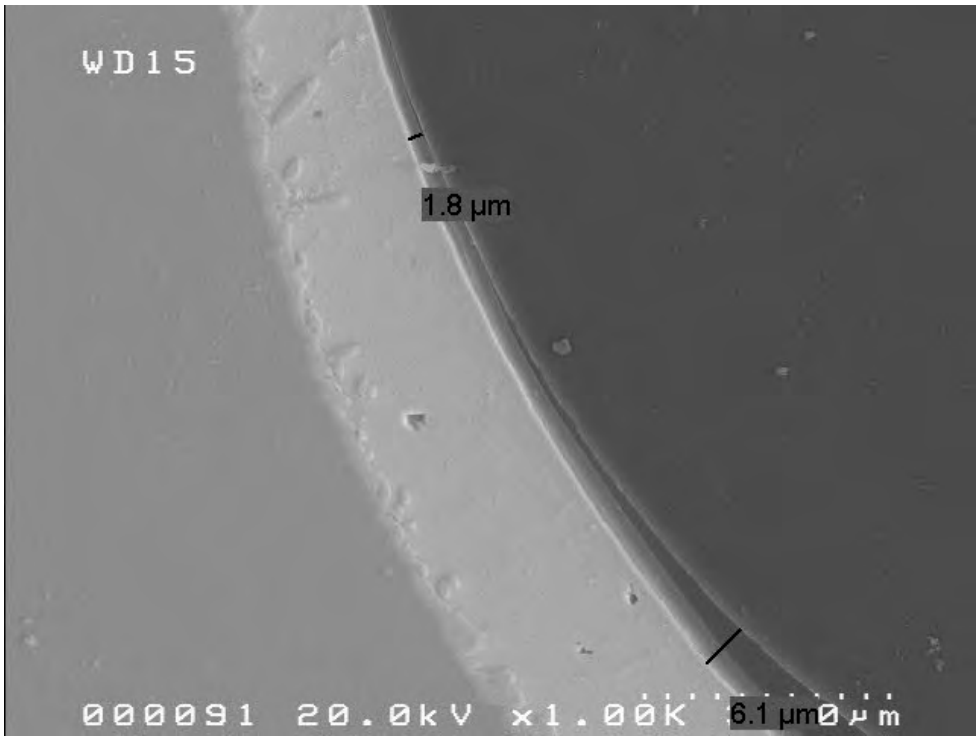


Figure 157: Batch B SEM cross-section image of PC40-UMF + 15.54%N3300 nanosilica dip+spray QFP44, location F, 1,000x (ref. Board 77).

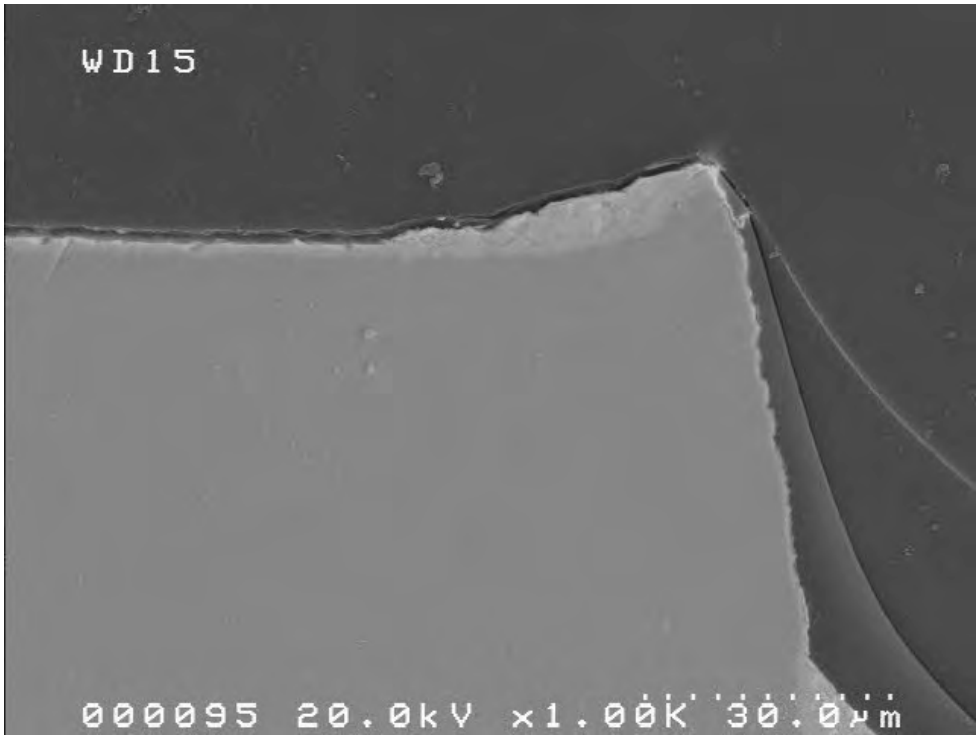


Figure 158: Batch B SEM cross-section image of PC40-UMF + 15.54%N3300 nanosilica dip+spray QFP44, location T, 1,000x (ref. Board 77).

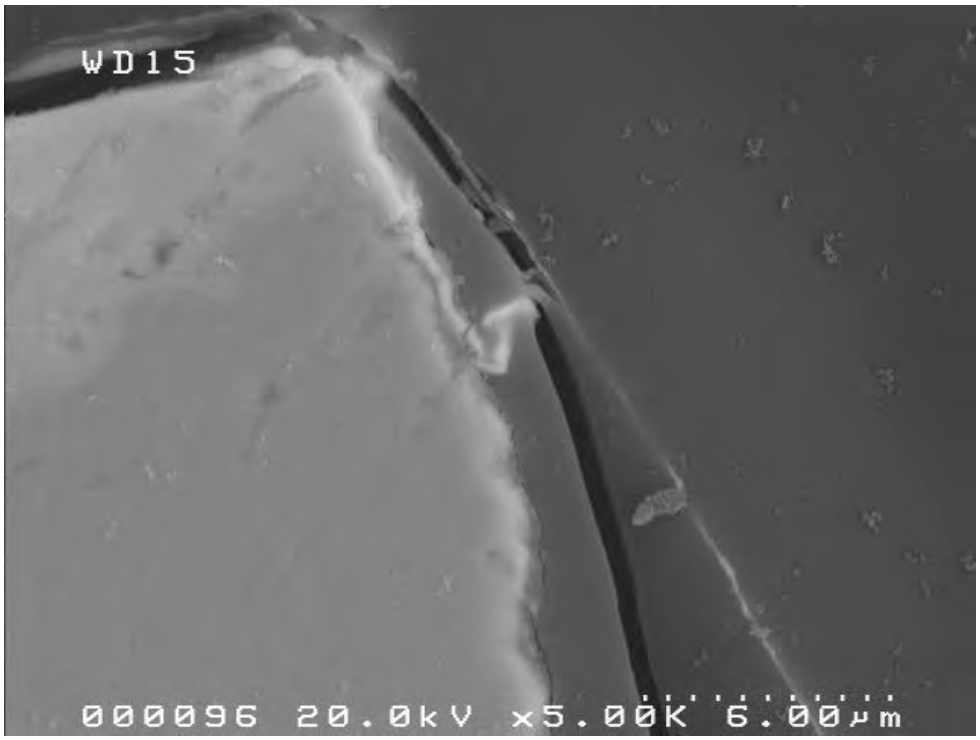


Figure 159: Batch B SEM cross-section image of PC40-UMF + 15.54%N3300 nanosilica dip+spray QFP44, location T, 5,000x (ref. Board 77).

2.1.5 PC40-UMF Batch B horizontal section

Similar to the PC18M evaluation, horizontal sections were performed on the PC40-UMF coated QFP44 to determine the coating variation around the perimeter of the device. For reference, the approximate section plane is located as shown in Figure 30 with the pin numbering being the same as Figure 32 and repeated below in Figure 160. The horizontal cross-sections for the batch B dip+spray with plasma etch between layers were made for the PC40-UMF (Figure 161 to Figure 178) and the PC40-UMF + 10%NNN2835 nanosilica (Figure 179 to Figure 204).

Note the nanosilica filled spray coating was always applied over an unfilled PC40-UMF dip, e.g. PC40-UMF dip, plasma etch, then (PC40-UMF + 10%NNN2835 nanosilica) spray.

The leads near the part corners had coating behind the leads more often than leads near the middle of the part (e.g. Figure 163). There was little or no coating on the lead corners, especially the side facing the package.

Some leads had dip coating bridging between the part and the leads and also between leads. When dip coating bridging was present, the spray tended to bridge between leads (e.g. Figure 170 and Figure 171).

Some leads had delamination between the dip and the spray layers (e.g. Figure 165) and sometimes there was delamination between the dip and the solder (e.g. Figure 177 and Figure 178).

There tended to be more delamination instances between the PC40-UMF dip and the PC40-UMF+10%NNN2835 spray layers (e.g. Figure 180, Figure 186 and Figure 204).

There were also some instances of delamination between the coating that bridged between the lead and the package and the lead which could be due to PC40-UMF shrinkage during cure (Figure 186).

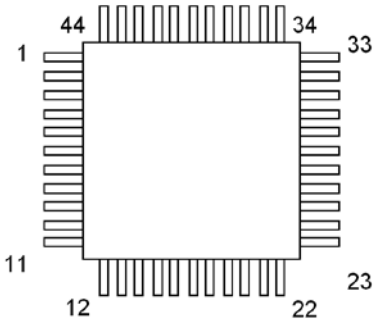


Figure 160: QFP44 pin numbering.

2.1.5.1 PC40-UMF Batch B dip+spray flat section

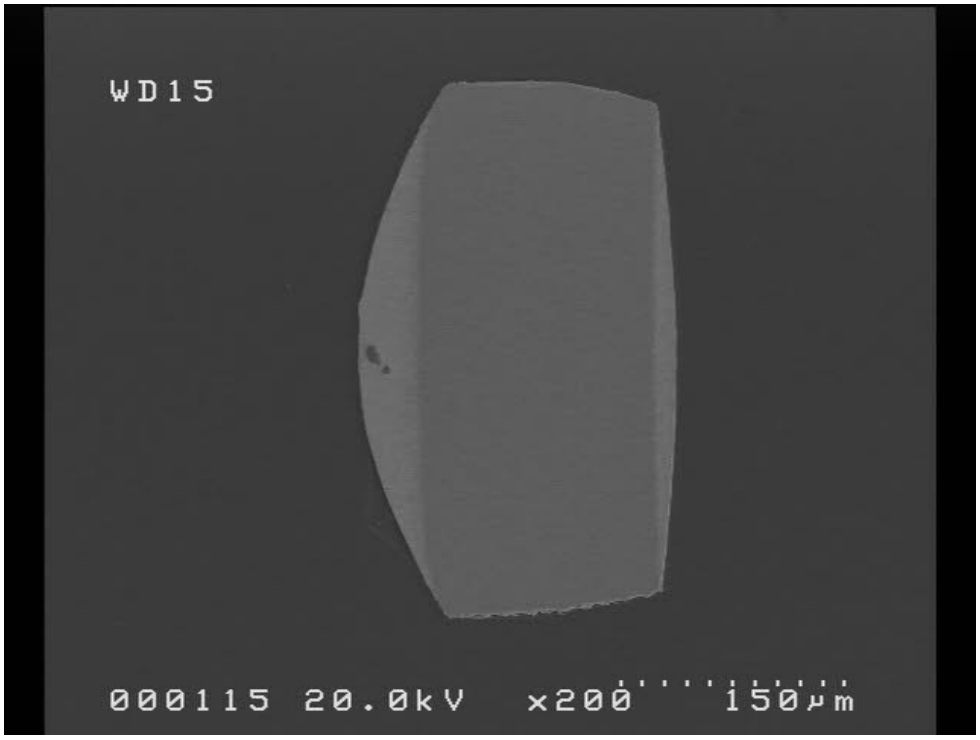


Figure 161: Batch B SEM image of the horizontal cross-section of PC40-UMF coating on a QFP44, lead 11, 200x (ref. Board 66, U3).

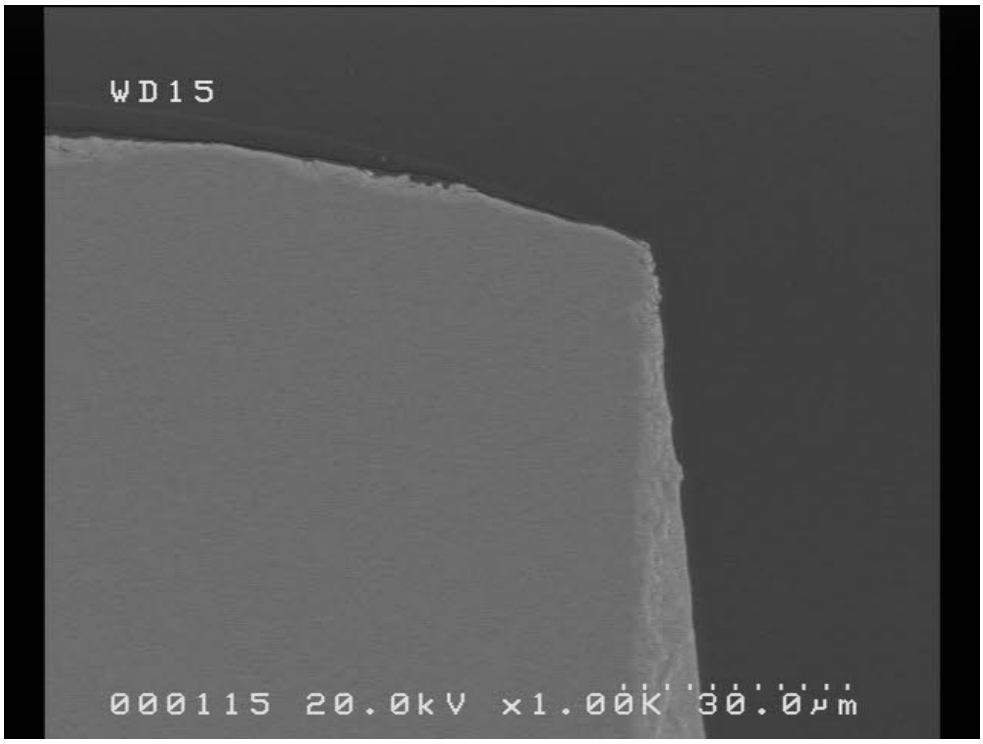


Figure 162: Batch B SEM image of the horizontal cross-section of PC40-UMF coating on a QFP44, lead 11, 1,000x (ref. Board 66, U3).

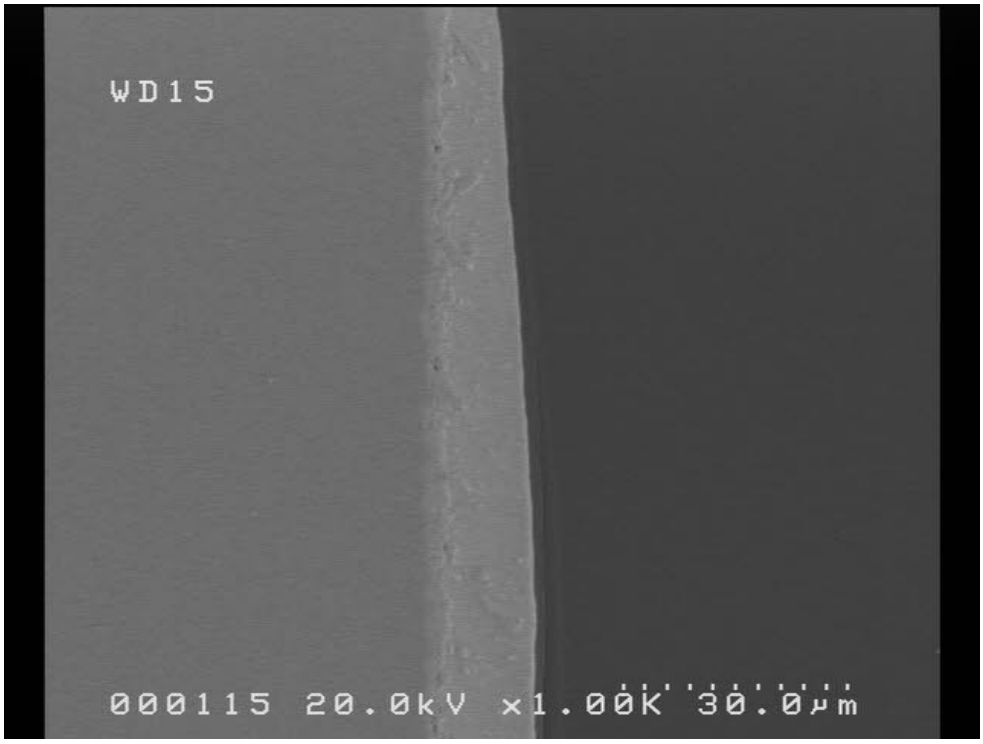


Figure 163: Batch B SEM image of the horizontal cross-section of PC40-UMF coating on a QFP44, lead 11, 1,000x (ref. Board 66, U3). The middle of the back of the lead is shown. There is a thin spray coating layer with delamination between the dip and the spray layers.

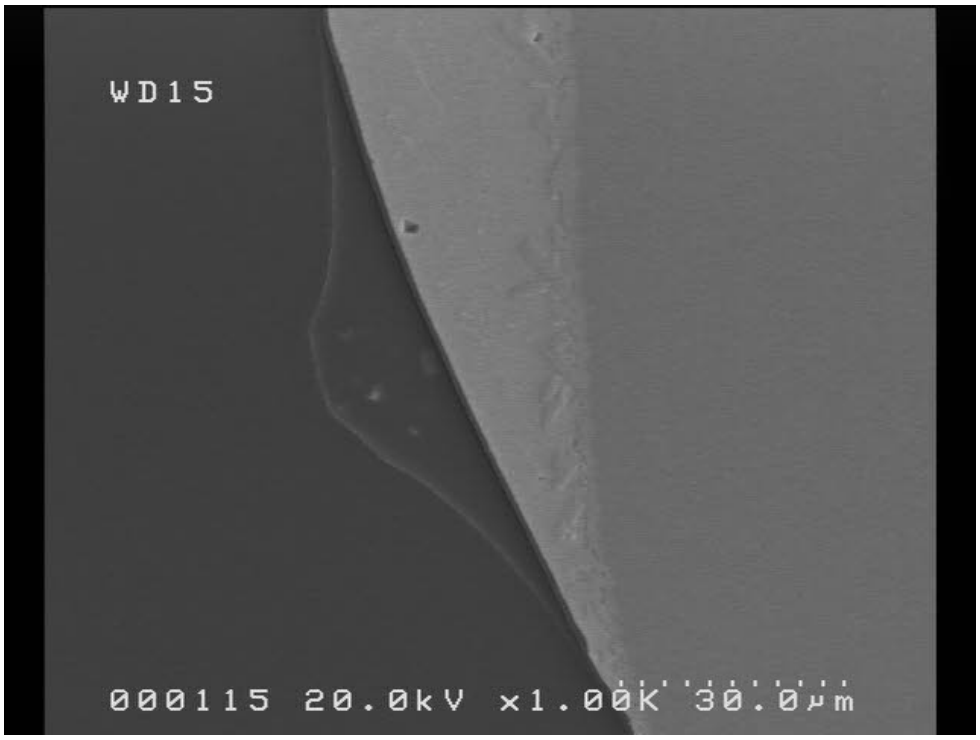


Figure 164: Batch B SEM image of the horizontal cross-section of PC40-UMF coating on a QFP44, lead 11, 1,000x (ref. Board 66, U3). Bump of spray coating on the dip coating with delamination between the dip and the spray layers.

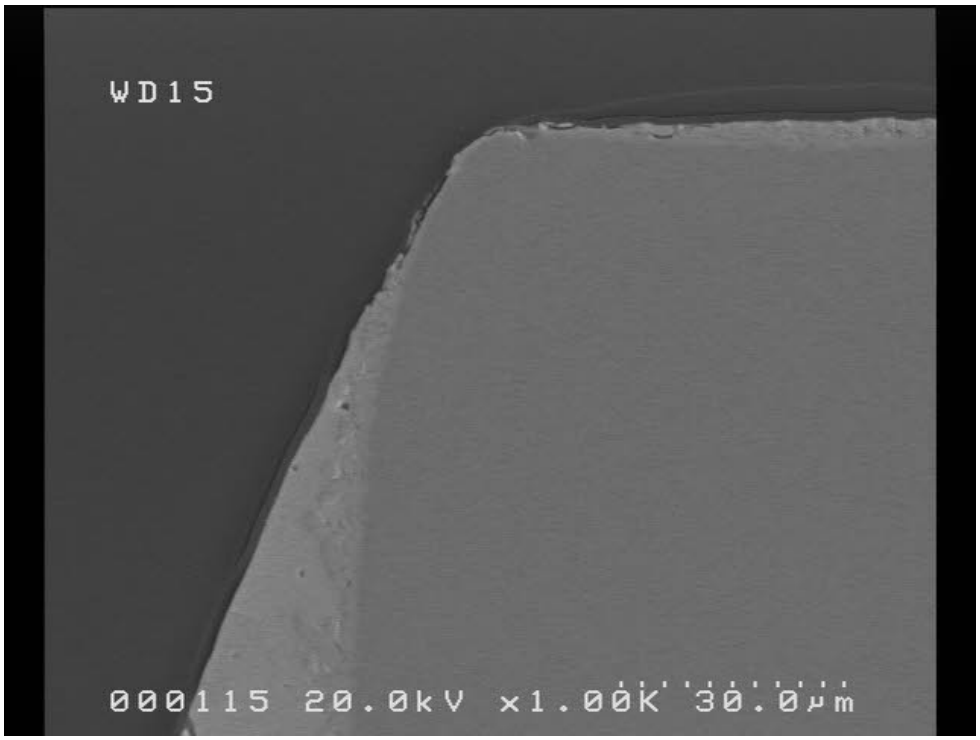


Figure 165: Batch B SEM image of the horizontal cross-section of PC40-UMF coating on a QFP44, lead 11, 1,000x (ref. Board 66, U3). Delamination is present between the dip and the spray layers.

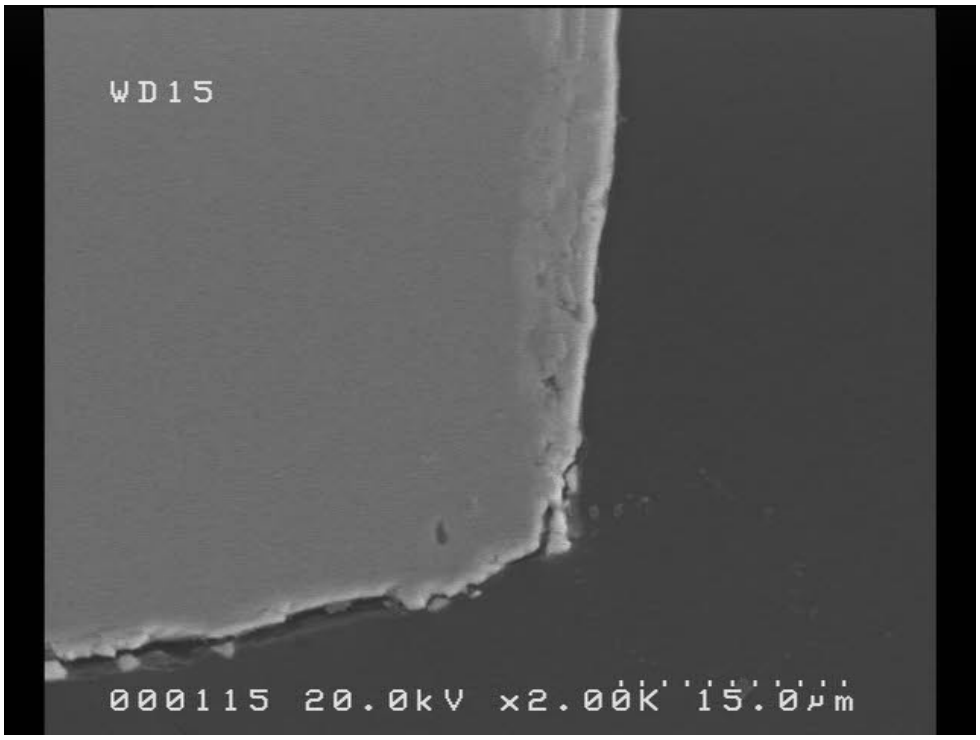


Figure 166: Batch B SEM image of the horizontal cross-section of PC40-UMF coating on a QFP44, lead 11, 2,000x (ref. Board 66, U3).

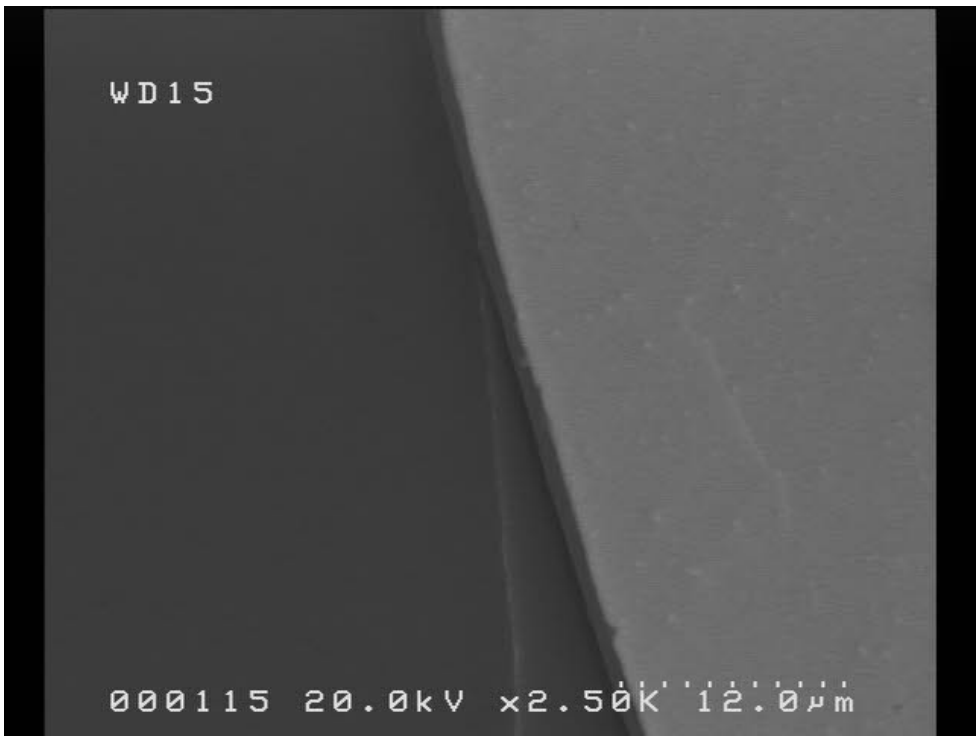


Figure 167: Batch B SEM image of the horizontal cross-section of PC40-UMF coating on a QFP44, lead 11, 2,500x (ref. Board 66, U3).

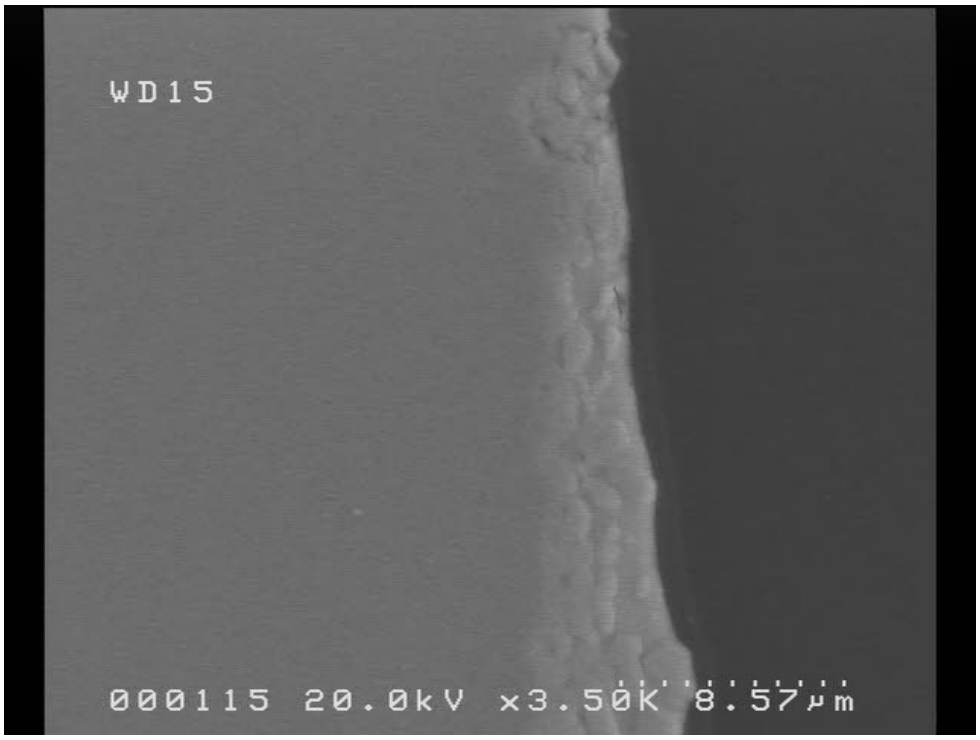


Figure 168: Batch B SEM image of the horizontal cross-section of PC40-UMF coating on a QFP44, lead 11, 3,500x (ref. Board 66, U3).

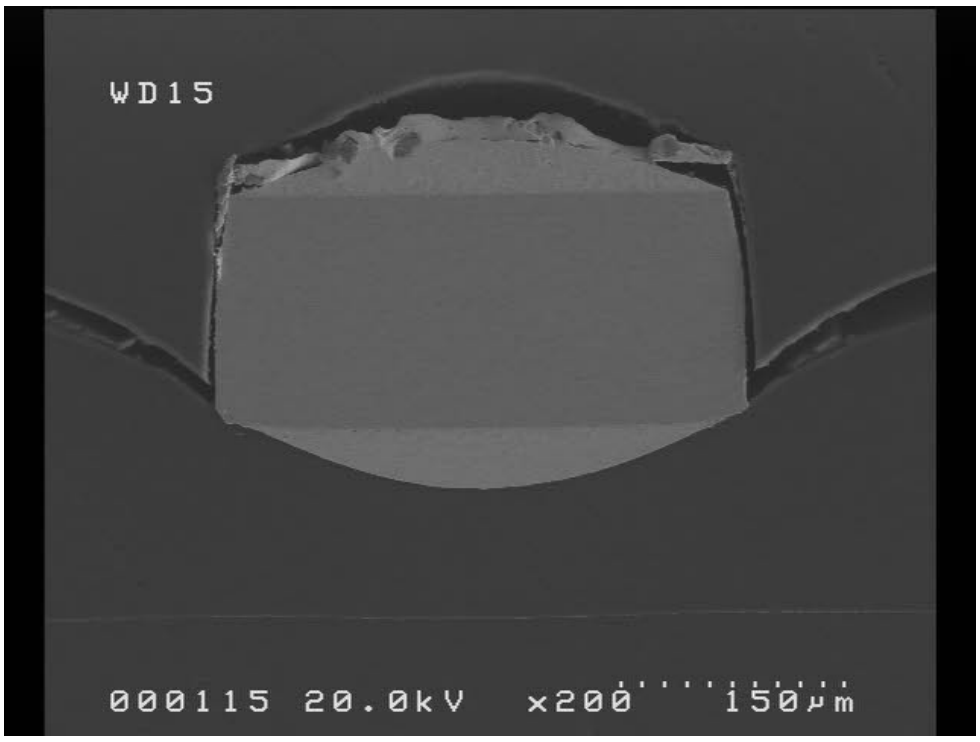


Figure 169: Batch B SEM image of the horizontal cross-section of PC40-UMF coating on a QFP44, lead 19, 200x (ref. Board 66, U3). Dip coating is bridging between the lead and the part at the image upper center. Spray coating appears to be bridging between leads at the image lower center. It is unclear what caused the large separation around the sides and the rear of the lead.

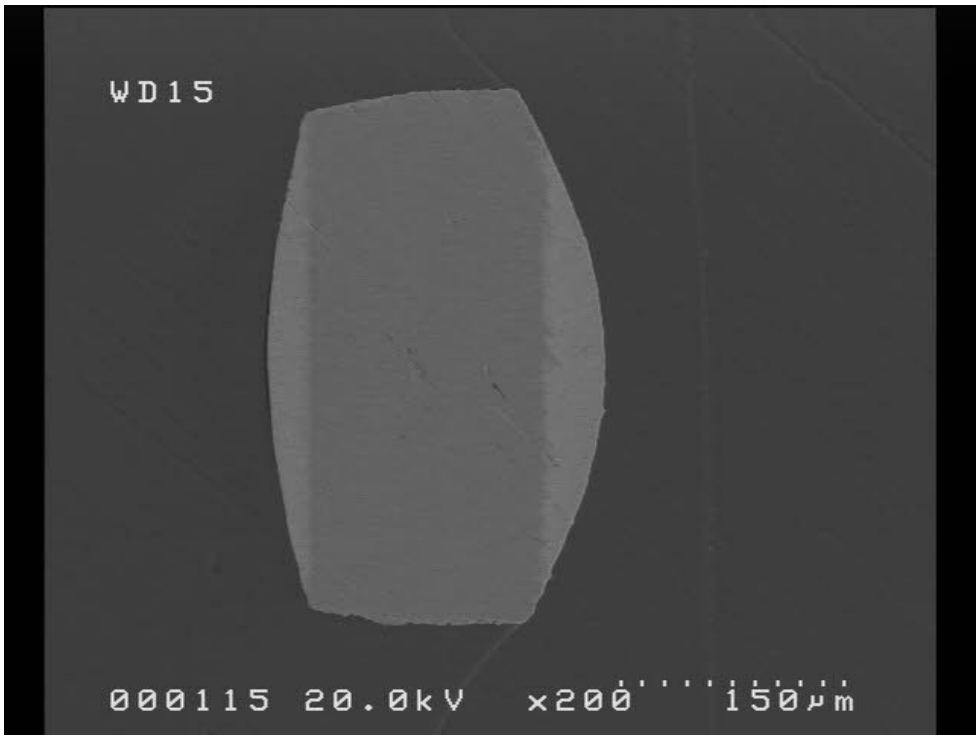


Figure 170: Batch B SEM image of the horizontal cross-section of PC40-UMF coating on a QFP44, lead 33, 200x (ref. Board 66, U3). Dip coating is bridging between the lead and the part at the image left center. Spray coating appears to be bridging between leads at the image right center.

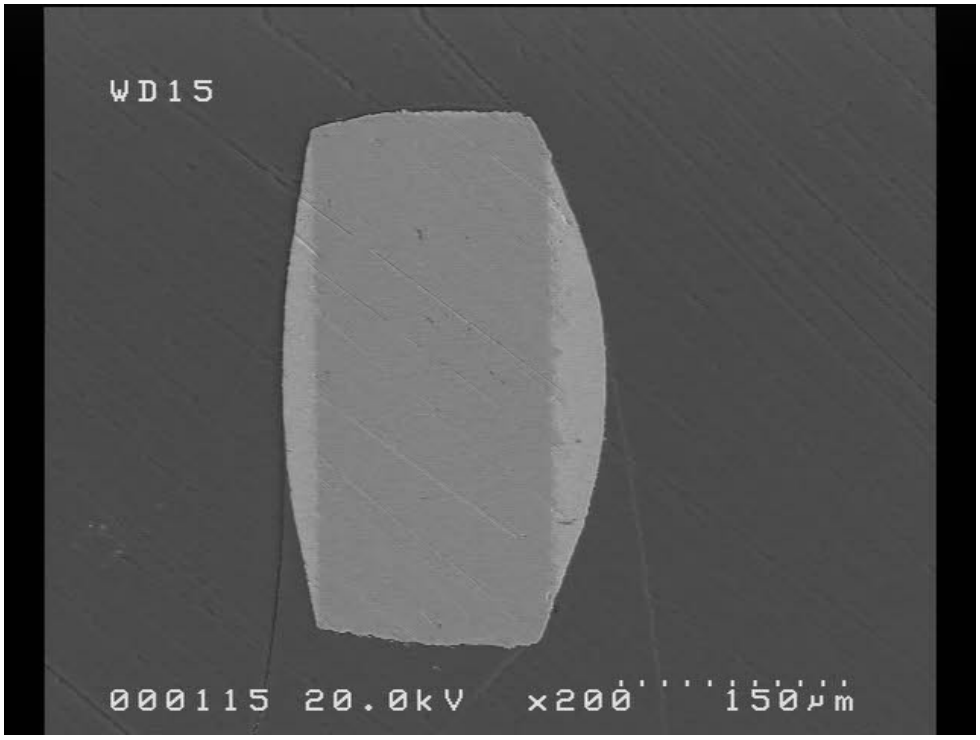


Figure 171: Batch B SEM image of the horizontal cross-section of PC40-UMF coating on a QFP44, lead 34, 200x (ref. Board 66, U3). Coating is bridging between leads on the lower part of the image.

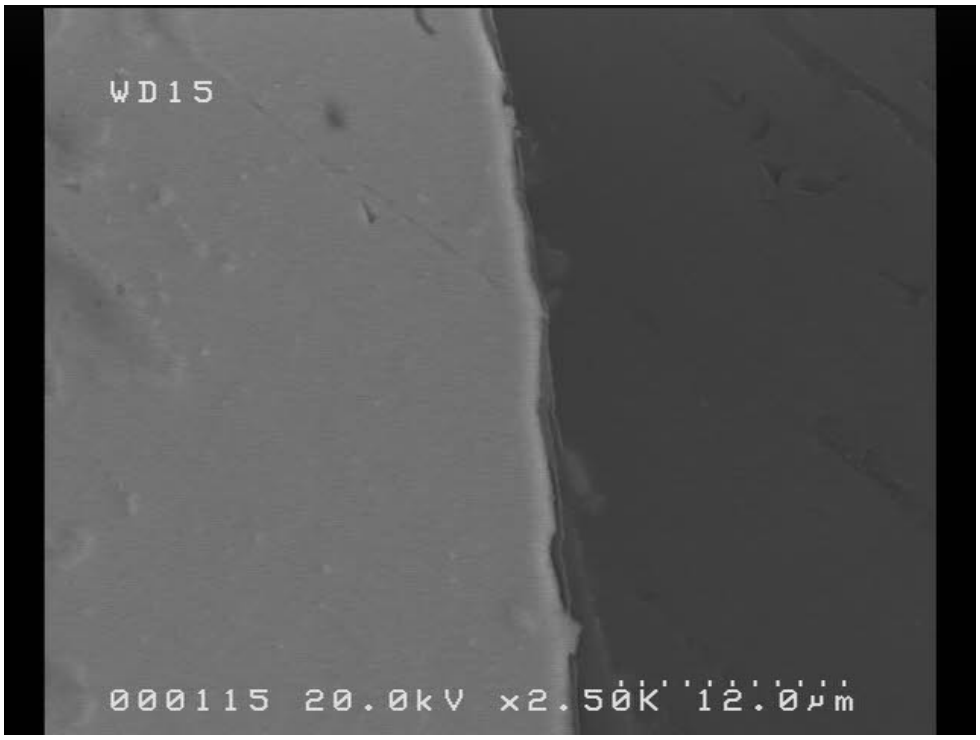


Figure 172: Batch B SEM image of the horizontal cross-section of PC40-UMF coating on a QFP44, lead 34, 2,500x (ref. Board 66, U3).

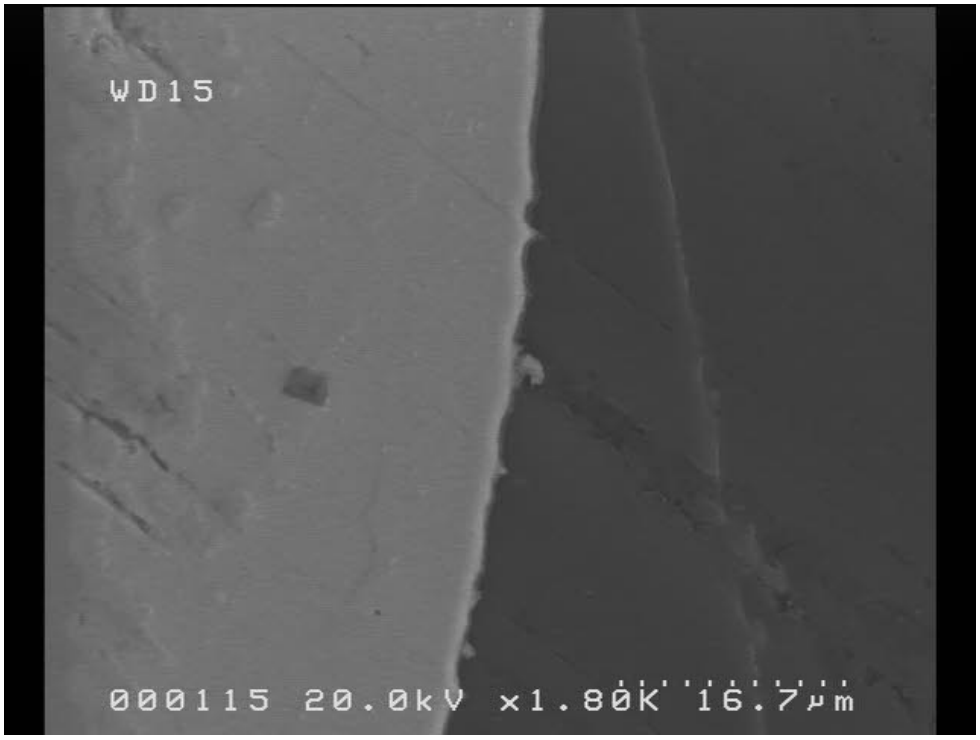


Figure 173: Batch B SEM image of the horizontal cross-section of PC40-UMF coating on a QFP44, lead 34, 1800x (ref. Board 66, U3).

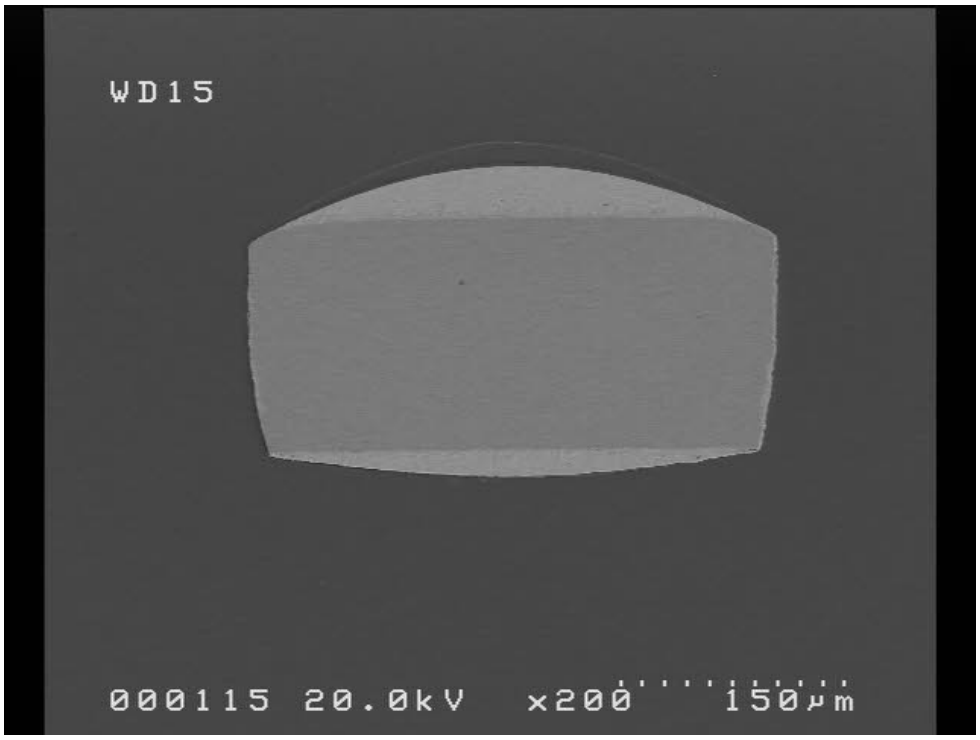


Figure 174: Batch B SEM image of the horizontal cross-section of PC40-UMF coating on a QFP44, lead 44, 200x (ref. Board 66, U3).

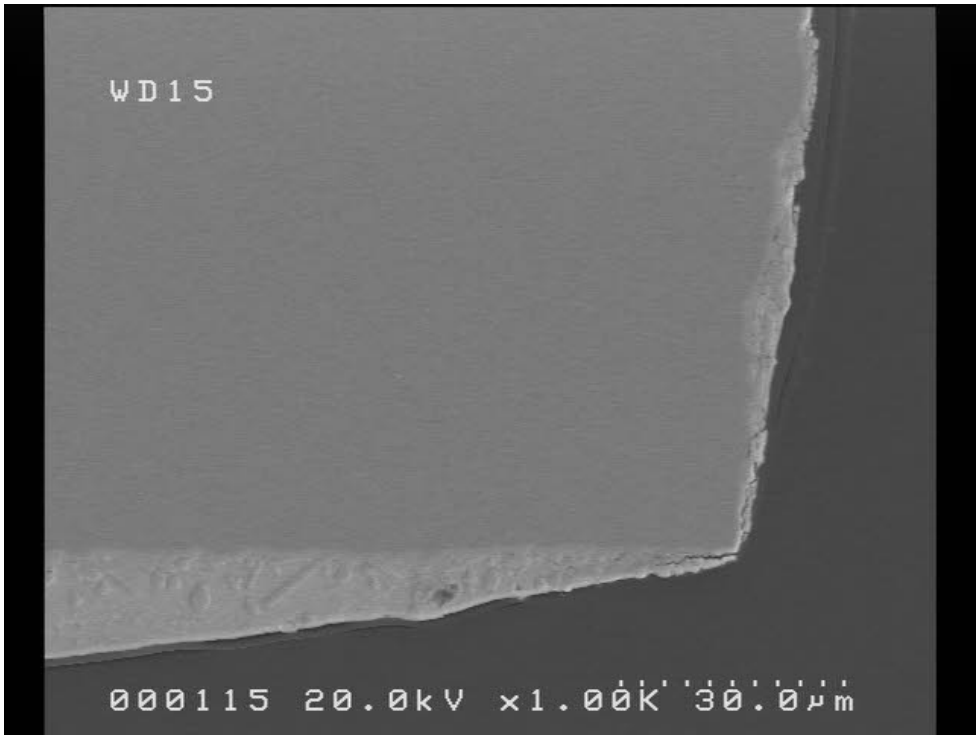


Figure 175: Batch B SEM image of the horizontal cross-section of PC40-UMF coating on a QFP44, lead 44, 1,000x (ref. Board 66, U3).

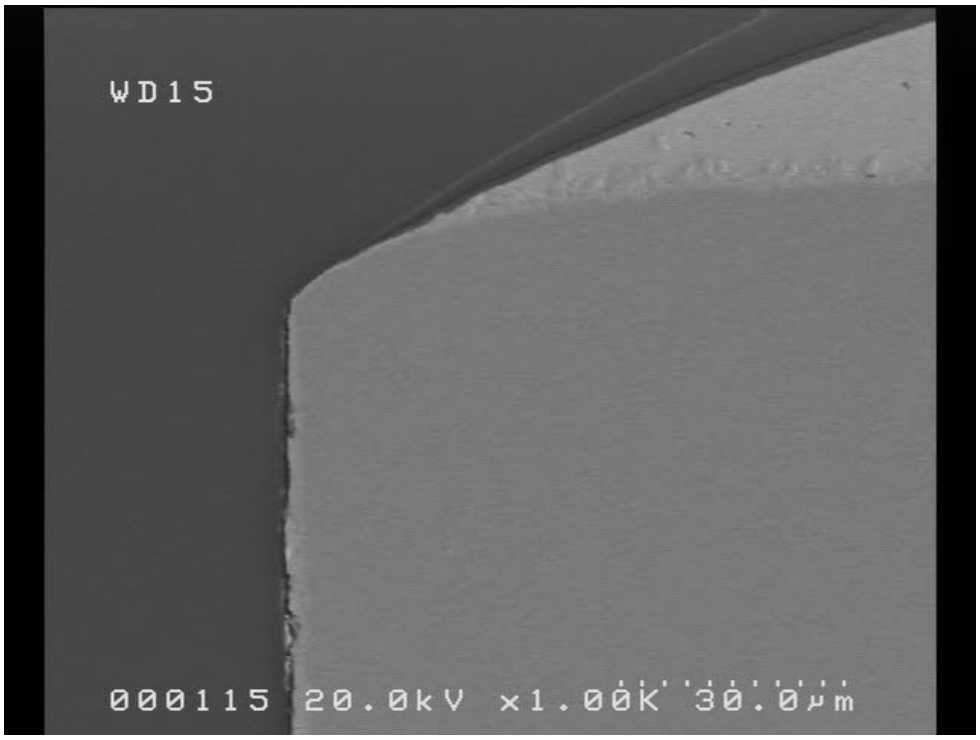


Figure 176: Batch B SEM image of the horizontal cross-section of PC40-UMF coating on a QFP44, lead 44, 1,000x (ref. Board 66, U3).

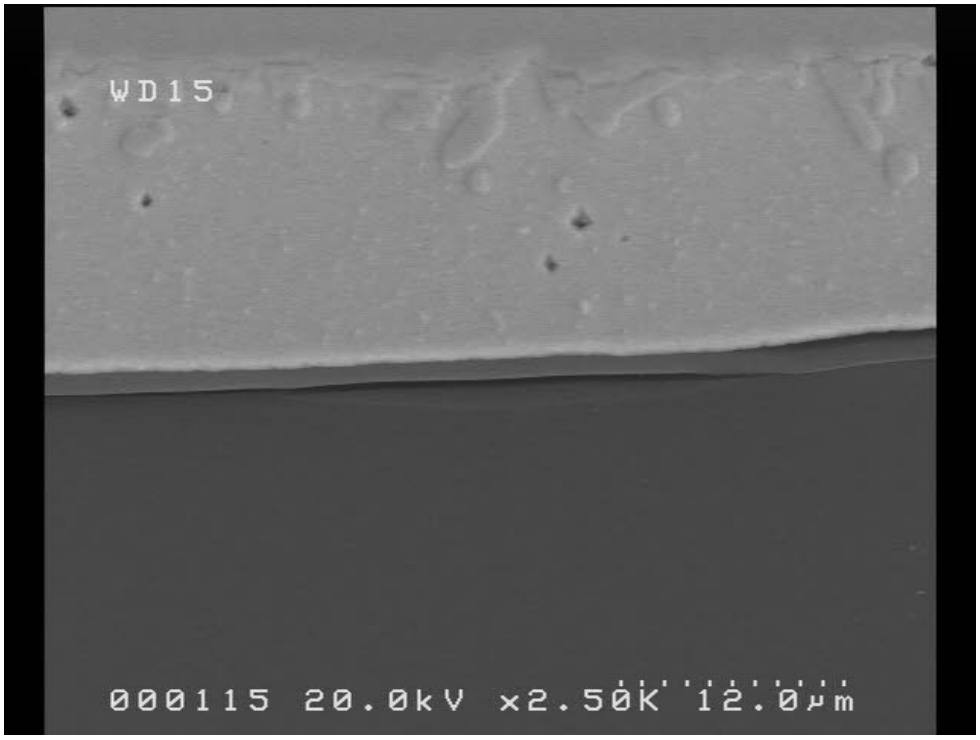


Figure 177: Batch B SEM image of the horizontal cross-section of PC40-UMF coating on a QFP44, lead 44, 2500x, 2 (ref. Board 66, U3).

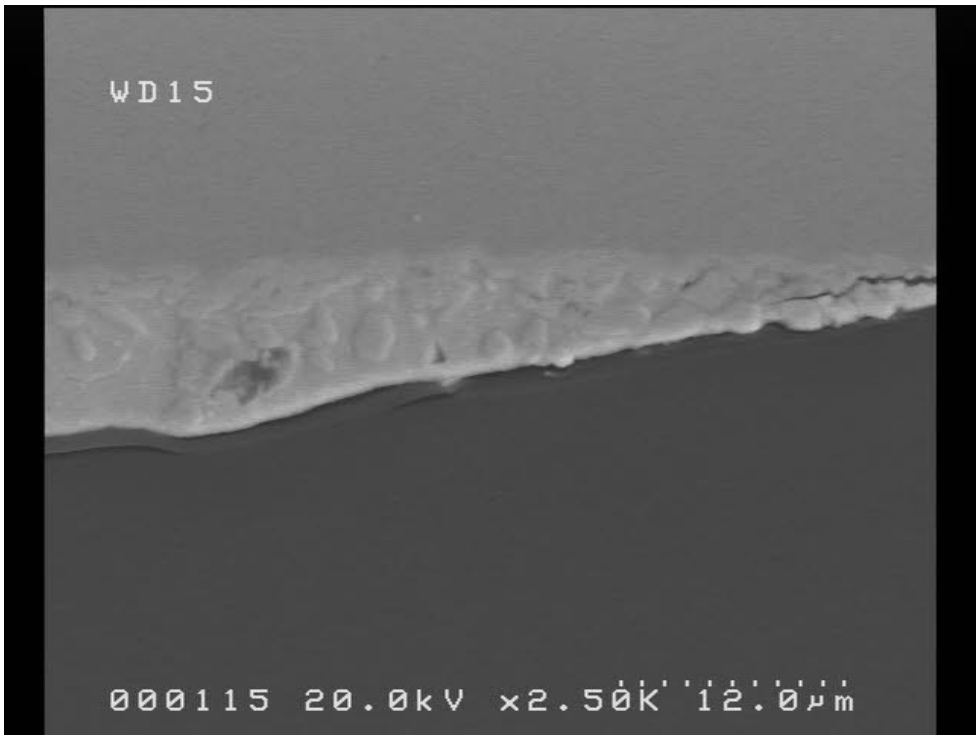


Figure 178: Batch B SEM image of the horizontal cross-section of PC40-UMF coating on a QFP44, lead 44, 2500x (ref. Board 66, U3).

2.1.5.2 PC40-UMF+10%NNN2835 nanosilica Batch B dip+spray flat section

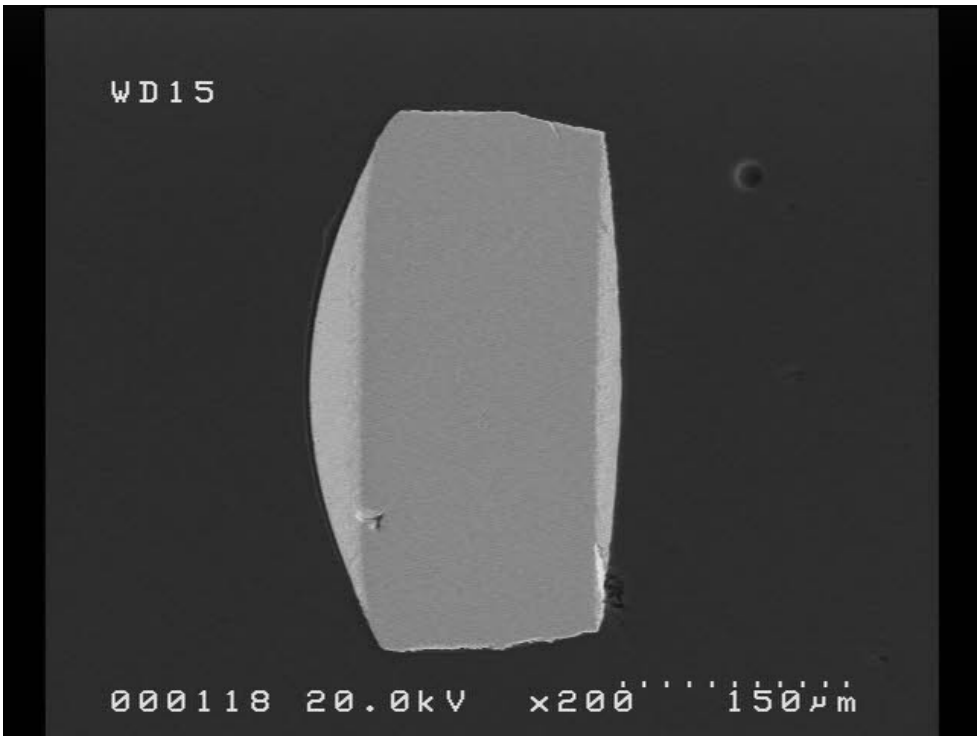


Figure 179: Batch B SEM image of the horizontal cross-section of PC40-UMF+10%NNN2835 coating on a QFP44, lead 11, 200x (ref. Board 62, U3).

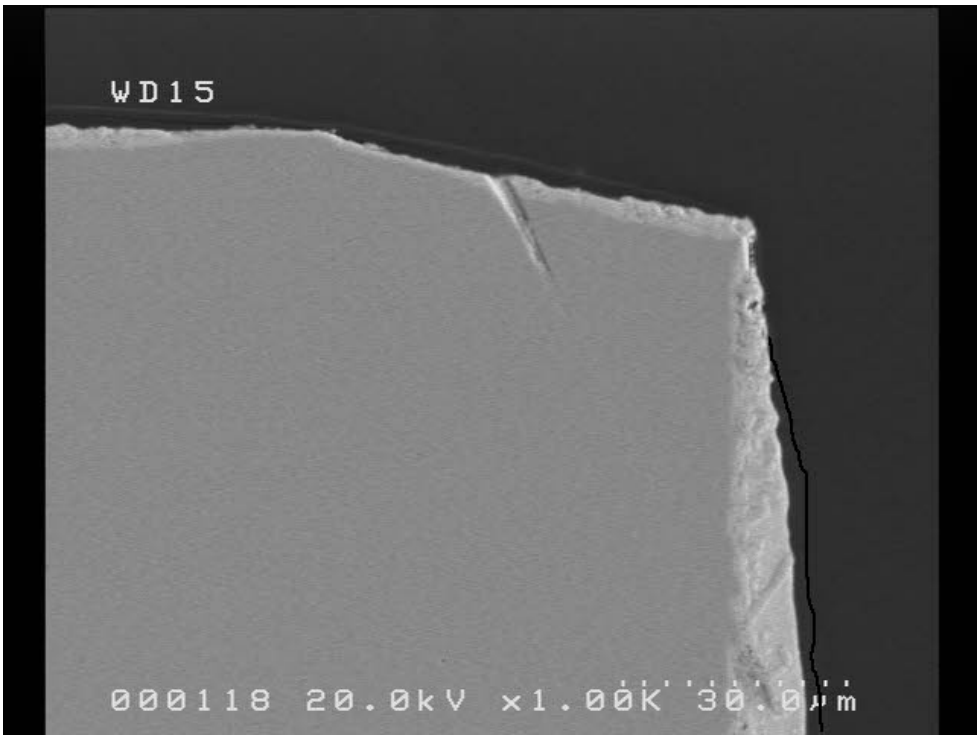


Figure 180: Batch B SEM image of the horizontal cross-section of PC40-UMF+10%NNN2835 coating on a QFP44, lead 11, 1,000x (ref. Board 62, U3).

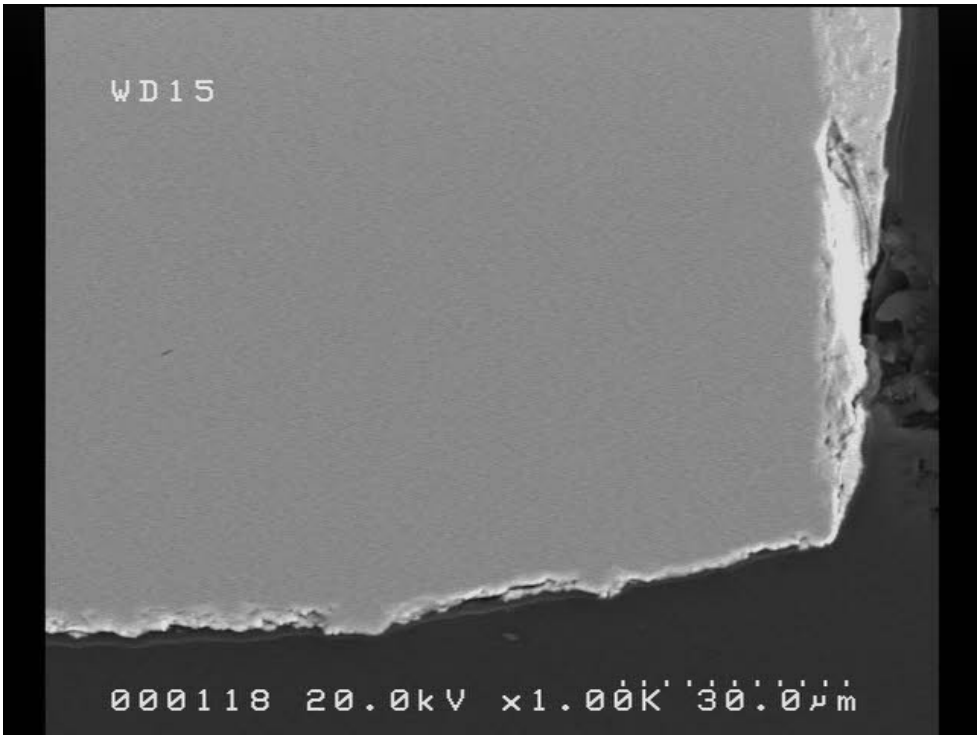


Figure 181: Batch B SEM image of the horizontal cross-section of PC40-UMF+10%NNN2835 coating on a QFP44, lead 11, 1,000x (ref. Board 62, U3).

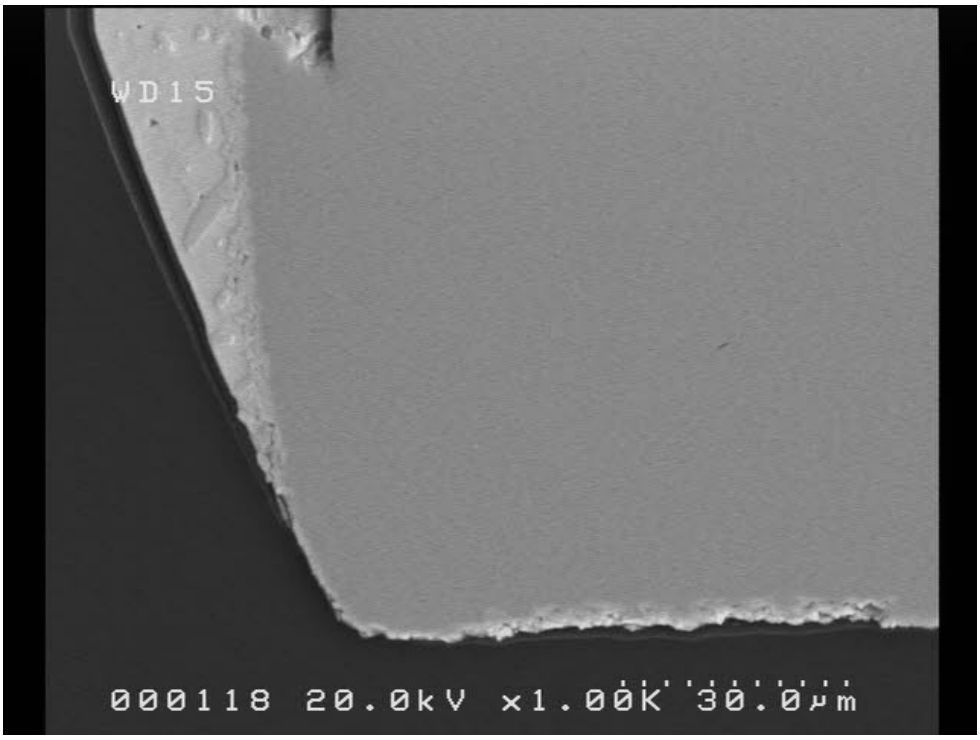


Figure 182: Batch B SEM image of the horizontal cross-section of PC40-UMF+10%NNN2835 coating on a QFP44, lead 11, 1,000x (ref. Board 62, U3).

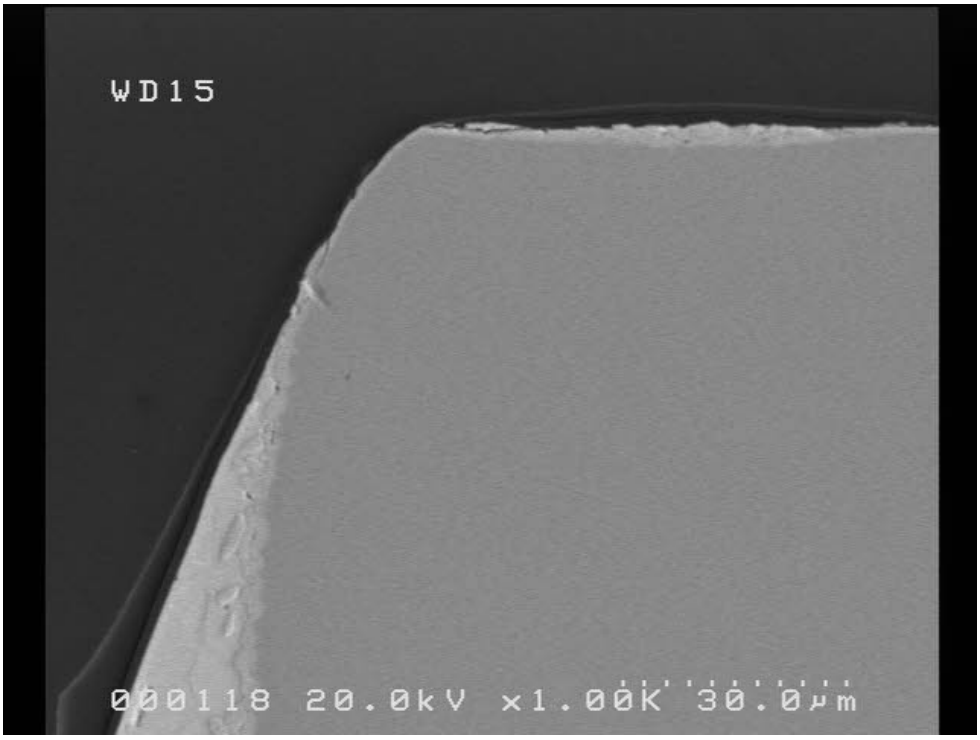


Figure 183: Batch B SEM image of the horizontal cross-section of PC40-UMF+10%NNN2835 coating on a QFP44, lead 11, 1,000x (ref. Board 62, U3).

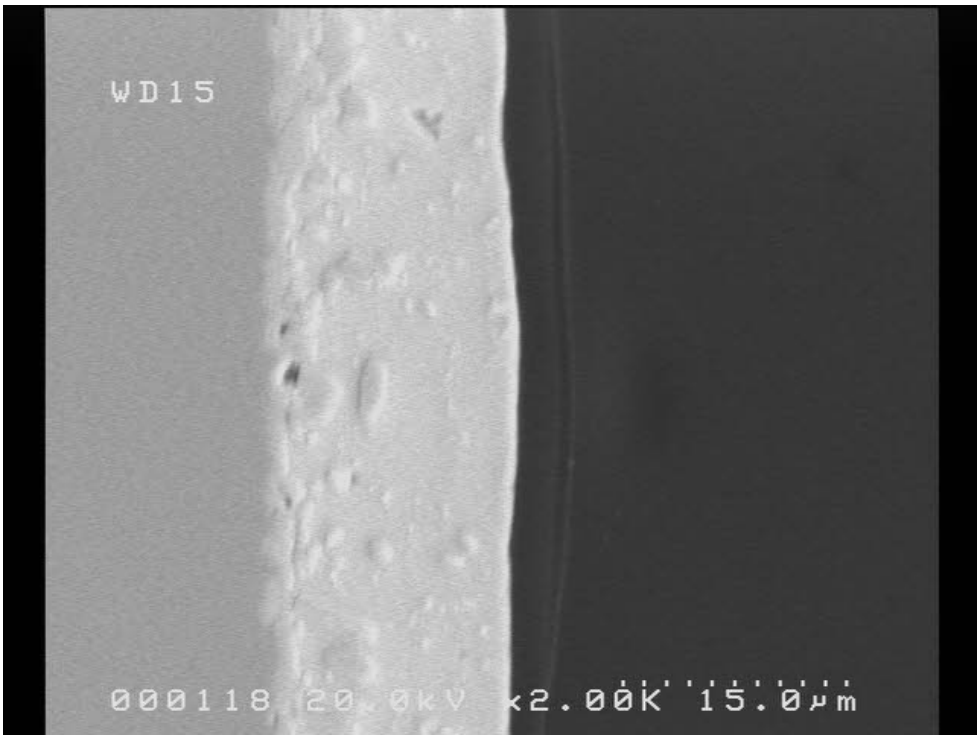


Figure 184: Batch B SEM image of the horizontal cross-section of PC40-UMF+10%NNN2835 coating on a QFP44, lead 11, 2,000x (ref. Board 62, U3).

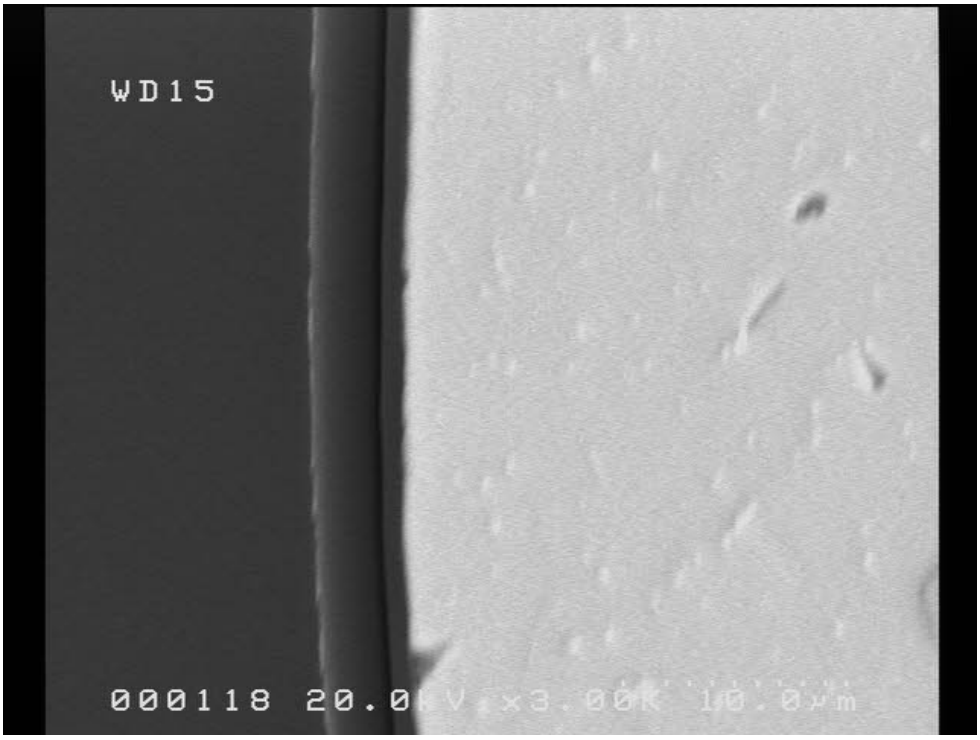


Figure 185: Batch B SEM image of the horizontal cross-section of PC40-UMF+10%NNN2835 coating on a QFP44, lead 11, 3,000x (ref. Board 62, U3).

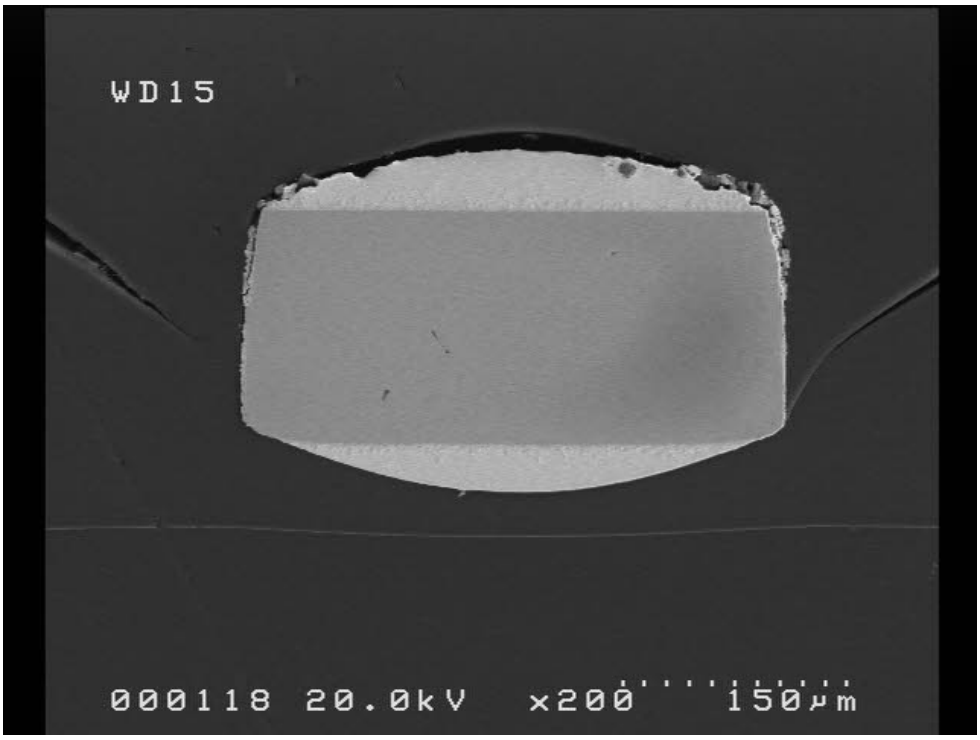


Figure 186: Batch B SEM image of the horizontal cross-section of PC40-UMF+10%NNN2835 coating on a QFP44, lead 19, 200x (ref. Board 62, U3). Dip coating is bridging between the lead and the part on the upper part of the image. Spray coating is bridging between leads in the image lower center. There is delamination between the dip and the spray layer along the bridging between leads. The delamination between the coating and the back of the lead (upper part of image) could be due to PC40-UMF shrinkage during cure.

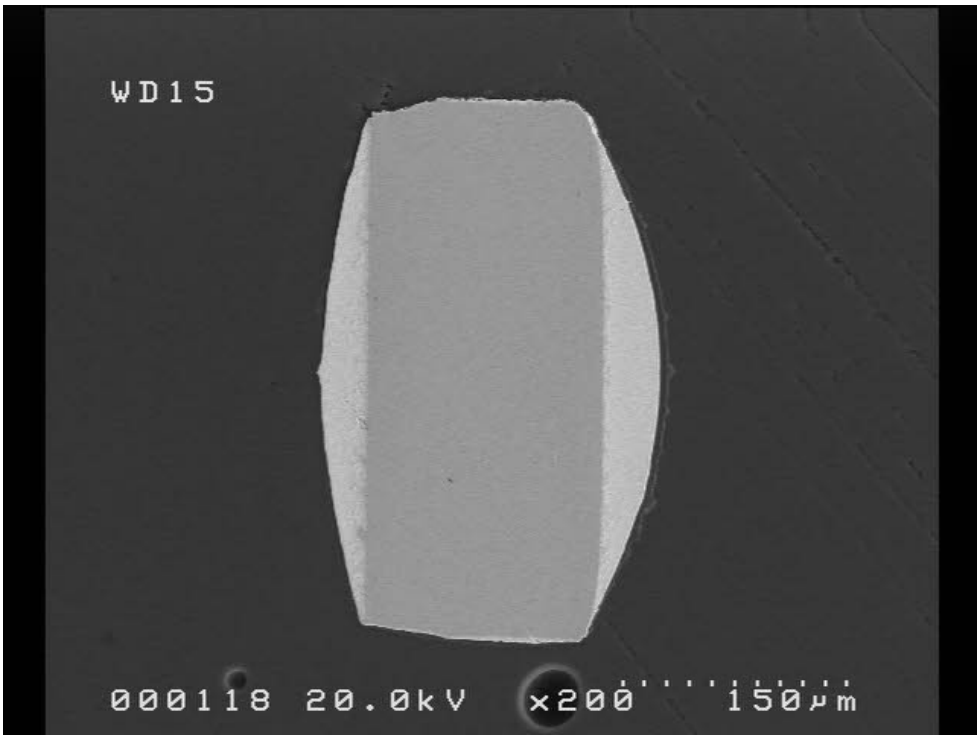


Figure 187: Batch B SEM image of the horizontal cross-section of PC40-UMF+10%NNN2835 coating on a QFP44, lead 33, 200x (ref. Board 62, U3).

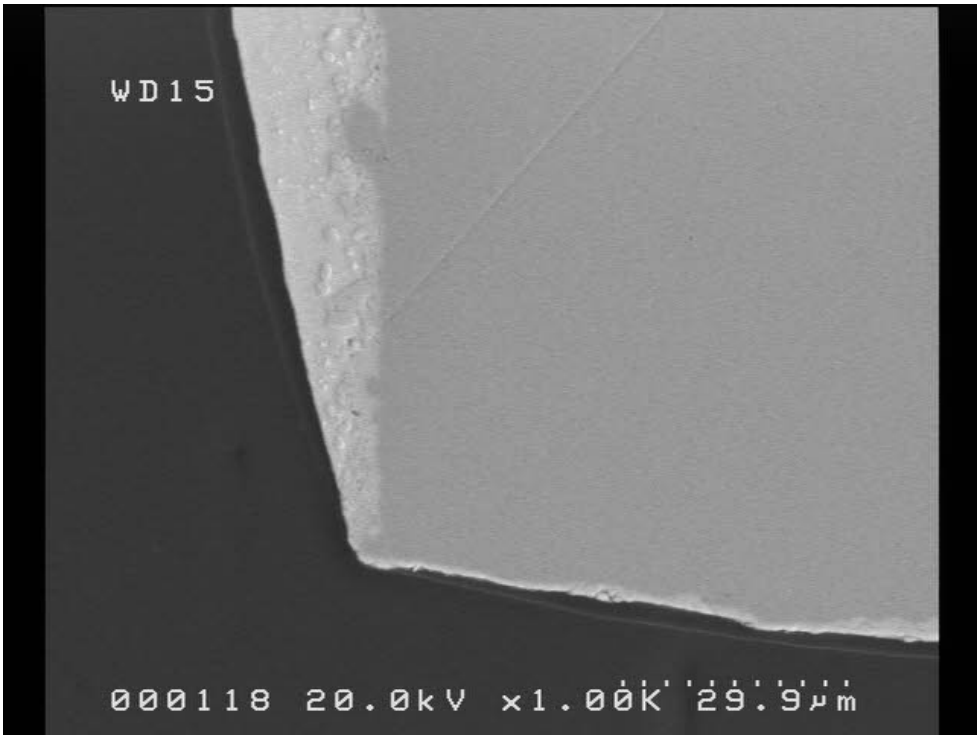


Figure 188: Batch B SEM image of the horizontal cross-section of PC40-UMF+10%NNN2835 coating on a QFP44, lead 33, 1000x (ref. Board 62, U3).

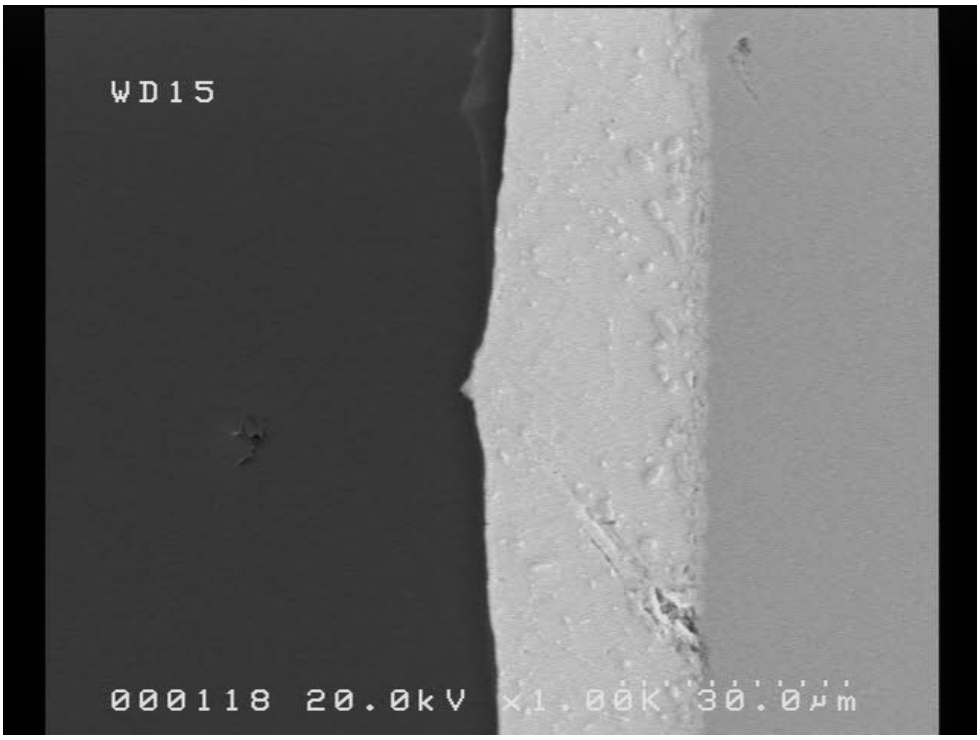


Figure 189: Batch B SEM image of the horizontal cross-section of PC40-UMF+10%NNN2835 coating on a QFP44, lead 33, 1,000x (ref. Board 62, U3).

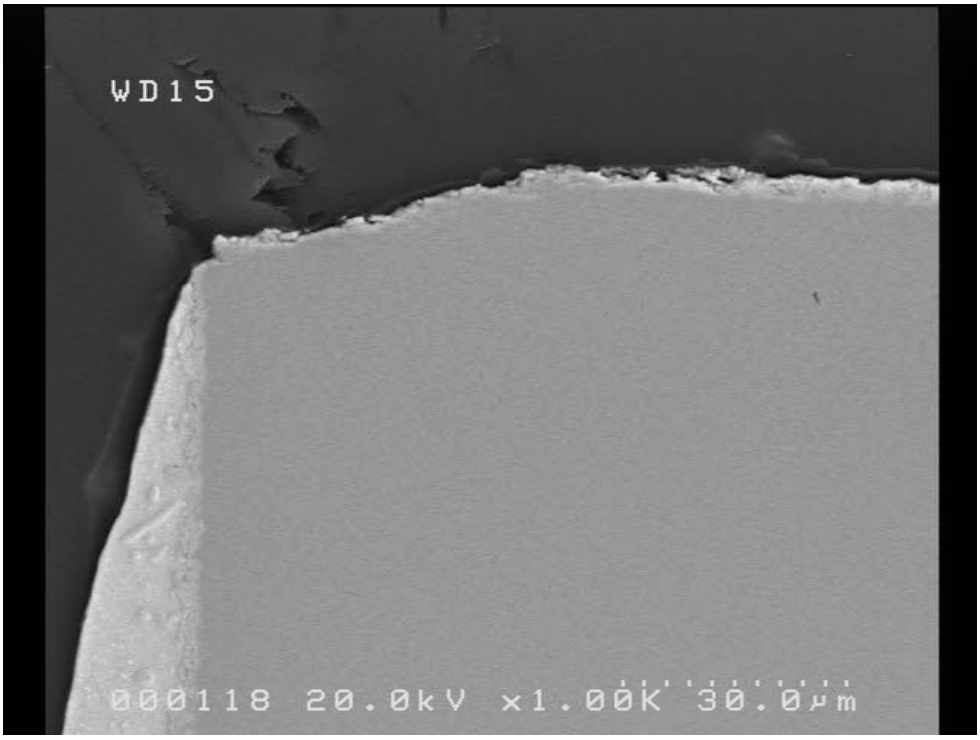


Figure 190: Batch B SEM image of the horizontal cross-section of PC40-UMF+10%NNN2835 coating on a QFP44, lead 33, 1,000x (ref. Board 62, U3).

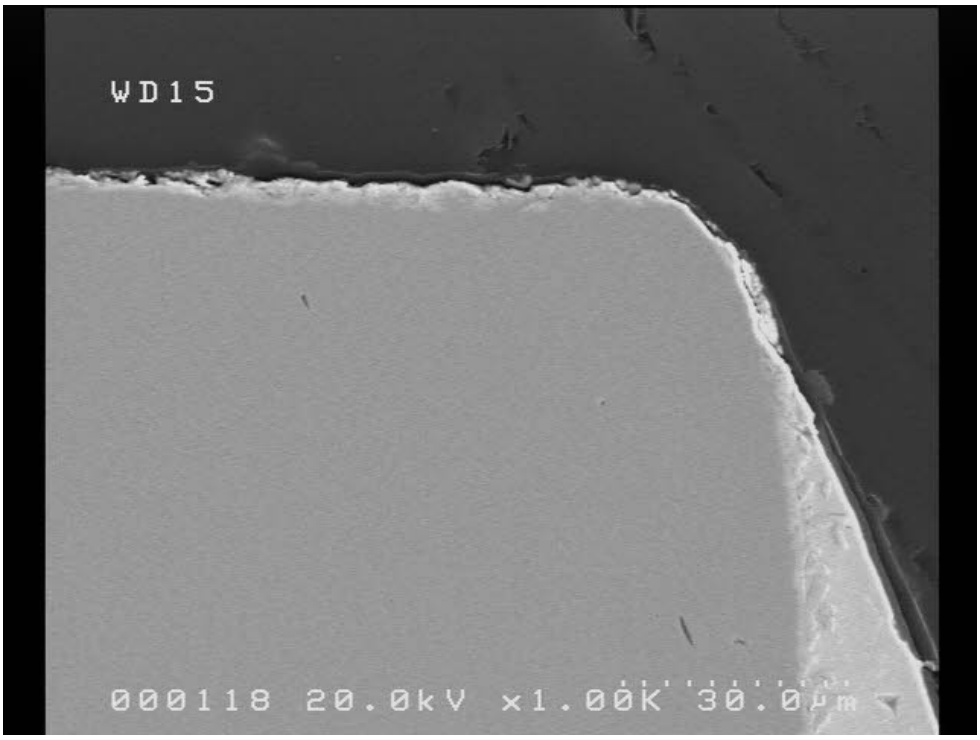


Figure 191: Batch B SEM image of the horizontal cross-section of PC40-UMF+10%NNN2835 coating on a QFP44, lead 33, 1,000x (ref. Board 62, U3).

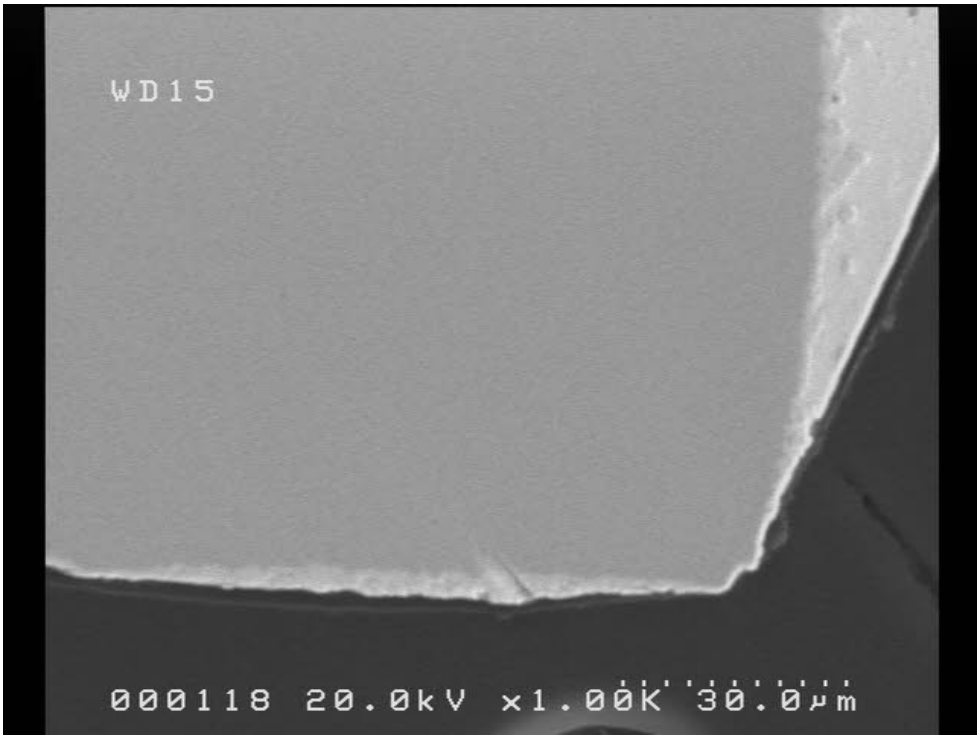


Figure 192: Batch B SEM image of the horizontal cross-section of PC40-UMF+10%NNN2835 coating on a QFP44, lead 33, 1,000x (ref. Board 62, U3).

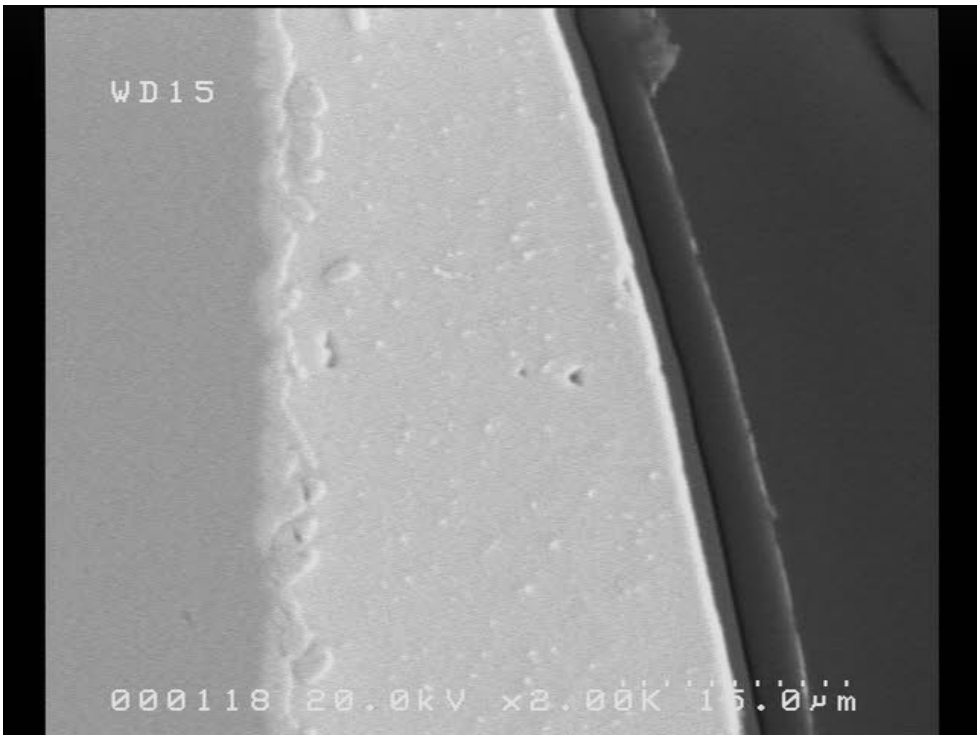


Figure 193: Batch B SEM image of the horizontal cross-section of PC40-UMF+10%NNN2835 coating on a QFP44, lead 33, 2,000x (ref. Board 62, U3). Delamination is present between the dip and spray layers.

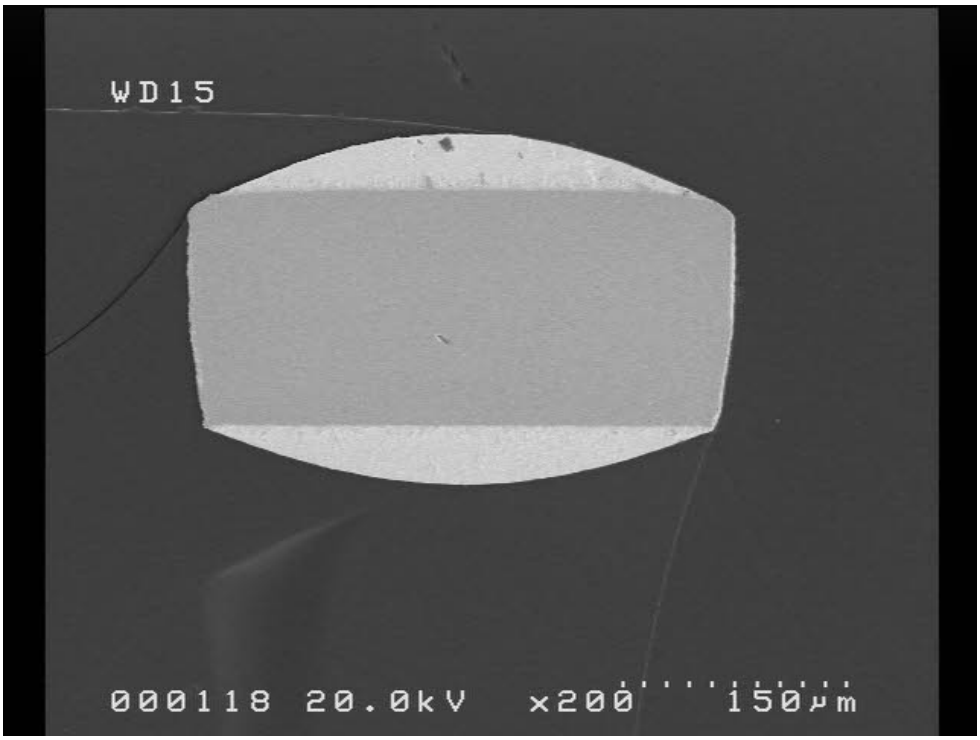


Figure 194: Batch B SEM image of the horizontal cross-section of PC40-UMF+10%NNN2835 coating on a QFP44, lead 34, 200x (ref. Board 62, U3). Dip coating is bridging to the package at the image left and bottom. Spray coating is bridging to the next lead on the left.

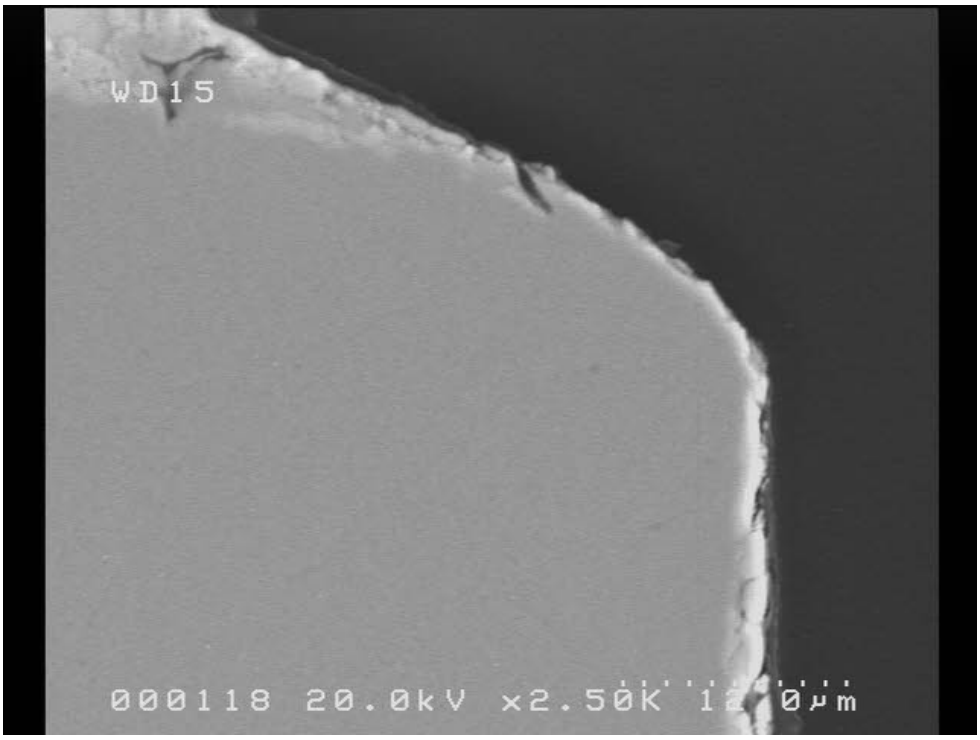


Figure 195: Batch B SEM image of the horizontal cross-section of PC40-UMF+10%NNN2835 coating on a QFP44, lead 34, 2,500x (ref. Board 62, U3).

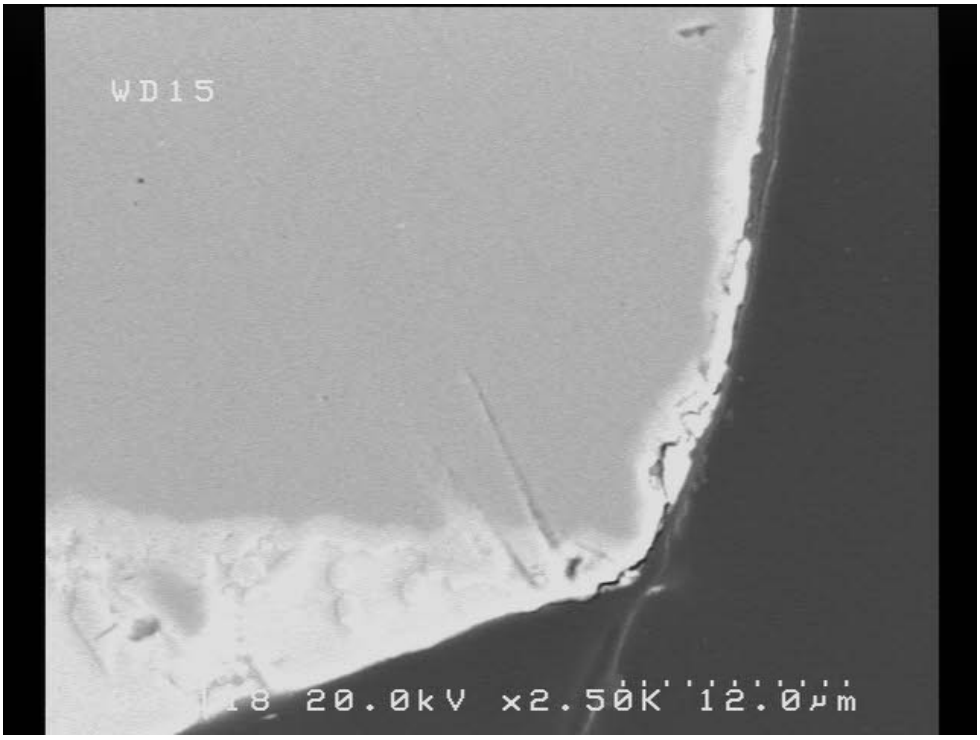


Figure 196: Batch B SEM image of the horizontal cross-section of PC40-UMF+10%NNN2835 coating on a QFP44, lead 34, 2,500x (ref. Board 62, U3).

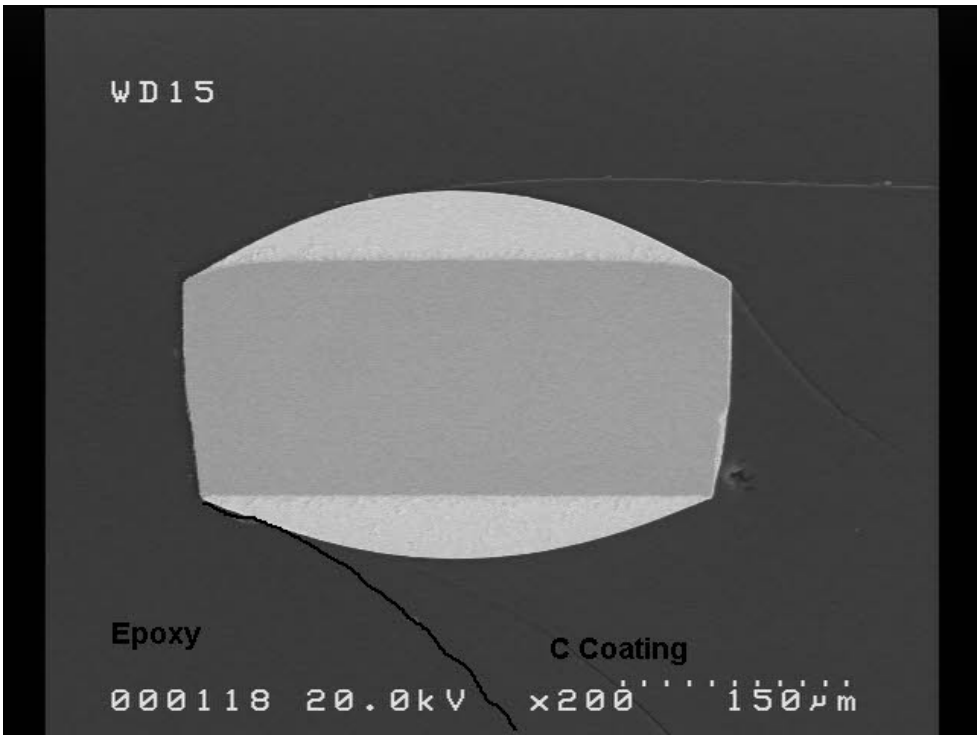


Figure 197: Batch B SEM image of the horizontal cross-section of PC40-UMF+10%NNN2835 coating on a QFP44, lead 39, 200x (ref. Board 62, U3). Dip coating bridging is bridging to the part body and the spray coating on top of it is bridging between leads. Epoxy to coating is highlighted by the added black line.

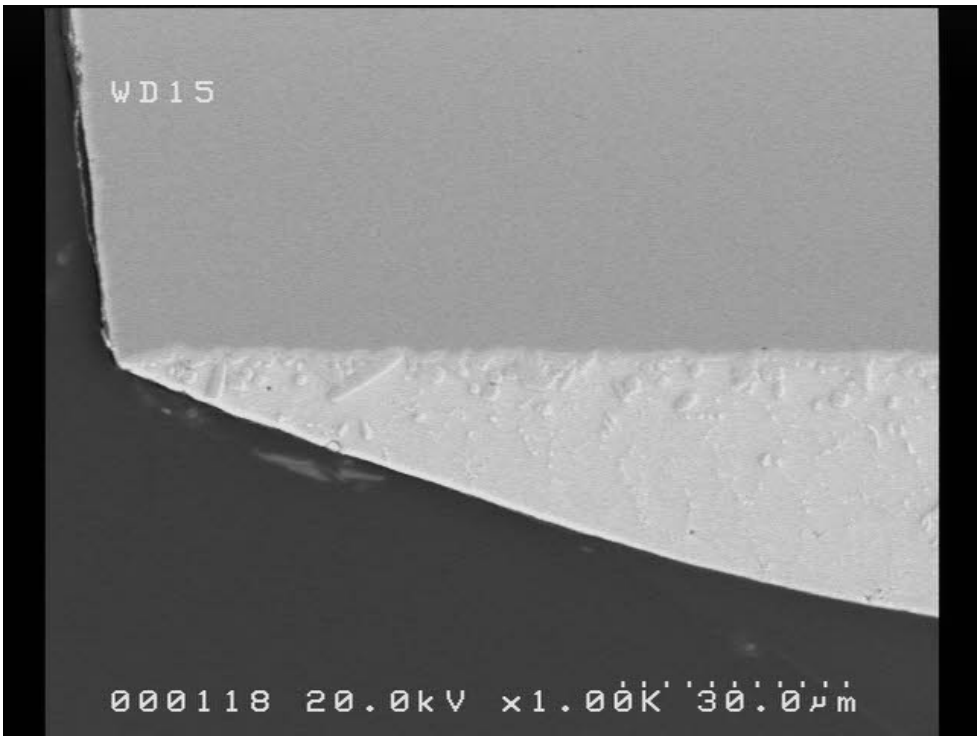


Figure 198: Batch B SEM image of the horizontal cross-section of PC40-UMF+10%NNN2835 coating on a QFP44, lead 39, 1,000x (ref. Board 62, U3).

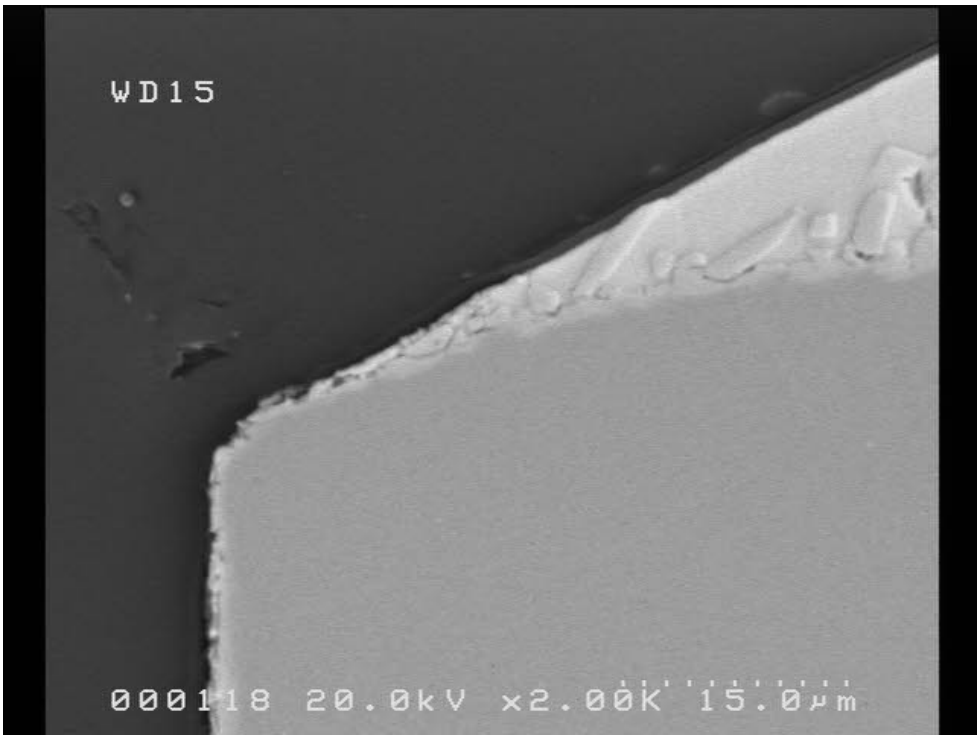


Figure 199: Batch B SEM image of the horizontal cross-section of PC40-UMF+10%NNN2835 coating on a QFP44, lead 39, 2,000x (ref. Board 62, U3).

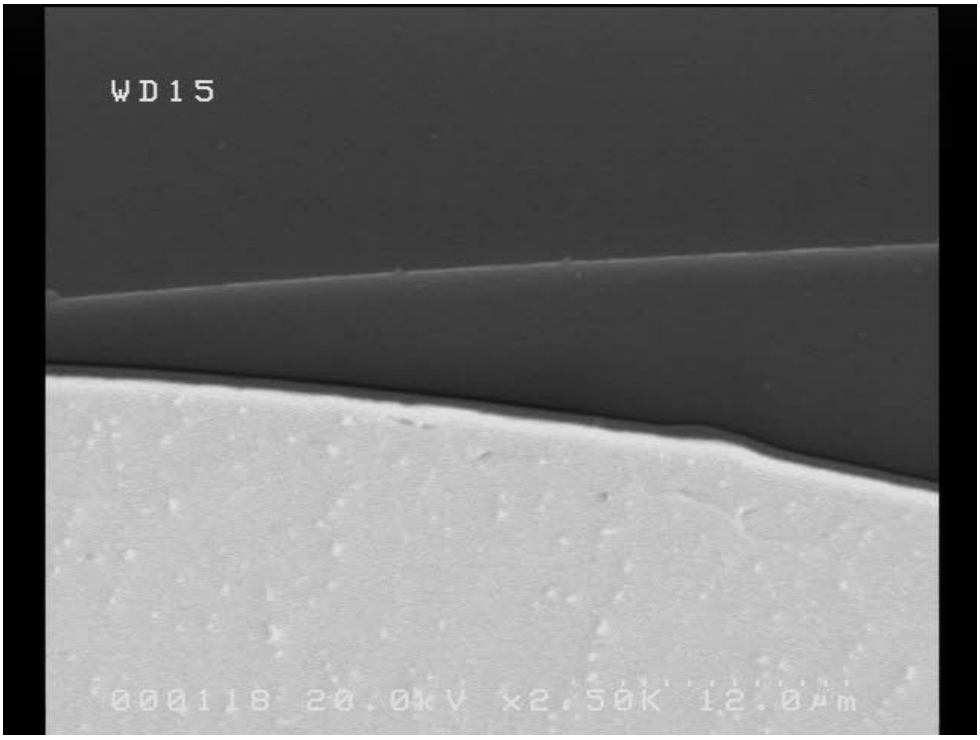


Figure 200: Batch B SEM image of the horizontal cross-section of PC40-UMF+10%NNN2835 coating on a QFP44, lead 39, 2,500x (ref. Board 62, U3).

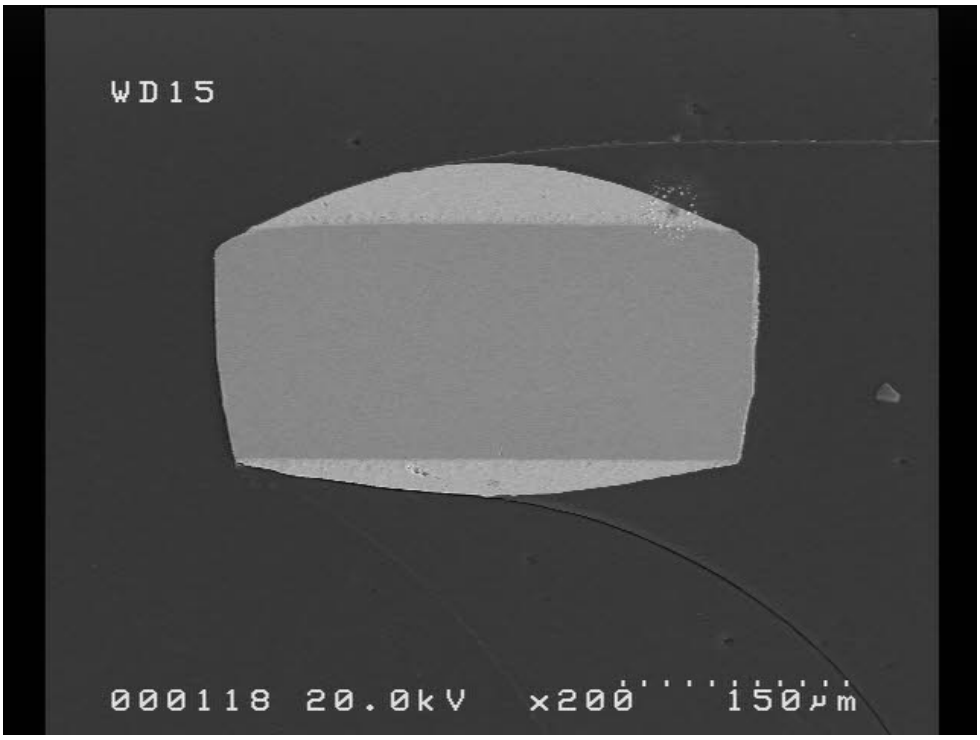


Figure 201: Batch B SEM image of the horizontal cross-section of PC40-UMF+10%NNN2835 coating on a QFP44, lead 44, 200x (ref. Board 62, U3). Coating is bridging to the next lead and to the package body on right side of the image.

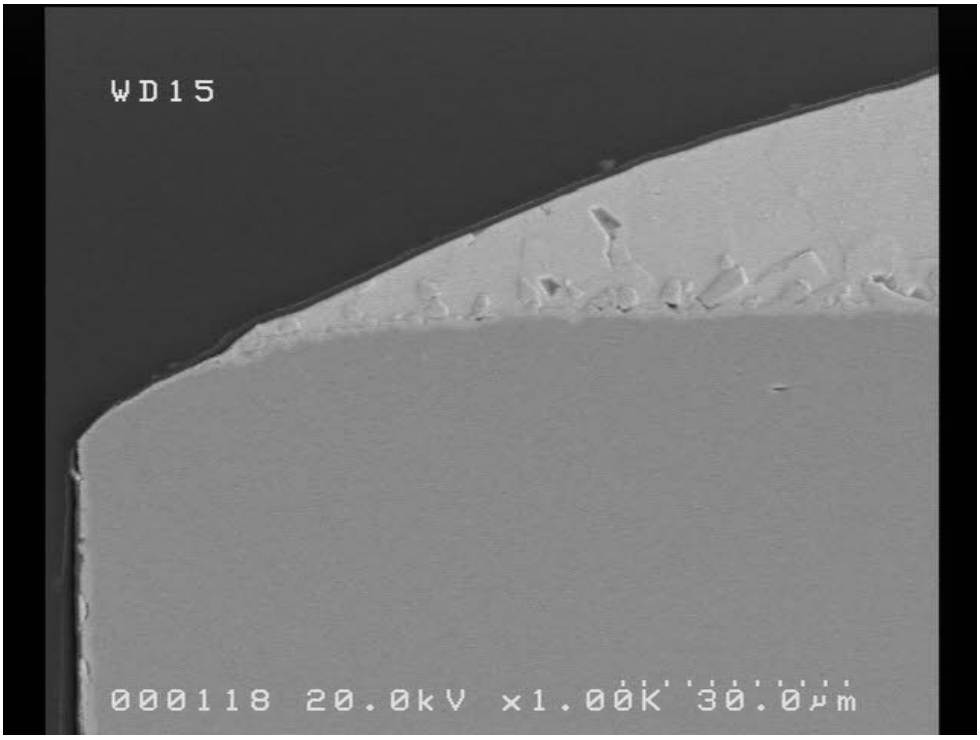


Figure 202: Batch B SEM image of the horizontal cross-section of PC40-UMF+10%NNN2835 coating on a QFP44, lead 44, 1,000x (ref. Board 62, U3).

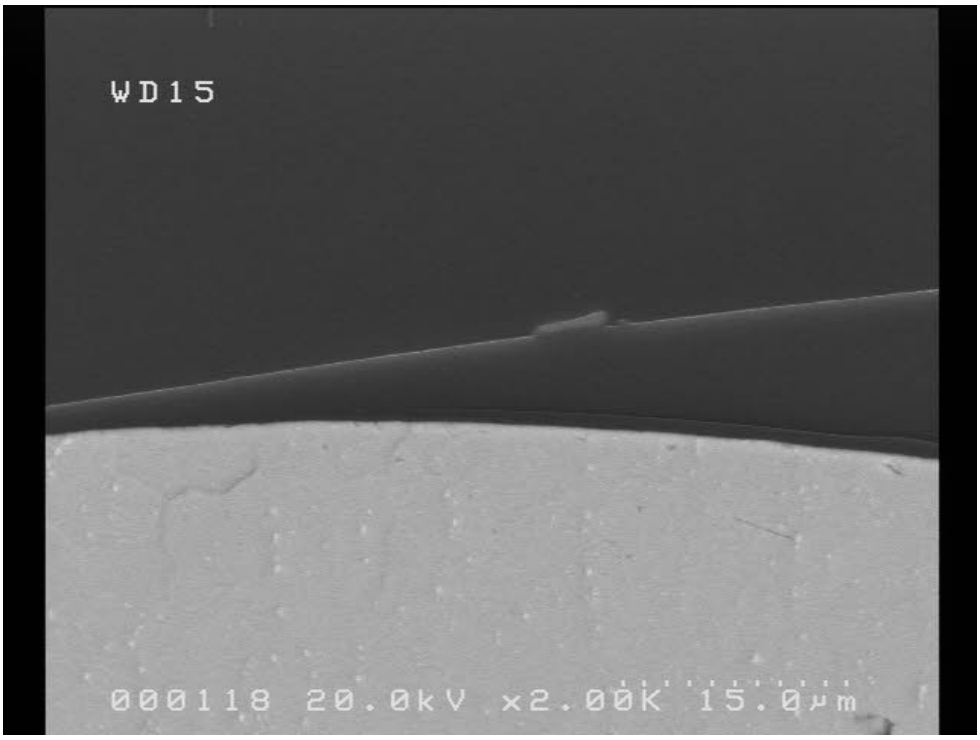


Figure 203: Batch B SEM image of the horizontal cross-section of PC40-UMF+10%NNN2835 coating on a QFP44, lead 44, 2000x (ref. Board 62, U3).

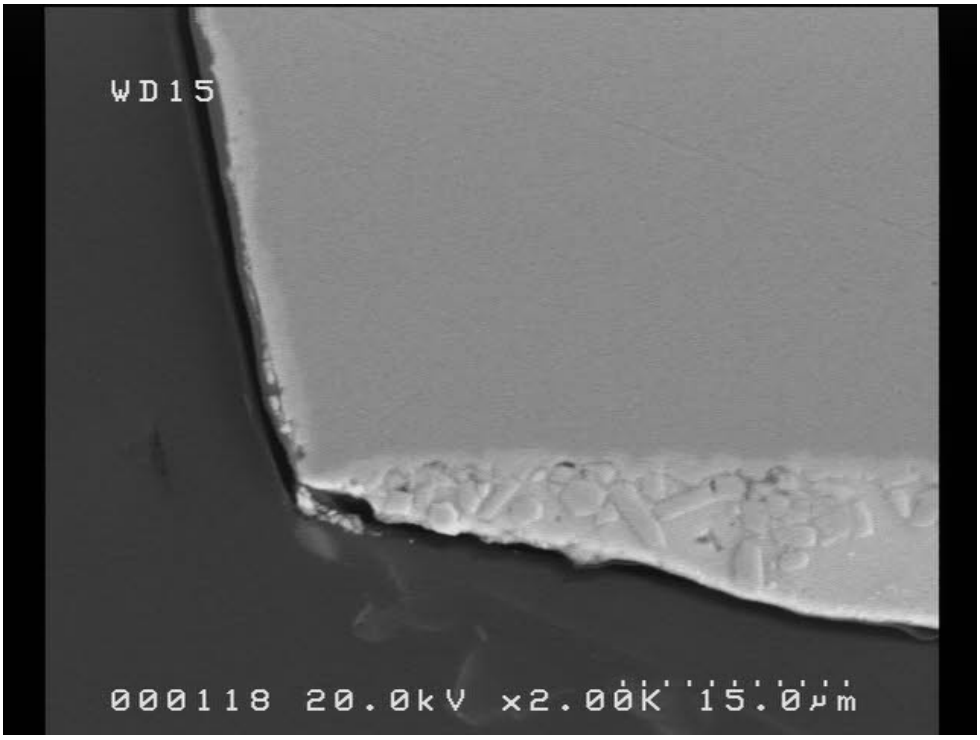


Figure 204: Batch B SEM image of the horizontal cross-section of PC40-UMF+10%NNN2835 coating on a QFP44, lead 44, 2,000x (ref. Board 62, U3).

2.2 PC40-UMF Batch C and D spray coating, standard and high viscosity

To avoid the poor wetting and adhesion between the dip and the spray layers encountered in batch A and B, a trial run of test assemblies were spray coated at Asymtek in Carlsbad, CA. The assemblies were coated with a either standard viscosity 256 cps (Batch C) or high viscosity 610 cps (Batch D) PC40-UMF unfilled coating materials. The same 2X-2Y spray settings were used for both. The PC40-UMF had a wet thickness of approximately 125 microns (5 mils) and a cured thickness of approximately 62.5 microns (2.5 mils).

2.2.1 Optical inspection of Batch C and D of PC40-UMF standard and high viscosity

The wetting was good for both the standard and the high viscosity PC40-UMF (Figure 205 and Figure 206).

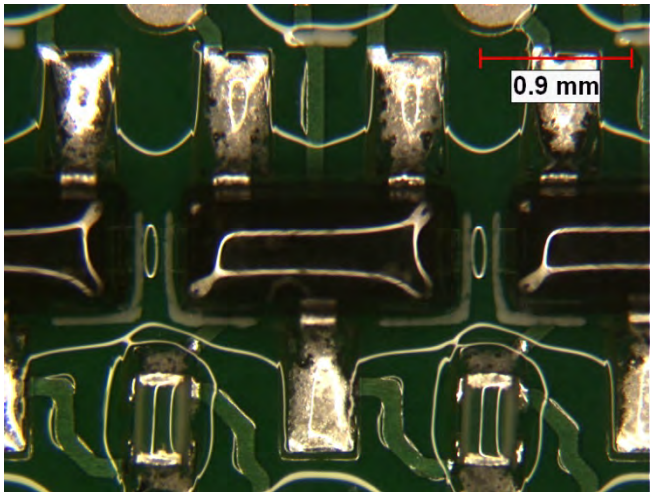


Figure 205: Optical image of PC40-UMF standard viscosity, SOT3, 25x (ref. Asymtech 8-2015).

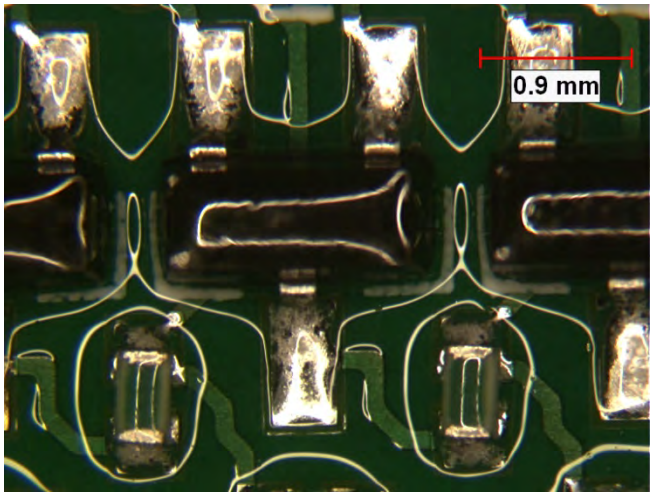


Figure 206: Optical image of PC40-UMF high viscosity, SOT3, 25x (ref. Asymtech 8-2015).

2.2.2 SEM inspection of Batch C and D with PC40-UMF standard and high viscosity

The batch C coverage of spray coated standard viscosity PC40-UMF was considerably better without the initial dip (Figure 207) as compared to the spray coating over an initial PC40-UMF dip (Figure 51 (b) or (c)).

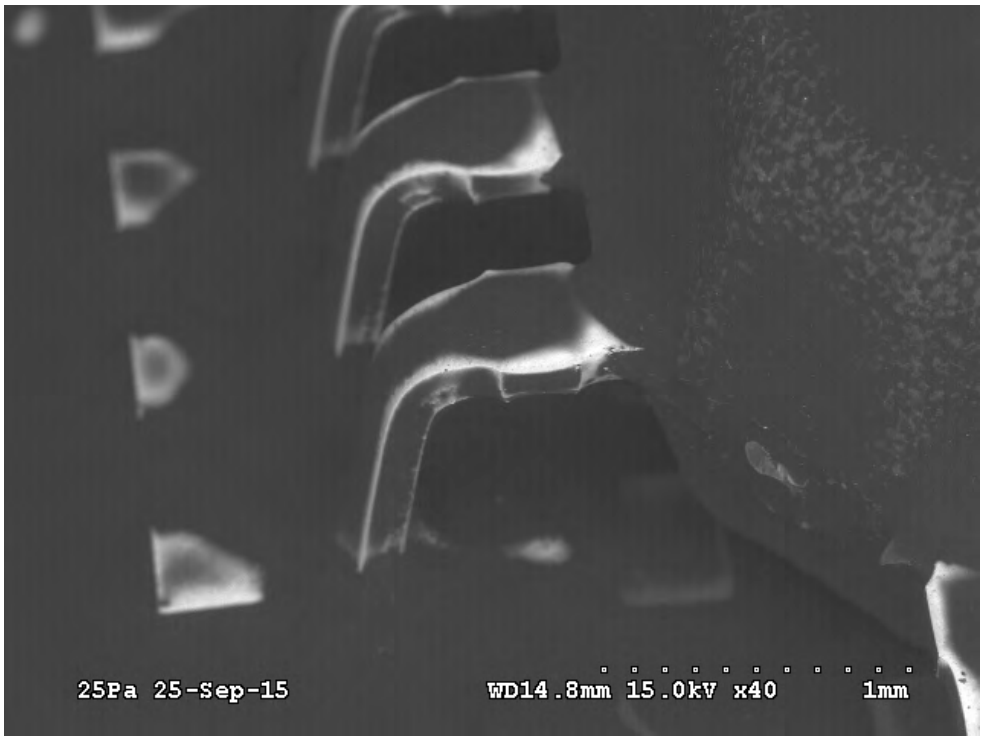


Figure 207: Batch C SEM image of PC40-UMF standard viscosity coated QFP44, 40x (ref. Asymtech 8-2015 QFP44 40x 4).

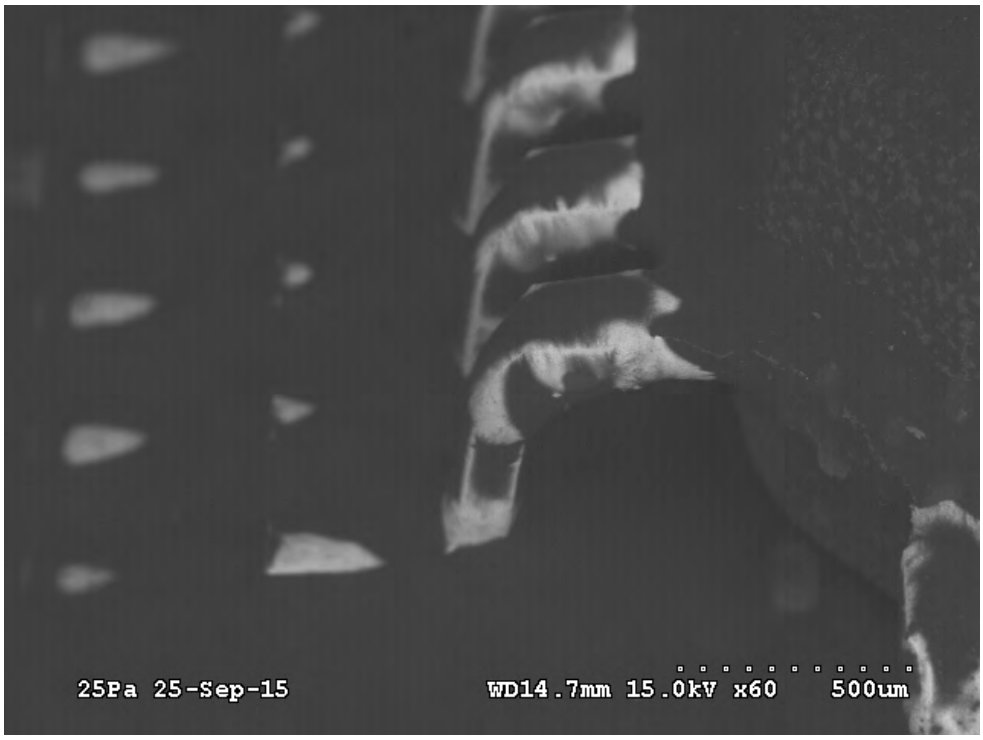


Figure 208: Batch C SEM image of PC40-UMF standard viscosity coated QFP64, 60x (ref Asymtech 8-2015).



Figure 209: Batch C SEM image of PC40-UMF standard viscosity coated PLCC44, 40x (ref. Asymtech 8-2015).



Figure 210: Batch D SEM image of PC40-UMF high viscosity coated QFP44, 40x (ref. Asymtech 8-2015).



Figure 211: Batch D SEM image of PC40-UMF high viscosity coated QFP64, 60x (ref. Asymtech 8-2015).



Figure 212: Batch D SEM image of PC40-UMF high viscosity coated PLCC, 40x (ref. Asymtech 8-2015).

2.2.3 Vertical cross-section inspection of Batch C and D with PC40-UMF and PC40-UMF high viscosity spray coating without initial dip coat

To obtain the coating thickness along the lead of a QFP44, a cross-section through pins 11 and 23 (see Figure 32) was made for both the standard viscosity and the high viscosity PC40-UMF materials. The thickness results are summarized in Figure 213 and cross-section images are provided in Figure 214 to Figure 243.

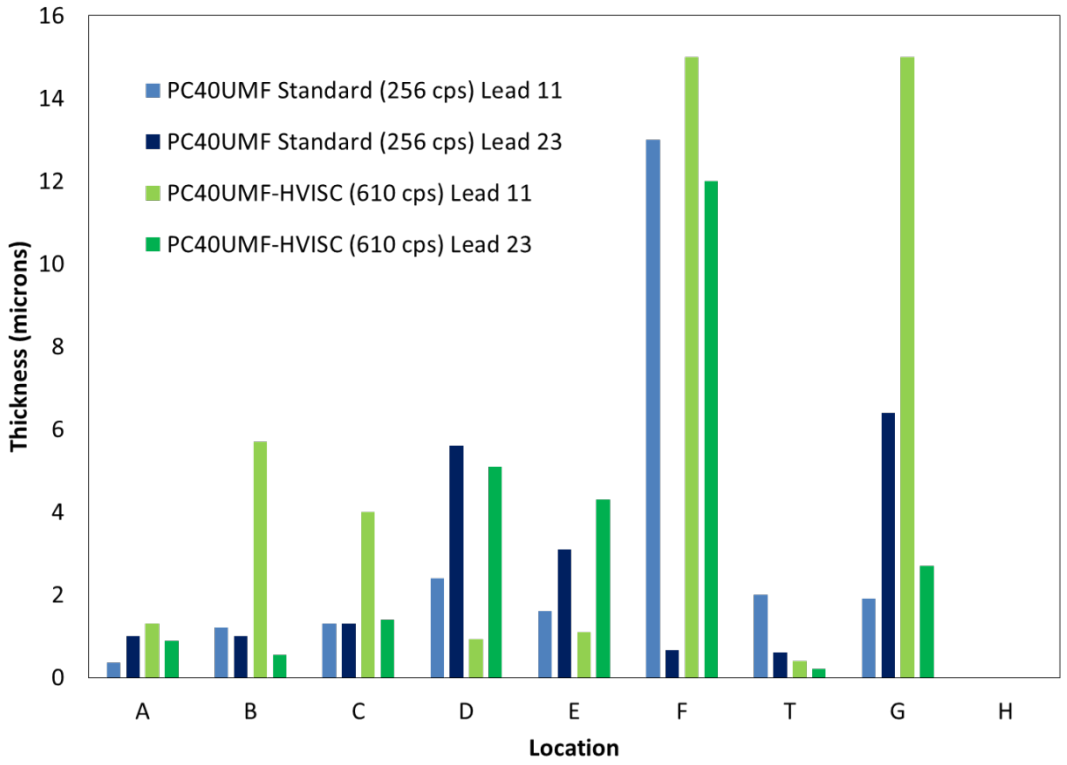


Figure 213: Thickness summary for the PC40-UMF standard and high viscosity spray coatings without an initial low viscosity dip.

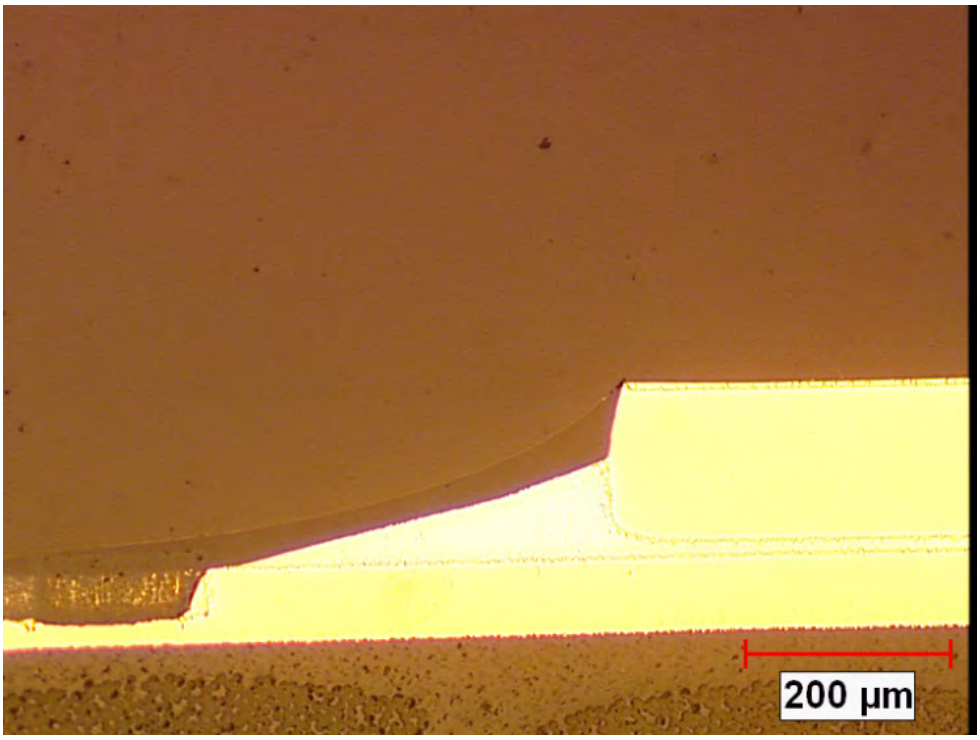


Figure 214: Optical cross-section image of the PC40-UMF standard viscosity coating on the QFP44 lead toe, 100x (ref. U2, lead 11).

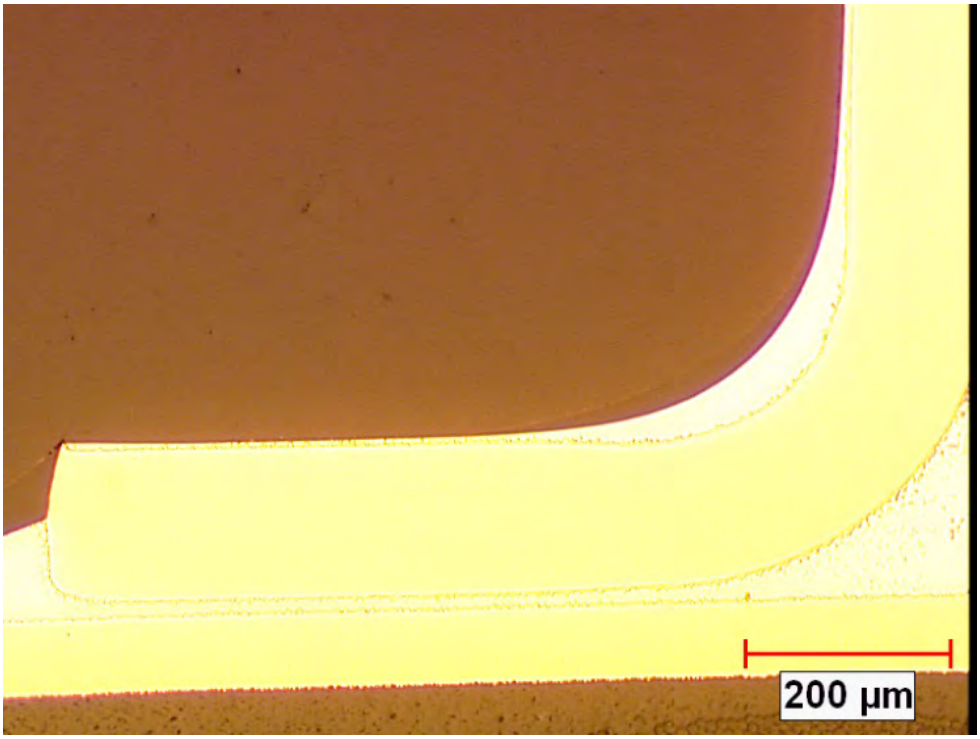


Figure 215: Optical cross-section image of the PC40-UMF standard viscosity coating on the QFP44 lead foot, 100x (ref. U2, lead 11).

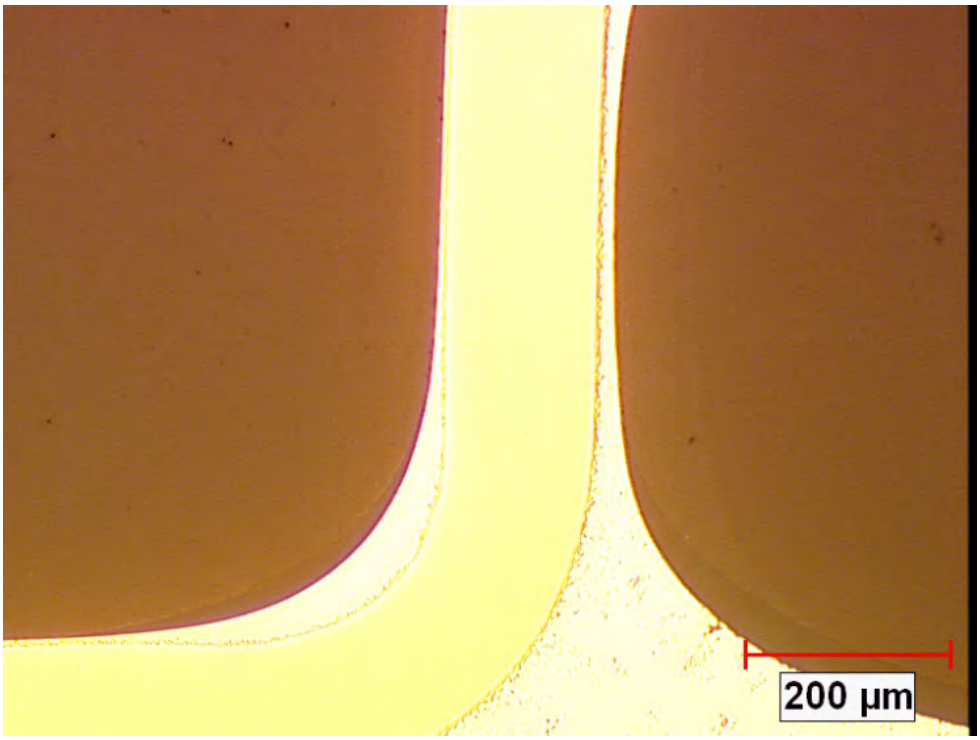


Figure 216: Optical cross-section image of the PC40-UMF standard viscosity coating on the QFP44 lower lead location, 100x (ref. U2, lead 11).

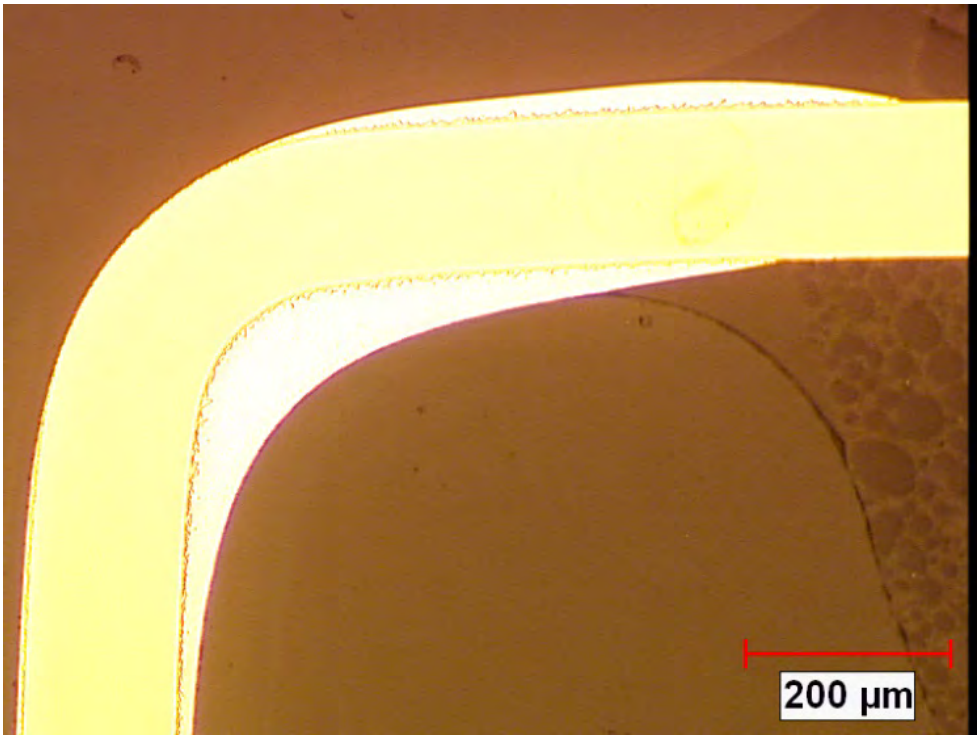


Figure 217: Optical cross-section image of the PC40-UMF standard viscosity coating on the QFP44 upper lead location, 100x (ref. U2, lead 11).

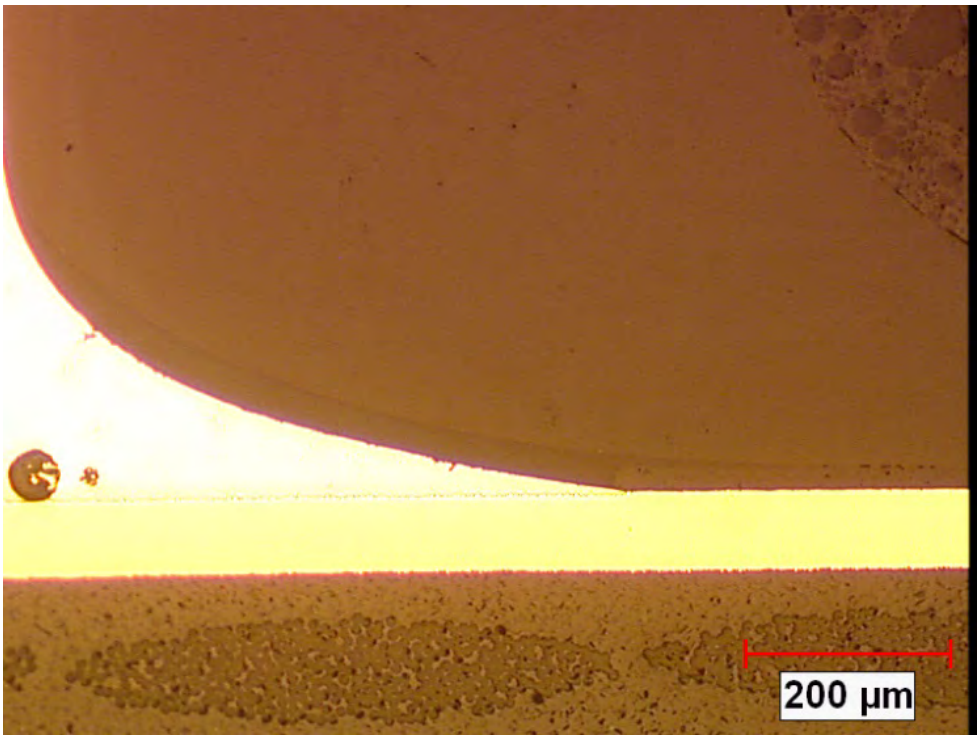


Figure 218: Optical cross-section image of the PC40-UMF standard viscosity coating on the QFP44 heel location, 100x (U2, lead 11).

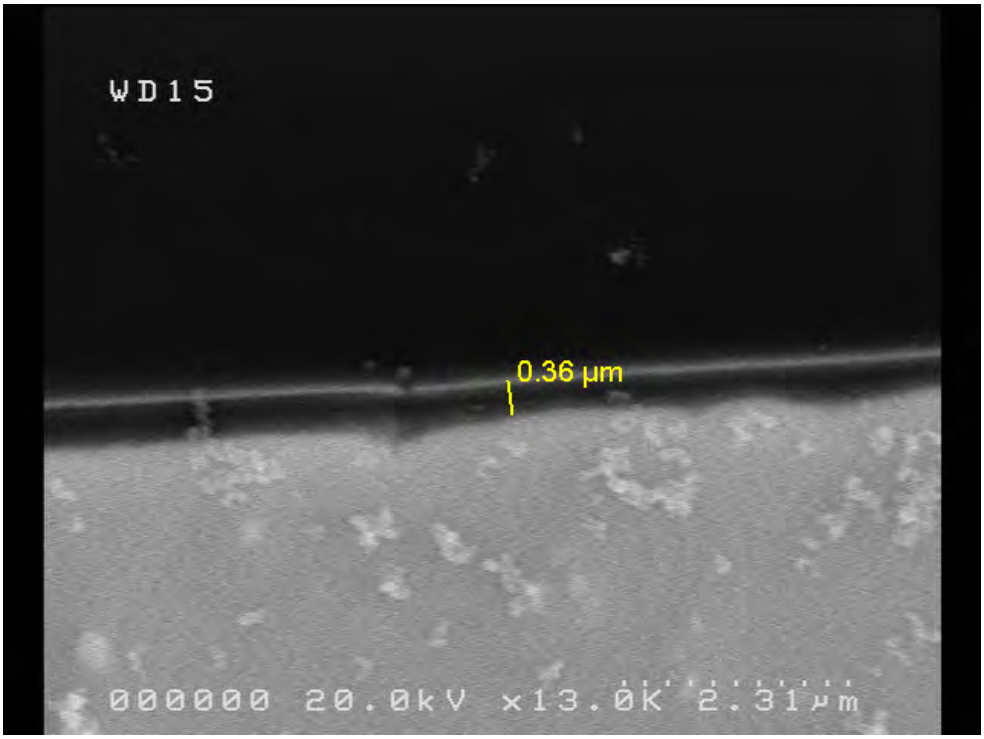


Figure 219: SEM Cross-section image of PC40-UMF standard viscosity coated QFP44, U2, lead 11, location A, 13,000x.

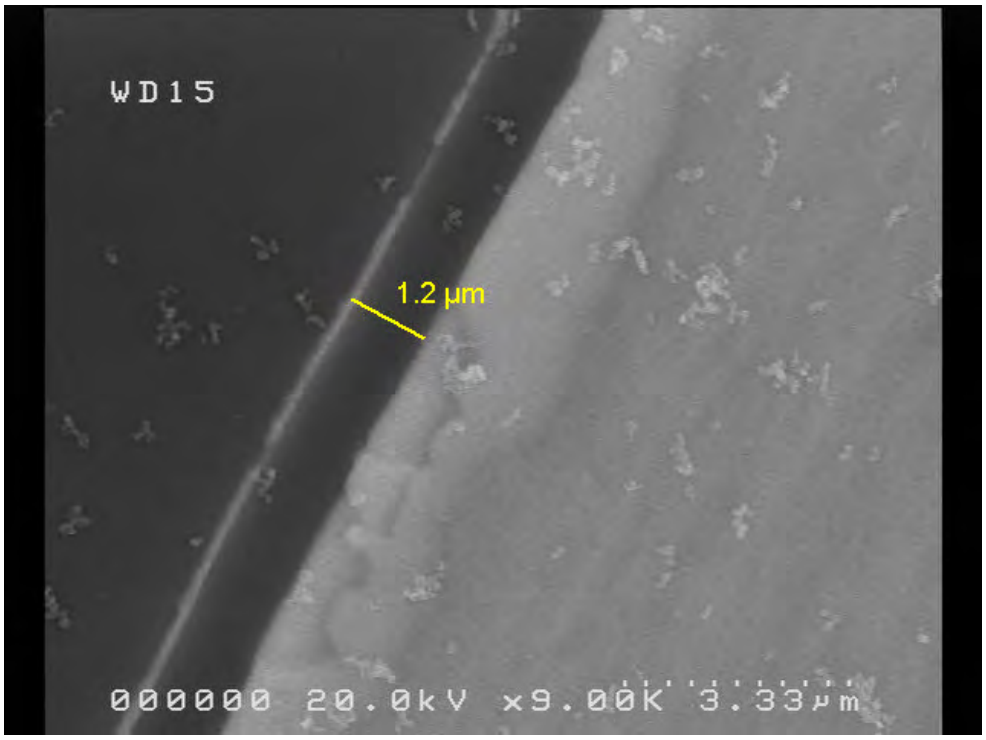


Figure 220: SEM Cross-section image of PC40-UMF standard viscosity coated QFP44, U2, lead 11, location B, 9,000x.



Figure 221: SEM Cross-section image of SEM Cross-section image of PC40-UMF standard viscosity coated QFP44, U2, lead 11, location C, 5,000x.

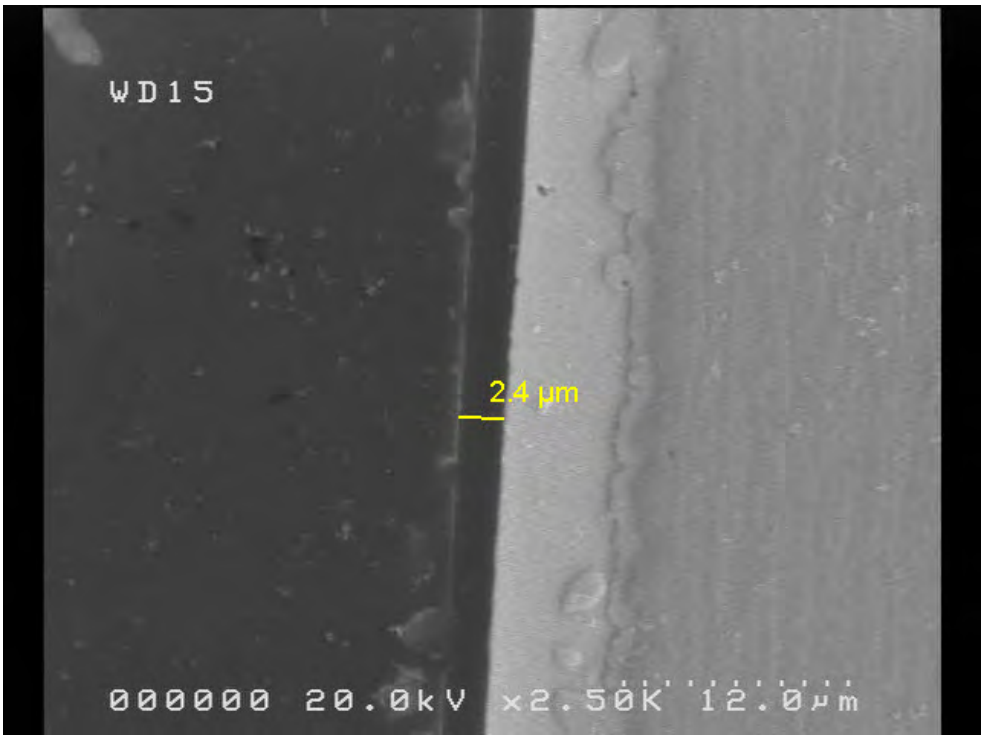


Figure 222: SEM Cross-section image of PC40-UMF standard viscosity coated, QFP44 U2, lead 11, location D, 2,500x.

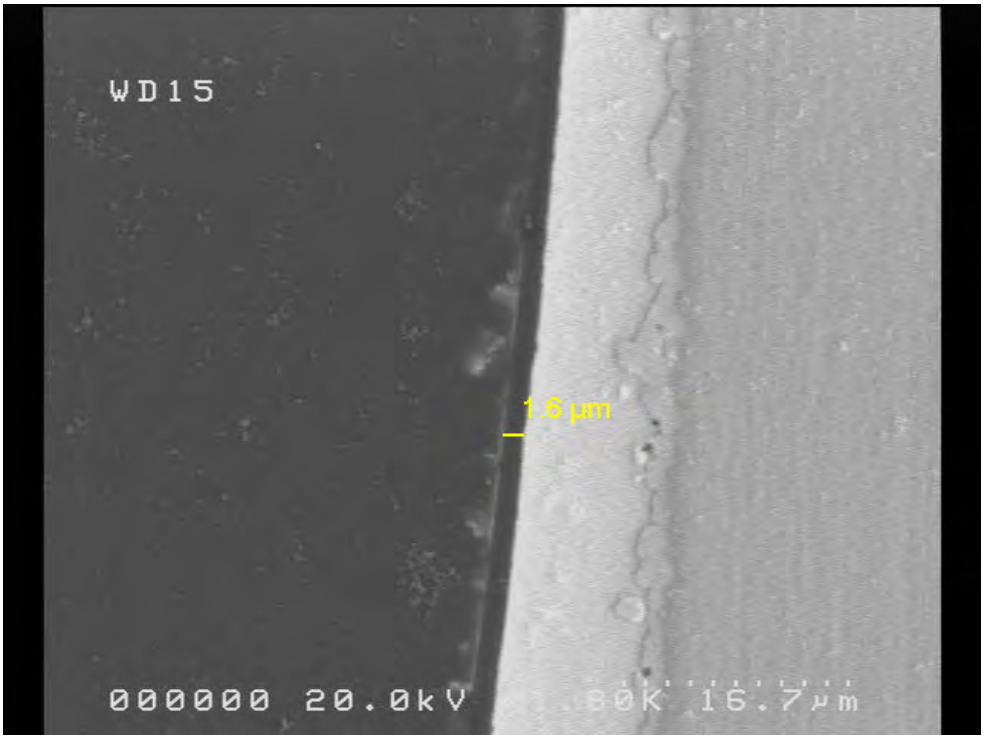


Figure 223: SEM Cross-section image of PC40-UMF standard viscosity coated QFP44, U2, lead 11, location E, 1,800x.



Figure 224: SEM Cross-section image of PC40-UMF standard viscosity coated QFP44, U2, lead 11, location F, 600x.

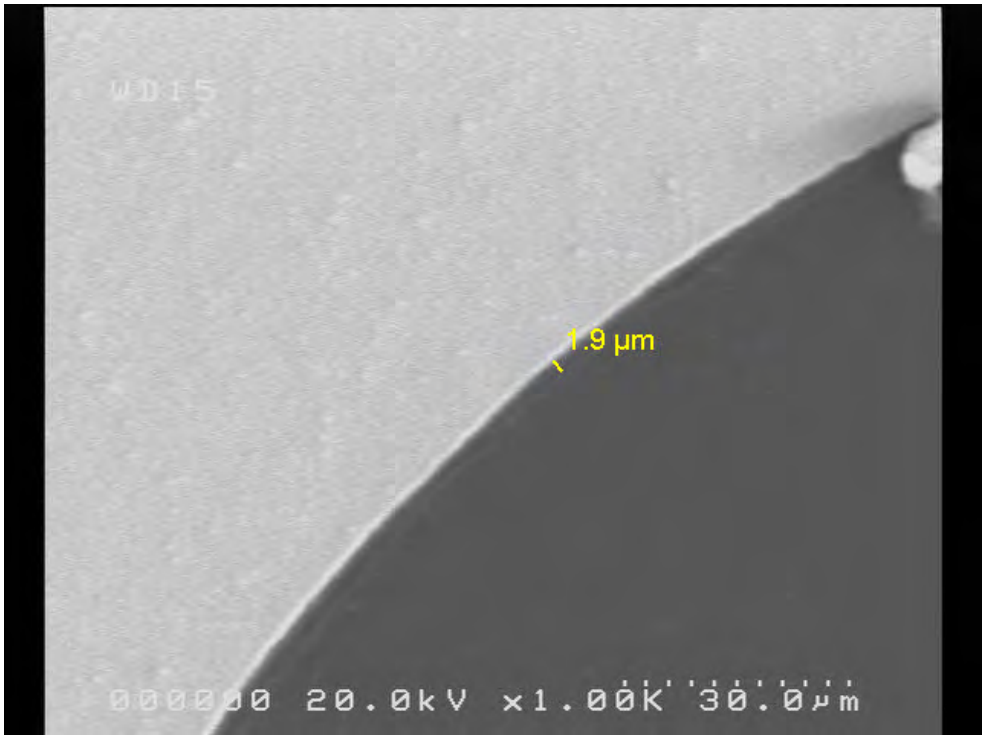


Figure 225: SEM Cross-section image of PC40-UMF standard viscosity coated QFP44, U2, lead 11, location G, 1,000x.

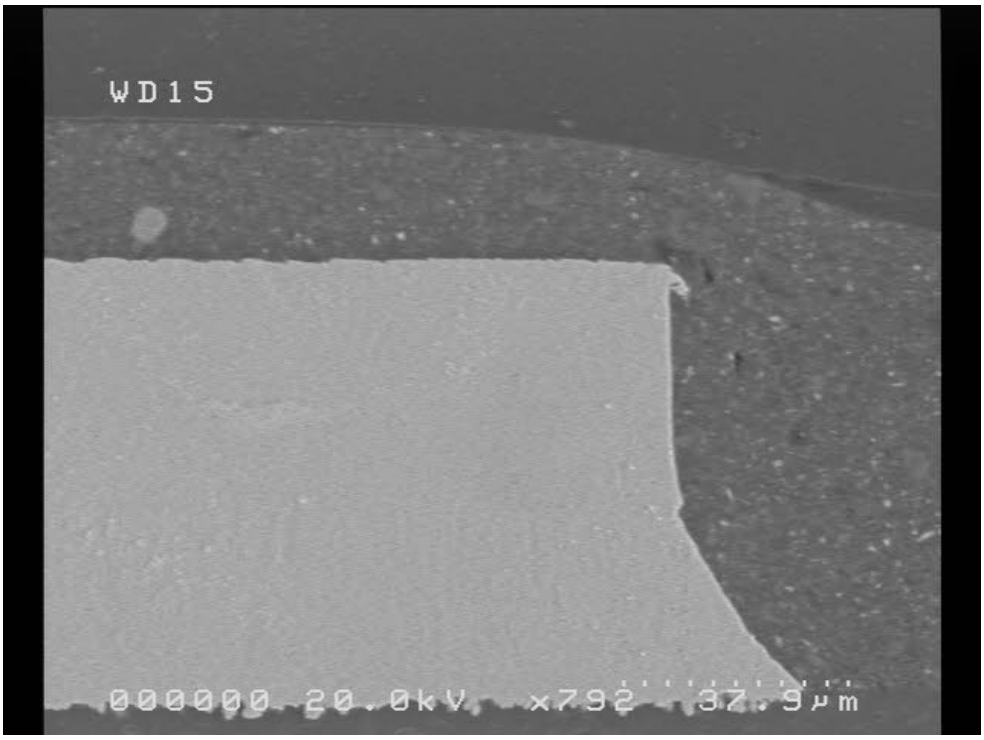


Figure 226: SEM Cross-section image of PC40-UMF standard viscosity coated QFP44, U2, lead 11, location H, 792x.

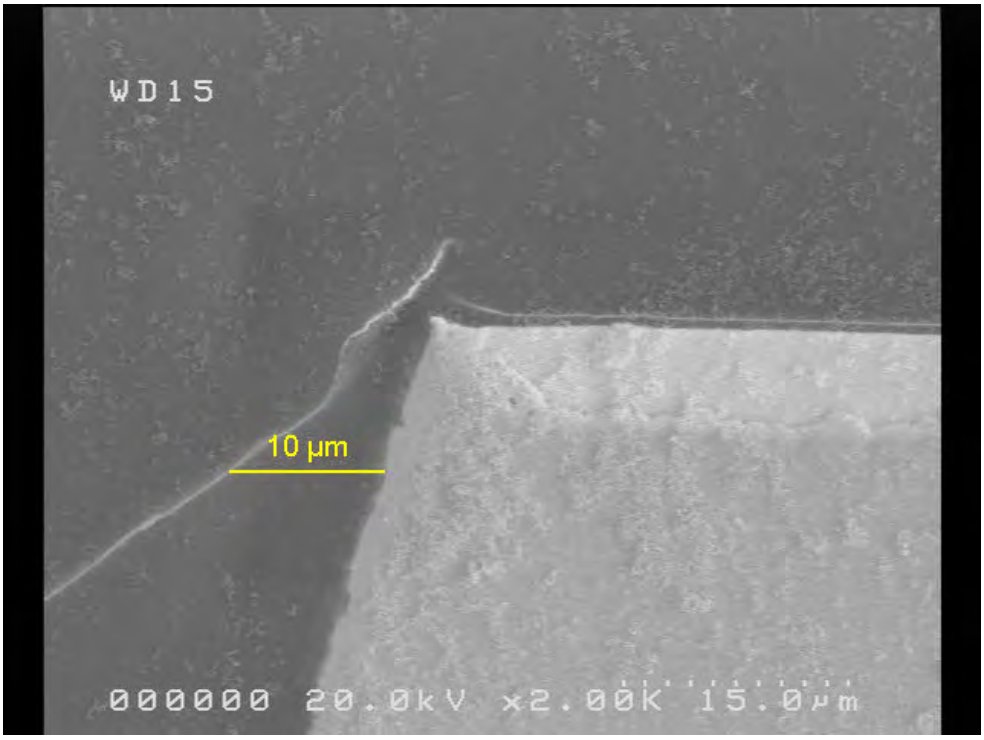


Figure 227: SEM Cross-section image of PC40-UMF standard viscosity coated QFP44, U2, lead 11, location T, 2000x. Coating is 10 microns in the fillet in front of the tip and two to three microns at the tip (Figure 228).

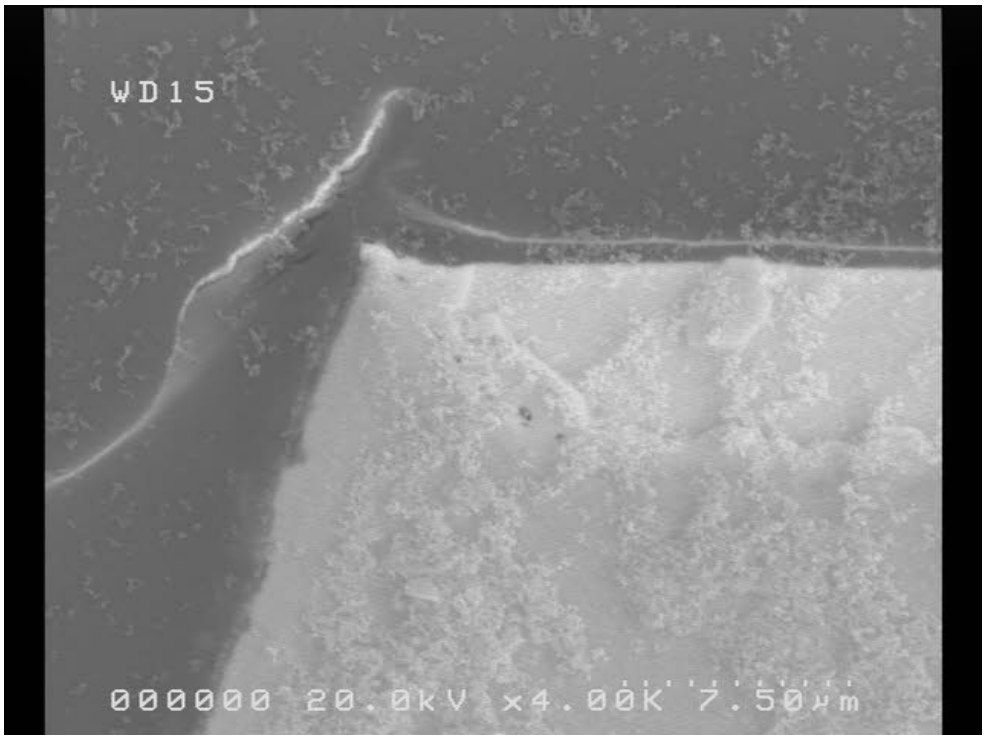


Figure 228: SEM Cross-section image of PC40-UMF standard viscosity coated QFP44, U2, lead 11, location T, 4000x.



Figure 229: SEM isometric image of PC40-UMF high viscosity coated QFP44, 40x (ref. U2, leads 1-3).

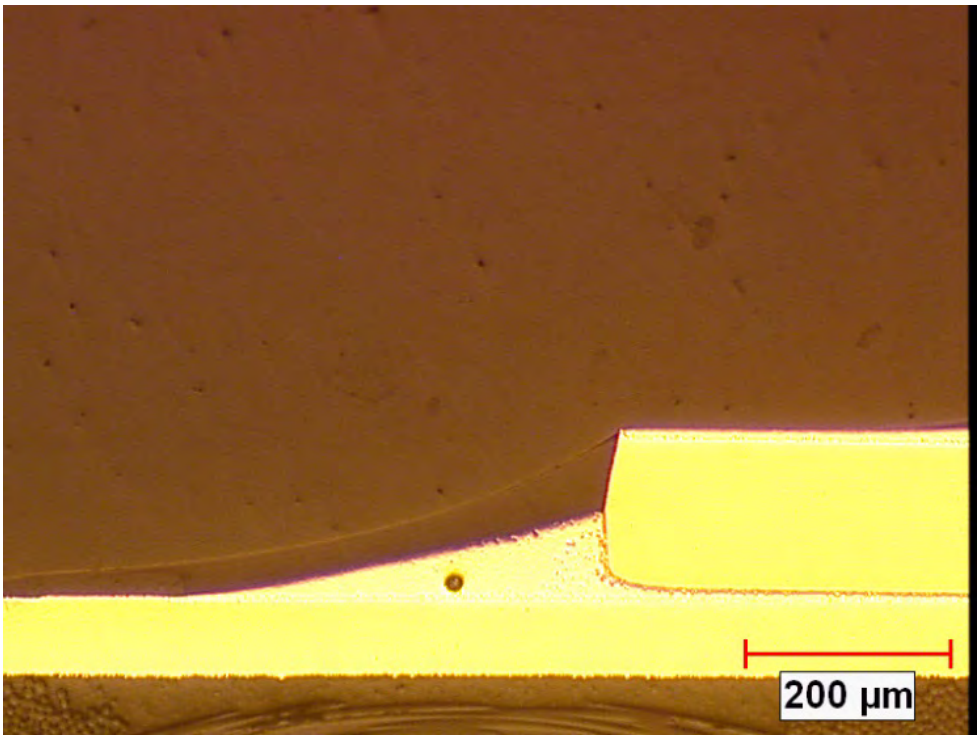


Figure 230: Optical cross-section image of the PC40-UMF high viscosity coating on the QFP44 lead toe, 100x (ref. U2, lead 11).

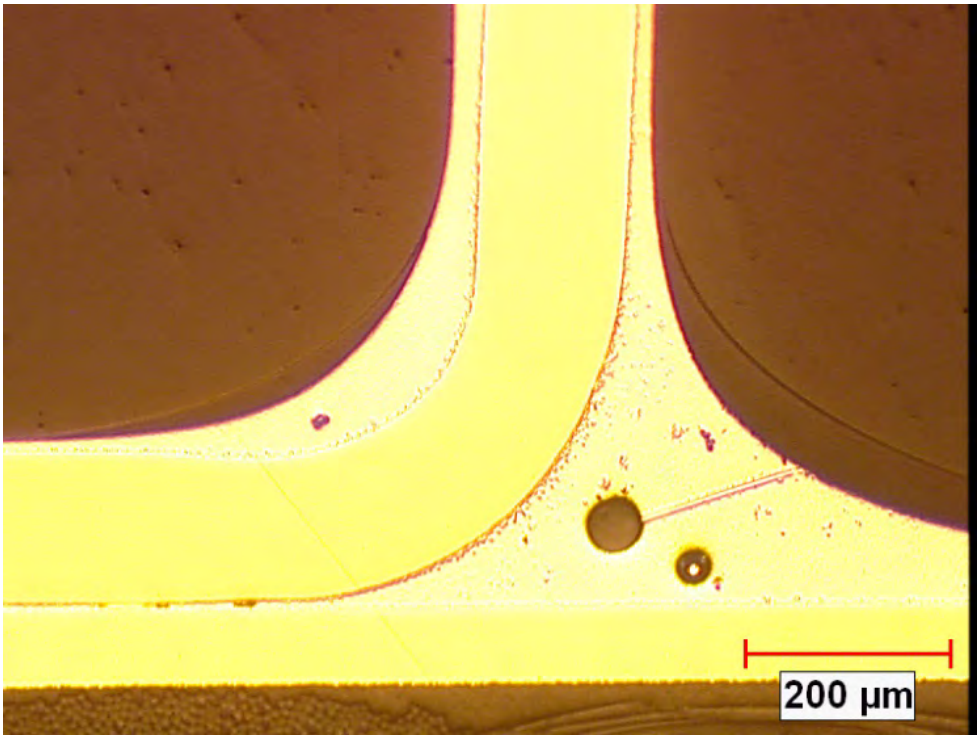


Figure 231: Optical cross-section image of the PC40-UMF high viscosity coating on the QFP44 lead foot, 100x (ref. U2, lead 11).

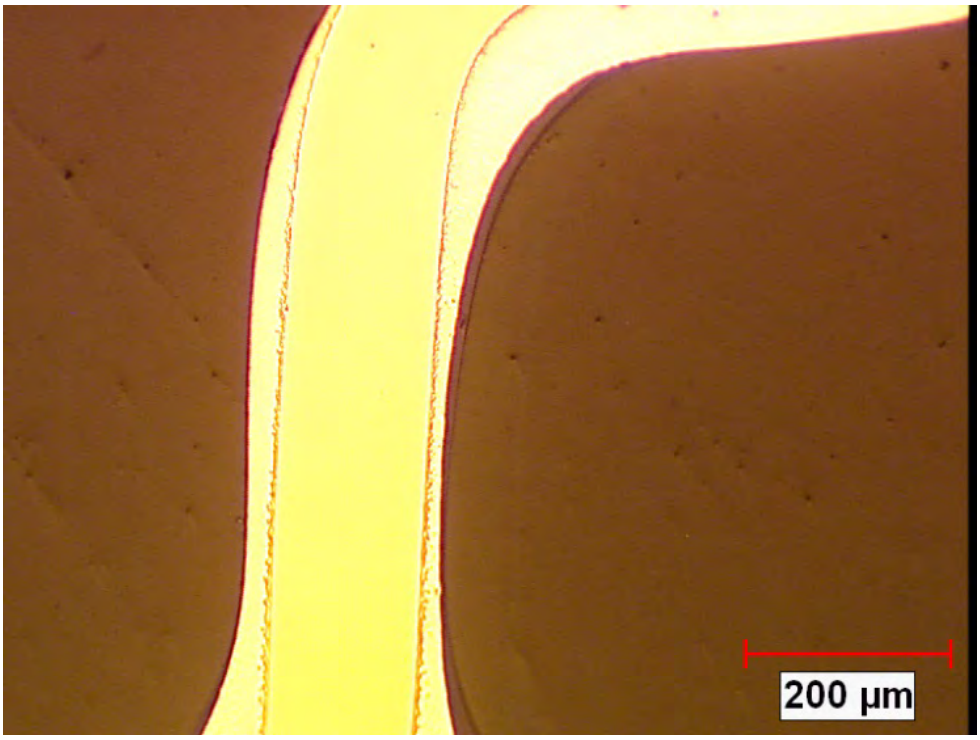


Figure 232: Optical cross-section image of the PC40-UMF high viscosity coating on the QFP44 middle lead location, 100x (ref. U2, lead 11).

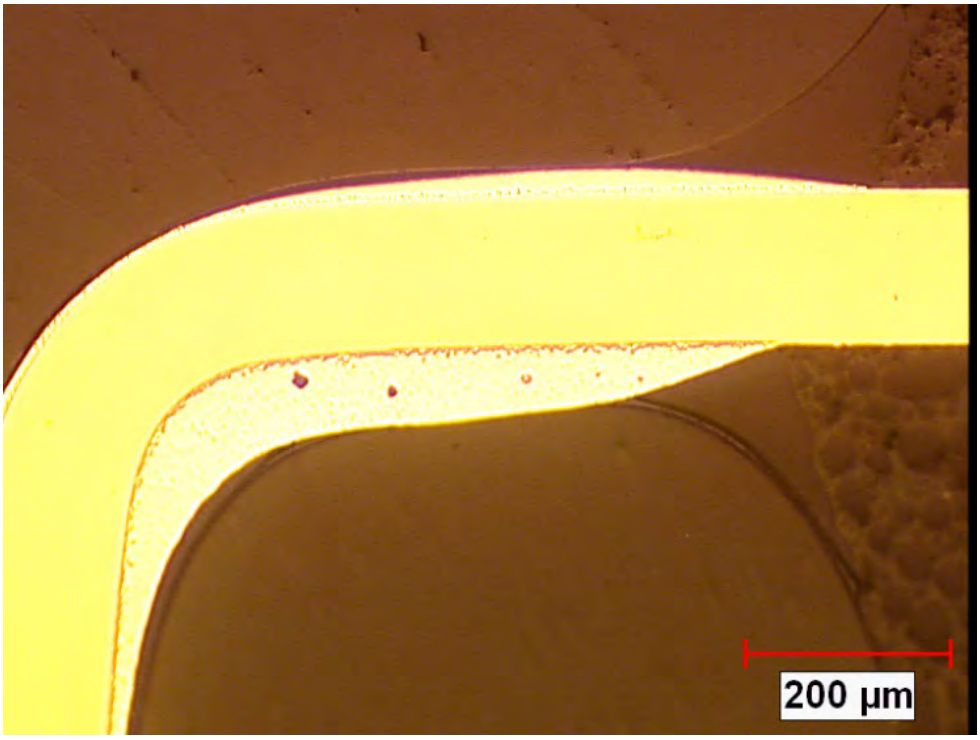


Figure 233: Optical cross-section image of the PC40-UMF high viscosity coating on the QFP44 upper lead location, 100x (ref. U2, lead 11).

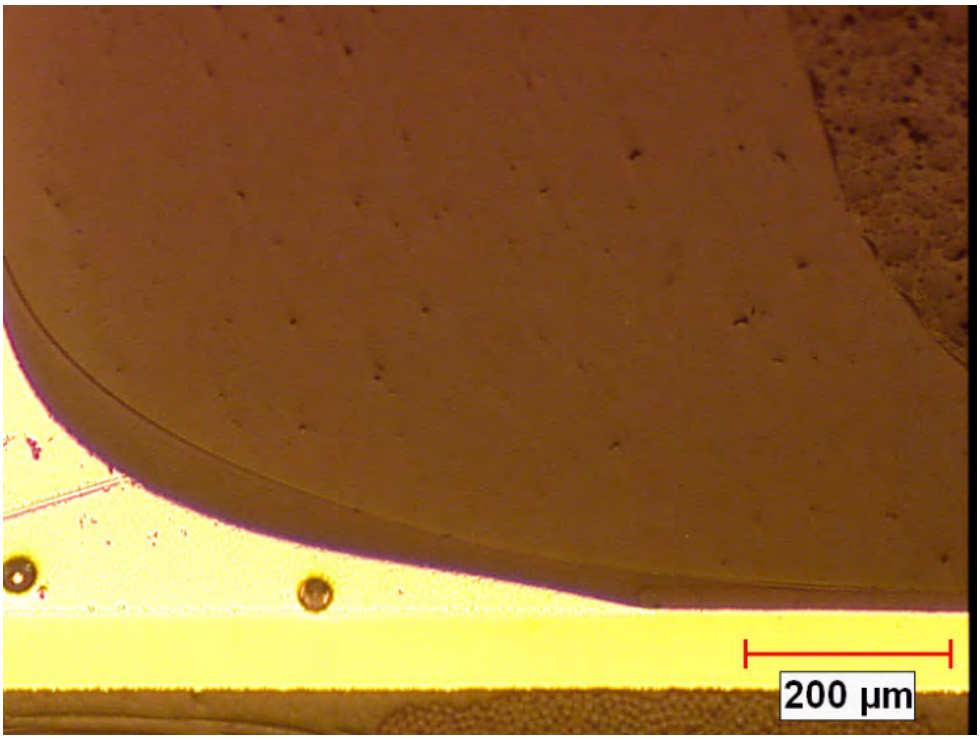


Figure 234: Optical cross-section image of the PC40-UMF high viscosity coating on the QFP44 heel location, 100x (ref. U2, lead 11).



Figure 235: SEM cross-section image of the PC40-UMF high viscosity coated QFP44, U2, lead 11, location A, 3,500x



Figure 236: SEM cross-section image of the PC40-UMF high viscosity coated QFP44, U2, lead 11, location B, 900x.



Figure 237: SEM cross-section image of the PC40-UMF high viscosity coated QFP44, U2, lead 11, location C, 1,000x.

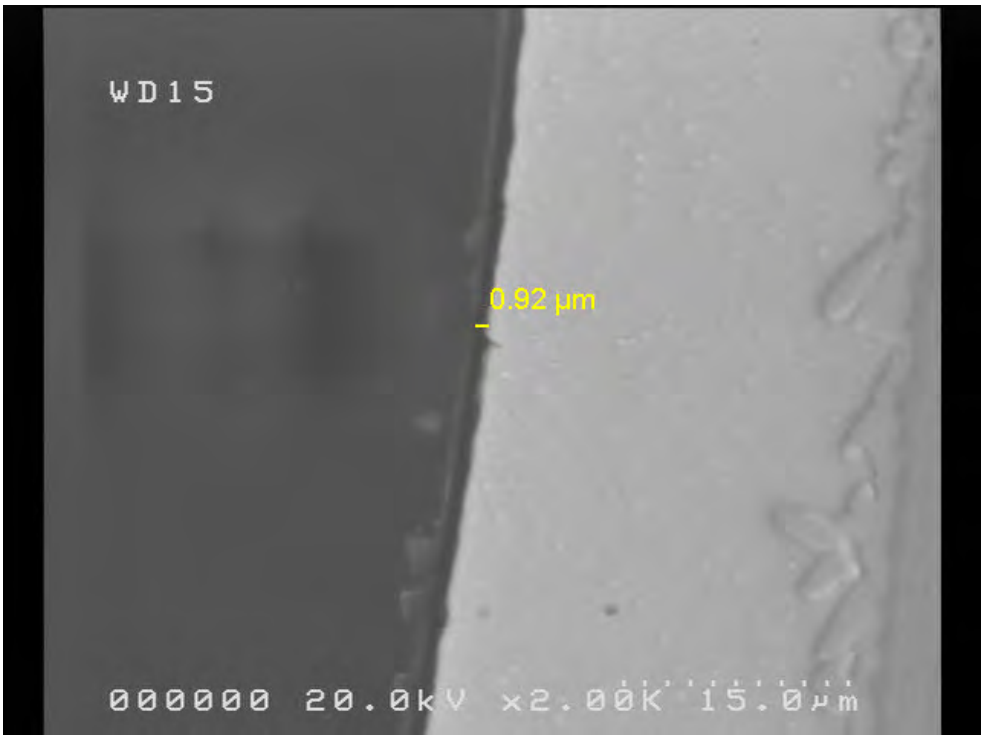


Figure 238: SEM cross-section image of the PC40-UMF high viscosity coated QFP44, U2, lead 11, location D, 2,000x.

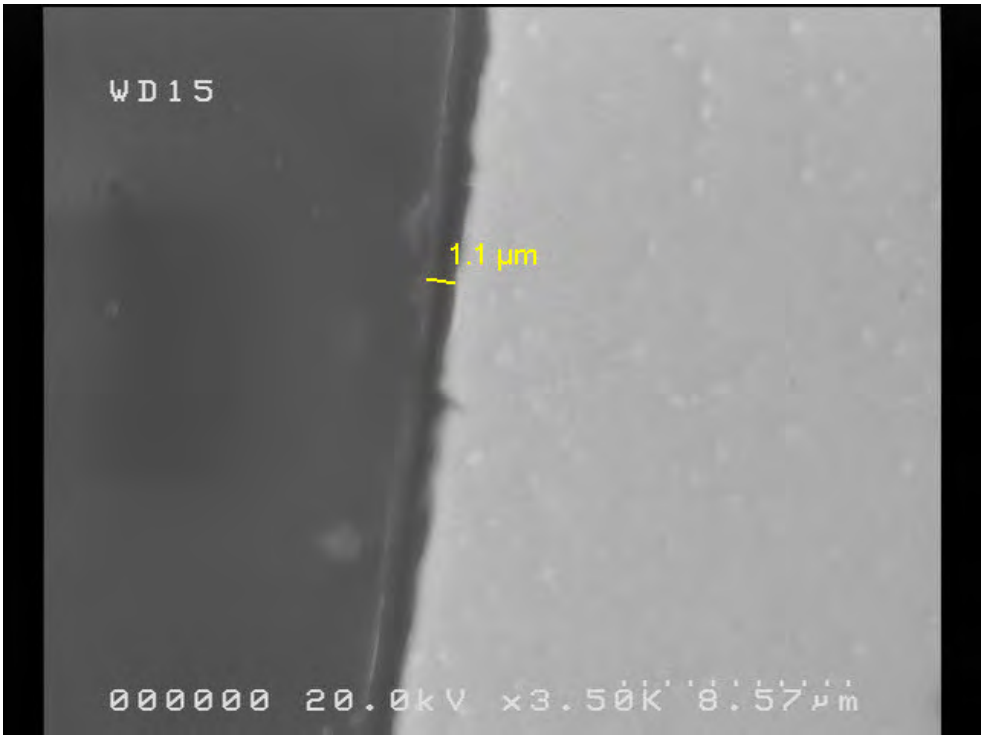


Figure 239: SEM cross-section image of the PC40-UMF high viscosity coated QFP44, U2, lead 11, location E, 3,500x.

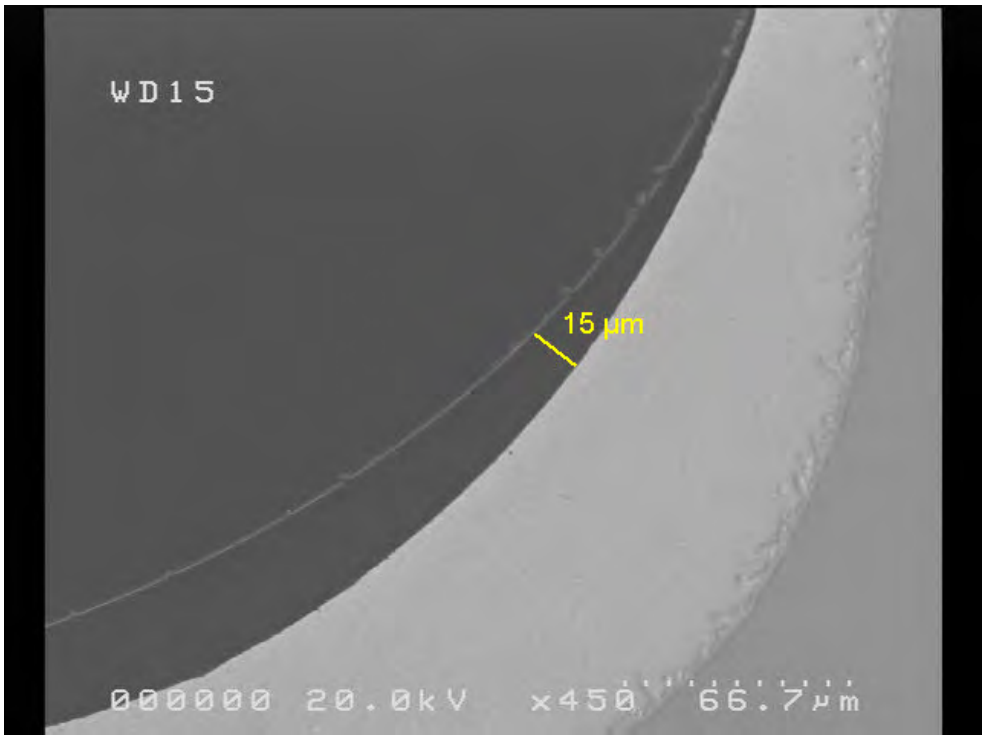


Figure 240: SEM cross-section image of the PC40-UMF high viscosity coated QFP44, U2, lead 11, location F, 450x.

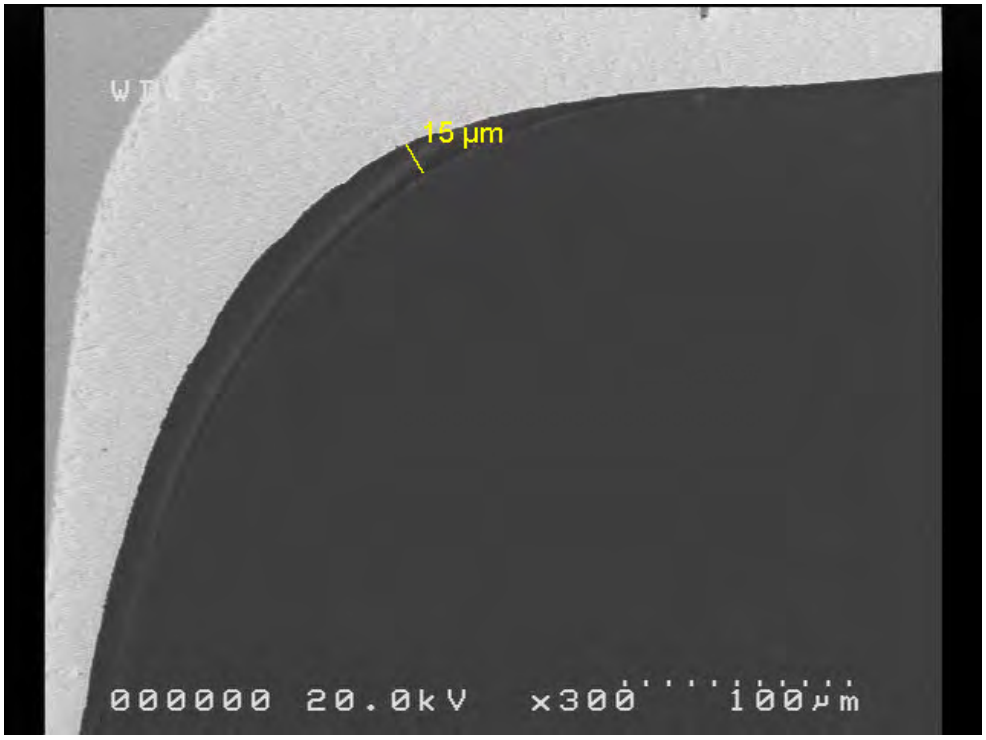


Figure 241: SEM cross-section image of the PC40-UMF high viscosity coated QFP44, U2, lead 11, location G, 300x.

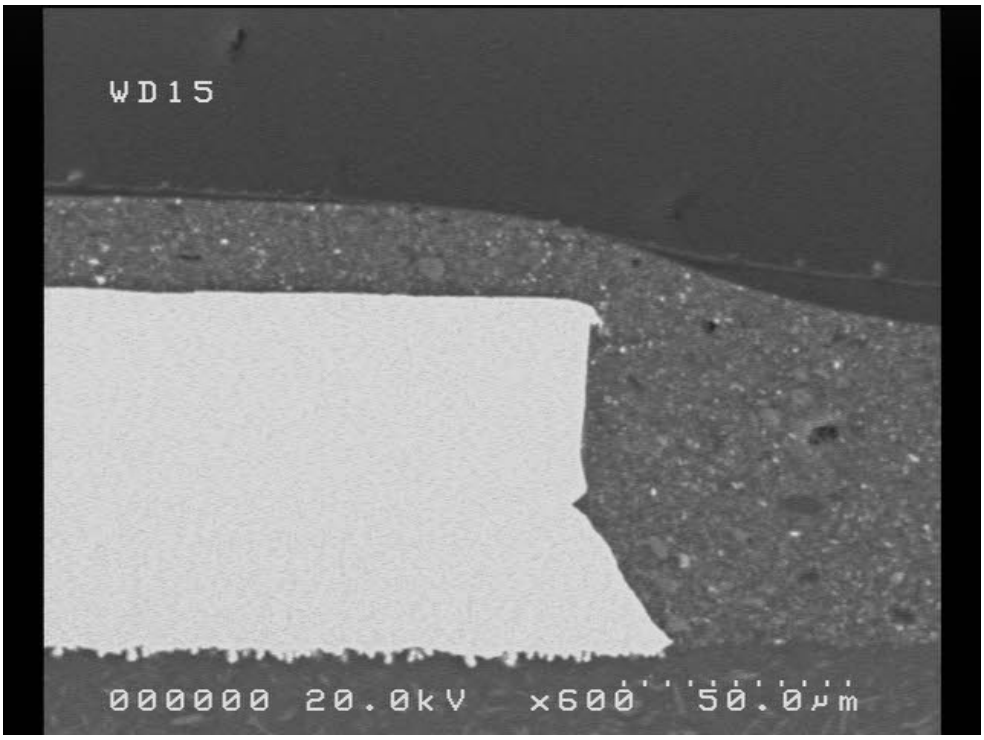


Figure 242: SEM cross-section image of the PC40-UMF high viscosity coated QFP44, U2, lead 11, location H, 600x.

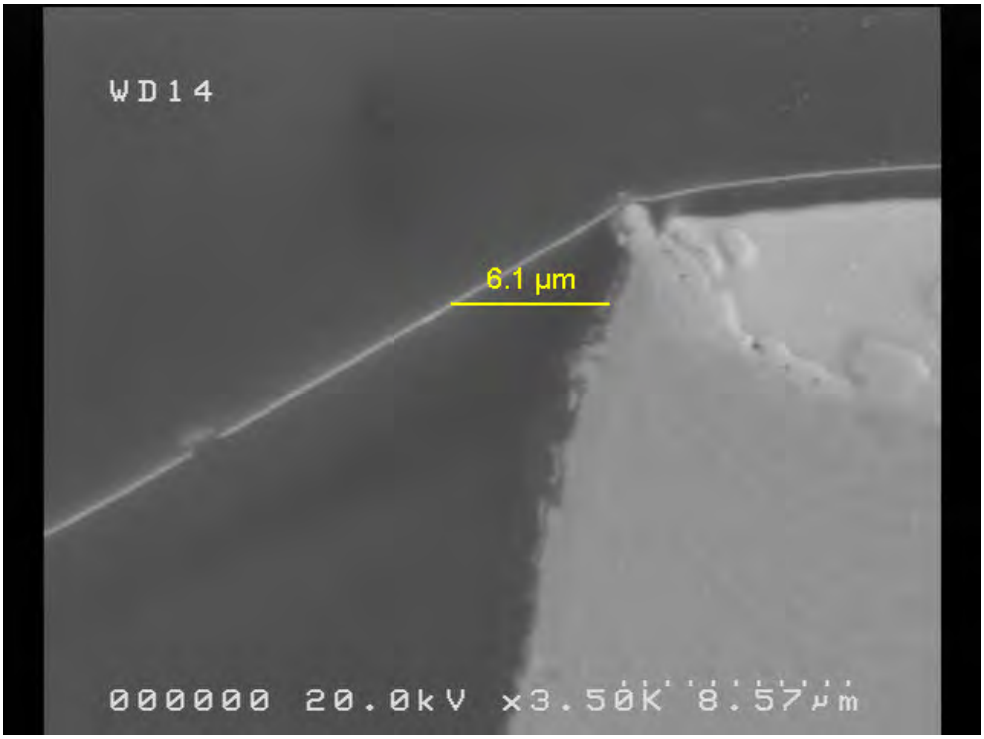


Figure 243: SEM cross-section image of the PC40-UMF high viscosity coated QFP44, U2, lead 11, T, 3,500x. Coating is 6.1 microns in the fillet in front of the tip and 0.4 microns at the tip not including the small burr location where it essentially zero (Figure 244).



Figure 244: SEM cross-section image of the PC40-UMF high viscosity coated QFP44, U2, lead 11, location T, 15,000x.

3. Reference coatings

3.1 Parylene C ™

SEM isometric images were obtained to show coverage. Cross – sections were only made on the Parylene ™ C with Adpro Plus as shown in the next section since the Parylene was deposited at the same time.

3.1.1 Parylene C ™ SEM

Isometric SEM images showing the coverage of Parylene C ™ coating are shown in Figure 245 to Figure 249. No thin regions were observed.

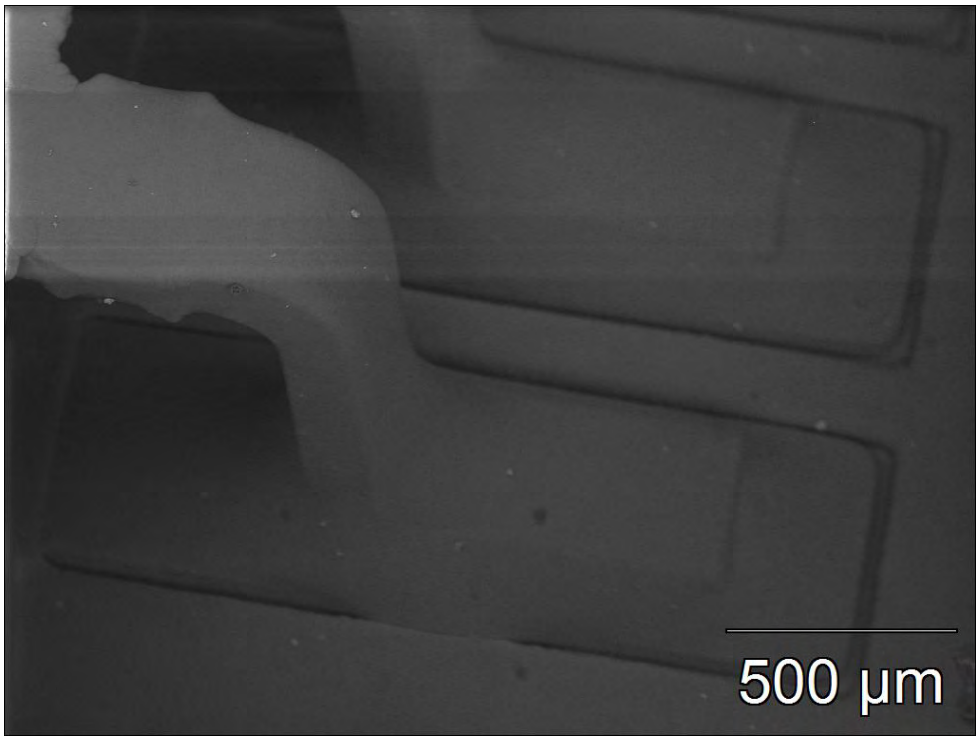


Figure 245: SEM image of Parylene C coated QFP44, U5, lead 23, 60x (ref. Board 2) (image taken after accelerated thermal cycling ref. Board 2).

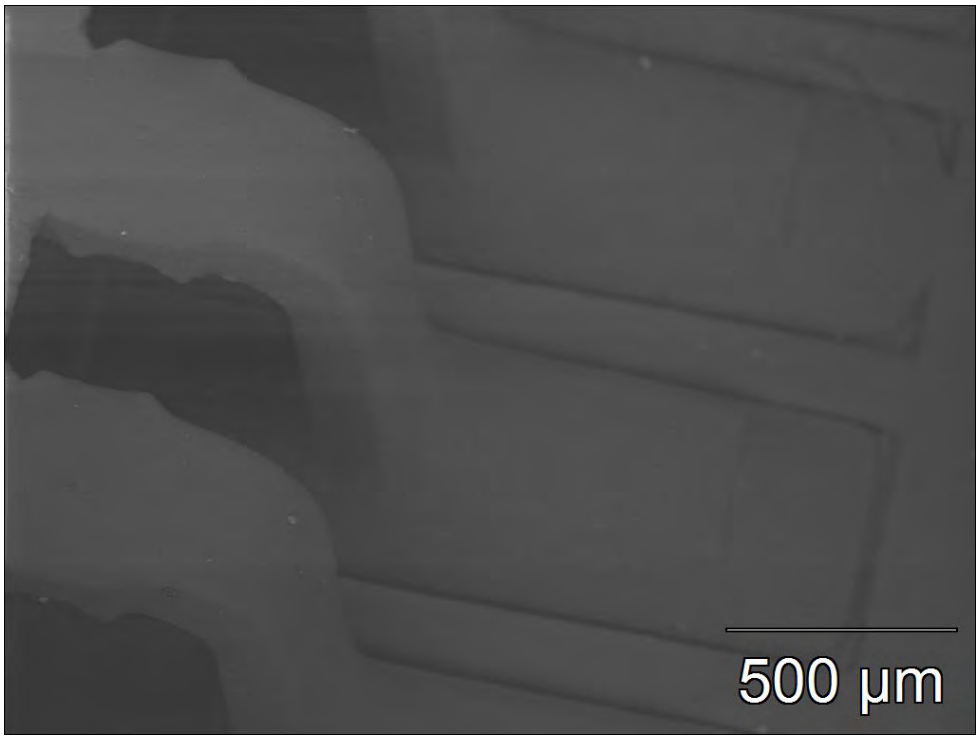


Figure 246: SEM image of Parylene C coated QFP44, U5, lead 24, 60x (image taken after accelerated thermal cycling ref. Board 2).

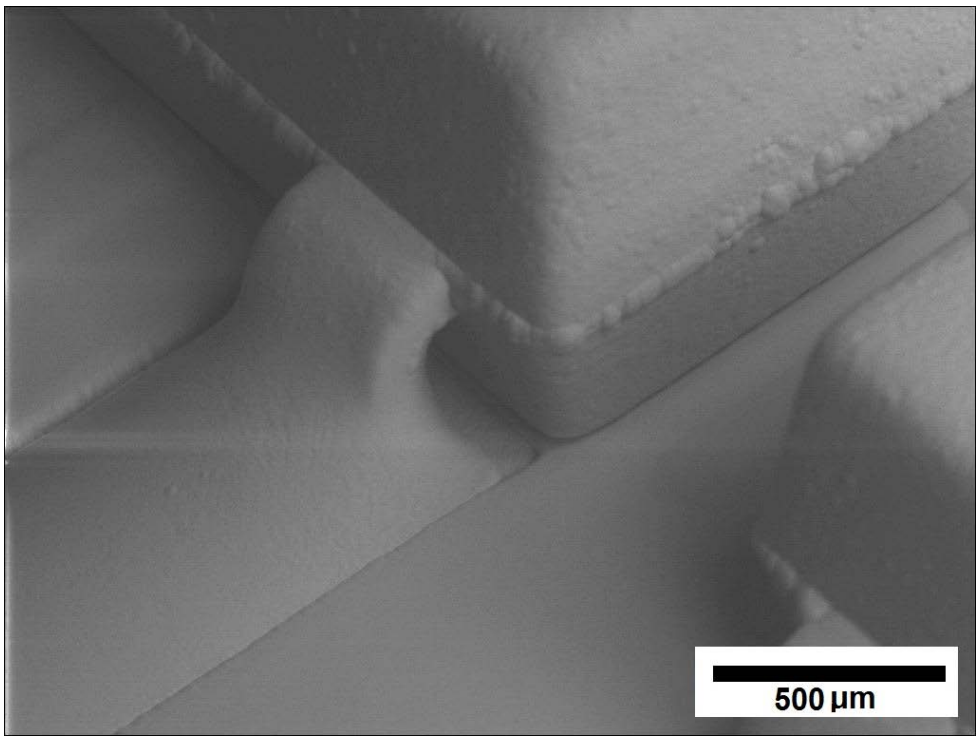


Figure 247: SEM image of Parylene C coated SOT3, 60x (image taken after accelerated thermal cycling ref. Board 207).

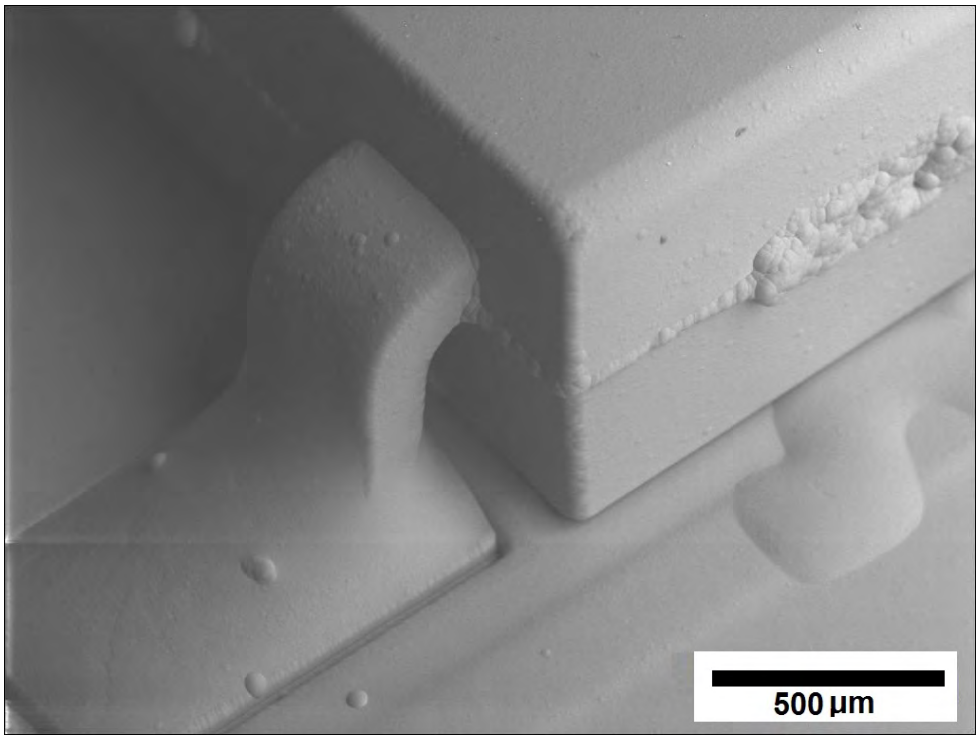


Figure 248: SEM image of Parylene C coated SOT5, 60x (image taken after accelerated thermal cycling ref. Board 207).

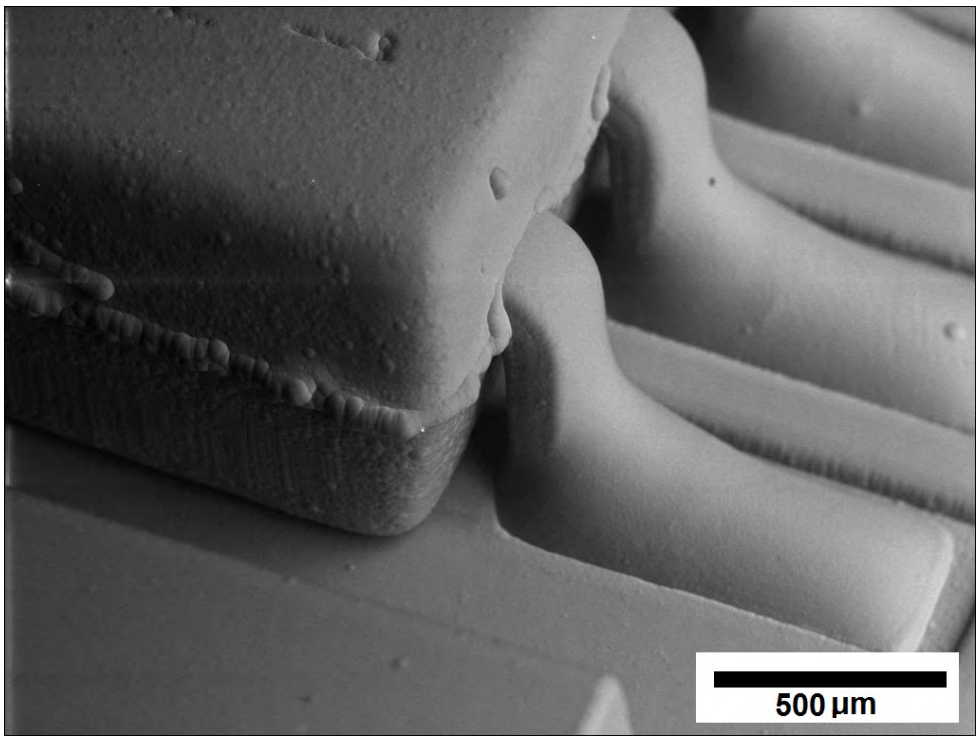


Figure 249: SEM image of Parylene C coated SOT6, 60x (image taken after accelerated thermal cycling ref. Board 207).

3.2 Parylene C ™ with Adpro plus

SEM isometric and cross – sections were made of the Parylene C ™ with Adpro plus coated samples.

3.2.1 Parylene C ™ with Adpro plus SEM

Isometric SEM images showing the coverage of parylene C ™ coating with the Adpro plus adhesion promoter are shown in Figure 250 and Figure 251. No thin regions were observed.

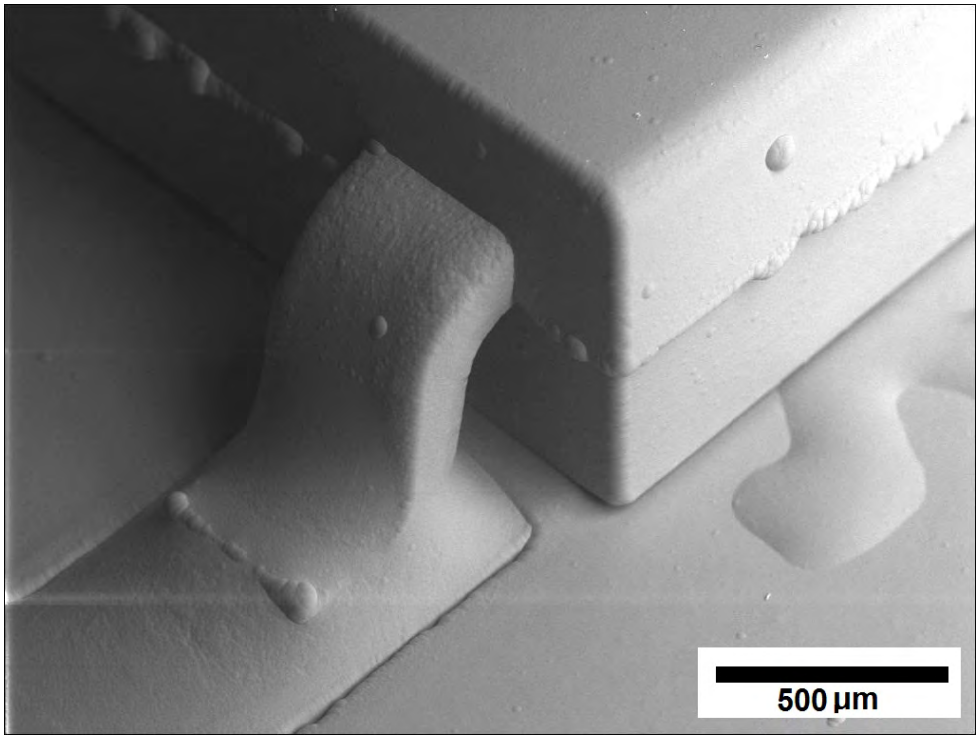


Figure 250: SEM image of Parylene C with Adpro plus coated SOT5, 60x (image taken after accelerated thermal cycling ref. Board 202).

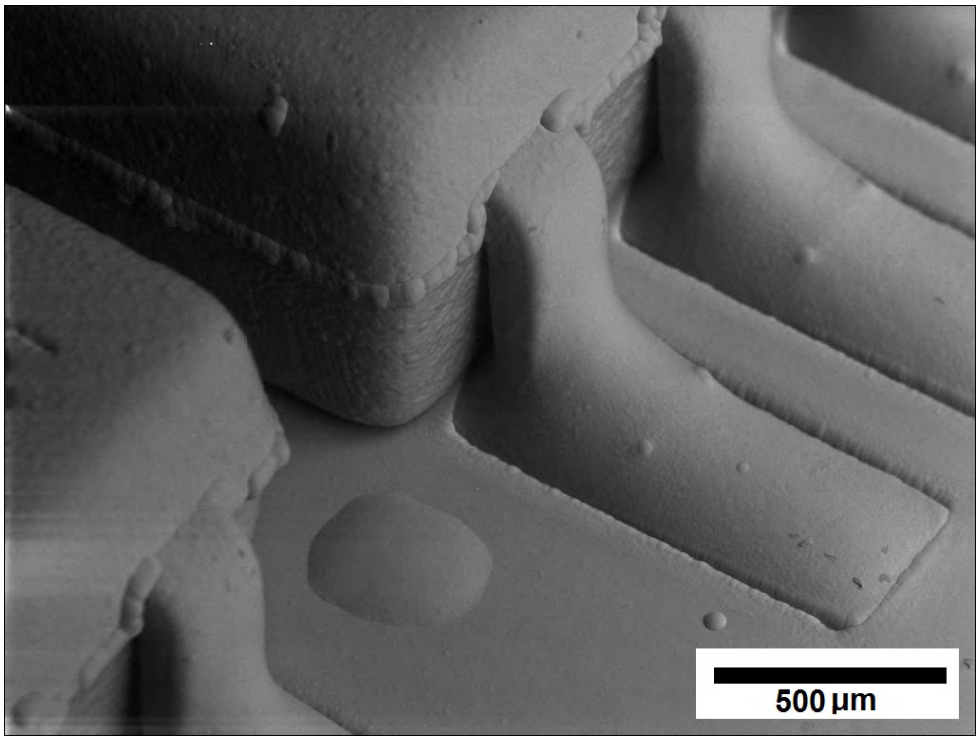


Figure 251: SEM image of Parylene C with Adpro plus coated SOT6, 60x (image taken after accelerated thermal cycling ref. Board 202).

3.2.2 Parylene C ™ with Adpro plus vertical cross-section coating thickness evaluation

The vertical cross-section coating thickness analysis was performed on the QFP44 components. The measurement locations are shown in Figure 23. The results summarized in Table 2 shows that the vacuum deposited coating thickness ranges from 27 to 30 microns. A typical overall cross-section is shown in Figure 252. Typical optical cross-section images at 100x are shown in Figure 253 to Figure 256. Typical SEM cross – section images are shown in Figure 257 to Figure 264.

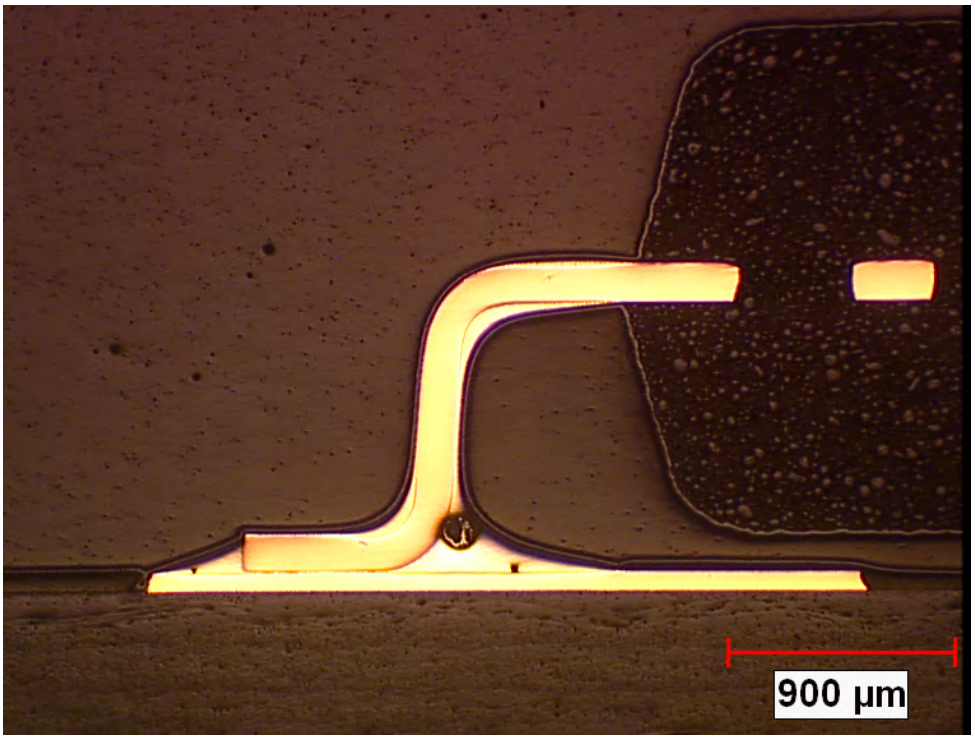


Figure 252: Optical cross-section view of Parylene C ™ with Adpro plus coated QFP44 lead, overall, 25x (ref. Board 1, left lead).

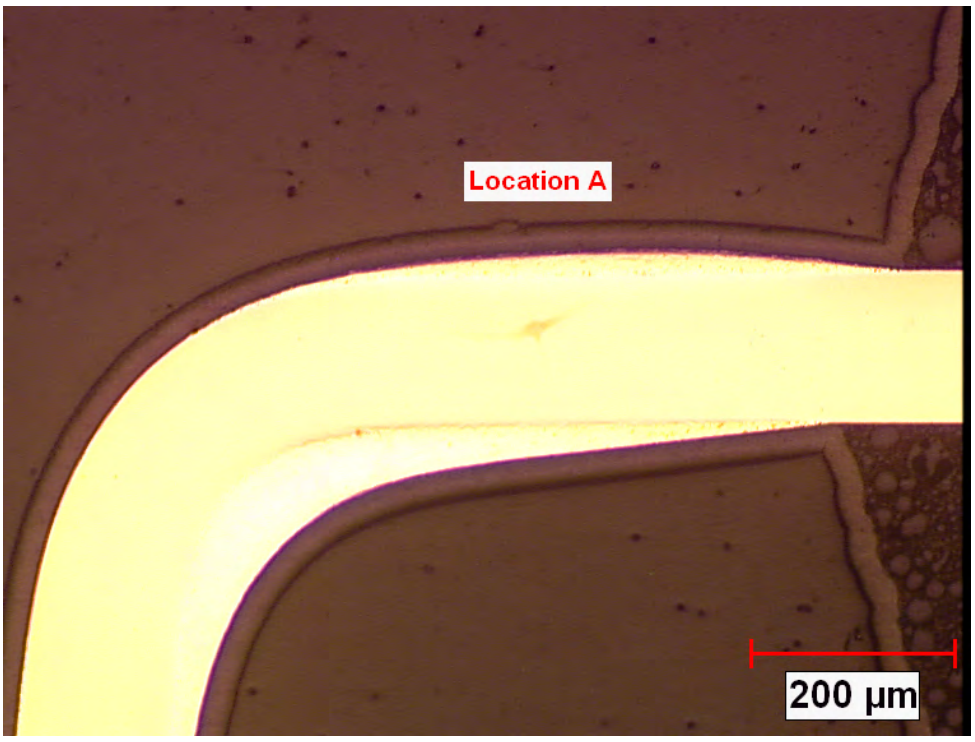


Figure 253: Optical cross-section view of Parylene C ™ with Adpro plus coated QFP44 lead, location A, 100x (ref. Board 1, left lead).

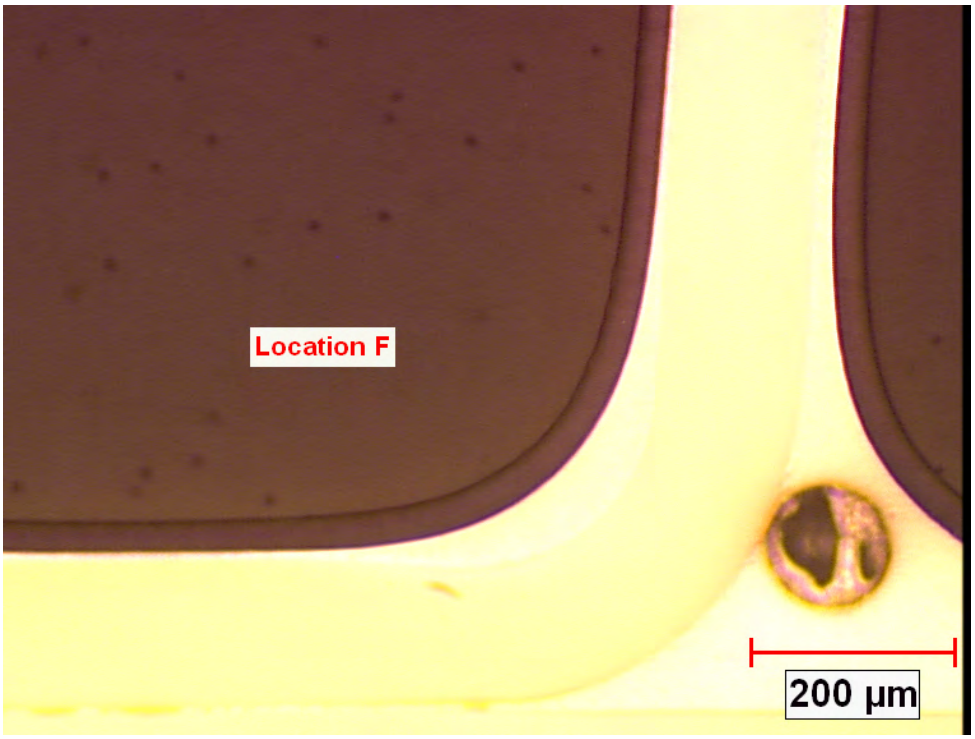


Figure 254: Optical cross-section view of Parylene C ™ with Adpro plus coated QFP44 lead, location F, 100x (ref. Board 1, left lead).

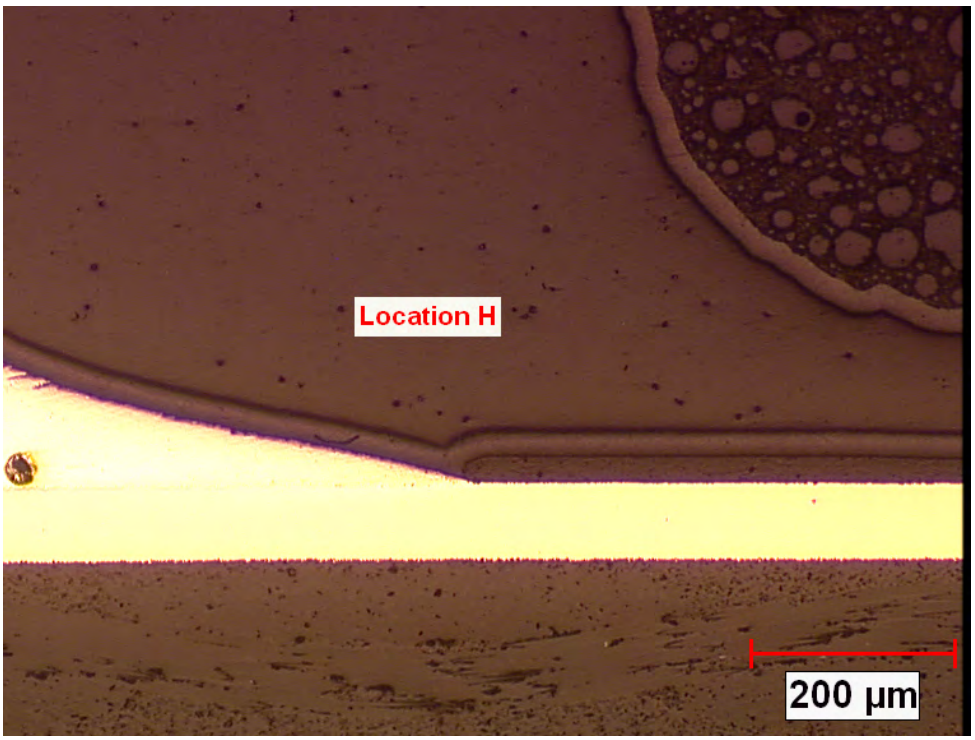


Figure 255: Optical cross-section view of Parylene C ™ with Adpro plus coated QFP44 lead, location H, 100x (ref. Board 1, left lead).

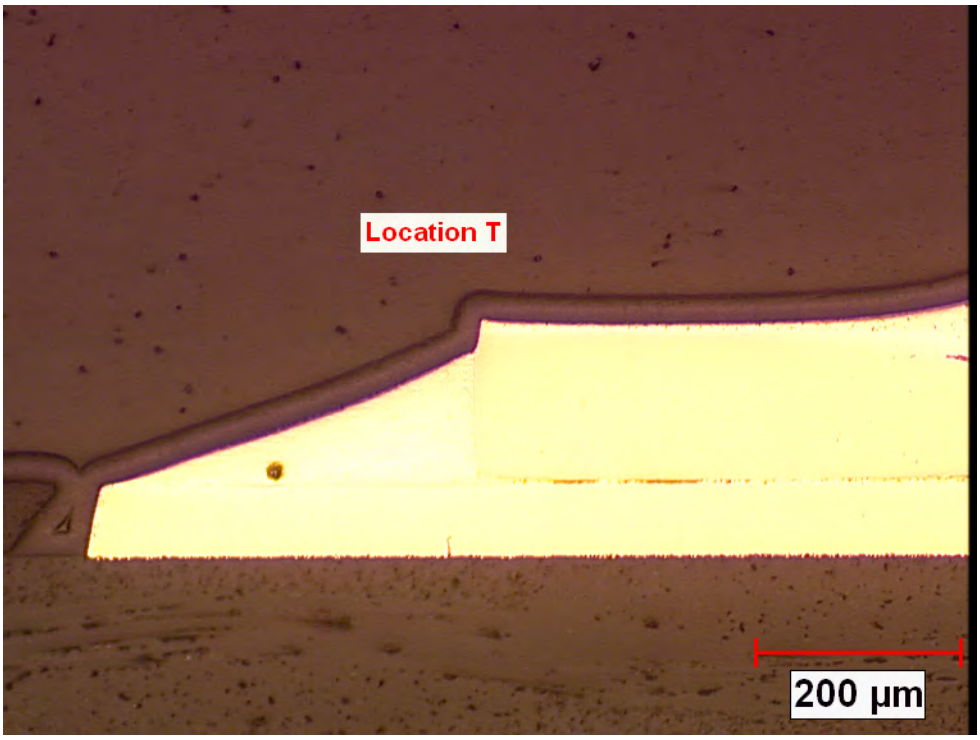


Figure 256: Optical cross-section view of Parylene C ™ with Adpro plus coated QFP44 lead, location T, 100x (ref. Board 1, left lead).

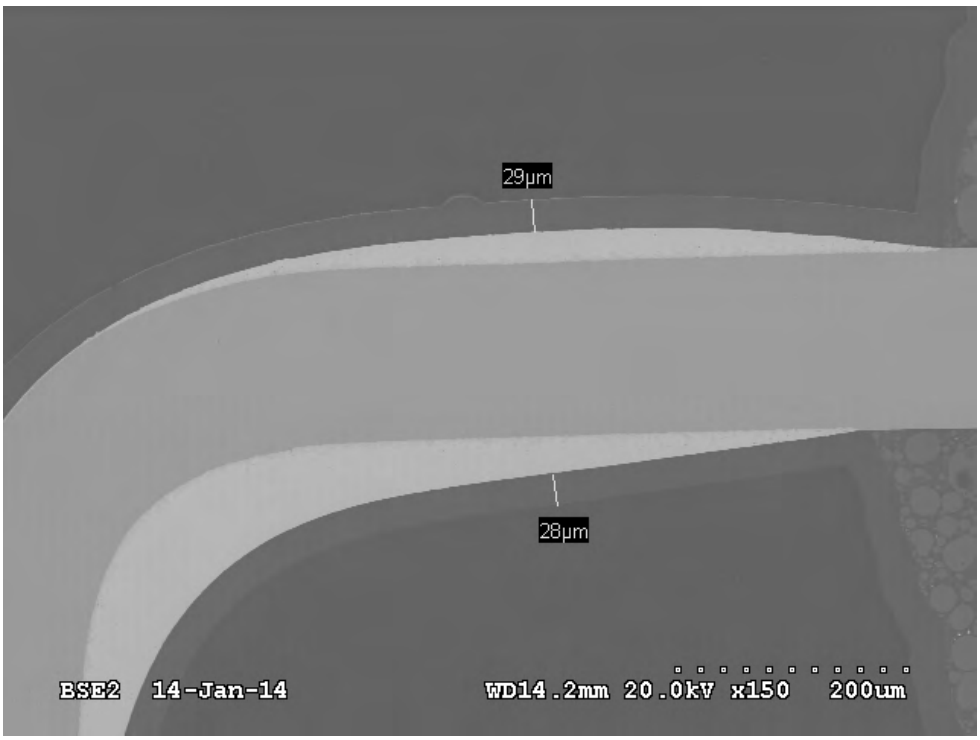


Figure 257: SEM cross-section view of Parylene C ™ with Adpro plus coated QFP44 lead, location A, 150x (ref. Board 1, left lead).

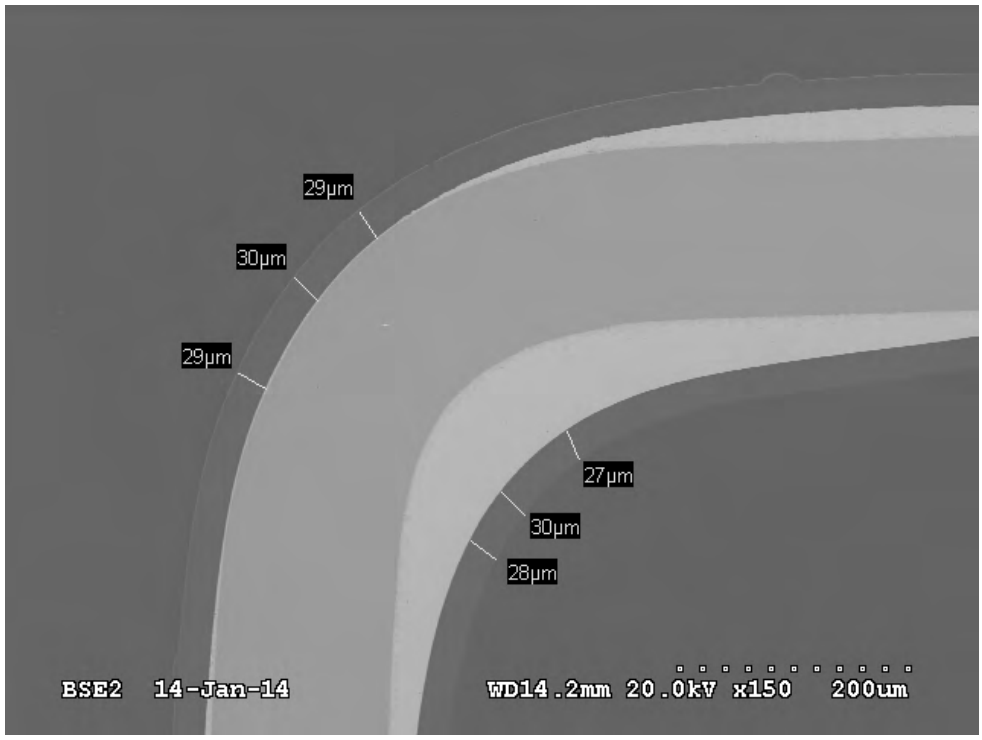


Figure 258: SEM cross-section view of Parylene C ™ with Adpro plus coated QFP44 lead, location B, 150x (ref. Board 1, left lead).

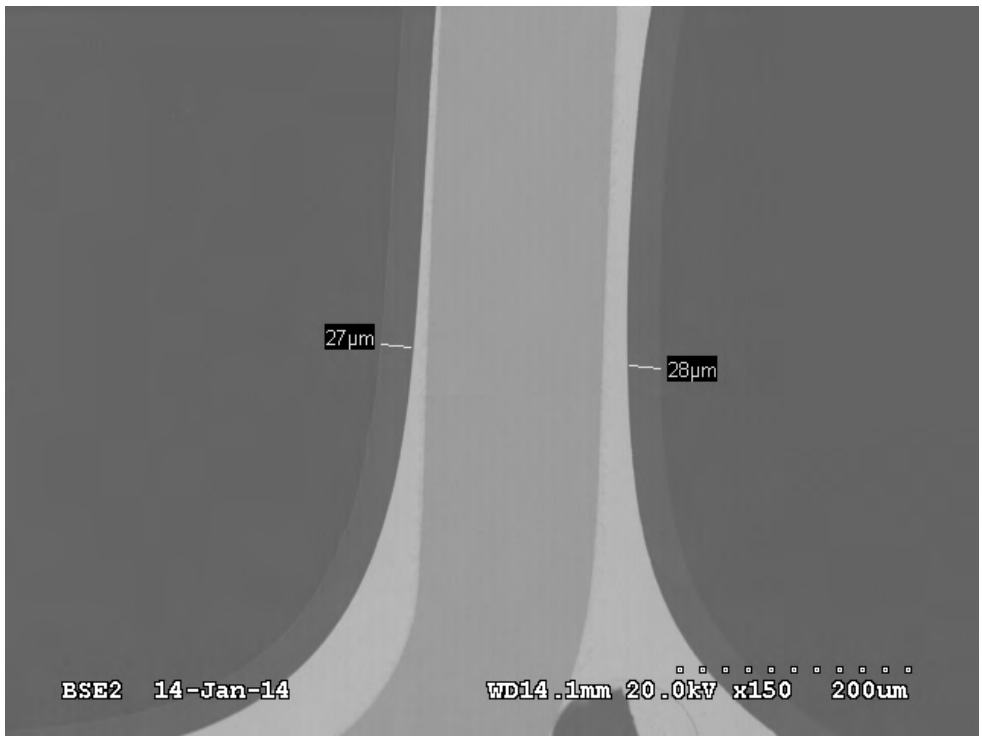


Figure 259: SEM cross-section view of Parylene C ™ with Adpro plus coated QFP44 lead, location E, 150x (ref. Board 1, left lead).

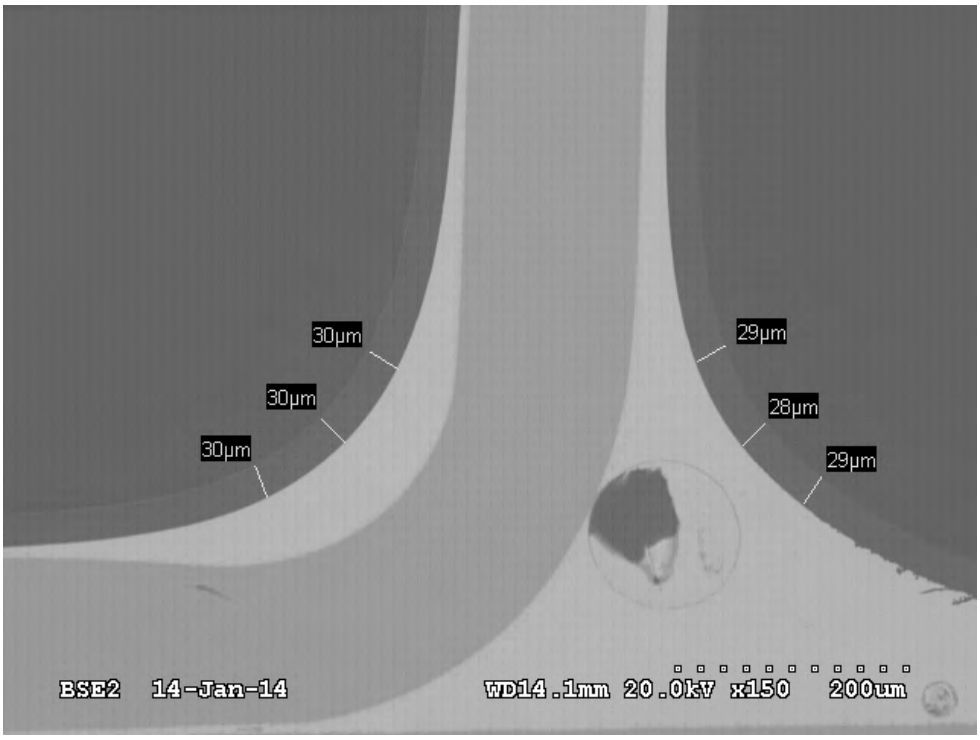


Figure 260: SEM cross-section view of Parylene C ™ with Adpro plus coated QFP44 lead, location F, 150x (ref. Board 1, left lead).

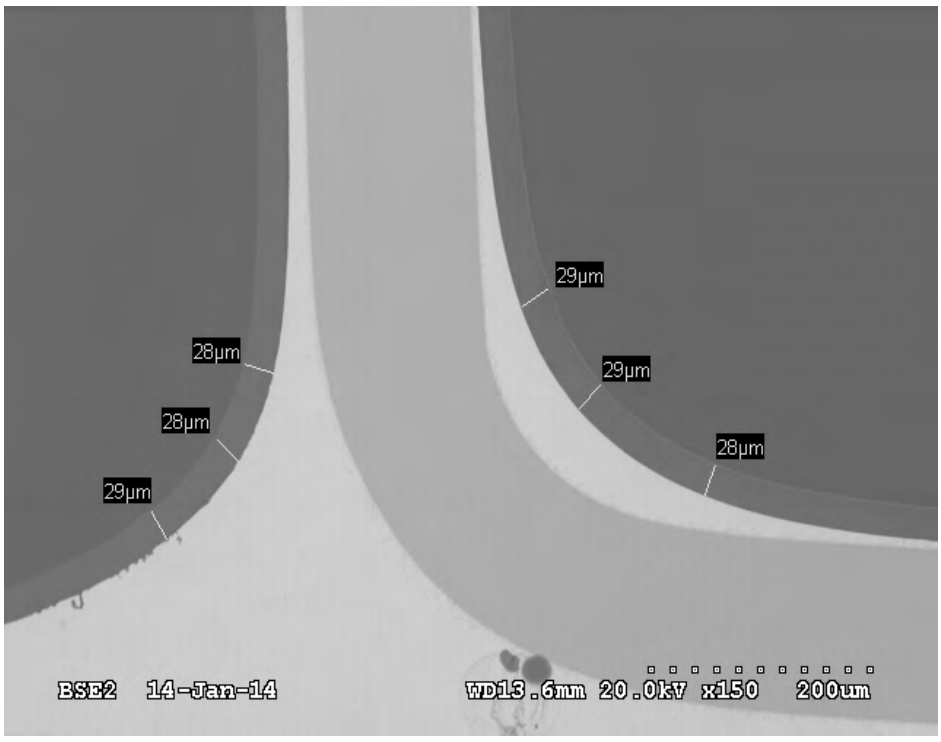


Figure 261: SEM cross-section view of Parylene C ™ with Adpro plus coated QFP44 lead, location F, 150x (ref. Board 1, right lead).

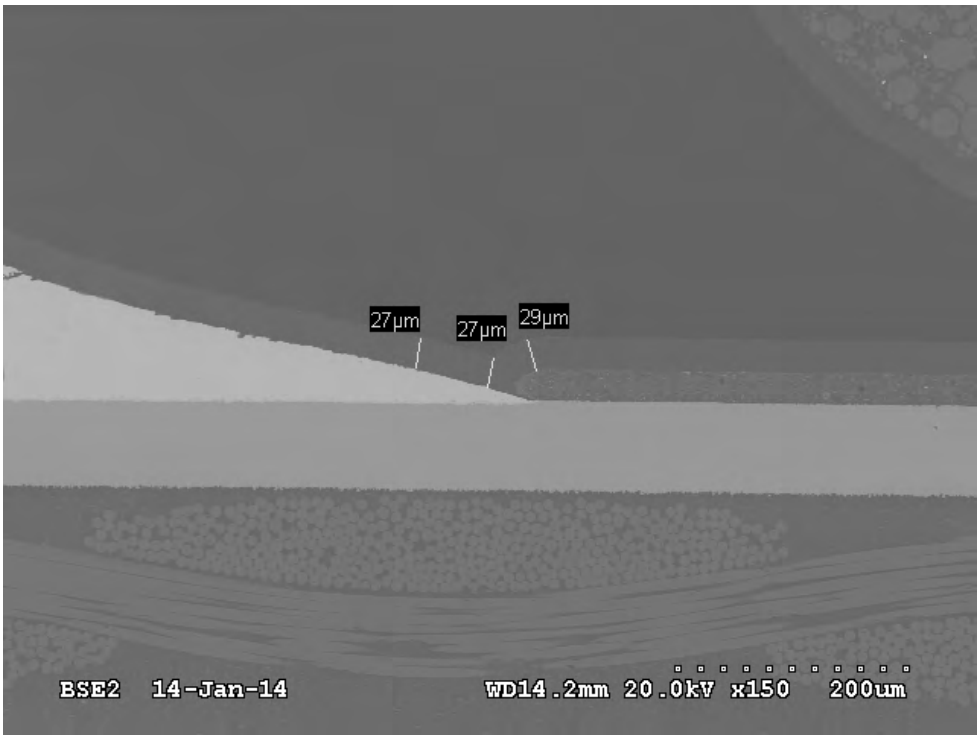


Figure 262: SEM cross-section view of Parylene C ™ with Adpro plus coated QFP44 lead, location H, 150x (ref. Board 1, left lead).



Figure 263: SEM cross-section view of Parylene C ™ with Adpro plus coated QFP44 lead, location T, 150x (ref. Board 1, left lead).

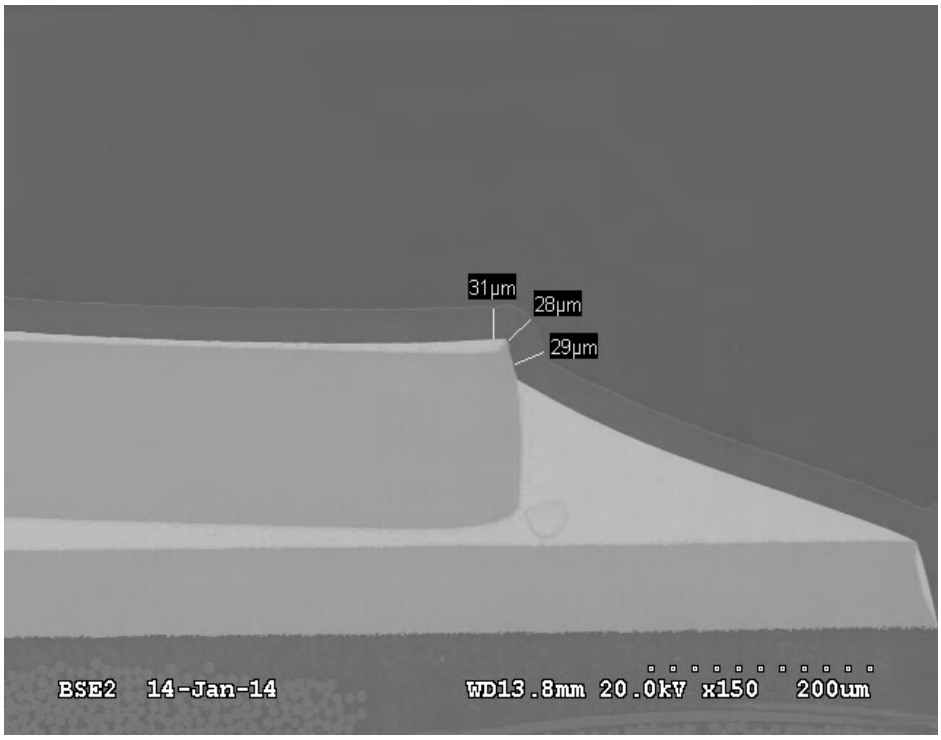


Figure 264: SEM cross-section view of Parylene C ™ with Adpro plus coated QFP44 lead, location T, 150x (ref. Board 1, right lead).

3.3 1B31LOC Acrylic

Some assemblies were coated with Humiseal 1B31LOC acrylic coating. The target coating thickness was 25 to 75 microns on a flat surface. SEM images were obtained on QFP44, QFP64 and PLCC devices. Some thinning of the coating along the lead edges and corners was observed (Figure 265 to Figure 267).

The cross – sections of the 1B31 was not successful because the solvents in the section potting compound attacked the coating.

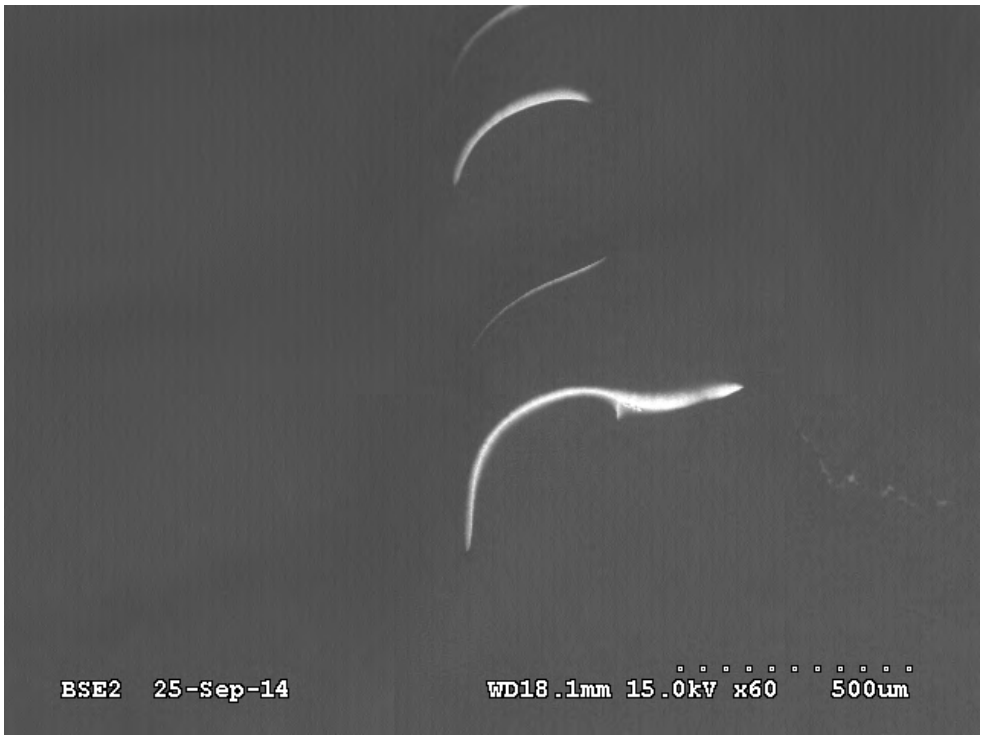


Figure 265: SEM image of 1B31LOC coated QFP44, 60x (ref. Board 82).



Figure 266: SEM image of 1B31LOC coated QFP64 showing thin coating on the lead knees, 60x (ref. Board 82).



Figure 267: SEM image of 1B31LOC coated PLCC, 30x (ref. Board 82).

4. Reference coating Parylene ™

The Parylene ™ C and Parylene ™ C with Adpro + coatings were very uniform on the leads and the package body (Figure 268 to Figure 272).

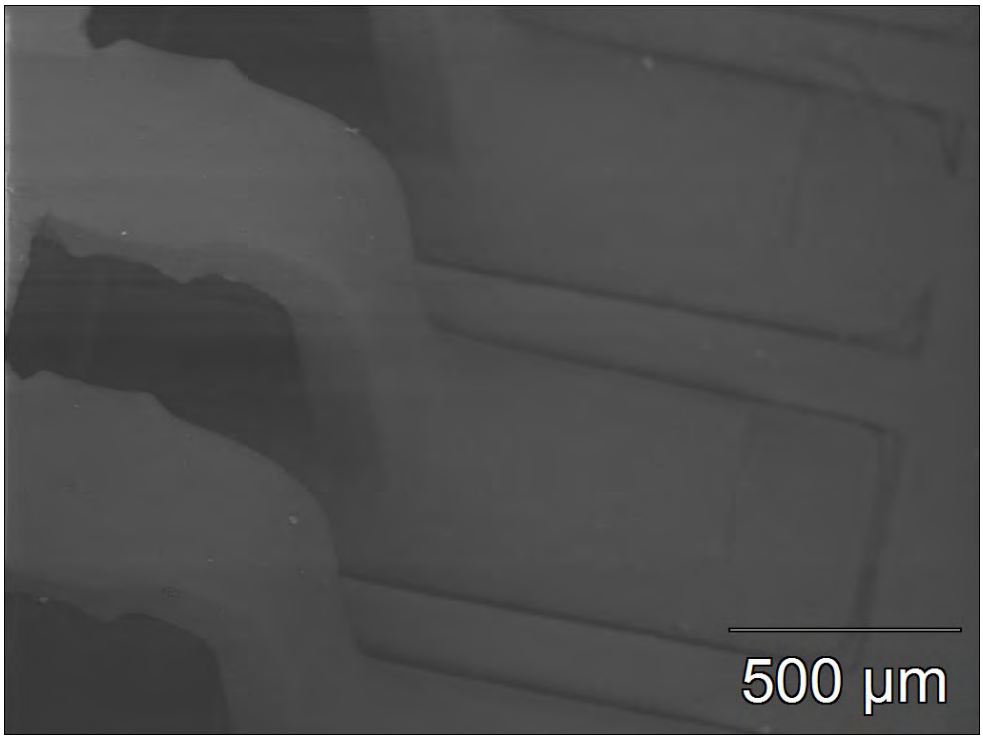


Figure 268: SEM image of Parylene ™ C coated QFP44, 60x (ref. Board 2, U5, lead 24).

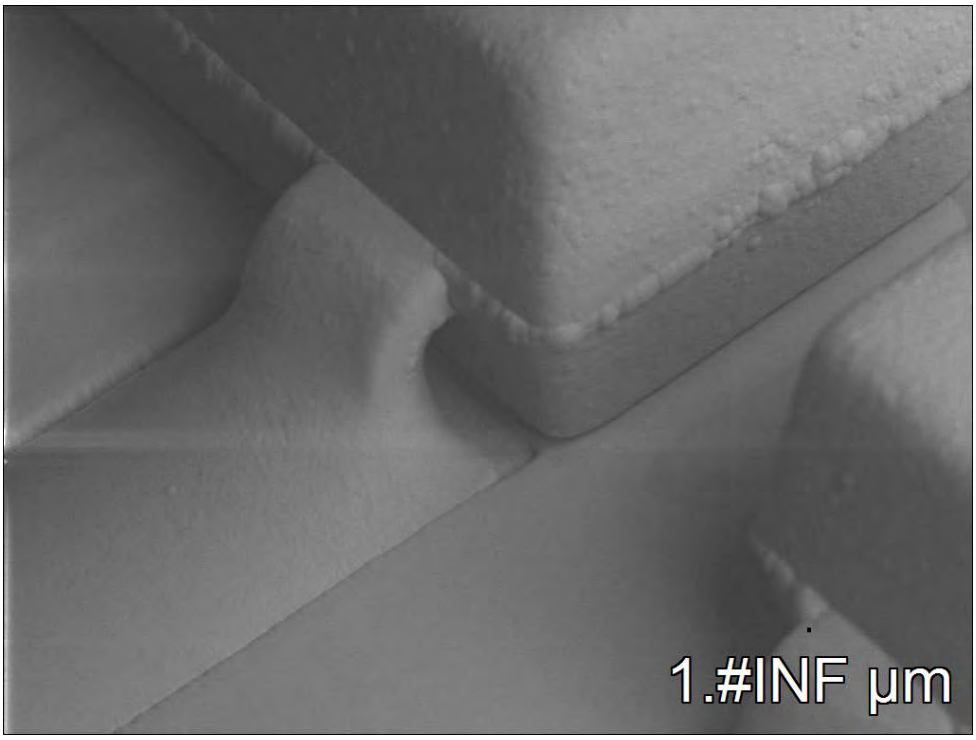


Figure 269: SEM image of Parylene ™ C coated SOT3, 60x (ref. Board 207). Note image taken after thermal cycling.

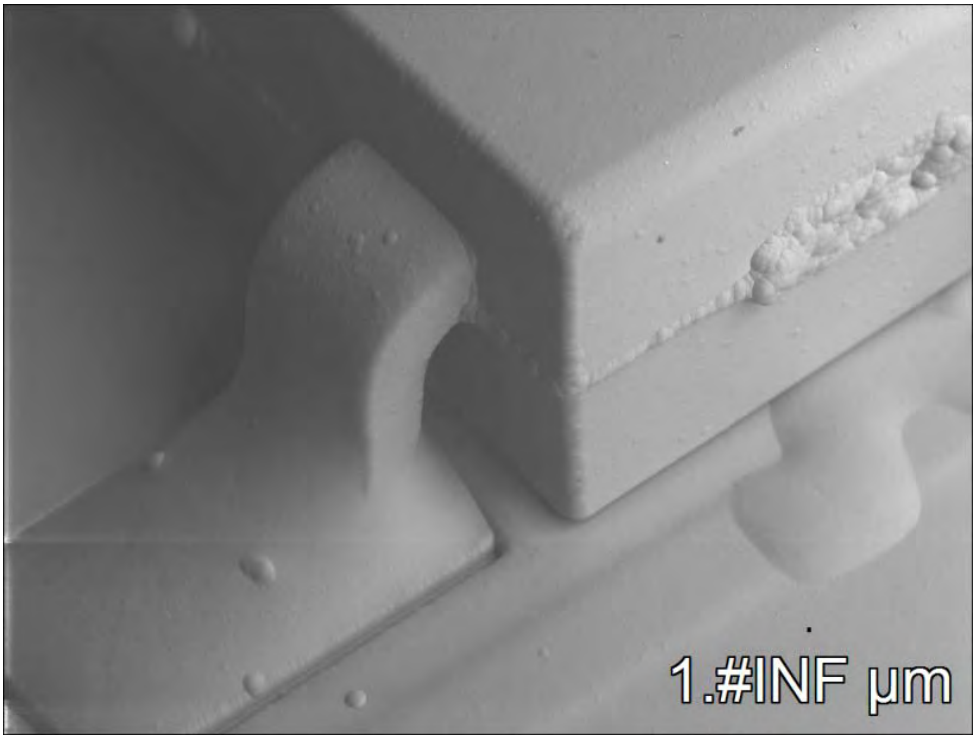


Figure 270: SEM image of Parylene ™ C coated SOT5, 60x (ref. Board 207). Note image taken after thermal cycling.

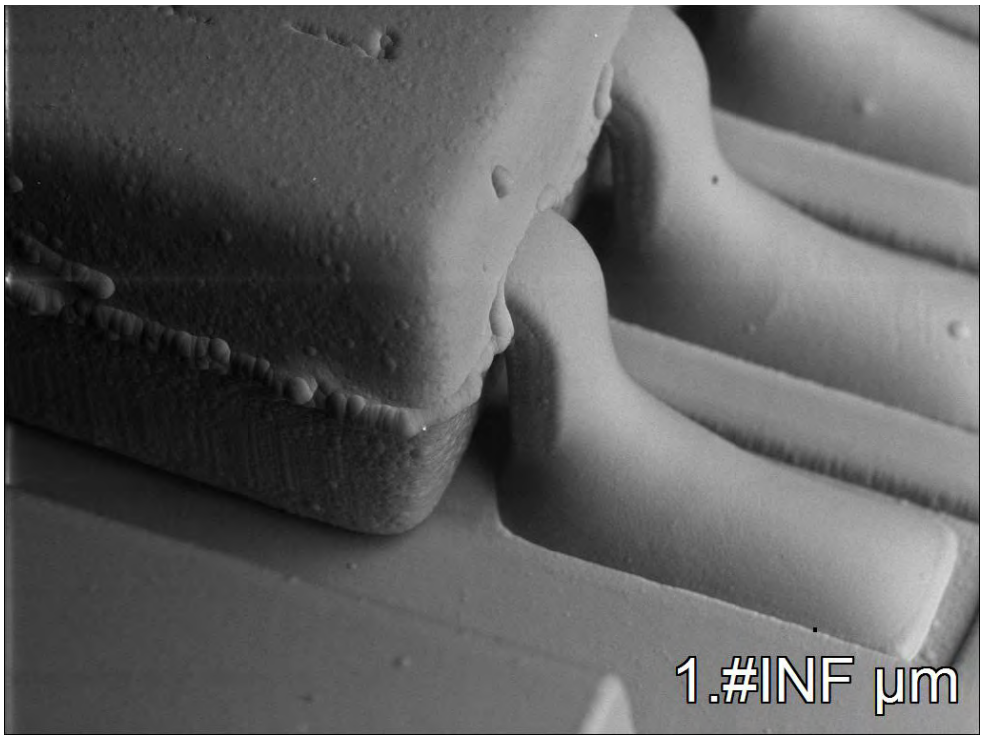


Figure 271: SEM image of Parylene ™ C coated SOT6, 60x (ref. Board 207). Note image taken after thermal cycling.

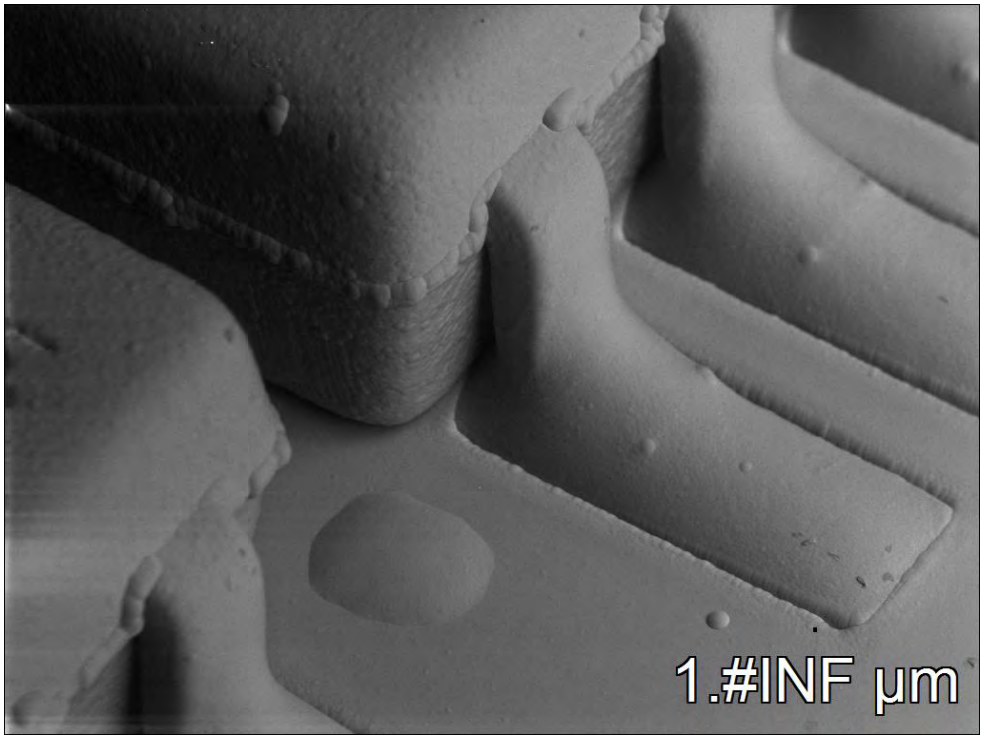


Figure 272: SEM image of Parylene ™ C with Adpro+ coated SOT6, 60x (ref. Board 202). Note image taken after thermal cycling.

4.1.1 Cross-section inspection of Parylene C with Adpro+ coating

The vacuum deposited Parylene™ C with Adpro+ was the most uniform, with a thickness range from 27 to 30 microns (Figure 273 to Figure 291) even at the back of the heel fillet (Figure 291). (Note Parylene™ C was not sectioned in the present evaluation, because it had previously shown excellent thickness uniformity).

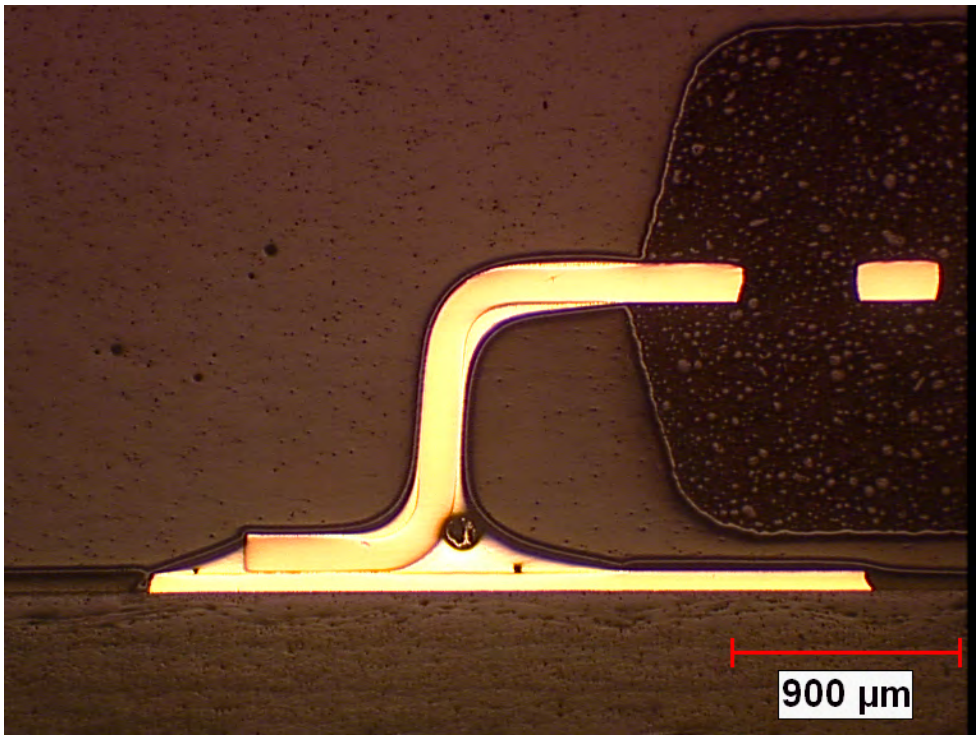


Figure 273: Optical overall cross-section image of Parylene ™ C with Adpro + coated QFP44, left lead, 25x.

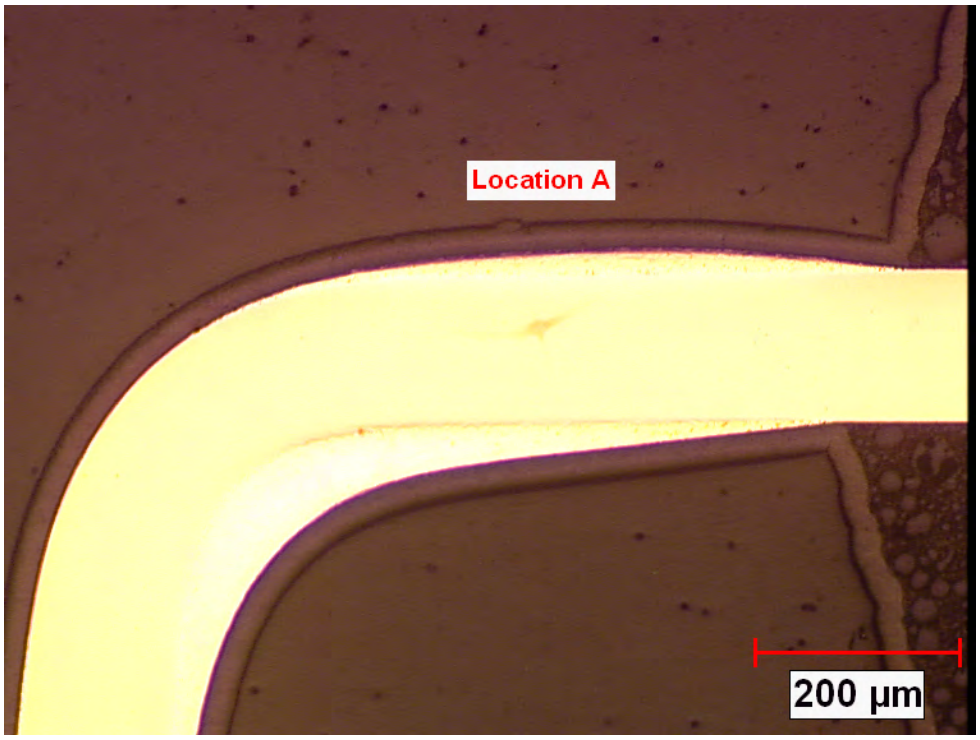


Figure 274: Optical cross-section image of Parylene ™ C with Adpro + coated QFP44, left lead, location A, 100x.

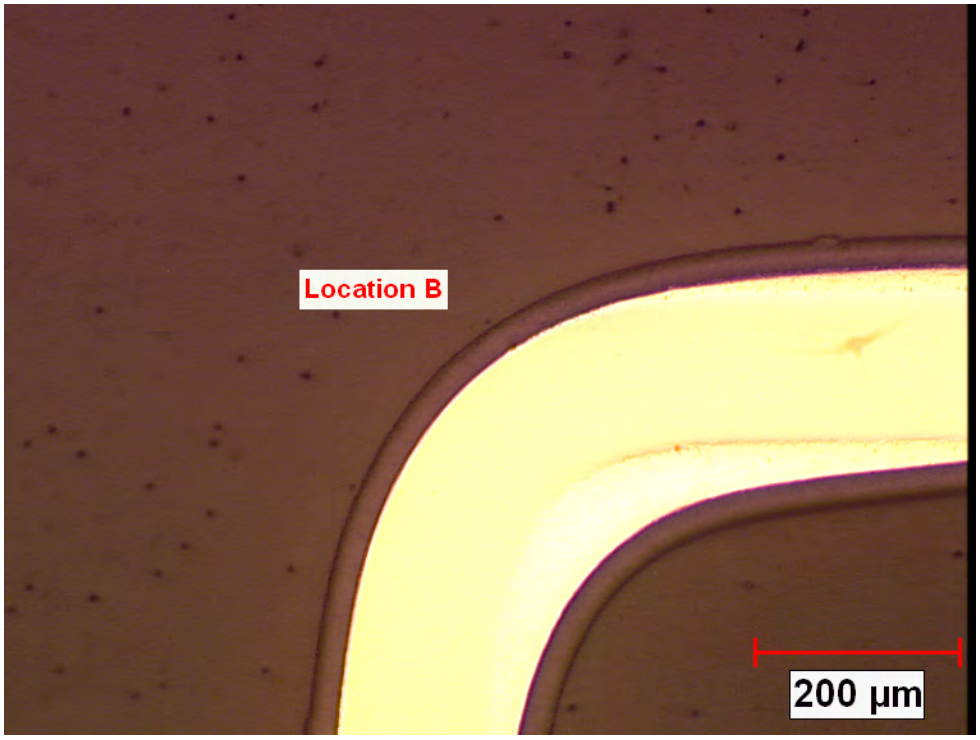


Figure 275: Optical cross-section image of Parylene ™ C with Adpro + coated QFP44, left lead, location B, 100x.

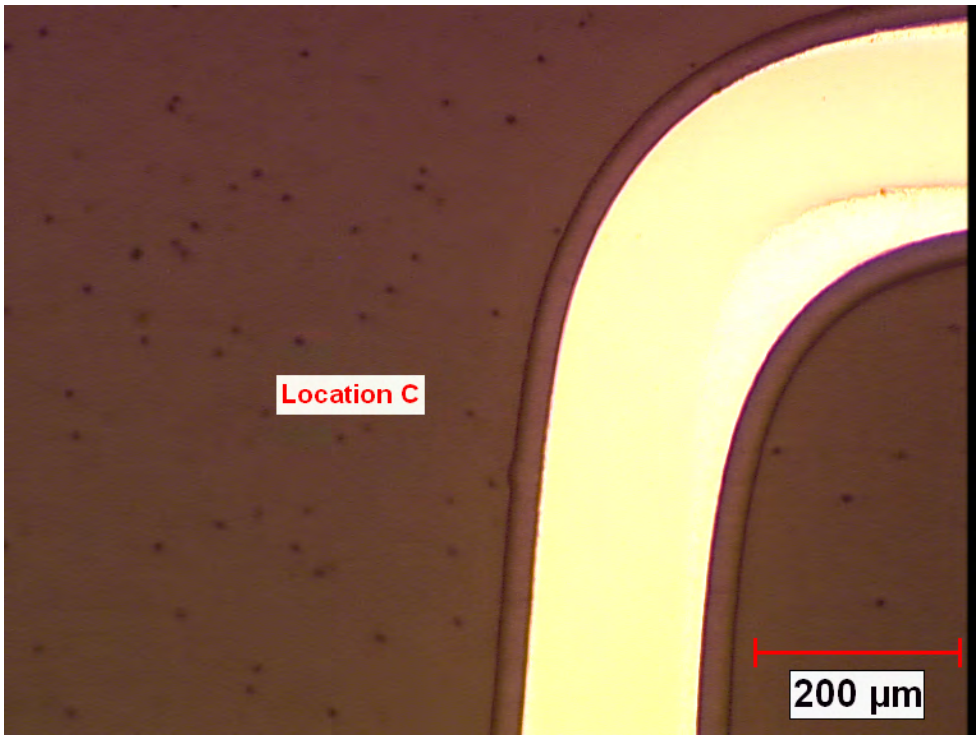


Figure 276: Optical cross-section image of Parylene ™ C with Adpro + coated QFP44, left lead, location C, 100x.

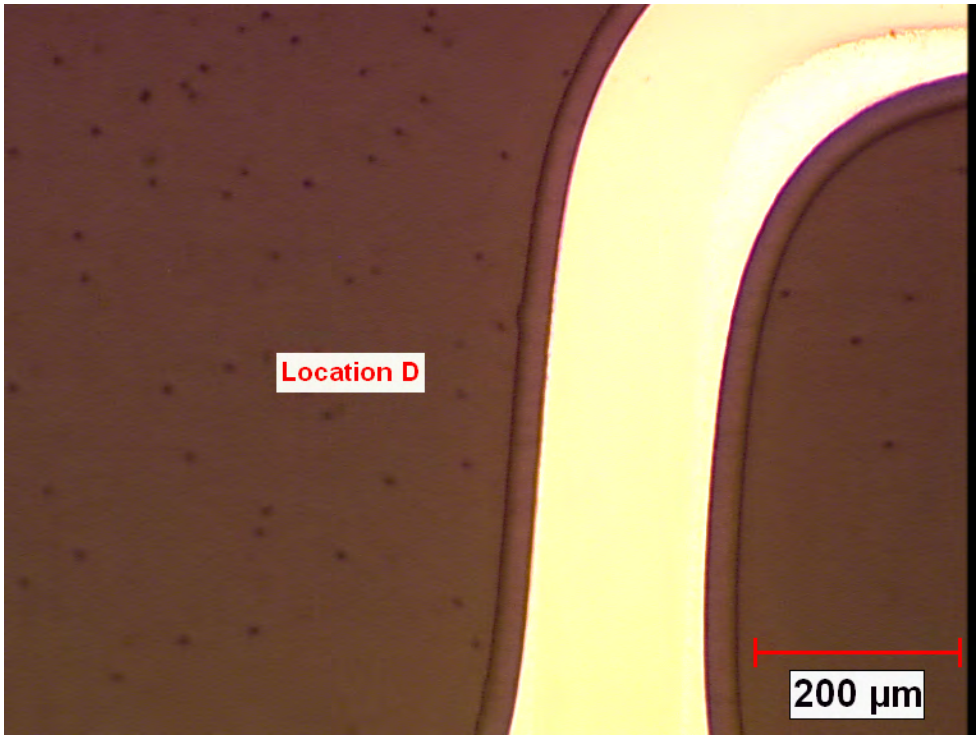


Figure 277: Optical cross-section image of Parylene ™ C with Adpro + coated QFP44, left lead, location D, 100x.

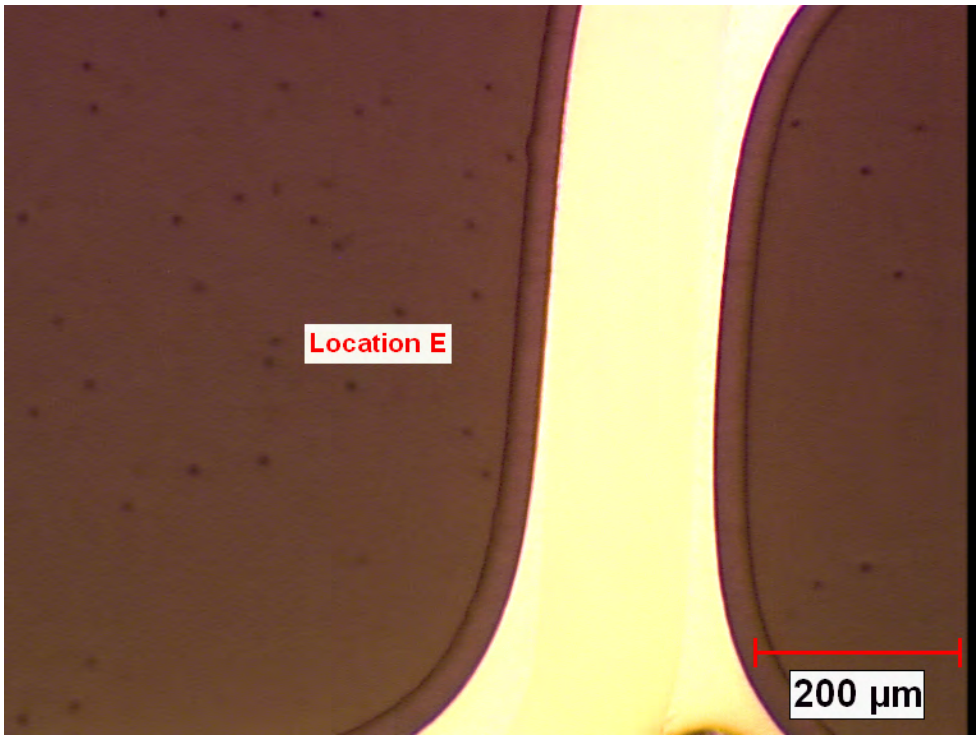


Figure 278: Optical cross-section image of Parylene ™ C with Adpro + coated QFP44, left lead, location E, 100x.

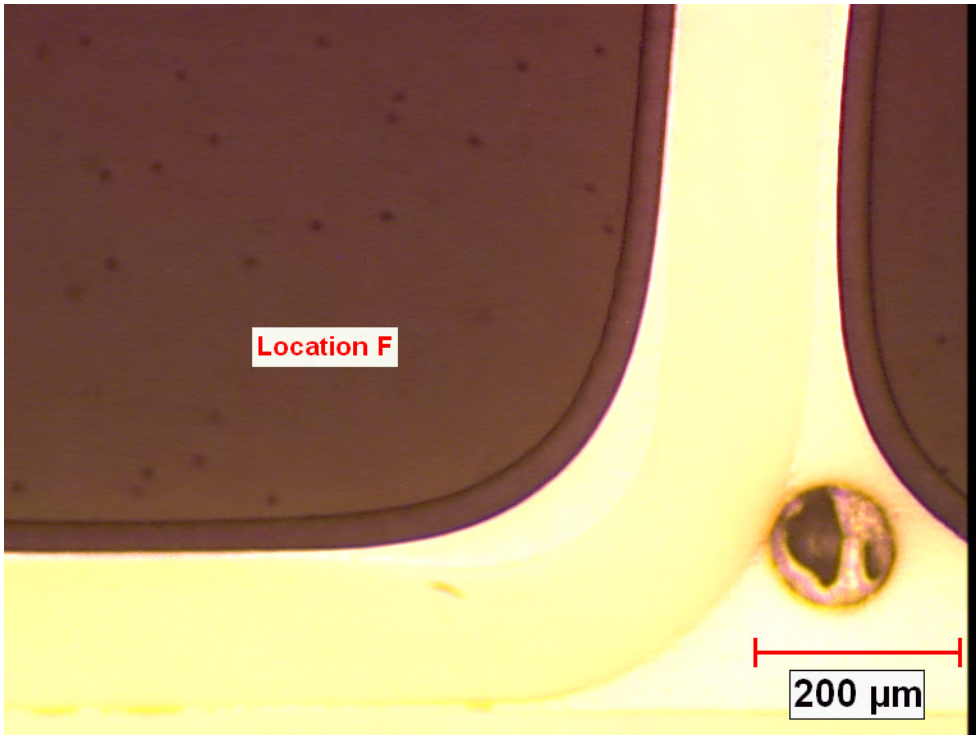


Figure 279: Optical cross-section image of Parylene ™ C with Adpro + coated QFP44, left lead, location F, 100x.

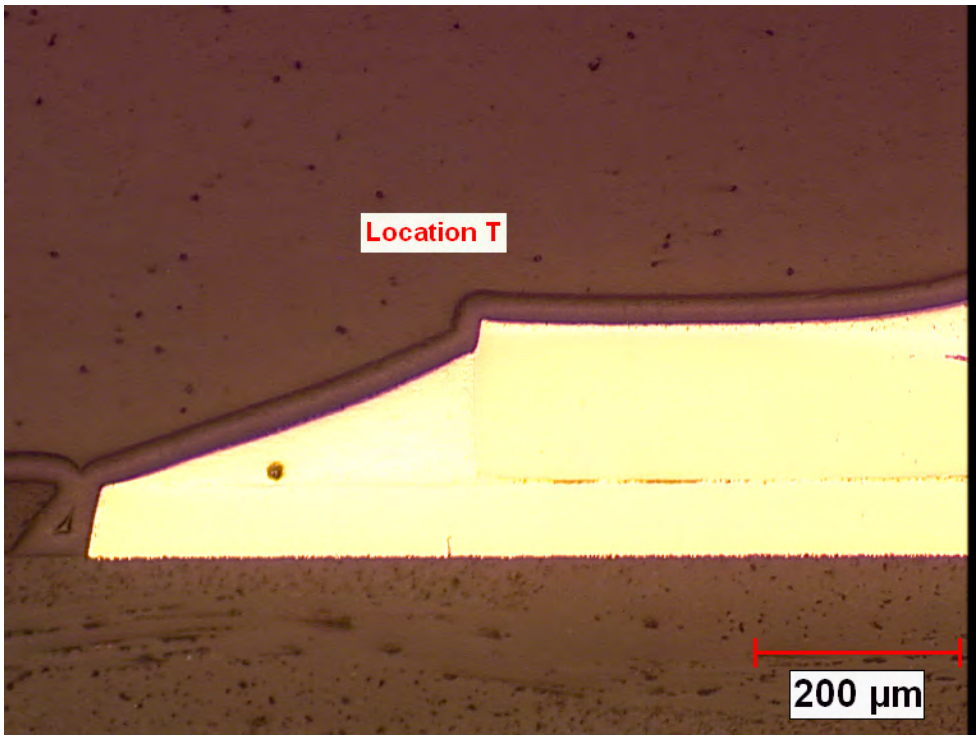


Figure 280: Optical cross-section image of Parylene ™ C with Adpro + coated QFP44, left lead, location T, 100x.

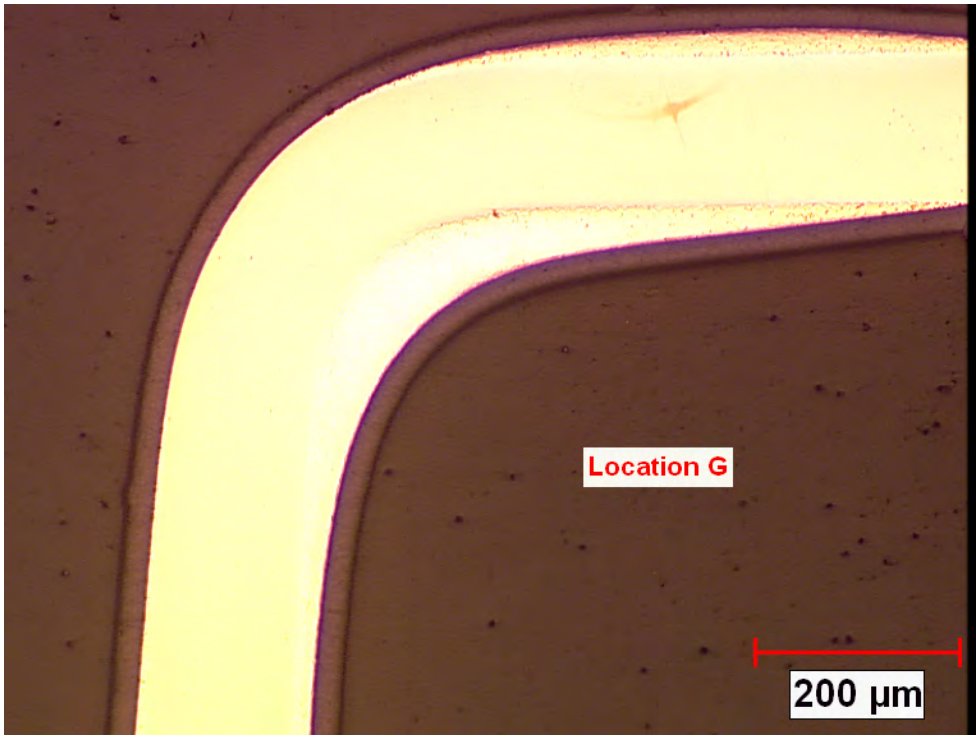


Figure 281: Optical cross-section image of Parylene ™ C with Adpro + coated QFP44, left lead, location G, 100x.

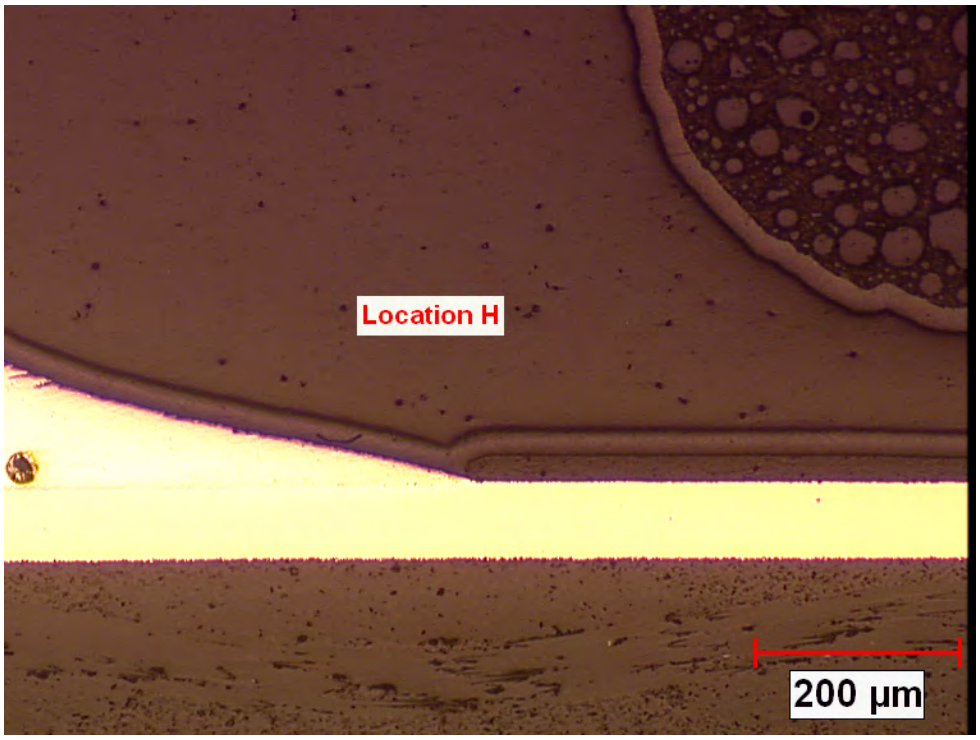


Figure 282: Optical cross-section image of Parylene ™ C with Adpro + coated QFP44, left lead, location H, 100x.

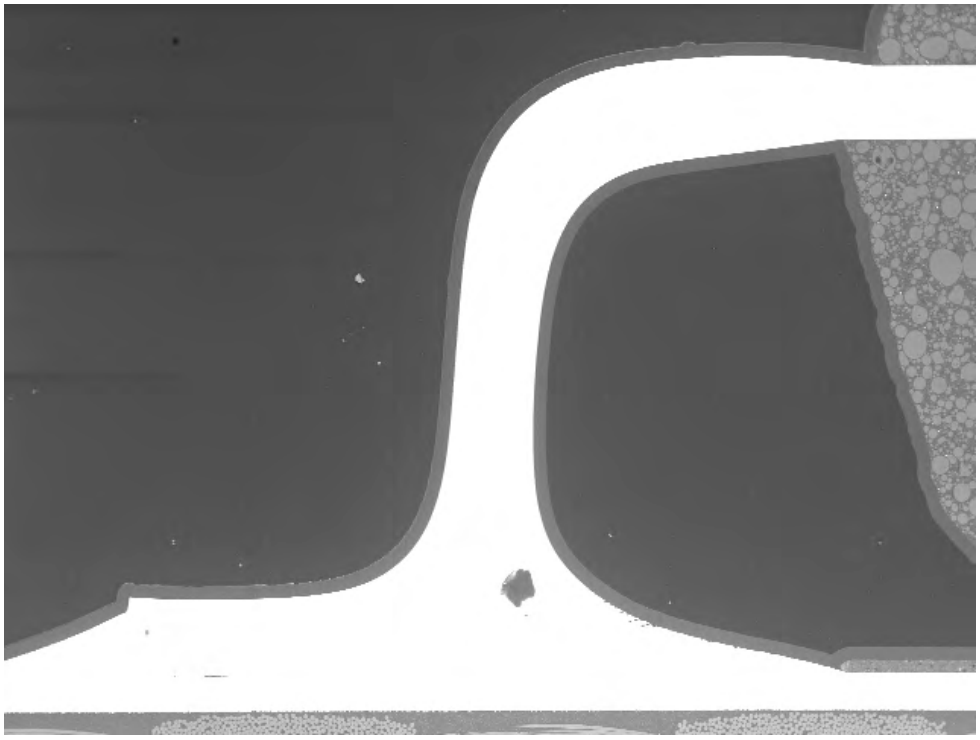


Figure 283: SEM overall cross-section image of the Parylene ™ C with Adpro + coated QFP44, left lead, 60x (ref. Board 1).

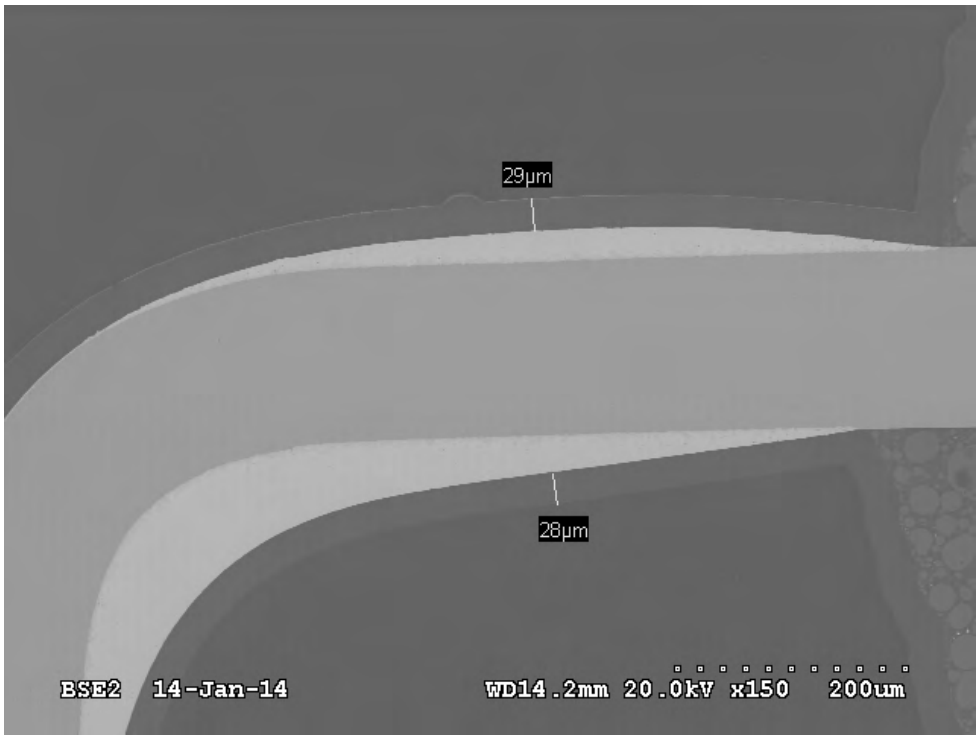


Figure 284: SEM cross-section image of the Parylene ™ C with Adpro + coated QFP44, left lead, location A, 150x (ref. Board 1).

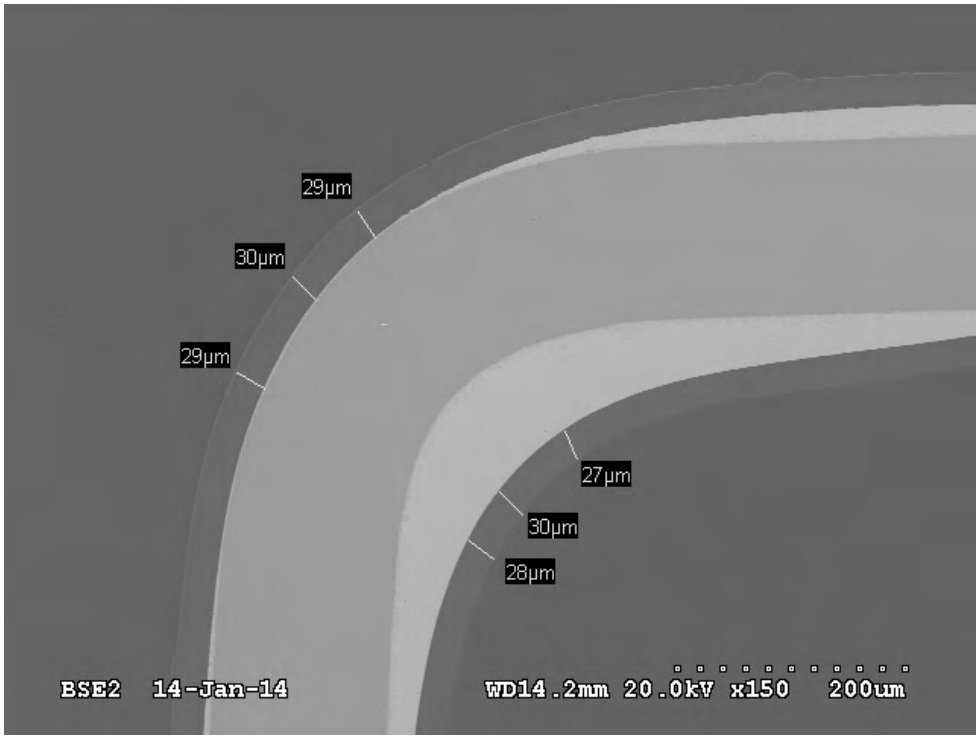


Figure 285: SEM cross-section image of the Parylene ™ C with Adpro + coated QFP44, left lead, location B, 150x (ref. Board 1).

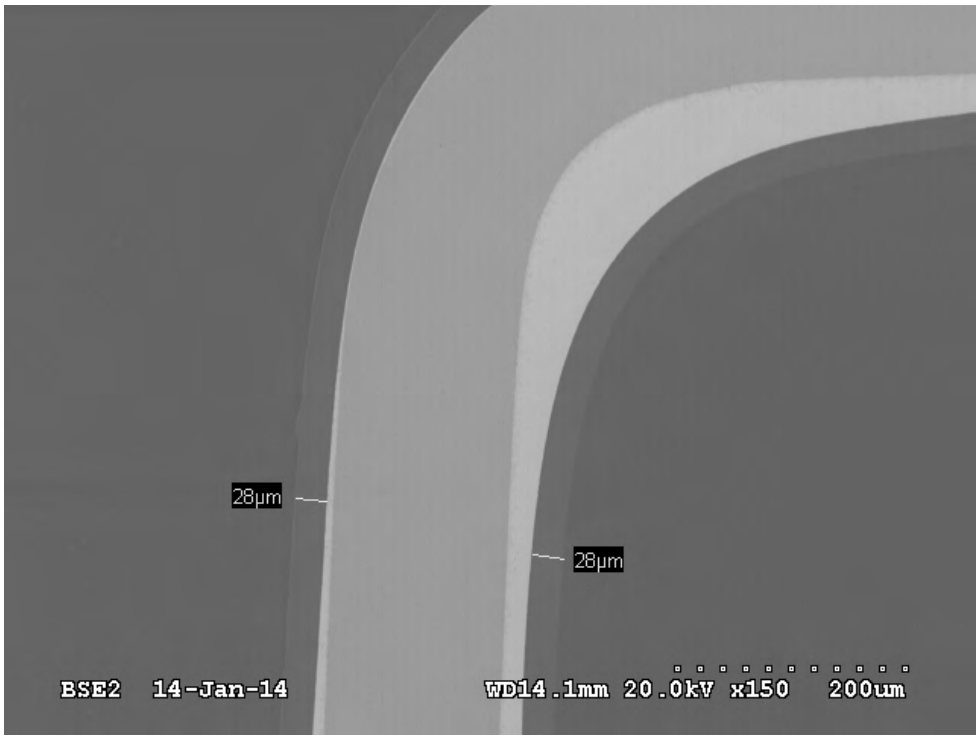


Figure 286: SEM cross-section image of the Parylene ™ C with Adpro + coated QFP44, left lead, location C, 150x (ref. Board 1).

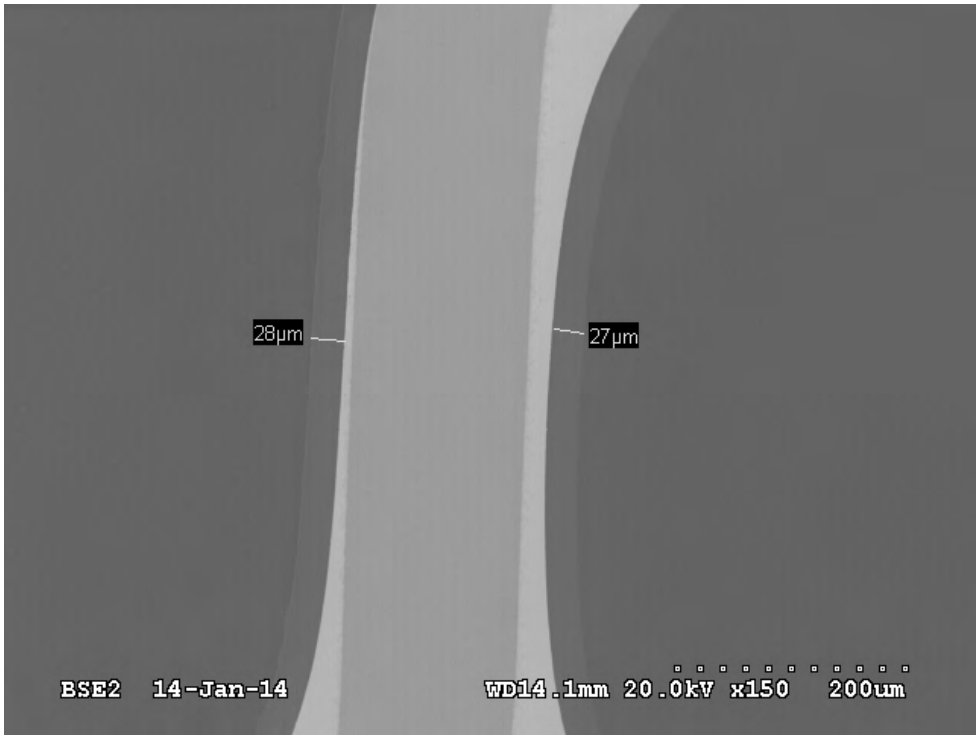


Figure 287: SEM cross-section image of the Parylene ™ C with Adpro + coated QFP44, left lead, location D, 150x (ref. Board 1).

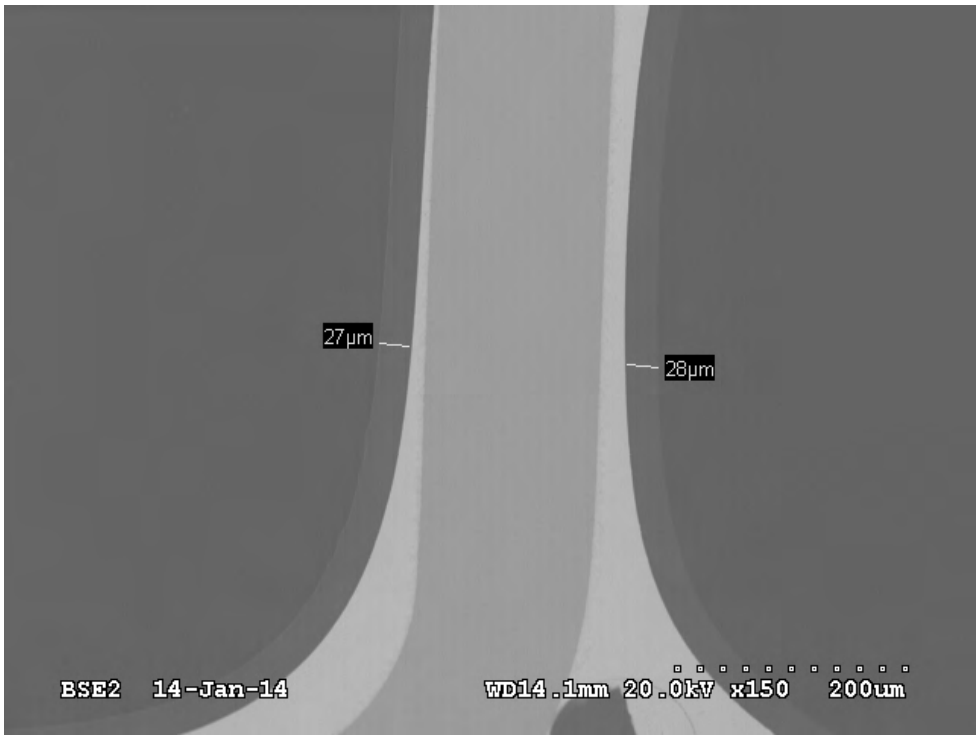


Figure 288: SEM cross-section image of the Parylene ™ C with Adpro + coated QFP44, left lead, location E, 150x (ref. Board 1).

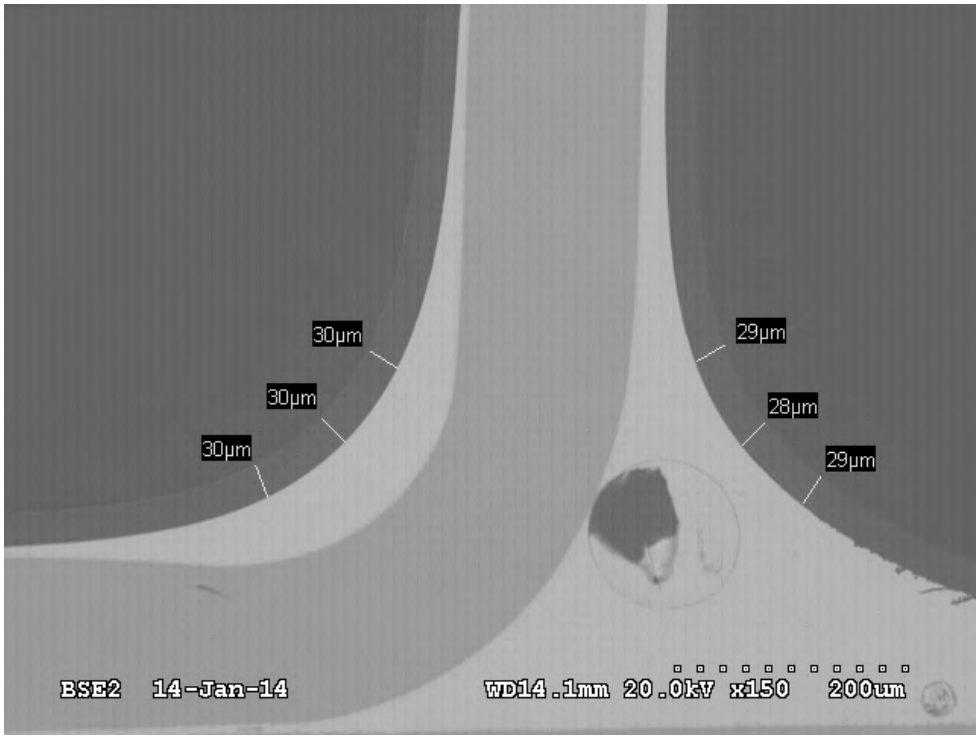


Figure 289: SEM cross-section image of the Parylene ™ C with Adpro + coated QFP44, left lead, location F, 150x (ref. Board 1).

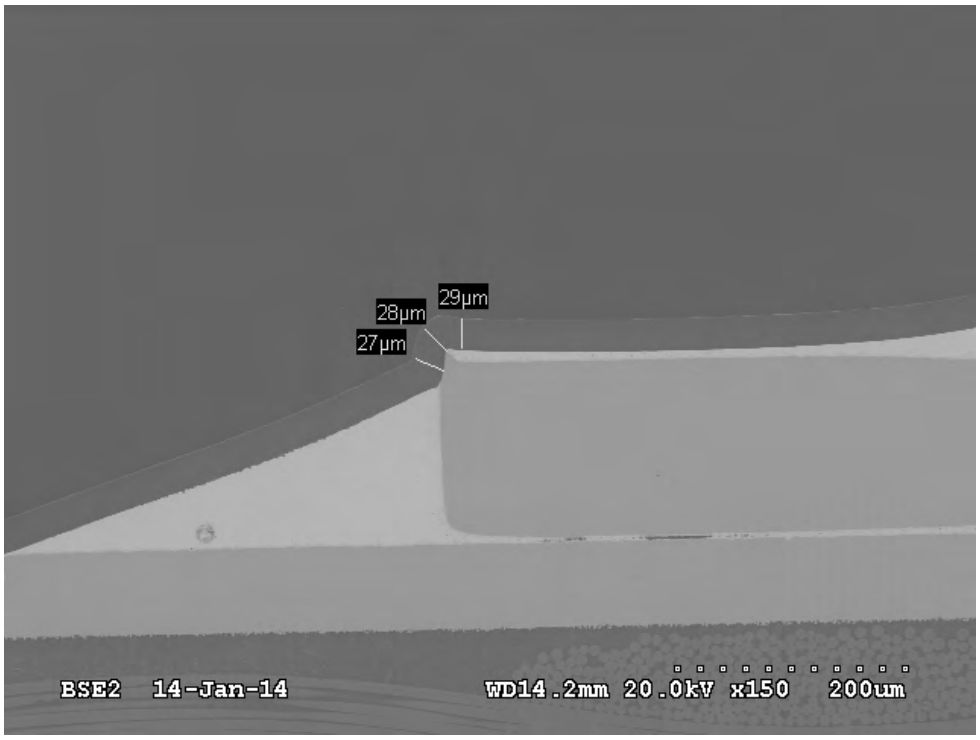


Figure 290: SEM cross-section image of the Parylene ™ C with Adpro + coated QFP44, left lead, location T, 150x (ref. Board 1).

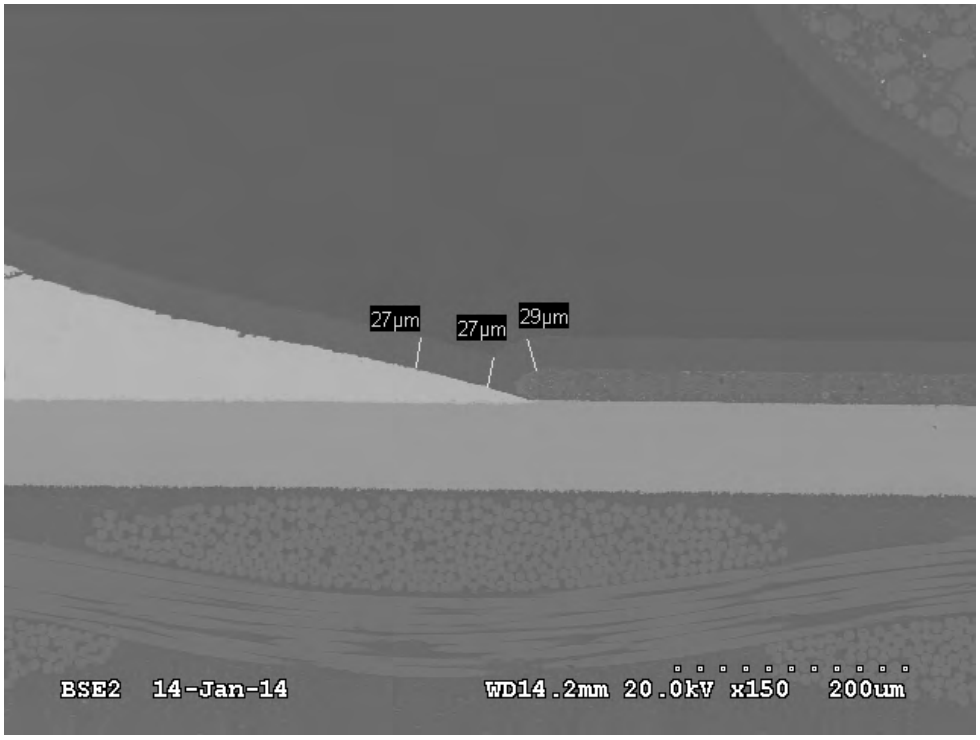


Figure 291: SEM cross-section image of the Parylene ™ C with Adpro + coated QFP44, left lead, location H, 150x (ref. Board 1).

5. Coating coverage summary

5.1 Coverage and thickness

The PC18M based coating vertical cross-section evaluation showed that coating thickness ranged from between 0.06 to 76 microns on the front of the lead and 0.5 to 103 microns on the back of the lead. The minimum and maximum for each coating type is given in Table 5. Location T in the front and location A1 in the back always had the thinnest coating.

Table 5: PC18M based coatings QFP44 minimum and maximum thicknesses (repeated from Table 3).

Coating	Min/Max	Front (micron)	Back (micron)
PC18M-mod	Min	0.06	0.8
	Max	76	103
PC18M+20%XP2742	Min	13	0.5
	Max	66	20
PC18M+20%X11102PMA	Min	10	0.5
	Max	73	18
Parylene C with Adpro+	Min	27	27
	Max	31	30

5.2 Role of coating solvent and coverage

The PC18M coating based coating generally exhibited better coverage than the PC40-UMF coating based coating. Comparing the coatings, one factor influencing coverage is the solvent dependent viscosity characteristics of the PC18M and the XP2742. Particularly for the PC18M based coatings, the coating starts with a high solvent concentration and low viscosity allowing the coating to flow readily behind the leads. Then as the solvent evaporates, the viscosity increases rapidly and to a high value, which tends to prevent the coating from flowing down and away from the vertical sides of the leads. The PC18M viscosity without solvent is very high (like molasses). The solvent dependent viscosity was also present in the PC40UFM based coatings, but to a lesser extent. The PC40-UMF had a small amount of solvent added to reduce its viscosity from 250 to 150 cps. It was also noted that the PC40-UMF coverage tended to improve slightly with increasing amounts of XP2742. The N3300 isocyanate resin in the XP2742 has a viscosity of 3,000 cps without solvent as compared to the PC40-UMF viscosity of 250 cps. So the improved coverage on the vertical surfaces observed might be due to the increased viscosity of the N3300 fraction as the solvent evaporates.

The amount of solvent loss is influenced by droplet size, droplet velocity and the solvent concentration in the surrounding air. Further work is needed to understand how these factors contribute to bubble formation and coating coverage.

5.3 Bubble formation

Understanding bubble formation in coatings is important because mechanical tensile testing had previously shown that bubbles are a defect site within the film that will reduce film elongation under load.

While it is postulated that coverage may be improved with the solvent dependent viscosity characteristic, it may also be related to the appearance of bubbles in the coating around the package by the leads (e.g. Figure 292) or on the package (e.g. Figure 293). The PC18M-mod and PC18M+20%XP2742 boards had the highest bubble density while the PC18M+11102PMA had few if any bubbles. Bubble propensity does not appear to be directly tied to a coating type, since there were some the PC18M spray coated assemblies with negligible bubble formation. The bubbling also does not appear to be related to the assembly or part type: one of five ball grid array boards (BGAs), three of seven QFPs and two of six SOTs exhibited large bubbles.

During coverage evaluation sectioning, two types of bubbles in the coating were observed; bubbles attached to the solder (Figure 294) and bubbles within the coating film (Figure 295). Bubbles attached to the solder are believed to be caused by coating flow over non – wetting regions of the solder. The bubbles trapped in the middle of the coating are likely created from vapor within the coating. Possible vapor sources are solvent or trapped CO_2 from the isocyanate reaction, but these would require that the bubble nucleation was more favorable than diffusion of the vapor to the surface. Alternatively, it could be due to a coalescence of microbubbles entrained in the coating during the spray process, not initially visible.

Generally it is more difficult to form a bubble in a liquid where one does not exist than it is to have small bubbles (not visible to the eye) coalesce into larger bubbles. In the present work, the bubbles were not visible after dip coating cure, after spraying or after the initial room temperature cure, but were visible to the unaided eye after the final elevated temperature oven cure. It appears that most of the bubbles were in the coating and not on the solder surface.

Several attempts to form bubbles with very thick cast films under various temperature humidity cure conditions were unable to reproduce the condition. It was noted that PC18M has very high viscosity when no solvent is present. Since the bubble formation was observed on both the 2X-2Y PC18M-mod spray coating and the 2X-2Y PC18M+20%XP2742 spray coating but not on the 4X-4Y PC18M+20%X11102PMA boards, the thickness of material applied during each spray pass and the manner that the solvent escapes may be related to the bubble formation.

The coating film formation during spray processing has a direct impact on the coating smoothness and bubble formation (Figure 296) [12]. Further work is needed, but the following bubble formation process is postulated. During the spray process, the coating droplets proceed from the nozzle to the assembly surface and loose solvent along the way. If the atomized droplet loses too much solvent, it might have a high enough viscosity to prevent micro air/solvent bubbles from escaping as the spray coating thickness is built up. Particularly for the PC18M based coatings, the coating starts with a high solvent concentration and low viscosity. Then as the solvent evaporates, the viscosity increases rapidly and to a high value, since the PC18M viscosity without solvent is very high (like molasses). Upon heating during the cure, the small gas bubbles coalesce to form larger bubbles that remain trapped under the surface (Figure 297).

The same mechanism is likely responsible for the rough coating surfaces observed during the layered coating processing using the PC18M based coatings [1]. In this case, the bubbles were able to break the free surface during curing leaving pits and craters ranging in size from one micron to 50 microns with some larger pits Figure 298 and Figure 299.

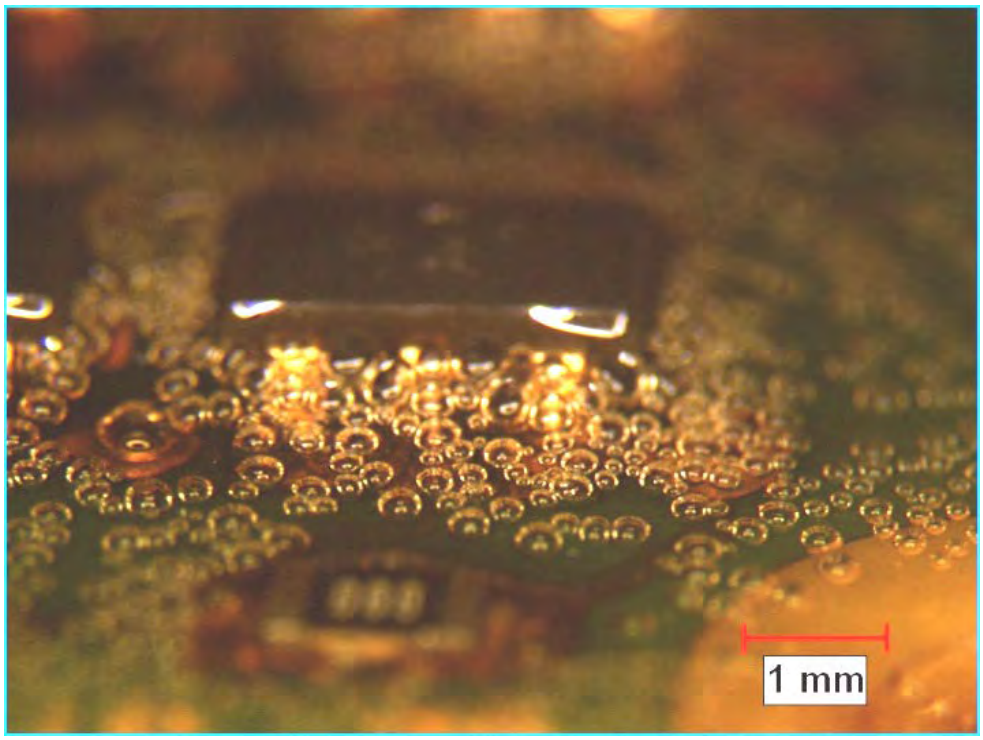


Figure 292: PC18M-mod SOT board 233 with large bubbles around the leads, 10x (note the photograph was taken after thermal cycling and 1,000 hours of 85°C/85%RH humidity (ATC+1000HTHH) environments). The color change in the second image is an artifact of the illumination used to highlight the bubbles (ref. Figure 7).

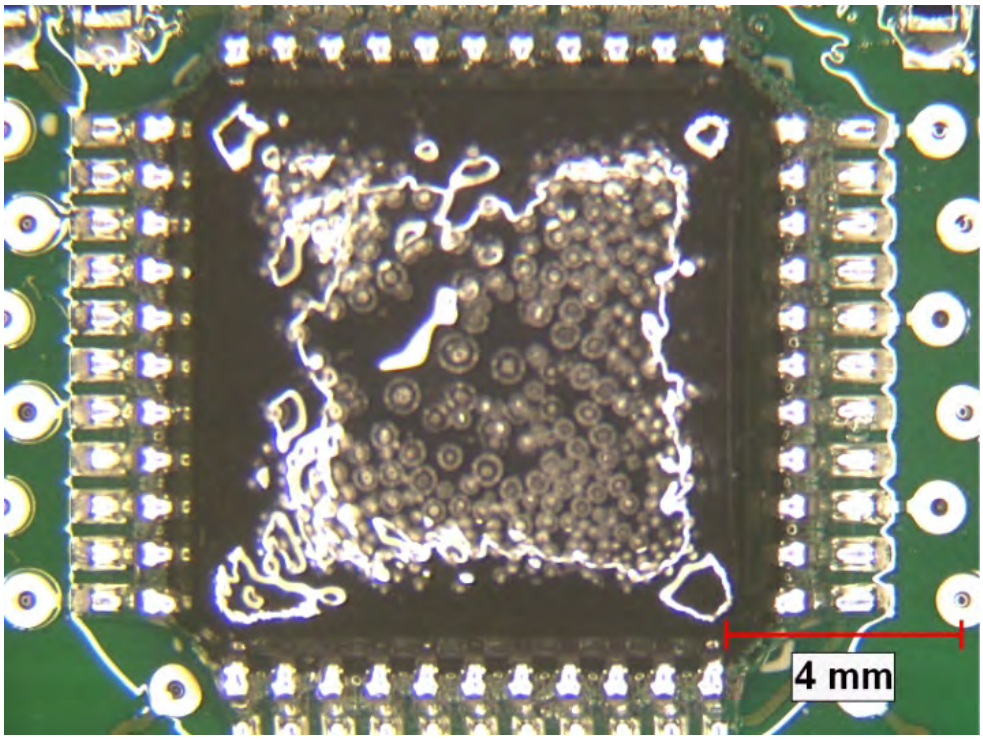


Figure 293: PC18M-mod QFP board 35 with large bubble density on top of the package, 10x (ref. Figure 8).

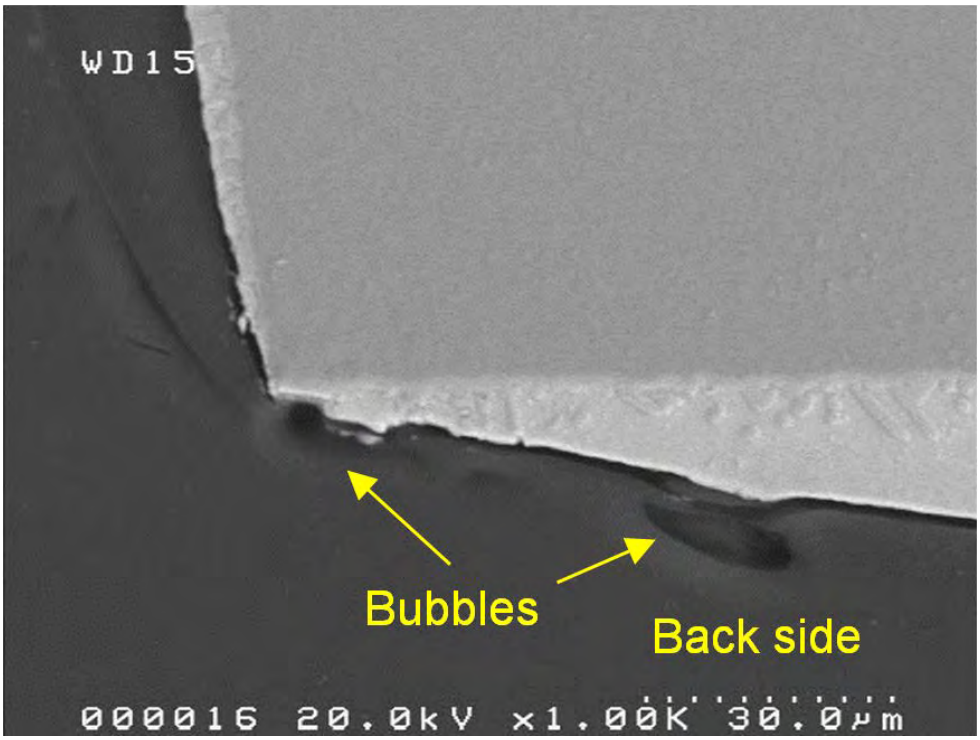


Figure 294: Horizontal cross-section, SEM, board 28, PC18M+20%X1102PMA, QFP44, U1, lead 39, 1,000x (ref. Figure 48).

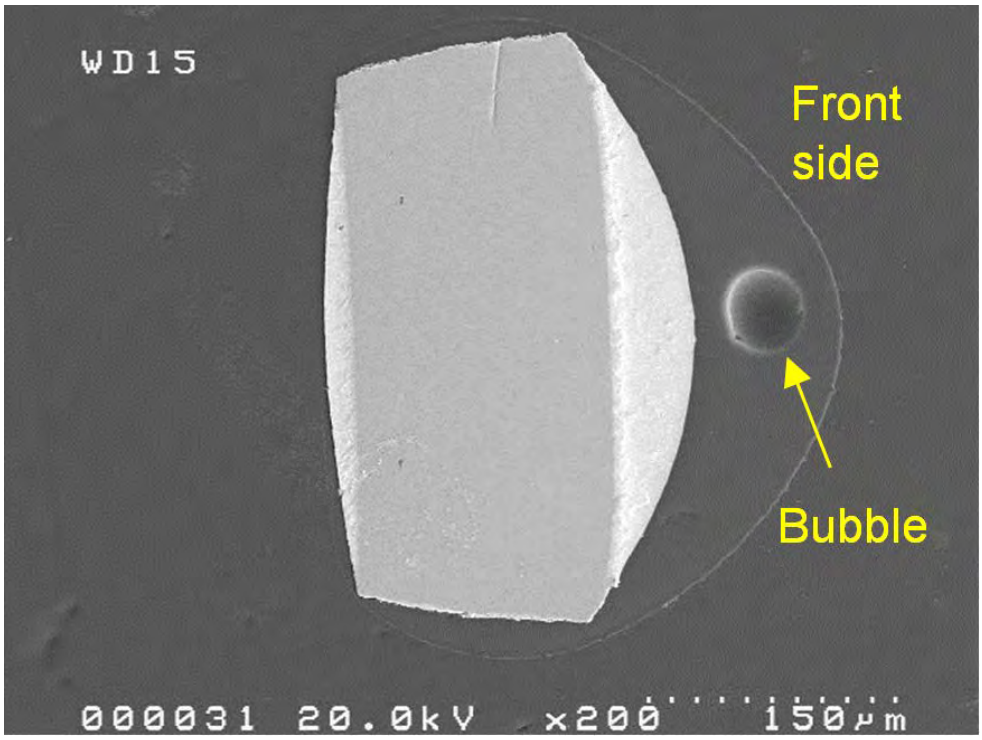


Figure 295: Horizontal cross section, SEM, board 21, PC18M+20%XP2742, QFP44, U1, lead 23, 200x (ref. Figure 37).

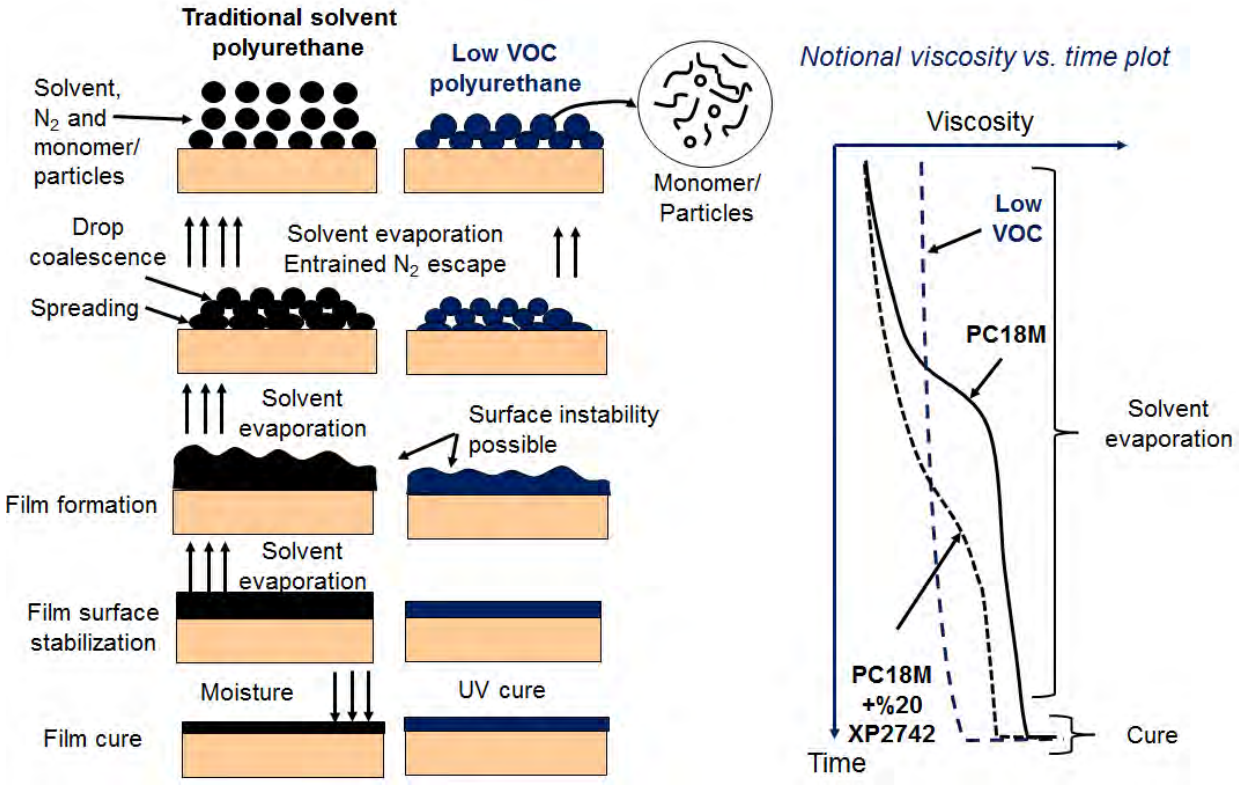


Figure 296: Coating film formation from spray coating process.

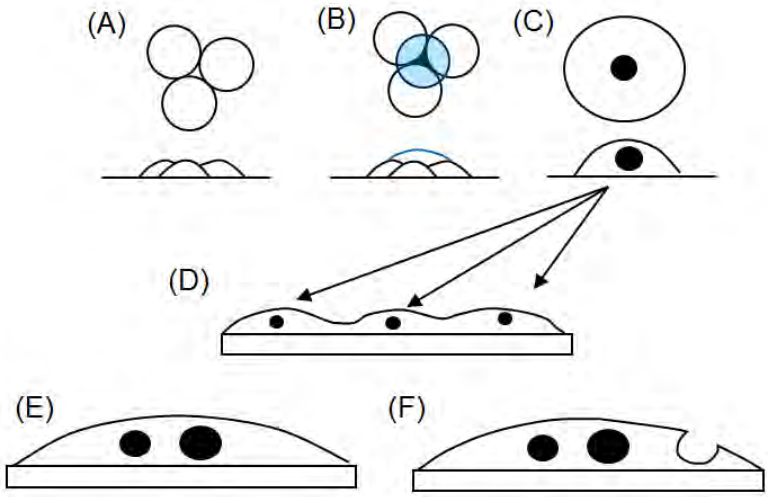


Figure 297: Spray drop deposition resulting in bubbles in the coating; (A) three deposited drops, (B) a fourth drop deposited on top of the initial three trapping some gas, (C) drop coalescence with a small entrained bubble, (D) multiple groups of the coalesced drops containing small bubbles, (E) during the heated portion of the cure there is a coalescence of small bubbles into larger bubbles, and (F) with drier films, having a higher some bubbles escape but the coating surface does not smooth out.

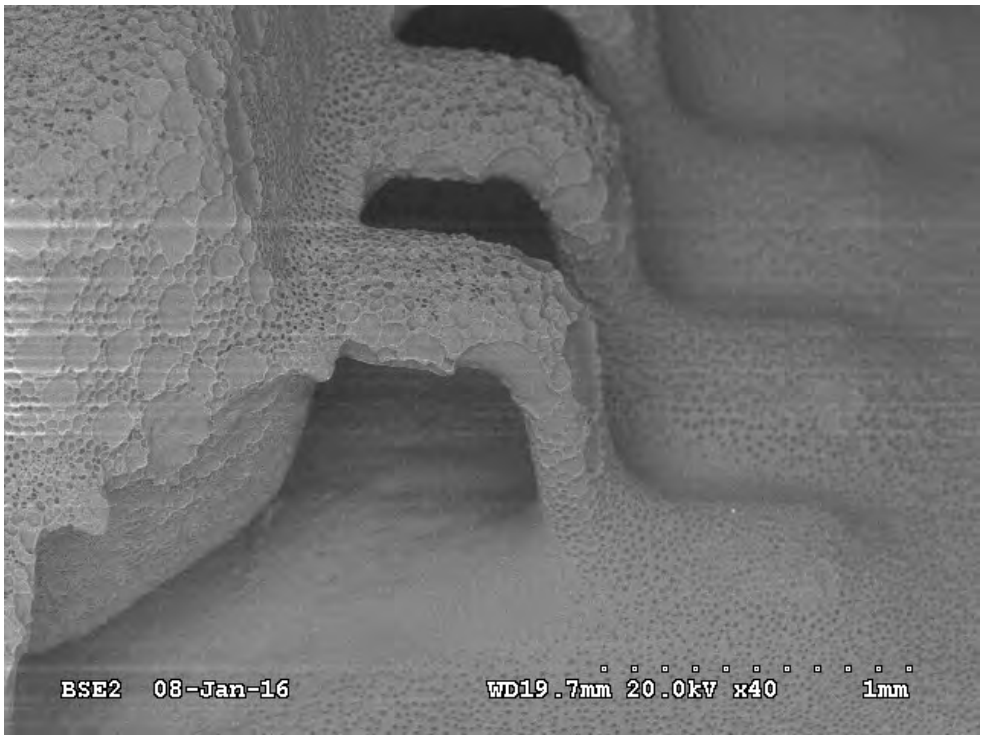


Figure 298: SEM image of PC18M dip two PC18M sprays, board A191, QFP44, with good overall coverage but still exhibiting surface roughness, 40x.

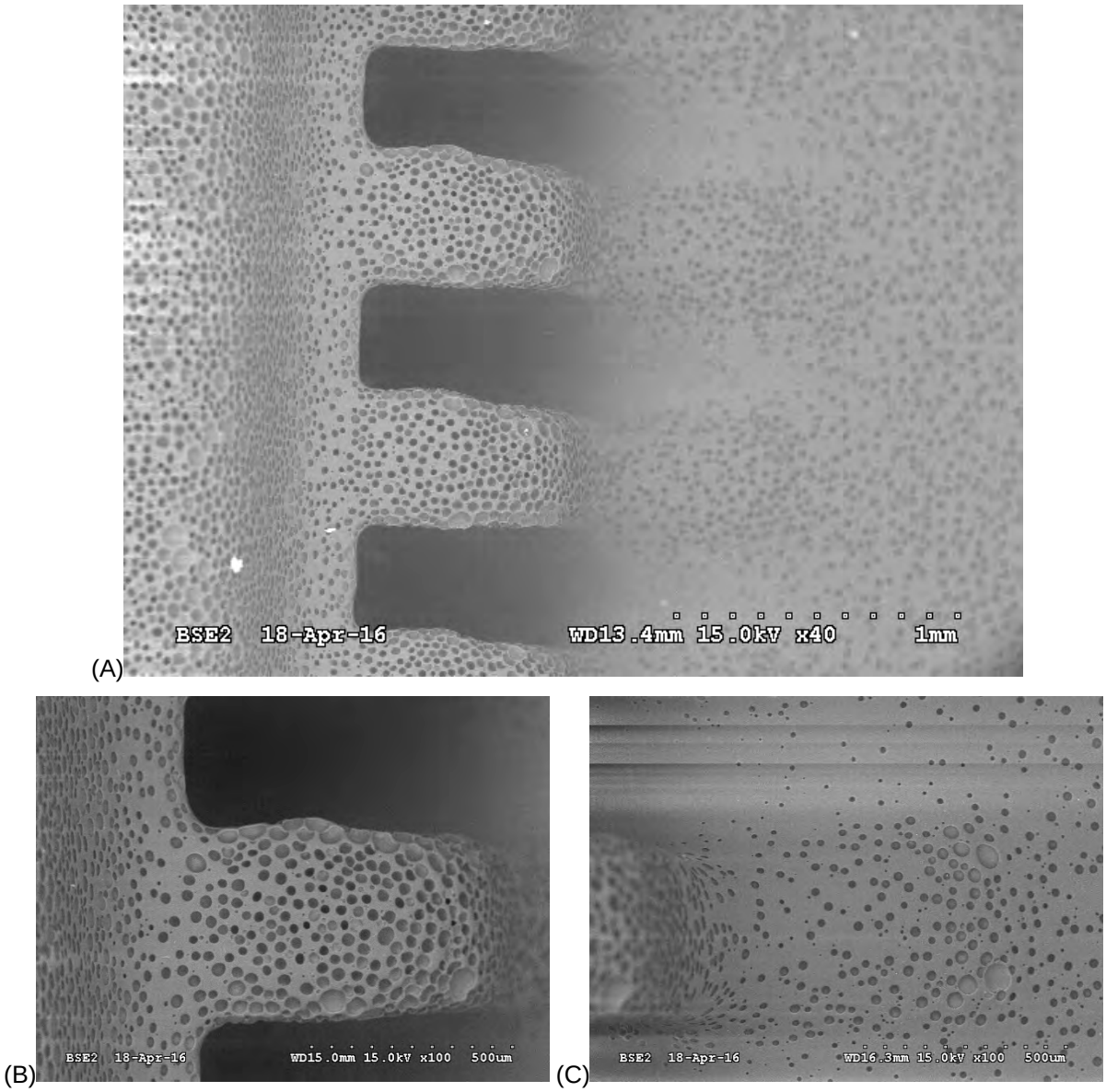
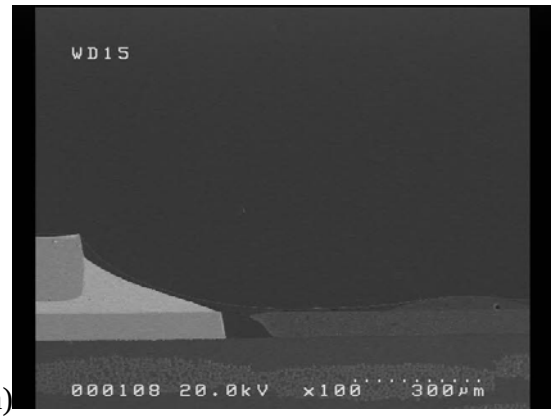


Figure 299: PC18M dip + two PC18M sprays, Board A023, QFP44 lead; (A) 40x and (B) top of lead, 100x, and (C) bottom of lead.

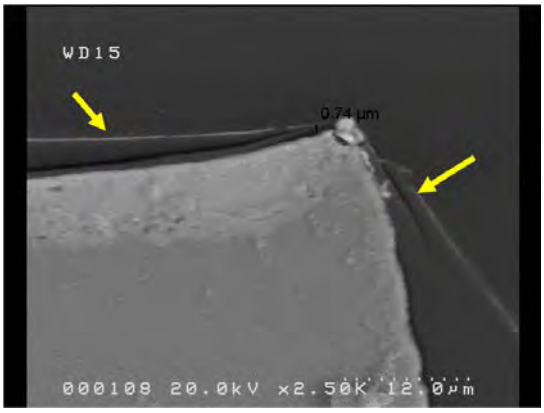
5.4 Interlayer adhesion

Another significant observation was the interlayer delamination on the PC40-UMF coated assemblies. Low adhesion observed between the PC40-UMF dip coating and the subsequent PC40-UMF based coating spray coating layers even with plasma etching to enhance wetting. (Figure 300 – Figure 302). Even with no nanosilica, separation occurred (Figure 301). Follow-on engineering tests revealed that using only a UV cure between layers rather than a UV and moisture cure combination increases interlayer adhesion. Interlayer adhesion improvement needs further work and other cure variations will be evaluated on the next group of PC40-UMF coated assemblies. The low interlayer adhesion may also be a factor during rework and may require the use of enhanced surface preparation.

(a)



(b)



(c)

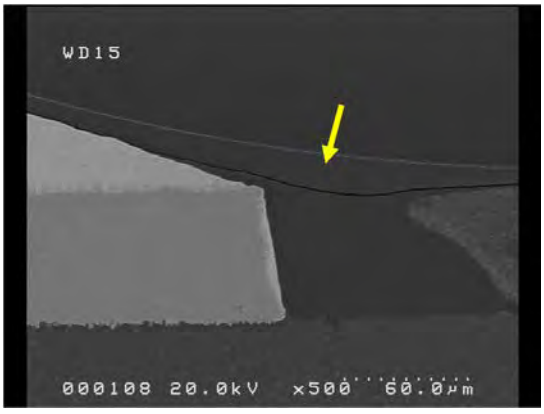
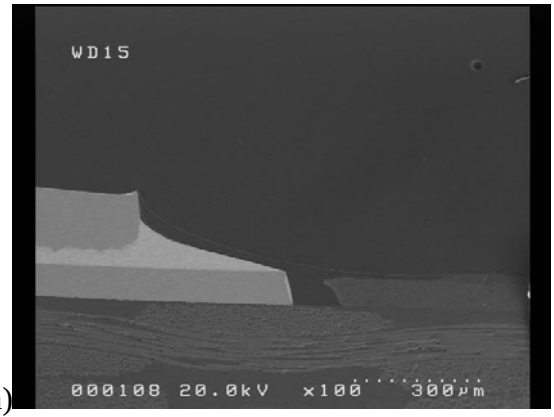
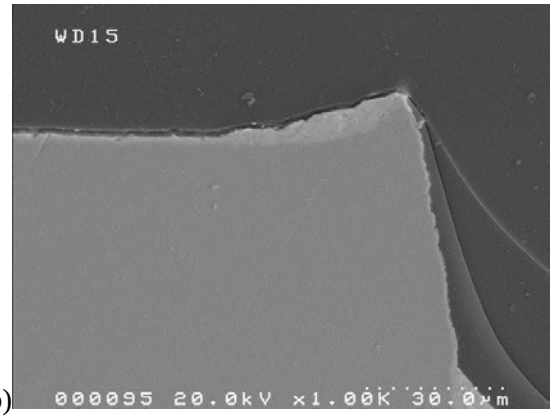


Figure 300: Batch A and B with interlayer delamination evident in the vertical section SEM image of PC40-UMF+30%NNN2835 nanosilica coating on QFP44 with a dip coat/plasma etch/spray coat; (a) overall of lead tip location T, (b) lead tip, and (c) between board pad and solder mask. Yellow arrows show delamination between dip and spray layers.

(a)



(b)



(c)



Figure 301: Batch B with interlayer delamination evident in the vertical section SEM image of PC40+15.54%N3300 coating on QFP44 location T; (a) 100x, (b) 1,000x, and (c) 5,000x. Yellow arrows highlight delamination between the dip and spray layers.

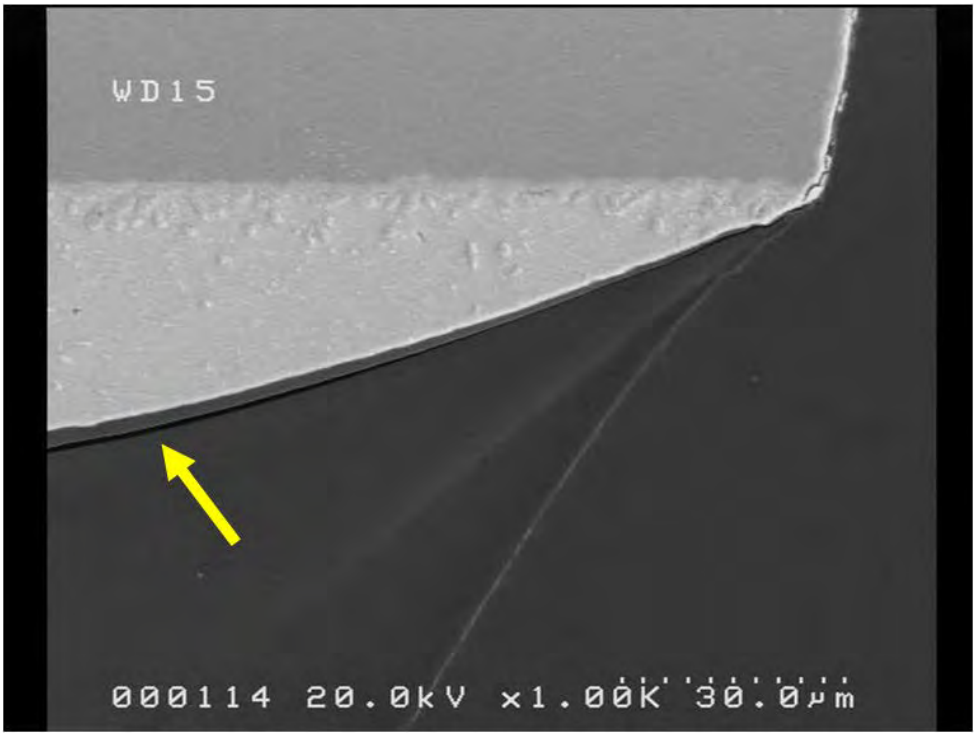


Figure 302: Batch A and B interlayer delamination (arrow) evident in the horizontal section SEM image of PC40-UMF coating on QFP44 with a dip coat/plasma etch/spray coat on U3, lead 11, 1,000x.

5.5 Dewetting spray coating over cured dip coat in the PC40-UMF system

The film stability and surface tension driven flow has been studies for decades and analysis of simplified free surface fluid flows such as flow down an inclined plane, fluid layer stability, drop spreading, contact line pinning, and flow enhancement on rough surfaces can provide insight into complex wetting processes [2] – [7]. For example, a stable oil layer can be obtained in a Teflon ™ pan if there is enough oil in the pan. In this case, the thick oil is stabilized by gravity [2]. As soon as the oil film is thinner than the capillary length of the liquid, λ_{cap}, the molecular forces dominate the gravitational forces and the film may dewet. The capillary length is described by

$$\lambda_{\mathrm{cap}} = \sqrt{\sigma_{\mathrm{lv}}/\rho g}$$

where σ_{lv} is the liquid vapor surface tension, ρ is the liquid density, and g is the acceleration of gravity. While this simplified equation does not include all the factors influencing the coating dewetting in Figure 303, it does describe a limiting condition for film stability.

(A) 

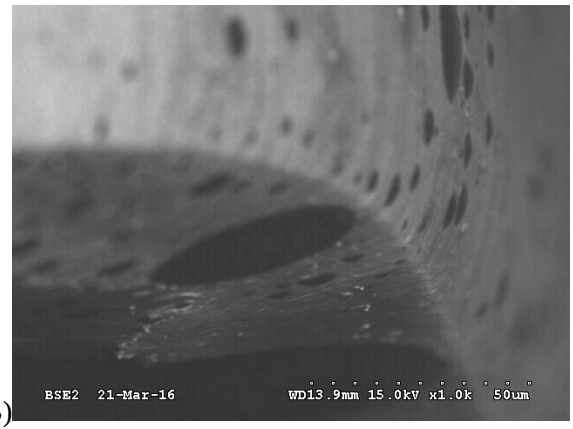
(B) 

Figure 303: SEM image of PC40-UMF coatings; (A) spray coated PC40-UMF directly on QFP44 leads showing no dewetting, 40x, and (B) dewetting on the knee and side of the lead of PC40-UMF spray coating over UV cured PC40-UMF dip coating on the side of a QFP44 lead, 1,000x (Ref for A: Batch C coating of PC40-UMF Asymtech 8-2015, and Ref. for B: baseline coating QFP44, U4, lead 12, Board 60 after HTHH1767).

5.6 Comparison with published work

Other researchers have evaluated coating coverage with respect to tin whisker growth [8] [9] [10] [11] and are discussed in more detail in the layered coating coverage results Appendix [1]. The PC18M with nanoparticles had better coverage than other polyurethane coating applied with standard processing.

6. Conclusions

The combination of SEM inspection with vertical and horizontal cross – sections provided a good assessment of coating coverage and thickness. The PC18M coating based coating generally exhibited better coverage than the PC40-UMF coating based coating. The PC18M+20%X11102PMA nanoalumina had the best coverage and the PC18M+20%XP2742 had the next best coverage and lack of bubbles.

One factor influencing coverage is the solvent dependent viscosity characteristics of the PC18M and the XP2742. The PC18M based coatings initially have a high solvent concentration and low viscosity allowing the coating to flow readily behind the leads. Then as the solvent evaporates, the viscosity increases, which tends to prevent the coating from flowing down and away from the vertical sides of the leads. Close control must be maintained on dip and spray coating viscosities. Increases in dip coating viscosity due to solvent drag out can result in excessive coating thickness build – up around parts and leads. Increase spray coating viscosity can result in bubbling or dry rough surfaces. The spray process is more complicated. The amount of solvent loss is influenced by droplet size, droplet velocity and the solvent concentration in the surrounding air. Further work is needed to understand how these factors contribute to bubble formation and coating coverage.

The adhesion between the dip coating and the subsequent spray coatings is dependent upon the coating type. The PC40-UMF exhibited delamination between layers indicating that cured coating surface energy is high which makes it difficult to bond additional layers to it. The interlayer adhesion for the PC18M based coatings was excellent.

7. Literature cited

[1] Appendix I from the current report: Coating coverage layered coating results

[2] R. Seemann, S. Herminghaus, C. Neto, S. Schlagowski, D. Podzimek, R. Konrad, H. Mantz, and K. Jacobs, Dynamics and structure formation of thin polymer melt films, J. Phys.: Condens. Matter 17, 2005, S267-S290 doi: 1088/0953-8984/17/9/001

[3] A. Oron, Three-Dimensional Nonlinear Dynamics of Thin Liquid Films, Physical Review Letters, Vol. 85, No. 10, 2000, pp. 2108 – 2111

[4] M. Schneider, C. Hager, U. Strohbeck, O. Tiedje, Causes for the formation of surface structures on paint films, 10th BYK-Gardner Users Meeting, Innsbruck, Austria, April 16-17, 2013.

[5] D. Bonn, J. Eggers, J. Indekeu, J. Meunier, and E. Rolley, Wetting and Spreading, Reviews of Modern Physics, Vol. 81, April-June 2009, pp. 739-805.

[6] B. Radoev, K. Stöckelhuber, R. Tsekov and P. Letocart, Wetting film dynamics and stability, Colloids Interface Science, Ser. 3, 2007, pp 151-172.

[7] L. Felton, Mechanisms of polymeric film formation, International Journal of Pharmaceuticals, Vol. 457, 2013, pp. 423 – 427.

[8] S. Han, S. Meschter, M. Osterman and M. Pecht, Evaluation of Effectiveness of Conformal Coatings as Tin Whisker Mitigation, Journal of Electronic Materials, DOI: 10.1007/s11664-012-2179-2, July 6, 2012.

[9] D. Hillman, IPC coating coverage round robin, to be presented at IPC APEX 2018.

[10] V. Kumar and L. Woody, Effect of Conformal Coating on Tin Whisker Growth, Proceedings of the 2007 IPC Apex Conference.

[11] J. Wilcox, M. Meilunas, Harsh Environment Reliability of Micro-Leadframe (QFN) Components and Conformal Coating Effects, Proceedings of the Surface Mount International Conference, Rosemont, IL, September 27-October 1, 2015.

[12] Appendix E from the current report: Assembly test vehicle coating process

SERDP WP2213
Final Report
Appendix G: Coupon whisker testing for baseline coating process

Appendix G: Table of Contents

1. Introduction 1

2. Cantilever beam coupon 1

2.1 PC18M+30%XP2742 nanosilica whisker test results 1

2.1.1 Method and samples review 1

2.1.2 SEM examination and cross – section results 1

2.1.3 Measurements from nodule cross – sections 5

2.1.4 Coating removal and tin inspection 7

2.1.5 Summary and discussion 8

2.1.6 Conclusions 12

3. SAC+REE Coupons 13

3.1 Method and samples review 13

3.2 PC18M based coatings whisker test results 14

3.3 PC40UMF+XP2742 based coatings whisker test results 17

3.4 Summary and discussion 26

3.5 Conclusions 26

4. Literature cited 27

Appendix G: List of Figures

Figure 1: Cantilever beam whisker coupon; (A) coated cantilever beam, and (B) cantilever beam installed in fixture (dimensions in mm). 1

Figure 2: Cantilever beam coupon whisker nodule with growth in non-coated areas after 2,500 (500+2,000) hours 60°C/60%RH; 100x, and 500x. 2

Figure 3: Cantilever beam coupon SEM inspection of thin coating region, areas after 2,500 (500+2,000) hours 60°C/60%RH showing a tin nodule under thicker coating and tin eruptions through thin coating. 3

Figure 4: Cantilever beam coupon longitudinal cross-section through thin coating region areas after 2,500 (500+2,000) hours 60°C/60%RH; (a) and (b) eruption through three micron coating, (c) cross-section region on sample, (d) nodule under seven micron coating and (e) nodule under 30 micron coating. ... 3

Figure 5: First ion beam polish of seven micron nominal coating. (A) back scatter electron image and (B) secondary electron image after 2,500 (500+2,000) hours 60°C/60%RH. 4

Figure 6: Second ion beam polish of seven micron nominal coating; (A) back scatter electron image, and (B) secondary electron image. Arrow shows separation between coating after 2,500 (500+2,000) hours 60°C/60%RH. 4

Figure 7: Whiskers growing from cantilever beam sample cross-sections two days after sectioning. 5

Figure 8: Measured tin dome height profiles for various coating thickness regions on the cantilever beam whisker test sample. 6

Figure 9: Typical measured tin and coating thickness values across the sample. The second ion beam mill section measurements from the seven micron thick coating shown. 6

Figure 10: Cantilever beam coupon inspection after coating removal after 2,500 (500+2,000) hours 60°C/60%RH. 8

Figure 11: Nanoindentation of Arathane 5750 on a glass slide. The as-received measurements were obtained after the initial cure of 6 hours at 85 °C. The measurements were repeated after an additional exposure of 10 hours at 90°C. 9

Figure 12: Nanoindentation testing results of PC18M filled with XP2742 (nanosilica); (A) elastic modulus, and (B) nanohardness. 10

Figure 13: Nanoindentation testing results of PC18M+20% XP2742 at room temperature, 50˚C, 85˚C, and 125˚C; (A) elastic modulus, and (B) nanohardness. 11

Figure 14: SAC+REE whisker coupon (dimensions in mm). 13

Figure 15: Typical SAC+REE whisker coupon. 13

Figure 16: SAC+REE non-coated coupon typical whisker growth after 1,000 hours 85°C/85%RH. 15

Figure 17: SAC+REE coupon with PC18M+ 20% X1102PMA growth after 1,000 hours 85°C/85%RH, 450x. 15

Figure 18: Close-up of SAC+REE coupon with PC18M+20%XP2742 after 1,000 hours 85°C/85%RH, 350x and 1,800x.Whiskers penetrated thin coating (estimated to be less than five microns). 16

Figure 19: SAC+REE coupon with PC18M-mod after 1,000 hours 85°C/85%RH, 250x.Whisker/nodule growth penetration where coating was thin. 17

Figure 20: Uncoated SAC+REE coupon after 1,000 hours 85C/85%RH; (A) 1,500x and (B) 2,000x. 18

Figure 21: SAC+REE coupon coated with PC40UMF after 1,000 hours 85C/85%RH; (A) 40x, (B) close up of corner, 400x, (c) and (d) close-up of eruption where coating begins to thin, 2,500x. 19

Figure 22: SAC+REE coupon coated with PC40UMF+15.54%N3300 after 1,000 hours 85C/85%RH; (A) 40x, and (B) close up of edge, 3,500x. 20

Figure 23: SAC+REE coupon coated with 100% N3300 after 1,000 hours 85C/85%RH; (A) 40x, (B) close up of coating edge, 3,500x. N3300 exhibited reduced wetting compared to the other samples. 21

Figure 24: SAC+REE coupon coated with PC40UMF+10%XP2742 after 1,000 hours 85C/85%RH; (A) 40x, and (B) close up of coating edge, 3,500x. 22

Figure 25: SAC+REE coupon coated with PC40UMF+30%XP2742 after 1,000 hours 85C/85%RH (composite image). 23

Figure 26: SAC+REE coupon coated with PC40UMF+50%XP2742 after 1,000 hours 85C/85%RH; (A) 40x, (B) close up of corner, 500x, and (C) higher magnification of corner, 2,500x. 24

Figure 27: SAC+REE coupon coated with 100%XP2742 after 1,000 hours 85C/85%RH; (A) 500x, and (B) close up of edge, 2,500x. 25

Appendix G: List of Tables

Table 1: Coating thickness and tin dome measurement summary. 7
Table 2: SAC+REE PC18M based test samples. 14
Table 3: SAC+REE PC40UMF+XP2742 test samples 17

Acronyms

Acronym	Definition
HTHH	High Temperature/High Humidity
REE	Rare Earth Element (Note only RE is used in a chemical formula)
RH	Relative Humidity
SAC	Sn-Ag-Cu alloy lead free solder
SEM	Scanning Electron Microscopy

1. Introduction

Coupon whisker tests were used for the baseline coating evaluation. The method details are provided in Appendix C [2]. Three coupon tests were performed. The first used a bright tin plated copper sample in a bent cantilever configuration. The second and third used a flat SAC+REE coated coupon. Later during the layered coating evaluation, a bright tin plated copper slotted coupon was used as described in [3].

2. Cantilever beam coupon

2.1 PC18M+30%XP2742 nanosilica whisker test results

2.1.1 Method and samples review

A brief description of the evaluation method and samples follows. The overall cantilever beam test coupon and test fixture are shown in Figure 1. Inspections were performed on PC18M+30%XP2742 nanosilica coating sample number four after 2,500 (500+2,000) hours at 60°C/60% Relative Humidity (RH). The coating was 100 microns thick in the center of sample and thinned to less than three microns near the internal beam edges.

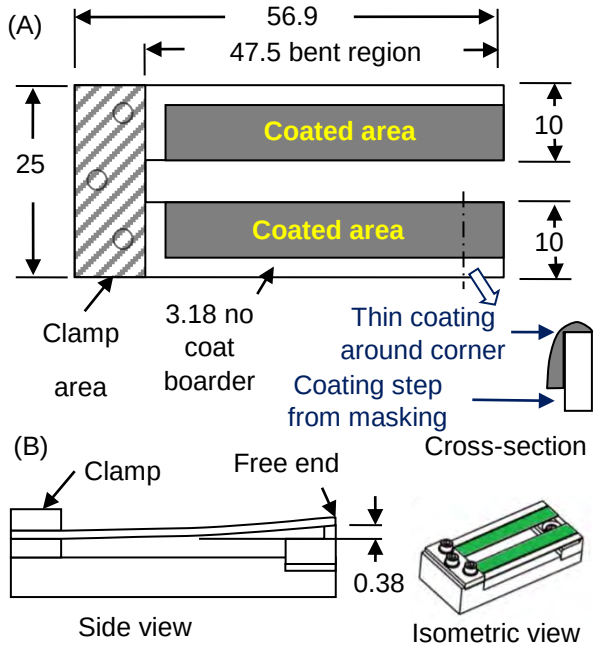


Figure 1: Cantilever beam whisker coupon; (A) coated cantilever beam, and (B) cantilever beam installed in fixture (dimensions in mm).

2.1.2 SEM examination and cross – section results

Scanning Electron Microscopy (SEM) examination showed that the non-coated areas grew eruptions and whiskers but that the adjacent thick coated areas had no eruptions or whisker growth (Figure 2). Where the coating was thin (~3 microns), nodules/odd shaped eruptions broke through the coating. Where the coating was a little thicker, there was evidence of nodule formation under the coating

(Figure 3 and Figure 4). Cross-sections indicated that Cu_6Sn_5 was present near the base of the eruptions where the original tin surface was located. Eruptions on the non-coated side of the cantilever beam have a similar Cu_6Sn_5 accumulation near the base of the eruption. Progressive ion milling was completed on the 7 micron thick coating region (Figure 5 and Figure 6). The second ion beam section revealed that the coating delaminated from the tin near the base of the tin dome.

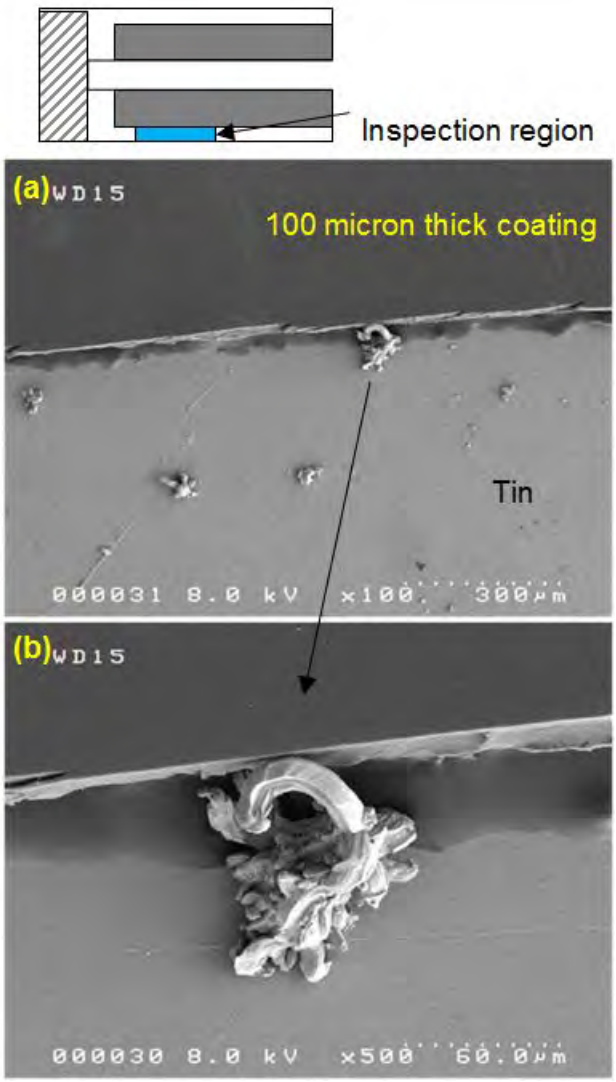


Figure 2: Cantilever beam coupon whisker nodule with growth in non-coated areas after 2,500 (500+2,000) hours 60°C/60%RH; 100x, and 500x.

Note that the cantilever beam tin films whiskers grew from the cross-sections after two days at room temperature, indicating that the tin film under the coating still had a high whisker propensity (Figure 7) at the time of the examination.

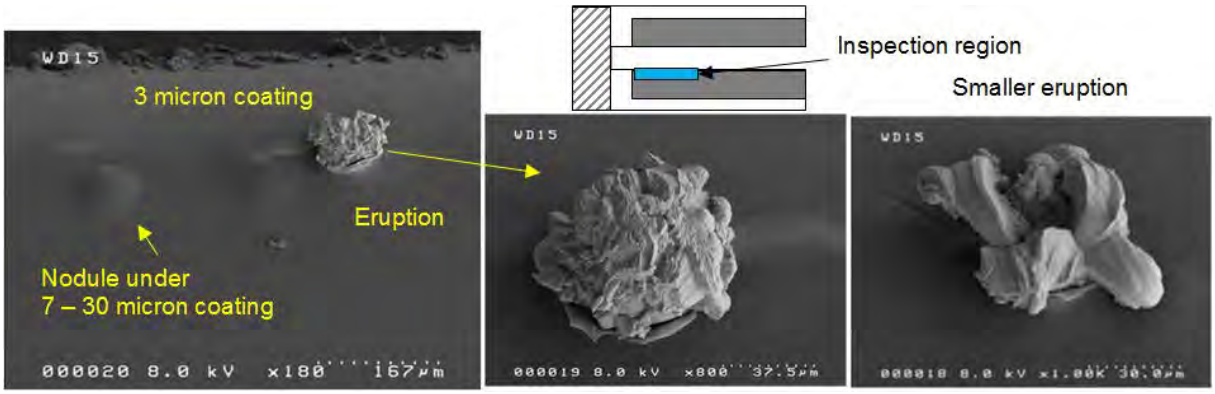


Figure 3: Cantilever beam coupon SEM inspection of thin coating region, areas after 2,500 (500+2,000) hours 60°C/60%RH showing a tin nodule under thicker coating and tin eruptions through thin coating.

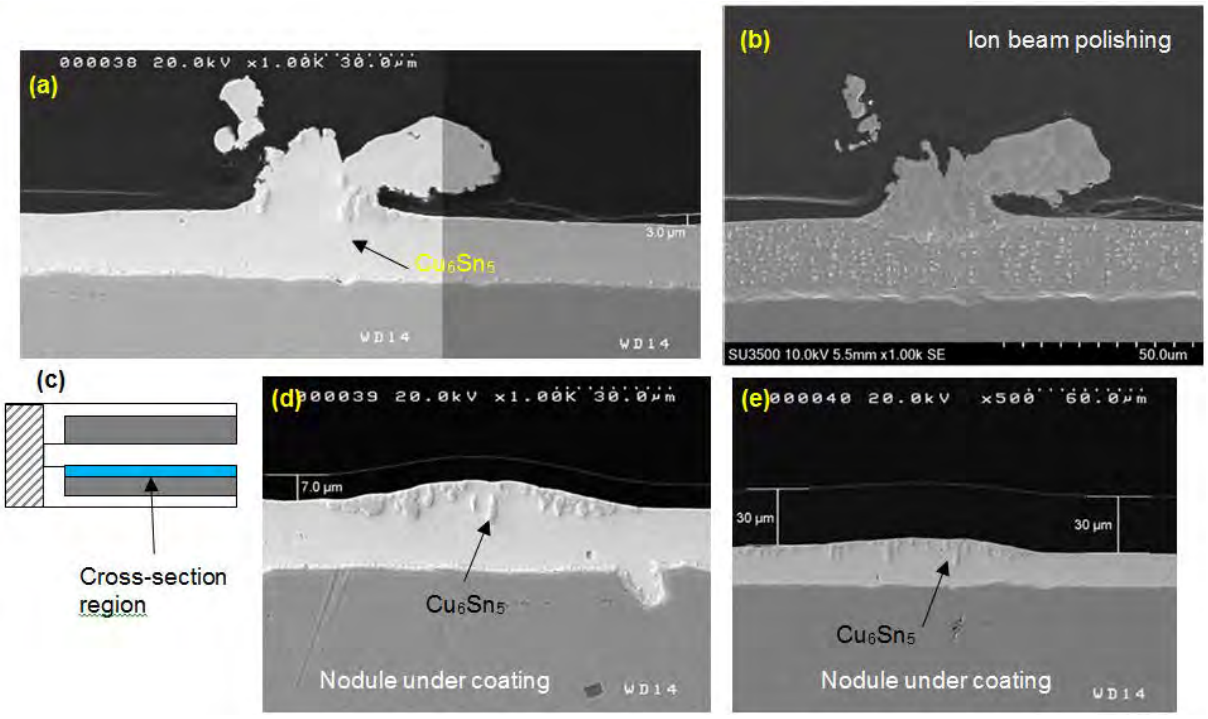
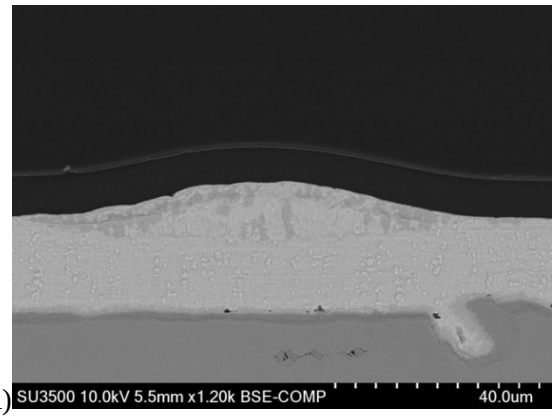


Figure 4: Cantilever beam coupon longitudinal cross-section through thin coating region areas after 2,500 (500+2,000) hours 60°C/60%RH; (a) and (b) eruption through three micron coating, (c) cross-section region on sample, (d) nodule under seven micron coating and (e) nodule under 30 micron coating.

(A) 

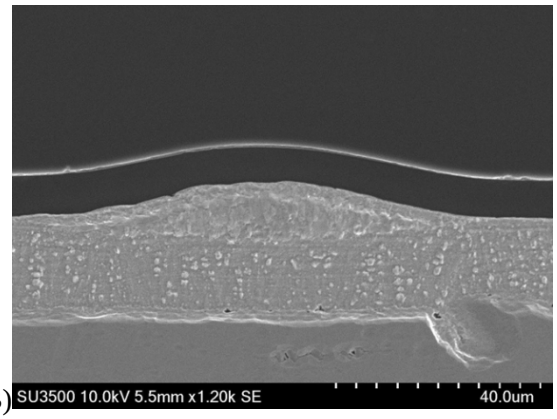
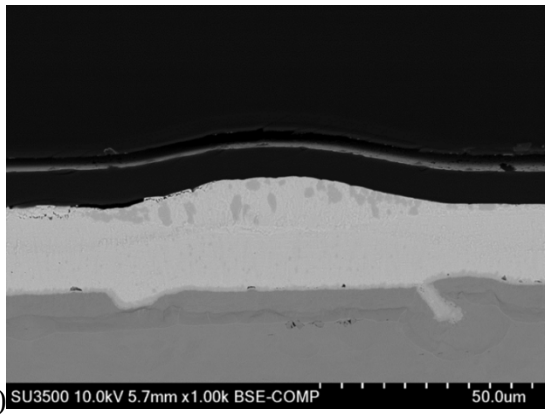
(B) 

Figure 5: First ion beam polish of seven micron nominal coating. (A) back scatter electron image and (B) secondary electron image after 2,500 (500+2,000) hours 60°C/60%RH.

(A) 

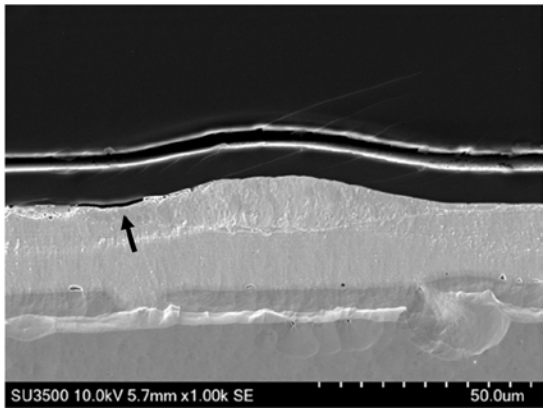
(B) 

Figure 6: Second ion beam polish of seven micron nominal coating; (A) back scatter electron image, and (B) secondary electron image. Arrow shows separation between coating after 2,500 (500+2,000) hours 60°C/60%RH.

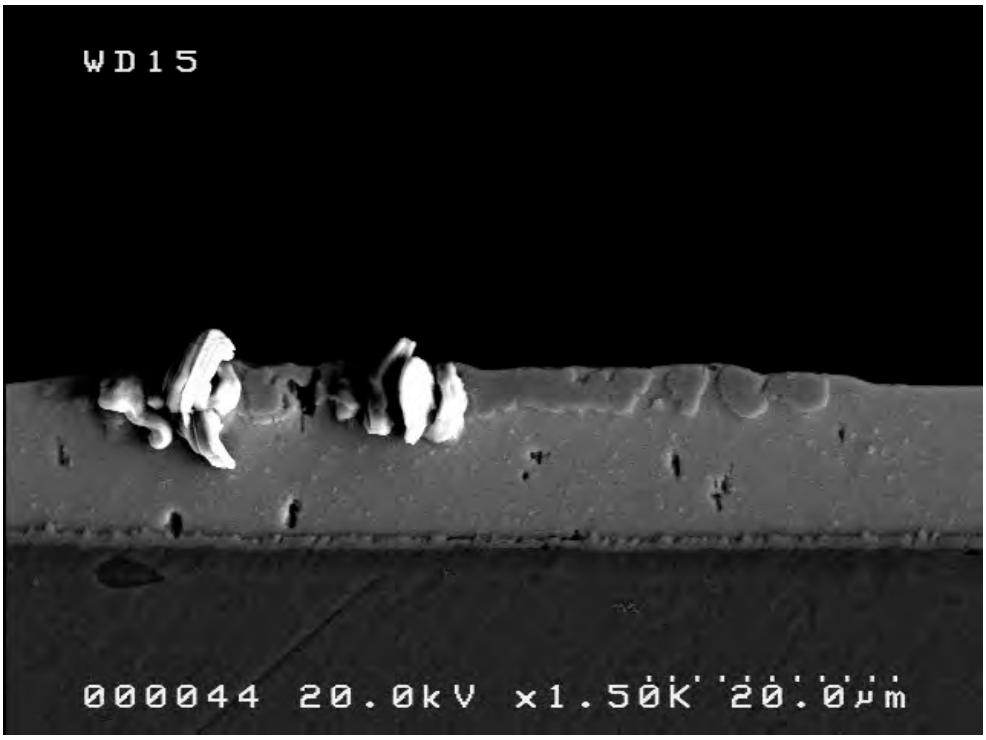


Figure 7: Whiskers growing from cantilever beam sample cross-sections two days after sectioning.

2.1.3 Measurements from nodule cross – sections

Measurements were obtained from the three nodule cross-sections to determine the nodule geometry and coating thickness profile. The dome heights were observed to be similar for the seven and 30 micron thick coating regions, but the diameters increased with increasing coating thickness (Figure 8). The coating typically thinned slightly near the apex of the tin dome (Figure 9). A summary of coating thicknesses and the tin dome diameter and height are given in Table 1.

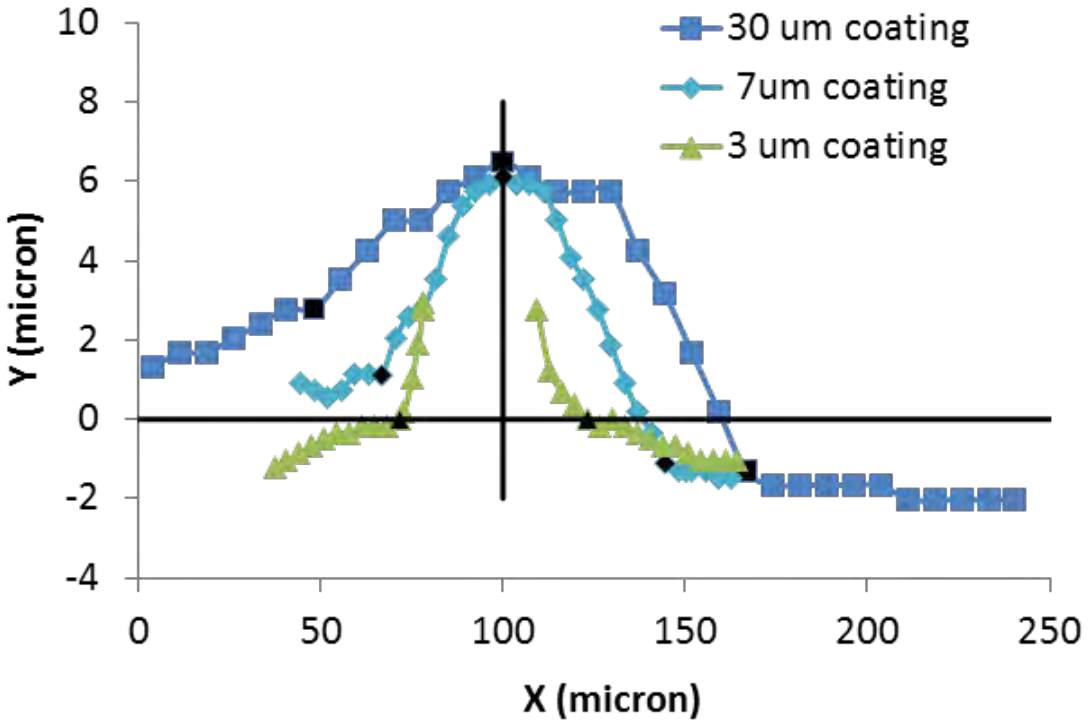


Figure 8: Measured tin dome height profiles for various coating thickness regions on the cantilever beam whisker test sample.

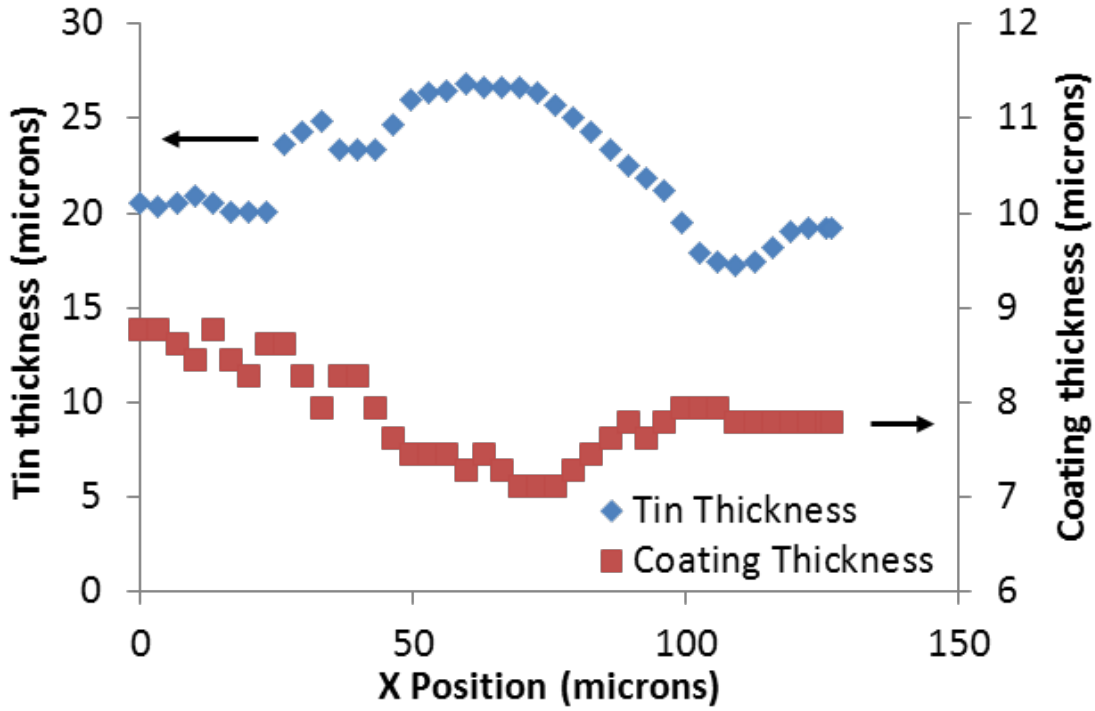


Figure 9: Typical measured tin and coating thickness values across the sample. The second ion beam mill section measurements from the seven micron thick coating shown.

Table 1: Coating thickness and tin dome measurement summary.

Nominal coating thickness	Average coating thickness in flat region (microns)	Minimum coating thickness at top of dome (microns)	Dome diameter (microns)	Dome height (microns)
3 um	3.4	Ruptured	51.6	Ruptured
7 um	8.2	7.1	79.5	6.8
30 um	30.2	28.5	118.5	5.7

2.1.4 Coating removal and tin inspection

The coating was removed on the cantilever beam sample with Uresolve™ solvent. The evaluation was performed on the cantilever arm opposite the one that was cross – sectioned. Under the 100 micron thick coating, very few if any tin nodules were observed (Figure 10). The occasional nodule occurrence may be indicative of poor coating adhesion sites.

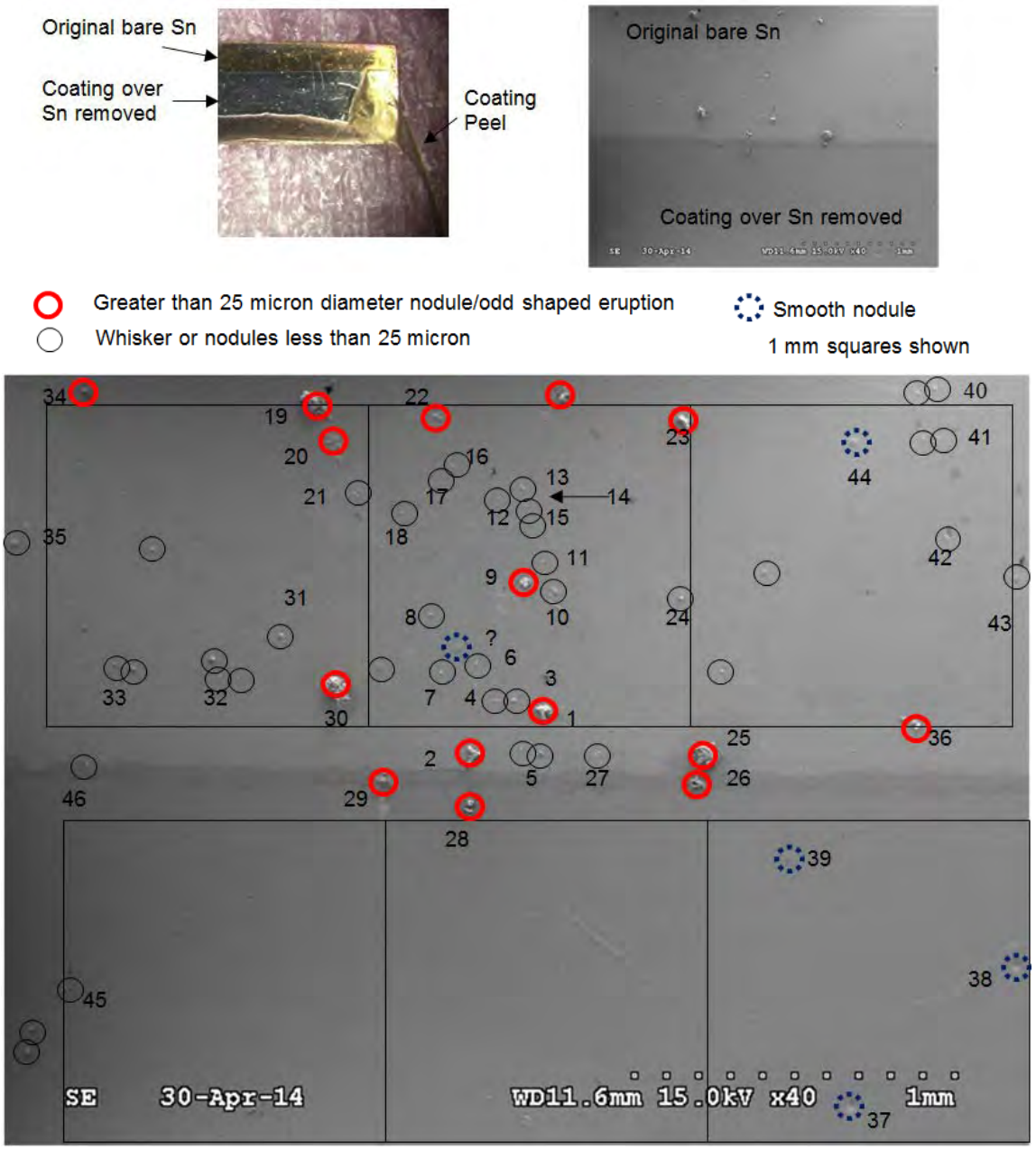


Figure 10: Cantilever beam coupon inspection after coating removal after 2,500 (500+2,000) hours 60°C/60%RH.

2.1.5 Summary and discussion

For the relatively high modulus high yield strength PC18M+30%XP2742 polyurethane coating, the tendency of the thicker coating regions to resist whisker penetration was not unexpected. The interesting observations were (1) tin dome diameter increased when the coating thickness increased and (2) the 100 micron coating thick almost complete inhibited whisker/nodule growth.

The relationship between coating rupture and coating thickness for a particular set of whisker/nodule diameters, coating modulus, coating strength, and coating strength was evaluated further in the model developed in Appendix M.

The nucleation inhibition observed with the rigid coating in the present work is in contrast to the behavior of the softer Arathane ™ 5750 tested by NASA [1]. On coupons of bright tin over brass, initial whisker/nodule growth under the coating was much greater than in the uncoated areas. The authors reported that at four months of exposure at 50°C, the coated side of the coupons exhibited four to five times more nodule and whisker growth than the uncoated side. However after a year, the density of growth on the non-coated side increased rapidly and was similar to the coated side. The authors also noted that a number of tin nodules appeared to be on the verge of breaking through the thinner regions of the coating, with the tin domes developing sharper tips over time.

In an effort to quantify the hardness differences between the PC18M+20%XP2742 and the Arathane ™ 5750, nanoindentation tests were performed on recently fabricated Arathane ™ 5750 coated glass slides. The results confirm that Arathane ™ 5750 is considerably less rigid (Figure 11) than the PC18M+30%XP2742 nanosilica filled coatings used in the present work (Figure 12). Even considering the fact that the whisker testing was above the PC18M glass transition temperature, the PC18M base coating modulus and hardness at 85°C (Figure 13 for PC18M+20%XP2742) are still expected to be orders of magnitude higher than the Arathane.

Thus, given that whisker growth is a surface stress relaxation phenomenon, it is reasonable that the presence of a more rigid coating on the tin surface could inhibit whisker nucleation provided the adhesion is adequate.

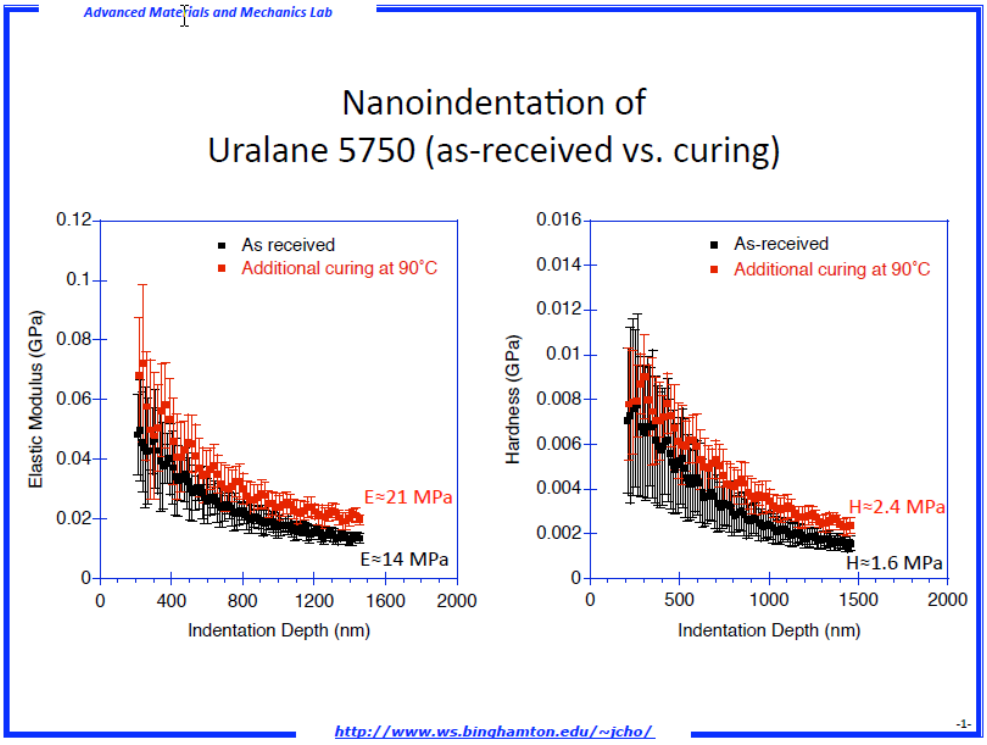


Figure 11: Nanoindentation of Arathane 5750 on a glass slide. The as-received measurements were obtained after the initial cure of 6 hours at 85 °C. The measurements were repeated after an additional exposure of 10 hours at 90°C.

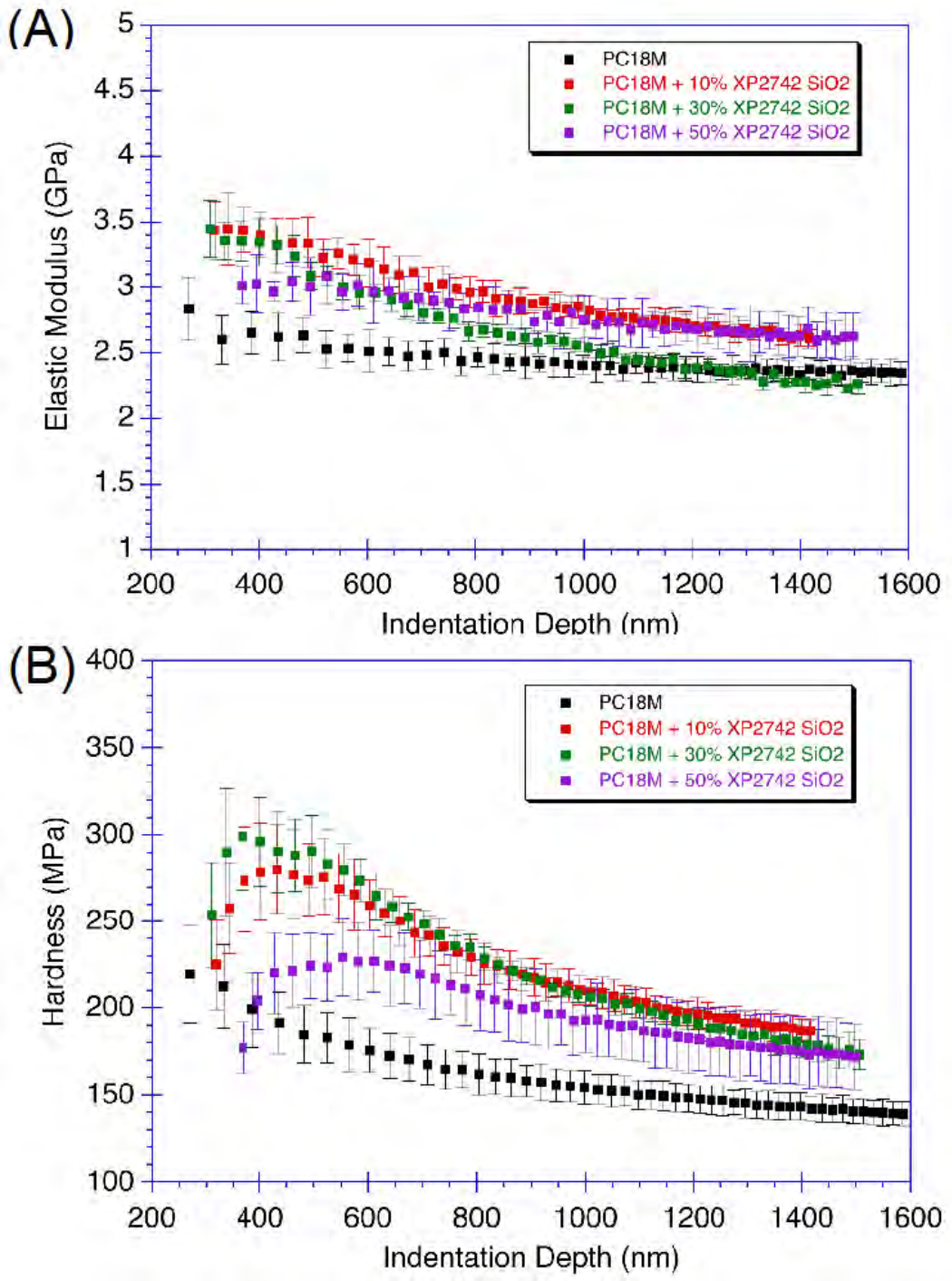


Figure 12: Nanoindentation testing results of PC18M filled with XP2742 (nanosilica); (A) elastic modulus, and (B) nanohardness.

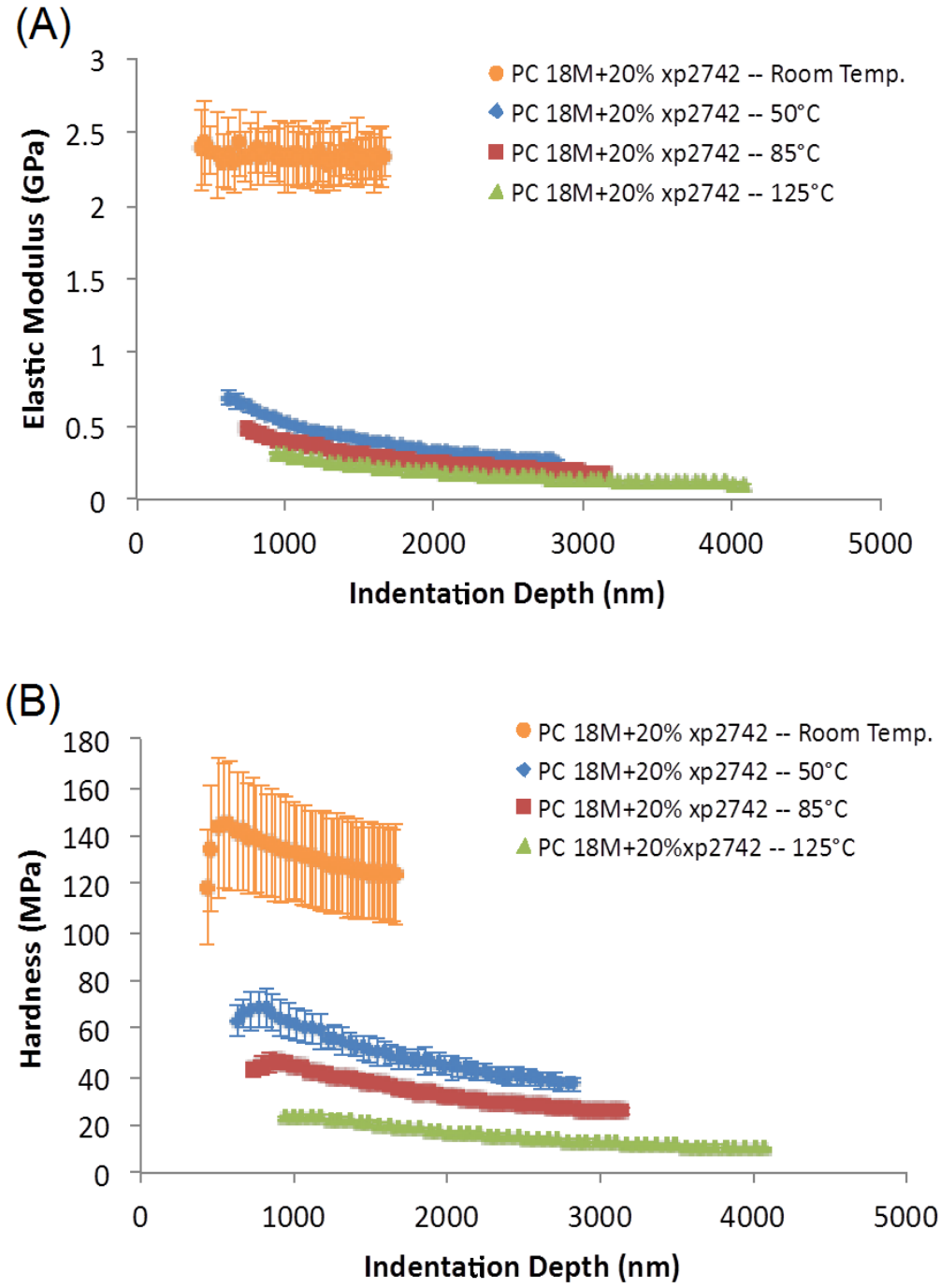


Figure 13: Nanoindentation testing results of PC18M+20% XP2742 at room temperature, 50˚C, 85˚C, and 125˚C; (A) elastic modulus, and (B) nanohardness.

2.1.6 Conclusions

For the relatively high modulus high yield strength PC18M+30%XP2742 polyurethane coating, the tendency of the thicker coating regions to resist whisker penetration was not unexpected. The interesting observations were (1) tin dome diameter increased when the coating thickness increased and (2) the 100 micron coating thick almost complete inhibited whisker/nodule growth.

The lack of nodule growth observed under the PC18M+30%XP2742 is in contrast to whisker/nodule growth under the softer Arathane ™ 5750 tested by NASA.

Thus, given that whisker growth is a surface stress relaxation phenomenon, it is reasonable that the presence of a more rigid coating on the tin surface could inhibit whisker nucleation provided the adhesion is adequate.

3. SAC+REE Coupons

3.1 Method and samples review

The addition of rare earth elements (REE) to Sn-Ag-Cu alloy lead free solder (SAC) is known to grow whiskers in high temperature high humidity environments. The SAC+REE coupon (Figure 10) was 0.2 to 0.3 mm thick and had notches to simulate coating lead corners, a hole for coating dipping and a corner chamfer to facilitate with sample orientation. A typical coupon is shown in Figure 15.

A summary of the coatings tested is given in Table 2.

The SAC+REE samples were exposed to 85°C/85%RH high temperature high humidity (HTHH) for 1,000 hours and examined in the scanning electron microscope (SEM).

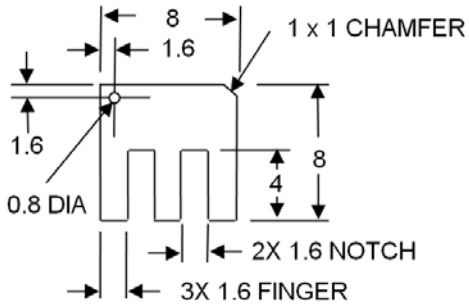


Figure 14: SAC+REE whisker coupon (dimensions in mm).

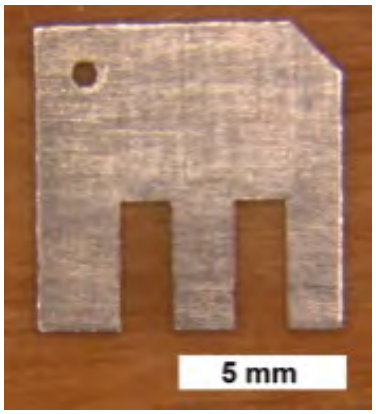


Figure 15: Typical SAC+REE whisker coupon.

Table 2: SAC+REE PC18M based test samples.

Coating	wt.% isocyanate in suspension (N3300 HDI trimer)	wt.% nanoparticle after cure
Uncoated	Not applicable	
PC18M-mod		0
PC18M+20%XP2742	10.36	6.74% SiO_2
PC18M+20%11102PMA	0	13.04% Al_2O_3
PC40UMF	0	0
PC40UMF+15.54%N3300	15.54	0
100% N3300	100	0
PC40UMF+10% XP2742	5.18	1.88% SiO_2
PC40UMF+30% XP2742	15.54	6.0% SiO_2
PC40UMF+50% XP2742	25.9	10.7% SiO_2
100% XP2742	51.8	26% SiO_2
Parylene™ C	Not applicable	
Parylene™ C with Adpro +	Not applicable	

3.2 PC18M based coatings whisker test results

The whisker growth was confirmed on non-coated specimens (Figure 16). After 1,000 hours 85°C/85%RH, none of the coating exhibited eruptions or whisker penetration where the coating was thick, but when the coating was thin on the edges, some eruption and whisker growth was observed (Figure 17 –Figure 19). None of the Parylene™ or Parylene™ with Adpro+ samples exhibited whisker growth.



Figure 16: SAC+REE non-coated coupon typical whisker growth after 1,000 hours 85°C/85%RH.

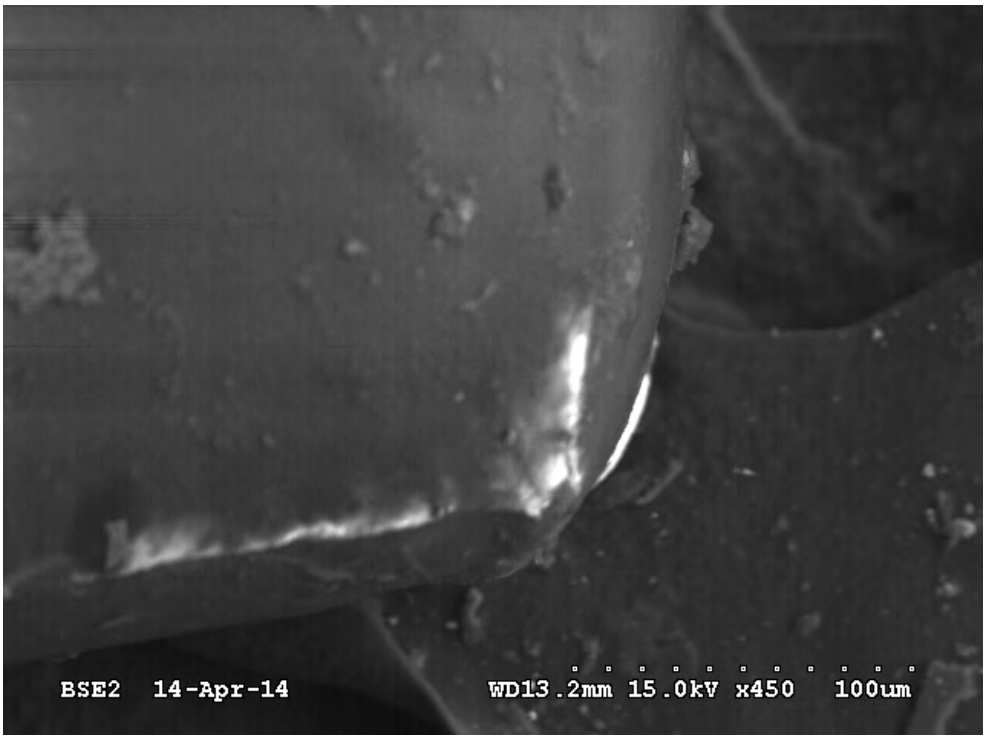


Figure 17: SAC+REE coupon with PC18M+ 20% X1102PMA growth after 1,000 hours 85°C/85%RH, 450x.

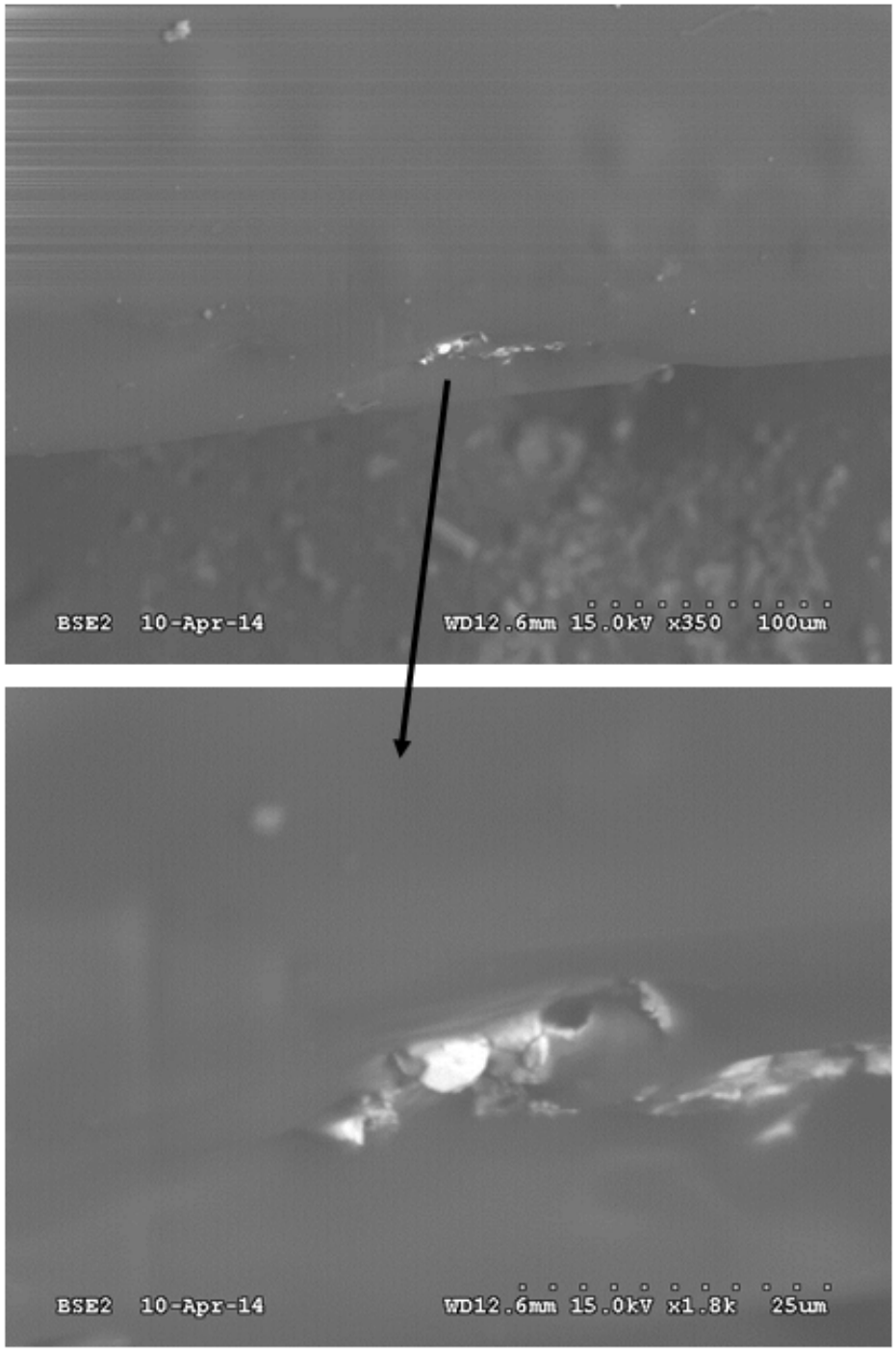


Figure 18: Close-up of SAC+REE coupon with PC18M+20%XP2742 after 1,000 hours 85°C/85%RH, 350x and 1,800x.Whiskers penetrated thin coating (estimated to be less than five microns).



Figure 19: SAC+REE coupon with PC18M-mod after 1,000 hours 85°C/85%RH, 250x.Whisker/nodule growth penetration where coating was thin.

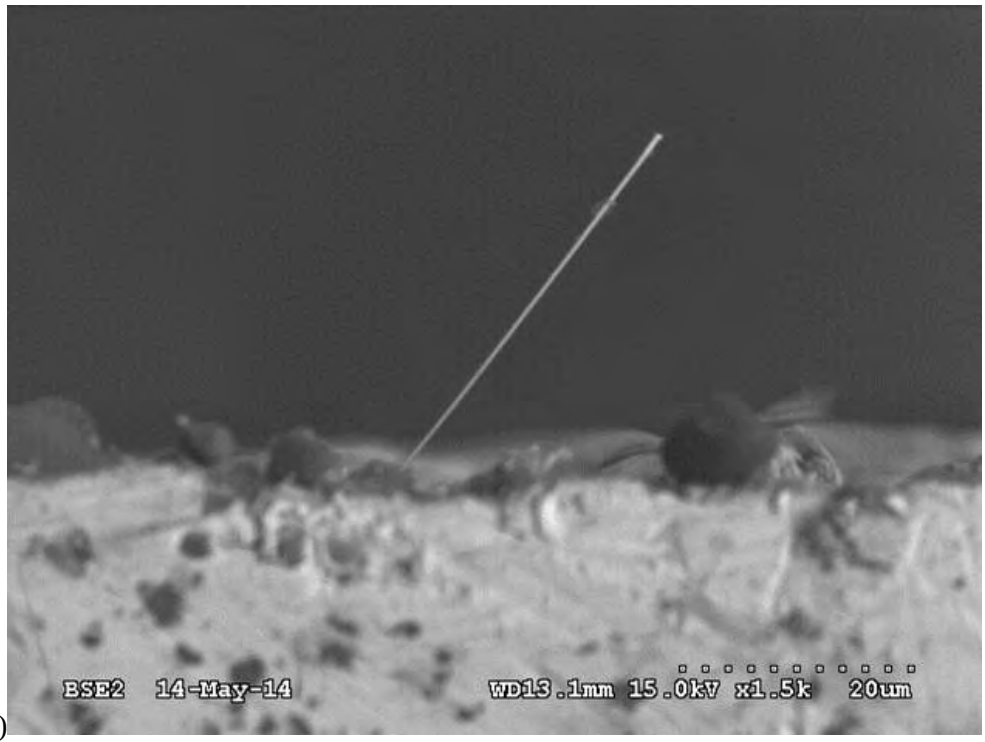
3.3 PC40UMF+XP2742 based coatings whisker test results

After 1,000 hours of 85°C/85%RH the samples were inspected. All the coatings provided some whisker mitigation as compared to the uncoated control (Figure 20). As shown in Figure 21 to Figure 27, the corner coverage was not as good as the PC18M family of coatings (e.g. Figure 17). None of the samples exhibited eruptions or whisker penetration through the coating where the coating was thick (~50 microns). Where the coatings were thinner near the edges, some eruption and whisker growth was observed.

Table 3: SAC+REE PC40UMF+XP2742 test samples.

Coating	wt.% nanosilica
PC40UMF	0
PC40UMF+15.54%N3300	0
100% N3300	0
PC40UMF+10% XP2742	1.88% SiO_2
PC40UMF+30% XP2742	6.0% SiO_2
PC40UMF+50% XP2742	10.7% SiO_2
100% XP2742	26% SiO_2

(A)



(B)

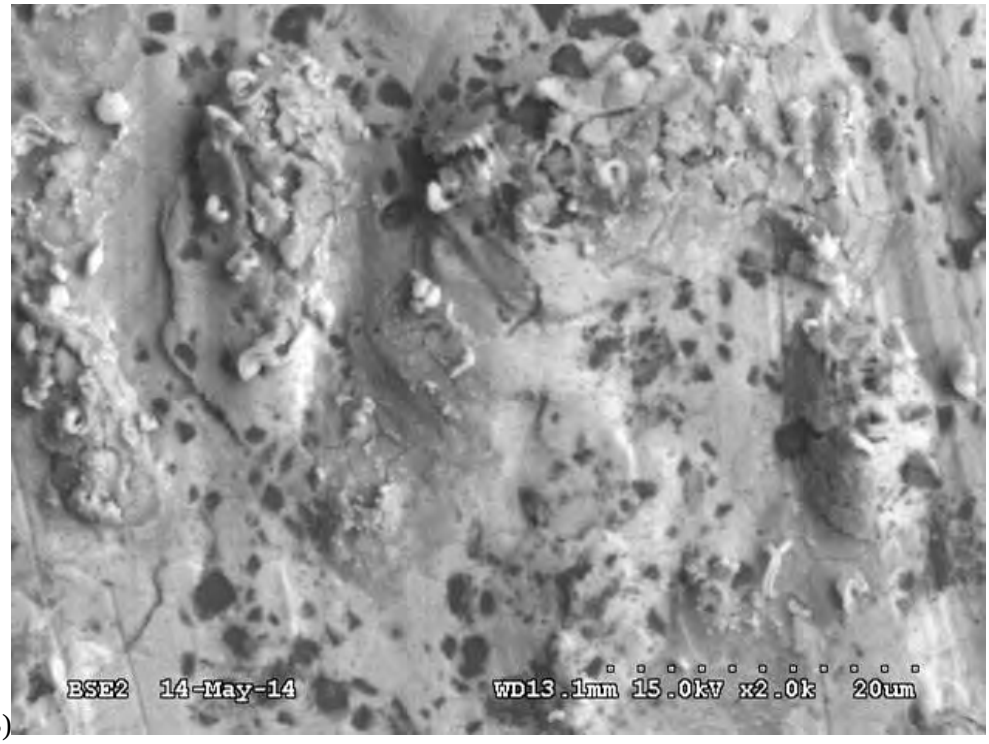


Figure 20: Uncoated SAC+REE coupon after 1,000 hours 85C/85%RH; (A) 1,500x and (B) 2,000x.



Figure 21: SAC+REE coupon coated with PC40UMF after 1,000 hours 85C/85%RH; (A) 40x, (B) close up of corner, 400x, (c) and (d) close-up of eruption where coating begins to thin, 2,500x.

(A)

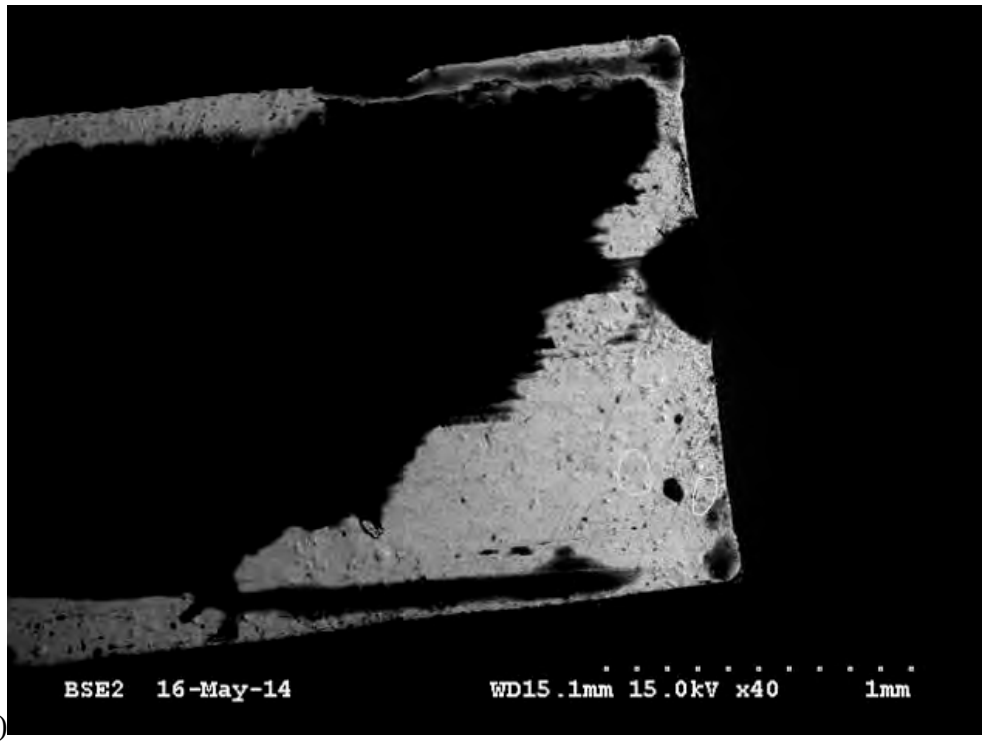


(B)



Figure 22: SAC+REE coupon coated with PC40UMF+15.54%N3300 after 1,000 hours 85C/85%RH; (A) 40x, and (B) close up of edge, 3,500x.

(A)



(B)

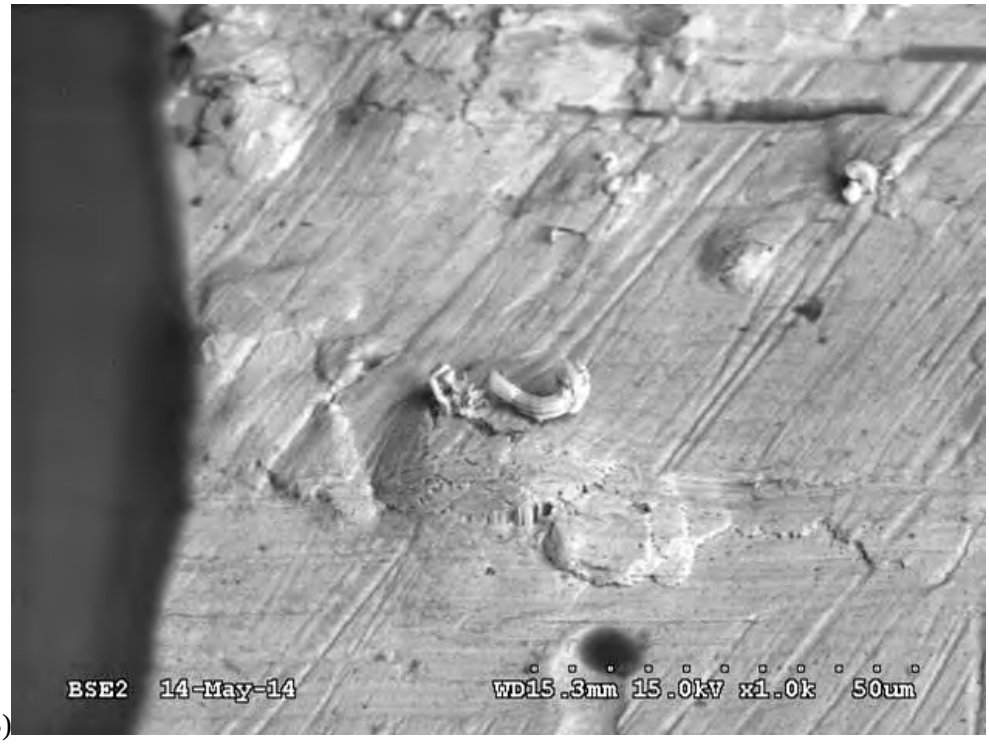
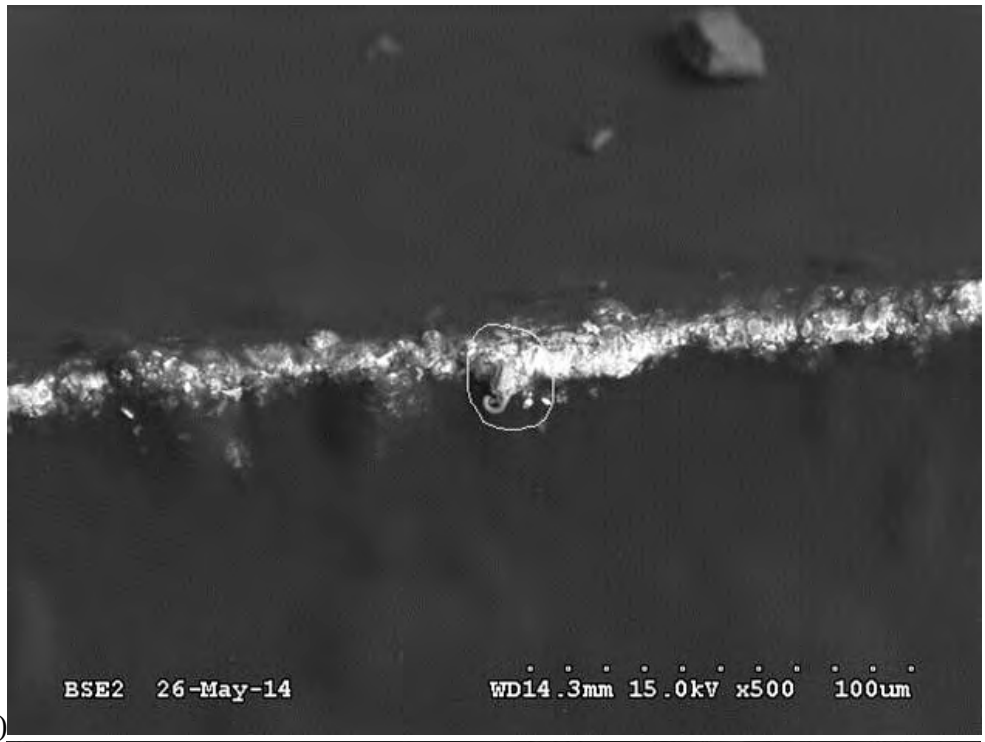


Figure 23: SAC+REE coupon coated with 100% N3300 after 1,000 hours 85C/85%RH; (A) 40x, (B) close up of coating edge, 3,500x. N3300 exhibited reduced wetting compared to the other samples.

(A)



(B)

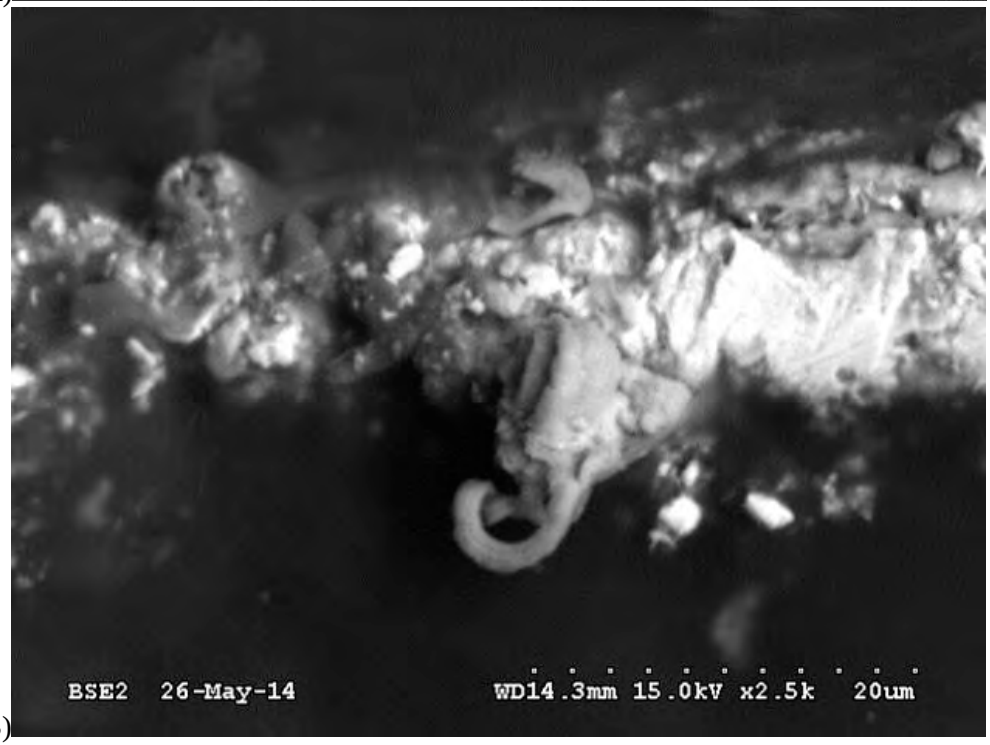


Figure 24: SAC+REE coupon coated with PC40UMF+10%XP2742 after 1,000 hours 85C/85%RH; (A) 40x, and (B) close up of coating edge, 3,500x.

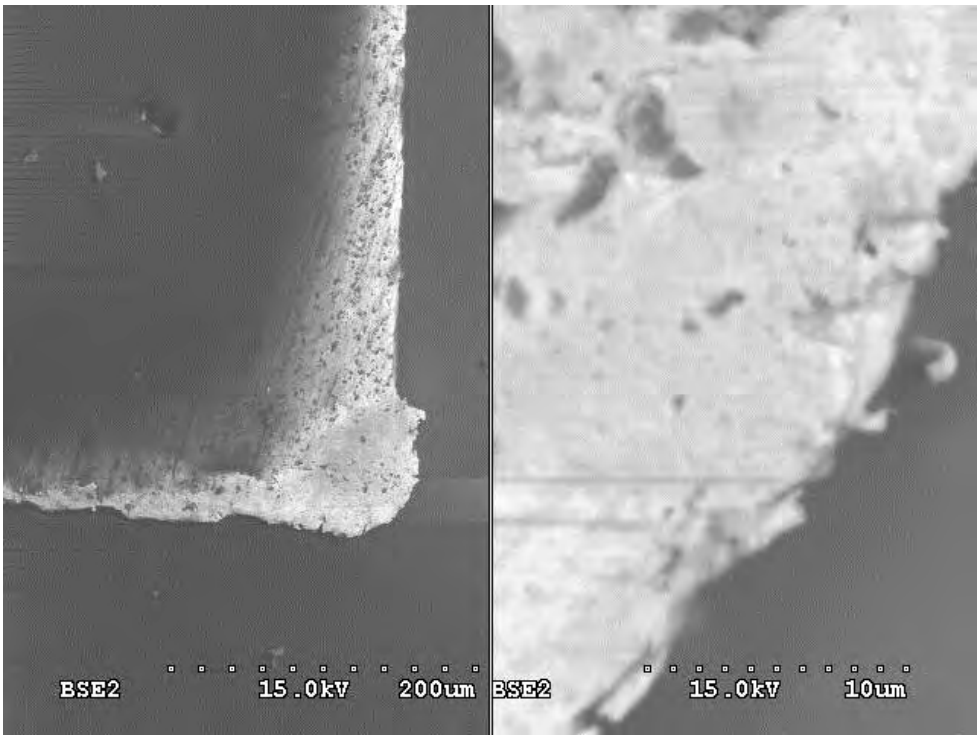
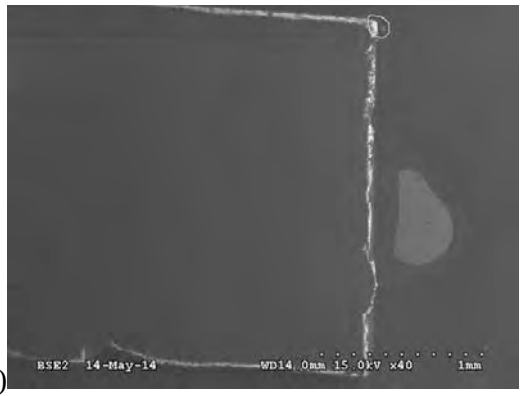
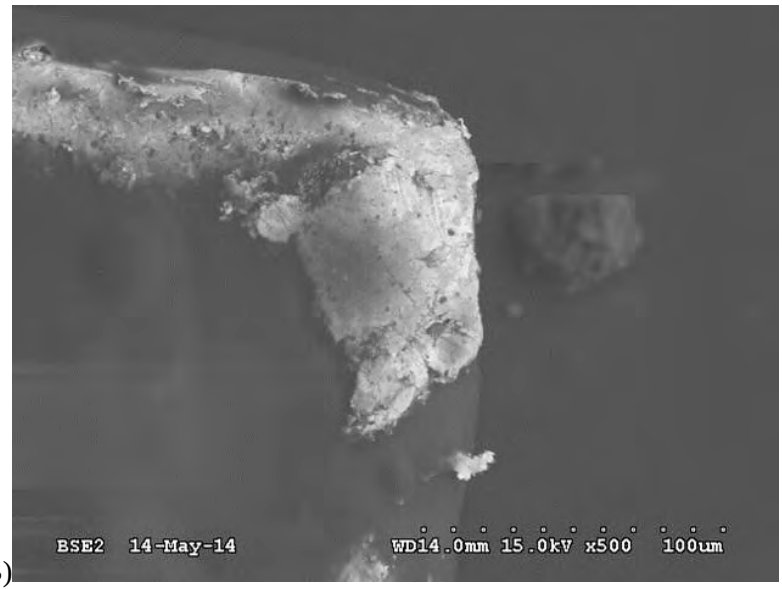


Figure 25: SAC+REE coupon coated with PC40UMF+30%XP2742 after 1,000 hours 85C/85%RH (composite image).

(A)



(B)



(C)

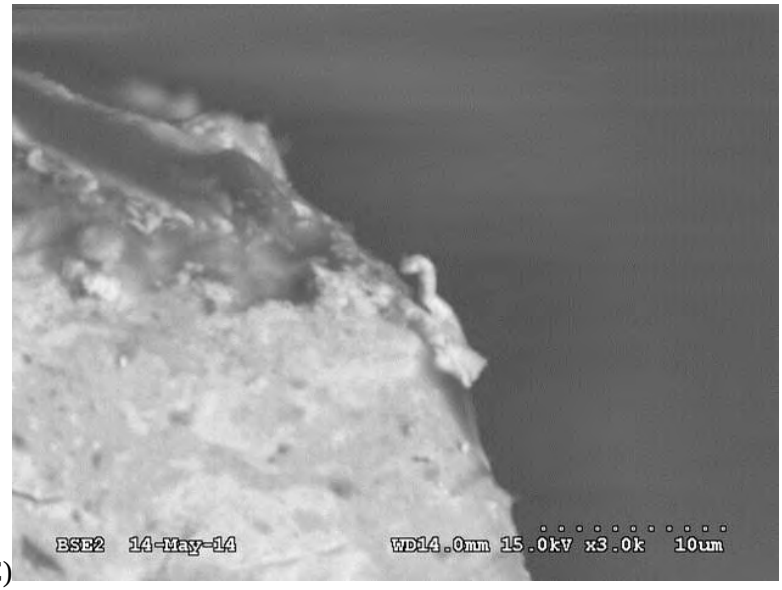
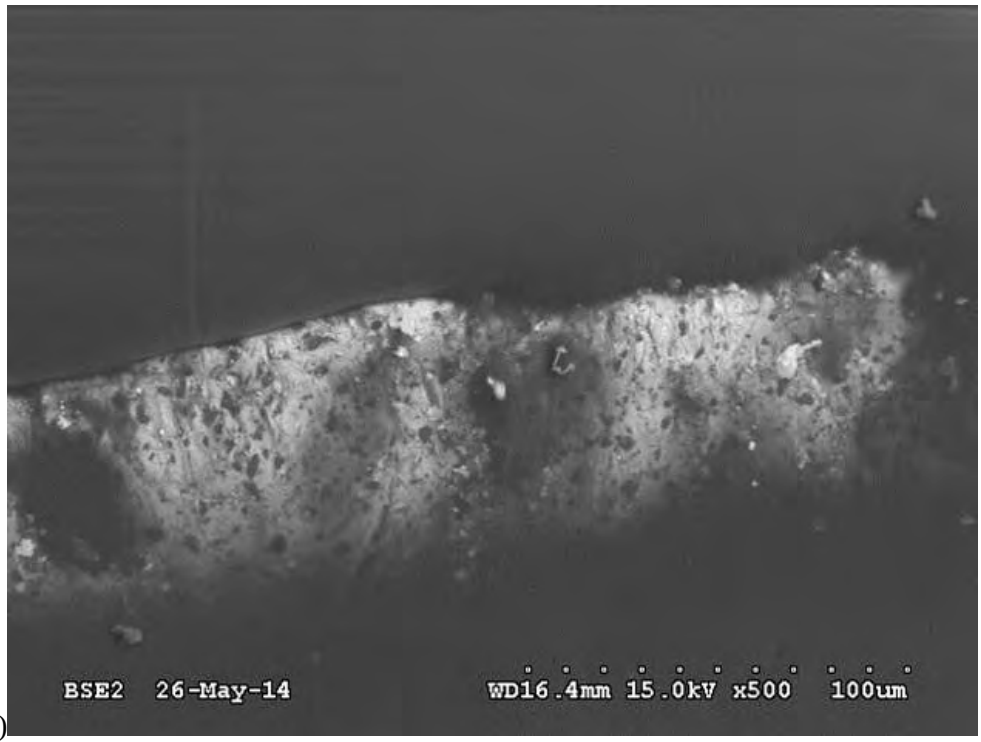


Figure 26: SAC+REE coupon coated with PC40UMF+50%XP2742 after 1,000 hours 85C/85%RH; (A) 40x, (B) close up of corner, 500x, and (C) higher magnification of corner, 2,500x.

(A)



(B)



Figure 27: SAC+REE coupon coated with 100%XP2742 after 1,000 hours 85C/85%RH; (A) 500x, and (B) close up of edge, 2,500x.

3.4 Summary and discussion

All the coatings had similar whisker penetration performance on the SAC+REE coated coupon over the 1,000 hour HTHH testing. Where the coating was thick, no whisker penetration was observed; where it was thin, whiskers and nodules were observed.

The 100%XP2742 and 100%N3300 materials did not wet as well as the other coatings.

3.5 Conclusions

The fine whisker growth that typically occurs from the oxidation of the rare earth element – tin intermetallic was suppressed by all the rigid coatings tested. These coupons were not able to significantly differentiate the whisker mitigation performance between these coatings.

4. Literature cited

[1] J.S. Kadesch and H. Leidecker, “Effects of Arathane Conformal Coating on Tin Whisker Growth”, Proceedings of IMAPS Nordic, The 37th IMAPS Nordic Annual Conference, pp. 108-116, September 10-13, 2000.
[2] Appendix C of the current report: Coating evaluation methods
[3] Appendix J of the current report: Layered coupon whisker testing

SERDP WP2213
Final report
Appendix H: Assembly whisker testing for baseline coating process

Appendix H: Table of Contents

1. Introduction 1

2. Baseline PC18M based coatings samples and environmental testing 1

2.1 Uncoated control assembly test results 1

2.2 PC18M based coatings whisker test results 10

2.2.1 SEM inspection of unfilled PC18M-mod 11

2.2.2 SEM inspection of PC18M+20%XP2742 nanosilica 16

2.2.3 SEM inspection of PC18M+20%X11102PMA nanoalumina 19

2.3 Parylene reference coating during baseline PC18M whisker test results 21

3. Baseline PC40-UMF based coating samples and environmental testing 24

3.1 Baseline PC40-UMF based coating whisker test results 24

3.1.1 Coating thickness 25

3.1.2 Coating type 25

3.1.3 Part type 25

3.1.4 SEM inspection of unfilled PC40UMF assemblies 26

3.1.5 SEM inspection of PC40-UMF+10%NNN2835 nanosilica assemblies 37

3.1.6 SEM inspection of PC40-UMF+30%NNN2835 nanosilica assemblies 47

3.2 Humiseal 1B31-LOC reference coating 60

3.2.1 SEM images Humiseal 1B31-LOC reference coating 60

4. Summary and Discussion 65

4.1 Comparison of coatings 65

4.2 Coating thickness 71

4.2.1 Excessively thick coating 71

4.2.2 Very thin coating with PC40-UMF base coating 72

4.3 Coating bubbles 72

4.4 Environmental exposure for coating whisker mitigation evaluation 72

4.5 Comparison of coating whisker performance with the literature 73

4.6 Whisker inspection 73

5. Conclusion 74

6. Literature cited 75

Appendix H: List of Figures

Figure 1: SEM image of an uncoated SOT6 lead, ATC, 180x (ref. board 237). Whiskers growing from top and lower solder fillet regions. 2

Figure 2: SEM image of an uncoated SOT3 lead, ATC, 1,000x (ref. board 237). Whisker growth occurred from a solder step between two tin grains. 2

Figure 3: SEM image of an uncoated SOT6 lead, ATC, 1,000x (ref. board 237). 3

Figure 4: SEM image of an uncoated SOT5 lead (lead 2), ATC+ HTHH1000, 100x (ref. board 238). Corrosion near the bottom of the joint and whisker growth from the boundary between tin grains were observed. 4

Figure 5: SEM image of an uncoated QFP44 lead, ATC+HTHH2000, 100x (ref. board 46). 5

Figure 6: SEM image of uncoated TQFP64 leads, ATC+HTHH2000, 100x (ref. board 46). 5

Figure 7: SEM image of an uncoated QFP44 lead top, HTHH2000, 100x (ref. Board 48). 6

Figure 8: SEM image of an uncoated QFP44 lead toe, HTHH2000, 100x (ref. Board 48). 6

Figure 9: SEM image of uncoated QFP64 top of leads, HTHH2000, 100x (ref. Board 48). 7

Figure 10: SEM image of uncoated QFP64 lead toes, HTHH2000, 100x (ref. Board 48). 7

Figure 11: SEM image of an uncoated QFP64 lead whisker growth, HTHH2000, 1500x (ref. Board 48). . 8

Figure 12: SEM image of an uncoated QFP64 lead whisker growth, HTHH2000, 2000x (ref. Board 48). . 8

Figure 13: SEM image of an uncoated QFP board PLCC lead, HTHH2000, 100x (ref. Board 48). 9

Figure 14: SEM image of an uncoated QFP board PLCC pad whiskering, HTHH2000, 100x, (ref. Board 48). 9

Figure 15: SEM image of an uncoated QFP board PLCC pad whisker, HTHH2000, 1000x (ref. Board 48). 10

Figure 16: SEM image of PC18M-mod coated SOT6 leads, ATC. 60x, small bubble density (ref. Board 211). 11

Figure 17: SEM image of PC18M-mod coated QFP44 leads, ATC, U2, Lead 17, 80x, large bubble density (ref. Board 34). 12

Figure 18: SEM image of PC18M-mod coated QFP44 leads, U2, Lead 14-15, ATC + 1000HTHH, 60x, small bubble density (ref. Board 15). 12

Figure 19: SEM image of PC18M-mod coated SOT package and leads, ATC+ HTHH1000, 40x (ref. Board 233). Large bubble density condition causing the coating to obscure the SOT leads. 13

Figure 20: SEM image of PC18M-mod coated SOT5 lead, ATC + 2000HTHH, 400x, small bubble density (ref. Board 215). 13

Figure 21: SEM image of PC18M-mod coated SOT5 leads, ATC+ HTHH2000, 40x, small bubble density (ref. Board 215). 14

Figure 22: SEM image of PC18M-mod coated SOT6 lead (lead 3), ATC + 2000HTHH, 150x, small bubble density (ref. Board 215). 15

Figure 23: SEM image of PC18M+20%XP2742 nanosilica coated SOT6 leads, ATC, 60x, medium coating bubble density (ref. Board 217). 16

Figure 24: SEM image of PC18M+20%XP2742 nanosilica coated chip resistor, ATC, 80x, medium coating bubble density (ref. Board 217). 16

Figure 25: SEM image of PC18M+20%XP2742 nanosilica coated SOT3 lead (lead 2), ATC+HTHH2000, 100x and 300x, medium bubble density (ref. Board 235). 17

Figure 26: SEM image of PC18M+20%XP2742 nanosilica coated SOT5 leads, ATC+HTHH2000, 40x, medium bubble density (ref. Board 235). 18

Figure 27: SEM image of PC18M+20%XP2742 nanosilica coated SOT6 leads, ATC+ 2000HTHH, 40x, medium bubble density (ref. Board 235). 18

Figure 28: SEM image of PC18M+20%X11102PMA nanoalumina coated SOT6 leads, ATC, 60x, small/no bubble density (ref. Board 222). 19

Figure 29: SEM image of PC18M+20%X11102PMA nanoalumina coated SOT3 leads, ATC+HTHH2000, 40x, small/no bubble density (ref. Board 228). 19

Figure 30: SEM image of PC18M+20%X11102PMA nanoalumina coated SOT3 lead, ATC + 2000HTHH, 100x, small/no bubble density (ref. Board 228). 20

Figure 31: SEM image of PC18M+20%X11102PMA nanoalumina coated SOT6 lead, ATC + 2000HTHH, 40x, small/no bubble density (ref. Board 228). 20

Figure 32: SEM image of PC18M+20%X11102PMA nanoalumina, SOT6, lead 4 (center lead from Figure 23), ATC+HTHH2000, 100x, small/no bubble density (ref. Board 228). 21

Figure 33: SEM image of Parylene™ C SOT3 leads, ATC + 2000HTHH, 40x (ref. Board 209)..... 22

Figure 34: SEM image of Parylene™ C with Adpro+ coated SOT6 leads, ATC+ 2000HTHH, 40x (ref. Board 206). 22

Figure 35: SEM image of a Parylene™ C & Adpro+ coated SOT3 lead, ATC+HTHH1000, 100x and 350x (ref. Board 204). Small coating crack evident at lead-to-package interface. 23

Figure 36: SEM image of PC40-UMF coated QFP44 lead, HTHH1767, 90x (ref. Board 60). A discontinuous film of discrete droplets and coating pull – away from the metal were observed. 26

Figure 37: SEM image of PC40-UMF coated QFP44 lead, HTHH1767, QFP44, 1,000x (ref. Board 60). Higher magnification view of coating pull away..... 26

Figure 38: SEM image of PC40-UMF coated QFP44 lead, HTHH1767, QFP44, U4, lead 11, 120x (ref. Board 60). 27

Figure 39: SEM image of PC40-UMF coated QFP44 lead, HTHH1767, QFP44, U4, lead 11, 500x (ref. Board 60). Corrosion region in circle is shown in Figure 40..... 27

Figure 40: SEM high magnification image of corrosion on PC40-UMF coated QFP44 lead, HTHH1767, QFP44, U4, lead 11, 4000x (ref. Board 60)..... 28

Figure 41: SEM image of PC40-UMF coated QFP44 lead front, HTHH1767, QFP44, U4, lead 12, 500x (ref. Board 60). 28

Figure 42: SEM image of PC40-UMF coated QFP44 lead side, HTHH1767, QFP44, U4, lead 12, 1,000x (ref. Board 60). 29

Figure 43: SEM image of PC40-UMF coated QFP44 lead, HTHH1767, QFP44, U4, lead 17, 120x (ref. Board 60). 29

Figure 44: SEM image of PC40-UMF coated QFP44 lead front whiskers, HTHH1767, QFP44, U4, lead 17, 500x (ref. Board 60). 30

Figure 45: SEM image of PC40-UMF coated QFP44 lead, HTHH1767, U4, lead 17, 600x (ref. Board 60). 30
Figure 46: SEM image of PC40-UMF coated QFP44 lead side whisker, HTHH1767, QFP44, U4, lead 17, 4,000x (ref. Board 60). 31
Figure 47: SEM image of PC40-UMF coated QFP44 lead front, HTHH1767, U4, lead 17, 3,500x (ref. Board 60). 31
Figure 48: SEM image of PC40-UMF coated SOT3 lead, HTHH1767, 40x (ref. Board 256)..... 32
Figure 49: SEM image of PC40-UMF coated SOT3 leads, HTHH1767, 40x (ref. Board 256). 32
Figure 50: SEM image of PC40-UMF coated SOT5 leads, HTHH1767, U01, 40x (ref. Board 256). 33
Figure 51: SEM image of PC40-UMF coated SOT5 lead, HTHH1767, U01, lead 2, 300x (ref. Board 256). 33
Figure 52: SEM image of PC40-UMF coated SOT5 lead, HTHH1767, U01, lead 2, 2,500x (ref. Board 256). 34
Figure 53: SEM image of PC40-UMF coated SOT5 lead, HTHH1767, U11, lead 4, 500x (ref. Board 256). 34
Figure 54: SEM image of PC40-UMF coated SOT5 lead, HTHH1767, U11, lead 4, 5,000x (ref. Board 256). 35
Figure 55: SEM image of PC40-UMF coated SOT5 lead, HTHH1767, U01, lead 5, 300x (ref. Board 256). 35
Figure 56: SEM image of PC40-UMF coated SOT5 lead, HTHH1767, U01, lead 5, 2,500x (ref. Board 256). 36
Figure 57: SEM image of PC40-UMF coated SOT5 lead, HTHH1767, U15, lead 5, 3,000x (ref. Board 256). 36
Figure 58: SEM image of PC40-UMF coated SOT6 leads, HTHH1767, 40x (ref. Board 256). 37
Figure 59: SEM image of PC40-UMF+10%NNN2835 nanosilica coated QFP44 lead, HTHH1767, U5, lead 1, 120x (ref. Board 65). Area in circle is shown in Figure 60. 37
Figure 60: SEM image of PC40-UMF+10%NNN2835 nanosilica coated QFP44 lead, HTHH1767, U5, lead 1, 500x (ref. Board 65). Area in circle shown in Figure 61. 38
Figure 61: SEM image of PC40-UMF+10%NNN2835 nanosilica coated QFP44 lead, HTHH1767, U5, lead 1, 3500x (ref. Board 65). 38
Figure 62: SEM image of PC40-UMF+10%NNN2835 nanosilica coated QFP44 lead, HTHH1767, U5, lead 1, 250x, and annotated (ref. Board 65). 39
Figure 63: SEM image of PC40-UMF+10%NNN2835 nanosilica coated QFP44 lead, HTHH1767, U5, lead 1, 3,000x (ref. Board 65). 39
Figure 64: SEM image of PC40-UMF+10%NNN2835 nanosilica coated QFP64 lead toe, HTHH1767, 700x, (ref. Board 65). 40
Figure 65: SEM image of PC40-UMF+10%NNN2835 nanosilica coated SOT3 leads, HTHH1767, U06, 40x (ref. Board 284). 40
Figure 66: SEM image of PC40-UMF+10%NNN2835 nanosilica coated SOT5 lead, HTHH1767, U06, lead 2, 250x (ref. Board 284). 41

Figure 67: SEM image of PC40-UMF+10%NNN2835 nanosilica coated SOT5 lead, HTHH1767, U06, lead 2, 3,000x (ref. Board 284). 41

Figure 68: SEM image of PC40-UMF+10%NNN2835 nanosilica coated SOT5 lead, HTHH1767, U14, lead 2, 250x (ref. Board 284). 42

Figure 69: SEM image of PC40-UMF+10%NNN2835 nanosilica coated SOT5 lead, HTHH1767, U14, lead 2, 3,000x (ref. Board 284). 42

Figure 70: SEM image of PC40-UMF+10%NNN2835 nanosilica coated SOT5 lead, HTHH1767, U15, lead 5, 250x (ref. Board 284). 43

Figure 71: SEM image of PC40-UMF+10%NNN2835 nanosilica coated SOT5 lead, HTHH1767, U15, lead 5, 3,500x (ref. Board 284). 43

Figure 72: SEM image of PC40-UMF+10%NNN2835 nanosilica coated SOT5 lead, HTHH1767, U16, lead 1, 250x (ref. Board 284). 44

Figure 73: SEM image of PC40-UMF+10%NNN2835 nanosilica coated SOT5 lead, HTHH1767, U16, lead 1, 4000x (ref. Board 284). 44

Figure 74: SEM image of PC40-UMF+10%NNN2835 nanosilica coated SOT6 lead, HTHH1767, U65, lead 2, 300x (ref. Board 284). 45

Figure 75: SEM image of PC40-UMF+10%NNN2835 nanosilica coated SOT6 lead, HTHH1767, U65, lead 2, 4,500x (ref. Board 284). 45

Figure 76: SEM image of PC40-UMF+10%NNN2835 nanosilica coated SOT6 lead, HTHH1767, U66, lead 3, 500x (ref. Board 284). 46

Figure 77: SEM image of PC40-UMF+10%NNN2835 nanosilica coated SOT6 lead, HTHH1767, U66, lead 3, 4000x (ref. Board 284). 46

Figure 78: SEM image of PC40-UMF+30%NNN2835 nanosilica coated QFP44 leads, HTHH1767, U5, 40x (ref. Board 70). 47

Figure 79: SEM image of PC40-UMF+30%NNN2835 nanosilica coated QFP44 lead, HTHH1767, U5, lead 2, 120x (ref. Board 70). 47

Figure 80: SEM image of PC40-UMF+30%NNN2835 nanosilica coated QFP44 lead, HTHH1767, U5, lead 2, 1,000x (ref. Board 70). 48

Figure 81: SEM image of PC40-UMF+30%NNN2835 nanosilica coated QFP44 lead, HTHH1767, U5, lead 2, 3,500x (ref. Board 70). 48

Figure 82: SEM image of PC40-UMF+30%NNN2835 nanosilica coated QFP44 lead, HTHH1767, U5, lead 3, 1000x (ref. Board 70). 49

Figure 83: SEM image of PC40-UMF+30%NNN2835 nanosilica coated QFP44 lead, HTHH1767, U5, lead 44, 120x (ref. Board 70). 49

Figure 84: SEM image of PC40-UMF+30%NNN2835 nanosilica coated QFP44 lead, HTHH1767, U5, lead 44, 500x (ref. Board 70). 50

Figure 85: SEM image of PC40-UMF+30%NNN2835 nanosilica coated QFP44 lead, HTHH1767, U5, lead 44, 1800x (ref. Board 70). 50

Figure 86: SEM image of PC40-UMF+30%NNN2835 nanosilica coated QFP44 lead, HTHH1767, U5, lead 44, 4,000x (ref. Board 70). 51

Figure 87: SEM image of PC40-UMF+30%NNN2835 nanosilica coated SOT3 leads, HTHH1767, U49, 40x (ref. Board 269). 51

Figure 88: SEM image of PC40-UMF+30%NNN2835 nanosilica coated SOT3 lead, HTHH1767, U49, 400x (ref. Board 269). 52

Figure 89: SEM image of PC40-UMF+30%NNN2835 nanosilica coated SOT3 lead, HTHH1767, U49, lead 2, 300x (ref. Board 269). 52

Figure 90: SEM image of PC40-UMF+30%NNN2835 nanosilica coated SOT3 lead, HTHH1767, U49, lead 2, 2,500x (ref. Board 269). 53

Figure 91: SEM image of PC40-UMF+30%NNN2835 nanosilica coated SOT5 leads, HTHH1767, U04, 40x (ref. Board 269). 53

Figure 92: SEM image of PC40-UMF+30%NNN2835 nanosilica coated SOT5 lead, HTHH1767, U04, lead 3, 250x (ref. Board 269). 54

Figure 93: SEM image of PC40-UMF+30%NNN2835 nanosilica coated SOT5 lead, HTHH1767, U04, lead 3, 2500x (ref. Board 269). 54

Figure 94: SEM image of PC40-UMF+30%NNN2835 nanosilica coated SOT5 lead, HTHH1767, U15, lead 5, 250x (ref. Board 269). 55

Figure 95: SEM image of PC40-UMF+30%NNN2835 nanosilica coated SOT5 lead, HTHH1767, U15, lead 5, 5,000x (ref. Board 269). 55

Figure 96: SEM image of PC40-UMF+30%NNN2835 nanosilica coated SOT6 lead, HTHH1767, U65, lead 2, 500x (ref. Board 269). 56

Figure 97: SEM image of PC40-UMF+30%NNN2835 nanosilica coated SOT6 lead, HTHH1767, U65, lead 2, 3,500x (ref. Board 269). 56

Figure 98: SEM image of PC40-UMF+30%NNN2835 nanosilica coated SOT6 lead, HTHH1767, U65, lead 3, 500x (ref. Board 269). 57

Figure 99: SEM image of PC40-UMF+30%NNN2835 nanosilica coated SOT6 lead, HTHH1767, U65, lead 3, 3500x (ref. Board 269). 57

Figure 100: SEM image of PC40-UMF+30%NNN2835 nanosilica coated SOT6 lead, HTHH1767, U70, 30x (ref. Board 269). 58

Figure 101: SEM image of PC40-UMF+30%NNN2835 nanosilica coated SOT6 lead, HTHH1767, U70, lead 6, 400x (ref. Board 269). 58

Figure 102: SEM image of PC40-UMF+30%NNN2835 nanosilica coated SOT6 lead, HTHH1767, U70, lead 6, 500x (ref. Board 269). 59

Figure 103: SEM image of PC40-UMF+30%NNN2835 nanosilica coated SOT6 lead, HTHH1767, U70, lead 6, 4,000x (ref. Board 269). 59

Figure 104: SEM image of 1B31-LOC acrylic coated QFP44 lead, HTHH1767, U5, lead 44, 120x (ref. Board 85). 60

Figure 105: SEM image of 1B31-LOC acrylic coated QFP44 lead, HTHH1767, U5, lead 44, 1,200x (ref. Board 85). 61

Figure 106: SEM image of 1B31-LOC acrylic coated QFP44 lead, HTHH1767, U5, lead 44, 4,000x (ref. Board 85). 61

Figure 107: SEM image of 1B31-LOC acrylic coated QFP44 lead, HTHH1767, U5, lead 10, 120x (ref. Board 85). 62

Figure 108: SEM image of 1B31-LOC acrylic coated QFP44 lead, HTHH1767, U5, lead 10, 500x (ref. Board 85). 62

Figure 109: SEM image of 1B31-LOC acrylic coated QFP44 lead, HTHH1767, U5, lead 10, 500x (ref. Board 85). 63

Figure 110: SEM image of 1B31-LOC acrylic coated QFP44 lead, HTHH1767, U5, lead 10, 4500x (ref. Board 85). 63

Figure 111: SEM image of 1B31-LOC acrylic coated SOT5 leads, HTHH1767, 40x (ref. Board 288). ... 64

Figure 112: SEM image of 1B31-LOC acrylic coated SOT5 lead, HTHH1767, 500x (ref. Board 288).... 64

Figure 113: SEM image of an uncoated SOT5 lead (lead 2), ATC+ HTHH1000, 100x (ref. board 238 Figure 4). Corrosion near the bottom of the joint and whisker growth from the boundary between tin grains were observed. 67

Figure 114: SEM image of uncoated TQFP64 leads, ATC+HTHH2000, 100x (ref. board 46 Figure 6)... 67

Figure 115: SEM image of uncoated QFP64 lead toes, HTHH2000, 100x (ref. Board 48 Figure 10)..... 67

Figure 116: SEM image of PC18M-mod coated SOT6 lead (lead 3), ATC + 2000HTHH, 150x, small bubble density (ref. Board 215 Figure 22)..... 68

Figure 117: SEM image of PC18M+20%XP2742 nanosilica coated SOT3 lead (lead 2), ATC+HTHH2000, 100x and 300x, medium bubble density (ref. Board 235 Figure 25)..... 68

Figure 118: SEM image of PC18M+20%X11102PMA nanoalumina, SOT6, lead 4 (center lead from Figure 23), ATC+HTHH2000, 100x, small/no bubble density (ref. Board 228 Figure 32). 69

Figure 119: SEM image of PC40-UMF coated QFP44 lead side, HTHH1767, QFP44, U4, lead 12, 1,000x (ref. Board 60 Figure 42). 69

Figure 120: SEM image of PC40-UMF+10%NNN2835 nanosilica coated SOT5 lead, HTHH1767, U16, lead 1, 4000x (ref. Board 284 Figure 73). 69

Figure 121: SEM image of PC40-UMF+30%NNN2835 nanosilica coated QFP44 lead, HTHH1767, U5, lead 44, 4,000x (ref. Board 70 Figure 86). 70

Figure 122: SEM image of 1B31-LOC acrylic coated QFP44 lead, HTHH1767, U5, lead 44, 4,000x (ref. Board 85 Figure 106)..... 70

Figure 123: SEM image of Parylene™ C SOT3 leads, ATC + 2000HTHH, 40x (ref. Board 209 Figure 33)..... 70

Figure 124: SEM image of a Parylene™ C & Adpro+ coated SOT3 lead, ATC+HTHH1000, 100x and 350x (ref. Board 204 Figure 35). Small coating crack evident at lead-to-package interface. 71

Figure 125: Schematic illustrating whisker buckling in a coating bubble. 72

Appendix H: List of Tables

Table 1: PC40-UMF base coating assembly whisker inspection summary. 24
Table 2: 1B31-LOC acrylic reference coating assembly whisker inspection summary. 60
Table 3: Comparison of baseline assembly coatings after environmental testing. 66

1. Introduction

The goal of the assembly whisker testing was to determine the coating whisker mitigation performance on actual assemblies with three dimensional features that are challenging to coat uniformly. The PC18M based coatings were evaluated in the first test group with uncoated assemblies and Parylene C ™ coated assemblies for reference. The low VOC PC40-UMF based coatings were evaluated in the second test group with Humiseal 1B31 acrylic coated boards as a control. The small outline transistor (SOT) and quad flat pack (QFP) boards were inspected with the scanning electron microscope (SEM) at various points in the environmental testing. The SOT3 and SOT6 parts have alloy-42 (Fe42Ni) leads and the remaining parts, SOT5, QFP44, QFP64 and plastic leaded chip carrier (PLCC) have copper alloy leads.

2. Baseline PC18M based coatings samples and environmental testing

The three PC18M-mod coating variations evaluated, each having an initial thinned PC18M-mod dip that was partially cured. Then the following spray coatings were applied on the dip coating layer; (1) PC18M-mod, (2) PC18M-mod+20%XP2742 nanosilica, and PC18M+20%X11102PMA nanoalumina coating. The following reference assemblies were tested at the same time: (1) uncoated and (2) Parylene C ™ coated assemblies with and without the Adpro + adhesion promoter. The boards were exposed to accelerated thermal cycling (ATC) and/or high temperature high humidity (HTHH). The following nomenclature was used to describe the conditions:

- **ATC:** 100 cycles -55 to +125°C followed by 233 cycles -20 to +80°C
- **ATC+HTHH1000:** 100 cycles -55 to +125°C followed by 233 cycles -20 to +80°C followed by 1,000 hours 85°C/85% Relative Humidity (RH)
- **ATC+HTHH2000:** 100 cycles -55 to +125°C followed by 233 cycles -20 to +80°C followed by 2,000 hours 85°C/85%RH
- **HTHH2000:** 2,000 hours 85°C/85%RH

2.1 Uncoated control assembly test results

The SEM images from the whisker inspection are shown in Figure 1 to Figure 15. The examination after ATC of the uncoated control boards showed that the alloy-42 lead terminations had more tin growths and solder steps (Figure 1 – Figure 3) than the Cu lead terminations. Inspections after the addition of 1,000 hours HTHH after ATC showed increased corrosion (Figure 4) that resulted whisker growth at the boundaries between tin grains even without a significant solder step (Figure 4). When ATC was followed by longer humidity exposure (ATC+HTHH2000), the lead terminations exhibited more whisker growth and more corrosion (Figure 5 and Figure 6). Only performing humidity, HTHH2000, was sufficient for whisker growth (Figure 7 to Figure 15).



Figure 1: SEM image of an uncoated SOT6 lead, ATC, 180x (ref. board 237). Whiskers growing from top and lower solder fillet regions.

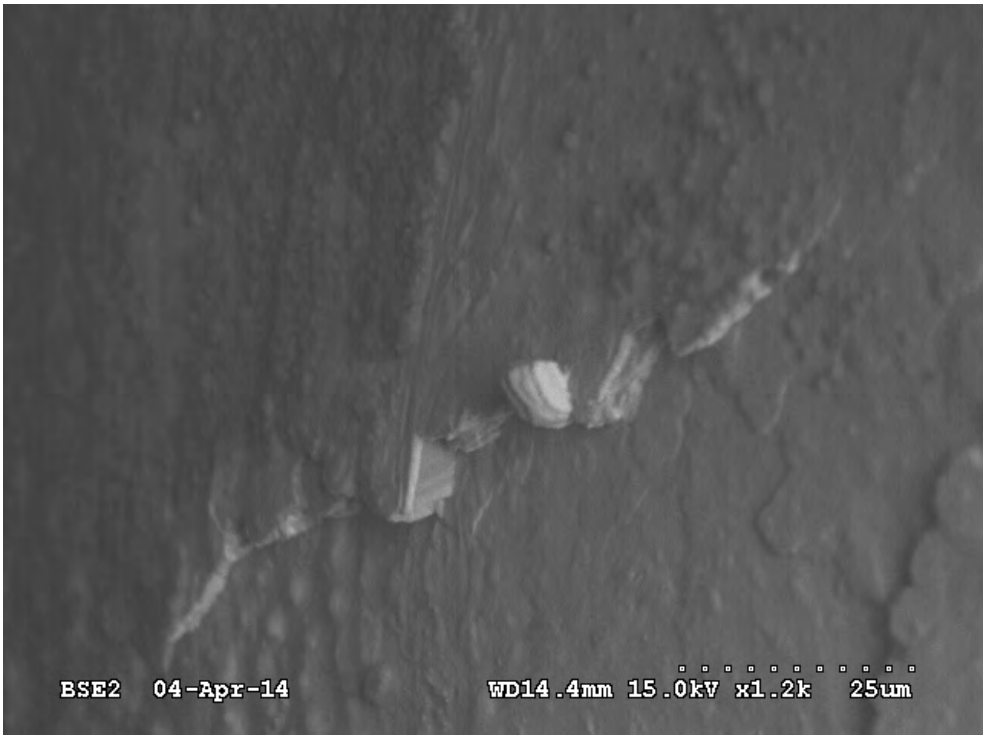


Figure 2: SEM image of an uncoated SOT3 lead, ATC, 1,000x (ref. board 237). Whisker growth occurred from a solder step between two tin grains.



Figure 3: SEM image of an uncoated SOT6 lead, ATC, 1,000x (ref. board 237).

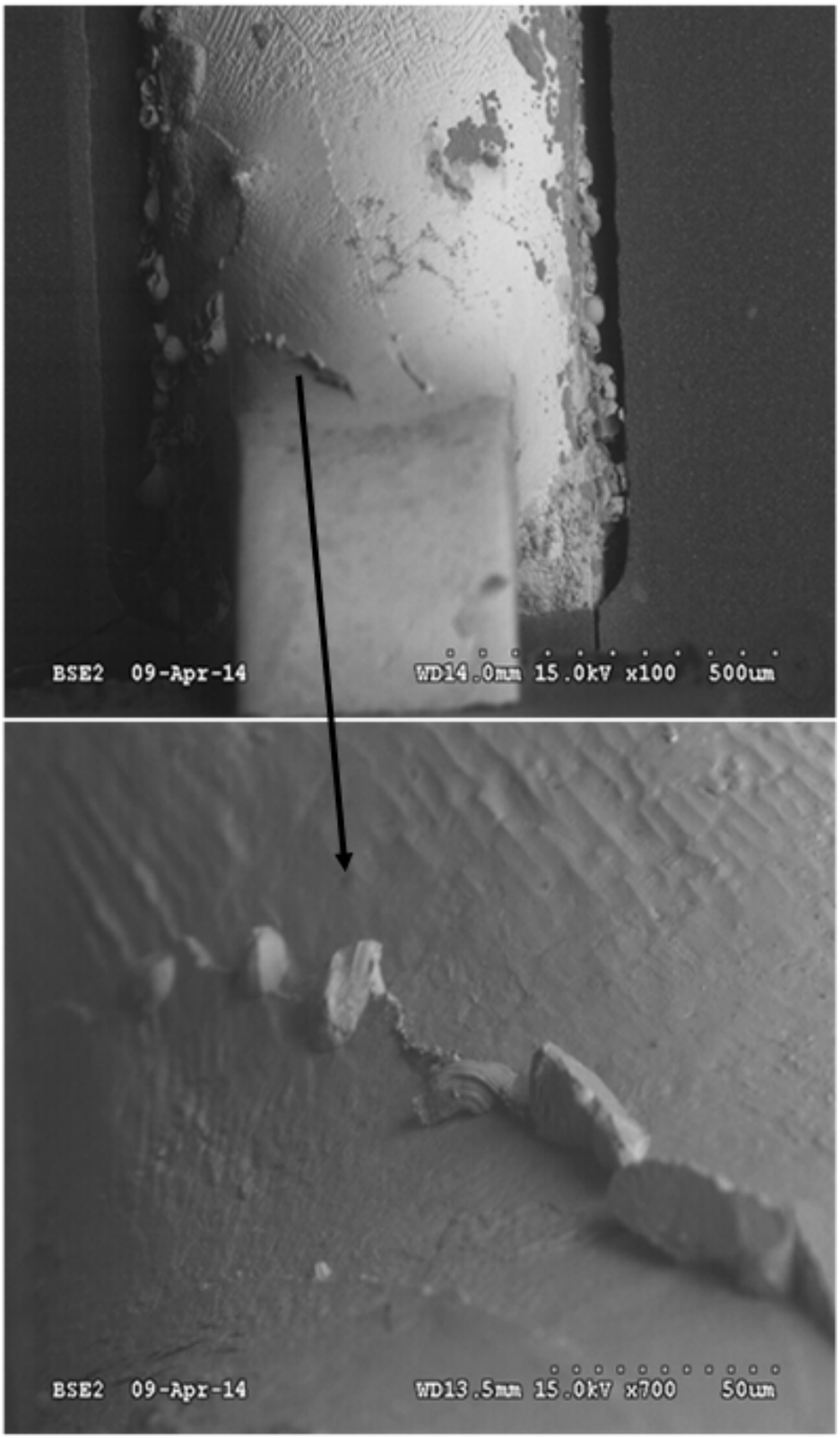


Figure 4: SEM image of an uncoated SOT5 lead (lead 2), ATC+ HTHH1000, 100x (ref. board 238). Corrosion near the bottom of the joint and whisker growth from the boundary between tin grains were observed.

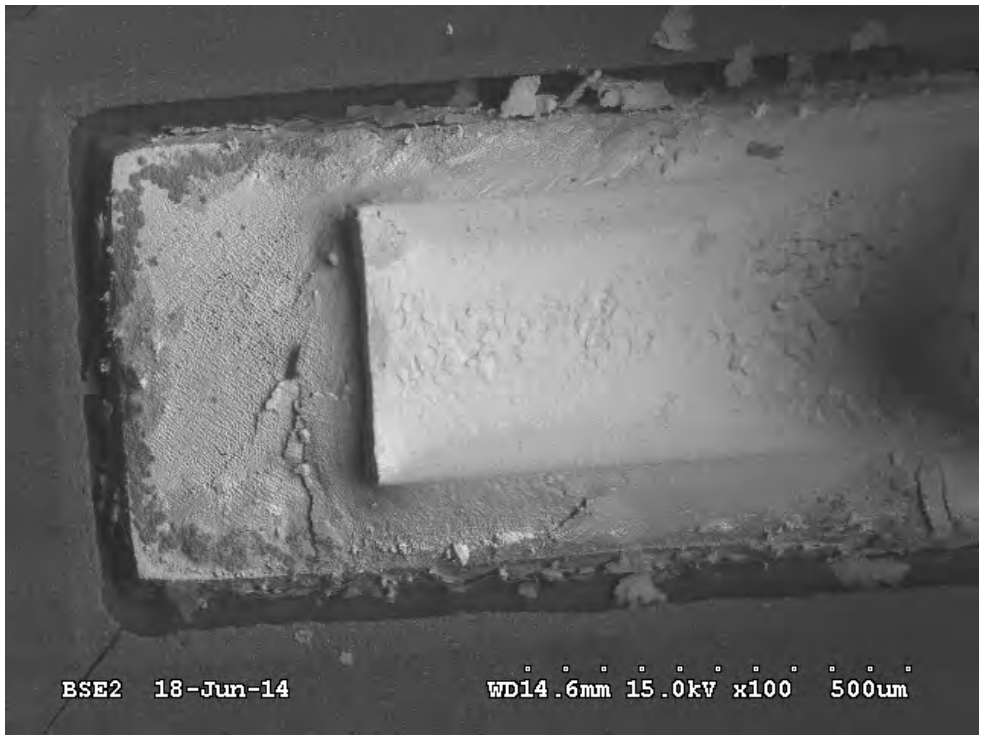


Figure 5: SEM image of an uncoated QFP44 lead, ATC+HTHH2000, 100x (ref. board 46).

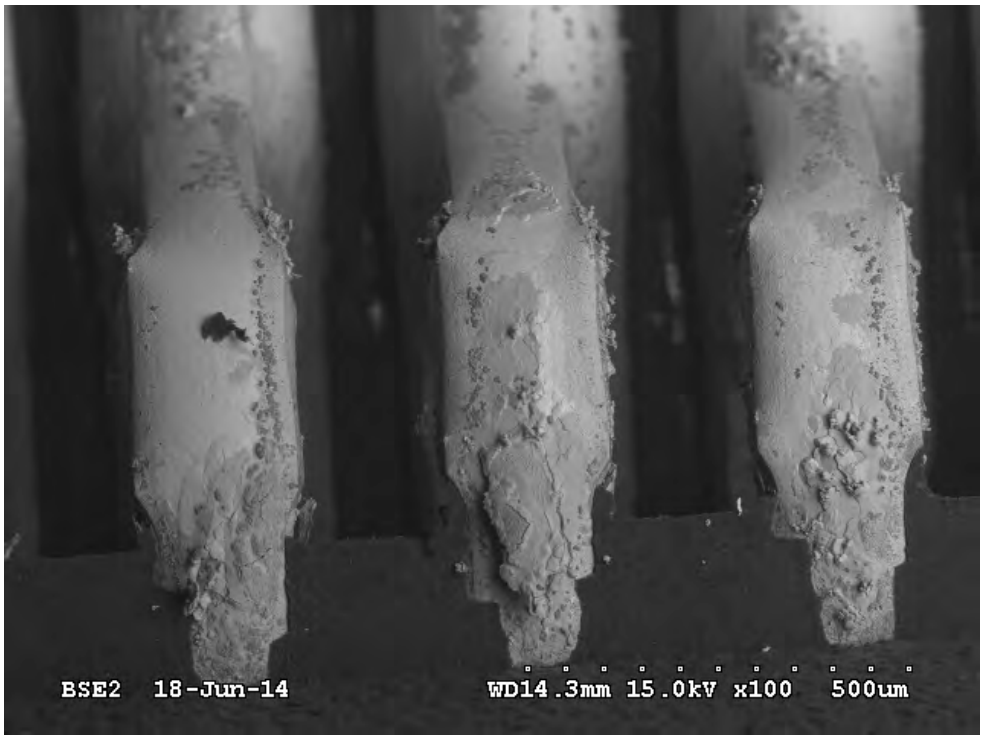


Figure 6: SEM image of uncoated TQFP64 leads, ATC+HTHH2000, 100x (ref. board 46).

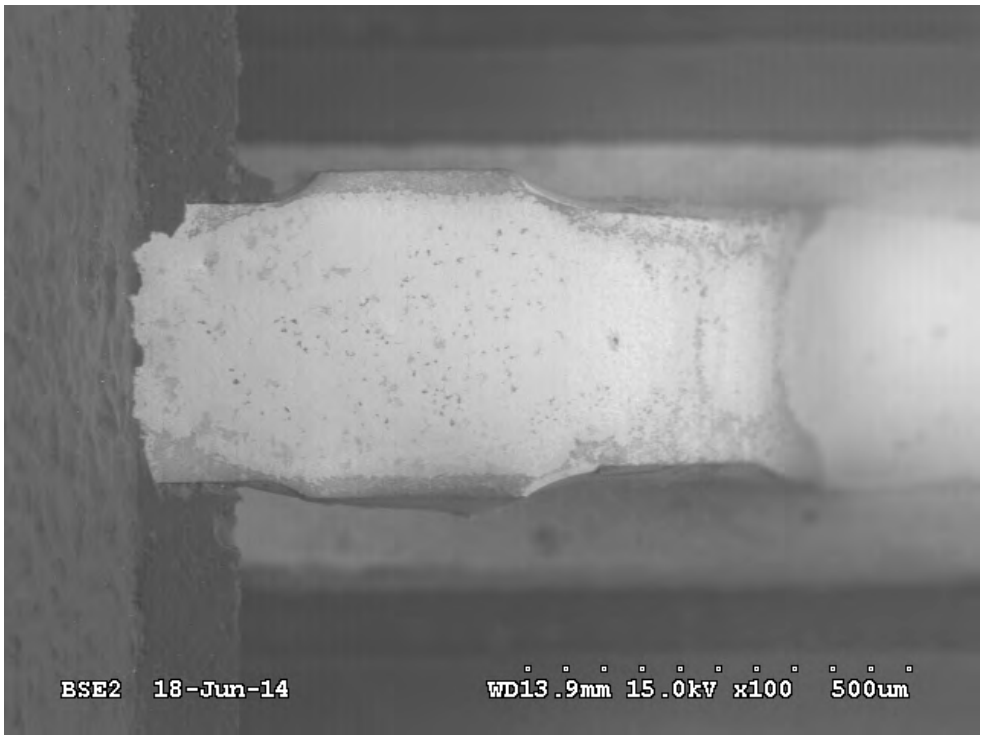


Figure 7: SEM image of an uncoated QFP44 lead top, HTHH2000, 100x (ref. Board 48).

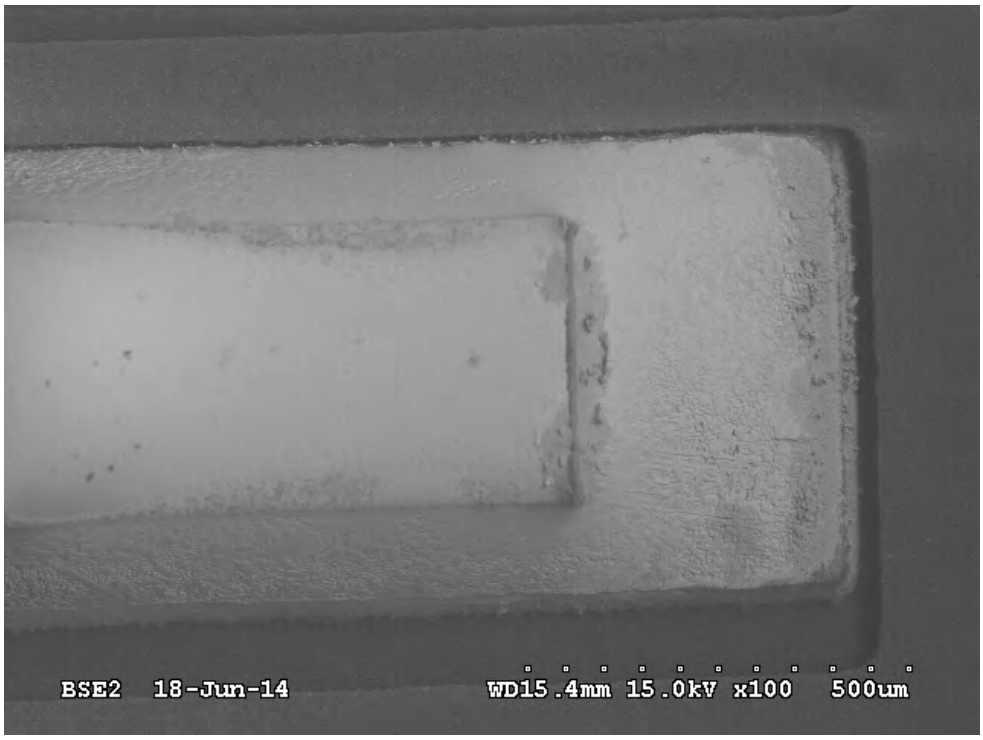


Figure 8: SEM image of an uncoated QFP44 lead toe, HTHH2000, 100x (ref. Board 48).



Figure 9: SEM image of uncoated QFP64 top of leads, HTHH2000, 100x (ref. Board 48).

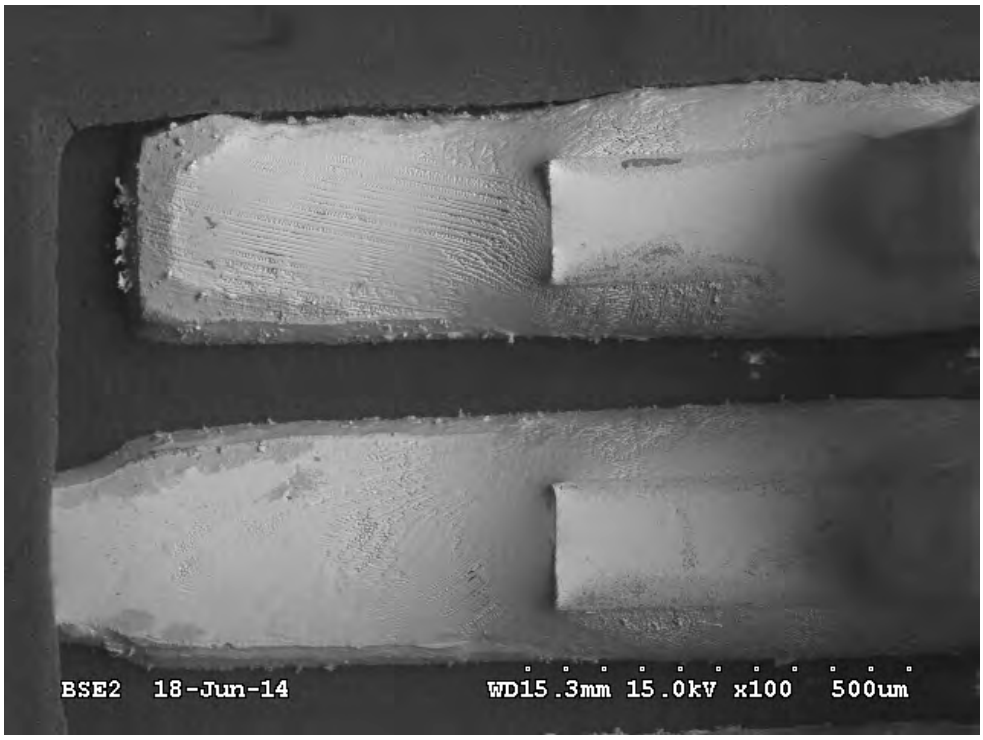


Figure 10: SEM image of uncoated QFP64 lead toes, HTHH2000, 100x (ref. Board 48).



Figure 11: SEM image of an uncoated QFP64 lead whisker growth, HTHH2000, 1500x (ref. Board 48).



Figure 12: SEM image of an uncoated QFP64 lead whisker growth, HTHH2000, 2000x (ref. Board 48).

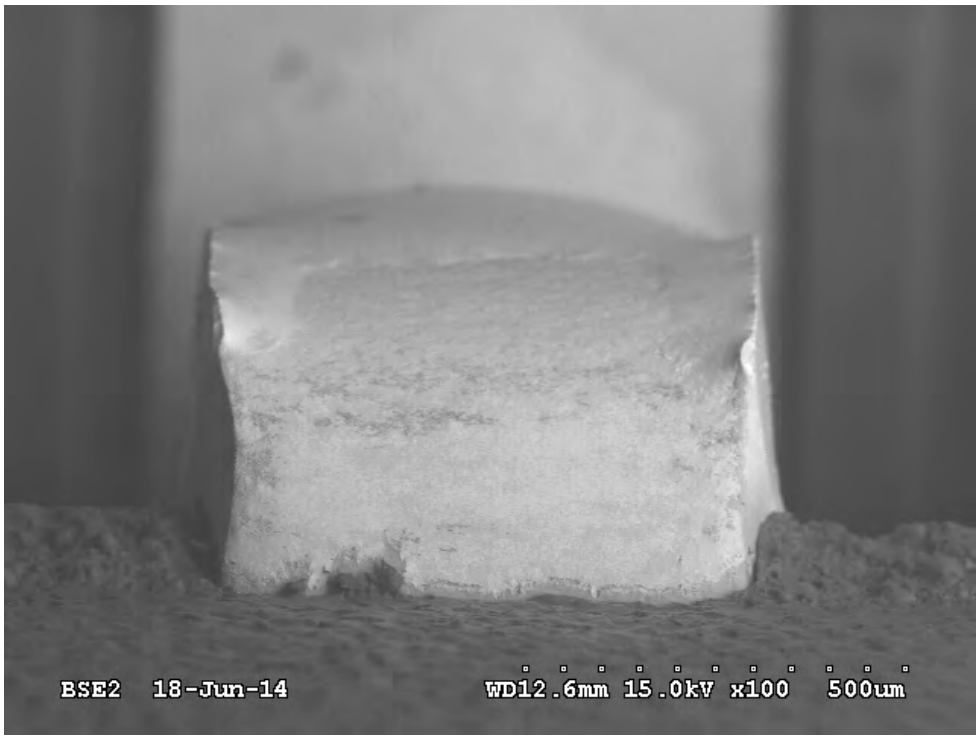


Figure 13: SEM image of an uncoated QFP board PLCC lead, HTHH2000, 100x (ref. Board 48).

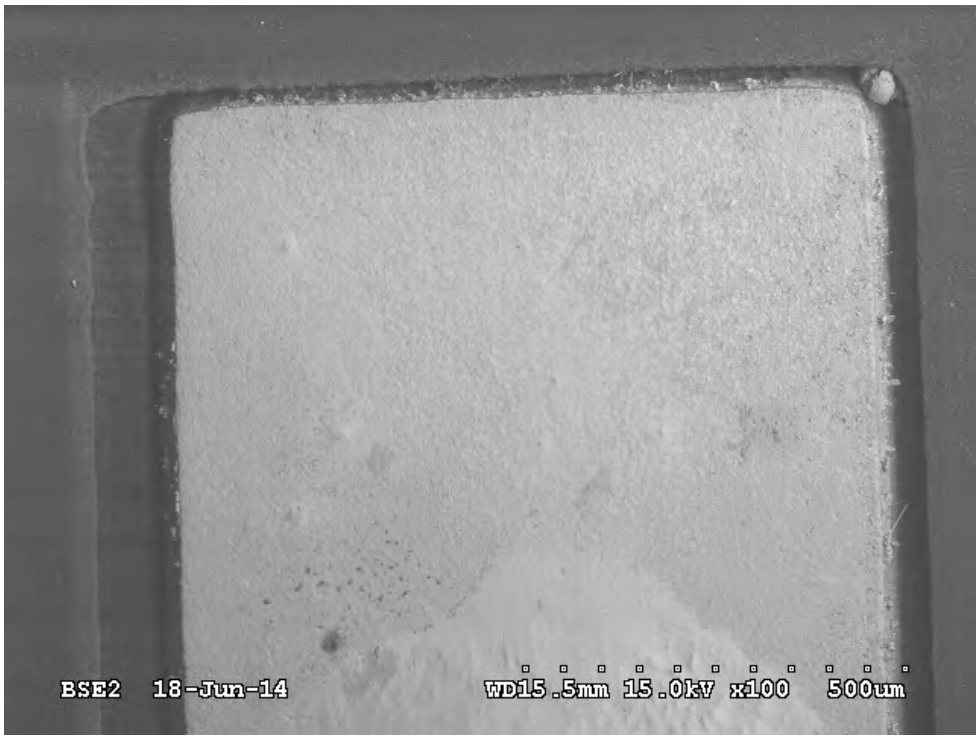


Figure 14: SEM image of an uncoated QFP board PLCC pad whiskering, HTHH2000, 100x, (ref. Board 48).



Figure 15: SEM image of an uncoated QFP board PLCC pad whisker, HTHH2000, 1000x (ref. Board 48).

2.2 PC18M based coatings whisker test results

The selected images from the SEM inspection results are given in Figure 16 to Figure 22 for the PC18M-mod, Figure 23 to Figure 27 for the PC18M+20%XP2742 nanosilica, and Figure 28 to Figure 32 for the PC18M+20%X11102PMA nanoalumina. The coated assemblies exhibited very little whisker growth or corrosion on the boards that went through ATC or ATC followed by HTHH. As was observed with the coupon tests, the whisker growth occurred where the coating was thin around the lead corners on the spray coated Polyurethane (PU) samples. Some of the spray coatings exhibited cracking after environmental exposure. The PC18M+20%X11102PMA nanoalumina did not crack, the PC18M+20%XP2742 nanosilica exhibited some cracking, and the PC18M-mod had greatest numbers of cracked coating regions. Generally, samples with good coverage without coating cracks showed no whisker growth or corrosion after ATC (Figure 28 and Figure 23) or after ATC+HTHH2000 (Figure 31 – Figure 34).

In some cases of conformal coat crack widths up to 100 microns were observed. The majority of the cases were on the unfilled PC18M-mod coated low thermal expansion leads after ATC (Figure 17 and Figure 16). After ATC+HTHH, coating cracking was observed both on alloy-42 lead and on Cu lead terminations (Note that large bubble density caused stress concentrations that resulted in more cracking) (Figure 19). The coating cracks did not generally grow from the exposed metal regions (Figure 20 and Figure 21). Note that the thin coating over the lead tip had instances of tin growth through the surface (Figure 21 and Figure 22). Not all lead termination coated with the PC18M-mod coating exhibited cracking (Figure 18).

Less cracks formed in the PC18M+20%XP2742 nanosilca coating. After ATC, a chip resistor (low thermal expansion ceramic) exhibited cracks around the perimeter (Figure 24), but there were no

cracks on the alloy-42 SOT6 (Figure 23). A small crack was observed in the PC18M+20%XP2742 nanosilica coated alloy-42 SOT3 after ATC+HTHH2000 (Figure 25).

The Parylene™ C with Adpro+ exhibited some instances of very small cracking (approximately one micron wide) at the lead-to-package interface (Figure 35) after thermal cycling. There were no whiskers or eruptions present in the microcrack region, and the crack may not go all the way to the underlying metal. The coating supplier indicated that small cracks can occur during assembly thermal cycling from the stresses arising from the various material thermal expansion coefficients. The enhanced Parylene™ C adhesion from the Adpro+ causes the substrate stresses to be transferred into the coating. Without the Adpro+, small regions of Parylene™ C debonding from the surface would likely occur in the high stress regions. A thinner Parylene™ C would be less susceptible to this type of cracking. Microcracking might be avoided with a 10 – 15 micron, rather than a 25 micron, thick coating when coated parts are subjected to high stress accelerated aging conditions.

There were no cracks observed during the SEM examination on any of the PC18M+20%X11102PMA nanoalumina samples.

2.2.1 SEM inspection of unfilled PC18M-mod

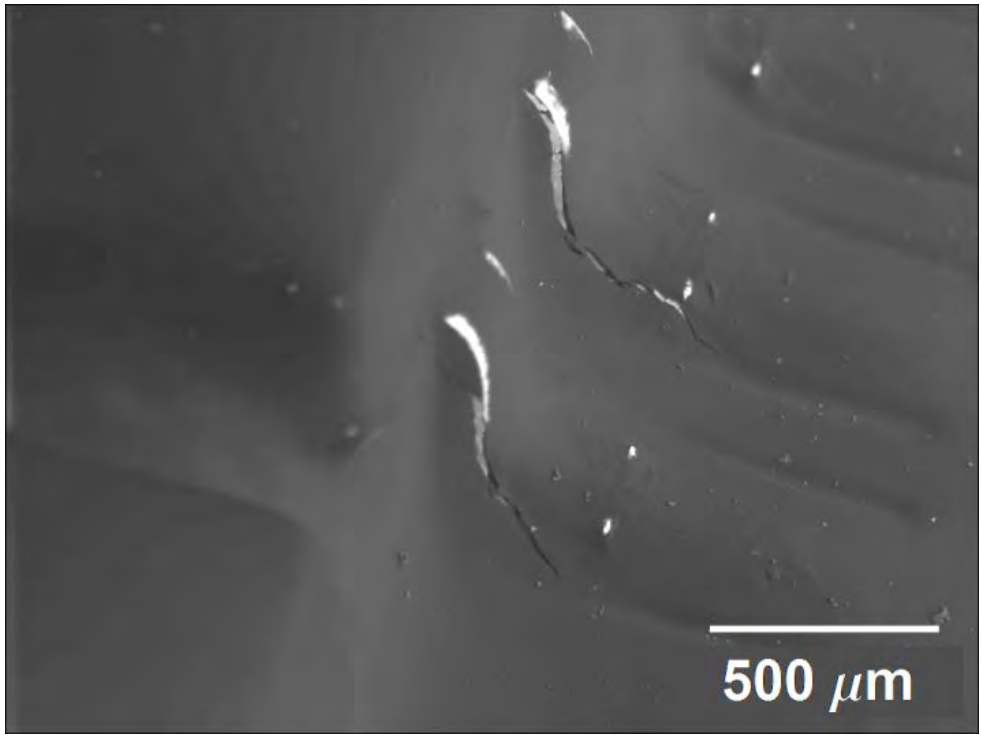


Figure 16: SEM image of PC18M-mod coated SOT6 leads, ATC. 60x, small bubble density (ref. Board 211).

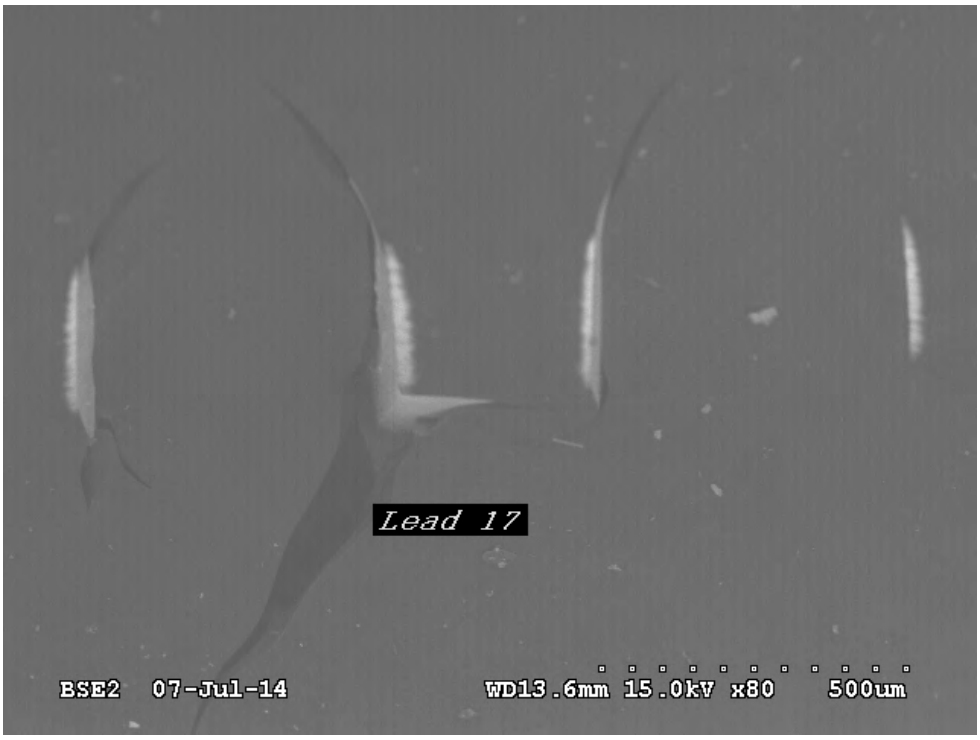


Figure 17: SEM image of PC18M-mod coated QFP44 leads, ATC, U2, Lead 17, 80x, large bubble density (ref. Board 34).



Figure 18: SEM image of PC18M-mod coated QFP44 leads, U2, Lead 14-15, ATC + 1000HTHH, 60x, small bubble density (ref. Board 15).



Figure 19: SEM image of PC18M-mod coated SOT package and leads, ATC+ HTHH1000, 40x (ref. Board 233). Large bubble density condition causing the coating to obscure the SOT leads.



Figure 20: SEM image of PC18M-mod coated SOT5 lead, ATC + 2000HTHH, 400x, small bubble density (ref. Board 215).

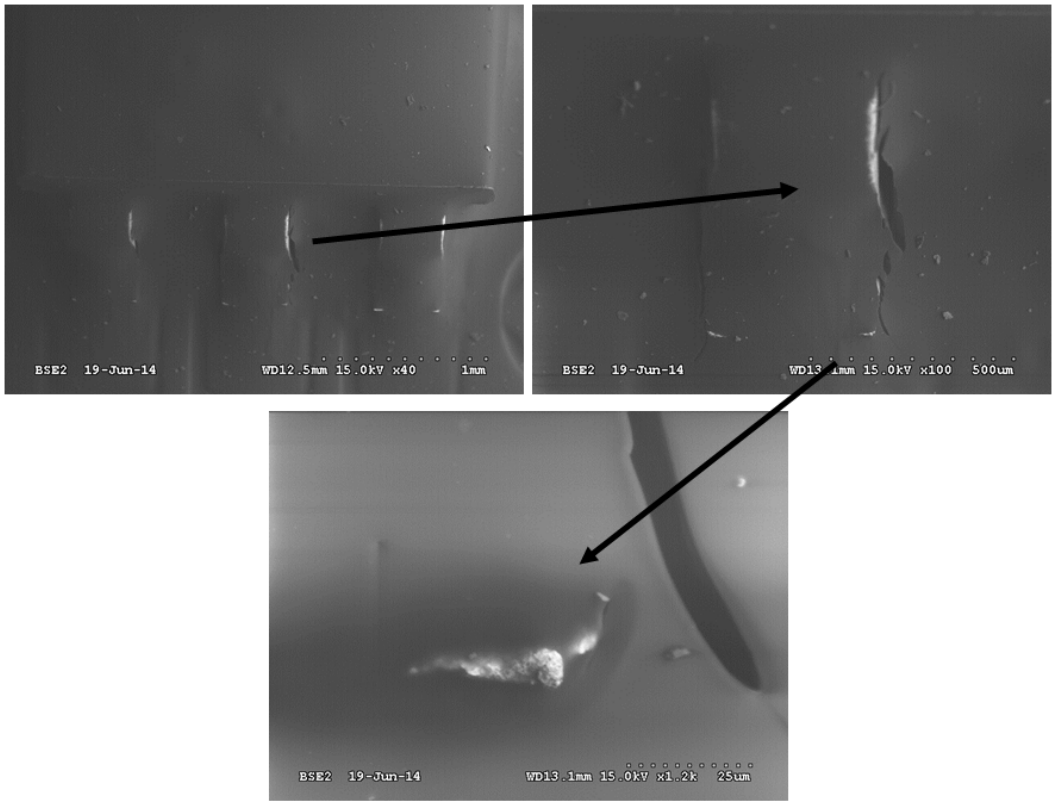


Figure 21: SEM image of PC18M-mod coated SOT5 leads, ATC+ HTHH2000, 40x, small bubble density (ref. Board 215).

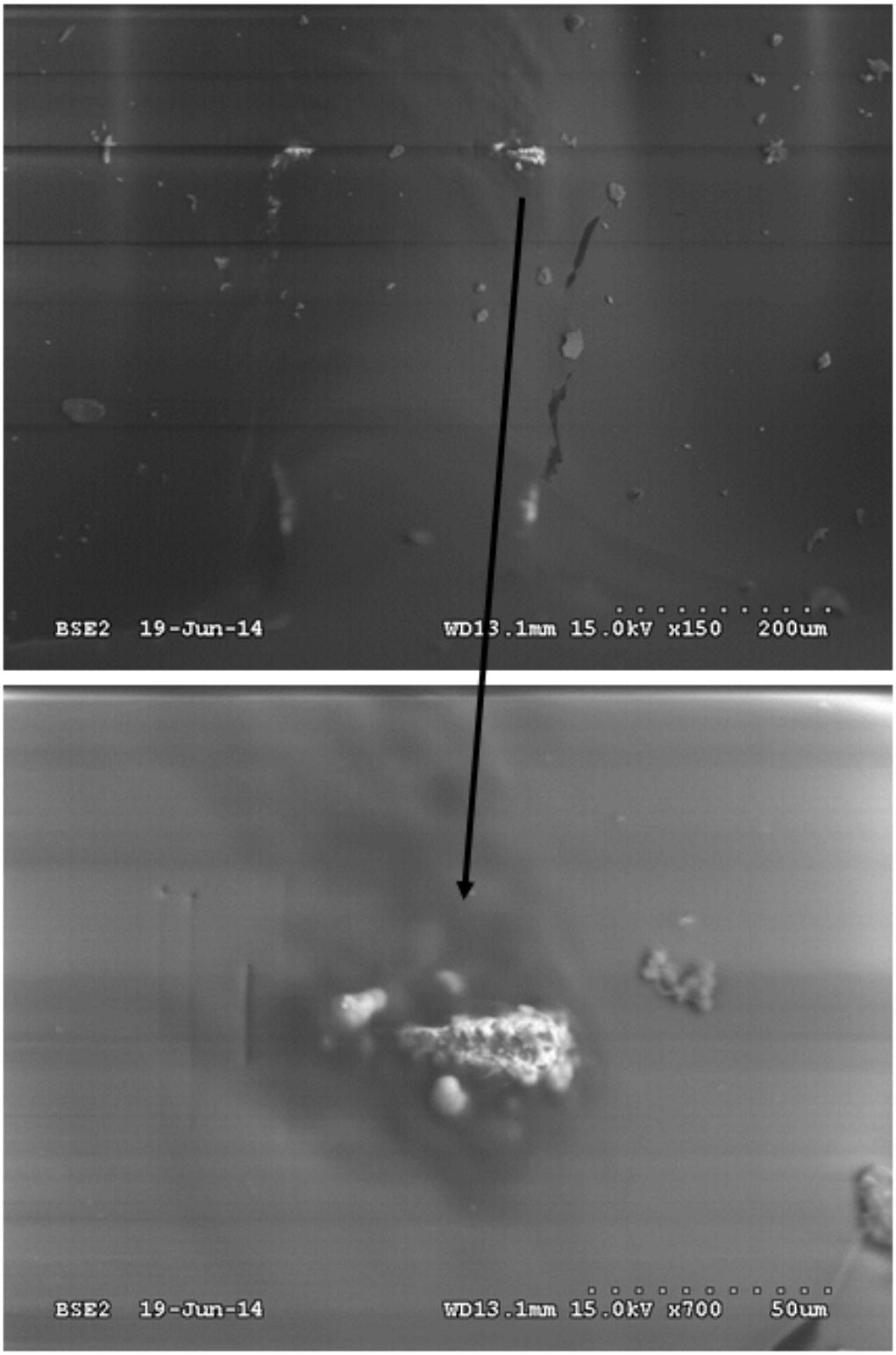


Figure 22: SEM image of PC18M-mod coated SOT6 lead (lead 3), ATC + 2000HTHH, 150x, small bubble density (ref. Board 215).

2.2.2 SEM inspection of PC18M+20%XP2742 nanosilica

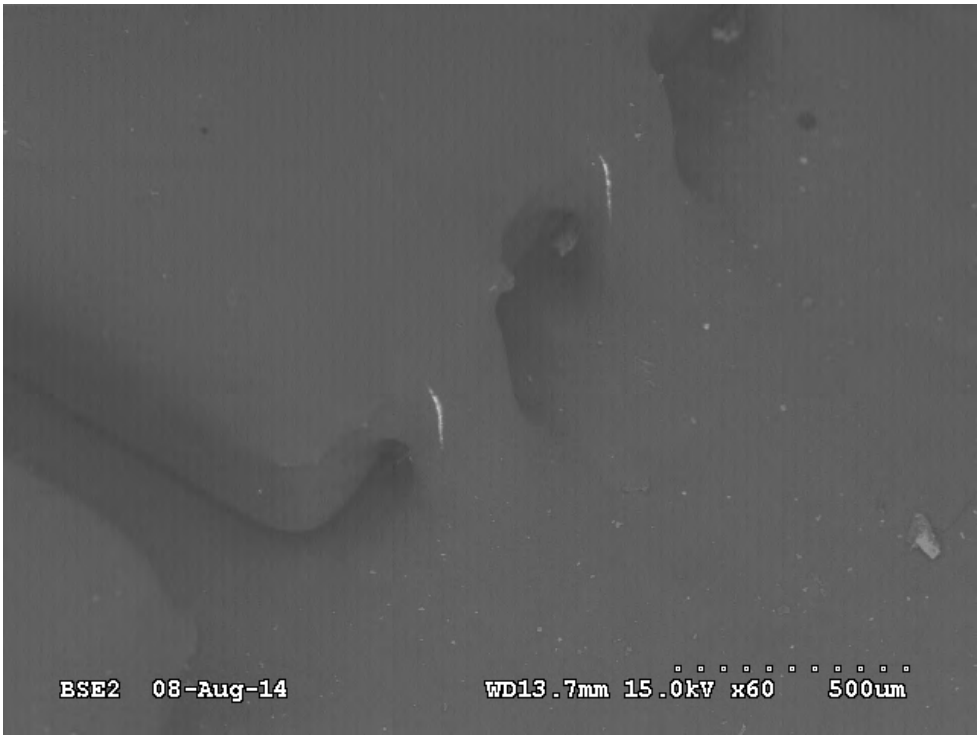


Figure 23: SEM image of PC18M+20%XP2742 nanosilica coated SOT6 leads, ATC, 60x, medium coating bubble density (ref. Board 217).

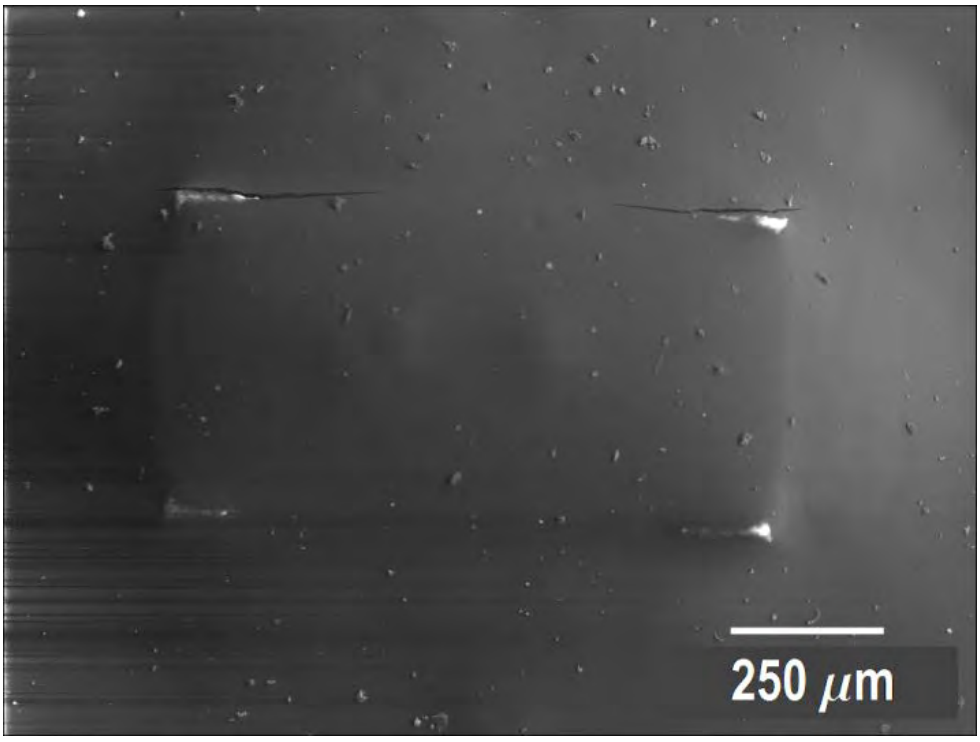


Figure 24: SEM image of PC18M+20%XP2742 nanosilica coated chip resistor, ATC, 80x, medium coating bubble density (ref. Board 217).

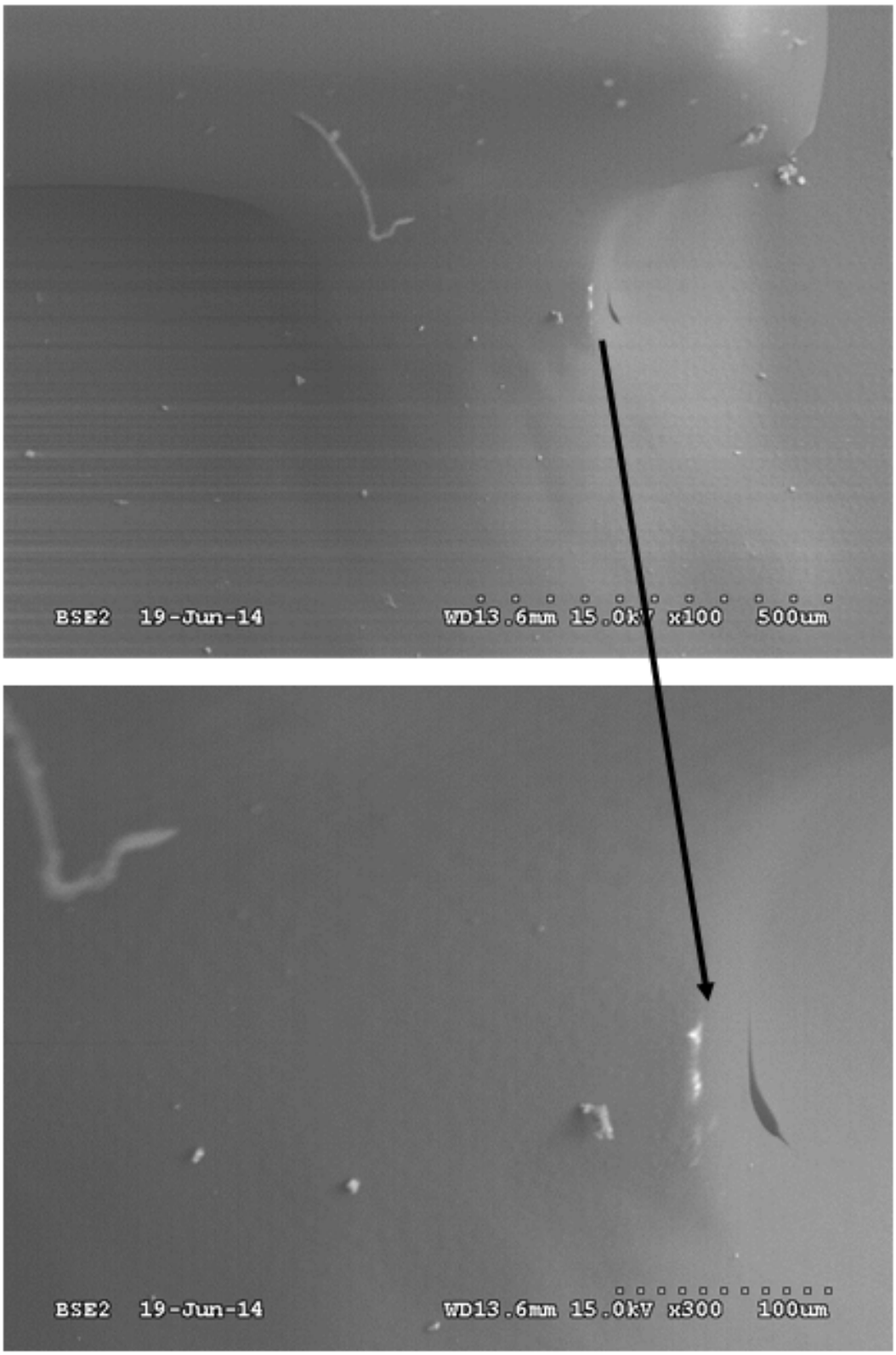


Figure 25: SEM image of PC18M+20%XP2742 nanosilica coated SOT3 lead (lead 2), ATC+HTHH2000, 100x and 300x, medium bubble density (ref. Board 235).

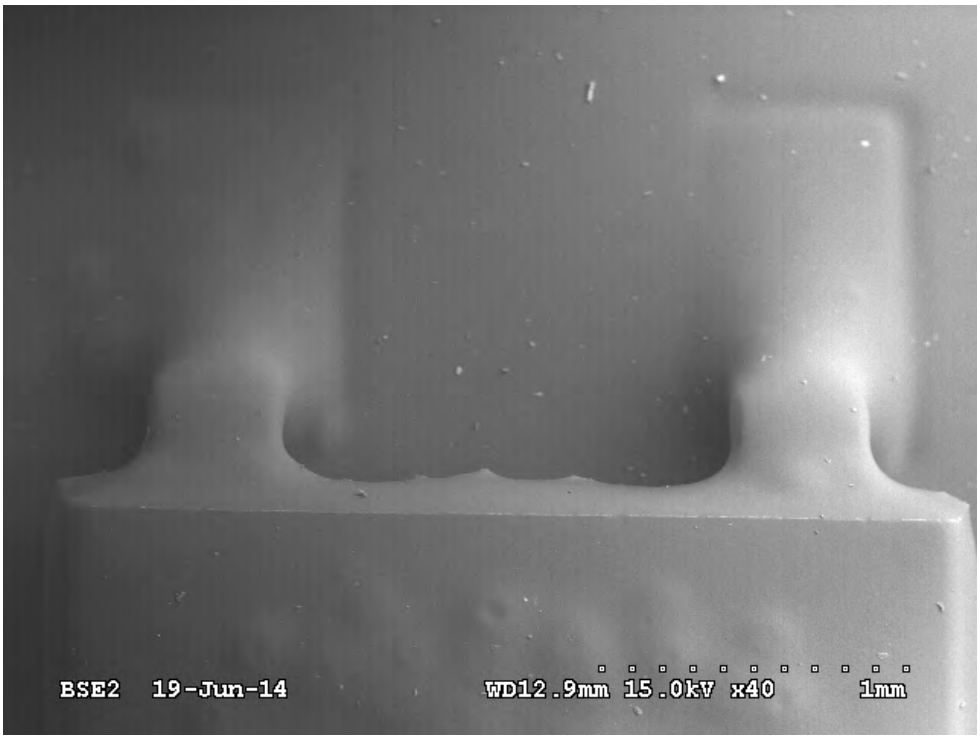


Figure 26: SEM image of PC18M+20%XP2742 nanosilica coated SOT5 leads, ATC+HTHH2000, 40x, medium bubble density (ref. Board 235).

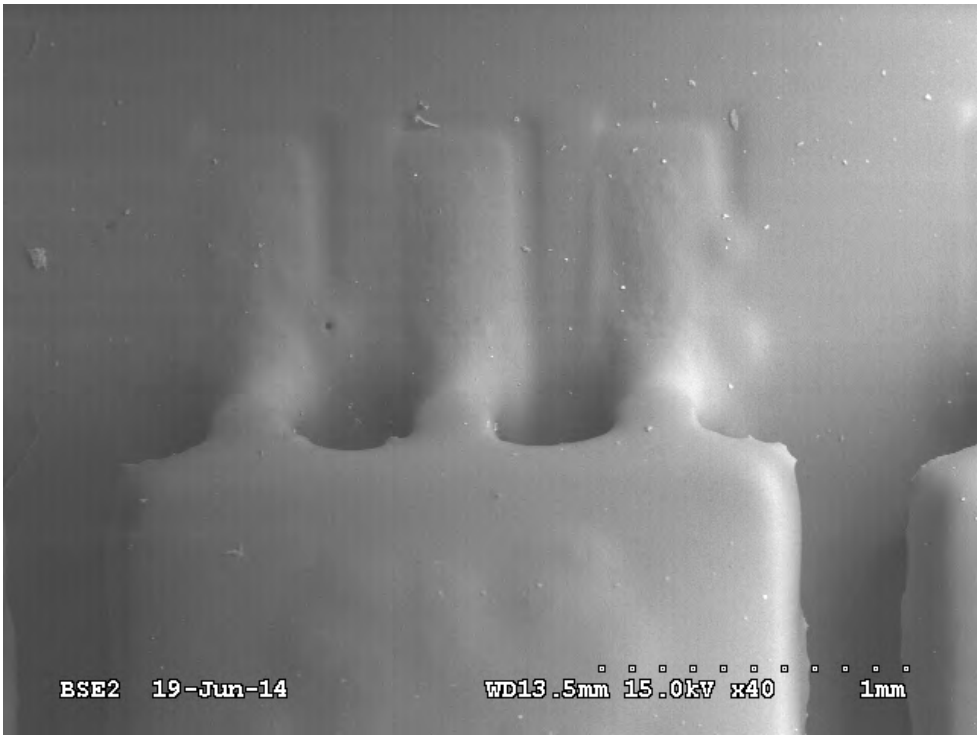


Figure 27: SEM image of PC18M+20%XP2742 nanosilica coated SOT6 leads, ATC+ 2000HTHH, 40x, medium bubble density (ref. Board 235).

2.2.3 SEM inspection of PC18M+20%X11102PMA nanoalumina

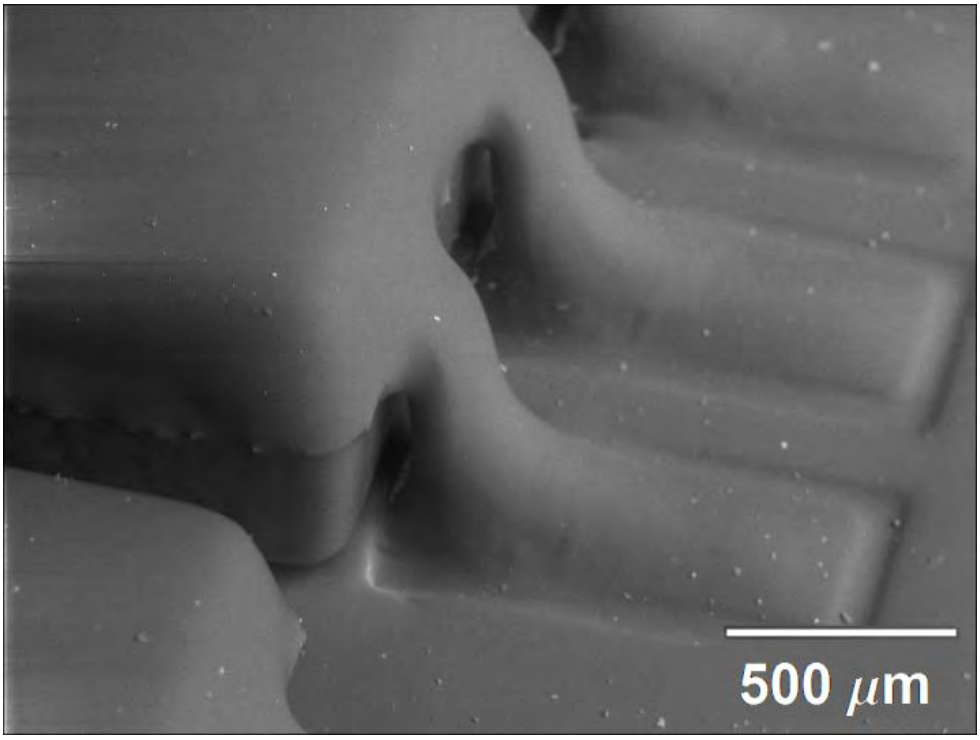


Figure 28: SEM image of PC18M+20%X11102PMA nanoalumina coated SOT6 leads, ATC, 60x, small/no bubble density (ref. Board 222).

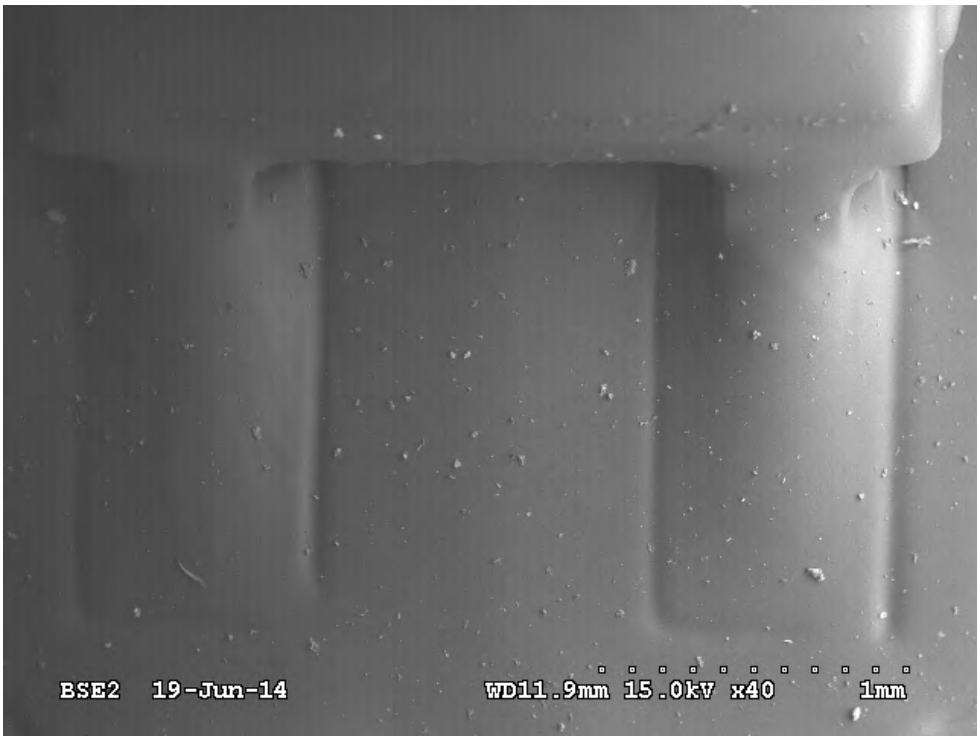


Figure 29: SEM image of PC18M+20%X11102PMA nanoalumina coated SOT3 leads, ATC+HTHH2000, 40x, small/no bubble density (ref. Board 228).

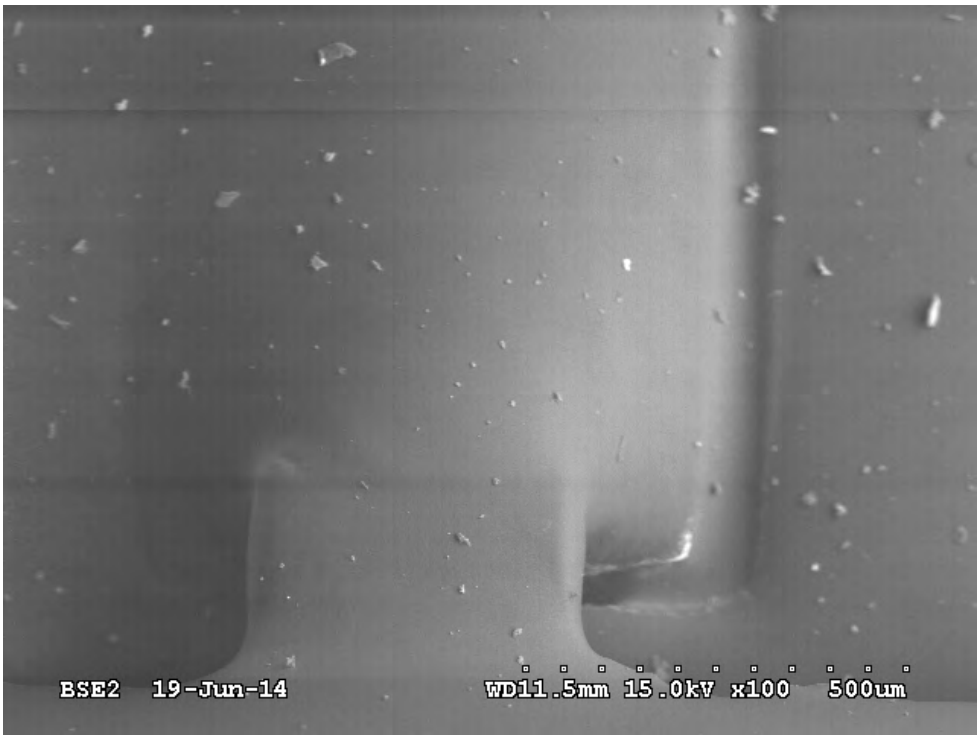


Figure 30: SEM image of PC18M+20%X11102PMA nanoalumina coated SOT3 lead, ATC + 2000HTHH, 100x, small/no bubble density (ref. Board 228).

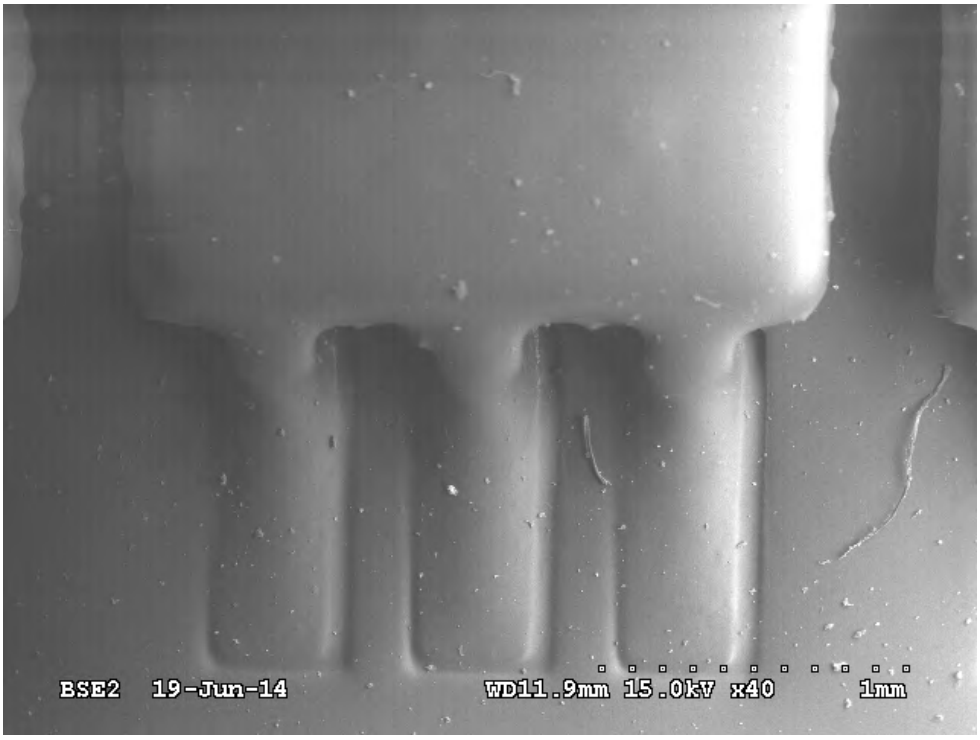


Figure 31: SEM image of PC18M+20%X11102PMA nanoalumina coated SOT6 lead, ATC + 2000HTHH, 40x, small/no bubble density (ref. Board 228).



Figure 32: SEM image of PC18M+20%X11102PMA nanoalumina, SOT6, lead 4 (center lead from Figure 23), ATC+HTHH2000, 100x, small/no bubble density (ref. Board 228).

2.3 Parylene reference coating during baseline PC18M whisker test results

Good coating integrity and no whisker growth was observed on either the Parylene ™ C or the Parylene ™ C with Adpro+ (Figure 33 and Figure 34). However, the Parylene™ C with Adpro+ exhibited some instances of very small cracking (approximately one micron wide) at the lead-to-package interface (Figure 35) after thermal cycling. There were no whiskers or eruptions present in the microcrack region, and the crack may not go all the way to the underlying metal. The coating supplier indicated that small cracks can occur during assembly thermal cycling from the stresses arising from the various material thermal expansion coefficients. The enhanced Parylene™ C adhesion from the Adpro+ causes the substrate stresses to be transferred into the coating. Without the Adpro+, small regions of Parylene™ C debonding from the surface would likely occur in the high stress regions. A thinner Parylene™ C would be less susceptible to this type of cracking. Microcracking might be avoided with a 10 – 15 micron, rather than a 25 micron, thick coating when coated parts are subjected to high stress accelerated aging conditions.

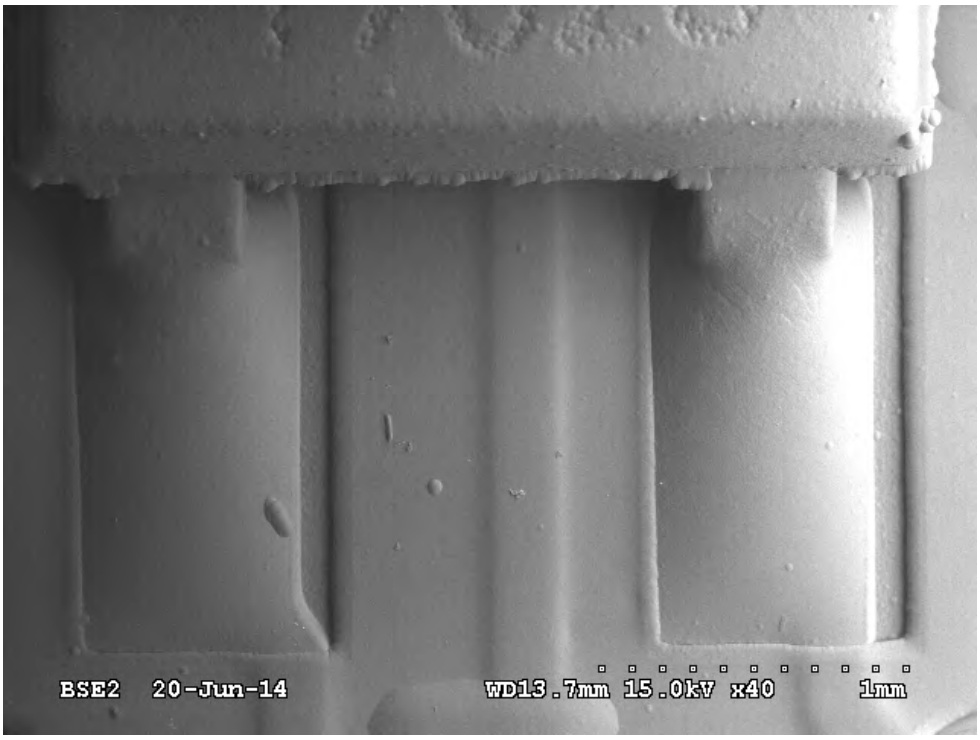


Figure 33: SEM image of Parylene™ C SOT3 leads, ATC + 2000HTHH, 40x (ref. Board 209).

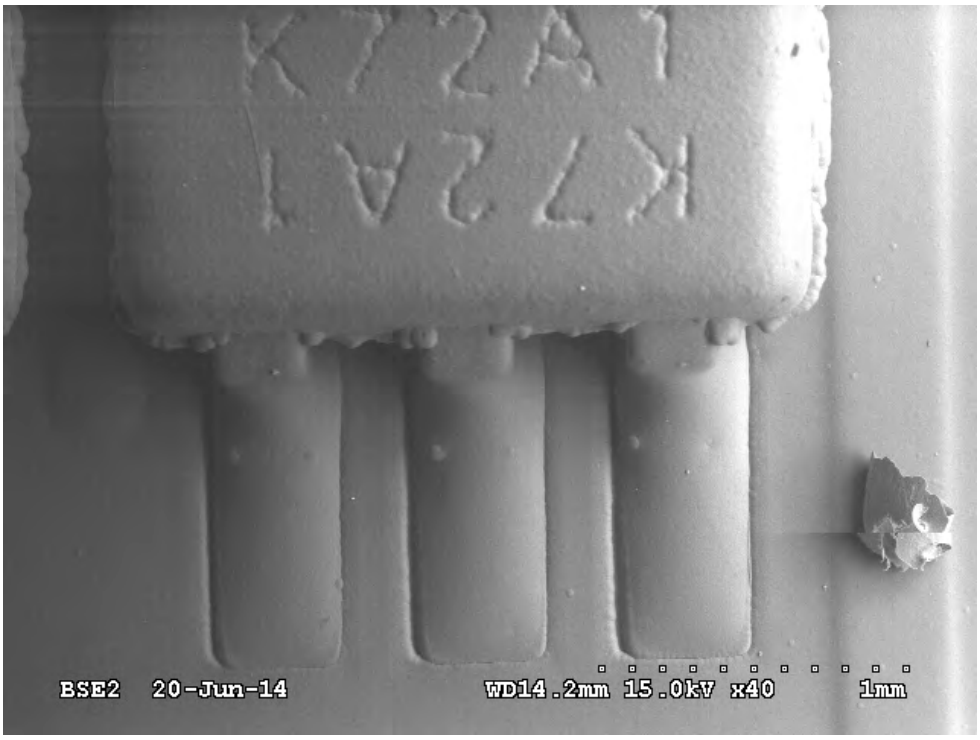


Figure 34: SEM image of Parylene™ C with Adpro+ coated SOT6 leads, ATC+ 2000HTHH, 40x (ref. Board 206).

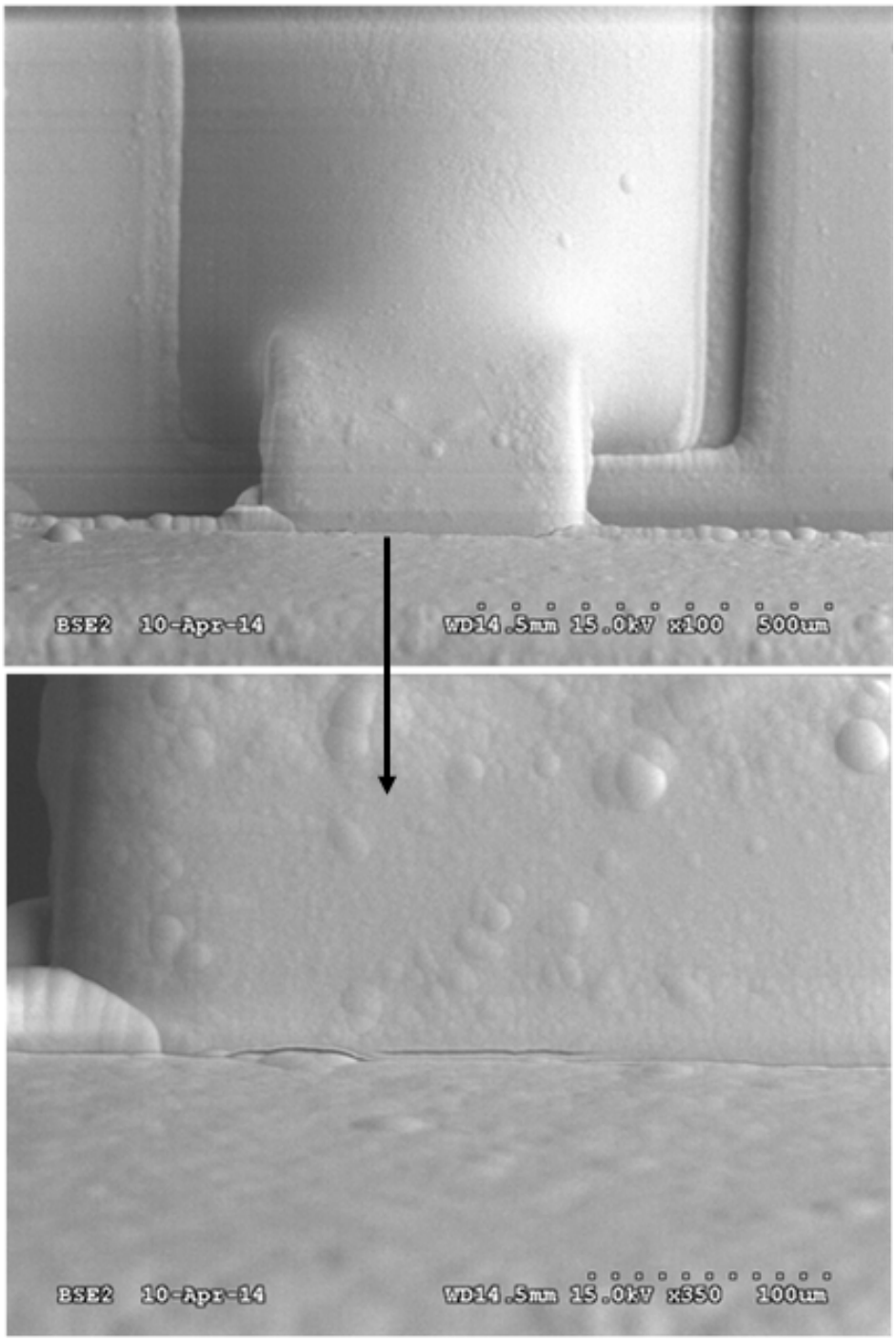


Figure 35: SEM image of a Parylene™ C & Adpro+ coated SOT3 lead, ATC+HTHH1000, 100x and 350x (ref. Board 204). Small coating crack evident at lead-to-package interface.

3. Baseline PC40-UMF based coating samples and environmental testing

The three PC40-UMF coating variations evaluated, each having an initial thinned PC40-UMF dip followed by plasma etching, were as follows; (1)PC40-UMF, (2) PC40-UMF+10%NNN2835 nanosilica, or (3) PC40-UMF+30%NNN2835 nanosilica. Note that the NNN2835 nanosilica suspension was made by Covestro (formerly Bayer Material Science) to be equivalent to the XP2742, but was prepared at a later time. Assemblies coated with 1B31 acrylic were tested at the same time for reference.

During the PC40-UMF coating process development, coverage and adhesion issues were encountered with the PC40-based coatings during the dip and spray process. Limited whisker testing was performed on these samples. The assemblies were part of the baseline coating build and test in the 2013-2014 time frame with the baseline PC18M samples, but not inspected. Then in 2015, these samples were included in the layered coating exposure for an additional 767 hours of 85C/85%RH and then inspected. The following nomenclature was used to define conditions:

- **HTHH1767:** 1,000 hours 85°C/85% RH then an additional 767 hours of 85°C/85% RH
  (Note: due to personnel changes and time elapsed, the records are unclear as to whether the samples were exposed to 100 cycles of -55 to +125°C and 200 cycles of -20 to +80°C thermal cycling)

3.1 Baseline PC40-UMF based coating whisker test results

The PC40-UMF based coatings included PC40-UMF (Figure 36 to Figure 58), PC40-UMF+ 10%NNN2835 nanosilica (Figure 59 to Figure 77), and PC40-UMF+30%NNN2835 nanosilica (Figure 78 to Figure 103). Whisker growth observations are summarized in Table 1. The summary of the SEM inspection results follows.

Table 1: PC40-UMF base coating assembly whisker inspection summary.

Board Label	Coating identifier	Board Type	Observations
60	2014 - Main (PC40-UMF)	QFP	Most whisker growth on QFP44; none on QFP64 and PLCC
65	2014 - Main (PC40-UMF+10% NNN2835 nanosilica)	QFP	On QFP44, no difference between 10% & 30% filler levels; no growth on QFP64 and PLCC
70	2014 - Main (PC40-UMF+30% NNN2835 nanosilica)	QFP	On QFP44, no difference between 10% & 30% fillers; no growth on QFP64 and PLCC, but some corrosion on QFP64
256	2014 - Main (PC40-UMF)	SOT	SOT5s show more growth than SOT3s and SOT6s.
284	2014 - Main (PC40-UMF+10%NNN2835 nanosilica)	SOT	SOT5s show more growth than SOT3s and SOT6s.
269	2014 - Main (PC40-UMF+30%NNN2835 nanosilica)	SOT	SOT5s show more growth than SOT3s and SOT6s.

3.1.1 Coating thickness

The PC40-UMF spray coating did not form a continuous thin film on the dip coating and formed discrete droplets. The droplets were especially pronounced on the knee and the vertical surfaces (Figure 36, Figure 38, and Figure 49).

No whisker growth was observed where the coating was thicker (greater than approximately three microns). Where the coating was thinner, whiskers and nodules were seen (e.g. Figure 41, Figure 42, Figure 43, Figure 46, Figure 67, Figure 75, Figure 77 Figure 81, Figure 86, Figure 90, and Figure 99). A range of corrosion was observed where the coating was thin. The majority was considered low (e.g. Figure 39 and Figure 40), but sometimes it was extensive (Figure 64 and Figure 76)

Some parts had very thick coating (greater than approximately 150 microns) and in some cases the coating nearly encapsulated the parts, especially of the lower profile SOT3 (Figure 50) and QFP64 (Figure 58). Also, when the coating was thick, it often pulled away from the lead leaving a substantial gap (e.g. Figure 36, Figure 37, and Figure 59) and cracked near the package body (Figure 48 and Figure 58). The pull-away was less evident with the PC40-UMF+30%NNN2835 nanosilica spray coating (Figure 94).

3.1.2 Coating type

All whiskers and corrosion were observed in thin areas that were of the initial PC40-UMF dip coating where the spray coating dewet. No significant differences in whisker mitigation were observed between the thick PC40-UMF and PC40-UMF with 10% or 30% nanosilica regions.

3.1.3 Part type

QFP44s had the more whisker growth than QFP64s and PLCCs. Board 85 had the least growth and board 60 had the most. SOT5s had more growth than SOT3s and SOT6s.

3.1.4 SEM inspection of unfilled PC40UMF assemblies

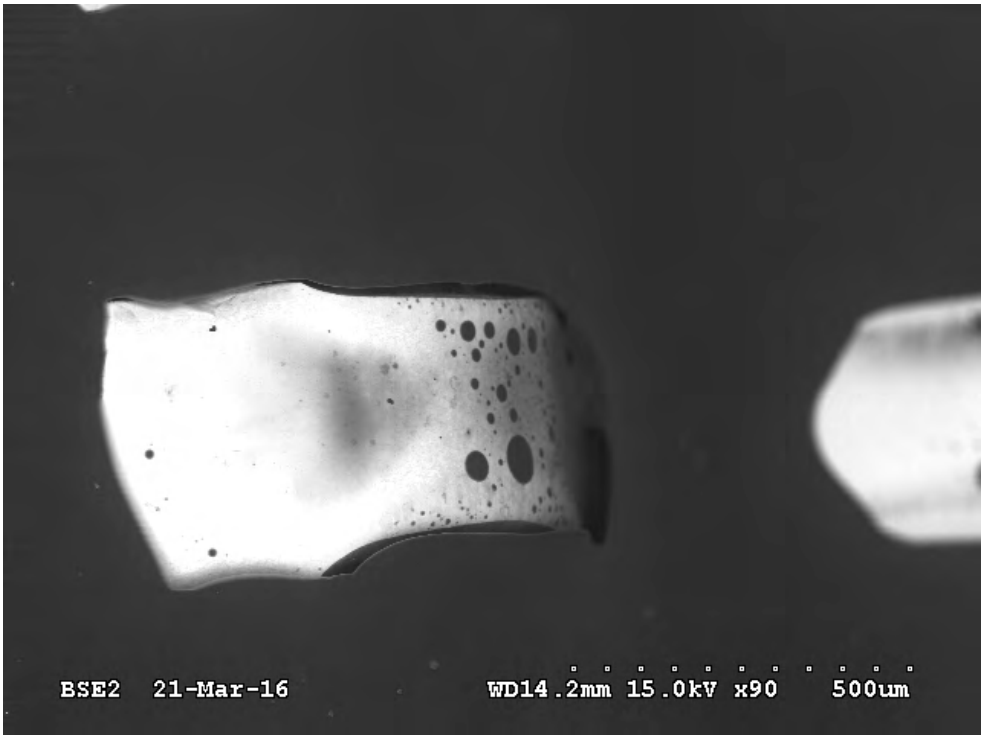


Figure 36: SEM image of PC40-UMF coated QFP44 lead, HTHH1767, 90x (ref. Board 60). A discontinuous film of discrete droplets and coating pull – away from the metal were observed.

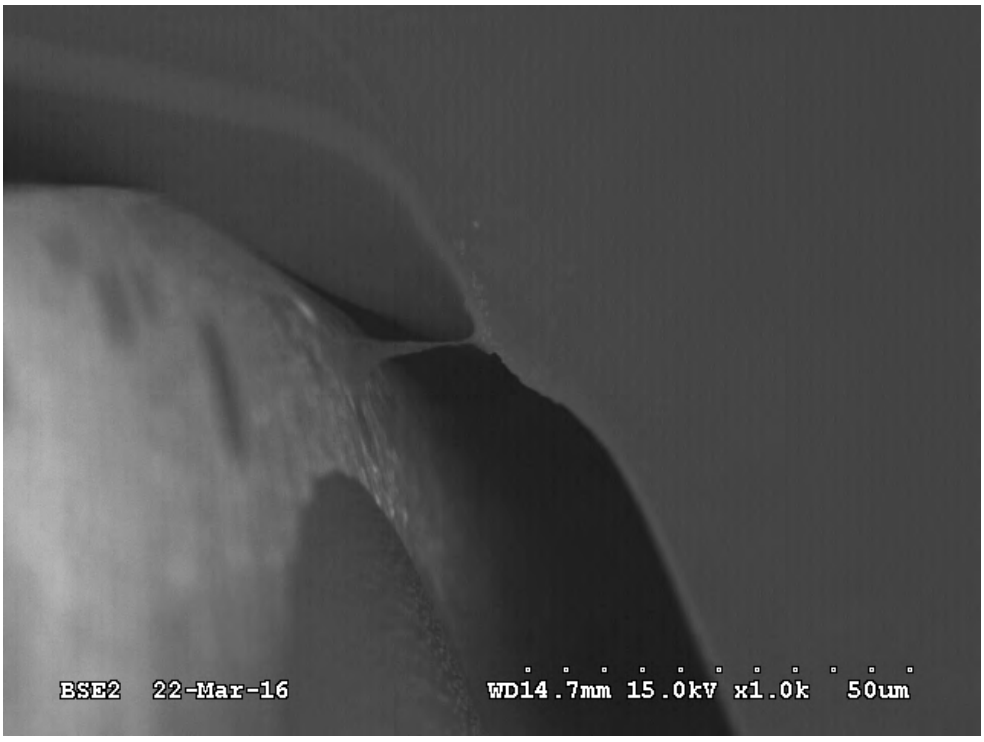


Figure 37: SEM image of PC40-UMF coated QFP44 lead, HTHH1767, QFP44, 1,000x (ref. Board 60). Higher magnification view of coating pull away.

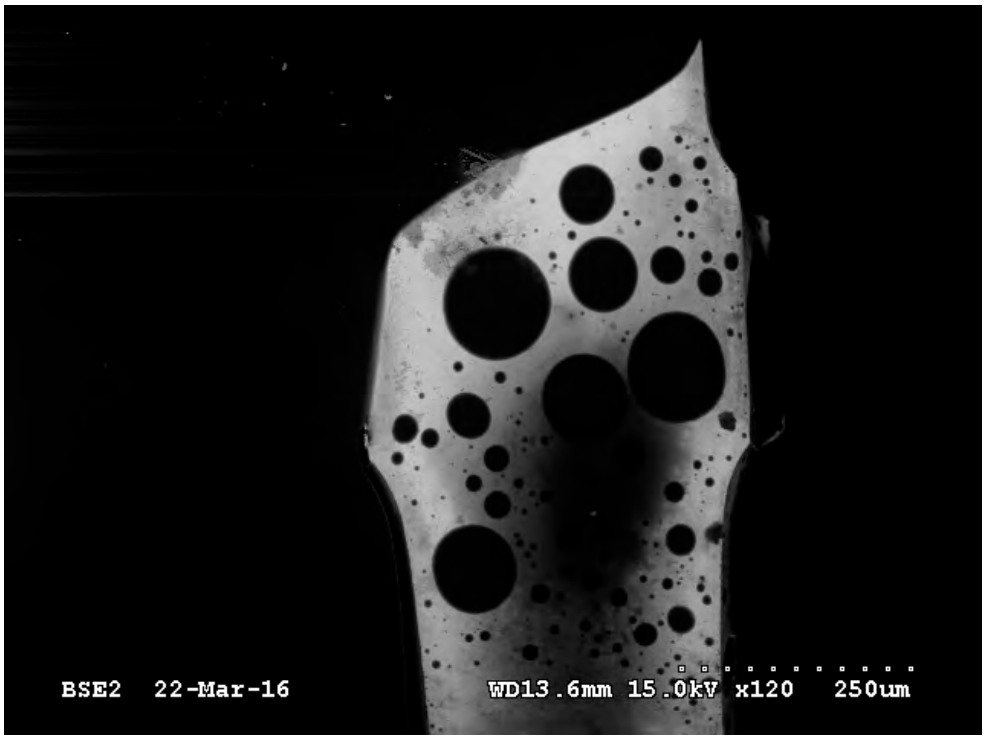


Figure 38: SEM image of PC40-UMF coated QFP44 lead, HTHH1767, QFP44, U4, lead 11, 120x (ref. Board 60).

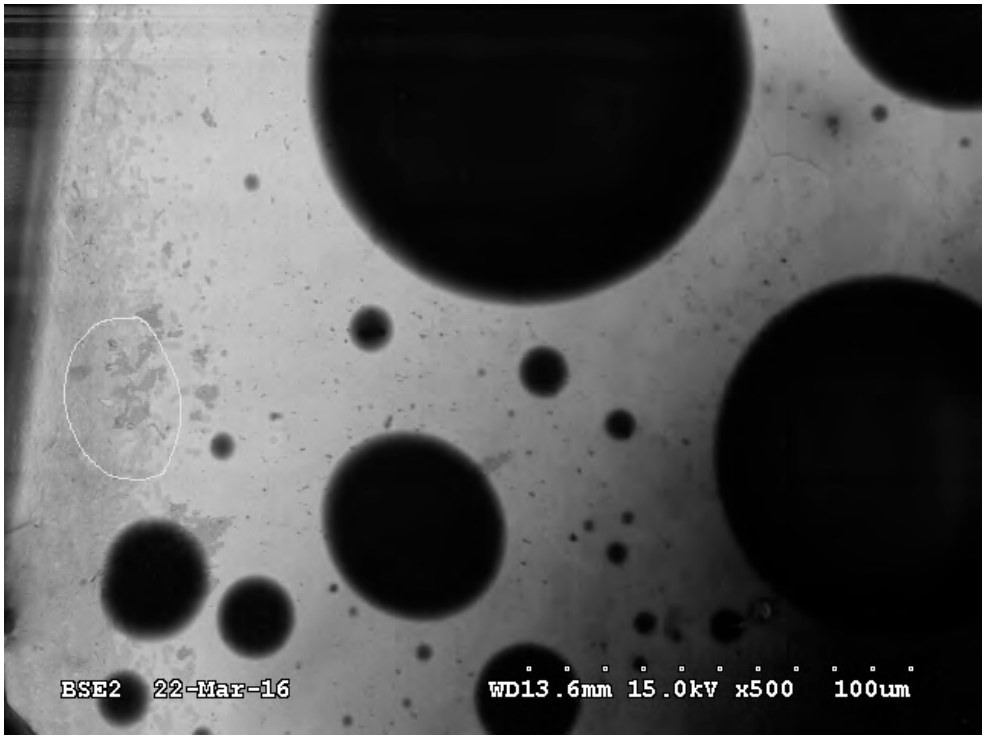


Figure 39: SEM image of PC40-UMF coated QFP44 lead, HTHH1767, QFP44, U4, lead 11, 500x (ref. Board 60). Corrosion region in circle is shown in Figure 40.



Figure 40: SEM high magnification image of corrosion on PC40-UMF coated QFP44 lead, HTHH1767, QFP44, U4, lead 11, 4000x (ref. Board 60).

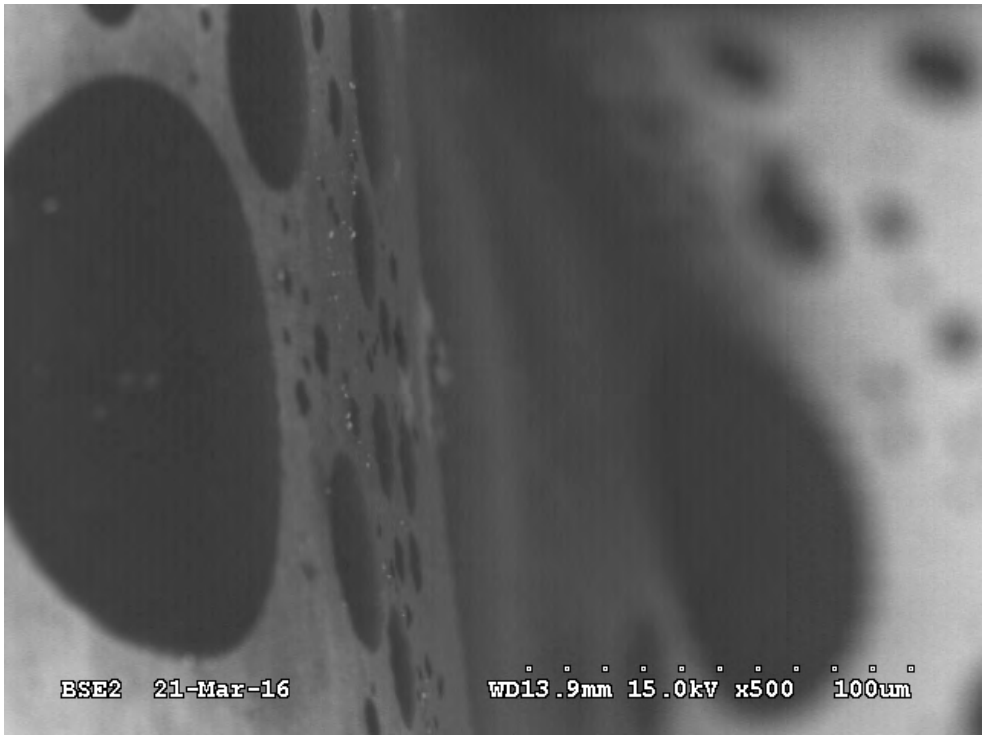


Figure 41: SEM image of PC40-UMF coated QFP44 lead front, HTHH1767, QFP44, U4, lead 12, 500x (ref. Board 60).

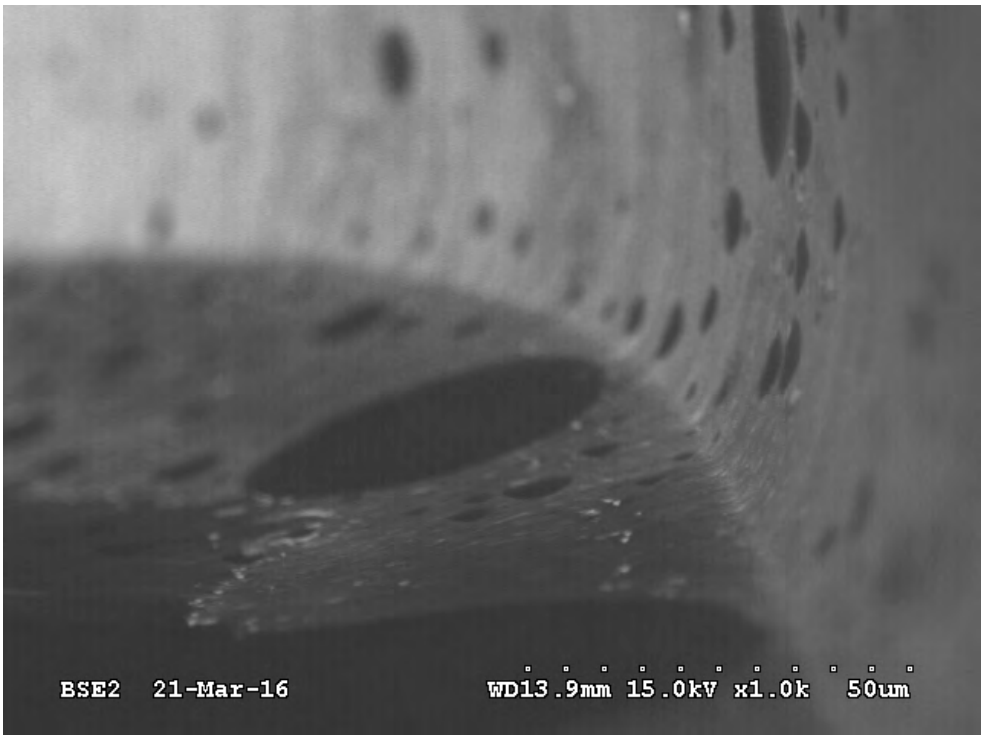


Figure 42: SEM image of PC40-UMF coated QFP44 lead side, HTHH1767, QFP44, U4, lead 12, 1,000x (ref. Board 60)**.**

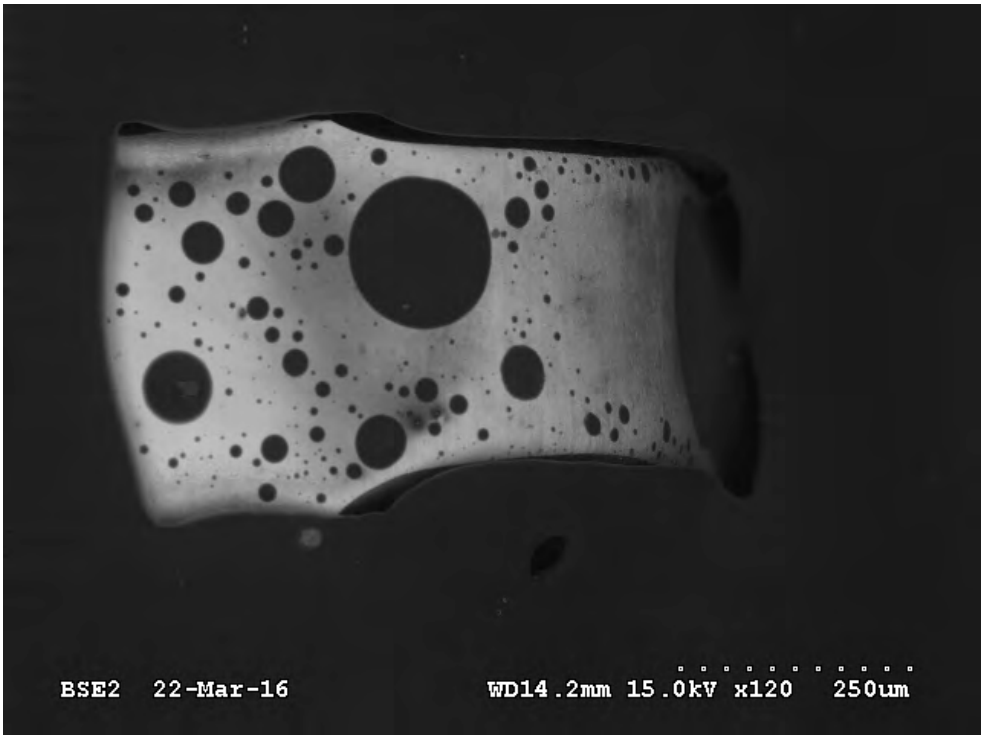


Figure 43: SEM image of PC40-UMF coated QFP44 lead, HTHH1767, QFP44, U4, lead 17, 120x (ref. Board 60).

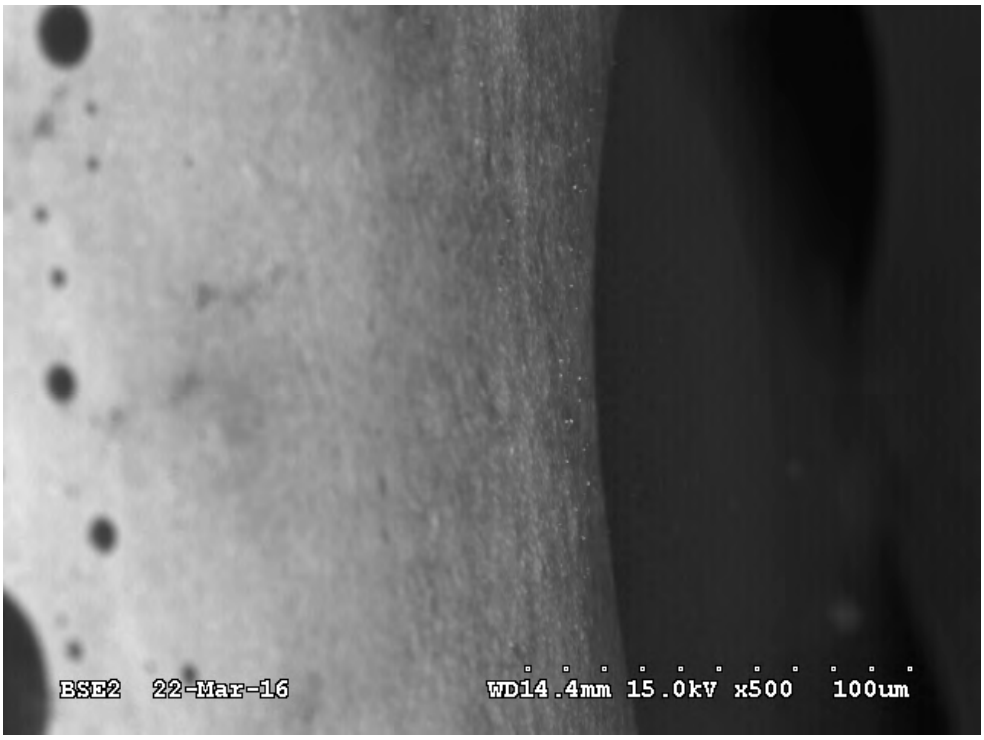


Figure 44: SEM image of PC40-UMF coated QFP44 lead front whiskers, HTHH1767, QFP44, U4, lead 17, 500x (ref. Board 60).

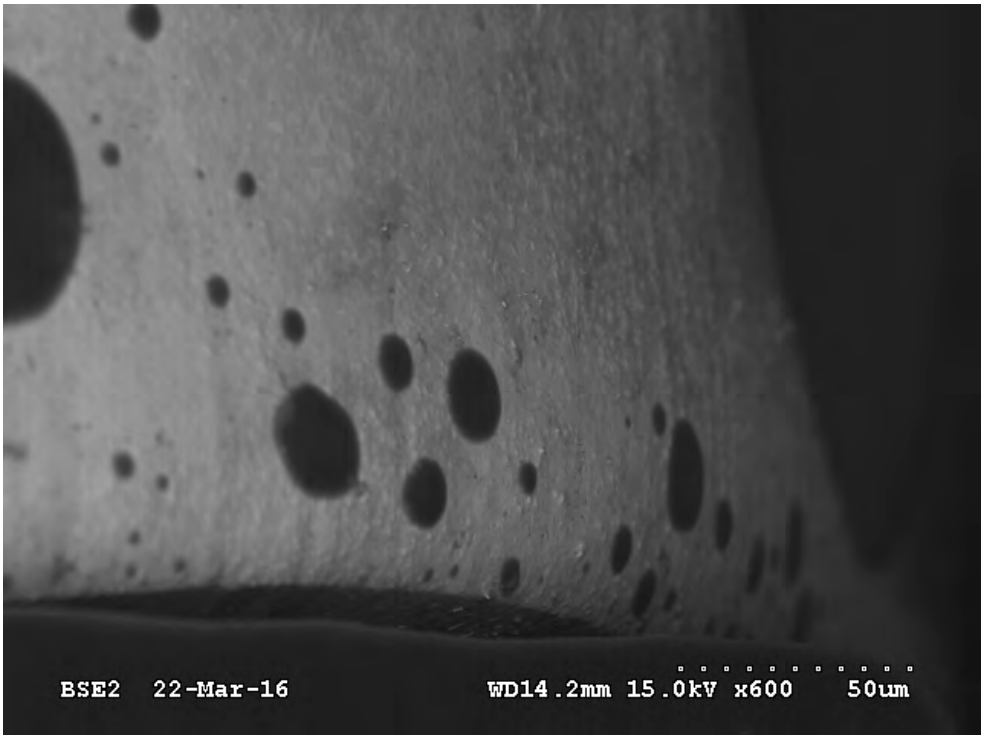


Figure 45: SEM image of PC40-UMF coated QFP44 lead, HTHH1767, U4, lead 17, 600x (ref. Board 60).

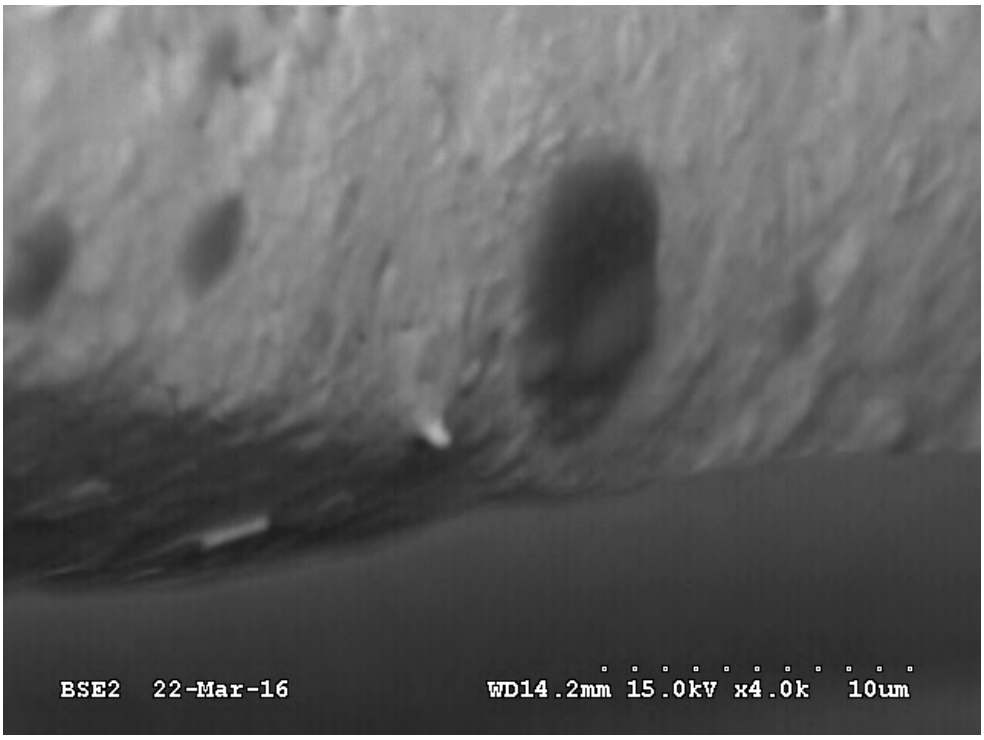


Figure 46: SEM image of PC40-UMF coated QFP44 lead side whisker, HTHH1767, QFP44, U4, lead 17, 4,000x (ref. Board 60).



Figure 47: SEM image of PC40-UMF coated QFP44 lead front, HTHH1767, U4, lead 17, 3,500x (ref. Board 60).

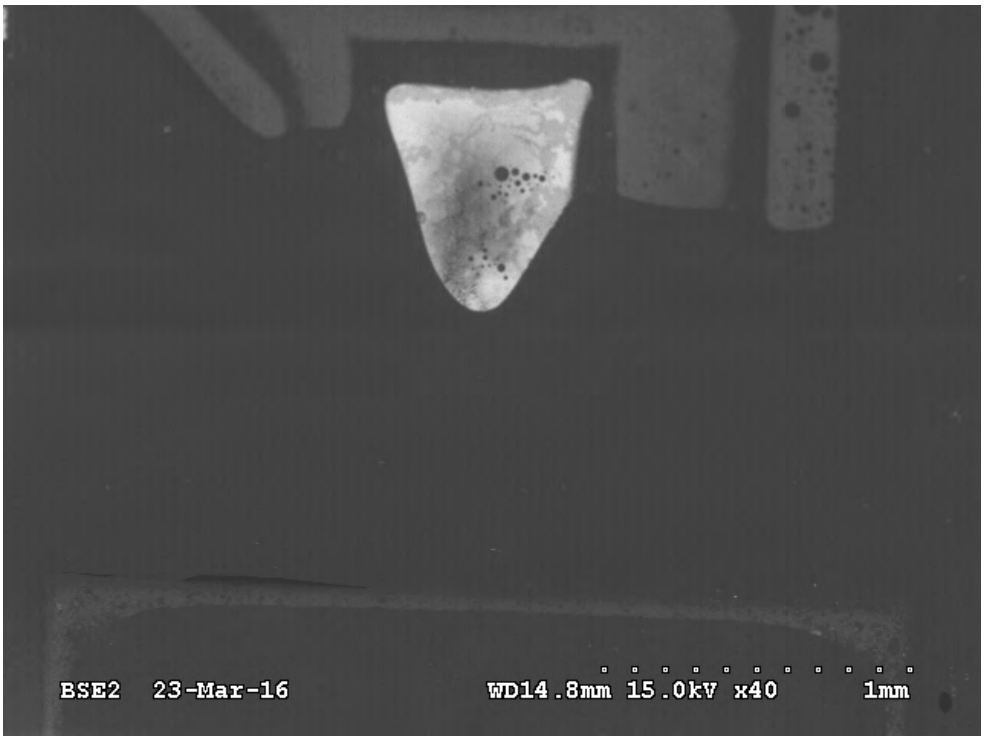


Figure 48: SEM image of PC40-UMF coated SOT3 lead, HTHH1767, 40x (ref. Board 256).

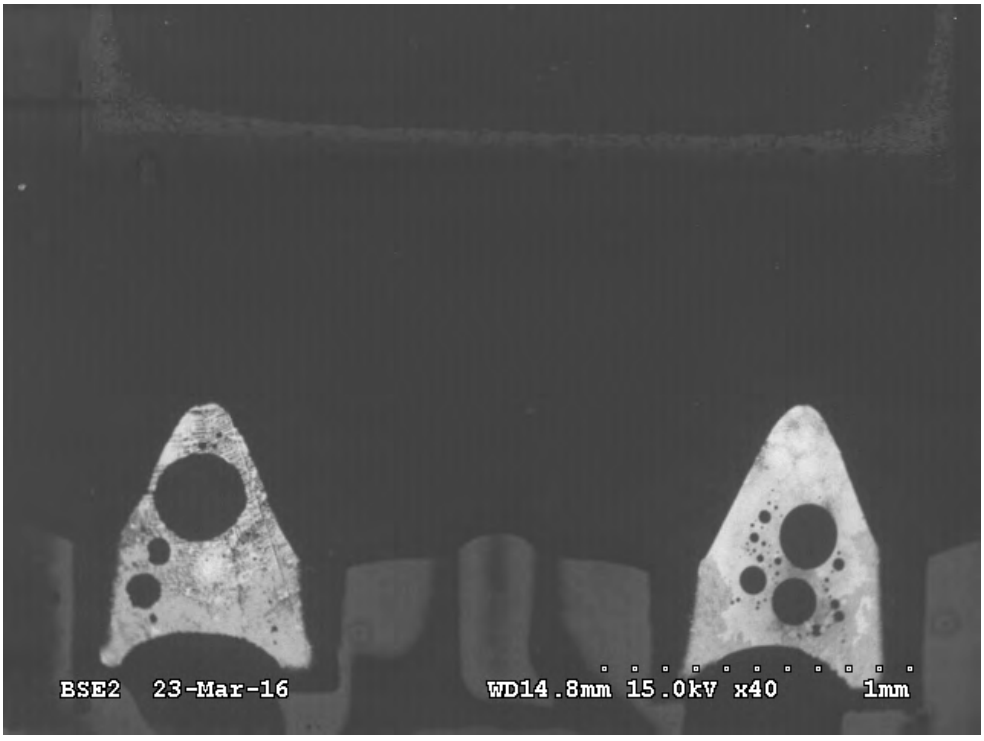


Figure 49: SEM image of PC40-UMF coated SOT3 leads, HTHH1767, 40x (ref. Board 256).

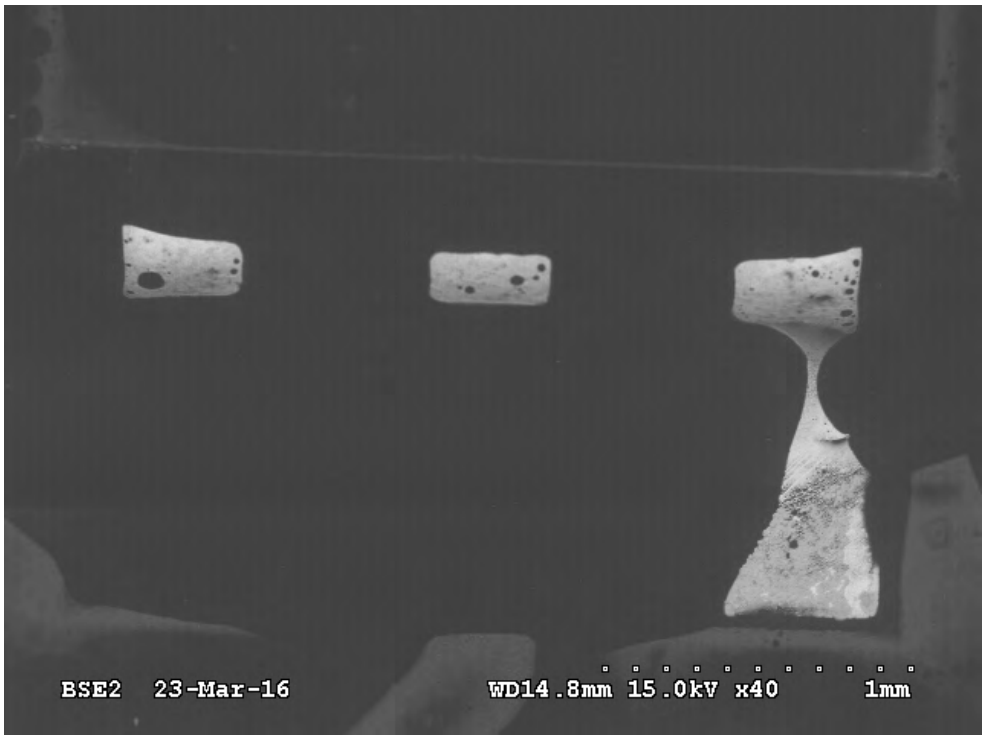


Figure 50: SEM image of PC40-UMF coated SOT5 leads, HTHH1767, U01, 40x (ref. Board 256).

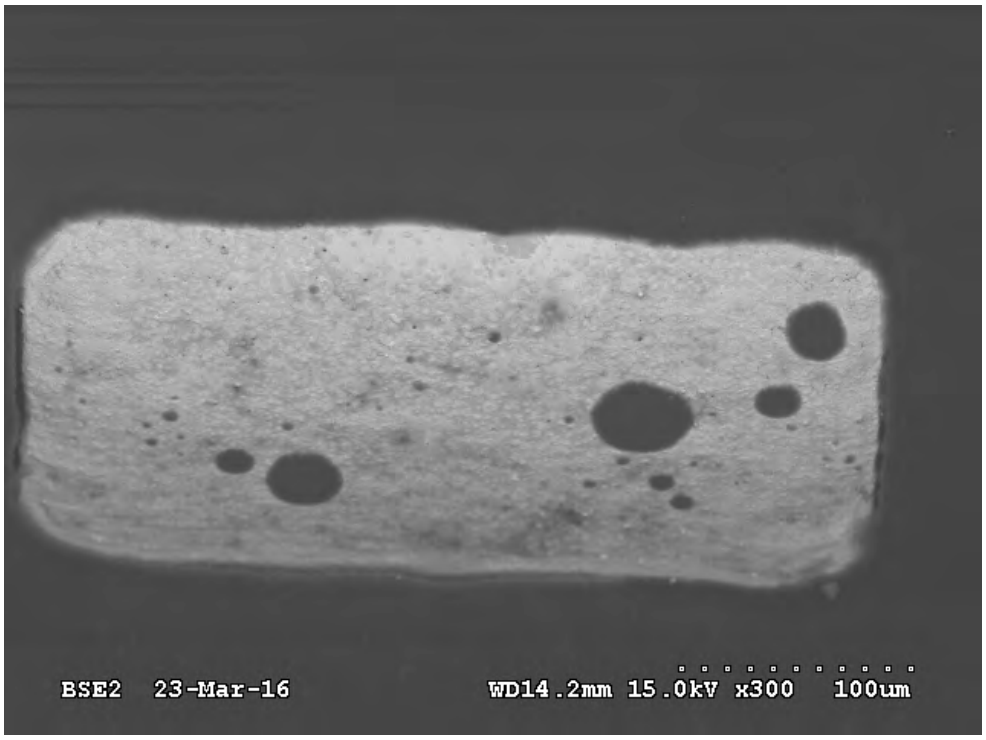


Figure 51: SEM image of PC40-UMF coated SOT5 lead, HTHH1767, U01, lead 2, 300x (ref. Board 256).

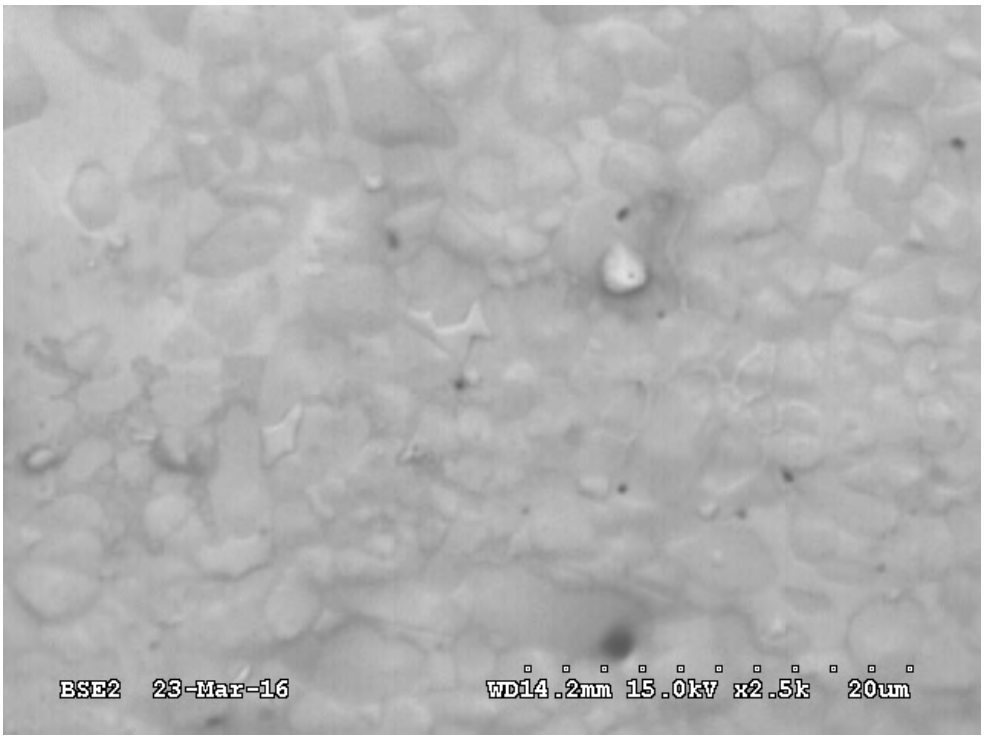


Figure 52: SEM image of PC40-UMF coated SOT5 lead, HTHH1767, U01, lead 2, 2,500x (ref. Board 256).

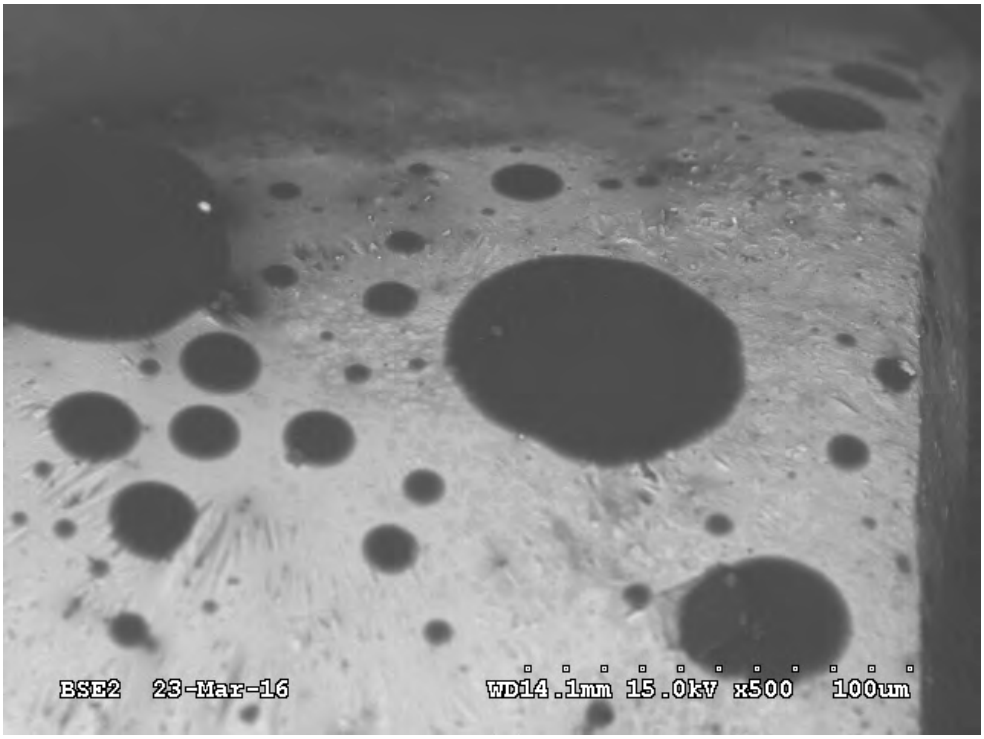


Figure 53: SEM image of PC40-UMF coated SOT5 lead, HTHH1767, U11, lead 4, 500x (ref. Board 256).



Figure 54: SEM image of PC40-UMF coated SOT5 lead, HTHH1767, U11, lead 4, 5,000x (ref. Board 256).

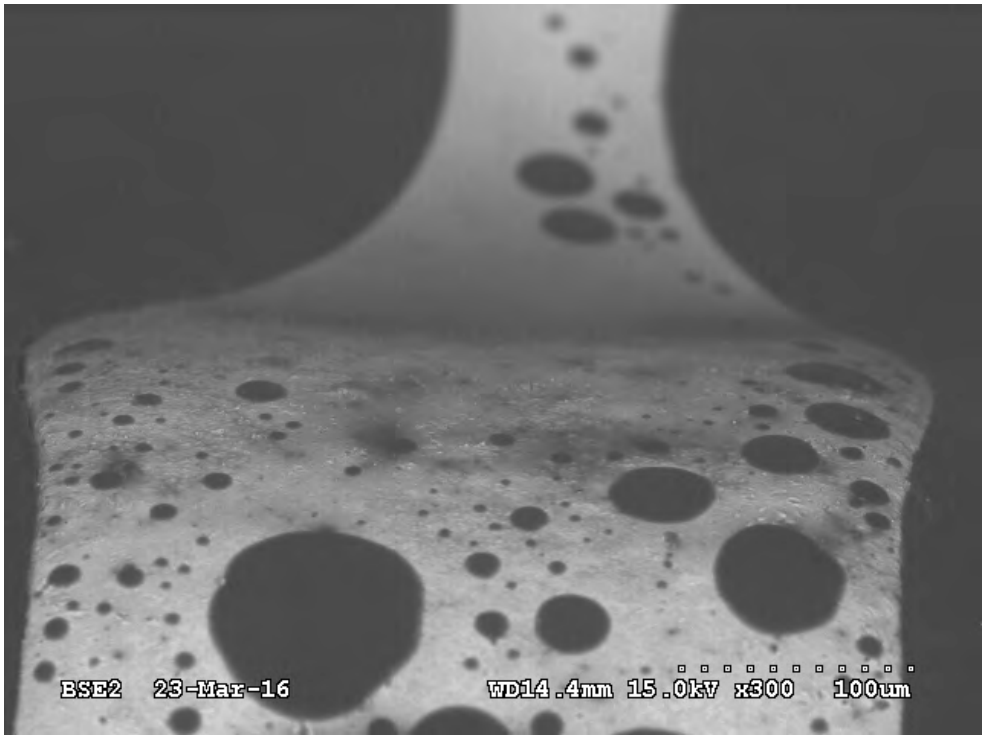


Figure 55: SEM image of PC40-UMF coated SOT5 lead, HTHH1767, U01, lead 5, 300x (ref. Board 256).

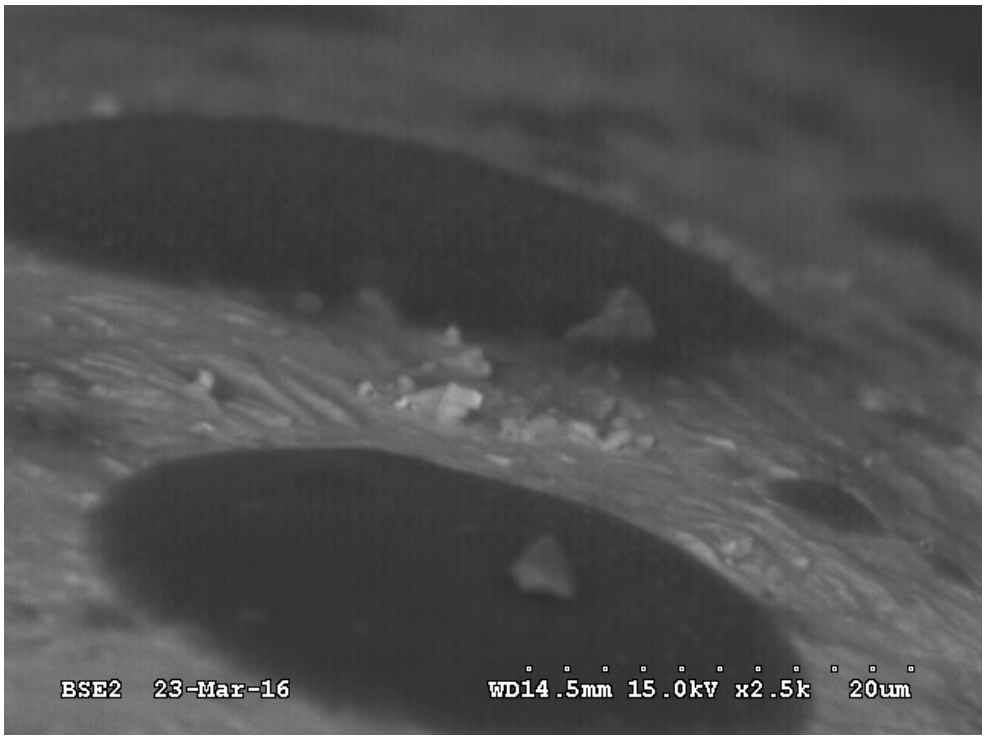


Figure 56: SEM image of PC40-UMF coated SOT5 lead, HTHH1767, U01, lead 5, 2,500x (ref. Board 256).



Figure 57: SEM image of PC40-UMF coated SOT5 lead, HTHH1767, U15, lead 5, 3,000x (ref. Board 256).

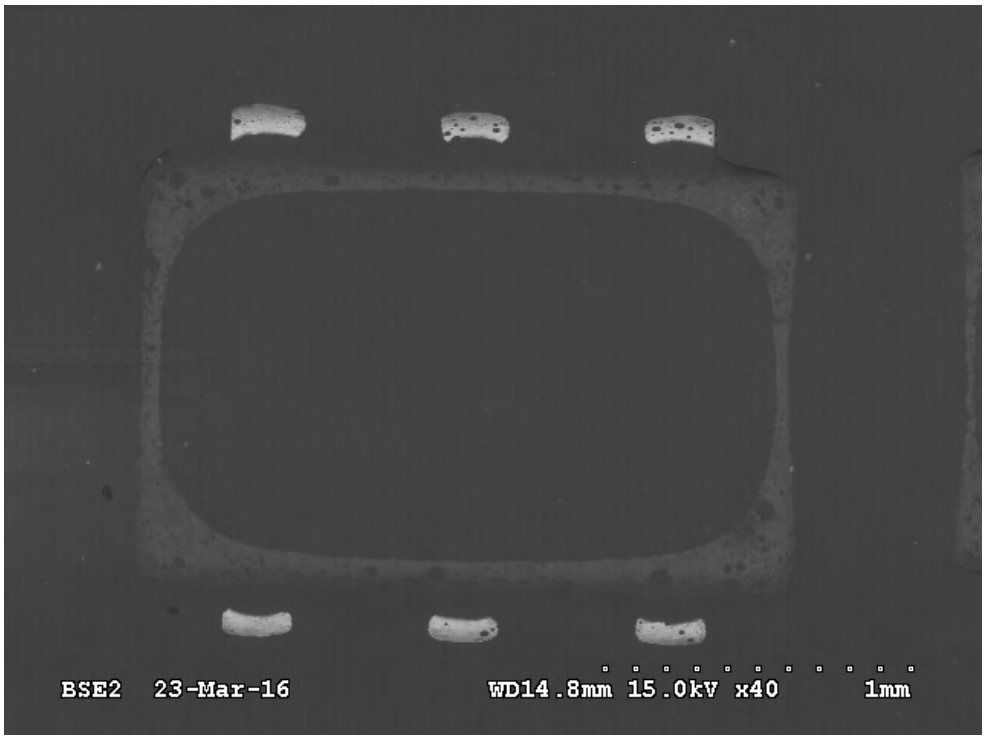


Figure 58: SEM image of PC40-UMF coated SOT6 leads, HTHH1767, 40x (ref. Board 256).

3.1.5 SEM inspection of PC40-UMF+10%NNN2835 nanosilica assemblies

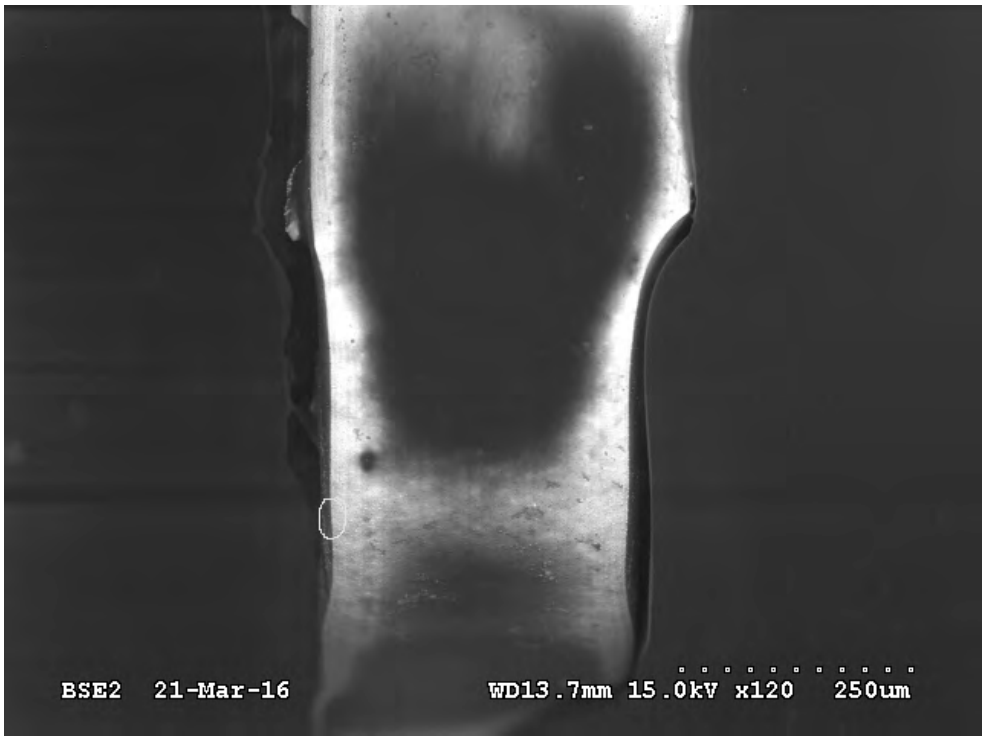


Figure 59: SEM image of PC40-UMF+10%NNN2835 nanosilica coated QFP44 lead, HTHH1767, U5, lead 1, 120x (ref. Board 65). Area in circle is shown in Figure 60.

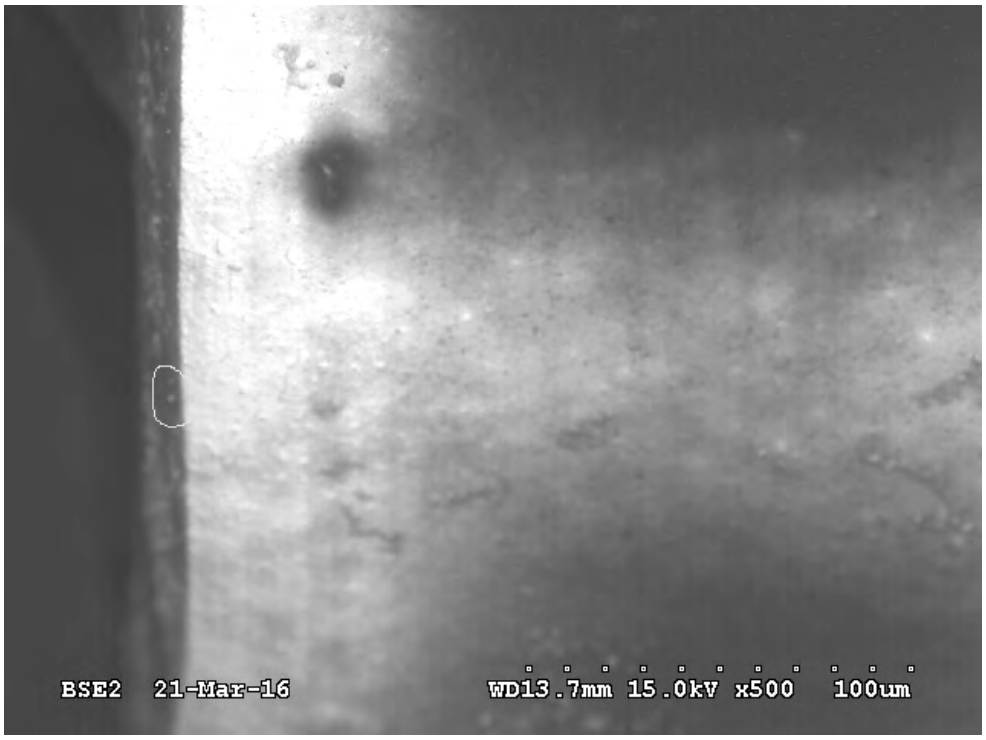


Figure 60: SEM image of PC40-UMF+10%NNN2835 nanosilica coated QFP44 lead, HTHH1767, U5, lead 1, 500x (ref. Board 65). Area in circle shown in Figure 61.



Figure 61: SEM image of PC40-UMF+10%NNN2835 nanosilica coated QFP44 lead, HTHH1767, U5, lead 1, 3500x (ref. Board 65).



Figure 62: SEM image of PC40-UMF+10%NNN2835 nanosilica coated QFP44 lead, HTHH1767, U5, lead 1, 250x, and annotated (ref. Board 65).

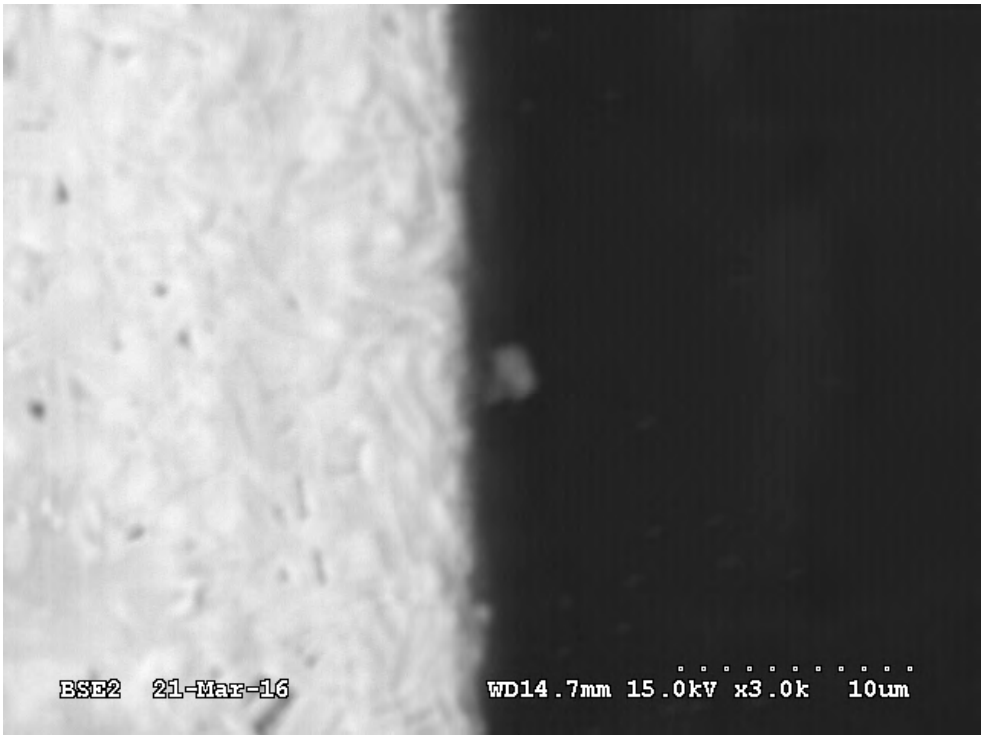


Figure 63: SEM image of PC40-UMF+10%NNN2835 nanosilica coated QFP44 lead, HTHH1767, U5, lead 1, 3,000x (ref. Board 65).

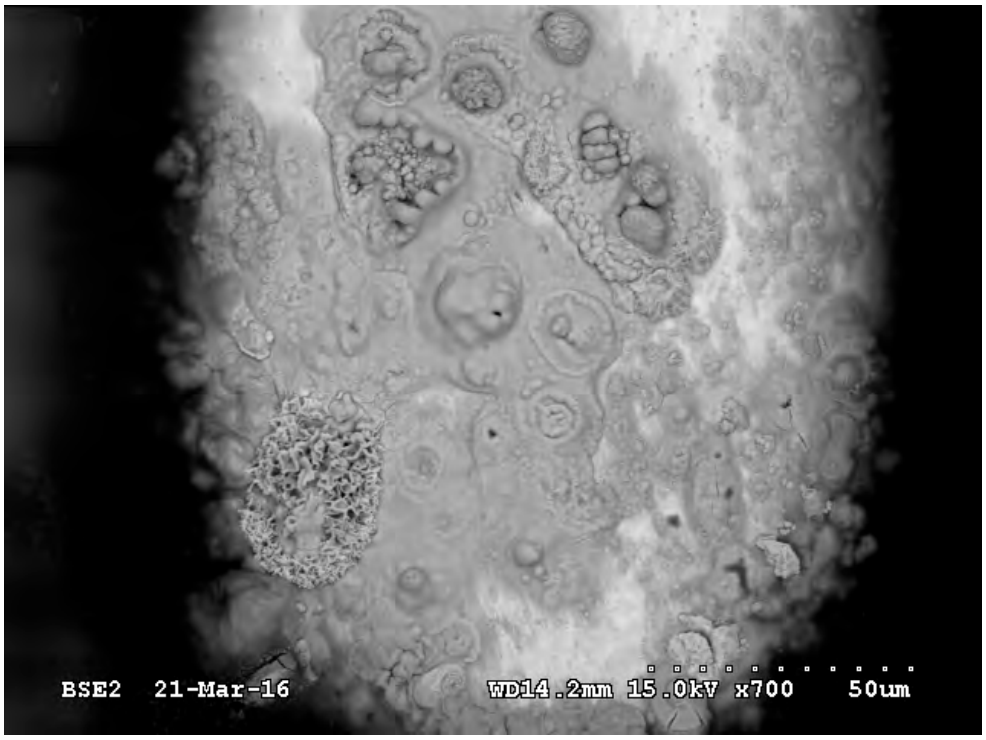


Figure 64: SEM image of PC40-UMF+10%NNN2835 nanosilica coated QFP64 lead toe, HTHH1767, 700x, (ref. Board 65).



Figure 65: SEM image of PC40-UMF+10%NNN2835 nanosilica coated SOT3 leads, HTHH1767, U06, 40x (ref. Board 284).

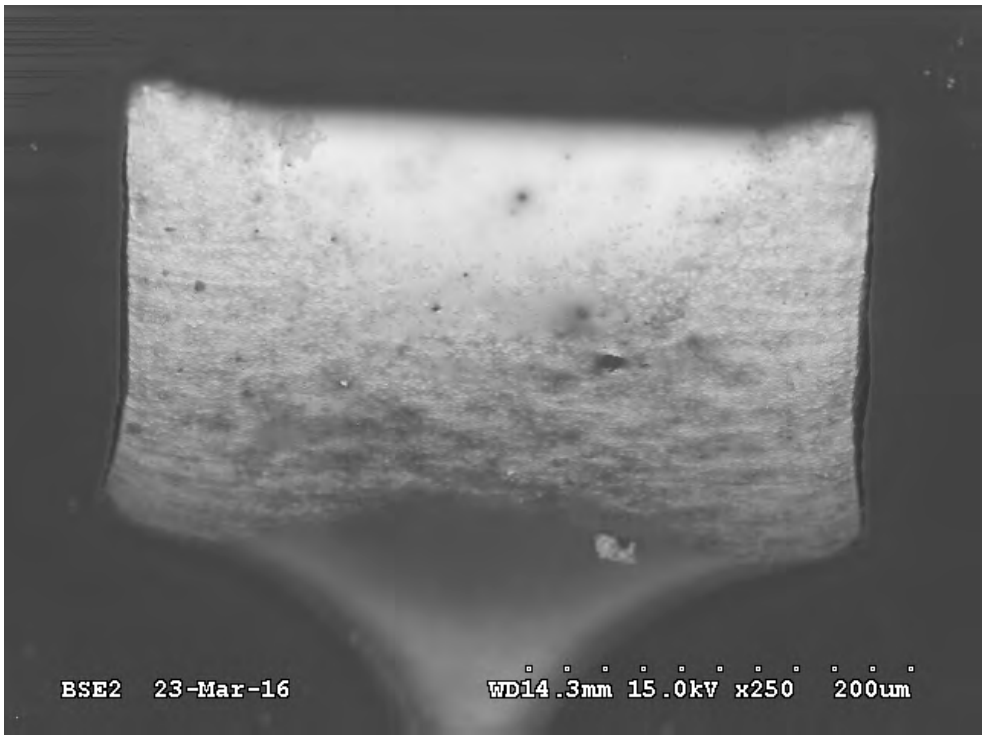


Figure 66: SEM image of PC40-UMF+10%NNN2835 nanosilica coated SOT5 lead, HTHH1767, U06, lead 2, 250x (ref. Board 284).



Figure 67: SEM image of PC40-UMF+10%NNN2835 nanosilica coated SOT5 lead, HTHH1767, U06, lead 2, 3,000x (ref. Board 284).

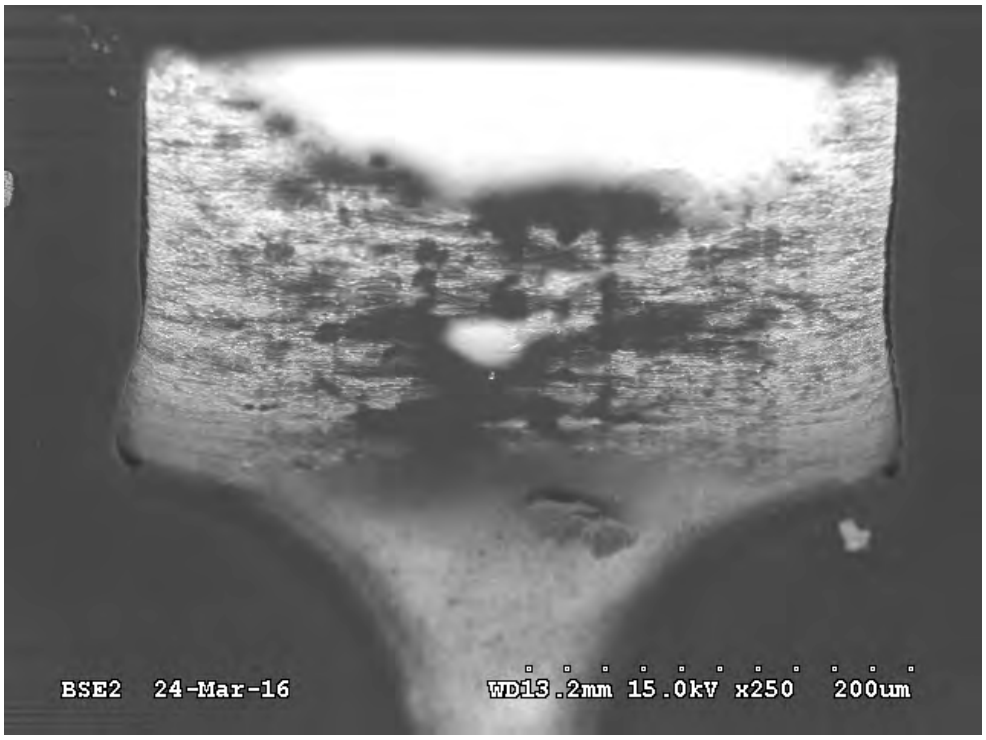


Figure 68: SEM image of PC40-UMF+10%NNN2835 nanosilica coated SOT5 lead, HTHH1767, U14, lead 2, 250x (ref. Board 284).

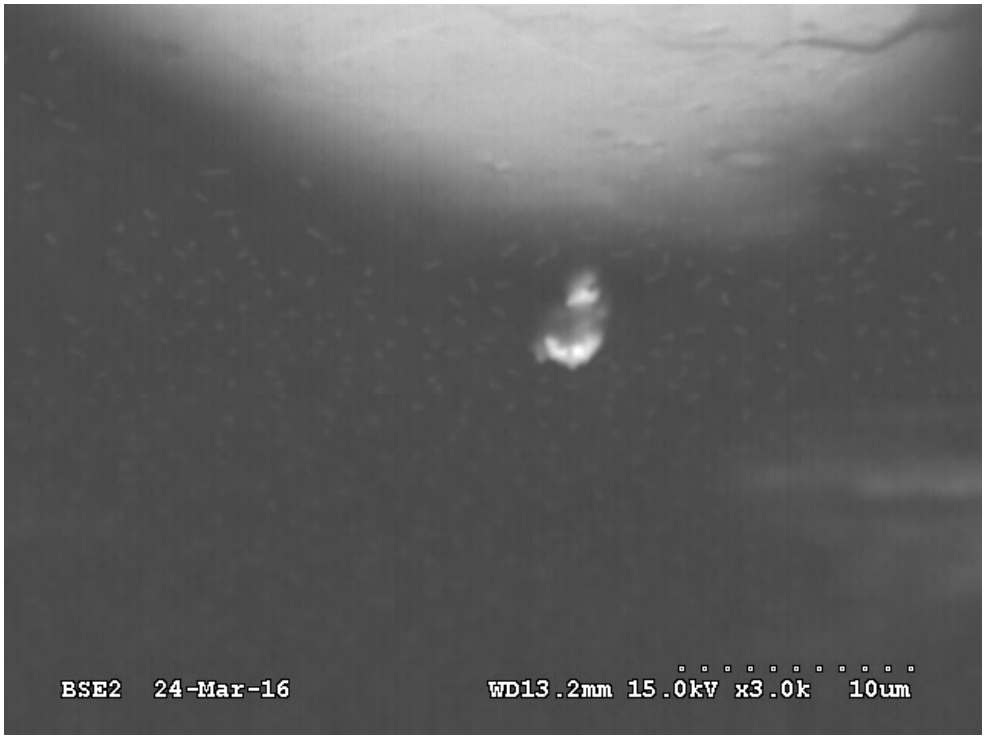


Figure 69: SEM image of PC40-UMF+10%NNN2835 nanosilica coated SOT5 lead, HTHH1767, U14, lead 2, 3,000x (ref. Board 284).

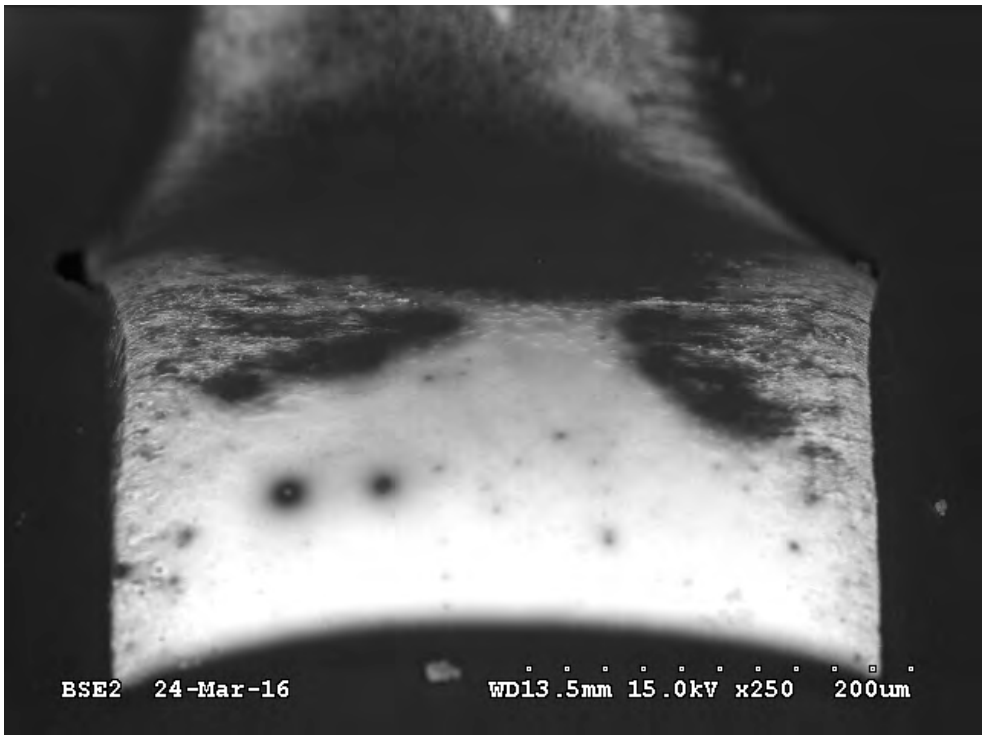


Figure 70: SEM image of PC40-UMF+10%NNN2835 nanosilica coated SOT5 lead, HTHH1767, U15, lead 5, 250x (ref. Board 284).

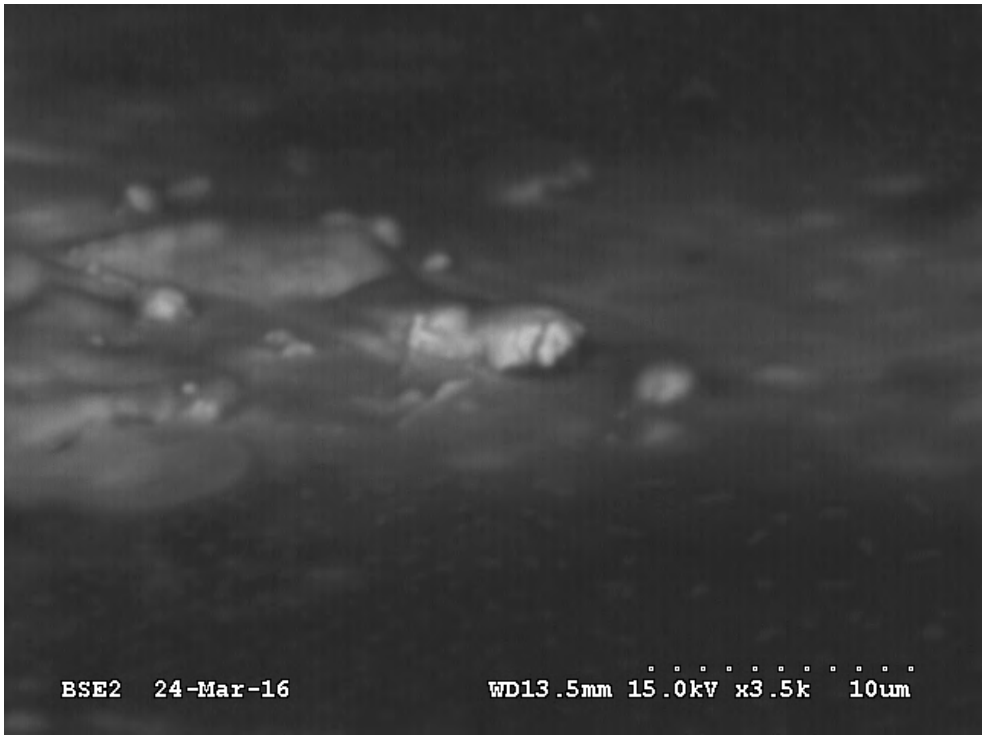


Figure 71: SEM image of PC40-UMF+10%NNN2835 nanosilica coated SOT5 lead, HTHH1767, U15, lead 5, 3,500x (ref. Board 284).

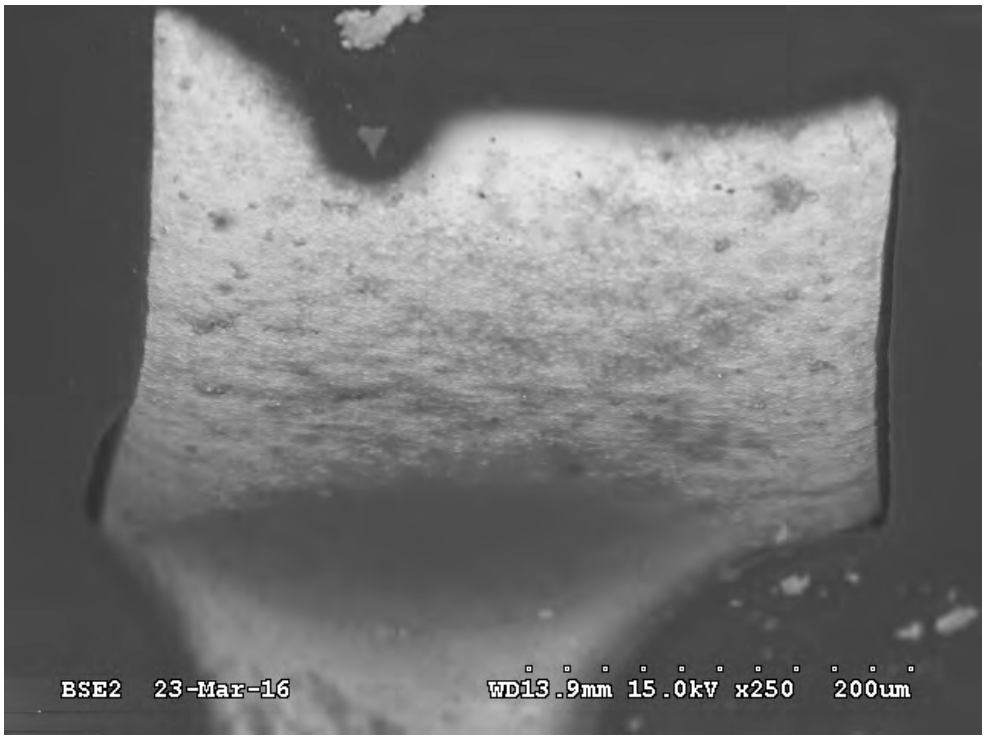


Figure 72: SEM image of PC40-UMF+10%NNN2835 nanosilica coated SOT5 lead, HTHH1767, U16, lead 1, 250x (ref. Board 284).

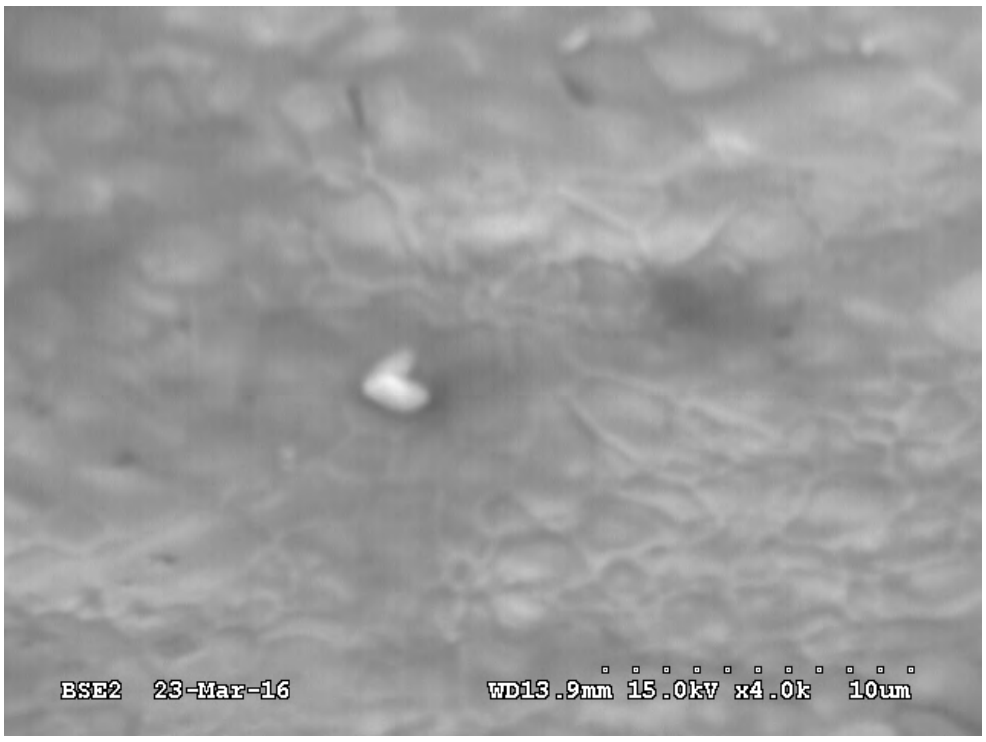


Figure 73: SEM image of PC40-UMF+10%NNN2835 nanosilica coated SOT5 lead, HTHH1767, U16, lead 1, 4000x (ref. Board 284).

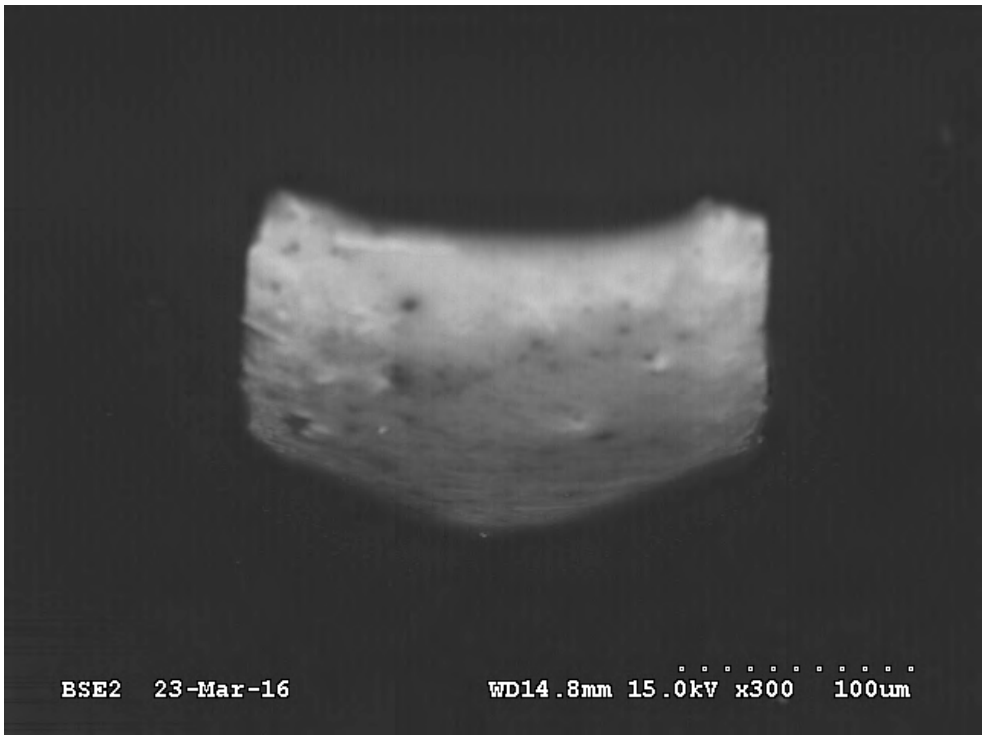


Figure 74: SEM image of PC40-UMF+10%NNN2835 nanosilica coated SOT6 lead, HTHH1767, U65, lead 2, 300x (ref. Board 284).

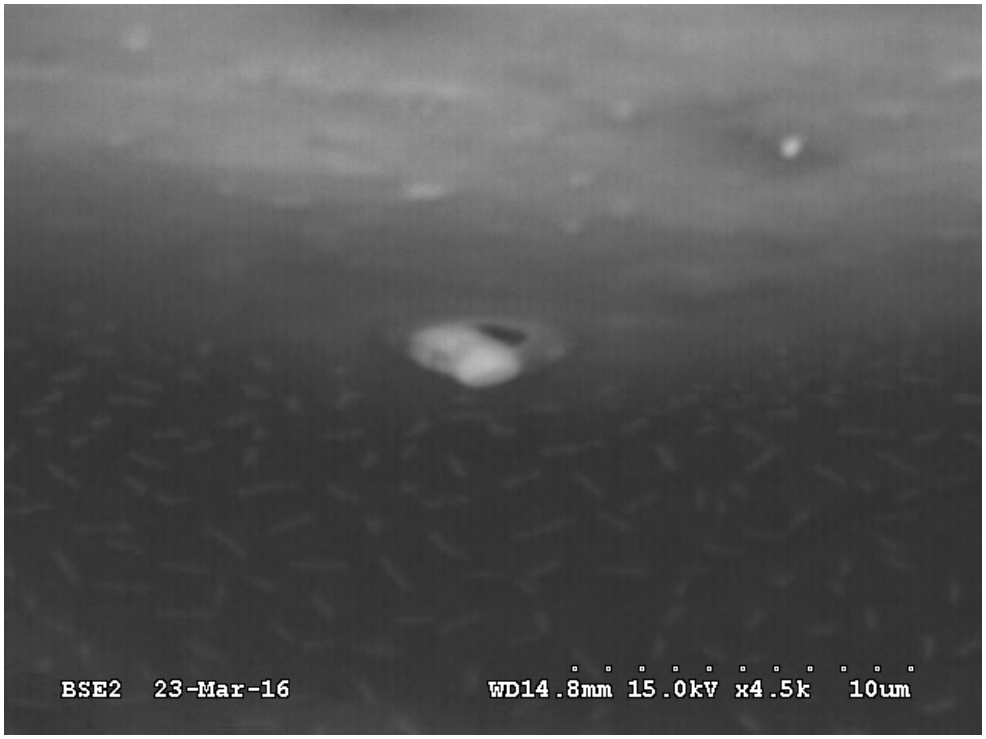


Figure 75: SEM image of PC40-UMF+10%NNN2835 nanosilica coated SOT6 lead, HTHH1767, U65, lead 2, 4,500x (ref. Board 284).

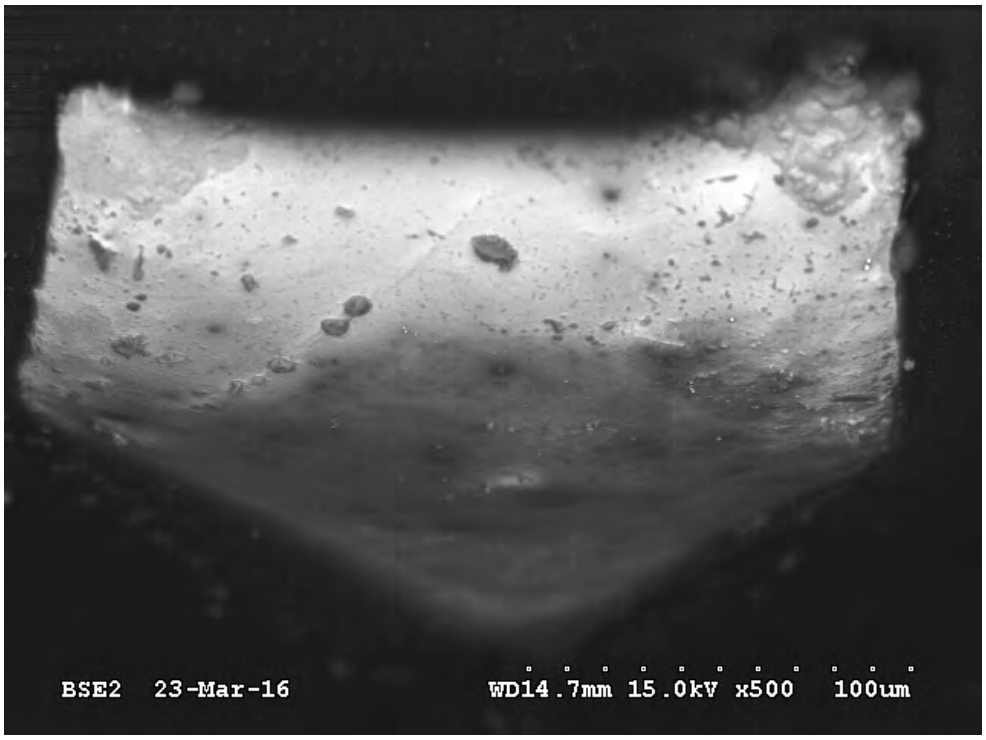


Figure 76: SEM image of PC40-UMF+10%NNN2835 nanosilica coated SOT6 lead, HTHH1767, U66, lead 3, 500x (ref. Board 284).



Figure 77: SEM image of PC40-UMF+10%NNN2835 nanosilica coated SOT6 lead, HTHH1767, U66, lead 3, 4000x (ref. Board 284).

3.1.6 SEM inspection of PC40-UMF+30%NNN2835 nanosilica assemblies

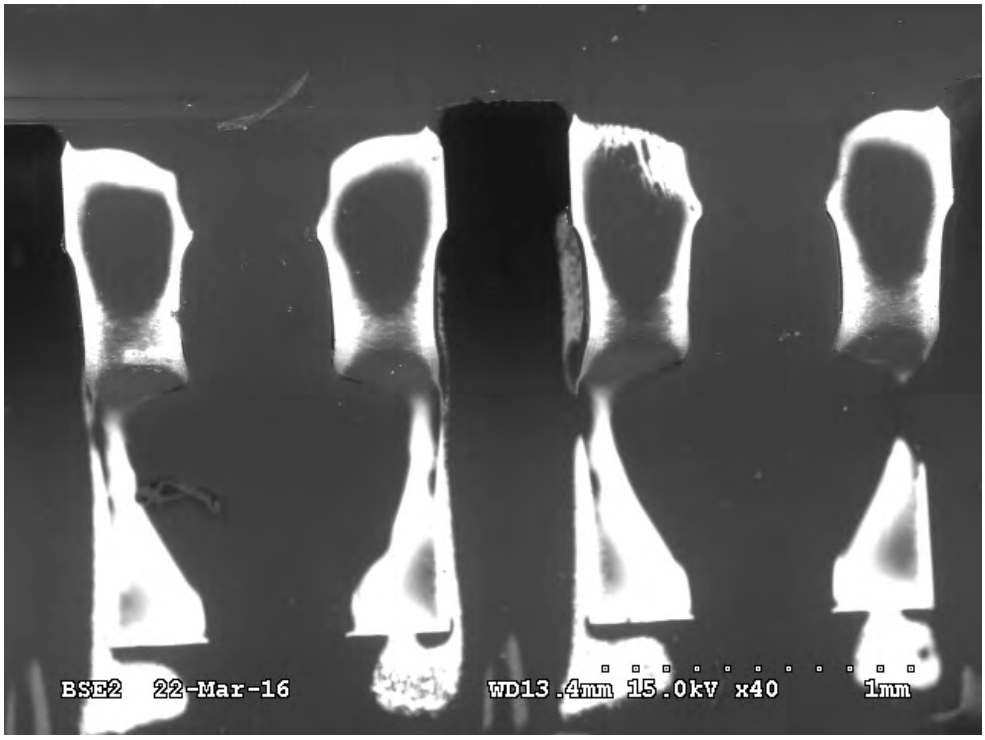


Figure 78: SEM image of PC40-UMF+30%NNN2835 nanosilica coated QFP44 leads, HTHH1767, U5, 40x (ref. Board 70).



Figure 79: SEM image of PC40-UMF+30%NNN2835 nanosilica coated QFP44 lead, HTHH1767, U5, lead 2, 120x (ref. Board 70).



Figure 80: SEM image of PC40-UMF+30%NNN2835 nanosilica coated QFP44 lead, HTHH1767, U5, lead 2, 1,000x (ref. Board 70).

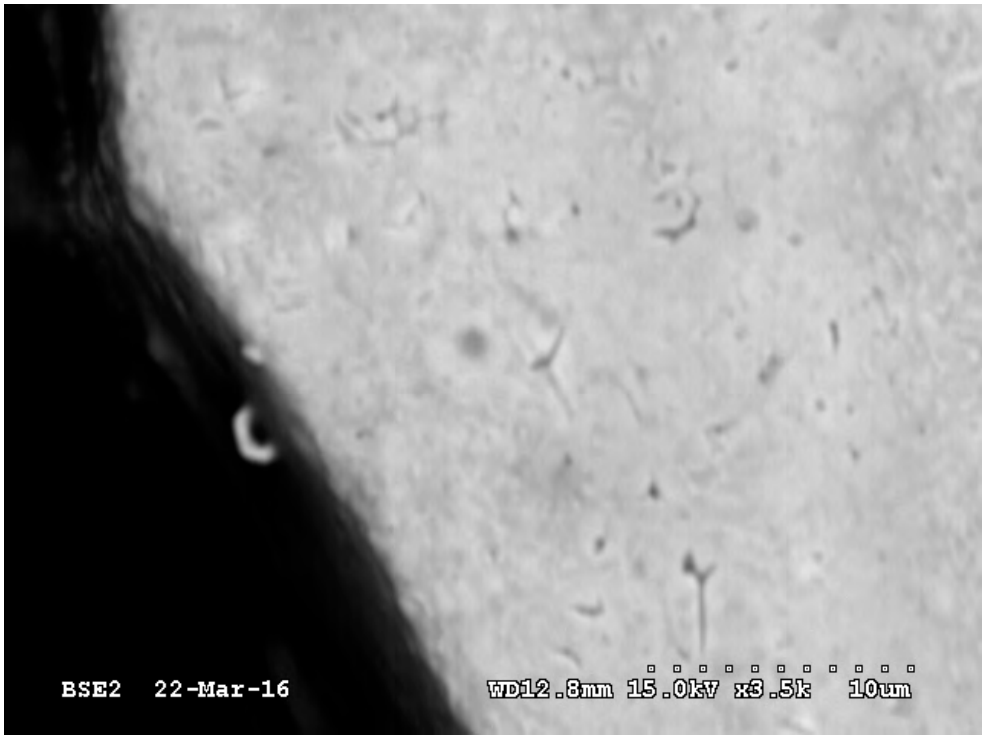


Figure 81: SEM image of PC40-UMF+30%NNN2835 nanosilica coated QFP44 lead, HTHH1767, U5, lead 2, 3,500x (ref. Board 70).

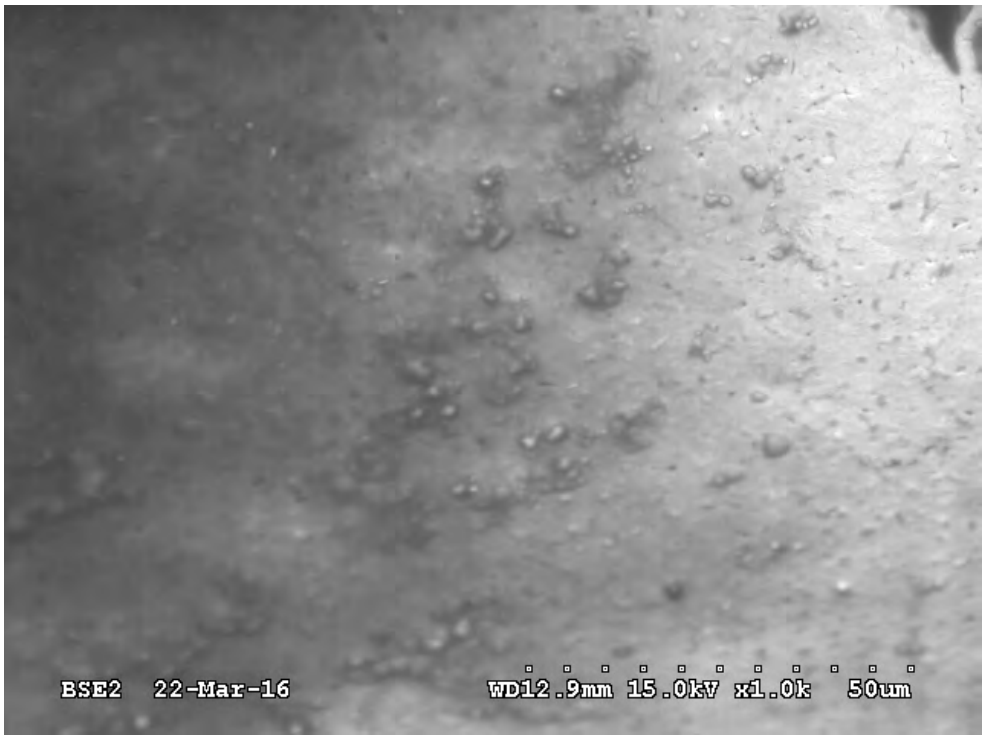


Figure 82: SEM image of PC40-UMF+30%NNN2835 nanosilica coated QFP44 lead, HTHH1767, U5, lead 3, 1000x (ref. Board 70).



Figure 83: SEM image of PC40-UMF+30%NNN2835 nanosilica coated QFP44 lead, HTHH1767, U5, lead 44, 120x (ref. Board 70).

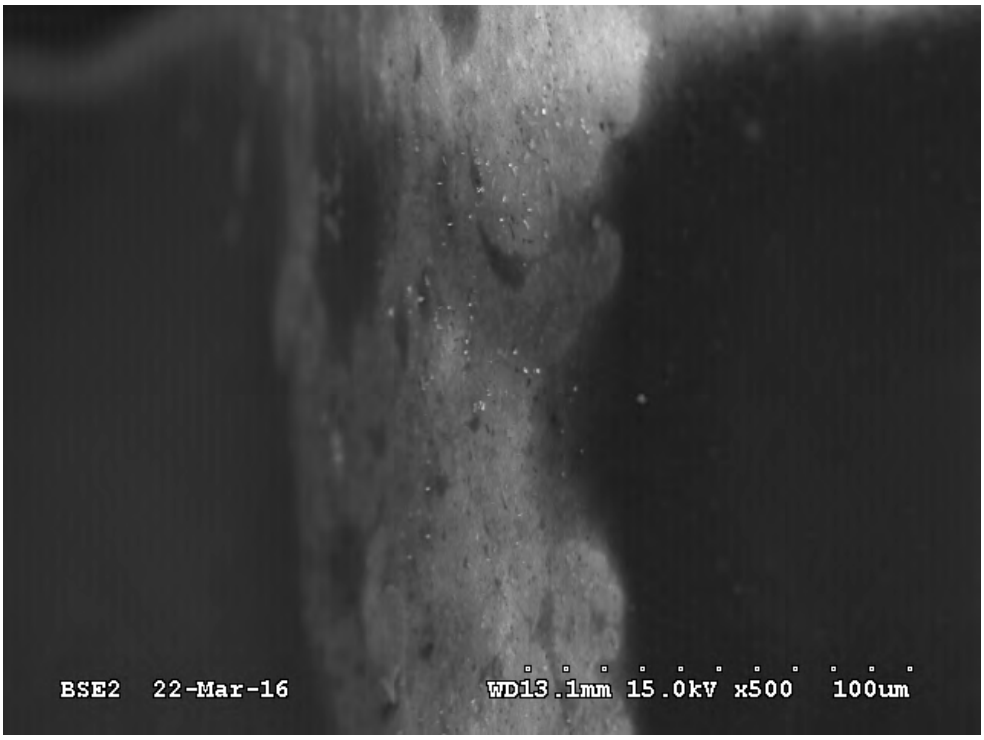


Figure 84: SEM image of PC40-UMF+30%NNN2835 nanosilica coated QFP44 lead, HTHH1767, U5, lead 44, 500x (ref. Board 70).

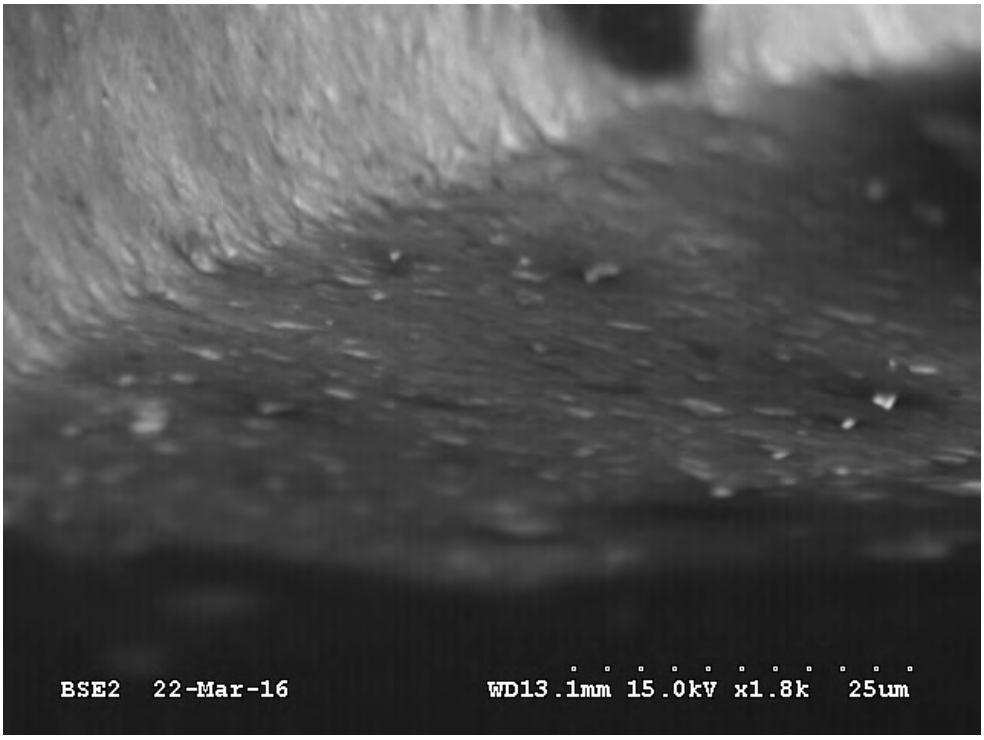


Figure 85: SEM image of PC40-UMF+30%NNN2835 nanosilica coated QFP44 lead, HTHH1767, U5, lead 44, 1800x (ref. Board 70).



Figure 86: SEM image of PC40-UMF+30%NNN2835 nanosilica coated QFP44 lead, HTHH1767, U5, lead 44, 4,000x (ref. Board 70).



Figure 87: SEM image of PC40-UMF+30%NNN2835 nanosilica coated SOT3 leads, HTHH1767, U49, 40x (ref. Board 269).

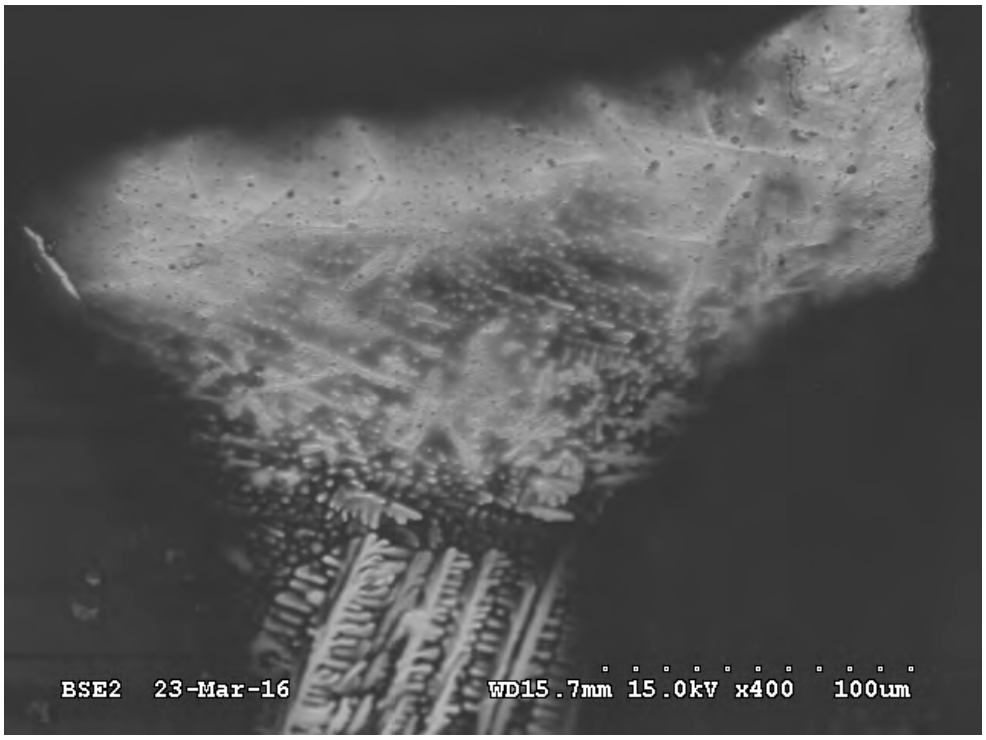


Figure 88: SEM image of PC40-UMF+30%NNN2835 nanosilica coated SOT3 lead, HTHH1767, U49, 400x (ref. Board 269).

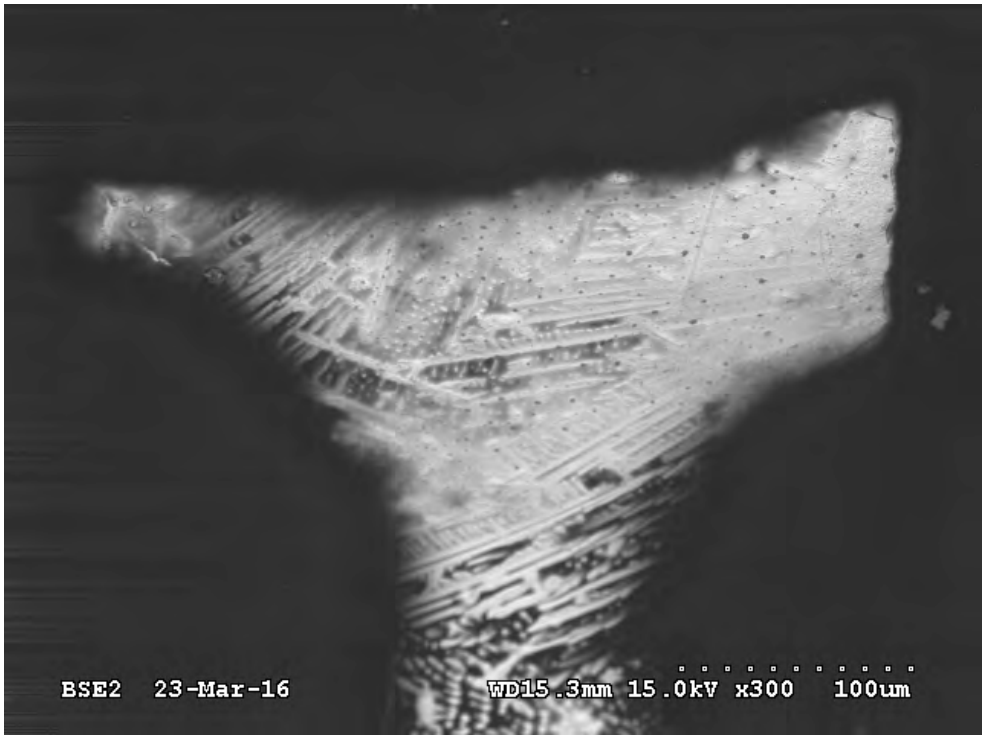


Figure 89: SEM image of PC40-UMF+30%NNN2835 nanosilica coated SOT3 lead, HTHH1767, U49, lead 2, 300x (ref. Board 269).

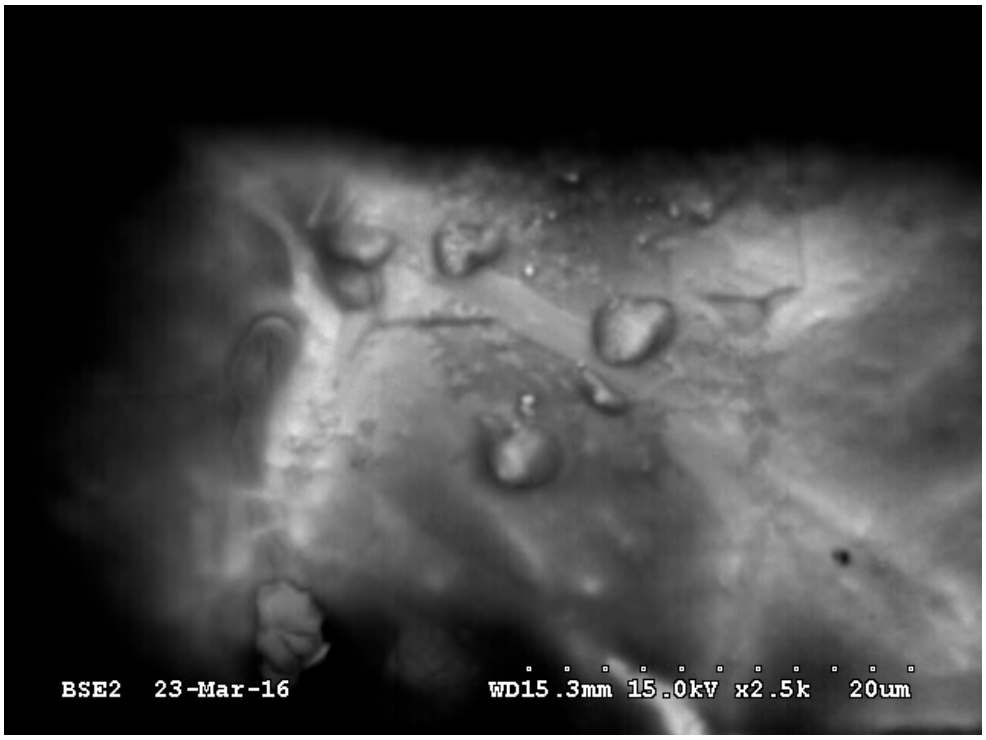


Figure 90: SEM image of PC40-UMF+30%NNN2835 nanosilica coated SOT3 lead, HTHH1767, U49, lead 2, 2,500x (ref. Board 269).

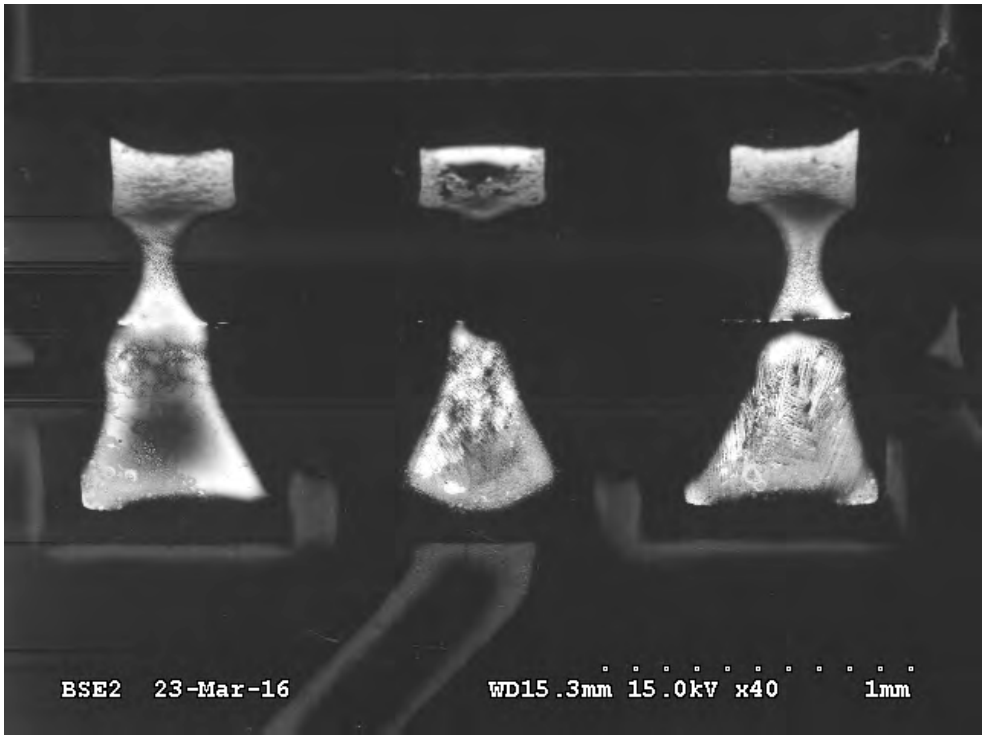


Figure 91: SEM image of PC40-UMF+30%NNN2835 nanosilica coated SOT5 leads, HTHH1767, U04, 40x (ref. Board 269).

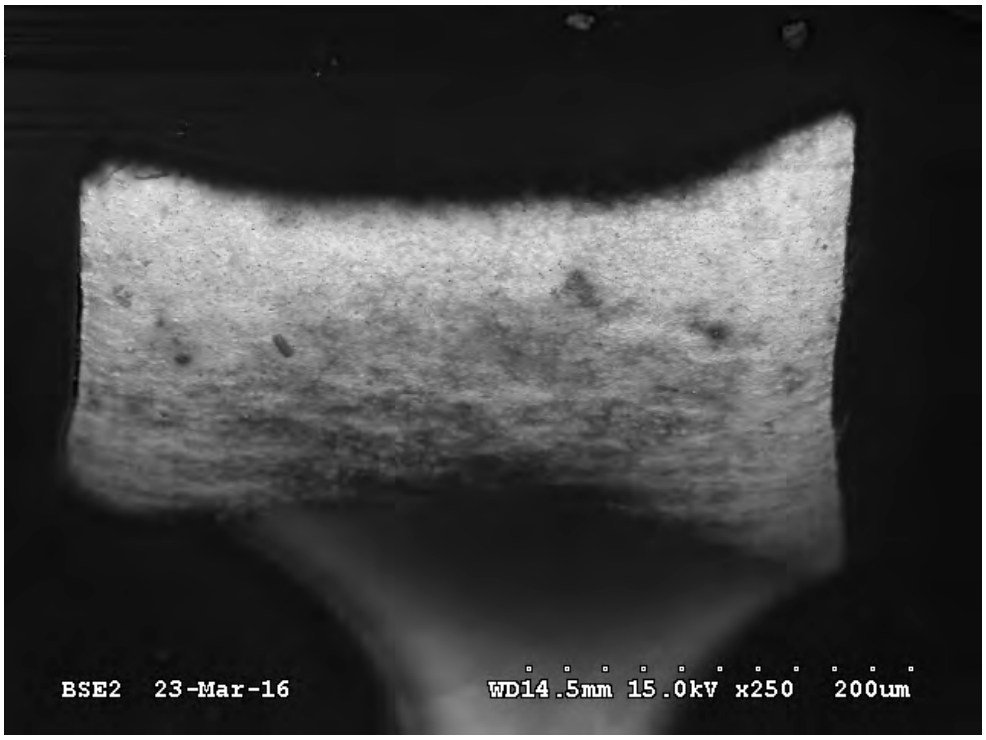


Figure 92: SEM image of PC40-UMF+30%NNN2835 nanosilica coated SOT5 lead, HTHH1767, U04, lead 3, 250x (ref. Board 269).

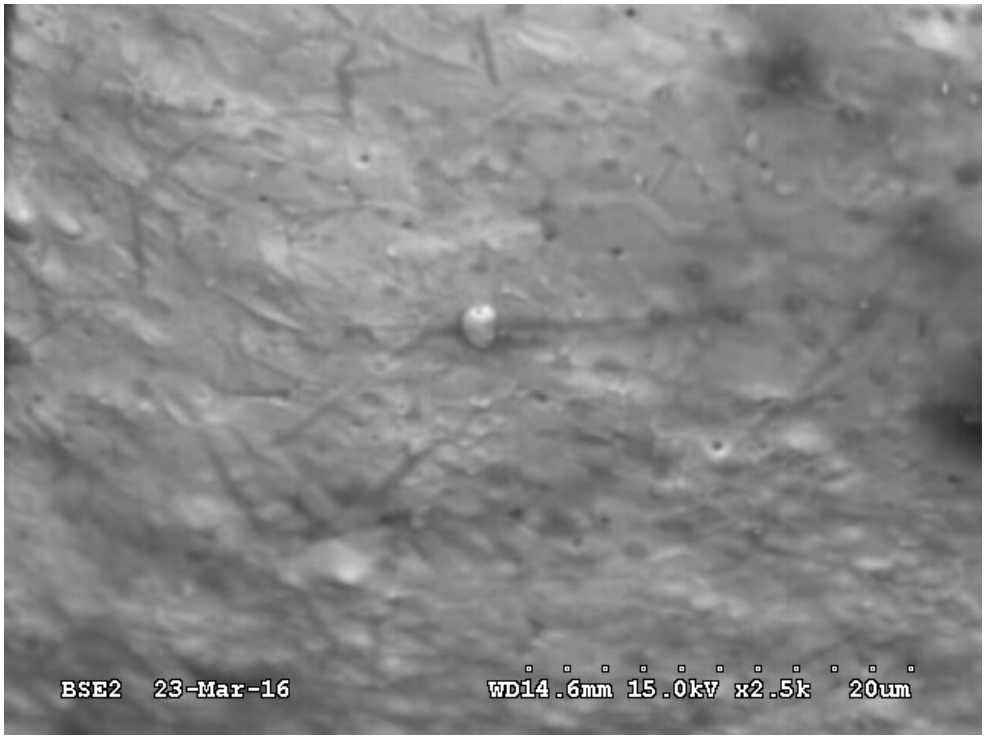


Figure 93: SEM image of PC40-UMF+30%NNN2835 nanosilica coated SOT5 lead, HTHH1767, U04, lead 3, 2500x (ref. Board 269).



Figure 94: SEM image of PC40-UMF+30%NNN2835 nanosilica coated SOT5 lead, HTHH1767, U15, lead 5, 250x (ref. Board 269).



Figure 95: SEM image of PC40-UMF+30%NNN2835 nanosilica coated SOT5 lead, HTHH1767, U15, lead 5, 5,000x (ref. Board 269).

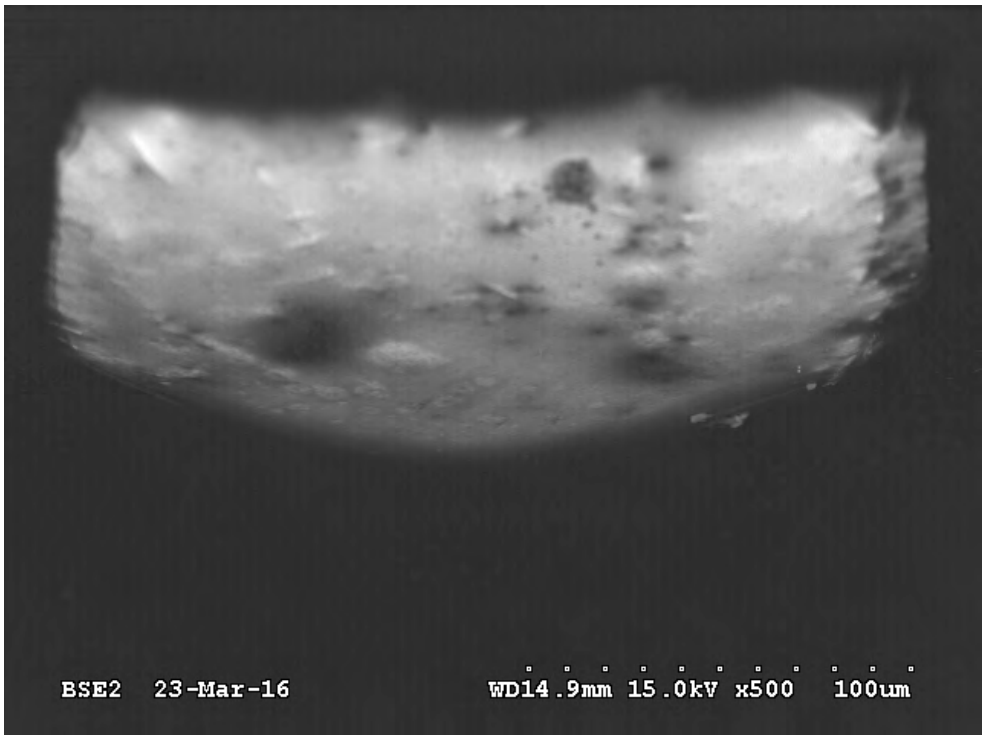


Figure 96: SEM image of PC40-UMF+30%NNN2835 nanosilica coated SOT6 lead, HTHH1767, U65, lead 2, 500x (ref. Board 269).



Figure 97: SEM image of PC40-UMF+30%NNN2835 nanosilica coated SOT6 lead, HTHH1767, U65, lead 2, 3,500x (ref. Board 269).

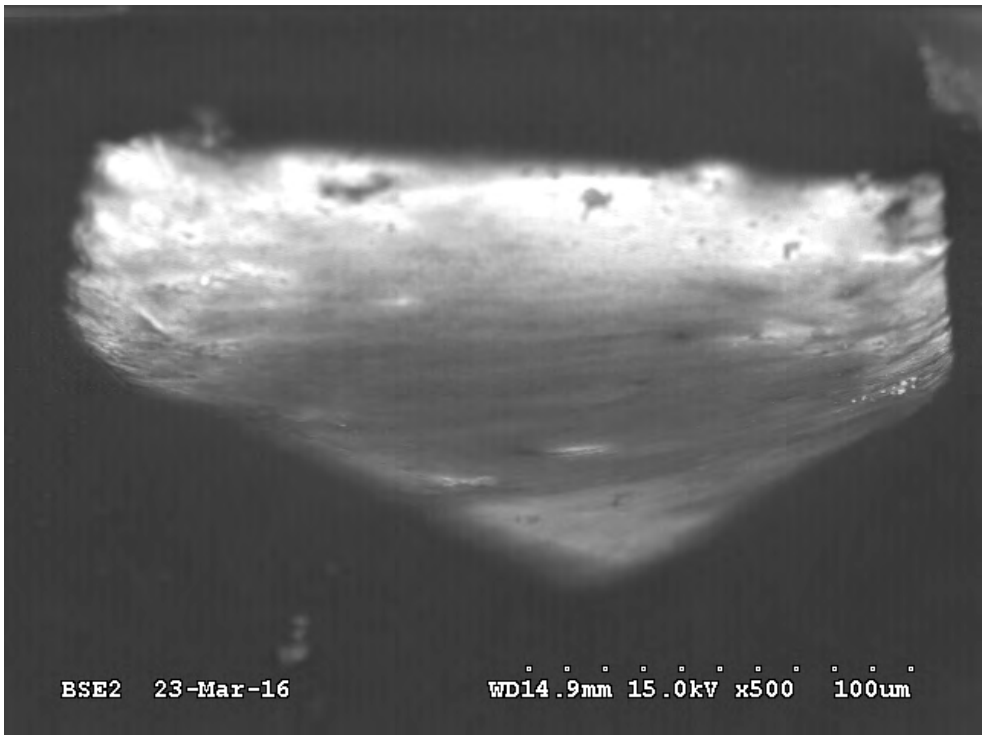


Figure 98: SEM image of PC40-UMF+30%NNN2835 nanosilica coated SOT6 lead, HTHH1767, U65, lead 3, 500x (ref. Board 269).

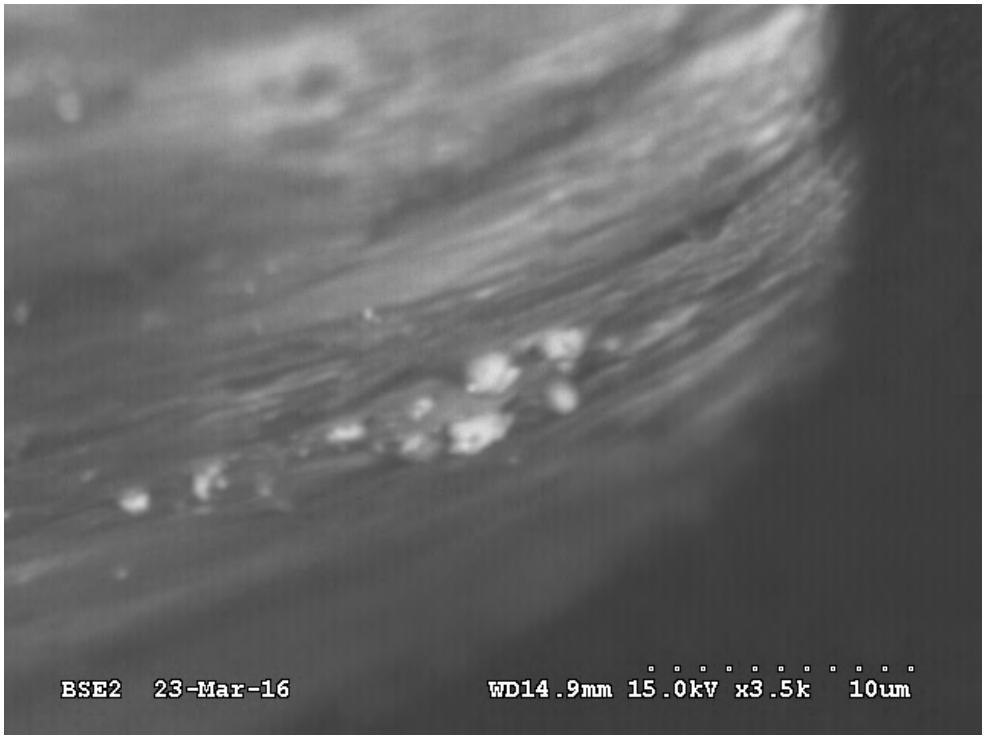


Figure 99: SEM image of PC40-UMF+30%NNN2835 nanosilica coated SOT6 lead, HTHH1767, U65, lead 3, 3500x (ref. Board 269).

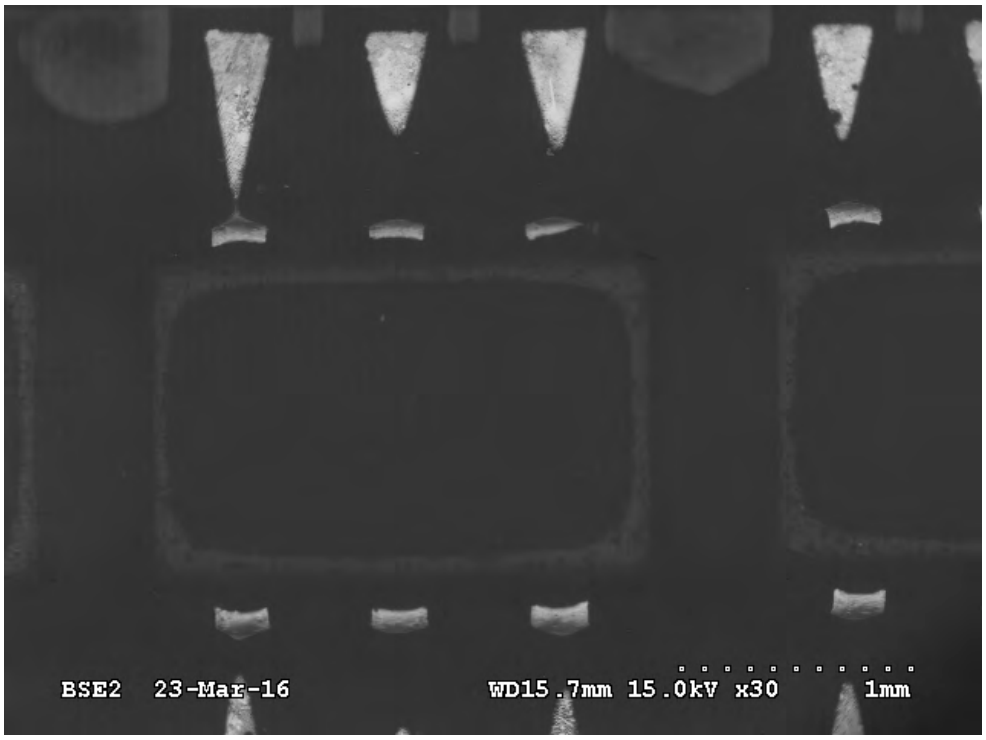


Figure 100: SEM image of PC40-UMF+30%NNN2835 nanosilica coated SOT6 lead, HTHH1767, U70, 30x (ref. Board 269).



Figure 101: SEM image of PC40-UMF+30%NNN2835 nanosilica coated SOT6 lead, HTHH1767, U70, lead 6, 400x (ref. Board 269).

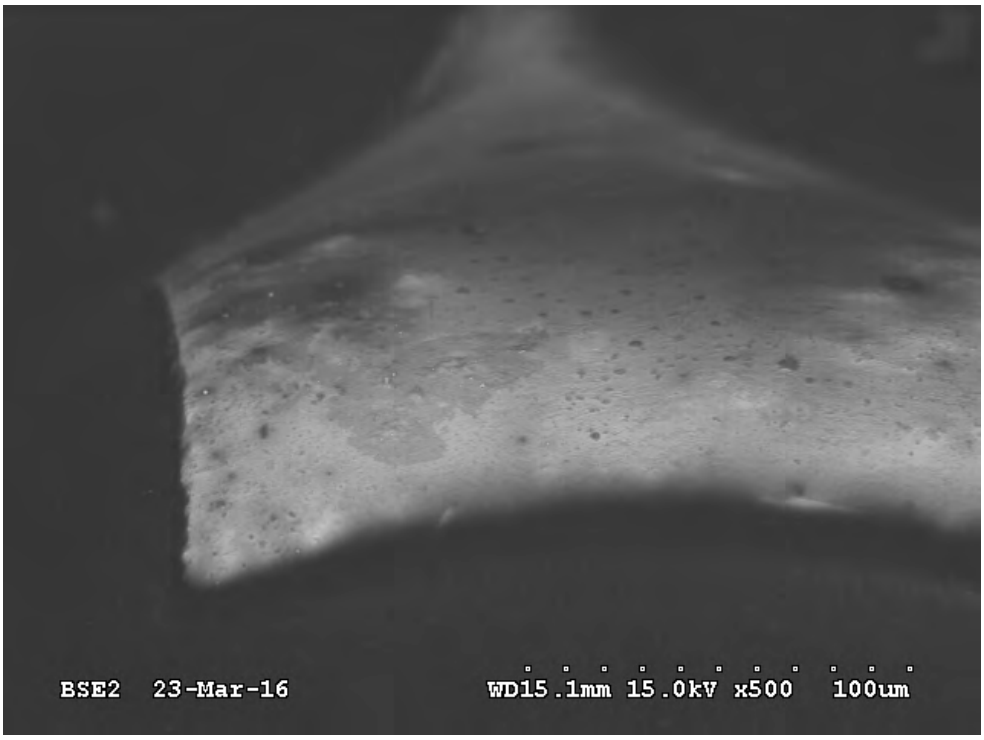


Figure 102: SEM image of PC40-UMF+30%NNN2835 nanosilica coated SOT6 lead, HTHH1767, U70, lead 6, 500x (ref. Board 269).



Figure 103: SEM image of PC40-UMF+30%NNN2835 nanosilica coated SOT6 lead, HTHH1767, U70, lead 6, 4,000x (ref. Board 269).

3.2 Humiseal 1B31-LOC reference coating

The 1B31-LOC acrylic reference coating was tested at the same time as the PC40-UMF based samples. The SEM inspection images are shown in Figure 104 to Figure 112 and summarized in Table 2. Although the 1B31-LOC coated boards samples size was limited (one QFP and SOT board), whisker growth was observed where it was thin (Figure 106). The 1B31 coated samples had less whisker growth than PC40-UMF based coatings, mostly because of the large thin areas due to the dewetting of the PC40-UMF spray coat from the thin dip coat layer.

Table 2: 1B31-LOC acrylic reference coating assembly whisker inspection summary.

Board label	Board type	Observations
85	QFP	Some whisker growth on QFP44 but less than PC40-UMF; none on QFP64 and PLCC
288	SOT	No growth, but debris seen.

3.2.1 SEM images Humiseal 1B31-LOC reference coating

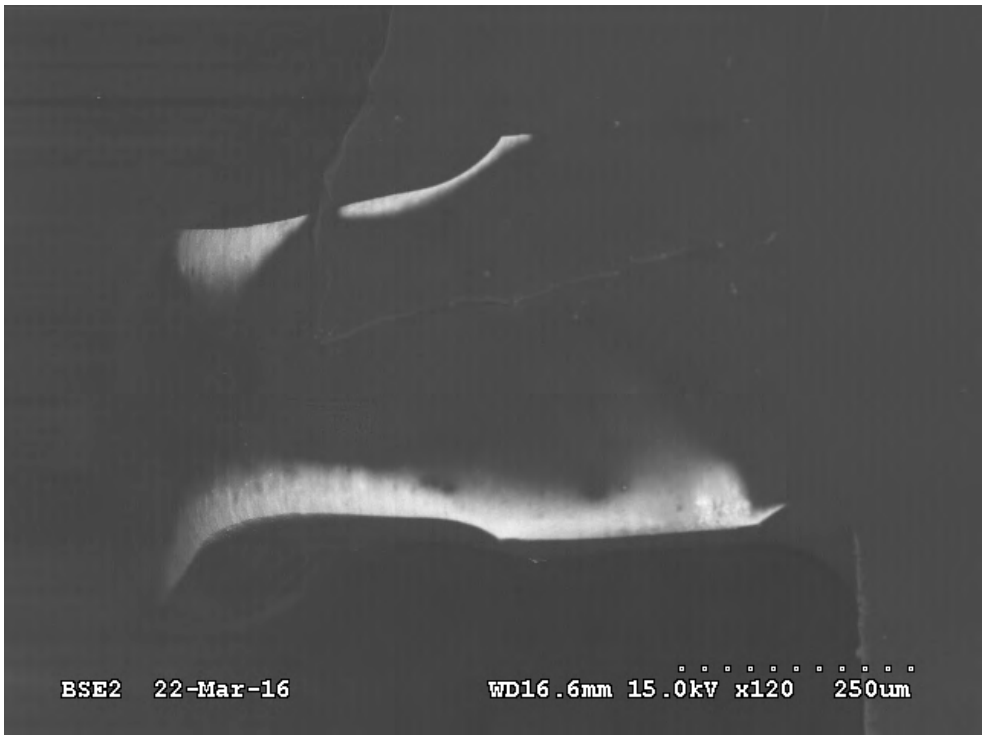


Figure 104: SEM image of 1B31-LOC acrylic coated QFP44 lead, HTHH1767, U5, lead 44, 120x (ref. Board 85).

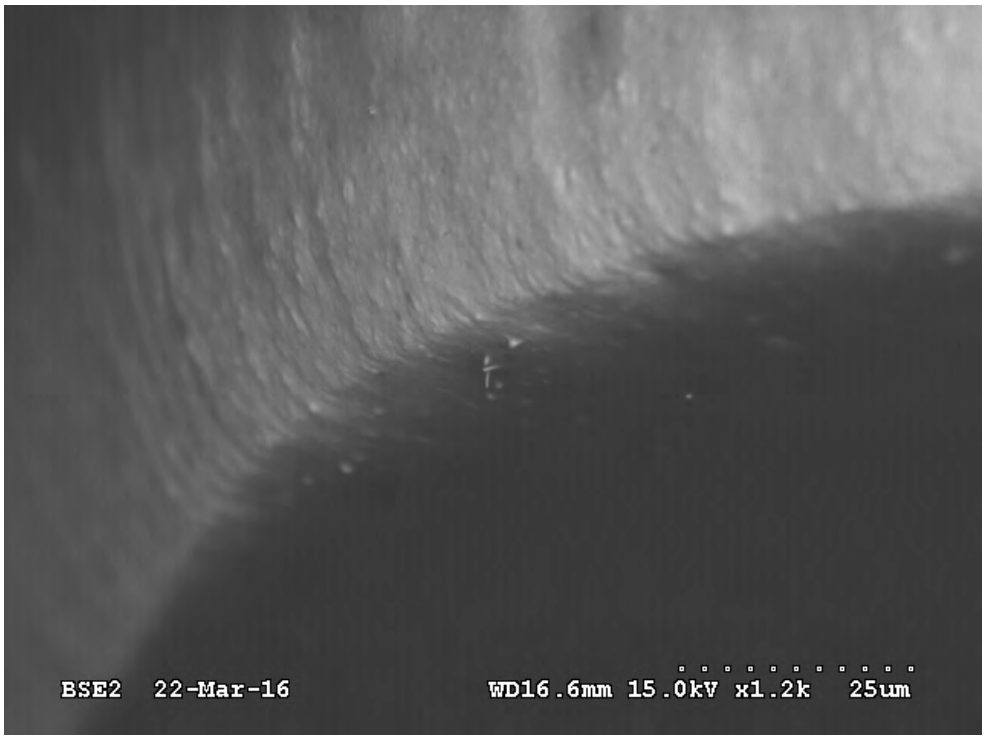


Figure 105: SEM image of 1B31-LOC acrylic coated QFP44 lead, HTHH1767, U5, lead 44, 1,200x (ref. Board 85).



Figure 106: SEM image of 1B31-LOC acrylic coated QFP44 lead, HTHH1767, U5, lead 44, 4,000x (ref. Board 85).



Figure 107: SEM image of 1B31-LOC acrylic coated QFP44 lead, HTHH1767, U5, lead 10, 120x (ref. Board 85).

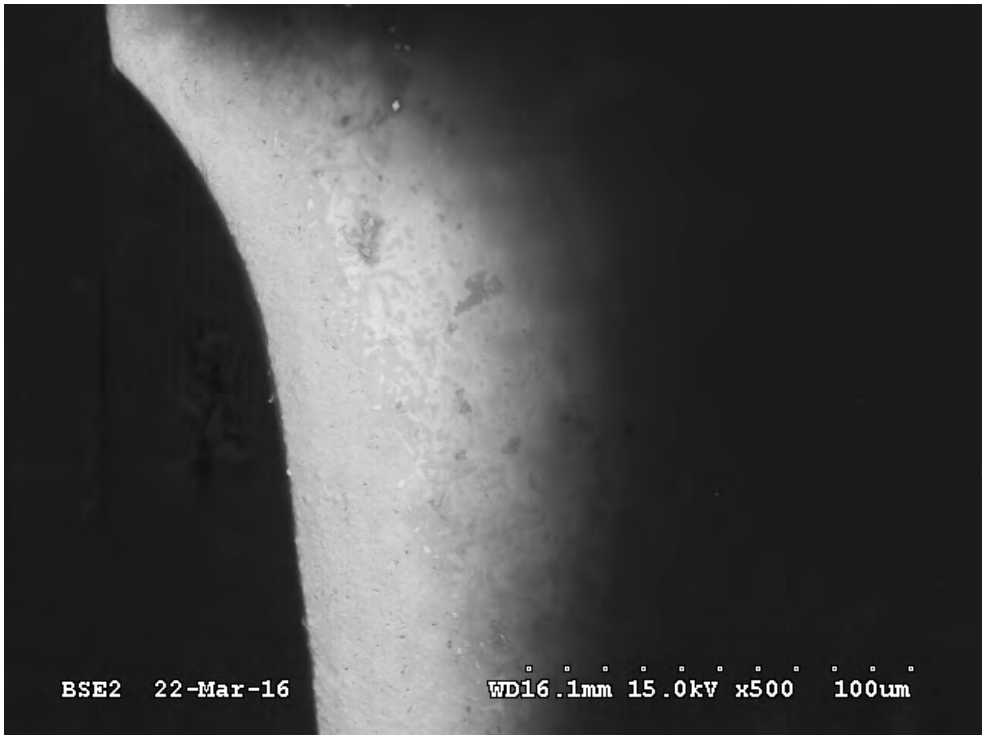


Figure 108: SEM image of 1B31-LOC acrylic coated QFP44 lead, HTHH1767, U5, lead 10, 500x (ref. Board 85).



Figure 109: SEM image of 1B31-LOC acrylic coated QFP44 lead, HTHH1767, U5, lead 10, 500x (ref. Board 85).



Figure 110: SEM image of 1B31-LOC acrylic coated QFP44 lead, HTHH1767, U5, lead 10, 4500x (ref. Board 85).



Figure 111: SEM image of 1B31-LOC acrylic coated SOT5 leads, HTHH1767, 40x (ref. Board 288).

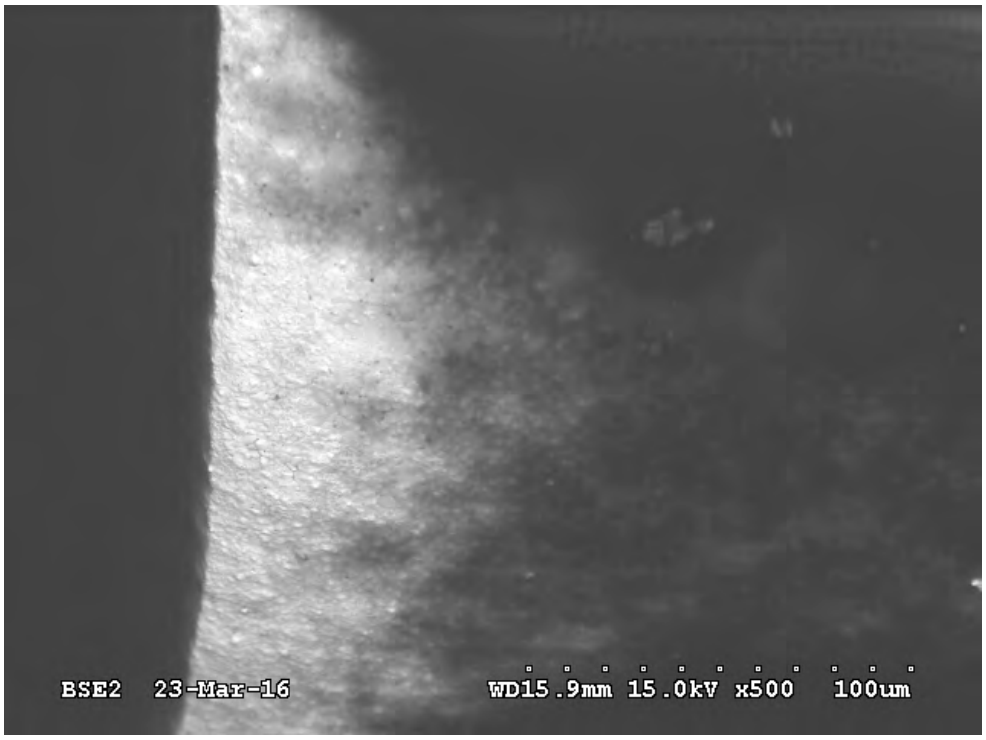


Figure 112: SEM image of 1B31-LOC acrylic coated SOT5 lead, HTHH1767, 500x (ref. Board 288).

4. Summary and Discussion

4.1 Comparison of coatings

Table 3 provides a comparison of uncoated and coated assemblies. The uncoated assemblies had significant tin growth and corrosion. The PC18M-mod coating had good coverage but some cracks and some corrosion on the exposed lead tips. The PC18M+20%XP2742 had a few exposed edges and some small cracks, but fewer than the PC18M-mod. The PC18M+20%11102PMA had the best coverage of the coatings tested and no cracks. All the PC40-UMF based coatings exhibited similar growth where the coating was thin. The PC40-UMF some whisker growth where the coating was thin and had very thin coating over a majority of the lead.

Unfortunately, the best performing spray coating, PC18M+X11102PMA nanoalumina, uses a nanoalumina suspension with significant shelf life issues, nanoparticles that are non – functional and tend to agglomerate in the cured coating, and a disinterested supplier not willing to improve the material at this time.

The 1B31 acrylic reference coating had larger thin areas than any of the PC18M-mod base coatings and exhibited whisker growth where the coating was thin.

The Parylene C ™ and Parylene C ™ with Adpro + adhesion promoter coatings had best coverage and no whisker growth. A hairline crack was observed with the Parylene C ™ with Adpro + adhesion promoter, which after discussion with the material supplier, is not unusual for a thicker coating like the one tested here.

Table 3: Comparison of baseline assembly coatings after environmental testing.

Initial dip	Spray coat	Whiskers/ corrosion	Coating coverage	Coating cracking	Reference
None	None	Whiskers and corrosion	Not applicable		Figure 113 Figure 114 Figure 115
Unfilled PC18M-mod	Unfilled PC18M-mod	No whiskers Corrosion where coating was thin	Thin coating on edges and lead tips	Coating cracks where thick No cracks where thin	Figure 116
	PC18M+ 20%XP2742 nanosilica	None	Thin coating on some lead tips	Smaller cracks than PC18M-mod where thick No cracks where thin	Figure 117
	PC18M+ 20%11102PMA nanoalumina	None	Lead tips covered	No cracks where thin	Figure 118
Unfilled PC40-UMF	Unfilled PC40-UMF	All PC40-UMF based coatings were similar Whiskers where coating was thin	Large thin regions On leads, the spray coating pooled on the dip coat	Cracks and separation where thick No cracks where thin	Figure 119
	PC40-UMF +10%XP2742 nanosilica		Large thin regions Spray coating spread more on dip coating		Figure 120
	PC40-UMF +30%XP2742 nanosilica				Figure 121
None	1B31 Acrylic Reference coating	Whiskers where coating was thin	Moderately large thin regions on lead sides and edges	None	Figure 122
None	Parylene C ™ Reference coating	None	Full coverage	None	Figure 123
None	Parylene C + Adpro plus Reference coating	None	Full coverage	Hairline crack at lead-to-package corner	Figure 124

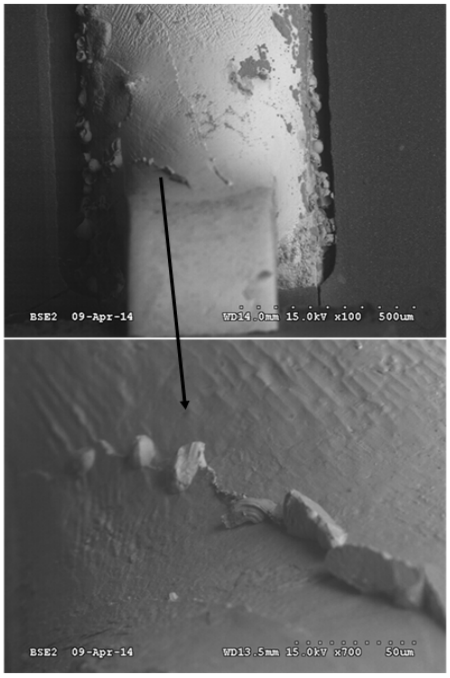


Figure 113: SEM image of an uncoated SOT5 lead (lead 2), ATC+ HTHH1000, 100x (ref. board 238 Figure 4). Corrosion near the bottom of the joint and whisker growth from the boundary between tin grains were observed.

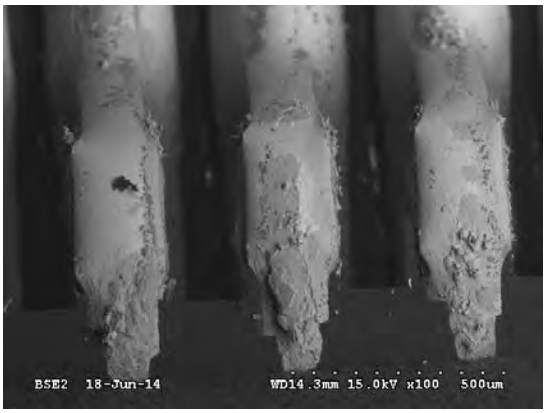


Figure 114: SEM image of uncoated TQFP64 leads, ATC+HTHH2000, 100x (ref. board 46 Figure 6).

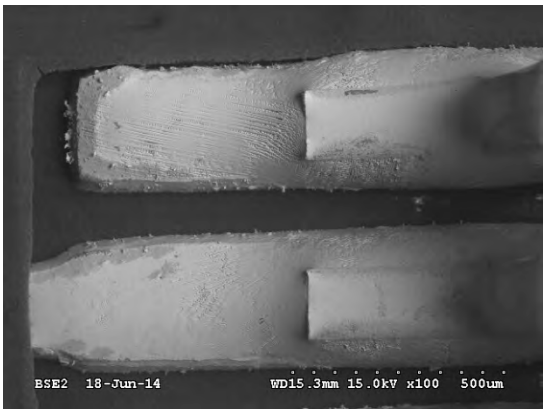


Figure 115: SEM image of uncoated QFP64 lead toes, HTHH2000, 100x (ref. Board 48 Figure 10).

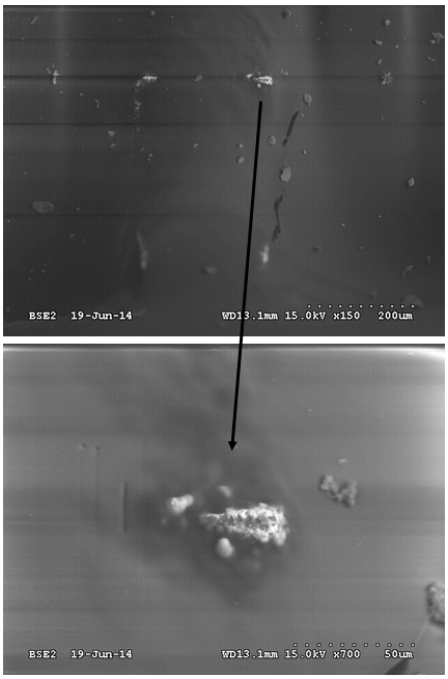


Figure 116: SEM image of PC18M-mod coated SOT6 lead (lead 3), ATC + 2000HTHH, 150x, small bubble density (ref. Board 215 Figure 22).

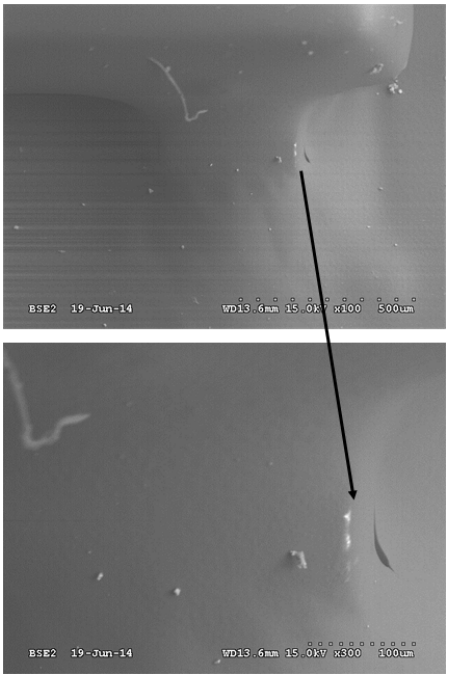


Figure 117: SEM image of PC18M+20%XP2742 nanosilica coated SOT3 lead (lead 2), ATC+HTHH2000, 100x and 300x, medium bubble density (ref. Board 235 Figure 25).

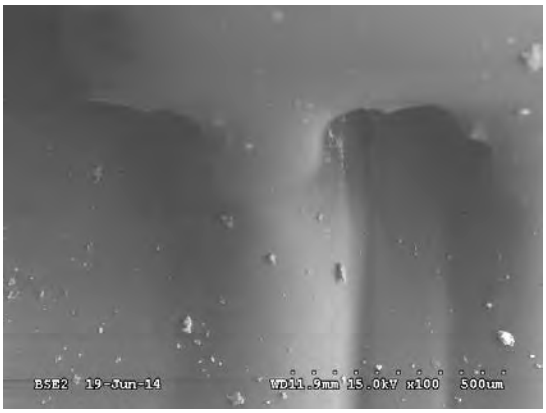


Figure 118: SEM image of PC18M+20%X11102PMA nanoalumina, SOT6, lead 4 (center lead from Figure 23), ATC+HTHH2000, 100x, small/no bubble density (ref. Board 228 Figure 32).

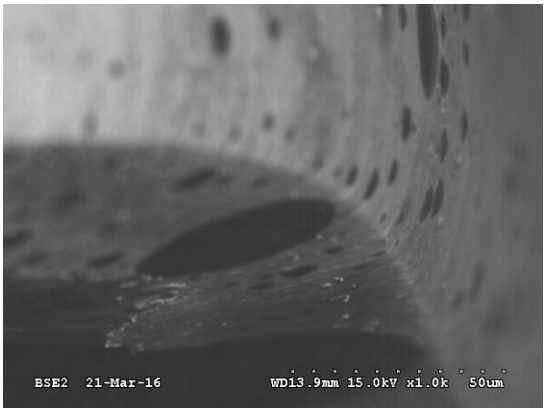


Figure 119: SEM image of PC40-UMF coated QFP44 lead side, HTHH1767, QFP44, U4, lead 12, 1,000x (ref. Board 60 Figure 42).

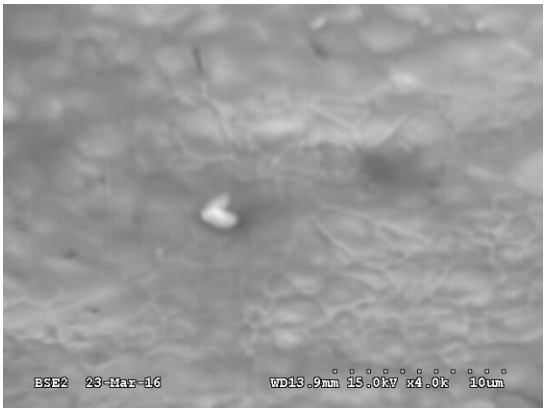


Figure 120: SEM image of PC40-UMF+10%NNN2835 nanosilica coated SOT5 lead, HTHH1767, U16, lead 1, 4000x (ref. Board 284 Figure 73).



Figure 121: SEM image of PC40-UMF+30%NNN2835 nanosilica coated QFP44 lead, HTHH1767, U5, lead 44, 4,000x (ref. Board 70 Figure 86).



Figure 122: SEM image of 1B31-LOC acrylic coated QFP44 lead, HTHH1767, U5, lead 44, 4,000x (ref. Board 85 Figure 106).

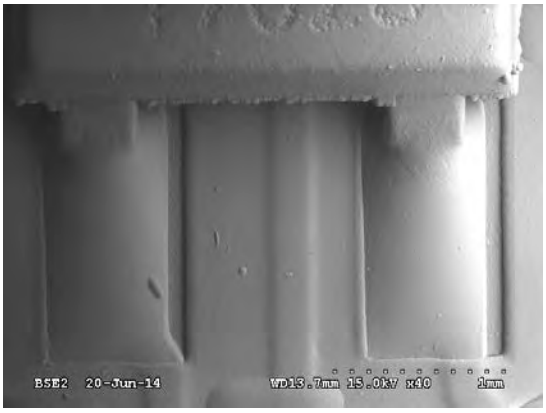


Figure 123: SEM image of Parylene™ C SOT3 leads, ATC + 2000HTHH, 40x (ref. Board 209 Figure 33).

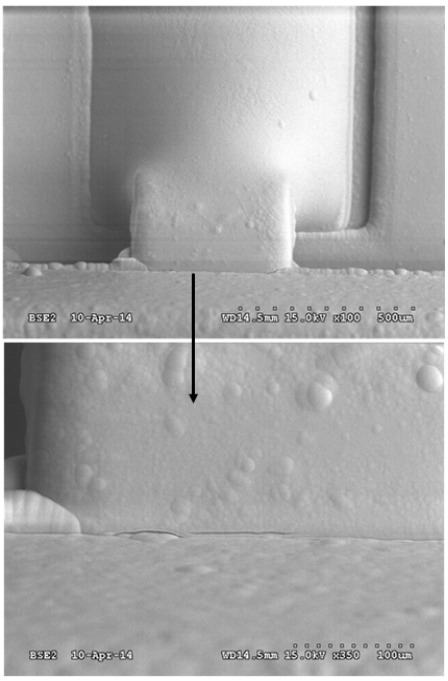


Figure 124: SEM image of a Parylene™ C & Adpro+ coated SOT3 lead, ATC+HTHH1000, 100x and 350x (ref. Board 204 Figure 35). Small coating crack evident at lead-to-package interface.

4.2 Coating thickness

Under conditions of limited thermal cycling and extended high temperature high humidity exposure with the relatively hard coatings tested here, the primary factor for whisker mitigation was coating coverage and thickness. The PC18M based coatings provided better whisker mitigation than the PC40-UMF based coatings, primarily because the PC18M based coatings had better coverage. There was no coating cracking or separation when the coating was relatively thin (~10 to 50 microns), did not fill between adjacent leads, or fill between the package and the leads. Regardless of the coating type, even thin coating on the order of three microns suppressed whisker growth and corrosion as compared to the uncoated assemblies.

4.2.1 Excessively thick coating

Where the coating was excessively thick cracking and pull away from the lead or part were observed. There were several causes for the excessive thickness (1) significant dip coat viscosity increasing with process time, (2) coating bubbles (PC18M-mod and PC18M+20%XP2742 only), and (3) dewetting causing in increased flow of spray material off the leads onto the board. The excessive dip coating tended to fill behind and between the leads (PC40-UMF based coatings only).

The PC18M-mod and the PC40-UMF coatings had differences in cracking behavior where the thickness was excessive. The PC18M-mod coating tended to crack in the coating adjacent to the leads, while the PC40-UMF had more instances of separation between the coating and the lead or package. Where the PC18M based coatings were thick, it cracked adjacent to the leads. The PC40-UMF based coating appeared to have lower adhesion to the lead or package than the PC18M and tended to pull away from the leads and packages. Some of the causes cracking/pull away include coating shrinkage during cure and thermal coefficient of expansion differences of the assembly materials.

4.2.2 Very thin coating with PC40-UMF base coating

The thin coating areas were most pronounced on the PC40-UMF based samples. There were many areas less than approximately three microns thick. These areas had reduced whisker mitigation and corrosion resistance. The material and process factors causing thin PC40-UMF areas are discussed in detail in the coating coverage evaluation appendix [1]. The primary factor was the high surface energy of the cured PC40-UMF dip coating made it difficult to apply another spray layer of PC40-UMF over it and obtain good adhesion, even with plasma etch. In addition, the PC40-UMF viscosity does not increase with solvent evaporation (because it has no solvents) and will thin on corners and vertical surfaces due to liquid surface tension and gravity forces.

4.3 Coating bubbles

While the higher viscosity of the PC18M based coating allowed better coverage, it was also susceptible to bubbles in the coating. The thick coating with bubbles prevented lead inspection because the parts and leads were buried under the coating. While the bubbles were cosmetically unappealing and reduce tensile properties, they did not appear to impact whisker mitigation. It might be possible that whisker growth into a coating bubble would improve whisker containment by allowing the whisker to grow longer and have an increased tendency to buckle (Figure 125). An extensive discussion on the process and material factors contributing to bubble formation is in Appendix F [1].

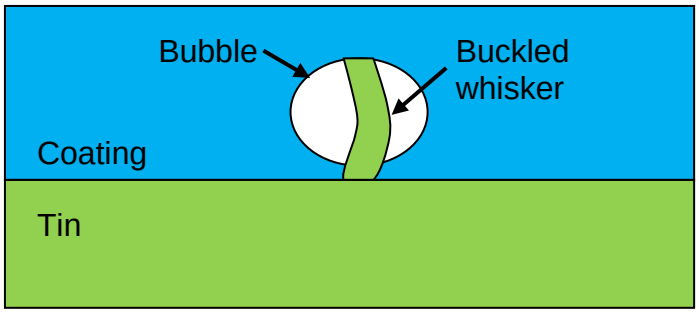


Figure 125: Schematic illustrating whisker buckling in a coating bubble.

4.4 Environmental exposure for coating whisker mitigation evaluation

While 2,000 hours of 85C/85%RH (2000HTHH) was sufficient to grow whiskers on uncoated assemblies, it is unclear if the environmental conditions were optimal for evaluating assembly coating whisker mitigation. Some whisker tests occur over many years [2] [3] [4], but few include thermal cycling [5]. The coating itself inhibits moisture transport to the tin surface. The longer tests could exceed the basic coating hydrolytic stability qualification requirements [6] [7] [8] (aging for 120 days at 85°C and 95%RH).

Even though the tin whisker mitigation is clearly improved with the coatings, unfortunately there is still no model available to correlate environmental testing conditions with service life.

4.5 Comparison of coating whisker performance with the literature

Consistent with the present results of the PC18M-mod polyurethane and the Parylene C ™, the testing by Woodrow [2] also showed that acrylic and silicone coatings had the lowest whisker penetration resistance while the urethane coatings and Parylene C ™ had the best [2].

Also in agreement with the present results, Han [5] evaluated a polyurethane acrylate (designated AR1) and the Humiseal 1B31 acrylic (designated AR2). The AR1 coating exhibited relatively poor coverage and significant whisker penetration where the coating was thin. The AR1 also exhibited whisker penetration.

4.6 Whisker inspection

The present inspection was time consuming and difficult. Examination of three dimensional lead and solder features on assemblies for whisker growth required extensive SEM stage manipulation, magnification changes, and focusing to obtain the images. In addition, there was no easy way to evaluate the metal under the coating since the SEM electron beam was blocked by thicker coating regions.

5. Conclusion

Under conditions of limited thermal cycling and extended high temperature high humidity exposure with the relatively hard coatings tested here, the primary factor for whisker mitigation was coating coverage and thickness. It is important to obtain consistent coating thickness on the leads for optimal whisker mitigation. Thick coatings provide better whisker mitigation than thin coatings. However, excessively thick coating regions exhibited cracking and separation from the leads.

The PC18M based coatings provided better whisker mitigation than the PC40-UMF based coatings, primarily because the PC18M based coatings had better coverage. There was no coating cracking or separation when the coating was relatively thin (~10 to 50 microns) and did not fill between adjacent leads or between the package and the leads. Regardless of the coating type, even thin coating on the order of three microns suppressed whisker growth and corrosion as compared to the uncoated assemblies.

Even though the tin whisker mitigation is clearly improved with the coatings, unfortunately there is still no model available to correlate environmental testing conditions with service life.

The present work highlights the difficulty of whisker inspections on assemblies. The whisker inspection on three dimensional assembly leads and solder was very challenging and time consuming. In addition, the tin under the thicker coating could not be examined. Optical methods have insufficient magnification and the SEM could not examine below the coating surface when it exceeded approximately three microns.

6. Literature cited

[1] Appendix F of the current report: Coating coverage baseline results
[2] T. Woodrow, E. Ledbury, Evaluation of Conformal Coatings as a Tin Whisker Mitigation Strategy, Part 2, Proceedings of the SMTA International Conference, September 24-28, 2006.
[3] L. Panashchenko, J. Brusse and H. Leidecker, Long Term Investigation of Urethane Conformal Coating Against Tin Whisker Growth Tenting of 2mil conformal coating, IPC Tin Whisker Conference Dec. 7, 2010.
[4] L. Woody and W. Fox, Tin Whisker Risk Management by Conformal Coating, SMT magazine, July 2014, pp. 40-58.
[5] S. Han, S. Meschter, M. Osterman and M. Pecht, Evaluation of Effectiveness of Conformal Coatings as Tin Whisker Mitigation, Journal of Electronic Materials, DOI: 10.1007/s11664-012-2179-2, July 6, 2012.
[6] MIL-I-46058, Insulating Compound, Electrical (for Coating Printed Circuit Assemblies), Military Specification, July 1972. Note that the Qualified Providers List (QPL) is still active, but MIL-I-46058 is inactive for new designs.
[7] IPC-CC-830, Qualification and Performance of Electrical Insulating Compound for Printed Wiring Assemblies, IPC-Association Connecting Electronics Industries, Bannockburn, Illinois, USA, Sept. 2008.
[8] IPC-TM-650, Method 2.6.11.1 Hydrolytic Stability - Conformal Coating, IPC-Association Connecting Electronics Industries, Bannockburn, Illinois, USA, July 2000.

SERDP WP2213
Final Report
Appendix I: Coating coverage layered coating results

Appendix I: Table of Contents

1. Introduction 1

2. Evaluation methods 1

2.1 Coverage and thickness 1

2.2 FE – SEM imaging of microtome sections 1

3. Layered coating assembly optical and SEM inspection results 2

3.1 Dip coating 2

3.2 Dip + one spray 2

3.3 Dip + two sprays 2

3.4 Baseline and layered coating comparison 2

4. Vertical cross-section coating thickness evaluation 13

4.1 Thickness of the enhanced (dip+25 micron spray + 25 micron spray) layer coating 13

4.2 Baseline (dip + 50 micron spray) and enhanced layered coating comparison 14

5. Horizontal cross-section coating thickness evaluation 33

6. FE – SEM images of microtome sections 39

6.1 Section one and two 39

6.2 Section three 49

7. Discussion 54

7.1 Dip coating 54

7.1.1 Back of lead dip coverage 54

7.2 Spray coating 54

7.2.1 Back of lead spray coating 56

7.3 Layered coating 56

7.4 Thickness comparison with other research 60

8. Summary 60

8.1 Process 61

8.2 Coverage and thickness 61

9. Conclusions 61

10. Literature cited 62

Appendix I: List of Figures

Figure 1: SEM image of unfilled PC18M dip coated QFP44, board A261, with the light gray color revealing thin coating coverage areas, 30x. 3

Figure 2: Optical image showing example of coating bridging between leads on the board A261, dip only, QFP44, 25x. 3

Figure 3: SEM image of PC18M dip + two (PC18M+20%XP2742) sprays board A336, TQFP64, 40x, with coating bridging. 4

Figure 4: Cross-section optical image of PC18M dip + two (PC18M+20XP2742) sprays, board A225, U1203, QFP44, lead 6-7 showing coating bridging, 100x. 4

Figure 5: SEM image of PC18M dip 1 spray, QFP44, board A156, exhibiting thin coating lead edges and backside of pad as well as surface roughness, 30x. 5

Figure 6: SEM image of PC18M dip + one (PC18M+20%XP2742) spray, board A348, QFP44, thin coating on edges and vertical surfaces of the leads and the printed wiring board vias, 30x..... 5

Figure 7: SEM image of PC18M dip two PC18M sprays, board A191, QFP44, with good overall coverage but still exhibiting surface roughness, 40x. 6

Figure 8: PC18M dip + two PC18M sprays, Board A023, QFP44 lead; (A) 40x and (B) top of lead, 100x, and (C) bottom of lead. 7

Figure 9: SEM image of PC18M dip + two (PC18M+20%XP2742) sprays, board A336, QFP44, 15KV, with good coverage on different leads than those shown in Figure 10, 60x. 8

Figure 10: SEM image of PC18M dip + two (PC18M+20%XP2742) sprays, board A336, QFP44, 15KV, good thick coverage, but arrows indicate small thin coverage areas, 40x. 8

Figure 11: PC18M dip + two (PC18M+20%XP2742) sprays, Board A347, QFP44 lead; (A) 40x, (B) top of lead, 100x, and (C) bottom of lead. The light areas at the lead tips are less than 50 microns long and approximately five microns wide. 9

Figure 12: Photographs illustrating the surface luster of QFP board; (A) PC18M dip only, (B) PC18M dip + two PC18M sprays, and (C) PC18M dip + two (PC18M+20%XP2742) sprays. 10

Figure 13: SEM image from ref. [1] [2] of the PC18M dip followed by a baseline PC18M spray. The image shows extended thin coverage regions (board A015, U2, QFP44 lead 23, 60x). 10

Figure 14: SEM image from ref. [1] [2] of the PC18M dip + baseline PC18M spray. The image shows extended thin coverage regions with measurements (board A011, U2, QFP44 lead 12, 80x). 11

Figure 15: SEM image from ref. [1] [2] of the PC18M dip + baseline PC18M-20%X2742 spray. The arrows indicate location of isolated thin coverage regions less than 50 microns (board A039, U2, QFP44 lead 23). 11

Figure 16: Vertical cross-section thickness measurement locations. 15

Figure 17: Vertical section comparison of location T coating thickness for the enhanced layered coating dip + 25 micron spray + 25 micron spray for a P18M dip with unfilled PC18M spray (left) or PC18M+20%XP2742 nanosilica spray (right). 17

Figure 18: Enhanced layered coating vertical section thickness plots comparing dip only, dip + 25 micron spray, and dip + 25 micron spray + 25 micron spray for a PC18M dip coating and PC18M+20%XP2742 nanosilica spray coating; (A) front of lead side and (B) back side. 18

Figure 19: Vertical section comparison of the dip + baseline 50 micron spray and the enhanced layered dip + 25 micron spray + 25 micron spray for a PC18M dip coating and PC18M+20%XP2742 nanosilica spray coating; (A) front of lead side and (B) back side. 19

Figure 20: Cross-section SEM image of PC18M dip only, board A179, U6, right A, 500x. 20

Figure 21: Cross-section SEM image of PC18M dip only, board A179, U6, right B, 500x..... 20

Figure 22: Cross-section SEM image of PC18M dip only, board A179, U6, right E, 1,000x..... 21

Figure 23: Cross-section SEM image of PC18M dip only, board A179 U6 left T, 1,000x. 21

Figure 24: Cross-section SEM image of PC18M dip only, board A179, U1, left lead, E1, 3,000x. 22

Figure 25: Cross-section SEM image of PC18M dip + one PC18M spray, board A012, U1, left A, 1,000x. 22

Figure 26: Cross-section SEM image of PC18M dip + one PC18M spray, board A012, U1, left B, 1,000x. 23

Figure 27: Cross-section SEM image of PC18M dip + one PC18M spray, board A012, U1, left E, 1,000x. 23

Figure 28: Cross-section SEM image of PC18M dip + one PC18M spray, board A012, U1, left T, 1,000x. 24

Figure 29: Cross-section SEM image of PC18M dip + one PC18M spray, board A012, U6, left E1, 1,500x. 24

Figure 30: Cross-section SEM image of PC18M dip + two PC18M sprays, board A191 U1, right A, 500x. 25

Figure 31: Cross-section SEM image of PC18M dip + two PC18M sprays, board A191 U1 right B, 500x. 25

Figure 32: Cross-section SEM image of PC18M dip + two PC18M sprays, board A191, U1 right E, 1,000x. 26

Figure 33: Cross-section SEM image of PC18M dip + two PC18M sprays, board A191, U1, right T, 1,000x. 26

Figure 34: Cross-section SEM image of PC18M dip + two PC18M sprays, board A191 U1, right lead, E1, 2,000x. 27

Figure 35: Cross-section SEM image of PC18M dip + one (PC18M+20XP2742) spray, board 334, U1, left A, 500x. 27

Figure 36: Cross-section SEM image of PC18M dip + one (PC18M+20XP2742) spray, board 334, U1, left B, 2,000x. 28

Figure 37: Cross-section SEM image of PC18M dip + one (PC18M+20XP2742) spray, board 334, U1, right G, 500x. 28

Figure 38: Cross-section SEM image of PC18M dip + one (PC18M+20XP2742) spray, board 334, U1, left E, 1,000x. 29

Figure 39: Cross-section SEM image of PC18M dip + one (PC18M+20XP2742) spray, board 334 U1 left T, 1,000x..... 29

Figure 40: Cross-section SEM image of PC18M dip + one (PC18M+20XP2742) spray, board 334 U1, left lead, E1, 3,000x. 30

Figure 41: Cross-section SEM image of PC18M dip + two (PC18M+20XP2742) sprays, board A225, U1, right A, 500x. 30

Figure 42: Cross-section SEM image of PC18M dip + two (PC18M+20XP2742) sprays, board A225, U1, right B, 1,000x. 31

Figure 43: Cross-section SEM image of PC18M dip + two (PC18M+20XP2742) sprays, board A225, U1, right E, 1,000x. 31

Figure 44: Cross-section SEM image of PC18M dip + two (PC18M+20XP2742) sprays, board A225, U1, right T, 1,000x. 32

Figure 45: Cross-section SEM image of PC18M dip + two (PC18M+20XP2742) sprays, board A225 U1, right E1, 1,000x. 32

Figure 46: Horizontal cross-section plane location for coating thickness evaluation. 33

Figure 47: QFP44 pin numbering. 33

Figure 48: Horizontal cross-section SEM image of corner leads, PC18M dip + two (PC18M+20XP2742) sprays, board A225, U3, 200x (enhancement added to highlight coating). 34

Figure 49: Cross-section SEM image of PC18M dip + two (PC18M+20XP2742) sprays, board A225, U3, lead 1; (A) 200x, (B) upper back corner, 900x, and (C) lower back corner, 900x. 35

Figure 50: Cross-section SEM image of PC18M dip + two (PC18M+20XP2742) sprays, board A225, U3, lead 22; (A) overall 200x, (B) back left corner, 600x and (C) back, 900x. 36

Figure 51: Cross-section SEM image of PC18M dip + two (PC18M+20XP2742) sprays, board A225, U3, lead 6; (A) 200x, and (B) upper back corner, 900x (enhancement added to highlight coating). 37

Figure 52: Cross-section SEM image of PC18M dip + two (PC18M+20XP2742) sprays, board A225, U3, lead 28; (A) overall, 200x, and, (B) back center and bottom corner, 900x (enhancement added to highlight coating). 38

Figure 53: QFP from board A225 examined using microtome sectioning. 39

Figure 54: Schematic showing microtome section locations. 39

Figure 55: Microtome section perpendicular to lead schematic; (A) materials and (B) locations examined. 40

Figure 56: FE – SEM images of microtome sections (A) section one, and (B) section two 41

Figure 57: FE – SEM of microtome section one at higher magnification; (A) top and (B) bottom. 42

Figure 58: FE – SEM of microtome section two at higher magnification; (A) front and (B) back. 43

Figure 59: FE – SEM of microtome section one outer and inner corners; (A) top right and (B) bottom left. 44

Figure 60: FE – SEM of microtome section one left side. 45

Figure 61: FE – SEM of microtome section two right back along the dip coating web to the adjacent lead. Arrow highlights particle filled spray coating droplets on the dip coating. 45

Figure 62: High magnification FE – SEM images of microtome section two front showing particle uniformity and a well adhered knit line between the two spray layers. 46

Figure 63: High magnification FE – SEM images of microtome section; (A) top of lead showing spray coating to dip coating interface and (B) image from the bottom right showing the spray coating microstructure. 47

Figure 64: Section one dip coat and spray coating thicknesses. 48

Figure 65: Section two dip coat and spray coating thicknesses. Note that a coating bridge between leads prevented measurements on the right side of the lead. 48

Figure 66: Microtome section three examination areas. 49

Figure 67: Overall FE – SEM image of microtome section three lead and coating..... 50

Figure 68: Typical FE – SEM image showing uniform particle distribution (Area C base shown). 50

Figure 69: Section three Area A FE – SEM image; (A) top, and (B) bottom. 51

Figure 70: Section three Area B FE – SEM image; (A) overall, (B) front, and (C) back with arrows showing the first spray layer covered by the second spray layer..... 52

Figure 71: Section three Area C FE – SEM image; (A) overall, (B) back of lead, (C) second location on back of lead with arrow indicating spray coating drop covered with additional spray coating. 53

Figure 72: PC18M-mod SOT board 233 baseline coating with large bubbles around the leads, 10x (note the photograph was taken after thermal cycling and 1,000 hours of 85°C/85%RH humidity (ATC+1000HTHH) environments). The color change in the second image is an artifact of the illumination used to highlight the bubbles [1]. 55

Figure 73: PC18M-mod QFP board 35 baseline coating with large bubble density on top of the package, 10x [1]..... 55

Figure 74: SEM image from the baseline coating test [1][2] of a SOT6 with varying degrees of coating fill around the parts, 60x; (A) board 211, PC18M dip + baseline PC18M spray and (B) board A217, PC18M dip + baseline (PC18M+20%XP2742). Note images taken after accelerated thermal cycling. 57

Figure 75: SEM image of PC18M dip + two PC18M sprays, board 243, SOT6, 60x, with thick coating behind leads. 58

Figure 76: SEM image of PC18M dip + two (PC18M+20%XP2742) sprays, board 51, SOT6, (A) leads almost filled, 40x, and (B) lead to body area filled. 59

Figure 77: 5-22arr IPC J-STD-001 conformal coating and material application industry assessment interim results. Actual minimum thicknesses on leads (solid line) much less than unencumbered flat surface (dashed line) process control measurement..... 60

Appendix I: List of Tables

Table 1: QFP44 SEM coating coverage inspection results. 12
Table 2: Vertical section layered coating front side and selected back side thickness measurements. 16
Table 3: Vertical section layered coating back side thickness measurements. 17
Table 4: Typical SEM layered coating cross-section images. 17

Acronyms

Acronym	Definition
EDX	Energy Dispersive X-ray Spectroscopy
FE SEM	Field Emission Scanning Electron Microscopy
FOD	Foreign Objects and Debris
QFP	Quad Flat Pack Electronic Packages
SEM	Scanning Electron Microscopy
SOT	Small Outline Transistor Electronic Packages

1. Introduction

In the present work, the layered coating approach was used to obtain better coverage than the baseline spray process [1] [2] and in turn improve whisker mitigation. The baseline spray process used a dip coat/partial cure/spray coat/final cure and the layered coating approach consists of a dip layer/partial cure/spray layer/partial cure/spray layer/full cure. Both the baseline and the layered coating process targeted a 25 to 75 micron thick coating on the flat surfaces in accordance with J-STD-001 Class 3 [3].

The layered process used the PC18M family of coating materials were selected for the layered process because of their superior interlayer adhesion as compared to the PC40-UMF materials [1]. As was done with the baseline coating, a thinned PC18M dip coat was used as the initial layer to apply some coating to the front and back of all the leads. For the spray layers, assemblies sprayed with PC18M were compared to PC18M+20%XP2742 nanosilica spray coats. The coating coverage was evaluated on the quad flat pack (QFP) and the small outline transistor (SOT) boards. The coverage and thickness obtained from assemblies with the "dip only" coat were compared to the "dip + spray" and the "dip + spray + spray" layer process.

2. Evaluation methods

2.1 Coverage and thickness

In the present work, the assemblies were evaluated from a mitigation perspective using a combination of optical and scanning electron microscope (SEM) inspection at magnifications up to 5,000x in conjunction with cross-sectioning. SEM imaging is an effective means of evaluating coating coverage over the metal surfaces, coating cracking, and tin whiskers [4]. With regard to coating coverage over metal, the SEM images can provide qualitative thickness information. The SEM image is dark when the coating is greater than approximately three microns thick and the electron beam cannot penetrate though the coating to the underlying metal. The SEM image becomes gray when the beam penetrates through the coating and interacts with the underlying metal. In this case, the coating is less than approximately three microns thick. The SEM image is brightest when directly imaging metal that either has no coating or very thin coating that the beam can easily penetrate. Note that some bright image regions on the leads evaluated with EDX (electron dispersive x-ray) were found to have a significant carbon peak, suggesting that some coating was present. Also, in a particular image the darkness also increases due to the incident electron beam angle with respect to the coating surface. So even if the coating thickness has not changed, some regions of the lead could be darker or lighter depending upon the orientation of the lead surface. In addition, comparing different images can be problematic because incident electron beam energy and brightness/contrast settings change for each image. Furthermore, non-conductive debris often appears as bright regions and can be difficult to differentiate from metal whiskers unless and EDX is used to verify the presence of tin.

2.2 FE – SEM imaging of microtome sections

To allow discrimination between the layers, microtome sections were obtained of potted leads. The microtome uses a highly polished hardened blade to slice through the materials of interest without conventional polishing media that could be embedded into the sample surface. The field emission scanning electron microscope (FE – SEM) is capable of imaging up to 100,000x and can resolve the 20 nanometer diameter nanosilica particles in the polyurethane matrix and can also reveal elements of the polyurethane structure.

3. Layered coating assembly optical and SEM inspection results

3.1 Dip coating

SEM examination of the “dip only” QFPs showed that the front and portions of the lead sides had coating thicker than approximately three microns (darker areas in Figure 1), while the corners and edges of the leads and the board pads were thin (light areas in Figure 1). The dip coating resulted in some bridging of the QFP44 and TQFP64 leads (Figure 2 to Figure 4). Cross – sectioning showed that the coating webs between leads were generally thin.

3.2 Dip + one spray

One spray layer of unfilled PC18M over the unfilled PC18M dip coating exhibited good coverage, but was rough (Figure 5).

The PC18M dip + one spray (PC18M+20%XP2742) nanosilica resulted in good coverage (Figure 6) and was smoother than the PC18M coating.

3.3 Dip + two sprays

The addition of a second spray and cure layer improved coverage for both the unfilled PC18M (Figure 7 and Figure 8) and the PC18M+20%XP2742 nanosilica filled spray (Figure 9). Although coverage was improved, there were some very small thin coating areas on some of the lead tips (Figure 10 and Figure 11) with the PC18M+20%XP2742 nanosilica filled spray.

The degree of surface roughness was greater on the PC18M dip + 2 spray layers of PC18M than on the PC18M dip + 2 spray layers of (PC18M+20%XP2742) QFPs. The unfilled PC18M spray surface appeared to have pits and craters that looked like popped microbubbles. Comparing the unfilled PC18M spray to the other coatings optically, it was duller (Figure 12).

3.4 Baseline and layered coating comparison

The layered coating coverage was generally better than the coverage obtained earlier with the baseline PC18M dip followed by a baseline 50 micron spray coating process (repeated here in Figure 13 to Figure 15) [1][2].

By counting the number of thin coating regions for various coatings, the layered spray coatings were measurably better than the baseline coatings (Table 1). While the current SEM results favor the unfilled PC18M without the nanoparticles, the roughness of the unfilled PC18M surface made it more difficult to examine the lead tips areas.

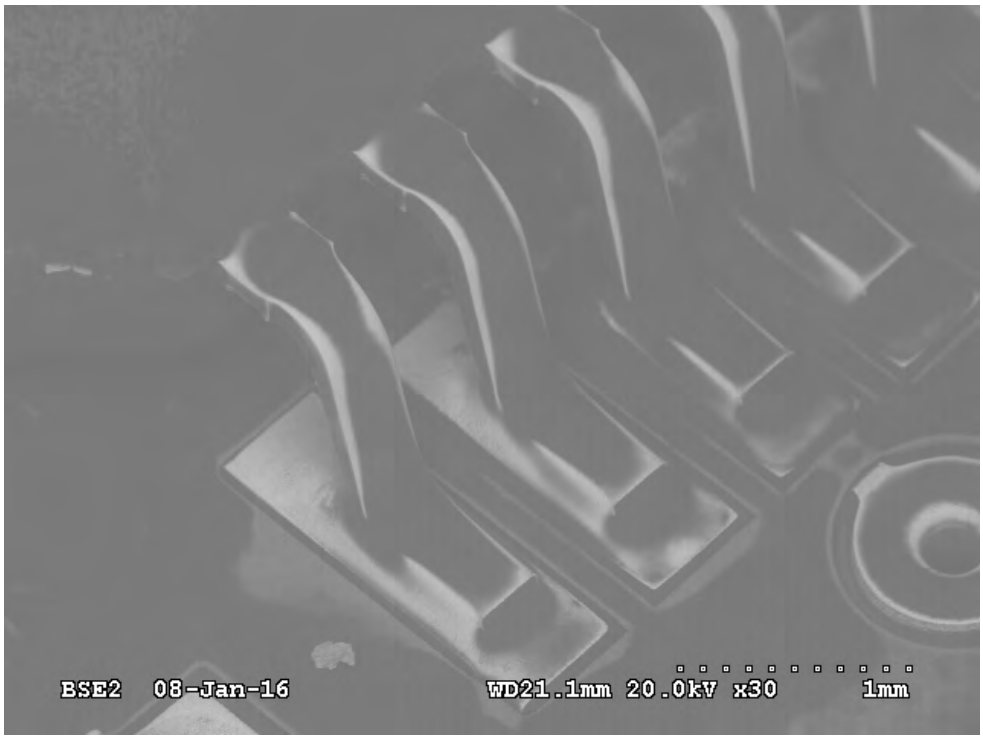


Figure 1: SEM image of unfilled PC18M dip coated QFP44, board A261, with the light gray color revealing thin coating coverage areas, 30x.

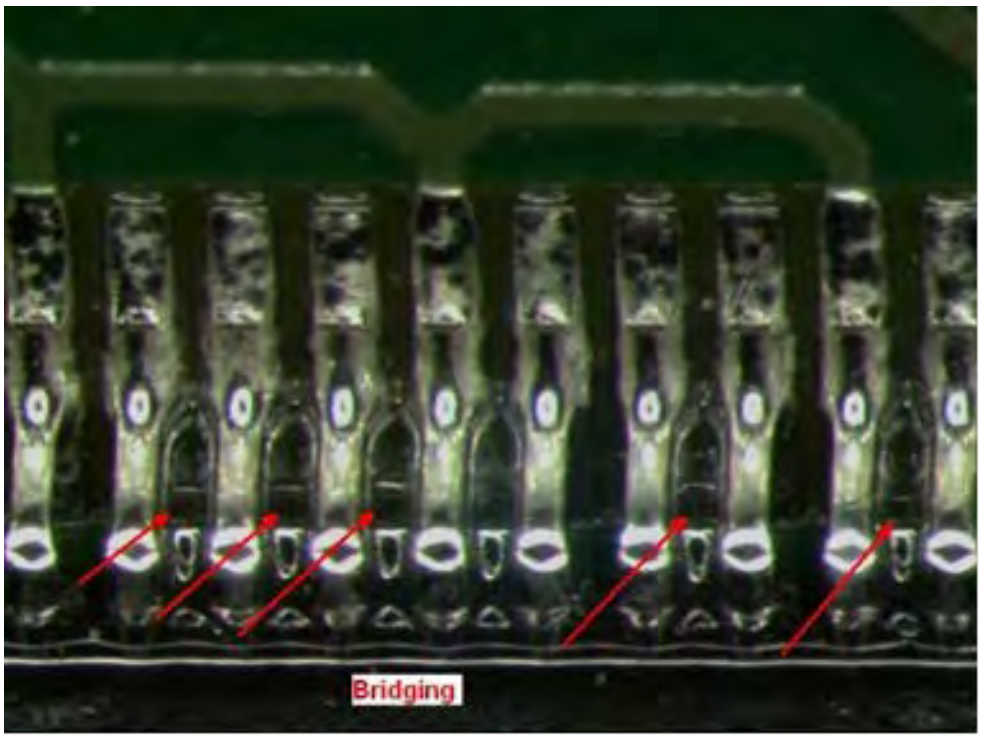


Figure 2: Optical image showing example of coating bridging between leads on the board A261, dip only, QFP44, 25x.

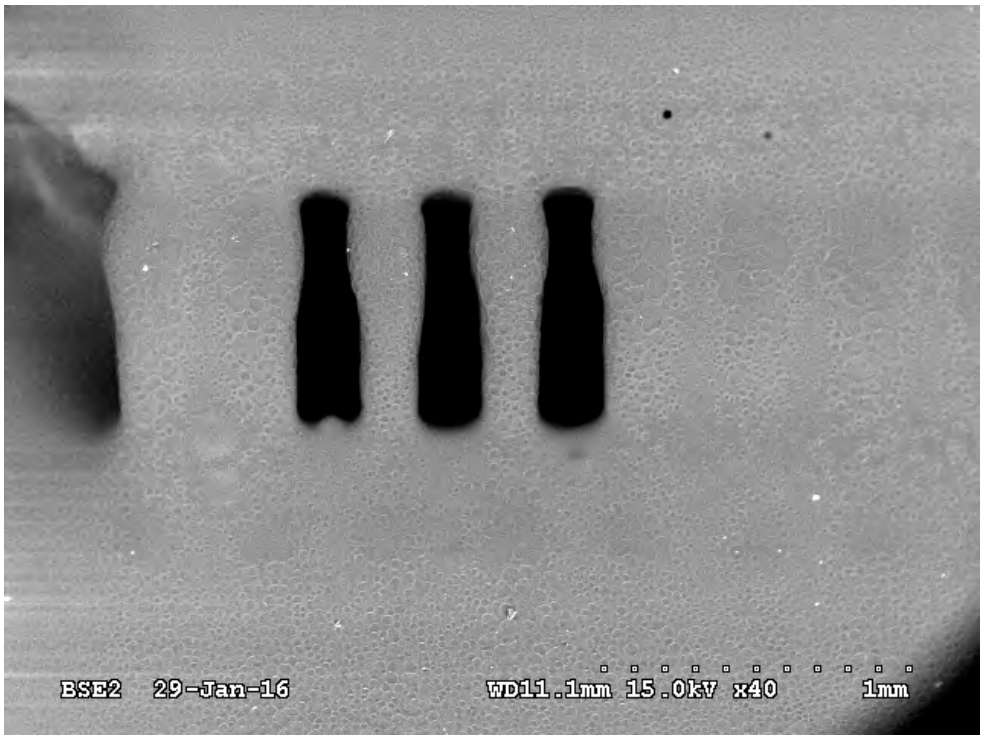


Figure 3: SEM image of PC18M dip + two (PC18M+20%XP2742) sprays board A336, TQFP64, 40x, with coating bridging.

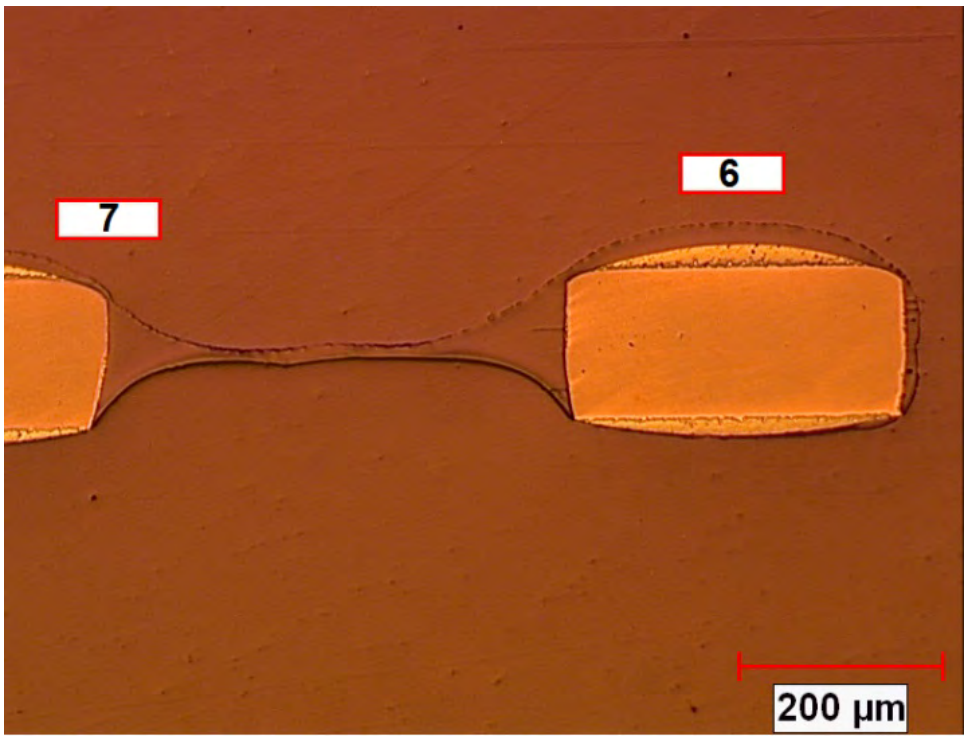


Figure 4: Cross-section optical image of PC18M dip + two (PC18M+20XP2742) sprays, board A225, U1203, QFP44, lead 6-7 showing coating bridging, 100x.

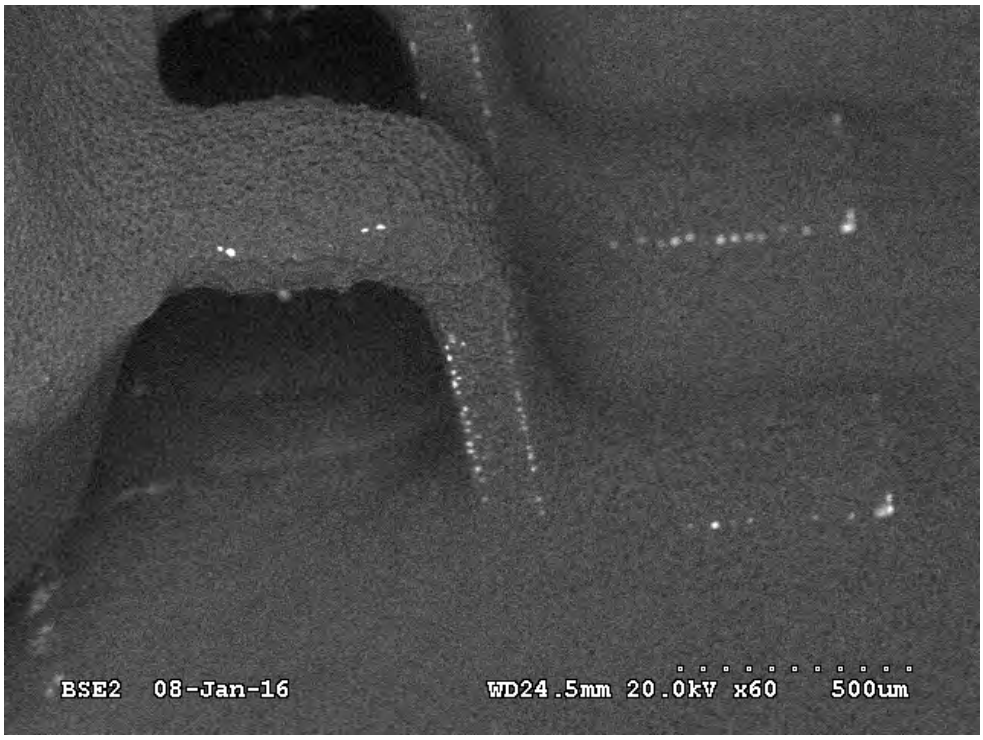


Figure 5: SEM image of PC18M dip 1 spray, QFP44, board A156, exhibiting thin coating lead edges and backside of pad as well as surface roughness, 30x.

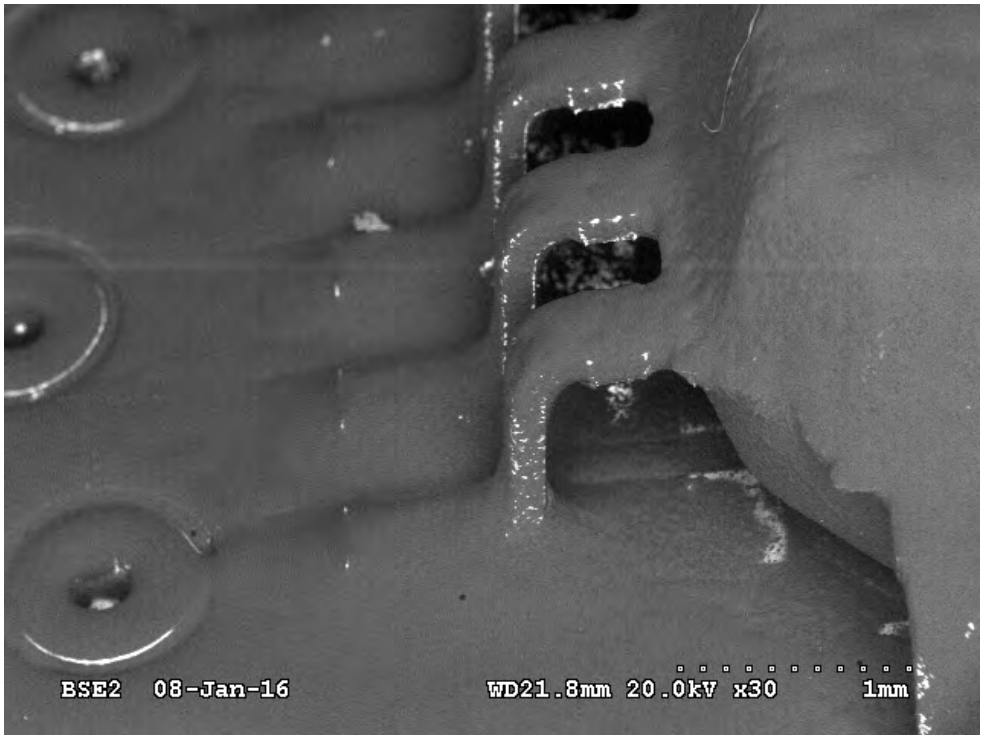


Figure 6: SEM image of PC18M dip + one (PC18M+20%XP2742) spray, board A348, QFP44, thin coating on edges and vertical surfaces of the leads and the printed wiring board vias, 30x.

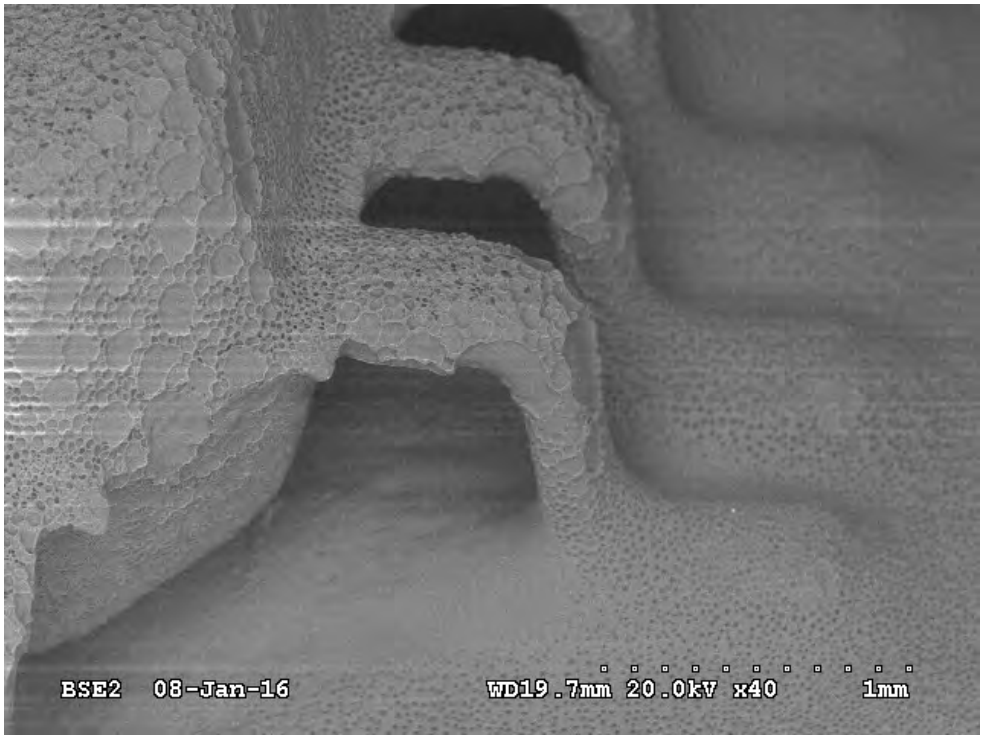


Figure 7: SEM image of PC18M dip two PC18M sprays, board A191, QFP44, with good overall coverage but still exhibiting surface roughness, 40x.

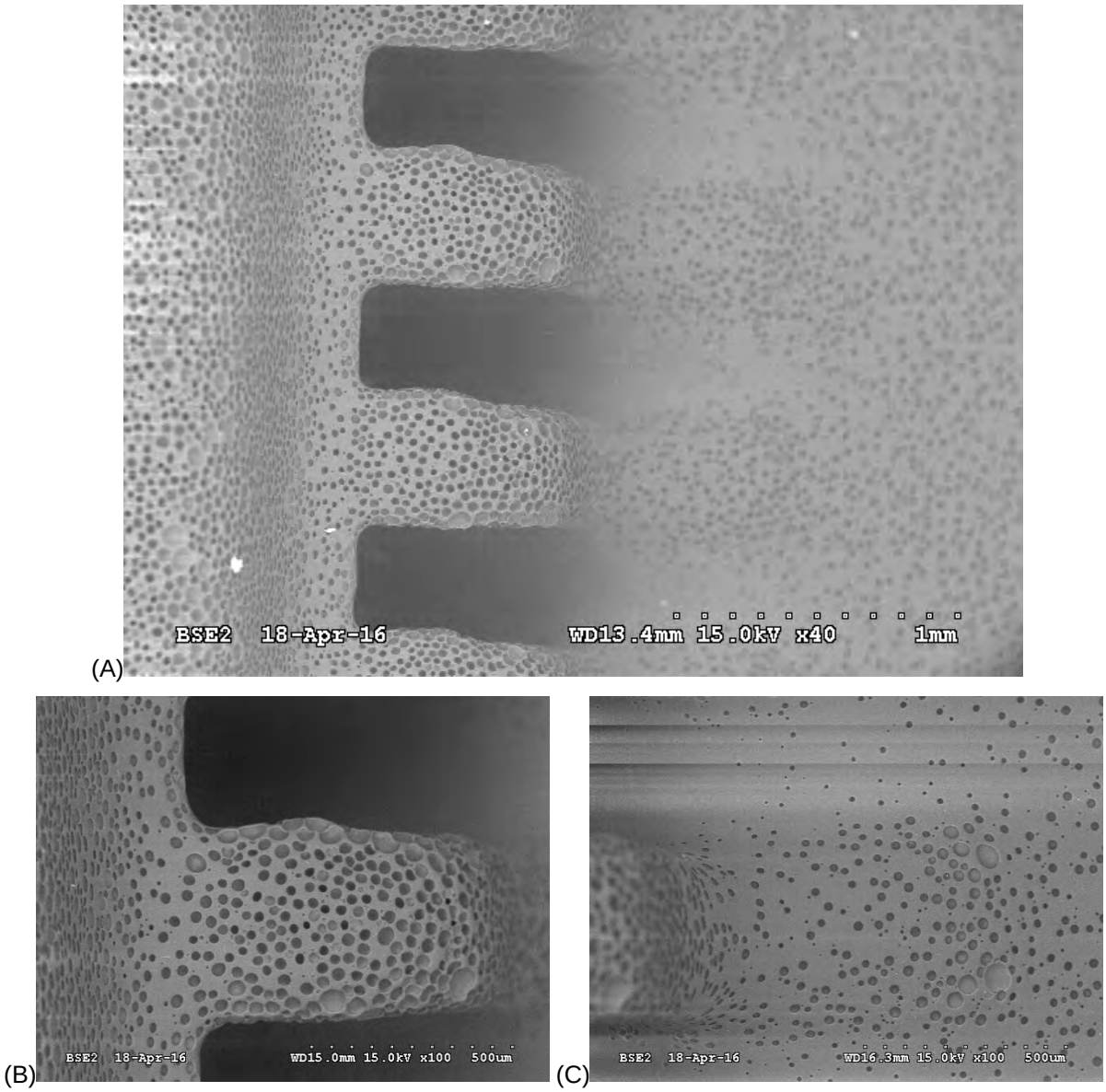


Figure 8: PC18M dip + two PC18M sprays, Board A023, QFP44 lead; (A) 40x and (B) top of lead, 100x, and (C) bottom of lead.

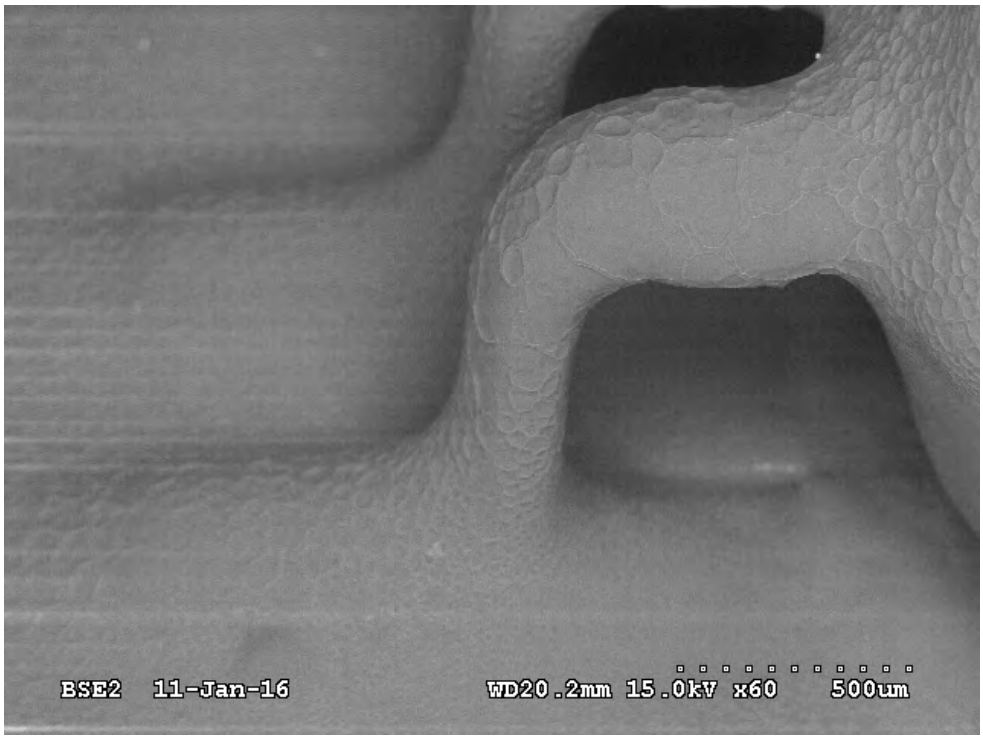


Figure 9: SEM image of PC18M dip + two (PC18M+20%XP2742) sprays, board A336, QFP44, 15KV, with good coverage on different leads than those shown in Figure 10, 60x.

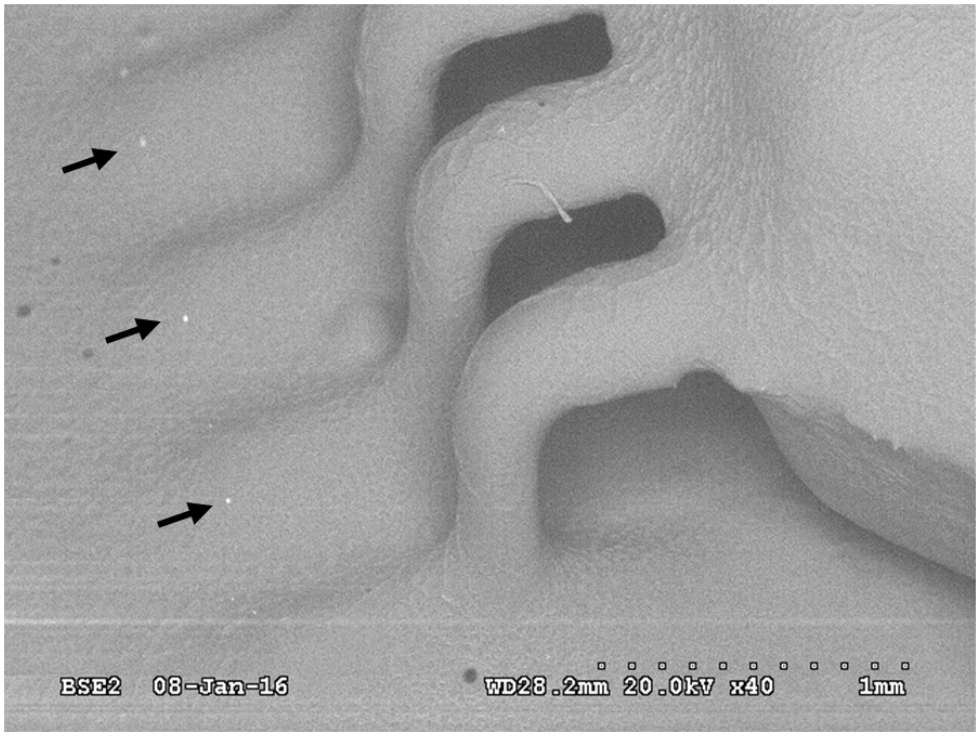
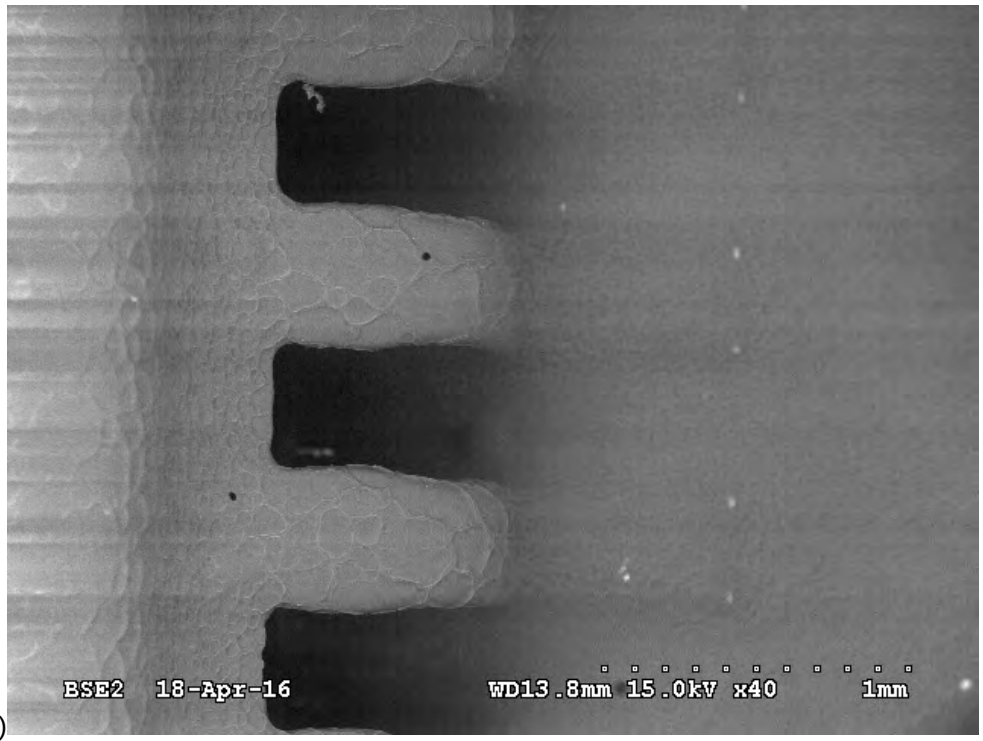


Figure 10: SEM image of PC18M dip + two (PC18M+20%XP2742) sprays, board A336, QFP44, 15KV, good thick coverage, but arrows indicate small thin coverage areas, 40x.

(A)



(B)



(C)

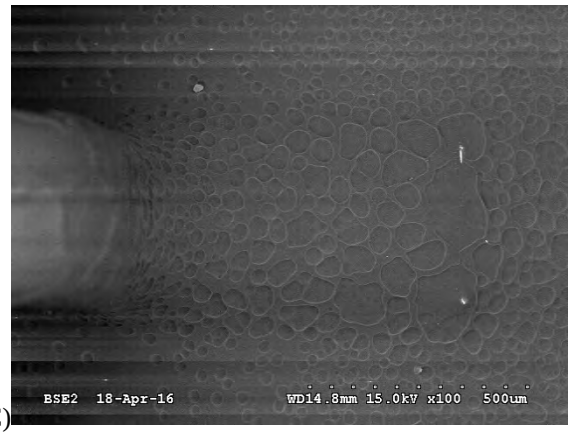


Figure 11: PC18M dip + two (PC18M+20%XP2742) sprays, Board A347, QFP44 lead; (A) 40x, (B) top of lead, 100x, and (C) bottom of lead. The light areas at the lead tips are less than 50 microns long and approximately five microns wide.

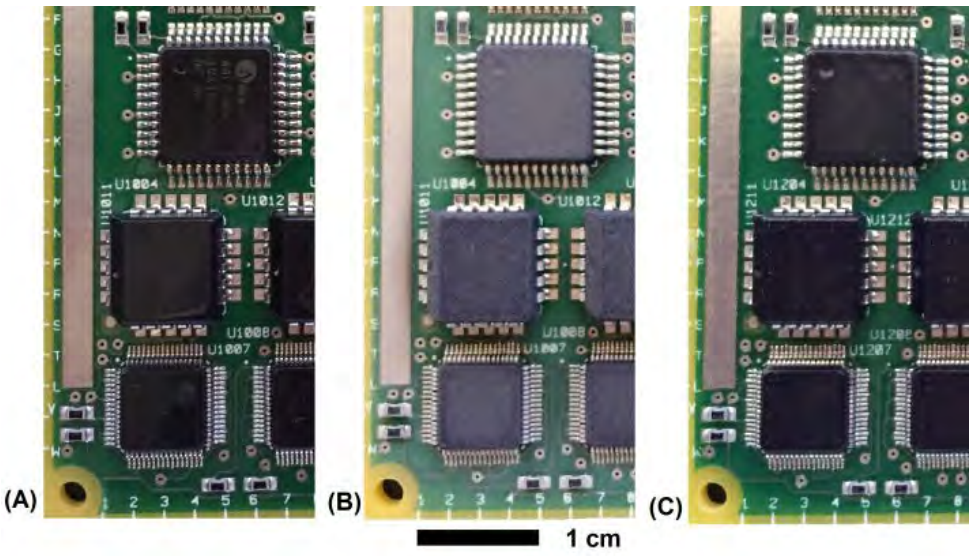


Figure 12: Photographs illustrating the surface luster of QFP board; (A) PC18M dip only, (B) PC18M dip + two PC18M sprays, and (C) PC18M dip + two (PC18M+20%XP2742) sprays.



Figure 13: SEM image from ref. [1] [2] of the PC18M dip followed by a baseline PC18M spray. The image shows extended thin coverage regions (board A015, U2, QFP44 lead 23, 60x).

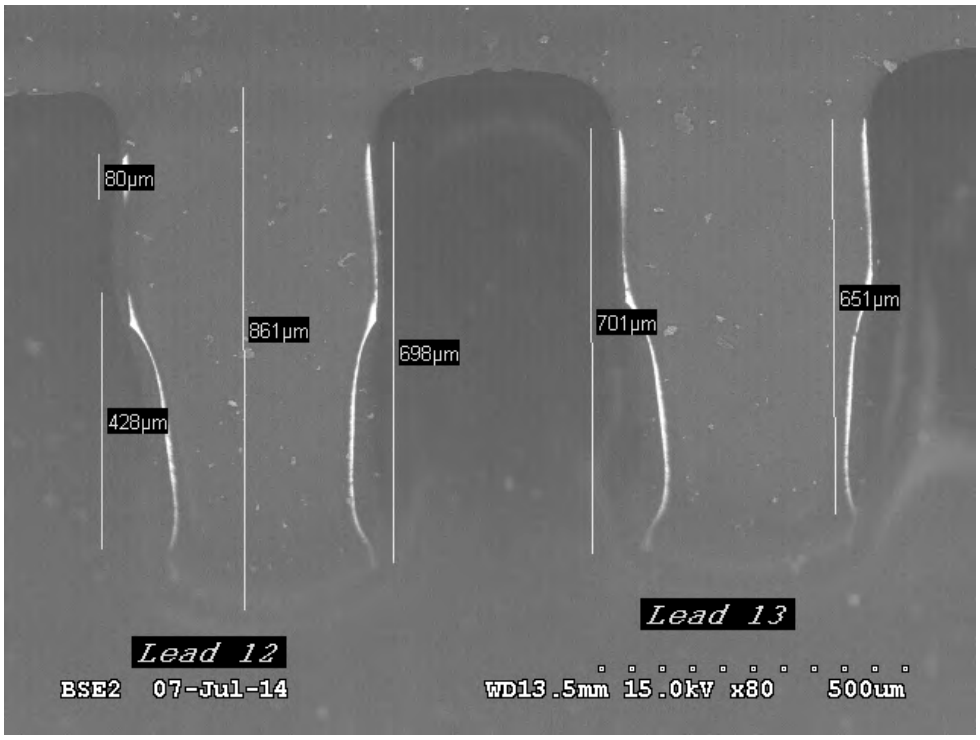


Figure 14: SEM image from ref. [1] [2] of the PC18M dip + baseline PC18M spray. The image shows extended thin coverage regions with measurements (board A011, U2, QFP44 lead 12, 80x).

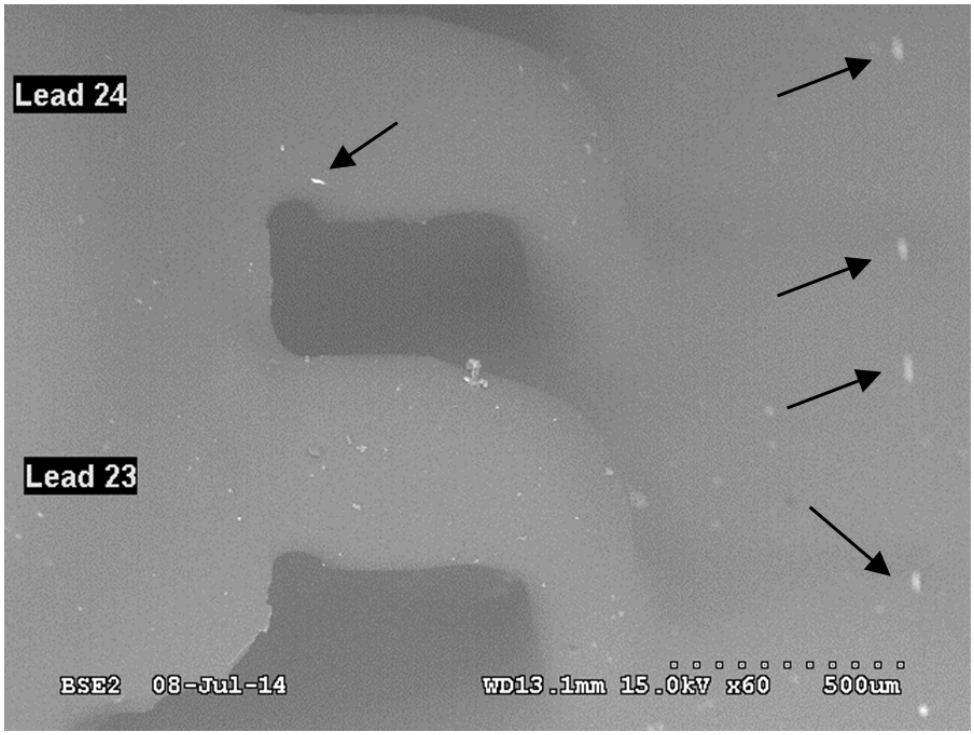


Figure 15: SEM image from ref. [1] [2] of the PC18M dip + baseline PC18M-20%X2742 spray. The arrows indicate location of isolated thin coverage regions less than 50 microns (board A039, U2, QFP44 lead 23).

Table 1: QFP44 SEM coating coverage inspection results.

Coating	Total leads inspected (1)	Total thin areas	Total less than 50 µm	Total greater than 50 µm
Baseline spray PC18M [1][2]	14	43	15	28
Baseline spray PC18M+20% XP2742 [1][2]	17	10	10	1
Layered PC18M dip + two spray PC18M (1)	11	3	3	0
Layered PC18M dip + two PC18M+20%XP2742	11	11	11	0
Note 1: The rough surface on the PC18M sprayed samples made it difficult to examine for thin coating.				

4. Vertical cross-section coating thickness evaluation

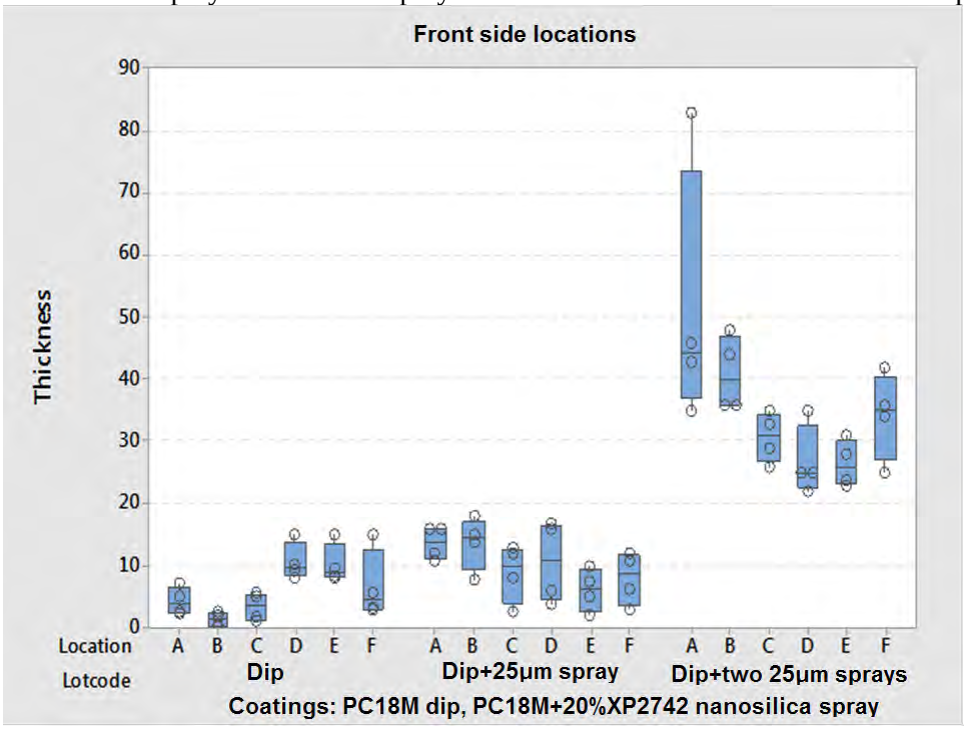
The vertical cross-section coating thickness analysis was performed on the QFP44 components. The measurement locations are shown in Figure 16. The tabular thickness data is given in Table 2 and Table 3. Selected figures showing front and the back side SEM cross-section images are summarized in Table 4.

The 2015 goal for the layered coating was to have the minimum coating thickness of 10 microns on the front and side lead surfaces along with less pooling at the bottom of the lead/package, and less coating thickness variation, both lead to lead and along the lead.

4.1 Thickness of the enhanced (dip+25 micron spray + 25 micron spray) layer coating

For the enhanced layer spray (PC18M dip + 25 micron spray + 25 micron spray), the lead tip location T thickness was more uniform with the PC18M+20%XP2742 nanosilica sprays than the unfilled PC18M spray was used (Figure 17). Due to the roughness of the layered PC18M spray samples, the thickness graphs focused on the layered PC18+20%XP2742 samples.

The enhanced layered coating progressive thickness increase from dip to dip + 25 micron spray to dip + 25 micron spray + 25 micron spray for the PC18M+20%XP2742 nanosilica spray is shown in (A)



(B)

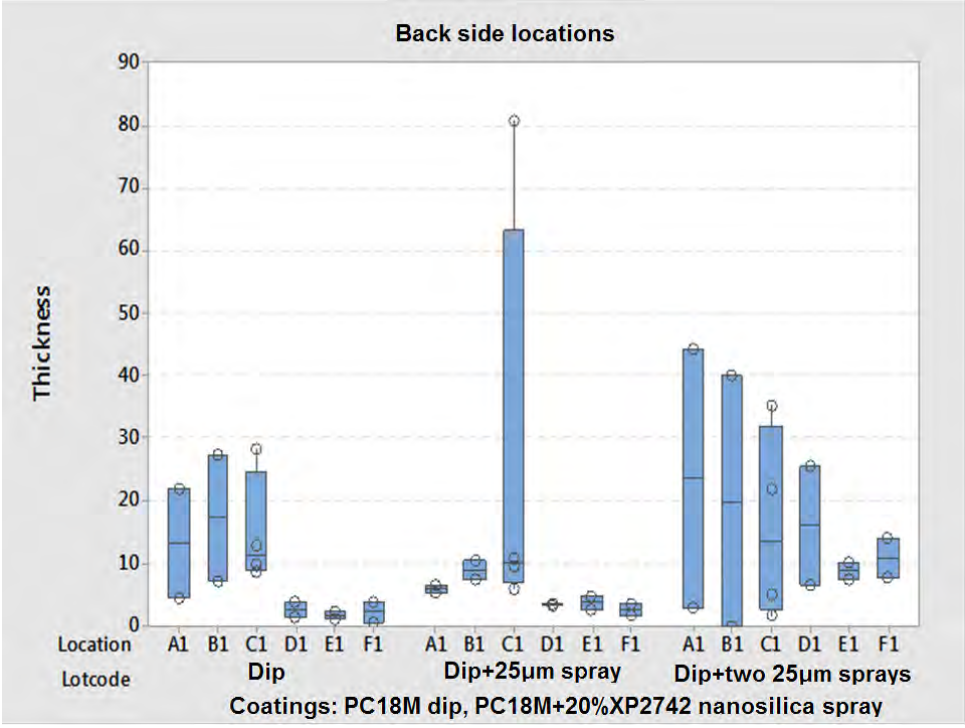
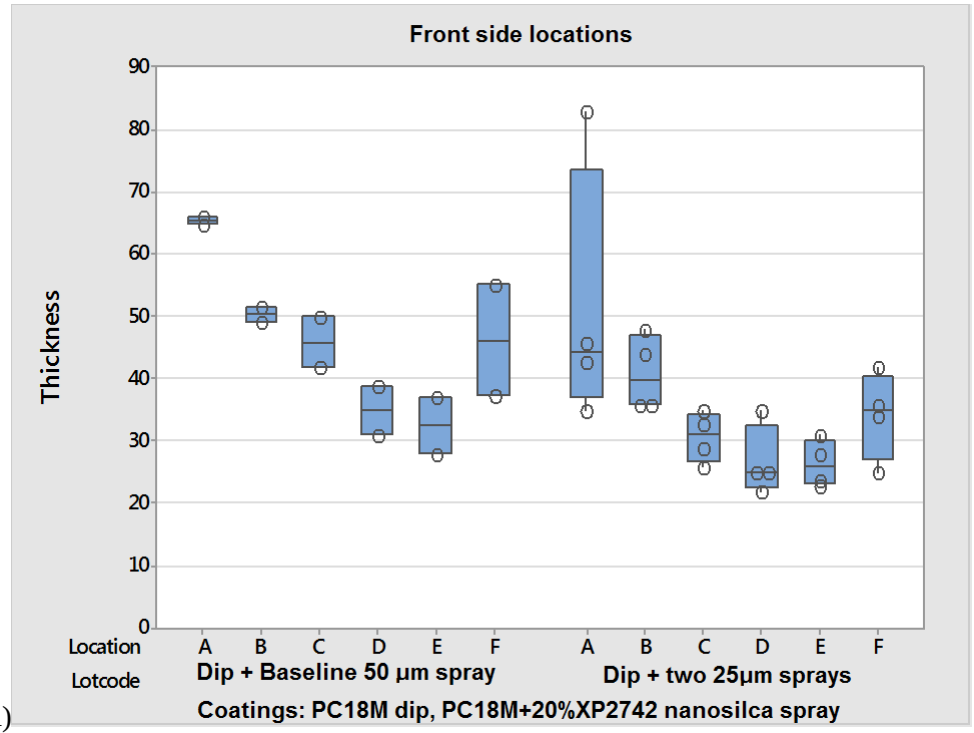


Figure 18. The dip + 25 micron spray + 25 micron spray minimum coating thickness of the on the lead front was above 20 microns and the maximum was approximately 85 microns in location A.

4.2 Baseline (dip + 50 micron spray) and enhanced layered coating comparison

(A)



(B)

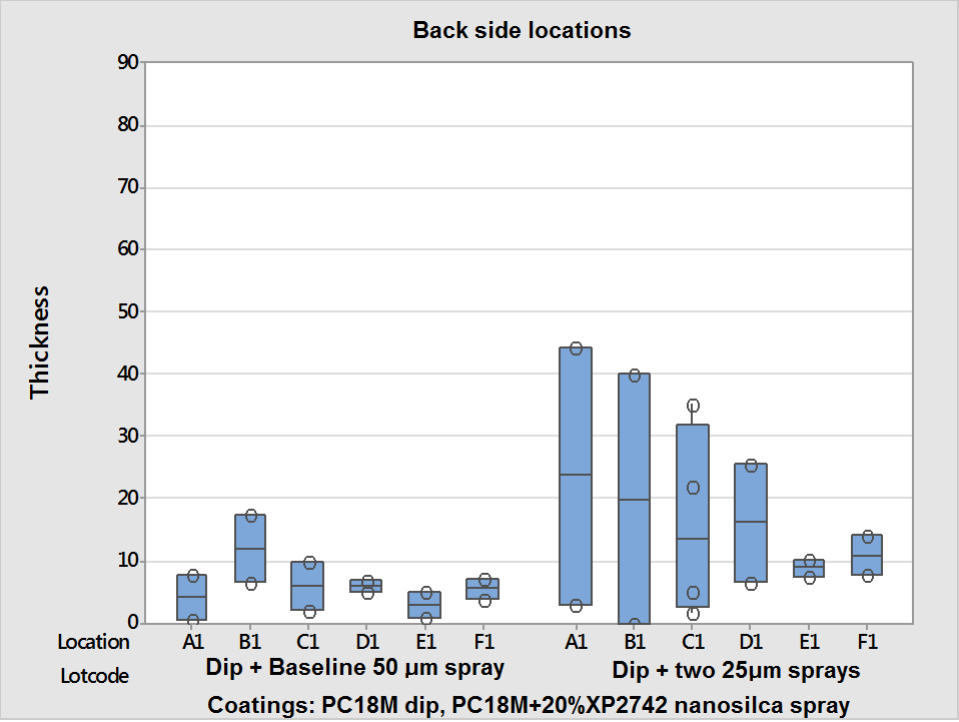


Figure 19 compares the baseline (dip + 50 micron spray) thickness with the enhanced (dip + 25 micron spray + 25 micron spray) layered coating. The average thickness on the back side of the leads for the layered coating was greater than the baseline. Although the thickness variation was larger for the layered coating, there might be a slight trend showing the layered coating having a tighter grouping of average thicknesses at the different lead the locations.

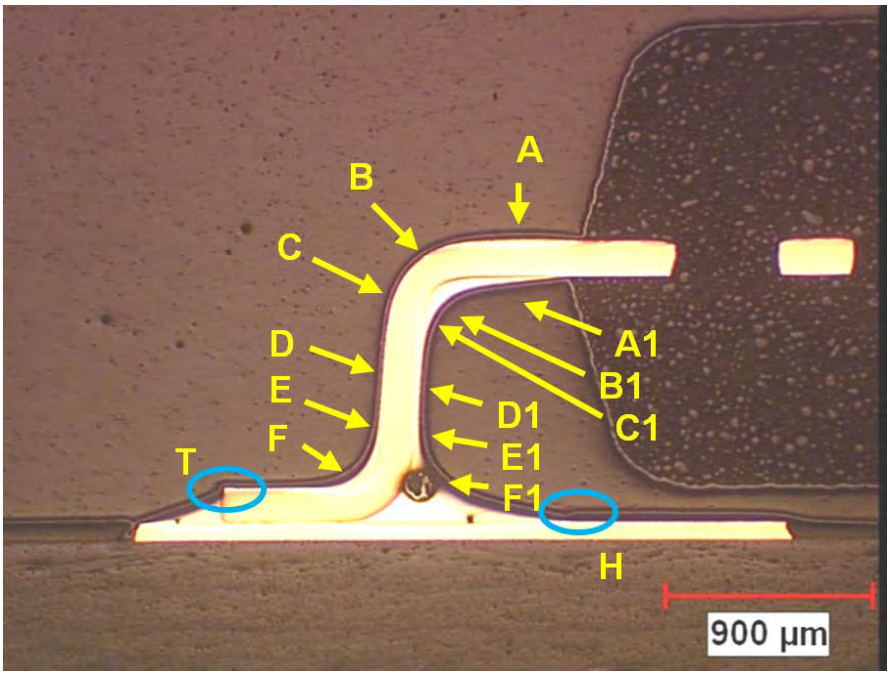


Figure 16: Vertical cross-section thickness measurement locations.

Table 2: Vertical section layered coating front side and selected back side thickness measurements.

Spray Coating	Process	Board Coupon	Part location	Lead	Location and thickness (microns)						
					A	B	C	D	E	F	T
PC18M+20 %XP2742	dip 1 spray	A334	U1	right	11	15	12	6	5	17	1
				left	12	18	13	16	10	2.9	4
			U6	right	16	7.8	2.7	3.9	2.1	6.3	1
				left	16	14	8.2	17	7.6	12	1
PC18M	dip 1 spray	A012	U1	right	15.7	9.8	11	17	13	14	5
				left	20	6.9	15	15	13	29	5
			U6	left	5.5	7.9	16	14	9.9	3.5	1
				right	4.9	6.4	21	17	20	26	0
PC18M+20 %XP2742	dip 2 sprays	A225	U1	Left	46	36	26	25	31	36	8
				right	43	44	35	35	28	42	17
			U6	right	35	36	29	22	23	25	8
				left	53	48	33	25	24	34	8
PC18M	dip 2 sprays	A191	U1	right	41	56	25	45	47	66	4.1
				left	54	24	21	23	20	53	1
			U6	right	34	43	26	25	29	25	24
				left	47	62	23	24	15	25	26
none	PC18M dip only	A179	U1	right	7.3	2.1	5.2	15	15	15	>1
				left	2.8	0.68	1.8	8.1	8.6	5.7	>1
			U6	right	2.3	0.24	1.1	9.4	9.7	2.9	>1
				left	5.2	2.6	5.6	10.2	8.1	3.4	>1

Table 3: Vertical section layered coating back side thickness measurements.

Spray Coating	Process	Board Coupon	Part location	Lead	Location and thickness (microns)					
					A1	B1	C1	D1	E1	F1
PC18M+20%XP2742	dip 1 spray	A334	U1	left	6.56	7.53	5.97	3.6	2.86	1.95
				right	5.38	10.65	9.59	3.38	4.91	3.64
PC18M	dip 1 spray	A012	U6	left	0	13.2	10.21	0	0	0
				right	3.85	6.16	11.34	1.26	4.7	7.75
PC18M+20%XP2742	dip 2 sprays	A225	U1	left	3.12	0	0	6.67	7.56	7.87
				right	44.4	40.1	35.3	25.8	10.28	14.1
PC18M	dip 2 sprays	A191	U6	left	9.11	13.34	14.6	8.22	6.7	7.16
				right	6.32	13.01	10.96	5.47	3.94	10.6
none	PC18M dip only	A179	U1	left	22	27.5	28.5	1.6	2.35	4.03
				right	4.67	7.38	8.76	3.99	1.06	0.6

Table 4: Typical SEM layered coating cross-section images.

Coating	Figures
PC18M dip only	Figure 20 to Figure 24
Dip + one PC18M spray	Figure 25 to Figure 29
Dip + two PC18M sprays	Figure 30 to Figure 34
Dip + one (PC18M+20%XP2742) spray	Figure 35 to Figure 40
Dip + two (PC18M+20%XP2742) sprays	Figure 41 to Figure 45

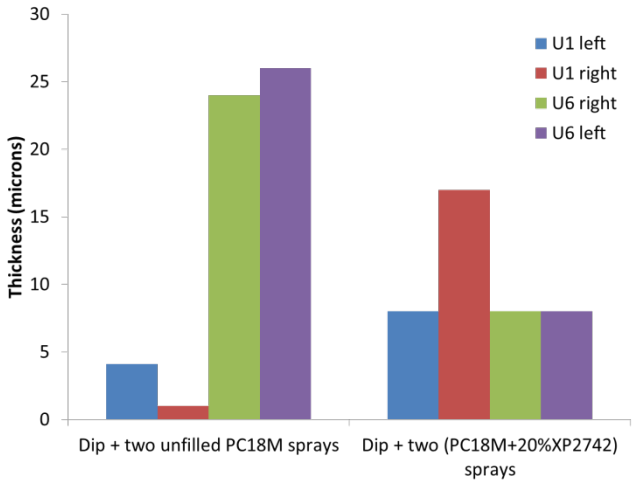
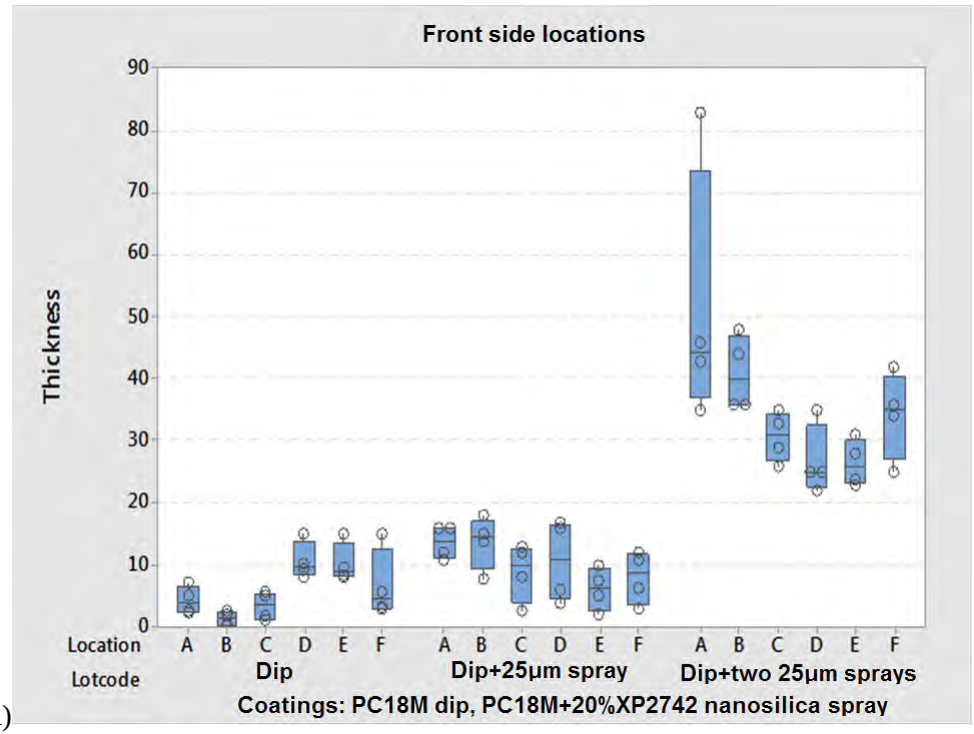


Figure 17: Vertical section comparison of location T coating thickness for the enhanced layered coating dip + 25 micron spray + 25 micron spray for a P18M dip with unfilled PC18M spray (left) or PC18M+20%XP2742 nanosilica spray (right).

(A)



(B)

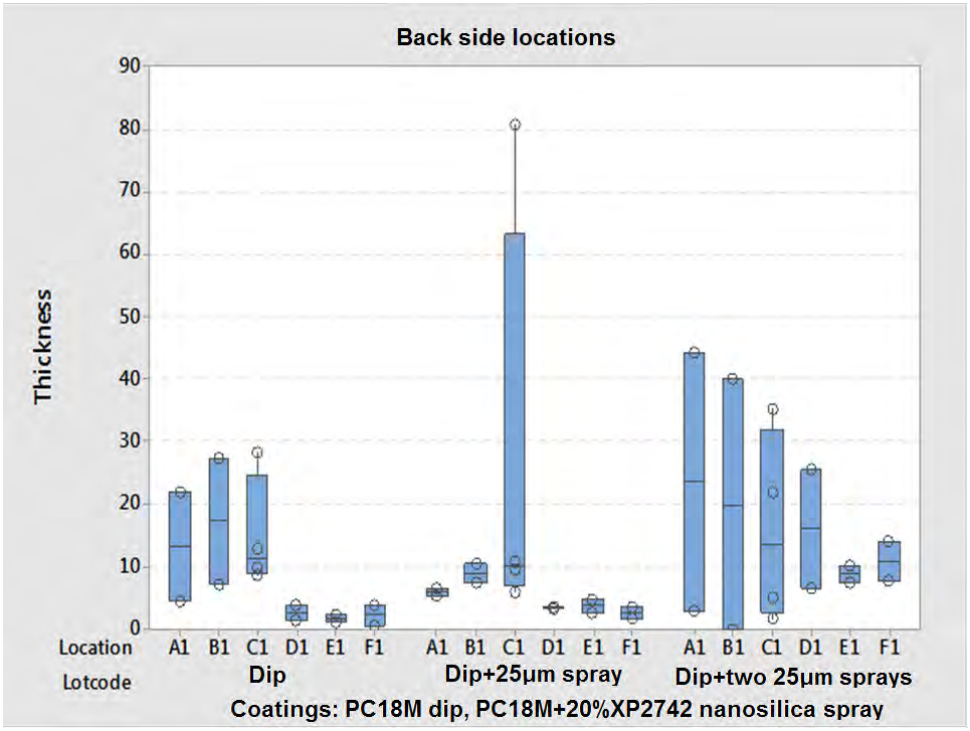
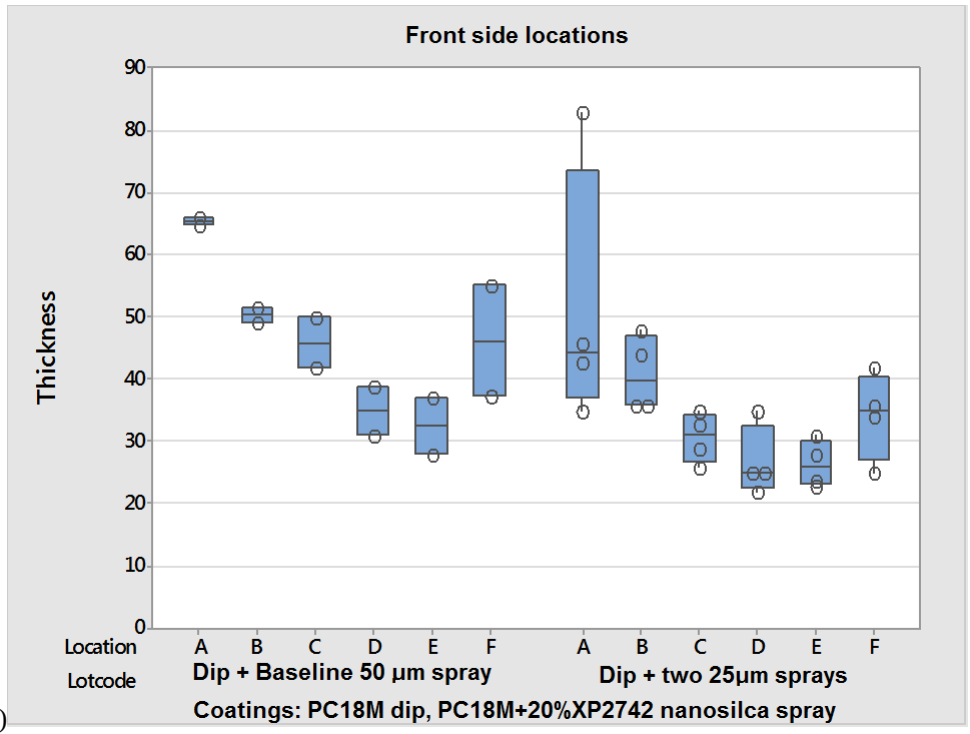


Figure 18: Enhanced layered coating vertical section thickness plots comparing dip only, dip + 25 micron spray, and dip + 25 micron spray + 25 micron spray for a PC18M dip coating and PC18M+20%XP2742 nanosilica spray coating; (A) front of lead side and (B) back side.

(A)



(B)

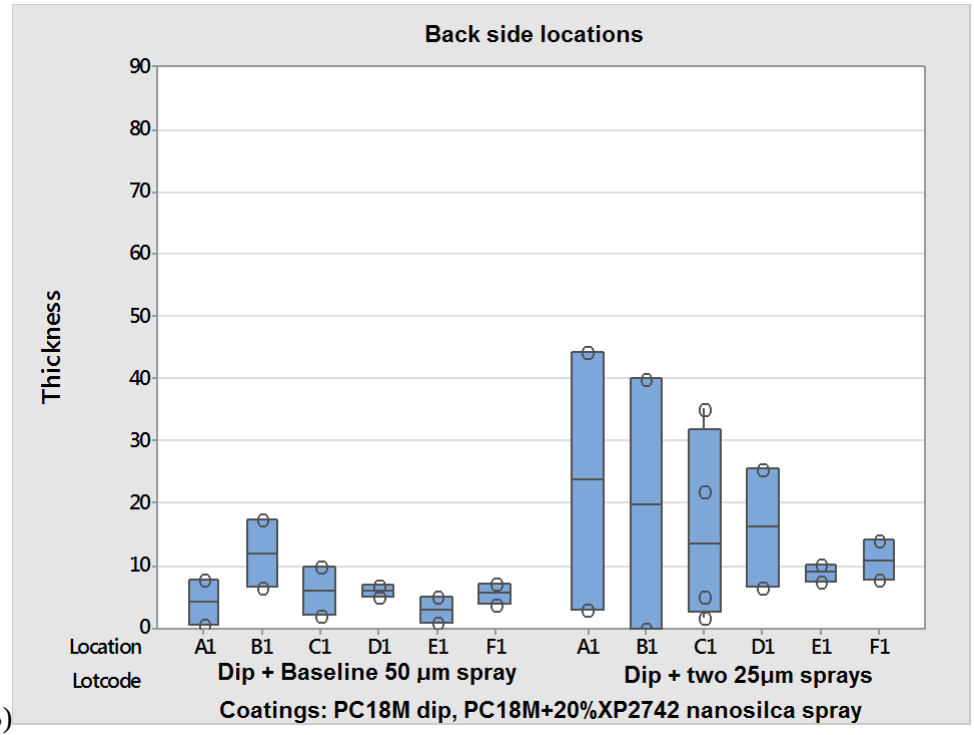


Figure 19: Vertical section comparison of the dip + baseline 50 micron spray and the enhanced layered dip + 25 micron spray + 25 micron spray for a PC18M dip coating and PC18M+20%XP2742 nanosilica spray coating; (A) front of lead side and (B) back side.

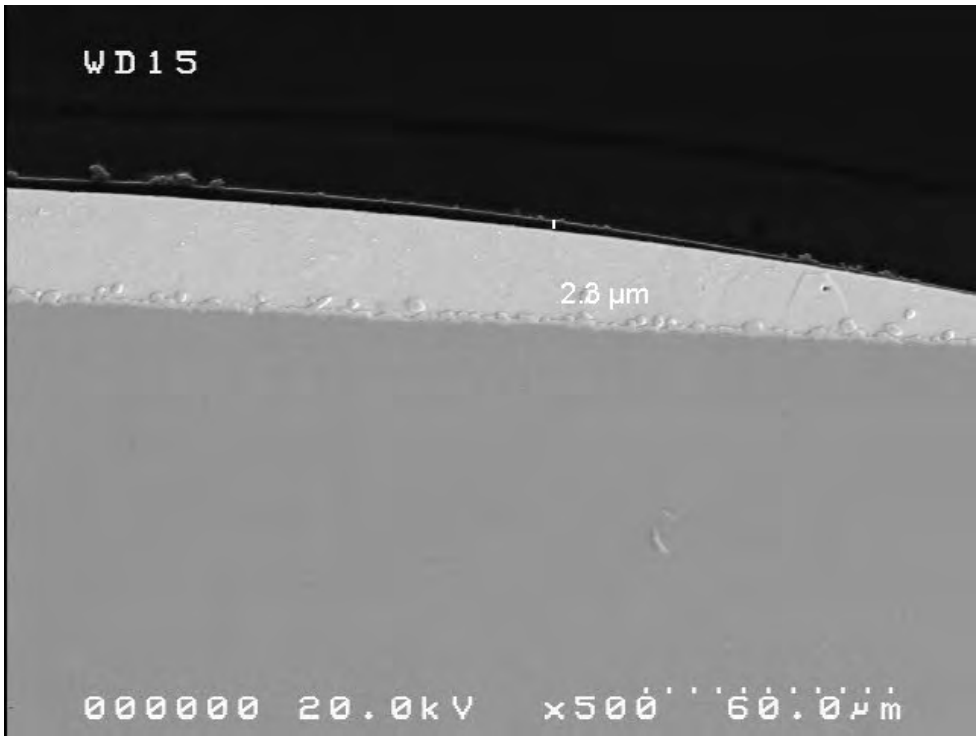


Figure 20: Cross-section SEM image of PC18M dip only, board A179, U6, right A, 500x.

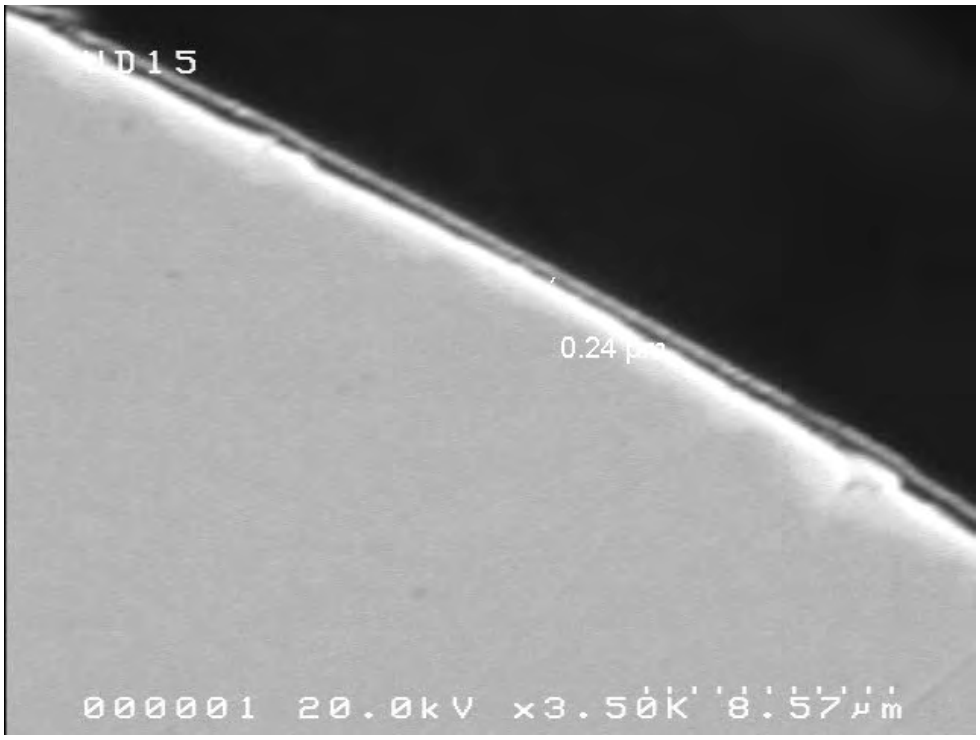


Figure 21: Cross-section SEM image of PC18M dip only, board A179, U6, right B, 500x.

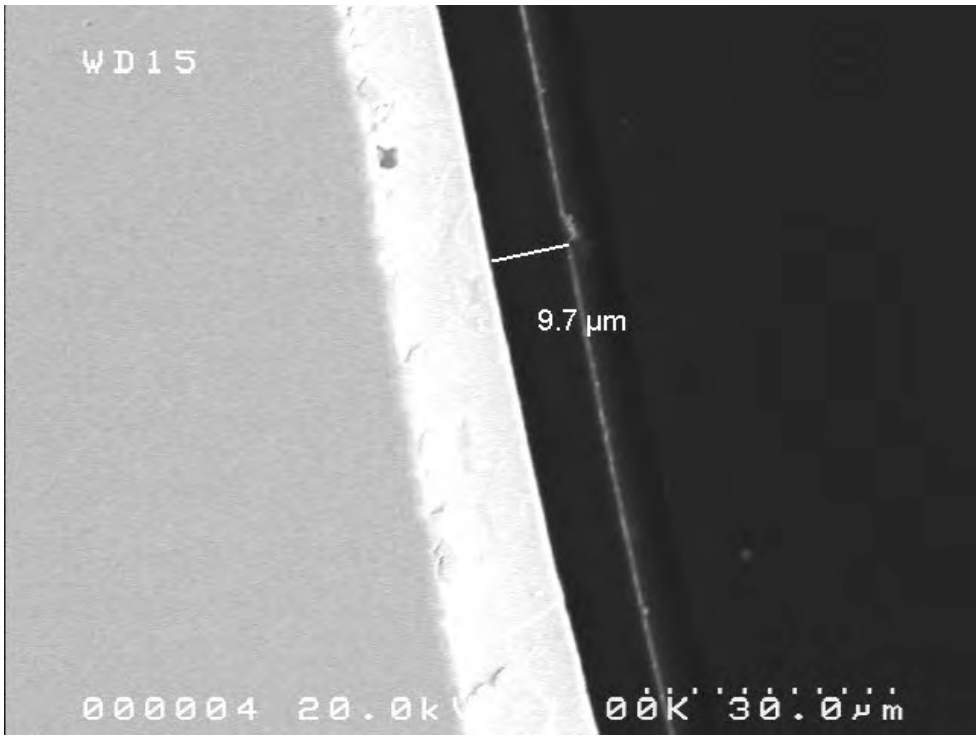


Figure 22: Cross-section SEM image of PC18M dip only, board A179, U6, right E, 1,000x.

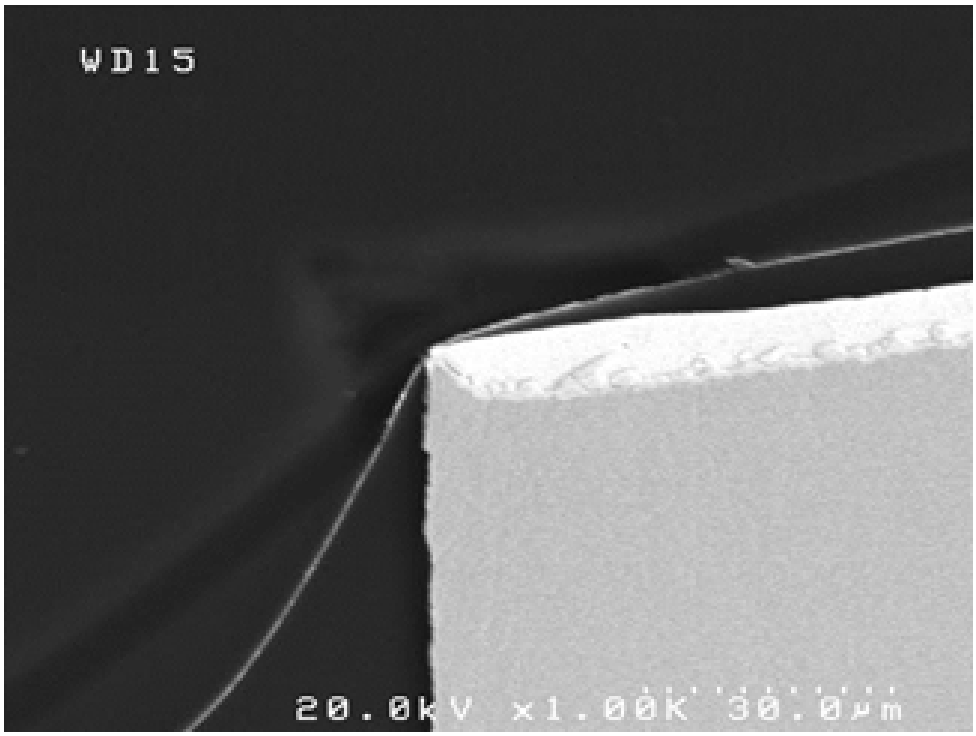


Figure 23: Cross-section SEM image of PC18M dip only, board A179 U6 left T, 1,000x.

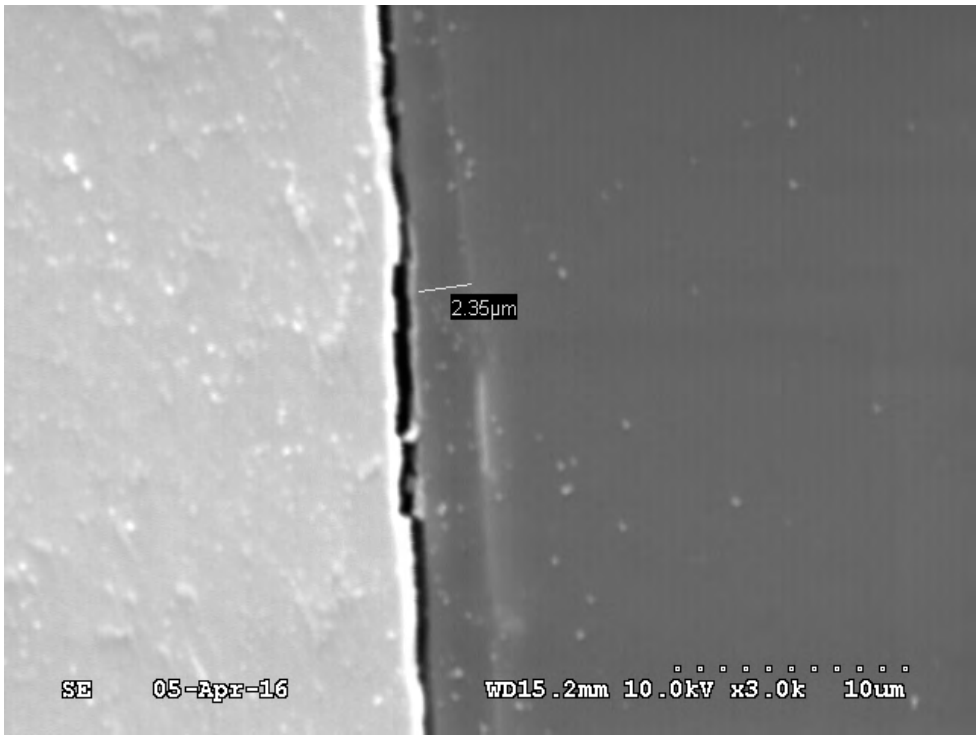


Figure 24: Cross-section SEM image of PC18M dip only, board A179, U1, left lead, E1, 3,000x.

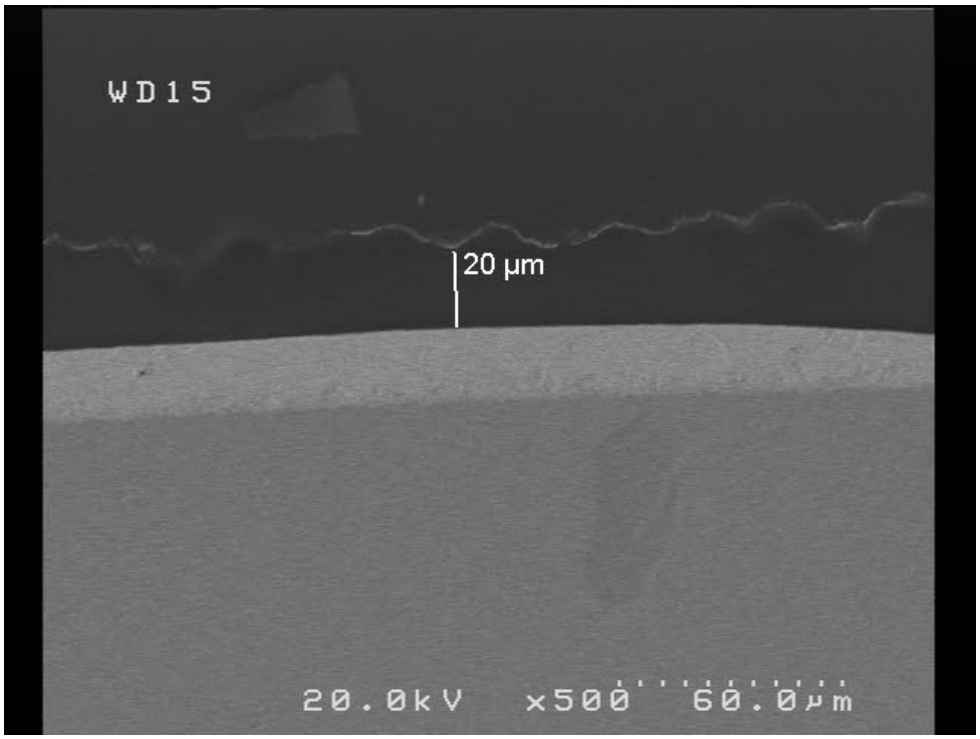


Figure 25: Cross-section SEM image of PC18M dip + one PC18M spray, board A012, U1, left A, 1,000x.

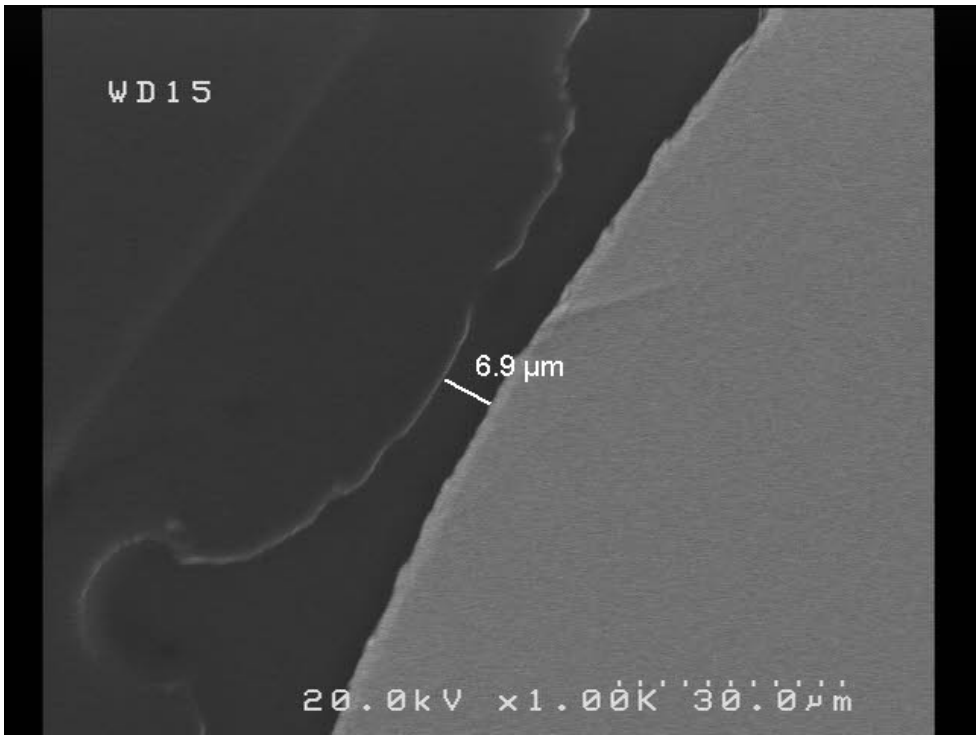


Figure 26: Cross-section SEM image of PC18M dip + one PC18M spray, board A012, U1, left B, 1,000x.

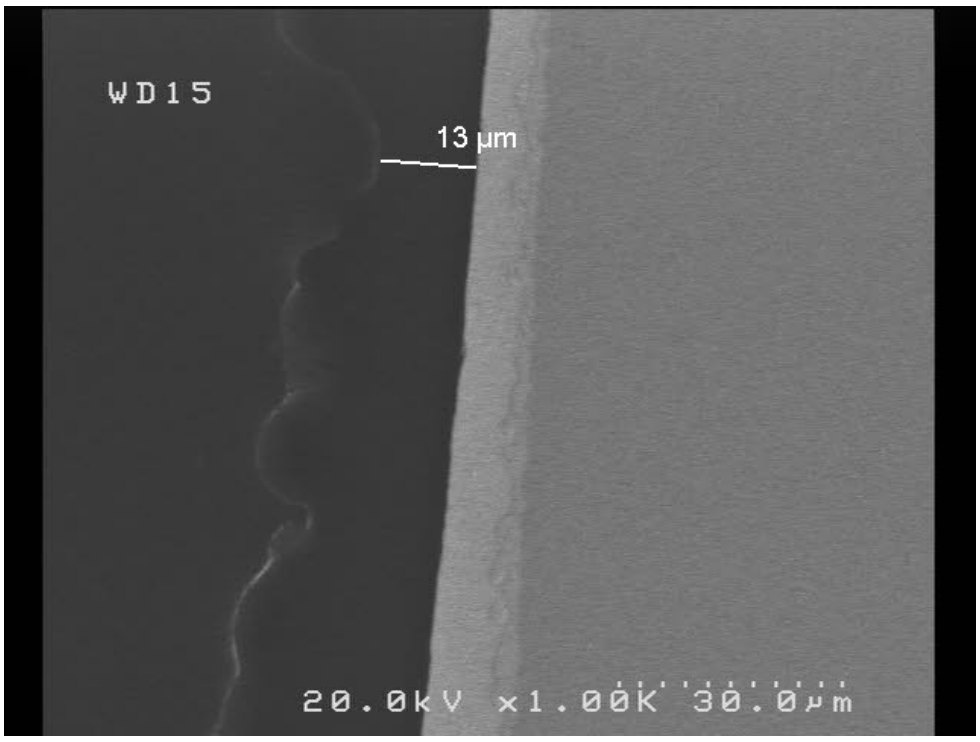


Figure 27: Cross-section SEM image of PC18M dip + one PC18M spray, board A012, U1, left E, 1,000x.

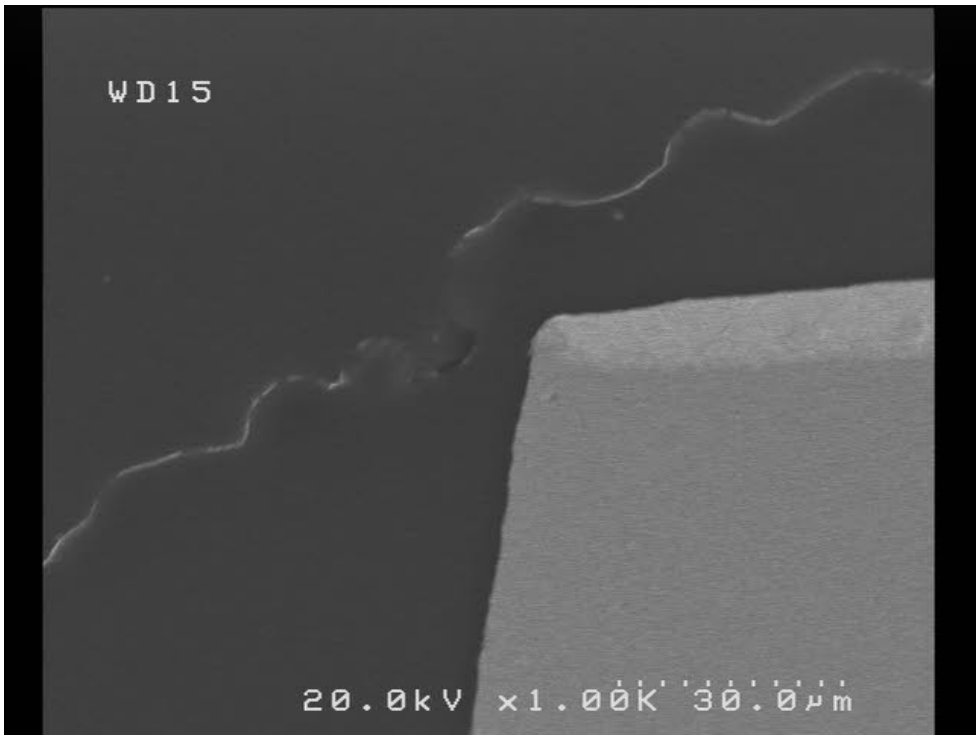


Figure 28: Cross-section SEM image of PC18M dip + one PC18M spray, board A012, U1, left T, 1,000x.

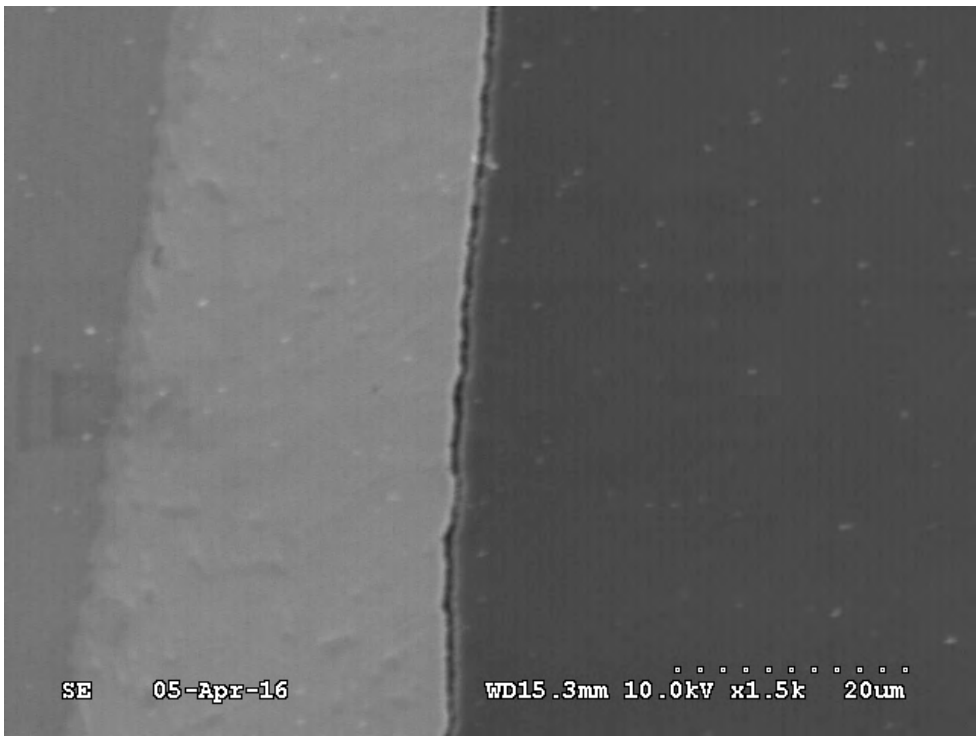


Figure 29: Cross-section SEM image of PC18M dip + one PC18M spray, board A012, U6, left E1, 1,500x.

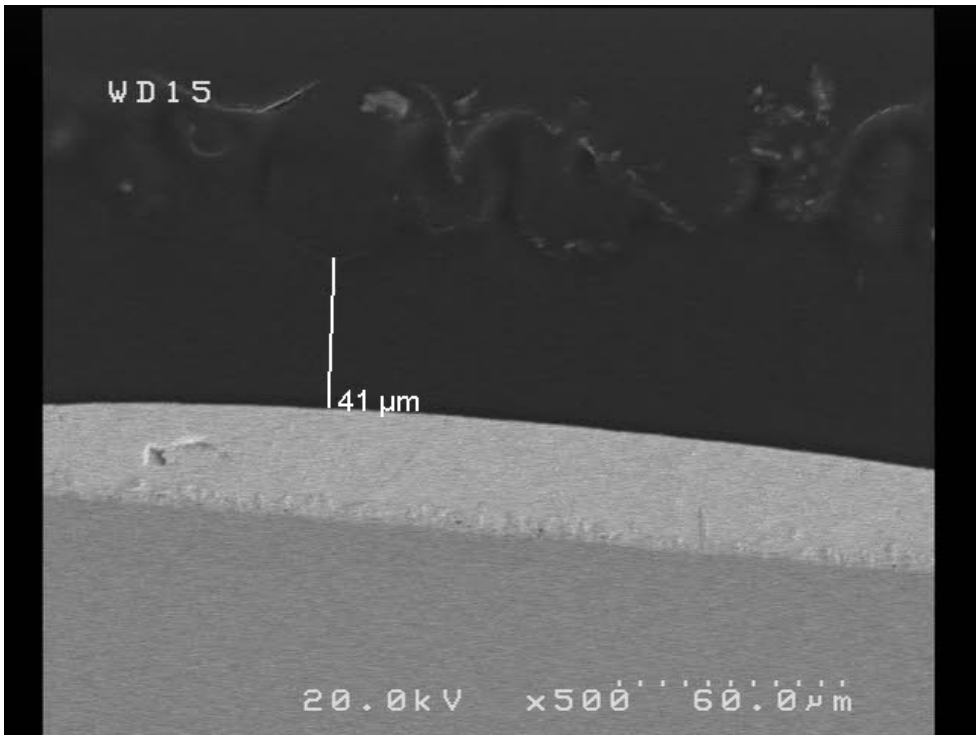


Figure 30: Cross-section SEM image of PC18M dip + two PC18M sprays, board A191 U1, right A, 500x.

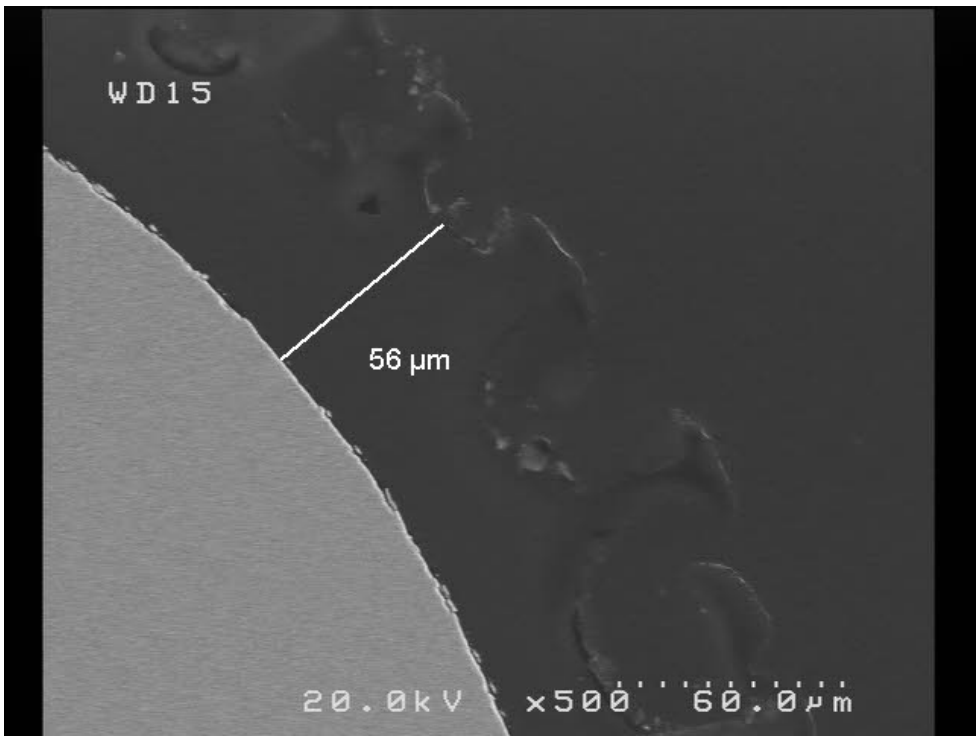


Figure 31: Cross-section SEM image of PC18M dip + two PC18M sprays, board A191 U1 right B, 500x.

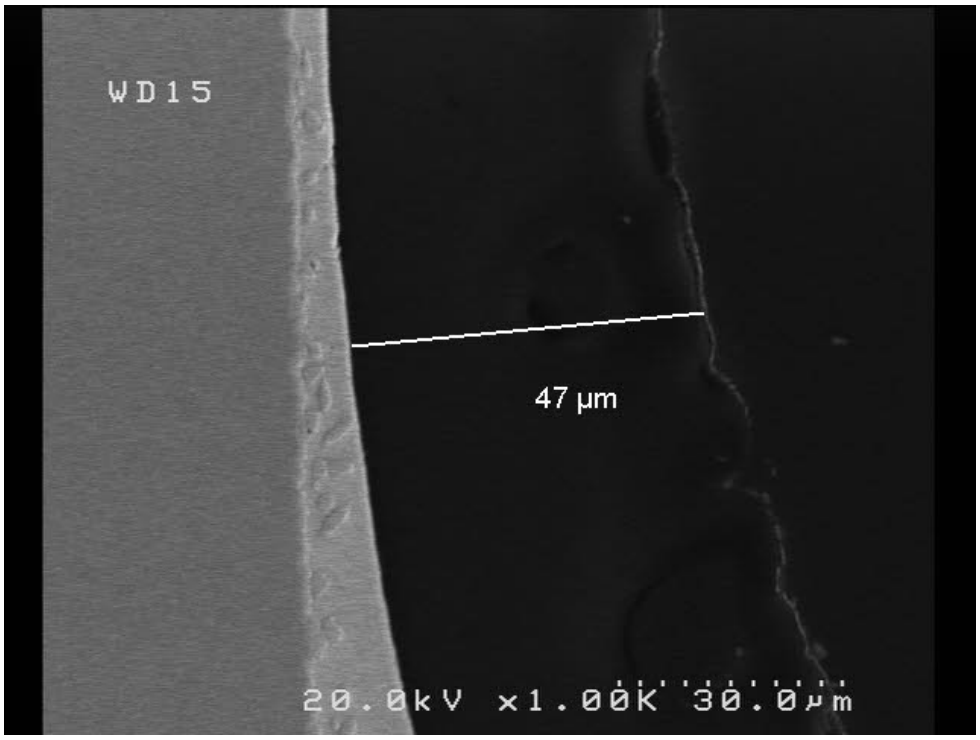


Figure 32: Cross-section SEM image of PC18M dip + two PC18M sprays, board A191, U1 right E, 1,000x.

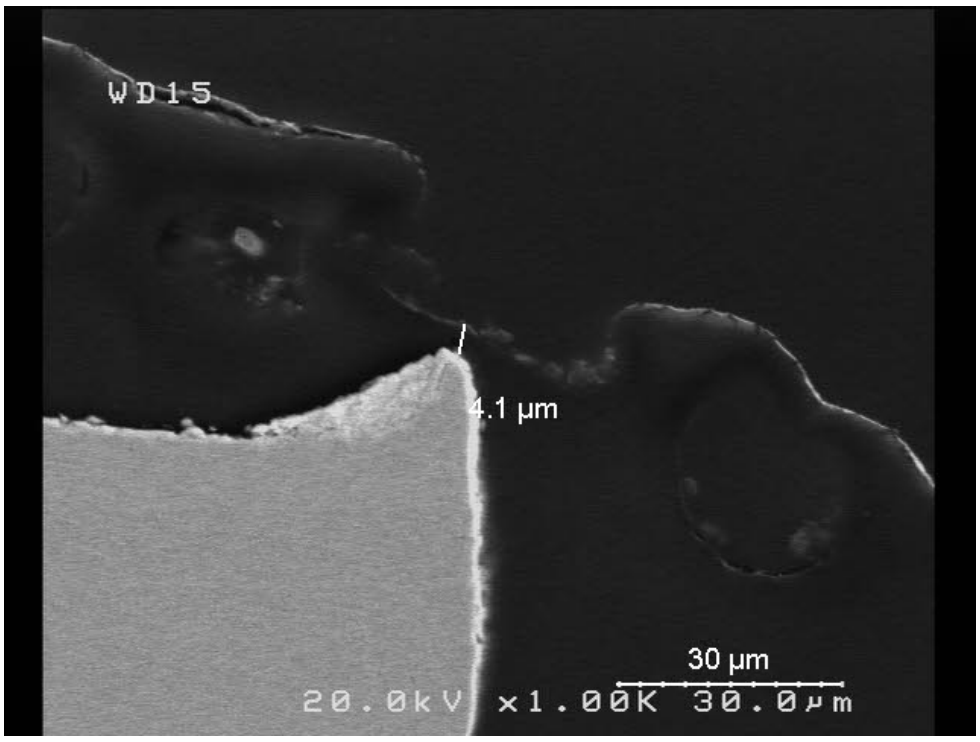


Figure 33: Cross-section SEM image of PC18M dip + two PC18M sprays, board A191, U1, right T, 1,000x.

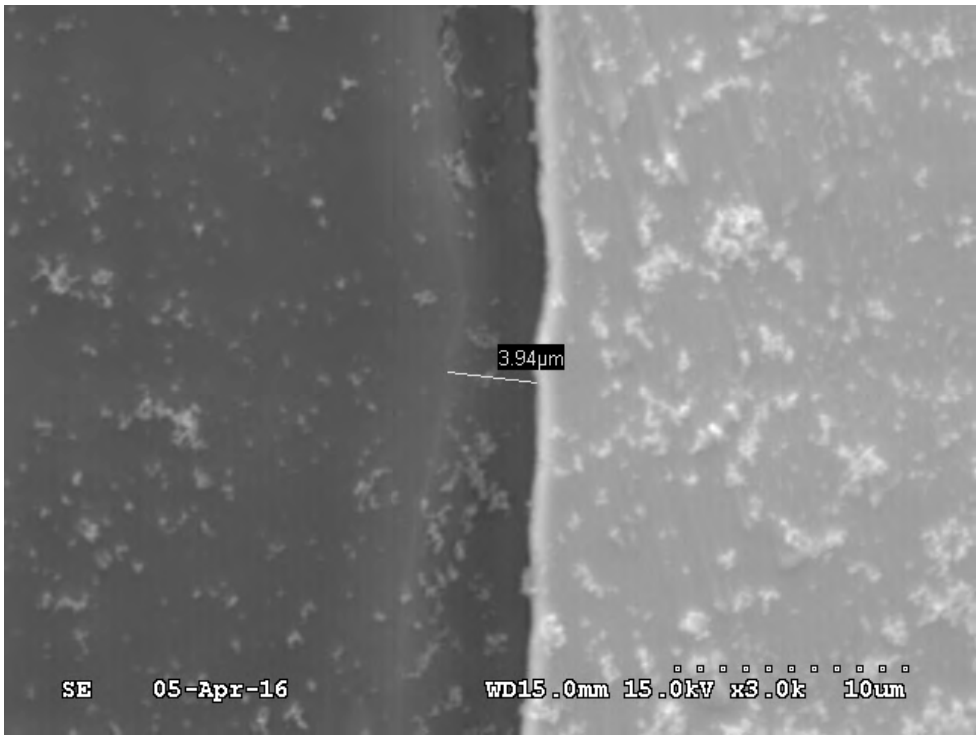


Figure 34: Cross-section SEM image of PC18M dip + two PC18M sprays, board A191 U1, right lead, E1, 2,000x.

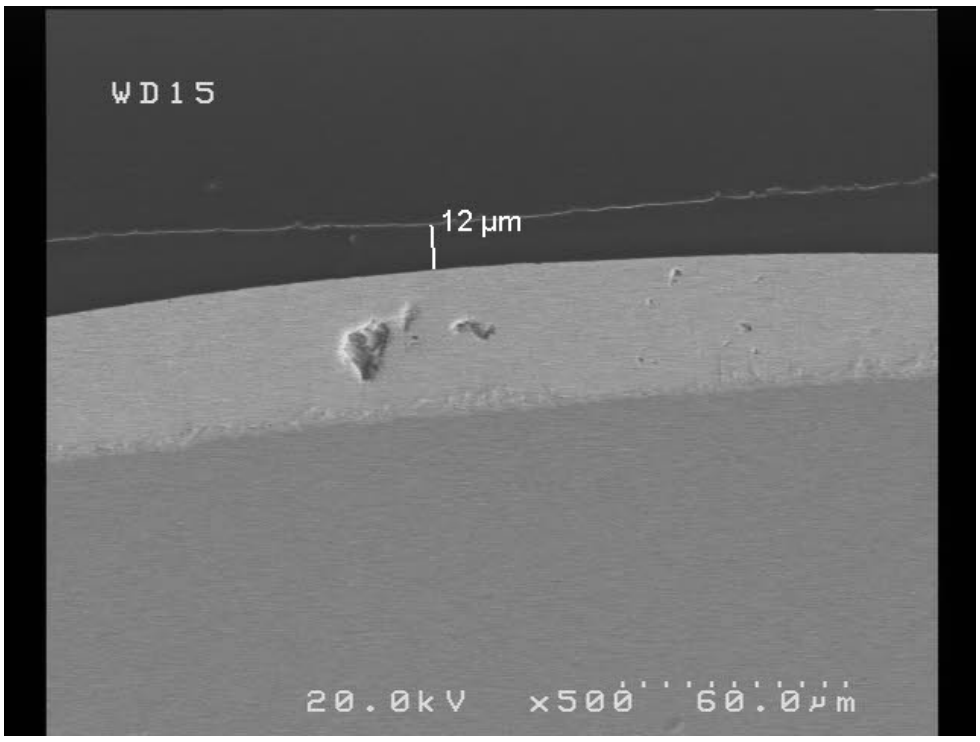


Figure 35: Cross-section SEM image of PC18M dip + one (PC18M+20XP2742) spray, board 334, U1, left A, 500x.

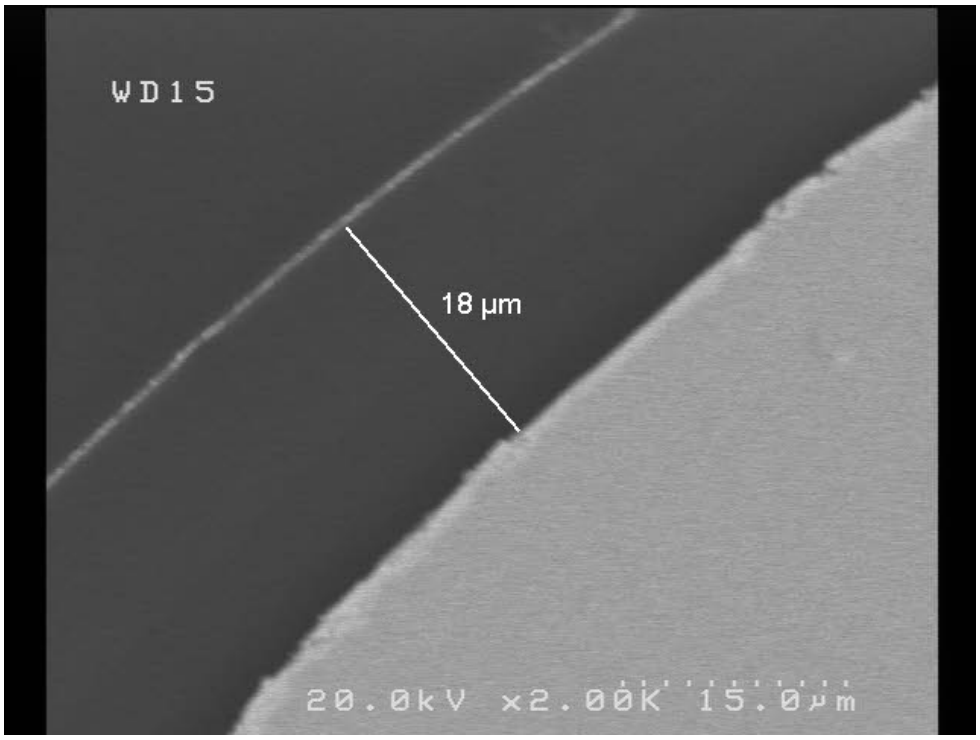


Figure 36: Cross-section SEM image of PC18M dip + one (PC18M+20XP2742) spray, board 334, U1, left B, 2,000x.

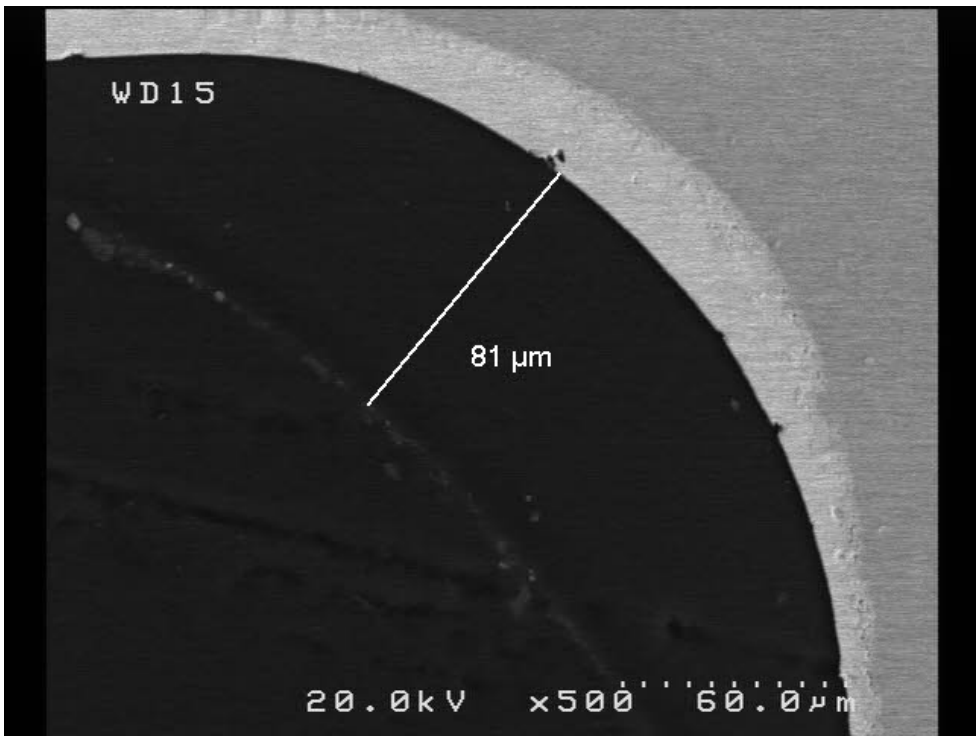


Figure 37: Cross-section SEM image of PC18M dip + one (PC18M+20XP2742) spray, board 334, U1, right G, 500x.

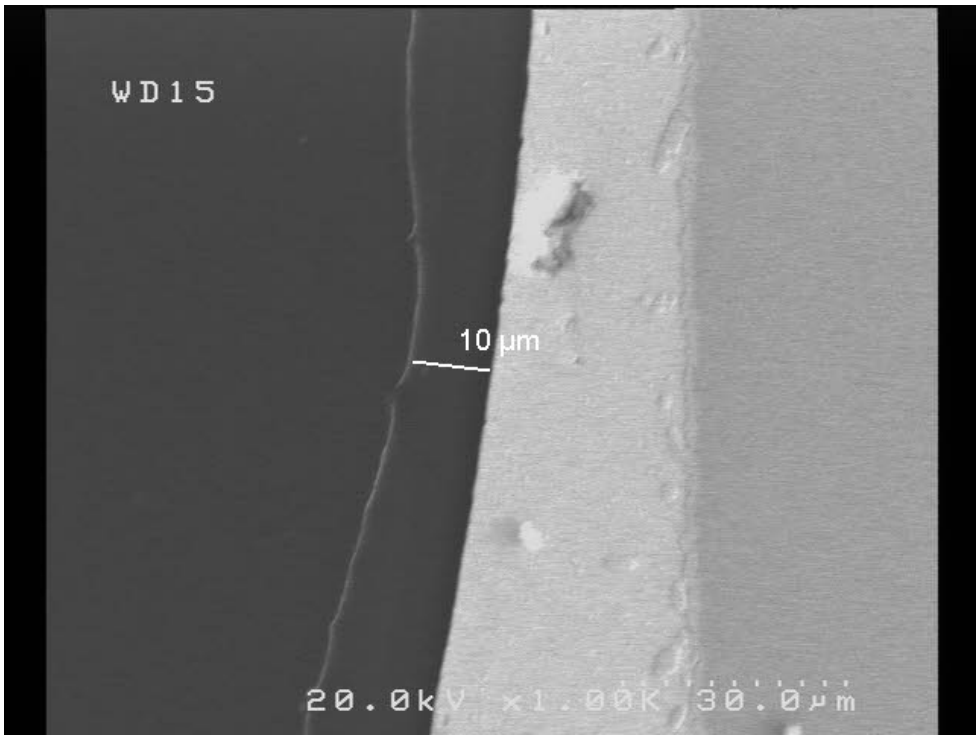


Figure 38: Cross-section SEM image of PC18M dip + one (PC18M+20XP2742) spray, board 334, U1, left E, 1,000x.

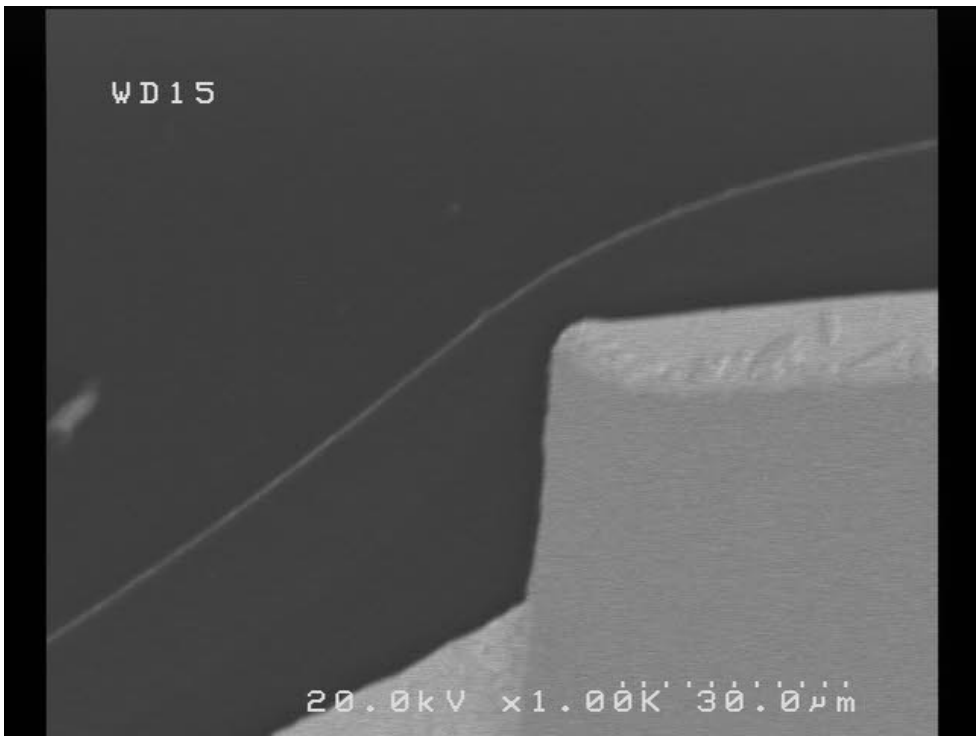


Figure 39: Cross-section SEM image of PC18M dip + one (PC18M+20XP2742) spray, board 334 U1 left T, 1,000x.

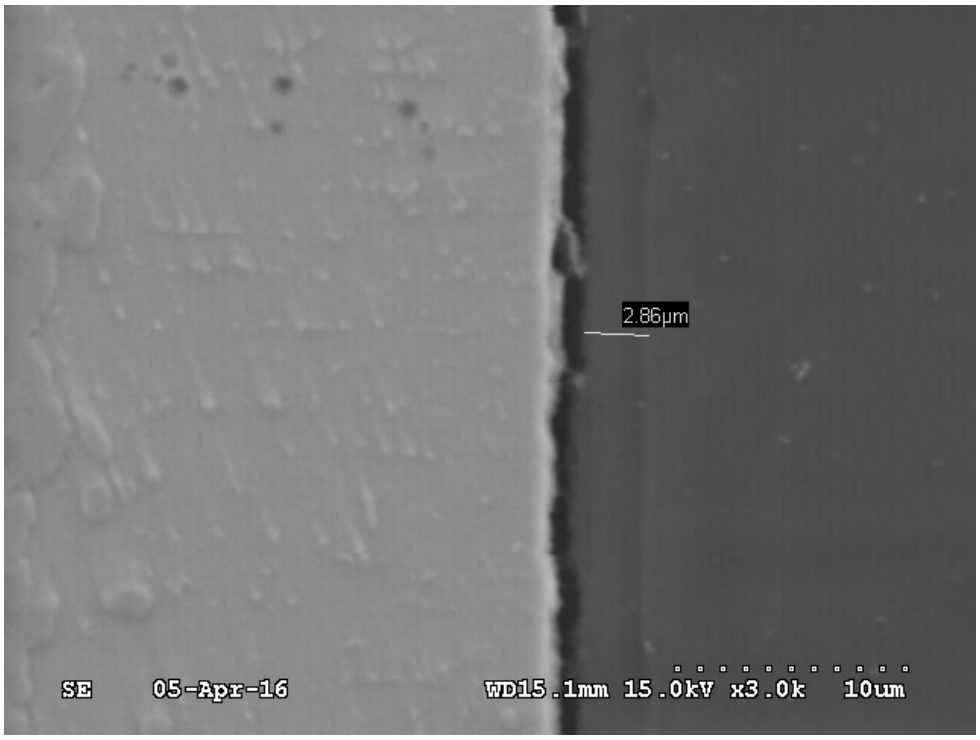


Figure 40: Cross-section SEM image of PC18M dip + one (PC18M+20XP2742) spray, board 334 U1, left lead, E1, 3,000x.

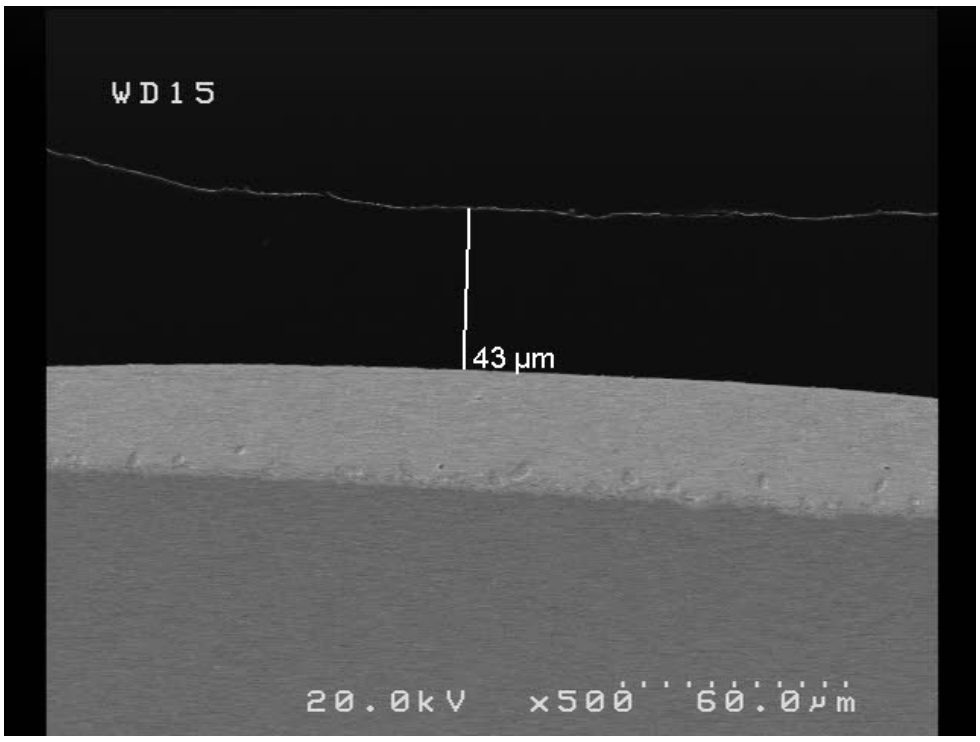


Figure 41: Cross-section SEM image of PC18M dip + two (PC18M+20XP2742) sprays, board A225, U1, right A, 500x.

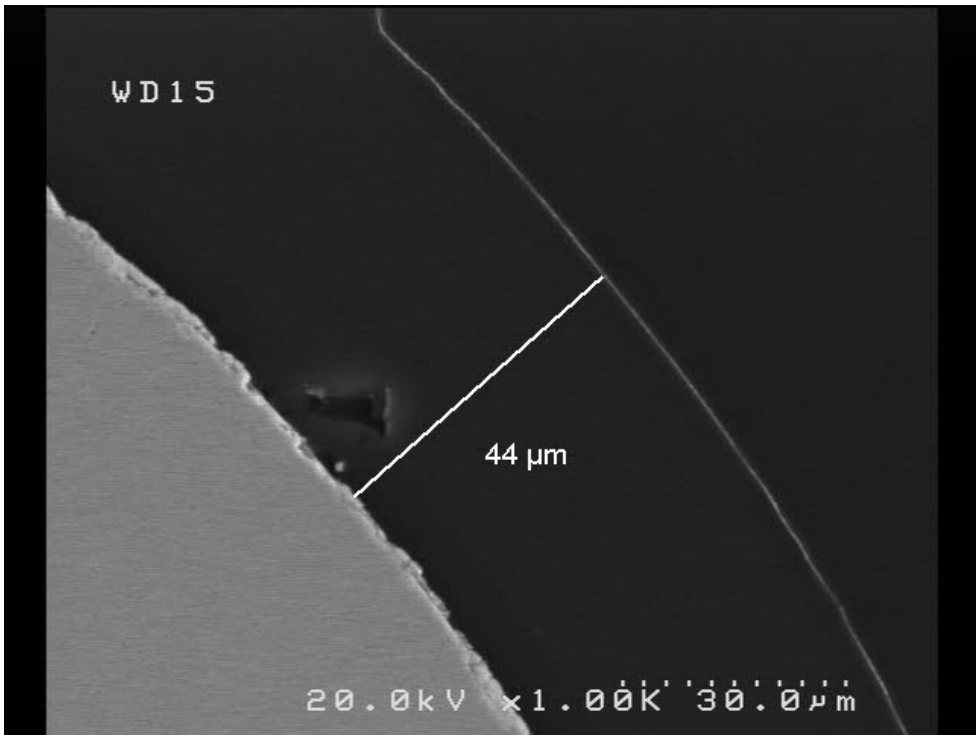


Figure 42: Cross-section SEM image of PC18M dip + two (PC18M+20XP2742) sprays, board A225, U1, right B, 1,000x.

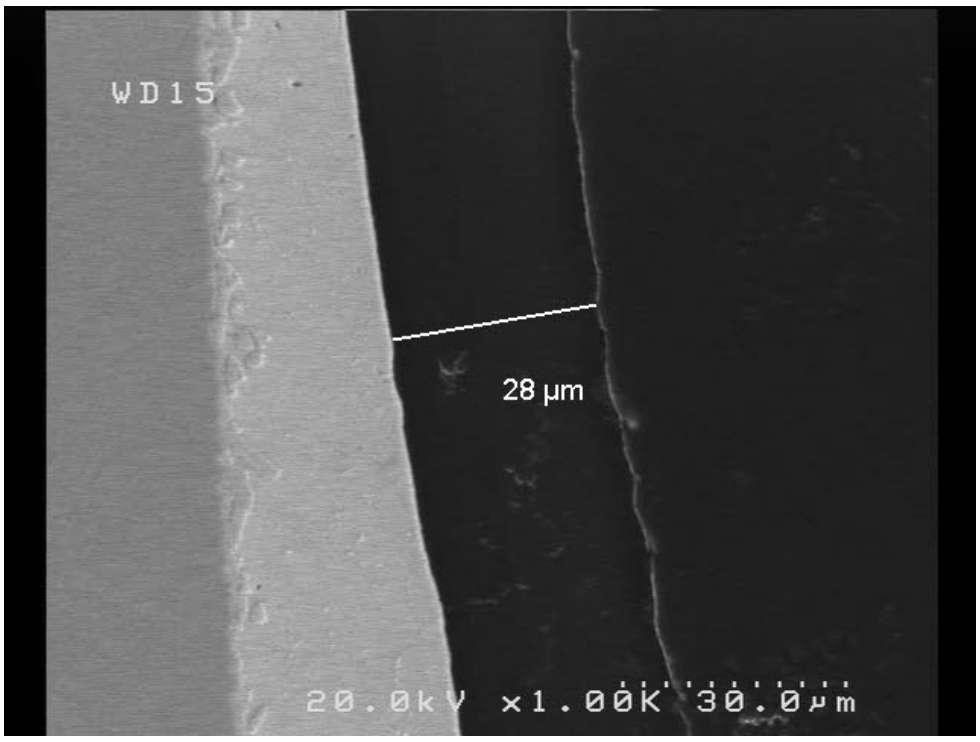


Figure 43: Cross-section SEM image of PC18M dip + two (PC18M+20XP2742) sprays, board A225, U1, right E, 1,000x.

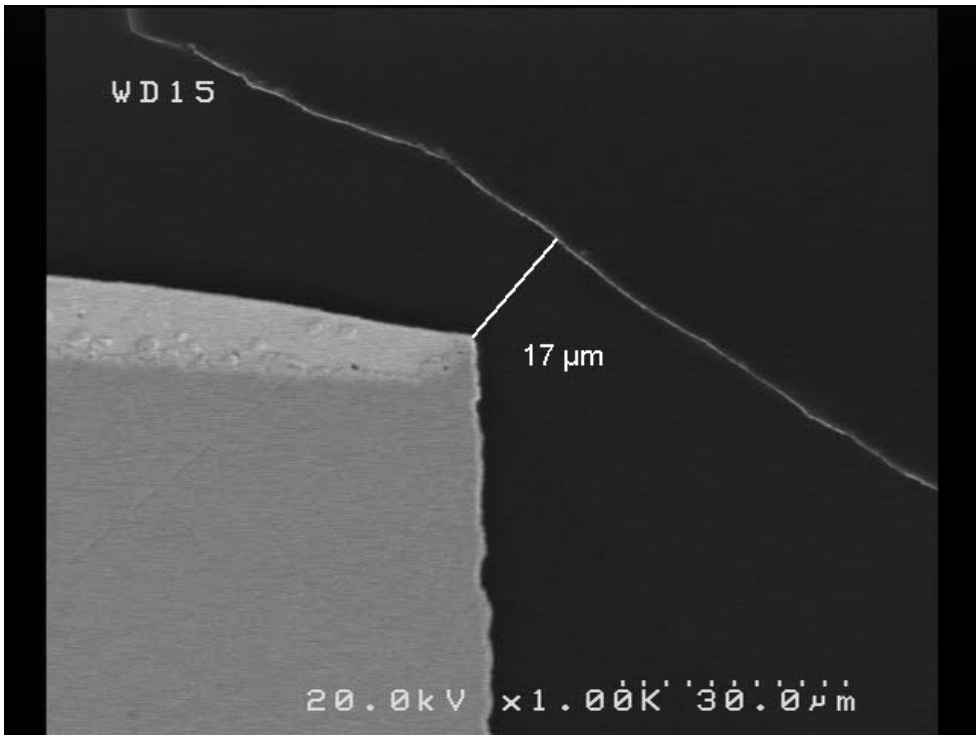


Figure 44: Cross-section SEM image of PC18M dip + two (PC18M+20XP2742) sprays, board A225, U1, right T, 1,000x.

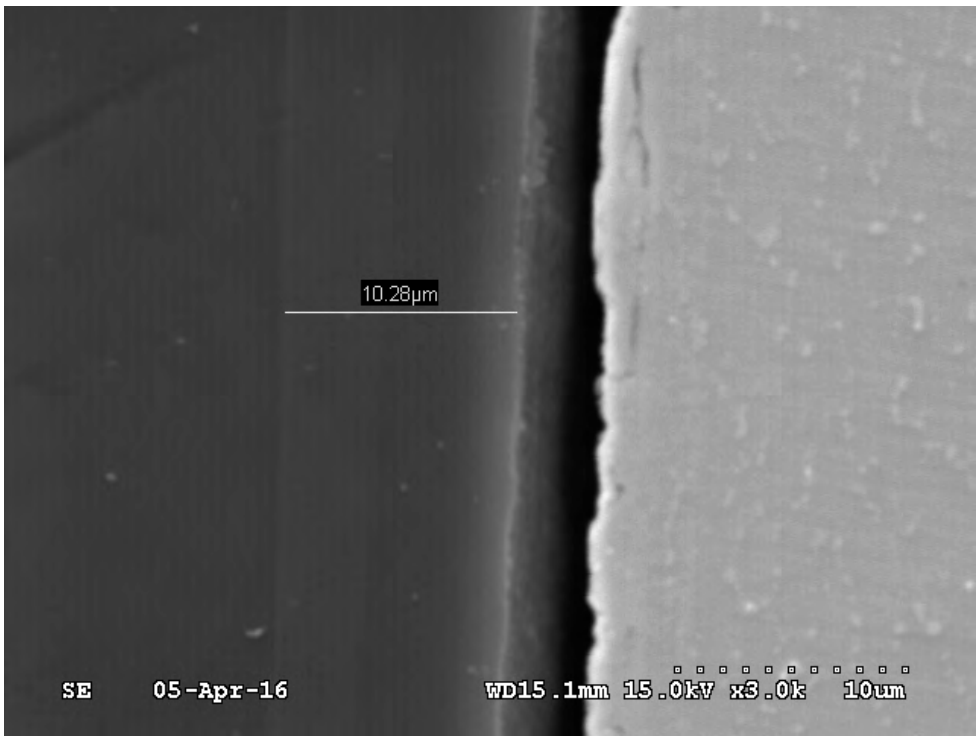


Figure 45: Cross-section SEM image of PC18M dip + two (PC18M+20XP2742) sprays, board A225 U1, right E1, 1,000x.

5. Horizontal cross-section coating thickness evaluation

For the PC18M dip + two (PC18M+20XP2742) sprays enhanced layered coating, the thickness of the coating was evaluated on the leads around the perimeter of the QFP44 with a horizontal section plane near located as shown in Figure 46 which is near location E of the vertical cross-section (Figure 16). The top of the chip resistors were used as a reference to keep the section plane parallel to the board and at a consistent height for the various boards that were sectioned. For the analysis, SEM images were obtained from corner and center leads on each side of the QFP (Figure 47). Sometimes the back of the lead had little or no sputtered gold over the conformal coating on the center leads, making it more difficult to differentiate between the coating and the potting compound. The coating coverage on the front and the sides of both the corner and center leads was good. The coverage on the back was more variable (Figure 48 to Figure 52).

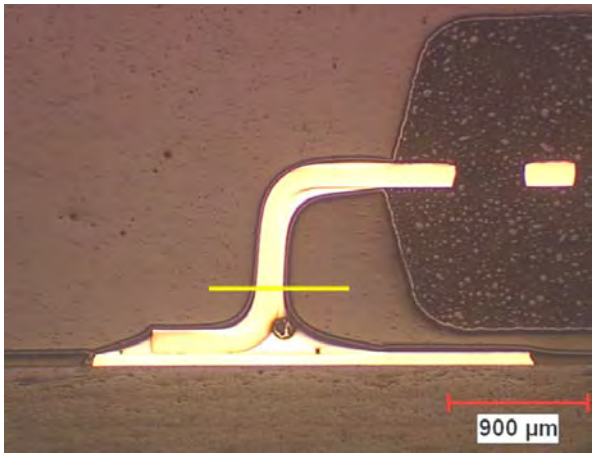


Figure 46: Horizontal cross-section plane location for coating thickness evaluation.

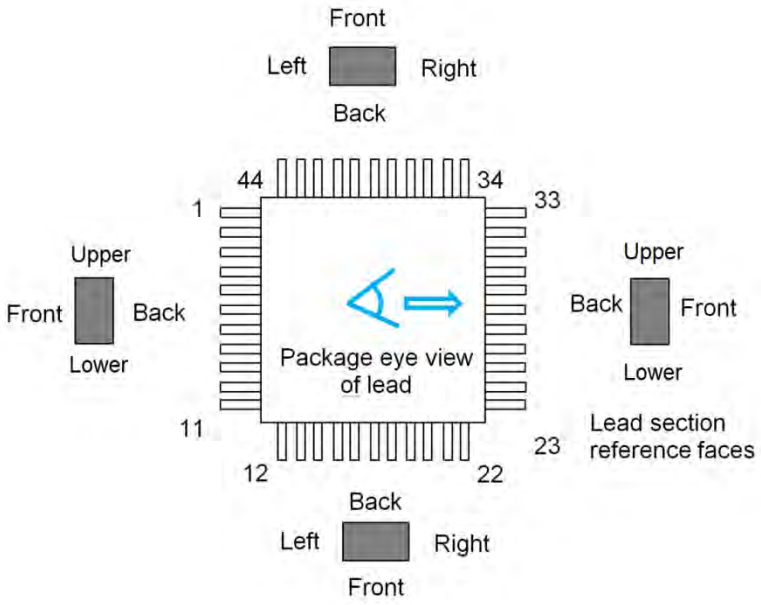


Figure 47: QFP44 pin numbering.

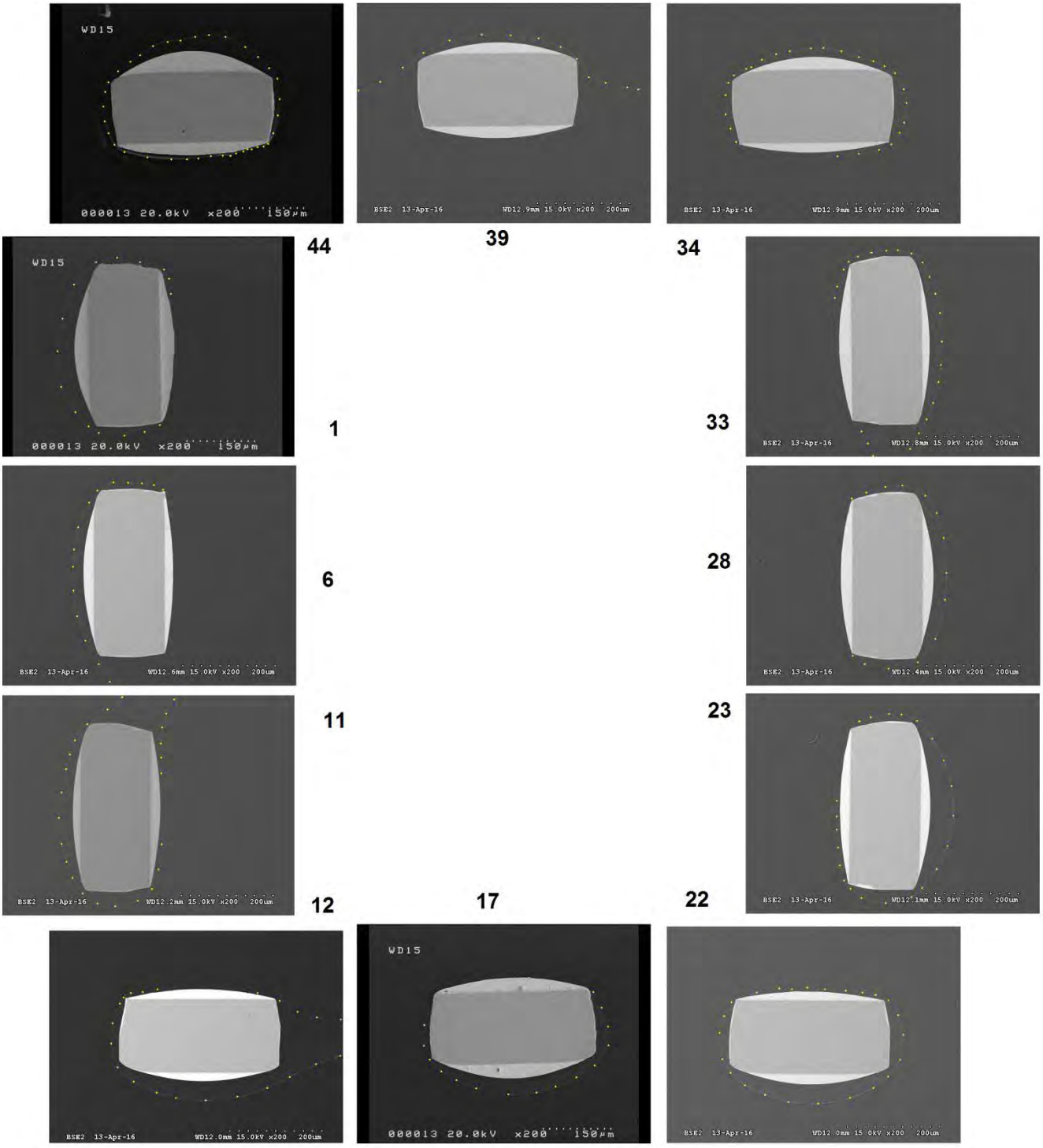
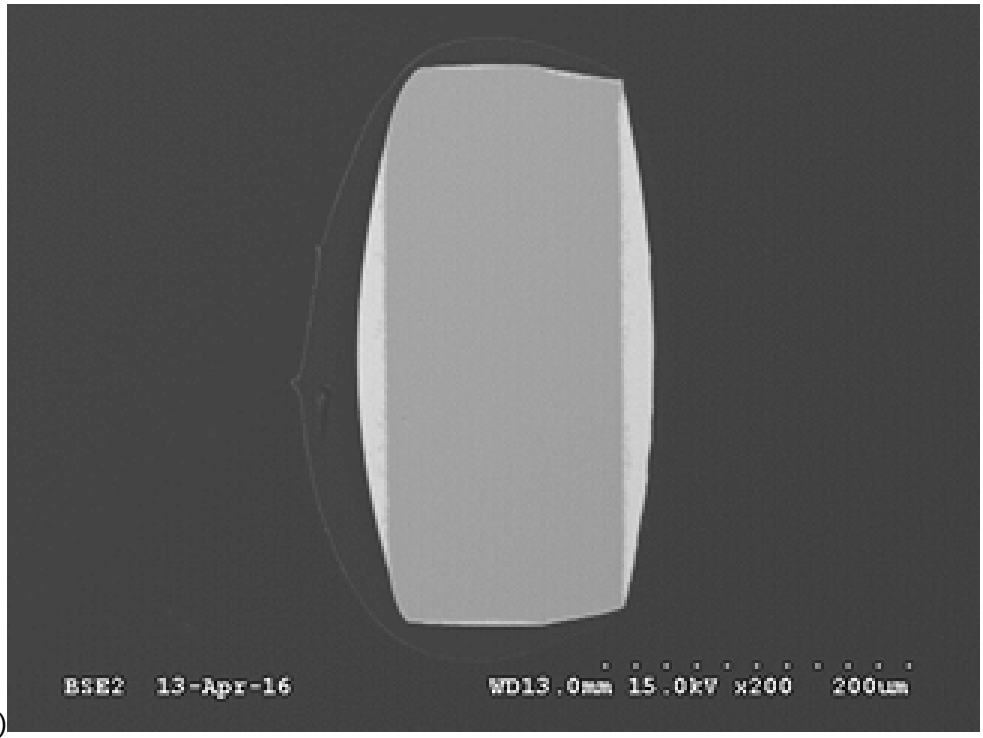
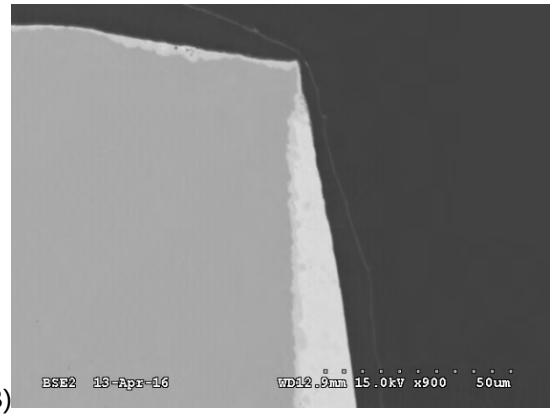


Figure 48: Horizontal cross-section SEM image of corner leads, PC18M dip + two (PC18M+20XP2742) sprays, board A225, U3, 200x (enhancement added to highlight coating).

(A)



(B)



(C)

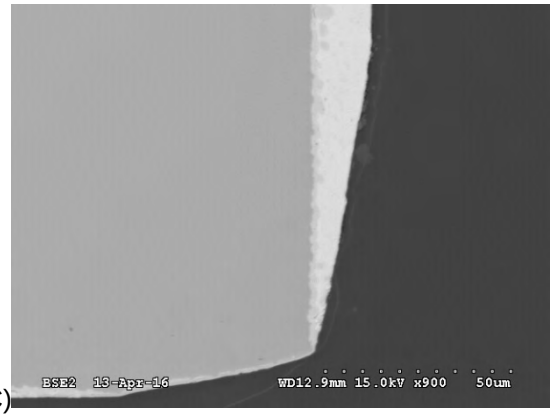
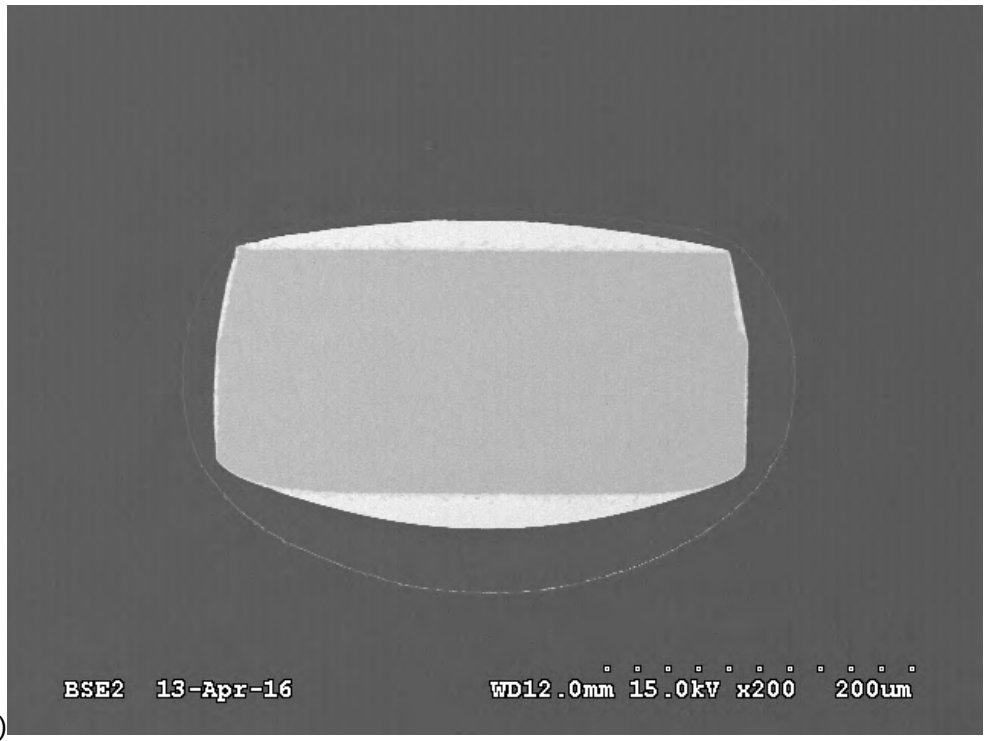
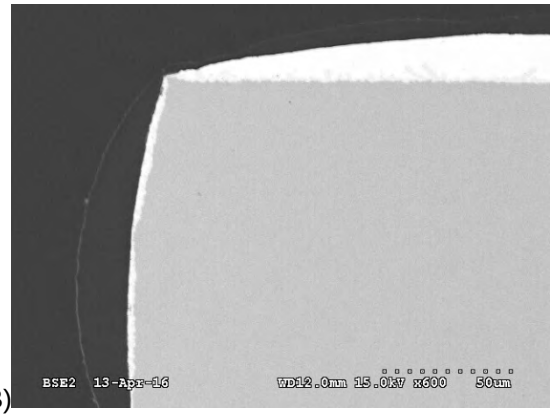


Figure 49: Cross-section SEM image of PC18M dip + two (PC18M+20XP2742) sprays, board A225, U3, lead 1; (A) 200x, (B) upper back corner, 900x, and (C) lower back corner, 900x.

(A)



(B)



(C)

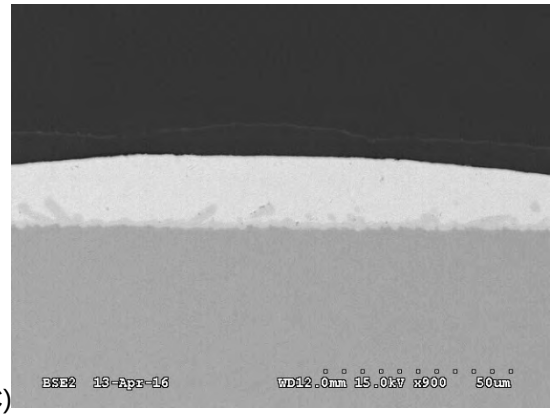
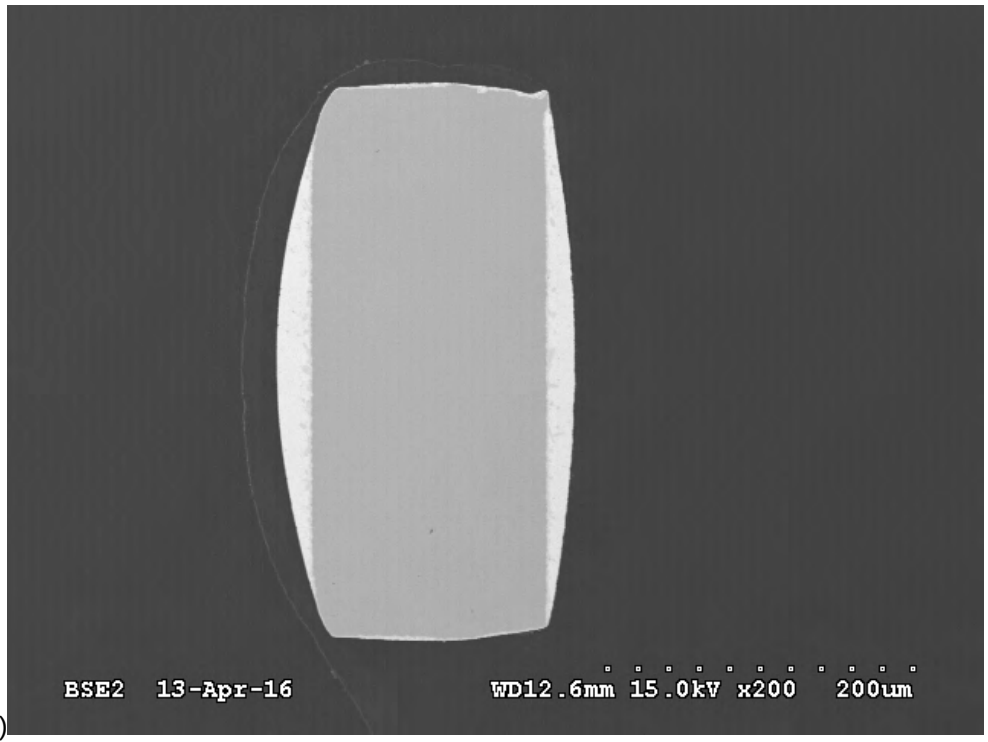


Figure 50: Cross-section SEM image of PC18M dip + two (PC18M+20XP2742) sprays, board A225, U3, lead 22; (A) overall 200x, (B) back left corner, 600x and (C) back, 900x.

(A)



(B)

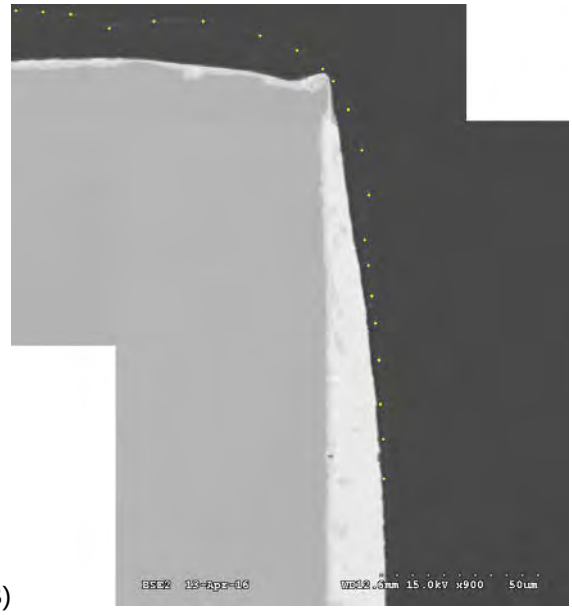
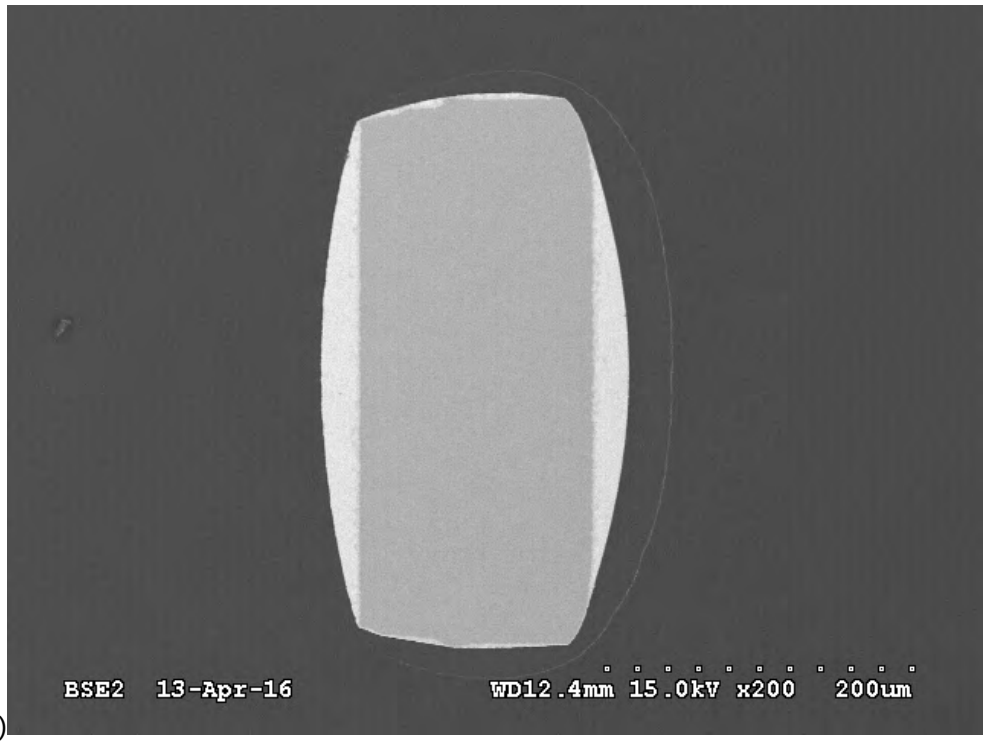


Figure 51: Cross-section SEM image of PC18M dip + two (PC18M+20XP2742) sprays, board A225, U3, lead 6; (A) 200x, and (B) upper back corner, 900x (enhancement added to highlight coating).

(A)



(B)

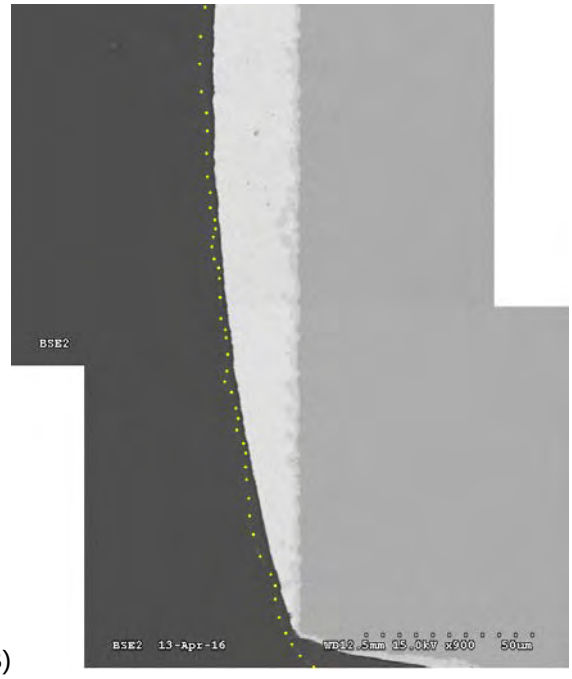


Figure 52: Cross-section SEM image of PC18M dip + two (PC18M+20XP2742) sprays, board A225, U3, lead 28; (A) overall, 200x, and, (B) back center and bottom corner, 900x (enhancement added to highlight coating).

6. FE – SEM images of microtome sections

A microtome section followed by a FE – SEM examination was used to examine the nanoparticles and layer thickness variation along the lead on a QFP44 with PC18M dip + two (PC18M+20%XP2742) sprays (Figure 53). Sections one and two are perpendicular to the lead and section three is along the length of the lead (Figure 54).

6.1 Section one and two

Section one and two locations correspond to locations A and D in the conventional vertical cross-sectioning (Figure 16). Leads from the middle of the row (not corner leads) were used for each section. The perpendicular section examined the sides and corners of the lead (Figure 55).



Figure 53: QFP from board A225 examined using microtome sectioning.

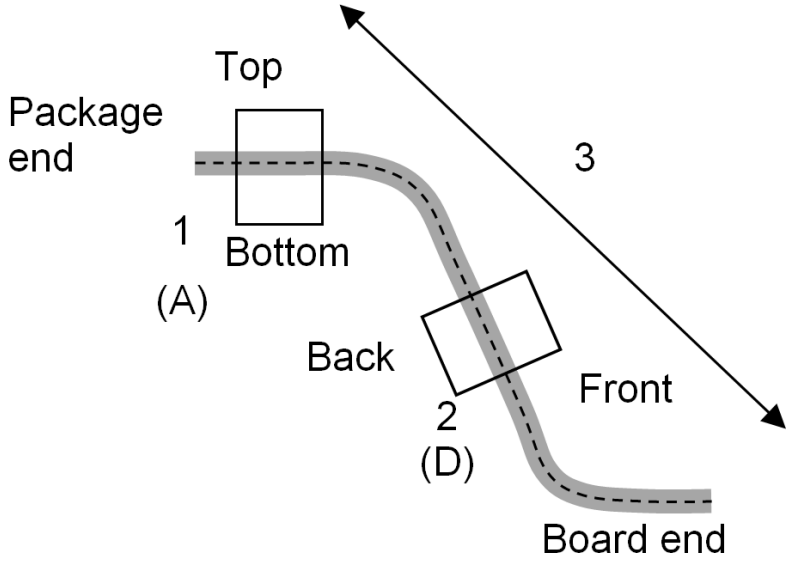


Figure 54: Schematic showing microtome section locations.

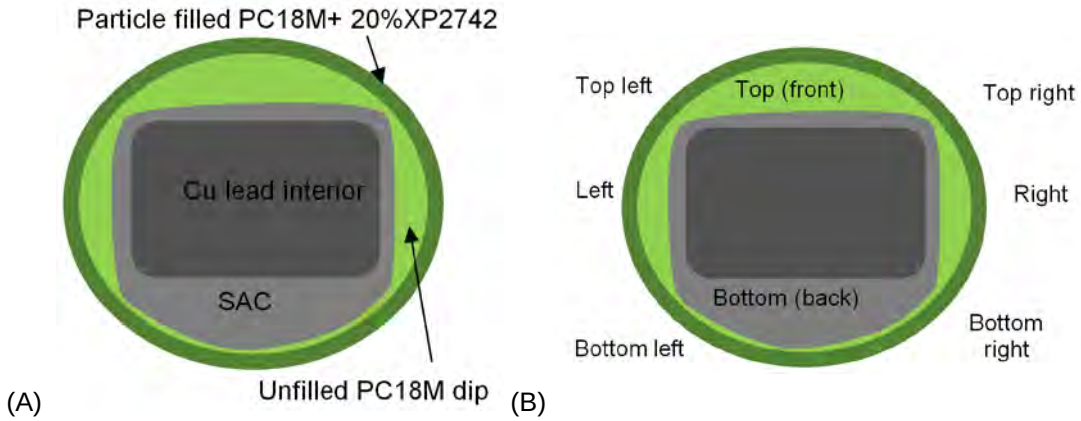


Figure 55: Microtome section perpendicular to lead schematic; (A) materials and (B) locations examined.

Generally, the nanosilica particles were well distributed with no agglomeration and good adhesion between layers and to the metal. The overall perpendicular cross-sections of section one and two (Figure 56) and the higher magnification images of top and bottom (Figure 57 and Figure 58) show that the side with the direct line-of-sight to the spray nozzle (top or front) has greater particle filled spray coating thickness than the shadowed side (bottom or back). Even though the right side of section two has a coating web bridging to the next lead, particle filled coating from the spray process was evident.

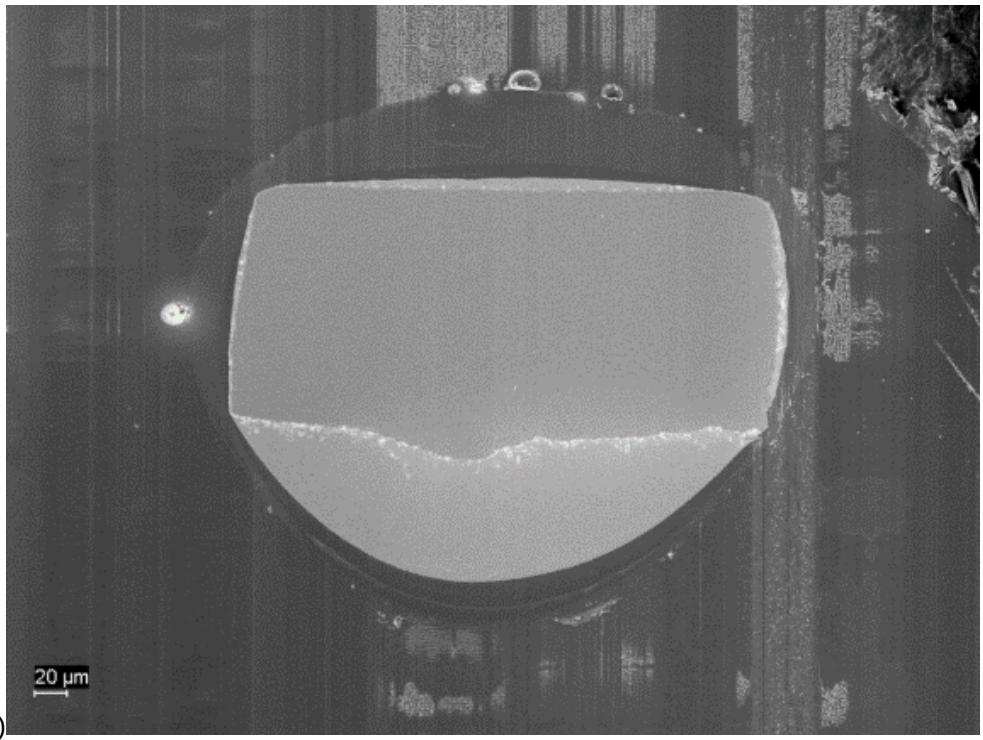
As expected, the corner coverage was better on the top and front side corners. The dip coating on the corners was approximately one micron thick. The spray coating added considerable the thickness build-up to the corners (Figure 59).

The coating thickness on the side consisted mostly of the particle filled spray coating build-up (Figure 60). The spray coating on the right side of section two along the back of the dip coating web had droplets of spray coating (Figure 61).

The particle uniformity and the knit line between the layers, both spray – to – spray layers and spray – to – dip layers, exhibited good adhesion (Figure 62 and Figure 63). The particle filled microstructure consisted of uniformly dispersed nanosilica particles (white specks) chemically bonded to an isotropic network structure in the polyurethane matrix (Figure 63). This has the benefits of increased flexibility and isotropic mechanical properties.

Measurements of the dip and spray coating thicknesses on sections one and two show that the top (or front) of the leads had the greatest amount of spray coating (Figure 64 and Figure 65). The sides and top (front) had a minimum of 10 microns of coating except in some instances of the bottom (back) corners. The very thin dip coating in the corners was covered by spray coating on the top (or front) and to a lesser extent bottom (or back) corners. In addition, there were often a few microns of spray coating on the bottom (back) in both sections.

(A)



(B)

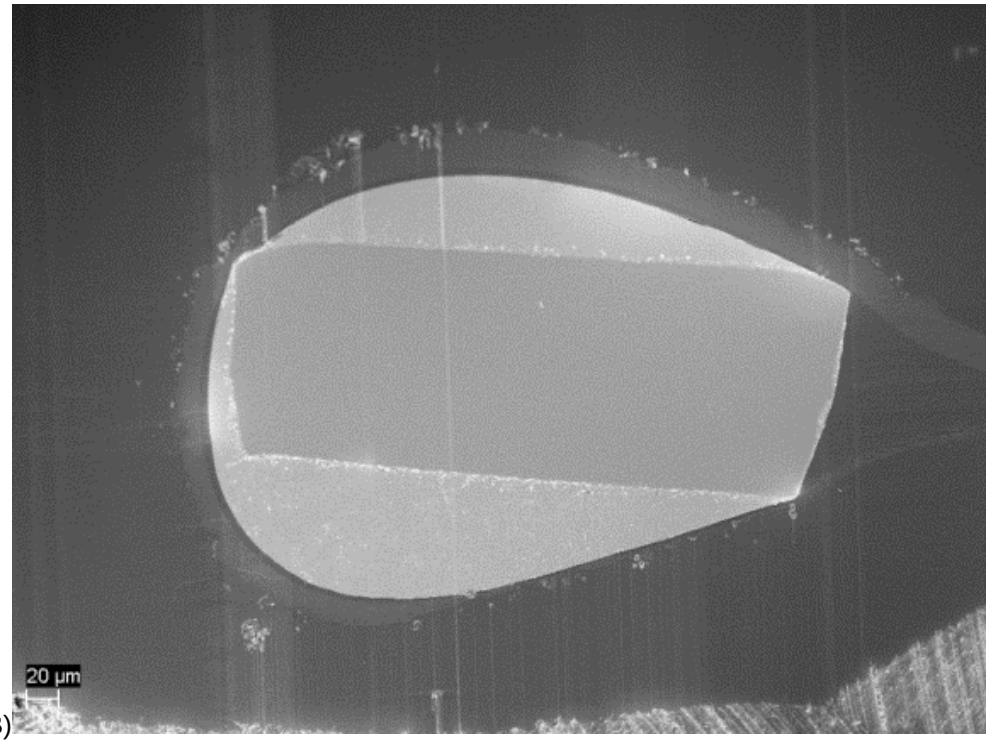


Figure 56: FE – SEM images of microtome sections (A) section one, and (B) section two.

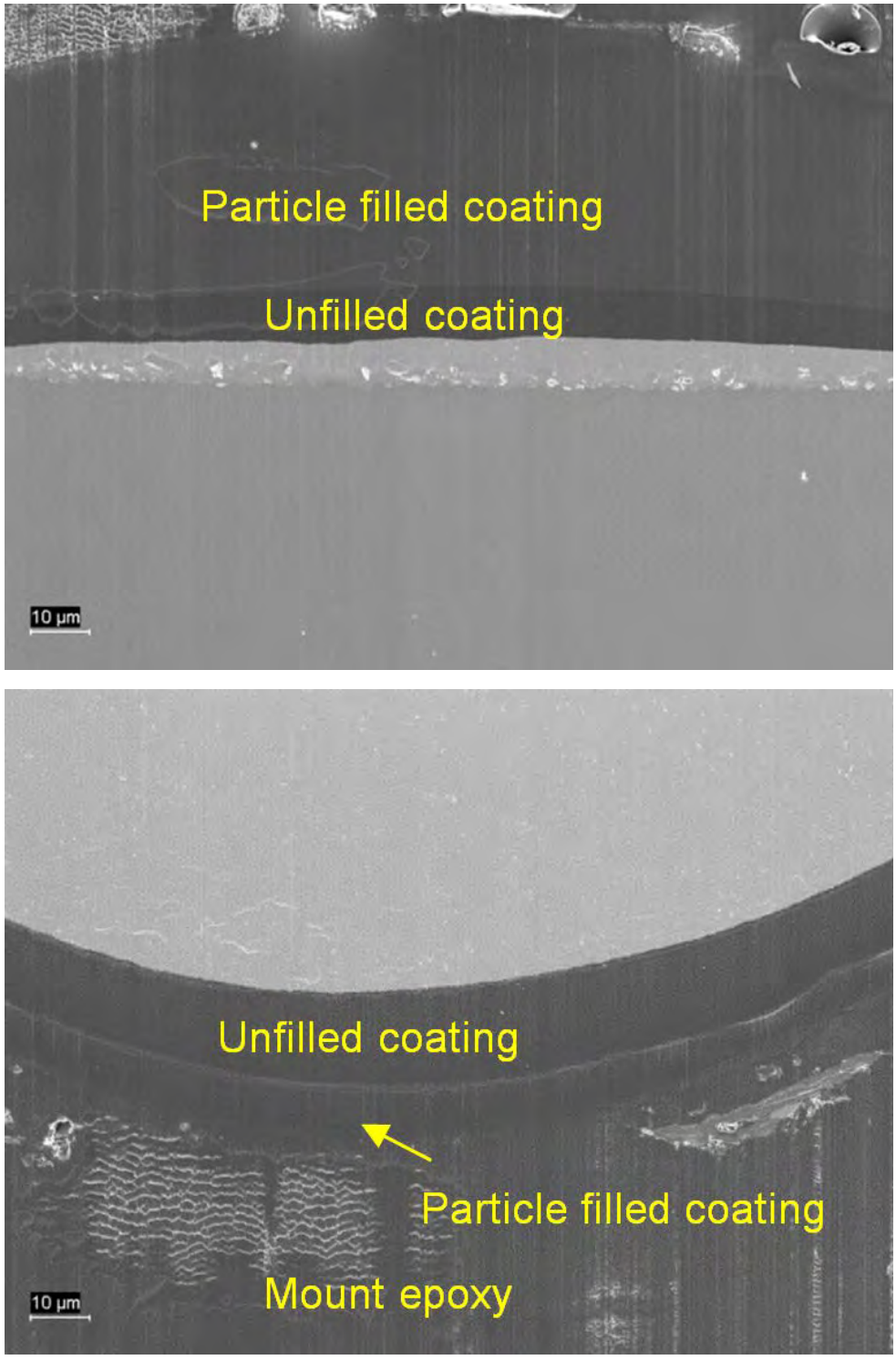


Figure 57: FE – SEM of microtome section one at higher magnification; (A) top and (B) bottom.

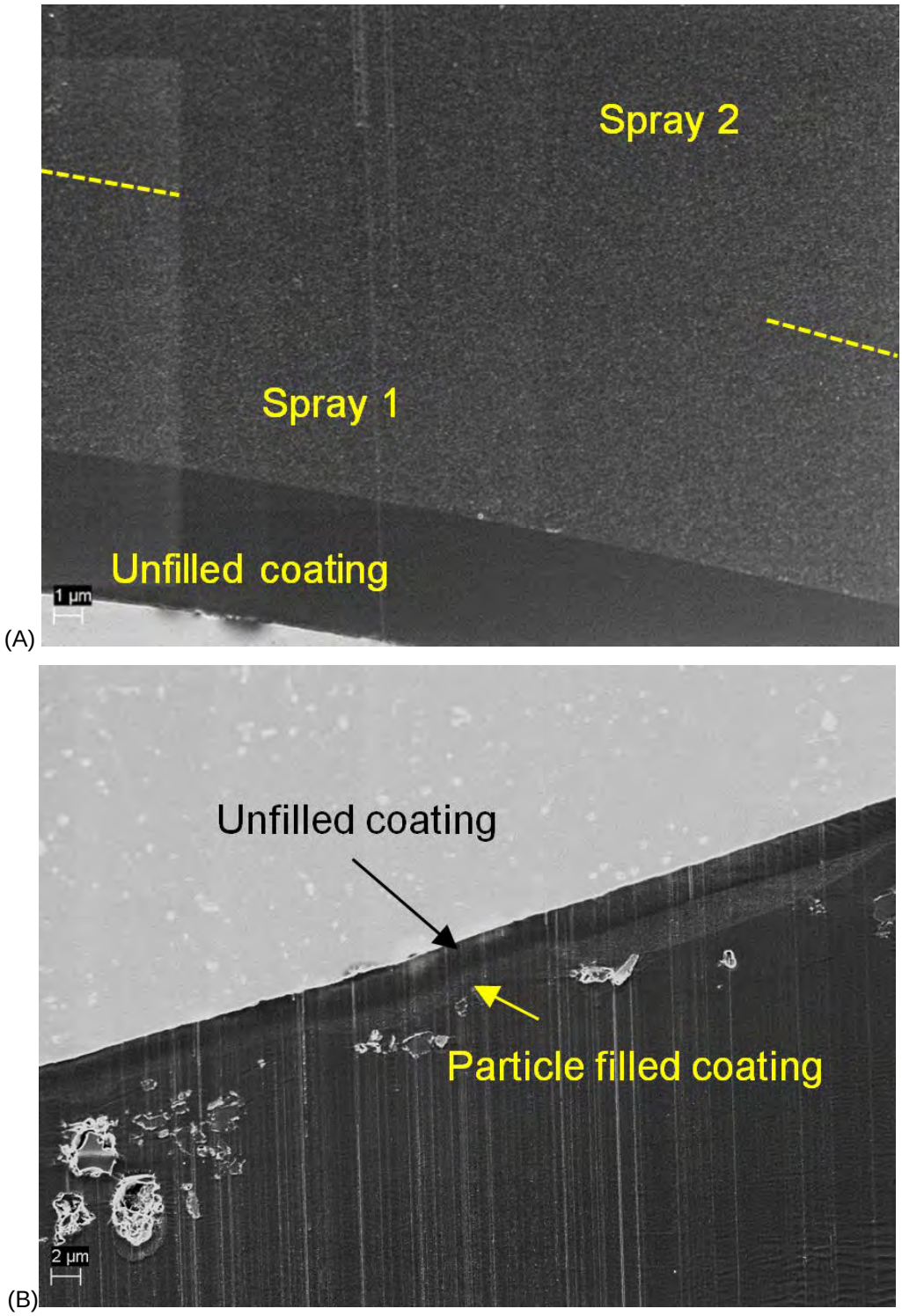
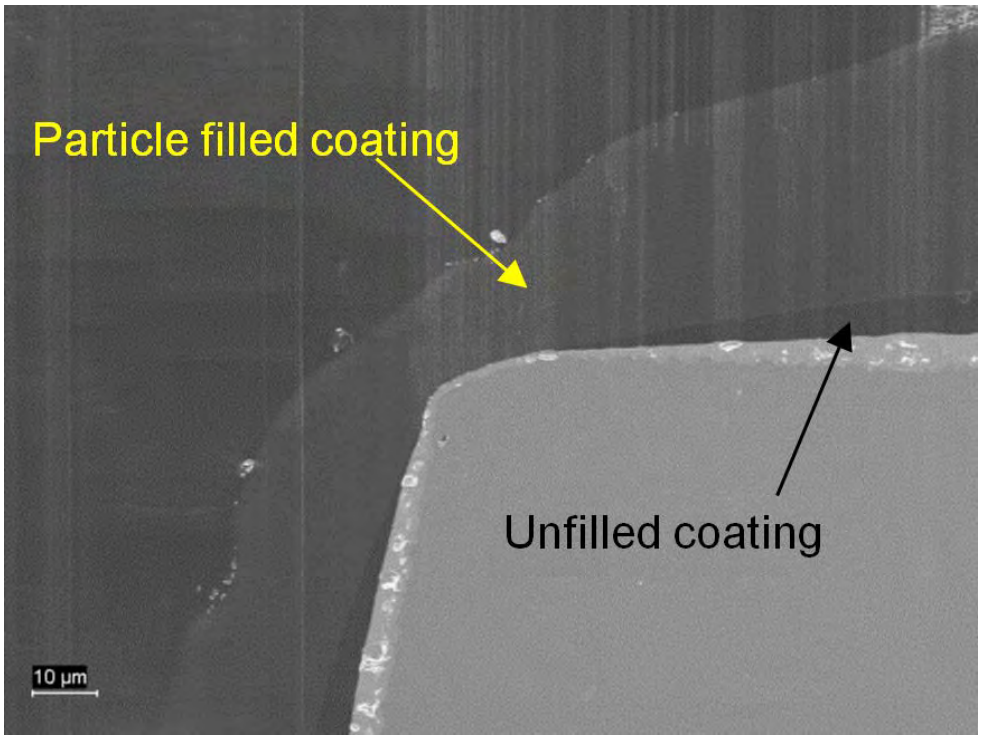


Figure 58: FE – SEM of microtome section two at higher magnification; (A) front and (B) back.

(A)



(B)

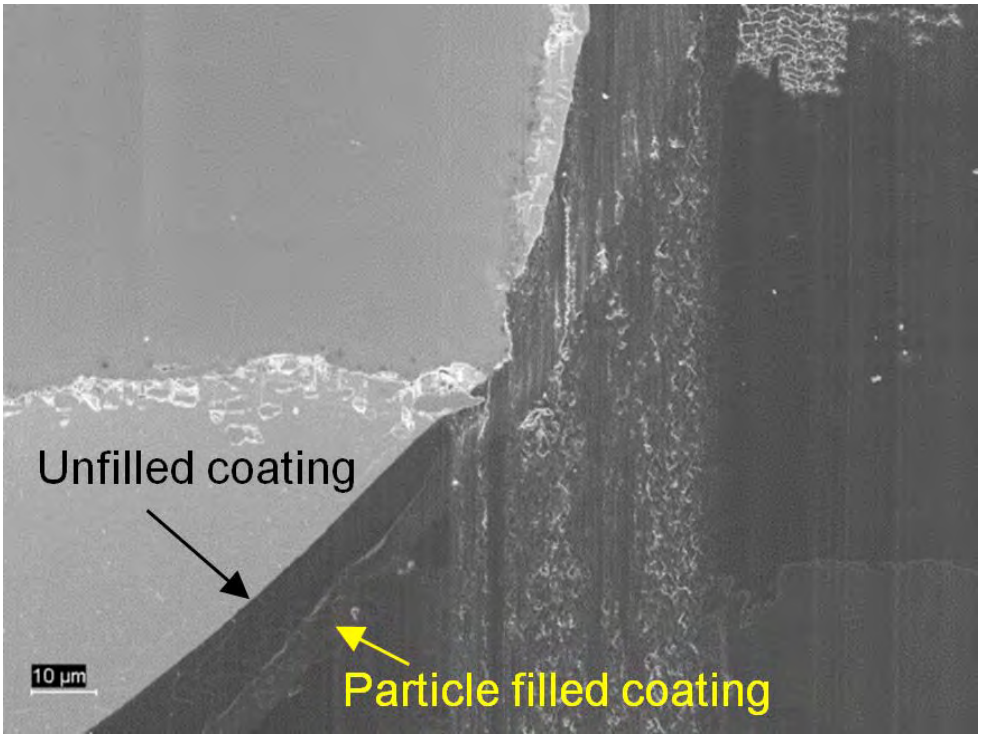


Figure 59: FE – SEM of microtome section one outer and inner corners; (A) top right and (B) bottom left.

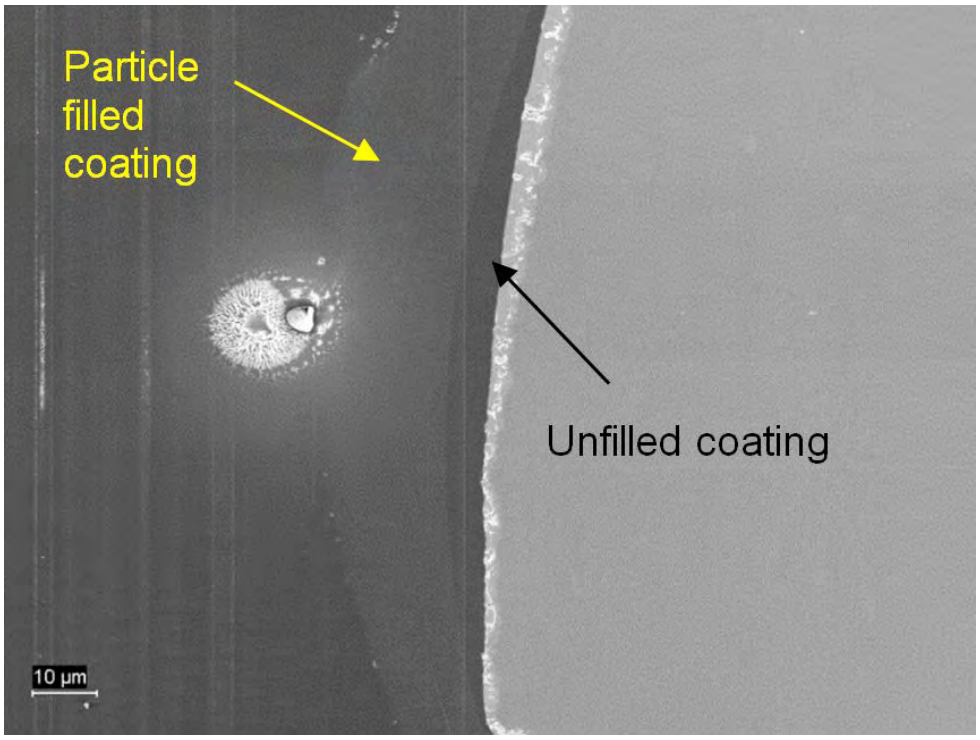


Figure 60: FE – SEM of microtome section one left side.

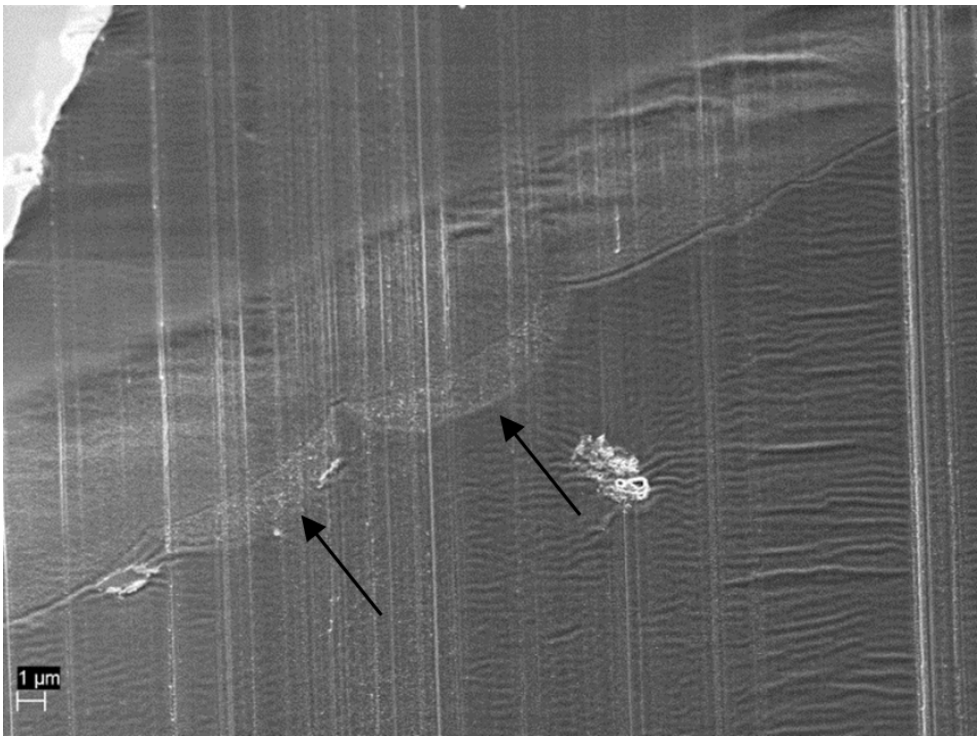


Figure 61: FE – SEM of microtome section two right back along the dip coating web to the adjacent lead. Arrow highlights particle filled spray coating droplets on the dip coating.

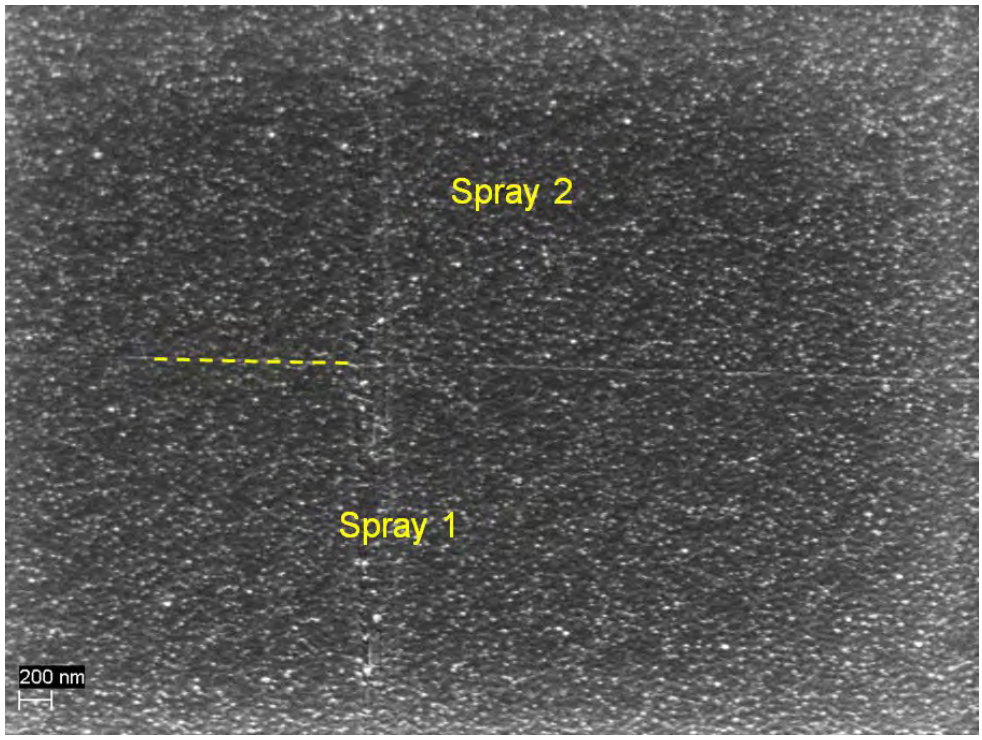
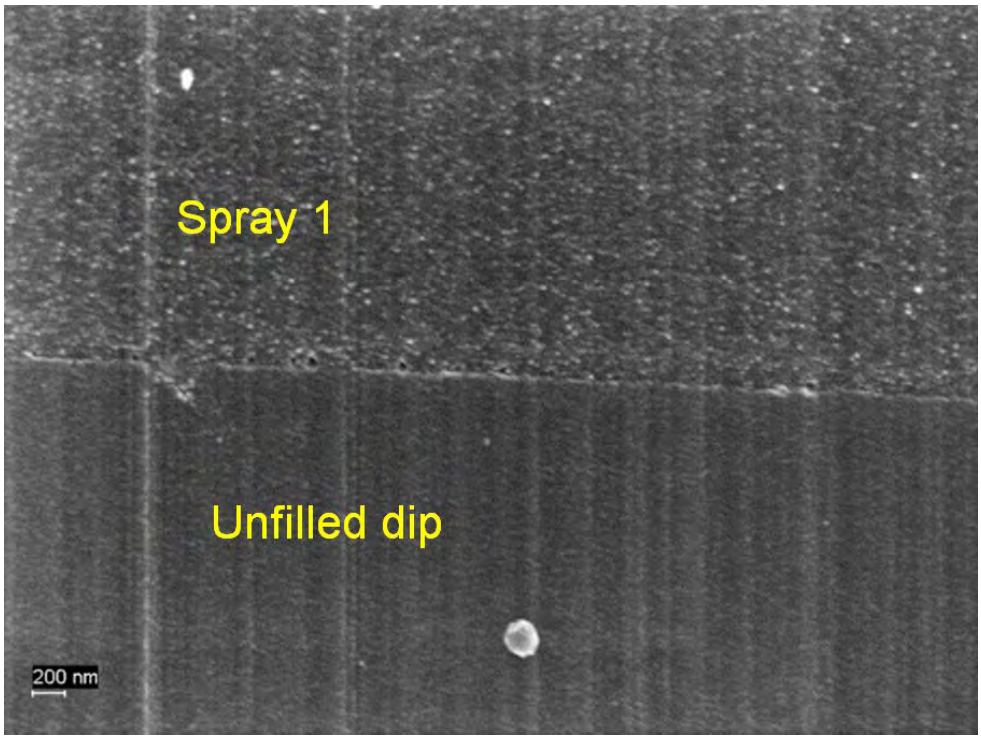


Figure 62: High magnification FE – SEM images of microtome section two front showing particle uniformity and a well adhered knit line between the two spray layers.

(A)



(B)

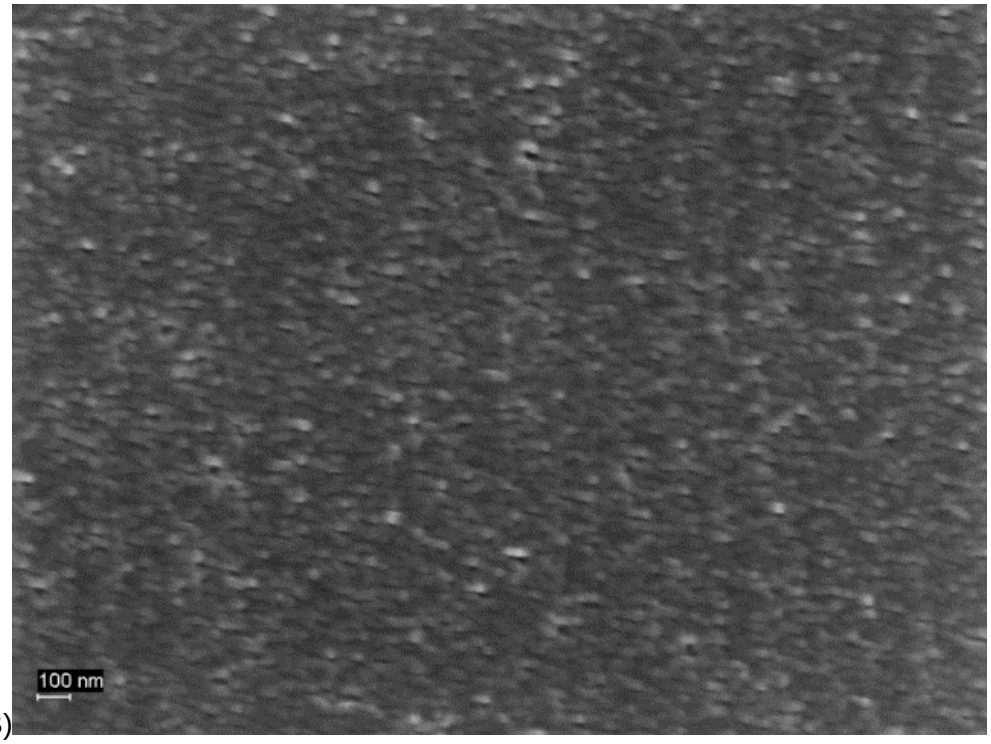


Figure 63: High magnification FE – SEM images of microtome section; (A) top of lead showing spray coating to dip coating interface and (B) image from the bottom right showing the spray coating microstructure.

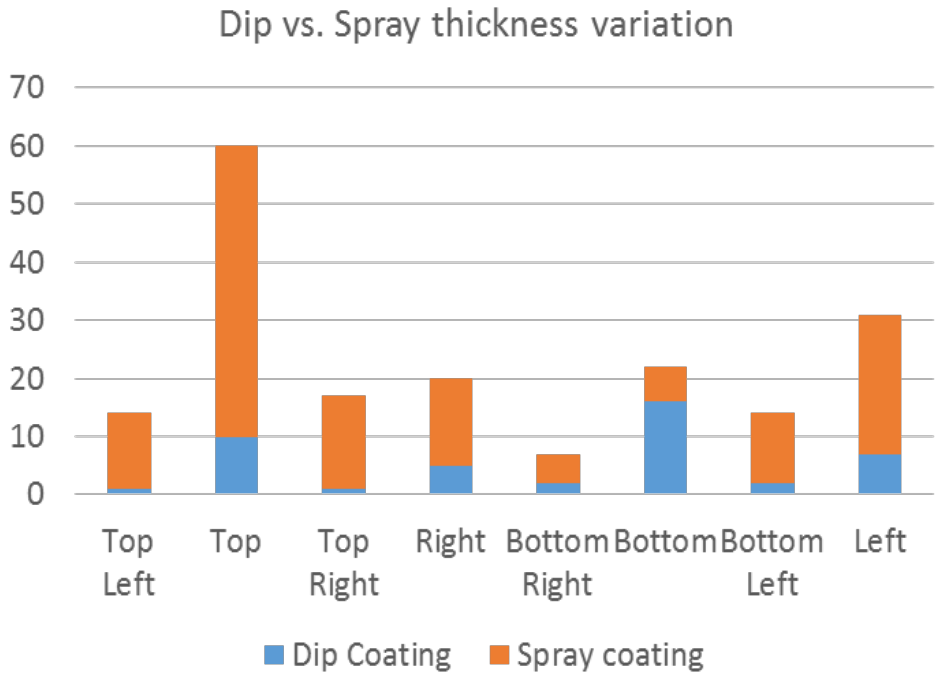


Figure 64: Section one dip coat and spray coating thicknesses.

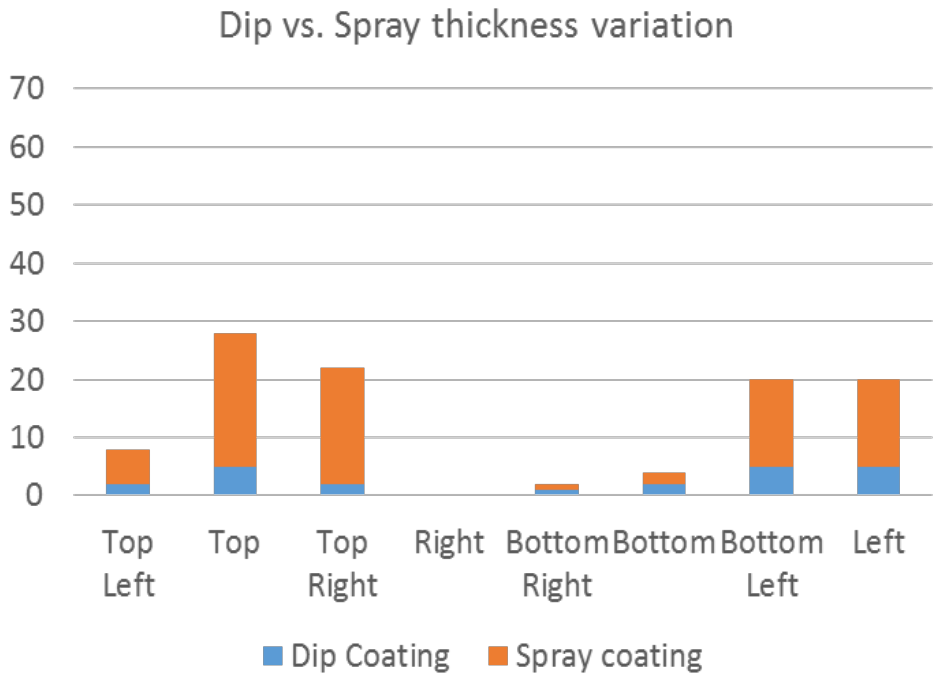


Figure 65: Section two dip coat and spray coating thicknesses. Note that a coating bridge between leads prevented measurements on the right side of the lead.

6.2 Section three

Microtome section three along the length of the lead was used to examine three areas (Figure 66). Note that the location of Area C aligns to microtome section 2 (Figure 54) which also approximately aligned to vertical section location D (Figure 16).

The overall section with the markers highlighting the coating thickness is shown in Figure 67. The thickest coating is in inside corners between the lead and the package and the inside radius made between the vertical part of the lead and the lead foot. The overall particle distribution throughout the section was uniform (e.g. Figure 68). Generally, the particle filled coating was thicker on the top or front of the lead than the bottom or back in all areas (Figure 69 to Figure 71).

At the lead – to – package region, area A (Figure 69), the coating fillet between the underside of the lead and the package was primarily unfilled dip coating with a thin layer of nanosilica spray coating. On the top side of the lead and the package corner, the fillet was smaller. In this area, the unfilled dip coating formed a fillet in the corner and became progressively thinner at locations further along the lead toward the knee. The top side nanosilica filled spray coating formed a relatively uniform layer on top of the dip coat layer.

At the lead knee, area B (Figure 70), the thickness of the unfilled dip on the back side of the lead was greater than the front side; while the nanosilica filled spray coat was thicker on the front than the back. There were also some distinct cured nanosilica droplets from the first spray layer that were covered over by additional nanosilica coating from the second spray layer. This may indicated that the first spray layer facilitated wetting behind the lead of the second spray layer.

At the midpoint of the lead, area C (Figure 71), there were more instances where nanosilica filled coating droplets from the first spray layer were covered by additional nanosilica filled coating from the second spray layer. In some areas the unfilled (dip) coating layer showed delamination from vertical portions of the back side of the lead, but that may have been from cutting motion of the microtome.

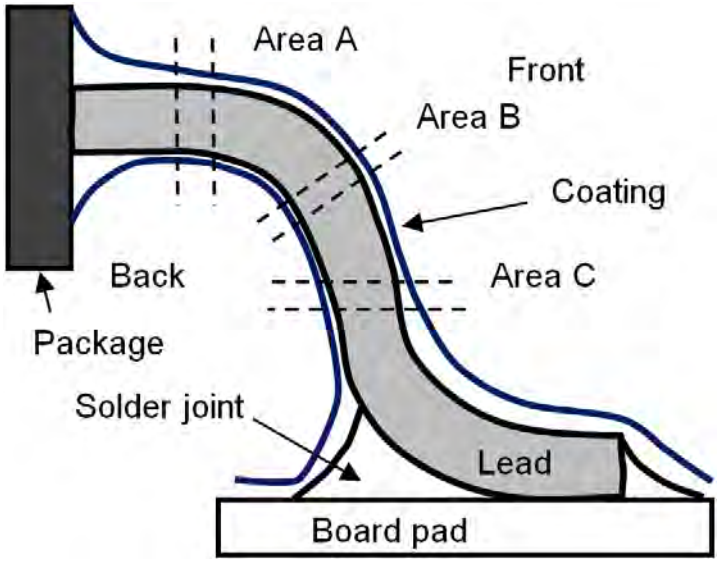


Figure 66: Microtome section three examination areas.

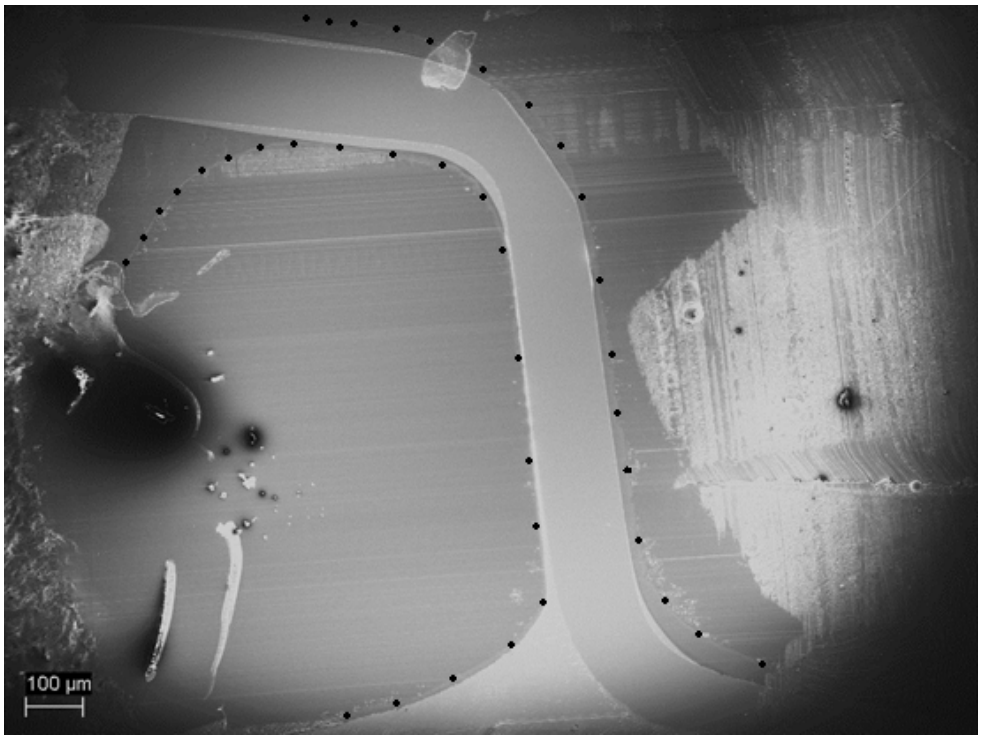


Figure 67: Overall FE – SEM image of microtome section three lead and coating.

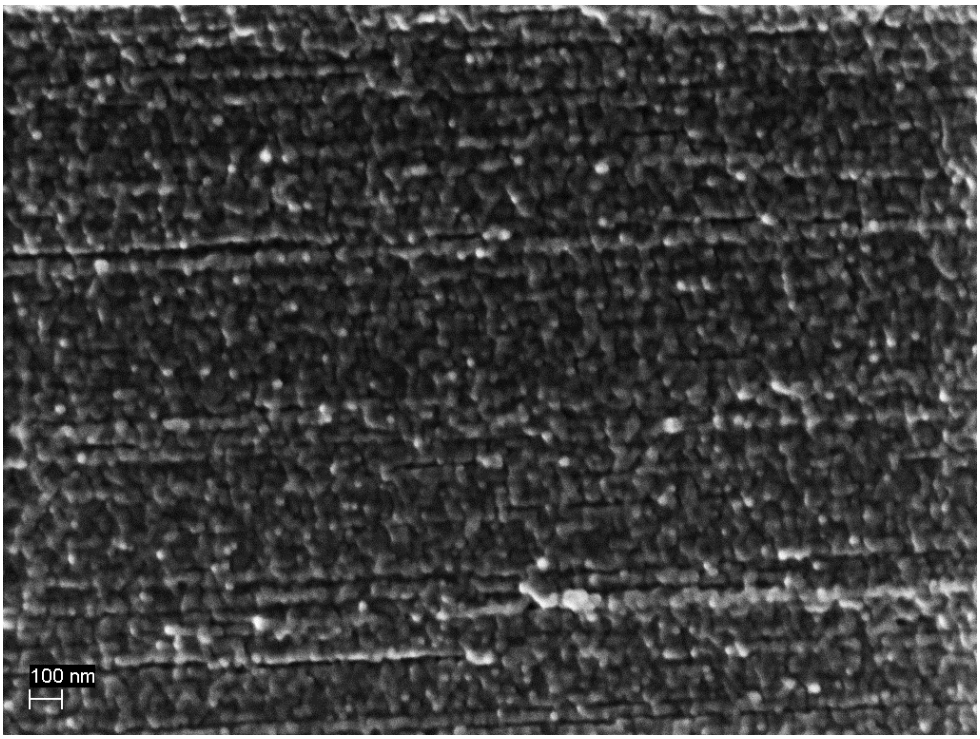


Figure 68: Typical FE – SEM image showing uniform particle distribution (Area C base shown).

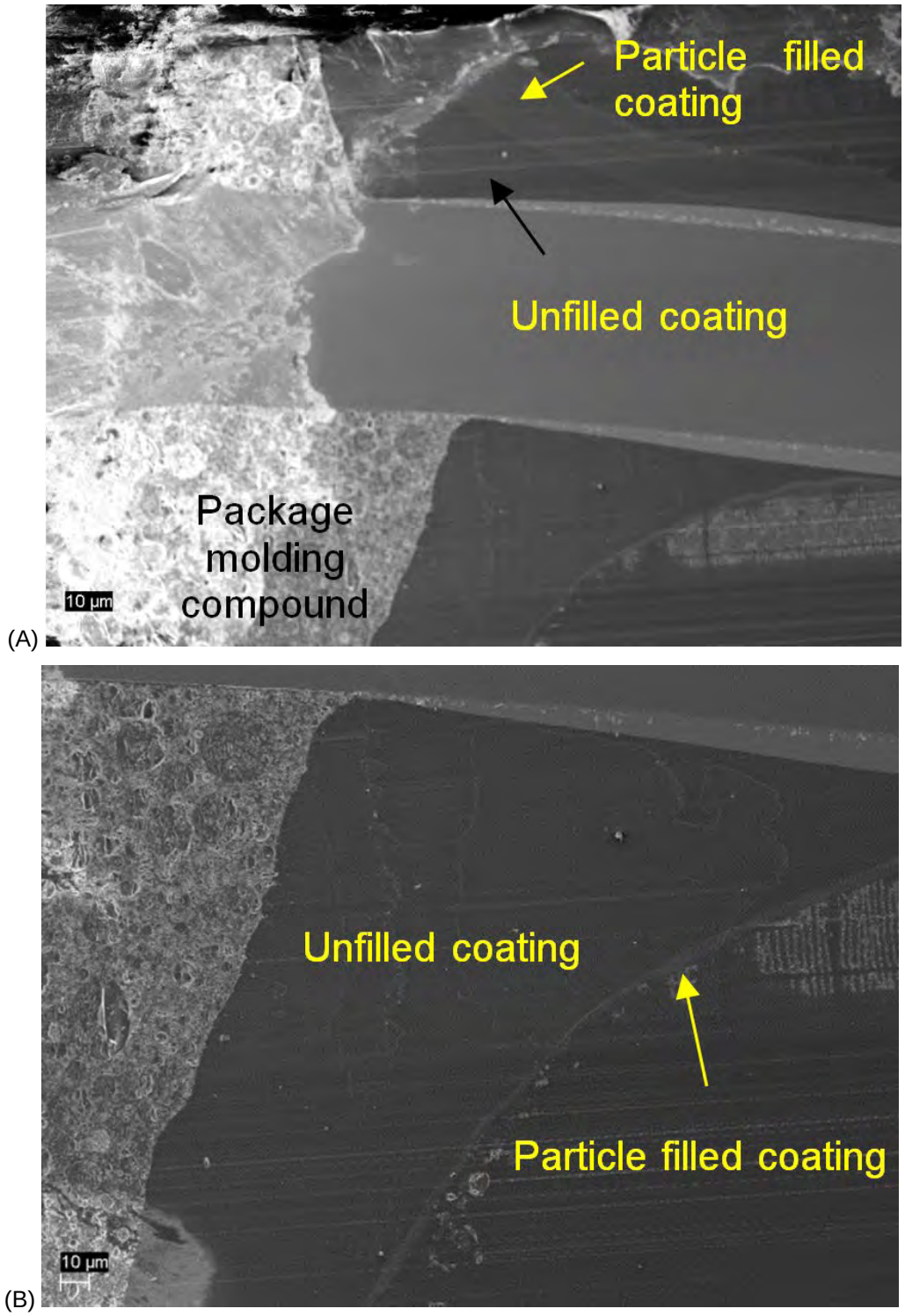


Figure 69: Section three Area A FE – SEM image; (A) top, and (B) bottom.

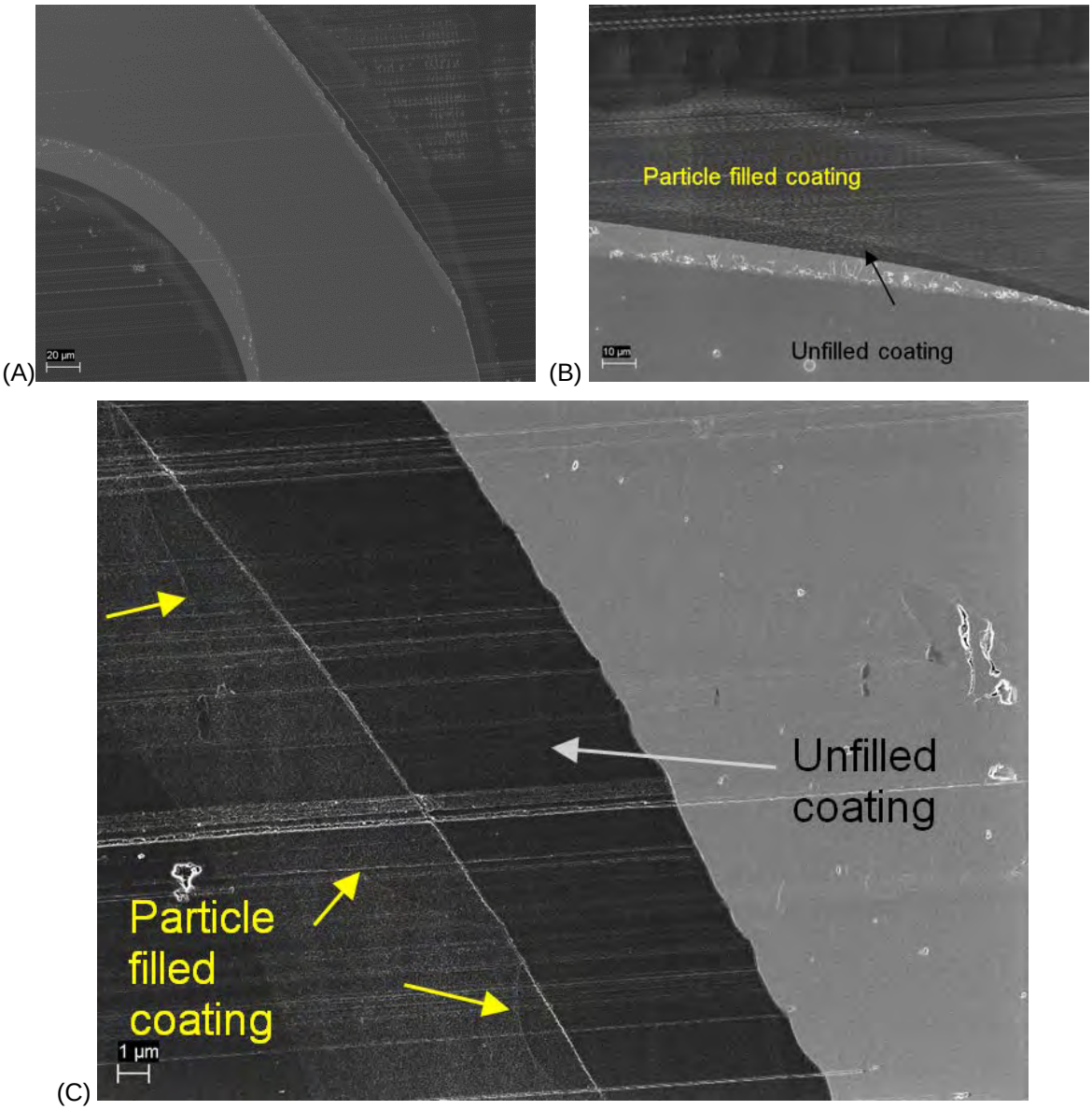


Figure 70: Section three Area B FE – SEM image; (A) overall, (B) front, and (C) back with arrows showing the first spray layer covered by the second spray layer.

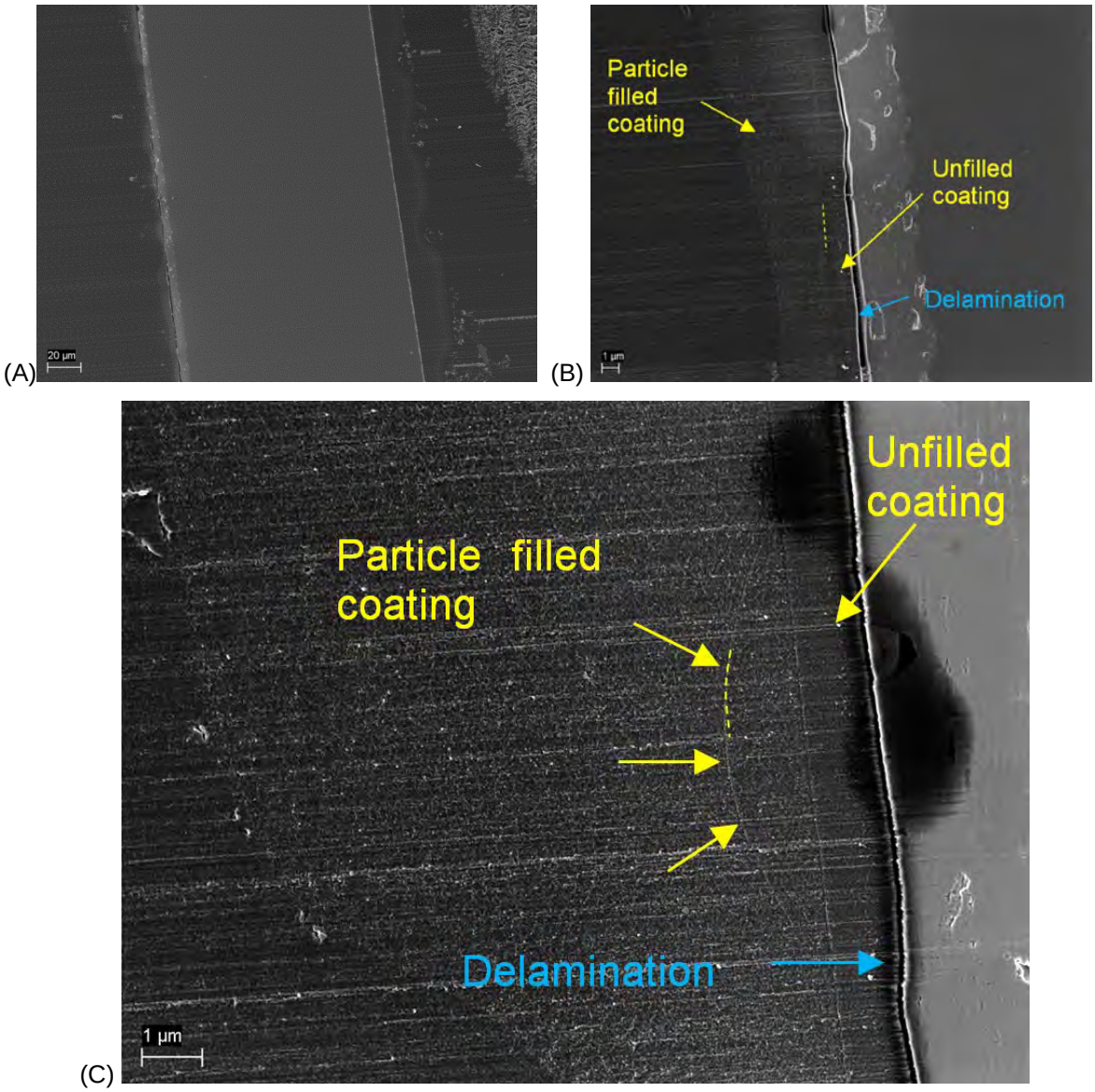


Figure 71: Section three Area C FE – SEM image; (A) overall, (B) back of lead, (C) second location on back of lead with arrow indicating spray coating drop covered with additional spray coating.

7. Discussion

7.1 Dip coating

The dip coating was applied, to ensure that there was some polyurethane on all surfaces in order to reduce potential shorting from detached whiskers, e.g. conductive foreign objects and debris (FOD), and from whiskers growing from other surfaces. After dip coating, some coating bridging between leads and fill behind leads was observed, particularly on the downward drainage side of the parts where the coating builds up. The drip time after board removal was approximately one minute, at which point the boards were removed and placed on a horizontal surface. It is possible that the bridging could have been avoided by shortening the drip time since the PC18M viscosity increases as solvent evaporates during the dripping phase.

7.1.1 Back of lead dip coverage

In some cases large dip coating thickness was observed at location B (Figure 37). The coating build-up on the inside corner of the lead is likely due to capillary action and a possible viscosity that has contributed to coating webbing.

7.2 Spray coating

After spray coating, a slightly dull coating appearance was observed on the PC18M sprayed assemblies. The dull finish was not rejectable per J-STD-001. Subsequent SEM examination of the coating surface revealed pits and craters ranging in size from one micron to 50 microns with some larger pits Figure 7 and Figure 8. It appears as though gas bubbles were escaping from the coating free surface while it was solidifying. The set-up of a spray process is largely empirical. Settings were established in order to maximize the number of spray passes to achieve a nominal dry thickness of 25 microns without being too dry. The highly atomized spray used in the present work met typical visual wetness criterion, but in hindsight may have been borderline. The characteristics of a dry coating are that it does not flow into a smooth film after spraying. The smoothing time after spray is typically on the order of minutes. Since lack of flow is due to reduced solvent content in the film, there may also have been some air entrained into the coating surface amongst the spray coating droplets.

The (PC18M+20%XP2742) spray coated samples exhibited a similar characteristic but to a much lower degree even though similar spray settings were used Figure 10 and Figure 11. The smoother surface is believe to be due the (PC18M+20%XP2742) having a lower coating viscosity than PC18M alone. The (PC18M+20%XP2742) has approximately 10 percent 3,300 cps viscosity HDI from the XP2742 nanoparticle suspension.

The phenomenon creating the rough surface appears to be related to the bubble formation observed during the baseline spray coating [**1**], but with a dryer spray and smaller coating droplets. The baseline coating process bubbles were observed in the coating around the package by the leads (e.g. Figure 72) or on the package (e.g. Figure 73).

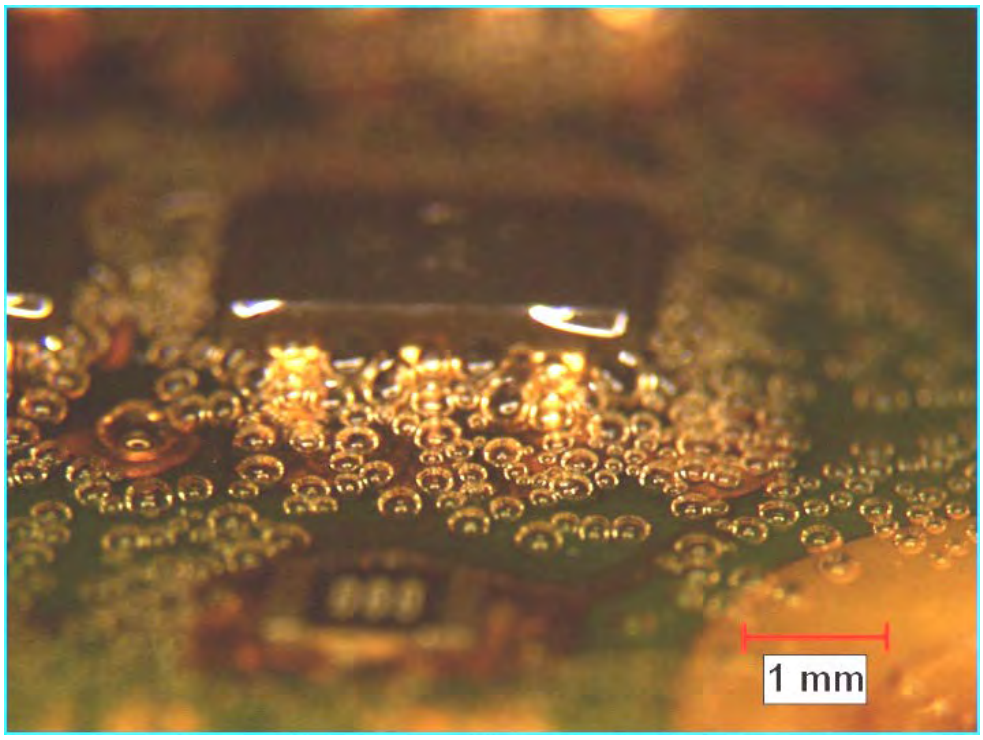


Figure 72: PC18M-mod SOT board 233 baseline coating with large bubbles around the leads, 10x (note the photograph was taken after thermal cycling and 1,000 hours of 85°C/85%RH humidity (ATC+1000HTHH) environments). The color change in the second image is an artifact of the illumination used to highlight the bubbles [1**].**

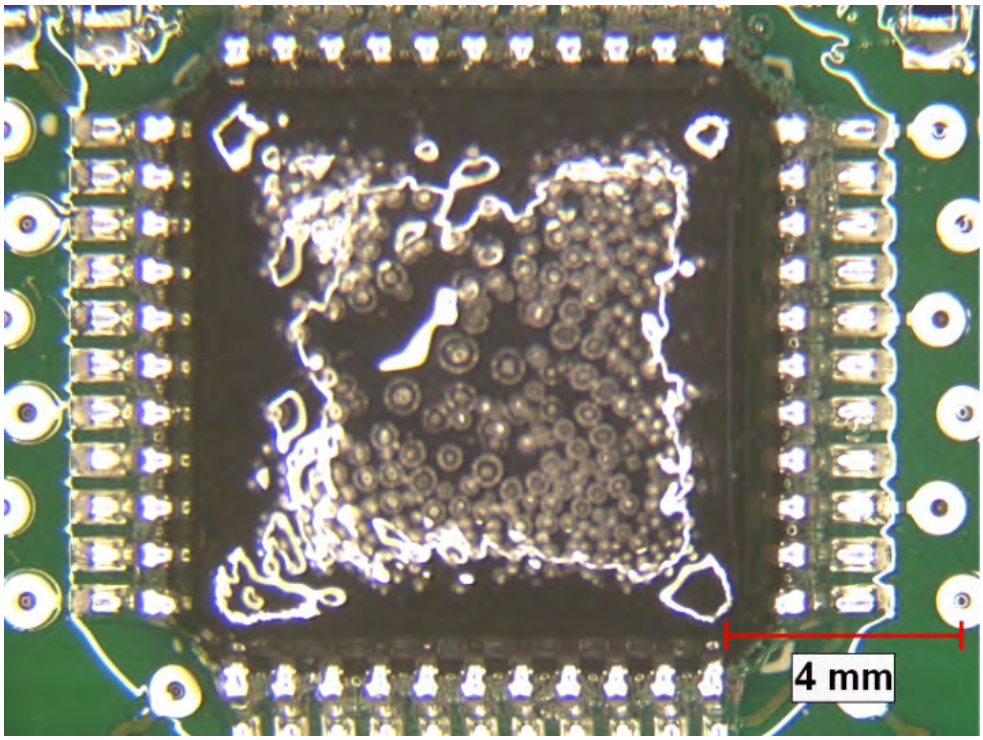


Figure 73: PC18M-mod QFP board 35 baseline coating with large bubble density on top of the package, 10x [1**].**

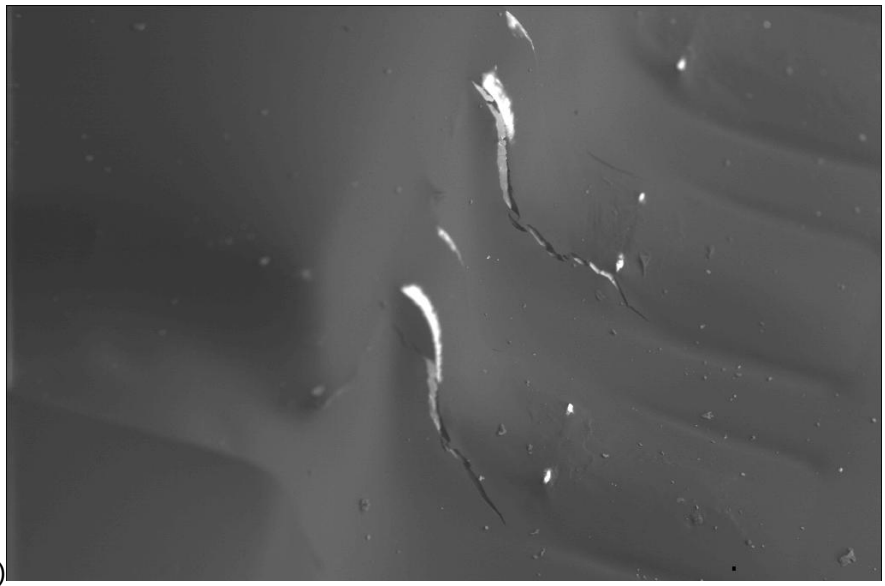
7.2.1 Back of lead spray coating

The observation of nanoparticle spray coating on the back of the leads and the back of the coating web between leads (Figure 58 and Figure 61) that are not in a line-of-sight with the spray nozzle suggests that “fog-like” coating particles from the atomized spray may be accumulating on the back side. The total spray time of the 1x-1y-1x-1y passes of one spray layer was approximately eight minutes. It is expected that particle filled coating coverage due to capillary action from the front side would not be made up of distinct “spreading droplets”.

7.3 Layered coating

The layered coating approach allows increased coating coverage and thickness on the leads while minimizing coating build-up around the package bodies. Since the coating coefficient of expansion is typically much higher than the copper leads or the solder, excessive coating build up around the package body can increase solder stresses during thermal cycling [5]. Variation in coating pooling around parts occurred in the baseline tests (Figure 74) and the layered coating work (Figure 75 and Figure 76). Contributors to coating pooling are heavy spray layers and high dip coating viscosity.

(A)



(B)



Figure 74: SEM image from the baseline coating test [1][2] of a SOT6 with varying degrees of coating fill around the parts, 60x; (A) board 211, PC18M dip + baseline PC18M spray and (B) board A217, PC18M dip + baseline (PC18M+20%XP2742). Note images taken after accelerated thermal cycling.

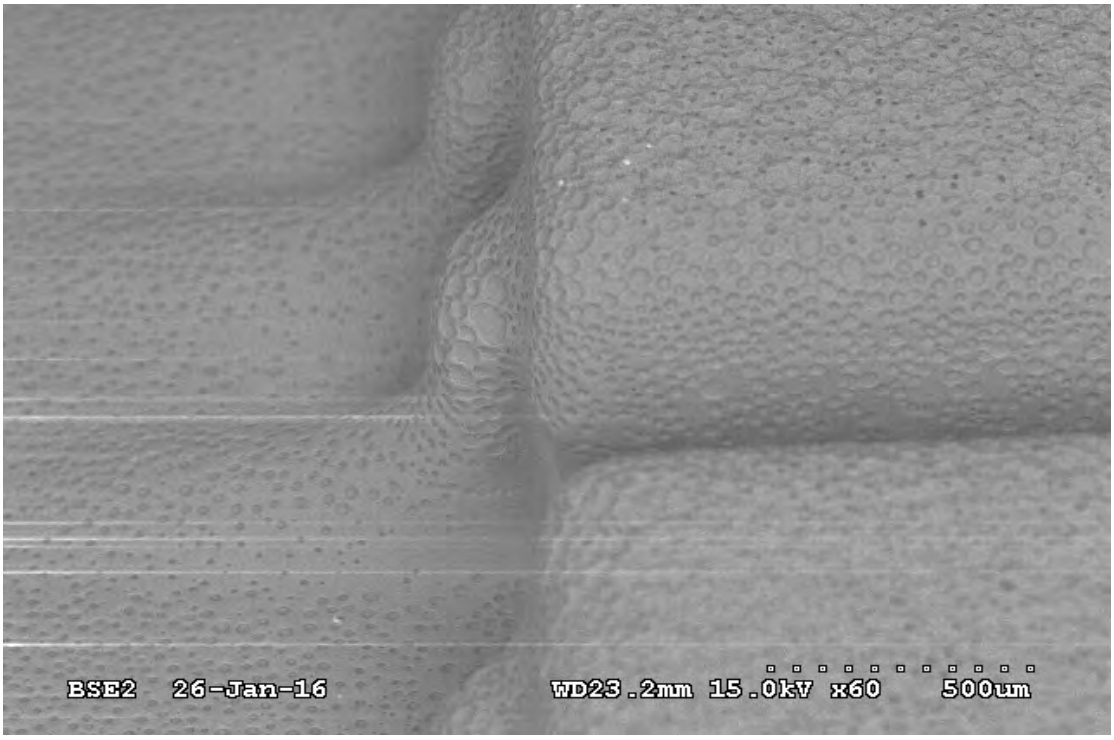
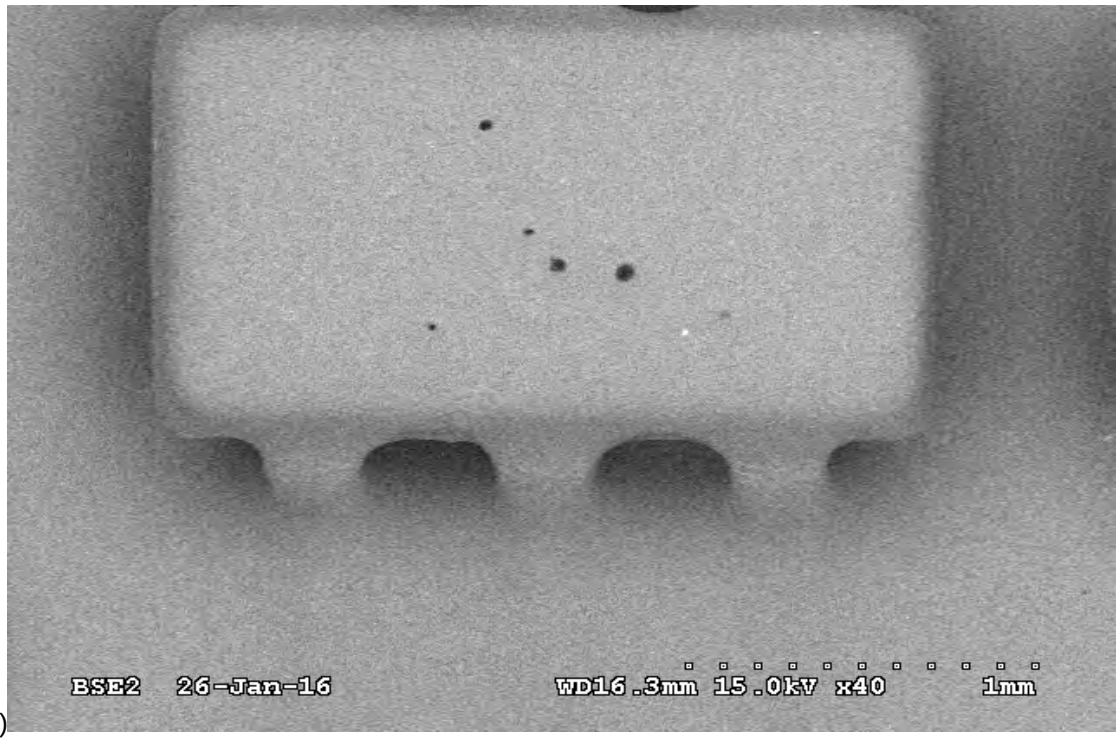


Figure 75: SEM image of PC18M dip + two PC18M sprays, board 243, SOT6, 60x, with thick coating behind leads.

(A)



(B)

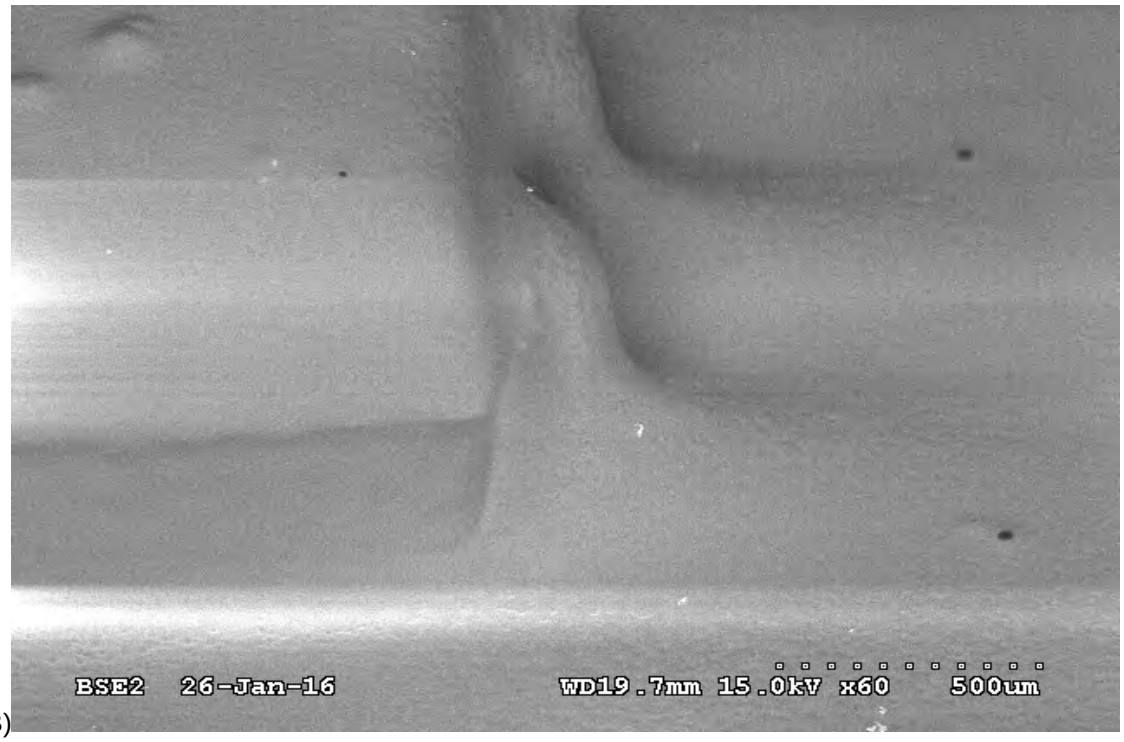


Figure 76: SEM image of PC18M dip + two (PC18M+20%XP2742) sprays, board 51, SOT6, (A) leads almost filled, 40x, and (B) lead to body area filled.

7.4 Thickness comparison with other research

The IPC round robin currently in its final year is evaluating the "state of the industry conformal coating coverage" [6] and has results on some polyurethane coatings. The QFP part is especially susceptible to thin coverage over the tip of the lead (location T, Figure 16). The lead tip thickness of the PC18M dip + two (PC18M+20%2742) spray was above the current industry results (Figure 77).

The present layered approach provided better coverage than that described by V. Kumar and L. Woody [7]. Kumar described the capability of automated conformal coating equipment to provide coating coverage of various packages, but did not indicate the coating type. The applied coating was targeted at 76 to 127 microns (three to five mils) and the flat control coupon thickness was 117 microns (4.6 mils). Thickness was only evaluated by cross-sectioning along the center of lead and optical microscopic measurements. The results showed that the back of the leads had 75 to 100 percent coverage with 12.7 to 20 microns (0.5 to 0.8 mils) of coating and the front of the leads had 100 percent coverage with 36 to 71 microns (1.4 to 2.8 mils).

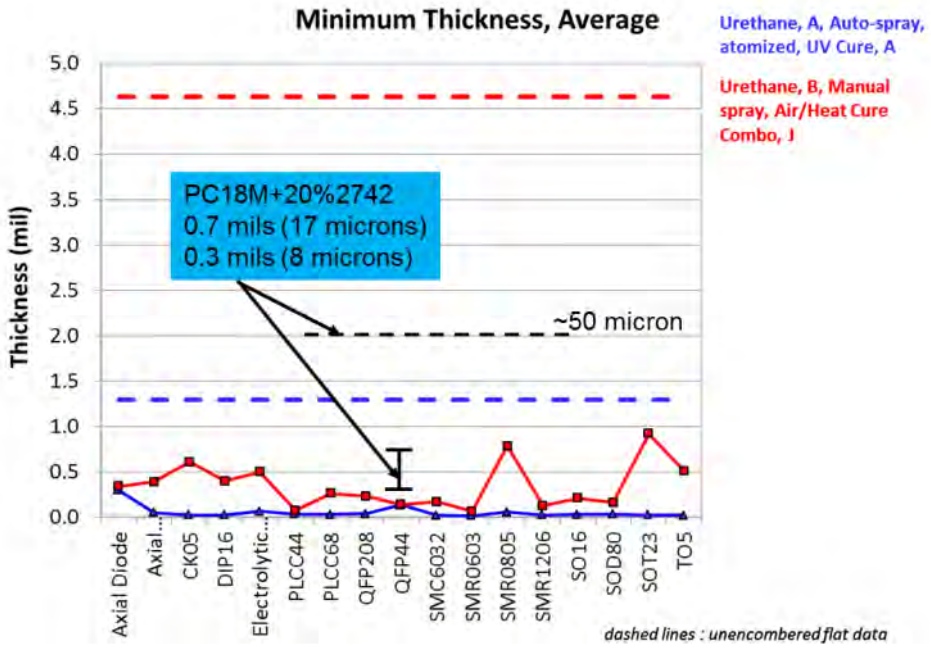


Figure 77: 5-22arr IPC J-STD-001 conformal coating and material application industry assessment interim results. Actual minimum thicknesses on leads (solid line) much less than unencumbered flat surface (dashed line) process control measurement.

8. Summary

Using conformal coating for whisker mitigation does not a guarantee elimination of whisker short circuit risk, but can greatly reduce it. Improving coverage, thickness consistency, and coating properties reduces whisker shorting risk. In contrast to the vacuum deposited Parylene™ coating, obtaining good coverage with the liquid coatings is still an industry challenge. In the present work, a layered coating approach was evaluated. Optical inspection at 100x for assembly inspection and SEM inspection at 1,000x or more was used for detailed analysis. Special microtome sectioning with FE – SEM examination was used to examine the build-up of the various layers and the nanoparticle distribution. These techniques may present a challenge in some supplier's production environments. The key observations from the present work include the following:

8.1 Process

Tight process controls are important for good coverage. This study showed the following:

- The solvent evaporation time during dip coating sample withdrawal needs careful monitoring to avoid lead-to-lead and lead-to-package coating bridging.
- A high degree of spray atomization can impact the coating surface smoothness, particularly when the coating material has a high viscosity that is strongly dependent upon solvent concentration.

8.2 Coverage and thickness

The enhanced inspection techniques used in this project are more comprehensive and address the coating performance aspects associated with tin whisker mitigation. The following observations were made during the examination:

- Layered coating coverage provided better coverage and thickness uniformity and thickness on corners than conventional spray without an excessive coating build-up around the packages
- All front and side areas had at least 15 micron thick coating
- Some lead tips had small areas, less than 50 microns long and ~ five microns wide, of thin coating (~three microns thick)
- The coating build-up on the back of the leads was primarily from the dip coat
- There was incomplete spray coverage (droplets and discontinuities) on the back of the leads
- Coating thickness on the vertical part of the lead was less than on the horizontal part near the package body due in part to a coating fillet between the lead and the package body.
- The spray coating contributed to an increased thickness on the front, front corners, and sides of the leads
- Spray coating built up the thinner dip coating at the corners and sides
- There was no discernable variation in nanoparticle distribution, even within thin or discontinuous coating regions
- Some interfaces between the first spray layer and the second spray layer were visible from high resolution FE – SEM imaging of the microtome sections; however, there was no indication of delamination
- The horizontal sectioning of the leads showed that the coating coverage was uniform lead-to-lead around the perimeter of the QFP (corner leads versus center leads).
- Further work is need on coating viscosity control during dipping to reduce coating webbing between fine pitch leads.
- The maximum coating thickness was 66 microns which is below the 75 micron thickness rule of thumb for rigid coatings to avoid coating cracking during thermal cycling

9. Conclusions

The layered coating method with intermediate partial cures steps is a promising method for obtaining enhanced thickness uniformity and control. The developed method can be used for polyurethane coatings with and without nanoparticles. The low viscosity dip provided some electrical insulation on all surfaces and the layered spray coating provided significant additional coating on all lead surfaces except for the back of the lead. The additional lead coating thickness was obtained without excessive coating build-up around part bodies which can negatively impact solder joint life when hard coating material is used. When using coating with a very high solvent dependent viscosity, process and material process controls have increased importance to avoid bubble entrapment and rough coating surfaces. It would be desirable to further reduce variation and increase back side thickness, but process/machine optimization or an entirely new liquid deposition technique may be needed.

10. Literature cited

[1] Appendix F of the current report: Coating coverage baseline results

[2] S. Meschter, J. Cho, S. Maganty, D. Starkey, M. Gomez, D. Edwards, A. Ekin, K. Elsken, J. Keeping, P. Snugovsky, Eva Kosiba, Zohreh Bagheri, and J. Kennedy, Strategic Environmental Research and Development Program (SERDP) Nanoparticle Enhanced Conformal Coating for Whisker Mitigation, Proceedings of SMTA International, Rosemont, IL, September 28-October 2, 2014.

[3] J-STD-001 Requirements for Soldered Electrical and Electronic Assemblies, IPC Association Connecting Electronics Industries, Bannockburn, IL

[4] S. Han, S. Meschter, M. Osterman and M. Pecht, Evaluation of Effectiveness of Conformal Coatings as Tin Whisker Mitigation, Journal of Electronic Materials, DOI: 10.1007/s11664-012-2179-2, July 6, 2012.

[5] J. Wilcox, M. Meilunas, Harsh Environment Reliability of Micro-Leadframe (QFN) Components and Conformal Coating Effects, Proceedings of the Surface Mount International Conference, Rosemont, IL, September 27-October 1, 2015.

[6] D. Hillman, IPC coating coverage round robin, to be presented at IPC APEX 2018.

[7] V. Kumar and L. Woody, Effect of Conformal Coating on Tin Whisker Growth, Proceedings of the 2007 IPC Apex Conference.

SERDP WP2213
Final report
Appendix J: Layered Coupon Whisker Testing

Appendix J: Table of Contents

1. Introduction 1

2. Experimental Procedure 1

2.1 Samples and materials description 1

2.2 Experimental methodology for evaluation of coated test coupons 3

2.2.1 Optical microscopy 3

2.2.2 Microtome 3

2.2.3 Scanning electron microscopy and energy dispersive x-ray spectroscopy 3

2.3 Results 3

2.3.1 Assessment of whisker mitigation ability of various coating schemes at different time steps 3

2.3.2 Tin-Copper interfacial reactions 8

2.3.3 Microstructure evolution of polyurethane coated coupons with zero hours, 2,500 hours and 5,250 hours HTHH storage 9

3. Discussion 14

3.1 Effect of HTHH storage on the tin-copper microstructure 14

3.2 Mechanism of lateral growth of tin protrusions 17

3.3 Effect of well-adhered conformal coating on tin: Cross – sectional analysis of Sn-plated Cu coupon with 4,000 hours HTHH storage 19

3.4 Effects of HTHH storage on polyurethane acrylate (PUA – PC40-UMF™), nanoparticle filled PC18M™, and bilayer (filled on unfilled PC18M™) conformal coatings 22

4. Summary of layered coating coupon whisker test results 24

5. Conclusions 25

6. Literature cited 26

Appendix J: List of Figures

Figure 1: (a) Schematic of a panel showing 18 individual tin-plated copper coupons attached with break-off tabs. (b) An individual coupon photograph. 2

Figure 2: As-coated 10 micron thick top surfaces of coupons optical images; (a) PU - PC18M, (b) PUA - PC40-UMF, (c) 20% nanosilica filled PC18M. 4

Figure 3: Bare tin coupon surface optical images; (a) Before HTHH exposure, (b) following 500 hours HTHH exposure. 4

Figure 4: SEM images of whisker growth (a) uncoated region thin whisker formation (initial stage) at 1500 hours HTHH storage, and (b) thin coverage vs. uncoated regions of the same coupon. 5

Figure 5: Low magnification overview images of 10 micron thick coatings following 4,000 hours HTHH storage; (a) PUA (PC40-UMF) (b) PU (PC18M).*(inset)* surface feature on PC18M coating. 5

Figure 6: 10 micron thick PUA following 4,000 hours HTHH storage; (a) SEM image of suspected tin protrusion region. (b) EDX on selected region in (a) showing no tin presence. 6

Figure 7: PU with 20% nanosilica suspension added; (a) Surface showing coarse micron sized domains (b) Single domain with bright out-of-plane protrusion (inset) EDX confirming silica. 6

Figure 8: 20 micron thick unfilled PUA coating after 4,000 hours HTHH storage. 7

Figure 9: Copper-tin phase diagram with two low temperature (<505K) IMC compounds noted [7]. 9

Figure 10: Over cross – sections of 20 micron thick PU conformal coating with (a) 0 hours HTHH storage, (b) 2,500 hours storage, and (c) 5,250 hours storage. 10

Figure 11: Zero hour cross – section SEM image of 20 micron thick unfilled PU; (a) overall view with various regions labelled (b) delamination between the coating and the tin indicative of poor adhesion, and (c) interfacial Cu_6Sn_5 formation noted between tin and copper. 11

Figure 12: Cross – section SEM image of 20 micron thick unfilled PU following 2,500 HTHH storage; (a) Cross – section of coating-tin-copper with revealed space (in box) between coating and tin (b) Close-up SEM image of delamination at coating-tin interface and attached tin on coating. 11

Figure 13: Cross – section SEM BSE images of IMC particles within tin under 20 micron PU; (a) 2,500 hours HTHH storage and (b) 5,250 hours storage; showing larger IMCs with time and interface IMC thickening. 12

Figure 14: 5,250 hours HTHH storage coupon cross – section with various key features labelled. 13

Figure 15: Cross – section examination of a representative coating-tin-copper interface in a coupon coated with 20 micron PU following 5,250 hours HTHH storage; (a) BSD image and (b) EDS spectrum obtained from the top (brighter) tin layer, and (c) EDS spectrum obtained from the bottom (darker) tin layer. 15

Figure 16: Cross – section SEM images of seven micron thick PC18M+30%XP2742 over bright tin on copper after 2,500 hours 60°C/60%RH (Celestica cross – section of the cantilever beam coupon [10]); (a) SE image with yellow arrow shows coating delamination from tin and red arrows shows fracture of a voided tin region below the coating and (b) BSE image showing the Cu_6Sn_5 intermetallic formation near the coating surface. 16

Figure 17: SEM cross – section image of a protrusive tin growth beginning to impinge on the conformal coating. 17

Figure 18: SEM cross – section images of tin growth under coating; (a) example of two well-developed protrusive growths from tin being deflected laterally by a conformal coating and (b) left branch of lateral growth from location ‘1’ in (a). 18

Figure 19: A mechanism of lateral protrusive tin growth from electroplated tin on copper substrate. 19

Figure 20: (a) Representative SEM cross – section of PU coated coupon following 4,000 HTHH storage and (b) a high magnification image of the well-adhered coating-tin interface. 20

Figure 21: Coating-tin interface in 4,000 hour HTHH storage coupon cross – section with oxide layer visible..... 21

Figure 22: Thickness measurements of primary tin plating and interfacial IMC formation from zero to 5,250 hours HTHH storage. 22

Figure 23: Representative cross – sectional microstructure developments in coated tin coupons following 4,000 hour HTHH storage; (a) 20 micron thick PC18M + 20%XP2742 nanosilica and (b) 20 micron thick unfilled PUA. 23

Figure 24: Cross – sectional microstructure development in a bilayer (filled PU on unfilled PU) coated coupons following 4,000 hour HTHH storage; (a) Tin plating on copper with secondary (lateral) growth and IMC formation and (b) Magnified view of unfilled and filled coatings with deformation noted at protrusion sites. 23

Appendix J: List of Tables

Table 1: Coating types for the 10, 20 and 50 micron schemes 2

Table 2: Coating types for the 10 + 10 micron thickness scheme 2

Table 3: Compiled summary of the PU, PUA and PU+nanosilica coating performance at various time-steps. 8

1. Introduction

The layered coupon evaluation was used to evaluate the influence long term high humidity on layered coating and to better understand the tin microstructural changes. The slotted coupon was used so that the coating thinning over corners could be evaluated as well.

2. Experimental Procedure

2.1 Samples and materials description

All the HTHH storage tests were performed on flat slotted test coupons, which were copper alloy sheets in accordance with ASTM B152, Type 110, 1/2 hard, 0.635 mm thick with waterjet cut slots finished by electroplating with bright acid tin in accordance with ASTM B545 paragraph 4.3.2 five to eight microns thick. The bright acid tin type of plating is a known tin whisker producing finish in contrast with matte tin finish which is more whisker resistant, and was thus used to further facilitate tin whisker growth [1].

The as-plated tin finish verified by cross – sectioning was confirmed to be around 8 microns thick. For the tin electrodeposition, panels containing 18 individual coupons attached by break-off tabs to a frame were used, as shown in the schematic in Figure 1(a). Individual coupons were 25.4 mm x 12.7 mm in dimension and are shown in Figure 1(b). The slots provide corners for the coating to flow over and thin. The slots are 1.27 mm wide by 7.62 mm long and form copper webs having widths similar to electronic component leads. The center slots create two copper webs 0.381 mm wide and the outer slots create two webs 0.762 mm wide. After water jet cutting, the exit side of the slots are deburred prior to plating using the following process while still in a panel: sand using 600 grit silicon carbide paper until top and bottom surfaces are smooth, then gently deburr slots using a scotchbright abrasive pad, and finally sand top and bottom surfaces again with 600 grit silicon carbide paper again.

Before conformal coating and HTHH test initiation, the coupons were rinsed with alcohol and acetone followed by deionized water and dried with pure dry nitrogen gas. As mentioned above, the tin-plated copper coupons were coated with PU and PUA resins of pre-determined thicknesses and subjected to HTHH storage after curing. The performance of the coatings and the tin coupons were studied in parallel by examining the cross – sections of the copper-tin-coating interface at various time steps.

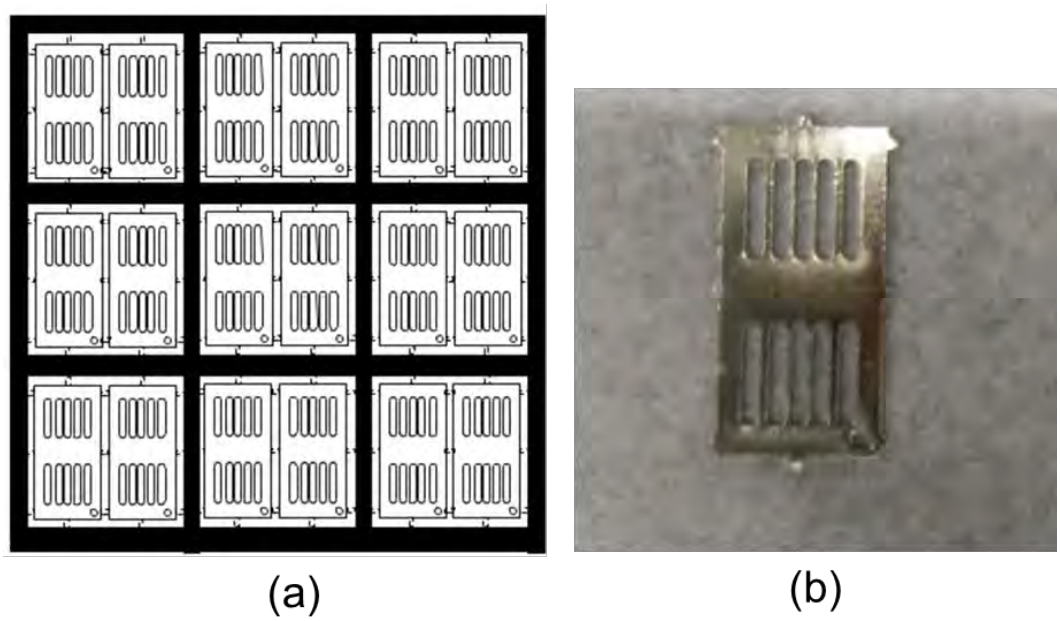


Figure 1: (a) Schematic of a panel showing 18 individual tin-plated copper coupons attached with break-off tabs. (b) An individual coupon photograph.

Two different commercially available polymer coatings, a PU, Hysol PC18M, and a PUA, Hysol PC40-UMF, both from Henkel Inc. (Irvine, CA) were used for this study. Additionally, a third coating composition consisting of PC18M™ with 20% of XP2742 suspension (hexamethylene diisocyanate (HDI), trimer with 20 nm mean diameter silica particles from Covestro Inc., Pittsburgh, PA) was also used for coating and evaluating the slotted tin test coupons. Different coating thicknesses were achieved by using polyimide (Kapton™, 3M Inc., St. Paul, Minnesota) tapes of varying thickness as walls on the sides of the coupons. The polymer resin was dispensed and spread through a manual doctor blade process using sharp edged glass slides. Three coating thicknesses of 10, 20 and 50 micron each with the fourth coating scheme of a dual coated layer of 10 micron thickness coated on a 10 micron pre-cured conformal coating were prepared. Table 1 shows the proposed coating types for the 10, 20 and 50 micron thicknesses. Table 2 shows the fourth coating thickness type (10 + 10 micron) with a dual coating scheme.

Table 1: Coating types for the 10, 20 and 50 micron schemes

10 micron thick	1) Unfilled PU	3) PU + 20% nanosilica	5) Unfilled PUA
20 micron thick	2) Unfilled PU	4) PU + 20% nanosilica	6) Unfilled PUA
50 micron thick	7) Unfilled PU	8) PU + 20% nanosilica	9) Unfilled PUA

Table 2: Coating types for the 10 + 10 micron thickness scheme

10) PU + 20% nanosilica on PU only base layer
11) PU + 20% nanosilica on PUA only base layer
12) Unfilled PUA on Unfilled PU base layer

Prepared coupons were transferred to the high-temperature and high-humidity chamber (Despatch® Ecosphere™) maintaining a steady condition of 85°C and 85% relative humidity (RH). These conditions of HTHH storage were chosen due to previously demonstrated ability to promote whisker growth in lead-free solder alloys [2][3][4]. Selected coupons were removed from storage and examined at various time steps which are reported along with their associated results throughout this study. Samples removed at the pre-designated time intervals were all stored at room temperature in a humidity controlled environment (below 10% RH). HTHH storage was terminated at the 5,250 hour mark (219 days).

2.2 Experimental methodology for evaluation of coated test coupons

2.2.1 Optical microscopy

Optical microscopy (OM) (Zeiss Axio Imager M1m) was utilized for surface analysis of coated coupons. Initial checks were made using OM to confirm and evaluate coating coverage on coupons; specifically, in case of the 0 hour case (as-coated) and 500 hour storage samples, with less probability of whisker formation and rupture of coatings.

2.2.2 Microtome

Cross – sections of the coupons for Scanning Electron Microscopy (SEM) viewing were prepared using an ultramicrotome (Leica™ EM UC7). Following sizing of the coupons for ultramicrotomy, using a low speed saw and traditional polishing operations, coupons were sliced using a diamond knife (Diatome™ Histo) with a precision edge. After slicing, regular SEM preparation and viewing were performed.

2.2.3 Scanning electron microscopy and energy dispersive x-ray spectroscopy

A scanning electron microscope (SEM) (Zeiss Supra 55 VP-SEM) was used for examining the top-surface of the coupons at the various time steps listed as well as observe the modification of the tin with respect to the growth of protrusions (whiskers and nodules), if any, at those time steps. Cross – sectional assessments of the interface between the tin and the coating were also facilitated through high-resolution field-emission SEM. Energy Dispersive X-ray Spectroscopy (EDS) (EDAX™ Pegasus EDS) was utilized for confirming materials as well as phase identification from cross – sectional samples.

2.3 Results

2.3.1 Assessment of whisker mitigation ability of various coating schemes at different time steps

Following initial coating of the coupons with the required resin, and the required curing steps, multiple coupons of similar type were placed in the HTHH chamber for each of the 12 compositions listed in Table 1 and Table 2: Coating types for the 10 + 10 micron thickness scheme 2. One coupon each from the 12 types tested was removed at time ‘0’ without exposure to HTHH conditions and examined in an optical microscope to evaluate the coverage and other surface features for the specific composition. Figure 2 shows representative as-coated surface conditions of 10 micron thick coating of the three primary compositions tested, i.e., unfilled PU, unfilled PUA and filled PU. While the PU compositions (filled and unfilled) appear to have a homogeneous coverage on the tin surface, the PUA coated sample has poor coverage around the edges of the slots.

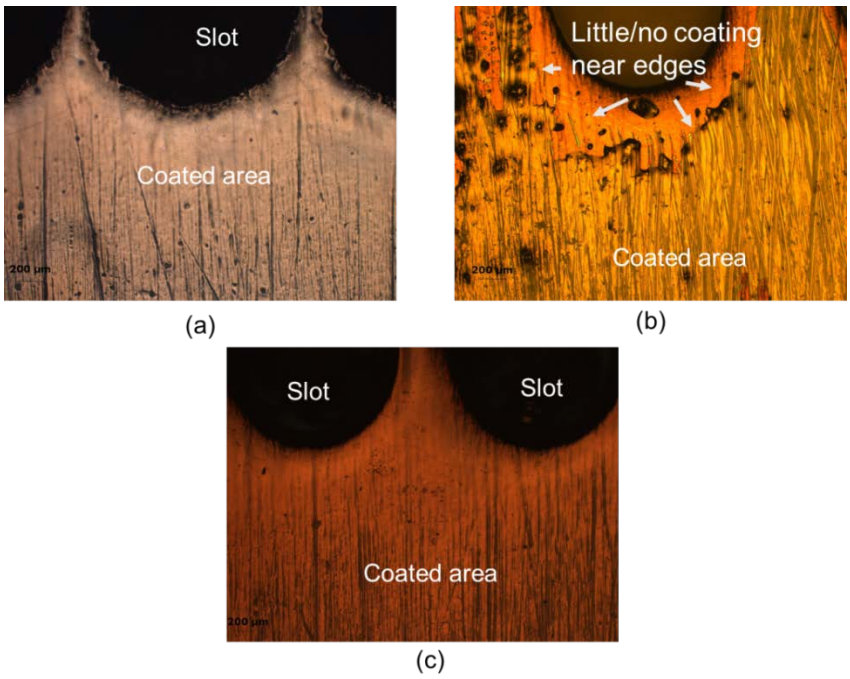


Figure 2: As-coated 10 micron thick top surfaces of coupons optical images; (a) PU - PC18M, (b) PUA - PC40-UMF, (c) 20% nanosilica filled PC18M.

Following the confirmation of coverage, each coupon was analyzed subsequently at 500, 1500, 2,500, and 4,000 hours to verify coating performance (rupture, or cracking) with respect to time of storage and coating condition. After 500 hours of HTHH storage, while whisker formation was not noted at the surface of the tin, the entire surface of the coupon was mostly convered by oxidation products of different thickness, as can be distinguished through the color variation from the OM image in Figure 3.

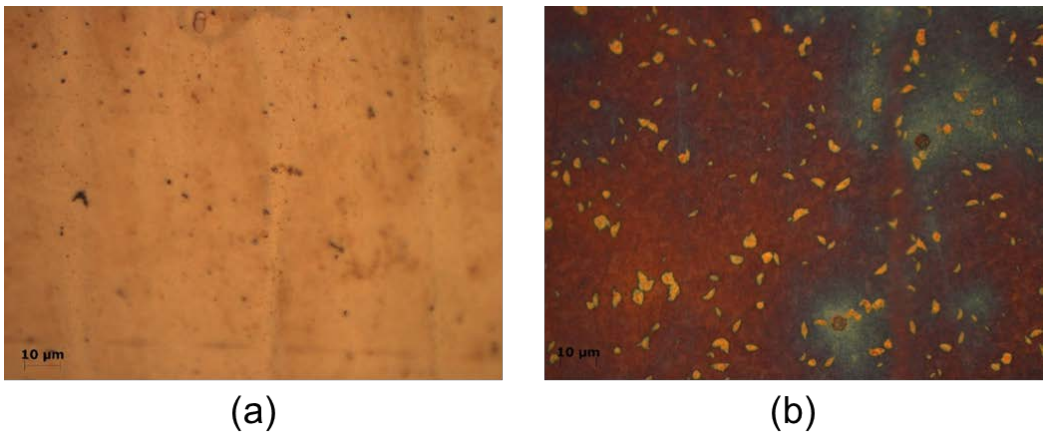


Figure 3: Bare tin coupon surface optical images; (a) Before HTHH exposure, (b) following 500 hours HTHH exposure.

SEM imaging of the coated coupons was performed at the succesive time-steps following HTHH exposure above 500 hours (1500 through 4,000 hours). Tin whisker formation in uncoated areas of coupons was first revealed at the 1500 hour time step. Figure 4 (a) shows uncoated regions of a 20 micron thick PU coated coupon with tiny whisker growth. Whisker aspect ratios are considerably large (filament-like), as can be seen in Figure 4; however, the diameter of the tin whisker is very small

(<100 nm diameter), such that it would not be visible through optical microscopy. This is also indicative of being in its initial stage of the growth. Spillover patches also formed while spreading the resin during the doctor blading process and were noted in the areas surrounding the polyimide tape walls on the coupon. These areas were much thinner (~3 micron in Figure 4 (b)) than the other coated areas but still showed no prortusions or rupture following 1500 hours storage.

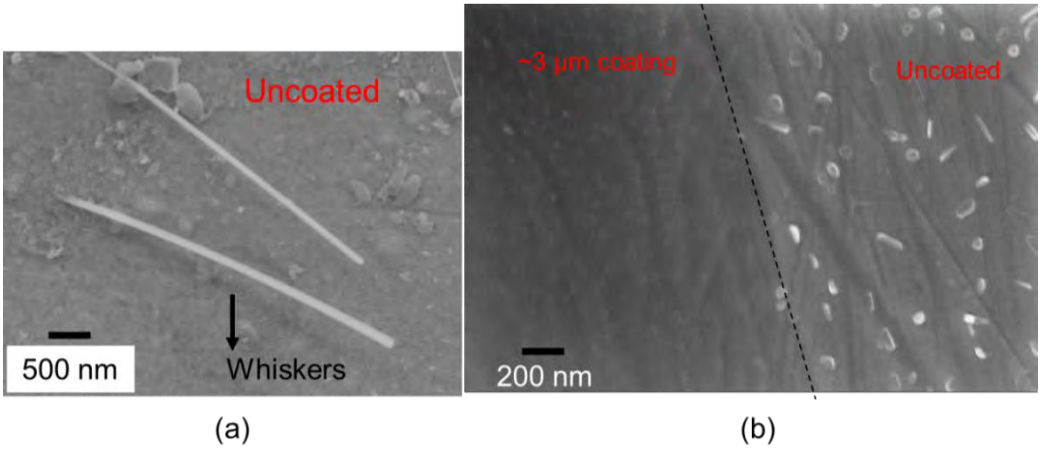


Figure 4: SEM images of whisker growth (a) uncoated region thin whisker formation (initial stage) at 1500 hours HTHH storage, and (b) thin coverage vs. uncoated regions of the same coupon.

Top view analyses of the coupon surfaces at 2,500 hours and 4,000 hours, with the thinnest coating thickness of 10 microns, revealed no rupture through the coating by protrusions of tin or other damage caused due to the long term HTHH storage. Figure 5 shows the representative views of the PU and PUA coupon surfaces following 4,000 hours storage at 85°C and 85% RH.

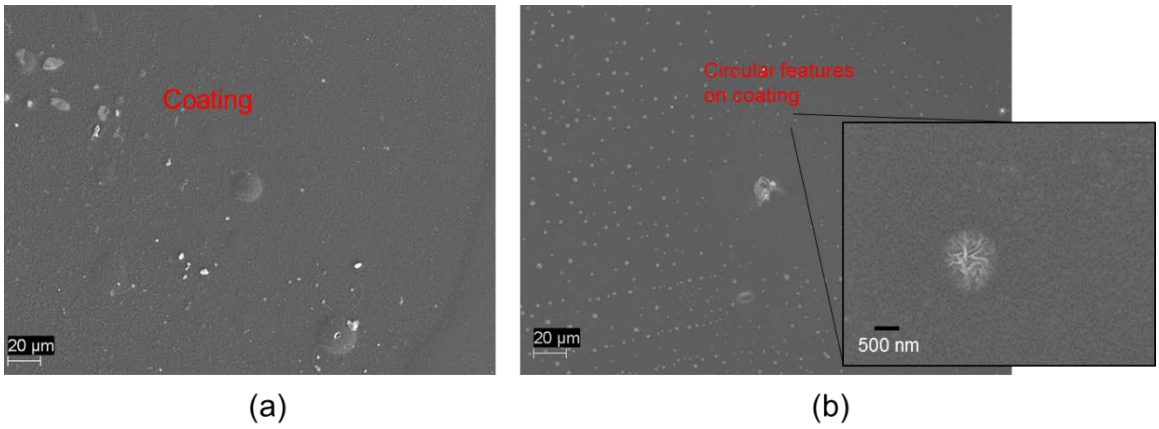


Figure 5: Low magnification overview images of 10 micron thick coatings following 4,000 hours HTHH storage; (a) PUA (PC40-UMF) (b) PU (PC18M).*(inset)* surface feature on PC18M coating.

While both PU and PUA surfaces showed some amount of surface particulate contamination following the 4,000 hours of extreme temperature and humidity storage, EDS analysis (Figure 6) confirmed the absence - tin in the coated regions. In the unfilled PU (PC18M) compositions, the top surface showed micron – sized (~ one to two micron) domains of coarse wormy networks integrated into the surrounding coating (Figure 5 (b)). These were noted in all stages of the storage and no correlation could be ascertained between the coating performance and the domains. Since these features were only

evident in the PU coatings which have a longer curing time involving moisture, it might be theorized that these features are artefacts of uneven cure during this moisture cure step.

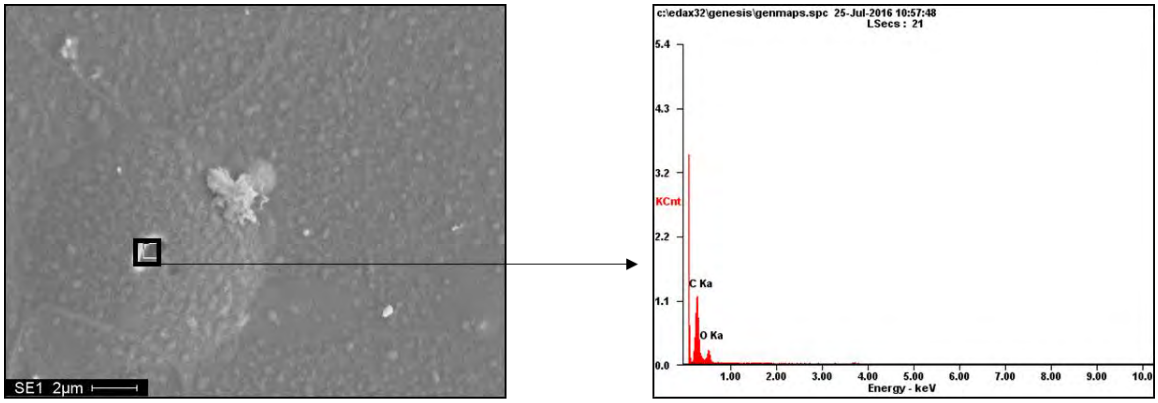


Figure 6: 10 micron thick PUA following 4,000 hours HTHH storage; (a) SEM image of suspected tin protrusion region. (b) EDX on selected region in (a) showing no tin presence.

The coarse wormy networks noted in the unfilled PU cases were also noted in the PU cases with the nanoparticle additions. Figure 7 shows these domains with a high-resolution image of a single domain with a protrusion also shown in Figure 7 (b). This protrusion was noted from EDS analysis to be an agglomeration of nanosilica on the top surface.

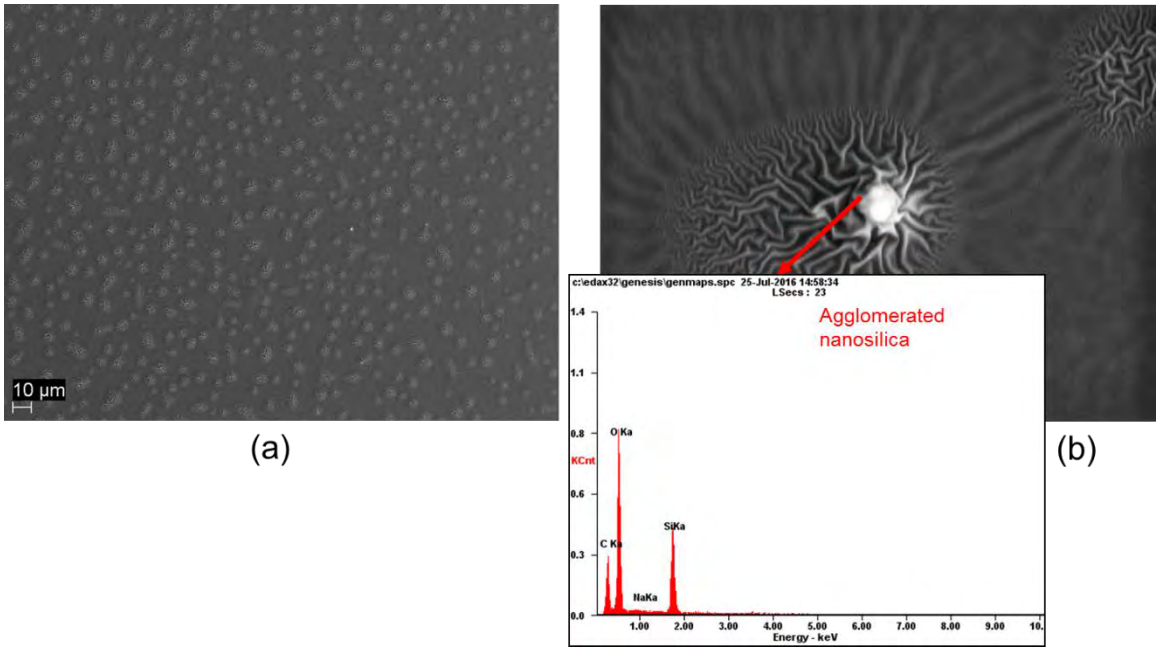


Figure 7: PU with 20% nanosilica suspension added; (a) Surface showing coarse micron sized domains (b) Single domain with bright out-of-plane protrusion (inset) EDX confirming silica.

Lastly, PUA coated coupons with 4,000 hour HTHH storage also showed no discernable difference on the top coating surface in the 20 micron thick coating case (Figure 8), even though some isolated tented areas were observed in the 10 micron case (see Figure 6).

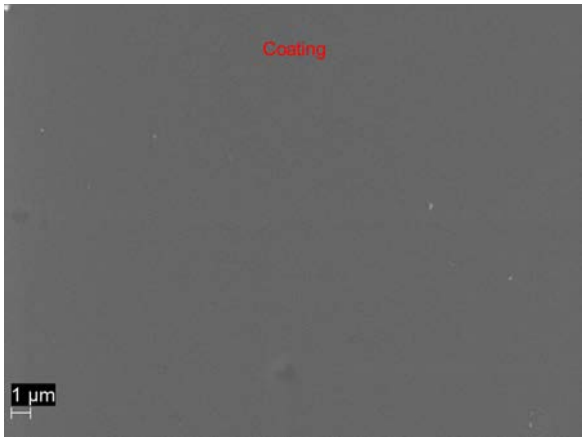


Figure 8: 20 micron thick unfilled PUA coating after 4,000 hours HTHH storage.

With the above results of the 4,000 hour assessments of the tin coupons, it was clear that the 10 micron thick conformal coatings of three different compositions showed robust performance at least with respect to rupture resistance at the extreme storage conditions tested. A comprehensive tabular report summarizing critical features noted for each time step is listed in Table 3. Further cross – sectional analysis on selected coupons from these compositions in addition to the bilayer (10-micron filled PU on top of 10-micron unfilled PU) coupon were performed and results are discussed in the forthcoming sections.

Table 3: Compiled summary of the PU, PUA and PU+nanosilica coating performance at various time-steps.

10, 20 and 50 µm thick coatings	500 hours	1500 hours	2500 hours	4000 hours
Plain PC18M	• Surface oxidation noted at 500 hours • No whisker formation in uncoated regions	• Whiskers noted at uncoated regions • No protrusions/tenting or rupturing in coated regions	• Whiskers noted at uncoated regions • No protrusions/tenting or rupturing in coated regions	• No whisker growth through the coatings • One 20µm sample showed tenting (candidate for cross-section)
Plain PC40UMF	• Surface oxidation noted at 500 hours • No whisker formation in uncoated regions	• Whiskers noted at uncoated regions • No protrusions/tenting or rupturing in coated regions	• Whiskers noted at uncoated regions • No protrusions/tenting or rupturing in coated regions	• 10 µm case shows tenting – not seen in 20 µm thickness • Isolated tenting noted; no rupture noted
PC18M + 20% XP2742	• Surface oxidation noted at 500 hours • No whisker formation in uncoated regions	• Whiskers noted at uncoated regions • No protrusions/tenting or rupturing in coated regions	• Whiskers noted at uncoated regions • No protrusions/tenting or rupturing in coated regions	• Similar performance as Plain PC18M case – no rupture/protrusions

2.3.2 Tin-Copper interfacial reactions

The strength of a tin joint with copper is controlled through the formation of intermetallic compounds, and from the copper-tin phase diagram (Figure 9) there is a possibility of two distinct intermetallic (IMC) phases forming at lower (below 505K) temperatures, an η-phase (Cu_6Sn_5) and an ε-phase (Cu_3Sn) [5]. During the initial stages of reaction between tin and copper, Cu dissolves rapidly into the Sn and forms a Cu_6Sn_5 phase at the Sn/Cu interface, per Eq. (1) below. The Cu_3Sn layer is formed between the Cu substrate and the Cu_6Sn_5 layer. The Cu atoms at the Cu/Cu_6Sn_5 interface react with Cu_6Sn_5 to form Cu_3Sn, according to Eq. (2). After a homogeneous Cu_3Sn layer forms, Cu atoms, denoted by [Cu] in Eq. (2), continuously diffuse through the Cu_3Sn layer and react with Cu_6Sn_5 to grow more Cu_3Sn at the Cu_3Sn/Cu_6Sn_5 interface through the consumption of some of the Cu_6Sn_5. There is also some Sn diffusion through the interfacial region, but Cu diffusion rates are shown to be higher, so Sn diffusion can be assumed to be negligible [6].

$$6Cu + 5Sn = Cu_6Sn_5 \qquad (1)$$

$$9[Cu] + Cu_6Sn_5 = 5Cu_3Sn \qquad (2)$$

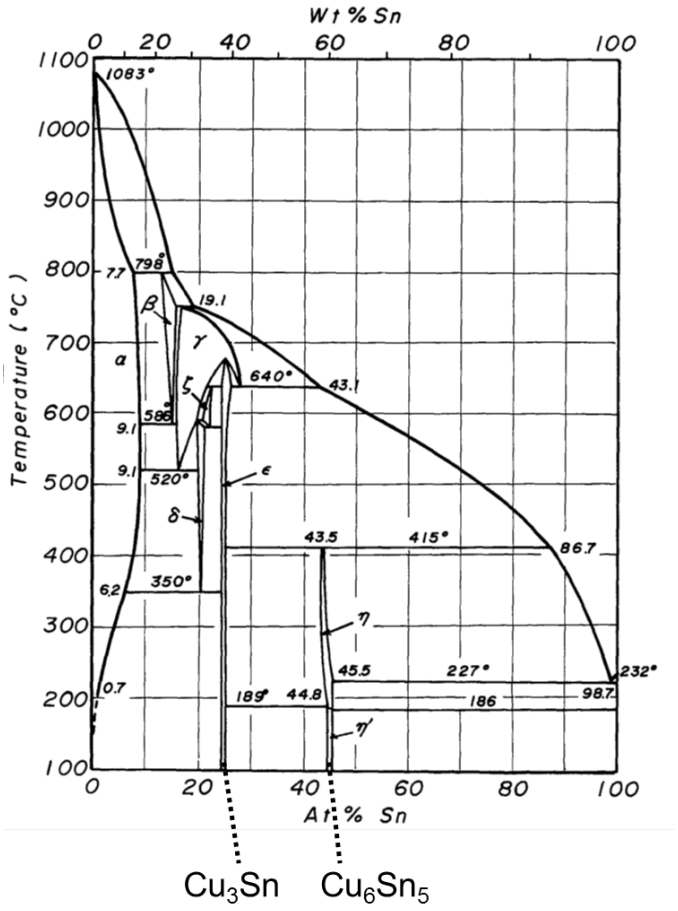


Figure 9: Copper-tin phase diagram with two low temperature (<505K) IMC compounds noted [7].

2.3.3 Microstructure evolution of polyurethane coated coupons with zero hours, 2,500 hours and 5,250 hours HTHH storage

Figure 10 shows a schematic representation of cross – sectional microstructure development between a coating and a copper substrate following storage in 85°C/85%RH, ranging from 0 to 5,250 hours. Of the- examples considered, the growths of intermetallics in tin-plated copper coupon cross – sections with 20 micron thick polyurethane (PU – PC18M) conformal coating after HTHH storage are shown. With an increase in HTHH storage time, significant intermetallic growth (of varying thickness) into the tin layer continuously along the interface between tin and copper was noted in every coupon. Additionally, some particulate - IMC growth was noted, which had no connection to bulk IMC at the interface. Some IMC particles were noted leading vertically toward the coating surface (Figure 10 (b) and (c)). A dramatic increase in total thickness (intermetallics and tin layer) of plating was observed.

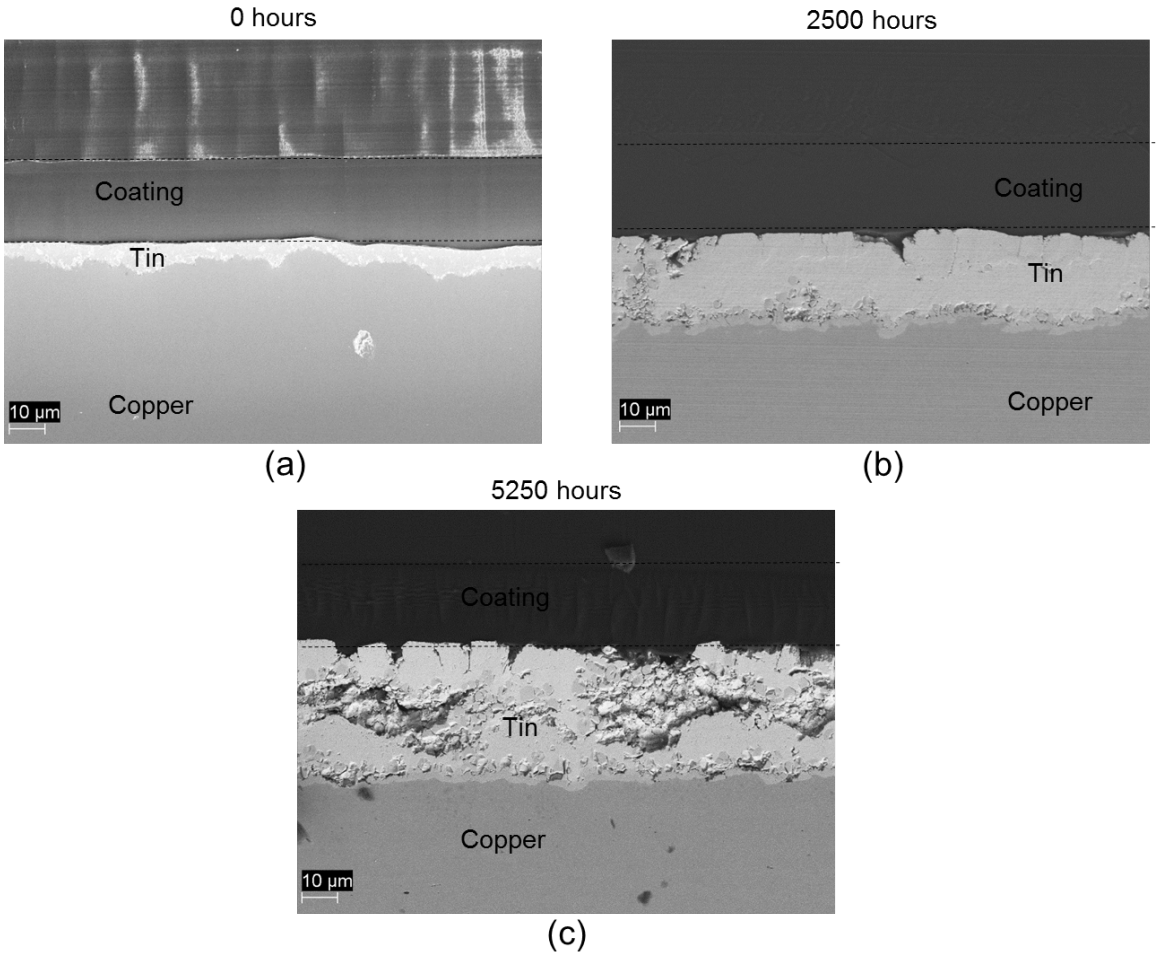


Figure 10: Over cross – sections of 20 micron thick PU conformal coating with (a) 0 hours HTHH storage, (b) 2,500 hours storage, and (c) 5,250 hours storage.

Figure 11(a) shows a more detailed cross – sectional image of the coating at the zero hour HTHH storage time step, with all the major regions denoted. Examination of this sample showed a homogeneous intermetallic layer at the interface of the copper and the plated tin. The high magnification SEM of the interface of the coating and the tin surface (Figure 11(b)) shows a continuous delamination of 100 to 200 nm. This split of the coating from the surface could have been caused during preparation of the cross – section, which involves a slicing operation using a sharp diamond edge and is indicative of weak adhesion between the coating and the tin layer in this case.

Following 2,500 hours HTHH exposure, a similarly prepared PC18M coated coupon, i.e., with 20 micron thickness, was removed from storage and examined. As noted in the zero hour coupon cross – section, a continuous interfacial intermetallic layer was observed; however, in this case with both Cu_6Sn_5 and an additional Cu_3Sn phase between the copper and the tin plating. In addition to this continuous layer, discrete Cu_6Sn_5 particles were noted interspersed within the tin layer. A concurrent increase in the interfacial IMC ($Cu_6Sn_5 + Cu_3Sn$) thickness is also noted. Some regions between the tin layer and the conformal coating appeared to have tin preferentially removed during microtome slicing, leaving spaces between the coating and the remaining tin layer. Further, such cracks which result in tin removal, propagated through the tin – coating interfacial region with a thin layer of tin remaining attached to the underside of the coating, indicative of weak interfacial adhesion due to formation of the reaction products at the interfacial region (Figure 12).

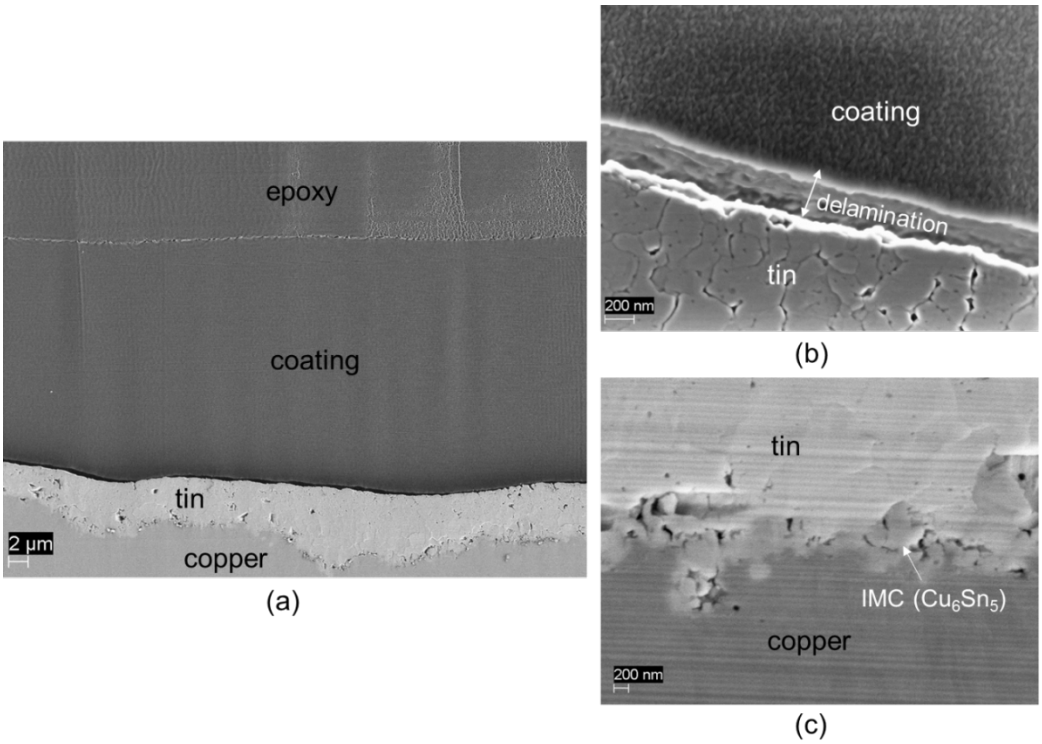


Figure 11: Zero hour cross – section SEM image of 20 micron thick unfilled PU; (a) overall view with various regions labelled (b) delamination between the coating and the tin indicative of poor adhesion, and (c) interfacial Cu_6Sn_5 formation noted between tin and copper.

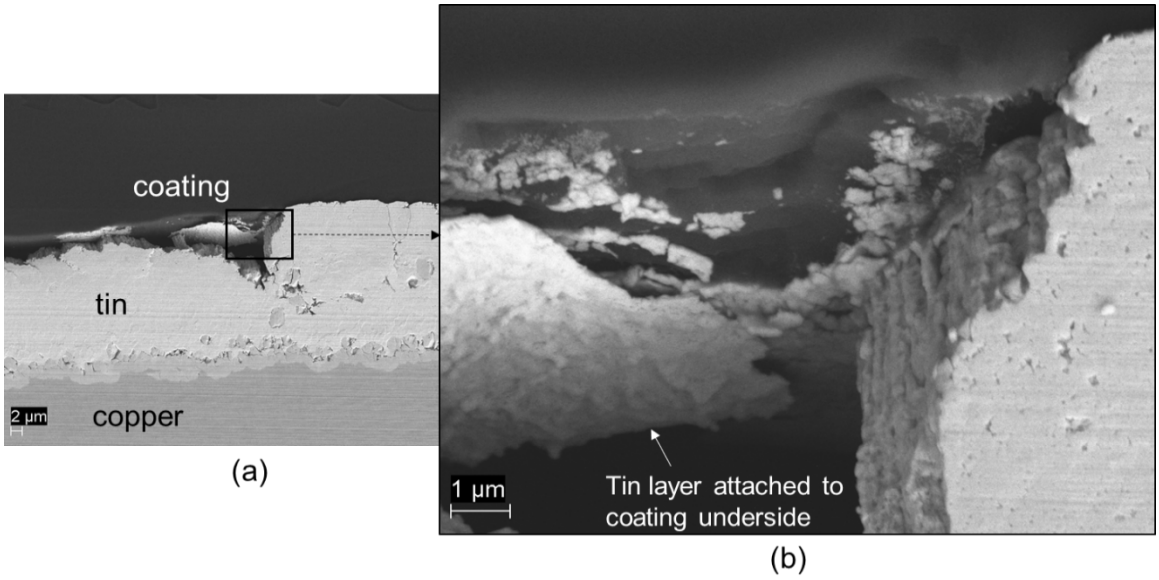


Figure 12: Cross – section SEM image of 20 micron thick unfilled PU following 2,500 HTHH storage; (a) Cross – section of coating-tin-copper with revealed space (in box) between coating and tin (b) Close-up SEM image of delamination at coating-tin interface and attached tin on coating.

Comparative back scatter electron (BSE) imaging of similarly located isolated IMC particles (with respect to Cu substrate) in Figure 13 of two coupons, following 2,500 hours and 5,250 hours storage, shows a larger intermetallic isolated particle size in the latter case, while a concurrent increase in the thickness of the interfacial IMC region can also be discerned. Red arrows in Figure 13 note IMC particles within the tin plating on the copper substrate. The interfacial region between the tin and the copper substrate can also be seen to ripen, with the more uniform Cu_3Sn forming between the Cu_6Sn_5 and the copper side of the interfacial region, and the scallop-like Cu_6Sn_5 forming into the tin plating.

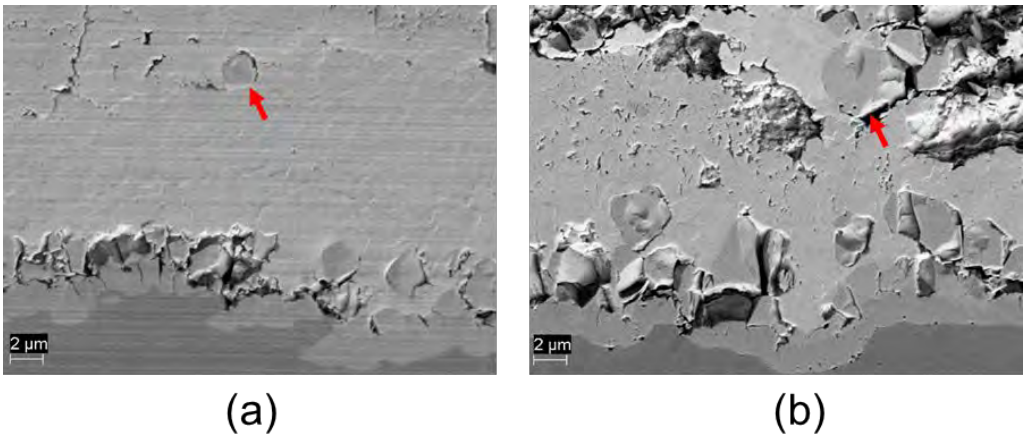


Figure 13: Cross – section SEM BSE images of IMC particles within tin under 20 micron PU; (a) 2,500 hours HTHH storage and (b) 5,250 hours storage; showing larger IMCs with time and interface IMC thickening.

Figure 14 shows a comprehensive view of the cross – section with 5,250 hours storage (point of experiment termination), with several critical features denoted. An additional development and coarsening of the discrete IMC's to form a layer of IMC's within the bulk tin as seen in Figure 14. A significant increase in the tin thickness from the original tin plating (< 10 micron) can be clearly observed. In contrast with the 2,500 hour storage case where discrete particle-like IMC's were noted interspersed within the tin layer, a more completely developed cluster of IMC's is visible above the original thickness of the tin layer plated on the copper substrate. Additionally, similar to the previous 2,500 hour storage case, the regions of removed tin were seen with a thin layer remaining attached to the underside of the coating. This is indicative of uneven adhesion at certain regions between the tin and the conformal coating with other regions having delamination initiated by the slicing motion of the microtome knife.

From the initial microstructural analysis of the corresponding stages of HTHH storage (time zero through 5,250 hours), it is evident that the nature of the IMC formation *within* the tin layer, in addition to interfacial IMC formation reactions, the nature of thickness increase in the tin plating, and the secondary layer of tin above the isolated clusters of IMC's noted in certain sections; all necessitate a more detailed analysis.

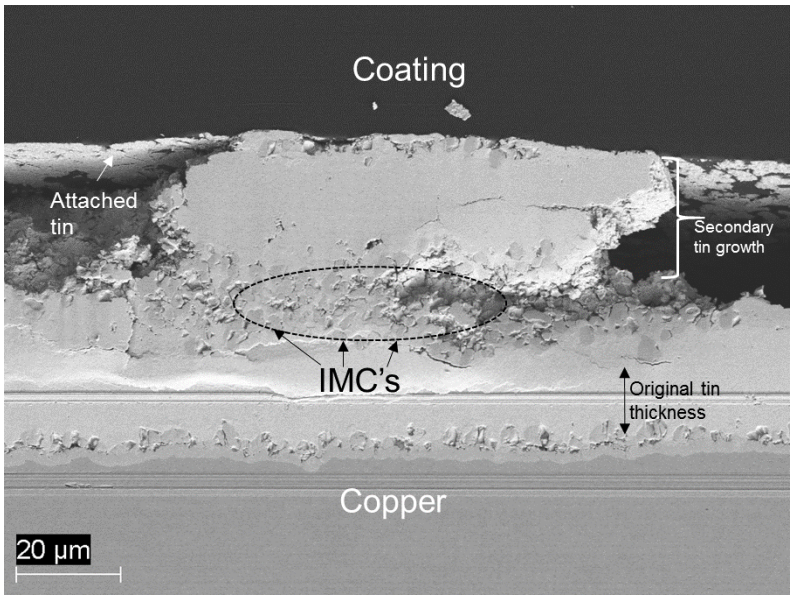


Figure 14: 5,250 hours HTHH storage coupon cross – section with various key features labelled.

3. Discussion

3.1 Effect of HTHH storage on the tin-copper microstructure

From Figure 13 and Figure 14, it is evident that there was a sustained growth of intermetallics, both at the interface of copper and tin and within the bulk tin with HTHH storage. In addition to this observation, a concurrent increase in the total thickness of the complex tin layer (including voids, intermetallics and pure tin) on the underlying copper substrate is seen. A closer look is therefore warranted at the various cross – sections to propose suggested mechanisms for this behavior, which includes the growth of intermetallics and a 'lateral' outward growth of tin away from the original tin layer and guided by the conformal coating.

It is well known that an atom such as Cu may diffuse easily into Sn by a rapid, interstitial mechanism, whereas Sn diffuses in Cu by a slower, substitutional mechanism [8]. This is further supported by considerations of the lattice parameters of tin, which is a relatively less densely packed tetragonal structure (a=b= 5.83Å & c= 3.18Å) and easily facilitates the accommodation of diffusing copper atoms within its lattice. Consequently, there is a concentration gradient established between the copper and tin layers which act as a diffusion couple stressed under high temperature and high humidity conditions. First, Cu_6Sn_5 formation was noted at the interface of tin and copper. As a result of the effects of continuing copper diffusion under increasing storage time from zero to 5,250 hours at 85°C and 85% RH, this was followed by thickening of the interface intermetallics along with increased incidence of copper within the bulk tin adjacent to growing Cu_6Sn_5. Reaction of copper with the Cu_6Sn_5 at the Cu/Cu_6Sn_5 interface eventually leads to Cu_3Sn formation first noted at the 2,500 hour examination step.

At the 2,500 hour time step, discrete particles of Cu_6Sn_5 begin to appear on the surface of tin plating. While copper diffusion on the whole is not restricted to grain boundaries but is rather throughout the bulk tin structure, an earlier work on the coupled copper-tin systems at room temperature has shown IMC (Cu_6Sn_5) growths to preferentially nucleate at triple junctions of tin grain boundaries and other regions of free surface availability [9]. In the case of the 2,500 and 5,250 hours HTHH storage samples, there is a significant availability of free surfaces at the interface between the coating and the tin layer caused due to the poor adhesion of the coating to the tin surface, as shown in Figure 11 and Figure 12. While there is in general an increased diffusion of copper atoms interstitially through the tin lattice, free surfaces and grain boundaries see an increased likeliness of intermetallic formation due to its accumulation. At such locations, the concentration of copper atoms within the tin is sufficient to initiate nucleation of the Cu_6Sn_5 intermetallic compound. Further, these particles continue to coarsen while newer particles nucleate and grow during the continual storage up to 5,250 hours as seen previously in Figure 14, forming more populated intermetallics at the coating-tin interface. Such a discrete layer of intermetallics is seen to significantly increase with the storage time.

Figure 15 (a) shows a backscattered electron detector (BSD) image of a cross – section after 5,250 hours HTHH storage. BSD facilitates atomic number contrast imaging with regions of darker contrast representing the presence of lower atomic number elements and can have different contrast with different grain orientation. As noted above, the formation of intermetallics in the bulk tin is preceded by a fast interstitial diffusion of Cu atoms into the Sn lattice. A clear demarcation in contrast can be noted from the copper substrate at the bottom toward the coating on the tin layer at the top. A complex tin 'band' of tin and IMC with higher copper concentration adjacent to the interfacial IMCs can be distinguished. Within the band, discrete particulate IMCs within the bulk tin, a region of the complex tin band showing a brighter contrast, and the unfilled PC18M coating at the top can all be noted in the BSD imaging.

EDS plots of the two different regions of tin, one adjacent to the coating (brighter contrast) and one adjacent to the copper (darker contrast) are shown in Figure 15(b) and Figure 15(c) respectively. Distinct peaks at 0.93 keV and 8.04 keV representing the copper Lα and Kα line, respectively in the X-ray spectrum were seen in the bottom tin layer, providing the confirmation of the presence of diffused copper in the tin region. Further, semi-quantitative analysis of the spectrum indicated a presence of around 3.7% Cu with a smaller amount detected from the upper tin layer (brighter contrast in BSD). It should be noted that the solubility of copper in tin at 85°C is very low (much less than 3.7 wt. %). The copper detected in the darker region of the band is likely to be primarily from the presence of nano – sized IMCs like those in Figure 13.

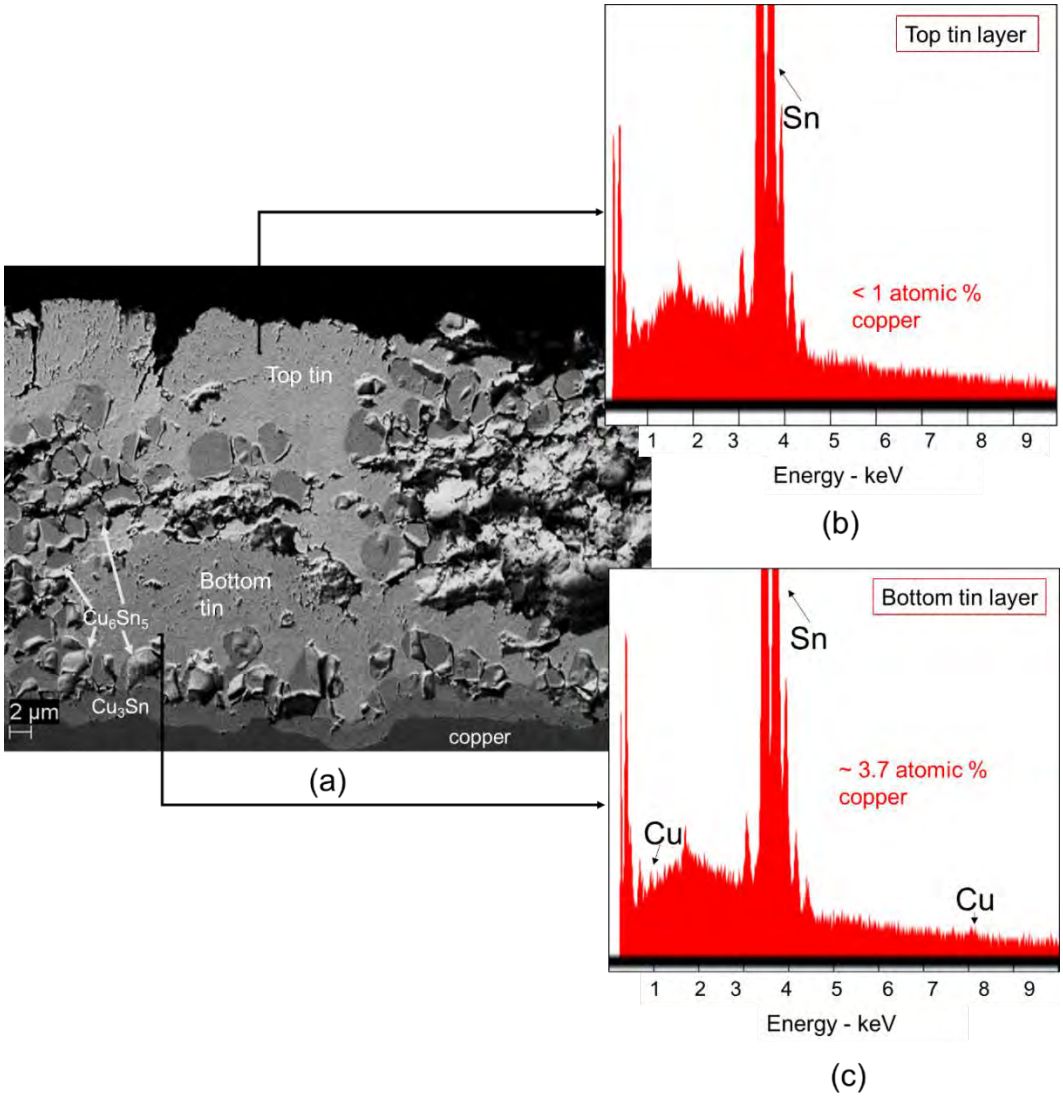


Figure 15: Cross – section examination of a representative coating-tin-copper interface in a coupon coated with 20 micron PU following 5,250 hours HTHH storage; (a) BSD image and (b) EDS spectrum obtained from the top (brighter) tin layer, and (c) EDS spectrum obtained from the bottom (darker) tin layer.

In 2014, similar tin and coating features were also observed during the cantilever beam coupon testing [10]. An ion polished conventional metallurgical cross – section of a typical tin nodule growing under PC18M+30%XP2742 nanosilica filled coating after 2,500 hours of 60°C/60%RH is repeated here in Figure 16. In this figure, the nodule is in an area where the PC18M+30%XP2742 nanosilica filled coating was seven microns thick and was bulging the coating. There is some coating delamination from the tin on the left side of the nodule Figure 16a where the tin is no longer adhered to the coating (yellow arrow). Adjacent to this delamination, the tin appears to have void defects, which caused a weakening of the tin and fracturing just below the coating (black arrows). In these regions, some tin remained adhered to the coating. Also on this sample, there were large Cu_6Sn_5 IMCs in the tin layer away from the copper interface and near the coating (Figure 16b).

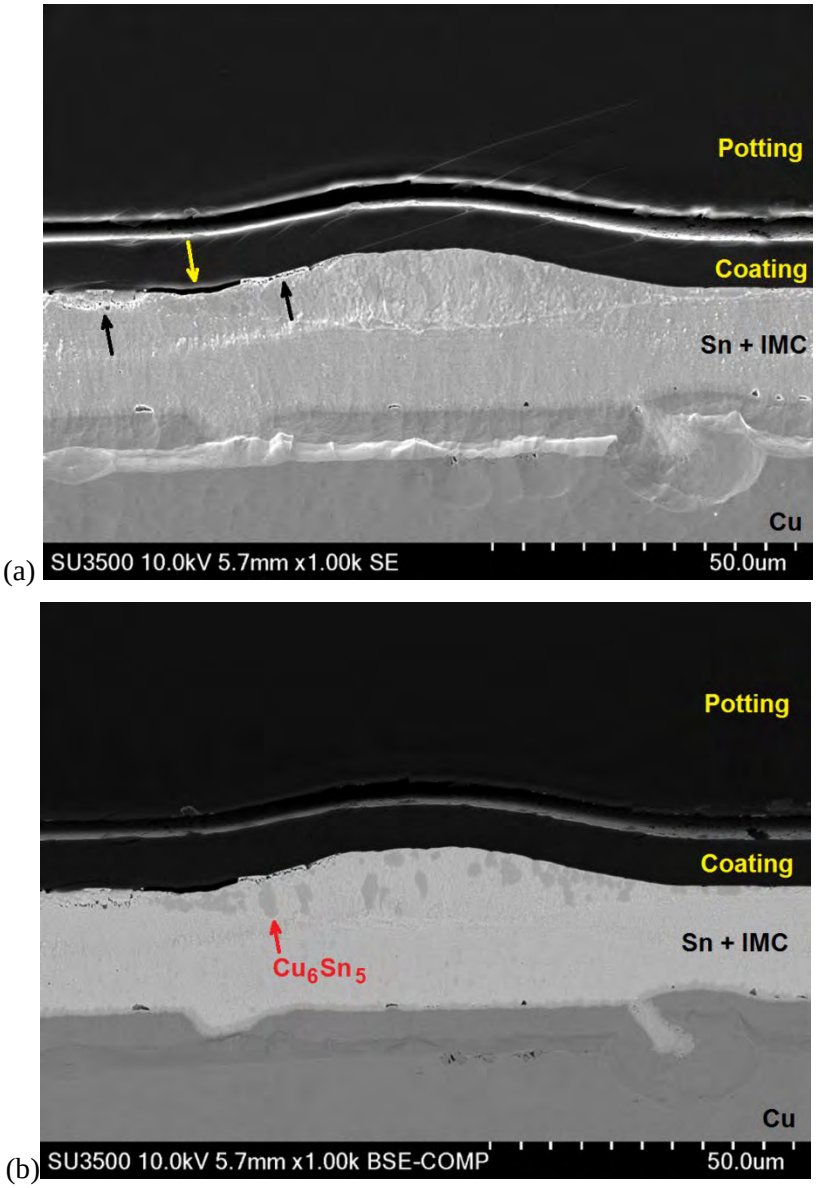


Figure 16: Cross – section SEM images of seven micron thick PC18M+30%XP2742 over bright tin on copper after 2,500 hours 60°C/60%RH (Celestica cross – section of the cantilever beam coupon [10]); (a) SE image with yellow arrow shows coating delamination from tin and red arrows shows

fracture of a voided tin region below the coating and (b) BSE image showing the Cu_6Sn_5 intermetallic formation near the coating surface.

3.2 Mechanism of lateral growth of tin protrusions

One of the most noted and commonly discussed sources of compressive stress in electroplated tin on copper is intermetallic compound (IMC) formation due to the reaction of Sn with Cu in the substrate metal [11]. Here, in the case of tin plated copper coupons, there is a clearly increasing presence of intermetallics and diffused copper regions in the tin plating with HTHH storage. Together with this, it is also observed that a secondary tin layer, above the complex tin and intermetallic layer formed from the original tin plating (discussed above), grows in thickness with storage time. The nature of this thickness increase is specifically due to an outward growth of tin and tin – copper intermetallic from the original plating layer region pushed laterally due to a barrier to vertical growth caused by the conformal coating. Figure 17 shows the initial stage of a protrusive tin growth beginning to interact with the conformal coating. The initial layer of IMC's formed on the top of the tin surface are also visible in this image.

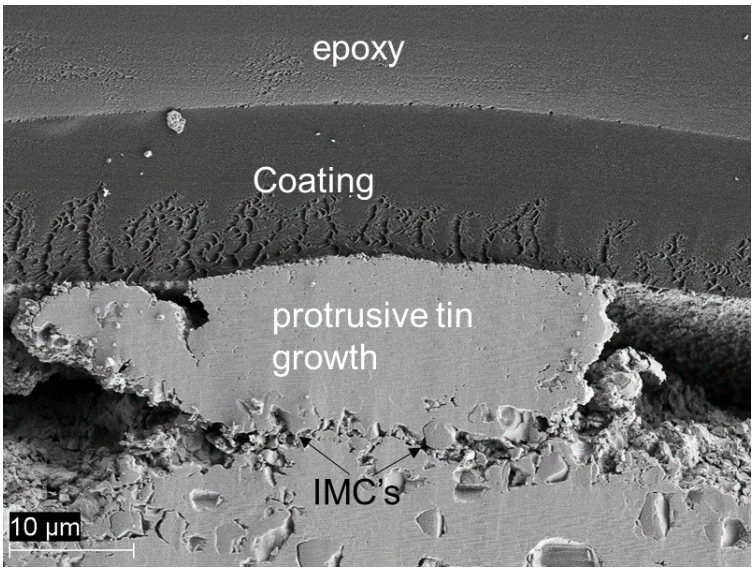


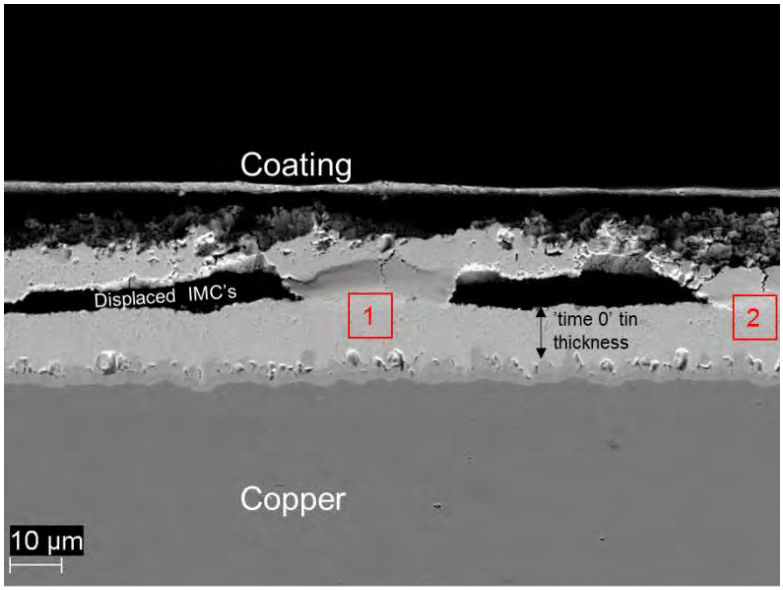
Figure 17: SEM cross – section image of a protrusive tin growth beginning to impinge on the conformal coating.

Figure 18(a) shows a BSD image of a tin plated copper coupon cross – section following 5,250 HTHH storage. A conformal coating of 20 micron unfilled PU - PC18M was applied to tin plated copper coupons prior to storage. In this micrograph, two locations shown by the numerals '1' and '2' in the tin layer denote regions which are the roots of outward tin protrusions originating from the original tin plating. Compared to Figure 17 this protrusion was in a much more advanced state of growth, leading to its advancement along the coating-tin interface.

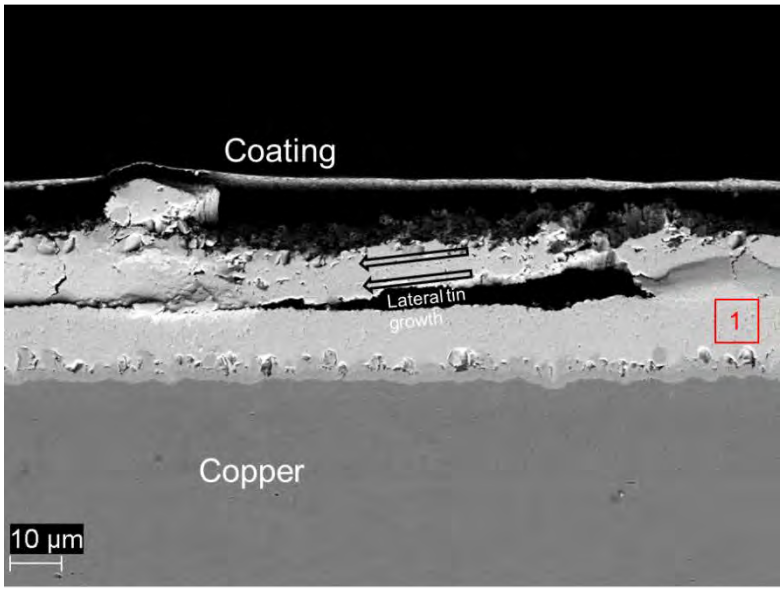
The thickness of the original (pure tin) region is labelled as 'time zero' thickness in Figure 18(a). It is seen that along with interfacial IMC developments which are expected and have been explained previously, there is also IMC formation on the top surface of the tin plating. The combined effect of steadily increasing compressive stress in the tin film from the effects of copper diffusion and intermetallic formation causes the outward protrusive growth of tin. These growths are subsequently

deflected laterally due to the blocking from conformal coating and follow a growth direction parallel to the surface of the original tin surface along the coating-tin interface.

Figure 18(b) shows the coupon cross – section adjacent to root location '1' in Figure 18(a). Laterally grown tin is continually pushed along the original tin plating and continues to grow in this orientation with continued storage. Empty spaces between this lateral protrusive growth and the tin layer correspond to IMC's which have been displaced during sample preparation.



(a)



(b)

Figure 18: SEM cross – section images of tin growth under coating; (a) example of two well-developed protrusive growths from tin being deflected laterally by a conformal coating and (b) left branch of lateral growth from location '1' in (a).

A schematic of the lateral growth mechanism is shown in Figure 19 by way of integrating the factors explained above. With no exposure to the HTHH conditions, i.e. immediately following the conformal coating, the cross – section consists simply of tin plated on copper. This microstructure eventually evolves at the interface to form an IMC layer consisting of the two phases, Cu_6Sn_5 and Cu_3Sn. The conformal coating is at the top of the tin surface. With sustained storage at the HTHH conditions (85°C/85%RH), copper diffusion is increased into the adjacent tin layer with IMC nucleation and growth with sufficient copper availability. In addition to these surface intermetallics, an embedment of copper atoms at the tin grain boundaries even without consequent IMC formation results in further compressive stress on the tin layer which needs to be relaxed. Concurrently, tin atoms are driven outward due to compressive stresses caused due to diffusion of copper as well as the steady growth of the intermetallics. A flux of mostly pure tin atoms is pushed upward and thus overall thickness is increased as a result of lateral growth of tin due to the restriction in further vertical growth due to the barrier in the form of the conformal coating.

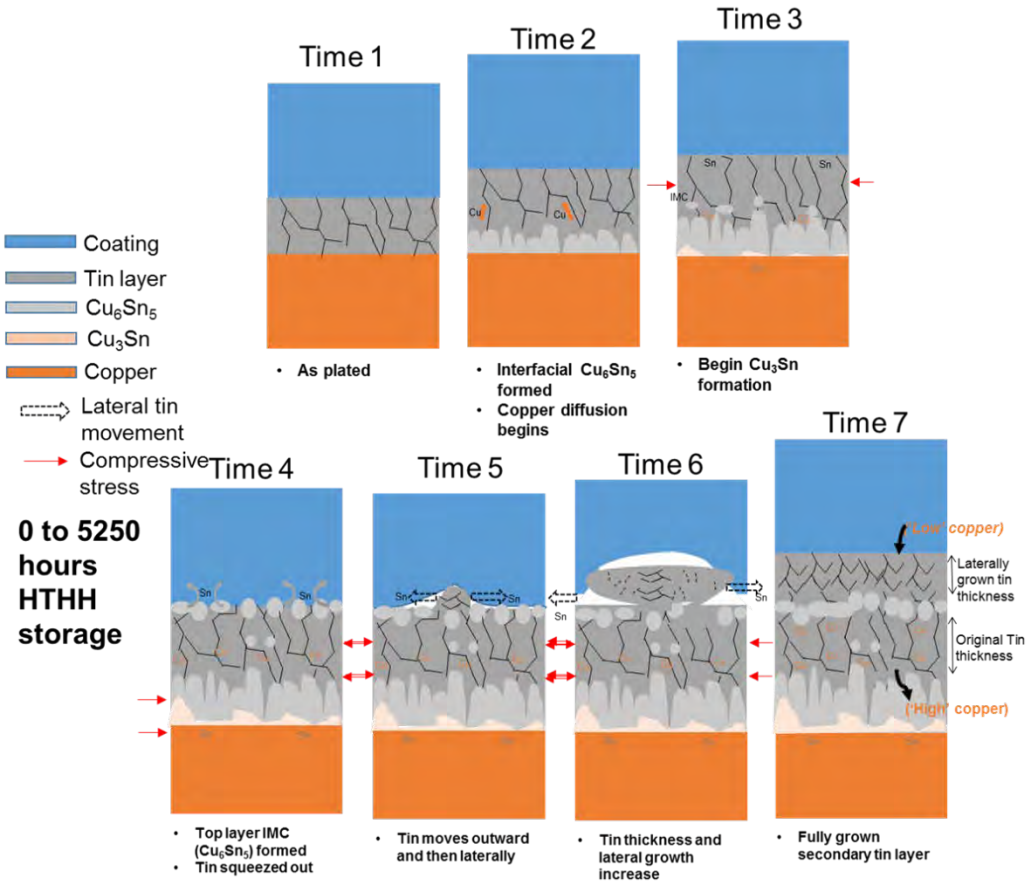


Figure 19: A mechanism of lateral protrusive tin growth from electroplated tin on copper substrate.

3.3 Effect of well-adhered conformal coating on tin: Cross – sectional analysis of Sn-plated Cu coupon with 4,000 hours HTHH storage

Cross – sectional analysis of 4,000 hour HTHH storage coupon coated with unfilled polyurethane (PU – PC18M) while demonstrating an increase of interfacial IMC thickness and a corresponding increase in the pure tin layer, did not show discrete particulate IMC formation within the bulk tin or a secondary lateral growth of plated Sn. This was an exception to the trend previously noted in coupons

exposed up to even 2,500 hours of HTHH storage. A more detailed look at the cross – section was undertaken in an attempt to understand the unusual (with respect to other coupon sections examined) microstructural characteristics.

At first, it may be recalled that similar coating thicknesses of the unfilled PU (PC18M) conformal coating, for zero, 2,500 and 5,250 hour HTHH storage, showed visibly poorer adhesion with delamination noted at the tin-coating interface. In this regard, Figure 20(a) shows an overview cross – section of the 4,000 hour HTHH section. As seen in this representative SEM micrograph, no delamination was visible between the tin layer and the conformal coating or in regions in the tin plating. High magnification imaging of the tin-coating interface also confirmed this observation, with homogeneous and consistent adhesion apparent between the coating and the tin at the sub – micron scale. The characteristic wormy networked microstructure of the PU is also noticeable (Figure 20(b)). Specifically, in this coupon, coating adhesion to the tin plating appeared to be robust and without delamination.

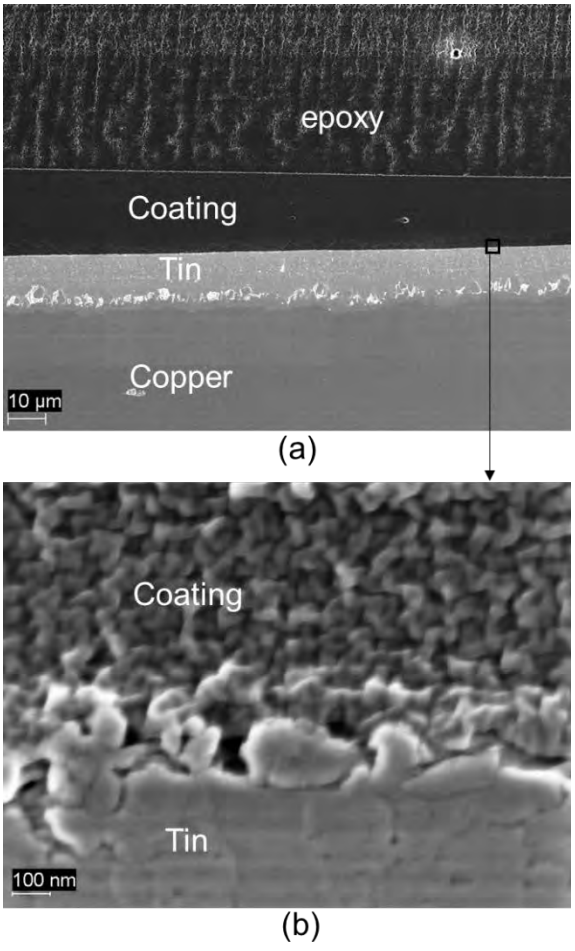


Figure 20: (a) Representative SEM cross – section of PU coated coupon following 4,000 HTHH storage and (b) a high magnification image of the well-adhered coating-tin interface.

Therefore, to better evaluate this well adhered interface, SEM imaging was performed using a BSD which is particularly sensitive to atomic numbers and therefore provides elemental contrast **(**Figure

21**).** This confirmed the presence of a clearly delineated, relatively thick and homogeneous layer of oxide (~30 nm) at the tin surface under the coating.

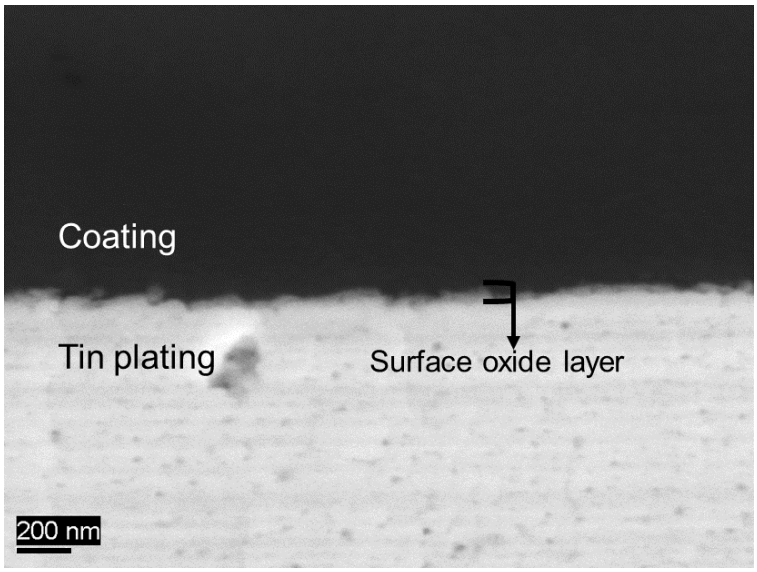


Figure 21: Coating-tin interface in 4,000 hour HTHH storage coupon cross – section with oxide layer visible.

A similar oxide layer was not observed for the other unfilled PC18M coated coupons examined in this study. Increased adhesion due to the presence of the very thin oxide layer could explain the lack of lateral tin growth and IMC formation in the tin plating layer. While the mechanisms of adhesion between metal surfaces and polyurethanes are not entirely understood, there is evidence in the case of aluminum and copper to show that the occurrence of native oxides plays a significant role in enhancing the adhesion of polyurethanes [12][13]. Due to the enhanced adhesion there is a reduced availability of free surfaces for, i) sufficient accumulation of copper atoms, and ii) the subsequent nucleation of the intermetallics following reaching a requisite concentration of the copper.

Figure 22 is the thickness comparison among primary tin layer and interfacial IMC layers at various time steps of the HTHH storage. The linear trend line (considering only the thickness of 0, 2,500 and 5,250 tin thickness; R^2= 94%) was plotted to compare *expected* thickness of primary Sn layer with the *measured* thickness, in the 4,000 hour storage case. While an increase in measured primary Sn thickness (i.e. original plating on copper) was noted in the 0, 2,500 and 5,250 hours HTHH storage coupons, in the 4,000 hour case, this measured thickness was significantly smaller (~23%) than predicted (from linear trend).

However, the interfacial IMC growth rates incorporating all four time steps (0-5,250 hours) were well matched with the growth rate exponents of Cu_6Sn_5 and Cu_3Sn (n = 0.17 and n = 0.46 respectively). The difference in tin thickness increase in the 4,000 hour cross – section between measured and expected values may therefore be attributed to the relative lack of volume expansion in the tin layer by the formation of discrete IMC's within the tin layer, as in the 2,500 and 5,250 hour cases. Diffusion of copper atoms into the tin lattice and accumulation at tin grain boundaries can also increase its thickness. The relative lack of compressive stress caused by the surface IMC growth reduces the need for pure tin atoms to push outward thereby negating the formation of protrusive growths in this case. Therefore, in comparison with the varying amounts of delamination noted in the other sections (0, 2,500 and 5,250 hours of HTHH storage) of same coating thickness and composition examined in this study, the better adhesion and lack of IMC formation afforded in part by the presence of the oxide layer in the 4,000 hour sample tended to restrict lateral tin layer growth.

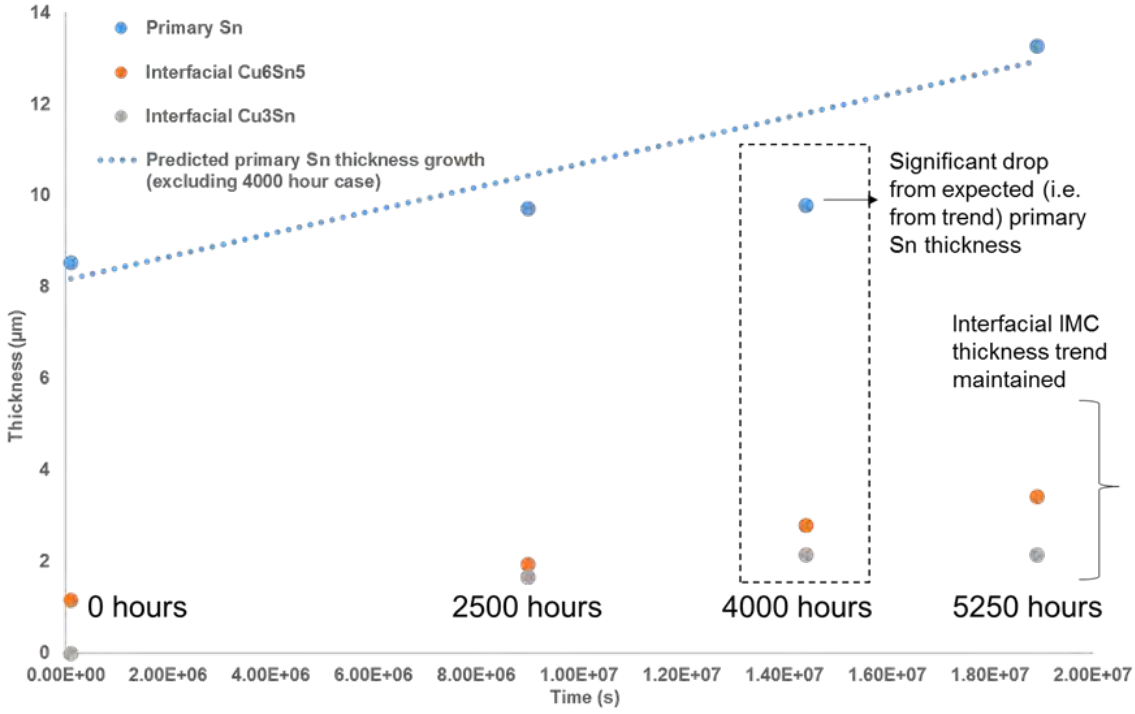


Figure 22: Thickness measurements of primary tin plating and interfacial IMC formation from zero to 5,250 hours HTHH storage.

3.4 Effects of HTHH storage on polyurethane acrylate (PUA – PC40-UMF™), nanoparticle filled PC18M™, and bilayer (filled on unfilled PC18M™) conformal coatings

In addition to unfilled polyurethane (PU – PC18M) coatings, HTHH storage tests were also conducted on unfilled polyurethane-acrylate (PUA – PC40-UMF) coatings as well as silica nanoparticle (20% suspension weight) filled PU coatings on the tin plated copper coupons. Another coupon, a bilayer conformal coating of 10 micron filled on 10 micron unfilled PU coating was also tested. On microelectronic components, the bilayer coating configuration may be used to afford more complete surface coverage; with the second coating run covering any ‘pinholes’ or other artefacts caused in the first coat. Further, an important effect of using two coatings with distinct mechanical properties is that the desirable properties of both the coatings may be utilized advantageously. For instance, in the bilayer configuration with a nanoparticle filled coating applied over unfilled coating layer, the filled coating may provide enhanced strength and stiffness while the unfilled coating could give more flexibility and ductility during plastic deformation.

The Figure 23 shows cross – sections show coupons coated with 20 micron filled PU and unfilled PUA following 4,000 hours HTHH storage. In both of these cases, similar to the unfilled PU cases, extensive interfacial IMC formation followed by tin growth was noted. The amount of lateral tin growth, however, is thicker in the case of PC40-UMF coated sample, compared to the filled PU coated sample. These differences could be caused due to adhesion effects and oxidation on the surface of the tin plating as explained in the earlier sections.

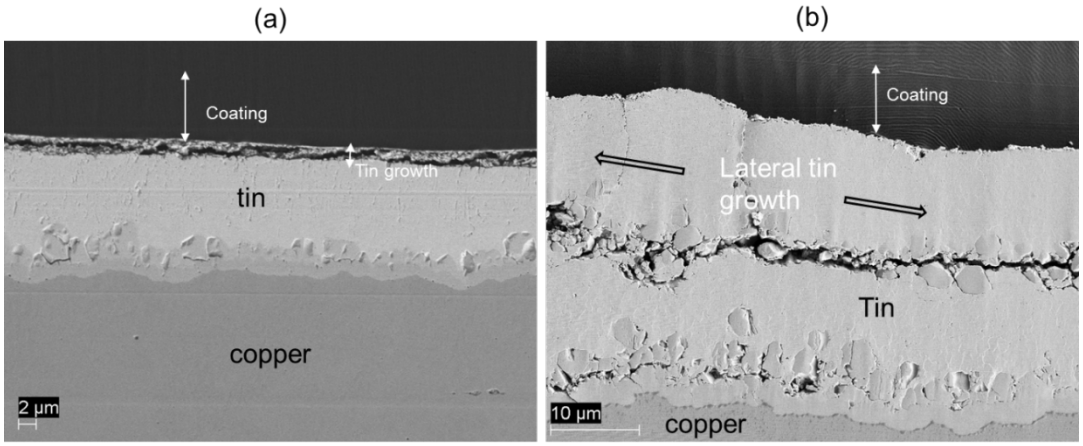


Figure 23: Representative cross – sectional microstructure developments in coated tin coupons following 4,000 hour HTHH storage; (a) 20 micron thick PC18M + 20%XP2742 nanosilica and (b) 20 micron thick unfilled PUA.

The lateral tin growth accompanied by the IMC formation at the interface was also noted in the case of bilayer coating coupon cross – section, as seen in Figure 24. Higher magnification images of the coating/tin interface showed a relatively higher deformation locally of the unfilled PU coating (PC18M) which was the first coating on tin (10 micron thickness). The second layer of filled PU of similar thickness was relatively less displaced. This may be explained by our previously reported nanoindentation measurements for the 'localized' matrix properties of the polyurethane coatings with and without nanoparticle additions which showed an increase of nanohardness in the case of 20% nanosilica suspension addition, to 210 MPa from about 160 MPa in the case of unfilled polyurethane, at a depth of one micron [14].

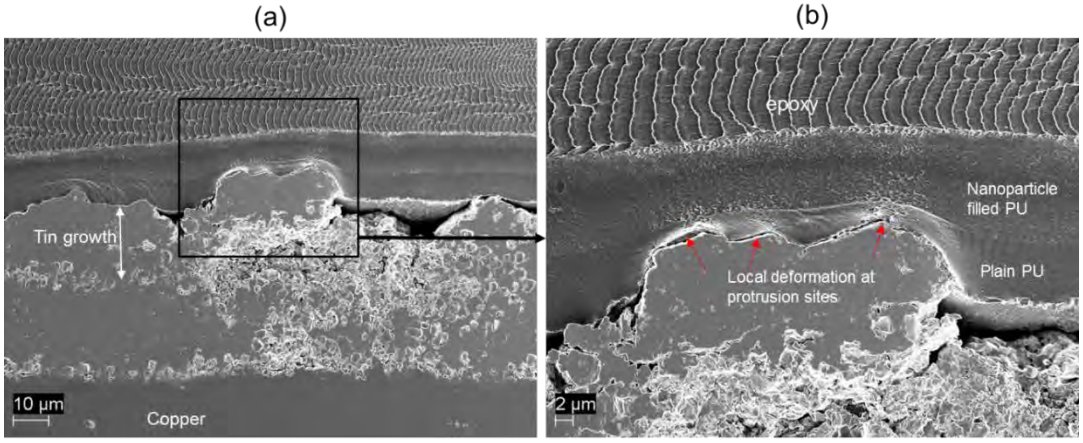


Figure 24: Cross – sectional microstructure development in a bilayer (filled PU on unfilled PU) coated coupons following 4,000 hour HTHH storage; (a) Tin plating on copper with secondary (lateral) growth and IMC formation and (b) Magnified view of unfilled and filled coatings with deformation noted at protrusion sites.

4. Summary of layered coating coupon whisker test results

High-temperature and high-humidity (HTHH @ 85°C/85%RH) storage testing of various conformal coatings applied to tin plated copper coupons was conducted for different time steps ranging from zero to 5,250 hours. The behavior of the conformal coatings was reported with respect to the mitigation of tin whisker and nodule growths originated from the surface of the tin plating as well as unique microstructural developments and features caused by the long-term storage. The effects of copper diffusion into the tin layer, followed by the formation of intermetallics in the tin-copper system was a critical factor in initiating protrusion-like growths from the surface of the tin plating.

All the polyurethane (PU) and polyurethane acrylate (PUA) coatings tested demonstrated their protection capabilities under HTHH storage up to 5,250 hours by showing no penetration of the tin whiskers or nodules through the coating layer. Cross-sectional analysis of selected coated coupons, however, showed that the poor adhesion due to the reaction between PU coatings and the top of the tin plating facilitated an availability of free surfaces at that interface, thereby causing diffused copper concentrations to reach critical levels necessary for intermetallic formation. Compressive stresses in the tin beneath this interface region (between coating and tin surface) and the growing interfacial intermetallic compounds caused protrusive growths to form and grow with increased storage time. Furthermore, the protrusive growths impinged upon the conformal coating which acted as a barrier to the vertical growth and forced the tin to grow into the interface between the coating and the tin, resulting in lateral growth.

Analysis of the lateral growth showed that extended storage (from 2,500 to 5,250 hours) resulted in an increase in the thickness of such secondary growth. The original tin plating thickness also showed an increasing linear trend with sustained storage time (0, 2,500 and 5,250 hours storage). However, when this trend was compared with the well-adhered coating case (4,000 hours HTHH storage) which showed no discrete intermetallic formation in bulk tin and no subsequent protrusions, the increase in tin plating thickness was significantly lower. The primary tin thickness increase can therefore have a critical dependence on the intermetallic formation at the tin surface (coating-tin interface) as well as diffused copper embedment along the grain boundaries of tin.

Other distinct coating compositions including PUA, nanosilica filled PU and bilayer (filled PU on unfilled PU) coatings all demonstrated similar tin microstructural developments (at 4,000 hours) with HTHH storage as in the unfilled PU cases although they displayed more substantial interfacial failure and tin lateral growth. The difference is believed to be due to interfacial adhesion, for which PU showed the highest adhesion. The beneficial effects of using coatings with different properties to construct bilayers was demonstrated via the distinct deformation behavior of filled PU versus unfilled PU coating under the stress during the tin protrusions.

5. Conclusions

Several aspects of tin whisker mitigation by conformal coatings were observed from the analysis of the various coupons with tin protrusions, in conjunction with a unique case which demonstrated a very homogeneous and strong adhesion between the coating and tin (20 micron thick PU with 4,000 hours HTHH storage). The following conclusions were made:

- Protection against whisker growth was demonstrated by all coatings that were at least 10 microns thick
  - All the polyurethane (PU) and polyurethane acrylate (PUA) coatings tested demonstrated their protection capabilities under HTHH storage up to 5,250 hours by showing no penetration of the tin whiskers or nodules through the coating layer.
- A new IMC formation phenomena was observed in the tin regions where nodules developed under the rigid coating
  - Large Cu_6Sn_5 intermetallic grain growth occurred near the coating/tin interface that was not attached to the lower copper substrate to tin interface
  - A complex layer of tin and IMC developed from original plated tin
  - Within the complex tin and IMC layer both small and large IMC grains as well as voids were observed
- Coating adhesion to the tin is important
  - PU showed the highest adhesion
  - Poor adhesion due to the reaction between PU coatings and the top of the tin plating facilitated an availability of free surfaces at that interface, thereby causing diffused copper concentrations to reach critical levels necessary for intermetallic formation.
  - Compressive stresses in the tin beneath this interface region (between coating and tin surface) and the growing interfacial intermetallic compounds caused protrusive growths to form and grow with increased storage time
  - The protrusive growths impinged upon the conformal coating which acted as a barrier to the vertical growth and forced the tin to grow into the interface between the coating and the tin, resulting in lateral growth available at the interface for IMC growth in that region
- The coating adhesion to the tin appeared to be limited by
  - Interfacial strength between the coating and the tin oxide on the tin surface
  - Strength of the tin below the coating, possibly impacted by voiding
  - Additional stress near the interface due to increased tin oxidation and the accumulation of Cu6Sn5 IMC near the coating/tin interface both which have greater volume than tin
- Layers high strength coating over a lower strength coating inhibited nodule penetration
  - The beneficial effects of using coatings with different properties to construct bilayers was demonstrated via the distinct deformation behavior of filled PU versus unfilled PU coating under the stress during the tin protrusions.

Following from the statements above it can be seen that a decrease in available free surfaces and grain boundaries (e.g., through a coarser grain structure of tin) would decrease the interfaces available for copper accumulation and subsequently the potential sites of intermetallic nucleation and growth, both of which contribute to complex tin and IMC layer thickness increase with time. Systematic annealing studies of tin and adhesion promoter (e.g., silane treatment) may be useful to assess the nature of this relationship between the adhesion and the tin whisker/nodule growth.

6. Literature cited

[1] Hillman D, Wilcox R, Lower N, Grossman D. Tin Whisker Inorganic Coating Evaluation (TWICE). In: *Proceedings* of *SMTA International*.; 2014:476-488.

[2] Meschter S, Snugovsky P, Bagheri Z, et al. Whisker Formation on SAC305 Soldered Assemblies. JOM J Miner Met Mater Soc. 2014;66(11):2320-2333. doi:10.1007/s11837-014-1183-9.

[3] Baated A, Kim KS, Suganuma K, et al. Effects of reflow atmosphere and flux on Sn whisker growth of Sn-Ag-Cu solders. J Mater Sci Mater Electron. 2010;21(10):1066-1075. doi:10.1007/s10854-010-0099-6.

[4] Panashchenko L, Osterman M. Examination of nickel underlayer as a tin whisker mitigator. Proc - Electron Components Technol Conf. 2009:1037-1043. doi:10.1109/ECTC.2009.5074139.

[5] Park MS, Arroyave R. Formation and Growth of Intermetallic Compound Cu(6)Sn(5) at Early Stages in Lead-Free Soldering. J Electron Mater. 2010;39(12):2574-2582. doi:DOI 10.1007/s11664-010-1353-7.

[6] Han C, Liu Q, Ivey DG. Interfacial Reactions Between Electrodeposited Sn-Cu, Sn-Ag-Cu Solders and Cu, Ni Substrates. J Microelectron Electron Pacakaging. 2010;7:48-57.

[7] Onishi, Masami and Fujibuchi H. Reaction-diffusion in the Cu-Sn system. Trans Japan Inst Met. 1975;16:539-547.

[8] Chromik RR, Cotts EJ. Thermodynamic and Kinetic Study of Phase Transformations in Solder/Metal Systems. In: MRS Proceedings. ; 1996:445.

[9] Baated A, Kim KS, Suganuma K. Effect of intermetallic growth rate on spontaneous whisker growth from a tin coating on copper. J Mater Sci Mater Electron. 2011;22(11):1685-1693. doi:10.1007/s10854-011-0346-5.

[10] Appendix G of this report: Coupon whisker testing for baseline coating process

[11] Tu KN. Cu/Sn interfacial reactions: Thin-film case versus bulk case. Mater Chem Phys. 1996;46(2-3):217-223. doi:10.1016/S0254-0584(97)80016-8.

[12] Mahan K, Sun Y, Han B, Han S, Osterman M. Adhesion and Puncture Strength of Polyurethane Coating Used to Mitigate Tin Whisker Growth. J Electron Packag. 2014;136. doi:10.1115/1.4026922.

[13] Nies C, Wehlack C, Ehbing H, Dijkstra DJ, Possart W. Adhesive Interactions of Polyurethane Monomers with Native Metal Surfaces. J Adhes. 2012;888:665-683. doi:10.1080/00218464.2012.682865.

[14] Appendix D of the current report: Coating Characterization Results



SERDP WP2213
Final Report
Appendix K: Assembly whisker testing for layered coating process

Appendix K: Table of Contents

1. Introduction 1
2. Detailed inspection results 1
2.1 QFP boards 2
2.1.1 QFP board layered PC18M dip + PC18M spray 3
2.1.2 QFP board layered dip + PC18M+20%XP2742 nanosilica 5
2.2 BGA Boards 7
2.2.1 BGA board unfilled PC18M dip only 7
2.2.2 BGA board layered unfilled PC18M spray 24
2.2.3 BGA board layered PC18M+20%XP2742 nanosilica 26
3. Layered coating assembly whisker test results summary 31
3.1 QFP Board summary 31
3.2 BGA board summary 33
4. Discussion 36
5. Conclusions 36
6. Literature cited 37

Appendix K: List of Figures

Figure 1: Board A023, QFP44, random lead, 3030HTHH, 40x, focused on lead foot (PC18M dip + two 25 micron PC18M sprays). 3

Figure 2: Board A023, QFP44, random lead, 3030HTHH, 40x, focused on lead top (PC18M dip + two 25 micron PC18M sprays). 3

Figure 3: Board A023, QFP44, random lead, 3030HTHH, 100x, lead foot (PC18M dip + two 25 micron PC18M sprays). 4

Figure 4: Board A023, QFP44, random lead, 3030HTHH, 100x, lead top (PC18M dip + two 25 micron PC18M sprays). 4

Figure 5: Board A347, QFP44, random lead, 3030HTHH, 40x, focused on lead foot (PC18M dip + two 25 micron PC18M+20%XP2742 nanosilica sprays). 5

Figure 6: Board A347, QFP44, random lead, 3030HTHH, 40x, focused on lead top (PC18M dip + two 25 micron PC18M+20%XP2742 nanosilica sprays). 5

Figure 7: Board A347, QFP44, random lead, 3030HTHH, 100x, focused on lead foot (PC18M dip + two 25 micron PC18M+20%XP2742 nanosilica sprays). 6

Figure 8: Board A347, QFP44, random lead, 3030HTHH, 100x, focused on lead top (PC18M dip + two 25 micron PC18M+20%XP2742 nanosilica sprays). 6

Figure 9: Board A377, BGA, U806, 3030HTHH, 40x (PC18M dip processed during the PC18M spray run)..... 7

Figure 10: Board A377, BGA, U806, C1, 3030HTHH, 180x (PC18M dip processed during the PC18M spray run). 8

Figure 11: Board A377, BGA, U806, C1, 3030HTHH, 3,000x, image 1 (PC18M dip processed during the PC18M spray run)..... 8

Figure 12: Board A377, BGA, U806, C1, 3030HTHH, 3,000x, image 2 (PC18M dip processed during the PC18M spray run)..... 9

Figure 13: Board A377, BGA, U806, C1, 3030HTHH, 3,000x, image 3 (PC18M dip processed during the PC18M spray run)..... 9

Figure 14: Board A377, BGA, U806, C2, 3030HTHH, 3,000x (PC18M dip processed during the PC18M spray run 10

Figure 15: Board A377, BGA, U806, C2, 3030HTHH, 500x (PC18M dip processed during the PC18M spray run). 10

Figure 16: Board A377, BGA, U806, F4, 3030HTHH, 180x (PC18M dip processed during the PC18M spray run). 11

Figure 17: Board A377, BGA, U806, F4, 3030HTHH, 3,500x (PC18M dip processed during the PC18M spray run). 11

Figure 18: Board A377, BGA, U806, H6, 3030HTHH, 3,500x (PC18M dip processed during the PC18M spray run). 12

Figure 19: Board A377, BGA, U806, H6, 3030HTHH, 500x (PC18M dip processed during the PC18M spray run). 12

Figure 20: Board A377, BGA, U808, B3, 3030HTHH, 180x (PC18M dip processed during the PC18M spray run). 13

Figure 21: Board A377, BGA, U808, B3, 3030HTHH, 3,500x (PC18M dip processed during the PC18M spray run). 13

Figure 22: Board A377, BGA, U808, G2, 3030HTHH, 180x (PC18M dip processed during the PC18M spray run). 14

Figure 23: Board A377, BGA, U808, G2, 3030HTHH, 2,000x (PC18M dip processed during the PC18M spray run). 14

Figure 24: EDX analysis of Board A377, 3030HTHH, Area (1) (PC18M dip processed during the PC18M spray run) 15

Figure 25: EDX analysis of Board A377, 3030HTHH, Area (2) (PC18M dip processed during the PC18M spray run) 16

Figure 26: EDX analysis of Board A377, 3030HTHH, Area (2) continued from Figure 25 (PC18M dip processed during the PC18M spray run) 17

Figure 27: Board A596, BGA, U507, 3030HTHH, 40x (PC18M dip processed during the PC18M+20%XP2742 nanosilica spray run). 18

Figure 28: Board A596, BGA, U507, A10, 3030HTHH, 180x (PC18M dip processed during the PC18M+20%XP2742 nanosilica spray run). 18

Figure 29: Board A596, BGA, U507, A10, 3030HTHH, 3,500x (PC18M dip processed during the PC18M+20%XP2742 nanosilica spray run). 19

Figure 30: Board A596, BGA, U507, A3, 3030HTHH, 180x (PC18M dip processed during the PC18M+20%XP2742 nanosilica spray run). 19

Figure 31: Board A596, BGA, U507, A3, 3030HTHH, 3,000x (PC18M dip processed during the PC18M+20%XP2742 nanosilica spray run). 20

Figure 32: Board A596, BGA, U508, E1, 3030HTHH, 2,500x (PC18M dip processed during the PC18M+20%XP2742 nanosilica spray run). 20

Figure 33: Board A596, BGA, U508, E1, 3030HTHH, 300x (PC18M dip processed during the PC18M+20%XP2742 nanosilica spray run). 21

Figure 34: Board A596, BGA, U508, F2, 3030HTHH, 180x (PC18M dip processed during the PC18M+20%XP2742 nanosilica spray run). 21

Figure 35: Board A596, BGA, U508, F2, 3030HTHH, 3,000x (PC18M dip processed during the PC18M+20%XP2742 nanosilica spray run). 22

Figure 36: Board A596, BGA, U508, G3, 3030HTHH, 180x (PC18M dip processed during the PC18M+20%XP2742 nanosilica spray run). 22

Figure 37: Board A596, BGA, U508, G3, 3030HTHH, 2,000x (PC18M dip processed during the PC18M+20%XP2742 nanosilica spray run). 23

Figure 38: Board A596, BGA, U508, G3, 3030HTHH, 500x (PC18M dip processed during the PC18M+20%XP2742 nanosilica spray run). 23

Figure 39: Board A307, BGA, U606, 3030HTHH, 40x (PC18M dip + 25 micron PC18M spray). 24

Figure 40: Board A307, BGA, U606, A2, 3030HTHH, 180x (PC18M dip + 25 micron PC18M spray)... 24

Figure 41: Board A296, BGA, U501, 3030HTHH, 40x (PC18M dip + two 25 micron PC18M sprays)… 25

Figure 42: Board A296, BGA, U501, 3030HTHH, A1, 180x (PC18M dip + two 25 micron PC18M sprays). 25

Figure 43: Board A593, BGA, U805, 3030HTHH, 40x (PC18M dip + 25 micron PC18M+20%XP2742 nanosilca spray). 26

Figure 44: Board A593, BGA, U805, K1, 3030HTHH, 180x (PC18M dip + 25 micron PC18M+20%XP2742 nanosilca spray). 26

Figure 45: Board A593, BGA, U508, K1, 3030HTHH, 300x (PC18M dip + 25 micron PC18M+20%XP2742 nanosilca spray). 27

Figure 46: Board A593, BGA, U508, K1, 3030HTHH, 300x, lighter contrast (PC18M dip + 25 micron PC18M+20%XP2742 nanosilca spray). 27

Figure 47: Board A593, BGA, U508, K1, 3030HTHH, 2,500x (PC18M dip + 25 micron PC18M+20%XP2742 nanosilca spray). 28

Figure 48: Board A392, BGA, U501, 3030HTHH, 40x (PC18M dip + two 25 micron PC18M+20%XP2742 nanosilca sprays). 28

Figure 49: Board A392, BGA, U501, 3030HTHH, 180x (PC18M dip + two 25 micron PC18M+20%XP2742 nanosilca sprays). 29

Figure 50: Board A392, BGA, U501, 3030HTHH, 300x (PC18M dip + two 25 micron PC18M+20%XP2742 nanosilca sprays). 29

Figure 51: Board A392, BGA, U501, 3030HTHH, 2,500x (PC18M dip + two 25 micron PC18M+20%XP2742 nanosilca sprays). 30

Figure 52: Uncoated board 48 QFP64 after 2,000h of HTHH; (A) 100x and (B) 1,500x. 31

Figure 53: SEM images comparing layer coated unfilled PC18M spray and PC18M+20%XP2742 nanosilica filled sprays in the dip + 2 spray QFP44 parts after HTHH testing for 3,030h. 32

Figure 54: SEM images of PC18M+20%XP2742 nanosilica spray layered coated BGA pads with increasing number of layers at various magnifications after HTHH testing for 3,030h.(A) (B) (C) dip, (D) (E) (F) dip + one spray, and (G) (H) (I) dip + two sprays with (A) (D) (G) 40x, (B) (E) (H) 180x and (C) (F) (I) 2,500x. 33

Figure 55: SEM images of layered coated BGA pads with increasing number of layers for unfilled PC18M sprays and PC18M+20%XP2742 nanosilica filled sprays after HTHH testing for 3,030h, 180x. (A) (B) (C) unfilled spray run and (D) (E) (F) nanosilica filled spray run with (A) (D) dip, (B) (E) dip+one spray, and (C) (D) dip + two sprays. 34

Figure 56: SEM image and electrodispersive x-ray (EDX) analysis of some nodules found on BGA pads from board A377, PC18M dip only. Note that the nodules in locations one and two are Ag_3Sn intermetallic with the surrounding Sn corroded away. 35

Appendix K: List of Tables

Table 1: Unfilled PC18M layered assembly batch coated with the PC18M dip + 2 sprays of PC18M exposed to 3,030 hrs of HTHH. 1

Table 2: Nanosilica filled PC18M layered assembly batch coated with the PC18M dip + 2 sprays of (PC18M+20%XP2742) exposed to 3,030 hrs of HTHH. 2

Acronyms

Acronym	Definition
BGA	Ball Grid Array
HTHH	High Temperature/High Humidity
QFP	Quad Flat Pack Electronic Packages
RH	Relative Humidity
SEM	Scanning Electron Microscopy

1. Introduction

The goal of the assembly whisker testing was to determine the coating whisker mitigation performance on actual assemblies with three dimensional features that are challenging to coat uniformly. The layered coating approach was developed in an effort to improve coverage over the baseline spray process and in turn improve whisker mitigation. The PC18M based coatings were selected for assembly layered coating testing from the results of the superior inter layer adhesion characteristics observed in prior testing.

The layered coating approach consisting of a dip layer, a partial cure, a spray layer, another partial cure, a final spray layer, and a full cure showed improved coverage over the baseline dip/partial cure/spray process [**1**][**2**][**3**]. The whisker mitigation capability of layer coated assemblies of layered unfilled PC18M spray coats was compared to PC18M+20%XP2742 nanosilica spray coats applied over a partially cured low viscosity PC18M dip coat. The quad flat pack (QFP) and the solder paste reflowed pads on the ball grid array (BGA) assemblies were evaluated over 3,030 hours of 85C/85%RH high temperature high humidity (3030HTHH) and examined in the scanning electron microscope (SEM). Note that thermal cycling was not performed because the evaluation focused on the QFP part leads which are difficult to coat. The QFP parts have copper leads which have the greatest whisker growth potential in high humidity.

2. Detailed inspection results

The QFP and BGA detailed inspection results are given in the next sections. The boards exposed to the HTHH environment are summarized in Table 1 and Table 2. Resource limitations restricted the inspection to the QFP44 parts and the BGA pads screened with SAC305 solder.

Table 1: Unfilled PC18M layered assembly batch coated with the PC18M dip + 2 sprays of PC18M exposed to 3,030 hrs of HTHH.

Coupon Type	Coupon ID	Dipping Lot	Spray runs	Post spray observations
QFP	A036	25	0	
SOT	A254	25	0	
BGA	A377	25	0	
QFP	A141	21	1	dull surface, many small bubbles, large bubbles
BGA	A307	22	1	
SOT	A328	21	1	
QFP	A023	20	2	
SOT	A206	20	2	
BGA	A296	18	2	

Table 2: Nanosilica filled PC18M layered assembly batch coated with the PC18M dip + 2 sprays of (PC18M+20%XP2742) exposed to 3,030 hrs of HTHH.

Coupon Type	Coupon ID	Dipping Lot	Spray runs	Post spray observations
SOT	A050	3	0	
QFP	A228	1	0	no bubbles
BGA	A596	9	0	
SOT	A134	11	1	
QFP	A275	12	1	duller coating, some microbubbles
BGA	A593	10	1	
SOT	A184	13	2	
QFP	A347	8	2	dull, many microbubbles, largish bubble but not visible at 4x mag
BGA	A392	15	2	

2.1 QFP boards

No whiskers were found on the any spray coated QFP44 leads after 3030 hours of HTHH. The unfilled spray coated PC18M dip + 2 sprays of PC18M and the nanosilica filled spray coated PC18M dip + 2 sprays of (PC18M+20%XP2742) assembly images are provided next.

2.1.1 QFP board layered PC18M dip + PC18M spray

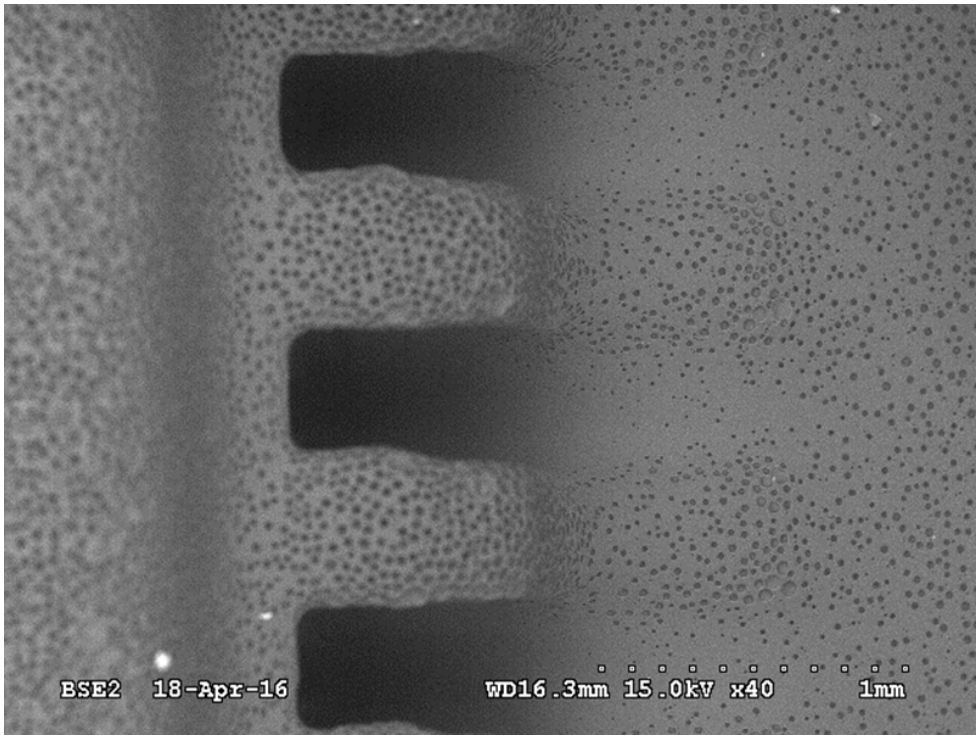


Figure 1: Board A023, QFP44, random lead, 3030HTHH, 40x, focused on lead foot (PC18M dip + two 25 micron PC18M sprays).

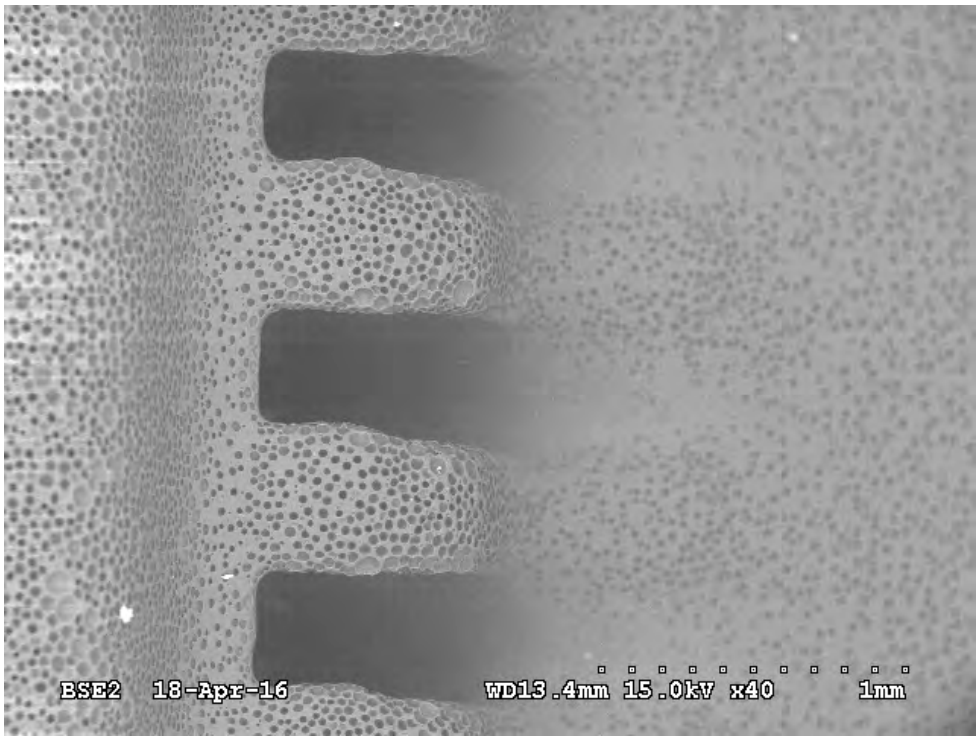


Figure 2: Board A023, QFP44, random lead, 3030HTHH, 40x, focused on lead top (PC18M dip + two 25 micron PC18M sprays).

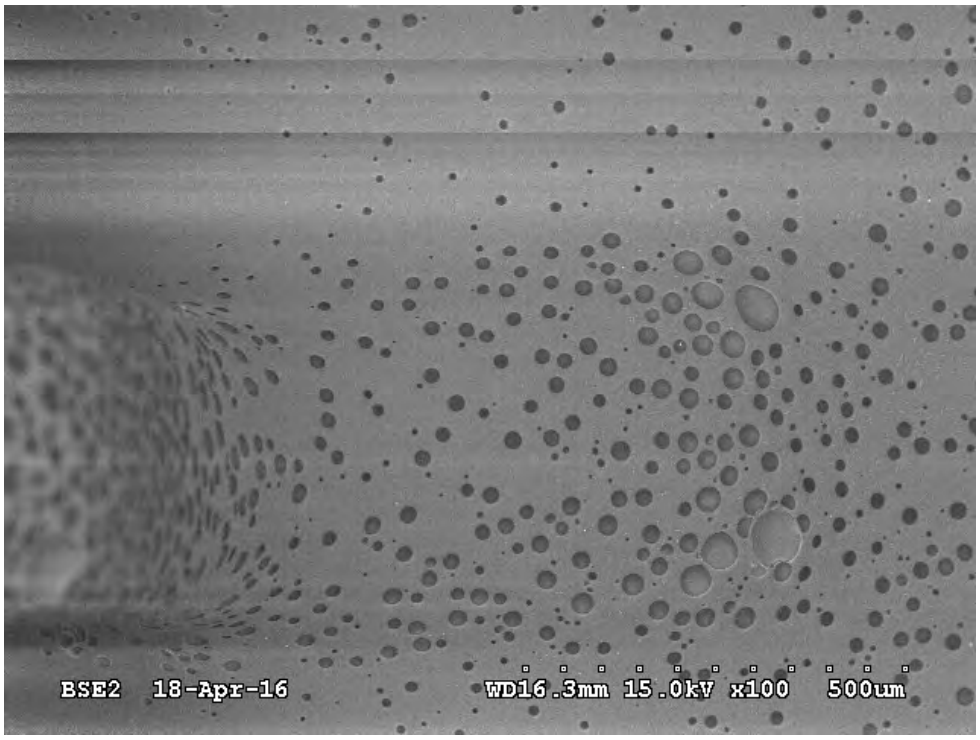


Figure 3: Board A023, QFP44, random lead, 3030HTHH, 100x, lead foot (PC18M dip + two 25 micron PC18M sprays).

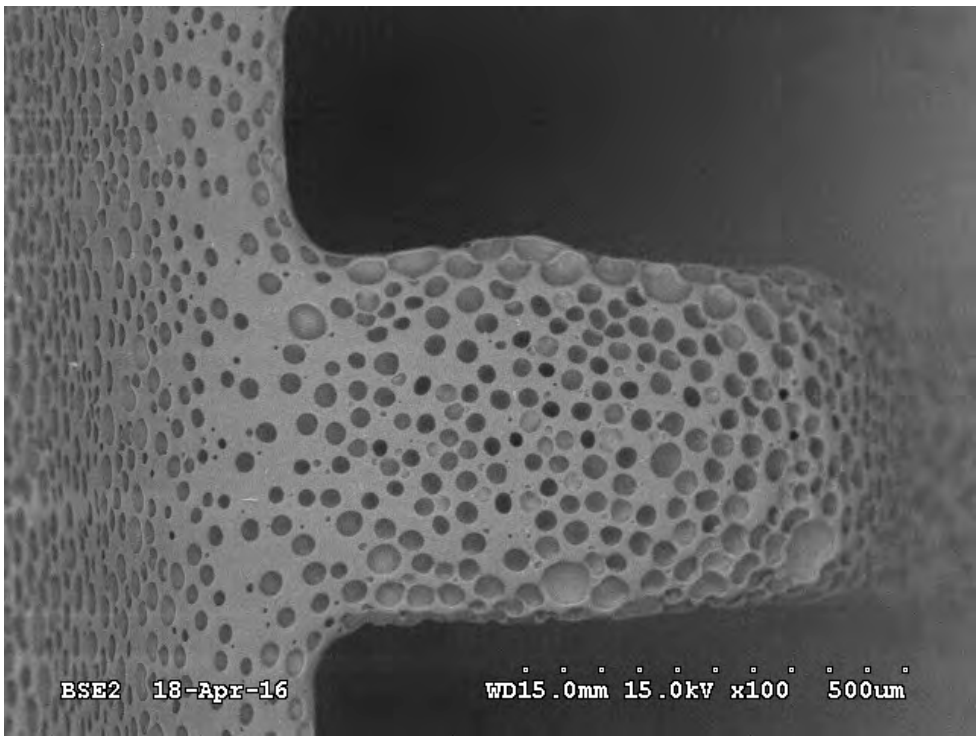


Figure 4: Board A023, QFP44, random lead, 3030HTHH, 100x, lead top (PC18M dip + two 25 micron PC18M sprays).

2.1.2 QFP board layered dip + PC18M+20%XP2742 nanosilica

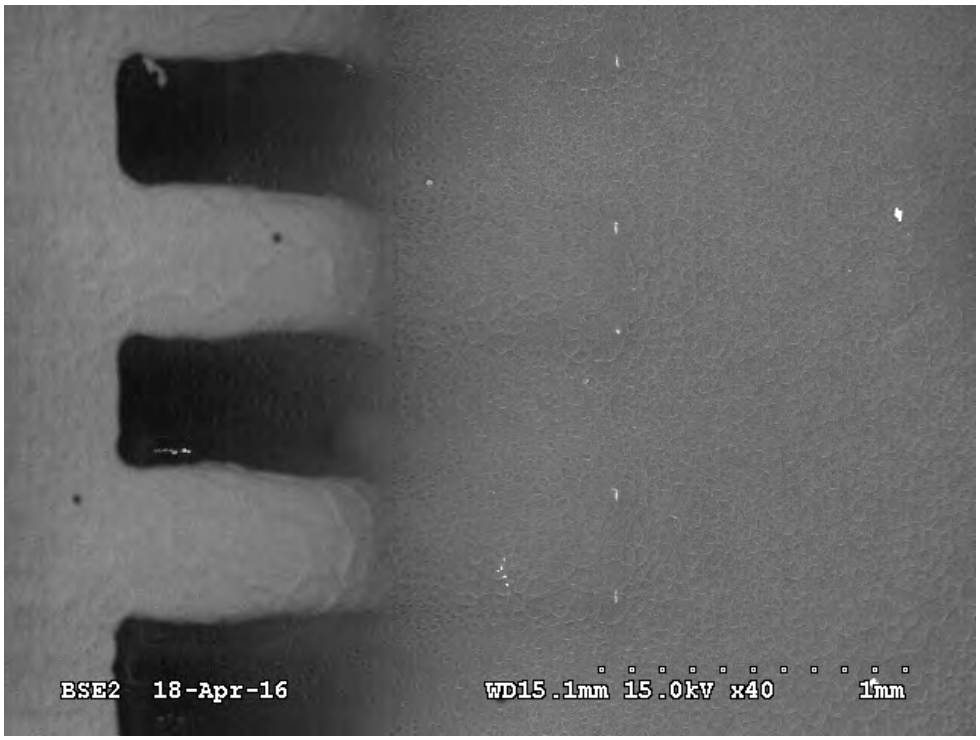


Figure 5: Board A347, QFP44, random lead, 3030HTHH, 40x, focused on lead foot (PC18M dip + two 25 micron PC18M+20%XP2742 nanosilica sprays).

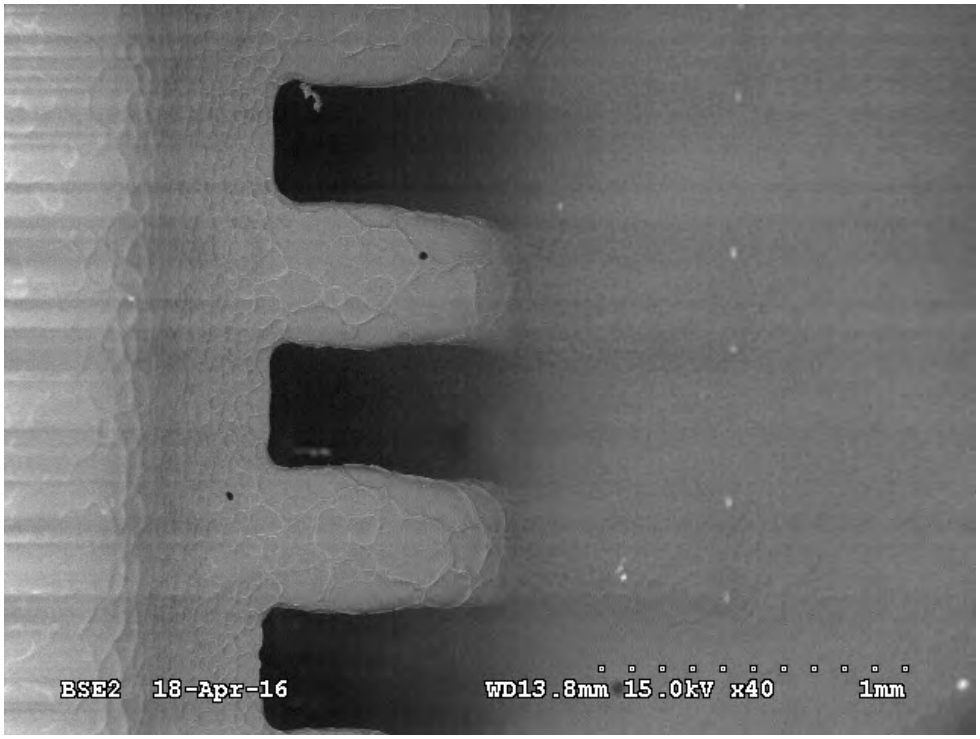


Figure 6: Board A347, QFP44, random lead, 3030HTHH, 40x, focused on lead top (PC18M dip + two 25 micron PC18M+20%XP2742 nanosilica sprays).

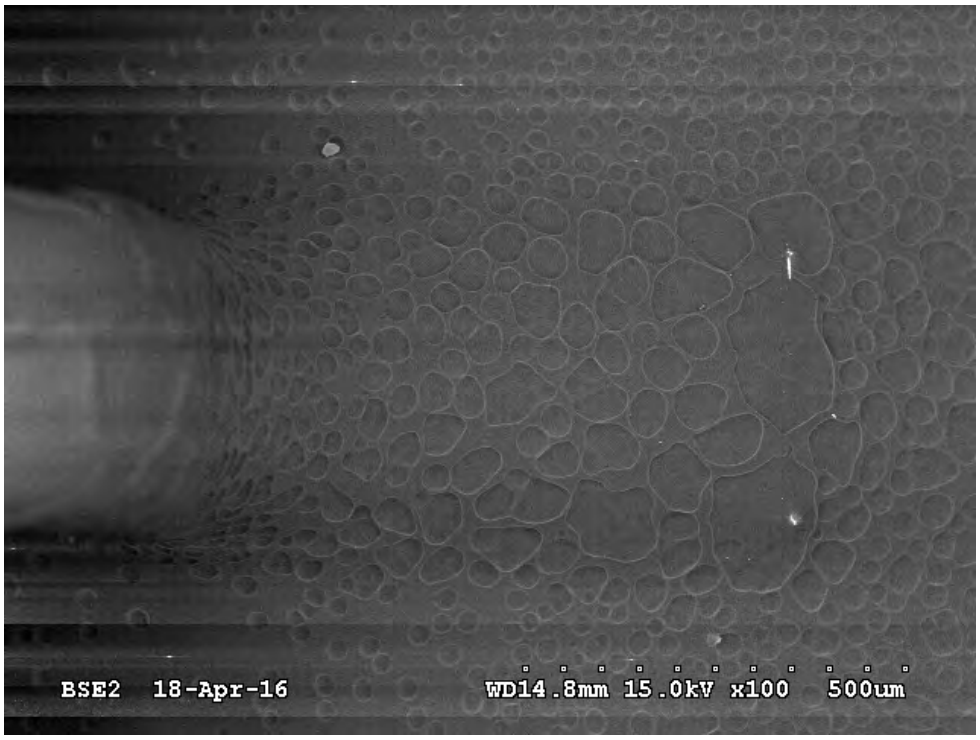


Figure 7: Board A347, QFP44, random lead, 3030HTHH, 100x, focused on lead foot (PC18M dip + two 25 micron PC18M+20%XP2742 nanosilica sprays).

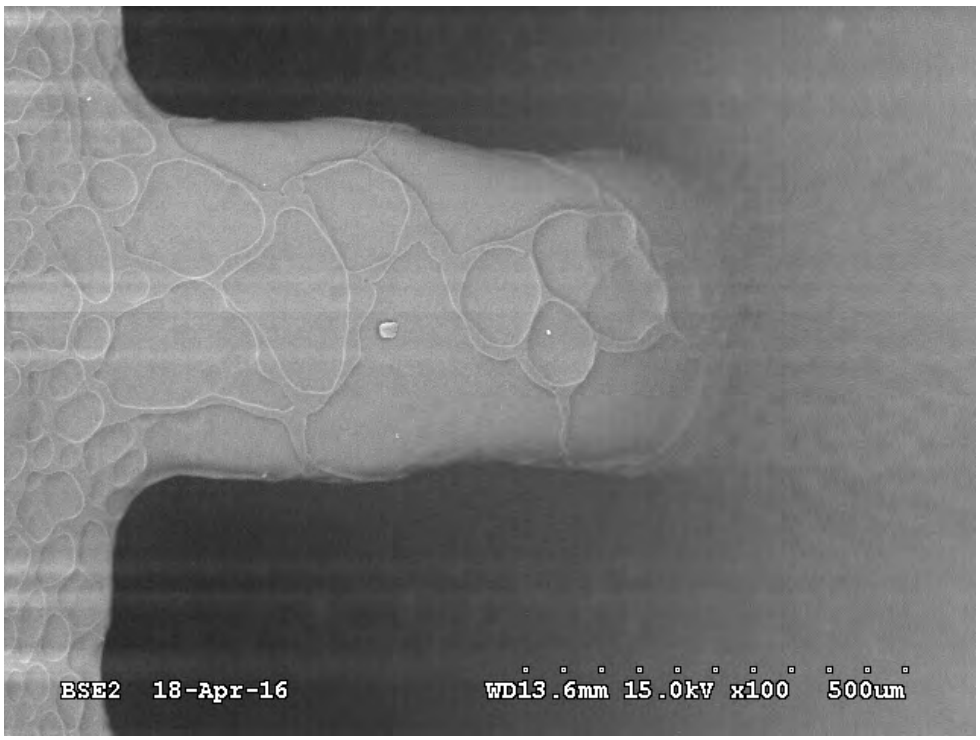


Figure 8: Board A347, QFP44, random lead, 3030HTHH, 100x, focused on lead top (PC18M dip + two 25 micron PC18M+20%XP2742 nanosilica sprays).

2.2 BGA Boards

Whiskers and corrosion were only found on the BGA solder pads coated with the dip coating. No whiskers were observed on any BGA solder pads that also had a spray coating.

2.2.1 BGA board unfilled PC18M dip only

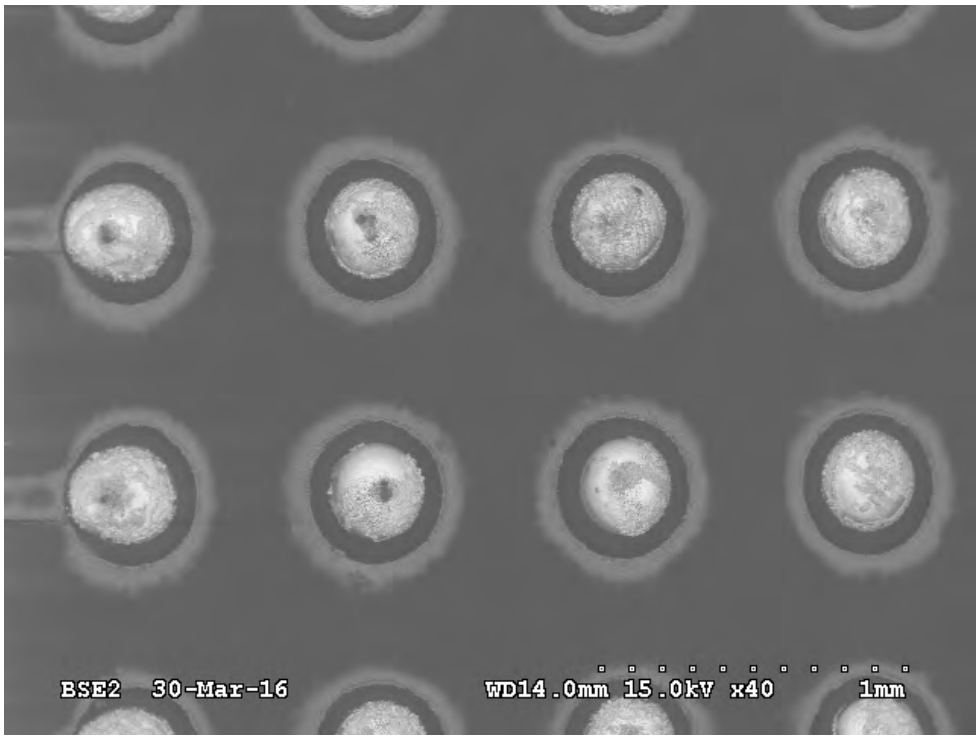


Figure 9: Board A377, BGA, U806, 3030HTHH, 40x (PC18M dip processed during the PC18M spray run).

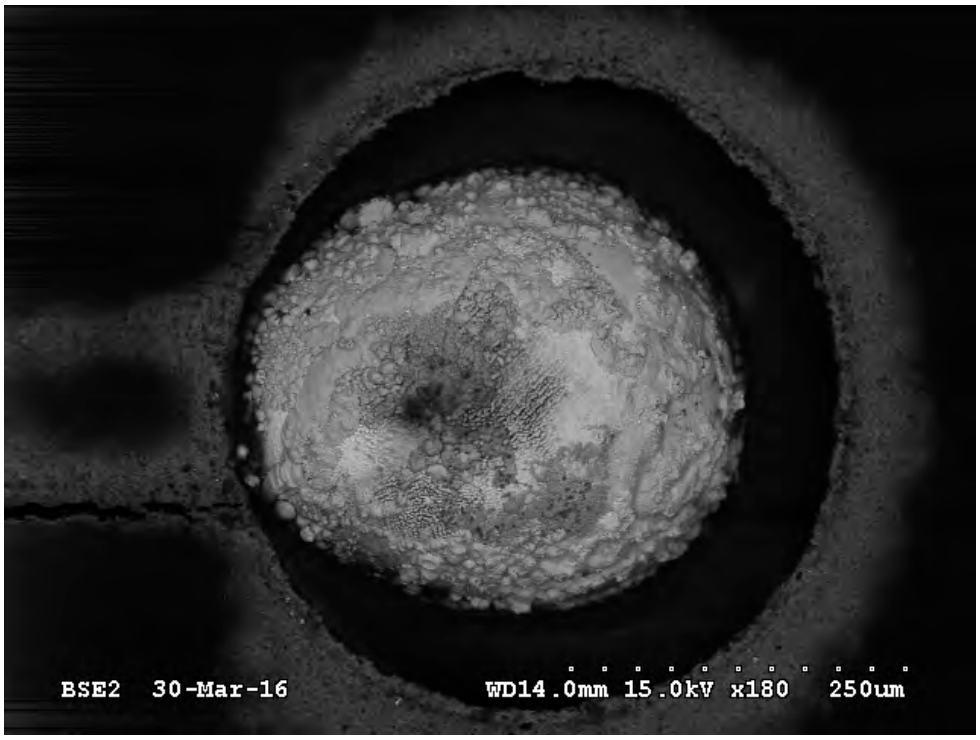


Figure 10: Board A377, BGA, U806, C1, 3030HTHH, 180x (PC18M dip processed during the PC18M spray run).

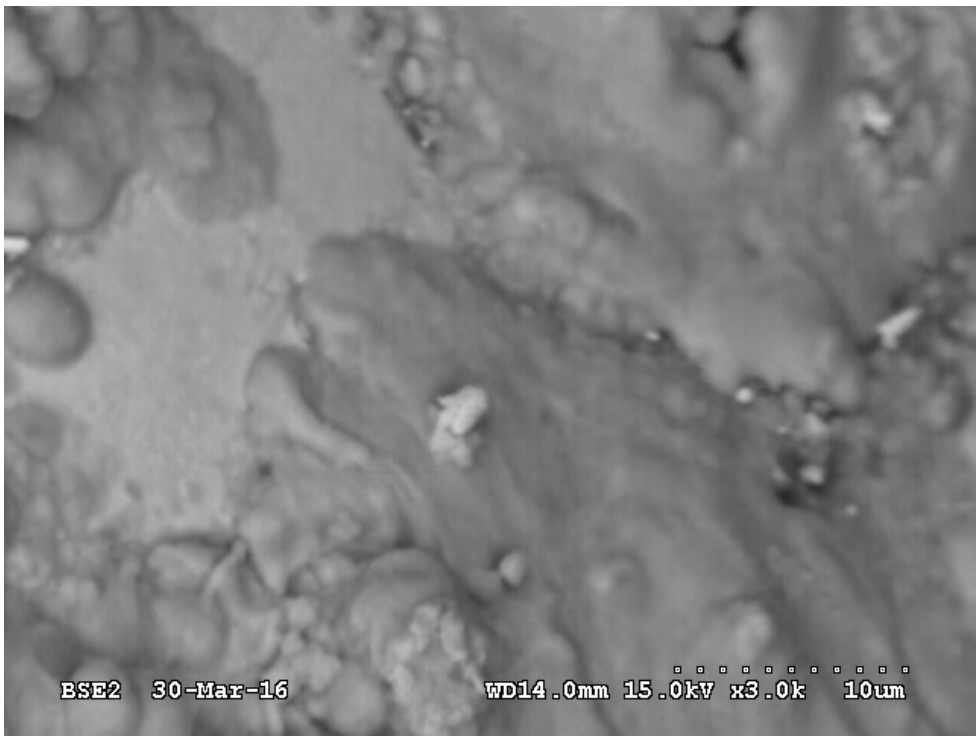


Figure 11: Board A377, BGA, U806, C1, 3030HTHH, 3,000x, image 1 (PC18M dip processed during the PC18M spray run).

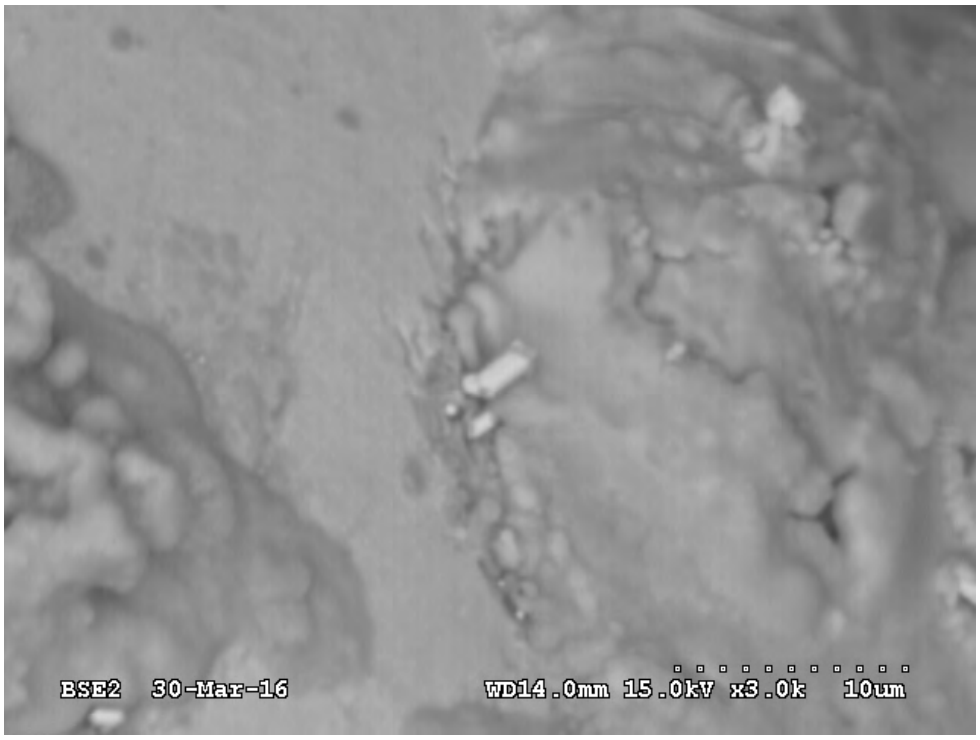


Figure 12: Board A377, BGA, U806, C1, 3030HTHH, 3,000x, image 2 (PC18M dip processed during the PC18M spray run).

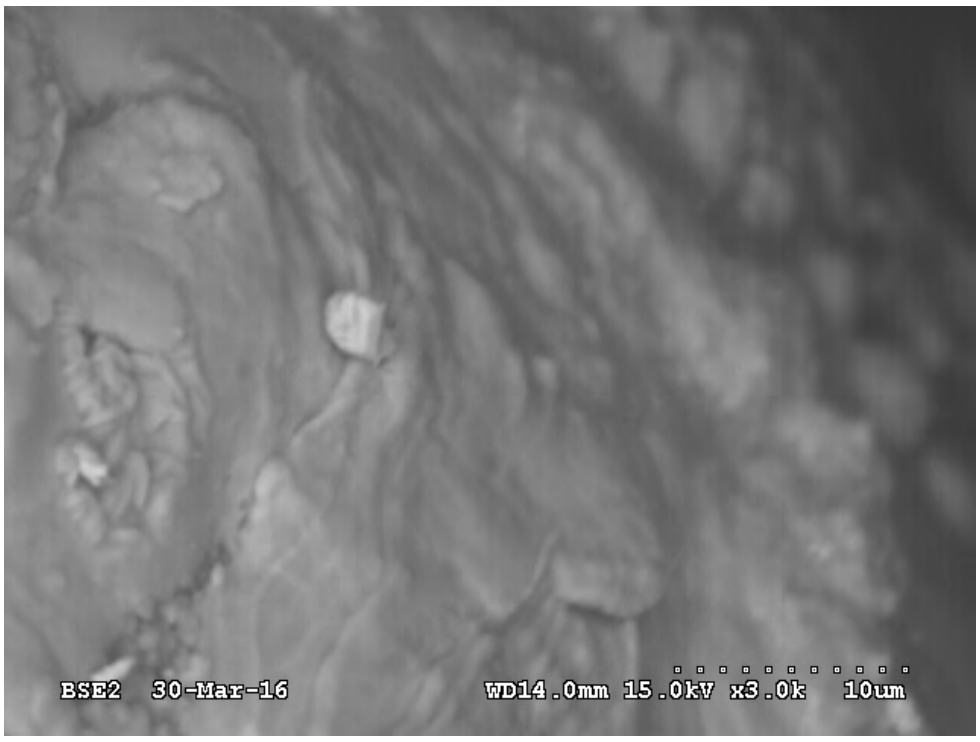


Figure 13: Board A377, BGA, U806, C1, 3030HTHH, 3,000x, image 3 (PC18M dip processed during the PC18M spray run).

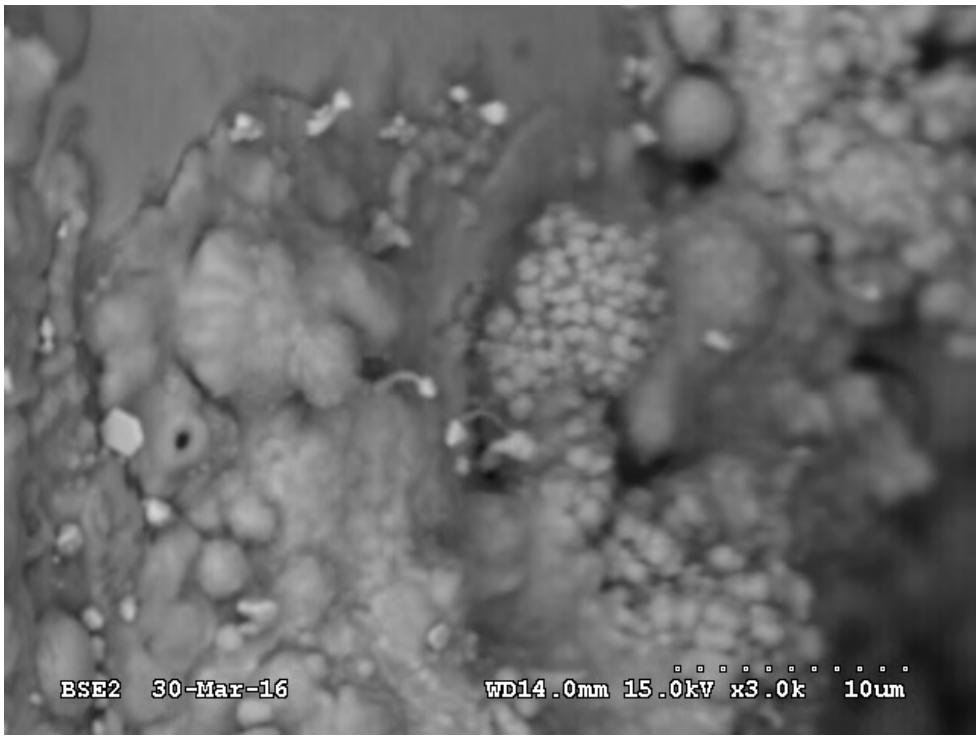


Figure 14: Board A377, BGA, U806, C2, 3030HTHH, 3,000x (PC18M dip processed during the PC18M spray run

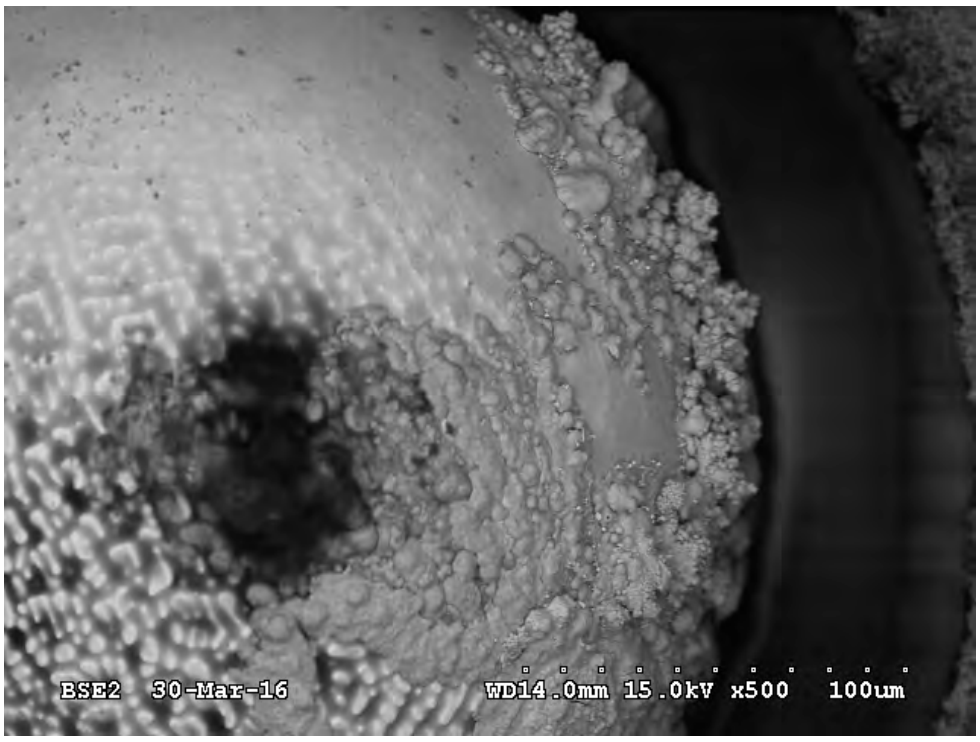


Figure 15: Board A377, BGA, U806, C2, 3030HTHH, 500x (PC18M dip processed during the PC18M spray run).

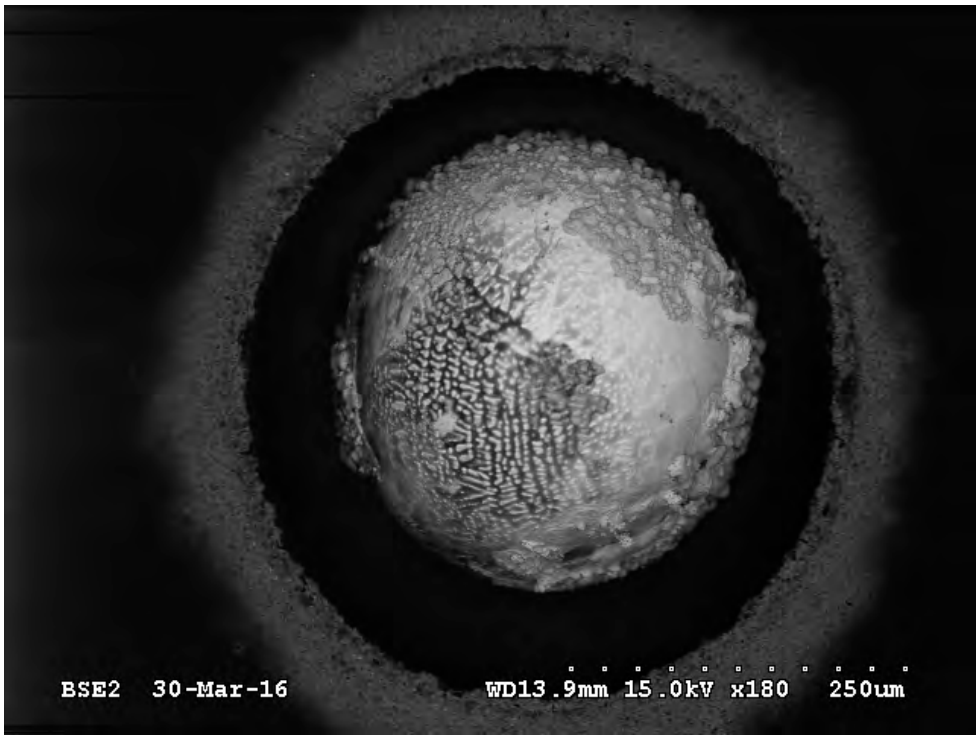


Figure 16: Board A377, BGA, U806, F4, 3030HTHH, 180x (PC18M dip processed during the PC18M spray run).



Figure 17: Board A377, BGA, U806, F4, 3030HTHH, 3,500x (PC18M dip processed during the PC18M spray run).



Figure 18: Board A377, BGA, U806, H6, 3030HTHH, 3,500x (PC18M dip processed during the PC18M spray run).

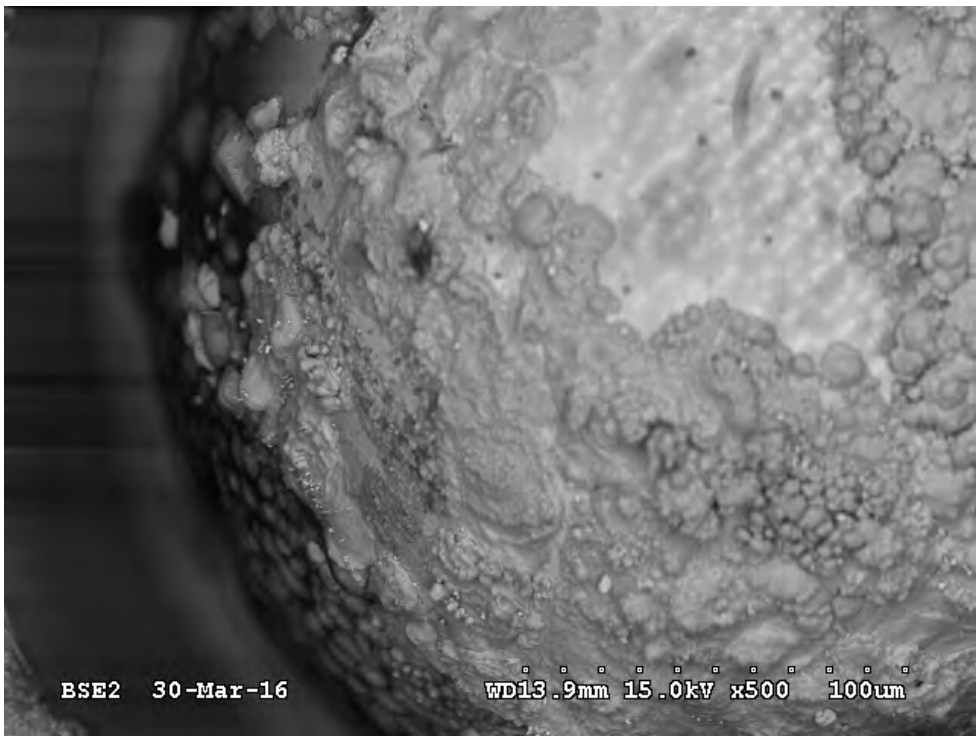


Figure 19: Board A377, BGA, U806, H6, 3030HTHH, 500x (PC18M dip processed during the PC18M spray run).

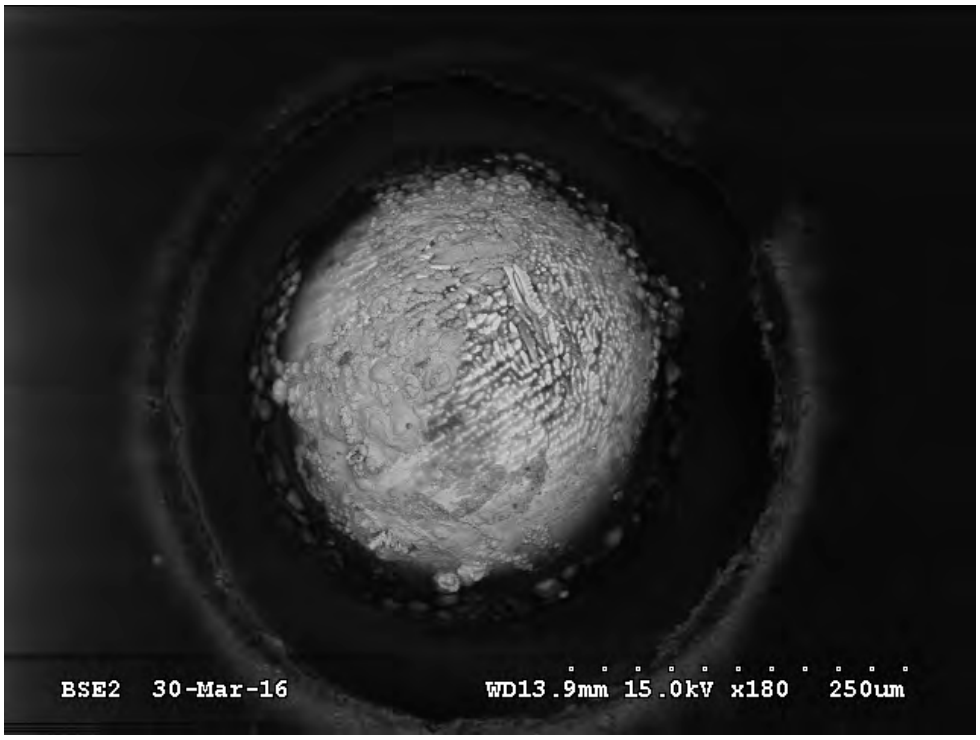


Figure 20: Board A377, BGA, U808, B3, 3030HTHH, 180x (PC18M dip processed during the PC18M spray run).



Figure 21: Board A377, BGA, U808, B3, 3030HTHH, 3,500x (PC18M dip processed during the PC18M spray run).



Figure 22: Board A377, BGA, U808, G2, 3030HTHH, 180x (PC18M dip processed during the PC18M spray run).

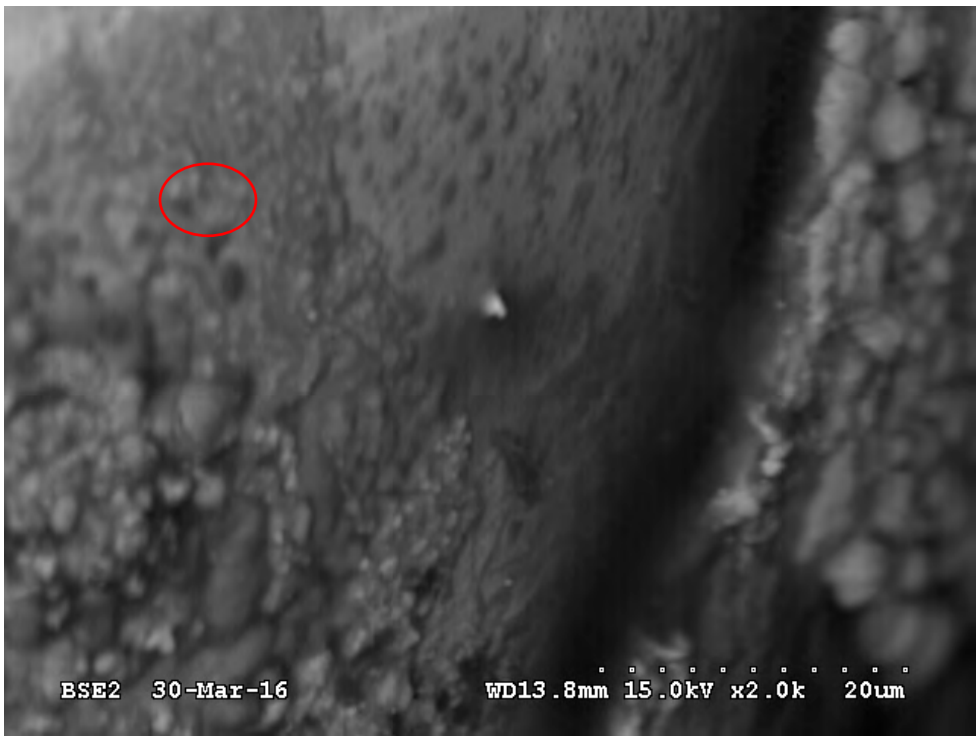
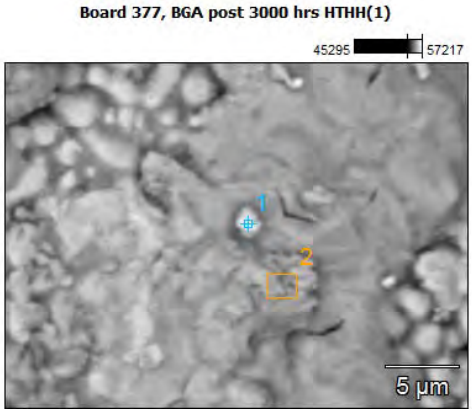
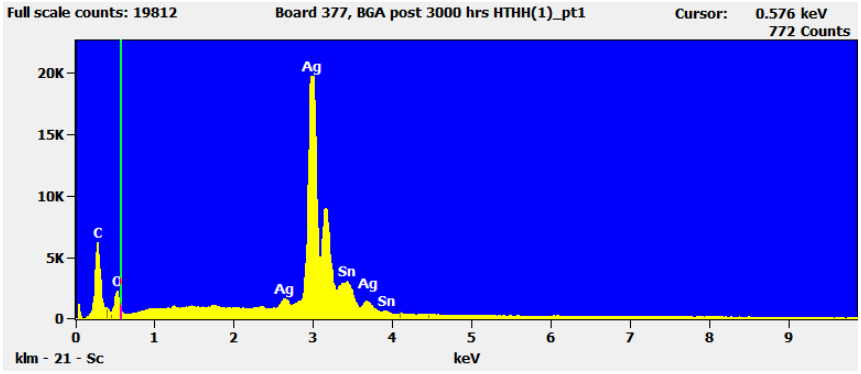
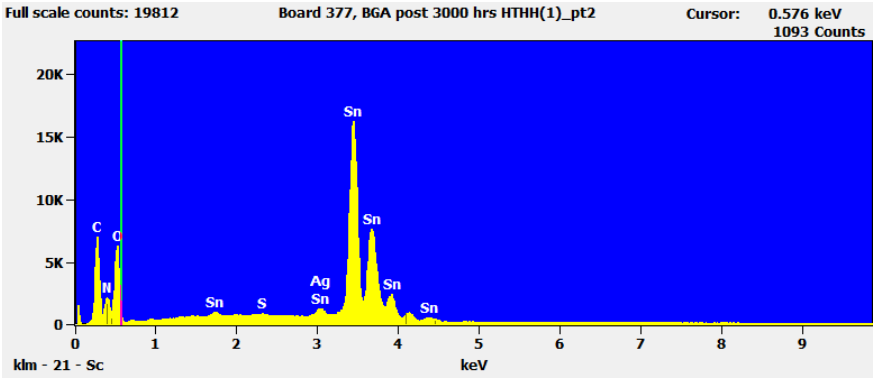


Figure 23: Board A377, BGA, U808, G2, 3030HTHH, 2,000x (PC18M dip processed during the PC18M spray run).







Weight %

	C	*N*	*O*	*S*	*Ag*	*Sn*
Board 377, BGA post 3000 hrs HTHH(1)_pt1	10.56		5.93		70.45	13.06
Board 377, BGA post 3000 hrs HTHH(1)_pt2	11.25	3.85	17.89	0.22	0.87	65.91

Atom %

	C	*N*	*O*	*S*	*Ag*	*Sn*
Board 377, BGA post 3000 hrs HTHH(1)_pt1	43.69		18.40		32.45	5.46
Board 377, BGA post 3000 hrs HTHH(1)_pt2	32.30	9.48	38.56	0.24	0.28	19.15

Figure 24: EDX analysis of Board A377, 3030HTHH, Area (1) (PC18M dip processed during the PC18M spray run)

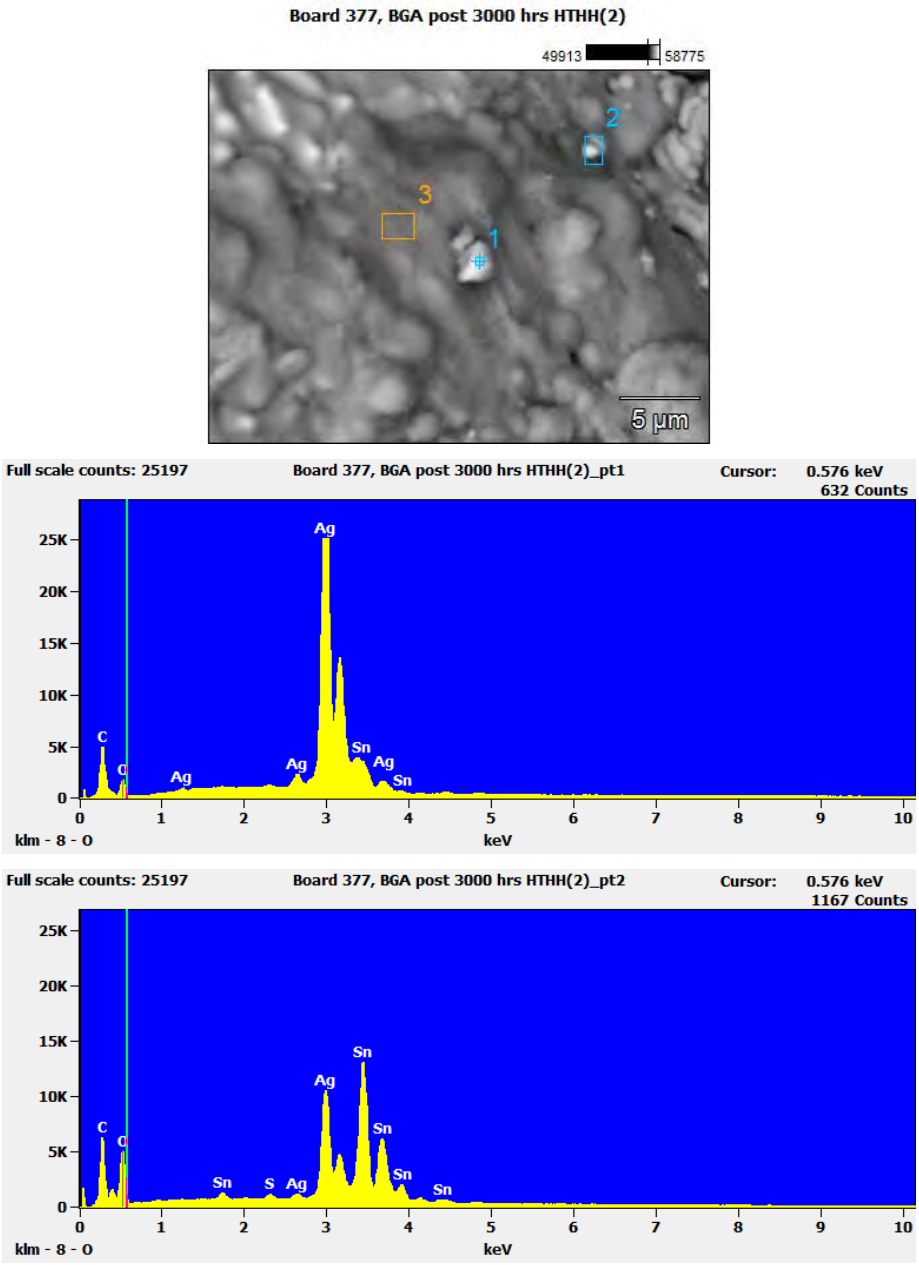
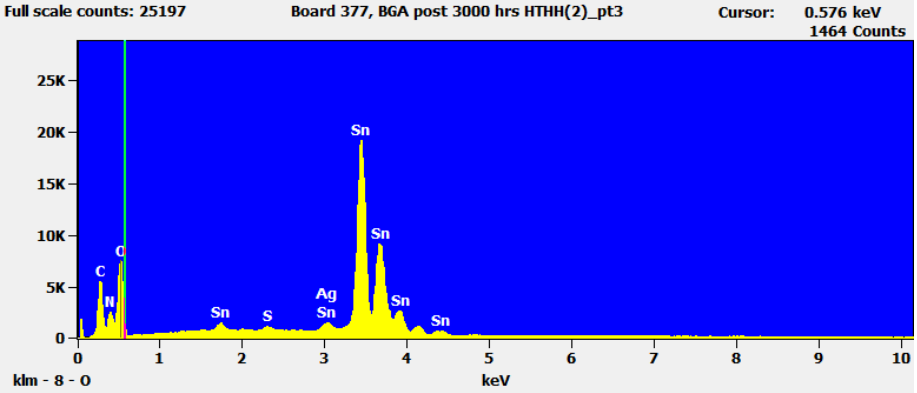


Figure 25: EDX analysis of Board A377, 3030HTHH, Area (2) (PC18M dip processed during the PC18M spray run).



Weight %

	C	N	O	S	Ag	Sn
Board 377, BGA post 3000 hrs HTHH(2)_pt1	8.80		6.75		74.11	10.33
Board 377, BGA post 3000 hrs HTHH(2)_pt2	12.49		18.20	0.42	24.22	44.67
Board 377, BGA post 3000 hrs HTHH(2)_pt3	11.48	7.39	26.76	0.37	0.94	53.07

Atom %

	C	N	O	S	Ag	Sn
Board 377, BGA post 3000 hrs HTHH(2)_pt1	38.00		21.87		35.62	4.51
Board 377, BGA post 3000 hrs HTHH(2)_pt2	37.24		40.76	0.47	8.04	13.48
Board 377, BGA post 3000 hrs HTHH(2)_pt3	26.37	14.56	46.17	0.32	0.24	12.34

Figure 26: EDX analysis of Board A377, 3030HTHH, Area (2) continued from Figure 25 (PC18M dip processed during the PC18M spray run).

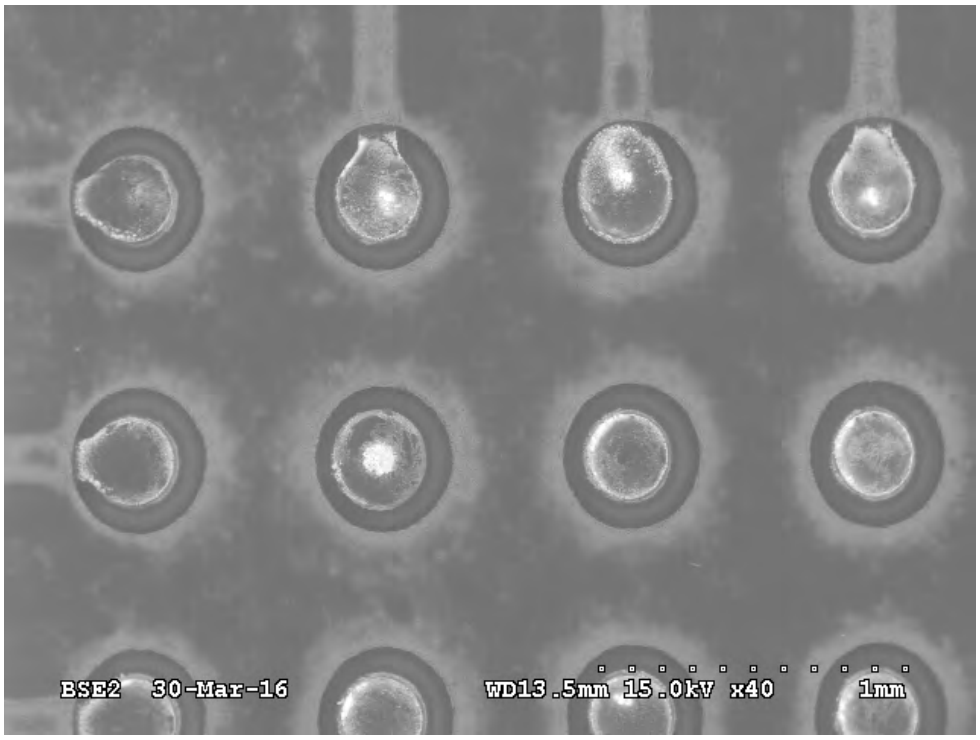


Figure 27: Board A596, BGA, U507, 3030HTHH, 40x (PC18M dip processed during the PC18M+20%XP2742 nanosilica spray run).

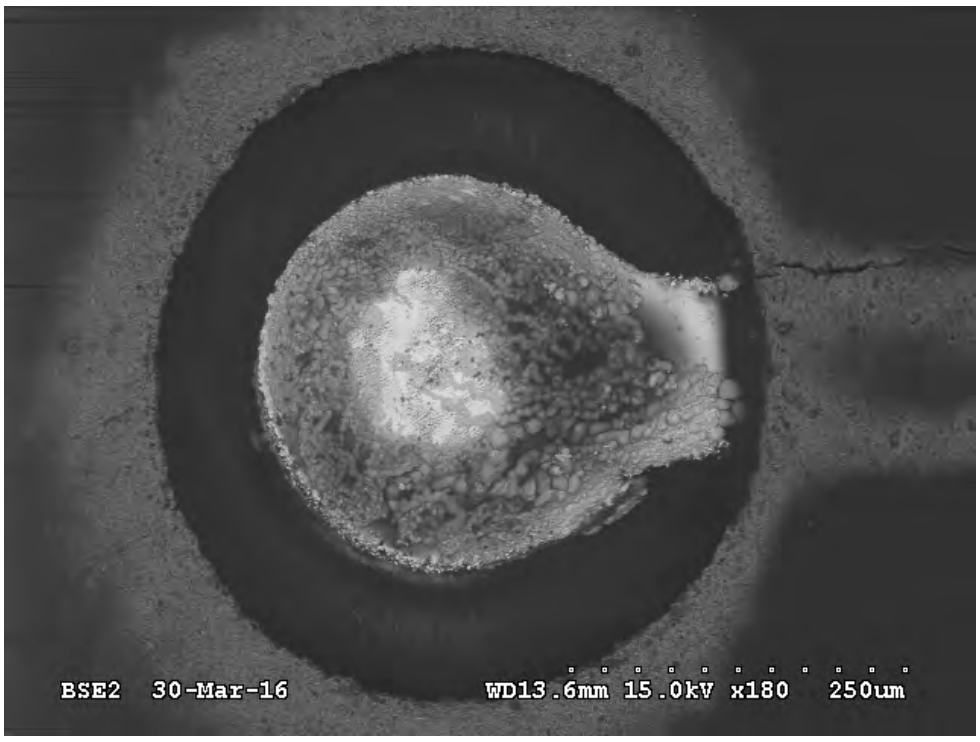


Figure 28: Board A596, BGA, U507, A10, 3030HTHH, 180x (PC18M dip processed during the PC18M+20%XP2742 nanosilica spray run).



Figure 29: Board A596, BGA, U507, A10, 3030HTHH, 3,500x (PC18M dip processed during the PC18M+20%XP2742 nanosilica spray run).

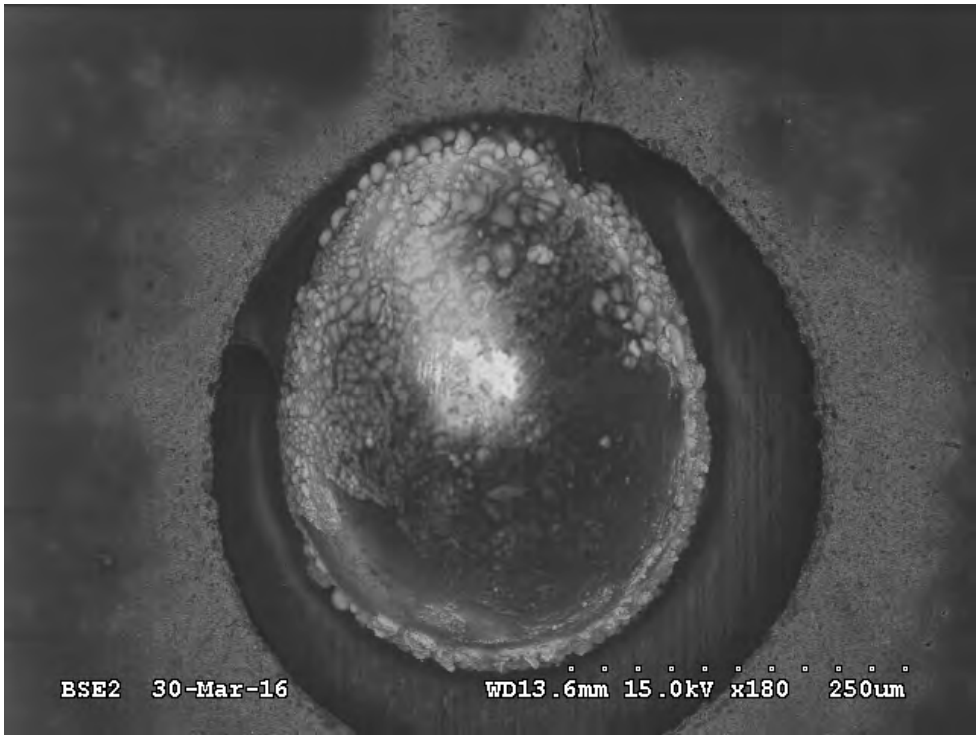


Figure 30: Board A596, BGA, U507, A3, 3030HTHH, 180x (PC18M dip processed during the PC18M+20%XP2742 nanosilica spray run).

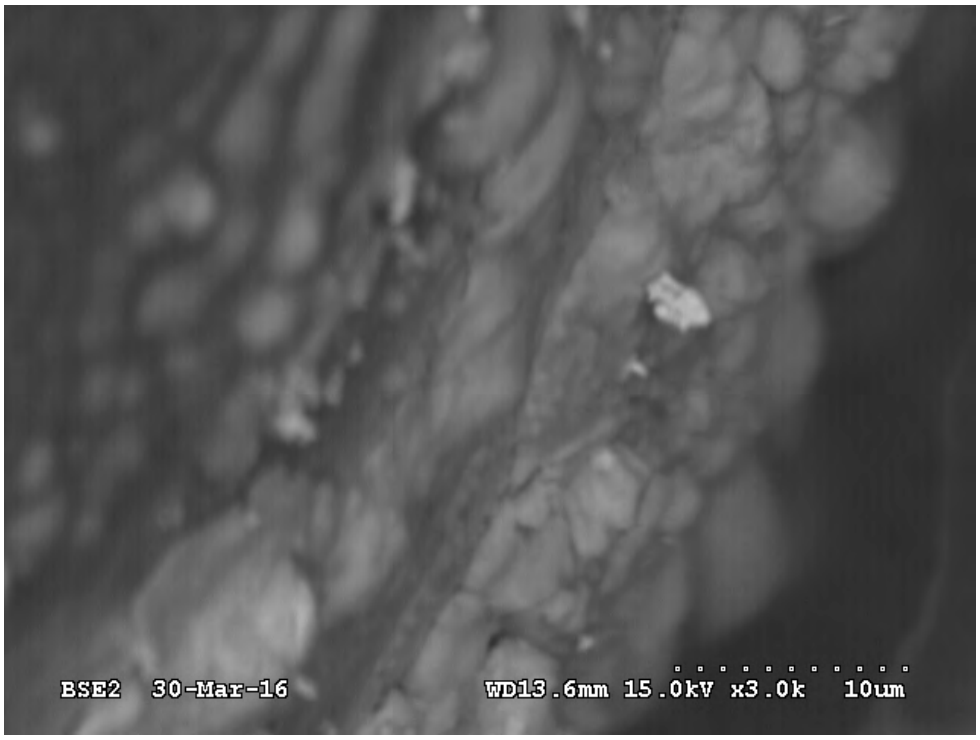


Figure 31: Board A596, BGA, U507, A3, 3030HTHH, 3,000x (PC18M dip processed during the PC18M+20%XP2742 nanosilica spray run).



Figure 32: Board A596, BGA, U508, E1, 3030HTHH, 2,500x (PC18M dip processed during the PC18M+20%XP2742 nanosilica spray run).

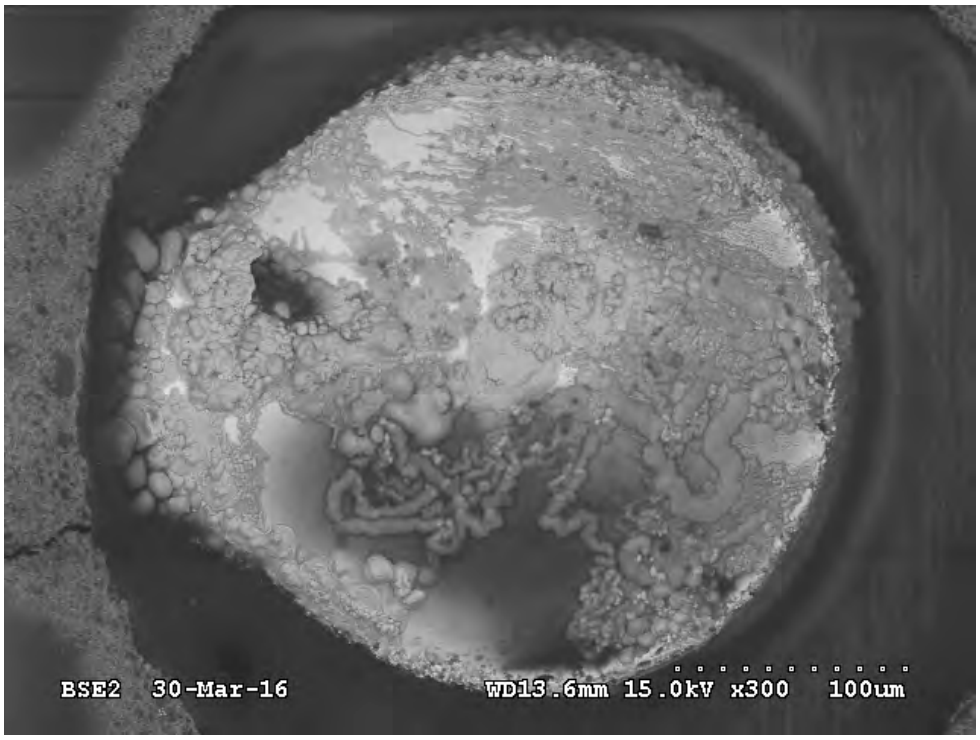


Figure 33: Board A596, BGA, U508, E1, 3030HTHH, 300x (PC18M dip processed during the PC18M+20%XP2742 nanosilica spray run).



Figure 34: Board A596, BGA, U508, F2, 3030HTHH, 180x (PC18M dip processed during the PC18M+20%XP2742 nanosilica spray run).

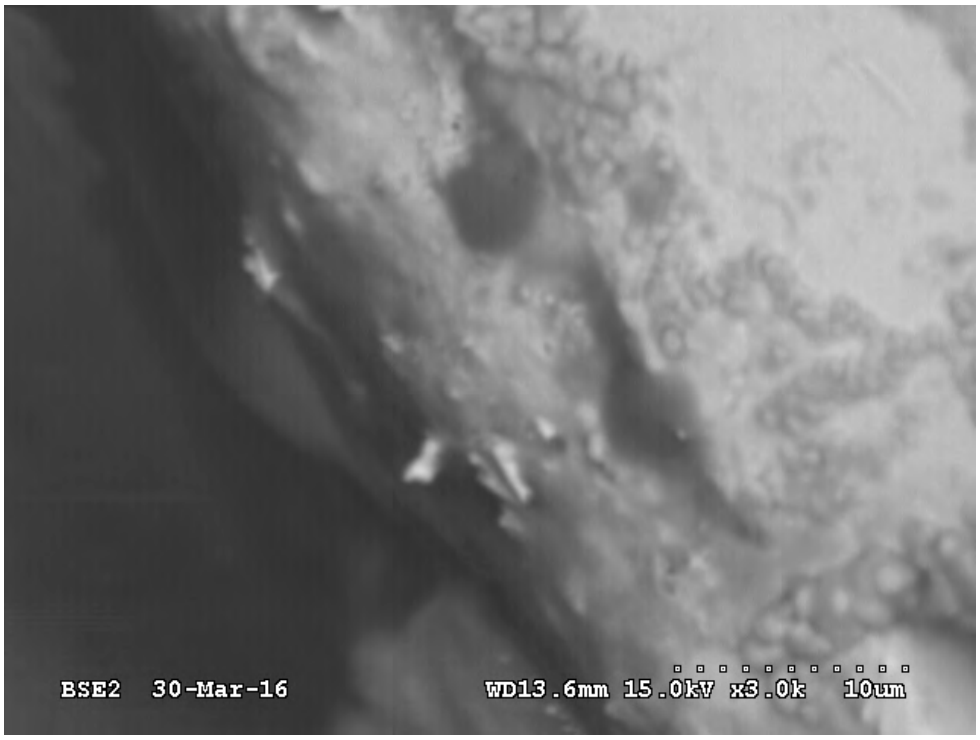


Figure 35: Board A596, BGA, U508, F2, 3030HTHH, 3,000x (PC18M dip processed during the PC18M+20%XP2742 nanosilica spray run).



Figure 36: Board A596, BGA, U508, G3, 3030HTHH, 180x (PC18M dip processed during the PC18M+20%XP2742 nanosilica spray run).

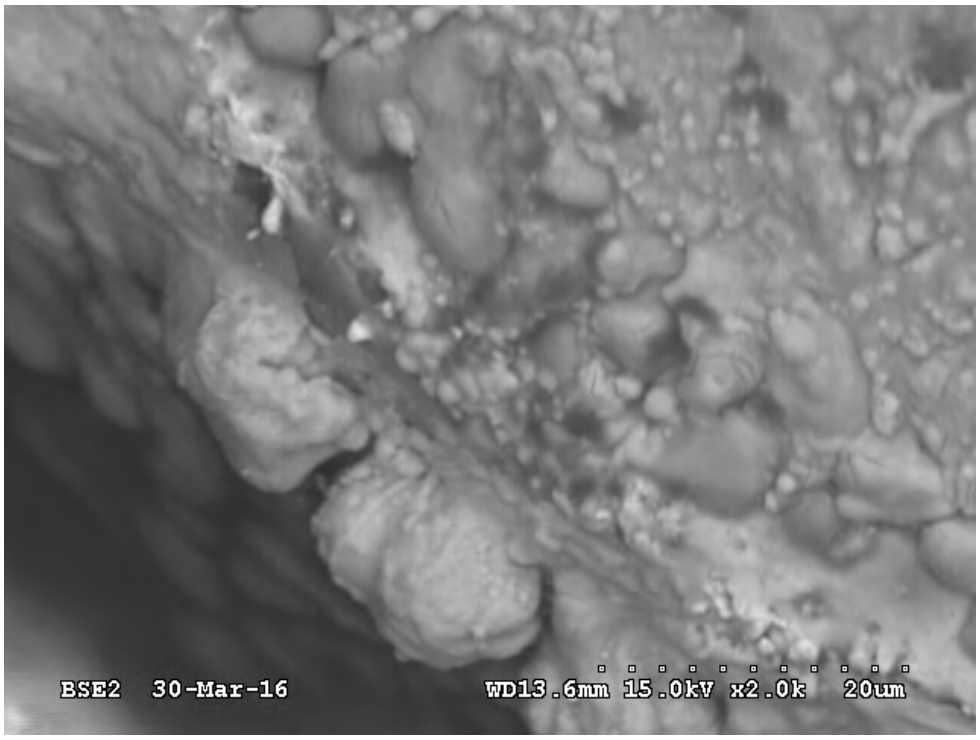


Figure 37: Board A596, BGA, U508, G3, 3030HTHH, 2,000x (PC18M dip processed during the PC18M+20%XP2742 nanosilica spray run).

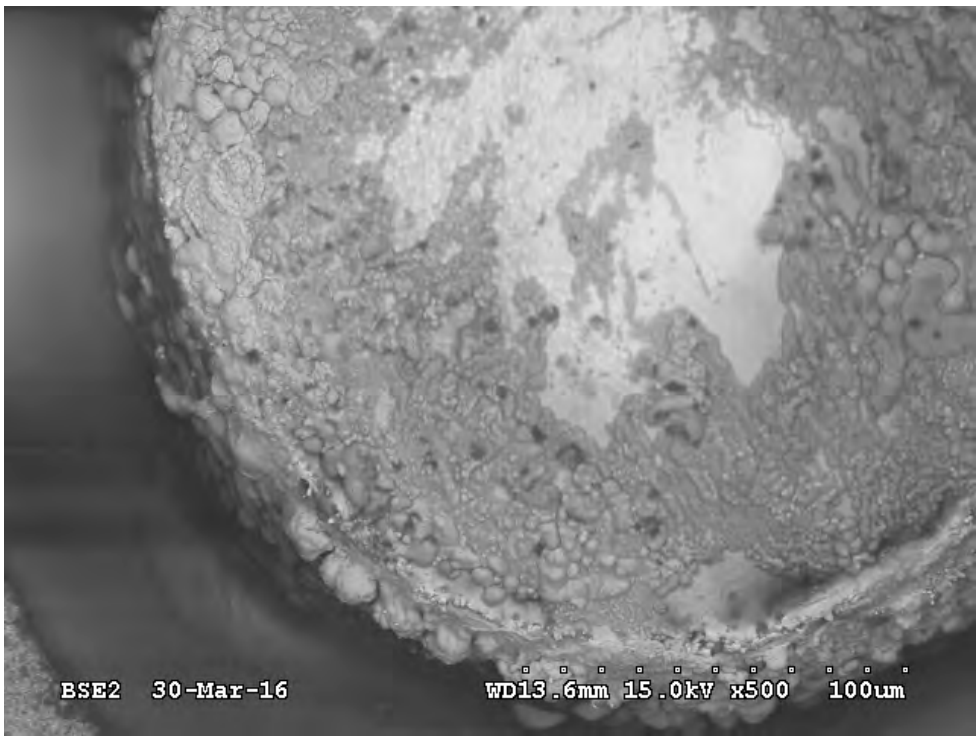


Figure 38: Board A596, BGA, U508, G3, 3030HTHH, 500x (PC18M dip processed during the PC18M+20%XP2742 nanosilica spray run).

2.2.2 BGA board layered unfilled PC18M spray

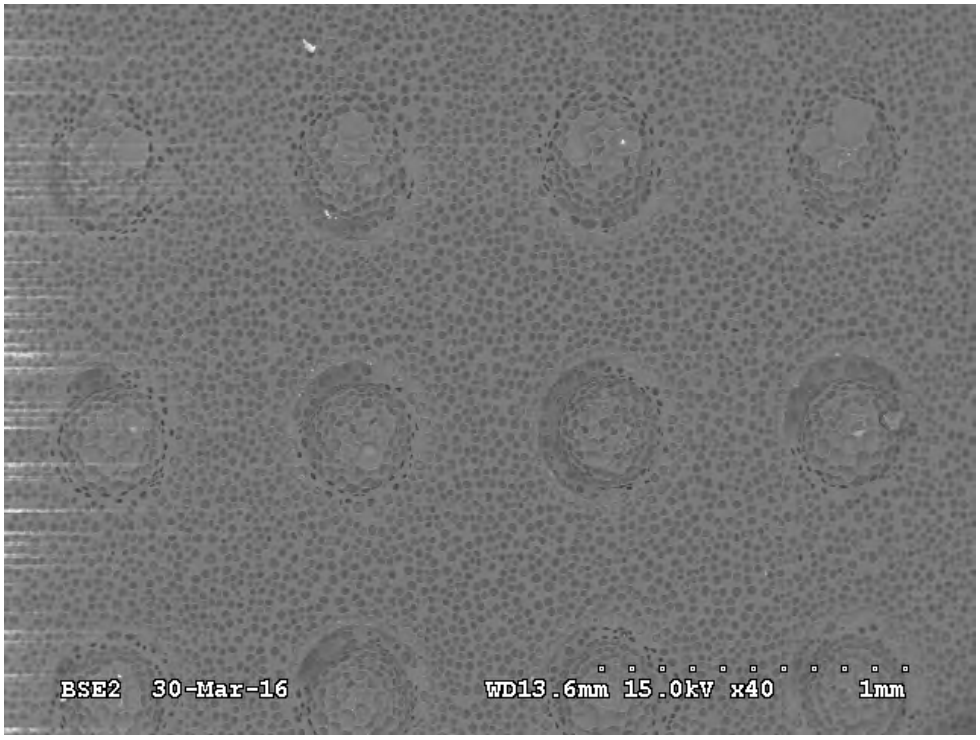


Figure 39: Board A307, BGA, U606, 3030HTHH, 40x (PC18M dip + 25 micron PC18M spray).



Figure 40: Board A307, BGA, U606, A2, 3030HTHH, 180x (PC18M dip + 25 micron PC18M spray).

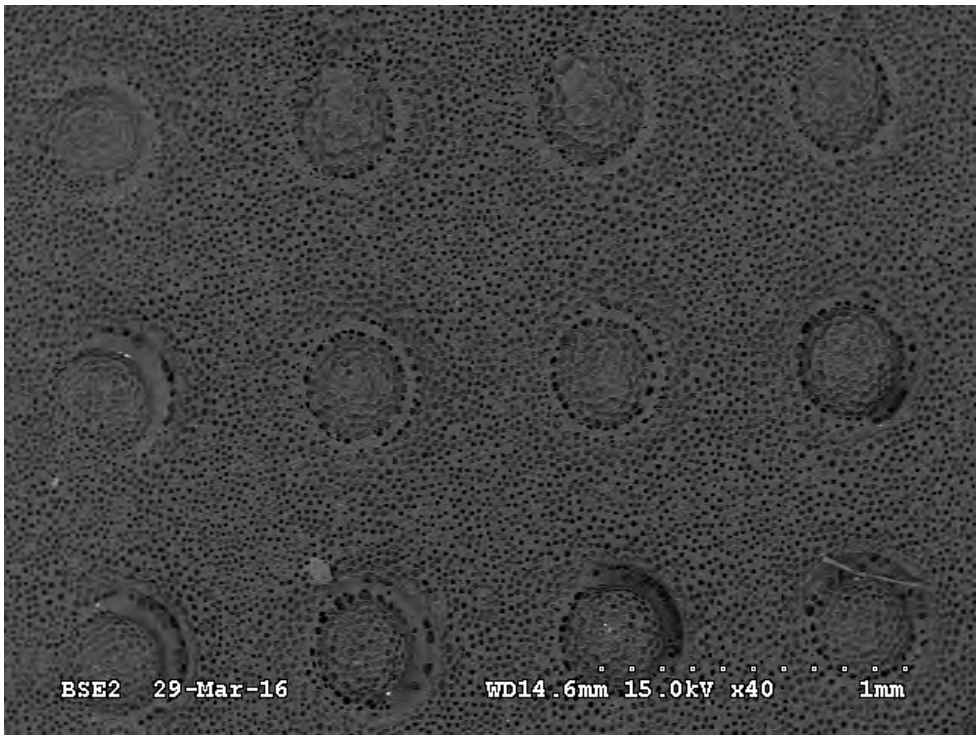


Figure 41: Board A296, BGA, U501, 3030HTHH, 40x (PC18M dip + two 25 micron PC18M sprays).

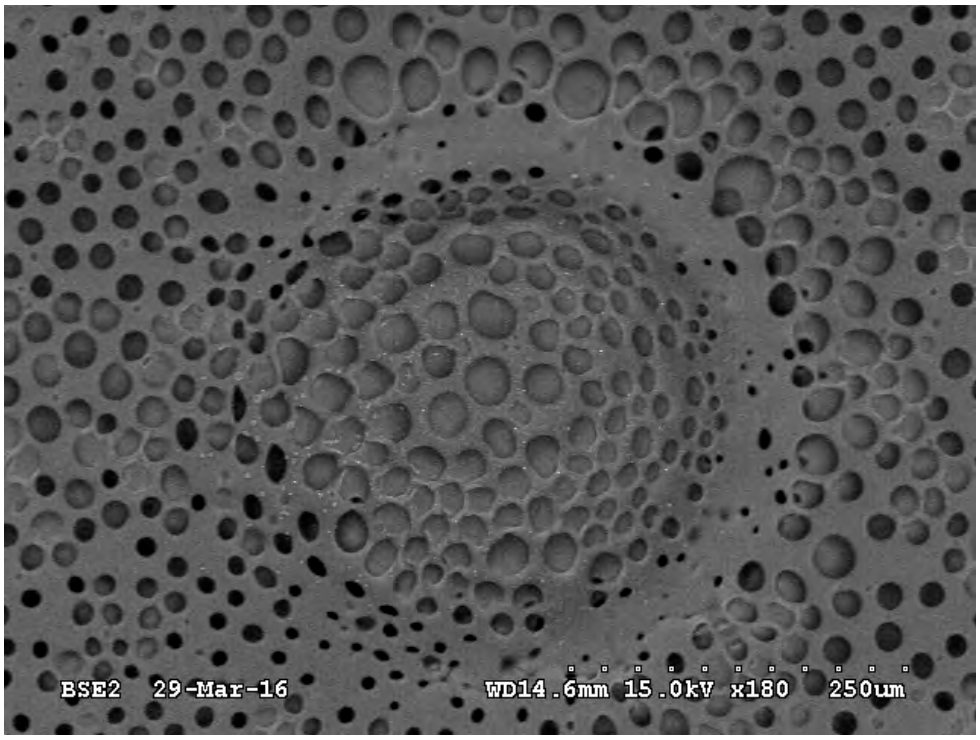


Figure 42: Board A296, BGA, U501, 3030HTHH, A1, 180x (PC18M dip + two 25 micron PC18M sprays).

2.2.3 BGA board layered PC18M+20%XP2742 nanosilica

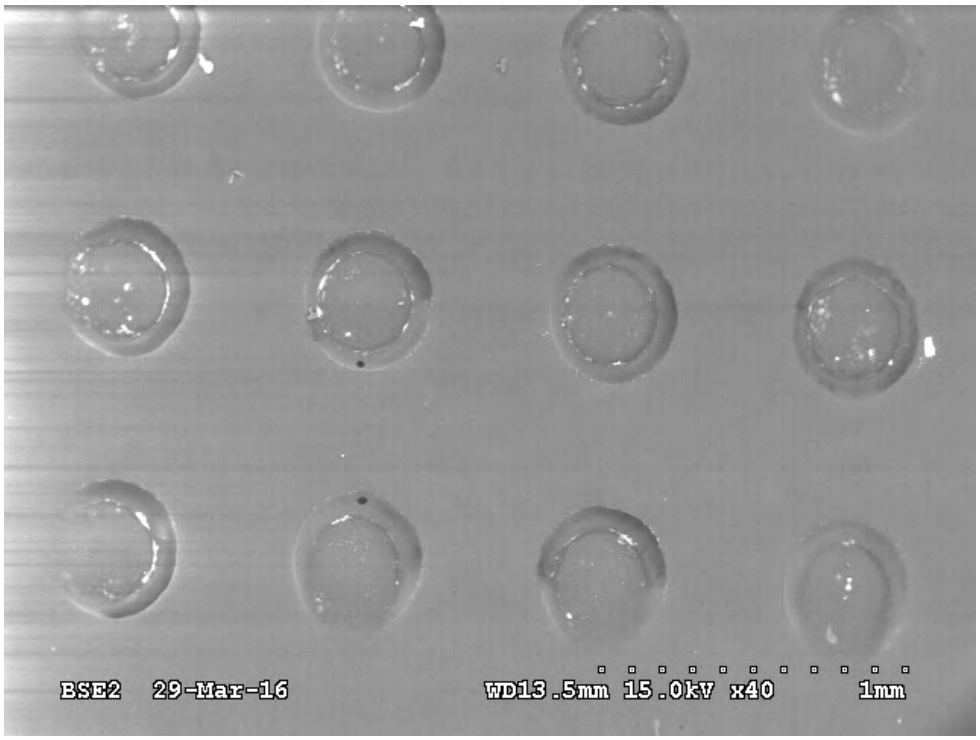


Figure 43: Board A593, BGA, U805, 3030HTHH, 40x (PC18M dip + 25 micron PC18M+20%XP2742 nanosilca spray).

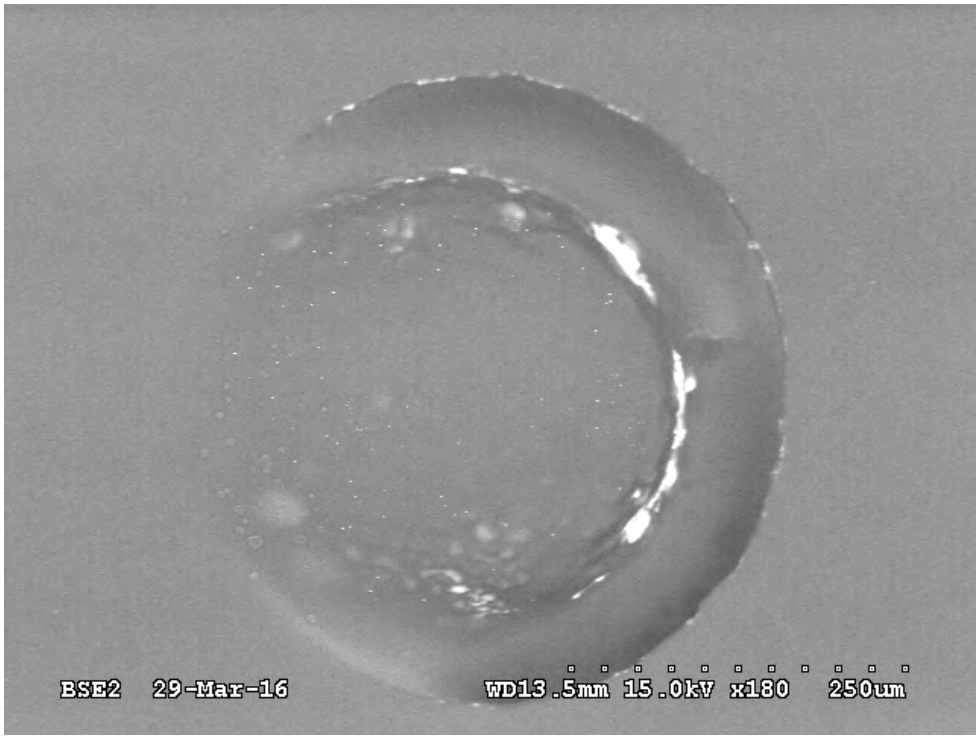


Figure 44: Board A593, BGA, U805, K1, 3030HTHH, 180x (PC18M dip + 25 micron PC18M+20%XP2742 nanosilca spray).

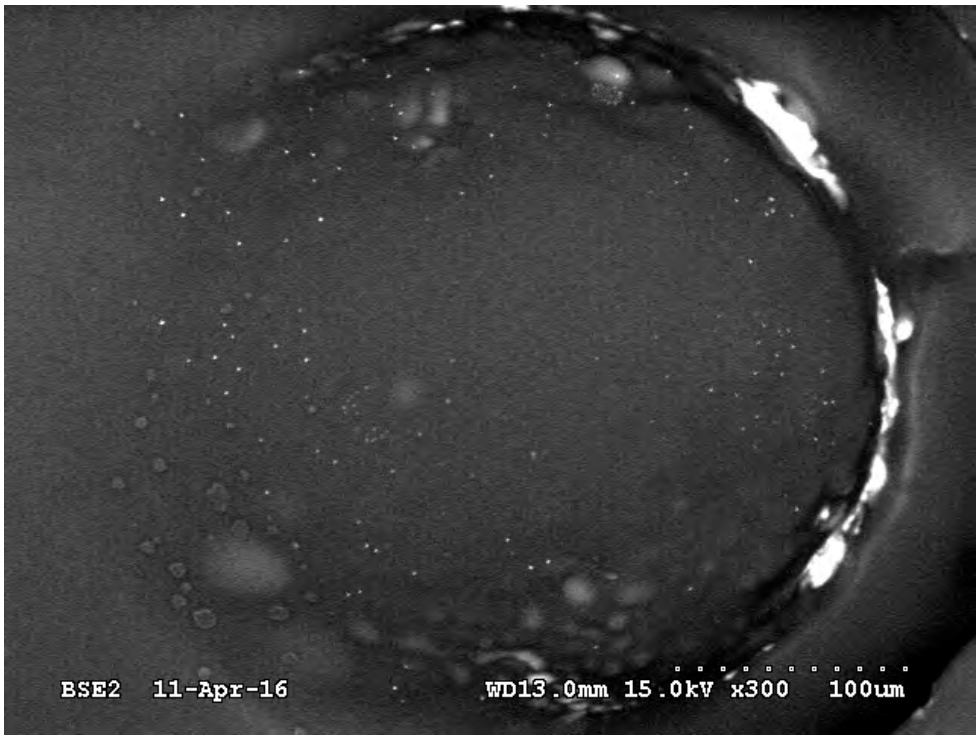


Figure 45: Board A593, BGA, U508, K1, 3030HTHH, 300x (PC18M dip + 25 micron PC18M+20%XP2742 nanosilca spray).

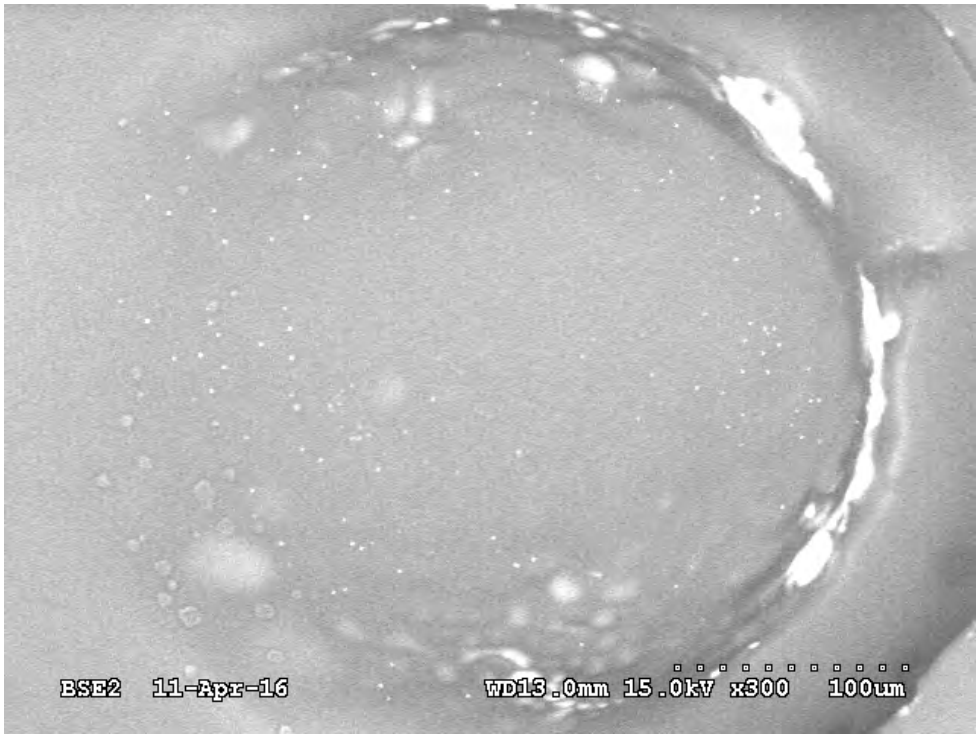


Figure 46: Board A593, BGA, U508, K1, 3030HTHH, 300x, lighter contrast (PC18M dip + 25 micron PC18M+20%XP2742 nanosilca spray).



Figure 47: Board A593, BGA, U508, K1, 3030HTHH, 2,500x (PC18M dip + 25 micron PC18M+20%XP2742 nanosilca spray).

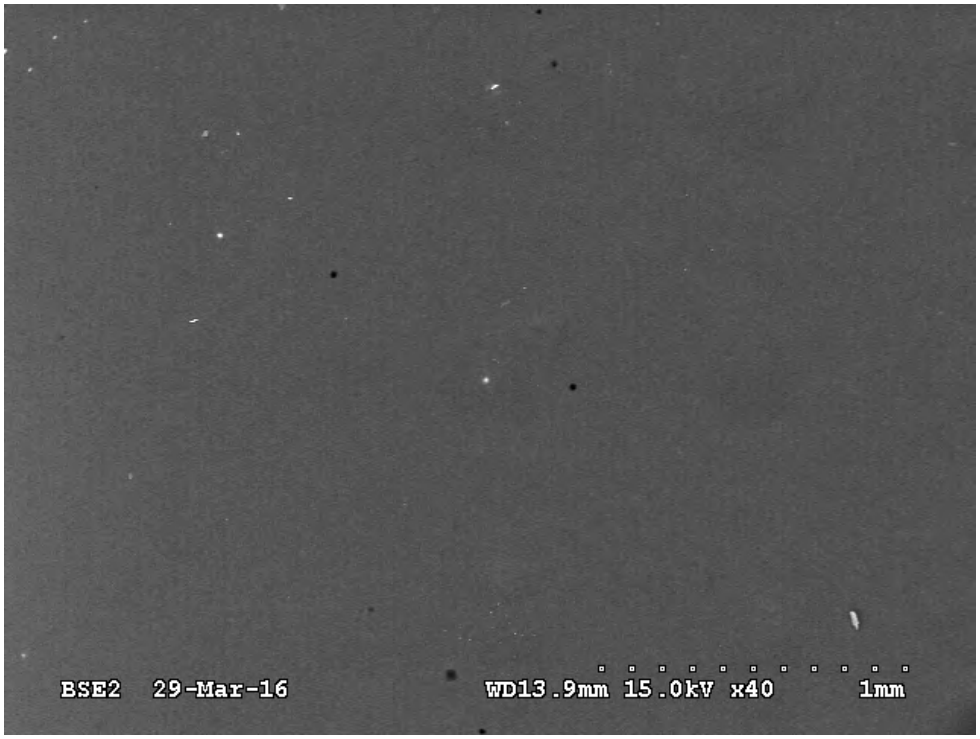


Figure 48: Board A392, BGA, U501, 3030HTHH, 40x (PC18M dip + two 25 micron PC18M+20%XP2742 nanosilca sprays).



Figure 49: Board A392, BGA, U501, 3030HTHH, 180x (PC18M dip + two 25 micron PC18M+20%XP2742 nanosilca sprays).

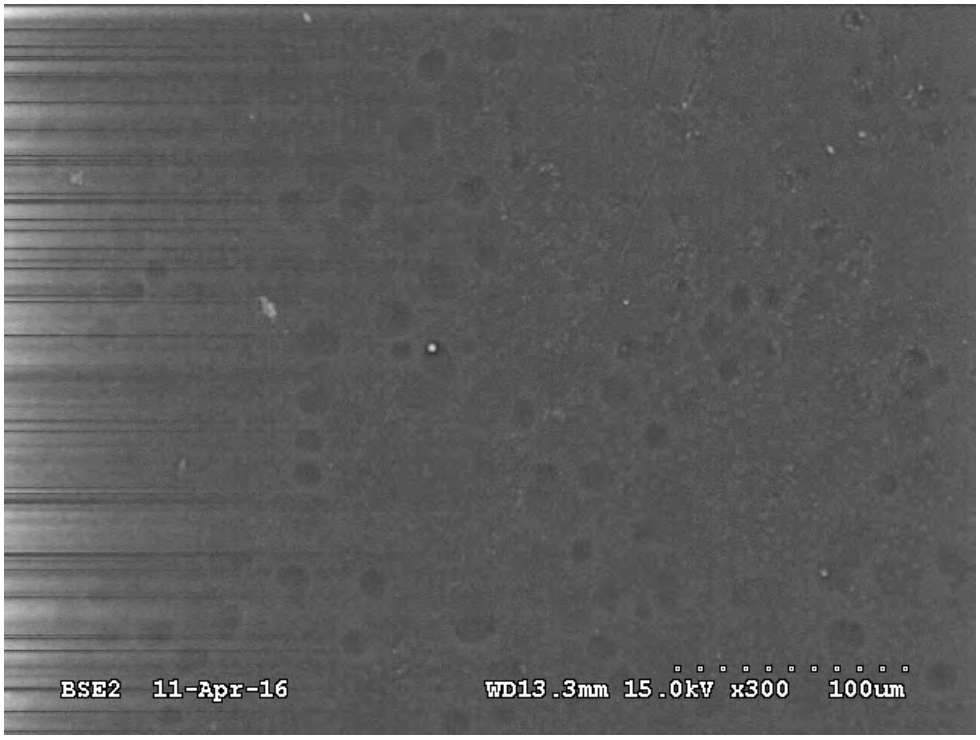


Figure 50: Board A392, BGA, U501, 3030HTHH, 300x (PC18M dip + two 25 micron PC18M+20%XP2742 nanosilca sprays).



Figure 51: Board A392, BGA, U501, 3030HTHH, 2,500x (PC18M dip + two 25 micron PC18M+20%XP2742 nanosilca sprays).

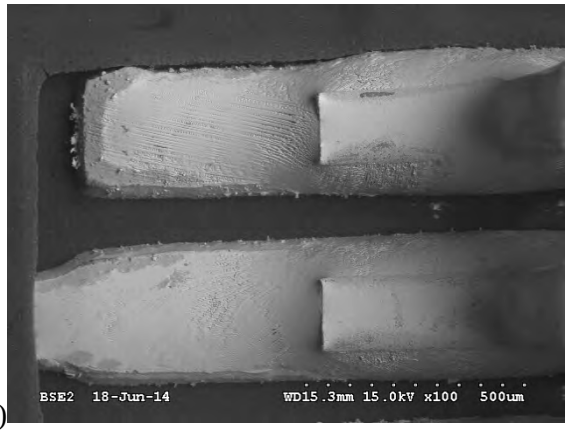
3. Layered coating assembly whisker test results summary

Layered coatings were applied in an effort to improve the coating coverage on corners, edges, behind leads and on vertical surfaces. The detailed materials and processes are given in prior appendices. Briefly, the layered coatings were formed through sequential dip or spray coating applications with partial cures between them. The base layer of both the unfilled and the nanosilica filled coatings is a low viscosity initial dip layer. Then additional layers are sprayed on using either unfilled PC18M or nanosilica filled PC18M+20%XP2742. The dip only boards were dipped then fully cured. The one spray layer coating sequence was: dip, partial cure, spray, and then full cure. The two spray layer coating sequence was: dip, partial cure, spray, partial cure, spray, and then full cure.

This appendix compares the whisker mitigation of layered unfilled and layered nanosilica filled coatings. The assemblies were exposed to an 85°C and 85 percent relative humidity (%RH) high temperature high humidity (HTHH) environment and examined after 3030 hours in the SEM. The inspection focused on the quad flat pack (QFP) because it contained part with the longest leads and the BGA boards because of the large number of solder bumps and the ease of inspection. A summary of the inspection is given next. The detailed inspection images are provided in Section 2.

3.1 QFP Board summary

During the baseline whisker testing [1] [2], uncoated SAC305 soldered QFPs were exposed to high temperature humidity. These boards exhibited corrosion and whisker growths after 2,000 hours of 85C/85%RH (Figure 52). In contrast to the uncoated boards, no corrosion or whisker growth was observed on the layer coated QFP44s assemblies using either the unfilled PC18M or the nanosilica filled PC18M+20%XP2742 (Figure 53). The presence of a rough coating surface and surface bubbles did not appear to impact whisker growth propagation to the surface.

(A) 

(B) 

Figure 52: Uncoated board 48 QFP64 after 2,000h of HTHH; (A) 100x and (B) 1,500x.

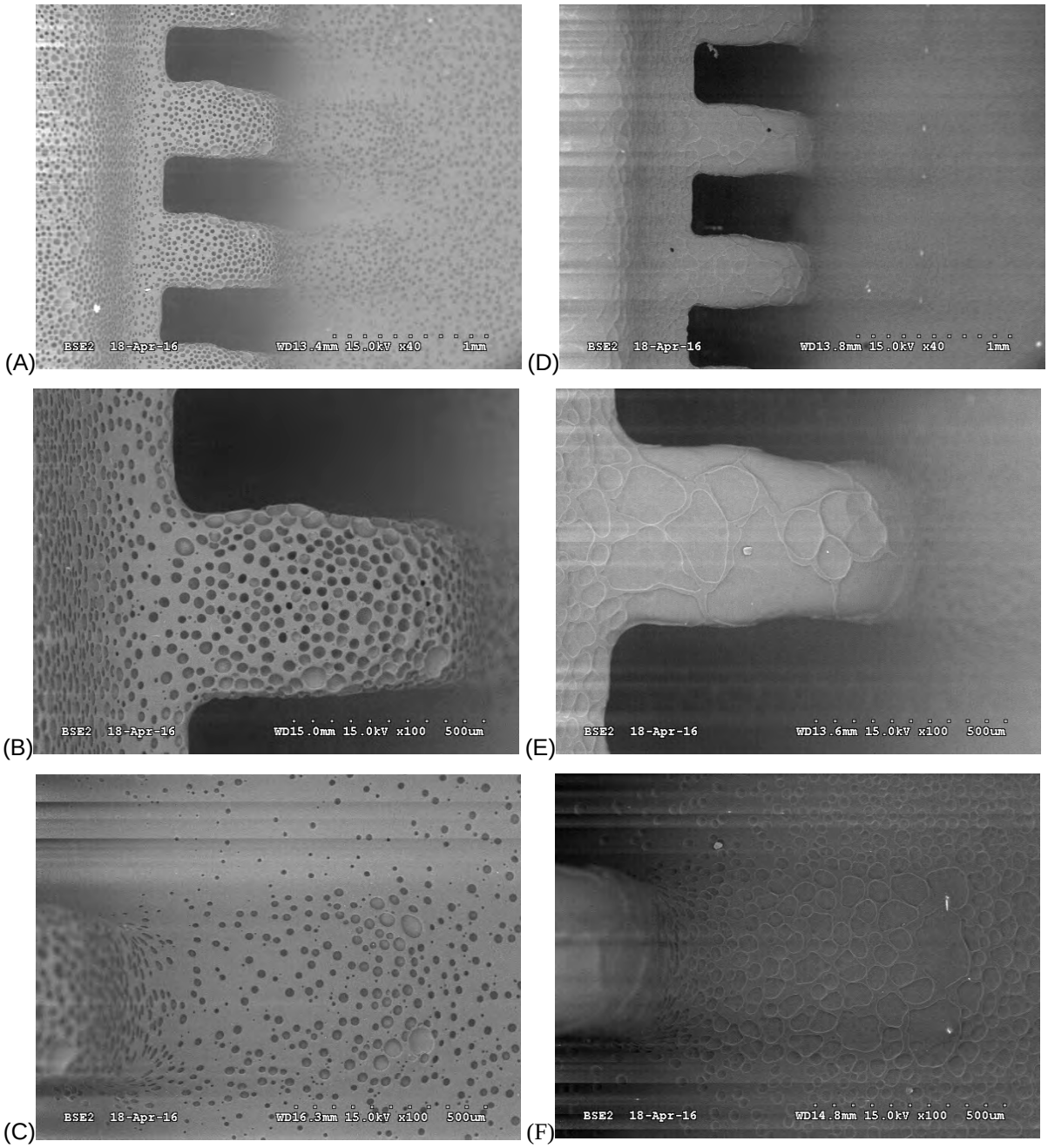


Figure 53: SEM images comparing layer coated unfilled PC18M spray and PC18M+20%XP2742 nanosilica filled sprays in the dip + 2 spray QFP44 parts after HTHH testing for 3,030h.

Extended Figure 53 caption: Images (A) (B) (C) are of unfilled PC18M dip + two unfilled PC18M sprays (board A023) and images (D) (E) (F) are of unfilled PC18M dip + two (PC18M+20%XP2742) nanosilica filled sprays (board A347). Image magnifications are: (A) (D) overall lead at 40x, (B) (E) lead top at 100x, and (C) (D) lead bottom at 100x.

3.2 BGA board summary

The BGA pads on this board were printed with a SAC305 solder paste and refllowed to form a small solder dome which caused thin coating areas when fewer layers were applied. The dip coat alone had the thinnest coating coverage. The dip/partial cure/spray layer combination increased the coating thickness, but there were still thin regions. The dip/partial cure/spray/partial cure/spray further increased the coating thickness. By increasing the number of layers a decrease in corrosion and whisker growth were observed (Figure 54). The PC18M "dip only" boards resulted in less than approximately three microns of coating on the BGA solder domes and exhibited extensive corrosion and whisker growth. In contrast, the PC18M dip + two sprays of either unfilled PC18M or (PC18M+20%XP2742 nanosilica filled) material had no corrosion or whisker growth (Figure 55).

In some instances, Ag_3Sn intermetallic nodules were observed because the surrounding tin had corroded away; reinforcing the importance of EDX verification when counting tin whiskers/nodules (Figure 56).

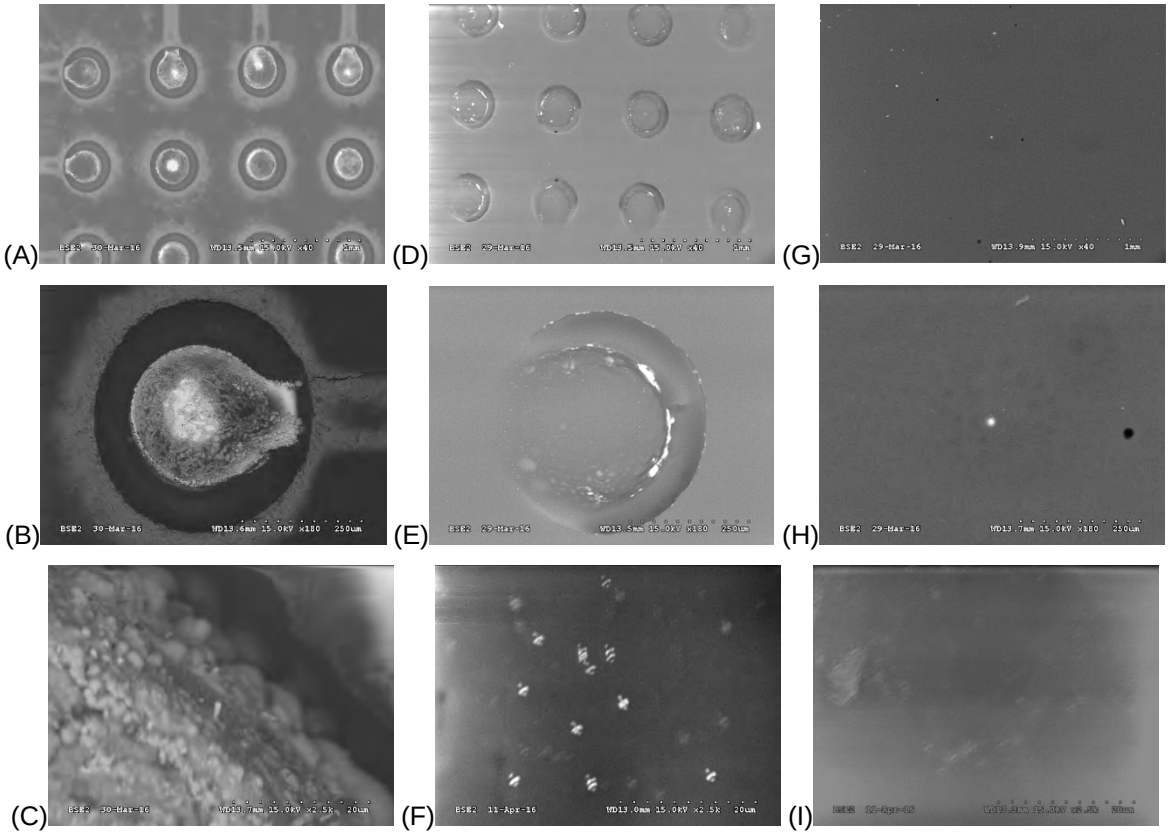


Figure 54: SEM images of PC18M+20%XP2742 nanosilica spray layered coated BGA pads with increasing number of layers at various magnifications after HTHH testing for 3,030h.(A) (B) (C) dip, (D) (E) (F) dip + one spray, and (G) (H) (I) dip + two sprays with (A) (D) (G) 40x, (B) (E) (H) 180x and (C) (F) (I) 2,500x.

Extended Figure 54 caption: (A) (B) (C) unfilled PC18M dip (board A596); (D) (E) (F) PC18M dip + one (PC18M+20%XP2742) nanosilica filled spray (board A593); (G) (H) (I) PC18M dip + two (PC18M+20%XP2742) nanosilica filled sprays (board A392). Note that the image (H) bright spot is debris and the dark spot is a hole.

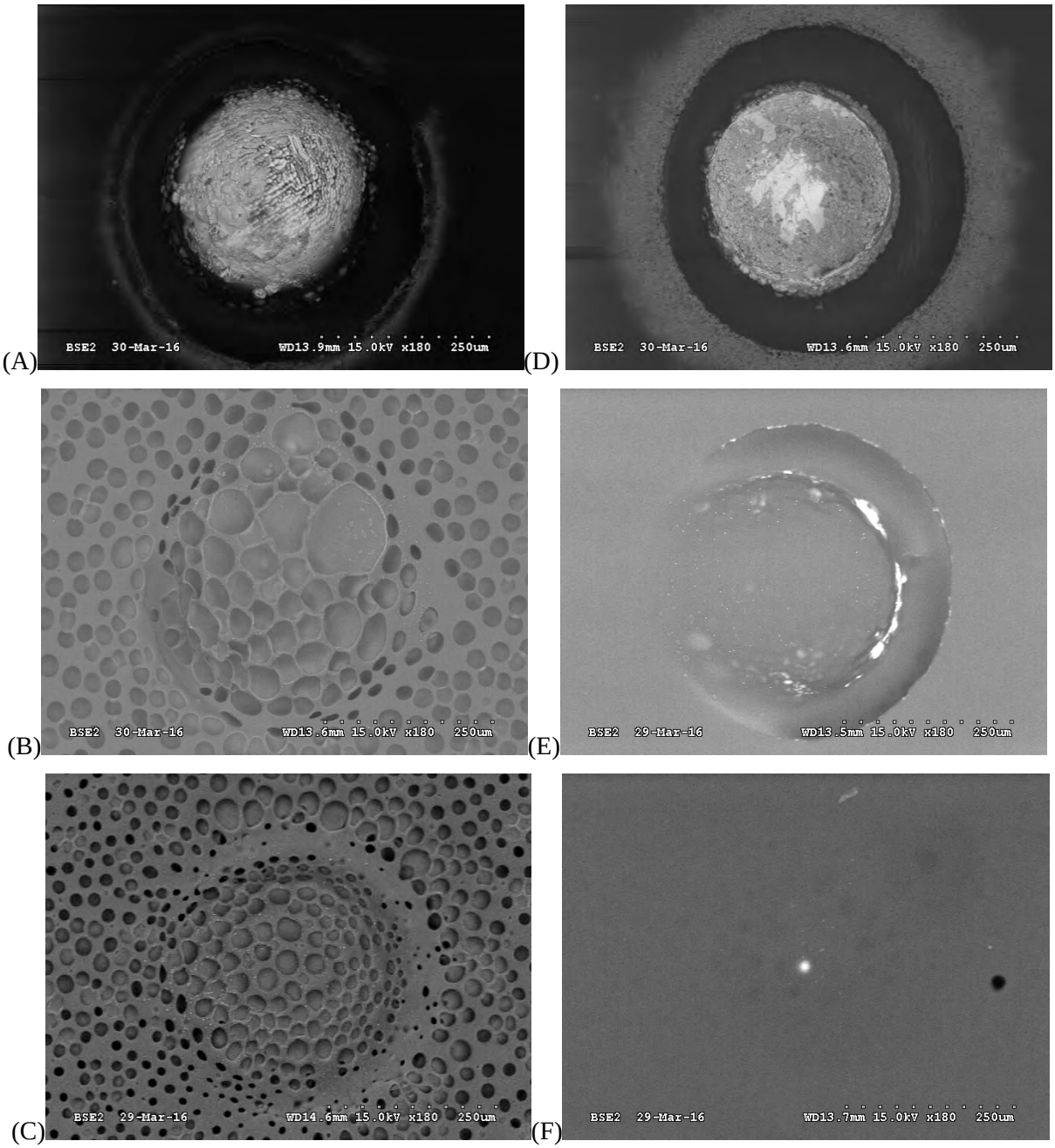


Figure 55: SEM images of layered coated BGA pads with increasing number of layers for unfilled PC18M sprays and PC18M+20%XP2742 nanosilica filled sprays after HTHH testing for 3,030h, 180x. (A) (B) (C) unfilled spray run and (D) (E) (F) nanosilica filled spray run with (A) (D) dip, (B) (E) dip+one spray, and (C) (D) dip + two sprays.

Extended Figure 55 caption: (A) unfilled PC18M dip processed with unfilled PC18M spray run (U808, B3, Board A377), (B) unfilled PC18M dip + two unfilled PC18M spray (U606, A2, Board A307), (C) unfilled PC18M dip + two unfilled PC18M sprays. (U501, A1, Board A296), (D) unfilled PC18M dip processed with the PC18M+20%XP2742 nanosilica filled spray run (U508, G3, Board A596), (E) unfilled PC18M dip + one (PC18M+20%XP2742) nanosilica filled spray (U805, K1, Board A593), and (F) unfilled PC18M dip + two (PC18M+20%XP2742) nanosilica filled sprays (U501, A1, Board A392). Note that the image (H) bright spot is debris and the dark spot is a hole.

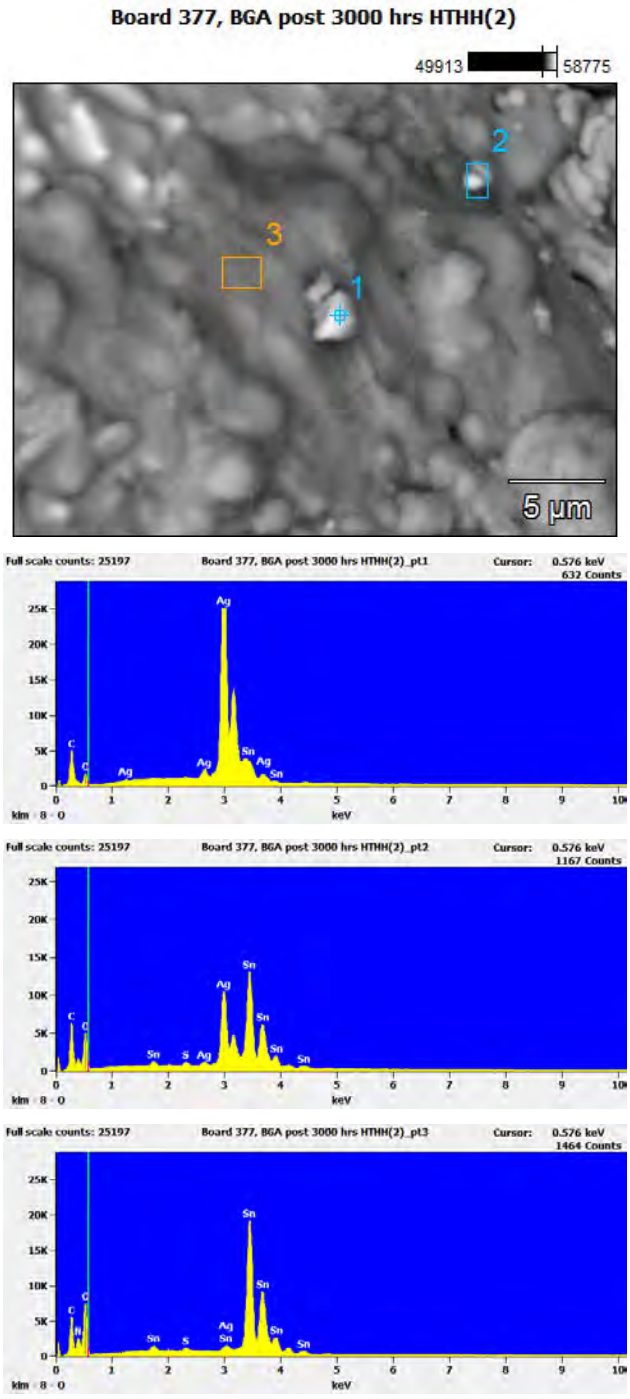


Figure 56: SEM image and electrodispersive x-ray (EDX) analysis of some nodules found on BGA pads from board A377, PC18M dip only. Note that the nodules in locations one and two are Ag_3Sn intermetallic with the surrounding Sn corroded away.

4. Discussion

No whisker growth or corrosion was observed where there was at least one layer of spray coating over the dip. Only the dip coated PC18M samples exhibited whisker growth or corrosion (Figure 54C). The successive layer thickness build-up from the dip/partial cure, to the first spray/partial cure, then the second spray/partial cure resulted in progressively better coverage [3]. As the coverage improved, there were fewer areas where the SEM beam could examine the tin though the coating (e.g. the coating was less than approximately three microns). The presence of a rough coating surface and surface bubbles, previously discussed [3], did not appear to negatively impact whisker mitigation effectiveness.

Even one additional spray layer significantly improved the coverage and the whisker/corrosion resistance. For example, the PC18M dip + one spray of PC18M+20%XP2742 nanosilica significantly improved the performance of the BGA pads. The PC18M dip + one spray of PC18M+20%XP2742 nanosilica only had a few areas of thin coating along the BGA PWB pad edge and a few solder tin dendrite tips (Figure 54 E and F).

On the QFP parts with the dip + 2 spray layer coating, only the lead tips had thin coating when examined with the SEM (Figure 53) and the BGA pads were fully covered (Figure 54 H and I). No whisker growth or corrosion was observed on the QFP lead tips.

5. Conclusions

The layered coating method provided good coverage. Increasing the number of layers, decreased the thin coating sites. No whisker growth or corrosion was observed on any of the dip + one or two spray layered assemblies regardless as to whether an unfilled PC18M spray or a filled PC18M+20%XP2742 nanoparticle spray was used.

6. Literature cited

[1] Appendix F of the current report: Coating coverage baseline results

[2] S. Meschter, J. Cho, S. Maganty, D. Starkey, M. Gomez, D. Edwards, A. Ekin, K. Elsken, J. Keeping, P. Snugovsky, Eva Kosiba, Zohreh Bagheri, and J. Kennedy, Strategic Environmental Research and Development Program (SERDP) Nanoparticle Enhanced Conformal Coating for Whisker Mitigation, Proceedings of SMTA International, Rosemont, IL, September 28-October 2, 2014.

[3] Appendix I of the current report: Coating coverage layered coating results

SERDP WP2213
Final Report
Appendix L: Rework evaluation

Appendix L: Table of Contents

1. Introduction 1

2. Coating removal method development 1

2.1 Assembly boards 1

2.2 Coating removal methods 2

2.2.1 Chemical removal process 2

2.2.2 Media blasting removal process 3

2.2.3 Thermal removal process 3

2.3 Celestica coating rework and replacement screening experiment 3

2.3.1 Coating removal testing 3

2.3.2 Coating re-application process 9

2.3.3 Coating removal conclusions 10

3. Assembly rework evaluation 11

3.1 Equipment and materials 11

3.1.1 Assembly boards 11

3.1.2 Coating materials 12

3.2 Celestica rework process for multilayer coatings 13

3.2.1 QFP44 Removal 13

3.2.2 QFP44 Recoating 13

3.2.3 Flat board rework 14

3.3 Environmental exposure and adhesion testing 14

3.3.1 Thermal cycling 14

3.3.2 Humidity 16

3.3.3 Inspection after environmental exposure 17

3.3.4 Rework coating thickness 28

3.3.5 Adhesion tape testing 31

3.3.6 Adhesion results 32

4. Detailed photographs and images 33

4.1 Photos prior to thermal cycling and humidity 33

4.2 Photos after environmental exposure 39

4.2.1 Optical images of unfilled PC18M 39

4.2.2 Optical images of filled PC18M+20%XP2742 45

4.3 SEM examination after environmental exposure 51

4.3.1 SEM of unfilled PC18M QFP-A023 rework 52

4.3.2 SEM of filled PC18M+20%XP2724 rework 57
4.4 Rework cross-sections 62
4.4.1 Cross-sections of unfilled PC18M QFP-A023 63
4.4.2 Cross-sections of filled PC18M+20%XP2742 QFP-A312 98
5. Rework summary 145
6. Rework conclusion 145
7. Literature cited 146

Appendix L: List of Figures

Figure 1: Assembled and coated boards after environmental exposure. 2

Figure 2: Areas reworked on boards 16 and 17. Red box shows parts removed and replaced after coating removal and the blue box shows parts where only the coating was removed. 4

Figure 3: Board 16, U1201, after coating removal, 7.5x. 5

Figure 4: Board 16, U1201, after coating removal, 25x angled image. Coating residue from thermal removal is at the top of leads. 5

Figure 5: Board 16, U1201, after coating removal, 15x angled image. Coating residue from thermal removal is at the top of leads. 5

Figure 6: Board 16, U1204, after coating removal, 7.5x. 6

Figure 7: Board 16, U1204, after coating removal, 25x angled image. A small amount of discolored residue after solvent removal is at the top of leads. 6

Figure 8: Board 16, U1205, after coating removal, 7.5x. 6

Figure 9: Board 16, U1205, after coating removal, 25x angled image. 7

Figure 10: Board 17, U1101, after coating removal, 7.5x. 7

Figure 11: Board 17, U1101, after coating removal, 7.5x angled image. 7

Figure 12: Board 17, U1101, after coating removal, 25x angled image. 8

Figure 13: Board 17, U1104, after coating removal, 7.5x. 8

Figure 14: Board 17, U1104, after coating removal, 25x angled image. 8

Figure 15: Board 17, U1105, after coating removal, overview, 7.5x 9

Figure 16: Board 17, U1105, after coating removal, 25x angled image. 9

Figure 17: Images of PC18M dipped and PC18M+20%XP2742 coated. 10

Figure 18: Images of PC18M+20%XP2742 with no pre – dip. 10

Figure 19: Sample placement in thermal cycling chamber. 15

Figure 20: Typical board temperature during thermal cycling. 15

Figure 21: Sample placement in humidity chamber. 16

Figure 22: Humidity cycling chart. 17

Figure 23: Optical image, board QFP-A034 unfilled PC18M after thermal cycling (A) overall part, (B) close-up of leads, and (C) isometric close-up of leads. 17

Figure 24: Optical image, board A312 filled PC18M-20%XP2742 after thermal cycling and humidity; (A) overall part and (B) close-up of leads. 18

Figure 25: SEM BSE unfilled PC18M QFP-A023 U1002 pins 44 to 40, 70x. 18

Figure 26: SEM BSE filled PC18M+20%XP2742 QFP-A312 U902 pins 23 to 26, 70X. 19

Figure 27: SEM BSE filled PC18M+20%XP2742 QFP-A312 non-reworked U903 adjacent to U902 pins 23 to 26, 67x. 19

Figure 28: SEM BSE filled PC18M+20%XP2742 QFP-A312 U902 pins 8 to 11, 70x. 20

Figure 29: Cross-section plane locations of unfilled PC18M coated QFP-A023. The cross-sections go through the right side of U1001 (not reworked) and both sides of U1002 (reworked). 21

Figure 30: Cross-section plane locations for PC18M+20%XP2742 coated QFP-A312. The cross-section planes go through the right side of U901 (non-reworked) and both sides of U902 (reworked). 21

Figure 31: Nomenclature used to define locations on the lead. 21

Figure 32: Good adhesion between old and new coatings. Rework coating from U902 flowed onto the toe of the adjacent non-reworked U901 lead 28 toe (nanosilica filled PC18M+20%XP2742, QFP-A312). 22

Figure 33: Preferred coating with good coverage on the lead with minimal coating fill behind the lead and minimal fill between the part and the board. Optical cross-section image, unfilled PC18M QFP-A023 U1002 Lead 1 shown, 50x. 22

Figure 34: SEM cross-section image, filled PC18M+20%XP2742 QFP-A312 U902, Lead 28 bend above foot, 1,000x. 23

Figure 35: Optical cross-section image, filled PC18M+20%XP2742 QFP-A312 U902, Lead 33 under part, 50x. 23

Figure 36: Optical cross-section image, filled PC18M+20%XP2742 QFP-A312 U902, Lead 1, 50x. 24

Figure 37: Optical cross-section image, filled PC18M+20%XP2742 QFP-A312 U902, Lead 1 heel, 200x. 24

Figure 38: SEM cross-section image, unfilled PC18M QFP-A023 U1002, Lead 28 toe, 330x. 25

Figure 39: SEM cross-section image, filled PC18M+20%XP2742 QFP-A312 U902, Lead 28 toe, 1,000x. 25

Figure 40: SEM cross-section image showing coating thinning over the lead tip (unfilled PC18M QFP-A023 U1002, Lead 6 toe, 330x shown). 26

Figure 41: Optical image showing the second solder reflow which occurred on the non-reworked U901 adjacent to the hot air reworked U902 part. (Filled PC18M+20%XP2742 QFP-A312, non-reworked U901, Lead 28, 50x shown.) 26

Figure 42: SEM cross-section image of Figure 42 showing the second solder reflow; (A) overall image and (B) higher magnification image showing with the broken original coating highlighted with yellow. (Filled PC18M+20%XP2742 QFP-A312, non-reworked U901, Lead 28 shown). 27

Figure 43: Coating thickness measurement locations. 28

Figure 44: Optical cross-section image, unfilled PC18M QFP-A023 U1002, Lead 6 measurements, C, 500x. Coating thickness is 10.5 microns. 29

Figure 45: SEM cross-section image, filled PC18M+20%XP2742 QFP-A312 U902, Lead 6 measurements, B, 1,930x. 29

Figure 46: Individual value plot comparing rework coating thickness by location, lead and side (front/back) for unfilled PC18M and filled PC18M+20%XP2742 (PC18M+NanoSi). 30

Figure 47: Box plot comparing rework coating thickness by location and by side (front/back) for unfilled PC18M and filled PC18M+20%XP2742 (PC18M+NanoSi). 30

Figure 48: Box plot comparing rework coating thickness by lead and side (front/back) for unfilled PC18M and filled PC18M+20%XP2742 (PC18M+NanoSi). 31

Figure 49: Board A235, post-TC+H, non-overlapped area, manual, before (left) and after (right) tape test. 32
Figure 50: BGA-A235 unfilled 1-spray before environmental exposure. 33
Figure 51: BGA-A296 unfilled 1-spray before environmental exposure. 34
Figure 52: BGA-A305 unfilled 2-spray before environmental exposure. 34
Figure 53: BGA-A392 filled 2-spray before environmental exposure. 35
Figure 54: BGA-A583 filled 1-spray before environmental exposure. 35
Figure 55: BGA-A593 filled 1-spray before environmental exposure. 36
Figure 56: QFP-A023 unfilled 2-spray before environmental exposure..... 36
Figure 57: QFP-A034 unfilled 2-spray before environmental exposure..... 37
Figure 58: QFP-A311 filled 1-spray before environmental exposure..... 37
Figure 59: QFP-A312 filled 2-spray before environmental exposure..... 38
Figure 60: QFP-A345 filled 2-spray before environmental exposure..... 38
Figure 61: QFP-A384 filled 2-spray before environmental exposure..... 39
Figure 62: BGA-A235 unfilled 1-spray after thermal cycling and humidity; (A) overall, (B) U611 area rework coating over existing coating, and (C) U612 area rework coating over stripped coating..... 40
Figure 63: BGA-A296 unfilled 1-spray after thermal cycling; (A) overall, (B) U511 area rework coating over existing coating, and (C) U512 area rework coating over stripped coating..... 41
Figure 64: BGA-A305 unfilled 2-spray after thermal cycling and humidity; (A) overall, (B) U911 area rework coating over existing coating, and (C) U912 area rework coating over stripped coating..... 42
Figure 65: QFP-A023 unfilled 2-spray after thermal cycling and humidity; (A) board overall, (B) reworked part overall, and (C) close-up of leads. 43
Figure 66: QFP-A034 unfilled 2-sprayafter thermal cycling; (A) board overall, (B) reworked part overall, (C) close-up of leads, and (D) isometric of end leads..... 44
Figure 67: BGA-A392 filled 2-spray after thermal cycling and humidity; (A) overall, (B) U511 area rework coating over existing coating, and (C) 512 area rework coating over stripped coating. 45
Figure 68: BGA-A583 filled 1-spray after thermal cycling and humidity; (A) overall, (B) U611 area rework coating over existing coating, and (C) U612 area rework coating over stripped coating..... 46
Figure 69: BGA-A593 filled 1-spray after thermal cycling; (A) overall, (B) U811 area rework coating over existing coating, and (C) U812 area rework coating over stripped coating..... 47
Figure 70: QFP-A311 filled 1-spray after thermal cycling and humidity; (A) board overall, (B) reworked part overall, and (C) close-up of leads. 48
Figure 71: QFP-A312 filled 2-spray after thermal cycling and humidity; (A) board overall, (B) reworked part overall, and (C) close-up of leads. 49
Figure 72: QFP-A345 filled 2 spray after thermal cycling and humidity; (A) board overall, (B) reworked part overall, and (C) close-up of leads. 50
Figure 73: QFP-A384 filled 2-spray after thermal cycling; (A) board overall, (B) reworked part overall, and (C) close-up of leads. 51
Figure 74: QFP pin numbering reference. 52

Figure 75: SEM BSE unfilled PC18M QFP-A023 U1002 pins 1 to 3, 70x. 52
Figure 76: SEM BSE unfilled PC18M QFP-A023 U1002 pins 8 to 11, 67x. 53
Figure 77: SEM BSE unfilled PC18M QFP-A023 U1002 pins 12 to 16, 70x. 53
Figure 78: SEM BSE unfilled PC18M QFP-A023 U1002 pins 18 to 22, 67x. 54
Figure 79: SEM BSE unfilled PC18M QFP-A023 U1002 pins, 23 to 26, 70x. 54
Figure 80: SEM BSE unfilled PC18M QFP-A023 U1002 pins, 23 to 28 composite, 70x. 55
Figure 81: SEM BSE unfilled PC18M QFP-A023 U1002 pins, 25 to 28, 69x. 55
Figure 82: SEM BSE unfilled PC18M QFP-A023 U1002 pins, 31 to 33, 70x. 56
Figure 83: SEM BSE unfilled PC18M QFP-A023 U1002 pins 38 to 34, 70x. 56
Figure 84: SEM BSE unfilled PC18M QFP-A023 U1002 pins 44 to 40, 70x. 57
Figure 85: SEM BSE filled PC18M+20%XP2742 QFP-A312 U902 pins 1 to 3, 69x. 57
Figure 86: SEM BSE filled PC18M+20%XP2742 QFP-A312 U902 pins 8 to 11, 70x. 58
Figure 87: SEM BSE filled PC18M+20%XP2742 QFP-A312 U902 pins 12 to 15, 70x. 58
Figure 88: SEM BSE filled PC18M+20%XP2742 QFP-A312 U902 pins 18 to 22, 70x. 59
Figure 89: SEM BSE filled PC18M+20%XP2742 QFP-A312 U902 pins 23 to 26, 70X. 59
Figure 90: SEM BSE filled PC18M+20%XP2742 QFP-A312 U902 pins 31 to 33, 70x. 60
Figure 91: SEM BSE filled PC18M+20%XP2742 QFP-A312 U903 side 1 to 12 adjacent to U902, 67x. 60
Figure 92: SEM BSE filled PC18M+20%XP2742 QFP-A312 U902 pins 38-34, 72x. 61
Figure 93: SEM BSE filled PC18M+20%XP2742 QFP-A312 U902 pins 44 to 40, 69x. 61
Figure 94: Thickness measurement locations (repeated from Figure 43). 62
Figure 95: Nomenclature used to define location on the lead. 63
Figure 96: QFP-A023 section planes through U1001 (not reworked) and U1002 (reworked). 63
Figure 97: Optical cross-section image, unfilled PC18M QFP-A023 U1002 Lead 1, 50x. 64
Figure 98: Optical cross-section image, unfilled PC18M QFP-A023 U1002 Lead 1 knee, 100x. 64
Figure 99: Optical cross-section image, unfilled PC18M QFP-A023 U1002 Lead 1, foot, 100x. 65
Figure 100: Optical cross-section image, unfilled PC18M QFP-A023 U1002 Lead 1 heel, 100x. 65
Figure 101: Optical cross-section image, unfilled PC18M QFP-A023 U1002, Lead 33, 50x. 66
Figure 102: Optical cross-section image, unfilled PC18M QFP-A023 U1002, Lead 33 knee, 100x. 66
Figure 103: Optical cross-section image, unfilled PC18M QFP-A023 U1002, Lead 33 foot, 100x. 67
Figure 104: Optical cross-section image, unfilled PC18M QFP-A023 U1002, Lead 33 heel, 100x. 67
Figure 105: Optical cross-section image, unfilled PC18M QFP-A023 U1002, overall stereoscope non-inverted, lead 6 (left) and lead 28 (right), 7.8x. 68
Figure 106: Optical cross-section image, unfilled PC18M QFP-A023 U1002, Lead 6 stereoscope non-inverted, 40x. 68
Figure 107: Optical cross-section image, unfilled PC18M QFP-A023 U1002, Lead 6, 50x. 69

Figure 108: Optical cross-section image, unfilled PC18M QFP-A023 U1002, Lead 6 knee, 100x. 69
Figure 109: Optical cross-section image, unfilled PC18M QFP-A023 U1002, Lead 6 foot, 100x. 70
Figure 110: Optical cross-section image, unfilled PC18M QFP-A023 U1002, Lead 6 heel, 100x. 70
Figure 111: Optical cross-section image, unfilled PC18M QFP-A023 U1002, Lead 28 stereoscope non-inverted, 40x. 71
Figure 112: Optical cross-section image, unfilled PC18M QFP-A023 U1002, Lead 28, 50x..... 71
Figure 113: Optical cross-section image, unfilled PC18M QFP-A023 U1002, Lead 28 knee, 100x. 72
Figure 114: Optical cross-section image, unfilled PC18M QFP-A023 U1002, Lead 28 foot, 100x. 72
Figure 115: Optical cross-section image, unfilled PC18M QFP-A023 U1002, Lead 28 heel, 100x. 73
Figure 116: SEM cross-section image, unfilled PC18M QFP-A023 U1002, Lead 6, 122x. 73
Figure 117: SEM cross-section image, unfilled PC18M QFP-A023 U1002, Lead 6 knee, 330x..... 74
Figure 118: SEM cross-section image, unfilled PC18M QFP-A023 U1002, Lead 6 toe, 330x. 74
Figure 119: SEM cross-section image, unfilled PC18M QFP-A023 U1002, Lead 28, 122x. 75
Figure 120: SEM cross-section image, unfilled PC18M QFP-A023 U1002, Lead 28 knee, 330x..... 75
Figure 121: SEM cross-section image, unfilled PC18M QFP-A023 U1002, Lead 28 heel, 330x..... 76
Figure 122: SEM cross-section image, unfilled PC18M QFP-A023 U1002, Lead 28 toe, 330x. 76
Figure 123: Optical cross-section image, unfilled PC18M QFP-A023 U1002, Lead 6 measurements, A, 500x. 77
Figure 124: Optical cross-section image, unfilled PC18M QFP-A023 U1002, Lead 6 measurements, A1, 500x. 77
Figure 125: Optical cross-section image, unfilled PC18M QFP-A023 U1002, Lead 6 measurements, B, 500x. 78
Figure 126: Optical cross-section image, unfilled PC18M QFP-A023 U1002, Lead 6 measurements, B1, 500x. 78
Figure 127: Optical cross-section image, unfilled PC18M QFP-A023 U1002, Lead 6 measurements, C, 500x. 79
Figure 128: Optical cross-section image, unfilled PC18M QFP-A023 U1002, Lead 6 measurements, C1, 500x. 79
Figure 129: Optical cross-section image, unfilled PC18M QFP-A023 U1002, Lead 6 measurements, D, 500x. 80
Figure 130: Optical cross-section image, unfilled PC18M QFP-A023 U1002, Lead 6 measurements, D1, 500x. 80
Figure 131: Optical cross-section image, unfilled PC18M QFP-A023 U1002, Lead 6 measurements, E, 500x. 81
Figure 132: Optical cross-section image, unfilled PC18M QFP-A023 U1002, Lead 6 measurements, E1, 500x. 81
Figure 133: Optical cross-section image, unfilled PC18M QFP-A023 U1002, Lead 6 measurements, F, 500x. 82

Figure 134: Optical cross-section image, unfilled PC18M QFP-A023 U1002, Lead 6 measurements, F1, 500x. 82

Figure 135: Optical cross-section image, unfilled PC18M QFP-A023 U1002, Lead 6 measurements, H, 500x. 83

Figure 136: Optical cross-section image, unfilled PC18M QFP-A023 U1002, Lead 6 measurements, T, 500x. 83

Figure 137: Optical cross-section image, unfilled PC18M QFP-A023 U1002, Lead 28 measurements, A, 500x. 84

Figure 138: Optical cross-section image, unfilled PC18M QFP-A023 U1002, Lead 28 measurements, A1, 500x. 84

Figure 139: Optical cross-section image, unfilled PC18M QFP-A023 U1002, Lead 28 measurements, B, 500x. 85

Figure 140: Optical cross-section image, unfilled PC18M QFP-A023 U1002, Lead 28 measurements, B1, 500x. 85

Figure 141: Optical cross-section image, unfilled PC18M QFP-A023 U1002, Lead 28 measurements, C, 500x. 86

Figure 142: Optical cross-section image, unfilled PC18M QFP-A023 U1002, Lead 28 measurements, C1, 500x. 86

Figure 143: Optical cross-section image, unfilled PC18M QFP-A023 U1002, Lead 28 measurements, D, 500x. 87

Figure 144: Optical cross-section image, unfilled PC18M QFP-A023 U1002, Lead 28 measurements, D1, 500x. 87

Figure 145: Optical cross-section image, unfilled PC18M QFP-A023 U1002, Lead 28 measurements, E, 500x. 88

Figure 146: Optical cross-section image, unfilled PC18M QFP-A023 U1002, Lead 28 measurements, E1, 500x. 88

Figure 147: Optical cross-section image, unfilled PC18M QFP-A023 U1002, Lead 28 measurements, F, 500x. 89

Figure 148: Optical cross-section image, unfilled PC18M QFP-A023 U1002, Lead 28 measurements, F1, 500x. 89

Figure 149: Optical cross-section image, unfilled PC18M QFP-A023 U1002, Lead 28 measurements, H, 500x. 90

Figure 150: Optical cross-section image, unfilled PC18M QFP-A023 U1002, Lead 28 measurements, H, 1000x. 90

Figure 151: Optical cross-section image, unfilled PC18M QFP-A023 U1002, Lead 28 measurements, T, 500x. 91

Figure 152: Optical cross-section image, unfilled PC18M QFP-A023 non-reworked U1001, Lead 33_50x. 91

Figure 153: Optical cross-section image, unfilled PC18M QFP-A023 non-reworked U1001, Lead 33 knee_100x. 92

Figure 154: Optical cross-section image, unfilled PC18M QFP-A023 non-reworked U1001, Lead 33 foot_100x. 92

Figure 155: Optical cross-section image, unfilled PC18M QFP-A023 non-reworked U1001, Lead 33 heel_100x. 93

Figure 156: Optical cross-section image, unfilled PC18M QFP-A023 non-reworked U1001, Overall lead 28 stereoscope non-inverted, 7.8x. 93

Figure 157: Optical cross-section image, unfilled PC18M QFP-A023 non-reworked U1001, Lead 28 stereomicroscope non-inverted, 40x. 94

Figure 158: Optical cross-section image, unfilled PC18M QFP-A023 non-reworked U1001, Lead 28_50x. 94

Figure 159: Optical cross-section image, unfilled PC18M QFP-A023 non-reworked U1001, Lead 28 knee_100x. 95

Figure 160: Optical cross-section image, unfilled PC18M QFP-A023 non-reworked U1001, Lead 28 foot_100x. 95

Figure 161: Optical cross-section image, unfilled PC18M QFP-A023 non-reworked U1001, Lead 28 heel_100x. 96

Figure 162: SEM cross-section image, unfilled PC18M QFP-A023 non-reworked U1001, Lead 28 122x. 96

Figure 163: SEM cross-section image, unfilled PC18M QFP-A023 non-reworked U1001, Lead 28 knee 330x. 97

Figure 164: SEM cross-section image, unfilled PC18M QFP-A023 non-reworked U1001, Lead 28 toe 330x. 97

Figure 165: SEM cross-section image, unfilled PC18M QFP-A023 non-reworked U1001, Lead 28 heel 330x. 98

Figure 166: Optical cross-section locations for PC18M+20%XP2742 QFP-A312 U901 (non-reworked) and U902 (reworked). 99

Figure 167: Cross-section plane locations for PC18M+20%XP2742 coated QFP-A312. The cross-section planes go through the right side of U901 (non-reworked) and both sides of U902 (reworked). 99

Figure 168: Optical cross-section image, filled PC18M+20%XP2742 QFP-A312 U902, Lead 1 knee, 100x. 100

Figure 169: Optical cross-section image, filled PC18M+20%XP2742 QFP-A312 U902, Lead 1 foot, 100x. 100

Figure 170: Optical cross-section image, filled PC18M+20%XP2742 QFP-A312 U902, Lead 1 heel, 100x. 101

Figure 171: Optical cross-section image, filled PC18M+20%XP2742 QFP-A312 U902, Lead 1 heel, 200x. 101

Figure 172: Optical cross-section image, filled PC18M+20%XP2742 QFP-A312 U902, Lead 33, 50x. 102

Figure 173: Optical cross-section image, filled PC18M+20%XP2742 QFP-A312 U902, Lead 33 knee, 100x. 102

Figure 174: Optical cross-section image, filled PC18M+20%XP2742 QFP-A312 U902, Lead 33 foot, 100x. 103

Figure 175: Optical cross-section image, filled PC18M+20%XP2742 QFP-A312 U902, Lead 33 heel, 100x. 103

Figure 176: Optical cross-section image, filled PC18M+20%XP2742 QFP-A312 U902, Lead 33 under part, 50x. 104

Figure 177: Optical cross-section image, filled PC18M+20%XP2742 QFP-A312 U902, overall stereoscope non-inverted, 7.8x. 104

Figure 178: Optical cross-section image, filled PC18M+20%XP2742 QFP-A312 U902, Lead 6 stereoscope non-inverted, 40x. 105

Figure 179: Optical cross-section image, filled PC18M+20%XP2742 QFP-A312 U902, Lead 6, 50x. .. 105

Figure 180: Optical cross-section image, filled PC18M+20%XP2742 QFP-A312 U902, Lead 6 knee, 100x. 106

Figure 181: Optical cross-section image, filled PC18M+20%XP2742 QFP-A312 U902, Lead 6 foot, 100x. 106

Figure 182: Optical cross-section image, filled PC18M+20%XP2742 QFP-A312 U902, Lead 6 heel, 100x. 107

Figure 183: Optical cross-section image, filled PC18M+20%XP2742 QFP-A312 U902, Lead 28 stereoscope non-inverted, 40x. 107

Figure 184: Optical cross-section image, filled PC18M+20%XP2742 QFP-A312 U902, Lead 28, 50x. 108

Figure 185: Optical cross-section image, filled PC18M+20%XP2742 QFP-A312 U902, Lead 28 knee, 100x. 108

Figure 186: Optical cross-section image, filled PC18M+20%XP2742 QFP-A312 U902, Lead 28 foot, 100x. 109

Figure 187: Optical cross-section image, filled PC18M+20%XP2742 QFP-A312 U902, Lead 28 heel 1, 100x. 109

Figure 188: SEM cross-section image, filled PC18M+20%XP2742 QFP-A312 U902, Lead 6, 121x..... 110

Figure 189: SEM cross-section image, filled PC18M+20%XP2742 QFP-A312 U902, Lead 6 knee, 330x. 110

Figure 190: SEM cross-section image, filled PC18M+20%XP2742 QFP-A312 U902, Lead 6 toe, 330x. 111

Figure 191: SEM cross-section image, filled PC18M+20%XP2742 QFP-A312 U902, Lead 6 heel, 330x. 111

Figure 192: SEM cross-section image, filled PC18M+20%XP2742 QFP-A312 U902, Lead 28, 119x... 112

Figure 193: SEM cross-section image, filled PC18M+20%XP2742 QFP-A312 U902, Lead 28 knee, 330x. 112

Figure 194: SEM cross-section image, filled PC18M+20%XP2742 QFP-A312 U902, Lead 28 toe, 330x. 113

Figure 195: SEM cross-section image, filled PC18M+20%XP2742 QFP-A312 U902, Lead 28 toe, 1,000x 113

Figure 196: SEM cross-section image, filled PC18M+20%XP2742 QFP-A312 U902, Lead 28 top bend above foot, 1,000x. 114

Figure 197: SEM cross-section image, filled PC18M+20%XP2742 QFP-A312 U902, Lead 28 heel, 330x. 114

Figure 198: SEM cross-section image, filled PC18M+20%XP2742 QFP-A312 U902, Lead 28 end of heel, 1,000x..... 115

Figure 199: Optical cross-section image, filled PC18M+20%XP2742 QFP-A312 U902, Lead 6 measurements, A, 500x..... 115

Figure 200: Optical cross-section image, filled PC18M+20%XP2742 QFP-A312 U902, Lead 6 measurements, A1, 500x..... 116

Figure 201: Optical cross-section image, filled PC18M+20%XP2742 QFP-A312 U902, Lead 6 measurements, B, 500x..... 116

Figure 202: SEM cross-section image, filled PC18M+20%XP2742 QFP-A312 U902, Lead 6 measurements, B, 1,930x..... 117

Figure 203: Optical cross-section image, filled PC18M+20%XP2742 QFP-A312 U902, Lead 6 measurements, B1, 500x..... 117

Figure 204: Optical cross-section image, filled PC18M+20%XP2742 QFP-A312 U902, Lead 6 measurements, C, 500x..... 118

Figure 205: Optical cross-section image, filled PC18M+20%XP2742 QFP-A312 U902, Lead 6 measurements, C1, 500x..... 118

Figure 206: Optical cross-section image, filled PC18M+20%XP2742 QFP-A312 U902, Lead 6 measurements, D, 500x..... 119

Figure 207: Optical cross-section image, filled PC18M+20%XP2742 QFP-A312 U902, Lead 6 measurements, D1, 500x..... 119

Figure 208: Optical cross-section image, filled PC18M+20%XP2742 QFP-A312 U902, Lead 6 measurements, E, 500x..... 120

Figure 209: Optical cross-section image, filled PC18M+20%XP2742 QFP-A312 U902, Lead 6 measurements, E1, 500x..... 120

Figure 210: Optical cross-section image, filled PC18M+20%XP2742 QFP-A312 U902, Lead 6 measurements, F, 500x..... 121

Figure 211: Optical cross-section image, filled PC18M+20%XP2742 QFP-A312 U902, Lead 6 measurements, F1, 500x..... 121

Figure 212: Optical cross-section image, filled PC18M+20%XP2742 QFP-A312 U902, Lead 6 measurements, H, 500x..... 122

Figure 213: Optical cross-section image, filled PC18M+20%XP2742 QFP-A312 U902, Lead 6 measurements, T, 500x..... 122

Figure 214: SEM cross-section image, filled PC18M+20%XP2742 QFP-A312 U902, Lead 6 measurements, T, 1,950x..... 123

Figure 215: Optical cross-section image, filled PC18M+20%XP2742 QFP-A312 U902, Lead 28 measurements, A, 500x..... 123

Figure 216: Optical cross-section image, filled PC18M+20%XP2742 QFP-A312 U902, Lead 28 measurements, A1, 500x..... 124

Figure 217: Optical cross-section image, filled PC18M+20%XP2742 QFP-A312 U902, Lead 28 measurements, B, 500x. 124

Figure 218: SEM cross-section image, filled PC18M+20%XP2742 QFP-A312 U902, Lead 28 measurements, B, 2,260x. 125

Figure 219: Optical cross-section image, filled PC18M+20%XP2742 QFP-A312 U902, Lead 28 measurements, B1, 500x. 125

Figure 220: Optical cross-section image, filled PC18M+20%XP2742 QFP-A312 U902, Lead 28 measurements, C, 500x. 126

Figure 221: Optical cross-section image, filled PC18M+20%XP2742 QFP-A312 U902, Lead 28 measurements, C1, 500x. 126

Figure 222: Optical cross-section image, filled PC18M+20%XP2742 QFP-A312 U902, Lead 28 measurements, D, 500x. 127

Figure 223: Optical cross-section image, filled PC18M+20%XP2742 QFP-A312 U902, Lead 28 measurements, D1, 500x. 127

Figure 224: Optical cross-section image, filled PC18M+20%XP2742 QFP-A312 U902, Lead 28 measurements, E, 500x. 128

Figure 225: Optical cross-section image, filled PC18M+20%XP2742 QFP-A312 U902, Lead 28 measurements, E1, 500x. 128

Figure 226: Optical cross-section image, filled PC18M+20%XP2742 QFP-A312 U902, Lead 28 measurements, F, 500x. 129

Figure 227: Optical cross-section image, filled PC18M+20%XP2742 QFP-A312 U902, Lead 28 measurements, F1, 500x. 129

Figure 228: Optical cross-section image, filled PC18M+20%XP2742 QFP-A312 U902, Lead 28 measurements, H, 500x. 130

Figure 229: Optical cross-section image, filled PC18M+20%XP2742 QFP-A312 U902, Lead 28 measurements, T, 500x. 130

Figure 230: Optical cross-section image, filled PC18M+20%XP2742 QFP-A312 U902, Lead 28 measurements, T, 1,000x. 131

Figure 231: SEM cross-section image, filled PC18M+20%XP2742 QFP-A312 U902, Lead 28 measurements, T, 2,450x. 131

Figure 232: Optical cross-section image, filled PC18M+20%XP2742 QFP-A312, non-reworked U901, Lead 33_50x. 132

Figure 233: Optical cross-section image, filled PC18M+20%XP2742 QFP-A312, non-reworked U901, Lead 33 knee_100x. 132

Figure 234: Optical cross-section image, filled PC18M+20%XP2742 QFP-A312, non-reworked U901, Lead 33 knee_200x. 133

Figure 235: Optical cross-section image, filled PC18M+20%XP2742 QFP-A312, non-reworked U901, Lead 33 foot_100x. 133

Figure 236: Optical cross-section image, filled PC18M+20%XP2742 QFP-A312, non-reworked U901, Lead 33 toe_100x. 134

Figure 237: Optical cross-section image, filled PC18M+20%XP2742 QFP-A312, non-reworked U901, Lead 33 heel_100x. 134

Figure 238: Optical cross-section image, filled PC18M+20%XP2742 QFP-A312, non-reworked U901, Lead 33 heel 1_200x. 135

Figure 239: Optical cross-section image, filled PC18M+20%XP2742 QFP-A312, non-reworked U901, Lead 33 heel 2_200x, ... 135

Figure 240: Optical cross-section image, filled PC18M+20%XP2742 QFP-A312, non-reworked U901, Overall 28 stereoscope non-inverted, 7.8x. 136

Figure 241: Optical cross-section image, filled PC18M+20%XP2742 QFP-A312, non-reworked U901, Lead 28 stereoscope non-inverted 40x. 136

Figure 242: Optical cross-section image, filled PC18M+20%XP2742 QFP-A312, non-reworked U901, Lead 28, 50x. 137

Figure 243: Optical cross-section image, filled PC18M+20%XP2742 QFP-A312, non-reworked U901, Lead 28 knee, 100x. 137

Figure 244: Optical cross-section image, filled PC18M+20%XP2742 QFP-A312, non-reworked U901, Lead 28 knee_200x. 138

Figure 245: Optical cross-section image, filled PC18M+20%XP2742 QFP-A312, non-reworked U901, Lead 28 foot, 100x. 138

Figure 246: Optical cross-section image, filled PC18M+20%XP2742 QFP-A312, non-reworked U901, Lead 28 foot, 200x. 139

Figure 247: Optical cross-section image, filled PC18M+20%XP2742 QFP-A312, non-reworked U901, Lead 28 toe, 100x 139

Figure 248: Optical cross-section image, filled PC18M+20%XP2742 QFP-A312, non-reworked U901, Lead 28 toe, 200x. 140

Figure 249: Optical cross-section image, filled PC18M+20%XP2742 QFP-A312, non-reworked U901, Lead 28 toe, 200x. 140

Figure 250: Optical cross-section image, filled PC18M+20%XP2742 QFP-A312, non-reworked U901, Lead 28 toe stereoscope non-inverted, 160x. 141

Figure 251: Optical cross-section image, filled PC18M+20%XP2742 QFP-A312, non-reworked U901, Lead 28 heel, 100x. 141

Figure 252: SEM cross-section image, filled PC18M+20%XP2742 QFP-A312, non-reworked U901, Lead 28, 121x. 142

Figure 253: SEM cross-section image, filled PC18M+20%XP2742 QFP-A312, non-reworked U901, Lead 28 knee, 330x. 142

Figure 254: SEM cross-section image, filled PC18M+20%XP2742 QFP-A312, non-reworked U901, Lead 28 toe, 330x. 143

Figure 255: SEM cross-section image, filled PC18M+20%XP2742 QFP-A312, non-reworked U901, Lead 28 heel, 330x. 143

Figure 256: SEM cross-section image, filled PC18M+20%XP2742 QFP-A312, non-reworked U901, Lead 28 heel, zoom 330x. Solder has reflowed after coating. The coating surface is highlighted with yellow dots. 144

Appendix L: List of Tables

Table 1: Assembly board history. 1
Table 2: Henkel AC0305 Solvent Composition. 2
Table 3: Cytec Conap S-13 Solvent Composition 2
Table 4: QFP parts reworked 3
Table 5: Assembly board history 11
Table 6: Unfilled PC18M rework coating material batch information. 12
Table 7: Solvent material batch information. 12
Table 8: Rework PC18M+20%XP2742 rework coating material batch information. 13
Table 9: Adhesion Rating of Reworked Coating. 32

Acronyms

Acronym	Definition
BGA	Ball Grid Array
BSE	Back Scatter Electron
FA	Failure Analysis
FOD	Foreign Object and Debris
FR4	Flame retardant type of printed circuit board laminate
HALT	Highly Accelerated Life Test
IPA	Isopropyl Alcohol
IPC	IPC Association Connecting Electronics Industries
QFP	Quad Flat Pack Electronic Packages
SAC	Sn-Ag-Cu alloy lead free solder
SAC305	Sn3Ag0.5Cu alloy lead free solder (composition is in weight percent)
SEM	Scanning Electron Microscope image
SMT	Surface Mount Technology
TC	Thermal Cycling
TGA	Thermogravimetric Analysis

1. Introduction

Rework is often required during high mix and low volume electronics manufacturing and for repair during service when parts need to be removed and replaced. The objective of the rework evaluation experiments is to determine whether the newly developed PC18M-based polyurethane coatings can be reworked. Several different coating removal methods were evaluated for ease of use. The application method focused on the commonly used brush coating technique.

2. Coating removal method development

The work described in the removal method development section encompasses coating removal experiments performed in 2015. The coating was removed from two boards in select locations using Celestica's modified conformal coating rework processes, while making observations as to the efficacy of the method.

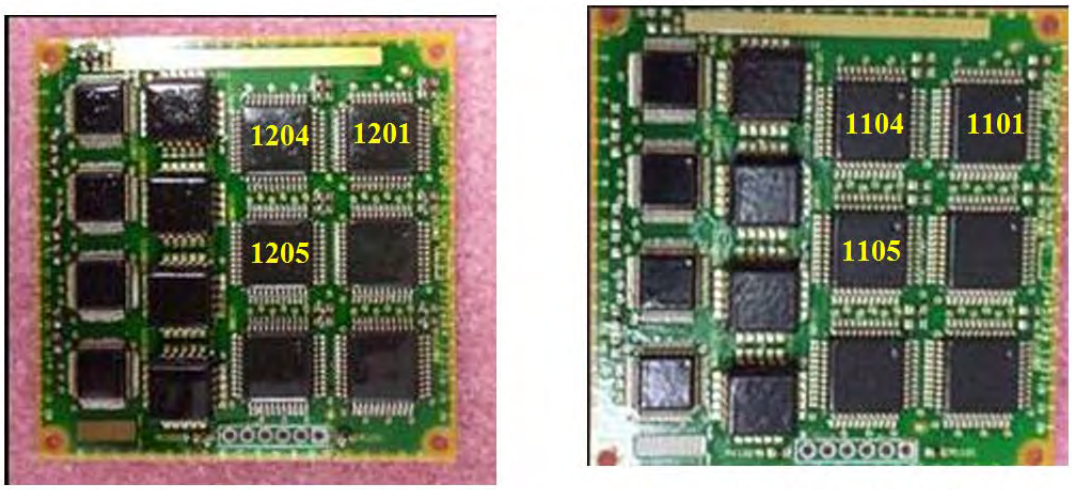
2.1 Assembly boards

Assembled WP 2213 Quad Flat Pack (QFP) boards were coated with PC18M-based coatings and aged in the WP 2213 project in 2013 [1]. The boards shown in Table 1 were selected for the rework process development trials. Both of these boards had been dip coated with PC18M at 30 cps prior to the baseline spray coating. The components were attached (soldered) using Sn3.0Ag0.5Cu alloy lead free solder (SAC305). The boards are shown in Figure 1, with the component reference designators superimposed on the images.

Table 1: Assembly board history.

Board #	Spray Coating	Board Type	ATC exposed (1)	85/85 exposed (2)
16	PC18M-Mod	QFP	Yes	Yes
17	PC18M-20% XP2742	QFP	No	Yes

Notes:
(1) 100 cycles – 55 to +125°C (10 minutes cold and 30 minutes at hot with 18 minute ramps) followed by 233 cycles -20 to +80°C (30 minutes at cold and hot with 10 minute ramps);
(2) 2,000 Hours 85°C/85%RH



(A) Board 16 PC18M (B) Board 17 PC18M+20%XP2742

Figure 1: Assembled and coated boards after environmental exposure.

2.2 Coating removal methods

Several common types of cured conformal coating removal are used at Celestica, depending on the coating material type and component fragility. These are: solvent based, media blasting, mechanical ablation, and thermal based methods for coating removal. Solvent based chemicals, similar if not identical to that used to thin the material, can be used for spot removal for acrylics and urethanes. Mechanical ablation and media blasting are the removal techniques commonly used for Parylene and hard epoxy type coatings. Thermal stripping is also possible, and requires knowledge of the thermal robustness of the assembly.

2.2.1 Chemical removal process

Chemical spot removal consists of applying a solvent in a controlled manner, using tools such as syringes and swabs, followed by rubbing and scraping as necessary. Henkel AC0305 and Conap S13 were both tried in this experiment. The solvent compositions are shown below in Table 2 and Table 3.The Henkel AC0305 is the solvent used for thinning PC18M coatings. Conap S13 was another solvent available in the factory.

Table 2: Henkel AC0305 Solvent Composition.

Chemical Name	CAS Number	Min %	Max %	Avg %	% Range
Xylene	1330-20-7	85.00%	90.00%	87.50%	85 - 90%
Ethyl Benzene	100-41-4	15.00%	20.00%	17.50%	15 - 20%

Table 3: Cytec Conap S-13 Solvent Composition

Chemical Name	CAS Number	% Range
Toluene	108-88-3	30 - 60%
Methoxypropyl acetate	2-108-65-6	30 - 60%

2.2.2 Media blasting removal process

Media blasting is “micro-sandblasting” with sodium bicarbonate or other fine powder type material such as walnut shells or silica. Sodium bicarbonate was used in these trials.

2.2.3 Thermal removal process

Thermal stripping uses a heated metal tip at 150 ± 10°C. The key elements of the process are as follows:

1. Cover plastic material and heat sensitive component with silicone – free masking tape before rework start.
2. Under a 30x scope, gently place the striping dull knife tip on coating surface. Do NOT place the dull thermal stripper tip on or near the solder joints of heat sensitive components. After heating for two to five seconds, the coating will soften.
3. With angle range within 30° to 60° gently strip the soften coating. Discard removed coating from the tip. Brush off waste conformal coat material particles on top of surface PCBA with using ESD horse hair brush.
4. Localized clean with IPA, remove masking tape ensuring the conformal coating is not damaged or delaminated. The coating on the components and the components shall not have discoloration.
5. Aqueous clean the assembly and inspect.

In order to determine the rework thermal process limits for a coating, cured coating samples can be analyzed by thermogravimetric analysis (TGA). This analysis will provide the decomposition temperature of the cured films, and is usually provided in the technical data sheets for a coating material by the coating supplier.

2.3 Celestica coating rework and replacement screening experiment

Standard site solder redress and part replacement was done. The solder iron temperature used was for SnPb at 371°C (700°F). The flux used was Kester 977 no clean for SnPb. The cleaning process was that for SnPb – unfluxed solder wick with Proclean alcohol – free flux remover.

The QFP part replacement was completed using the SRT tool using a SnPb reflow profile (that is, the temperature for part replacement was cooler than for replacement with a SnAgCu alloy lead free solder (SAC) profile). The rework was done with SnPb solder.

2.3.1 Coating removal testing

Coating removal, part removal, and part replacement was done in the Celestica A&D Toronto factory by engineering and operations staff in September 2015. The solvent, thermal and media blaster removal methods were evaluated on QFP boards. Three QFP44 parts were reworked on each board (Table 4).

Table 4: QFP parts reworked

Board	Part Designator	Coating Removal Method	Part Replaced	Coating removal comments
16	U1201	Thermal stripper	Yes	Removes coating.
16	U1204	AC0305	Yes	Softens coating, but will not remove it. Needs to be scraped off. Better than SG13.
16	U1205	S13	No	Softens coating slowly. Will not

Board	Part Designator	Coating Removal Method	Part Replaced	Coating removal comments
				remove completely. Needs to be scraped off.
17	U1101	Media Blaster	Yes	Removes coating.
17	U1104	AC0305	Yes	Softens coating slowly. Will not remove completely. Needs to be scraped off.
17	U1105	AC0305	No	Softens coating slowly. Will not remove completely. Needs to be scraped off.

The reworked boards are shown in Figure 2. The part highlighted in blue on both boards, U1205 and U1105, had the coating removed by the method shown in Table 4. The part itself was not removed.

The parts highlighted in red had the coating removed by the method shown in Table 4, then the part was removed, replaced, and the coating was reapplied. The rework was done with SnPb solder. Components were reused in the rework process as fresh components were not readily available.

Higher magnification images of the reworked parts are shown in Figure 3 through Figure 16. There is some residual coating between the leads near the body of the component on U1201, which was thermally reworked, and on U1204, which had some thermal rework after AC0305. See Figure 4, Figure 5 and Figure 7 for images of these residues. The intent of the overall rework experiment was to verify the adhesion between old and new coatings on the card – i.e. around the component - so contamination directly on the component is not relevant to this study. There were no other notable observations.

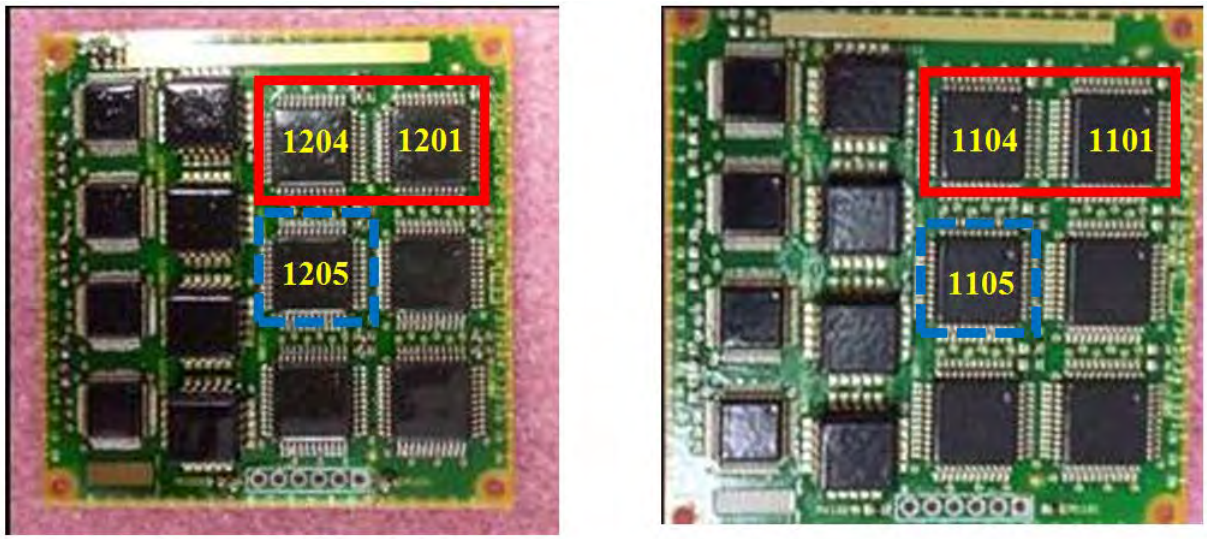


Figure 2: Areas reworked on boards 16 and 17. Red box shows parts removed and replaced after coating removal and the blue box shows parts where only the coating was removed.

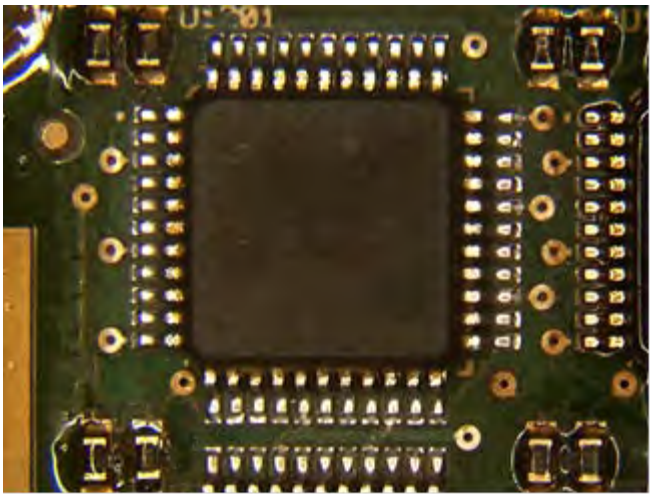


Figure 3: Board 16, U1201, after coating removal, 7.5x.

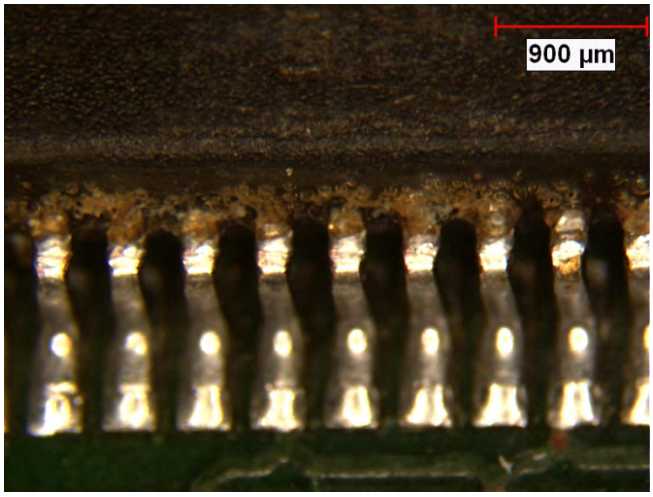


Figure 4: Board 16, U1201, after coating removal, 25x angled image. Coating residue from thermal removal is at the top of leads.

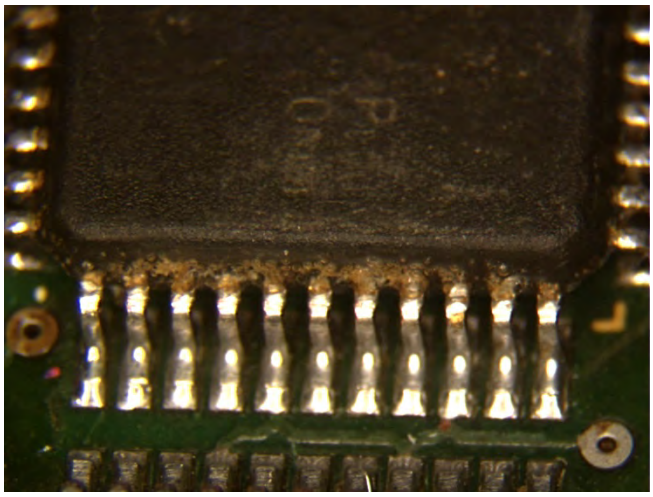


Figure 5: Board 16, U1201, after coating removal, 15x angled image. Coating residue from thermal removal is at the top of leads.

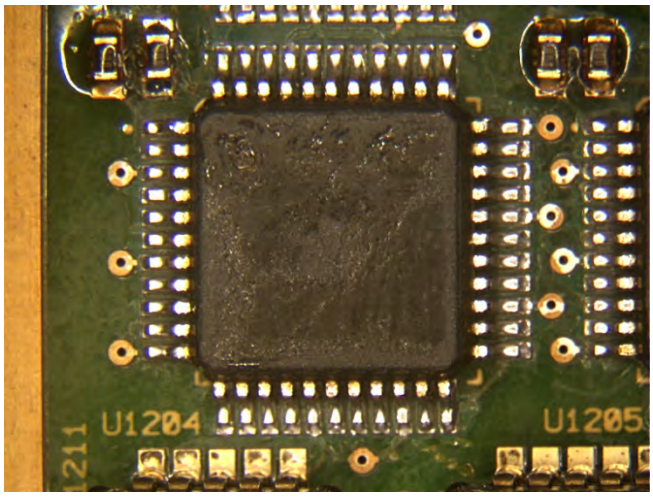


Figure 6: Board 16, U1204, after coating removal, 7.5x.

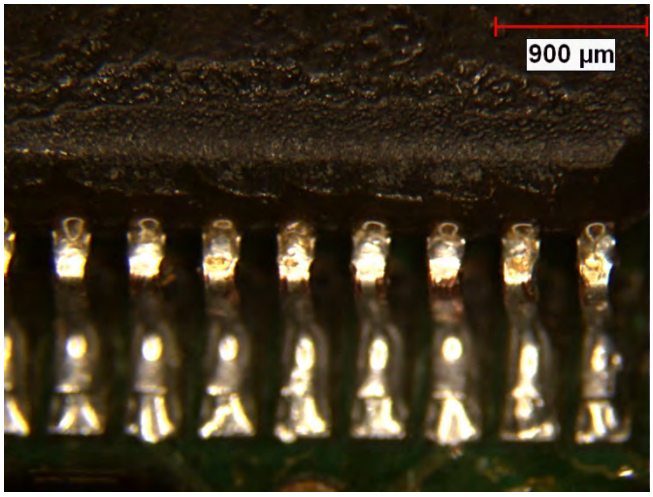


Figure 7: Board 16, U1204, after coating removal, 25x angled image. A small amount of discolored residue after solvent removal is at the top of leads.

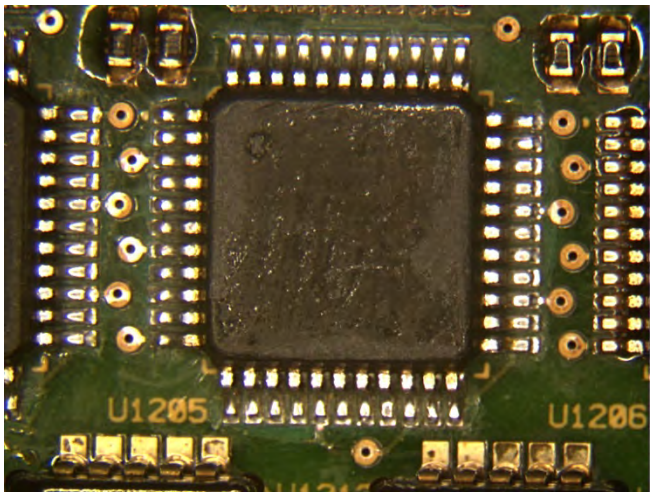


Figure 8: Board 16, U1205, after coating removal, 7.5x.

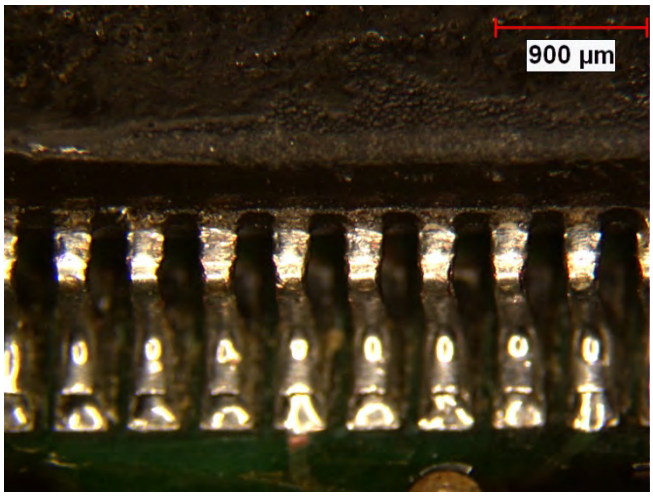


Figure 9: Board 16, U1205, after coating removal, 25x angled image.

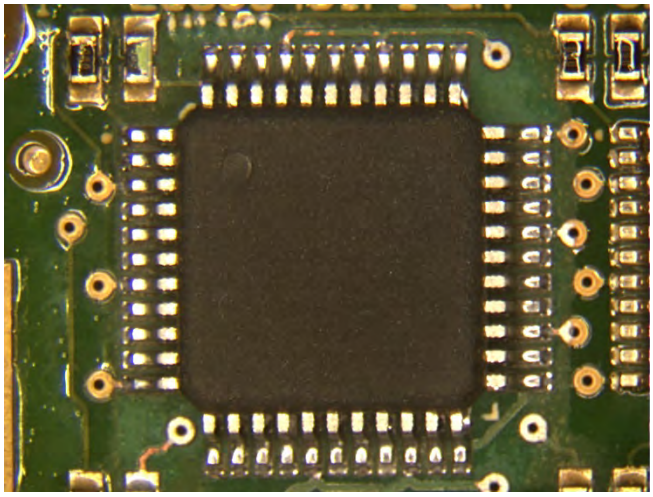


Figure 10: Board 17, U1101, after coating removal, 7.5x.

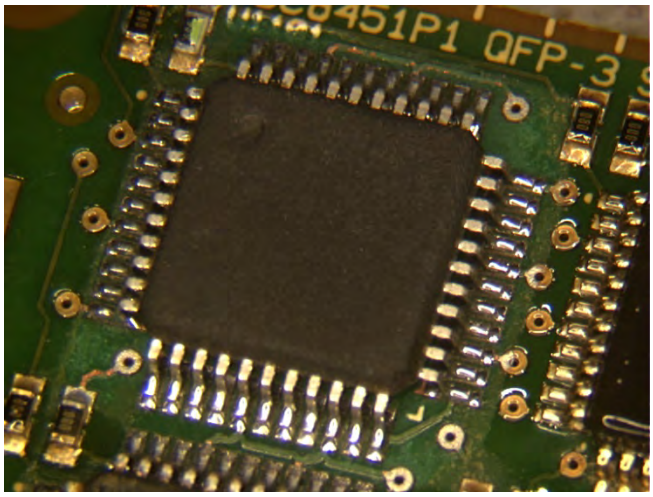


Figure 11: Board 17, U1101, after coating removal, 7.5x angled image.

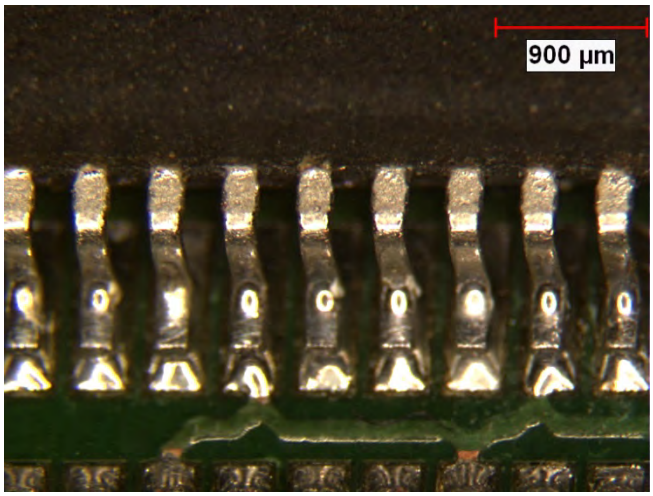


Figure 12: Board 17, U1101, after coating removal, 25x angled image.

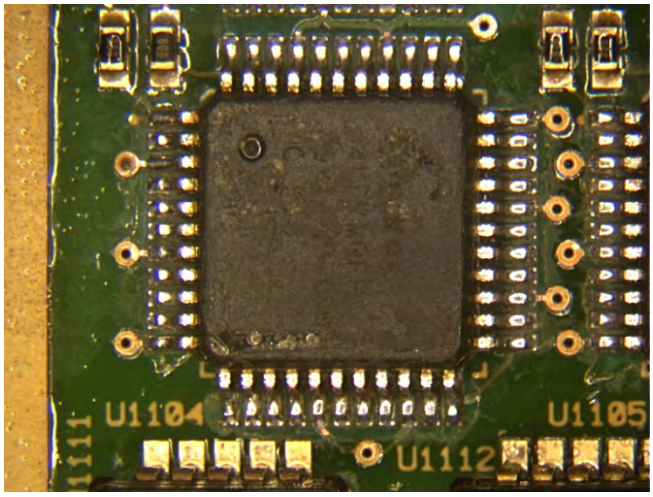


Figure 13: Board 17, U1104, after coating removal, 7.5x.

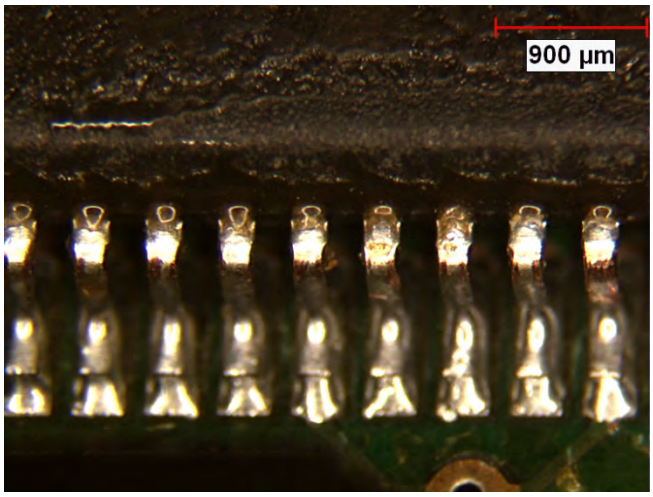


Figure 14: Board 17, U1104, after coating removal, 25x angled image.

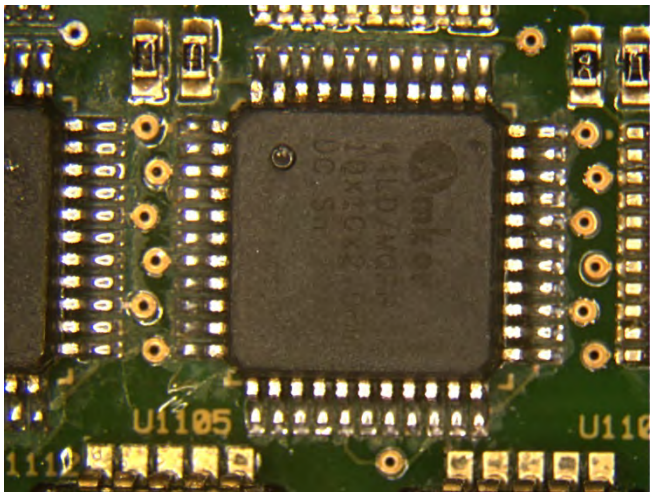


Figure 15: Board 17, U1105, after coating removal, overview, 7.5x.

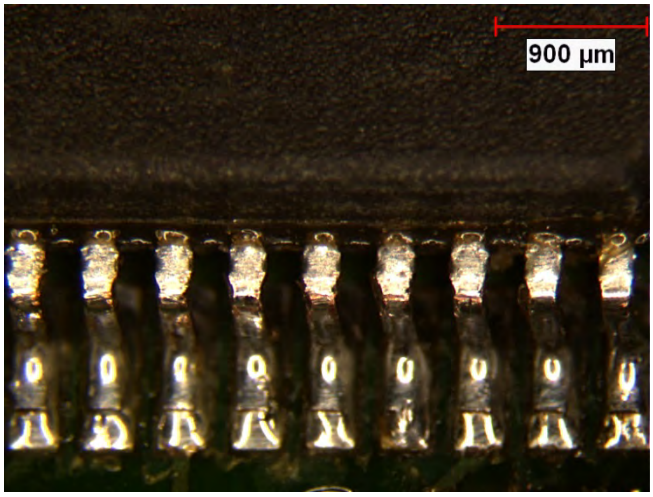


Figure 16: Board 17, U1105, after coating removal, 25x angled image.

2.3.2 Coating re-application process

The reworked cards were provided to Henkel for replacement of the coating with one of the experimental coatings. One reworked test board was dip coated with PC18M thinned to 30cPs with AC0305, dried and cured for two hours at 60C/60%RH and one was not pre-dipped. Both boards were brush coated in reworked area with PC18M+20%XP2784, dried overnight, then cured at 60°C/60%RH for two hours.

These boards were then thermal shock cycled at Henkel from -55C to 125°C (15 minute dwells, shuttle basket transition from cold to hot) for 100 cycles. No delamination, bubbling or cracking were seen on these reworked test boards (see Figure 17 and Figure 18) [1].

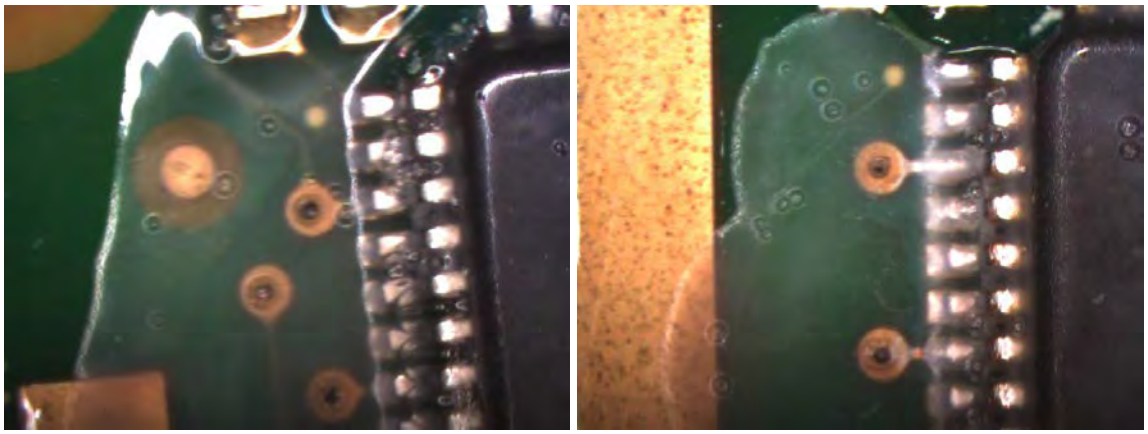


Figure 17: Images of PC18M dipped and PC18M+20%XP2742 coated.

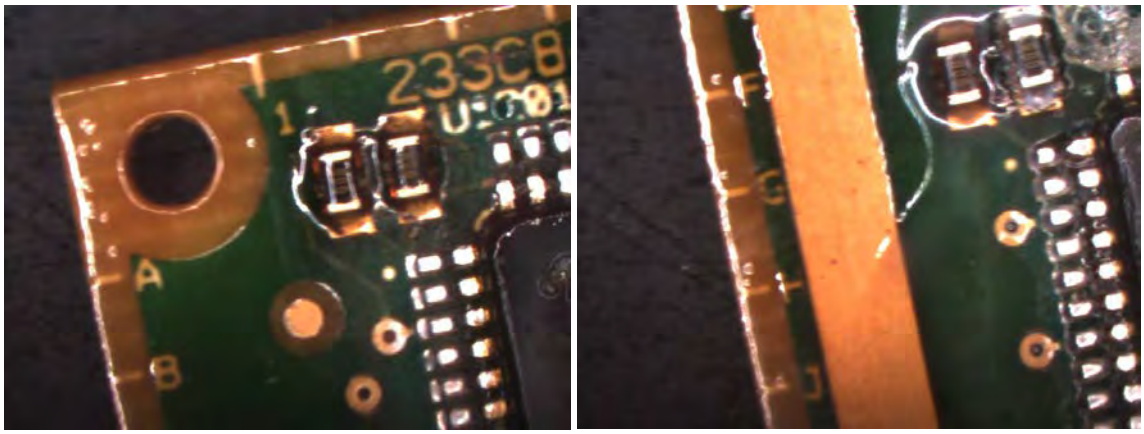


Figure 18: Images of PC18M+20%XP2742 with no pre – dip.

2.3.3 Coating removal conclusions

Solvent removal with Henkel AC0305, thermal stripping or media blasting all are feasible coating removal methods for aged PC18M and PC18M+20%XP2742. The thermal stripping method was selected for the final assembly QFP testing and the media blaster was selected for the flat board rework.

3. Assembly rework evaluation

A larger board matrix of assemblies was evaluated. The rework coating adhesion was evaluated on unaged and humidity aged boards with two coating removal methods.

3.1 Equipment and materials

3.1.1 Assembly boards

Assembled boards that had been coated as shown in Table 5 were selected. The components had been attached (soldered) using SAC305.

Table 5: Assembly board history

Spray coating type (Note 1)	Board Type	Board ID	Dipping Lot	Spray runs (Note 2)	Follow-on environment test after rework (Note 3)
Unfilled PC18M	QFP	A023 (Note 4)	20	2	TC+H
Unfilled PC18M	QFP	A034	24	2	TC Only
Unfilled PC18M	BGA	A235	19	1	TC+H
Unfilled PC18M	BGA	A296 (Note 4)	18	2	TC Only
Unfilled PC18M	BGA	A305	21	2	TC+H
Unfilled PC18M	BGA	A307 (Note 4)	22	1	TC+H
Filled XP2742	QFP	A311	6	1	TC+H
Filled XP2742	QFP	A312	6	2	TC+H
Filled XP2742	QFP	A345	7	2	TC+H
Filled XP2742	QFP	A384	14	2	TC Only
Filled XP2742	BGA	A392 (Note 4)	15	2	TC+H
Filled XP2742	BGA	A583	14	1	TC+H
Filled XP2742	BGA	A593 (Note 4)	10	1	TC Only
Unfilled PC18M dip only (Note 5)	BGA	A596 (Note 4)	9	0	TC+H

Notes

Note 1: Spray type after the low viscosity unfilled PC18M dip coat and partial cure

Note 2: The number of spray runs with partial cures between them (e.g. Board A23 with two spray runs has the following layers: low viscosity unfilled PC18M dip coat/partial cure/spray/partial cure/spray/full cure).

Note 3: The boards were environmentally stressed using thermal cycling (TC) or TC and humidity (TC+H) as described in 3.3 and 3.3.2 below.

Note 4: Older boards for comparison: Assembled WP 2213 QFP boards were coated with PC18M-based coatings and aged for 3,030h at 85°C and 85%RH during whisker testing earlier in the WP 2213 project in 2015 [3].

Note 5: PC18M dip only sample with no spray processed during the XP2742 spray coating sample batch.

3.1.2 Coating materials

The rework coating material batch information is given in Table 6 to

Table 8. The unfilled PC18M was mixed with the solvent to obtain the appropriate viscosity. The target dilution of the PC18M based on the coatings used in 2015 was 70%. A viscosity of 50 cps was used in the rework coating, rather than 30 cps as was used in the dip coating process. The low viscosity unfilled PC18M was applied with a syringe to flood coat the part and the 50 cps flow characteristics were satisfactory.

The viscosity of the PC18M and the PC18M 20% XP2742 for the coatings used in 2015 was 150 cps at start of process. The coatings used in this rework trial were diluted to 350 cps with AC0305, since the automated spray equipment was not going to be used, and it was known that the sprayed coatings increased in viscosity during the usage time, so an intermediate value would likely be acceptable. There was an option to dilute the coating if needed, but it coated well at 350 cps. Bubbles were observed in the coatings; a lower viscosity would avoid bridging, however, the higher viscosity was expected to provide better coverage.

Table 6: Unfilled PC18M rework coating material batch information.

Sample name:	Loctite Hysol Stycast PC18M
Lot code:	OX5H006076
Incoming viscosity:	nominal from supplier unknown
Date of manufacture	06/12/2015
Packaging	1 gallon can
History	opened 2015, Oct. 14, and repurged / resealed
Re-opened date	11/21/2016
Packaging	1 gallon can

Table 7: Solvent material batch information.

Diluent name	Loctite Hysol AC0305
Lot code:	OX5J001293
Incoming viscosity:	n/a
Date of manufacture	6/18/2015
Packaging	1 gallon can
History	received 2015, unopened
Re-opened date	11/21/2016
Packaging	1 gallon can

Table 8: Rework PC18M+20%XP2742 rework coating material batch information.

Sample:	PC18M 20% 2742
Sample name:	Loctite CCP-20601-26
Lot code:	XO5APR16
Incoming viscosity:	nominal from supplier unknown, > 3000 cps
Date of manufacture	Mar-16
Packaging	100 mL received, sealed with black tape in dark plastic container.

3.2 Celestica rework process for multilayer coatings

There were two varieties of boards provided for the rework process. The first board has multiple components mounted but only a single QFP44 was reworked. The second board, a partially populated Ball Grid Array (BGA) board, has domed solder from the SMT screening and reflow processes but does not have any components. This second board will be used to compare the adhesion of the reworked coatings to aged coating on bare FR4 epoxy.

The team decided to use thermal stripping as the removal method for the QFP boards and the media blaster for the BGA boards.

3.2.1 QFP44 Removal

The QFP44 devices were removed using an Air Vac DRS25-XLT semi-automated hot gas rework machine. The softened residual coating from under the device was then cleaned from the footprint area to allow for attachment of a new device to the solder pads. The new devices were attached using standard manual soldering techniques as described in Section 2.3.

3.2.2 QFP44 Recoating

Appropriate dilutions of the coating materials were provided. A 30 cc syringe with an 18 gauge plastic tip was loaded with the ~50 cps PC18M material. In this case, the syringe acts to keep the very low viscosity material from flowing freely over the board. Light manual pressure was applied to the plunger to allow some material to escape as the end of the tip was run over the knees of the solder leads. This effectively flooded the four edges of the device. The boards were left to air dry at room temperature for 35 minutes in the flat orientation. Then loaded into a preheated, vented oven with a pan of water and held at 60 °C for two hours.

The boards were removed from the oven and allowed to cool to room temperature. They were then brush coated with the more viscous unfilled PC18M or PC18M+20%XP2742 nanosilica filled coating and left to air dry at room temperature for 35 minutes followed by 2 hours at 60 °C and elevated humidity. The boards were then allowed to cool and air dry at room temperature for 24 hrs before being packed for shipping.

3.2.3 Flat board rework

An area 25 mm by 60 mm at the lower end of the BGA card was identified as the test area. Inside that zone a smaller area approximately 20 mm by 25 mm was identified for coating removal. The entire board except for the removal area was masked with tape and the coating was removed by media blasting with sodium bicarbonate powder. Once the coating was removed the mask was removed by hand and the perimeter of the removed area was chased with a 700°F solder iron to remove the step at the margin of media blasting.

The entire 25 mm by 60 mm area was brush coated with the 50 cps material, air dried for 35 minutes and then heat cured in a high humidity oven at 60 °C for two hours in the flat orientation. The boards were then cooled to room temperature, brush coated with the more viscous unfilled PC18M or PC18M+20%XP2742 nanosilica filled material and air dried for 35 minutes then heat cured in a high humidity oven at 60 °C for two hours in the flat orientation.

3.3 Environmental exposure and adhesion testing

After the rework coating was applied and cured, the samples were sent back to BAE Systems for environmental exposure, photography and analysis. The SEM and cross-section boards: QFP-A023 and QFP-A031 were submitted to the BAE Systems Failure Analysis (FA) lab for SEM back-scatter inspection for coating coverage and cross-sectioning.

Time line was as follows:

- 12/6/2016 received samples from Celestica
- 12/9/2016 to 12/16/2016 Thermal cycling
- 12/27/2016 to 1/5/2017 Humidity
- 1/9/2017 to 1/18/2017 Inspection in FA Lab and photographs
- 1/20/2017 BGA rework boards sent back to Celestica for adhesion testing

3.3.1 Thermal cycling

The samples were at room temperature and humidity conditions for approximately a week prior to starting thermal cycling. One hundred thermal cycles from -55 to 125 °C were performed in a highly accelerated life test (HALT) chamber with liquid nitrogen cooling. The sample placement in the chamber is shown in Figure 19. The total cycle time was 96 minutes. The cycle used a dwell time of 30 minutes and a ramp rate of 10 °C/min (for a total ramp time of 18 minutes). Two boards were instrumented with type K thermocouples and were monitored during thermal cycling (see Figure 20). The cycling started December 14, 2016 and was completed December 16, 2016.

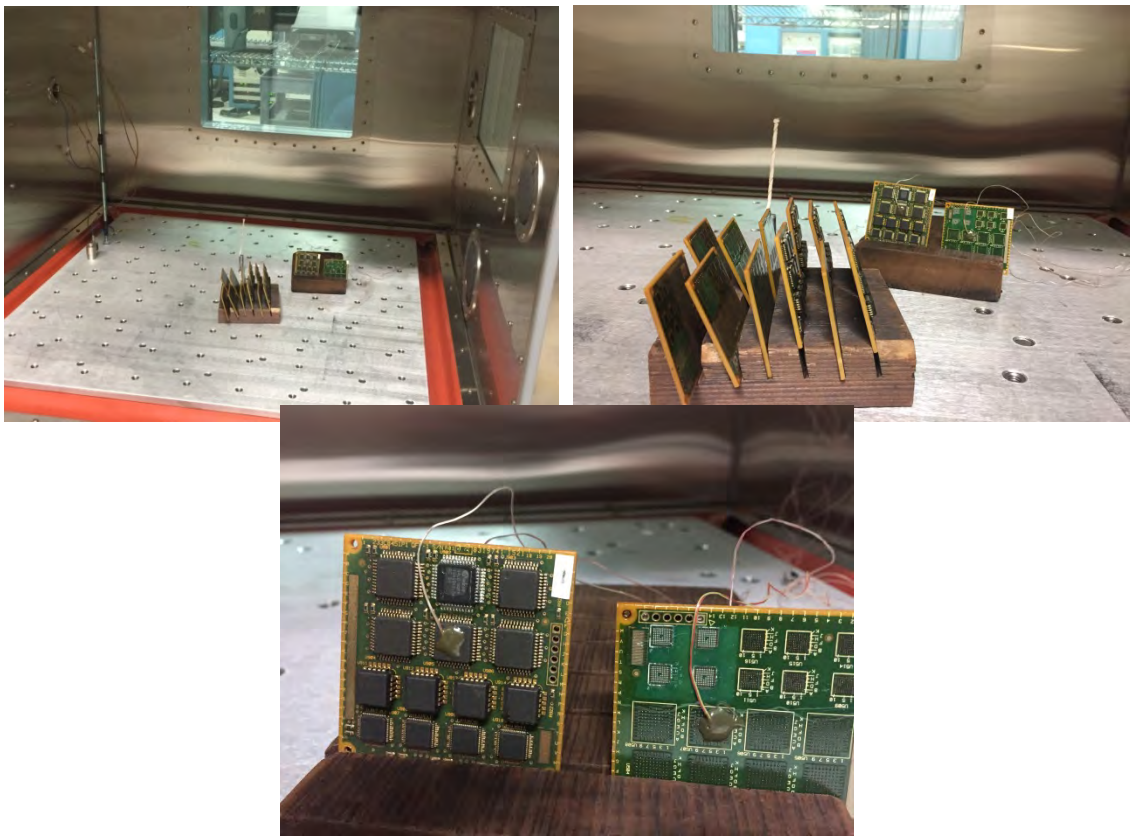


Figure 19: Sample placement in thermal cycling chamber.

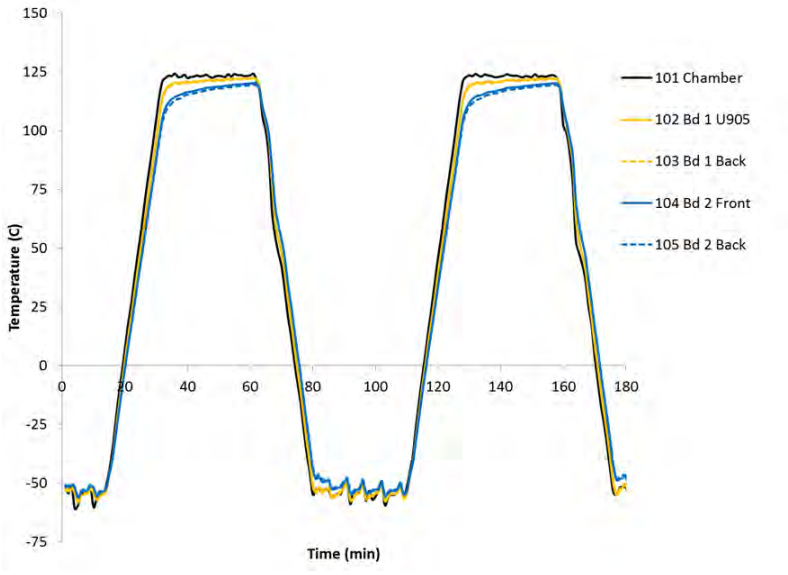


Figure 20: Typical board temperature during thermal cycling.

3.3.2 Humidity

A modified MIL-STD-810 method 507 humidity test was performed for 10 days. The sample placement in the chamber is shown in Figure 21. The test used a 24 hour cycle consisting of a ramp from 38 °C to 65 °C in 2 hours, then a hold at 65 °C for 6 hours, followed by a ramp from 65 °C to 38 °C in 16 h while continually maintaining 95 percent relative humidity (see Figure 22). The humidity exposure started on 12/27/2016 and completed 1/5/2017 at 3:30 PM.



Figure 21: Sample placement in humidity chamber.

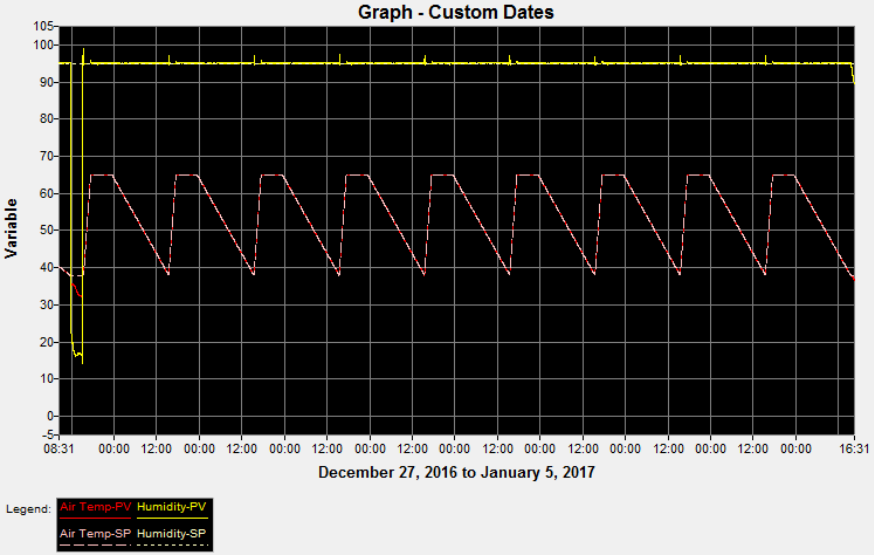


Figure 22: Humidity cycling chart.

3.3.3 Inspection after environmental exposure

3.3.3.1 Optical

No abnormalities in the surface appearance were visually noted after thermal cycling and before the tape testing (see Figure 23 and Figure 24). Some bubbles were evident in the coating. Additional optical images before and after environmental exposure are shown in sections 4.1 and 4.2.

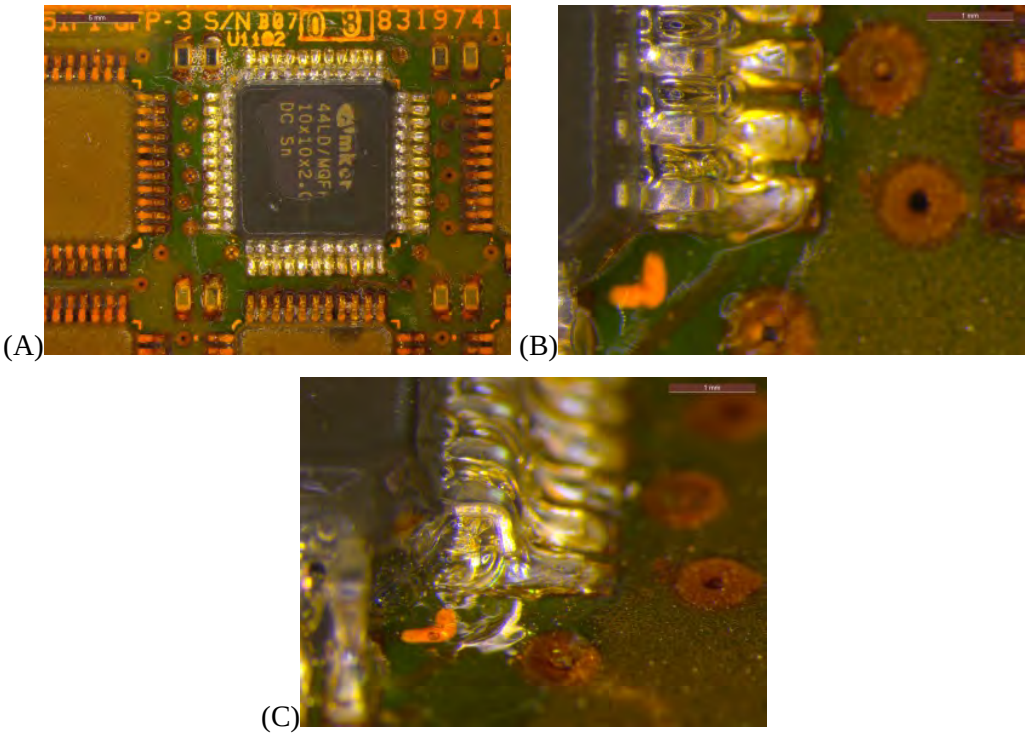


Figure 23: Optical image, board QFP-A034 unfilled PC18M after thermal cycling (A) overall part, (B) close-up of leads, and (C) isometric close-up of leads.

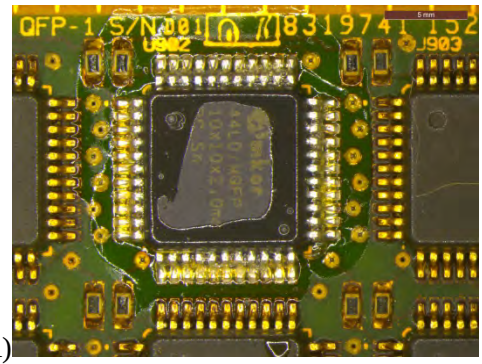
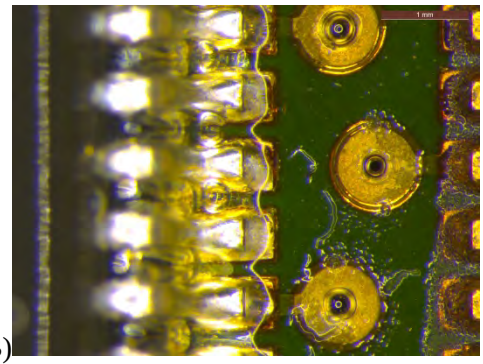
(A)  (B) 

Figure 24: Optical image, board A312 filled PC18M-20%XP2742 after thermal cycling and humidity; (A) overall part and (B) close-up of leads.

3.3.3.2 SEM Inspection

The reworked assemblies were examined with the scanning electron microscope (SEM) using back scatter electron (BSE) imaging. Undesirable bubbles in the coating and coating bridging between leads were evident. Some of the lead corners near the knee tended to have thin coating regions on both the unfilled PC18M sample and the nanosilica filled PC80+20%XP2742 sample coatings (Figure 25 and Figure 26). There were some coating cracks. The cracks were located in the coating along a line adjacent to the lead corners. The cracks seemed more predominant on the unfilled sample than the filled sample. Some coating cracks along the leads were also evident in the non-reworked leads (Figure 27). The rework coating has smoothed the rough original coating surface (Figure 27). Some undesirable fibrous foreign object and debris (FOD) were found on the assembly after rework (Figure 28). Additional images from the SEM examination are shown in section 4.3.

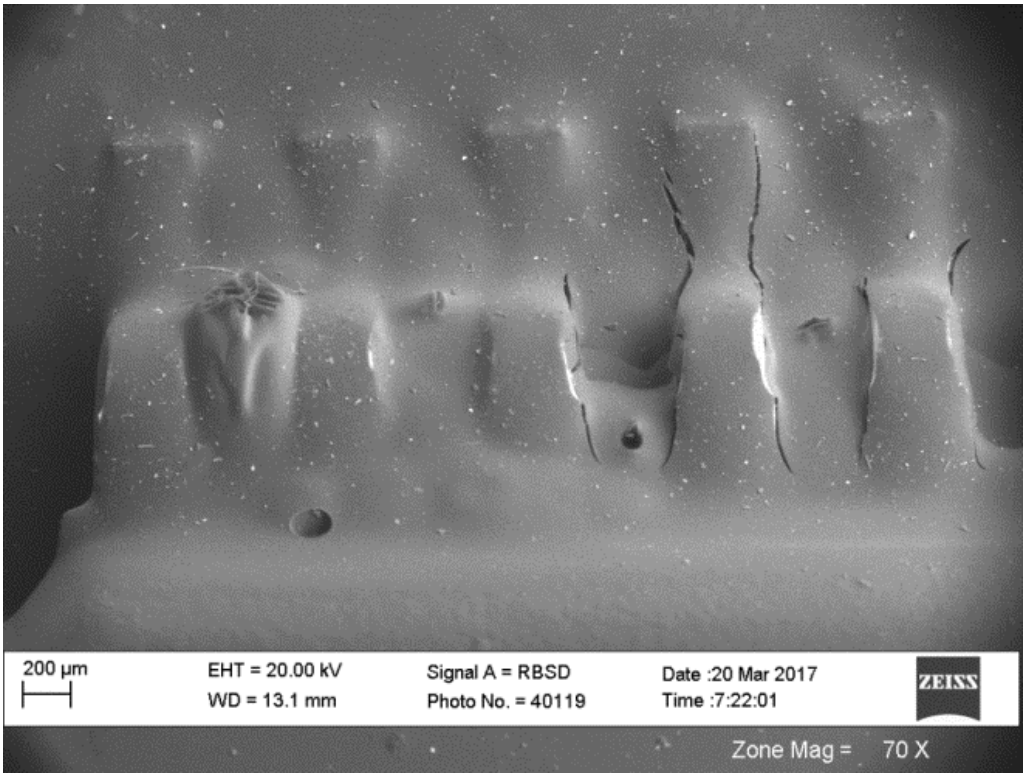


Figure 25: SEM BSE unfilled PC18M QFP-A023 U1002 pins 44 to 40, 70x.

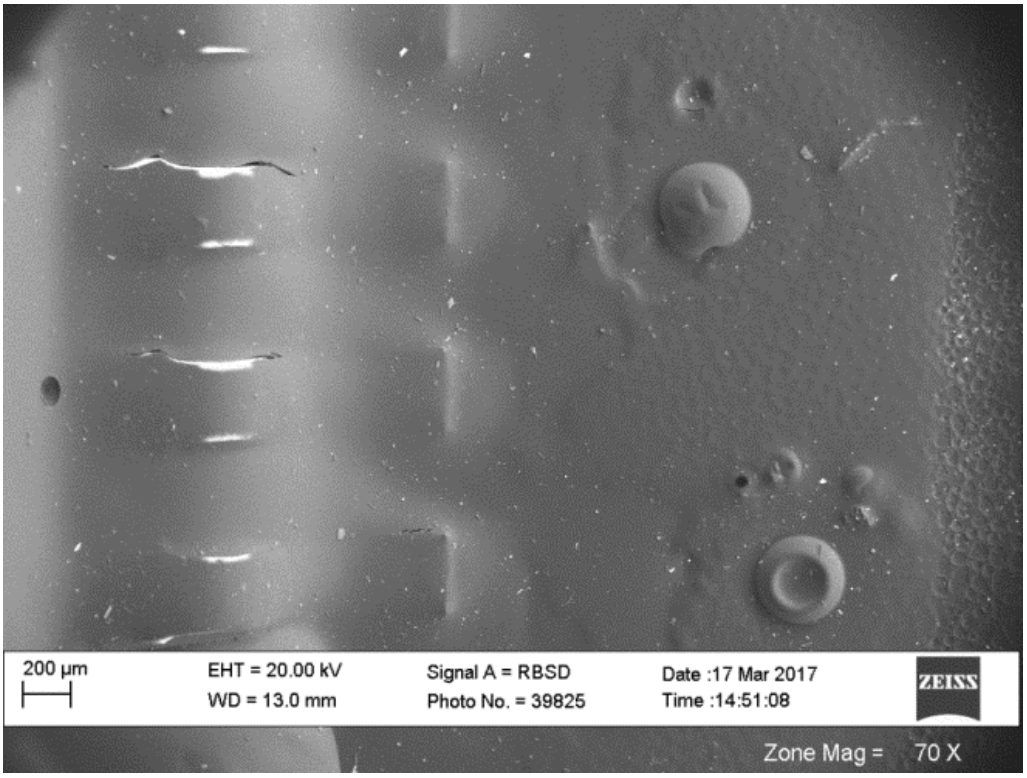


Figure 26: SEM BSE filled PC18M+20%XP2742 QFP-A312 U902 pins 23 to 26, 70X.

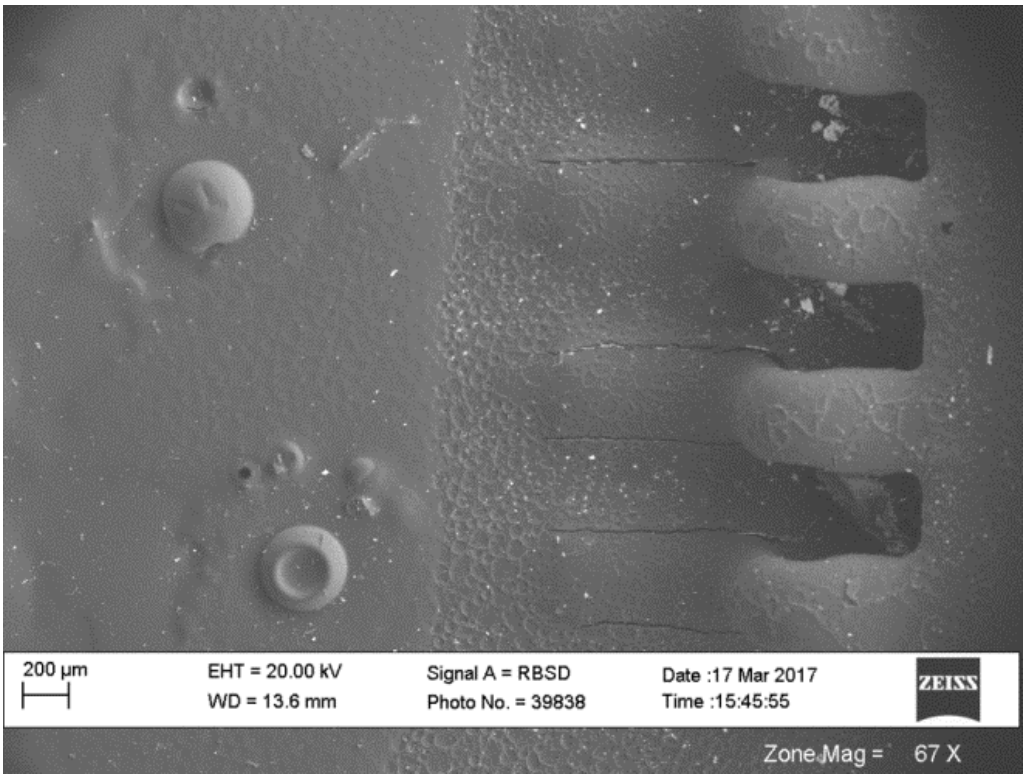


Figure 27: SEM BSE filled PC18M+20%XP2742 QFP-A312 non-reworked U903 adjacent to U902 pins 23 to 26, 67x.

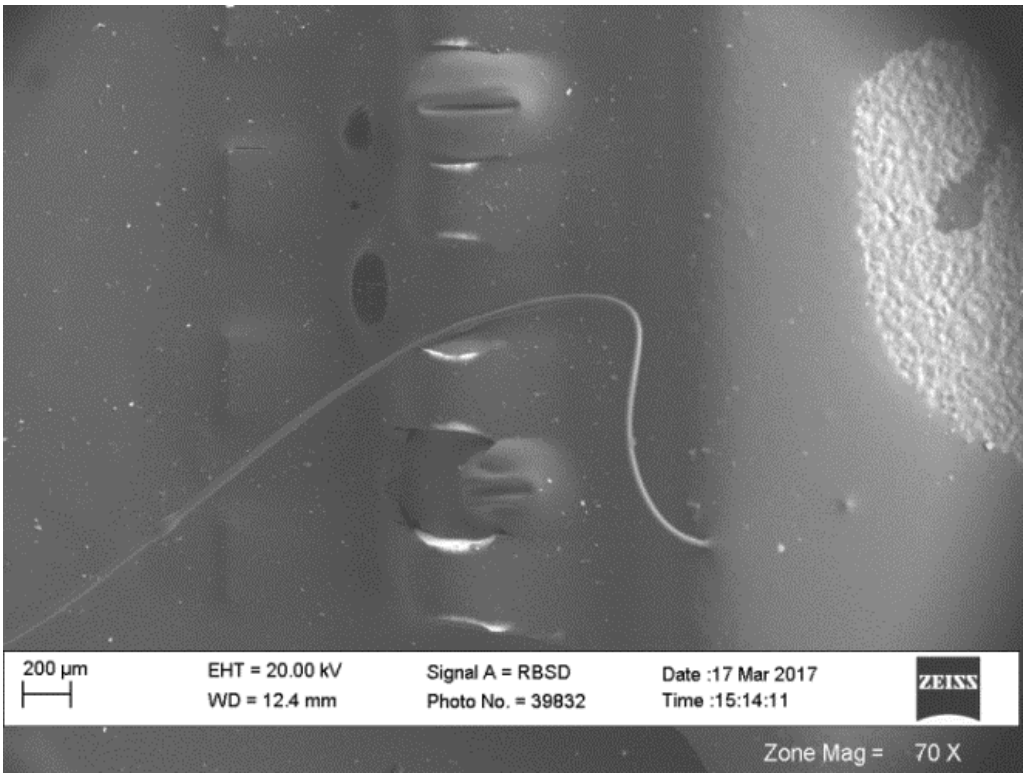


Figure 28: SEM BSE filled PC18M+20%XP2742 QFP-A312 U902 pins 8 to 11, 70x.

3.3.3.3 Cross-section inspection

Cross-sections were made of the unfilled PC18M and the nanosilica filled PC18M+20%XP2742 (Figure 29 and Figure 30). The cross-section images compare the lead knee, foot and heel of the reworked parts with the unfilled and filled coatings (Figure 31).

Typically good adhesion was observed between original and rework coating on the part adjacent to the reworked site (Figure 32). The preferred coating situation having good coverage on the lead with minimal coating fill behind the lead and minimal fill between the part and the board was sometimes observed (Figure 33). The nanosilica filled coating can be seen on top of the unfilled syringe flood coat near the foot (Figure 34).

In some instances, significant coating flowed between the part and the board (Figure 35) and significantly filled between the lead and the package body (Figure 36). Since the thermal coefficient of expansion of the conformal coating is much higher than the leads and the solder, thermal cycling can cause solder fractures (Figure 36 and Figure 37).

The coating over the lead tip, when sufficiently thick, does not fracture (Figure 38). If the coating becomes thinner, the stress concentration of the lead tip can crack the coating (Figure 39). In some cases, the coating can become so thin that the lead tip has less than a micron of coating coverage (Figure 40).

Additional cross-section optical and SEM images are shown in section 4.4.

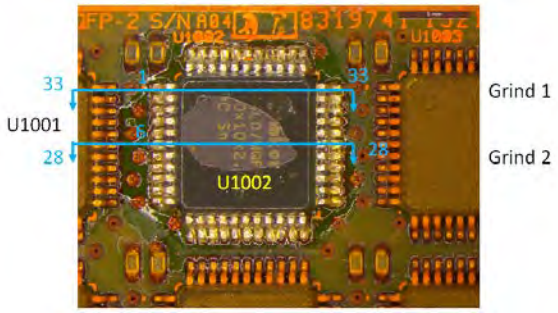


Figure 29: Cross-section plane locations of unfilled PC18M coated QFP-A023. The cross-sections go through the right side of U1001 (not reworked) and both sides of U1002 (reworked).

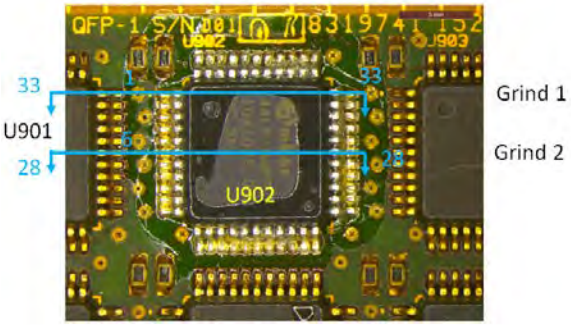


Figure 30: Cross-section plane locations for PC18M+20%XP2742 coated QFP-A312. The cross-section planes go through the right side of U901 (non-reworked) and both sides of U902 (reworked).

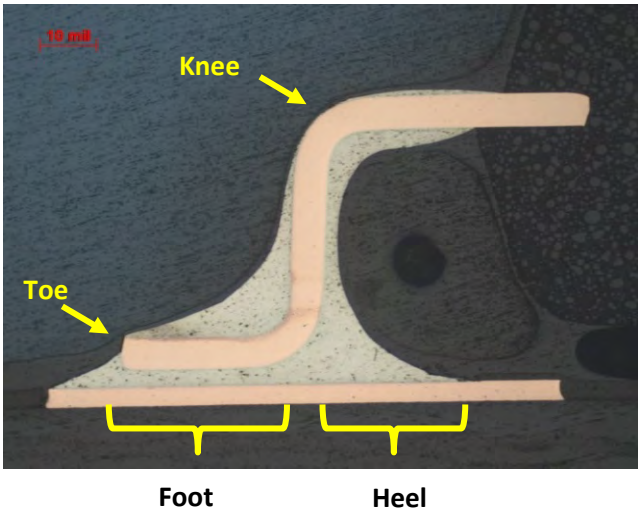


Figure 31: Nomenclature used to define locations on the lead.

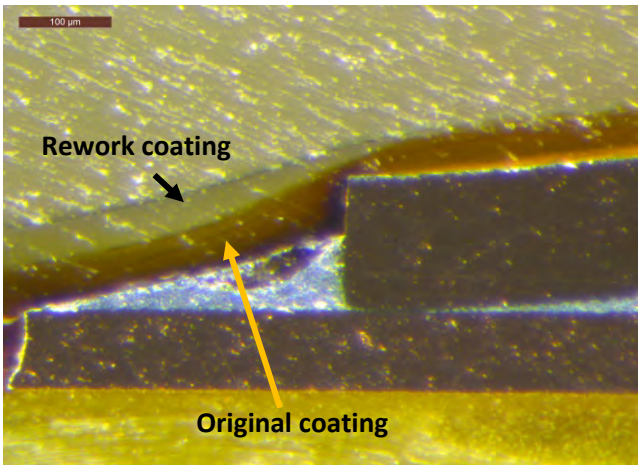


Figure 32: Good adhesion between old and new coatings. Rework coating from U902 flowed onto the toe of the adjacent non-reworked U901 lead 28 toe (nanosilica filled PC18M+20%XP2742, QFP-A312).

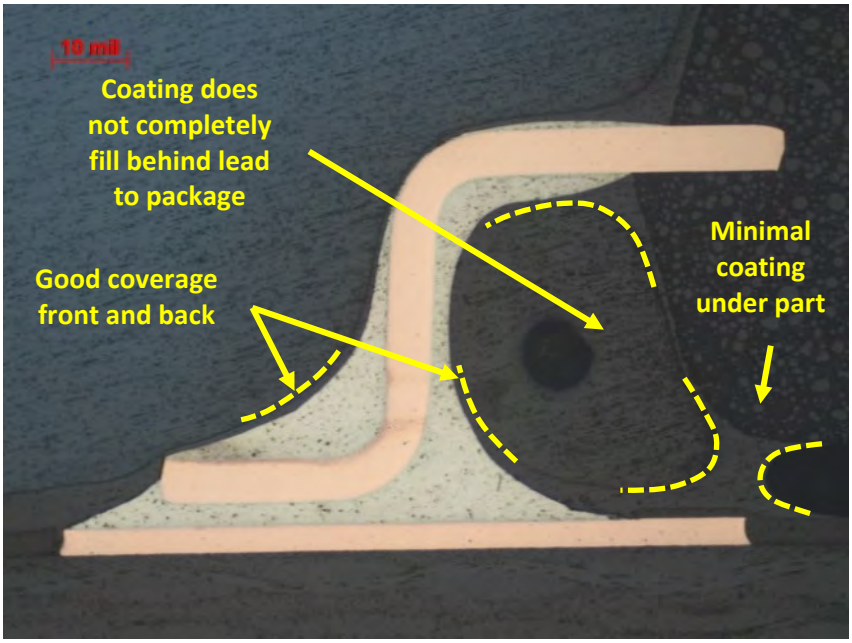


Figure 33: Preferred coating with good coverage on the lead with minimal coating fill behind the lead and minimal fill between the part and the board. Optical cross-section image, unfilled PC18M QFP-A023 U1002 Lead 1 shown, 50x.

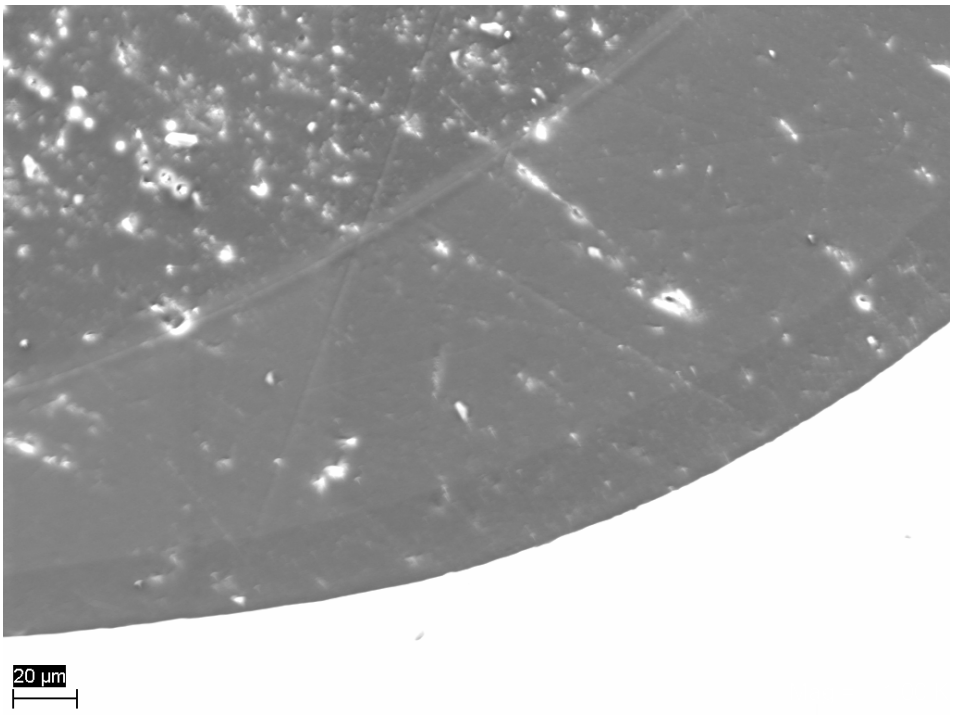


Figure 34: SEM cross-section image, filled PC18M+20%XP2742 QFP-A312 U902, Lead 28 bend above foot, 1,000x.



Figure 35: Optical cross-section image, filled PC18M+20%XP2742 QFP-A312 U902, Lead 33 under part, 50x.

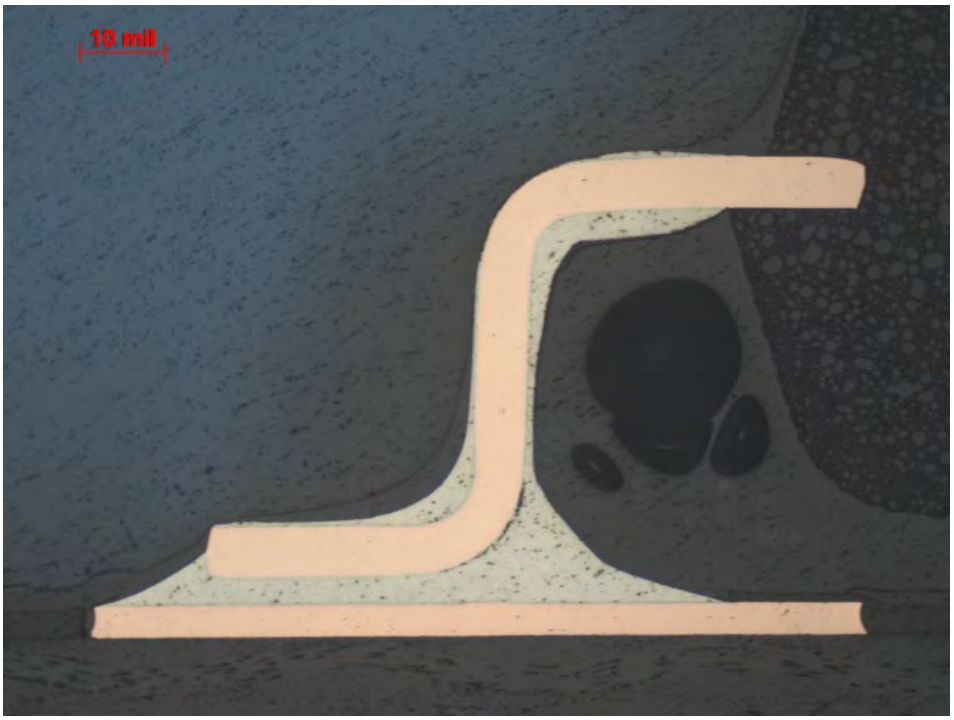


Figure 36: Optical cross-section image, filled PC18M+20%XP2742 QFP-A312 U902, Lead 1, 50x.

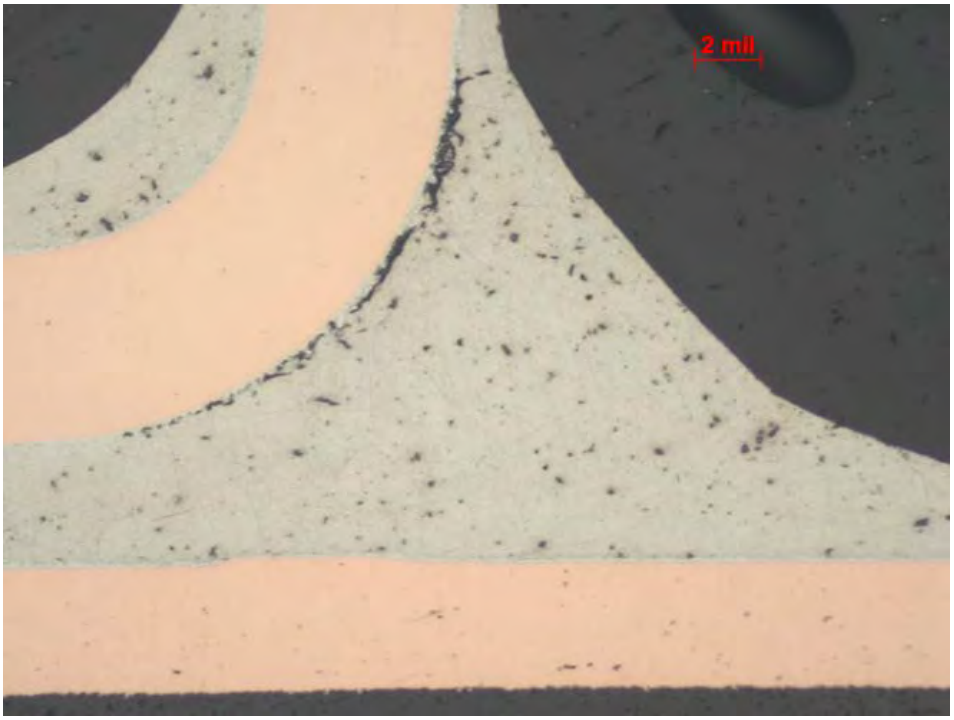


Figure 37: Optical cross-section image, filled PC18M+20%XP2742 QFP-A312 U902, Lead 1 heel, 200x.

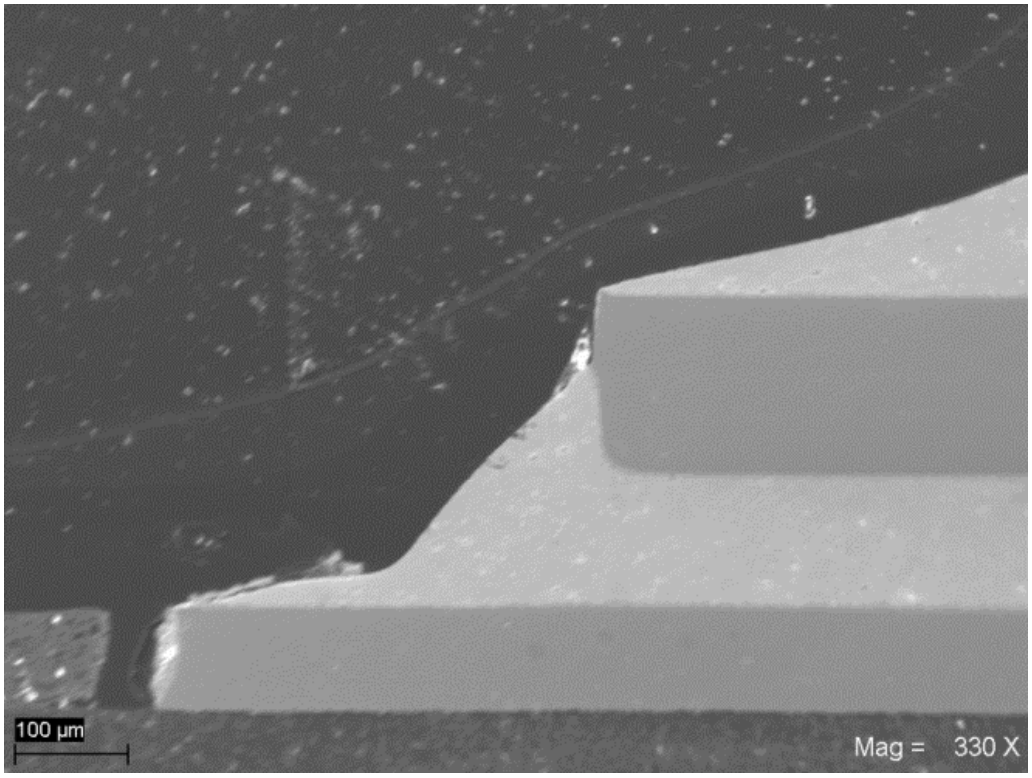


Figure 38: SEM cross-section image, unfilled PC18M QFP-A023 U1002, Lead 28 toe, 330x.

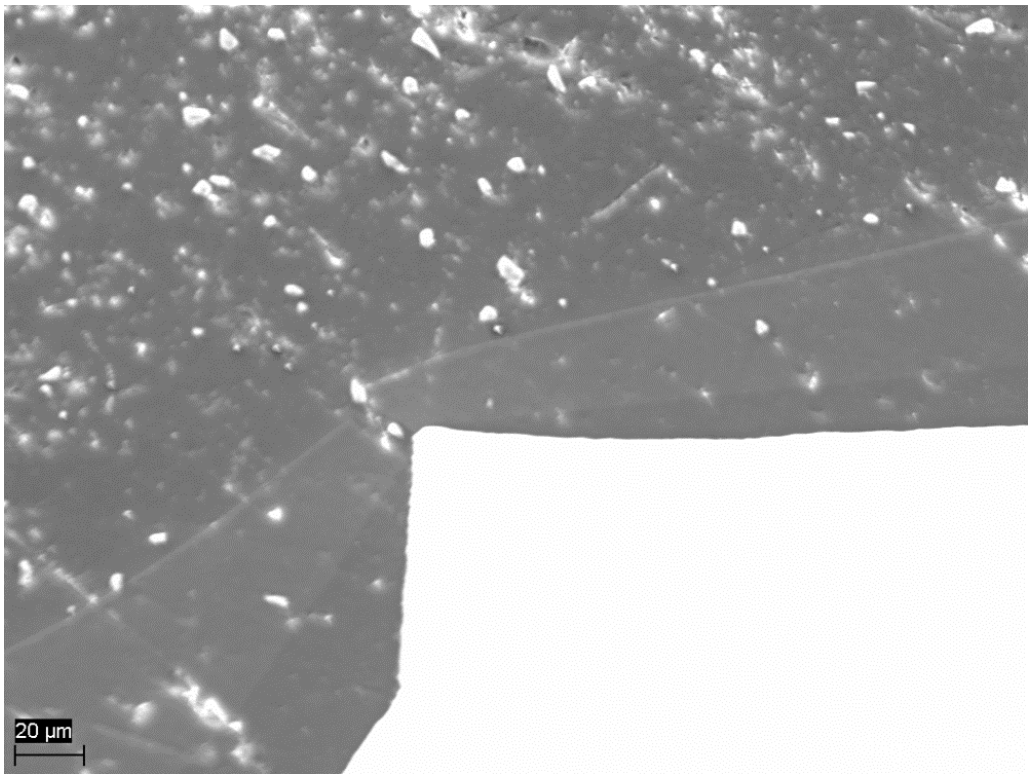


Figure 39: SEM cross-section image, filled PC18M+20%XP2742 QFP-A312 U902, Lead 28 toe, 1,000x.

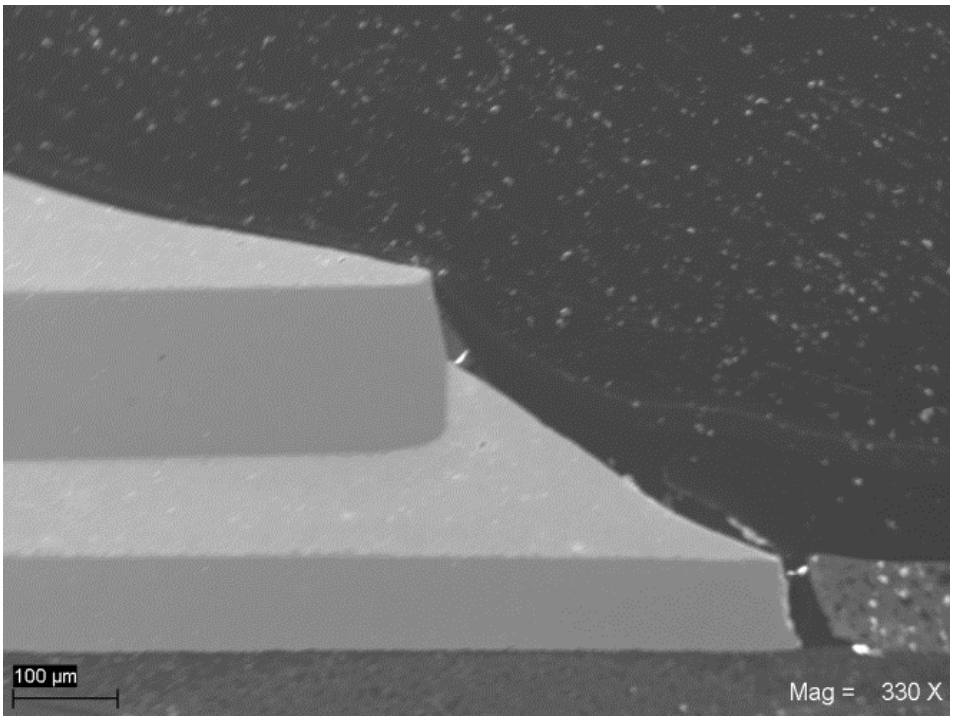


Figure 40: SEM cross-section image showing coating thinning over the lead tip (unfilled PC18M QFP-A023 U1002, Lead 6 toe, 330x shown).

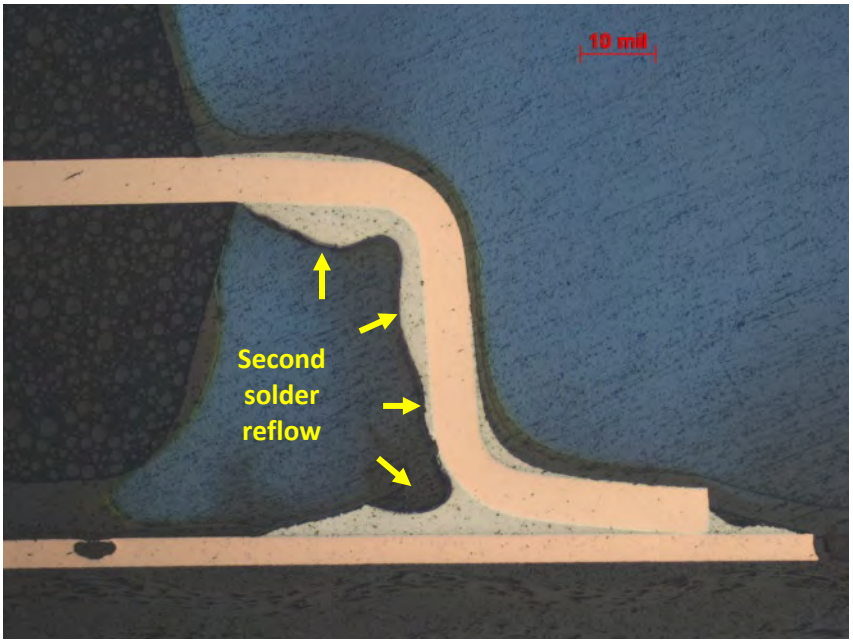
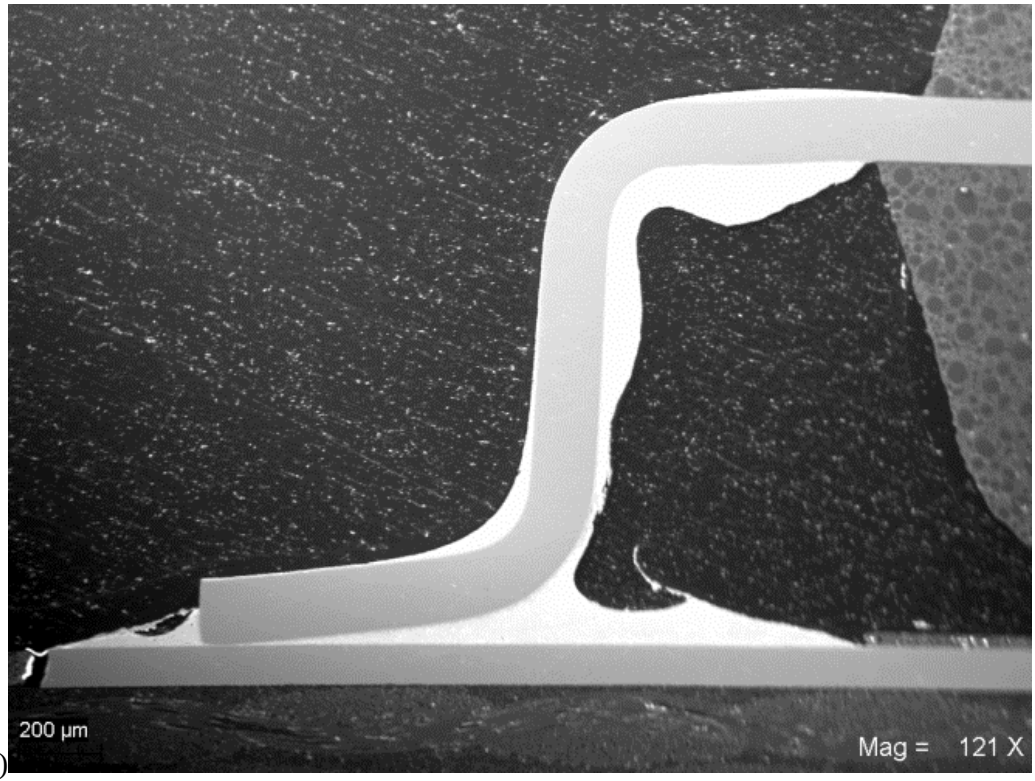


Figure 41: Optical image showing the second solder reflow which occurred on the non-reworked U901 adjacent to the hot air reworked U902 part. **(**Filled PC18M+20%XP2742 QFP-A312, non-reworked U901, Lead 28, 50x shown.)

(A)



(B)

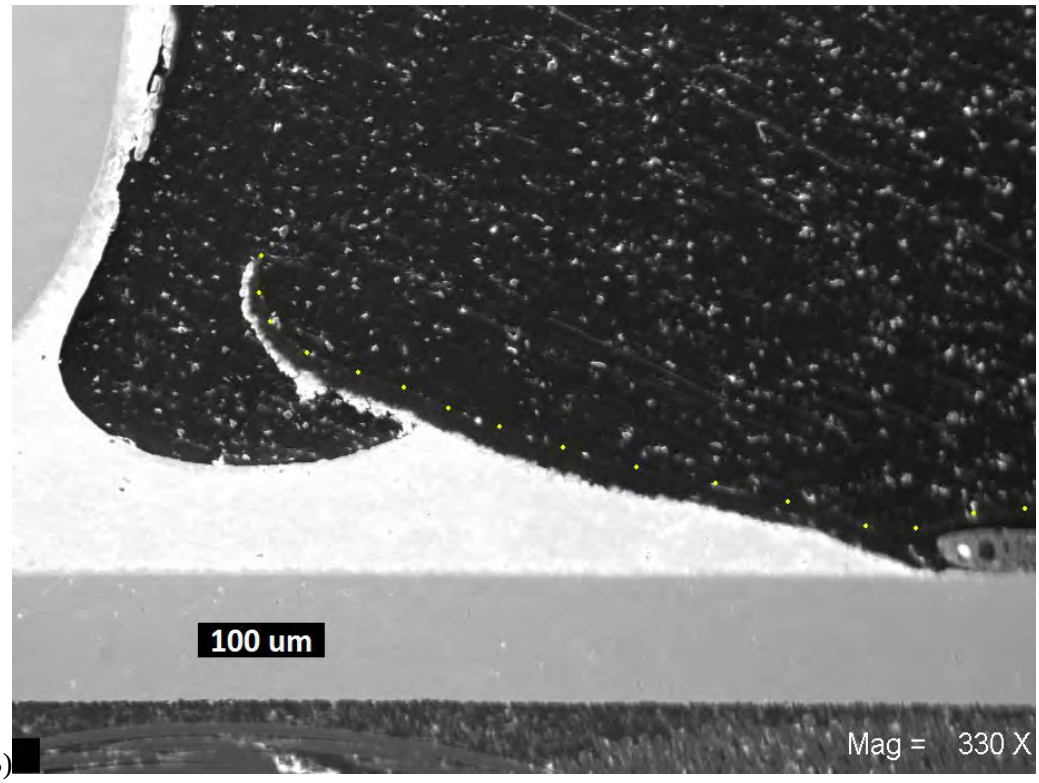


Figure 42: SEM cross-section image of Figure 42 showing the second solder reflow; (A) overall image and (B) higher magnification image showing with the broken original coating highlighted with yellow. (Filled PC18M+20%XP2742 QFP-A312, non-reworked U901, Lead 28 shown).

3.3.4 Rework coating thickness

The rework coating thickness was measured on the QFP center leads six and 28. The coating thicknesses at the locations shown Figure 43 were measured. When the coating was sufficiently thick, high magnification optical images were used for the measurement. In cases where the coating thickness could not be resolved, the sample was examined in the SEM (note that the sample was Au sputter coated prior to potting so that the coating surface could be distinguished from the potting when imaged in the SEM). Typical optical and SEM measurements are shown in Figure 44 and Figure 45.

Plots of coating thickness are shown in Figure 46 to Figure 48. Locations B, T and H had the thinnest coating. Significant coating build-up on the inside of the bend radius above the foot (locations D to F) was evident on several leads.

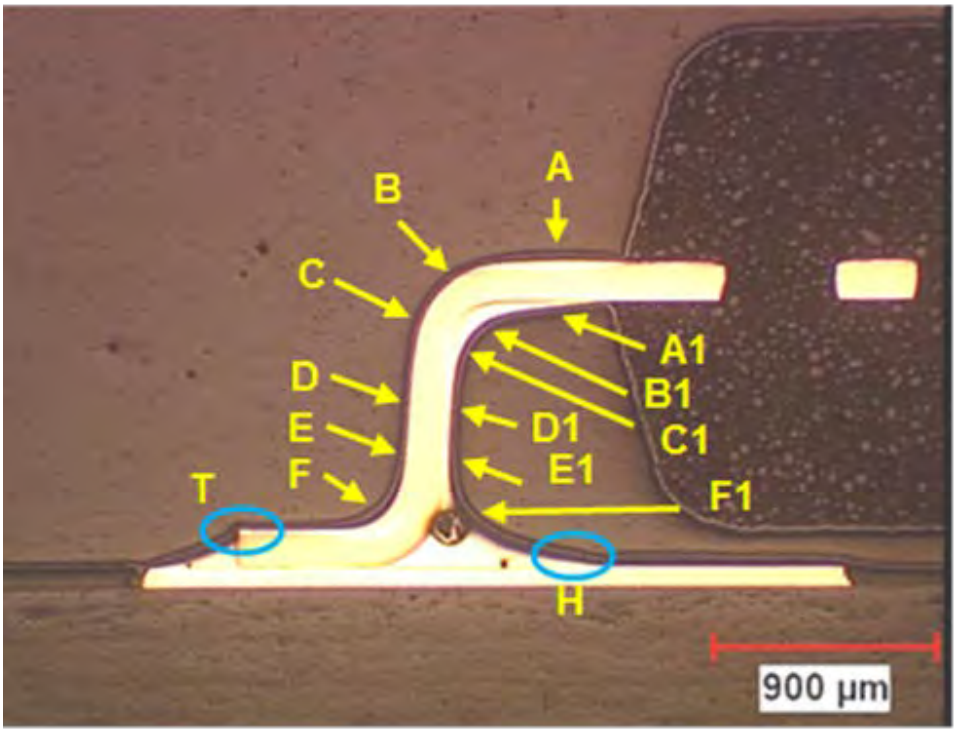


Figure 43: Coating thickness measurement locations.

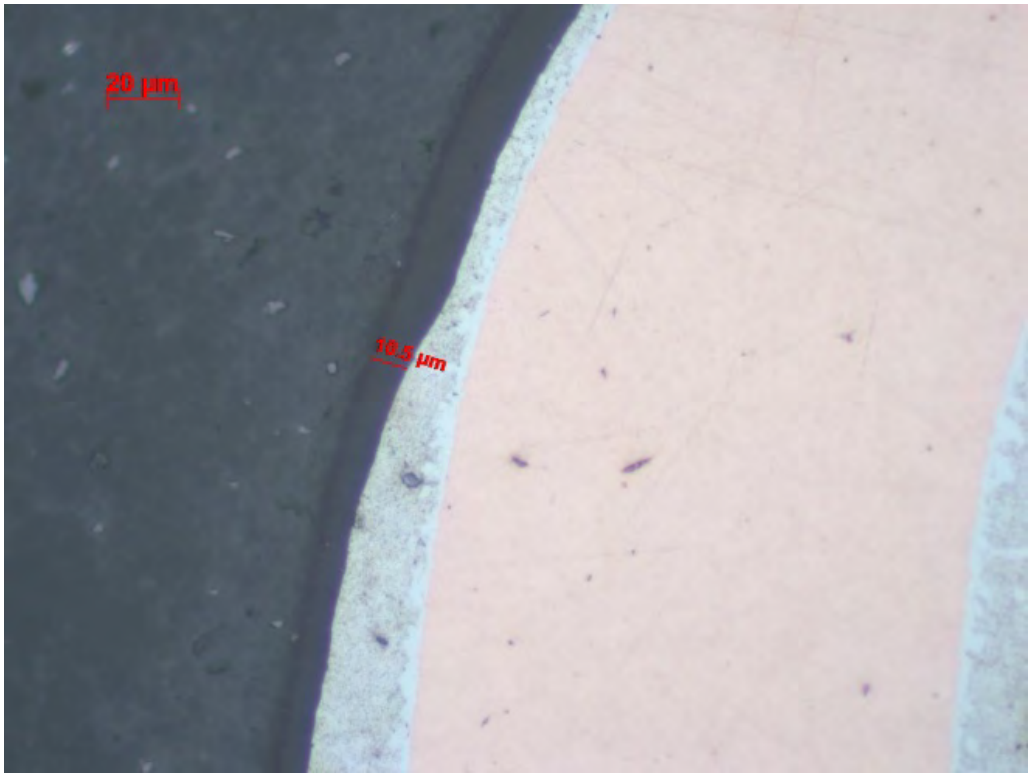


Figure 44: Optical cross-section image, unfilled PC18M QFP-A023 U1002, Lead 6 measurements, C, 500x. Coating thickness is 10.5 microns.

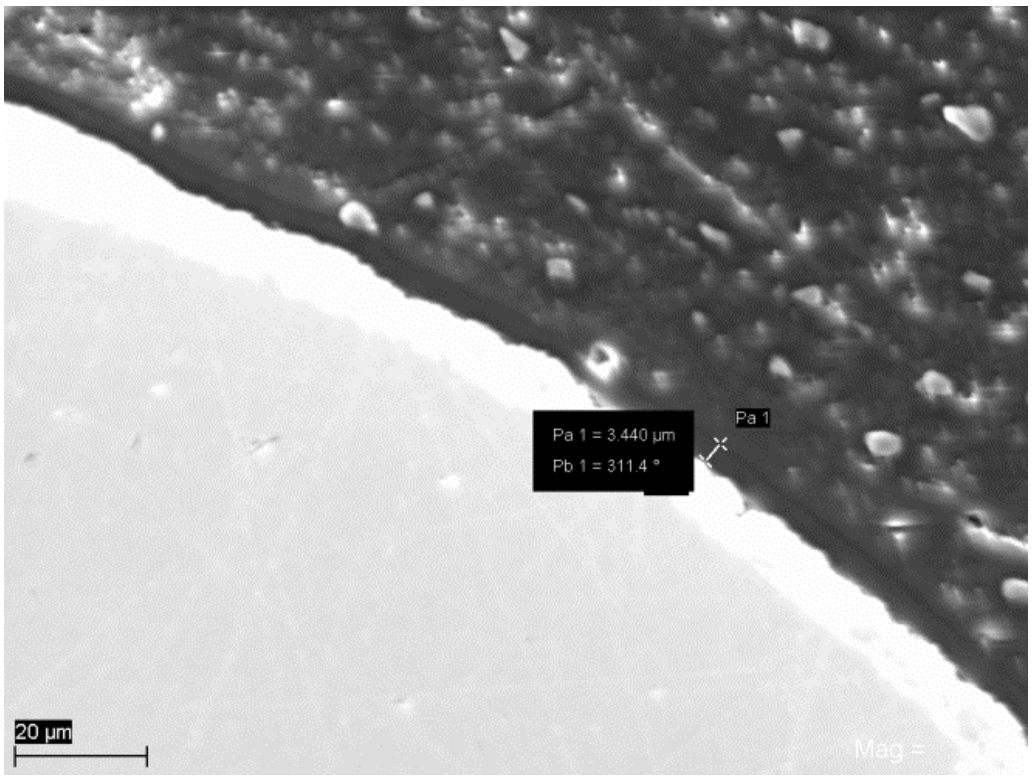


Figure 45: SEM cross-section image, filled PC18M+20%XP2742 QFP-A312 U902, Lead 6 measurements, B, 1,930x.

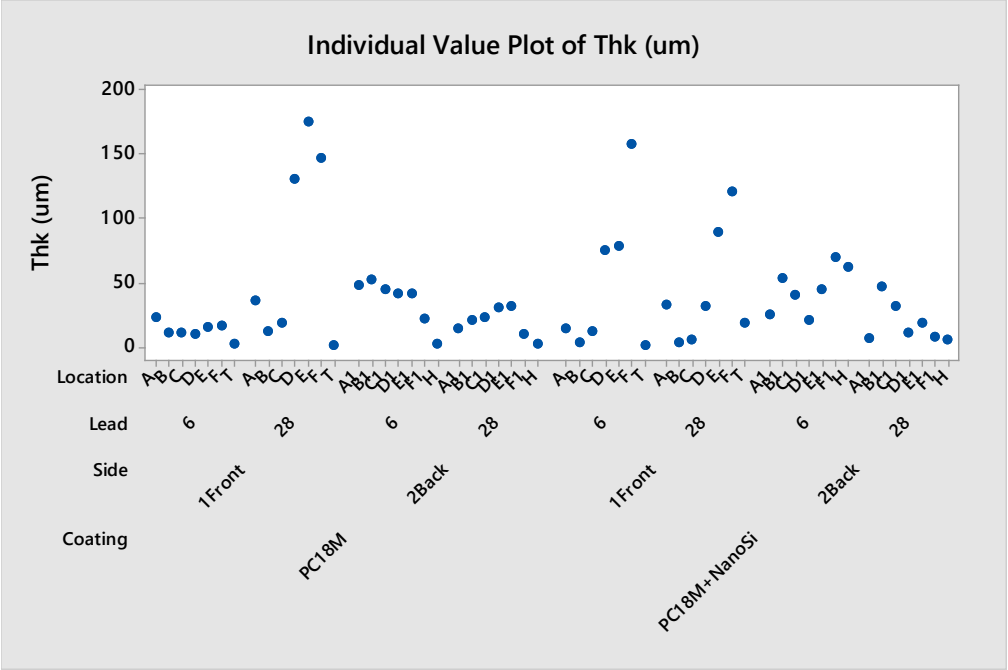


Figure 46: Individual value plot comparing rework coating thickness by location, lead and side (front/back) for unfilled PC18M and filled PC18M+20%XP2742 (PC18M+NanoSi).

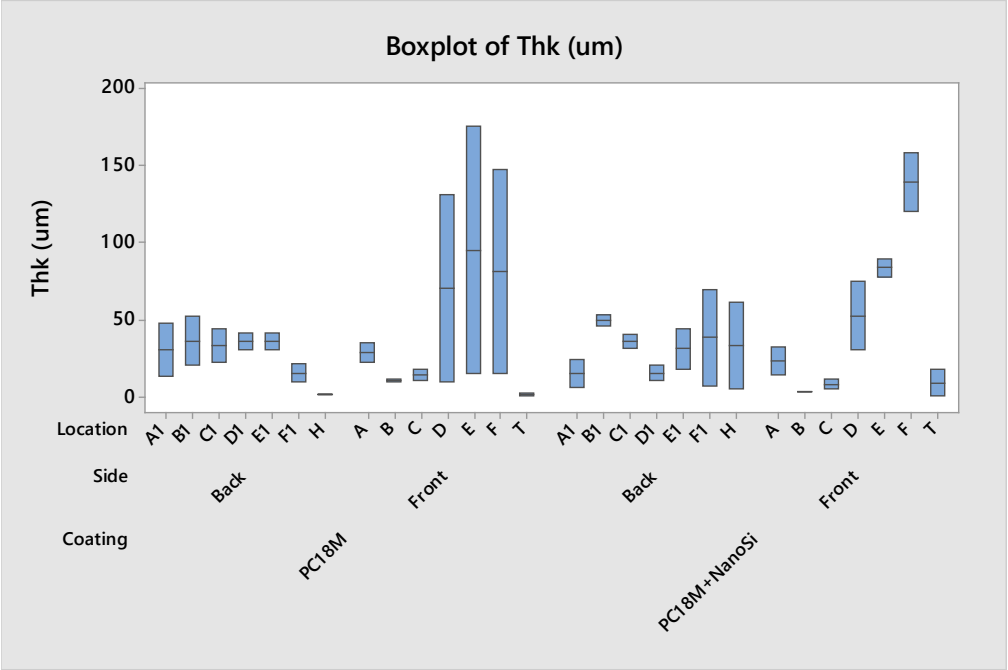


Figure 47: Box plot comparing rework coating thickness by location and by side (front/back) for unfilled PC18M and filled PC18M+20%XP2742 (PC18M+NanoSi).

Note that each box represents two data points.

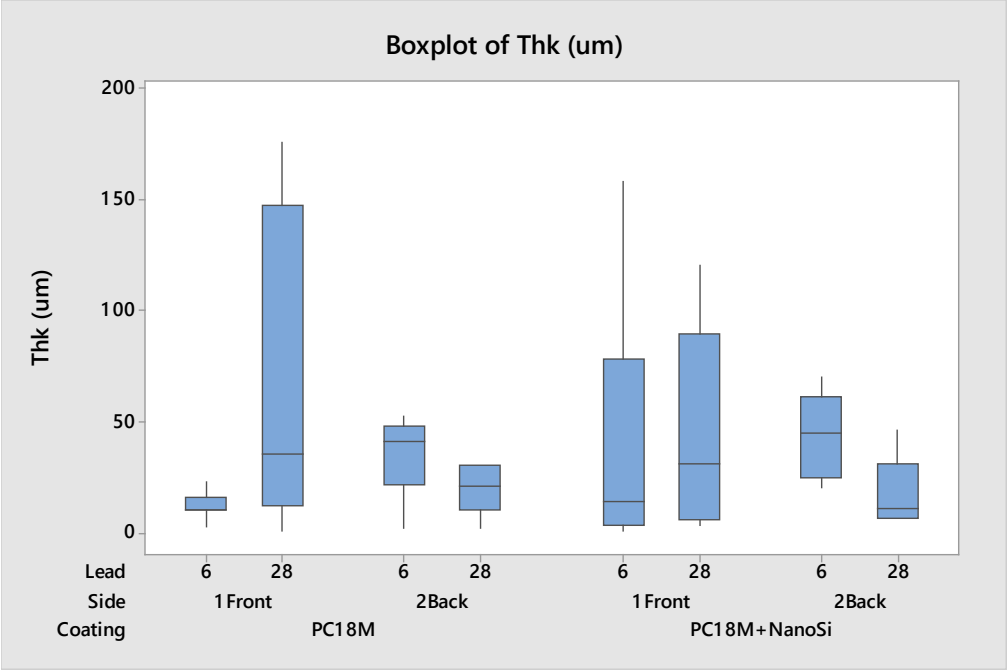


Figure 48: Box plot comparing rework coating thickness by lead and side (front/back) for unfilled PC18M and filled PC18M+20%XP2742 (PC18M+NanoSi).

3.3.5 Adhesion tape testing

The IPC-TM-650 2.4.1.6 Adhesion, Polymer coating test method [4] is a procedure for "determining whether the adhesion of a polymer coating to an inorganic or ceramic substrate is above an adequate level." This test is also commonly used for conformal coating adhesion testing.

According to the test method, the coating was patterned in a 10 x 10 grid of 1 mm squares. This patterning was created manually with an exacto knife, as the IPC Association Connecting Electronics Industries (IPC) patterning tool did not scribe the coating surface properly, due to the uneven topology of the substrate surface. Due to the complexity of the sample, (solder pads, not just solder mask), even the manual scribing was non-uniform, therefore, on most test sites, the full 100 squares could not be created. On some samples only a few squares were visible, therefore, the pattern lines were re-scribed.

Two grids per board were scribed, one in the non-overlapped area, and one in the overlapped area. An example of the scribed area is shown below in Figure 49.

Since the sample boards had already been through thermal cycling as described above in 3.3, scribing after a boiling water test was not performed, as the thermal cycling was deemed a more appropriate test of adhesion.

3.3.6 Adhesion results

On the squares that were created, adhesion by the tape test at room temperature gave good results (see Figure 49). The results are tabulated in Table 9.

A data file with all the images is available [5].

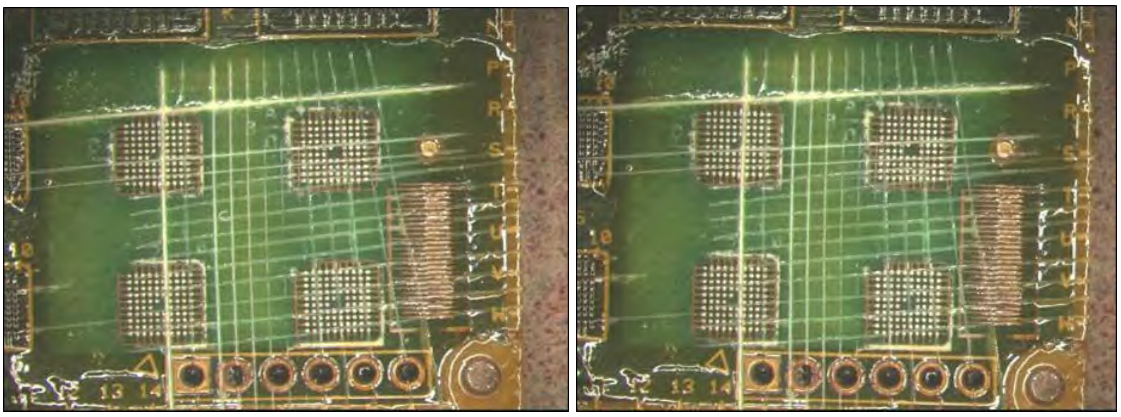


Figure 49: Board A235, post-TC+H, non-overlapped area, manual, before (left) and after (right) tape test.

Table 9: Adhesion Rating of Reworked Coating.

Board ID	Spray Coating Type	Coating Area	IPC Adhesion Rating	Comments
A305	Unfilled	overlapped	4	Manually scribed
A305	Unfilled	non-overlapped	4	Manually scribed
A235	Unfilled	overlapped	5	Manually scribed
A235	Unfilled	non-overlapped	5	Manually scribed
A296	Unfilled	overlapped	5	Manually scribed
A296	Unfilled	non-overlapped	5	Manually scribed
A307	Unfilled	overlapped	5	Manually scribed
A307	Unfilled	non-overlapped	5	Manually scribed
A596	Unfilled	overlapped	5	Manually scribed
A596	Unfilled	non-overlapped	5	Manually scribed
A593	Filled	overlapped	5	Manually scribed
A593	Filled	non-overlapped	5	Manually scribed

4. Detailed photographs and images

4.1 Photos prior to thermal cycling and humidity

Prior to environmental exposure, the figures showing the unfilled and filled samples are:

- Unfilled PC18M
  - BGA boards: Figure 50 to Figure 52
  - QFP boards: Figure 56 and Figure 57
- Nanosilica filled PC18M+20%XP2742
  - BGA boards: Figure 53 to Figure 55
  - QFP boards: Figure 58 to Figure 61

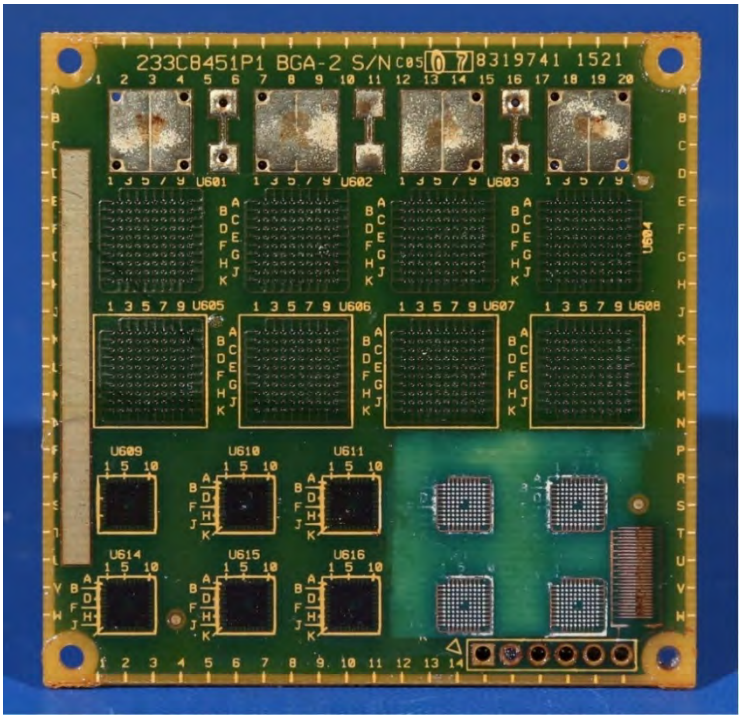


Figure 50: BGA-A235 unfilled 1-spray before environmental exposure.

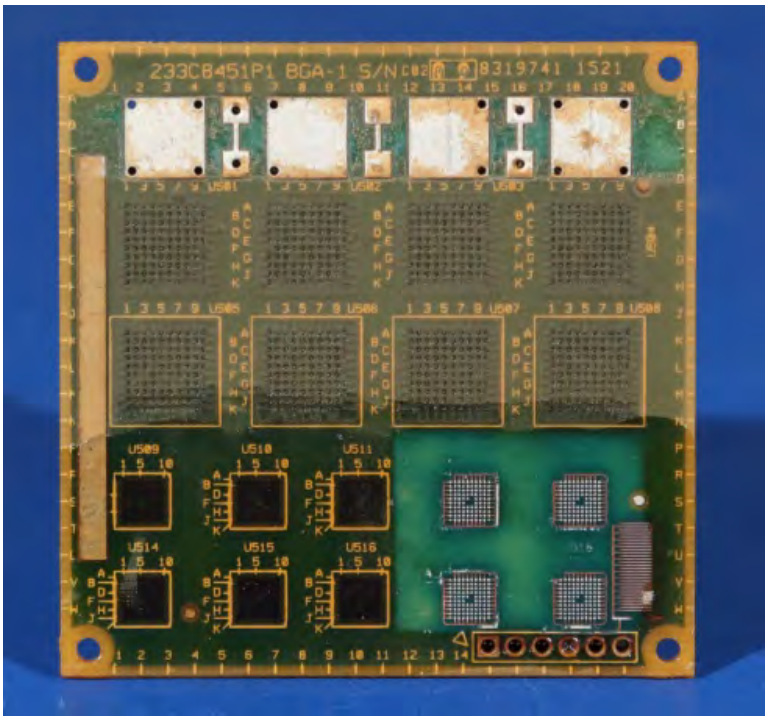


Figure 51: BGA-A296 unfilled 1-spray before environmental exposure.

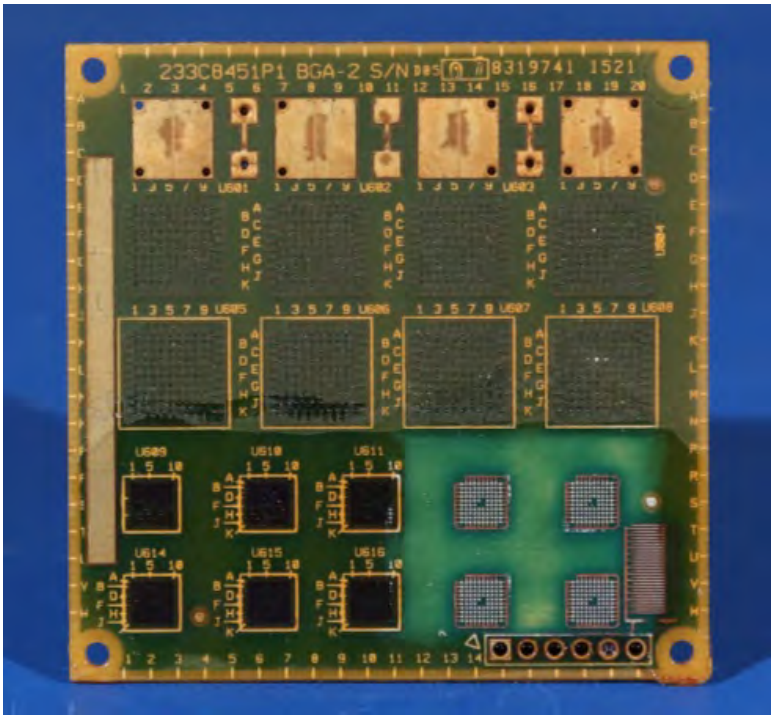


Figure 52: BGA-A305 unfilled 2-spray before environmental exposure.

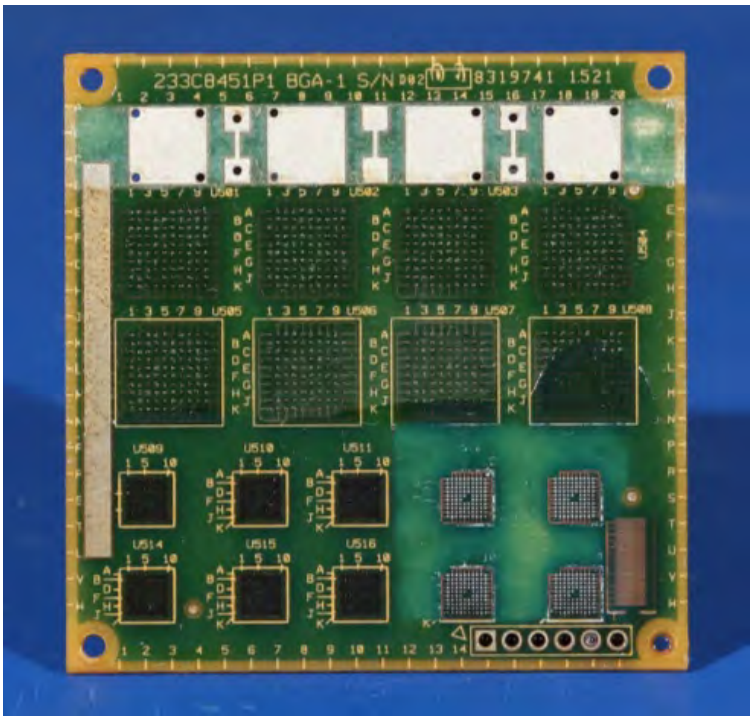


Figure 53: BGA-A392 filled 2-spray before environmental exposure.

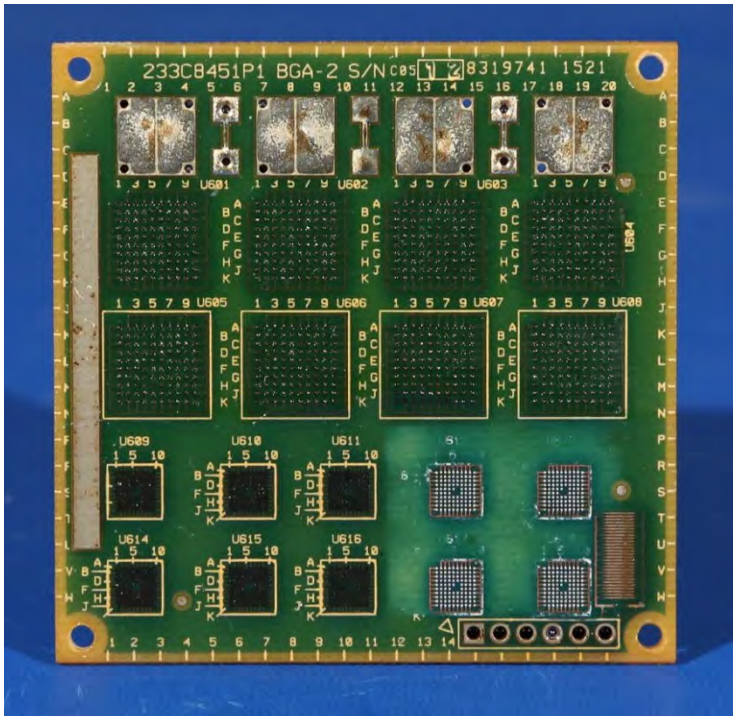


Figure 54: BGA-A583 filled 1-spray before environmental exposure.

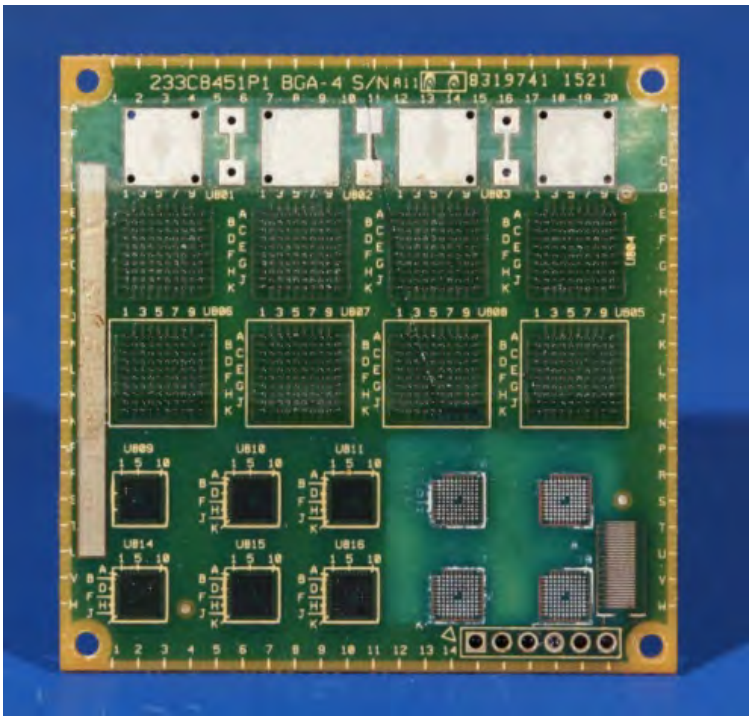


Figure 55: BGA-A593 filled 1-spray before environmental exposure.

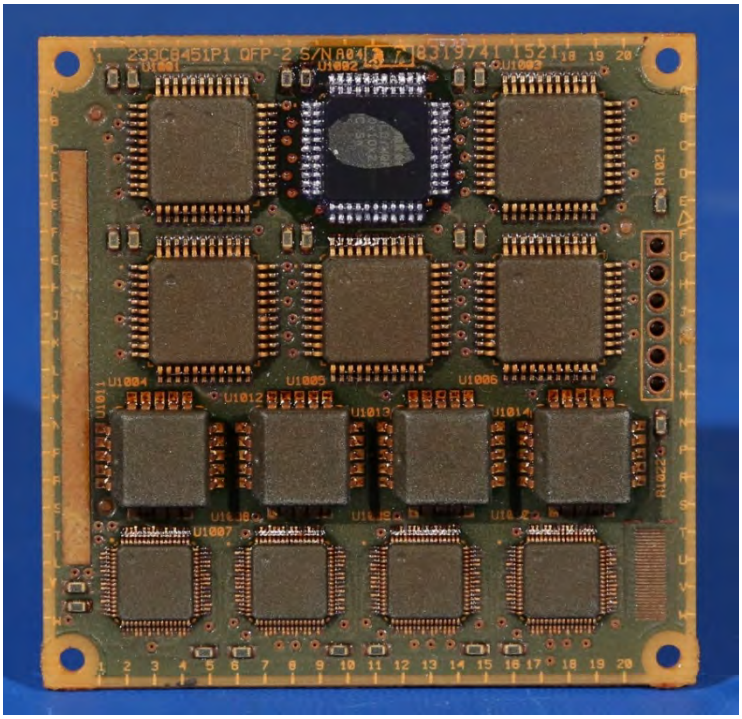


Figure 56: QFP-A023 unfilled 2-spray before environmental exposure.

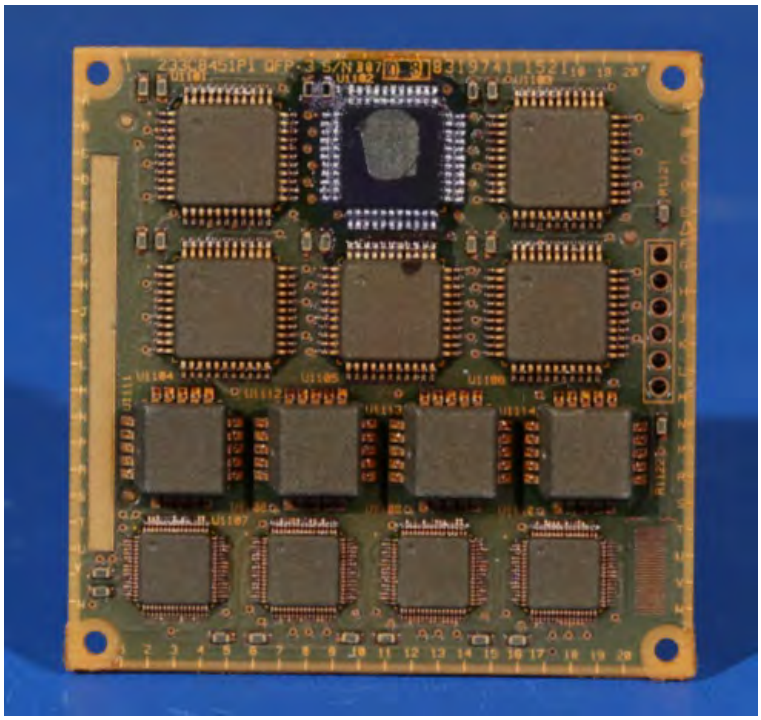


Figure 57: QFP-A034 unfilled 2-spray before environmental exposure.

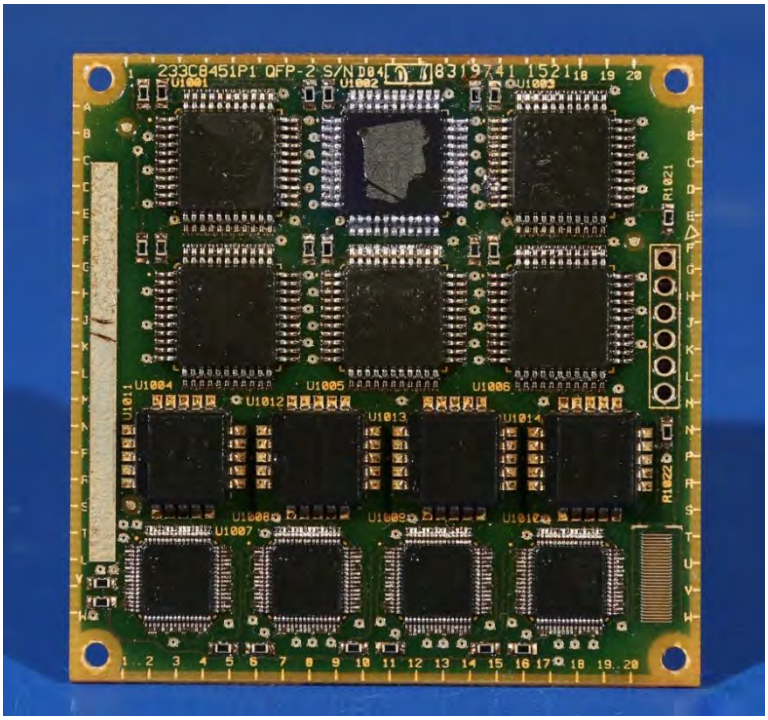


Figure 58: QFP-A311 filled 1-spray before environmental exposure.

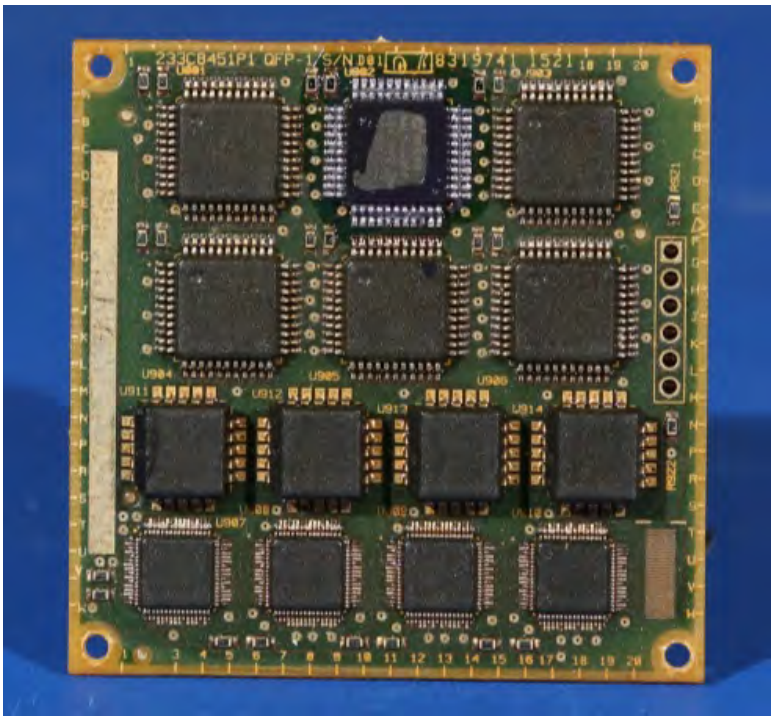


Figure 59: QFP-A312 filled 2-spray before environmental exposure.

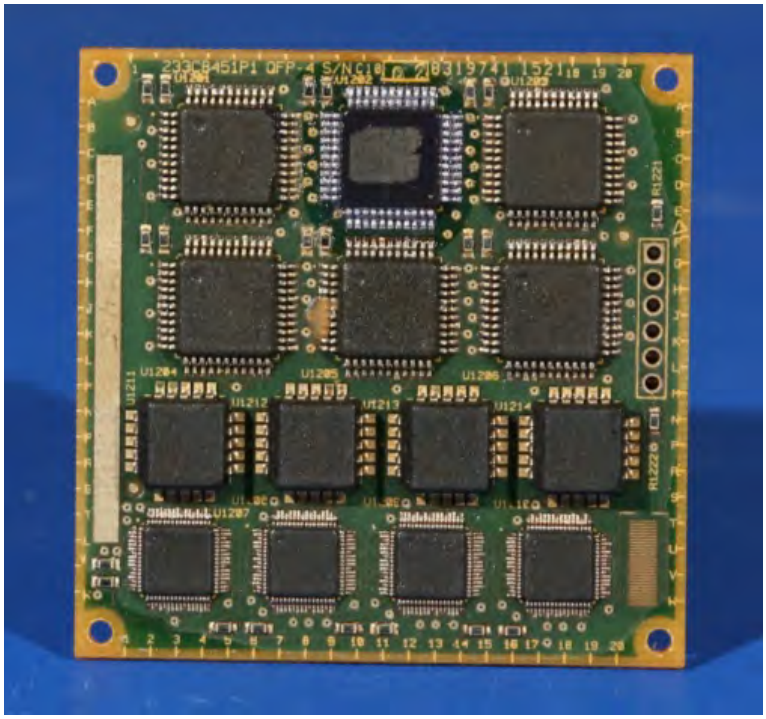


Figure 60: QFP-A345 filled 2-spray before environmental exposure.

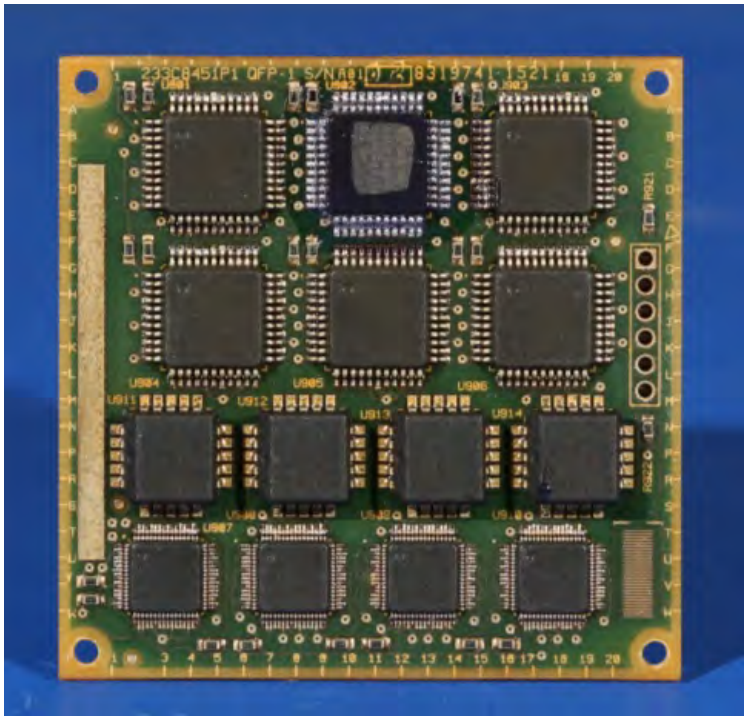


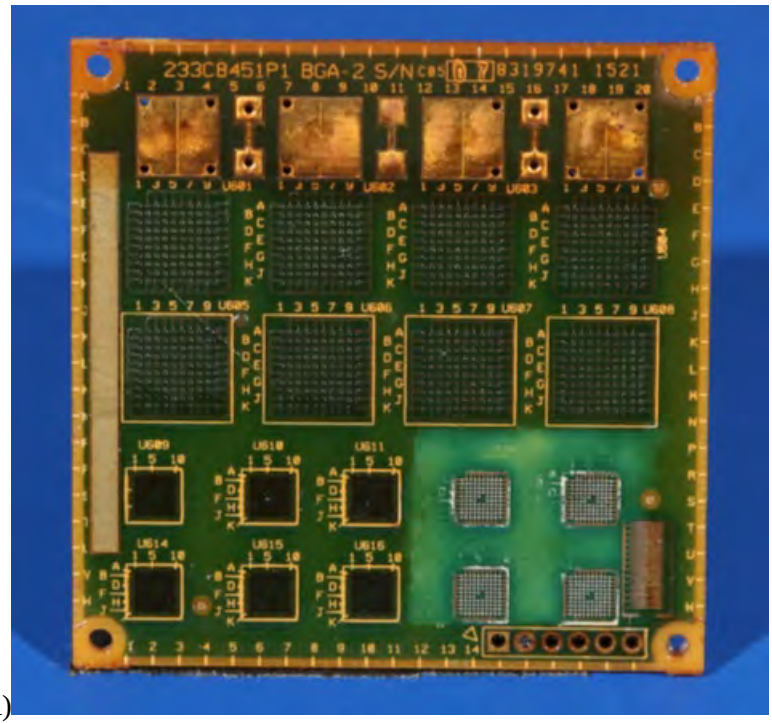
Figure 61: QFP-A384 filled 2-spray before environmental exposure.

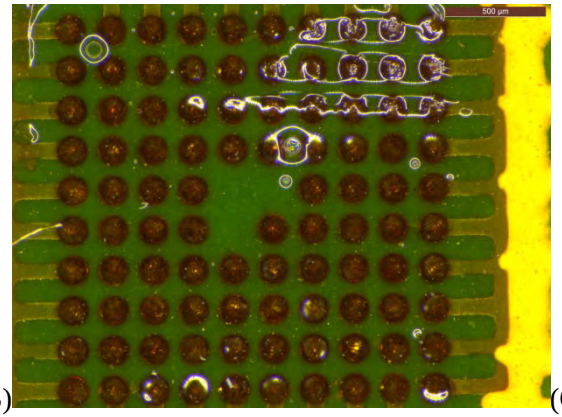
4.2 Photos after environmental exposure

4.2.1 Optical images of unfilled PC18M

After environmental exposure, the figures showing the unfilled and the filled samples are:

- Unfilled PC18M
  - BGA boards: Figure 62 to Figure 64
  - QFP boards: Figure 65 and Figure 66
- Nanosilica filled PC18M+20%XP2742
  - BGA boards: Figure 67 to Figure 69
  - QFP boards: Figure 70 to Figure 73

(A) 

(B) 

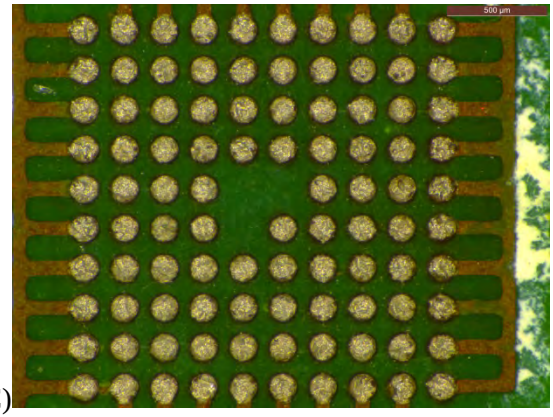
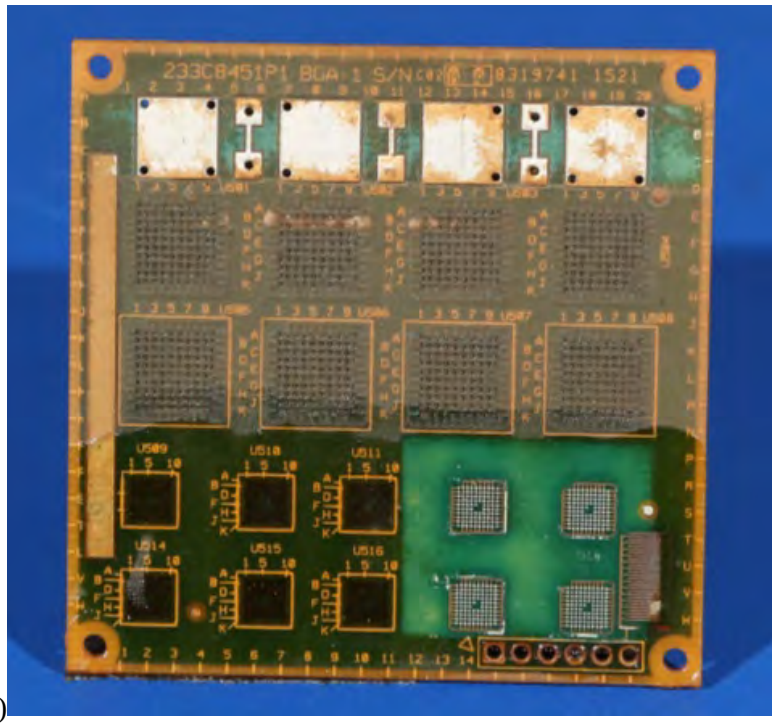
(C) 

Figure 62: BGA-A235 unfilled 1-spray after thermal cycling and humidity; (A) overall, (B) U611 area rework coating over existing coating, and (C) U612 area rework coating over stripped coating.

(A) 

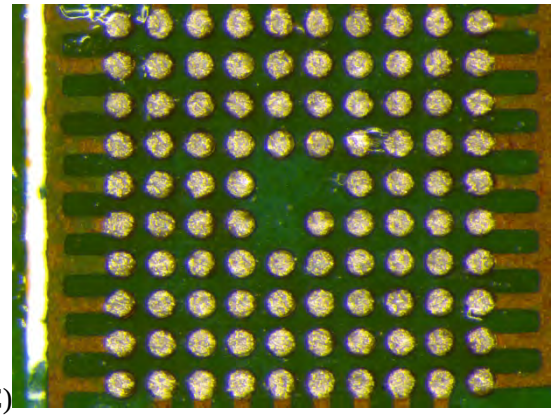
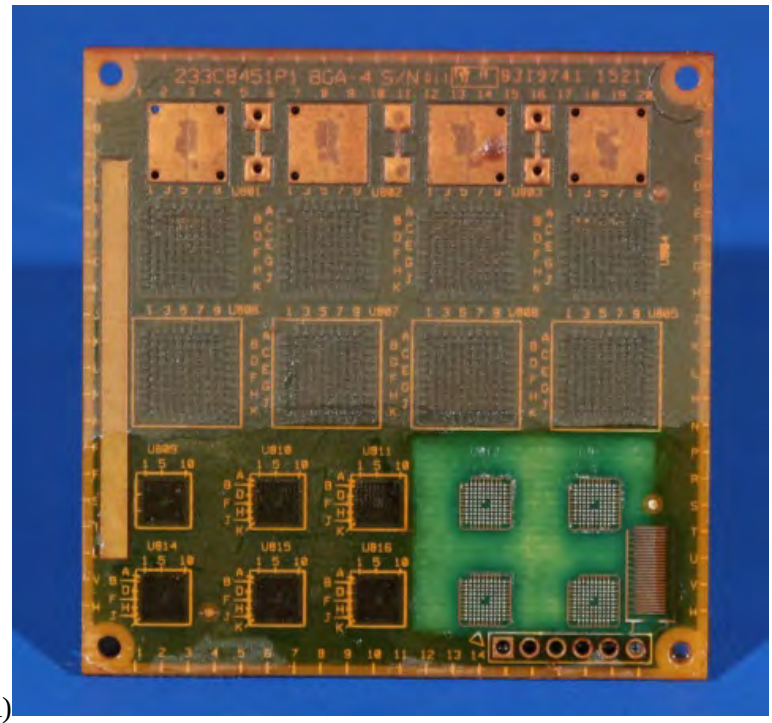
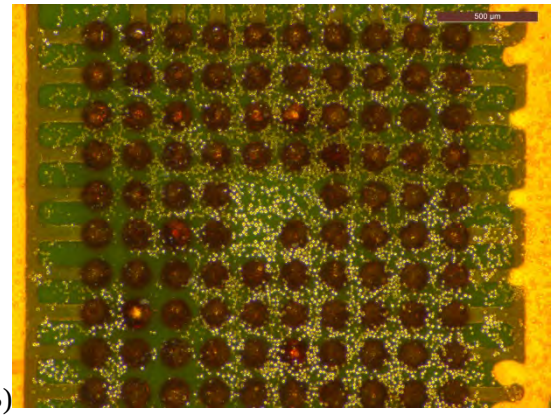
(B)  (C) 

Figure 63: BGA-A296 unfilled 1-spray after thermal cycling; (A) overall, (B) U511 area rework coating over existing coating, and (C) U512 area rework coating over stripped coating.

(A) 

(B) 

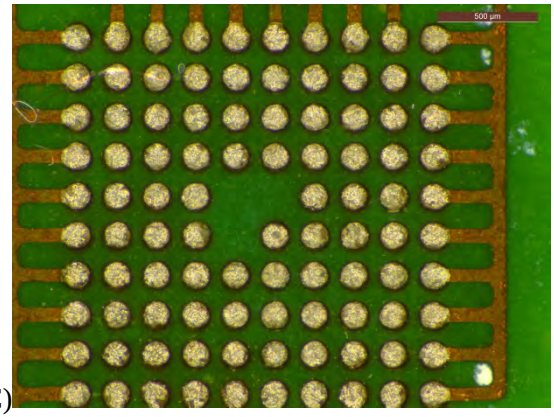
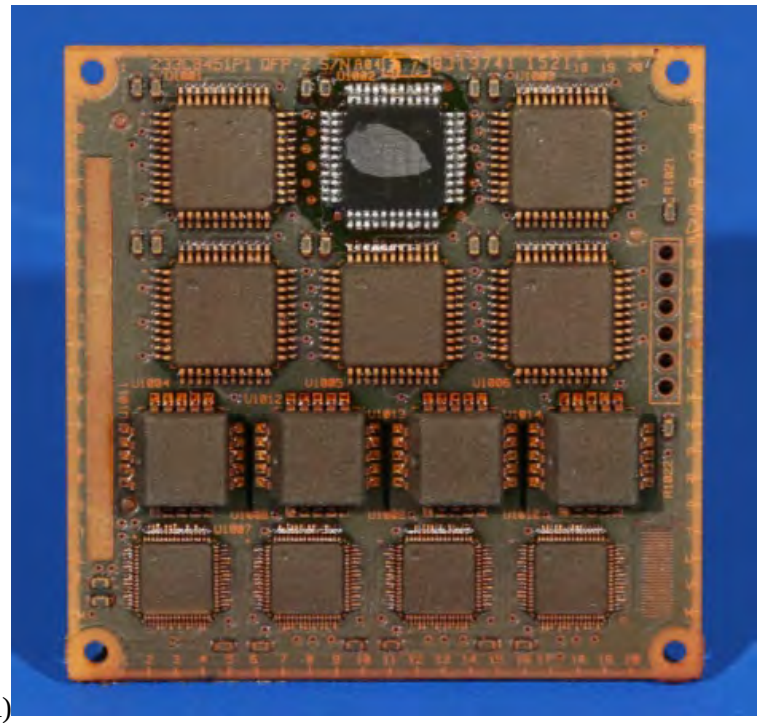
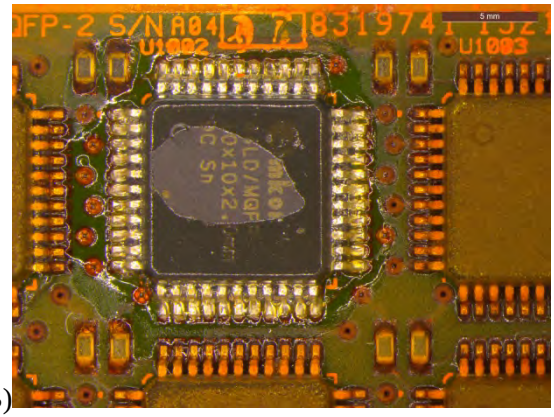
(C) 

Figure 64: BGA-A305 unfilled 2-spray after thermal cycling and humidity; (A) overall, (B) U911 area rework coating over existing coating, and (C) U912 area rework coating over stripped coating.

(A) 

(B) 

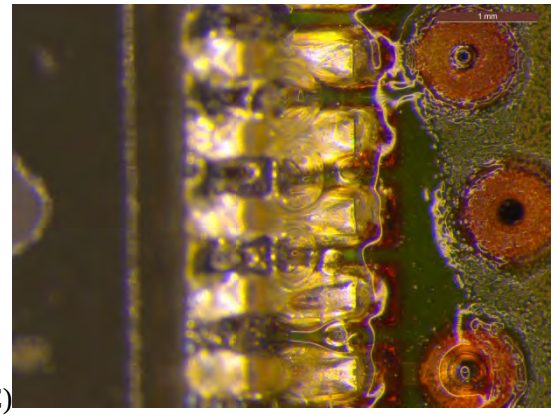
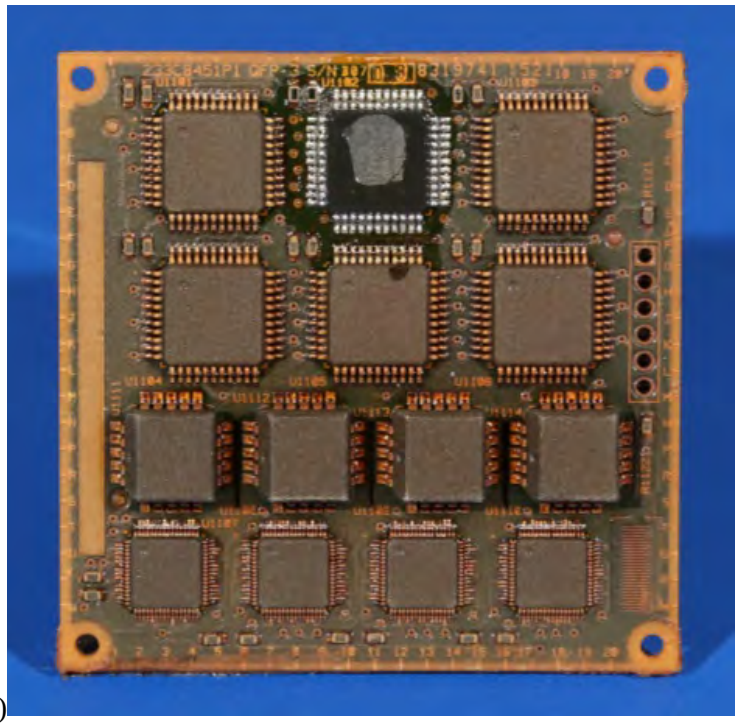
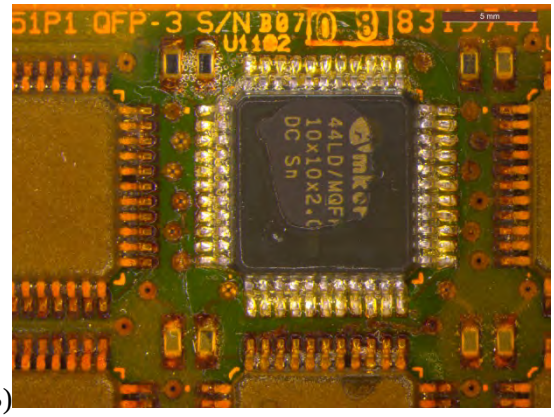
(C) 

Figure 65: QFP-A023 unfilled 2-spray after thermal cycling and humidity; (A) board overall, (B) reworked part overall, and (C) close-up of leads.

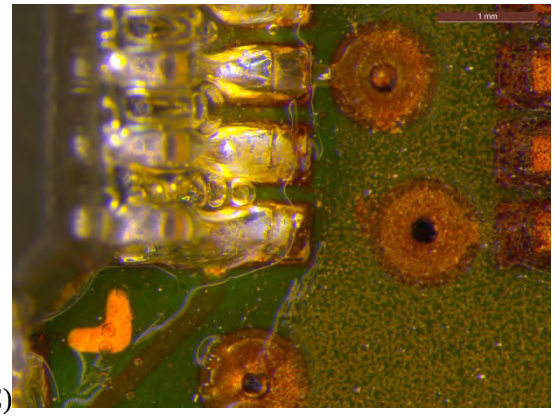
(A)



(B)



(C)



(D)

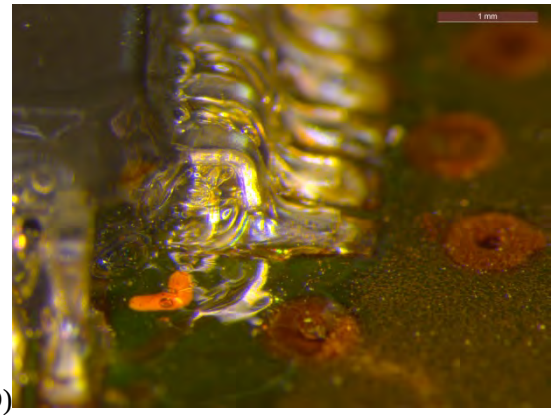
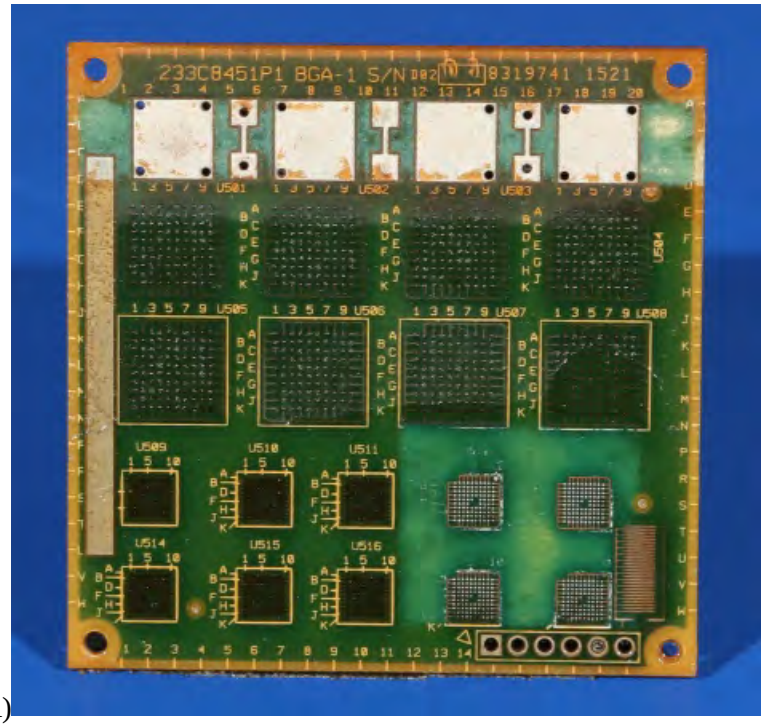


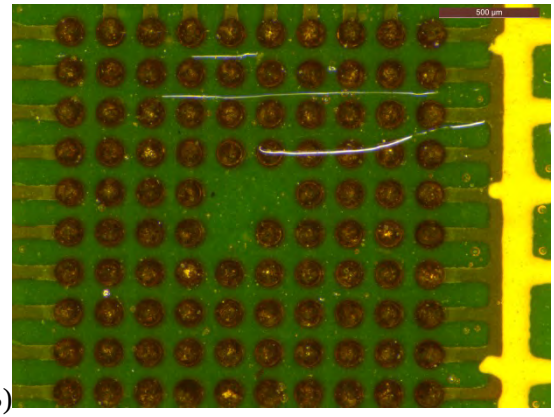
Figure 66: QFP-A034 unfilled 2-sprayafter thermal cycling; (A) board overall, (B) reworked part overall, (C) close-up of leads, and (D) isometric of end leads.

4.2.2 Optical images of filled PC18M+20%XP2742

(A)



(B)



(C)

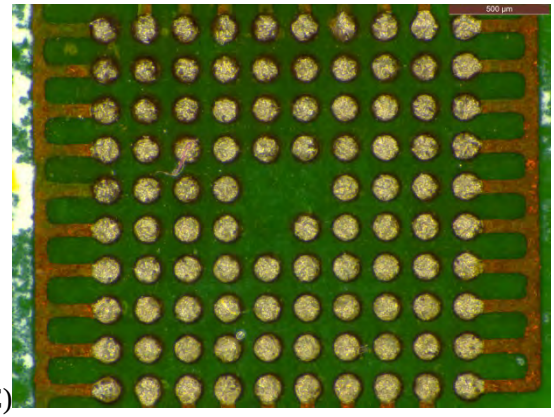
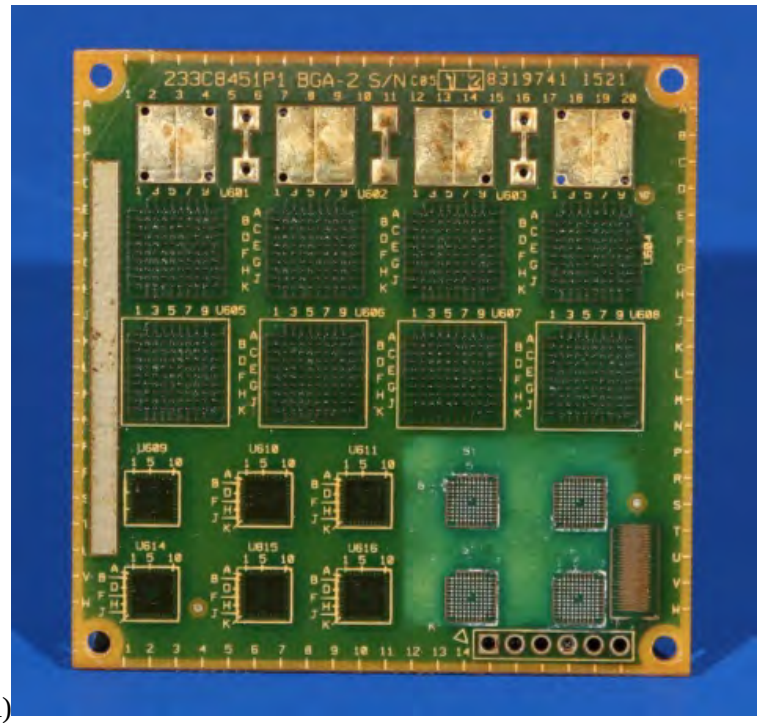
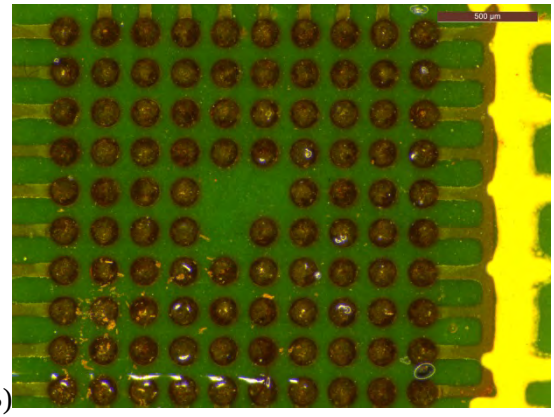


Figure 67: BGA-A392 filled 2-spray after thermal cycling and humidity; (A) overall, (B) U511 area rework coating over existing coating, and (C) 512 area rework coating over stripped coating**.**

(A) 

(B) 

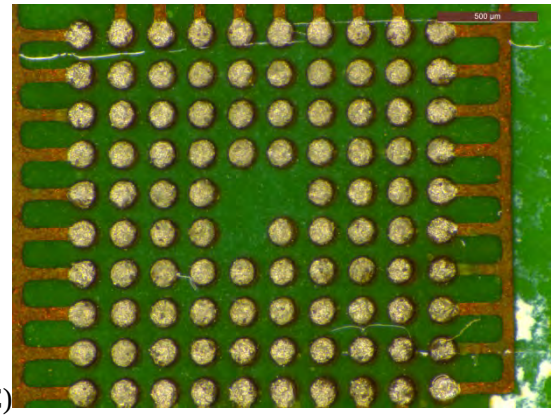
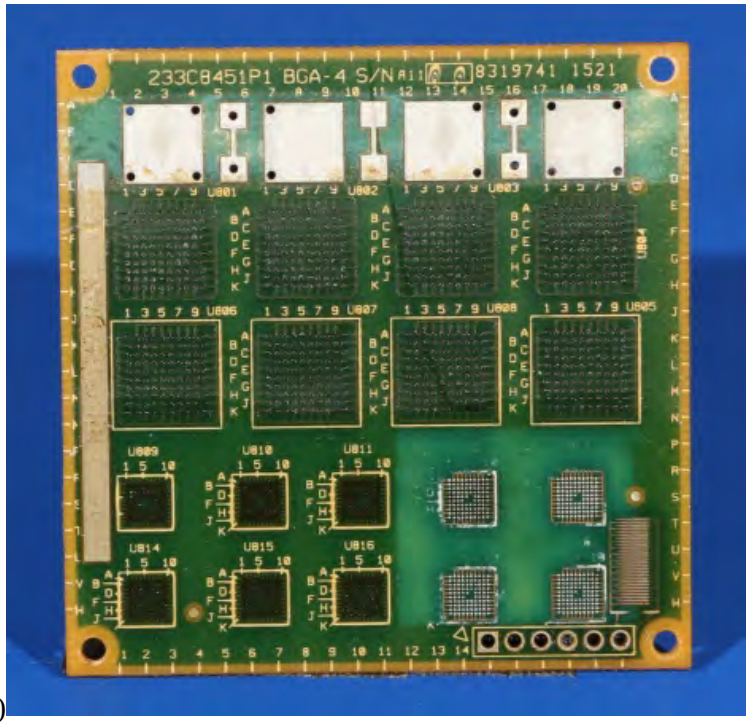
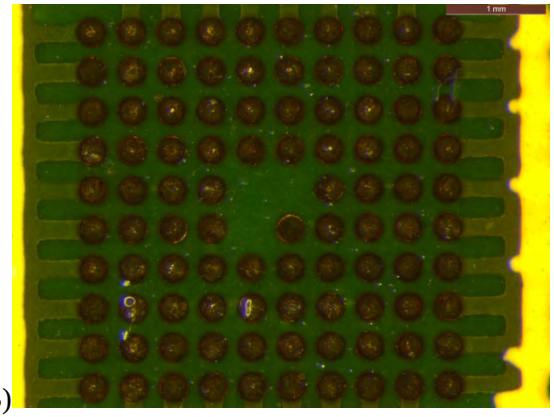
(C) 

Figure 68: BGA-A583 filled 1-spray after thermal cycling and humidity; (A) overall, (B) U611 area rework coating over existing coating, and (C) U612 area rework coating over stripped coating.

(A) 

(B) 

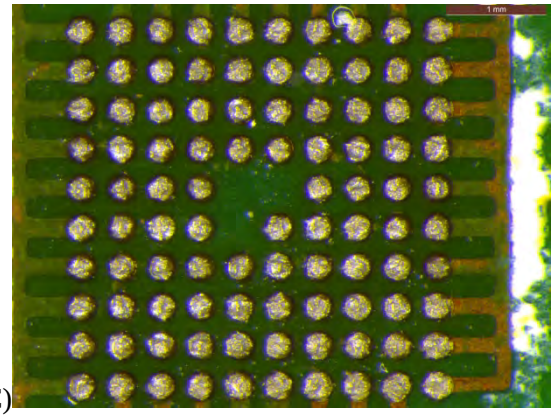
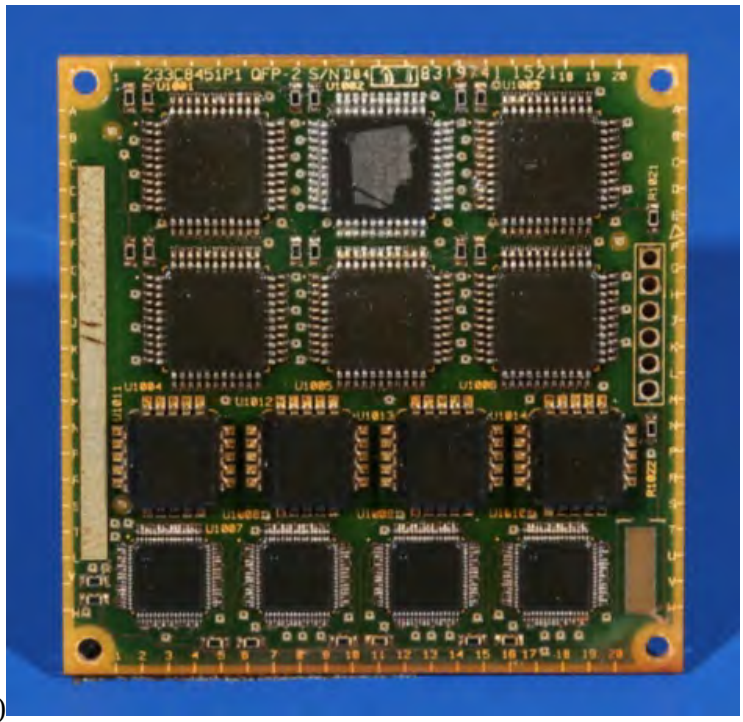
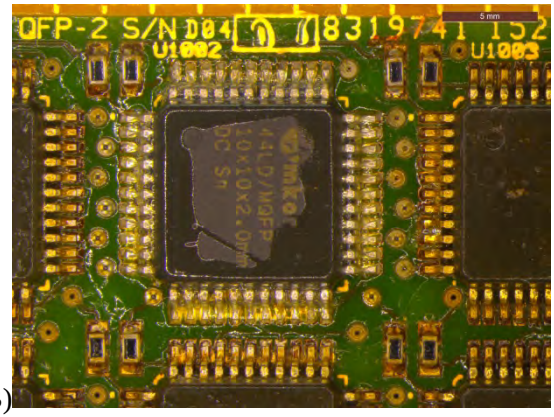
(C) 

Figure 69: BGA-A593 filled 1-spray after thermal cycling; (A) overall, (B) U811 area rework coating over existing coating, and (C) U812 area rework coating over stripped coating.

(A) 

(B) 

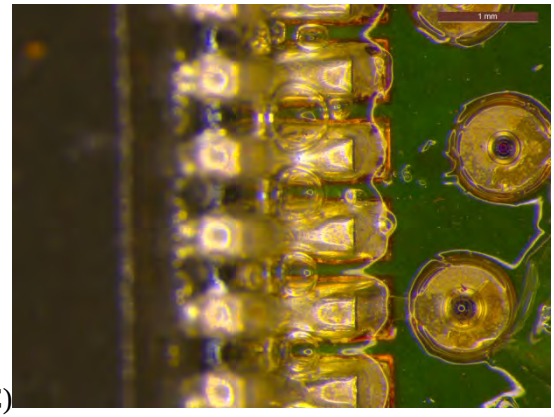
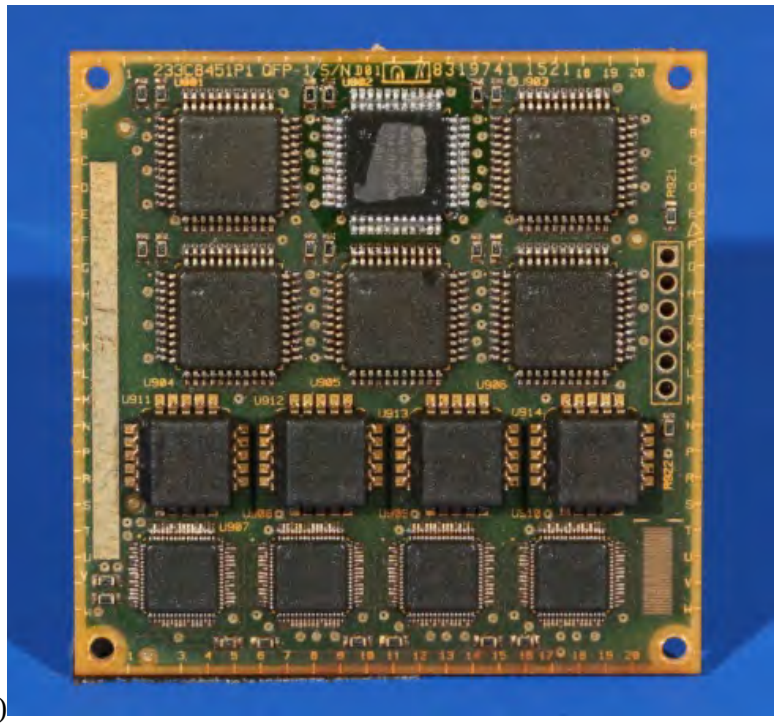
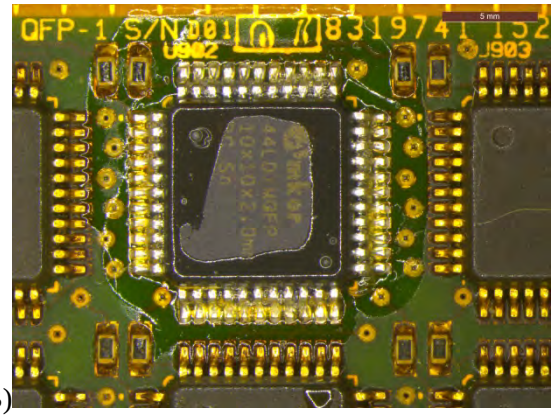
(C) 

Figure 70: QFP-A311 filled 1-spray after thermal cycling and humidity; (A) board overall, (B) reworked part overall, and (C) close-up of leads.

(A) 

(B) 

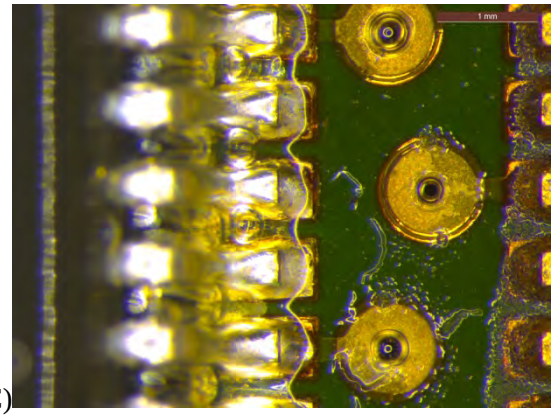
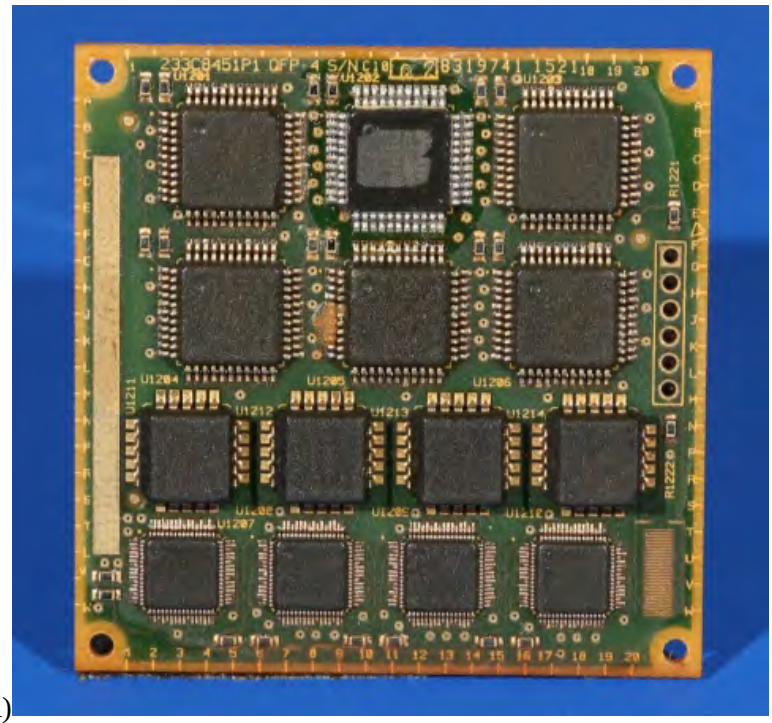
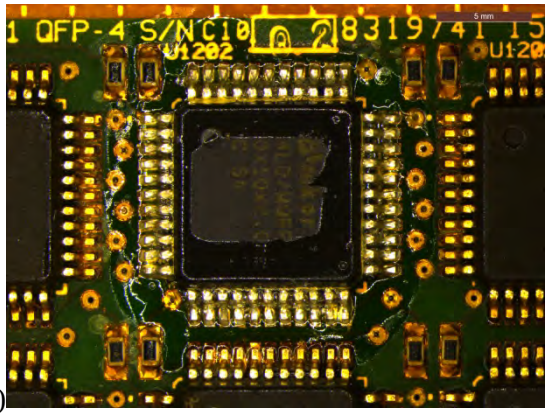
(C) 

Figure 71: QFP-A312 filled 2-spray after thermal cycling and humidity; (A) board overall, (B) reworked part overall, and (C) close-up of leads**.**

(A)



(A)



(B)

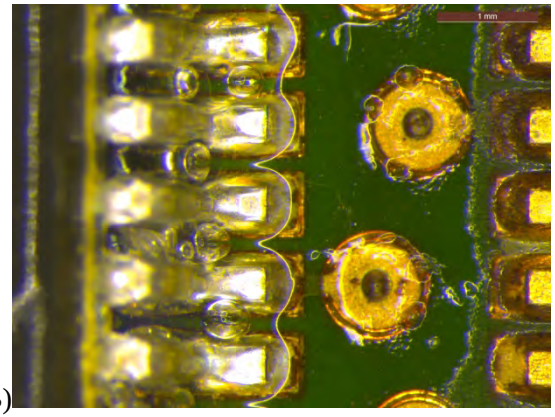
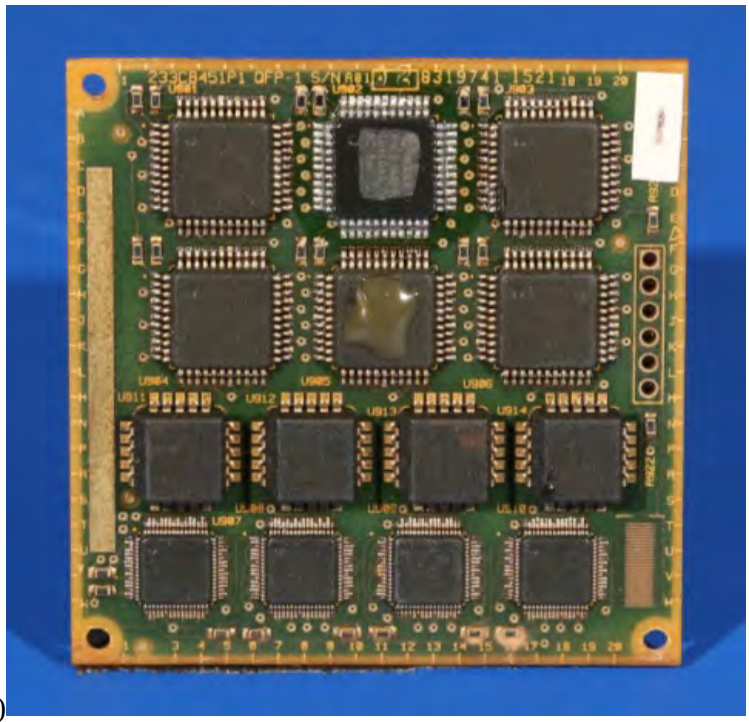
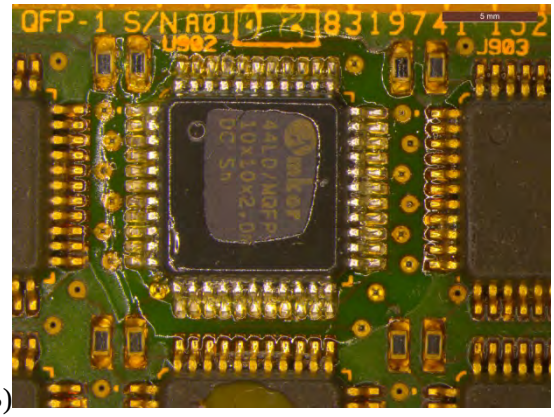


Figure 72: QFP-A345 filled 2 spray after thermal cycling and humidity; (A) board overall, (B) reworked part overall, and (C) close-up of leads.

(A) 

(B) 

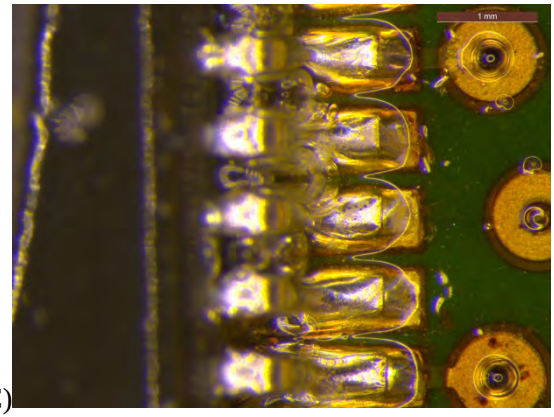
(C) 

Figure 73: QFP-A384 filled 2-spray after thermal cycling; (A) board overall, (B) reworked part overall, and (C) close-up of leads.

4.3 SEM examination after environmental exposure

The QFP pin numbering is shown in Figure 74. SEM BSE images of the unfilled PC18M reworked QFP part after environmental exposure are shown in:

- Unfilled PC18M: Figure 75 to Figure 84
- Nanosilica filled PC18M+20%XP2742: Figure 85 to Figure 93.

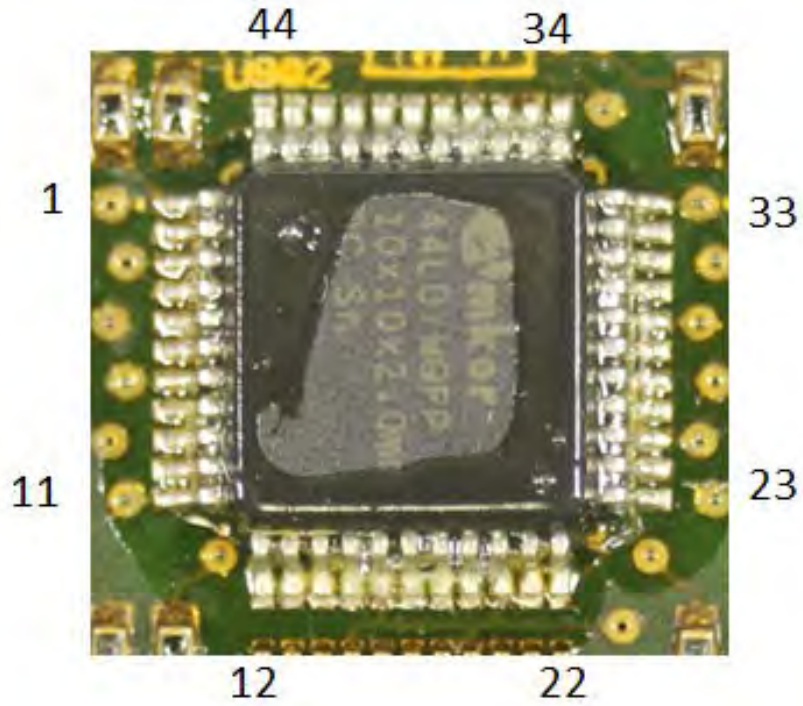


Figure 74: QFP pin numbering reference.

4.3.1 SEM of unfilled PC18M QFP-A023 rework

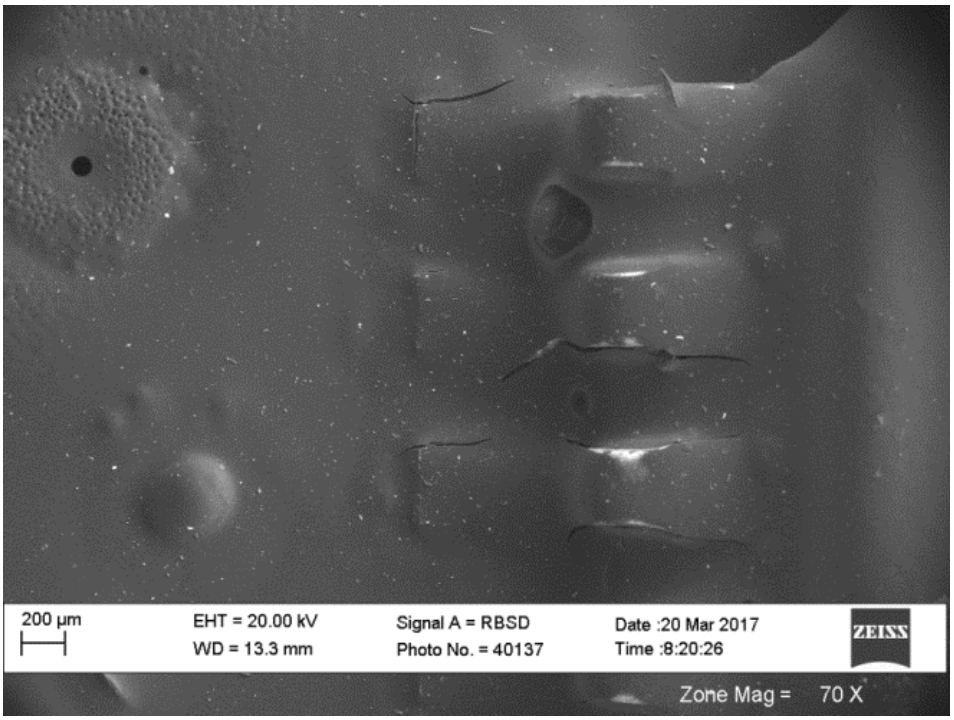


Figure 75: SEM BSE unfilled PC18M QFP-A023 U1002 pins 1 to 3, 70x.

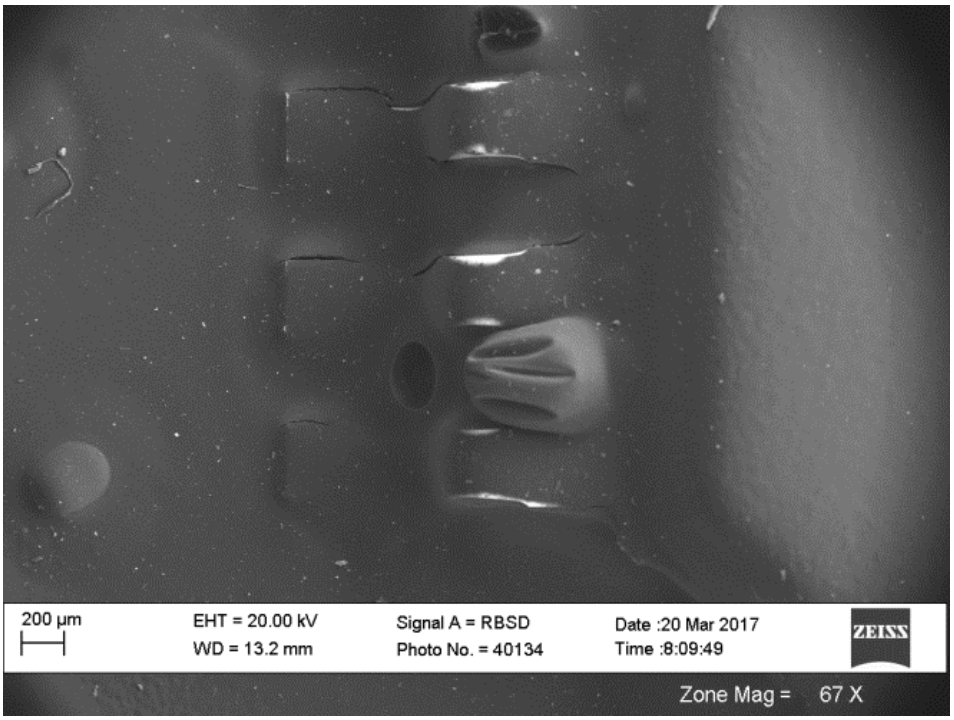


Figure 76: SEM BSE unfilled PC18M QFP-A023 U1002 pins 8 to 11, 67x.

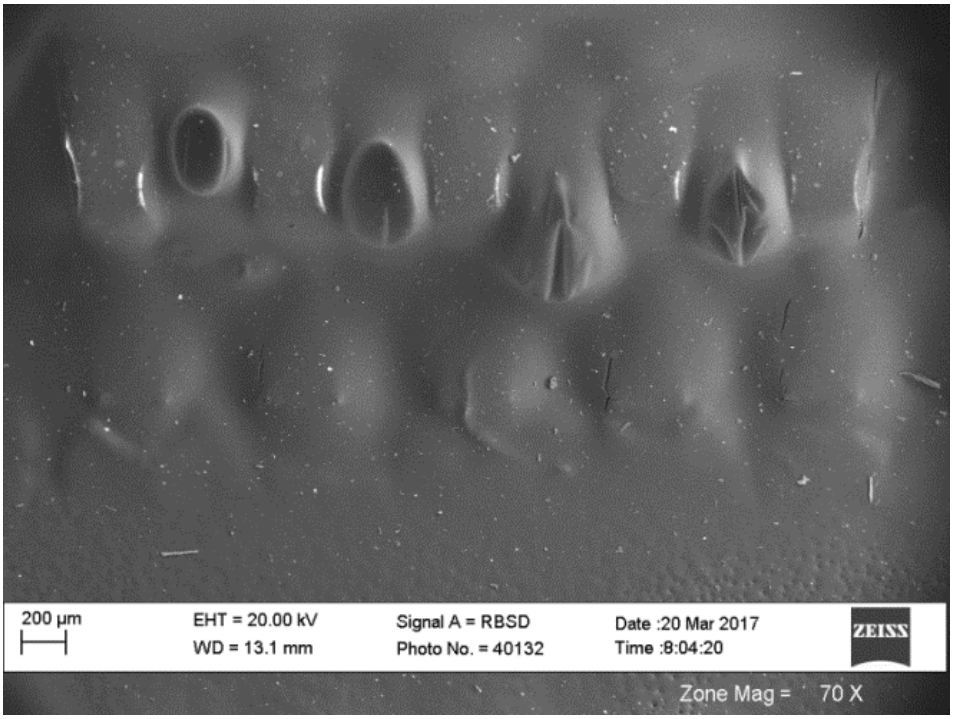


Figure 77: SEM BSE unfilled PC18M QFP-A023 U1002 pins 12 to 16, 70x.

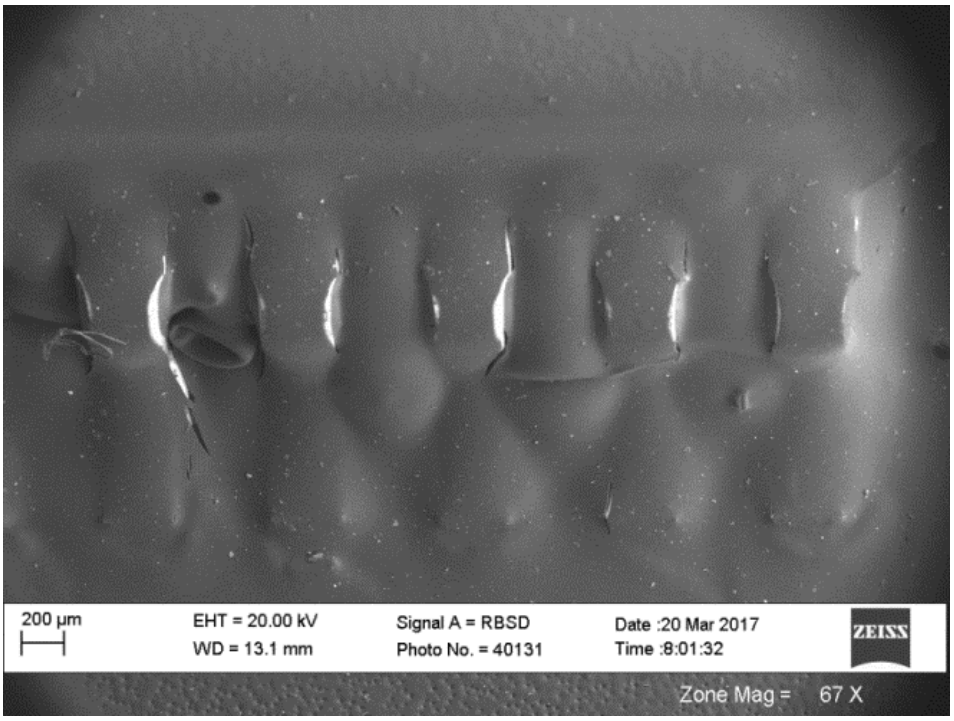


Figure 78: SEM BSE unfilled PC18M QFP-A023 U1002 pins 18 to 22, 67x.

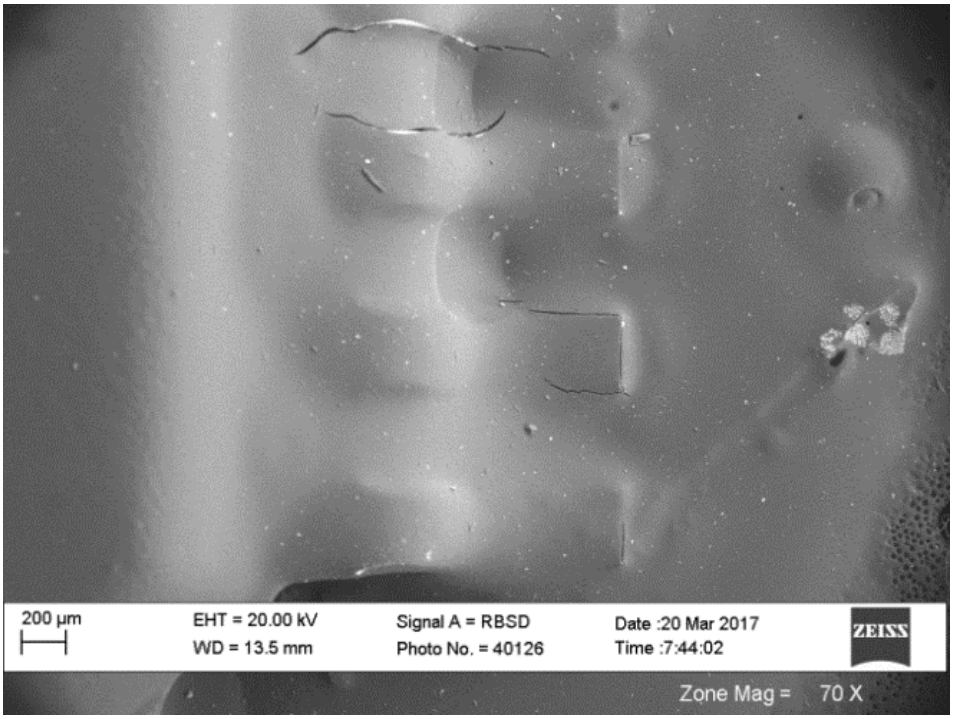


Figure 79: SEM BSE unfilled PC18M QFP-A023 U1002 pins, 23 to 26, 70x.

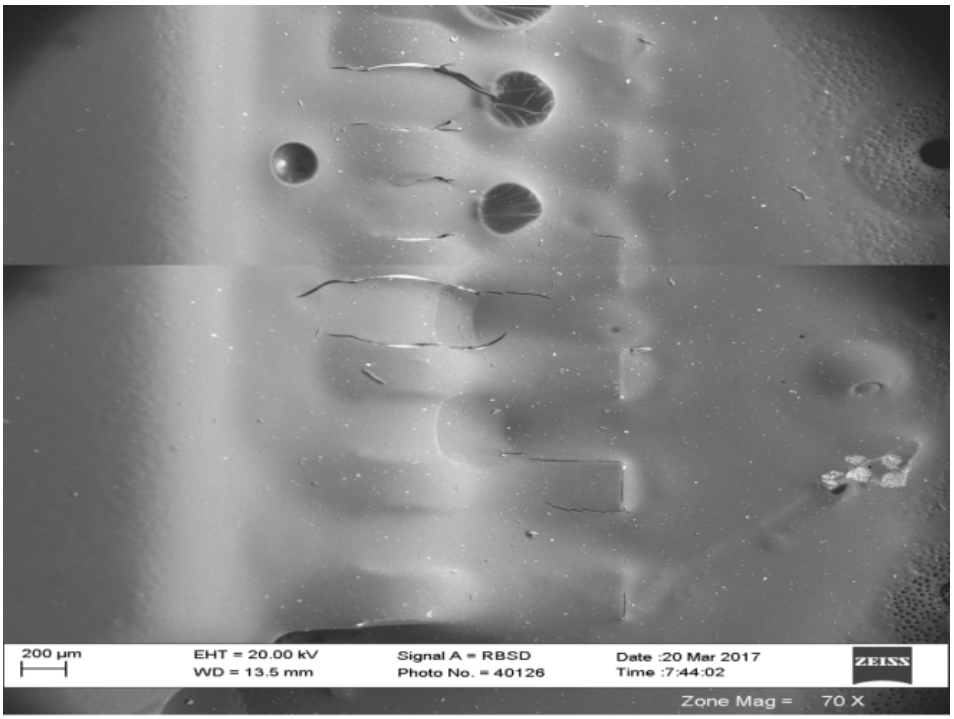


Figure 80: SEM BSE unfilled PC18M QFP-A023 U1002 pins, 23 to 28 composite, 70x.

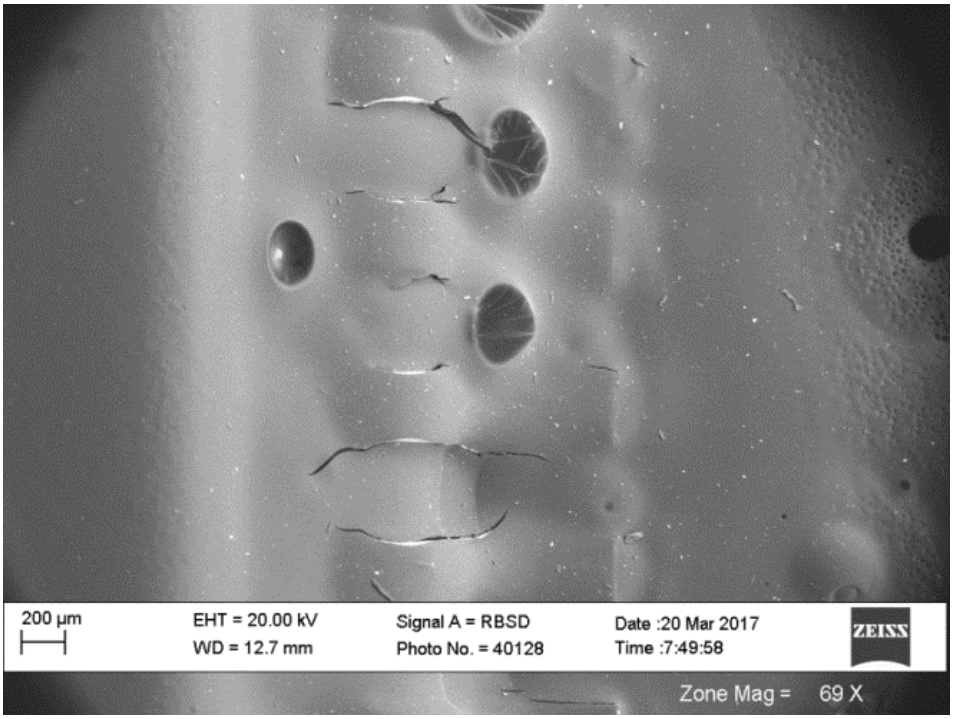


Figure 81: SEM BSE unfilled PC18M QFP-A023 U1002 pins, 25 to 28, 69x.

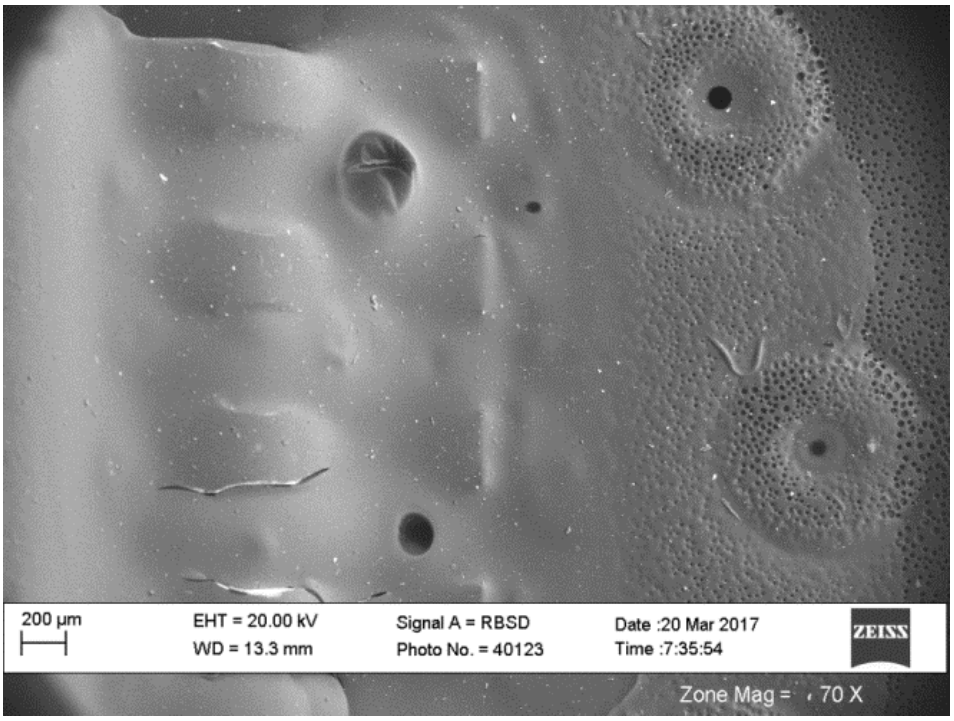


Figure 82: SEM BSE unfilled PC18M QFP-A023 U1002 pins, 31 to 33, 70x.

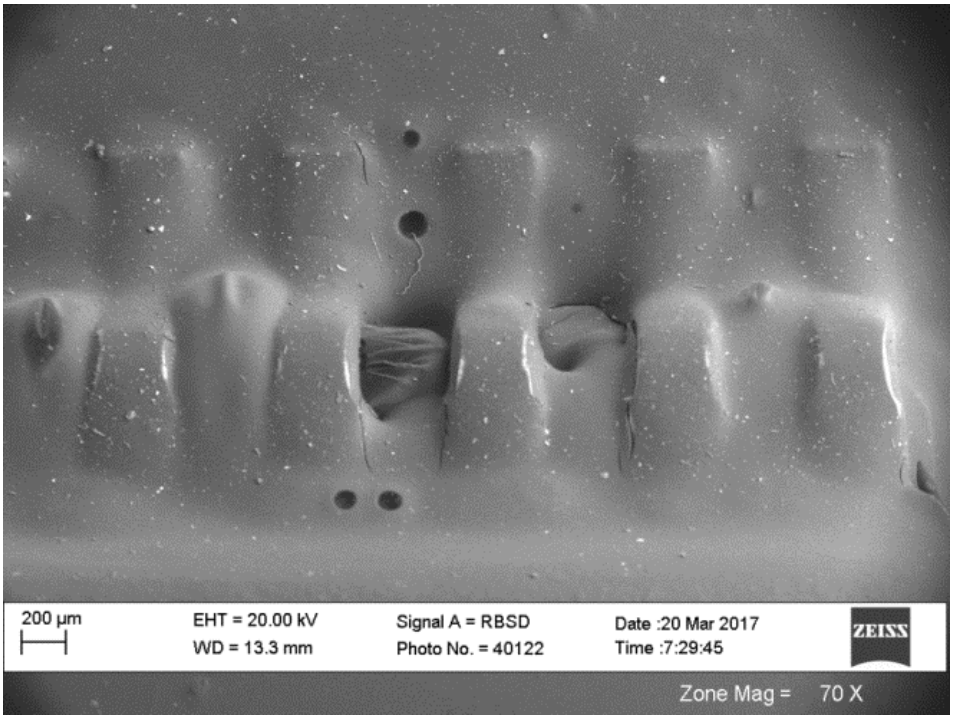


Figure 83: SEM BSE unfilled PC18M QFP-A023 U1002 pins 38 to 34, 70x.

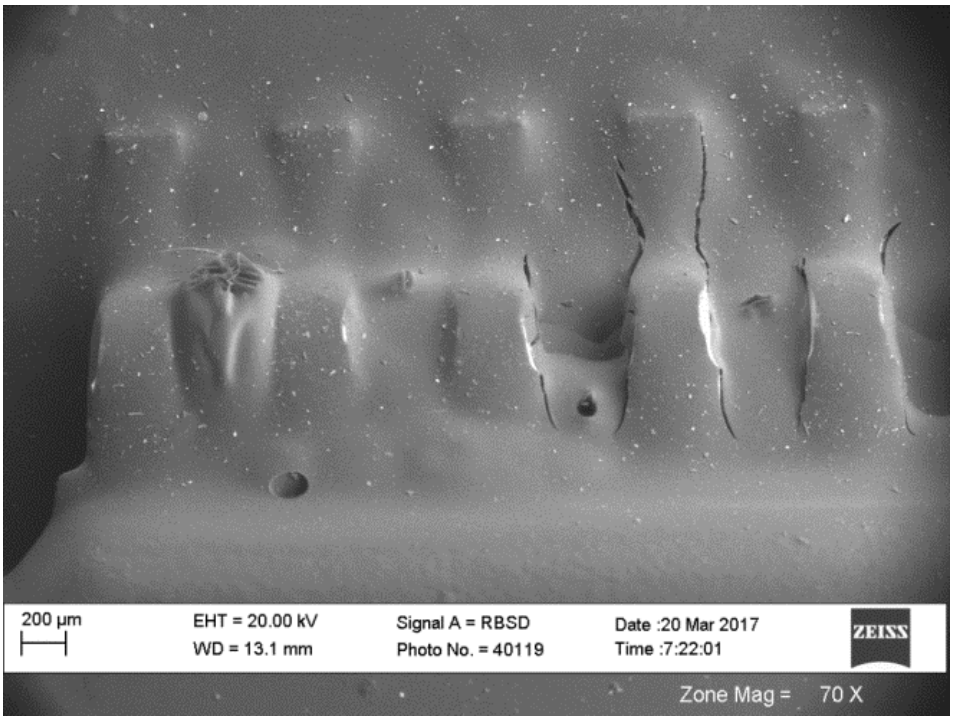


Figure 84: SEM BSE unfilled PC18M QFP-A023 U1002 pins 44 to 40, 70x.

4.3.2 SEM of filled PC18M+20%XP2724 rework

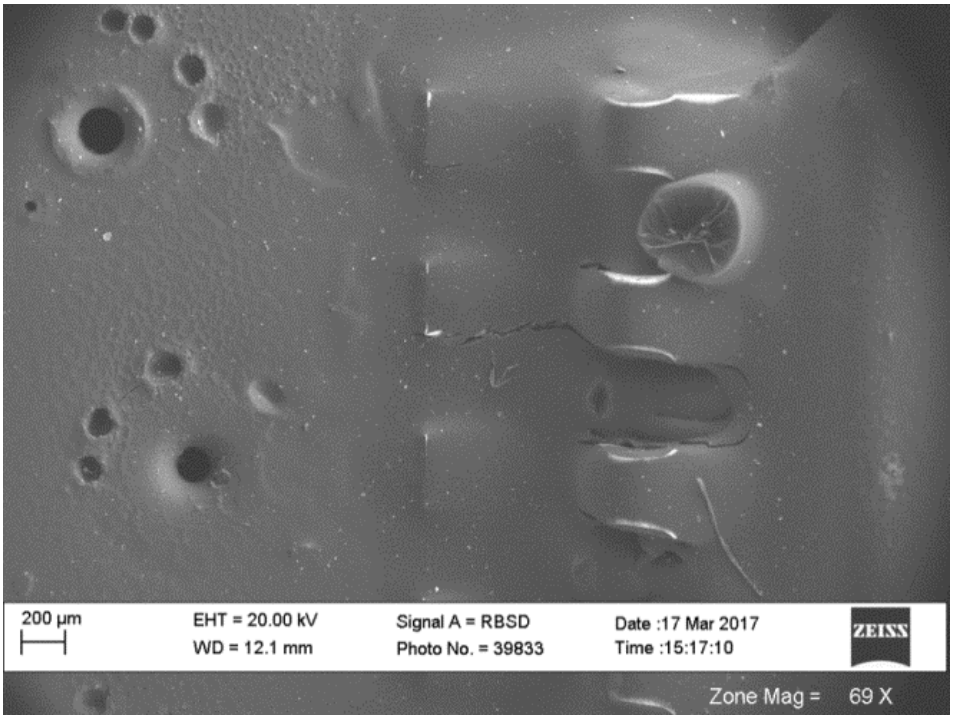


Figure 85: SEM BSE filled PC18M+20%XP2742 QFP-A312 U902 pins 1 to 3, 69x.

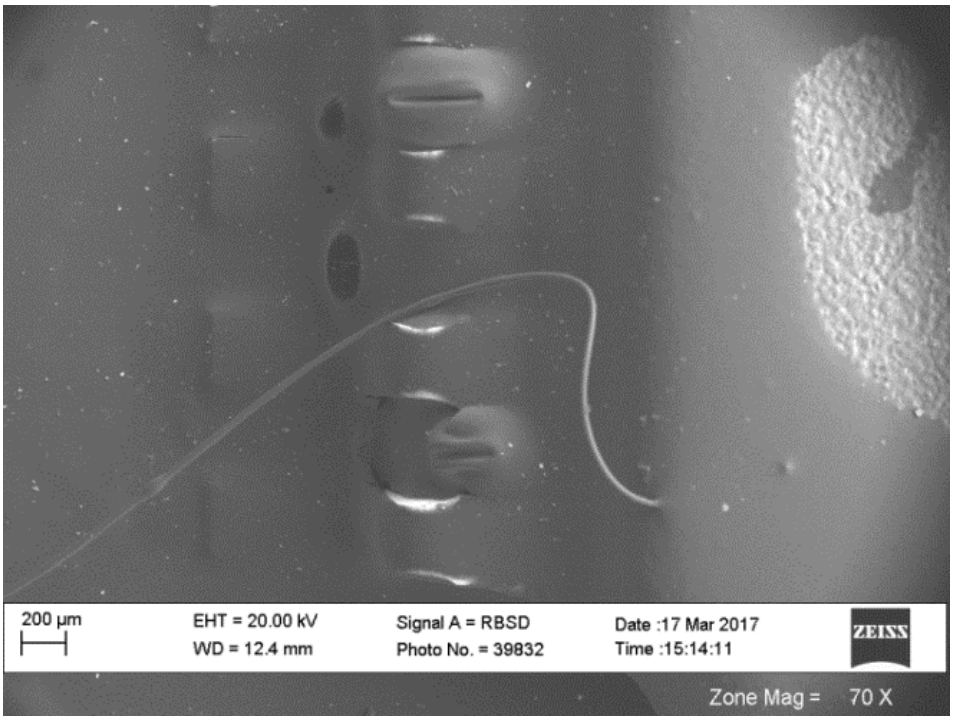


Figure 86: SEM BSE filled PC18M+20%XP2742 QFP-A312 U902 pins 8 to 11, 70x.

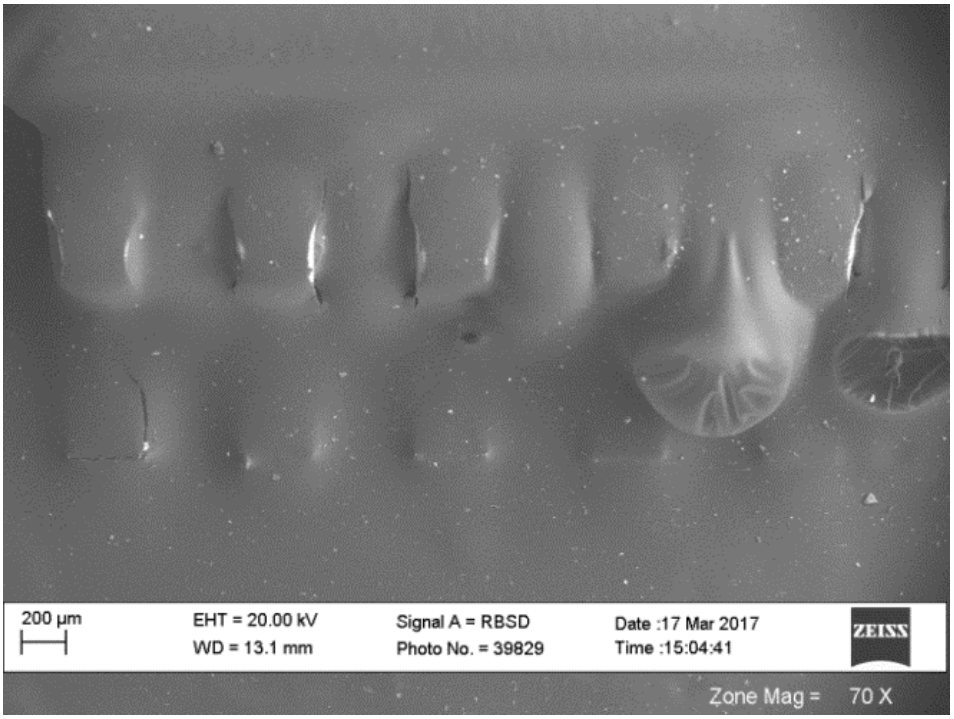


Figure 87: SEM BSE filled PC18M+20%XP2742 QFP-A312 U902 pins 12 to 15, 70x.

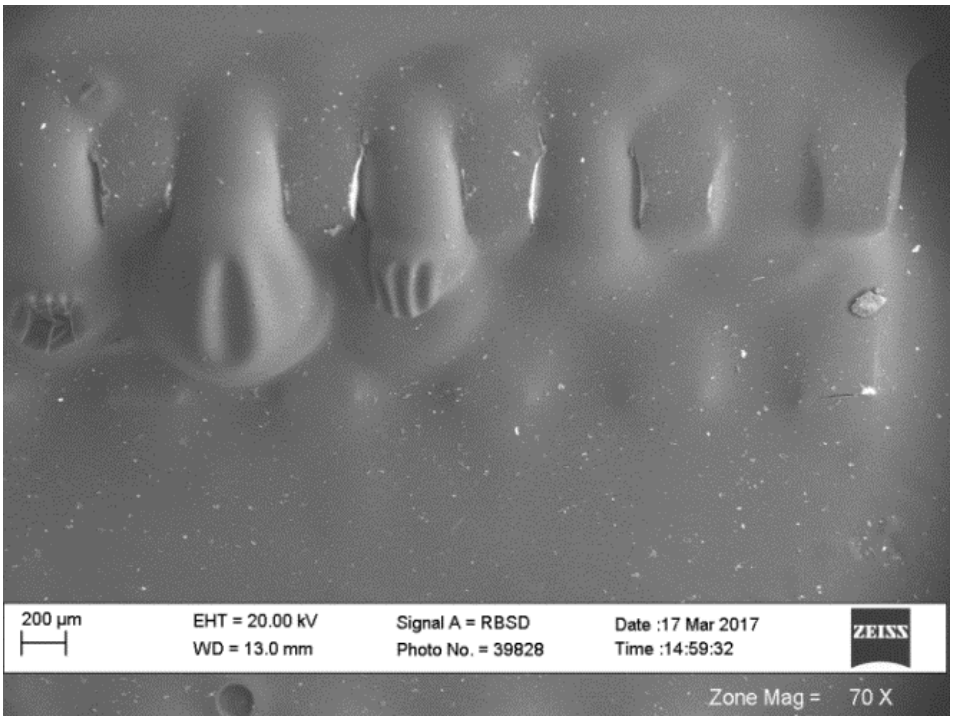


Figure 88: SEM BSE filled PC18M+20%XP2742 QFP-A312 U902 pins 18 to 22, 70x.

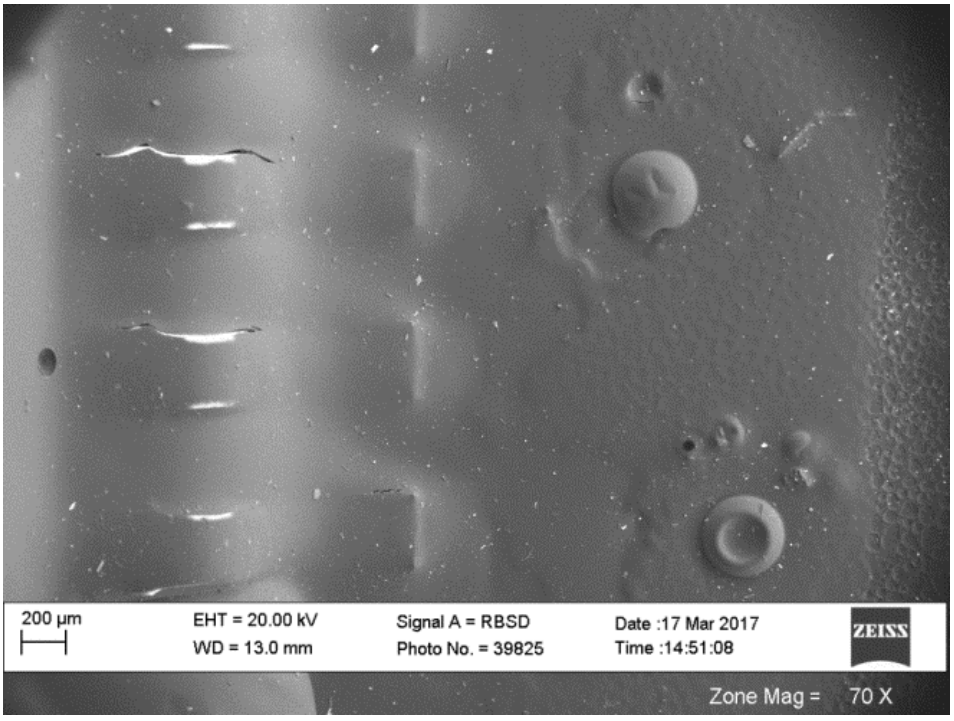


Figure 89: SEM BSE filled PC18M+20%XP2742 QFP-A312 U902 pins 23 to 26, 70X.

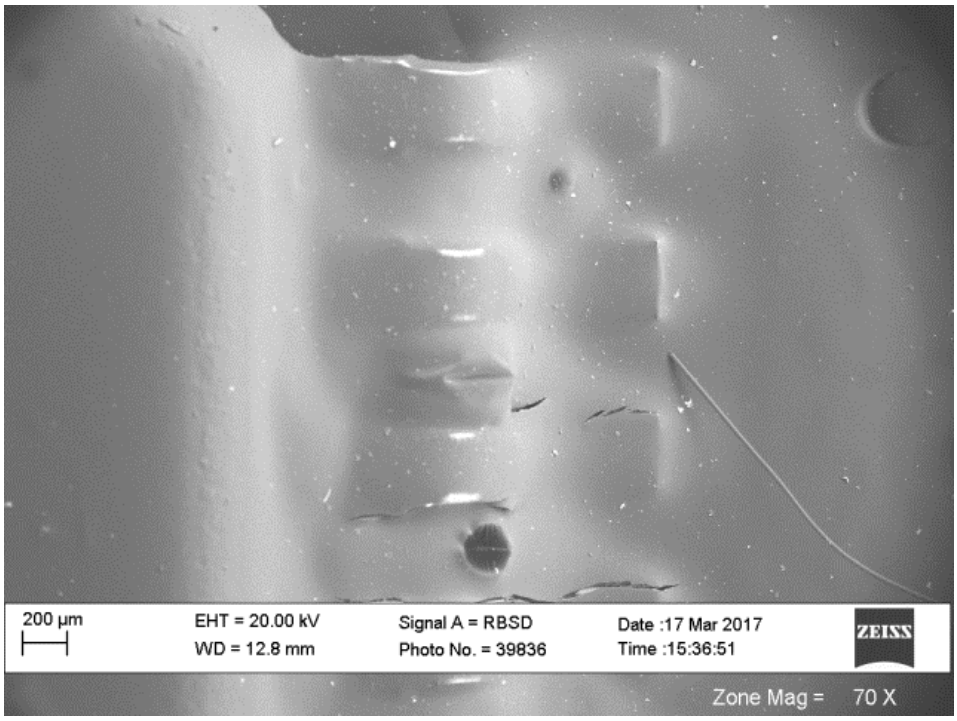


Figure 90: SEM BSE filled PC18M+20%XP2742 QFP-A312 U902 pins 31 to 33, 70x.

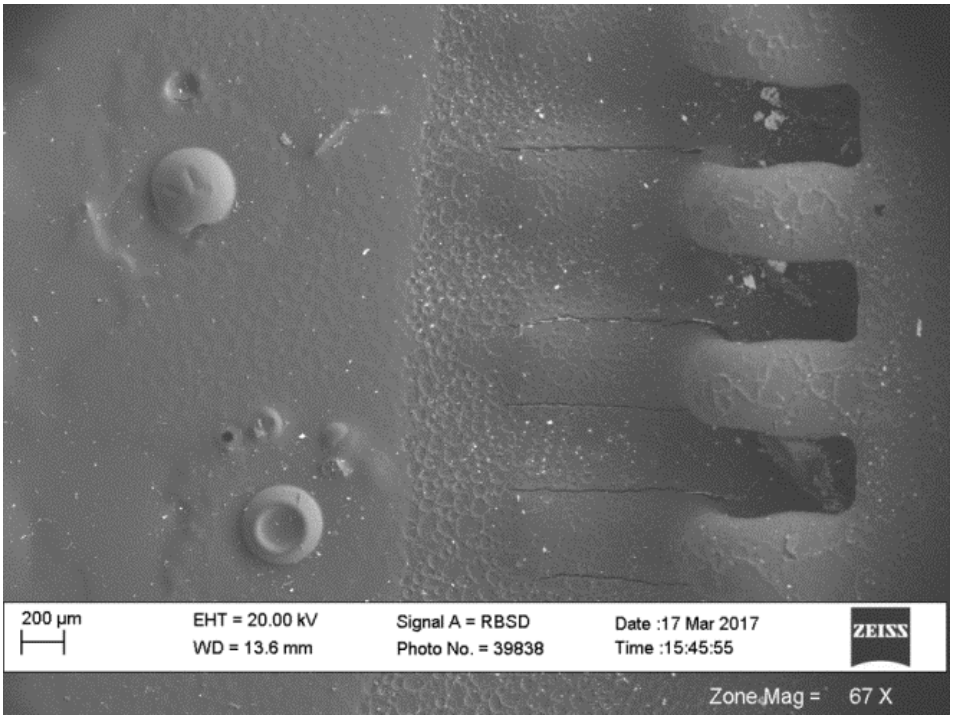


Figure 91: SEM BSE filled PC18M+20%XP2742 QFP-A312 U903 side 1 to 12 adjacent to U902, 67x.

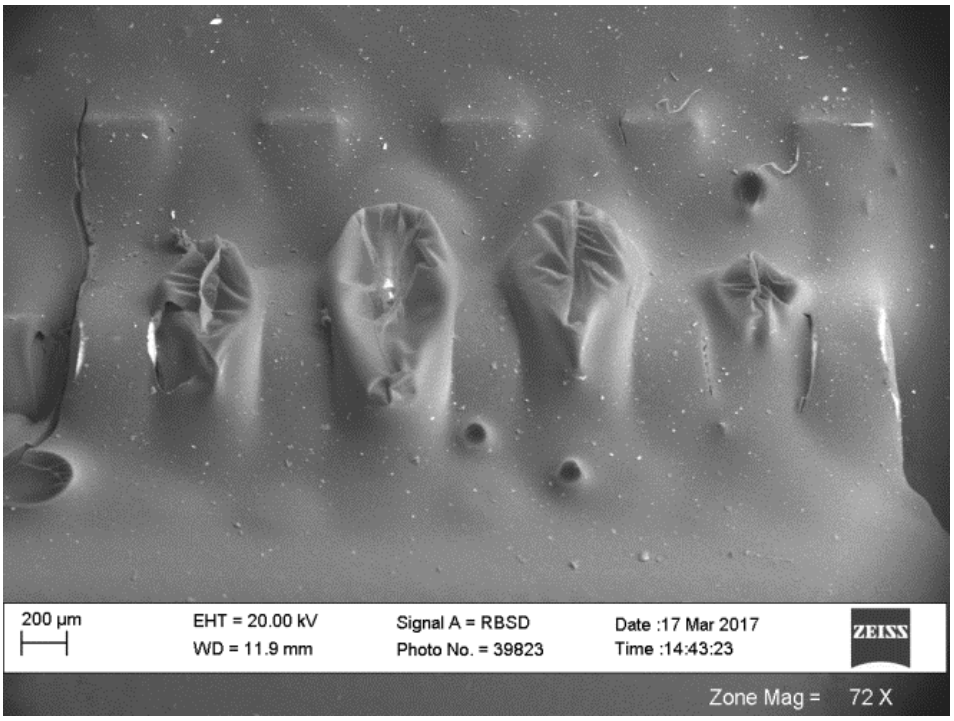


Figure 92: SEM BSE filled PC18M+20%XP2742 QFP-A312 U902 pins 38-34, 72x.

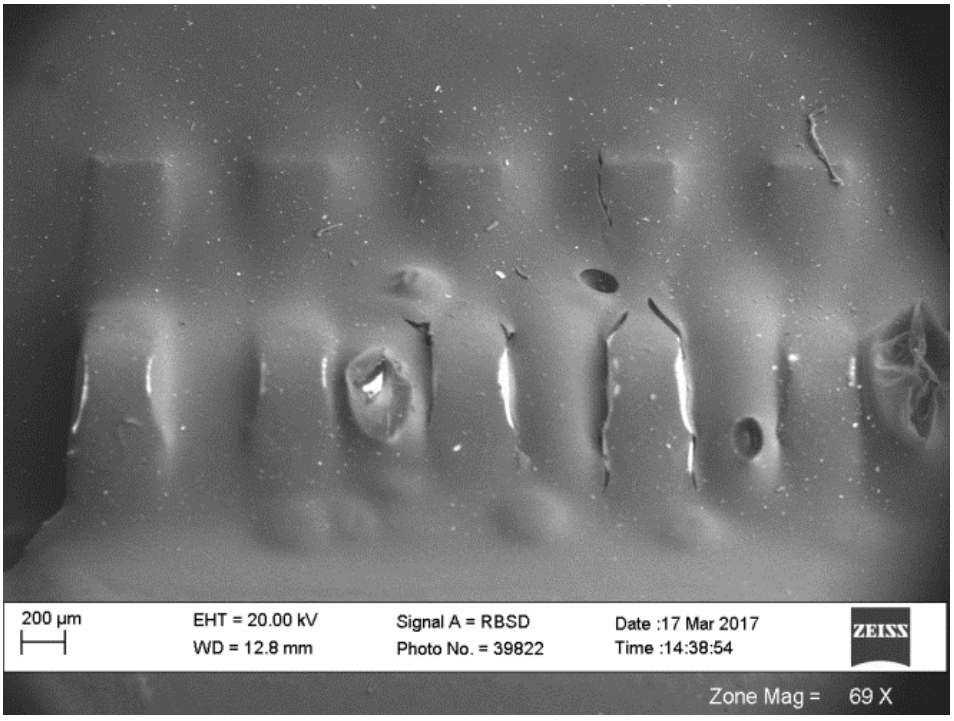


Figure 93: SEM BSE filled PC18M+20%XP2742 QFP-A312 U902 pins 44 to 40, 69x.

4.4 Rework cross-sections

Cross-section optical, SEM and coating thickness measurement images are presented for the reworked parts for both the unfilled PC18M and nanosilica filled PC18M+20%XP2742 coatings. Selected images are also presented for adjacent non-reworked QFPs for comparison. Note that unless otherwise specified, the optical cross-section images were taken on a metallurgical microscope and are inverted. The lead location nomenclature is defined in Figure 95. The thickness location definitions are given in Figure 94.

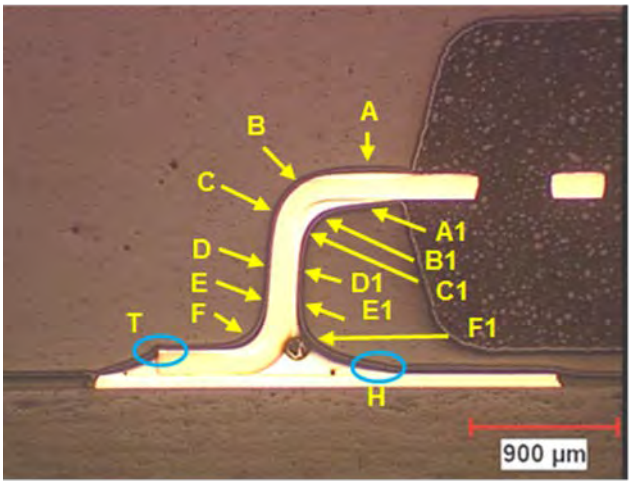


Figure 94: Thickness measurement locations (repeated from Figure 43).

The following images are provided:

- Unfilled PC18M
  - Reworked part optical: Figure 97 to Figure 115
  - Reworked part SEM: Figure 116 to Figure 122
  - Reworked part coating thickness measurements: Figure 123 to Figure 151.
  - Adjacent non-reworked part optical: Figure 151 to Figure 161.
  - Adjacent non-reworked part SEM: Figure 162 to Figure 165
- Nanosilica filled PC18M+20%XP2742
  - Reworked part optical: Figure 167 to Figure 187
  - Reworked part SEM: Figure 188 to Figure 198
  - Reworked part coating thickness measurements: Figure 199 to Figure 231
  - Adjacent non-reworked part optical: Figure 232 to Figure 251
  - Adjacent non-reworked part SEM: Figure 252 to Figure 256

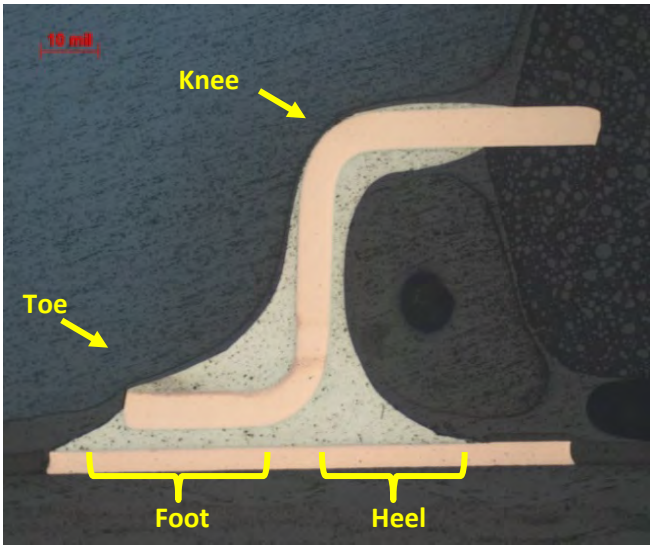


Figure 95: Nomenclature used to define location on the lead.

4.4.1 Cross-sections of unfilled PC18M QFP-A023

The cross-section plane locations and numbers of the unfilled PC18M pins that were sectioned are shown in Figure 96.

o

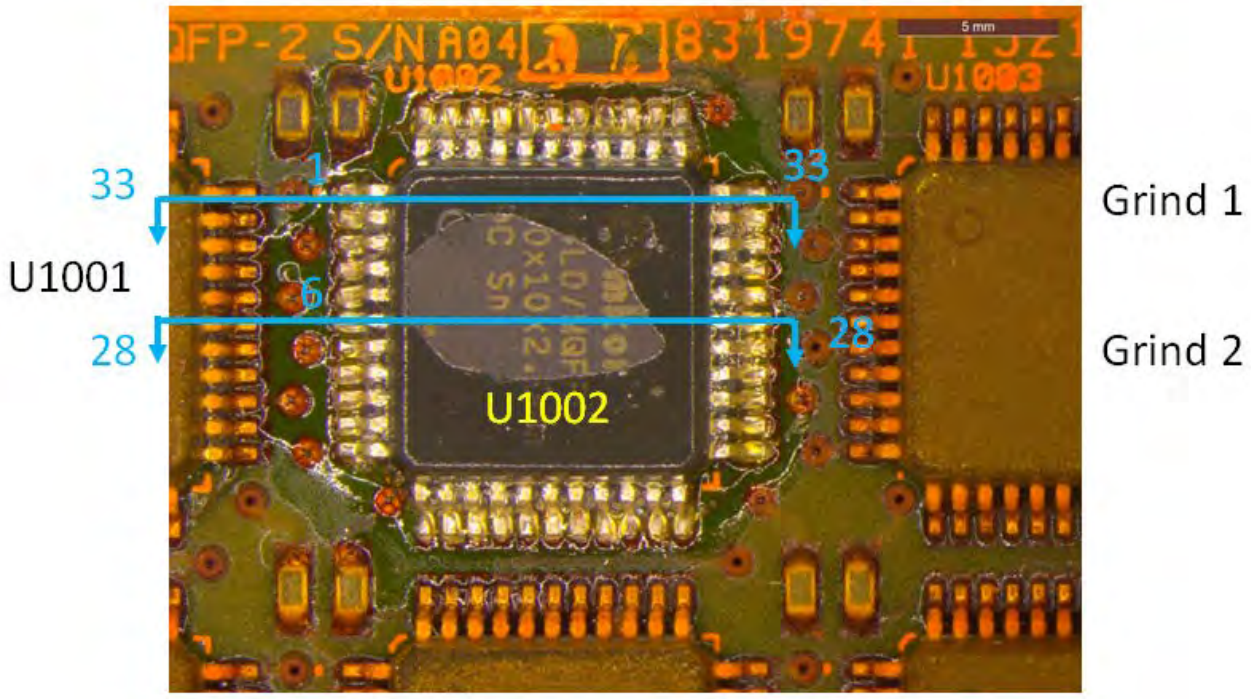


Figure 96: QFP-A023 section planes through U1001 (not reworked) and U1002 (reworked).

4.4.1.1 Optical cross-sections of unfilled PC18M QFP-A023 U1002 (reworked)

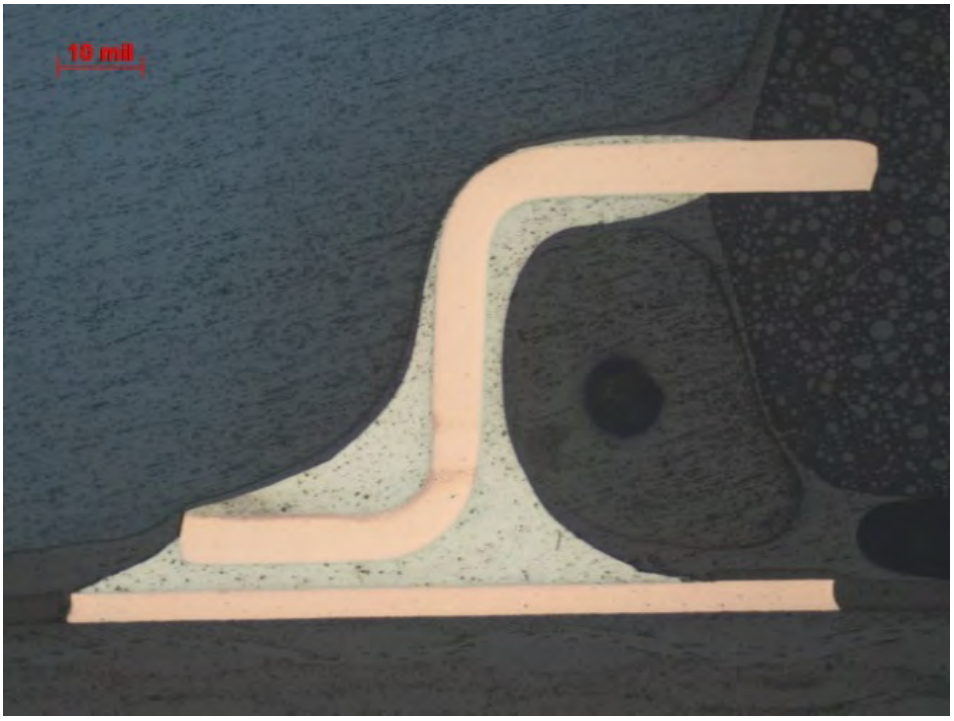


Figure 97: Optical cross-section image, unfilled PC18M QFP-A023 U1002 Lead 1, 50x.



Figure 98: Optical cross-section image, unfilled PC18M QFP-A023 U1002 Lead 1 knee, 100x.



Figure 99: Optical cross-section image, unfilled PC18M QFP-A023 U1002 Lead 1, foot, 100x.

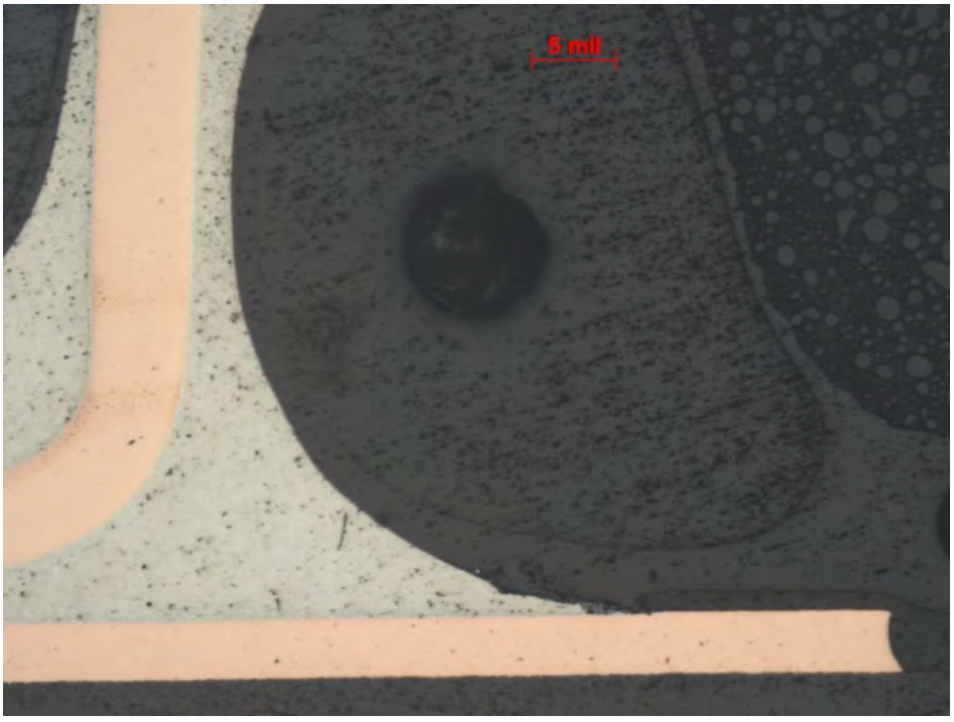


Figure 100: Optical cross-section image, unfilled PC18M QFP-A023 U1002 Lead 1 heel, 100x.

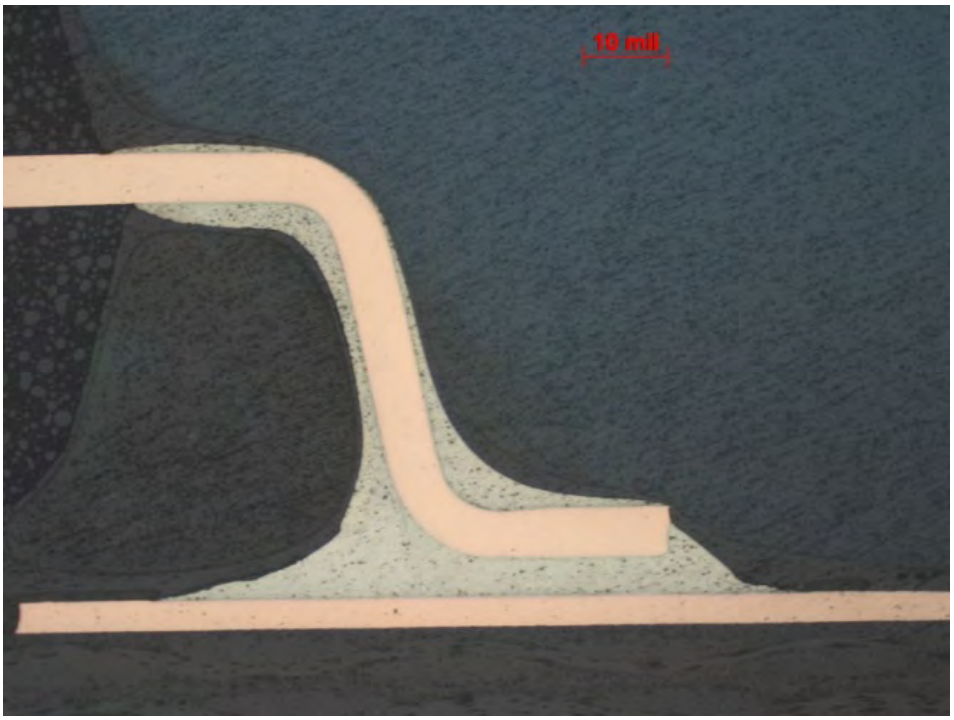


Figure 101: Optical cross-section image, unfilled PC18M QFP-A023 U1002, Lead 33, 50x.

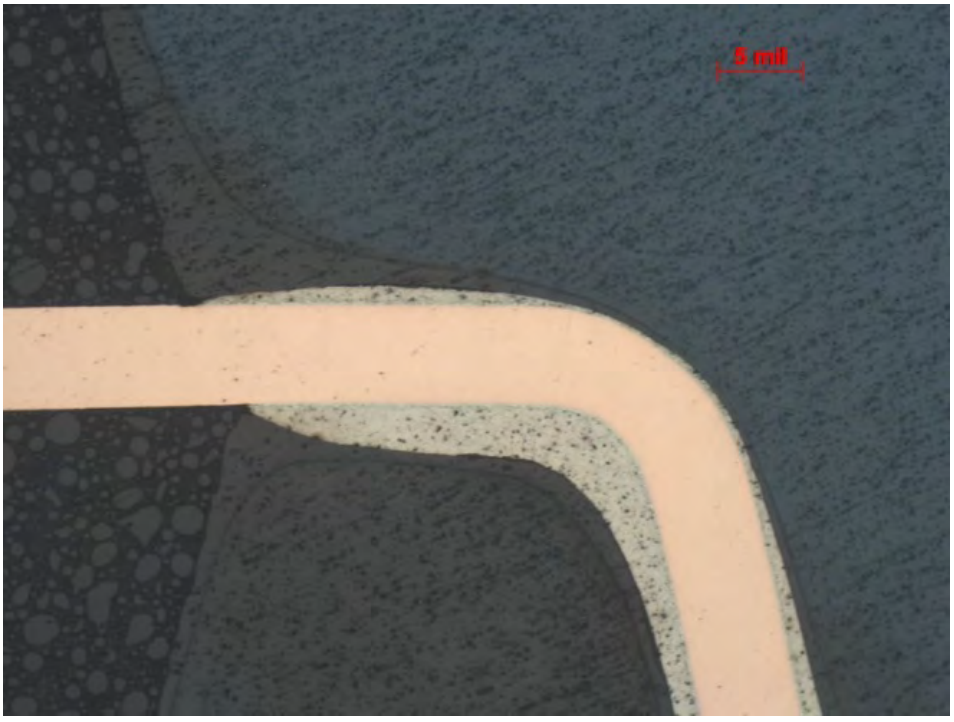


Figure 102: Optical cross-section image, unfilled PC18M QFP-A023 U1002, Lead 33 knee, 100x.

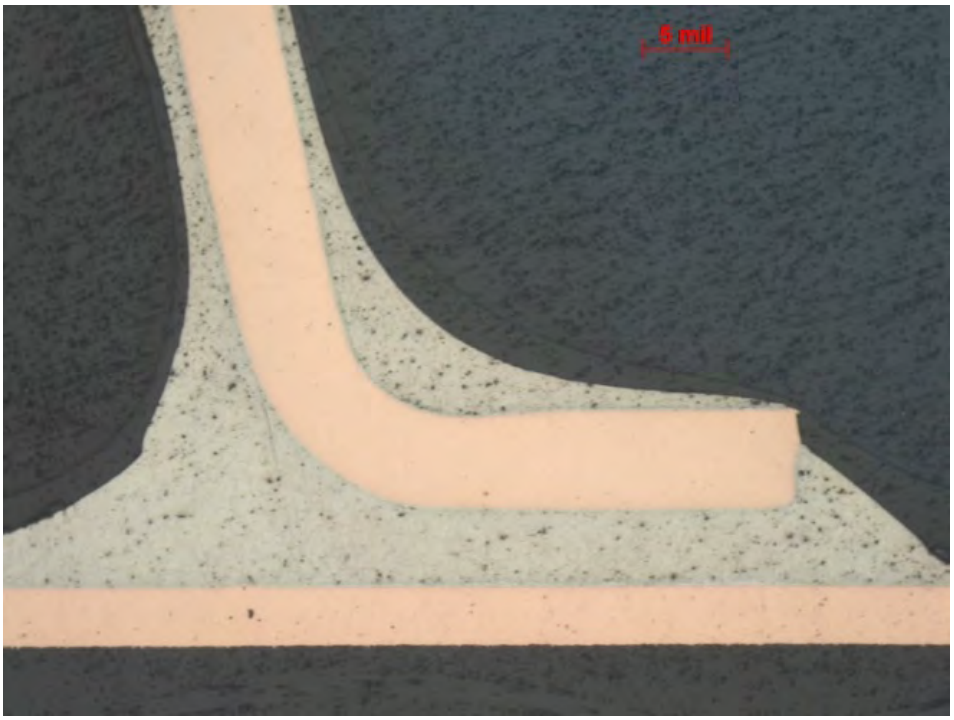


Figure 103: Optical cross-section image, unfilled PC18M QFP-A023 U1002, Lead 33 foot, 100x.

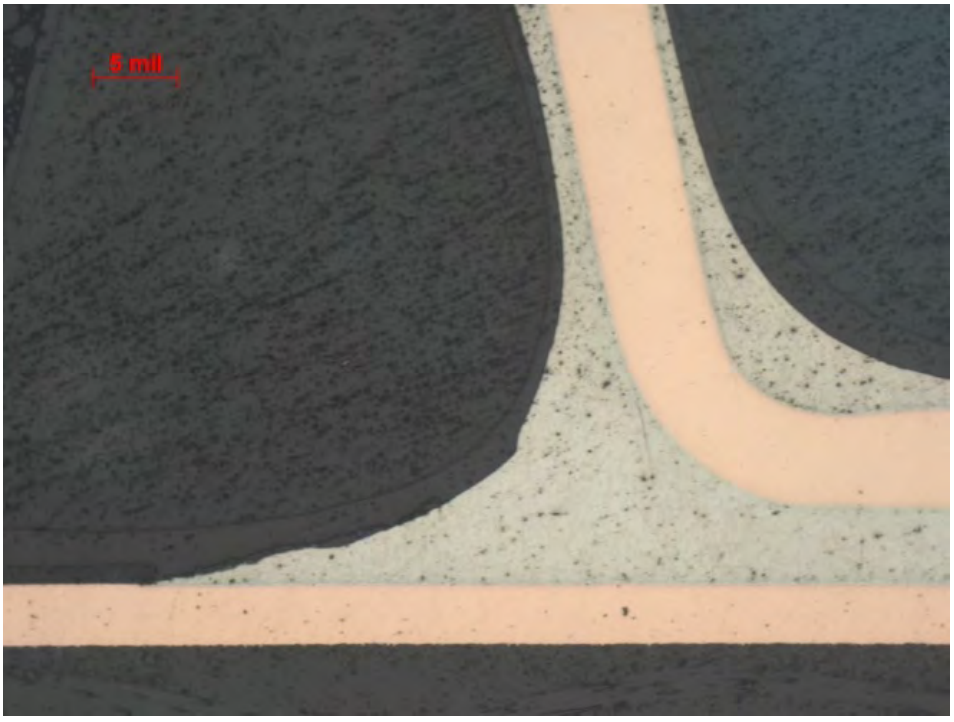


Figure 104: Optical cross-section image, unfilled PC18M QFP-A023 U1002, Lead 33 heel, 100x.

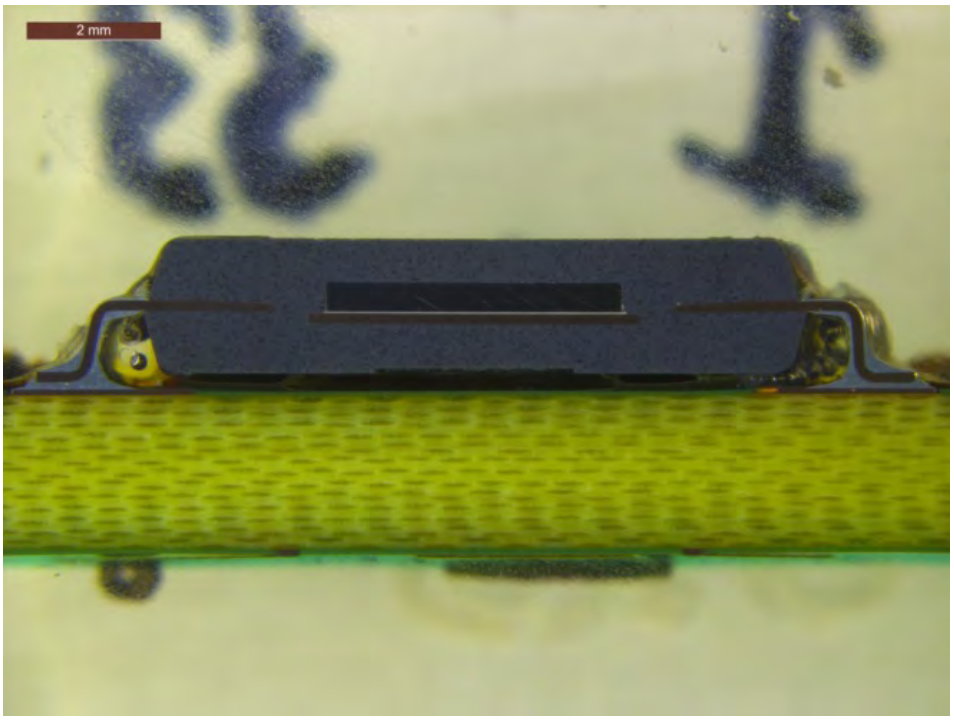


Figure 105: Optical cross-section image, unfilled PC18M QFP-A023 U1002, overall stereoscope non-inverted, lead 6 (left) and lead 28 (right), 7.8x.

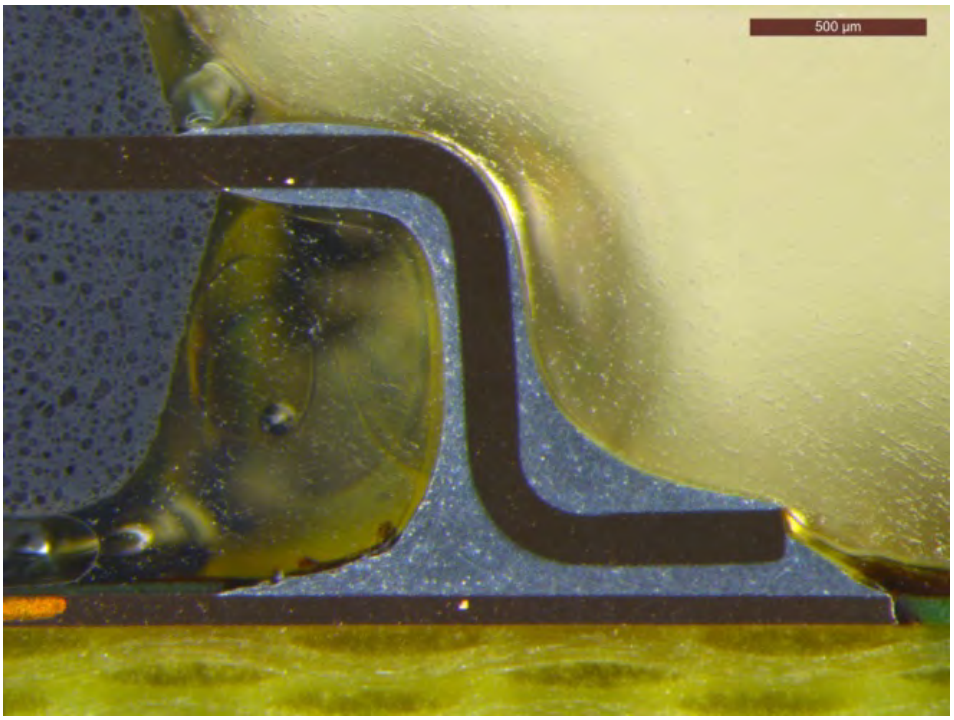


Figure 106: Optical cross-section image, unfilled PC18M QFP-A023 U1002, Lead 6 stereoscope non-inverted, 40x.

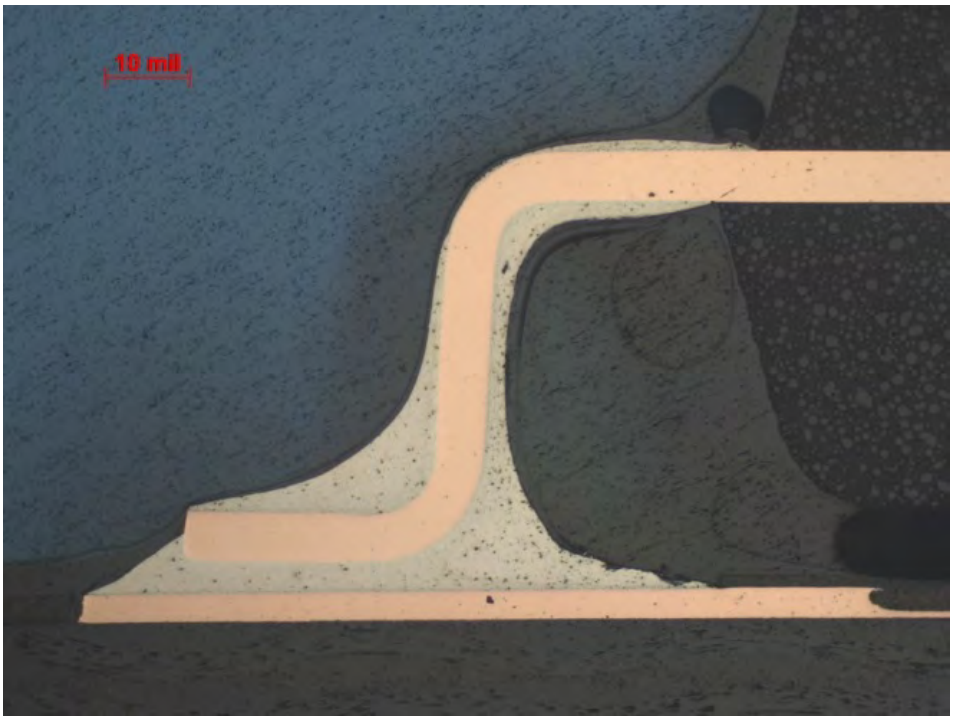


Figure 107: Optical cross-section image, unfilled PC18M QFP-A023 U1002, Lead 6, 50x.



Figure 108: Optical cross-section image, unfilled PC18M QFP-A023 U1002, Lead 6 knee, 100x.

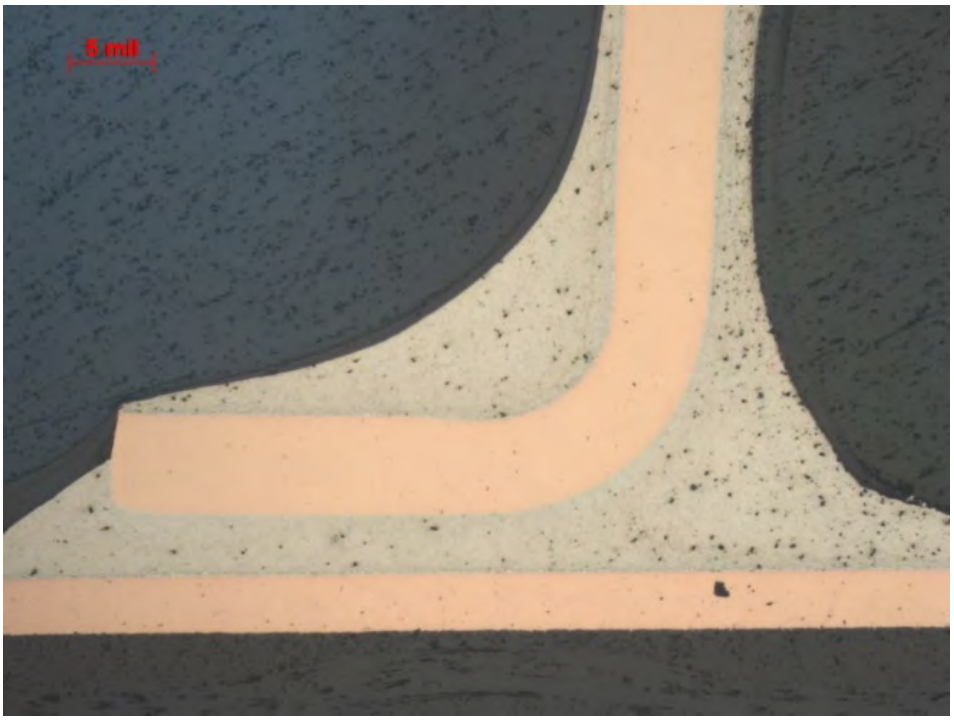


Figure 109: Optical cross-section image, unfilled PC18M QFP-A023 U1002, Lead 6 foot, 100x.

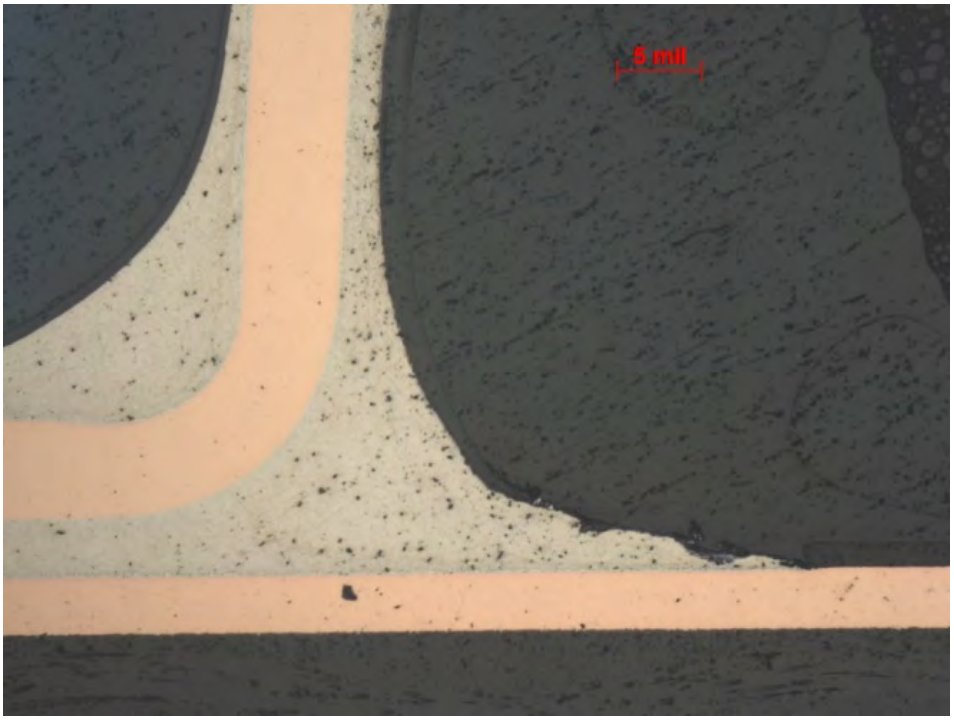


Figure 110: Optical cross-section image, unfilled PC18M QFP-A023 U1002, Lead 6 heel, 100x.

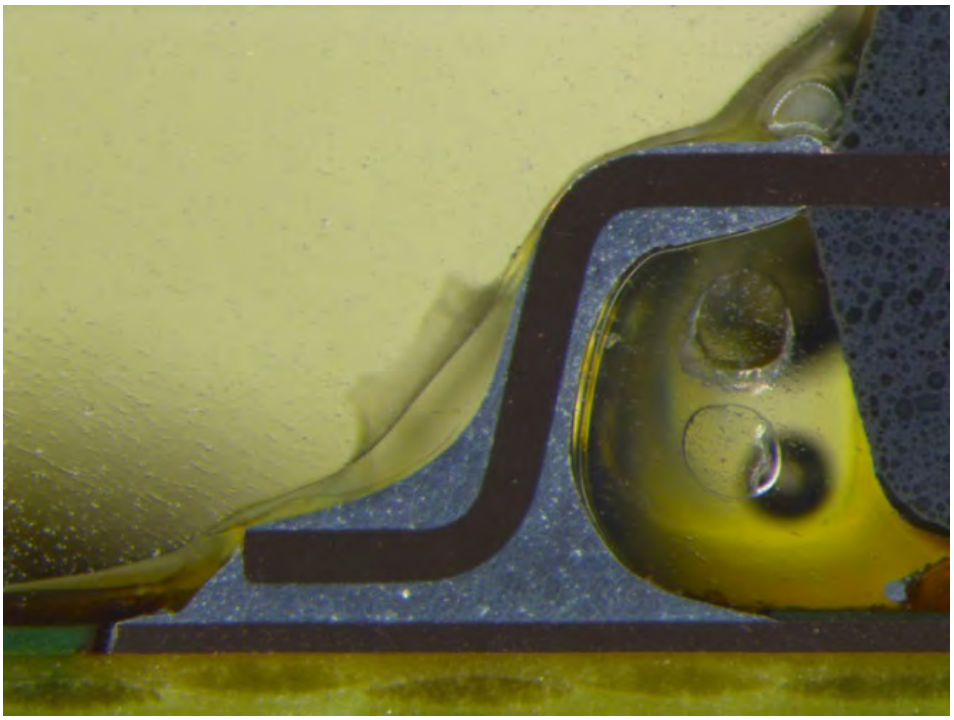


Figure 111: Optical cross-section image, unfilled PC18M QFP-A023 U1002, Lead 28 stereoscope non-inverted, 40x.

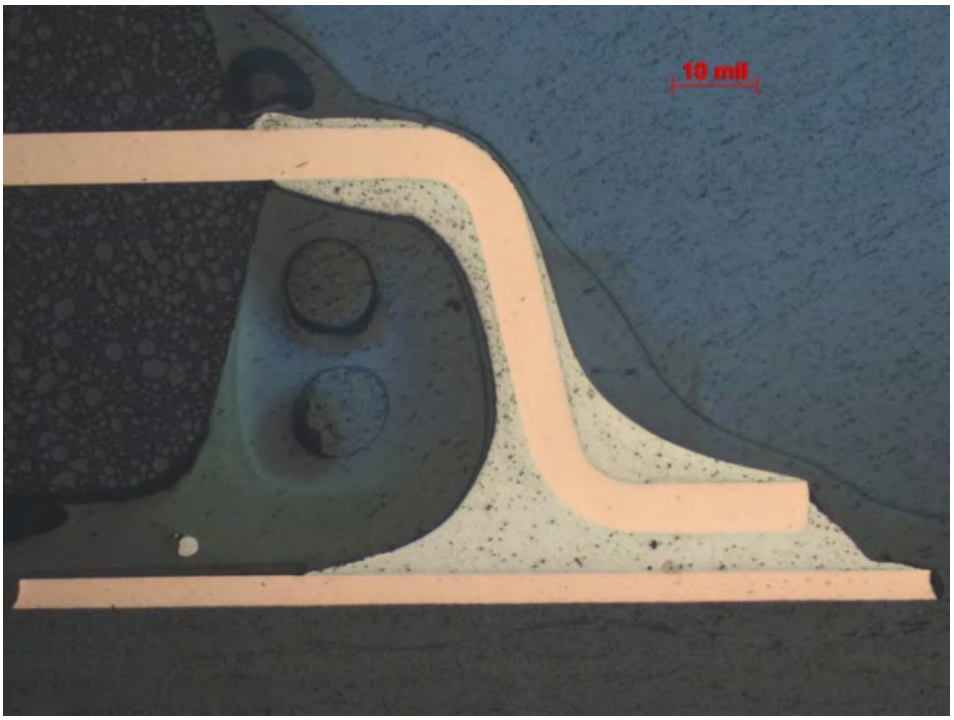


Figure 112: Optical cross-section image, unfilled PC18M QFP-A023 U1002, Lead 28, 50x.

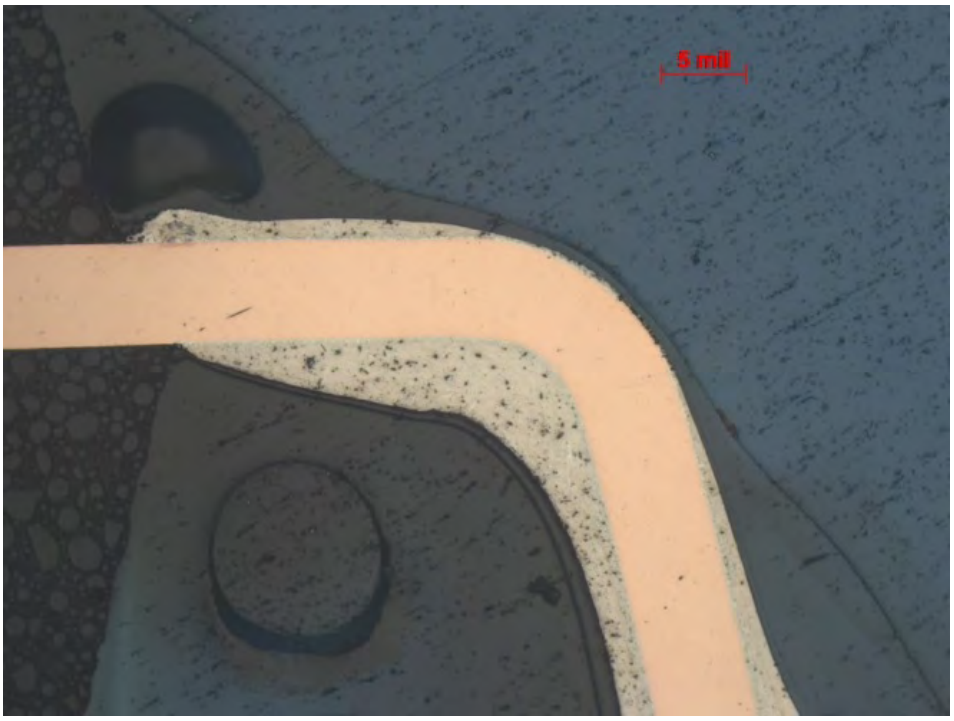


Figure 113: Optical cross-section image, unfilled PC18M QFP-A023 U1002, Lead 28 knee, 100x.

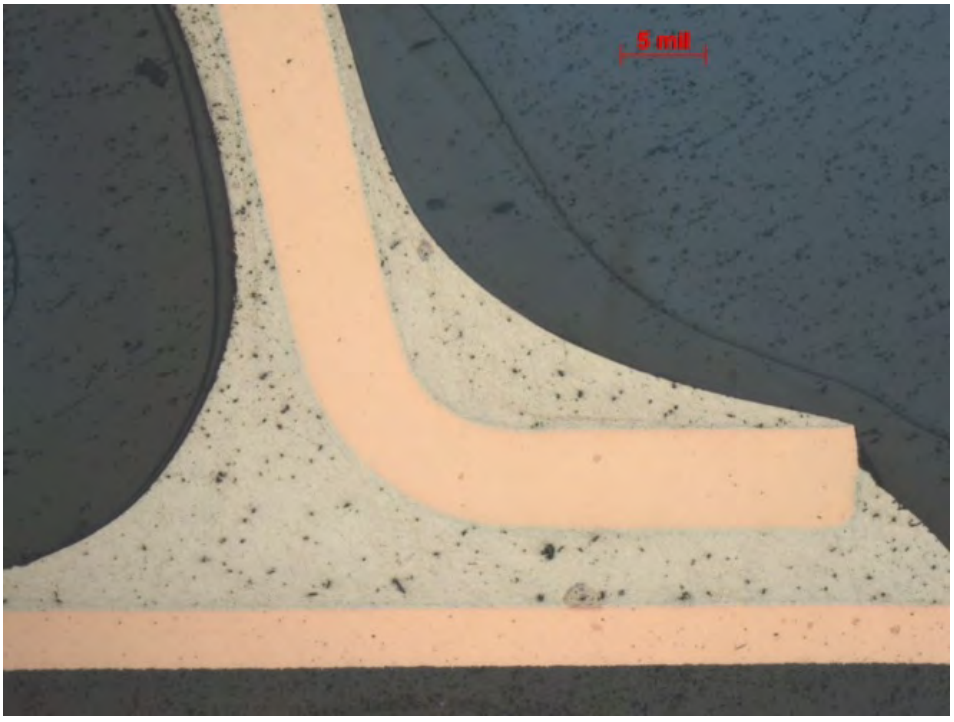


Figure 114: Optical cross-section image, unfilled PC18M QFP-A023 U1002, Lead 28 foot, 100x.

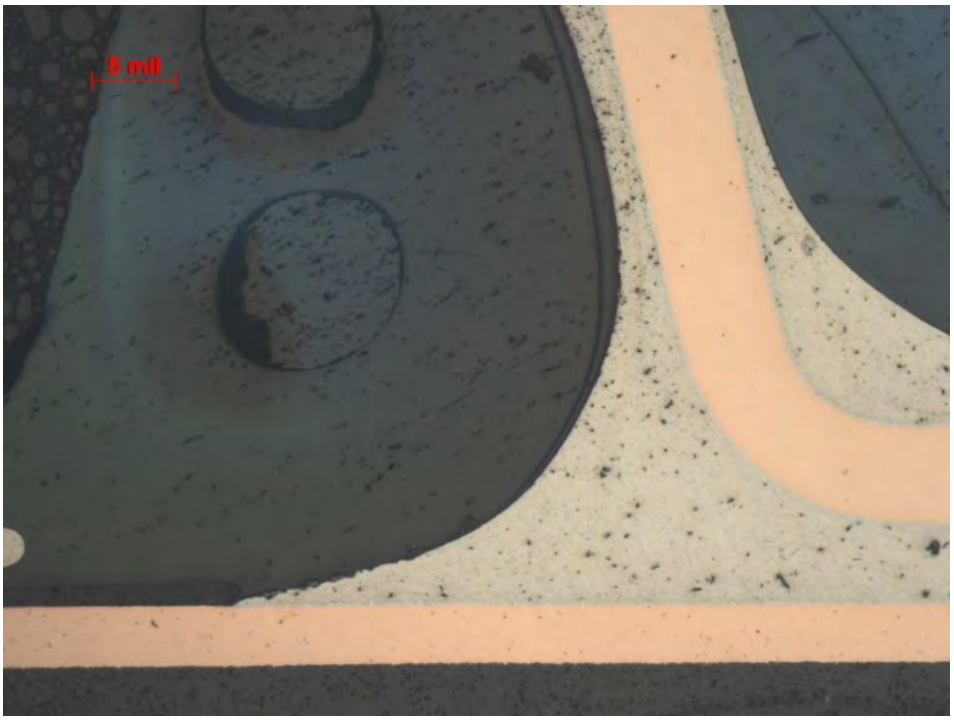


Figure 115: Optical cross-section image, unfilled PC18M QFP-A023 U1002, Lead 28 heel, 100x.

4.4.1.2 SEM cross-sections of unfilled PC18M QFP-A023 U1002 (reworked)

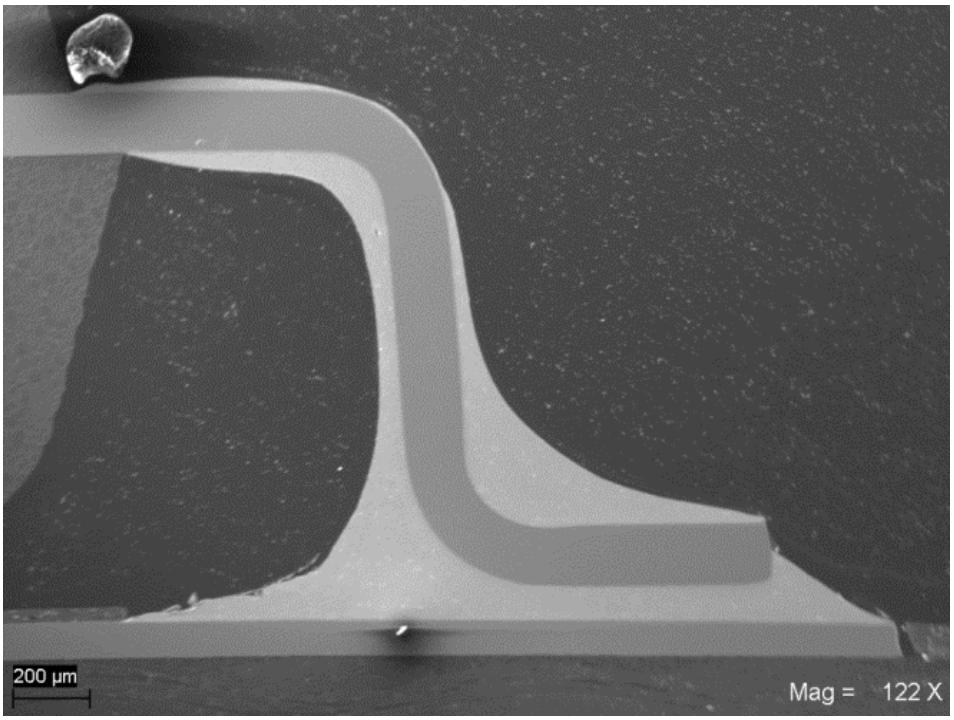


Figure 116: SEM cross-section image, unfilled PC18M QFP-A023 U1002, Lead 6, 122x.

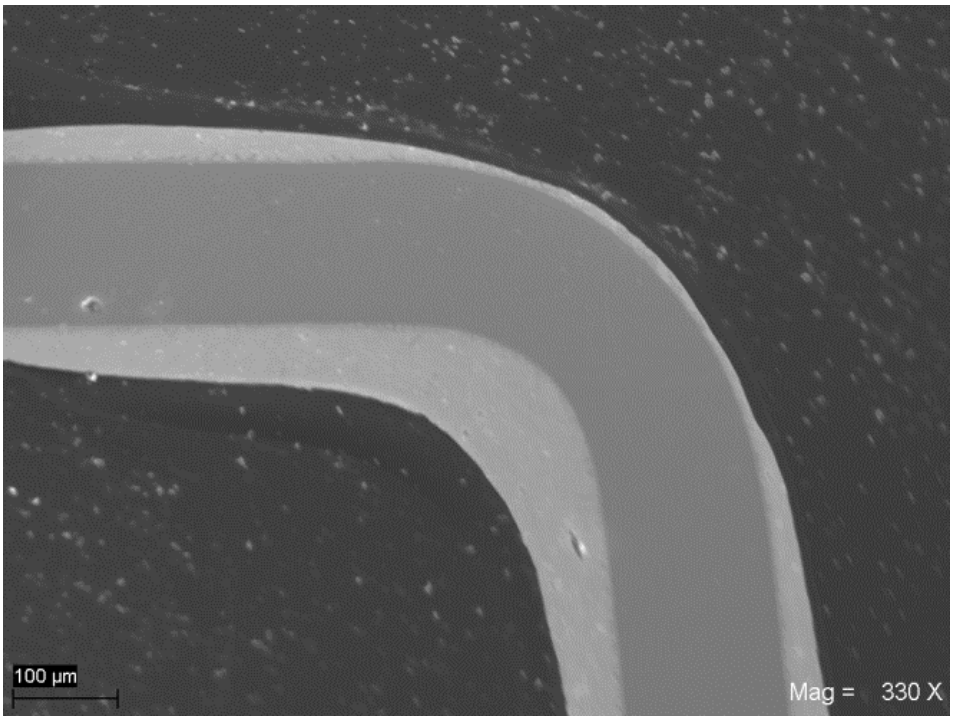


Figure 117: SEM cross-section image, unfilled PC18M QFP-A023 U1002, Lead 6 knee, 330x.

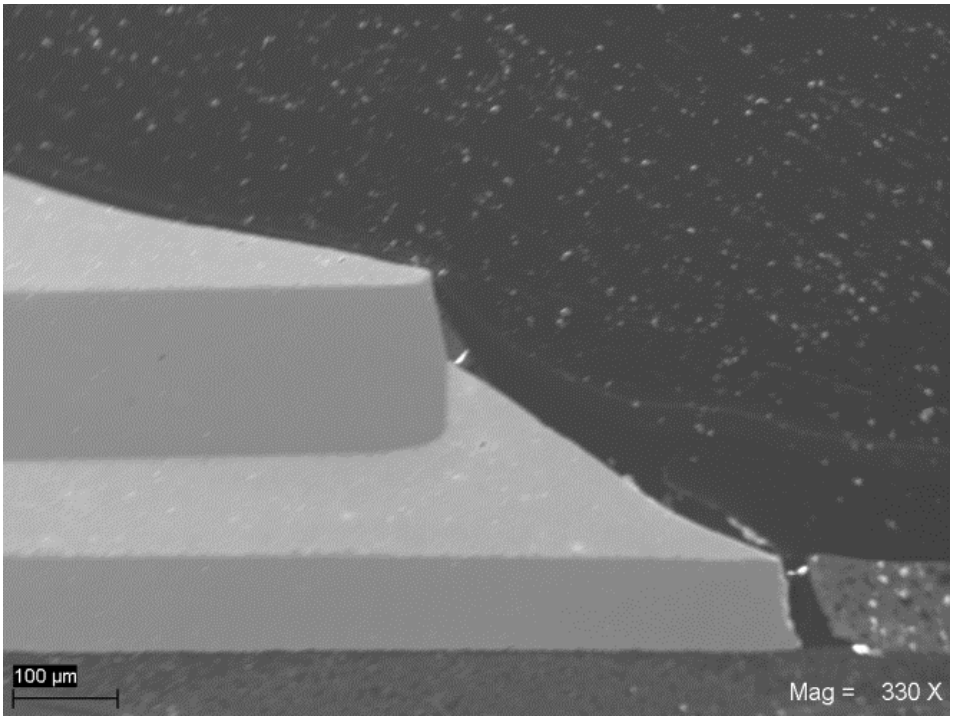


Figure 118: SEM cross-section image, unfilled PC18M QFP-A023 U1002, Lead 6 toe, 330x.

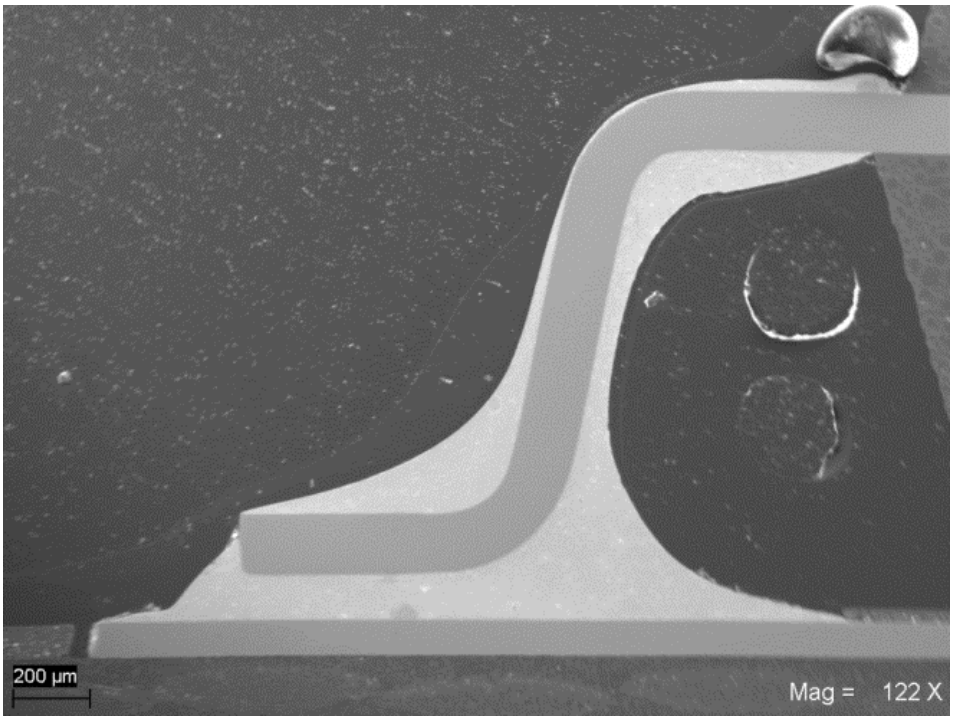


Figure 119: SEM cross-section image, unfilled PC18M QFP-A023 U1002, Lead 28, 122x.

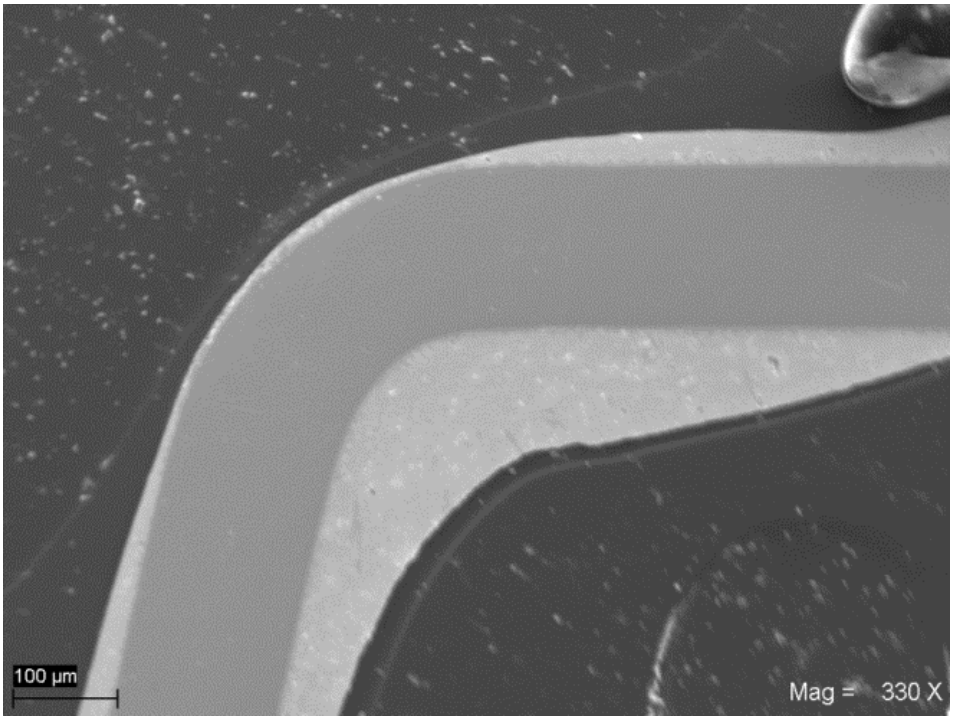


Figure 120: SEM cross-section image, unfilled PC18M QFP-A023 U1002, Lead 28 knee, 330x.

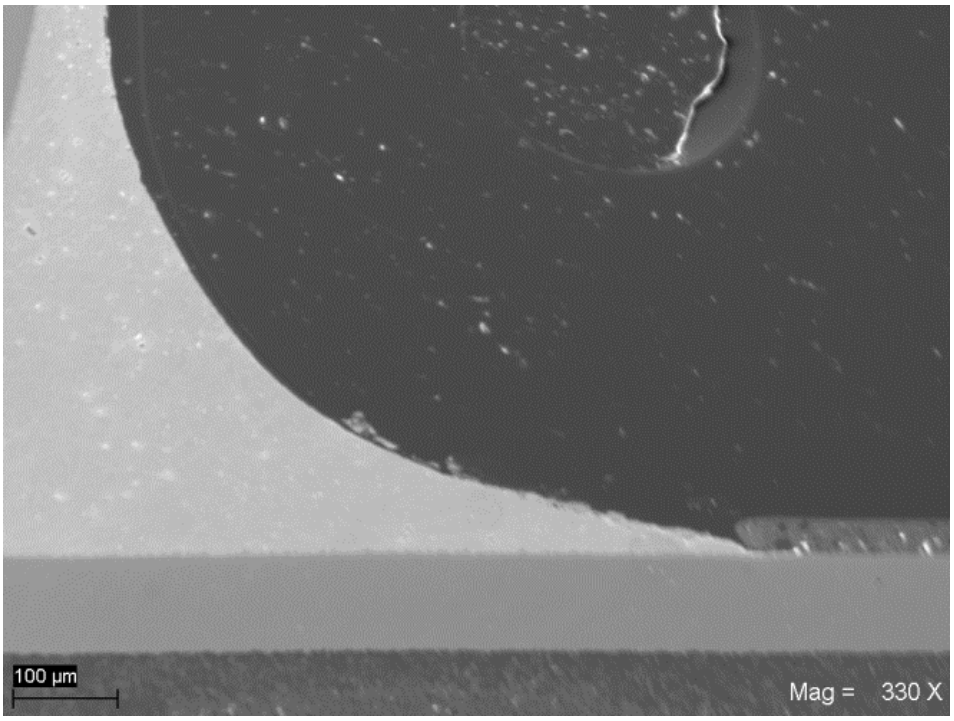


Figure 121: SEM cross-section image, unfilled PC18M QFP-A023 U1002, Lead 28 heel, 330x.

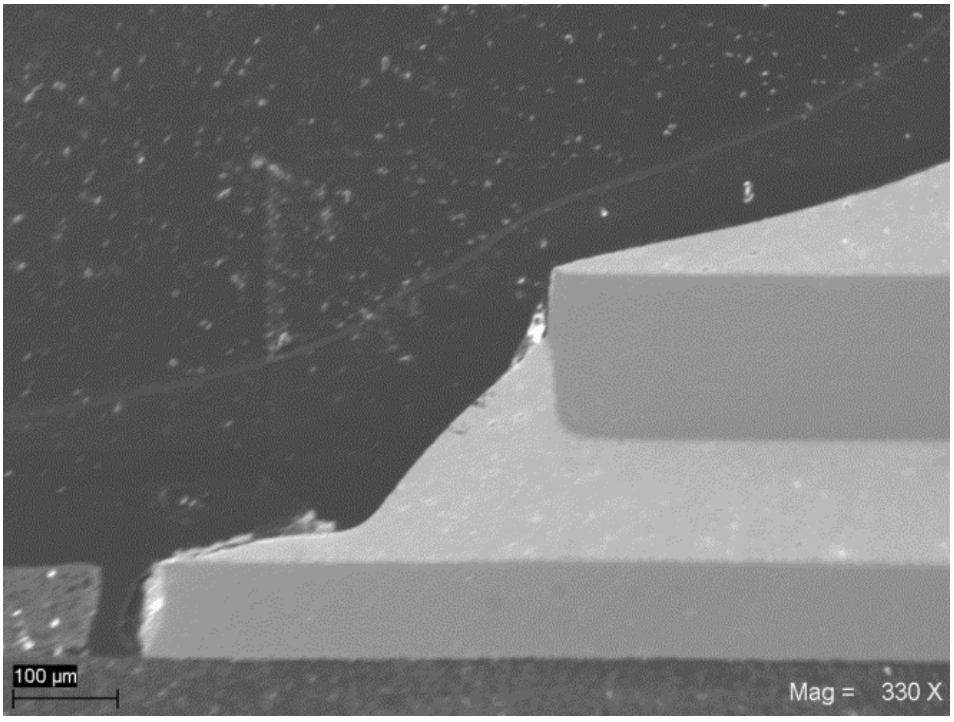


Figure 122: SEM cross-section image, unfilled PC18M QFP-A023 U1002, Lead 28 toe, 330x.

4.4.1.3 Coating thickness measurements of unfilled PC18M QFP-A023 U1002

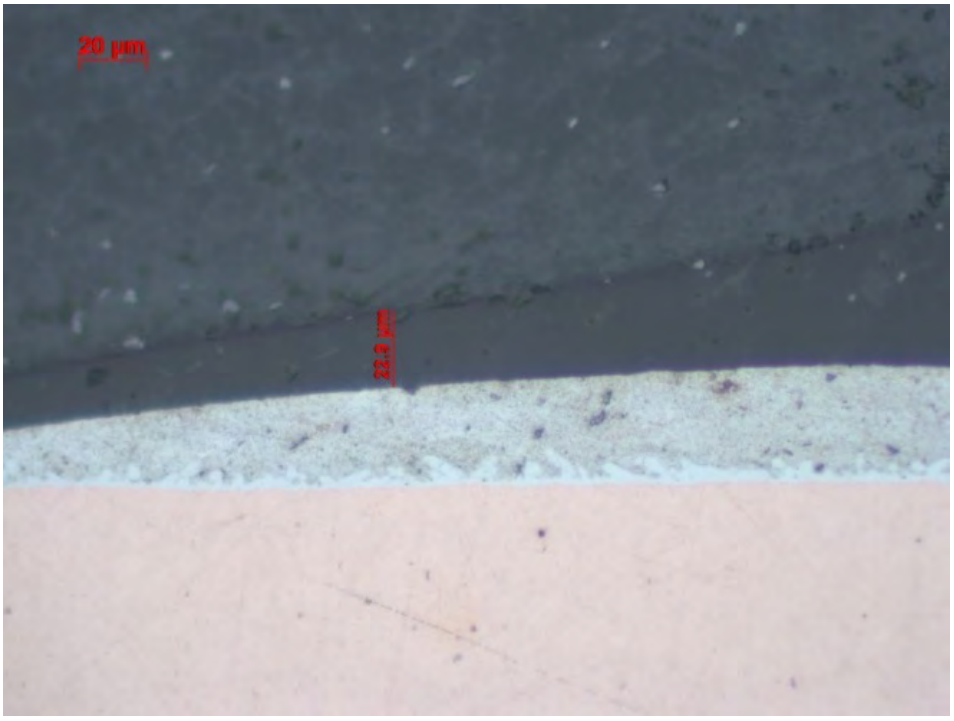


Figure 123: Optical cross-section image, unfilled PC18M QFP-A023 U1002, Lead 6 measurements, A, 500x.

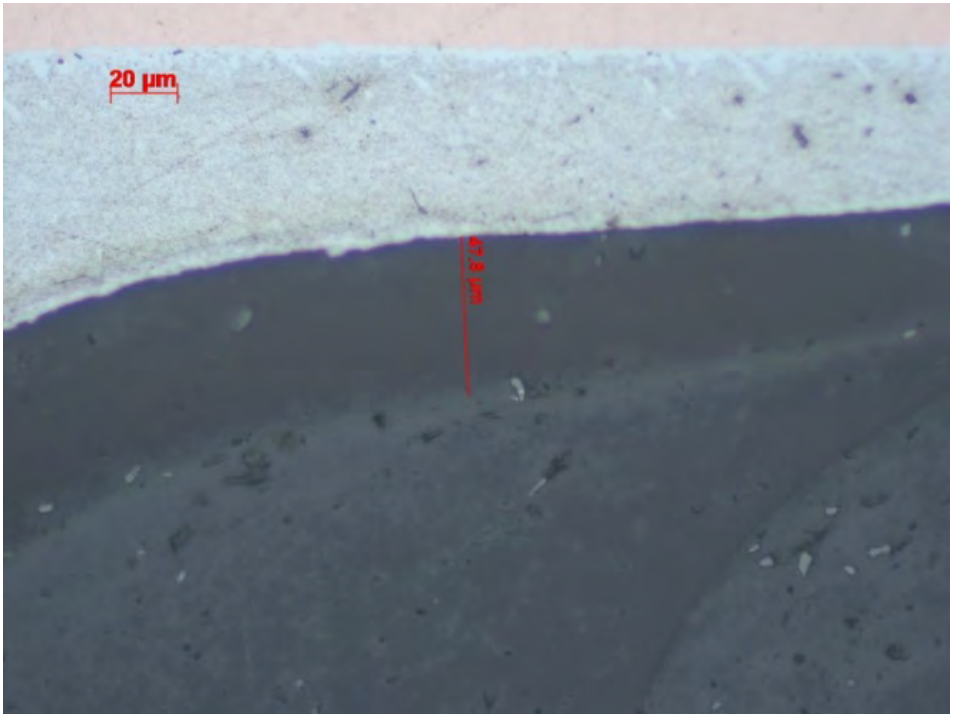


Figure 124: Optical cross-section image, unfilled PC18M QFP-A023 U1002, Lead 6 measurements, A1, 500x.

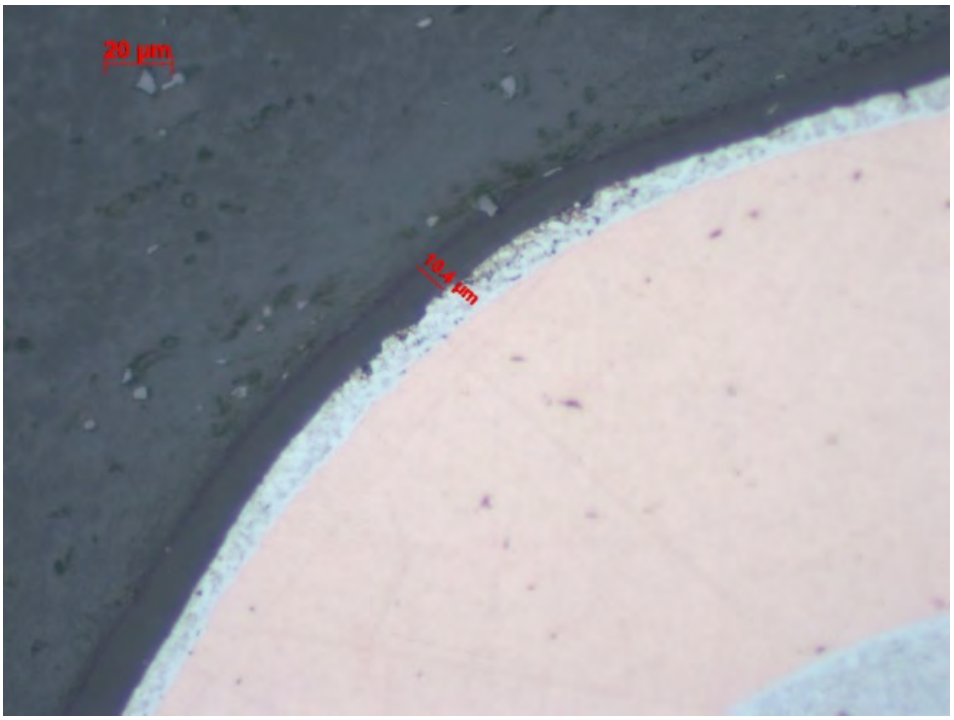


Figure 125: Optical cross-section image, unfilled PC18M QFP-A023 U1002, Lead 6 measurements, B, 500x.

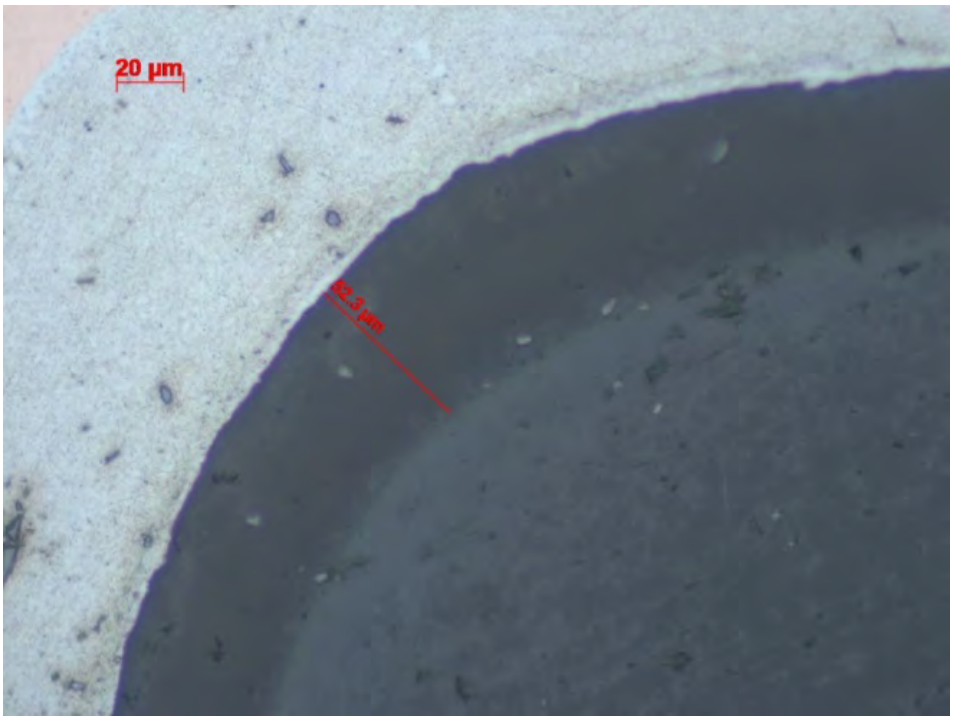


Figure 126: Optical cross-section image, unfilled PC18M QFP-A023 U1002, Lead 6 measurements, B1, 500x.

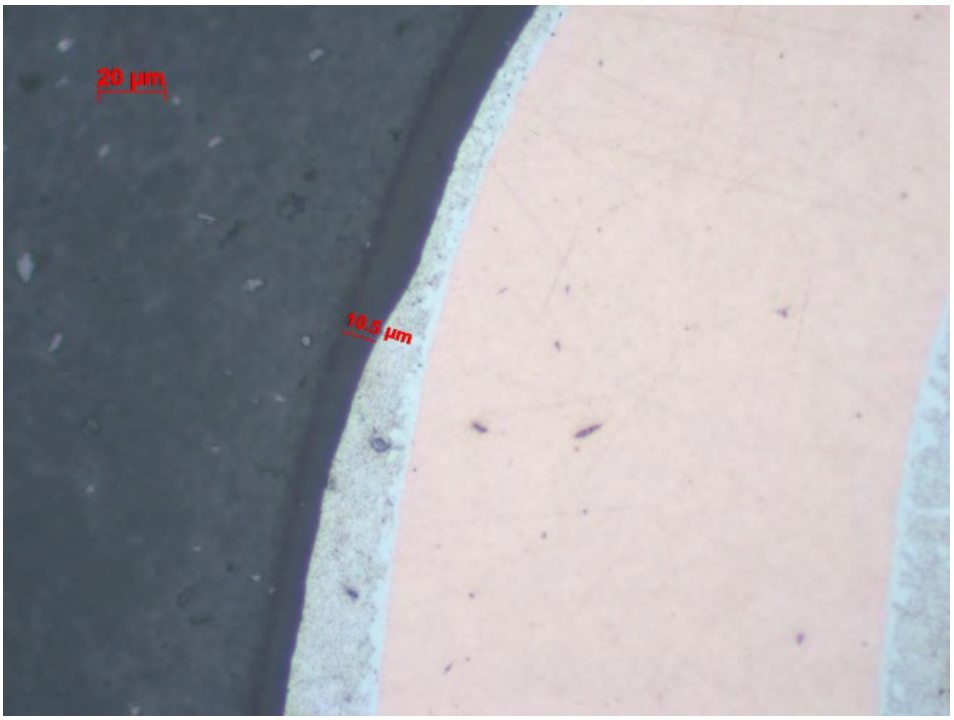


Figure 127: Optical cross-section image, unfilled PC18M QFP-A023 U1002, Lead 6 measurements, C, 500x.

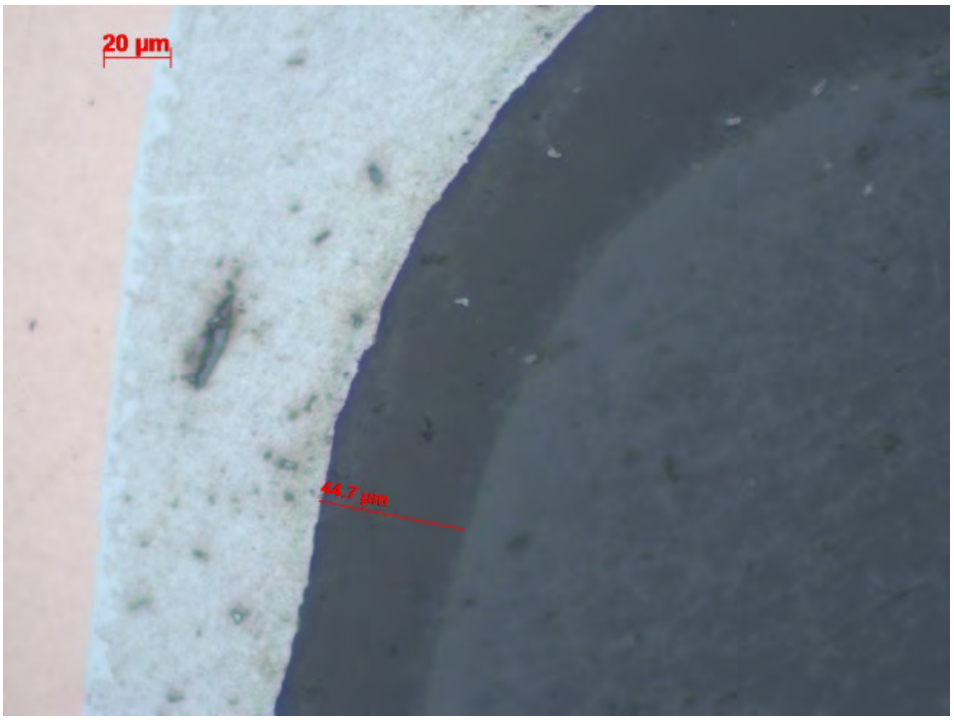


Figure 128: Optical cross-section image, unfilled PC18M QFP-A023 U1002, Lead 6 measurements, C1, 500x.

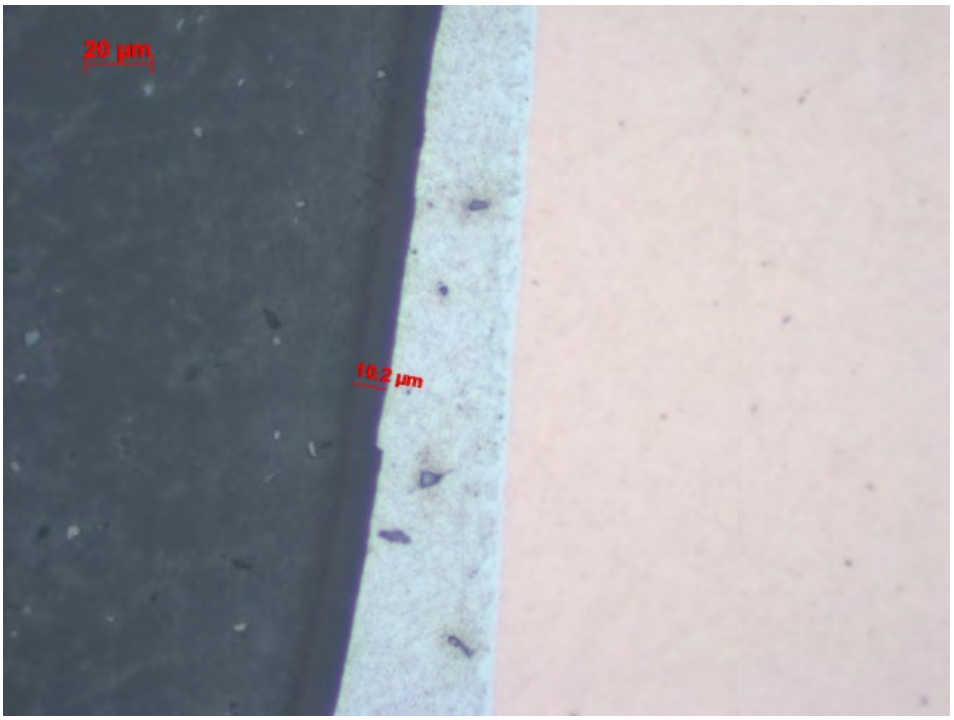


Figure 129: Optical cross-section image, unfilled PC18M QFP-A023 U1002, Lead 6 measurements, D, 500x.

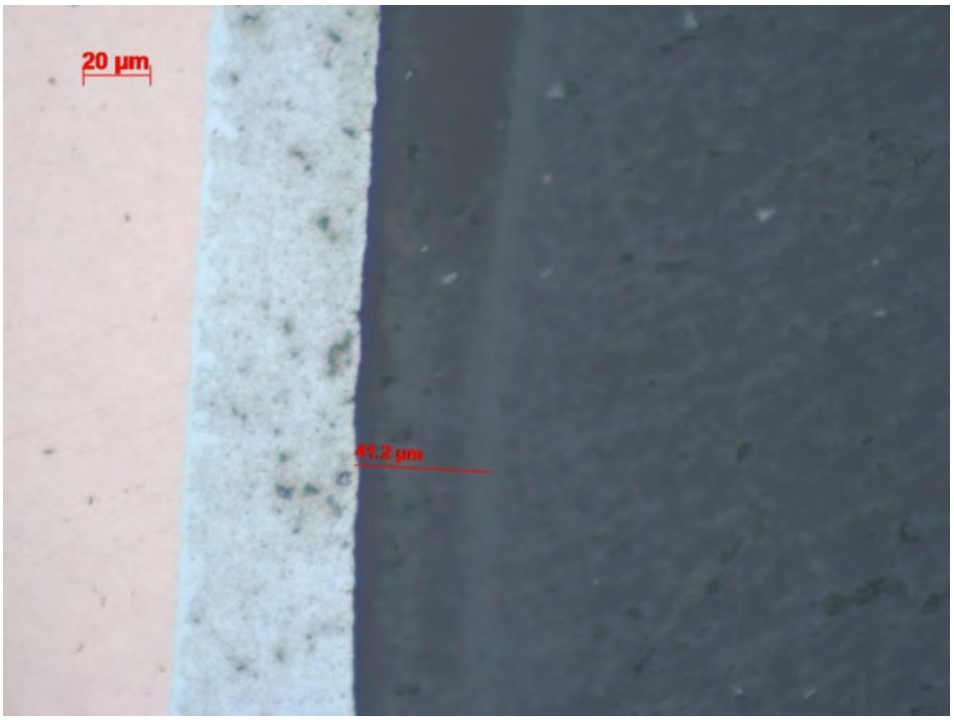


Figure 130: Optical cross-section image, unfilled PC18M QFP-A023 U1002, Lead 6 measurements, D1, 500x.

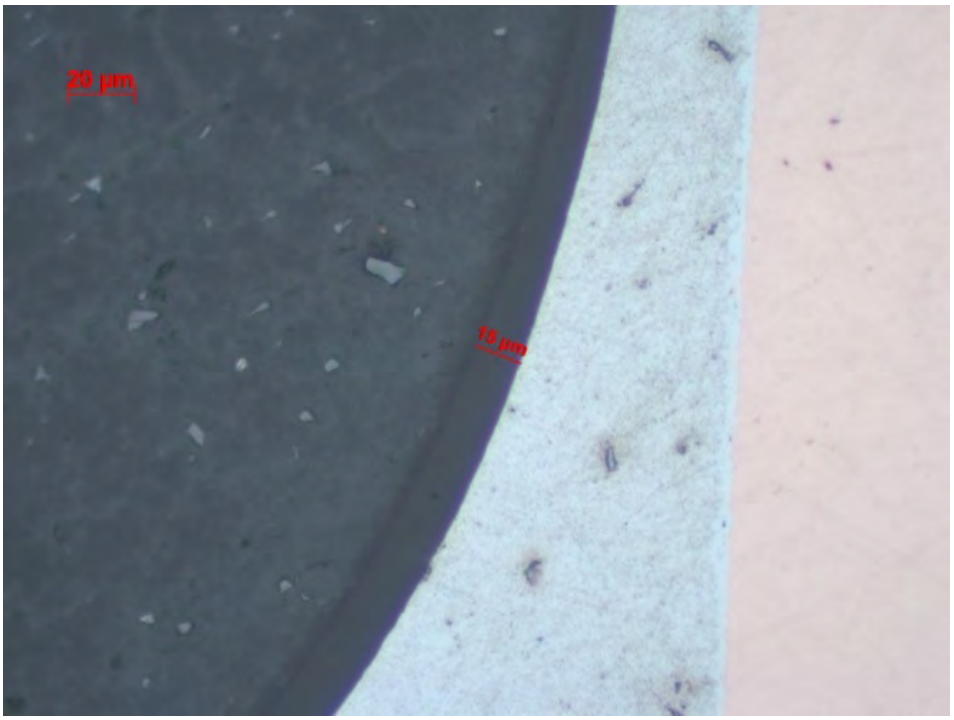


Figure 131: Optical cross-section image, unfilled PC18M QFP-A023 U1002, Lead 6 measurements, E, 500x.

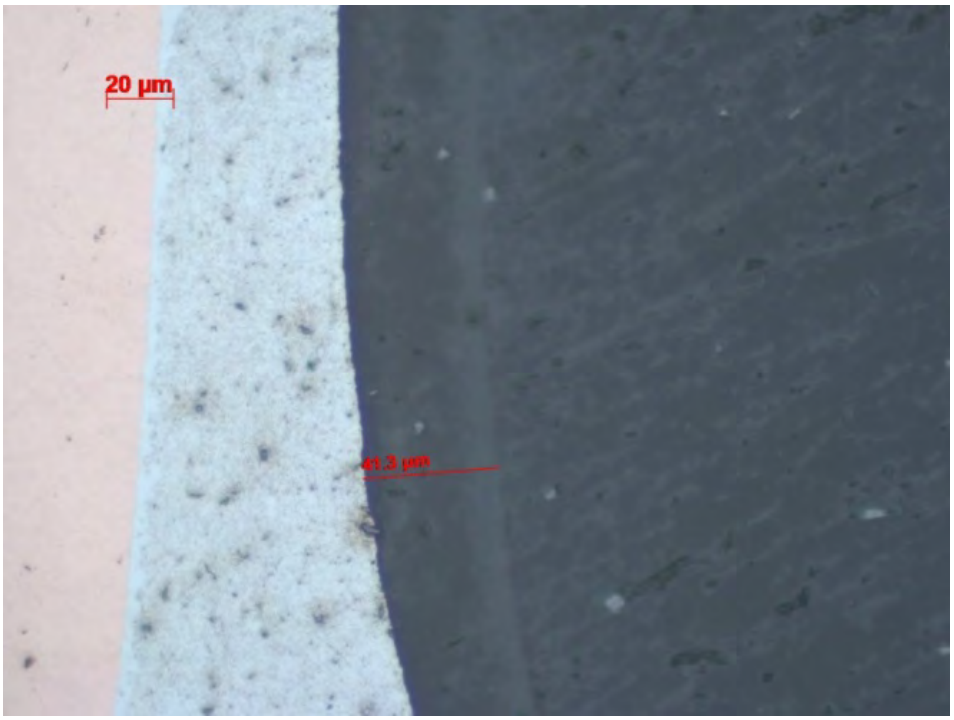


Figure 132: Optical cross-section image, unfilled PC18M QFP-A023 U1002, Lead 6 measurements, E1, 500x.

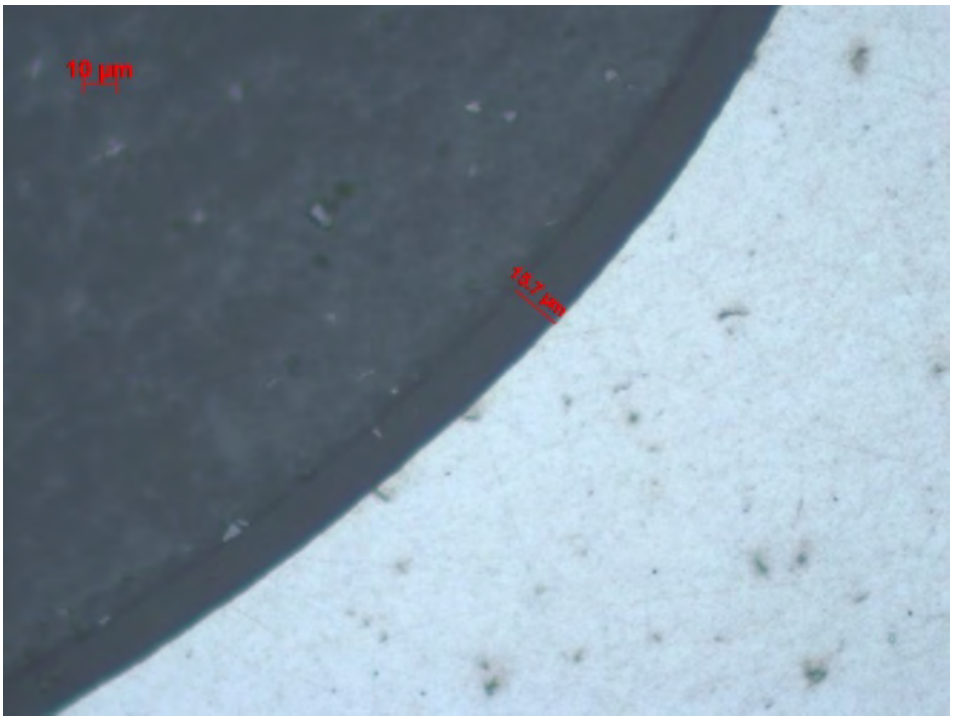


Figure 133: Optical cross-section image, unfilled PC18M QFP-A023 U1002, Lead 6 measurements, F, 500x.

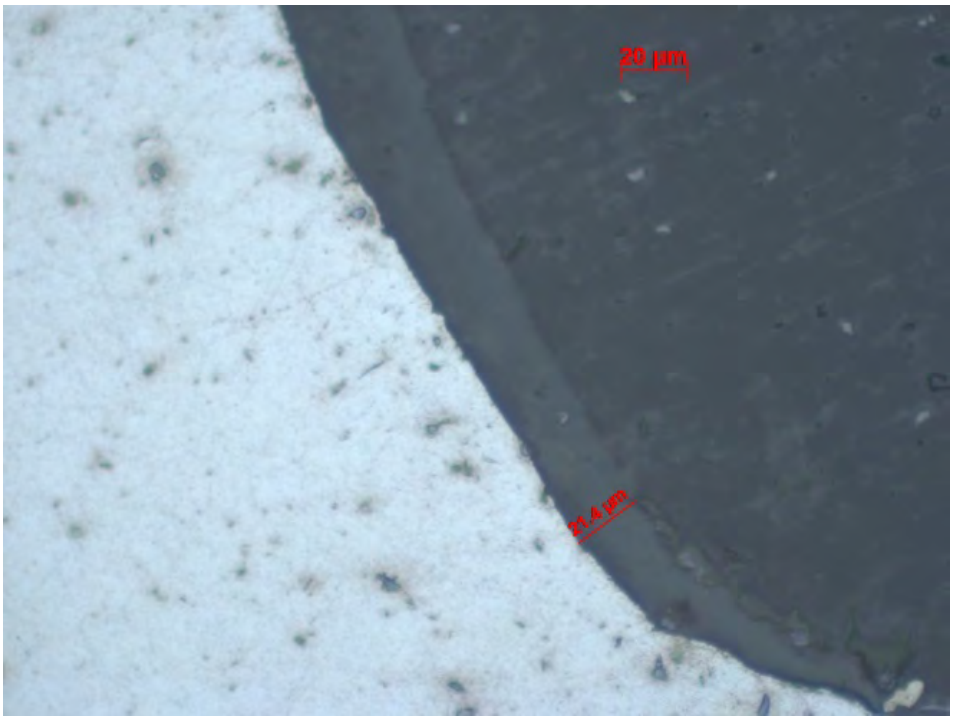


Figure 134: Optical cross-section image, unfilled PC18M QFP-A023 U1002, Lead 6 measurements, F1, 500x.

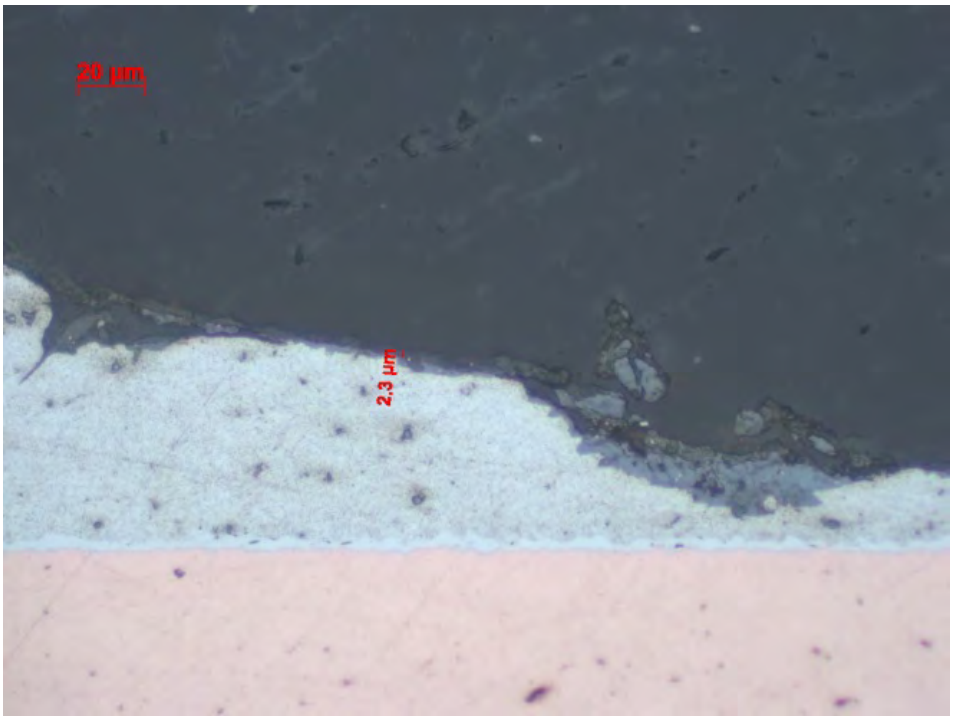


Figure 135: Optical cross-section image, unfilled PC18M QFP-A023 U1002, Lead 6 measurements, H, 500x.

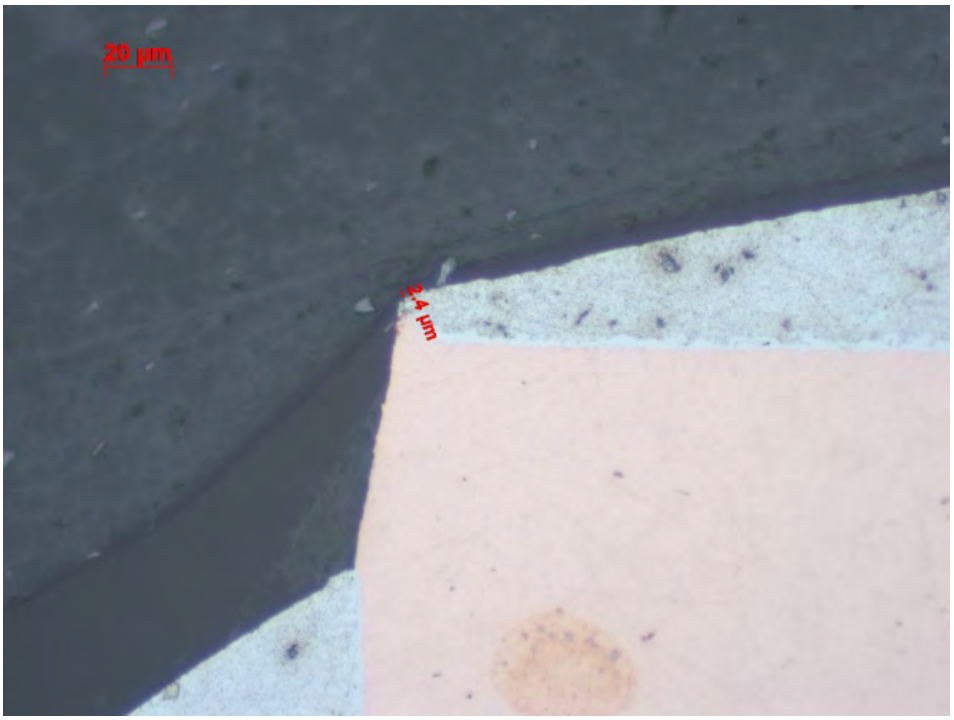


Figure 136: Optical cross-section image, unfilled PC18M QFP-A023 U1002, Lead 6 measurements, T, 500x.

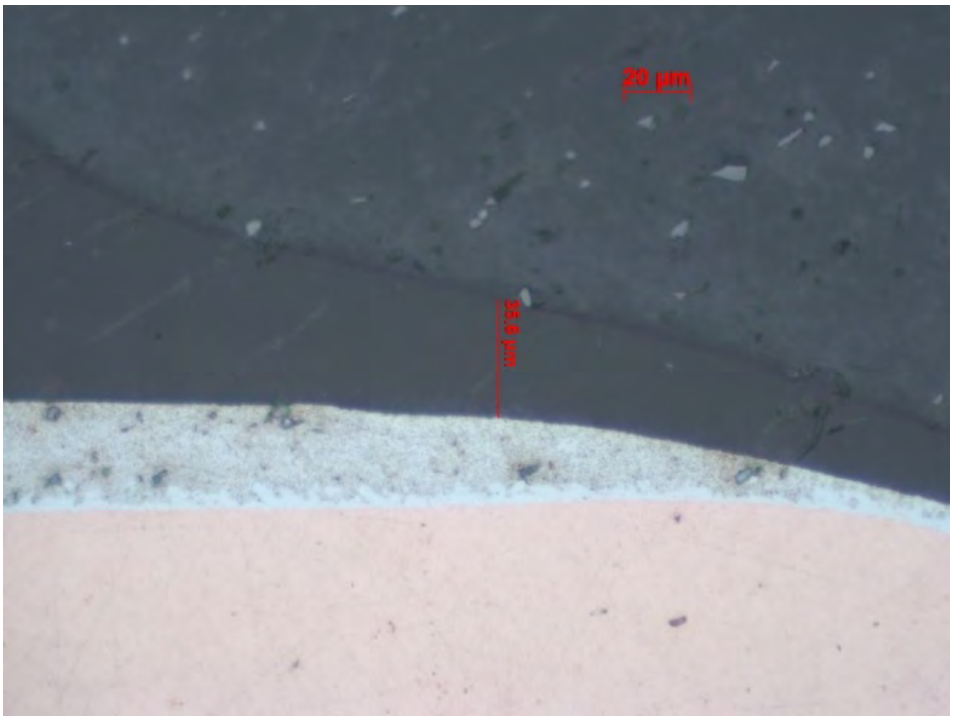


Figure 137: Optical cross-section image, unfilled PC18M QFP-A023 U1002, Lead 28 measurements, A, 500x.

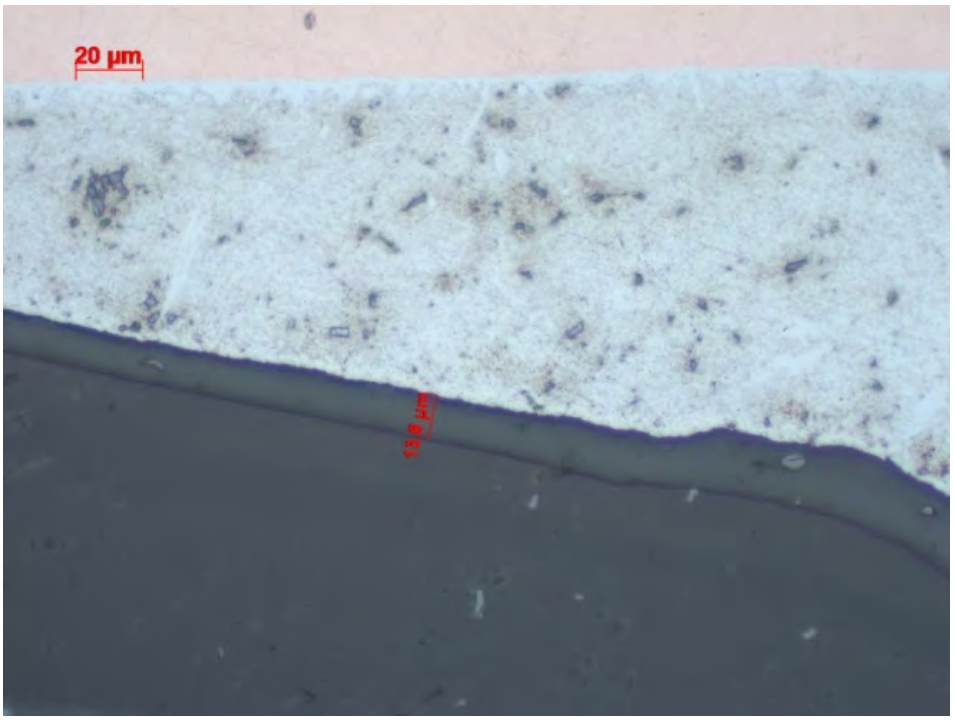


Figure 138: Optical cross-section image, unfilled PC18M QFP-A023 U1002, Lead 28 measurements, A1, 500x.

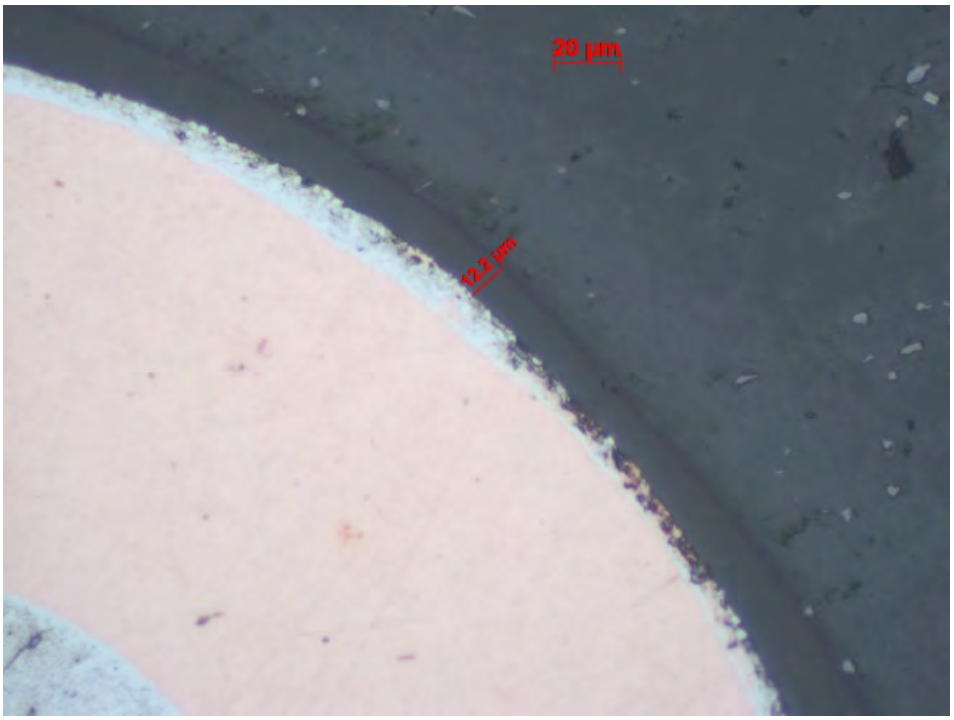


Figure 139: Optical cross-section image, unfilled PC18M QFP-A023 U1002, Lead 28 measurements, B, 500x.

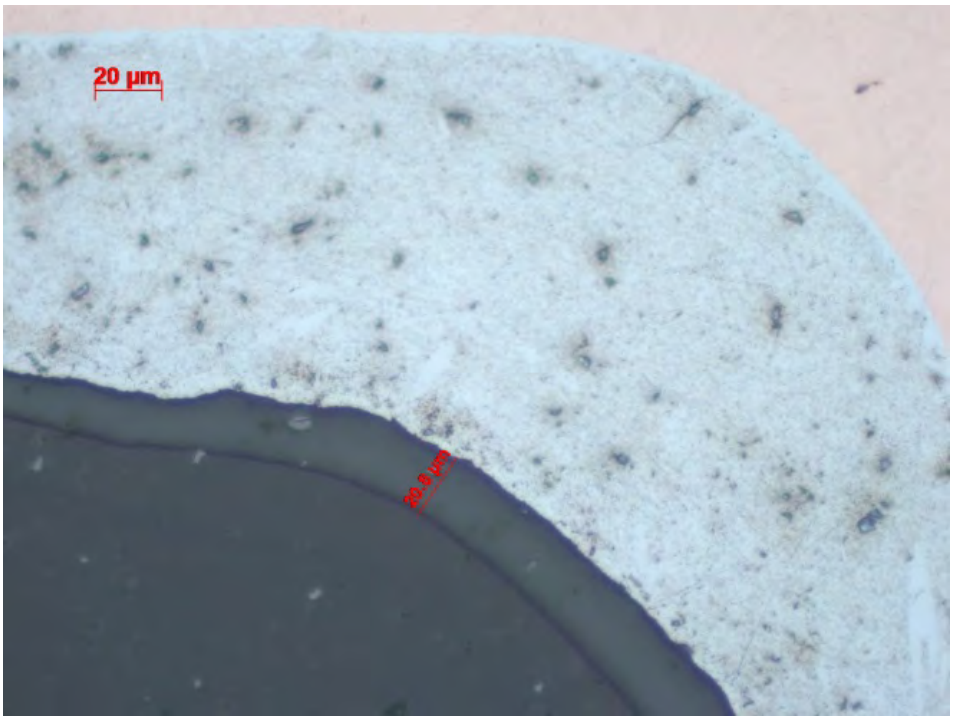


Figure 140: Optical cross-section image, unfilled PC18M QFP-A023 U1002, Lead 28 measurements, B1, 500x.

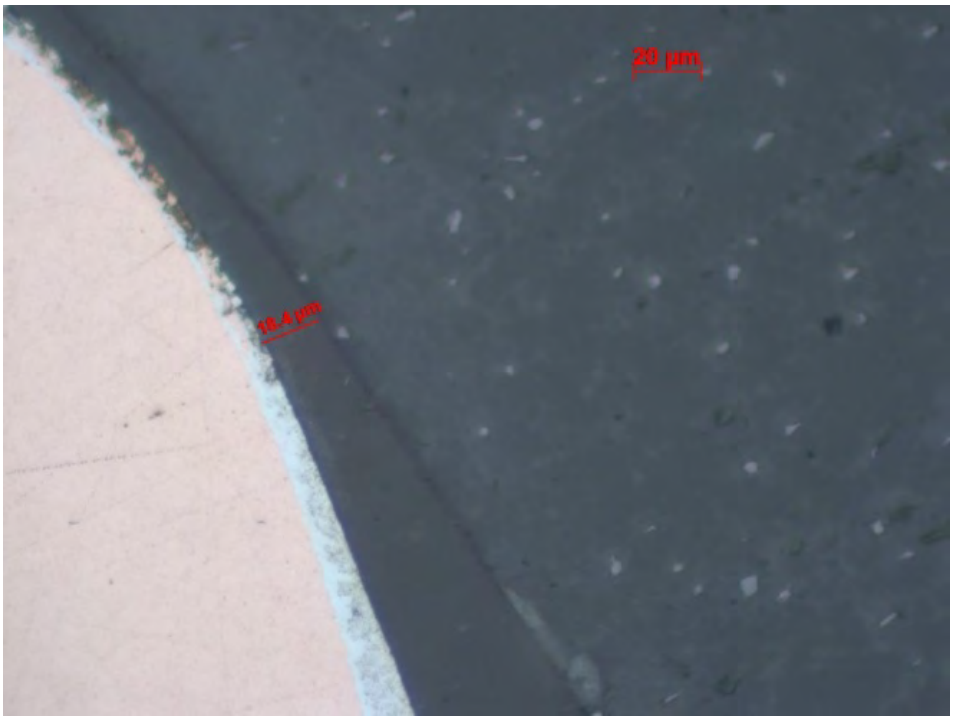


Figure 141: Optical cross-section image, unfilled PC18M QFP-A023 U1002, Lead 28 measurements, C, 500x.

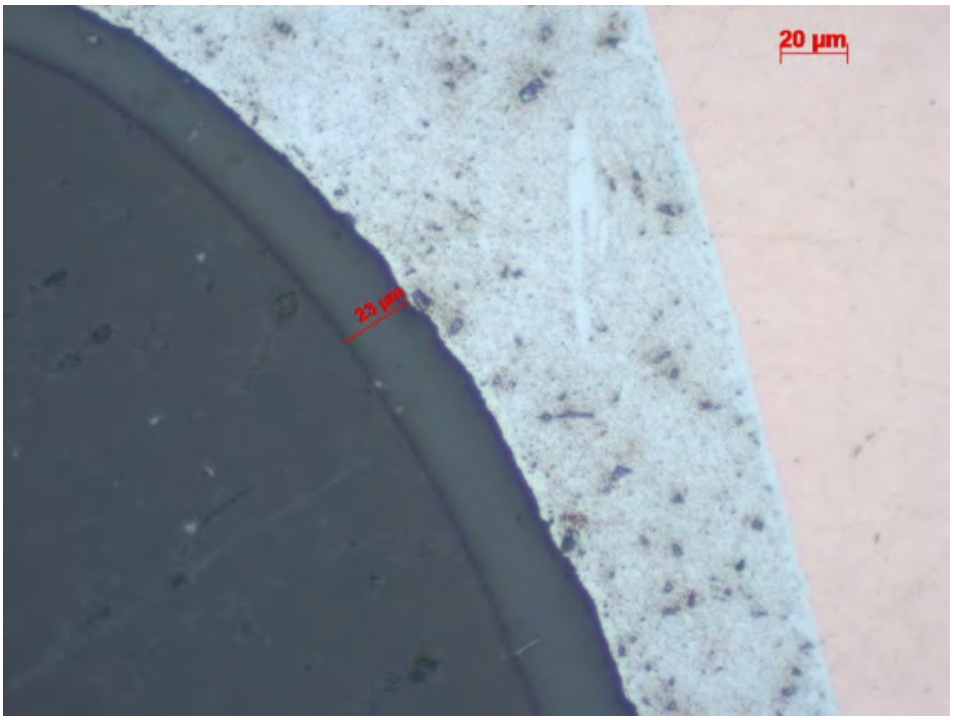


Figure 142: Optical cross-section image, unfilled PC18M QFP-A023 U1002, Lead 28 measurements, C1, 500x.

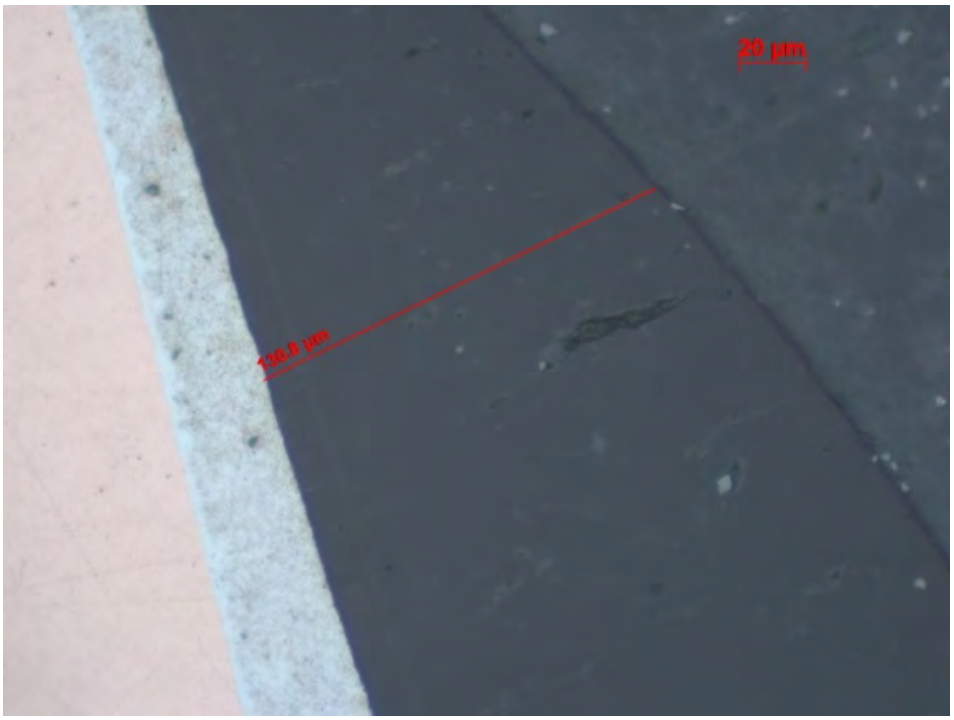


Figure 143: Optical cross-section image, unfilled PC18M QFP-A023 U1002, Lead 28 measurements, D, 500x.

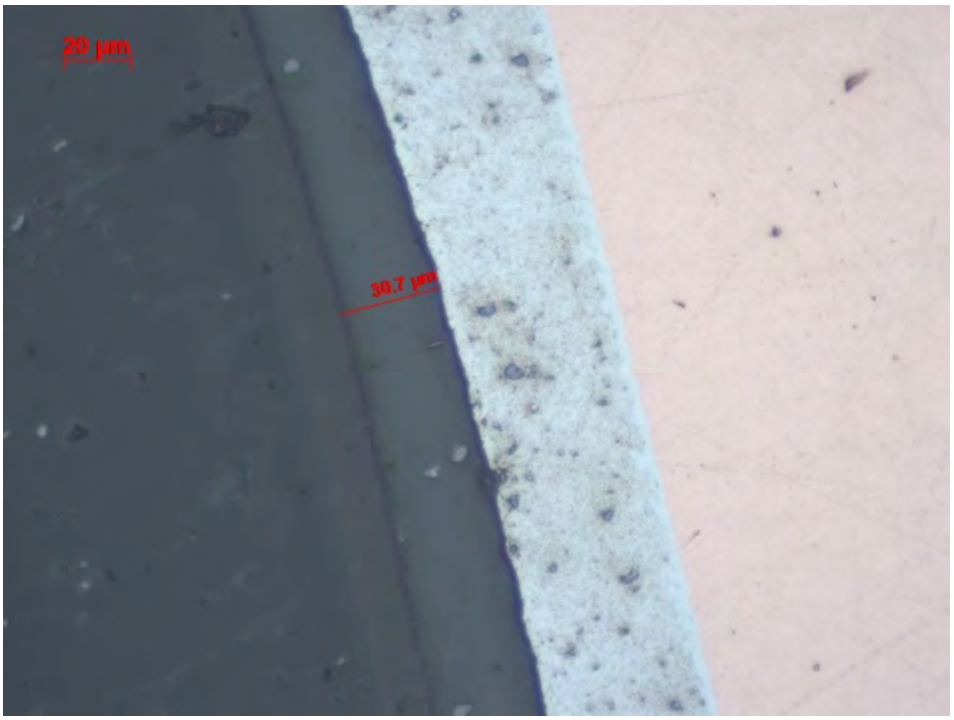


Figure 144: Optical cross-section image, unfilled PC18M QFP-A023 U1002, Lead 28 measurements, D1, 500x.



Figure 145: Optical cross-section image, unfilled PC18M QFP-A023 U1002, Lead 28 measurements, E, 500x.

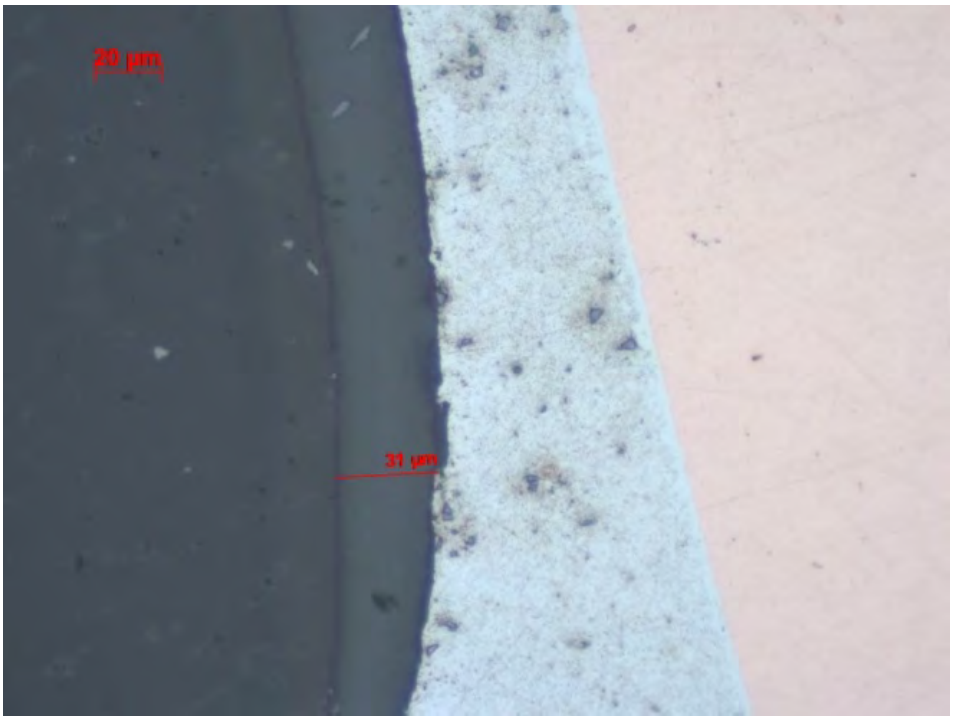


Figure 146: Optical cross-section image, unfilled PC18M QFP-A023 U1002, Lead 28 measurements, E1, 500x.

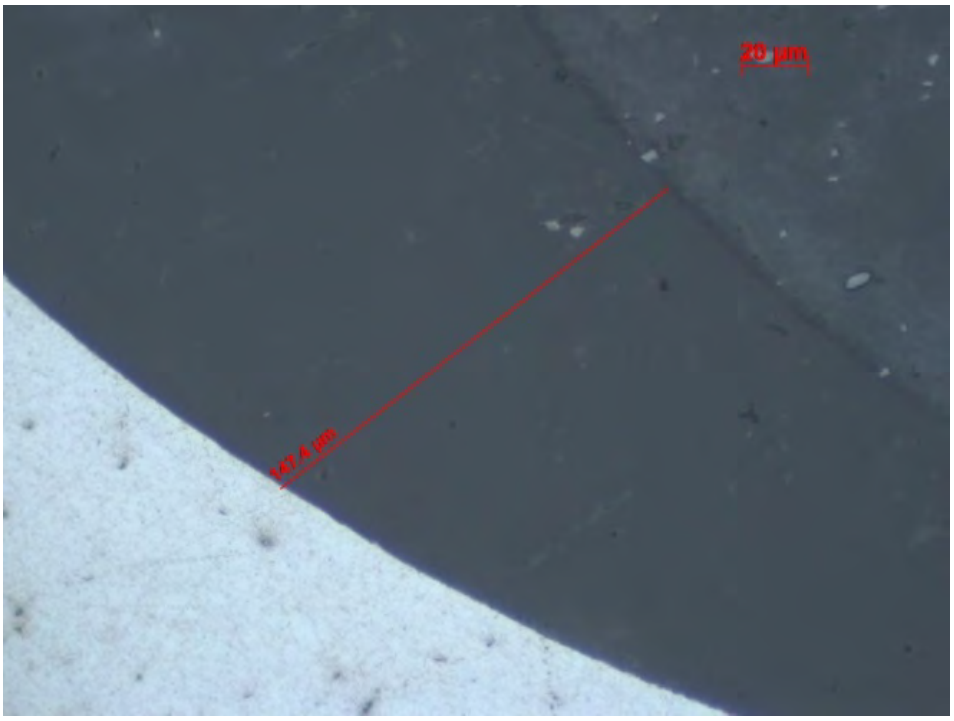


Figure 147: Optical cross-section image, unfilled PC18M QFP-A023 U1002, Lead 28 measurements, F, 500x.

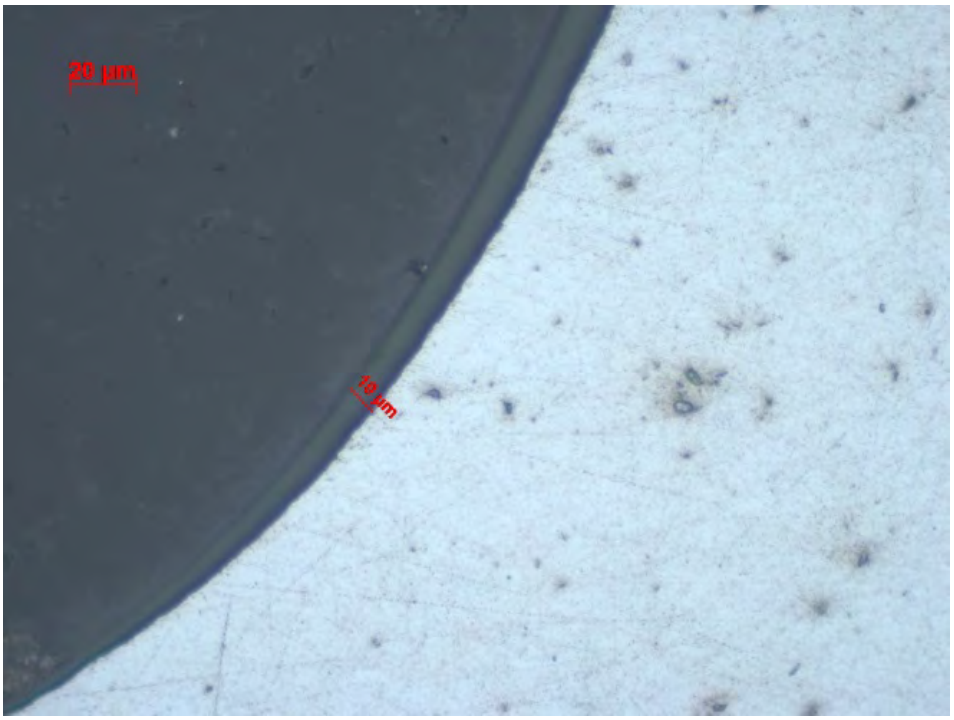


Figure 148: Optical cross-section image, unfilled PC18M QFP-A023 U1002, Lead 28 measurements, F1, 500x.

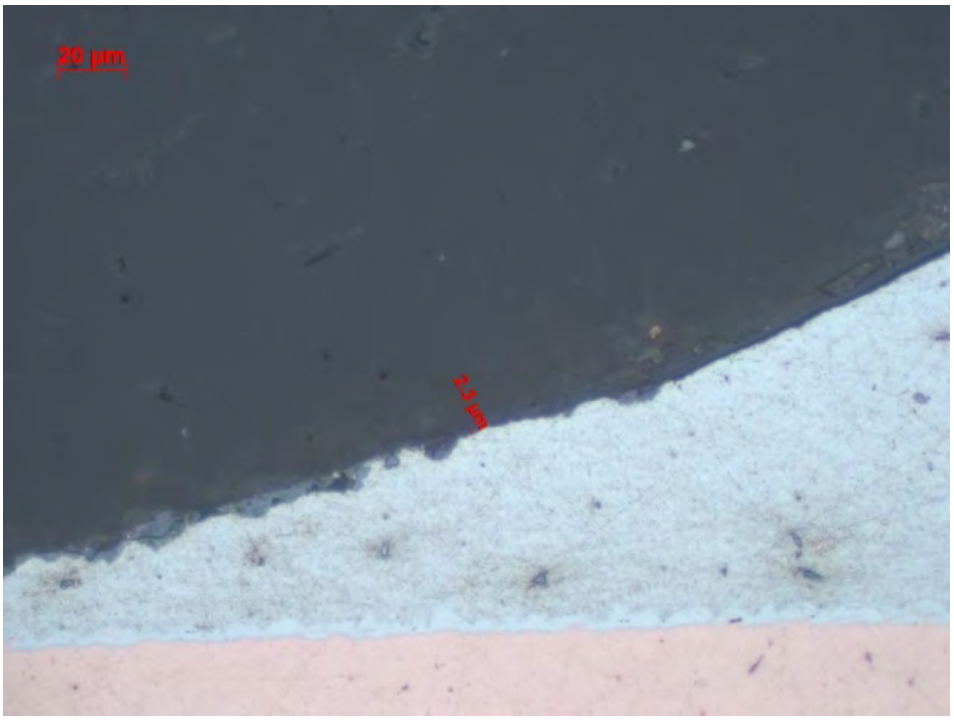


Figure 149: Optical cross-section image, unfilled PC18M QFP-A023 U1002, Lead 28 measurements, H, 500x.

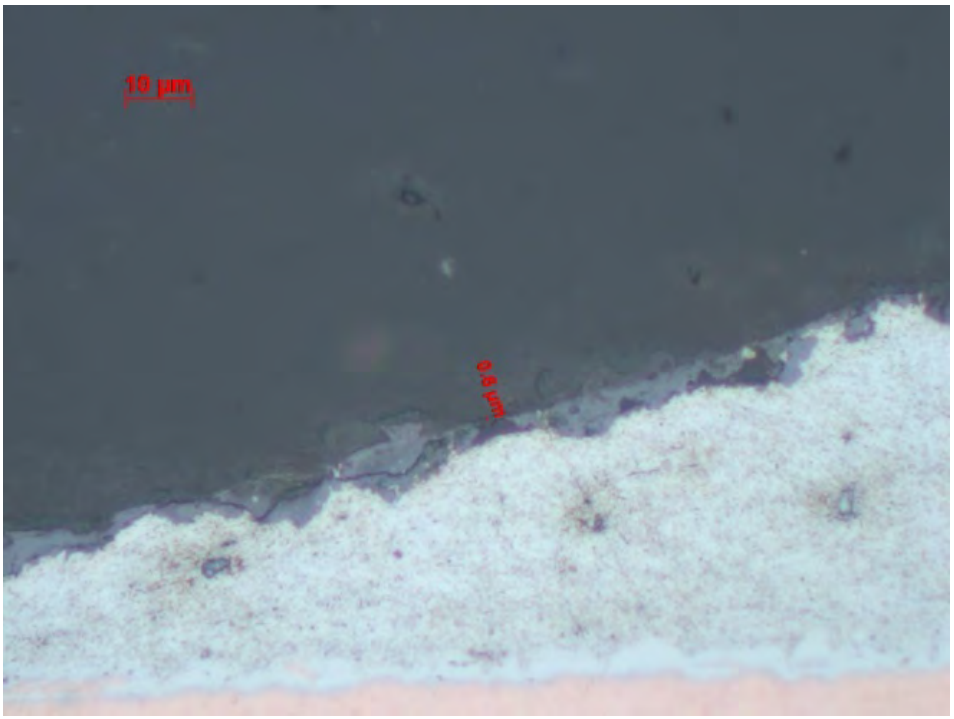


Figure 150: Optical cross-section image, unfilled PC18M QFP-A023 U1002, Lead 28 measurements, H, 1000x.

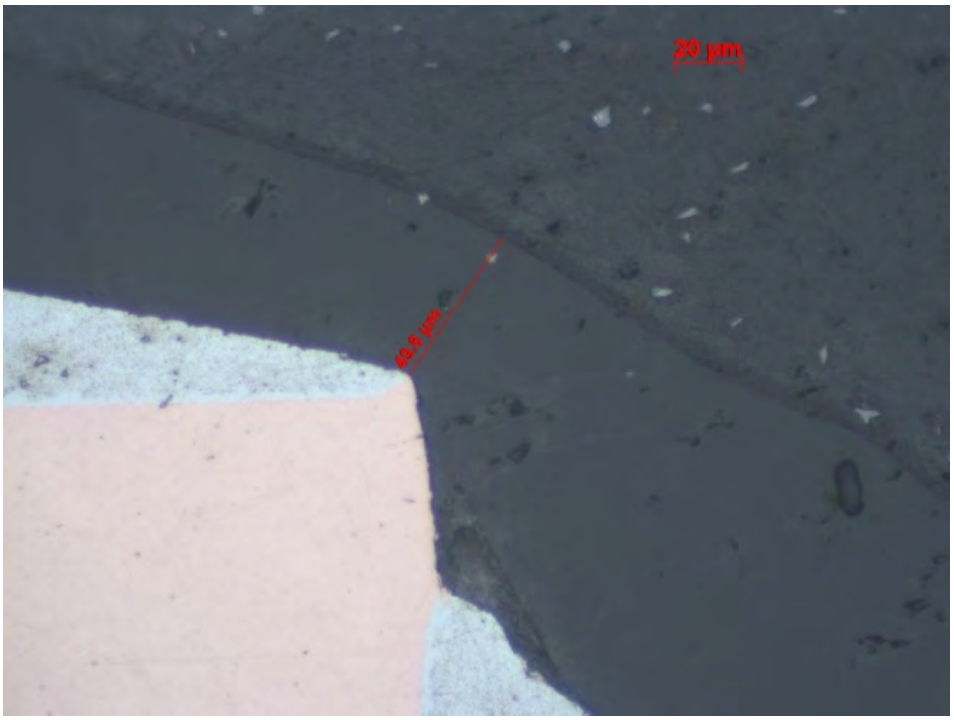


Figure 151: Optical cross-section image, unfilled PC18M QFP-A023 U1002, Lead 28 measurements, T, 500x.

4.4.1.4 Optical cross-sections, unfilled PC18M, QFP-A023 non-reworked U1001



Figure 152: Optical cross-section image, unfilled PC18M QFP-A023 non-reworked U1001, Lead 33_50x.

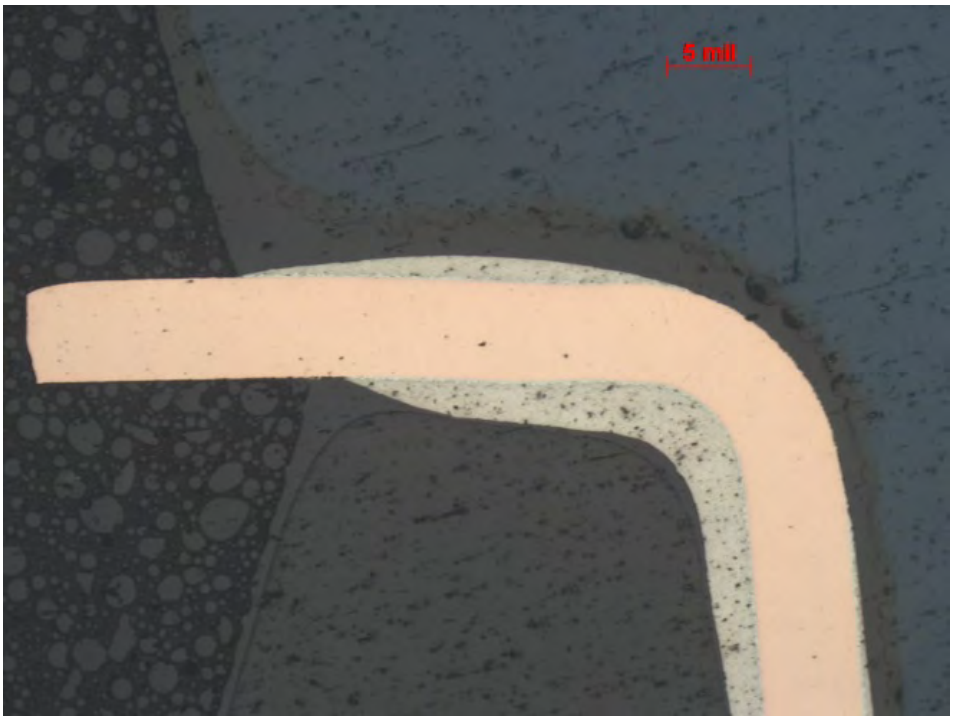


Figure 153: Optical cross-section image, unfilled PC18M QFP-A023 non-reworked U1001, Lead 33 knee_100x.



Figure 154: Optical cross-section image, unfilled PC18M QFP-A023 non-reworked U1001, Lead 33 foot_100x.

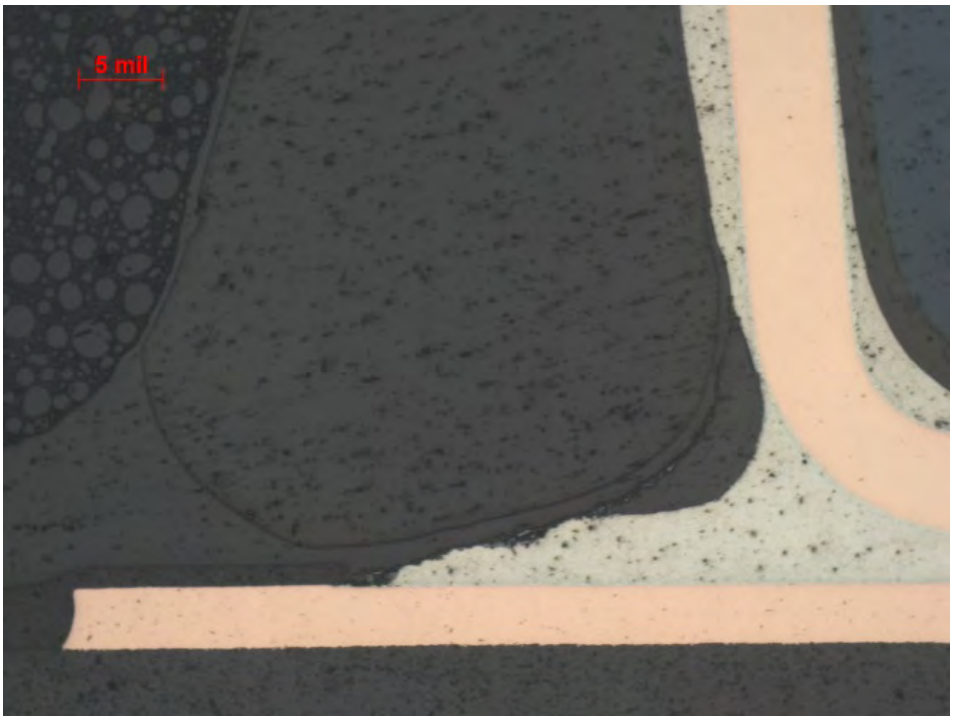


Figure 155: Optical cross-section image, unfilled PC18M QFP-A023 non-reworked U1001, Lead 33 heel_100x.

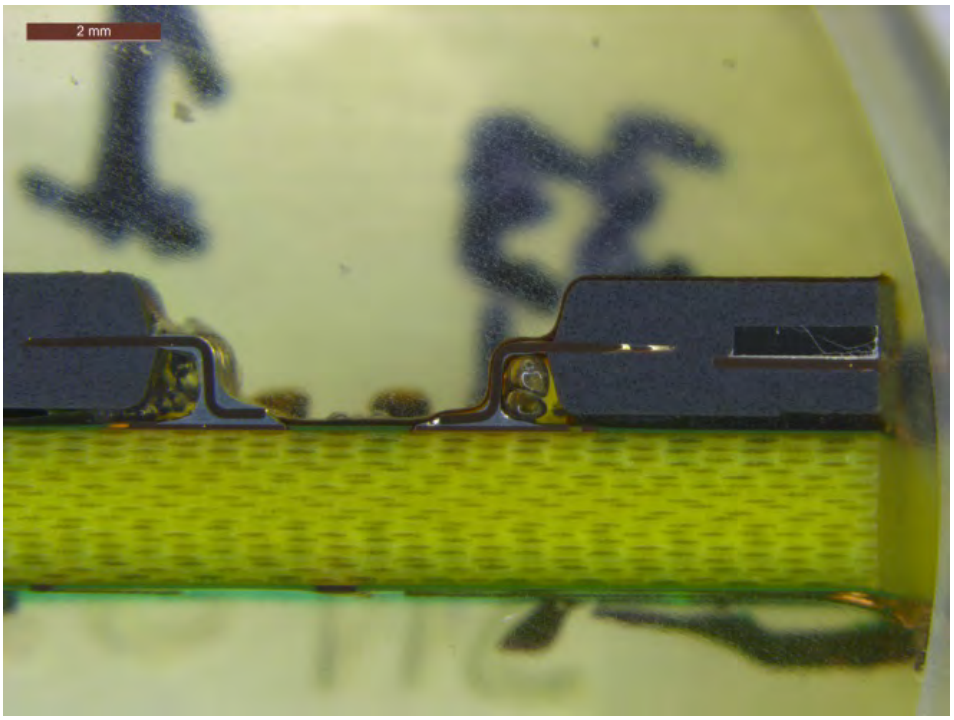


Figure 156: Optical cross-section image, unfilled PC18M QFP-A023 non-reworked U1001, Overall lead 28 stereoscope non-inverted, 7.8x.

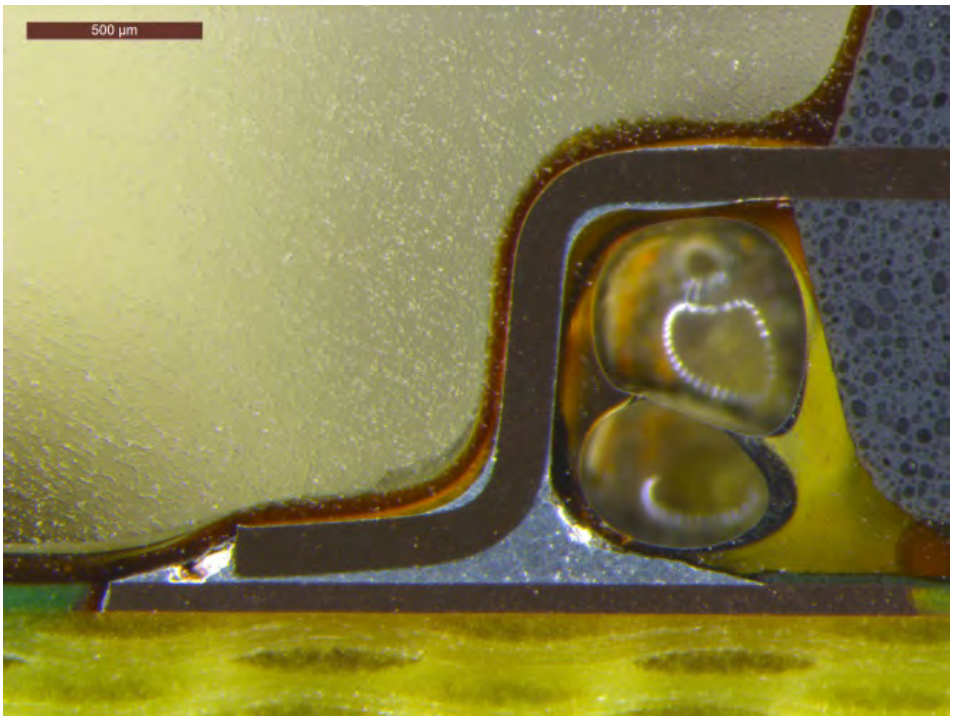


Figure 157: Optical cross-section image, unfilled PC18M QFP-A023 non-reworked U1001, Lead 28 stereomicroscope non-inverted, 40x.

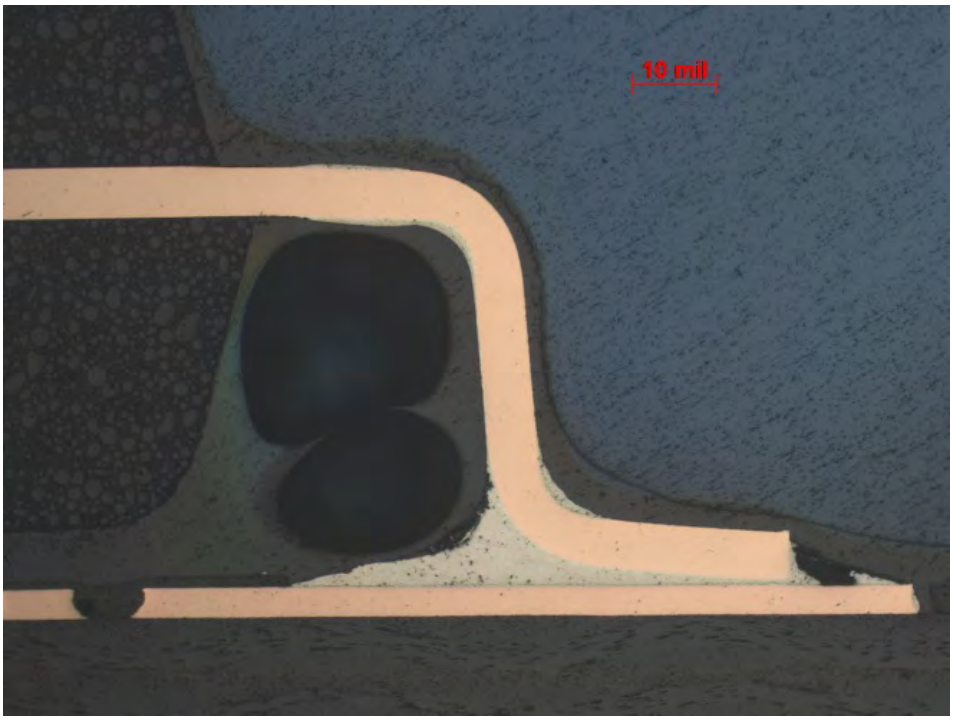


Figure 158: Optical cross-section image, unfilled PC18M QFP-A023 non-reworked U1001, Lead 28_50x.



Figure 159: Optical cross-section image, unfilled PC18M QFP-A023 non-reworked U1001, Lead 28 knee_100x.

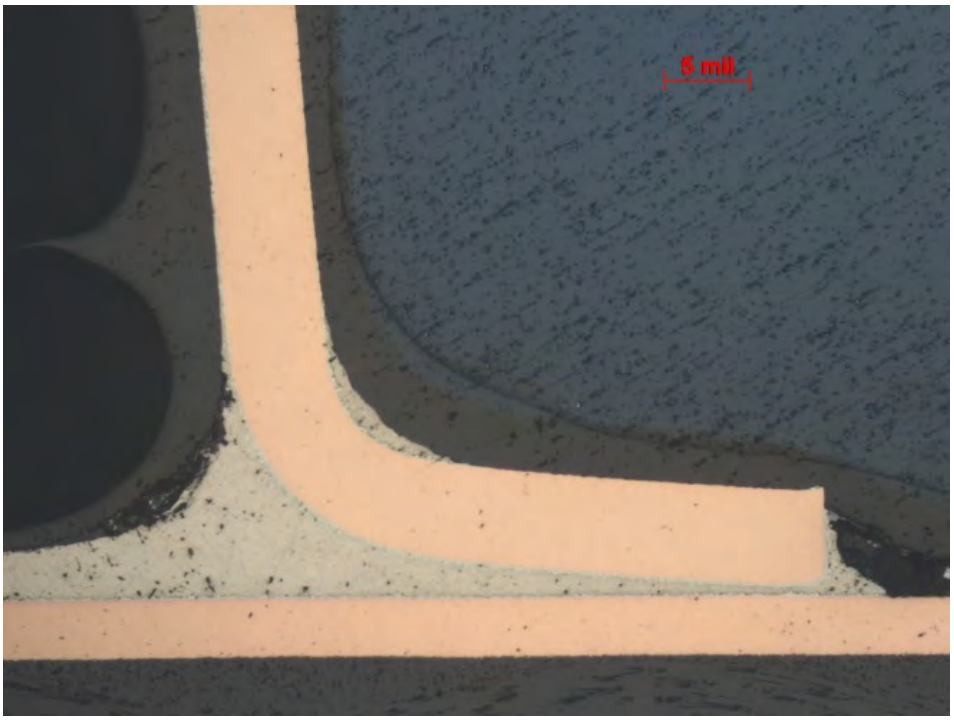


Figure 160: Optical cross-section image, unfilled PC18M QFP-A023 non-reworked U1001, Lead 28 foot_100x.



Figure 161: Optical cross-section image, unfilled PC18M QFP-A023 non-reworked U1001, Lead 28 heel_100x.

4.4.1.5 SEM cross-sections, unfilled PC18M, QFP-A023 non-reworked U1001

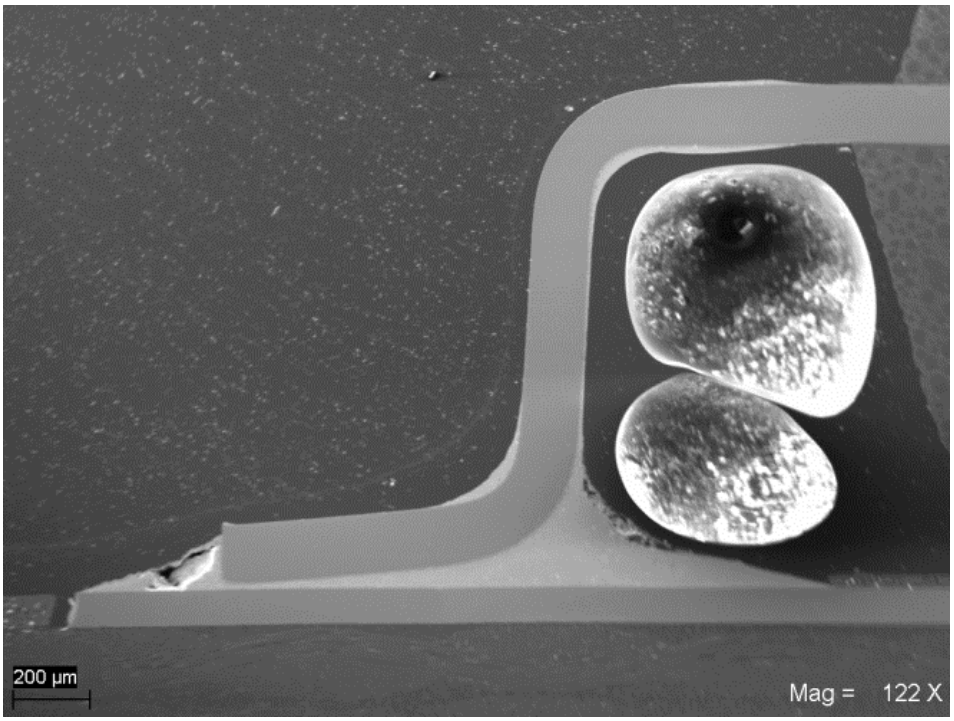


Figure 162: SEM cross-section image, unfilled PC18M QFP-A023 non-reworked U1001, Lead 28 122x.

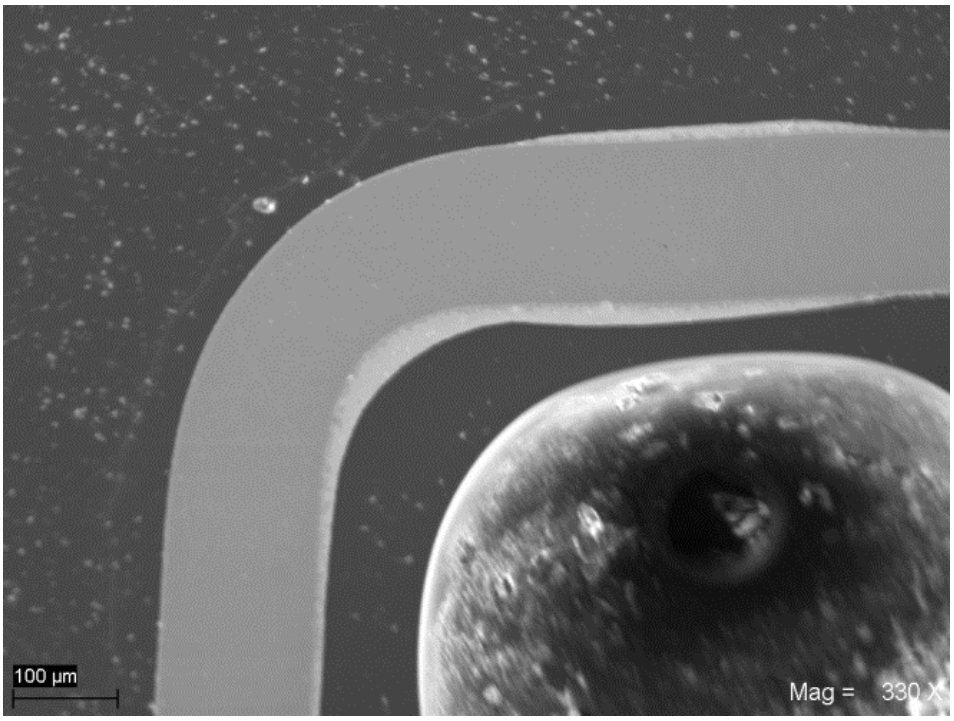


Figure 163: SEM cross-section image, unfilled PC18M QFP-A023 non-reworked U1001, Lead 28 knee 330x.

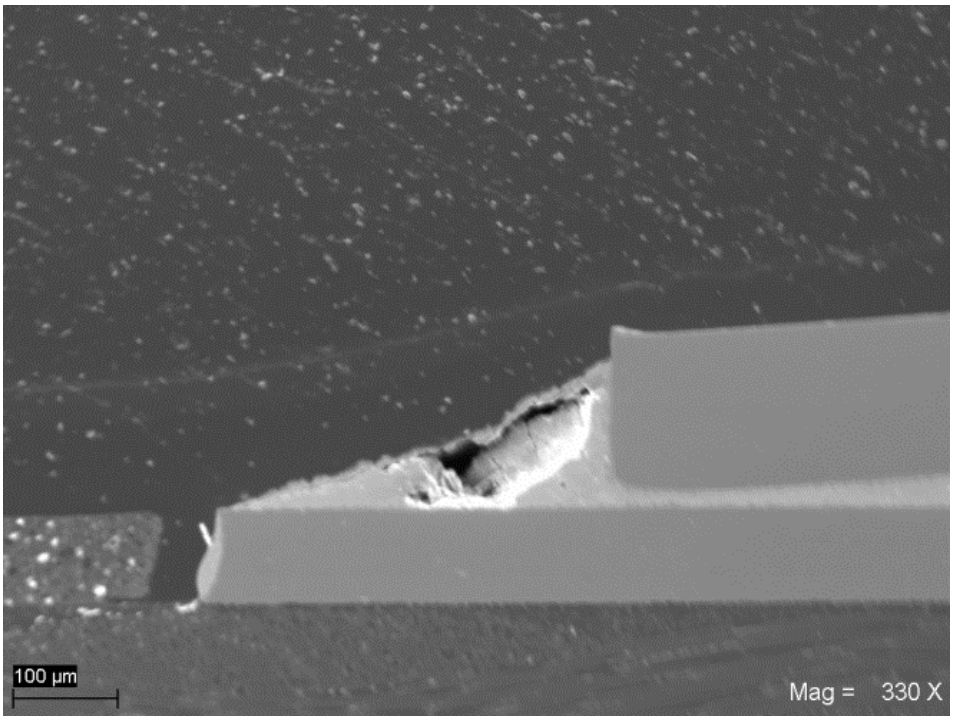


Figure 164: SEM cross-section image, unfilled PC18M QFP-A023 non-reworked U1001, Lead 28 toe 330x.

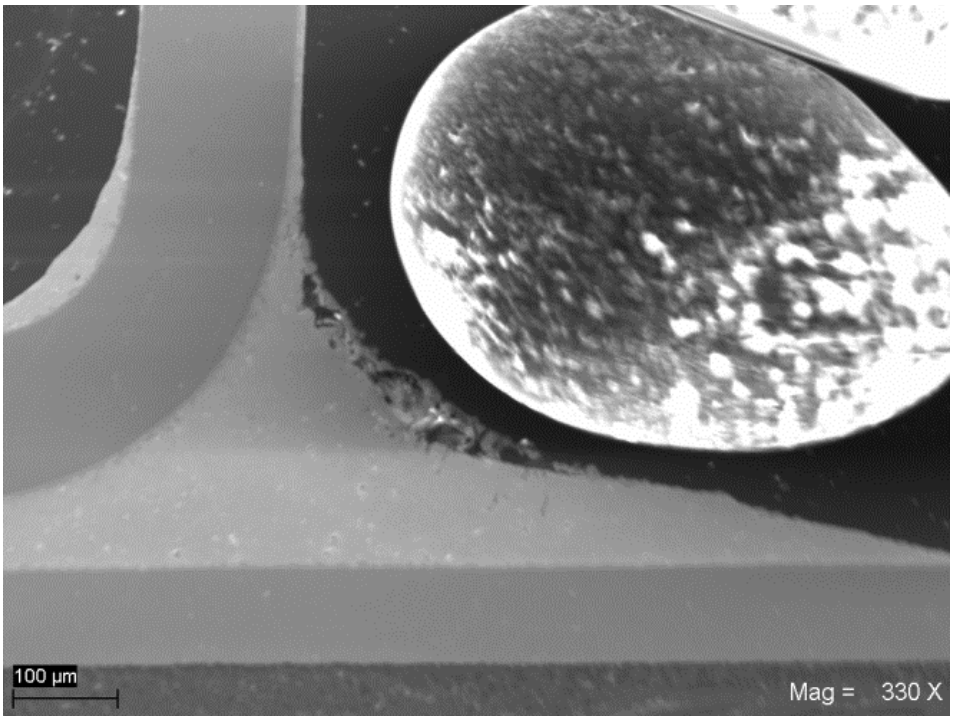


Figure 165: SEM cross-section image, unfilled PC18M QFP-A023 non-reworked U1001, Lead 28 heel 330x.

4.4.2 Cross-sections of filled PC18M+20%XP2742 QFP-A312

The cross-section plane locations and numbers of the nanosilica filled PC18M+20%XP2742 pins that were sectioned are shown in Figure 166.

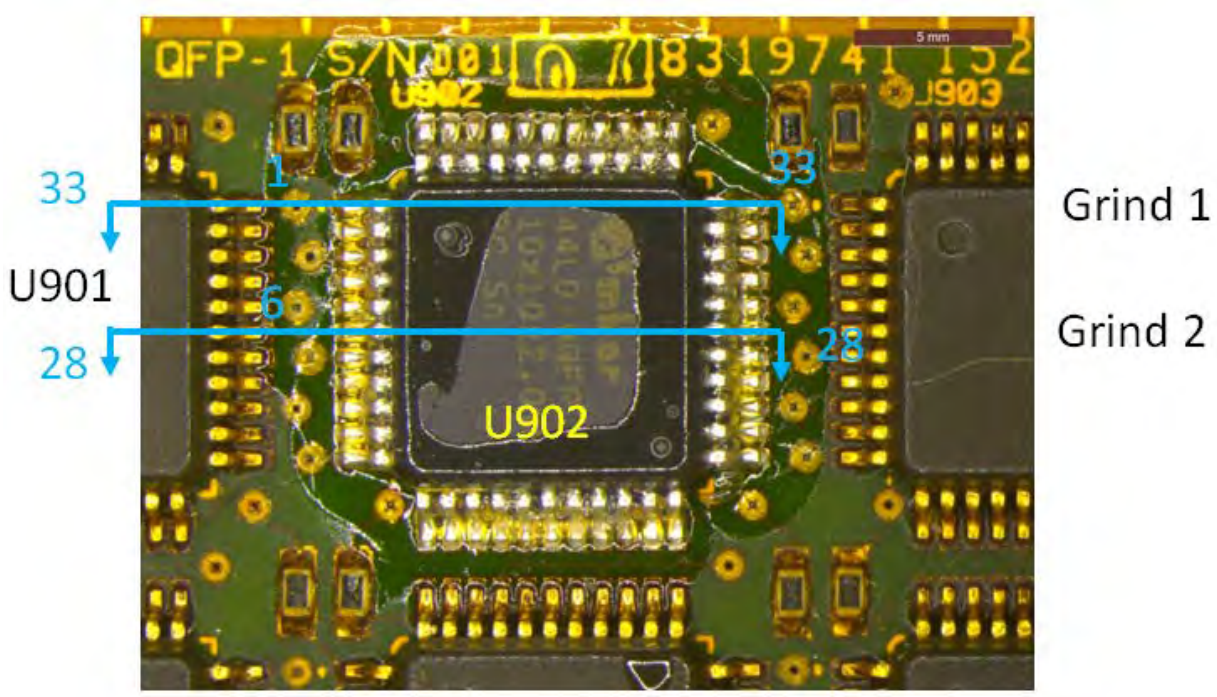


Figure 166: Optical cross-section locations for PC18M+20%XP2742 QFP-A312 U901 (non-reworked) and U902 (reworked).

4.4.2.1 Optical cross-sections filled PC18M+20%XP2742 QFP-A312 U902

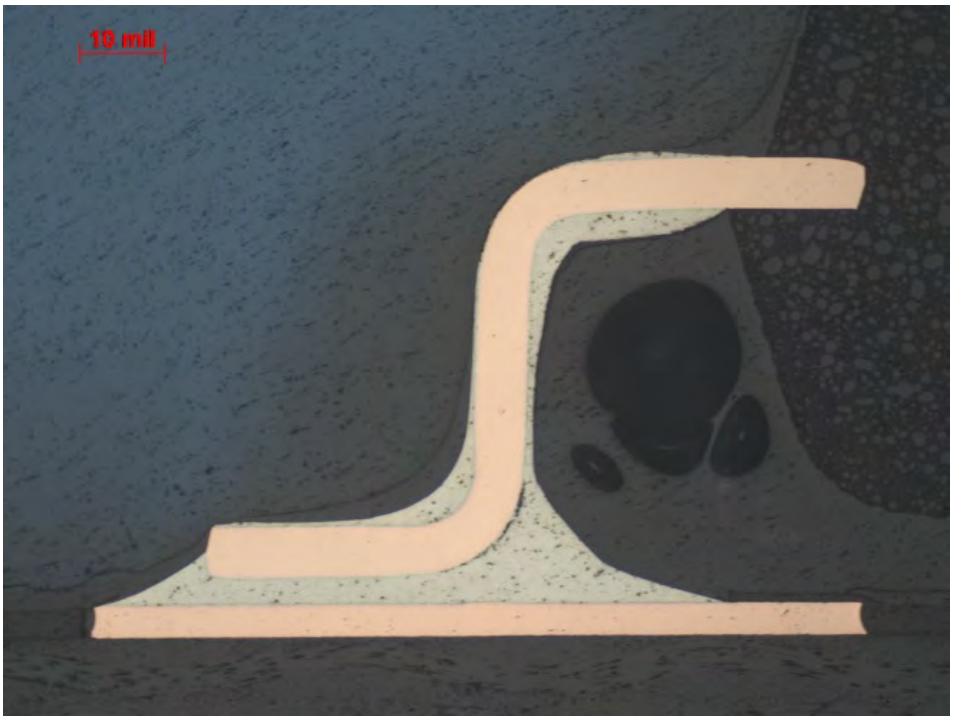


Figure 167: Cross-section plane locations for PC18M+20%XP2742 coated QFP-A312. The cross-section planes go through the right side of U901 (non-reworked) and both sides of U902 (reworked).

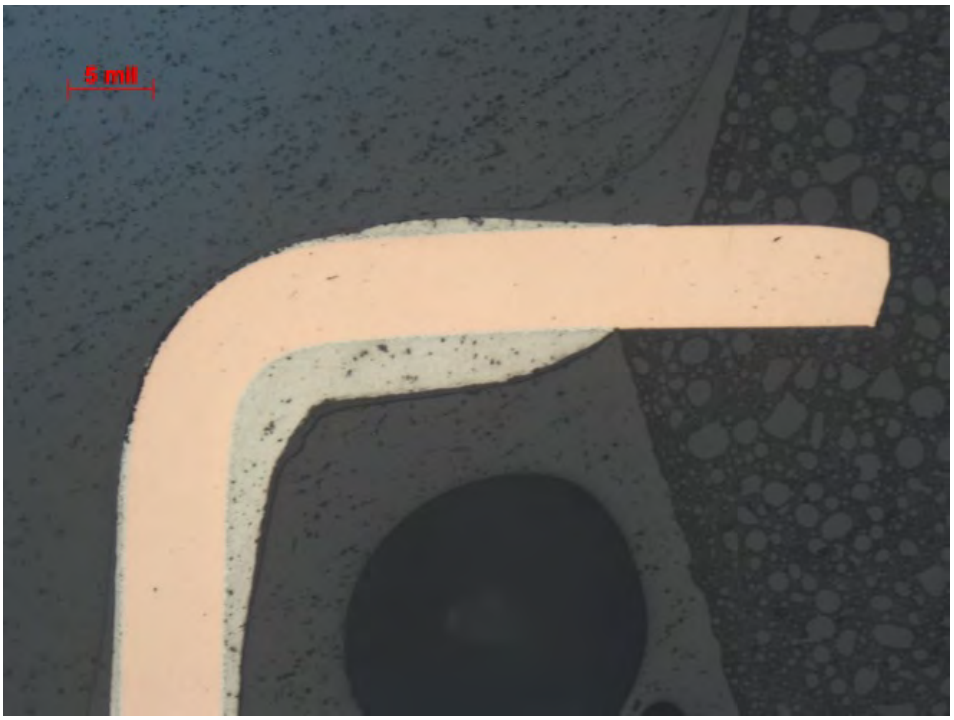


Figure 168: Optical cross-section image, filled PC18M+20%XP2742 QFP-A312 U902, Lead 1 knee, 100x.

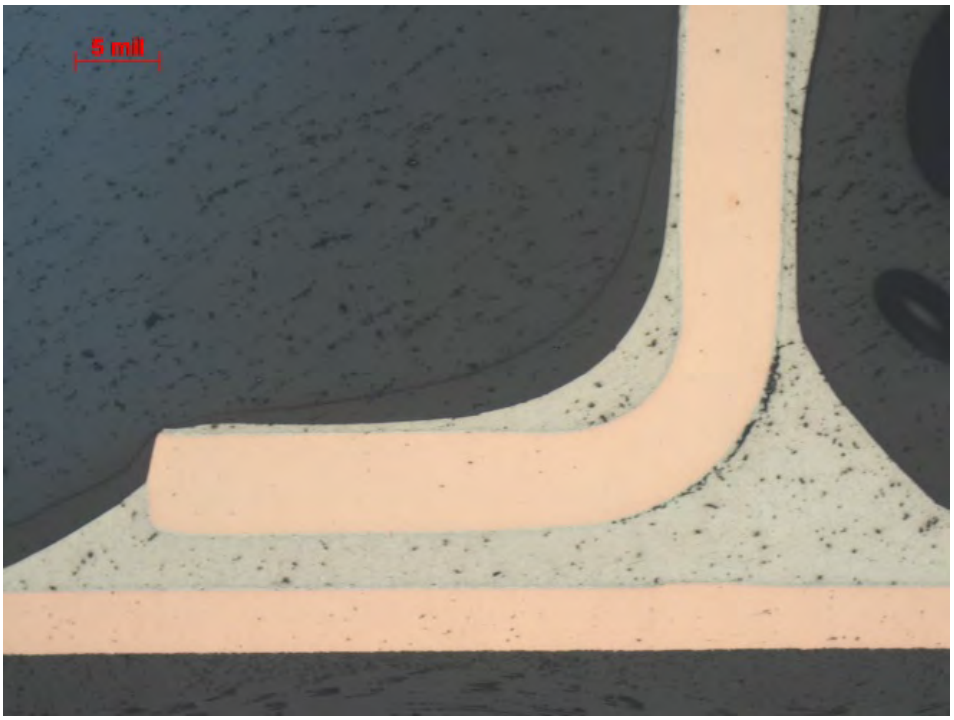


Figure 169: Optical cross-section image, filled PC18M+20%XP2742 QFP-A312 U902, Lead 1 foot, 100x.

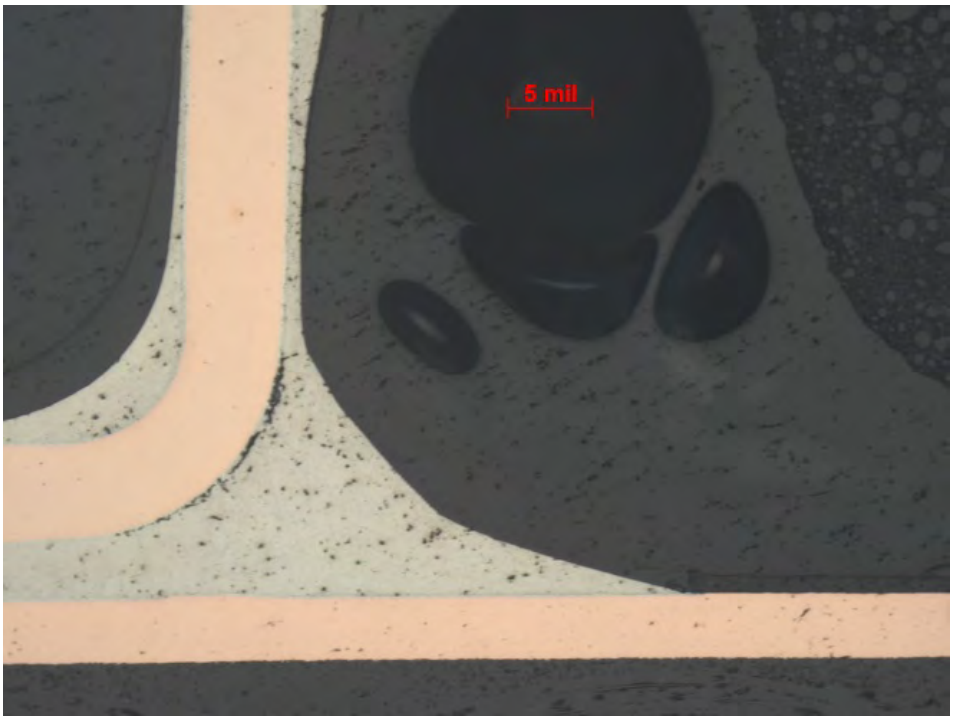


Figure 170: Optical cross-section image, filled PC18M+20%XP2742 QFP-A312 U902, Lead 1 heel, 100x.

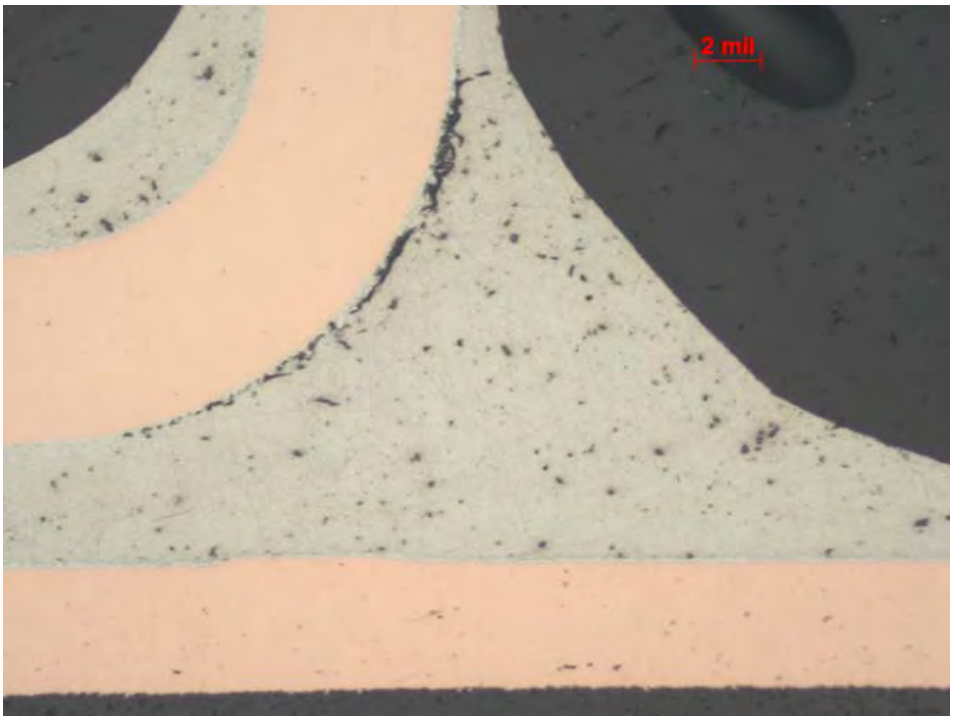


Figure 171: Optical cross-section image, filled PC18M+20%XP2742 QFP-A312 U902, Lead 1 heel, 200x.

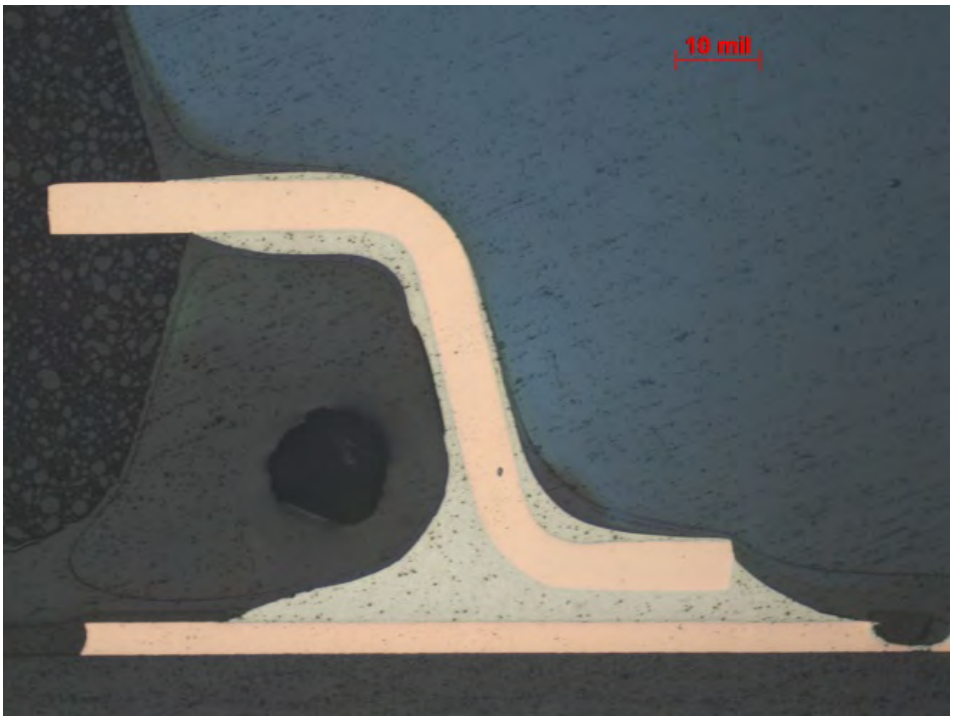


Figure 172: Optical cross-section image, filled PC18M+20%XP2742 QFP-A312 U902, Lead 33, 50x.



Figure 173: Optical cross-section image, filled PC18M+20%XP2742 QFP-A312 U902, Lead 33 knee, 100x.

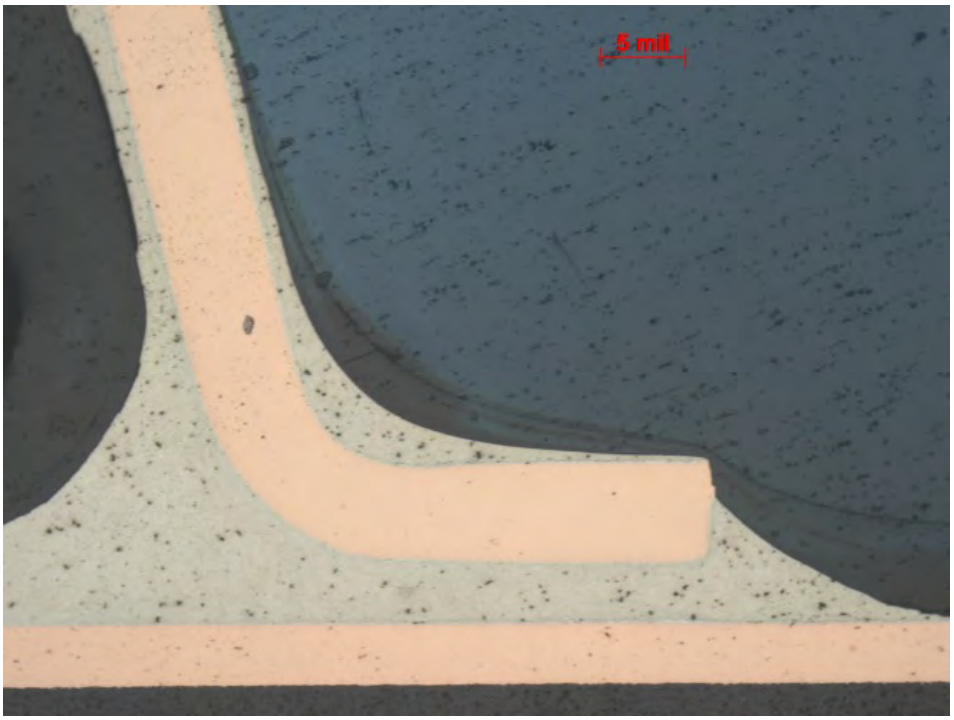


Figure 174: Optical cross-section image, filled PC18M+20%XP2742 QFP-A312 U902, Lead 33 foot, 100x.

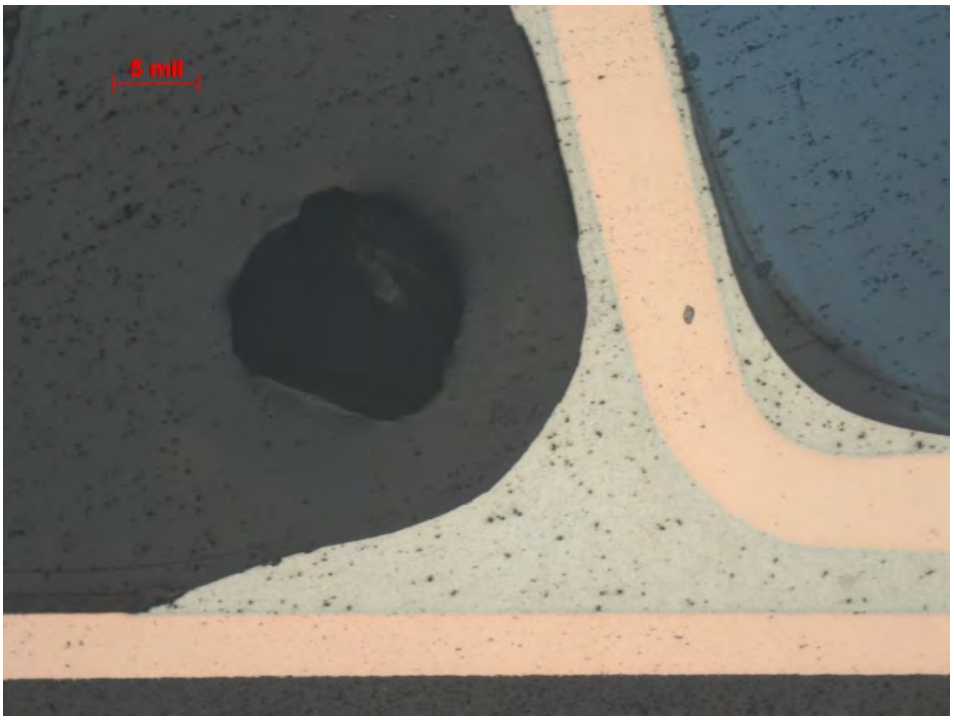


Figure 175: Optical cross-section image, filled PC18M+20%XP2742 QFP-A312 U902, Lead 33 heel, 100x.



Figure 176: Optical cross-section image, filled PC18M+20%XP2742 QFP-A312 U902, Lead 33 under part, 50x.

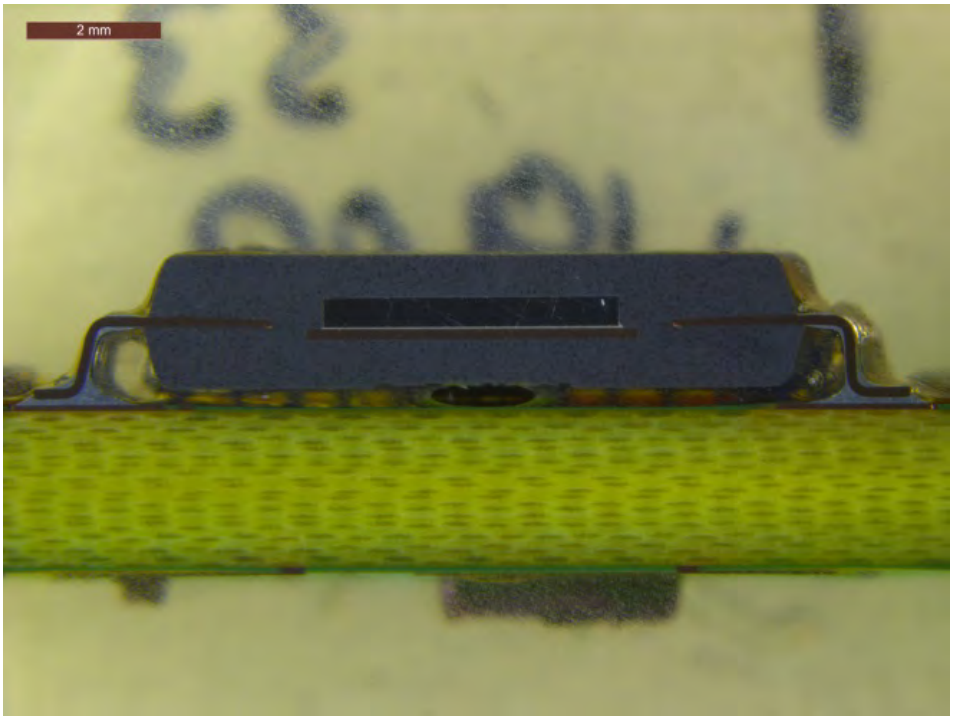


Figure 177: Optical cross-section image, filled PC18M+20%XP2742 QFP-A312 U902, overall stereoscope non-inverted, 7.8x.

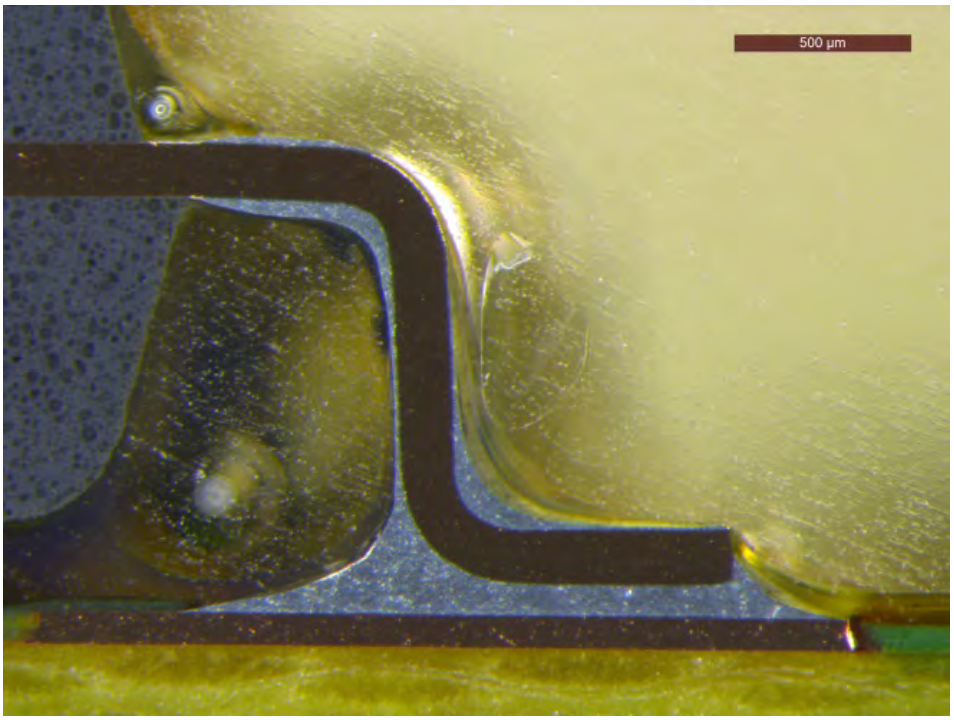


Figure 178: Optical cross-section image, filled PC18M+20%XP2742 QFP-A312 U902, Lead 6 stereoscope non-inverted, 40x.

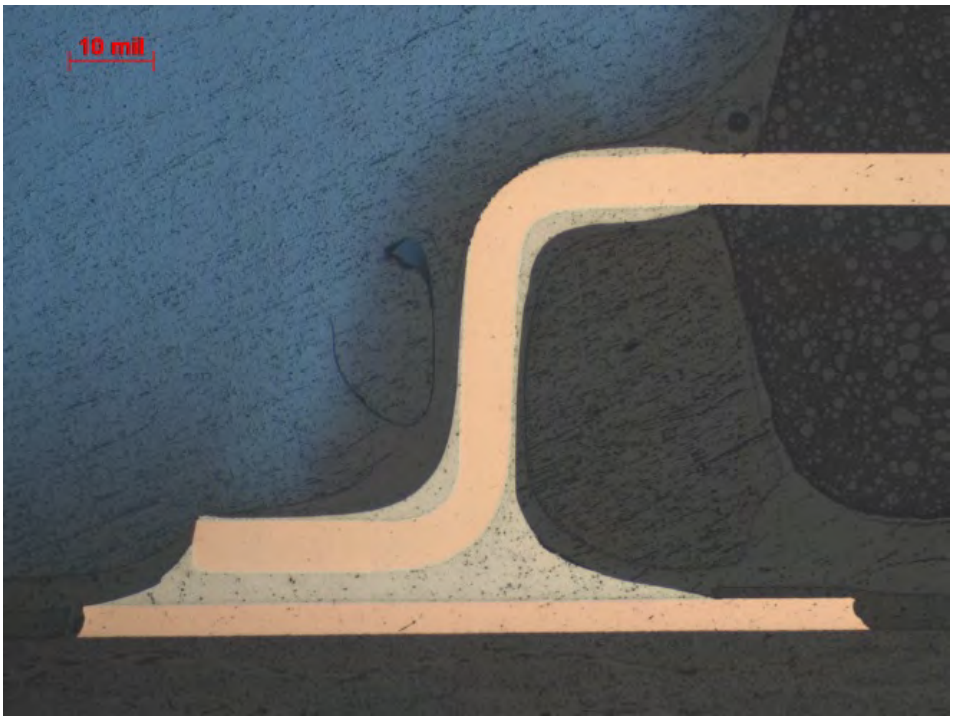


Figure 179: Optical cross-section image, filled PC18M+20%XP2742 QFP-A312 U902, Lead 6, 50x.

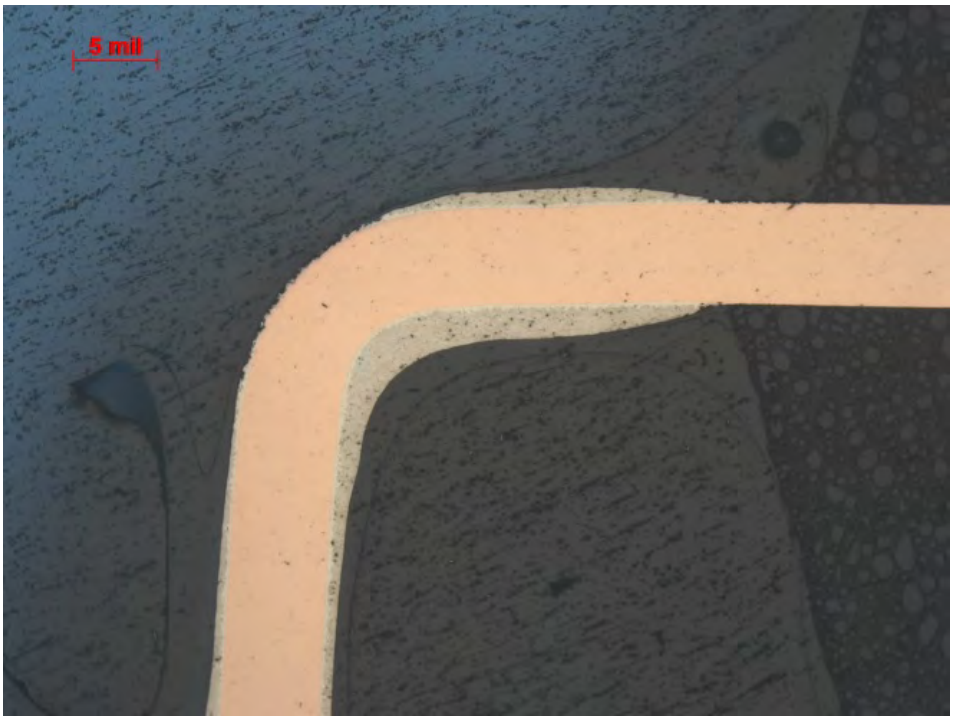


Figure 180: Optical cross-section image, filled PC18M+20%XP2742 QFP-A312 U902, Lead 6 knee, 100x.

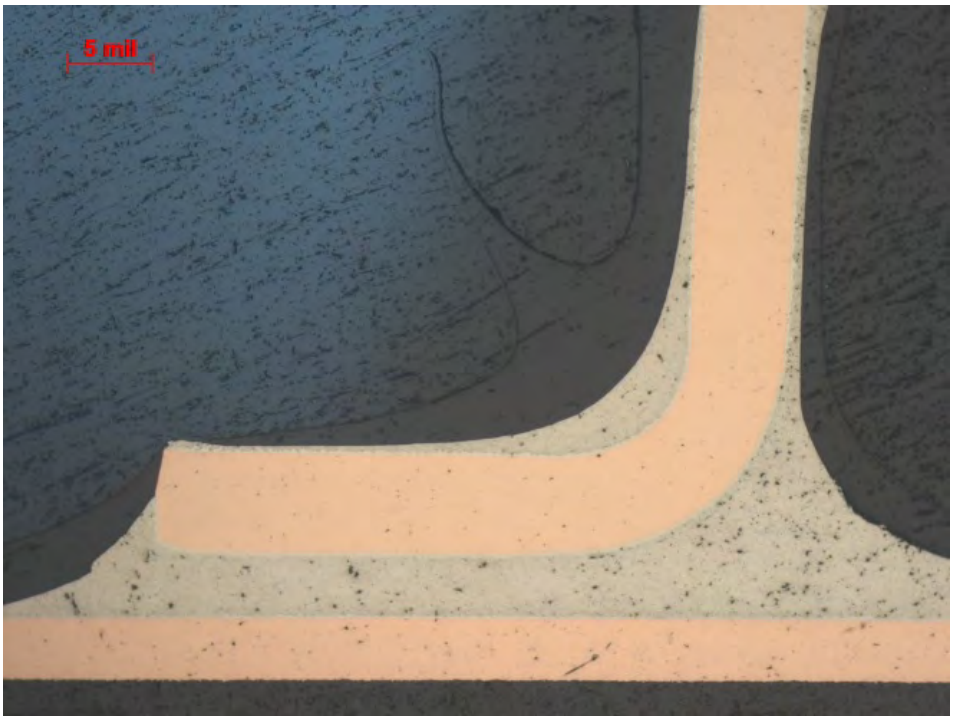


Figure 181: Optical cross-section image, filled PC18M+20%XP2742 QFP-A312 U902, Lead 6 foot, 100x.

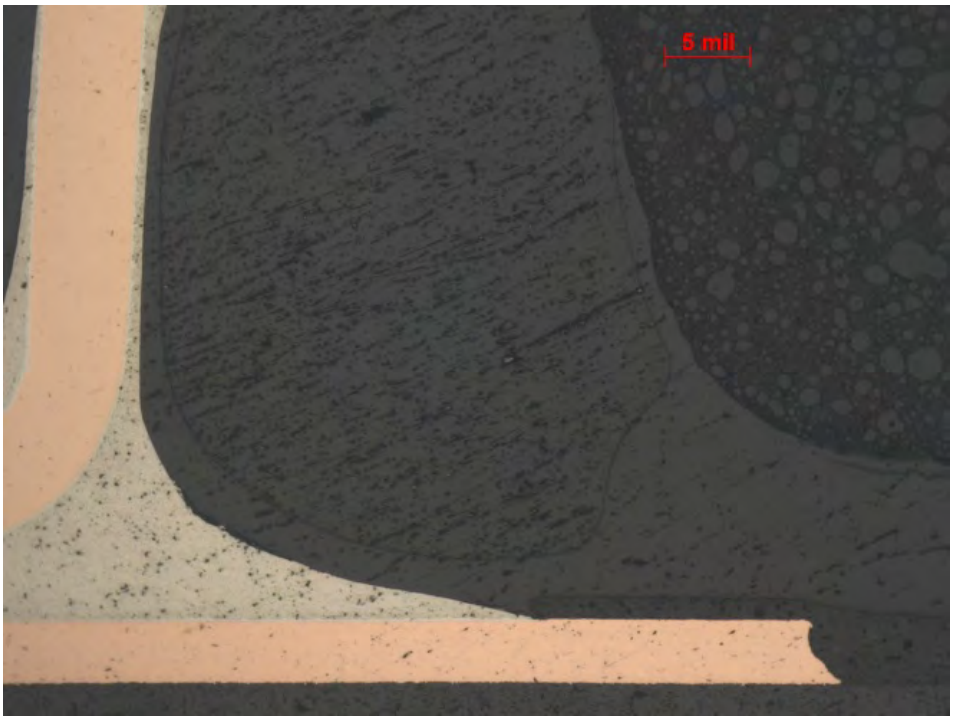


Figure 182: Optical cross-section image, filled PC18M+20%XP2742 QFP-A312 U902, Lead 6 heel, 100x.

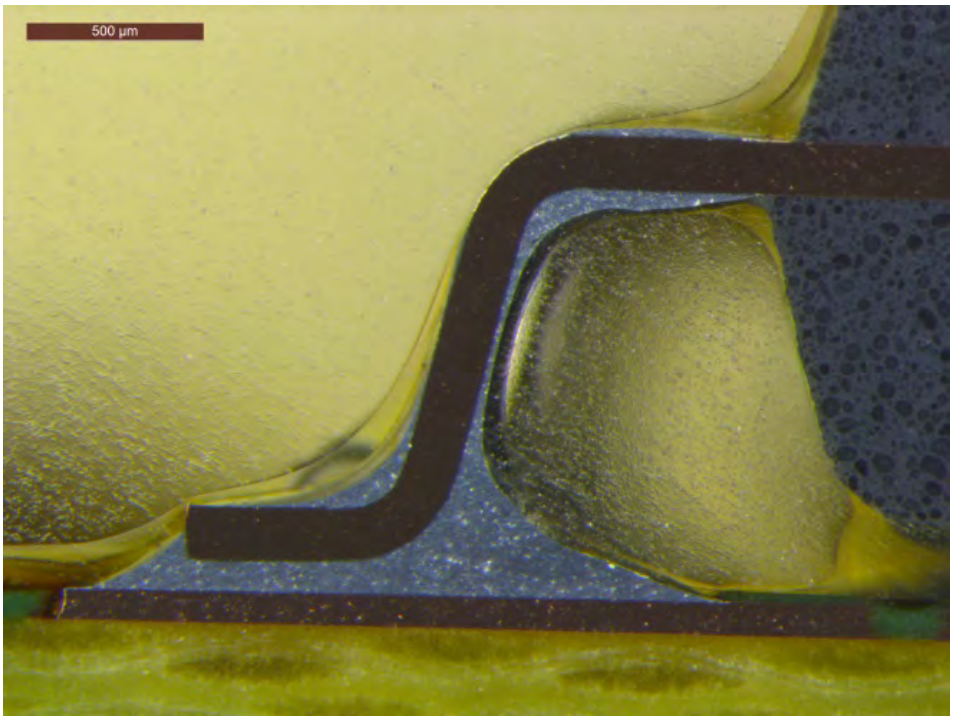


Figure 183: Optical cross-section image, filled PC18M+20%XP2742 QFP-A312 U902, Lead 28 stereoscope non-inverted, 40x.

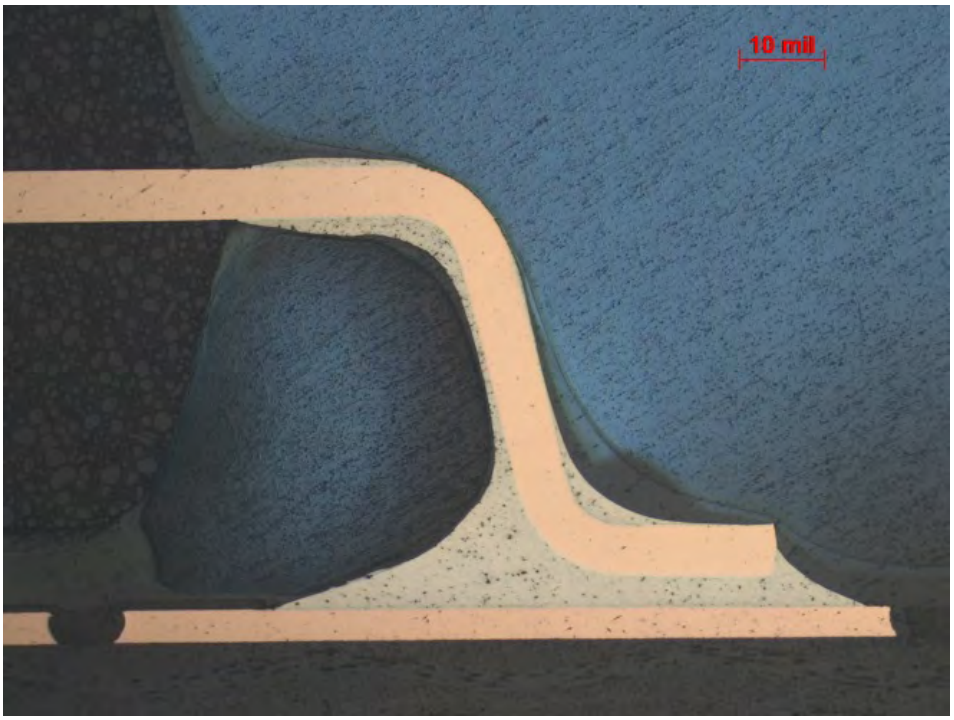


Figure 184: Optical cross-section image, filled PC18M+20%XP2742 QFP-A312 U902, Lead 28, 50x.

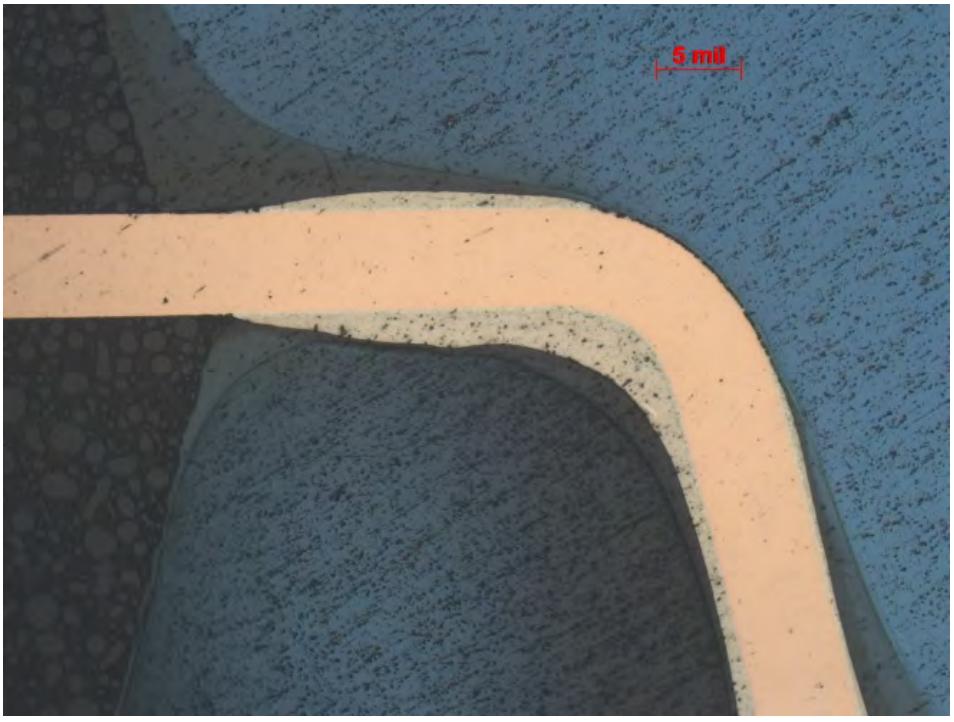


Figure 185: Optical cross-section image, filled PC18M+20%XP2742 QFP-A312 U902, Lead 28 knee, 100x.

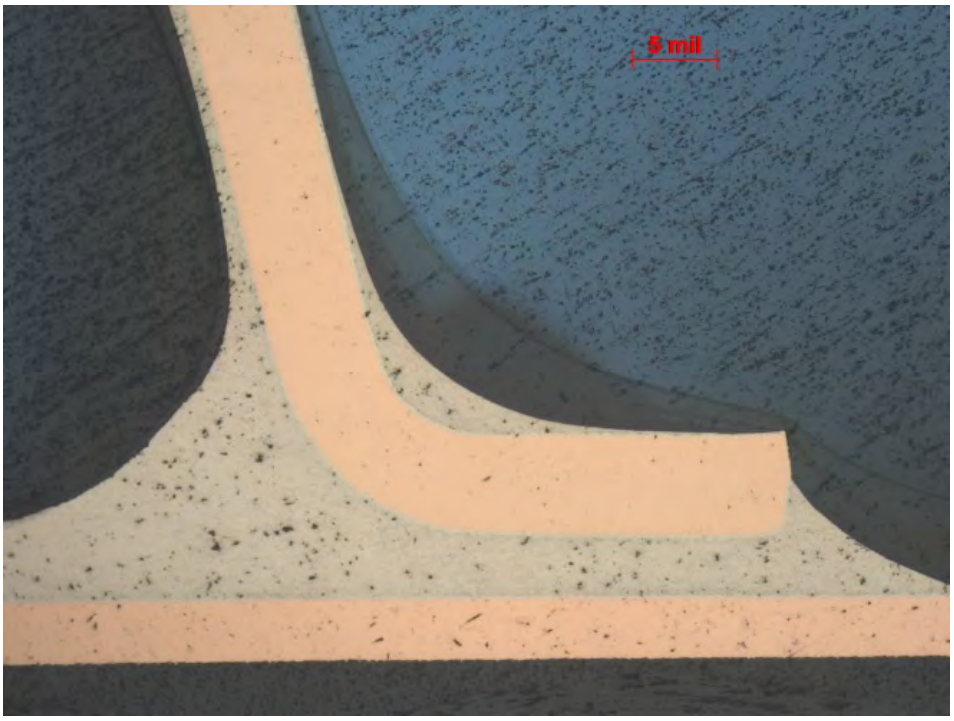


Figure 186: Optical cross-section image, filled PC18M+20%XP2742 QFP-A312 U902, Lead 28 foot, 100x.

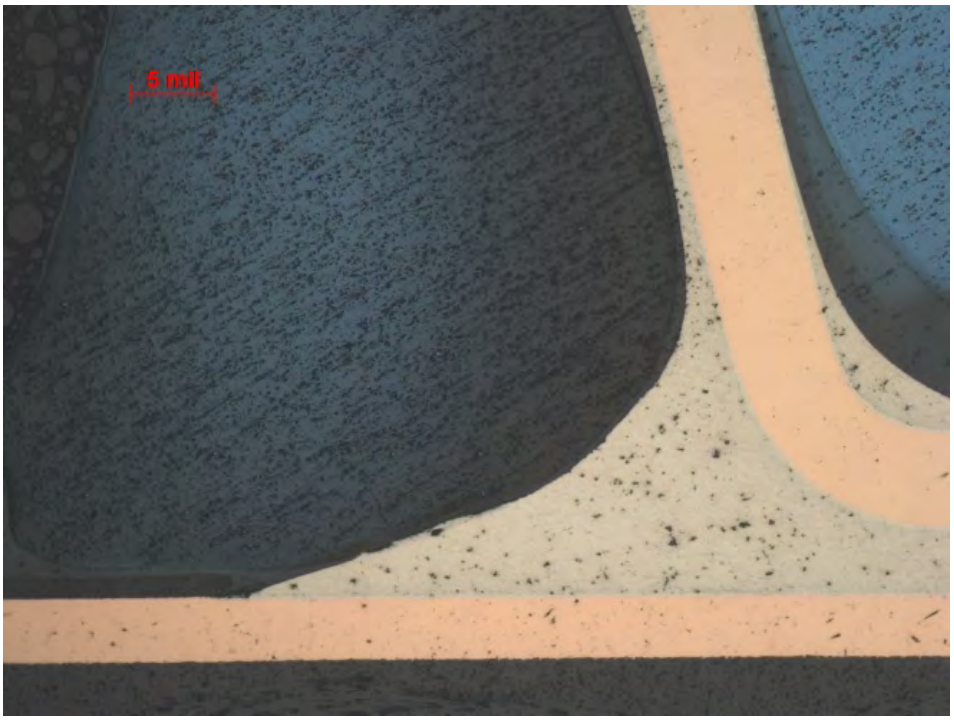


Figure 187: Optical cross-section image, filled PC18M+20%XP2742 QFP-A312 U902, Lead 28 heel 1, 100x.

4.4.2.2 SEM cross-sections filled PC18M+20%XP2742 QFP-A312 U902

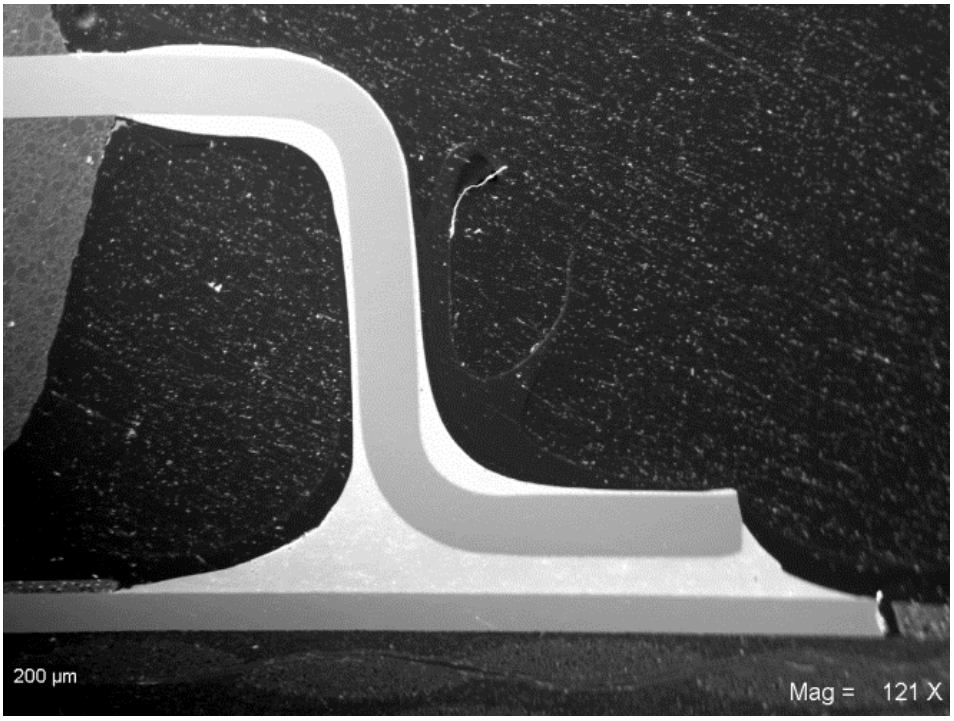


Figure 188: SEM cross-section image, filled PC18M+20%XP2742 QFP-A312 U902, Lead 6, 121x.

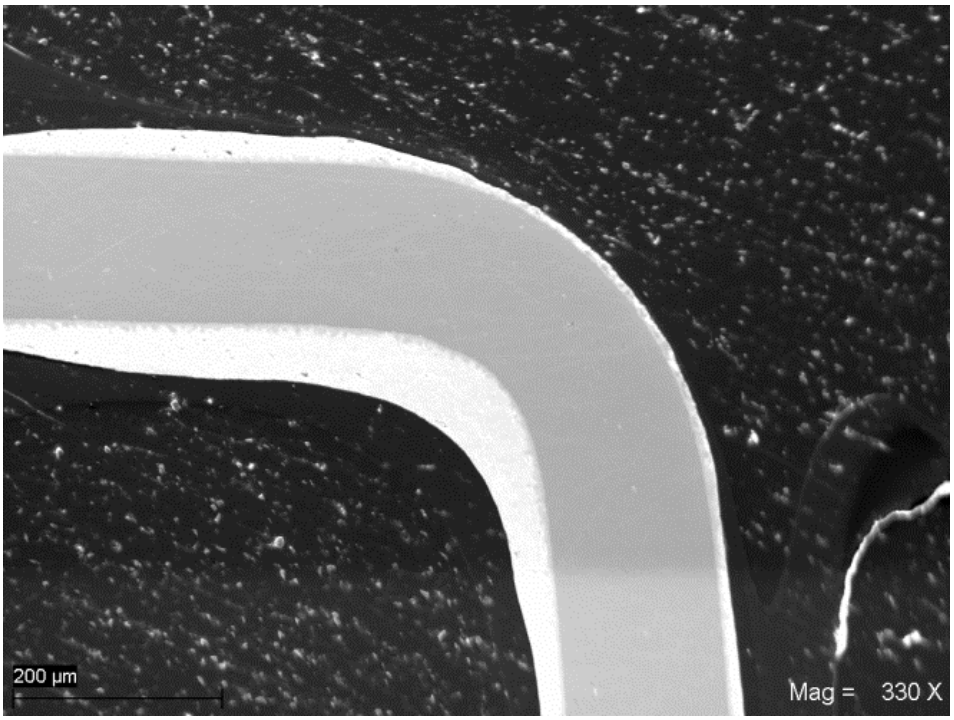


Figure 189: SEM cross-section image, filled PC18M+20%XP2742 QFP-A312 U902, Lead 6 knee, 330x.

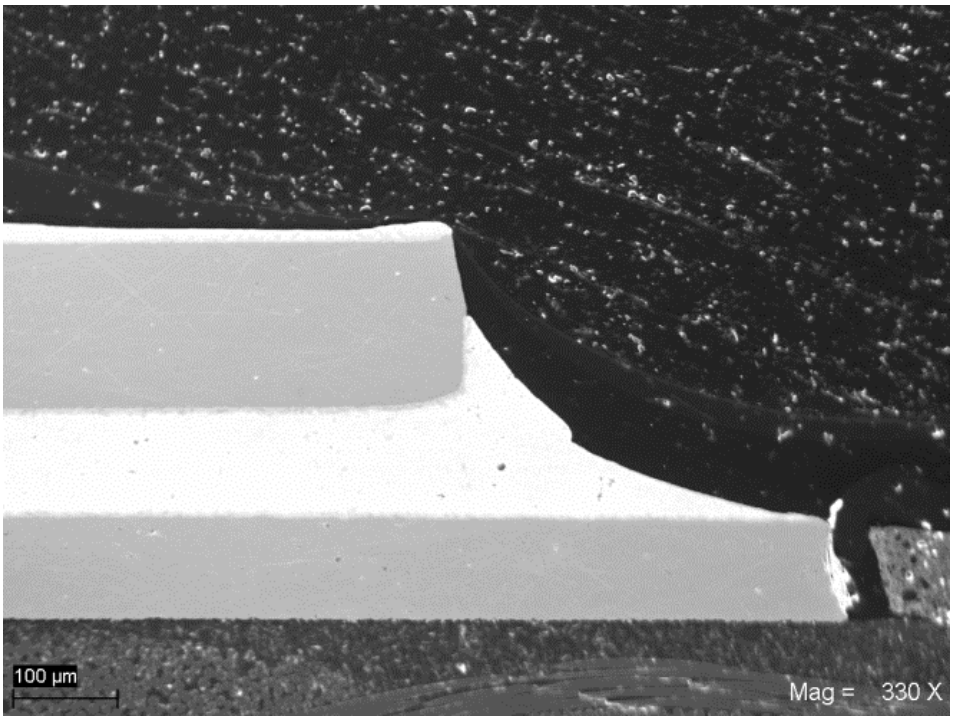


Figure 190: SEM cross-section image, filled PC18M+20%XP2742 QFP-A312 U902, Lead 6 toe, 330x.

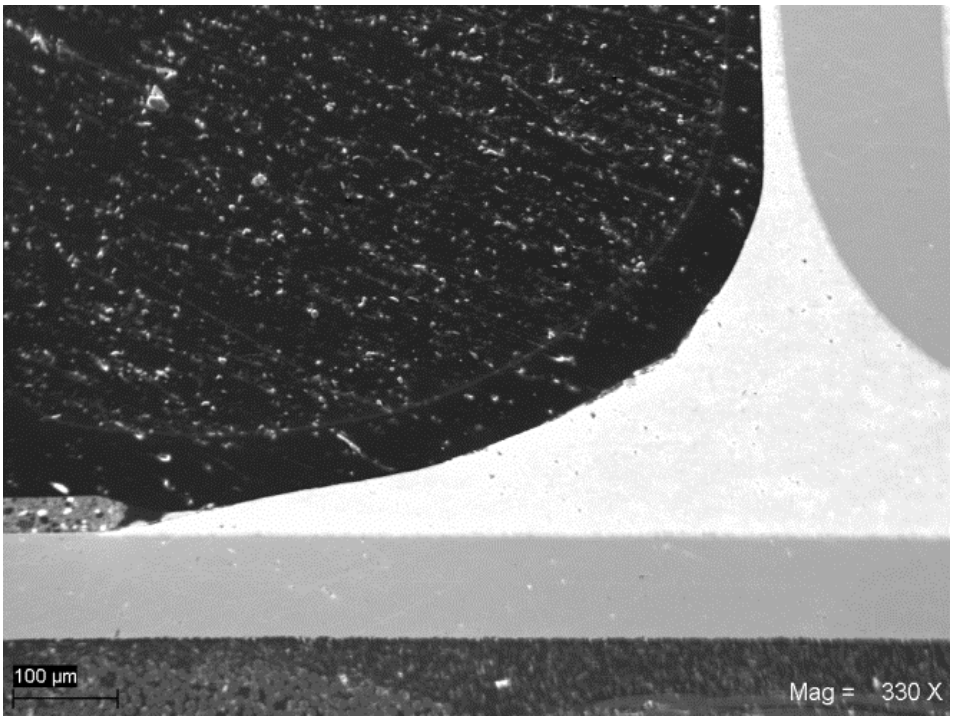


Figure 191: SEM cross-section image, filled PC18M+20%XP2742 QFP-A312 U902, Lead 6 heel, 330x.



Figure 192: SEM cross-section image, filled PC18M+20%XP2742 QFP-A312 U902, Lead 28, 119x.

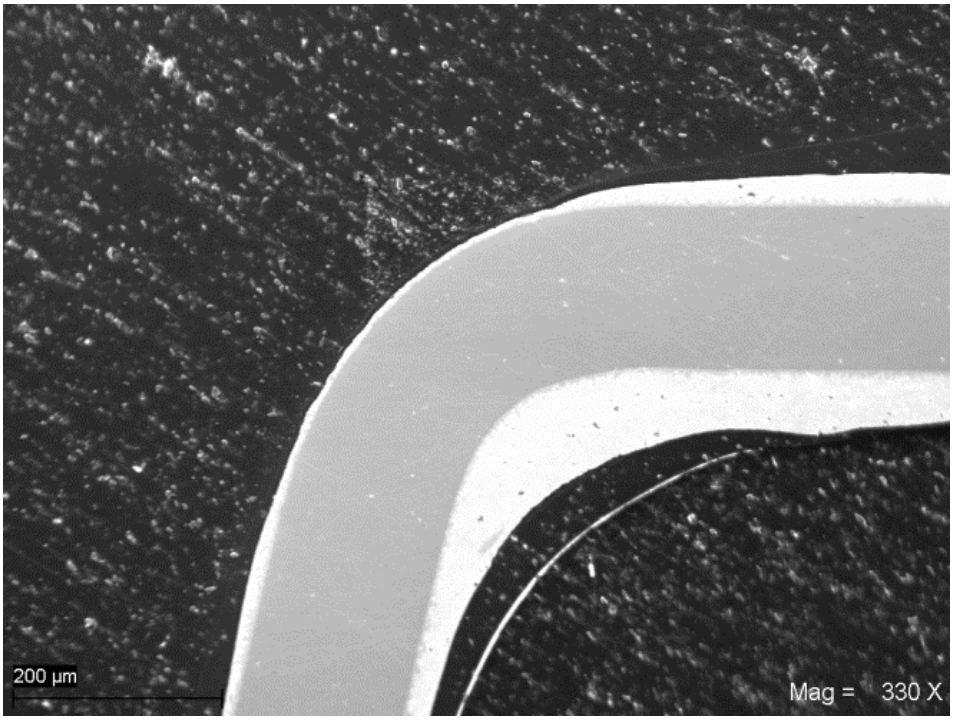


Figure 193: SEM cross-section image, filled PC18M+20%XP2742 QFP-A312 U902, Lead 28 knee, 330x.

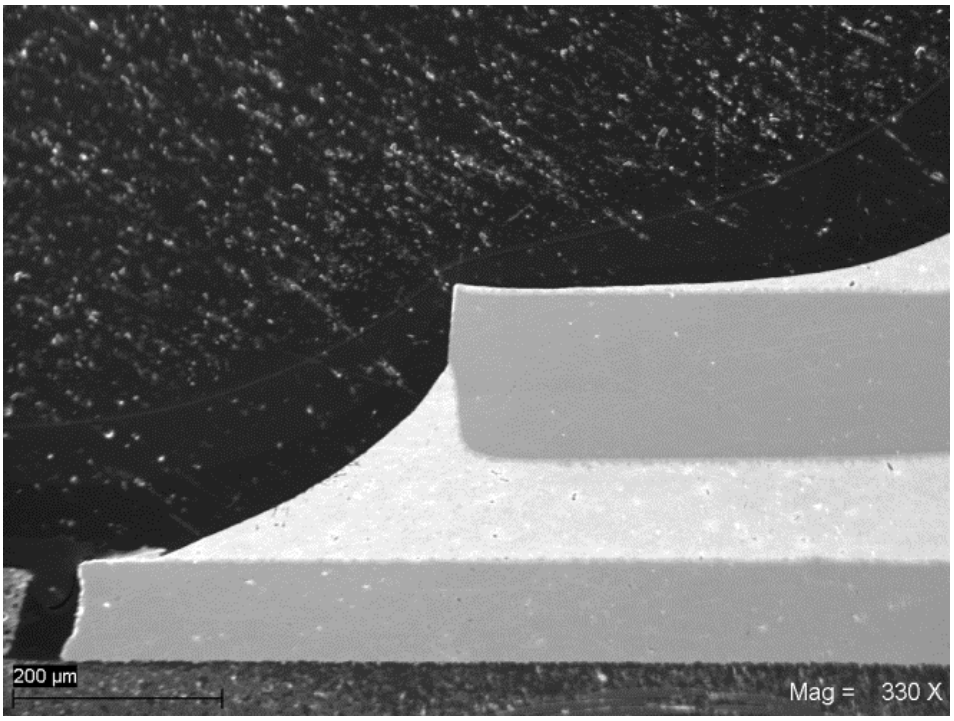


Figure 194: SEM cross-section image, filled PC18M+20%XP2742 QFP-A312 U902, Lead 28 toe, 330x.

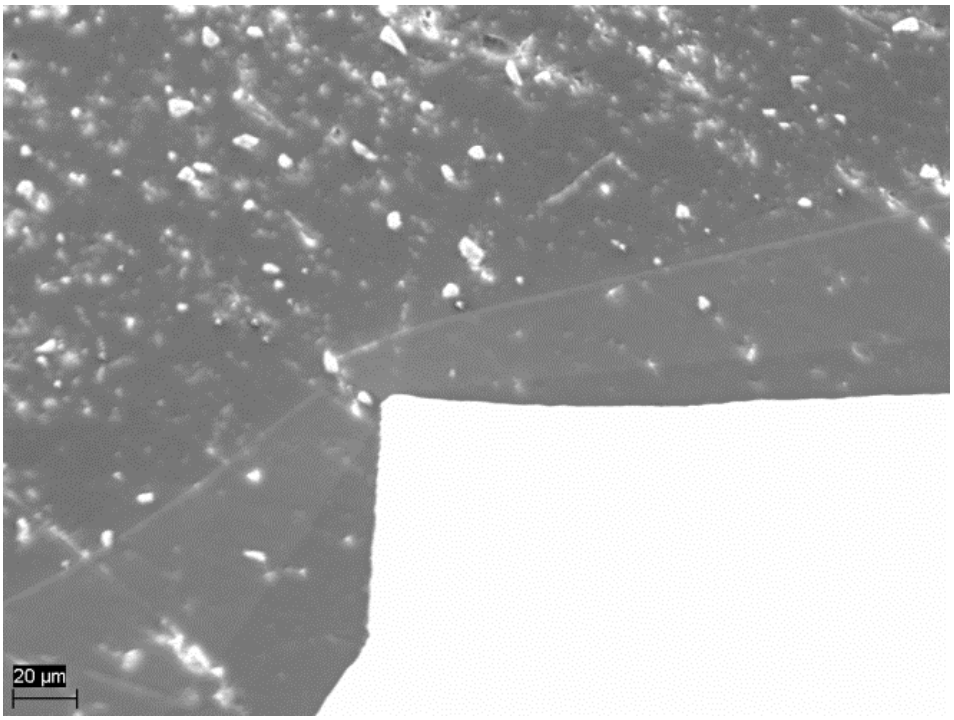


Figure 195: SEM cross-section image, filled PC18M+20%XP2742 QFP-A312 U902, Lead 28 toe, 1,000x

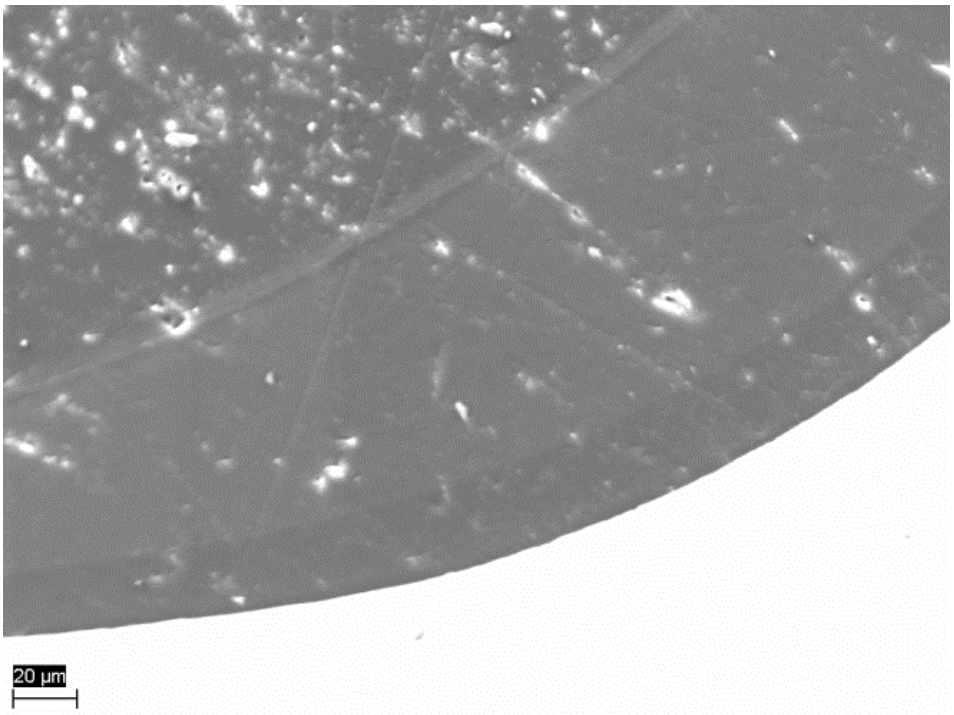


Figure 196: SEM cross-section image, filled PC18M+20%XP2742 QFP-A312 U902, Lead 28 top bend above foot, 1,000x.

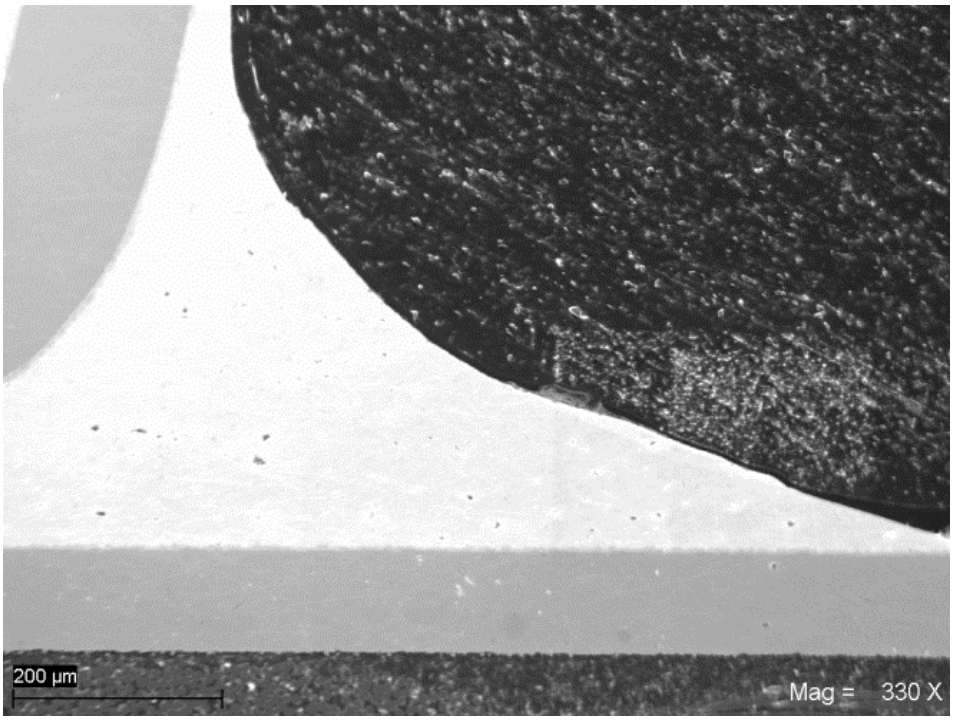


Figure 197: SEM cross-section image, filled PC18M+20%XP2742 QFP-A312 U902, Lead 28 heel, 330x.

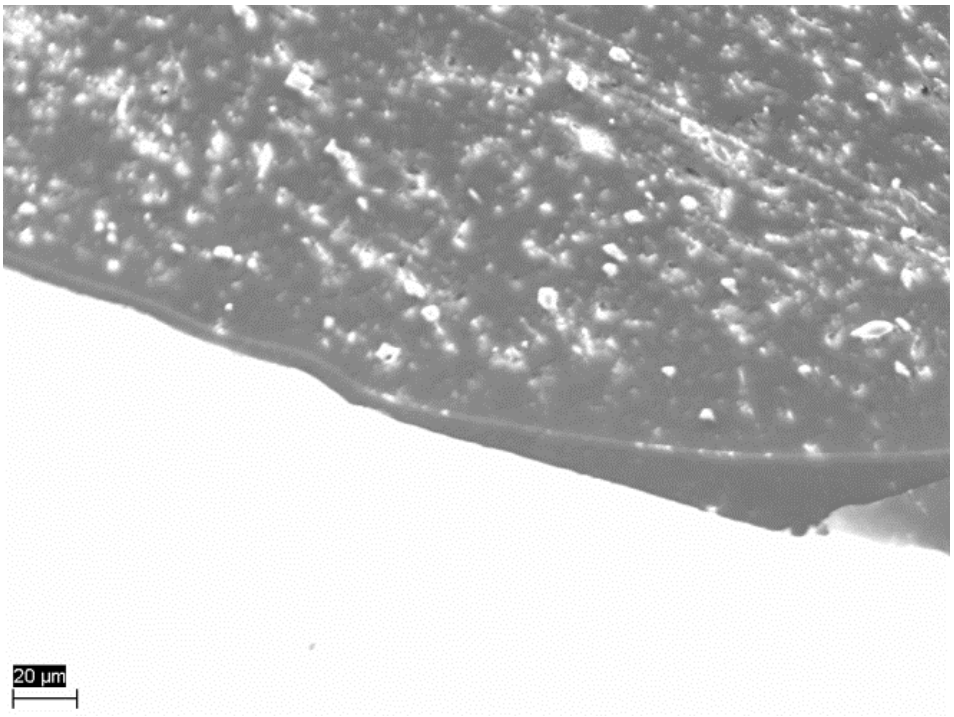


Figure 198: SEM cross-section image, filled PC18M+20%XP2742 QFP-A312 U902, Lead 28 end of heel, 1,000x.

4.4.2.3 Coating thickness measurements filled PC18M+20%XP2742 QFP-A312 U902

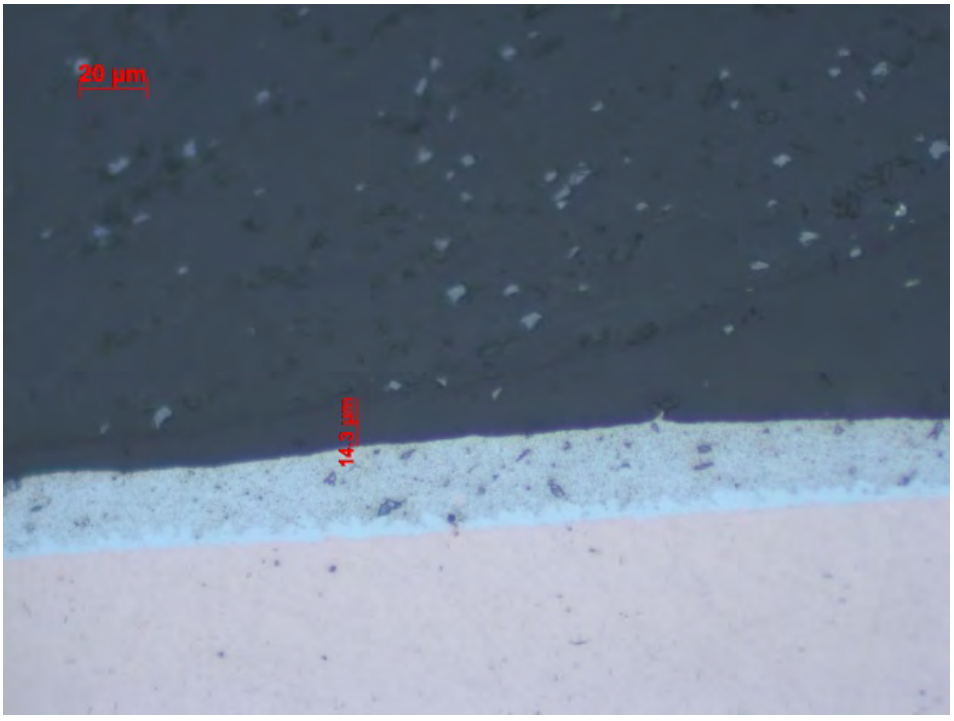


Figure 199: Optical cross-section image, filled PC18M+20%XP2742 QFP-A312 U902, Lead 6 measurements, A, 500x.

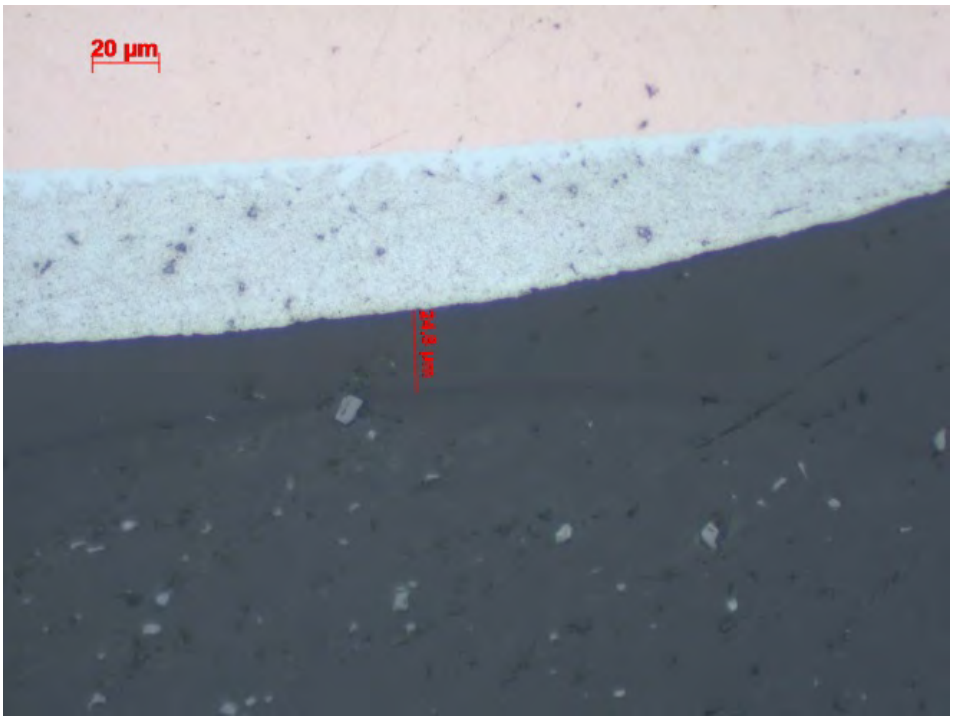


Figure 200: Optical cross-section image, filled PC18M+20%XP2742 QFP-A312 U902, Lead 6 measurements, A1, 500x.

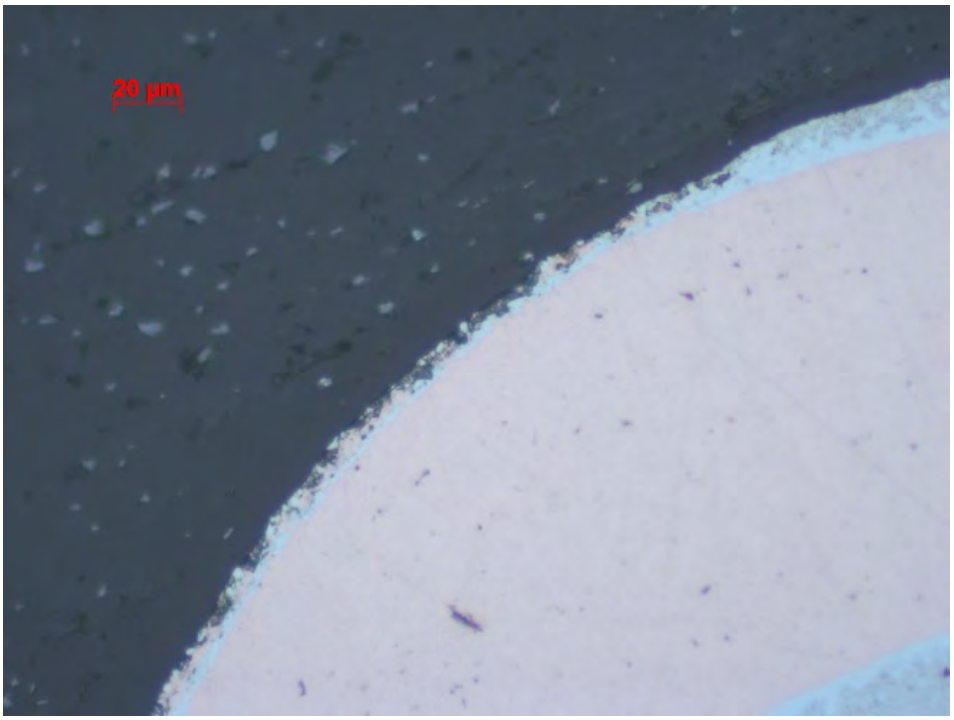


Figure 201: Optical cross-section image, filled PC18M+20%XP2742 QFP-A312 U902, Lead 6 measurements, B, 500x

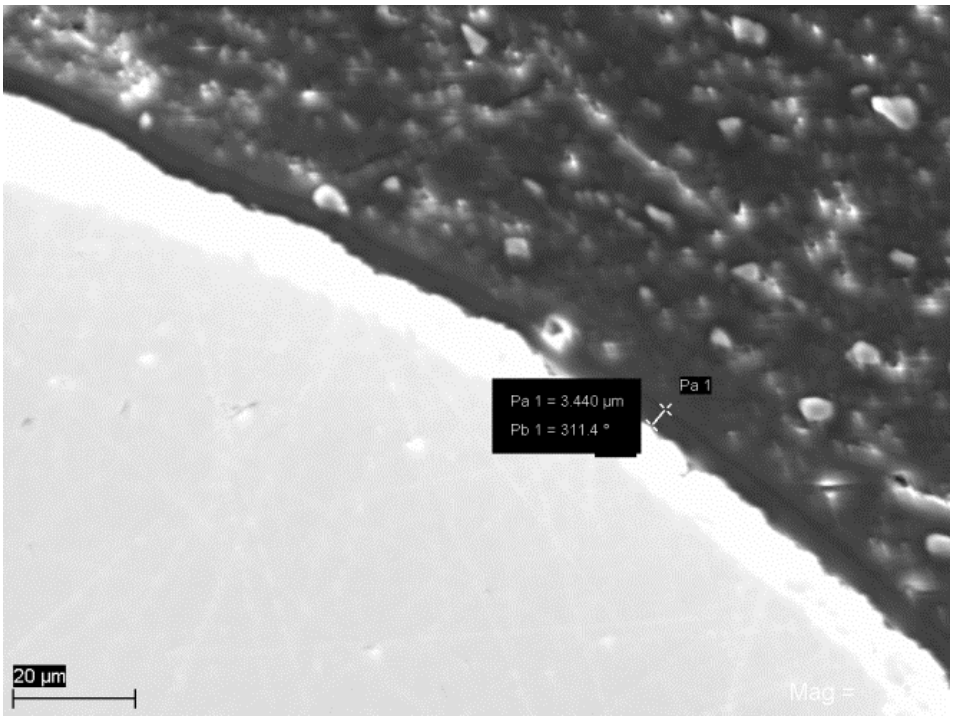


Figure 202: SEM cross-section image, filled PC18M+20%XP2742 QFP-A312 U902, Lead 6 measurements, B, 1,930x.

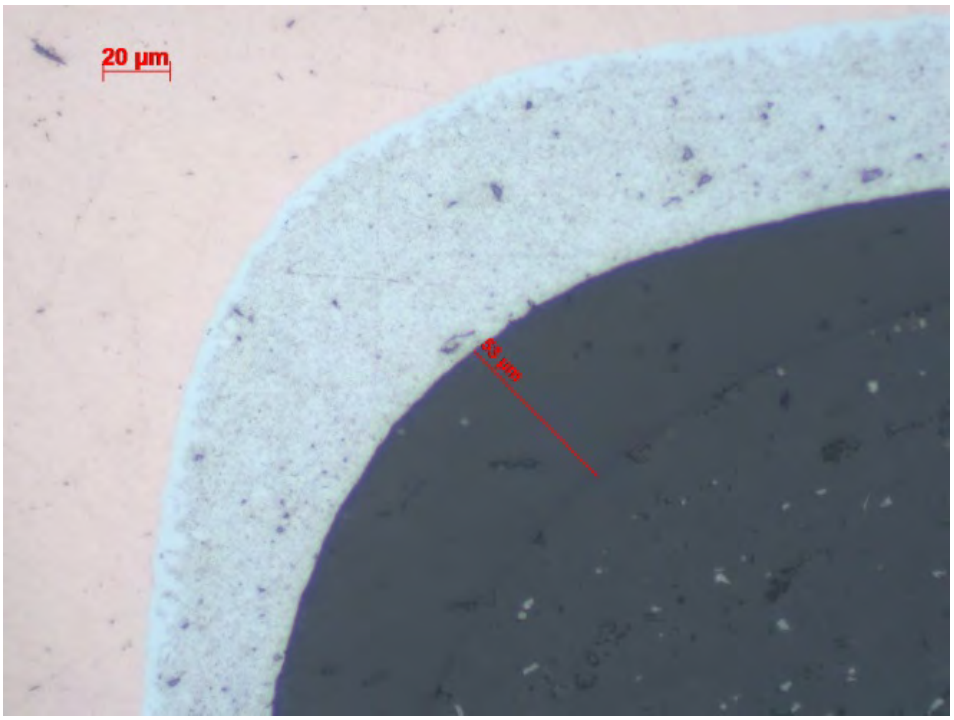


Figure 203: Optical cross-section image, filled PC18M+20%XP2742 QFP-A312 U902, Lead 6 measurements, B1, 500x.

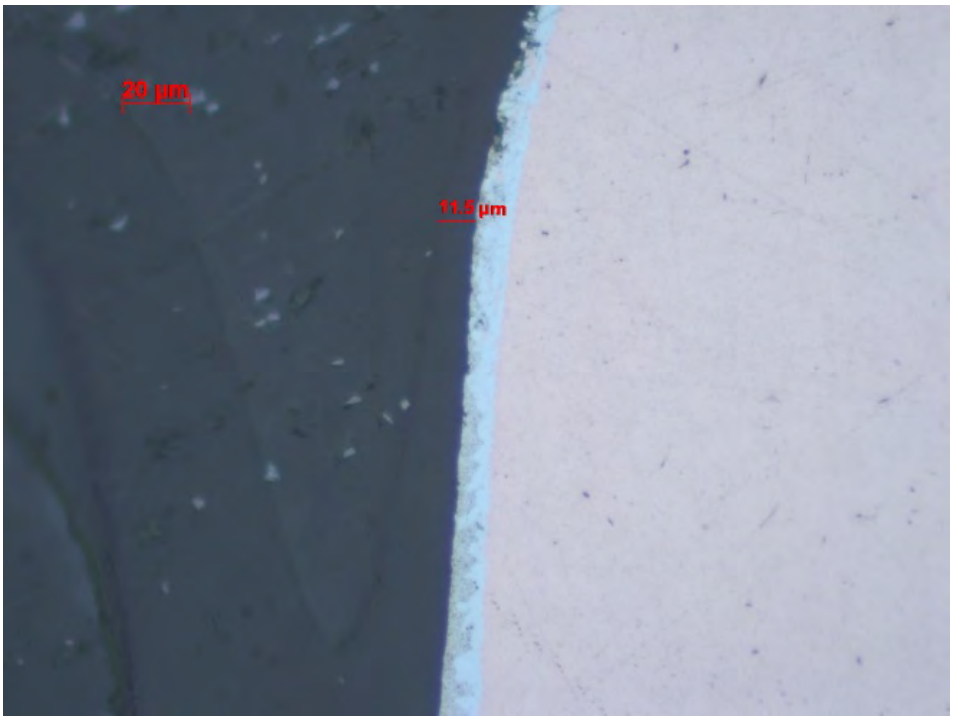


Figure 204: Optical cross-section image, filled PC18M+20%XP2742 QFP-A312 U902, Lead 6 measurements, C, 500x.

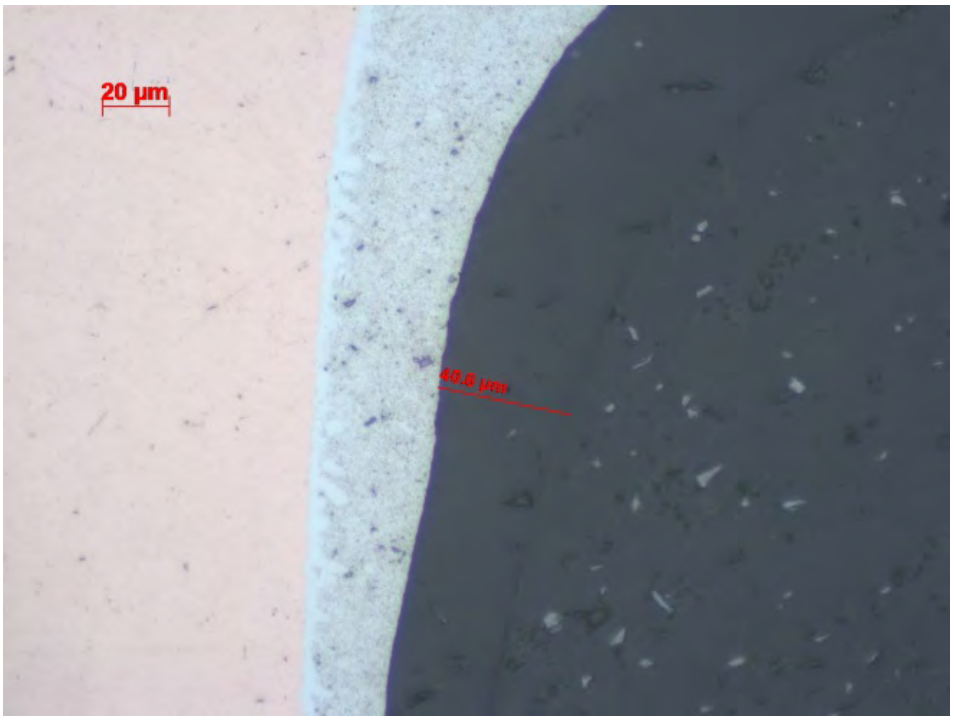


Figure 205: Optical cross-section image, filled PC18M+20%XP2742 QFP-A312 U902, Lead 6 measurements, C1, 500x.

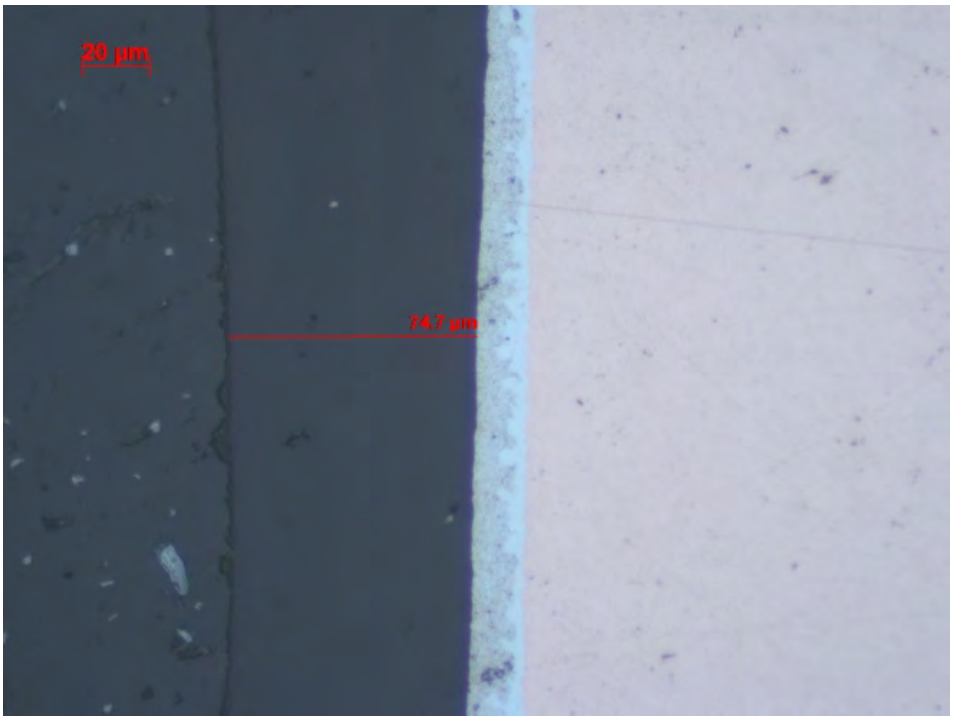


Figure 206: Optical cross-section image, filled PC18M+20%XP2742 QFP-A312 U902, Lead 6 measurements, D, 500x.

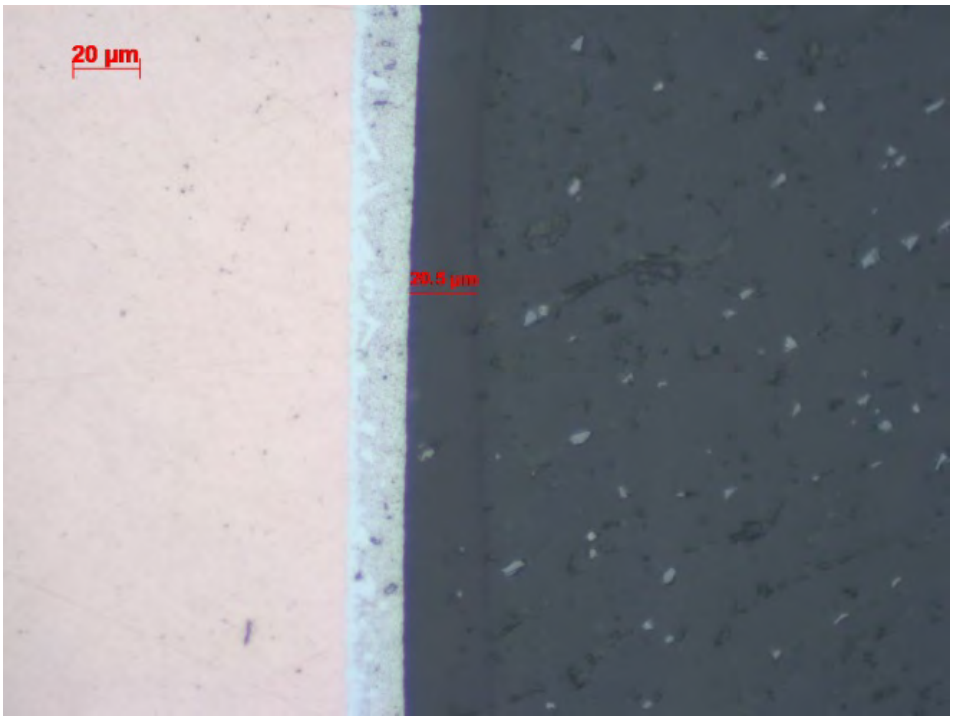


Figure 207: Optical cross-section image, filled PC18M+20%XP2742 QFP-A312 U902, Lead 6 measurements, D1, 500x.

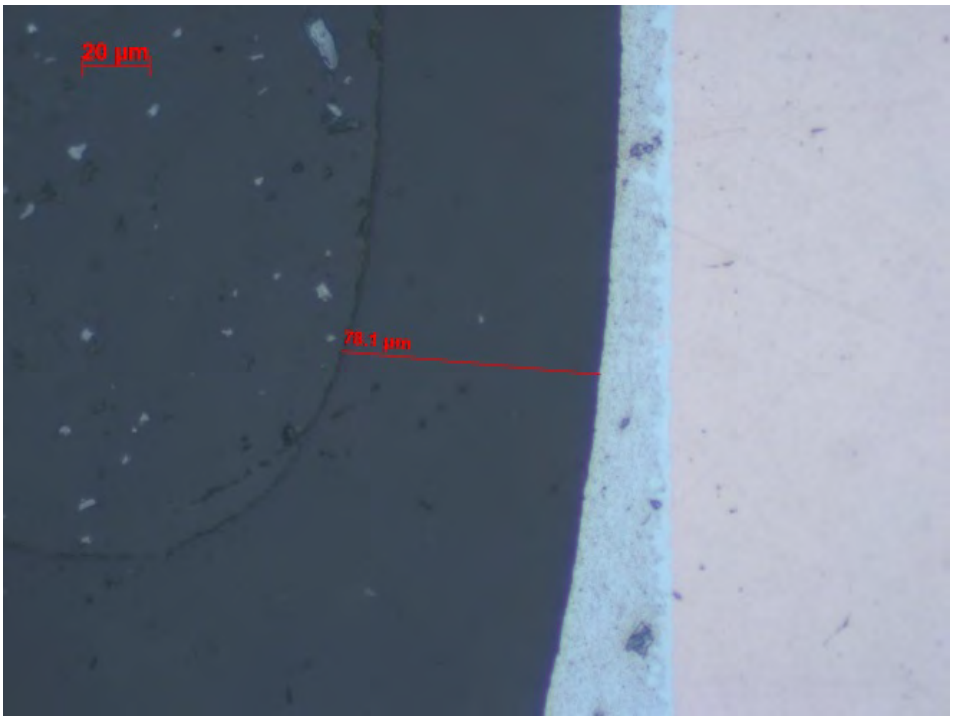


Figure 208: Optical cross-section image, filled PC18M+20%XP2742 QFP-A312 U902, Lead 6 measurements, E, 500x.

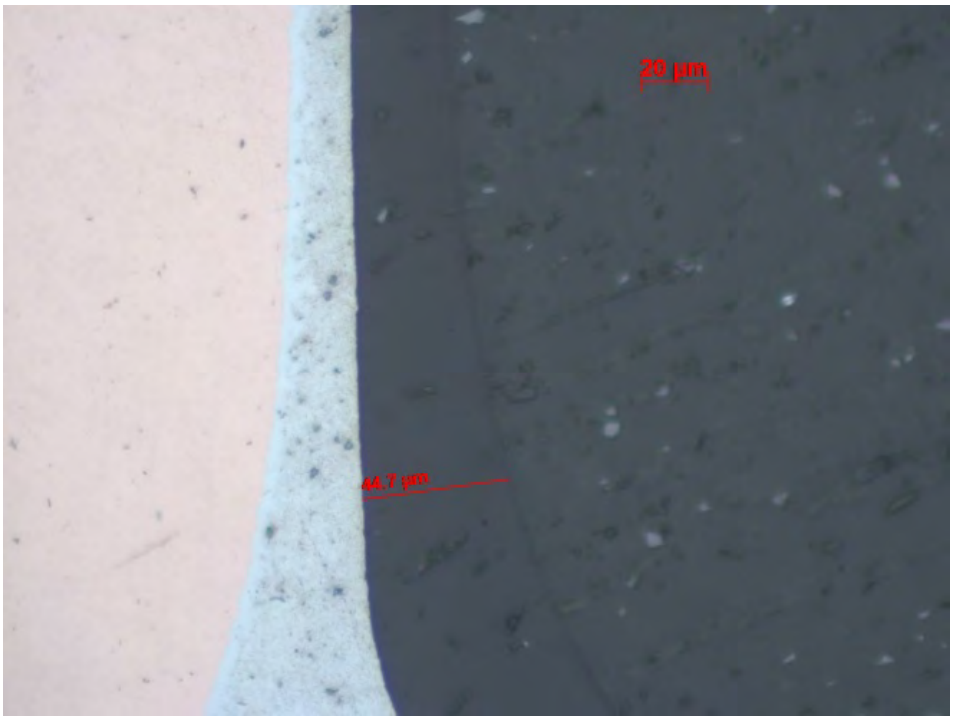


Figure 209: Optical cross-section image, filled PC18M+20%XP2742 QFP-A312 U902, Lead 6 measurements, E1, 500x.

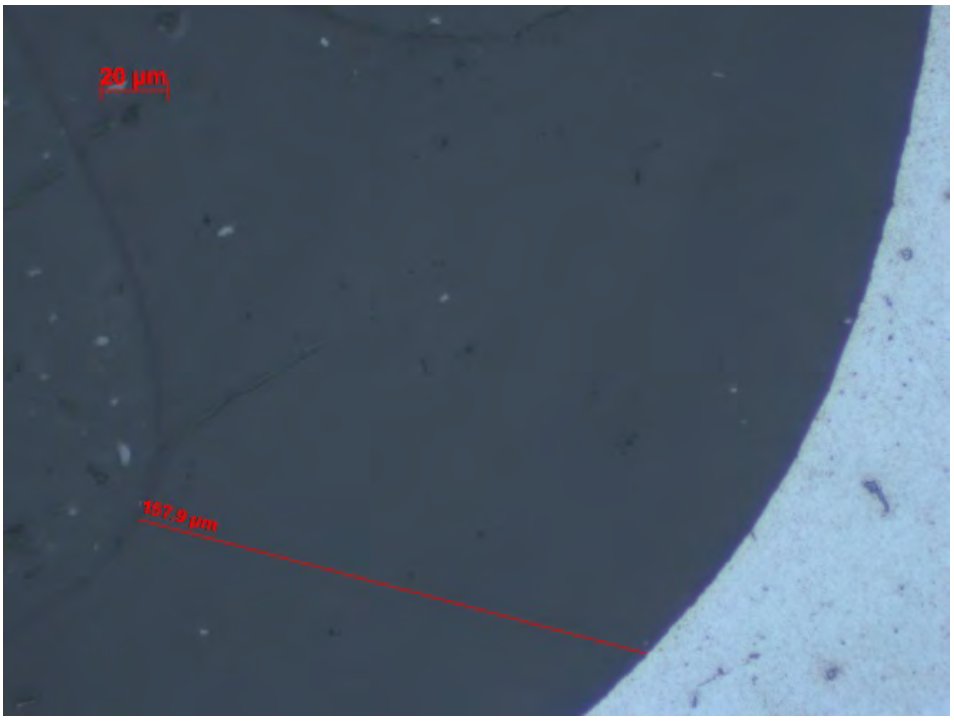


Figure 210: Optical cross-section image, filled PC18M+20%XP2742 QFP-A312 U902, Lead 6 measurements, F, 500x.

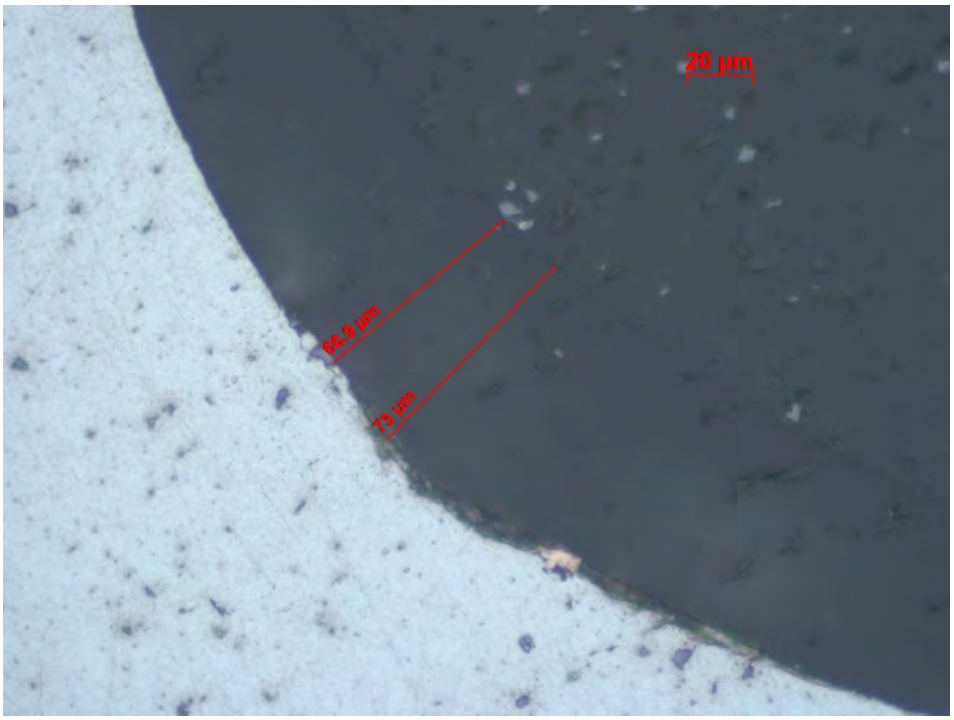


Figure 211: Optical cross-section image, filled PC18M+20%XP2742 QFP-A312 U902, Lead 6 measurements, F1, 500x.

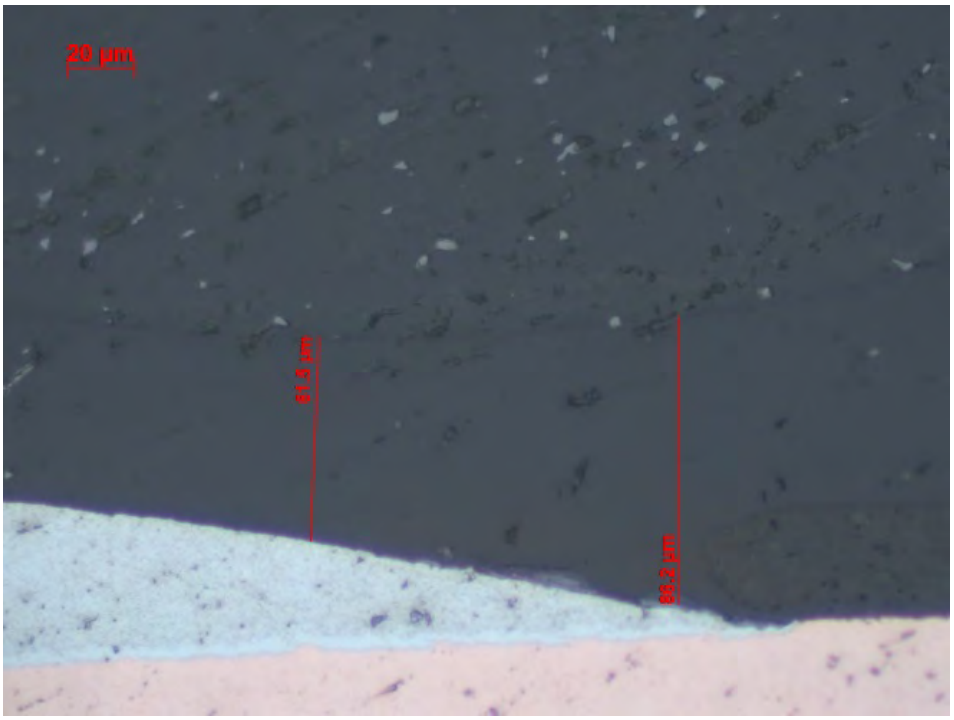


Figure 212: Optical cross-section image, filled PC18M+20%XP2742 QFP-A312 U902, Lead 6 measurements, H, 500x.

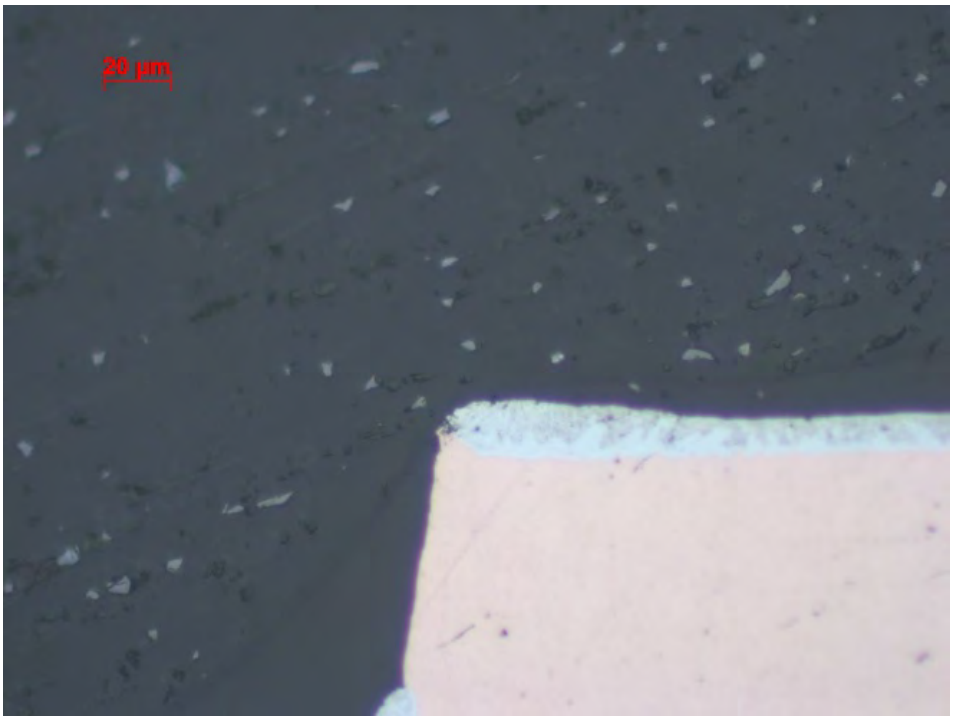


Figure 213: Optical cross-section image, filled PC18M+20%XP2742 QFP-A312 U902, Lead 6 measurements, T, 500x.

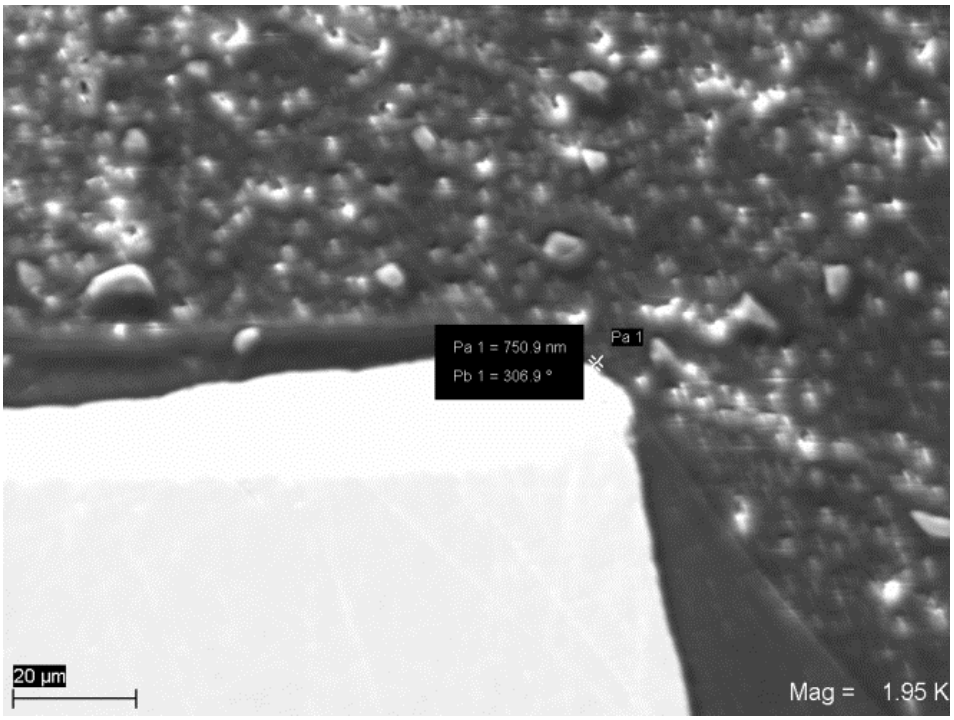


Figure 214: SEM cross-section image, filled PC18M+20%XP2742 QFP-A312 U902, Lead 6 measurements, T, 1,950x.

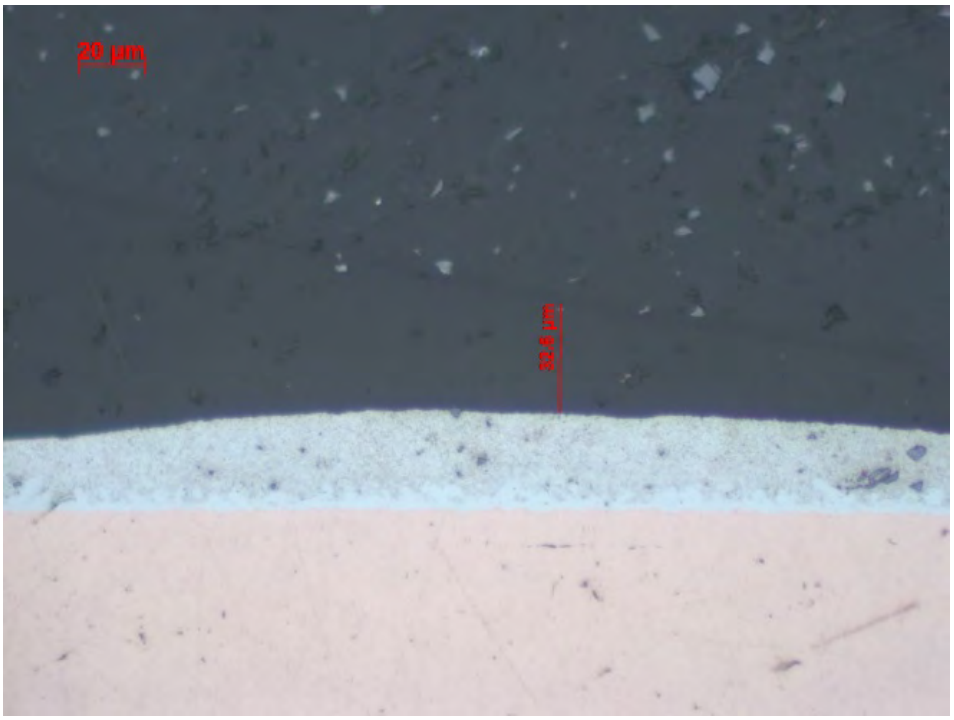


Figure 215: Optical cross-section image, filled PC18M+20%XP2742 QFP-A312 U902, Lead 28 measurements, A, 500x.

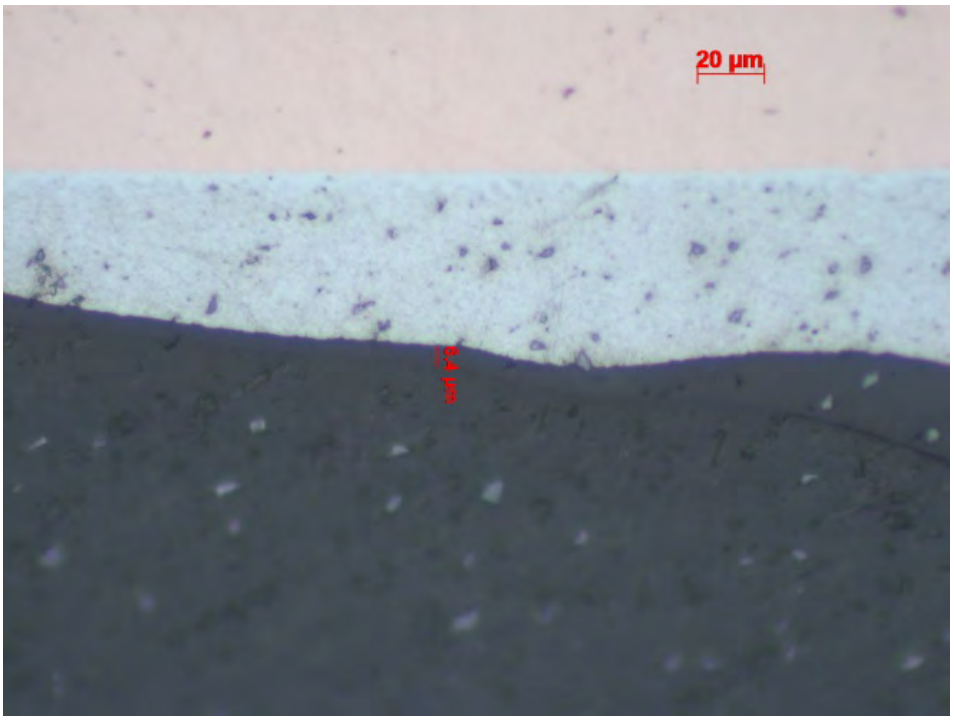


Figure 216: Optical cross-section image, filled PC18M+20%XP2742 QFP-A312 U902, Lead 28 measurements, A1, 500x.

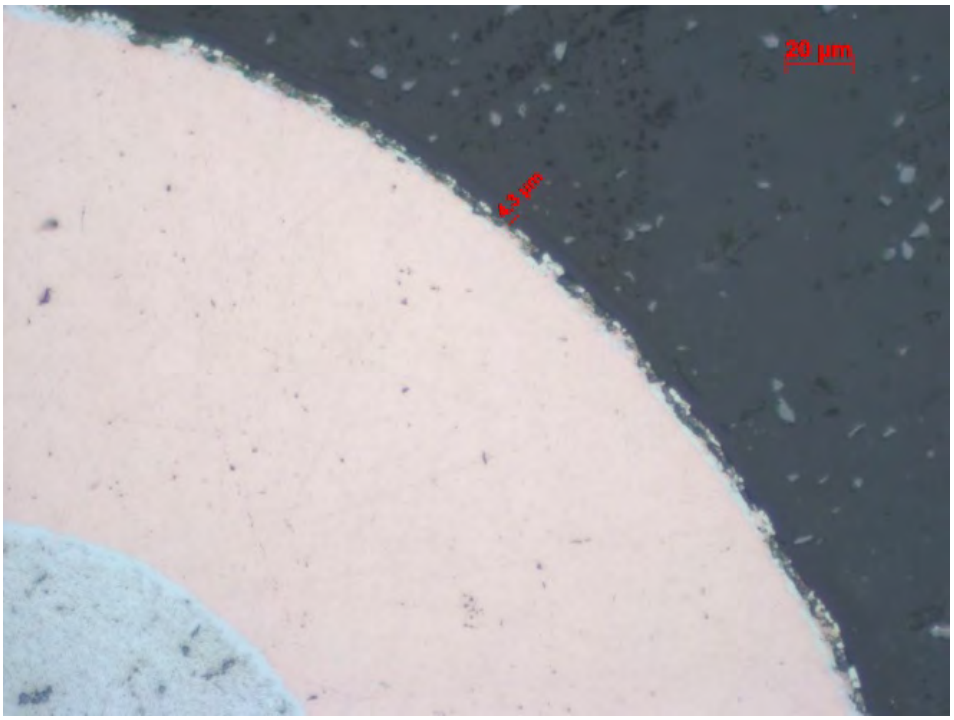


Figure 217: Optical cross-section image, filled PC18M+20%XP2742 QFP-A312 U902, Lead 28 measurements, B, 500x.

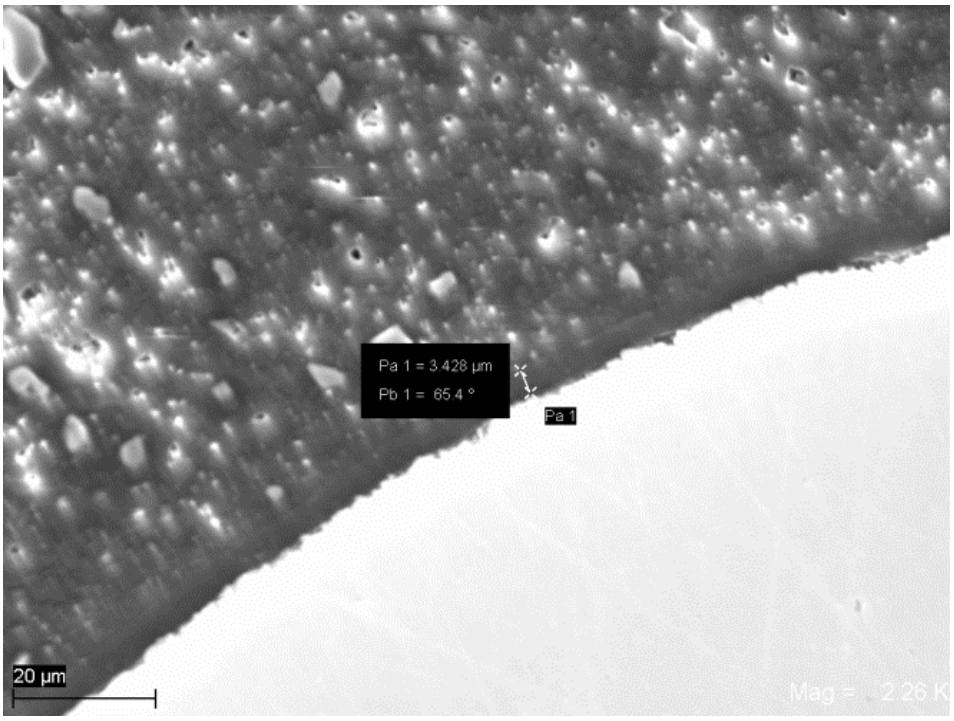


Figure 218: SEM cross-section image, filled PC18M+20%XP2742 QFP-A312 U902, Lead 28 measurements, B, 2,260x.

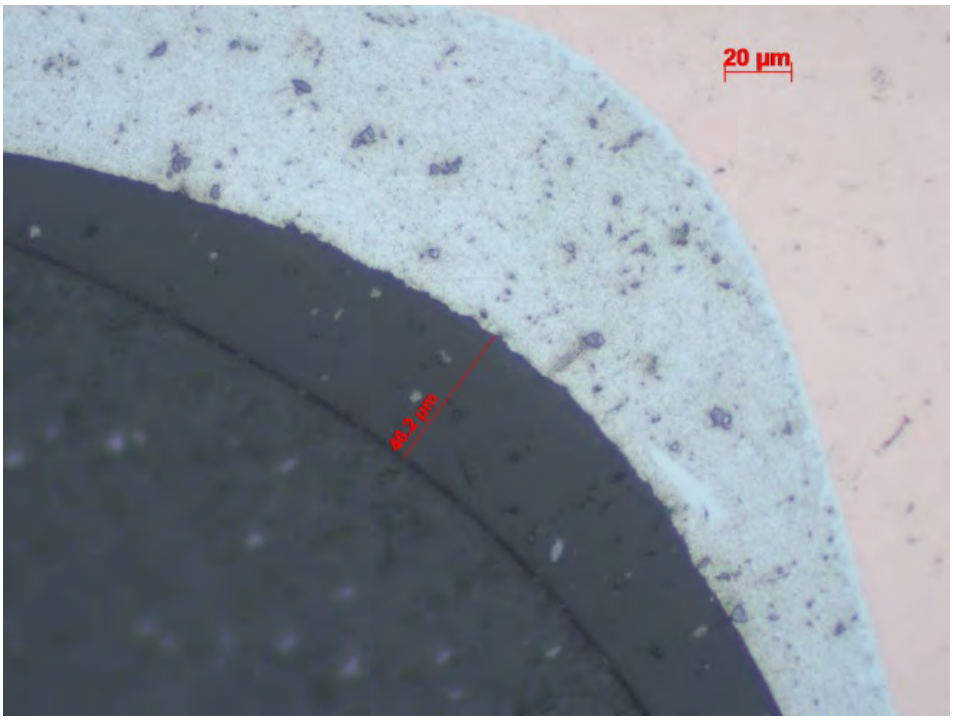


Figure 219: Optical cross-section image, filled PC18M+20%XP2742 QFP-A312 U902, Lead 28 measurements, B1, 500x.

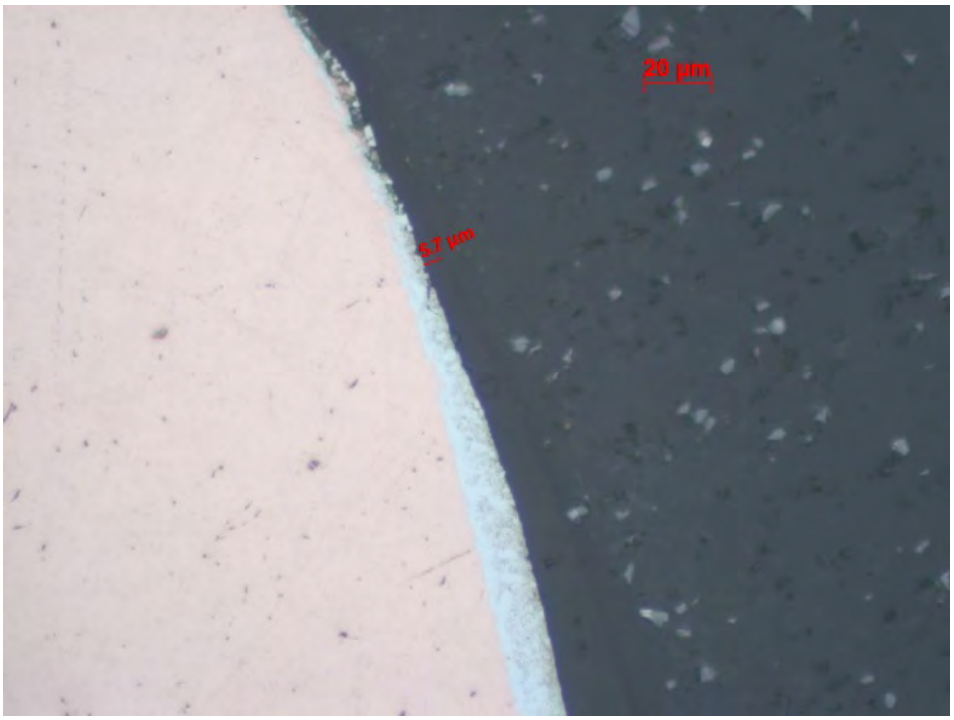


Figure 220: Optical cross-section image, filled PC18M+20%XP2742 QFP-A312 U902, Lead 28 measurements, C, 500x.

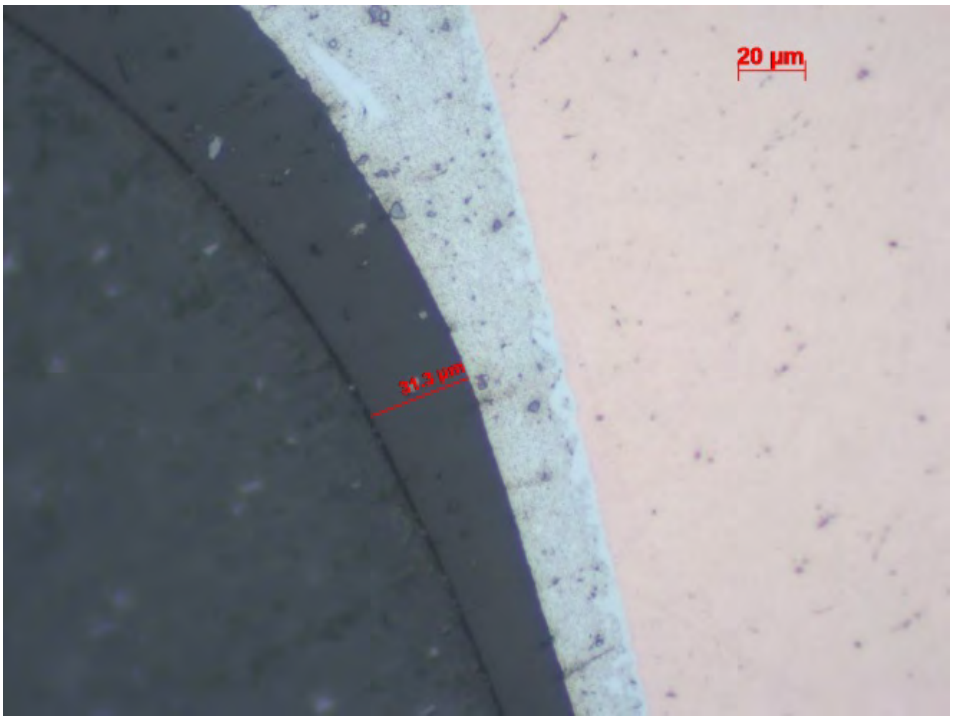


Figure 221: Optical cross-section image, filled PC18M+20%XP2742 QFP-A312 U902, Lead 28 measurements, C1, 500x.

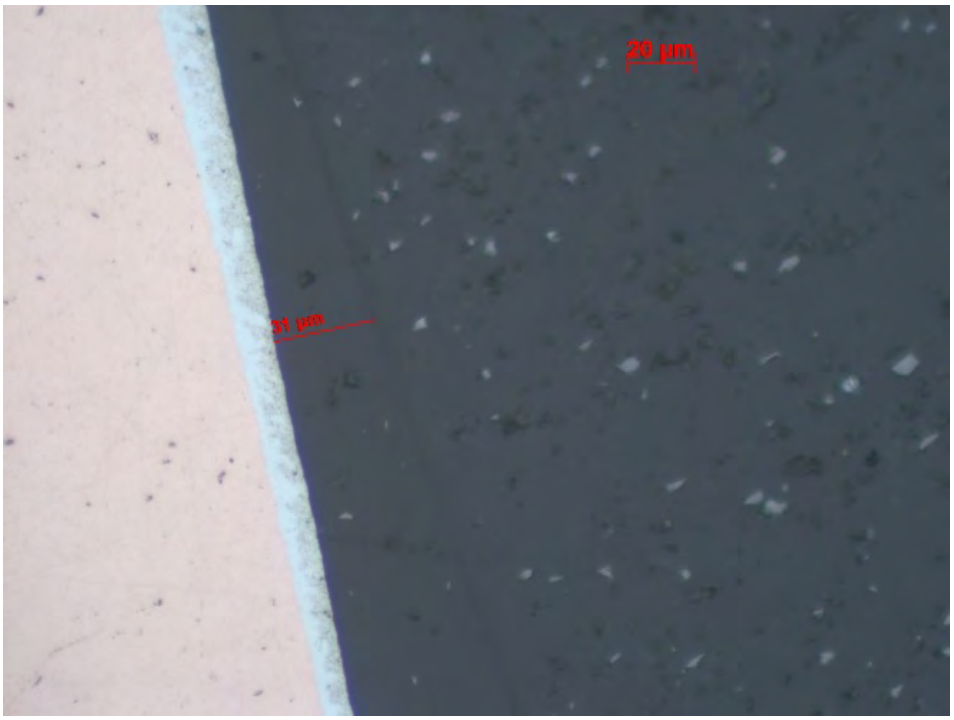


Figure 222: Optical cross-section image, filled PC18M+20%XP2742 QFP-A312 U902, Lead 28 measurements, D, 500x.

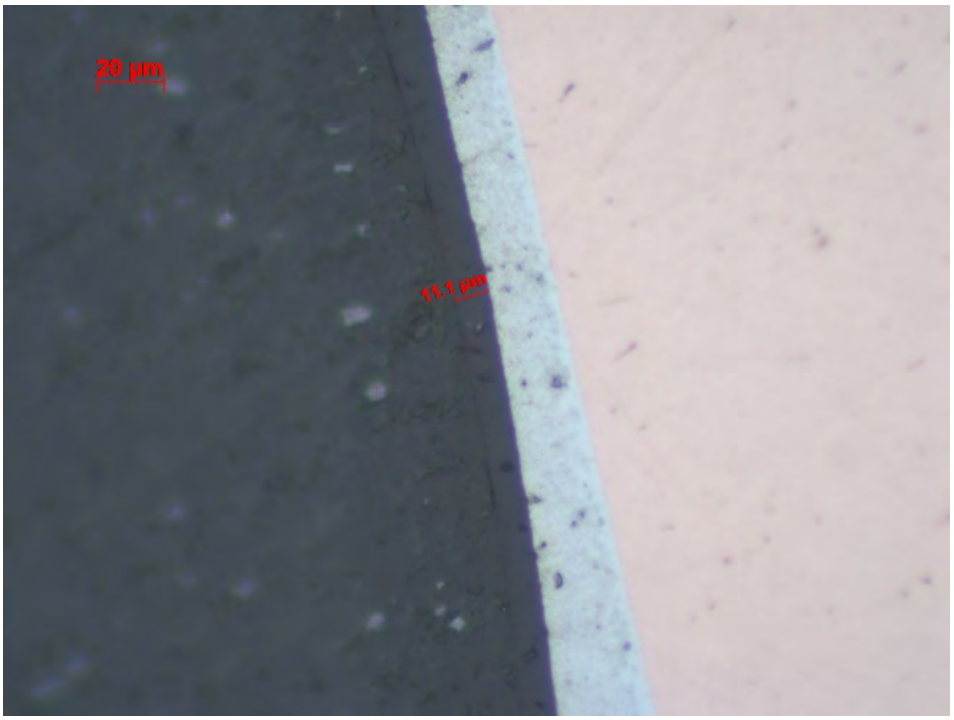


Figure 223: Optical cross-section image, filled PC18M+20%XP2742 QFP-A312 U902, Lead 28 measurements, D1, 500x.



Figure 224: Optical cross-section image, filled PC18M+20%XP2742 QFP-A312 U902, Lead 28 measurements, E, 500x.

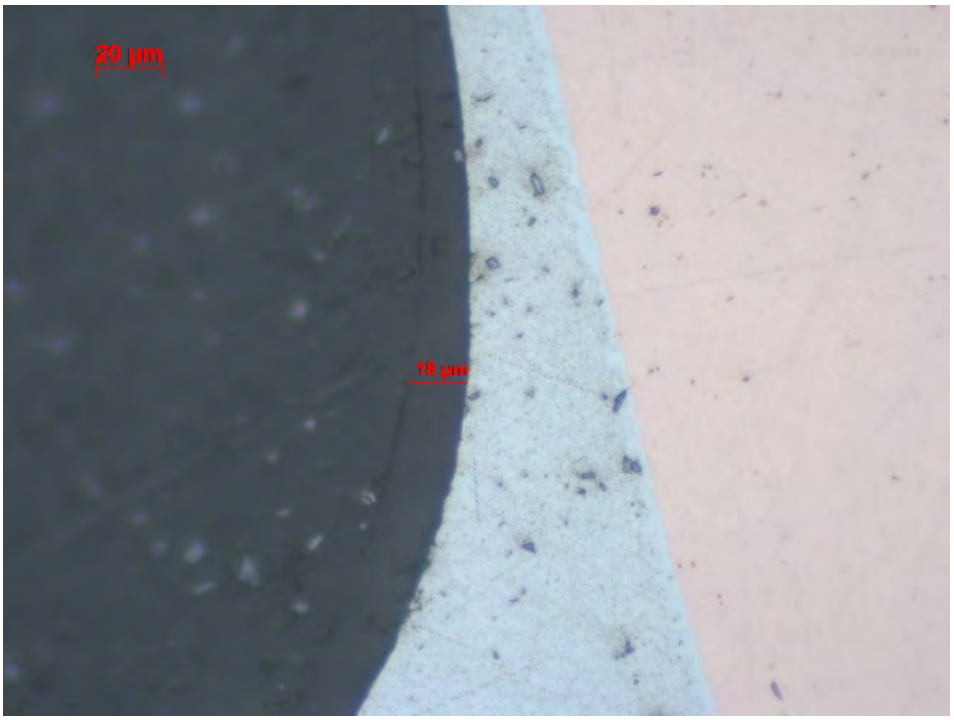


Figure 225: Optical cross-section image, filled PC18M+20%XP2742 QFP-A312 U902, Lead 28 measurements, E1, 500x.

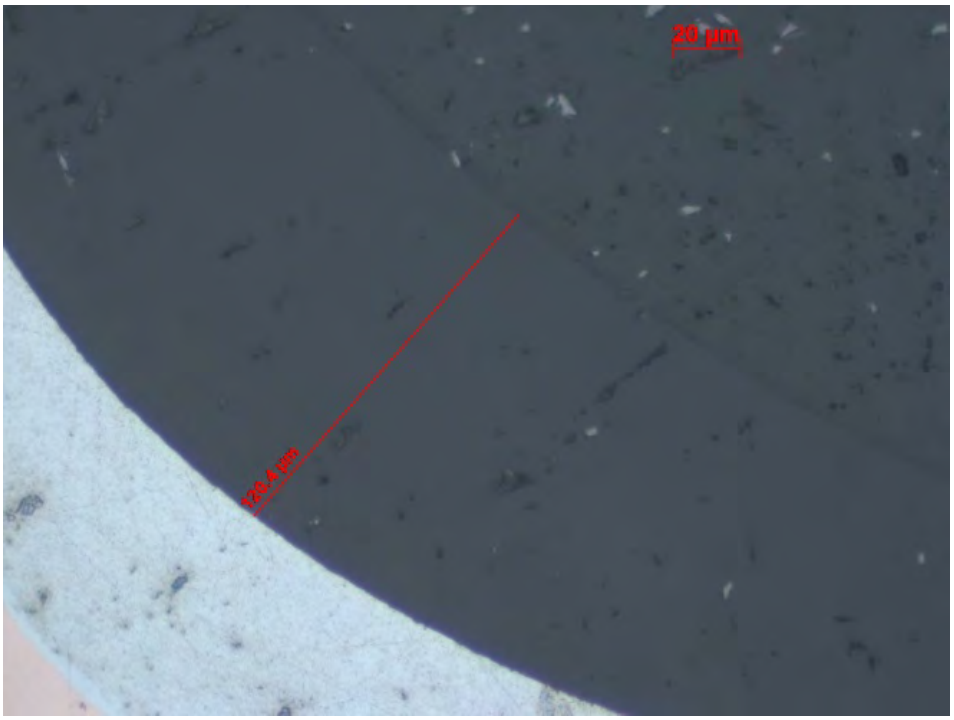


Figure 226: Optical cross-section image, filled PC18M+20%XP2742 QFP-A312 U902, Lead 28 measurements, F, 500x.

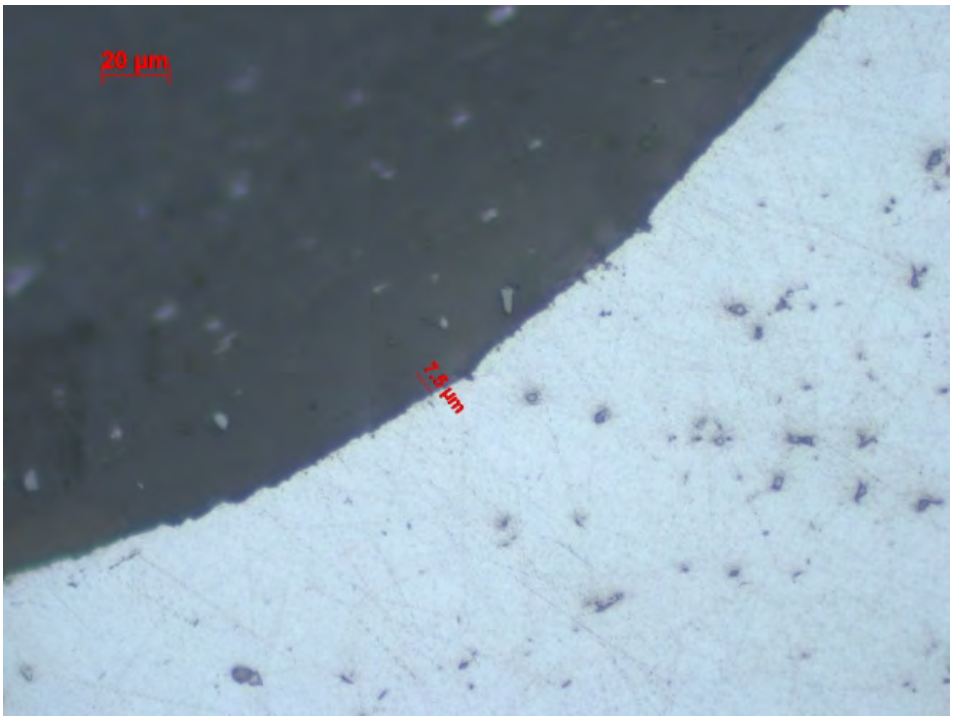


Figure 227: Optical cross-section image, filled PC18M+20%XP2742 QFP-A312 U902, Lead 28 measurements, F1, 500x.

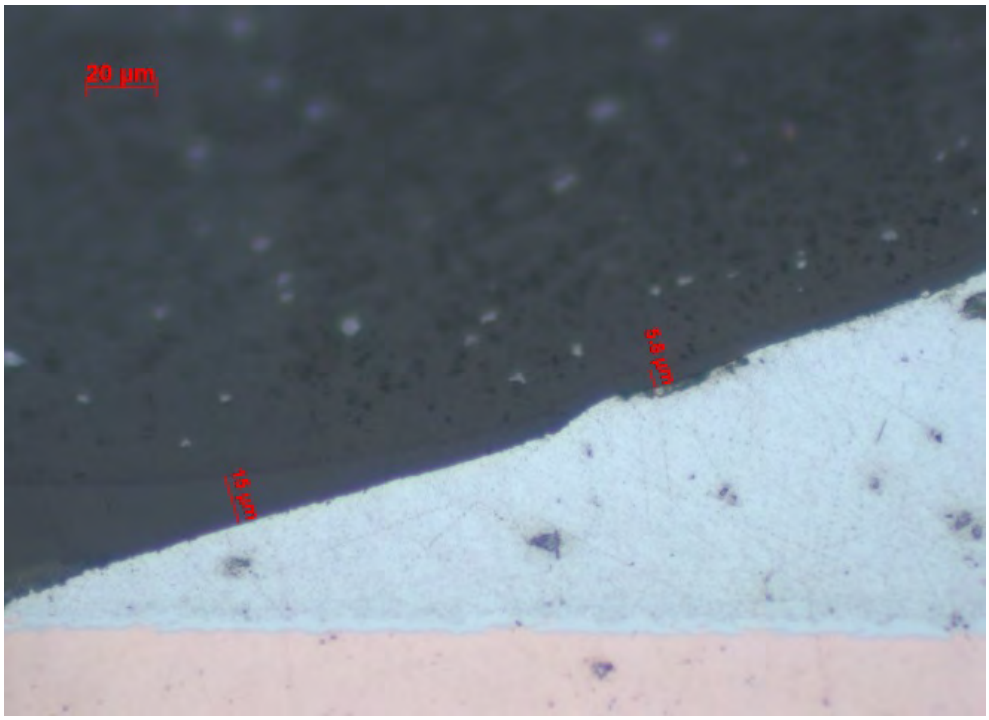


Figure 228: Optical cross-section image, filled PC18M+20%XP2742 QFP-A312 U902, Lead 28 measurements, H, 500x.

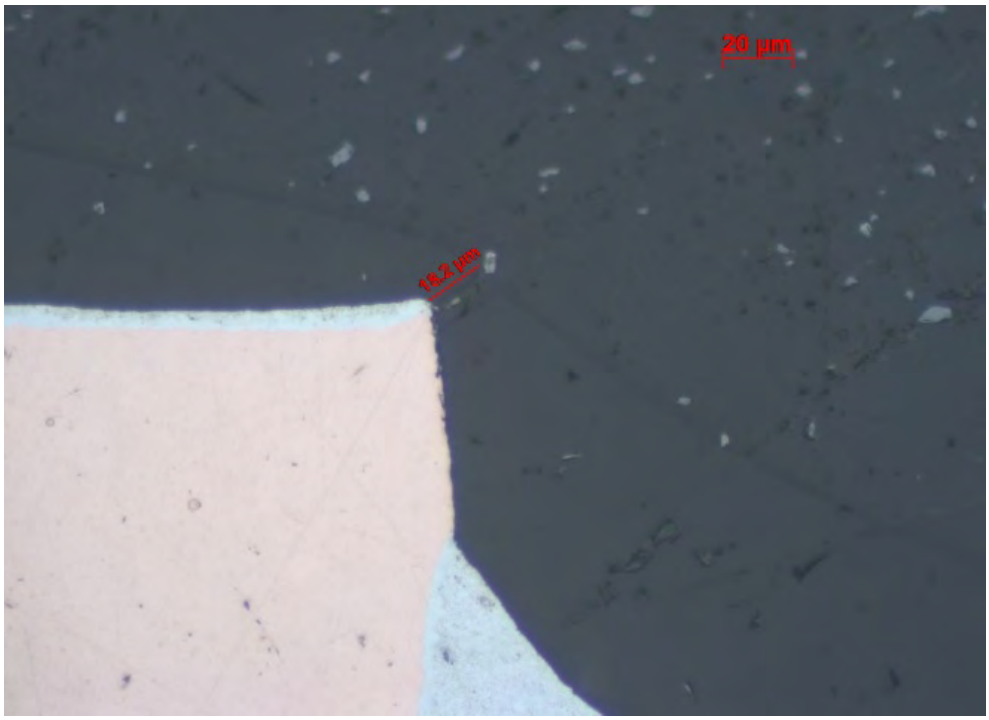


Figure 229: Optical cross-section image, filled PC18M+20%XP2742 QFP-A312 U902, Lead 28 measurements, T, 500x.

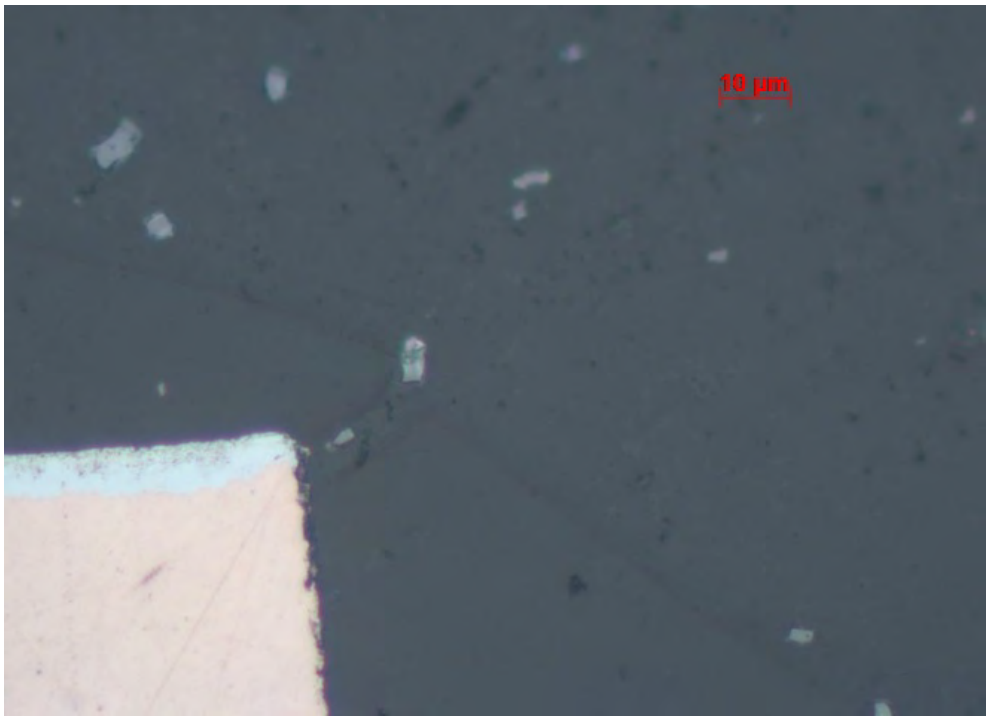


Figure 230: Optical cross-section image, filled PC18M+20%XP2742 QFP-A312 U902, Lead 28 measurements, T, 1,000x.

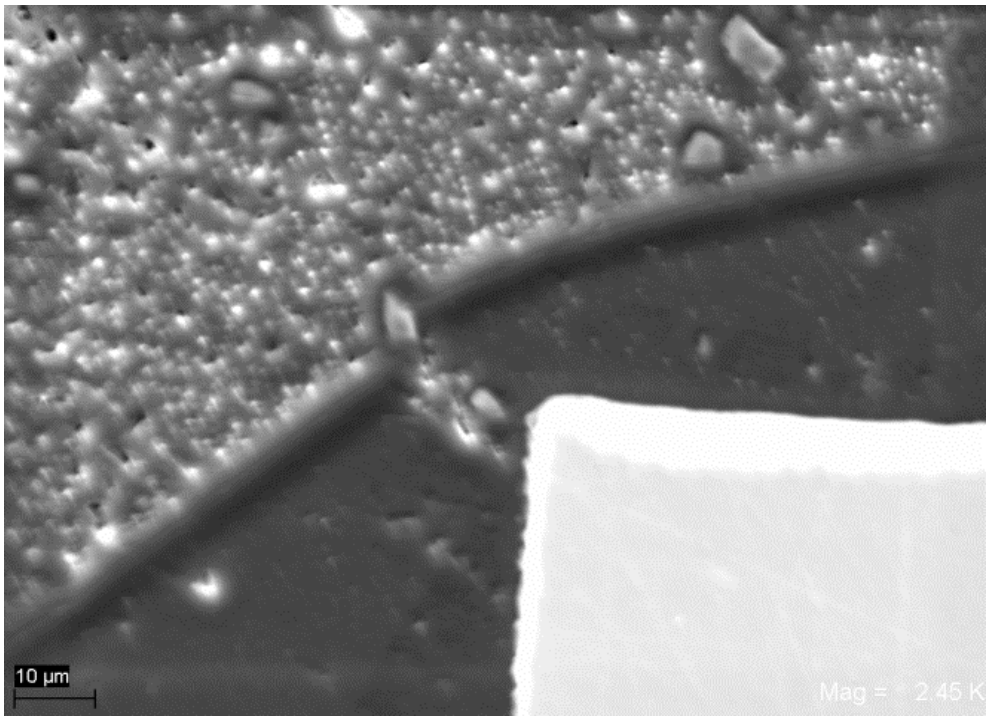


Figure 231: SEM cross-section image, filled PC18M+20%XP2742 QFP-A312 U902, Lead 28 measurements, T, 2,450x.

4.4.2.4 Optical cross-sections filled PC18M+20%XP2742 QFP-A312 non-reworked U901

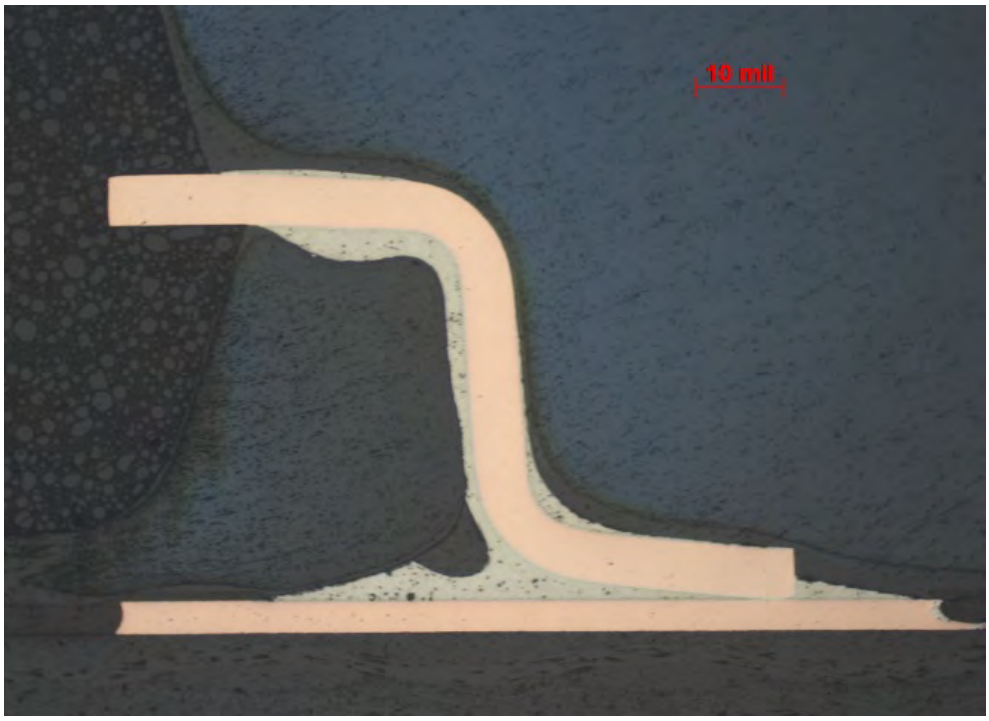


Figure 232: Optical cross-section image, filled PC18M+20%XP2742 QFP-A312, non-reworked U901, Lead 33_50x.

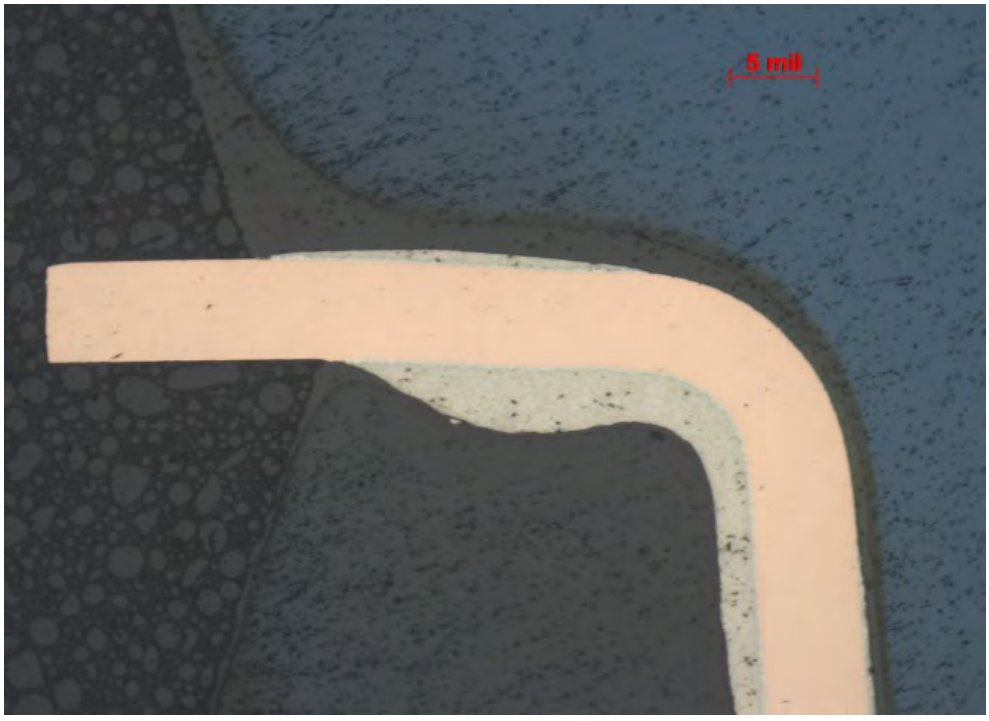


Figure 233: Optical cross-section image, filled PC18M+20%XP2742 QFP-A312, non-reworked U901, Lead 33 knee_100x.

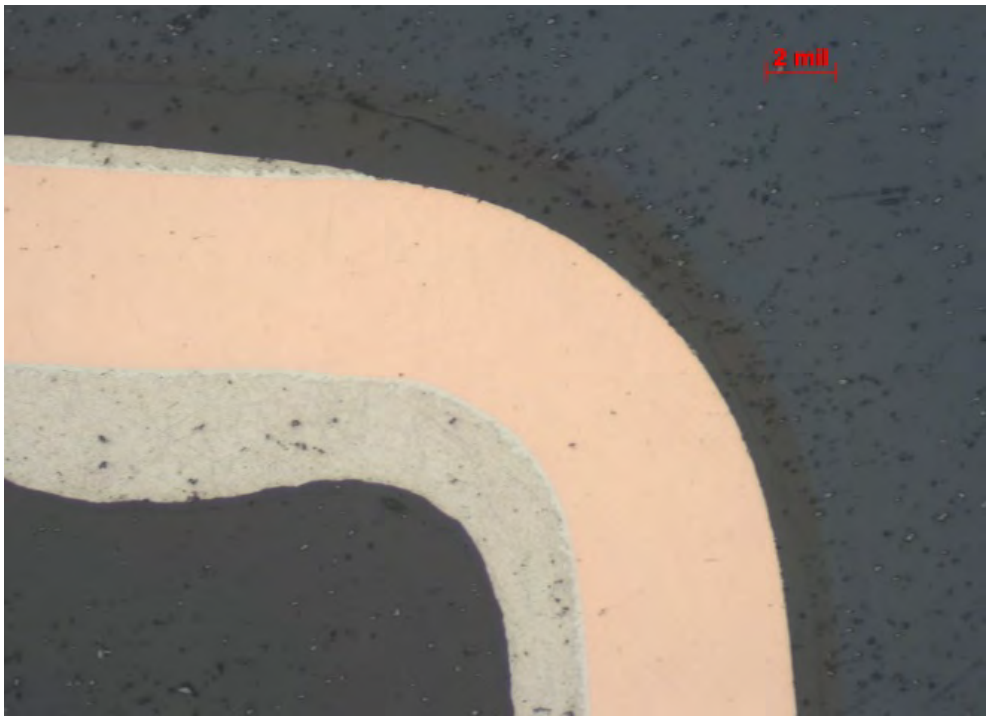


Figure 234: Optical cross-section image, filled PC18M+20%XP2742 QFP-A312, non-reworked U901, Lead 33 knee_200x.

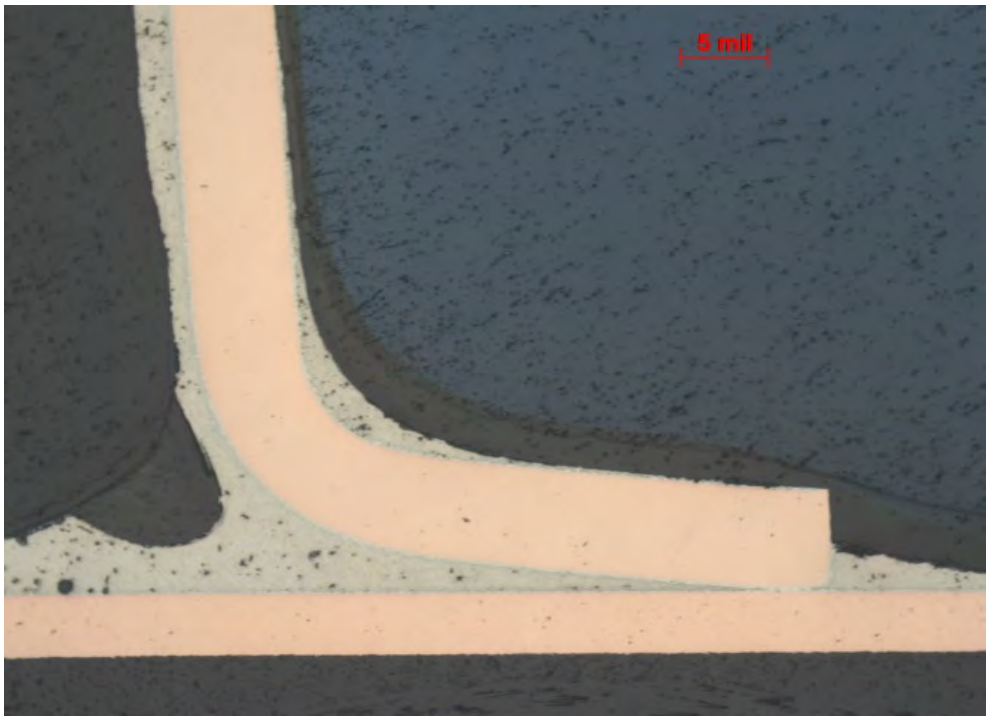


Figure 235: Optical cross-section image, filled PC18M+20%XP2742 QFP-A312, non-reworked U901, Lead 33 foot_100x.

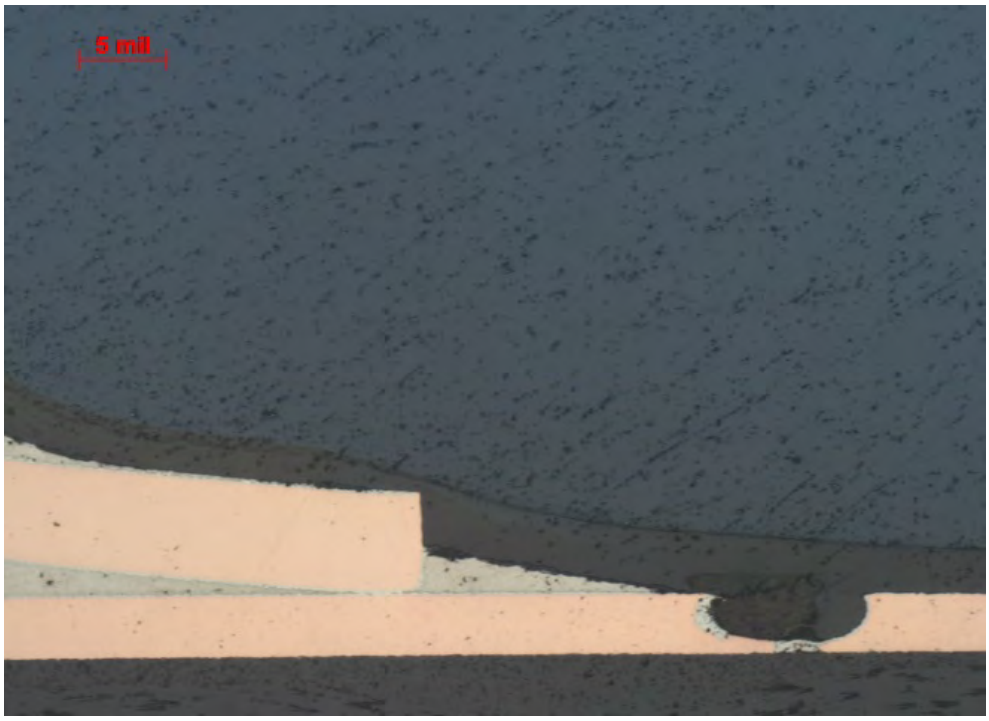


Figure 236: Optical cross-section image, filled PC18M+20%XP2742 QFP-A312, non-reworked U901, Lead 33 toe_100x.



Figure 237: Optical cross-section image, filled PC18M+20%XP2742 QFP-A312, non-reworked U901, Lead 33 heel_100x.

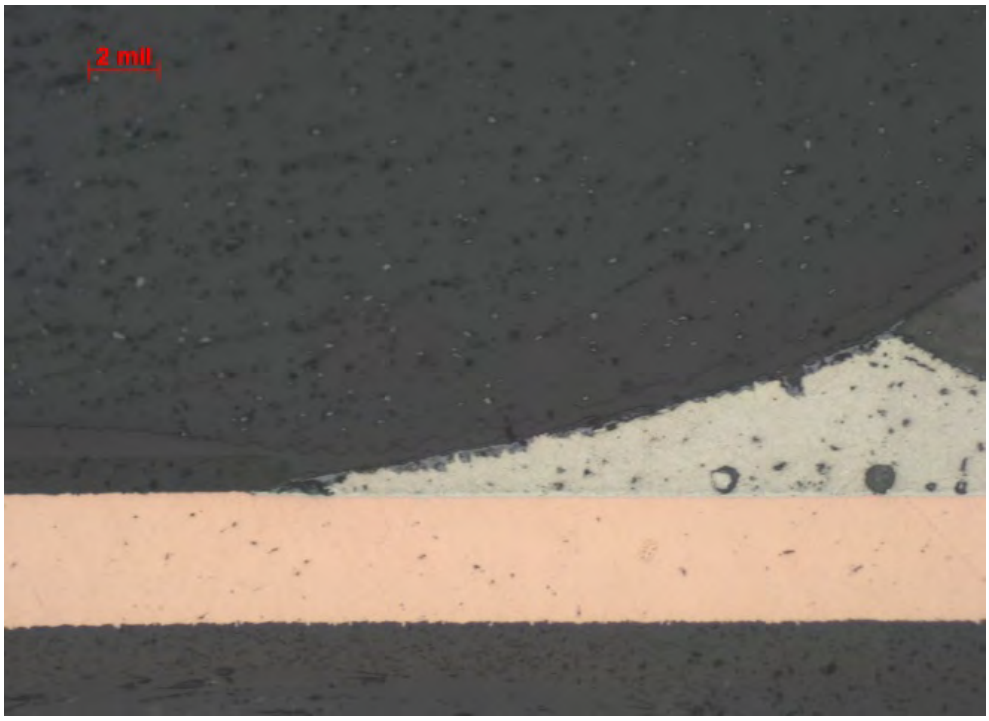


Figure 238: Optical cross-section image, filled PC18M+20%XP2742 QFP-A312, non-reworked U901, Lead 33 heel 1_200x.

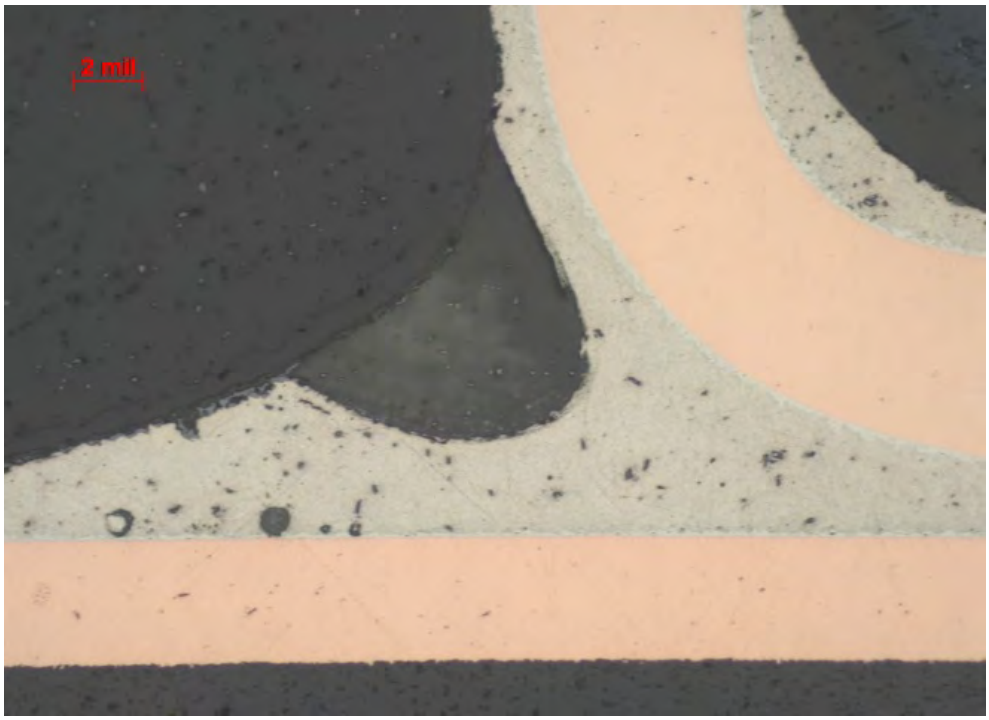


Figure 239: Optical cross-section image, filled PC18M+20%XP2742 QFP-A312, non-reworked U901, Lead 33 heel 2_200x,

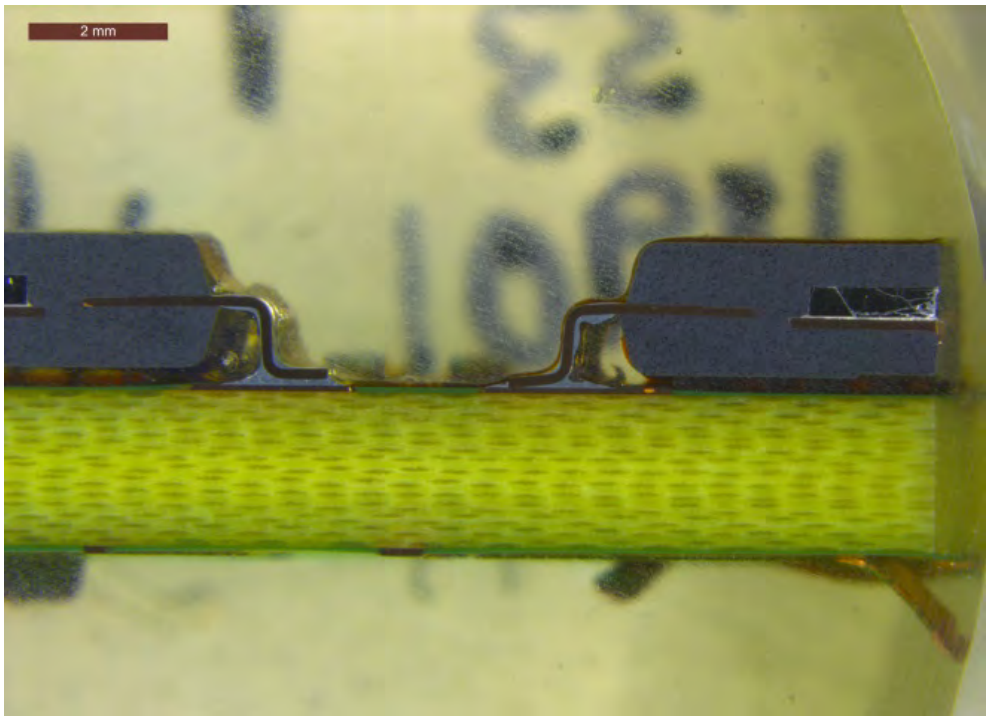


Figure 240: Optical cross-section image, filled PC18M+20%XP2742 QFP-A312, non-reworked U901, Overall 28 stereoscope non-inverted, 7.8x.

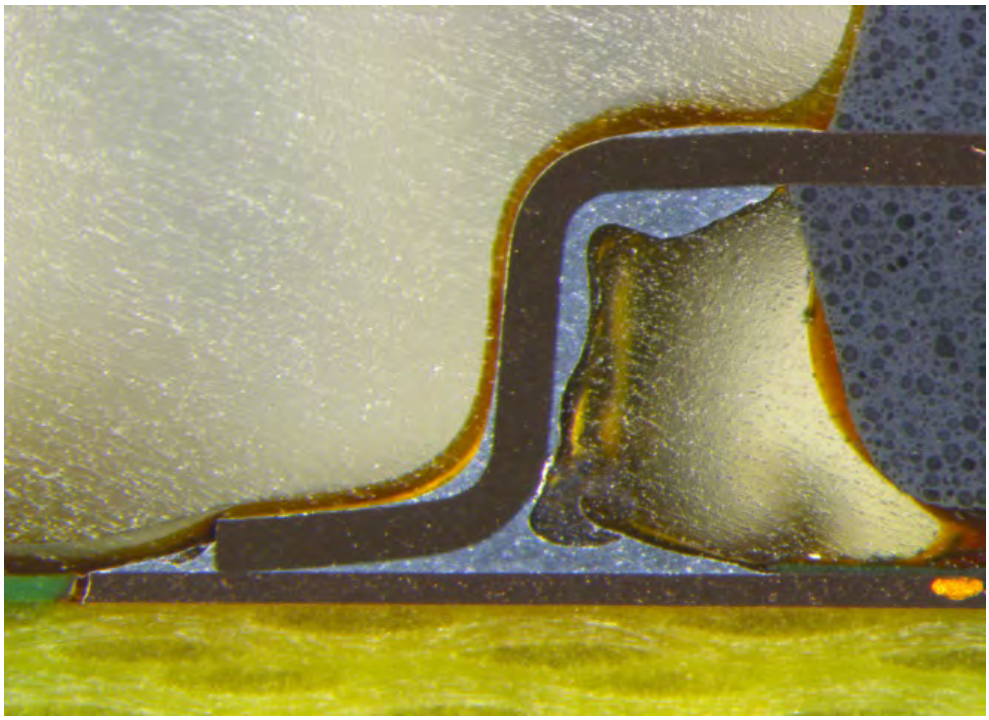


Figure 241: Optical cross-section image, filled PC18M+20%XP2742 QFP-A312, non-reworked U901, Lead 28 stereoscope non-inverted 40x.

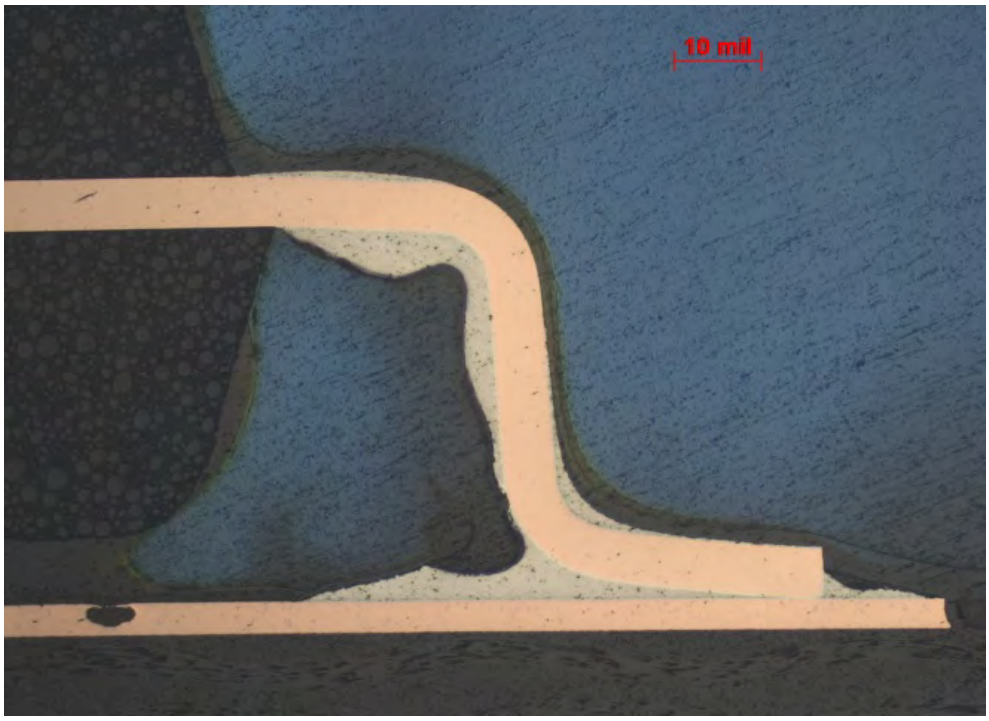


Figure 242: Optical cross-section image, filled PC18M+20%XP2742 QFP-A312, non-reworked U901, Lead 28, 50x.

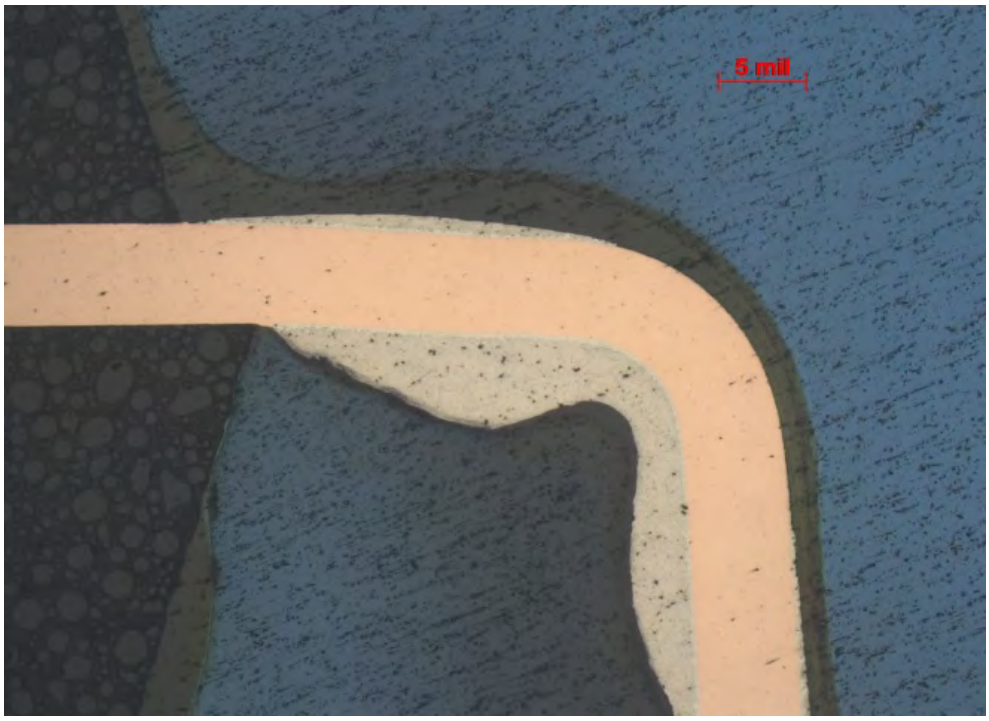


Figure 243: Optical cross-section image, filled PC18M+20%XP2742 QFP-A312, non-reworked U901, Lead 28 knee, 100x.

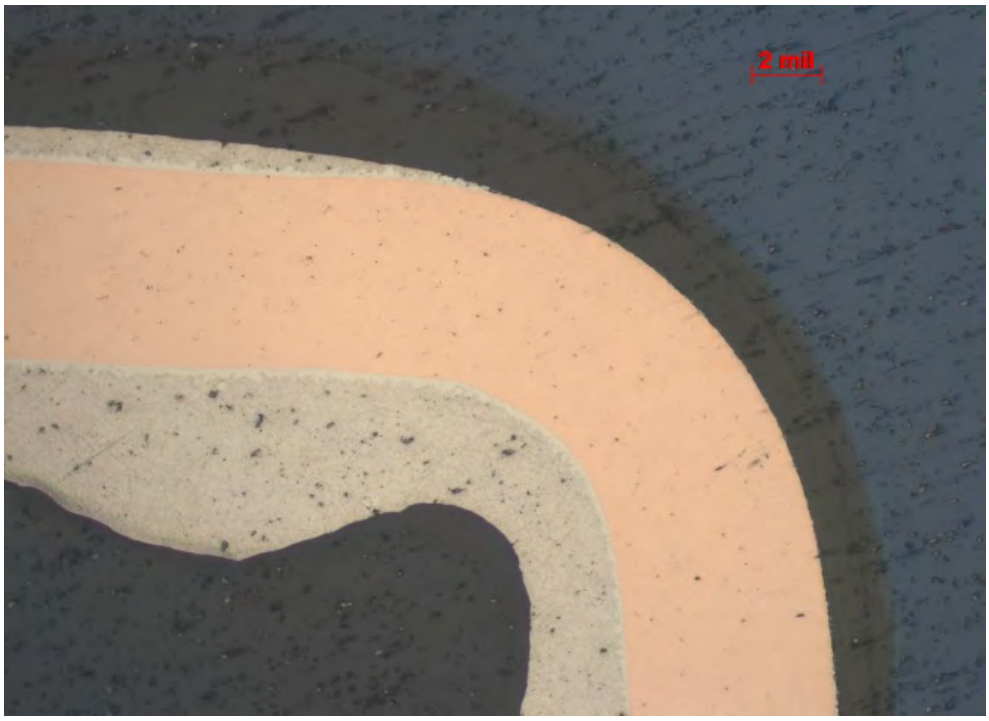


Figure 244: Optical cross-section image, filled PC18M+20%XP2742 QFP-A312, non-reworked U901, Lead 28 knee_200x.

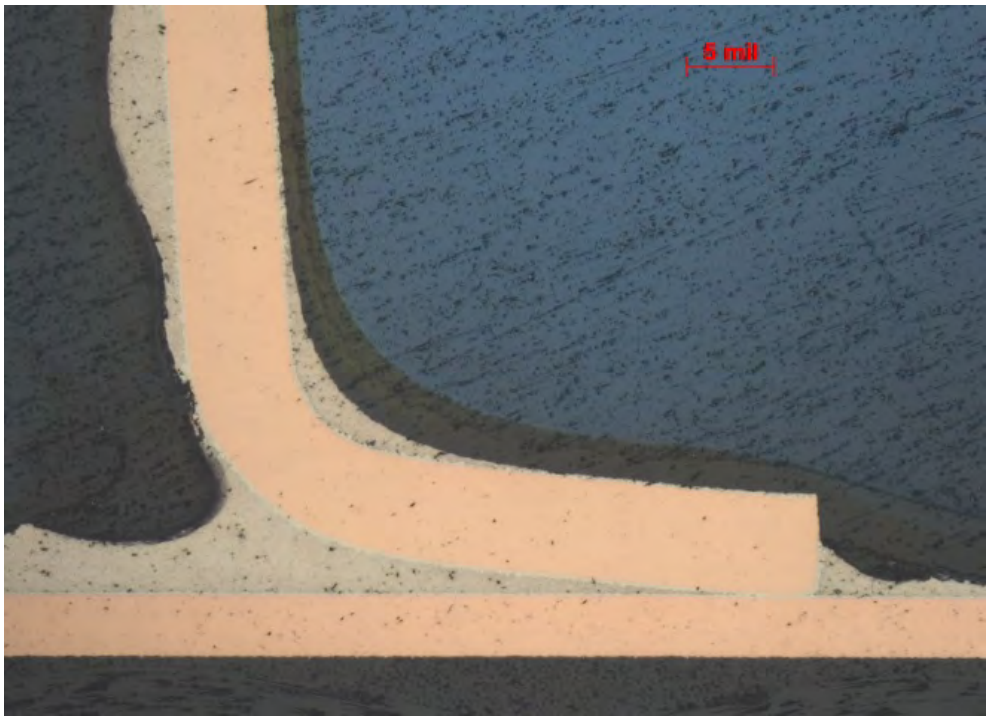


Figure 245: Optical cross-section image, filled PC18M+20%XP2742 QFP-A312, non-reworked U901, Lead 28 foot, 100x.

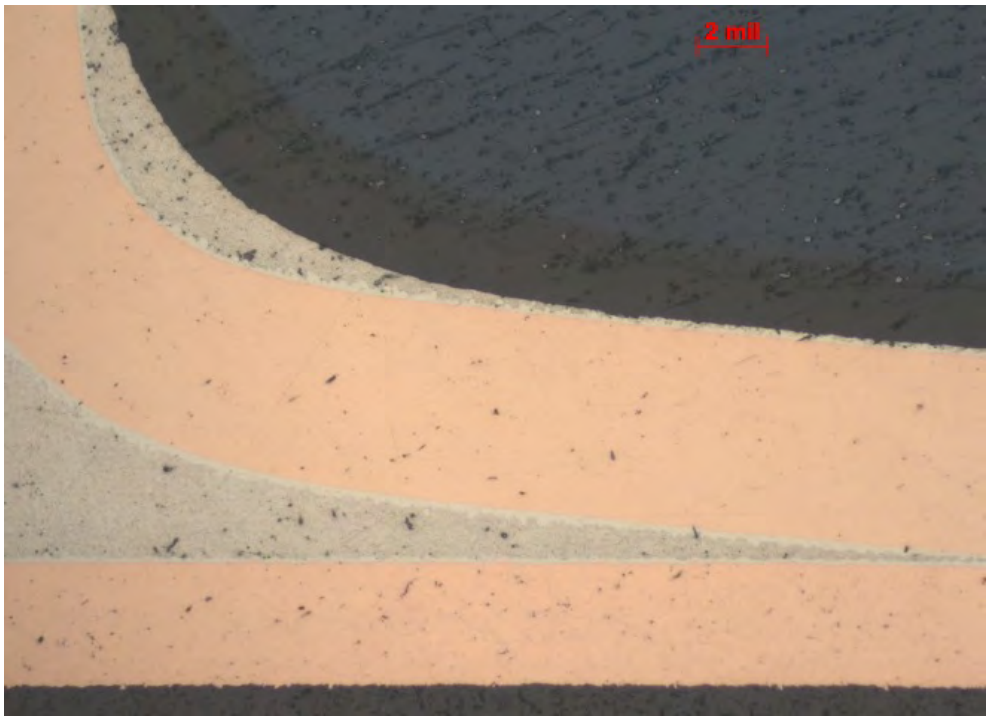


Figure 246: Optical cross-section image, filled PC18M+20%XP2742 QFP-A312, non-reworked U901, Lead 28 foot, 200x.

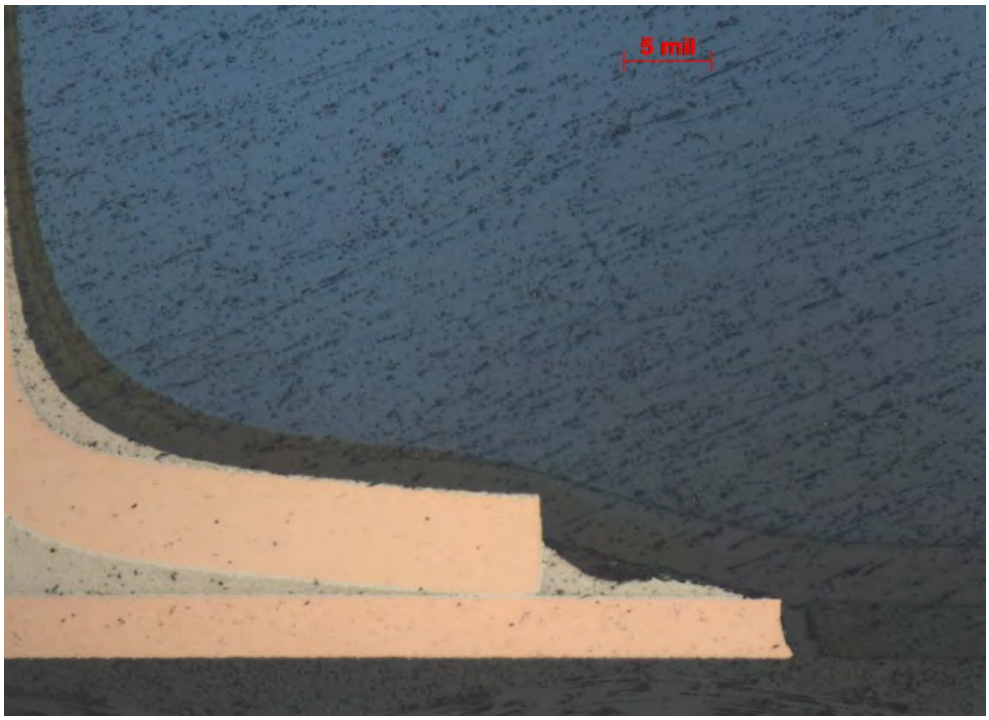


Figure 247: Optical cross-section image, filled PC18M+20%XP2742 QFP-A312, non-reworked U901, Lead 28 toe, 100x

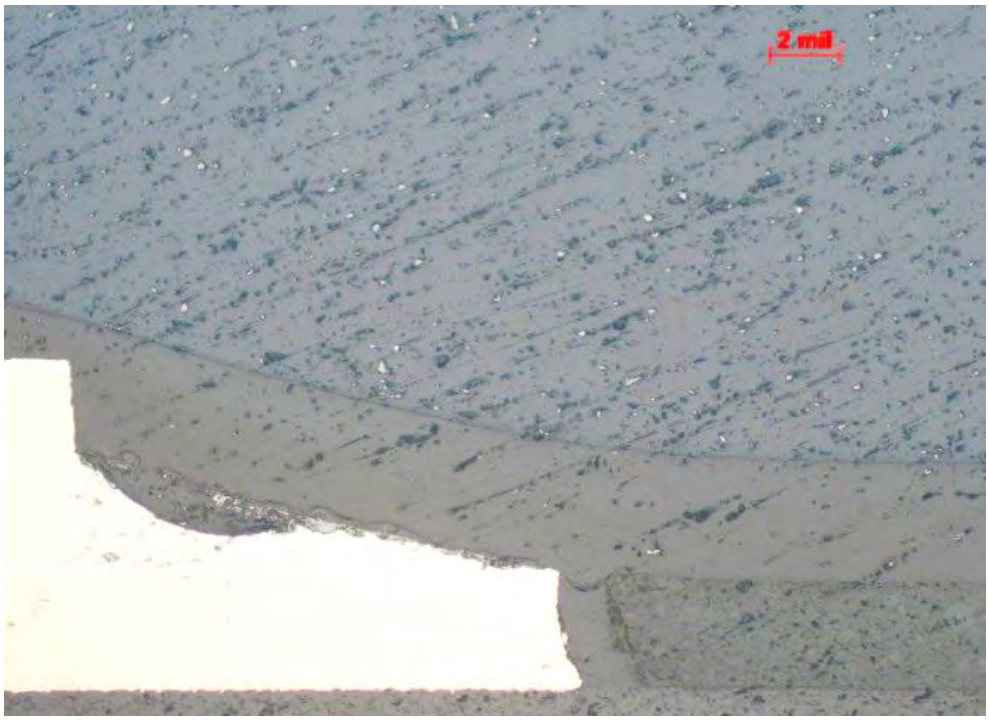


Figure 248: Optical cross-section image, filled PC18M+20%XP2742 QFP-A312, non-reworked U901, Lead 28 toe, 200x.



Figure 249: Optical cross-section image, filled PC18M+20%XP2742 QFP-A312, non-reworked U901, Lead 28 toe, 200x.

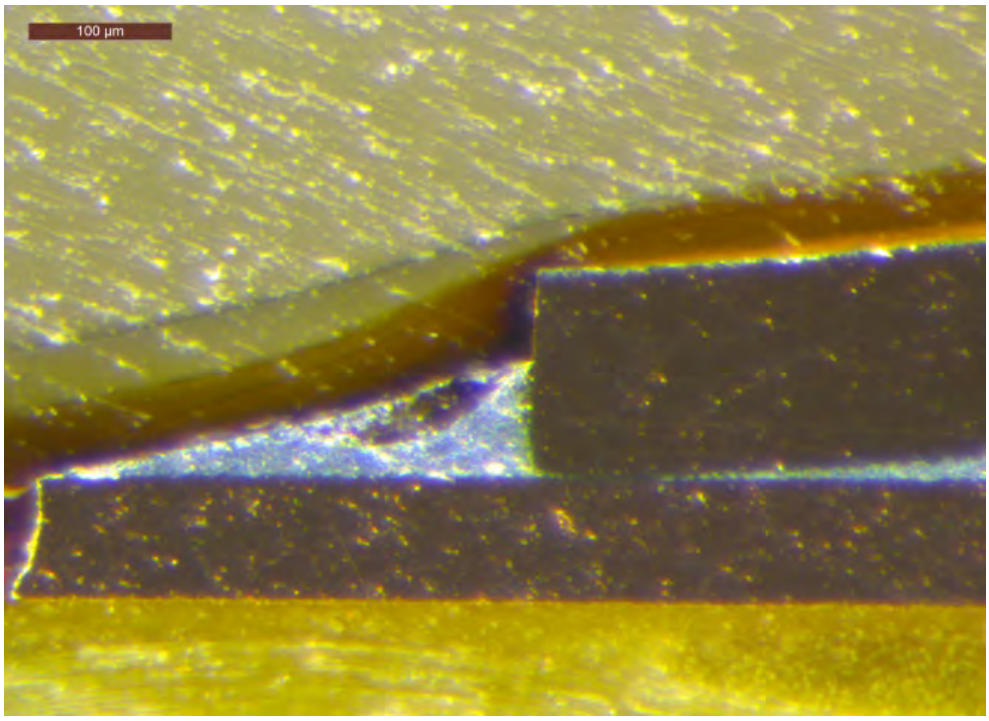


Figure 250: Optical cross-section image, filled PC18M+20%XP2742 QFP-A312, non-reworked U901, Lead 28 toe stereoscope non-inverted, 160x.

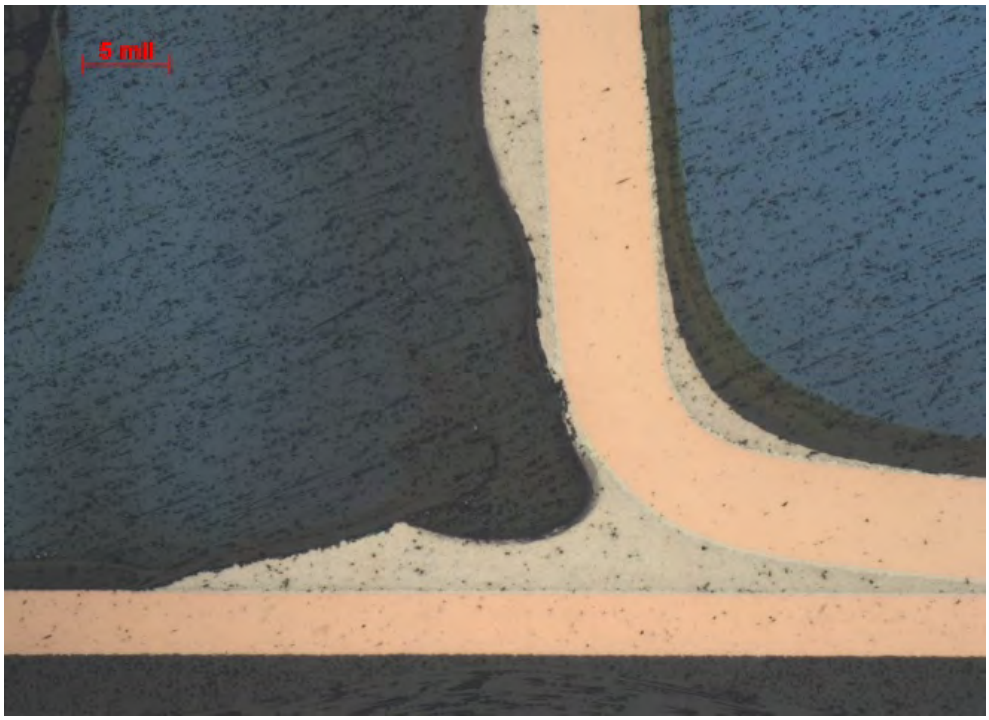


Figure 251: Optical cross-section image, filled PC18M+20%XP2742 QFP-A312, non-reworked U901, Lead 28 heel, 100x.

4.4.2.5 SEM cross-sections filled PC18M+20%XP2742 QFP-A312 non-reworked U901

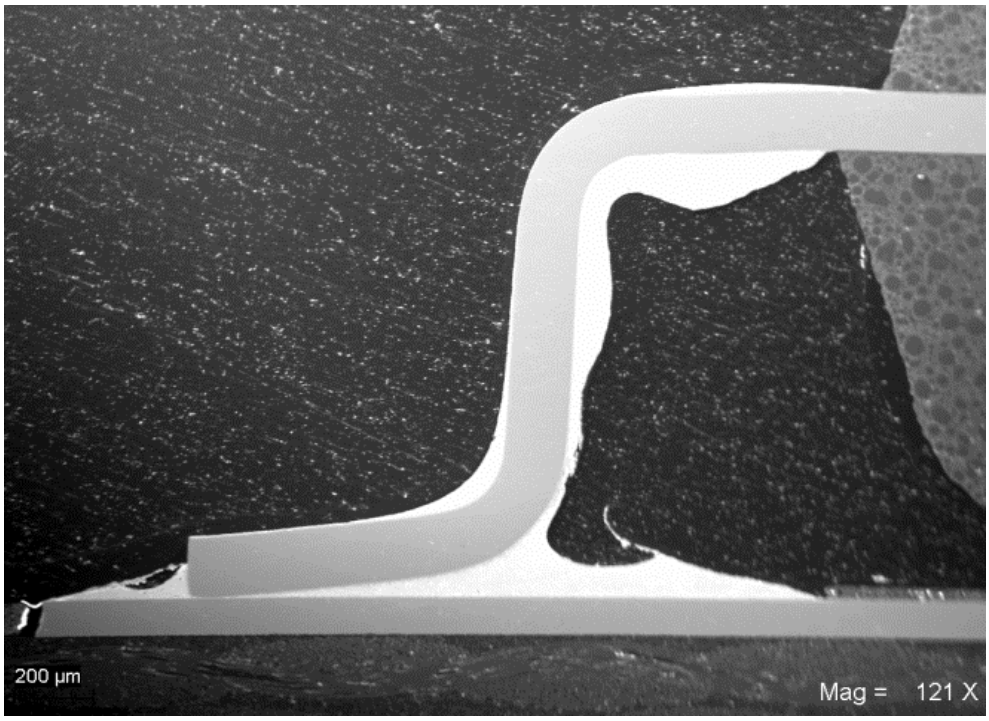


Figure 252: SEM cross-section image, filled PC18M+20%XP2742 QFP-A312, non-reworked U901, Lead 28, 121x.

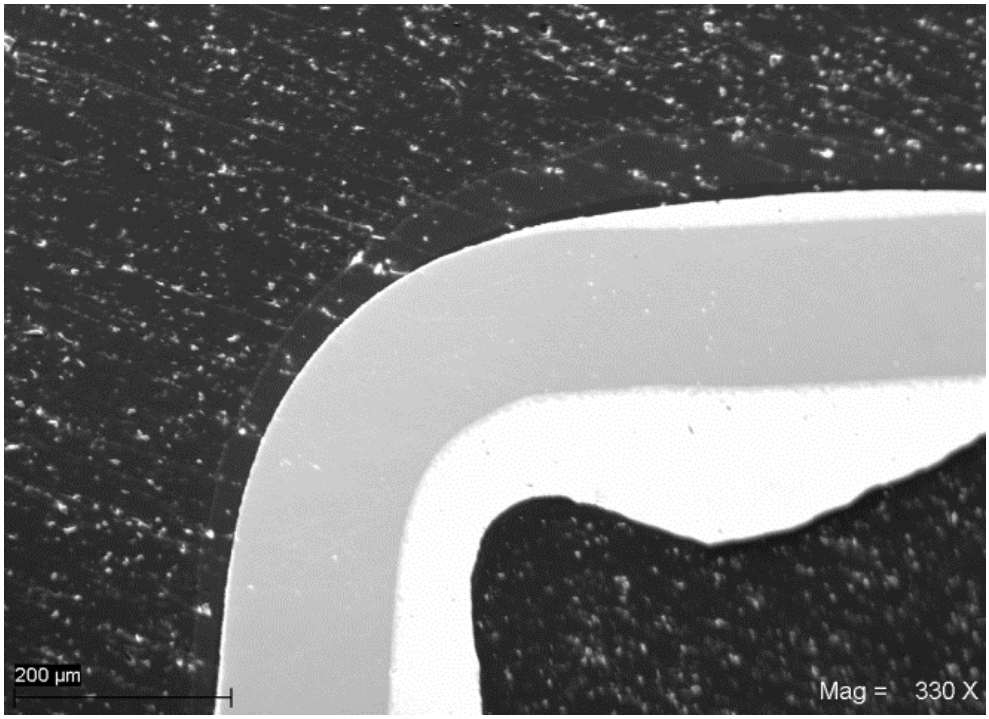


Figure 253: SEM cross-section image, filled PC18M+20%XP2742 QFP-A312, non-reworked U901, Lead 28 knee, 330x.

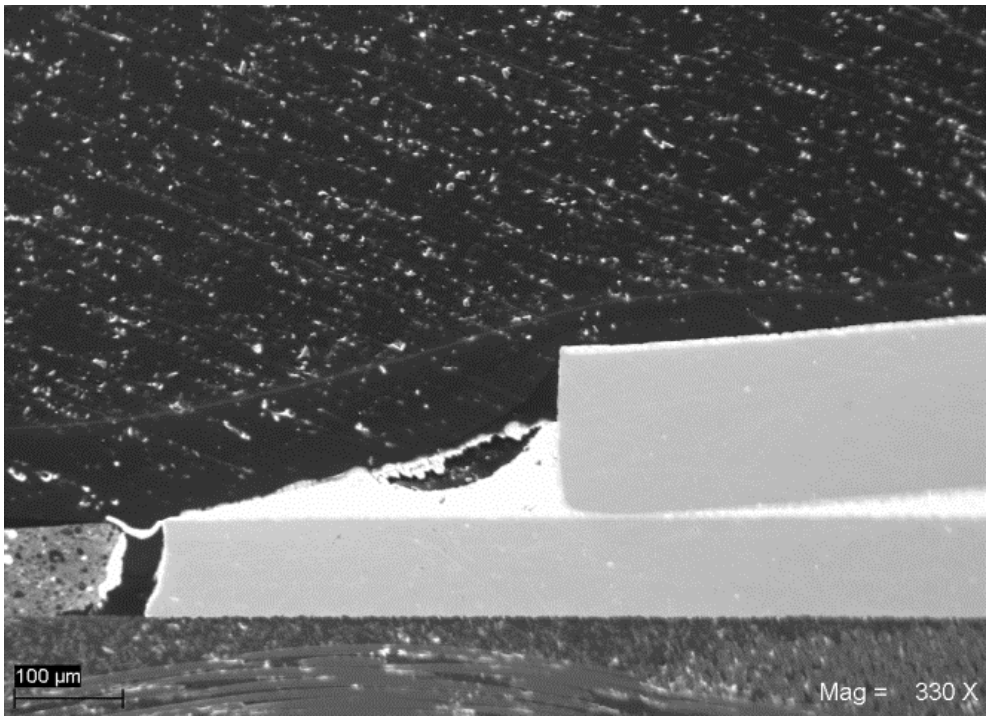


Figure 254: SEM cross-section image, filled PC18M+20%XP2742 QFP-A312, non-reworked U901, Lead 28 toe, 330x.

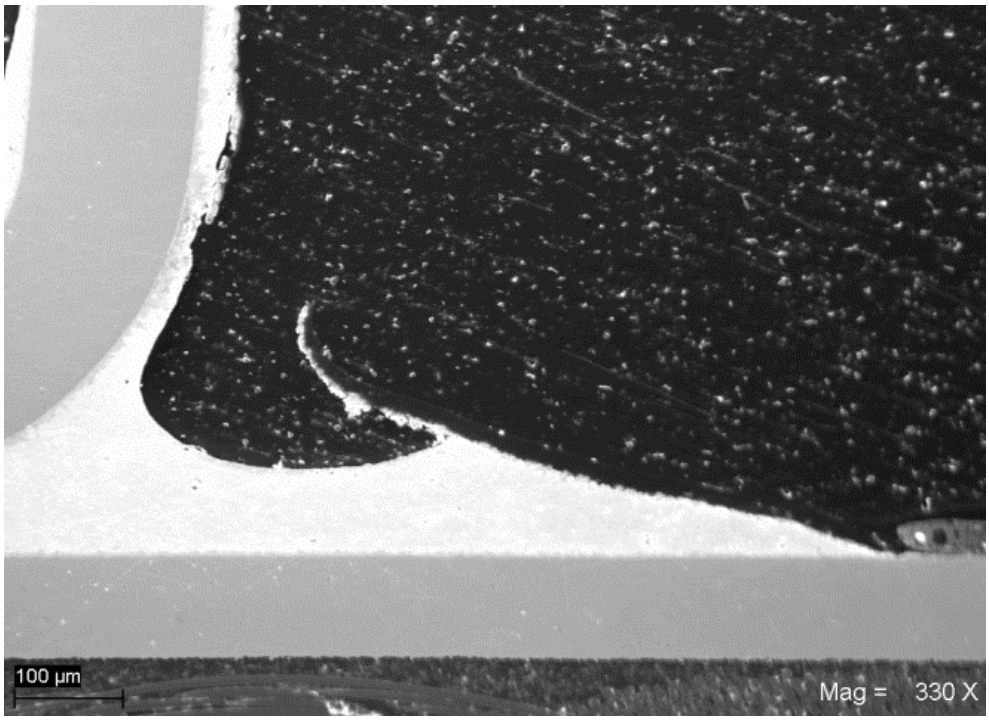


Figure 255: SEM cross-section image, filled PC18M+20%XP2742 QFP-A312, non-reworked U901, Lead 28 heel, 330x.

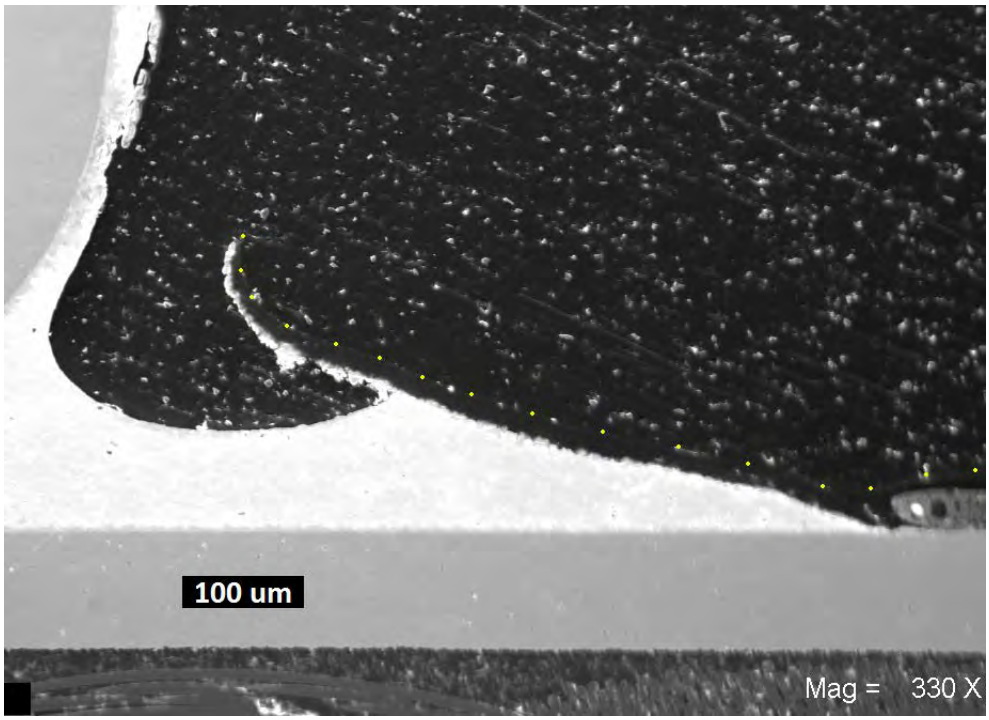


Figure 256: SEM cross-section image, filled PC18M+20%XP2742 QFP-A312, non-reworked U901, Lead 28 heel, zoom 330x. Solder has reflowed after coating. The coating surface is highlighted with yellow dots.

5. Rework summary

The newly developed nano-reinforced coatings were both removable by standard manufacturing methods, and localized re-coatings were successful using typical brush application process. Using the thermal removal and the media blaster removal method, the rework coating adhesion to both the solder and the adjacent old coating was acceptable.

6. Rework conclusion

The PC18M and newly developed nano-reinforced coatings were both removable by standard manufacturing methods, and localized re-coatings were successful using typical brush application process. Using the thermal removal and the media blaster removal method, the rework coating adhesion to both the solder and the adjacent old coating was acceptable. The viscosity of the brush coating needed to be reduced to reduce the reworked coating thickness and prevent cracking. Note also that the rework coating wet into the original rough layered coating surface indicating that the initial cause for the roughness was not poor wetting. The coating materials have the basic adhesion characteristics for a successful rework, but further work is needed to refine the method.

7. Literature cited

[1] Appendix G in this report; Coupon whisker testing for baseline coating process

[2] SERDP: Re-Coating of Reworked Test Boards" by Dave Edwards, Dec. 15, 2015.

[3] Appendix K of this report, Assembly whisker testing for layered coating process

[4] IPC-TM-650 2.4.1.6 Adhesion; Polymer coating test method

[5] Prakash Kapadia, Adhesion Test Images, issued within Celestica on Feb. 9, 2017 and updated Feb. 21, 2017.

SERDP WP2213
Final Report
Appendix M: Coating tin whisker mitigation modeling

Appendix M: Table of Contents

1. Coating tin whisker mitigation modeling approach 1
1.1 Assumptions 1
1.2 Symbols and nomenclature 1
2. Analysis and modeling 2
2.1 Coating FEA to determine coating deflection 3
2.2 Classical deflection calculations 3
2.3 Energy release rate calculations to determine coating blistering 7
2.3.1 Deflection calculation 7
2.3.2 Volume change and energy calculation 8
2.3.3 Energy release rate calculation 9
3. Analysis results 10
3.1 Comparison of Classical and Finite-Element Deflection Calculations 10
3.2 Analysis results for coating rupture 11
3.3 Energy release rate calculation results 11
4. A simple experiment 12
4.1 Coating formulation 12
4.2 Cantilever beam whisker coupon 13
4.3 Whisker coupon environmental exposure and inspection results 13
5. Discussion 17
6. Summary 17
7. Conclusions 17
8. Literature cited 18

Appendix M: List of Figures

Figure 1: Schematic diagram of tin growth forming a dome in the coating. 1

Figure 2: Coating tensile data simplified model. 2

Figure 3: Finite element model (Diam. = 45 µm, Thick. = 7 µm shown). 3

Figure 4: Model boundary conditions. 3

Figure 5: Plastic hinge stress versus position. 4

Figure 6: Deflection versus pressure comparison of the elastic/perfectly plastic FEA and classical models for the pressure which yields the maximum tensile stress at maximum elongation.. 10

Figure 7: Deflection versus pressure comparison of the FEA and classical models for the pressure which yields the maximum tensile stress at maximum elongation. 10

Figure 8: Coating strength required versus coating thickness. 11

Figure 9: Energy release rate versus coating thickness. 12

Figure 10: Cantilever beam whisker coupon; (A) coated cantilever beam, and (B) cantilever beam installed in fixture (dimensions in mm). 13

Figure 11: Cantilever beam coupon SEM inspection of thin coating region, areas after 2,500 (500+2,000) hours 60°C/60%RH showing a tin nodule under thicker coating and tin eruptions through thin coating 14

Figure 12: Cantilever beam coupon longitudinal cross-section through thin coating region areas after 2,500 (500+2,000) hours 60°C/60%RH; (a) and (b) eruption through three micron coating, (c) cross-section region on sample, (d) nodule under seven micron coating and (e) nodule under 30 micron coating. 15

Figure 13: Second ion beam polish of seven micron nominal coating; (A) back scatter electron image, and (B) secondary electron image. Arrow shows separation between coating after 2,500 (500+2,000) hours 60°C/60%RH. 15

Figure 14: Cantilever beam coupon inspection after coating removal after 2,500 (500+2,000) hours 60°C/60%RH. 16

Appendix M: List of Tables

Table 1: Coating thickness and tin dome measurement summary. 15

Acronyms

Acronym	Definition
ANSYS	Mechanical finite element analysis tool for structural analysis
FEA	Finite Element Analysis
MPa	Mega Pascal unit of stress
SEM	Scanning Electron Microscope

1. Coating tin whisker mitigation modeling approach

The factors influencing tin nodule formation and/or tin nodule/whisker suppression under coating are not captured with a whisker buckling type of model. The development of a whisker or nodule under the coating causes pressure to be applied to the coating. The pressure application diameter could vary several orders of magnitude depending upon the type of tin growth. The diameter of a tin whisker can range from less than a micron to 20 microns. In the case of a nodule or an odd shaped eruption, the diameter can be on the order of 100 microns.

In this analysis, a combination of finite element, classical plate deflection, and adhesion models are used to examine the critical pressure that a tin nodule/whisker can exert on a coating before rupture or delamination occur (Figure 1).

Coating analysis was based on three approaches:

A. Non-linear finite element analysis (FEA) to calculate the deflection in the coating to determine if the coating will rupture
B. Classical non-linear (plastic hinge) analysis to determine the deflection in the coating for comparison to the previous approach
C. Classical analysis to determine the energy release rate to delaminate the coating to determine in the coating will blister

1.1 Assumptions

The following assumptions were used in the analysis:

- The pressure exerted as a tin whisker develops is equal to the yield strength of tin
- Membrane deflection under pressure is neglected in the energy release rate calculations because the thinner coatings typically affected by membrane behavior would likely rupture and therefore not be influenced by delamination
- The outer boundary of the disk used in the energy release calculation is fixed initially but then limited to a critical bending moment value defined by plastic hinge behavior
- Yielding for the plastic hinge is elastic/perfectly plastic

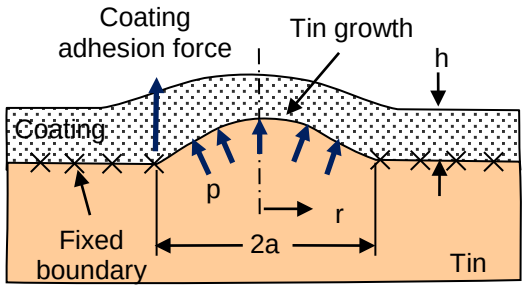


Figure 1: Schematic diagram of tin growth forming a dome in the coating.

1.2 Symbols and nomenclature

a = Outer radius of whisker/radius of applied pressure

r = Variable radius

E = Modulus of elasticity

ν = Poisson's ratio

h = Coating thickness

w = Deflection (subscripts described in text)

M_a, M_{crit} = Moment at radius a, critical plastic hinge moment

p = Pressure applied from whisker

p_{crit} = Critical whisker pressure

σ_r, σ_θ = Radial, circumferential stress

σ_1, σ_2, σ_3 = Principal stresses

σ_{vm} = Von Mises stress

σ_{crit} = Critical stress

τ_{rv} = Radial-vertical shear stress

K_s = Shear Stress effectiveness factor

K_m = Plastic hinge moment factor

G = Energy release rate, shear modulus (temporary variable)

2. Analysis and modeling

The analysis is based on applying pressure in a circular area to represent the nascent tin whisker in a method similar to that used by B.T. Han [1] using the yield strength of tin (11 MPa [2]) as the applied pressure. Coating data was based on measurements by Cho [3][4] simplified into a bilinear curve (see Figure 2). The numerical value of the elastic modulus for coating below the yield point was 500 MPa; the yield stress was taken as 34.5 MPa, and the tangent modulus as 7.29 MPa. The Poisson's ratio for the coating was estimated as 0.4999 based on the "rubbery" nature of the material and to attempt to maximize the indentation stiffness based on high measured hardness values.

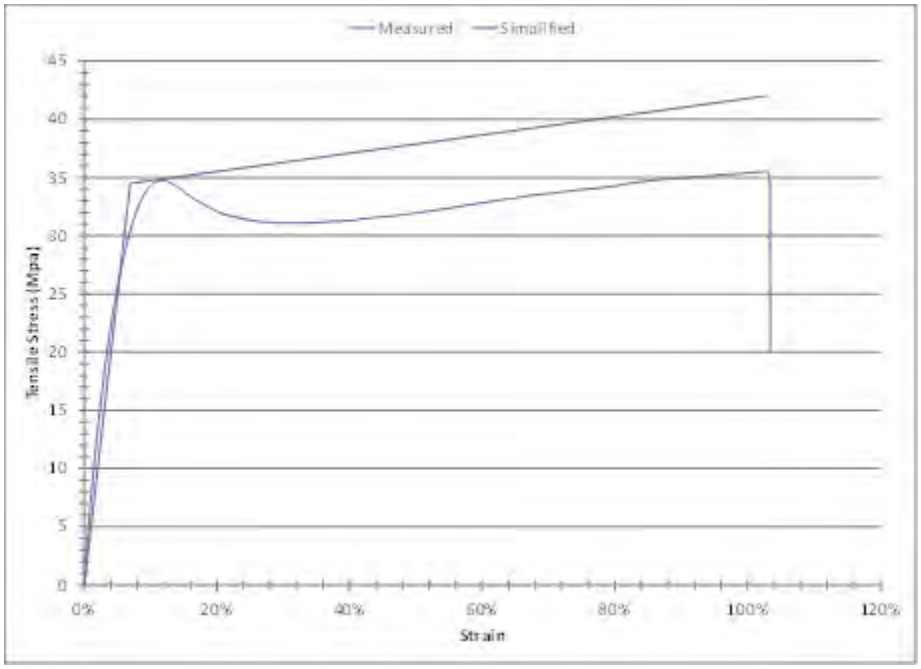


Figure 2: Coating tensile data simplified model.

2.1 Coating FEA to determine coating deflection

The coating was modeled using axisymmetric 8-node rectangular parabolic elements using approximately 30,713 nodes and 10,080 elements (see Figure 3). The actual node and element count varied based upon the specific geometry which was automatically generated based on dimensions using an ANSYS macro. Symmetry constraints were applied along the right boundary (centerline), the left boundary was fixed, and pressure was applied to the lower surface (red arrow) to represent the action of the tin "nodule/whisker" (see Figure 4). The initial analysis was conducted for nodule/whisker diameters of 15, 30, and 45 microns and coating thicknesses of three and seven microns. Because the coating properties were nonlinear, an iterative solution was required.

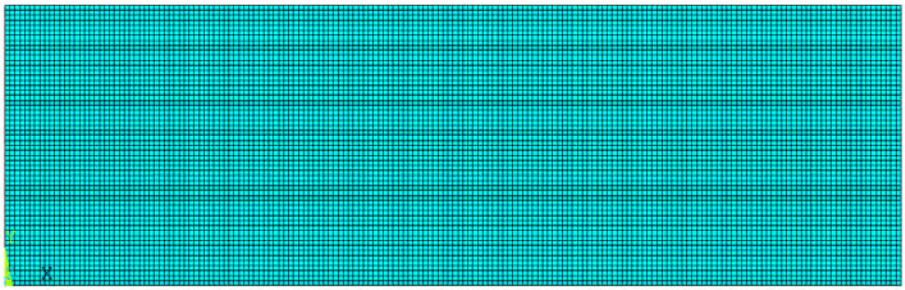


Figure 3: Finite element model (Diam. = 45 µm, Thick. = 7 µm shown).

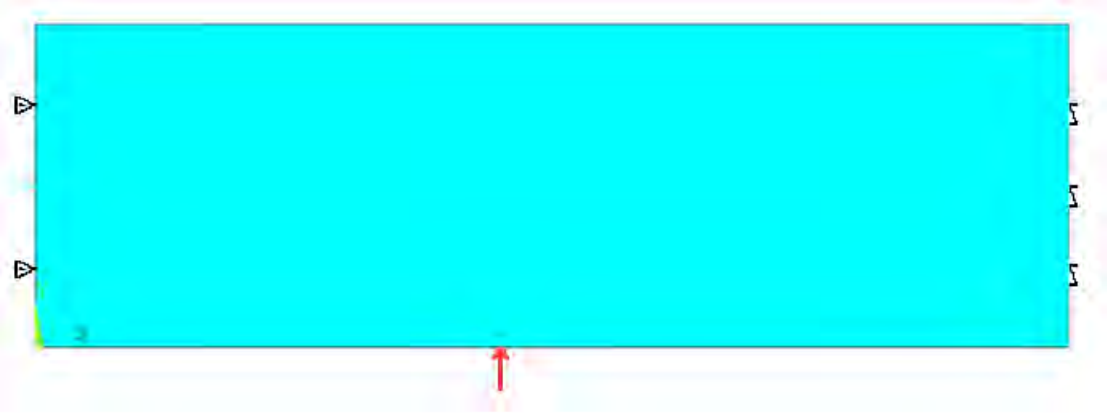


Figure 4: Model boundary conditions.

2.2 Classical deflection calculations

Coating deflection was determined analytically by considering the coating as an axisymmetric disk with both shear and bending deflection included. Bending deflection relationships included a bending moment applied along the outer edge to allow consideration of a plastic hinge. A plastic hinge is a consideration for beams in bending where the bending stress is considered to increase up to the yield stress and then remain constant at the yield stress, e.g. elastic-perfectly plastic (see Figure 5). Once the cross-section is fully yielded (half in compression and half in tension at yield stress), the beam is considered a plastic hinge allowing unlimited bending rotation at a critical moment. The critical moment for a rectangular cross-section is 1.5 times the moment where yielding begins.

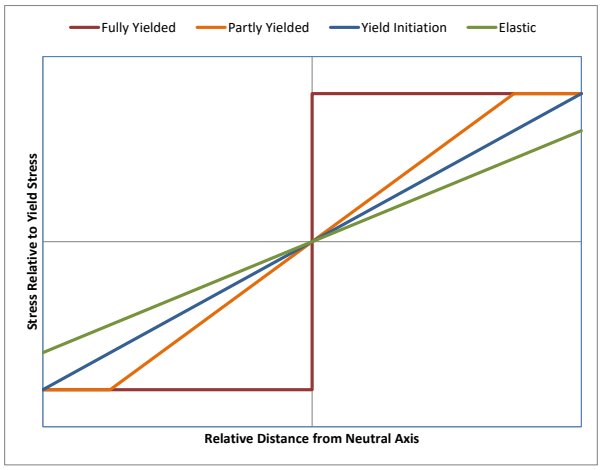


Figure 5: Plastic hinge stress versus position.

Bending deflection for a disk with uniform pressure and a variable edge moment is given by the following equations:

General Deflection due to bending:

$$w_b = \frac{\left(a^2 - r^2\right)\cdot\left[(\nu + 5)\cdot a^2 - r^2\cdot(\nu + 1)\right]}{64\cdot D\cdot(\nu + 1)}\cdot p + \frac{M_a\cdot\left(a^2 - r^2\right)}{2\cdot D\cdot(\nu + 1)}$$

Deflection at center (r = 0):

$$w_b = \frac{a^4\cdot(\nu + 5)}{64\cdot D\cdot(\nu + 1)}\cdot p + \frac{a^2 M_a}{2\cdot D\cdot(\nu + 1)}$$

Plate stiffness:

$$D = \frac{E\cdot h^3}{12\cdot\left(1 - \nu^2\right)}$$

Moment at edge for fixed edge (limited by plastic hinge):

$$M_a = -\frac{a^2\cdot p}{8}$$

The above equations correctly predict deflection for the simply supported case ($M_a = 0$) and the fixed edge case ($M_a = -a^2p/8$). When yielding occurs, the moment is limited by the plastic hinge effect described above. Although the bending deflection equations produce good results for thin disks of coating, thicker coatings require consideration of shear deflection as follows:

General deflection due to shear:

$$w_s = \frac{p\cdot\left(a^2 - r^2\right)}{4\cdot G\cdot h}$$

Deflection at center (r = 0):

$$w_s = \frac{a^2 \cdot p}{4 \cdot G \cdot h}$$

Shear modulus:

$$G = \frac{E}{2 \cdot (1 + \nu)}$$

It should be noted that the above shear deflection equations produce results 2/3 of the values given by Volterra and Gaines [5] this is because the reference used the peak shear stress (1.5 times average) in the cross-section to calculate deflection but better agreement with finite-element results is obtained by using the average shear stress. Stresses due to bending at the outside edge of disk are given by the following relationships:

Radial stress:

$$\sigma_r = \frac{6 \cdot M_a}{h^2}$$

Circumferential stress:

$$\sigma_\theta = \frac{\left[3 \cdot a^2 \cdot (1 - \nu)\right] \cdot p + 24 \cdot M_a}{4 \cdot h^2}$$

Initial attempts at plastic hinge calculations using the above equations compared well to finite-element results for thin coatings but showed considerable divergence for thicker coatings. Including shear stress given by the following equation improved agreement:

Radial-vertical shear stress:

$$\tau_{rv} = \frac{K_s \cdot a \cdot p}{2 \cdot h}$$

The K_s factor in the above equation is the shear stress effectiveness factor, and represents the effectiveness of shear in the Von Mises stress calculations. Theoretically the shear stress in a rectangular cross-section varies from zero at the top and bottom edges (where bending stress is highest) to 1.5 times average shear stress at the centerline. Although shear has no effect on the maximum Von Mises stress when yielding first occurs (because shear stress is zero, shear becomes important as the region of yielding moves toward the center of the cross-section. The specific value of K_s is empirically derived from the critical pressure determined by finite-element analysis. The shear stress is combined with the radial stress to determine the principal stresses, which are in turn used to determine the Von Mises stress as follows:

$$\sigma_1 = \frac{\sigma_r}{2} + \sqrt{\left(\frac{\sigma_r}{2}\right)^2 + \tau_{rv}^2}$$

$$\sigma_2 = \frac{\sigma_r}{2} - \sqrt{\left(\frac{\sigma_r}{2}\right)^2 + \tau_{rv}^2}$$

$$\sigma_3 = \sigma_\theta$$

$$\sigma_3 = \frac{\left[3 \cdot a^2 \cdot (1 - \nu)\right] \cdot p + 24 \cdot M_a}{4 \cdot h^2}$$

Substituting:

$$\sigma_3 = \frac{\left[3 \cdot a^2 \cdot (1 - \nu)\right] \cdot p + 24 \cdot M_a}{4 \cdot h^2}$$

$$\sigma_2 = \frac{3 \cdot M_a}{h^2} - \sqrt{\frac{K_s^2 \cdot a^2}{4 \cdot h^2} \cdot p^2 + \frac{9 \cdot M_a^2}{h^4}}$$

$$\sigma_3 = \frac{\left[3 \cdot a^2 \cdot (1 - \nu)\right] \cdot p + 24 \cdot M_a}{4 \cdot h^2}$$

Von Mises Stress:

$$2 \cdot \sigma_{vm}^2 = (\sigma_1 - \sigma_2)^2 + (\sigma_1 - \sigma_3)^2 + (\sigma_2 - \sigma_3)^2$$

Substituting:

$$2 \cdot \sigma_{vm}^2 = \left[\frac{3 \cdot \left(3 \cdot \nu^2 - 6 \cdot \nu + 3\right)}{8 \cdot h^4} \cdot a^4 + \frac{3 \cdot K_s^2}{2 \cdot h^2} \cdot a^2\right] \cdot p^2 - \frac{9 \cdot M_a \cdot a^2 \cdot (\nu - 1)}{h^4} \cdot p + \frac{72 \cdot M_a^2}{h^4}$$

Solving for M_a and using a critical stress for the Von Mises stress can derive a critical moment, which is used to establish the critical plastic hinge moment:

$$M_a = \left[\frac{a^2 \cdot (\nu - 1)}{16}\right] \cdot p - \frac{\sqrt{64 \cdot h^4 \cdot \sigma_{vm}^2 - p^2 \cdot \left[a^4 \cdot \left(27 \cdot \nu^2 - 54 \cdot \nu + 27\right) + 48 \cdot K_s^2 \cdot a^2 \cdot h^2\right]}}{48}$$

$$M_{crit} = K_m \cdot M_a$$

$$\sigma_{vm} = \sigma_{crit}$$

$$M_{crit} = K_m \cdot \left[\left[\frac{a^2 \cdot (\nu - 1)}{16} \right] \cdot p - \frac{\sqrt{64 \cdot h^4 \cdot \sigma_{crit}{}^2 - p^2 \cdot \left[a^4 \cdot \left(27 \cdot \nu^2 - 54 \cdot \nu + 27 \right) + 48 \cdot K_s{}^2 \cdot a^2 \cdot h^2 \right]}}{48} \right]$$

The K_m in the above equation represents the ratio between the plastic hinge moment and that at which yield initiates. Theoretically, for a rectangular cross section in pure bending with elastic-perfectly plastic material behavior this value is 1.5 but stress combinations and the specific stress-strain curve can cause some variation. The specific value of K_m is empirically derived from the deflection obtained by finite-element analysis. From the above equations, it can be seen that there is a critical pressure that results in an unstable (imaginary) result. This critical pressure is obtained by setting the relationship under the radical to zero and solving for pressure:

$$0 = 64 \cdot h^4 \cdot \sigma_{crit}{}^2 - p^2 \cdot \left[a^4 \cdot \left(27 \cdot \nu^2 - 54 \cdot \nu + 27 \right) + 48 \cdot K_s{}^2 \cdot a^2 \cdot h^2 \right]$$

$$p_{crit} = \frac{8 \cdot \sqrt{3} \cdot h^2 \cdot \sigma_{crit}}{3 \cdot a \cdot \sqrt{\left[9 \cdot (\nu - 1)^2 \right] \cdot a^2 + 16 \cdot K_s{}^2 \cdot h^2}}$$

2.3 Energy release rate calculations to determine coating blistering

Energy release rate was determined by using the following steps by modeling the coating as an axisymmetric model of a disk:

1. Calculate the deflection of the coating in terms of thickness, radius, pressure, and material properties considering bending, shear, and bulk compression (membrane deflection is neglected as described in the assumptions)
2. Use the calculated deflection to determine the change in volume of the front surface of the coating and the energy absorbed by the coating
3. Differentiate the energy with respect to radius and divide by circumference to determine the energy release rate

2.3.1 Deflection calculation

The bending deflection of a circular plate with radius=a fixed at the edge with a uniform pressure is given by [5]:

$$w = \frac{p \cdot a^4}{64 \cdot D} \cdot \left(\frac{r^4}{a^4} - 2 \cdot \frac{r^2}{a^2} + 1 \right)$$

$$w_{max} = \frac{a^4 \cdot p}{64 \cdot D}$$

The shear deflection for a similar plate is given by:

$$w = \frac{p \cdot h^2}{24 \cdot D} \cdot \frac{\left(a^2 - r^2\right)}{(1 - \nu)}$$

$$w_{max} = \frac{a^2 \cdot h^2 \cdot p}{24 \cdot D \cdot (1 - \nu)}$$

The total deflection is obtained by summing the individual deflections and expressing the plate stiffness (D) in terms of the elastic modulus (E):

$$D = \frac{E \cdot h^3}{12 \cdot \left(1 - \nu^2\right)}$$

$$w = \frac{3 \cdot p \cdot \left(a^2 - r^2\right) \cdot (1 + \nu)}{4 \cdot E \cdot h} + \frac{3 \cdot p \cdot \left(a^2 - r^2\right)^2 \cdot \left(1 - \nu^2\right)}{24 \cdot E \cdot h^3}$$

2.3.2 Volume change and energy calculation

The volume change of the surface of the coating is determined by integrating the deflection over the radius as follows:

$$\Delta V = 2 \cdot \pi \cdot \int_0^a \left[\frac{3 \cdot p \cdot \left(a^2 - r^2\right) \cdot (1 + \nu)}{4 \cdot E \cdot h} + \frac{3 \cdot p \cdot \left(a^2 - r^2\right)^2 \cdot \left(1 - \nu^2\right)}{24 \cdot E \cdot h^3} \right] \cdot r \, dr$$

$$\Delta V = \frac{\pi \cdot a^4 \cdot p \cdot (\nu + 1) \cdot \left(a^2 - a^2 \cdot \nu + 9 \cdot h^2\right)}{24 \cdot E \cdot h^3}$$

The coating energy is then calculated as follows:

$$U = \frac{p \cdot \Delta V}{2}$$

$$U = \frac{\pi \cdot a^4 \cdot p^2 \cdot (\nu + 1) \cdot \left(a^2 - a^2 \cdot \nu + 9 \cdot h^2\right)}{48 \cdot E \cdot h^3}$$

2.3.3 Energy release rate calculation

The energy release rate is determined by differentiating with respect to the radius of the applied pressure (a) and dividing by the circumference as follows:

$$G = \frac{\frac{d}{da}U}{2\cdot\pi\, a} = \frac{\frac{\pi\cdot a^3\cdot p^2\cdot(\nu+1)\cdot\left(a^2-a^2\cdot\nu+6\cdot h^2\right)}{8\cdot E\cdot h^3}}{2\cdot\pi\cdot a}$$

$$G = \frac{a^2\cdot p^2\cdot(\nu+1)\cdot\left(a^2-a^2\cdot\nu+6\cdot h^2\right)}{16\cdot E\cdot h^3}$$

3. Analysis results

3.1 Comparison of Classical and Finite-Element Deflection Calculations

Finite-element results were compared to the classical relationships described above for the coating thickness values and nodule diameters. Values of K_s and K_m were adjusted for best agreement on critical pressure and deflection respectively. These comparisons are plotted in Figure 6 and Figure 7.

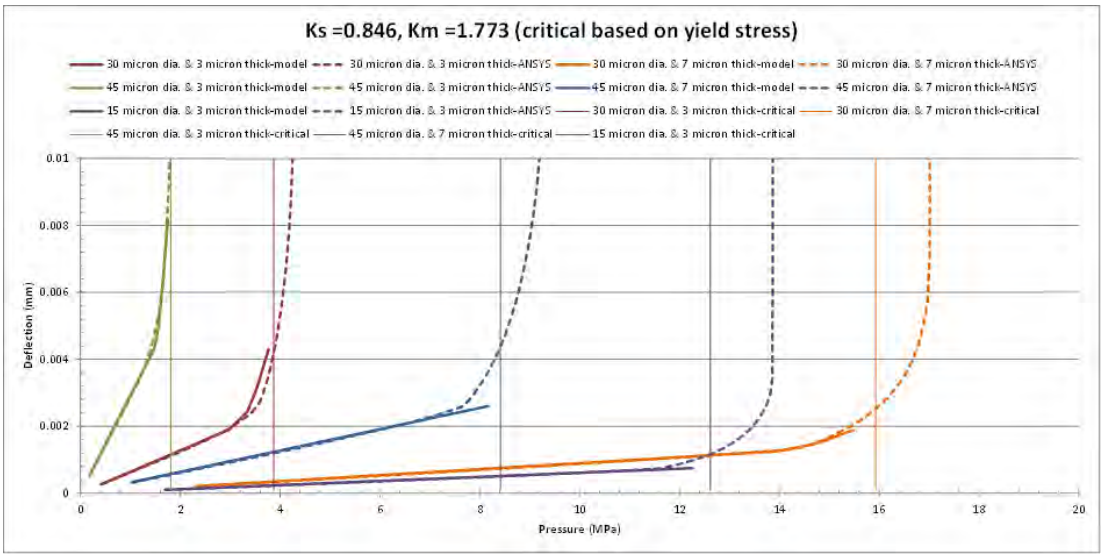


Figure 6: Deflection versus pressure comparison of the elastic/perfectly plastic FEA and classical models for the pressure which yields the maximum tensile stress at maximum elongation.

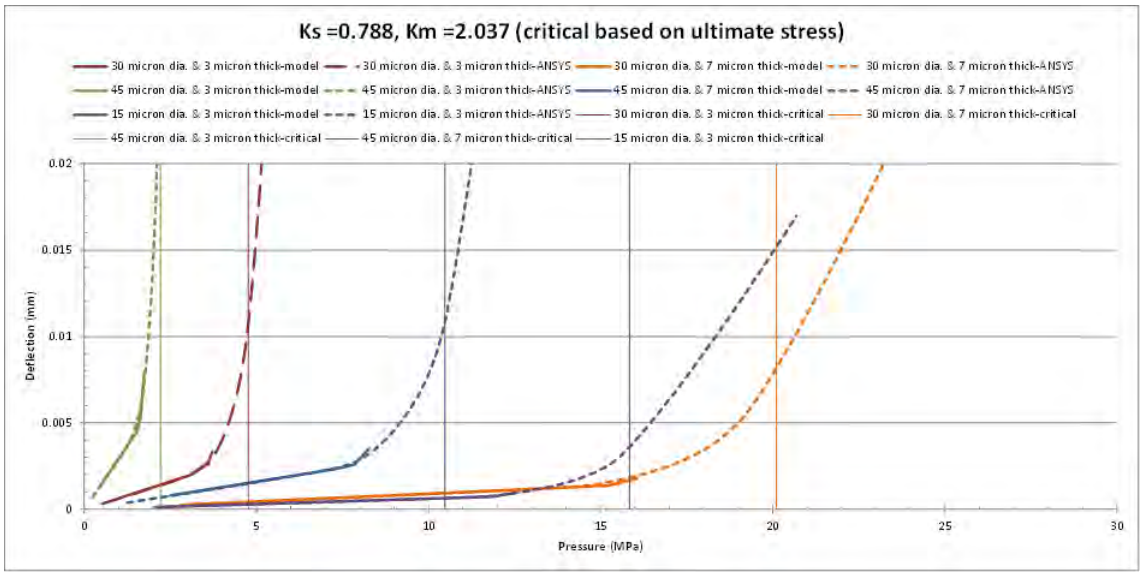


Figure 7: Deflection versus pressure comparison of the FEA and classical models for the pressure which yields the maximum tensile stress at maximum elongation.

3.2 Analysis results for coating rupture

From the plots in the previous section, it is clear that there is a critical pressure where the coating deflection becomes unstable as confirmed by both classical and FEA. Analysis was conducted by solving the critical pressure equation for the critical stress to determine the minimum coating strength required for seven nodule/whisker diameters (up to 120 microns) as a function of thickness (see Figure 8). Here it can be seen that for a rubbery ($\nu = 0.4999$) coating with a Ks value of 0.846 and a pressure of 11 MPa (tin yield strength [2]), the coating will not fail with a coating thickness greater than 5.5 micron and a strength greater than 34.5 MPa for nodules less than 30 microns in diameter. Tensile data for the current coatings under study is provided in [3][4].

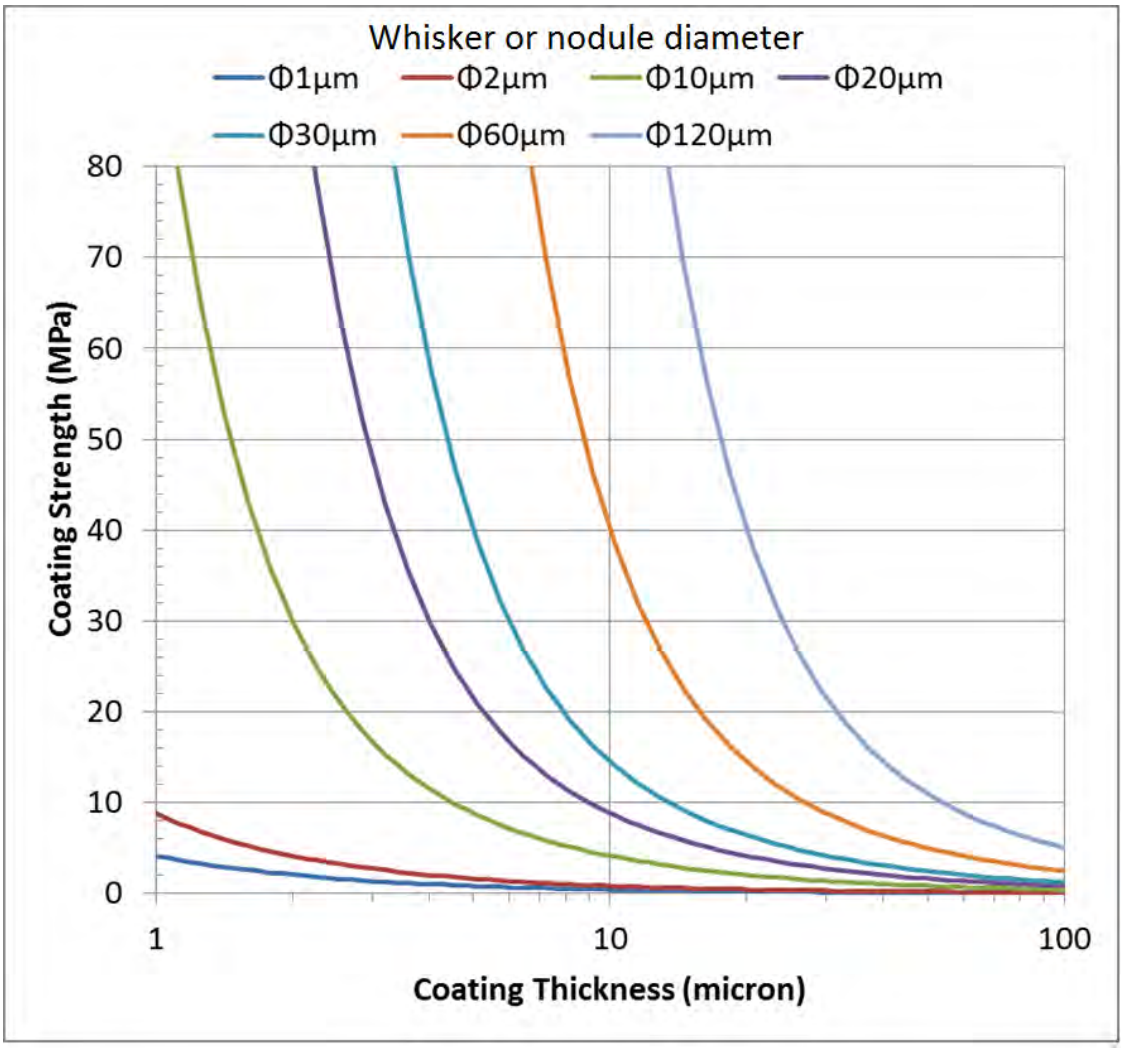


Figure 8: Coating strength required versus coating thickness.

3.3 Energy release rate calculation results

Similar to the coating rupture approach, the minimum energy release rate is calculated for the same five nodule diameters (up to 30 microns) as a function of thickness (see Figure 9). Here it can be seen that for a rubbery ($\nu = 0.4999$) coating with an elastic modulus of 500 MPa and a pressure of 11 MPa (tin yield strength), the coating will not delaminate with a coating thickness greater than 4.5 micron and the critical adhesion energy of polyurethane of 14-15 J/m^2 [6] for nodules less than 30 microns in diameter. The critical adhesion energy of the coatings being evaluated in the present work is provided in [3][6][7]. The

initial testing [6] indicated that the 14-15 J/m^2 critical adhesion energy is a lower limit since during testing the interface between the epoxy and the polyurethane failed before the polyurethane to tin interface. Additional testing using plasma etch and improved epoxy material yielded a critical interfacial energy of 57.8 J/m^2 for the PC18M polyurethane [7]. It was also noted that using plasma etch and a silane treatment the critical interfacial energy increased to 22.4 J/m^2 for the PC40-UMF polyurethane acrylate.

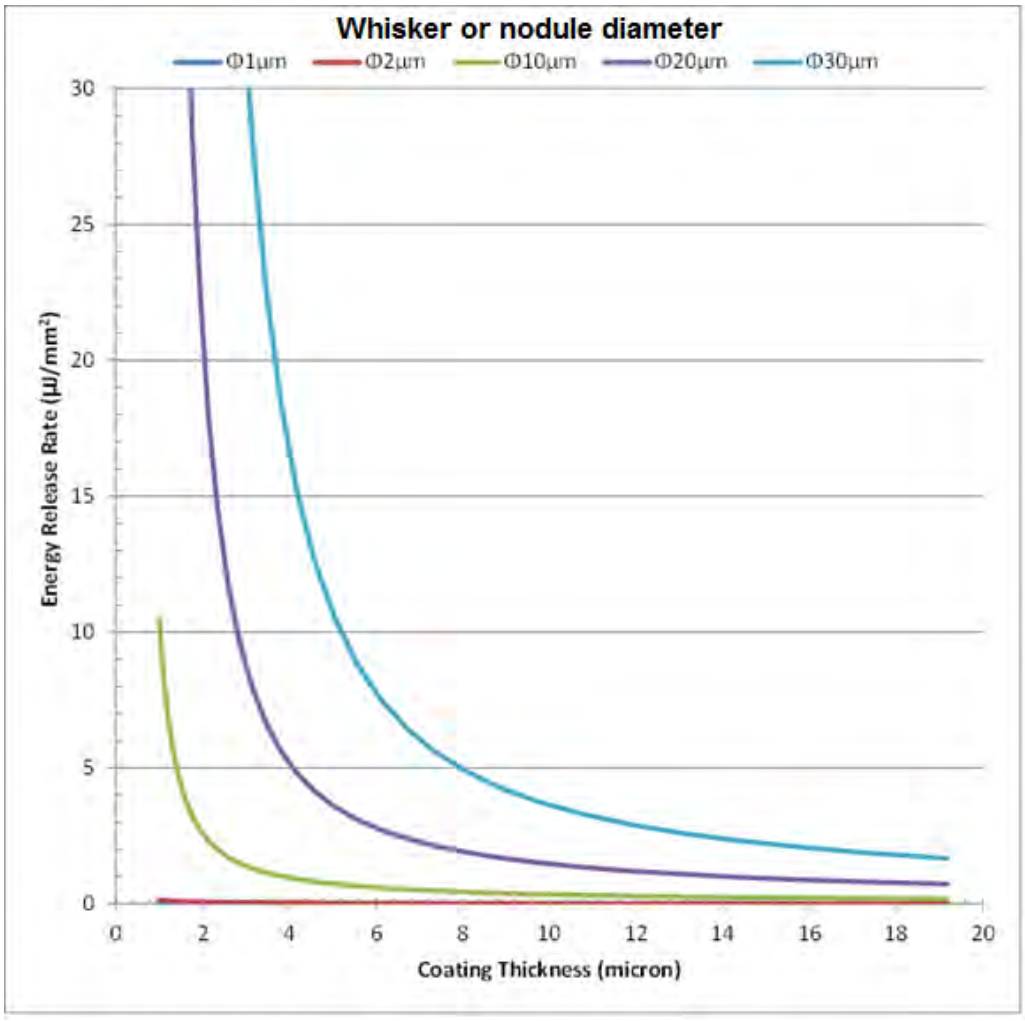


Figure 9: Energy release rate versus coating thickness.

4. A simple experiment

One of the first whisker growth experiments was the coated cantilever beam coupon. The results are presented in Appendix G [9] and key points pertinent to the modeling are presented next.

4.1 Coating formulation

This whisker coupon work used the PC18M+30%XP2742 (9.75wt% nanosilica) coating because it had the highest elastic modulus and tensile strength of the initial compositions tested [3][4]. Subsequent properties testing on the PC18M+20%XP2742 showed that it had a more optimal balance between strength and consistent elongation. The PC18M+20%XP2742 (6.74wt% nanosilica) was eventually used for the assembly coverage and whisker testing [3].

4.2 Cantilever beam whisker coupon

The cantilever beam coupon used bright tin plating over C110 alloy copper (see Figure 10). The plating was specified to be five to eight microns thick. The coupons were solvent cleaned and then draw coated with PC18M+30%XP2742 using shims and a doctor blade to obtain a final nominal thickness of 100 microns. After liquid coating application, the samples were air dried for a minimum of 30-45 minutes and then cured for a minimum of two hours at 60 ºC in an oven having a minimum relative humidity of 30 percent in accordance with the PC18M datasheet. After coating air drying, the tape was removed along two long edges of the coupon exposing uncoated tin plating. The coating was 100 microns thick in the center of sample and thinned to less than three microns near the internal beam edges.

The coupons were then installed in an aluminum fixture that clamped one end and raised the other end. The 0.38 mm free end displacement resulted in a bending preload of 11.4 MPa near the clamp.

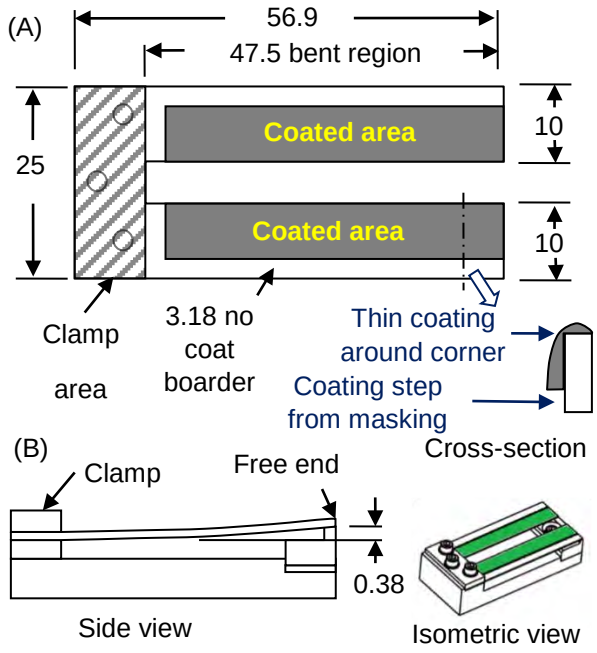


Figure 10: Cantilever beam whisker coupon; (A) coated cantilever beam, and (B) cantilever beam installed in fixture (dimensions in mm).

4.3 Whisker coupon environmental exposure and inspection results

Optical inspection up to 100x, scanning electron microscope (SEM) inspection up to 2,000x and metallurgical cross-sectioning methods were used to evaluate the sample.

The coated coupon was initially placed in 60°C/60%RH for 500 hours and inspected. There were small whiskers and nodules on the non-coated areas and no whiskers or nodules under the coating. The sample was returned to the humidity environment for a total of 2,500 hours (500+2,000 hours).

Where the coating was thin (~three microns), odd shaped eruptions broke through the coating; and when the coating was a little thicker (~seven to 30 microns), there was evidence of nodule formation under the coating (see Figure 11). The cross-sections verified that the nodules were tin dome-like structures. The tin dome diameter was smaller when the coating was thinner (Figure 12). The curvature change between the flat tin surface and the beginning of the nodule is an area that is susceptible to delamination (Figure 13).

A summary of coating thicknesses and the tin dome diameter and height are given in Table 1.

The coating was removed on the cantilever beam sample with Uresolve™ solvent. The evaluation was performed on the cantilever arm opposite the one that was cross – sectioned. Under the 100 micron thick coating, very few if any tin nodules were observed (Figure 14). The occasional nodule occurrence may be indicative of poor coating adhesion sites.

These experimental results were consistent with the modeling.

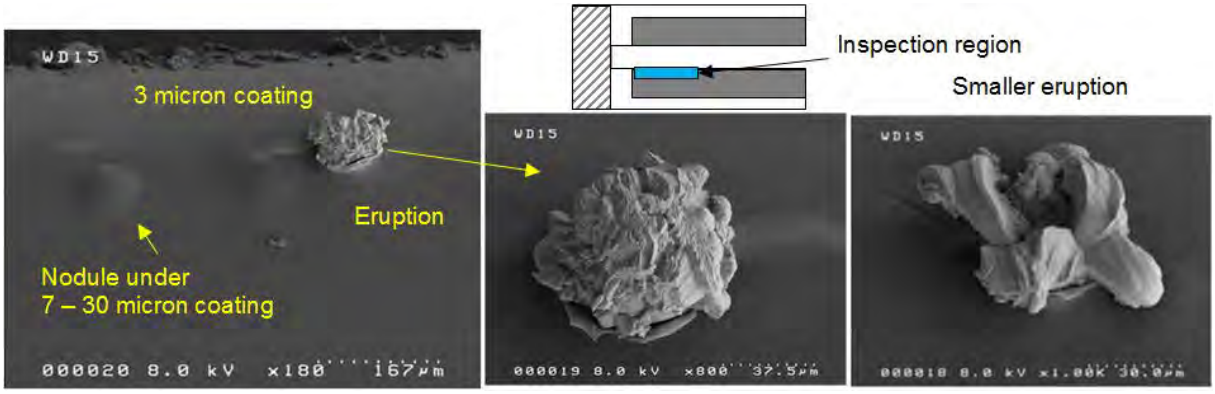


Figure 11: Cantilever beam coupon SEM inspection of thin coating region, areas after 2,500 (500+2,000) hours 60°C/60%RH showing a tin nodule under thicker coating and tin eruptions through thin coating.

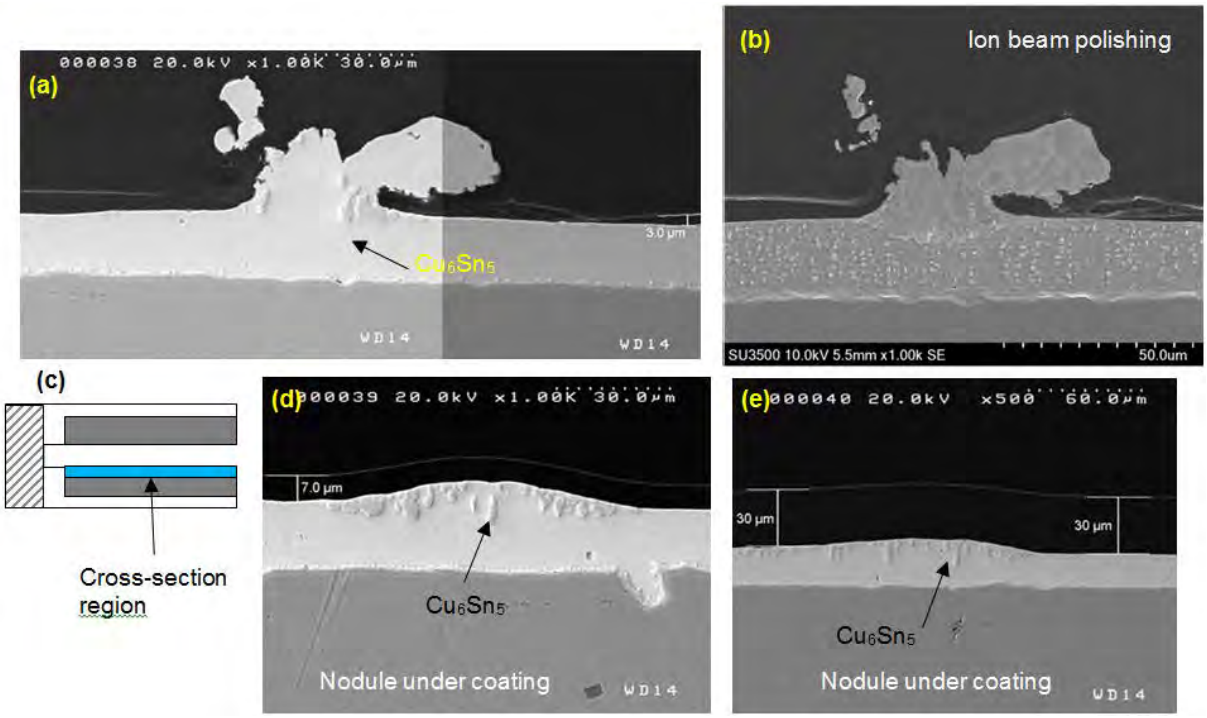


Figure 12: Cantilever beam coupon longitudinal cross-section through thin coating region areas after 2,500 (500+2,000) hours 60°C/60%RH; (a) and (b) eruption through three micron coating, (c) cross-section region on sample, (d) nodule under seven micron coating and (e) nodule under 30 micron coating.

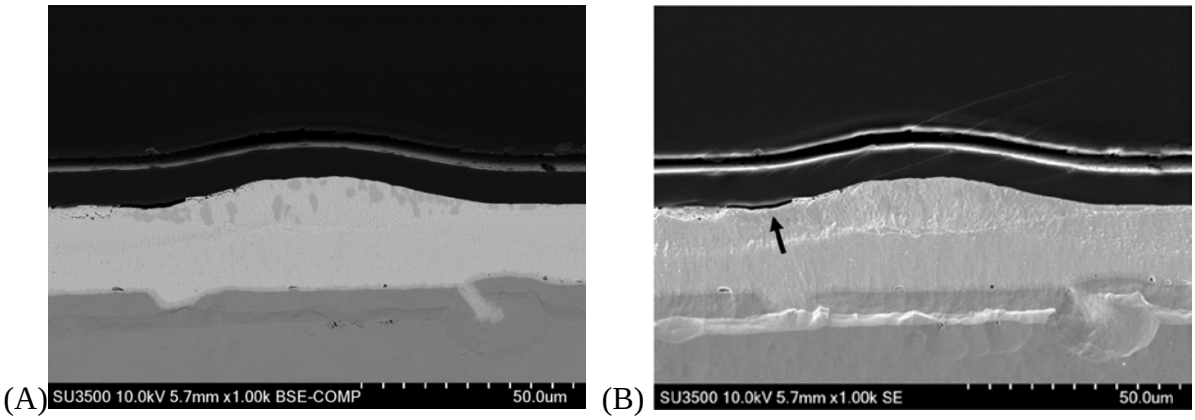


Figure 13: Second ion beam polish of seven micron nominal coating; (A) back scatter electron image, and (B) secondary electron image. Arrow shows separation between coating after 2,500 (500+2,000) hours 60°C/60%RH.

Table 1: Coating thickness and tin dome measurement summary.

Nominal coating thickness	Average coating thickness in flat region (microns)	Minimum coating thickness at top of dome (microns)	Dome diameter (microns)	Dome height (microns)
3 um	3.4	Ruptured	51.6	Ruptured

7 um	8.2	7.1	79.5	6.8
30 um	30.2	28.5	118.5	5.7

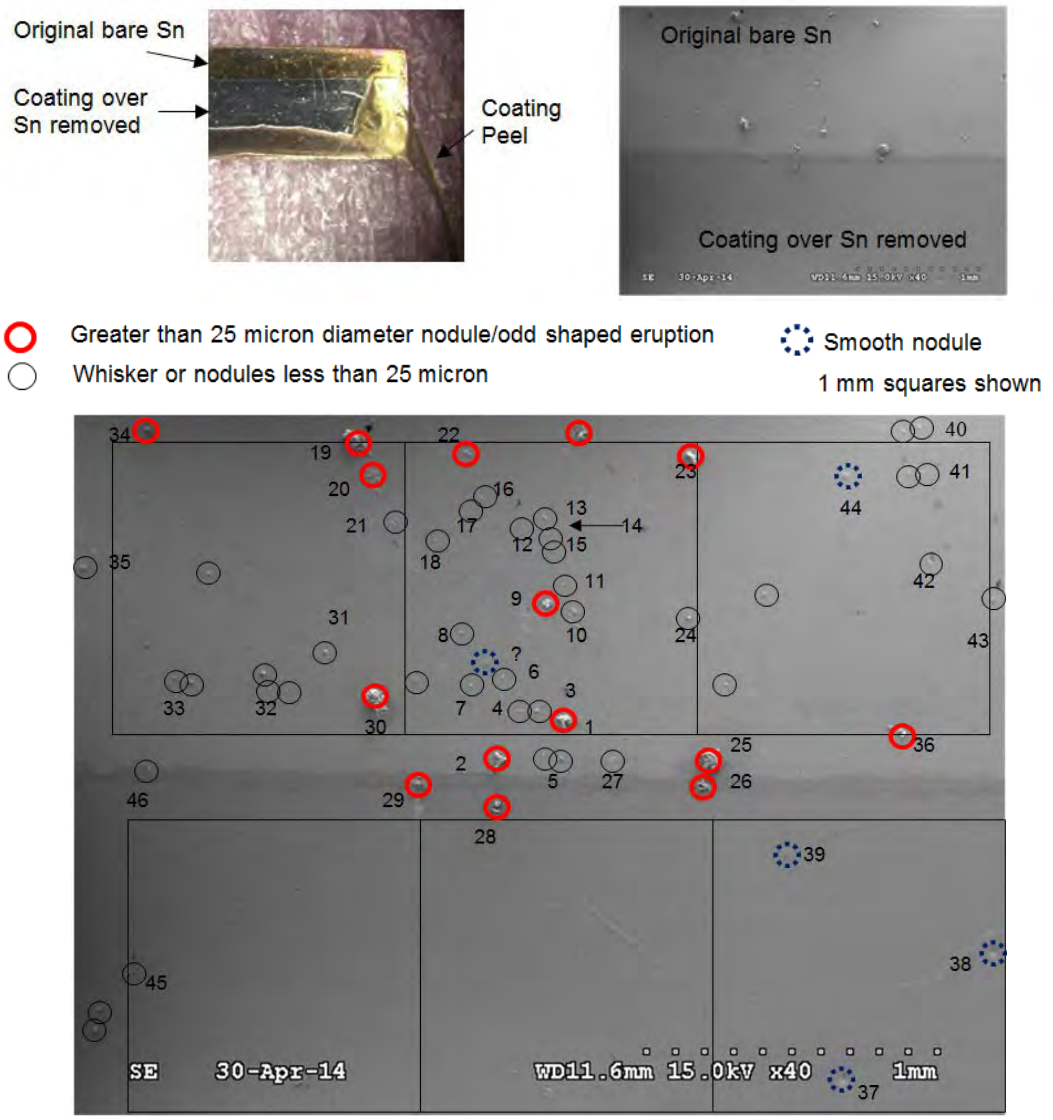


Figure 14: Cantilever beam coupon inspection after coating removal after 2,500 (500+2,000) hours 60°C/60%RH.

5. Discussion

The evaluation of coating mitigation for whisker growth is complex and often requires many years of effort [8] to [15]. In the present work, the relationship between coating rupture and coating thickness for various whisker/nodule diameters, coating strength, and coating adhesion for a high modulus coating was evaluated.

The ability of the thicker coating regions to resist whisker penetration was not unexpected. However, the model predicted what the experiment showed; when the coating is thin enough to be deformed by a tin dome, the tin dome diameter increased when the coating thickness increased.

As was discussed in Appendix G, the lack of nodule growth, e.g. infinite nodule diameter, observed under the PC18M+30%XP2742 is in contrast to whisker/nodule growth under the softer Arathane ™ 5750 tested by NASA [13]. It is reasonable that the presence of a more rigid coating on the tin surface could inhibit whisker nucleation, since whisker growth is a surface stress relaxation phenomenon.

6. Summary

The modeling showed reasonable correlation with the experimental whisker coupon results. The FEA modeling predicted rupture of a three micron thick coating which was consistent with the rigid coating experimental observations.

If the nodule/whisker diameter was larger, the coating needed to be thicker and/or stronger to provide mitigation. From a practical perspective, after coating rupture, whiskers could grow from the uncoated tin nodule at the rupture site. Furthermore, during high humidity or corrosive environments, further coating delamination due to corrosion, corrosion induced whisker growth and/or electrical leakage may occur at the rupture site.

Just a word of caution when it comes to conformal coating electronic assemblies: care must be used when applying coating because depending upon the coating hardness and thickness, while mitigating whisker growth, it can negatively impact the solder joint thermal cycling reliability if not implemented properly [16][17].

7. Conclusions

The following conclusions can be made

- There is a combination of coating thickness, strength, and adhesion that can provide whisker mitigation
- In contrast to smaller diameter whiskers, larger diameter tin nodule formations have greater potential to rupture the coating
- The whisker growth surface stress relaxation phenomena causing formation of the tin filament structure is altered in the presence of a coating having high adhesion, high strength, and sufficient thickness
- Although rigid coatings can inhibit tin nodule/whisker formation they need to be evaluated for potential impacts to solder joint thermal cycling fatigue reliability

8. Literature cited

[1] B.T. Han, C. Jang, K. Mahan, S. Han, M. Osterman, Long Term Reliability Evaluation of Conformal Coatings for Tin Whisker Failure Mitigation, University of Maryland, 2010.

[2] matweb.com; “Tin, Sn”

[3] Appendix D of this report, Coating Characterization Results.

[4] J. Cho, S. Meschter, S. Maganty, D. Starkey, M. Gomez, D. Edwards, A. Ekin, K. Elsken, J. Keeping, P. Snugovsky, J. Kennedy, and M. Romansky, Polyurethane Conformal Coatings Filled with Hard Nanoparticles for Tin Whisker Mitigation, SMTA International Conference on Soldering and Reliability, Toronto, Ontario, Canada, May 13-15, 2014.

[5] E. Volterra, and J, Gaines, Advanced Strength of Materials; Prentice Hall, 1971

[6] M. Roma, S. Maganty, R. Roeder, J. Cho, S. Meschter,“Evaluation of Interfacial Adhesion of Polyurethane Conformal Coatings Used for Tin Whisker Mitigation”, Materials Science and Technology 2014 Conference and Exhibition, October 12-16, 2014, Pittsburgh, PA.

[7] F. Dong, S. Meschter, J. Cho, Study of Tin Whisker Growth under Polyurethane Based Conformal Coatings, Materials Science and Technology 2017 Conference and Exhibition, Oct. 8 – 12, 2017, Pittsburg, PA.

[8] J. Cho, S. Meschter, S. Maganty, D. Starkey, M. Gomez, D. Edwards, A. Ekin, K. Elsken, J. Keeping, P. Snugovsky, and J. Kennedy, Characterization of Hybrid Conformal Coatings used for Mitigating Tin Whisker Growth, SMTA International Conference on Soldering and Reliability, Toronto, Ontario, Canada, May 14-17, 2013.

[9] Appendix G of this report, Coupon whisker testing for baseline coating process.

[10] D. Hillman, Tin Whiskers Inorganic Coating Evaluation, 7th International Symposium on Tin Whiskers, Nov. 12-13, 2013, Costa Mesa, CA.

[11] L. Woody and W. Fox, Tin Whisker Risk Management by Conformal Coating, SMT magazine, July 2014, pp. 40-58.

[12] T. Woodrow, E. Ledbury, Evaluation of Conformal Coatings as a Tin Whisker Mitigation Strategy, Part 2, Proceedings of the SMTA International Conference, September 24-28, 2006.

[13] J. Kadesch, H. Leidecker, Effects of Conformal Coat on Tin Whisker Growth, Proceedings of IMAPS Nordic, The 37th IMAPS Nordic Annual Conference, pp. 108-116, September, 10-13, 2000

[14] L. Panashchenko, J. Brusse and H. Leidecker, Long Term Investigation of Urethane Conformal Coating Against Tin Whisker Growth Tenting of 2mil conformal coating, IPC Tin Whisker Conference Dec. 7, 2010.

[15] S. Meschter, J. Cho, S. Maganty, D. Starkey, M. Gomez, D. Edwards, A. Ekin, K. Elsken, J. Keeping, P. Snugovsky, and J. Kennedy, Nanoparticle Enhanced Conformal Coating for Whisker Mitigation, SMTA International, Sept/Oct 2014

[16] G. Caswell, C. Tulkoff and N. Blattau, The Effect of Coating and Potting on the Reliability of QFN Devices, DFR Solutions

[17] J. Wilcox, M. Meilunas and M. Anselm., Harsh Environment Reliability and Conformal Coat, SMTAi 2015

WP2213
Final Report
Appendix N: Simulated power cycling thermal cycling (PCTC)

Appendix N: Table of Contents

1. PCTC Background 1

1.1 PCTC Test overview 1

1.2 Sample preparation 1

1.3 Coating thickness 2

1.3.1 Coating process development screening experiment 3

1.3.2 Whisker test assembly coating thickness 9

1.4 Whisker inspection results at 1,797 prior to starting the 6,000 PCTC cycle test 28

1.5 Metallurgical observations at 1,797 PCTC cycles 29

1.6 Coating inspection at 1,797 PCTC cycles 32

2. Test vehicles, environmental exposure and inspection methods for 6,000 PCTC test 38

2.1 Test vehicles and environmental exposure 38

2.2 Inspection method 38

3. Results after 6,000 PCTC cycles 40

3.1 Whisker statistics for 6,000 PCTC cycle samples 40

3.2 Metallurgical observations for uncoated 6,000 PCTC samples 50

3.3 Coating integrity and whisker mitigation results for 6,000 PCTC cycle test 74

4. PCTC Discussion 86

4.1 Whisker statistics discussion 86

4.2 Metallurgical observations discussion for uncoated 6,000 PCTC samples 87

4.3 Coating integrity and whisker mitigation discussion for 6,000 PCTC cycle test 92

5. Conclusions for the 6,000 PCTC cycle test 96

6. Literature cited 97

Appendix N: List of Figures

Figure 1: Typical contamination regions on intentionally contaminated (SOT6 shown). 1

Figure 2: Cross-section planes used for coating thickness measurement. 3

Figure 3: Coating measurement locations used for process development. 4

Figure 4: Screening experiment left and right lead coating thicknesses for the following combinations of viscosity and spray passes: (A) 250 cps UV40 1x-1y and 2x-2y spray passes and (B) 100 cps UV40-100 3x-3y and 6x-6y spray passes. 5

Figure 5: Screening experiment average, maximum and minimum UV40 coating thicknesses for the four UV40 coating variations comparison of 250 cps and 100 cps coatings. The following combinations of viscosity and spray passes are presented: 250 cps UV40 1x-1y and 2x-2y spray passes and 100 cps UV40-100 3x-3y and 6x-6y spray passes. Graph (A) shows average thickness, (B) maximum thickness, and (C) minimum thickness. 6

Figure 6: Optical image of a cross-section showing the typical coating measurements of a flat unencumbered area of the board. The three measurements from left to right are 60.4 microns (2.38 mils), 65.5 microns (2.58 mils) and 62.5 microns (2.46 mils). 7

Figure 7: Typical coating screening experiment high magnification SEM cross – section images for thickness measurement (location B sample 11 shown). 7

Figure 8: Typical coating screening experiment high magnification SEM cross – section image showing thin coating and separation (location T sample 14 shown) 8

Figure 9: Typical coating screening experiment high magnification SEM cross – section image showing coating thickness behind the lead (location G sample 5 shown); (A) SEM image showing the solder and (B) SEM image with increased brightness and contrast showing coating. 8

Figure 10: Typical coating screening experiment high magnification SEM cross – section image showing a region with no measureable coating. 9

Figure 11: Typical optical image of a coated part 9

Figure 12: Overall composite SEM image of the SOT3 coating cross – section. Thickness at arrow is 0.8 microns (see Figure 14). Note the light line above the coating is the gold sputtered layer. 10

Figure 13: SEM image of the SOT3 coating cross – section with decreased brightness that shows the lead in the solder. 11

Figure 14: High magnification SEM image of the SOT3 coating cross – section in the lead knee region showing 0.8 micron (800 nm) thick coating, 3,000x. 12

Figure 15: Close-up SEM image of the SOT3 cross – sectioned solder joint in the toe region, 100x. 12

Figure 16: Composite SEM image of the SOT5 coating cross – section (plane A Figure 2), 100x. There is a coating void behind lead leaving an uncoated region. The coating on the knee is 1.3 microns (see Figure 29). 13

Figure 17: Images of the SOT5 coating cross – section with reduced brightness to show lead; (A) optical and (B) SEM. 14

Figure 18: High magnification SEM image of the SOT5 coating in the knee region, 2,000x. 15

Figure 19: High magnification SEM image of the SOT5 coating in foot region, 1,000x. 15

Figure 20: Overall SOT5 front grind coating cross – section images obtained by grinding into the vertical part of the lead from the toe (see Figure 2 plane B); (A) optical, 25x, and (B) deeper grind plane SEM, 100x. The approximate location of the section plane is shown in Figure 21. 16

Figure 21: SEM image of the SOT5 cross – section annotated to show the approximate front section plane location. 17

Figure 22: High magnification images of the SOT5 coating front grind cross – section of the top corners of the lead in section plane B; (A) 1,000x and (B) 3,000x. 18

Figure 23: High magnification images of the SOT5 front grind coating cross – section of the left of the lead in section plane B, 1,500x. 19

Figure 24: SEM image of the overall SOT6 coating cross – section (plane A Figure 2). Note that there was no coating behind the lead. 20

Figure 25: Overall SOT6 coating cross – section images showing the lead; (A) Optical, 100x, and (B) SEM image with reduced brightness. 21

Figure 26: SEM image of the SOT6 coating cross – section in the knee region. At its thinnest location, the conformal coating is only 0.3 microns; (A) 1,000x and (B) 3,500x. 22

Figure 27: SEM image of the SOT6 coating cross – section between the shin region and the foot, 1,000x. 23

Figure 28: First front grind of the SOT6 coating cross – section images obtained by grinding into the vertical part of the lead from the toe (see Figure 2 plane B); (A) optical,25x, and (B) SEM, 100x.... 24

Figure 29: High magnification SEM images of the SOT6 cross – section of the top of lead of Figure 28, 1,000x and 3,000x. The coating on the corner is 0.15 microns. 25

Figure 30: Overall deeper second front grind SOT6 coating cross – section images; (A) optical, 25x, and (B) SEM, 100x. The arrow shows where the height of the conformal coating on the side of the lead between leads is 560 microns. 26

Figure 31: SEM image of the SOT6 coating front grind cross – section at the top of lead, 1,800x. 27

Figure 32: SEM image of the SOT6 coating front grind cross – section at the top corner of lead, 5,000x. 27

Figure 33: SOT3 maximum whisker length results after a total of 1,797 PCTC cycles. 28

Figure 34: SEM images showing whisker growth on alloy-42 lead solder joint after a total of 1,797 PCTC cycles; (A) overall view highlighting whisker growth where the lead exits the top of the solder joint with (B) and (C) showing higher magnification whisker growth images. 28

Figure 35: Box plot comparing whisker length (microns) for lead alloy, part contamination and board contamination combinations after 1,797 PCTC cycles where no flux was applied. 29

Figure 36: Whiskers observed on the SOT3 part with 1-1 contamination without flux after 1,797 PCTC cycles. 30

Figure 37: Whiskers observed on the SOT6 part with 1-1 contamination with flux applied after 1,797 PCTC cycles. 30

Figure 38: Competing mechanisms of stress relaxation (SOT3, 0-0 contamination level) after 1,797 PCTC cycles. 31

Figure 39: Micro-cracks (red arrows) in SAC305 fillets observed after 1,797 PCTC cycles; (A) SOT3 0-0 contamination level, (B) SOT3 1-1 contamination level with whisker adjacent to Ag_3Sn IMC and (C) SOT3 1-0 contamination level with whisker growing from primary tin dendrite triple junction Micro-cracks. 32

Figure 40: SEM image of a SOT3 with conformal coating with a 1-1 contamination level after 1,797 PCTC cycles, 40x (ref. B-SOT-PC-1-1-cc-3, SOT3). 33

Figure 41: SEM image of a SOT3 lead with conformal coating with a 1-1 contamination level after 1,797 PCTC cycles, 100x (ref. B-SOT-PC-1-1-cc-3, SOT3, 2). 33

Figure 42: SEM image of a SOT3 lead with conformal coating with a 1-1 contamination level after 1,797 PCTC cycles, 1,500x (ref. B-SOT-PC-1-1-cc-3, SOT3). 34

Figure 43: SEM image of a SOT6 lead and solder joint with conformal coating with a 1-1 contamination level after 1,797 PCTC cycles, 100x, and (ref. B-SOT-PC-1-1-cc-2, SOT6). 34

Figure 44: SEM image of a SOT6 solder joint with conformal coating with a 1-1 contamination level after 1,797 PCTC cycles, 400x (ref. B-SOT-PC-1-1-cc-2, SOT6). 35

Figure 45: SEM image of SOT6 leads with conformal coating with a 1-1 contamination level after 1,797 PCTC cycles, 45x (ref. B-SOT-PC-1-1-cc-3, SOT6). 35

Figure 46: SEM image of a SOT6 solder joint with conformal coating with a 1-1 contamination level after 1,797 PCTC cycles, 100x (ref. B-SOT-PC-1-1-cc-3, SOT6). 36

Figure 47: SEM image of a SOT6 solder joint with conformal coating with a 1-1 contamination level after 1,797 PCTC cycles, 350x (ref. B-SOT-PC-1-1-cc-3, SOT6). 36

Figure 48: SEM image of a SOT6 solder joint with conformal coating with a 1-1 contamination level after 1,797 PCTC cycles, 500x (ref. B-SOT-PC-1-1-cc-3, SOT6). Close up of solder joint shown in Figure 47. 37

Figure 49: SEM image of a SOT6 solder joint with conformal coating with a 1-1 contamination level after 1,797 PCTC cycles, 1,000x (ref. B-SOT-PC-1-1-cc-3, SOT6). 37

Figure 50: Whisker location definition. The hatched region 2 indicates the thick solder region on the lead and includes the thinner solder that wet onto the board pad. Areas 1, 3, 4 and 5 represent the thin solder or tin regions above the thick solder area. 39

Figure 51: Whisker angle measurement definition 39

Figure 52: Box plot of whisker length after 6,000 PCTC cycles for different contamination levels and lead alloys. 44

Figure 53: Probability plot of whisker length for alloy 42 leads after 6,000 PCTC cycles. 44

Figure 54: Probability plot of whisker length for various contamination levels after 6,000 PCTC cycles. 45

Figure 55: Probability plot of whisker diameter for alloy 42 leads after 6,000 PCTC cycles. 45

Figure 56: Scatter plot of length versus diameter of whiskers from terminations with different lead alloy materials after 6,000 PCTC cycles. 46

Figure 57: Scatter plot of ln(diameter) versus ln(length) of whiskers from terminations with different lead alloy materials after 6,000 PCTC cycles. 46

Figure 58: Scatter plot of ln(diameter) versus ln(length) of whiskers from SOT3, SOT5 and SOT6 part terminations after 6,000 PCTC cycles. 47

Figure 59: Scatter plot of whisker diameter versus length of whiskers at various locations after 6,000 PCTC cycles. 47

Figure 60: Histogram of whisker growth location after 6,000 PCTC cycles. Note location 2 only has whiskers from 2B as defined in Figure 50. 48

Figure 61: Histogram of whisker angle after 6,000 PCTC cycles. Whiskers oriented parallel to the growth surface are defined to have angle of zero and whiskers perpendicular to the growth surface have an angle of 90 degrees. 48

Figure 62: Probability plot for the length of new whiskers that grew between 1,797 and 6,000 cycles..... 49

Figure 63: Probability plot for the diameter of new whiskers that grew between 1,797 and 6,000 cycles. 49

Figure 64: Scatter plot of length change versus previous length for whiskers that grew longer between 1,797 and 6,000 cycles..... 50

Figure 65: SEM image of SOT3, U27, lead 1, no conformal coating, 1-1 contamination level after 6,000 PCTC cycles, 100x (ref. A-SOT-PC-1-1-ncc-1, SOT3, U27, lead 1). 51

Figure 66: Close-up SEM image of a whisker nucleation site on the SOT3 shown in Figure 65, 2,000x. (ref. A-SOT-PC-0-0-ncc-1, SOT3, U27, lead 1). 51

Figure 67: SEM image of the SOT3, U37, lead 1, no conformal coating, 0-0 contamination level, after 6,000 PCTC cycles, 100x (ref. A-SOT-PC-0-0-ncc-1, SOT3, U37, lead 1)..... 52

Figure 68: Close-up SEM image of a whisker nucleation site on the SOT3 from Figure 67, 3,000x. (ref. A-SOT-PC-0-0-ncc-1, SOT3, U37, lead 1). Whisker growth is occurring from between two tin grains. 52

Figure 69: SEM image of the SOT3, U33, lead 1, no conformal coating, 0-0 contamination level, after 6,000 PCTC cycles (ref. A-SOT-PC-0-0-ncc-1, SOT3, U33, lead 1). 53

Figure 70: Close up image of deformation growth on the SOT3 from Figure 69, 2,000x (ref. A-SOT-PC-0-0-ncc-1). The growth deformation is approximately 2 microns high and is near an Ag_3Sn intermetallic platelet in location 4. 53

Figure 71: SEM image of the SOT3, U20, lead 1, no conformal coating, 1-0 contamination level after 6,000 PCTC cycles, 100x (ref. A-SOT-PC-1-0-ncc-3)..... 54

Figure 72: Close-up SEM image of the pad edge growths on the left side of Figure 71, 1,000x. (ref. A-SOT-PC-1-0-ncc-3, SOT3, U20, lead 1, 1,000x). 54

Figure 73: SEM image of the SOT3, U58, lead 3, no conformal coating, 1-1 contamination level, after 6,000 PCTC cycles, 100x (ref. A-SOT-PC-1-1-ncc-1, SOT3, U58, lead 3)..... 55

Figure 74: Close-up SEM image of a whisker nucleation site on the SOT3 shown in Figure 73, 2,000x. (ref. A-SOT-PC-1-1-ncc-1, SOT3, U58, lead 3). 55

Figure 75: SEM image of the SOT3, U44, lead 1, no conformal coating, 0-0 contamination level after 6,000 PCTC cycles, 100x (ref. A-SOT-PC-0-0-ncc-1, SOT3, U44, lead 1)..... 56

Figure 76: Close-up SEM image of a whisker nucleation site on the SOT3, 2,000x (A-SOT-PC-0-0-ncc-1, SOT3, U44, lead 1). 56

Figure 77: SEM image of the SOT3, U63, lead 2, no conformal coating, 1-1 contamination level after 6,000 PCTC cycles, 100x (ref. A-SOT-PC-1-1-ncc-1, SOT3, U63, lead 2)..... 57

Figure 78: Close-up SEM images of a whisker nucleation and deformation growths on the SOT3 shown in Figure 77; (A) 500x, (B) 1,800x, and (C) 2,500x. 58

Figure 79: SEM image of the SOT6, U68, lead 1, no conformal coating, 1-1 contamination level after 6,000 PCTC cycles, 100x (ref. A-SOT-PC-1-1-ncc-1)..... 59

Figure 80: Close-up SEM image of the SOT6 shown in Figure 79, 1,500x (ref. A-SOT-PC-1-1-ncc-1, SOT6, U68, lead 1). 59

Figure 81: SEM image of the SOT6, U71, lead 4, no conformal coating, 1-0 contamination level after 6,000 PCTC cycles, 100x (ref. A-SOT-PC-1-0-ncc-3)..... 60

Figure 82: Close-up SEM image of the right side of the SOT6 lead shown in Figure 81, 1,500x (ref. A-SOT-PC-1-0-ncc-3, U71, lead 4)..... 60

Figure 83: Close-up SEM image of the left side of the SOT6 lead shown in Figure 81, 1,500x (ref. A-SOT-PC-1-0-ncc-3, U71, lead 4)..... 61

Figure 84: Close-up SEM image of the center-left side of the SOT6 lead shown in Figure 81, 2,500x (ref. A-SOT-PC-1-0-ncc-3, U71, lead 4)..... 61

Figure 85: SEM image of the SOT6, U68, lead 2 (right) and 3 (left), no conformal coating, 1-1 contamination level after 6,000 PCTC cycles, 100x (A-SOT-PC-1-1-ncc-1, SOT6, U68, lead 2-3).. 62

Figure 86: Close-up SEM image of a whisker nucleation site on the SOT6 shown in Figure 85, 1,000x (ref. A-SOT-PC-1-1-ncc-1, SOT6, U68, lead 2)..... 62

Figure 87: Close-up SEM image of a whisker on the SOT6 lead shown in Figure 85, 2,500x (ref. A-SOT-PC-1-1-ncc-1, SOT6, U68, lead 2). Note that the whisker diameter is decreasing from the tip to the base..... 63

Figure 88: SEM image of the SOT6, U71, lead 4 (left) and lead 5 (right), no conformal coating, 0-1 contamination level, after 6,000 PCTC cycles 100x (ref. A-SOT-PC-0-1-ncc-1, SOT6, U71, lead 4-5)..... 63

Figure 89: Close up SEM image of the whisker on the SOT6 lead 5 shown in Figure 88, 1,000x (A-SOT-PC-0-1-ncc-1, SOT6, U71, lead 5, 1,000x)..... 64

Figure 90: SEM image of cracks and deformation around the lead tip of the SOT3, U27, lead 3, no conformal coating, 1-0 contamination level after 6,000 PCTC cycles, 100x (ref. A-SOT-PC-1-0-ncc-1). The surface whisker growth and solder cracking are located near the lead tip which is just under the solder..... 64

Figure 91: Close up SEM image of the SOT3 lead shown in Figure 90, 2,000x (ref. A-SOT-PC-1-0-ncc-1, U27, lead 3)..... 65

Figure 92: Close up SEM image of growth along the grain boundary for the SOT3 lead shown in Figure 90, 3,000x, (ref. A-SOT-PC-1-0-ncc-1, U27, lead 3)..... 65

Figure 93: Close up SEM image of a whisker near a solder crack in the SOT3 solder joint shown in Figure 90, 3,000x (ref. A-SOT-PC-1-0-ncc-1, U27, lead 3)..... 66

Figure 94: Close up SEM image of a second whisker near a solder crack in the SOT3 solder joint shown in Figure 90, 3,000x (ref. A-SOT-PC-1-0-ncc-1, U27, lead 3)..... 66

Figure 95: Close up SEM image of a third whisker near a solder joint crack in the SOT3 lead shown in Figure 90, 3,000x (ref. A-SOT-PC-1-0-ncc-1, U27, lead 3)..... 67

Figure 96: SEM image of the SOT3, U31, lead 1, no conformal coating, 1-1 contamination level after 6,000 PCTC cycles, 100x (ref. A-SOT-PC-1-1-ncc-1)..... 67

Figure 97: Close up SEM image of pad edge extrusions on the SOT3 solder joint shown in Figure 96, 200x (ref. A-SOT-PC-1-1-ncc-1, U31 lead 1)..... 68

Figure 98: Close up SEM image of various growths on the SOT3 lead shown in Figure 96, 500x (ref. A-SOT-PC-1-1-ncc-1, U31 lead 1)..... 68

Figure 99: Close up SEM image of deformation and whisker growth along a grain boundary on the SOT3 lead shown in Figure 96, 700x (ref. A-SOT-PC-1-1-ncc-1, U31 lead 1)..... 69

Figure 100: Close up SEM image of whisker growth adjacent to an Ag_3Sn intermetallic plate and grain boundary slip regions on the SOT3 lead shown in Figure 96, 1,500x (ref. A-SOT-PC-1-1-ncc-1, U31 lead 1). 69

Figure 101: Close up SEM image of whisker growth and grain boundary slip regions on the SOT3 lead shown in Figure 96, 1,000x (ref. A-SOT-PC-1-1-ncc-1, U31 lead 1). 70

Figure 102: Close up SEM image of the upper whisker shown in Figure 101, 1,500x. In addition to whisker growth, deformation growth and grain boundary deformation are present (ref. A-SOT-PC-1-1-ncc-1, SOT3 U31 lead 1). 70

Figure 103: Close up SEM image of grain boundary slip regions, grain recrystallization, multiple whisker nucleation sites and whisker growth on the SOT3 lead shown in Figure 96, 2,000x (ref. A-SOT-PC-1-1-ncc-1, U31 lead 1). 71

Figure 104: Close up SEM image of grain boundary slip regions, solder cracks, grain recrystallization, and whisker growth on the SOT3 lead shown in Figure 96, 2,500x (ref. A-SOT-PC-1-1-ncc-1, U31 lead 1). 71

Figure 105: Close up SEM image of grain boundary slip regions and a whisker with an increasing whisker base diameter on the SOT3 lead shown in Figure 96, 3,000x (ref. A-SOT-PC-1-1-ncc-1, U31 lead 1). 72

Figure 106: SEM image of the SOT5, U24, lead 2, no conformal coating, 1-0 contamination level after 6,000 PCTC cycles, 100x (ref A-SOT-PC-1-0-ncc-1, SOT5, U24, lead 2) 72

Figure 107: Close up SEM image of the SOT5 lead shown in Figure 106, 2,500x (ref. A-SOT-PC-1-0-ncc-1, SOT5, U24, lead 2). 73

Figure 108: SEM image of the SOT5, U11, lead 2, no conformal coating, 0-1 contamination level after 6,000 PCTC cycles, 100x (ref. A-SOT-PC-0-1-ncc-3, SOT5, U11, lead 2) 73

Figure 109: Close up SEM image of the SOT5 lead shown in Figure 108, 1,500x (ref. A-SOT-PC-0-1-ncc-3, SOT5, U11, lead 2). 74

Figure 110: SEM image of coating on SOT6 leads from board 3 after 6,000 PCTC cycles (ref. B-SOT-PC-1-1-cc-3, SOT6), 45x. 75

Figure 111: SEM image of coating on SOT6 leads from board 3 after 6,000 PCTC cycles, 100x (ref. B-SOT-PC-1-1-cc-3, SOT6). 75

Figure 112: Intermediate magnification SEM image of coating on a SOT6 lead from board 3 after 6,000 PCTC cycles, 250x (ref. B-SOT-PC-1-1-cc-3, SOT6). 76

Figure 113: High magnification SEM image of coating on a SOT6 lead from board 3 after 6,000 PCTC cycles, 300x (ref. B-SOT-PC-1-1-cc-3, SOT6). 76

Figure 114: Higher magnification SEM image of coating on a SOT6 lead from board 3 after 6,000 PCTC cycles, 1,000x (ref. B-SOT-PC-1-1-cc-3, SOT6). 77

Figure 115: SEM image of coating on SOT6 leads from board 2 after 6,000 PCTC cycles, 45x (ref. B-SOT-PC-1-1-cc-2, SOT6). Arrows highlight coating cracks. 77

Figure 116: Close-up SEM image of coating on a SOT3 lead after 6,000 PCTC cycles, 100x; (A) normal contrast and (B) high contrast. Lead knee is toward the bottom of the image (ref. B-SOT-PC-1-1-cc-2, SOT3). 78

Figure 117: Higher magnification SEM image of the coating crack on the left side of the SOT3 lead show in Figure 116 after 6,000 PCTC cycles, 500x (ref. B-SOT-PC-1-1-cc-2, SOT3). 79

Figure 118: SEM image of coating on the SOT3 part from board 3 after 6,000 PCTC cycles, 40x (ref. B-SOT-PC-1-1-cc-3, SOT3). 79

Figure 119: Higher magnification SEM image of coating on the upper SOT3 lead shown in Figure 118 illustrating coating cracks after 6,000 PCTC cycles, 250x (ref. B-SOT-PC-1-1-cc-3, SOT3). 80

Figure 120: High magnification SEM image of coating on a SOT3 lead near the knee illustrating coating cracks and separation between the coating and the knee after 6,000 PCTC cycles, 1,000x. (ref. B-SOT-PC-1-1-cc-3, SOT3). 80

Figure 121: SEM image of coating with cracks on SOT6 leads from board 2 after 6,000 PCTC cycles, 100x, image 2; (A) normal contrast and (B) high contrast (ref. B-SOT-PC-1-1-cc-2, SOT6). 81

Figure 122: SEM image of coating on a SOT6 lead from board 2 showing some coating cracks after 6,000 PCTC cycles, 350x; (A) normal contrast and (B) high contrast (ref. B-SOT-PC-1-1-cc-2, SOT6). ... 82

Figure 123: SEM image of coating on a SOT6 lead from board 2 with the interdendritic solder spaces filled with coating and no whiskers, 6,000 cycles, 400x (ref. B-SOT-PC-1-1-cc-2, SOT6). 83

Figure 124: Higher magnification SEM image of coating on a SOT6 lead from board 2 showing that the interdendritic solder spaces are filled with coating and there are no whiskers 6,000 cycles, 1,000x (ref. B-SOT-PC-1-1-cc-2, SOT6). 83

Figure 125: SEM image of coating on a SAC+Re paste reflowed on a BGA solder pad after 6,000 PCTC cycles, 180x (ref. C-BGA-PC-0-0-cc-1). 84

Figure 126: SEM image of coating on SAC+Re paste reflowed on another BGA solder pad after 6,000 PCTC cycles 6,000 cycles, 200x (ref. C-BGA-PC-0-0-cc-1). 84

Figure 127: High magnification SEM image of coating on a SAC+Re paste reflowed on a BGA solder pad after 6,000 PCTC cycles, 1,000x (ref. C-BGA-PC-0-0-cc-1). 85

Figure 128: Stress conditions that promote whisker growth. 86

Figure 129: Box plot comparing whisker length (microns) after 1,797 and 6,000 PCTC cycles for lead alloy, part contamination and board contamination combinations; (A) 1,797 PCTC cycles from Figure 35 and (B) 6,000 PCTC cycles from Figure 52. 86

Figure 130: SOT3 maximum whisker length for the three last PCTC inspection intervals. 87

Figure 131: Competing mechanisms of stress relaxation (SOT3, 0-0 contamination level after 1,797 PCTC cycles shown) 88

Figure 132: Whisker formation as a result of dynamic recrystallization (DRX) [3][4][5]. 89

Figure 133: High magnification SEM image comparison of whisker growth at 1,797 and 6,000 cycles SOT6 (A) after 1797 cycles, and (B) after 6,000 cycles 2,500x (ref. Image B A-SOT-PC-1-0-ncc-3, SOT6, U71, lead 4). 89

Figure 134: Close up SEM image of grain boundary slip regions, cracks, grain recrystallization, and whisker growth after 6,000 cycles on a SOT3 lead region with increasing amount of solder cracking; (A) no cracks, 3,000x, (B) small cracks, 2,500x and (C) large crack, 3,000x (ref. A-SOT-PC-1-1-ncc-1, SOT3, U31 lead 1 and A-SOT-PC-1-0-ncc-1, SOT3, U27, lead 3). 89

Figure 135: Close-up SEM images of whiskers with a decreasing whisker diameter; (A) on a SOT6 lead, 2,500x and (B) a SOT5 lead shown in Figure 108 (ref. A-SOT-PC-1-1-ncc-1, SOT6, U68, lead 2 and A-SOT-PC-0-1-ncc-3, SOT5, U11, lead 2). 90

Figure 136: Close up SEM image of grain boundary slip regions and whisker with an increasing whisker base diameter on the SOT3 lead, 3,000x (ref. A-SOT-PC-1-1-ncc-1, SOT3, U31 lead 1). 90

Figure 137: Close up SEM image of the SOT5 lead shown in Figure 106, 2,500x (ref. A-SOT-PC-1-0-ncc-1, SOT5, U24, lead 2). 91

Figure 138: SEM image of the SOT3, U20, lead 1, no conformal coating, 1-0 contamination level after 6,000 PCTC cycles; (A) 100x and (B) high magnification image of pad edge growth highlighted by arrow, 1,000x (ref. A-SOT-PC-1-0-ncc-3). 91

Figure 139: Close up SEM image of growth after 6,000 cycles along the grain boundary on the front of the lead for the SOT3 lead shown in Figure 90, 3,000x, (ref. A-SOT-PC-1-0-ncc-1, SOT3, U27, lead 3). 92

Figure 140: SEM image of coating on two SOT6 leads from board 3 after 6,000 PCTC cycles; (A) 100x and (B) higher magnification image of right lead knee showing whisker nucleation,1,000x (ref. B-SOT-PC-1-1-cc-3, SOT6). 93

Figure 141: Higher magnification SEM image of coating on right SOT6 lead shown in Figure 140 after 6,000 PCTC cycles, 1,000x. Some whisker nucleation is evident (ref. B-SOT-PC-1-1-cc-3, SOT6). 93

Figure 142: Higher magnification SEM image of coating on a SOT6 lead from board 2 with interdendritic solder spaces filled with coating and no whiskers 6,000 cycles , 1,000x (ref. B-SOT-PC-1-1-cc-2, SOT6). 94

Figure 143: SEM image of coating on SOT6 leads from board 2 after 6,000 PCTC cycles, 45x (ref. B-SOT-PC-1-1-cc-2, SOT6). Arrows highlight coating cracks near the lead knee. 94

Figure 144: SEM image of coating on a SOT3 lead after 6,000 PCTC cycles; (A) 100x and (B) higher magnification image of cracks near the knee highlighted by arrow in A, 500x (ref. B-SOT-PC-1-1-cc-2, SOT3). 95

Appendix N: List of Tables

Table 1: UV40 QFP44 process development screening experiment coating thickness results..... 4

Table 2: PCTC +50 to +85°C cycling dates and parameters 38

Table 3: Summary of whisker growth for SOT6, SOT3 and SOT5 parts after 6,000 PCTC cycles..... 41

Table 4: Summary of additional whisker growth between 1,797 and 6,000 PCTC cycles for SOT6, SOT3 and SOT5 parts. 41

Table 5: Summary of part inspection results for the four contamination variants after 6,000 PCTC cycles. 41

Table 6: SOT6 observations for the top 10 longest whiskers after 6,000 PCTC cycles. 42

Table 7: SOT3 observations for the top 10 longest whiskers after 6,000 PCTC cycles. 42

Table 8: Summary of non-whisker deformation grain growths and pad edge growths after 6,000 PCTC cycles. 43

Table 9: Subset of protrusion edge growths (PEGs) which were included in the 6,000 PCTC Table 8 results. 43

Table 10: Whisker count by location after 6,000 PCTC cycles.. 43

Table 11: Whisker density by location (whiskers/mm^2) after 6,000 PCTC cycles. 43

Acronyms

Acronym	Definition
BGA	Ball Grid Array
CTE	Coefficient of Thermal Expansion
IMC	Intermetallic
IPC	IPC Association Connecting Electronics Industries
JEDEC	Joint Electron Devices Engineering Council
PCTC	Simulated power cycling thermal cycling
PLCC	Plastic Leaded Chip Carrier Electronic Package
ppm	Parts per million
QFP	Quad Flat Pack Electronic Packages
ROL0	Low-rosin Halide-free flux
ROL1	Rosin based flux with halide content below 0.05%
ROLO	Low activity organic acid flux
SAC	Sn-Ag-Cu alloy lead free solder
SAC305	Sn3Ag0.5Cu alloy lead free solder (composition is in weight percent)
SEM	Scanning Electron Microscopy
SERDP	Strategic Environmental Research and Development Program
SOT	Small Outline Transistor Electronic Packages
TQFP	Thin Quad Flat Pack Electronic Packages

1. PCTC Background

1.1 PCTC Test overview

The simulated power cycling thermal cycling (PCTC) environment replicates the thermal conditions where an electronic assembly is maintained at a high temperature and the power is turned on and off simulating high temperature operation. During the WP1753 PCTC testing, 1797 thermal cycles from +50 to +85C with inspections from September 2011 to January 2012 [1]. Four contamination levels were compared: (0 – 0) clean components and cleaned assemblies, (1 – 0) contaminated components and cleaned assemblies, (0 – 1) cleaned components and contaminated assemblies, and (1 – 1) contaminated components and contaminated assemblies.

In the original testing, the following inspection intervals were used:

- Doubled cycle count between inspection intervals
- Cycles 0 -250 from Sept-13-2011 to Sept-21-2011
  - First inspection (250 Cycles)
- Cycles 251 -730 from Oct-4-2011 to Nov-1-2011
  - Second inspection (250 + 500 Cycles) (actual count: 250 + 480)
- Cycles 731 – 1,797 from Dec-1-2011 to Jan-29-2012
  - Third inspection (250+500+1,000 Cycles) (actual count: 250 + 480 + 1067)

1.2 Sample preparation

For the cleaned parts, the intention was to have the level of contamination 10 times below typical acceptable industry levels. The intentionally contaminated parts were first cleaned, then immersed in an aqueous solution of NaCl, and then dried. For the contaminated parts, the goal was to have the part level contamination equal to 3.0 µg/in^2 Cl^-, but more contamination was trapped by SOT5, SOT6 TQFP64 and PLCC20 because they had rougher lead surfaces and greater numbers of gaps than the SOT3s. After intentional contamination, the contamination segregated on the tin surface to the rough regions, grain boundaries, and plating gaps as shown in Figure 1.

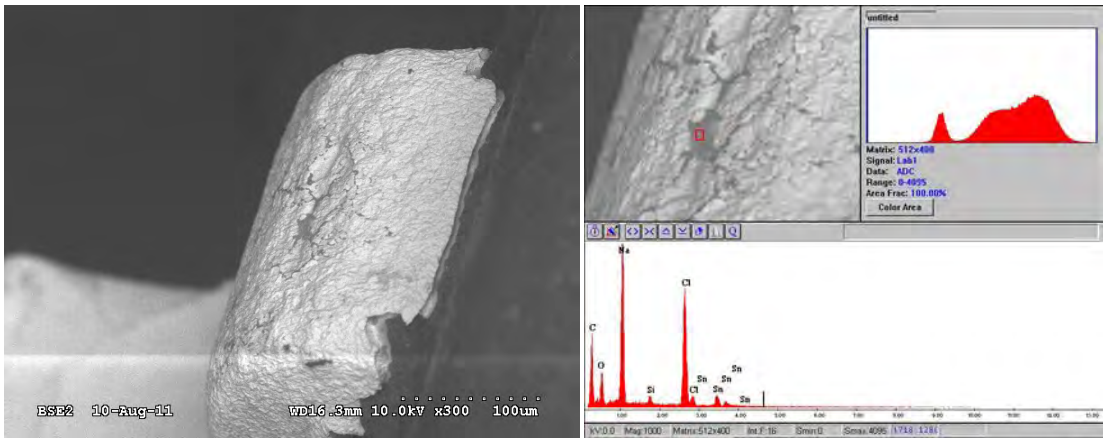


Figure 1: Typical contamination regions on intentionally contaminated (SOT6 shown)**.**

Following the part cleaning/contamination processes, the SAC305 assembly soldering was performed. The boards on the panels were soldered in accordance with J-STD-001 Class 3, using SAC305 (Sn3Ag0.5Cu) alloy. Convection reflow in air was done with a 245 °C peak temperature using a paste with a ROL1 flux cleanable no-clean solder paste.

Each board was populated entirely either with clean parts or contaminated parts. After soldering and flux residue cleaning, selected boards were contaminated at the assembly level to 10 µg/in^2 Cl- (1.55 µg/cm^2 sodium chloride (NaCl) equivalent ionic or ionizable flux residue) to simulate the maximum level of contamination allowed by the J-STD-001 ionic residues test [2]. The assemblies were immersed in a solution of 160 +/- 10 ppm NaCl and then baked dry in an oven. The assembly contamination level of the intentionally contaminated assemblies was 5.2 ppm Cl- by ion chromatography with a total concentration of 12.5 µg/in^2 (1.94 µg/cm^2) equivalent Cl- as measured by resistivity of solvent extraction.

In the Cycles 731 - 1797 portion of the experiment, one board of the three board replicates had selected parts contaminated with a ROLO, no-clean flux used for rework. The flux was not cleaned off in order to simulate instances where flux would be trapped under parts during a typical rework. The flux residue stimulated whisker growth. The small outline transistor board parts with alloy-42 (Fe-42Ni) lead frames had the longest whiskers.

Conformal coated assemblies were also evaluated. Coating is a primary mitigation against the detrimental effects of whisker growth. The coating was a dual cure ultraviolet (UV) and humidity acrylic/urethane (AR/UR) blend (Humiseal UV40, Chase Corp.) qualified to both IPC-CC-830 and MIL-I-46058. The coating was applied with a machine spray process using multiple overlapping X – Y spray passes to achieve a thickness of 75 microns +/- 25 microns (3 mils +/- 1 mil) on a free and unencumbered surface.

1.3 Coating thickness

Additional information from the initial WP1753 project coating process development and characterization is presented next. Initially, a screening experiment was performed to identify the coating viscosity and process parameters for the final assemblies.

Coverage was determined using a combination of visual inspection accordance with J-STD-001 and cross-sectioning. The cross-sections were examined using optical microscopy up to 100x and scanning electron microscopy up to 3,000x to determine the coating thickness on the leads. A new method was developed for the cross-section inspection where the components were gold sputter coated before potting to allow precise definition between the epoxy potting and the coating surface in the Scanning Electron Microscopy (SEM). The section planes shown in Figure 2 allow the coating thickness to be determined behind the lead (Plane A) and on the sides of the lead (Plane B).

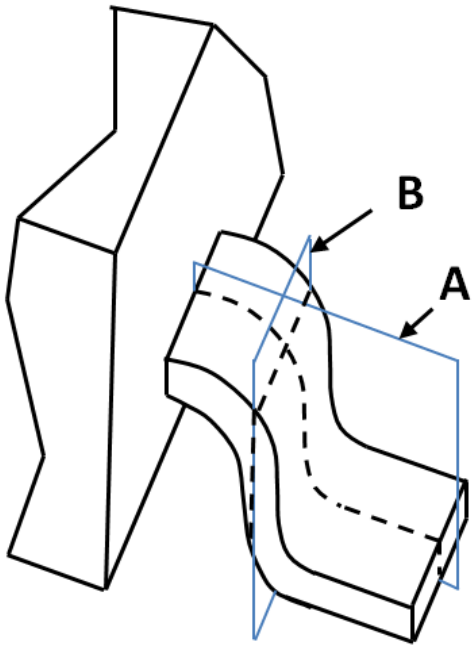


Figure 2: Cross-section planes used for coating thickness measurement.

1.3.1 Coating process development screening experiment

The QFP44 part on the lead-free IPC-7711/21 Rework and Repair Training board part number 405-2435 from STI Electronics (Madison, AL) was used for the coating thickness characterization.

Two viscosity variants (250 and 100 cps) of the Humiseal UV40 were evaluated. Both the UV40 (250 cps) and the UV40-100 (100 cps) coatings were sprayed on an automated Asymtek spray machine at Asymtek's Ohio laboratory. The number of x and y direction sprays, atomization and flow control were set to achieve a nominal thickness of 50 microns on a flat unencumbered surface after curing. The UV40 (250 cps) was spray coated with 1-x direction pass and 1-y direction pass (designated UV40-1x-1y) and 2-x direction and 2-y direction passes (designated UV40-2x-2y). The lower viscosity UV-40-100 was sprayed with 3-x and 3-y (designated UV40-100-3x-3y) passes and 6x-6y (designated UV40-100-6x-6y) passes.

Visual inspection showed good coverage. The screening experiment coating thickness from a single cross-section plane with a left and a right lead are shown in Table 1 using the locations from Figure 3. The variation between the left and right lead is plotted in Figure 4. Plots of the average, maximum, and minimum coating thickness are shown in Figure 5. A typical optical cross – section image from a flat unencumbered board area is shown in Figure 6. Typical SEM images from the cross – section measurements are: knee region (Figure 7), toe region with thin coating and separation (Figure 8), behind the lead with different contrasts needed to see the solder and the coating (Figure 9), and a region with no measureable coating (Figure 10).

On the front of the lead regions A, E and T tended to have thinner coating. On the back of the lead, regions G and H were difficult to coat. The largest thickness variation was observed with the 100 cps UV40-100 6x-6y sample at location H where the left lead had 27.8 microns but the right lead had no coating.

Based in part on the smaller thickness variation in regions A and B and the lower amount of pooling in the H region, the 250cps UV40 with a 2x-2y was selected for the primary tin whisker test boards.

Table 1: UV40 QFP44 process development screening experiment coating thickness results.

Abbreviations: R=Right, L=Left lead, Seprt.= Separation

		Thickness (microns) at location										
No.	Type	Flat coupon	Lead	A	B	C	D	E	F	G	T	H
2	UV40-1x-1y	60.96	R	<0.2	8.4	3	2.3	<0.1	<0.1	<0.1	<0.1	2.3
			L	<0.1	3.7	2.6	0.4	1.8	<0.2	0	<0.1	<0.2
			Avg	**<0.15**	**6.05**	**2.8**	**1.35**	**<0.95**	**<0.15**	**0.05**	**<0.1**	**<1.25**
5	UV40-2x-2y	66.04	R	<0.1	5.9	4.6	1.6	0.3	<0.2	0.4	<0.2	0.9
			L	0.7	6.7	5.8	3	0.7	0.7	1	<0.2	<0.2
			Avg	**<0.4**	**6.3**	**5.2**	**2.3**	**0.5**	**0.45**	**0.7**	**<0.2**	**0.55**
11	UV40-100-3x-3y	60.96	R	1.3	5.2	2.5	2	None	None	None	0.5	None
			L	<0.2	2.9	3.7	0.2	<0.2	<0.2	None	None	None
			Avg	**<0.75**	**4.05**	**3.1**	**1.1**	**<0.1**	**<0.1**	**0**	**0.25**	**0**
14	UV40-100-6x-6y	63.5	R	0.3	1.6	5.7	0.8	<0.2	0.3	None	<0.2 (Seprt.)	None
			L	0.8	0.7	2.9	<0.2	<0.2	None	None	0.9	27.8
			Avg	**0.55**	**1.15**	**4.3**	**<0.5**	**<0.2**	**0.15**	**0**	**0.55**	**13.9**

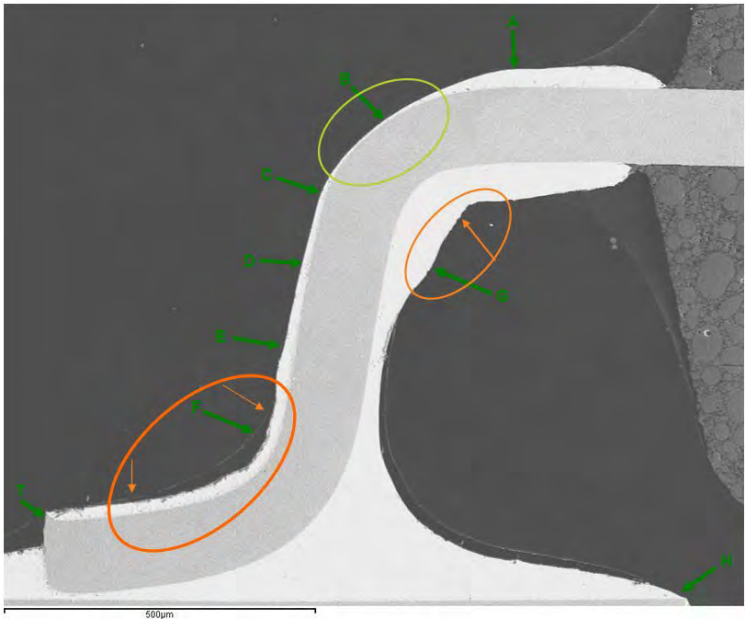
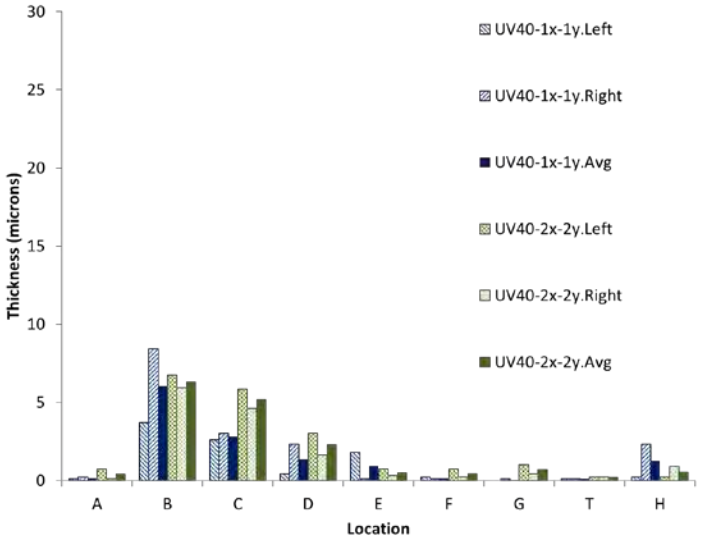
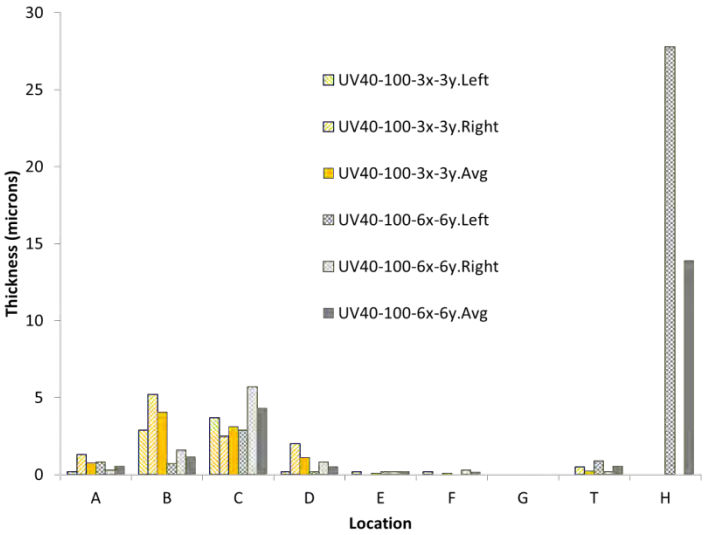


Figure 3: Coating measurement locations used for process development.

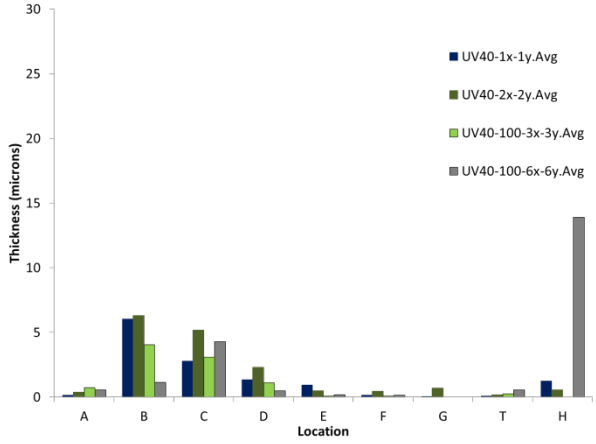


(A)

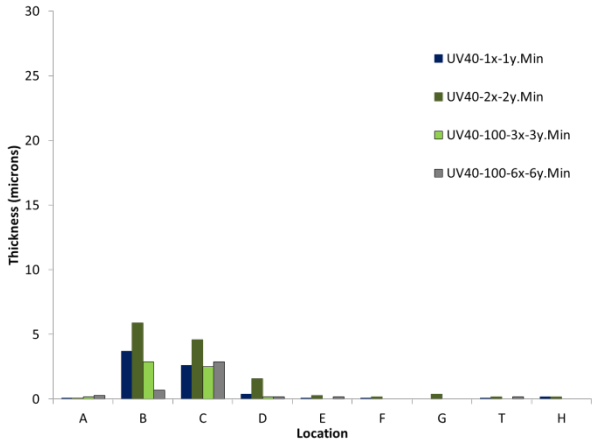


(B)

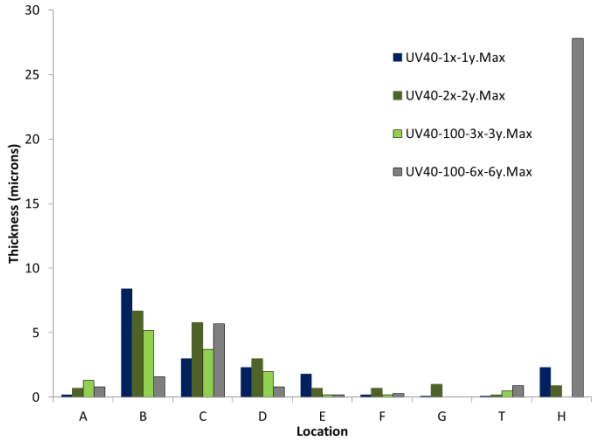
Figure 4: Screening experiment left and right lead coating thicknesses for the following combinations of viscosity and spray passes: (A) 250 cps UV40 1x-1y and 2x-2y spray passes and (B) 100 cps UV40-100 3x-3y and 6x-6y spray passes.



(A)



(B)



(C)

Figure 5: Screening experiment average, maximum and minimum UV40 coating thicknesses for the four UV40 coating variations comparison of 250 cps and 100 cps coatings. The following combinations of viscosity and spray passes are presented: 250 cps UV40 1x-1y and 2x-2y spray passes and 100 cps UV40-100 3x-3y and 6x-6y spray passes. Graph (A) shows average thickness, (B) maximum thickness, and (C) minimum thickness.

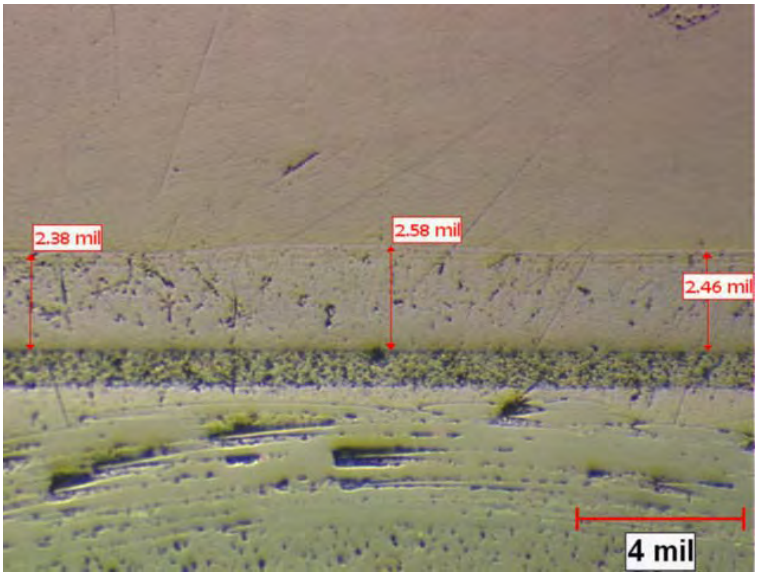


Figure 6: Optical image of a cross-section showing the typical coating measurements of a flat unencumbered area of the board. The three measurements from left to right are 60.4 microns (2.38 mils), 65.5 microns (2.58 mils) and 62.5 microns (2.46 mils).

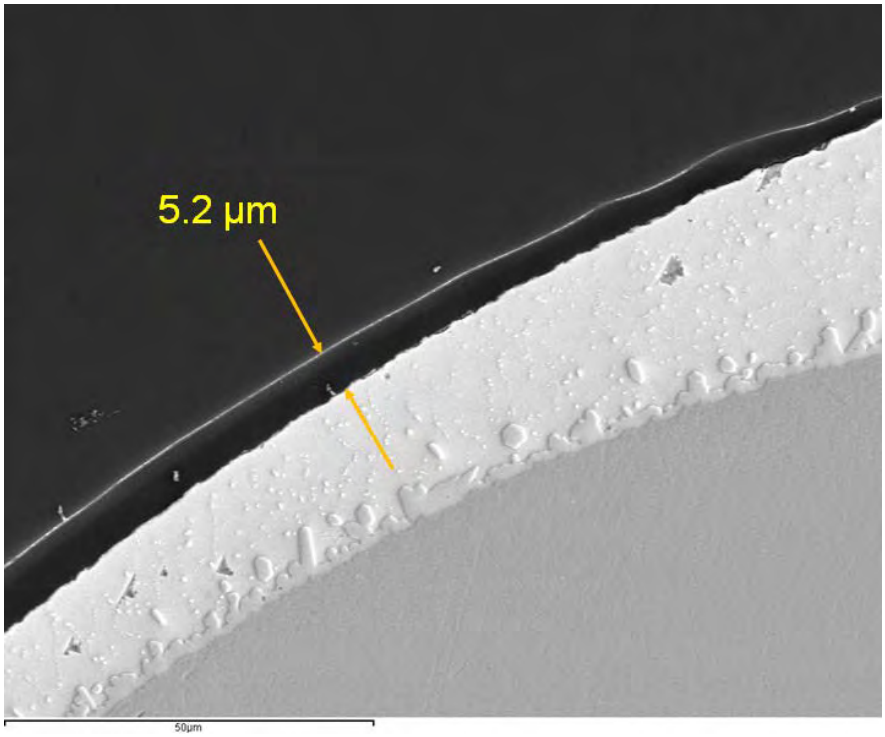


Figure 7: Typical coating screening experiment high magnification SEM cross – section images for thickness measurement (location B sample 11 shown).

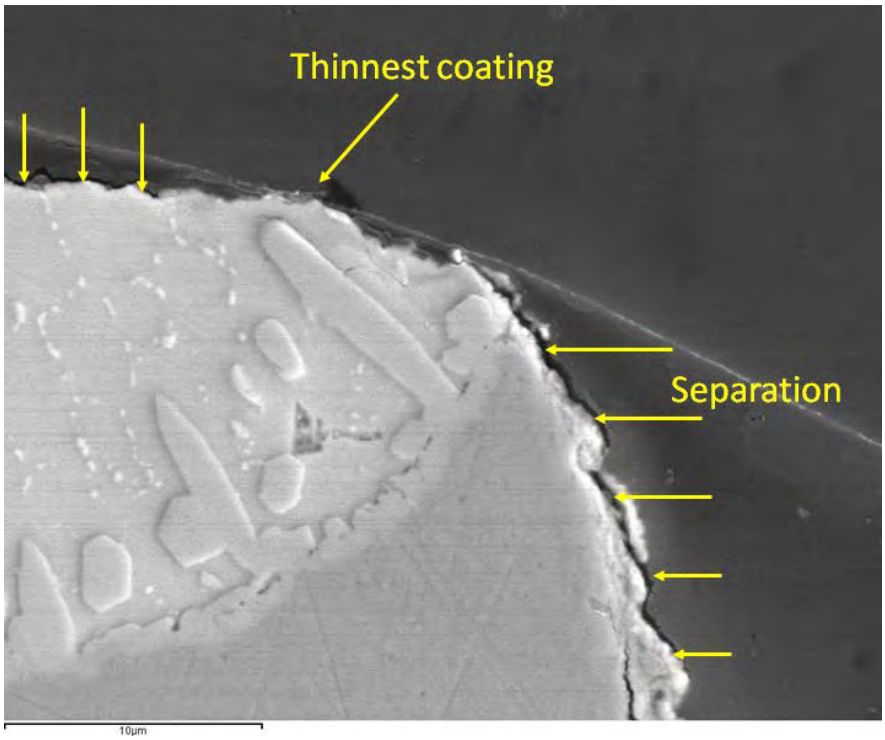


Figure 8: Typical coating screening experiment high magnification SEM cross – section image showing thin coating and separation (location T sample 14 shown).

(A) (B)

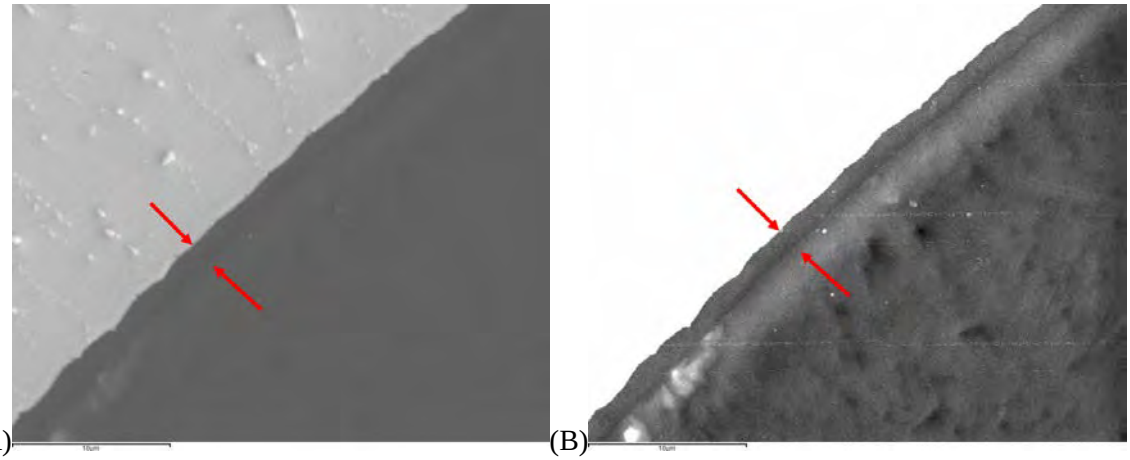


Figure 9: Typical coating screening experiment high magnification SEM cross – section image showing coating thickness behind the lead (location G sample 5 shown); (A) SEM image showing the solder and (B) SEM image with increased brightness and contrast showing coating.



Figure 10: Typical coating screening experiment high magnification SEM cross – section image showing a region with no measureable coating.

1.3.2 Whisker test assembly coating thickness

Visual inspection in accordance with J-STD-001 Class 3 of the UV40 coating on the board shows full coverage (Figure 11).

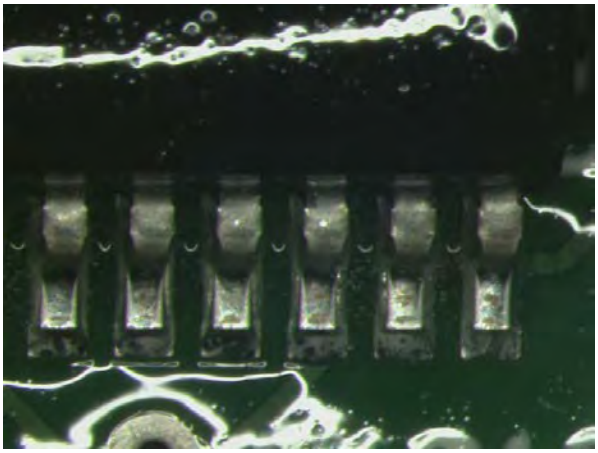


Figure 11: Typical optical image of a coated part.

1.3.2.1 SOT3 Coating thickness

The SOT3 coating thickness was examined in section planes A of Figure 2. The side profile section plane A images are shown in Figure 12 to Figure 15. Section B plane was not examined. The SOT3 coating thickness was examined in section planes A and B of Figure 2. The side profile section

showed that the conformal coating covered everywhere on the lead with a minimum thickness of 0.8 micron. However, there was no coating behind the lead since there was no space between the solder and the plastic body.

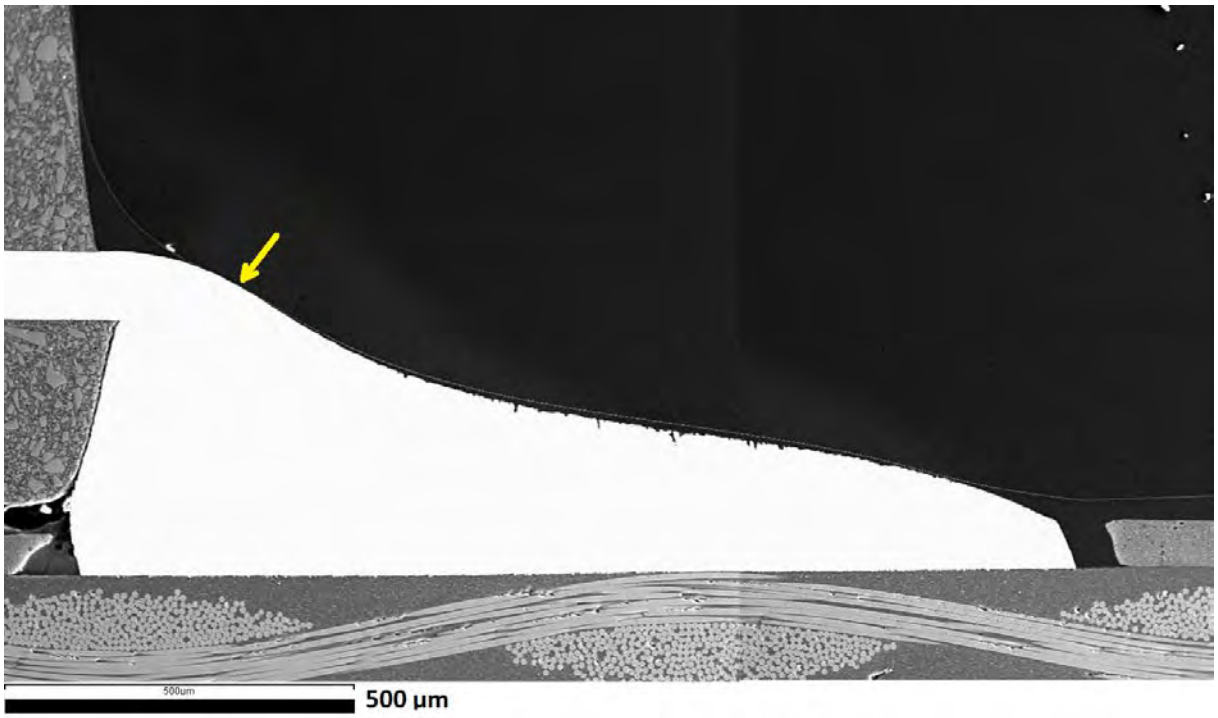


Figure 12: Overall composite SEM image of the SOT3 coating cross – section. Thickness at arrow is 0.8 microns (see Figure 14). Note the light line above the coating is the gold sputtered layer.

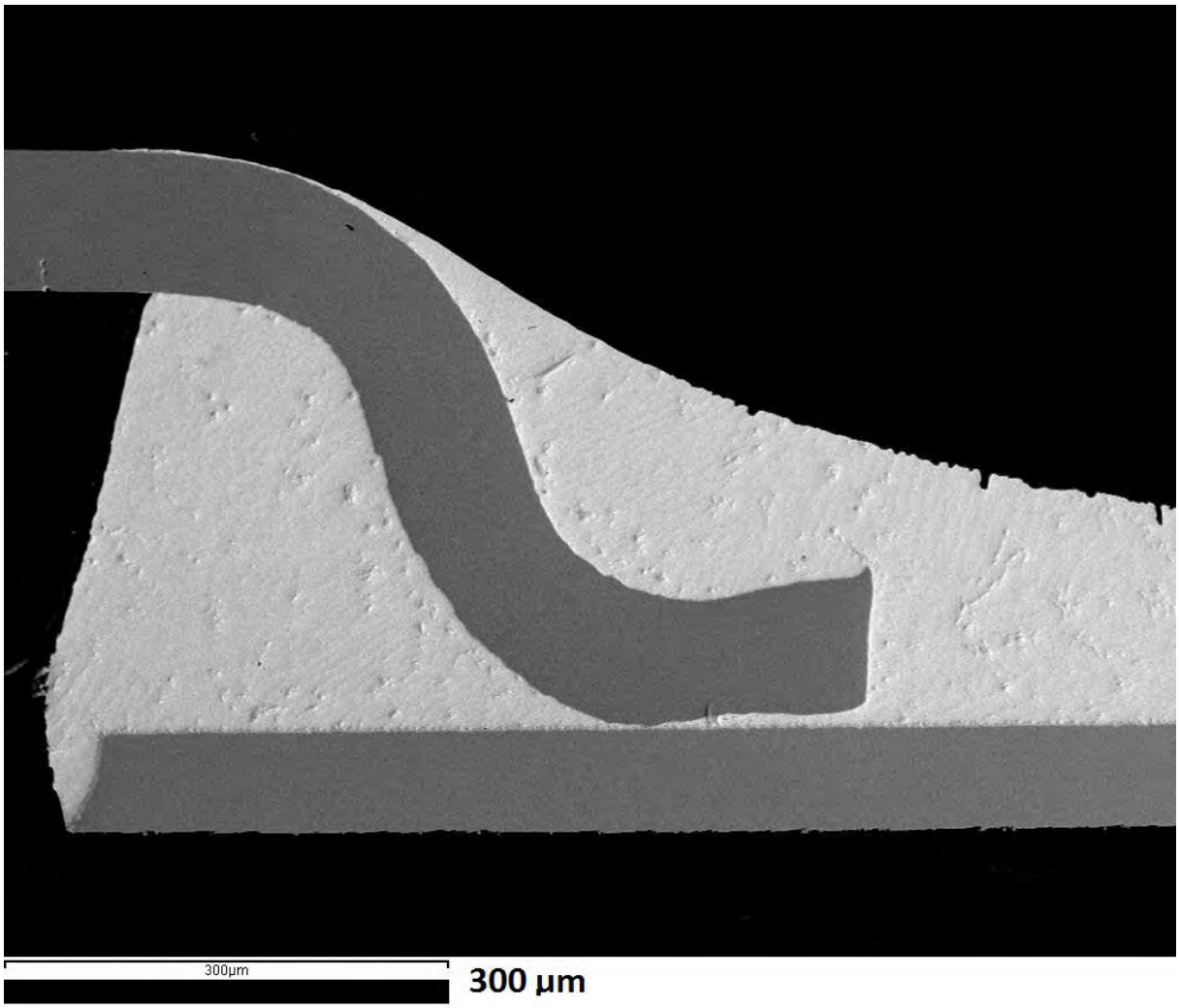


Figure 13: SEM image of the SOT3 coating cross – section with decreased brightness that shows the lead in the solder.

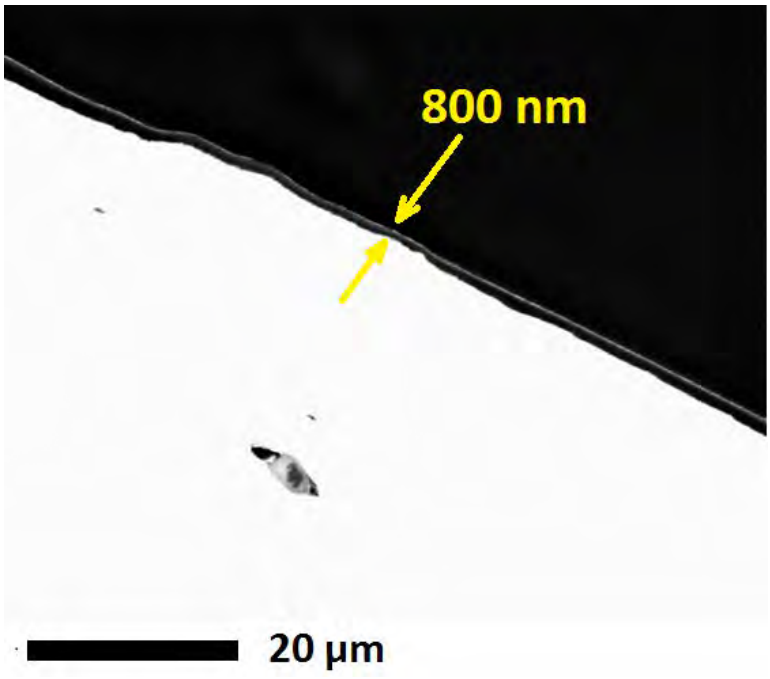


Figure 14: High magnification SEM image of the SOT3 coating cross – section in the lead knee region showing 0.8 micron (800 nm) thick coating, 3,000x.

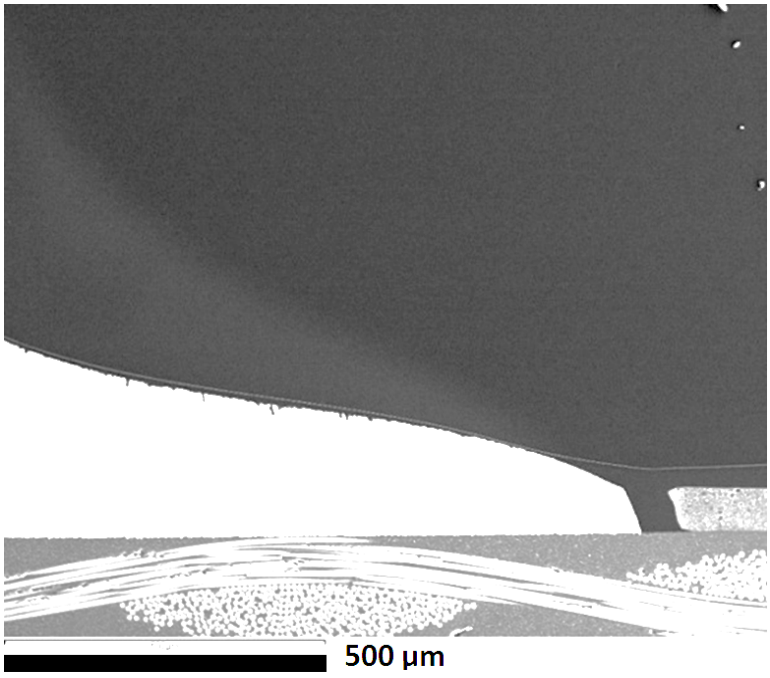


Figure 15: Close-up SEM image of the SOT3 cross – sectioned solder joint in the toe region, 100x.

1.3.2.2 SOT5 Coating thickness

The SOT5 coating thickness was examined in section planes A and B of Figure 2. The side profile section plane A images are shown in Figure 16 and Figure 18 and front section plane B images are given in Figure 28 and Figure 29. The conformal coating covered the front of the lead when examined in the side view (plane A). A minimum thickness of about 1.3 microns was observed on the knee, but the back side of the lead was not covered. From the front section (plane B), there was thick coating between leads almost to the top of the lead. Good coverage was observed up to the knee of the lead and then very thin coating about 0.15 micron on the corner.

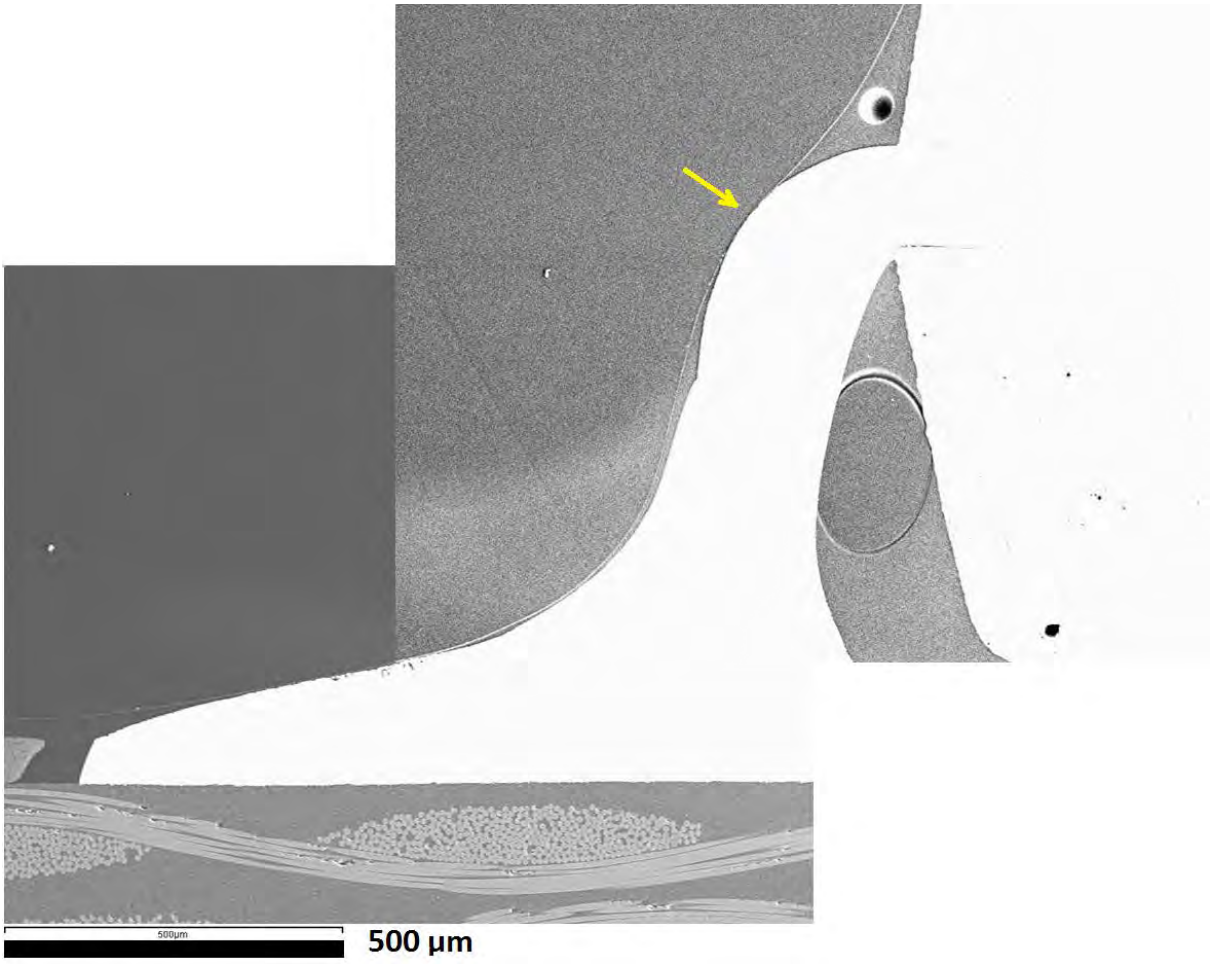


Figure 16: Composite SEM image of the SOT5 coating cross – section (plane A Figure 2), 100x. There is a coating void behind lead leaving an uncoated region. The coating on the knee is 1.3 microns (see Figure 29).

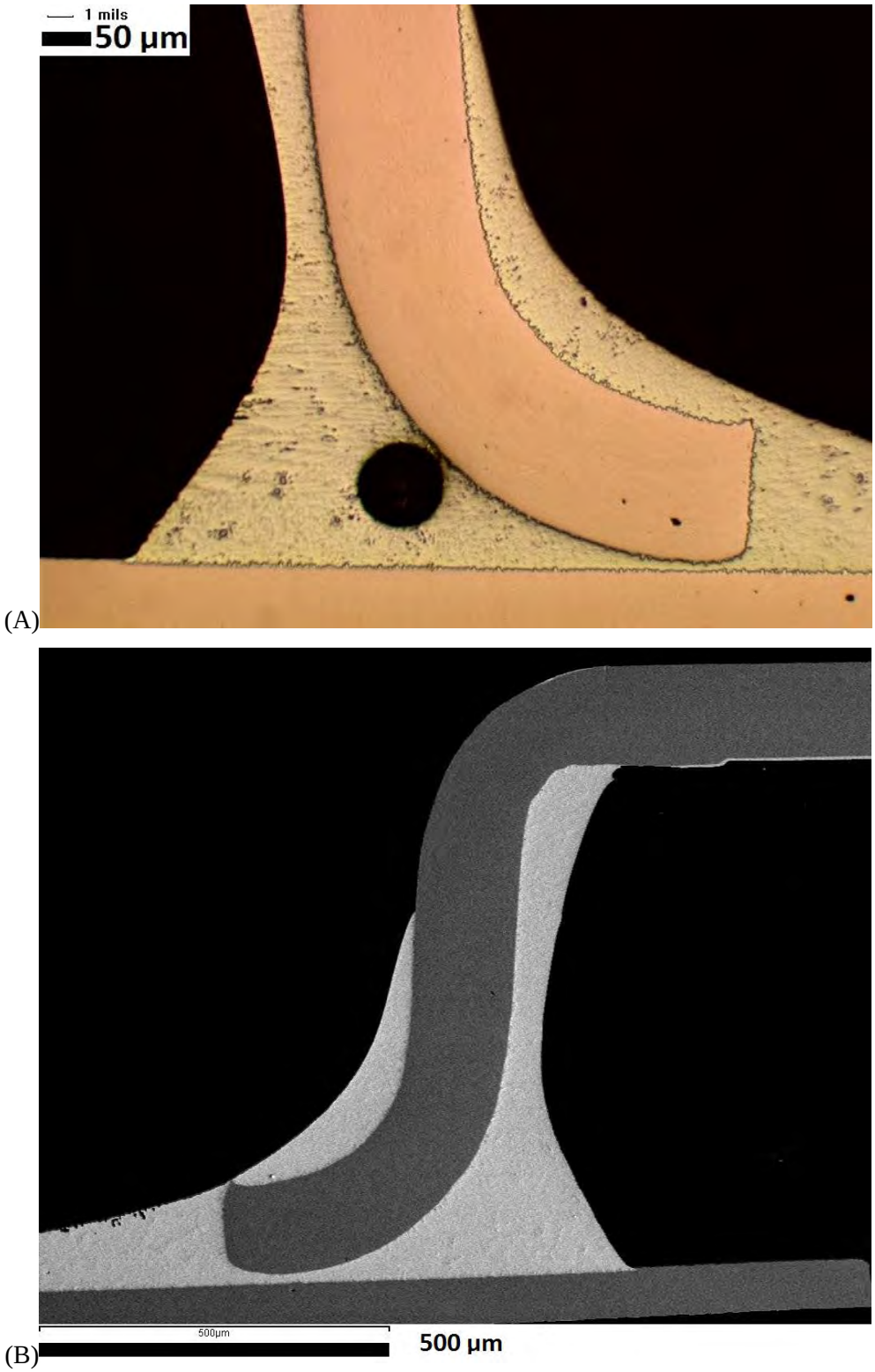


Figure 17: Images of the SOT5 coating cross – section with reduced brightness to show lead; (A) optical and (B) SEM.

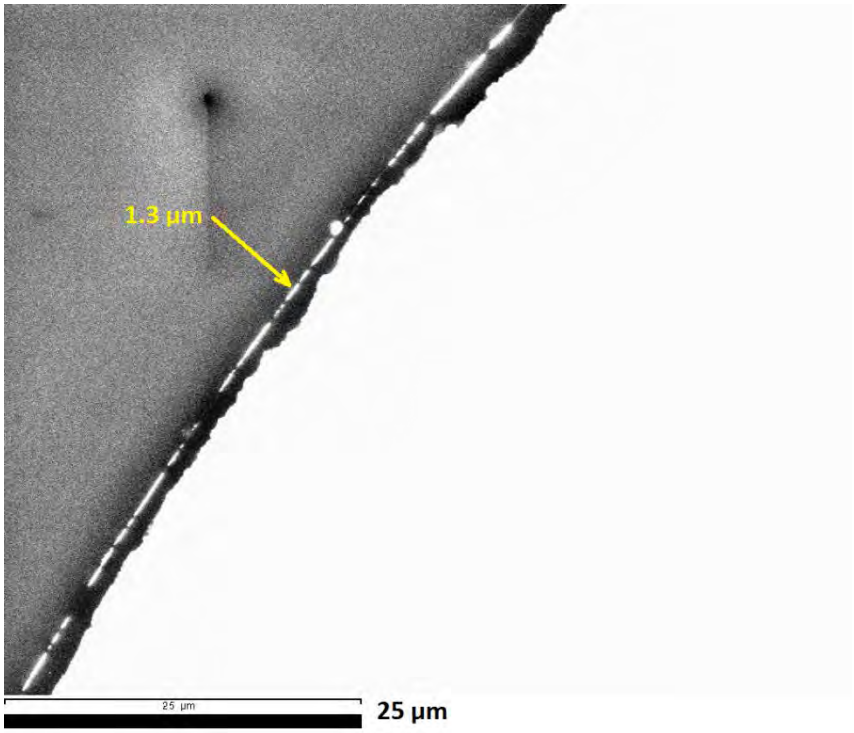


Figure 18: High magnification SEM image of the SOT5 coating in the knee region, 2,000x.

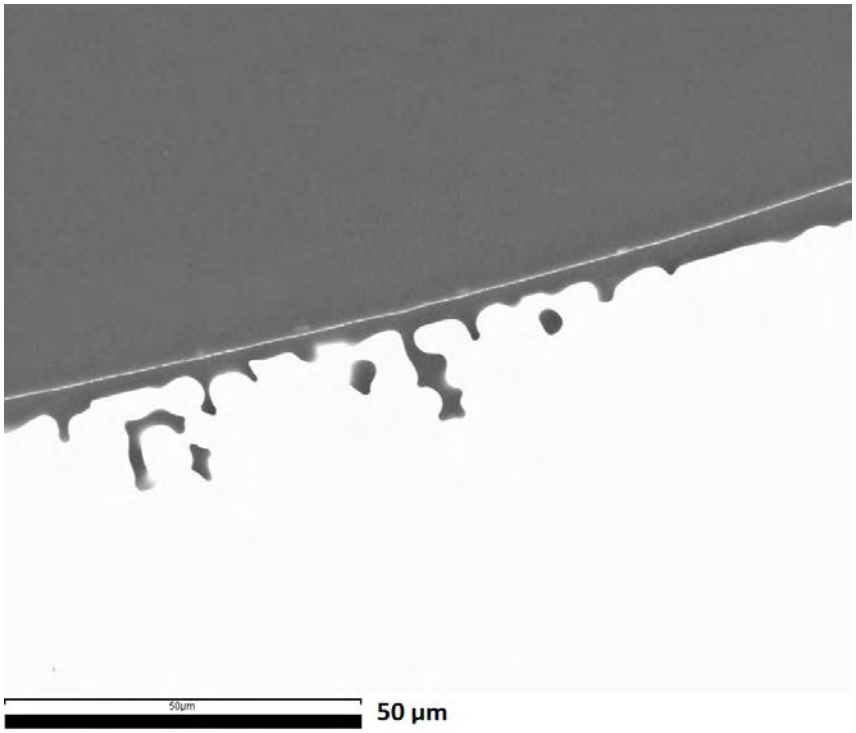
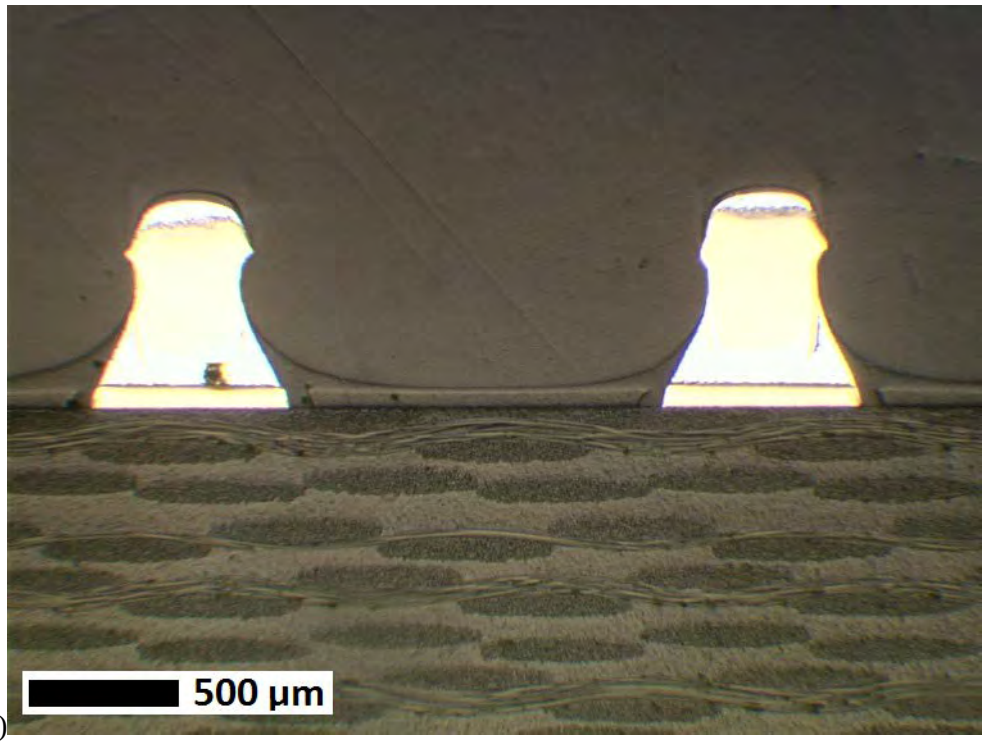


Figure 19: High magnification SEM image of the SOT5 coating in foot region, 1,000x.

(A)



(B)

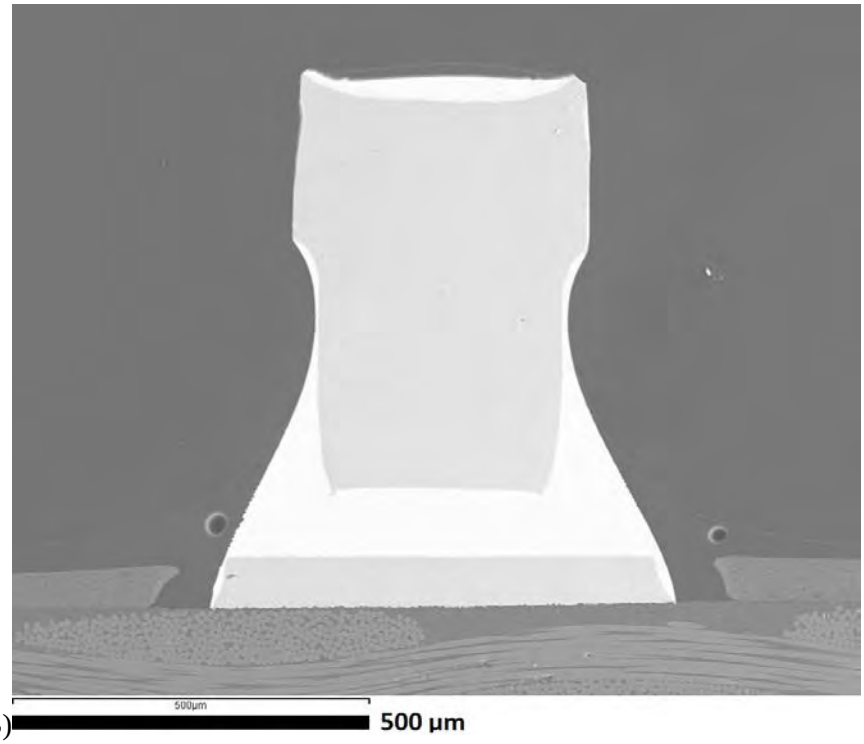


Figure 20: Overall SOT5 front grind coating cross – section images obtained by grinding into the vertical part of the lead from the toe (see Figure 2 plane B); (A) optical, 25x, and (B) deeper grind plane SEM, 100x. The approximate location of the section plane is shown in Figure 21.

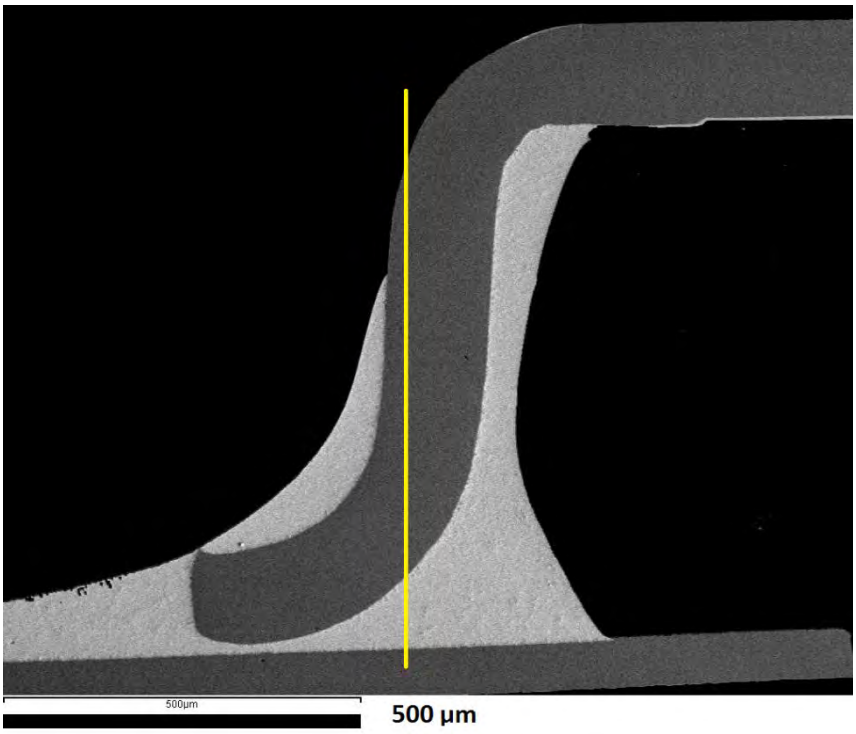


Figure 21: SEM image of the SOT5 cross – section annotated to show the approximate front section plane location.

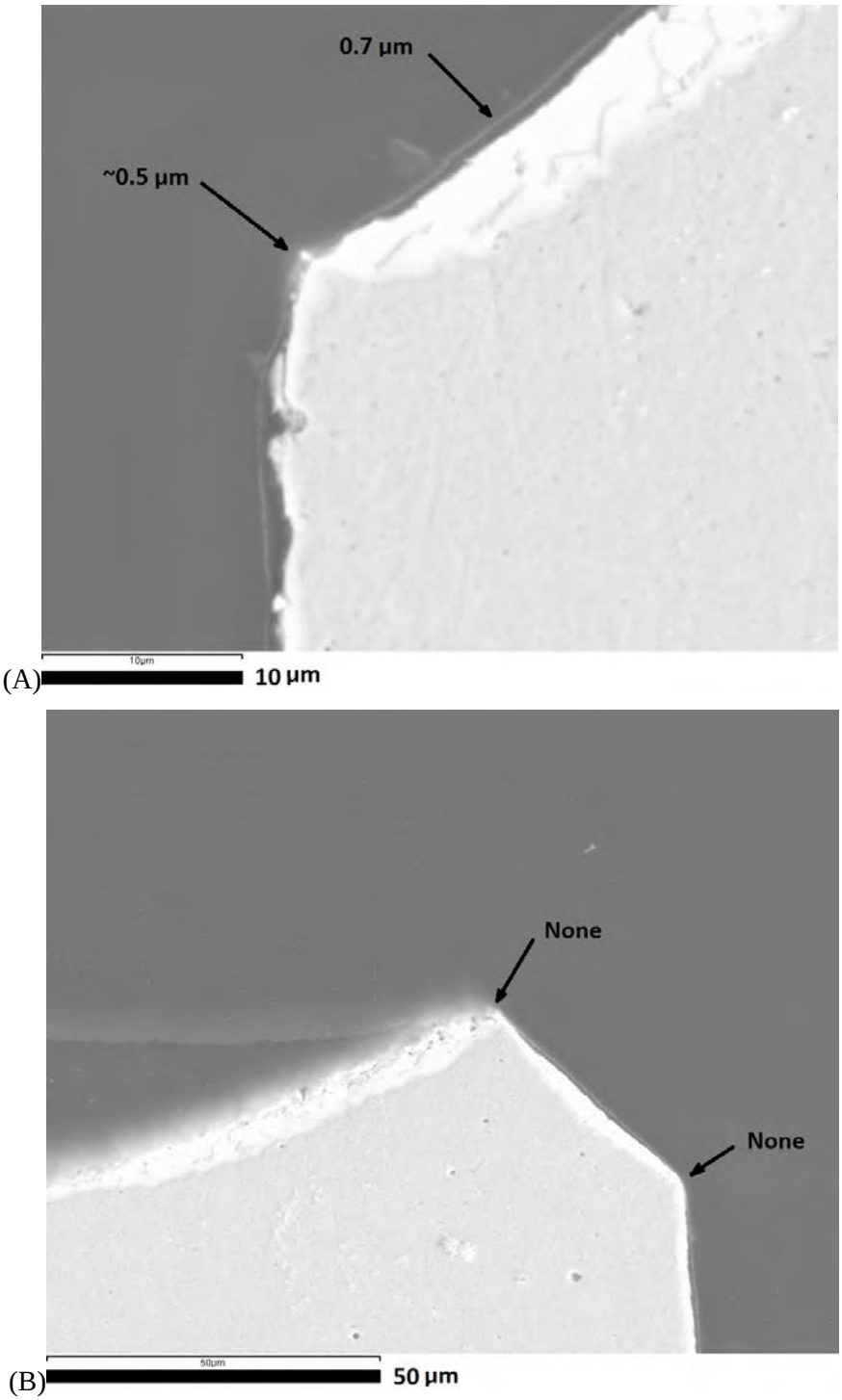


Figure 22: High magnification images of the SOT5 coating front grind cross – section of the top corners of the lead in section plane B; (A) 1,000x and (B) 3,000x.

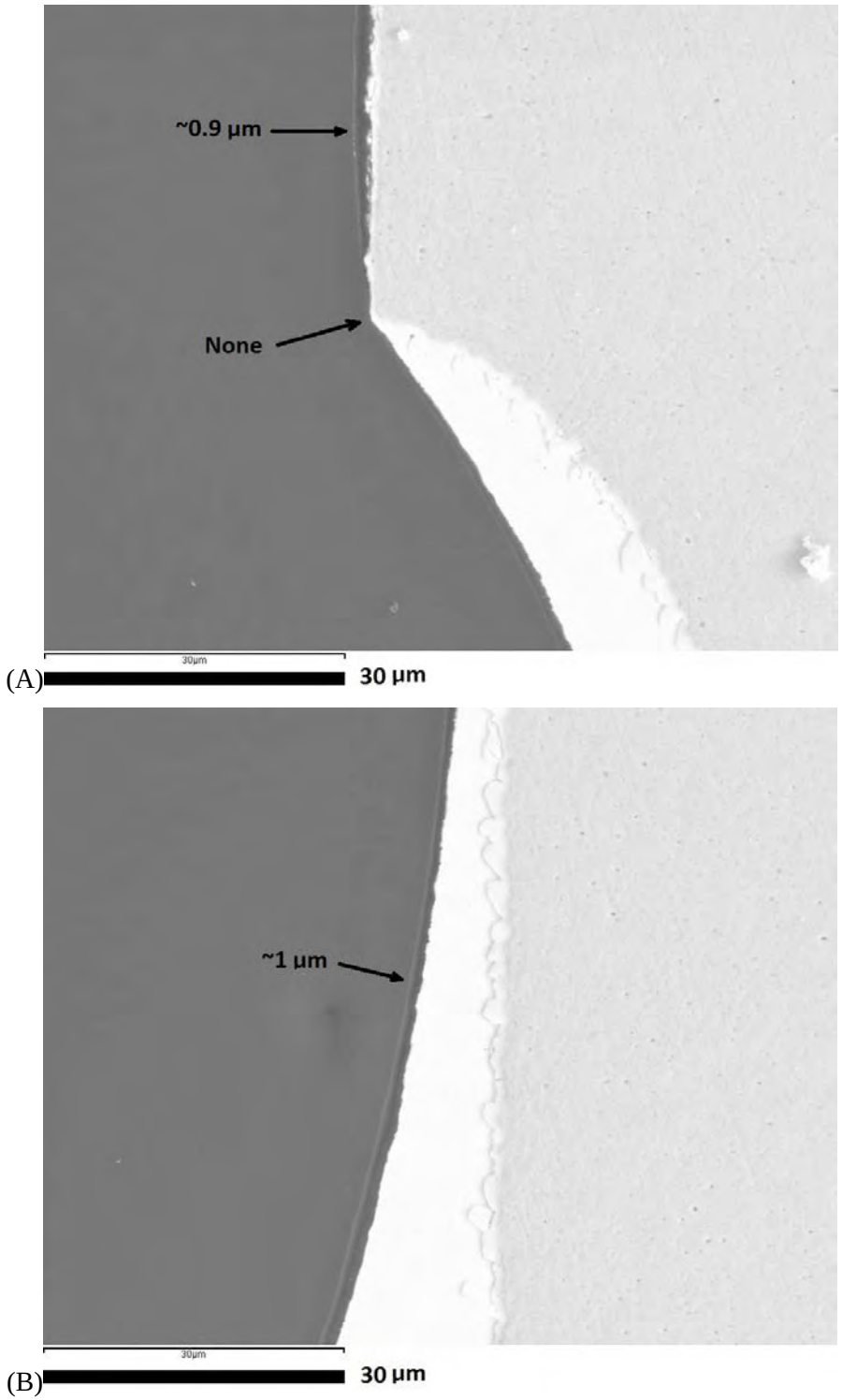


Figure 23: High magnification images of the SOT5 front grind coating cross – section of the left of the lead in section plane B, 1,500x.

1.3.2.3 SOT6 Coating thickness

The SOT6 coating thickness was examined in section planes A and B of Figure 2. Side profile section plane A images are shown in Figure 25 and Figure 27 and front grind section plane B images are given in Figure 28 and Figure 32. Generally, very thin coating was seen on the knee, only about 0.3 microns. The back side of the lead was not covered. The front grind showed that the coating between the leads was very thick and built up almost to the top of lead at the knee but the coating thickness on the top corners was very thin, only about 0.1 microns.

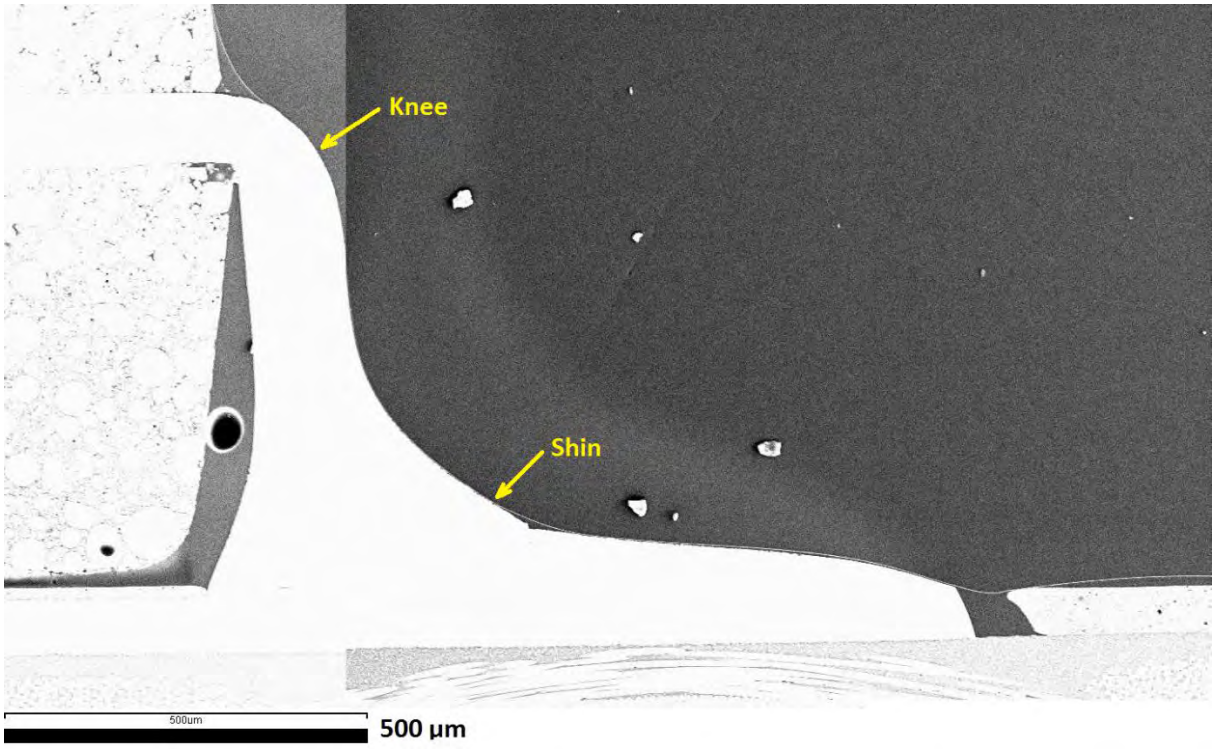
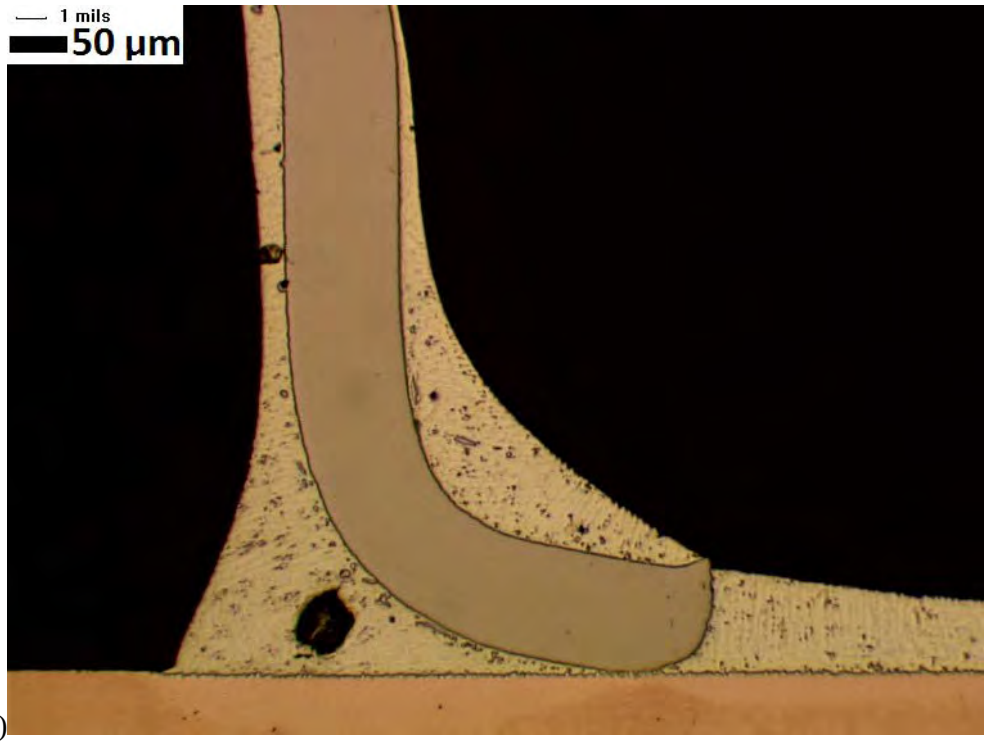


Figure 24: SEM image of the overall SOT6 coating cross – section (plane A Figure 2). Note that there was no coating behind the lead.

(A)



(B)

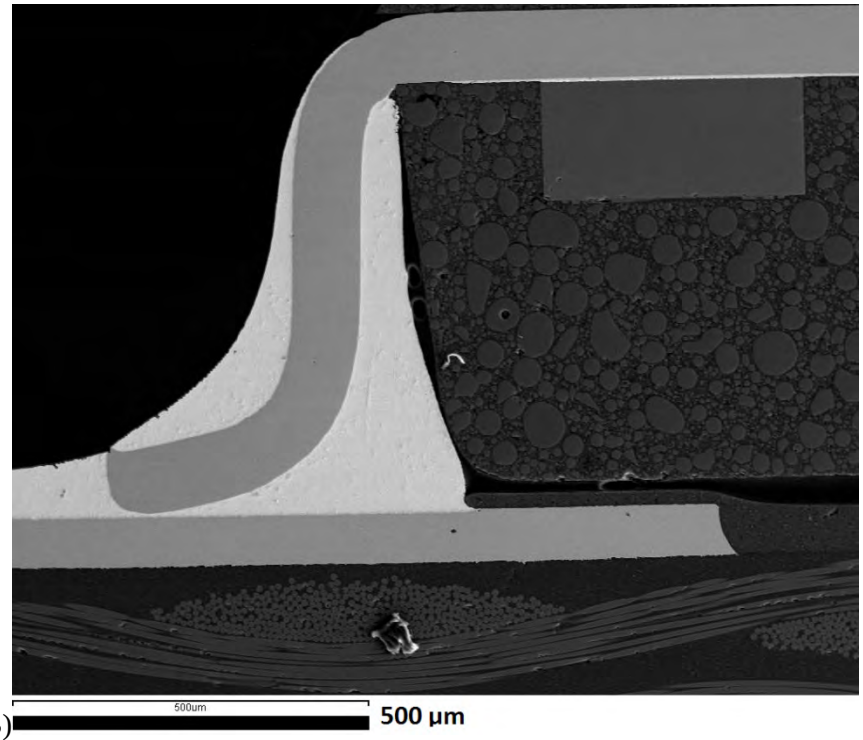


Figure 25: Overall SOT6 coating cross – section images showing the lead; (A) Optical, 100x, and (B) SEM image with reduced brightness.

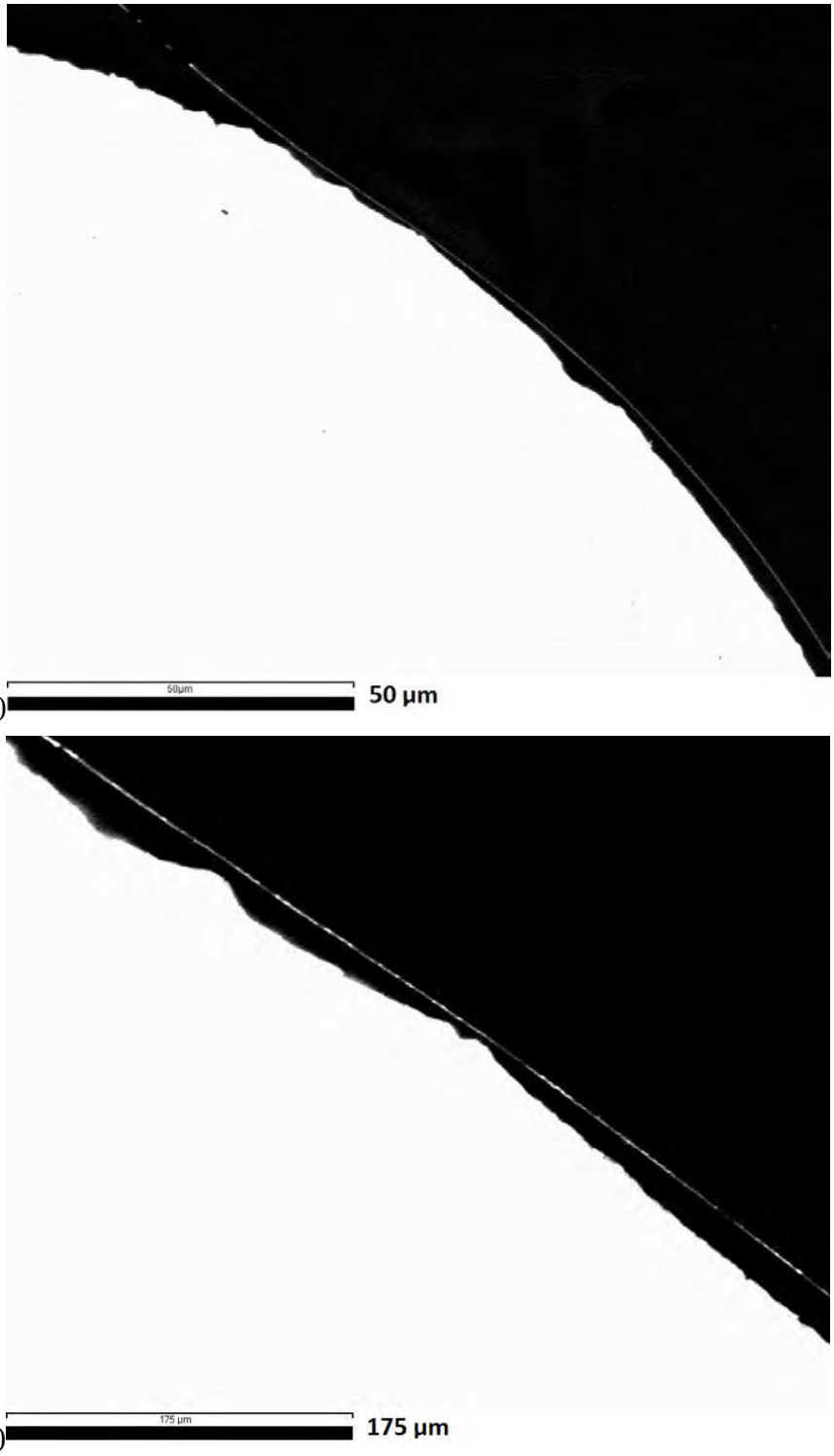


Figure 26: SEM image of the SOT6 coating cross – section in the knee region. At its thinnest location, the conformal coating is only 0.3 microns; (A) 1,000x and (B) 3,500x.

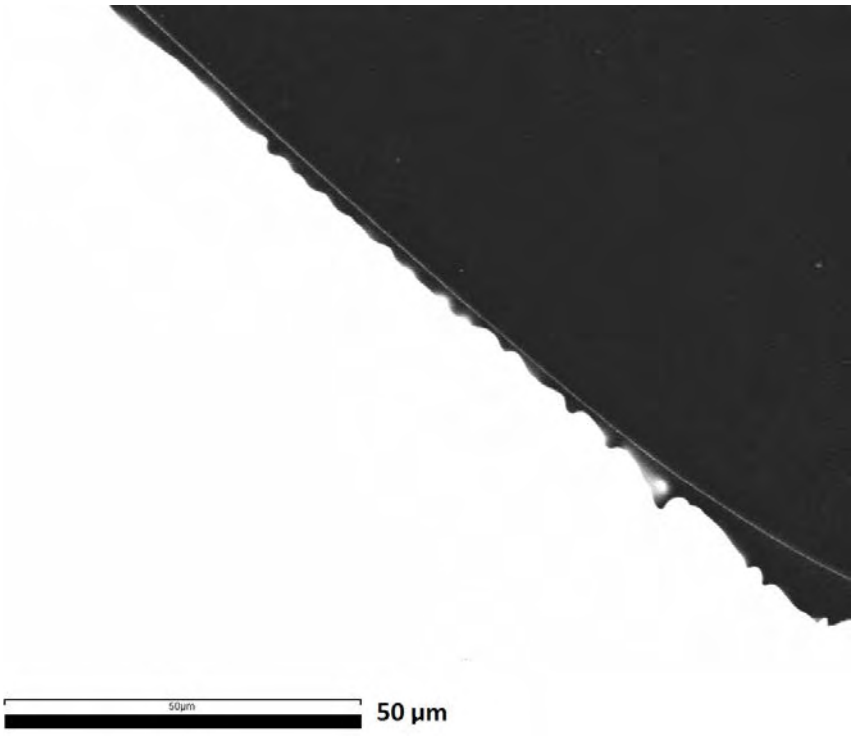
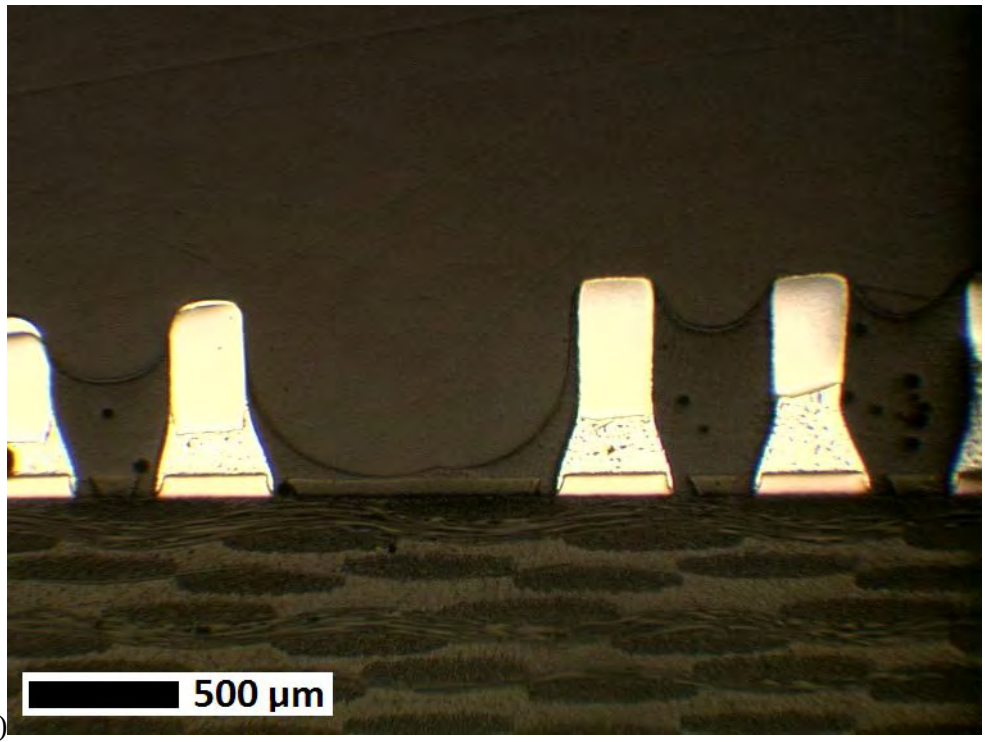


Figure 27: SEM image of the SOT6 coating cross – section between the shin region and the foot, 1,000x.

(A)



(B)

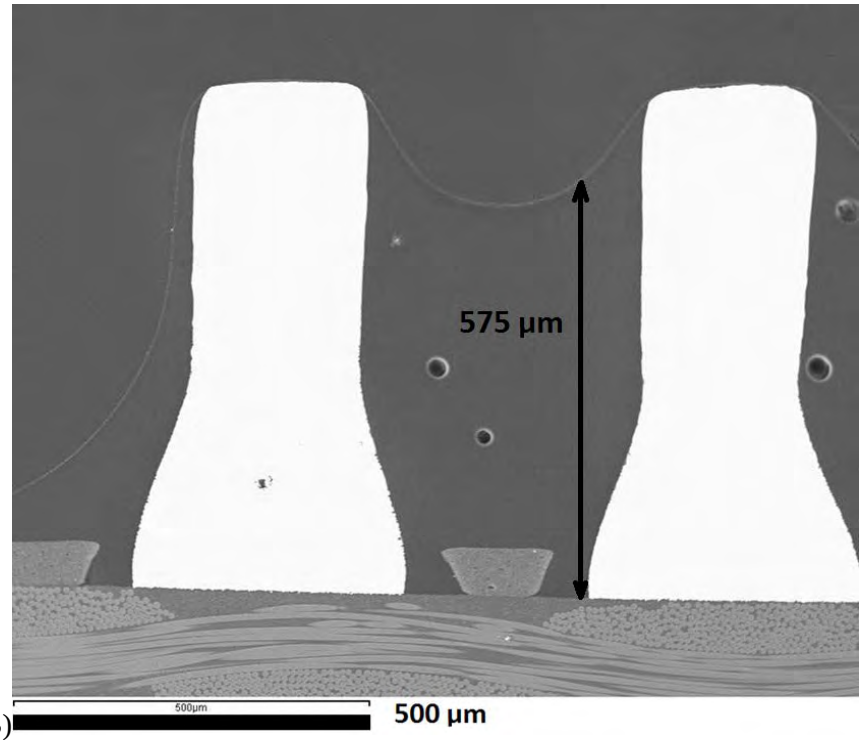


Figure 28: First front grind of the SOT6 coating cross – section images obtained by grinding into the vertical part of the lead from the toe (see Figure 2 plane B); (A) optical,25x, and (B) SEM, 100x.

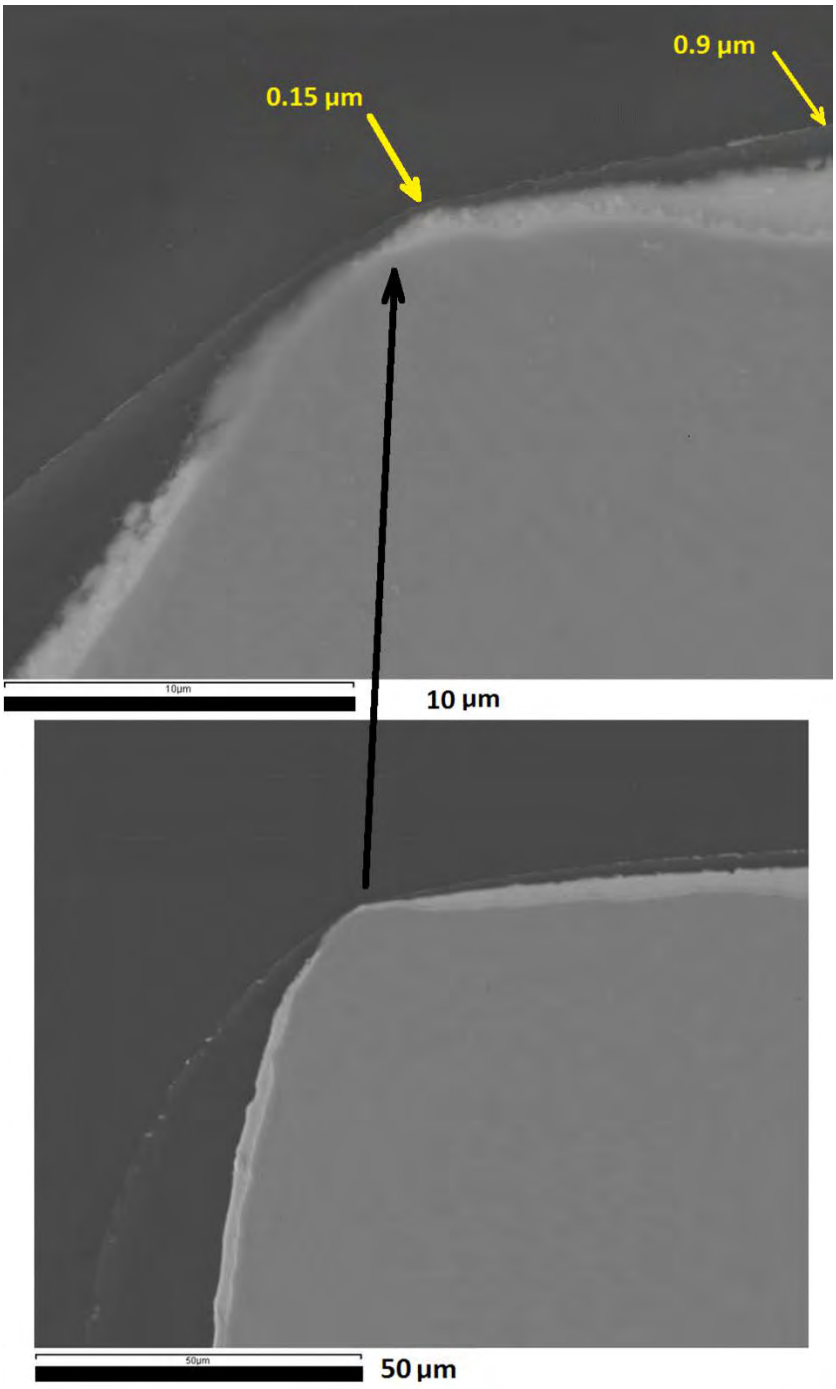
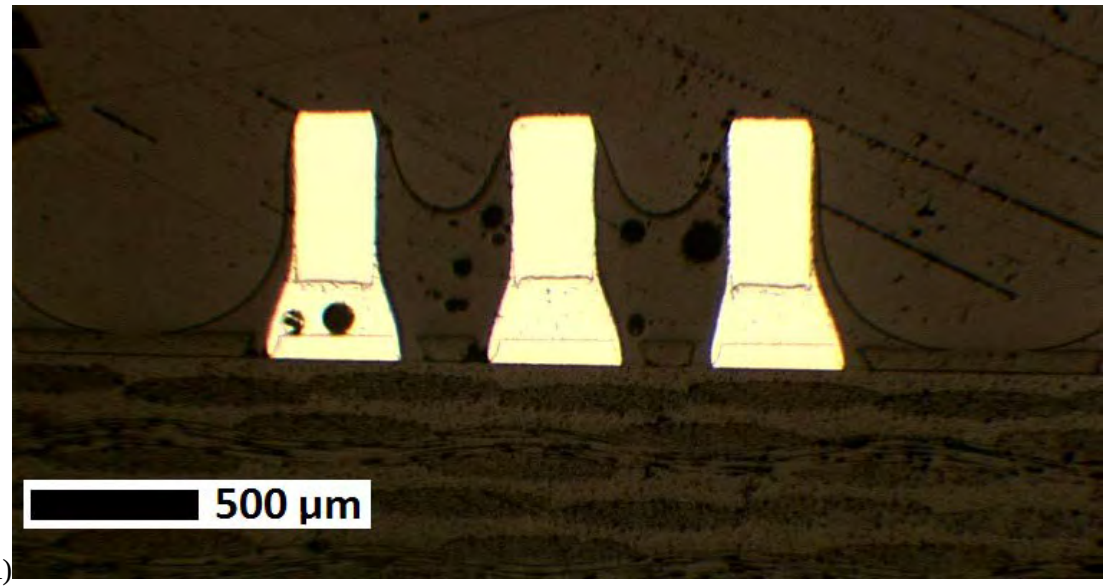


Figure 29: High magnification SEM images of the SOT6 cross – section of the top of lead of Figure 28, 1,000x and 3,000x. The coating on the corner is 0.15 microns.

(A)



(B)

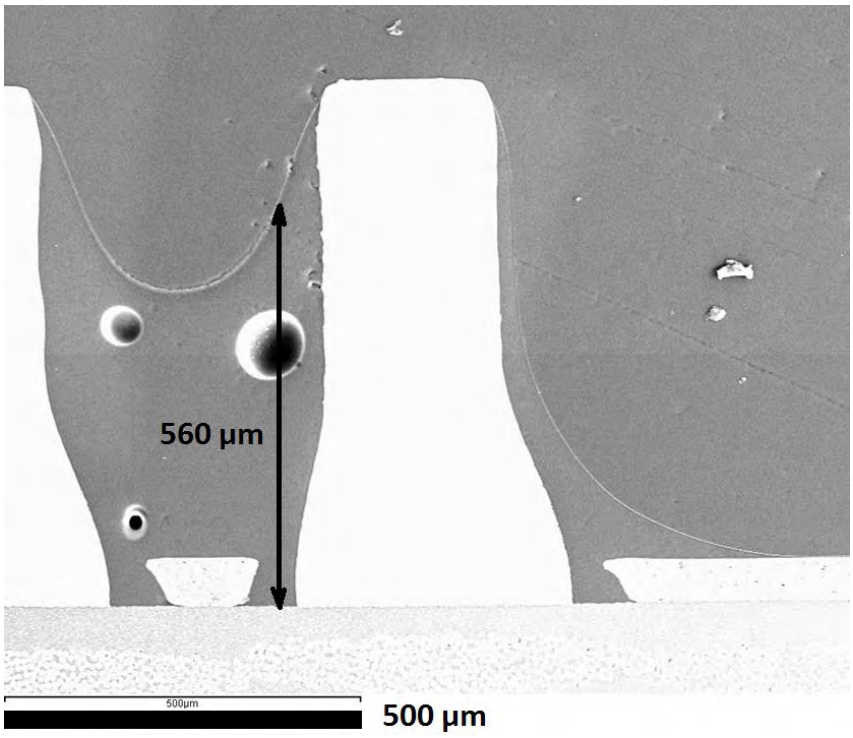


Figure 30: Overall deeper second front grind SOT6 coating cross – section images; (A) optical, 25x, and (B) SEM, 100x. The arrow shows where the height of the conformal coating on the side of the lead between leads is 560 microns.

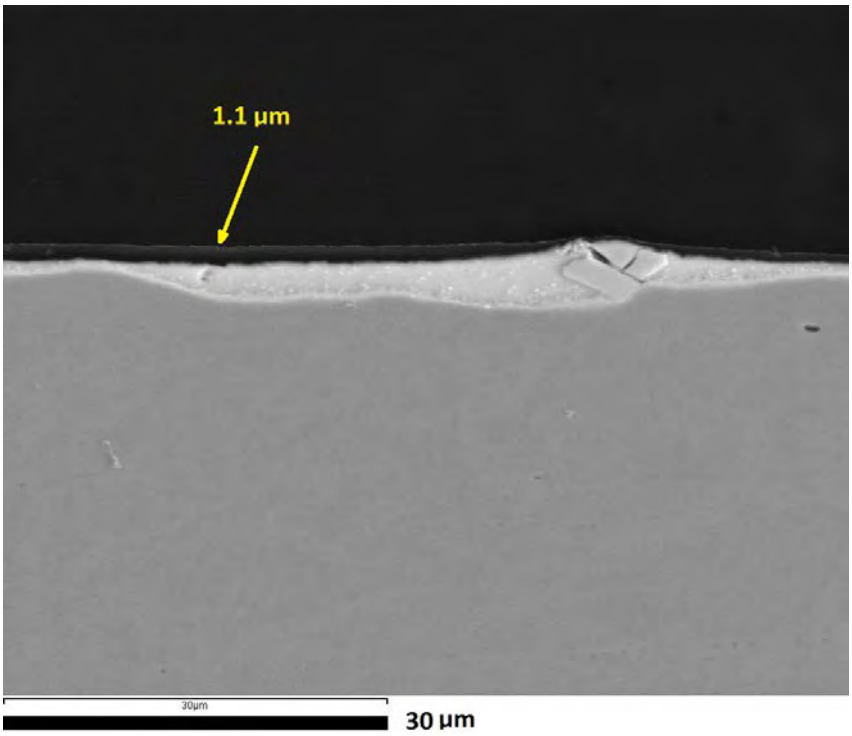


Figure 31: SEM image of the SOT6 coating front grind cross – section at the top of lead, 1,800x.

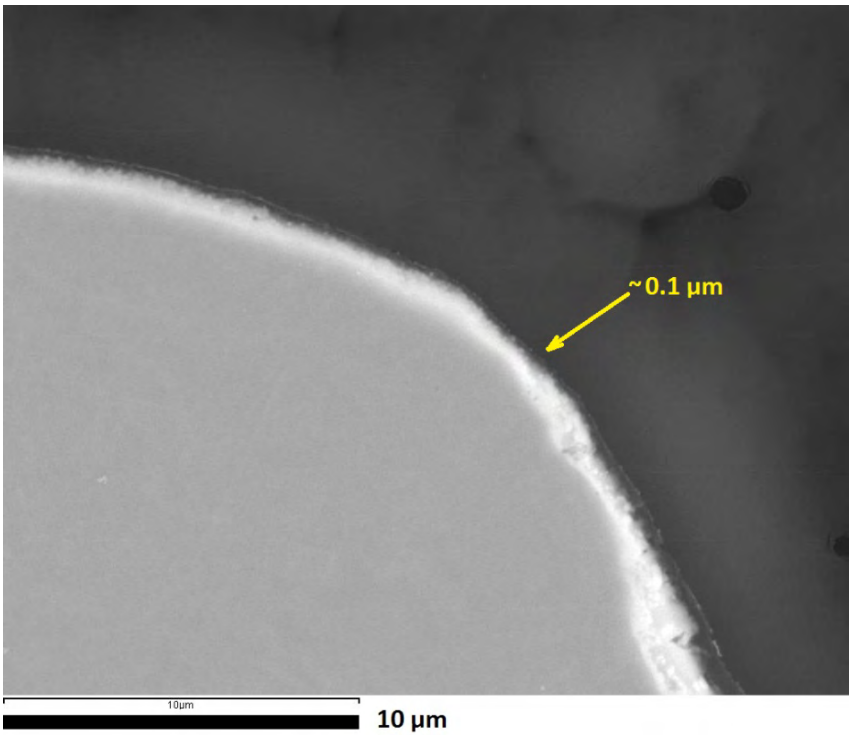


Figure 32: SEM image of the SOT6 coating front grind cross – section at the top corner of lead, 5,000x.

1.4 Whisker inspection results at 1,797 prior to starting the 6,000 PCTC cycle test

Whisker inspections were performed after 250, 730 (250 + 480), and 1,797 (250 + 480 + 1067) cycles from +50 to 85°C with a one hour cycle with 15 minute ramps and dwells. No whiskers were observed at the 250 cycle inspection. At the 730 and 1,797 cycle inspections, whisker nucleation and growth were observed. The maximum whisker length was 19.4 microns after 1,797 cycles on the SOT3 part with the 1-1 contamination level (Figure 33). The whiskers grew in the region where the lead exits the solder fillet and the solder is thin (Figure 34). Contamination level had a slight impact on whisker length (Figure 35).

No cracks or whiskers were observed on the coated samples (Figure 40 to Figure 49).

The primary goal of the extended testing to 6,000 cycles was to evaluate changes in the conformal coated samples and a secondary goal was to determine if whisker growth continued.

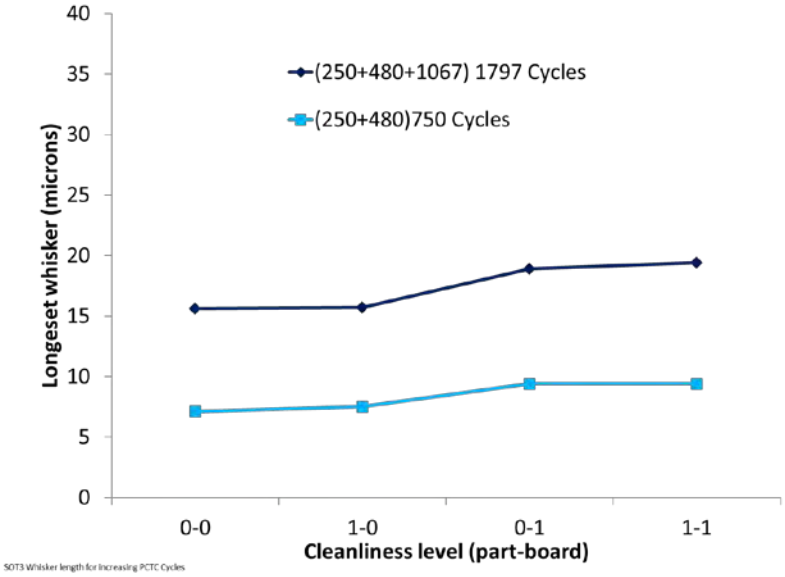


Figure 33: SOT3 maximum whisker length results after a total of 1,797 PCTC cycles.

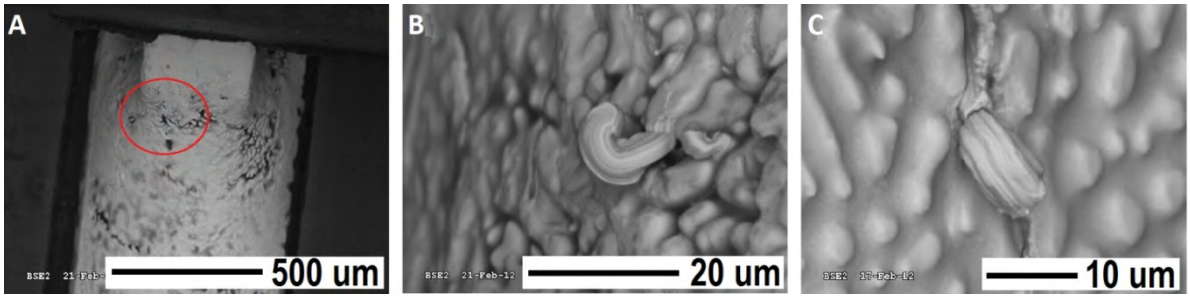


Figure 34: SEM images showing whisker growth on alloy-42 lead solder joint after a total of 1,797 PCTC cycles; (A) overall view highlighting whisker growth where the lead exits the top of the solder joint with (B) and (C) showing higher magnification whisker growth images.

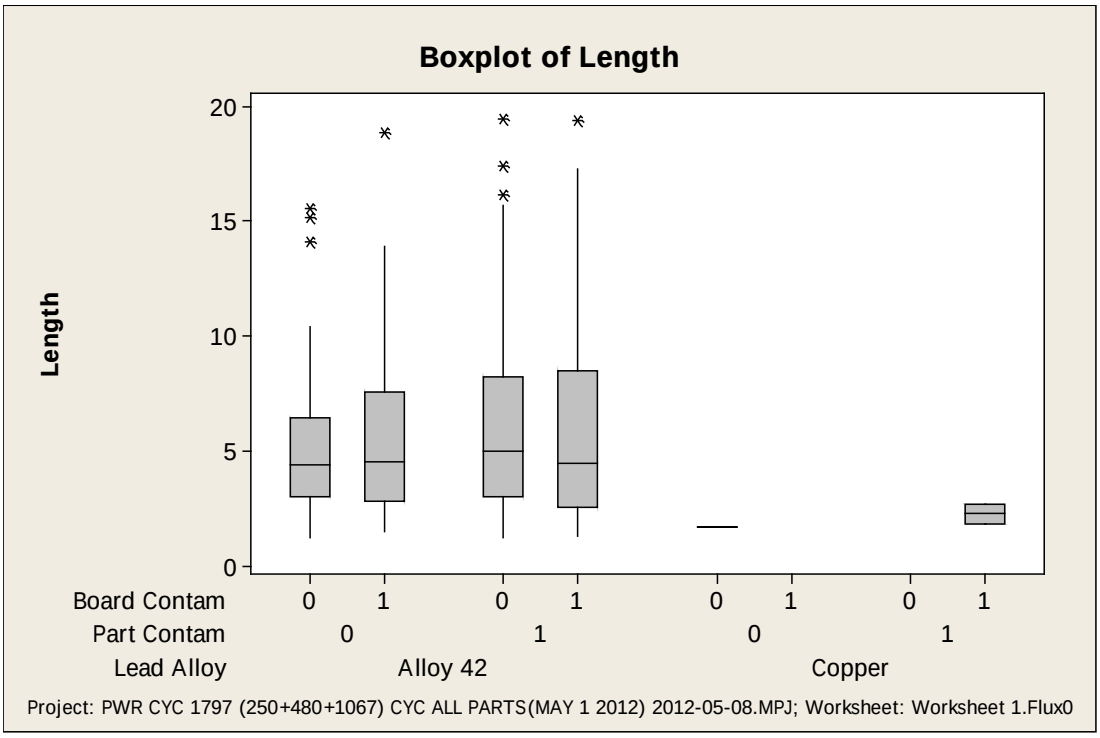


Figure 35: Box plot comparing whisker length (microns) for lead alloy, part contamination and board contamination combinations after 1,797 PCTC cycles where no flux was applied.

1.5 Metallurgical observations at 1,797 PCTC cycles

As is seen in Figure 36 and Figure 37, in some cases, the whiskers grew from between the tin dendrites. Figure 38 illustrates that there are several stress relaxation mechanisms occurring. In addition to whisker growth, there is grain boundary sliding, crack formation and grain recrystallization. The micro-cracks (Figure 39) that have formed to relieve the stresses often occur between the primary tin dendrites, around the Cu_6Sn_5 Intermetallic (IMC), and in some cases through Ag_3Sn IMC after thermal cycling.

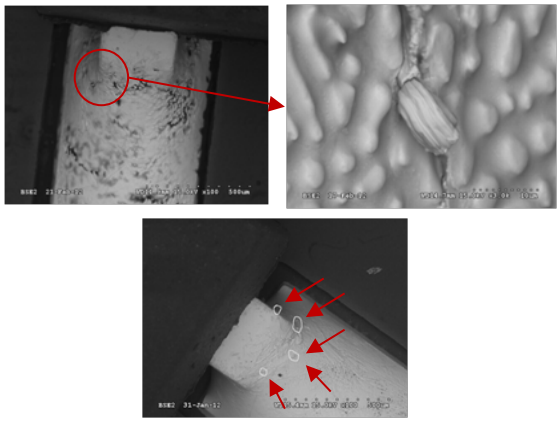


Figure 36: Whiskers observed on the SOT3 part with 1-1 contamination without flux after 1,797 PCTC cycles.

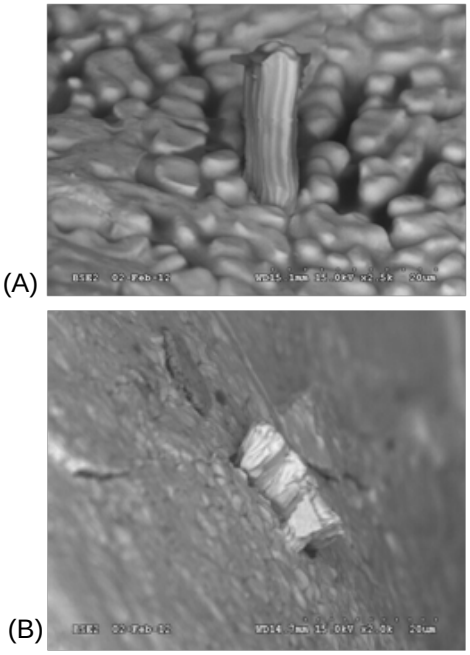


Figure 37: Whiskers observed on the SOT6 part with 1-1 contamination with flux applied after 1,797 PCTC cycles.

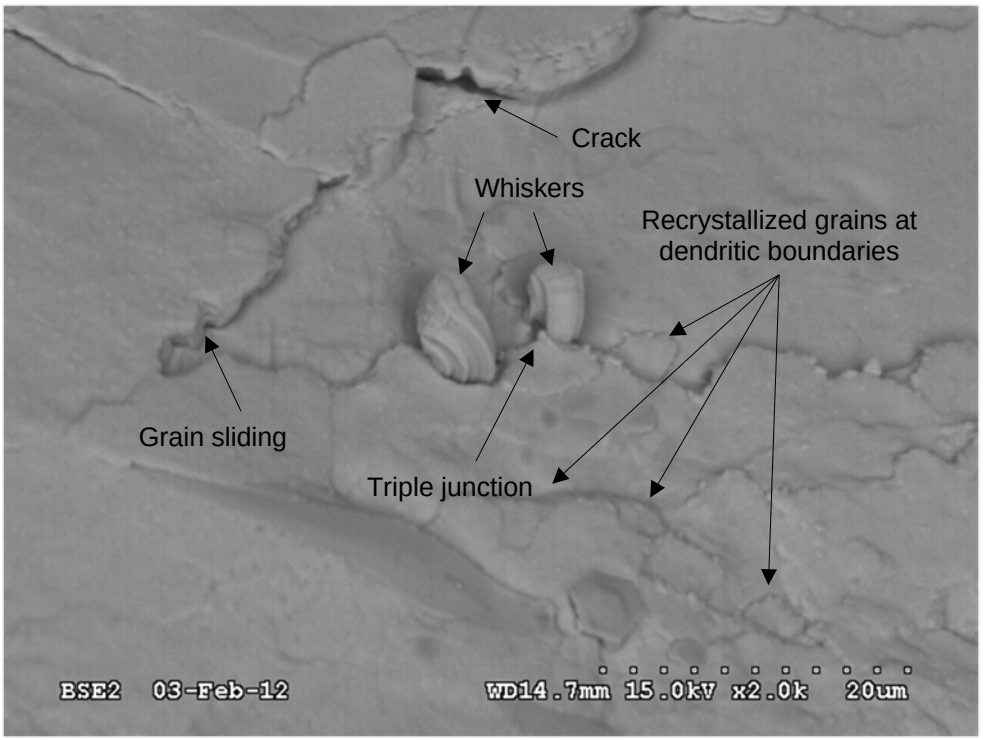


Figure 38: Competing mechanisms of stress relaxation (SOT3, 0-0 contamination level) after 1,797 PCTC cycles.

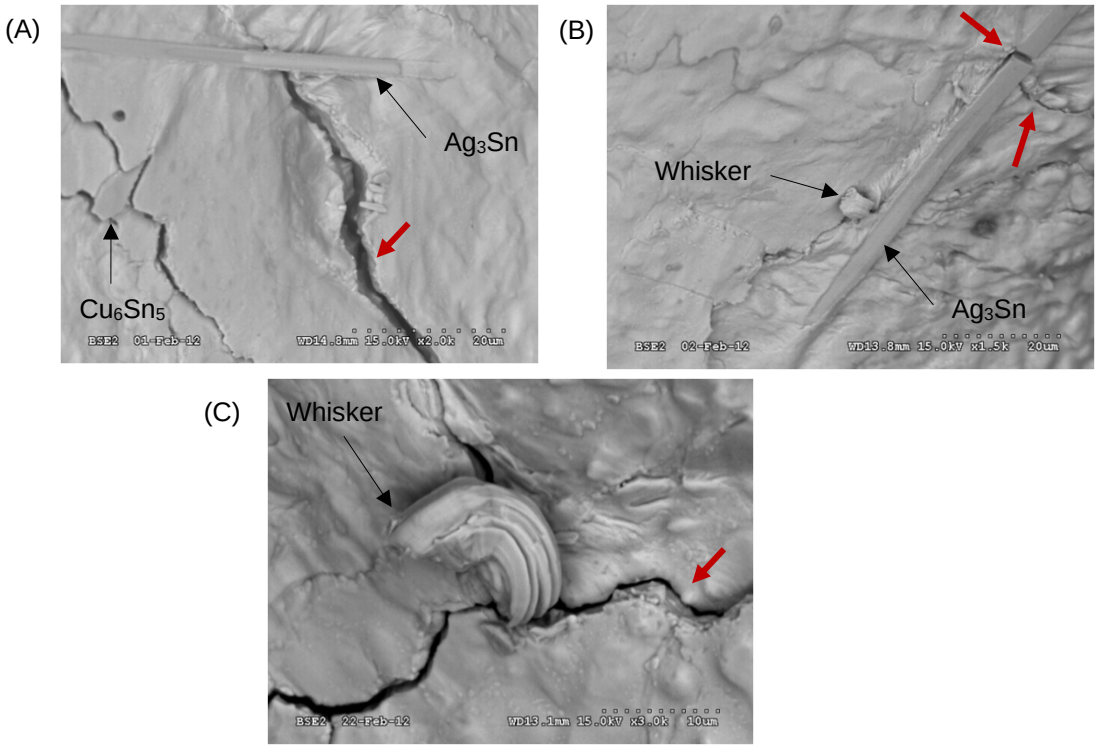


Figure 39: Micro-cracks (red arrows) in SAC305 fillets observed after 1,797 PCTC cycles; (A) SOT3 0-0 contamination level, (B) SOT3 1-1 contamination level with whisker adjacent to Ag_3Sn IMC and (C) SOT3 1-0 contamination level with whisker growing from primary tin dendrite triple junction Micro-cracks.

1.6 Coating inspection at 1,797 PCTC cycles

Typical inspection photos at the 1,797 cycle interval are shown in Figure 40 to Figure 49. There was no evidence of tin whiskers, other tin growths, or coating cracking. The coating wicked into the solder joint interdendritic spaces (Figure 49).



Figure 40: SEM image of a SOT3 with conformal coating with a 1-1 contamination level after 1,797 PCTC cycles, 40x (ref. B-SOT-PC-1-1-cc-3, SOT3).



Figure 41: SEM image of a SOT3 lead with conformal coating with a 1-1 contamination level after 1,797 PCTC cycles, 100x (ref. B-SOT-PC-1-1-cc-3, SOT3, 2).

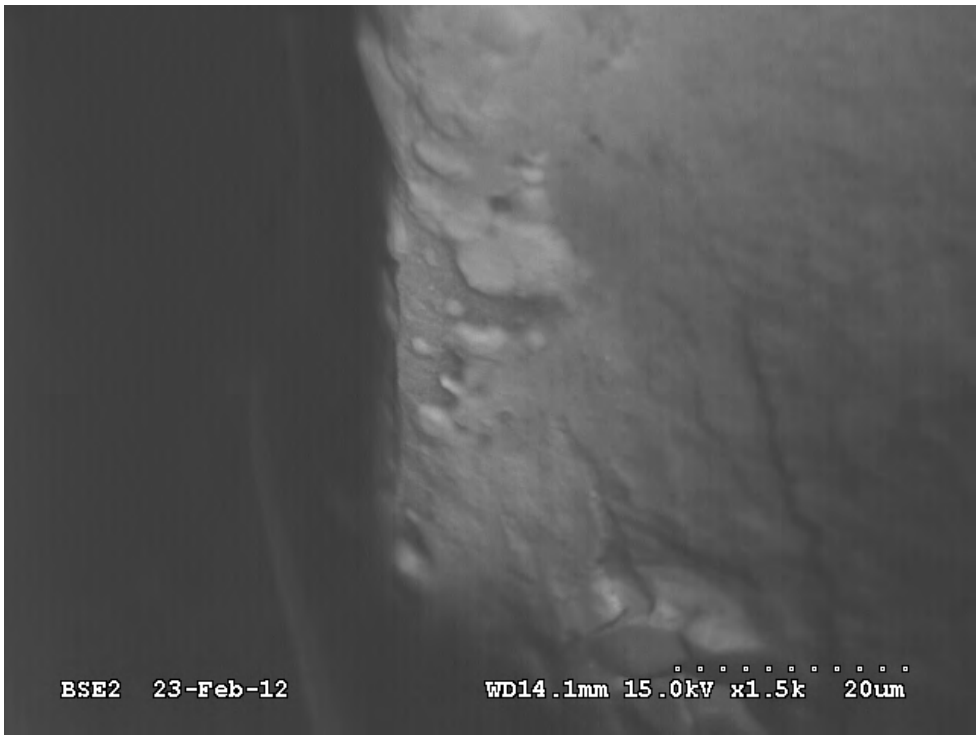


Figure 42: SEM image of a SOT3 lead with conformal coating with a 1-1 contamination level after 1,797 PCTC cycles, 1,500x (ref. B-SOT-PC-1-1-cc-3, SOT3).



Figure 43: SEM image of a SOT6 lead and solder joint with conformal coating with a 1-1 contamination level after 1,797 PCTC cycles, 100x, and (ref. B-SOT-PC-1-1-cc-2, SOT6).

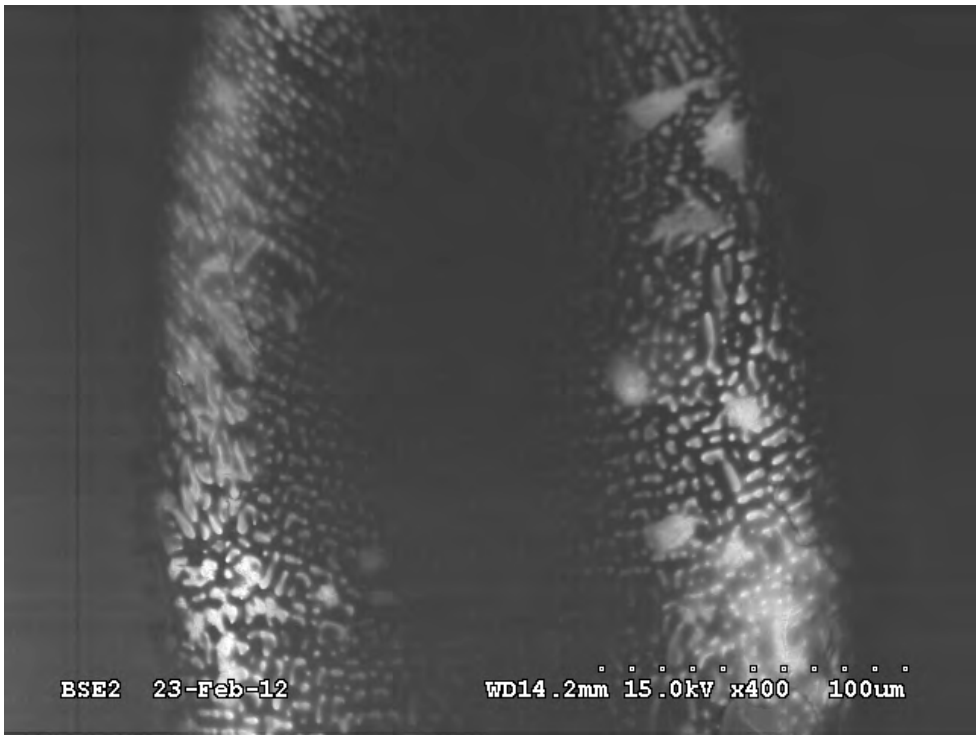


Figure 44: SEM image of a SOT6 solder joint with conformal coating with a 1-1 contamination level after 1,797 PCTC cycles, 400x (ref. B-SOT-PC-1-1-cc-2, SOT6).



Figure 45: SEM image of SOT6 leads with conformal coating with a 1-1 contamination level after 1,797 PCTC cycles, 45x (ref. B-SOT-PC-1-1-cc-3, SOT6).



Figure 46: SEM image of a SOT6 solder joint with conformal coating with a 1-1 contamination level after 1,797 PCTC cycles, 100x (ref. B-SOT-PC-1-1-cc-3, SOT6).

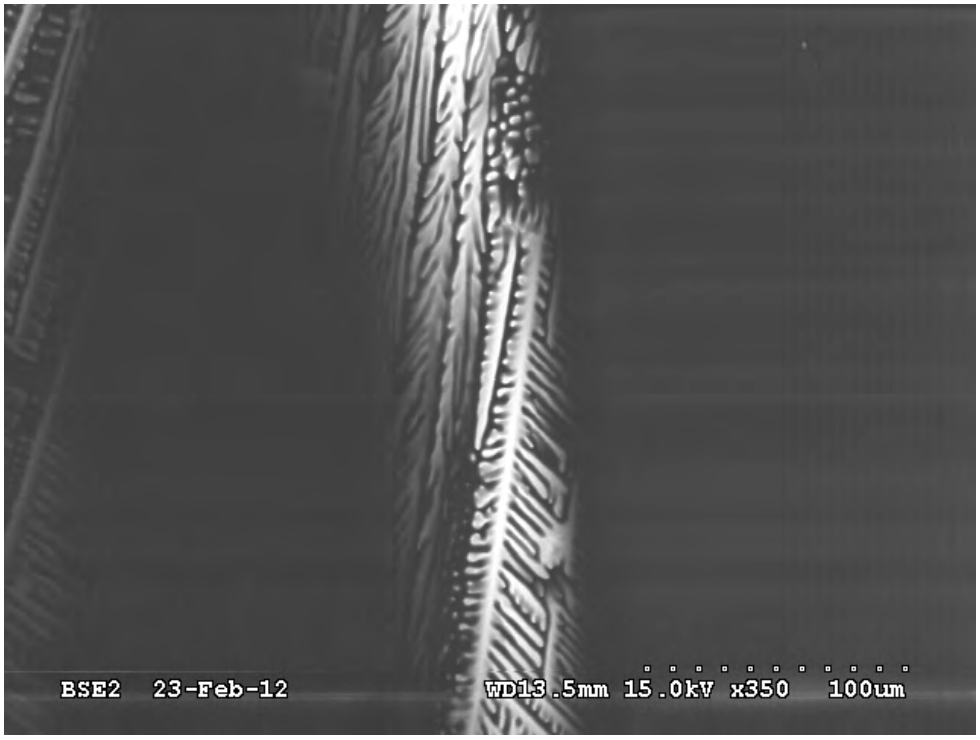


Figure 47: SEM image of a SOT6 solder joint with conformal coating with a 1-1 contamination level after 1,797 PCTC cycles, 350x (ref. B-SOT-PC-1-1-cc-3, SOT6).

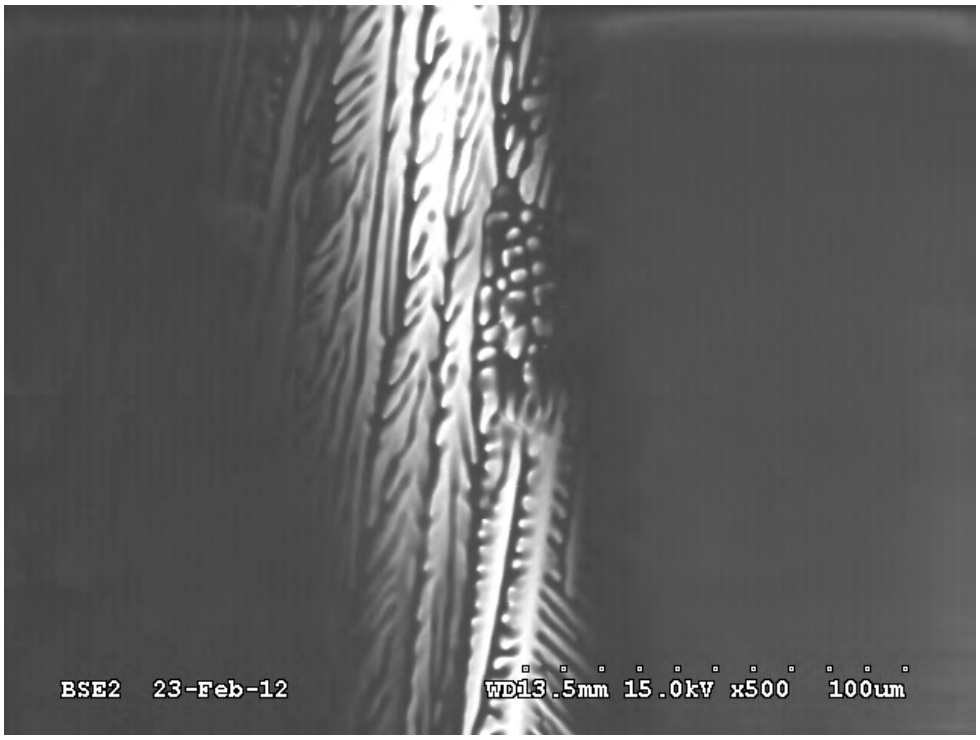


Figure 48: SEM image of a SOT6 solder joint with conformal coating with a 1-1 contamination level after 1,797 PCTC cycles, 500x (ref. B-SOT-PC-1-1-cc-3, SOT6). Close up of solder joint shown in Figure 47.



Figure 49: SEM image of a SOT6 solder joint with conformal coating with a 1-1 contamination level after 1,797 PCTC cycles, 1,000x (ref. B-SOT-PC-1-1-cc-3, SOT6).

2. Test vehicles, environmental exposure and inspection methods for 6,000 PCTC test

2.1 Test vehicles and environmental exposure

In the original testing, four of the original 20 boards were cross-sectioned after 1,797 cycles and there were 20 available for extended testing. The extended PCTC cycling test added 4797 cycles to the boards to obtain a total of 6,000 cycles. After a baseline inspection, the extended cycling started in January 2016 and finished in October 2016. The PCTC cycle is over a nominal temperature range of 50 to 85°C with 10 minute dwells and 33 minute dwells for a total of 88 minutes, except for the 250 first cycles (Table 2). During the extended cycling, the under shoot at the low temperature was reduced slightly compared to the original cycles. The overall duration of the environmental exposure was four years and one month. The evaluation consisted of four months of original testing (1 to 1,797 cycles), then 36 months room temperature storage, followed by nine months of extended testing (1,798 to 6,000 cycles).

Table 2: PCTC +50 to +85°C cycling dates and parameters

Original testing	Dates	Chamber	Measured maximum and minimum temperatures (°C)	Time (minutes) for ramps(R), hot dwell (HD), cold dwell(CD) and total cycle
Cycles 0 - 250	Sept-13-2011 to Sept-21-2011	101VTH	89 to 46	11R, 12HD, 11R, 12CD Total = 46
Cycles 251 - 730	Oct-4-2011 to Nov-1-2011	101VTH	89 to 46	33R, 12HD ,33R, 10CD Total = 88
Cycles 731 - 1797	Dec-1-2011 to Jan-29-2012	101VTH	89 to 46	33R, 12HD, 33R, 10CD Total = 88
Extended testing				
Cycles 1798 - 2245	Jan-12-2016 to Feb-16-2016	104TCV	89 to 48	33R, 12HD, 33R, 10CD Total = 88
Cycles 2246 - 6000	Feb-18-2016 to Oct-2016	101VTH	89 to 48	33R, 12HD, 33R, 10CD Total = 88

2.2 Inspection method

Whisker length, diameter, location, and angle measurements were made with the SEM at magnifications up to 3,000x. The growth location and growth angle are defined in Figure 50 and Figure 51, respectively. Given that the whiskers were short and stubby, a whisker was counted with lengths down 0.8 microns with (length:diameter) ratios as small as 1:2 (shorter length than the diameter) as long as there were striation indicative of typical whisker growth. The 1,797 cycle images were compared to the 6,000 cycle images to obtain instances of new whisker growth and for existing whiskers increases in length and changes in orientation were noted.

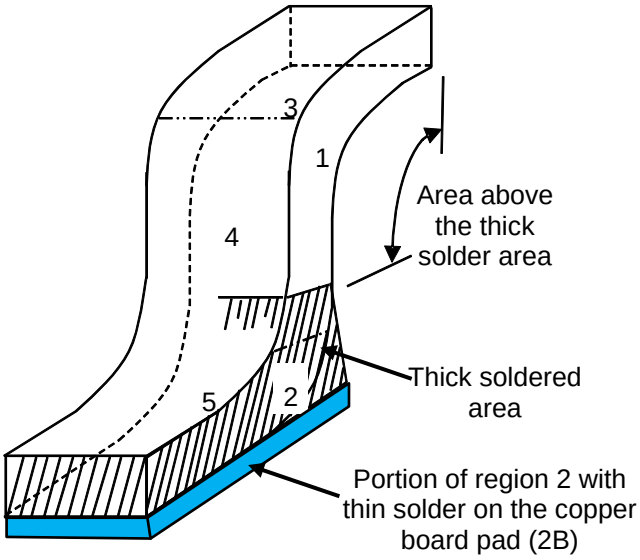


Figure 50: Whisker location definition. The hatched region 2 indicates the thick solder region on the lead and includes the thinner solder that wet onto the board pad. Areas 1, 3, 4 and 5 represent the thin solder or tin regions above the thick solder area.

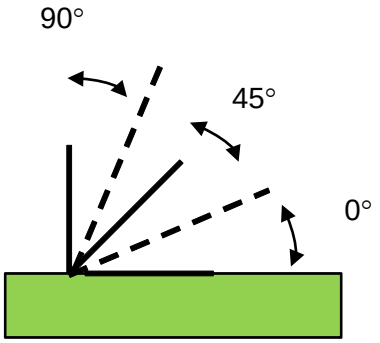


Figure 51: Whisker angle measurement definition

3. Results after 6,000 PCTC cycles

This section provides whisker, length, diameter, and location data from the uncoated sample whisker inspection. Then a metallurgical review of the uncoated samples is provided, followed by the an examination of the conformally coated samples.

3.1 Whisker statistics for 6,000 PCTC cycle samples

The inspection results are provided in Table 3 to Table 11 and in plots given in Figure 52 to Figure 64. Selected SEM images are provided in Figure 65 to Figure 109 for uncoated assemblies and in Figure 110 to Figure 127 for coated assemblies.

Tabular data review

The whiskers were generally kinked (Figure 66), but some were straight (Figure 68). The alloy 42 leads on the SOT3 and SOT6 parts exhibited the greatest whisker growth (Table 3). The Cu leads on the SOT5 part had very few whiskers. All the whiskers were shorter than 40 microns. Within the whisker count, there were a number of new whiskers and existing whiskers that grew longer (Table 4 and Table 5).

Examining the top ten longest whiskers from the SOT6 and SOT3 parts (Table 6 and Table 7), the whiskers were primarily a combination of new whiskers and existing whiskers that have grown longer. The longest whisker on the SOT6 part happened to be a new whisker while the on the SOT3 part it was an existing whisker that grew longer. In both cases, the longest whisker was from a 1 – 1 contamination level assembly. It was noted during the inspection that two whiskers observed at 1,797 disappeared when examined at 6,000 cycles.

In addition to whiskers, there were growths that appeared to be deformation extrusions (Figure 70) between grains and pad edge extrusions of solder (Figure 72). The instances of other growths are provided in Table 8 and Table 9.

The whisker count and whisker density at the various locations (ref. Figure 50) on the lead are given in Table 10 and Table 11. The SOT6 L4 location had the most whiskers.

Plotted data review

A box plot of whisker length for the various cleanliness levels and lead alloys (Figure 52) shows that the average whisker length is similar for all cleanliness levels, but the 1 – 1 (purposely contaminated part soldered to a purposely contaminated board) had the longest whiskers. It should be noted that the whisker length reported at 6,000 cycles did not include board with the longest whiskers at 1,797 cycles which was removed for sectioning.

A probability plot of whisker length for all the data (Figure 53) shows a reasonably good fit to a lognormal distribution and that contamination level did not have a strong influence on the lognormal parameters (Figure 54).

The whisker diameter also fit a lognormal distribution well (Figure 55). Examining the relationship between whisker diameter and whisker length is done using scatter plots of length versus diameter and ln(length) versus ln(diameter) shown in Figure 56, Figure 57, Figure 58, and Figure 59. There was no strong relationship between whisker length and diameter.

A histogram of whisker growth at the various locations is illustrated in Figure 60 for the alloy 42 and copper leads. Overall, the greatest number of whiskers grew from locations 4 and 5.

A histogram of growth angle (Figure 61) shows that the whiskers growth angle was fairly uniform.

The results from the new whiskers and whiskers that grew longer from 1,797 to 6,000 PCTC cycles are reviewed next. The lognormal probability plots of new whisker length and diameter show a relatively good fit (Figure 62 and Figure 63). For whiskers that grew longer, there is no strong correlation between the previous length and the amount of length change as shown by the Figure 64 scatter plot.

Table 3: Summary of whisker growth for SOT6, SOT3 and SOT5 parts after 6,000 PCTC cycles.

Part type	Part Count	Parts with whiskers	% Parts with whiskers	Total leads	Leads with whiskers	% leads with whiskers	# Total whiskers	Max whisker (um)
SOT6	27	27	100%	162	110	69%	261	29.9
SOT3	50	47	94%	150	98	65%	258	**33.5**
SOT5	48	10	4%	240	12	5%	22	7.7
Total	125	84	67%	552	220	40%	541	

Table 4: Summary of additional whisker growth between 1,797 and 6,000 PCTC cycles for SOT6, SOT3 and SOT5 parts.

Part type	# Total whiskers	# New whiskers	# Longer whiskers	Max length change (um)
SOT6	261	138	32	22
SOT3	258	83	50	23.7
SOT5	22	9	0	0
Total	541	230	82	

Table 5: Summary of part inspection results for the four contamination variants after 6,000 PCTC cycles.

Part type	Clean-liness (Part-Board)	Max whisker (um)	# Parts	# Parts w/ whiskers	% Parts with whiskers	# Leads	# Leads with whiskers	% Leads with whiskers	# Whiskers	# New whiskers	# Existing whiskers that grew longer
SOT6	0-0	23.2	4	4	100%	24	14	50%	37	16	5
SOT3		22.5	10	10	100%	30	23	77%	60	27	6
SOT5		0	9	3	33%	45	3	7%	6	0	0
SOT6	1-0	26	9	9	100%	54	41	71%	123	60	12
SOT3		25.5	16	15	94%	48	29	60%	71	17	18
SOT5		6.6	16	3	19%	80	3	4%	5	3	0
SOT6	0-1	29.3	10	10	100%	60	38	56%	64	35	4
SOT3		25.6	16	15	94%	48	27	50%	70	24	14
SOT5		7.7	15	3	20%	75	5	7%	10	5	0
SOT6	1-1	29.9	4	4	100%	24	17	65%	37	27	4
SOT3		33.5	8	7	88%	24	19	79%	57	15	12
SOT5		0	8	1	13%	40	1	3%	1	0	0

Table 6: SOT6 observations for the top 10 longest whiskers after 6,000 PCTC cycles.

Clean-liness (Part-Board)	Brd	Ref Des	Lead	Loc-ation	Length (um)	Dia. (um)	Angle	1797-6000 Change	Orient chg	Prev length (um)	Length chg (um)	Comments
0-1	1	U68	3	L4	21.7	10.4	90	Longer	N	6.6	15.1	Was 6.6 um
0-0	1	U72	1	L4	22	28.9	90	Longer	N	0.1	21.9	Grew significantly before it was too short to measure
0-1	3	U77	3	L4	22.2	19.8	45	Longer	N	5.2	17	Was 5.2 um
0-0	1	U65	5	L4	23.2	9.8-2.3	90	New				
0-1	3	U77	1	L5	25.4	14.7	90	New				
1-0	3	U70	1	L3	26	8.4	45	Longer	N	4	22	It was short, was not measured before, < 4 um
1-1	1	U77	5	L5	27.9	7.8	0	New				
0-1	3	U72	4	L4	28.9	15.6-6.5	90	New				
0-1	1	U71	5	L4	29.3	24	45	New				
1-1	1	U68	2	L4	29.9	18.7	90	New				

Table 7: SOT3 observations for the top 10 longest whiskers after 6,000 PCTC cycles.

Clean-liness (Part-Board)	Brd	Ref Des	Lead	Loc-ation	Length (um)	Dia. (um)	Angle	1797-6000 Change	Orient chg	Prev length (um)	Length chg (um)	Comments
0-1	3	U61	3	L4	20.3	17.4	45	New				
0-0	1	U58	2	L1	20.7	8.4	45	Longer	N	14.8	5.9	Changed, was 14.8 um
0-0	1	U37	2	L3	22.5	9.2	0	New				
0-1	3	U61	3	L5	23.7	18.7	45	New				
1-1	1	U27	2	L3	24	2.9	0	Same	N			Same as before
1-1	1	U27	2	L3	25.3	5.2	0	Longer	N	1.6	23.7	Was 1.6 um
1-0	3	U40	2	L4	25.4	5.4-9.5	0	New				
1-0	3	U40	3	L3	25.5	10-14.7	45	Longer	N	3.3	22.2	It was 3.3 um before
0-1	3	U15	3	L5	25.6	11.6	45	New				
1-1	1	U27	1	L3	33.5	6.6	0	Longer	N	9.9	23.6	Changed, was 9.9

Table 8: Summary of non-whisker deformation grain growths and pad edge growths after 6,000 PCTC cycles.

		Contamination (part-board)			
Part type	Total	0-0	1-0	0-1	1-1
SOT6	26	0	3	21	2
SOT3	13	4	3	2	3
SOT5	2	0	1	1	0
Total	41	4	7	24	5

Table 9: Subset of protrusion edge growths (PEGs) which were included in the 6,000 PCTC Table 8 results.

	Contamination (part-board)			
Part type	0-0	1-0	0-1	1-1
SOT6	0	0	0	0
SOT3	0	1	2	3
SOT5	0	1	1	0

Table 10: Whisker count by location after 6,000 PCTC cycles..

Part	L1	L2(B)	L3	L4	L5	Total
SOT6	13	5	14	153	76	261
SOT3	65	1	51	65	76	258
SOT5	1	0	13	7	1	22

Table 11: Whisker density by location (whiskers/mm^2) after 6,000 PCTC cycles.

Part	L1	L2	L3	L4	L5
SOT6	112.1	33.5	384.6	1312.2	569.7
SOT3	753.2	5.1	771.6	978.9	242.2
SOT5	5.4	0.0	239.0	33.1	4.1

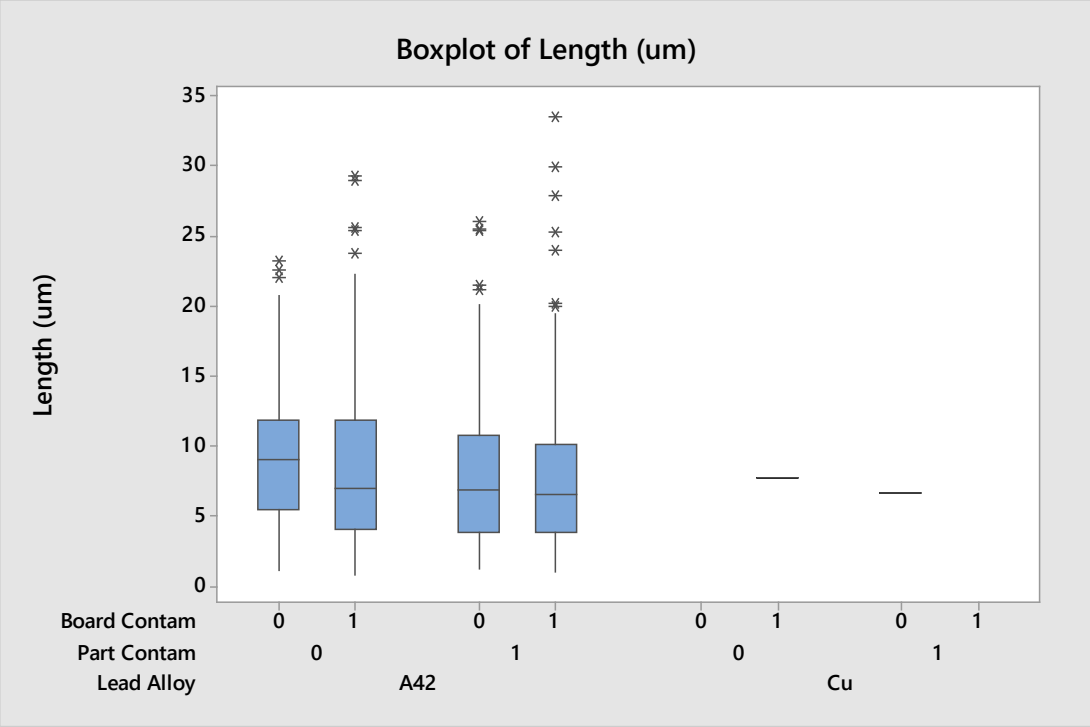


Figure 52: Box plot of whisker length after 6,000 PCTC cycles for different contamination levels and lead alloys.

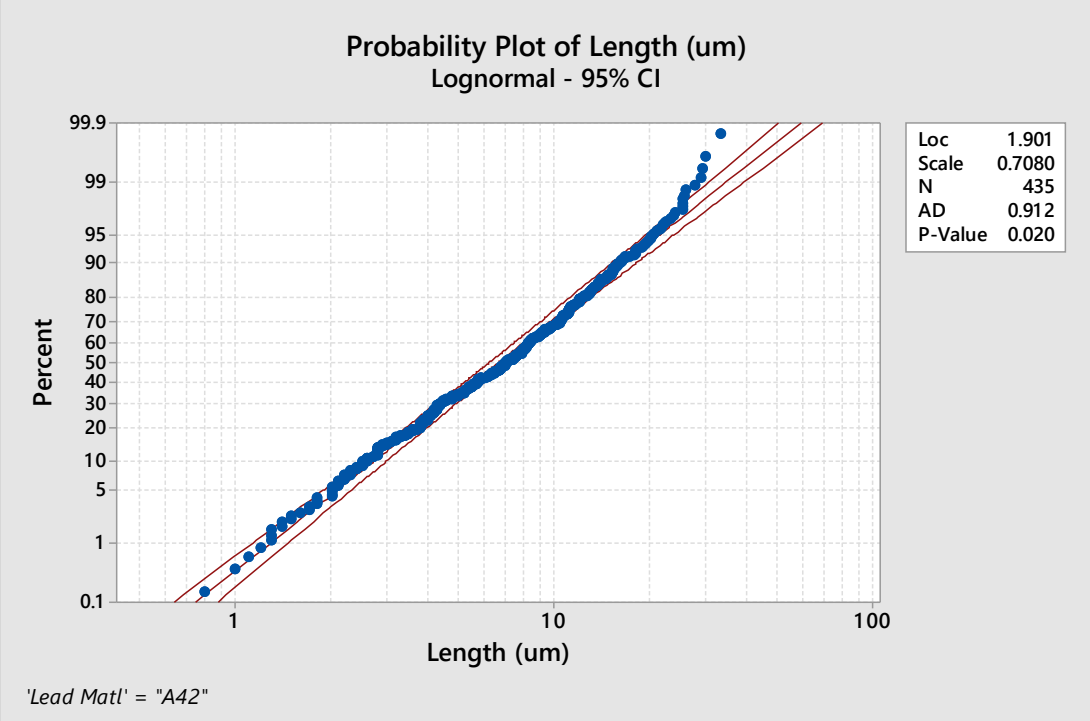


Figure 53: Probability plot of whisker length for alloy 42 leads after 6,000 PCTC cycles.

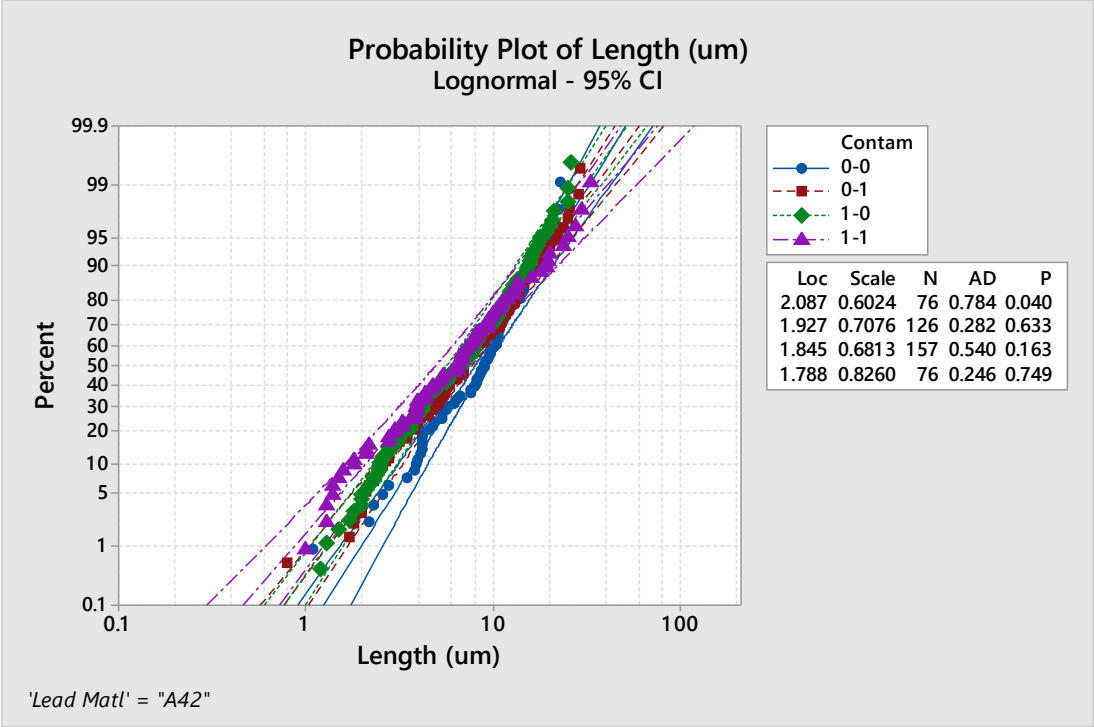


Figure 54: Probability plot of whisker length for various contamination levels after 6,000 PCTC cycles.

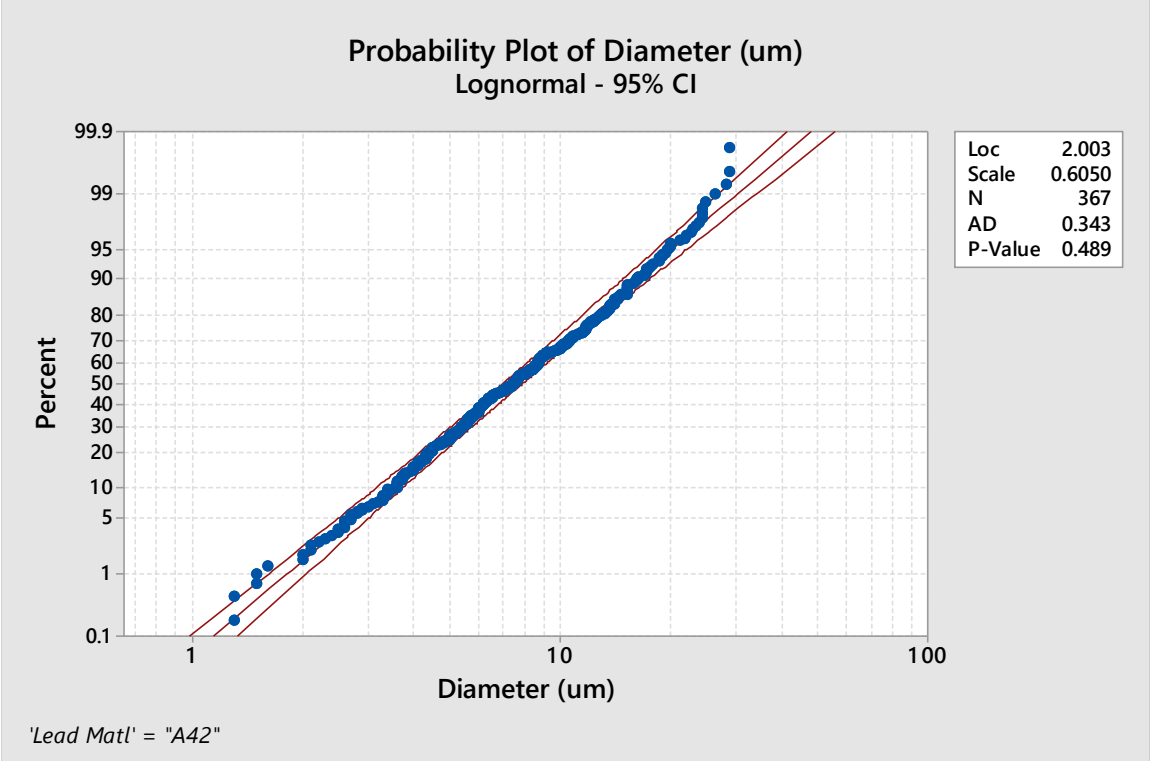


Figure 55: Probability plot of whisker diameter for alloy 42 leads after 6,000 PCTC cycles.

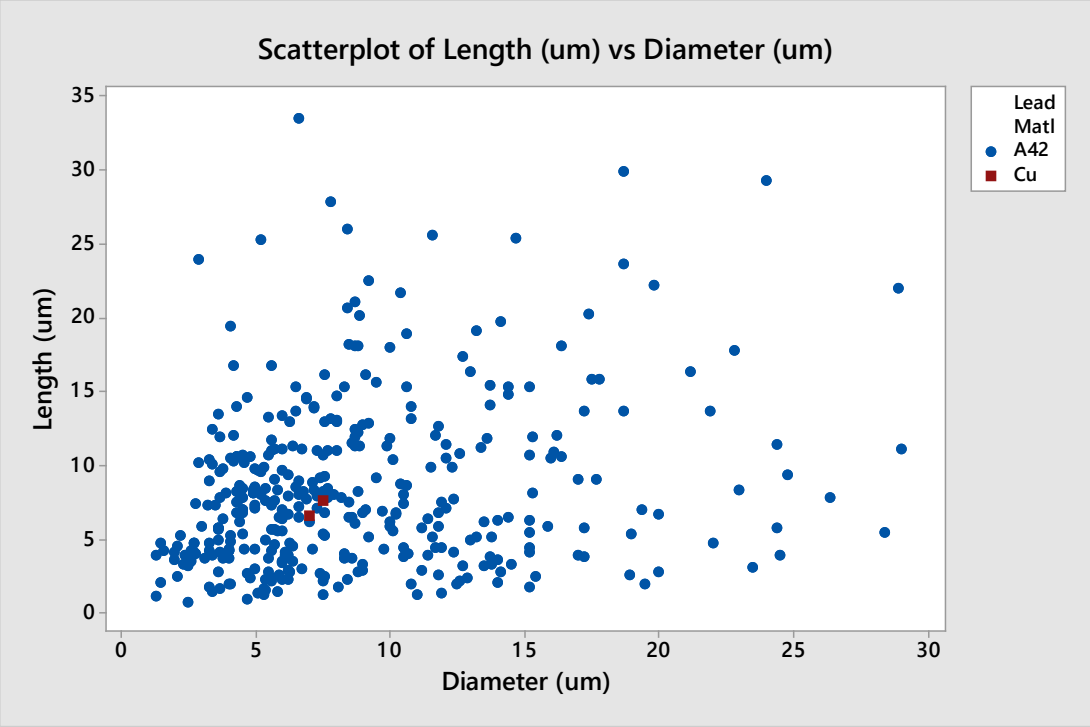


Figure 56: Scatter plot of length versus diameter of whiskers from terminations with different lead alloy materials after 6,000 PCTC cycles.

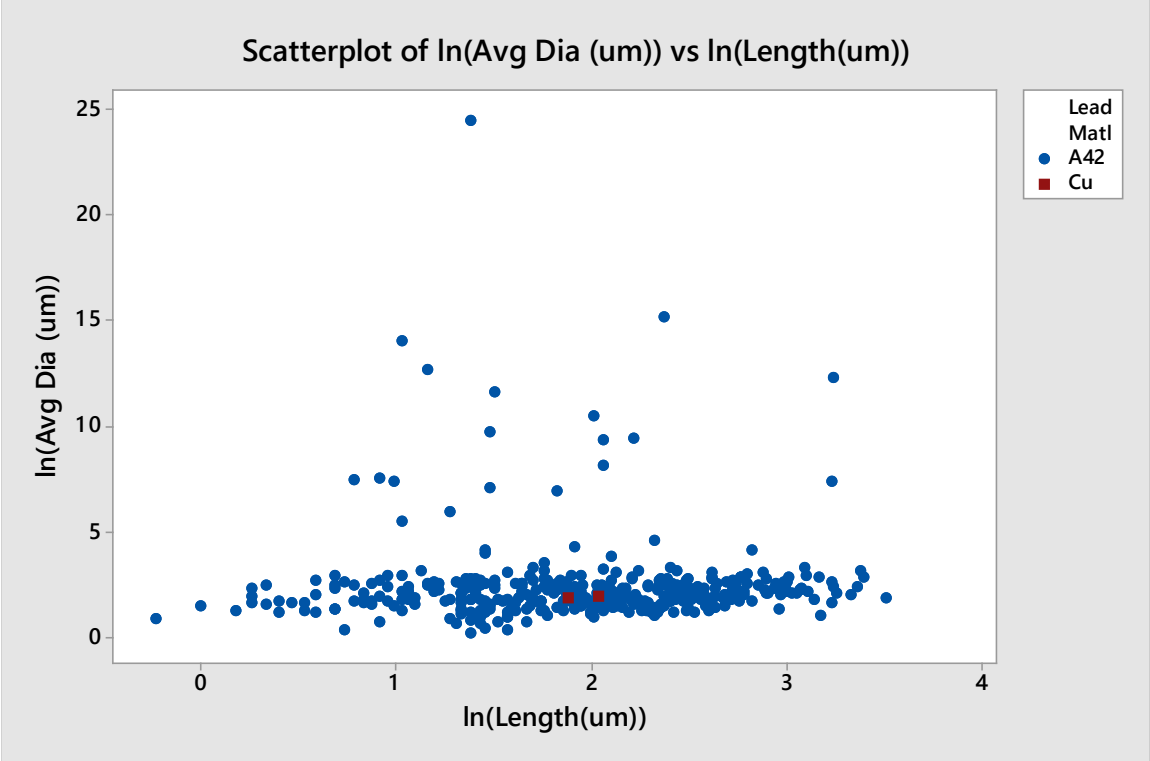


Figure 57: Scatter plot of ln(diameter) versus ln(length) of whiskers from terminations with different lead alloy materials after 6,000 PCTC cycles.

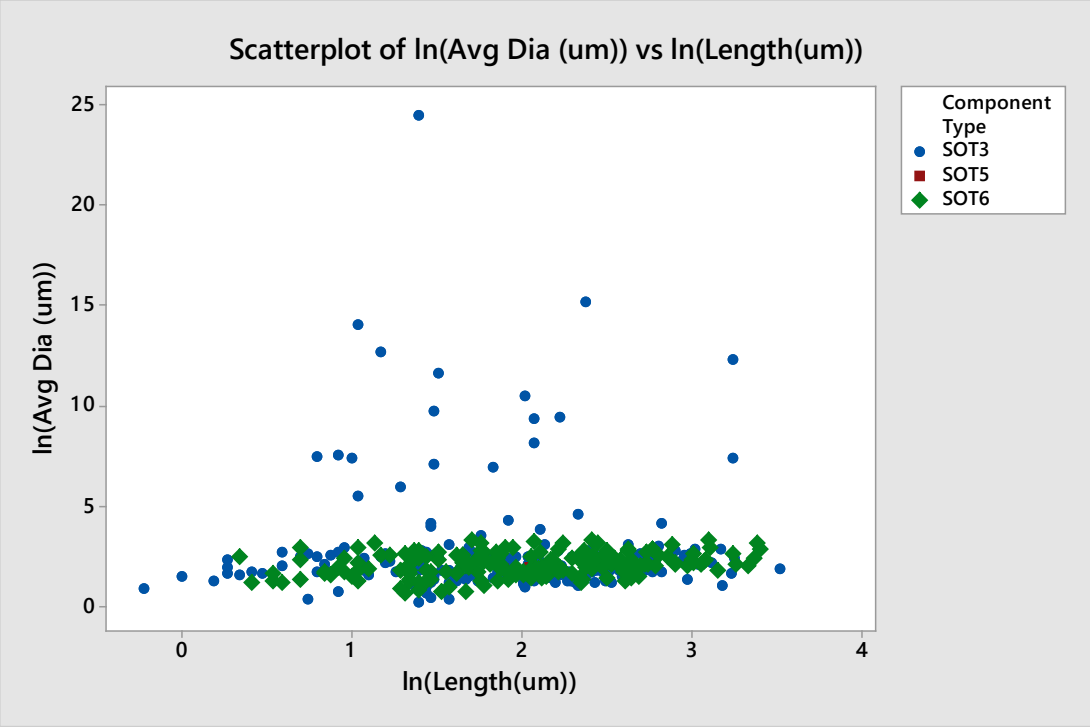


Figure 58: Scatter plot of ln(diameter) versus ln(length) of whiskers from SOT3, SOT5 and SOT6 part terminations after 6,000 PCTC cycles.

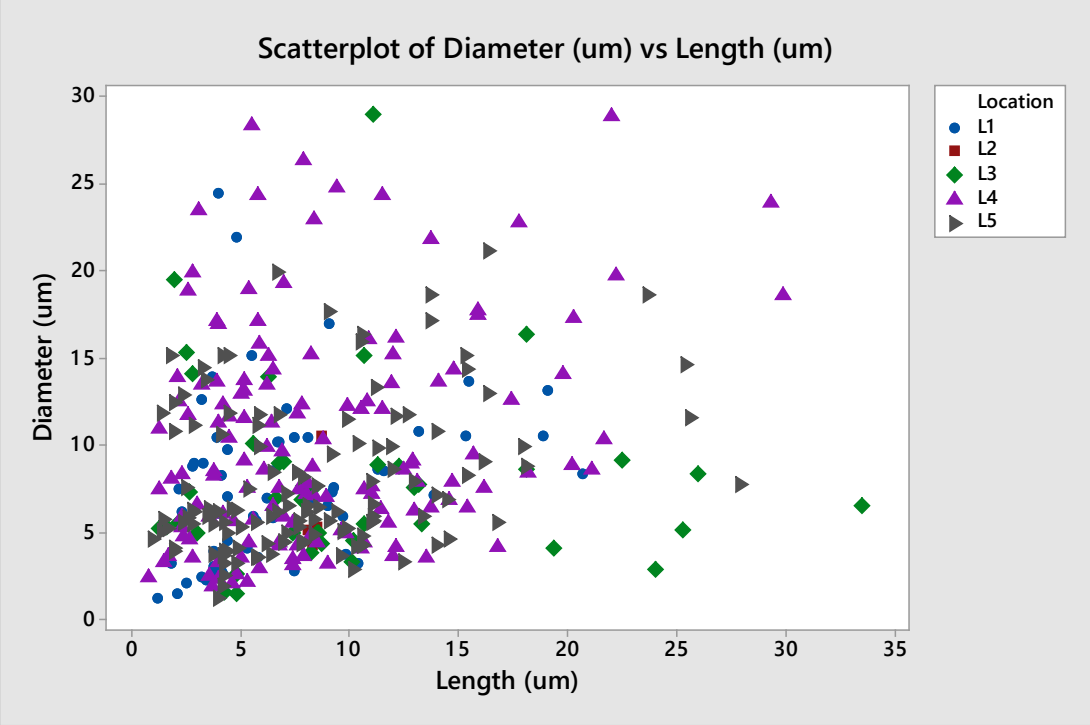


Figure 59: Scatter plot of whisker diameter versus length of whiskers at various locations after 6,000 PCTC cycles.

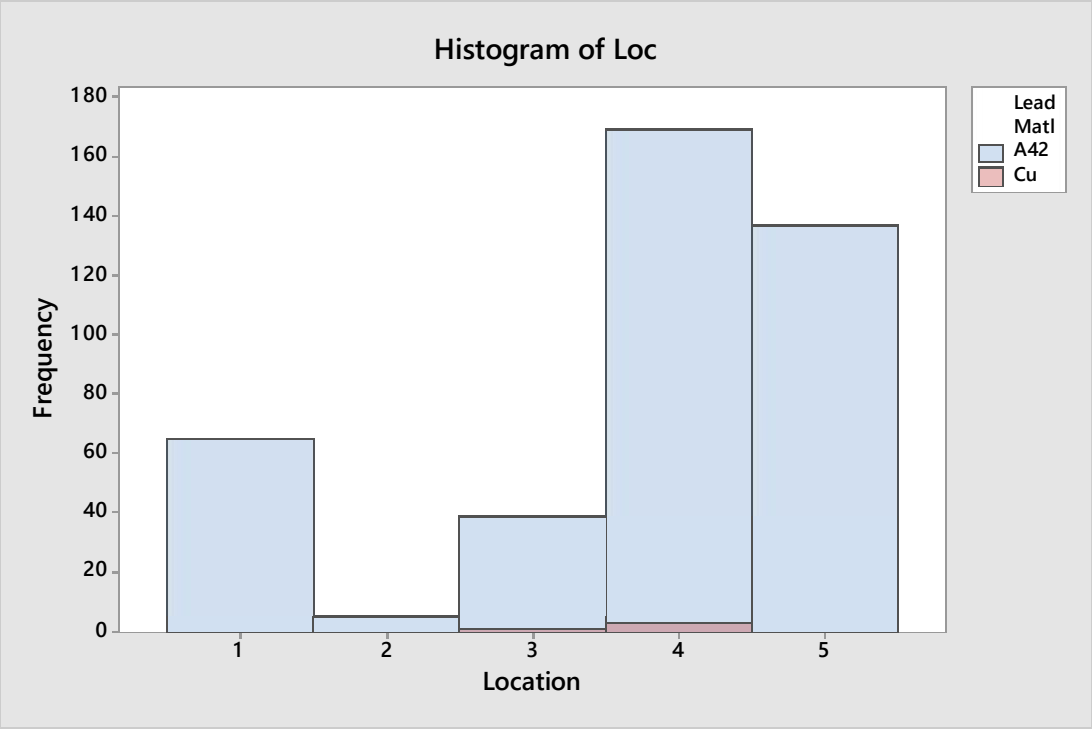


Figure 60: Histogram of whisker growth location after 6,000 PCTC cycles. Note location 2 only has whiskers from 2B as defined in Figure 50.

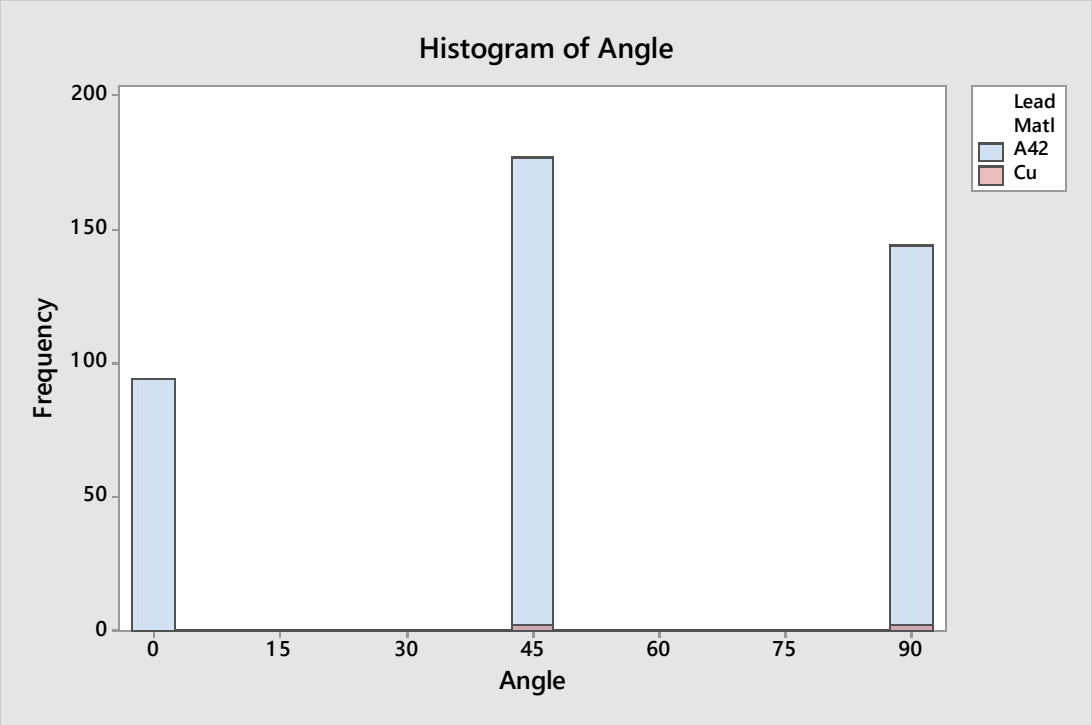


Figure 61: Histogram of whisker angle after 6,000 PCTC cycles. Whiskers oriented parallel to the growth surface are defined to have angle of zero and whiskers perpendicular to the growth surface have an angle of 90 degrees.

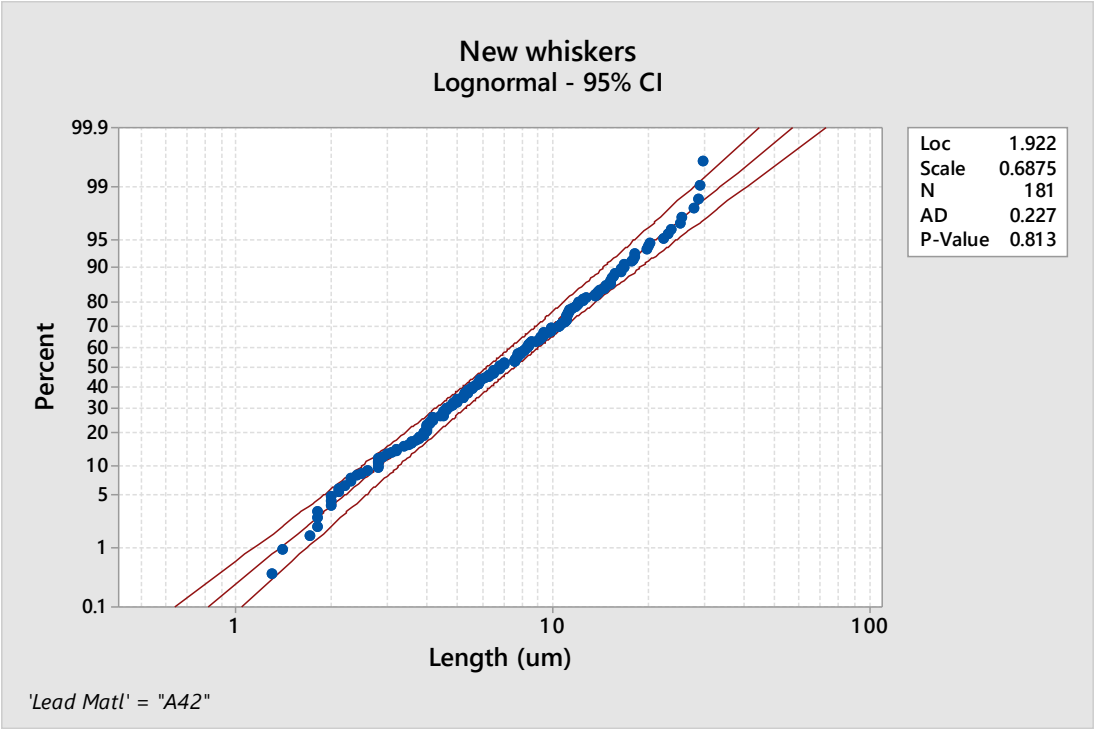


Figure 62: Probability plot for the length of new whiskers that grew between 1,797 and 6,000 cycles.

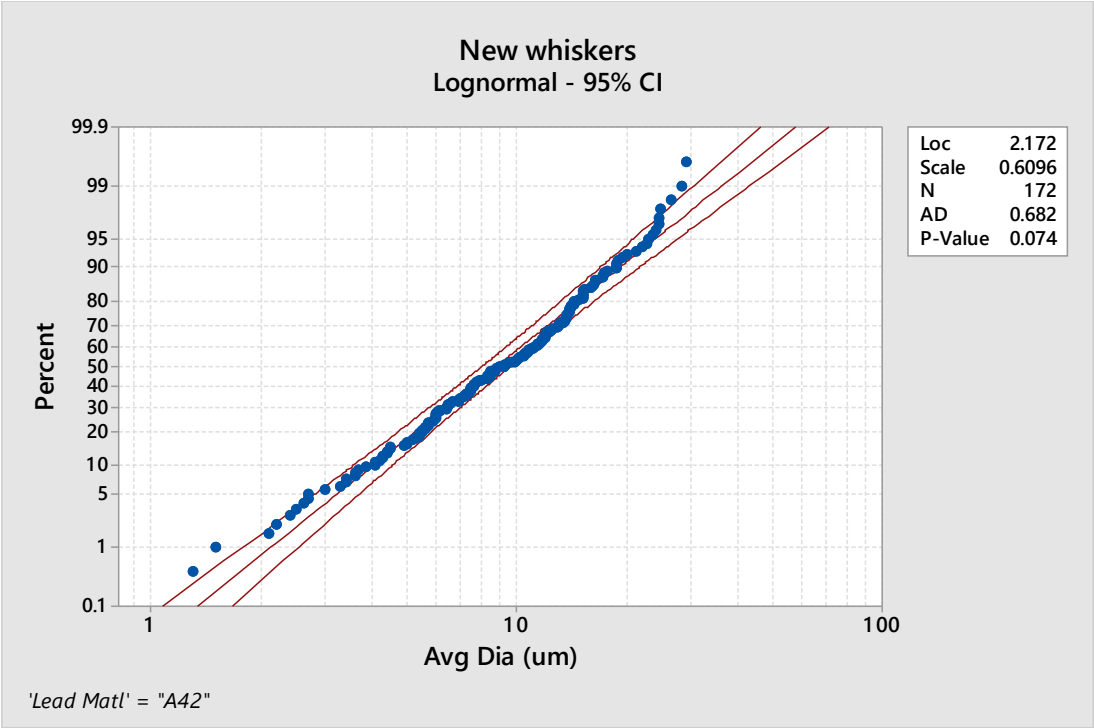


Figure 63: Probability plot for the diameter of new whiskers that grew between 1,797 and 6,000 cycles.

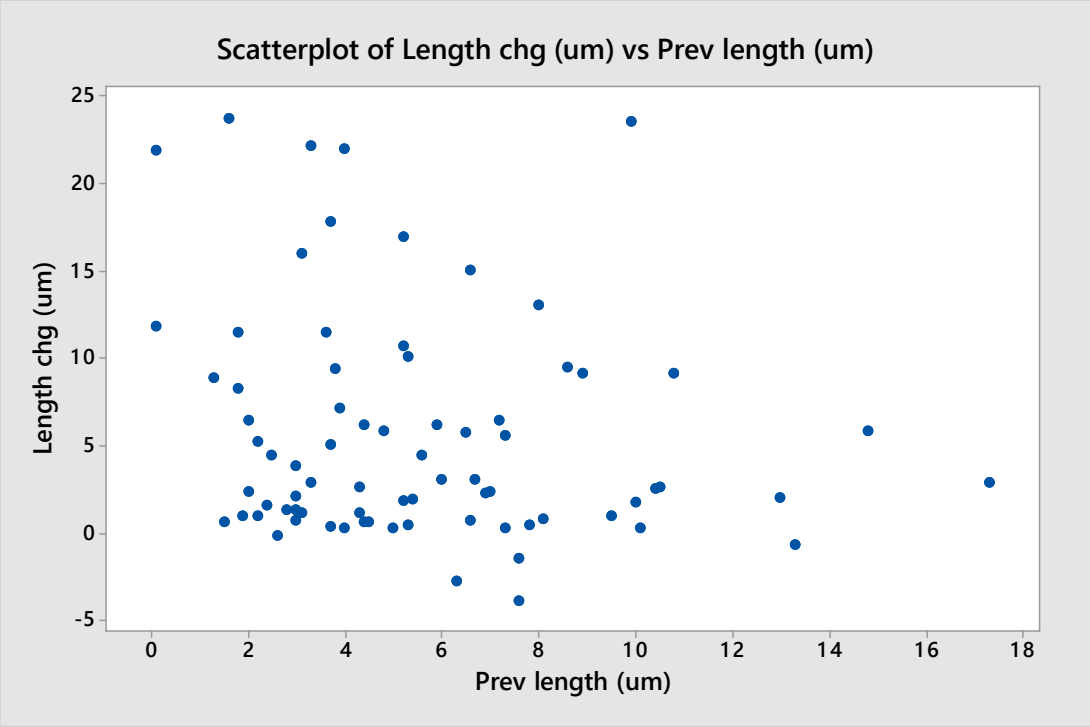


Figure 64: Scatter plot of length change versus previous length for whiskers that grew longer between 1,797 and 6,000 cycles.

3.2 Metallurgical observations for uncoated 6,000 PCTC samples

As was previously observed after 1,797 PCTC cycles, the whiskers at 6,000 PCTC cycles grew where the solder was thin. In some cases, they grew adjacent to Ag_3Sn intermetallic (IMC) (Figure 66 and Figure 74) and sometimes they grew from between the tin dendrites (Figure 68). In addition, there were other stress relaxation mechanisms occurring such as deformation growth (Figure 70), pad edge growth (Figure 72), grain boundary sliding, crack formation and grain recrystallization (Figure 77 and Figure 78). In some cases on the SOT6 lead, a very pronounced whisker visible at 100x grew in the in the upper center part of the lead (Figure 85 and Figure 86; Figure 88 and Figure 89).

Some whiskers had diameter decreases or increases during growth. An example of whisker diameter decrease from the tip to the base is shown in Figure 89 and Figure 105, while an increasing diameter whisker is given in Figure 107.

There were instances where significant deformation and whisker growth were observed near the lead tip (Figure 90 to Figure 95) rather than where the lead exits the solder.

While some leads had one or two whiskers, sometimes a single lead had numerous deformation growth, whisker sites and pad edge growth (Figure 96 to Figure 105). Often the whiskers grew next to a crack between tin grains suggesting that the stresses promoting whisker growth, while small, can eventually result in solder fatigue cracks. A range of solder crack sizes and adjacent whisker growths were observed; (1) no cracks with initial recrystallization and whisker growth from between tin grains with no cracks (Figure 90), (2) small solder cracks with many whiskers (Figure 103 and Figure 104), and (3) large cracks with whiskers on the crack edges (Figure 94).

Although the vast majority of whisker growth occurred on the alloy 42 leads, the copper leads on the SOT5 device grew a limited number of very short whiskers (Figure 109).

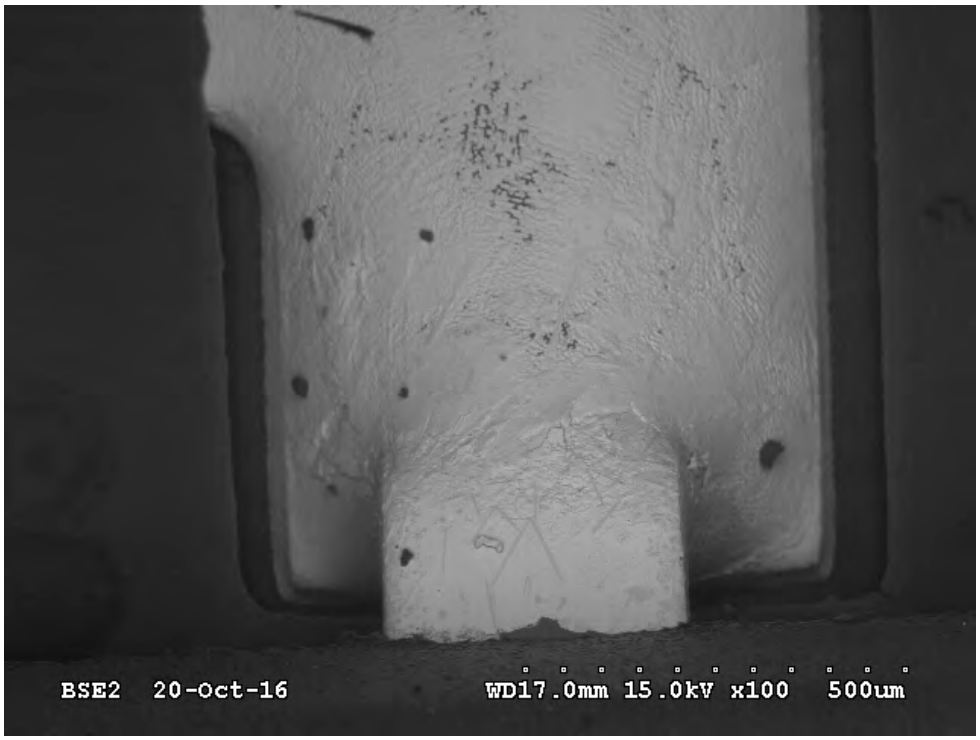


Figure 65: SEM image of SOT3, U27, lead 1, no conformal coating, 1-1 contamination level after 6,000 PCTC cycles, 100x (ref. A-SOT-PC-1-1-ncc-1, SOT3, U27, lead 1).

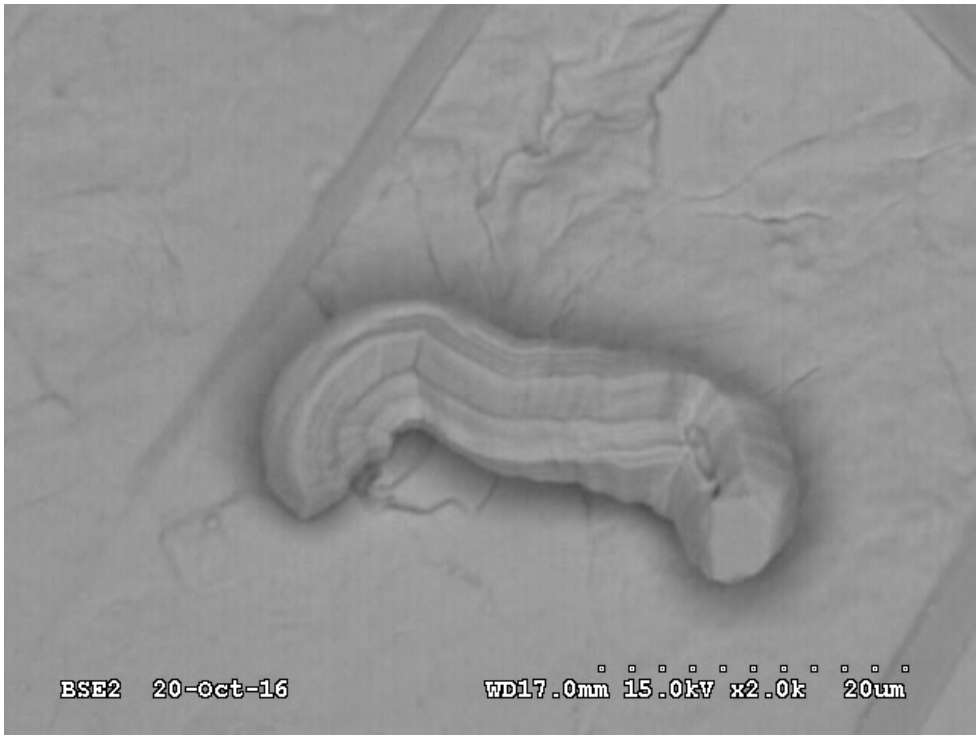


Figure 66: Close-up SEM image of a whisker nucleation site on the SOT3 shown in Figure 65, 2,000x. (ref. A-SOT-PC-0-0-ncc-1, SOT3, U27, lead 1).

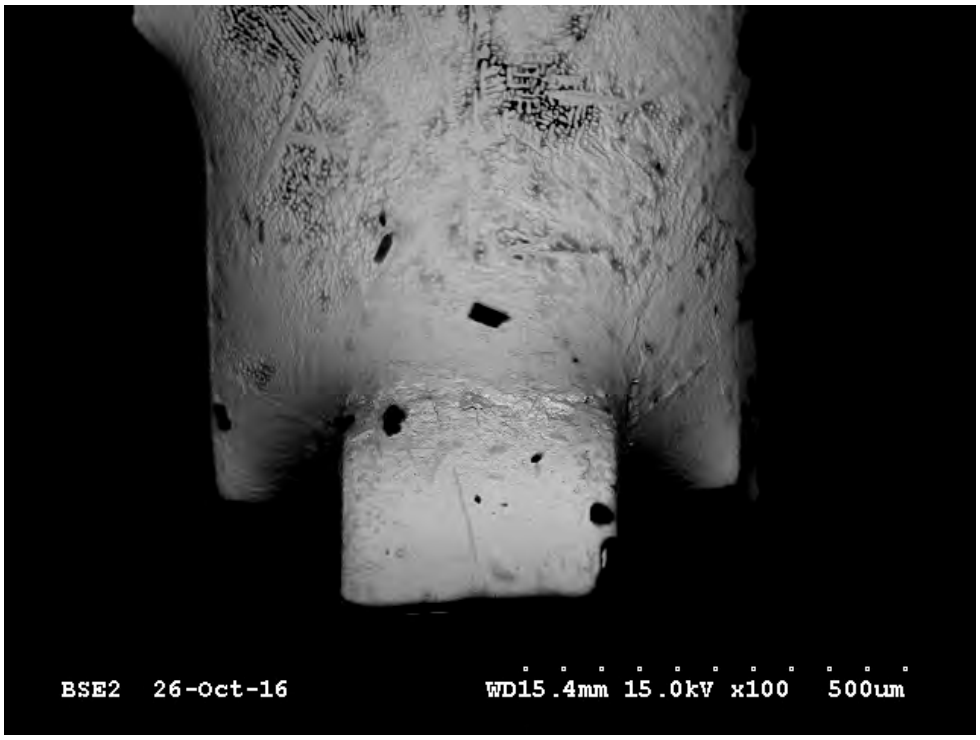


Figure 67: SEM image of the SOT3, U37, lead 1, no conformal coating, 0-0 contamination level, after 6,000 PCTC cycles, 100x (ref. A-SOT-PC-0-0-ncc-1, SOT3, U37, lead 1).

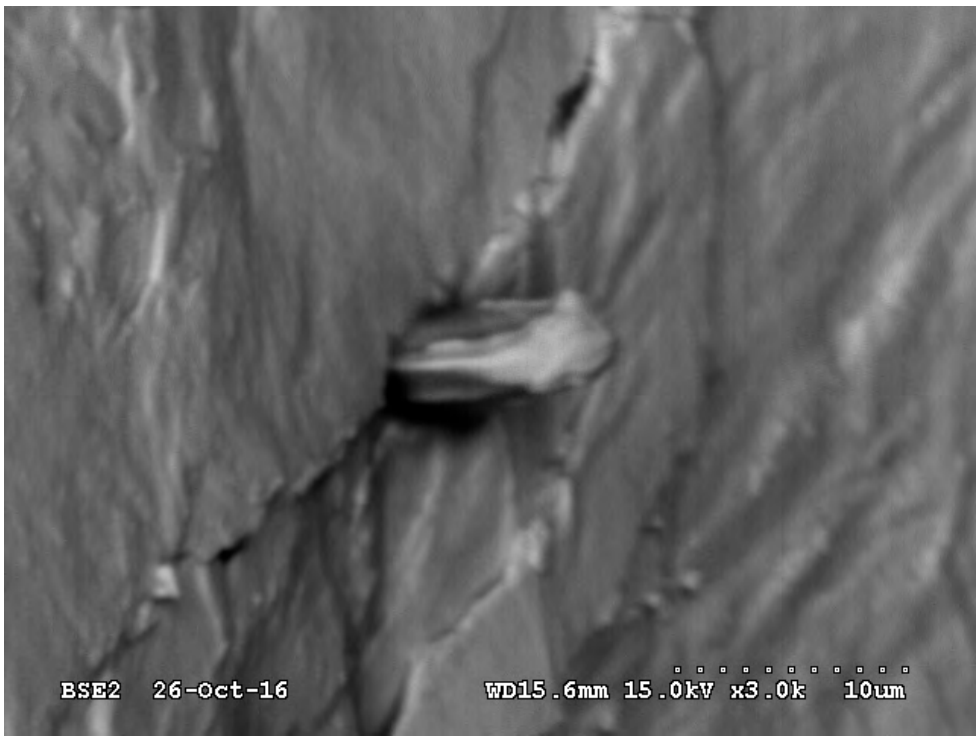


Figure 68: Close-up SEM image of a whisker nucleation site on the SOT3 from Figure 67, 3,000x. (ref. A-SOT-PC-0-0-ncc-1, SOT3, U37, lead 1). Whisker growth is occurring from between two tin grains.

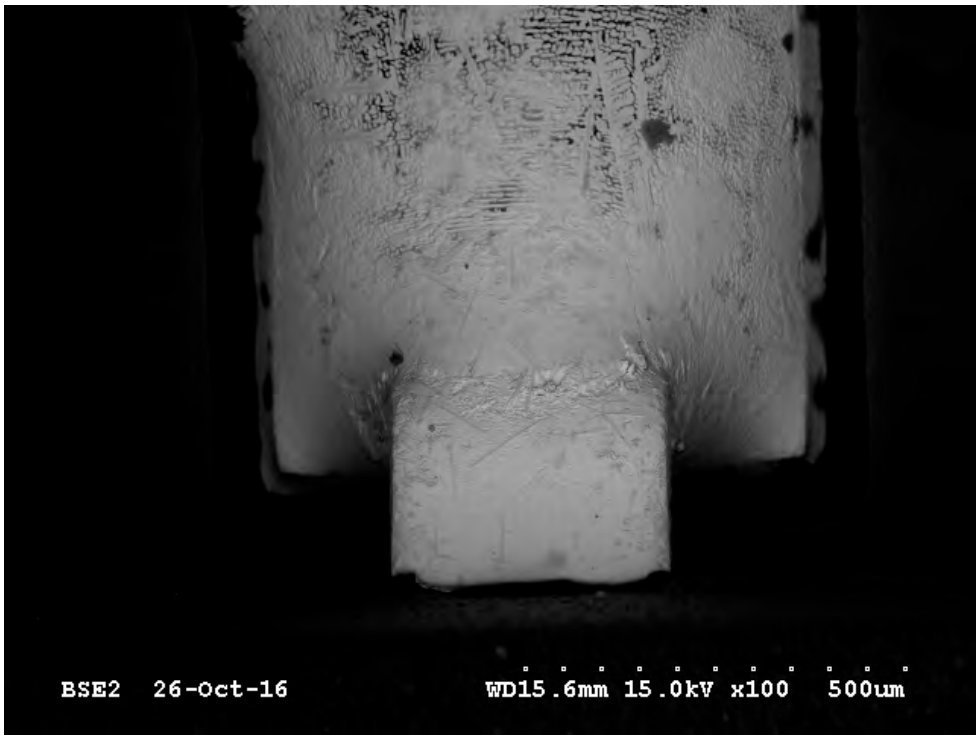


Figure 69: SEM image of the SOT3, U33, lead 1, no conformal coating, 0-0 contamination level, after 6,000 PCTC cycles (ref. A-SOT-PC-0-0-ncc-1, SOT3, U33, lead 1).



Figure 70: Close up image of deformation growth on the SOT3 from Figure 69, 2,000x (ref. A-SOT-PC-0-0-ncc-1). The growth deformation is approximately 2 microns high and is near an Ag_3Sn intermetallic platelet in location 4.

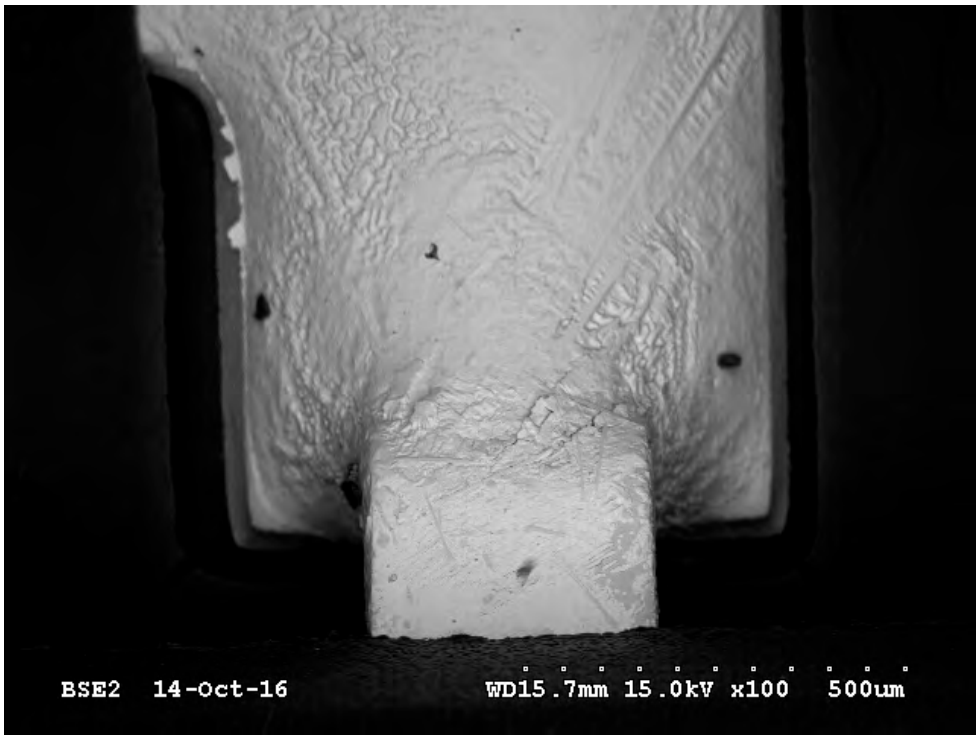


Figure 71: SEM image of the SOT3, U20, lead 1, no conformal coating, 1-0 contamination level after 6,000 PCTC cycles, 100x (ref. A-SOT-PC-1-0-ncc-3).

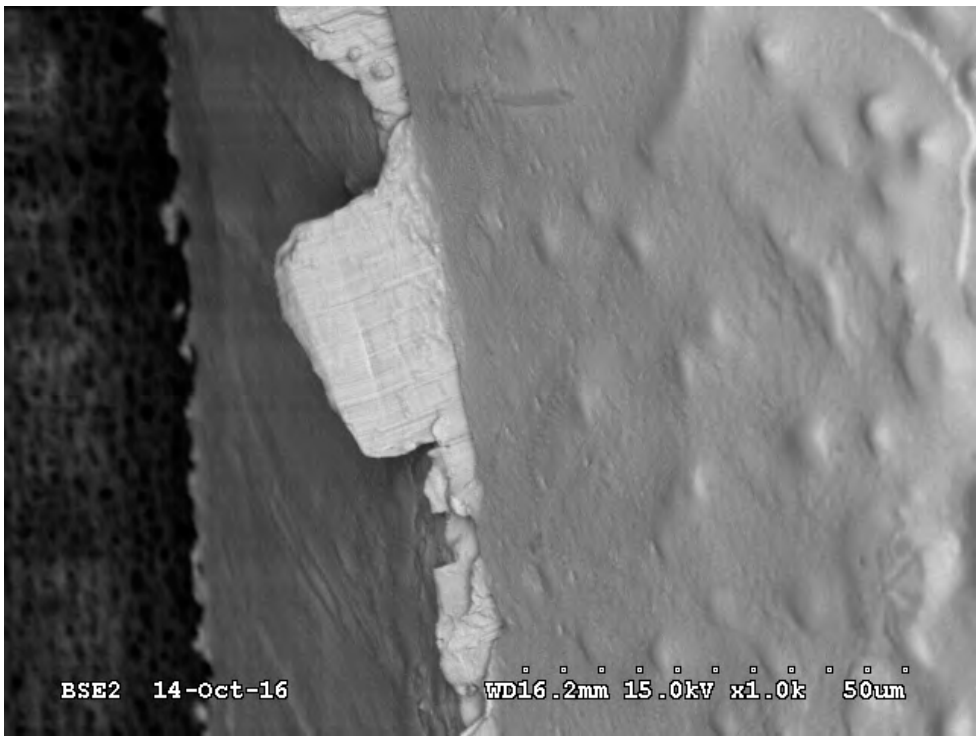


Figure 72: Close-up SEM image of the pad edge growths on the left side of Figure 71, 1,000x. (ref. A-SOT-PC-1-0-ncc-3, SOT3, U20, lead 1, 1,000x).



Figure 73: SEM image of the SOT3, U58, lead 3, no conformal coating, 1-1 contamination level, after 6,000 PCTC cycles, 100x (ref. A-SOT-PC-1-1-ncc-1, SOT3, U58, lead 3).



Figure 74: Close-up SEM image of a whisker nucleation site on the SOT3 shown in Figure 73, 2,000x. (ref. A-SOT-PC-1-1-ncc-1, SOT3, U58, lead 3).

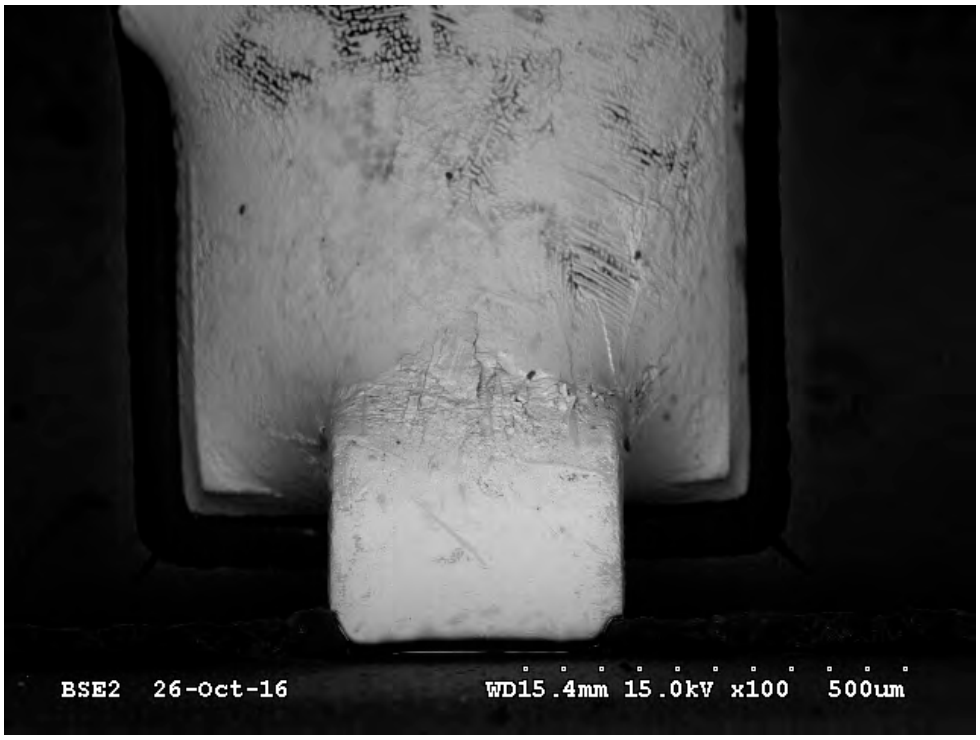


Figure 75: SEM image of the SOT3, U44, lead 1, no conformal coating, 0-0 contamination level after 6,000 PCTC cycles, 100x (ref. A-SOT-PC-0-0-ncc-1, SOT3, U44, lead 1).



Figure 76: Close-up SEM image of a whisker nucleation site on the SOT3, 2,000x (A-SOT-PC-0-0-ncc-1, SOT3, U44, lead 1).

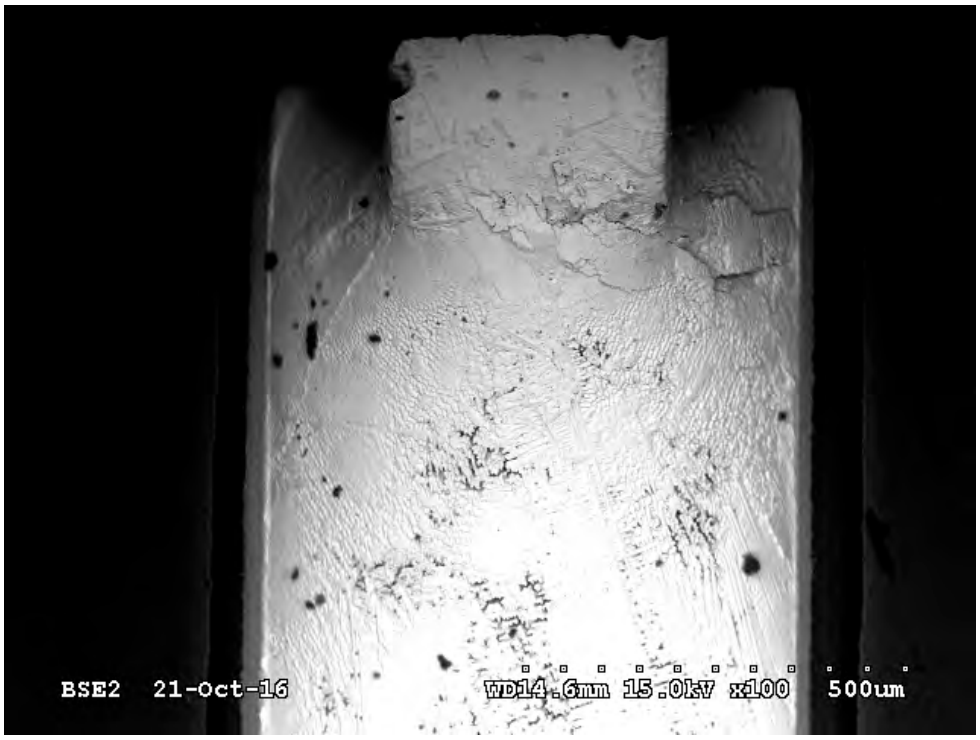
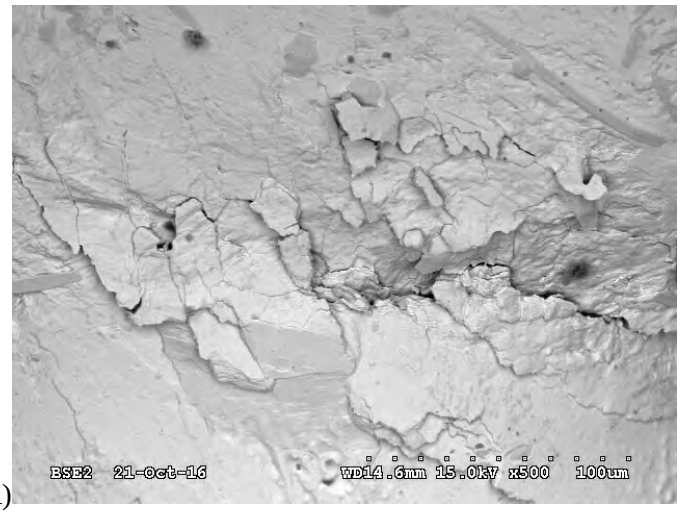
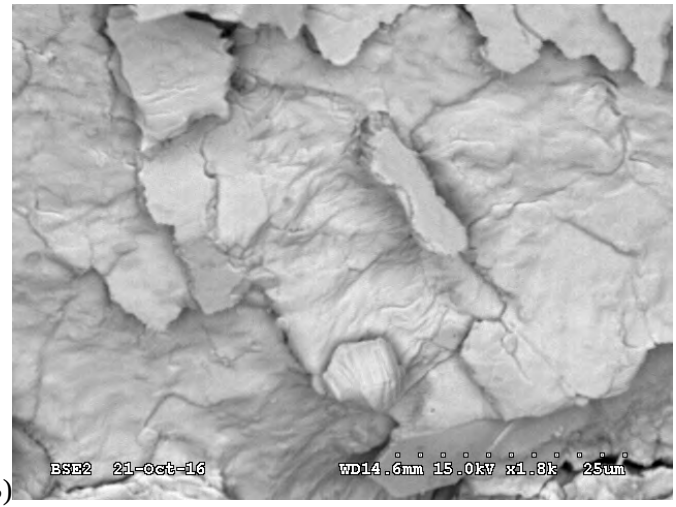


Figure 77: SEM image of the SOT3, U63, lead 2, no conformal coating, 1-1 contamination level after 6,000 PCTC cycles, 100x (ref. A-SOT-PC-1-1-ncc-1, SOT3, U63, lead 2).

(A)



(B)



(C)

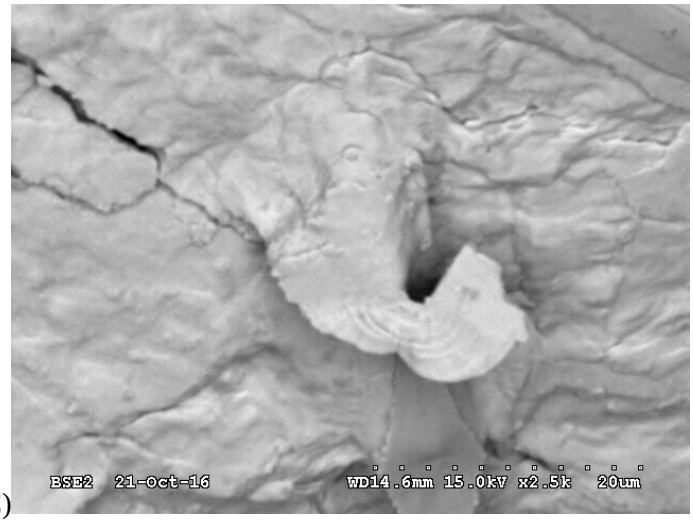


Figure 78: Close-up SEM images of a whisker nucleation and deformation growths on the SOT3 shown in Figure 77; (A) 500x, (B) 1,800x, and (C) 2,500x.

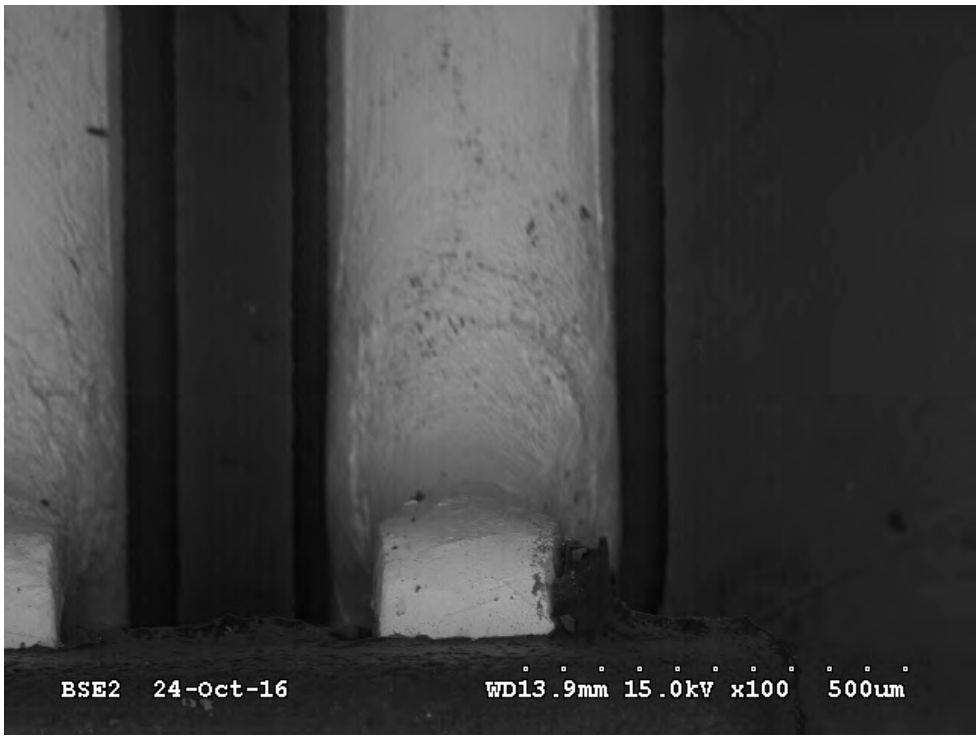


Figure 79: SEM image of the SOT6, U68, lead 1, no conformal coating, 1-1 contamination level after 6,000 PCTC cycles, 100x (ref. A-SOT-PC-1-1-ncc-1).



Figure 80: Close-up SEM image of the SOT6 shown in Figure 79, 1,500x (ref. A-SOT-PC-1-1-ncc-1, SOT6, U68, lead 1).



Figure 81: SEM image of the SOT6, U71, lead 4, no conformal coating, 1-0 contamination level after 6,000 PCTC cycles, 100x (ref. A-SOT-PC-1-0-ncc-3).

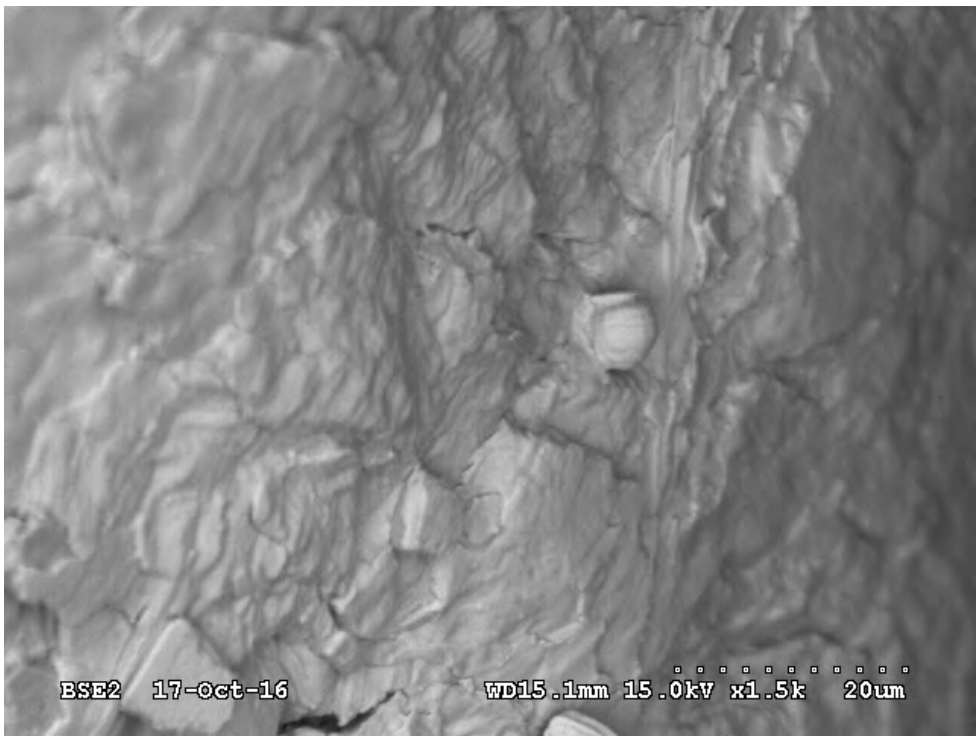


Figure 82: Close-up SEM image of the right side of the SOT6 lead shown in Figure 81, 1,500x (ref. A-SOT-PC-1-0-ncc-3, U71, lead 4).



Figure 83: Close-up SEM image of the left side of the SOT6 lead shown in Figure 81, 1,500x (ref. A-SOT-PC-1-0-ncc-3, U71, lead 4).

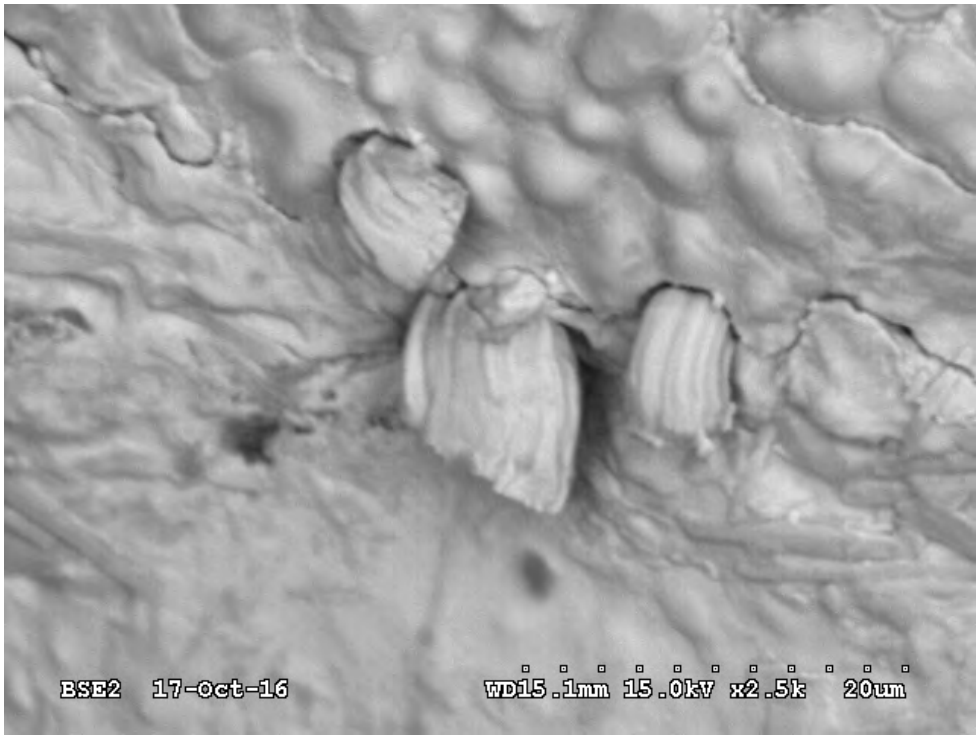


Figure 84: Close-up SEM image of the center-left side of the SOT6 lead shown in Figure 81, 2,500x (ref. A-SOT-PC-1-0-ncc-3, U71, lead 4).

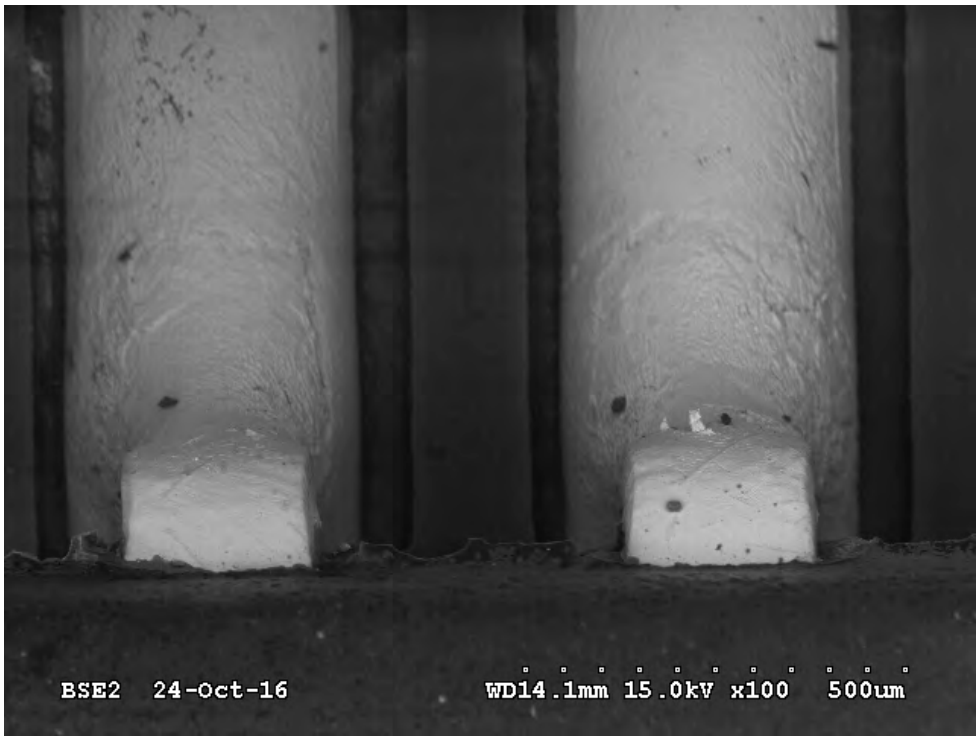


Figure 85: SEM image of the SOT6, U68, lead 2 (right) and 3 (left), no conformal coating, 1-1 contamination level after 6,000 PCTC cycles, 100x (A-SOT-PC-1-1-ncc-1, SOT6, U68, lead 2-3).



Figure 86: Close-up SEM image of a whisker nucleation site on the SOT6 shown in Figure 85, 1,000x (ref. A-SOT-PC-1-1-ncc-1, SOT6, U68, lead 2)



Figure 87: Close-up SEM image of a whisker on the SOT6 lead shown in Figure 85, 2,500x (ref. A-SOT-PC-1-1-ncc-1, SOT6, U68, lead 2). Note that the whisker diameter is decreasing from the tip to the base.

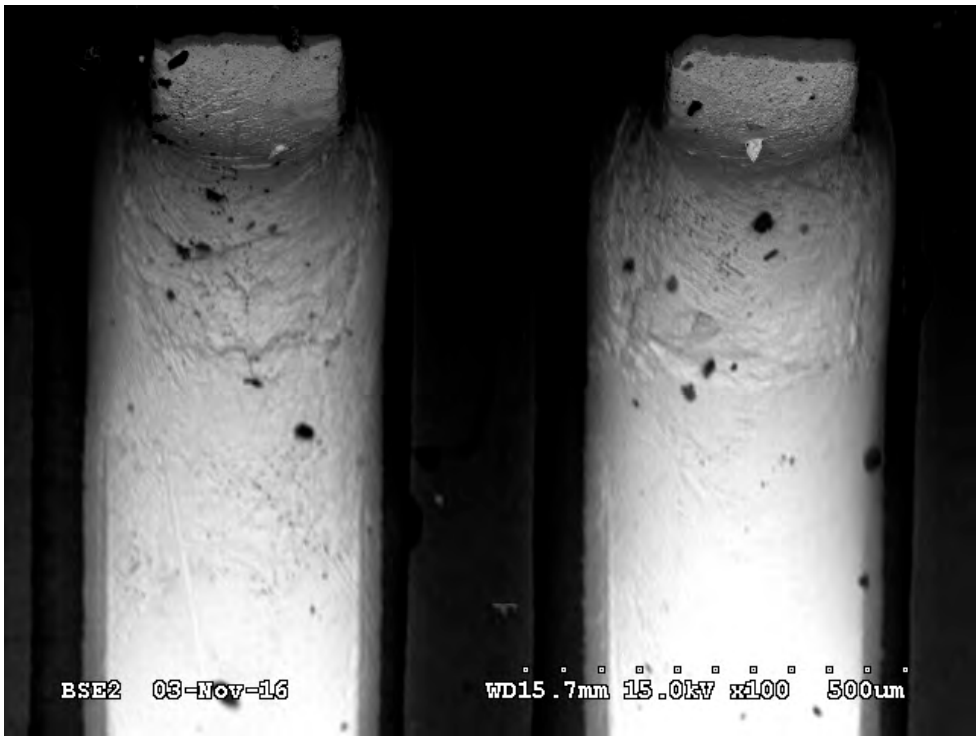


Figure 88: SEM image of the SOT6, U71, lead 4 (left) and lead 5 (right), no conformal coating, 0-1 contamination level, after 6,000 PCTC cycles 100x (ref. A-SOT-PC-0-1-ncc-1, SOT6, U71, lead 4-5).



Figure 89: Close up SEM image of the whisker on the SOT6 lead 5 shown in Figure 88, 1,000x (A-SOT-PC-0-1-ncc-1, SOT6, U71, lead 5, 1,000x).

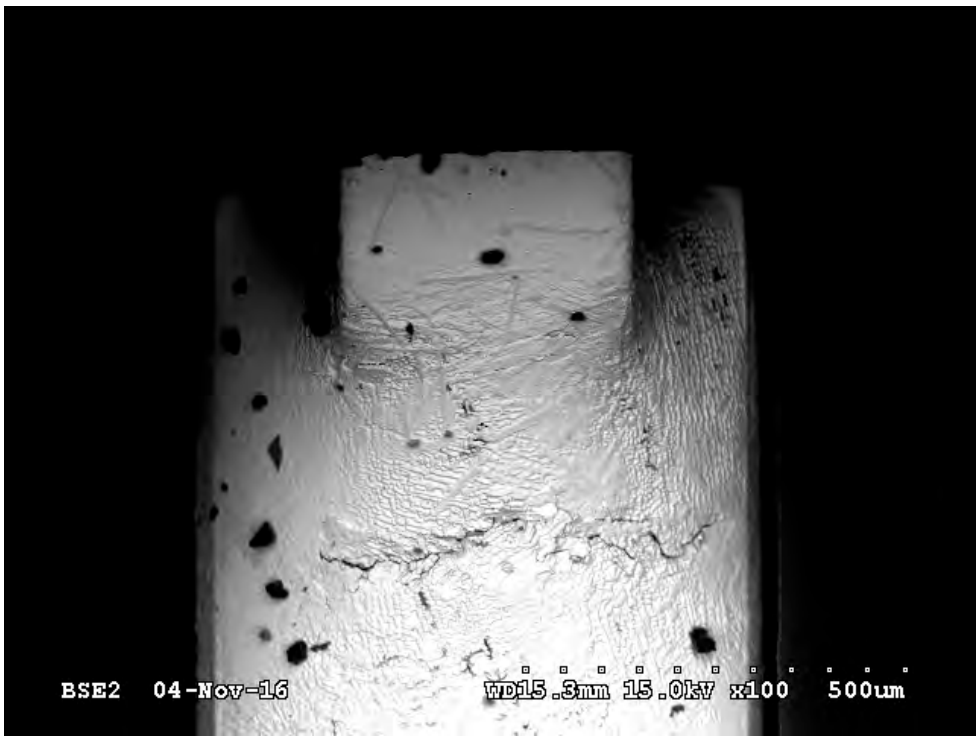


Figure 90: SEM image of cracks and deformation around the lead tip of the SOT3, U27, lead 3, no conformal coating, 1-0 contamination level after 6,000 PCTC cycles, 100x (ref. A-SOT-PC-1-0-ncc-1). The surface whisker growth and solder cracking are located near the lead tip which is just under the solder.

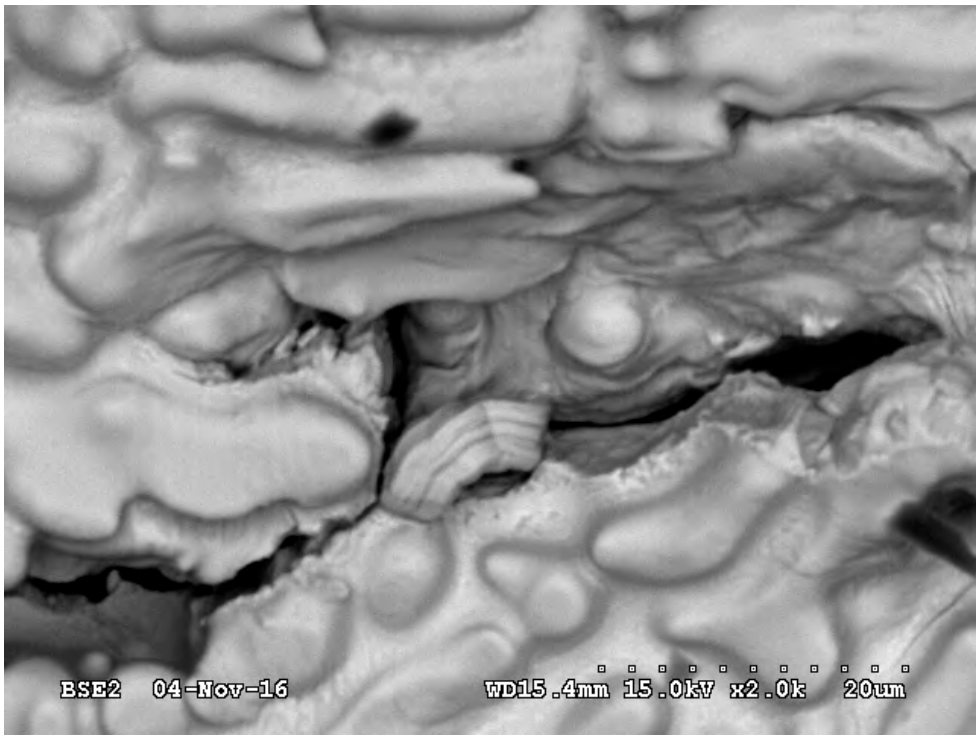


Figure 91: Close up SEM image of the SOT3 lead shown in Figure 90, 2,000x (ref. A-SOT-PC-1-0-ncc-1, U27, lead 3).

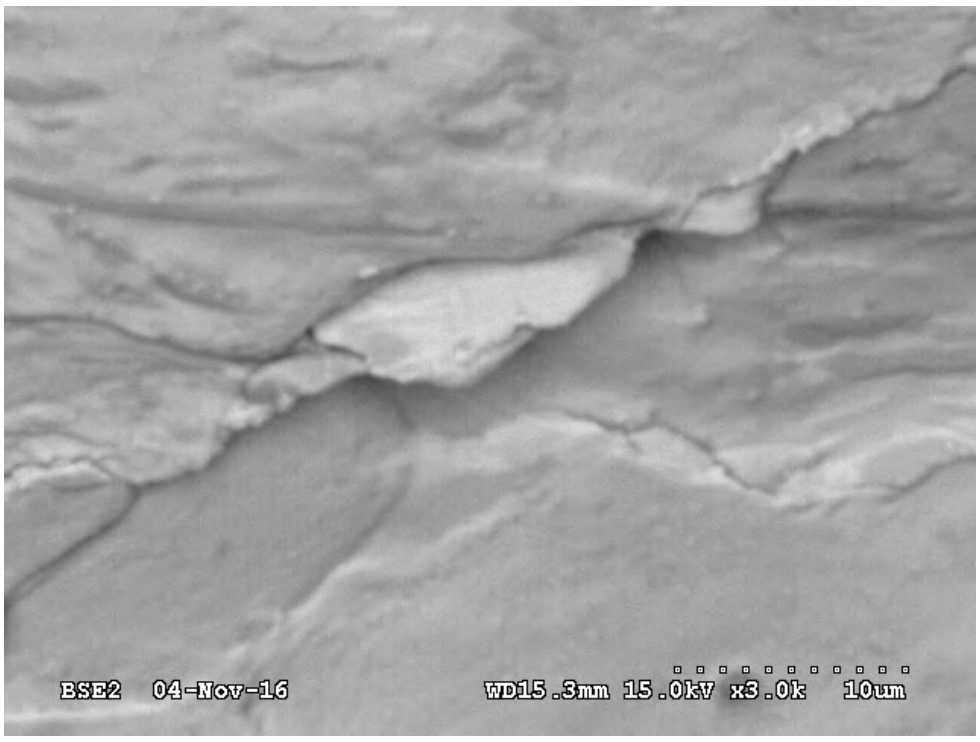


Figure 92: Close up SEM image of growth along the grain boundary for the SOT3 lead shown in Figure 90, 3,000x, (ref. A-SOT-PC-1-0-ncc-1, U27, lead 3).

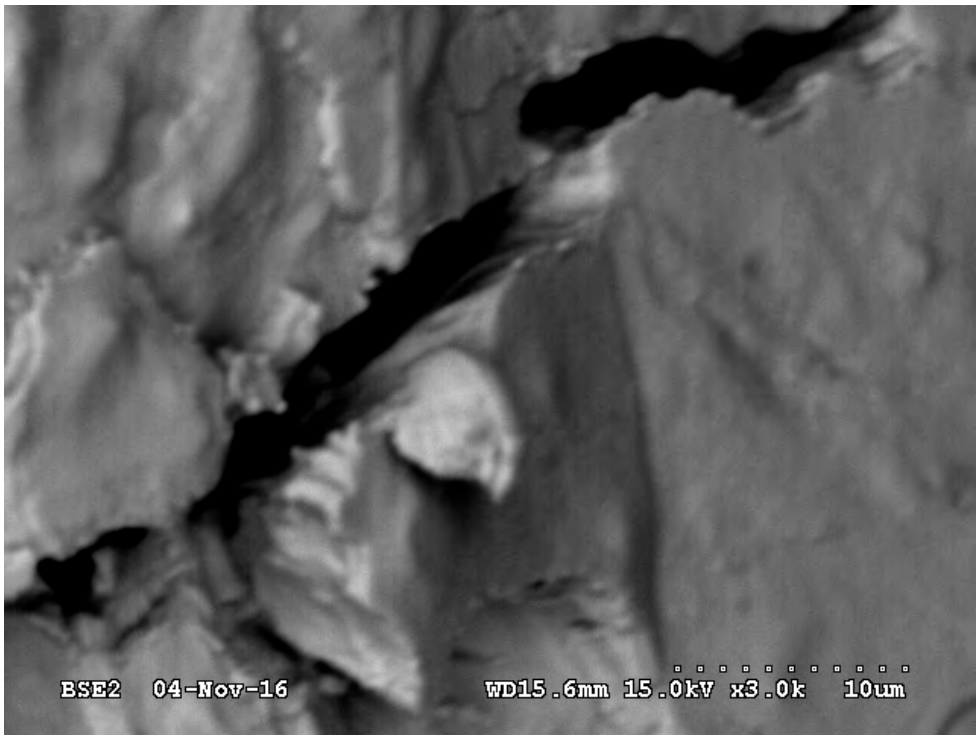


Figure 93: Close up SEM image of a whisker near a solder crack in the SOT3 solder joint shown in Figure 90, 3,000x (ref. A-SOT-PC-1-0-ncc-1, U27, lead 3).

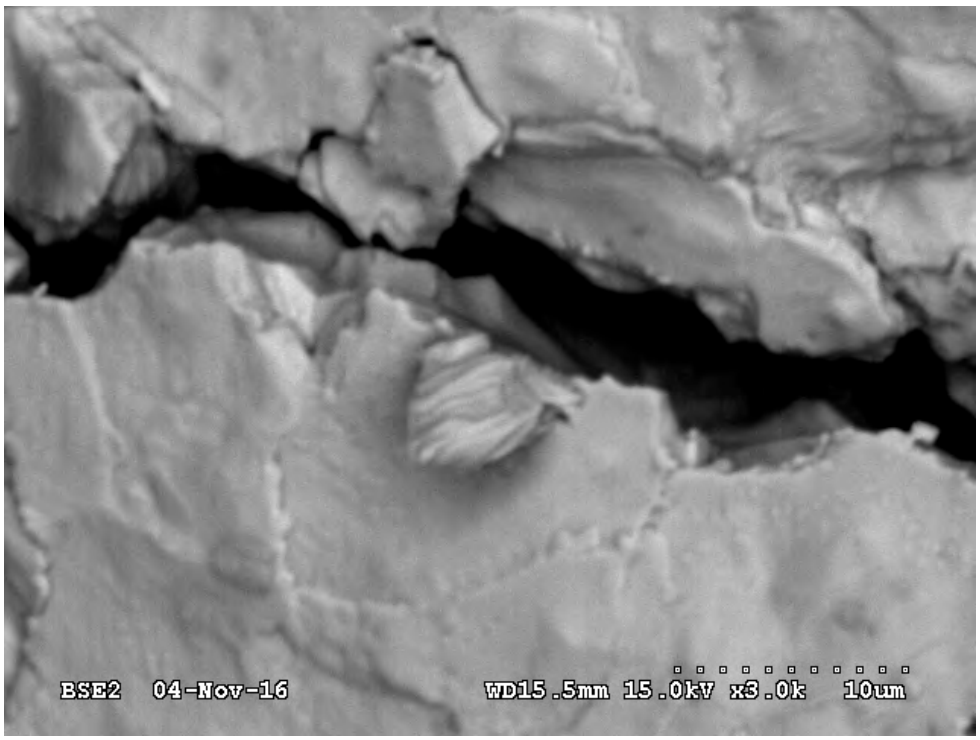


Figure 94: Close up SEM image of a second whisker near a solder crack in the SOT3 solder joint shown in Figure 90, 3,000x (ref. A-SOT-PC-1-0-ncc-1, U27, lead 3).

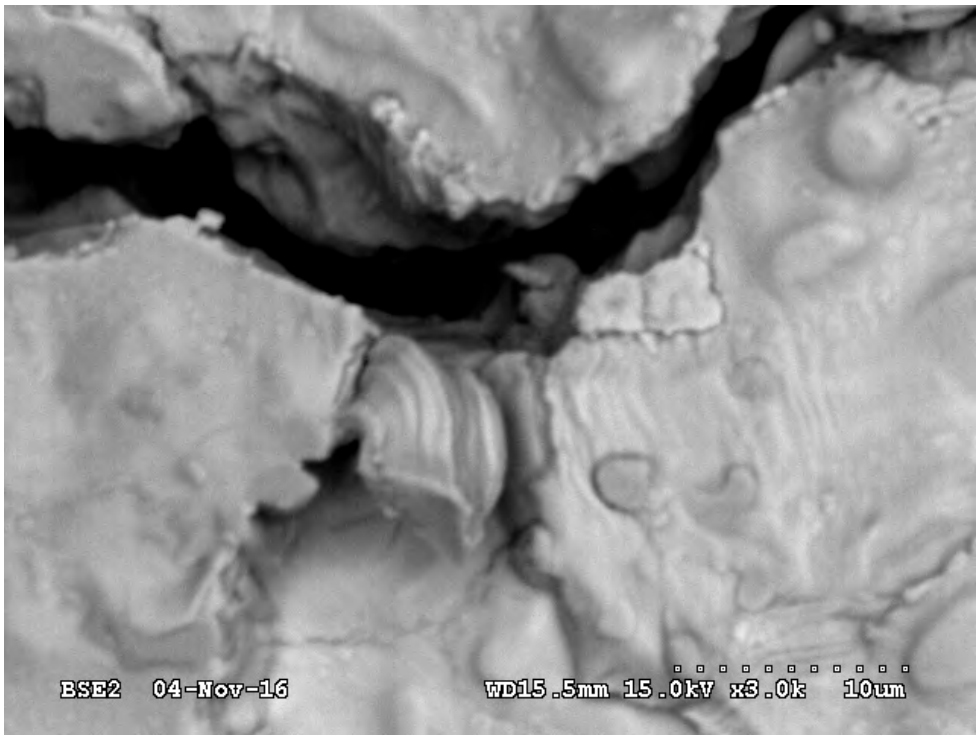


Figure 95: Close up SEM image of a third whisker near a solder joint crack in the SOT3 lead shown in Figure 90, 3,000x (ref. A-SOT-PC-1-0-ncc-1, U27, lead 3).

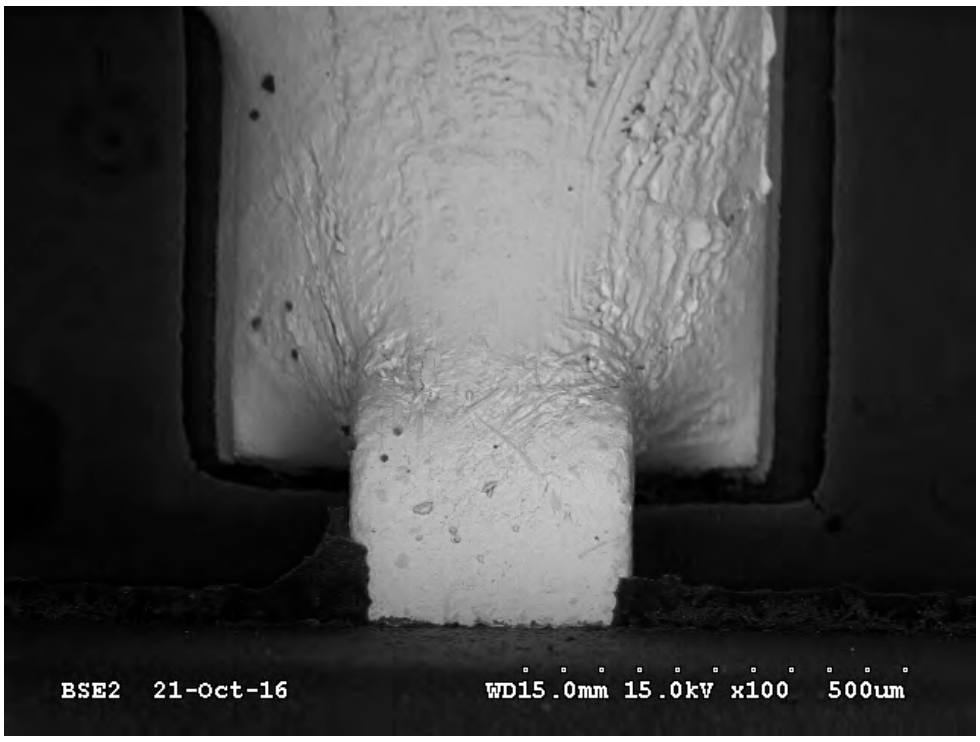


Figure 96: SEM image of the SOT3, U31, lead 1, no conformal coating, 1-1 contamination level after 6,000 PCTC cycles, 100x (ref. A-SOT-PC-1-1-ncc-1).

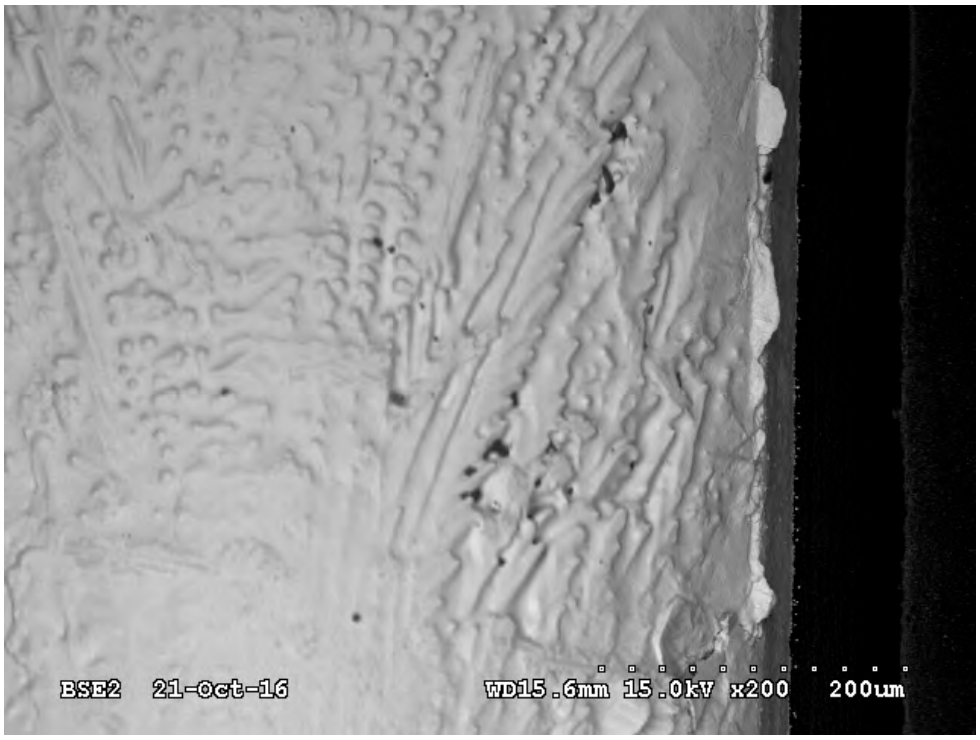


Figure 97: Close up SEM image of pad edge extrusions on the SOT3 solder joint shown in Figure 96, 200x (ref. A-SOT-PC-1-1-ncc-1, U31 lead 1).

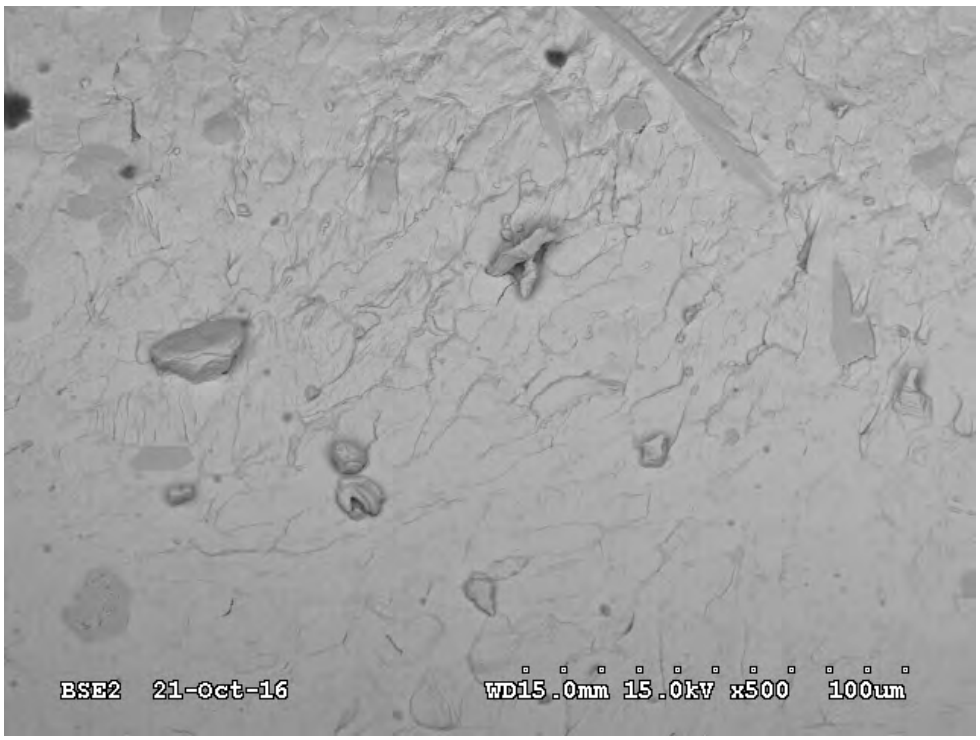


Figure 98: Close up SEM image of various growths on the SOT3 lead shown in Figure 96, 500x (ref. A-SOT-PC-1-1-ncc-1, U31 lead 1).

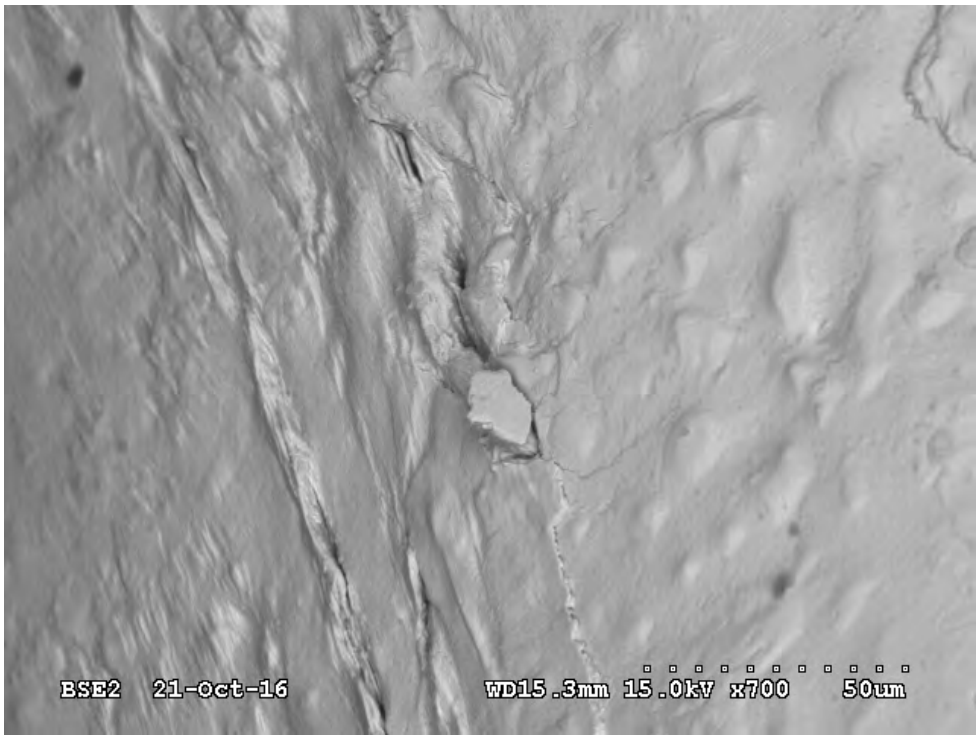


Figure 99: Close up SEM image of deformation and whisker growth along a grain boundary on the SOT3 lead shown in Figure 96, 700x (ref. A-SOT-PC-1-1-ncc-1, U31 lead 1).

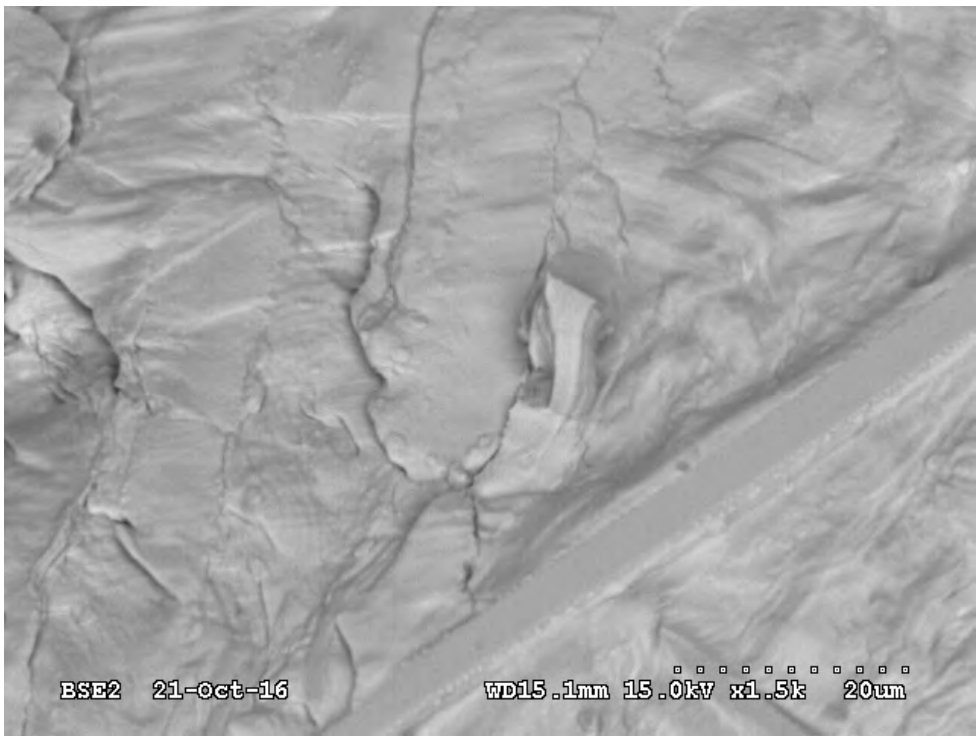


Figure 100: Close up SEM image of whisker growth adjacent to an Ag_3Sn intermetallic plate and grain boundary slip regions on the SOT3 lead shown in Figure 96, 1,500x (ref. A-SOT-PC-1-1-ncc-1, U31 lead 1).

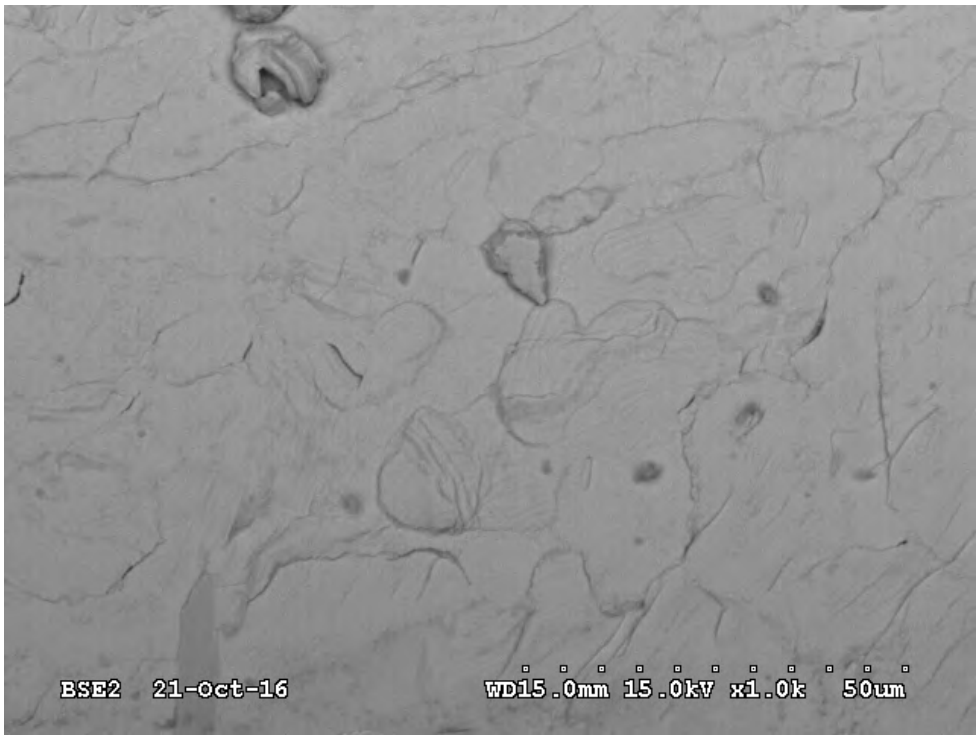


Figure 101: Close up SEM image of whisker growth and grain boundary slip regions on the SOT3 lead shown in Figure 96, 1,000x (ref. A-SOT-PC-1-1-ncc-1, U31 lead 1).

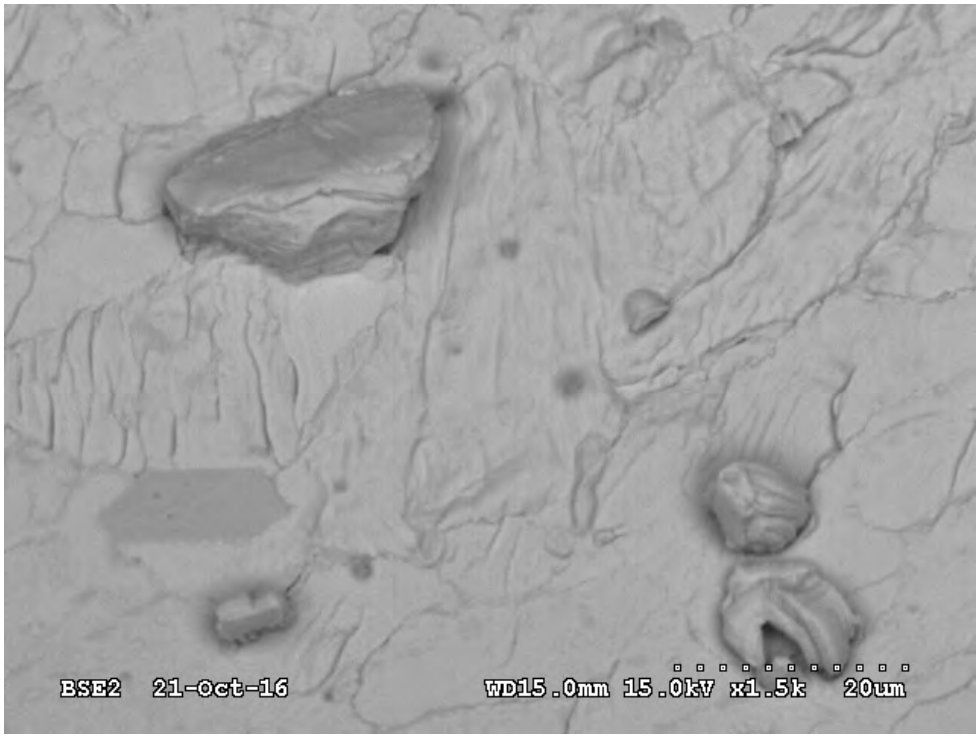


Figure 102: Close up SEM image of the upper whisker shown in Figure 101, 1,500x. In addition to whisker growth, deformation growth and grain boundary deformation are present (ref. A-SOT-PC-1-1-ncc-1, SOT3 U31 lead 1).

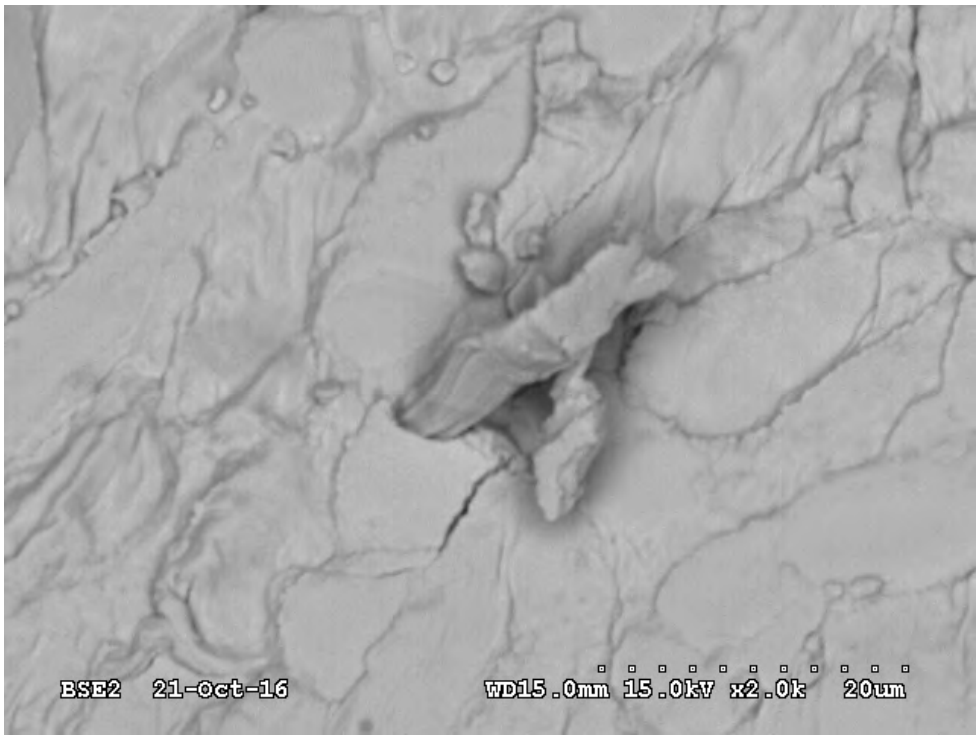


Figure 103: Close up SEM image of grain boundary slip regions, grain recrystallization, multiple whisker nucleation sites and whisker growth on the SOT3 lead shown in Figure 96, 2,000x (ref. A-SOT-PC-1-1-ncc-1, U31 lead 1).



Figure 104: Close up SEM image of grain boundary slip regions, solder cracks, grain recrystallization, and whisker growth on the SOT3 lead shown in Figure 96, 2,500x (ref. A-SOT-PC-1-1-ncc-1, U31 lead 1).

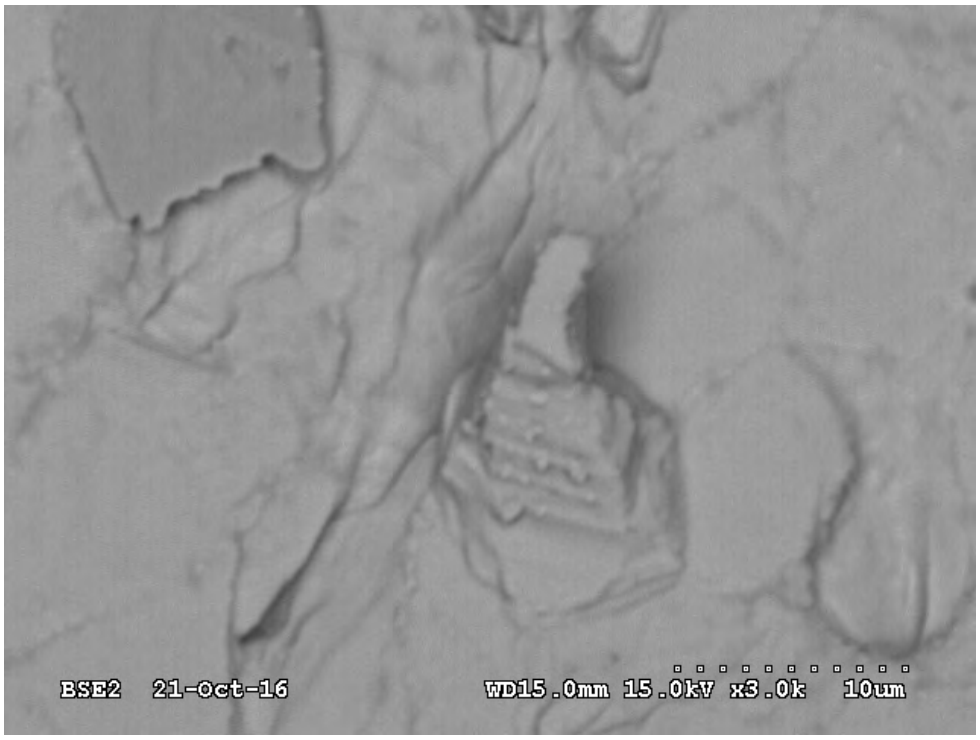


Figure 105: Close up SEM image of grain boundary slip regions and a whisker with an increasing whisker base diameter on the SOT3 lead shown in Figure 96, 3,000x (ref. A-SOT-PC-1-1-ncc-1, U31 lead 1).

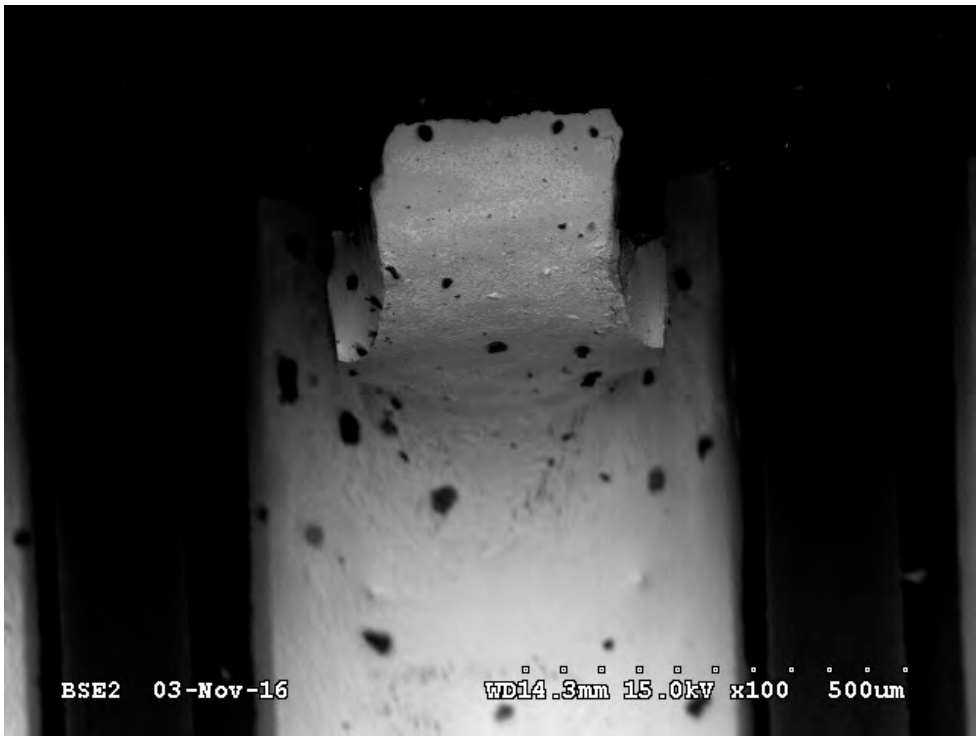


Figure 106: SEM image of the SOT5, U24, lead 2, no conformal coating, 1-0 contamination level after 6,000 PCTC cycles, 100x (ref A-SOT-PC-1-0-ncc-1, SOT5, U24, lead 2).

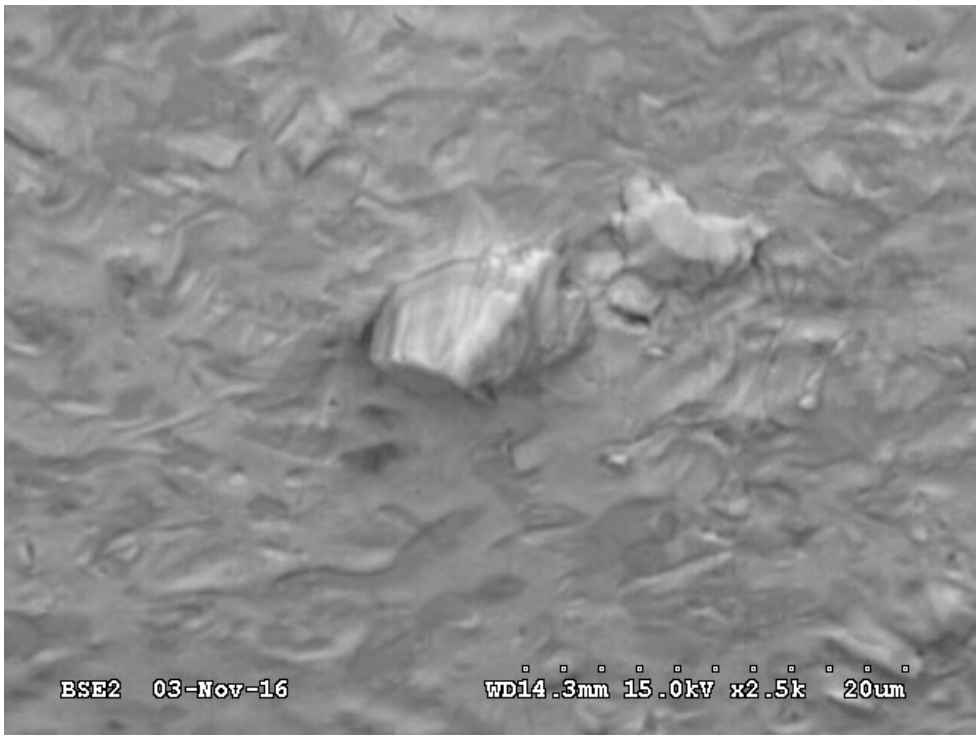


Figure 107: Close up SEM image of the SOT5 lead shown in Figure 106, 2,500x (ref. A-SOT-PC-1-0-ncc-1, SOT5, U24, lead 2).

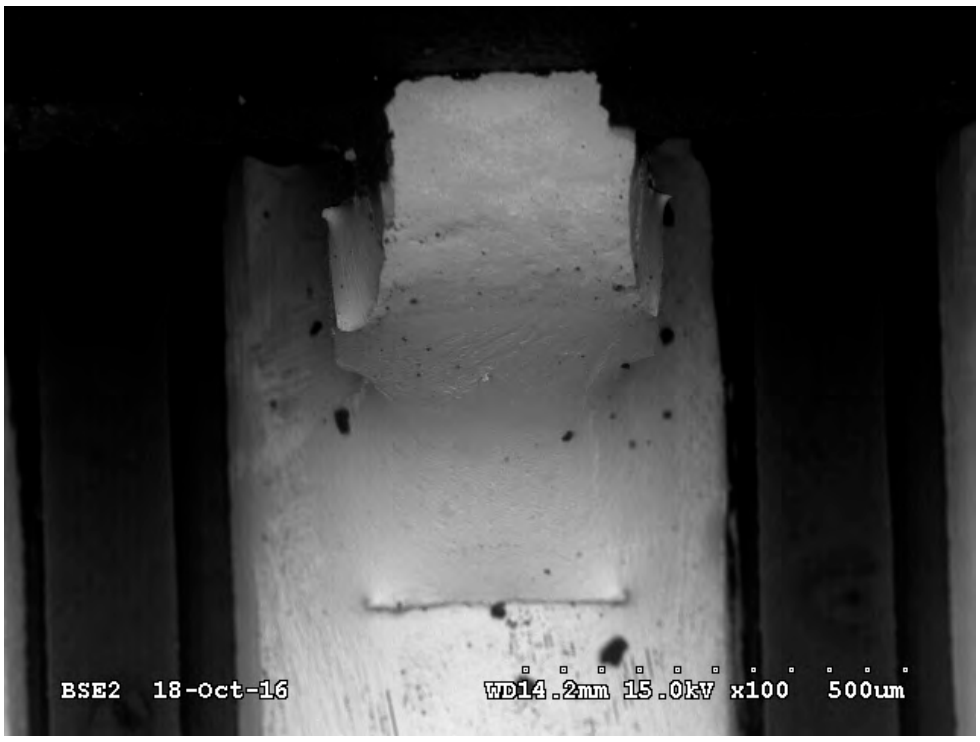


Figure 108: SEM image of the SOT5, U11, lead 2, no conformal coating, 0-1 contamination level after 6,000 PCTC cycles, 100x (ref. A-SOT-PC-0-1-ncc-3, SOT5, U11, lead 2).

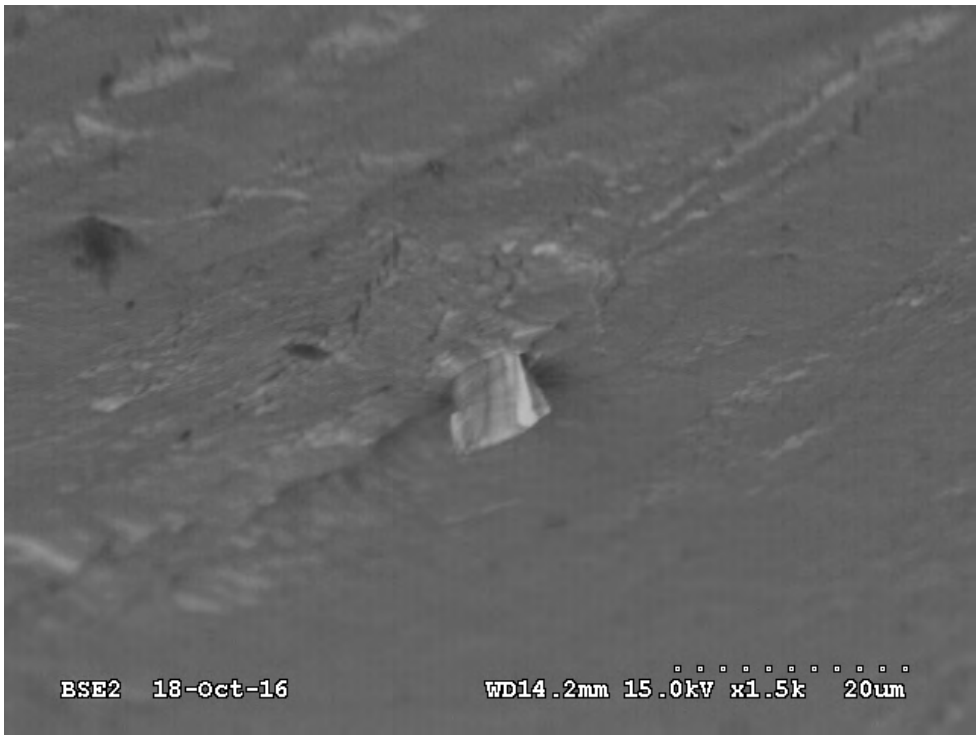


Figure 109: Close up SEM image of the SOT5 lead shown in Figure 108, 1,500x (ref. A-SOT-PC-0-1-ncc-3, SOT5, U11, lead 2).

3.3 Coating integrity and whisker mitigation results for 6,000 PCTC cycle test

Overall the coating retarded whisker growth even where it was thin. While there were cases where the coating did not develop cracks (Figure 111 to Figure 114), there were instances were where coating cracks developed. These cracks were usually located near the leads where the coating was thicker. These cracks often required magnifications 100x or greater to see (Figure 116, Figure 117, Figure 119, Figure 120, Figure 115 and Figure 121). In some cases, the cracks continued and went along the lead-to-package interface region (Figure 122).

While the coating retarded whisker growth even where it was thin (Figure 120), on some leads whisker nucleation occurred (Figure 114).

The coating wicked into the solder interdendritic grooves and no cracking was observed in these areas (Figure 124). Note that the coating adhesion in these areas is both mechanical and chemical.

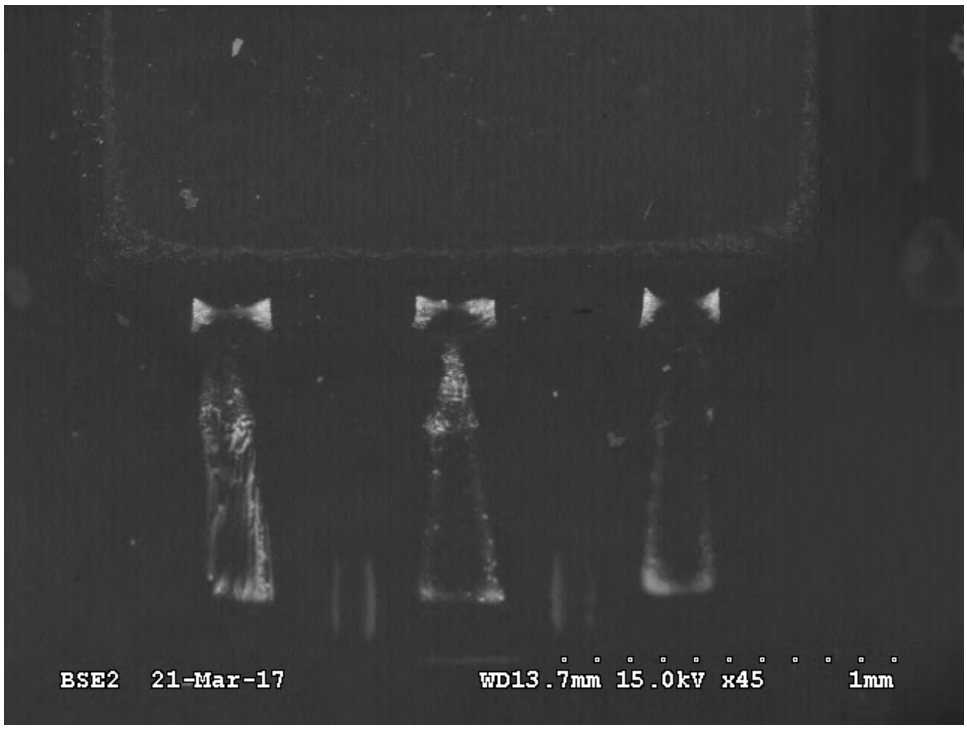


Figure 110: SEM image of coating on SOT6 leads from board 3 after 6,000 PCTC cycles (ref. B-SOT-PC-1-1-cc-3, SOT6), 45x.



Figure 111: SEM image of coating on SOT6 leads from board 3 after 6,000 PCTC cycles, 100x (ref. B-SOT-PC-1-1-cc-3, SOT6).

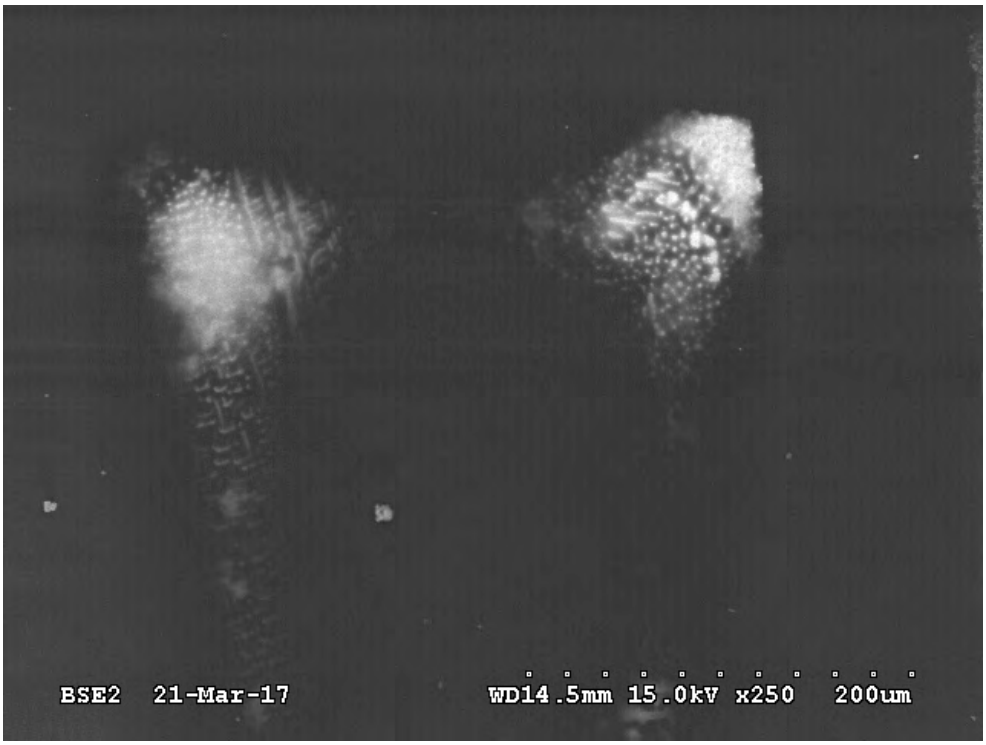


Figure 112: Intermediate magnification SEM image of coating on a SOT6 lead from board 3 after 6,000 PCTC cycles, 250x (ref. B-SOT-PC-1-1-cc-3, SOT6).

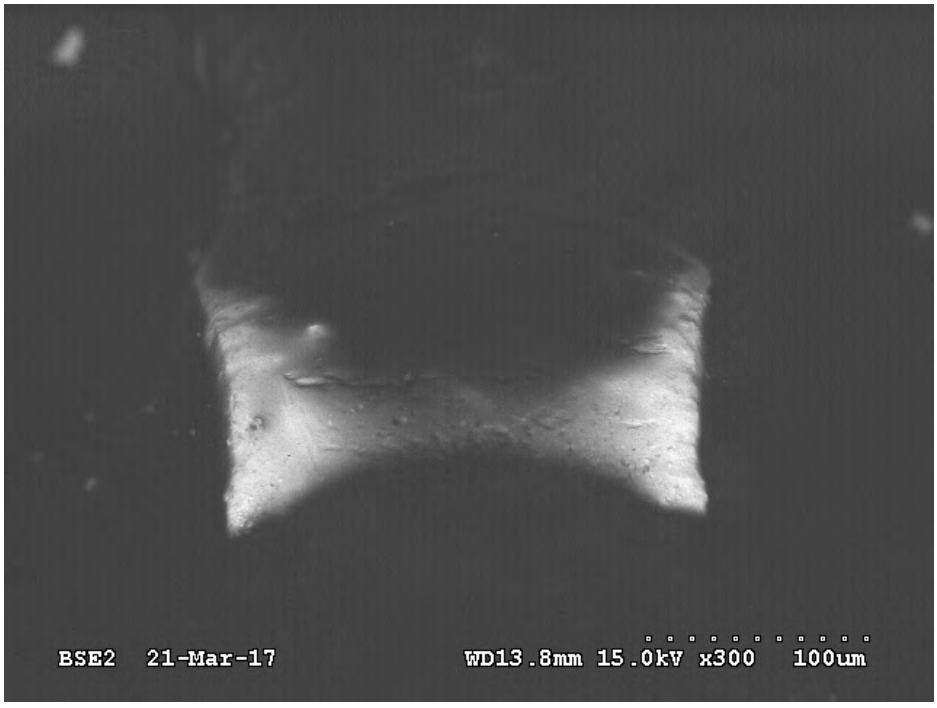


Figure 113: High magnification SEM image of coating on a SOT6 lead from board 3 after 6,000 PCTC cycles, 300x (ref. B-SOT-PC-1-1-cc-3, SOT6).

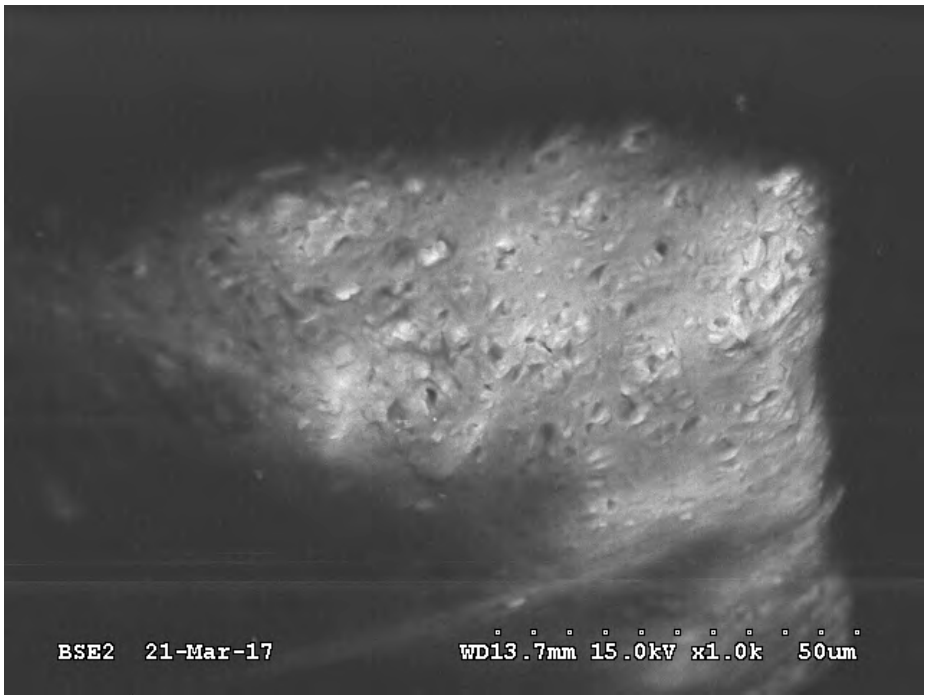


Figure 114: Higher magnification SEM image of coating on a SOT6 lead from board 3 after 6,000 PCTC cycles, 1,000x (ref. B-SOT-PC-1-1-cc-3, SOT6).

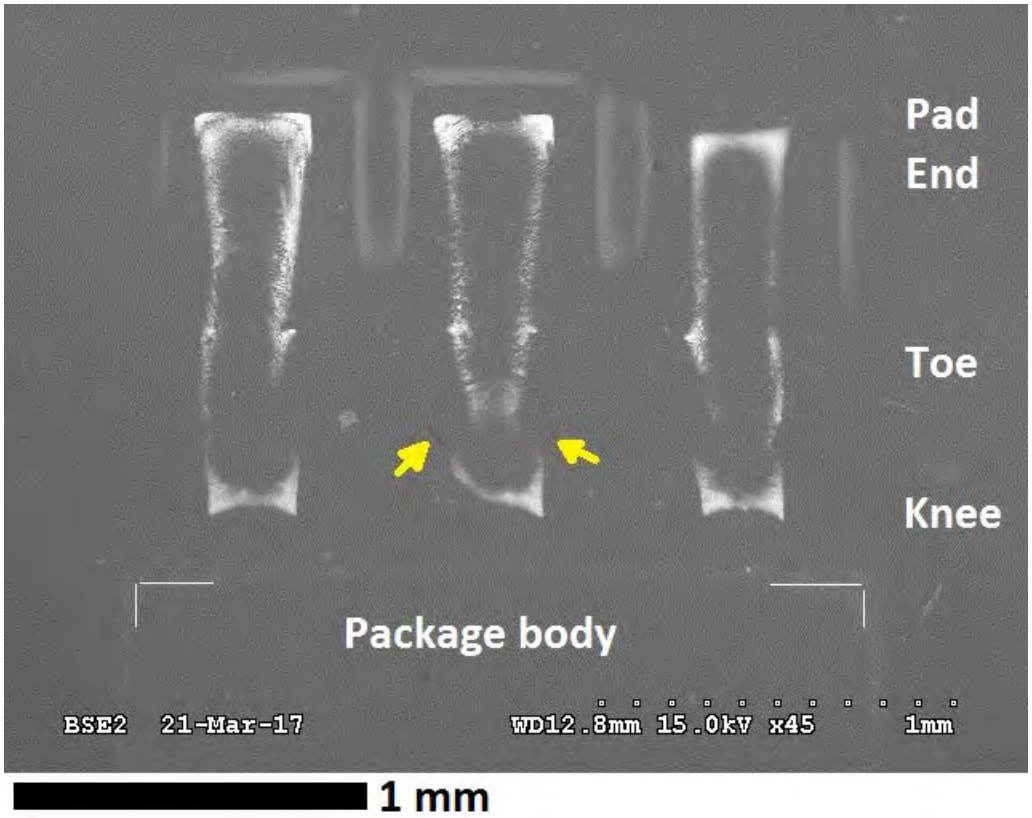
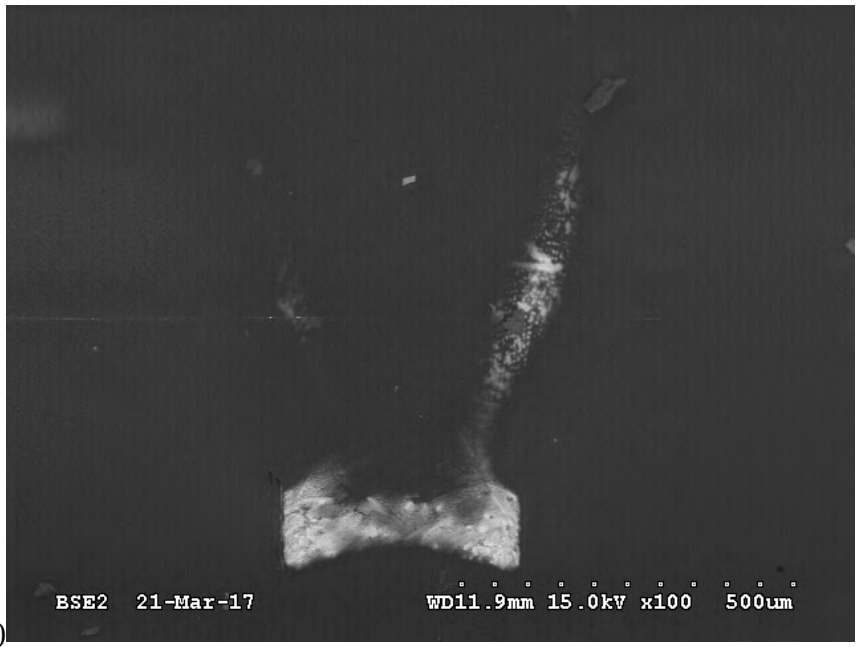


Figure 115: SEM image of coating on SOT6 leads from board 2 after 6,000 PCTC cycles, 45x (ref. B-SOT-PC-1-1-cc-2, SOT6). Arrows highlight coating cracks.

(A)



(B)



Figure 116: Close-up SEM image of coating on a SOT3 lead after 6,000 PCTC cycles, 100x; (A) normal contrast and (B) high contrast. Lead knee is toward the bottom of the image (ref. B-SOT-PC-1-1-cc-2, SOT3).

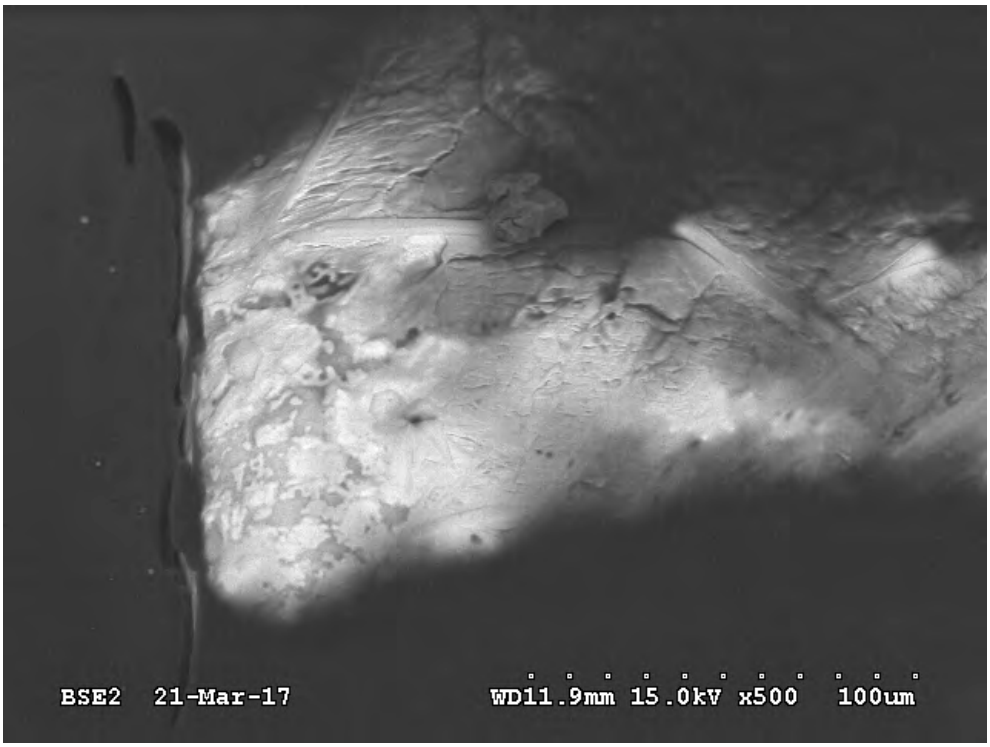


Figure 117: Higher magnification SEM image of the coating crack on the left side of the SOT3 lead show in Figure 116 after 6,000 PCTC cycles, 500x (ref. B-SOT-PC-1-1-cc-2, SOT3).

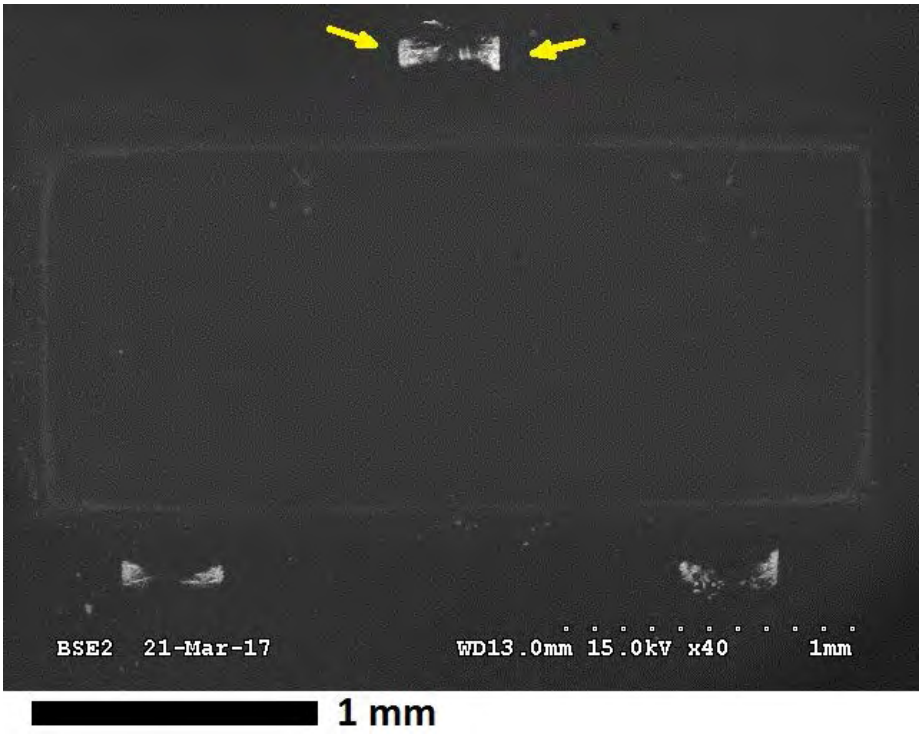


Figure 118: SEM image of coating on the SOT3 part from board 3 after 6,000 PCTC cycles, 40x (ref. B-SOT-PC-1-1-cc-3, SOT3).

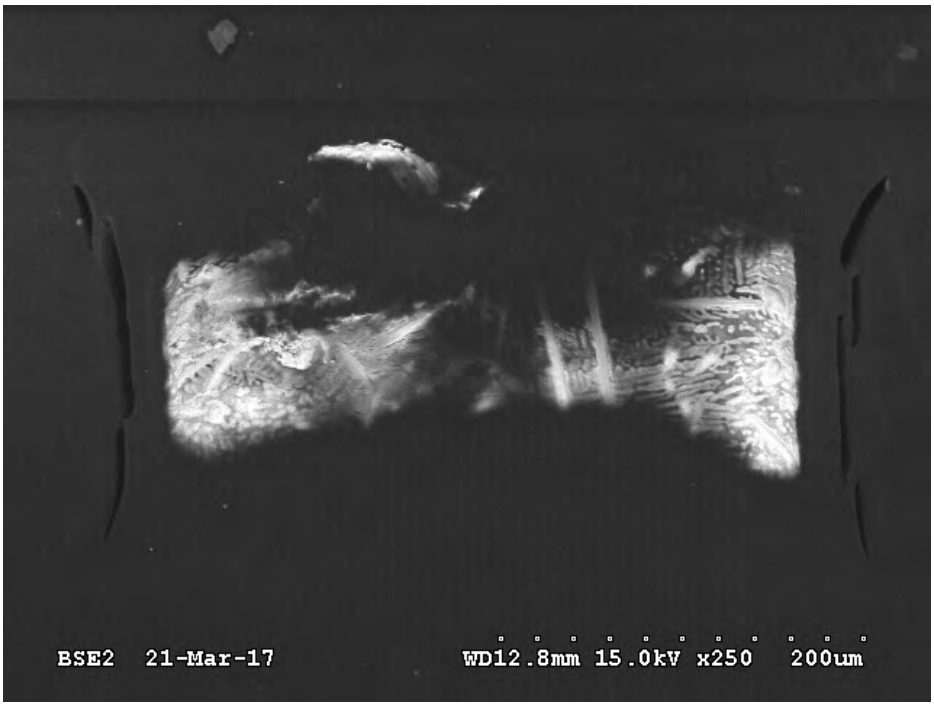
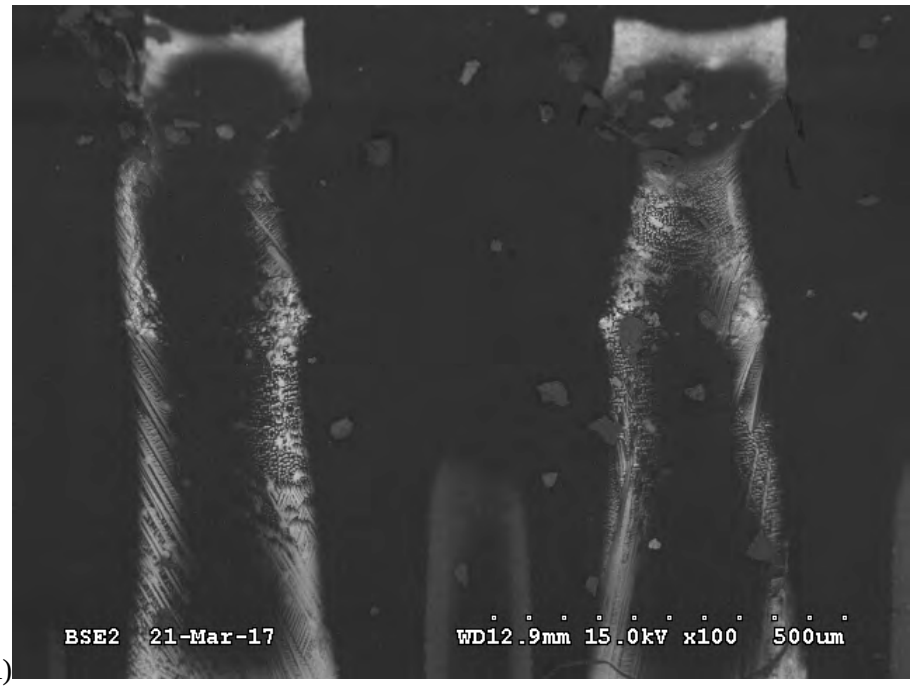


Figure 119: Higher magnification SEM image of coating on the upper SOT3 lead shown in Figure 118 illustrating coating cracks after 6,000 PCTC cycles, 250x (ref. B-SOT-PC-1-1-cc-3, SOT3).



Figure 120: High magnification SEM image of coating on a SOT3 lead near the knee illustrating coating cracks and separation between the coating and the knee after 6,000 PCTC cycles, 1,000x. (ref. B-SOT-PC-1-1-cc-3, SOT3).

(A)

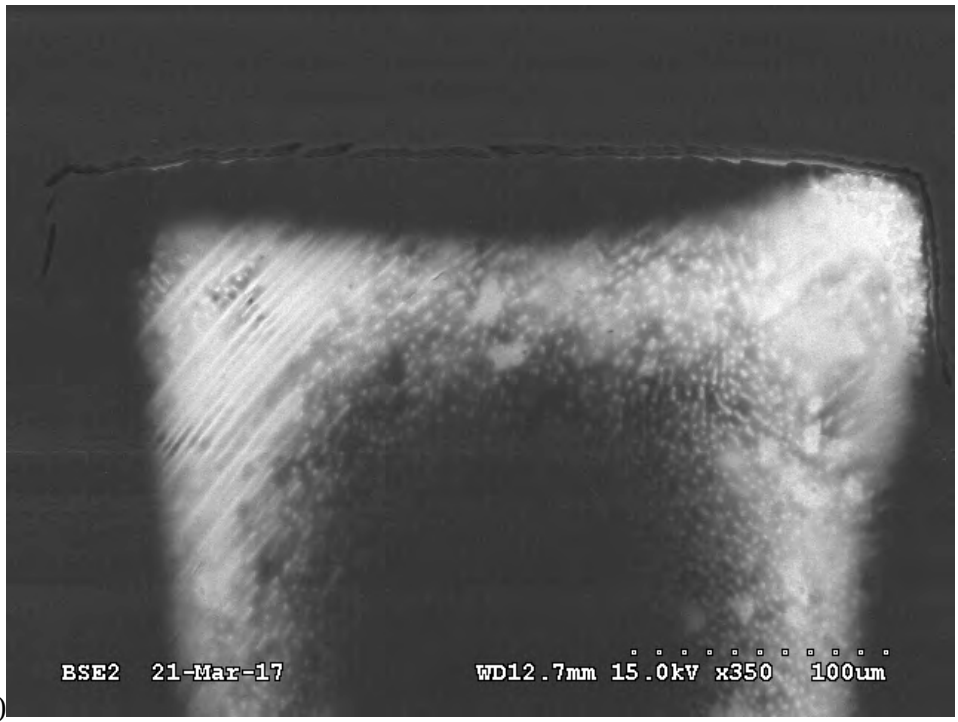


(B)



Figure 121: SEM image of coating with cracks on SOT6 leads from board 2 after 6,000 PCTC cycles, 100x, image 2; (A) normal contrast and (B) high contrast (ref. B-SOT-PC-1-1-cc-2, SOT6).

(A)



(B)

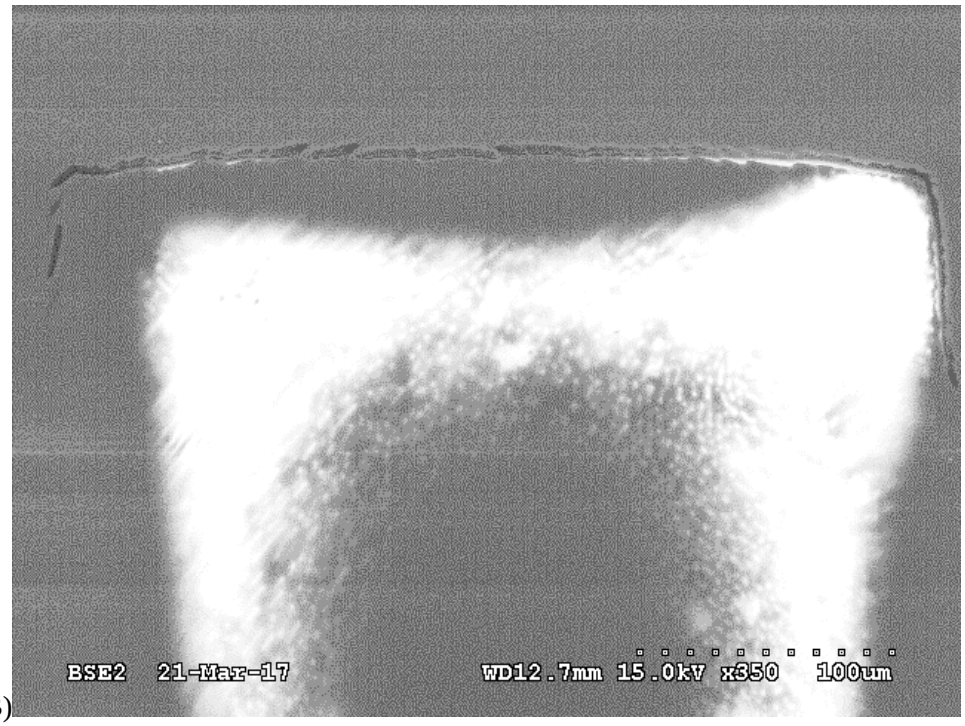


Figure 122: SEM image of coating on a SOT6 lead from board 2 showing some coating cracks after 6,000 PCTC cycles, 350x; (A) normal contrast and (B) high contrast (ref. B-SOT-PC-1-1-cc-2, SOT6).



Figure 123: SEM image of coating on a SOT6 lead from board 2 with the interdendritic solder spaces filled with coating and no whiskers, 6,000 cycles, 400x (ref. B-SOT-PC-1-1-cc-2, SOT6).

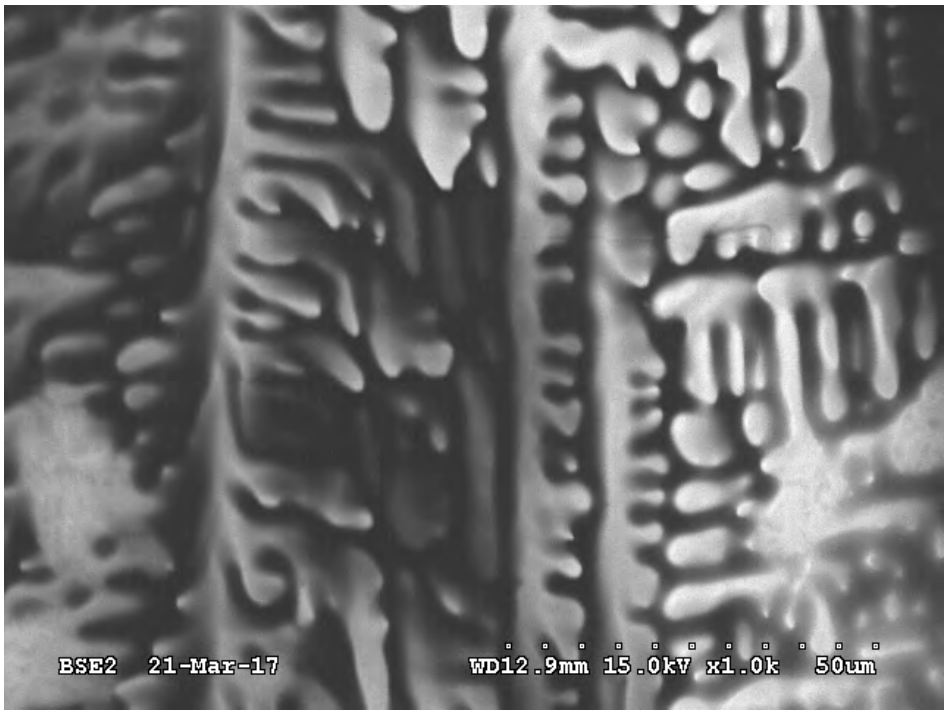


Figure 124: Higher magnification SEM image of coating on a SOT6 lead from board 2 showing that the interdendritic solder spaces are filled with coating and there are no whiskers 6,000 cycles, 1,000x (ref. B-SOT-PC-1-1-cc-2, SOT6).

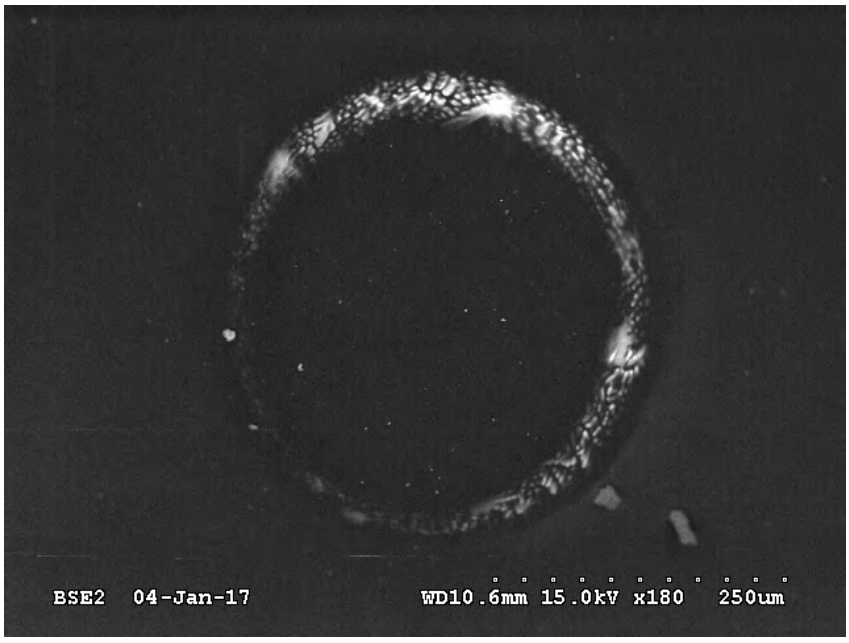


Figure 125: SEM image of coating on a SAC+Re paste reflowed on a BGA solder pad after 6,000 PCTC cycles, 180x (ref. C-BGA-PC-0-0-cc-1).

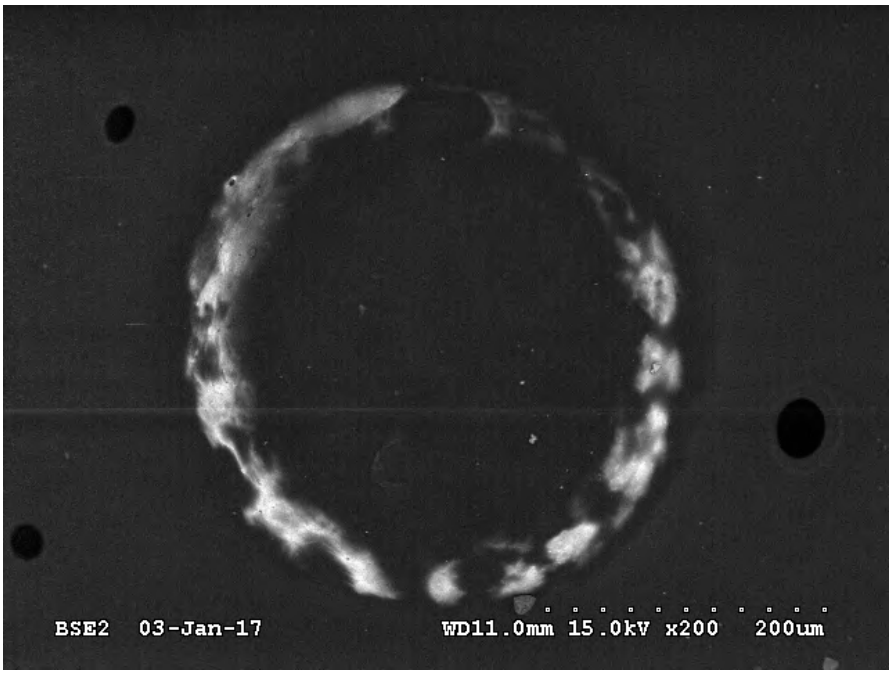


Figure 126: SEM image of coating on SAC+Re paste reflowed on another BGA solder pad after 6,000 PCTC cycles 6,000 cycles, 200x (ref. C-BGA-PC-0-0-cc-1).

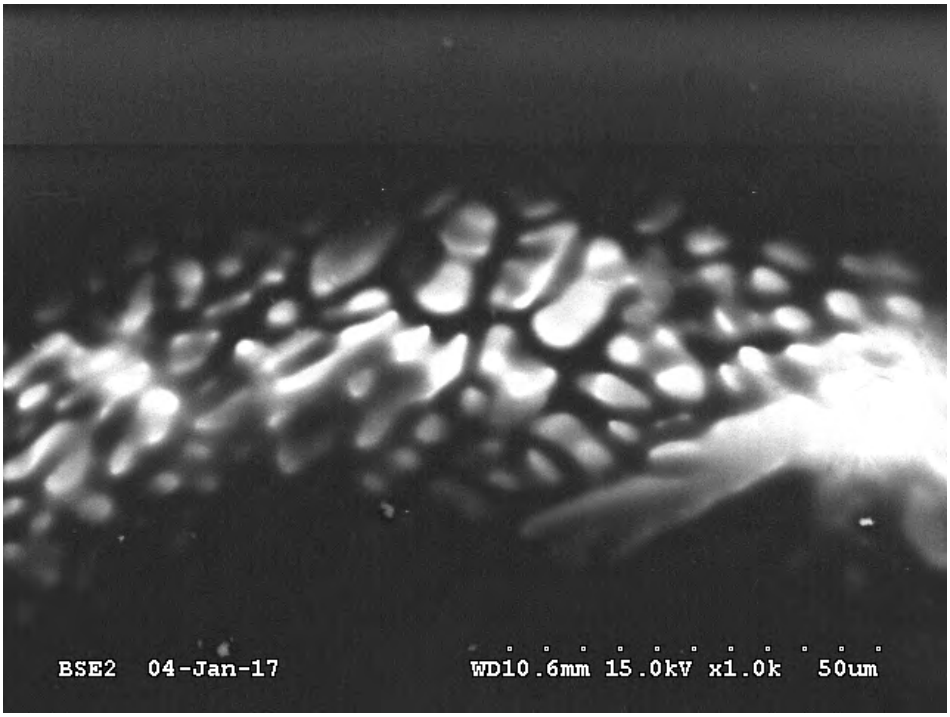


Figure 127: High magnification SEM image of coating on a SAC+Re paste reflowed on a BGA solder pad after 6,000 PCTC cycles, 1,000x (ref. C-BGA-PC-0-0-cc-1).

4. PCTC Discussion

4.1 Whisker statistics discussion

There are many stresses conditions that promote whisker growth (Figure 128). During PCTC cycling, the whisker growth stress was predominantly from the coefficient of thermal expansion differences between the low expansion leads and higher expansion lead-free solder and tin. Over the interval from 1,797 to 6,000 PCTC cycles, some whiskers remained unchanged, some grew longer, and some new whiskers grew. The box plots in Figure 129 show that mean and the maximum whisker length increased between 1,797 PCTC cycles to 6,000 cycles. It should be noted that the whisker length reported at 6,000 cycles did not include board with the longest whiskers at 1,797 cycles which was removed for sectioning. The trend of increasing whisker length with increasing cycle count continued through the 6,000 PCTC cycles (Figure 130). The 0 – 0 contamination level had shorter maximum whisker lengths throughout the test and the 1 – 1 contamination level had the longest.

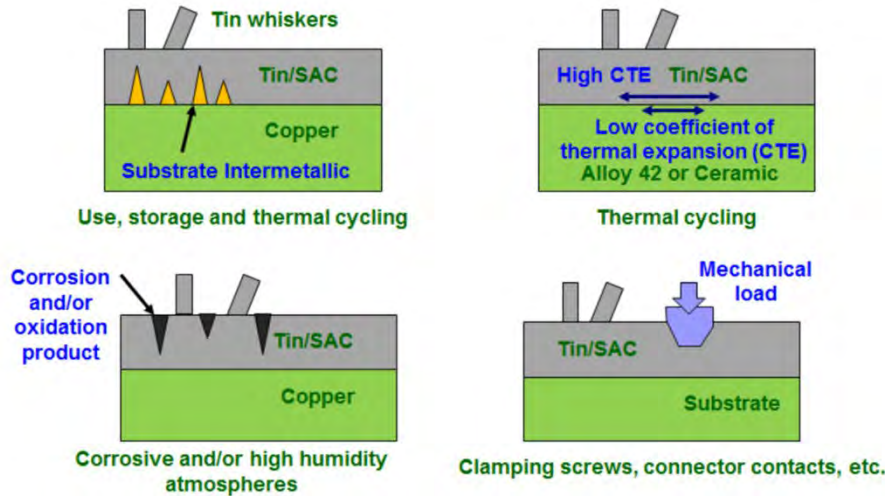
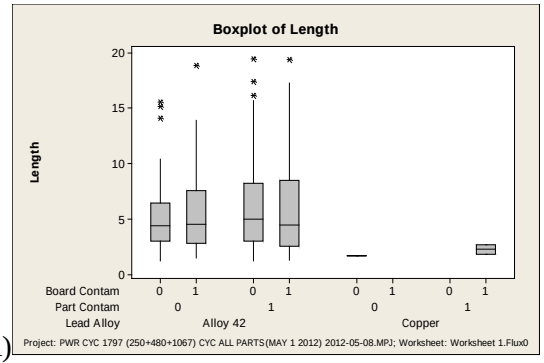


Figure 128: Stress conditions that promote whisker growth.

(A)



(B)

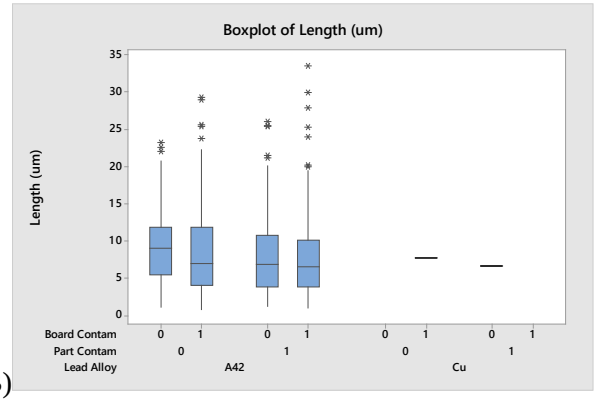


Figure 129: Box plot comparing whisker length (microns) after 1,797 and 6,000 PCTC cycles for lead alloy, part contamination and board contamination combinations; (A) 1,797 PCTC cycles from Figure 35 and (B) 6,000 PCTC cycles from Figure 52.

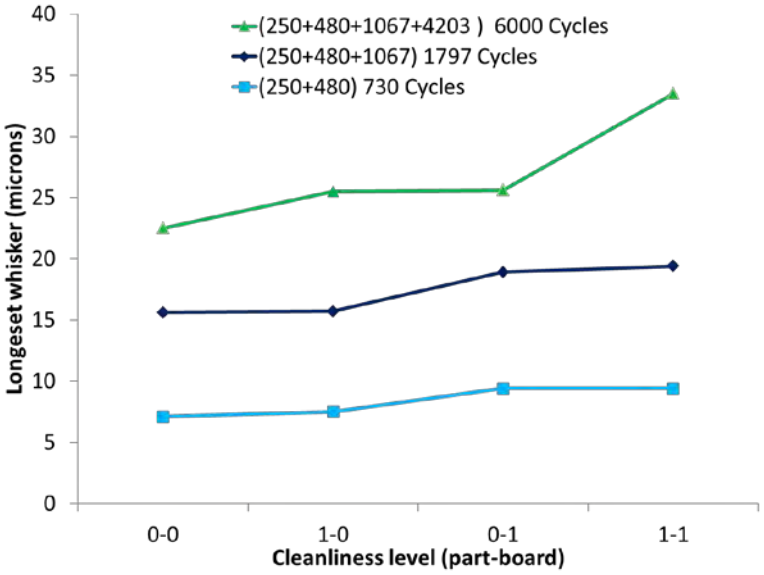


Figure 130: SOT3 maximum whisker length for the three last PCTC inspection intervals.

4.2 Metallurgical observations discussion for uncoated 6,000 PCTC samples

The whiskers mainly grow where the solder is thin at the lead above the main solder joint and around the toe. During PCTC cycling, there are several stress relaxation mechanisms occurring. In addition to whisker growth, there is grain boundary sliding, crack formation and grain recrystallization (Figure 131). The dynamic recrystallization theory proposed by Vianco and Rejent [3][4] suggests that there is an optimal combination of stress, strain rate, grain size and temperature conditions for whisker growth (Figure 132). If the stresses are too high other non-whisker growth stress relaxation mechanisms occur if the stresses are too low, whiskers would not form.

The whisker growth between tin dendrites at 1,797 PCTC cycles was similar in some cases to the 6,000 PCTC (Figure 133). As was seen initially at 1,797 PCTC cycles, sometimes the whiskers were observed next to small solder cracks between tin grains. At the 6,000 PCTC cycle inspection, larger cracks were also observed suggesting that the cyclic stresses promoting whisker growth, while small, can eventually result in solder fatigue cracks. A progression of whisker growth and crack formation during thermal cycling is postulated as follows: (1) initial tin grain recrystallization, whisker nucleation, and whisker growth in the region between tin grains (Figure 134A), (2) then after more cycling the initiation of solder cracks less than a micron wide which could result in decreased whisker growth rate due to reduction of stress from the crack gaps (Figure 134B), and (3) then after more cycling the formation of very large cracks (~ 5 microns) where a whisker growth slows significantly or stops due to a reduction in stress and/or a reduction in mass tin transport to the whisker (Figure 134C).

There is similarity between the tin recrystallization observed during PCTC cycling in the present work and ball grid thermal cycling fatigue studies. The recrystallization of primary Sn grains and subsequent crack formation between these recrystallized grains was discussed by Borgesen et.al. [6] in the SERDP WP1752 final report section titled “Thermal Mismatch Induced Fatigue of SnAgCu”. In this section, thermal cycling of SnAgCu based ball grid array or chip scale package assemblies tended to lead to dynamic recrystallization of the Sn grains and the formation of a network of grain boundaries across the high strain region. As documented in detail in their publication [7] failure analysis, fatigue cracks propagate through the recrystallized region along or very near the new grain boundaries, which is also suggested by others [8][9][10].

A variation in whisker diameter along the length of some whiskers was also observed. Some whisker growths had a smaller diameter at the base than the tip (Figure 135) suggesting that the grain at the whisker root was decreasing with increasing cycling. If this process continued, it would be possible that the whisker root grain would eventually disappear causing the whisker to fall off. Conversely, some whiskers had a larger diameter at the base than the tip (Figure 136 and Figure 137) indicating that the whisker root grain was increasing with increasing cycling. Susan et al. [11] whisker work on thin film tin showed that when the whisker diameter increases, whisker growth stopped. In the current work, sometimes growth seemed to stop (Figure 136) and sometimes additional whisker growth continued to develop after the whisker base diameter increased. Increasing and decreasing whisker diameters were also reported in the WP1753 project [1].

Unique pad edge growths were also observed at the 6,000 PCTC inspection. The thin flat tin sheets were growing laterally from the interface region between the solder and the copper pad (Figure 138). They were similar in appearance to flat tin growths observed between grains (Figure 139). The pad edge growths were on the order of 10 microns long, 20 microns wide and a few microns thick. Pad edge growth was observed on both alloy 42 and copper lead terminations.

Although the vast majority of whisker and pad edge growth occurred on the alloy 42 lead terminations, the SOT5 copper lead terminations did exhibit some growth (Figure 109). The SOT5 whisker growth could be due to different coefficients of thermal expansion (CTE) between the different tin grain orientations. As is discussed by Borgesen et.al. [6] and Tegehall [12], β-tin is one of the most anisotropic metals. The CTE varies between 15 (a- and b-axes) and 30 ppm/K (c-axis) at 25 and between 20 and 40 ppm/K at 125^{0}C. The elastic modulus varies between 22 (a- and b-axes) and 69 GPa (c-axis) at 25^{0}C. Tin is stiffest in the direction in which it also expands the most.

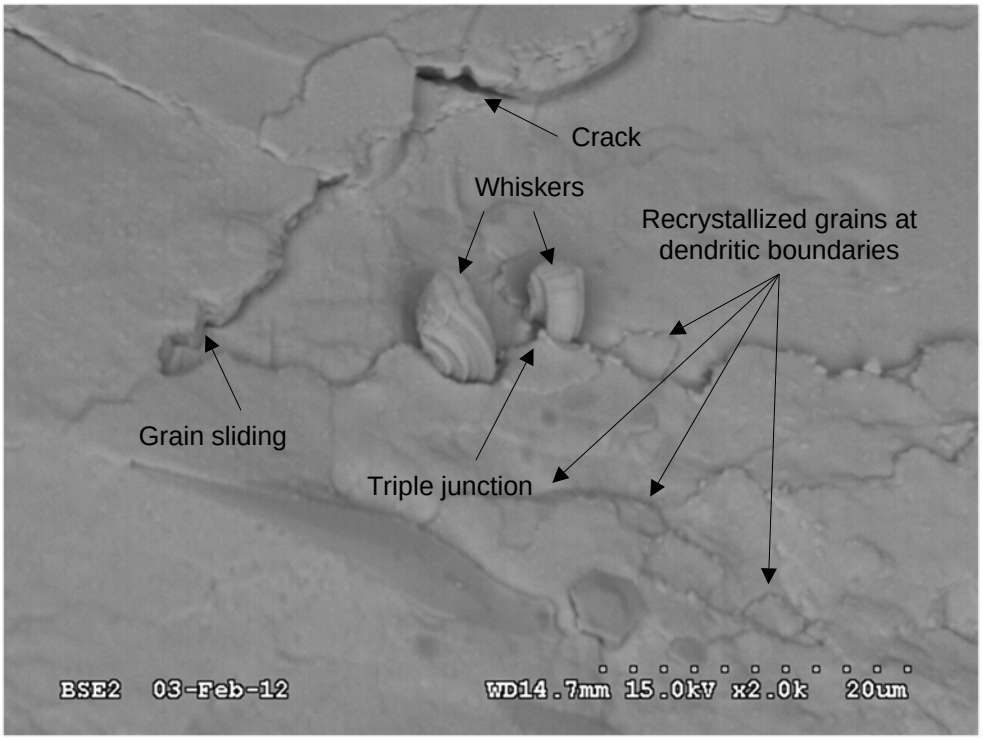
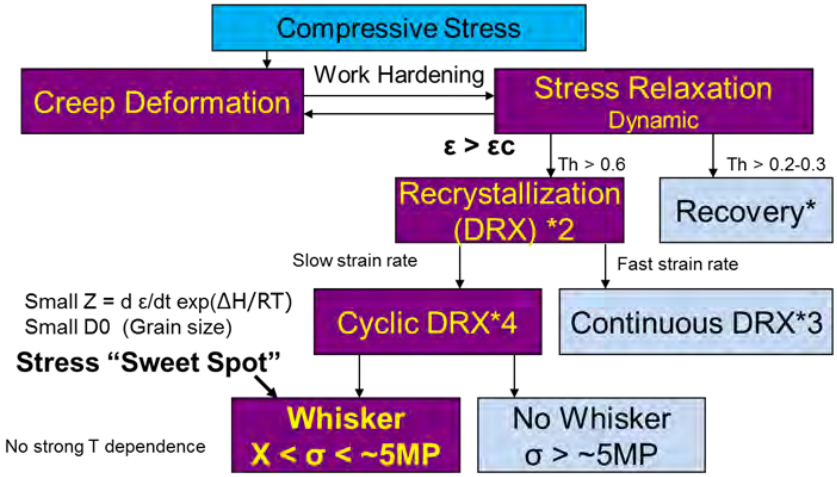


Figure 131: Competing mechanisms of stress relaxation (SOT3, 0-0 contamination level after 1,797 PCTC cycles shown).



*Recovery - rearrangement and annihilation of dislocations and formation of dislocation subgrain walls, takes place at 0.2-0.3 of the homologous temperature (Th), -172°C to -122°C for Sn
*2Recrystalliation – Grain nucleation and growth, takes place at Th > 0.6, 30°C for Sn
*3 Continuous DRX – Single nucleation, very limited grain growth
*4 Cyclic DRX – Multiple nucleation, extensive grain growth

Figure 132: Whisker formation as a result of dynamic recrystallization (DRX) [3][4][5].

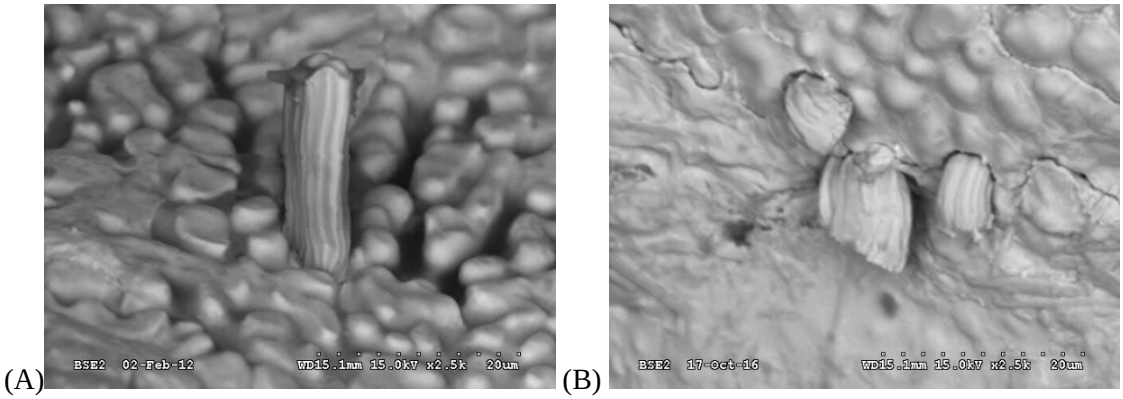


Figure 133: High magnification SEM image comparison of whisker growth at 1,797 and 6,000 cycles SOT6 (A) after 1797 cycles, and (B) after 6,000 cycles 2,500x (ref. Image B A-SOT-PC-1-0-ncc-3, SOT6, U71, lead 4).

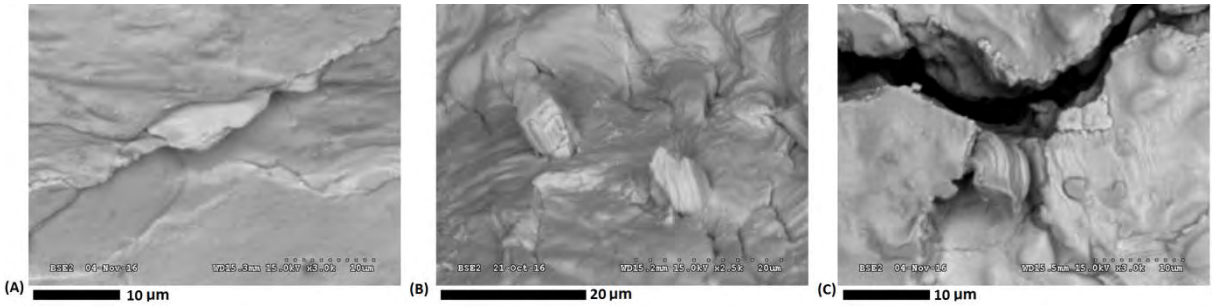


Figure 134: Close up SEM image of grain boundary slip regions, cracks, grain recrystallization, and whisker growth after 6,000 cycles on a SOT3 lead region with increasing amount of solder cracking; (A) no cracks, 3,000x, (B) small cracks, 2,500x and (C) large crack, 3,000x (ref. A-SOT-PC-1-1-ncc-1, SOT3, U31 lead 1 and A-SOT-PC-1-0-ncc-1, SOT3, U27, lead 3).

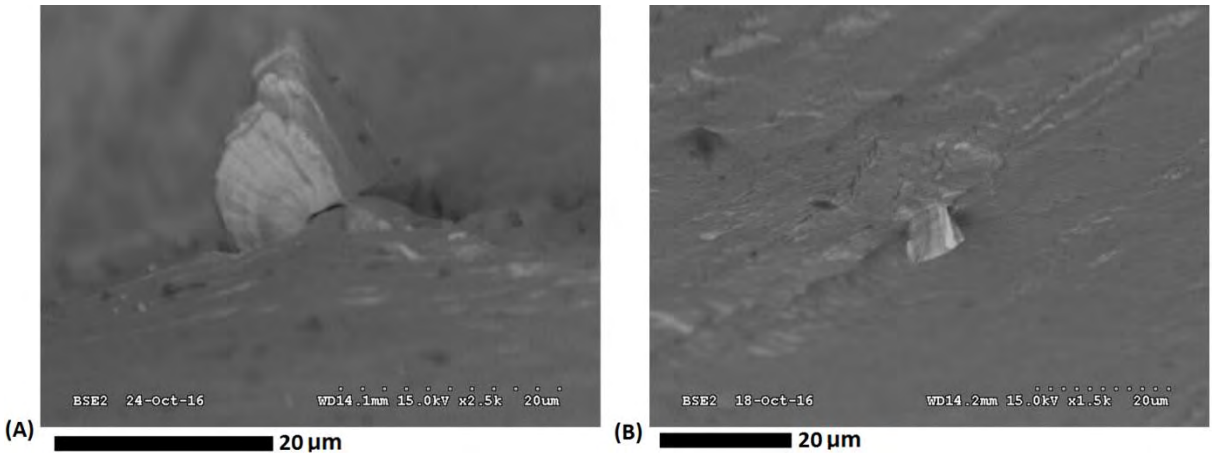


Figure 135: Close-up SEM images of whiskers with a decreasing whisker diameter; (A) on a SOT6 lead, 2,500x and (B) a SOT5 lead shown in Figure 108 (ref. A-SOT-PC-1-1-ncc-1, SOT6, U68, lead 2 and A-SOT-PC-0-1-ncc-3, SOT5, U11, lead 2).

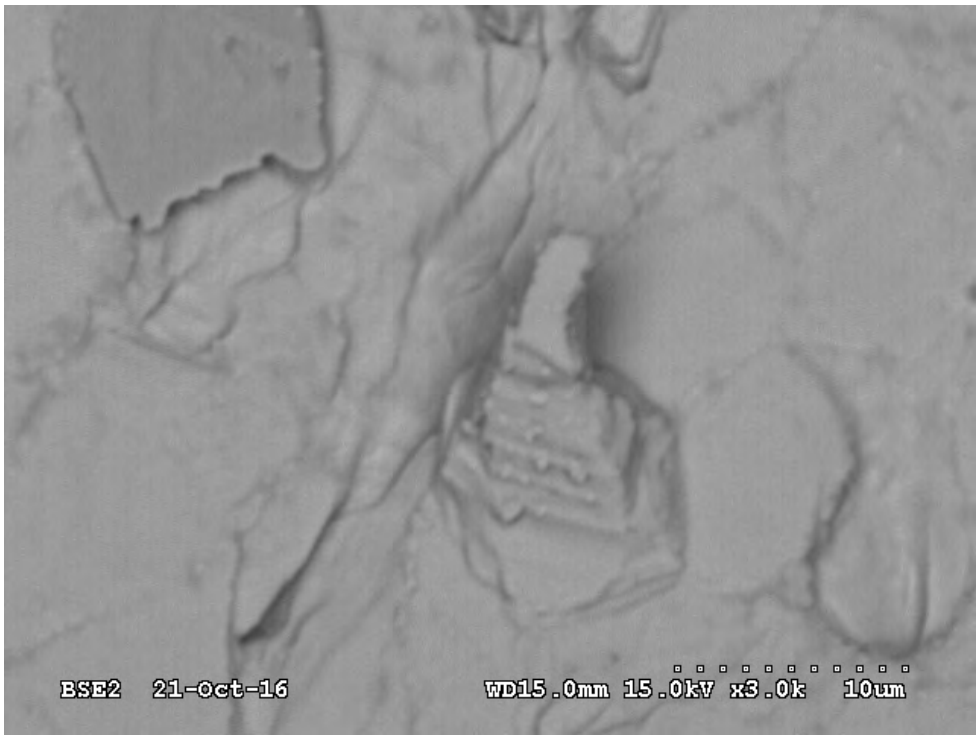


Figure 136: Close up SEM image of grain boundary slip regions and whisker with an increasing whisker base diameter on the SOT3 lead, 3,000x (ref. A-SOT-PC-1-1-ncc-1, SOT3, U31 lead 1).

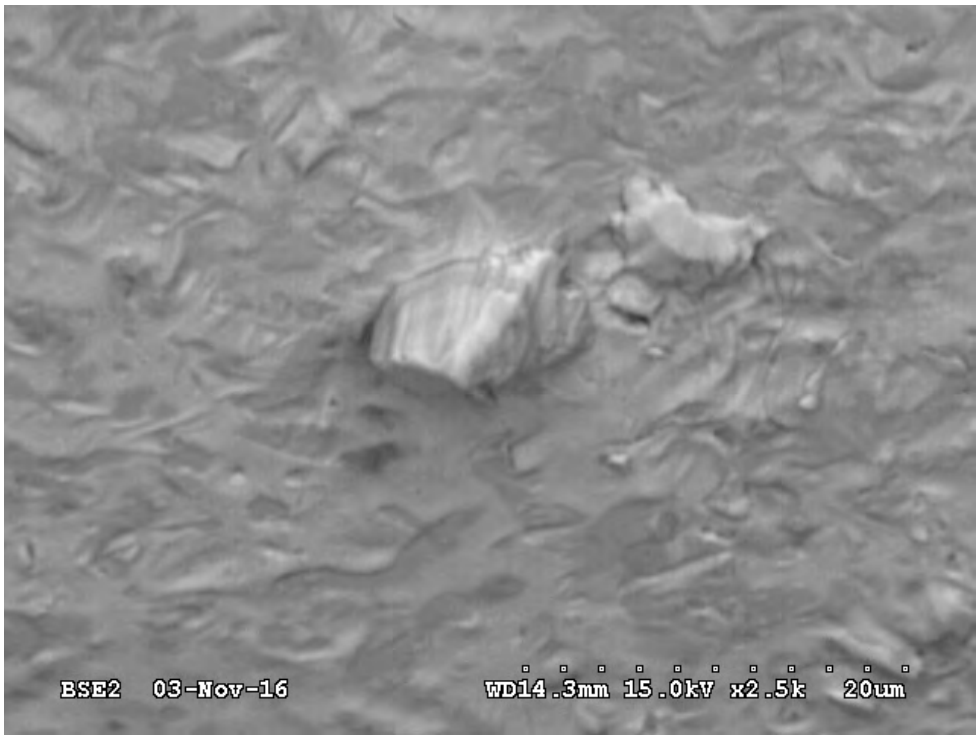


Figure 137: Close up SEM image of the SOT5 lead shown in Figure 106, 2,500x (ref. A-SOT-PC-1-0-ncc-1, SOT5, U24, lead 2).

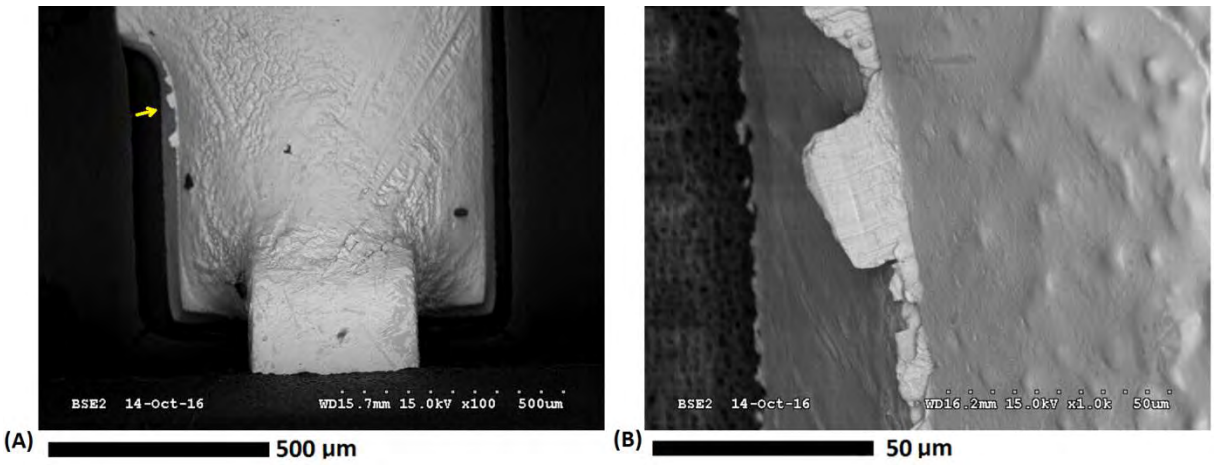


Figure 138: SEM image of the SOT3, U20, lead 1, no conformal coating, 1-0 contamination level after 6,000 PCTC cycles; (A) 100x and (B) high magnification image of pad edge growth highlighted by arrow, 1,000x (ref. A-SOT-PC-1-0-ncc-3).

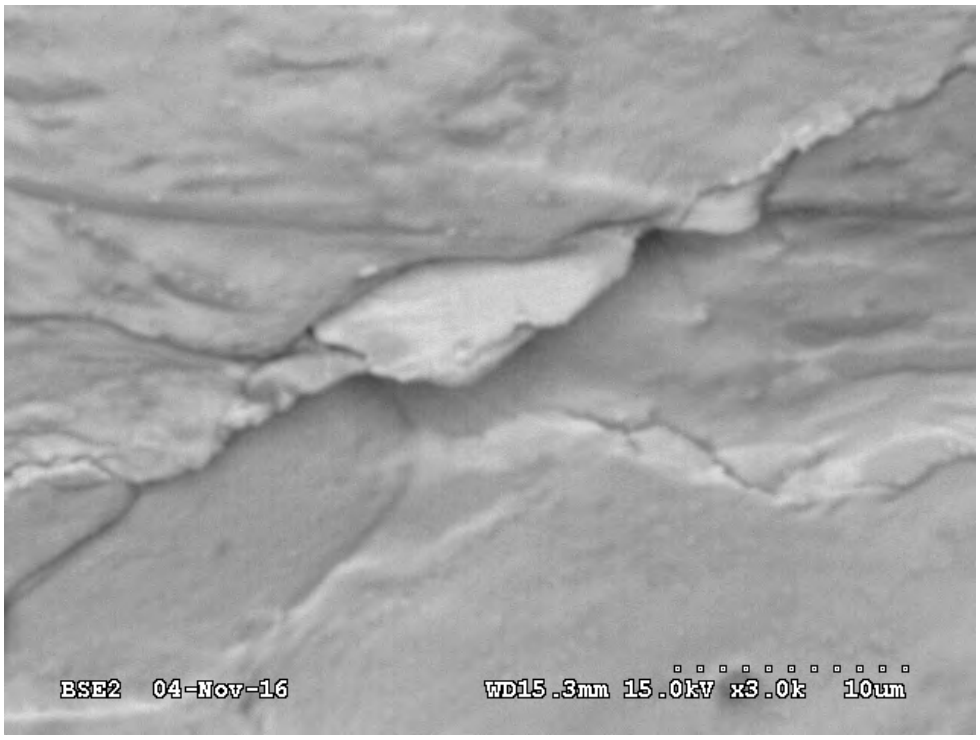


Figure 139: Close up SEM image of growth after 6,000 cycles along the grain boundary on the front of the lead for the SOT3 lead shown in Figure 90, 3,000x, (ref. A-SOT-PC-1-0-ncc-1, SOT3, U27, lead 3).

4.3 Coating integrity and whisker mitigation discussion for 6,000 PCTC cycle test

No whiskers penetrated coating where it was thicker than approximately three microns (e.g the approximate coating thickness where the SEM beam cannot penetrate through the coating and image the underlying solder).

Although the coating obscured the majority of the tin surface from SEM examination, it was thin enough (less than approximately three microns) on the knee and at the toe to examine the metal. The solder areas with thin coating did have some whisker nucleation (Figure 140 and Figure 141).

The coating wicked thoroughly into the solder interdendritic grooves (Figure 142). The coating adhesion in these areas is both mechanical and chemical.

Some coating cracking was observed. The cracks were located along the lead near the lead knee where the coating fillets were thick (Figure 143). The cracks were sometimes accompanied by separation of the coating from the lead (Figure 144).

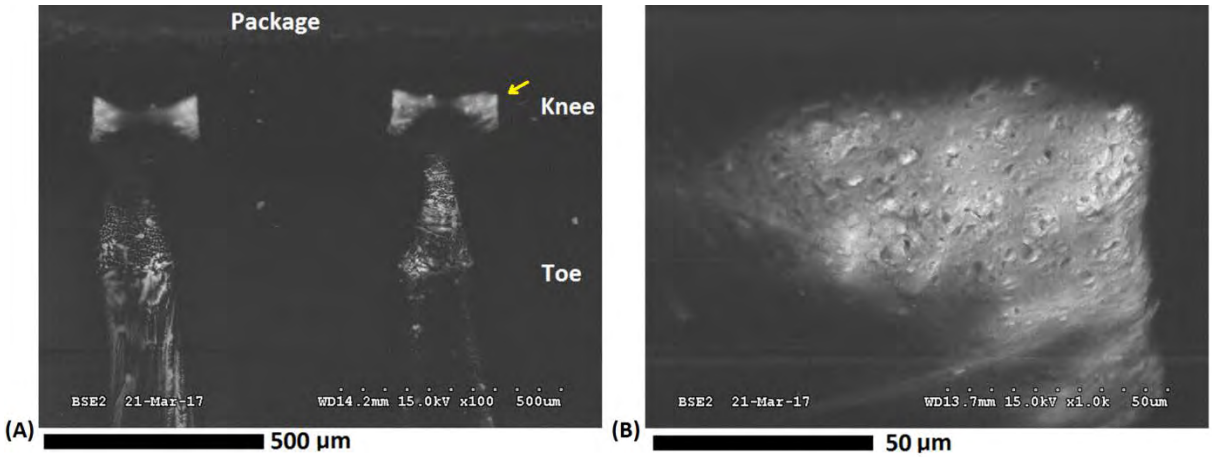


Figure 140: SEM image of coating on two SOT6 leads from board 3 after 6,000 PCTC cycles; (A) 100x and (B) higher magnification image of right lead knee showing whisker nucleation,1,000x (ref. B-SOT-PC-1-1-cc-3, SOT6).

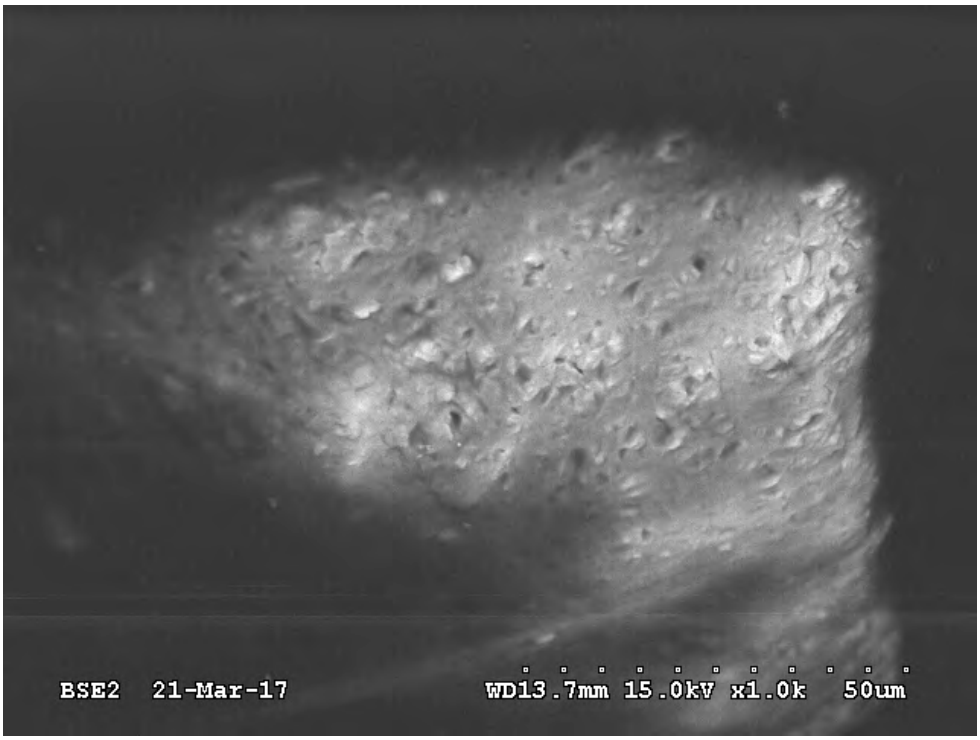


Figure 141: Higher magnification SEM image of coating on right SOT6 lead shown in Figure 140 after 6,000 PCTC cycles, 1,000x. Some whisker nucleation is evident (ref. B-SOT-PC-1-1-cc-3, SOT6).

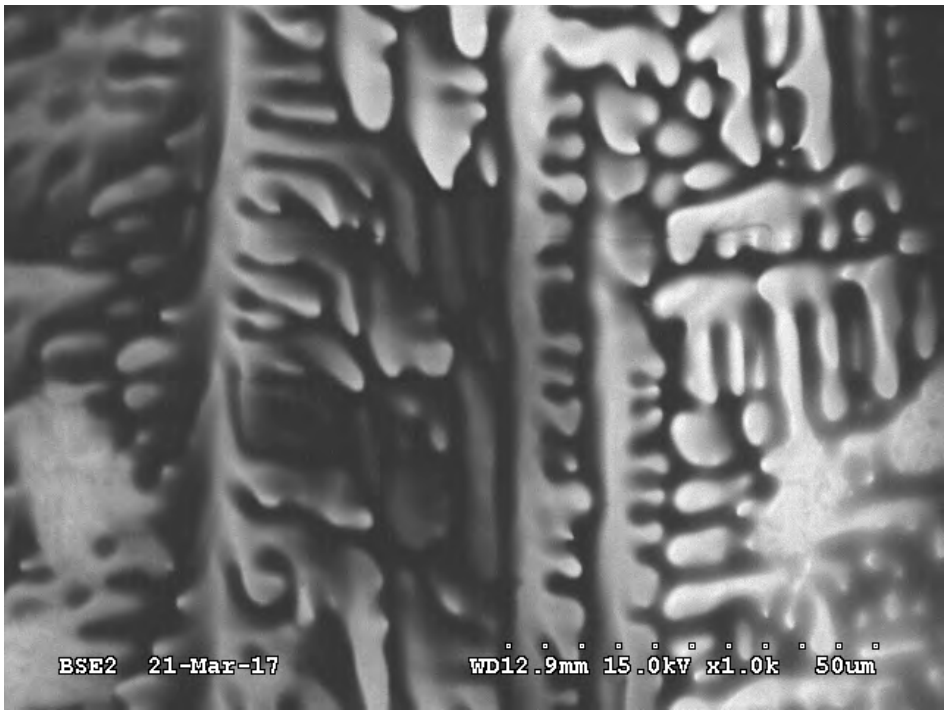


Figure 142: Higher magnification SEM image of coating on a SOT6 lead from board 2 with interdendritic solder spaces filled with coating and no whiskers 6,000 cycles , 1,000x (ref. B-SOT-PC-1-1-cc-2, SOT6).

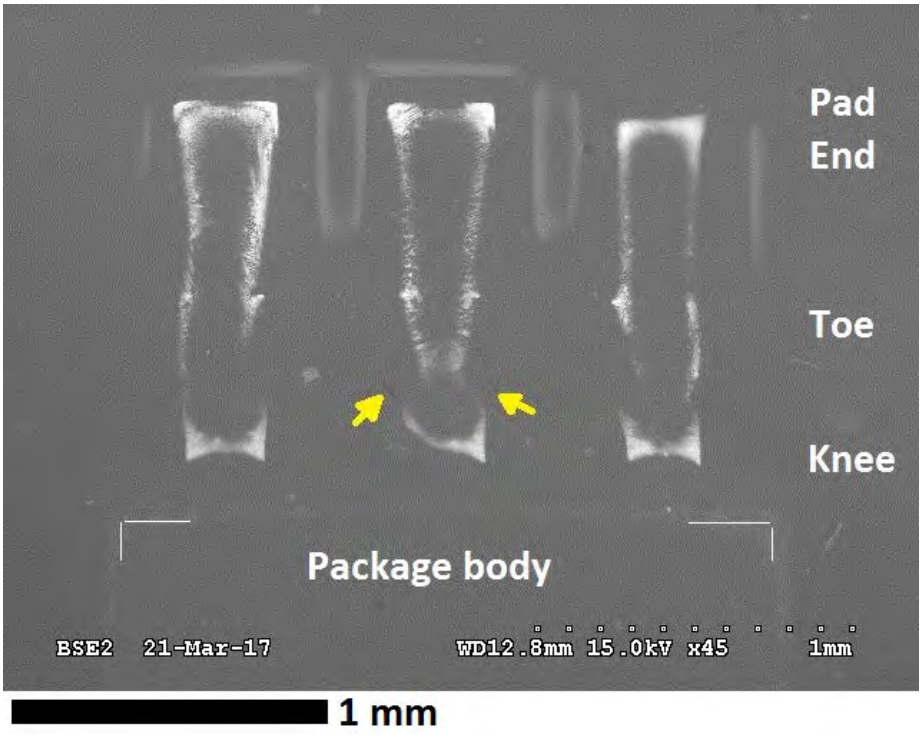


Figure 143: SEM image of coating on SOT6 leads from board 2 after 6,000 PCTC cycles, 45x (ref. B-SOT-PC-1-1-cc-2, SOT6). Arrows highlight coating cracks near the lead knee.

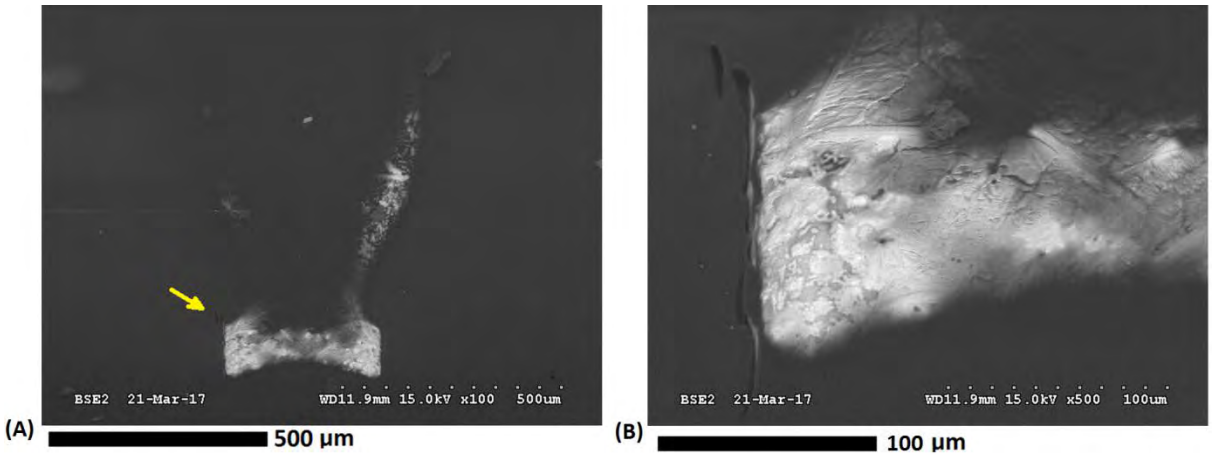


Figure 144: SEM image of coating on a SOT3 lead after 6,000 PCTC cycles; (A) 100x and (B) higher magnification image of cracks near the knee highlighted by arrow in A, 500x (ref. B-SOT-PC-1-1-cc-2, SOT3).

5. Conclusions for the 6,000 PCTC cycle test

The PCTC environment replicates the high temperature operation conditions where an electronic assembly is maintained at a high temperature and the power is turned on and off. The overall duration of the PCTC test was four years and one month. The evaluation consisted of four months of the original testing (1 to 1,797 cycles), then 36 months room temperature storage, followed by nine months of extended testing (1,798 to 6,000 cycles).

The whisker growth on the uncoated samples was almost entirely on the SOT3 and SOT6 SAC305 soldered alloy 42 lead tin and thin solder regions. In addition, to whisker growth, there was deformation induced tin growth and unique pad edge growth. The pad edge growths were thin sheet like layers of tin on the order of 10 microns long, 20 microns wide and a few microns thick protruding from the solder immediately above the printed circuit board copper pads.

The primary whisker stresses were from the coefficient of thermal expansion difference between the alloy 42 and the SAC305 solder tin. There was also sufficient cyclic stress to cause solder fatigue fractures that were not present at the 1,797 cycle inspection. The cyclic stresses caused recrystallization at the interfaces between the primary tin dendrites, then whisker nucleation and growth, followed by progressively increasing crack growth in the grain boundary area, until the cracks became so large that the whisker growth slowed or stopped altogether. It is hypothesized that the cyclic stress induced recrystallization observed here is similar to what was observed during ball grid array/chip scale package SAC305 thermal cycling [6].

No whiskers penetrated the coating regions thicker than approximately three microns. The solder areas with thin coating less than approximately three microns did have some whisker nucleation. In addition, some coating cracking was observed. The cracks were located along the lead near the lead knee where the coating fillets were thick. The cracks were sometimes accompanied by separation of the coating from the lead.

6. Literature cited

[1] S. Meschter and P. Snugovsky, SERDP WP1753 Final Report: Tin whisker testing and modeling, November 2015.

[2] J-STD-001, Requirements for Soldered Electrical and Electronic Assemblies, Joint JEDEC Solid State Technology Association/IPC Association Connecting Electronics Industries document, April 2010.

[3] P.T. Vianco, and J.A. Rejent, "Dynamic Recrystallization (DRX) as the Mechanism for Sn Whisker Development Part I: A Model", Journal of Electronic Materials, Volume 38, Number 9, pp. 1815-1825, September 2009.

[4] P.T. Vianco, and J.A. Rejent, Dynamic Recrystallization (DRX) as the Mechanism for Sn Whisker Development. Part II: Experimental Study, Journal of Electronic Materials, Volume 38, Number 9, pp 1826-1837, September 2009.

[5] P. Snugovsky, Flow Diagram for the Vianco and Rejent Dynamic Recrystallization (DRX) Mechanism for Tin Whisker Growth in the presentation Whisker formation on SAC305, Lead-free Solder Workshop at the 2014TMS Annual Meeting.

[6] P. Borgesen, I. Dutta, and E. Cotts, SERDP WP1752 Final Report: Microstructurally Adaptive Constitutive Relations and Reliability Assessment Protocols for Lead Free Solder, October 30, 2014.

[7] L. Yin, L. Wentlent, L. Yang, B. Arfaei, A. Qasaimeh, and P. Borgesen, "Recrystallization and Precipitate Coarsening in Pb-free Solder Joints during Thermo-mechanical Fatigue", J. Electronic Materials 41, Issue 2 (2012) pp. 241-252.

[8] J. Sundelin, S. Nurmi, and T. Lepistö, "Recrystallization behaviour of SnAgCu solder joints", Mater. Sci. Eng. A- Struct. 474, 201 (2008).

[9] T. Mattila and J. Kivilahti, "The Role of Recrystallization in the Failure of SnAgCu Solder Interconnections Under Thermomechanical Loading", IEEE Trans. Compon. Pack T., 33, 629 (2010).

[10] B. Zhou, T. R. Bieler, T-K. Lee, and K-C. Liu, "Crack Development in a Low-Stress PBGA Package due to Continuous Recrystallization Leading to Formation of Orientations with [001] Parallel to the Interface", Journal of Electronic Materials 39 (2010) 2669-2679.

[11] D. F. Susan, J. R. Michael, W. G. Yelton, B. B. McKenzie, R. P. Grant, J. Pillars, and M. A. Rodriguez, Understanding and Predicting Metallic Whisker Growth and its Effects on Reliability: LDRD Final Report, SANDIA REPORT SAND2012-0519 Sandia National Laboratories Albuquerque, New Mexico, January 2012 http://prod.sandia.gov/techlib/access-control.cgi/2012/120519.pdf .

[12] Per-Erik Tegehall and Andreas Lövberg, Review of the impact of microstructure of Pb-free solder joints on assessment of fatigue lives of the solder joints, Presentation at IPC-PERM Meeting #34, Andover, MA, November 7-9, 2017.